

Enclosure 3 to E-54806

NUHOMS[®] HD System UFSAR, Revision 7
(Public Version)

Non-Proprietary Version

**UPDATED FINAL SAFETY ANALYSIS REPORT
FOR THE
NUHOMS[®] HD
Horizontal Modular Storage System
For Irradiated Nuclear Fuel
Revision 7**

By
TN Americas LLC ⁽¹⁾
Columbia, MD

⁽¹⁾ TN Americas LLC, formerly Transnuclear, Inc. (herein referred to as AREVA TN, Transnuclear, Inc., Transnuclear, or TN)

REVISION LOG SHEET

FSAR Revision	Date	Record of Changes/FCNs
0	2/23/07	None
1	10/3/07	FCNs 721030-004 Rev. 0, 008 Rev. 1, 009 Rev. 1, 010 Rev. 1, 012 Rev. 1, 016 Rev. 1, 037 Rev. 0, 054 Rev. 0, 056 Rev. 0, 057 Rev. 0, 058 Rev. 2, 060 Rev. 1, 064 Rev. 1, 081 Rev. 1, 082 Rev. 0, 084 Rev. 0, 085 Rev. 0, 087 Rev. 0, 089 Rev. 1, 105 Rev. 0, 107 Rev. 0, 108 Rev. 1, 109 Rev. 0, 116 Rev. 0, 117 Rev. 0, 119 Rev. 0, 121 Rev. 0, 122 Rev. 0, 123 Rev. 0, 124 Rev. 0, 126 Rev. 1
2	10/02/09	FCNs 721030-124 R-1, 143 R-0, 162 R-0, 166 R-0, 168 R-0, 171 R-0, 186 R-0, 188 R-1, 189 R-2, 191 R-0, 217 R-0, 219 R-0, 223 R-0, 227 R-0, 231 R-0
3	9/30/11	FCNs 721030-203 R-0, 721030-234 R-0, 721030-244 R-0, 721030-252 R-0, 721030-256 R-0, R-1, and R-2, 721030-257 R-0, 721030-262 R-0, 721030-265 R-0, 721030-267 R-1, 721030-284 R-0, 721030-287 R-1, 721030-289 R-0, 721030-294 R-0, 721030-296 R-0, 721030-305 R-0, 721030-306 R-0, 721030-309 R-0
4	9/30/13	FCNs 721030-255 R-0, 721030-274 R-0, 721030-308 R-0, 721030-318 R-0, 721030-319 R-0, 721030-325 R-0, 721030-344 R-0, 721030-347 R-0
5	9/30/15	FCNs 721030-348 R-0, 721030-349 R-0, 721030-356 R-0, 721030-364 R-0, 721030-382 R-0, 721030-384 R-0, 721030-385 R-0
6	9/28/17	FCNs 721030-406 R-0, 407 R-1, 415 R-0, 424 R-0, 432 R-0, 433 R-0, 437 R-0, 442 R-0, 443 R-0, 444 R-1
7	9/30/19	FCNs 721030-447 R-0, 721030-455 R-0, 721030-458 R-0

TABLE OF CONTENTS

1.	GENERAL INFORMATION	1-1
1.1	Introduction	1-2
1.2	General Description of the NUHOMS® HD System	1-4
1.2.1	NUHOMS® HD System Characteristics	1-4
1.2.2	Operational Features	1-9
1.2.3	32PTH DSC Contents	1-14
1.3	Identification of Agents and Contractors	1-15
1.4	Generic Cask Arrays	1-16
1.5	Supplemental Data	1-17
1.5.1	References	1-17
1.5.2	Drawings	1-17
2.	PRINCIPAL DESIGN CRITERIA	2-1
2.1	Spent Fuel to be Stored	2-1
2.1.1	Detailed Payload Description	2-1
2.2	Design Criteria for Environmental Conditions and Natural Phenomena	2-6
2.2.1	Tornado and Wind Loadings	2-6
2.2.2	Water Level (Flood) Design	2-8
2.2.3	Seismic Design	2-9
2.2.4	Snow and Ice Loadings	2-9
2.2.5	Tsunami	2-9
2.2.6	Lightning	2-9
2.2.7	Combined Load Criteria	2-10
2.2.8	Burial under Debris	2-11
2.2.9	Thermal Conditions	2-11
2.3	Safety Protection Systems	2-13
2.3.1	General	2-13
2.3.2	Protection by Multiple Confinement Barriers and Systems	2-13
2.3.3	Protection by Equipment and Instrumentation Selection	2-15
2.3.4	Nuclear Criticality Safety	2-15
2.3.5	Radiological Protection	2-16
2.3.6	Fire and Explosion Protection	2-17
2.3.7	Acceptance Tests and Maintenance	2-18

2.4	Decommissioning Considerations.....	2-19
2.5	Structures, Systems and Components Important to Safety	2-20
2.5.1	Dry Shielded Canister	2-20
2.5.2	Horizontal Storage Module.....	2-20
2.5.3	ISFSI Basemat and Approach Slabs	2-21
2.5.4	Transfer Equipment	2-21
2.5.5	Auxiliary Equipment.....	2-21
2.6	References	2-22
3.	STRUCTURAL EVALUATION.....	3-1
3.1	Structural Design	3-1
3.1.1	Discussion	3-1
3.1.2	Design Criteria	3-12
3.2	Weights.....	3-15
3.2.1	32PTH DSC Weight	3-16
3.2.2	OS187H Transfer Cask Weight	3-17
3.2.3	HSM-H Weight.....	3-18
3.3	Mechanical Properties of Materials	3-19
3.3.1	32PTH-DSC Material Properties	3-19
3.3.2	HSM-H Material Properties.....	3-20
3.3.3	OS187H Transfer Cask Material Properties	3-21
3.4	General Standards for 32PTH DSC, HSM-H, and OS187H TC.....	3-22
3.4.1	Chemical and Galvanic Reactions	3-22
3.4.2	Positive Closure	3-27
3.4.3	Lifting Devices.....	3-28
3.4.4	Heat	3-28
3.4.5	Cold.....	3-28
3.5	Fuel Rods General Standards for 32PTH DSC.....	3-29
3.5.1	Fuel Rod Temperature Limits	3-29
3.5.2	Fuel Assembly Thermal and Irradiation Growth	3-29
3.5.3	Fuel Rod Integrity During Drop Scenario	3-31
3.5.4	Fuel Unloading.....	3-32
3.6	Normal Conditions of Storage and Transfer.....	3-33
3.6.1	32PTH DSC Normal Conditions Structural Analysis.....	3-33
3.6.2	HSM-H Normal Conditions Structural Analysis	3-37
3.6.3	OS187H Transfer Cask Normal Conditions Structural Analysis	3-38

3.7	Off Normal and Hypothetical Accident Conditions	3-41
3.7.1	32PTH DSC Off Normal and Accident Conditions Structural Analysis.....	3-41
3.7.2	HSM-H Off Normal and Accident Conditions Structural Analysis	3-47
3.7.3	OS187H Transfer Cask Off Normal and Accident Conditions Structural Analysis.....	3-48
3.8	References.....	3-52
3.9	Appendices.....	3-55
Appendix 3.9.1	32PTH DSC (Canister and Basket) Structural Analysis	
Appendix 3.9.2	OS187H Transfer Cask Body Structural Analysis	
Appendix 3.9.3	OS187H Transfer Cask Top Cover and RAM Access Cover Bolt Analyses	
Appendix 3.9.4	OS187H Transfer Cask Lead Slump and Inner Shell Buckling Analysis	
Appendix 3.9.5	OS187H Transfer Cask Trunnion Analysis	
Appendix 3.9.6	OS187H Transfer Cask Shield Panel Structural Analysis	
Appendix 3.9.7	OS187H Transfer Cask Impact Analysis	
Appendix 3.9.8	Damaged Fuel Cladding Structural Evaluation	
Appendix 3.9.9	HSM-H Structural Analysis	
Appendix 3.9.10	OS187H Transfer Cask Dynamic Impact Analysis	
Appendix 3.9.11	32PTH DSC Dynamic Amplification Factor (DAF) Calculation	
3.10	ASME Code Alternatives	3-56
4.	THERMAL EVALUATION.....	4-1
4.1	Discussion.....	4-1
4.2	Summary of Thermal Properties of Materials	4-3
4.3	Thermal Evaluation for Normal and Off-Normal Conditions	4-9
4.3.1	Thermal Models for Normal and Off-Normal Conditions.....	4-9
4.3.2	Maximum Temperatures for Normal and Off-Normal Conditions.....	4-20
4.3.3	Minimum Temperatures for Normal and Off-Normal Conditions	4-21
4.3.4	Maximum Internal Pressures for Normal and Off-Normal Conditions	4-21
4.3.5	Maximum Thermal Stresses for Normal and Off-Normal Conditions	4-21
4.3.6	Evaluation of Thermal Performance for Normal and Off-Normal Conditions	4-21
4.4	Thermal Evaluation for Accident Conditions	4-23
4.4.1	Thermal Models for Accident Conditions	4-23

4.4.2	Maximum Temperatures for Accident Conditions	4-28
4.4.3	Maximum Internal Pressures for Accident Conditions.....	4-29
4.4.4	Maximum Thermal Stresses for Accident Conditions.....	4-29
4.4.5	Evaluation of Thermal Performance for Accident Conditions	4-29
4.5	Thermal Evaluation for Loading and Unloading Conditions.....	4-30
4.5.1	Vacuum Drying.....	4-30
4.5.2	Reflooding.....	4-34
4.6	Maximum Internal Pressure.....	4-36
4.6.1	Average Gas Temperature	4-37
4.6.2	Amount of Initial Helium Backfill.....	4-38
4.6.3	Free Gas within Fuel Assemblies / BPRA.....	4-39
4.6.4	Total Amount of Gas within DSC	4-39
4.6.5	Maximum DSC Internal Pressures.....	4-40
4.6.6	Maximum Pressure in Annulus.....	4-40
4.7	Axial Decay Heat Profile	4-41
4.8	Effective Fuel Properties	4-44
4.8.1	Discussion	4-44
4.8.2	Summary of Material Properties.....	4-44
4.8.3	Effective Fuel Conductivity.....	4-46
4.8.4	Effective Fuel Density and Specific Heat.....	4-47
4.8.5	Conclusion	4-48
4.8.6	Effect of Irradiation on UO ₂ Thermal Conductivity	4-50
4.9	Effective Conductivity of Fluids in the Transfer Cask.....	4-53
4.9.1	Effective Conductivity in the Shielding Panel.....	4-53
4.9.2	Effective Water Conductivity in Annulus between TC and DSC.....	4-55
4.10	Justification of the Assumed Hot Gap Sizes	4-57
4.10.1	Radial Gap between Basket Rails and DSC shell.....	4-57
4.10.2	Radial Gap between Lead and the Cask Structural Shell	4-58
4.11	Heat Transfer Coefficients	4-60
4.11.1	Total heat Transfer Coefficient to Ambient.....	4-60
4.11.2	Free Convection Coefficients	4-60
4.12	Effective Conductivity of Air in Closed Cavity of HSM-H.....	4-68
4.13	Thermal-Hydraulic Equations for the HSM-H.....	4-69
4.14	Thermal Evaluation of DSC Containing Damaged Fuel.....	4-72
4.14.1	Normal / Off-Normal Conditions.....	4-72
4.14.2	Accident Conditions.....	4-72
4.14.3	Effective Properties of Damaged Fuel	4-74

4.14.4	Evaluation of DSC Thermal Performance with Damaged Fuel.....	4-75
4.15	References.....	4-77
4.16	Appendices.....	4-79
Appendix 4.16.1	Heat Transfer Coefficient Macros	
Appendix 4.16.2	Heat Generation Rate as a Function of Spent Fuel Parameters	
Appendix 4.16.3	Addition of CE 16x16 Fuel Assemblies	
Appendix 4.16.4	Effect of Change in Minimum Off-Normal Ambient Temperature to -21°F	
Appendix 4.16.5	Effect of Dose Reduction Hardware on Airflow Analysis for HSM-H	
5.	SHIELDING EVALUATION.....	5-1
5.1	Discussion and Results.....	5-3
5.2	Source Specification.....	5-5
5.2.1	Gamma Sources	5-8
5.2.2	Neutron Source	5-8
5.2.3	Fuel Qualification	5-9
5.3	Model Specification.....	5-14
5.3.1	Description of the Radial and Axial Shielding Configurations	5-14
5.3.2	Shield Regional Densities	5-15
5.4	Shielding Evaluation.....	5-17
5.4.1	Computer Programs	5-17
5.4.2	Spatial Source Distribution	5-17
5.4.3	Cross-Section Data.....	5-18
5.4.4	Flux-to-Dose-Rate Conversion	5-18
5.4.5	Model Geometry	5-18
5.4.6	Methodology	5-18
5.4.7	Assumptions.....	5-19
5.4.8	Normal Condition Models	5-20
5.4.9	Impact on Dose Rates from Gaps between HSM-Hs in the ISFSI	5-24
5.4.10	Impact on Dose Rates with the Addition of Dose Reduction Hardware (DRH).....	5-25
5.5	Supplemental Information	5-26
5.5.1	References.....	5-26
5.5.2	Sample Input Files	5-27

6.	CRITICALITY EVALUATION	6-1
6.1	Discussion and Results.....	6-2
6.2	Spent Fuel Loading	6-4
6.3	Model Specification.....	6-6
6.3.1	Description of Criticality Analysis Model	6-6
6.3.2	Package Regional Densities	6-8
6.4	Criticality Calculation	6-9
6.4.1	Calculational Method.....	6-9
6.4.2	Fuel Loading Optimization	6-14
6.4.3	Criticality Results.....	6-26
6.5	Critical Benchmark Experiments.....	6-28
6.5.1	Benchmark Experiments and Applicability	6-28
6.5.2	Results of the Benchmark Calculations	6-29
6.6	Supplemental Information	6-30
6.6.1	References.....	6-30
6.6.2	KENO Input Files	6-31
7.	CONFINEMENT	7-1
7.1	Confinement Boundary	7-1
7.1.1	Confinement Vessel	7-1
7.1.2	Confinement Penetrations	7-2
7.1.3	Seals and Welds	7-2
7.1.4	Closure	7-2
7.2	Requirements for Normal Conditions of Storage	7-3
7.2.1	Release of Radioactive Material	7-3
7.2.2	Pressurization of Confinement Vessel	7-3
7.3	Confinement Requirements for Hypothetical Accident Conditions	7-4
7.3.1	Fission Gas Products.....	7-4
7.3.2	Release of Contents.....	7-4
7.4	Supplemental Data.....	7-5
7.4.1	Confinement Monitoring Capability.....	7-5
7.4.2	References.....	7-5
8.	OPERATING PROCEDURES.....	8-1
8.1	Procedures for Loading the DSC and Transfer to the HSM-H.....	8-1
8.1.1	Narrative Description.....	8-1

8.2	Procedures for Unloading the DSC	8-10
8.2.1	DSC Retrieval from the HSM-H.....	8-10
8.2.2	Removal of Fuel from the DSC	8-11
8.3	Supplemental Information	8-14
8.3.1	Other Operating Systems	8-14
8.3.2	Operation Support System	8-14
8.3.3	Surveillance and Maintenance	8-14
8.4	References	8-15
9.	ACCEPTANCE TESTS AND MAINTENANCE PROGRAM.....	9-1
9.1	Acceptance Criteria	9-1
9.1.1	Visual Inspection and Non-Destructive Examination (NDE).....	9-1
9.1.2	Structural and Pressure Tests	9-1
9.1.3	Leak Tests	9-2
9.1.4	Components	9-3
9.1.5	Shielding Integrity	9-3
9.1.6	Thermal Acceptance	9-3
9.1.7	Neutron Absorber Tests	9-4
9.2	Maintenance Program	9-6
9.2.1	Inspection.....	9-6
9.2.2	Tests	9-7
9.2.3	Repair, Replacement, and Maintenance.....	9-8
9.3	Marking	9-8
9.4	Pre-Operational Testing and Training Exercise.....	9-8
9.5	Specification for Neutron Absorbers	9-9
9.5.1	Specification for Thermal Conductivity Testing of Neutron Absorbers	9-9
9.5.2	Specification for Acceptance Testing of Neutron Absorbers by Neutron Transmission.....	9-10
9.5.3	Specification for Qualification Testing of Metal Matrix Composites.....	9-12
9.5.4	Specification for Process Controls for Metal Matrix Composites.....	9-14
9.6	References	9-16
10.	RADIATION PROTECTION	10-1
10.1	Ensuring That Occupational Radiation Exposures Are As Low As Reasonably Achievable (ALARA).....	10-1
10.1.1	Policy Considerations	10-1

10.1.2	Design Considerations	10-1
10.1.3	Operational Considerations.....	10-3
10.2	Radiation Protection Design Features	10-4
10.2.1	NUHOMS® HD System Design Features.....	10-4
10.2.2	Offsite Dose Calculations	10-4
10.3	Estimated Onsite Collective Dose Assessment	10-8
10.3.1	DSC Loading, Transfer and Storage Operations	10-8
10.3.2	DSC Retrieval Operations.....	10-8
10.3.3	Fuel Unloading Operations	10-9
10.3.4	Maintenance Operations	10-9
10.3.5	Doses During ISFSI Array Expansion.....	10-9
10.4	References	10-10
11.	ACCIDENT ANALYSIS.....	11-1
11.1	Introduction.....	11-1
11.2	Off-Normal Operation.....	11-2
11.2.1	Off-Normal Transfer Load.....	11-3
11.2.2	Extreme Temperature.....	11-5
11.2.3	Radiological Impact from Off-Normal Operations.....	11-6
11.3	Postulated Accident	11-7
11.3.1	Cask Drop	11-8
11.3.2	Earthquake	11-10
11.3.3	Tornado Wind and Tornado Missiles Effect on HSM-H.....	11-11
11.3.4	Tornado Wind and Tornado Missiles Effect on Transfer Cask	11-18
11.3.5	Flood	11-25
11.3.6	Blockage of HSM-H Air Inlet and Outlet Openings	11-25
11.3.7	Lightning.....	11-26
11.3.8	Fire/Explosion.....	11-27
11.4	References	11-28
12.	OPERATING CONTROLS AND LIMITS.....	12-1
13.	QUALITY ASSURANCE	13-1
13.1	Introduction.....	13-2
13.2	“Important-to-Safety & “Safety Related” NUHOMS® HD System Components	13-3
13.3	Description of TN 10CFR 72, Subpart G QA Program	13-5
13.3.1	Project Organization	13-5

13.3.2	QA Program	13-5
13.3.3	Design Control	13-5
13.3.4	Procurement Document Control	13-6
13.3.5	Procedures, Instructions, and Drawings.....	13-6
13.3.6	Document Control.....	13-6
13.3.7	Control of Purchased Items and Services	13-6
13.3.8	Identification and Control of Materials, Parts, and Components.....	13-7
13.3.9	Control of Special Processes.....	13-7
13.3.10	Inspection	13-7
13.3.11	Test Control	13-7
13.3.12	Control of Measuring and Test Equipment	13-7
13.3.13	Handling, Storage and Shipping.....	13-7
13.3.14	Inspection and Test Status	13-8
13.3.15	Control of Nonconforming Items	13-8
13.3.16	Corrective Action	13-8
13.3.17	Records	13-8
13.3.18	Audits and Surveillances	13-8
13.4	Conditions of Approval Records	13-9
13.5	Supplemental Information	13-10
13.5.1	References.....	13-10
14.	DECOMMISSIONING	14-1
14.1	Decommissioning Considerations.....	14-1
14.2	Supplemental Information	14-4
14.2.1	References.....	14-4

APPENDIX A 32PTH TYPE 1 DSC AND OS187H TYPE 1 TC

APPENDIX B 32PTH TYPE 2 DSC AND OS187H TYPE 2 TC

CHAPTER 1
GENERAL INFORMATION

TABLE OF CONTENTS

1. GENERAL INFORMATION	1-1
1.1 Introduction.....	1-2
1.2 General Description of the NUHOMS® HD System	1-4
1.2.1 NUHOMS® HD System Characteristics	1-4
1.2.2 Operational Features	1-8
1.2.3 32PTH DSC Contents	1-12
1.3 Identification of Agents and Contractors	1-13
1.4 Generic Cask Arrays	1-14
1.5 Supplemental Data.....	1-15
1.5.1 References	1-15
1.5.2 Drawings	1-15

LIST OF TABLES

Table 1-1	Key Design Parameters of the NUHOMS® HD System Components	1-16
Table 1-2	Known Fabricated NUHOMS® Transfer Casks Licensed for Use Under CoC 1030.....	1-17

LIST OF FIGURES

Figure 1-1	NUHOMS® HD System Horizontal Storage Module (HSM-H).....	1-18
Figure 1-2	NUHOMS® HD 32PTH DSC.....	1-19
Figure 1-3	NUHOMS® HD System Components, Structures, and Transfer Equipment – Elevation View (Typical)	1-20
Figure 1-4	NUHOMS® HD System Components, Structures, and Transfer Equipment – Plan View (Typical).....	1-21
Figure 1-5	DELETED	1-22
Figure 1-6	OS187H On-Site Transfer Cask	1-23
Figure 1-7	Transport Trailer for OS187H Transfer Cask (Typical).....	1-24
Figure 1-8	Cask Support Skid for OS187H Transfer Cask (Typical)	1-25
Figure 1-9	Typical Double Module Row HSM-H ISFSI Layout.....	1-26
Figure 1-10	Typical Single Module Row HSM-H ISFSI Layout	1-27
Figure 1-11	Typical Combined Single and Double Module Row HSM-H ISFSI Layout	1-28

1. GENERAL INFORMATION

This Safety Analysis Report (SAR) describes the design and forms the licensing basis for 10CFR 72[1], Subpart L certification of the NUHOMS[®] HD dry spent fuel storage system. The NUHOMS[®] HD System provides for the horizontal storage of high burnup spent Pressurized Water Reactor (PWR) fuel assemblies in a dry shielded canister (DSC) that is placed in a Horizontal Storage Module (HSM-H) utilizing an OS187H transfer cask (TC). The NUHOMS[®] HD System is designed to be installed in an Independent Spent Fuel Storage Installation (ISFSI) at power reactor sites under the provision of a general license in accordance with 10CFR 72, Subpart K. This system has been specifically optimized for high thermal loads, limited space, and needs for superior radiation shielding performance.

The QA program applicable to this design satisfies the requirements of 10CFR 72, Subpart G and is described in Chapter 13. The format of this SAR follows the guidance of NRC Regulatory Guide 3.61[2]. To facilitate NRC review of this application, this SAR has been prepared in compliance with the information and methods defined in NUREG-1536 [3], “Standard Review Plan for Dry Cask Storage Systems” and the associated Interim Staff Guidance (ISGs).

The NUHOMS[®] HD System is an improved version of the Standardized NUHOMS[®] System described in Certificate of Compliance (C of C) 72-1004 [4]. The 32PTH DSC included in this application is similar to the 24PTH DSC previously included in the license for the Standardized NUHOMS[®] System [5]. The HSM-H is virtually identical to the HSM-H in the 24PTH amendment. The OS187H TC is very similar to the previously licensed OS197 TC but with a slightly larger diameter and closures containing seals.

The NUHOMS[®] HD System has been designed for enhanced heat rejection capabilities, and to permit storage of Control Components (CCs) with the fuel and/or damaged spent fuel assemblies. Protection afforded to the public is equivalent to or has been increased relative to standardized HSM designs [5] by substantially reducing radiation dose rates. Details of the system design, analyses, operation, and margins are provided in the remainder of this SAR.

The NUHOMS[®] HD system also includes two longer length DSCs and corresponding TCs, designated the 32PTH Type 1 DSC and OS187H Type 1 TC and 32PTH Type 2 DSC and OS187H Type 2 TC, respectively. A detailed description of the 32PTH Type 2 DSC and OS187H Type 2 TC is provided in Appendix B. A detailed description of the 32PTH Type 1 DSC and OS187H Type 1 TC are provided in Appendix A. The 32PTH Type 1 DSC and 32PTH Type 2 DSC are stored in an HSM-H with a slightly increased support rail length and optional bolted spacer. The design details of these additional HD system components are provided in the drawings shown in Section A.1.5 and Section B.1.5.

1.1 Introduction

The type of fuel to be stored in the NUHOMS[®] HD System is Light Water Reactor (LWR) fuel of the PWR type. The NUHOMS[®] HD System accommodates up to 32 PWR fuel assemblies with zircaloy, (zirlo, M5) cladding, uranium dioxide (UO₂), and CCs. Provisions have been made, as discussed in Chapter 2, for storage of up to sixteen damaged fuel assemblies in the 32PTH DSC. The physical and radiological characteristics of these payloads are provided in Chapter 2.

The NUHOMS[®] HD System consists of the following components as shown in Figure 1-1, Figure 1-2, and Figure 1-6:

- A Horizontal Storage Module (HSM-H) that provides spent fuel decay heat removal, physical and radiological protection for the 32PTH DSC. The HSM-H consists primarily of thick concrete walls, a steel support structure for the 32PTH DSC, and a thick concrete door. Each HSM-H includes provisions for thermal monitoring instrumentation. The HSM-H is virtually identical to the HSM-H for the NUHOMS[®] 24PTH DSC included in UFSAR Revision 9 [5].
- A Dry Shielded Canister (32PTH DSC) that provides confinement, an inert environment, structural support, and criticality control for 32 PWR fuel assemblies. The 32PTH DSC shell is a welded stainless steel pressure vessel that includes thick shield plugs at either end to maintain occupational exposures ALARA. The 32PTH DSC basket consists of stainless steel square tubes and support strips for structural support, and geometry control; and aluminum/borated aluminum for heat transfer and criticality control. The 32PTH DSC is very similar to the 24PTH DSC.
- The OS187H TC provides shielding and protection from potential hazards during the DSC closure operations and transfer to the HSM-H. It also provides a helium environment around the DSC during transfer operations. It is very similar to the previously licensed OS197 transfer cask for the Standardized NUHOMS[®] System.
- HSM-Hs are arranged in arrays to minimize space and maximize self-shielding. The 32PTH DSC is longitudinally restrained to prevent movement during seismic events. Arrays are fully expandable to permit modular expansion in support of operating power plants.
- The HSM-H provides the bulk of the radiation shielding for the 32PTH DSC. The HSM-Hs can be arranged in either a single-row or a back-to-back arrangement. Thick concrete supplemental shield walls are used at either end of an HSM-H array and along the back wall of single-row arrays to minimize radiation dose rates both onsite and offsite.

Approval of the NUHOMS[®] HD System components described above is sought under the provisions of 10CFR 72, Subpart L for use under the general license provisions of 10CFR 72, Subpart K. The components are intended for storage on a reinforced concrete pad at a nuclear power plant. In addition to these components, the system requires use of an onsite transfer cask,

transfer trailer, and other auxiliary equipment that is described in this SAR. Similar equipment was previously licensed under C of C 72-1004 [5]. Sufficient information for the transfer system and auxiliary equipment is included in this SAR to demonstrate that means for safe operation of the system are provided.

1.2 General Description of the NUHOMS[®] HD System

The NUHOMS[®] HD System provides for the horizontal, dry storage of canisterized Spent Fuel Assemblies (SFAs) in a concrete HSM-H. The storage system components consist of a reinforced concrete HSM-H and a stainless steel 32PTH DSC confinement vessel which holds the SFAs. The general arrangement of the NUHOMS[®] HD System components is shown in Figure 1-3 and Figure 1-4. The confinement boundary is defined in Section 7.1 of Chapter 7 and is shown in Figure 7-1. This SAR addresses the design and analysis of the storage system components, including the 32PTH DSC, the OS187H TC, and the HSM-H, which are important to safety in accordance with 10CFR 72.

In addition to these storage system components, the NUHOMS[®] HD System also utilizes transfer equipment to move the 32PTH DSCs from the plant's fuel/reactor building, where they are loaded with SFAs and readied for storage, to the HSM-Hs where they are stored. This transfer system consists of a transfer cask, a lifting yoke, a hydraulic ram system, a prime mover for towing, a transfer trailer, a cask support skid, and a skid positioning system. This transfer system interfaces with the existing plant fuel pool, the cask handling crane, the site infrastructure (i.e. roadways and topography) and other site specific conditions and procedural requirements. Auxiliary equipment such as a cask/canister annulus seal, a vacuum drying system and a welding system are also used to facilitate canister loading, draining, drying, inerting, and sealing operations. Similar transfer system and auxiliary equipment have been previously licensed under C of C 72-1004 [5].

During dry storage of the spent fuel, no active systems are required for the removal and dissipation of the decay heat from the fuel. The NUHOMS[®] HD System is designed to transfer the decay heat from the fuel to the canister and from the canister to the surrounding air by conduction, radiation and natural convection.

Each canister is identified by a Model Number, XXX-32PTH-YYY-Z, where XXX typically identifies the site for which the 32PTH DSC was fabricated, Z designates the basket type, and YYY is a sequential number corresponding to a specific canister. The basket types are described in SAR drawing no. 10494-72-10.

The NUHOMS[®] HD System components do not include receptacles, valves, sampling ports, impact limiters, protrusions, or pressure relief systems.

The alternate DSC design and the alternate TC design, designated the 32PTH Type 1 DSC and the OS187H Type 1 TC, respectively, as well as the modifications required for the HSM-H to accommodate the 32PTH Type 1 DSC, are discussed in detail in Appendix A. The alternate DSC design and the alternate TC designated the 32PTH Type 2 DSC and OS187H Type 2 TC, respectively, as well as modifications required for the HSM-H to accommodate the 32PTH Type 2 DSC, are discussed in detail in Appendix B.

1.2.1 NUHOMS[®] HD System Characteristics

1.2.1.1 Dry Shielded Canister (32PTH DSC)

The key design parameters of the 32PTH DSC are listed in Table 1-1. The cylindrical shell, the inner top cover/shield plug¹ (including vent and siphon cover plates), and shell bottom form the

¹ See Chapter 1 drawings for option 2 and option 3 designs and Chapter 7 for confinement boundary definitions.

pressure retaining confinement boundary for the spent fuel. The inner top cover/shield plug¹ and shell bottom provide shielding for the 32PTH DSC so that occupational doses at the ends are minimized during drying, sealing, handling, and transfer operations.

The cylindrical shell and inner bottom cover plate confinement boundary welds are fully compliant to Subsection NB of the ASME Code and are made during fabrication. The confinement boundary weld between the shell and the inner top cover/shield plug¹ (including siphon/vent cover welds) and structural attachment weld between the shell and the outer top cover plate are in accordance with Alternatives to the ASME code as described in Section 3.10.

Both siphon and vent covers are welded after drying operations are complete. There are no credible accidents that could breach the confinement boundary of the 32PTH DSC as documented in Chapters 3 and 11.

The 32PTH DSC is designed for a maximum heat load of 34.8 kW. The internal basket assembly contains a storage position for each fuel assembly. The criticality analysis credits the fixed borated neutron absorbing material placed between the fuel assemblies. The analysis takes credit for soluble boron during loading operations. Sub-criticality during wet loading, drying, sealing, transfer, and storage operations is maintained through the geometric separation of the fuel assemblies by the basket assembly, the boron loading of the pool water, and the neutron absorbing capability of the 32PTH DSC materials, as applicable. Based on poison material and boron loading, several basket types are provided, as shown on drawing 10494-72-10 and described in Chapter 6.

Structural support for the PWR fuel is provided by the basket fuel compartments and support strips. The support strips are located periodically over the full length of the basket with allowance provided for thermal growth. Stainless steel transition rails are provided at the basket periphery for support and heat transfer.

Dimensions of the 32PTH DSC components described in the text and provided in figures and tables of this SAR are nominal dimensions for general system description purposes. Actual design dimensions are contained in the drawings in Section 1.5.2 of this SAR. For a discussion of the contents authorized to be stored in this DSC, see Section 2.1.1 of this SAR.

1.2.1.2 Horizontal Storage Module (HSM-H)

Each HSM-H provides a self-contained modular structure for storage of spent fuel canisterized in a 32PTH DSC. The HSM-H is constructed from reinforced concrete and structural steel. The thick concrete roof and walls provide substantial neutron and gamma shielding. Contact doses for the HSM-H are designed to be ALARA. The key design parameters of the HSM-H are listed in Table 1-1.

The nominal thickness of the HSM-H roof is four feet for biological shielding. Separate shield walls at the end of a module row in conjunction with the module wall, provide a minimum thickness of four feet for shielding. Similarly, an additional shield wall is used at the rear of the module if the ISFSI is configured as single module arrays. Sufficient shielding is provided by

¹ See Chapter 1 drawings for option 2 and option 3 designs and Chapter 7 for confinement boundary definitions.

thick concrete side walls between HSM-Hs in an array to minimize doses in adjacent HSMs during loading and retrieval operations.

An array of pipes are provided in the front inlets and at the side inlets and outlets of the HSM-H module. In addition, the roof vent caps are lined with steel plates. These features are optional and assist in a reduction of the HSM-H dose rates. The fabrication details of the dose reduction hardware are shown on drawing 10494-72-120, included in Section 1.5.2.

The HSM-Hs provide an independent, passive system with substantial structural capacity to ensure the safe dry storage of SFAs. To this end, the HSM-Hs are designed to ensure that normal transfer operations and postulated accidents or natural phenomena do not impair the 32PTH DSC or pose a hazard to the public or plant personnel.

The HSM-H provides a means of removing spent fuel decay heat by a combination of radiation, conduction and convection. Ambient air enters the HSM-H through ventilation inlet openings located on both sides of the lower front wall of the HSM-H and circulates around the 32PTH DSC and the heat shields. Air exits through air outlet openings located on each side of the top of the HSM-H. The HSM-H is designed to remove up to 34.8 kW of decay heat from the 32PTH DSC.

Decay heat is rejected from the 32PTH DSC to the HSM-H air space by convection and then removed from the HSM-H by natural circulation air flow. Heat is also radiated from the 32PTH DSC surface to the heat shields and HSM-H walls where the natural convection air flow and conduction through the walls aids in the removal of the decay heat. The passive cooling system for the HSM-H is designed to assure that SFA peak cladding temperatures during long term storage remain below acceptable limits to ensure fuel cladding integrity.

The HSM-Hs are installed on a load bearing foundation which consists of a reinforced concrete basemat on a subgrade suitable to support the loads. The HSM-Hs are not tied to the basemat.

Dimensions of the HSM-H components described in the text and provided in figures and tables of this SAR are nominal dimensions for general system description purposes. Actual design dimensions are contained in the drawings in Section 1.5.2 of this SAR.

1.2.1.3 Transfer Systems

1.2.1.3.1 OS187H On-Site Transfer Cask

The OS187H transfer cask (TC) used in the NUHOMS® HD System provides shielding and protection from potential hazards during 32PTH DSC loading and closure operations and transfer to the HSM-H. The key design parameters of the TC are listed in Table 1-1. The TC included in this SAR is the NUHOMS® cask which is limited to on-site use under 10CFR 72. The OS187H transfer cask is very similar to the OS197 and OS197H transfer casks described in the FSAR for the Standard NUHOMS® Storage System [5]. An alternate TC design, designated the OS187H Type 1 TC, is discussed in detail in Appendix A. An alternate TC design, designated the OS187H Type 2 TC, is discussed in detail in Appendix B.

The OS187H TC has a 186.6 inch cavity length, a 70.5 inch inside diameter and a payload capacity of 121,000 pounds (wet) and 109,000 pounds (dry). The TC is designed to meet the requirements of 10CFR72 for on-site transfer of the DSC from the plant's fuel pool to the

HSM-H. As shown in Figure 1-6, the TC is constructed from two concentric stainless steel shells with a bolted and gasketed top cover plate and a welded bottom end assembly. The TC also includes an outer steel jacket which is filled with water to provide neutron shielding. The top and bottom end assemblies also incorporate a solid neutron shield material.

The TC is designed to provide sufficient shielding to ensure dose rates are ALARA. Two top lifting trunnions are provided for handling the TC using a lifting yoke and overhead crane. Lower trunnions are provided for rotating the cask from/to the vertical and horizontal positions on the support skid/transport trailer. A gasketed cover plate is provided to seal the bottom hydraulic ram access penetration of the cask during loading. The TC lid is also provided with gaskets so that a helium environment can be maintained during DSC transfer operations.

Table 1-2 provides a listing of known fabricated NUHOMS® transfer casks that have design compatibility with the TC design basis models indicated on the table.

1.2.1.3.2 Transfer Equipment

Transfer Trailer: The typical transfer trailer for the NUHOMS® HD System consists of a heavy industrial trailer used to transfer the empty cask, support skid and the loaded transfer cask between the plant's fuel/reactor building and the ISFSI. The trailer is designed to ride as low to the ground as possible to minimize the overall HSM-H height and the transfer cask height during 32PTH DSC transfer operations. The trailer is equipped with four hydraulic leveling jacks to provide vertical alignment of the cask with the HSM-H. The trailer is towed by a conventional heavy haul truck tractor or other suitable prime mover. Figure 1-7 shows the typical trailer.

Cask Support Skid: The cask support skid for the NUHOMS® HD System is shown in Figure 1-8 and is essentially the same as described in the FSAR [5] for the standard NUHOMS® System. Key design features include:

The skid is mounted on a surface with sliding support bearings and hydraulic positioners to provide alignment of the cask with the HSM-H. Brackets with locking bolts are provided to prevent movement during trailer towing.

The hydraulic ram may be mounted on the skid or, as an option, the ram can be set-up using a frame structure bolted to the cask bottom and a rear support tripod.

The cask support skid is mounted on a low profile heavy haul industrial trailer.

The plant's fuel/reactor building crane or other suitable lifting device is used to lower the cask onto the support skid which is secured to the transfer trailer. Specific details of this operation and the fuel/reactor building arrangement are covered by the provisions of the plant's 10CFR 50 operating license.

Hydraulic Ram: The hydraulic ram system consists of a hydraulic cylinder with a capacity and a reach sufficient for 32PTH DSC insertion into and retrieval from the HSM-H. The design of the ram support system provides a direct load path for the hydraulic ram reaction forces during 32PTH DSC insertion and retrieval. The system uses a rear ram support for alignment of the ram

to the 32PTH DSC, and trunnions as the front support. The design provides positive alignment of the major components during 32PTH DSC insertion and retrieval.

1.2.2 Operational Features

This section provides a discussion of the sequence of operations involving the NUHOMS[®] HD System components.

1.2.2.1 Dry Run Operations

A dry run utilizing a 32PTH DSC loaded with mock-up fuel assemblies will be performed prior to loading the first canister by each licensee to demonstrate the adequacy of training, familiarity of system components and operational procedures. Mock-up fuel assemblies shall provide a representation of the maximum fuel assembly cross sectional envelope and provide a reasonable approximation of fuel assembly length and weight. The licensee shall determine the quantity of mock-up fuel assemblies required for the dry run to demonstrate that the loading and unloading processes are sound and the operations personnel are adequately trained.

The loading and unloading operations which have an impact on safety will be verified and recorded according to the requirements detailed in Chapter 8. The operations include loading and identifying fuel assemblies, ensuring the fuel assemblies meet the fuel acceptance criteria, drying, backfilling and pressurizing the canister, gas sampling and transferring the loaded canister to the HSM-H. Additionally, the ability to weld the top cover plates and open a sealed canister shall be demonstrated.

1.2.2.2 SFA Loading Operations

The primary operations (in sequence of occurrence) for the NUHOMS[®] HD System are:

1. Transfer Cask Preparation
2. 32PTH DSC Preparation
3. Place 32PTH DSC in Transfer Cask
4. Fill Transfer Cask/32PTH DSC Annulus with Clean Water and Seal
5. Fill 32PTH DSC Cavity with Fuel Pool Water (may be accomplished in step 6)
6. Lift Transfer Cask and Place in Fuel Pool
7. Spent Fuel Loading
8. Top Shield Plug Placement
9. Lifting Transfer Cask from Pool (DSC water may be drained and replaced with helium during draindown)
10. Inner Top Cover/Top Shield Plug Assembly Sealing
11. Vacuum Drying and Backfilling
12. Pressure Test

13. Leak Test
14. Outer Top Cover Plate Sealing
15. Transfer Cask/32PTH DSC Annulus Draining and Transfer Cask Top Cover Plate Placement
16. Backfill Transfer Cask Cavity with Helium
17. Place Loaded Transfer Cask on Transfer Skid/Trailer
18. Move Loaded Transfer Cask to HSM-H
19. Transfer Cask/HSM-H Preparation and Alignment
20. Insertion of 32PTH DSC into HSM-H
21. HSM-H Closure

These operations are described in the following paragraphs. The descriptions are intended to be generic and are described in greater detail in Chapter 8. Plant specific requirements may affect these operations and are to be addressed by the licensee.

Transfer Cask Preparation: Transfer cask preparation includes exterior washdown and interior decontamination. These operations are performed on the decontamination pad/pit outside the fuel pool area. The operations are similar to those for a shipping cask which are performed by plant personnel using existing procedures.

32PTH DSC Preparation: The internals and externals of the 32PTH DSC are inspected and cleaned if necessary. This ensures that the 32PTH DSC will meet plant cleanliness requirements for placement in the spent fuel pool.

Place 32PTH DSC in Transfer Cask: The empty 32PTH DSC is inserted into the transfer cask.

Fill Transfer Cask/32PTH DSC Annulus with Water and Seal: The transfer cask/32PTH DSC annulus is filled with uncontaminated water and is then sealed prior to placement in the pool. This prevents contamination of the 32PTH DSC outer surface and the transfer cask inner surface by the pool water.

Fill 32PTH DSC Cavity with Water: The 32PTH DSC cavity is filled with pool water to prevent an in-rush of water as the transfer cask is lowered into the pool.

Lift Transfer Cask and Place in Fuel Pool: The transfer cask, with the water-filled 32PTH DSC inside, is then lowered into the fuel pool. The transfer cask liquid neutron shield, if provided, may be left unfilled to meet hook weight limitations.

Spent Fuel Loading: Spent fuel assemblies are placed into the 32PTH DSC. This operation is identical to that presently used at plants for shipping cask loading.

Inner Top Cover/Shield Plug Placement: This operation consists of placing the inner top cover/shield plug into the 32PTH DSC using the plant's crane or other suitable lifting device.

Lifting Transfer Cask from Pool: The loaded transfer cask is lifted out of the pool and placed (in the vertical position) on the drying pad in the decontamination pit. This operation is similar to that used for shipping cask handling operations.

Inner Top Cover/Shield Plug¹ Sealing: The water contained in the space above the inner top cover plate/shield plug¹ is drained. The inner top cover plate/shield plug¹ is welded to the shell. This weld provides the top (confinement) seal for the 32PTH DSC.

Vacuum Drying and Backfilling: The initial blowdown of the 32PTH DSC is accomplished by pressurizing the vent port with helium. The water in the cavity is forced out of the siphon tube and routed back to the fuel pool or to the plant's liquid radwaste processing system via appropriate size flexible hose or pipe, as appropriate. The cavity water may also be removed by pumping out the water using the siphon port/tube and replaced by helium. The 32PTH DSC is then evacuated to remove the residual liquid water and water vapor, and helium in the cavity. When the system pressure has stabilized, the 32PTH DSC is backfilled with helium.

Pressure Test: Perform a pressure test of inner top cover/shield plug¹ weld by backfilling the DSC cavity with helium.

After the pressure test, remove the helium lines then the vent and siphon cover plates are installed and welded to the inner top cover/shield plug¹.

Leak Test: Perform a leak test of the inner top cover/shield plug¹ to the DSC shell weld and siphon/vent cover welds using a temporary test head or any other alternative means.

Outer Top Cover Plate Sealing: After helium backfilling, the 32PTH DSC outer top cover plate is installed by using a partial penetration weld between the outer top cover plate and the DSC shell.

The outer cover plate to shell weld and inner top cover plate/shield plug¹ weld provide redundant seals at the upper end of the 32PTH DSC.

Transfer Cask/32PTH DSC Annulus Draining and Transfer Cask Top Cover Plate Placement: The transfer cask/32PTH DSC annulus is drained. A swipe is then taken over the 32PTH DSC exterior at the top cover plate and the upper portion of the shell. Demineralized water is flushed through the transfer cask/32PTH DSC annulus, as required, to remove any contamination left on the 32PTH DSC exterior. The transfer cask top cover plate is installed, using the plant's crane or other suitable lifting device, and bolted closed.

Backfill Transfer Cask Cavity with Helium: The TC cavity is evacuated and the cavity/annulus is backfilled to a positive pressure with helium.

Place Loaded Transfer Cask on Transfer Skid/Trailer: The transfer cask is lifted onto the transfer cask support skid and downended onto the transfer trailer from the vertical to horizontal position. Trunnions must be seated completely onto the trunnion bearings. The trunnion closure plates are then installed (optional).

¹ See Chapter 1 drawings for option 2 and option 3 designs and Chapter 7 for confinement boundary definitions.

Move Loaded Transfer Cask to HSM: The transfer trailer is towed to the ISFSI along a predetermined route on a prepared road surface. Upon entering the ISFSI the cask is positioned and aligned with the designated HSM-H into which the 32PTH DSC is to be transferred.

Transfer Cask/HSM Preparation and Alignment: At the ISFSI with the cask positioned in front of the HSM-H, the transfer cask top cover plate is removed. The HSM-H door is removed and the transfer trailer is then backed into close proximity with the HSM-H. The skid positioning system is then used for the final alignment and docking of the transfer cask with the HSM-H and the cask restraint installed.

Insertion of 32PTH DSC into HSM: After final alignment of the transfer cask, HSM-H, and hydraulic ram, the 32PTH DSC is pushed into the HSM-H by the hydraulic ram.

HSM Closure: Install 32PTH DSC axial retainer and install HSM-H door.

1.2.2.3 Identification of Subjects for Safety and Reliability Analysis

1.2.2.3.1 Criticality Prevention

Criticality is controlled by utilizing the fixed borated neutron absorbing material in the 32PTH DSC basket and the pool water boron loading. During storage, with the cavity dry and sealed from the environment, criticality control measures within the installation are not necessary because water cannot enter the canister during storage.

1.2.2.3.2 Chemical Safety

There are no chemical safety hazards associated with operations of the NUHOMS[®] HD System. The coating materials used in the design of the 32PTH DSC are chosen to minimize hydrogen generation. Hydrogen monitoring is required during sealing operations to ensure hydrogen concentration levels remain within acceptable limits.

1.2.2.3.3 Operation Shutdown Modes

The NUHOMS[®] HD System is a totally passive system so that consideration of operation shutdown modes is unnecessary.

1.2.2.3.4 Instrumentation

The NUHOMS[®] HD System is a totally passive system. No safety-related instrumentation is necessary. The maximum temperatures and pressures are conservatively bounded by analyses. Therefore, there is no need for monitoring the internal cavity of the 32PTH DSC for pressure or temperature during normal operations. The 32PTH DSC is conservatively designed to perform its confinement function during all worst case normal, off-normal, and accident conditions.

1.2.2.3.5 Maintenance and Surveillance

All maintenance and surveillance tasks are described in Chapter 9.

1.2.3 32PTH DSC Contents

The 32PTH DSC is designed to store up to 32 intact PWR Westinghouse 15x15 (WE 15x15), Westinghouse 17x17 (WE 17x17) Combustion Engineering 14x14 (CE 14x14) and Combustion Engineering 16x16 (CE 16x16) class fuel assemblies. The 32PTH DSC is designed to store up to 32 Control Components (CCs). Authorized CCs include Burnable Poison Rod Assemblies (BPRAs), Thimble Plug Assemblies (TPAs), Control Rod Assemblies (CRAs), Control Element Assemblies (CEAs), Rod Cluster Control Assemblies (RCCAs), Axial Power Shaping Rod Assemblies (APSRAs), Orifice Rod Assemblies (ORAs), Vibration Suppression Inserts (VSIs), Neutron Source Assemblies (NSAs) and neutron sources. Non-fuel hardware that is positioned within the fuel assembly after the fuel assembly is discharged from the core such as Guide Tubes or Instrument Tube Tie Rods or Anchors, Guide Tube Inserts, BPRA Spacer Plates or devices that are positioned and operated within the fuel assembly during reactor operation such as those listed above are also considered as CCs.

Reconstituted assemblies containing up to 10 replacement irradiated stainless steel rods per assembly or an unlimited number of lower enrichment UO₂ rods, or Zr rods (or Zr pellets), or unirradiated stainless steel rods are acceptable for storage in 32PTH DSC as intact fuel assemblies with a slightly longer cooling time than that required for a standard assembly. The maximum number of reconstituted fuel assemblies with irradiated stainless steel rods per DSC is 4, and 32 for all other reconstituted fuel assemblies.

The 32PTH DSC is also designed for storage of up to 16 damaged fuel assemblies, and remaining intact assemblies, utilizing top and bottom end caps. A description of the fuel assemblies including the damaged fuel assemblies is provided in Chapter 2.

The 32PTH DSC is qualified for storage of WE 15x15 and WE 17x17 fuel assemblies containing Instrument Tube Tie Rods (ITTRs) as described in Chapter 2.

The maximum allowable assembly average initial enrichment of the fuel to be stored is 5.00 weight % U-235 and the maximum assembly average burnup is 60,000 MWd/MTU. The fuel must be cooled at least 5 years prior to storage.

The criticality control features of the NUHOMS[®] HD System are designed to maintain the neutron multiplication factor k-effective (including uncertainties and calculational bias) at less than 0.95 under normal, off-normal, and accident conditions.

The quantity and type of radionuclides in the SFAs are described and tabulated in Chapter 5. Chapter 6 covers the criticality safety of the NUHOMS[®] HD System and its parameters. These parameters include rod pitch, rod outside diameter, material densities, moderator ratios, and geometric configurations. The maximum pressure buildup in the 32PTH DSC cavity is addressed in Chapter 4.

1.3 Identification of Agents and Contractors

The prime contractor for design and procurement of the NUHOMS[®] HD System components is Transnuclear, Inc. (TN). TN will subcontract the fabrication, testing, on-site construction, and QA services as necessary to qualified firms on a project specific basis in accordance with TN QA program requirements.

The design activities for the NUHOMS[®] HD Safety Analysis Report were performed by TN and subcontractors in accordance with TN QA program requirements. TN is responsible for the design and analysis of the 32PTH DSC, the HSM-H, the on-site TC, and the associated transfer equipment.

Closure activities associated with welding the top cover plates on the 32PTH DSC following fuel loading are typically performed by the licensee under the licensee's NRC approved QA program.

1.4 Generic Cask Arrays

The 32PTH DSC containing the SFAs is transferred to, and stored in a HSM-H in the horizontal position. Multiple HSM-Hs are grouped together to form arrays whose size is determined to meet plant-specific needs. Arrays of HSM-Hs are arranged within the ISFSI site on a concrete basemat(s) with the entire area enclosed by a security fence. Individual HSM-Hs are arranged adjacent to each other. The decay heat for each HSM-H is primarily removed by internal natural circulation flow and conduction through the HSM-H walls. Figures 1-9, 1-10, and 1-11 show typical layouts for NUHOMS[®] 32PTH ISFSIs which are capable of modular expansion to any capacity. These are typical layouts only and do not represent limitations in number of modules, number of rows, and orientation of modules in rows. An empty module is required at the end of an array to allow for future expansion. Back to back module configurations require expansion in pairs. Expansion can be accomplished as necessary by the licensee provided the criteria of 10CFR 72.104, 10CFR 72.106 and Chapter 12 are met. The parameters of interest in planning the installation layout are the configuration of the HSM-H array and an area in front of each HSM-H to provide adequate space for backing and aligning the transfer trailer.

1.5 Supplemental Data

1.5.1 References

1. Title 10, Code of Federal Regulations, Part 72, “Licensing Requirements for the Storage of Spent Fuel in an Independent Spent Fuel Storage Installation.”
2. U.S. Nuclear Regulatory Commission, Regulatory Guide 3.61, Standard Format and Content for a Topical Safety Analysis Report for a Spent Fuel Dry Storage Cask, February 1989.
3. U.S. Nuclear Regulatory Commission, “Standard Review Plan for Dry Cask Storage Systems,” NUREG 1536, U.S. NRC, January 1997.
4. NRC Certificate of Compliance 72-1004, NUHOMS[®] General License Spent Fuel Storage System, Amendment No. 8, December, 2005.
5. Updated Final Safety Analysis Report for the Standardized NUHOMS[®] Horizontal Modular Storage System for Irradiated Nuclear Fuel, Revision 14, USNRC Docket No. 72-1004.
6. Title 10, Code of Federal Regulations, Part 50, “Domestic Licensing of Production and Utilization Facilities.”

1.5.2 Drawings

- 32PTH DSC: 10494-72-(1 to 12) (PROPRIETARY)
- OS187H: 10494-72-(15 to 21) (PROPRIETARY)
- Damaged Fuel End Caps: 10494-72-30 (PROPRIETARY)
- HSM-H: 10494-72-(100 to 110, 120) (PROPRIETARY)

Drawings for the 32PTH Type 1 DSC and OS187H Type 1 TC are shown in Appendix A, Section A.1.5.2.

Drawings for the 32PTH Type 2 DSC and OS187H Type 2 TC are shown in Appendix B, Section B.1.5.2.

Table 1-1
Key Design Parameters of the NUHOMS[®] HD System Components

Dry Shielded Canister (32PTH DSC)^(a)	
Overall Length (in)	185.75 (max)
Outside Diameter (in)	69.75
Cavity Length (in)	164.5 (min)
Shell Thickness (in)	0.5
Design Weight of Loaded 32PTH DSC (lbs.)	108,800
Materials of Construction	Stainless Steel Shell Assembly and Internals, Carbon Steel and/or Stainless Steel Shield Plugs, Aluminum
Neutron Absorbing Material	Boral [™] , borated aluminum, metal matrix composite (MMC) as specified in Chapter 9
Internal Atmosphere	Helium

Horizontal Storage Module (HSM-H):	
Overall length (without back shield wall)	20'-8"
Overall width (without end shield walls)	9'-8"
Overall height	18' 6"
Total Weight not including 32PTH DSC (lbs.)	306,000
Materials of Construction	Reinforced Concrete and Structural Steel
Heat Removal	Conduction, Convection, and Radiation

On-Site Transfer Cask (OS187H)^(b)	
Overall Length (in)	197.1
Outside Diameter (in)	92.2
Cavity Length (in)	186.6
Lead Thickness (in)	3.60 (nom)
Gross Weight (including 32PTH DSC) (tons)	114.5
Materials of Construction	Stainless Steel Shell Assemblies and closures with lead shielding
Internal Atmosphere	Helium

^(a) See Appendix A for 32 PTH Type 1 DSC and Appendix B for 32PTH Type 2 DSC.

^(b) See Appendix A for OS187H Type 1 TC and Appendix B for OS187H Type 2 TC.

Table 1-2
Known Fabricated NUHOMS® Transfer Casks Licensed for Use Under CoC 1030

Fabricated NUHOMS® transfer casks (TCs) listed in the table below have design compatibility with the TC design basis models indicated. These fabricated TCs may have been fabrication-certified to one or more of the indicated compatible amendments. Determination of the fabrication-certification, the maintenance history, and current condition of these casks, in order to determine suitability for use under a particular amendment, would be achieved through contractual agreement between general licensees and the owner of the TC in question.

Fabricated TC Serial Number*	TC Design Basis Model	Amendment TC Design Initially Licensed Under	Amendments Currently Licensed Under	Design Variants Licensed
OS187-1	OS187	0	0, 1, and 2	none
OS187-2				
OSTC-1	OS187 Type 1	0#	0#, 1#, and 2#	none
OSTC-3				

* These fabricated casks are to the best of TN Americas LLC's knowledge as of this UFSAR revision.

Added pursuant to 10 CFR 72.48 provisions.

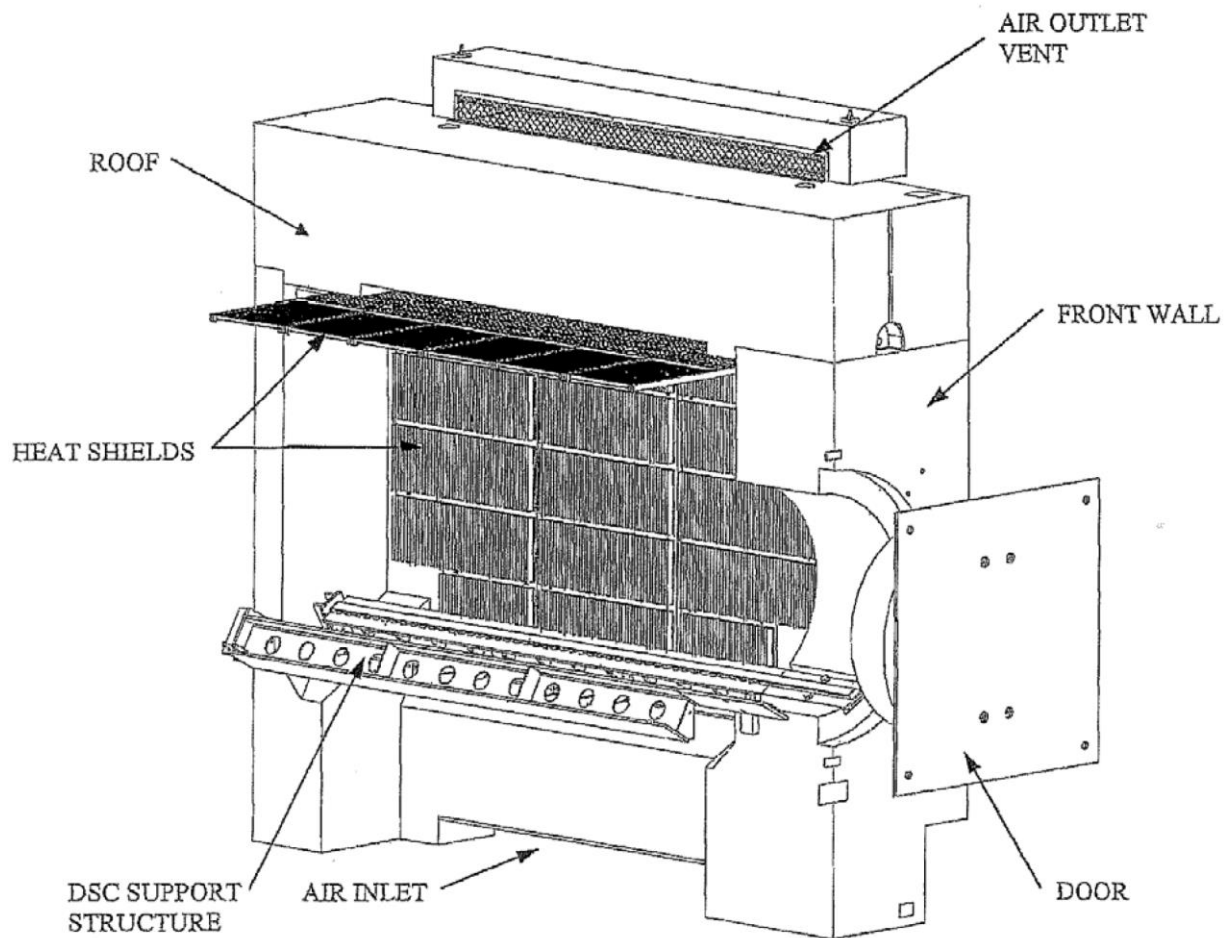


Figure 1-1
NUHOMS® HD System Horizontal Storage Module (HSM-H)

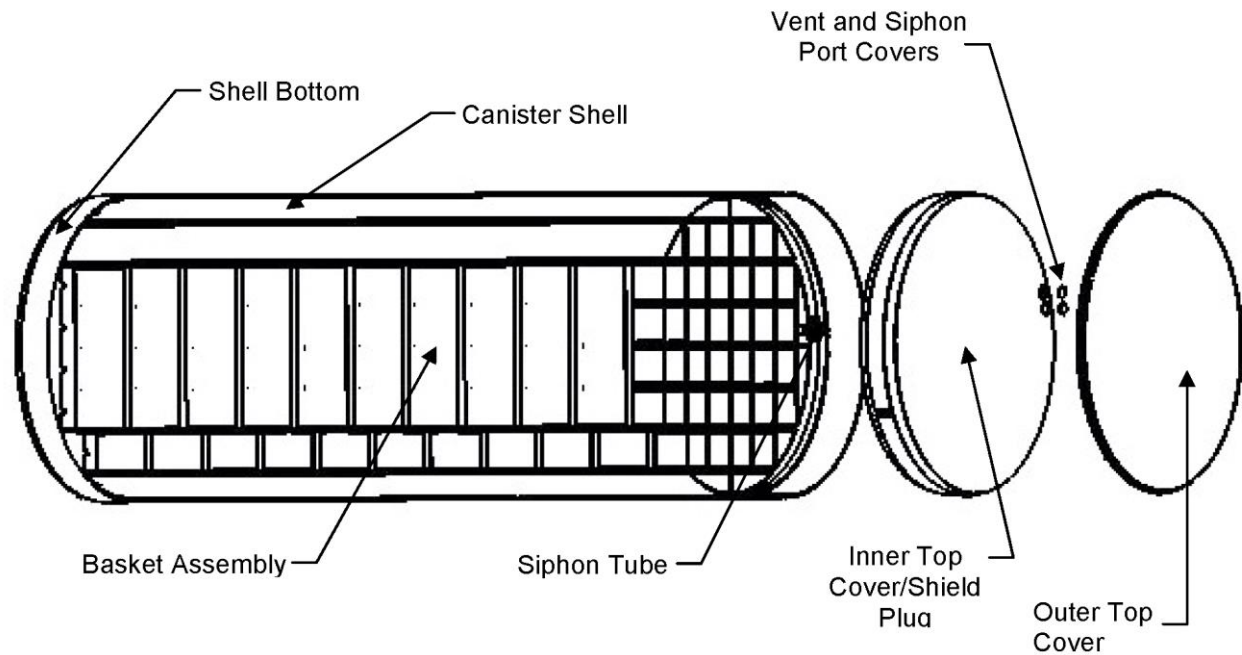


Figure 1-2
NUHOMS[®] HD 32PTH DSC

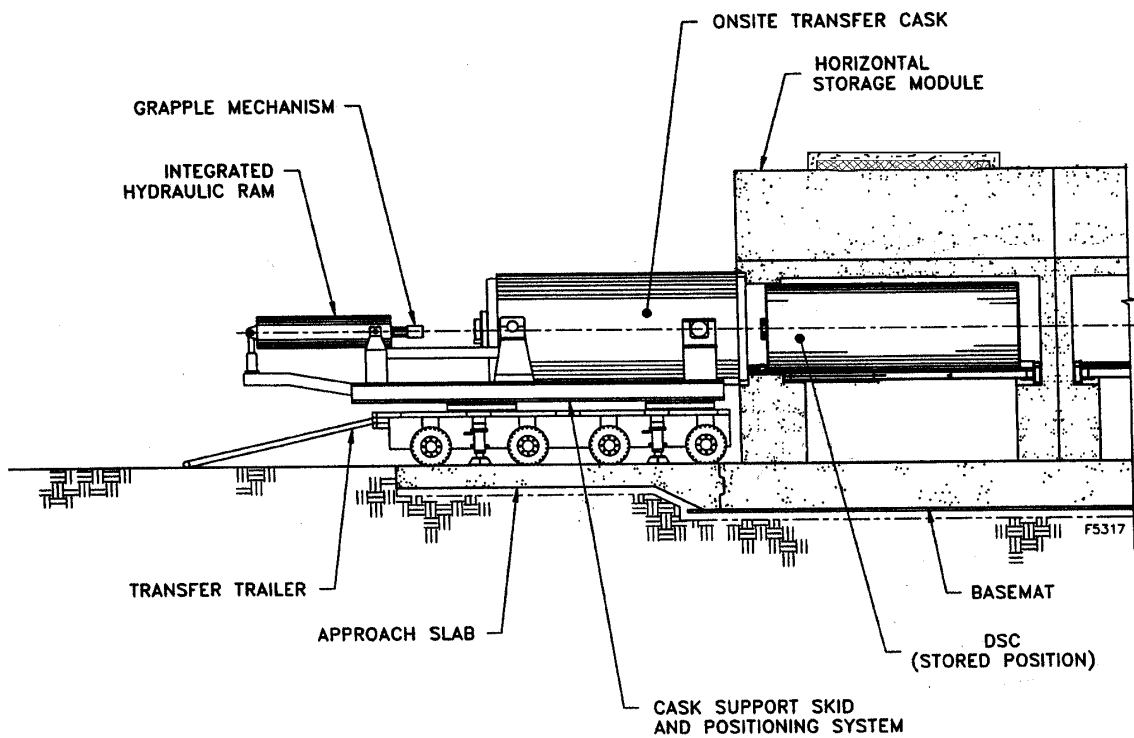


Figure 1-3
NUHOMS® HD System Components, Structures, and
Transfer Equipment – Elevation View (Typical)

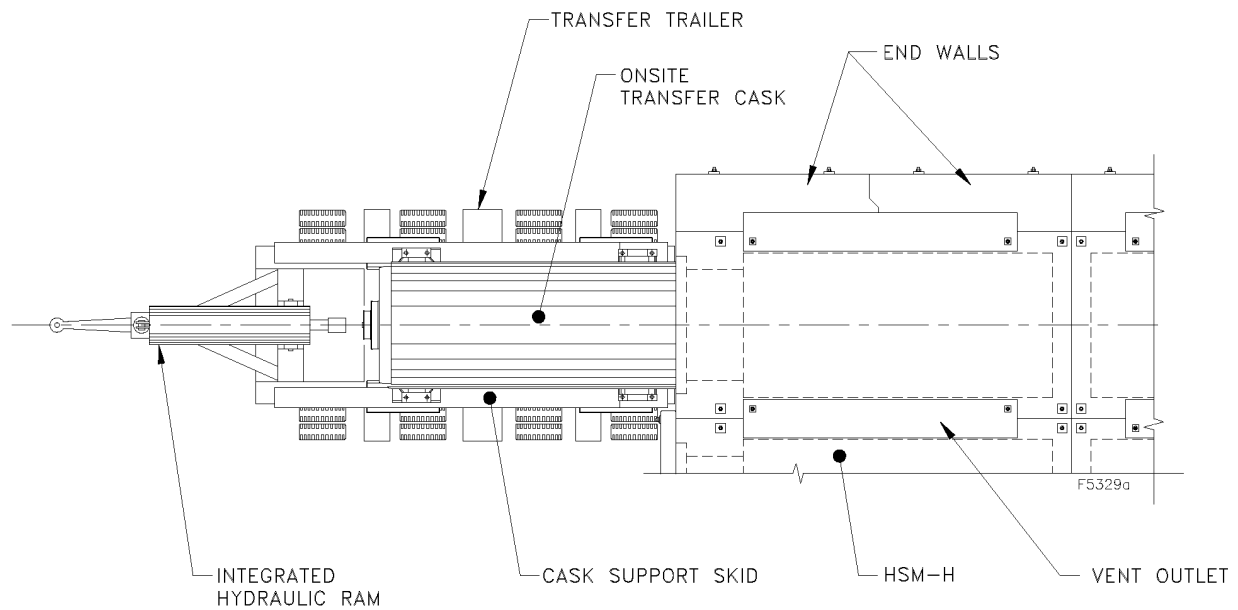


Figure 1-4
NUHOMS® HD System Components, Structures, and
Transfer Equipment – Plan View (Typical)

THIS FIGURE HAS BEEN DELETED

**Figure 1-5
DELETED**

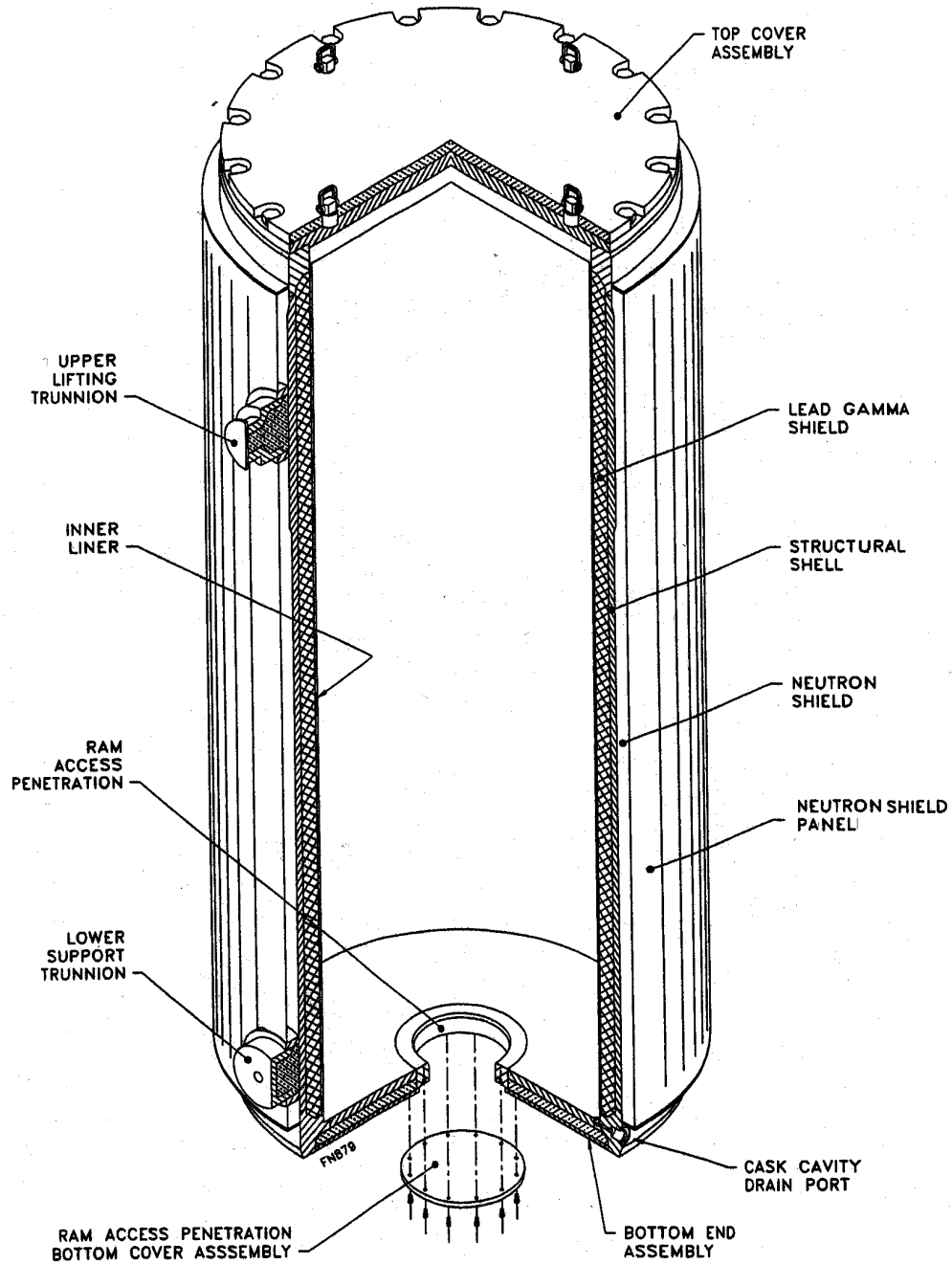


Figure 1-6
OS187H On-Site Transfer Cask

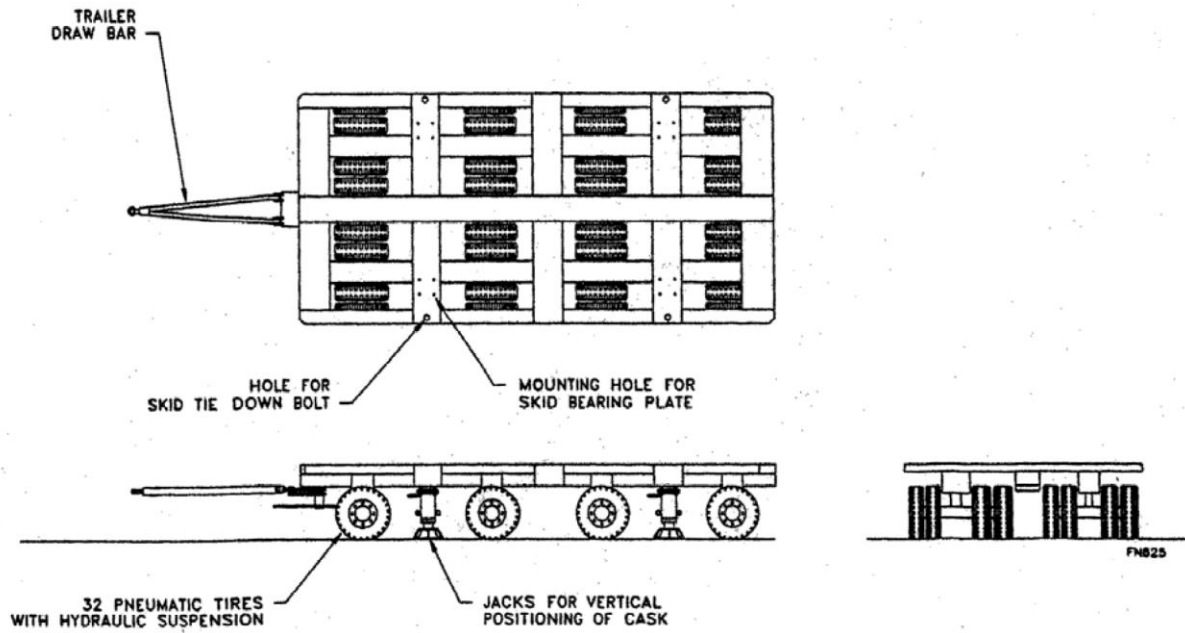


Figure 1-7
Transport Trailer for OS187H Transfer Cask (Typical)

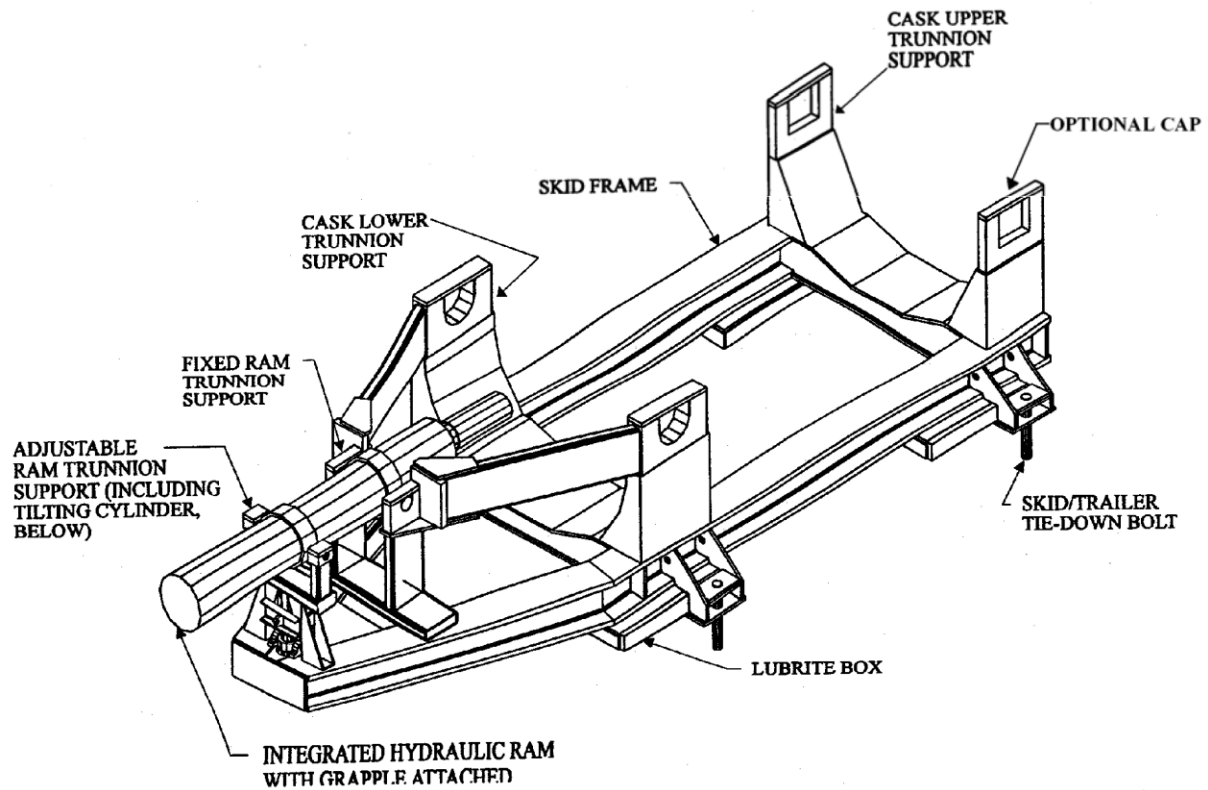


Figure 1-8
Cask Support Skid for OS187H Transfer Cask (Typical)



1. LOCATION OF ENTRANCE TO ISFSI TO BE COMPATIBLE WITH PLANT SITE ROADS.
2. NUMBER OF MODULES DETERMINED BY USER BASED ON PLANT DISCHARGE RATES AND DRY STORAGE NEEDS.
3. HSM ARRAYS CAN BE EXPANDED BY ADDING ADDITIONAL HSM UNITS. THIS CAN BE DONE WITH OR WITHOUT RELOCATING END SHIELD WALLS.

Page 1-26

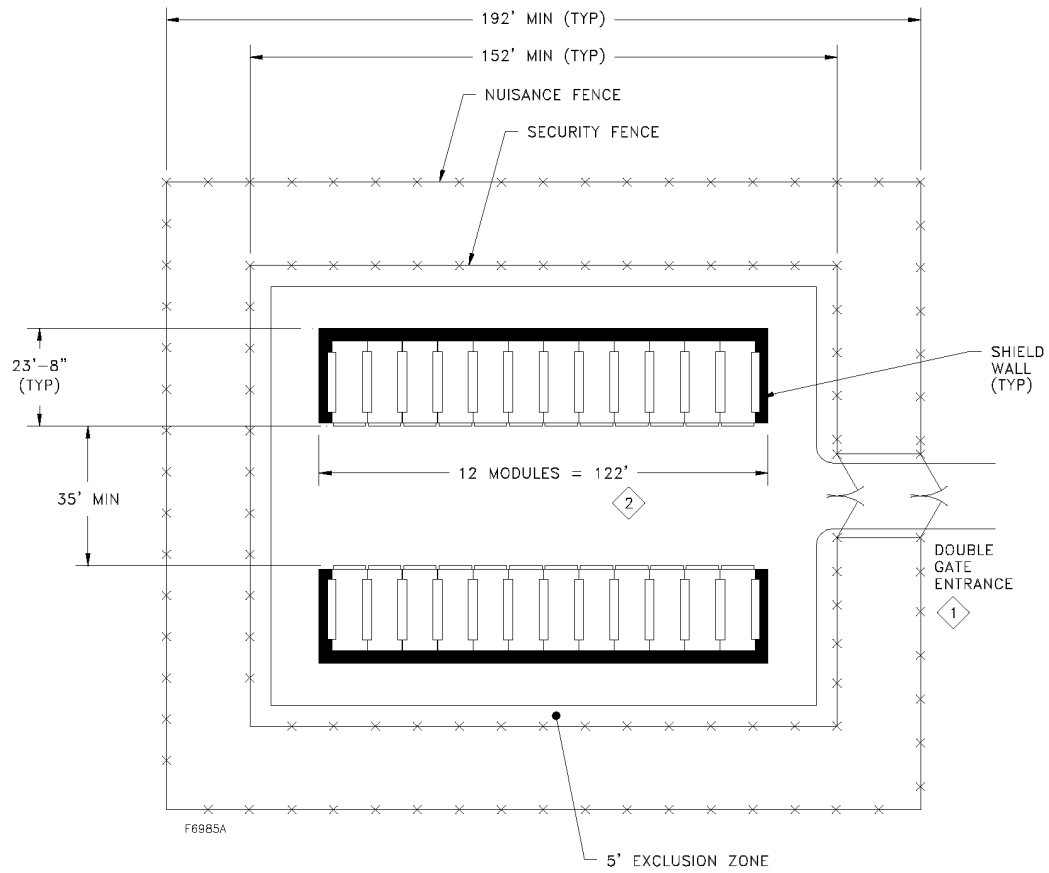
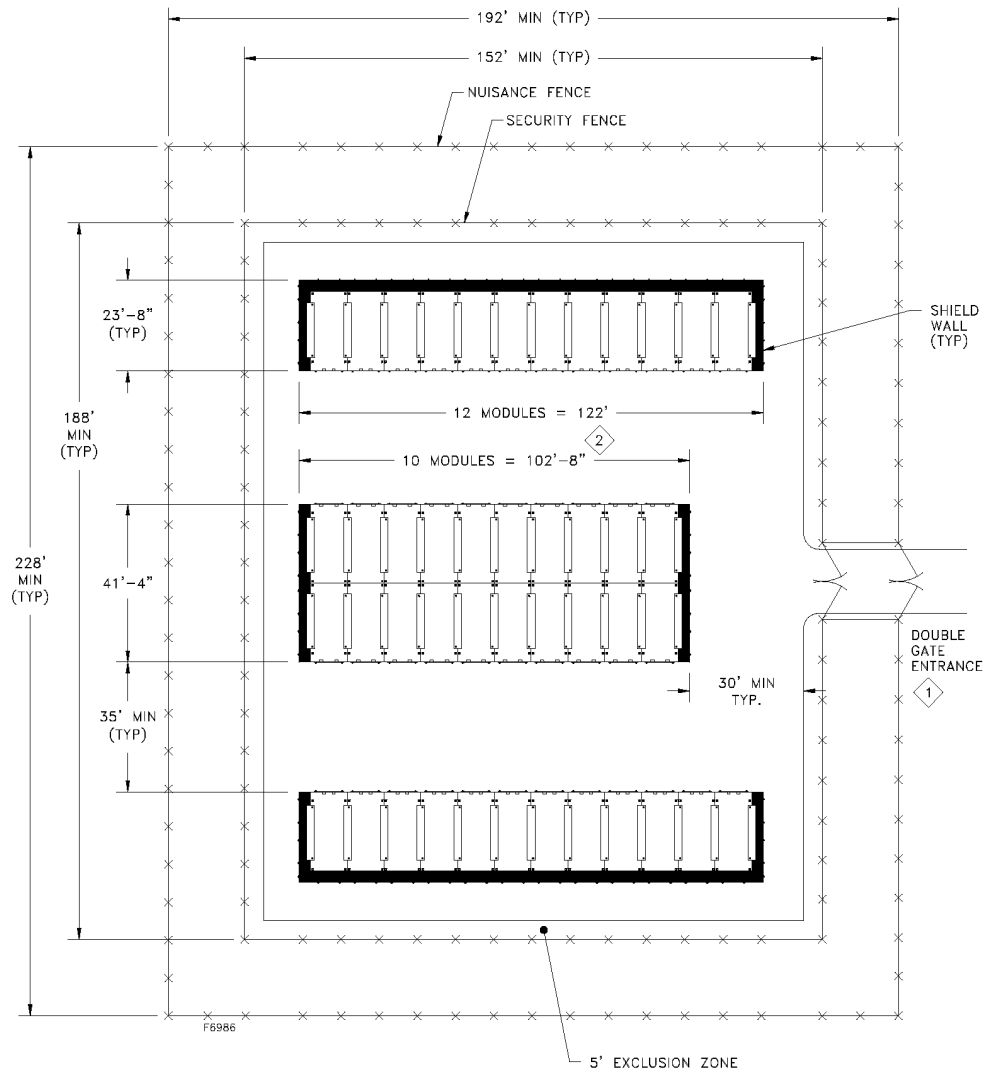


Figure 1-10
Typical Single Module Row HSM-H ISFSI Layout



NOTES:

- 1 LOCATION OF ENTRANCE TO ISFSI TO BE COMPATIBLE WITH PLANT SITE ROADS.
- 2 NUMBER OF MODULES DETERMINED BY USER BASED ON PLANT DISCHARGE RATES AND DRY STORAGE NEEDS.
3. HSM ARRAYS CAN BE EXPANDED BY ADDING ADDITIONAL HSM UNITS. THIS CAN BE DONE WITH OR WITHOUT RELOCATING END SHIELD WALLS.

Figure 1-11
Typical Combined Single and Double Module Row HSM-H ISFSI Layout

**Proprietary and Security Related Information
for Drawing 10494-72-1, Rev. 3
Withheld Pursuant to 10 CFR 2.390**

**Proprietary and Security Related Information
for Drawing 10494-72-2, Rev. 4
Withheld Pursuant to 10 CFR 2.390**

**Proprietary and Security Related Information
for Drawing 10494-72-3, Rev. 4
Withheld Pursuant to 10 CFR 2.390**

**Proprietary and Security Related Information
for Drawing 10494-72-4, Rev. 3
Withheld Pursuant to 10 CFR 2.390**

**Proprietary and Security Related Information
for Drawing 10494-72-5, Rev. 3
Withheld Pursuant to 10 CFR 2.390**

**Proprietary and Security Related Information
for Drawing 10494-72-6, Rev. 3
Withheld Pursuant to 10 CFR 2.390**

**Proprietary and Security Related Information
for Drawing 10494-72-7, Rev. 2
Withheld Pursuant to 10 CFR 2.390**

**Proprietary and Security Related Information
for Drawing 10494-72-8, Rev. 2
Withheld Pursuant to 10 CFR 2.390**

**Proprietary and Security Related Information
for Drawing 10494-72-9, Rev. 3
Withheld Pursuant to 10 CFR 2.390**

**Proprietary and Security Related Information
for Drawing 10494-72-10, Rev. 2
Withheld Pursuant to 10 CFR 2.390**

**Proprietary and Security Related Information
for Drawing 10494-72-11, Rev. 3
Withheld Pursuant to 10 CFR 2.390**

**Proprietary and Security Related Information
for Drawing 10494-72-12, Rev. 3
Withheld Pursuant to 10 CFR 2.390**

**Proprietary and Security Related Information
for Drawing 10494-72-15, Rev. 2
Withheld Pursuant to 10 CFR 2.390**

**Proprietary and Security Related Information
for Drawing 10494-72-16, Rev. 2
Withheld Pursuant to 10 CFR 2.390**

**Proprietary and Security Related Information
for Drawing 10494-72-17, Rev. 3
Withheld Pursuant to 10 CFR 2.390**

**Proprietary and Security Related Information
for Drawing 10494-72-18, Rev. 1
Withheld Pursuant to 10 CFR 2.390**

**Proprietary and Security Related Information
for Drawing 10494-72-19, Rev. 2
Withheld Pursuant to 10 CFR 2.390**

**Proprietary and Security Related Information
for Drawing 10494-72-20, Rev. 2
Withheld Pursuant to 10 CFR 2.390**

**Proprietary and Security Related Information
for Drawing 10494-72-21, Rev. 2
Withheld Pursuant to 10 CFR 2.390**

**Proprietary and Security Related Information
for Drawing 10494-72-30, Rev. 2
Withheld Pursuant to 10 CFR 2.390**

**Proprietary and Security Related Information
for Drawing 10494-72-100, Rev. 7
Withheld Pursuant to 10 CFR 2.390**

**Proprietary and Security Related Information
for Drawing 10494-72-101, Rev. 1
Withheld Pursuant to 10 CFR 2.390**

**Proprietary and Security Related Information
for Drawing 10494-72-102, Rev. 1
Withheld Pursuant to 10 CFR 2.390**

**Proprietary and Security Related Information
for Drawing 10494-72-103, Rev. 1
Withheld Pursuant to 10 CFR 2.390**

**Proprietary and Security Related Information
for Drawing 10494-72-104, Rev. 3
Withheld Pursuant to 10 CFR 2.390**

**Proprietary and Security Related Information
for Drawing 10494-72-105, Rev. 1
Withheld Pursuant to 10 CFR 2.390**

**Proprietary and Security Related Information
for Drawing 10494-72-106, Rev. 1
Withheld Pursuant to 10 CFR 2.390**

**Proprietary and Security Related Information
for Drawing 10494-72-107, Rev. 2
Withheld Pursuant to 10 CFR 2.390**

**Proprietary and Security Related Information
for Drawing 10494-72-108, Rev. 4
Withheld Pursuant to 10 CFR 2.390**

**Proprietary and Security Related Information
for Drawing 10494-72-109, Rev. 1
Withheld Pursuant to 10 CFR 2.390**

**Proprietary and Security Related Information
for Drawing 10494-72-110, Rev. 0
Withheld Pursuant to 10 CFR 2.390**

**Proprietary and Security Related Information
for Drawing 10494-72-120, Rev. 0
Withheld Pursuant to 10 CFR 2.390**

CHAPTER 2
PRINCIPAL DESIGN CRITERIA

TABLE OF CONTENTS

2.	PRINCIPAL DESIGN CRITERIA	2-1
2.1	Spent Fuel to be Stored.....	2-1
2.1.1	Detailed Payload Description	2-1
2.2	Design Criteria for Environmental Conditions and Natural Phenomena	2-6
2.2.1	Tornado and Wind Loadings	2-6
2.2.2	Water Level (Flood) Design	2-8
2.2.3	Seismic Design	2-9
2.2.4	Snow and Ice Loadings	2-9
2.2.5	Tsunami	2-9
2.2.6	Lightning	2-9
2.2.7	Combined Load Criteria	2-10
2.2.8	Burial under Debris	2-11
2.2.9	Thermal Conditions	2-11
2.3	Safety Protection Systems	2-13
2.3.1	General	2-13
2.3.2	Protection by Multiple Confinement Barriers and Systems	2-13
2.3.3	Protection by Equipment and Instrumentation Selection	2-15
2.3.4	Nuclear Criticality Safety	2-15
2.3.5	Radiological Protection	2-16
2.3.6	Fire and Explosion Protection	2-17
2.3.7	Acceptance Tests and Maintenance	2-18
2.4	Decommissioning Considerations.....	2-19
2.5	Structures, Systems and Components Important to Safety	2-20
2.5.1	Dry Shielded Canister	2-20
2.5.2	Horizontal Storage Module	2-20
2.5.3	ISFSI Basemat and Approach Slabs.....	2-21
2.5.4	Transfer Equipment	2-21
2.5.5	Auxiliary Equipment	2-21
2.6	References	2-22

LIST OF TABLES

Table 2-1	Fuel to be Stored in the 32PTH DSC	2-24
Table 2-2A	Maximum Allowable Assembly Average Burnup as a Function of Assembly Average Initial Enrichment	2-26
Table 2-2B	For Assembly Average Initial Enrichment Greater Than or Equal to 1.50 wt. % U-235	2-27
Table 2-2C	For Assembly Average Initial Enrichment Less Than 1.50 wt. % U-235	2-28
Table 2-2D	Example Tables Which May Be Used to Verify Proper Use of the Equation from Table 2-2B	2-29
Table 2-3	Spent Fuel Assembly Physical Characteristics	2-31
Table 2-4	Maximum Control Component Source Terms	2-31
Table 2-5	NUHOMS [®] HD System Major Components and Safety Classification	2-32
Table 2-6	Maximum Planar Average Initial Enrichment for Intact and Damaged Fuel Loading	2-33

LIST OF FIGURES

Figure 2-1	Heat Load Zones	2-35
Figure 2-2	Location of Damaged Assemblies	2-36

2. PRINCIPAL DESIGN CRITERIA

The design criteria described herein for the 32PTH DSC and the OS187H TC are also applicable to the 32PTH Type 1 DSC and the OS187H Type 1 TC discussed in Appendix A. Design criteria applicable specifically to the 32PTH Type 1 DSC and the OS187H Type 1 TC are described in Appendix A, Chapter A.2. Design criteria applicable specifically to the 32PTH Type 2 DSC and OS187H Type 2 are described in Appendix B, Chapter B.2.

2.1 Spent Fuel to be Stored

The NUHOMS[®] HD System components have currently been designed for the storage of 32 intact and or up to 16 damaged with remaining intact, Westinghouse 15x15 (WE 15x15), Combustion Engineering 16x16 (CE 16x16), Westinghouse 17x17 (WE 17x17), and Combustion Engineering 14x14 (CE 14x14) class PWR fuel assemblies. Equivalent reload fuel assemblies that are enveloped by the fuel assembly design characteristics listed in Table 2-1 for a given assembly class are also acceptable. WE 15x15 and WE 17x17 class fuel assemblies containing Instrument Tube Tie Rods (ITTRs) are also qualified for storage in the NUHOMS[®] HD System. Additional payloads may be defined in future amendments to this application.

The thermal and radiological characteristics for the PWR spent fuel were generated using the SCALE computer code package [1]. The physical characteristics for the PWR fuel assembly types are shown in Table 2-3. Free volume in the 32PTH DSC cavity is addressed in Chapter 4. Specific gamma and neutron source spectra are given in Chapter 5.

Although analyses in this UFSAR are performed only for the design basis fuel, any other intact or damaged PWR fuel that falls within the geometric, thermal, and nuclear limits established for the design basis fuel can be stored in the 32PTH DSC.

2.1.1 Detailed Payload Description

The NUHOMS[®] HD System is designed to store intact (including reconstituted) and/or damaged PWR fuel assemblies as specified in Table 2-1 and Table 2-3. The fuel to be stored is limited to a maximum planar average initial enrichment of 5.0 wt. % U-235. The maximum allowable assembly average burnup is limited to 60 GWd/MTU and the minimum cooling time is 5 years. The system is also designed to store Control Components (CCs) with thermal and radiological characteristics as listed in Table 2-4. Authorized CCs include Burnable Poison Rod Assemblies (BPRAs), Thimble Plug Assemblies (TPAs), Control Rod Assemblies (CRAs), Control Element Assemblies (CEAs), Rod Cluster Control Assemblies (RCCAs), Axial Power Shaping Rod Assemblies (APSRAs), Orifice Rod Assemblies (ORAs), Vibration Suppression Inserts (VSIs), Neutron Source Assemblies (NSAs) and Neutron Sources.

Nonfuel hardware that are positioned within the fuel assembly after the fuel assembly is discharged from the core such as Guide Tubes or Instrument Tube Tie Rods or Anchors, Guide Tube Inserts, BPRA Spacer Plates or devices that are positioned and operated within the fuel assembly during reactor operation such as those listed above are also considered to be authorized CCs. The cladding materials for the CCs include stainless steel, nickel based alloys such as Inconel, zirconium based alloys such as Zircaloy, M5, or Zirlo. The internal component materials include non-fuel materials like Inconel, B₄C, Ag-In-Cd, Al₂O₃, etc.

Reconstituted assemblies containing up to 10 replacement irradiated stainless steel rods per assembly or an unlimited number of lower enrichment UO₂ rods, or Zr rods, or Zr pellets, or unirradiated stainless steel rods are acceptable for storage in 32PTH DSC as intact fuel assemblies with a slightly longer cooling time than that required for a standard assembly. The stainless steel rods are assumed to have two-thirds the irradiation time as the same irradiation history as the entire fuel assembly. The reconstituted rods can be at any location in the fuel assemblies. The maximum number of reconstituted fuel assemblies with irradiated stainless steel replacement rods per DSC is 4 and 32 for all other reconstituted fuel assemblies.

The NUHOMS[®] HD System is also authorized to store fuel assemblies containing Blended Low Enriched Uranium (BLEU) fuel material. Fuel pellets containing BLEU fuel material are no different than UO₂ fuel pellets except for the presence of a higher quantity of cobalt impurity. The consideration of cobalt impurity only affects the gamma source terms for fuel assemblies located in the DSC periphery. This does not affect any criticality, thermal or structural analysis inputs for evaluation of fuel assemblies with BLEU material. The qualification of fuel assemblies containing BLEU fuel pellets will require an additional cooling time of 2.5 years to ensure that the source terms calculated with UO₂ material are bounding.

Some versions of Westinghouse WE 15x15 and WE 17x17 class fuel assemblies, fabricated with 304 stainless steel guide tube sleeves, have been found to be susceptible to Intergranular Stress Corrosion Cracking (IGSCC). This corrosion may potentially result in failure of the bulge joints that connect the top nozzle to the guide tubes when the fuel assembly is lifted [18]. Therefore, the fuel assemblies fabricated with these sleeves risk top nozzle separation from the assembly when moved or lifted for loading/unloading into or out of the DSC using the standard fuel handling tools and procedures.

A resolution for this issue is to install a Westinghouse designed component called the Instrument Tube Tie Rod (ITTR) in each of these fuel assemblies. The ITTR consists of a long stainless steel tube that is inserted in the instrument tube, through the top nozzle and extends through the bottom nozzle. The bottom portion of the ITTR is fitted with an expanding tip that secures it to the bottom nozzle. The top end of the ITTR extending above the top nozzle is threaded to accept a locknut that, when installed, ties the top and bottom nozzles together. The ITTR is designed to be capable of carrying the entire weight of the fuel assembly during handling.

As noted in the NEI Letter to the NRC [18], the ITTR hardware does not need to be explicitly listed in the cask's "Approved Contents" in the CoC and a revision to the "Approved Contents" in the CoC is not necessary because they are non-separable constituent hardware, integral to the fuel assembly. TN has reviewed the addition of ITTRs to WE 15x15 and WE 17x17 fuel assemblies and determined that all the requirements specified in [18] for this change are met.

The addition of ITTRs to the WE 15x15 and WE 17x17 fuel assemblies does not alter any of the physical characteristics (unirradiated length, MTU/assembly, number of fuel rods and number of guide/instrument tubes) as listed in Table 2-1.

The NRC has reviewed closure form I-10-01 [18] and determined, as documented in the NRC Letter to the NEI [20], that it accurately documents the resolution of the RIRP Top Nozzle SCC Issue [18].

Structural, thermal, shielding and criticality analysis of the addition of ITTRs to the WE 15x15 and WE 17x17 fuel assemblies is provided in Sections 3.6, 4.6, 5.1 and 6.3, respectively. The

32PTH DSC may store up to 32 PWR fuel assemblies arranged in accordance with a heat load zoning configuration as shown in Figure 2-1, with a maximum decay heat of 1.5 kW per assembly and a maximum heat load of 34.8 kW per DSC, (33.8 kW per DSC for CE 14x14).

The 32PTH DSC can accommodate up to 16 damaged fuel assemblies as defined in Chapter 12. Damaged fuel assemblies shall be placed into the sixteen inner most basket fuel compartments, as shown in Figure 2-2, which contain top and bottom end caps that confine any loose material and gross fuel particles to a known, sub-critical volume during normal, off-normal and accident conditions and to facilitate handling and retrievability. Reactor records, visual/videotape records, fuel sipping, ultrasonic examination, and radio chemistry are examples of techniques utilized by utilities to identify damaged fuel.

The end caps are sized to fit inside the fuel compartment (see drawing 10494-72-30). The bottom end cap is slid into the fuel compartment before loading the fuel, utilizing a special tool.

After fuel loading, a top end cap is placed into the fuel compartment. The end caps are not “attached” to the basket, but are a slip/friction fit into the basket compartment. The fuel assembly is thus enclosed/confined by the fuel compartment walls and the end caps. The DSC inner top cover prevents any significant movement of the top end cap. The damaged fuel assemblies can be retrieved simply by removing the top end cap and grappling the fuel assembly by normal means.

The NUHOMS[®]-32TH DSC basket is designed with three alternate poison materials: Borated Aluminum alloy, Boron Carbide/Aluminum Metal Matrix Composite (MMC) and Boral[®].

The NUHOMS[®]-32PTH DSC basket is analyzed for seven alternate basket configurations, depending on the boron loadings and poison materials.

A summary of the alternate poison loadings considered for each poison material as a function of basket types is presented below:

NUHOMS [®] -32PTH DSC Basket Type	Minimum B10 Areal Density, g/cm ²	
	Natural or Enriched Boron Aluminum Alloy / Metal Matrix Composite (MMC) (Type I)	Boral [®] (Type II)
A	0.007	0.009
B	0.015	0.019
C	0.020	0.025
D	0.032	N/A
E	0.050	N/A

Table 2-2B shows a parametric equation that can be utilized to qualify spent fuel assemblies for the defined decay heat load zones. The decay heat load can be calculated based on a fuel assembly’s burnup, cool time, and initial enrichment parameters. This table ensures that the fuel assembly decay heat load is within the appropriate zone. The development of this equation is provided in Appendix 4.16.2.

The maximum fuel cladding temperature limit of 400°C (752°F) is set for normal conditions of storage and all short term operations from the spent fuel pool to the ISFSI pad including vacuum drying and helium backfilling of the NUHOMS[®]-32PTH DSC per Interim Staff Guidance (ISG) No. 11, Revision 3 [15]. In addition, the change in fuel cladding temperature is restricted to less than 65 °C (117 °F) and is limited to less than 10 cycles during DSC drying, backfilling and transfer operations [15].

The maximum fuel cladding temperature limit is set to 570°C (1058°F) for accidents or off-normal thermal transients [15].

Calculations were performed to determine the fuel assembly type which was most limiting for each of the analyses including shielding, criticality, thermal and confinement. These evaluations are performed in Chapters 5 and 6. The fuel assembly classes considered are listed in Table 2-1. It was determined that the Framatome ANP Advanced MK BW 17x17 (a WE 17x17 Class Assembly) is the enveloping fuel design for the shielding, thermal and confinement source term calculation because of its total assembly weight and highest initial heavy metal loading. The bounding source term for shielding analysis is described in Table 2-3. Table 2-4 presents the thermal and radiological source terms for the CCs.

These values are consistent with the cumulative exposures and cooling times of the fuel assemblies. The gamma spectra for the bounding fuel assembly and CCs are presented in Chapter 5.

The shielding evaluation is performed assuming 32 fuel assemblies with the parameters corresponding to a decay heat of (1.5kW) per fuel assembly. Any fuel assembly that is thermally qualified by Table 2-2B or Table 2-2C is also acceptable from a shielding perspective since the maximum decay heat load is 1.5 kW and only eight (8) are allowed in the 32PTH DSC. The shielding analysis assumes 32, 1.5 kW assemblies are in the 32PTH DSC. Minimum initial enrichments are defined for each of the zones to assure the shielding evaluation is bounding.

For criticality safety, the WE 17x17 is the most reactive assembly type for a given enrichment. This assembly is used to determine the most reactive configuration in the DSC. Using this most reactive configuration, criticality analysis for all other fuel assembly classes is performed to determine the maximum enrichment allowed as a function of the soluble boron concentration and fixed poison plate loading. These results are shown in Table 2-6 and the analyses results are presented in Chapter 6.

For calculating the maximum internal pressure in the NUHOMS[®]-32PTH DSC, it is assumed that 1% of the fuel rods are damaged for normal conditions, up to 10% of the fuel rods are damaged for off normal conditions, and 100% of the fuel rods will be damaged following a design basis accident event. A minimum of 100% of the fill gas and 30% of the fission gases within the ruptured fuel rods are assumed to be available for release into the DSC cavity, consistent with NUREG-1536 [17].

The maximum internal pressures used in the structural analysis for the NUHOMS[®]-32PTH DSC are 15 and 20 psig for normal and off-normal storage and transfer conditions respectively and 120 and 70 psig during transfer and storage accident conditions respectively.

The structural integrity of the fuel cladding due to the side drop is analyzed in Section 3.5.3. The end and corner drops are not considered credible during storage and transfer. The structural integrity of the fuel cladding due to these loads will be addressed by the users under their site license (10CFR50).

2.2 Design Criteria for Environmental Conditions and Natural Phenomena

The 32PTH DSC and HSM-H form a self-contained, independent, passive system, which does not rely on any other systems or components for its operation. The criterion used in the design of the 32PTH DSC and HSM-H ensures that their exposure to credible site hazards does not impair their safety functions.

The design criteria satisfy the requirements of 10CFR Part 72 [2]. They include the effects of normal operation, natural phenomena and postulated man-made accidents. The criteria are defined in terms of loading conditions imposed on the 32PTH DSC. The loading conditions are evaluated to determine the type and magnitude of loads induced on the 32PTH DSC. The combinations of these loads are then established based on the conditions that can be superimposed. The load combinations are classified by Service Level consistent with Section III of the ASME Boiler and Pressure Vessel Code [3]. The stresses resulting from the application of these loads are then evaluated based on the rules for a Class I nuclear component prescribed by Subsection NB of the Code for the 32PTH DSC Shell Assembly important to safety components. Subsections NG and NF of the Code apply to the 32PTH DSC Basket Assembly. The HSM-H loads and load combinations are developed in accordance with the requirements of ANSI 57.9 [4] and ASCE 7-95 [5]. The HSM-H component stresses are evaluated based on the applicable ACI and AISC standards specified.

2.2.1 Tornado and Wind Loadings

The NUHOMS® HD System is designed to resist the most severe tornado and wind loads specified by NRC Regulatory Guide 1.76 [6] and NUREG-0800 [7]. The HSM-H is designed to safely withstand tornado missiles as defined by 10CFR 72.122(b) (2). Extreme wind effects are much less severe than the specified design basis tornado wind forces, which are used in load combinations specifying extreme wind for the design of the HSM-H.

There are no credible wind loads applied to the 32PTH DSC as the HSM-H and transfer cask provide the required environmental protection. The case of the canister inside the HSM-H is evaluated in Chapter 3 for the associated pressure drop condition.

Since the NUHOMS® HD System on-site transfer cask (TC) is used infrequently and for short durations, the possibility of a tornado funnel cloud enveloping the TC/32PTH DSC during transit to the HSM-H is a low probability event. Nevertheless, the TC is designed for the effects of tornadoes, in accordance with 10CFR 72.122 which includes design for the effects of worst case tornado winds and missiles [7]. Analyses are presented in Chapter 11.

2.2.1.1 Applicable Design Parameters

The design basis tornado (DBT) intensities used for the HSM-H are obtained from NRC Regulatory Guide 1.76 [6]. Region I intensities are utilized since they result in the most severe loading parameters. The maximum wind speed is 360 mph which is the sum of the rotational speed of 290 mph plus the maximum translational speed of 70 mph. The radius of the maximum rotational speed is 150 feet, the pressure drop across the tornado is 3.0 psi, and the rate of pressure drop is 2.0 psi per second.

2.2.1.2 Determination of Forces on Structures

The effects of a DBT are evaluated for the HSM-H. Tornado loads are generated for three separate loading phenomena:

1. Pressure or suction forces created by drag as air impinges and flows past the HSM-H with a maximum tornado wind speed of 360 mph,
2. Suction forces due to a tornado generated pressure drop or differential pressure load of 3 psi, and
3. Impact forces created by tornado-generated missiles impinging on the HSM-H.

The determination of the DBT velocity pressure is in accordance with the requirements of ASCE 7-95 [5]. The resistance to overturning and sliding of the HSM-H under these design pressures is evaluated in Chapter 3, Appendix 3.9.9.

2.2.1.3 Tornado Missiles

The determination of impact forces created by DBT generated missiles for the HSM-H is based on the criteria provided by NUREG-0800 [7], Section 3.5.1.4, III.4. Accordingly, eight types of missiles are postulated:

1. The utility wooden pole, 13.5" diameter, 35' long missile weighing 1500 lbs at a horizontal velocity of 294 fps.
2. The armor piercing artillery shell 8" diameter, weighing 276 lbs at a horizontal velocity of 185 fps.
3. The steel pipe missile 12" diameter, Schedule 40, 30' long weighing 1500 lbs at a horizontal velocity of 205 fps.
4. The massive automobile missile weighing 4000 lbs at a horizontal velocity of 195 fps traveling through the air not more than 25 ft above the ground and having contact area of 20 square ft.
5. Wood plank missiles traveling end on, 200 lbs, traveling at 440 fps.
6. Steel Pipe 3" diameter, Sch 40, weighing 115 lbs, traveling at 268 fps.
7. Steel Pipe 6" diameter, Sch 40, 285 lbs, traveling at 230 fps.
8. Steel rod, 1" diameter, 3' long weighing 8 lbs traveling at 317 fps.

In determining the overall effects of a DBT missile impact, overturning, and sliding of the HSM-H, the force due to the deformable massive missile impact is applied to the structure at the most adverse location. Conservation of momentum is used to demonstrate that sliding and/or tipping

of a single module will not result in an unacceptable condition for the module. The coefficient of restitution is conservatively assumed to be zero so that 100% of the missile energy is transferred to the module.

The missile energy is assumed to be dissipated as sliding friction, or an increase in potential energy due to raising the center of gravity with the force evenly distributed over the impact area. These overall effects are evaluated in Chapters 3, Appendix 3.9.9.

For the local damage analysis of the HSM-H for DBT missiles, the postulated missiles shall be used for the evaluation of concrete penetration, scabbing and perforation thickness. The modified NDRC empirical formula shall be used for this evaluation as recommended in NUREG-0800, Section 3.5.3.

Evaluation for the effects of small diameter solid spherical missiles on the 32PTH DSC is not required, as there are no openings in the HSM-H which lead directly to the canister.

2.2.2 Water Level (Flood) Design

The 32PTH DSC and HSM-H are designed for an enveloping design basis flood, postulated to result from natural phenomena such as tsunamis, and seiches, as specified by 10CFR 72.122(b). For the purpose of this generic evaluation, a flood height of 50 feet with a water velocity of 15 fps is used. The 32PTH DSC is subjected to an external hydrostatic pressure equivalent to the 50 feet head of water or 21.7 psi. The HSM-H is evaluated for the effects of a water current of 15 fps impinging on the sides of a submerged HSM-H. For the flood case that submerges the HSM-H, the inside of the HSM-H will be rapidly filled with water through the HSM-H vents. Therefore, the HSM-H components are not evaluated for the resulting static head of water. The effects of flooding and submergence on the canister are addressed in Chapters 3, 4 and 11.

2.2.2.1 Flood Elevations

It is anticipated that the 32PTH DSC and HSM-H will be located on flood-dry sites. However, as stated above, the HSM-H and 32PTH DSC are designed for a flood elevation 50 ft. above the base of the HSM-H.

2.2.2.2 Phenomena Considered in Design Load Calculations

The HSM-H is designed to withstand loads from forces developed by the probable maximum flood including dynamic phenomena such as momentum and drag. The 32PTH DSC is designed for the hydrostatic head equal to 50 ft. water submergence.

2.2.2.3 Flood Force Application

All flood loadings and effects from floods on the NUHOMS[®] HD System are discussed in Chapters 3 and 11.

2.2.2.4 Flood Protection

Flood protection measures for the NUHOMS[®] HD System are discussed in Chapters 3 and 11.

2.2.3 Seismic Design

Seismic design criteria are dependent on the specific site location. These criteria are established based on the general requirements as stated in 10 CFR 72.102.

The design earthquake (DE) for use in the design of the casks must be equivalent to the safe shutdown earthquake (SSE) for a co-located nuclear power plant, the site of which has been evaluated under the criteria of 10 CFR Part 100, Appendix A[8].

2.2.3.1 Input Criteria

The seismic design criteria for the HSM-H are based on the NRC Regulatory Guide 1.60 (R.G.) [9]. Reactor site design response spectra seismic zero period acceleration (ZPA) levels for systems using HSM-H modules are 0.30g horizontal and 0.20g vertical. The results of the frequency analysis of the HSM-H structure (which includes a simplified model of the DSC) yield a lowest frequency of 23.2 Hz in the transverse direction and 28.4 Hz in the longitudinal direction. The lowest vertical frequency exceeds 33 Hz. Thus, based on the R.G. 1.60 response spectra amplifications, the corresponding seismic accelerations used for the design of the HSM-H are 0.37g and 0.33g in the transverse and longitudinal directions respectively and 0.20g in the vertical direction. The corresponding accelerations applicable to the DSC are 0.41g and 0.36g in the transverse and longitudinal directions, respectively, and 0.20g in the vertical direction.

2.2.4 Snow and Ice Loadings

Snow and ice loads for the HSM-H are derived from ASCE 7-95 [5]. The maximum 100 year roof snow load, specified for most areas of the continental United States for an unheated structure, of 110 psf is assumed. There are no credible snow and ice loads applied to the 32PTH DSC as the HSM-H and TC provide the environmental protection. Snow and ice loads for the TC with a loaded 32PTH DSC are negligible due to the smooth curved surface of the cask, the heat rejection of the SFAs, and the infrequent short term use of the cask.

2.2.5 Tsunami

Specific analyses including analyses for tip-over are not done for tsunamis as they are typically bounded by the tornado, wind and flooding load conditions. The licensee should evaluate site-specific impacts of a tsunami.

2.2.6 Lightning

A lightning strike will not cause a significant thermal effect on the HSM-H or stored 32PTH DSC. The effects on the HSM-H resulting from a lightning strike are discussed in Chapter 11.

2.2.7 Combined Load Criteria

2.2.7.1 Horizontal Storage Module

The reinforced concrete HSM-H is designed to meet the requirements of ACI 349-97 [10]. The alternate temperature criteria of NUREG-1536 will be utilized as discussed in Chapters 3 (Appendix 3.9.9) and 11. The ultimate strength method of analysis is utilized with the appropriate strength reduction factors as described in Chapter 3 (Appendix 3.9.9). The load combinations specified in ANSI 57.9-1984 [4] are used for combining normal operating, off-normal, and accident loads for the HSM-H. All seven load combinations specified are considered and the governing combinations and the appropriate load factors are presented in Chapter 3 (Appendix 3.9.9).

The resulting HSM-H load combinations and load factors are also presented in Chapter 3 (Appendix 3.9.9). The effects of duty cycle on the HSM-H are considered and found to have negligible effect on the design. The corresponding structural design evaluation for the 32PTH DSC support structure is presented in Chapter 3 (Appendix 3.9.9).

2.2.7.2 32PTH DSC

The 32PTH DSC is designed by analysis to meet the stress intensity allowables of the ASME Boiler and Pressure Vessel Code (1998 Edition with 2000 Addenda) Section III, Division I, Subsection NB including alternatives to ASME code specified in SAR Section 3.10, NG and NF for Class 1 components and supports [3]. The 32PTH DSC is conservatively designed by utilizing linear elastic or non-linear elastic-plastic analysis methods. The load combinations considered for the 32PTH DSC normal, off-normal and postulated accident loadings are described in Chapter 3. ASME Code Service Level A allowables are used for normal and off-normal operating conditions. Service Level D allowables are used for accident conditions such as a postulated cask drop accident. Using these acceptance criteria ensures that in the event of a design basis drop accident, the 32PTH DSC confinement boundary is not breached. Normal operational stresses are combined with the appropriate off-normal and accident stresses. It is assumed that only one postulated accident condition occurs at any one time. The structural evaluation for the 32PTH DSC is documented in Chapter 3.

2.2.7.3 Transfer Cask

The on-site transfer cask is a pressure retaining component (maintain helium backfill) and is designed by analysis to meet the stress allowables of the ASME Code, Subsection NC for Class 2 components. The cask is designed by utilizing linear elastic analysis methods. The load combinations considered for the transfer cask, normal, off-normal, and postulated accident loadings are defined in Chapter 3. Service Level A allowables are used for all normal operating and off-normal conditions. Service Level D allowables are used for load combinations which include postulated accident loadings. Allowable stress limits for upper lifting trunnions are developed to meet the requirements of ANSI N14.6 [11] for non-redundant lifting. The appropriate dead load and thermal stresses are combined with the calculated drop accident scenario stresses to determine the worst case design stresses. The transfer cask structural analyses are presented in Chapter 3.

2.2.8 Burial under Debris

Debris resulting from natural phenomena or accidents that may affect system performance are to be determined by the licensee. Such debris can result from floods, wind storms and land slides. The principal effect is typically on thermal performance. See Chapters 4 and 11 for a generic evaluation of HSM-H blocked vent event.

2.2.9 Thermal Conditions

The NUHOMS[®] HD System component temperatures and thermal gradients are affected by the following thermal conditions:

- Fuel Loading
- Decay Heat
- Beginning of Storage Unloading
- Ambient Variations (including solar insolation)
- Lightning
- Fire

The thermal conditions which are of concern structurally are the temperature distributions in the system and the differential thermal expansion of interfacing components. See detailed analyses in Chapters 3, 4 and 11.

2.2.9.1 Fuel Loading

The 32PTH DSC/transfer cask is loaded in a spent fuel pool under water. The 32PTH DSC inner surfaces are cooled by pool water and the 32PTH DSC outer surface is cooled by water contained in the 32PTH DSC/transfer cask annulus; therefore, the thermal gradients established during fuel loading will be negligible. During DSC processing, draining and vacuum drying, DSC component temperatures increase. DSC component temperatures are evaluated in Chapter 4.

2.2.9.2 Decay Heat

After the 32PTH DSC/transfer cask is loaded and removed from the pool, the temperatures will gradually reach steady state conditions. The temperature gradients in the 32PTH DSC/TC have an insignificant effect on structural integrity.

The 32PTH DSC is designed for zoned loading as a function of decay heat. Four zones are designated: 1a, 1b, 2 and 3, with the maximum decay heat in zone 3. Details of the zone loading are discussed and evaluated in Chapter 4.

Thermal analysis calculations were performed for different ambient and decay heat load conditions. The methods used to obtain these results are discussed in Chapter 4. The effect on structural integrity is addressed in Chapters 3 and 11.

2.2.9.3 Beginning of Storage Unloading

Beginning of storage unloading would occur if it were necessary to place the 32PTH DSC back into the pool at the beginning of storage after it had been loaded and reached thermal equilibrium. Prior to unloading fuel, the 32PTH DSC and fuel would be cooled by circulating water through the 32PTH DSC. Therefore, cool water would contact the hotter 32PTH DSC inner surfaces. The thermal gradients in the 32PTH DSC body due to this condition are small and would have an insignificant effect on the cask body. The fuel cladding stresses during beginning of storage unloading is evaluated in Chapters 3 and 4.

2.2.9.4 Ambient Variations

Because the combined HSM-H and 32PTH DSC thermal inertia is large, the 32PTH DSC temperature response to changes in atmospheric conditions will be relatively slow. Ambient temperature variations due to changes in atmospheric conditions i.e., sun, ice, snow, rain and wind will not affect the performance of the 32PTH DSC. The cyclical variation of insolation during a day will also create insignificant thermal gradients. The analysis provided in Appendix 4.16.4 demonstrates that the thermal analyses with -20°F ambient temperature bound those for -21°F ambient temperature. Therefore, the results of the structural analyses in Chapter 3 and thermal analyses in Chapter 4, including the appendices with -20°F ambient temperature cases, are also applicable to -21°F ambient temperature cases.

The thermal effects due to ambient variations and conditions are discussed in further detail in Chapter 4.

2.2.9.5 Lightning

Thermal effects due to lightning are discussed in Chapter 11.

2.2.9.6 Fire

It is demonstrated in Chapter 11 that the 32PTH DSC will maintain confinement integrity during and after the postulated fire accident.

2.3 Safety Protection Systems

2.3.1 General

The NUHOMS[®] HD System is designed to provide long term storage of spent fuel. The canister materials are selected such that degradation is not expected during the storage period. The 32PTH DSC shell and bottom end assembly confinement boundary weld is made during fabrication of the 32PTH DSC in accordance with the subsection NB of the ASME code. The top shield plug and bottom provide shielding for the 32PTH DSC so that occupational doses are minimized during drying, sealing, and handling operations. The confinement boundary weld between the DSC shell and inner top cover/shield plug¹ (including siphon/vent cover welds) and structural attachment weld between the DSC shell and outer top cover plate are in accordance with alternatives to the ASME code as described in SAR Section 3.10.

The NUHOMS[®] HD System is designed for safe and secure, long-term confinement and dry storage of SFAs. The key elements of the NUHOMS[®] HD System and their operation which require special design consideration are:

- A. Minimizing the contamination of the 32PTH DSC exterior by fuel pool water.
- B. The 32PTH DSC confinement boundaries and welds as defined in SAR Section 7.1.
- C. Minimizing personnel radiation exposure during 32PTH DSC loading, closure, and transfer operations.
- D. Design of the HSM-H, OS187H TC, and 32PTH DSC for postulated accidents.
- E. Design of the HSM-H passive ventilation system for effective decay heat removal to ensure the integrity of the fuel cladding. The HSM-H is designed with no active safety systems.
- F. Design of the 32PTH DSC to ensure subcriticality.
- G. Design of the OS187H TC for shielding, protection, and efficient operability.

2.3.2 Protection by Multiple Confinement Barriers and Systems

2.3.2.1 Confinement Barriers and Systems

The radioactive material which the NUHOMS[®] HD System confines is the spent fuel assemblies and the associated contaminated or activated materials.

During fuel loading operations, the radioactive material in the plant's fuel pool is prevented from contacting the 32PTH DSC exterior by filling the cask/32PTH DSC annulus with uncontaminated, demineralized water prior to placing the cask and 32PTH DSC in the fuel pool. In addition, the cask/32PTH DSC annulus opening at the top of the cask is sealed using an inflatable seal to prevent pool water from entering the annulus. This procedure minimizes the likelihood of contaminating the 32PTH DSC exterior surface. The combination of the above operations assures that the 32PTH DSC surface loose contamination levels are within those

¹ See Chapter 1 drawings for option 2 and option 3 designs and Chapter 7 for confinement boundary definitions.

required for shipping cask externals. Compliance with these contamination limits is assured by taking surface swipes of the upper end of the 32PTH DSC before transferring the cask from the fuel building.

Once inside the 32PTH DSC, the SFAs are confined by the 32PTH DSC confinement boundary. The fuel cladding integrity is ensured by maintaining the storage cladding temperatures below levels which are known to cause degradation of the cladding. In addition, the SFAs are stored in an inert atmosphere to prevent degradation of the cladding, specifically cladding rupture due to oxidation and its resulting volumetric expansion of the fuel. Thus, a helium atmosphere for the 32PTH DSC is incorporated in the design to protect the fuel cladding integrity by inhibiting the ingress of oxygen into the cavity.

Helium is known to leak through valves, mechanical seals, and escape through very small passages because it has a small atomic diameter, is an inert element, and exists in a monatomic species. Helium will not, to any practical extent, diffuse through stainless steel. For this reason the 32PTH DSC has been designed as a welded confinement pressure vessel with no mechanical or electrical penetrations and meets the leak-tight criteria as described in Chapter 9. See Chapter 7 for a detailed discussion of the confinement boundary design.

The 32PTH DSC itself has a series of barriers to ensure the confinement of radioactive materials. The cylindrical shell is fabricated from rolled ASME stainless steel plate which is joined with full penetration welds that are 100% inspected by non-destructive examination. All top and bottom end closure welds are multiple-layer welds. This effectively eliminates any pinhole leaks which might occur in a single pass weld, since the chance of pinholes being in alignment on successive weld passes is not credible. Furthermore, the cover plates are sealed by separate, redundant closure welds. Pressure boundary welds and welders are qualified in accordance with Section IX of the ASME B&PV Code and inspected according to the appropriate articles of Section III, Division 1, Subsection NB including alternatives to ASME Code as specified in SAR Section 3.10. These criteria ensure that the as-deposited weld filler metal is as sound as the parent metal of the pressure vessel.

Pressure monitoring instrumentation is not used since penetration of the pressure boundary would be required. The penetration itself would then become a potential leakage path and by its presence compromise the integrity of the 32PTH DSC design. The shell and welded cover plates provide total confinement of radioactive materials. Once the 32PTH DSC is sealed, there are no credible events, as discussed in Chapter 11, which could fail the cylindrical shell or the closure plates which form the confinement boundary.

2.3.2.2 32PTH DSC Cooling

The HSM-H provides a means of removing spent fuel decay heat by a combination of radiation, conduction, and natural convection. The passive convective ventilation system is driven by the pressure difference due to the stack buoyancy effect (ΔP_s) provided by the temperature difference between the 32PTH DSC and the ambient air outlet. This pressure difference is larger than the flow pressure drop (ΔP_f) at the design air inlet and outlet temperatures.

There are no radioactive releases of effluents during normal and off-normal storage operations. Also, there are no credible accidents which cause releases of radioactive effluents from the

32PTH DSC. Therefore, an off-gas monitoring system is not required for the HSM-H. The only time an off-gas system is required is during 32PTH DSC drying operations. During this operation, the spent fuel pool or plant's radwaste system is used to process the helium evacuated from the 32PTH DSC.

During transfer of the DSC from the reactor building to the HSM, cooling of the DSC is maintained by utilizing a helium environment inside the transfer cask.

2.3.3 Protection by Equipment and Instrumentation Selection

2.3.3.1 Equipment

The HSM-H, 32PTH DSC, and transfer cask encompass equipment which is important to safety. Other equipment important to safety associated with the NUHOMS[®] 32PTH System includes the equipment required for handling operations within the plant's fuel/reactor building. This equipment is regulated by the plant's 10CFR 50 [16] operating license.

2.3.3.2 Instrumentation

The NUHOMS[®] HD System is a totally passive system. No safety-related instrumentation is necessary for monitoring the 32PTH DSC. The maximum temperatures and pressures are conservatively bounded by analyses. Therefore, there is no need for monitoring the internal cavity of the 32PTH DSC for pressure or temperature during normal operations. The 32PTH DSC is conservatively designed to perform its confinement function during all worst case normal, off-normal, and postulated accident conditions.

2.3.4 Nuclear Criticality Safety

2.3.4.1 Control Methods for Prevention of Criticality

The design criteria for criticality is that an upper sub-critical limit (USL) of 0.95 minus statistical uncertainties and bias, shall be limiting for all postulated arrangements of fuel within the canister. The 32PTH DSC incorporates borated aluminum material(s) as fixed neutron absorbing materials to provide criticality control. Criticality control is discussed in Chapter 6.

The 32PTH DSC is designed to assure an ample margin of safety against criticality under the conditions of fresh fuel (fuel without burnup credit) in a canister flooded with borated pool water. The methods of criticality control are in accordance with the requirements of 10CFR 72.124 [2].

Criticality analysis is performed using the SCALE computer code package [1] which is widely used for criticality analysis of shipping casks, fuel storage pools and storage systems.

Benchmark problems are run to verify the codes, methodology and cross section library and to determine calculational bias and uncertainties. Chapter 6 of the SAR presents the NUHOMS[®] HD System criticality analyses.

In the criticality calculation, the fuel assemblies and canister geometries are explicitly modeled. Each fuel pin and each guide tube is represented within each assembly.

Reactivity analyses were performed for CE 14x14, CE 16x16, WE 15x15, and WE 17x17 class fuel assemblies. These analyses do not credit the neutron absorption capability of the CCs where applicable.

2.3.4.2 Error Contingency Criteria

Provision for error contingency is built into the criterion used in Section 2.3.4.1. The criterion is common practice for licensing submittals. Because conservative assumptions are made in modeling, it is not necessary to introduce additional contingency for error.

2.3.4.3 Verification Analysis-Benchmarking

Evaluation and verification against critical benchmarking experiments are described in Chapter 6, Section 6.5.

2.3.5 Radiological Protection

The NUHOMS[®] HD System ISFSI is designed to maintain on-site and off-site doses as low as reasonably achievable (ALARA) during transfer operations and long-term storage conditions. ISFSI operating procedures, shielding design, and access controls provide the necessary radiological protection to assure radiological exposures to station personnel and the public are ALARA. Further details concerning on-site and off-site dose rates resulting from NUHOMS[®] 32PTH HD System, ISFSI operations and the ISFSI ALARA evaluation are provided in Chapter 10.

2.3.5.1 Access Control

The NUHOMS[®] HD System ISFSI will typically be located within the owner controlled area of an operating plant. A separate protected area consisting of a double fenced, double gated, lighted area may be installed around the ISFSI. Access is then controlled by locked gates, and guards are stationed when the gates are open. The licensee's Security Plan must describe the devices employed to detect unauthorized access to the facility. The specific procedures for controlling access to the ISFSI site and the restricted area within the site per 10CFR 72, Subpart H shall be addressed by the licensee's physical security and safeguards contingency plans. The system will not require the continuous presence of operators or maintenance personnel.

In addition to the controlled access, a method of providing a security tamper seal on the HSM-H door may be included after insertion of a loaded 32PTH DSC. This may be, but is not limited to, one of the following:

- Tack welding the HSM-H access door
- Tack welding 2 or more closure bolts on the HSM-H access door
- Tamper seals

2.3.5.2 Shielding

Shielding has the objective of assuring that radiation dose rates at key locations are at acceptable levels for those locations. Three locations are of particular interest:

1. Immediate Vicinity of the HSM-H
2. Restricted Area Boundary
3. Controlled Area Boundary

Dose rates in the immediate vicinity of the HSM-H are important for consideration of occupational exposure. Because of the passive nature of storage with this system, occupational tasks related to the system are infrequent and short in duration. Expected personnel exposures due to operational and maintenance activities are discussed in Chapter 10, Section 10.3. The estimated occupational doses for personnel comply with applicable requirements (occupational dose limits).

Restricted area boundaries may be selected so that monitoring of radiation exposure to people outside the restricted area is not required. Dose rates at the controlled area boundary are in accordance with applicable regulatory guides.

2.3.5.3 Radiological Alarm System

There are no radiological alarms required for the NUHOMS[®] HD System. There are no credible events which result in releases of radioactive products or unacceptable increases in direct radiation.

2.3.6 Fire and Explosion Protection

The NUHOMS[®] HD System HSM-H and 32PTH DSC do not contain flammable materials. The concrete and steel used for their fabrication can withstand any credible fire hazard. There is no fixed fire suppression system within the boundaries of the ISFSI. An evaluation of the system engulfed in a minor fuel fire is provided in Chapter 11. Due to the large thermal mass of the HSM-H, any minor fires in the vicinity of the ISFSI would raise the HSM-H temperature by only a few degrees and will not affect the confinement capability of the 32PTH DSC.

ISFSI initiated explosions are not considered credible since explosive materials are not present in the fission product or cover gases within the 32PTH DSC cavity. Externally initiated explosions are considered to be bounded by the design basis tornado generated missile load analysis. As indicated in Chapter 11, overpressures of a few psi can be conservatively postulated to occur at the ISFSI as a result of accidents involving explosive materials which are stored or transported near the site. This impact is significantly less than that postulated to result from the tornado wind loading and missile impact analysis, as described in Section 2.2.1, and is well within the design basis of the HSM-H. The licensee will evaluate the site specific external hazards to demonstrate these are bounded by the tornado effects.

2.3.7 Acceptance Tests and Maintenance

2.3.7.1 Acceptance Test

The acceptance tests and criteria for visual inspections, leak testing of components, valves, gaskets, shielding integrity, thermal acceptance and neutron absorbers are discussed in Chapter 9.

2.3.7.2 Maintenance Program

Because of their passive nature, the storage modules will require little, if any, maintenance over the lifetime of the ISFSI. The maintenance program is discussed in Chapter 9.

2.4 Decommissioning Considerations

The 32PTH DSC is designed to interface with a 10CFR 71 [13] transportation system for the eventual off-site transport of canisters by the DOE to either a monitored retrievable storage facility (MRS) or a permanent geologic repository, as discussed in Chapter 14.

Decommissioning of the NUHOMS® HD System ISFSI will be performed in a manner consistent with the decommissioning of the plant itself since all NUHOMS® HD System components are constructed of materials similar to those found in existing plants. The 32PTH DSC is compatible with wet or dry unloading facilities.

If the fuel is removed from the 32PTH DSC at the plant prior to shipment, the 32PTH DSC will likely be internally contaminated by crud from the spent fuel and may be slightly activated by spontaneous neutron emissions from the spent fuel. The 32PTH DSC internals may be cleaned to remove surface contamination and disposed of as low-level waste. Alternatively, if the contamination and activation levels are small enough (to be determined on a case-by-case basis), it may be possible to decontaminate the 32PTH DSC and dispose of it as commercial scrap.

While the intent for the NUHOMS® HD System includes the eventual disposal of each 32PTH DSC should fuel removal be required, current closure weld designs do not preclude future development of a non-destructive closure removal technique that allows for reuse of the 32PTH DSC shell/basket assembly. Economic and technical conditions existing at the time of fuel removal would be assessed prior to making a decision to reuse the 32PTH DSC.

The exact decommissioning plan for the ISFSI will be dependent on the DOE's fuel transportation system capability and requirements for a specific plant. Because of the minimal contamination of the outer surface of the 32PTH DSC, no contamination is expected on the internal surfaces of an HSM-H. It is anticipated that the prefabricated HSM-Hs can be dismantled and disposed of using commercial demolition and disposal techniques. Alternatively, the HSM-Hs may be refurbished and reused at another site or at the MRS for storage of intact 32PTH DSCs transported from the plant.

2.5 Structures, Systems and Components Important to Safety

Table 2-5 provides a list of major NUHOMS[®] HD System ISFSI components and their classification. Table 2-5 identifies all structures, systems and components that are “Important To Safety” (ITS). Components are classified in accordance with the criteria of 10CFR 72. Structures, systems, and components classified as ITS are defined in 10CFR 72.3 as those features of the ISFSI whose function is:

- A. To maintain the conditions required to store spent fuel safely.
- B. To prevent damage to the spent fuel container during handling and storage.
- C. To provide reasonable assurance that spent fuel can be received, handled, packaged, stored, and retrieved without undue risk to the health and safety of the public.

These criteria are applied to the NUHOMS[®] HD System components in determining their classification in the paragraphs which follow.

2.5.1 Dry Shielded Canister

The 32PTH DSC provides fuel assembly support required to maintain the fuel geometry for criticality control. Accidental criticality inside a 32PTH DSC could lead to off-site doses comparable with the limits in 10CFR 100 [8] which must be prevented. The 32PTH DSC also provides the confinement boundary for radioactive materials. Therefore, the 32PTH DSC is designed to remain intact under all accident conditions identified in Chapters 3 and 11 without losing its function to provide confinement of the spent fuel assemblies. The 32PTH DSC is designed, constructed, and tested in accordance with a QA program incorporating a graded quality approach for ITS requirements as defined by 10CFR 72, Subpart G, paragraph 72.140(b) and described in Chapter 13.

The welding materials required making the closure welds on the 32PTH DSC inner and outer top cover plates shall be fabricated to the same ASME Code criteria as the 32PTH DSC shell (Subsection NB, Class 1).

2.5.2 Horizontal Storage Module

The HSM-H is considered ITS since it provides physical protection and shielding for the spent fuel container (32PTH DSC) during storage. The reinforced concrete HSM-H is designed in accordance with ACI 349-97 [10] and built to ACI-318 [14]. The level of testing, inspection, and documentation provided during construction and maintenance is in accordance with the quality assurance requirements as defined in 10CFR 72, Subpart G and as described in Chapter 13. Thermal instrumentation for monitoring HSM-H concrete temperatures is considered “Not Important To Safety” (NITS).

2.5.3 ISFSI Basemat and Approach Slabs

The ISFSI basemat and approach slabs are considered NITS and are designed, constructed, maintained, and tested as commercial grade items.

Licensees are required to perform an assessment to confirm that the license seismic criteria described in Section 2.2.3 are met.

2.5.4 Transfer Equipment

2.5.4.1 Transfer Cask and Yoke

The on-site transfer cask OS-187H is ITS since it protects the spent fuel canister (32PTH DSC) during handling and is part of the primary load path used while handling the 32PTH DSC in the fuel/reactor building. An accidental drop of a loaded transfer cask (weighing approximately 115 tons) has the potential for creating conditions in the plant which must be evaluated. These possible drop conditions are evaluated with respect to the impact on the 32PTH DSC in Chapters 3 and 11. Therefore, the transfer cask is designed, constructed, and tested in accordance with a QA program incorporating a graded quality approach for ITS requirements as defined by 10CFR 72, Subpart G, paragraph 72.140(b) and described in Chapter 13.

A lifting yoke is used for handling the transfer cask within the fuel/reactor building and it is used by the licensee (utility) under their 10CFR 50 [16] program requirement.

Due to site unique requirements, rigid or sling lifting members may be used to augment the lifting yoke. These members shall be designed, fabricated and tested in accordance with the same requirements as the cask lifting yoke.

2.5.4.2 Other Transfer Equipment

The NUHOMS[®] HD System transfer equipment (i.e., ram, skid, transfer trailer) are necessary for the successful loading of the 32PTH DSC into the HSM-H. However, the analyses described in Chapter 11 demonstrate that the performance of these items are not required to provide reasonable assurance that spent fuel can be received, handled, packaged, stored, and retrieved without undue risk to the health and safety of the public. Therefore, these components are considered NITS and need not comply with the requirements of 10CFR 72. These components are designed, constructed, and tested in accordance with good industry practices.

2.5.5 Auxiliary Equipment

The vacuum drying system and the automated welding system are NITS. Performance of these items is not required to provide reasonable assurance that spent fuel can be received, handled, packaged, stored, and retrieved without undue risk to the health and safety of the public. Failure of any part of these systems may result in a delay of operations, but will not result in a hazard to the public or operating personnel. These components are designed, constructed, and tested in accordance with good industry practices.

2.6 References

1. Oak Ridge National Laboratory, RSIC Computer Code Collection, "SCALE: A Modular Code System for Performing Standardized Computer Analysis for Licensing Evaluations for Workstations and Personal Computers," NUREG/CR-0200, Revision 6, ORNL/NUREG/CSD-2/V2/R6.
2. U.S. Government, "Licensing Requirements for the Storage of Spent Fuel in an Independent Spent Fuel Storage Installation (ISFSI)," Title 10 Code of Federal Regulations, Part 72, Office of the Federal Register, Washington, D.C.
3. American Society of Mechanical Engineers, ASME Boiler and Pressure Vessel Code, Section III, Division 1, 1998 Edition through 2000 Addenda.
4. American National Standards Institute, American Nuclear Society, ANSI/ANS 57.9-1984, Design Criteria for an Independent Spent Fuel Storage Installation (Dry Storage Type).
5. American Society of Civil Engineers, ASCE 7-95, Minimum Design Loads for Buildings and Other Structures, (formerly ANSI A58.1).
6. U.S. Atomic Energy Commission, "Design Basis Tornado for Nuclear Power Plants," Regulatory Guide 1.76 (1974).
7. NUREG-0800, Standard Review Plan, Section 3.3.1, "Wind Loading" and Section 3.5.1.4 "Missiles Generated by Natural Phenomenon."
8. U.S. Government, "Reactor Site Criteria," Title 10 Code of Federal Regulations, Part 100, Office of the Federal Register, Washington, D.C.
9. U.S. Atomic Energy Commission, "Design Response Spectra for Seismic Design of Nuclear Power Plants," Regulatory Guide 1.60, Revision 1 (1973).
10. American Concrete Institute, Code Requirements for Nuclear Safety Related Concrete Structures and Commentary, ACI 349-97, and ACI 349R-97, American Concrete Institute, Detroit, Michigan.
11. American National Standards Institute, ANSI N14.6-1993, American National Standard for Special Lifting Device for Shipping Containers Weighing 10,000 lbs. or More for Nuclear Materials.
12. DELETED.
13. U.S. Government, "Packaging and Transportation of Radioactive Material," Title 10 Code of Federal Regulations, Part 71, Office of the Federal Register, Washington, D.C.

14. American Concrete Institute, "Building Code Requirements for Structural Concrete," ACI 318-95.
15. US NRC, Interim Staff Guidance -11, Rev 3, "Cladding Considerations for the Transportation and Storage of Spent Fuel," dated November 17, 2003.
16. U.S. Government, "Domestic Licensing of Production and Utilization Facilities," Title 10 Code of Federal Regulations, Part 50, Office of the Federal Register, Washington, D.C.
17. NUREG-1536, "Standard Review Plan for Dry Cask Storage Systems," 1997.
18. NEI Spent Fuel Storage and Transportation Regulatory Issue Resolution Protocol (RIRP) I-10-01, "PWR Fuel Top Nozzle Stress Corrosion Cracking."
19. NEI Letter to NRC, dated 02-22-2012, "RIRP Issue Closure Form Top Nozzle SCC I-10-01," ML 120540821.
20. NRC Letter to NEI dated 4-17-2012, "Response to NEI Letter Regarding Regulatory Issue Resolution Protocol Issue Closure Form for Top Nozzle Stress Corrosion Cracking," ML 1209A137.

Table 2-1
Fuel to be Stored in the 32PTH DSC

Physical Parameters: Fuel Class	Intact or damaged unconsolidated Westinghouse 17x17 (WE 17x17), Westinghouse 15x15 (WE 15x15), Combustion Engineering 16x16 (CE 16x16) and Combustion Engineering 14x14 (CE 14x14) class PWR assemblies (with or without control components) that are enveloped by the fuel assembly design characteristics listed in Table 2-3. Reload fuel manufactured by the same or other vendors but enveloped by the design characteristics listed in Table 2-3 is also acceptable. Damaged fuel assemblies beyond the definition contained below are not authorized for storage.
Damaged Fuel	Damaged PWR fuel assemblies are assemblies having missing or partial fuel rods or fuel rods with known or suspected cladding defects greater than hairline cracks or pinhole leaks. The extent of cladding damage in the fuel rods is to be limited such that a fuel assembly needs to be handled by normal means. Damaged assemblies shall also contain top and bottom end fittings or nozzles or tie plates depending on the fuel type.
Reconstituted Fuel Assemblies: <ul style="list-style-type: none"> Maximum No. of Reconstituted Assemblies per DSC With Irradiated Stainless Steel Rods Maximum No. of Irradiated Stainless Steel Rods per Reconstituted Fuel Assembly Maximum No. of Reconstituted Assemblies per DSC with unlimited number of low enriched UO₂ rods, or Zr Rods or Zr Pellets or Unirradiated Stainless Steel Rods 	<div>4</div> <div>10</div> <div>32</div>
Control Components (CCs)	<ul style="list-style-type: none"> Up to 32 CCs are authorized for storage in 32PTH DSC. Authorized CCs include Burnable Poison Rod Assemblies (BPRAs), Thimble Plug Assemblies (TPAs), Control Rod Assemblies (CRAs), Control Element Assemblies (CEAs), Rod Cluster Control Assemblies (RCCAs), Axial Power Shaping Rod Assemblies (APSRAs), Orifice Rod Assemblies (ORAs), Vibration Suppression Inserts (VSIs), Neutron Source Assemblies (NSAs) and Neutron Sources. Non-fuel hardware that are positioned within the fuel assembly after the fuel assembly is discharged from the core such as Guide Tubes or Instrument Tube Tie Rods or Anchors, Guide Tube Inserts, BPRA Spacer Plates or devices that are positioned and operated within the fuel assembly during reactor operation such as those listed above are also considered to be authorized CCs Design basis thermal and radiological characteristics for the CCs are listed in Table 2-4.

Table 2-1
Fuel to be Stored in the 32PTH DSC
(Concluded)

Number of Intact Assemblies	≤ 32
Number and Location of Damaged Assemblies	Up to 16 damaged fuel assemblies with balance intact fuel assemblies, or dummy assemblies are authorized for storage in 32PTH DSC. Damaged fuel assemblies are to be placed in the center 16 locations as shown in Figure 2-2. The DSC basket cells that store damaged fuel assemblies are provided with top and bottom end caps to assure retrievability.
Maximum Assembly plus CC Weight	1610 lb
Thermal/Radiological Parameters: Burnup, Enrichment, and Minimum Cooling Time for the 32PTH DSC	Per Table 2-2A, Table 2-2B, and Table 2-2C The licensee is responsible for ensuring that uncertainties in fuel enrichment and burnup are correctly accounted for during fuel qualification.
Maximum Planar Average Initial Fuel Enrichment	Per Table 2-6
Maximum Decay Heat Limits for Heat Load Zones 1a, 1b, 2 and 3 fuel.	Per Figure 2-1
Decay Heat per DSC	≤ 34.8 kW for WE 15x15, WE 17x17 and CE 16x16 class fuel assemblies
	≤ 33.8 kW for CE 14x14 class fuel assemblies
Minimum Boron Loading	Per Table 2-6

Table 2-2A
Maximum Allowable Assembly Average Burnup as a Function of Assembly Average Initial Enrichment

Assembly Average Initial Enrichment (X2) (wt. % U-235)	Maximum Assembly Average Burnup (X1) (GWd/MTU)
$0.2 \leq X2 < 0.3$	20
$0.3 \leq X2 < 0.7$	25
$0.7 \leq X2 < 1.5$	32
$1.5 \leq X2 < 2.5$	55
$2.5 \leq X2 < 5.00$	60

Table 2-2B
For Assembly Average Initial Enrichment Greater Than or Equal to 1.50 wt. % U-235

For an assembly average initial enrichment greater than or equal to 1.50 wt. % U-235, the equation shown below to calculate the decay heat shall be employed. Table 2-2D provides example tables, which may be used at the discretion of the user, to verify the proper use of the equation.

The Decay Heat (DH) in watts is expressed as:

$$F1 = A + B \cdot X1 + C \cdot X2 + D \cdot X1^2 + E \cdot X1 \cdot X2 + F \cdot X2^2$$

$$DH = F1 \cdot \text{Exp}(\{[1 - (5/X3)]^G\} \cdot [(X3/X1)^H] \cdot [(X2/X1)^I])$$

where,

- F1 Intermediate Function
- X1 Assembly Average Burnup in GWd/MTU
- X2 Assembly Average Initial Enrichment in wt. % U-235 ($1.5 \leq X2 \leq 5.0$)
- X3 Cooling Time in Years (minimum 5 yrs)

A=13.69479	B= 25.79539	C= -3.547739	D= 0.307917	E= -3.809025
F= 14.00256	G= -0.831522	H= 0.078607	I= -0.095900	

- When irradiated stainless steel rods are present in the reconstituted fuel assembly, the decay heat is calculated with using an X3 value, which corresponds to the actual cooling time minus 1 year. This restriction is applicable only when the cooling time of the reconstituted fuel assembly is less than 10 years. This fuel assembly is qualified if X3 is greater than 5 years. Further, this calculated decay heat shall be employed to determine the applicable Heat Load Zone shown in Figure 2-1.
- For a fuel assembly containing BLEU fuel material, the decay heat is calculated using an X3 value, which corresponds to the actual cooling time of BLEU fuel minus 2.5 years. This fuel assembly is qualified if X3 is greater than 5 years. Further, this calculated decay heat shall be employed to determine the applicable Heat Load Zone shown in Figure 2-1.
- The calculated decay heat with actual cooling time shall be employed to determine the total heat load of the DSC as shown in Figure 2-1.
- Any fuel assembly that is qualified from a thermal standpoint is also qualified from a radiological standpoint.
- Any fuel assembly with a burnup and enrichment combination that is encompassed by that specified in Table 2-2A is qualified from a radiological standpoint.
- The qualification of fuel assemblies with assembly average initial enrichment between 0.2 wt. % U-235 and 1.5 wt. % U-235 as a function of burnup and cooling time is specified in Table 2-2C.

Table 2-2C
For Assembly Average Initial Enrichment Less Than 1.50 wt. % U-235

For an assembly average initial enrichment less than 1.5 wt. % U-235, the following qualification shall be employed.

Assembly Average Initial Enrichment Range (wt. % U-235)	Maximum Assembly Average Burnup BU (GWd/MTU)	Cooling Time (Years)	Decay Heat (Watts)
0.7 ≤ X2 < 1.5	32	5	1100
	32	6	900
	32	7	780
	32	10	620
0.3 ≤ X2 < 0.7	25	5	970
	25	6	800
	25	7	690
	25	10	540
0.2 ≤ X2 < 0.3	20	5	652

Notes:

1. For an assembly average enrichment between 0.2 and 0.3 wt. % U-235, fuel assemblies with an average burnup below 20 GWd/MTU and a cooling time greater than 5 years are qualified for storage anywhere in the basket.
2. For an assembly average enrichment between 0.3 and 0.7 wt. % U-235, fuel assemblies with an average burnup below 25 GWd/MTU and a cooling time greater than 6 years are qualified for storage anywhere in the basket.
3. For an assembly average enrichment between 0.7 and 1.5 wt. % U-235, fuel assemblies with an average burnup below 32 GWd/MTU and a cooling time greater than 7 years are qualified for storage anywhere in the basket.
4. For fuel assemblies containing BLEU fuel material, the cooling time used in the table corresponds to the actual cooling time of BLEU fuel minus 2.5 years. For example, an assembly average enrichment between 0.7 and 1.5 wt. % U-235 containing BLEU fuel material, fuel assemblies with an assembly average burnup below 32 GWd/MTU and a cooling time greater than 7.5 years, the maximum decay heat is less than or equal to 1100 Watts.

Table 2-2D
Example Tables Which May Be Used to Verify Proper Use of the Equation from
Table 2-2B

Example fuel qualification tables for the various heat load zones that provide the maximum allowable assembly average burnup (GWd/MTU) as a function of assembly average initial enrichment (wt. % U-235) and cooling time (years) are shown below. These examples may be used at the discretion of the user to verify proper use of the equation from Table 2-2B. See Appendix 4.16.2 for additional details.

Examples for Zone 1a -1050 watts (Burnup GWd/MTU)

Assembly Average Initial Enrichment (wt. % U-235)	Minimum Cooling Time ⁽¹⁾					
	5 Years	6 Years	7 Years	8 Years	10 Years	15 Years
1.50	32.8	37.2	40.7	43.7	48.1	55.2
2.50	34.7	39.2	42.7	45.6	50.0	57.0
3.00	35.5	40.1	43.6	46.5	51.0	57.9
3.50	36.2	40.9	44.5	47.4	52.0	58.9
4.00	36.8	41.5	45.3	48.3	52.8	59.9
4.50	37.2	42.1	45.9	49.0	53.7	60.0

Examples for Zone 1b -800 watts (Burnup GWd/MTU)

Assembly Average Initial Enrichment (wt. % U-235)	Minimum Cooling Time ⁽¹⁾					
	5 Years	6 Years	7 Years	8 Years	10 Years	15 Years
1.50	26.3	30.0	32.9	35.4	39.2	45.2
2.00	27.1	30.8	33.8	36.2	40.0	46.0
2.50	27.7	31.5	34.5	37.0	40.8	46.7
3.00	28.2	32.1	35.2	37.7	41.5	47.5
3.50	28.5	32.5	35.7	38.3	42.2	48.3
4.00	28.5	32.9	36.2	38.8	42.8	49.0
4.50	28.5	33.0	36.4	39.2	43.3	49.7

Table 2-2D
Example Tables Which May Be Used to Verify Proper Use of the Equation from
Table 2-2B

(Concluded)

Examples for Zone 2 -1100 watts (Burnup GWd/MTU)

Assembly Average Initial Enrichment (wt. % U-235)	Minimum Cooling Time ⁽¹⁾					
	5 Years	6 Years	7 Years	8 Years	10 Years	15 Years
1.60	34.2	39.8	42.4	45.4	50.0	57.3
2.50	36.0	40.6	44.2	47.2	51.7	58.9
3.00	36.9	41.5	45.2	48.2	52.8	59.9
3.50	37.6	42.4	46.1	49.1	53.7	60.0
4.00	38.3	43.1	46.9	50.0	54.7	60.0
4.50	38.7	43.8	47.7	50.8	55.6	60.0

Examples for Zone 3 -1500 watts (Burnup GWd/MTU)

Assembly Average Initial Enrichment (wt. % U-235)	Minimum Cooling Time ⁽¹⁾			
	5 Years	6 Years	7 Years	8 Years
3.50	47.9	53.5	57.8	60.0
4.00	48.9	54.6	59.0	60.0
4.25	49.4	55.1	59.5	60.0
4.50	49.9	55.6	60.0	60.0

Note:

- For fuel assemblies containing BLEU fuel material, the minimum cooling time shall be the cooling time shown above plus 2.5 years.

Table 2-3
Spent Fuel Assembly Physical Characteristics

Assembly Class		WE 17x17	WE 15x15	CE 14x14	CE 16x16
Maximum Unirradiated Length (in) ⁽¹⁾	32PTH	162.6	162.6	162.6	162.6
	32PTH Type 1 32PTH Type 2	170.0	170.0	170.0	170.0
Fissile Material		UO ₂	UO ₂	UO ₂	UO ₂
Cladding Material ⁽³⁾		Zircaloy / Zirlo / M5	Zircaloy / Zirlo / M5	Zircaloy / Zirlo / M5	Zircaloy / Zirlo / M5
Maximum MTU/Assembly ⁽²⁾		0.476	0.476	0.476	0.476
Maximum Number of Fuel Rods		264	204	176	236
Maximum Number of Guide/ Instrument Tubes		25	21	5	5

Notes:

1. Maximum Assembly + Control Component Length (unirradiated)
2. The maximum MTU/assembly is based on the shielding analysis. The listed value is higher than the actual.
3. All zirconium-based alloys are acceptable.

Table 2-4
Maximum Control Component Source Terms

Parameter	Limit
Maximum Gamma Source Term (γ/sec/DSC)	7.36E+15
Maximum Decay Heat (Watts/Control Component)	9

Note:

NSAs and Neutron Sources shall be stored only in the interior compartments of the basket. Interior compartments are those that are completely surrounded by other compartments, including the corners. There are 12 interior compartments in the 32PTH DSC.

Table 2-5
NUHOMS® HD System Major Components and Safety Classification

Component	10CFR 72 Classification⁽¹⁾
Dry Shielded Canister (32PTH DSC)	
Fuel compartment	Important to Safety
Poison Plate	Important to Safety
Basket Plate	Important to Safety
Basket Rail	Important to Safety
Weld Studs	Important to Safety
Shell	Important to Safety
Outer Top Cover Plate	Important to Safety
Top Shield Plug/Inner Top Cover	Important to Safety
Shell Bottom	Important to Safety
Bottom Shield Plug (alternate design)	Important to Safety
DSC Support Ring	Important to Safety
Siphon and Vent Port Cover Plates	Important to Safety
Grapple Ring and Grapple Support	Important to Safety
Weld Filler Metal	Important to Safety
Horizontal Storage Module (HSM-H)	
Reinforced Concrete	Important to Safety
32PTH DSC Support Structure	Important to Safety
Thermal Instrumentation (if used)	Not Important to Safety
ISFSI Basemat and Approach Slabs	Not Important to Safety
Transfer Equipment	
On-site OS187H	Important to Safety
Transfer Cask	
Cask Lifting Yoke	See Note 2
Transfer Trailer/Skid	Not Important to Safety
Ram Assembly	Not Important to Safety
Dry Film Lubricant	Not Important to Safety
Auxiliary Equipment	
Vacuum Drying System	Not Important to Safety
Automatic Welding System	Not Important to Safety
Transfer Cask/DSC Annulus Seal	Not Important to Safety

- (1) Structures, systems and components "important to safety" are defined in 10CFR 72.3 as those features of the ISFSI whose function is (1) to maintain the conditions required to store spent fuel safely, (2) to prevent damage to the spent fuel container during handling and storage, or (3) to provide reasonable assurance that spent fuel can be received, handled, packaged, stored, and retrieved without undue risk to the health and safety of the public.
- (2) Safety classification shall be per existing plant-specific requirements under the user's 10CFR 50 heavy loads program.

Table 2-6
Maximum Planar Average Initial Enrichment for Intact and Damaged Fuel Loading

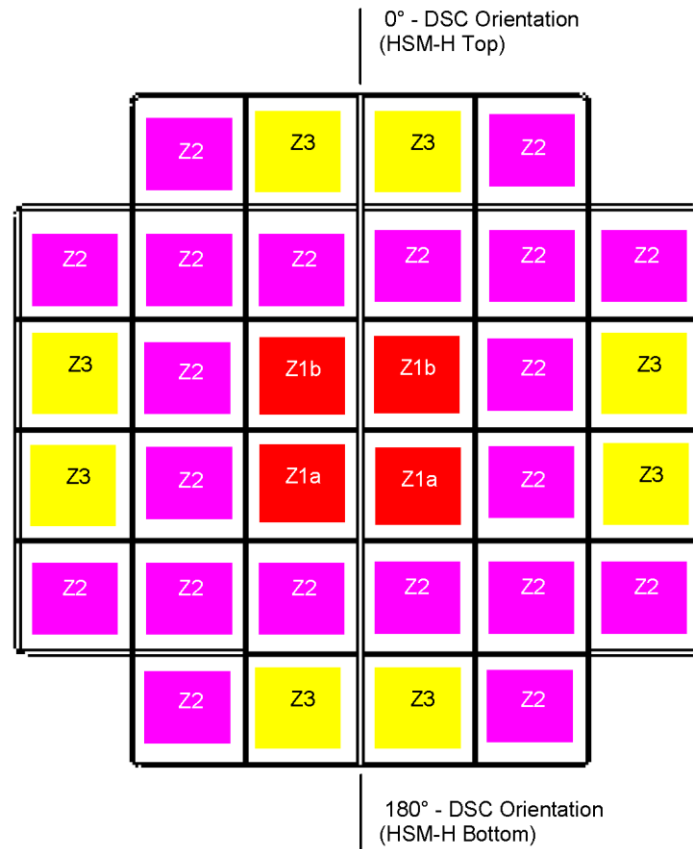
Assembly Class	Maximum Planar Average Initial Enrichment ⁽²⁾ of U-235 as a Function of Soluble Boron Concentration and Fixed Poison Loading (Basket Type)					
	Basket Type ⁽¹⁾	Minimum Soluble Boron Concentration				
		2000 ppm	2300 ppm	2400 ppm	2500 ppm	2800 ppm
CE 14x14 Intact Fuel Assembly (without CCs)	A	4.05	4.40	4.45	4.55	4.60
	B	4.55	4.90	5.00	5.00	5.00
	C	4.70	5.00	5.00	5.00	5.00
	D	5.00	5.00	5.00	5.00	5.00
	E	5.00	5.00	5.00	5.00	5.00
CE 14x14 Intact Fuel Assembly (with⁽³⁾ CCs)	A	3.95	4.25	4.35	4.45	4.55
	B	4.35	4.70	4.80	4.90	5.00
	C	4.50	4.85	5.00	5.00	5.00
	D	4.75	5.00	5.00	5.00	5.00
	E	5.00	5.00	5.00	5.00	5.00
CE 16x16 Intact Fuel Assembly (without CCs)	A	3.90	5.00	4.20	4.30	4.60
	B	4.30	4.60	4.70	4.80	5.00
	C	4.50	4.80	4.90	5.00	5.00
	D	4.80	5.00	5.00	5.00	5.00
	E	5.00	5.00	5.00	5.00	5.00
CE 16x16 Intact Fuel Assembly (with⁽³⁾ CCs)	A	3.80	4.00	4.10	4.20	4.50
	B	4.20	4.50	4.60	4.70	5.00
	C	4.40	4.70	4.80	4.90	5.00
	D	4.70	4.90	5.00	5.00	5.00
	E	4.90	5.00	5.00	5.00	5.00
WE 15x15 Intact Fuel Assembly (with and without CCs)	A	3.50	3.70	3.80	3.90	4.05
	B	3.80	4.10	4.20	4.30	4.50
	C	3.95	4.25	4.35	4.45	4.70
	D	4.20	4.50	4.70	4.80	5.00
	E	4.50	4.80	4.90	5.00	5.00
WE 17x17 Intact Fuel Assembly (with and without CCs)	A	3.50	3.70	3.80	3.90	4.00
	B	3.80	4.10	4.20	4.30	4.45
	C	3.95	4.25	4.35	4.45	4.65
	D	4.20	4.50	4.60	4.70	4.95
	E	4.45	4.70	4.90	5.00	5.00

Table 2-6
Maximum Planar Average Initial Enrichment for Intact and Damaged Fuel Loading
(Concluded)

Assembly Class	Maximum Planar Average Initial Enrichment ⁽²⁾ of U-235 as a Function of Soluble Boron Concentration and Fixed Poison Loading (Basket Type)					
	Basket Type ⁽¹⁾	Minimum Soluble Boron Concentration				
		2000 ppm	2300 ppm	2400 ppm	2500 ppm	2800 ppm
CE 14x14 Damaged Fuel Assembly (without CCs)	A	3.90	4.20	4.25	4.35	4.40
	B	4.35	4.70	4.80	4.90	4.90
	C	4.50	4.85	4.95	5.00	5.00
	D	4.85	5.00	5.00	5.00	5.00
	E	5.00	5.00	5.00	5.00	5.00
CE 14x14 Damaged Fuel Assembly (with⁽³⁾ CCs)	A	3.70	3.95	4.05	4.10	4.20
	B	4.10	4.40	4.50	4.60	4.65
	C	4.20	4.55	4.65	4.75	4.90
	D	4.50	4.85	5.00	5.00	5.00
	E	4.75	5.00	5.00	5.00	5.00
CE 16x16 Damaged Fuel Assembly (without CCs)	A	3.65	3.90	4.00	4.05	4.30
	B	4.05	4.30	4.40	4.50	4.80
	C	4.20	4.50	4.60	4.70	5.00
	D	4.50	4.80	4.90	5.00	5.00
	E	4.75	5.00	5.00	5.00	5.00
CE 16x16 Damaged Fuel Assembly (with⁽³⁾ CCs)	A	3.60	3.80	3.90	4.00	4.20
	B	3.95	4.20	4.30	4.40	4.70
	C	4.10	4.40	4.50	4.60	4.90
	D	4.40	4.70	4.80	4.90	5.00
	E	4.65	4.90	5.00	5.00	5.00
WE 15x15 Damaged Fuel Assembly (with and without CCs)	A	3.40	3.60	3.70	3.80	3.95
	B	3.75	4.00	4.10	4.20	4.35
	C	3.85	4.15	4.25	4.35	4.50
	D	4.10	4.40	4.50	4.60	4.80
	E	4.35	4.70	4.80	4.90	5.00
WE 17x17 Damaged Fuel Assembly (with and without CCs)	A	3.40	3.60	3.70	3.80	3.95
	B	3.75	4.00	4.10	4.20	4.35
	C	3.85	4.15	4.25	4.35	4.55
	D	4.10	4.40	4.50	4.60	4.80
	E	4.30	4.65	4.80	4.90	5.00

Notes:

1. The fixed poison loading requirements as a function of Basket Type are specified in Section 2.1.1.
2. Linear interpolation is allowed between adjacent maximum planar average initial enrichments and soluble boron concentration levels.
3. Applicable for fuel assemblies with CCs that extend into the active fuel region.



For CE 14x14 Class Fuel Assemblies

Q_{zi} is the maximum decay heat per assembly in zone i

Total Decay Heat ≤ 33.8 kW

4 fuel assemblies in zone 1 with $Q_{z1} \leq 0.775$ kW

20 fuel assemblies in zone 2 with $Q_{z2} \leq 1.068$ kW

8 fuel assemblies in zone 3 with $Q_{z3} \leq 1.5$ kW

For other Class Fuel Assemblies:

Q_{zi} is the maximum decay heat per assembly in zone i

Total Decay Heat ≤ 34.8 kW

4 fuel assemblies in zone 1 with

total decay heat ≤ 3.2 kW

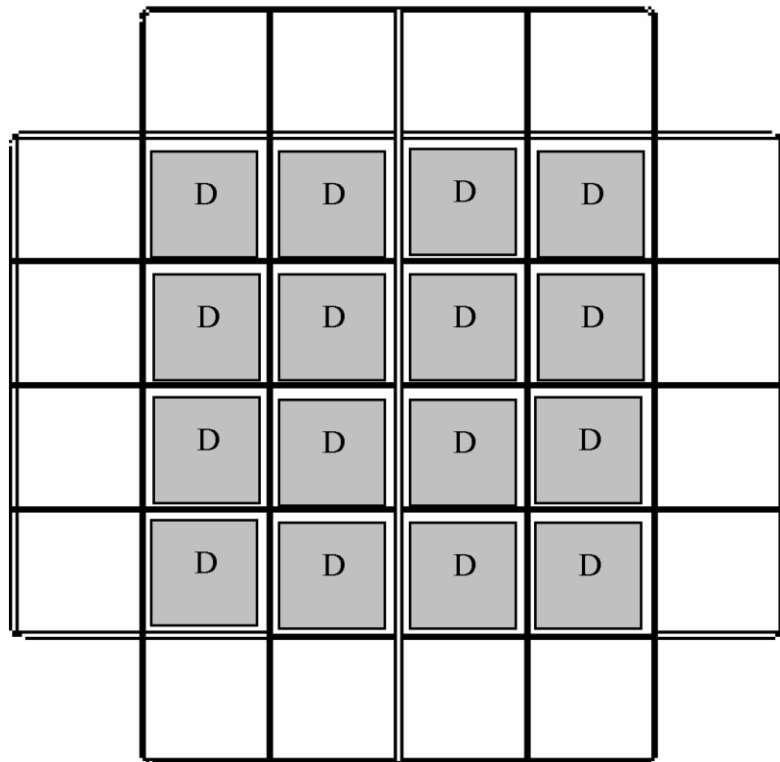
$Q_{z1a} \leq 1.05$ kW in the lower compartments

$Q_{z1b} \leq 0.8$ kW in the upper compartments

20 fuel assemblies in zone 2 with $Q_{z2} \leq 1.1$ kW

8 fuel assemblies in zone 3 with $Q_{z3} \leq 1.5$ kW

Figure 2-1
Heat Load Zones



Up to 16 damaged assemblies with the remaining intact assemblies.

Figure 2-2
Location of Damaged Assemblies

CHAPTER 3 STRUCTURAL EVALUATION

TABLE OF CONTENTS

3. STRUCTURAL EVALUATION	3-1
3.1 Structural Design	3-1
3.1.1 Discussion	3-1
3.1.2 Design Criteria	3-12
3.2 Weights.....	3-15
3.2.1 32PTH DSC Weight	3-16
3.2.2 OS187H Transfer Cask Weight	3-17
3.2.3 HSM-H Weight.....	3-18
3.3 Mechanical Properties of Materials	3-19
3.3.1 32PTH-DSC Material Properties	3-19
3.3.2 HSM-H Material Properties	3-20
3.3.3 OS187H Transfer Cask Material Properties	3-21
3.4 General Standards for 32PTH DSC, HSM-H, and OS187H TC	3-22
3.4.1 Chemical and Galvanic Reactions	3-22
3.4.2 Positive Closure	3-27
3.4.3 Lifting Devices.....	3-28
3.4.4 Heat	3-28
3.4.5 Cold.....	3-28
3.5 Fuel Rods General Standards for 32PTH DSC.....	3-29
3.5.1 Fuel Rod Temperature Limits.....	3-29
3.5.2 Fuel Assembly Thermal and Irradiation Growth	3-29
3.5.3 Fuel Rod Integrity During Drop Scenario	3-31
3.5.4 Fuel Unloading.....	3-32
3.6 Normal Conditions of Storage and Transfer.....	3-33
3.6.1 32PTH DSC Normal Conditions Structural Analysis.....	3-33
3.6.2 HSM-H Normal Conditions Structural Analysis	3-37
3.6.3 OS187H Transfer Cask Normal Conditions Structural Analysis	3-38
3.7 Off Normal and Hypothetical Accident Conditions	3-41
3.7.1 32PTH DSC Off Normal and Accident Conditions Structural Analysis.....	3-41
3.7.2 HSM-H Off Normal and Accident Conditions Structural Analysis	3-47
3.7.3 OS187H Transfer Cask Off Normal and Accident Conditions Structural Analysis.....	3-48

3.8	References	3-52
3.9	Appendices.....	3-55
Appendix 3.9.1	32PTH DSC (Canister and Basket) Structural Analysis	
Appendix 3.9.2	OS187H Transfer Cask Body Structural Analysis	
Appendix 3.9.3	OS187H Transfer Cask Top Cover and RAM Access Cover Bolt Analyses	
Appendix 3.9.4	OS187H Transfer Cask Lead Slump and Inner Shell Buckling Analysis	
Appendix 3.9.5	OS187H Transfer Cask Trunnion Analysis	
Appendix 3.9.6	OS187H Transfer Cask Shield Panel Structural Analysis	
Appendix 3.9.7	OS187H Transfer Cask Impact Analysis	
Appendix 3.9.8	Damaged Fuel Cladding Structural Evaluation	
Appendix 3.9.9	HSM-H Structural Analysis	
Appendix 3.9.10	OS187H Transfer Cask Dynamic Impact Analysis	
Appendix 3.9.11	32PTH DSC Dynamic Amplification Factor (DAF) Calculation	
3.10	ASME Code Alternatives	3-56

LIST OF TABLES

Table 3-1	Codes and Standards for the Fabrication and Construction of Principal Components.....	3-59
Table 3-2	Summary of Stress Criteria for Subsection NB Pressure Boundary Components.....	3-60
Table 3-3	Summary of Stress Criteria for Subsection NG Components	3-62
Table 3-4	Summary of Stress Criteria for Subsection NC Components	3-63
Table 3-5	SA-240 Type 304/SA-182 F304 Temperature Dependent Material Properties.....	3-64
Table 3-6	HSM-H Concrete Temperature Dependent Material Properties	3-65
Table 3-7	HSM-H Reinforcing Steel Properties at Temperature.....	3-66
Table 3-7A	Material Data for ASTM A-992 Steel	3-67
Table 3-7B	Material Data for ASTM A-36 Steel	3-68
Table 3-8	SA-240 Type XM-19 Temperature Dependent Material Properties	3-69
Table 3-9	SA-540 Grade B24 Class 1 Temperature Dependent Material Properties	3-70
Table 3-10	ASTM B-29, Chemical Lead Temperature Dependent Material Properties	3-71
Table 3-11	Resin Material Properties	3-72
Table 3-12	Input Data for Fuel Rod Cladding Side Drop ANSYS Runs	3-73
Table 3-13	Maximum Fuel Rod Cladding Axial Stresses During 75g Side Drop.....	3-74
Table 3-14	Summary of OS187H Transfer Cask Top Cover Bolt Stress Analysis	3-75
Table 3-15	Summary of OS187H Transfer Cask RAM Access Cover Bolt Stress Analysis	3-76

LIST OF FIGURES

Figure 3-1	Potential Versus pH Diagram for Aluminum-Water System	3-77
Figure 3-2	Finite Element Model and Boundary Conditions WE 15x15 and WES 15x15	3-78
Figure 3-3	Bending stress – WE 15x15 and WES 15x15	3-79
Figure 3-4	Bending stress – WE 17x17 and WEV 17x17.....	3-80
Figure 3-5	Bending stress – MK BW 17x17	3-81
Figure 3-6	Bending stress – WEO 17x17.....	3-82
Figure 3-7	Bending stress – CE 14x14.....	3-83

3. STRUCTURAL EVALUATION

The structural evaluation described in this chapter 3.0 is applicable to the 32PTH DSC, the OS187H TC, and the HSM-H. See Appendix A, Chapter A.3 for descriptions of the structural evaluation for the 32PTH Type 1 DSC, OS187H Type 1 TC, and HSM-H changes required to accommodate the 32PTH Type 1 DSC. See Appendix B, Chapter B.3 for descriptions of the structural evaluation of the 32PTH Type 2 DSC, OS187H Type 2 TC and HSM-H changes required to accommodate the 32PTH Type 2 DSC.

3.1 Structural Design

This chapter, including its appendices, presents the structural evaluation of the NUHOMS[®] HD System.

The NUHOMS[®] HD system consists of the 32PTH DSC basket and shell assemblies, the HSM-H, and the OS187H Transfer Cask. The 32PTH DSC is a new dual purpose canister that is designed to accommodate up to 32 intact PWR fuel assemblies (or up to 16 damaged assemblies, with the remaining intact) with total heat load of up to 34.8 kW. The HSM-H is an enhanced version of the NUHOMS[®] Standardized HSM and incorporates design features to enable storage of the higher heat load 32PTH DSC. The OS187H is the modified version of OS197 transfer cask with a redesigned shielding panel to improve the thermal performance, shortened the cavity length and increased inside diameter to accommodate the larger diameter of 32PTH DSC.

The overall design bases for the NUHOMS[®] HD system are described in Chapters 1 and 2. This Chapter discusses the structural design criteria and associated design bases applicable to the 32PTH DSC, HSM-H, and OS187H transfer cask. This Chapter also describes the ability of these components to perform their design function during normal and off-normal operating conditions, as well as under postulated accident conditions and extreme natural phenomena events.

3.1.1 Discussion

The NUHOMS[®] HD system consists of the 32PTH DSC, a high-integrity stainless steel dry shielded canister that provides for the dry storage of spent fuel assemblies in an inert atmosphere; the HSM-H, a massive reinforced concrete storage module that houses and provides environmental protection and shielding to the 32PTH DSC; and the OS187H transfer cask, a stainless steel cask, with lead shielding, that handles and protects the 32PTH DSC during transfer to and from the HSM-H.

Multiple HSM-Hs are grouped together to form arrays in single or double rows to provide storage capacity consistent with available site space and reactor SFA discharge rates. The HSM-H is placed next to, and in contact with, an adjacent module(s) to form a continuous single or double row arrays.

For purposes of the structural analyses and agreement with the criteria set forth in Regulatory Guide 3.61 [1] and NUREG 1536 [2], a single NUHOMS[®] HD System 32PTH DSC plus an HSM-H form the cask cited in [1] and [2].

The codes and standards used for the design, fabrication, and construction of the NUHOMS® HD system components, equipment, and structures are summarized in Table 3-1 and are identified throughout the SAR. Alternatives to the ASME Code [4] are provided in Section 3.10.

3.1.1.1 General Description of the 32PTH DSC

The principal characteristics of the 32PTH DSC are described in Chapter 1, Section 1.2.1. The drawings in Section 1.5 provide the principal dimensions and design parameters of the 32PTH DSC. For purposes of the structural analysis, the 32PTH DSC is divided into the 32PTH DSC shell assembly and the internal basket assembly.

A. DSC Canister (Shell) Assembly Description

The canister shell assembly and details are shown on drawings 10494-72-2 through 10494-72-7 in Chapter 1, Section 1.5. The shell assembly is a high integrity stainless steel (SA-240 Type 304 or SA-182 Type F304) welded pressure vessel that provides confinement of radioactive materials, encapsulates the fuel in an inert atmosphere (the canister is backfilled with Helium before being seal welded closed), and provides biological shielding (in axial direction).

The remaining 32PTH DSC shell assembly components include the solid stainless steel top shield plug, the grapple ring assembly, support ring, and the lifting blocks. The outer top cover, top shield plug and shell bottom provide biological shielding during fuel loading operations and storage of a loaded 32PTH DSC. The grapple ring assembly is welded to the shell bottom or outer bottom cover plate for the purpose of inserting/extracting the 32PTH DSC to and from the Horizontal Storage Module (HSM-H). The support ring, welded to the cylindrical shell, supports the top shield plug. Four lifting blocks are welded to the inside of the shell bottom and are used in conjunction with a lifting fixture to lift the unloaded 32PTH DSC into the transfer cask prior to fuel loading operations.

All primary components of the 32PTH DSC are constructed from Type 304 stainless steel. The 32PTH DSC cylindrical shell and shell bottom assembly (which includes the shell bottom and the grapple ring assembly), and the internal basket assembly, are shop-fabricated (and assembled) components. The top shield plug and outer top cover plate is installed at the plant after the spent fuel assemblies have been loaded into the 32PTH DSC internal basket.

The 32PTH DSC shell assembly is designed, fabricated, examined and tested in accordance with the requirements of Subsection NB of the ASME Code including alternatives to ASME code specified in Section 3.10. The circumferential and longitudinal shell plate weld seams are multi-layer full penetration butt welds. The butt weld joints are fully radiographed and inspected according to the requirements of NB-5000 of the ASME Boiler and Pressure Vessel Code. The full penetration inner bottom cover plate to shell weld is inspected to the same Code standards.

The 32PTH DSC top closure is designed, fabricated and inspected using alternatives to ASME code specified in Section 3.10. The outer top cover plate and inner top cover/shield plug (including option 2 or option 3 inner top cover as described in Chapter 1 drawings) are sealed by separate, redundant closure welds. The inner top cover/shield plug (including option 2 or option 3 design welds as described in Chapter 1 drawings) is welded to the 32PTH DSC shell to form the confinement boundary at the top end of the 32PTH DSC, as shown in Chapter 7, Figure 7-1.

The outer top cover plate provides structural support to the confinement boundary. All closure welds are multiple layer welds. This effectively eliminates any pinhole leaks which may occur in a single-pass weld, since the chance of pinholes being in alignment on successive weld passes is negligibly small. Also, both welds are examined by multi-level liquid penetrant to effectively eliminate through wall leaks.

The top shield plug of the 32PTH DSC incorporates a vent and a siphon port, with two small-diameter tubing penetrations into the 32PTH DSC cavity for draining and filling operations. One penetration, the vent port, is terminated at the bottom of the shield plug assembly. The other port is attached to a siphon tube, which continues to the bottom of the 32PTH DSC cavity. The vent and siphon ports terminate in normally closed quick-connect fittings. Both ports are used to remove water from the 32PTH DSC during the drying and sealing operations.

During fabrication, the 32PTH DSC shell and bottom assemblies are leak tested to an acceptance criterion of 1×10^{-7} ref. cm^3/sec as defined in ANSI N14.5 [6]. The welds between the DSC shell and the inner top cover/shield plug (including siphon/vent cover and option 2 or option 3 inner top cover welds as described in Chapter 1 drawings) are also leak tested to an acceptance criteria of 1×10^{-7} ref. cm^3/sec at the field after the fuel assemblies are loaded into the canister.

The stringent design and fabrication requirements described above ensure that the pressure retaining confinement function is maintained for the design life of the 32PTH DSC. Pressure monitoring instrumentation is not used since penetration of the pressure boundary would be required. The penetration itself would then become a potential leakage path and, by its presence, compromise the leaktightness of the 32PTH DSC design.

During draining, backfilling, and leak testing, a “Strongback Device” may be installed to minimize deformation of the inner top cover plate during blowdown. The strongback is bolted to the top flange of the transfer cask and provides support to the inner cover plate during those operations that may involve significant pressurization of the 32PTH DSC cavity.

Transfer of the 32PTH DSC from the transfer cask into the HSM-H is performed using a hydraulic ram that applies a load to the bottom cover plate assembly, at the center of the DSC.

Frictional loads during 32PTH DSC transfer are reduced by application of a dry film lubricant to the nitronic surface on the support rails of the HSM-H and the transfer cask. The lubricant chosen for this application is a tightly adhering inorganic lubricant with an inorganic binder. The dry film lubricant provides a thin, clean, dry, layer of lubricating solids that is intended to reduce wear, and prevent galling in metals. It is applied as a thin sprayed coating, similar to paint, using a carefully controlled process. The lubricant is not affected by water and is designed to be highly resistant to aggressive chemicals. This product is designed for radiation service and has a low coefficient of sliding friction for stainless steel.

B. Fuel Basket Assembly Description

The details of the 32PTH DSC basket are shown in drawings 10494-72-8 through 10494-72-12 on Chapter 1, Section 1.5. The 32PTH DSC basket is a welded assembly of stainless steel fuel compartment boxes, and designed to accommodate 32 PWR fuel assemblies. The sections of the stainless steel fuel compartments are fusion welded to Type 304 stainless steel structural plates,

sandwiched between the box sections. The fusion welds are spaced intermittently along the box sections. Neutron poison plates, composed of a boron-aluminum alloy (or a boron carbide aluminum metal matrix composite), are sandwiched between the sections of the stainless steel walls of the adjacent box and the adjacent stainless steel plates. The Type 304 stainless steel members are the primary structural components. The neutron poison plates provide criticality control and a heat conduction path from the fuel assemblies to the canister shell. The bottom rows of plates which are 304 SST (no poison) are also sandwiched between the fuel compartment box sections, and provide structural support to the basket.

Stainless steel rails are oriented parallel to the axis of the canister and attached to the periphery of the basket to establish and maintain basket orientation and to support the basket.

The nominal open dimension of each fuel compartment cell is 8.70 inches \times 8.70 inches, which provides clearance around the fuel assemblies. The overall length of the fuel basket is 162.00 inches, which is less than the canister cavity length of the canister (164.50 inches minimum) to allow for thermal expansion, tolerances, and access to the top of the fuel assemblies.

The basket structure is open at each end. Therefore, longitudinal fuel assembly loads are applied directly on the DSC body and not on the fuel basket structure. The fuel assemblies are laterally supported by the stainless steel fuel compartments and structural plates, and the fuel basket is laterally supported by the rails and the canister shell.

The circumferential orientation of the basket, relative to the canister shell, is maintained by the four lifting blocks attached to the bottom closure assembly of the canister. The four canister lifting blocks mate with the hollow portions of the basket outer support rails, without interfering with the spent fuel assemblies. During normal transfer conditions, the DSC rests on four transfer support rails, attached to the inside surface of the NUHOMS®-OS187H Transfer Cask.

3.1.1.2 General Description of the HSM-H

The details of the HSM-H module are shown in drawings 10494-72-100 through 10494-72-110 in Chapter 1, Section 1.5. The HSM-H is a free standing reinforced concrete structure designed to provide environmental protection and radiological shielding for the 32PTH DSC. Each HSM-H provides a self contained modular structure for the storage of a 32PTH DSC containing up to 32 PWR fuel assemblies. The HSM-H provides heat rejection from the spent fuel decay heat by a combination of radiation, conduction and convection.

The HSM-H is a reinforced concrete structure consisting of two separate units: a base storage unit, where the 32PTH canister is stored, and a roof that serves to provide environmental protection and radiation shielding. The roof is attached to the base unit by four vertical ties or by four angle brackets. Three-foot thick shield walls are installed behind each HSM-H (single row array only) and at the ends of each row to provide additional environmental protection and radiological shielding.

The HSM-H module design for 32PTH canister is identical to the HSM-H design for 24PTH canister except the following modifications:

- 1 The module for the 32PTH canister is designed such that the center line of the loaded 32PTH canister is approximately four inches higher compared to that of the 24PTH canister.
- 2 The diameter of the door openings in the front and rear of the front wall are approximately four inches and two inches larger for the 32PTH canister compared to those of the 24PTH canister.
- 3 The transfer cask docking surface in the module for the 32PTH canister transfer cask is approximately half inch wider compared to the cask docking surface for the 24PTH canister transfer cask.
- 4 The diameters of the front inner circular steel plate and rear circular concrete block of the shielded door for the 32PTH canister are approximately four inches and two inches larger compared to those of the 24PTH canisters.
- 5 For the 32PTH design the spacers at the canister stop plate of the module will be provided similar to the 24PTH short cavity design.

The drawings in Chapter 1, Section 1.5 provide the principal dimensions and design parameters of the HSM-H. The dimension differences between the HSM-H to be used for storing the 32PTH canister and 24PTH canister are listed in the following tables. Dimensions for the 24PTH canister are detailed in the Standardized NUHOMS[®] UFSAR [40].

TN drawing No. 10494-72-104 (for 32PTH data)

Dimension	HSM-H	
	System Type	
	For 32PTH Canister	For 24PTH Canister
A	8' – 10"	8' – 6"
B	Ø 5' – 11 5/8"	Ø 5' – 9"
C	Ø 7' – 5"	Ø 7' – 1 1/2"

TN drawing No. 10494-72-107 (for 32PTH data)

Dimension	HSM-H	
	System Type	
	For 32PTH Canister	For 24PTH Canister
A	34.88"	33.60"

TN drawing No. 10494-72-108 (for 32PTH data)

Dimension	HSM-H	
	System Type	
	For 32PTH Canister	For 24PTH Canister
A	8' – 1 1/2"	7' – 3 3/4"
B	Ø 7' – 3"	Ø 6' – 11 1/2"
C	Ø 5' – 8 5/8"	Ø 5' – 6"
D	Ø 7' – 7 1/4"	Ø 7' – 3 3/4"
E	1' – 10 1/2"	1' – 10 1/2"

The design of the HSM-H for the 32PTH DSC is the same as the HSM-H documented in Appendix P of the CoC 1004 UFSAR with certain adjustments to accommodate the larger diameter 32PTH DSC. Analyses performed for HSM-H with 24PTH DSC used bounding values to envelop both 24PTH DSC and 32PTH DSC.

3.1.1.3 General Description of the OS187H On-Site Transfer Cask

The NUHOMS[®]-OS187H On-Site Transfer Cask consists of a structural shell, gamma shielding material, and solid and liquid (water) neutron shield. The OS187H is the modified version of OS197 transfer cask with a redesigned shielding panel to improve the thermal performance, shortened the cavity length and increased inside diameter to accommodate the larger diameter of 32PTH DSC. The cavity between the DSC and the transfer cask contains an inert gas during transfer operations. Sets of upper and lower trunnions, welded to the structural shell of the cask that provide support, lifting, and rotation capability for the OS187H transfer cask.

The overall dimensions of the OS187H transfer cask are 197.07 inches long and 92.20 inches in diameter. The transfer cask structural shell is 82.70 inches in diameter. The transfer cask cavity is 186.60 inches long and 70.50 inches in diameter. Detailed design drawings for the OS187H Transfer Cask are provided in drawings 10494-72-15 through 10494-72-21 on Chapter 1, Section 1.5. The materials used to fabricate the transfer cask are shown in the Parts List on Drawing 10494-72-15. Where more than one material has been specified for a component, the most limiting properties are used in the analyses in the subsequent chapters of this Safety Analysis Report.

The gross weight of the loaded transfer cask is 114.8 tons including a maximum payload of 54.78 tons. Section 3.2.2 summarizes the weights of the NUHOMS[®]-OS187H packaging components. Trunnions, welded to the structural shell of the transfer cask, are provided for lifting and handling operations, including rotation of the packaging between the horizontal and vertical orientations. The OS187H cask transfers the DSC in the horizontal orientation, on a specially designed transfer skid, with the lid end facing the direction of travel.

The transfer cask is fabricated primarily of stainless steel. Non-stainless steel members include the cast lead shielding between the inner radial shell and the structural shell, the o-ring seals, the resin and water neutron shield material and the carbon steel closure bolts. The lead is poured into

the annulus in a molten state using a carefully controlled procedure. The top cover is bolted to the top flange by 24-1 1/2 in. diameter high strength bolts and sealed with O-ring. A cover plate is provided to seal the bottom hydraulic ram access penetration of the cask (by 12-1/2 in. high strength bolts with O-ring) during fuel loading and transferring the canister to the ISFSI.

Drawing 10494-72-15 provides the part list for the NUHOMS[®]-OS187H transfer cask. Drawing 10494-72-16 shows the overall configuration of the NUHOMS[®]-OS187H transfer cask. Drawing 10494-72-17 shows the details of the transfer cask top cover. The remaining drawings (10494-72-18 through 10494-72-21) show the details of the remaining individual components that make up the transfer cask.

The following sections provide physical and functional descriptions of each major component of the transfer cask. Detail drawings showing dimensions of significance to the safety analyses, welding and NDE information, as well as a complete materials list are provided in Chapter 1, Section 1.5. Reference to these drawings is made in the following physical description sections, and in general, throughout this SAR.

A. Transfer Cask Body and Structural Components

The shell or cask body cylinder assembly is an open ended (at the top) cylindrical unit with an integral closed bottom end. This assembly consists of concentric inner shell and outer shell (both SA -240 Type 304), welded to massive closure flanges (SA-182 Type F304N) at the top and bottom ends. The inner shell is 0.50 inches thick and has a 70.50 inch inside diameter. The outer shell is the primary structural shell and is 1.5 inches to 2.0 inches thick, and has an 82.70 inch outside diameter. The annulus between the shells is filled with lead shielding. The lead gamma shield is 3.60 inch thick and is poured into the annulus in a molten state using a carefully controlled procedure.

The transfer cask bottom end assembly consists of a 2.00 inch bottom end plate and a 0.75 inch bottom neutron shield plate, that sandwich a 2.25 inch thick resin neutron shield. The RAM access penetration at the center of the bottom end assembly is used during insertion/removal operations to and from the HSM-H. The RAM access penetration is four inches thick in the radial direction and 4.25 inches thick in the axial direction. A cover plate is provided to seal the bottom hydraulic ram access penetration of the cask (by 12-1/2 in. high strength bolts with O-ring) during fuel loading and transferring the canister to the ISFSI.

The transfer cask top cover consists of a 3 inch thick structural plate constructed from SA-240, Type XM-19, and a top radial neutron shield constructed from resin encased in a 0.25 inch thick SA-240 Type 304 stainless steel shell. The top cover is fastened to the top flange of the transfer cask body with 24-1.5 inch diameter SA-540 Grade B24 Class 1 high strength steel bolts. The top closure is designed to maintain confinement of the 32PTH DSC inside the transfer cask during all normal, off normal and hypothetical accident conditions.

The transfer cask body provides additional radiation shielding and structural support for the 32PTH DSC. It also maintains an inert atmosphere (helium) in the cask cavity. Helium assists in heat removal during transfer operations and provides a non-reactive environment. To preclude air in-leakage, the cask cavity is pressurized with helium to above atmospheric pressure.

The NUHOMS[®]-OS187H transfer cask is designed, fabricated, examined and tested in accordance with the requirements of Subsection NC [7] of the ASME Code to the maximum practical extent. Alternatives to the ASME Code are discussed in Section 3.10.

B. Gamma and Radial Neutron Shielding

The lead and steel shells of the transfer cask provide shielding between the DSC and the exterior surface of the package for the attenuation of gamma radiation.

Axial neutron shielding is primarily provided by a borated polyester resin compound. The resin compound is cast into stainless steel cavities on the outside surface of the top closure and bottom assembly.

The resin material is an unsaturated polyester cross-linked with styrene, with about 50% weight mineral and fiberglass reinforcement. The components are polyester resin, styrene monomer, alpha methyl styrene, aluminum oxide, zinc borate, and chopped fiberglass which produce the elemental resin composition is shown in Chapter 5, Table 5-17.

Radial neutron shielding is primarily provided by liquid water enclosed in a radial outer stainless steel shield shell. The shield shell around the neutron shield consists of a cylindrical shell section, with closure plates at each end. The closure plates are welded to the outer surface of the structural shell of the cask body. The outer shield shell has no structural function other than to provide an enclosure for the neutron shield water. The shell is made of SA-240 Type 304 stainless steel.

C. Tiedown and Lifting Devices

There are four trunnions welded to the exterior of the structural shell of the transfer cask. There are two front trunnions located on opposite sides of the cask near the top closure, and two rear trunnions located similarly, near the bottom of the cask. The two top trunnions are used to first lift the cask, containing a canister and an empty basket, into a fuel pool for loading of the spent fuel. After the spent fuel has been loaded into the basket, the cask is lifted to a decontamination area. After draining and drying of the pool water, welding of the canister cover, and bolting of the cask cover, the cask is placed in a trailer for transfer to ISFSI. The cask is vertically lifted onto the trailer and is initially supported by the bottom trunnions which are mated to transfer trailer. Then the cask is allowed to pivot about the bottom trunnions, into a horizontal position until the top trunnions rest on their supports in the trailer.

The top trunnions are constructed from SA-182 Type FXM-19 and the bottom trunnions are constructed from SA-182 Type 304. Both materials are stainless steel forgings. The top trunnions are designed fabricated and tested in accordance with ANSI N14.6 [8] as single failure proof lifting devices. Consequently they are designed with a factor of safety of six against the material yield strength and a factor of ten against the material ultimate strength.

D. Operational Features

The NUHOMS[®]-OS187H transfer cask is not considered to be operationally complex and is designed to be compatible with spent fuel pool loading/unloading methods. All operational

features are readily apparent from inspection of the General Arrangement Drawings provided in Chapter 1, Section 1.5. The sequential steps to be followed for cask loading, testing, and unloading operations are provided in Chapter 8.

3.1.1.4 Discussion of NUHOMS[®] HD System Drop Analysis

All lifting of the TC loaded with the DSC must be made within the existing heavy loads requirements and procedures of the licensed nuclear power plant. The TC design has been reviewed under 10 CFR Part 72 and found to meet NUREG-0612 [5] and ANSI N14.6 [8].

The transfer cask is transported to the ISFSI in a horizontal configuration. Therefore the only credible drop accident during storage or transfer operations is a side drop. The transfer cask, canister and fuel cladding are analyzed for these credible accidents in the following sections.

In addition, a vertical or corner drop accident may be credible under 10CFR50 during loading onto trailer or during transport operations governed under 10CFR71. The transfer cask and canister have been evaluated for these postulated accidents. However, the fuel cladding integrity has not been demonstrated for these accident scenarios. An additional safety review by the user is required to demonstrate fuel cladding integrity under 10CFR50 or to demonstrate that the drop accidents are not credible.

The drop analyses of the NUHOMS[®] HD components are performed in the following Appendices.

Appendix 3.9.1

This appendix describes the detail analysis of the canister and basket for all the loading conditions. For the drop loads, the canister is analyzed for the 75g side and end drops. The canister end closure welds are analyzed for the 22g corner drop.

The basket is analyzed for 75g the side and end drops. The basket is not analyzed for the 22g corner drop since the 75g end drop analysis bounds the 22g corner drop.

Appendix 3.9.2

This appendix describes the detail analysis of the TC for all the loading conditions. For the drop loads, the TC is analyzed for the 75g side and end drops. The results for the TC corner drop using LS-DYNA is reported in Appendix 3.9.10.

Appendix 3.9.3

This appendix describes the detail analysis of the TC top cover bolt and ram cover bolt due to the 22g corner drop. The stress analysis is performed in accordance with NUREG/CR-6007.

Appendix 3.9.4

This appendix describes the detailed analysis of the TC lead slump and inner shell buckling analysis. A 75g end drop load is used for these analyses.

Appendix 3.9.8

This appendix describes the detailed structural analysis of the fuel cladding due to the following loads.

10CFR72 (Normal & Off-Normal loads):

1g down (dead weight), transfer loads (1g longitudinal, 1g transverse, and 1g vertical).

10CFR71 (Normal loads): 30g (1 foot side drop)

1 foot end drop will be addressed in the 10CFR71 application.

3.1.2 Design Criteria

This section specifies the design requirements of the NUHOMS[®] HD system. The system consists of the Transportable Dry Shielded Canister (DSC), the Horizontal Storage Module, HSM-H and the OS-187H onsite transfer cask. The system is designed for high burnup fuel, up to 60 GWD/MTU, with a maximum assembly average initial enrichment of 5 wt. % U-235. The design will be based on the NUHOMS[®] design concept of horizontal storage, and is intended for use with a compatible transport cask.

General design requirements include structural, thermal, nuclear criticality safety, confinement/containment, and radiological protection criteria.

The overall storage system consists of three major components:

- 32PTH Dry Storage Container
- 32PTH Horizontal Storage Module
- OS187H Transfer Cask

The reinforced concrete 32PTH HSM-H, including the 32PTH-DSC support structure, the 32PTH-DSC, and the structural components of the OS187H transfer cask are important to safety of NUHOMS[®] HD System components. Consequently, they are designed and analyzed to perform their intended functions under the extreme environmental and natural phenomena specified in 10CFR 72.122 [3] and ANSI 57.9 [9]. These include tornado and wind, seismic, and flood design criteria.

This section addresses component specific design criteria, loads, and load combinations for the structural analyses of the 32PTH DSC, 32PTH HSM-H and the OS187H Transfer Cask.

3.1.2.1 32PTH DSC Structural Design Criteria

3.1.2.1.1 32PTH DSC Stress Criteria

A. 32PTH DSC Shell Stress Limits

The stress limits for the DSC shell are taken from the ASME Boiler and Pressure Vessel Code, Section III, Subsection NB, Article NB-3200 for Level A through D Service Limits [12]. In accordance with NB-3225, Appendix F [13] is used for accident condition loads (Level D).

The stress due to each load shall be identified as to the type of stress induced, e.g. membrane, bending, etc., and the classification of stress, e.g. primary, secondary, etc.

Stress limits for Level A through D service loading conditions are summarized in Table 3-2. Local yielding is permitted at the point of contact where Level D load is applied. If elastic stress limits cannot be met, the plastic system analysis approach and acceptance criteria of Appendix F of Section III shall be used.

The allowable stress intensity value, S_m , as defined by the Code, is to be based on the calculated (or a bounding) temperature for each service load condition.

B. 32PTH DSC Basket Stress Limits

The basket fuel compartment tube wall thickness is established to meet heat transfer, nuclear criticality, and structural requirements. The basket structure must provide sufficient rigidity to maintain a sub-critical configuration under the applied loads.

The stress analyses of the basket do not take credit for the poison plates except for through thickness compression. However, the weight of the poison plate is considered when determining stresses in the stainless steel.

The basis for the stainless steel fuel compartment section stress allowables is the ASME Code, Section III, Subsection NG [14]. Stress limits for Level A through D service loading conditions are summarized in Table 3-3.

Alternatively, and in accordance with NG-3222 and Note 9 to Figure NG-3221-1, the Limit Analysis provisions of NG-3228 may be used for Level A Service Limits.

The basket shall be evaluated under Level D Service loadings in accordance with the Level D Service limits for components in Appendix F [13] of Section III of the Code. The hypothetical impact accidents are evaluated as short duration Level D conditions.

For fusion welds between the stainless steel plates and the stainless steel fuel compartments shall be qualified by testing. The required minimum tested capacity of the weld connection shall be based on a margin of safety (test to design) of 2.0, corrected for temperature difference between testing and basket operating conditions and the maximum weld load at any weld location in the basket. This margin of safety, 2, is larger than the ASME Code-implied margin of safety for level D loads. The minimum capacity shall be determined by shear test (pull test) of individual

specimen made from production material. In addition to the ASME Code requirements for weld qualification, as part of the weld qualification procedure, in order to verify proper machine setting and operation, a shear test (pull test) of test coupon from each welding machine will be performed prior to the start of each working shift.

3.1.2.1.2 32PTH DSC Stability Criteria

The critical loads for buckling of the DSC shell, basket, and transfer cask shell will be calculated using ANSYS finite element Nonlinear Buckling Analysis. This technique employs a nonlinear static analysis with gradually increased loads to seek the load level at which the structure becomes unstable. Using nonlinear option, the model can include features such as plastic material behavior, gaps and large-deflection response. Reasonable safety factors for the allowable buckling loads will be provided to take into account material and geometrical imperfections.

3.1.2.2 HSM-H Structural Design Criteria

The HSM-H concrete and steel components shall be designed to the requirements of ACI 349 [15] and the AISC Manual of Steel Construction [16], respectively, meeting the load combinations in accordance with the requirements of ANSI 57.9 [9]. A detail design criteria is described in Appendix 3.9.9.

3.1.2.3 OS187H Transfer Cask Structural Design Criteria

The OS187H TC is designed to meet the criteria of ASME Code Subsection NC [7] for Class 2 components. Service Level A allowables are used to for all normal operating and off-normal loadings. Service Level D allowables are used for load combinations that include postulated accidents loadings. The OS187H Transfer Cask allowable stresses for normal and accident conditions are summarized in Table 3-4.

3.2 Weights

The nominal DSC, HSM-H and OS187H Transfer Cask geometry is used to compute the weights of the NUHOMS[®] HD system components.

The following densities are used to compute the component weights.

NUHOMS[®] HD Component Material Densities

Material	Density (lb./in³.)	Reference
Stainless Steel	0.29	10
Aluminum	0.098	10
Water	0.0361	10
Lead	0.41	10
Resin (neutron shield) ⁽¹⁾	0.065	Table 5-17, Chapter 5

Note:

- (1) The actual resin density from Table 5-17 is 0.057 lb/in³. However, a higher density of 0.065 lb/in³ is utilized to conservatively compute higher neutron resin weight.

3.2.1 32PTH DSC Weight

The total weight of the loaded 32PTH DSC is 109.56 kips (54.78 tons). The weights of the major individual subassemblies are listed in following table.

32PTH DSC Summary of Nominal Component Weights

Component	Nominal Weight (lbs. x 1000)
Canister Shell	5.86
Outer Top Cover Plate	2.14
Top Shield Plug and Support Ring	10.71
Bottom Shield Plug	9.42
Grapple Ring	0.06
Total Canister Assembly	28.19
Fuel Compartments (32)	10.02
Aluminum Plates	3.73
Poison Plates	0.55
Stainless Steel Plates	1.94
Small Support Rails (4)	3.24
½ Large Support Rails (8)	10.38
Total Fuel Basket	29.85
Total Empty DSC (Basket & Canister)	58.04
Fuel Assembly Weight (32) @ 1610 lbs/assembly	51.52
Total Loaded DSC Weight	109.56

3.2.2 OS187H Transfer Cask Weight

The total weight of the loaded NUHOMS®-OS187H Transfer Cask is 229.5 kips (114.8 tons). The weights of the major individual subassemblies are listed in following table.

OS187H Transfer Cask Summary of Nominal Component Weights

Component	Nominal Weight (lbs. x 1000)
Structural Shell	20.85
Inner Shell	5.86
Lead Gamma Shield	62.37
Top Flange	3.18
Bottom Flange	3.37
Top Cover Assembly	5.20
Bottom Assembly	3.46
Neutron Shield Panel	4.29
Radial Neutron Shield (water)	8.46
Upper Trunnion Pair	1.61
Lower Trunnion Pair	1.27
Total Empty Transfer Cask Weight	119.95
Total Transfer Cask with Empty DSC Weight	178.00
Total Transfer Cask with Loaded DSC Weight	229.5

Note: 250.0 kips is conservatively used for trunnion analysis.

3.2.3 HSM-H Weight

The following table summarizes the weights of the loaded HSM-H single module.

Summary Weights of 32PTH HSM-H

Component	Nominal Weight (lbs. x 1000)
HSM-H Single Module Weight (empty)	306.1
Total Empty DSC (Basket & Canister)	58.04
Fuel Assembly Weight (32)	51.52
Total Loaded HSM-H Weight	415.66

3.3 Mechanical Properties of Materials

3.3.1 32PTH-DSC Material Properties

The principal material of construction for the 32PTH DSC is Type 304 stainless steel. The 32PTH DSC cylindrical shell, cover plates and shield plugs are constructed from SA-240 Type 304 stainless steel for plate material and SA-182 F304 for forging material. The 32PTH DSC basket assembly fuel compartments and structural plate assemblies are also constructed from SA-240 Type 304 or equivalent stainless steel. Table 3-5 contains the ASME Code material properties for SA-240 Type 304 and SA-182 F304 stainless steel materials.

The neutron absorber plates are constructed from boron carbide/aluminum metal matrix composite material and the aluminum thermal conduction plates are constructed from B-209 (Type 1100 Aluminum). No structural credit is taken for either the neutron absorber plates or the aluminum thermal conducting plates, except for through the thickness load transmission.

3.3.1.1 Radiation Effects on 32PTH DSC Materials

Gamma radiation has no significant effect on metals. The effect of fast neutron irradiation of metals is a function of the integrated fast neutron fluence, which is on the order of 1×10^{15} neutrons/cm² inside the 32PTH DSC after 50 years. Studies on fast neutron damage in stainless steel, and low alloy steels rarely evaluate damage below 10^{17} n/cm² because it is not significant [17]. Extrapolation of the data available down to the 10^{15} range confirms that there will be no measurable neutron damage to any of the 32PTH DSC metallic components.

3.3.1.2 DSC Weld Material

Welding processes, welders and welding materials used for the welding of the 32PTH DSC meet the requirements of the appropriate ASME Section III subsections and Section IX. Non-Code welds meet the provisions of Section IX of the ASME Code or AWS D1.1 [18] or D1.6 [19]. Weld metal material properties meet the requirements of Section II of the ASME Code or associated AWS requirements.

3.3.1.3 DSC Material Brittle Fracture

Brittle fracture is not a concern for the stainless steel components, which comprises all structural components of the DSC.

3.3.2 HSM-H Material Properties

The temperature dependent material properties for concrete and reinforcing steel are provided in Tables 3-6 and 3-7. The material properties of the ASTM A992 steel used for fabrication of the rail support structures are listed in 3-7A. The material properties for type 304 used for the heat shield support plate are provided in Table 3-5. The A-36 steel used for rail assembly extension plate is provided Table 3-7B.

3.3.2.1 Radiation Effects on HSM-H Concrete

The accumulated neutron flux over a 40 year service life of the HSM-H is estimated to be 1.5×10^{14} neutrons/cm². From the study by Hilsdorf, Kropp, and Koch [20], the compressive strength and modulus of elasticity of concrete is not affected by a neutron flux of this magnitude.

The gamma energy flux deposited in the HSM-H concrete is 1.7×10^9 MeV/cm²-sec. or 3.0×10^{-4} watt/cm². According to ANSI/ANS-6.4-1977 [21], the temperature rise in concrete due to this level of radiation is negligible. Thus, radiation effects on concrete strength are not evaluated further for the HSM-H design.

3.3.2.2 HSM-H Materials Durability

As shown in Table 3-5 through Table 3-7B, all materials meet the appropriate requirements of the ASME Code, ACI Code, and ASTM Standards. The durability of the steel components is well beyond the design life of the applicable components. The specifications controlling the mix of concrete, specified minimum concrete strength requirements, and fabrication control ensure durability of the materials for this application.

3.3.3 OS187H Transfer Cask Material Properties

The principal material of construction for the OS187H transfer cask is Type 304 stainless steel. The transfer cask structural, inner and outer neutron shield shells and the bottom closure assembly are constructed from SA-240 Type 304 stainless steel. The primary structural member of the top cover plate is constructed from SA-240 Type XM-19 stainless steel. Table 3-5 contains the ASME Code material properties for SA-240 Type 304 stainless steel material. ASME Code material properties for the top cover material (SA-240 Type XM-19) are given in Table 3-8.

The transfer cask top cover and ram access cover bolts are constructed from SA-540 Grade B24 Class 1. ASME Code material properties for SA-540 Grade B24 Class 1 are given in Table 3-9.

Material properties for ASTM B-29 (Chemical Lead), which is used for the transfer cask radial gamma shield, are given in Table 3-10.

The outer radial neutron shield consists of a SA-240 Type 304 stainless steel shell that contains the neutron absorbing material (water). The top and bottom axial neutron absorber resin material is, described in Section 3.1.1.3 B. No structural credit is taken for the neutron absorber material, except for through the thickness load transmission. Material Properties for the resin are given in Table 3-11.

3.3.3.1 Radiation Effects on the Transfer Cask Materials

Gamma radiation has no significant effect on metals. The effect of fast neutron irradiation of metals is a function of the integrated fast neutron fluence, which is on the order of 1×10^{15} neutrons/cm² inside the cask after 50 years. Studies on fast neutron damage in stainless steel, and low alloy steels rarely evaluate damage below 10^{17} n/cm² because it is not significant [17]. Extrapolation of the data available down to the 10^{15} range confirms that there will be no measurable neutron damage to any of the cask metallic components.

3.3.3.2 Transfer Cask Weld Material

Welding processes, welders and welding materials used for the welding of the 32PTH DSC meet the requirements of the appropriate ASME Section III subsections and Section IX. Non-Code welds meet the provisions of Section IX of the ASME Code or AWS D1.1 [18] or D1.6 [19]. Weld metal material properties meet the requirements of Section II of the ASME Code or associated AWS requirements.

3.3.3.3 Transfer Cask Brittle Fracture

Brittle fracture is not a concern for the stainless steel components, which comprises all structural components of the cask.

3.4 General Standards for 32PTH DSC, HSM-H, and OS187H TC

3.4.1 Chemical and Galvanic Reactions

The materials of the DSC shell and basket assemblies, the HSM-H, and the transfer cask components have been reviewed to determine whether chemical, galvanic or other reactions among the materials, contents and environment might occur during any phase of loading, unloading, handling or storage.

The canister, transfer cask, and HSM-H are exposed to the following environments:

- During loading and unloading, the canister is inside of the transfer cask. Thus, the exterior of the canister will not be exposed to pool water. The annulus between the transfer cask and canister is filled with clean water and sealed.
- The interior surfaces of the canister, top shield plug, and the basket will be exposed to (borated) pool water. The transfer cask and canister are kept in the spent fuel pool for only about 6 hours to load or unload fuel, and 2 hours to lift the loaded transfer cask/canister out of the spent fuel pool. An additional 12 to 24 hours is typically needed to decontaminate the cask, weld the DSC cover, and drain the water.
- The canister is vacuum dried before storage. It is then backfilled with helium, thus providing a non-corrosive environment. During storage, the interior of the canister is exposed only to the helium environment. The dry helium environment does not support chemical or galvanic reactions.
- During storage, the exterior of the canister is protected by the concrete HSM-H. The HSM-H is vented, so the exterior of the canister is exposed to the atmosphere. The exterior is exposed to the weather.

Materials used for the DSC, transfer cask, and HSM-H are shown in the parts lists of the drawings provided in Chapter 1, Section 1.5.

Within the canister, there is a basket with support rails made from SA-240 Type 304 stainless steel with aluminum inserts. The basket structure consists of an assembly of stainless steel tubes (fuel compartments) separated by aluminum and neutron absorber plates. The basket fuel compartments are constructed from Type 304 stainless steel. The neutron absorber is borated aluminum alloy or composite sandwiched. The neutron poison plates are not welded or bolted to the fuel compartments, but are held in place by the fuel compartments and the stainless steel structural plates. The aluminum thermal conduction plates are constructed from Type 1100 aluminum.

The only potential galvanic couples are the low alloy steel transfer cask bolts and hoist rings with stainless steel, and stainless steel with aluminum in the DSC. The lid, test, drain cover, and ram cover bolts will be exposed to the weather or pool water for only a short period during DSC transfer. Galvanic corrosion during transfer will be negligible and will have no adverse affect on design functions. Furthermore, the bolts are subject to periodic inspection per Section 9.2.1. The couple of stainless steel and aluminum is discussed in Section 3.4.1.2.

Typical water chemistry in a PWR spent fuel pool is as follows:

pH (77 °F)	4.5 – 9.0
Chloride, max	0.15 ppm
Fluoride, max	0.1 ppm
Dissolved Air, max	Saturated
Lithium, max	2.5 ppm
Boric Acid	2,100 – 2,600 ppm
Pool Temperature Range	40 – 140 °F

3.4.1.1 Behavior of Austenitic Stainless Steel (DSC and Transfer Cask)

With the exception of the low alloy and aluminum parts noted above, all exposed surfaces of the transfer cask and the canister are stainless steel Type 304, Nitronic 60, or XM-19. Stainless steel does not exhibit general corrosion when immersed in borated water.

The chloride ion concentration and exposure duration are too short to cause stress corrosion cracking in the stainless steel welds, which may have residual fabrication stresses. Although stress corrosion cracking can take place at very low chloride concentrations and temperatures such as those in spent fuel pools (less than 10 ppb and 160 °F, respectively), the effect of low chloride concentration and low temperature is to greatly increase the initiation time, that is, the period during which the corrodent is breaking down the passive oxide film on the stainless steel surface. Below 60 °C (140 °F), stress corrosion cracking of austenitic stainless steel does not occur at all. At 100 °C (212 °F), chloride concentration on the order of 15% is required to initiate stress corrosion cracking [24]. At 288 °C (550 °F), with tensile stress at 100% of yield in PWR water containing 100 ppm O₂, time to crack is about 40 days in sensitized 304 stainless steel [24]. Thus, the combination of low chlorides, low temperature and short time of exposure to the corrosive environment eliminates the possibility of stress corrosion cracking in the fuel compartment welds.

3.4.1.2 Behavior of Aluminum (DSC Basket)

Aluminum is used for many applications in spent fuel pools. In order to understand the corrosion resistance of aluminum within the normal operating conditions of spent fuel storage pools, a discussion of each of the types of corrosion is addressed separately. None of these corrosion mechanisms are expected to occur in the short time period that the cask is submerged in the spent fuel pool.

General Corrosion

General corrosion is a uniform attack of the metal over the entire surfaces exposed to the corrosive media. The severity of general corrosion of aluminum depends upon the chemical nature and temperature of the electrolyte and can range from superficial etching and staining to dissolution of the metal. Figure 3-1 shows a potential -pH diagram for aluminum in high purity water at 77 °F [25]. The potential for aluminum coupled with stainless steel and the limits of pH for BWR pools are shown in the diagram to be well within the passivation domain. The passivated surface of aluminum (hydrated oxide of aluminum) affords protection against corrosion in the domain shown because the coating is insoluble, non-porous and adherent to the

surface of the aluminum. The protective surface formed on the aluminum is known to be stable up to 275 °F and in a pH range of 4.5 to 8.5 [25].

Galvanic Corrosion

Galvanic corrosion is a type of corrosion which could cause degradation of dissimilar metals exposed to a corrosive environment for a long period of time.

Galvanic corrosion is associated with the current of a galvanic cell consisting of two dissimilar conductors in an electrolyte. The two dissimilar conductors of interest in this discussion are aluminum and stainless steel in deionized water. There is less galvanic current flow between the aluminum-stainless steel couple than the potential difference on stainless steel which is known as polarization. It is because of this polarization characteristic that stainless steel is compatible with aluminum in all but severe marine, or high chloride, environmental conditions [26].

Pitting Corrosion

Pitting corrosion is the forming of small sharp cavities in a metal surface. The first step in the development of corrosion pits is a local destruction of the protective oxide film. Pitting will not occur on commercially pure aluminum when the water is kept sufficiently pure, even when the aluminum is in electrical contact with stainless steel. Pitting and other forms of localized corrosion occur under conditions like those that cause stress corrosion, and are subject to an induction time which is similarly affected by temperature and the concentration of oxygen and chlorides. As with stress corrosion, at the low temperatures and low chloride concentrations of a spent fuel pool, the induction time for initiation of localized corrosion will be greater than the time that the cask internal components are exposed to the aqueous environment.

Crevice Corrosion

Crevice corrosion is the corrosion of a metal that is caused by the concentration of dissolved salts, metal ions, oxygen or other gases in crevices or pockets remote from the principal fluid stream, with a resultant build-up of differential galvanic cells that ultimately cause pitting. Crevice corrosion could occur at the contact surfaces between the aluminum plates, neutron absorber, and fuel compartment tubes.

Due to the short time in the spent fuel pool, this type of corrosion is not expected to be significant.

Intergranular Corrosion

Intergranular corrosion is corrosion occurring preferentially at grain boundaries or closely adjacent regions without appreciable attack of the grains or crystals of the metal itself. Intergranular corrosion does not occur with commercially pure aluminum and other common work hardened aluminum alloys.

Stress Corrosion

Stress corrosion is failure of the metal by cracking under the combined action of corrosion and high stresses approaching the yield stress of the metal. During normal operations there are negligible loads, mostly compressive, imposed on the aluminum parts.

3.4.1.3 Behavior of Aluminum Based Neutron Poison (DSC Basket)

The aluminum component of the borated aluminum is a ductile metal having a high resistance to corrosion. Its corrosion resistance is provided by the buildup of a protective oxide film on the metal surface when exposed to a corrosive environment. As stated above for aluminum, once a stable film develops, the corrosion process is arrested at the surface of the metal. The film remains stable over a pH range of 4.5 to 8.5.

Tests were performed by Eagle Picher [29] which concluded that borated aluminum exhibits a strong corrosion resistance at room temperature in deionized water. Satisfactory long-term usage in these environments is expected. At high temperature, the borated aluminum still exhibits high corrosion resistance in the pure water environment.

From tests on pure aluminum, it was found that borated aluminum was more resistant to uniform corrosion attack than pure aluminum.

An alternate neutron poison material is a boron carbide / aluminum composite, which is a matrix of full-density aluminum with a fine dispersion of boron carbide particles throughout. The corrosion behavior is similar to that of the base aluminum alloy.

The third neutron poison material is Boral[™]. The faces of the Boral sheet are 1100 aluminum, while the aluminum/boron carbide core is exposed at the edges of the sheet. There are no chemical, galvanic or other reactions that could reduce the areal density of boron in any of the poison plate materials for the 32PTH DSC. Boral[™] is a proven neutron poison used extensively in spent fuel storage racks. The short term exposure of the material to borated water in the spent fuel storage canisters will have significantly less effect on the Boral[™] than that experienced in spent fuel pools.

3.4.1.4 Behavior of HSM Materials

The exterior of the HSM-H is exposed to the weather. The interior is dry, and is subject to the thermal and radiological environment created by the decay of the spent fuel stored in the DSC. Chapter 4 demonstrates that the concrete remains below its operational temperature limit under all normal and off-normal conditions.

If an ISFSI site is located in a coastal salt water marine atmosphere, then any load-bearing carbon steel DSC support structure rail components of any associated HSM-H shall be procured with a minimum of 0.20 percent copper content for corrosion resistance.

The sliding surface of the support rails for the DSC consists of Nitronic[®] 60 or equivalent stainless steel. Carbon steel embedments in the HSM-H concrete are coated to protect them from corrosion or they may be stainless steel. Other carbon steel components such as bolts, nuts, tie

plates, etc., are also coated. Bird screens are stainless steel. For the side heat shield with fins, the side facing the DSC is made of anodized aluminum. The side facing the HSM-H concrete is plain aluminum surface.

Because of the coatings and the dry environment, degradation of concrete or steel parts inside the HSM-H is unlikely. Exterior parts or surfaces are also visible and accessible, and if any degradation occurs from exposure to weather, it can be corrected.

3.4.1.5 Lubricants, Sealants, and Cleaning Agents

Lubricants may be used to coat the slide rails, the threads and shoulders of bolts, o-rings, and the contact areas of the trunnions. Lubricants are generally selected from the list of materials approved for contact with the pool water at the facility where wet loading occurs.

Sealants may be used at pipe threads, e.g., at quick connect fittings.

The transfer cask and DSC are cleaned during fabrication using procedures approved by Transnuclear. After loading, exterior surfaces of the cask will be decontaminated using procedures and decontamination agents approved at the loading facility.

The cleaning agents, sealants, and lubricants have no significant effect on the cask and canister materials.

3.4.1.6 Hydrogen Generation

There is no mechanism for galvanic corrosion in the space between the DSC and the transfer cask, because both the inner shell of the TC and the outer shell of the DSC are stainless steel, and because the canister is sealed before the lid is placed on the transfer cask. Therefore, any concern for hydrogen generation applies solely inside the canister during wet loading.

Monitoring of the hydrogen concentration before and during welding operations will be performed to ensure that the hydrogen concentration does not exceed 2.4%. If the concentration exceeds 2.4%, welding operations will be suspended and the DSC will be purged with an inert gas.

Numerous NUHOMS[®] canisters fabricated using aluminum, neutron absorber, and stainless steel have been loaded in both borated and deionized water. Hydrogen monitoring has measured hydrogen in the range 0-2%, well below the 4% lower limit of flammability, provided that sufficient plenum space is provided between the water in the DSC and the inner top cover/shield.

3.4.1.7 Polymers (Transfer Cask and DSC)

The transfer cask lid and port cover o-rings may be fluorocarbon, silicone, EPDM, or other material with a service temperature range from -15 °F to 300 °F. Accident conditions assume the loss of the transfer cask seal, whose function is to retain helium, not radionuclides. All sealing surfaces are stainless steel 304 or XM-19. Quick connect fittings and the neutron shield pressure relief valve also contain elastomer seals. The o-rings and quick connect fittings are subject to periodic inspection per Section 9.2.1.

The axial neutron shield is a proprietary reinforced polymer. The fire retardant mineral fill makes it self-extinguishing. Furthermore, the material is contained inside a steel shell, so that it is retained in place and isolated from sources of ignition. The trunnion plugs include polypropylene neutron shielding in Type 304 or Type XM-19 stainless steel. Polypropylene is slow burning to non-burning according to Table 24, Section 1 of the Handbook of Plastics and Elastomers [32].

Chapter 4 demonstrates that the transfer cask o-rings and solid neutron shielding remain below the upper limit of their service temperature. Polymers such as these used in the transfer cask have been demonstrated to be adequate for use in continuous thermal and radiation environments of spent fuel storage for 40 years duration. The intermittent usage of the transfer cask is less challenging for these materials.

The DSC uses o-rings at the connection of the drain tube to the inner top cover/shield, and in the quick connect fittings. The long term exposure to the thermal and radiation environment inside the DSC is likely to cause hardening of these seals. These seals do not provide any confinement function for either helium or radionuclides, and their function is not essential to refueling and fuel removal operations.

3.4.1.8 Coatings (Transfer Cask)

Corrosion-resistant coatings are optional on transfer cask alloy steel bolts.

3.4.1.9 Effect of Degradation Mechanisms on the Performance of the System

For the environment and materials of the NUHOMS[®] HD system, there is no chemical, galvanic, thermal, or radiological reaction or degradation mechanism that would have a measurable adverse effect on design functions. There are no significant reactions that could reduce the overall integrity of the HSM, transfer cask, canister, or the spent fuel during storage. There are no reactions that would cause binding of the mechanical surfaces or of the fuel to fuel compartments.

3.4.2 Positive Closure

Positive closure is provided by the redundant closure welds for the inner top cover / shield and outer top cover plate and by the leak-tight DSC shell assembly.

3.4.3 Lifting Devices

There are no permanent lifting devices used for lifting a loaded DSC. The loaded DSC is always inside a transfer/transportation cask during handling.

The evaluation of lifting devices is performed in the transfer system (see Appendix 3.9.5).

3.4.4 Heat

3.4.4.1 Summary of Pressures and Temperatures

Temperatures and pressures for the 32PTH DSC, HSM-H and OS187H Transfer Cask are described in Chapter 4. Section 4.3 and Section 4.4 describe the thermal evaluations performed for normal, off-normal, and accident conditions. Section 4.5 describes the thermal evaluations during fuel loading/unloading operations. Maximum and minimum temperatures for the various components of the NUHOMS[®] HD System for normal, off-normal, and accident conditions are summarized in Table 4-1 to 4-6. These temperatures are used for the structural evaluations documented in Sections 3.6 and 3.7. Stress allowables for the cask components are a function of component temperature. The temperatures used to perform the structural analysis are based on actual calculated temperatures or conservatively selected higher temperatures.

Table 4-10 provides a summary of the maximum 32PTH DSC pressures for normal, off-normal and accident conditions. The pressures used in the 32PTH DSC stress analyses in Appendix 3.9.1 bound those summarized in Table 4-10.

3.4.4.2 Differential Thermal Expansion

Potential interference due to differential thermal expansion between the 32PTH DSC shell assembly, the basket assembly, and transfer cask components is evaluated in Appendix 3.9.1, Section 3.9.1.4.

3.4.4.3 Stress Calculations

The stress analyses have been performed using the acceptance criteria presented in Section 3.1.2. The structural analyses for the 32PTH DSC, the HSM-H and OS187H Transfer Cask are summarized in Sections 3.6 and 3.7, for normal, off-normal, and hypothetical accident conditions, respectively.

3.4.5 Cold

The 32PTH DSC and OS187H TC lifting, structural, and confinement materials are Type 304 and Type XM-19 stainless steels that are not subject to brittle fracture, so they do not impose a limit on low temperature operations. Cask lid and ram access port seal o-ring operating temperatures are -15 to -40 F depending on the material. The seal function is not confinement of radioactive material, but retention of helium for heat rejection. At very low ambient temperatures, this is not a concern, so the seal operating temperature lower limit does not impose an operations limit on the NUHOMS[®] HD system.

For operations below 32 °F, operations shall make provision to prevent freezing of water in the neutron shield.

3.5 Fuel Rods General Standards for 32PTH DSC

This section provides the temperature criteria used in the 32PTH DSC thermal evaluation for the safe storage and handling of SFA's in accordance with the requirements of 10CFR 72. This section also contains the analysis of the thermal and irradiation growth of the fuel assemblies to ensure adequate space exists within the 32PTH DSC cavity for the fuel assemblies to grow thermally under all conditions.

In addition, this section provides an evaluation of the fuel rod stresses and critical buckling loads due to accident drop loads.

3.5.1 Fuel Rod Temperature Limits

The fuel rod temperature limits during transfer operation and storage are defined by Interim Staff Guidance, ISG-11, revision 3 [39]. The temperature limits are summarized in the following table.

Transfer		Storage	
Normal/Off Normal	Accident	Normal	Off Normal/Accident
752°F	1058°F	752°F	1058°F

3.5.2 Fuel Assembly Thermal and Irradiation Growth

The thermal and irradiation growth of the fuel assemblies were calculated to ensure there is adequate space for the fuel assemblies to grow within the 32PTH DSC canister cavity. Detail thermal expansion evaluations of canister cavity versus lengths of basket and fuel assembly, canister ID vs. basket OD, canister OD vs. transfer cask ID, and overall length of canister vs. transfer cask cavity length are included in Appendix 3.9.1, Section 3.9.1.4.

The extreme metal temperatures for the fuel cladding and canister under different cases are obtained from Chapter 4 for computation of the differential length growth. These temperatures are conservatively rounded and used in this calculation as listed in the following table.

Thermal Expansion Evaluation Cases

Cases \ Component Temperature	Length Growth Between Fuel Cladding and Canister	
	Fuel Cladding Temp. (°F)	Canister (DSC Shell) Temp. (°F)
Vacuum Drying	750	210
Transfer	730	390
Storage – Off Normal	700	310
Storage – Blocked Vent	810	500

The following table summarizes the minimum gap between the canister cavity and the fuel assembly in the above thermal cases.

	Thermal Load Cases			
	Vacuum Drying	Transfer	Storage – Off Normal	Storage – Blocked Vent
Fuel assembly length	162.4 in.	162.4 in.	162.4 in.	162.4 in.
Total thermal growth	0.4 in.	0.38 in.	0.36 in.	0.43 in.
Irradiation growth	1.25 in.	1.25 in.	1.25 in.	1.25 in.
Total fuel assembly length after thermal growth	164.05 in.	164.03 in.	164.01 in.	164.08 in.
Min. canister cavity length	164.5 in.	164.5 in.	164.5 in.	164.5 in.
Canister thermal growth	0.2 in.	0.5 in.	0.3 in.	0.69 in.
Canister cavity length after thermal growth	164.7 in.	165.0 in.	164.8 in.	165.19 in.
Min. calculated gap	0.65 in.	0.97 in.	0.79 in.	1.11 in.

Based on the evaluations, there is adequate space within the 32PTH DSC cavity for thermal and irradiation growth of the fuel assemblies and spacers.

3.5.3 Fuel Rod Integrity During Drop Scenario

The purpose of this section is to calculate zircaloy clad fuel cladding stresses due to a transfer cask side drop.

3.5.3.1 Side Drop

The fuel rod side impact stresses are computed by treating the fuel rod as a continuous beam supported at locations of spacer grids. Continuous beam theory is used to determine the maximum bending moment in the entire beam. An ANSYS [33] finite element model of the fuel rod is created for each fuel type, using PIPE16 elements. The details of the finite element model geometry and equivalent densities are given computed in Table 3-12. The dimensions (lengths) of the fuel cladding for each fuel type are taken from reference [11]. The weight of fuel pellets is incorporated in the cladding model by using equivalent densities. The weights of the top and

bottom end fittings are distributed to the top and bottom spans of the fuel rod cladding models (Span L_T and Span L_B in Table 3-12). The typical details of finite element model and boundary conditions of fuel types WE 15x15 and WES 15x15 are shown on Figure 3-2.

The maximum bending stress corresponding to the maximum bending moment in the cladding tubes is calculated. The fuel gas internal pressure is also considered in the calculation. The cladding axial tensile stress due to the gas pressure is added to the bending stress due to the 75g drop load. In this elastic analysis, the 75g side drop load is applied as an acceleration. The maximum bending stresses for the fuel cladding from the ANSYS analyses are shown on Figures 3-3 to 3-7 and also summarized in Table 3-13.

3.5.3.2 End Drop

The structural integrity of the fuel cladding due to the end drop loading condition will be evaluated by the user under the 10CFR50 site license.

3.5.3.3 Results

Side Drop

Table 3-13 summarizes the maximum bending stresses in various specified fuel cladding during the 75g side drop of their transfer cask. All of the combined stresses are less than the yield strength of the irradiated cladding material (93,950 psi) with ample margin of safety. The maximum combined stress was calculated to be 76,931 psi in the cladding of the WE 15x15 fuel. It is less than the cladding yield strength of 93,950 psi at 725 °F.

3.5.4 Fuel Unloading

For unloading operations, the DSC will be filled with the spent fuel pool water through the siphon port. During this filling, the DSC vent port is maintained open with effluents routed to the plant's off-gas monitoring system.

When the pool water is added to a DSC cavity containing hot fuel and basket components, some of the water will flash to steam causing internal cavity pressure to rise. The steam pressure is released through the vent port. The initial flow rate of the reflood water must be controlled such that the internal pressure in the DSC cavity does not exceed 20 psig. This is assured by monitoring the maximum internal pressure in the DSC cavity during reflood event. The reflood of the DSC is considered as a "Service Level D" event and the design pressure of the DSC is 120 psig. Therefore, there is sufficient margin in the DSC internal pressure during the reflooding event to assure that the DSC will not be over pressurized.

The maximum fuel cladding temperature during reflooding process is significantly less than the vacuum drying condition owing to the presence of water/steam in the DSC cavity. Hence, the peak cladding temperature during the reflooding operation will be less than 734°F calculated in Chapter 4, Section 4.5.1.

To evaluate the effects of the thermal loads on the fuel cladding during reflooding operations, a conservative high fuel rod temperature of 750 °F and a conservative low quench water

temperature of 50 °F are used. These evaluations are performed in Chapter 4, Section 4.5.2. The calculated maximum fuel cladding stress is 25,910 psi. This calculated maximum stress is much less than the claddings yield stress of 69,500 psi. Therefore, cladding integrity is maintained during reflooding operation.

3.6 Normal Conditions of Storage and Transfer

This section presents the structural analyses of the 32PTH DSC, the HSM-H and the OS187H Transfer Cask subjected to normal conditions of storage and transfer. The analyses performed evaluate these three major NUHOMS[®] HD System components for the design criteria described in Section 3.1.2 of this chapter.

The 32PTH DSC is subjected to both storage and transfer loading conditions, while the HSM-H is only subjected to storage loading conditions and the OS187H Transfer Cask is only subjected to transfer loading conditions.

Numerical analyses have been performed for the normal and accident conditions, as well as for the lifting loads. In general, numerical analyses have been performed for the regulatory events. These analyses are summarized in the main body of this section, and described in detail in Appendices 3.9.1 through 3.9.9.

The detailed structural analysis of the NUHOMS[®] HD System is included in the following appendices:

Appendix 3.9.1	32PTH DSC (Canister and Basket) Structural Analysis
Appendix 3.9.2	OS187H Transfer Cask Body Structural Analysis
Appendix 3.9.3	OS187H Transfer Cask Top Cover and RAM Access Cover Bolts Analyses
Appendix 3.9.4	OS187H Transfer Cask Lead Slump and Inner Shell Buckling Analyses
Appendix 3.9.5	OS187H Transfer Cask Trunnion Analysis
Appendix 3.9.6	OS187H Transfer Cask Shield Panel Structural Analysis
Appendix 3.9.7	OS187H Transfer Cask Impact Analysis
Appendix 3.9.8	Damaged Fuel Cladding Structural Evaluation
Appendix 3.9.9	HSM-H Structural Analysis

The structural integrity of the fuel cladding due to the end and corner drops has not been demonstrated and should be addressed by the users under their 10CFR50 programs.

3.6.1 32PTH DSC Normal Conditions Structural Analysis

Details of the structural analysis of the 32PTH DSC are provided on Appendix 3.9.1. The Fuel Basket and Canister are analyzed independently. The Fuel Basket is analyzed in Appendix 3.9.1, Section 3.9.1.2, while the Canister is analyzed in Appendix 3.9.1, Section 3.9.1.3. Three separate finite element models are constructed for the structural evaluation of the fuel basket while four finite element models are used for the structural evaluation of the canister shell.

3.6.1.1 32PTH DSC Fuel Basket Normal Condition Structural Evaluation

The fuel basket stress analysis is performed for normal condition loads during fuel transfer and storage. The detailed stress analysis is presented in Appendix 3.9.1, Section 3.9.1.2.3. A summary of the fuel basket load cases is provided in Appendix 3.9.1, Section 3.9.1.2.2.

The basket stress analysis is performed using a finite element method for the transfer handling, storage dead weight, and both transfer and storage thermal load cases. A 3-dimensional cross-section finite element model is utilized to evaluate the effect of transverse inertial loads on the fuel basket. The finite element model is described in detail in Appendix 3.9.1, Section 3.9.1.2.3.A. Analytical calculations are used for the vertical dead weight load case.

The mechanical properties of structural materials used in the basket, rail and canister are shown in the Appendix 3.9.1, Tables 3.9.1-1 and 3.9.1-2 as a function of temperature. All structural components of the fuel basket and support rails are constructed from SA-240, Type 304 stainless steel, with properties taken from AMSE B&PV Code [10].

ANSYS nonlinear elastic stress analyses are conducted for computing the elastic stresses in the fuel basket model. The nonlinearity of analysis results from the gaps in the model. In general, for each load case, the maximum total load is applied in small steps. The automatic time stepping program option "Autots" is activated. This option lets the program decide the actual size of the load-substep for a converged solution. Where shell elements are used, the shell middle surface nodal stress intensity is the membrane stress intensity and top or bottom surface stress intensity is the membrane plus bending stress intensity.

The calculated stresses in the 32PTH DSC fuel basket under normal conditions are summarized and compared with the corresponding ASME code allowable stresses for transfer load cases in Appendix 3.9.1, Table 3.9.1-3 and storage load cases in Appendix 3.9.1, Table 3.9.1-5.

The fusion weld is qualified by a pull test (shear). The required minimum test load is 17.1 kips. This load corresponds to the maximum fusion weld loads generated during a 75g hypothetical accident impact with a safety factor of 2 and a correction for material strength for room temperature testing. The maximum force generated in the fusion welds due to transfer load is 1415 lb (Appendix 3.9.1) and thermal load in fusion weld during transfer is 631 lb (Appendix 3.9.1). The combined load is 2,046 lb (2.05 kip). This combined load is much smaller than the required test load of 17.1 kips.

Based on the results of these analyses, the design of the 32PTH DSC basket is structurally adequate with respect to normal condition transfer and storage loads.

3.6.1.2 32PTH DSC Canister Shell Normal Condition Structural Evaluation

This section summarizes the evaluation of the structural adequacy of the 32PTH DSC canister under all applied normal condition loads. Detail evaluation of the stresses generated in the canister is presented in Appendix 3.9.1, Section 3.9.1.3.2. The DSC canister shell buckling evaluation is presented in Appendix 3.9.1, Section 3.9.1.3.3.

An enveloping technique of combining various individual loads in a single analysis is used in this evaluation for several load combinations. This approach greatly reduces the number of computer runs while remains conservative. However, for some load combinations, the stress intensities under individual loads are added to obtain resultant stress intensities for the specified combined loads. This stress addition at the stress intensity level for the combined loads, instead of at component stress level, is also a conservative way to reduce numbers of analysis runs.

The ANSYS calculated stresses are the total stresses of the combined membrane, bending, and peak stresses. These total stresses are conservatively taken to be membrane stresses (P_m) as well as membrane plus bending stresses ($P_L + P_b$) and are evaluated against their corresponding ASME code stress limits. In the case where the total stresses, evaluated in this manner, exceed the ASME allowable stresses, a detailed stress linearization is performed to separate the membrane, bending, and peak stresses. The linearized stresses are then compared to their proper Code allowable stresses. ASME B&PV Code Subsection NB [12] is used for evaluation of loads under normal conditions. The thermal stress intensities are classified as secondary stress intensities, Q , for code evaluations.

Material properties obtained from Reference 10 for the 32PTH DSC canister materials, taken at the highest metal temperature of 500° F (from thermal evaluation presented in Chapter 4). The ANSYS Multilinear Kinematic Hardening material option of inelastic analysis is employed in the analyses of all canister accident side drops. A multi-linear stress-strain curve for type 304 stainless steel at 500° F is constructed using the yield and tensile stress values taken from Reference 10.

Elastic and elastic-plastic analyses are performed to calculate the stresses in the 32PTH DSC canister under the transfer and storage loads. These detail load cases are summarized in Appendix 3.9.1, Tables 3.9.1-9, 3.9.1-10 and 3.9.1-19.

The calculated stresses in the canister shell due to normal transfer loading conditions are summarized in Appendix 3.9.1, Tables 3.9.1-11, 12, 15, and 16. The stresses due to normal storage loading conditions are summarized in Appendix 3.9.1, Tables 3.9.1-20, and 21.

An alternate 32PTH DSC canister design with a composite top and/or bottom is also evaluated for their structural adequacy.

Details of the structural evaluation of the alternate canister composite bottom design under loads of normal conditions are provided in Appendix 3.9.1, Section 3.9.1.3.4. For the alternate canister composite bottom design, the stresses in the canister under the normal transfer loading conditions are summarized in Appendix 3.9.1, Tables 3.9.1-24, 25, 26, and 27. The loads under the normal storage conditions are bounded by the loads under the normal transfer conditions.

Under the loads of both the normal transfer and storage conditions, the stresses generated in the canister will not be significantly different between the canister designs with a one-piece top and with a composite top. SAR Drawing 10494-72-4, Rev. 0 shows the alternate composite top.

As described in Chapter 8, Section 8.1.1.3, operation steps 7 and 13, a maximum of 15 psig pressure may be applied at the canister vent port to assist draining of the water. Conservatively, the canister is structurally evaluated for a 60 psig internal pressure using the 2-D ANSYS finite element model described in Appendix 3.9.1, Section 3.9.1.3.2. The outer cover plate of the canister is removed from the 2-D model, since it is not yet installed during the application of this helium pressure. The maximum primary stress intensity and the maximum primary plus secondary stress intensity in the canister due to the 60 psig pressure load (conservatively used for stress calculation) are calculated to be 8,247 psi and 26,070 psi, respectively. Their corresponding stress limits as per ASME B&PV Code Subsection NB [12] are 16,400 psig and 49,200 psi, respectively. Based on this analysis, it concluded that the application of 15 psig pressure to the canister is conservative and acceptable.

Based on the results of these analyses, the design of the 32PTH DSC canister is structurally adequate with respect to both transfer and storage loads under the normal conditions.

The 32PTH DSC is also qualified for storage of WE 15x15 and WE 17x17 class fuel assemblies containing Instrument Tube Tie Rods (ITTRs).

The ITTR has been designed by Westinghouse to carry the entire weight of WE 15x15 or WE 17x17 class fuel assemblies during lifting/handling. In the event of a potential failure of all of the Type 304 stainless steel sleeves, the ITTR provides a load path that bypasses the sleeve bulge joint and allows the fuel assembly to be handled by the top nozzle using standard fuel handling tools.

Westinghouse has performed proprietary analyses [41, 42, 43 and 44] to document the acceptability of the ITTR to support the dead load of the FA during lifting operations. The Westinghouse analyses were performed under three types of loading conditions: 1g lifting, 2g lifting and lateral translation in fuel pool water with up to a recommended velocity of 2.0 ft/sec. The Westinghouse analyses demonstrate that the ITTR concept meets the design goal of no elastic yield of the ITTR or the FA components under all the three scenarios and allows for these FAs containing ITTRs to be handled using standard fuel handling tools and procedures described in Chapters 8 and A.8.

The maximum allowed fuel assembly weight is 1,610 lbs per Section 3.2.1. The combined weight of the ITTR and the WE 15x15 or WE 17x17 class fuel assembly used in the Westinghouse evaluations documented in [41, 42, 43 and 44] is less than this weight. Hence, the structural analysis presented in Section 3.6 above remains bounding for the WE 15x15 and WE 17x17 class fuel assemblies containing ITTRs.

3.6.2 HSM-H Normal Conditions Structural Analysis

The design of the HSM-H for 32PTH DSC is the same as the HSM-H documented in Appendix P of the CoC 1004 UFSAR with certain adjustments to accommodate larger diameter 32PTH DSC. Analyses performed for HSM-H with 24PTH DSC used bounding values to envelop both 24PTH DSC and 32PTH DSC. Following table shows how the bounding loads are used for structural evaluation of the HSM-H.

	Weight	Thermal
24PTH DSC (loaded weight)	93.7 kips	40.8 kw
32PTH DSC (loaded weight)	109.56 kips	34.8 kw
Weight used for HSM-H structural evaluation to envelop both 24PTH & 32PTH	110.0 kips (max.) ⁽¹⁾ 72.0 kips (min.) ⁽²⁾	
Thermal load used for HSM-H structural evaluation to envelop both 24PTH & 32PTH		40.8 kw

Notes:

1. Maximum weight is used for structural evaluation of the HSM-H.
2. Minimum weight is used for stability evaluation of the HSM-H.

Detail geometry descriptions, material properties, loadings, and structural evaluation of the HSM-H as presented in Appendix P of the CoC 1004 UFSAR is reproduced and included in Appendix 3.9.9 of this chapter.

3.6.3 OS187H Transfer Cask Normal Conditions Structural Analysis

Details of the structural analysis of the OS187H Transfer Cask are provided in Appendices 3.9.2 through 3.9.7. The contents of each of these appendices are as follows.

- 3.9.2 OS187H Transfer Cask Body Structural Analysis
- 3.9.3 OS187H Transfer Cask Lid and RAM Access Cover Bolt Analyses
- 3.9.4 OS187H Transfer Cask Lead Slump and Inner Shell Buckling Analyses
- 3.9.5 OS187H Transfer Cask Trunnion Analysis
- 3.9.6 OS187H Transfer Cask Shield Panel Structural Analysis
- 3.9.7 OS187H Transfer Cask Impact Analysis

3.6.3.1 Structural Analysis of the Transfer Cask Body under Normal Conditions

The details of the structural analyses of the NUHOMS®-OS187H Transfer Cask body including the cylindrical shell assembly and bottom assembly, the top cover, and the local stresses at the trunnion/cask body interface are presented in Appendix 3.9.2. The specific methods, models and assumptions used to analyze the cask body for the various individual loading conditions specified in 10CFR72 [3] are described in that appendix.

The OS187H transfer cask body structural analyses generally use static or quasistatic linear elastic methods. The stresses and deformations due to the applied loads are generally determined using the ANSYS [33] computer program.

Table 3.9.2-1 of Appendix 3.9.2 Summarizes the maximum stresses in the Transfer Cask Body computed for normal conditions of transfer. The maximum stresses in each component are listed

along with the normal loading condition that generates the stress. The results are evaluated against the ASME Code [7] design criteria described in Section 3.1.2 of this chapter.

Based on the results of these analyses, the design of the OS187H transfer cask is structurally adequate with respect to normal condition (Level A) transfer loads.

3.6.3.2 Transfer Cask Top Cover and RAM Access Cover Bolt Normal Condition Analysis

The detailed calculations for the top cover and RAM access cover bolts are presented in Appendix 3.9.3. The analysis is based on NUREG/CR-6007 [34]. The bolts are analyzed for the following normal loading conditions: operating pre-load, gasket seating load, internal pressure, and temperature changes.

The bolt preload is calculated to withstand the worst case load combination and to maintain a clamping (compressive) force on the closure joint, under normal conditions. Based upon the load combination results (see Appendix 3.9.3, Sections 3.9.3.3 and 3.9.3.8), it is shown that a positive (compressive) load is maintained on the clamped joint for all normal condition load combinations.

A summary of the calculated Top Cover bolt stresses is listed in Table 3-14 of this chapter. The calculations result in a maximum average tensile stress of 37.4 ksi, which is below the allowable tensile stress of 92.4 ksi for normal conditions. The maximum average shear stress in the bolts is due to torsion during pre-loading. This stress is 6.8 ksi, which is well below the allowable shear stress of 55.4 ksi. The maximum combined stress intensity due to tension plus shear plus bending is 74.0 ksi., which is also less than the maximum allowable stress intensity of 124.7 ksi.

A summary of the calculated RAM access bolt stresses is listed in Table 3-15 of this chapter. The analysis results in a maximum average tensile stress of 45.2 ksi, which is below the allowable tensile stress of 92.4 ksi for normal conditions. The maximum normal condition shear stress is 8.0 ksi, which is well below the allowable shear stress of 55.4 ksi. The maximum combined stress intensity due to tension plus shear plus bending is 97.0 ksi., which is also less than the maximum allowable stress intensity of 124.7 ksi.

3.6.3.3 Transfer Cask Normal Condition Trunnion Analysis

Appendix 3.9.5 presents the evaluation of the trunnion stresses in the NUHOMS[®]-OS187H Transfer Cask due to all applied loads during fuel loading and transfer operations.

NUHOMS[®] -OS187H transfer cask has two top trunnions constructed from SA-182 Gr. FXM19 and two bottom trunnions constructed from SA-182 Gr. F304. Both sets of trunnions are welded to the structural shell of the transfer cask, which is constructed from Type 304 stainless steel. The two top trunnions are used to first lift the cask, containing a canister and an empty basket, into a fuel pool for loading of the spent fuel. After the spent fuel has been loaded into the basket, the cask is lifted to a decontamination area. After draining and drying of the pool water, welding of the canister cover, and bolting of the cask lid, the cask is placed in a trailer for transfer to onsite HSM. The cask is vertically lifted onto the trailer and is initially supported by the bottom trunnions which are mated to transfer trailer. Then the cask is allowed to pivot about the bottom trunnions, into a horizontal position until the top trunnions rest on their supports in the trailer.

Throughout the operation the maximum total load is applied to the cask top trunnions. After the cask has been placed on the trailer, it is supported by all four trunnions and is subject to a set of specified design handling loads.

Based on the loading and transfer scenario described above, the top trunnions are analyzed for 6g vertical lifting loads, and both sets of trunnions are evaluated for the prescribed set of transfer handling loads.

The transfer cask shell and trunnions are assumed to be at 300° F during transfer. This assumption is conservative based on the thermal evaluation performed in Chapter 4.

The calculated maximum trunnion stresses are summarized in Appendix 3.9.5, Table 3.9.5-1 and compared with their corresponding allowable stresses. Table 3.9.5-1 shows that all calculated trunnion stresses are less than their corresponding allowable stresses. Therefore, the NUHOMS[®]-OS187H Transfer Cask top and bottom trunnions are structurally adequate to withstand loads during lifting and transfer operations.

3.6.3.4 Transfer Cask Shield Panel Structural Analysis for Normal Conditions

Appendix 3.9.6 presents the evaluation of the stresses in the NUHOMS[®]-OS187H Transfer Cask neutron shield shell due to all applied loads during fuel loading and transfer operations.

A finite element model was built for the structural analysis of the outer neutron shield shell, end closure, central plates and structural shell. These structural components were modeled with two dimensional axisymmetric elements. The same finite element model is used for all loading conditions.

Table 3.9.6-1 of Appendix 3.9.6 summarizes the calculated stresses for the transfer cask lifting and transfer loads. Based on the results of the analysis, it is concluded that the outer shell structure is structurally adequate for the specified transfer loads.

3.7 Off Normal and Hypothetical Accident Conditions

This section presents the structural analyses of the 32PTH DSC, the HSM-H and the OS187H Transfer Cask subjected to off normal and hypothetical accident conditions of storage and transfer. The analyses are summarized in Sections 3.7.1, 3.7.2 and 3.7.3 of this chapter and are evaluated against the design criteria described in Section 3.1.2 of this chapter.

The 32PTH DSC is subjected to both storage and transfer loading conditions, while the HSM-H is only subjected to storage loading conditions and the OS187H Transfer Cask is only subjected to transfer loading conditions.

The structural integrity of the fuel cladding due to the end and corner drops has not been demonstrated and should be addressed by the users under their 10CFR50 programs.

3.7.1 32PTH DSC Off Normal and Accident Conditions Structural Analysis

Details of the structural analysis of the 32PTH DSC are provided in Appendix 3.9.1. The Fuel Basket and Canister are analyzed independently. The Fuel Basket is analyzed in Appendix 3.9.1, Section 3.9.1.2, while the Canister is analyzed in Section 3.9.1.3. Three separate finite element models are constructed for the structural evaluation of the fuel basket, while four finite element models are used for the structural evaluation of the canister shell.

3.7.1.1 32PTH DSC Fuel Basket Off Normal and Accident Condition Structural Analysis

3.7.1.1.1 32PTH Fuel Basket Off Normal and Accident Condition Stress Analysis

The fuel basket stress analyses are performed for off normal and accident condition loads during fuel transfer and storage. The detailed stress analysis is presented in Appendix 3.9.1, Section 3.9.1.2.3. A summary of the fuel basket load cases is provided in Section 3.9.1.2.2.

The basket stress analyses are performed using a finite element method for the transfer side drop impact loads, as well as, storage seismic loads, and both transfer and storage thermal load cases. A 3-dimensional cross-section finite element model is utilized to evaluate the effect of transverse inertial loads on the fuel basket. The finite element model is described in detail in Appendix 3.9.1, Section 3.9.1.2.3.A. Analytical calculations are used for the axisymmetric transfer end drop load case.

The mechanical properties of structural materials used in the basket, rail and canister are shown in the Appendix 3.9.1, Tables 3.9.1-1 and 3.9.1-2 as a function of temperature. All structural components of the fuel basket and support rails are constructed from SA-240, Type 304 stainless steel, with properties taken from AMSE B&PV Code [10].

Nonlinear elastic stress analyses are conducted for computing the elastic stresses in the fuel basket model. The nonlinearity of analysis results from the gaps in the model. In general, for each load case, the maximum total load is applied in small steps. The ANSYS automatic time

stepping program option "Autots" is activated. This option lets the program decide the actual size of the load-substep for a converged solution. Where shell elements are used, the shell middle surface nodal stress intensity is the membrane stress intensity and the top or bottom surface stress intensity is the membrane plus bending stress intensity.

The calculated stresses in the 32PTH DSC fuel basket is summarized and compared with their corresponding ASME code allowable stresses. Tables 3.9.1-4a and 3.9.1-4b of Appendix 3.9.1 show these summaries for the transfer accident loads and Table 3.9.1-5 for the storage accident loads.

The maximum shear load in the fusion welds during the accident loading condition is calculated in Appendix 3.9.1. The calculated maximum shear force during side drop is 7,208 lb.

The fusion weld is qualified by a pull test (shear). The minimum test load is 17.1 kips. This test load includes a safety factor of 2 and a correction for material strength for room temperature testing.

Based on the results of these analyses, the design of the 32PTH DSC basket is structurally adequate with respect to off-normal and accident conditions of transfer and storage loads.

3.7.1.1.2 32PTH DSC Fuel Basket Accident Condition Buckling Analysis

Buckling analysis of the fuel basket plates and support rails are only performed for the bounding hypothetical accident condition impact loads. The accident condition buckling evaluation is presented in detail in Appendix 3.9.1, Section 3.9.1.2.4.

The NUHOMS[®] 32PTH1 basket with stainless steel rail design provided for the standardized NUHOMS[®] system in CoC 1004 (see UFSAR [40]) is identical to the NUHOMS[®] 32PTH basket design for the NUHOMS[®] HD system. The buckling evaluation for the 32PTH1 basket performed in Section U.3.7.4.3.3 of the CoC 1004 UFSAR [40] is applicable also to the NUHOMS[®] HD system. The used pressure on the basket panels due to the fuel assembly load for the evaluation is 1.24 psi. However, the actual fuel assembly load calculated in in Section 3.9.1.2.3, B.2 is 1.1856 psi.

Based on the evaluation performed in [40], the basket assembly structure will properly support and position the fuel assemblies under the drop accident stability loads.

3.7.1.1.3 32PTH DSC Fuel Basket Support Rail Accident Condition Buckling Analysis

This section removed.

3.7.1.2 32PTH DSC Canister Shell Off Normal and Accident Condition Structural Evaluation

3.7.1.2.1 32PTH Canister Shell Off Normal and Accident Condition Stress Analysis

An enveloping technique of combining various individual loads in a single analysis is used in this evaluation for several load combinations. This approach greatly reduces the number of computer runs while remains conservative. However, for some load combinations, the stress

intensities under individual loads are added to obtain resultant stress intensities for the specified combined loads. This stress addition at the stress intensity level for the combined loads, instead of at component stress level, is also a conservative way to reduce numbers of analysis runs.

The ANSYS calculated stresses are the total stresses of the combined membrane, bending, and peak stresses. These total stresses are conservatively taken to be membrane stresses (P_m) as well as membrane plus bending stresses ($P_L + P_b$) and are evaluated against their corresponding ASME code stress limits. In the case where the total stresses, evaluated in this manner, exceed the ASME allowable stresses, a detailed stress linearization is performed to separate the membrane, bending, and peak stresses. The linearized stresses are then compared to their proper Code allowable stresses. ASME B&PV Code Subsection NB [12] is used for evaluation of loads under off normal conditions and Appendix F [13] for evaluation of loads under hypothetical accident conditions. The thermal stress intensities are classified as secondary stress intensities, Q , for code evaluations.

Material properties obtained from Reference 10 for the 32PTH DSC canister materials, taken at the highest metal temperature of 500° F (from thermal evaluation presented in Chapter 4). The ANSYS Multilinear Kinematic Hardening material option of inelastic analysis is employed in the analyses of all canister accident side drops. A multi-linear stress-strain curve for type 304 stainless steel at 500° F is constructed using the yield and tensile stress values taken from [10].

Elastic and elastic-plastic analyses are performed to calculate the stresses in the 32PTH DSC canister under the transfer and storage loads. These load cases are summarized in Appendix 3.9.1, Tables 3.9.1-9, 3.9.1-10 and 3.9.1-19. All side drop loads are analyzed by elastic-plastic analyses and the rest by elastic analyses.

The calculated stresses in the canister shell due to off-normal and accident transfer loading conditions are summarized in Appendix 3.9.1, Tables 3.9.1-12, 13, 14, 16, 17, and 18. The stresses due to accident storage loading conditions are summarized in Appendix 3.9.1, Tables 3.9.1-20, and 21.

The alternate 32PTH DSC canister design with the composite bottom is also evaluated for the worst case accident condition loads, which bounds all possible applied loads to the canister. Details of the Alternate canister design structural evaluation are provided in Appendix 3.9.1, Section 3.9.1.3.4.

For the alternate canister composite bottom design, the stresses in the off-normal and accident transfer loading conditions are summarized in Appendix 3.9.1, Tables 3.9.1-28 to 35. The loads under the off normal and accident storage conditions are bounded by the loads under the off normal and accident transfer conditions, except the bottom end drop load.

For the alternate canister composite top design, as shown in SAR Drawing 10494-72-4, Rev. 0, only the bottom end drop load, out of all specified off-normal and accident loads, will generate significantly different stresses in the composite top from that in the one-piece top. Therefore a 2-D finite element model is created for the canister with the alternate composite top and is analyzed for a 75g bottom end drop load. The maximum primary membrane plus bending stress intensity in the entire canister is calculated to be 22,003 psi. The limit for a general primary

membrane stress intensity is given 40,600 psi by ASME B&PV Code Appendix F [13]. The calculated maximum primary membrane plus bending stress intensity of 22,003 psi is less than the limit for a general primary membrane stress intensity of 40,600 psi. Therefore, the alternate canister composite top design is structurally adequate.

Based on the results of these analyses, the design of the 32PTH DSC canister is structurally adequate with respect to off-normal and accident condition transfer and storage loads.

3.7.1.2.2 32PTH DSC Canister Shell Accident Condition Buckling Analysis

This section summarizes the evaluation of 32PTH DSC canister against buckling under a vertical end drop during transfer operations. The detail of the DSC canister shell buckling analysis is provided in Appendix 3.9.1, Section 3.9.1.3.3. A finite element plastic analysis with large displacement option is performed to monitor occurrence of canister shell buckling under the specified loads.

The thermal evaluation presented in Chapter 4 shows that the metal temperatures of the entire canister are below 500° F during the transfer operations. The material properties of the canister at 500° F are therefore conservatively used for the canister buckling analysis.

The following two hypothetical accident load cases for the canister are considered in this buckling analysis.

Buckling Load Case 1: 15 psig external pressure and 75g axial acceleration due to 30 foot hypothetical accident condition drop

Buckling Load Case 2: 30 psig internal pressure and 75g axial acceleration due to 30 foot hypothetical accident condition drop

The two-dimensional axisymmetric finite element model of the canister described in Appendix 3.9.1, Section 3.9.1.3.2.D.2 for the DSC canister stress analysis is used for this analysis. Since the top end of the canister is heavier than the bottom end, it is a more severe case when the canister drops on its bottom end. A bottom end drop is therefore chosen for analysis in this calculation.

For each load case, a quasi-static plastic analysis consisting of two load steps is performed to monitor the buckling of canister. The first load step applies external pressure or internal pressure alone. A subsequent inertial load of 150g is added in the second load step. The outer surface of the canister bottom is held in order to simulate the case that the canister drops on a rigid cask bottom face.

In the load step 1, the stepped external or internal pressure is applied as a static load.

In the load step 2, the weight of the canister internals (basket and fuel assemblies) is accounted for by applying an equivalent internal pressure on the canister bottom. This inertial load is uniformly distributed over the bottom surface of the canister cavity.

A multilinear stress-strain relationship (with kinematic hardening) is used to obtain stresses and deflections beyond the elastic limit of the material. The large deflection option in ANSYS is activated to monitor the buckling response.

The ANSYS program stops at the first load sub-step that fails to result in a converged solution, corresponding to buckling of the structure. When the structure buckles and the ANSYS solution fails to converge, the loads applied in the last converged load sub-step are considered to be the critical buckling load for the structure. The 150g drop loads applied in load step 2 is ramped in small sub-steps (1g load increment in each sub-step).

In both load cases, converged solutions are obtained up to 113.24g load. This load is much higher than the required 75g load in either Load Case 1 or 2. The analysis shows that the canister does not buckle up to an end drop load of 113.24g, which is well beyond the design 75g load. It is, therefore, concluded that buckling of the canister will not occur during a hypothetical accident end drop.

3.7.2 HSM-H Off Normal and Accident Conditions Structural Analysis

The design of the HSM-H for 32PTH DSC is the same as the HSM-H documented in Appendix P of the CoC 1004 UFSAR with certain adjustments to accommodate the larger diameter 32PTH DSC. Analyses performed for HSM-H with 24PTH DSC used bounding values to envelop both 24PTH DSC and 32PTH DSC. Following table shows how the bounding loads are used for structural evaluation of the HSM-H.

	Weight	Thermal
24PTH DSC (loaded weight)	93.7 kips	40.8 kw
32PTH DSC (loaded weight)	109.56 kips	34.8 kw
Weight used for HSM-H structural evaluation to envelop both 24PTH & 32PTH	110.0 kips (max.) ⁽¹⁾ 72.0 kips (min.) ⁽²⁾	
Thermal load used for HSM-H structural evaluation to envelop both 24PTH & 32PTH		40.8 kw

Notes:

1. Maximum weight is used for structural evaluation of the HSM-H.
2. Minimum weight is used for stability evaluation of the HSM-H.

Detail geometry descriptions, material properties, loadings, and structural evaluation of the HSM-H presented in Appendix P of the CoC 1004 UFSAR is reproduced and included in Appendix 3.9.9 of this Chapter.

3.7.3 OS187H Transfer Cask Off Normal and Accident Conditions Structural Analysis

3.7.3.1 Structural Analysis of the Transfer Cask Body for Off-Normal and Accident Conditions

The details of the structural analyses of the NUHOMS®-OS187H Transfer Cask body including the cylindrical shell assembly and bottom assembly, the top cover, and the local stresses at the trunnion/cask body interface are presented in Appendix 3.9.2. The specific methods, models

and assumptions used to analyze the cask body for the various individual loading conditions specified in 10CFR72 [3] are described in that appendix.

The OS187H transfer cask body structural analyses generally use static or quasistatic linear elastic methods. The stresses and deformations due to the applied loads are generally determined using the ANSYS [33] computer program.

The maximum stresses in each of the major components of the transfer cask are reported for each load case and load combination in Appendix 3.9.2, Table 3.9.2-1. The results are evaluated against the ASME Code [7] design criteria described in Section 3.1.2 of this chapter.

Based on the results of these analyses, the design of the OS187H transfer cask is structurally adequate with respect to off normal and hypothetical accident transfer loads.

3.7.3.2 Transfer Cask Top Cover and RAM Access Cover Bolt Accident Condition Analysis

The detailed calculations for the top cover and RAM access cover bolts are presented in Appendix 3.9.3. The analysis is based on NUREG/CR-6007 [34]. The bolts are analyzed for the hypothetical accident condition impact loads and load combinations.

A summary of the calculated top cover bolt stresses is listed in Appendix 3.9.3, Section 3.9.3.5. The calculations result in a maximum average tensile stress of 106.6 ksi, which is below the allowable tensile stress of 115.5 ksi for accident conditions. The maximum average shear stress in the bolts is due to torsion during pre-loading. This stress is 6.8 ksi, which is well below the allowable shear stress of 69.3 ksi.

A summary of the calculated RAM access bolt stresses is listed in Appendix 3.9.3, Section 3.9.3.10. The analysis results in a maximum average tensile stress of 45.2 ksi, which is below the allowable tensile stress of 115.5 ksi for accident conditions. The maximum accident shear stress is 9.5 ksi, which is well below the allowable shear stress of 69.3 ksi.

3.7.3.3 Transfer Cask Lead Slump Analysis

Appendix 3.9.4 presents the details of the OS187H Transfer Cask lead slump evaluation. The load considered is a 75g top and bottom end drop load in hot (115° F) ambient environments.

During a hypothetical accident condition end drop, permanent deformation of the lead gamma shield may occur. The lead gamma shield is supported by friction between the lead and transfer cask shells, in addition to bearing at the end of the lead column.

A nonlinear finite element analysis is performed in order to quantify the amount of lead slump generated during an end drop event. A 2-dimensional axisymmetric ANSYS finite element model is constructed for this purpose. The displacement results are used to determine the maximum size of the axial gap that develops between the lead gamma shield column and the structural shell of the transfer cask.

Figures 3.9.4-14 and 3.9.4-15 of Appendix 3.9.4 show the deformed shape of the transfer cask for 75g top and bottom end drops. The maximum calculated lead slump is 0.833 inches and

occurs during the 75g bottom end drop in the 115°F hot ambient environment. The effect of this cavity size on the shielding ability of the transport package is evaluated in Chapter 5.

3.7.3.4 Transfer Cask Inner Containment Buckling Analysis

Appendix 3.9.4 also presents the details of the evaluation of the structural adequacy of the OS187H Transfer Cask inner shell with respect to buckling. The load considered includes lateral pressure of lead and a 75g top and bottom end drop load in hot (115° F) ambient environments.

An ANSYS elastic-plastic buckling analysis is performed for the transfer cask end drop cases. A 200g drop load, which is greater than the design load of 75g, is applied to the ANSYS model. This 200g drop load was ramped in small increments by many load sub-steps. The ANSYS solution was set to stop and exit at any load sub-step that fails to result in a converged solution. The failure of convergence represents the onset of buckling of the structure. Once the ANSYS solution fails to converge, the loads applied in the last converged load sub-step will be considered the critical buckling load for the structure.

The ANSYS solutions have converged at 189g for the top end drop and 178g for the bottom end drop. This indicates that the transfer cask will not buckle during 75g end drop conditions

3.7.3.5 Transfer Cask Trunnion Analysis

Appendix 3.9.5 presents the evaluation of the trunnion stresses in the NUHOMS[®]-OS187H Transfer Cask due to all applied loads during fuel loading and transfer operations.

The loads applied to the transfer cask trunnions only occur during normal condition loading and fuel transfer. There are no hypothetical accident condition events that cause loads to be applied to the trunnions.

The calculated maximum normal condition trunnion stresses are summarized in Table 3.9.5-1 and compared with their corresponding allowable stresses.

3.7.3.6 Transfer Cask Shield Panel Structural Analysis for Accident Conditions

Appendix 3.9.6 presents the evaluation of the stresses in the NUHOMS[®]-OS187H Transfer Cask neutron shield shell due to all applied loads during fuel loading and transfer operations.

The neutron shield shell is only designed to withstand normal condition transfer cask lifting and fuel transfer loads. Consequently, the neutron shield shell is only analyzed for these loads, and is not analyzed to hypothetical accident condition events.

The calculated maximum normal condition neutron shield shell stresses are summarized in Table 3.9.6-1 of Appendix 3.9.6.

3.7.3.7 Transfer Cask Impact Analysis

In spite of the incredible nature of any scenario that could lead to a drop accident for the Transfer Cask, a conservative range of drop scenarios are developed and evaluated. These bounding

scenarios assure that the integrity of the DSC and spent fuel cladding is not compromised. Analyses of these scenarios demonstrate that the Transfer Cask will maintain the structural integrity of the DSC pressure containment boundary. Therefore, there is no potential for a release of radioactive materials to the environment due to a cask drop.

Appendix 3.9.7 presents the computation of the peak decelerations of NUHOMS[®] OS187H Transfer Cask during impact, subsequent to the hypothetical accident drop onto the concrete pad/soil system during transfer operations. The analytical methodology described in Reference 35 is used to perform this evaluation.

The hypothetical accident condition drop consists of an 80 inch end drop, side drop, and center of gravity (C.G.) over corner drop. The transfer cask is assumed rigid as compared to the flexibility of the concrete slab/soil system, which consists of a 36 inch thick concrete pad, with #11 rebar on 12 spacing, the at top and bottom and 2" coverage.

The following table summarizes the results of the analysis described in detail in Appendix 3.9.7.

Drop Orientation	Peak Deceleration (gs)	Target Penetration Depth (in.)
End Drop	49	3.10
Side Drop	44	2.5
Corner Drop	16	6.5

The ranges of drop scenarios conservatively selected for design are:

- 1 A horizontal side drop from a height of 80 inches (75g horizontal drop).
- 2 Vertical end drops for the NUHOMS[®] HD system are non-mechanistic and thus, no end drops are postulated for the 32PTH DSC. However, 75g vertical end drop analyses are performed as a means of enveloping the 16g corner drop (in conjunction with the 75g horizontal side drop).
- 3 An oblique corner drop from a height of 80 inches at an angle of 30° to the horizontal, onto the top or bottom corner of the Transfer Cask. This case is not specifically evaluated. The side drop and end drop cases envelop the corner drop.

3.8 References

1. NRC Regulatory Guide 3.61, Standard Format and Content for a Topical Safety Analysis Report for a Spent Fuel Dry Storage Cask, February 1989.
2. NUREG-1536, "Standard Review Plan for Dry Cask Storage Systems - Final Report," U.S. Nuclear Regulatory Commission, Office of Nuclear Material Safety and Safeguards, January 1997.
3. Title 10, Code of Federal Regulations, Part 72, "Licensing Requirements for the Storage of Spent Fuel in an Independent Spent Fuel Storage Installation."
4. American Society of Mechanical Engineers, Boiler & Pressure Vessel Code, Section III, 1998 through 2000 Addenda.
5. NUREG -0612, "Control of Heavy Loads at Nuclear Power Plants," July 1980.
6. American National Standards Institute, ANSI N14.5-1997, Leakage Tests on Packages for Shipment of Radioactive Materials.
7. American Society of Mechanical Engineers, ASME Boiler and Pressure Vessel Code, Section III, Subsection NC, 1998 through 2000 addenda.
8. American National Standards Institute, ANSI N14.6, American National Standard for Special Lifting Devices for Shipping Containers Weighing 10,000 Pounds or More for Nuclear Materials, 1993.
9. American National Standards Institute, American Nuclear Society, ANSI/ANS 57.9-1984, Design Criteria for an Independent Spent Fuel Storage Installation (Dry Storage Type).
10. American Society of Mechanical Engineers, ASME Boiler and Pressure Vessel Code, Section II, Parts A, B, C and D, 1998, through 2000 addenda.
11. DOE/ET/47912-3, Volume 3, September 1981, Nuclear Assurance Corporation, "Domestic Light Water Reactor Fuel Design Evolution".
12. American Society of Mechanical Engineers, ASME Boiler and Pressure Vessel Code, Section III, Subsection NB, 1998 through 2000 addenda.
13. ASME Boiler and Pressure Vessel Code, Section III, Division 1, Appendices, 1998, through 2000 addenda

14. American Society of Mechanical Engineers, ASME Boiler and Pressure Vessel Code, Section III, Subsection NG, 1998 through 2000 Addenda.
15. American Concrete Institute, ACI 349-97 and 349R-97, Code Requirements for Nuclear Safety Related Concrete Structures and Commentary.
16. American Institute of Steel Construction, AISC Manual of Steel Construction, Ninth Edition.
17. Regulatory Guide 1.99, "Radiation Embrittlement of Reactor Vessel Materials," Revision 2, May 1988.
18. AWS D1.1 – 1998, Structural Welding Code-Steel.
19. AWS D1.6 – 1999, Structural Welding Code-Stainless Steel.
20. H. K. Hilsdorf, J. Kropp, and H. J. Koch, "The Effects of Nuclear Radiation on the Mechanical Properties of Concrete," Paper 55-10, Douglas McHenry International Symposium on Concrete and Concrete Structures, American Concrete Institute, Detroit, MI (1978).
21. American Nuclear Society, "American National Standard Guidelines on the Nuclear Analysis and Design of Concrete Radiation Shielding for Nuclear Power Plants," ANSI/ANS-6.4-1977, American National Standards Institute, Inc., (1977).
22. "An Assessment of Stress-Strain Data Suitable for Finite Element Elastic-Plastic Analysis of Shipping Containers", NUREG/CR-0481
23. Baumeister & Marks, *Standard Handbook for Mechanical Engineers*, 7th Edition.
24. G. Wranglen, *An Introduction to Corrosion and Protection of Metals*, Chapman and Hall, 1985, pp. 109-112.
25. V. Brooks and Perkins, Boral Product Performance Report 624.
26. Pacific Northwest Laboratory Annual Report - FY 1979, Spent Fuel and Fuel Pool Component Integrity, May, 1980.
27. G. Wranglen, "An Introduction to Corrosion and Protection of Metals", Chapman and Hall, 1985, pp. 109-112.
28. A.J. McEvily, Jr., ed., "Atlas of Stress Corrosion and Corrosion Fatigue Curves", ASM Int'l, 1995, p. 185.

29. Baratta, et al. "Evaluation of Dimensional Stability and Corrosion Resistance of Borated Aluminum", Final Report submitted to Eagle-Picher Industries, Inc. by the Nuclear Engineering Department, Pennsylvania State University.
30. Hydrogen Generation Analysis Report for TN-68 Cask Materials, Test Report No. 61123-99N, Rev 0, Oct 23, 1998, National Technical Systems.
31. AMS-R-83485, "Rubber, Fluorocarbon, Improved Performance at Low Temperatures"
32. Harper, Charles A., ed., "Handbook of Plastics and Elastomers," McGraw-Hill, 1975
33. ANSYS Users Manual, Rev. 5.6 and 6.0, 1998
34. NUREG/CR-6007 "Stress Analysis of Closure Bolts for Shipping Casks", By Mok, Fischer, and Hsu, Lawrence Livermore National Laboratory, 1992.
35. Rashid, Nickel and James, "Structural Design of Concrete Storage Pads for Spent Fuel Casks", EPRI NP-7551, August 1991.
36. "Handbook of Concrete Engineering," Mark Fintel, September 1974
37. UCID – 21246, "Dynamic Impact Effects on Spent Fuel Assemblies," Lawrence Livermore National Laboratory, October 20, 1987.
38. K. J. Geelhood and C. E. Beyer, "PNNL Stress/Strain Correlation for Zircaloy", March 2005.
39. USNRC Spent Fuel Project Office, Interim Staff Guidance, ISG-11, Revision 3, "Cladding Considerations for the Transportation and Storage of Spent Fuel."
40. Updated Final Safety Analysis Report (UFSAR), for the Standardized NUHOMS[®] Horizontal Modular Storage System for Irradiated Nuclear Fuel, NUH003.0103, Rev. 12.
41. Westinghouse Calculation No. CN-NFPE-10-194, Rev. 2, "Stress Analysis of the use of the Instrument Tube Tie Rod for 15x15 Westinghouse Fuel," (Proprietary).
42. Westinghouse Calculation No. CN-NFPE-07-55, Rev. 1, "Stress Analysis of use of the Instrument Tube Tie Rod at the Farley Plant," (Proprietary).
43. Westinghouse Calculation No. CN-NFPE-09-70, Rev. 1, "Stress Analysis of use of the Instrument Tube Tie Rod and Removable Top Nozzle ITTR Adapter Plate with 17x17 Fuel Assembly and 1137E32 Top Nozzle," (Proprietary).
44. Westinghouse Calculation No. CN-NFPE-11-6, Rev.0, "FEA Analysis of use of Instrument Tube Tie Rod with 17x17 Top Nozzle 1101E77 and Bottom Nozzle 1100E39," (Proprietary).

3.9 Appendices

The detailed structural analyses of the NUHOMS[®] HD system are included in the following appendices:

Appendix 3.9.1	32PTH DSC (Canister and Basket) Structural Analysis
Appendix 3.9.2	OS187H Transfer Cask Body Structural Analysis
Appendix 3.9.3	OS187H Transfer Cask Top Cover and RAM Access Cover Bolt Analyses
Appendix 3.9.4	OS187H Transfer Cask Lead Slump and Inner Shell Buckling Analysis
Appendix 3.9.5	OS187H Transfer Cask Trunnion Analysis
Appendix 3.9.6	OS187H Transfer Cask Shield Panel Structural Analysis
Appendix 3.9.7	OS187H Transfer Cask Impact Analysis
Appendix 3.9.8	Damaged Fuel Cladding Structural Evaluation
Appendix 3.9.9	HSM-H Structural Analysis
Appendix 3.9.10	OS187H Transfer Cask Dynamic Impact Analysis
Appendix 3.9.11	32PTH DSC Dynamic Amplification Factor (DAF) Calculation

3.10 ASME Code Alternatives

The confinement boundary of the 32PTH DSC canister shell, the inner top cover/shield plug, the inner bottom cover, the siphon vent block, and the siphon/vent port cover plate are designed, fabricated and inspected in accordance with the ASME Code Subsections NB to the maximum practical extent. The basket is designed, fabricated and inspected in accordance with ASME Code Subsection NG to the maximum practical extent. Other canister components (such as outer bottom cover and shield plugs) are not governed by the ASME Code.

ASME Code Alternatives for the 32PTH DSC

Reference ASME Code Section/Article	Code Requirement	Alternatives, Justification & Compensatory Measures
NCA	All	Not compliant with NCA
NB-1100	Requirements for Code Stamping of Components	The canister shell, the inner top cover/shield plug, the inner bottom cover, and the siphon/vent port cover are designed & fabricated in accordance with the ASME Code, Section III, Subsection NB to the maximum extent practical. However, Code Stamping is not required. As Code Stamping is not required, the fabricator is not required to hold an ASME "N" or "NPT" stamp, or to be ASME Certified.
NB-2130	Material must be supplied by ASME approved material suppliers	Material is certified to meet all ASME Code criteria but is not eligible for certification or Code Stamping if a non-ASME fabricator is used. As the fabricator is not required to be ASME certified, material certification to NB-2130 is not possible. Material traceability & certification are maintained in accordance with TN's NRC approved QA program.
NB-4121	Material Certification by Certificate Holder	
NB-4243 and NB-5230	Category C weld joints in vessels and similar weld joints in other components shall be full penetration joints. These welds shall be examined by UT or RT and either PT or MT	The shell to the outer top cover weld, the shell to the inner top cover/shield plug weld (including option 2 or option 3 inner top cover as described in the SAR), and the siphon/vent cover welds, are all partial penetration welds. As an alternative to the NDE requirements of NB-5230, for Category C welds, all of these closure welds will be multi-layer welds and receive a root and final PT examination, except for the shell to the outer top cover weld. The shell to the outer top cover weld will be a multi-layer weld and receive multi-level PT examination in accordance with the guidance provided in ISG-15 for NDE. The multi-level PT examination provides reasonable assurance that flaws of interest will be identified. The PT examination is done by qualified personnel, in accordance with Section V and the acceptance standards of Section III, Subsection NB-5000. All of these welds will be designed to meet the guidance provided in ISG-15 for stress reduction factor.
NB-5520	NDE personnel must be qualified to a specific edition of SNT-TC-1A	Permit use of a more recent edition of SNT-TC-1A.

ASME Code Alternatives for the 32PTH DSC (continued)

Reference ASME Code Section/Article	Code Requirement	Alternatives, Justification & Compensatory Measures
NB-2531	Vent & siphon Port Cover; straight beam UT per SA-578 for all plates for vessel	SA-578 applies to 3/8" and thicker plate only; allow alternate UT techniques to achieve meaningful UT results.
NB- 6000	All completed pressure retaining systems shall be pressure tested	<p>The 32PTH is not a complete or "installed" pressure vessel until the top closure is welded following placement of Fuel Assemblies within the DSC. Due to the inaccessibility of the shell and lower end closure welds following fuel loading and top closure welding, as an alternative, the pressure testing of the DSC is performed in two parts. The DSC shell, shell bottom, including all longitudinal and circumferential welds, is pneumatically tested and examined at the fabrication facility.</p> <p>The shell to the inner top cover/shield plug closure weld (including option 2 or option 3 inner top cover as described in the SAR) are pressure tested and examined for leakage in accordance with NB-6300 in the field. The siphon/vent cover welds will not be pressure tested; these welds and the shell to the inner top cover/shield plug closure weld (including option 2 or option 3 inner top cover as described in the SAR) are helium leak tested after the pressure test.</p> <p>Per NB-6324 the examination for leakage shall be done at a pressure equal to the greater of the Design pressure or three-fourths of the test pressure. As an alternative, if the examination for leakage of these field welds, following the pressure test, is performed using helium leak detection techniques, the examination pressure may be reduced to 1.5 psig. This is acceptable given the significantly greater sensitivity of the helium leak detection method.</p>
NB-7000	Overpressure Protection	No overpressure protection is provided for the 32PTH DSC. The function of the 32PTH DSC is to contain radioactive materials under normal, off-normal, and hypothetical accident conditions postulated to occur during transportation. The 32PTH DSC is designed to withstand the maximum internal pressure considering 100% fuel rod failure at maximum accident temperature. The 32PTH DSC is pressure tested in accordance with the requirements of 10CFR71 and TN's approved QA program.
NB-8000	Requirements for nameplates, stamping & reports per NCA-8000	The 32PTH DSC nameplates provide the information required by 10CFR71, 49CFR173, and 10CFR72 as appropriate. Code stamping is not required for the 32PTH DSC. QA Data packages are prepared in accordance with the requirements of 10CFR71, 10CFR72, and TN's approved QA program.
NB-1132	Attachments with a pressure retaining function, including stiffeners, shall be considered part of the component.	Outer bottom cover, bottom plate, bottom casing plate, side casing plate, top shield plug casing plate, lifting posts, grapple ring and grapple ring support are outside code jurisdiction; these components together are much larger than required to provide stiffening for the confinement boundary cover. These component welds are subject to root and final PT examinations.

ASME Code Alternatives for the 32PTH DSC Fuel Basket

Reference ASME Code Section/Article	Code Requirement	Alternatives, Justification & Compensatory Measures
NG/NF-1100	Requirement for Code Stamping of Components	The 32PTH DSC baskets are designed & fabricated in accordance with the ASME Code, Section III, Subsection NG to the maximum extent practical as described in the SAR, but Code Stamping is not required. As Code Stamping is not required, the fabricator is not required to hold an ASME N or NPT stamp or be ASME Certified.
NG/NF-2130	Material must be supplied by ASME approved material suppliers	Material is certified to meet all ASME Code criteria but is not eligible for certification or Code Stamping if a non-ASME fabricator is used. As the fabricator is not required to be ASME certified, material certification to NG/NF-2130 is not possible. Material traceability & certification are maintained in accordance with TN's NRC approved QA program. The poison material and aluminum plates are not used for structural analysis, but to provide criticality control and heat transfer. They are not ASME Code Class I materials. See note 1.
NG/NF-4121	Material Certification by Certificate Holder	
NG/NF-8000	Requirements for nameplates, stamping & reports per NCA-8000	The 32PTH DSC nameplates provide the information required by 10CFR71, 49CFR173, and 10CFR72 as appropriate. Code stamping is not required for the 32PTH DSC. QA Data packages are prepared in accordance with the requirements of 10CFR71, 10CFR72, and TN's approved QA program.
NCA	All	Not compliant with NCA.

Note:

1. Because Subsection NCA does not apply, the NCA-3820 requirements for accreditation or qualification of material organizations do not apply. CMTR's shall be provided using NCA-3862 for guidance.

Table 3-1
Codes and Standards for the Fabrication and Construction of Principal Components

Component, Equipment, Structure	Code of Construction
32PTH DSC Shell Assembly	ASME Code, Section III, Subsection NB (1998 Edition through 2000 Addenda, including alternatives to the ASME code specified in SAR Section 3.10)
32PTH DSC Basket	ASME Code, Section III, Subsection NG (1998 Edition through 2000 Addenda)
Transfer Cask	ASME Code, Section III, Subsection NC (1998 Edition through 2000 Addenda)
HSM-H	<ul style="list-style-type: none">- ACI 349-97 (Concrete)- AISC Ninth Edition (Structural Steel)- AWS D1.1 (Structural Welds)- ASCE 7-95 (Loads)- ANSI 57.9-84 (Loads & Load Combinations)

Table 3-2
Summary of Stress Criteria for Subsection NB Pressure Boundary Components

Loadings	Stress Category	Notes
Design [NB-3221]	$P_m \leq 1.0S_m$ $P_L \leq 1.5S_m$ $P_m \text{ (or } P_L) + P_b \leq 1.5S_m$ $F_p \leq 1.5S_y$	
Service Level A [NB-3222]	$P_m \text{ (or } P_L) + P_b + Q \leq 3.0S_m$	Notes 1 & 2
Service Level B [NB-3223]	$P_m \leq 1.0S_m$ $P_L \leq 1.5S_m$ $P_m \text{ (or } P_L) + P_b \leq 1.5S_m$ $P_m \text{ (or } P_L) + P_b + Q \leq 3.0S_m \text{ (Note 1)}$	Note 3
Service Level C [NB-3224]	$P_m \leq \max(1.2S_m, 1.0S_y)$ $P_L \leq \max(1.8S_m, 1.5S_y)$ $P_m \text{ (or } P_L) + P_b \leq \max(1.8S_m, 1.5S_y)$	

continued...

Table 3-2
Summary of Stress Criteria for Subsection NB Pressure Boundary Components
(continued)

Loadings	Stress Category	Notes
Carbon Steel Components (e.g., shield plugs)		
Level D Elastic Analysis [NB-3225, App. F]	$P_m \leq 0.7S_u$ $P_m \text{ (or } P_L) + P_b \leq 1.0S_u$	Note 4
Level D Plastic Analysis [NB-3225, App. F]	$P_m \leq 0.7S_u$ $P_m \text{ (or } P_L) + P_b \leq 0.9S_u$	Note 4
Austenitic Steel Components (e.g., Shell)		
Level D Elastic Analysis [NB-3225, App. F]	$P_m \leq \min (2.4S_m, 0.7S_u)$ $P_m \text{ (or } P_L) + P_b \leq \min (3.6S_m, 1.0S_u)$	Note 5
Level D Plastic Analysis [NB-3225, App. F]	$P_m \leq \max (0.7S_u, S_y + (S_u - S_y)/3)$ $P_m \text{ (or } P_L) + P_b \leq 0.9S_u$	Note 5

Notes:

1. This limit may be exceeded provided the criteria of NB-3228.5 are satisfied.
2. There are no specific limits on primary stresses for Level A events. However, the stresses due to primary loads during normal service must be computed and combined with the effects of other loadings in satisfying other limits. See NB-3222.1.
3. The 10% increase in allowables from NB-3223(a) may be applicable for load combinations for which the pressure exceeds the design pressure.
4. Criteria listed are for carbon steel components (e.g., shield plugs).
5. Criteria listed are for austenitic parts including shells, cover plates, and the grapple assembly.

Table 3-3
Summary of Stress Criteria for Subsection NG Components

Loadings	Stress Category (5)	Notes
Design [NG-3221]	$P_m \leq 1.0S_m$ $P_m + P_b \leq 1.5S_m$	
Level A [NG-3222]	$P_m \leq 1.0S_m$ (Note 6) $P_m + P_b \leq 1.5S_m$ (Note 6) $P_m + P_b + Q \leq 3.0S_m$ (Note 4)	
Level B [NG-3223] ⁽¹⁾	$P_m \leq 1.0S_m$ (Note 6) $P_m + P_b \leq 1.5S_m$ (Note 6) $P_m + P_b + Q \leq 3.0S_m$ (Note 4)	Note 1
Level C Elastic Analysis [NG-3224]	$P_m \leq 1.5S_m$ $P_m + P_b \leq 2.25S_m$	Notes 2 & 3
Level D Elastic Analysis [NG-3225, App. F]	$P_m \leq \min (2.4S_m, 0.7S_u)$ $P_m + P_b \leq \min (3.6S_m, 1.0S_u)$	
Level D Plastic Analysis [NG-3225, App. F]	$P_m \leq \max (0.7S_u, S_y + (S_u - S_y)/3)$ $P_m + P_b \leq 0.9S_u$	

Notes:

1. There are no pressure loads on the basket, therefore the 10% increase permitted by NG-3223(a) for pressures exceeding the design pressure are not included.
2. Evaluation of secondary stresses not required for Level C and D events.
3. Criteria listed are for elastic analyses, other analysis methods permitted by NG-3224.1 are acceptable if performed in accordance with the appropriate paragraph of NG-3224.1.
4. This limit may be exceeded provided the requirements of NG-3228.3 are satisfied, see NG-3222.2 and NG-3228.3.
5. As appropriate, the special stress limits of NG-3227 should be applied.
6. In accordance with NG-3222 and Note 9 of Figure NG-3221-1, the Limit Analysis provisions of NG-3228 may be used.
7. The weld strength of each fusion weld nugget shall have a minimum capacity of 16.5 kips (70°F). The minimum capacity shall be determined by shear tests using test specimens made from production materials.

Table 3-4
Summary of Stress Criteria for Subsection NC Components
(OS187H Transfer Cask)

Service Level	Stress Category	Stress Criteria
A (Normal Conditions)	Primary Membrane Stress, P_m	S_m
	Primary Membrane + Bending Stress, $P_m + P_b$	$1.5 S_m$
	Primary + Secondary Stress, $P_m + P_b + Q$	$3 S_m$
D (Accident Conditions)	Primary Membrane Stress, P_m	Lesser of $2.4 S_m$ or $0.7 S_u$
	Primary Local Membrane Stress, P_L	150% of P_m Stress Limit
	Primary Membrane + Bending Stress, $P_m + P_b$	Lesser of $3.6 S_m$ or S_u

Table 3-5
SA-240 Type 304/SA-182 F304 Temperature Dependent Material Properties

Temp. °F	Ultimate S_u (ksi)	Yield S_y (ksi)	Allow. S_m (ksi)	E (10^6 psi)	α (10^{-6} °F ⁻¹)	Density, ρ (lb./in. ³)*	Poisson, ν (10^{-6})*
70	75.0	30.0	20.0	28.3	8.5	0.29	0.3
200	71.0	25.0	20.0	27.6	8.9	0.29	0.3
300	66.2	22.4	20.0	27.0	9.2	0.29	0.3
400	64.0	20.7	18.7	26.5	9.5	0.29	0.3
500	63.4	19.4	17.5	25.8	9.7	0.29	0.3
600	63.4	18.4	16.4	25.3	9.8	0.29	0.3
700	63.4	17.6	16.0	24.8	10.0	0.29	0.3

*Material Properties taken from Reference 23

Table 3-6
HSM-H Concrete Temperature Dependent Material Properties

Material	Temperature (°F)	28 Day Compressive Strength, f_c (ksi)	Modulus of Elasticity, E (1.0E3 ksi)	Coefficient of Thermal Expansion, α ($\times 10^{-6} \text{ } ^\circ\text{F}^{-1}$)
Concrete Normal Weight 5000 psi Strength	100	5.0	4.0	5.5
	200	5.0	3.6	5.5
	300	4.8	3.3	5.5
	400	4.5	3.0	5.5
	500	4.5	2.9	5.5

Table 3-7
HSM-H Reinforcing Steel Properties at Temperature

Material	Temperature °F	Yield Strength (ksi)	Modulus of Elasticity E (1.0 E3 ksi)
Reinforcing Steel, ASTM A615 Grade 60 ⁽¹⁾	100	60.0	29.0
	200	57.0	28.4
	300	54.0	27.8
	400	51.0	27.3
	500	51.0	27.0

Note

(1) Reinforcing steel data obtained from Handbook of Concrete Engineering [36].

Table 3-7A
Material Data for ASTM A-992 Steel

Material	Temperature (°F)	Yield Strength, f_y (ksi)	Modulus of Elasticity, $E^{(1)}$ (ksi)	$\alpha_{AVG}^{(1)}$ ($1 \times 10^{-6} \text{ } ^\circ\text{F}^{-1}$)
ASTM A-992 Steel	70	50.0	29,500	--
	100	50.0	--	5.53
	200	45.6	28,800	5.89
	400	42.8	27,700	6.61
	500	40.4	27,300	6.91
	600	36.9	26,700	7.17
	700	36.0	25,500	7.41

(1) E and α are assumed to be same as that of ASTM A36 steel. Yield strength f_y of ASTM A-992 material is assumed to vary with temperature in same proportion as A-36 steel.

Table 3-7B
Material Data for ASTM A-36 Steel

Material	Temperature (°F)	Stress Properties (ksi)			Elastic Modulus (x1.0E3 ksi) (E)	Average Coefficient of Thermal Expansion ⁽¹⁾ (x10 ⁻⁶ in./in.-°F)
		Stress Intensity (S _m)	Yield Strength (S _y)	Ultimate Strength (S _u)		
Carbon Steel ASTM A-36	70	-	36.0	58.0	29.5	--
	100	19.3	36.0	58.0	-	5.53
	200	19.3	32.8	58.0	28.8	5.89
	400	19.3	30.8	58.0	27.7	6.61
	500	19.3	29.1	58.0	27.3	6.91
	600	17.7	26.6	58.0	26.7	7.17
	700	17.3	25.9	58.0	25.5	7.41

Table 3-8
SA-240 Type XM-19 Temperature Dependent Material Properties

Temp. °F	Ultimate S_u (ksi)	Yield S_y (ksi)	Allow. S_m (ksi)	E (10^6 psi)	α (10^{-6} °F ⁻¹)	Density, ρ (lb./in. ³)	Poisson, ν (10^{-6})
70	100.0	55.0	33.3	28.3	8.2	0.29	0.3
200	99.4	47.1	33.2	27.6	8.5	0.29	0.3
300	94.2	43.3	31.4	27.0	8.8	0.29	0.3
400	91.1	40.7	30.2	26.5	8.9	0.29	0.3
500	89.1	38.8	29.7	25.8	9.1	0.29	0.3
600	87.7	37.4	29.2	25.3	9.2	0.29	0.3

*Material Properties taken from Reference 23

Table 3-9
SA-540 Grade B24 Class 1 Temperature Dependent Material Properties

Temp. °F	Ultimate S_u (ksi)	Yield S_y (ksi)	Allow. S_m (ksi)	E (10^6 psi)	α (10^{-6} °F ⁻¹)	Density, ρ (lb./in. ³) [*]	Poisson, ν (10^{-6}) [*]
70	165.0	150.0	50.0	27.8	6.4	0.29	0.3
200	165.0	143.4	47.8	27.1	6.7	0.29	0.3
300	165.0	138.6	46.2	26.7	6.9	0.29	0.3
400	165.0	134.4	44.8	26.1	7.1	0.29	0.3
500	165.0	130.2	43.4	25.7	7.3	0.29	0.3
600	165.0	124.2	41.4	25.2	7.4	0.29	0.3

^{*}Material Properties taken from Reference 23

Table 3-10
ASTM B-29, Chemical Lead Temperature Dependent Material Properties

Temp. °F	E (10^6 psi)	α (10^{-6} °F ⁻¹)	Density, ρ (lb./in. ³) [*]	Poisson, ν (10^{-6}) [*]
70	2.35	16.21	0.41	0.45
200	2.28	16.70	0.41	0.45
300	2.06	17.34	0.41	0.45
400	1.92 ^{**}	18.12	0.41	0.45
500	1.78 ^{**}	18.90	0.41	0.45
600	1.64 ^{**}	19.68	0.41	0.45

^{*}Material Properties taken from Reference 23

^{**}Extrapolated from available Reference 22 Data.

Table 3-11
Resin Material Properties

Temperature	Modulus of Elasticity⁽¹⁾ E (psi)	Coefficient of Thermal Expansion⁽²⁾, α (in./in.°F)	Density⁽³⁾, ρ (lb./in.³)	Poisson's Ratio⁽⁴⁾
Room Temperature	0.16×10^6	—	0.065	0.20

- (1) The modulus of elasticity utilized is lower than that of commercially available glass filled, polyester based polymers. Typical values are 0.25×10^6 psi.
- (2) The coefficient of thermal expansion for the resin material is not used in the transfer cask structural analysis. The resin material is not a structural component, and since the resin has a very low Modulus of Elasticity (relative to stainless steel) it's thermal expansion is not expected to affect the stresses in the structural components significantly.
- (3) A conservative density value of 0.065 lb/in^3 is utilized to estimate a higher mass for the resin while the actual density per Table 5-17 is 0.057 lb/in^3 .
- (4) A Poisson's ratio of 0.20, which is closer to that of concrete (0.17) is utilized.

Table 3-12
Input Data for Fuel Rod Cladding Side Drop ANSYS Runs

Item	WE & WES 15x15	WE 17x17	MK BW 17x17	WEV 17x17	WEO 17x17	CE 14x14
Number of Supports ⁽¹⁾	7	8	8	8	8	8
Number Of Spans ⁽¹⁾	6	7	7	7	7	7
Total Length, L (in) ⁽¹⁾	152.152	151.635	151.635	151.635	151.635	147.174
Span L ₁ (in) ⁽¹⁾	22.657	22.93	22.93	22.93	22.93	17.36
Span L ₂ (in) ⁽¹⁾	24.69	19.05	19.05	19.05	19.05	17.36
Span L ₃ (in) ⁽¹⁾	24.69	19.05	19.05	19.05	19.05	17.36
Span L ₄ (in) ⁽¹⁾	24.69	19.05	19.05	19.05	19.05	17.36
Span L ₅ (in) ⁽¹⁾	24.69	19.05	19.05	19.05	19.05	17.36
Span L ₆ (in) ⁽¹⁾	17.46	18.95	18.95	18.95	18.95	17.36
Span L ₇ (in) ⁽¹⁾	-	19.19	19.19	19.19	19.19	17.36
Span L _B (in) ⁽¹⁾	1.775	1.204	1.204	1.204	1.204	8.495
Span L _T (in) ⁽¹⁾	1.00	1.161	1.161	1.161	1.161	5.159
Cladding Tube, D _O (in)	0.4193	0.3713	0.3713	0.3713	0.3573	0.4373
Cladding Tube, t _(Corroded) (in) ⁽⁸⁾	0.0216	0.0198	0.0213	0.0198	0.0198	0.0253
Cladding Tube, D _i (in)	0.3761	0.3317	0.3287	0.3317	0.3177	0.3867
Cladding Tube Volume, V _t (in ³ /in) ⁽²⁾	0.026987	0.02186	0.02342	0.02186	0.020994	0.032747
Tube Weight, w ₁ (lb/in) ⁽³⁾	0.006315	0.005116	0.00548	0.005116	0.004913	0.007663
Fuel Pellet, D (in)	0.3659	0.3225	0.3195	0.3225	0.3088	0.3765
Pellet Weight, w ₂ (lb/in) ⁽⁴⁾	0.040378	0.031368	0.030787	0.031368	0.028759	0.042751
(Tube+Pellet) w _s (lb/in)	0.046693	0.036484	0.036267	0.036484	0.033672	0.050414
Tube Eqv. Density, ρ _e (lb/in ³) ⁽⁵⁾	1.730	1.669	1.549	1.669	1.604	1.540
Weight Bottom Fitting, W _B (lb)	12.566	12.566	12.566	12.566	12.566	12.566
Weight Top Fitting, W _T (lb)	17.416	18.012	18.012	18.012	18.012	18.012
Tube _{Bot} Eqv. Density, ρ _B (lb/in ³) ⁽⁶⁾	3.02	3.48	3.24	3.48	3.49	1.80
Tube _{Top} Eqv. Density, ρ _T (lb/in ³) ⁽⁷⁾	4.89	4.36	4.06	4.36	4.41	2.13

Notes:

(1) Number of supports and span lengths are taken from [11]. Support grids are 1.5 in. wide.

(2) $V_t = \pi/4[D_o^2 - D_i^2] \times 1.0$ (3) $W_1 w_1 = V_t \times \rho_{tube} = V_t \times 0.234 \text{ lb/in}$ (4) $W_2 w_2 = \pi/4[D^2] \times 1.0 \times \rho_{Pellet} = \pi/4[D^2] \times 0.384 \text{ lb/in}$ (5) $\rho_e = w_s / V_t$ (6) $\rho_B = [w_s + W_B / (\text{No. of tubes} \times L_B)] / V_t$ (7) $\rho_T = [w_s + W_T / (\text{No. of tubes} \times L_T)] / V_t$

(8) Clad thickness reduced by 0.0027 in to account for an assumed oxide layer of 120 microns

Table 3-13
Maximum Fuel Rod Cladding Axial Stresses During 75g Side Drop

Fuel Assembly Type	WE & WES 15x15	WE 17x17	MK BW 17x17	WEV 17x17	WEO 17x17	CE 14x14
Fuel Cladding OD, D (in)	0.4193	0.3713	0.3713	0.3713	0.3573	0.4373
Clad Thick. (Corr.), t (in) ⁽¹⁾	0.0216	0.0198	0.0213	0.0198	0.0198	0.0253
Average Radius, R (in) ⁽²⁾	0.1989	0.1758	0.1725	0.1758	0.1688	0.2060
Fuel Pallet OD, D _P (in) ⁽¹⁾	0.3659	0.3225	0.3195	0.3225	0.3088	0.3765
Number of Spans, N ⁽⁸⁾	6	7	7	7	7	7
Max. Span Length (in) ⁽⁸⁾	24.69	22.93	22.93	22.93	22.93	17.36
No. of Rods, N ⁽¹⁾	204	264	264	264	264	176
Cladding Tube Weight (lb/in) ⁽³⁾	0.006315	0.005116	0.00548	0.005116	0.004913	0.007663
Fuel Pellet Weight (lb/in) ⁽⁴⁾	0.040378	0.031368	0.030787	0.031368	0.028759	0.042751
W _S , [Tube + Pellet] (lb/in)	0.046693	0.036484	0.036267	0.036484	0.033672	0.050414
30 Foot Side Drop - Equivalent g load	75	75	75	75	75	75
Max. Bending Stress, S _b (psi) ⁽⁵⁾	66,642	63,230	59,160	63,230	63,442	47,725
Internal Pressure, P (psi)	2,235	2,235	2,235	2,235	2,235	2,235
Pressure Axial Stress, S _{press.} (psi) ⁽⁶⁾	10,289	9,921	9,183	9,921	9,525	9,100
S _{Max} = S _b + S _{press.} (psi)	76,931	73,151	68,343	73,151	72,967	56,825
Allowable Stress, S _{all} = S _y (psi) ⁽⁷⁾	93,950	93,950	93,950	93,950	93,950	93,950
Factor of Safety, (S _y / S _{Max})	1.22	1.28	1.37	1.28	1.29	1.65

Notes:

(1) Reduction of wall thickness by 0.0027 inch

(2) $R = (D-t)/2$ (3) Cladding Tube Weight = $[\pi / 4 \times (D^2 - (D - 2t)^2)] \times \rho_t = [\pi / 4 \times (D^2 - (D - 2t)^2)] \times 0.234$ lb/in.(4) Fuel Pellet Weight = $[(\pi / 4) \times D_p^2] \times \rho_p = [(\pi / 4) \times D_p^2] \times 0.384$ lb/in.

(5) See Figures 3-3 to 3-7.

(6) $S_{pressure} = (P \times R) / (2 \times t)$ (7) Yield strength of high burn up Zircaloy cladding tube at 725 °F based on reference [38] with a strain rate at 0.5 s⁻¹.

(8) From Table 3-12

Table 3-14
Summary of OS187H Transfer Cask Top Cover Bolt Stress Analysis

Stress Type	Normal Condition		Accident Condition	
	Stress	Allowable	Stress	Allowable
Average Tensile (ksi.)	37.4	92.4	106.6	115.5
Shear (ksi)	6.8	55.4	6.8	69.3
Combined (ksi)	74.0	124.7	Not Required [1]	
Interaction Equation $R_t^2 + R_s^2 < 1$	0.179	1	0.862	1
Bearing (ksi) Allowable (ksi) (S_y of lid material)	11.5	43.3	Not Required [1]	

Table 3-15
Summary of OS187H Transfer Cask RAM Access Cover Bolt Stress Analysis

Stress Type	Normal Condition		Accident Condition	
	Stress	Allowable	Stress	Allowable
Average Tensile (ksi.)	45.2	92.4	45.2	115.5
Shear (ksi)	8.0	55.4	9.5	69.3
Combined (ksi)	97.0	124.7	Not Required [1]	
Interaction E.Q. $R_t^2 + R_s^2 < 1$	0.548	1	0.282	1
Bearing (ksi) Allowable (ksi) (S_y of lid material)	10.1	22.4	Not Required [1]	

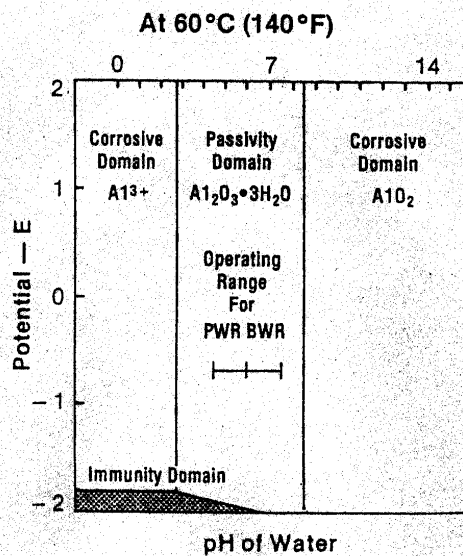
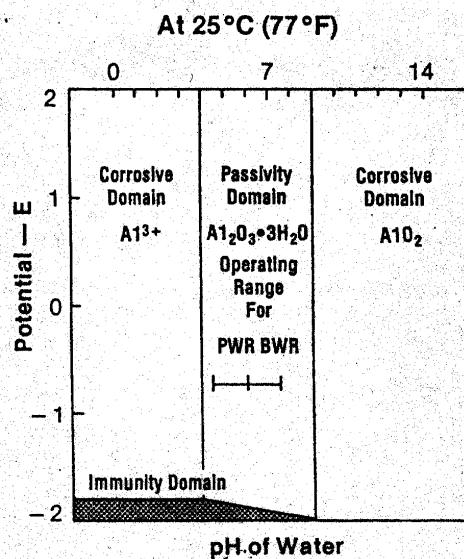


Figure 3-1
Potential Versus pH Diagram for Aluminum-Water System

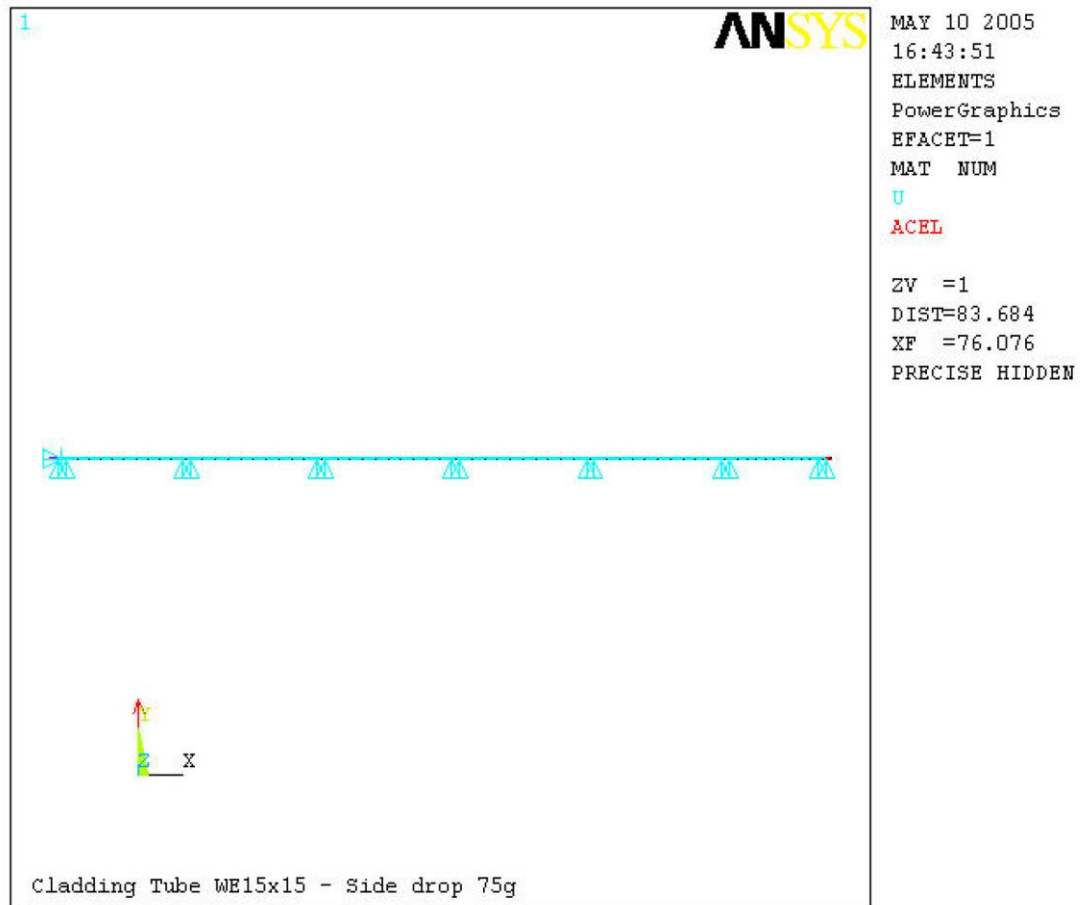


Figure 3-2
Finite Element Model and Boundary Conditions WE 15x15 and WES 15x15

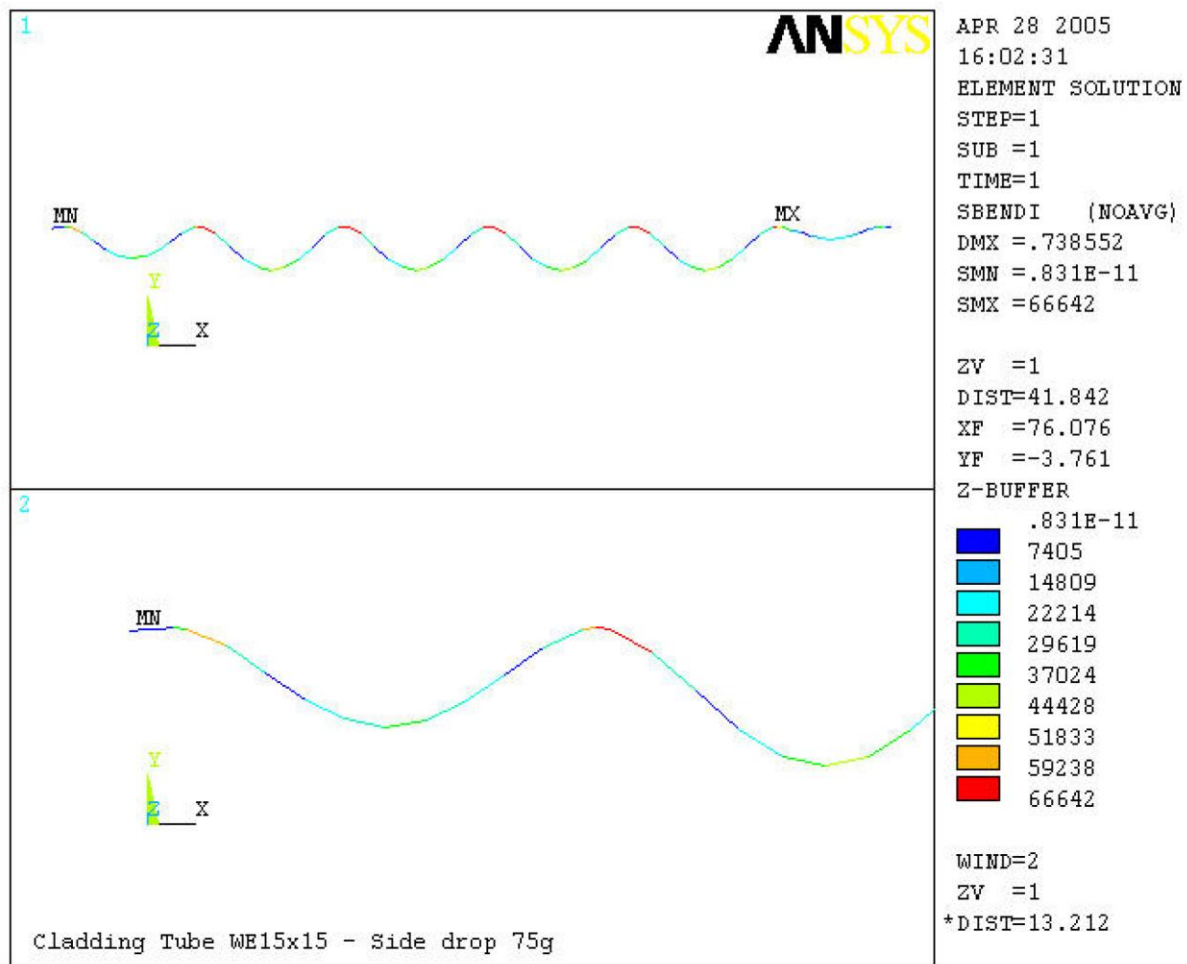


Figure 3-3
Bending stress – WE 15x15 and WES 15x15
(The bottom figure is enlarged view of span)

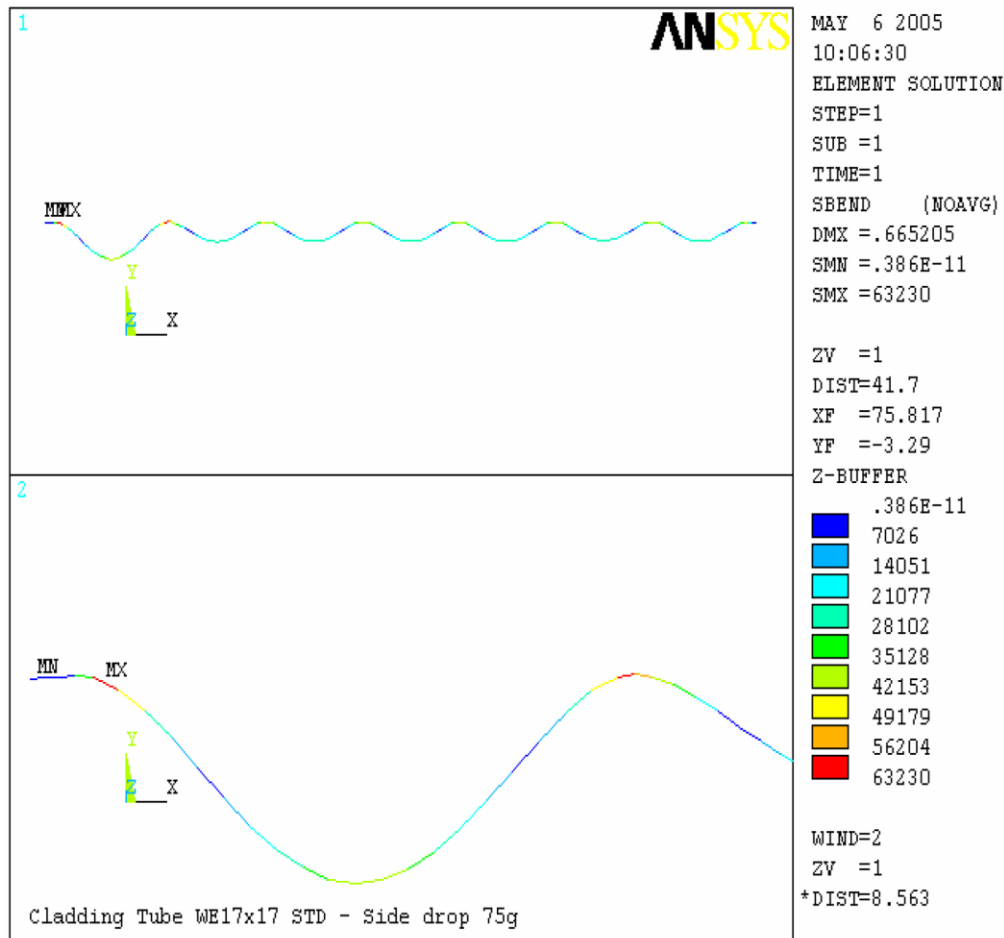


Figure 3-4
Bending stress – WE 17x17 and WEV 17x17
(The bottom figure is an enlarged view of the span)

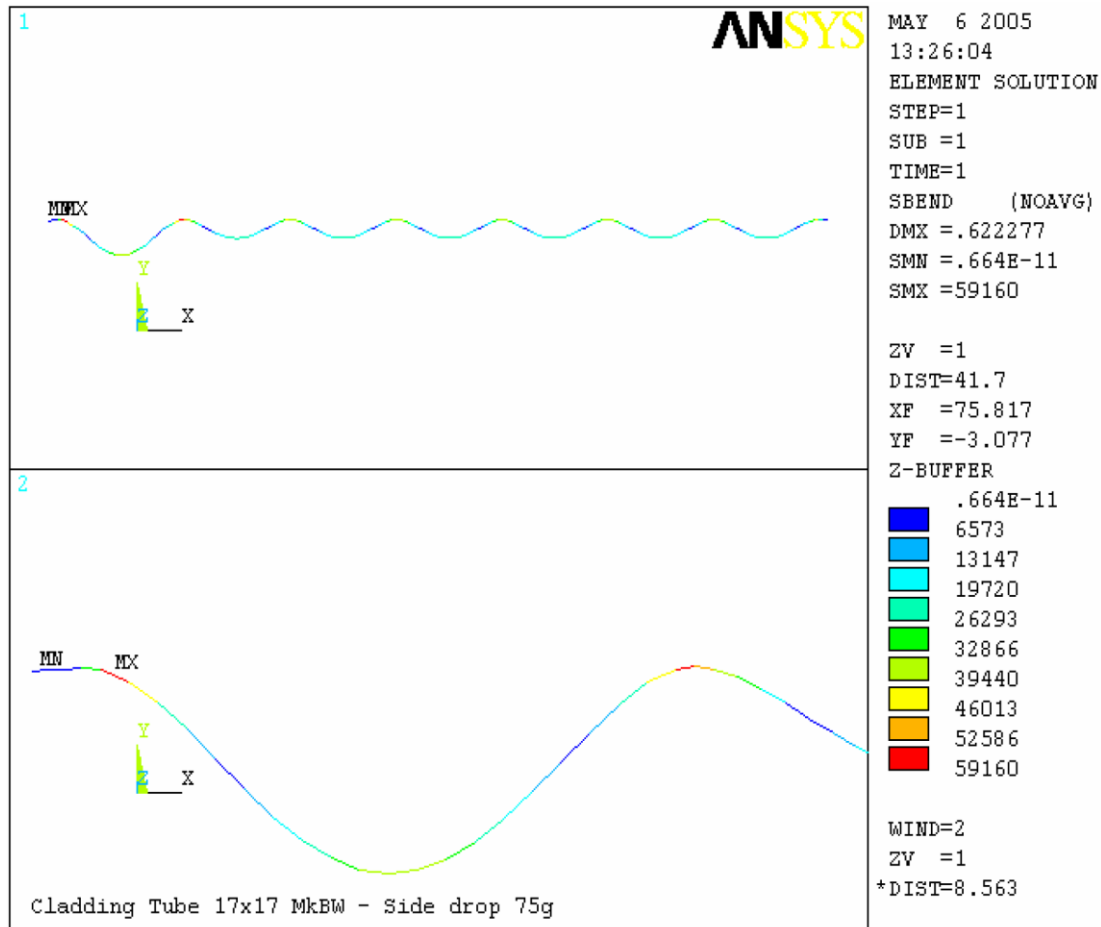


Figure 3-5
Bending stress – MK BW 17x17
(The bottom figure is an enlarged view of the span)

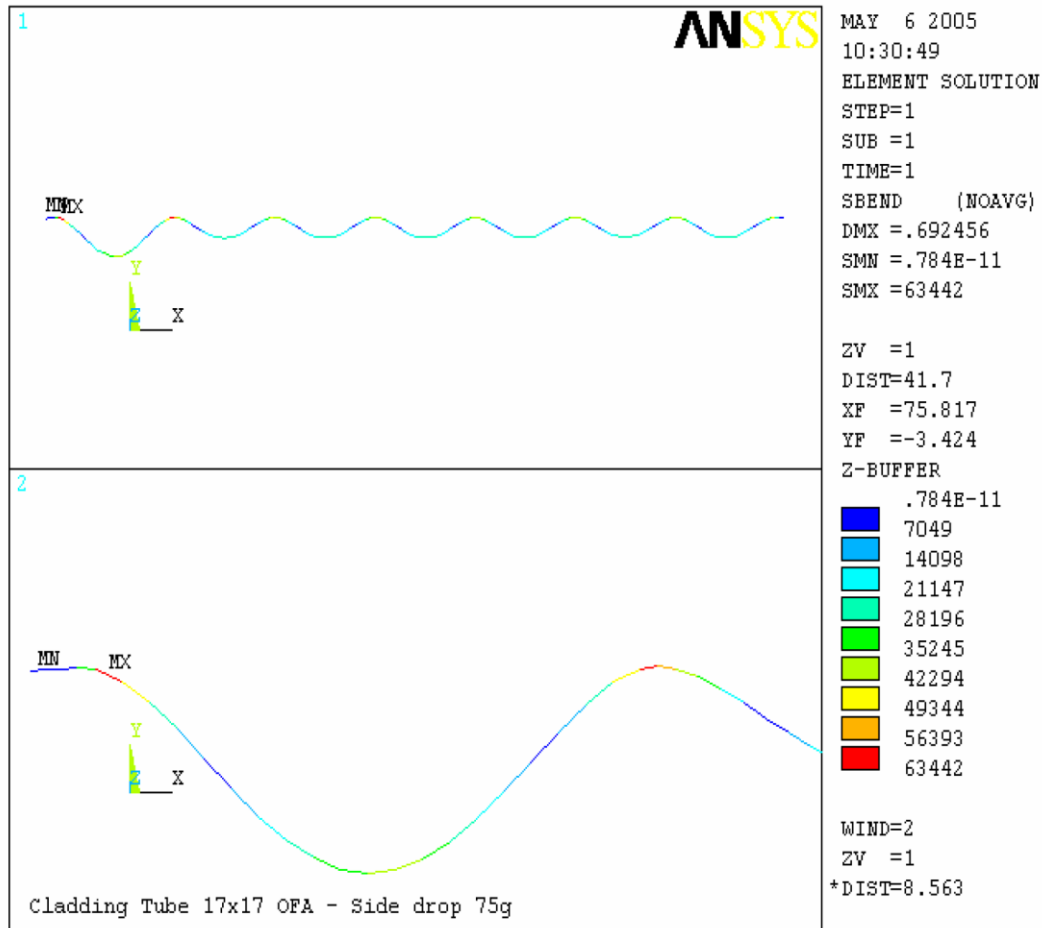


Figure 3-6
Bending stress – WEO 17x17
(The bottom figure is an enlarged view of the span)

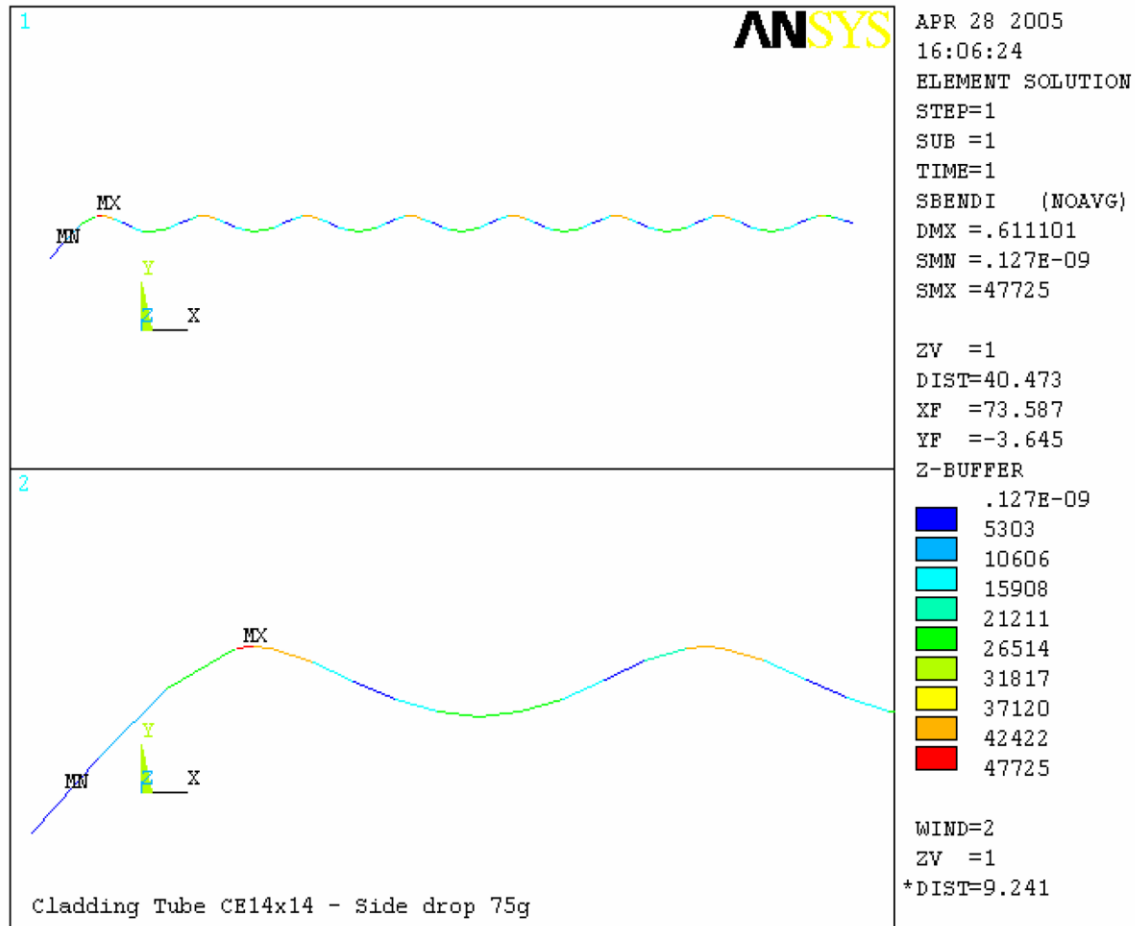


Figure 3-7
Bending stress – CE 14x14
(The bottom figure is an enlarged view of the span)

APPENDIX 3.9.1
32PTH DSC (CANISTER AND BASKET) STRUCTURAL ANALYSIS

TABLE OF CONTENTS

3.9.1	32PTH DSC (CANISTER AND BASKET) STRUCTURAL ANALYSIS	3.9.1-1
3.9.1.1	Introduction.....	3.9.1-1
3.9.1.2	32PTH DSC Fuel Basket Structural Evaluation.....	3.9.1-2
3.9.1.2.1	Approach.....	3.9.1-2
3.9.1.2.2	Loading Conditions.....	3.9.1-5
3.9.1.2.3	Fuel Basket Stress Analysis	3.9.1-7
3.9.1.2.4	32PTH DSC Fuel Basket Buckling Analysis.....	3.9.1-27
3.9.1.3	32PTH DSC Shell Structural Evaluation	3.9.1-30
3.9.1.3.1	Approach.....	3.9.1-30
3.9.1.3.2	DSC Canister Shell Stress Analysis.....	3.9.1-30
3.9.1.3.3	DSC Shell Buckling Evaluation.....	3.9.1-58
3.9.1.3.4	Evaluation of Alternate DSC Bottom Closure Assembly Design	3.9.1-61
3.9.1.4	32PTH DSC and OS187H Transfer Cask Thermal Expansion Evaluation.....	3.9.1-75
3.9.1.4.1	Introduction.....	3.9.1-75
3.9.1.4.2	Approach.....	3.9.1-75
3.9.1.4.3	Mechanical Properties of Materials	3.9.1-75
3.9.1.4.4	Thermal Expansion Computation	3.9.1-76
3.9.1.4.5	Thermal Expansion Analysis Conclusions	3.9.1-82
3.9.1.5	References	3.9.1-83

LIST OF TABLES

Table 3.9.1-1	Temperature Dependent Material Properties	3.9.1-85
Table 3.9.1-2	SA-240, Type 304, Thermal Material Properties.....	3.9.1-86
Table 3.9.1-3	Summary of Stresses in Fuel Compartments, Rails and Canister for Transfer Loads	3.9.1-87
Table 3.9.1-4(a)	Summary of Calculated Stresses in the Fuel Basket and Canister Shell due to 75g Drop Loads.....	3.9.1-88
Table 3.9.1-4(b)	Summary of Linearized Stresses in 7/8 inch Square Bars for 75g Side Drop Loads.....	3.9.1-89
Table 3.9.1-5	Summary of Stresses in Fuel Compartments, Support Rails and Canister Shell for Storage Loads	3.9.1-90
Table 3.9.1-6	Temperature Dependent Coefficients of Thermal Expansion	3.9.1-91
Table 3.9.1-7	ASME Subsection NB Code Allowable Stresses for the 32PTH DSC Canister (for Transfer Loads).....	3.9.1-92
Table 3.9.1-8	ASME Code Allowable Stresses for the 32PTH DSC Canister for Storage Loads.....	3.9.1-93
Table 3.9.1-9	32PTH DSC Canister Load Combinations during Transfer	3.9.1-94
Table 3.9.1-10	32PTH DSC Canister Load Combinations during Lifting, Testing, and Hydraulic Loads.....	3.9.1-95
Table 3.9.1-11	Summary of Calculated Stresses for Testing Condition Loads	3.9.1-96
Table 3.9.1-12	Summary of Calculated Stress for Normal and Off-Normal Condition Transfer Loads	3.9.1-97
Table 3.9.1-13	Summary of Calculated Stresses for Accident Condition Transfer Loads (Elastic Analysis)	3.9.1-98
Table 3.9.1-14	Summary of Stresses for Accident Condition Transfer Loads (Elastic / Plastic Analysis).....	3.9.1-99
Table 3.9.1-15	Summary of Calculated Stress at the End Closure Welds for Testing Condition Loads.....	3.9.1-100
Table 3.9.1-16	Summary of Calculated Stress at the End Closure Welds for Normal and Off-Normal Condition Transfer Loads	3.9.1-101
Table 3.9.1-17	Summary of Calculated Stresses at the End Closure Welds for Accident Condition Transfer Loads (Elastic Analysis)	3.9.1-102
Table 3.9.1-18	Summary of Calculated Stresses at End Closure Welds for Accident Condition Transfer Loads (Elastic/Plastic Analysis).....	3.9.1-103
Table 3.9.1-19	32PTH DSC Canister Load Combinations during Storage.....	3.9.1-104
Table 3.9.1-20	Summary of Calculated Stresses for Normal and Accident Condition Loads ⁽¹⁾ (Canister in horizontal storage position).....	3.9.1-105

Table 3.9.1-21	Summary of Calculated Stresses for Normal and Accident Conditions of Storage Loads (At End Closure Welds) ⁽¹⁾	3.9.1-106
Table 3.9.1-22	ASME Code Allowable Stresses for the Alternate Canister Bottom Assembly Design (Subsection NF)	3.9.1-107
Table 3.9.1-23	ASME Code Allowable Stresses for the Weld between the Canister Shell and the Bottom Outer Cover as per Subsection NF	3.9.1-108
Table 3.9.1-24	Summary of Calculated Stresses in the Alternate Canister Design for Normal Condition Loads (Subsection NB components)	3.9.1-109
Table 3.9.1-25	Summary of Calculated Stresses in the Alternate Canister Design for Normal Condition Loads (Subsection NF components)	3.9.1-110
Table 3.9.1-26	Summary of Calculated Stresses in the Alternate Canister Design for Normal Condition Loads (Subsection NF welds)	3.9.1-111
Table 3.9.1-27	Summary of Calculated Stresses in the Alternate Canister Design at the End Closure Welds for Normal Condition Loads	3.9.1-112
Table 3.9.1-28	Summary of Calculated Stresses in the Alternate Canister Design for Off-Normal Condition Loads (Subsection NB components)	3.9.1-113
Table 3.9.1-29	Summary of Calculated Stresses in the Alternate Canister Design for Off-Normal Condition Loads (Subsection NF components)	3.9.1-114
Table 3.9.1-30	Summary of Calculated Stresses in the Alternate Canister Design for Off-Normal Condition Loads (Subsection NF weld)	3.9.1-115
Table 3.9.1-31	Summary of Calculated Stresses in the Alternate Canister Design at the End Closure Welds for Off-Normal Condition Loads	3.9.1-116
Table 3.9.1-32	Summary of Calculated Stresses in the Alternate Canister Design for Accident Condition Loads (Subsection NB components)	3.9.1-117
Table 3.9.1-33	Summary of Calculated Stresses in the Alternate Canister Design for Accident Condition Loads (Subsection NF components)	3.9.1-118
Table 3.9.1-34	Summary of Calculated Tensile Stresses Normal to the NF Weld Throat In the Alternate Canister Design for Accident Condition Loads (Subsection NF welds)	3.9.1-119
Table 3.9.1-35	Summary of Calculated Stresses in the Alternate Canister Design for Accident Condition Loads (Top End Closure Welds)	3.9.1-120

LIST OF FIGURES

Figure 3.9.1-1	32PTH DSC Basket – 3D Cross Section Finite Element Model	3.9.1-121
Figure 3.9.1-2	32PTH DSC Basket Cross Section Finite Element Model – Fuel Compartments	3.9.1-122
Figure 3.9.1-3	32PTH DSC Basket Cross Section Finite Element Model – Center and Outer Plates	3.9.1-123
Figure 3.9.1-4	32PTH DSC Basket Cross Section Finite Element Model – Support Rails	3.9.1-124
Figure 3.9.1-5	32PTH DSC Basket Cross Section Finite Element Model – 7/8 inch Square Bars	3.9.1-125
Figure 3.9.1-6	32PTH DSC Basket Cross Section Finite Element Model – Canister and Gap Elements	3.9.1-126
Figure 3.9.1-7	32PTH DSC Basket FEM – Transfer Handling Loads Boundary Conditions	3.9.1-127
Figure 3.9.1-8	Fuel Compartments Finite Element Model – Thermal Analysis	3.9.1-128
Figure 3.9.1-9	Support Rail Finite Element Model – Thermal Analysis.....	3.9.1-129
Figure 3.9.1-10	Finite Element Model Boundary Conditions for Dead Weight Storage Load	3.9.1-130
Figure 3.9.1-11	DELETED.....	3.9.1-131
Figure 3.9.1-12	DELETED.....	3.9.1-132
Figure 3.9.1-13	DELETED.....	3.9.1-133
Figure 3.9.1-14	DELETED.....	3.9.1-134
Figure 3.9.1-15	DELETED.....	3.9.1-135
Figure 3.9.1-16	2-D Canister Axisymmetrical Thermal and Stress Finite Element Model	3.9.1-136
Figure 3.9.1-17	Top End of the 2-D Axisymmetrical Canister Model.....	3.9.1-137
Figure 3.9.1-18	Bottom End of the 2-D Axisymmetrical Canister Model	3.9.1-138
Figure 3.9.1-19	3-D DSC Canister Top End Assembly Finite Element Model	3.9.1-139
Figure 3.9.1-20	3-D DSC Canister Bottom End Assembly Finite Element Model.....	3.9.1-140
Figure 3.9.1-21	32PTH DSC Canister Finite Element Model used for Pressure Test Analysis.....	3.9.1-141
Figure 3.9.1-22	DELETED.....	3.9.1-142
Figure 3.9.1-23	2-D Axisymmetric Finite Element Model of the Alternate Canister Bottom Assembly.....	3.9.1-143
Figure 3.9.1-24	DELETED.....	3.9.1-144

Figure 3.9.1-25	DELETED.....	3.9.1-145
Figure 3.9.1-26	DELETED.....	3.9.1-146
Figure 3.9.1-27	Canister Finite Element Model	3.9.1-147
Figure 3.9.1-28	Loading Condition for DSC Corner Drop	3.9.1-148
Figure 3.9.1-29	Boundary Condition for DSC Corner Drop	3.9.1-149
Figure 3.9.1-30	Maximum Stress Intensities in DSC Shell.....	3.9.1-150
Figure 3.9.1-31	Maximum Stress Intensities in DSC Outer Top Cover.....	3.9.1-151
Figure 3.9.1-32	Maximum Stress Intensities in DSC Inner Top Cover	3.9.1-152

3.9.1 32PTH DSC (CANISTER AND BASKET) STRUCTURAL ANALYSIS

3.9.1.1 Introduction

Each NUHOMS®-32PTH DSC consists of a fuel basket and a canister body (cylindrical shell, outer top cover plate, top shield plug/inner cover, and shell bottom or shell bottom assembly). The 32PTH DSC canister body is provided with four alternate shell bottom assembly configurations. The primary confinement boundary for the 32PTH DSC consists of DSC shell, the top shield plug/inner cover plate, and shell bottom or inner bottom cover plate of the shell bottom assembly.

The Canister shell thickness is 0.50 inches, and the top and bottom closure assemblies are 12.0 inches and 8.75 inches, respectively. The Canister is constructed entirely from SA-240 Type 304 stainless steel and SA-182 Type F304. There are no penetrations through the confinement vessel. The draining and venting systems are covered by the port plugs and the outer cover plate and the top shield plug are welded to the cylindrical shell with multi-layer welds. The canister cavity is pressurized above atmospheric pressure with helium. The 32PTH DSC shell assembly geometry and the materials used for its analysis and fabrication are shown on drawings 10492-72-1 to 12 included in Chapter 1.

The basket structure consists of assemblies of stainless steel fuel compartments and support rails. The borated aluminum or boron carbide/aluminum metal matrix composite plates (neutron poison plates) provide the necessary criticality control and also provide the heat conduction paths from the fuel assemblies to the cask cavity wall. This method of construction forms a very strong structure of compartment assemblies which provide for storage of 32 PWR fuel assemblies. The open dimension of each fuel compartment is 8.70 in. × 8.70 in., which provides clearance around the fuel assemblies.

The Fuel Basket and Canister are analyzed separately. The Fuel Basket is analyzed in Section 3.9.1.2, while the Canister is analyzed in Section 3.9.1.3. Three separate finite element models are constructed for the structural evaluation of the fuel basket, while four finite element models are used for the structural evaluation of the canister shell.

A 3-dimensional cross-section finite element model is utilized to evaluate the effect of transverse inertial loads on both the basket and canister radial shell. A 3-dimensional model of a fuel compartment section is used to perform a buckling evaluation for the basket during lateral impact loads. Three-dimensional models of support rails are used to perform both thermal stress and buckling analyses.

A 2-dimensional axisymmetric model of the DSC canister shell is used to evaluate axial inertial loads as well as internal, external and thermal loads. Two 3-dimensional finite element models of the DSC canister bottom cover assembly and top cover assembly are utilized to evaluate the effects of transverse inertial loads on them. Also, a finite element model of the alternate canister composite bottom cover assembly is constructed to evaluate the structural adequacy of this alternate design.

3.9.1.2 32PTH DSC Fuel Basket Structural Evaluation

3.9.1.2.1 Approach

The Fuel Basket is evaluated for normal and accident condition impact and thermal loads. The basket stress analysis is performed using a finite element method for the side drop and thermal load cases and classical hand calculations for the end drop load cases. Buckling of the basket assembly structure, when subjected to lateral impact loads, is also evaluated. A summary of the basket load cases is provided in Section 3.9.1.2.2. Stress and buckling analyses are provided in Sections 3.9.1.2.3 and 3.9.1.2.4, respectively.

A. Material Properties

The mechanical properties of structural materials used in the basket, rail and canister are shown in the Table 3.9.1-1 as a function of temperature. All structural components of the fuel basket and support rails are constructed from SA-240, Type 304 or equivalent stainless steel, with properties taken from AMSE B&PV Code [1]. The yield and ultimate strengths of the structural steel, shown in Table 3.9.1-1, are the minimum values specified in the material specifications. In general, the temperatures chosen for the evaluation of material properties for each component of the DSC bound the maximum temperatures computed in Chapter 4.

B. Design Criteria

For normal conditions, the basis for the basket allowable stress is the ASME Code, Section III, Subsection NG [2]. The primary membrane stress intensity and membrane plus bending stress intensities are limited to S_m (S_m is the code allowable stress intensity) and $1.5 S_m$, respectively, at any location in the basket for Level A (Normal Service) load combinations. The average shear stress is limited to $0.6 S_m$.

The ASME Code provides a $3S_m$ limit on primary plus secondary stress intensity for Level A conditions. This limit is specified to prevent ratcheting and distortion of a structure under primary plus secondary loads.

For accident conditions, stresses are evaluated as short duration Level D conditions as per ASME B&PV Code, Section III, Appendix F [3]. When evaluating the stainless steel basket results from the elastic analysis, the general primary membrane stress intensity in, P_m , shall not exceed $2.4S_m$ or $0.7S_u$ and membrane plus bending stress intensity ($P_m + P_b$) is limited to the smaller of $3.6S_m$ or $1.0S_u$. The average primary shear stress is limited to the smaller of $0.42S_u$ or $2(0.6S_m)$.

When evaluating the results from the non-linear elastic-plastic analysis, the general primary membrane stress intensity, P_m , shall not exceed $0.7S_u$ and the maximum stress intensity at any location (P_l or $P_m + P_b$) shall not exceed $0.9S_u$. The average primary shear stress is limited to $0.42S_u$ or $2(0.6S_m)$.

The acceptability of a component, against buckling, is described in Section 3.1.2.1.2 of Chapter 3.

For fusion welds between the stainless steel plates and the stainless steel fuel compartment are qualified by testing. The required minimum tested capacity of the weld connection (each weld) shall be 17.1 kips (at room temperature). This value is based on a margin of safety (test to design) of 2.0, corrected for temperature difference and the maximum weld load of 7208 lbs calculated from a 75g side drop. This margin of safety, 2, is larger than the ASME Code-implied margin of safety for level D loads. The minimum capacity shall be determined by shear test (pull test) of individual specimen made from production material. In addition to the ASME Code requirements for weld qualification, as part of the weld qualification procedure, in order to verify proper machine setting and operation, a shear test (pull test) of test coupon from each welding machine will be performed prior to the start of each working shift.

The allowable stresses for both normal and accident conditions are summarized in the following table.

Loading Condition	Stress Category	Stress Criteria
Normal Conditions, Elastic Analysis	Membrane Stress, P_m	S_m
	Membrane + Bending Stress, $P_m + P_b$	$1.5 S_m$
	Average Shear Stress	$0.6 S_m$
	Primary + Secondary Stress, $P_m + P_b + Q$	$3 S_m$
Accident Conditions, Elastic Analysis	Membrane Stress, P_m	$\min\{2.4S_m \text{ or } 0.7S_u\}$
	Membrane + Bending Stress, $P_m + P_b$	$\min\{3.6S_m \text{ or } 1.0S_u\}$
	Average Shear Stress	$\min\{1.2S_m \text{ or } 0.42S_u\}$
Accident Conditions, Elastic-Plastic Analysis	Membrane Stress, P_m	$0.7 S_u$
	Membrane + Bending Stress, $P_m + P_b$	$0.9 S_u$
	Average Shear Stress	$\min\{1.2S_m \text{ or } 0.42S_u\}$

3.9.1.2.2 Loading Conditions

The transfer and storage basket loads are summarized in the tables below.

Basket Transfer Loads in Transfer Cask

Loading	Basket Orientation	Service Level	Load	Enveloped Load for Analysis	Load Combination
Dead Weight (DW)	Vertical ⁽¹⁾	A	1g Down (Axial)	1g Down (Axial)	1g Down (Axial)
Dead Weight (DW)	Horizontal ⁽²⁾	A	1g Down	2g Axial + 2g Trans. + 2 g Vertical	A = 2g Axial + 2g Trans. + 2 g Vertical
Handling load in Transfer Cask	Horizontal ⁽²⁾	A	DW +1g Axial		A + Thermal (115 °F amb.) A + Thermal (-20 °F amb.)
			DW + 1g Trans.		
			DW +1g Vert.		
			DW +0.5g Axial + 0.5g Trans. + 0.5 g Vert.		
Thermal	Vertical ⁽¹⁾	A	Vacuum Dry	Vacuum Dry	DW + Vacuum Dry
Thermal	Horizontal ⁽²⁾	A	Thermal Stress (115 °F amb.)	Thermal Stress (115 °F amb.)	Thermal Stress (115 °F amb.)
Thermal	Horizontal ⁽²⁾	A	Thermal Stress (-20 °F amb.)	Thermal Stress (-20 °F amb.)	Thermal Stress (-20 °F amb.)
Accident Side Drop	Horizontal	D	44g Transverse ⁽³⁾	75g Transverse	75g Transverse
Accident End Drop	Vertical	D	49g Vertical ⁽³⁾	75g Vertical	75g Vertical

⁽¹⁾ Canister supported at the bottom.

⁽²⁾ Canister supported at transfer cask rails.

⁽³⁾ Impact accelerations computed in Appendix 3.9.7.

Basket Storage Loads in HSM-H

Loading	Basket Orientation	Service Level	Load	Enveloped Load for analysis	Load Combinations
Dead Weight (DW)	Horizontal ⁽¹⁾	A	1g Down	1g Down	1g Down
Seismic Loads	Horizontal ⁽¹⁾	C ⁽²⁾	0.43g Axial + 0.43g Trans. + 0.20g Vertical +DW	0.65g Axial + 0.65 Trans.+ 1.30g Vertical	0.65g Axial + 0.65 Trans.+ 1.30g Vertical 0.65g Axial + 0.65 Trans.+ 1.30g Vertical Thermal (-20 °F amb.) 0.65g Axial + 0.65 Trans.+ 1.30g Vertical Thermal (115 °F amb.)
Thermal	Horizontal	A	Thermal (-20 °F ambient)	Thermal (-20 °F ambient)	Thermal
Thermal	Horizontal	A	Thermal (115 °F ambient)	Thermal (115 °F ambient)	Thermal
Thermal	Horizontal	D ⁽²⁾	Thermal (Blocked Vent)	Thermal (Blocked Vent)	1g Down + Thermal (Blocked Vent)

(1) Canister Supported at HSM-H Rails and axially restrained by seismic restraint devices.

(2) Level C and D loads are conservatively treated as Level A loads.

3.9.1.2.3 Fuel Basket Stress Analysis

A. 3D Cross Section Finite Element Model Description

A three-dimensional finite element model of the basket fuel compartments, peripheral rails and canister is constructed using ANSYS [10] SHELL43 elements. The overall finite element model of the basket, peripheral rails and canister is shown in Figure 3.9.1-1. For conservatism, the strength of aluminum plates in the basket was neglected by excluding these from the finite element model. However, their weight was accounted for by increasing the basket plates and peripheral rail material densities. Because of the large number of plates in the basket and large size of the basket, certain modeling approximations were necessary. In view of continuous support of fuel compartment tubes by the peripheral rails along the entire basket length during a side drop, only a 15.0" long slice of the basket and rail was modeled. At the two cut faces of the model, symmetry boundary conditions were applied ($UZ = ROTX = ROTY = 0$). The fuel compartment tubes, structural plates, support rails, square bars, and canister shell are included in the model and are shown individually in Figure 3.9.1-2 through Figure 3.9.1-6.

Radial gap elements (CONTAC 52) are used to simulate the interface between the basket peripheral rails and inner side of the canister and between canister outer radius and cask inner radius. Each gap element contains two nodes; one on each surface of the structure. The gap nodes specified at the inner side of cask are restrained in x, y and z directions. The gap size at each gap element is determined by the difference between the basket rails radius and the inside radius of the canister and between the canister outer radius and the inside radius of the cask. A sensitivity analysis of gap size and fusion weld effectiveness study have shown that the difference of the gaps and fusion weld effectiveness will have no significant impact to the results of the analysis. Radial gap (and link) elements are generated using a small ANSYS macro. Actual gap sizes for the gap element, at each radial location, were determined and input into the model as real constants using another small ANSYS macro. This macro accepts the drop orientation and model geometry as inputs and determines the circumferential position of each gap element. The macro then computes the appropriate real constants and applies to appropriate gap elements. At the operating temperatures, the initial gap sizes will be lower. Thus use of room temperature gap sizes is conservative. Figure 3.9.1-6 shows the locations of both sets of gap elements.

During drops on cask rails (180° side drop), the initial gaps between the canister and the cask are modified using the ANSYS macro. Two 3 inch wide and 0.12 inch thick rails are welded to the cask inside at 12° on both sides of vertical center line and another set of two rails are welded at 38° on both sides of the vertical center line. For the 180° side drop onto the rails, the initial gaps at the two inner rail locations are assumed closed. In-between these two rail locations, the initial gaps are set to 0.12 inches. On the other two rail locations, the gap statuses are initially set to open, and the gap sizes are generated by macro and decreased by the rail thickness.

The connections between the stainless steel fuel compartment tubes (with intermediate aluminum plates), between the tubes and stainless steel plates as well as between the tubes and rails are made with node couplings. The nodes of various plates are coupled together in the out-of-plane direction so that they will bend in unison under surface pressure or other lateral loading to simulate the through-the-thickness support provided by the aluminum plates. The fusion welds, connecting the fuel compartment and plates, are modeled by coupling nodes in all directions. The bolts connecting the peripheral rails with the plates are also modeled by coupling nodes (in x , y and z directions).

Material Nonlinearities

The basket fuel compartments, structural plates, peripheral rails and canister shell are constructed from SA-240, Type 304 or equivalent stainless steel. A bilinear stress-strain relationship, with kinematic hardening, was used for each component to simulate a correct nonlinear material behavior at the maximum operating temperature. The following elastic and inelastic material properties are used in the analysis:

Material Property	Basket Fuel Compartments, and Center Plates at 700 °F	Peripheral Rails, Sq. Bars and Outer Plates at 550 °F	Canister at 500 °F
Modulus of Elasticity, E (psi)	24.8×10^6	25.6×10^6	25.8×10^6
Yield Strength, F_y (psi)	17,600	18,900	19,400
Tangent Modulus, E_t (psi)	5% of $E = 1.24 \times 10^6$	5% of $E = 1.28 \times 10^6$	5% of $E = 1.29 \times 10^6$

Gap Element Nonlinearities

Gap elements (CONTAC 52) are used to model the actual surface clearance between the basket rails and canister inside as well as between canister outside and cask inside. The gap elements introduce nonlinearities in the analysis depending whether they are open or closed. Initially, at the contact surface, gaps are closed. For the remaining periphery, the gaps are open. Actual gap size at each rail nodal location was computed using ANSYS macro for each basket orientation. The gap element spring constant, K_n , is calculated as:

$$K_n = f E h \quad [10]$$

Where f is a factor usually between 0.01 and 100, E is the material modulus of elasticity (25.8×10^6 psi), and h is a typical “target length” or typical element size [typical element length ≈ 1.2 in., typical element width ≈ 1.9 in. typical target length $h = (1.2 \times 1.9)^{0.5} = 1.51$ in.]. Therefore,

$$K_n = 25.8 \times 10^6 \times 1.51 \times f = 0.39 \times 10^6 \text{ to } 3,900 \times 10^6 \text{ lb./in.}$$

Thus, there is very wide range for K_n value. The structure responded well for a spring constant value of 1.0×10^6 lb/in. and is used in previous similar analyses. Further, to help convergence, ANSYS elements LINK8 were inserted coincident with the CONTAC52 elements. To assure that these elements do not transfer a substantial load between the surfaces, a very low elastic modulus ($E = 1000$ psi), a small area (0.1 in^2) and zero density (to zero their inertial loading contribution to the structure) are used in the analysis.

B. Fuel Basket Stress Analysis for Transfer Loads

B.1. Dead Weight, 1g Down (Cask Vertical)

During 1g down loading, the fuel assemblies and fuel compartment are forced against the bottom of the canister/transfer cask. It is important to note that, for any vertical or near vertical loading, the fuel assemblies react directly against the bottom of the cask and not through the basket structure as in lateral loading. It is the dead weight of basket only that causes axial compressive stress during an end drop. Axial compressive stresses are computed as if only the compartment tubes will withstand all the weight. A conservative basket weight of 30.0 kips. (Actual weight is 29.854 kips) is used in the end drop stress calculations.

Total weight of the basket assembly = 30.0 kips

Compressive Stress in Fuel Compartments

$$\text{Section area of compartment tubes} = 32 \times [9.075^2 - 8.7^2] = 213.3 \text{ in}^2$$

$$\text{Area of 1 in} \times 1 \text{ in drain slots} = 32 \times 4 \text{ slots/compartment} \times [1.0'' \times 0.1875''] = 24.0 \text{ in}^2$$

$$\text{Area of 4 lifting slots} = 8 \times 7.7 \times 0.1875 = 11.55 \text{ in}^2$$

$$\text{Area of 8 corner notches} = 8 \times 1.0 \times 0.1875 = 1.5 \text{ in}^2$$

$$\text{Stress due to 1g} = -30.0 / [(213.3 - (24 + 11.55 + 1.5))] = -.1702 \text{ ksi}$$

Shear Stress in Rail Stud

During vertical basket orientation, the rail will support its own weight. Therefore, there will be no load on rail studs.

B.2. Handling Loads (Cask Horizontal)

During normal conditions of transfer, the basket and canister shell is resting on two rails in OS187H Transfer Cask (3 in wide \times 0.12 in thick) at 12° on either side of basket centerline. The radial contact elements between the pads and canister are assumed to be initially closed. The canister and rail nodes at one location are held in circumferential direction to avoid rigid-body motion of the model. In-between the two rail locations, initial gaps are set to 0.12 inches. On the other two rail locations (at 38° on either side of basket centerline); the macro generated gaps are decreased by rail thickness and are initially open.

Loading

The basket pressure is evaluated using fuel assembly weight distributed over an effective length of 144 inches corresponding to the active fuel assembly length. The used pressure on the basket panels in the analysis bounds the maximum pressure calculated when considering the individual skeleton parts (cladding tubes, fuel pellets, support grid and end fittings), as calculated below:

$$\text{Fuel assembly weight} = \text{Wt. of Fuel Rods} + \text{Wt. Skeleton}$$

The pressure on the basket panels due to the fuel assembly weight

$$= \text{No. of Fuel Rods (Fuel Cladding Weight + Fuel Pellet Weight) / Panel span} + \text{Fuel Skeleton Weight / (Panel span} \times \text{fuel assembly length)}$$

$$= n(\rho_c \pi (d_{co}^2 - d_{ci}^2) / 4 + \rho_f \pi d_f^2 / 4) / W + W_{\text{Skeleton}} / (L \times W)$$

Where,

$$n = \text{No. of fuel rods for Westinghouse 17x17 Standard} = 264$$

$$\rho_c = \text{Density of fuel cladding} = 0.234 \text{ lb/in}^3 \text{ Ref. [16]}$$

$$\rho_f = \text{Density of fuel pellet} = 0.382 \text{ lb/in}^3 \text{ Ref. [16]}$$

$$d_{co} = \text{Outer diameter of fuel cladding} = 0.374 \text{ in. Ref. [17]}$$

d_{ci} = Inner diameter of fuel cladding = $0.374 - 2 \times 0.0225 = 0.329$ in. Ref. [17]

W = Panel span = 8.8874"

$W_{Skeleton}$ = Weight of the fuel assembly skeleton assumed = $50 \text{ kg} \times 2.2 = 110 \text{ lb}$

L = Length on the fuel assembly, conservatively assumed to be the active fuel assembly length = 144", Ref. [17].

The pressure on the basket panels is calculated below:

$$= 264 \left\{ (0.234 \times \pi \times (0.374^2 - 0.329^2) / 4) \right\} + 110 / (144 \times 8.8874)$$

$$= 1.0996 + 0.0860 = 1.1856 \text{ psi}$$

However, in the evaluation it is conservatively assumed that fuel assembly weight of 1585 lb is distributed along 144 inches of active fuel length (active basket length is 162 inches) i.e.

Pressure P_v on horizontal plate for 1g acceleration =

$$= \text{Fuel assembly wt.} / (\text{Panel span} \times \text{Panel length})$$

$$= 1,585 \text{ lb} / (8.8874" \times 144") = 1.238489 \text{ psi}$$

The vertical and transverse loads, resulting from the fuel assembly weight, are applied as pressure on horizontal and vertical faces of plates (see Figure 3.9.1-7). The pressure for 2g acceleration is calculated conservatively, as shown below:

$$\begin{aligned} \text{Pressure, } P_v, \text{ on horizontal plates} &= P_h \text{ on vertical plates} \\ &= \text{Fuel wt.} \times \text{acceleration} / (\text{Panel span} \times \text{Panel length}) \\ &= 1,585 \text{ lb.} \times 2.0 / (8.8874 \text{ in} \times 144 \text{ in}) = 2.477 \text{ psi} \end{aligned}$$

The inertia load due to fuel compartments, rails and canister dead weight is simulated using the density and appropriate acceleration in vertical and transverse directions.

The steel panels and peripheral rail material density is modified to account for the aluminum plates, which are not modeled. The equivalent densities of these components are the following:

Fuel Compartments:	Equivalent Density, $\rho = 0.424 \text{ lb/in}^3$
Large Peripheral Rails:	Equivalent Density, $\rho = 0.50 \text{ lb/in}^3$
Small Peripheral Rails:	Equivalent Density, $\rho = 0.488 \text{ lb/in}^3$

Since only a 15 inch length of the basket is modeled, the acceleration in axial direction is increased to account for the entire 144 inch length.

$$\text{Axial acceleration for } 2g \text{ load} = 2.0g \times 144/15.0 = 19.2g$$

To simulate the axial stress due to the above acceleration, only one side of basket is restrained in z-direction.

For (2g axial + 2g Transverse + 2g Vertical) handling load, the pressures and accelerations are applied simultaneously:

Therefore the acceleration applied to the model is: accel,-2.0, 2.0, 19.2

Analysis and Results

A nonlinear elastic stress analysis was conducted for computing the elastic stresses in the basket model. The nonlinearity of analysis resulted from the gaps in the model. The total load was applied in small steps. The automatic time stepping program option "Autots" was activated. This option lets the program decide the actual size of the load-substep for a converged solution. The shell middle surface nodal stress intensity is the membrane stress intensity and top or bottom surface stress intensity is the membrane plus bending stress intensity.

Analysis of Fusion Welds for Handling Loads

The maximum fusion weld load was computed using the finite element model side drop load case. The finite element model is modified by replacing the fusion weld couplings with PIPE20 elements.

A static nonlinear stress run is made and results of the run are post-processed in order to extract the axial (FX) and shear (FY and FZ) forces in the pipe elements. The maximum shear force in anyplace of the pipe elements for the 2g handling load is 1415 lbs. The thermal loads in the fusion welds are calculated in Section B.3 below. The maximum combined shear force due to handling load and thermal load is 2.05 kips. The fusion weld load capacity is qualified for 75g accident load by test and is 17.1 kips. The transfer loads (2g) are much smaller than the 75g load. Thus by comparison, fusion welds capacity is judged to be much higher than the combined handling and thermal loads.

B.3. Thermal Loads during Transfer

Generally, thermal stresses develop in the basket if its free thermal expansion is constrained by the peripheral rails or canister. The thermal expansion calculations in Section 3.9.1.4.4 show that the basket rails are free to grow due to the maximum operating temperature in the canister. The rails are attached to the basket with bolts in slotted holes. Thus rails also permit free thermal growth of basket boxes. Aluminum and poison plates are sandwiched by the compartment tubes. A thermal expansion gaps are provided to allow the aluminum/poison plates free to grow in the axial direction while oversize slots are provided to allow aluminum/poison plates free to grow in the radial direction (see TN drawing 10494-72-8). However, some thermal stresses in basket and rails can develop due to radial gradients (hot at center and cooler at periphery) for normal thermal conditions. Basket and Rail thermal stresses are therefore calculated for the 115 °F (hot normal), -20 °F (cold normal) ambient and vacuum drying process.

Thermal Stresses in Basket Fuel Compartments during Transfer

A three-dimensional finite element model of the basket is used for thermal and stress analyses of the basket, using ANSYS. This finite element model is described in Section 3.9.1.2.3A. Due to symmetry of temperature distribution, only a ¼ model (see Figure 3.9.1-8) is used in this analysis. The rails and canister are removed from the model, as they have no effect on the fuel compartment thermal stresses. The support rails are analyzed separately for the thermal loads.

In order to model realistic contact between the fuel compartments, the couplings are replaced by contact elements. The couplings at the fusion weld locations are replaced by pipe elements.

Two finite element analyses are required to compute the thermal stresses in the fuel basket. The first analysis is a thermal analysis that computes the temperature distribution at each node of the structural model, given the temperature distribution in the thermal model described in Chapter 4. The second finite element analysis computes the thermal stress distribution caused by the temperature distribution computed in the first analysis.

The four-node element SHELL57 (Thermal Shell) and LINK33 (Thermal Conduction Bar) are used in the thermal analysis. These elements are replaced by stress elements SHELL43 and PIPE20 in the stress analysis.

Thermal Analyses

Thermal analyses of a gross model of 32PTH DSC Canister, Basket, and OS187H Cask is conducted for hot and cold normal ambient conditions and for vacuum drying and transfer cask backfill operations in Chapter 4. Steady-state thermal analyses of the basket structural model are conducted to obtain the nodal temperatures by impressing the temperatures computed in the Chapter 4 analyses as the boundary conditions for 115 °F, -20 °F ambient and vacuum drying cases.

In Chapter 4, the basket and rail temperatures are computed for vacuum drying and TC backfill operations. The table below provides the maximum basket and rail temperatures and thermal gradients from these operations.

	Assumed in this Analysis Max. Temp (°F)	TC Backfill from Table 4-8 at 40 hours, Max. Temp (°F)
Basket Fuel Compartments	697	734
Basket Rails	531	591
Thermal Gradient, ΔT	166	143

From the above table, it is judged that the assumed temperature gradient (shown above in column 2) case will be critical for stresses due to the highest thermal gradient and is selected for the analysis.

Thermal material properties for material (type 304 stainless steel), taken from Reference 1, are reproduced in Table 3.9.1-2.

The thermal analysis resulting temperature distributions for -21 °F and 115 °F ambient and vacuum drying conditions closely match the temperature distributions presented in Chapter 4.

Thermal Stress Analysis

Elastic stress analyses of the basket structure are conducted in order to compute the thermal stresses. The nodal temperature distribution from the thermal analysis results is applied to obtain the thermal stresses in the model. The resulting nodal stress intensity distribution in the basket fuel compartments reveals that the maximum thermal stress occurs during the vacuum drying load case, and is 9.86 ksi.

Thermal Stresses in Support Rails during Transfer

The temperature distribution and the thermal stresses in peripheral rails are computed using the same methodology as given above for the fuel compartments. The finite element model of the rails is taken from the full basket model described in Section 3.9.1.2.3A and is shown in Figure 3.9.1-9.

The resulting nodal stress intensity distribution in the support rails reveals that the maximum thermal stress occurs during the vacuum drying load case, and is 18.70 ksi.

Thermal Load in Fusion Welds during Transfer

The forces in x , y and z global directions in the PIPE elements (modeling the fusion welds) for the critical vacuum dry thermal load case are tabulated for stress computation. The thermal analysis results show that the thermal loads in the fusion welds are quite small. The maximum shear force, $\underline{F}_{\text{weld}}$, is:

$$\underline{F}_{\text{weld}} = \sqrt{611^2 + 150^2} = 631 \text{ lbs.}$$

This force is combined with the force generated from 2g handling load calculated above, therefore, the total load is:

$$1,415 \text{ lb} + 631 \text{ lb} = 2,046 \text{ lb} \approx 2.05 \text{ kips}$$

This load is much smaller compared to the weld capacity of 17.1 kips from test.

B.4. Summary of Fuel Basket Stresses for Normal Condition Transfer Loads

Table 3.9.1-3 summarizes basket stress analysis results and compares them with the Code allowable stresses. For the Normal thermal condition allowable stresses, the fuel compartment temperature is taken to be 700° F uniform, the peripheral rail temperature is taken to be 600 °F uniform and canister temperature is taken to be 500 °F uniform. Based on the results of these analyses, the basket and rails are structurally adequate for normal transfer condition loads.

B.5. 75g Hypothetical Accident Condition Side Drop during Transfer

In this section, stresses are evaluated in 32PTH DSC Basket for 75g transfer accident condition side and end drop impact loads.

The basket temperature is taken as 700 °F, uniform. The rail temperature is taken as 550 °F, uniform, and the canister temperature is taken as 500 °F uniform. These temperatures conservatively bound the temperature distributions computed in Chapter 4.

The 3-dimensional finite element model described in Section 3.9.1.2.3A is also used to compute the stresses due to the 75g accident drop.

Loadings

The basket structure is analyzed for 75g side drops in 0°, 30°, 45°, and 180° (on rails) orientations. Due to the basket structure symmetry, these orientations are assumed to bound all possible maximum stress cases.

The load resulting from the fuel assembly weight is applied as pressure on the fuel compartment plates of the basket. For the 180° (drop on support rails) and 0° orientations, the pressure act only on the horizontal plates while for all other orientations, the pressure is divided into components to act on both horizontal and vertical plates of the basket. The pressures for the different orientations are calculated below for 1g and 75g accelerations:

0° and 180° drops

The resulting pressure on the basket panel bounds maximum pressure (i.e., 1.1856 psi) calculated in 3.9.1.2.3, Section B.2. However, conservatively a pressure value of 1.238489 psi for 1g acceleration is used in the evaluation.

$$\text{Pressure, } p \text{ for } 75g = 75 \times 1.238489 = 92.8867 \text{ psi.}$$

30° drop

$$p_h \text{ on vertical plates for } 1g = p \sin 30^\circ = 1.238489 \times 0.5 = 0.619244 \text{ psi.}$$

$$p_v \text{ on horizontal plates for } 1g = p \cos 30^\circ = 1.238489 \times 0.86603 = 1.072563 \text{ psi}$$

$$p_h \text{ on vertical plates for } 75g = 75 \times 0.619244 = 46.4433 \text{ psi}$$

$$p_v \text{ on horizontal plates for } 75g = 75 \times 1.072563 = 80.4422 \text{ psi}$$

45° drop

$$p_v \text{ on horizontal plates} = p \cos 45^\circ = 1.238489 \times 0.7071 = 0.875736 \text{ psi}$$

$$p_h \text{ on vertical plates} = p \sin 45^\circ = 1.238489 \times 0.7071 = 0.875736 \text{ psi}$$

$$p_v = p_h \text{ for } 75g = 75 \times 0.875736 = 65.680 \text{ psi}$$

The inertia loads due to the basket and peripheral rail dead weights are simulated by applying the density and appropriate acceleration in the runs.

The aluminum plate weight is accounted for by increasing the densities of stainless steel basket fuel compartments, large rails and small rails, as in Section 3.9.1.2.3B.2.

Finite Element Analysis

A nonlinear static stress analysis of the structural basket is conducted for computing the stresses for 0°, 30°, 45° and 180° (drop rails) drop orientations. The maximum load of 75g was applied in each analysis. The automatic time stepping program option "Autots" was activated. This option lets the program decide the actual size of the load-substep for a converged solution.

Displacements, Stresses and Forces at each node of model (for each converged substep load) were written in ANSYS result files. The program stops at the load substep when it fails to result in a converged solution. In all side drop cases, the program gave converged solutions up to 75g load. Results were extracted at the last load sub-step of 75g for evaluation.

Shear Load in Fusion Welds due to 75g Side Drop

The maximum fusion weld load was computed using the finite element model. The finite element model is modified by replacing the fusion weld couplings with PIPE20 elements.

A static nonlinear stress run is made and results of the run are post-processed in order to extract the axial (FX) and shear (FY and FZ) forces in the pipe elements. Reviewing the details of pipe element forces (at 'i' node and 'j' node of each pipe element) show that the axial (FX) and shear (FZ) loads are not significant.

Conservatively, the maximum shear load in a fusion weld is computed by vectorially adding the maximum FY and maximum FZ (irrespective of their locations in the finite element model) as follows.

Maximum Force, FY = 7,197 lb.

Maximum Force, FZ = 393 lb.

Maximum Shear Force = $[7,197^2 + 393^2]^{1/2} = 7,208 \text{ lb.}$

From the above, it is seen that the maximum shear load on a fusion weld is 7,208 lb. The fusion weld capacity (by test) is to match or exceed this maximum weld load.

For the fusion weld load capacity test at room temperature, it is determined to include a safety factor of 2 and a correction for material strength for room temperature testing. Therefore, the Required Minimum Fusion Weld Test Load = $7,208 \times (2) \times (F_{tu} \text{ at room temperature} / F_{tu} \text{ at } 700^\circ\text{F}) = 7,208 (2.0) (75.0 \text{ ksi}/63.4 \text{ ksi}) = 17,054 \text{ lbs} \approx 17.1 \text{ kips}$

Square Bar Stresses due to 75g Side Drop

Four 7/8 inch square bars are welded to the small rails. These square bars are modeled with SOLID45 Elements in finite element model shown in Figure 3.9.1-5.

From the nodal stress intensity distribution in the bars for 0°, 30°, 45° and 180° (on rails) side drops, it is seen that the maximum nodal stresses are local and secondary (surrounded by a low stress area) in nature and can be neglected in the accident stress evaluation. However, for conservatism, stresses are considered primary and are linearized at the highest nodal stress intensity locations to compute P_m and $P_m + P_b$.

Summary of Side Drop Results

The Table 3.9.1-4(a) and Table 3.9.1-4(b) summarizes the accident condition basket structural analysis maximum stress intensities for the various side drops and compares them with the material code allowable stresses at 700 °F for the basket, 550 °F for the support rails and 500 °F for the canister shell. The shell element middle surface nodal stress intensity is the membrane stress intensity and the maximum of the top or bottom surface stress intensity is the membrane plus bending stress intensity. All stresses in the basket components are below the allowables.

Rail Stud Stresses due to 75g Side Drop

It is observed from the stress summary table (Table 3.9.1-4(a)) that the maximum rail stresses occurred during the 180° side drop (drop on rails). Stresses in other basket components are also quite high during this drop orientation. In other side drop orientations stresses were somewhat lower. Therefore, the maximum shear stresses in the rail studs are expected to occur during a 180° side drop. The rail stud stresses are therefore computed for this side drop. These stresses will bound the stud stresses for the other basket drop orientations.

For the small rails, due to the enlarged holes in rails mounting spacers, the top small rail will slide and will be supported by the fuel compartment. The bottom small rail will also slide and be supported by the canister and in turn supported by the transfer cask. There are no loads to be carried by the studs. Therefore stress evaluations of the small rail studs are not critical.

For the large rail (A180) studs, the rails also will slide during the drop and will be supported by the canister and in turn will be supported by the transfer cask. However, for conservatism, the shear stresses are considered in the rail plate/stud weld (O.D. = 0.75 in, I.D. = $0.75 - (2 \times 0.31) = 0.13$ in) by assuming all the weight of the rail will be carried by the studs. There are 11 stud rows over the entire basket length.

Weight of 8 half-rails = 10378 lb. (Section 3.2.1)

Weight of one half-rail = $10378/8 = 1297.3$ lb

Number of Studs supporting the half-rail = $11 \text{ rows} \times 2 \text{ studs/row} = 22$

Weld area of one stud, $A = \pi/4 (0.75^2 - 0.13^2) = 0.4285 \text{ in}^2$

Weld Shear Stress for 75g = $(1297.3 \times 75) / (22 \times 0.4285) = 10,321 \text{ psi} \approx 10.3 \text{ ksi}$

Allowable Shear Stress (at 550 °F) = $1.2 S_m = 0.8 \times 1.2 \times 16.95 = 16.27 \text{ ksi} > 10.3 \text{ ksi}$.

The design is adequate.

B.6. 75g Hypothetical Accident Condition End Drop during Transfer

During an end drop, the fuel assemblies and fuel compartments are forced against the bottom of the canister/transfer cask. It is important to note that, for any vertical or near vertical loading, the fuel assemblies react directly against the bottom or top end of the canister/transfer cask and not through the basket structure as in lateral loading. It is the dead weight of the basket only that causes axial compressive stress during an end drop. Axial compressive stresses are conservatively computed assuming that all loads act on the compartment tubes during an end drop. A conservative basket weight of 30.0 kips. (Actual weight is 29.85 kips from Section 3.2.1) is used in the end drop stress calculations.

Compressive Stress in Fuel Compartments due to 75g End Drop

Section area, A , of the fuel compartment tubes is,

$$A = 32 \times [9.075^2 - 8.7^2] = 213.3 \text{ in}^2$$

Area of 1×1 inch drain slots, A_s , is,

$$A_s = 32 \times 4 \text{ slots/compartment} \times [1.0 \text{ in} \times 0.1875 \text{ in}] = 24.0 \text{ in}^2$$

Area of .5 x .5 inch fuel compartment notches, A_n , is,

$$A_n = 8 \times [(.5+.5) \text{ in} \times 0.1875 \text{ in}] = 1.5 \text{ in}^2$$

Area of Basket Type 1 lifting slots, A_1 , is,

$$A = 8 \times [7.7 \text{ in} \times 0.1875 \text{ in}] = 11.55 \text{ in}^2$$

Stress due to 1g load, σ_{1g} , is,

$$\sigma_{1g} = -30.0 / (213.3 - 24.0 - 11.55 - 1.5) = -0.17 \text{ ksi}$$

At 75g the compressive stress, σ_{75g} , is,

$$\sigma_{75g} = -0.17 \text{ ksi} \times 75 = -12.8 \text{ ksi}$$

Stress in Rail Stud due to 75g End Drop

During the 75g end drop, the rail will support its own weight by contact with the bottom or top of canister / transfer cask. Therefore, there will not be any stresses in rail studs during an end drop.

C. Fuel Basket Stress Analysis for Storage Loads

This section evaluates the elastic stresses in the 32PTH DSC fuel basket due to HSM-H storage loads including, dead weight, seismic and thermal loads. The basket stresses are then compared with the code allowable stresses.

During normal condition of storage, the fuel compartment temperature is taken to be 700° F, uniform, the rail temperature is taken as 550 °F, uniform, and the canister temperature is taken as 500 °F, uniform. These temperatures are considered conservative based on the thermal evaluation presented in Chapter 4.

During the blocked vent hypothetical accident case, the fuel compartment and support rail temperatures are taken to be 800 °F and 650°F, respectively. These temperatures are also conservatively based on the thermal evaluation in Chapter 4.

C.1. Dead Weight Analysis during Storage

The three-dimensional finite element model of the basket fuel compartments, rails and canister shell used to compute stresses for storage loads is described in Section 3.9.1.2.3A. The finite element model, boundary conditions, and real constants are described in detail in that section.

The canister shell is resting on two support pads (3 inches wide) inside the HSM-H at 30° on either side of canister/basket centerline (canister/basket in 180° orientation). The radial contact elements at the pad locations are assumed closed. The canister shell nodes at one location coincident with the pad are held in circumferential direction to avoid rigid-body motion of the model. The gap elements between inside surface of the canister shell and basket rails are assumed to be closed at 180° (bottom) orientation and the remaining initial gaps were suitably modified (from 0.0 inch gaps at the bottom, to 0.25 inch gaps at the top) using an ANSYS macro. The node couplings, boundary conditions and loading are shown in Figure 3.9.1-10. For clarity, only the front view of the model is shown and rotational displacement boundary conditions are not shown in this figure.

Dead Weight Applied Load

Dead Weight Load (1g) is applied as pressure on the horizontal faces of fuel compartment plates (see Figure 3.9.1-10). The pressures for the 1g acceleration are calculated below.

The resulting pressure on the basket panel bounds the maximum pressure (i. e., 1.1856 psi) calculated in Section 3.9.1.2.3B.2. However, conservatively a pressure value of 1.2385 psi for 1g acceleration is used in the evaluation.

Pressure, p_v on horizontal plates is 1.2385 psi.

The inertial load due to the basket rails and canister dead weight is simulated applying density and 1g acceleration in vertical direction. The aluminum plate weights are accounted for by increasing the basket fuel compartment plate and rail densities.

Dead Weight Finite Element Analysis

An ANSYS elastic nonlinear stress analysis is conducted to compute stresses in the basket and canister model. The nonlinearity of analysis results from the gaps elements in the model. The total load is applied in small steps. The automatic time stepping program option "Autots" is activated. This option lets the program decide the actual size of the load sub-step for a converged solution. Displacements, stresses and forces at the final load sub-step are written to ANSYS result files.

C.2. Seismic Load Analysis for Storage

An elastic static analysis of seismic loads is conducted using the finite element model described in Section 3.9.1.2.3A. The lowest natural frequency of the fuel basket is computed by modal finite element analyses to be 82.7 Hz. This shows that the basket structure is relatively rigid and therefore, the ground seismic loads will not be appreciably amplified. However, 0.65g axial + 0.65g transverse + 1.3g vertical loads are conservatively used in the static stress analysis. These loads translate into the following applied pressures in horizontal and vertical plates and accelerations.

The vertical and transverse loads, resulting from the fuel assembly weight, are applied as pressure on horizontal and vertical faces of plates. The pressures on the horizontal and vertical plates of the fuel compartments are calculated below as follows.

The pressure, p_v on the horizontal plates due to the vertical 1.3g acceleration is,

$$p_v = 1.3 \times (1.2385) = 1.610 \text{ psi}$$

The pressure, p_h on the vertical plates due to the transverse 0.65g acceleration is,

$$p_h = 0.65 \times (1.2385) = 0.805 \text{ psi}$$

The inertia load due to the fuel compartments, rails and canister dead weights are simulated using the density and appropriate acceleration in the vertical, transverse and axial directions. As described in Section 3.9.1.2.3A, the steel panels and peripheral rail material density are modified to account for the aluminum plates, which are not modeled. Since only a 15 inch length of the basket is modeled, the acceleration in axial direction is increased to account for the entire 144 inch length.

The axial acceleration for the 0.65g load, a_{axial} , is,

$$a_{axial} = 0.65g \times 144/15.0 = 6.24g$$

To simulate the axial stress due to the above acceleration, only one side of the basket is restrained in z-direction. The above loads and boundary conditions are applied to the finite element model using a method similar to that described for the dead weight load case.

For (1.3g vertical + 0.65g transverse + 0.65g axial) seismic load, the calculated pressures and the following accelerations are applied simultaneously.

Acceleration applied to the model: 1.3g (vertical), -0.65g (transverse), and 6.24g (axial)

Seismic Load Finite Element Analysis

A nonlinear elastic stress analysis was conducted for computing the elastic stresses in the basket model. The nonlinearity of analysis results from the gap elements in the model. The total load is applied in small steps. Again, the automatic time stepping program option "Autots" is activated. The detailed displacements, stresses and forces for each computer run, at the final load sub-step, are written to ANSYS result files. The shell middle surface nodal stress intensity is the membrane stress intensity and top or bottom surface stress intensity is the membrane plus bending stress intensity.

C.3. Thermal Loads during Storage

For the thermal stress analysis, temperatures are assumed to be symmetric about a 90° basket model.

Generally, thermal stresses develop in the basket if its free thermal expansion is constrained by the peripheral rails or canister. The thermal expansion calculations in Section 3.9.1.4.4 show that the basket rails are free to grow due to the maximum operating temperature in the canister. Also, the peripheral rails are attached to the fuel compartments with bolts in slotted holes. Thus rails also permit free thermal growth of the fuel compartments boxes. Aluminum and poison plates are sandwiched by the compartment tubes. A thermal expansion gaps are provided to allow the aluminum/poison plates free to grow in the axial direction while oversize slots are provided to allow aluminum/poison plates free to grow in the radial direction (see TN drawing 10494-72-8). However, some thermal stresses in fuel compartments and rails can develop due to radial gradients (hot at center and cooler at periphery) due to normal and accident condition thermal conditions. The fuel compartments and support rail thermal stresses are therefore calculated for the 115 °F (hot environment), -20 °F (cold environment) ambient and HSM blocked vent accident conditions.

Thermal Stresses in the Basket Fuel Compartments

A 3-dimensional finite element model of the basket is used for the thermal and stress analyses of the fuel basket. This finite element model is described in Section 3.9.1.2.3A. Due to symmetry of temperature distribution, only a ¼ model (see Figure 3.9.1-8) is used in this analysis. The rails and canister are removed from the model, as they have no effect on the fuel compartment thermal stresses. The support rails are analyzed separately.

In order to model realistic contact between the fuel compartments, the couplings are replaced by contact elements. The couplings at the fusion weld locations are replaced by pipe elements.

Two finite element analyses are required to compute the thermal stresses in the fuel basket. The first analysis is a thermal analysis that computes the temperature distribution at each node of the structural model, given the temperature distribution in the thermal model described in Chapter 4. The second finite element analysis computes the thermal stress distribution caused by the temperature distribution computed in the first analysis.

The four-node element SHELL57 (Thermal Shell) and LINK33 (Thermal Conduction Bar) are used in the thermal analysis. These elements are replaced by stress elements SHELL43 and PIPE20 in the stress analysis.

Thermal Analyses

Thermal analyses of the gross finite element model of the 32PTH DSC and fuel basket is conducted for both hot and cold normal ambient conditions as well as for the HSM blocked vent accident in Chapter 4. Steady-state thermal analyses of the detailed basket model, shown in Figure 3.9.1-8, are conducted to obtain the nodal temperatures by impressing the temperature distribution (computed in Chapter 4) as the boundary conditions for hot, cold and vent blockage cases. Thermal analyses of a gross model of NUHOMS[®] 32PTH Cask, DSC and Basket were conducted for hot and cold normal conditions and for HSM blocked vent accident in Chapter 4. Below are given the maximum basket and rail temperatures and thermal gradients for all cases from Chapter 4.

	115 °F Ambient With Fins Max. Temp. (°F)	-20 °F Ambient With Fins Max. Temp. (°F)	34 Hours After Blockage with Fins Max. Temp. (°F)
Basket Fuel Compartments	656	565	801
Basket Rails	511	418	662
Thermal Gradient, ΔT	145	147	139

Thermal material properties for material (type 304 stainless steel), taken from Reference 1, are reproduced in Table 3.9.1-2.

The thermal analysis resulting temperature distributions for each thermal load case closely match the temperature distributions presented in Chapter 4.

Thermal Stress Analyses

Elastic stress analyses of the fuel compartment structure are conducted for computing the thermal stresses in the fuel basket. The nodal temperature distribution from the above thermal analysis results are applied to obtain the thermal stresses in the model.

The resulting displacements and stresses in the model are written to ANSYS result files. The critical stresses are summarized in Table 3.9.1-5. It is seen from Table 3.9.1-5, that the maximum thermal stress intensities in fuel compartments are developed in -20 °F ambient case.

Thermal Stresses in Peripheral Rails during Storage

Temperature distribution and thermal stresses in peripheral rails are computed using the same methodology as given above for the fuel compartments. The finite element model of the support rails is extracted from the model described in Section 3.9.1.2.3A and is shown in Figure 3.9.1-9.

The resulting thermal stress intensities for the 115 °F, -20 °F, and blocked vent cases are summarized in Table 3.9.1-5.

Fusion Welds Evaluation for Thermal Storage Loads

The forces in the X, Y and Z global directions, in the PIPE elements (modeling the fusion welds), for the critical -20 °F case are post processed from the ANSYS result files.

Review of the ANSYS results files reveal that the thermal loads are quite small. The maximum shear load in a fusion weld is computed by vectorially adding the maximum FY and maximum F8 (irrespective of their location) for dead weight:

$$\text{Maximum shear force} = [282^2 + 8.4^2]^{1/2} = 282 \text{ lb.}$$

The maximum shear force in the fusion weld is for seismic + normal thermal load, 1,967 lbs.

The fusion weld load capacity, qualified by load test (for 75g horizontal drop accident) is 17.1 kips. The storage seismic and thermal loads are much smaller than the test load. Thus by comparison, fusion welds capacity is judged to be adequate for the storage loads.

C.4. Summary of Fuel Basket Stresses for Storage Loads

Table 3.9.1-5 summarizes the fuel basket stress analysis results and compares them with the code allowable stresses.

For the normal condition thermal load cases, the fuel compartment temperature is taken to be 700° F uniform, the peripheral rail temperature is taken to be 600 °F uniform and the canister shell temperature is taken to be 500 °F uniform. For the HSM vent blockage hypothetical accident condition the fuel compartment temperature is taken to be 800° F uniform and the peripheral rail temperature is taken to be 650 °F.

Based on the results of these analyses, the basket and rails are structurally adequate for the normal and accident condition storage loads.

3.9.1.2.4 32PTH DSC Fuel Basket Buckling Analysis

This Section evaluates the 32PTH DSC basket design with respect to buckling.

A. Basket Fuel Compartment Buckling Analysis

NUHOMS[®] 32PTH1 basket design for the Standardized NUHOMS[®] Horizontal Modular Storage System for Irradiated Nuclear Fuel (CoC 1004) is identical to NUHOMS[®] 32PTH design. The buckling evaluation for 32PTH1 basket is performed in Section U.3.7.4.3.3 [19]. The fuel assembly load is calculated using a fuel assembly weight of 11 lb/in, resulting in a 1.24 psi pressure on the basket panels for 1g. However, the actual pressure on the basket panels calculated in Section 3.9.1.2.3 is 1.1856 psi for 1g. Thus, the evaluation performed in Section U.3.7.4.3 [19] bounds the buckling evaluation for the NUHOMS[®] 32PTH basket.

B. Finite Element Buckling Analysis

Finite Element model

The finite element basket model and material properties for the buckling analysis is described in Section U.3.7.4.3.1 [19]. Basket assembly buckling analysis loads are described in Section U.3.7.4.3.3 [19].

Result

Figure U.3.7-28 [19] shows a representative deformed shape plot for the 95g load case (45° drop orientation). The critical tube is at the bottom corner location where the maximum lateral deflection occurs in the outer ligament of this tube, directly adjacent to the R45 rail. As shown by these results, the basket assembly has sufficient margin against buckling type failure. Therefore, the basket structure will properly support and position the fuel assembly under the accident condition drop loads.

3.9.1.3 32PTH DSC Shell Structural Evaluation

3.9.1.3.1 Approach

This section evaluates the structural adequacy of the 32PTH DSC Canister under all applicable normal and hypothetical accident condition loads. Evaluation of the stresses generated in the canister is presented in Section 3.9.1.3.2, and the DSC canister shell buckling evaluation is presented in Section 3.9.1.3.3.

3.9.1.3.2 DSC Canister Shell Stress Analysis

A. Methodology

An enveloping technique of combining various individual loads in a single analysis is used in this evaluation for several load combinations. This approach greatly reduces the number of computer runs while remains to be conservative. However, for some load combinations, the stress intensities under individual loads are added to obtain resultant stress intensities for the specified combined loads. This stress addition at the stress intensity level for the combined loads, instead of at component stress level, is also a conservative way to reduce numbers of analysis runs.

The ANSYS calculated stresses are the total stresses of the combined membrane, bending, and peak stresses. These total stresses are conservatively taken to be membrane stresses (P_m) as well as membrane plus bending stresses ($P_L + P_b$) and are evaluated against their corresponding ASME code stress limits. In the case where the total stresses, evaluated in this manner, exceed the ASME allowable stresses, a detailed stress linearization is performed to separate the membrane, bending, and peak stresses. The linearized stresses are then compared to their proper Code allowable stresses. ASME B&PV Code Subsection NB [8] is used for evaluation of loads under normal conditions and Appendix F [3] for evaluation of loads under hypothetical accident conditions.

The thermal stress intensities are classified as secondary stress intensities, Q , for code evaluations. The hypothetical accident blocked vent and flood loads (Service Level D) are conservative evaluated as normal loads.

B. Canister Material Properties

Material properties obtained from Reference 1 for the NUHOMS[®] 32 PTH canister materials, taken at the highest metal temperature of 500 °F (from thermal evaluation presented in Chapter 4), are summarized here.

Elastic Material Properties

1. Canister Shell, Support Ring of Shield Plug, Outer Top Cover, and Bottom Grapple Ring (SA-240 Type 304) @ 500° F.

$$E = 25.8 \times 10^6 \text{ psi.}$$

$$S_y = 19.4 \text{ ksi.}$$

$$S_u = 63.4 \text{ ksi.}$$

$$S_m = 17.5 \text{ ksi.}$$

$$\nu = 0.3$$

$$\rho = 0.29 \text{ lb}_f / \text{in}^3$$

Temperature dependent coefficients of thermal expansion are as follows.

Temperature °F	α_D (in./in. °F ⁻¹)
70	8.5×10^{-6}
100	8.6×10^{-6}
150	8.8×10^{-6}
200	8.9×10^{-6}
250	9.1×10^{-6}
300	9.2×10^{-6}
350	9.3×10^{-6}
400	9.5×10^{-6}
500	9.7×10^{-6}

2. Top Shield Plug and Shell Bottom (SA-182 F304, plate thickness > 5 in) @ 500 °F.

$$E = 25.8 \times 10^6 \text{ psi.}$$

$$S_y = 19.4 \text{ ksi.}$$

$$S_u = 59.2 \text{ ksi.}$$

$$S_m = 17.5 \text{ ksi.}$$

$$\nu = 0.3$$

$$\rho = 0.29 \text{ lb}_f / \text{in}^3$$

Temperature dependent coefficients of thermal expansion are as follows.

Temperature °F	α_T (in./in. °F ⁻¹)
70	8.5×10^{-6}
100	8.6×10^{-6}
150	8.8×10^{-6}
200	8.9×10^{-6}
250	9.1×10^{-6}
300	9.2×10^{-6}
350	9.3×10^{-6}
400	9.5×10^{-6}
500	9.7×10^{-6}

Elastic-Plastic Material Properties

The ANSYS Multilinear Kinematic Hardening material option of inelastic analysis is employed in the analyses of all canister accident side drops. A multi-linear stress-strain curve for Type 304 stainless steel at 500 °F is constructed using the yield and tensile stress values taken from Reference 1 and the elongation value from Reference 9. The stress-strain curve used for all canister materials is as follows.

Point	1	2	3	4	5
Strain (in/in)	0.0004845	0.000768	0.001164	0.00275	0.46
Stress (psi)	12,500	14,660	17,120	19,400	63,400

C. DSC Canister Stress Criteria

Allowable stresses given in ASME B&PV Code Subsection NB [8] and Appendix F [3] are used to evaluate the calculated stresses in the canister under normal, off-normal, and accident conditions, respectively. The allowable stresses for the transfer load case, evaluated at 500 °F for both normal and accident conditions are summarized in Table 3.9.1-7. The allowable stresses for the storage load cases, evaluated at 450 °F for normal conditions and 550 °F for accident condition, are summarized in Table 3.9.1-8.

D. DSC Shell Stress Analysis for Transfer Loads

The evaluation of the stresses generated in the NUHOMS[®] 32 PTH canister during transfer operations is presented here. During fuel transfer, the canister is oriented horizontally inside the OS187H Transfer Cask. The OS187H Transfer Cask is mounted to the transfer skid and transferred from the fuel building to the ISFSI.

The maximum temperature in the canister under vacuum drying operation is calculated to be 511 °F in the thermal stress (see Chapter 4). This temperature occurs in the shell center where stresses are low. The maximum temperature in critical stress areas (top and bottom canister regions) are below 500 °F. However, the stress evaluations are conservatively performed at 500 °F.

D.1. Canister Transfer Load Cases

Elastic and elastic-plastic analyses are performed to calculate the stresses in the NUHOMS[®] 32 PTH canister under the transfer loads. These load cases are summarized in Table 3.9.1-9 and Table 3.9.1-10. All side drop loads are analyzed by elastic-plastic analyses and the rest by elastic analyses.

D.2. DSC Canister Finite Element Model Descriptions

Canister Thermal Model

There are three thermal load cases considered in this section. They are: a) vacuum drying, b) decay heat with ambient temperatures at 115 °F, and c) at -20 °F. An ANSYS 2-D thermal model is created using Thermal SOLID55 elements to calculate the metal temperatures in the canister for the vacuum drying load case.

For the cases with decay heat loads, no thermal models are created. The canister metal temperatures which are calculated in Chapter 4 are extracted and directly applied as temperature loads to the 2-D stress model using ANSYS macros.

2-D Canister Stress Models

A two-dimensional (2-D) axisymmetric ANSYS finite element model, constructed from PLANE42 elements, is used for the elastic analyses of all axisymmetrical loading on the canister. Only elastic properties of the canister materials are used in the analysis. The Canister Lifting Blocks are not simulated in the model. The effect of the omitted weight of the lifting blocks is negligible. ANSYS contact elements CONTAC12 are generated by connecting the nodes of two adjacent solids along their boundary. The real constant of each contact element is defined by the actual initial gap at each contact element.

At the weld locations between two joined solids, the contacting nodes are coupled in all directions without creation of contact elements. These coupled-nodes are applied to the welds between the shell and the support ring of the top shield plug and between the shell and the top shield plug. The larger ½ inch weld between the shell and the top cover is fully modeled with PLANE42 elements. The normal stiffness of all contact elements are calculated using guidelines

in the ANSYS 6.0 manual [10]. The applied boundary conditions for this 2-D model under each load case are described in the following sections. Figure 3.9.1-16, Figure 3.9.1-17, and Figure 3.9.1-18 show the ANSYS 2-D finite element model, which includes the canister shell, bottom, top shield plug and its support ring, and outer top cover. This model is used for analyses of all axisymmetric loads during the transfer operations of the canister.

The normal stiffness, K_N , for the contact elements were estimated according to the ANSYS manual [10] as follows.

$$K_N \approx f E h$$

Where,

f = Factor that controls contact compatibility (ranging between 0.01 to 100), use 1

E = Young's Modulus, use 25.8×10^6 psi

h = Average radius where contact to occur (for 2-D axisymmetrical model), use 34 in.

$$K_N = 1 \times 25.8 \times 10^6 \times 34 = 8.8 \times 10^8 \text{ lb/in}$$

3-D Canister Stress Model

A three-dimensional (3-D) ANSYS stress model is created from the axisymmetrical 2-D stress model using ANSYS elements SOLID45 and CONTAC52. The 3-D model is used for the analysis of accident side drops. To help reduce the ANSYS run time and assure numerical convergence, the whole canister is split into two portions, namely, the top and the bottom end sections. These two sections are represented by two different ANSYS models. Each end model includes the canister shell at a length beyond which the un-modeled shell will have no significant impact on the stress levels at the junction between the shell and its end closures. The DSC canister top end assembly finite element model is shown in Figure 3.9.1-19 and the canister bottom end assembly model is shown in Figure 3.9.1-20.

These 3-D models are used for analyses of side drops only. The postulated side drops will occur when the canister is nesting inside the OS187H transfer cask during transfer. Two side drops with the impact points located at 0° (i.e. the cask drops onto a target at 180° opposite to its four canister support pads) and at 180° (i.e. the cask drops onto a target between its two bottom canister support pads) are analyzed.

Load cases 6, 7, 10, and 11 consider the side drop loads at 0° and load cases 8, 9, 12, and 13 at 180° (see Table 3.9.1-9). Elastic-plastic analyses, using multi-linear hardening material properties, are performed for both side drops. In addition to the contact elements generated from the 2-D model, new contact elements radially connecting the inner diameter of the cask and the outer diameter of the canister are generated. The nodes of these contact elements are located either on the inner diameter of the cask or on the outer diameter of the canister at the moment when the cask hits the side drop target. The actual gaps between these contact element nodes at this moment were calculated and input for the contact element real constants. The contact element nodes located on the inner diameter of the cask are held fixed in all directions, simulating a rigid cask on which the canister drops.

A weak link element with a cross-section area of 0.1 in² and a Young's modulus of 1 psi is added to each contact element in the model to help numerical convergence. Zero density of these link elements is used to avoid adding any non-existing weights. This model does not calculate the stress levels in the middle section of the canister shell, which are calculated and evaluated in Section 3.9.1.2.3.

Only half of the canister in circumferential direction is included in the 3-D model. Symmetry boundary conditions are applied to the plane of symmetry (global Cartesian x - y plane) during a side drop. Symmetry boundary conditions are also applied to the cut-off plane at the canister shell to provide proper diametrical rigidity of the shell during side drops.

During the 75g side drop, the canister internals are accounted for by applying a cosine varying pressure distribution on the inside surface of the canister shell. Assuming that the canister internals react upon 90° arc of the inside surface, then the inertial load of the internals, $P_{(\theta)}$, which varies with angle, θ , ($\theta = 0$ is at the impact point), is governed by the following expression.

$$P_{(\theta)} = P_{max} \cos(2\theta) \quad (0^\circ < \theta < 45^\circ)$$

Where P_{max} is the maximum pressure at the impact point ($\theta = 0$). Assuming the axial length of the applied load is L , the inside radius of the canister shell is R , and the load distribution, $P_{(\theta)}$ above, then the total inertial load generated by the internals, F , is the following.

$$F = \int_{-\frac{\pi}{4}}^{\frac{\pi}{4}} P_{max} \cos(2\theta) \cos(\theta) LR d\theta$$

or,

$$F = \frac{P_{max} LR}{2} \int_{-\frac{\pi}{4}}^{\frac{\pi}{4}} \cos((2+1)\theta) + \cos((2-1)\theta) d\theta$$

By integrating we get the following.

$$F = \left[\frac{P_{max} LR}{2} \right] \left[\frac{\sin(3\theta)}{3} + \sin(\theta) \right] \Bigg|_{-\frac{\pi}{4}}^{\frac{\pi}{4}}$$

Therefore,

$$F = \left[\frac{P_{\max} LR}{2} \right] \left[\frac{\sin\left(\frac{3\pi}{4}\right)}{3} + \sin\left(\frac{\pi}{4}\right) - \frac{\sin\left(\frac{-3\pi}{4}\right)}{3} - \sin\left(\frac{-\pi}{4}\right) \right]$$

$$F = P_{\max} LR \left[\frac{\sin\left(\frac{3\pi}{4}\right)}{3} + \sin\left(\frac{\pi}{4}\right) \right]$$

The canister shell inner diameter, $R = 34.375$ in., the axial length of the applied load, $L = 164.88$ in. (Max. canister length 185.75 in – top 12.12 in – bottom 8.75 in). The total applied force, F , is equal to the inertial load of the canister internals, which is the following.

Basket weight = 29,854 lb,
32 Fuel assembly weights = 51,520 lb

Total weight of canister internals = 29,854 lb + 51,520 lb = 81,374 lb, ... used 81,000 in the evaluation. This results in a negligible increase of less than 0.5%.

Then,

$$F = 81,000 \times 75g = 6,075,000 \text{ lb.}$$

Therefore, P_{\max} is the following.

$$P_{\max} = \frac{6,075,000}{(164.88)(34.375)} \left[\frac{\sin\left(\frac{3\pi}{4}\right)}{3} + \sin\left(\frac{\pi}{4}\right) \right]^{-1} = 1136.87 \text{ psi.}$$

The equivalent pressure applied on the canister inside shell surface is therefore,

$$P_{(\theta)} = 1136.87 \cos(2\theta) ,$$

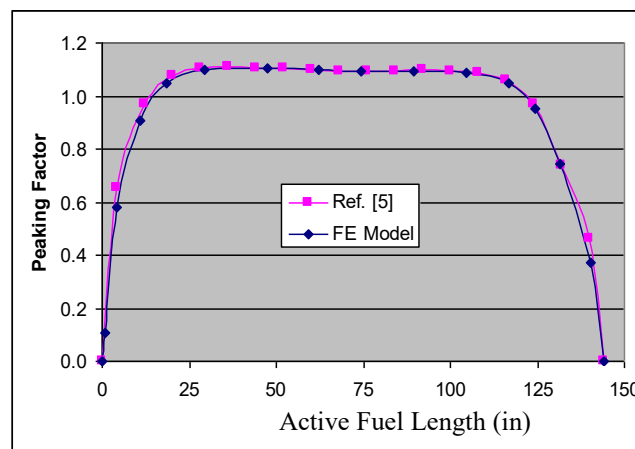
Where, θ is the angle from the bottom ($\theta = 0$) of the horizontal canister shell to the center of the shell element, up to 45° .

D.3. Canister Finite Element Analysis for Transfer Loads

All analyzed load cases in this section are identified in Table 3.9.1-9 and Table 3.9.1-10 and are described in detail in the following sections.

Transfer Load Case 1: Deadweight + 15 psig external pressure + Thermal (Vacuum Drying)

The metal temperature profile in the canister shell is assumed to be of the same shape as that of the decay heat peaking factor reported in Chapter 4. The distribution of the decay heat along the fuel effective length for normal condition is shown in the following figure.



The vacuum drying evaluation in Chapter 4 shows a maximum metal temperature of 515 °F in the canister. A steady-state thermal calculation using a 2-D canister thermal model is performed to calculate the temperature distribution throughout the canister. In this model the maximum temperature of 522 °F is applied to the canister shell in locations corresponding to that between 26 inches and 125 inches of the active fuel length, where the maximum decay heat peaking factor occurs. Also an ambient temperature of 100 °F is applied to the outer surfaces of the canister top and bottom plates. A steady-state thermal analysis is conducted to calculate the temperature profile in the canister. This temperature profile is then used as the thermal load for the stress analysis. The stress analysis of this load case contains two load steps. Load step 1 includes the primary loads of 1g down deadweight and an external pressure of 15 psig. Load step 2 includes these primary loads plus the secondary thermal loads from the thermal analysis.

For load step 1, the maximum stress intensity in the canister shell is 1,637 psi. The maximum stress intensity in the area of closure weld between the shell and the top shield plug is 1,341 psi., and the maximum stress intensity in the area of closure weld between the shell and the top cover plate is 410 psi.

The following load step 2 is run based on maximum temperature. Since the maximum temperature increased to 522 °F, a scale factor of 1.05 $[(522-70) / (511-70) = 1.03]$ is used for the load step 2 which includes primary loads of 1g down deadweight, an external pressure of 15 psig and secondary thermal loads.

For load step 2, the maximum stress intensity in the canister shell is 18,720 psi. The maximum stress intensity in the area of closure weld between the shell and the top is 2,114 psi., and the maximum stress intensity in the area of closure weld between the shell and the top cover plate is 413psi.

Transfer Load Case 2: Handling, 2g Axial + 2g Transverse + 2g Vertical + 30 psig Int. Pressure + Thermal (115 °F ambient)

The handling loads applied to the canister in the horizontal orientation are analyzed in Section 3.9.1.2.3. It is judged that under the relatively light handling loads the maximum stresses in the canister will occur in the shell section and can be obtained from the results calculated in Section 3.9.1.2.3. Therefore only the axisymmetric loads, internal pressure of 30 psig and the 115 °F ambient environment loads are analyzed in this section. The calculated stress intensities from these two computations are then conservatively added for comparison with the corresponding ASME Code allowable stresses.

The maximum primary membrane stress intensity and primary membrane plus bending stress intensity in the canister shell under the handling load of 2g are calculated, in Section 3.9.1.2.3, to be 880 psi and 9,740 psi, respectively.

The stress analysis of this load case contains two load steps. Load step 1 includes the primary loads of 30 psig internal pressure. Load step 2 includes this primary load plus the secondary thermal load from the thermal analysis.

The maximum primary stress intensity in the canister was calculated to be 3,332 psi in Load Step 1 analysis. The maximum primary stress intensity in the area of closure weld between the shell and the top shield plug is calculated to be 3,134 psi. The maximum primary stress intensity in the area of closure weld between the shell and the top cover plate is calculated to be 656 psi.

The maximum primary plus secondary stress intensity in the canister is calculated to be 36,219 psi under load step 2. The maximum primary plus secondary stress intensity in the area of closure weld between the shell and the top shield plug is calculated to be 3,646 psi. The maximum primary plus secondary stress intensity in the area of closure weld between the shell and the top cover plate is calculated to be 1,292 psi.

The maximum primary stress intensities in the canister shell calculated in Section 3.9.1.2.3 are to be added to these maximum primary and primary plus secondary stress intensities calculated under this Load Case for combined load evaluation per ASME stress limits. The direct addition of stresses at the stress intensities level, instead of at the component level, as well as the addition of the maximum stress intensities at different locations is very conservative. This enveloping technique is used to minimize the computer runs.

Transfer Load Case 3: Handling 2g Axial + 2g Transverse + 2g Vertical + 15 psig Ext. Pressure + Thermal (-20 °F ambient)

The same methodology described for load case 2 is used in this load case.

The maximum stress intensity in the canister for the primary load of 15 psig external pressure in load step 1, is calculated to be 1,666 psi. The maximum stress intensity in the area of the closure weld between the shell and the top shield plug is calculated to be 1,232 psi. The maximum stress intensity in the area of closure weld between the shell and the top cover plate is calculated to be 344 psi.

The maximum stress intensity in the canister for the primary load of 15 psig internal pressure plus the secondary temperature load in load step 2, is calculated to be 35,001 psi. The maximum stress intensity in the area of closure weld between the shell and the top shield plug is calculated to be 2,247 psi. The maximum stress intensity in the area of closure weld between the shell and the top cover plate is calculated to be 1,514 psi.

Transfer Load Case 4: 120 psig internal pressure and hypothetical accident fire.

Stresses in the canister under an internal pressure of 120 psig are calculated in this Load Case. ASME code [3] requires only primary stresses be evaluated under accident conditions. The secondary thermal stresses are therefore not calculated. The ANSYS 2-D model is used for analysis of this axisymmetrical pressure load.

The maximum calculated stress in the entire canister for the pressure load is 13,329 psi. This maximum stress intensity is conservatively treated both as primary membrane stress intensity and as primary membrane plus bending stress intensity and so evaluated against ASME code limits at the maximum metal temperature of the canister.

The maximum metal temperature in the canister during fire accident is calculated to be 790 °F (see Chapter 4). Canister material properties at 800 °F are used for the ANSYS model. The maximum stress intensity in the area of the closure weld between the shell and the shield plug is calculated to be 12,379 psi. The maximum stress intensity in the area of closure weld between the shell and the top cover plate is calculated to be 2,613 psi.

Transfer Load Case 5: 25 psig external pressure and flood hypothetical accident

The external pressure of 25 psig on the canister is analyzed using material properties taken at 500 °F for the entire model.

The maximum stress intensity in the canister for this load case is calculated to be 2,777 psi. The maximum stress intensity in the area of closure weld between the shell and the top shield plug is calculated to be 2,051 psi. The maximum stress intensity in the area of closure weld between the shell and the top cover plate is calculated to be 573 psi.

Transfer Load Case 6: Accident Condition 75g side drop at 0° (No Rail) at ambient temperature of 115 °F (75g side drop + 30 psig internal pressure) – Top End Portion of Canister

The canister internal pressure of 30 psig plus a side acceleration of 75g is analyzed in this load case. A multi-linear elastic-plastic stress-strain curve for material 304 SS at 500 °F is applied to all materials. The stress-strain curve is obtained from Reference 9. ASME code requires only primary stresses be evaluated under accident conditions. The values of the thermal expansion coefficients for all materials are therefore set to 0 to eliminate any secondary thermal stresses in the canister.

The maximum stress intensity in the canister for this load case is calculated to be 27,990 psi. The maximum stress intensity in the area of closure weld between the shell and the top shield plug is calculated to be 25,841 psi. The maximum stress intensity in the area of closure weld between the shell and the top cover plate is calculated to be 27,566 psi.

Transfer Load Case 7: Accident condition 75g side drop at 0° (No Rail) at ambient temperature of 115 °F (75g side drop + 30 psig internal pressure) – Bottom End Portion of Canister

The methodology of the analysis and stress evaluation used in this load case is the same as that described for Load Case 6.

The maximum stress intensity in the canister for this load case is calculated to be 19,976 psi.

Transfer Load Case 8: Accident 75g side drop at 180° (drop between two transfer cask bottom support pads) at ambient temperature of 115 °F (75g side drop + 30 psig internal pressure) – Top End Portion of Canister

The same methodology of the analysis and stress evaluation used for Load Case 6 is used for this load case except that the gaps between the canister and the rigid cask are different due to the orientation of the transfer cask support pads.

The maximum stress intensity in the canister for this load case is calculated to be 28,869 psi. The maximum stress intensity in the area of closure weld between the shell and the top shield plug is calculated to be 23,242 psi. The maximum stress intensity in the area of closure weld between the shell and the top cover plate is calculated to be 27,220 psi.

Transfer Load Case 9: **Accident 75g side drop at 180° (drop between two cask bottom rails) at ambient temperature of 115 °F (75g side drop + 30 psig internal pressure) – Bottom End Portion of Canister**

The same methodology of the analysis and stress evaluation used for Load Case 7 is used for this load case except that the gaps between the canister and the rigid cask are different.

The maximum stress intensity in the canister for this load case is calculated to be 22,666 psi.

Transfer Load Case 10: **Accident 75g side drop at 0° (drop at no cask rail) at ambient temperature of -20 °F (75g side drop + 15 psig external pressure) – Top End Portion of Canister**

The same methodology of the analysis and stress evaluation used for Load Case 6 is used for this load case except that external pressure instead of internal pressure is applied.

The maximum stress intensity in the canister for this load case is calculated to be 28,402 psi. The maximum stress intensity in the area of closure weld between the shell and the top shield plug is calculated to be 25,618 psi. The maximum stress intensity in the area of closure weld between the shell and the top cover plate is calculated to be 27,493 psi.

Transfer Load Case 11: **Accident 75g side drop at 0° (drop at no cask rail) at ambient temperature of -20 °F (75g side drop + 15 psig external pressure) – Bottom End Portion of Canister**

The same methodology of the analysis and stress evaluation used for Load Case 7 are used for this load case except external pressure instead of internal pressure is applied.

The maximum stress intensity in the canister for this load case is calculated to be 19,381 psi.

Transfer Load Case 12: Accident 75g side drop at 180° (drop between two cask bottom rails) at ambient temperature of -20 °F (75g side drop + 15 psig external pressure) – Top End Portion of Canister

The same methodology of the analysis and stress evaluation used for Load Case 8 is used for this load case except that external pressure instead of internal pressure is applied.

The maximum stress intensity in the canister for this load case is calculated to be 29,354 psi. The maximum stress intensity in the area of closure weld between the shell and the top shield plug is calculated to be 23,073 psi. The maximum stress intensity in the area of closure weld between the shell and the top cover plate is calculated to be 27,306 psi.

Transfer Load Case 13: Accident 75g side drop at 180° (drop between two cask bottom rails) at ambient temperature of -20 °F (75g side drop + 15 psig external pressure) – Bottom End Portion of Canister

The same methodology of the analysis and stress evaluation used for Load Case 9 is used for this load case except that the external pressure instead of the internal pressure is applied.

The maximum stress intensity in the canister is calculated to be 22,650 psi.

Transfer Load Case 14: Accident 75g Top End Drop (75g + Internal pressure of 30 psig)

The weight of the canister internals (basket and fuel assemblies) during end drop is accounted for by applying equivalent pressures on canister components that support them. The actual weights of the canister basket and fuel assemblies are 29,854 lb and 51,520 lb. (see Section 3.2.1).

Therefore, the total actual weight of the canister internals is 81,374 lb. The weight of the canister internals used in the analysis is 81,000 lb. This results in a negligible increase of less than 0.5%.

The canister cavity inner radius at the top end is 34.375 in. The pressure load equivalent to the inertial load of the internals at 75g under accident condition, P_{ia} , is,

$$P_{ia} = [81,000 / (\pi \times 34.375^2)] \times 75g = 1636.481 \text{ psi.}$$

The top face of the canister outer top cover is held in the axial direction in order to simulate the rigid support provided by the transfer cask top cover. An inertial load of 75g in the negative y-direction is applied to the model. An internal pressure of 30 psig and the metal temperatures from the 115 °F ambient condition are also included in this analysis. The temperatures in the canister are only applied so that the proper temperature dependent material properties are used. However, the values of thermal expansion coefficients for all materials are set to 0 to eliminate the secondary thermal stresses, which are not required for evaluation under an accident condition per Reference 3.

The maximum stress intensity in the canister for this load case is calculated to be 15,539 psi. The maximum stress intensity in the area of closure weld between the shell and the top shield plug is calculated to be 4,907 psi. The maximum stress intensity in the area of closure weld between the shell and the top cover plate is calculated to be 5,641 psi.

Transfer Load Case 15: Accident 75g Bottom End Drop (75g + Internal pressure of 30 psig)

The weight of the canister internals used in this analysis is 81,000 lb. The canister cavity inner radius at the bottom end is 34.375 in. The pressure load equivalent to the weight of the internals under the accident condition 75g drop, P_{ia} , is,

$$P_{ia} = [81,000 / (\pi \times 34.375^2)] \times 75g = 1636.481 \text{ psi.}$$

The bottom face of the canister is held in the axial direction in order to simulate the rigid support provided by the transfer cask bottom. An inertial load of 75g in the positive y-direction is applied to the model. An internal pressure of 30 psig and the metal temperatures from the 115 °F ambient condition are included in this analysis. The temperatures in the canister are only applied so that the proper temperature dependent material properties are used. However, the values of thermal expansion coefficients for all materials are set to 0 to eliminate the secondary thermal stresses, which are not required for evaluation under an accident condition per Reference 3.

The maximum stress intensity in the canister for this load case is calculated to be 16,492 psi. The maximum stress intensity in the area of closure weld between the shell and the top shield plug is calculated to be 5,295 psi. The maximum stress intensity in the area of closure weld between the shell and the top cover plate is calculated to be 8,714 psi.

Transfer Load Case 16: Accident 75g Top End Drop (75g + External pressure of 15 psig)

This load case is similar to Load Case 14 with different pressure loadings and metal temperatures. An external pressure of 15 psig and the metal temperatures from the -20 °F ambient condition are applied in this analysis. The temperatures in the canister are only applied so that the proper temperature dependent material properties are used. However, the values of thermal expansion coefficients for all materials are set to 0 to eliminate the secondary thermal stresses, which are not required for evaluation under an accident condition per Reference 3.

The maximum stress intensity in the canister for this load case is calculated to be 18,545 psi. The maximum stress intensity in the area of closure weld between the shell and the top shield plug is calculated to be 7,916 psi. The maximum stress intensity in the area of closure weld between the shell and the top cover plate is calculated to be 6,135 psi.

Transfer Load Case 17: Accident 75g Bottom End Drop in Accident Condition (75g + External Pressure of 15 psig)

This load case is similar to Load Case 15 with different pressure loadings and metal temperatures. An external pressure of 15 psig and the metal temperatures from the -20 °F ambient condition are applied in this analysis. The temperatures in the canister are only applied so that the proper temperature dependent material properties are used. However, the values of thermal expansion coefficients for all materials are set to 0 to eliminate the secondary thermal stresses, which are not required for evaluation under an accident condition per Reference 3.

The maximum stress intensity in the canister for this load case is calculated to be 19,956 psi. The maximum stress intensity in the area of closure weld between the shell and the top shield plug is calculated to be 12,319 psi. The maximum stress intensity in the area of closure weld between the shell and the top cover plate is calculated to be 6,279 psi.

Transfer Load Case 18: Fabrication Test Condition (DW + 23.5 psig Internal Pressure + 155 kips Axial Load)

After the canister bottom is welded to the shell a pressure test is conducted by applying an internal pressure of 23.5 psig with a top seal plate being held by an axial force of 155 kips. The canister bottom may be made, as an option, of composite plates. For each of these options the inner plate, which is to be first welded to the shell and tested, has a minimum thickness of 1.69 inches. An ANSYS model, shown in Figure 3.9.1-21, is generated that simulates the canister shell with this thin bottom inner plate for analysis of pressure and axial loads under the test condition. The deadweight load on the horizontal canister is manually analyzed using Roark's formulas [7]. The stresses calculated from both manual and ANSYS analyses are conservatively added for ASME Code stress evaluation.

1. 1g deadweight load

It is conservatively assumed that the horizontal shell's own weight is line supported at its base.

From Case 15 of Table 17 in Roark's Formulas for Stress & Strains, 6th Edition.

$$R \text{ (mean radius)} = \frac{1}{2} (69.75 \text{ in.} - 0.5 \text{ in.}) = 34.625 \text{ in.}$$

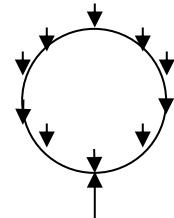
$$t \text{ (wall thickness)} = 0.5 \text{ in.}$$

$$\rho \text{ (density)} = 0.29 \text{ lb/in}^3$$

Take unit length ($L = 1 \text{ in.}$) of shell,

The weight per unit length of circumference of shell, w , is,

$$\begin{aligned} w &= (2 \times \pi \times R \times t \times L \times \rho) / (2 \times \pi \times R) \\ &= t \times L \times \rho = 0.5 \times 1 \text{ in.} \times 0.29 \text{ lb/in}^3 = 0.145 \text{ lb/in} \end{aligned}$$



$2\pi R w$ (Line support)

For a thin ring, $I = \frac{t^3}{12(1-\nu^2)} = 0.01145$, where $\nu = 0.3$

$$K_T = 1 + \frac{I}{AR^2} \approx 1 \quad K_2 = 1 - \alpha = 1 - \frac{I}{AR^2} \approx 1$$

$$\text{Max. } -M = -wR^2(1.6408 - K_2) = -0.145 \times 34.625^2 (1.6408 - 1) = -111.4 \text{ in-lb/in}$$

or,

$$\text{Max. } +M = (3/2) wR^2 = 1.5 \times .145 \times 34.625^2 = 260.76 \text{ in-lb/in}$$

$$\text{Max. bending stress, } \sigma_b = (6M)/(t^2) = (6 \times 260.76) / (0.5^2) = 6,258 \text{ psi}$$

$$N = N_A \cos(x) + V_A \sin(x) + LT_N$$

$$V_A = 0$$

$$LT_N = -Wr(x)(\sin(x))$$

$$N_A = wR/2 = 2.51 \text{ lb/in}$$

$$N = 2.51 \cos(x) - 0.145 \times 34.625 \times (x) \times \sin(x) \text{ lb/in}$$

$$N_{\max} = 2.51 \text{ lb/in at } x = 0^\circ.$$

$$\text{Max. membrane stress, } \sigma_m = N_{\max} / t = (2.51 \text{ lb/in}) / (0.5 \text{ in}) = 5 \text{ psi}$$

2. 23.5 psig internal pressure + 155 kips axial load

An internal pressure of 23.5 psig is applied while an axial force of 155 kips is applied to a seal plate on the top of the shell. The net force applied to the entire circumference of the shell at the top will be 67,763 lb ($155,000 \text{ lb} - 23.5 \text{ lb/in}^2 \times [\pi/4 \times 68.75^2] \text{ in}^2 = 67,763 \text{ lb}$). A nodal force of 22,586 lb ($67,763 / 3 = 22,586 \text{ lb}$) is applied at each node on the top end of the shell.

Figure 3.9.1-21 shows the model with the applied pressure of 23.5 psig and the nodal forces of 67,763 lb.

The maximum stress intensity in the canister is calculated to be 18,437 psi under these testing loads.

The resultant stresses calculated in (1) and (2) are conservatively added and evaluated against ASME Code allowable stresses in Table 3.9.1-11.

Transfer Load Case 19: Normal 80 kip Push Hydraulic Load (Internal Pressure of 30 psig + 80 kip Push + Thermal load of 115 °F ambient)

During transfer of the canister from the transfer cask to the HSM a normal maximum push force of 80 kip is applied by a hydraulic ram over an area of 9 inch diameter on the canister bottom. A uniform pressure of 1,257.52 psig $[= 80,000 \text{ lb} / ((\pi/4) \times 9^2)]$ is applied over this area. The periphery of the top cover outer surface is held as boundary condition. The sustained loads of an internal pressure of 30 psig plus the equivalent push load pressure of 1,257.5 psi are applied in load step 1. The sustained loads plus the temperature load from fuel decay heat are applied in load step 2.

The maximum stress intensity for load step 1 is calculated to be 7,238 psi. The maximum stress intensity in the area of closure weld between the shell and the top shield plug is calculated to be 3,123 psi. The maximum stress intensity in the area of closure weld between the shell and the top cover plate is calculated to be 669 psi.

The maximum stress intensity in the canister for load step 2 is calculated to be 34,916 psi. The maximum stress intensity in the area of closure weld between the shell and the top shield plug is calculated to be 3,602 psi. The maximum stress intensity in the area of closure weld between the shell and the top cover plate is calculated to be 1,267 psi.

Transfer Load Case 20: Normal 60 kip Pull Hydraulic Load (Internal Pressure of 30 psig + 60 kip Pull + Thermal of 115 °F ambient)

During retrieval of the canister from the HSM into the transfer cask a normal maximum pull force of 60 kips is applied by a hydraulic ram over an annulus area of 12.62 inches outer diameter and 10 inches inner diameter on the inside surface of grapple ring. A uniform pressure of 1,289.04 psig $[= 60,000 \text{ lb} / ((\pi/4) \times (12.62^2 - 10^2))]$ is applied over this area. The periphery of the top cover outer surface is held as boundary condition. The sustained loads of an internal pressure of 30 psig plus the equivalent pull load pressure of 1,289.04 psi are applied in load step 1. The sustained loads plus the temperature load from fuel decay heat are applied in the load step 2.

The maximum stress intensity in the canister is calculated to be 11,484 psi for load step 1. The maximum stress intensity in the area of closure weld between the shell and the top shield plug is calculated to be 3,134 psi. The maximum stress intensity in the area of closure weld between the shell and the top cover plate is calculated to be 656 psi.

The maximum stress intensity in the canister is calculated to be 36,753 psi for load step 2. The maximum stress intensity in the area of closure weld between the shell and the top shield plug is calculated to be 3,646 psi. The maximum stress intensity in the area of closure weld between the shell and the top cover plate is calculated to be 1,292 psi.

Transfer Load Case 21: Off-Normal 80 kip Push Hydraulic Load (Internal Pressure of 30 psig + 80 kip Push + Thermal load of 115 °F ambient)

The same 80 kip push hydraulic load analyzed in load case 19 is also designated as an off-normal condition. Evaluation of this load in load case 19 as normal condition covers this off-normal condition.

Transfer Load Case 22: Off-Normal 80 kip Pull Hydraulic Load (Internal Pressure of 30 psig + 80 kip Pull + Thermal of 115 °F ambient)

During retrieval the canister from the HSM into the transfer cask a normal maximum pull force of 80 kips is applied by a hydraulic ram over an annulus area of 12.62 inches outer diameter and 10 inches inner diameter on the inside surface of grapple ring. A uniform pressure of 1,718.72 psig $[= 80,000 \text{ lb} / ((\pi/4) \times (12.62^2 - 10^2))]$ is applied over this area. The periphery of the top cover outer surface is held as boundary condition. The sustained loads of an internal pressure of 30 psig plus the equivalent pull load pressure of 1,718.72 psi are applied in load step 1. The sustained loads plus the temperature load from fuel decay heat are applied in the load step 2.

The maximum stress intensity in the canister, other than the grapple ring and its support, is calculated to be 3,134 psi for load step 1. The maximum stress intensity in the area of closure weld between the shell and the top shield plug is calculated to be 657 psi. The maximum stress intensity in the area of closure weld between the shell and the top cover plate is calculated to be 1,794 psi.

The maximum stress intensity in the grapple ring and its support is calculated to be 15,301 psi for load step 1. The calculated total stress intensities in the grapple ring and its support are further linearized to separate the membrane, bending, from the peak stress intensities. The maximum primary membrane stress in the grapple ring and its support is calculated, by stress linearization, to be 5,249 psi and the membrane plus bending stress intensity is 13,790 psi.

The maximum stress intensity in the canister is calculated to be 36,931 psi for load step 2. The maximum stress intensity in the area of closure weld between the shell and the top shield plug is calculated to be 3,646 psi. The maximum stress intensity in the area of closure weld between the shell and the top cover plate is calculated to be 1,292 psi.

Transfer Load Case 23: Accident 110 kip Push Hydraulic Load (Internal Pressure of 30 psig + 110 kip Push)

The maximum accident hydraulic force applied by the ram to push the canister from its transfer cask to the HSM is set at 110 kips. The load will be applied over an area with a 9 inch diameter on the canister bottom. A uniform pressure of 1,729.1 psig $[= 110,000 \text{ lb} / ((\pi/4) \times 9^2)]$ is applied over this area in the 2-D ANSYS canister model. The periphery of the canister top cover outer surface is held as boundary condition. The sustained loads of an internal pressure of 30 psig plus the equivalent push force pressure of 1,729.1 psi are applied as the loading. The secondary temperature load is not required by ASME code for an accident condition analysis.

The maximum stress intensity in the canister for this load case is calculated to be 9,854 psi. The maximum stress intensity in the area of closure weld between the shell and the top shield plug is

calculated to be 3,132 psi. The maximum stress intensity in the area of closure weld between the shell and the top cover plate is calculated to be 686 psi.

Transfer Load Case 24: Accident 110 kip Pull Hydraulic Load (Internal Pressure of 30 psig + 110 kip Pull)

The maximum accident condition hydraulic force applied by the ram to pull the canister out of the HSM into the transfer cask is set at 110 kips. This pull force is applied over an annulus area of 12.62 inches outer diameter and 10 inches inner diameter on the inside surface of grapple ring. A uniform pressure of 2363.25 psig $[=110,000 \text{ lb} / ((\pi/4) \times (12.62^2 - 10^2))]$ is applied over this area in the 2-D ANSYS canister model. The periphery of the top cover outer surface is held as a boundary condition. The sustained loads of an internal pressure of 30 psig plus the equivalent pull force pressure of 2363.25 psi are applied as loading. The secondary temperature load is not required by ASME code for an accident condition analysis.

The maximum calculated stress intensity in the canister for this load case is calculated to be 21,025 psi. The maximum stress intensity in the area of closure weld between the shell and the top shield plug is calculated to be 3,134 psi. The maximum stress intensity in the area of closure weld between the shell and the top cover plate is calculated to be 656 psi.

Transfer Load Case 25: Canister Lifting

ANSI N16.4 [11] is used as guide for evaluation of the canister lifting blocks. It requires that a load bearing member of a lifting device shall be capable of lifting six and ten times the weight of the canister without exceeding the material yield and ultimate strengths respectively. The combined shear stress or maximum tensile stress at any point in the device shall not exceed the material minimum tensile yield strength and the material ultimate tensile strength for 6g and 10g lifting loads, respectively. Since the ultimate tensile strength of the canister and its lifting block material exceeds 10/6 times their minimum tensile yield strength (i.e. $S_u / S_y > 10/6$), the 6g lifting load is the critical load for stress evaluation.

The empty canister weight is 28,191 lb. Therefore, the total lifting load is $28,191 \text{ lb} \times 6 = 169,146 \text{ lb}$.

Lifting Block Weld Stresses

It is conservatively assumed that the full lift load acts on the throat area of the 5/16 in. all-around weld of each 2.5 in. × 2.5 in. square lifting block. There are four lifting blocks welded to the inside surface of canister bottom. The total throat area of the welds in all four blocks is,

$$\text{Weld throat area} = (5/16 \text{ in} \times \cos 45^\circ) \times 2.5 \text{ in} \times 4 \times 4 = 8.84 \text{ in}^2$$

Therefore, the maximum shear stress in the weld, τ_w , is,

$$\tau_w = 169,146 \text{ lb} / 8.84 \text{ in}^2 = 19,134 \text{ psi} < S_y$$

Lifting Block thread stresses

Each lifting block has internal threads of 1-1/4-7UNC-2B and a minimum thread length of 2 inches.

For each block, the thread stripping shear area = 2.9441 in² / in of engagement [12].

For an engaging length of 2 inches, the total stripping shear area for 4 blocks is,

$$A = 2.9441 \text{ in}^2 \times 2 \text{ in.} \times 4 = 23.55 \text{ in}^2$$

Since the thread stripping shear area is greater than area of the weld shear area in above, the design thread shear area is acceptable.

Max. Tensile stress in Lift Block

For each block, the cross-section area, A_b , is,

$$A_b = 2.5 \text{ in} \times 2.5 \text{ in} = 6.25 \text{ in}^2$$

The major diameter of a 1-1/4-7UNC-2B thread is 1.25 in. [13]

The minimum cross-section area, A_{min} , is,

$$A_{min} = 6.25 \text{ in}^2 - \pi/4 \times (1.25 \text{ in})^2 = 5.02 \text{ in}^2$$

Therefore, the maximum membrane tensile stress, P_m , is,

$$P_m = 169,146 \text{ lb} / (5.02 \text{ in}^2 \times 4) = 8,424 \text{ psi} < S_y$$

Where,

$$S_y = 30,000 \text{ psi for SA-240 Gr.304 at } 70^\circ \text{F.}$$

Therefore, it is concluded that the design lift blocks for the canister is structurally adequate.

Shear stress at the canister end closure welds

There are two closure welds in the canister design. One weld joins the canister shell and the inner top cover/shield plug (including option 2 or option 3 inner top cover as described in the Chapter 1 drawings). Another weld joins the canister shell and its outer cover. Since the radiographic examination of these two closure welds is not feasible, ISG-15 [14] requires a design stress reduction factor be used in the design calculation. For multi pass inspection, a stress reduction factor of 0.8 is recommended by ISG-15. However, for conservatism, a stress reduction factor of 0.7 is used in the evaluation of the stresses at these two welds in this section.

The allowable shear stresses at the closure welds based on Subsection NB [8] and Appendix F [3] are listed in the following table and are used to compare with the calculated maximum shear stresses.

ASME Code Allowable for Weld Stresses (304 SS 500 °F)

Loading Condition	Stress Type	Stress Limits	Allowable Stress (ksi)
Normal	Shear	$(0.6 S_m)^{(1)} \times 0.7^{(3)}$	$(0.6 \times 17.5) \times 0.7 = 7.35$
Accident	Shear	$(0.42 S_u)^{(2)} \times 0.7^{(3)}$	$(0.42 \times 63.4) \times 0.7 = 18.64^{(4)}$
			$(0.42 \times 59.2) \times 0.7 = 17.4^{(5)}$

Notes:

1. Shear allowable from Subsection NB, NB-3227.2.
2. Shear allowable from Appendix F, F-1341.2.
3. The allowables were reduced ($\times 0.7$) to include the quality factor from ISG-15 based on PT or MT of root and final layers.
4. For SA-240, Type 304
5. For SA-182, F304

Loading Conditions

The canister end closure welds are included in the ANSYS [10] finite element models and described in Appendix 3.9.1, Section 3.9.1.3.2. A total of 24 transfer load cases (Appendix 3.9.1, Section D.3) are analyzed by using these two models.

The most critical shear stress at the end closure welds for these analyzed load cases occurs for the 75g side drop + 30 psi internal pressure and the 75g side drop + 15 psi external pressure cases. The ANSYS result files for these two load cases are postprocessed to get the maximum shear stresses at the canister end closure weld locations. These shear stresses are compared with the above ASME code shear stress criteria.

The weld stresses at outer top cover and inner top cover plates are summarized and compared with code allowables in the following table.

Summary of Weld Shear Stresses and Allowables

Weld	Load	Stress Type	Maximum Stress (ksi)	Allowable (ksi)	Factor of Safety
Between Outer Top Cover and Shell	75g Side Drop + 30 psig Internal Pressure	Shear	13.78	18.64	1.35
	75g Side Drop +15 psig External Pressure	Shear	13.68	18.64	1.36
Between Inner Top Cover and Shell	75g Side Drop + 30 psig Internal	Shear	13.30	17.4	1.31
	75g Side Drop +15 psig External Pressure	Shear	13.38	17.4	1.30

The canister corner drop load case is analyzed as follows.

- Finite Element Model

The 3D canister finite element model as described in Appendix 3.9.1, Section 3.9.1.3.2 is used for calculating the canister corner drop. The finite element model is shown on Figure 3.9.1-27.

- Loading and Boundary Conditions

The transfer cask cavity length is 186.6” and the canister length is 185.75”. The gap between the inside surface of the transfer cask lid and outer surface of the canister outer top cover is 0.85”. For storage the end drop is not a creditable event. The transfer cask is transferred in a horizontal position held by the transfer trailer. During the rotation of the transfer cask from vertical to horizontal, the cask could slide into the ground and incur a corner drop if a non-single failure proof crane is used. The only possible corner drop impact to the bottom of the transfer cask. However, for weld shear stress calculation it is conservatively assumed that the internal weight (basket + fuel assemblies) will impact the inner surface of the canister inner top cover without any support from transfer cask lid.

The maximum axial G load calculated from LS-DYNA as described in Appendix 3.9.11 is 21g (Appendix 3.9.11, Section 3.9.11.6). For conservatism an axial g load of 22g is used for the analysis.

This inertial load is uniformly distributed over the inner surface of the canister inner top cover with a radius of 34.375 in. This equivalent uniform pressure, P_{in} , exerted on the canister inner top cover by the weight of the internals under a 22g load is calculated as follows.

$$P = [(81,500 \times 22) / (\pi \times 34.375^2)] = 483 \text{ psi.}$$

The canister internal pressure of 30 psi is also added to the above calculated inertial pressure, therefore the total pressure used for the analysis is 513 psi.

The loading and boundary condition plots are shown on Figure 3.9.1-28 and Figure 3.9.1-29, repetitively. This boundary condition shows that all the internal loads impact to the inner surface of the canister inner top cover without any support from the transfer cask lid.

- Analysis Results

The results of the analyses are summarized in the following table.

Summary of Weld Shear Stresses and Allowables

Load Case	Weld	Stress Type	Maximum Stress (ksi)	Allowable (ksi)	Factor of Safety
Canister Corner Drop + 30 psi Internal Pressure	Between Outer Top Cover and Shell	Shear	9.60	18.64	1.94
	Between Inner Top Cover and Shell	Shear	9.66	17.4	1.80

Summary of DSC Component Maximum Stress Intensities and Allowables

Load Case	Component	Stress Type	Calculated Max. Stress Intensity (Ksi)	Allowable Membrane Stress Intensity (Ksi) ⁽¹⁾	Factor of Safety
Canister Corner Drop + 30 psi	Canister Shell	$P_L + P_b$	20.46	44.38	2.17
	Canister Outer Top Cover	$P_L + P_b$	16.39	44.38	2.71
	Canister Inner Top Cover	$P_L + P_b$	15.83	41.44	2.62

Note:

1. Allowable stresses are taken from Appendix 3.9.1, Table 3.9.1-7. Since the calculated maximum membrane plus bending stress intensity ($P_L + P_b$) is less than the allowable membrane stress intensity (P_m), therefore only maximum membrane plus bending stress intensity ($P_L + P_b$) is reported.

The ANSYS maximum stress intensity plots for canister shell, canister outer top cover, and canister inner top cover are shown on Figure 3.9.1-30, Figure 3.9.1-31 and Figure 3.9.1-32, respectively.

D.4. Summary of the Stress Calculation Results for All Transfer Load Cases

Table 3.9.1-11 through Table 3.9.1-18 summarize the calculated maximum stress intensities in the canister and compared with ASME code stress intensity allowables.

Based on the results of these analyses, the design of the 32PTH DSC Canister is structurally adequate under transfer loads of testing, normal (Service Level A), and accident (Level D) conditions.

E. DSC Shell Stress Analysis for Storage Loads

This section evaluates the structural adequacy of the 32PTH DSC Canister when it is in the horizontal storage position within a HSM-H. This section considers storage loads on the canister under both normal and hypothetical accident conditions.

The evaluation of the stresses in the canister for storage loads employs an ANSYS 2-D axisymmetrical model to analyze three thermal conditions specified for the canister during storage. This 2-D model is the same model described in Section 3.9.1.3.2D.2 used to compute stresses due to axisymmetric transfer loads. The analyses of axisymmetric loads such as internal and external pressure loads for transfer conditions are also valid for a horizontal storage canister. Their results are therefore used in this section for stress combinations and evaluations.

The fuel basket stress analysis for storage loads (Section 3.9.1.2.3C) uses an ANSYS 3-D model, which includes the DSC canister shell, to calculate the non-axisymmetrical seismic and deadweight loads. The calculated stress intensities in the canister under the seismic and deadweight loads from Section 3.9.1.2.3C are used in this section for stress combinations and evaluations.

The temperatures in the canister under 115 °F and -20 °F ambient conditions of and under HSH-H blocked vent conditions for 48 hours are computed in Chapter 4. These temperatures are imposed on the stress model in this evaluation for thermal stress calculations.

E.1. Canister Storage Load Cases

The storage load cases considered in this section are summarized in Table 3.9.1-19.

E.2. DSC Canister Finite Element Model Descriptions

The 2-D axisymmetrical thermal and stress models described in Section 3.9.1.3.2D.2 for the canister transfer load analysis are also used for the storage load analysis. Figure 3.9.1-16, Figure 3.9.1-17 and Figure 3.9.1-18 show this model. This model is used in this section to evaluate the three specified thermal cases for storage, which are the -20 °F and 115 °F ambient conditions, and the blocked vent hypothetical accident condition. The temperature profiles in the canister for the three storage thermal cases are calculated in Chapter 4.

E.3. Canister Finite Element Analysis for Storage Loads

All individual load cases specified in Table 3.9.1-19 are described in details in the following sections.

Storage Load Case 1 Deadweight (1g Down)

The canister shell and fuel basket containing the fuel assemblies, resting horizontally on the rails of a HSM-H is analyzed in Section 3.9.1.2.3C. for storage loads. The maximum primary membrane and membrane plus bending stress intensities in the canister shell due to the deadweight load are calculated to be 0.4 ksi, and 4.05 ksi, respectively (see Table 3.9.1-5).

Storage Load Case 2: Internal Pressure of 30 psig

The internal pressure of 30 psig applied on the canister is analyzed in load step1 of transfer load case 2 in Section 3.9.1.3.2D. The maximum membrane plus bending stress intensities in the canister, calculated in Section 3.9.1.3.2D is 3.33 ksi.

Storage Load Case 3: Seismic Loads (0.65g Axial + 0.65g Transverse + 1.3g Vertical Down)

The seismic loads on the canister, containing the basket and the fuel assemblies and resting on the rails of a HSM-H, are analyzed in Section 3.9.1.2.3C. The maximum primary membrane and membrane plus bending stress intensities are calculated in Section 3.9.1.2.3C to be 0.63 ksi, and 6.08 ksi, respectively (see Table 3.9.1-5). This specified seismic load includes a 1g deadweight load.

Storage Load Case 4: Thermal Load at -20 °F Ambient

The maximum temperature in the canister for this thermal case is calculated in Chapter 4 to be 318 °F. The temperatures in the canister calculated in Chapter 4 are applied to the stress model in order to compute the thermal stress intensities in the canister. The maximum secondary thermal stress intensity is calculated to be 20.60 ksi. The 20.60 ksi stress is calculated based on canister maximum temperature of 324 °F. Since the revised temperature of 318 °F is less than 324 °F, therefore 20.60 ksi is conservatively used for load combination and compare with the allowables.

Storage Load Case 5: Thermal Load at 115 °F Ambient

The thermal load case with the canister stored in the HSM-H fins, described in Chapter 4, is selected for this evaluation. The maximum temperature in the canister for this thermal case is calculated in Chapter 4 to be 407 °F. The same procedure used for calculating the thermal stress intensities for the load case 4 is repeated for the 115 °F ambient thermal load. The secondary thermal stress intensity is calculated to be 18.48 ksi. The 18.48 ksi stress is calculated based on canister maximum temperature of 434 °F. Since the revised temperature of 407 °F is less than 434 °F, therefore 18.48 ksi is conservatively used for load combination and compare with the allowables.

Storage Load Case 6: Blocked Vent Thermal Accident Condition

The thermal evaluation presented in Chapter 4 reports four thermal cases for the canister stored in the HMS with blocked vent. The maximum temperature of 600 °F in the canister is reached after 34 hours of complete vent blockage in a HSM with fins. The 34 hour vent blockage is a conservative scenario, since the vent is visually checked at least every 24 hours. However, this case is reported in thermal evaluation and is therefore selected for analysis in this section. The same procedure used for obtaining the thermal load in load case 4 is used in this load case. The secondary thermal stress intensity is calculated to be 15.50 ksi.

Storage Load Case 7: Accident Internal Pressure of 70 psig (In the Event of Blocked Vent)

The internal pressure of 70 psig in the canister is analyzed for enveloping the accident condition internal pressures during the blocked vent scenario. The maximum primary membrane plus bending stress intensity in the canister is calculated to be 7.77 ksi.

Storage Load Case 8: Accident Flood Load (Enveloped by External Pressure of 30 psig)

The hypothetical accident condition flood load is enveloped by an external pressure of 30 psig. The maximum primary membrane plus bending stress intensity in canister is calculated to be 3.33 ksi.

Shear Stresses in the Canister End Closure Welds due to Storage Loads

Since the transfer loads are much higher than the storage loads, therefore the end closure weld shear stresses calculated from transfer loads bound the storage loads.

E.4. Summary of the Stress Calculation Results for All Storage Load Cases

Table 3.9.1-20 and Table 3.9.1-21 summarize the calculated stresses in the entire canister and their corresponding ASME code evaluations.

Based on the results of this calculation, the 32PTH DSC canister is structurally adequate under all normal (Service Level A), off-normal (Service Level C), and hypothetical accident (Service Level D) conditions during storage.

3.9.1.3.3 DSC Shell Buckling Evaluation

This section evaluates the structural adequacy of 32PTH DSC canister against buckling during a vertical end drop during transfer operations.

A. Approach

A finite element plastic analysis with large displacement option is performed to monitor occurrence of canister shell buckling under the specified loads.

The thermal evaluation presented in Chapter 4 show that the metal temperatures of the entire canister are below 500 °F during the transfer operations. The material properties of canister at 500 °F are therefore conservatively used in this calculation.

B. Material Properties used for Canister Buckling Evaluation

The material properties of the canister materials, SA-240 Gr. 304 and SA-182 F304 (with thickness > 5 inches) stainless steel, at 500°F are as follows.

Property	@ 500° F
S_m (ksi)	17.5
S_y (ksi)	19.4
S_u (ksi)	59.2*
E (psi)	25.8×10^6

* Lesser value of S_u for materials SA-240 Gr. 304 and SA-182 F304 is used.

For the plastic finite element analysis, a multilinear modulus of elasticity is used. The following material stress-strain relation for SA-240 Gr. 304 is used:

Stress (at 500° F) (psi)	Strain (in /in)
12,500	0.0004845
14,660	0.0007680
17,120	0.001164
19,400	0.002750
59,200	0.46

C. Finite Element Buckling Analysis

The following three hypothetical accident load cases for the canister are considered in this buckling analysis.

Buckling Load Case 1: Corner drop + 15 psig external pressure

Buckling Load Case 2: Corner drop + 0 psig internal pressure

Buckling Load Case 3: Corner drop + 30 psig internal pressure

The two-dimensional axisymmetric finite element model of the canister described in Appendix 3.9.1, Section 3.9.1.3.2D.2 for the DSC canister stress analysis is used for this analysis. The gap element real constants, node couplings and displacement boundary conditions are also the same as those used in Section 3.9.1.3.2D.2. The weight of canister's outer top cover plus the top shield plug and its support ring is 12,847 lb, and the bottom shield plug is 9,420 lb (Chapter 3, Section 3.2.1). Since the top end of the canister is heavier than the bottom end, it is a more severe case when the canister drops on its bottom end. A drop on the bottom end is therefore chosen for analysis in this calculation.

For storage application, the end drop is not a credible event. The transfer cask is transferred in a horizontal position held by the transfer trailer. In the axial direction it is possible to slide into the ground and incur a corner drop. The maximum g load calculated by the LS-DYNA as described in Appendix 3.9.11 is 21g. For conservatism, 75g end drop is used for canister buckling analysis.

For load case with external pressure or internal pressure, a quasi-static plastic analysis consisting of two load steps is performed to monitor the buckling of canister. The first load step applies external pressure or internal pressure alone. A subsequent inertial load of 300g is added in the second load step. The outer surface of the canister bottom is held in order to simulate the case that the canister drops on a rigid cask bottom face.

In the load step 1, the stepped external or internal pressure is applied as a static load.

In the load step 2, the weight of the canister internals (basket and fuel assemblies) is accounted for by applying an equivalent internal pressure on the canister bottom. The actual total weight of the canister internals is 81,374 lb (basket 29,854 lb + fuel assemblies 51,520 lb) (Chapter 3, Section 3.2.1). A total weight of 81,500 lb for the canister internals is conservatively used in this analysis. This inertial load is uniformly distributed over the bottom surface of the canister cavity with a radius of 34.375 in. This equivalent uniform pressure, P_{in} , exerted on the canister bottom by the weight of the internals under a 1g load is calculated as follows.

$$P_{in} = [81,500 / (\pi \times 34.375^2)] = 21.954 \text{ psi.}$$

An equivalent pressure of 6586.2 psig on the canister bottom corresponding to the 300g load ($P_{in} = 300 \times 21.954 = 6586.2$ psi) is therefore applied to the canister bottom along with the 300g acceleration load in the load step 2.

A stress-strain relationship (with kinematic hardening) is used to obtain stresses and deflections beyond the elastic limit of the material. The large displacement option in ANSYS is activated to monitor the buckling response.

D. Summary Canister Buckling Analysis Results

The following table summarizes the last converged load for the three load cases:

Load Case	Last Converged Load (g)	G load calculated From Appendix 3.9.11 Section 3.9.11.6	G Load Used For Basket Structural Analysis	Factor of Safety
1	175	21	75	2.33
2	176	21	75	2.35
3	177	21	75	2.36

The analysis shows that the critical buckling load for the canister end drop is 175g, which is well beyond the design 75g load. It is, therefore, concluded that buckling of the canister will not occur during a hypothetical accident end drop.

3.9.1.3.4 Evaluation of Alternate DSC Bottom Closure Assembly Design

This section evaluates the optional composite bottom assembly design of the canister. The same transfer loads and evaluation methodology used in Section 3.9.1.3.2D are used in this evaluation, because the applied transfer loads bound all possible canister loads, including storage loads.

A. Approach

This analysis is performed to evaluate the structural adequacy of the optional composite canister bottom, relative to the one-piece canister bottom assembly. The same methodology used for the analysis of the solid canister bottom assembly, described in Section 3.9.1.3.2 is employed in this evaluation.

An enveloping technique of combining various individual loads in a single analysis is used. The ANSYS calculated total stresses are conservatively taken to be membrane stresses (P_m) as well as membrane plus bending stresses ($P_L + P_b$) or ($P_m + P_b$) and are accordingly evaluated against their corresponding ASME code stress limits. In case that the total stresses exceed the ASME allowable stresses, detailed stress linearization are then performed to separate the membrane, bending, and peak stresses from the total stresses, for their specific code evaluations. ASME B&PV Code Subsection NB [8] and NF [5], as designated for each canister component, are used to evaluate loads under normal conditions, and Appendix F [3] to evaluate loads under hypothetical accident conditions.

There are four optional composite bottom designs, designated Optional T1, T2, T3 and T4. The canister transfer loads specified in Table 3.9.1-9 are analyzed in this section by following the methodology used in Section 3.9.1.3.2. The analysis of the solid canister bottom assembly subject to side drop loads shows that the maximum stresses occurred at the junction between the canister shell and the solid bottom assembly. During the side drop of the canister, the stiff canister bottom prevents its connected flexible shell from flattening. This incompatible deformation between the two creates a maximum stress at their junction. Should the canister bottom become less stiff as in a composite design, it would better conform to the shell deformation and result in a less maximum stress at the junction. The side drop analysis of the canister with one-piece bottom design, presented in Section 3.9.1.3.2, will therefore bound the more flexible optional bottom designs. Therefore, the side drop load to the canister with the optional composite bottom designs are not analyzed in this section. All other transfer loads are analyzed for the canister with the optional composite bottom. The Optional T3 composite bottom design, which is structurally equivalent to the Optional T4 design, is selected for stress evaluations in this section, since it provides the least rigidity among all optional bottom designs.

B. Material Properties use for the Alternate Canister Design

Mechanical properties obtained from Reference 1 for 32PTH DSC canister materials, at the highest metal temperature of 500° F, from the transfer thermal analysis presented in Chapter 4, are used in this calculation, and are as follows.

1. Canister Shell, Support Ring of Shield Plug, Outer Top Cover, and Bottom Grapple Ring (SA-240 Type 304) @ 500° F.

$$E = 25.8 \times 10^6 \text{ psi.}$$

$$S_y = 19.4 \text{ ksi.}$$

$$S_u = 63.4 \text{ ksi.}$$

$$S_m = 17.5 \text{ ksi.}$$

$$\nu = 0.3$$

$$\rho = 0.29 \text{ lb}_f / \text{in}^3$$

Temperature dependent coefficients of thermal expansion are as follows.

Temperature °F	α_T (in./in. °F ⁻¹)
70	8.5×10^{-6}
100	8.6×10^{-6}
150	8.8×10^{-6}
200	8.9×10^{-6}
250	9.1×10^{-6}
300	9.2×10^{-6}
350	9.3×10^{-6}
400	9.5×10^{-6}
500	9.7×10^{-6}

2. Top Shield Plug and Shell Bottom (SA-182 F304, plate thickness > 5 in) @ 500° F.

$$E = 25.8 \times 10^6 \text{ psi.}$$

$$S_y = 19.4 \text{ ksi.}$$

$$S_u = 59.2 \text{ ksi.}$$

$$S_m = 17.5 \text{ ksi.}$$

$$\nu = 0.3$$

$$\rho = 0.29 \text{ lb}_f / \text{in}^3$$

Temperature dependent coefficients of thermal expansion are as follows.

Temperature °F	α_T (in./in. °F ⁻¹)
70	8.5×10^{-6}
100	8.6×10^{-6}
150	8.8×10^{-6}
200	8.9×10^{-6}
250	9.1×10^{-6}
300	9.2×10^{-6}
350	9.3×10^{-6}
400	9.5×10^{-6}
500	9.7×10^{-6}

3. Bottom Shield Plug Shield Plug in Optional Composite Bottom Design (SA-36) @ 500° F.

$$E = 27.3 \times 10^6 \text{ psi.}$$

$$S_y = 29.3 \text{ ksi.}$$

$$S_u = 58 \text{ ksi.}$$

$$S_m = 19.3 \text{ ksi.}$$

$$\nu = 0.3$$

$$\rho = 0.29 \text{ lb}_f / \text{in}^3$$

Temperature dependent coefficients of thermal expansion are as follows.

Temperature °F	α_T (in./in. °F ⁻¹)
70	6.4×10^{-6}
100	6.5×10^{-6}
200	6.7×10^{-6}
250	6.8×10^{-6}
300	6.9×10^{-6}
350	7.0×10^{-6}
400	7.1×10^{-6}
500	7.3×10^{-6}

C. Alternate Canister Design Stress Design Criteria

Allowable stresses given in ASME B&PV Code Subsection NB [8], NF [5], and Appendix F [3] are used to evaluate the calculated stresses in the canister under normal, off-normal and accident conditions. The allowable stresses for all materials, taken at 500 °F, are summarized in Table 3.9.1-7 for NB components and Table 3.9.1-22 for NF components. Table 3.9.1-23 summarizes the allowable stresses for the weld between the canister shell and the bottom outer cover. This weld is designated a Subsection NF weld. Figure 3.9.1-23 shows the boundary between Code designations for Subsection NB and NF. All stresses are evaluated at metal temperature of 500 °F for all load conditions except for the accident fire condition in Transfer Load Case 4.

D. Alternate Canister Design Evaluation Load Cases

Elastic finite element analyses are performed in order to compute the stresses in the 32PTH DSC canister subjected to the transfer loads. These load cases are tabulated in Table 3.9.1-9 and Table 3.9.1-10.

E. Alternate Canister Design Finite Element Model Description

The 2-D ANSYS thermal and stress models described in Section 3.9.1.3.2D.2 is modified with a composite bottom design, as shown in Figure 3.9.1-23. The Optional T3 design is selected as the representative of the four composite bottom designs.

Thermal Model

There are three thermal load cases considered in this evaluation. They are vacuum drying and decay heat with ambient temperatures at 115 °F and -20 °F. The ANSYS 2-D thermal model is created using thermal SOLID55 elements to calculate the metal temperatures in the canister for the vacuum drying case.

For the thermal load cases with decay heat loads, no thermal models are created. The canister metal temperatures which are calculated in Chapter 4 are extracted and directly applied to the 2-D stress model.

Stress Models

A two-dimensional axisymmetric ANSYS finite element model, constructed from PLANE42 elements, is used for the elastic analyses of all axisymmetrical loads on the canister. Only elastic properties of the canister materials are used in the analysis. The canister lifting blocks are not simulated in the model. The effect of the omitted weight of the lifting blocks is negligible. ANSYS CONTAC12 elements are generated connecting the nodes of two adjacent solids along their boundary. The actual initial gap for each contact element is input by its real constant.

At the welds between two joined solids, the contacting nodes are coupled in all directions without creation of contact elements. These coupled-nodes are applied between the shell and the support ring of the top shield plug and between the shell and the top shield plug. The larger ½ inch weld between the shell and the top cover is fully modeled with PLANE42 elements. The

normal stiffness of all contact elements is calculated using guidelines in the ANSYS 6.0 manual [10] in the following way.

$$K_n = f E h$$

Where f is a factor usually between 0.01 and 100, E is the material modulus of elasticity (25.8×10^6 psi), and h is the average radius where contact occurs (34 inches is used). Therefore,

$$K_n = 1 \times 25.8 \times 10^6 \times 34 \times f = 8.8 \times 10^8 f$$

Thus, there is very wide range for K_n value. The structure responded well for a spring constant value of 8.8×10^6 lb/in ($f = 1$).

The applied boundary conditions for this 2-D model under each load case are described in the following sections.

F. Alternate Canister Design Finite Element Analysis

All analyzed load cases in this calculation are identified in Table 3.9.1-9 and Table 3.9.1-10 and are described in details in the following sections.

Transfer Load Case 1: **Deadweight + 15 psig external pressure + Thermal (Vacuum drying)**

The same methodology used to calculate the canister metal temperature profile in the standard canister design for the transfer load case described in Section 3.9.1.3.2D.3 is used in this load case.

The stress analysis of this load case contains two load steps. Load step 1 includes the primary loads of 1g down deadweight and an external pressure of 15 psig. Load step 2 includes these primary loads plus the secondary thermal loads from the thermal analysis.

The maximum stress intensity in the canister for load case 1 is calculated to be 1,657 psi and 331 psi in NB components and NF components, respectively. The maximum stress intensity in the area of closure weld between the shell and the top shield plug is calculated to be 1,341 psi. The maximum stress intensity in the area of closure weld between the shell and the top cover plate is calculated to be 410 psi. The maximum tensile stress normal to the effective throat of the weld between the shell and the bottom outer cover plate is calculated to be 0 psi as it is compressive.

The maximum stress intensity in the canister for load case 2 is calculated to be 14,668 psi and 6,369 psi in NB components and NF components, respectively. The maximum stress intensity in the area of closure weld between the shell and the top shield plug is calculated to be 2,112 psi. The maximum stress intensity in the area of closure weld between the shell and the top cover plate is calculated to be 420 psi.

Transfer Load Case 2: Handling 2g Axial + 2g Transverse + 2g Vertical + 30 psig Int. Pressure + Thermal (115 °F ambient)

The axisymmetrical loads due to an internal pressure of 30 psig and the temperature distribution due to the 115 °F ambient environment are analyzed in this load case. The calculated stress intensities for this load case are added to the stress intensities in the canister shell computed in Section 3.9.1.2.3B for the transfer loads. This is the same procedure used in Section 3.9.1.3.2D for the standard canister design. The combined stress intensities are evaluated against ASME code allowable stresses.

The maximum primary membrane stress intensity and primary membrane plus bending stress intensity in canister shell due to the 2g handling load, computed in Section 3.9.1.3.2D, are 880 psi and 9,740 psi, respectively.

The maximum stress intensity in the canister due to the primary load of 30 psig internal pressure in load step 1 is calculated to be 3,831 psi and 4,067 psi in NB components and NF components respectively. The maximum stress intensity in the area of closure weld between the shell and the top shield plug is calculated to be 3,134 psi. The maximum stress intensity in the area of closure weld between the shell and the top cover plate is calculated to be 656 psi. The maximum tensile stress normal to the effective throat of the weld between the shell and the bottom outer cover plate is calculated to be 1,502 psi. These maximum stress intensities calculated in this load case are added directly to the maximum stress intensities in the shell calculated in Section 3.9.1.2.3B for combined load evaluations. The direct addition of stresses at the stress intensities level, instead of at component level, as well as addition of maximum stress intensities at different location is a conservative enveloping approach. This enveloping technique is used to minimize the computer runs.

The maximum stress intensities in the canister due to the primary load of 30 psig internal pressure plus the secondary temperature load in load step 2 are calculated to be 35,266 psi and 4,729 psi in NB components and NF components, respectively. The maximum stress intensity in the area of closure weld between the shell and the top shield plug is calculated to be 3,646 psi. The maximum stress intensity in the area of closure weld between the shell and the top cover plate is calculated to be 1,292 psi. These calculated maximum stress intensities are to be added to the maximum shell stress intensity calculated in Section 3.9.1.2.3B for ASME code stress evaluation as described above for load step 1.

Transfer Load Case 3: Handling 2g Axial + 2g Transverse + 2g Vertical + 30 psig Ext. Pressure + Thermal (-20 °F ambient)

The same methodology used in Transfer Load Case 2 is used for this load case.

The maximum stress intensity in the canister due to the primary load of external pressure of 15 psig in load step 1 is calculated to be 1,772 psi and 540 psi in NB components and NF components, respectively. The maximum stress intensity in the area of closure weld between the shell and the top shield plug is calculated to be 1,232 psi. The maximum stress intensity in the area of closure weld between the shell and the top cover plate is calculated to be 344 psi. The maximum tensile stress normal to the effective throat of the weld between the shell and the bottom outer cover plate is calculated to be 23 psi.

The maximum stress intensities in the canister due to the primary load of 15 psig internal pressure plus the secondary temperature load in load step 2 are calculated to be 27,619 psi and 12,448 psi in NB components and NF components, respectively. The maximum stress intensity in the area of closure weld between the shell and the top shield plug is calculated to be 2,247 psi. The maximum stress intensity in the area of closure weld between the shell and the top cover plate is calculated to be 1,514 psi.

Transfer Load Case 4: 120 psig internal pressure during the accident fire

Stresses in the canister under an internal pressure of 120 psig are calculated in this load case. ASME code [3] requires only primary stresses be evaluated under accident conditions. The secondary thermal stresses are therefore not calculated. ANSYS 2-D model is used for analysis of this axisymmetrical pressure load.

The maximum stress intensity in the canister for this load case is calculated to be 15,389 psi and 16,570 psi in NB components and NF components, respectively. The maximum stress intensity in the area of closure weld between the shell and the top shield plug is calculated to be 12,502 psi. The maximum stress intensity in the area of closure weld between the shell and the top cover plate is calculated to be 2,628 psi. The maximum tensile stress normal to the effective throat of the weld between the shell and the bottom outer cover plate is calculated to be 6,249 psi. This maximum stress intensity is conservatively treated both as primary membrane stress intensity and as primary membrane plus bending stress intensity and so evaluated against ASME code limits at the maximum metal temperature of the canister. The maximum metal temperature in the canister during fire accident is calculated to be 790 °F in Chapter 4. Canister material properties taken at 800 °F are used in the ANSYS model.

Transfer Load Case 5: 25 psig external pressure during flood accident

The external pressure of 25 psig on the canister is analyzed using material properties taken at 500 °F for the entire model.

The maximum stress intensity in the canister for this load case is calculated to be 2,953 psi and 900 psi in NB components and NF components, respectively. The maximum stress intensity in the area of closure weld between the shell and the top shield plug is calculated to be 2,054 psi. The maximum stress intensity in the area of closure weld between the shell and the top cover plate is calculated to be 573 psi. The maximum tensile stress normal to the effective throat of the weld between the shell and the bottom outer cover plate is calculated to be 39 psi.

Transfer Load Cases 6 through 13:

Side drop Load cases 6 through 13 depicted in Table 3.9.1-9 are not analyzed in this calculation as explained in Section 3.9.1.3.4A. These loads are bounded by Transfer Load Cases 6 through 13 analyzed in Section 3.9.1.3.2D.

Transfer Load Case 14: Accident 75g Top End Drop (75g + Internal pressure of 30 psig)

The weight of the canister internals (basket and fuel assemblies) during an end drop is accounted for by applying equivalent pressures on the canister surfaces that support them. The actual weights of the canister basket and fuel assemblies are 29,854 lb and 51,520 lb, respectively. Therefore, the total actual weight of the canister internals is 81,374 lb. The weight of the canister internals used in this analysis is 81,000 lb. This results in a negligible increase of less than 0.5%. The canister cavity inner radius at the top end is 34.375 in. The pressure load equivalent to the inertial load of the internals at 75g, P_{ia} , is,

$$P_{ia} = [81,000 / (\pi \times 34.375^2)] \times 75g = 1636.481 \text{ psi.}$$

The top end face of the canister outer top cover is held in the axial direction in order to simulate the rigid support provided by the transport cask lid. An inertial load of 75g in the negative y-direction is applied to the model. An internal pressure of 30 psig and the metal temperatures from the 155 °F ambient thermal analysis performed in Chapter 4 are also included in this analysis. The temperatures in the canister are applied for proper use of material properties. However, the value of thermal expansion coefficients of all materials are set to 0 in order to eliminate secondary thermal stresses, which are not required for evaluation under accident conditions according to Reference 3.

The maximum stress intensity in the canister for this load case is calculated to be 15,645 psi and 6,337 psi in NB components and NF components, respectively. The maximum stress intensity in the area of closure weld between the shell and the top shield plug is calculated to be 4,814 psi. The maximum stress intensity in the area of closure weld between the shell and the top cover plate is calculated to be 5,578 psi. The maximum tensile stress normal to the effective throat of the weld between the shell and the bottom outer cover plate is calculated to be 483 psi.

Transfer Load Case 15: Accident 75g Bottom End Drop (75g + Internal pressure of 30 psig)

The weight of the canister internals used in this analysis is 81,000 lb. The canister cavity inner radius at the bottom end is 34.375 in. The pressure load equivalent to the weight of the internals during a 75g accident condition end drop, P_{ia} , is,

$$P_{ia} = [81,000 / (\pi \times 34.375^2)] \times 75g = 1636.481 \text{ psi.}$$

The bottom end face of the canister is held in the axial direction in order to simulate the rigid support provided by the transfer cask bottom. An inertial load of 75g in the positive y-direction is applied to the model. An internal pressure of 30 psig and the metal temperatures from the 115 °F ambient thermal analysis presented in Chapter 4 are also included in this analysis. The temperatures in the canister are applied for proper use of material properties. However, the value of thermal expansion coefficients of all materials were set to 0 to eliminate the secondary thermal stresses, which are not required for evaluation under a accident condition per Reference 3.

The maximum stress intensity in the canister for this load case is calculated to be 16,584 psi and 9,024 psi in NB components and NF components, respectively. The maximum stress intensity in the area of closure weld between the shell and the top shield plug is calculated to be 8,582 psi. The maximum stress intensity in the area of closure weld between the shell and the top cover plate is calculated to be 5,283 psi. The maximum tensile stress normal to the effective throat of the weld between the shell and the bottom outer cover plate is calculated to be 596 psi.

Transfer Load Case 16: Accident 75g Top End Drop (75g + External pressure of 15 psig)

This load case is similar to Transfer Load Case 14 with different pressure loadings and metal temperatures. An external pressure of 15 psig and the metal temperatures from the -20 °F ambient thermal analysis from Chapter 4 are applied in this analysis. The temperatures in the canister are applied for proper use of material properties. However, the value of thermal expansion coefficients of all materials are set to 0 to eliminate the secondary thermal stresses, which are not required for evaluation for accident conditions as per Reference 3.

The maximum stress intensity in the canister for this load case is calculated to be 18,685 psi and 6,992 psi in NB components and NF components, respectively. The maximum stress intensity in

the area of closure weld between the shell and the top shield plug is calculated to be 7,808 psi. The maximum stress intensity in the area of closure weld between the shell and the top cover plate is calculated to be 6,085 psi. The maximum tensile stress normal to the effective throat of the weld between the shell and the bottom outer cover plate is calculated to be 598 psi.

Transfer Load Case 17: Accident 75g Bottom End Drop in Accident Condition (75g + Extern. Press. of 15 psig)

This load case is similar to Transfer Load Case 15 with different pressure loadings and metal temperatures. An external pressure of 15 psig and the metal temperatures from the -20 °F ambient thermal analysis in Chapter 4 are applied in this analysis. The temperatures in the canister are applied for proper use of material properties. However, the value of thermal expansion coefficients of all materials are set to 0 to eliminate the secondary thermal stresses, which are not required for evaluation for accident conditions as per Reference 3.

The maximum stress intensity in the canister for this load case is calculated to be 20,081 psi and 9,121 psi in NB components and NF components, respectively. The maximum stress intensity in the area of closure weld between the shell and the top shield plug is calculated to be 12,153 psi. The maximum stress intensity in the area of closure weld between the shell and the top cover plate is calculated to be 6,265 psi. The maximum tensile stress normal to the effective throat of the weld between the shell and the bottom outer cover plate is calculated to be 432 psi.

Transfer Load Case 18: Fabrication Test Condition (DW + 23.5 psig Internal Pressure + 155 kips Axial Load)

This load case is equivalent to the fabrication test load case analyzed for the standard canister design presented in Section 3.9.1.3.2D, and is therefore not reevaluated.

Transfer Load Case 19: Normal 80 kip Push Hydraulic Load (Internal Pressure of 30 psig + 80 kip Push + Thermal load of 115 °F ambient)

In the event of transferring the canister from the transfer cask to the HSM-H a normal maximum push force of 80 kip will be applied by a hydraulic ram over an area with a 9 inch diameter on the canister bottom. A uniform pressure of 1,257.52 psig $[= 80,000 \text{ lb} / ((\pi/4) \times 9^2)]$ is applied over this area. The periphery of the top cover outer surface is held as a boundary condition. The sustained loads of an internal pressure of 30 psig plus the equivalent push load pressure of 1,257.52 psi are applied in load step 1. The sustained loads plus the temperature load from fuel decay heat are applied in load step 2.

The maximum stress intensity in the canister for load step 1 is calculated to be 7,238 psi and 2,499 psi in NB components and NF components, respectively. The maximum stress intensity in the area of closure weld between the shell and the top shield plug is calculated to be 3,123 psi. The maximum stress intensity in the area of closure weld between the shell and the top cover plate is calculated to be 669 psi. The maximum tensile stress normal to the effective throat of the weld between the shell and the bottom outer cover plate is calculated to be 152 psi.

The maximum stress intensities in the canister for load case 2 are calculated to be 33,189 psi and 6,394 psi in NB components and NF components, respectively. The maximum stress intensity in the area of closure weld between the shell and the top shield plug is calculated to be 3,602 psi. The maximum stress intensity in the area of closure weld between the shell and the top cover plate is calculated to be 1,267 psi.

Transfer Load Case 20: Normal 60 kip Pull Hydraulic Load (Internal Pressure of 30 psig + 60 kip Pull + Thermal of 115 °F ambient)

In the event of retrieving the canister from the HSM into the transfer cask a normal maximum pull force of 60 kips will be applied by a hydraulic ram over an annulus area with a 12.62 inch outer diameter and a 10 inch inner diameter on the inside surface of grapple ring. A uniform pressure of 1,289.04 psig $[= 60,000 \text{ lb} / ((\pi/4) \times (12.62^2 - 10^2))]$ is applied over this area. The periphery of the top cover outer surface is held as boundary condition. The sustained loads of an internal pressure of 30 psig plus the equivalent pull load pressure of 1289.04 psi are applied in load step 1. The sustained loads plus the temperature load from fuel decay heat are applied in the load step 2.

The maximum primary stress intensity in the canister for load step 1 is calculated to be 4,115 psi in NB components. The maximum primary stress intensity in the area of closure weld between the shell and the top shield plug is calculated to be 3,110 psi. The maximum primary stress intensity in the area of closure weld between the shell and the top cover plate is calculated to be 603 psi. The maximum tensile stress normal to the effective throat of the weld between the shell and the bottom outer cover plate is calculated to be 12,498 psi.

The maximum stress intensity in the canister NF components is calculated to be 30,046 psi at the junction between the shell and the bottom cover plate, which is a gross structural discontinuity according to NF-3121.14 of Reference 5. Bending stress at a gross structural discontinuity is a secondary stress as per NF-3121.3 of Reference 5. The allowable primary plus secondary stress intensity for loads under Normal condition (Service Level A) is $2S_y$ per Table NF-3522(b)-1 of Reference 5.

The calculated maximum total stress intensities in the grapple ring and its support for load case 1 are linearized to separate the membrane and bending stresses from the peak stress intensities. The maximum primary membrane stress in the grapple ring and its support is computed, by stress linearization, to be 10,410 psi and the membrane plus bending stress is computed to be 24,790 psi.

The maximum primary plus secondary stress intensities in the canister for load case 2 are calculated to be 35,029 psi and 30,340 psi in NB components and NF components, respectively.

The maximum stress intensity in the area of closure weld between the shell and the top shield plug is calculated to be 3,660 psi. The maximum stress intensity in the area of closure weld between the shell and the top cover plate is calculated to be 1,311 psi.

Transfer Load Case 21: Off-Normal 80 kip Push Hydraulic Load (Internal Pressure of 30 psig + 80 kip Push + Thermal load of 115 °F ambient)

The Transfer Load Case 19 of normal 80 kip push hydraulic load is also designated as an off-normal load case. The stresses calculated in Transfer Load Case 19 are then used for evaluations against the allowable stresses of this off-normal load case.

Transfer Load Case 22: Off-Normal 80 kip Pull Hydraulic Load (Internal Pressure of 30 psig + 80 kip Pull + Thermal of 115 °F ambient)

In the event of retrieving the canister from the HSM into the transfer cask an off-normal maximum pull force of 80 kips will be applied by a hydraulic ram over an annulus area with a 12.62 inch outer diameter and 10 inch inner diameter on the inside surface of grapple ring. A uniform pressure of 1,718.72 psig $[= 80,000 \text{ lb} / ((\pi/4) \times (12.62^2 - 10^2))]$ is applied over this area. The periphery of the top cover outer surface is held as boundary condition. The sustained loads of an internal pressure of 30 psig plus the equivalent pull load pressure of 1,718.72 psi are applied in load step 1. The sustained loads plus the temperature load from fuel decay heat are applied in the load step 2.

The maximum stress intensity in the canister for load step 1 is calculated to be 4,223 psi in NB components. The maximum stress intensity in the area of closure weld between the shell and the top shield plug is calculated to be 3,110 psi. The maximum stress intensity in the area of closure weld between the shell and the top cover plate is calculated to be 603 psi. The maximum tensile stress normal to the effective throat of the weld between the shell and the bottom outer cover plate is calculated to be 16,407 psi.

The calculated total stress intensities in the grapple ring and its support are linearized to separate the membrane and bending stresses from the peak stress intensities. The maximum primary membrane stress in the grapple ring and its support is calculated, by stress linearization, to be 13,860 psi and the membrane plus bending stress is calculated to be 33,010 psi.

The primary plus secondary stress intensities calculated in the NF components under load step 2 are not required to be evaluated for Service Level C and D loads as per Table NF-3522(b)-1 of Reference 5. The maximum primary plus secondary stress intensity in the canister NB components for load step 2 is calculated to be 34,905 psi. The maximum primary plus secondary stress intensity in the area of closure weld between the shell and the top shield plug is calculated to be 3,660 psi. The maximum primary plus secondary stress intensity in the area of closure weld between the shell and the top cover plate is calculated to be 1,311 psi.

Transfer Load Case 23: Accident 110 kip Push Hydraulic Load (Internal Pressure of 30 psig + 110 kip Push)

The hypothetical accident condition maximum hydraulic force applied by the ram to push the canister from the transfer cask to the HSM is set at 110 kips. The load is applied over an area with a 9 inch diameter on the canister bottom. A uniform pressure of 1,729.1 psig [= 110,000 lb / $((\pi/4) \times 9^2)$] is applied over this area in the 2-D ANSYS canister model. The periphery of the canister top cover outer surface is held as a boundary condition. The sustained loads of an internal pressure of 30 psig plus the equivalent push force pressure of 1,729.1 psi are applied as the loading. The secondary temperature load is not required by ASME code for analysis in an accident condition.

The maximum stress intensity in the canister for this load case is calculated to be 9,854 psi and 3,565 psi in NB components and NF components, respectively. The maximum stress intensity in the area of closure weld between the shell and the top shield plug is calculated to be 3,132 psi. The maximum stress intensity in the area of closure weld between the shell and the top cover plate is calculated to be 688 psi. The maximum tensile stress normal to the effective throat of the weld between the shell and the bottom outer cover plate is calculated to be 135 psi.

Transfer Load Case 24: Accident 110 kip Pull Hydraulic Load (Internal Pressure of 30 psig + 110 kip Pull)

The accident maximum hydraulic force applied by the ram to pull the canister out of the HSM into the transfer cask is set at 110 kips. This pull force is applied over an annulus area with a 12.62 inch outer diameter and a 10 inch inner diameter on the inside surface of grapple ring. A uniform pressure of 2363.25 psig [= 110,000 lb / $((\pi/4) \times (12.62^2 - 10^2))$] is applied over this area in the 2-D ANSYS canister model. The periphery of the top cover outer surface is held as a boundary condition. The sustained loads of an internal pressure of 30 psig plus the equivalent pull force pressure of 2363.25 psi are applied as loading. The secondary temperature load is not required by ASME code for analysis in an accident condition.

The maximum stress intensity in the canister NB components for this load case is calculated to be 4,393 psi. The maximum stress intensity in the area of closure weld between the shell and the top shield plug is calculated to be 3,132 psi. The maximum stress intensity in the area of closure weld between the shell and the top cover plate is calculated to be 656 psi. The maximum tensile stress normal to the effective throat of the weld between the shell and the bottom outer cover plate is calculated to be 21,928 psi.

The calculated total stress intensities in the grapple ring and its support are linearized to separate the membrane and bending stresses from the peak stress intensities. The maximum primary membrane stress in the grapple ring and its support is calculated, by stress linearization, to be 19,090 psi and the membrane plus bending stress is calculated to be 45,480 psi.

Transfer Load Case 25: Canister Lifting

During the lifting of the canister the most weights, except the weight of the bottom inner plate to which the lifting blocks are attached, are transmitted through the shell and its connected bottom inner plate to the lifting blocks. Since the four 2.5" square lifting blocks are very close to the canister shell (1.5 inch from the edge of the block to the inner diameter of the shell), the load path of the bottom inner plate between the shell and the blocks is relatively rigid. It is therefore judged that the lifting blocks are the weakest link in the composite bottom design, as in the one-piece bottom design case, during a lifting operation. The total canister weight is the same for both composite and one-piece bottom canisters. Analysis of the lifting blocks in Transfer Load Case 25 of Section 3.9.1.3.2D for canister with one-piece bottom is therefore also valid for the canister with the optional composite bottom designs.

Stresses in the Canister End Closure Welds due to Storage Loads

There are two closure welds in the alternate canister design. One weld joins the canister shell and the top shield plug. Another weld joins the canister shell and its outer cover. Since the radiographic examinations of these two closure welds are not feasible, Reference 14 requires a design stress reduction factor be used in the design calculation. The design stress reduction factor of 0.8 from Table 1 of Reference 14 is used in evaluation of the ANSYS calculated stresses at these two welds. Table 3.9.1-27, Table 3.9.1-31, Table 3.9.1-35 summarize these reported stress intensities at the welds and their evaluations. Only the higher of the calculated stress intensities in these two closure welds is reported in the summary Tables.

G. Summary of the Stress Calculation Results for the Alternate Canister Design

Table 3.9.1-24 through Table 3.9.1-35 summarize the calculated stress intensities in the alternate canister design and their corresponding ASME code evaluations for all bounding transfer load cases.

Based on the results of these analyses, the 32PTH DSC alternate canister composite bottom assembly is structurally adequate with respect to normal, off-normal, and hypothetical accident conditions.

3.9.1.4 32PTH DSC and OS187H Transfer Cask Thermal Expansion Evaluation

3.9.1.4.1 Introduction

The purpose of this section is to determine the thermal growths among components of fuel cladding, basket, canister, and transfer cask in the 32PTH DSC. This thermal expansion calculation covers events of Vacuum Drying, Transfer, Storage, and Storage with Blocked Vent.

3.9.1.4.2 Approach

The temperatures of the fuel cladding, basket, canister, and transfer cask under various events are calculated in the thermal analyses of Chapter 4. Transient thermal analyses are conducted for the vacuum drying and blocked vent events. Steady-state thermal analyses are conducted for the normal and off-normal conditions during transfer and Storage. This section computes the thermal expansions at the steady-state temperatures in the events of Transfer and Storage.

In the vacuum drying load case, the profiles of transient temperature versus time computed in Chapter 4 are studied for selection of the critical time points at which the corresponding component temperatures would generate a minimum clearance between two nested components. For the blocked vent load case, the maximum temperatures from Chapter 4 are used in this calculation.

The cold dimensions of each pair of nested components are so determined, based on design tolerances, which generates a minimum cold clearance between the two components.

Unless otherwise stated, nominal dimensions of basket, canister, and cask are used for the thermal expansion calculations.

3.9.1.4.3 Mechanical Properties of Materials

The coefficient of thermal expansion of structural materials used for the fuel basket, canister shell, and transfer cask are provided in Table 3.9.1-6 as a function of temperature. The properties of SA-240 Gr.304 are taken from Reference 1, and the zircaloy properties are taken from Reference 4.

3.9.1.4.4 Thermal Expansion Computation

A. Thermal Expansion between the Length of Fuel Assembly and Canister Cavity

The extreme metal temperatures for the fuel cladding and canister under different cases are obtained from Chapter 4 for computation of the differential length growth. These temperatures are conservatively rounded and used in this calculation as listed in the following table.

Cases \ Component Temperature	Length Growth Between Fuel Cladding and Canister	
	Fuel Cladding Temp., T_F (°F)	Canister (DSC Shell) Temp., T_C (°F)
Vacuum Drying	760 ⁽¹⁾	210
Transfer	730	390
Storage – Off Normal	700	280
Storage – Blocked Vent	830	590

Note

- 1: As shown in Chapter 4, Table 4-8, the fuel cladding temperature during vacuum drying does not exceed 752 °F. This is a conservative value used for determining the clearances.

The spent fuel type was assumed to be Westinghouse 17×17 Standard. An examination of the fuel cladding temperature and DSC shell temperature in the above table shows that the largest temperature difference corresponds to the vacuum drying case and the smallest temperature difference corresponds to the storage blocked vent case. These two cases are selected as the controlling cases to analyze the thermal expansion between the fuel assemblies and the DSC shell as follows.

The length of the spent fuel assembly when hot is,

$$L_F = L_T + (L_Z \times \alpha_Z + L_S \times \alpha_S) \Delta T$$

Where,

L_F = Hot length of PWR fuel assembly, in.

L_T = Total length of fuel assembly at room temperature = 162.4 in.

L_Z = Length of Zircaloy guide tube \cong 144 in.

α_Z = Zircaloy axial coefficient of thermal expansion (in./in.°F)

L_S = Length of stainless steel per fuel assembly $\cong 18.4$ in.

α_S = Stainless steel coefficient of thermal expansion (in./in.°F)

$$\Delta T = T_F - 70 \text{ (°F)}$$

Allowing 1.25 inch for irradiation growth of the spent fuel assembly, the total assembly length including thermal expansion is:

$$L_{F, \text{irrad}} = L_F = \Delta L_{\text{irrad}}$$

Where:

$L_{F, \text{irrad}}$ = Hot length of PWR fuel assembly with irradiation growth (in)

ΔL_{irrad} = irradiation growth = 1.25 in.

The minimum length of the canister cavity at room temperature is 164.5 inches. The minimum length of the canister cavity is,

$$L_{CH} = L_{CC} + L_{CC} \times \alpha_C \times \Delta T$$

Where,

L_{CH} = Hot length of canister cavity, in.

L_{CC} = Minimum canister cavity length at room temperature = 164.5 in.

α_C = Stainless steel coefficient of thermal expansion (in./in.°F)

$$\Delta T = T_C - 70 \text{ (°F)}$$

The results of the calculation for the thermal expansion between the fuel assembly and the DSC cavity for 32PTH DSC are summarized below.

Event	T_F (°F)	α_Z (in/in-°F)	α_S (in/in-°F)	T_C (°F)	α_C (in/in-°F)	L_F (in)	$L_{F, \text{irrad}}$ (in)	L_{CH} (in)	$L_{CH} - L_{FHT}$ (in)
Vacuum Drying	760	3.01E-06	10.0E-06	210	8.94E-06	162.83	164.08	164.71	0.63
Storage Accident	830	3.01E-06	10.1E-06	590	9.80E-06	162.87	164.12	165.34	1.22

As shown in the above table, adequate clearance has been provided between the PWR spent fuel assemblies and the canister cavity length to permit free thermal expansion.

B. Thermal Expansion between the Outer Diameter of the Basket and the Inner Diameter of the Canister Cavity

The following spreadsheet is used to compute the relative thermal expansions between the fuel basket outer diameter and the DSC canister cavity inner diameter. All maximum and minimum component temperatures are taken from the thermal evaluation performed in Chapter 4.

The maximum outer diameter of the basket at room temperature, D_b , is computed as follows.

$$D_b = 68.53 \text{ in.} - 0.16 \text{ in. min. gap} = 68.370 \text{ in.}$$

The minimum inner diameter of the DSC canister cavity at room temperature, D_c , is computed as follows.

$$D_c = (69.75 \text{ in.} - 0.12 \text{ in.}) - 2 \times (0.50 \text{ in.} + 0.05 \text{ in.}) = 68.530 \text{ in.}$$

Thermal Expansion between the O.D. of Basket and I.D. of Canister Cavity

Max. OD of cold basket = 68.370 inch [68.53 – .16 min. gap = 68.37]

Min. ID of cold canister cavity = 68.530 inch [(69.75 – .12) – 2 × (.50 + .05) = 68.53]

Event	Case	T _{CNH} ⁽²⁾ (°F)	α _{CN} (in/in-°F)	T _{BKH} ⁽³⁾ (°F)	α _{BK} (in/in-°F)	D _{CNH} (in)	D _{BKH} (in)	D _{CNH} - D _{BKH} (in)
Vacuum Drying	TC Backfill	500	9.700E-06	550	9.800E-06	68.816	68.692	0.124
Transfer (34.8 kW)	115 °F Amb. Basket Type I, Conf. # 1	460	9.620E-06	640	9.880E-06	68.787	68.755	0.032
	115 °F Amb. Basket Type I, Conf. # 2	460	9.620E-06	625	9.850E-06	68.787	68.744	0.043
	115 °F Amb. Basket Type I, Conf. # 3	460	9.620E-06	630	9.860E-06	68.787	68.748	0.040
	115 °F Amb. Basket Type I, Conf. # 4	460	9.620E-06	640	9.880E-06	68.787	68.755	0.032
	-20 °F Amb. Basket Type I, Conf. # 1	390	9.460E-06	570	9.800E-06	68.737	68.705	0.032
	115 °F Amb. Basket Type II, Conf. # 1	460	9.620E-06	640	9.880E-06	68.787	68.755	0.032
	115 °F Amb. HSM-H w/ Finned Side Shield	400	9.500E-06	600	9.800E-06	68.745	68.725	0.020
Storage (34.8 kW)	-20 °F Amb. HSM-H w/ Finned Side Shield	280	9.160E-06	505	9.710E-06	68.662	68.659	0.003
Storage Blocked Vent (34.8 kW)	34 hours after Blockage HSM-H w/ Finned Side Shield	590	9.800E-06	740	1.000E-05	68.879	68.828	0.051

Note :

(1) Not Used.

(2) Canister temperatures are conservatively decreased from the values calculated in thermal analyses.

(3) Basket temperatures are conservatively increased from the values calculated in thermal analyses.

$$D_{CNH} = 68.53 \times [1 + \alpha_{CN} \times (T_{CNH} - 70)]$$

$$D_{BKH} = 68.37 \times [1 + \alpha_{BK} \times (T_{BKH} - 70)]$$

T_{CNH} = Temperature of hot canister

α_{CN} = Thermal expansion coefficient of canister at T_{CNH} temperature

T_{BKH} = Temperature of hot basket

α_{BK} = Thermal expansion coefficient of basket at T_{BKH} temperature

D_{CNH} = ID of hot canister at T_{CNH} temperature

D_{BKH} = OD of hot basket at T_{BKH} temperature

D_{CNH} - D_{BKH} = diametrical clearance between the ID of the canister and the OD of the basket

C. Thermal Expansion between the Length of Basket and Canister Cavity

The maximum basket length at room temperature, $L_b = 162.120$ inches.

The minimum canister cavity length at room temperature, $L_c = 164.50$ inches.

Max. cold basket length = 162.120 inch

Min. cold canister cavity length = 164.500 inch

Event	Case	$T_{CNH}^{(1)}$ (°F)	α_{CN} (in/in-°F)	$T_{BKH}^{(2)}$ (°F)	α_{BK} (in/in-°F)	L_{CNH} (in)	L_{BKH} (in)	$L_{CNH} - L_{BKH}$ (in)
Vacuum Drying	TC Backfill	500	9.700E-06	550	9.800E-06	165.186	162.883	2.304
Transfer (34.8 kW)	115 °F Amb. Basket Type I, Conf. # 1	460	9.620E-06	640	9.880E-06	165.117	163.033	2.084
	115 °F Amb. Basket Type I, Conf. # 2	460	9.620E-06	625	9.850E-06	165.117	163.006	2.111
	115 °F Amb. Basket Type I, Conf. # 3	460	9.620E-06	630	9.860E-06	165.117	163.015	2.102
	115 °F Amb. Basket Type I, Conf. # 4	460	9.620E-06	640	9.880E-06	165.117	163.033	2.084
	-20 °F Amb. Basket Type I, Conf. # 1	390	9.460E-06	570	9.800E-06	164.998	162.914	2.084
	115 °F Amb. Basket Type II, Conf. # 1	460	9.620E-06	640	9.880E-06	165.117	163.033	2.084
Storage (34.8 kW)	115 °F Amb. HSM-H w/ Finned Side Shield	400	9.500E-06	600	9.800E-06	165.016	162.962	2.054
	-20 °F Amb. HSM-H w/ Finned Side Shield	280	9.160E-06	505	9.710E-06	164.816	162.805	2.012
Storage Blocked Vent (34.8 kW)	34 hours after Blockage HSM-H w/ Finned Side Shield	590	9.800E-06	740	1.000E-05	165.338	163.206	2.132

Note:

(1) Canister temperatures are conservatively decreased from the values calculated in thermal analyses.

(2) Basket temperatures are conservatively increased from the values calculated in thermal analyses.

Where,

$$L_{CNH} = 164.5 \times [1 + \alpha_{CN} \times (T_{CNH} - 70)]$$

$$L_{CNH} = 162.12 \times [1 + \alpha_{BK} \times (T_{BKH} - 70)]$$

T_{CNH} = Temperature of canister

α_{CN} = Thermal expansion coefficient of canister at T_{CNH} temperature

T_{BKH} = Average of temperatures of hot basket and basket rail

α_{BK} = Thermal expansion coefficient of basket at T_{BKH} temperature

L_{CNH} = Length of hot canister cavity at T_{CNH} temperature

L_{BKH} = Length of hot basket at T_{BKH} temperature

$L_{CNH} - L_{BKH}$ = Hot clearance between the length of the canister cavity and the length of the basket

D. Thermal Expansion between the Outer Diameter of the Canister and the Inner Diameter of the Cask Body

Max. OD of cold canister = 69.870 inch

Min. ID of cold cask cavity = 70.350 inch

Event	Case	T _{CKH} ⁽¹⁾ (°F)	α _{CK} (in/in-°F)	T _{CNH} ⁽²⁾ (°F)	α _{CN} (in/in-°F)	D _{CKH} (in)	D _{CNH} (in)	D _{CNH} - D _{BKH} (in)
Vacuum Drying	TC Backfill	265	9.130E-06	525	9.750E-06	70.475	70.180	0.295
Transfer (34.8 kW)	115 °F Amb.	330	9.260E-06	485	9.670E-06	70.519	70.150	0.369
	-20 °F Amb.	240	9.060E-06	500	9.700E-06	70.458	70.161	0.297

Note:

(1) Cask temperatures are conservatively decreased from the values calculated in thermal analyses.

(2) Canister temperatures are conservatively increased from the values calculated in thermal analyses.

Where,

$$D_{CKH} = 70.35 \times [1 + \alpha_{CK} \times (T_{CKH} - 70)]$$

$$D_{CNH} = 69.87 \times [1 + \alpha_{CN} \times (T_{CNH} - 70)]$$

T_{CKH} = Temperature of hot cask outer structural shell

α_{CK} = Thermal expansion coefficient of cask inner liner at T_{CKH} temperature

T_{CNH} = Temperature of hot canister shell

α_{CN} = Thermal expansion coefficient of canister shell at T_{CNH} temperature

D_{CKH} = ID of hot cask inner liner at T_{CKH} temperature

D_{CNH} = OD of hot canister shell at T_{CNH} temperature

D_{CKH} - D_{CNH} = diametrical hot clearance between the ID of the cask inner liner and the OD of the canister shell

E. Thermal Expansion between the Length of the Canister and the Transfer Cask Cavity

Max. length of cold canister = 185.750 inch
 Min. length of cold cask cavity = 186.550 inch [186.60 – .05 = 186.55]

Event	Case	T _{CKH} ⁽¹⁾ (°F)	α _{CK} (in/in-°F)	T _{CNH} ⁽²⁾ (°F)	α _{CN} (in/in-°F)	L _{CKH} (in)	L _{CNH} (in)	L _{CKH} - L _{CNH} (in)
Vacuum Drying	TC Backfill	265	9.130E-06	525	9.750E-06	186.882	186.574	0.308
Transfer (34.8 kW)	115 °F Amb.	330	9.260E-06	485	9.670E-06	186.999	186.495	0.504
	-20 °F Amb.	240	9.060E-06	500	9.700E-06	186.837	186.525	0.313

Note:

- (1) Cask temperatures are conservatively decreased from the values calculated in thermal analyses.
 (2) Canister temperatures are conservatively increased from the values calculated in thermal analyses.

$$L_{CKH} = 186.55 \times [1 + \alpha_{CK} \times (T_{CKH} - 70)]$$

$$L_{CNH} = 185.75 \times [1 + \alpha_{CN} \times (T_{CNH} - 70)]$$

T_{CKH} = Temperature of hot cask structural shell

α_{CK} = Thermal expansion coefficient of cask structural shell at T_{CKH} temperature

T_{CNH} = Temperature of hot canister

α_{CN} = Thermal expansion coefficient of canister at T_{CNH} temperature

L_{CKH} = Length of hot cask cavity at T_{CKH} temperature

L_{CNH} = Length of hot canister at T_{CNH} temperature

L_{CKH} - L_{CNH} = diametrical hot clearance between the length of the cask cavity and the length of the canister

3.9.1.4.5 Thermal Expansion Analysis Conclusions

This evaluation demonstrates that adequate clearance is provided between the 32PTH DSC fuel basket and canister shell, and between the 32PTH DSC canister and the OS187H Transfer Cask to permit free thermal expansions among these components due to all specified design and service conditions.

A condition may exist where the gap between the DSC basket and shell is reduced below the minimum specified in the design drawings due to local distortion of the shell, thereby constituting controlling locations for basket to shell gap. These local conditions involve the potential for a zero basket to shell gap which could impose loads on the shell due to differential thermal expansion between the basket and shell. This condition has been specifically evaluated in the design basis analytical model and demonstrated to satisfy ASME Code stress allowable values such that design basis compliance for the DSC confinement boundary is maintained.

3.9.1.5 References

1. American Society of Mechanical Engineers, ASME Boiler and Pressure Vessel Code, Section II, Part D, 1998, through 2000 addenda.
2. American Society of Mechanical Engineers, ASME Boiler and Pressure Vessel Code, Section III, Subsection NG, 1998 through 2000 addenda.
3. American Society of Mechanical Engineers, ASME Boiler and Pressure Vessel Code, Section III, Appendix F, 1998 through 2000 addenda.
4. NUREG/CR-0497-Rev 2, MATPRO-Version 11 (Revision 2), A handbook of materials properties for use in the analysis of light water reactor fuel rod behavior.
5. American Society of Mechanical Engineers, ASME Boiler and Pressure Vessel Code, Section III, Division 1, Subsection NF, 1998, through 2000 addenda.
6. Manual of Steel Construction, Ninth Edition, American Institute of Steel Construction, Inc., 1989.
7. Roark, Formulas for Stress and Strain, Sixth Edition.
8. American Society of Mechanical Engineers, ASME Boiler and Pressure Vessel Code, Section III, Division 1, Subsection NB, 1998, through 2000 addenda.
9. NUREG/CR-0481 SAND77-1872 R-7, "An Assessment of Stress-Strain Data Suitable for Finite-Element Elastic-Plastic Analysis of Shipping Containers," September 1978.
10. ANSYS User's Manual, Rev 6.0.
11. American National Standard ANSI N14.6 – 1993, "American National Standard for Radioactive Materials – Special Lifting Devices for Shipping Containers Weighing 10000 pounds (4500 kg) or More."
12. "Table speeds calculation of Strength of Threads," R. C. Boucher, Product Engineering, November 27, 1961.
13. Machinery's Handbook, 24th Edition.
14. USNRC Spent Fuel Project Office, Interim Staff Guidance – 15, "Materials Evaluation."
15. Roark, Formulas for Stress and Strain, Fourth Edition.
16. UCID-21246, "Dynamic Impact Effects on Spent Fuel Assemblies," Lawrence Livermore National Library, October 20, 1987.

17. DOE/RW-0184, "Characteristics of Spent Fuel, Highlevel Waste, and Other Radioactive Wastes Which May Require Long-Term Isolation," Volume 3 of 6, December 1987.
18. SCALE NUREG/CR-0200, Volume 3, Revision 5.
19. Updated Final Safety Analysis Report (UFSAR), for the Standardized NUHOMS[®] Horizontal Modular Storage System for Irradiated Nuclear Fuel, NUH003.0103, Rev. 12.

Table 3.9.1-1
Temperature Dependent Material Properties

Component	Material	Temp. °F	Ultimate S_u (ksi)	Yield S_y (ksi)	Allow. S_m (ksi)	E (106 psi)	α (10⁻⁶ oF⁻¹)
Basket, Plates, Rails And Canister	SA-240 Stainless Steel 304	70	75.0	30.0	20.0	28.3	8.5
		200	71.0	25.0	20.0	27.6	8.9
		300	66.2	22.4	20.0	27.0	9.2
		400	64.0	20.7	18.7	26.5	9.5
		500	63.4	19.4	17.5	25.8	9.7
		600	63.4	18.4	16.4	25.3	9.8
		700	63.4	17.6	16.0	24.8	10.0

Table 3.9.1-2
SA-240, Type 304, Thermal Material Properties

Temperature (°F)	Conductivity (Btu/hr-in- °F)	Specific Heat (Btu/lbm- °F)	Density (lb/in³)
200	0.775	0.1224	0.29
300	0.817	0.1258	0.29
400	0.867	0.1294	0.29
500	0.908	0.1317	0.29
600	0.942	0.1334	0.29
700	0.983	0.135	0.29
800	1.017	0.136	0.29
900	1.058	0.137	0.29
1000	1.100	0.139	0.29

Table 3.9.1-3
Summary of Stresses in Fuel Compartments, Rails and Canister for Transfer Loads

Loading	Component	Service Level	Stress Classification	Loads	Stress (ksi)	Allow. Stress (ksi)
Dead Weight (Cask Vert.)	Fuel Comp. & Plates	A	P_m	1g Axial	0.17	16.0
		A	$P_m + P_b$		0.17	24.0
	Rail	A	P_m		0.16	16.4
		A	$P_m + P_b$		0.16	24.6
Handling Loads (Cask Horiz.)	Fuel Comp. & Plates	A	P_m	2g Vert. + 2g Trans. + 2g Axial	6.98	16.0
		A	$P_m + P_b$		9.98	24.0
	Rail	A	P_m		3.15	16.4
		A	$P_m + P_b$		13.8	24.6
	Canister	A	P_m		0.88	17.5
		A	$P_m + P_b$		9.74	26.25
Thermal	Fuel Comp. & Plates	A	Q	115 °F Amb.	8.48	48.0
	Rail	A	Q	115 °F Amb.	14.2	49.2
	Fuel Comp. & Plates	A	Q	-20 °F Amb.	8.69	48.0
	Rail	A	Q	-20 °F Amb.	14.40	49.2
	Fuel Comp. & Plates	A	Q	Vacuum Drying (Proc. A)	9.86	48.0
	Rail	A	Q	Vacuum Drying (Proc. A)	18.50	49.2
Handling Load + Normal Thermal	Fuel Comp. & Plates	A	$P_m + P_b + Q$	Primary plus Secondary	18.70	48.0
	Rails	A	$P_m + P_b + Q$	Primary plus Secondary	28.20	49.2
DW + Vacuum Drying Thermal	Fuel Comp. & Plates	A	$P_m + P_b + Q$	Primary plus Secondary	10.00	48.0
	Rails	A	$P_m + P_b + Q$	Primary plus Secondary	18.70	49.2

Table 3.9.1-4(a)
Summary of Calculated Stresses in the Fuel Basket and Canister Shell
due to 75g Drop Loads

Drop Orientation	Component	Stress Category	Max. Stress (ksi)	Allowable Stress (ksi)
0° Side Drop	Fuel Compartment and Plates	P_m	24.5	44.38
		$P_m + P_b$	25.6	57.06
	Rails	P_m	22.0	44.38
		$P_m + P_b$	22.3	57.06
	Canister	P_m	4.61	44.38
		$P_m + P_b$	10.9	57.06
30° Side Drop	Fuel Compartment and Plates	P_m	28.3	44.38
		$P_m + P_b$	29.7	57.06
	Rails	P_m	20.6	44.38
		$P_m + P_b$	22.1	57.06
	Canister	P_m	4.81	44.38
		$P_m + P_b$	11.3	57.06
45° Side Drop	Fuel Compartment and Plates	P_m	26.4	44.38
		$P_m + P_b$	27.6	57.06
	Rails	P_m	19.8	44.38
		$P_m + P_b$	22.7	57.06
	Canister	P_m	4.53	44.38
		$P_m + P_b$	12.1	57.06
180° Side Drop (on Rails)	Fuel Compartment and Plates	P_m	25.5	44.38
		$P_m + P_b$	31.8	57.06
	Rails	P_m	13.6	44.38
		$P_m + P_b$	37.1	57.06
	Canister	P_m	13.2	44.38
		$P_m + P_b$	36.8	57.06
End Drop	Fuel Comp.	P_m	12.8	44.38

Table 3.9.1-4(b)
Summary of Linearized Stresses in 7/8 inch Square Bars for 75g Side Drop Loads

Drop Orientation	Max. Nodal Stress Intensity (ksi) ($P_m + P_b$)	Stress Category	Allowable Stress (ksi)
0° Side Drop	27.5	P_m	44.38
		$P_m + P_b$	57.06
30° Side Drop	24.7	P_m	44.38
		$P_m + P_b$	57.06
45° Side Drop	24.7	P_m	44.38
		$P_m + P_b$	57.06
180° (on rails) Side Drop	41.8	P_m	44.38
		$P_m + P_b$	57.06

All the Max. Nodal Stress Intensities ($P_m + P_b$) are below the P_m allowable.

Table 3.9.1-5
Summary of Stresses in Fuel Compartments, Support Rails and Canister Shell
for Storage Loads

Loading	Component	Service Level	Stress Classification	Applied Loads	Calculated Stress (ksi)	Allowable Stress (ksi)
Dead Weight (Cask Horiz.)	Fuel Compartment	A	P_m	1g Down	1.03	16.0
		A	$P_m + P_b$		2.93	24.0
	Rail	A	P_m		0.68	16.4
		A	$P_m + P_b$		4.37	24.6
	Canister Shell	A	P_m		0.38	17.5
		A	$P_m + P_b$		4.05	26.25
Seismic Loads (Cask Horiz.)	Fuel Compartment	A	P_m	0.65g Axial + 0.65g Trans.+ 1.30g Vertical	8.80	16.0
		A	$P_m + P_b$		9.80	24.0
	Rail	A	P_m		3.18	16.4
		A	$P_m + P_b$		12.70	24.6
	Canister Shell	A	P_m		0.63	17.5
		A	$P_m + P_b$		6.08	26.25
Thermal	Fuel Compartment	A	Q	115 °F Amb. (with fins)	7.98	48.0
	Rail	A	Q		13.5	49.2
	Fuel Compartment	A	Q	-20 °F Amb. (with fins)	8.38	48.0
	Rail	A	Q		13.7	49.2
	Fuel Compartment	A	Q	HSM Vent Blockage	7.04	45.6
	Rail	A	Q		8.68	48.6
Seismic Load + Normal Thermal	Fuel Compartment	A	$P_m + P_b + Q$	Primary plus Secondary	18.18	48.0
	Rails	A	$P_m + P_b + Q$		26.4	49.2
DW + Vent Blockage Thermal	Fuel Compartment	A	$P_m + P_b + Q$	Primary plus Secondary	9.97	45.6
	Rails	A	$P_m + P_b + Q$		13.05	48.6

Table 3.9.1-6
Temperature Dependent Coefficients of Thermal Expansion

Component	Material	Temperature (°F)	α (10^{-6} in/in/°F)
Basket, Canister, And Transfer Cask	SA-240 Gr. 304	70	8.50
		100	8.60
		150	8.80
		200	8.90
		250	9.10
		300	9.20
		350	9.30
		400	9.50
		450	9.60
		500	9.70
		550	9.80
		600	9.80
		650	9.90
		700	10.0
		750	10.0
		800	10.1
Fuel Cladding	Zircaloy	850	10.1
		700	2.70*
		730	2.73*
		750	2.79*
		810	2.70*

* Axial thermal expansion coefficient is taken from Reference 4.

Table 3.9.1-7
ASME Subsection NB Code Allowable Stresses for the 32PTH DSC Canister
(for Transfer Loads)

Loading Condition	Stress Category		Stress Limits	Material	Allowable Stress (ksi.)
Normal and Off-Normal Conditions ⁽¹⁾	Elastic Analysis	Membrane Stress, P_m	S_m	SA-240 Type 304	17.5
				SA-182 Type F304	17.5
		Membrane + Bending Stress, $P_L + P_b$	$1.5 S_m$	SA-240 Type 304	26.25
				SA-182 Type F304	26.25
		Membrane + Bending Stress + Secondary stress $P_L + P_b + Q$	$3 S_m$	SA-240 Type 304	52.5
				SA-182 Type F304	52.5
Accident Conditions	Elastic Analysis	Membrane Stress, P_m	Lesser of $2.4 S_m$ and $0.7 S_u$	SA-240 Type 304	42
				SA-182 Type F304	41.44
		Membrane + Bending Stress, $P_L + P_b$	Lesser of $3.6 S_m$ and S_u	SA-240 Type 304	63
				SA-182 Type F304	59.2
	Elastic / Plastic Analysis	Membrane Stress, P_m	Greater of $0.7 S_u$ and $[S_y + 1/3 (S_u - S_y)]$	SA-240 Type 304	44.38
				SA-182 Type F304	41.44
		Membrane + Bending Stress, $P_L + P_b$	$0.9 S_u$	SA-240 Type 304	57.06
				SA-182 Type F304	53.28

Notes:

1. Normal condition allowable stresses are conservatively used for off-normal loads.

Table 3.9.1-8
ASME Code Allowable Stresses for the 32PTH DSC Canister
for Storage Loads

Loading Condition	Stress Category	Stress Limits	Material	Allowable Stress (ksi.)
Normal Conditions ⁽¹⁾ (At max. temperature of 450 °F for both cases of ambient at -20 °F and 115 °F)	Membrane Stress (P_m)	S_m	SA-240 Type 304	18.1
			SA-182 Grade F304	18.1
	Membrane + Bending Stress ($P_L + P_b$)	$1.5 S_m$	SA-240 Type 304	27.15
			SA-182 Grade F304	27.15
	Membrane + Bending Stress + Secondary stress ($P_L + P_b + Q$)	$3 S_m$	SA-240 Type 304	54.3
			SA-182 Grade F304	54.3
Accident Conditions ⁽²⁾ (At max. temperature of 600 °F for case of Blocked Vent)	Membrane Stress (P_m)	Lesser of $2.4 S_m$ and $0.7 S_u$	SA-240 Type 304	39.36
			SA-182 Grade F304	39.36
	Membrane + Bending Stress ($P_L + P_b$)	Lesser of $3.6 S_m$ and S_u	SA-240 Type 304	59.04
			SA-182 Grade F304	59.04

Notes:

1. Stress limit per Reference 8
2. Stress limits per Reference 3

Table 3.9.1-9
32PTH DSC Canister Load Combinations during Transfer

Loading	Canister w/Transfer Cask Orientation	Service Level	Load for Analysis	Load Combinations	Analyzed Load Case No.	ANSYS Model
Dead Weight	Vertical ⁽¹⁾	A	1 _g Down (Axial)	1 _g Down + 15 psig Ext. Press. + Thermal (Vacuum Dry)	1	2-D
External Pressure	Vertical ⁽¹⁾	A	15 psig			
Thermal	Vertical ⁽¹⁾	A	Vacuum Dry			
Dead Weight	Horizontal ⁽²⁾	A	2 _g Axial + 2 _g Trans. + 2 _g Vertical	A = 2 _g Axial + 2 _g Trans. + 2 _g Vertical	2	2-D
Handling load in Transfer Cask	Horizontal ⁽²⁾	A		A+ 30 psig Int. Pressure + Thermal (115 °F)	3	2-D
				A+ 15 psig Ext. Pressure + Thermal (-20 °F)		
Internal Pressure	Horizontal ⁽²⁾	A	30 psig ⁽⁶⁾	Pressure Stress	[2] ⁽⁵⁾	2-D
Ext. Press.	Horizontal ⁽²⁾	A	15 psig	Pressure Stress	[3] ⁽⁵⁾	2-D
Thermal	Horizontal ⁽²⁾	A	Thermal Stress (-20 °F Ambient)	Thermal Stress	[3] ⁽⁵⁾	2-D
Thermal	Horizontal ⁽²⁾	A	Thermal Stress (115 °F Ambient)	Thermal Stress	[2] ⁽⁵⁾	2-D
Internal Pressure	Horizontal	D	120 psig ⁽³⁾	Pressure Stress	4	2-D
External Pressure	Horizontal	D	25 psig ⁽⁴⁾	Pressure Stress	5	2-D
Side Drop	Horizontal	D	75 _g Multiple Orientations (0°, 30°, 45°, impact on two rails, impact on one rails) Drop angles are enveloped by 0° (no rail) and 180° (two rails)	75 _g side drop at 0° (no rail) + 30 psig Int. Press. of Top / Bottom ends	6 / 7	3-D
				75 _g side drop at 180° (two rails) + 30 psig Int. Press. of Top / Bottom ends	8 / 9	3-D
				75 _g side drop at 0° (no rail) + 15 psig Ext. Press. of Top / Bottom ends	10 / 11	3-D
				75 _g side drop at 180° (two rails) + 15 psig Ext. Press. of Top / Bottom ends	12 / 13	3-D
Corner Drop	Horizontal	D	Enveloped by 75 _g Side Drop and 75 _g End Drop			
End Drop	Vertical	D	75 _g End Drop	75 _g Top/Bottom + 30 psig Int. Pressure	14 / 15	2-D
				75 _g Top/Bottom + 15 psig Ext. Pressure	16 / 17	2-D

Notes:

- Transfer cask supported at the bottom.
- Transfer cask supported at 4 trunnion location.
- Under accident fire condition.
- Under accident flood condition.
- [#] indicates this individual load case is enveloped in the analyzed load case No. #
- From Chapter 4, Table 4-10, the maximum normal operating pressure is 6.4 psig during transfer operation. However, a design pressure of 15 psig is used. Conservatively, 30 psig is used for structural evaluation of the canister.

Table 3.9.1-10
32PTH DSC Canister Load Combinations during Lifting, Testing, and Hydraulic Loads

Loading	Canister w/Transfer Cask Orientation	Service Level	Load for Analysis	Load Combinations	Analyzed Load Case No.	ANSYS Model
Dead Weight	Horizontal	A	1 _g	1 _g + 23.5 psig Int. Pressure + 155 kips Axial Loads	18	2-D
Test Pressure	Horizontal	A	23.5 psig ⁽³⁾			
Seal Plate Axial Load	Horizontal	A	155 kips			
Hydraulic Loads ^{(1) (2)} (Push/Pull)	Horizontal	A	80 / 60 kips	30 psig Int. Pressure + 80 kips push / 60 kips pull + Thermal (115 °F)	19 / 20	2-D
Hydraulic Loads ^{(1) (2)} (Push/Pull)	Horizontal	C	80 / 80 kips	30 psig Int. Pressure + 80 kips + Thermal (115 °F)	21 / 22	2-D
Hydraulic Loads ^{(1) (2)} (Push/Pull)	Horizontal	D	110 / 110 kips	30 psig Int. Pressure + 110 kips	23 / 24	2-D
Lifting	Vertical	A	6g	6 _g	25	Manual

Notes:

1. The hydraulic push loads are applied at the canister bottom surface within the grapple ring support.
2. The hydraulic pull loads are applied at the inner surface of the grapple ring.
3. From Chapter 4, Table 4-10, the maximum normal operating pressure is 6.4psig during transfer operation. The canister is conservatively evaluated at higher test pressures.

Table 3.9.1-11
Summary of Calculated Stresses for Testing Condition Loads

Load Case	Combination of Loads	Canister Orientation	Stress Limits (NB-3226) ⁽¹⁾	
			$P_m < 0.8 S_y$ ($0.8 S_y = 24,000$ psi)	$P_m + P_b < 1.35 S_y$ ($1.35 S_y = 40,500$ psi)
18	DW + 23.5 psig Int. Press. + 155 kip Axial Load	Horizontal	18,442 psi ⁽²⁾	24,695 psi ⁽³⁾

Notes:

1. Yield stress, $S_y = 30,000$ psi, is taken at test temperature of 100 °F for both material SA-240 Gr.304 and SA-182 F304.
2. $P_m = 18,437$ psi + 5 psi (Deadweight, in Load Case 18) = 18,442 psi
3. $P_m + P_b = 18,437$ psi + 6,258 psi (Dead weight, in Load Case 18) = 24,695 psi

Table 3.9.1-12
Summary of Calculated Stress for Normal and Off-Normal Condition Transfer Loads

Load Case	Combination Of Loads	Canister Orientation	Stress Intensity Limits (NB-3220) ⁽¹⁾		
			$P_m < S_m$ ($S_m = 17,500$ psi)	$P_L + P_b < 1.5 S_m$ ($1.5 S_m = 26,250$ psi)	$P_L + P_b + Q < 3 S_m$ ($3 S_m = 52,500$ psi)
1	1 _g down + 15 psig Ext. Press. + Vac. Dry Thermal	Vertical	1,637	1,637	19,574 ⁽²⁾
2	Handling 2 _g + 30 psig Int. Press. + Thermal (115 °F)	Horizontal	880 + 3,332 = 4,212	9,740 + 3,332 = 13,072	9,740 + 36,219 = 45,959
3	Handling 2g's + 15 psig Ext. Press. + Thermal (-20 °F)	Horizontal	880 + 1,666 = 2,546	9,740 + 1,666 = 11,406	9,740 + 35,001 = 44,741
19	30 psig Int. Press. + 80 kip push + Thermal (115 °F)	Horizontal	7,238	7,238	34,916
20	30 psig Int. Press. + 60 kip pull + Thermal (115 °F)	Horizontal	11,484	11,484	36,753
21	30 psig Int. Press. + 80 kip push + Thermal (115 °F)	Horizontal	7,238	7,238	34,916
22	30 psig Int. Press. + 80 kip pull + Thermal (115 °F)	Horizontal	5,249	13,790	36,931

Notes:

- Design stress intensity, S_m is taken at 500 °F of material SA-240 Gr.304 and SA-182 F304.
- A scale factor of 1.05 is used, $19,574 = 1,637 + (18,720 - 1,637) \times 1.05$

Table 3.9.1-13
Summary of Calculated Stresses for Accident Condition Transfer Loads (Elastic Analysis)

Load Case	Combination Of Loads	Canister Orientation	Stress Intensity Limits ⁽¹⁾	
			$P_m < 0.7 S_u$ ⁽²⁾ ($0.7 S_u = 41,440$ psi)	$P_L + P_b < S_u$ ⁽³⁾ ($S_u = 59,200$ psi)
4	120 psig internal pressure under fire accident	Horizontal	13,329 ⁽⁴⁾	13,329 ⁽⁴⁾
5	25 psig external pressure under flood accident	Horizontal	2,777	2,777
14	Top End Drop 75_g + 30 psig Int. Press.	Vertical	15,539	15,539
15	Bottom End Drop 75_g + 30 psig Int. Press.	Vertical	16,492	16,492
16	Top End Drop 75_g + 15 psig Ext. Press.	Vertical	18,545	18,545
17	Bottom End Drop 75_g + 15 psig Ext. Press.	Vertical	19,956	19,956
23	30 psig Int. Press. + 110 kip push + Thermal (115 °F)	Horizontal	9,854	9,854
24	30 psig Int. Press. + 110 kip pull + Thermal (115 °F)	Horizontal	21,025	21,025

Notes:

- See Table 3.9.1-7 for allowable stress intensities. Lesser values of allowable stresses for material SA-182 Type F304 are also used for material SA-240 Type 304.
- $0.7 S_u$ is the lesser value of $2.4 S_m$ and $0.7 S_u$, which is specified as Stress intensity limit in Reference 3.
- S_u is the lesser value of $3.6 S_m$ and S_u , which is specified as Stress intensity limit in Reference 3.
- For metal temperature of 800 °F under accident fire, allowable stress intensities, $P_m < 2.4 S_m$ ($2.4 \times 15,200$ psi = 36,480 psi), $P_L + P_b < 3.6 \times S_m$ ($3.6 \times 15,200$ psi = 54,720 psi).

Table 3.9.1-14
Summary of Stresses for Accident Condition Transfer Loads (Elastic / Plastic Analysis)

Load Case	Combination Of Loads	Canister Orientation	Stress Intensity Limits ⁽¹⁾	
			$P_m < 0.7 S_u$ ⁽²⁾ ($0.7 S_u = 41,440$ psi)	$P_L + P_b < 0.9 S_u$ ⁽³⁾ ($0.9 S_u = 53,280$ psi)
6	Side Drop 75g at 0° + 30 psig Int. Press. (Top End)	Horizontal	27,990	27,990
7	Side Drop 75g at 0° + 30 psig Int. Press. (Bottom End)	Horizontal	19,976	19,976
8	Side Drop 75g at 180° + 30 psig Int. Press. (Top End)	Horizontal	28,869	28,869
9	Side Drop 75g at 180° + 30 psig Int. Press. (Bottom End)	Horizontal	22,666	22,666
10	Side Drop 75g at 0° + 15 psig Ext. Press. (Top End)	Horizontal	28,402	28,402
11	Side Drop 75g at 0° + 15 psig Ext. Press. (Bottom End)	Horizontal	19,381	19,381
12	Side Drop 75g at 180° + 15 psig Ext. Press. (Top End)	Horizontal	29,354	29,354
13	Side Drop 75g at 180° + 15 psig Ext. Press. (Bottom End)	Horizontal	22,650	22,650

Notes:

- See Table 3.9.1-7 for allowable stress intensities. Lesser value of allowable stresses for material SA-182 Type F304 was also used for material SA-240 Type 304.
- $0.7 S_u$ is the greater value of $[S_y + 1/3 (S_u - S_y)]$ and $0.7 S_u$, which is specified as stress intensity limit in Reference 3.
- $0.9 S_u$ is the value specified as Stress intensity limit in Reference 3.

Table 3.9.1-15
Summary of Calculated Stress at the End Closure Welds for Testing Condition Loads

Load Case	Combination of Loads	Canister Orientation	Stress Limits (NB-3226) ⁽¹⁾	
			$P_m < 0.8 S_y$ ($0.8 S_y = 24,000$ psi)	$P_m + P_b < 1.35 S_y$ ($1.35 S_y = 40,500$ psi)
18	DW + 23.5 Psig Int. Press. + 155 kip Axial Load	Horizontal	No closure welds	No closure welds

Notes:

- Yield stress, $S_y = 30,000$ psi, is taken at test temperature of 100 °F for both material SA-240 Gr.304 and SA-182 F304.

Table 3.9.1-16
Summary of Calculated Stress at the End Closure Welds
for Normal and Off-Normal Condition Transfer Loads

Load Case	Combination Of Loads	Canister Orientation	Stress Intensity Limits (NB-3220) ⁽¹⁾		
			$P_m < 0.8S_m$ ($0.8S_m = 14,000$ psi)	$P_L + P_b < 0.8(1.5 S_m)$ ($1.2S_m=21,000$ psi)	$P_L + P_b + Q < 0.8(3 S_m)$ ($2.4 S_m = 42,000$ psi)
1	1g down + 15 psig Ext. Press. + Vac. Dry Thermal	Vertical	1,341	1,341	2153 ⁽²⁾
2	Handling 2g's + 30 psig Int. Press. + Thermal (115 °F)	Horizontal	880 + 3,134 = 4,014	9,740 + 3,134 = 12,874	9,740 + 4,160 = 13,900
3	Handling 2g's + 15 psig Ext. Press. + Thermal (-20 °F)	Horizontal	880 + 1,234 = 2,114	9,740 + 1,234 = 10,974	9,740 + 2,318 = 12,058
19	30 psig Int. Press.+80 kip push + Thermal (115 °F)	Horizontal	3,123	3,123	3,602
20	30 psig Int. Press. + 60 kip pull + Thermal (115 °F)	Horizontal	3,134	3,134	3,646
21	30 psig Int. Press.+80 kip push + Thermal (115 °F)	Horizontal	3,123	3,123	3,602
22	30 psig Int. Press.+ 80 kip pull + Thermal (115 °F)	Horizontal	3,134	3,134	3,646

Notes:

- Design stress intensity, S_m is taken at 500 °F of material SA-240 Gr.304 and SA-182 F304.
- A scale factor of 1.05 is used, $2153 = 1341 + (2114 - 1341) \times 1.05$

Table 3.9.1-17
Summary of Calculated Stresses at the End Closure Welds
for Accident Condition Transfer Loads (Elastic Analysis)

Load Case	Combination Of Loads	Canister Orientation	Stress Intensity Limits ⁽¹⁾	
			$P_m < 0.8 (0.7 S_u) (2)$ ($0.8 \times 0.7 S_u = 33,152$ psi)	$P_L + P_b < 0.8 S_u (3)$ ($0.8 S_u = 47,360$ psi)
4	120 psig internal pressure under fire accident	Horizontal	12,379 ⁽⁴⁾	12,379 ⁽⁴⁾
5	25 psig external pressure under flood accident	Horizontal	2,051	2,051
14	Top End Drop 75 _g + 30 psig Int. Press.	Vertical	5,641	5,641
15	Bottom End Drop 75 _g + 30 psig Int. Press.	Vertical	8,714	8,714
16	Top End Drop 75 _g + 15 psig Ext. Press.	Vertical	7,916	7,916
17	Bottom End Drop 75 _g + 15 psig Ext. Press.	Vertical	12,319	12,319
23	30 psig Int. Press. + 110 kip push + Thermal (115 °F)	Horizontal	3,132	3,132
24	30 psig Int. Press. + 110 kip pull + Thermal (115 °F)	Horizontal	3,134	3,134

Notes:

- See Table 3.9.1-7 for allowable stress intensities. Lesser values of allowable stresses for material SA-182 Type F304 was also used for material SA-240 Type 304.
- $0.7 S_u$ is the lesser value of $2.4 S_m$ and $0.7 S_u$, which is specified as Stress intensity limit in Reference 3.
- S_u is the lesser value of $3.6 S_m$ and S_u , which is specified as Stress intensity limit in Reference 3.
- For metal temperature of 800 °F under accident fire, allowable stress intensities, $P_m < 0.8 \times 2.4 S_m$ ($0.8 \times 2.4 \times 15,200$ psi = 29,184 psi), $P_L + P_b < 0.8 \times 3.6 \times S_m$ ($0.8 \times 3.6 \times 15,200$ psi = 43,776 psi).

Table 3.9.1-18
Summary of Calculated Stresses at End Closure Welds for Accident Condition Transfer
Loads
(Elastic/Plastic Analysis)

Load Case	Combination of Loads	Canister Orientation	Stress Intensity Limits (Ref. 9) ⁽¹⁾	
			$P_m < 0.8 (0.7 S_u)$ ⁽²⁾ ($0.8 \times 0.7 S_u = 41,440$ psi)	$P_L + P_b < 0.8 (0.9 S_u)$ ⁽³⁾ ($0.8 \times 0.9 S_u = 53,280$ psi)
6	Side Drop 75 _g at 0° + 30 psig Int. Press. (Top End)	Horizontal	27,566	27,566
8	Side Drop 75 _g at 180° + 30 psig Int. Press. (Top End)	Horizontal	27,220	27,220
10	Side Drop 75 _g at 0° + 15 psig Ext. Press. (Top End)	Horizontal	27,493	27,493
12	Side Drop 75 _g at 180° + 15 psig Ext. Press. (Top End)	Horizontal	27,306	27,306

Note:

1. See Table 3.9.1-7 for allowable stress intensities. Lesser value of allowable stresses for material SA-182 Type F304 was also used for material SA-240 Type 304.
2. $0.7 S_u$ is the greater value of $[S_y + 1/3 (S_u - S_y)]$ and $0.7 S_u$, which is specified as stress intensity limit in Reference 3.
3. $0.9 S_u$ is the value specified as Stress intensity limit in Reference 3.

Table 3.9.1-19
32PTH DSC Canister Load Combinations during Storage

Loading	Canister Orientation	Service Level	Load	Enveloped Load for Analysis	Load Combinations
Dead Weight (DW)	Horizontal ⁽¹⁾	A	1g Down	.65g Axial + .65g Trans. + 1.3g Vertical (See Note 2)	.65g Axial + .65g Trans. + 1.3g Vertical Down
Seismic Loads	Horizontal ⁽¹⁾	C ⁽²⁾	0.43g Axial + 0.43g Trans. +0.20g Vertical		.65g Axial + .65g Trans. + 1.3g Vertical Down + 30 psig + Thermal (115 °F)
					.65g Axial + .65g Trans. + 1.3g Vertical Down + 30 psig + Thermal (-20 °F)
Internal Pressure	Horizontal ⁽¹⁾	A	15 psig	30 psig	Pressure
Thermal	Horizontal ⁽¹⁾	A	Thermal (-20 °F ambient)	Thermal (-20 °F ambient)	Thermal
Thermal	Horizontal ⁽¹⁾	A	Thermal (115 °F ambient)	Thermal (115 °F ambient)	Thermal
Thermal	Horizontal ⁽¹⁾	D ⁽²⁾	Blocked Vent	Blocked Vent	1g Down + 70 psig Int. Pressure + Thermal (Blocked Vent)
Internal Pressure	Horizontal ⁽¹⁾	D ⁽²⁾	< 67 psig due to Blocked Vent	Enveloped by 70 psig inter pressure	
Flood	Horizontal ⁽¹⁾	D ⁽²⁾	50 ft Water (≈22 psig)	Enveloped by 30 psig external pressure design	

Notes:

1. Canister supported at HSM rails and axial restrained by the seismic restraint devices.
2. Levels C and D loads are conservatively treated as Level A loads and so evaluated.

Table 3.9.1-20
Summary of Calculated Stresses for Normal and Accident Condition Loads ⁽¹⁾
(Canister in horizontal storage position)

Load Case	Applied Loads	Stress Intensity Limits			
		$P_m < S_m$ ($S_m = 18.1$ ksi)	$P_L + P_b < 1.5 S_m$ ($1.5 S_m = 27.15$ ksi)	Q	$P_L + P_b + Q < 3 S_m$ ($3 S_m = 54.3$ ksi)
1	Deadweight (1g down) ⁽²⁾	0.4	4.05	---	---
2	30 psig Internal Pressure	3.33	3.33	---	---
3	Seismic (.65g Axial + .65g Trans. + 1.3g Vertical Down) ⁽³⁾	0.63	6.08	---	---
4	Thermal (-20 °F)	---	---	20.60	---
5	Thermal (115 °F)	---	---	18.48	---
6	Thermal (Blocked Vent)	---	---	15.50	---
7	Accident 70 psig Internal Pressure	7.77	7.77	---	---
8	Accident Flood (Enveloped by ext. pressure of 30 psig)	3.33	3.33	---	---
3 + 4	30 psig Internal Pressure + Seismic + Thermal (-20 °F)	$3.33 + 0.63$ = 3.96	$3.33 + 6.08$ = 9.41	20.60	$3.33 + 6.08 +$ $20.60 = 30.01$
3 + 5	30 psig Internal Pressure + Seismic + Thermal (115 °F)	$3.33 + 0.63$ = 3.96	$3.33 + 6.08$ = 9.41	18.48	$3.33 + 6.08 +$ $18.48 = 27.89$
1 + 6 + 7	Deadweight + 70 psig Int. Pressure + Thermal (Blocked Vent) ⁽⁴⁾	$0.4 + 7.77$ = 8.17	$4.05 + 7.77$ = 11.82	15.50	$4.05 + 7.77 +$ $15.50 = 27.32$ ⁽⁵⁾
1 + 8	Deadweight + Flood (30 psig ext. pressure)	$0.4 + 3.33$ = 3.73	$4.05 + 3.33$ = 7.38	---	---

Notes:

1. Accident loads are conservatively treated as Normal loads since the allowable stress intensities for accident loads are higher than those for normal loads as indicated in Table 3.9.1-8.
2. The maximum stress intensities are obtained from Table 3.9.1-5.
3. Seismic load includes 1g down Deadweight. The maximum stress intensities are obtained from Table 3.9.1-5.
4. Seismic event is assumed not to occur with accident event of blocked vent.
5. For blocked vent accident condition, $3 S_m = 49.2$ ksi (600 °F)

Table 3.9.1-21
Summary of Calculated Stresses for Normal and Accident Conditions of Storage Loads
(At End Closure Welds)⁽¹⁾

Load Case	Combination of Loads	Stress Intensity Limits			
		$P_m < 0.7S_m$ [$0.7S_m = 12.67 \text{ ksi}$]	$P_L + P_b < 0.7 (1.5S_m)$ [$0.7 (1.5S_m) = 19.0 \text{ ksi}$]	Q	$P_L + P_b + Q < 0.7(3S_m)$ [$0.7 (3S_m) = 38.0 \text{ ksi}$]
1	Deadweight (1g down) ⁽²⁾	0.4	4.05	---	---
2	30 psig Internal Pressure	3.33	3.33	---	---
3	Seismic (.65g Axial + .65g Trans. + 1.3g Vertical Down) ⁽³⁾	0.63	6.08	---	---
4	Thermal (-20 °F)	---	---	20.60	---
5	Thermal (115 °F)	---	---	18.48	---
6	Thermal (Blocked Vent)	---	---	15.5	---
7	Accident 70 psig Internal Pressure	7.77	7.77	---	---
8	Accident Flood (Enveloped by ext. pressure of 30 psig)	3.33	3.33	---	---
3 + 4	30 psig Internal Pressure + Seismic + Thermal (-20 °F)	$3.33 + 0.63 = 3.96$	$3.33 + 6.08 = 9.41$	20.60	$3.33 + 6.08 + 20.60 = 30.01$
3 + 5	30 psig Internal Pressure + Seismic + Thermal (115 °F)	$3.33 + 0.63 = 3.96$	$3.33 + 6.08 = 9.41$	18.48	$3.33 + 6.08 + 18.48 = 27.89$
1 + 6 + 7	Deadweight + 70 psig Internal Pressure + Thermal (Blocked Vent) ⁽⁴⁾	$0.4 + 7.77 = 8.17$	$4.05 + 7.77 = 11.82$	15.50	$4.05 + 7.77 + 15.50 = 27.32^{(5)}$
1 + 8	Deadweight + Flood (30 ext. pressure)	$0.4 + 3.33 = 3.73$	$4.05 + 3.33 = 7.38$	---	---

Notes:

1. Accident loads are conservatively treated as normal condition loads since the allowable stress intensities for accident loads are higher than those for normal loads as indicated in Table 3.9.1-8.
2. The maximum stress intensities are obtained from Table 3.9.1-5.
3. Seismic load includes 1g down Deadweight. The maximum stress intensities are obtained from Table 3.9.1-5.
4. Seismic event is assumed not to occur with accident event of blocked vent
5. For blocked vent accident condition, $0.7 (3 S_m) = 34.44 \text{ ksi}$ (600 °F)

Table 3.9.1-22
ASME Code Allowable Stresses for the Alternate Canister Bottom Assembly Design
(Subsection NF)

Loading Condition	Stress Category	Stress Limit	Material	Allowable Stress (ksi.)
Normal Conditions ⁽¹⁾	Membrane Stress Intensity , P_m	S_m	SA-240 Type 304	17.5
			SA-182 Type F304	17.5
			SA-36	19.3
	Membrane + Bending Stress Intensity , $P_m + P_b$	$1.5 S_m$	SA-240 Type 304	26.25
			SA-182 Type F304	26.25
			SA-36	28.95
	Primary + Secondary Stress Intensity, $P_m + P_b + Q$	$2 S_y$	SA-182 Type F304	38.8
			SA-182 Type F304	38.8
			SA-36	58.6
Off-Normal Condition ⁽²⁾	Membrane Stress Intensity, P_m	$1.5 S_m$	SA-240 Type 304	26.25
			SA-182 Type F304	26.25
			SA-36	28.95
	Membrane + Bending Stress Intensity, $P_m + P_b$	$2.25 S_m$	SA-240 Type 304	39.38
			SA-182 Type F304	39.38
			SA-36	43.43
Accident Conditions ⁽³⁾	Membrane Stress Intensity , P_m	The largest of $1.2 S_y$, $1.5 S_m$, and $0.7 S_u$	SA-240 Type 304	44.38
			SA-182 Type F304	41.44
			SA-36	40.6
	Membrane + Bending Stress Intensity , $P_m + P_b$	The largest of $1.8 S_y$, $2.25 S_m$, and $1.0 S_u$	SA-240 Type 304	63.4
			SA-182 Type F304	59.2
			SA-36	58

Notes:

1. Service Level A limits per Paragraph NF-3221.2 of Reference 5.
2. Service Level C limits per Paragraph NF-3221.2 of Reference 5.
3. Service Level D limits per Paragraph F-1332 of Reference 3.

Table 3.9.1-23
ASME Code Allowable Stresses for the Weld between the Canister Shell
and the Bottom Outer Cover as per Subsection NF

Loading Condition	Stress Category	Stress Limit	Material	Allowable Stress (ksi.)
Normal Conditions ⁽¹⁾	Membrane Stress Intensity , P_m	S_m	SA-240 Type 304	17.5
	Membrane + Bending Stress Intensity , $P_m + P_b$	$1.5 S_m$	SA-240 Type 304	26.25
	Tensile stress normal to the effective weld throat	$0.3 S_u$	SA-240 Type 304	19.02
Off-Normal Condition ⁽²⁾	Membrane Stress Intensity, P_m	$1.5 S_m$	SA-240 Type 304	26.25
	Membrane + Bending Stress Intensity, $P_m + P_b$	$2.25 S_m$	SA-240 Type 304	39.375
	Tensile stress normal to the effective weld throat	$1.5 \times 0.3 S_u$	SA-240 Type 304	28.53
Accident Conditions ⁽³⁾	Membrane Stress Intensity , P_m	The largest of $1.2 S_y$, $1.5 S_m$, and $0.7 S_u$	SA-240 Type 304	44.38
	Membrane + Bending Stress Intensity , $P_m + P_b$	The largest of $1.8 S_y$, $2.25 S_m$, and $1.0 S_u$	SA-240 Type 304	63.4
	Tensile stress normal to the effective weld throat	$2 \times 0.3 S_u$ ⁽⁴⁾	SA-240 Type 304	38.04

Notes:

1. Service Level A limits per Paragraph NF-3226.2 of Reference 5.
2. Service Level C limits per Paragraph NF-3226.2 of Reference 5.
3. Service Level D limits per Paragraph F-1332 of Reference 3.
4. Service Level D limits per Paragraph F-1334 of Reference 3.

Table 3.9.1-24
Summary of Calculated Stresses in the Alternate Canister Design
for Normal Condition Loads (Subsection NB components)

Load Case	Combination of Loads	Canister Orientation	Stress Intensity Limits (NB-3222) ⁽¹⁾		
			$P_m < S_m$ ($S_m = 17,500$ psi)	$P_L + P_b < 1.5 S_m$ ($1.5 S_m = 26,250$ psi)	$P_L + P_b + Q < 3 S_m$ ($3 S_m = 52,500$ psi)
1	1 _g down + 15 psig Ext. Press. + Vac. Dry Thermal	Vertical	1,657	1,657	14,668
2	Handling 2 _g + 30 psig Int. Press. + Thermal (115 °F)	Horizontal	880 + 3,831 = 4,711 ⁽²⁾	9,740 + 3,831 = 13,571 ⁽²⁾	9,740 + 35,266 = 45,006 ⁽²⁾
3	Handling 2 _g + 15 psig Ext. Press. + Thermal (-20 °F)	Horizontal	880 + 1,772 = 2,652 ⁽²⁾	9,740 + 1,772 = 11,512 ⁽²⁾	9,740 + 27,619 = 37,359 ⁽²⁾
19	30 psig Int. Press. + 80 kip push + Thermal (115 °F)	Horizontal	7,238	7,238	33,189
20	30 psig Int. Press. + 60 kip pull + Thermal (115 °F)	Horizontal	4,115	4,115	35,029

Notes:

- Design stress intensity, S_m is taken at 500 °F of material SA-240 Gr.304 and SA-182 F304; see Table 3.9.1-7 for allowable stresses.
- Maximum stress intensity in the canister due to pressure and thermal loads from this evaluation are conservatively added to the maximum stress intensity due to the 2_g transfer load from Table 3.9.1-3.

Table 3.9.1-25
Summary of Calculated Stresses in the Alternate Canister Design
for Normal Condition Loads (Subsection NF components)

Load Case	Combination Of Loads	Canister Orientation	Stress Intensity Limits (NF-3221.2) ⁽¹⁾		
			$P_m < S_m$ ($S_m = 17,500$ psi)	$P_m + P_b < 1.5 S_m$ ($1.5S_m = 26,250$ psi)	$P_m + P_b + Q < 2 S_y$ ($2 S_y = 38,800$ psi)
1	1g down + 15 psig Ext. Press. + Vac. Dry Thermal	Vertical	331	331	6,369
2	Handling 2g's + 30 psig Int. Press. + Thermal (115 °F)	Horizontal	$880 + 4,067$ $= 4,947^{(2)}$	$9,740 + 4,067$ $= 13,807^{(2)}$	$9,740 + 4,729$ $= 14,469^{(2)}$
3	Handling 2g's + 15 psig Ext. Press. + Thermal (-20 °F)	Horizontal	$880 + 540$ $= 1,420^{(2)}$	$9,740 + 540$ $= 10,280^{(2)}$	$9,740 + 12,448$ $= 22,188^{(2)}$
19	30 psig Int. Press. + 80 kip push + Thermal (115 °F)	Horizontal	2,499	2,499	6,394
20	30 psig Int. Press. + 60 kip pull + Thermal (115 °F)	Horizontal	$10,410^{(3)}$	$24,790^{(3)}$	30,340

Notes:

- Design stress intensity (S_m) and yield stress (S_y) are taken at 500 °F for all materials, see Table 3.9.1-22 for allowable stresses.
- Maximum stress intensity in the canister due to pressure and thermal loads from this evaluation are conservatively added to the maximum stress intensity due to the 2g transfer load from Table 3.9.1-3.
- Linearized stress intensities through the thickness of the component plates.

Table 3.9.1-26
Summary of Calculated Stresses in the Alternate Canister Design
for Normal Condition Loads (Subsection NF welds)

Load Case	Combination of Loads	Canister Orientation	Stress Intensity Limits ⁽¹⁾ (NF-3226.2)
			$S_x < 0.3 S_u$ ($0.3 S_u = 19,020$ psi)
1	1g down + 15 psig Ext. Press. + Vac. Dry Thermal	Vertical	0
2	Handling 2g + 30 psig Int. Press. + Thermal (115 °F)	Horizontal	9,740 + 1,502 = 11,242 ⁽²⁾
3	Handling 2g's + 15 psig Ext. Press. + Thermal (-20 °F)	Horizontal	9,740 + 23 = 9,763 ⁽²⁾
19	30 psig Int. Press. + 80 kip push + Thermal (115 °F)	Horizontal	152
20	30 psig Int. Press. + 60 kip pull + Thermal (115 °F)	Horizontal	12,498

Notes:

1. Tensile strength, S_u , is taken at 500 °F for material SA-240 Gr.304, see Table 3.9.1-23 for allowable stresses.
2. Maximum stress intensity in the canister due to pressure and thermal loads from this evaluation are conservatively added to the maximum stress intensity due to the 2g transfer load from Table 3.9.1-3.

Table 3.9.1-27
Summary of Calculated Stresses in the Alternate Canister Design
at the End Closure Welds for Normal Condition Loads

Load Case	Combination of Loads	Canister Orientation	Stress Intensity Limits ⁽¹⁾ (NB-3222)		
			$P_m < 0.8S_m$ ($0.8S_m = 14,000$ psi)	$P_L + P_b < 0.8(1.5 S_m)$ ($1.2S_m = 21,000$ psi)	$P_L + P_b + Q < 0.8(3 S_m)$ ($2.4 S_m = 42,000$ psi)
1	1g down + 15 psig Ext. Press. + Vac. Dry Thermal	Vertical	1,341	1,341	2,112
2	Handling 2g + 30 psig Int. Press. + Thermal (115 °F)	Horizontal	$880 + 3,134 = 4,014^{(2)}$	$9,740 + 3,134 = 12,874^{(2)}$	$9,740 + 3,646 = 13,386^{(2)}$
3	Handling 2g + 15 psig Ext. Press. + Thermal (-20 °F)	Horizontal	$880 + 1,232 = 2,112^{(2)}$	$9,740 + 1,232 = 10,972^{(2)}$	$9,740 + 2,247 = 11,987^{(2)}$
19	30 psig Int. Press.+80 kip push + Thermal (115 °F)	Horizontal	3,123	3,123	3,602
20	30 psig Int. Press. + 80 kip pull + Thermal (115 °F)	Horizontal	3,110	3,110	3,660

Notes:

- Design stress intensity, S_m is taken at 500 °F for material SA-240 Gr.304; see Table 3.9.1-7 for allowable stresses.
- Maximum stress intensity in the canister due to pressure and thermal loads from this evaluation are conservatively added to the maximum stress intensity due to the 2g transfer load from Table 3.9.1-3.

Table 3.9.1-28
Summary of Calculated Stresses in the Alternate Canister Design
for Off-Normal Condition Loads (Subsection NB components)

Load Case	Combination of Loads	Canister Orientation	Stress Intensity Limits ⁽¹⁾ (NB-3222)		
			$P_m < S_m$ (S_m) = 17,500 psi)	$P_L + P_b < 1.5 S_m$ ($1.5 S_m$) = 26,250 psi)	$P_L + P_b + Q < 3 S_m$ ($3 S_m$) = 52,500 psi)
21	30 psig Int. Press. + 80 kip push + Thermal (115 °F)	Horizontal	7,238	7,238	33,819
22	30 psig Int. Press. + 80 kip pull + Thermal (115 °F)	Horizontal	4,223	4,223	34,905

Notes:

- Design stress intensity, S_m is taken at 500 °F for material SA-240 Gr.304, see Table 3.9.1-7 for allowable stresses.

Table 3.9.1-29
Summary of Calculated Stresses in the Alternate Canister Design
for Off-Normal Condition Loads (Subsection NF components)

Load Case	Combination of Loads	Canister Orientation	Stress Intensity Limits ⁽¹⁾ (NF-3221.2)	
			$P_m < 1.5 S_m$ ($1.5S_m = 26,250$ psi)	$P_m + P_b < 2.25 S_m$ ($2.25S_m = 39,380$ psi)
21	30 psig Int. Press. + 80 kip push + Thermal (115 °F)	Horizontal	2,499	2,499
22	30 psig Int. Press. + 80 kip pull + Thermal (115 °F)	Horizontal	13,860 ⁽²⁾	33,010 ⁽²⁾

Notes:

- Design stress intensity, S_m is taken at 500 °F for material SA-240 Gr.304, see Table 3.9.1-22 for allowable stresses.
- Linearized stress intensities through the thickness of the component plates.

Table 3.9.1-30
Summary of Calculated Stresses in the Alternate Canister Design
for Off- Normal Condition Loads (Subsection NF weld)

Load Case	Combination of Loads	Canister Orientation	Stress Intensity Limits ⁽¹⁾ (NF-3226.2)
			$S_x < 1.5 \times 0.3 S_u$ ($0.45 S_u = 28,530$ psi)
21	30 psig Int. Press. + 80 kip push + Thermal (115 °F)	Horizontal	152
22	30 psig Int. Press. + 80 kip pull + Thermal (115 °F)	Horizontal	16,407

Note:

1. Tensile strength, S_u , is taken at 500 °F for material SA-240 Gr.304; see Table 3.9-23 for allowable stresses.

Table 3.9.1-31
Summary of Calculated Stresses in the Alternate Canister Design
at the End Closure Welds for Off-Normal Condition Loads

Load Case	Combination of Loads	Canister Orientation	Stress Intensity Limits ⁽¹⁾ (NB-3222)		
			$P_m < 0.8S_m$ ($0.8S_m$ = 14,000 psi)	$P_L + P_b < 0.8(1.5 S_m)$ ($1.2S_m = 21,000$ psi)	$P_L + P_b + Q < 0.8(3 S_m)$ ($2.4 S_m = 42,000$ psi)
21	30 psig Int. Press. + 80 kip push + Thermal (115 °F)	Horizontal	3,123	3,123	3,602
22	30 psig Int. Press. + 80 kip pull + Thermal (115 °F)	Horizontal	3,110	3,110	3,660

Notes:

- Design stress intensity, S_m is taken at 500 °F for material SA-240 Gr.304, see Table 3.9.1-7 for allowable stresses.

Table 3.9.1-32
Summary of Calculated Stresses in the Alternate Canister Design
for Accident Condition Loads (Subsection NB components)

Load Case	Combination of Loads	Canister Orientation	Stress Intensity Limits ⁽¹⁾	
			$P_m < 0.7 S_u$ ($0.7 S_u = 41,440$ psi)	$P_L + P_b < S_u$ ($S_u = 59,200$ psi)
4	120 psig internal pressure under fire accident	Horizontal	15,389 ⁽²⁾	15,389 ⁽²⁾
5	25 psig external pressure under flood accident	Horizontal	2,953	2,953
14	Top End Drop 75_g + 30 psig Int. Press.	Vertical	15,645	15,645
15	Bottom End Drop 75_g + 30 psig Int. Press.	Vertical	16,584	16,584
16	Top End Drop 75_g + 15 psig Ext. Press.	Vertical	18,685	18,685
17	Bottom End Drop 75_g + 15 psig Ext. Press.	Vertical	20,081	20,081
23	30 psig Int. Press. + 110 kip push + Thermal (115 °F)	Horizontal	9,854	9,854
24	30 psig Int. Press. + 110 kip pull + Thermal (115 °F)	Horizontal	4,393	4,393

Notes:

1. Lesser values of allowable stresses for material SA-182 Type F304 is also used for material SA-240 Type 304. See Table 3.9.1-7 for allowable stress intensities.
2. For metal temperature of 800 °F under accident fire, allowable stress intensities, $P_m < 2.4 S_m$ ($2.4 \times 15,200$ psi = 36,480 psi), $P_L + P_b < 3.6 \times S_m$ ($3.6 \times 15,200$ psi = 54,720 psi), where $S_m = 15,200$ psi for both SA240-304 and SA182-F304 at 800 °F.

Table 3.9.1-33
Summary of Calculated Stresses in the Alternate Canister Design
for Accident Condition Loads (Subsection NF components)

Load Case	Combination of Loads	Canister Orientation	Stress Intensity Limits ⁽¹⁾	
			$P_m < 0.7 S_u$ ($0.7 S_u = 40,600$ psi)	$P_m + P_b < S_u$ ($S_u = 58,000$ psi)
4	120 psig internal pressure under fire accident	Horizontal	16,570 ⁽²⁾	16,570 ⁽²⁾
5	25 psig external pressure under flood accident	Horizontal	900	900
14	Top End Drop 75 _g + 30 psig Int. Press.	Vertical	6,337	6,337
15	Bottom End Drop 75 _g + 30 psig Int. Press.	Vertical	9,024	9,024
16	Top End Drop 75 _g + 15 psig Ext. Press.	Vertical	6,992	6,992
17	Bottom End Drop 75 _g + 15 psig Ext. Press.	Vertical	9,121	9,121
23	30 psig Int. Press. + 110 kip push + Thermal (115 °F)	Horizontal	3,565	3,565
24	30 psig Int. Press. + 110 kip pull + Thermal (115 °F)	Horizontal	19,090 ⁽³⁾	45,480 ⁽³⁾

Notes:

- Least values of allowable stresses for materials SA-240 Type 304, SA-182 Type F304, and SA-36 are used for stress evaluations. See Table 3.9.1-22 for allowable stress intensities.
- For metal temperature of 800 °F under accident fire, allowable stress intensities, $P_m < 0.7 S_u$ ($0.7 \times 53,300$ psi = 37,310 psi) and $P_m + P_b < S_u$ ($1 \times 53,300$ psi = 53,300 psi), where $S_u = 53,300$ psi of SA-36 at 800 °F (the least tensile strength value at 800 °F of SA-240 Type 304, SA-182 Type F304, and SA-36)
- Linearized stress intensities through the thickness of the component plates.

Table 3.9.1-34
Summary of Calculated Tensile Stresses Normal to the NF Weld Throat
In the Alternate Canister Design for Accident Condition Loads
(Subsection NF welds)

Load Case	Combination of Loads	Canister Orientation	Tensile Stress Limits ⁽¹⁾
			$S_x < 2 \times 0.3 S_u$ ($0.6 S_u = 38,040 \text{ psi}$)
4	120 psig internal pressure under fire accident	Horizontal	6,249 ⁽²⁾
5	25 psig external pressure under flood accident	Horizontal	39
14	Top End Drop 75_g + 30 psig Int. Press.	Vertical	483
15	Bottom End Drop 75_g + 30 psig Int. Press.	Vertical	596
16	Top End Drop 75_g + 15 psig Ext. Press.	Vertical	598
17	Bottom End Drop 75_g + 15 psig Ext. Press.	Vertical	432
23	30 psig Int. Press. + 110 kip push + Thermal (115 °F)	Horizontal	135
24	30 psig Int. Press. + 110 kip pull + Thermal (115 °F)	Horizontal	21,928

Notes:

- See Table 3.9.1-23 for allowable tensile stresses.
- For metal temperature of 800 °F under accident fire, allowable stress intensities, $S_x < 2 \times 0.3 S_u$ ($= 0.6 \times 62,800 \text{ psi} = 37,680 \text{ psi}$), where $S_u = 62,800 \text{ psi}$ at 800 °F for SA-240 Type 304.

Table 3.9.1-35
Summary of Calculated Stresses in the Alternate Canister Design
for Accident Condition Loads (Top End Closure Welds)

Load Case	Combination of Loads	Canister Orientation	Stress Intensity Limits ⁽¹⁾	
			$P_m < 0.8 \times 0.7 S_u$ (0.56 S_u =33,152 psi)	$P_L + P_b < 0.8 \times S_u$ (0.8 S_u =47,360 psi)
4	120 psig internal pressure under fire accident	Horizontal	12,502 ⁽²⁾	12,502 ⁽²⁾
5	25 psig external pressure under flood accident	Horizontal	2,054	2,054
14	Top End Drop 75 _g + 30 psig Int. Press.	Vertical	5,578	5,578
15	Bottom End Drop 75 _g + 30 psig Int. Press.	Vertical	8,582	8,582
16	Top End Drop 75 _g + 15 psig Ext. Press.	Vertical	7,808	7,808
17	Bottom End Drop 75 _g + 15 psig Ext. Press.	Vertical	12,153	12,153
23	30 psig Int. Press. + 110 kip push + Thermal (115 °F)	Horizontal	3,132	3,132
24	30 psig Int. Press. + 110 kip pull + Thermal (115 °F)	Horizontal	3,132	3,132

Notes:

1. Lesser values of allowable stresses for material SA-182 Type F304 is also used for material SA-240 Type 304. See Table 3.9.1-7 for allowable stress intensities.
2. For maximum metal temperature at 800 °F under accident fire condition, allowable stress intensities are $P_m < 0.8 \times 2.4 S_m$ ($0.8 \times 2.4 \times 15,200$ psi = 29,184 psi) and $P_L + P_b < 0.8 \times 3.6 \times S_m$ ($0.8 \times 3.6 \times 15,200$ psi = 43,776 psi).

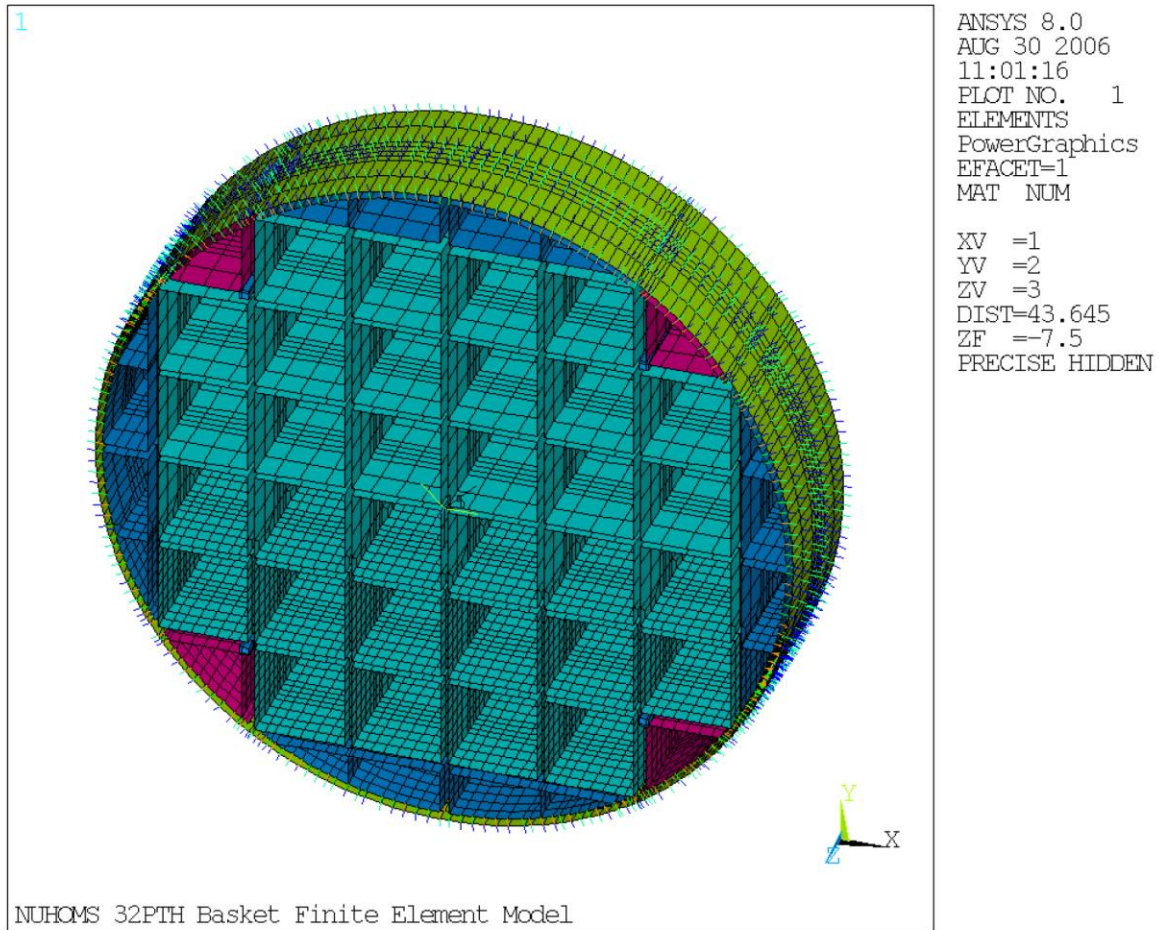


Figure 3.9.1-1
32PTH DSC Basket – 3D Cross Section Finite Element Model

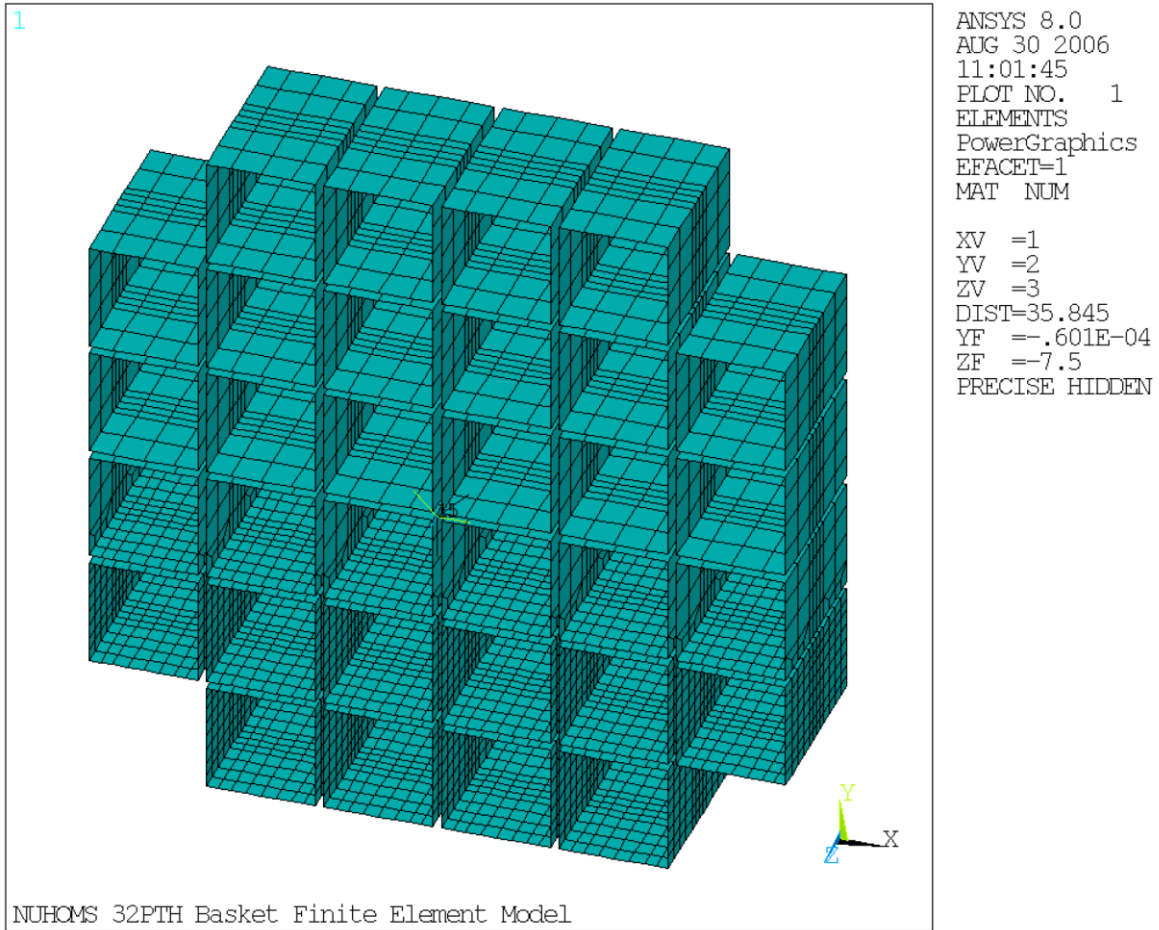


Figure 3.9.1-2
32PTH DSC Basket Cross Section Finite Element Model – Fuel Compartments

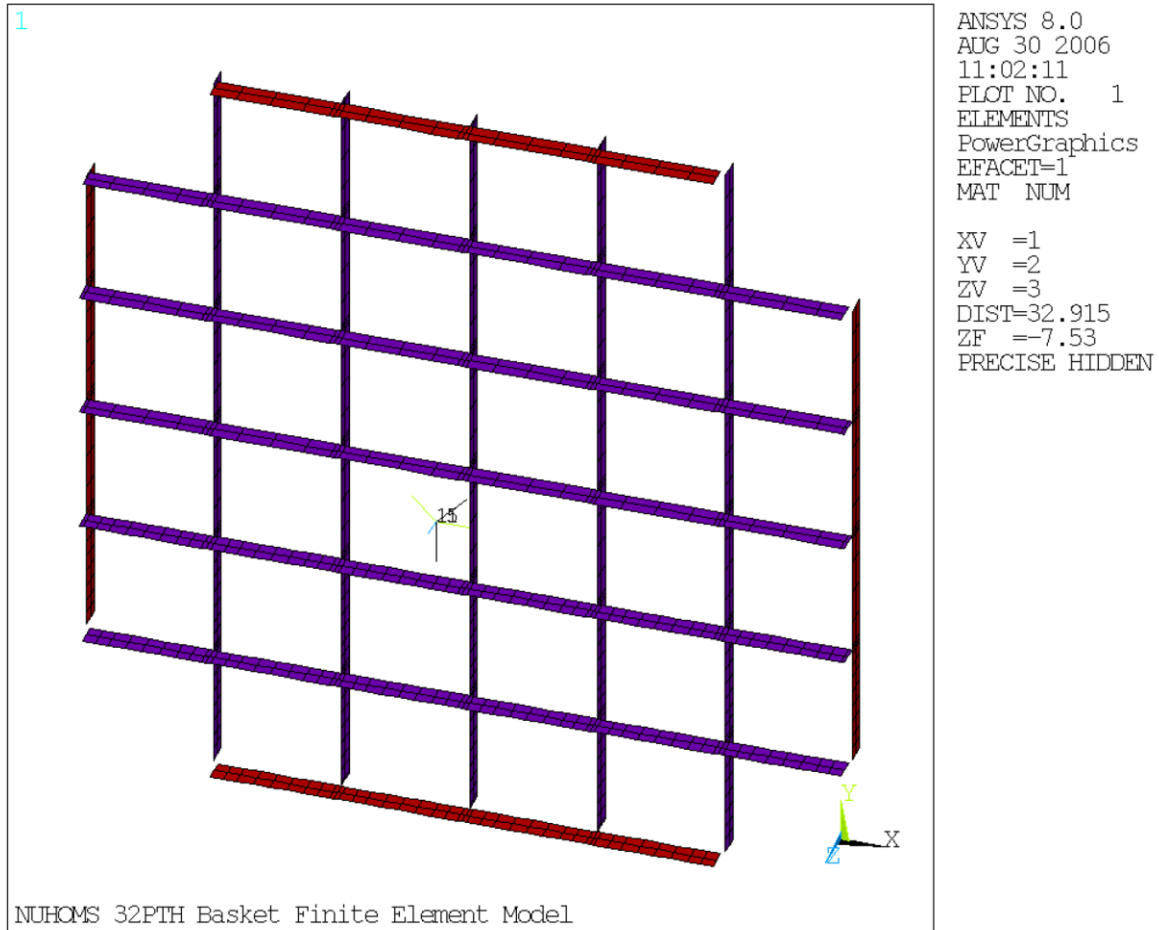


Figure 3.9.1-3
32PTH DSC Basket Cross Section Finite Element Model – Center and Outer Plates

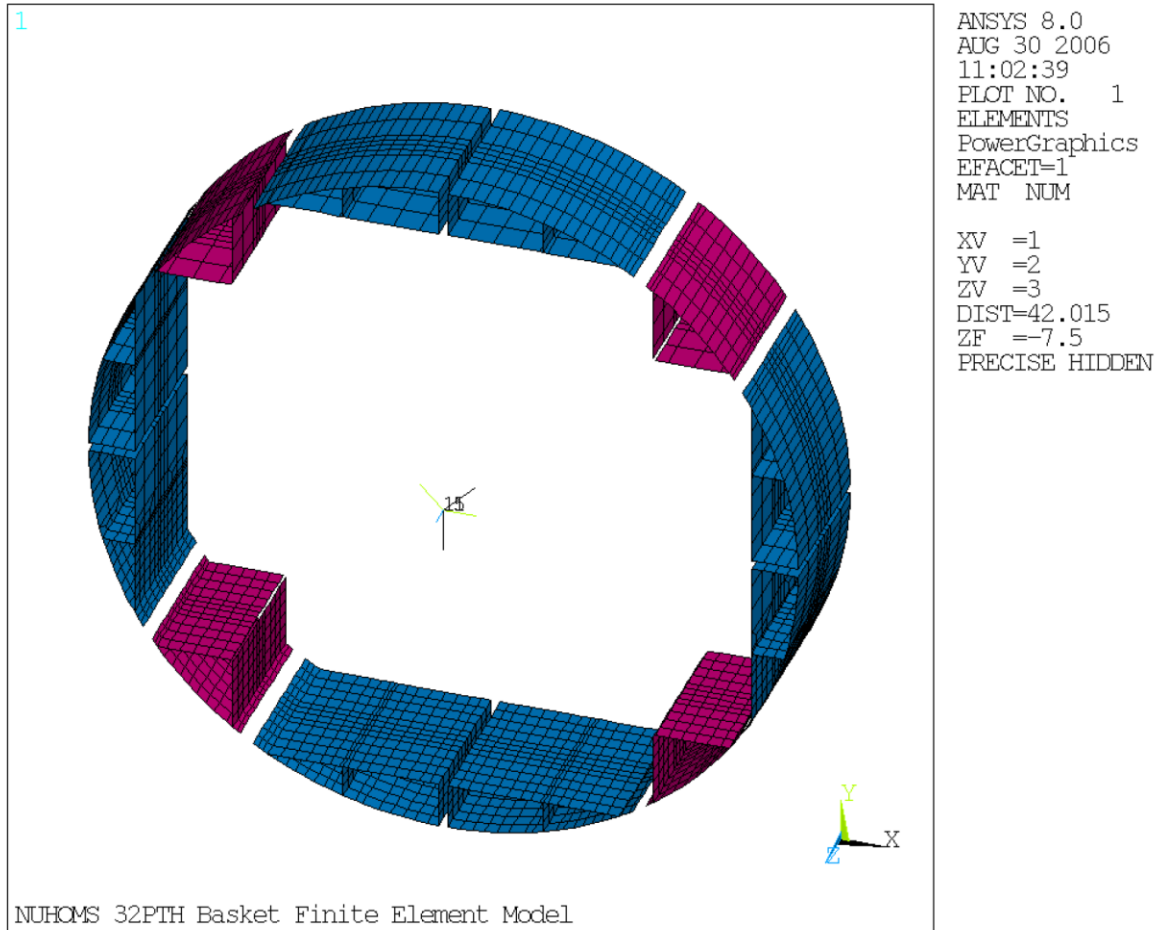


Figure 3.9.1-4
32PTH DSC Basket Cross Section Finite Element Model – Support Rails

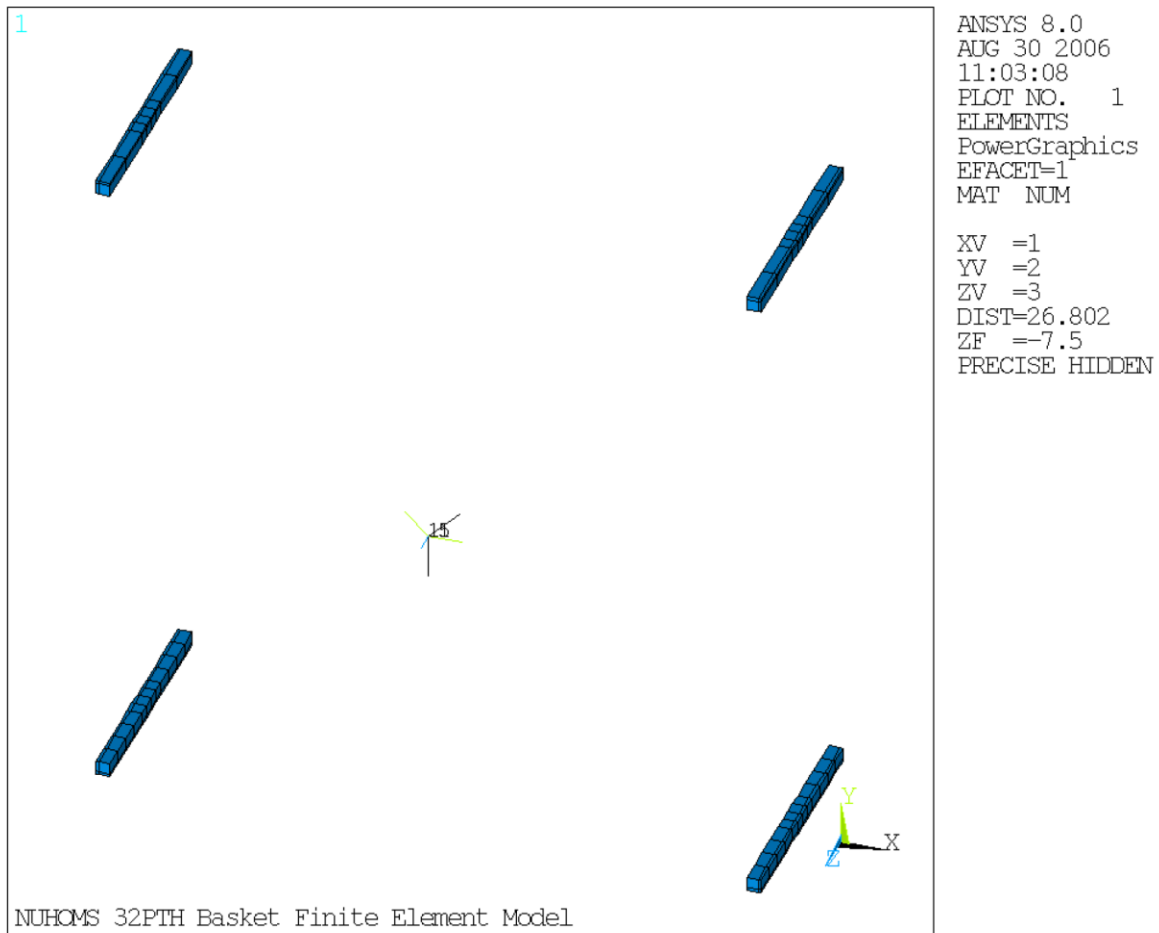


Figure 3.9.1-5
32PTH DSC Basket Cross Section Finite Element Model – 7/8 inch Square Bars

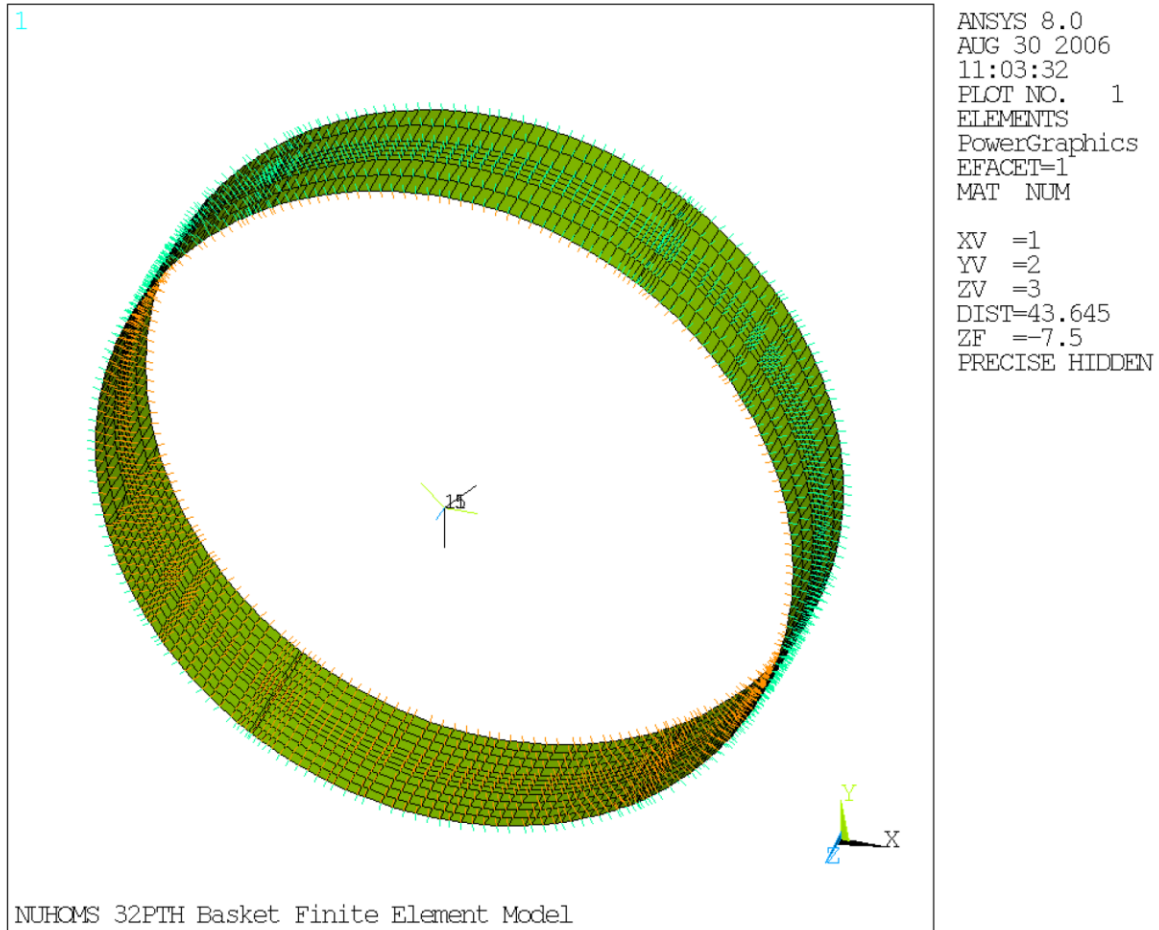


Figure 3.9.1-6
32PTH DSC Basket Cross Section Finite Element Model –
Canister and Gap Elements

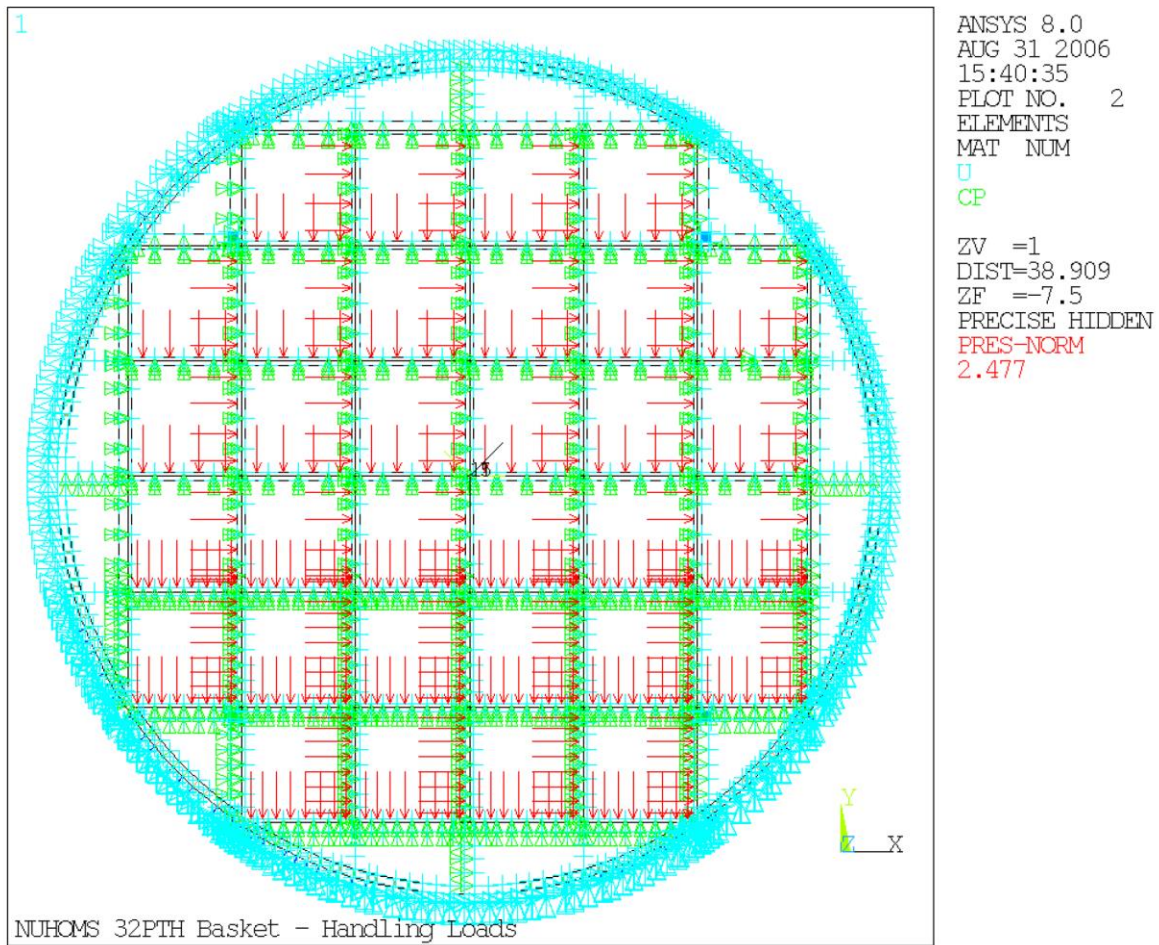


Figure 3.9.1-7
32PTH DSC Basket FEM – Transfer Handling Loads Boundary Conditions

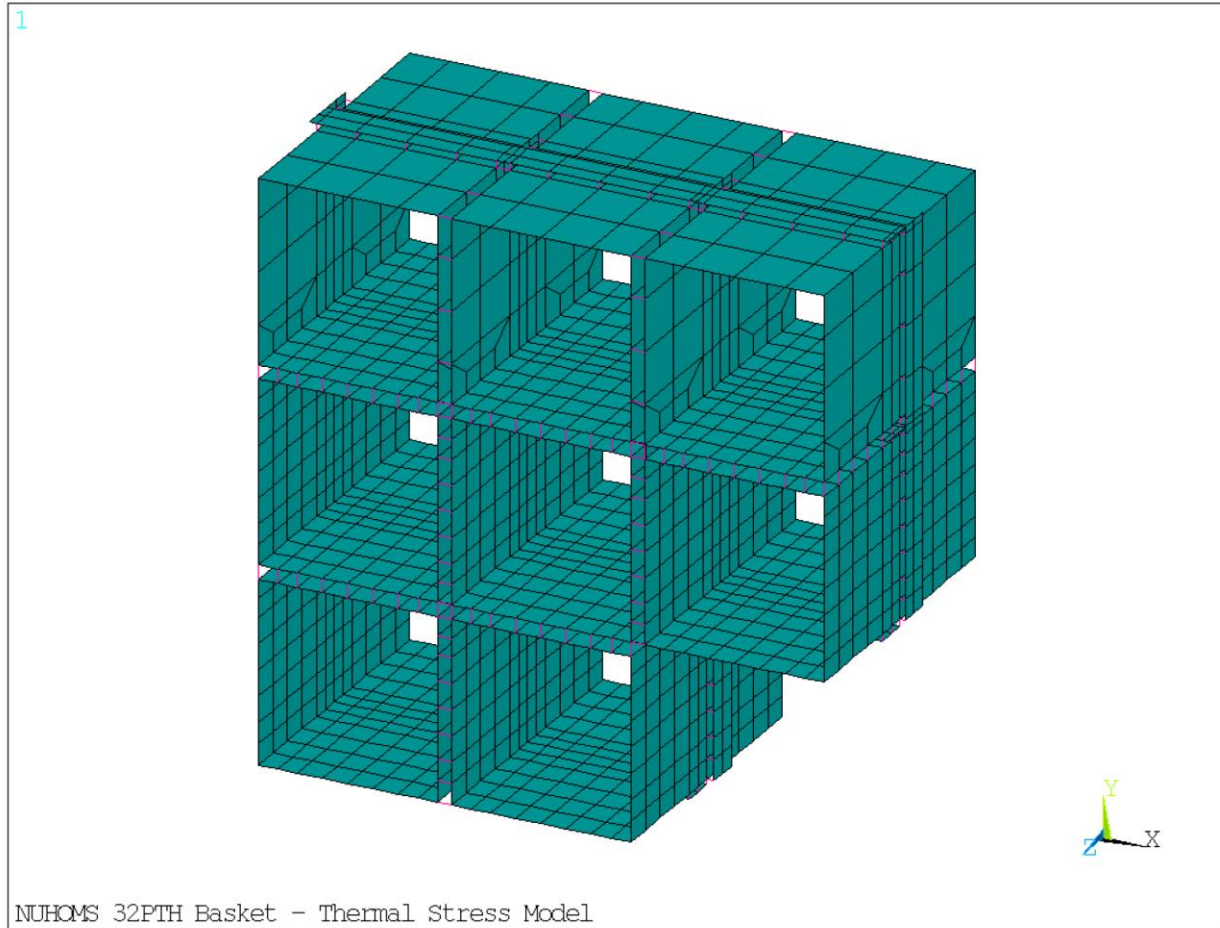


Figure 3.9.1-8
Fuel Compartments Finite Element Model – Thermal Analysis

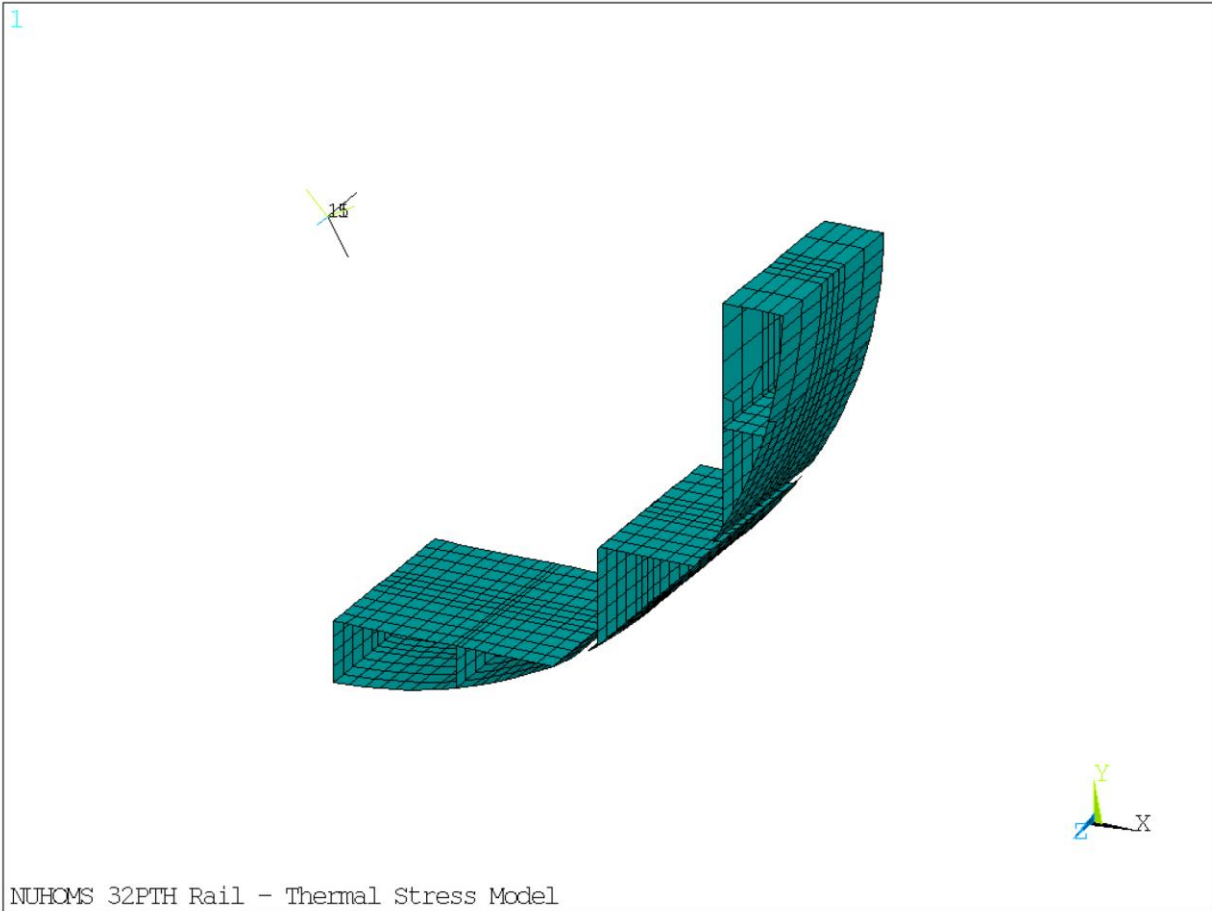


Figure 3.9.1-9
Support Rail Finite Element Model – Thermal Analysis

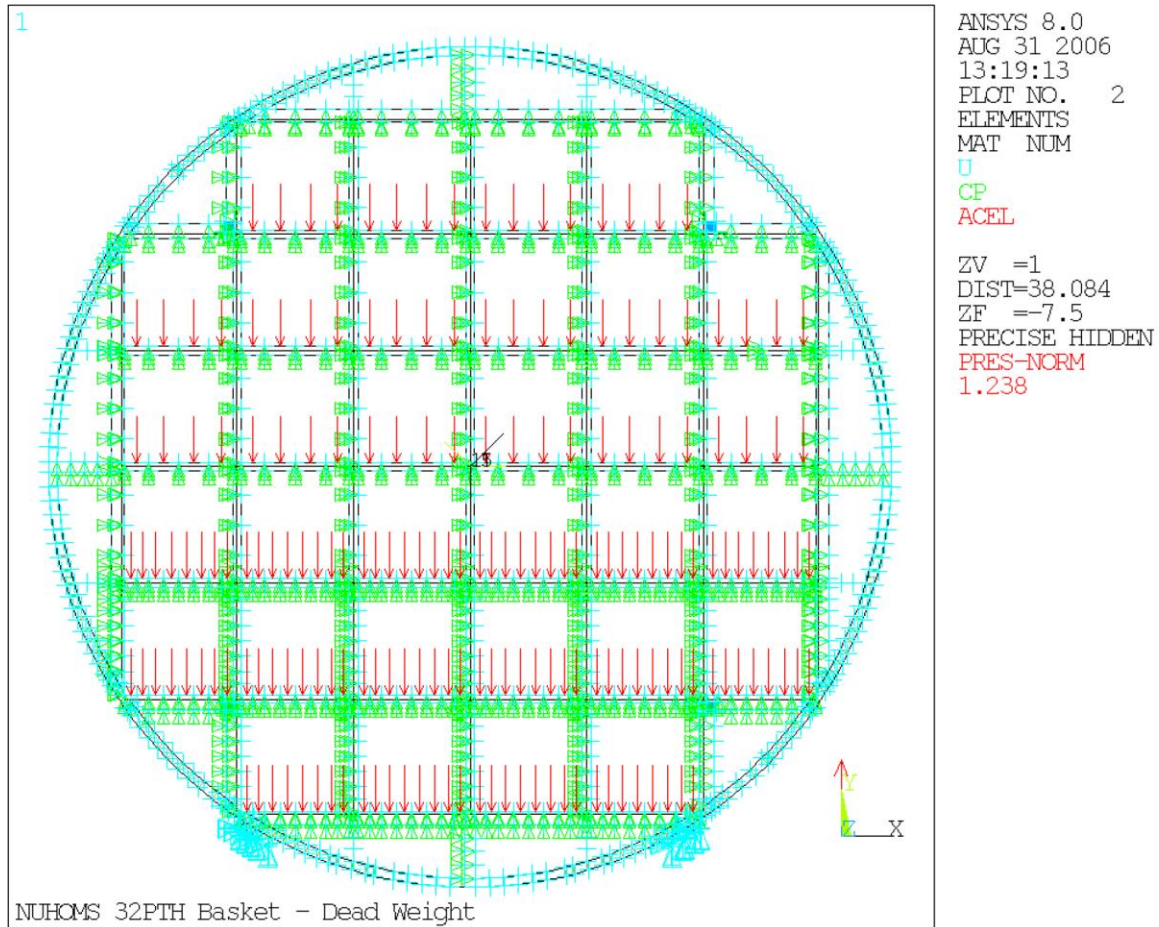


Figure 3.9.1-10
Finite Element Model Boundary Conditions for Dead Weight Storage Load

Figure Deleted in its Entirety

Figure 3.9.1-11
DELETED

Figure Deleted in its Entirety

Figure 3.9.1-12
DELETED

Figure Deleted in its Entirety

Figure 3.9.1-13
DELETED

Figure Deleted in its Entirety

Figure 3.9.1-14
DELETED

Figure Deleted in its Entirety

Figure 3.9.1-15
DELETED

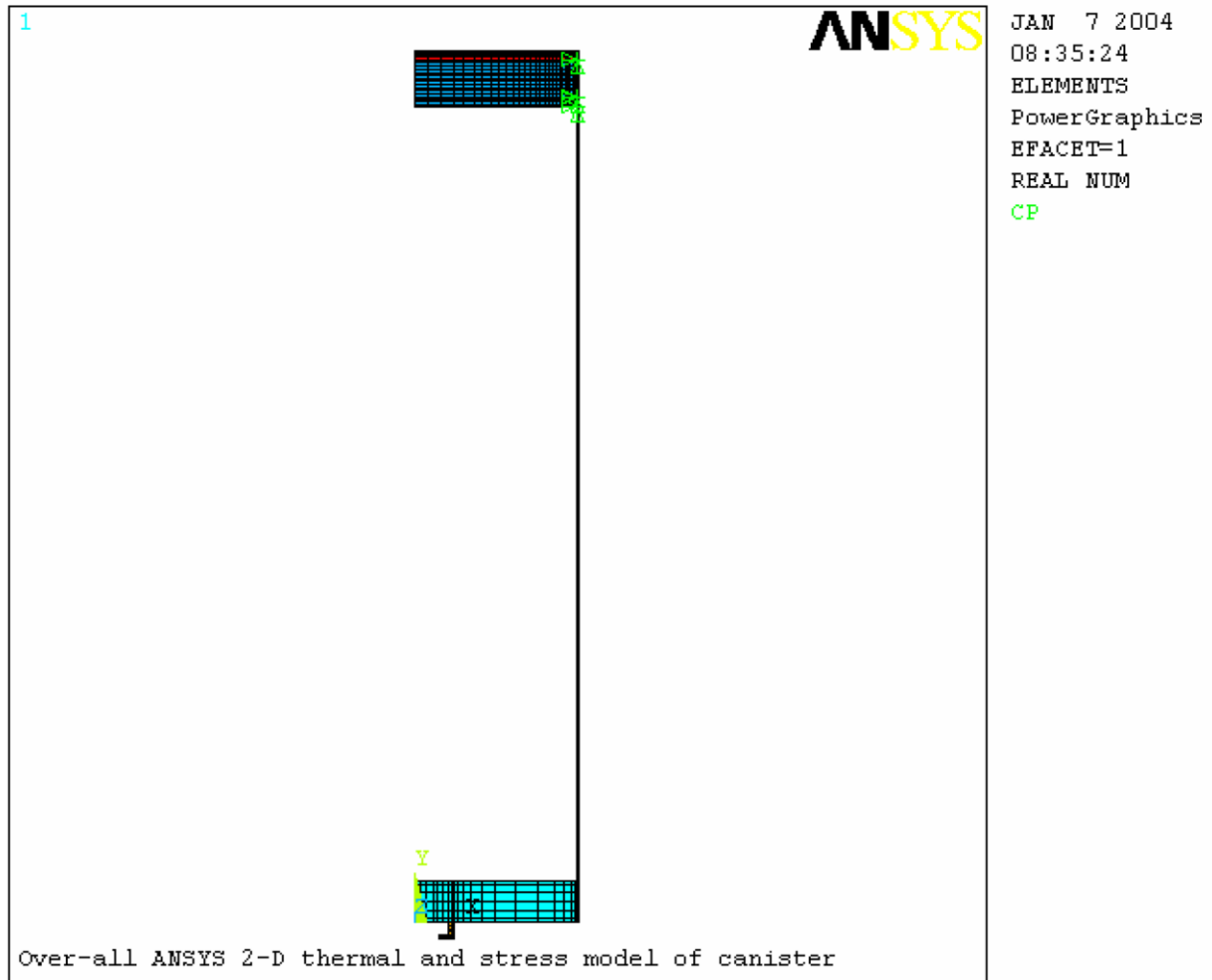


Figure 3.9.1-16
2-D Canister Axisymmetrical Thermal and Stress Finite Element Model

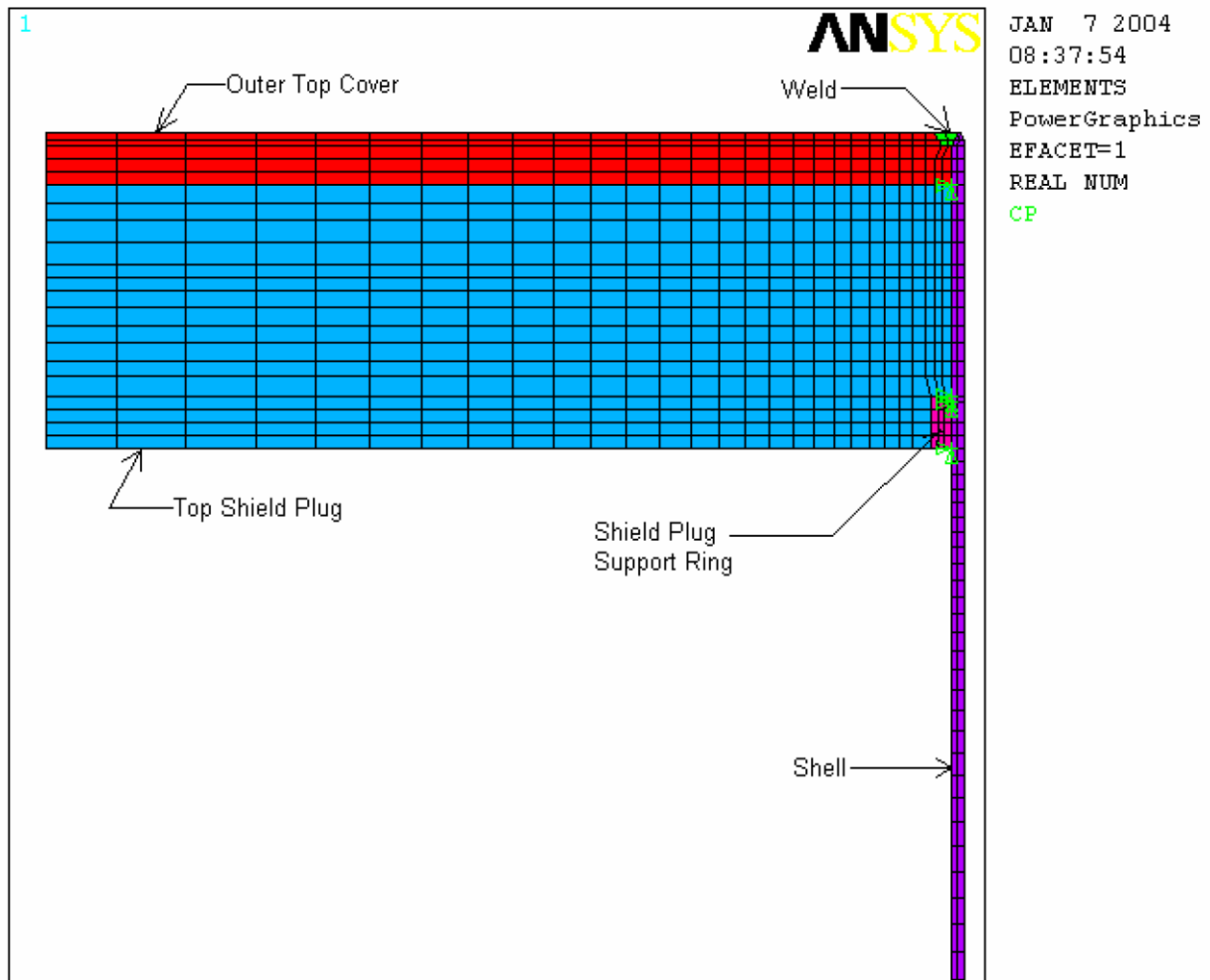


Figure 3.9.1-17
Top End of the 2-D Axisymmetrical Canister Model

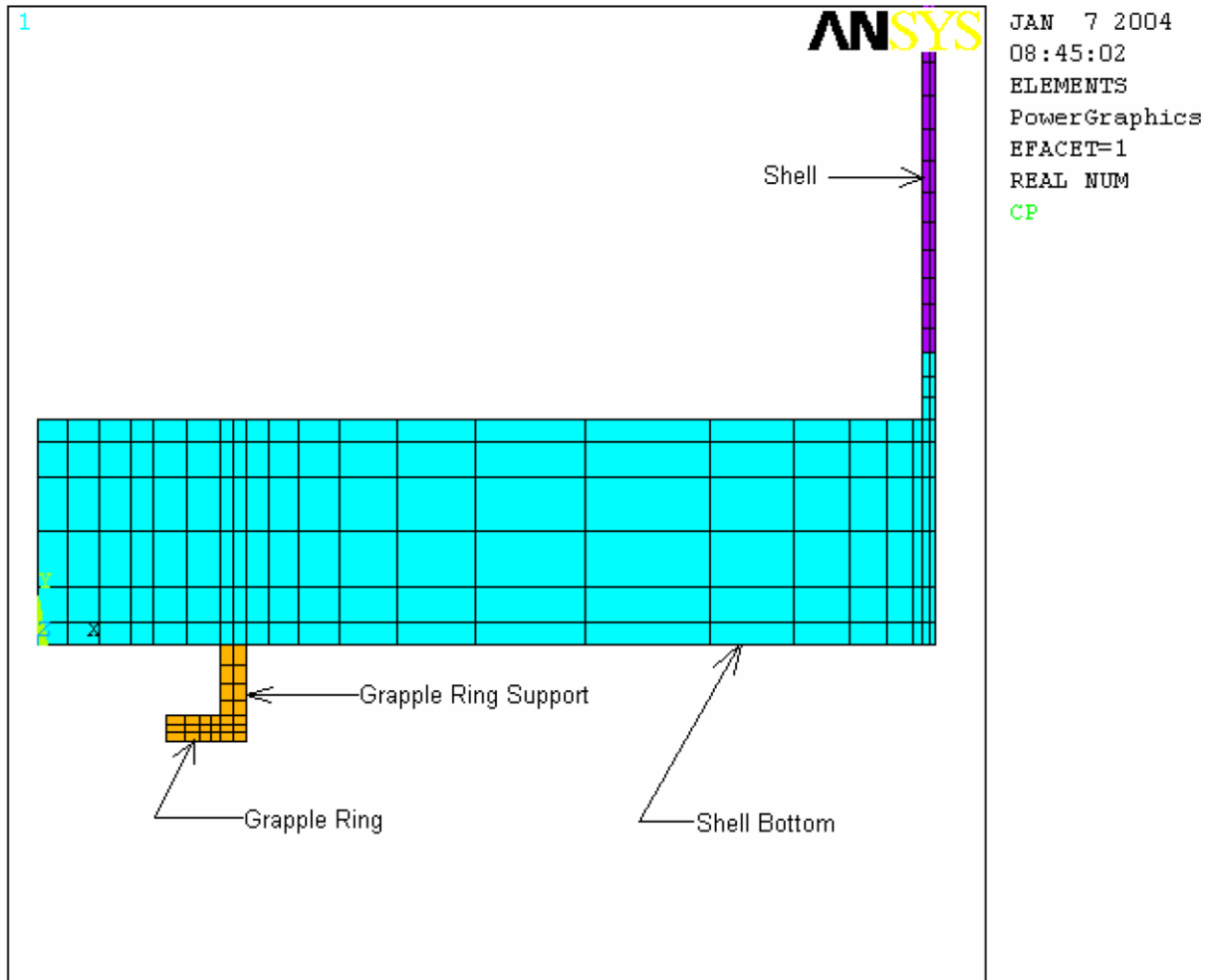


Figure 3.9.1-18
Bottom End of the 2-D Axisymmetrical Canister Model

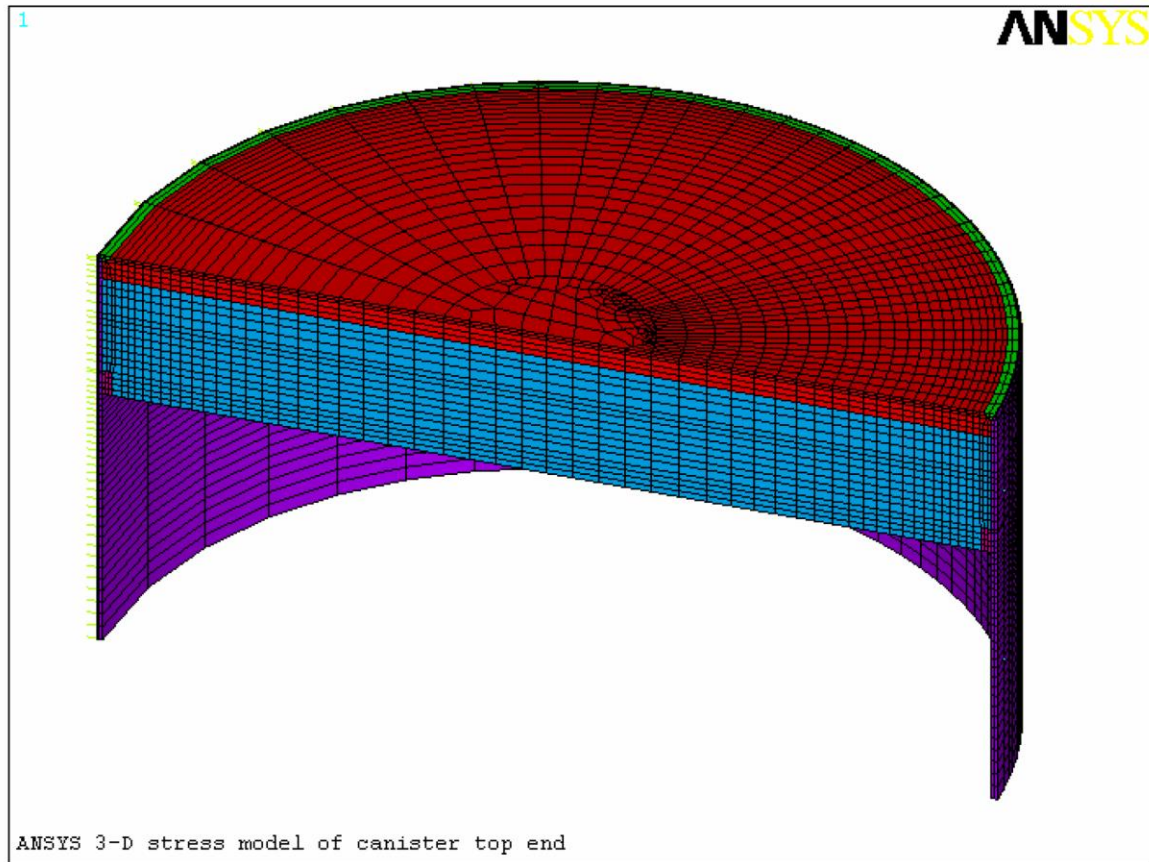


Figure 3.9.1-19
3-D DSC Canister Top End Assembly Finite Element Model

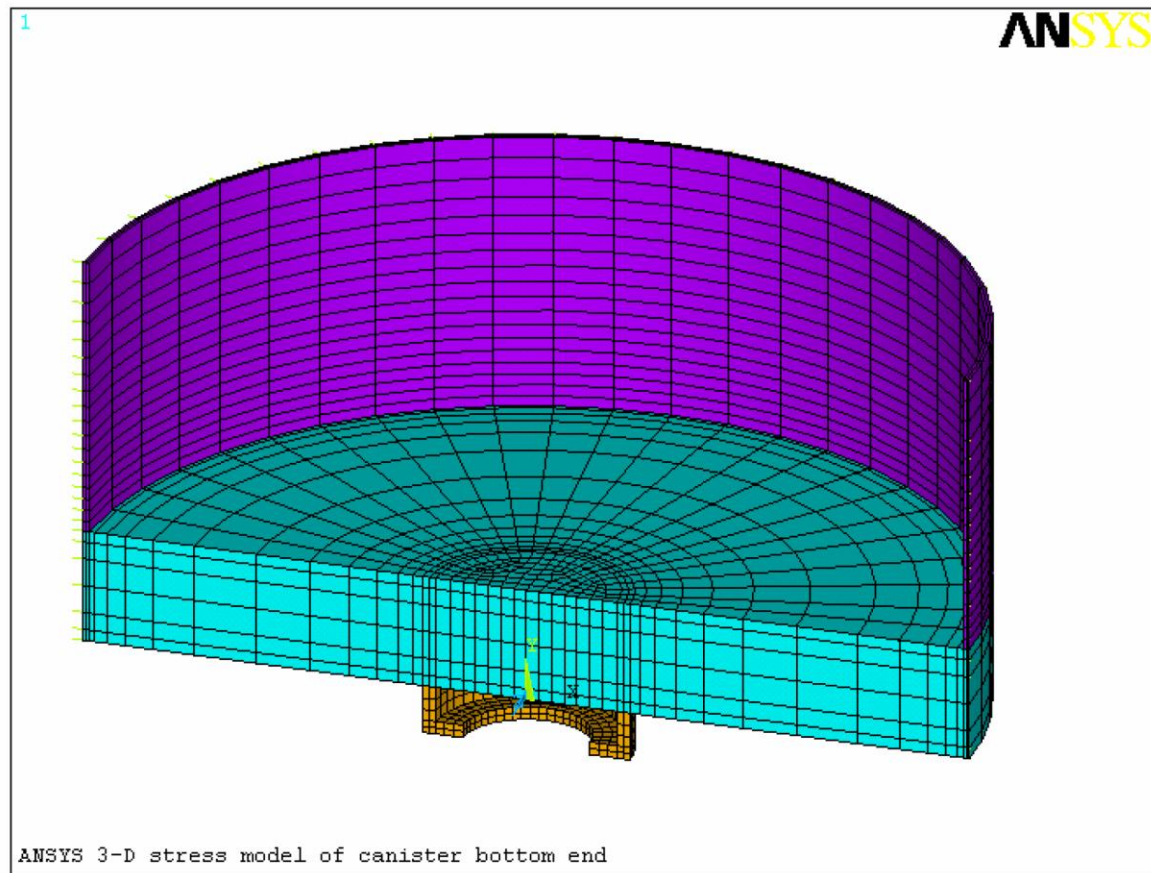


Figure 3.9.1-20
3-D DSC Canister Bottom End Assembly Finite Element Model

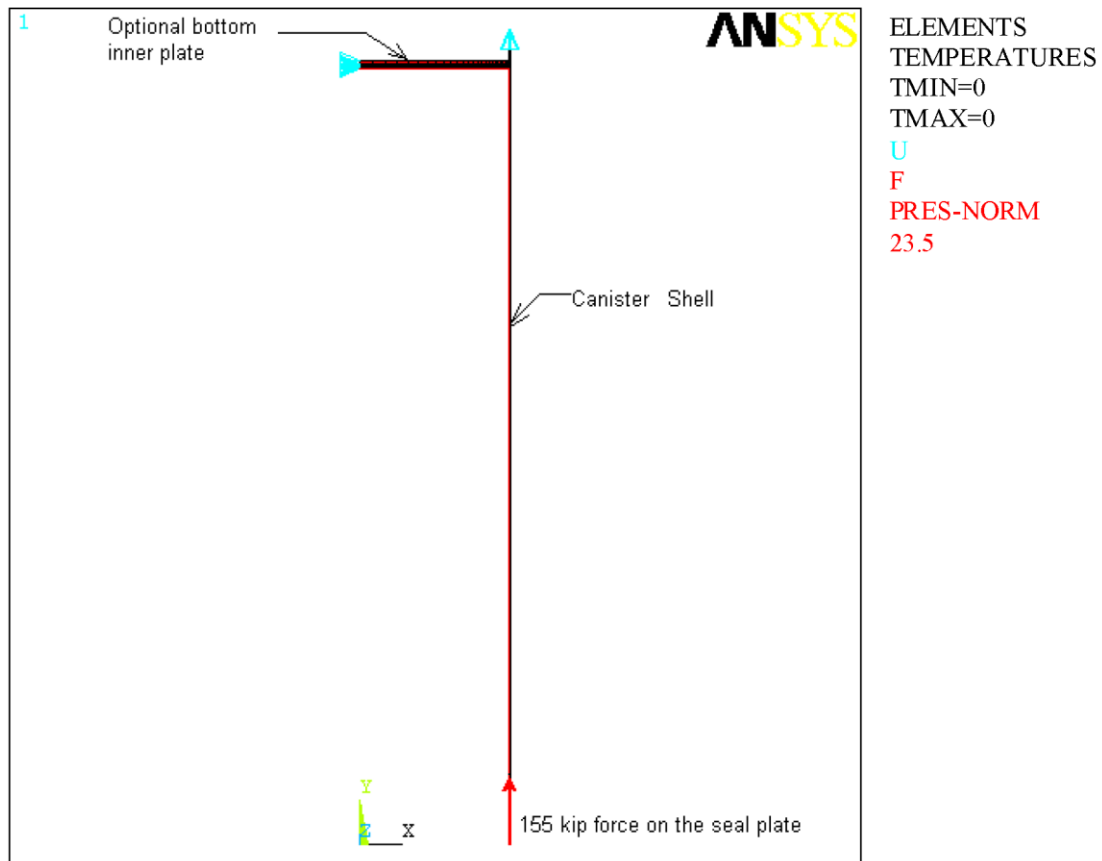


Figure 3.9.1-21
32PTH DSC Canister Finite Element Model used for Pressure Test Analysis

Figure Deleted in its Entirety

Figure 3.9.1-22
DELETED

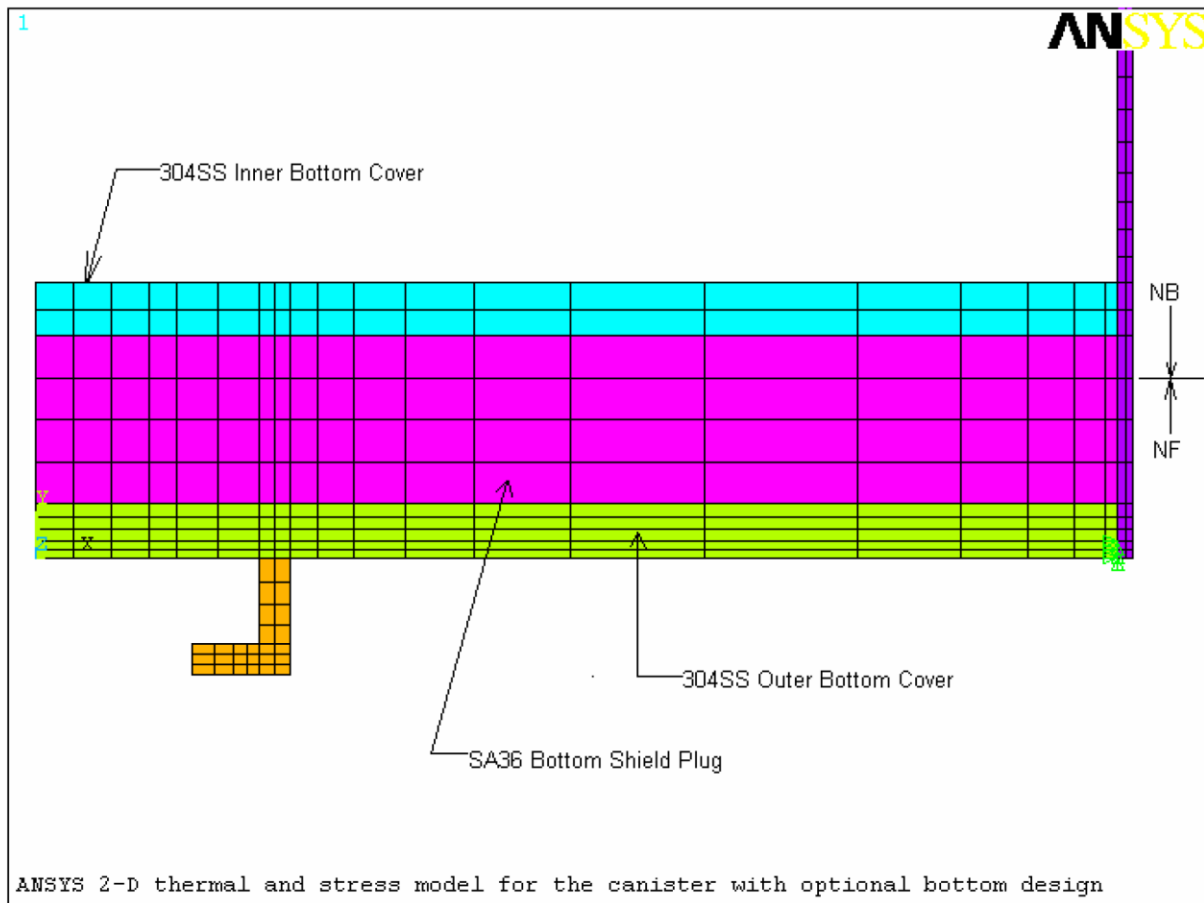


Figure 3.9.1-23
2-D Axisymmetric Finite Element Model of the Alternate Canister Bottom Assembly

Figure Deleted in its Entirety

Figure 3.9.1-24
DELETED

Figure Deleted in its Entirety

**Figure 3.9.1-25
DELETED**

Figure Deleted in its Entirety

Figure 3.9.1-26
DELETED

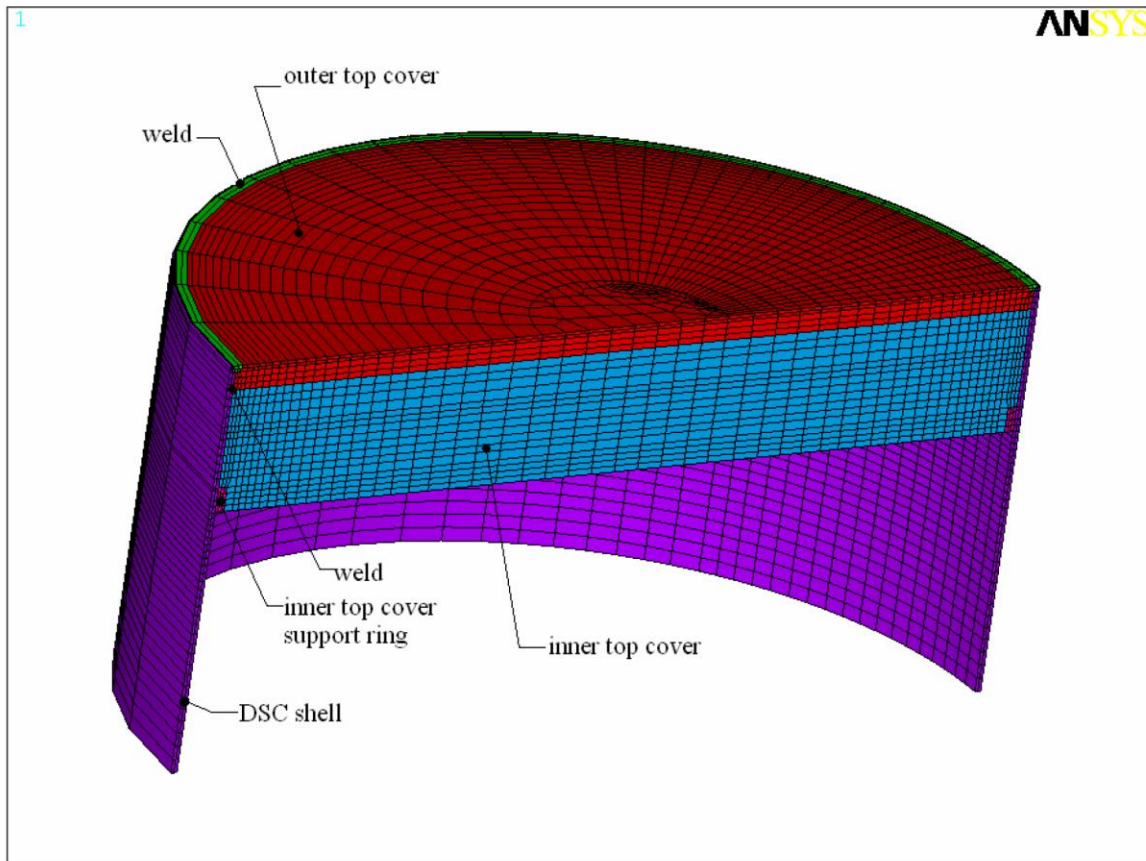


Figure 3.9.1-27
Canister Finite Element Model

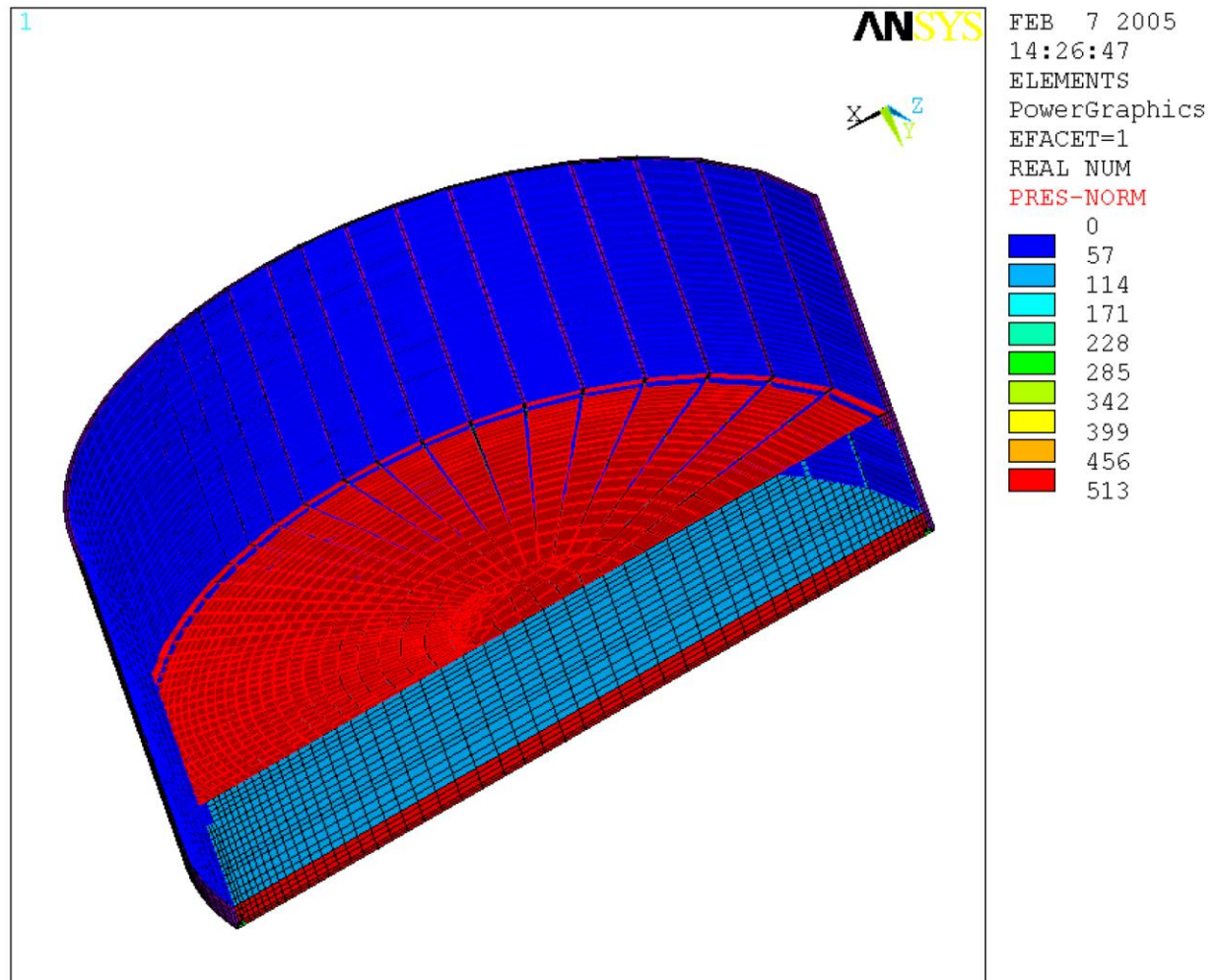


Figure 3.9.1-28
Loading Condition for DSC Corner Drop

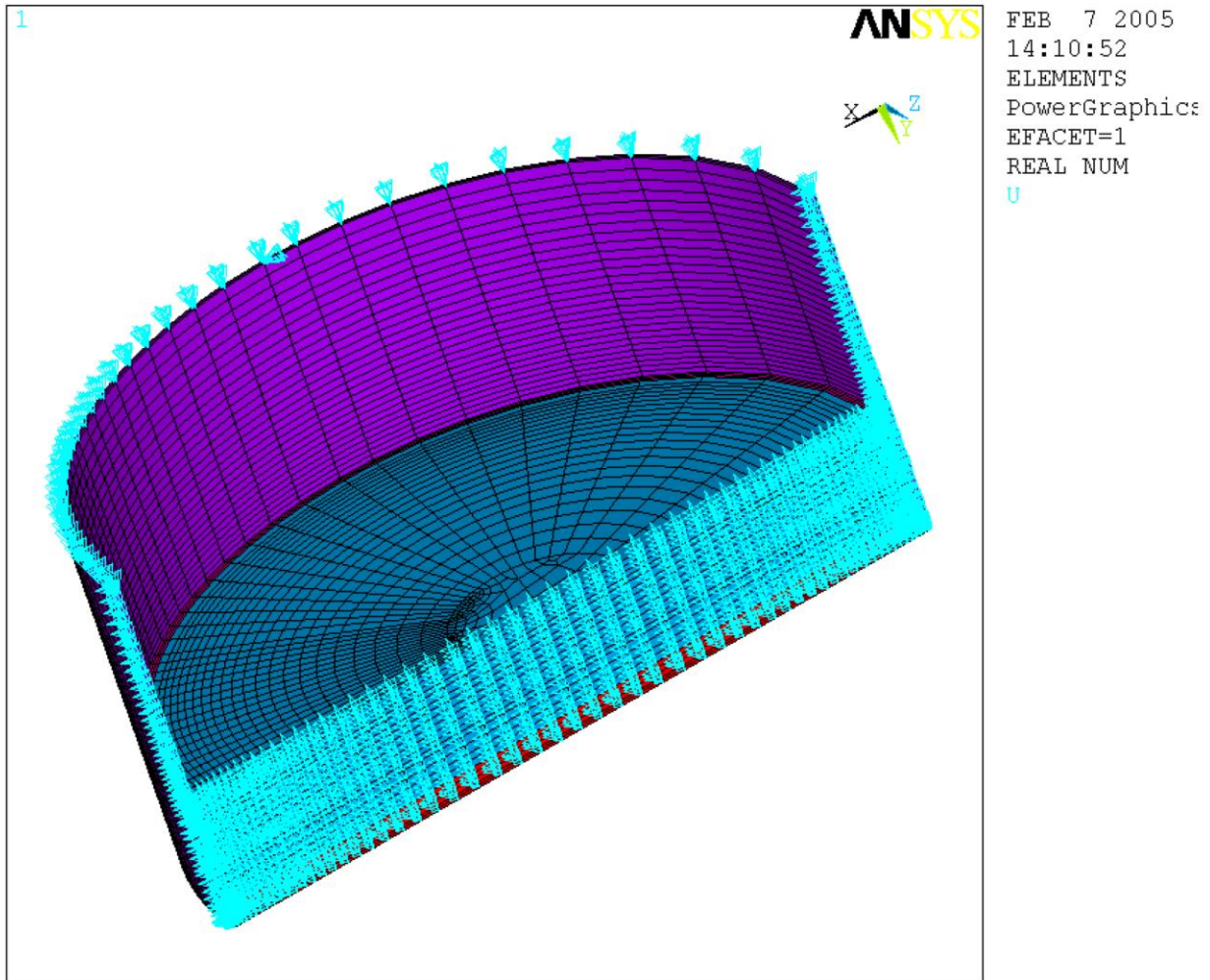


Figure 3.9.1-29
Boundary Condition for DSC Corner Drop

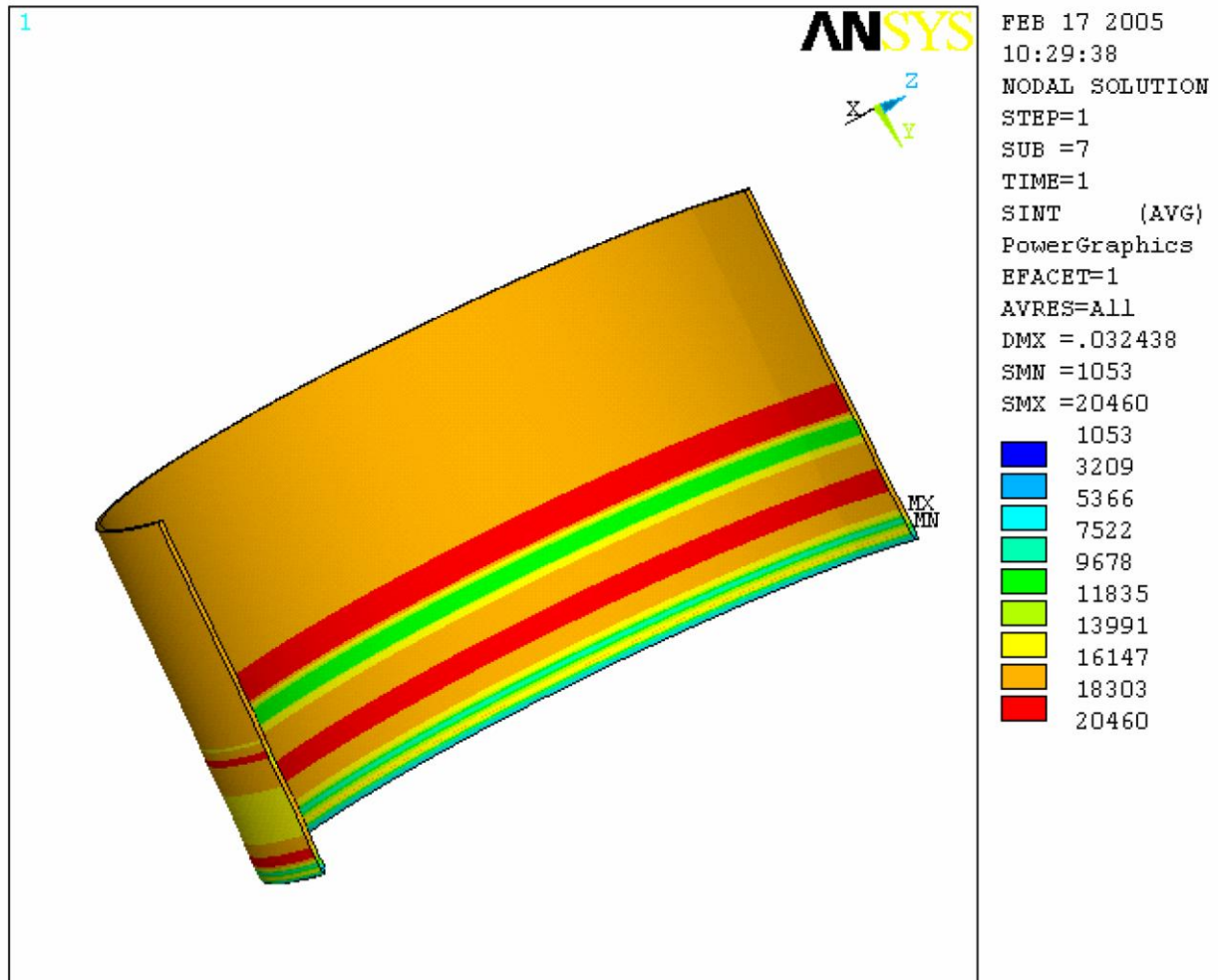


Figure 3.9.1-30
Maximum Stress Intensities in DSC Shell

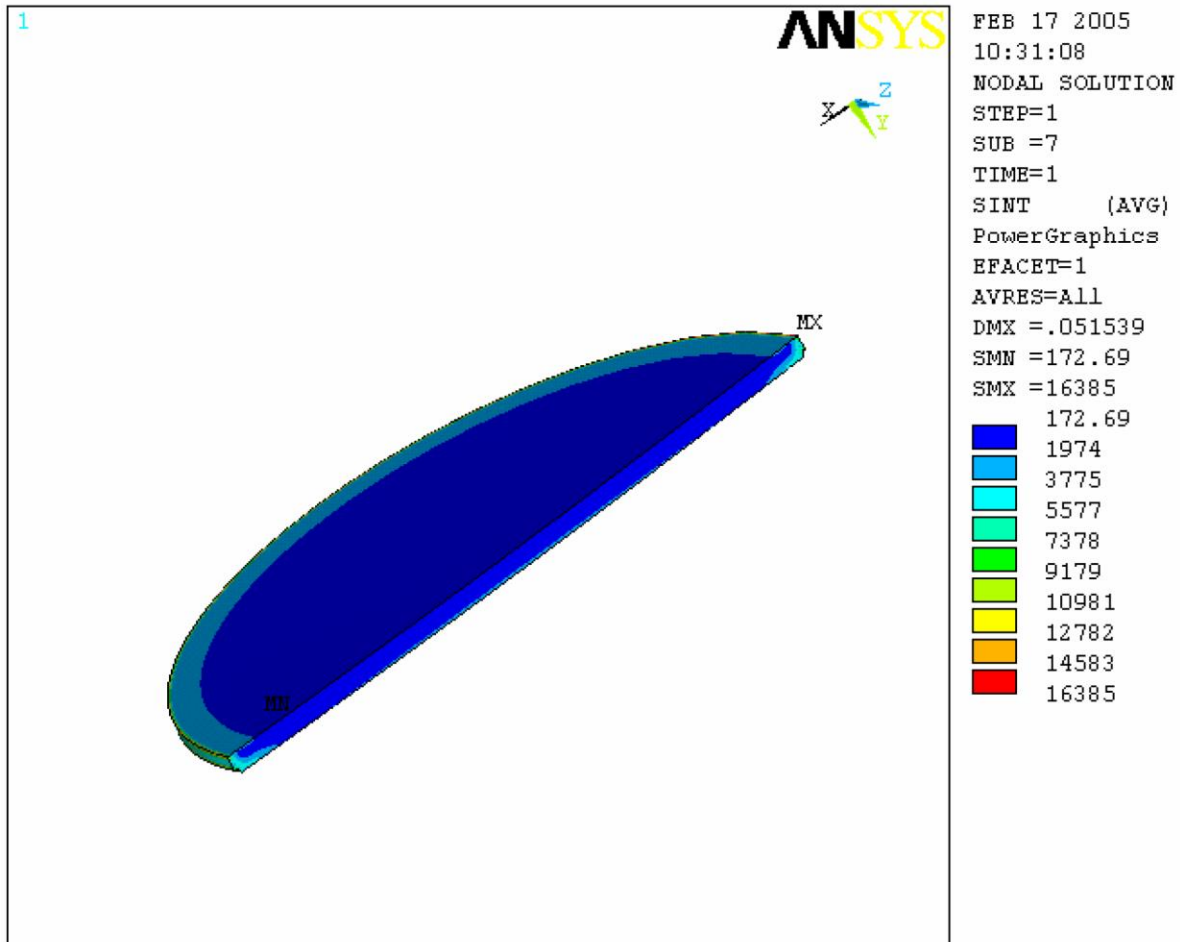


Figure 3.9.1-31
Maximum Stress Intensities in DSC Outer Top Cover

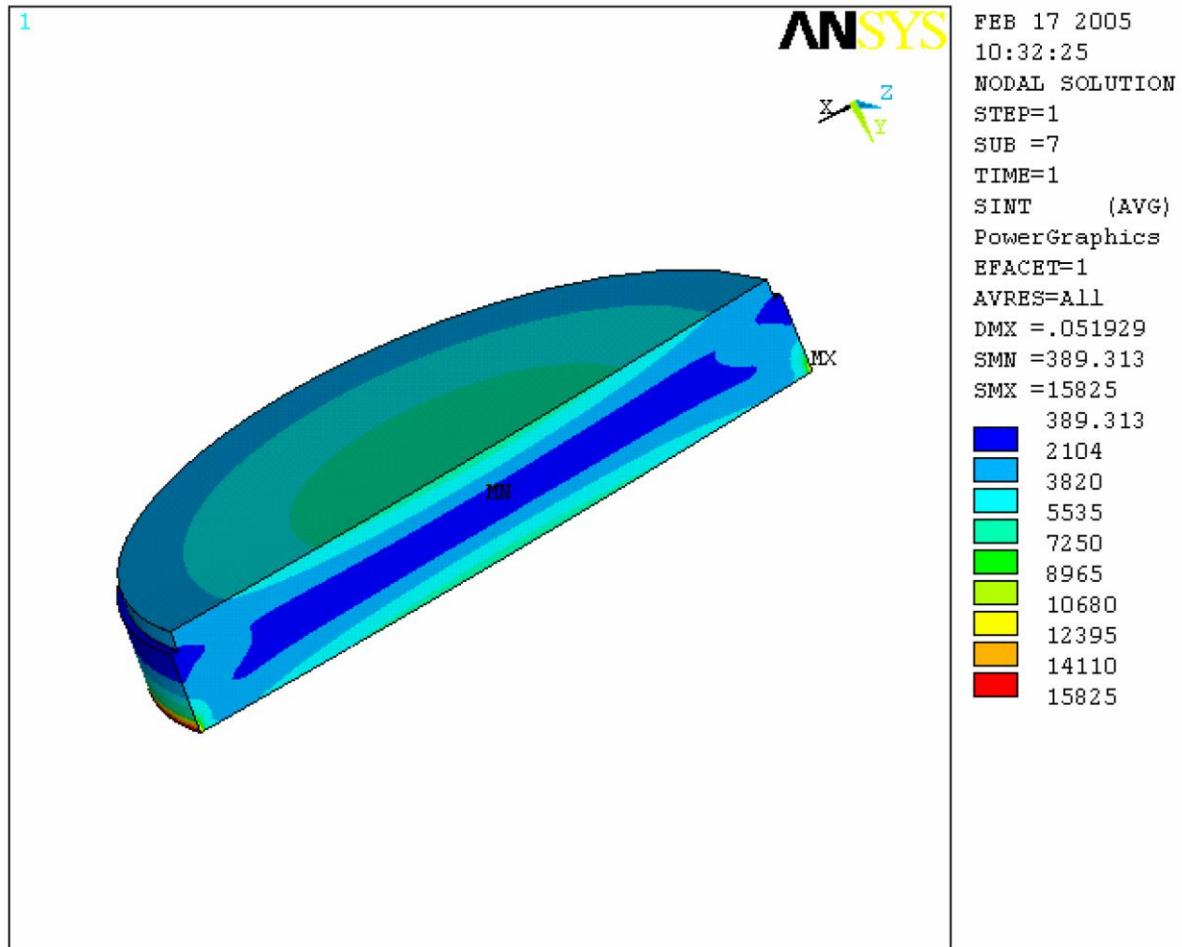


Figure 3.9.1-32
Maximum Stress Intensities in DSC Inner Top Cover

APPENDIX 3.9.2 OS187H TRANSFER CASK BODY STRUCTURAL ANALYSIS

TABLE OF CONTENTS

3.9.2	OS187H TRANSFER CASK BODY STRUCTURAL ANALYSIS	3.9.2-1
3.9.2.1	Introduction.....	3.9.2-1
3.9.2.1.1	OS187H Transfer Cask Geometry Description	3.9.2-1
3.9.2.1.2	Transfer Cask Component Weights	3.9.2-3
3.9.2.1.3	Stress Criteria.....	3.9.2-4
3.9.2.1.4	Material Properties.....	3.9.2-5
3.9.2.2	ANSYS Analysis.....	3.9.2-7
3.9.2.2.1	Geometry Description.....	3.9.2-7
3.9.2.2.2	Allowable Stresses	3.9.2-7
3.9.2.2.3	ANSYS Cask Finite Element Models.....	3.9.2-9
3.9.2.2.4	Load Cases	3.9.2-17
3.9.2.3	ANSYS Analysis Results and Reporting Methodology	3.9.2-28
3.9.2.4	Transfer Cask Trunnion Local Stresses	3.9.2-29
3.9.2.4.1	Approach.....	3.9.2-29
3.9.2.4.2	Load Cases	3.9.2-30
3.9.2.4.3	Material Properties.....	3.9.2-31
3.9.2.4.4	Stress Criteria.....	3.9.2-31
3.9.2.4.5	Stress Computation	3.9.2-32
3.9.2.4.6	Stress Intensity Calculation.....	3.9.2-38
3.9.2.4.7	Local Shell Stress Results.....	3.9.2-38
3.9.2.4.8	Local Shell Stress Conclusions.....	3.9.2-38
3.9.2.5	Stress and Deflection of Transfer Cask Inner Shell Support Rails....	3.9.2-39
3.9.2.6	References.....	3.9.2-41

LIST OF TABLES

Table 3.9.2-1	Summary of OS-187H Transfer Cask Stress Analysis	3.9.2-42
Table 3.9.2-2	Computation Spreadsheet for the 6g Lifting, Top Trunnion, Local Stresses at Trunnion Pad	3.9.2-45
Table 3.9.2-3	Computation Spreadsheet for the 6g Lifting, Top Trunnion, Local Stresses at Pad - Shell Intersection	3.9.2-46
Table 3.9.2-4	Computation Spreadsheet for the (DW + 1.0g Axial) Transfer Load, Bottom Trunnion – Local Shell Stresses	3.9.2-47

Table 3.9.2-5	Computation Spreadsheet for the (DW + 1.0g Vertical) Transfer Load, Bottom Trunnion – Local Shell Stresses	3.9.2-48
Table 3.9.2-6	Computation Spreadsheet for the (DW + 1.0g transverse) Transfer Load, Bottom Trunnion – Local Shell Stresses	3.9.2-49
Table 3.9.2-7	Computation Spreadsheet for the (DW + 0.5g axial + 0.5g vertical + 0.5g trans.) Transfer Load, Bottom Trunnion – Local Shell Stresses....	3.9.2-50
Table 3.9.2-8	NUHOMS [®] -OS187H Transfer Cask Local Shell Stresses and Allowables	3.9.2-51

LIST OF FIGURES

Figure 3.9.2-1	NUHOMS®-OS187H Transfer Cask Key Components and Dimensions (Drawing Not to Scale).....	3.9.2-52
Figure 3.9.2-2	2-Dimensional Finite Element Model, Element Plot.....	3.9.2-53
Figure 3.9.2-3	3-Dimensional Finite Element Model, Element Plot.....	3.9.2-54
Figure 3.9.2-3A	Cask Top Cover / Flange / Bolt Model.....	3.9.2-55
Figure 3.9.2-3B	Cask Bottom Ram Access/Cover/Bolt Model	3.9.2-55
Figure 3.9.2-3C	Cask Top Cover / Flange CONTAC52 Element Representation.....	3.9.2-56
Figure 3.9.2-3D	Cask Shell / Lead CONTAC52 Element Representation	3.9.2-56
Figure 3.9.2-3E	Cask Bottom Access / Shell / Flange / Lead CONTAC52 Element Representation.....	3.9.2-57
Figure 3.9.2-4	115°F Ambient Temperature Distribution.....	3.9.2-58
Figure 3.9.2-5	-20°F Ambient Temperature Distribution.....	3.9.2-59
Figure 3.9.2-6	6g Lifting Boundary Conditions (3D Model)	3.9.2-60
Figure 3.9.2-7	30 psi Internal Pressure Boundary Conditions (2D Model)	3.9.2-61
Figure 3.9.2-8	Transfer Loads Boundary Conditions (3D Model).....	3.9.2-62
Figure 3.9.2-9	75g Bottom End Drop Boundary Conditions (2D Model).....	3.9.2-63
Figure 3.9.2-10	75g Top End Drop Boundary Conditions (2D Model)	3.9.2-64
Figure 3.9.2-11	75g Side Drop Boundary Conditions (3D Model).....	3.9.2-65
Figure 3.9.2-12	Local Trunnion Stress Computation Sheet	3.9.2-66
Figure 3.9.2-13	3D - Model of Transfer Cask	3.9.2-67
Figure 3.9.2-14	Canister/Cask Top Cover/Flange/CONTAC52 Element Representation.....	3.9.2-68
Figure 3.9.2-15	Canister/ Cask Shell /Lead /CONTAC52 Element Representation	3.9.2-69
Figure 3.9.2-16	Canister/ Cask Bottom Access/Shell/ Flange/ Lead /CONTAC52 Element Representation	3.9.2-70
Figure 3.9.2-17	Transfer Cask Inner Shell & Rails	3.9.2-71
Figure 3.9.2-18	Drop Sketch for Initial Impact @ both 168° and 192° Rails (Load Case 1)	3.9.2-72
Figure 3.9.2-19	Drop Sketch for Initial Impact @ 168° Rail (Load Case 2)	3.9.2-73
Figure 3.9.2-20	Inner Shell Stress Intensity Plot (Load Case 1)	3.9.2-74
Figure 3.9.2-21	Outer Shell Stress Intensity Plot (Load Case 1).....	3.9.2-75
Figure 3.9.2-22	Inner Shell Stress Intensity Plot (Load Case 2)	3.9.2-76

Figure 3.9.2-23	Outer Shell Stress Intensity Plot (Load Case 2).....	3.9.2-77
-----------------	--	----------

3.9.2 OS187H TRANSFER CASK BODY STRUCTURAL ANALYSIS

3.9.2.1 Introduction

This appendix presents the structural analyses of the NUHOMS[®]-OS187H Transfer Cask body including the top cover, cylindrical shell assembly, bottom assembly, and the local stresses at the trunnion/cask body interface. The specific methods, models, and assumptions used to analyze the cask body for the various individual loading conditions specified in 10CFR72 [1] are described. The maximum stresses in each of the major components of the transfer cask are reported for each load case and load combination in Section 3.9.2.2.4. The results are evaluated against the ASME Code [2] design criteria described in Section 3.9.2.1.3.

The OS187H transfer cask body structural analyses generally use static linear elastic methods. The stresses and deformations due to the applied loads are generally determined using the ANSYS [4] computer program.

Other components associate with the transfer cask are described and analyzed in the following Appendices:

- Appendix 3.9.3 – OS187H transfer cask top cover and RAM access cover bolt analyses
- Appendix 3.9.4 – OS187H transfer cask lead slump and inner shell buckling analyses
- Appendix 3.9.5 – OS187H transfer cask trunnion analysis
- Appendix 3.9.6 – OS187H transfer cask shield shell panel structural analyses

The analysis methods described in this appendix and used to evaluate the cask body for the loading conditions are:

ANSYS Analysis

- Axisymmetric and
- Asymmetric Loads

3.9.2.1.1 OS187H Transfer Cask Geometry Description

Key dimensions of the transfer cask are shown in Figure 3.9.2-1. The shell, or cask body cylinder assembly, is an open ended (at the top) cylindrical unit with an integral closed bottom end. This assembly consists of concentric inner shell (SA-240, Type 304) and an outer shell (SA-240, Type 304) welded to a massive closure flange (SA-182, Type F304N) at the top and bottom ends. The annulus between the shells is filled with lead shielding. The lead is poured into the annulus in a molten state using a carefully controlled procedure. The top cover is bolted to the top flange by 24-1 1/2 in. diameter high strength bolts and sealed with O-ring. A cover plate is provided to seal the bottom hydraulic ram access penetration of the cask (by 12-1/2 in. high strength bolt with O-ring) during fuel loading and transferring the canister to the ISFSI.

Two lifting trunnions are provided for handling the transfer cask in the plant's fuel/reactor building using a lifting yoke and an overhead crane. Lower support trunnions are provided on the cask for pivoting the transfer cask from/to the vertical and horizontal positions on the support skid/transport trailer.

The overall dimensions of the OS187H transfer cask are 197.07 inches long and 92.20 inches in diameter. The transfer cask structural shell is 82.70 inches in diameter. The transfer cask cavity is 186.60 inches long and 70.50 inches in diameter. A detailed physical description of the transfer cask is provided in Chapter One. Chapter One also contains reference drawings of the NUHOMS[®]-OS187H cask which are the source of dimensions and other information used to develop analysis models.

The gross weight of the loaded transfer cask is 114.8 tons (229.5 kips) including a maximum payload of 54.78 tons (109.56 kips). Sections 3.9.2.1.2 and Figure 3.9.2-1 summarize the component weights and key dimensions of the NUHOMS[®]-OS187H transfer cask.

This appendix evaluates the structural integrity of the OS187H Transfer Cask main structural members during all normal and hypothetical accident condition loadings.

3.9.2.1.2 Transfer Cask Component Weights

The following tables summarize the component weights of the NUHOMS[®]-OS187H Transfer Cask as well as the dry loaded NUHOMS[®]-DSC weight, that are used for the transfer cask structural evaluation.

OS-187H Transfer Cask Component Weights

Transfer Cask Component	Weight (lb. x 1000)
Structural Shell	20.85
Inner Shell	5.86
Lead Gamma Shield	62.37
Top Flange	3.18
Bottom Flange	3.37
Top Cover	5.20
Bottom Assembly	3.46
Neutron Shield Panel (including water)	12.75
Upper Trunnions (2)	1.61
Lower Trunnions (2)	1.27
Total Transfer Cask Weight	119.92

Dry Loaded 32PTH DSC Weight

Transfer Cask Payload	Weight (lb. x 1000)	Weight Used for Analysis (lb. x 1000)
32PTH Canister	28.19	
32PTH Basket	29.85	
Fuel Assemblies (32)	51.52	
Total 32PTH DSC Weight	109.56	115.00

3.9.2.1.3 Stress Criteria

The resulting stresses are compared with the allowable stresses set forth by ASME B&PV Code, Section III, Subsection NC [2] for normal conditions and ASME B&PV Code, Section III, Appendix F [3] for accident conditions. The allowable stresses for both normal and accident conditions are summarized in the following table.

Service Level	Stress Category	Stress Criteria
A (Normal Conditions)	Primary Membrane Stress, P_m	S_m
	Primary Membrane + Bending Stress, $P_m + P_b$	$1.5 S_m$
	Primary + Secondary Stress, $P_m + P_b + Q$	$3 S_m$
D (Accident Conditions)	Primary Membrane Stress, P_m	Lesser of $2.4 S_m$ or $0.7 S_u$
	Primary Local Membrane Stress, P_L	150% of P_m Stress Limit
	Primary Membrane + Bending Stress, $P_m + P_b$	Lesser of $3.6 S_m$ or S_u

3.9.2.1.4 Material Properties

The NUHOMS[®]-OS187H Transfer Cask is primarily constructed from SA-240 Type 304 stainless steel. The top cover is constructed to SA-240 Type XM-19. SA-540 Grade B24 Class 1 is used for the top cover and bottom cover bolts. Chemical lead is used for radial gamma shielding, a proprietary polyester based polymer resin material is used for the solid axial neutron shielding, and liquid water is used for radial neutron shielding.

Since various temperature distributions are applied to the transfer cask model, temperature dependent Modulus of Elasticity, E , and Coefficient of Thermal Expansion, α , are used to model each material. The following material properties are used in the transfer cask model.

Transfer Cask Body (SA-240, type 304 Stainless Steel)

Temperature	Modulus of Elasticity, E (psi) [6]	Coefficient of Thermal Expansion, α (in./in.°F) [6]	Density, ρ (lb./in ³ .) [7]	Poisson's ratio, ν [7]
70 °F	28.3×10^6	8.5×10^{-6}	0.29	0.3
200 °F	27.6×10^6	8.9×10^{-6}	0.29	0.3
300 °F	27.0×10^6	9.2×10^{-6}	0.29	0.3
400 °F	26.5×10^6	9.5×10^{-6}	0.29	0.3
500 °F	25.8×10^6	9.7×10^{-6}	0.29	0.3
600 °F	25.3×10^6	9.8×10^{-6}	0.29	0.3

Top Cover (SA-240, type XM-19 Stainless Steel)

Temperature	Modulus of Elasticity, E (psi) [6]	Coefficient of Thermal Expansion, α (in./in.°F) [6]	Density, ρ (lb./in ³ .) [7]	Poisson's ratio, ν [7]
70 °F	28.3×10^6	8.2×10^{-6}	0.29	0.3
200 °F	27.6×10^6	8.5×10^{-6}	0.29	0.3
300 °F	27.0×10^6	8.8×10^{-6}	0.29	0.3
400 °F	26.5×10^6	8.9×10^{-6}	0.29	0.3
500 °F	25.8×10^6	9.1×10^{-6}	0.29	0.3
600 °F	25.3×10^6	9.2×10^{-6}	0.29	0.3

Top Cover Bolts and RAM Access Cover Bolts (SA-540 Grade B24 Class 1)

Temperature	Modulus of Elasticity, E (psi) [6]	Coefficient of Thermal Expansion, α (in./in.°F) [6]	Density, ρ (lb./in ³ .) [7]	Poisson's ratio, ν [7]
70 °F	27.8×10^6	6.4×10^{-6}	0.29	0.3
200 °F	27.1×10^6	6.7×10^{-6}	0.29	0.3
300 °F	26.7×10^6	6.9×10^{-6}	0.29	0.3
400 °F	26.1×10^6	7.1×10^{-6}	0.29	0.3
500 °F	25.7×10^6	7.3×10^{-6}	0.29	0.3
600 °F	25.2×10^6	7.4×10^{-6}	0.29	0.3

Gamma Shield (ASTM B-29, Chemical Lead)

Temperature	Modulus of Elasticity, E (psi) [8]	Coefficient of Thermal Expansion, α (in./in.°F) [8]	Density, ρ (lb./in ³ .) [7]	Poisson's ratio, ν [7]
70 °F	2.35×10^6	16.21×10^{-6}	0.41	0.45
200 °F	2.28×10^6	16.70×10^{-6}	0.41	0.45
300 °F	2.06×10^6	17.34×10^{-6}	0.41	0.45
400 °F	$1.92 \times 10^{6*}$	$18.12 \times 10^{-6*}$	0.41	0.45

* Extrapolated from available Reference 8 Data.

The resin material properties used to model the bottom neutron shield plate for the axisymmetric load cases are taken from Chapter 3, Table 3-11.

3.9.2.2 ANSYS Analysis

3.9.2.2.1 Geometry Description

The top cover, inner shell, structural shell, and bottom assembly are the primary structural members of the cask. Key components and dimensions of the confinement vessel are shown in Figure 3.9.2-1. Chapter 1 contains reference drawings of the NUHOMS®-OS187H transfer cask which are the source of dimensions and other information used to develop analysis models.

3.9.2.2.2 Allowable Stresses

Allowable stresses are based on the material properties of each component taken at their corresponding maximum temperatures. Based on the 115°F hot ambient thermal analysis performed in Chapter 4, and shown in Figure 3.9.2-4, the maximum temperatures of the various transfer cask components are as shown in the following table.

Transfer Cask Component	Maximum Temperature	Temperature Used to Compute Allowable Stress
Structural Shell	280	300 °F
Top Cover	196	300 °F
Inner Shell	340	400 °F
Bottom End Plates**	216	300 °F
RAM access and Cover	197	200 °F

* Includes outer structural shell and top and bottom flanges.

** Includes Bottom End Plate and Bottom Neutron Shield Plate

The NUHOMS®-OS187H transfer cask is broken down into 5 major components for ease of stress evaluation as seen in the table above. The above table also lists the temperatures used to determine the allowable stress for each major component. The temperature chosen for each component is conservatively higher than the maximum temperature experienced during the 115 °F hot ambient condition.

The following transfer cask component allowable stresses are computed based on the stress criteria and component temperatures described above, and the material properties provided in Reference 6.

Transfer Cask Component	Service Level	Stress Category	Allowable Stress
Structural Shell*	A	P_m	20.00
		$(P_m \text{ or } P_L) + P_b$	30.00
		$P_L + P_b + Q$	60.00
	D	P_m	46.34
		P_L	66.20
		$(P_m \text{ or } P_L) + P_b$	66.20
Top Cover	A	P_m	31.40
		$(P_m \text{ or } P_L) + P_b$	47.10
		$P_L + P_b + Q$	94.20
	D	P_m	65.94
		P_L	94.20
		$(P_m \text{ or } P_L) + P_b$	94.20
Inner Shell	A	P_m	18.70
		$(P_m \text{ or } P_L) + P_b$	28.05
		$P_L + P_b + Q$	56.10
	D	P_m	44.80
		P_L	64.00
		$(P_m \text{ or } P_L) + P_b$	64.00
Bottom End Plates**	A	P_m	20.00
		$(P_m \text{ or } P_L) + P_b$	30.00
		$P_L + P_b + Q$	60.00
	D	P_m	46.34
		P_L	66.20
		$(P_m \text{ or } P_L) + P_b$	66.20
RAM access and Cover	A	P_m	20.00
		$(P_m \text{ or } P_L) + P_b$	30.00
		$P_L + P_b + Q$	60.00
	D	P_m	48.00
		P_L	71.00
		$(P_m \text{ or } P_L) + P_b$	71.00

* Includes outer structural shell and top and bottom flanges.

** Includes Bottom End Plate and Bottom Neutron Shield Plate

3.9.2.2.3 ANSYS Cask Finite Element Models

Two separate FEMs were constructed. The first is a 2-dimensional, axisymmetric representation of the cask, which is constructed with plane elements. The second model is a 180°, 3-dimensional “brick” element representation.

A. 2-Dimensional Finite Element Model Description

A 2-dimensional axisymmetric ANSYS [4] finite element model, constructed primarily from PLANE42 elements, is used to analyze all axisymmetric load cases. The Basic dimensions of the transfer cask are provided in Figure 3.9.2-1. An element plot of the 2-dimensional FEM is shown in Figure 3.9.2-2.

Model Material Properties

The elastic material properties listed above are used to model the transfer cask materials. For all load cases, except for the -20 °F Ambient load cases, the temperature distribution for the 115 °F Ambient condition is applied to the finite element model. Figure 3.9.2-4 shows the 115 °F ambient temperature distribution as applied to the 2-dimensional model. The 115 °F Ambient temperature distribution is used to determine the appropriate temperature dependent material property to be used at each node. However, non-zero coefficients of thermal expansion are used only in the load cases where thermal stresses are to be evaluated. For all other load cases, all material coefficients of thermal expansion are set to zero, so that no thermal stresses are induced.

Unmodeled Components

Only the structural steel section of the top cover (3 in. thick.) is modeled. The top neutron shield resin, the ¼ in. thickness top cover outer plate, and hoist ring standoffs are not modeled since they are not intended to provide any structural support. However, their inertial load is accounted for by increasing the density of the structural portion of the top cover. The weight of the unmodeled portion of the top cover assembly is as follows.

Weight of unmodeled top cover components = 678 lb. (resin) + 422 lb. (1/4” top cover outer plate) + 20 lb. (standoffs) = 1,120 lb.

The volume and weight of the structural steel portion of the top cover is 14,051 in.³ and 4,075 lb. respectively. Therefore the density of the top cover, ρ_l , is increased as follow.

$$\rho_l = [1,120 \text{ lb.} + 4,075 \text{ lb.}] / 14,051 \text{ in.}^3 = 0.37 \text{ lb./in.}^3$$

For conservatism, the density of the top cover used in this analysis is increased to 0.38 lb./in.³

The radial neutron shield (water) and neutron shield panel are also not modeled, because they are not considered structural components of the transfer cask. Therefore, the density of the structural shell of the transfer cask is increased to account for the unmodeled components. The weight of the unmodeled radial neutron shield assembly is 12,746 lb.

The volume and weight of the structural shell is 71,895 in.³ and 20,850 lb. respectively. Therefore the density of the structural shell, ρ_s , is increased as follow.

$$\rho_l = [12,746 \text{ lb.} + 20,850 \text{ lb.}] / 71,895 \text{ in.}^3 = 0.47 \text{ lb./in.}^3$$

For conservatism, the density of the structural shell used in this analysis is increased to 0.49 lb./in.³

Top Cover and RAM Access Cover Bolts

The top cover and RAM access cover bolts are modeled with axisymmetric BEAM3 elements, and are only used in the model to simulate the overall behavior of the closure joints. The stresses in the top cover and RAM access cover bolts are evaluated separately in Appendix 3.9.3. The element real constants are computed in the following way for the top cover and RAM access cover bolts.

Top Cover Bolts

There are 24, 1½ in - 8UN 2A bolts used to mount the transfer cask top cover to the flange. However, the size used to model the transfer cask top cover bolts is 1½ in. - 10UN 2A bolts, which have a negligible difference in geometry relative to that of the 1½ in - 8UN 2A bolts. The bolt diameter used for stress analysis, D_{tc} , is computed using formulae given in Table 5.1 of Reference 9, as follows.

$$D_{tc} = 1.50 - 0.9743(1/10) = 1.403 \text{ in.}$$

The total tensile stress area for all 24 top cover bolts, A_{tc2d} , is computed as follows.

$$A_{tc2d} = (\pi/4) \times 1.403^2 \times 24 \text{ bolts} = 1.546 \times 24 \text{ bolts} = 37.104 \text{ in.}^2$$

The total moment of inertia of all 24 top cover bolts, I_{tc2d} , is,

$$I_{tc2d} = (\pi/64) \times 1.403^4 \times 24 \text{ bolts} = 4.565 \text{ in.}^4$$

The total height of the top cover bolts, H_{tc2d} , is computed assuming the following equivalent height method.

$$H_{tc2d} = \sqrt{A_{tc2d}} = \sqrt{1.546} = 1.243 \text{ in.}$$

RAM Access Cover Bolts

There are 12, ½ in - 13UNC 2A bolts used to mount the transfer cask RAM access cover to the bottom of the cask. The bolt diameter used for stress analysis, D_{ra} , is computed as follows.

$$D_{ra} = 0.50 - 0.9743(1/13) = 0.425 \text{ in.}$$

The total tensile stress area for all 12 RAM access cover bolts, A_{ra2d} , is computed as follows.

$$A_{ra2d} = (\pi/4) \times 0.425^2 \times 12 \text{ bolts} = 0.142 \times 12 \text{ bolts} = 1.704 \text{ in.}^2$$

The total moment of inertia of all 12 RAM access cover bolts, I_{ra2d} , is,

$$I_{ra2d} = (\pi/64) \times 0.425^4 \times 12 \text{ bolts} = 0.01922 \text{ in.}^4$$

The height of the RAM access cover bolts, H_{ra2d} , used in the model is,

$$H_{ra2d} = \sqrt{0.142} = 0.3768 \text{ in.}$$

For both the top cover bolts and the RAM access cover bolts, a bolt preload stress of 25,000 psi. is used. This bolt preload stress is applied to the model by placing an initial strain in the beam elements that are used to model the bolts.

Contact Elements

CONTAC12 elements are placed between all surfaces of the top flange and top cover, between the RAM access cover and RAM access penetration that contact each other, and between the lead gamma shielding and the inner and structural shells. These contact elements are used to model the reaction forces that occur between these surfaces.

The contact elements introduce nonlinearities in the analysis depending whether they are open or closed. Initially, at all contact surfaces, the gaps are closed. The contact element spring constant, K_n , is calculated in the following way.

$$K_n = f E h [4]$$

Where,

f = A factor usually between 0.01 to 100.

E = Modulus of elasticity (27.0×10^6 psi for SA-240, type 304 @ 300°F)

h = contact target length (i.e., the square root of target area).

Typical element length $\approx 1/2$ in.

Typical element width ≈ 1 in.

Typical target length, $h = (0.5 \times 1.0)^{0.5} = 1.22$ in.

Therefore,

$$K_n = 27.0 \times 10^6 \times 1.22 \times f \approx 3.29 \times 10^5 \text{ to } 3.29 \times 10^9 \text{ lb./in}$$

Thus, there is very wide range for K_n value. For the 2-D finite element model, the structure responded well with a spring constant value of 1.0×10^6 lb/in. for the lead shield contact elements and 1.0×10^7 lb/in. for the top cover and RAM access cover contact elements.

Boundary Conditions

Separate sets of boundary conditions are required for the various loading cases analyzed. The boundary condition sets are used to prevent rigid body motion and are assigned based on the specific loading configuration. In each of the boundary condition sets, displacement constraints are fixed such that no displacement is permitted in the prescribed direction.

B. 3-Dimensional Finite Element Model Description

A 3-dimensional axisymmetric ANSYS [4] finite element model, constructed primarily from SOLID45 elements, is used to analyze all non-axisymmetric load cases. The 3-dimensional model represents 180° of the full 360° cask, or a half model. An element plot of the 3-dimensional FEM is shown in Figure 3.9.2-3, Figure 3.9.2-3A, Figure 3.9.2-3B, Figure 3.9.2-3C, Figure 3.9.2-3D, and Figure 3.9.2-3E.

Model Material Properties

The elastic material properties listed in the material properties section are used to model the transfer cask materials. As in the 2-dimensional finite element model, the temperature distribution for the 115 °F Ambient condition is applied to the finite element model unless otherwise stated. The 115 °F Ambient temperature distribution however, is used to determine the appropriate temperature dependent material property to be used at each node. But, material coefficients of thermal expansion are only used for thermal stress load cases.

Modeled Component Weights

Only the structural steel section of the top cover is modeled. The top neutron shield resin, top cover outer plate (1/4" thick.), and hoist ring standoffs are not modeled since they are not intended to provide any structural support. However, their inertial load is accounted for by increasing the density of the structural portion of the top cover. The weight of the unmodeled portion of the top cover assembly is as follows.

Weight of unmodeled top cover components = 678 lb. (resin) + 422 lb. (top cover outer plate) + 20 lb. (standoffs) = 1,120 lb.

The volume and weight of the structural steel portion of the lid are 14,051 in.³ and 4,075 lb. respectively. Therefore the density of the top cover, ρ_l , is increased as follow.

$$\rho_l = [1,120 \text{ lb.} + 4,075 \text{ lb.}] / 14,051 \text{ in.}^3 = 0.37 \text{ lb./in.}^3$$

For conservatism, the density of the unmodeled top cover components used in this analysis is increased 0.38 lb./in.³

The radial neutron shield (water) and shield panel are not modeled, because they are not considered structural components of the transfer cask. Therefore, the density of the structural shell of the transfer cask is increased to account for the unmodeled components. The weight of the unmodeled radial neutron shield assembly is 12,746 lb.

The volume and weight of the structural shell are 71,895 in.³ and 20,850 lb. respectively. Therefore the density of the structural shell, ρ_s , is increased as follow.

$$\rho_s = [12,746 \text{ lb.} + 20,850 \text{ lb.}] / 71,895 \text{ in.}^3 = 0.47 \text{ lb./in.}^3$$

For conservatism, the density of the structural shell used in this analysis is increased to 0.53 lb./in.³

The bottom neutron shield (resin) is also not modeled, because it is not considered a structural component for the non-axisymmetric load cases. Therefore, the density of the bottom end plate, bottom neutron shield plate, and the bottom flange is increased to account for the unmodeled component. The weight of the unmodeled bottom neutron shield is 551 lb.

The volume and weight of the bottom end plate, bottom neutron shield plate, and the bottom flange are 19,871 in.³ and 5,763 lb. respectively. Therefore the density of the cask bottom components, ρ_b , is increased as follow.

$$\rho_b = [5,763 \text{ lb.} + 551 \text{ lb.}] / 19,871 \text{ in.}^3 = 0.318 \text{ lb./in.}^3$$

For conservatism, the density of the bottom components used in this analysis is increased to 0.32 lb./in.³

Top Cover and RAM Access Cover Bolts

The top cover and RAM access cover bolts are modeled with BEAM4 elements, and are only used in the model to simulate the overall behavior of the closure joints. The stresses in the top cover and RAM access cover bolts are evaluated separately in Appendix 3.9.3. The element real constants are computed in the following way for the top cover and RAM access cover bolts.

Top Cover Bolts

There are 24, 1½ in - 8UN 2A bolts used to mount the transfer cask top cover to the cask flange. However, the size used to model the transfer cask top cover bolts is 1½ in. - 10UN 2A bolts, which have a negligible difference in geometry relative to that of the 1½ in - 8UN 2A bolts. The bolt diameter used for stress analysis, computed above, is $D_{tc} = 1.403$ in. The tensile stress area for a single top cover bolt, A_{tc3d} , is computed as follows.

$$A_{tc3d} = (\pi/4) \times 1.403^2 = 1.546 \text{ in.}^2$$

The moment of inertia for a single top cover bolt, I_{tc3d} , is,

$$I_{tc3d} = (\pi/64) \times 1.403^4 = 0.190 \text{ in.}^4$$

The height for a single top cover bolt, H_{tc3d} , is computed assuming the following equivalent height method.

$$H_{tc3d} = \sqrt{A_{tc3d}} = \sqrt{1.546} = 1.243 \text{ in.}$$

RAM Access Cover Bolts

There are 12, ½ in - 13UNC 2A bolts used to mount the transfer cask RAM access cover to the bottom of the cask. The bolt diameter used for stress analysis, computed above is $D_{ra} = 0.425$ in.

The tensile stress area for a single RAM access cover bolt, A_{ra3d} , is computed as follows.

$$A_{ra3d} = (\pi/4) \times 0.425^2 = 0.142 \text{ in.}^2$$

The moment of inertia for a single RAM access cover bolt, I_{ra3d} , is,

$$I_{ra3d} = (\pi/64) \times 0.425^4 = 0.00160 \text{ in.}^4$$

The height for a single RAM access cover bolt, H_{ra3d} , is,

$$H_{ra3d} = \sqrt{0.142} = 0.3768 \text{ in.}$$

The top cover bolt and RAM access cover bolt preload strain, ε_b , used in the finite element model, is the same as that used in the 2-dimensional model. Again, the preload strain is applied to the model bolt elements to simulate a preload stress of 25,000 psi, due to the applied preload torque.

Contact Elements

CONTAC52 elements are placed between all surfaces of the top flange and top cover, between the RAM access cover and RAM access penetration that contact each other, and between the lead gamma shielding and the inner and structural shells. These contact elements are used to model the reaction forces that occur between closure surfaces. LINK8 elements with a very low Modulus of Elasticity and density are placed in all locations where CONTAC52 elements exist in order to maintain overall stability of the model. This is only required in the 3-dimensional model.

The contact elements introduce nonlinearities in the analysis depending whether they are open or closed. Initially, at all contact surfaces, the gaps are closed. The contact element spring constant, K_n , is calculated in the following way.

$$K_n = f E h [4]$$

Where,

f = A factor usually between 0.01 to 100.

E = Modulus of elasticity (27.0×10^6 psi for SA-240, type 304 @ 300°F)

h = contact target length (i.e., the square root of target area).

Typical element length $\approx 1/2$ in.

Typical element width ≈ 1 in.

Typical target length, $h = (0.5 \times 1.0)^{0.5} = 1.22$ in.

Therefore,

$$K_n = 25.8 \times 10^6 \times 1.22 \times f \approx 3.39 \times 10^5 \text{ to } 3.39 \times 10^9 \text{ lb./in}$$

Thus, there is very wide range for K_n value. For the 3-D finite element model, the structure responded well with a spring constant value of 1.0×10^7 lb/in. for the lead shield contact elements and 1.0×10^8 lb/in. for the top cover and RAM access cover contact elements.

3.9.2.2.4 Load Cases

The following two tables describe the normal (Level A) and accident (Level D) condition load cases analyzed in this calculation. The load cases considered consist of 115 °F hot ambient and -20 °F cold ambient environments, 30 psig internal, vacuum drying conditions, transfer loads, and 75g accident condition end and side drops. The normal and accident load conditions are summarized in the following table.

Summary of Normal and Accident Load Conditions

Load Case Number	Loading Condition	Service Level	Applied Load
1	6g Vertical Lifting	A	Cask vertical, supported at top trunnions, 6g vertical accel. + 30 psi. internal pressure.
1A	6g Vertical Lifting + Thermal Loads	A	Cask vertical, supported at top trunnions, 6g vertical accel. + 30 psi. internal pressure + 115 °F ambient.
2	Vacuum Drying	A	Cask vertical, supported at cask bottom, 15 psi. external pressure + vacuum drying thermal loads
3	30 psi. Internal Pressure	A	30 psi. internal pressure
4	115°F Ambient Hot Thermal Environment	A	115 °F ambient environment
5	-20°F Ambient Cold Thermal Environment	A	-20 °F ambient environment
6	Transfer Inertial Loads (2g Vertical + 2g Transverse + 2g Axial)	A	Cask horizontal, supported at top and bottom trunnions, 2g acceleration in all directions
6A	Transfer Loads + Internal Pressure	A	Cask horizontal, supported at top and bottom trunnions, 2g acceleration in all directions + 30 psi. internal pressure
6B	Transfer Loads + 115 °F Ambient + Internal Pressure	A	Cask horizontal, supported at top and bottom trunnions, 2g acceleration in all directions +30 psi. internal pressure + 115 °F ambient
6C	Transfer Loads + -20 °F Ambient + Internal Pressure	A	Cask horizontal, supported at top and bottom trunnions, 2g acceleration in all directions + 30 psi internal pressure + -20 °F ambient
7	75g Bottom End Drop + Internal Pressure	D	Cask vertical, supported at bottom, 75g vertical up acceleration + 30 psi. internal pressure
8	75g Top End Drop + Internal Pressure	D	Cask vertical, supported at top, 75g vertical down acceleration + 30 psi. internal pressure
9	75g Side Drop + Internal Pressure	D	Cask horizontal, supported on side, 75g transverse acceleration + 30 psi. internal pressure
10	Transfer Thermal Accident (Fire)	D	30 psi. internal pressure + thermal accident loads

Method of Applying Load to the Cask Body

Pressures applied in the axial direction are calculated based on load divided by pressure area calculation. For example, to calculate the pressure applied due to internal loading on the inner surface of the bottom transfer cask due to an end drop on the bottom end, divide the total applied load by the cross-sectional area of the inner surface of the bottom transfer cask.

Pressures applied in the radial direction in the 3-dimensional finite element model are based on cosine distributed pressure functions. These pressure distributions simulate the internal cask contents applying pressure to the inner cask wall. The pressure distribution is assumed to be in the longitudinal direction over a specified length and vary with a cosine distribution around the circumference of the cask.

The following sections describe the boundary conditions used for each individual load case and load combination.

Load Case 1: 6g Lifting (3-D FEM)

The 6g Lifting Load case consists of the loaded transfer cask in the vertical position, supported by the top two trunnions. A 6g vertical acceleration is conservatively used to bound the normal lifting load. An internal pressure of 30 psi. is also conservatively applied to the model to bound any possible pressure build up inside the cask.

The weight of the transfer cask internals (canister, basket, and fuel assemblies) is accounted for by applying equivalent pressures. The weight of the cask internals used in this analysis is 115,000 lb. The transfer cask inner radius is 35.25 in., and the inner radius of the ram access penetration is 10.00 in. The inertial load of the transfer cask internals reacts against the annular surface bounded by these two radii during a lifting. Therefore the area of the reaction surface, A_{6gi} , is as follows.

$$A_{6gi} = \pi(35.25^2 - 10.00^2) = 3,589.47 \text{ in}^2.$$

The pressure equivalent to the inertial load of the internals during a 6g lift, P_{6gi} , is,

$$P_{6gi} = [115,000 / 3,589.47] \times 6 \text{ gs} = 192.229 \text{ psi.}$$

Symmetry displacement boundary conditions are applied along the y-axis of the 3-dimensional axisymmetric model.

A depiction of the 6g Lifting load case boundary conditions is provided in Figure 3.9.2-6.

Load Case 2: Vacuum Drying

The stresses generated during the vacuum drying process are computed by hand in the following way.

The applied loads used to calculate the maximum stress in the transfer cask during vacuum drying include a 15 psi external pressure, a maximum radial temperature gradient, and a 1g axial (gravity) load. The stresses generated in the transfer cask shell by these three loads are computed using hand calculations. Since the primary load during vacuum drying is caused by the radial temperature gradient, the maximum transfer cask stress is computed for the outer radial structural shell.

A uniform 15 psi pressure is applied to the external radial surface of the cask, generating a hoop stress in the cask structural shell. The hoop stress, σ_p , in the shell is computed in the following way.

$$\begin{aligned}\sigma_p &= \text{external pressure} \times \text{the mean structural shell radius} / \text{the minimum structural shell thickness} \\ &= 15 \text{ psi} \times (78.70 + 1.50)/2 \text{ in.} / 1.50 \text{ in.} = 401 \text{ psi.}\end{aligned}$$

The stress generated in the structural shell by the 1g axial load is conservatively computed assuming that the weight of the entire transfer cask is taken by the cross sectional area of the structural shell. The weight of the transfer cask is conservatively taken to be 250,000 lb., which is higher than the actual weight (229, 520 lb.). The 1g axial stress in the structural shell, σ_g , is computed as follows.

$$\begin{aligned}\sigma_g &= 1g \times \text{maximum transfer cask weight} / \text{minimum cross sectional area of the structural shell} \\ &= 1g \times 250,000 / [(\pi/4) \times (81.70^2 - 78.70^2)] = 661 \text{ psi.}\end{aligned}$$

The maximum hoop stress generated by the radial thermal gradient during the vacuum drying process will occur in the outer structural shell due to the thermal expansion of the lead gamma shield. From Chapter 4, the maximum temperature difference between the lead gamma shield and the structural shell occurs during the drying process C at 42 hours, when the lead and structural shell are at 271 °F and 217 °F, respectively.

The change in the outer radius of the lead gamma shield, ΔR_l , is computed as follows.

$$\begin{aligned}\Delta R_l &= R_l \times \alpha_l \times \Delta T_l = 39.35 \text{ in.} \times 17.34 \times 10^{-6} \text{ in./in.}^\circ\text{F} (@300^\circ\text{F}) \times (271 - 70)^\circ\text{F} \\ &= 0.1372 \text{ in.}\end{aligned}$$

The change in the inner radius of the structural shell, ΔR_s , is computed as follows.

$$\begin{aligned}\Delta R_s &= R_s \times \alpha_s \times \Delta T_s = 39.35 \text{ in.} \times 9.2 \times 10^{-6} \text{ in./in.}^\circ\text{F} (@300^\circ\text{F}) \times (217 - 70)^\circ\text{F} \\ &= 0.0532 \text{ in.}\end{aligned}$$

Therefore the differential radial expansion between the lead and structural shell, ΔR , is as follows.

$$\Delta R = 0.1372 \text{ in.} - 0.0532 \text{ in.} = 0.084 \text{ in.}$$

Therefore, the lead cylinder, if it were free, would grow 0.084 in. more than the inner surface of the structural shell. If all of the differential expansion is accommodated in the lead, the lead strain, ε_l , would be the following.

$$\varepsilon_l = \Delta R / R_l = 0.084 \text{ in.} / 39.35 \text{ in.} = 0.00213 \text{ in./in.}$$

If the lead remained linear elastic, the maximum hoop stress in the lead would be,

$$\sigma_l = E_l \times \varepsilon_l = 2.06 \times 10^6 \text{ psi. (@300°F)} \times 0.00213 \text{ in./in.} = 4,388 \text{ psi.}$$

Conservatively assuming that the lead remains linear elastic, the interference pressure on the outer structural shell required to exert an average hoop stress of 4,388 psi. in the lead can be determined in the following way.

$$P_{interface} = \sigma_l \times \text{lead thickness} / R_{interface} = 4,388 \text{ psi.} \times 3.60 \text{ in.} / 39.35 \text{ in.} = 401 \text{ psi.}$$

This interference pressure would generate the following hoop stress in the structural shell.

$$\sigma_s = P_{interface} \times R_{interface} / t_s = 401 \text{ psi.} \times 39.35 / 1.50 = 10,520 \text{ psi.}$$

The total combine maximum stress intensity, σ , in the transfer cask during vacuum drying operations is then,

$$\sigma = 401 \text{ psi.} + 661 \text{ psi.} + 10,520 \text{ psi.} = 11,582 \text{ psi.}$$

Load Case 3: 30 psi Internal Pressure (2-D FEM)

A uniform 30 psi pressure is applied to all internal surfaces of the transfer cask up to the top cover and RAM access cover seal locations. Symmetry displacement boundary conditions are applied along the y -axis of the 2-dimensional axisymmetric model, and transfer cask is held in the y -direction at one location to prevent rigid body motion. A depiction of the Internal Pressure load case boundary conditions is provided in Figure 3.9.2-7.

Load Case 4: 115 °F Ambient Hot Thermal Environment (2-D FEM)

The temperature distribution resulting from a 115°F Ambient Environment, shown in Figure 3.9.2-4, is computed in Chapter 4, and is applied to all nodes of the transfer cask model. An ANSYS macro is used to assign each node of the transfer cask model to a node in the ANSYS thermal model (described in Chapter 4) that is closest to that node. The macro then applies these nodal temperatures to the transfer cask model. The temperature dependant coefficients of thermal expansion are applied to each of the corresponding material types, in order to induce thermal stresses in the model.

Symmetry displacement boundary conditions are applied along the y -axis of the 2-dimensional axisymmetric model, and transfer cask is held in the y -direction at one location to prevent rigid body motion.

Load Case 5: -20 °F Ambient Cold Thermal Environment (2-D FEM)

The temperature distribution resulting from a -20 °F Ambient Environment, shown in Figure 3.9.2-5, is computed in Chapter 4, and is applied to all nodes of the transfer cask model. Again, an ANSYS macro is used to assign each node of the transfer cask model to a node in the ANSYS thermal model (described in Chapter 4) that is closest to that node. The macro then applies these nodal temperatures to the transfer cask model. The temperature dependent coefficients of thermal expansion are applied to each corresponding material types, in order to induce thermal stresses in the model.

Symmetry displacement boundary conditions are applied along the y -axis of the 2-dimensional axisymmetric model, and transfer cask is held in the y -direction at one location to prevent rigid body motion.

Load Case 6: Transfer Loads (3-D FEM)

The Transfer load case consists of the loaded transfer cask in the horizontal position, supported at both top and bottom trunnions. An acceleration of 2g in all directions is applied to the transfer cask model in order to bound all possible transfer accelerations, and an internal pressure of 30 psi. is conservatively applied to the model to bound any possible pressure build up inside the cask.

The vertical and transverse accelerations are combined, so that a single horizontal acceleration is applied to the finite element model in the following way.

$$\text{Horizontal Acceleration} = [2g^2 \text{ transverse} + 2g^2 \text{ vertical}]^{1/2} = 2.828g$$

The horizontal inertial load of the transfer cask internals is accounted for by applying a cosine varying pressure on the inside surface of the cask inner shell. Assuming that the transfer cask internals react upon 90° arc of the inside surface, then the inertial load of the internals, $P_{(\theta)}$, which varies with angle, θ , ($\theta = 0$ is at the impact point), is governed by the following expression.

$$P_{(\theta)} = P_{\max} \cos(2\theta)$$

Where P_{\max} is the maximum load at the impact point ($\theta = 0$). Assuming the axial length of the applied load is L , the inside radius of the cask inner shell is R , and the load distribution, $P_{(\theta)}$ above, then the total inertial load generated by the internals, F , is the following.

$$F = \int_{-\frac{\pi}{4}}^{\frac{\pi}{4}} P_{\max} \cos(2\theta) \cos(\theta) LR d\theta$$

or,

$$F = \frac{P_{\max} LR}{2} \int_{-\frac{\pi}{4}}^{\frac{\pi}{4}} \cos((2+1)\theta) + \cos((2-1)\theta) d\theta$$

By integrating we get the following.

$$F = \left[\frac{P_{\max} LR}{2} \right] \left[\frac{\sin(3\theta)}{3} + \sin(\theta) \right]_{-\frac{\pi}{4}}^{\frac{\pi}{4}}$$

Therefore,

$$F = \left[\frac{P_{\max} LR}{2} \right] \left[\frac{\sin\left(\frac{3\pi}{4}\right)}{3} + \sin\left(\frac{\pi}{4}\right) - \frac{\sin\left(\frac{-3\pi}{4}\right)}{3} - \sin\left(\frac{-\pi}{4}\right) \right]$$

$$F = P_{\max} LR \left[\frac{\sin\left(\frac{3\pi}{4}\right)}{3} + \sin\left(\frac{\pi}{4}\right) \right]$$

The transfer cask inner shell inner diameter, $R = 35.25$ in., and the axial length of the applied load, $L = 183.6$ in. The total applied force, F , is equal to the inertial load of the cask internals, which is the following.

$$F = 115,000 \text{ lb.} \times \sqrt{8} g = 325,269 \text{ lb.}$$

Therefore, P_{\max} is the following.

$$P_{\max} = \frac{325,269}{(183.60)(35.25)} \left[\frac{\sin\left(\frac{3\pi}{4}\right)}{3} + \sin\left(\frac{\pi}{4}\right) \right]^{-1} = 53.307 \text{ psi.}$$

The axial inertial load of the transfer cask internals is accounted for by applying a pressure on the inside surface of the cask top cover. For a 2g inertial load, the applied axial pressure, P_a , is as follows.

$$P_a = 115,000 \text{ lb.} \times 2g / [\pi \times 35.70^2] = 57.444 \text{ psi}$$

Symmetry displacement boundary conditions are applied along the y-axis of the 3-dimensional axisymmetric model.

A depiction of the Transfer Loads load case boundary conditions is provided in Figure 3.9.2-8.

Load Case 7: 75g Bottom End Drop (2-D FEM)

The weight of the transfer cask internals (canister, basket, and fuel assemblies) is accounted for by applying equivalent pressures. The actual weights of the canister, basket, and fuel assemblies are 28.19 kips, 29.85 kips, and 51.52 kips, respectively. Therefore, the total actual weight of the cask internals is 109.56 kips. For conservatism, the weight of the cask internals used in this analysis is increased to 115 kips. The transfer cask inner radius is 35.25 in., and the inner radius of the ram access penetration is 10.00 in. The inertial load of the transfer cask internals reacts against the annular surface bounded by these two radii during a bottom end drop. The area of this reaction surface, A_{bi} , is as follows.

$$A_{bi} = \pi(35.25^2 - 10.00^2) = 3,589.47 \text{ in}^2.$$

The pressure equivalent to the inertial load of the internals under accident conditions, P_{bi} , is,

$$P_{in} = [115,000 / 3,589.47] \times 75 \text{ gs} = 2,403.86 \text{ psi.}$$

Symmetry displacement boundary conditions are applied along the y-axis of the 2-dimensional axisymmetric model. The bottom end of the transfer cask is held in the axial direction in order to simulate the rigid reaction force generated by the impact target. A 75 g inertial load in the positive y-direction is also applied to the model for the accident condition load case.

Local Trunnion Stress Computation Sheet A depiction of the Bottom End Drop load case boundary conditions is provided in Figure 3.9.2-9.

Load Case 8: 75g Top End Drop (2-D FEM)

The weight of the transfer cask internals (canister, basket, and fuel assemblies) is accounted for by applying equivalent pressures. The weight of the canister internals used in this analysis is 115,000 lb. The inertial load of the transfer cask internals reacts against the inside surface of the top cover assembly during a top end drop. The outer radius of the inside surface of the transfer cask top cover assembly is 35.70 in. Therefore the area of the reaction surface, A_{bi} , is as follows.

$$A_{bi} = \pi(35.70^2) = 4,003.93 \text{ in}^2.$$

The pressure equivalent to the inertial load of the internals under accident conditions, P_{bi} , is,

$$P_{in} = [115,000 / 4,003.93] \times 75 \text{ gs} = 2,154.13 \text{ psi}.$$

Symmetry displacement boundary conditions are applied along the y-axis of the 2-dimensional axisymmetric model. The outer surface of the top cover is held in the axial direction in order to simulate the rigid reaction force generated by the impact target. A 75 g inertial load in the negative y-direction is also applied to the model for the accident condition load case.

A depiction of the Top End Drop load case boundary conditions is provided in Figure 3.9.2-10.

Since the top end vertical drop will induce much higher shear stress in the weld between the transfer cask inner shell and top flange, therefore this load case used to calculate the weld stresses. The ANSYS run result file from this load case are post processed to get the maximum shear stress at this weld location.

The maximum shear stress is 5,034 psi and the allowable shear stress is $0.42 S_u$ ($0.42 \times 64,000 = 26,880$ psi, for 304 SS at 400°F). Factor of safety = $26,880/5,034 = 5.34$

Load Case 9: 75g Side Drop (3-D FEM)

During the 75g Side Drop load case, the loaded transfer cask is dropped onto a concrete target generating a transverse acceleration of 75g.

The impact side of the transfer cask is supported in the cask radial direction along the entire length of the cask. The radial support spans 15° of the model. The radial support is intended to model the reaction of the concrete target during impact.

The inertial load of the transfer cask internals is accounted for by applying a cosine varying pressure on the inside surface of the cask inner shell using the same method that was used for the Transfer Loads case. The total applied force, F , is equal to the inertial load of the cask internals, which is the following.

$$F = 115,000 \text{ lb.} \times 75g = 8,625,000 \text{ lb.}$$

Therefore, using the formula derived for the Transfer Loads case, P_{\max} is the following.

$$P_{\max} = \frac{8,625,000}{(183.60)(35.25)} \left[\frac{\sin\left(\frac{3\pi}{4}\right)}{3} + \sin\left(\frac{\pi}{4}\right) \right]^{-1} = 1,413.53 \text{ psi.}$$

Symmetry displacement boundary conditions are applied along the y-axis of the 3-dimensional axisymmetric model. An internal pressure of 30 psi. is conservatively to the model to bound any possible pressure build up inside the cask.

A depiction of the 75g Side Drop load case boundary conditions is provided in Figure 3.9.2-11.

Load Case 10: Transfer Thermal Accident (Fire)

The stresses generated during the thermal accident are computed by hand, and use the thermal stresses generated from the Transfer Loads load case, computed with ANSYS.

The applied loads used to calculate the maximum stress in the transfer during fire accident event, include a maximum radial temperature gradient, and normal conditions transfer loads. The stresses generated in the transfer cask shell by the temperature gradient are computed using hand calculations. The resulting stresses caused by the thermal temperature gradient are added to the stresses computed for the transfer load case. Since the primary load for the fire accident is caused by the radial temperature gradient, the maximum transfer cask stress is computed for the outer radial structural shell.

The maximum stress generated by the radial thermal gradient fire accident will occur in the outer structural shell due to the thermal expansion of the lead gamma shield. From Chapter 4, the maximum temperature difference between the lead gamma shield and the structural shell occurs when the lead and structural shell are at 618 °F and 553 °F, respectively.

The change in the outer radius of the lead gamma shield, ΔR_l , is computed as follows.

$$\begin{aligned} \Delta R_l &= R_l \times \alpha_l \times \Delta T_l = 39.35 \text{ in.} \times 19.68 \times 10^{-6} \text{ in./in.}^\circ\text{F} (@600^\circ\text{F}) \times (618 - 70)^\circ\text{F} \\ &= 0.4243 \text{ in.} \end{aligned}$$

The change in the inner radius of the structural shell, ΔR_s , is computed as follows.

$$\begin{aligned} \Delta R_s &= R_s \times \alpha_s \times \Delta T_s = 39.35 \text{ in.} \times 9.8 \times 10^{-6} \text{ in./in.}^\circ\text{F} (@600^\circ\text{F}) \times (553 - 70)^\circ\text{F} \\ &= 0.1863 \text{ in.} \end{aligned}$$

Therefore the differential radial expansion between the lead and structural shell, ΔR , is as follows.

$$\Delta R = 0.4243 \text{ in.} - 0.1863 \text{ in.} = 0.238 \text{ in.}$$

Therefore, the lead cylinder, if it were free, would grow 0.238 in. more than the inner surface of the structural shell. If all of the differential expansion is accommodated in the lead, the lead strain, ε_l , would be the following.

$$\varepsilon_l = \Delta R / R_l = 0.238 \text{ in.} / 39.35 \text{ in.} = 0.006 \text{ in./in.}$$

If the lead remained linear elastic, the residual hoop stress in the lead would be,

$$\sigma_l = E_l \times \varepsilon_l = 1.64 \times 10^6 \text{ psi. (@600°F)} \times 0.006 \text{ in./in.} = 9,840 \text{ psi.}$$

Conservatively assuming that the lead remains linear elastic, the interference pressure on the outer structural shell required to exert an average hoop stress of 9,840 psi. in the lead can be determined in the following way.

$$P_{\text{interface}} = \sigma_l \times \text{lead thickness} / R_{\text{interface}} = 9,840 \text{ psi.} \times 3.60 \text{ in.} / 39.35 \text{ in.} = 900 \text{ psi.}$$

This interference pressure would generate the following hoop stress in the structural shell.

$$\sigma_s = P_{\text{interface}} \times R_{\text{interface}} / t_s = 900 \text{ psi.} \times 39.35 / 1.50 = 23,610 \text{ psi.} \approx 23.61 \text{ ksi}$$

The total combine maximum stress, σ , in the transfer cask during the fire accident is then,

$$\begin{aligned} \sigma &= 5.02 \text{ ksi (stress due to 30 psi internal pressure from load case 3)} + 23.61 \text{ ksi} \\ &= 28.63 \text{ ksi} \end{aligned}$$

3.9.2.3 ANSYS Analysis Results and Reporting Methodology

The maximum nodal stress intensities in various components of the NUHOMS®-OS187H Transfer Cask are extracted from the ANSYS results files for all load cases. These stresses are compared to the normal and accident condition allowable stresses set forth by ASME B&PV Code Subsection NC [2]. Allowable Stresses are derived from material properties taken from Reference 6 at the various component temperatures listed in the Material Properties section. A summary of the maximum transfer cask component stresses and corresponding allowable stresses are presented in Table 3.9.2-1.

The maximum nodal stress intensities ($P_m + P_b$) are conservatively compared to the allowable membrane stress intensities, unless otherwise stated. In load cases where the nodal stress intensity exceeds the membrane allowable stress, individual membrane and membrane plus bending stresses are computed by linearizing the maximum component stresses through the thickness of the component. The resulting linearized stresses are then compared to their corresponding P_m and $P_m + P_b$ allowable stresses.

For the load combinations involving mechanical loads and thermal loads (i.e. 6g Lifting plus 115 °F ambient), the maximum stresses from the mechanical load case and the maximum stress from the thermal load case are simply summed for each of the major cask components. This method of computing the maximum load combination stresses is very conservative, because, in general, the maximum stress caused by a mechanical load and the maximum stress caused by a thermal load will not occur at the same location in the transfer cask.

Typically, fictitious stresses at nodes where point contact exists with a beam element used to model a transfer cask bolt is ignored. These unrealistic stresses usually occur in the top cover at locations where the top cover bolts are fixed to the cover by node coupling (in all degrees of freedom) at a single node.

3.9.2.4 Transfer Cask Trunnion Local Stresses

The purpose of this section is to evaluate the local stress intensities in the NUHOMS[®]-OS187H Transfer Cask radial shells near the top and bottom trunnions, due to all applied loads during fuel loading and transfer operations.

3.9.2.4.1 Approach

The NUHOMS[®]-OS187H Transfer Cask has two top trunnions made of SA-182 Gr. FXM19 (22Cr-13Ni-5Mn Forging) and two bottom trunnions made of SA-182 Gr. F304. The transfer cask radial shells are made of SA-240, Gr. 304 (18Cr-8Ni).

The two top trunnions are used to first lift the cask, containing an empty DSC into a fuel pool for loading of the spent fuel. After the spent fuel has been loaded into the DSC, the cask is lifted to a decontamination area. After draining and drying of the pool water, welding of the canister cover, and bolting of the cask top cover, the cask is placed on a trailer for transfer to onsite HSM-H.

The transfer cask is vertically lifted into the trailer and rests its bottom trunnions on a support frame mounted to the top of the trailer. Then the cask is allowed to rotate, using the bottom trunnion supports as the pivot points, into a horizontal position until the top trunnions rest on their supports on the trailer. Throughout the operation the maximum total load is applied to the cask top trunnions. After the cask has been placed in the trailer, it is supported by all four trunnions and is subject to a set of specified handling loads.

The following two load cases are analyzed for the four cask trunnions and adjoining shell:

- a) Lifting Loads (Cask lifted from the pool to the decontamination area and then to the trailer)

The two top trunnions are analyzed for vertical 6 g and 10g loads as required by ANSI N14.6 [11]. The two bottom trunnions are not used during lifting of the cask.

- b) Handling Loads (Cask in a horizontal position inside trailer)

All four trunnions rest on the supports in the trailer. These four trunnions are designed to resist the following transfer loads:

DW (dead weight) + 1g Axial

DW + 1g Transverse

DW + 1g Vertical

DW + 1/2g Axial + 1/2g Transverse + 1/2g Vertical

(Directions are relative to a horizontal cask)

All four trunnions carry the axial and vertical loads while only one top trunnion and one bottom trunnion on the same side of the cask will carry the transverse load. The bottom trunnion has the same cross section geometry as the top trunnion. However, the structural shell near the bottom trunnion is thinner (1.5 inches) than the shell near the top trunnion (2 inches). Also, there is a 1 inch thick reinforcing pad at top trunnion location. Thus, the bottom trunnion is critical with respect to stress generated by the handling load. The transfer loads are therefore analyzed only for the weaker bottom trunnions.

The outer neutron shield cylinder and structural cylinder are welded to the trunnion. Therefore, both cylinders resist the trunnion loads. However, for conservatism, support of outer shell is neglected in the analysis.

The trunnions and cask shells are assumed to be at a 300° F uniform temperature during transfer, which is conservative compared to the maximum temperature computed in Chapter 4 for the 115 °F ambient environment condition (see Figure 3.9.2-4).

The following calculations are based on the method described in Reference 10. A spreadsheet, based on Figure 3.9.2-12 taken from Reference 10, was created to aid in the computation. Table 3.9.2-2 through Table 3.9.2-7 are hardcopies of this spreadsheet for the various load cases analyzed. Typical parameters used in the spread sheet are hand calculated for load case 2D (DW + 0.5g Axial + 0.5g Vertical + 0.5g Transverse in Table 3.9.2-7) to illustrate the calculation process.

3.9.2.4.2 Load Cases

The weights of NUHOMS[®]-OS187H Transfer Cask components are the same as the component weights listed in Section 3.9.2.1.2. The weight for the NUHOMS[®]-OS187H Transfer Cask is 241,330 lb., including the loaded DSC and water in the canister and annulus. However, for conservatism, a weight of 250,000 lb. is used in this analysis.

The following moment arms are used for the two load cases:

Load Case	g Load	Moment Arm Length	Reaction Support
Lifting	6g axial	9.750 in.*	Top two trunnions only
Transfer Loads	DW +1g Axial DW+1g vertical DW+1g transverse DW + 0.5g Axial + 0.5g Vertical + 0.5g Transverse	7.135 in.**	All four top and bottom trunnions

* $[105.96 \text{ (trunnion outside)} - 2 \times 0.38 \text{ in. (trunnion lip)} - 3.00 \text{ in. (average outer shoulder width)} - 82.70 \text{ in. (shell outer diameter)}] / 2 = 9.75 \text{ in.}$

** $[49.61 - 81.7/2 - 3.25/2] = 7.135 \text{ in.}$

3.9.2.4.3 Material Properties

The following pertinent material properties are taken from Reference 6 at 300 °F.

Property	SA-240, Type 304 stainless steel (cask shells and pad)
S_m	20 ksi
S_v	22.4 ksi
S_u	66.2

3.9.2.4.4 Stress Criteria

All load cases analyzed are normal condition (Level A) load cases. According to ASME Code, Section III, Subsection NC [2], the maximum allowable local membrane (P_l) and local membrane plus bending ($P_l + P_b$) stress intensities for normal conditions are $1.5S_m$ and $3.0S_m$ respectively.

The transfer cask radial shells are constructed from SA-240, Type 304 stainless steel. The shell material properties are conservatively taken at 300 °F, which bounds the maximum inner shell and structural shell temperatures generated during the 115 °F ambient transfer condition.

Therefore, the maximum allowable membrane and membrane plus bending stress intensities are as follows.

Stress Category	S_m for SA-240 Type 304 at 300 °F [6]	Stress Criteria	Maximum Allowable Stress
P_m	20.0 ksi.	$1.5S_m$	30.0 ksi.
$P_m + P_b$	20.0 ksi.	$3.0S_m$	60.0 ksi.

3.9.2.4.5 Stress Computation

Note that all calculation results performed here are rounded to significant figures, even though the results computed in the attached spreadsheets (Table 3.9.2-2 through Table 3.9.2-7) are not rounded.

Load Case 1. 6g Lifting

The 6g lifting loads are as follows.

Direction	g-load
Longitudinal	6.0g
Vertical	0.0g
Lateral	0.0g

At the top trunnions the g-load per trunnion is:

$$6.0g \text{ (Axial)} / 2 = 3.0 g \text{ Axial per trunnion.}$$

The following analytical method is taken from Reference 10. See Figure 3.9.2-12 for derivation of the following terms and equations.

Trunnion loads:

$$P = 0.0 \text{ lb.}$$

$$M_L = 3.0 \times 1.1 \times 250,000 \times 9.75 = 8,043,750 \text{ in. lb.}$$

$$M_C = 0.0 \text{ in. lb.}$$

$$M_T = 0.0 \text{ in. lb.}$$

$$V_L = 3.0 \times 1.1 \times 250,000 = 825,000 \text{ lb.}$$

$$V_C = 0.0 \text{ lb.}$$

The following parameters based on the nominal geometry and Reference 10 formulae are calculated as follows.

At Trunnion – Pad intersection:

$$\text{Trunnion radius, } r_0 = 8.575 \text{ in.}$$

$$\text{Mean radius, } R_m = 39.35 + 3.0/2 = 40.85 \text{ in.}$$

$$\text{Shell and Pad thickness, } T = 2.0 + 1.0 = 3.0 \text{ in}$$

At Pad – Shell intersection:

$$\text{Trunnion Pad radius, } r_0 = 13.575 \text{ in.}$$

$$\text{Mean radius, } R_m = 39.35 + 2.0/2 = 40.35 \text{ in.}$$

$$\text{Shell thickness, } T = 2.0 \text{ in}$$

Shell stresses are calculated at Trunnion-Pad intersection (in Table 3.9.2-2) and at Pad – Shell intersection (in Table 3.9.2-3).

Load Case 2.

Transfer Loads

Load Case 2A.

DW + 1g Axial

The transfer loads are as follows:

Direction	g-load
Axial	1.0g
Vertical (DW)	1.0g
Lateral	0g

The top trunnion carries no axial load because it rests on a sliding support.

At the top and bottom trunnions the g-load per trunnion is:

1.0g (axial) / 2 sides / 1 set of trunnions = 0.5g axial per bottom trunnion.

1.0g (vertical) / 2 sides / 2 sets of trunnions = 0.25g vertical per top and bottom trunnion

Due to the above loads, stresses in the bottom trunnion locations will be critical since shell thickness at the bottom trunnion intersection is thinner relative to that of the top trunnions.

Trunnion loads:

$$P = 0 \text{ lb.}$$

$$M_L = 0.5 \times 250,000 \times 7.135 = 891,875 \text{ in. lb.}$$

$$M_C = 0.25 \times 250,000 \times 7.135 = 445,938 \text{ in. lb.}$$

$$M_T = 0.0 \text{ in. lb.}$$

$$V_L = 0.5 \times 250,000 = 125,000 \text{ lb.}$$

$$V_C = 0.25 \times 250,000 = 62,500 \text{ lb.}$$

At bottom trunnion locations:

$$\text{Trunnion radius, } r_0 = 8.575 \text{ in.}$$

$$\text{Mean radius, } R_m = 39.35 + 1.5/2 = 40.1 \text{ in.}$$

$$\text{Shell thickness, } T = 1.5 \text{ in}$$

See Table 3.9.2-4 for shell stress calculations and results.

Load Case 2B.*DW + 1g Vertical*

The transfer loads are as follows:

Direction	g-load
Axial	0g
Vertical (DW)	1.0g + 1.0g = 2.0g
Transverse	0g

At the top and bottom trunnions the g-load per trunnion is:

$$2.0g \text{ (vertical)} / 2 \text{ sides} / 2 \text{ set trunnions} = 0.5g \text{ vertical per trunnion}$$

Trunnion loads:

$$P = 0 \text{ lb.}$$

$$M_L = 0 \text{ in. lb.}$$

$$M_C = 0.5 \times 250,000 \times 7.135 = 891,875 \text{ in. lb.}$$

$$M_T = 0.0 \text{ in. lb.}$$

$$V_L = 0 \text{ lb.}$$

$$V_C = 0.5 \times 250,000 = 125,000 \text{ lb.}$$

At bottom trunnion locations:

$$\text{Trunnion radius, } r_0 = 8.575 \text{ in.}$$

$$\text{Mean radius, } R_m = 39.35 + 1.5/2 = 40.1 \text{ in.}$$

$$\text{Shell thickness, } T = 1.5 \text{ in}$$

See Table 3.9.2-5 for shell stresses calculations and results.

Load Case 2C.*DW + 1g Transverse*

The transfer loads are as follows:

Direction	g-load
Axial	0g
Vertical (DW)	1.0g
Transverse	1.0g

At the top and bottom trunnions the *g*-load per trunnion is:

$$1.0g \text{ (vertical)} / 2 \text{ sides} / 2 \text{ set trunnions} = 0.25g \text{ vertical per trunnion}$$

$$1.0g \text{ (transverse)} / 2 \text{ sides} / 1 \text{ set trunnions} = 0.5g \text{ transverse per trunnion}$$

Trunnion loads:

$$P = 0.5 \times 250,000 = 125,000 \text{ lb.}$$

$$M_L = 0 \text{ in. lb.}$$

$$M_C = 0.25 \times 250,000 \times 7.135 = 445,938 \text{ in. lb.}$$

$$M_T = 0.0 \text{ in. lb.}$$

$$V_L = 0 \text{ lb.}$$

$$V_C = 0.25 \times 250,000 = 62,500 \text{ lb.}$$

At bottom trunnion locations:

$$\text{Trunnion radius, } r_0 = 8.575 \text{ in.}$$

$$\text{Mean radius, } R_m = 39.35 + 1.5/2 = 40.1 \text{ in.}$$

$$\text{Shell thickness, } T = 1.5 \text{ in}$$

See Table 3.9.2-6 for shell stresses calculations and results.

Load Case 2D.

$$DW + 0.5g \text{ Axial} + 0.5g \text{ Vertical} + 0.5g \text{ Transverse}$$

The transfer loads are as follows:

Direction	g-load
Axial	0.5g
Vertical (DW)	1.0g + 0.5 = 1.5g
Transverse	0.5g

The top trunnion carries no axial load because it rests on a sliding support.

At the top and bottom trunnions the g-load per trunnion is:

$$0.5g \text{ (axial)} / 2 \text{ sides} / 1 \text{ set of trunnions} = 0.25g \text{ axial per bottom trunnion}$$

$$1.5g \text{ (vertical)} / 2 \text{ sides} / 2 \text{ sets of trunnions} = 0.375g \text{ vertical per trunnion}$$

$$0.5g \text{ (transverse)} / 2 \text{ sides} / 1 \text{ set of trunnions} = 0.25g \text{ axial per trunnion}$$

Trunnion loads:

$$P = 0.25 \times 250,000 = 62,500 \text{ lb.}$$

$$M_L = 0.25 \times 250,000 \times 7.135 = 445,938 \text{ in. lb.}$$

$$M_C = 0.375 \times 250,000 \times 7.135 = 668,906 \text{ in. lb.}$$

$$M_T = 0.0 \text{ in. lb.}$$

$$V_L = 0.25 \times 250,000 = 62,500 \text{ lb.}$$

$$V_C = 0.375 \times 250,000 = 93,750 \text{ lb.}$$

At bottom trunnion locations:

$$\text{Trunnion radius, } r_0 = 8.575 \text{ in.}$$

$$\text{Mean radius, } R_m = 39.35 + 1.5/2 = 40.1 \text{ in.}$$

$$\text{Shell thickness, } T = 1.5 \text{ in}$$

See Table 3.9.2-7 for shell stress calculations and results.

These transfer load case parameter values are determined from tables in Reference 10. The following calculated parameters for load case 2D are given here to illustrate the typical procedure used in spreadsheet Table 3.9.2-2 through Table 3.9.2-7.

$$\gamma = R_m/T = 26.7333$$

$$\beta = 0.875 \times r_0/R_m = 0.1871$$

$$\frac{P}{R_m T} = \frac{62,500}{40.1(1.5)} = 1,039$$

$$\frac{6P}{T^2} = \frac{6(62,500)}{1.5^2} = 166,667$$

$$\frac{M_C}{R_M^2 \beta T} = \frac{668,906}{40.1^2 (0.1871)(1.5)} = 1,482$$

$$\frac{6M_C}{R_M \beta T^2} = \frac{6(668,906)}{40.1(0.1871)(1.5^2)} = 237,747$$

$$\frac{M_L}{R_M^2 \beta T} = \frac{445,938}{40.1^2 (0.1871)(1.5)} = 988$$

$$\frac{6M_L}{R_M \beta T^2} = \frac{6(445,938)}{40.1(0.1871)(1.5^2)} = 158,498$$

$$\tau_{X\phi} \text{ for } V_C = \frac{V_C}{\pi r_0 T} = \frac{93,750}{\pi(8.575)(1.5)} = 2,320$$

$$\tau_{X\phi} \text{ for } V_L = \frac{V_L}{\pi r_0 T} = \frac{62,500}{\pi(8.575)(1.5)} = 1,546$$

It may be noted that some numbers in hand calculation do not exactly match the spreadsheet (Table 3.9.2-7) numbers. The reason is that hand calculation results are rounded as compared to the results in the spreadsheets.

3.9.2.4.6 Stress Intensity Calculation

Membrane plus bending Stress intensities are calculated in the following way.

$$S.I. = \text{Max. of} \left\{ \begin{array}{l} \frac{1}{2} \left[(\sigma_x + \sigma_\phi) \pm \sqrt{(\sigma_x - \sigma_\phi)^2 + 4\tau^2} \right] \\ \sqrt{(\sigma_x - \sigma_\phi)^2 + 4\tau^2} \end{array} \right.$$

In order to calculate the membrane or bending stress intensity, only those components associated with membrane or bending stress, respectively, are summed to calculate σ_ϕ , σ_x and τ .

3.9.2.4.7 Local Shell Stress Results

The Table 3.9.2-8 summarizes the maximum stress intensities for both loading conditions.

3.9.2.4.8 Local Shell Stress Conclusions

All calculated local membrane stresses are less than the allowable local membrane stress of 30,000 psi., and all local membrane plus bending stress intensities are less than the allowable local membrane plus bending stress of 60,000 psi. Therefore, the NUHOMS®-OS187H Transfer Cask shells adjoining the trunnions are structurally adequate with respect to local stresses generated during lifting and transfer operations.

3.9.2.5 Stress and Deflection of Transfer Cask Inner Shell Support Rails

The 3D finite element model used for side drop analyses as described in Appendix 3.9.2, Section 3.9.2.2.3B is modified as follows and used to calculate the stresses and deflections of the transfer cask inner shell along the support rail locations.

Finite Element Model Modifications

1. Including the 3" wide x 0.12 thick rails in the 3D transfer cask inner shell (SHELL 43 element).
2. Including canister shell (SOLID 45 element) in the 3D model.
3. Gap element (CONTACT 52) is used between the canister shell and transfer cask inner shell and between the canister shell and inner shell rail.

Radial gap elements (CONTACT 52) are used to simulate the interface between the outer radius of the canister and inner radius of the cask inner shell. Each gap element contains two nodes; one on each surface of the structure. The gap size at each gap element is determined by the difference between the canister outer radius and the inside radius of the cask (canister outer radius = 34.875" and cask inner radius = 35.25" to give a 0.375 inch mean gap). Radial gap elements are generated using a ANSYS macro. Actual gap sizes for the gap element, at each radial location, were determined and input into the model as real constants using another ANSYS macro. This macro accepts the drop orientation and model geometry as inputs and determines the circumferential position of each gap element. The macro then computes the appropriate real constants and applies to appropriate gap elements.

During drops on cask rails (180° side drop), the initial gaps between the canister and the cask are modified using the ANSYS macro. Two 3 inch wide and 0.12 inch thick rails are welded to the cask inner shell at 12° on both sides of the vertical center line of the model and another set of two rails are welded at 38° on both sides of the same vertical center line. For the 180° side drop onto the rails, the initial gaps at the two inner rail locations are assumed closed (0 gap). In-between these two rail locations, the initial gaps are set to 0.12 inches. On the other two rail locations, the gaps are initially set to open, and the gap sizes are generated by macro with consideration of the rail thickness.

The ANSYS 3D finite element models including cask shell, lead, rails, canister, and gap elements are shown on Figure 3.9.2-13 to Figure 3.9.2-17.

Loadings

Pressures applied in the radial direction to the inner surface of the canister in the 3-dimensional finite element model are based on a cosine distribution. This pressure distribution simulates the load which the internal canister contents exert on the inner canister wall. Two drop orientations are analyzed.

The canister initial impacts on two rails (168° and 192°). See Figure 3.9.2-18.

The canister initial impacts on one rail (168°). See Figure 3.9.2-19.

Materials

In order to properly calculate the deflections of the rails, elastic and inelastic material properties of the canister and cask at the temperatures are used for analysis.

Results

The following table summarizes the maximum stress intensities at the transfer cask inner and outer shells for the above two drop load cases.

Summary of Maximum Stress Intensities and Allowables

Load Case	Component	Stress Category	Calculated Max. Stress Intensity (Ksi)	Allowable Membrane Stress Intensity (Ksi) ⁽¹⁾	Factor of Safety
Impact on Two Rails	Inner Shell	$P_L + P_b$	40.35	44.8	1.11
	Outer Shell	$P_L + P_b$	37.54	46.34	1.23
Impact on One Rail	Inner Shell	$P_L + P_b$	36.11	44.8	1.24
	Outer Shell	$P_L + P_b$	38.41	46.34	1.21

Note:

1. Allowable stresses are taken from Appendix 3.9.2, Section 3.9.2.2. Since the calculated maximum membrane plus bending stress intensity ($P_L + P_b$) is less than the allowable membrane stress intensity (P_m), therefore only maximum membrane plus bending stress intensity ($P_L + P_b$) is reported.

All the calculated stresses are less than the code allowables and the calculated maximum deflection in the rail is 0.02", this small deflection will not affect the retrieving of the canister from the transfer cask after an accident drop.

The maximum stress intensity plots of the cask inner shell and outer shell for the impact to the two rails load case are shown on Figure 3.9.2-20 and Figure 3.9.2-21, respectively. The maximum stress intensity plots of the inner shell and outer shell for the impact to the one rail load case are shown on Figure 3.9.2-22 and Figure 3.9.2-23, respectively.

3.9.2.6 References

1. 10CFR Part 72, Licensing Requirement for Storage of Spent Fuel in an Independent Spent Fuel Storage Installation.
2. ASME Code Section III, Subsection NC and Appendices, 1998, through 2000 addenda.
3. American Society of Mechanical Engineers, ASME Boiler and Pressure Vessel Code, Section III, Appendix F, 1998, through 2000 addenda.
4. ANSYS Users Manual, Rev. 5.6, 1998.
5. Not used.
6. American Society of Mechanical Engineers, ASME Boiler and Pressure Vessel Code, Section II, Part D, 1998, through 2000 addenda.
7. Baumeister & Marks, Standard Handbook for Mechanical Engineers, 7th Edition.
8. An Assessment of Stress-Strain Data Suitable for Finite Element Elastic-Plastic Analysis of Shipping Containers, NUREG/CR-0481.
9. Stress Analysis of Closure Bolts for Shipping Casks, NUREG/CR-6007, April 1992.
10. Welding Research Council (WRC), Local Stresses in Spherical and Cylindrical Shells Due To External Loadings, Bulletin 107.
11. Special Lifting Devices for Shipping Containers Weighing 10,000 Pounds or More, ANSI N14.6, 1993.

Table 3.9.2-1
Summary of OS-187H Transfer Cask Stress Analysis

Load Case Number	Loading Condition	Service Level	Component		Maximum Stress Intensity (ksi)	Allowable Membrane Stress Intensity (ksi)
1	6g Vertical Lifting	A	Structural Shell	P_m	12.13	20.00
				$P_m + P_b$	27.75	30.00
			Top Cover		7.49	31.40
			Inner Shell		15.39	18.70
			Bottom End plates	P_m	14.68	20.00
				$P_m + P_b$	28.51	30.00
			RAM Acc. and Cover	P_m	13.08	20.00
				$P_m + P_b$	20.48	30.00
1A	6g Vertical Lifting + Thermal Loads	A	Structural Shell		46.69	60.00 ⁽¹⁾
			Top Cover		16.05	94.20 ⁽¹⁾
			Inner Shell		36.60	56.10 ⁽¹⁾
			Bottom End plates		38.79	60.00 ⁽¹⁾
			RAM Access and Cover		33.42	60.00 ⁽¹⁾
2	Vacuum Drying	A	Structural Shell		11.58	60.00 ⁽¹⁾
3	30 psi. Internal Pressure	A	Structural Shell		5.02	20.00
			Top Cover		5.54	31.40
			Inner Shell		4.41	18.70
			Bottom End plates		5.16	20.00
			RAM Access and Cover		4.71	20.00
4	115°F Ambient Hot Thermal Environment	A	Structural Shell		19.04	60.00 ⁽¹⁾
			Top Cover		8.56	94.20 ⁽¹⁾
			Inner Shell		21.21	56.10 ⁽¹⁾
			Bottom End plates		10.28	60.00 ⁽¹⁾
			RAM Access and Cover		12.94	60.00 ⁽¹⁾

Table 3.9.2-1 (continued)
Summary of OS-187H Transfer Cask Stress Analysis

Load Case Number	Loading Condition	Service Level	Component	Maximum Stress Intensity (ksi)	Allowable Membrane Stress Intensity (ksi)
5	-20°F Ambient Cold Thermal Environment	A	Structural Shell	18.32	60.00 ⁽¹⁾
			Top Cover	7.30	94.20 ⁽¹⁾
			Inner Shell	24.84	56.10 ⁽¹⁾
			Bottom End plates	10.53	60.00 ⁽¹⁾
			RAM Access and Cover	11.73	60.00 ⁽¹⁾
6	Transfer Inertial Loads (2g Vertical + 2g Transverse + 2g Axial)	A	Structural Shell	11.18	20.00
			Top Cover	17.60	31.40
			Inner Shell	6.06	18.70
			Bottom End plates	1.76	20.00
			RAM Access and Cover	2.89	20.00
6A	Transfer Loads + Internal Pressure	A	Structural Shell	9.49	20.00
			Top Cover	17.69	31.40
			Inner Shell	5.40	18.70
			Bottom End plates	4.75	20.00
			RAM Access and Cover	4.15	20.00
6B	Transfer Loads + 115° F Ambient + Internal Pressure	A	Structural Shell	28.53	60.00 ⁽¹⁾
			Top Cover	26.25	94.20 ⁽¹⁾
			Inner Shell	26.61	56.10 ⁽¹⁾
			Bottom End plates	15.03	60.00 ⁽¹⁾
			RAM Access and Cover	17.09	60.00 ⁽¹⁾
6C	Transfer Loads + -20° F Ambient + Internal Pressure	A	Structural Shell	27.81	60.00 ⁽¹⁾
			Top Cover	24.99	94.20 ⁽¹⁾
			Inner Shell	30.24	56.10 ⁽¹⁾
			Bottom End plates	15.28	60.00 ⁽¹⁾
			RAM Access and Cover	15.88	60.00 ⁽¹⁾
7	75g Bottom End Drop + Internal Pressure	D	Structural Shell	35.16	46.34
			Top Cover	10.07	65.94
			Inner Shell	13.02	44.80
			Bottom End plates	28.23	46.34
			RAM Access and Cover	38.46	48.00

Table 3.9.2-1 (concluded)
OS-187H Transfer Cask Maximum Stresses

Load Case Number	Loading Condition	Service Level	Component	Maximum Stress Intensity (ksi)	Allowable Membrane Stress Intensity (ksi)
8	75g Top End Drop + Internal Pressure	D	Structural Shell	19.11	46.34
			Top Cover	27.89	65.94
			Inner Shell	10.07	44.80
			Bottom End plates	6.56	46.34
			RAM Access and Cover	4.83	48.00
9	75g Side Drop + Internal Pressure	D	Structural Shell	P_m	42.95
				$(P_m \text{ or } P_L) + P_b$	58.17
			Top Cover	P_m	60.38
				P_L	77.81 ⁽⁴⁾
				$(P_m \text{ or } P_L) + P_b$	91.90
			Inner Shell	P_m	33.43
				$(P_m \text{ or } P_L) + P_b$	49.86
			Bottom End plates	P_m	43.88
				P_L	51.26 ⁽⁴⁾
				$(P_m \text{ or } P_L) + P_b$	48.28
			RAM Access and Cover	P_m	37.14
				$(P_m \text{ or } P_L) + P_b$	47.74
10	Transfer Thermal Accident (Fire)	D	Structural Shell	28.63	58.32 ⁽²⁾

(1) $P_L + P_b + Q$ allowable stress.

(2) $S_m = 16.2$ ksi. For SA-240 type 304 at a temperature of 650° F. (the maximum transfer cask temperature is 618° F during the thermal accident [Chapter 4]). The allowable is taken as $3.6S_m$.

(3) Membrane plus bending $[(P_m \text{ or } P_L) + P_b]$ allowable stress.

(4) Stresses at the edge of the impact target support at the 15° location are considered local and are compared to P_L allowable stresses.

Table 3.9.2-2
Computation Spreadsheet for the 6g Lifting, Top Trunnion,
Local Stresses at Trunnion Pad

Table 2 - 6g Lifting, Top Trunnion Pad

Transfer Loads applied to the NUHOMS-OS187H Transfer Cask

Applied Loads

W	250000
P	0
ML	8043750
MC	0
MT	0
VL	825000
VC	0

Geometry

T	3
r0	8.575
Rm	40.85

Geometric Parameters

gamma	13.6167
beta	0.1837

from fig	read curves for	multiplier	abs. stress values	column # =	1	2	3	4	5	6	7	8
					Au	Al	Bu	Bl	Cu	Cl	Du	DI
3C AND 4C	0	0	0	0	0	0	0	0	0	0	0	0
1C AND 2C-1	0	0	0	0	0	0	0	0	0	0	0	0
3A	0	0	0	0	0	0	0	0	0	0	0	0
1A	0	0	0	0	0	0	0	0	0	0	0	0
3B	1.4	8748	12247	0	-12247	-12247	12247	12247	0	0	0	0
1B OR 1B-1	0.046	714702	32876	0	-32876	32876	32876	-32876	0	0	0	0
Summation of phi stresses => sigma phi =					-45123	20629	45123	-20629	0	0	0	0
3C AND 4C	0	0	0	0	0	0	0	0	0	0	0	0
1C-1 AND 2C	0	0	0	0	0	0	0	0	0	0	0	0
4A	0	0	0	0	0	0	0	0	0	0	0	0
2A	0	0	0	0	0	0	0	0	0	0	0	0
4B	0.48	8748	4199	0	-4199	-4199	4199	4199	0	0	0	0
2B OR 2B-1	0.072	714702	51459	0	-51459	51459	51459	-51459	0	0	0	0
Summation of X stresses => sigma X =					-55658	47260	55658	-47260	0	0	0	0
Shear stress due to torsion MT					0	0	0	0	0	0	0	0
Shear stress due to load VC					0	0	0	0	0	0	0	0
Shear stress due to load VL					10208	0	0	0	-10208	-10208	10208	10208
Summation of shear stresses tau =					0	0	0	0	-10208	-10208	10208	10208
stress intensities =>					55658	47260	55658	47260	20416	20416	20416	20416
membrane components of sigma phi =>					-12247	-12247	12247	12247	0	0	0	0
membrane components of sigma X =>					-4199	-4199	4199	4199	0	0	0	0
tau =>					0	0	0	0	-10208	-10208	10208	10208
membrane stress intensities =>					12247	12247	12247	12247	20416	20416	20416	20416

Table 3.9.2-3
Computation Spreadsheet for the 6g Lifting, Top Trunnion,
Local Stresses at Pad - Shell Intersection

Table 6. (6g Lifting Test)-Top Trunnion (Local stresses at pad - shell intersection)

Transfer Loads applied to the NUHOMS-OS187H Transfer Cask

Applied Loads		Geometry		Geometric Parameters	
W	250000	T	2	gamma	20.1750
P	0	r0	13.575	beta	0.2944
ML	8043750	Rm	40.35		
MC	0				
MT	0				
VL	825000				
VC	0				

		column # =				1	2	3	4	5	6	7	8
from fig	read curves for	multiplier	abs. stress values			Au	Al	Bu	Bl	Cu	Cl	Du	DI
3C AND 4C	0	0	0	0	0	0	0	0	0	0	0	0	0
1C AND 2C-1	0	0	0	0	0	0	0	0	0	0	0	0	0
3A	0	0	0	0	0					0	0	0	0
1A	0	0	0	0	0					0	0	0	0
3B	2	8391	16783			-16783	-16783	16783	16783				
1B OR 1B-1	0.024	1015785	24379			-24379	24379	24379	-24379				
Summation of phi stresses => sigma phi =						-41162	7596	41162	-7596	0	0	0	0
3C AND 4C	0	0	0	0	0	0	0	0	0	0	0	0	0
1C-1 AND 2C	0	0	0	0	0	0	0	0	0	0	0	0	0
4A	0	0	0	0	0					0	0	0	0
2A	0	0	0	0	0					0	0	0	0
4B	0.84	8391	7049			-7049	-7049	7049	7049				
2B OR 2B-1	0.043	1015785	43679			-43679	43679	43679	-43679				
Summation of X stresses => sigma X =						-50728	36630	50728	-36630	0	0	0	0
Shear stress due to torsion MT						0	0	0	0	0	0	0	0
Shear stress due to load VC						0	0	0	0				
Shear stress due to load VL						9672				-9672	-9672	9672	9672
Summation of shear stresses tau =						0	0	0	0	-9672	-9672	9672	9672
stress intensities =>						50728	36630	50728	36630	19345	19345	19345	19345
membrane components of sigma phi =>						-16783	-16783	16783	16783	0	0	0	0
membrane components of sigma X =>						-7049	-7049	7049	7049	0	0	0	0
tau =>						0	0	0	0	-9672	-9672	9672	9672
membrane stress intensities =>						16783	16783	16783	16783	19345	19345	19345	19345

Table 3.9.2-4
Computation Spreadsheet for the (DW + 1.0g Axial) Transfer Load,
Bottom Trunnion – Local Shell Stresses

Applied Loads			Geometry			Geometric Parameters							
W	250000		T	1.5		gamma	26.7333						
P	0		r0	8.575		beta	0.1871						
ML	891875		Rm	40.1									
MC	445938												
MT	0												
VL	125000												
VC	62500												

from fig	read curves for	multiplier	abs. stress values	column # =	1	2	3	4	5	6	7	8
					Au	Al	Bu	Bl	Cu	Cl	Du	DI
3C AND 4C	3.5	4.5	0	0	0	0	0	0	0	0	0	0
1C AND 2C-1	0.088	0.054	0	0	0	0	0	0	0	0	0	0
3A	1.1		988	1087					-1087	-1087	1087	1087
1A	0.09		158490	14264					-14264	14264	14264	-14264
3B	3		1976	5929	-5929	-5929	5929	5929				
1B OR 1B-1	0.034		316979	10777	-10777	10777	10777	-10777				
Summation of phi stresses => sigma phi =					-16706	4849	16706	-4849	-15351	13177	15351	-13177
3C AND 4C	3.5	4.5	0	0	0	0	0	0	0	0	0	0
1C-1 AND 2C	0.084	0.052	0	0	0	0	0	0	0	0	0	0
4A	1.7		988	1680					-1680	-1680	1680	1680
2A	0.044		158490	6974					-6974	6974	6974	-6974
4B	1		1976	1976	-1976	-1976	1976	1976				
2B OR 2B-1	0.05		316979	15849	-15849	15849	15849	-15849				
Summation of X stresses => sigma X =					-17825	13873	17825	-13873	-8653	5294	8653	-5294
Shear stress due to torsion MT					0	0	0	0	0	0	0	0
Shear stress due to load VC					1547	1547	-1547	-1547				
Shear stress due to load VL					3093				-3093	-3093	3093	3093
Summation of shear stresses tau =					1547	1547	-1547	-1547	-3093	-3093	3093	3093
stress intensities =>					18910	14131	18910	14131	16561	14246	16561	14246
membrane components of sigma phi =>					-5929	-5929	5929	5929	-1087	-1087	1087	1087
membrane components of sigma X =>					-1976	-1976	1976	1976	-1680	-1680	1680	1680
tau =>					1547	1547	-1547	-1547	-3093	-3093	3093	3093
membrane stress intensities =>					6462	6462	6462	6462	6215	6215	6215	6215

Table 3.9.2-5
Computation Spreadsheet for the (DW + 1.0g Vertical) Transfer Load,
Bottom Trunnion – Local Shell Stresses

Table 3. (Transfer Loads)-Bottom Trunnion DW + 1.0 Vertical

Transfer Loads applied to the NUHOMS-OS187H Transfer Cask

Applied Loads		Geometry		Geometric Parameters	
W	250000	T	1.5	gamma	26.7333
P	0	r0	8.575	beta	0.1871
ML	0	Rm	40.1		
MC	891875				
MT	0				
VL	0				
VC	125000				

from fig	read curves for	multiplier	abs. stress values	column # =	1	2	3	4	5	6	7	8
					Au	Al	Bu	Bl	Cu	Cl	Du	DI
3C AND 4C	3.5	4.5	0	0	0	0	0	0	0	0	0	0
1C AND 2C-1	0.088	0.054	0	0	0	0	0	0	0	0	0	0
3A	1.1		1976	2174					-2174	-2174	2174	2174
1A	0.09		316979	28528					-28528	28528	28528	-28528
3B	3		0	0	0	0	0	0				
1B OR 1B-1	0.034		0	0	0	0	0	0				
Summation of phi stresses => sigma phi =					0	0	0	0	-30702	26354	30702	-26354
3C AND 4C	3.5	4.5	0	0	0	0	0	0	0	0	0	0
1C-1 AND 2C	0.084	0.052	0	0	0	0	0	0	0	0	0	0
4A	1.7		1976	3360					-3360	-3360	3360	3360
2A	0.044		316979	13947					-13947	13947	13947	-13947
4B	1		0	0	0	0	0	0				
2B OR 2B-1	0.05		0	0	0	0	0	0				
Summation of X stresses => sigma X =					0	0	0	0	-17307	10588	17307	-10588
Shear stress due to torsion MT					0	0	0	0	0	0	0	0
Shear stress due to load VC					3093	3093	-3093	-3093				
Shear stress due to load VL					0				0	0	0	0
Summation of shear stresses tau =					3093	3093	-3093	-3093	0	0	0	0
stress intensities =>					6187	6187	6187	6187	30702	26354	30702	26354
membrane components of sigma phi =>					0	0	0	0	-2174	-2174	2174	2174
membrane components of sigma X =>					0	0	0	0	-3360	-3360	3360	3360
tau =>					3093	3093	-3093	-3093	0	0	0	0
membrane stress intensities =>					6187	6187	6187	6187	3360	3360	3360	3360

Table 3.9.2-6
Computation Spreadsheet for the (DW + 1.0g transverse) Transfer Load,
Bottom Trunnion – Local Shell Stresses

Table 2. (Transfer Loads)-Bottom Trunnion- DW + 1.0g Transverse

Transfer Loads applied to the NUHOMS-OS187H Transfer Cask

Applied Loads		Geometry		Geometric Parameters	
W	250000	T	1.5	gamma	26.7333
P	125000	r0	8.575	beta	0.1871
ML	0	Rm	40.1		
MC	445938				
MT	0				
VL	0				
VC	62500				

from fig	read curves for	multiplier	abs. stress values	column # =	1	2	3	4	5	6	7	8
					Au	Al	Bu	Bl	Cu	Cl	Du	DI
3C AND 4C	3.5	4.5	2078	7273	9352	-9352	-9352	-9352	-9352	-7273	-7273	-7273
1C AND 2C-1	0.088	0.054	333333	29333	18000	-18000	18000	-18000	18000	-29333	29333	-29333
3A	1.1		988	1087						-1087	-1087	1087
1A	0.09		158490	14264						-14264	14264	-14264
3B	3		0	0	0	0	0	0				
1B OR 1B-1	0.034		0	0	0	0	0	0				
Summation of phi stresses => sigma phi =					-27352	8648	-27352	8648	-51958	35237	-21256	8883
3C AND 4C	3.5	4.5	2078	7273	9352	-7273	-7273	-7273	-7273	-9352	-9352	-9352
1C-1 AND 2C	0.084	0.052	333333	28000	17333	-28000	28000	-28000	28000	-17333	17333	-17333
4A	1.7		988	1680						-1680	-1680	1680
2A	0.044		158490	6974						-6974	6974	-6974
4B	1		0	0	0	0	0	0				
2B OR 2B-1	0.05		0	0	0	0	0	0				
Summation of X stresses => sigma X =					-35273	20727	-35273	20727	-35338	13275	-18032	2688
Shear stress due to torsion MT					0	0	0	0	0	0	0	0
Shear stress due to load VC					1547	1547	1547	-1547	-1547			
Shear stress due to load VL					0				0	0	0	0
Summation of shear stresses tau =					1547	1547	-1547	-1547	0	0	0	0
stress intensities =>					35565	20921	35565	20921	51958	35237	21256	8883
membrane components of sigma phi =>					-9352	-9352	-9352	-9352	-8360	-8360	-6187	-6187
membrane components of sigma X =>					-7273	-7273	-7273	-7273	-11031	-11031	-7672	-7672
tau =>					1547	1547	-1547	-1547	0	0	0	0
membrane stress intensities =>					10176	10176	10176	10176	11031	11031	7672	7672

Table 3.9.2-7
Computation Spreadsheet for the (DW + 0.5g axial + 0.5g vertical + 0.5g trans.) Transfer Load, Bottom Trunnion – Local Shell Stresses

Applied Loads			Geometry		Geometric Parameters								
W	250000		T	1.5	gamma	26.7333							
P	62500		r0	8.575	beta	0.1871							
ML	445938		Rm	40.1									
MC	668906												
MT	0												
VL	62500												
VC	93750												
			column # =			1	2	3	4	5	6	7	8
from fig	read curves for		multiplier	abs. stress	values	Au	Al	Bu	Bl	Cu	Cl	Du	DI
3C AND 4C	3.5	4.5	1039	3637	4676	-4676	-4676	-4676	-4676	-3637	-3637	-3637	-3637
1C AND 2C-1	0.088	0.054	166667	14667	9000	-9000	9000	-9000	9000	-14667	14667	-14667	14667
3A	1.1		1482	1630						-1630	-1630	1630	1630
1A	0.09		237734	21396						-21396	21396	21396	-21396
3B	3		988	2964		-2964	-2964	2964	2964				
1B OR 1B-1	0.034		158490	5389		-5389	5389	5389	-5389				
Summation of phi stresses => sigma phi =						-22029	6749	-5323	1900	-41330	30796	4723	-8736
3C AND 4C	3.5	4.5	1039	3637	4676	-3637	-3637	-3637	-3637	-4676	-4676	-4676	-4676
1C-1 AND 2C	0.084	0.052	166667	14000	8667	-14000	14000	-14000	14000	-8667	8667	-8667	8667
4A	1.7		1482	2520						-2520	-2520	2520	2520
2A	0.044		237734	10460						-10460	10460	10460	-10460
4B	1		988	988		-988	-988	988	988				
2B OR 2B-1	0.05		158490	7924		-7924	7924	7924	-7924				
Summation of X stresses => sigma X =						-26549	17300	-8724	3427	-26322	11932	-363	-3950
Shear stress due to torsion MT					0	0	0	0	0	0	0	0	0
Shear stress due to load VC					2320	2320	2320	-2320	-2320				
Shear stress due to load VL					1547					-1547	-1547	1547	1547
Summation of shear stresses tau =						2320	2320	-2320	-2320	-1547	-1547	1547	1547
stress intensities =>						27528	17787	9900	5106	41488	30922	5952	9192
membrane components of sigma phi =>						-7640	-7640	-1712	-1712	-5267	-5267	-2006	-2006
membrane components of sigma X =>						-4625	-4625	-2649	-2649	-7195	-7195	-2156	-2156
tau =>						2320	2320	-2320	-2320	-1547	-1547	1547	1547

Table 3.9.2-8
NUHOMS®-OS187H Transfer Cask Local Shell Stresses and Allowables

Load Case Number	Load	Maximum Local Stress		Allowable (ksi)	Reference Table
		Type	Magnitude (ksi)		
1	6g Lifting (Pad)	P_l	20.42	30.0	Table 3.9.2-2
		$P_l + P_b$	55.66	60.0	Table 3.9.2-2
	6g Lifting (Shell)	P_l	19.35	30.0	Table 3.9.2-3
		$P_l + P_b$	50.73	60.0	Table 3.9.2-3
2A.	Transfer, DW + 1g Axial	P_l	6.46	30.0	Table 3.9.2-4
		$P_l + P_b$	18.91	60.0	Table 3.9.2-4
2B.	Transfer, DW + 1g Vertical	P_l	6.19	30.0	Table 3.9.2-5
		$P_l + P_b$	30.70	60.0	Table 3.9.2-5
2C.	Transfer, DW + 1g Transverse	P_l	11.03	30.0	Table 3.9.2-6
		$P_l + P_b$	51.96	60.0	Table 3.9.2-6
2D.	Transfer, DW + 0.5g Axial + 0.5g Vertical + 0.5g Transverse	P_l	8.90	30.0	Table 3.9.2-7
		$P_l + P_b$	41.48	60.0	Table 3.9.2-7

Proprietary Information on This Page
Withheld Pursuant to 10 CFR 2.390

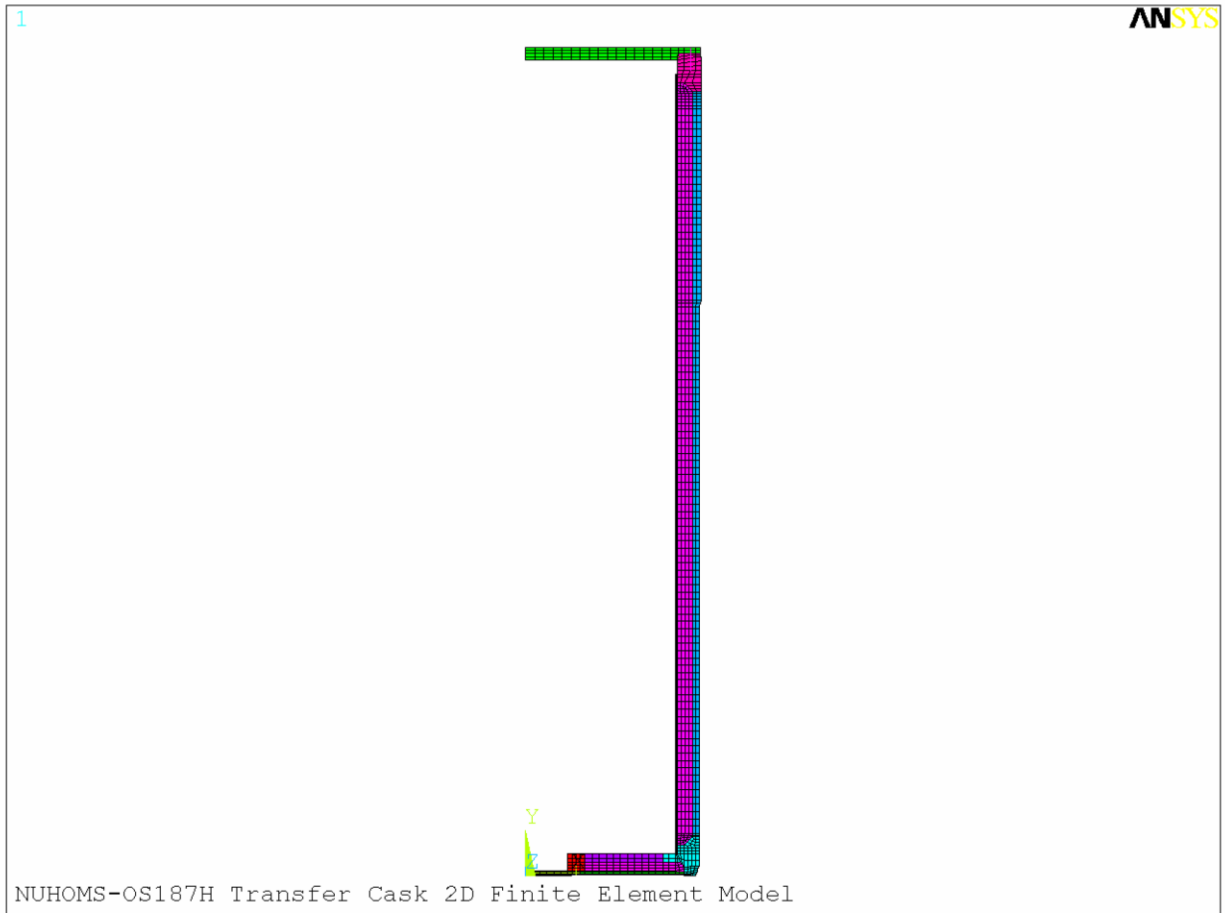


Figure 3.9.2-2
2-Dimensional Finite Element Model, Element Plot

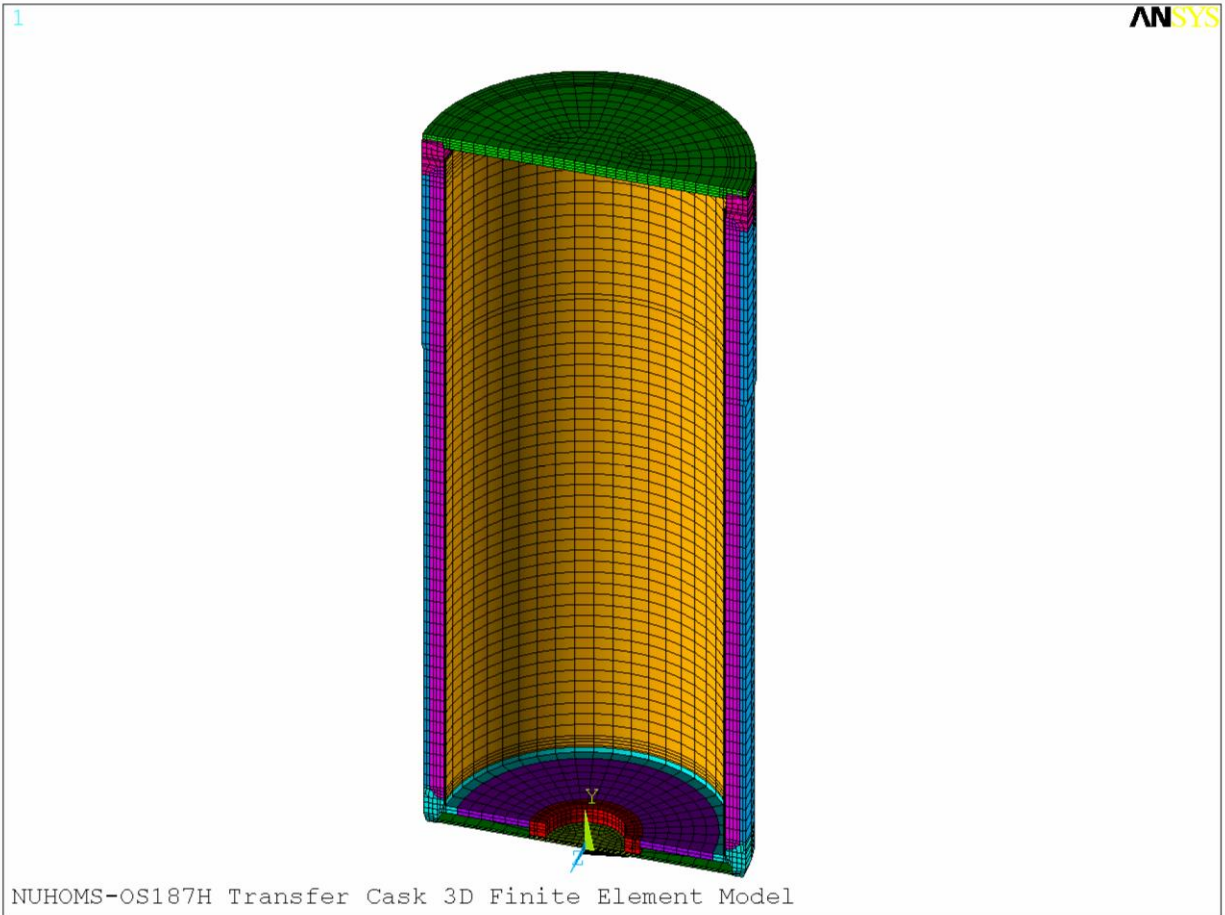


Figure 3.9.2-3
3-Dimensional Finite Element Model, Element Plot

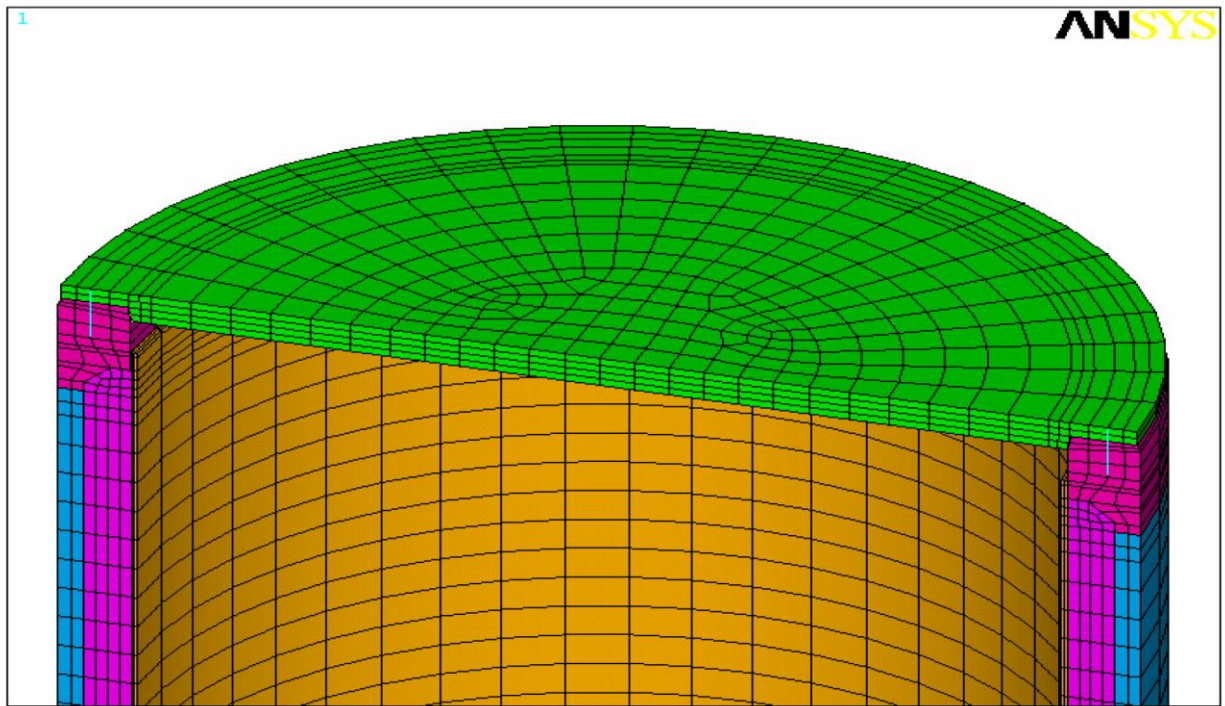


Figure 3.9.2-3A
Cask Top Cover / Flange / Bolt Model

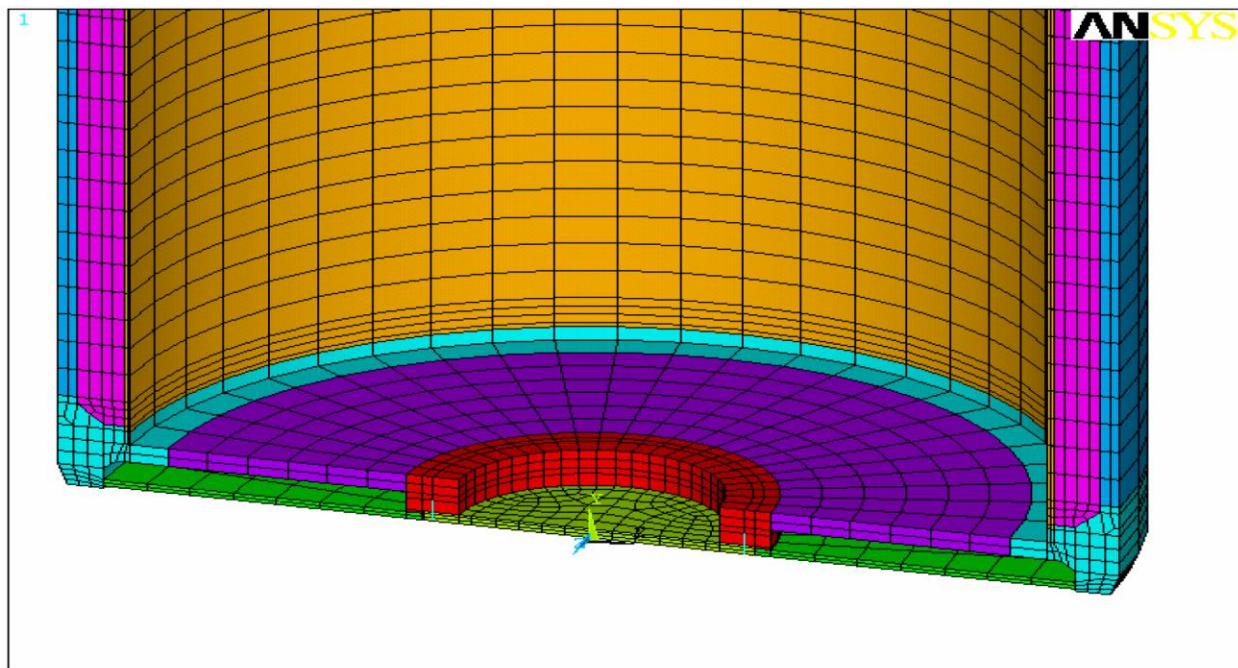


Figure 3.9.2-3B
Cask Bottom Ram Access/Cover/Bolt Model

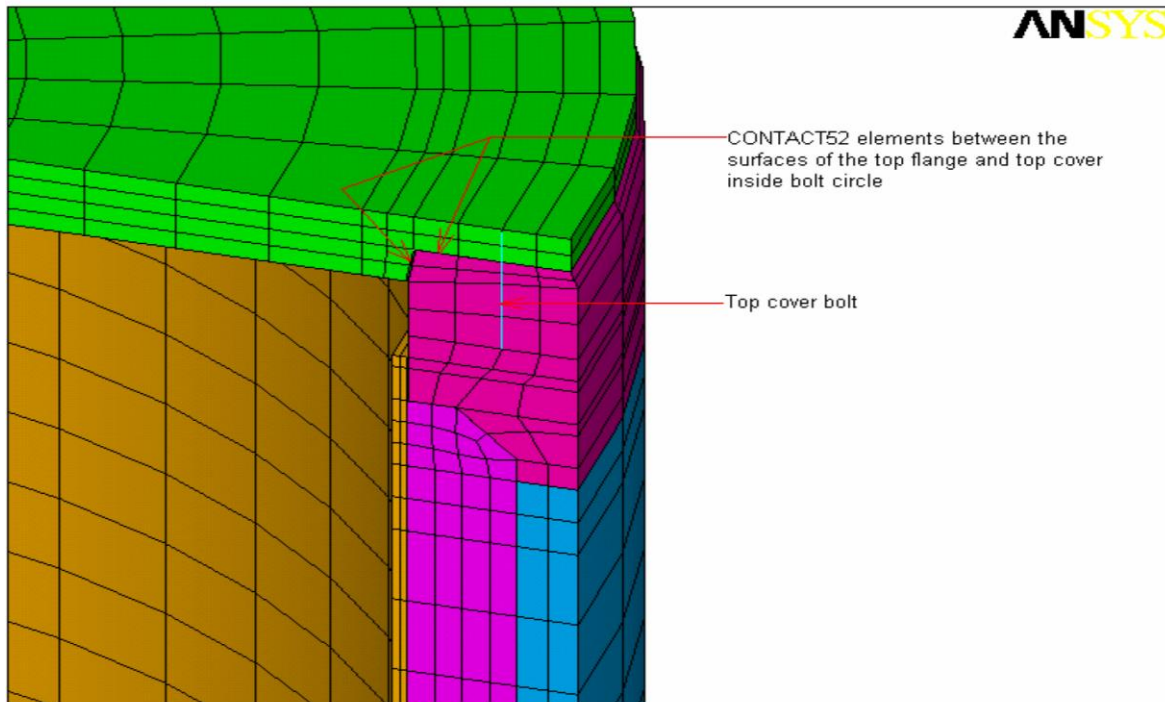


Figure 3.9.2-3C
Cask Top Cover / Flange CONTACT52 Element Representation

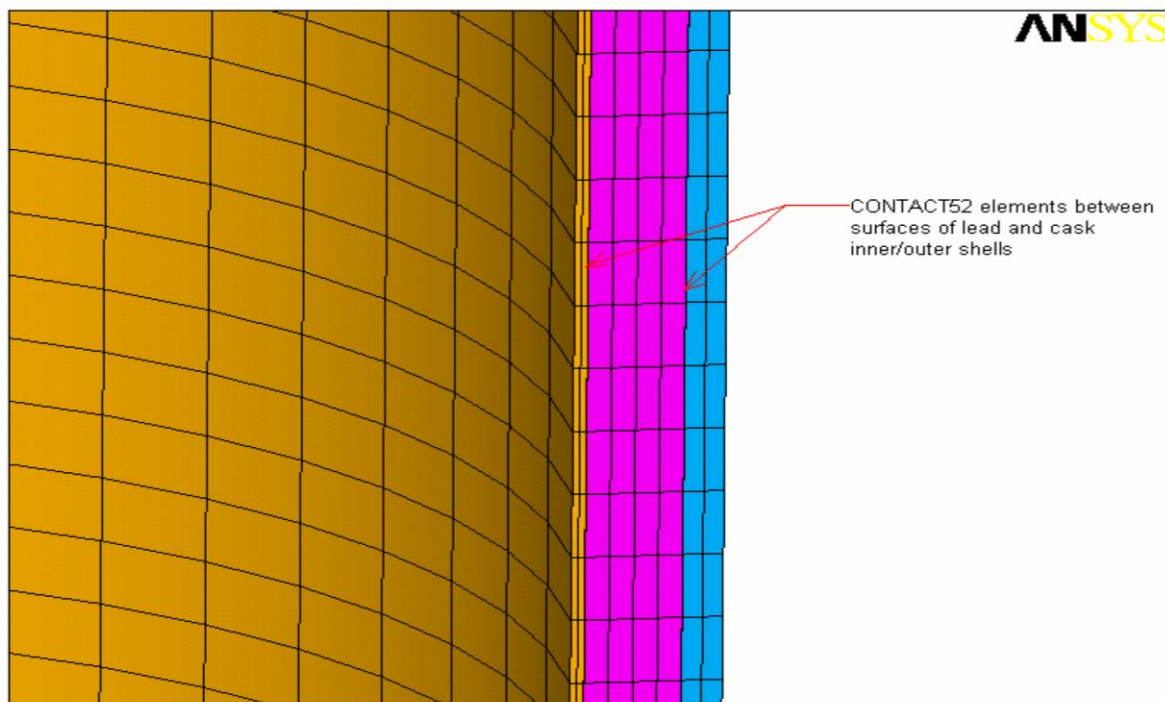


Figure 3.9.2-3D
Cask Shell / Lead CONTACT52 Element Representation

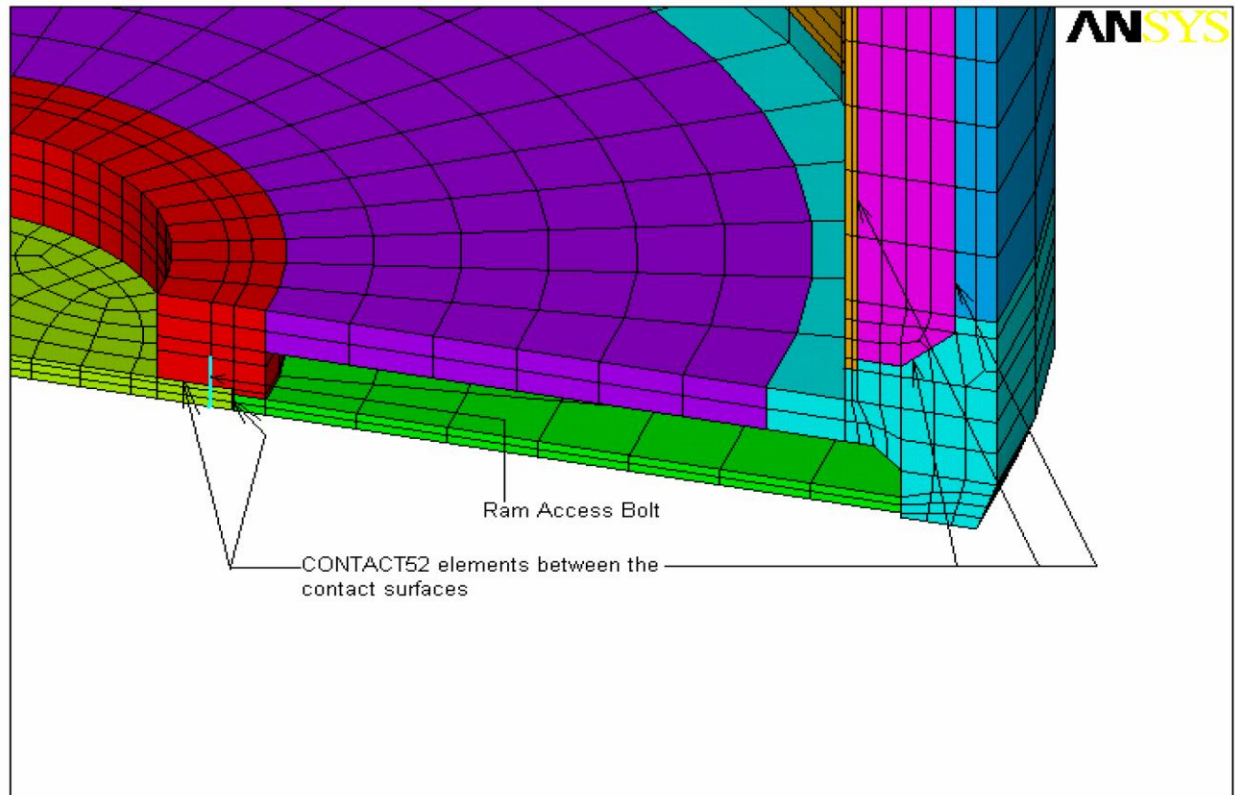


Figure 3.9.2-3E
Cask Bottom Access / Shell / Flange / Lead CONTACT52 Element Representation

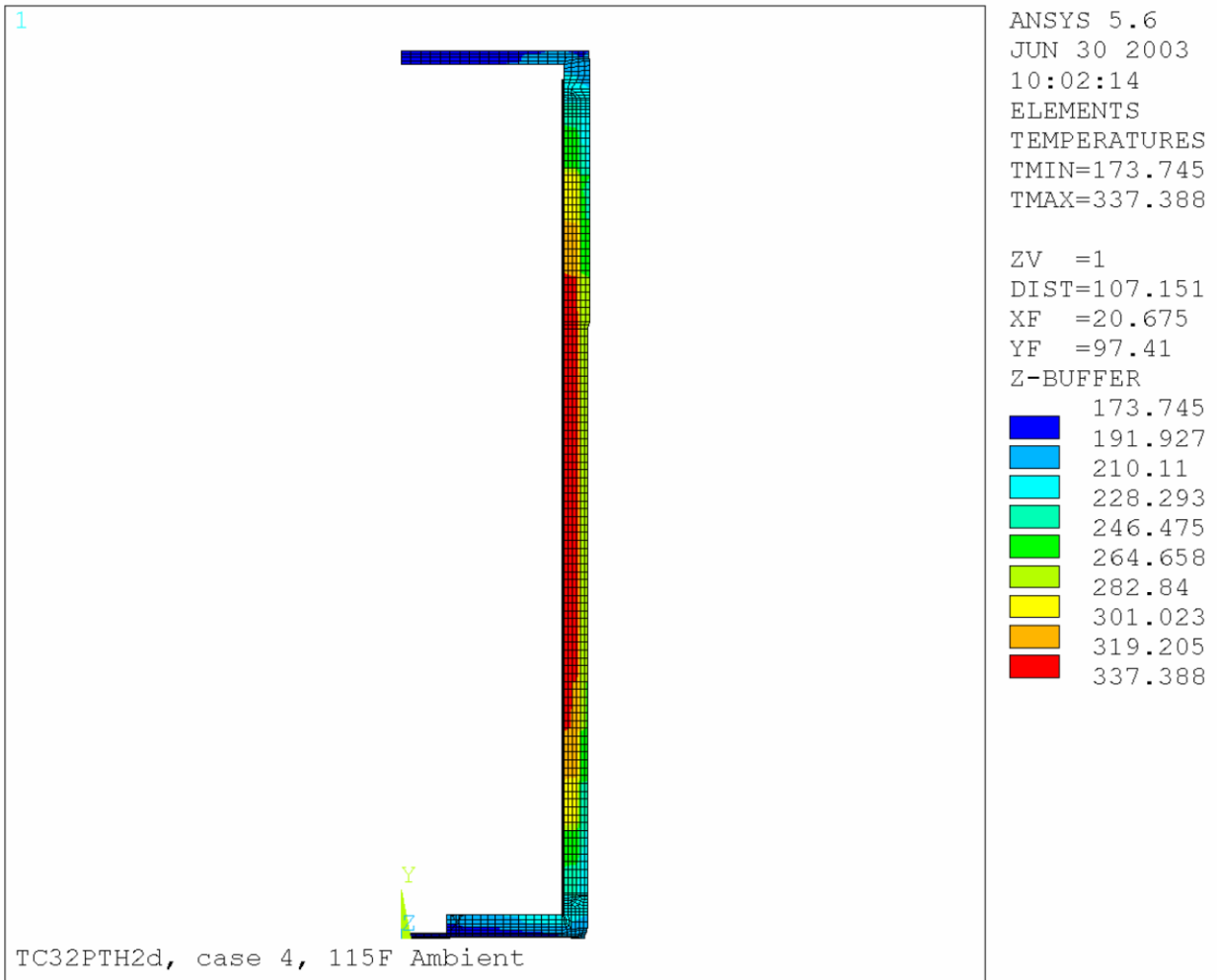


Figure 3.9.2-4
115°F Ambient Temperature Distribution

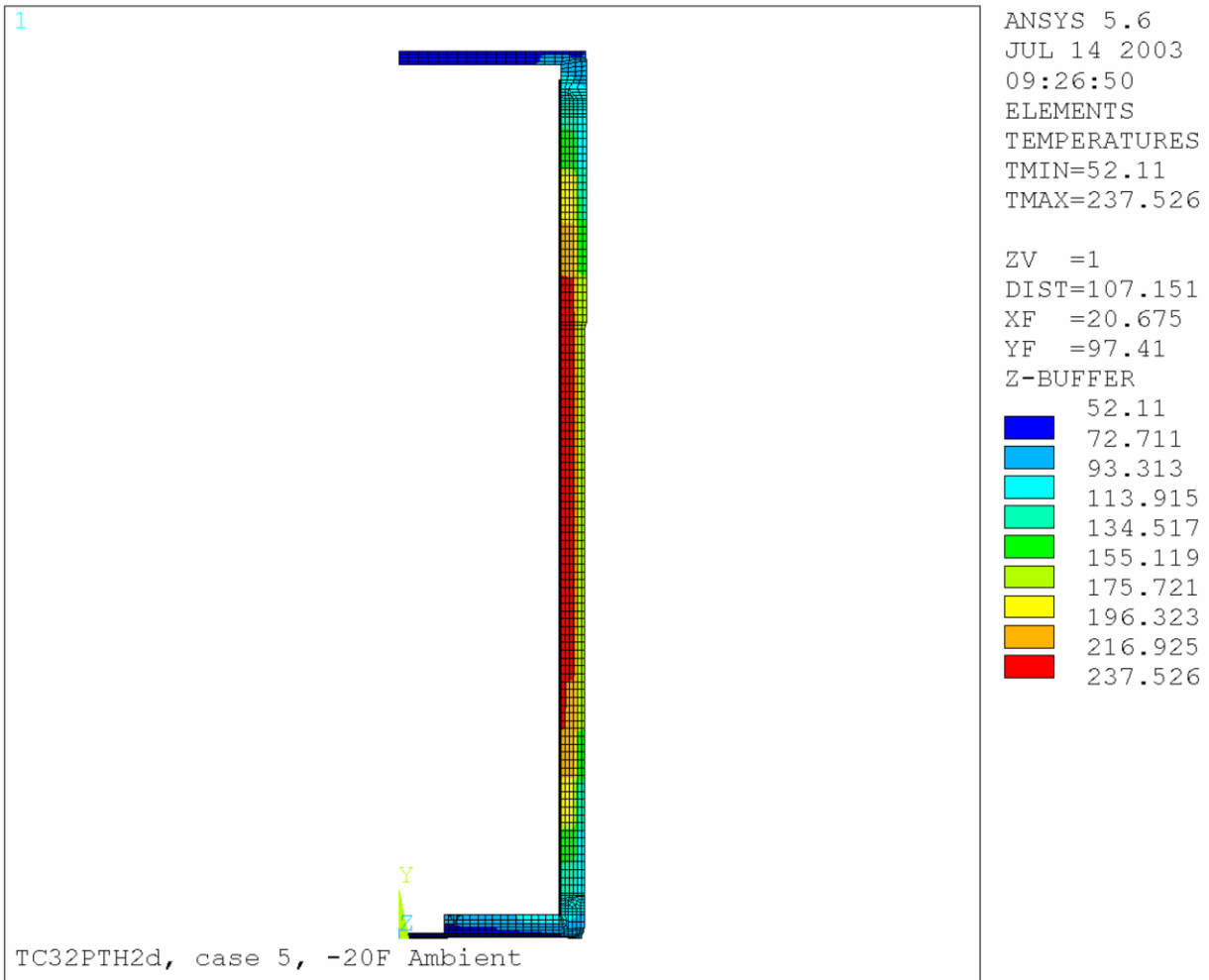


Figure 3.9.2-5
-20°F Ambient Temperature Distribution

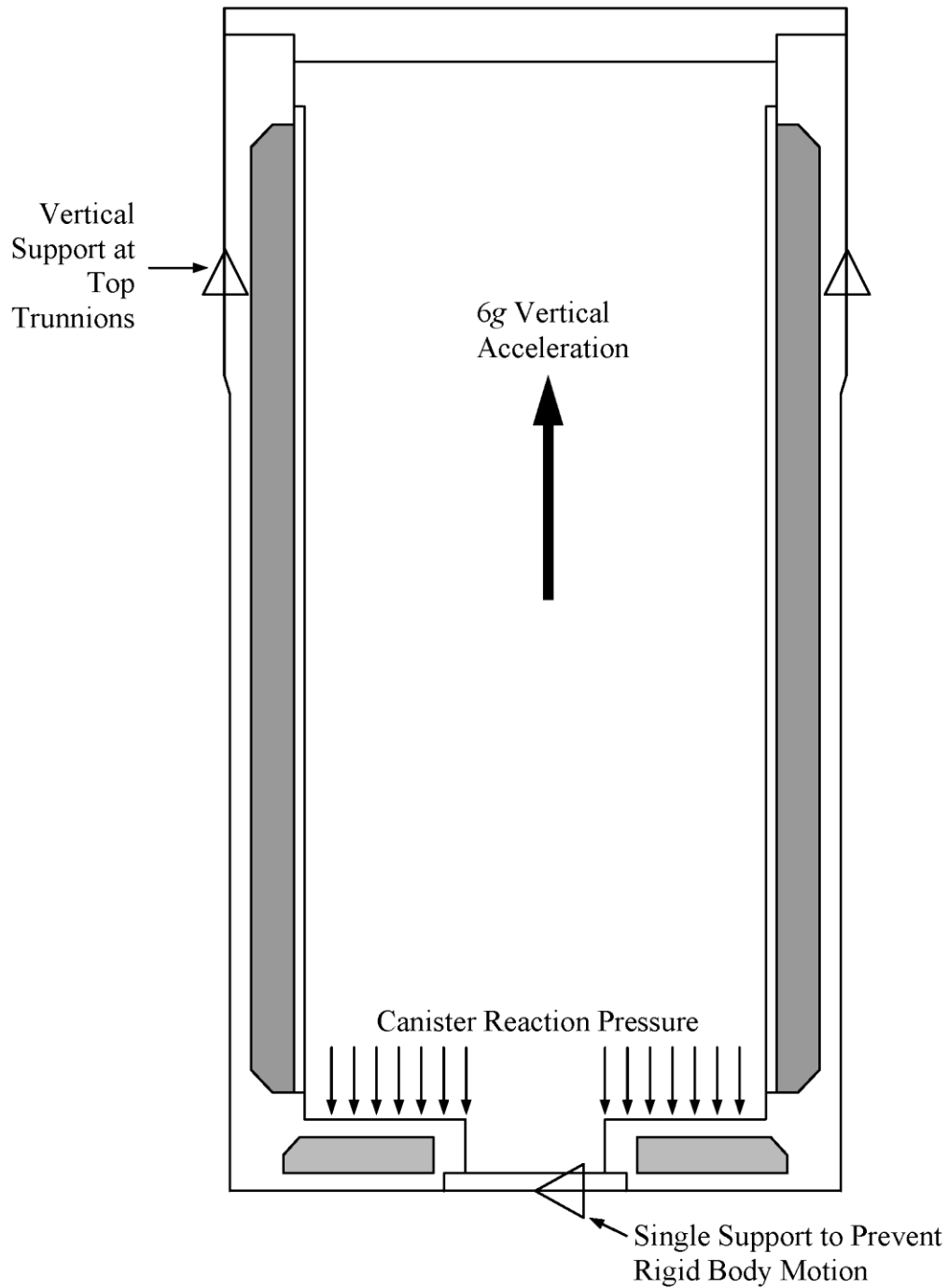


Figure 3.9.2-6
6g Lifting Boundary Conditions
(3D Model)

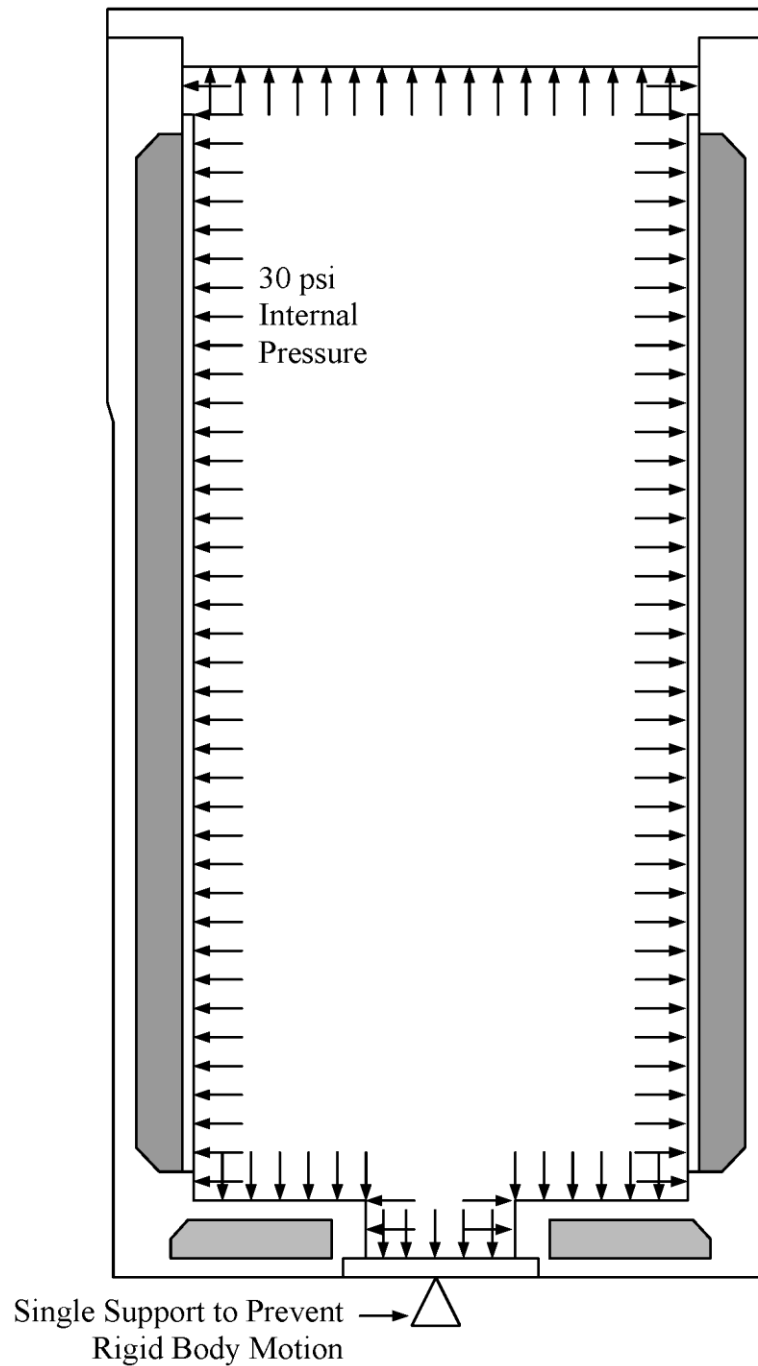


Figure 3.9.2-7
30 psi Internal Pressure Boundary Conditions (2D Model)

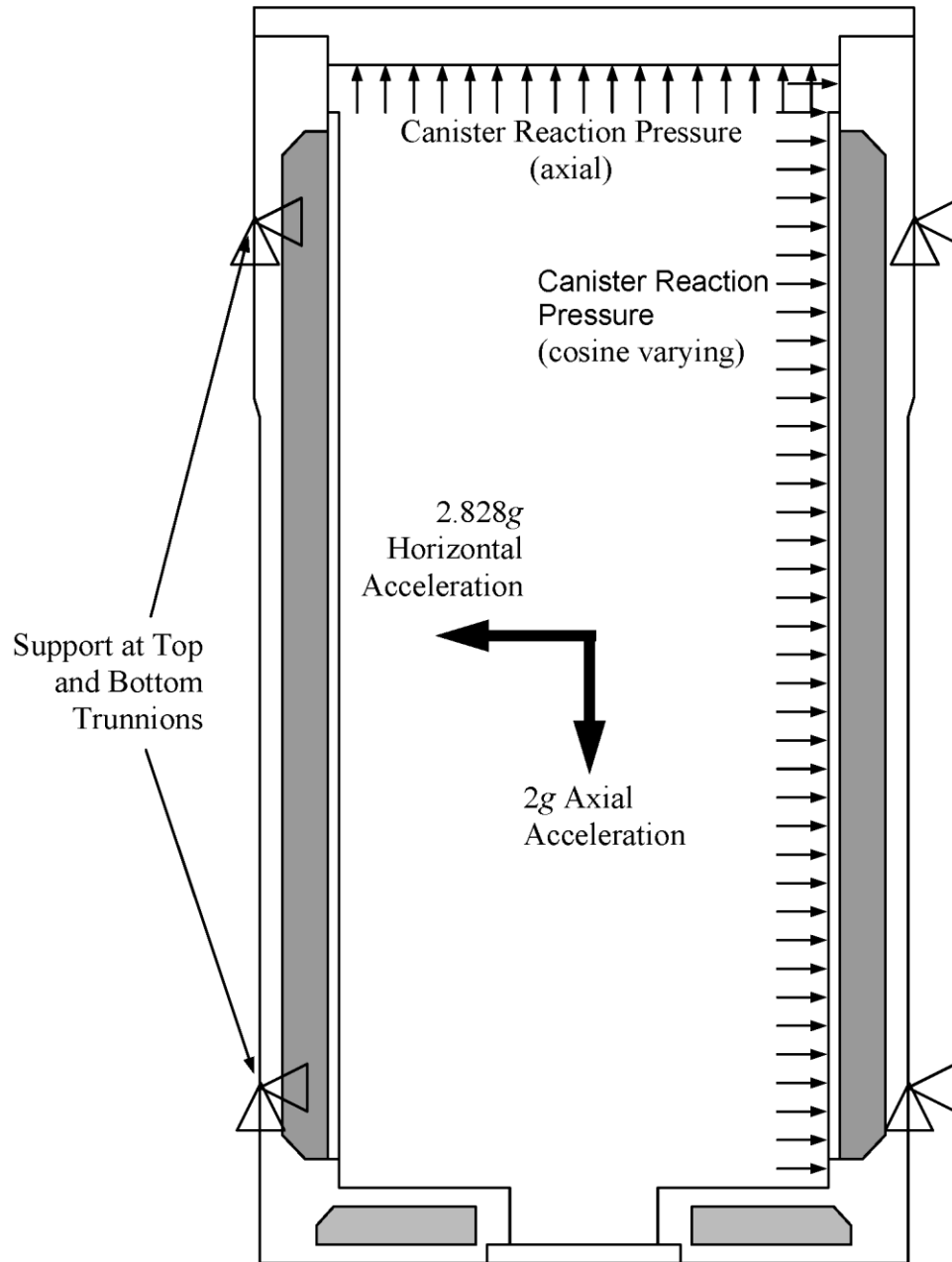


Figure 3.9.2-8
Transfer Loads Boundary Conditions
(3D Model)

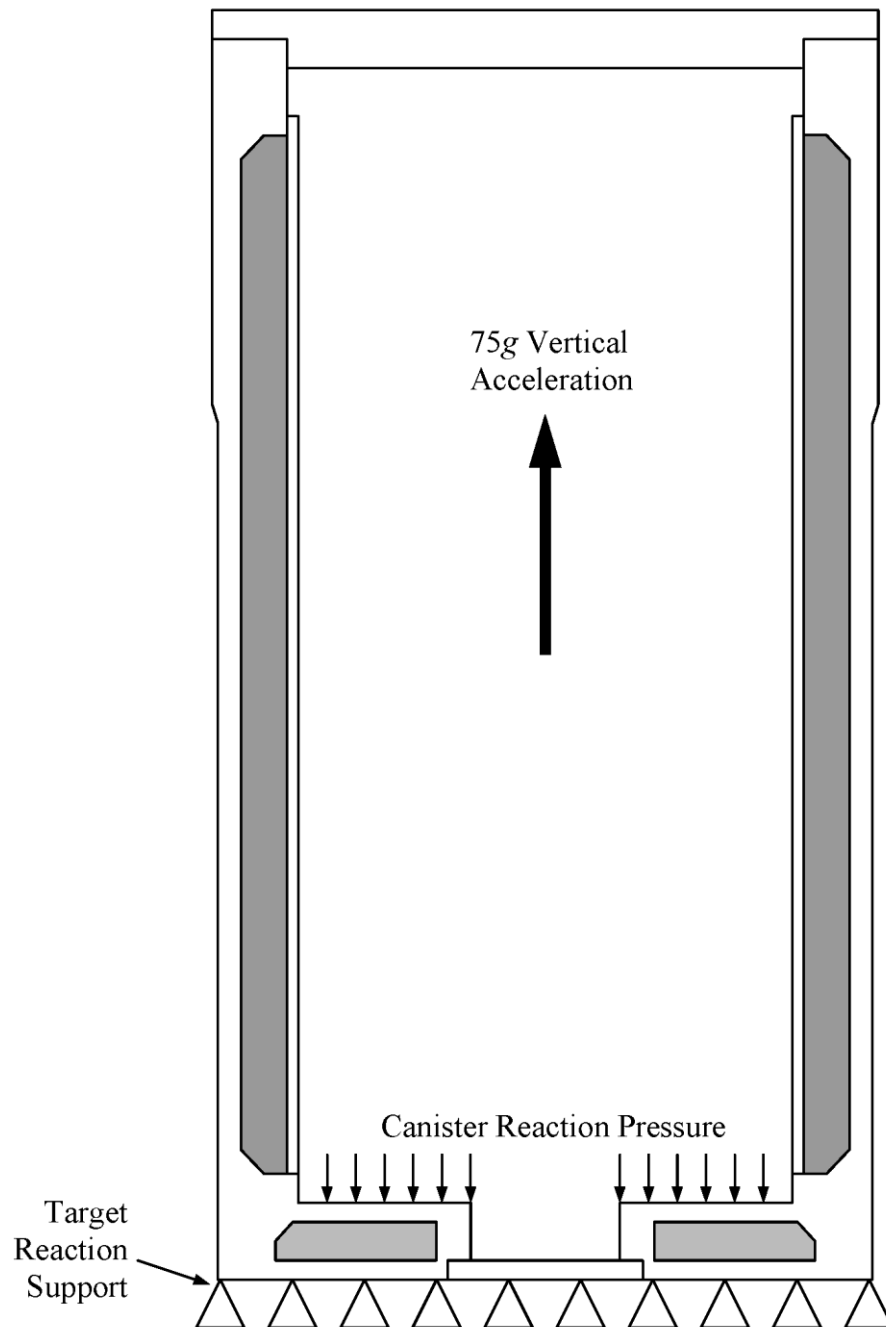


Figure 3.9.2-9
75g Bottom End Drop Boundary Conditions
(2D Model)

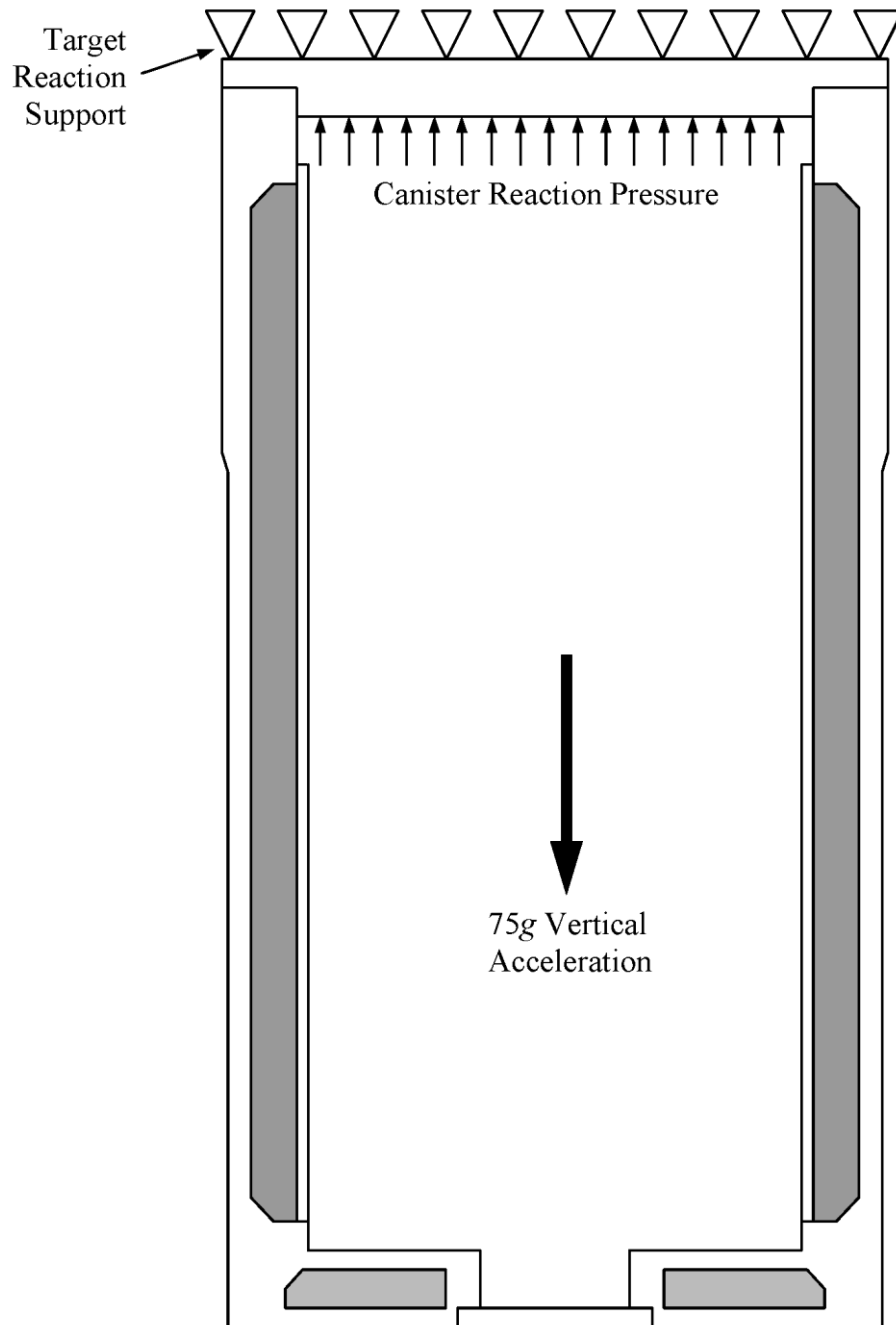


Figure 3.9.2-10
75g Top End Drop Boundary Conditions
(2D Model)

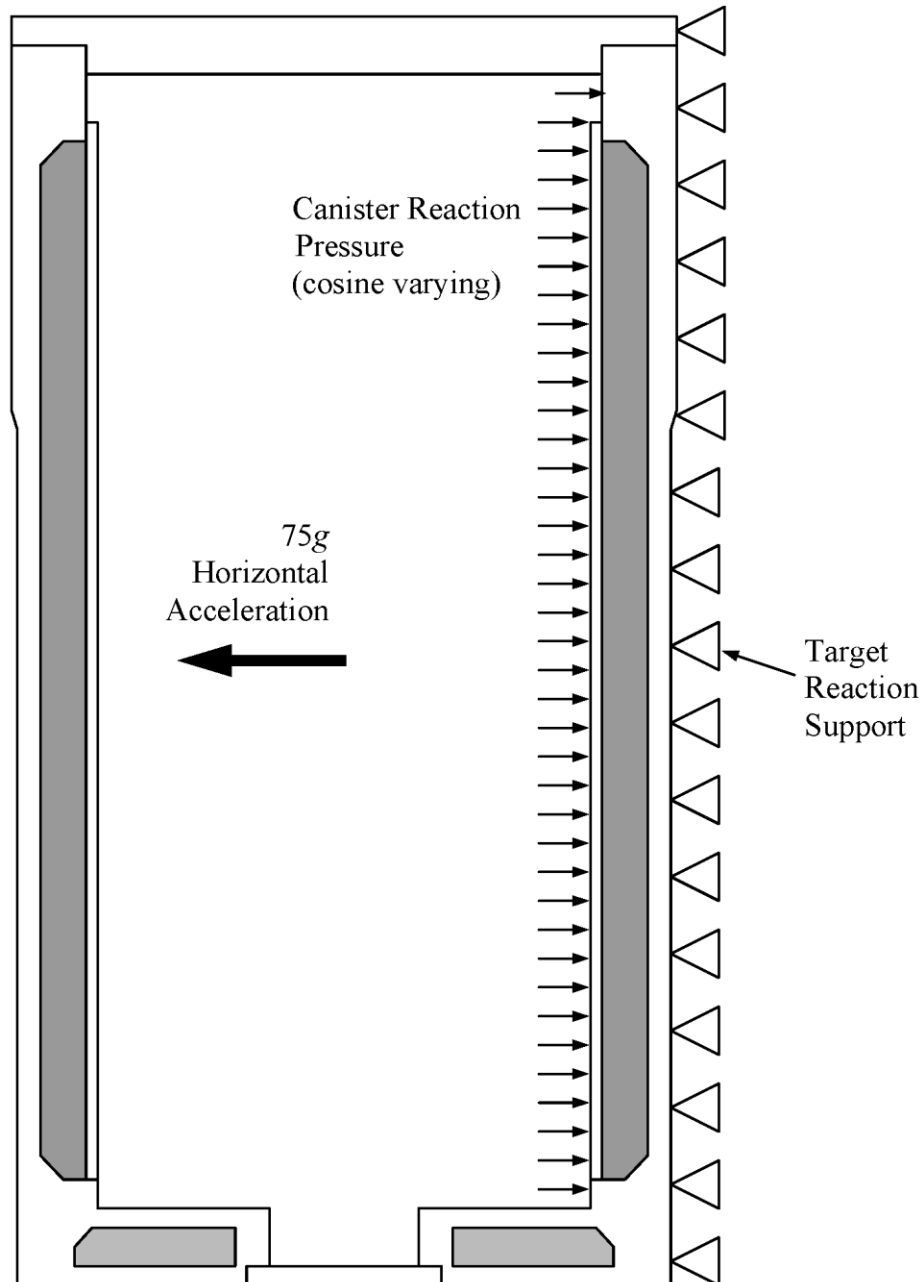


Figure 3.9.2-11
75g Side Drop Boundary Conditions
(3D Model)

1. APPLIED LOADS

MAJOR LOAD P _____ LB. VESSEL THICKNESS T _____ IN. $7 \cdot \frac{P}{T}$ _____

CIRC. MOMENT M_c _____ IN-LB. ATTACHMENT MAJOR IN L _____ IN. $P \cdot 10 \cdot R \cdot \frac{P}{T}$ _____

LONG. MOMENT M_L _____ IN-LB. VESSEL MAJOR IN L _____ IN.

TORSION MOMENT M_T _____ IN-LB.

SHEAR LOAD V _____ LB.

* NOTE: ENTER ALL FORCE VALUES IN ACCORDANCE WITH SIGN CONVENTION

2. GEOMETRY

3. GEOMETRIC PARAMETERS

FROM FIG.	READ VALUES FOR	COMPUTE ABSOLUTE VALUES OF STRESS AND ENTER RESULT	STRESSES - P LOAD 3 OPPOSITE THAT SHOWN, REVERSE SIGNS SHOWN					
			M_c	M_L	M_T	V	S_x	S_y
30 AND 40	$\frac{M_c}{I}$	$\left(\frac{M_c}{I}\right) \cdot \frac{P}{T}$	+	+	+	+	+	+
10 AND 20-1	$\frac{M_L}{I}$	$\left(\frac{M_L}{I}\right) \cdot \frac{P}{T}$	+	-	+	+	+	-
34	$\frac{M_T}{J}$	$\left(\frac{M_T}{J}\right) \cdot \frac{P}{T}$	+	+	+	+	+	+
14	$\frac{V}{A}$	$\left(\frac{V}{A}\right) \cdot \frac{P}{T}$	+	+	+	+	+	+
38	$\frac{M_c}{I}$	$\left(\frac{M_c}{I}\right) \cdot \frac{P}{T}$	+	+	+	+	+	+
18 AND 1-1	$\frac{M_L}{I}$	$\left(\frac{M_L}{I}\right) \cdot \frac{P}{T}$	+	+	+	+	+	+
ADD ALGEBRAICALLY FOR SUMMATION OF 8 STRESSES OF 8.								
30 AND 40	$\frac{M_c}{I}$	$\left(\frac{M_c}{I}\right) \cdot \frac{P}{T}$	+	+	+	+	+	+
10 AND 20	$\frac{M_L}{I}$	$\left(\frac{M_L}{I}\right) \cdot \frac{P}{T}$	+	+	+	+	+	+
44	$\frac{M_T}{J}$	$\left(\frac{M_T}{J}\right) \cdot \frac{P}{T}$	+	+	+	+	+	+
24	$\frac{V}{A}$	$\left(\frac{V}{A}\right) \cdot \frac{P}{T}$	+	+	+	+	+	+
48	$\frac{M_c}{I}$	$\left(\frac{M_c}{I}\right) \cdot \frac{P}{T}$	+	+	+	+	+	+
18 AND 1-1	$\frac{M_L}{I}$	$\left(\frac{M_L}{I}\right) \cdot \frac{P}{T}$	+	+	+	+	+	+
ADD ALGEBRAICALLY FOR SUMMATION OF 8 STRESSES OF 8.								
SHEAR STRESS DUE TO TORSION M_T			+	+	+	+	+	+
SHEAR STRESS DUE TO LOAD V			+	+	+	+	+	+
SHEAR STRESS DUE TO LOAD V			+	+	+	+	+	+
ADD ALGEBRAICALLY FOR SUMMATION OF SHEAR STRESSES 7.			+	+	+	+	+	+

PRESSURE STRESS

LONGITUDINAL BENDING STRESS

TOTAL HOUSING STRESS

TOTAL SURFACE STRESS

LONGITUDINAL σ_x

CIRCUMFERENTIAL σ_y

NOZZLE NO. _____

PPMS LOAD CODE _____

ANALYSIS POINT _____

COMPARISON SHEET FOR LOCAL STRESSES IN CYLINDRICAL SHELLS

Figure 3.9.2-12
Local Trunnion Stress Computation Sheet

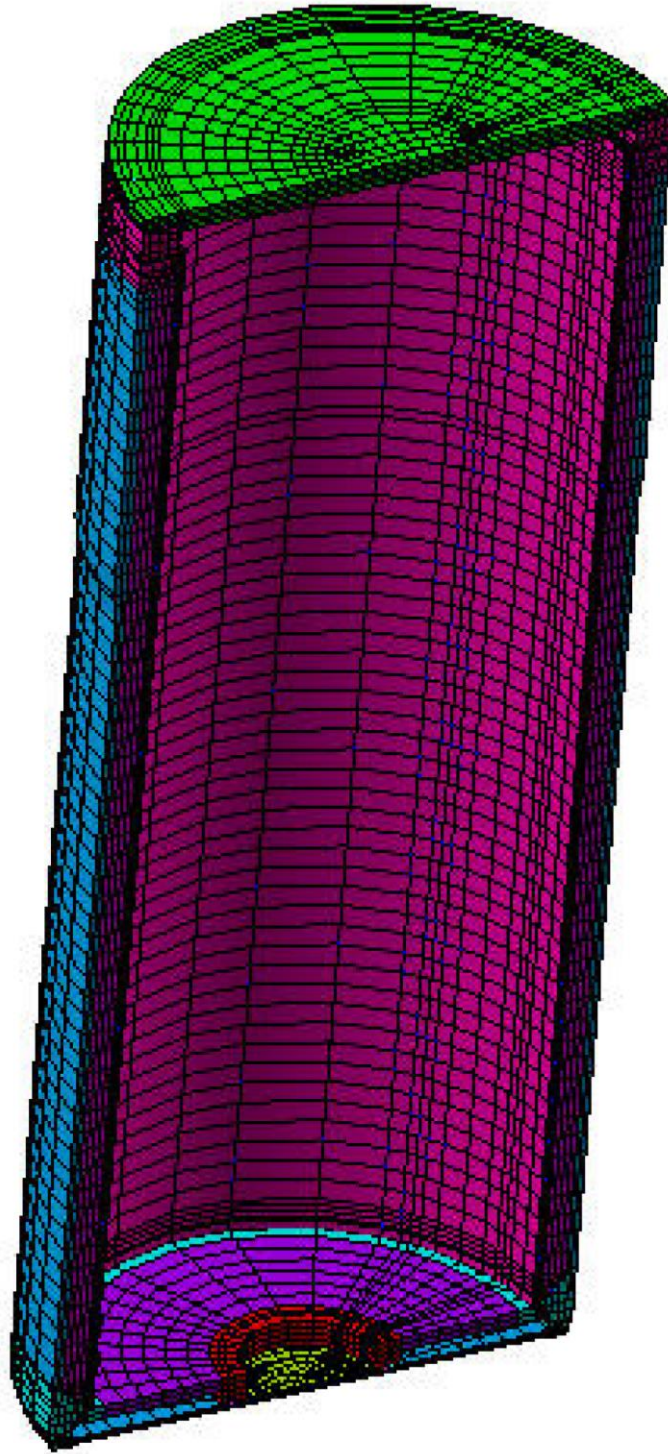


Figure 3.9.2-13
3D - Model of Transfer Cask

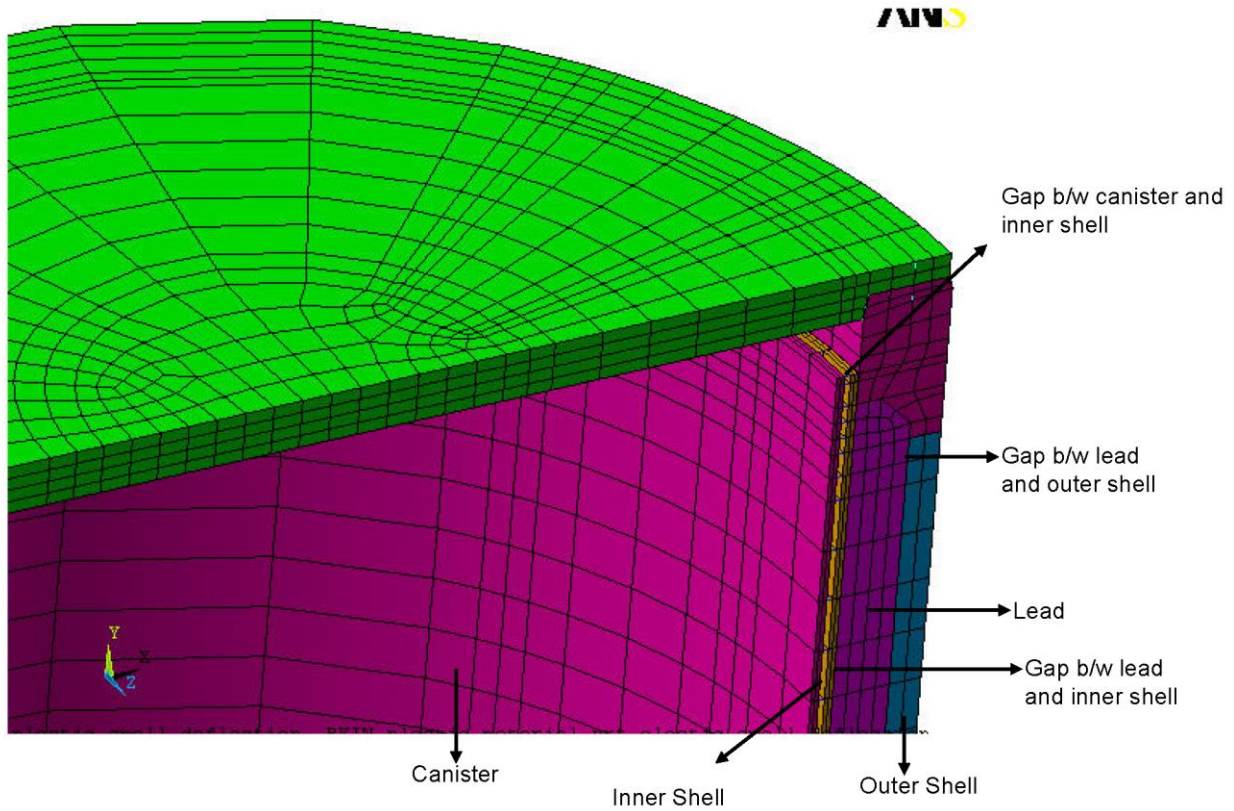


Figure 3.9.2-14
Canister/Cask Top Cover/Flange/CONTAC52 Element Representation

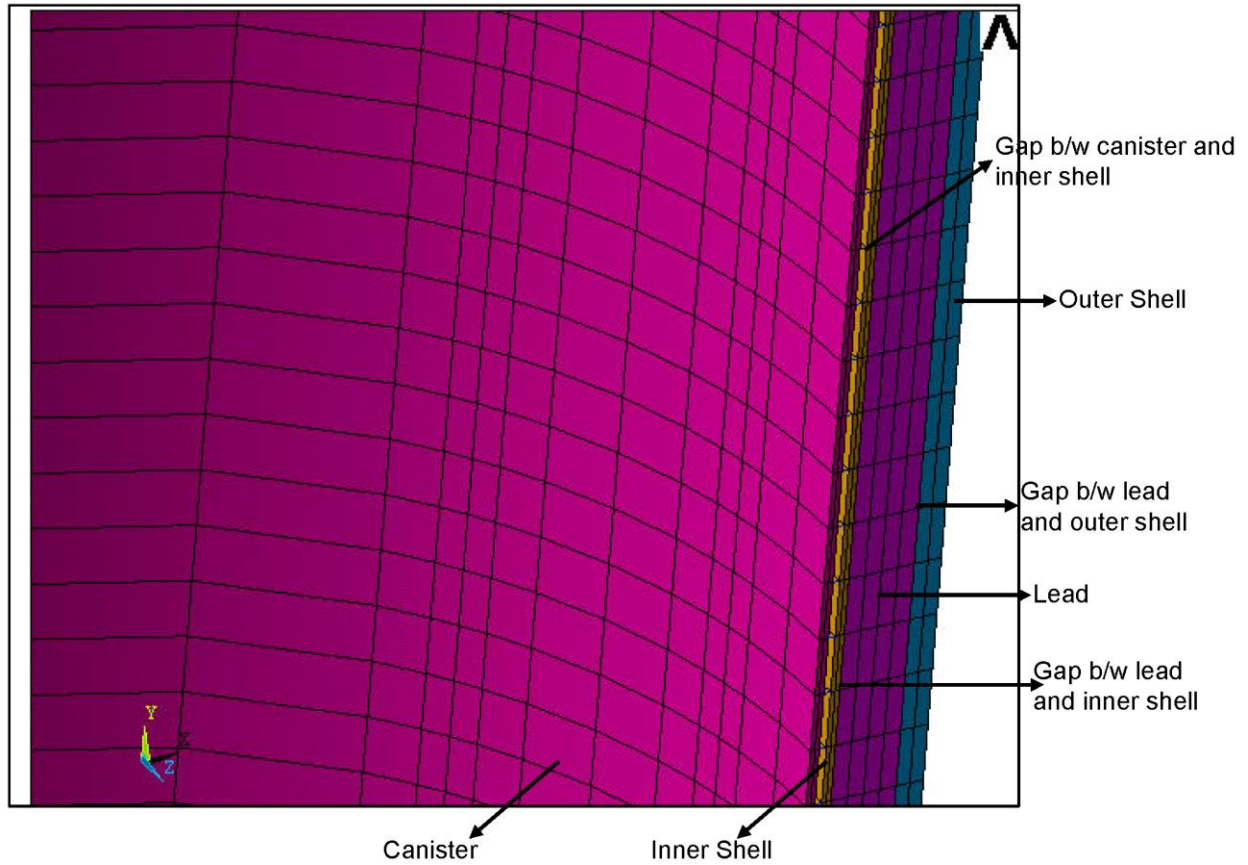


Figure 3.9.2-15
Canister/ Cask Shell /Lead /CONTAC52 Element Representation

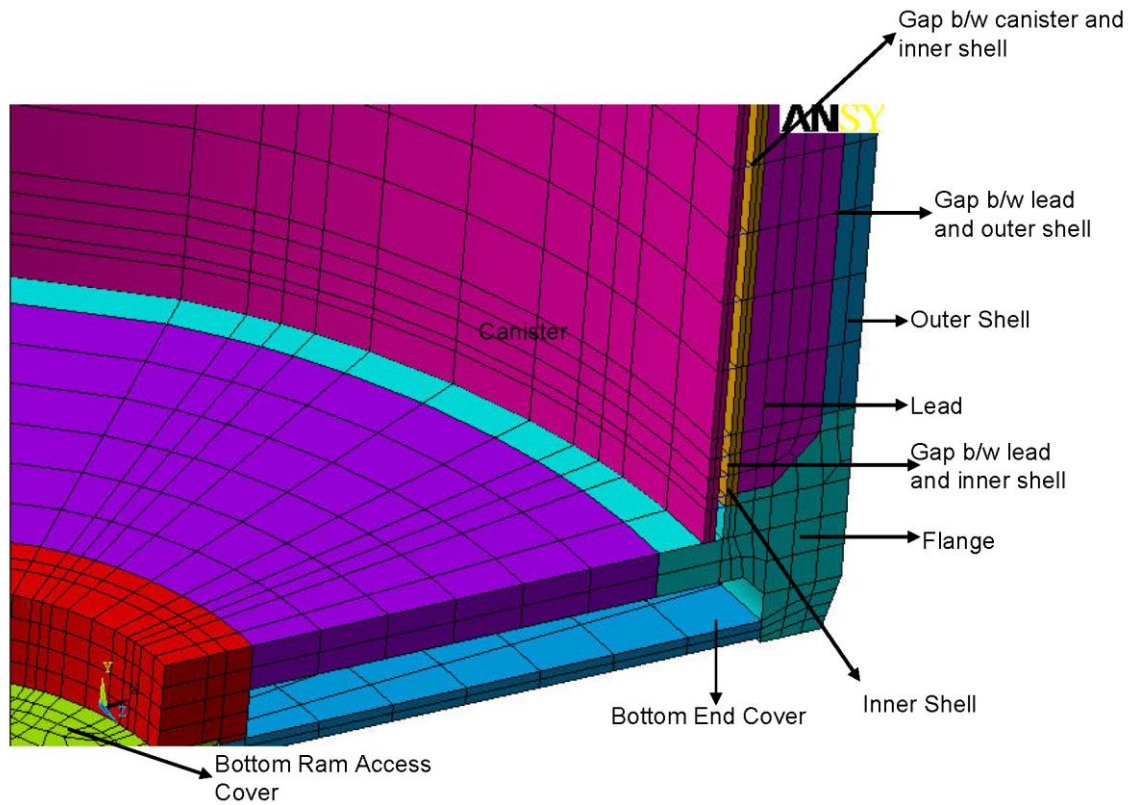


Figure 3.9.2-16
Canister/ Cask Bottom Access/Shell/ Flange/ Lead /CONTAC52 Element Representation

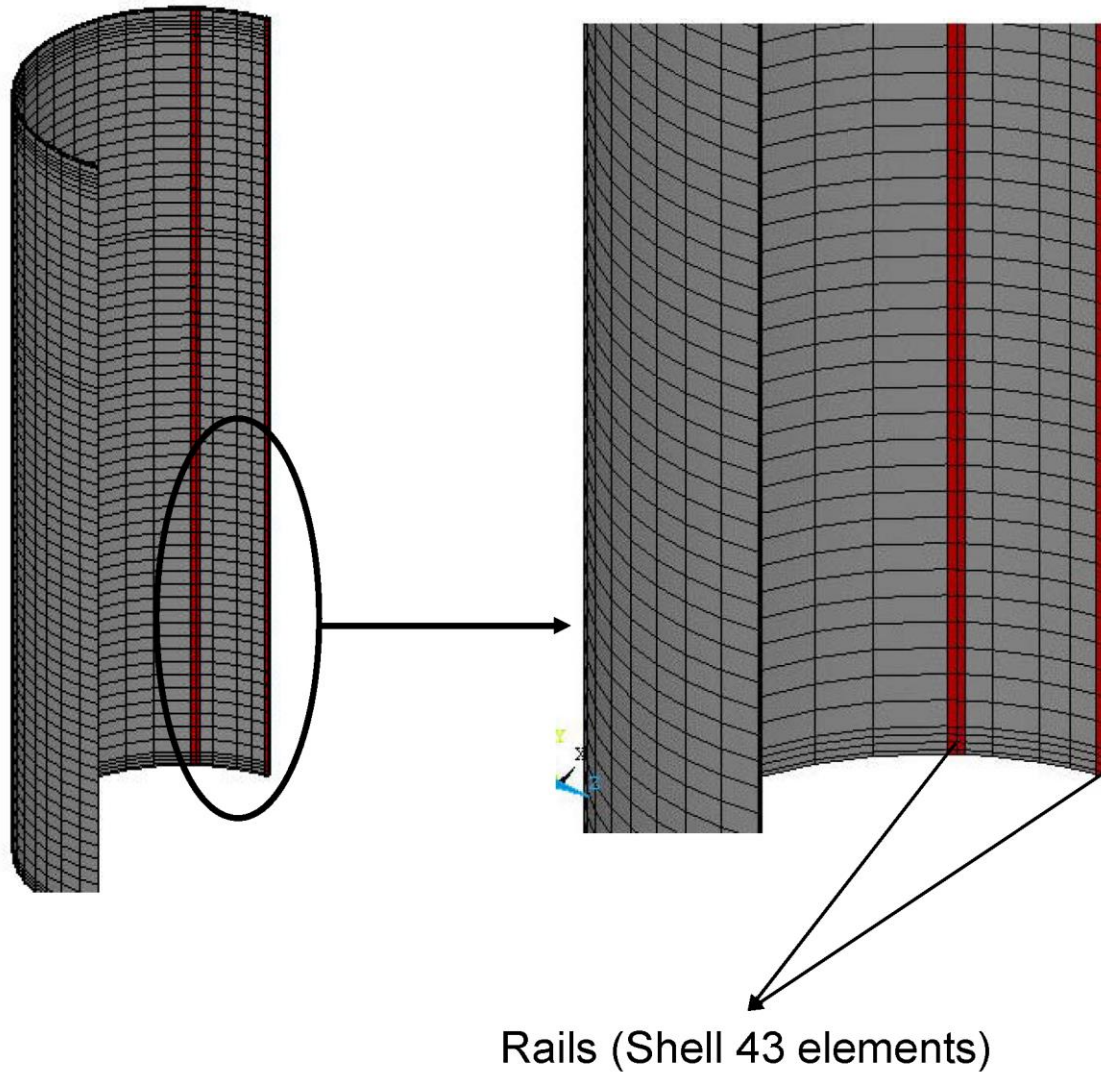


Figure 3.9.2-17
Transfer Cask Inner Shell & Rails

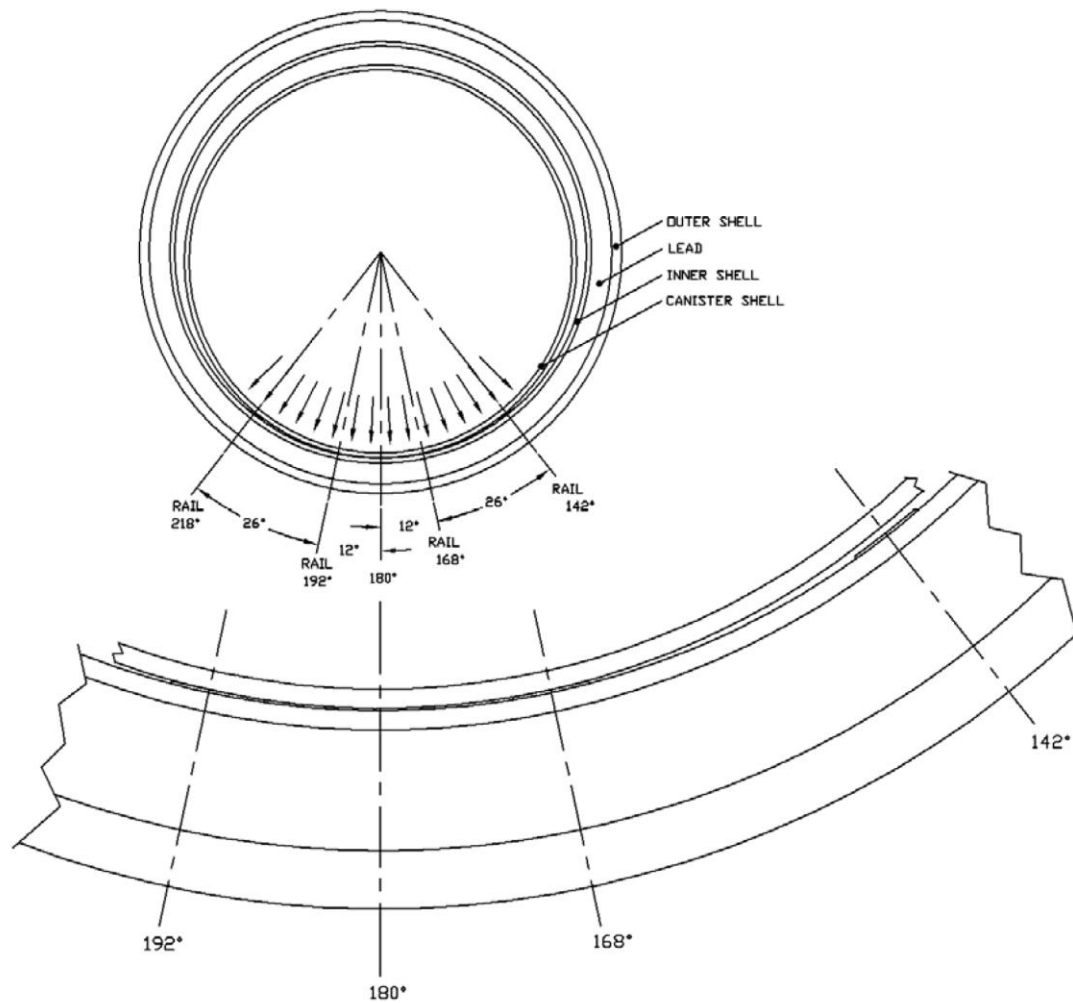


Figure 3.9.2-18
Drop Sketch for Initial Impact @ both 168° and 192° Rails (Load Case 1)

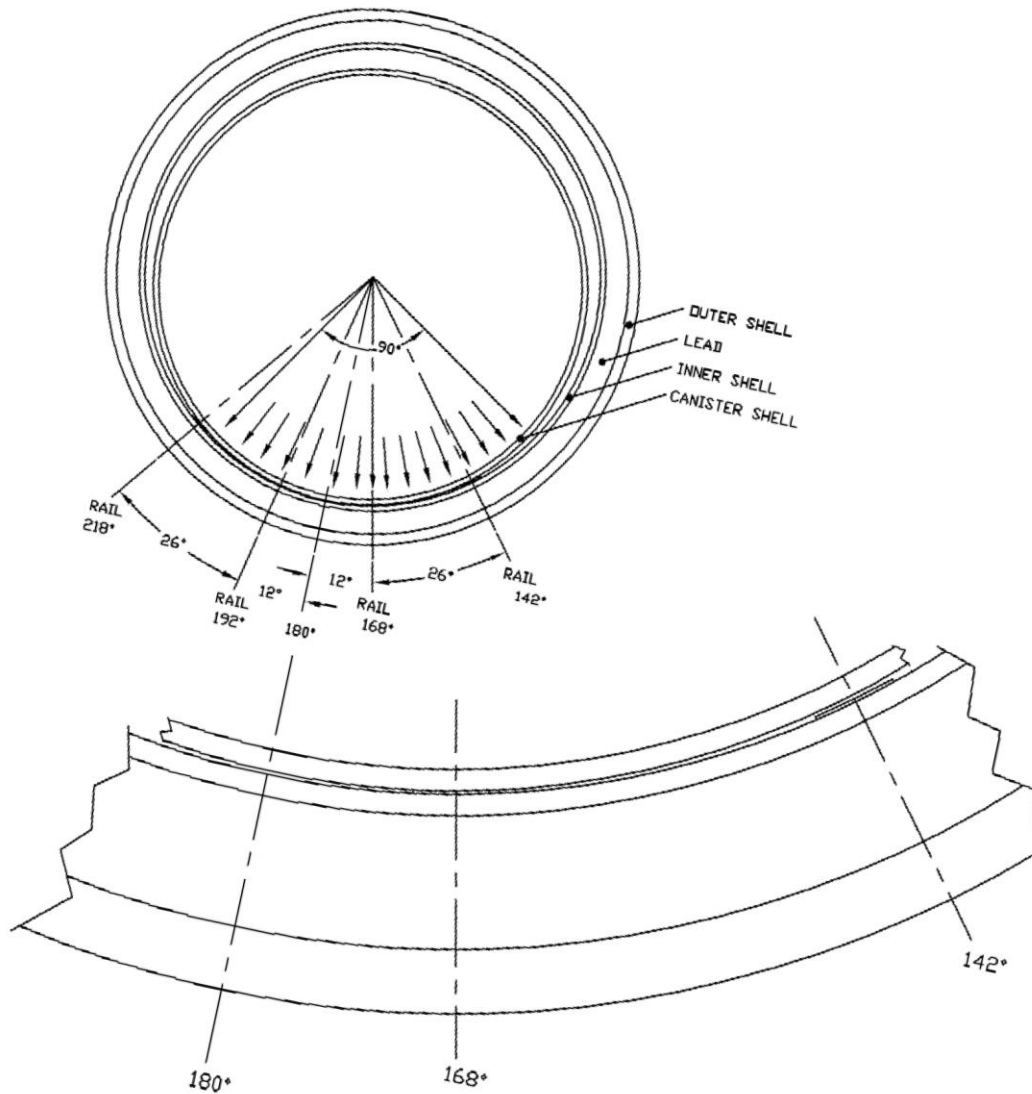


Figure 3.9.2-19
Drop Sketch for Initial Impact @ 168° Rail (Load Case 2)

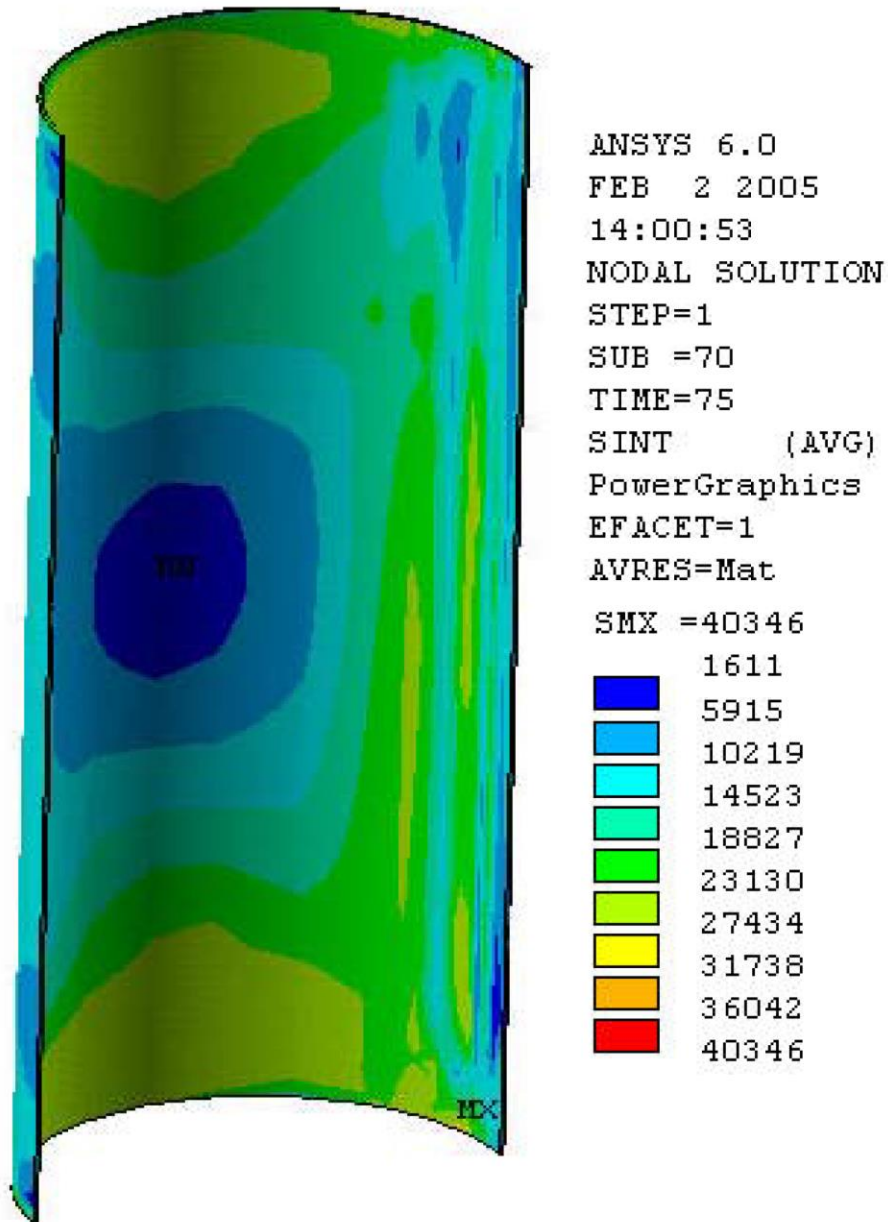


Figure 3.9.2-20
Inner Shell Stress Intensity Plot (Load Case 1)

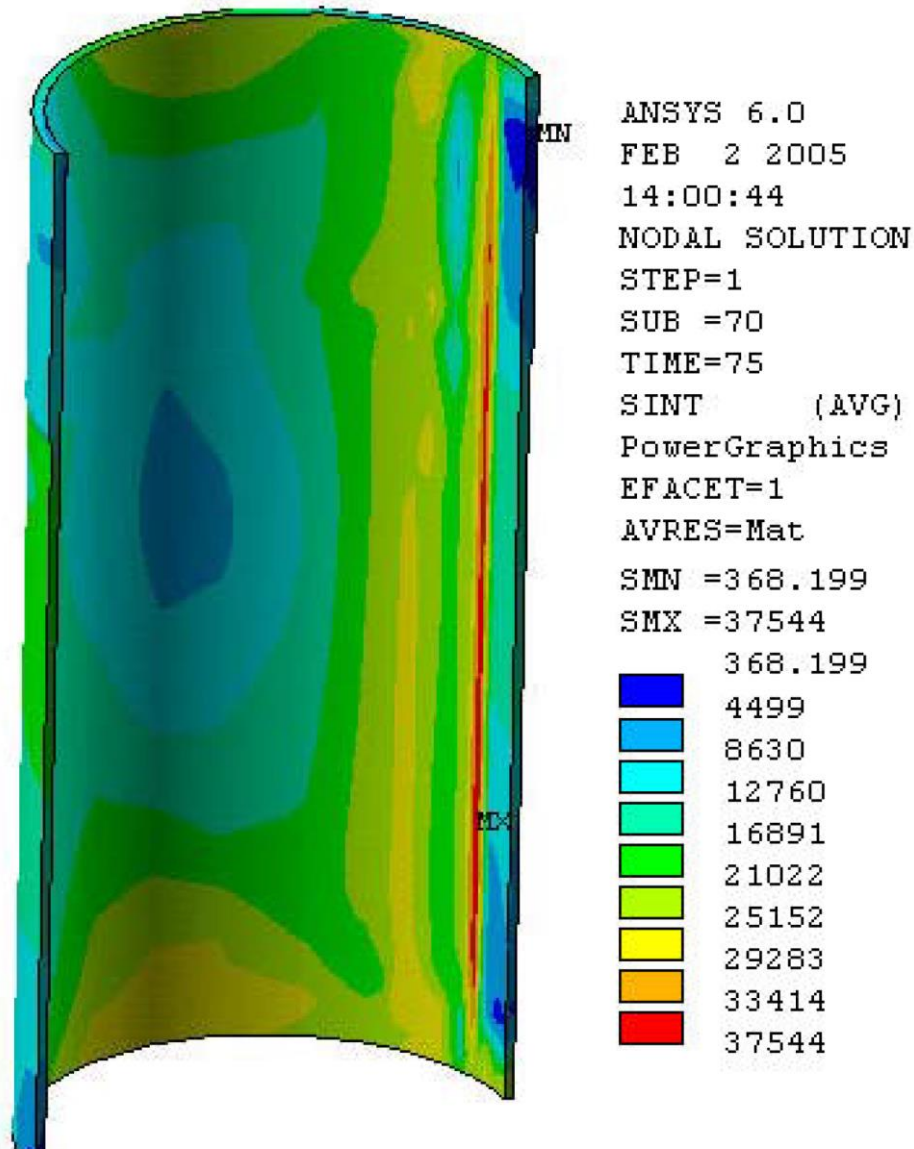


Figure 3.9.2-21
Outer Shell Stress Intensity Plot (Load Case 1)

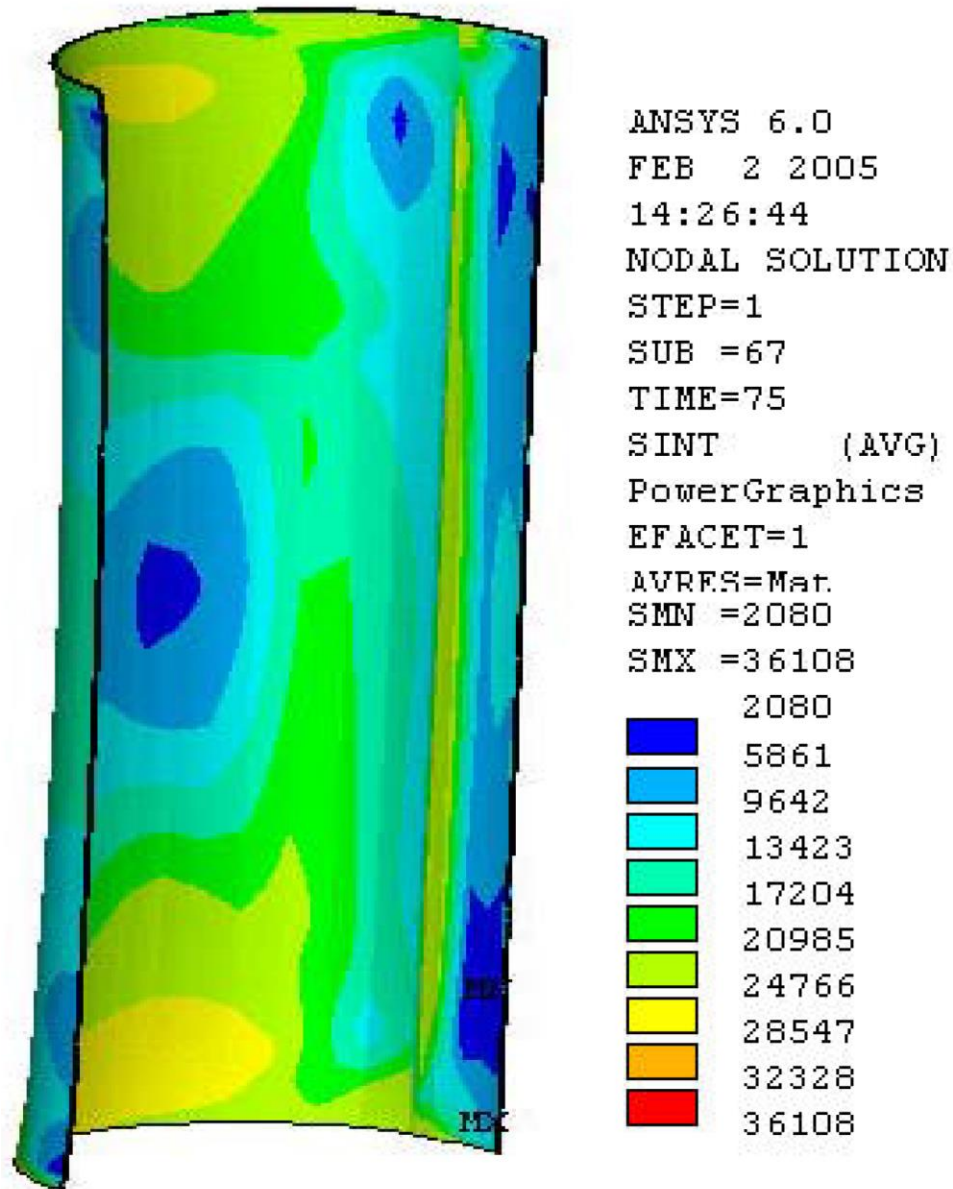


Figure 3.9.2-22
Inner Shell Stress Intensity Plot (Load Case 2)

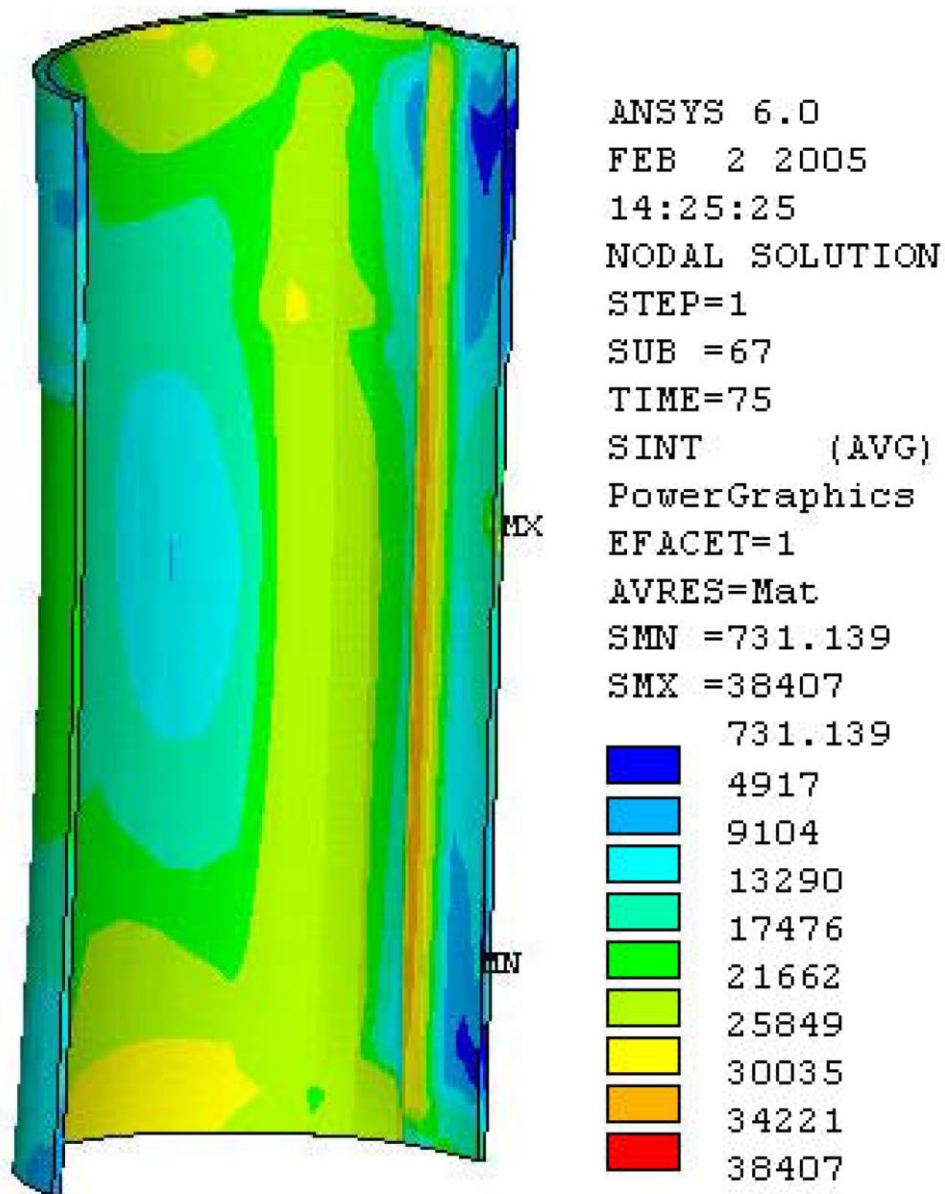


Figure 3.9.2-23
Outer Shell Stress Intensity Plot (Load Case 2)

APPENDIX 3.9.3
OS187H TRANSFER CASK TOP COVER AND RAM COVER BOLT ANALYSES

TABLE OF CONTENTS

3.9.3 OS187H TRANSFER CASK TOP COVER AND RAM ACCESS COVER BOLT ANALYSES	3.9.3-1
3.9.3.1 Introduction.....	3.9.3-1
3.9.3.2 Top Cover Bolt Load Calculations.....	3.9.3-3
3.9.3.3 Top Cover Bolt Load Combinations	3.9.3-8
3.9.3.4 Top Cover Bolt Stress Calculations.....	3.9.3-10
3.9.3.5 Top Cover Bolt Analysis Results	3.9.3-13
3.9.3.6 Minimum Engagement Length for Top Cover Bolt and Flange	3.9.3-14
3.9.3.7 RAM Access Cover Bolt Calculations.....	3.9.3-16
3.9.3.8 RAM Access Cover Bolt Load Combinations	3.9.3-21
3.9.3.9 RAM Access Cover Bolt Stress Calculations.....	3.9.3-23
3.9.3.10 RAM Access Cover Bolt Analysis Results	3.9.3-26
3.9.3.11 Minimum Engagement Length for RAM Access Cover Bolt	3.9.3-27
3.9.3.12 Brittle Fracture Analysis of Top Cover Bolt	3.9.3-29
3.9.3.13 Conclusions.....	3.9.3-32
3.9.3.14 References	3.9.3-33

LIST OF TABLES

Table 3.9.3-1	Design Parameters for Top cover Bolt Analysis	3.9.3-34
Table 3.9.3-2	Design Parameters for Ram Access Cover Bolt Analysis.....	3.9.3-35
Table 3.9.3-3	Bolt Data.....	3.9.3-36
Table 3.9.3-4	Allowable Stresses in Closure Bolts for Normal Conditions	3.9.3-37
Table 3.9.3-5	Allowable Stresses in Closure Bolts for Hypothetical Accident Conditions	3.9.3-38

LIST OF FIGURES

Figure 3.9.3-1	Effect of Tempering Temperature on Notch Toughness	3.9.3-39
Figure 3.9.3-2	Correlation Between Notch Toughness and Yield Strength	3.9.3-40
Figure 3.9.3-3	Singular Integral Equation and Asymptotic Approximation for Brittle Fracture Evaluation	3.9.3-41

3.9.3 OS187H TRANSFER CASK TOP COVER AND RAM ACCESS COVER BOLT ANALYSES

3.9.3.1 Introduction

This calculation evaluates the top cover bolts and RAM access cover bolts of the NUHOMS[®]-OS187H Transfer Cask under normal and accident conditions. Also evaluated in this calculation is the bolt thread engagement length. The stress analysis is performed in accordance with NUREG/CR-6007 [1].

The NUHOMS[®]-OS187H transfer cask top cover closure arrangement is shown in drawings 10494-72-16 and 17. The 3.0 inch thick cover is bolted directly to the end of the vessel top flange by 24 high strength steel 1.50 inch diameter bolts. Close fitting alignment pins ensure that the top cover is centered in the vessel. The top cover bolt material is SA-540 Gr. B24 class 1 which has a minimum yield strength of 150 ksi at room temperature [2].

The OS-187H Transfer Cask RAM access cover arrangement is shown in drawings 10494-72-16 and 18. The 1.0 inch thick cover is bolted directly to the end of the RAM access penetration ring by 12 high strength 0.50 inch diameter bolts. The RAM access cover bolt material is SA-540 Gr B24 Class 1, which has a minimum yield strength of 150 ksi at room temperature [2].

The following ways to minimize bolt forces and bolt failures for shipping casks are taken directly from NUREG/CR-6007, page xiii [1]. All of the following design methods are employed in the NUHOMS[®]-OS187H transfer cask closure system.

- Use materials with similar thermal properties for the closure bolts, the top cover, and the cask wall to minimize the bolt forces generated by fire accident
- Apply sufficiently large bolt preload to minimize fatigue and loosening of the bolts by vibration.
- Lubricate bolt threads to reduce required preload torque and to increase the predictability of the achieved preload.
- Use closure top cover design which minimizes the prying actions of applied loads.
- When choosing a bolt preload, pay special attention to the interactions between the preload and thermal load and between the preload and the prying action.

The following evaluations are presented in this section:

- Top over and RAM cover bolt torque
- Bolt preload
- Gasket seating load
- Pressure load
- Temperature load
- Impact load
- Thread engagement length evaluation
- Bearing stress
- Load combinations for normal and accident conditions
- Bolt stresses and allowable stresses

3.9.3.2 Top Cover Bolt Load Calculations

The design parameters of the top cover are summarized in Table 3.9.3-1. The top cover bolt data and material allowables are presented in Table 3.9.3-3 through Table 3.9.3-5. A temperature of 300° F is used in the top cover bolt region during normal and accident conditions. The following load cases are considered in the analysis.

- Preload + Temperature Load (normal condition)
- Pressure Load (normal condition)
- Pressure + 80 inch Corner Drop (accident condition)

Symbols and terminology used in this analysis are taken from NUREG/CR-6007 [1] and are reproduced in Table 3.9.3-1.

3.9.3.2.1 Top Cover Bolt Preload and Bolt Torque

A bolt torque range of 450 to 580 ft. lb. has been selected.

Using the minimum torque,

$$F_a = Q/KD_b = 450 \times 12 / (0.132 \times 1.50) = 27,270 \text{ lb.}, \text{ and}$$

$$\text{Preload stress} = F_a / \text{Stress Area (Table 3.9.3-3)} = 27,270 / 1.406 = 19,400 \text{ psi.}$$

Using the maximum torque,

$$F_a = Q/KD_b = 580 \times 12 / (0.132 \times 1.50) = 35,150 \text{ lb.}, \text{ and}$$

$$\text{Preload stress} = F_a / \text{Stress Area (Table 3.9.3-3)} = 35,150 / 1.406 = 25,000 \text{ psi.}$$

Residual torsional moment for minimum torque of 450 ft. lb. is,

$$M_{tr} = 0.5Q = .5(450 \times 12) = 2,700 \text{ in. lb.}$$

Residual torsional moment for maximum torque of 580 ft. lb. is,

$$M_{tr} = 0.5Q = .5(580 \times 12) = 3,480 \text{ in. lb.}$$

Residual tensile bolt force for maximum torque,

$$F_{ar} = F_a = 35,150 \text{ lb.}$$

3.9.3.2.2 Top Cover Gasket Seating Load

Since a self energizing o-ring is used, the gasket seating load is negligible.

3.9.3.2.3 Pressure Loads ([1], Table 4.3)

Axial force per bolt due to internal pressure is

$$F_a = \frac{\pi D_{lg}^2 (P_{li} - P_{lo})}{4 N_b}$$

D_{lg} (median lid seal diameter) = 74.19 in. Then,

$$F_a = \frac{\pi(74.19^2)(30 - 0)}{4(24)} = 5,404 \text{ lb./bolt.}$$

The fixed edge closure lid force is,

$$F_f = \frac{D_{lb}(P_{li} - P_{lo})}{4} = \frac{77.70(30)}{4} = 582.8 \text{ lb. in.}^{-1}.$$

The fixed edge closure lid moment is,

$$M_f = \frac{(P_{li} - P_{lo})D_{lb}^2}{32} = \frac{30(77.70^2)}{32} = 5,660 \text{ in. lb. in.}^{-1}.$$

The shear bolt force per bolt is,

$$F_s = \frac{\pi E_l t_l (P_{li} - P_{lo}) D_{lb}^2}{2 N_b E_c t_c (1 - N_{ul})} = \frac{\pi (27.0 \times 10^6) (3.0) (30) (77.70)^2}{2 (24) (27.0 \times 10^6) (5.575) (1 - 0.3)} = 9,113 \text{ lb./bolt.}$$

The top cover shoulder takes this shear force, so that $F_s = 0$.

3.9.3.2.4 Temperature Loads

From Reference 2, the top cover bolt material is SA-540, Grade B24, which is 2 Ni 3/4Cr 1/3Mo. The top cover is constructed from of SA-240 Type XM-19, which is 23Cr 13Ni 5Mn, and the flange is constructed from of SA-240 Type 304, which is 18Cr 8Ni. Therefore the bolts have a coefficient of thermal expansion of $6.9 \times 10^{-6} \text{ in./in.}^\circ\text{F}^{-1}$ at 300°F , the lid has a coefficient of thermal expansion of $8.8 \times 10^{-6} \text{ in./in.}^\circ\text{F}^{-1}$ at 300°F , and the flange has a coefficient of thermal expansion of $9.2 \times 10^{-6} \text{ in./in.}^\circ\text{F}^{-1}$ at 300°F .

Therefore, the tensile load in the bolt due to different thermal expansion is,

$$F_a = 0.25 \pi D_b^2 E_b (a_l T_l - a_b T_b)$$

$$F_a = 0.25(\pi)(1.50^2)(26.7 \times 10^6)[(8.8 \times 10^{-6})(230) - (6.9 \times 10^{-6})(230)] = 20,620 \text{ lb.}$$

Even though the top cover and flange are constructed from different materials, the shear force per bolt, F_s , due to a temperature change of 230° F is, 0 psi, since the clearance holes in the lid are oversized (1.688 in. diameter) allowing the lid to grow in the radial direction.

$$F_s = 0.$$

The temperature difference between the inside and outside of the top cover will always be less than one degree (see Chapter 4). Consequently, the resulting bending moment is negligible.

$$M_f = 0.$$

3.9.3.2.5 Impact Loads ([1], Table 4.5)

The non-prying tensile bolt force per bolt, F_a , is,

$$F_a = \frac{1.34 \sin(xi)(DLF)(ai)(W_l + W_c)}{N_b} = \frac{1.34 \sin(xi)(1.1)(ai)(115,500)}{24} = 7,094(ai) \sin(xi) \text{ lb./bolt.}$$

Note: $W_l + W_c$ is conservatively assumed to be 115,500 lbs. [see Table 3.9.3-1]

The shear bolt force is,

$$F_s = \frac{\cos(xi)(ai)(W_l)}{N_b} = \frac{5,500(ai) \cos(xi)}{24} = 229.2(ai) \cos(xi) \text{ lb./bolt.}$$

The lid shoulder during normal and accident condition drops takes shear force. Therefore,

$$F_s = 0.$$

The fixed-edge closure lid force, F_f , is,

$$F_f = \frac{1.34 \sin(xi)(DLF)(ai)(W_l + W_c)}{\pi D_{lb}} = \frac{1.34 \sin(xi)(1.1)(ai)(115,500)}{\pi(77.70)} = 697.4 \sin(xi)(ai) \text{ lb. in.}^{-1}$$

The fixed-edge closure lid moment, M_f , is,

$$M_f = \frac{1.34 \sin(xi)(DLF)(ai)(W_l + W_c)}{8\pi} = \frac{1.34 \sin(xi)(1.1)(ai)(115,500)}{8\pi} = 6,774 \sin(xi)(ai) \text{ in.lb.in}^{-1}$$

The accident condition impact load is taken to be the axial acceleration due to corner drop. The following accident condition corner drop acceleration and impact angle bound the 15.9g C.G. over corner drop acceleration computed in Appendix 3.9.7.

$$ai = 25 \text{ gs, and } xi = 60^\circ$$

Therefore,

$$F_a = 7,094 \times 25 \times \sin(60^\circ) = 153,600 \text{ lb./bolt}$$

$$F_s = 0 \text{ lb./bolt}$$

$$F_f = 697.4 \times 25 \times \sin(60^\circ) = 15,100 \text{ lb./bolt, and}$$

$$M_f = 6,774 \times 25 \times \sin(60^\circ) = 146,700 \text{ lb./bolt.}$$

The top cover individual load is summarized in the following table.

Top Cover Bolt Individual Load Summary

Load Case	Applied Load		Non-Prying Tensile Force, F_a (lb.)	Torsional Moment, M_t (in. lb.)	Prying Force, F_f (lb.in. ⁻¹)	Prying Moment, M_f (in. lb. in. ⁻¹)
Preload	Residual	Minimum Torque	27,270	2,700	0	0
		Maximum Torque	35,150	3,480	0	0
Gasket	Seating Load		0	0	0	0
Pressure	50 psig Internal		5,404	0	582.8	5,660
Thermal	300°F		20,620	0	0	0
Impact	Accident Condition Drop		153,600	0	15,100	146,700

3.9.3.3 Top Cover Bolt Load Combinations ([1], Table 4.9)

A summary of normal and accident condition load combinations is presented in the following table.

Top Cover Bolt Normal and Accident Load Combinations

Load Case	Combination Description		Non-Prying Tensile Force, F_a (lb.)	Torsional Moment, M_t (in. lb.)	Prying Force, F_f (lb.in. ⁻¹)	Prying Moment, M_f (in. lb. in. ⁻¹)
1.	Preload + Temperature (Normal Condition)	Minimum Torque	47,890	2,700	0	0
		Maximum Torque	55,770	3,480	0	0
2.	Pressure (Normal Condition)		5,404	0	582.8	5,660
3.	Pressure + Accident Impact (Accident Condition)		159,000	0	15,680	152,400

Additional Prying Bolt Force

It is shown in the above table, Top Cover Bolt Normal and Accident Load Combinations, that all loading conditions cause outward acting loads only. Outward acting loads generate no additional prying bolts forces, because the gap between the lid and flange at the outer edge prevents the creation of a prying moment.

Bolt Bending Moment ([1], Table 2.2)

The maximum bending bolt moment, M_{bb} , generated by the applied load is evaluated as follows:

$$M_{bb} = \left(\frac{\pi D_{lb}}{N_b} \right) \left[\frac{K_b}{K_b + K_l} \right] M_f$$

The K_b and K_l are based on geometry and material properties and are defined in Reference 1, Table 2.2. By substituting the values given above,

$$K_b = \left(\frac{N_b}{L_b} \right) \left(\frac{E_b}{D_{lb}} \right) \left(\frac{D_b^4}{64} \right) = \left(\frac{24}{1.5} \right) \left(\frac{26.7 \times 10^6}{77.70} \right) \left(\frac{1.50^4}{64} \right) = 4.349 \times 10^5, \text{ and}$$

$$K_l = \frac{E_l t_l^3}{3 \left[(1 - N_{ul}^2) + (1 - N_{ul})^2 \left(\frac{D_{lb}}{D_{lo}} \right)^2 \right] D_{lb}} = \frac{27.0 \times 10^6 (3.0^3)}{3 \left[(1 - 0.3^2) + (1 - 0.3)^2 \left(\frac{77.70}{82.20} \right)^2 \right] 77.70}$$

$$= 2.320 \times 10^6$$

Therefore,

$$M_{bb} = \left(\frac{\pi 77.70}{24} \right) \left[\frac{4.349 \times 10^5}{4.349 \times 10^5 + 2.320 \times 10^6} \right] M_f = 1.606 M_f.$$

For load case 2, $M_f = 5,660$ in. lb. Substituting this value into the equation above gives,

$$M_{bb} = 9,090 \text{ in. lb. / bolt.}$$

3.9.3.4 Top Cover Bolt Stress Calculations ([1], Table 5.1)

3.9.3.4.1 Average Tensile Stress

A summary of the applied loads for the transfer cask lid bolts is provided in the Top Cover Bolt Normal and Accident Load Combinations Table in Section 3.9.3.3.

For the normal condition load cases, the applied bolt preload maintains closure of the transfer cask top cover. The closure force per bolt generated by the minimum lid bolt torque, with or without the additional closure force generated by thermal loads, is greater than the normal condition forces trying to open the top cover.

For accident conditions, the impact loads may instantaneously relax pressure on the top cover seals. However the accident condition loads will not cause lid bolt failure, as shown below and immediately following the accident impact, the top closure seal will be reseated by the bolt preload.

Normal Condition

$$S_{ba} = 1.2732 \frac{F_a}{D_{ba}^2} = 1.2732 \frac{55,770}{1.378^2} = 37,390 \text{ psi.} = 37.4 \text{ ksi.}$$

Accident Condition

$$S_{ba} = 1.2732 \frac{F_a}{D_{ba}^2} = 1.2732 \frac{159,000}{1.378^2} = 106,600 \text{ psi.} = 106.6 \text{ ksi.}$$

3.9.3.4.2 Bending Stress

Normal Condition

$$S_{bb} = 10.186 \frac{M_{bb}}{D_{ba}^3} = 10.186 \frac{9,090}{1.378^3} = 35,390 \text{ psi.} = 35.4 \text{ ksi.}$$

3.9.3.4.3 Shear Stress

For both normal and accident conditions, the average shear stress caused by shear bolt force F_s is,

$$S_{bs} = 0.$$

For normal and accident conditions the maximum shear stress caused by the torsional moment M_t is,

$$S_{bt} = 5.093 \frac{M_t}{D_{ba}^3} = 5.093 \frac{3,480}{1.378^3} = 6,773 \text{ psi.} = 6.8 \text{ ksi.}$$

3.9.3.4.4 Maximum Combined Stress Intensity

The maximum combined stress intensity is calculated in the following way (Ref. 1, Table 5.1).

$$S_{bi} = [(S_{ba} + S_{bb})^2 + 4(S_{bs} + S_{bt})^2]^{0.5}$$

For normal conditions combine tension, shear, bending, and residual torsion.

$$S_{bi} = [(37,390 + 35,390)^2 + 4(0 + 6,773)^2]^{0.5} = 74,030 \text{ psi.} = 74.0 \text{ ksi.}$$

3.9.3.4.5 Stress Ratios

In order to meet the stress ratio requirement, the following relationship must hold for both normal and accident conditions.

$$R_t^2 + R_s^2 < 1$$

Where R_t is the ratio of average tensile stress to allowable average tensile stress, and R_s is the ratio of average shear stress to allowable average shear stress.

For normal conditions

$$R_t = 37,390/92,400 = 0.405,$$

$$R_s = 6,773/55,400 = 0.122,$$

$$R_t^2 + R_s^2 = (0.405)^2 + (0.122)^2 = 0.179 < 1.$$

For accident conditions

$$R_t = 106,600/115,500 = 0.923,$$

$$R_s = 6,773/69,300 = 0.098,$$

$$R_t^2 + R_s^2 = (0.923)^2 + (0.098)^2 = 0.862 < 1.$$

3.9.3.4.6 Bearing Stress (Under Bolt Head)

A standard 1.50 in. washer placed under the head of each top cover bolt. The inside and outside diameter of a standard 1.50 in. washer is 1.50 in. and 3.00 in. respectively. The diameter of the bolt clearance hole in the top cover is 1.688 in. Therefore, the total bearing area under the top cover bolts, A_b , is the following.

$$A_b = (\pi/4) [3.00^2 - 1.688^2] = 4.831 \text{ in.}^2$$

According to Reference 1, bearing stresses are only required to be evaluated for normal condition loads. For normal conditions, the maximum bearing stress under the washer, σ_b , is the following.

$$\sigma_b = 55,770 \text{ lb.} / 4.831 \text{ in.}^2 = 11,540 \text{ psi.}$$

The normal condition allowable bearing stress on the cover is taken to be the yield stress of the cover material at 300° F. The cover is manufactured out of SA-240 Type XM-19, which has a yield stress of 43.3 ksi. at 300° F.

3.9.3.5 Top Cover Bolt Analysis Results

A summary of the stresses calculated above is listed in the following table:

Summary of Top Cover Bolt Stresses and Allowables

Stress Type	Normal Condition		Accident Condition	
	Stress	Allowable	Stress	Allowable
Average Tensile (ksi.)	37.4	92.4	106.6	115.5
Shear (ksi)	6.8	55.4	6.8	69.3
Combined (ksi)	74.0	124.7	Not Required [1]	
Interaction Equation $R_t^2 + R_s^2 < 1$	0.179	1	0.862	1
Bearing (ksi) Allowable (ksi) (S_y of lid material)	11.5	43.3	Not Required [1]	

3.9.3.6 Minimum Engagement Length for Top Cover Bolt and Flange

For a 1 1/2" – 8UN – 2A bolt, the material is SA-540 GR. B24 CL.1, with

$$S_u = 165 \text{ ksi.}, \text{ and} \\ S_y = 150 \text{ ksi (at room temperature)}$$

The helicoil insert is neglected in the thread engagement length computation. It is conservative to neglect the helicoil insert, because it has a much higher tensile strength (200 ksi. [3]) than the flange material. The flange material is constructed from type 304 stainless steel and has the following material properties.

$$S_u = 75 \text{ ksi.}, \text{ and} \\ S_y = 30 \text{ ksi (at room temperature)}$$

The minimum engagement length, L_e , for the bolt and flange is [4],

$$L_e = \frac{2A_t}{3.1416 K_{n \max} \left[\frac{1}{2} + .57735 n (E_{s \min} - K_{n \max}) \right]}$$

Where,

$$A_t = \text{tensile stress area} = 1.491 \text{ in.}^2, \\ n = \text{number of threads per inch} = 8, \\ K_{n \max} = \text{maximum minor diameter of internal threads} = 1.390 \text{ in. [4]} \\ E_{s \min} = \text{minimum pitch diameter of external threads} = 1.4093 \text{ in. [4]}$$

Substituting the values given above,

$$L_e = \frac{2(1.491)}{(3.1416)1.390 \left[\frac{1}{2} + .57735 (8)(1.4093 - 1.390) \right]} = 1.159 \text{ in.}$$

$$J = \frac{A_s \times S_{ue}}{A_n \times S_{ui}} \text{ . [5]}$$

Where, S_{ue} is the tensile strength of external thread material, and S_{ui} is the tensile strength of internal thread material.

$$A_s = \text{shear area of external threads} = 3.1416 n L_e K_{n \max} [1/(2n) + .57735 (E_{s \min} - K_{n \max})]$$

$$A_n = \text{shear area of internal threads} = 3.1416 n L_e D_{s \min} [1/(2n) + .57735 (D_{s \min} - E_{n \max})]$$

For the bolt / Helicoil insert connection:

$$E_{n\ max} = \text{maximum pitch diameter of internal threads} = 1.4283 \text{ in. [4]}$$

$$D_{s\ min} = \text{minimum major diameter of external threads} = 1.4828 \text{ in. [4]}$$

Therefore,

$$A_s = 3.1416(8)(1.159)(1.390)[1/(2 \times 8) + .57735 (1.4093 - 1.390)] = 2.982 \text{ in.}^2$$

$$A_n = 3.1416(8)(1.159)(1.4828)[1/(2 \times 8) + .57735 (1.4828 - 1.4283)] = 4.059 \text{ in.}^2$$

So,

$$J = \frac{2.982(165.0)}{4.059(75.0)} = 1.616$$

$$Q = L_e J = (1.159)(1.616) = 1.873 \text{ in.}$$

The actual minimum engagement length:

$$4.50 \text{ in. bolt length} - 1.50 \text{ in. cover thickness} - 0.180 \text{ in. washer thickness} = 2.82 \text{ in.} > 1.873 \text{ in.}$$

3.9.3.7 RAM Access Cover Bolt Calculations

The design parameters of the RAM access cover bolts are summarized in Table 3.9.3-2. The RAM access cover bolt data and material allowables are presented in Table 3.9.3-3 through Table 3.9.3-5. A temperature of 300° F is used in the RAM access cover bolt region during normal and accident conditions. The following load cases are considered in the analysis.

- Preload + Temperature Load (normal condition)
- Pressure Load (normal condition)
- Pressure + 80 inch Corner Drop (accident condition)

Symbols and terminology used in this analysis are taken from NUREG/CR-6007 [1] and are reproduced in Table 3.9.3-2.

3.9.3.7.1 RAM Access Cover Bolt Preload and Bolt Torque

A bolt torque range of 15 to 20 ft. lb. has been selected.

Using the minimum torque,

$$F_a = Q/KD_b = 15 \times 12 / (0.132 \times 0.50) = 2,727 \text{ lb.}, \text{ and}$$

$$\text{Preload stress} = F_a / \text{Stress Area (Table 3.9.3-3)} = 2,727 / 0.142 = 19,204 \text{ psi.}$$

Using the maximum torque,

$$F_a = Q/KD_b = 20 \times 12 / (0.132 \times 0.50) = 3,636 \text{ lb.}, \text{ and}$$

$$\text{Preload stress} = F_a / \text{Stress Area (Table 3.9.3-3)} = 3,636 / 0.142 = 25,610 \text{ psi.}$$

Residual torsional moment for minimum torque of 15 ft. lb. is,

$$M_{tr} = 0.5Q = .5(15 \times 12) = 90 \text{ in. lb.}$$

Residual torsional moment for maximum torque of 20 ft. lb. is,

$$M_{tr} = 0.5Q = .5(20 \times 12) = 120 \text{ in. lb.}$$

Residual tensile bolt force for maximum torque,

$$F_{ar} = F_a = 3,636 \text{ lb.}$$

3.9.3.7.2 RAM Access Cover Gasket Seating Load

Since a self energizing o-ring is used, the gasket seating load is negligible.

3.9.3.7.3 Pressure Loads ([1], Table 4.3)

Axial force per bolt due to internal pressure is

$$F_a = \frac{\pi D_{lg}^2 (P_{li} - P_{lo})}{4N_b}.$$

D_{lg} (median cover seal diameter) = 21.16 in. Then,

$$F_a = \frac{\pi(21.16^2)(30 - 0)}{4(12)} = 879.1 \text{ lb./bolt.}$$

The fixed edge cover force is,

$$F_f = \frac{D_{lb}(P_{li} - P_{lo})}{4} = \frac{23.50(30)}{4} = 176.3 \text{ lb. in.}^{-1}.$$

The fixed edge cover moment is,

$$M_f = \frac{(P_{li} - P_{lo})D_{lb}^2}{32} = \frac{30(23.50^2)}{32} = 517.7 \text{ in. lb. in.}^{-1}.$$

The shear bolt force per bolt is,

$$F_s = \frac{\pi E_l t_l (P_{li} - P_{lo}) D_{lb}^2}{2 N_b E_c t_c (1 - N_{ul})} = \frac{\pi (27.0 \times 10^6) (1.0) (30) (23.50)^2}{2 (12) (27.0 \times 10^6) (4.0) (1 - 0.3)} = 774.5 \text{ lb./bolt.}$$

The radial growth of the access ring due to an internal pressure of 30 psi is, δ_r , is given by the following equation.

$$\delta_r = \frac{Pr^2}{Et}$$

Where, P is the applied pressure (30 psi.), r is the mean radius of the RAM access penetration (12.00 in.), E is the material modulus of elasticity (27.0×10^6 psi. @ 300° F [2]), and t is the radial thickness of the penetration (4.00 in.). Therefore,

$$\delta_r = \frac{(30)(12.00)^2}{(27 \times 10^6)(4.00)} = 4.00 \times 10^{-5} \text{ in.}$$

Since the radial growth due to internal pressure is less than the RAM access bolt clearance (0.563 in. – ½ in. bolt = 0.063 in.), no shear force is generated in the RAM access cover bolts. Therefore,

$$F_s = 0.$$

3.9.3.7.4 Temperature Loads

The cover bolt material is SA-540 Grade B24 Class 1, which is 2Ni ¾ Cr 1/3 Mo. The RAM access penetration and cover are both constructed from of SA-240 Type 304, which is 18Cr 8Ni. Therefore the bolts have a coefficient of thermal expansion of 6.9×10^{-6} in./in. °F⁻¹ at 300° F, the RAM access penetration and cover has a coefficient of thermal expansion of 9.2×10^{-6} in./in. °F⁻¹ at 300° F. The tensile load in the bolt due to different thermal expansion is,

$$F_a = 0.25 \pi D_b^2 E_b (a_l T_l - a_b T_b)$$

$$F_a = 0.25(\pi)(0.50^2)(26.7 \times 10^6)[(9.2 \times 10^{-6})(230) - (6.9 \times 10^{-6})(230)] = 2,773 \text{ lb./bolt}$$

The shear force per bolt, F_s , due to a temperature change of 230° F is 0 lb, since there is negligible differential thermal expansion between the RAM access penetration and cover, which are both constructed from the same material, and since the clearance holes in the cover are oversized (0.563 in. diameter). Therefore,

$$F_s = 0.$$

The temperature difference between the inside and outside of the cover will always be less than one degree (see Chapter 4). Consequently, the resulting bending moment is negligible.

$$M_f = 0.$$

3.9.3.7.5 Impact Loads ([1], Table 4.5)

The DSC inside the NUHOMS®-OS187H Transfer Cask is supported in the axial direction at the bottom of the cask by the bottom end plate. During a free drop event, the inertial load of the transfer cask internals is transferred through the bottom end plate, bottom neutron shield, and neutron shield plate to the impact target. Consequently, only the inertial load of the RAM access cover itself generates loads in the bolts.

The non-prying tensile bolt force per bolt, F_a , is,

$$F_a = \frac{1.34 \sin(xi)(DLF)(ai)(W_l + W_c)}{N_b} = \frac{1.34 \sin(xi)(1.1)(ai)(200)}{12} = 24.57(ai) \sin(xi) \text{ lb./bolt.}$$

Note: $W_l + W_c$ is assumed to be only the weight of the RAM access cover, $W_c = 200$ lbs. [see Table 3.9.3-2]

The shear bolt force is,

$$F_s = \frac{\cos(xi)(ai)(W_l)}{N_b} = \frac{200(ai) \cos(xi)}{12} = 16.67(ai) \cos(xi) \text{ lb./bolt.}$$

The fixed-edge cover force, F_f , is,

$$F_f = \frac{1.34 \sin(xi)(DLF)(ai)(W_l + W_c)}{\pi D_{lb}} = \frac{1.34 \sin(xi)(1.1)(ai)(200)}{\pi(23.50)} = 3.993 \sin(xi)(ai) \text{ lb. in.}^{-1}$$

The fixed-edge cover moment, M_f , is,

$$M_f = \frac{1.34 \sin(xi)(DLF)(ai)(W_l + W_c)}{8\pi} = \frac{1.34 \sin(xi)(1.1)(ai)(200)}{8\pi} = 11.73 \sin(xi)(ai) \text{ in.lb.in}^{-1}$$

The accident condition impact load is taken to be the axial acceleration due to corner drop. The following accident condition corner drop acceleration and impact angle bound the 15.9g C.G. over corner drop acceleration computed in Appendix 3.9.7.

$$ai = 25 \text{ gs, and } xi = 60^\circ$$

Therefore,

$$\begin{aligned} F_a &= 24.57 \times 25 \times \sin(60^\circ) = 531.9 \text{ lb./bolt} \\ F_s &= 16.67 \times 25 \times \cos(60^\circ) = 208.4 \text{ lb./bolt,} \\ F_f &= 3.993 \times 25 \times \sin(60^\circ) = 86.45 \text{ lb./in., and} \\ M_f &= 11.73 \times 25 \times \sin(60^\circ) = 254.0 \text{ in.lb./in.} \end{aligned}$$

The ram cover bolt individual load is summarized in the following table.

Ram Access Cover Bolt Individual Load Summary

Load Case	Applied Load		Non-Prying Tensile Force, F_a (lb.)	Torsional Moment, M_t (in. lb.)	Shear Force, F_s (lb.)	Prying Force, F_f (lb.in. ⁻¹)	Prying Moment, M_f (in. lb. in. ⁻¹)
Preload	Residual	Minimum Torque	2,727	90	0	0	0
		Maximum Torque	3,636	120	0	0	0
Gasket	Seating Load		0	0	0	0	0
Pressure	30 psig Internal		879.1	0	0	176.3	517.7
Thermal	300°F		2,773	0	0	0	0
Impact	Accident Condition Drop		531.9	0	208.4	86.45	254.0

3.9.3.8 RAM Access Cover Bolt Load Combinations ([1], Table 4.9)

A summary of normal and accident condition load combinations is presented in the following table.

Ram Access Cover Bolt Normal And Accident Load Combinations

Load Case	Combination Description		Non-Prying Tensile Force, F_a (lb.)	Torsional Moment, M_t (in. lb.)	Shear Force, F_s (lb.)	Prying Force, F_f (lb.in. ⁻¹)	Prying Moment, M_f (in. lb. in. ⁻¹)
1.	Preload + Temperature (Normal Condition)	Minimum Torque	5,500	90	0	0	0
		Maximum Torque	6,409	120	0	0	0
2.	Pressure (Normal Condition)		879.1	0	0	176.3	517.7
3.	Pressure + Accident Impact (Accident Condition)		1,411	0	208.4	262.8	771.7

Additional Prying Bolt Force

It is shown in the above table, Ram Access Cover Bolt Normal and Accident Load Combinations, that all loading conditions cause outward acting loads only. Outward acting loads generate no additional prying bolts forces, because the gap between the cover and the ram access penetration ring at the outer edge prevents the creation of a prying moment.

Bolt Bending Moment ([1], Table 2.2)

The maximum bending bolt moment, M_{bb} , evaluated for normal conditions only, is evaluated as follows:

$$M_{bb} = \left(\frac{\pi D_{lb}}{N_b} \right) \left[\frac{K_b}{K_b + K_l} \right] M_f$$

The K_b and K_l are based on geometry and material properties and are defined in Reference 1, Table 2.2. By substituting the values given above,

$$K_b = \left(\frac{N_b}{L_b} \right) \left(\frac{E_b}{D_{lb}} \right) \left(\frac{D_b^4}{64} \right) = \left(\frac{12}{0.34} \right) \left(\frac{26.7 \times 10^6}{23.50} \right) \left(\frac{0.50^4}{64} \right) = 3.916 \times 10^4, \text{ and}$$

$$K_l = \frac{E_l t_l^3}{3 \left[(1 - N_{ul}^2) + (1 - N_{ul})^2 \left(\frac{D_{lb}}{D_{lo}} \right)^2 \right] D_{lb}} = \frac{27.0 \times 10^6 (1.00^3)}{3 \left[(1 - 0.3^2) + (1 - 0.3)^2 \left(\frac{23.50}{25.45} \right)^2 \right] 23.50}$$

$$= 2.884 \times 10^5$$

Therefore,

$$M_{bb} = \left(\frac{\pi 23.50}{12} \right) \left[\frac{3.619 \times 10^4}{3.619 \times 10^4 + 2.884 \times 10^5} \right] M_f = 0.7355 M_f$$

For load case 2, $M_f = 517.7 \text{ in.lb./in.}$ Substituting this value into the equation above gives,

$$M_{bb} = 380.8 \text{ in. lb. / bolt.}$$

3.9.3.9 RAM Access Cover Bolt Stress Calculations ([1], Table 5.1)

3.9.3.9.1 Average Tensile Stress

A summary of the applied loads for the transfer cask RAM access cover bolts is provided in the Ram Access Cover Bolt Normal and Accident Load Combinations Table in Section 3.9.3.8.

For both normal and accident condition load cases, the applied bolt preload maintains closure of the transfer cask RAM access cover. The closure force per bolt generated by the minimum RAM access cover bolt torque, with or without the additional closure force generated by thermal loads, is greater than all loads trying to open the RAM access cover.

Normal Condition

$$S_{ba} = 1.2732 \frac{F_a}{D_{ba}^2} = 1.2732 \frac{6,409}{0.425^2} = 45,180 \text{ psi.} = 45.2 \text{ ksi.}$$

Accident Condition

$$S_{ba} = 1.2732 \frac{F_a}{D_{ba}^2} = 1.2732 \frac{6,409}{0.425^2} = 45,180 \text{ psi.} = 45.2 \text{ ksi.}$$

3.9.3.9.2 Bending Stress

Normal Condition

$$S_{bb} = 10.186 \frac{M_{bb}}{D_{ba}^3} = 10.186 \frac{380.8}{0.425^3} = 50,530 \text{ psi.} = 50.5 \text{ ksi.}$$

3.9.3.9.3 Shear Stress

For normal conditions, the average shear stress caused by shear bolt force F_s is,

$$S_{bs} = 0.$$

For accident conditions, the average shear stress caused by shear bolt force F_s is,

$$S_{bs} = 1.2732 \frac{F_s}{D_{ba}^2} = 1.2732 \frac{208.4}{0.425^2} = 1,469 \text{ psi.} = 1.5 \text{ ksi.}$$

For normal and accident conditions the maximum shear stress caused by the torsional moment M_t is,

$$S_{bt} = 5.093 \frac{M_t}{D_{ba}^3} = 5.093 \frac{120}{0.425^3} = 7,961 \text{ psi.} = 8.0 \text{ ksi.}$$

3.9.3.9.4 Maximum Combined Stress Intensity

The maximum combined stress intensity is calculated in the following way (Ref. 1, Table 5.1).

$$S_{bi} = [(S_{ba} + S_{bb})^2 + 4(S_{bs} + S_{bt})^2]^{0.5}$$

For normal conditions combine tension, shear, bending, and residual torsion.

$$S_{bi} = [(45,180 + 50,530)^2 + 4(0 + 7,961)^2]^{0.5} = 97,030 \text{ psi.} = 97.0 \text{ ksi.}$$

3.9.3.9.5 Stress Ratios

In order to meet the stress ratio requirement, the following relationship must hold for both normal and accident conditions.

$$R_t^2 + R_s^2 < 1$$

Where R_t is the ratio of average tensile stress to allowable average tensile stress, and R_s is the ratio of average shear stress to allowable average shear stress.

For normal conditions

$$R_t = 45,180/92,400 = 0.740,$$

$$R_s = 0/55,400 = 0,$$

$$R_t^2 + R_s^2 = (0.740)^2 + (0)^2 = 0.548 < 1.$$

For accident conditions

$$R_t = 45,180/115,500 = 0.531,$$

$$R_s = 1,469/69,300 = 0.021,$$

$$R_t^2 + R_s^2 = (0.531)^2 + (0.021)^2 = 0.282 < 1.$$

3.9.3.9.6 Bearing Stress (Under Bolt Head)

A ½ in. standard washer is placed under the head of each RAM access cover bolt. The inside and outside diameter the washer is 0.531 in. and 1.062 in. respectively. The diameter of the bolt clearance hole in the cover is 0.563 in. Therefore, the total bearing area under the top cover bolts, A_b , is the following.

$$A_b = (\pi/4) [1.062^2 - 0.563^2] = 0.637 \text{ in.}^2$$

According to Reference 1, bearing stresses are only required to be evaluated for normal condition loads. For normal conditions, the maximum bearing stress under the washer, σ_b , is the following.

$$\sigma_b = 6,409 \text{ lb.} / 0.637 \text{ in.}^2 = 10,060 \text{ psi.}$$

The normal condition allowable bearing stress on the cover is taken to be the yield stress of the cover material at 300° F. The cover is manufactured out of SA-240 Type 304, which has a yield stress of 22.4 ksi. at 300° F.

3.9.3.10 RAM Access Cover Bolt Analysis Results

A summary of the stresses calculated above is listed in the following table:

Summary Of Stresses And Allowables

Stress Type	Normal Condition		Accident Condition	
	Stress	Allowable	Stress	Allowable
Average Tensile (ksi.)	45.2	92.4	45.2	115.5
Shear (ksi)	8.0	55.4	9.5	69.3
Combined(ksi)	90.7	124.7	Not Required [1]	
Interaction E.Q. $R_t^2 + R_s^2 < 1$	0.548	1	0.282	1
Bearing (ksi) Allowable (ksi) (S _y of lid material)	10.1	22.4	Not Required [1]	

3.9.3.11 Minimum Engagement Length for RAM Access Cover Bolt

For a 1/2"– 13UNC – 2A bolt, the material is SA-540 GR. B24 CL.1, with

$$S_u = 165 \text{ ksi.}, \text{ and}$$

$$S_y = 150 \text{ ksi (at room temperature)}$$

The RAM access penetration and threaded insert material are both constructed from type 304 stainless steel and have the following material properties.

$$S_u = 75 \text{ ksi.}, \text{ and}$$

$$S_y = 30 \text{ ksi (at room temperature)}$$

The minimum engagement length, L_e , for the bolt and flange is [4],

$$L_e = \frac{2A_t}{3.1416 K_{n \max} \left[\frac{1}{2} + .57735 n (E_{s \min} - K_{n \max}) \right]}.$$

Where,

$$A_t = \text{tensile stress area} = 0.142 \text{ in.}^2,$$

$$n = \text{number of threads per inch} = 13$$

$$K_{n \max} = \text{maximum minor diameter of internal threads} = 0.434 \text{ in. [4]}$$

$$E_{s \min} = \text{minimum pitch diameter of external threads} = 0.4435 \text{ in. [4]}$$

Substituting the values given above,

$$L_e = \frac{2(0.142)}{(3.1416)0.434 \left[\frac{1}{2} + .57735 (13)(0.4435 - 0.434) \right]} = 0.365 \text{ in.}$$

$$J = \frac{A_s \times S_{ue}}{A_n \times S_{ui}} \quad [4]$$

Where, S_{ue} is the tensile strength of external thread material, and S_{ui} is the tensile strength of internal thread material.

$$A_s = \text{shear area of external threads} = 3.1416 n L_e K_{n \max} [1/(2n) + .57735 (E_{s \min} - K_{n \max})]$$

$$A_n = \text{shear area of internal threads} = 3.1416 n L_e D_{s \min} [1/(2n) + .57735 (D_{s \min} - E_{n \max})]$$

For the bolt / Helicoil insert connection:

$E_{n\ max}$ = maximum pitch diameter of internal threads = 0.4565 in. [4]

$D_{s\ min}$ = minimum major diameter of external threads = 0.4876 in. [4]

Therefore,

$$A_s = 3.1416(13)(0.365)(0.434)[1/(2 \times 13) + .57735 (0.4435 - 0.434)] = 0.2843 \text{ in.}^2$$

$$A_n = 3.1416(13)(0.365)(0.4876)[1/(2 \times 13) + .57735 (0.4876 - 0.4565)] = 0.4101 \text{ in.}^2$$

So,

$$J = \frac{0.2843(165.0)}{0.4101(75.0)} = 1.525$$

$$Q = L_e J = (0.365)(1.525) = 0.557 \text{ in.}$$

The actual minimum engagement length is,

1.25 in. bolt length – 1.00 in. cover thickness + 0.66 in. cover counter bore – 0.125 in. washer thickness = 0.785 in. > 0.557 in.

3.9.3.12 Brittle Fracture Analysis of Top Cover Bolt

The transfer cask and its attachment bolts are designed and fabricated per ASME Subsection NC Code [6]. The fracture toughness requirements for the bolting material are specified in Section NC-2332.3. This section indicates that in order to meet the fracture toughness requirements, a Charpy V-notch test shall be performed. The test shall be performed at or below the Lowest Service Metal Temperature, and all three specimens shall meet the requirements of Table NC-2332.3-1. The size of lid bolt is 1.5" diameter, based on Table NC-2332.3-1 the required C_v value is 25 mils (lateral expansions).

In addition to the above Charpy V-notch test, a brittle fracture evaluation is performed to demonstrate that the brittle fracture is not a concern for the lid bolts.

The lid bolt is fabricated from SA-540 Gr. B24 Cl. 1 and has the following material properties.

Material Grade	Yield Strength, ksi (Room Temperature)	Ultimate Tensile Strength, ksi (Room Temperature)
SA-540 Gr. B24 Cl. 1	150	165

In accordance with the ASME Code, Section II, Part A [7], the bar stocks of these materials are quenched and fully tempered (1000 – 1100°F or higher) to produce a strong and tough microstructure.

ASM Metal Handbook [8], Figure 26 (reproduced here in Figure 3.9.3-1) shows that a 4340 steel tempered at 1035°F for 1 ½ hours to produce a yield strength of 158 ksi exhibits a very low Charpy impact transition temperature (< -20°F) and an upper shelf energy of about 45 ft-lbs at -20°F.

Figure 31 (reproduced here in Figure 3.9.3-2) shows that a medium carbon low alloy steel tempered to a yield strength of 107 ksi (like SA-193, Grade B7) would have an upper shelf energy of about 52 ft-lbs and absorb about 48 ft-lbs at -20°F while material at a yield strength of 149 ksi (like SA-540 Gr. B24 Cl. 1) would have an upper shelf energy of 35 ft-lbs and absorb about 30 ft-lbs at -20°F.

The following table summarizes the equivalent impact energy of the SA-540 Gr. B24 Cl. 1 at -20°F and the Charpy values used for the brittle fracture evaluation.

Summary of the Equivalent Impact Energy

Material Grade	Yield Strength (ksi)	Charpy Value, -20°F (Ft-lbs)	Charpy Value Used for Brittle Fracture Evaluation (Ft-lbs)
4340 Steel Tempered at 1035°F for 1 ½ Hours (Figure 3.9.3-1)	158	45	
Medium-Carbon Low Alloy (Figure 3.9.3-2)	149	30	
SA-540 Gr. B24 Cl. 1	150		20**

** By comparison with the similar yield strength materials, lower values are conservatively used for SA-540 Gr. B24 Cl.1 brittle fracture evaluations.

A brittle fracture evaluation of the lid bolt is performed based on a service temperature of –20°F. The work includes the following:

- Methodology
- Stress
- Material fracture toughness
- Fracture toughness criteria
- Allowable flaw calculations
- NDE Inspection Plan

Methodology

The allowable flaw sizes were performed using the Singular Integral Equation and Asymptotic Approximation [9] (see Figure 3.9.3-3). The total applied stress intensity K_{applied} is calculated based on the following equations.

$$\sigma_{\text{net}} = P/(\pi a^2)$$

$$K_{\text{applied}} = \sigma_{\text{net}} (\pi a)^{1/2} F_1(a/b) \quad (\text{see Figure 3.9.3-3 for definitions})$$

Stress

The maximum tensile stress for the lid bolt is 106.6 ksi and is calculated in Appendix 3.9.3, Section 3.9.3.5. The maximum net tensile stress is calculated based on 0.025" deep 360° circumferential crack.

$$\sigma_{\text{net}} = 106.6 [1.5/(1.5-2 \times 0.025)]^2 = 114.08 \text{ ksi}$$

Material Fracture Toughness

The Charpy impact value may be transformed into a fracture toughness value by using the empirical relation developed in Section 4.2 of NUREG/CR-1815 [10] as follows:

$$K_{id} = [5E(C_v)]^{1/2}$$

Where

K_{id} = Dynamic Fracture Toughness, psi \cdot (in)^{1/2}

E = Modulus of Elasticity, 26.7×10^6 psi

C_v = Charpy Impact Value, 20 ft-lbs

Substituting the values given above,

$$K_{id} = [5E(C_v)]^{1/2} = [5 \times 26.7 \times 10^6 (20)]^{1/2} = 51,672 \text{ psi-in}^{1/2}$$

Fracture Toughness Criteria

Using the method described in the ASME Code, Section XI, IWB-3613 [11], the limiting fracture toughness values are reduced by a factor of $\sqrt{2}$ for the accident condition and are calculated as follows:

$$K_{allowable} \leq 51,672/\sqrt{2} = 36.54 \text{ ksi-}\sqrt{\text{in}}$$

Allowable Flaw Size Calculation

Using the above load definitions, fracture toughness values and assumed flaw size (0.025"), the total applied stress intensity K_I (applied) is calculated based on the Singular Integral Equation and Asymptotic Approximation (see Figure 3.9.3-3).

$$K_{applied} = \sigma_{net} (\pi a)^{1/2} F_1(a/b)$$

$$2b = 1.5''$$

$$b = 0.75''$$

$$2a = 1.5'' - 2 \times 0.025'' = 1.45''$$

$$a = 0.725''$$

$$a/b = 0.725/0.75 = 0.97$$

$$F_1(a/b) = 0.18$$

$$K_{applied} = 114.08 (\pi \times 0.725)^{1/2} (0.18) = 30.99 \text{ ksi-}\sqrt{\text{in}} \leq 36.54 \text{ ksi-}\sqrt{\text{in}}$$

NDE Inspection Plan

The results of the fracture toughness analysis show that the critical flaws in the attachment bolts which would result in unstable crack growth or brittle fracture are larger than those generally observed in the bolt and bar stock.

The allowable flaw size for the attachment bolts is 0.025 in. The attachment bolts are fabricated per ASME Subsection NC code and only visual inspection is required by this code. In order to detect the surface indication, a PT or MT will be performed using NB code paragraph NB-2583.3. The requirement is that any linear nonaxial indications are unacceptable and therefore assuming 0.025" deep 360° circumferential crack for brittle fracture evaluation is conservative.

The liquid penetrant or magnetic particle method will be used in accordance with Section V, Article 6 of ASME Code [12].

3.9.3.13 Conclusions

1. Top cover and RAM access cover bolt stresses meet the acceptance criteria of NUREG/CR-6007 "Stress Analysis of Closure Bolts for Shipping Casks" [1].
2. The top cover and RAM cover bolt, insert, and flange thread engagement length is acceptable.

3.9.3.14 References

1. Stress Analysis of Closure Bolts for Shipping Cask, NUREG/CR-6007, 1992.
2. American Society of Mechanical Engineers, ASME Boiler and Pressure Vessel Code, Section II, Part D, 1998 through 2000 addenda.
3. Helicoil Catalog, Heli-Coil 8-Pitch Inserts, Bulletin 913B.
4. Machinery Handbook, 21st Ed, Industrial Press, 1979.
5. Baumeister, T., Marks, L. S., *Standard Handbook for Mechanical Engineers*, 7th Edition, McGraw-Hill, 1967.
6. American Society of Mechanical Engineers, ASME Boiler and Pressure Vessel Code, Section III, Division 1, Subsection NC, 1998, through 2000 addenda.
7. American Society of Mechanical Engineers, ASME Boiler and Pressure Vessel Code, Section II, Part A, 1998, through 2000 addenda.
8. American Society for Metals (ASM) Metal Handbook (Volume 1), “Notch Toughness of Steels Section,” 9th Edition, 1978.
9. Singular Integral Equation (Bueckner) and Asymptotic Approximation (Bentheim)
10. NUREG/CR-1815 “Recommendation for Protecting Against Failure by Brittle Fracture in Ferritic Steel Shipping Containers Up to Four Inches Thick” Lawrence Livermore National Laboratory, June 15, 1981.
11. American Society of Mechanical Engineers, ASME Boiler and Pressure Vessel Code, Section XI, 1989.
12. American Society of Mechanical Engineers, ASME Boiler and Pressure Vessel Code, Section V, Article 6, 1998 through 2000 addenda.

Table 3.9.3-1
Design Parameters for Top cover Bolt Analysis

- D_b Nominal diameter of closure bolt; 1.500 in.
- K Nut factor for empirical relation between the applied torque and achieved preload is 0.132
- Q Applied torque for the preload (in.-lb.)
- D_{lb} Closure lid diameter at bolt circle, 77.70 in.
- D_{lg} Closure lid diameter at the seal = 74.19 in.
- E_c Young's modulus of cask wall material, 27.0×10^6 psi. @ 300° F.
- E_l Young's modulus of lid material, 27.0×10^6 psi. @ 300° F.
- N_b Total number of closure bolts, 24
- N_{ul} Poisson's ratio of closure lid, 0.3, [5].
- P_{ei} Inside pressure of cask, 30 psig.
- D_{lo} Closure lid diameter at outer edge, 82.20 in.
- P_{li} Pressure inside the closure lid, 30 psig.
- t_c Thickness of flange, 5.575 in.
- t_l Thickness of lid, 3.0in./1.5 in.
- a_b Thermal coefficient of expansion, bolt material, 6.9×10^{-6} in. in.⁻¹ °F⁻¹ at 300°F
- a_c Thermal coefficient of expansion, cask, 9.2×10^{-6} in. in.⁻¹ °F⁻¹ at 300°F
- a_l Thermal coefficient of expansion, lid, 8.8×10^{-6} in. in.⁻¹ °F⁻¹ at 300°F
- E_b Young's modulus of bolt material, 26.7×10^6 psi. at 300°F
- ai Maximum rigid-body impact acceleration (g) of the cask
- DLF Dynamic load factor to account for any difference between the rigid body acceleration and the acceleration of the contents and closure lid = 1.1
- W_c weight of contents = 51,520 lb. (fuel) + 29,854 lb. (basket) + 28,191 lb. (canister) = 109,560 lbs., conservatively use 110,000 lbs.
- W_l weight of closure lid = 5,195 lb., conservatively use 5,500 lb.
- $W_c + W_l$ 110,000 + 5,500 = 115,500 lbs.
- xi Impact angle between the cask axis and target surface
- S_{yl} Yield strength of closure lid material, 43.3 ksi. @ 300° F.
- S_{ul} Ultimate strength of closure lid, 94.2 ksi @ 300° F.
- S_{yb} Yield strength of bolt material (see Table 3.9.3-3).
- S_{ub} Ultimate strength of bolt material (see Table 3.9.3-4).
- P_{lo} Pressure outside the lid.
- P_{co} Pressure outside the cask, 0 psig. (worst case scenario)
- L_b Bolt length between the top and bottom surfaces of closure, 1.50 in.

Table 3.9.3-2
Design Parameters for Ram Access Cover Bolt Analysis

- D_b Nominal diameter of closure bolt; 0.50 in.
- K Nut factor for empirical relation between the applied torque and achieved preload is 0.132
- Q Applied torque for the preload (in.-lb.)
- D_{lb} RAM access cover diameter at bolt circle, 23.50 in.
- D_{lg} RAM access cover diameter at the seal = 21.16 in.
- E_c Young's modulus of RAM access penetration wall material, 27.0×10^6 psi. @ 300° F.
- E_l Young's modulus of cover material, 27.0×10^6 psi. @ 300° F.
- N_b Total number of closure bolts, 12
- N_{ul} Poisson's ratio of closure RAM access cover, 0.3, [5].
- P_{ci} Inside pressure of RAM access penetration, 30 psig.
- D_{lo} Cover diameter at outer edge, 25.45 in.
- D_{li} Cover diameter at inner edge, 20.00 in.
- P_{li} Pressure inside the cover, 30 psig.
- t_c Thickness of RAM access penetration, 4.00 in.
- t_l Thickness of cover, 1.0 in.
- a_b Thermal coefficient of expansion, bolt material, 6.9×10^{-6} in. in.⁻¹ °F⁻¹ at 300°F
- a_c Thermal coefficient of expansion, RAM access penetration, 9.2×10^{-6} in. in.⁻¹ °F⁻¹ at 300°F
- a_l Thermal coefficient of expansion, cover, 9.2×10^{-6} in. in.⁻¹ °F⁻¹ at 300°F
- E_b Young's modulus of bolt material, 26.7×10^6 psi. at 300°F
- a_i Maximum rigid-body impact acceleration (g) of the cask
- DLF Dynamic load factor to account for any difference between the rigid body acceleration and the acceleration of the contents and cover = 1.1.
- W_c the inertial load of the transfer cask contents does not affect the cover bolts.
- W_l weight of RAM access cover = 148 lb., conservatively use 200 lb.
- $W_c + W_l$ 0 + 200 = 200 lbs.
- α_i Impact angle between the cask axis and target surface.
- S_{yl} Yield strength of closure cover material, 22.4 ksi. @ 300° F.
- S_{ul} Ultimate strength of closure lid, 66.2 ksi @ 300° F.
- S_{yb} Yield strength of bolt material (see Table 3.9.3-4).
- S_{ub} Ultimate strength of bolt material (see Table 3.9.3-5).
- P_{lo} Pressure outside the cover, 0 psig. (worst case scenario)
- P_{co} Pressure outside the RAM access penetration, 0 psig. (worst case scenario)
- L_b Bolt length between the top and bottom surfaces of closure, 0.34 in.

Table 3.9.3-3
Bolt Data ([1], Table 5.1)

Top cover Bolts

Bolt: 1 1/2"– 8UN – 2A

N : no of threads per inch = 8

p : Pitch = $1/8" = .125$ in.

D_b : Nominal Diameter = 1.50 in.

D_{ba} : Bolt diameter for stress calculations = $D_b - .9743p = 1.50 - .9743 (0.125)$
= 1.378 in.

Stress Area = $\pi/4 (1.378)^2 = 1.491 \text{ in}^2$

Ram Closure Bolts:

Bolt: 1/2"– 13UNC – 2A

N : no of threads per inch = 13

p : Pitch = $1/13" = .0769$ in.

D_b : Nominal Diameter = 0.50 in.

D_{ba} : Bolt diameter for stress calculations = $D_b - .9743p = 0.50 - .9743 (0.0769)$
= 0.425 in.

Stress Area = $\pi/4 (0.425)^2 = 0.142 \text{ in}^2$

Table 3.9.3-4
Allowable Stresses in Closure Bolts for Normal Conditions

(MATERIAL: SA-540 Gr. B24 CL.1)

Temperature (°F)	Yield Stress ⁽¹⁾ (ksi)	Normal Condition Allowables		
		$F_{tb}^{(2,4)}$ (ksi)	$F_{vb}^{(3,4)}$ (ksi)	S.I. ⁽⁵⁾ (ksi)
100	150	100.0	60.0	135.0
200	143.4	95.6	57.4	129.1
300	138.6	92.4	55.4	124.7
400	134.4	89.6	53.8	121.0
500	130.2	86.8	52.1	117.2
600	124.2	82.8	49.7	111.8

Notes:

1. Yield stress values are from ASME Code, Section II, Table 4 (Ratio: $S_y = 3S_m$) [2]
2. Allowable Tensile stress, $F_{tb} = 2/3 S_y$ (Ref. 1, Table 6.1)
3. Allowable shear stress, $F_{vb} = 0.4 S_y$ (Ref. 1, Table 6.1)
4. Tension and shear stresses must be combined using the following interaction equation:

$$\frac{\sigma_{tb}^2}{F_{tb}^2} + \frac{\tau_{vb}^2}{F_{vb}^2} \leq 1.0 \text{ [1]}$$

Stress intensity from combined tensile, shear and residual torsion loads, $S.I. \leq 0.9 S_y$
 (Ref. 1, Table 6.1)

Table 3.9.3-5
Allowable Stresses in Closure Bolts for Hypothetical Accident Conditions

(MATERIAL: SA-540 Gr. B24 Cl.1)

Temperature (°F)	Yield Stress ⁽¹⁾ (ksi)	Accident Condition Allowables		
		$0.6 S_y^{(3)}$ (ksi)	$F_{tb}^{(2,4)}$ (ksi)	$F_{vb}^{(3,4)}$ (ksi)
100	150.0	90.0	115.5	69.3
200	143.4	86.0	115.5	69.3
300	138.6	83.2	115.5	69.3
400	134.4	80.6	115.5	69.3
500	130.2	78.1	115.5	69.3
600	124.2	74.5	115.5	69.3

Notes:

1. Yield and tensile stress values are from ASME Code, [2] Table 4, Note that S_u is 165.0 ksi at all temperatures of interest.
2. Allowable Tensile stress, $F_{tb} = \text{MINIMUM}(0.7 S_u, S_y)$, where $0.7 S_u = 0.7 (165.0) = 115.5$ ksi. (Ref. 1, Table 6.3)
3. Allowable shear stress, $F_{vb} = \text{MINIMUM}(0.42 S_u, 0.6 S_y)$, where $0.42 S_u = 0.42 (165.0) = 69.3$ ksi. (Ref. 1, Table 6.3)
4. Tension and shear stresses must be combined using the following interaction equation:

$$\frac{\sigma_{tb}^2}{F_{tb}^2} + \frac{\tau_{vb}^2}{F_{vb}^2} \leq 1.0 \quad [1]$$

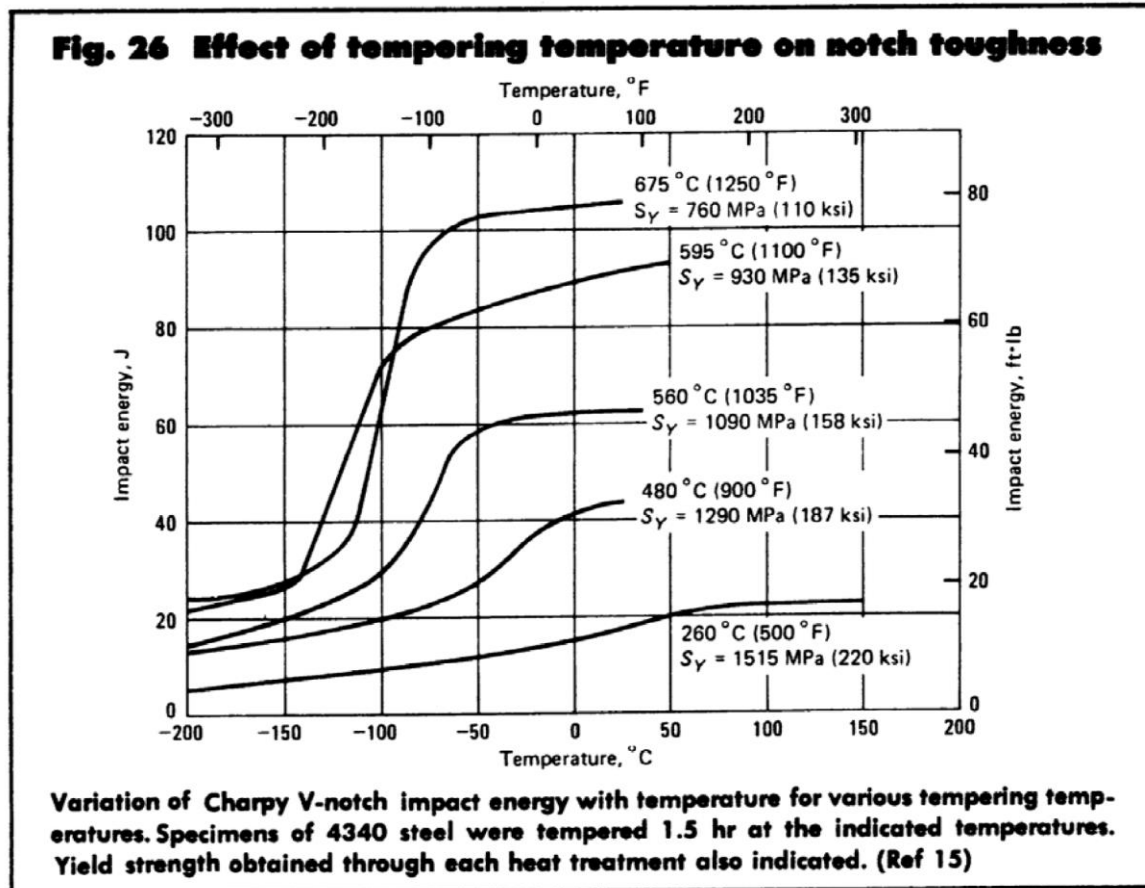


Figure 3.9.3-1
Effect of Tempering Temperature on Notch Toughness

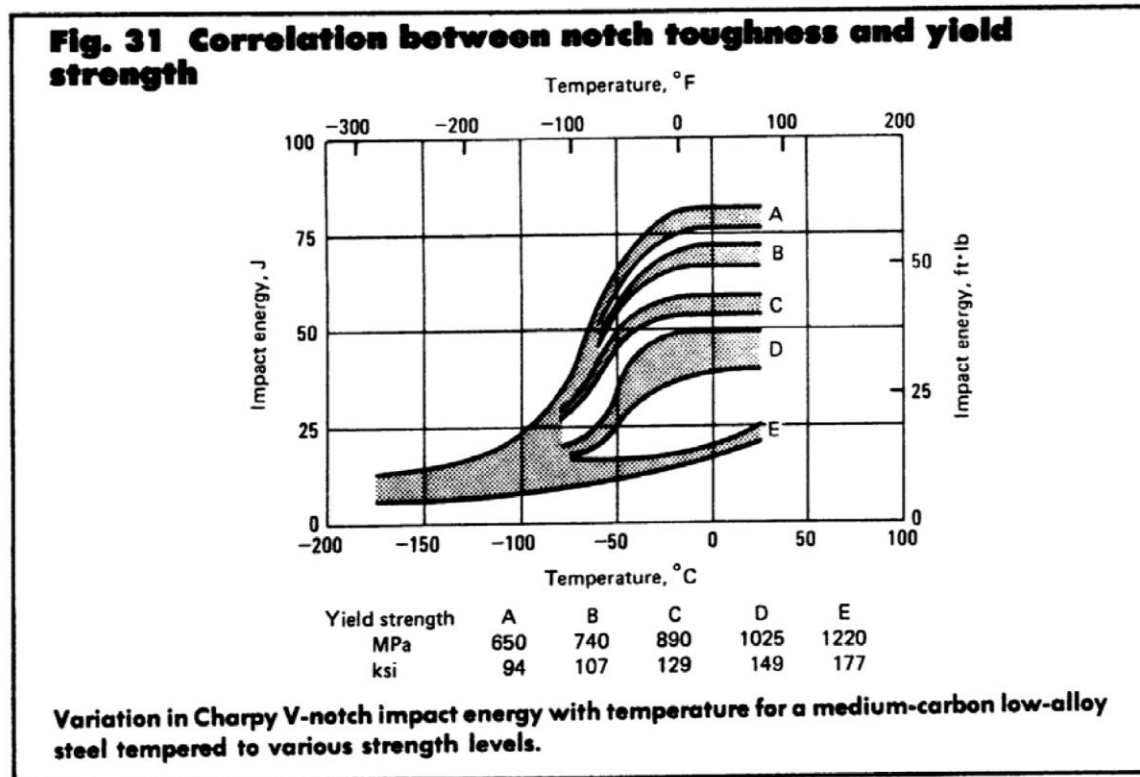


Figure 3.9.3-2
Correlation Between Notch Toughness and Yield Strength

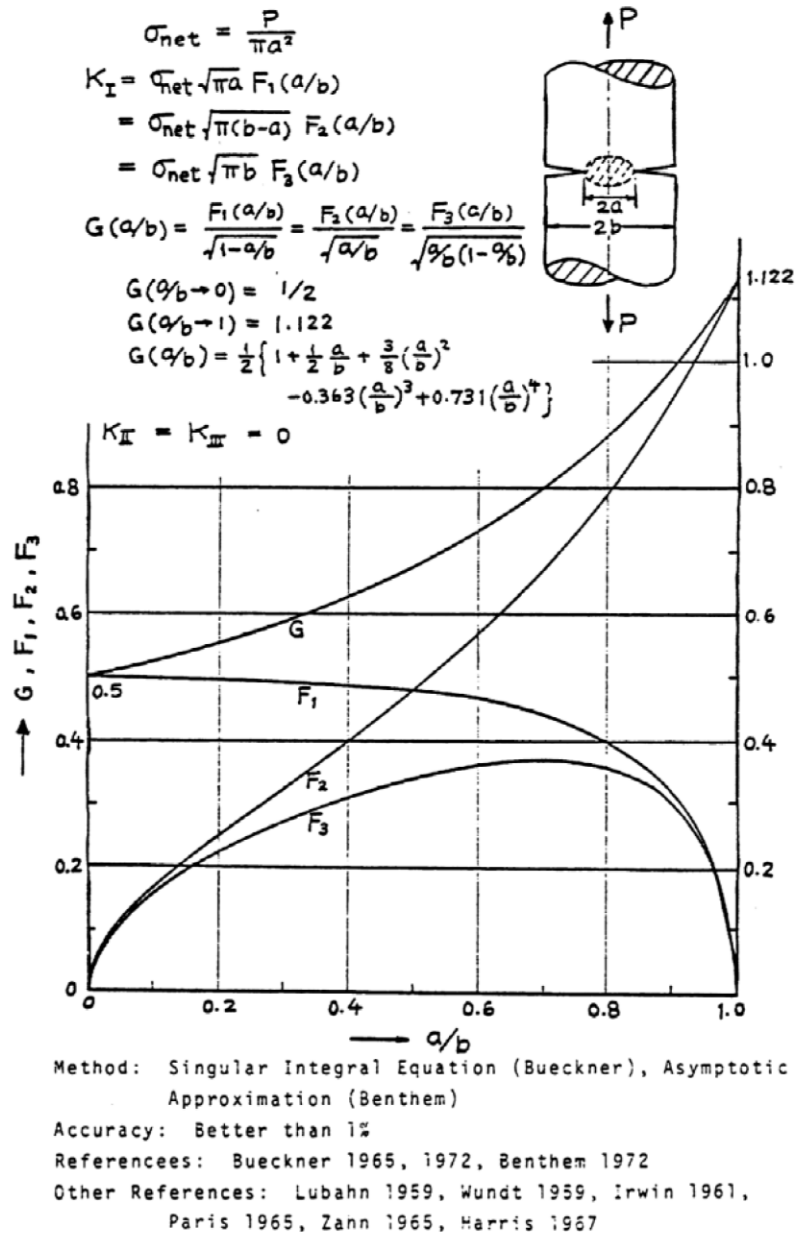


Figure 3.9.3-3
Singular Integral Equation and Asymptotic Approximation for Brittle Fracture Evaluation

APPENDIX 3.9.4 OS187H TRANSFER CASK LEAD SLUMP AND INNER SHELL BUCKLING ANALYSIS

TABLE OF CONTENTS

3.9.4 OS187H TRANSFER CASK LEAD SLUMP AND INNER SHELL BUCKLING ANALYSIS	3.9.4-1
3.9.4.1 Introduction.....	3.9.4-1
3.9.4.2 Material Properties	3.9.4-2
3.9.4.3 Finite Element Model	3.9.4-6
3.9.4.4 FEA Results	3.9.4-11
3.9.4.5 Conclusions.....	3.9.4-12
3.9.4.6 References	3.9.4-13

LIST OF FIGURES

Figure 3.9.4-1	Loads and Boundary Conditions for Transfer Cask Bottom End Drop Model (Top End, 115° F Ambient Case)	3.9.4-14
Figure 3.9.4-2	Loads and Boundary Conditions for Transfer Cask Bottom End Drop Model (Bottom End, 115° F Ambient Case)	3.9.4-15
Figure 3.9.4-3	Loads and Boundary Conditions for Transfer Cask Bottom End Drop Model (Top End, -20° F Ambient Case).....	3.9.4-16
Figure 3.9.4-4	Loads and Boundary Conditions for Transfer Cask Bottom End Drop Model (Bottom End, -20° F Ambient Case)	3.9.4-17
Figure 3.9.4-5	Loads and Boundary Conditions for Transfer Cask Top End Drop Model (Top End, 115° F Ambient Case)	3.9.4-18
Figure 3.9.4-6	Loads and Boundary Conditions for Transfer Cask Top End Drop Model (Bottom End, 115° F Ambient Case)	3.9.4-19
Figure 3.9.4-7	Loads and Boundary Conditions for Transfer Cask Top End Drop Model (Top End, -20° F Ambient Case).....	3.9.4-20
Figure 3.9.4-8	Loads and Boundary Conditions for Transfer Cask Top End Drop Model (Bottom End, -20° F Ambient Case)	3.9.4-21
Figure 3.9.4-9	Deformed Shape of Transfer Cask for 75g Bottom End Drop (Top End, 115° F Ambient Case)	3.9.4-22
Figure 3.9.4-10	Deformed Shape of Transfer Cask for 75g Bottom End Drop (Top End, -20° F Ambient Case).....	3.9.4-23
Figure 3.9.4-11	Deformed Shape of Transfer Cask for 75g Top End Drop (Bottom End, 115° F Ambient Case)	3.9.4-24

Figure 3.9.4-12	Deformed Shape of Transfer Cask for 75g Top End Drop (Bottom End, -20° F Ambient Case).....	3.9.4-25
Figure 3.9.4-13	Construction of Collapse Load for Transfer Cask Bottom End Drop ...	3.9.4-26
Figure 3.9.4-14	Transfer Cask Top End Drop Deformation Plot (at 189.625g)	3.9.4-27
Figure 3.9.4-15	Transfer Cask Bottom End Drop Deformation Plot (at 178.375g).....	3.9.4-28
Figure 3.9.4-16	Lateral Force Exerted on Inner Shell (Transfer Cask Top End Drop)...	3.9.4-29
Figure 3.9.4-17	Lateral Force Exerted on Inner Shell (Transfer Cask Bottom End Drop)	3.9.4-30

3.9.4 OS187H TRANSFER CASK LEAD SLUMP AND INNER SHELL BUCKLING ANALYSIS

3.9.4.1 Introduction

The purpose of this Appendix is to evaluate the structural adequacy of the OS187H Transfer Cask inner shell with respect to buckling, and to determine the extent of lead slump. The load considered includes lead lateral pressure and a 75g top and bottom end drop load in hot (115° F) ambient environments. The calculations for the component stresses and their evaluations under these loads were conducted and reported in Appendix 3.9.2 and Appendix 3.9.3 for the top cover and ram cover bolts.

During a hypothetical accident condition end drop, permanent deformation of the lead gamma shield may occur. The lead gamma shield is supported by friction between the lead and transfer cask shells, in addition to bearing at the end of the lead column.

A nonlinear finite element analysis is performed in order to quantify the amount of lead slump generated during an end drop event. A 2-dimensional axisymmetric ANSYS [1] finite element model is constructed for this purpose. The results of the finite element analysis provide both stresses and displacements generated during the end drop event. The displacement results are used in this section to determine the maximum size of the axial gap that develops between the lead gamma shield column and the structural shell of the transfer cask. The effect of this cavity size on the shielding ability of the transfer package is evaluated in Chapter 5. Both stress and displacement distributions computed by the finite element analysis are also used to perform a buckling evaluation of inner containment shell of the OS187H transfer cask.

An ANSYS elastic-plastic buckling analysis is performed for the transfer cask end drop cases. A 200g drop load, which is greater than the design load of 75g, is applied to the ANSYS model. This 200g drop load was ramped in small increments by many load sub-steps. The ANSYS solution was set to stop and exit at any load sub-step that fails to result in a converged solution. The failure of convergence represents the onset of buckling of the structure.

3.9.4.2 Material Properties

The maximum normal condition temperature in each transfer cask component from Chapter 4 was used to obtain the tangent modulus of the material. The following table summarizes the maximum transfer cask component temperatures taken from Chapter 4.

Cask Component	Material	Temperature Used in Analysis
Lid	SA-240 Type XM-19	300 °F
Inner Shell	SA-240 Type 304	350 °F
Top and Bottom Flanges, Ram Access Penetration Ring	SA-182 Gr. F304N	300 °F
Outer Structural Shell, Bottom Neutron Shield plate, Bottom End and Cover plates	SA-240 Type 304	300 °F
Top Lid and Bottom RAM access Cover Bolts	SA-540-Gr. B24 Cl.1	300 °F
Gamma Shield	B-29, Chemical Lead	350 °F

The following is a summary of the transfer cask material properties evaluated at the temperatures listed above.

A. Lid Material (SA-240 Type XM-19)

Temperature	Modulus of Elasticity, E (psi) [2]	Density, ρ (lb./in.3) [3]	Poisson's ratio, ν [3]
70° F	28.3×10^6	0.29	0.3
200° F	27.6×10^6	0.29	0.3
300° F	27.0×10^6	0.29	0.3
400° F	26.5×10^6	0.29	0.3

@ 300° F,

$$E = 27.0 \times 10^6 \text{ psi. [2]}$$

$$S_y = 43.3 \text{ ksi. [2]}$$

$$S_u = 94.2 \text{ ksi. [2]}$$

$$\text{Tangent Modulus, } E_T = 5\% \text{ of } E = 0.05 \times 27.0 \times 10^6 \text{ psi} = 1.35 \times 10^6 \text{ psi}$$

B. Inner Shell (SA-240 Type 304)

Temperature	Modulus of Elasticity, E (psi) [2]	Density, ρ (lb./in.3) [3]	Poisson's ratio, ν [3]
70° F	28.3×10^6	0.29	0.3
200° F	27.6×10^6	0.29	0.3
300° F	27.0×10^6	0.29	0.3
400° F	26.5×10^6	0.29	0.3

@ 350° F,

$$E = 26.75 \times 10^6 \text{ psi. [2]}$$

$$S_y = 21.55 \text{ ksi. [2]}$$

$$S_u = 65.1 \text{ ksi. [2]}$$

$$\text{Tangent Modulus, } E_T = 5\% \text{ of } E = 0.05 \times 26.75 \times 10^6 \text{ psi} = 1.34 \times 10^6 \text{ psi}$$

C. Top and Bottom Flanges, and Ram Access Penetration Ring (SA-182 Gr. F304N)

Temperature	Modulus of Elasticity, E (psi) [2]	Density, ρ (lb./in.3) [3]	Poisson's ratio, ν [3]
70° F	28.3×10^6	0.29	0.3
200° F	27.6×10^6	0.29	0.3
300° F	27.0×10^6	0.29	0.3
400° F	26.5×10^6	0.29	0.3

@ 300° F,

$$E = 27.0 \times 10^6 \text{ psi. [2]}$$

$$S_y = 25 \text{ ksi. [2]}$$

$$S_u = 76.1 \text{ ksi. [2]}$$

$$\text{Tangent Modulus, } E_T = 5\% \text{ of } E = 0.05 \times 27.0 \times 10^6 \text{ psi} = 1.35 \times 10^6 \text{ psi}$$

D. Outer Structural Shell, Bottom Neutron Shield plate, Bottom End plate, and Bottom cover plate (SA-240 Type 304)

Temperature	Modulus of Elasticity, E (psi) [2]	Density, ρ (lb./in.3) [3]	Poisson's ratio, ν [3]
70° F	28.3×10^6	0.29	0.3
200° F	27.6×10^6	0.29	0.3
300° F	27.0×10^6	0.29	0.3
400° F	26.5×10^6	0.29	0.3

@ 300° F,

$$E = 27.0 \times 10^6 \text{ psi. [2]}$$

$$S_y = 22.4 \text{ ksi. [2]}$$

$$S_u = 66.2 \text{ ksi. [2]}$$

$$\text{Tangent Modulus, } E_T = 5\% \text{ of } E = 0.05 \times 27.0 \times 10^6 \text{ psi} = 1.35 \times 10^6 \text{ psi}$$

E. Bolts for Top Lid and Bottom RAM Access Cover (SA-54 Gr. 24 CL 1)

Temperature	Modulus of Elasticity, E (psi) [2]	Density, ρ (lb./in.3) [3]	Poisson's ratio, ν [3]
70° F	27.8×10^6	0.29	0.3
200° F	27.1×10^6	0.29	0.3
300° F	26.7×10^6	0.29	0.3
400° F	26.1×10^6	0.29	0.3

@ 300° F,

$$E = 26.7 \times 10^6 \text{ psi. [2]}$$

$$S_y = 138.6 \text{ ksi. [2]}$$

$$S_u = 165 \text{ ksi. [2]}$$

$$\text{Tangent Modulus, } E_T = 5\% \text{ of } E = 0.05 \times 26.7 \times 10^6 \text{ psi} = 1.335 \times 10^6 \text{ psi [3]}$$

F. Chemical Lead (B-29)

Temperature	Modulus of Elasticity, E (psi) [2]	Density, ρ (lb./in.3) [3]	Poisson's ratio, ν [3]
70° F	2.49×10^6	0.41	0.45
200° F	2.28×10^6	0.41	0.45
300° F	2.06×10^6	0.41	0.45
400° F	1.78×10^6 *	0.41	0.45

* Extrapolated from available Reference 4 Data.

@ 350° F,

Multi-linear Stress/Strain Curve: [4] [5]

Strain (in/in)	Stress (psi)
	350° F
0.000485	1,208*
0.030	1,500
0.100	2,100
0.300	2,400
0.500	2,700

* Values adjusted for consistence with modulus of elasticity listed in above table.

3.9.4.3 Finite Element Model

3.9.4.3.1 Approach

A 2-dimensional axisymmetric ANSYS [1] finite element model, constructed primarily from PLANE42 elements, is used in this analysis. Beam3 elements are used to model the lid and RAM port cover bolts. Contact elements are used to model the interaction between the lead gamma shield and the cask inner and outer shells. The coefficient of sliding friction for lead on mild steel varies from 0.3 for lubricated surfaces to 0.95 for dry surfaces [3]. A lower bound coefficient of static friction of 0.25 is conservatively used for this buckling analysis.

In order to determine the buckling load of the inner shell and the amount of lead slump settling, an elastic-plastic analysis is required. The material properties of the lid, bottom, inner shell and outer shell of the transfer cask are modeled with bilinear stress-strain curves, while the lead material is modeled with a multilinear stress-strain curve. Above tables list these material properties.

3.9.4.3.2 Unmodeled Components

Only the structural steel section of the top cover is modeled. The top neutron shield resin, top cover plate, and hoist ring standoffs are not modeled since they are not intended to provide any structural support. However, their inertial load is accounted for by increasing the density of the structural portion of the top cover. The weight of the unmodeled portion of the top cover assembly is as follows.

$$\begin{aligned}\text{Weight of unmodeled lid components} &= 678 \text{ lb. (resin)} + 422 \text{ lb. (cover plate)} + 20 \text{ lb. (standoffs)} \\ &= 1,120 \text{ lb.}\end{aligned}$$

The volume and weight of the structural steel portion of the lid is $14,051 \text{ in.}^3$ and $4,075 \text{ lb.}$ respectively. Therefore the weight of the structural steel portion of the lid, ρ_l , is the following.

$$\rho_l = [1,120 \text{ lb.} + 4,075 \text{ lb.}] / 14,051 \text{ in.}^3 = 0.37 \text{ lb./in.}^3$$

For conservatism, the density of the top cover used in this analysis is increased 0.38 lb./in.^3

The radial neutron shield and shell are also not modeled, because they are not considered structural components of the transfer cask. Therefore, the density of the outer structural steel shell of the transfer cask is increased to account for the un-modeled components. The weight of the un-modeled radial neutron shield assembly is $12,746 \text{ lb.}$

The volume and weight of the outer structural shell is 71,895 in.³ and 20,850 lb. respectively. Therefore the weight of the structural steel portion of the lid, ρ_s , is the following.

$$\rho_l = [12,746 \text{ lb.} + 20,850 \text{ lb.}] / 71,895 \text{ in.}^3 = 0.47 \text{ lb./in.}^3$$

For conservatism, the density of the outer structural steel shell used in this analysis is increased 0.49 lb./in.³

3.9.4.3.3 Attachment Bolt Modeling

The top cover and RAM access cover bolts are modeled with axisymmetric BEAM3 elements. The top cover and RAM access bolts are constructed from SA-540 grade B24 class 1 material. The element real constants are computed in the following way for the top cover and RAM access bolts.

There are 24, 1½ in - 8UN 2A bolts used to mount the transfer cask top cover. The bolt diameter used for stress analysis, D_{tc} , is computed using formulae given in Table 5.1 of Reference 6, as follows.

$$D_{tc} = 1.50 - 0.9743(1/8) = 1.378 \text{ in.}$$

The total tensile stress area for all 24 top cover bolts, A_{tc2d} , is computed as follows.

$$A_{tc2d} = (\pi/4) \times 1.378^2 \times 24 \text{ bolts} = 1.491 \times 24 \text{ bolts} = 35.793 \text{ in.}^2$$

The total moment of inertia of all 24 top cover bolts, I_{tc2d} , is,

$$I_{tc2d} = (\pi/64) \times 1.378^4 \times 24 \text{ bolts} = 4.248 \text{ in.}^4$$

The total height of the top cover bolts, H_{tc2d} , is computed assuming the following equivalent height method.

$$H_{tc2d} = \sqrt{A_{tc2d}} = \sqrt{1.491} = 1.221 \text{ in.}$$

There are 12, ½ in - 13UNC 2A bolts used to mount the transfer cask RAM access cover. The bolt diameter used for stress analysis, D_{ra} , is computed as follows.

$$D_{ra} = 0.50 - 0.9743(1/13) = 0.425 \text{ in.}$$

The total tensile stress area for all 12 RAM access cover bolts, A_{ra2d} , is computed as follows.

$$A_{ra2d} = (\pi/4) \times 0.425^2 \times 12 \text{ bolts} = 0.142 \times 12 \text{ bolts} = 1.704 \text{ in.}^2$$

The total moment of inertia of all 12 RAM access cover bolts, I_{ra2d} , is,

$$I_{ra2d} = (\pi/64) \times 0.425^4 \times 12 \text{ bolts} = 0.01922 \text{ in.}^4$$

The height of the RAM access cover bolts, H_{ra2d} , used in the model is,

$$H_{ra2d} = \sqrt{0.142} = 0.3768 \text{ in.}$$

For both the top cover bolts and the RAM access cover bolt, a bolt preload stress of 25,000 psi. is used. Since the top cover bolts and RAM access cover bolts are constructed from the same material, SA-540, type B24. Both sets of bolts are torqued to the same preload stress, and their corresponding preload strains, ε_b , used in the finite element model are computed as follows.

$$\varepsilon_b = \text{preload stress} / \text{bolt modulus of elasticity}$$

3.9.4.3.4 Contact Elements

CONTAC12 elements are places between all surfaces of the top flange and lid as well as the RAM access cover and RAM access penetration that contact each other. These contact elements are used to model the reaction forces that occur between closure surfaces.

The contact elements introduce nonlinearities in the analysis depending whether they are open or closed. Initially, at all contact surfaces, the gaps are closed. The contact element spring constant, K_n , is calculated in the following way.

$$K_n = f E h [7]$$

Where,

f = A factor usually between 0.01 to 100.

E = Modulus of elasticity (27.0×10^6 psi for SA-240, type 304 @ 300°F [2])

h = contact target length (i.e., the square root of target area).

Typical element length $\approx 1/2$ in.

Typical element width ≈ 1 in.

Typical target length, $h = (0.5 \times 1.0)^{0.5} = 1.22$ in.

$$K_n = 27.0 \times 10^6 \times 1.22 \times f \approx 3.29 \times 10^5 \text{ to } 3.29 \times 10^9 \text{ lb./in}$$

Thus, there is very wide range for K_n value. For the 2-D finite element model, an upper value of 3×10^9 lb/in was used to minimize penetrations in the contact elements.

3.9.4.3.5 Bottom End Drop Boundary Conditions

The weight of the transfer cask internals (canister, basket, and fuel assemblies) is accounted for by applying equivalent pressures. The actual weights of the canister, basket, and fuel assemblies

are 28.19 kips, 29.85 kips, and 51.52 kips, respectively. Therefore, the total actual weight of the cask internals is 109.56 kips. For conservatism, the weight of the cask internals used in this analysis is increased to 115.00 kips. The transfer cask inner radius is 35.25 in., and the inner radius of the ram access penetration is 10.00 in. The inertial load of the transfer cask internals reacts against the annular surface bounded by these two radii during a bottom end drop. The area of this reaction surface, A_{bi} , is as follows.

$$A_{bi} = \pi(35.25^2 - 10.00^2) = 3,589.47 \text{ in}^2.$$

The pressure equivalent to the inertial load of the internals under accident conditions, P_{bi} , is,

$$P_{in} = [115,000 / 3,589.47] \times 200 \text{ gs} = 6407.63 \text{ psi}.$$

Symmetry displacement boundary conditions are applied along the y -axis of the 2-dimensional axisymmetric model. The bottom end of the transfer cask is held in the axial direction in order to simulate the rigid reaction force generated by the impact target. A 200 g inertial load in the positive y -direction is also applied to the model for the accident condition load case. The loading and boundary conditions are shown on Figure 3.9.4-1 to Figure 3.9.4-4.

3.9.4.3.6 Top End Drop Boundary Conditions

The weight of the transfer cask internals (canister, basket, and fuel assemblies) is accounted for by applying equivalent pressures. The weight of the canister internals used in this analysis is 115.00 kips. The inertial load of the transfer cask internals reacts against the inside surface of the top cover assembly during a top end drop. The outer radius of the inside surface of the transfer cask top cover assembly is 35.70 in. Therefore the area of the reaction surface, A_{bi} , is as follows.

$$A_{bi} = \pi(35.70^2) = 4,003.93 \text{ in}^2.$$

The pressure equivalent to the inertial load of the internals under accident conditions, P_{bi} , is,

$$P_{in} = [115,000 / 4,003.93] \times 200 \text{ gs} = 5744.36 \text{ psi}.$$

Symmetry displacement boundary conditions are applied along the y -axis of the 2-dimensional axisymmetric model. The outer surface of the top cover is held in the axial direction in order to simulate the rigid reaction force generated by the impact target. A 200g inertial load in the negative y -direction is also applied to the model for the accident condition load case. The loading and boundary conditions are shown on Figure 3.9.4-5 to Figure 3.9.4-8.

3.9.4.3.7 Thermal Loads

The temperature distributions applied to the finite element models are taken from Chapter 4.

3.9.4.4 FEA Results

- Shell Buckling

ANSYS nonlinear buckling analysis was performed. Maximum loads of 200g were applied in the following two load cases.

- 1) Top end drop with lateral pressure of lead in hot ambient (115°F)
- 2) Bottom end drop with lateral pressure of lead in hot ambient (115°F)

The automatic time stepping program option "Autots" was activated. This option lets the program decide the actual size of the load-substep for a converged solution. The program stops at the load substep when it fails to result in a converged solution. The last load step, with a converged solution, is the buckling load for the structure.

The following table summarizes the last converged load for all two load cases:

Load Cases	Last Converged Load (g)	G load calculated From Appendix 3.9.10 LS-DYNA CG Over Corner Analysis(1)	G Load Used For Cask Structural Analysis	Factor of Safety
Top End Drop (Hot)	189	15.5	75	2.52
Bottom End Drop (Hot)	178	15.5	75	2.37

Note:

1. For storage the end drop is not a creditable event. The transfer cask is transferred in the horizontal position held by the transfer trailer. In the axial direction it is possible to slide into the ground and incur a corner drop. The maximum g load calculated by the LS-DYNA as described in Appendix 3.9.10 is 15.5g. For conservatism 75g is used for inner shell buckling analysis.

The ANSYS displacement plots for the last converged load steps for the above two load cases are shown on Figure 3.9.4-14 and Figure 3.9.4-15.

The lateral pressure of the lead vs. g load at a typical location in the middle section of the cask during the top and bottom end drops are shown in Figure 3.9.4-16 and Figure 3.9.4-17, respectively. These figures show that the pressure load increases as the g load increases.

- Lead Slump

The ANSYS solutions have converged at different load sub-steps for each end drop as described in the above table. The lead slump at 75g load is extracted from its corresponding time in each drop solution. The calculated maximum lead slumps in each case are listed in the following table.

Load Combination	Lead Slump Cavity Length
75g Top End Drop, Hot Environment	0.809 in.
75g Bottom End Drop, Hot Environment	0.833 in.

3.9.4.5 Conclusions

The analysis indicates that the transfer cask will not buckle during 75g end drops. The table above shows that the maximum longitudinal gap, caused by lead slump, is 0.833 inches, and occurs during accident condition bottom end drop, in the hot environment. The effect of the gap on the shielding ability of the NUHOMS®-OS187H transfer cask is analyzed in Chapter 7.

3.9.4.6 References

1. ANSYS User's Manual, Rev 6.0
2. American Society of Mechanical Engineers, ASME Boiler and Pressure Vessel Code, Section II, Part D and Section III, Subsection NB and Appendix F, 1998, through 2000 addenda.
3. Baumeister & Marks, Standard Handbook for Mechanical Engineers, 7th Edition.
4. An Assessment of Stress-Strain Data Suitable for Finite-Element Elastic-Plastic Analysis of Shipping Containers, NUREG/CR-0481.
5. A Survey of Strain Rate Effects for some Common Structural Materials Used in Radioactive Material Packaging and Transportation Systems, U.S. Energy Research and Development Administration, Battelle Columbus Laboratories, August 1976.
6. "Stress Analysis of Closure Bolts for Shipping Casks", NUREG/CR-6007, April 1992
7. ANSYS User's Manual, Rev 5.6

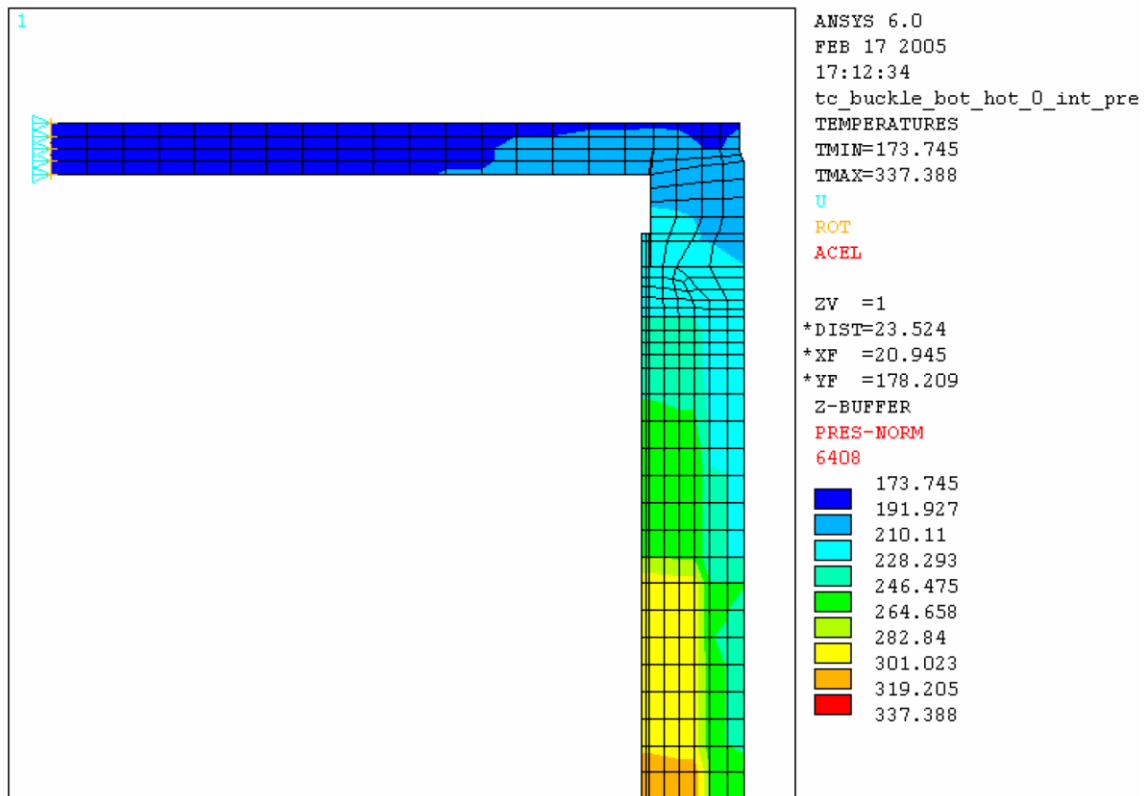


Figure 3.9.4-1
Loads and Boundary Conditions for Transfer Cask Bottom End Drop Model
(Top End, 115° F Ambient Case)

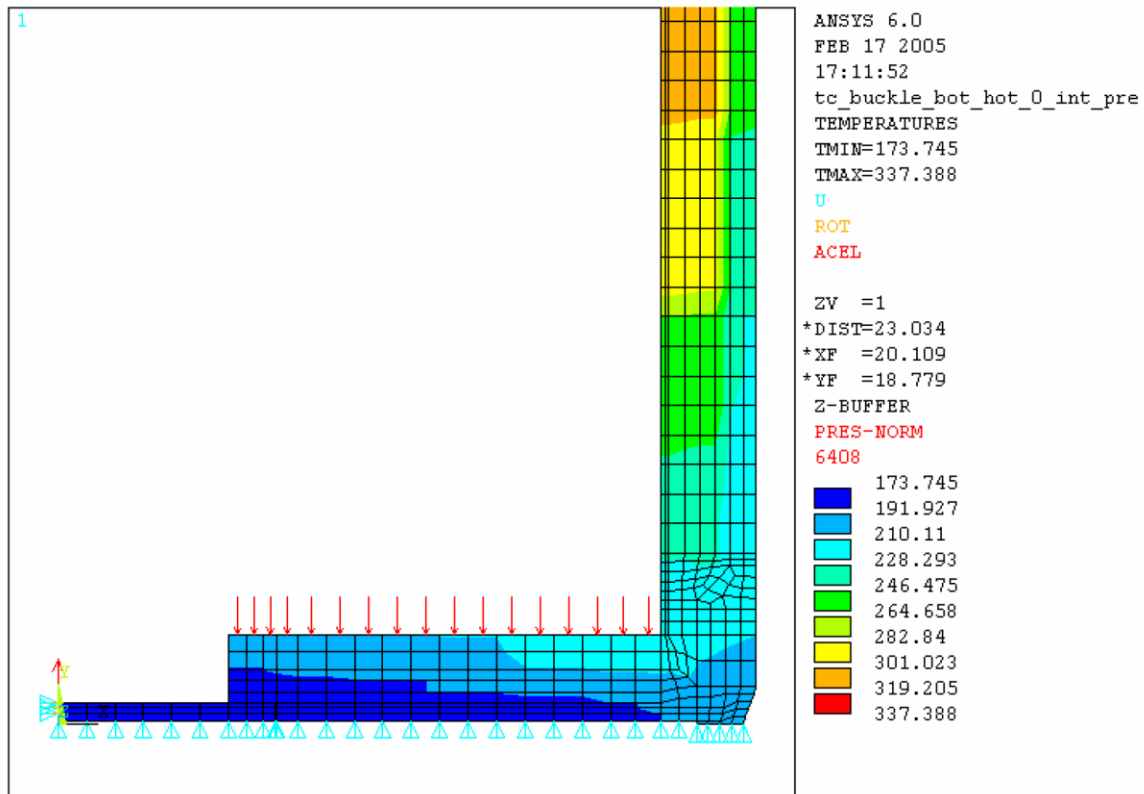


Figure 3.9.4-2
Loads and Boundary Conditions for Transfer Cask Bottom End Drop Model
(Bottom End, 115° F Ambient Case)

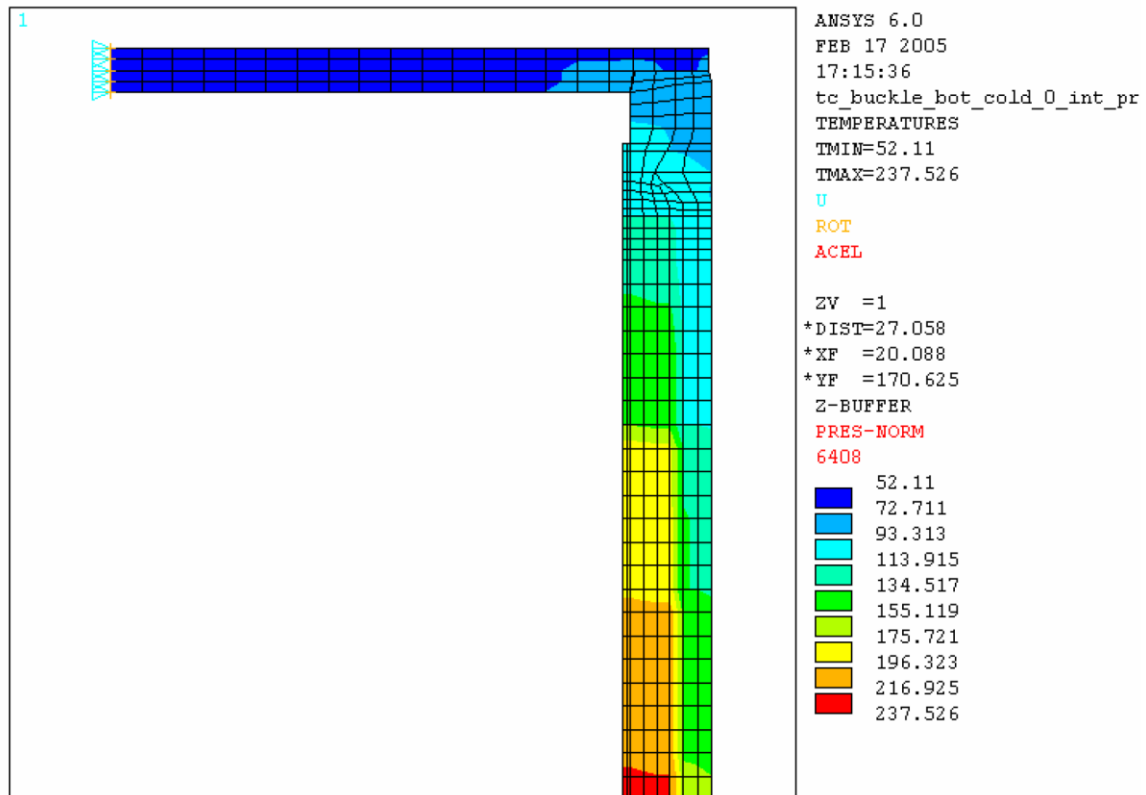


Figure 3.9.4-3
Loads and Boundary Conditions for Transfer Cask Bottom End Drop Model
(Top End, -20° F Ambient Case)

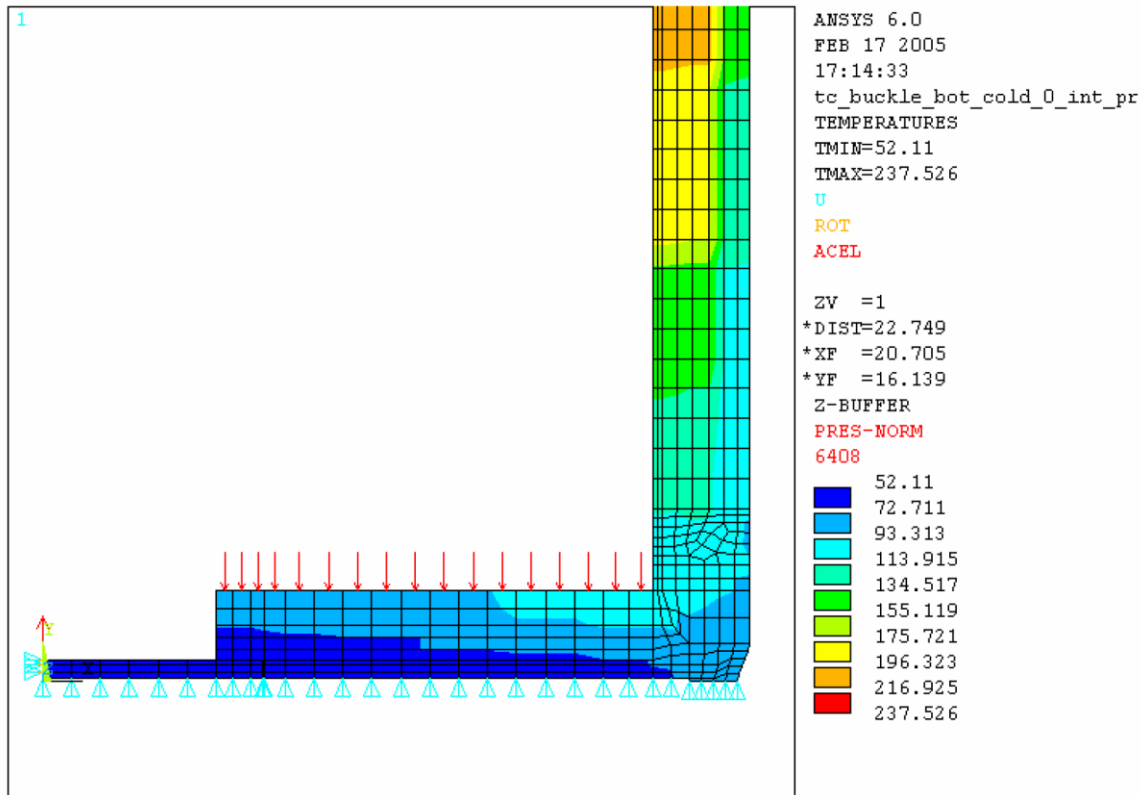


Figure 3.9.4-4
Loads and Boundary Conditions for Transfer Cask Bottom End Drop Model
(Bottom End, -20° F Ambient Case)

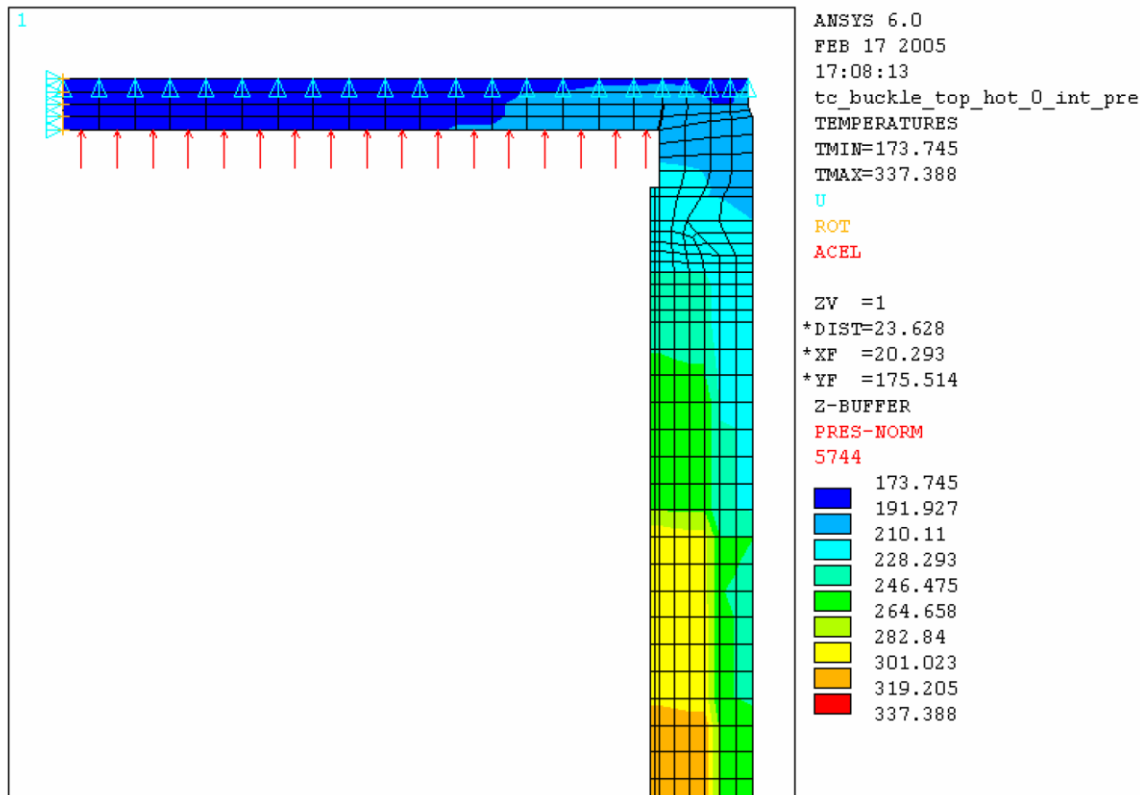


Figure 3.9.4-5
Loads and Boundary Conditions for Transfer Cask Top End Drop Model
(Top End, 115° F Ambient Case)

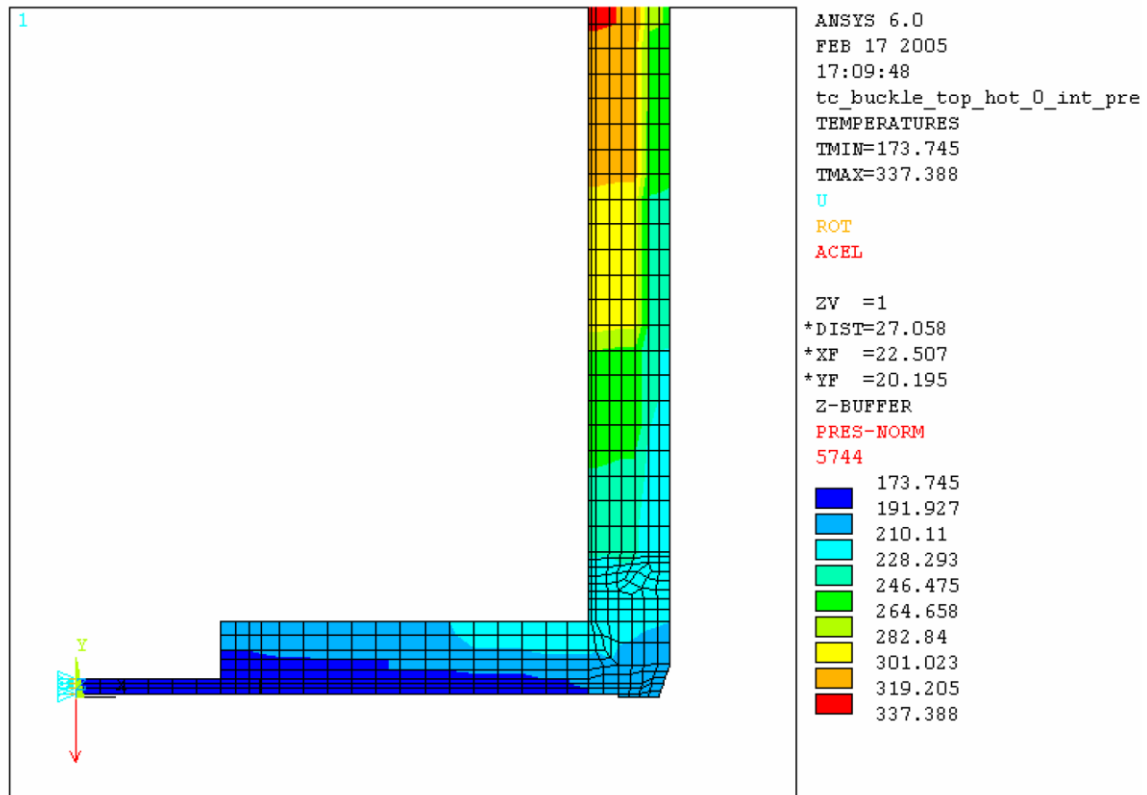


Figure 3.9.4-6
Loads and Boundary Conditions for Transfer Cask Top End Drop Model
(Bottom End, 115° F Ambient Case)

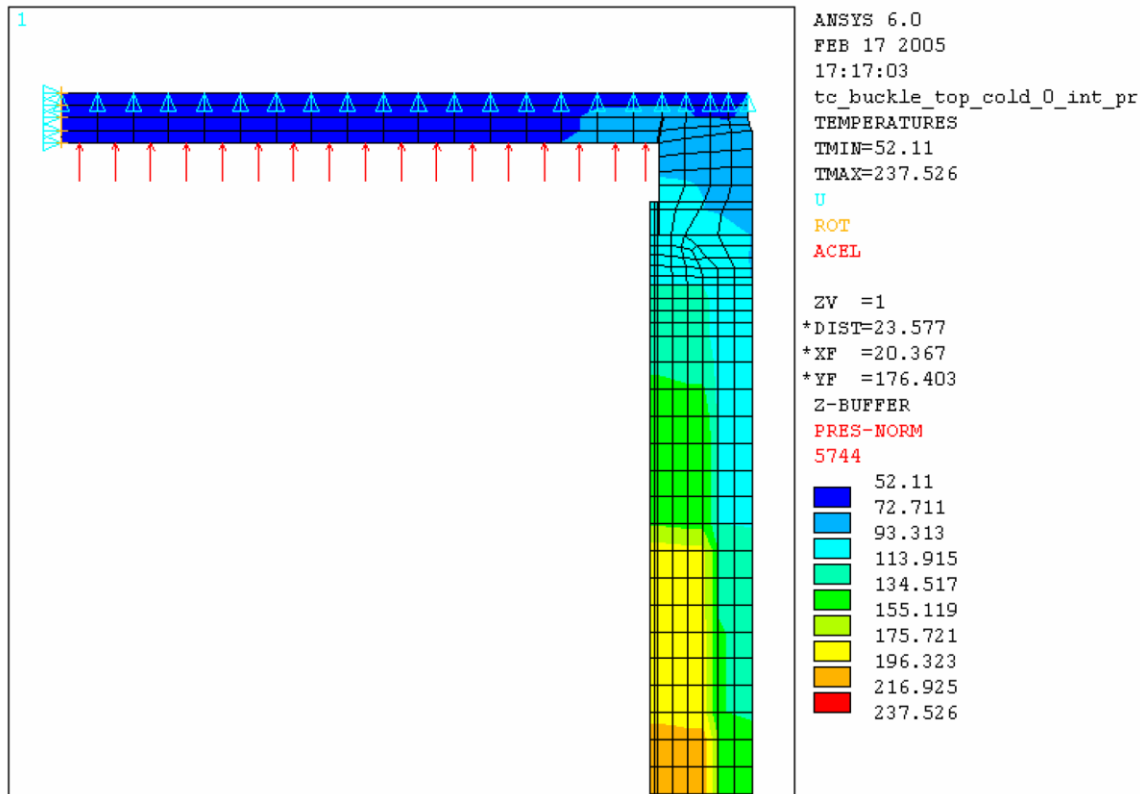


Figure 3.9.4-7
Loads and Boundary Conditions for Transfer Cask Top End Drop Model
(Top End, -20° F Ambient Case)

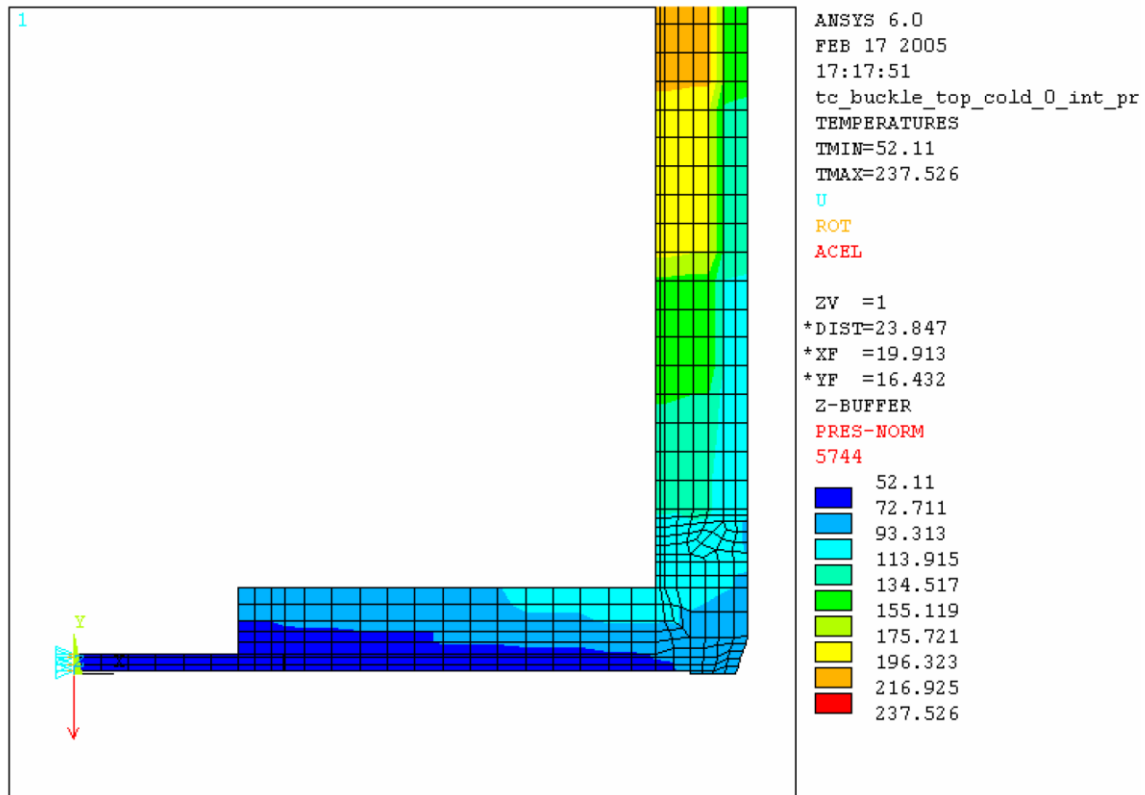


Figure 3.9.4-8
Loads and Boundary Conditions for Transfer Cask Top End Drop Model
(Bottom End, -20° F Ambient Case)

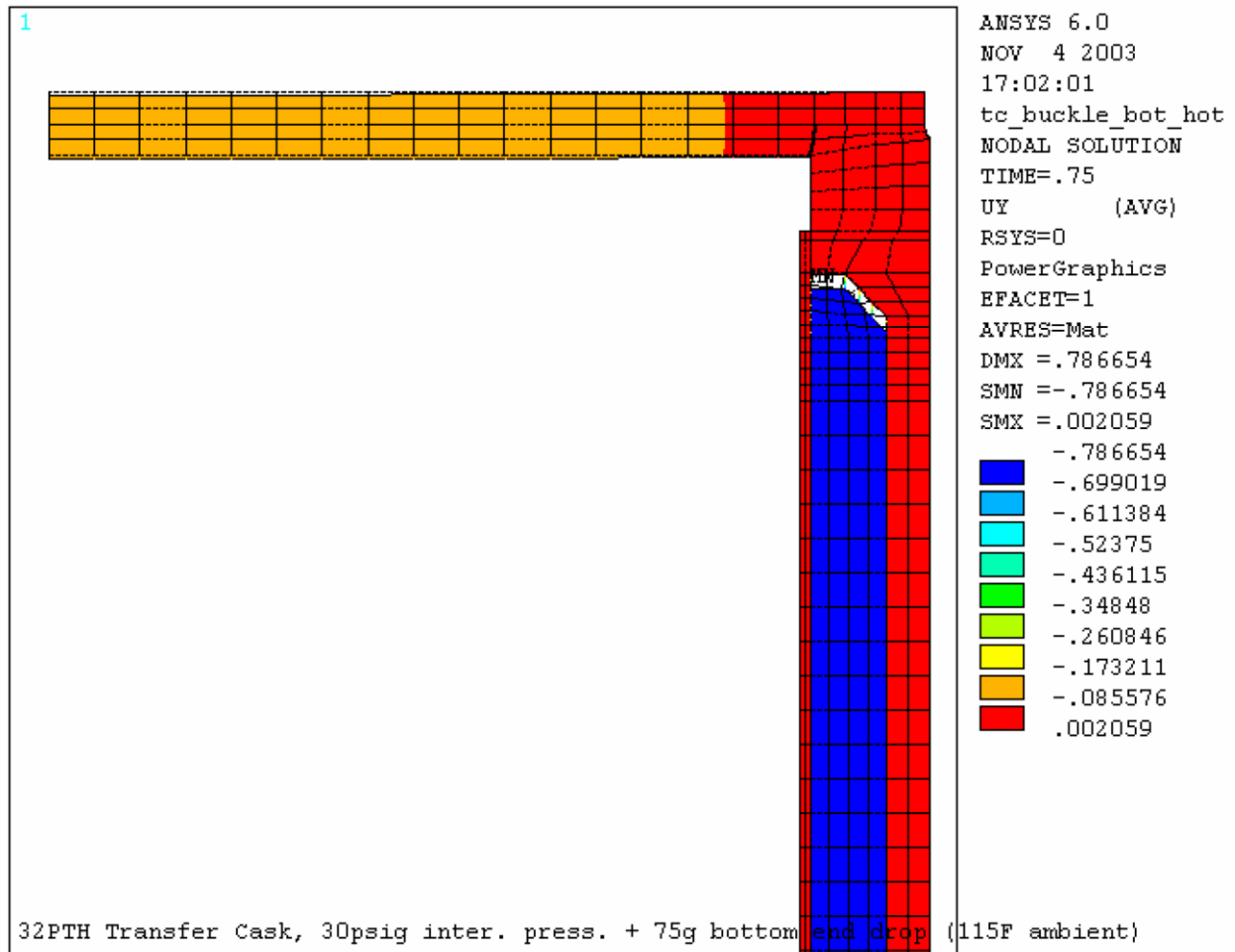


Figure 3.9.4-9
Deformed Shape of Transfer Cask for 75g Bottom End Drop
(Top End, 115° F Ambient Case)

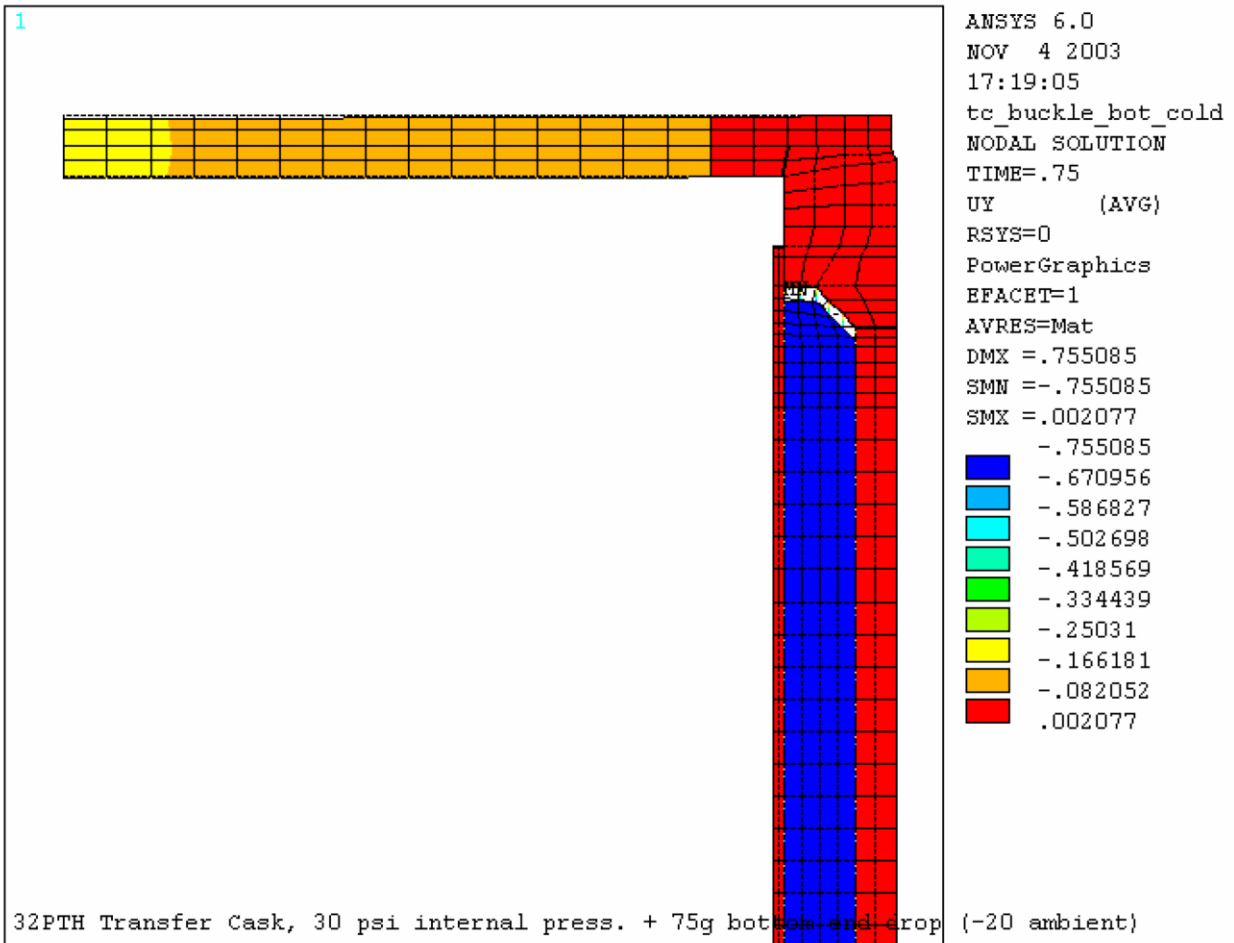


Figure 3.9.4-10
Deformed Shape of Transfer Cask for 75g Bottom End Drop
(Top End, -20° F Ambient Case)

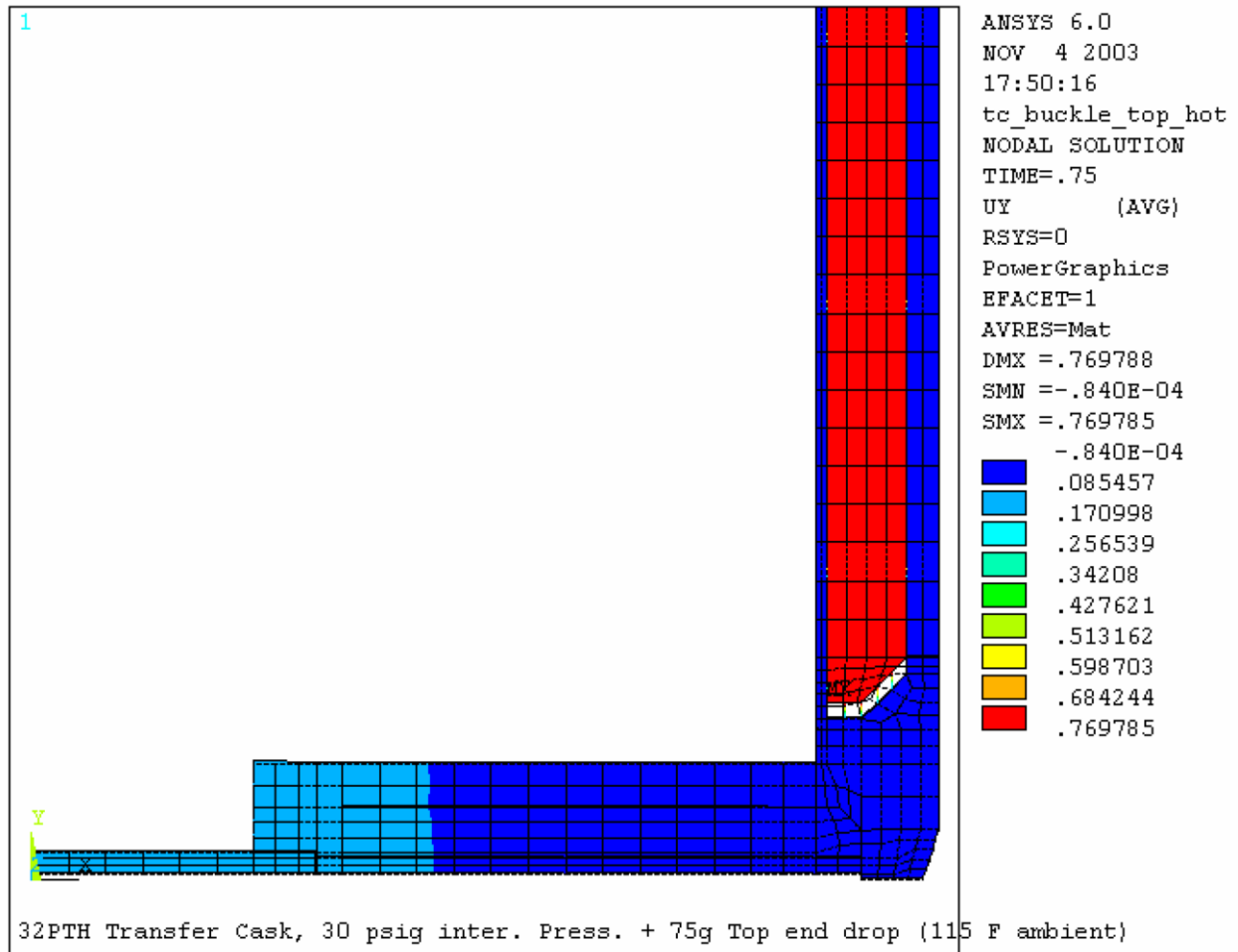


Figure 3.9.4-11
Deformed Shape of Transfer Cask for 75g Top End Drop
(Bottom End, 115° F Ambient Case)

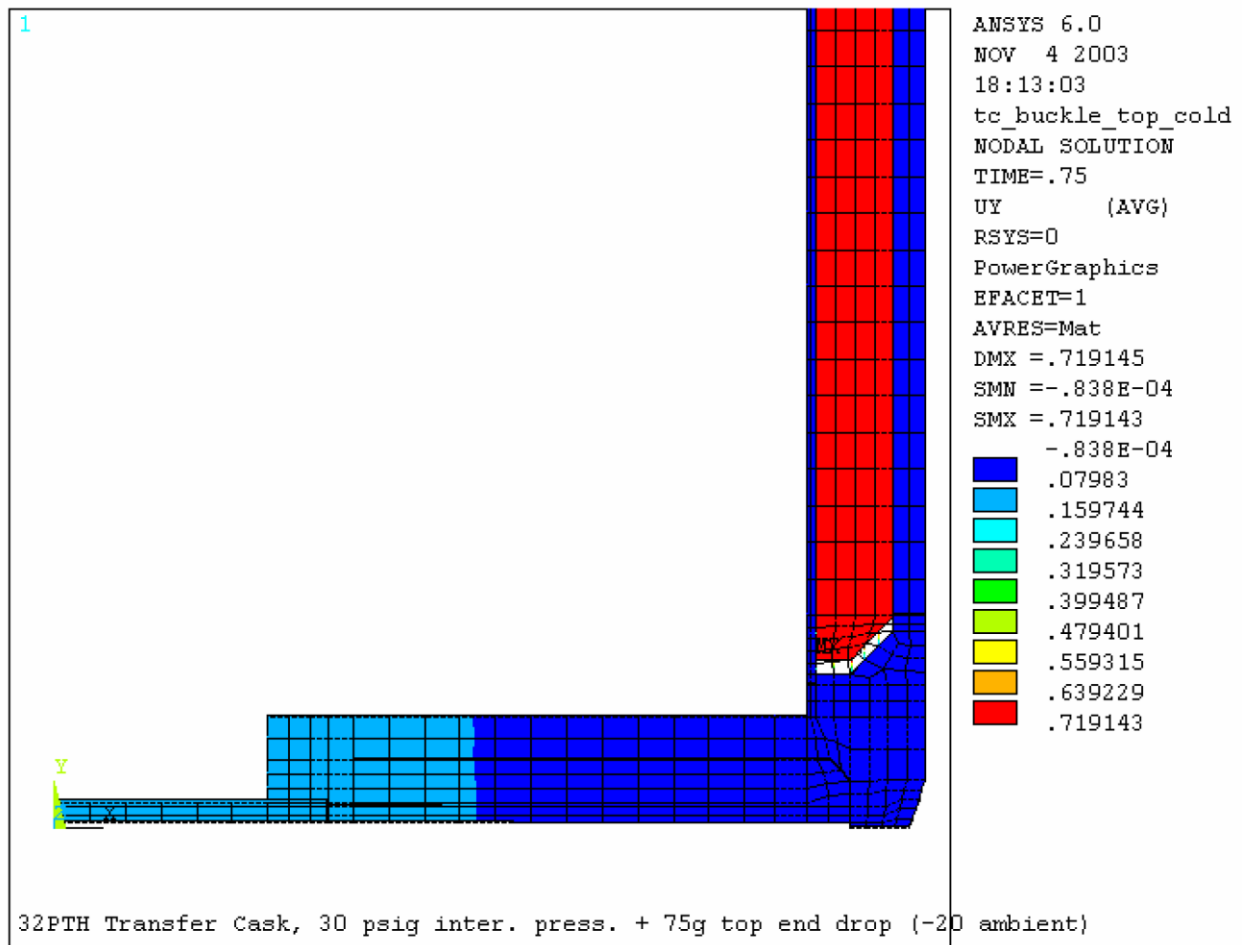


Figure 3.9.4-12
Deformed Shape of Transfer Cask for 75g Top End Drop
(Bottom End, -20° F Ambient Case)

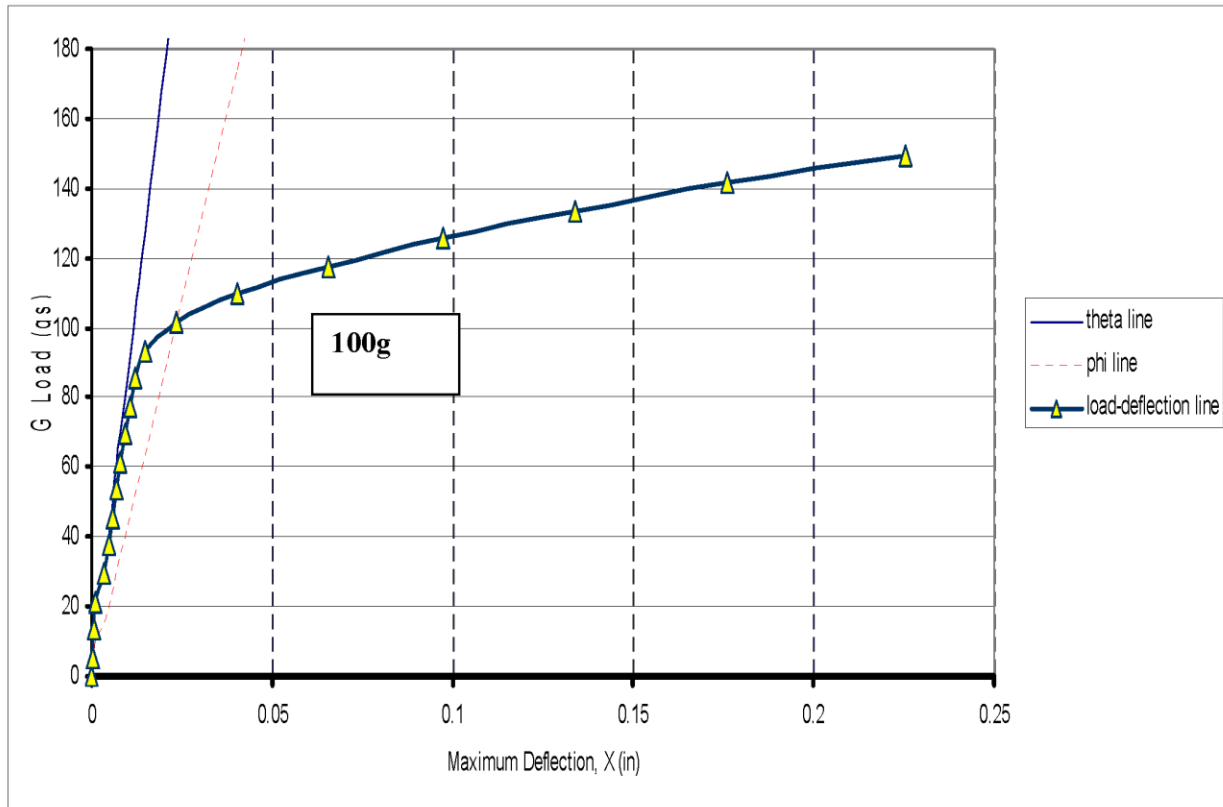


Figure 3.9.4-13
Construction of Collapse Load for Transfer Cask Bottom End Drop

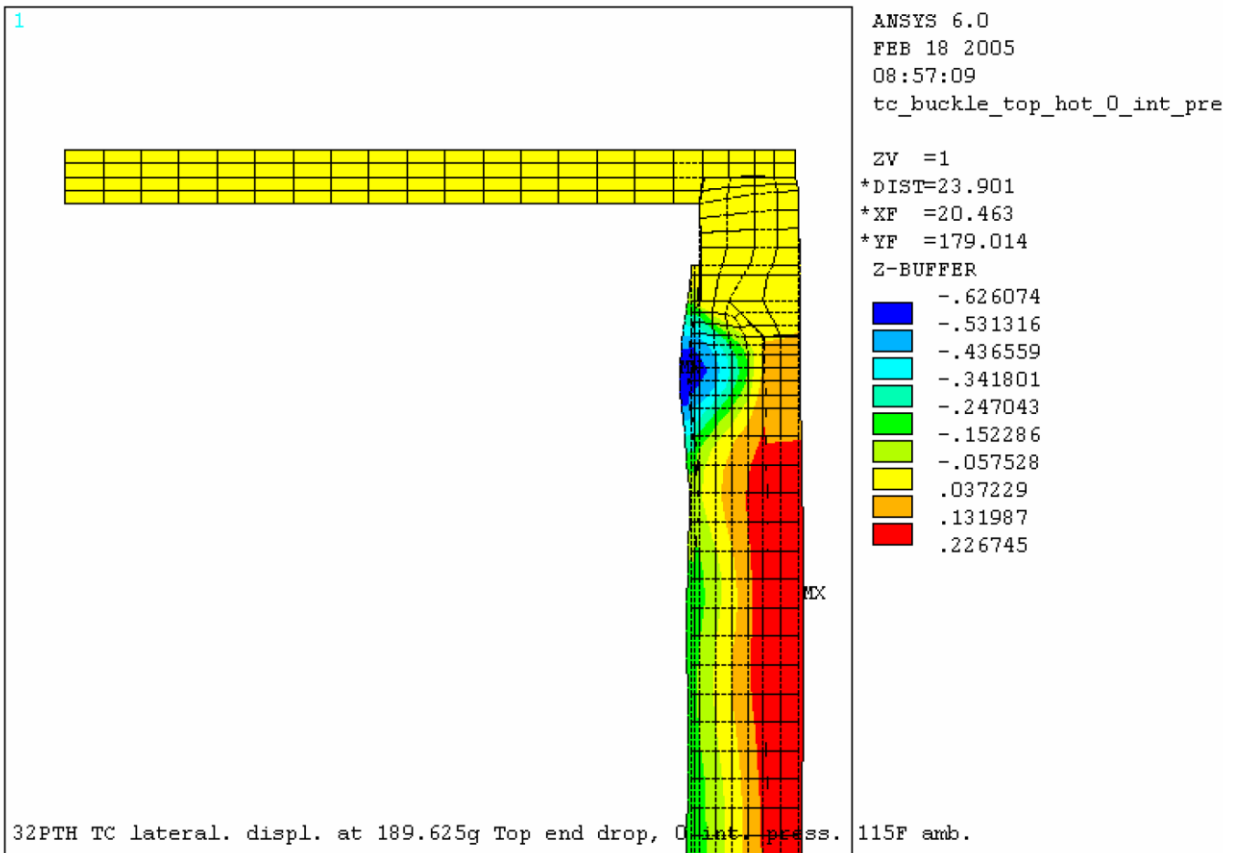


Figure 3.9.4-14
Transfer Cask Top End Drop Deformation Plot (at 189.625g)

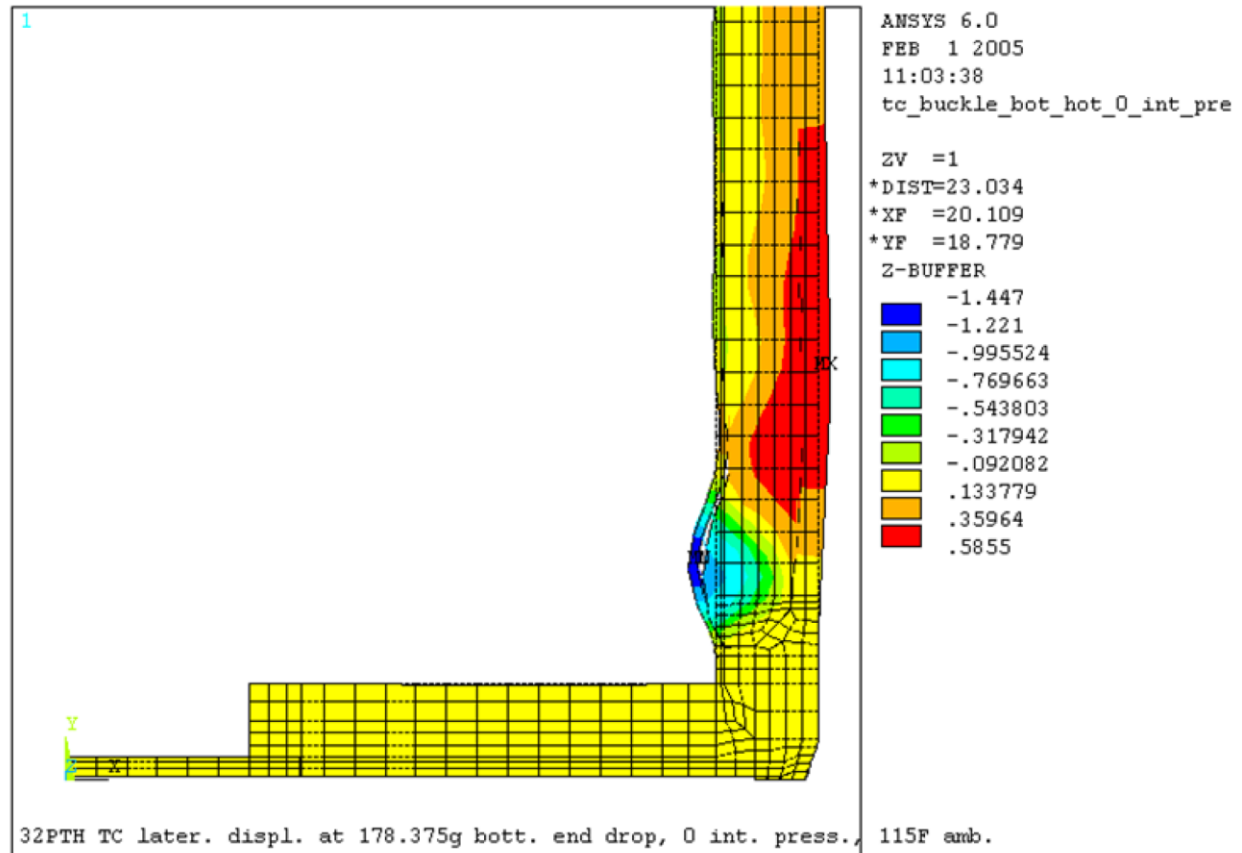


Figure 3.9.4-15
Transfer Cask Bottom End Drop Deformation Plot (at 178.375g)

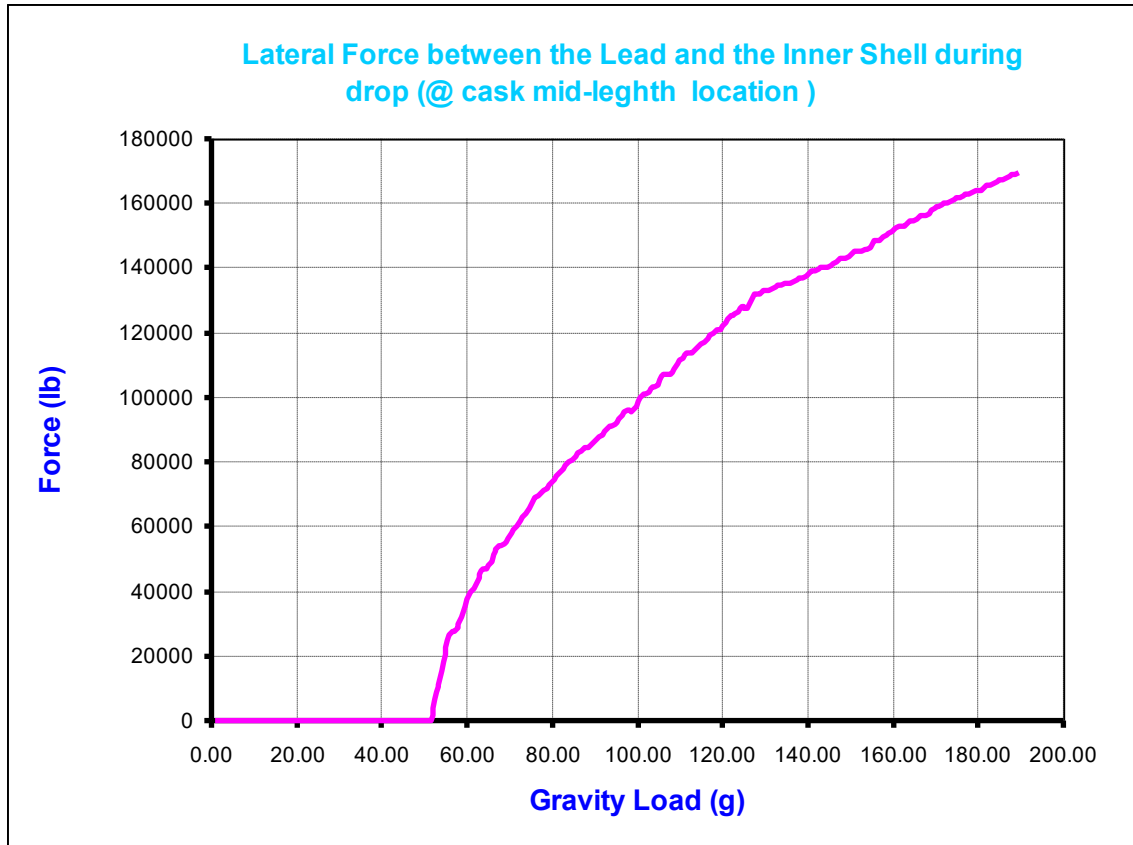


Figure 3.9.4-16
Lateral Force Exerted on Inner Shell (Transfer Cask Top End Drop)

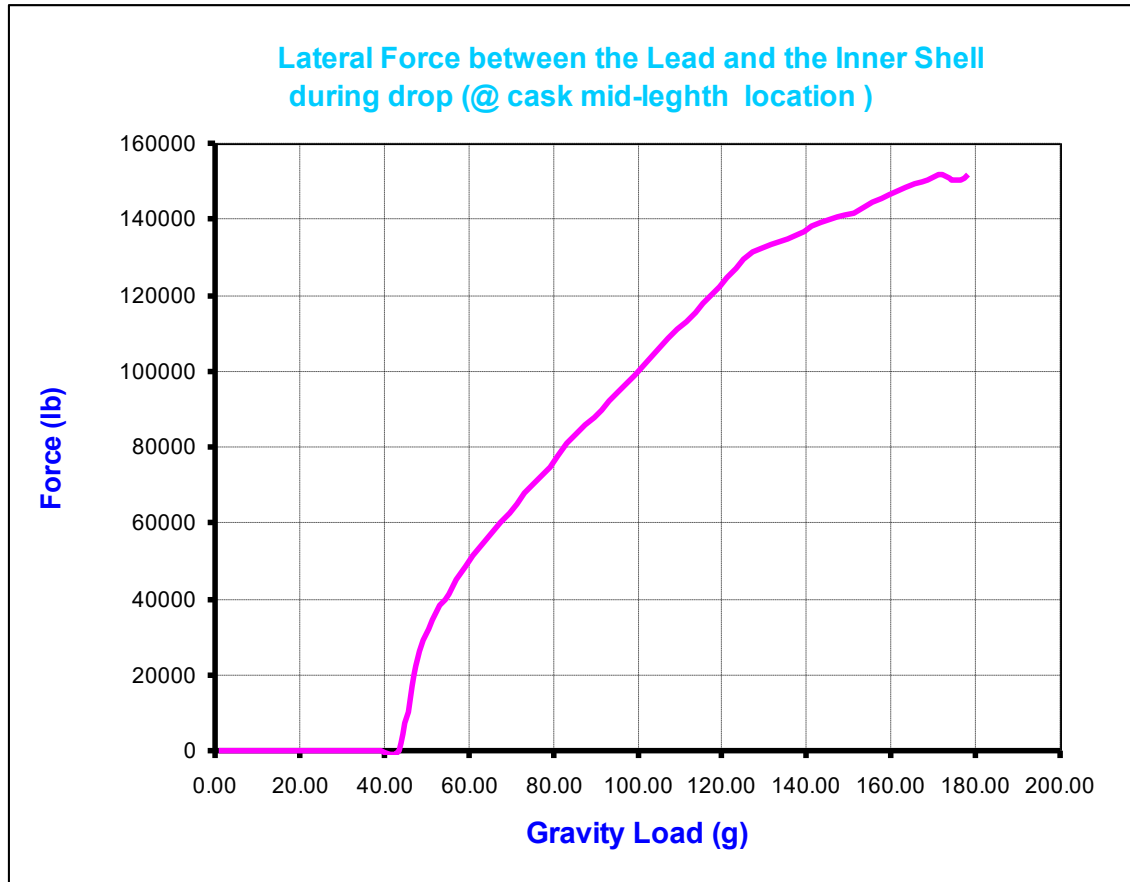


Figure 3.9.4-17
Lateral Force Exerted on Inner Shell (Transfer Cask Bottom End Drop)

APPENDIX 3.9.5
OS187H TRANSFER CASK TRUNNION ANALYSIS

TABLE OF CONTENTS

3.9.5	OS187H TRANSFER CASK TRUNNION ANALYSIS	3.9.5-1
3.9.5.1	Introduction.....	3.9.5-1
3.9.5.2	Component Weights.....	3.9.5-2
3.9.5.3	Load Cases.....	3.9.5-2
3.9.5.4	Material Properties.....	3.9.5-3
3.9.5.5	Stress Criteria.....	3.9.5-3
3.9.5.6	Stress Computation.....	3.9.5-3
3.9.5.7	Summary of Computed Stresses.....	3.9.5-13
3.9.5.8	Conclusions.....	3.9.5-13
3.9.5.9	References.....	3.9.5-14

LIST OF TABLES

Table 3.9.5-1	Summary of Computed and Allowable Trunnion Stresses.....	3.9.5-15
---------------	--	----------

LIST OF FIGURES

Figure 3.9.5-1	OS187H Transfer Cask Bottom Trunnion (Top View)	3.9.5-16
Figure 3.9.5-2	OS187H Transfer Cask Top Trunnion (Top View).....	3.9.5-17
Figure 3.9.5-3	Opening in the Lifting Yoke Arm Geometry.....	3.9.5-18

3.9.5 OS187H TRANSFER CASK TRUNNION ANALYSIS

3.9.5.1 Introduction

This appendix presents the evaluation of the NUHOMS[®]-OS187H Transfer Cask Trunnion stresses due to all applied loads during fuel loading and transfer operations.

NUHOMS[®] OS187H transfer cask has two top trunnions constructed from SA-182 Gr. FXM19 (22Cr-13Ni-5Mn Forging) and two bottom trunnions constructed from SA-182 Gr. F304. The cask shells are made of SA-240, Gr. 304 (18Cr-8Ni) stainless steel. The two top trunnions are used to first lift the cask, containing a canister and an empty basket, into a fuel pool for loading of the spent fuel. After the spent fuel has been loaded into the basket, the cask is lifted to a decontamination area. After draining and drying of the pool water, welding of the canister cover, and bolting of the cask lid, the cask is placed in a trailer for transfer to onsite HSM. The cask is vertically lifted onto the trailer and is initially supported by the bottom trunnions which are mated to transfer trailer. Then the cask is allowed to pivot about the bottom trunnions, into a horizontal position until the top trunnions rest on their supports in the trailer. Throughout the operation the maximum total load is applied to the cask top trunnions. After the cask has been placed on the trailer, it is supported by all four trunnions and is subject to a set of specified design handling loads.

The following two load cases are analyzed for the four transfer cask trunnions:

- A. Lifting Loads (Cask lifted from the pool to the decontamination area and then to the trailer). The two top trunnions are analyzed for 6g and 10g vertical loads as required by ANSI N14.6 [1]. The two bottom trunnions are not used during lifting of the cask.
- B. Handling Loads (Cask in a horizontal position on transfer trailer). All four trunnions rest on the supports on the trailer. The four trunnions are designed to resist the following transfer loads:

DW (Dead Weight) + 1g Axial

DW + 1g Transverse

DW + 1g Vertical

DW + ½g Axial + ½g Transverse + ½g Vertical

(Directions are relative to a horizontal cask)

The transfer cask shell and trunnions are assumed to be at 300° F during transfer. This assumption is conservative based on the thermal evaluation performed in Chapter 4.

3.9.5.2 Component Weights

The weight of the NUHOMS®-OS187H Transfer Cask is 229.52 kips, including the loaded DSC (Section 3.2). However, for conservatism, a weight of 250.00 kips. is used in this analysis.

3.9.5.3 Load Cases

The following moment arms are used for the two load cases:

Load Case	g Load	Moment Arm Length	Reaction Support
Lifting	6g and 10g longitudinal	9.750 in.*	Top two trunnions only
Transfer Loads	DW +1g Axial DW+1g vertical DW+1g transverse DW + 0.5g Axial + 0.5g Vertical + 0.5g Trans.	7.135 in.**	All four top and bottom trunnions

* See Figure 3.9.5-2 ($11.63'' - 0.38'' - 1.5'' = 9.75''$)

** See Figure 3.9.5-1 ($8.76'' - 1.625'' = 7.135''$)

3.9.5.4 Material Properties

The following material properties, used for the trunnion stress analysis, are taken from Reference 2 at 300°F.

Property	SA-182, Gr. FXM-19 (Top Trunnions)	SA-182, Gr. F304 (Bottom Trunnions, t >5")
S_m	31.4 ksi	20 ksi
S_y	43.3 ksi	22.4 ksi
S_u	94.2 ksi	66.2 ksi

3.9.5.5 Stress Criteria

ANSI N14.6 requires the maximum tensile and shear stresses in the lifting trunnion due to 6g and 10g load be checked against the material yield and ultimate stresses respectively. The handling loads are normal condition (Level A) loads and are compared with the allowable stresses in ASME Code, Section III, Subsection NC [3].

3.9.5.6 Stress Computation

3.9.5.6.1 Lifting Load Stresses in Top Trunnions

The top trunnion material (SA-182 Gr. FXM19) ultimate and yield stresses at 300° F are 94,200 psi and 43,300 psi respectively. Since the ratio of two design lifting loads for each top trunnion is 1.667 (10g / 6g), is less than the ratio of the allowable stresses, 2.175 (94,200psi / 43,300 psi), it is not necessary to check stresses in the trunnions for the higher 10g design load.

The 6g Vertical load on one top trunnion, F_1 , is,

$$F_1 = 250,000 \text{ lb} \times 6g \times 1.1 \times 1/2 = 825,000 \text{ lb}$$

A dynamic load factor, DLF, of 1.1 is used in this calculation.

The 2.5 inch thick lifting yoke plate is to be positioned in the middle of the 3 inch wide top trunnion groove. Therefore, the lift weight acts at the center of the 3 inch trunnion groove. (See Figure 3.9.5-2 for the load location)

A. Stresses at trunnion Section A-A (See Figure 3.9.5-2)

The cross-section area, A_{A-A} , and area moment of inertia, I_{A-A} are the following.

$$A_{A-A} = \pi/4 (8.75^2 - 4^2) = 47.57 \text{ in}^2$$

$$I_{A-A} = \pi/64 (8.75^4 - 4^4) = 275.17 \text{ in}^4$$

$$M_{A-A} = F_1 \times L_{A-A} = 825,000 \text{ lb} \times (3 / 2) = 1,237,500 \text{ in-lb.}$$

The average shear stress, τ_{avg} , is,

$$\tau_{\text{avg}} = F_1 / A_{A-A} = 825,000 \text{ lb} / 47.57 \text{ in}^2 = 17,343 \text{ psi}$$

The maximum bending stress, σ_b , is,

$$\begin{aligned} \sigma_b &= (M_{A-A} / I_{A-A}) \times (H_{A-A} / 2) \\ &= (1,237,500 \text{ in-lb} / 275.17 \text{ in}^4) (8.75 / 2) = 19,675 \text{ psi} \end{aligned}$$

The combined shear stress, τ_{max} ,

$$\begin{aligned} \tau_{\text{max}} &= 0.5 \times [(\sigma_b^2 + 4(\tau_{\text{avg}})^2)]^{0.5} \\ &= 0.5 \times [19,675^2 + 4(17,343)^2]^{0.5} \\ &= 19,940 \text{ psi} < S_y \end{aligned}$$

The maximum tensile stress, σ_{max} , is the following.

$$\begin{aligned} \sigma_{\text{max}} &= \sigma_b / 2 + \tau_{\text{max}} \\ &= 19,675 / 2 + 19,940 = 29,778 \text{ psi} < S_y \end{aligned}$$

B. Stresses at trunnion Section B-B (See Figure 3.9.5-2)

Cross-section Area, A_{B-B} , Area Moment of Inertia, I_{B-B} , are the following.

$$A_{B-B} = \pi/4 (12^2 - 4^2) = 100.53 \text{ in}^2$$

$$I_{B-B} = \pi/64 (12^4 - 4^4) = 1,005 \text{ in}^4$$

$$M_{B-B} = 825,000 \text{ lb} \times (3" / 2 + 3.25") = 3,918,750 \text{ in-lb.}$$

The average shear stress, τ_{avg} , is,

$$\tau_{\text{avg}} = F_1 / A_{B-B} = 825,000 \text{ lb} / 100.53 \text{ in}^2 = 8,207 \text{ psi}$$

The maximum bending stress, σ_b , is,

$$\begin{aligned}\sigma_b &= (M_{B-B} / I_{B-B}) \times (H_{B-B} / 2) \\ &= (3,918,750 \text{ in-lb} / 1,005 \text{ in}^4) (12 / 2) = 23,396 \text{ psi}\end{aligned}$$

The combined shear stress, τ_{\max} ,

$$\begin{aligned}\tau_{\max} &= 0.5 \times [(\sigma_b^2 + 4(\tau_{\text{avg}})^2)^{0.5}] \\ &= 0.5 \times [23,396^2 + 4(8,207)^2]^{0.5} \\ &= 14,289 \text{ psi} < S_y\end{aligned}$$

The maximum tensile stress, σ_{\max} , is the following.

$$\begin{aligned}\sigma_{\max} &= \sigma_b / 2 + \tau_{\max} \\ &= 22,396 / 2 + 14,289 = 25,987 \text{ psi} < S_y\end{aligned}$$

C. Stresses at Section C-C (See Figure 3.9.5-2)

Cross-section Area, A_{B-B} , Area Moment of Inertia, I_{B-B} , are the following.

$$A_{C-C} = \pi/4 (17.15^2 - 4^2) = 218.44 \text{ in}^2$$

$$I_{C-C} = \pi/64 (17.15^4 - 4^4) = 4,234 \text{ in}^4$$

$$M_{C-C} = F_1 \times L_{C-C} = 825,000 \text{ lb} \times (11.63'' - 0.38'' - 3'' / 2) = 8,043,750 \text{ in-lb.}$$

The average shear stress, τ_{avg} , is,

$$\tau_{\text{avg}} = F_1 / A_{C-C} = 825,000 \text{ lb} / 218.44 \text{ in}^2 = 3,777 \text{ psi}$$

The maximum bending stress, σ_b , is,

$$\begin{aligned}\sigma_b &= (M_{C-C} / I_{C-C}) \times (H_{C-C} / 2) \\ &= (8,043,750 \text{ in-lb} / 4,234 \text{ in}^4) (17.15 / 2) = 16,291 \text{ psi}\end{aligned}$$

The combined shear stress, τ_{\max} ,

$$\begin{aligned}\tau_{\max} &= 0.5 \times [(\sigma_b^2 + 4(\tau_{\text{avg}})^2)^{0.5}] \\ &= 0.5 \times [16,291^2 + 4(3,777)^2]^{0.5} \\ &= 8,979 \text{ psi} < S_y\end{aligned}$$

The maximum tensile stress, σ_{\max} , is the following.

$$\begin{aligned}\sigma_{\max} &= \sigma_b / 2 + \tau_{\max} \\ &= 16,291 / 2 + 8,979 = 17,125 \text{ psi} < S_y\end{aligned}$$

D. Bearing Stresses at Trunnion

The following dimensions refer to the Figure 3.9.5-3.

$$\text{Length AO} = 6.5 \text{ in.}, \text{BC} = 4.75 \text{ in.}, \text{OC} = 5 \text{ in.}, \text{FC} = 4.375 \text{ in.}$$

Therefore,

$$\text{DO} = \text{AO} - \text{AD} = \text{AO} - \text{BC} = 6.5 \text{ in.} - 4.75 \text{ in.} = 1.75 \text{ in.}$$

$$\angle \text{DCO} = \sin^{-1}(\text{DO}/\text{CO}) = 20.4873^\circ$$

$$\angle \text{BCE} = 90^\circ - \angle \text{DCO} = 90^\circ - 20.4873^\circ = 69.5127^\circ$$

During lifting, the 2.5 inch thick lifting arm plate will generate bearing stress in the outer end of the trunnion. The contact between the lifting arm plate and the trunnion is to encompass 69.51° . The projected bearing stress area, A_{br} , is,

$$A_{br} = 2 \times 4.375 \text{ in.} \times \sin 69.51^\circ \times 2.5 \text{ in.} = 20.491 \text{ in.}^2$$

The bearing stress, σ_{br} , is then,

$$\sigma_{br} = 825,000 \text{ lb} / 20.491 \text{ in.}^2 = 40,262 \text{ psi} < S_y$$

3.9.5.6.2 Handling Load Stresses

All four trunnions carry the axial and vertical loads while only one top trunnion and one bottom trunnion on the same side of the cask will carry the transverse load. The axial load is carried only by the bottom trunnions because the top trunnions rest on sliding supports.

A. DW (1g vertical) + 1g Axial

At the top and bottom trunnions the g -loads per trunnion are:

$$1.0g \text{ (axial)} / 2 \text{ sides} / 1 \text{ set trunnions} = 0.5g \text{ axial per bottom trunnion.}$$

$$1.0g \text{ (vertical)} / 2 \text{ sides} / 2 \text{ set trunnions} = 0.25g \text{ vertical per trunnion}$$

The bottom trunnions have a larger inner diameter (8 inch diameter of material is removed to reduce the weight, see Figure 3.9.5-1) than the top trunnions (4 inch diameter, see Figure 3.9.5-2). Also, the bottom trunnions material has lower yield and ultimate strengths relative to the top trunnions, and therefore has lower allowable stresses. Thus, the bottom trunnions are critical with respect to stress generated by the handling load. The transfer loads are therefore analyzed only for the weaker bottom trunnions, which are shown in Figure 3.9.5-1.

$$\text{The vector sum of } 0.25g \text{ vertical and } 0.5g \text{ axial} = [0.25^2 + 0.5^2]^{1/2} g = 0.559g$$

Therefore, the lateral load at each bottom trunnion, F_1 , is,

$$F_1 = 250,000\text{lb} \times 0.559g = 139,750 \text{ lb.}$$

Stresses at Trunnion Section B-B (See Figure 3.9.5-1)

The cross-section Area, A_{B-B} , is,

$$A_{B-B} = \pi/4 (12^2 - 8^2) = 62.83 \text{ in}^2$$

Area Moment of Inertia, I_{B-B} , is,

$$I_{B-B} = \pi/64 (12^4 - 8^4) = 816.81 \text{ in}^4$$

Therefore, the bending moment, M_{B-B} , is,

$$M_{B-B} = 139,750 \text{ lb} \times (3.25 \text{ in.} / 2) = 227,100 \text{ in-lb.}$$

The maximum shear stress due to bending for a hollow circular section, τ_{\max} , is the following.

$$\tau_{\max} = 2F_1 / A_{B-B} = 2 \times 139,750 \text{ lb} / 62.83 \text{ in}^2 = 4,450 \text{ psi}$$

The maximum bending stress due to lateral load, σ_x , is,

$$\begin{aligned} \sigma_x &= (M_{B-B} / I_{B-B}) \times (H_{B-B} / 2) \\ &= (227,100 \text{ in-lb} / 816.61 \text{ in}^4) (12 \text{ in.} / 2) = 1,670 \text{ psi.} \end{aligned}$$

The stress intensity, $S.I.$, is then,

$$S.I. = [(\sigma_x^2 + 4(\tau_{\max})^2)]^{0.5} = [1,670^2 + 4(4,450)^2]^{0.5} \\ = 9,055 \text{ psi} < S_m$$

The stress intensity, $S.I.$, calculated here is conservatively considered to be primary membrane stress, P_m , and is evaluated against its allowable stress, S_m , as per ASME B&PV Section III-NC [3].

$$S_m = 20,000 \text{ psi (for SA-182 Gr.F304 at } 300^\circ \text{ F)}$$

Stresses at Section C-C (See Figure 3.9.5-1)

Cross-section Area, A_{C-C} , is,

$$A_{C-C} = \pi/4 (17.15^2 - 8^2) = 180.74 \text{ in}^2.$$

Area Moment of Inertia, I_{C-C} , is,

$$I_{C-C} = \pi/64 (17.15^4 - 8^4) = 4,045 \text{ in}^4.$$

The bending moment, M_{C-C} , is then,

$$M_{C-C} = F \times L_{C-C} \\ = 139,750 \text{ lb} \times (8.75 \text{ in.} - 3.25 \text{ in.} / 2) = 995,720 \text{ in-lb.}$$

The maximum shear stress due to bending for a hollow circular section, τ_{\max} , is the following.

$$\tau_{\max} = 2 F / A_{C-C} = 2 \times 139,750 \text{ lb} / 180.74 \text{ in}^2 = 1550 \text{ psi.}$$

The maximum bending stress due to lateral load, σ_x , is,

$$\sigma_x = (M_{C-C} / I_{C-C}) \times (H_{C-C} / 2) + F_a / A_{C-C} \\ = (995,720 \text{ in-lb} / 4,045 \text{ in}^4) (17.15 \text{ in.} / 2) = 2,111 \text{ psi}$$

The stress intensity, $S.I.$, is,

$$S.I. = [(\sigma_x^2 + 4(\tau_{\max})^2)]^{0.5} \\ = [2,111^2 + 4(1550)^2]^{0.5} = 3,751 \text{ psi} < S_m$$

B. DW (1g vertical) + 1g Vertical

At the top and bottom trunnions the *g*-load per trunnion is:

$$2.0g \text{ (vertical)} / 2 \text{ sides} / 2 \text{ set trunnions} = 0.5g \text{ vertical per trunnion}$$

The lateral load at each bottom trunnion, F_1 is the following.

$$F_1 = 250,000\text{lb} \times 0.5g = 125,000 \text{ lb.}$$

Stresses are calculated from Case A by multiplying with a factor $125,000/88,500 = 1.4124$

Stresses at trunnion Section B-B (See Figure 3.9.5-1)

Maximum Stress Intensity, *S.I.*, is,

$$S.I. = 1.4124 \times 5,732 = 8,096 \text{ psi.} < S_m$$

Stresses at trunnion Section C-C (See Figure 3.9.5-1)

Maximum Stress Intensity, *S.I.*, is,

$$S.I. = 1.4124 \times 2,371 = 3,349 \text{ psi.} < S_m$$

C. DW (1g vertical) + 1g Transverse

At the top and bottom trunnions the *g*-loads per trunnion are:

$$1.0g \text{ (transverse)} / 1 \text{ side} / 2 \text{ set trunnions} = 0.5g \text{ transverse per trunnion.}$$

$$1.0g \text{ (vertical)} / 2 \text{ sides} / 2 \text{ set trunnions} = 0.25g \text{ vertical per trunnion}$$

Lateral load at each bottom trunnion, F_1 , is,

$$F_1 = 250,000\text{lb} \times 0.25 = 62,500 \text{ lb}$$

Axial Load at bottom trunnion, F_2 , is,

$$F_2 = 250,000\text{lb} \times 0.5 = 125,000 \text{ lb}$$

Stresses at trunnion Section B-B (See Figure 3.9.5-1)

Therefore, the bending moment, M_{B-B} , is,

$$M_{B-B} = 62,500 \text{ lb} \times (3.25 \text{ in.} / 2) = 101,563 \text{ in-lb.}$$

The maximum shear stress due to bending for a hollow circular section, τ_{\max} , is the following.

$$\tau_{\max} = 2F_1 / A_{B-B} = 2 \times 62,500 \text{ lb} / 62.83 \text{ in}^2 = 1,989 \text{ psi.}$$

The maximum normal stress, σ_x , is,

$$\begin{aligned} \sigma_x &= \text{max. bending stress due to lateral load} + \text{normal stress due to axial load} \\ &= (M_{B-B} / I_{B-B}) \times (H_{B-B} / 2) + F_2 / A_{B-B} \\ &= (101,563 \text{ in-lb} / 816.61 \text{ in}^4) (12 \text{ in.} / 2) + 125,000 \text{ lb} / 62.83 \text{ in}^2 \\ &= 746 + 1989 = 2,735 \text{ psi.} \end{aligned}$$

The stress intensity, $S.I.$, is,

$$\begin{aligned} S.I. &= [(\sigma_x^2 + 4(\tau_{\max})^2)]^{0.5} = [2,735^2 + 4(1,989)^2]^{0.5} \\ &= 4,828 \text{ psi} < S_m \end{aligned}$$

Stresses at Section C-C (See Figure 3.9.5-1)

The bending moment, M_{C-C} , is,

$$\begin{aligned} M_{C-C} &= F_1 \times L_{C-C} \\ &= 62,500 \text{ lb} \times (8.75 \text{ in.} - 3.25 \text{ in.} / 2) = 445,313 \text{ in-lb.} \end{aligned}$$

The maximum shear stress due to bending for a hollow circular section, τ_{\max} , is the following.

$$\tau_{\max} = 2F / A_{C-C} = 2 \times 62,500 \text{ lb} / 180.74 \text{ in}^2 = 692 \text{ psi.}$$

The maximum normal stress, σ_x , is,

$$\begin{aligned} \sigma_x &= \text{max. bending stress due to lateral load} + \text{normal stress due to axial load} \\ &= (M_{C-C} / I_{C-C}) \times (H_{C-C} / 2) + F_a / A_{C-C} \\ &= (445,313 \text{ in-lb} / 4,045 \text{ in}^4) (17.15 \text{ in.} / 2) + 125,000 \text{ lb} / 180.74 \text{ in}^2 \\ &= 944 + 692 = 1,636 \text{ psi.} \end{aligned}$$

The stress intensity, $S.I.$, is,

$$\begin{aligned} S.I. &= [(\sigma_x^2 + 4(\tau_{\max})^2)]^{0.5} \\ &= [1,636^2 + 4(692)^2]^{0.5} = 2,143 \text{ psi} < S_m \end{aligned}$$

D. DW + 0.5g Axial + 0.5g Vertical + 0.5g Transverse

At the top and bottom trunnions the g -loads per trunnion are:

$$0.5g \text{ (axial)} / 2 \text{ sides} / 1 \text{ set trunnions} = 0.25g \text{ axial per trunnion}$$

$$0.5g \text{ (transverse)} / 1 \text{ side} / 2 \text{ set trunnions} = 0.25g \text{ transverse per trunnion}$$

$$1.5g \text{ (vertical)} / 2 \text{ sides} / 2 \text{ set trunnions} = 0.375g \text{ vertical per trunnion}$$

The vector sum of 0.375g vertical and 0.125g axial = $[0.375^2 + 0.25^2]^{1/2} g = 0.451g$

Lateral Load at each bottom trunnion, F_1 , is,

$$F_1 = 250,000\text{lb} \times 0.451g = 112,750 \text{ lb}$$

Transverse Load at bottom trunnion, F_2 , is,

$$F_2 = 250,000\text{lb} \times 0.25g = 62,500 \text{ lb}$$

Where, the load, F_2 , acts as an axial load on the bottom trunnion.

Stresses at trunnion Section B-B (See Figure 3.9.5-1)

The bending moment, M_{B-B} , is,

$$M_{B-B} = 112,750 \text{ lb} \times (3.25 \text{ in.} / 2) = 183,219 \text{ in-lb.}$$

The maximum shear stress due to bending for a hollow circular section, τ_{\max} , is the following.

$$\tau_{\max} = 2F_1 / A_{B-B} = 2 \times 112,750 \text{ lb} / 62.83 \text{ in}^2 = 3,590 \text{ psi.}$$

The maximum normal stress, σ_x , is,

$$\begin{aligned} \sigma_x &= \text{max. bending stress due to lateral } (F_1) \text{ load} + \text{normal stress due to } F_2 \text{ load} \\ &= (M_{B-B} / I_{B-B}) \times (H_{B-B} / 2) + F_2 / A_{B-B} \\ &= (183,219 \text{ in-lb} / 816.61 \text{ in}^4) (12 \text{ in.} / 2) + 62,500 \text{ lb} / 62.83 \text{ in}^2 \\ &= 1,347 + 995 = 2,342 \text{ psi.} \end{aligned}$$

The stress intensity, $S.I.$, is,

$$\begin{aligned} S.I. &= [(\sigma_x^2 + 4(\tau_{\max})^2)]^{0.5} = [2,342^2 + 4(3,590)^2]^{0.5} \\ &= 7,553 \text{ psi.} < S_m \end{aligned}$$

Stresses at Section C-C (See Figure 3.9.5-1)

The bending moment, M_{C-C} , is,

$$\begin{aligned} M_{C-C} &= F_1 \times L_{C-C} \\ &= 112,750 \text{ lb} \times (8.75 \text{ in.} - 3.25 \text{ in.} / 2) = 803,344 \text{ in-lb.} \end{aligned}$$

The maximum shear stress due to bending for a hollow circular section, τ_{\max} , is the following.

$$\tau_{\max} = 2F_1 / A_{C-C} = 2 \times 112,750 \text{ lb} / 180.74 \text{ in}^2 = 1,248 \text{ psi.}$$

The maximum normal stress, σ_x , is,

$$\begin{aligned} \sigma_x &= \text{max. bending stress due to lateral load} + \text{normal stress due to axial load} \\ &= (M_{C-C} / I_{C-C}) \times (H_{C-C} / 2) + F_2 / A_{C-C} \\ &= (803,344 \text{ in-lb} / 4,045 \text{ in.}^4) (17.15 \text{ in.} / 2) + 62,500 \text{ lb} / 180.74 \text{ in.}^2 \\ &= 1,703 + 346 = 2,050 \text{ psi.} \end{aligned}$$

The stress intensity, $S.I.$, is,

$$\begin{aligned} S.I. &= [(\sigma_x^2 + 4(\tau_{\max})^2)]^{0.5} \\ &= [2,050^2 + 4(1,248)^2]^{0.5} = 3,230 \text{ psi.} < S_m \end{aligned}$$

3.9.5.7 Summary of Computed Stresses

The calculated maximum trunnion stresses are summarized in Table 3.9.5-1 and compared with their corresponding allowable stresses.

3.9.5.8 Conclusions

Table 3.9.5-1 shows that all calculated trunnion stresses are less than their corresponding allowable stresses. Therefore, the NUHOMS[®]-OS187H Transfer Cask top and bottom trunnions are structurally adequate to withstand loads during lifting and transfer operations.

3.9.5.9 References

1. “Special Lifting Devices for Shipping Containers Weighing 10,000 Pounds or More”, ANSI N14.6, 1993.
2. American Society of Mechanical Engineers, ASME Boiler and Pressure Vessel Code, Section II, Part D, 1998, through 2000 addenda.
3. American Society of Mechanical Engineers, ASME Boiler and Pressure Vessel Code, Section III, Division 1, Subsection NC, 1998, through 2000 addenda.

Table 3.9.5-1
Summary of Computed and Allowable Trunnion Stresses

Case Number	Load	Maximum Stress		Allowable (ksi)
		Type	Magnitude (ksi)	
1	Lifting 6g	Shear	19.9	43.3 ⁽²⁾
		Tensile	29.8	43.3 ⁽²⁾
2	Lifting ⁽¹⁾ 10g	Shear	33.2	94.2 ⁽⁴⁾
		Tensile	49.6	94.2 ⁽⁴⁾
3	Handling DW + 1.0g Axial	P_m	9.1	20.0 ⁽³⁾
		$P_m + P_b$	9.1	20.0 ⁽³⁾
4	Handling DW + 1.0g Vertical	P_m	8.1	20.0 ⁽³⁾
		$P_m + P_b$	8.1	20.0 ⁽³⁾
5	Handling DW + 1.0g Transverse	P_m	4.8	20.0 ⁽³⁾
		$P_m + P_b$	4.8	20.0 ⁽³⁾
6	Handling DW + 0.5g Axial + 0.5g Vertical + 0.5g Transverse	P_m	7.6	20.0 ⁽³⁾
		$P_m + P_b$	7.6	20.0 ⁽³⁾

Notes:

- (1) Stresses in the trunnions are obtained by direct ratio from 6g load.
- (2) Yield stress, S_y , for top trunnion material SA-182-FXM19 at 300° F per ANSI N14.6 [1] criterion.
- (3) Design Stress Intensity, S_m , for bottom trunnion material SA-182-F304 at 300° F per ASME Section III-NC [3] criterion. Conservatively, $P_m + P_b$ is compared with S_m .
- (4) Ultimate stress, S_u , for trunnion material SA-182-FXM19 at 300° F per ANSI N14.6 [1] criterion.

Proprietary Information on Pages 3.9.5-16 and 3.9.5-17
Withheld Pursuant to 10 CFR 2.390

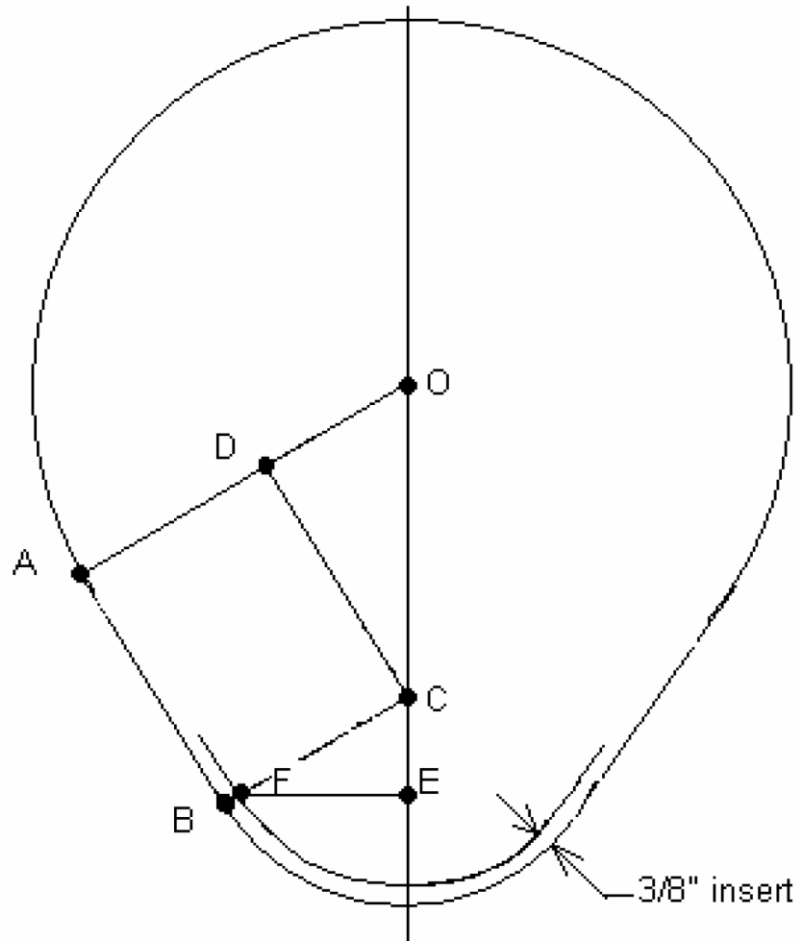


Figure 3.9.5-3
Opening in the Lifting Yoke Arm Geometry

APPENDIX 3.9.6
OS187H TRANSFER CASK SHIELD PANEL STRUCTURAL ANALYSIS

TABLE OF CONTENTS

3.9.6	OS187H TRANSFER CASK SHIELD PANEL STRUCTURAL ANALYSIS..	3.9.6-1
3.9.6.1	Introduction.....	3.9.6-1
3.9.6.2	Material Properties.....	3.9.6-1
3.9.6.3	Component Weights.....	3.9.6-2
3.9.6.4	Stress Criteria.....	3.9.6-2
3.9.6.5	Load Cases.....	3.9.6-3
3.9.6.6	Stress Calculations.....	3.9.6-3
3.9.6.7	Conclusions.....	3.9.6-7
3.9.6.8	References.....	3.9.6-8

LIST OF TABLES

Table 3.9.6-1	Summary of Calculated and Allowable Neutron Shield Shell Stresses...	3.9.6-9
---------------	--	---------

LIST OF FIGURES

Figure 3.9.6-1	Neutron Shield Shell Finite Element Model	3.9.6-10
Figure 3.9.6-2	Neutron Shield Shell Finite Element Model, Top Plate Region	3.9.6-11
Figure 3.9.6-3	Neutron Shield Shell Finite Element Model, Bottom Plate Region	3.9.6-12
Figure 3.9.6-4	Neutron Shield Shell Finite Element Model, 3g Lifting Boundary Conditions	3.9.6-13
Figure 3.9.6-5	3g Lifting Stress Intensity Distribution.....	3.9.6-14
Figure 3.9.6-6	Neutron Shield Shell Finite Element Model, Transfer Loads Boundary Conditions	3.9.6-15
Figure 3.9.6-7	Transfer Loads Stress Intensity Distribution	3.9.6-16
Figure 3.9.6-8	Cold Ambient Environment Temperature Distribution	3.9.6-17
Figure 3.9.6-9	Hot Ambient Environment Temperature Distribution.....	3.9.6-18
Figure 3.9.6-10	Transfer Loads plus Cold Ambient Condition Stress Intensity Distribution	3.9.6-19
Figure 3.9.6-11	Transfer Loads plus Hot Ambient Condition Stress Intensity Distribution	3.9.6-20

3.9.6 OS187H TRANSFER CASK SHIELD PANEL STRUCTURAL ANALYSIS

3.9.6.1 Introduction

The purpose of this appendix is to present the evaluation of the stresses in the NUHOMS® - OS187H Transfer Cask neutron shield shell due to all applied loads during fuel loading and transfer operations.

A finite element model was built for the structural analysis of the outer neutron shield shell, end closure, central plates and structural shell. These components were modeled with the ANSYS Solid PLANE42 elements with axisymmetric option. The top and bottom closure plate welds were also modeled with PLANE42 elements. Double nodes were created at the central plate and shell intersections. These nodes were coupled to simulate the weld effect. Figure 3.9.6-1, Figure 3.9.6-2 and Figure 3.9.6-3 show the overall finite element model and its details. The same finite element model is used for all loading conditions.

3.9.6.2 Material Properties

The transfer cask shell is assumed to be at 300° F uniform temperature during transfer operations. This assumption is conservative based on the thermal evaluations performed in Chapter 4.

All shell components are constructed from stainless steel SA-240, Grade 304. The following mechanical and thermal material properties taken from Reference 1 are used in the analysis:

Material	Temp. °F	S _u (ksi)	S _y (ksi)	S _m (ksi)	E (10 ⁶ psi)	α (10 ⁻⁶) (in/in/°F)	Conductivity (Btu/hr-in-°F)	Density (lb/in ³)
SA-240 Stainless Steel 304	70	75.0	30.0	20.0	28.3	8.5	0.7217	0.29
	200	71.0	25.0	20.0	27.6	8.9	0.775	0.29
	300	66.2	22.4	20.0	27.0	9.2	0.8167	0.29
	400	64.0	20.7	18.7	26.5	9.5	0.8667	0.29

3.9.6.3 Component Weights

The weight of the NUHOMS[®]-OS187H Transfer Cask neutron shield shell, including the cylindrical shell, the top and bottom support rings, and the 15 central support rings is 4,288 lb. The weight of the neutron shield shell water is 8,458 lb (the transfer component weights are tabulated in Section 3.2). However, for conservatism, a weight of 8,500 lb. is used for the weights of water in this analysis.

For the transfer cask in the vertical orientation, the inertial force due to water weight is applied as pressure in the following way.

The weight of the neutron shield water, W is 8,500 lb. The maximum hydrostatic pressure at the bottom of the neutron shield shell, W_h , is,

$$W_h = 62.4 \text{ lb/ft}^3 \times 177.24 \text{ in} / 12^3 = 6.4 \text{ psi. ... say 6.5 psi}$$

This hydrostatic pressure is linear with the axial height of the shield shell and is 0 psi at the top.

In addition to the water weight pressure, an additional internal uniform pressure of 40 psig is used in all load cases.

3.9.6.4 Stress Criteria

All load cases are analyzed and results evaluated to the requirements of ASME Code, Subsection NC [2] as normal condition (Level A) load cases. According to Reference 2, the maximum allowable membrane (P_m) and membrane plus bending ($P_m + P_b$) stress intensities for normal conditions are S_m and $1.5 S_m$ respectively. Also, average pure shear is limited to $0.6 S_m$. The maximum primary plus secondary stress is limited to $3.0 S_m$.

The transfer cask inner shell and structural shell are constructed from SA-240, Type 304 stainless steel. Therefore, the maximum allowable membrane and membrane plus bending stress intensities (at 300 °F) are as follows:

Stress Category	Stress Criteria	Maximum Allowable Stress
P_m	S_m	20.0ksi.
$P_m + P_b$	$1.5S_m$	30.0 ksi.
$P_m + P_b + Q$	$3.0 S_m$	60.0 ksi.
Pure Shear	$0.6S_m$	12.0 ksi.

3.9.6.5 Load Cases

The following load cases are considered. When transfer the loaded cask to ISFSI, the transfer loads are 1g axial, 1g transverse, and 1g vertical. For conservatism, a bounding 2g axial + 2g transverse + 2g vertical is used for stress calculations.

Load Case	Applied Load
3g Lifting (Cask Vertical)	40 psi. pressure + hydrostatic pressure + 3g longitudinal
Transfer Loads (Cask Horizontal)	40 psi. pressure + water pressure + 2g longitudinal + 2g vertical + 2g transverse 40 psi. pressure + water pressure + 2g longitudinal + 2g vertical + 2g transverse + Cold Thermal 40 psi. pressure + water pressure + 2g longitudinal + 2g vertical + 2g transverse + Hot Thermal

3.9.6.6 Stress Calculations

3.9.6.6.1 3g Lifting Load Case

The pressure at the bottom plate due to the 3g lifting load for water = $3 \times 6.5 = 19.5$ psi

The ANSYS elastic stress run is made by applying a 40 psi internal pressure and a 19.5 psi hydrostatic pressure. The loading and boundary conditions are shown in Figure 3.9.6-4. A 3g vertical acceleration is applied to account for the inertia loads. As shown in Figure 3.9.6-4, an internal pressure of 59.5 psi. (40 psi. + 19.5 psi.) is applied at the bottom of the shield shell. This pressure tapers linearly to 40 psi at the top.

The resulting stress intensity distribution in the various shell components is shown in Figure 3.9.6-5. It is seen that the maximum nodal stress intensity in the shell model is 24,123 psi. This maximum stress occurs in weld between the bottom plate and cylinder. These stresses are linearized through the shell thickness and presented in Table 3.9.6-1.

3.9.6.6.2 Transfer Load Condition

During transfer operations, the cask is in the horizontal position and the neutron shield shell is subjected to 40 psi internal pressure and transfer handling loads (2g vertical + 2g lateral + 2g axial).

The vertical and lateral loads are combined in the following way.

$$g_{transverse} = (2.0^2 + 2.0^2)^{1/2} = 2.83g$$

The stress due to the 2.83g inertia load conservatively assumes that the weight of the shell structure (4,288 lb.) and water (8,500 lb.) are uniformly distributed only over the 177.24 inch length and a 60° arch. Therefore, the equivalent pressure applied to the outer shell is,

$$p_{vl} = [(4,288 + 8,500) \times 2.83] / [2 \pi (45.913)(177.24)] \times (360^\circ/60^\circ) = 4.25 \text{ psi. ... say 5 psi}$$

Again, the 5 psi load on the 60° sector is conservatively assumed to act on the full 360°. This pressure is added to 40 psi. pressure and applied to the cylinder.

For 2g axial acceleration, the pressure due to the water inertial load on the top plate is,

$$p_a = 8,500 \times 2.0 / [\pi \times (45.913^2 - 41.35^2)] = 13.6 \text{ psi. ... say 14 psi}$$

Therefore, a pressure of 54 psi. (40 + 14) is applied to the top plate. Also, there is a 40 psi. pressure applied to the bottom plate.

An ANSYS elastic stress run is made by applying the above calculated pressures to the finite element model. The boundary conditions are shown in Figure 3.9.6-6. The resulting stress intensity distribution is shown in Figure 3.9.6-7. It is seen that the maximum nodal stress intensity in the shell model is 20,137 psi. This maximum stress occurs in the outer shell near the bottom plate weld. These stresses are linearized through the shell thickness and presented in Table 3.9.6-1.

3.9.6.6.3 Thermal Analyses

The thermal analysis of the neutron shield shell model is conducted for both cold and hot environmental conditions. Steady-state ANSYS thermal analyses of the model are conducted to obtain the nodal temperatures by impressing the temperatures as the boundary conditions for both cold and hot conditions. Two-dimensional thermal elements (PLANE55) are used in the analyses. Temperature dependent thermal material properties are also used in the analysis

The resulting temperature distributions for cold and hot ambient cases are shown Figure 3.9.6-8 and Figure 3.9.6-9, respectively.

3.9.6.6.4 Thermal Stress Analyses

Elastic stress analyses of the shield shell structure are conducted in order to evaluate the transfer plus thermal loads. The loads and boundary conditions of model are shown in Figure 3.9.6-6.

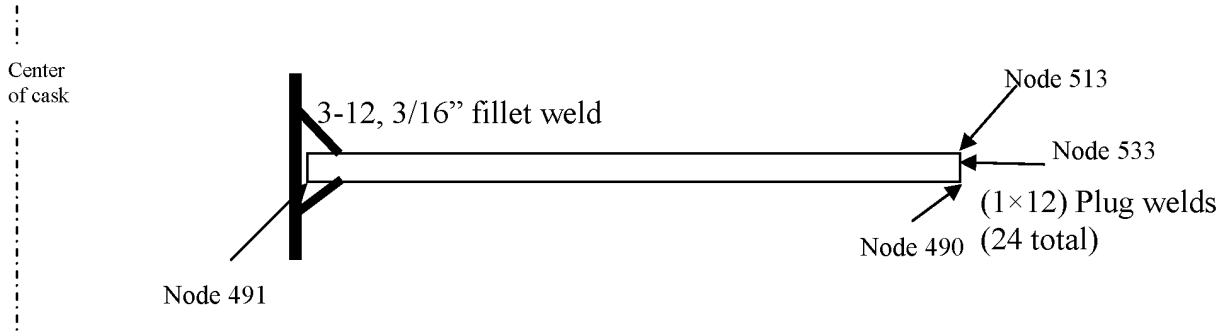
The nodal temperature distribution from the above thermal analyses results is applied to obtain the thermal stresses in the model.

The nodal stress intensity distribution is plotted Figure 3.9.6-10 for cold condition, and in Figure 3.9.6-11 for 115° F hot ambient case. The critical stress intensities are summarized in Table 3.9.6-1.

It is seen from these figures that the maximum thermal stress intensities are generated in the cold ambient case. The maximum nodal stress intensity in the shell model is 26,045 psi. This maximum stress occurs in the outer shell near the bottom plate weld. Cold and hot stresses are linearized through the shell thickness, and the maximum stresses are summarized and evaluated in Table 3.9.6-1.

3.9.6.6.5 Weld Stresses at Center Support Plates

The center support plates are attached to the cask structural shell by 3/16 inch fillet (3-12) stitch-welds, and to the outer neutron shield cylinder by 1 inch × 0.12 inch plug welds (24 plug welds for each plate). It is seen from stress intensity distribution in Figure 3.9.6-10 that the maximum stress intensity (13,417 psi) occurs during the transfer load plus cold ambient load case. The maximum stressed center support plate is located close to the bottom end closure plate. The maximum weld stresses are also expected to occur at this plate. The following fillet and plug weld stresses are calculated from the nodal forces.

Fillet Weld Stresses

The maximum nodal forces at node 491 (from ANSYS result file) are:

$$F_x = 124,800 \text{ lb.} \quad F_y = -11,840 \text{ lb.}$$

The fillet weld tensile/shear area, A_f is,

$$A_f = 3/12 [\pi(81.7) \times 3/16 \times 2] = 24.06 \text{ in}^2$$

Therefore, the tensile stress, σ_f is,

$$\sigma_f = 124,800 / 24.06 = 5,187 \text{ psi}$$

And the shear stress, τ_f , is,

$$\tau_f = 11,840 / 24.06 = 492 \text{ psi}$$

The maximum stress intensity, $S.I._f$, is,

$$S.I._f = [(5,187)^2 + 4 \times (492^2)]^{0.5} = 5,280 \text{ psi,}$$

Which is less than the allowable stress, $S_m = 20.0 \text{ ksi}$. The maximum shear stress, $\tau_{f\max}$, is,

$$\tau_{f\max} = [(5,187/2)^2 + 492^2]^{0.5} = 2,640 \text{ psi}$$

Which is less than the allowable shear stress, $0.6S_m = 0.6(20.0) = 12.0 \text{ ksi}$.

Plug Weld Stress

The maximum forces in the plug weld are the following.

Node	F_x (lb.)	F_y (lb.)
533	0	0
513	-110,100	-130,700
490	59,850	123,800
Total	-50,250	-6,900

The fillet weld shear area, A_b is,

$$A_b = 24 \text{ plugs} \times (1.0 \times 0.12) = 2.88 \text{ in}^2$$

Therefore, the tensile stress, σ_b is,

$$\sigma_b = 50,250/2.88 = 17,448 \text{ psi}$$

And the shear stress, τ_b , is,

$$\tau_b = 6,900/2.88 = 2,396 \text{ psi}$$

The maximum stress intensity, $S.I._b$, is,

$$S.I._b = [(17,448)^2 + 4 \times (2,396^2)]^{0.5} = 18,094 \text{ psi}$$

Which is less than the allowable stress, $S_m = 20.0$ ksi. The maximum shear stress, $\tau_{b\max}$, is,

$$\tau_{b\max} = [(17,448/2)^2 + 2,396^2]^{0.5} = 9,047 \text{ psi}$$

Which is less than the allowable shear stress, $0.6S_m = 0.6(20.0) = 12.0$ ksi.

3.9.6.7 Conclusions

Based on the results of the analysis, it is concluded that the outer shell structure is structurally adequate for the specified transfer loads.

3.9.6.8 References

1. American Society of Mechanical Engineers, ASME Boiler and Pressure Vessel Code, Section II, Part D, 1998, through 2000 addenda.
2. American Society of Mechanical Engineers, ASME Boiler and Pressure Vessel Code, Section III, Division 1, Subsection NC, 1998, through 2000 addenda.

Table 3.9.6-1
Summary of Calculated and Allowable Neutron Shield Shell Stresses

Load Case	Stress Category	Maximum Stress (ksi)	Allowable Stress (ksi)
3g Lifting	P_m	9.11	20.0
	$P_m + P_b$	21.47	30.0
Transfer Load	P_m	1.52	20.0
	$P_m + P_b$	15.99	30.0
	$P_m + P_b + Q$ (Cold)	21.21	60.0
	$P_m + P_b + Q$ (Hot)	20.6	60.0

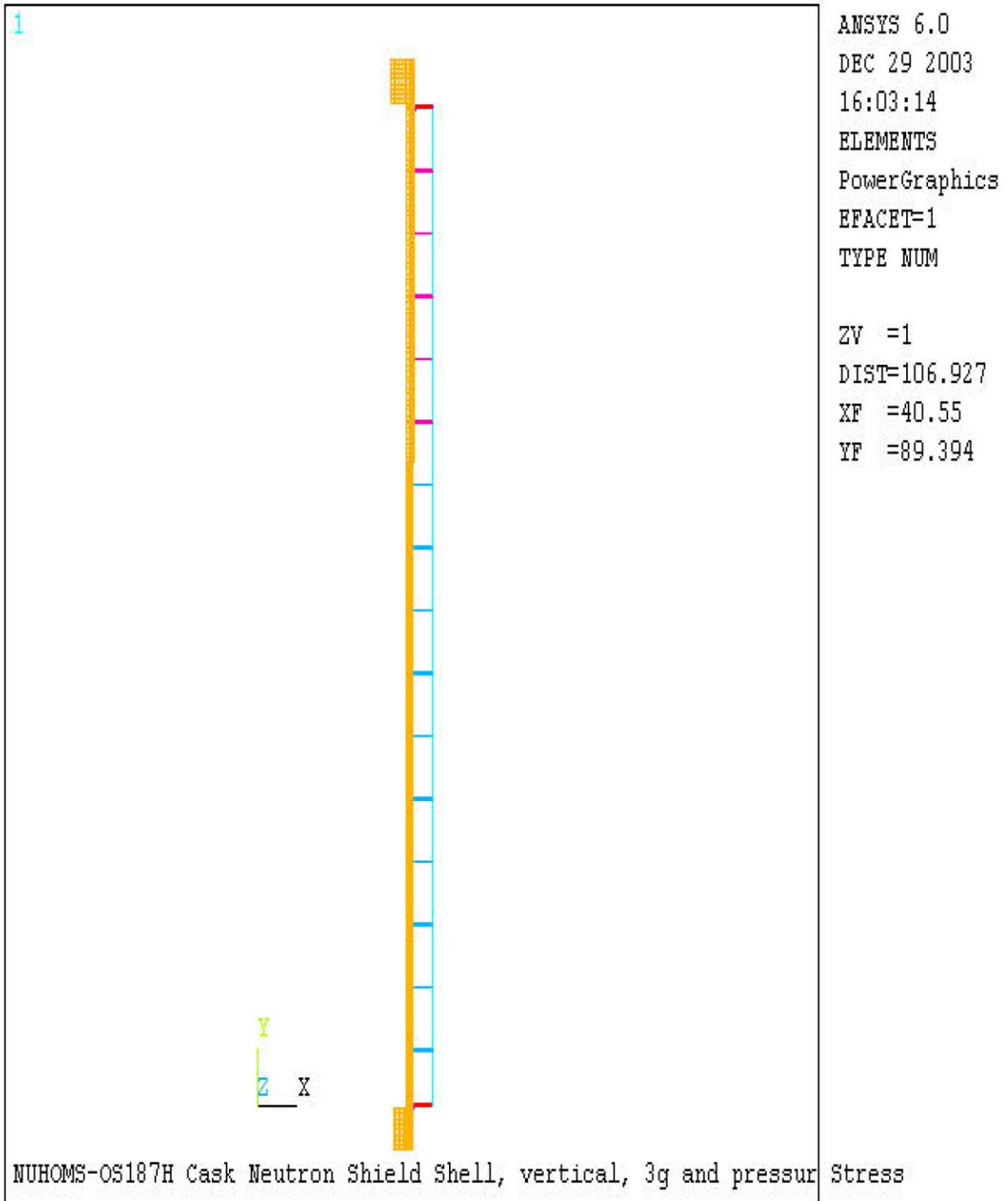


Figure 3.9.6-1
Neutron Shield Shell Finite Element Model

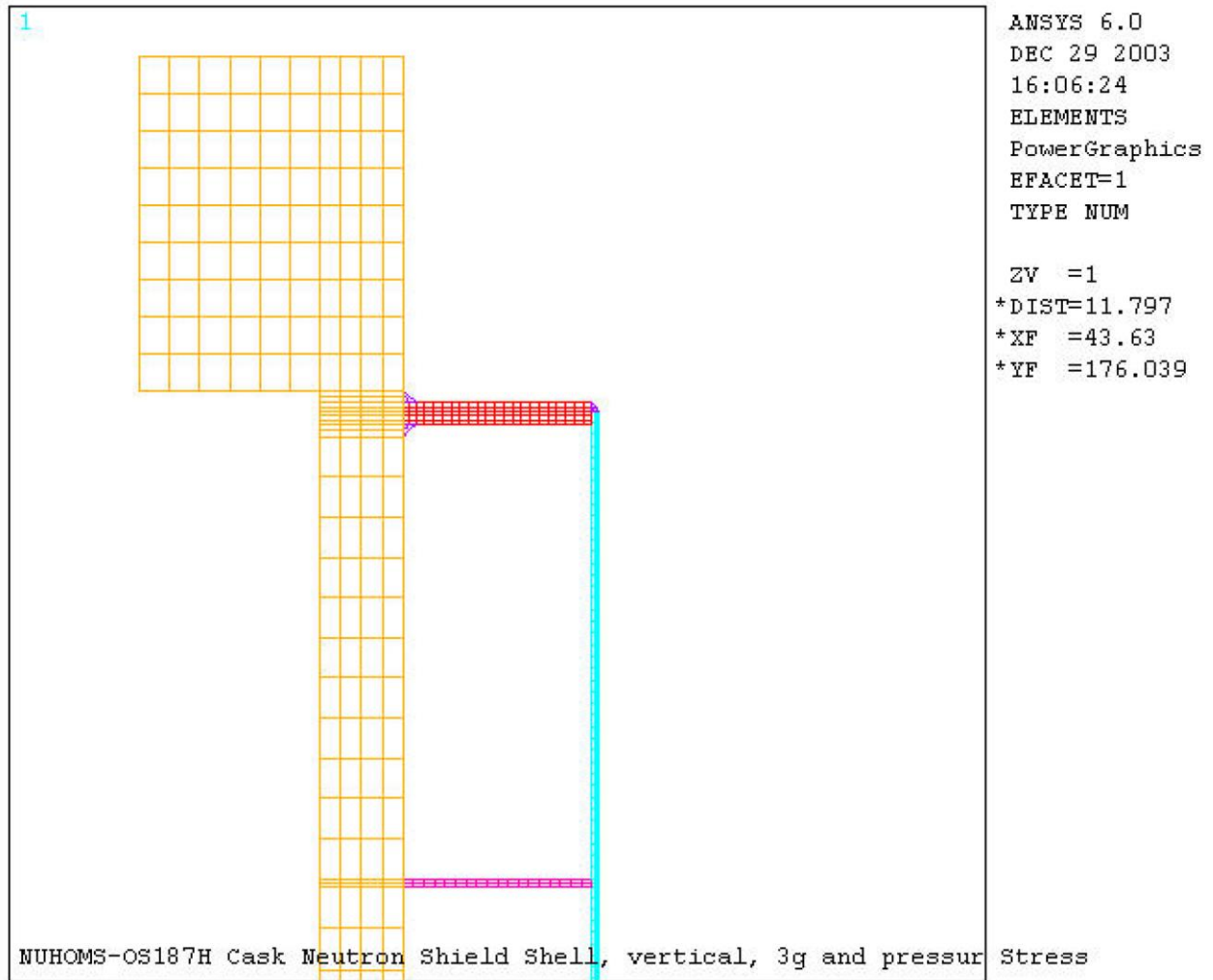


Figure 3.9.6-2
Neutron Shield Shell Finite Element Model, Top Plate Region

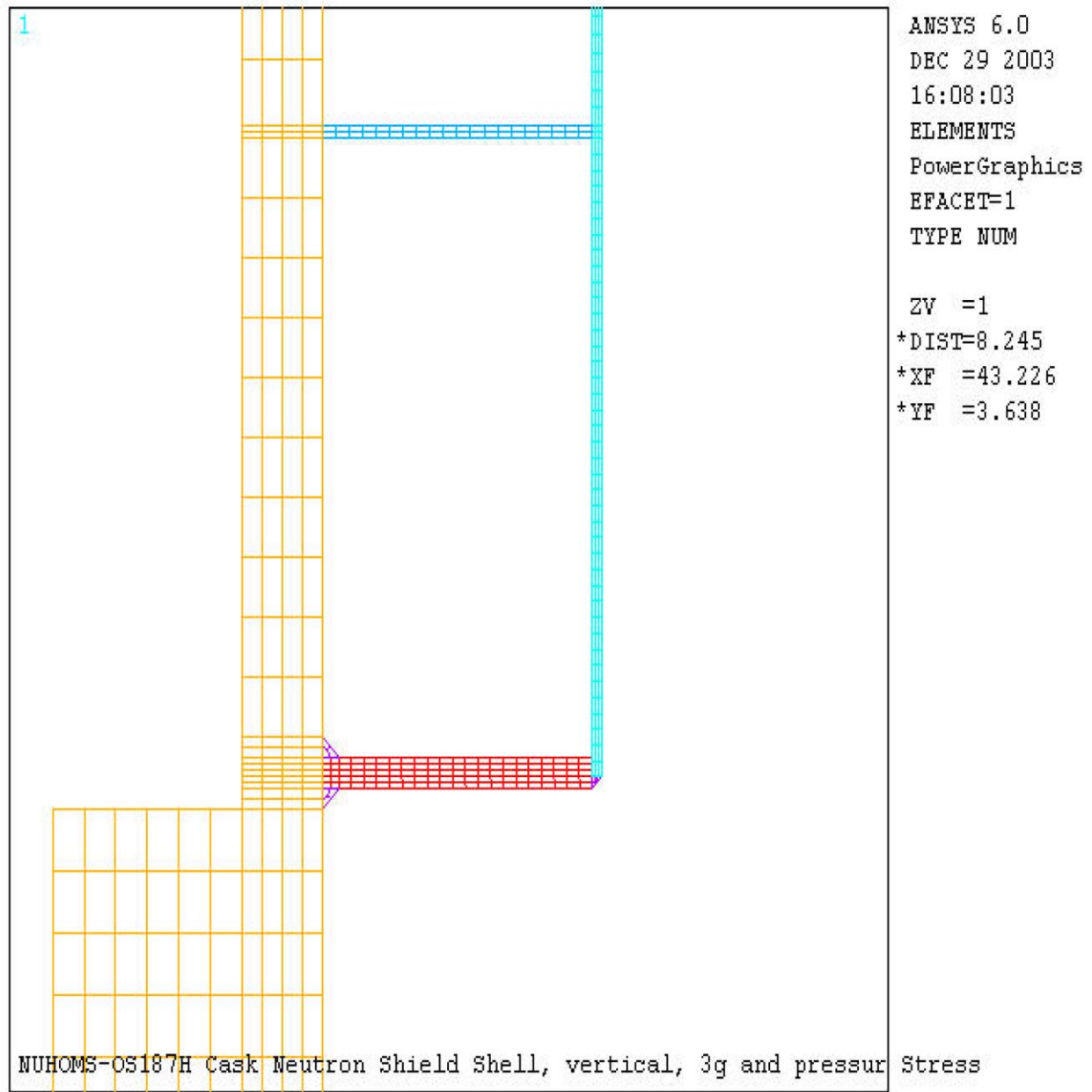


Figure 3.9.6-3
Neutron Shield Shell Finite Element Model, Bottom Plate Region

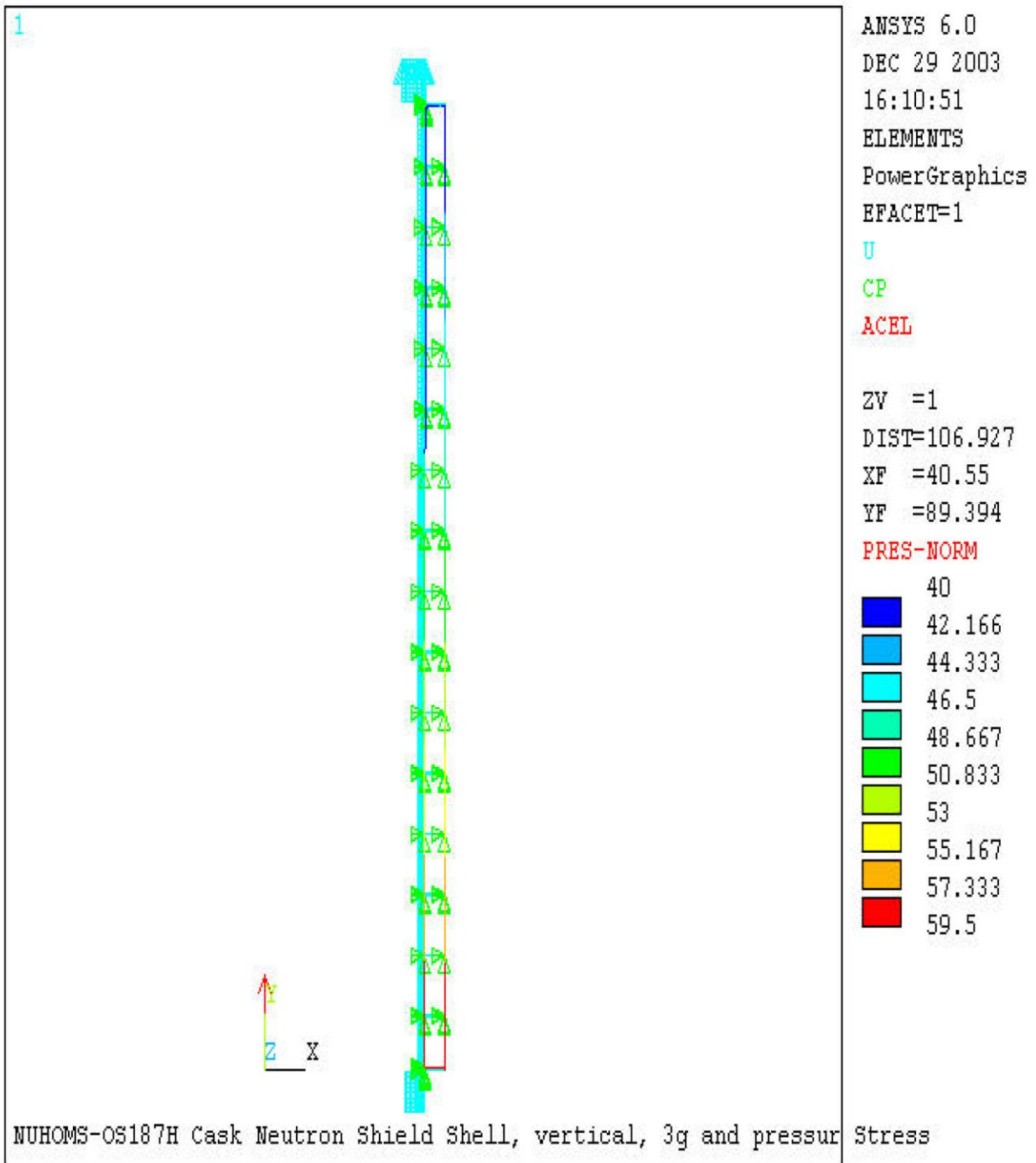


Figure 3.9.6-4
Neutron Shield Shell Finite Element Model, 3g Lifting Boundary Conditions

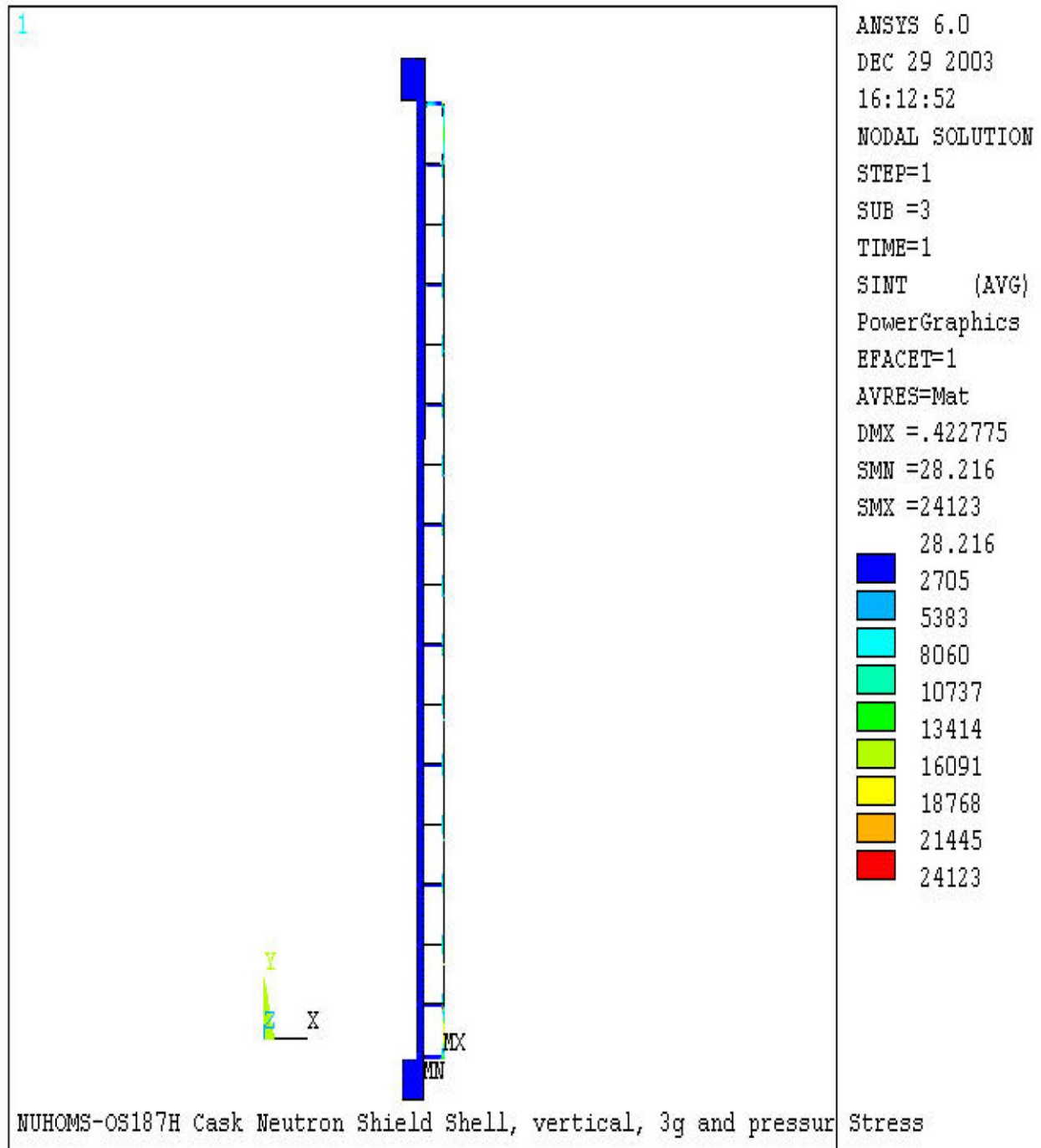


Figure 3.9.6-5
3g Lifting Stress Intensity Distribution

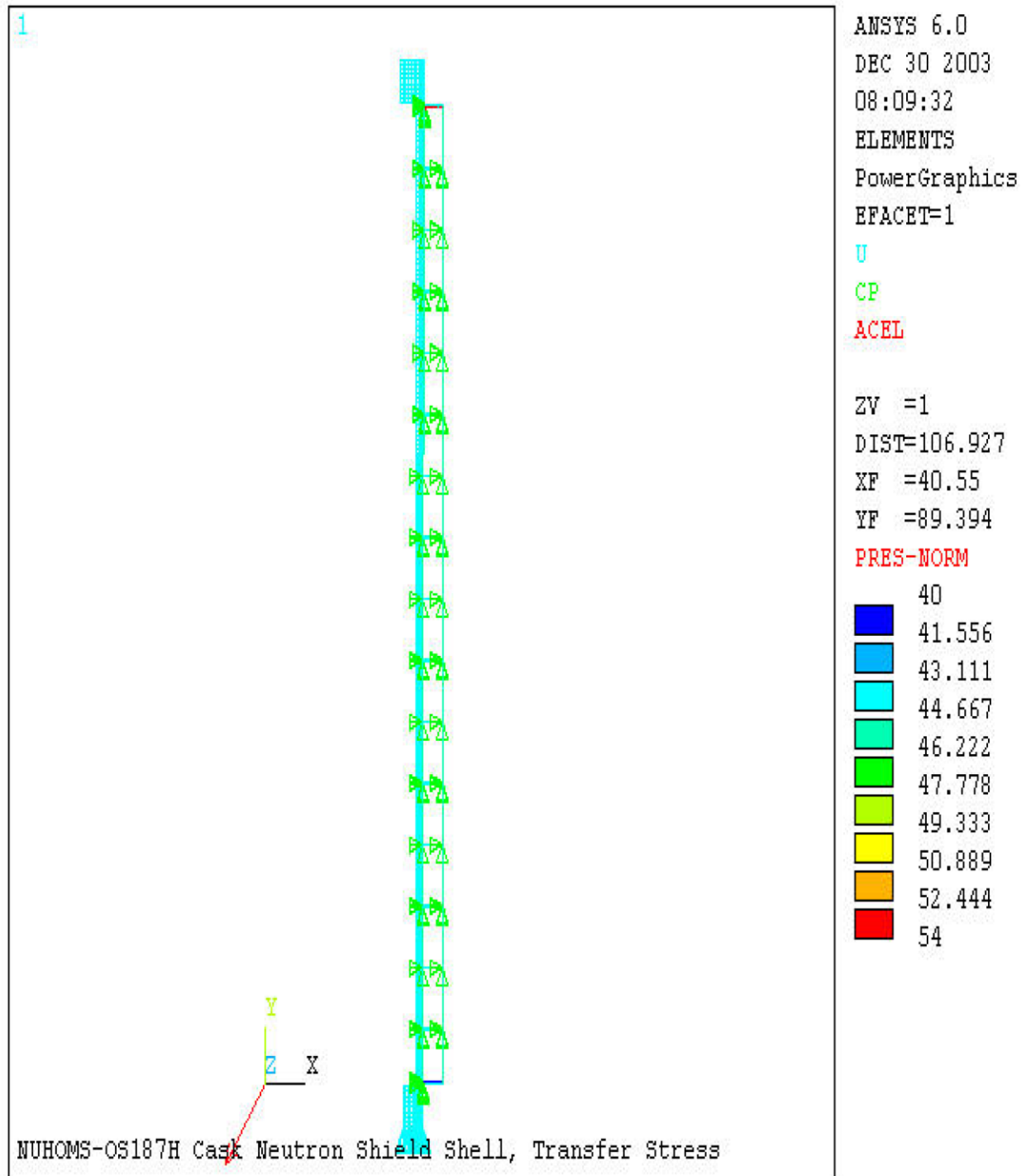


Figure 3.9.6-6
Neutron Shield Shell Finite Element Model, Transfer Loads Boundary Conditions

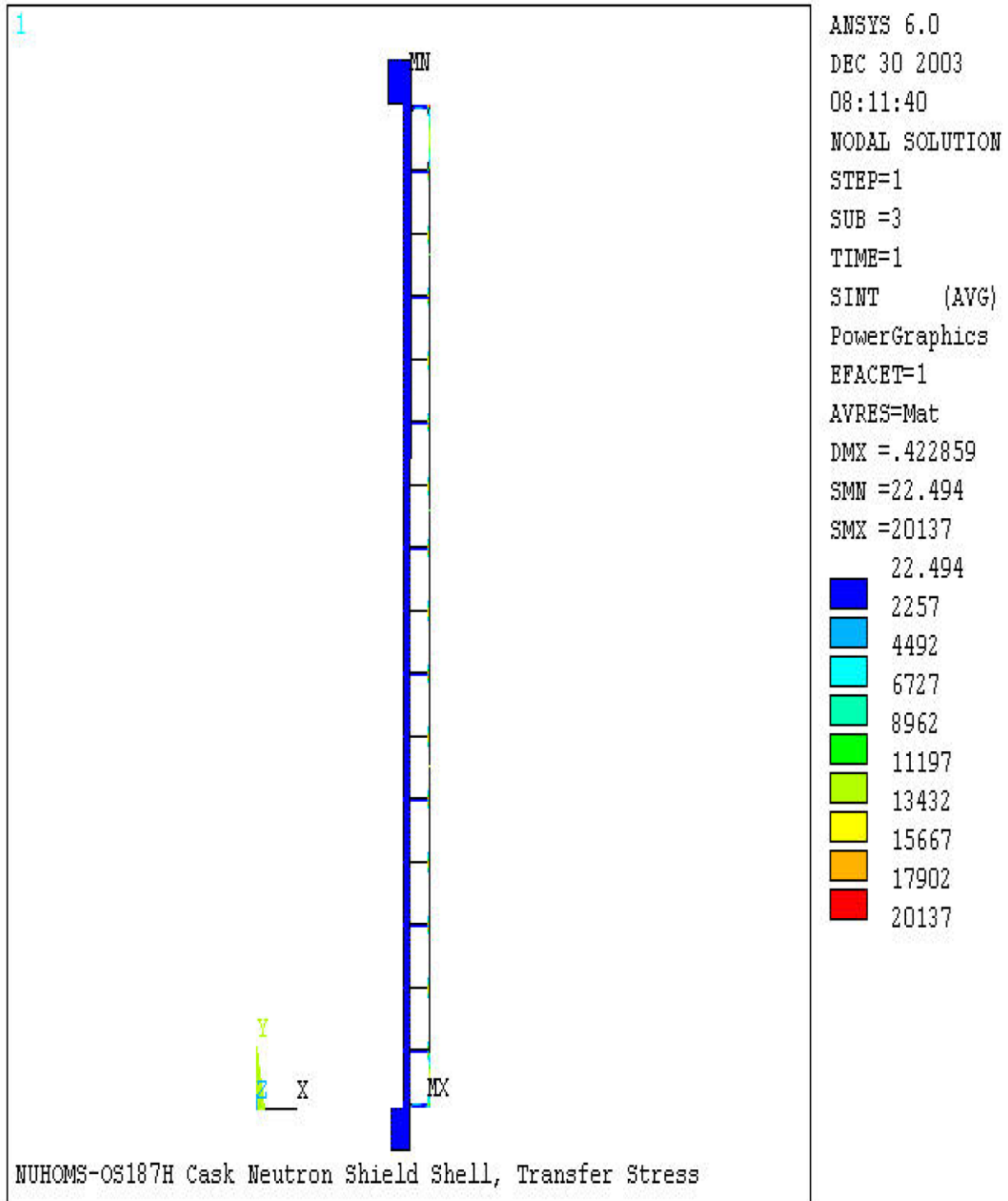


Figure 3.9.6-7
Transfer Loads Stress Intensity Distribution

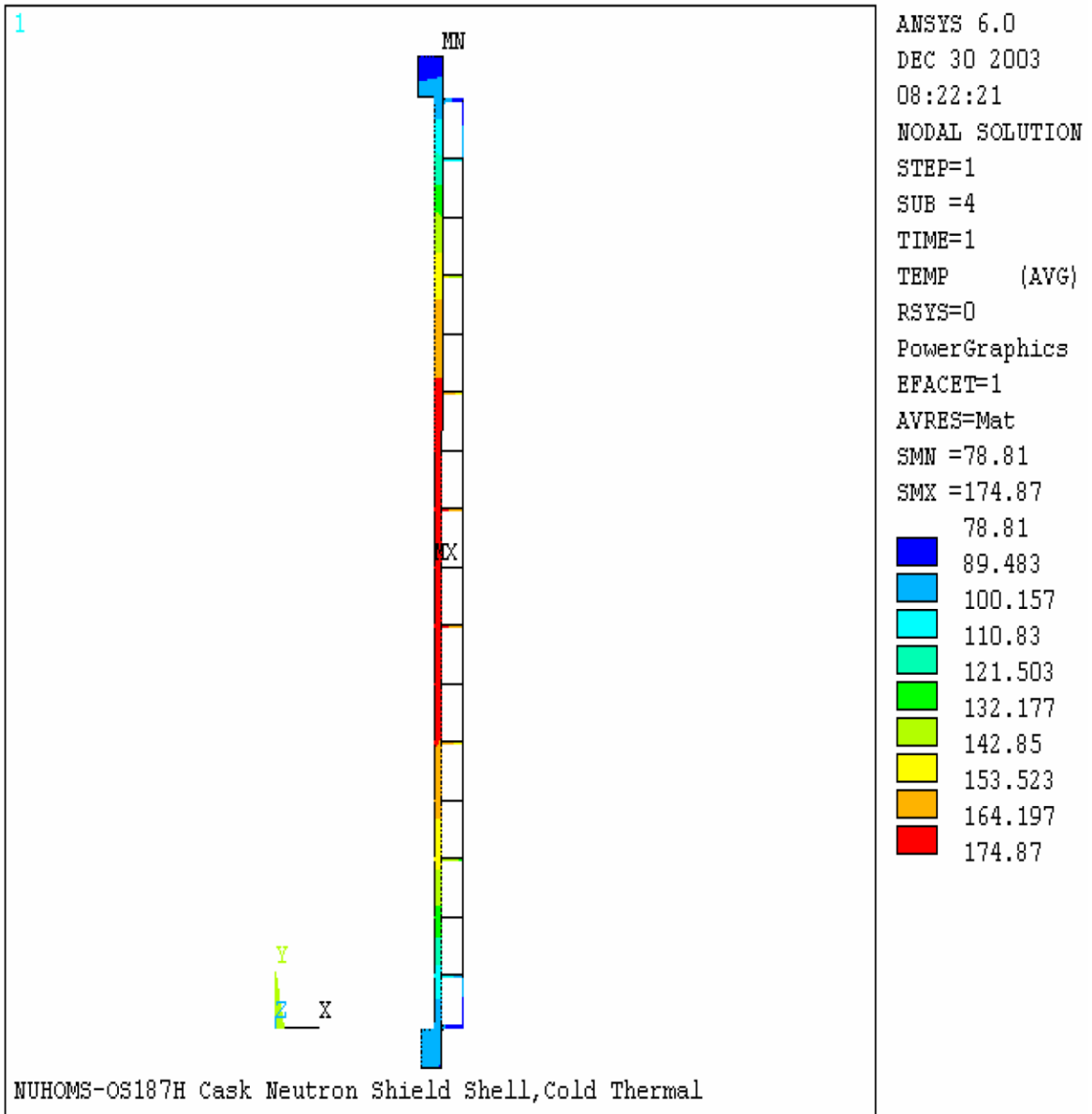


Figure 3.9.6-8
Cold Ambient Environment Temperature Distribution

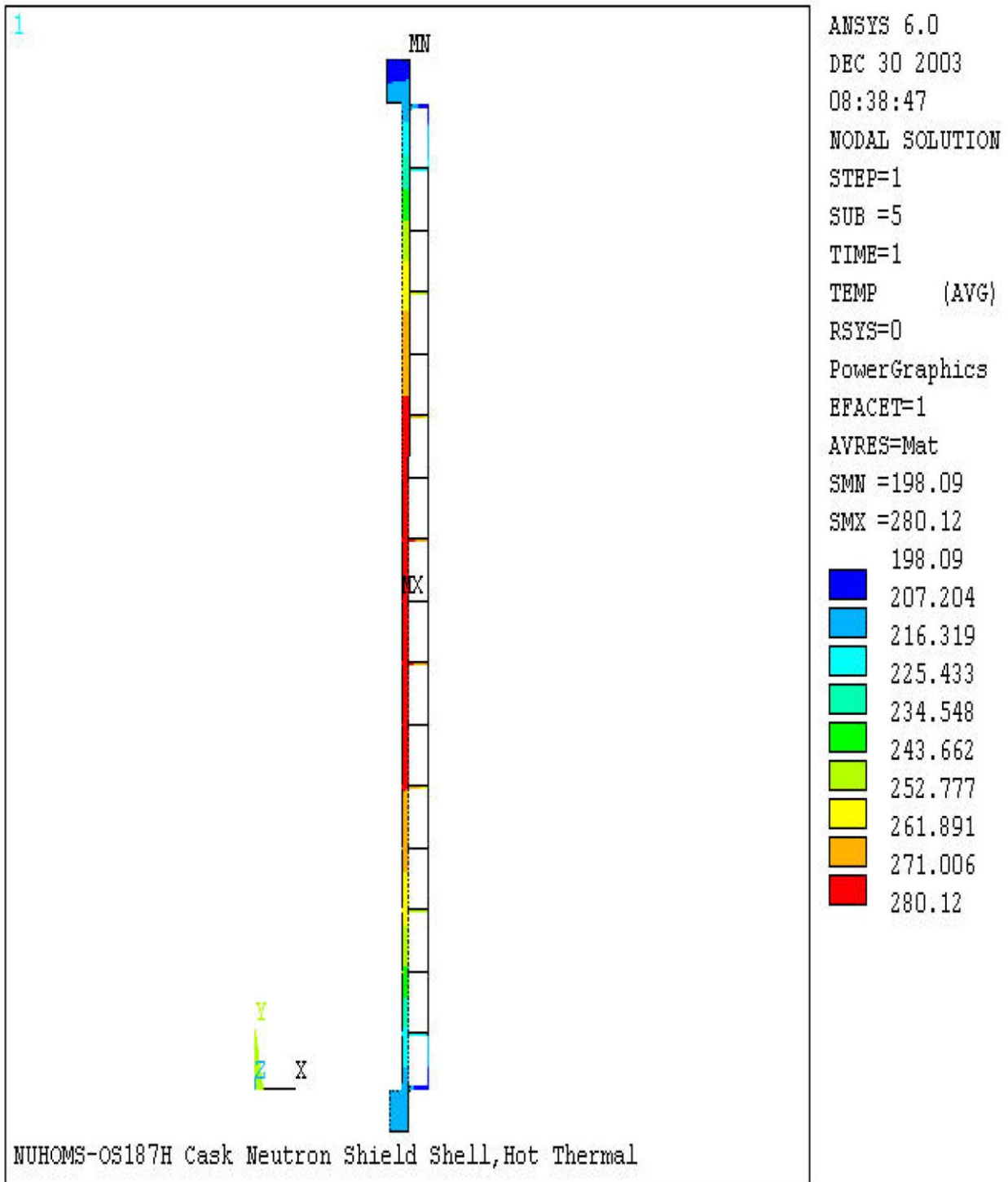


Figure 3.9.6-9
Hot Ambient Environment Temperature Distribution

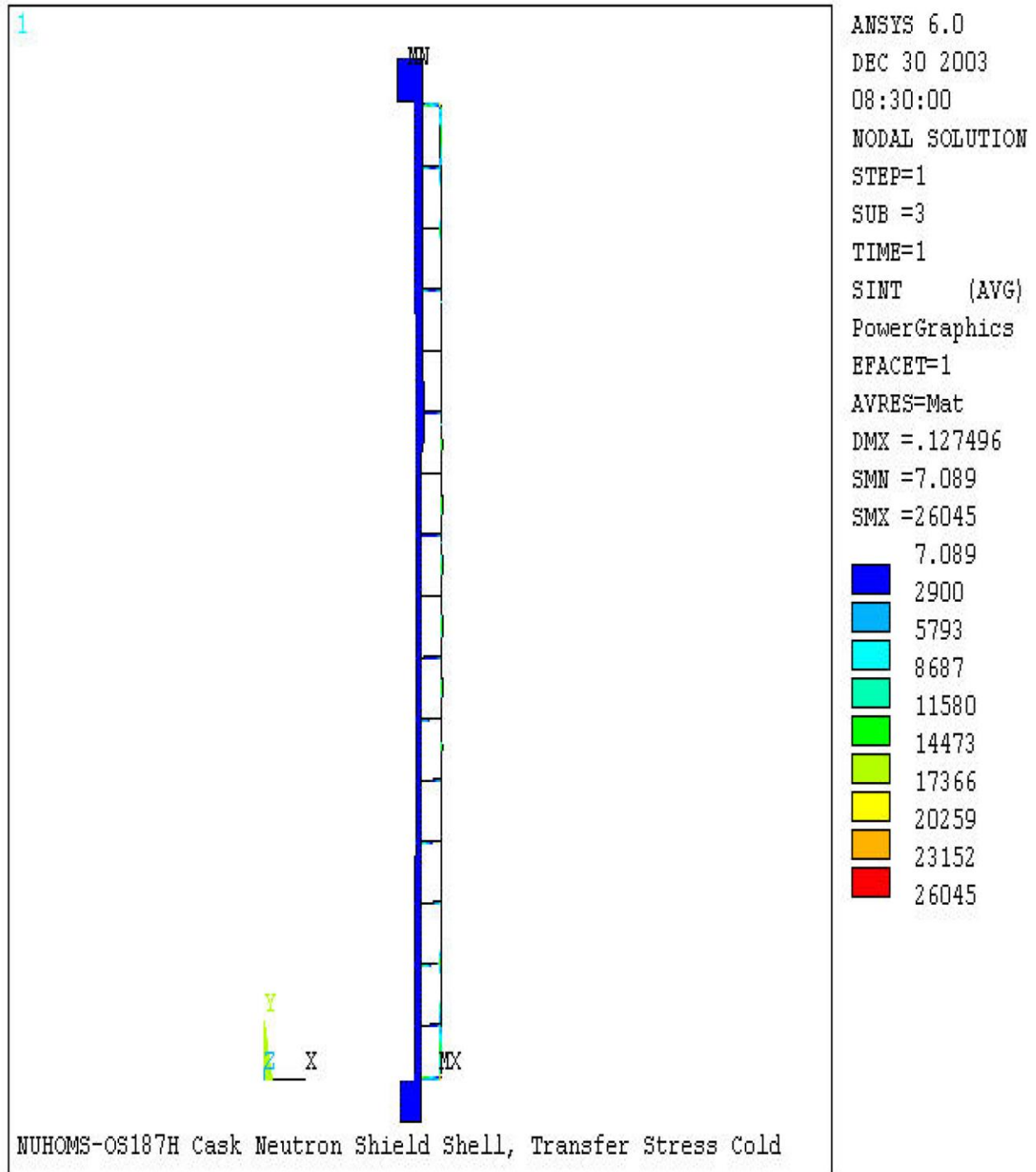


Figure 3.9.6-10
Transfer Loads plus Cold Ambient Condition Stress Intensity Distribution

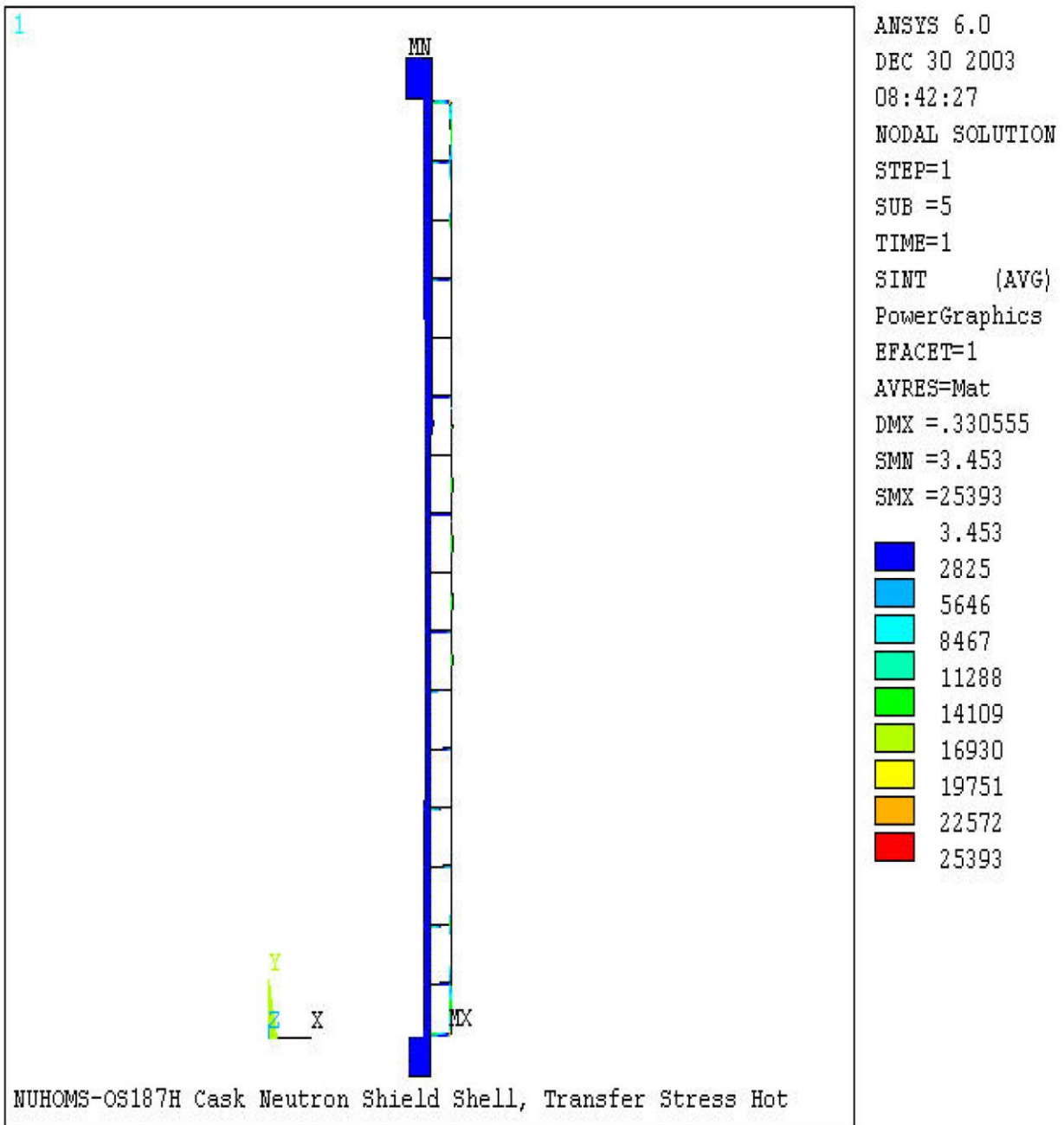


Figure 3.9.6-11
Transfer Loads plus Hot Ambient Condition Stress Intensity Distribution

APPENDIX 3.9.7
OS187H TRANSFER CASK IMPACT ANALYSIS

TABLE OF CONTENTS

3.9.7	OS187H TRANSFER CASK IMPACT ANALYSIS.....	3.9.7-1
3.9.7.1	Introduction.....	3.9.7-1
3.9.7.2	Material Properties.....	3.9.7-1
3.9.7.3	Component Weights.....	3.9.7-2
3.9.7.4	Geometry and Nomenclature.....	3.9.7-2
3.9.7.5	Ultimate Capacity of Slab	3.9.7-3
3.9.7.6	End Drop Impact Analysis.....	3.9.7-4
3.9.7.7	Side Drop Impact Analysis.....	3.9.7-6
3.9.7.8	Corner Drop Impact Analysis.....	3.9.7-8
3.9.7.9	Conclusions.....	3.9.7-9
3.9.7.10	References	3.9.7-10

LIST OF TABLES

Table 3.9.7-1	Spreadsheet for 80 inch Side Drop Impact Load Calculations (Using Non-Linear S vs. g relationship)	3.9.7-11
Table 3.9.7-2	C. G. Over Corner Drop – L Calculations	3.9.7-12
Table 3.9.7-3	C. G. Over Corner Drop – Area Calculations	3.9.7-13
Table 3.9.7-4	C. G. Over Corner Drop – Energy Calculations	3.9.7-14

LIST OF FIGURES

Figure 3.9.7-1	Force vs. Displacement – End Drop	3.9.7-15
Figure 3.9.7-2	S vs. g Curve for 80 inch Height Side Drop	3.9.7-16
Figure 3.9.7-3	Geometry of C. G. Over Corner Drop	3.9.7-17
Figure 3.9.7-4	Geometry of C. G. Over Corner Drop	3.9.7-18
Figure 3.9.7-5	Geometry of the C. G. Over Corner Drop - Area Calculation	3.9.7-19
Figure 3.9.7-6	C. G. Over Corner Drop – L Dimension Calculation	3.9.7-20

3.9.7 OS187H TRANSFER CASK IMPACT ANALYSIS

3.9.7.1 Introduction

The purpose of this appendix is to present the evaluation of the peak decelerations of NUHOMS® OS187H Transfer Cask during impact, subsequent to the hypothetical accident drop onto the concrete pad/soil system during transfer operations. The hypothetical accident condition drop consists of 80 inch end drop, side drop and center of gravity (C.G.) over corner drop. The 80 inch end drop and CG over corner drop are not credible events under 10CFR72 storage and transfer operations. However, these analyses are included to support credible accidents under 10CFR50. The fuel cladding integrity has not been demonstrated for these accident scenarios. An additional safety review by the user is required to demonstrate fuel cladding integrity under 10CFR50.

For the impact analysis, the transfer cask is assumed rigid as compared to the flexibility of the concrete slab/soil system. The methodology described in Reference 1 is used in this evaluation.

The cask is approximated by a cylinder 197.07 inches long and 81.7 inches in diameter. The effect of the outer shield shell, which is very thin relative to the main structural body of the transfer cask, is neglected. Also, small variations around top cover and cylinder are neglected. The stiffness variation due to the neglected items of the transfer cask is negligible.

The OS187H Transfer Cask is assumed to impact a 36 inch thick concrete pad, with #11 rebar on 12" spacing, at top and bottom of the pad, and 2" coverage.

3.9.7.2 Material Properties

The following material properties, taken from Reference 1, are assumed to model the design basis concrete pad and soil foundation.

E_c = Concrete elastic modulus = 3.6×10^6 psi.

σ_u = Ultimate concrete strength = 4,000 psi.

E_s = Sub-soil modulus = 60,000 psi. (higher value gives higher g load)

S_y = Rebar yield strength = 60,000 psi.

ν_c = Poisson's ratio of concrete = 0.17

ν_s = Poisson's ratio of soil = 0.49

3.9.7.3 Component Weights

The 32PTH DSC and OS187H Transfer Cask component weights are tabulated in Section 3.2. The following component weights relevant to this analysis are summarized below.

Empty Canister Weight = 28.19 kips

Fuel Basket Weight = 29.85 kips

Fuel Assembly Weight (32) = 51.52 kips

Transfer Cask Weight = 119.95 kips

Total Weight, $W = 229.52$ kips.

For conservative estimating the g load, a lower weight, 226.9 kips, is used for the impact analysis (lower weight gives higher g load).

3.9.7.4 Geometry and Nomenclature

The technical data used for transfer cask and concrete slab/soil system are:

W = Weight of cask = 226,900 lbs

R = Cask outer radius = $81.7/2 = 40.85$ in

A = cask foot print area = $\pi (40.85)^2 = 5,242.4$ in²

L = cask length = 197.07 in.

E_c = Concrete elastic modulus = 3.6×10^6 psi

σ_u = Ultimate concrete strength = 4,000 psi

ν_c = Poisson's ratio of concrete = 0.17

h_c = Concrete pad thickness = 36 inches

S_y = Rebar yield strength = 60,000 psi

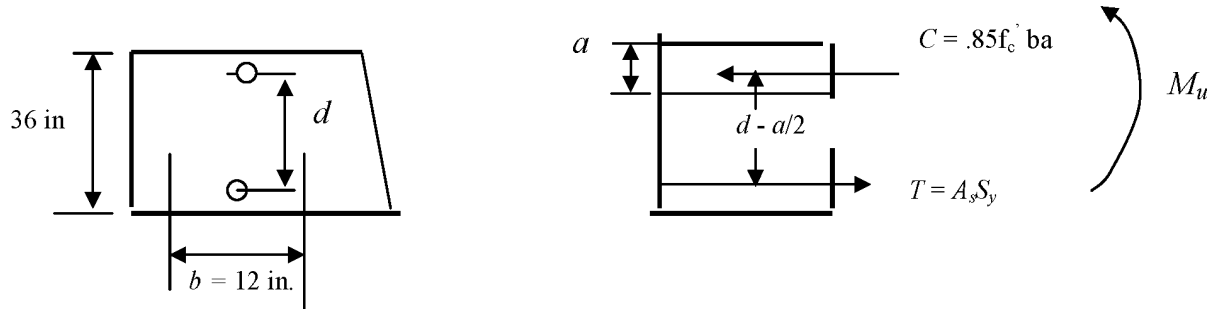
E_s = Sub-soil modulus = 60,000 psi (high value of E_s gives higher g load)

ν_s = Poisson's ratio of soil = 0.49

A_s = Rebar (#11) area = $\pi/4 (1.41)^2 = 1.56$ in²

3.9.7.5 Ultimate Capacity of Slab

The ultimate bending capacity of reinforced cement concrete slab, M_u , is computed based on a 1 foot wide pad with a thickness of 36 in., #11 Rebar @ 12 inch spacing and a 2 inch cover. For a 36 inch thick concrete slab, the steel in compression zone is assumed to have no effect and is neglected.



Average depth of steel, d , is the following.

$$d = 36 - 4 - 1.41 = 30.59 \text{ in}$$

Therefore,

$$C = T = A_s S_y = 0.85 f'_c b a$$

$$a = A_s S_y / 0.85 f'_c b = 1.56 \times 60,000 / 0.85 \times 4000 \times 12 = 2.294 \text{ in}$$

$$M_u = A_s S_y (d - a/2) = 1.56 \times 60,000 (30.59 - 2.294/2) = 2.7559 \times 10^6 \text{ in-lb/ft width of slab}$$

3.9.7.6 End Drop Impact Analysis

The results of EPRI NP-7551 report [1] are presented in terms of a target hardness number, S . In general this is given by the following.

$$S = \frac{M_u \sigma_u A}{W^2 \delta_e}$$

Where,

M_u = Ultimate moment capacity of 1 foot section of slab = 2.7559×10^6 in-lb/ft

σ_u = Ultimate concrete strength = 4,000 psi

A = Area of impact surface = 5,242.4 in²

W = Weight of cask = 226,900 lbs

δ_e = Deflection of cask under weight of cask (1g), in

The deflection, δ_e , is given as:

$$\delta_e = \frac{W}{2Rk} (1 - e^{-\beta R} \cos(\beta R))$$

Where,

$$k = \frac{\pi E_s}{1 - \nu_s^2} = \frac{\pi(60,000)}{1 - 0.49^2} = 248,053 \text{ psi/in}$$

$$\beta = \left(\frac{E_s}{4D_c} \right)^{1/4} = \left(\frac{60,000}{4 \times 14,413 \times 10^6} \right)^{1/4} = 0.03194$$

$$D_c = \frac{E_c h^3}{12(1 - \nu_c^2)} = \frac{3.6(10)^6 (36)^3}{12(1 - 0.17^2)} = 14,413 \times 10^6 \text{ in-lbs}$$

Therefore,

$$\delta_e = \frac{226,900}{2 \times 40.85 \times 248,053} (1 - e^{-0.03194 \times 40.85} \cos 0.03194 \times 40.85) = 0.0104 \text{ in}$$

Then,

$$S = \frac{M_u \sigma_u A}{W^2 \delta_e} = \frac{2.7559 \times 10^6 \times 4,000 \times 5,242.4}{226,900^2 \times 0.0104} \approx 10.793 \times 10^4$$

Conservatively using upper bound of Figure 28 from Reference 1 for an 80 inch drop height, the peak force is 49g (\times weight). To calculate the maximum deformation of the concrete, the force-deformation curve (Figure 3.9.7-1) is obtained by interpolating the data shown on Figure 14 of the EPRI report [1]. From Figure 3.9.7-1, the displacement at the end of elastic phase is about 0.4 inch and elastic-plastic displacement is about 1.0 inch.

We now use energy method to compute final deformation. Using the force – displacement plot on Figure 3.9.7-1 (interpolating $S = 107,930$). It is assumed that displacements beyond 1 inch are fully plastic.

Let x be the final plastic deformation. Then, the energy absorbed by target, E_{ab} , is equal to the Area under the Curve (see Figure 3.9.7-1). Therefore,

$$E_{ab} = W [(27.5 \times 0.4/2) + (27.5 + 39.0)/2 (0.66 - 0.44) + (39.0 + 48.3)/2 (1.0 - 0.66) + 49(x - 1.0)]$$

The potential energy of the drop, E_{drop} , is,

$$E_{drop} = W [H + x + 1] = W [81 + x]$$

Equating $E_{ab} = E_{drop}$, gives the following.

$$5.5 + 8.65 + 14.84 + 49x - 49 = 81 + x$$

$$\Rightarrow x = 2.10 \text{ in}$$

Therefore, the total displacement is,

$$\text{Displacement} = 1.0 + 2.10 = 3.10 \text{ in}$$

3.9.7.7 Side Drop Impact Analysis

The side drop analysis is conducted in the same manner as for the end drop, except that the expression for δ_e varies, and the target area changes as the depth of penetration increases. Using Reference 1 to evaluate δ_e , we get,

$$I_c = \frac{Lh^3}{12} = 197.07 \times \frac{36^3}{12} = 766,208 \text{ in}^4$$

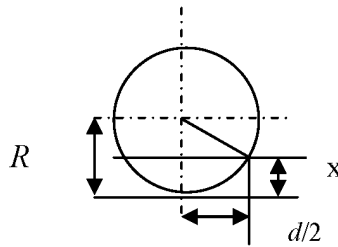
$$\beta = \left(\frac{E_s}{4E_c I_c} \right)^{1/4} = \left(\frac{60,000}{4 \times 3.6 \times 10^6 \times 766,208} \right)^{1/4} = 0.00859 \text{ in}^{-1}$$

$$k = E_s = 60,000 \text{ lb/in}^2$$

$$\delta_e = \frac{W\beta}{2k} = \frac{226,900 \times 0.00859}{2 \times 60,000} = 0.01624 \text{ in}$$

$$S = \frac{M_u \sigma_u A}{W^2 \delta_e} = \frac{2.7559 \times 10^6 \times 4,000 \times A}{226,900^2 \times 0.01624} = 13.18464 A$$

The following sketch shows the geometry of the transfer cask side drop



Where,

$$d/2 = [R^2 - (R - x)^2]^{0.5} = [2Rx - x^2]^{0.5}$$

The impact surface area, A , as a function of the penetration depth is,

$$A = 2 \times 197.07 [81.7 x - x^2]^{0.5} = 394.14 \times [81.7 x - x^2]^{0.5}$$

$$S = 13.18464 A$$

The following data is obtained from Figure 28 of Reference 1.

Target Hardness, S	Acceleration, g
0	6
10,000	17.5
20,000	25.0
30,000	29.8
40,000	33.5
50,000	37.0
60,000	40.0
70,000	43.3
80,000	46.0
90,000	47.8
100,000	49.0

This S vs. g curve is plotted in Figure 3.9.7-2. A spread sheet solution is carried out by incrementing x (penetration depth) to obtain the absorbed energy equal to drop energy. The following steps are carried out on the spreadsheet:

1. Select x
2. Compute Area, $A = 394.14 \times [81.7 x - x^2]^{0.5}$
3. Compute $S = 13.18464 A$
4. Obtain g from Figure 3.9.7-2 for computed S
5. Compute Force, $F = W \times g$
6. Compute Energy Increment, $\Delta E = [1/2(F_i + F_{i-1})] (x_i - x_{i-1})$
7. Add ΔE to the previous to obtain current total absorbed energy
8. Compute total drop energy = $W (80 + x)$
9. Keep incrementing x until total absorbed energy is equal to the drop energy.

The resulting spreadsheet for the side drop impact is given on Table 3.9.7-1.

From Table 3.9.7-1, it is seen that, when the target deformation is 2.46 inches, the total absorbed energy is approximately equal to the drop energy. The g load at this deformation is 44g.

3.9.7.8 Corner Drop Impact Analysis

The C. G. over corner drop is performed in a similar manner as the side drop. For the corner drop, both δ_e and impact area are a function of the penetration depth into the target.

$$\delta_e = \frac{W\beta}{2k} = \frac{226,900 \times \beta}{2 \times 60,000} = 1.8908 \beta$$

And

$$\beta = \left(\frac{E_s}{4E_c I_c} \right)^{1/4} = \left(\frac{60,000}{4 \times 3.6 \times 10^6} \right)^{1/4} \times \left(\frac{1}{I_c} \right)^{1/4} = \frac{0.254}{I_c^{1/4}}$$

$$I_c = \frac{Lh^3}{12} = L \times \frac{36^3}{12} = 3,888 L$$

The geometry relations used to evaluate of the impact area as a function of the deformation into the target are shown in Figure 3.9.7-3 to Figure 3.9.7-6. The area, A, as a function of deformation is shown in Figure 3.9.7-5. Table 3.9.7-3 tabulates the results of the ‘area vs. deformation’ calculations, using a small ANSYS input file.

The next quantity that is needed is the deflection, δ_e . This deflection will occur as a result of only a small portion of the transfer cask being in contact with the target surface, with the area increasing as δ_e increases. The above L dimension calculation is developed in Figure 3.9.7-6.

$$L = 2 \left[\left(\frac{2R\delta_e}{\cos 67.48^\circ} \right) - \left(\frac{\delta_e^2}{\cos^2 67.48^\circ} \right) \right]^{1/2} \quad (\text{See Figure 3.9.7-3 for drop angle calculation})$$

$$= 2[213.316\delta_e - 6.8166\delta_e^2]^{1/2}$$

To solve for L, iteratively, this is done in the spreadsheet given in Table 3.9.7-2. Which give

$$\delta_e = 0.03922, \quad L = 5.7815 \text{ in}$$

Using Reference 1, the target hardness number, S , is

$$S = \frac{M_u \sigma_u A}{W^2 \delta_e} = \frac{2.7559 \times 10^6 \times 4,000 \times A}{226,900^2 \times 0.03922} = 5.4594 A$$

A spread sheet solution is carried out by incrementing Δ (penetration depth as shown in Figure 3.9.7-3) to obtain the Absorbed Energy that is equal to Drop Energy. The following steps are carried out in the spreadsheet:

1. Select Δ
2. Obtain Area, A , from Table 3.9.7-3
3. Compute $S = 5.4594 A$
4. Obtain g from Figure 3.9.7-2
5. Compute Force, $F = W \times g$
6. Compute Energy Increment, $\Delta E = [1/2(F_i + F_{i-1})] (\Delta_i - \Delta_{i-1})$
7. Add ΔE to the previous to obtain current total absorbed energy
8. Compute total drop energy = $W (80 + x)$
9. Keep incrementing x till total absorbed energy is equal to the drop energy

The spreadsheet is given on Table 3.9.7-4. It is seen from this table that at a target deformation of 6.5 inches, the total absorbed energy is equal to the drop energy and the g load for this deformation is 15.9g.

3.9.7.9 Conclusions

The following table summarizes the results of the analysis described above.

Drop Orientation	Peak Deceleration (gs)	Target Penetration Depth (in.)
End Drop	49	3.10
Side Drop	44	2.5
Corner Drop	15.9	6.5

3.9.7.10 References

1. “Structural Design of Concrete Storage Pads for Spent Fuel Casks”, EPRI NP-7551, August 1991 by Rashid, Nickell and James.

Table 3.9.7-1
Spreadsheet for 80 inch Side Drop Impact Load Calculations
(Using Non-Linear S vs. g relationship)

x	A	S	g	F	ΔE	Energy Absorbed	Drop Energy
0	0	0	0	0	0	0	18,152,000
0.5	2511.4	33,112	31.0	7,033,900	1,758,475	1,758,475	18,265,450
1	3540.7	46,683	36.0	8,168,400	3,800,575	5,559,050	18,378,900
1.5	4323.0	56,997	39.0	8,849,100	4,254,375	9,813,425	18,492,350
2	4976.2	65,609	42.0	9,529,800	4,594,725	14,408,150	18,605,800
2.1	5095.9	67,187	42.5	9,643,250	958,653	15,366,803	18,628,490
2.2	5212.5	68,725	42.9	9,734,010	968,863	16,335,666	18,651,180
2.3	5326.3	70,225	43.2	9,802,080	976,804	17,312,470	18,673,870
2.4	5437.4	71,690	43.5	9,870,150	983,612	18,296,082	18,696,560
2.42	5459.3	71,979	43.7	9,915,530	197,857	18,493,938	18,701,098
2.44	5481.2	72,267	43.8	9,938,220	198,538	18,692,476	18,705,636
2.46	5502.9	72,554	43.9	9,960,910	198,991	18,891,467	18,710,174
2.5	5546.0	73,123	44.0	9,983,600	398,890	19,290,357	18,719,250
2.51	5556.8	73,264	44.1	10,006,290	99,949	19,390,307	18,721,519
2.52	5567.5	73,405	44.15	10,017,635	100,120	19,490,426	18,723,788
2.53	5578.2	73,546	44.2	10,028,980	100,233	19,590,659	18,726,057
2.54	5588.8	73,687	44.24	10,038,056	100,335	19,690,995	18,728,326
2.55	5599.5	73,827	44.28	10,047,132	100,426	19,791,421	18,730,595

Table 3.9.7-2
C. G. Over Corner Drop – L Calculations

L_{initial}	I_c	β	δ_e	L_{final}
6	23328	0.020552	0.0388606	5.75475522
5.9	22939.2	0.020639	0.0390243	5.766842939
5.8	22550.4	0.020727	0.0391914	5.779163276
5.7	22161.6	0.020818	0.0393622	5.791724835
5.75	22356	0.020772	0.0392763	5.785413347
5.76	22394.88	0.020763	0.0392593	5.784158456
5.77	22433.76	0.020754	0.0392422	5.782906012
5.78	22472.64	0.020745	0.0392253	5.781656007
5.781	22476.53	0.020744	0.0392236	5.78153114
5.7815	22478.47	0.020744	0.0392227	5.781468716

Table 3.9.7-3
C. G. Over Corner Drop – Area Calculations

Δ	Δ_{CL}	α_{max}	α_{min}	Area, A
0.5	-15.146	37.942	36.529	19.361
1	-14.646	38.150	35.323	54.494
1.5	-14.146	38.357	34.117	99.620
2	-13.646	38.564	32.911	152.613
2.5	-13.146	38.772	31.705	212.213
3	-12.646	38.979	30.500	277.544
3.5	-12.146	39.186	29.294	347.950
4	-11.646	39.394	28.088	422.905
4.5	-11.146	39.601	26.882	501.977
5	-10.646	39.808	25.676	584.796
5.5	-10.146	40.015	24.470	671.043
6	-9.646	40.223	23.264	760.435
6.5	-9.146	40.430	22.058	852.716
7	-8.646	40.637	20.852	947.656
7.5	-8.146	40.845	19.646	1045.042
8	-7.646	41.052	18.440	1144.679
8.5	-7.146	41.259	17.234	1246.381
9	-6.646	41.467	16.028	1349.978
9.5	-6.146	41.674	14.822	1455.306
10	-5.646	41.881	13.617	1562.209
10.5	-5.146	42.089	12.411	1670.539
11	-4.646	42.296	11.205	1780.153
11.5	-4.146	42.503	9.999	1890.915
12	-3.646	42.710	8.793	2002.689
12.5	-3.146	42.918	7.587	2115.347
13	-2.646	43.125	6.381	2228.761
13.5	-2.146	43.332	5.175	2342.808
14	-1.646	43.540	3.969	2457.364
14.5	-1.146	43.747	2.763	2572.310
15	-0.646	43.954	1.557	2687.526
15.5	-0.146	44.162	0.351	2802.894
16	0.354	44.369	-0.855	2918.295
16.5	0.854	44.576	-2.060	3033.611
17	1.354	44.784	-3.266	3148.725
17.5	1.854	44.991	-4.472	3263.517
18	2.354	45.198	-5.678	3377.868
18.5	2.854	45.406	-6.884	3491.655
19	3.354	45.613	-8.090	3604.757
19.5	3.854	45.820	-9.296	3717.048
20	4.354	46.027	-10.502	3828.400

Table 3.9.7-4
C. G. Over Corner Drop – Energy Calculations

Δ	AREA, A	S	g	Force, F	Energy Inc.	Total energy	Drop Energy
0.00	0	0	-	0	0	0	18,152,000
0.50	19.361	105.70	14.04	3,186,193	796,548	796,548	18,265,450
1.00	54.494	297.50	14.12	3,203,602	1,597,449	2,393,997	18,378,900
1.50	99.620	543.87	14.22	3,225,961	1,607,391	4,001,388	18,492,350
2.00	152.613	833.18	14.33	3,252,219	1,619,545	5,620,933	18,605,800
2.50	212.213	1158.55	14.46	3,281,750	1,633,492	7,254,425	18,719,250
3.00	277.544	1515.23	14.61	3,314,122	1,648,968	8,903,393	18,832,700
3.50	347.950	1899.60	14.76	3,349,007	1,665,782	10,569,175	18,946,150
4.00	422.905	2308.81	14.92	3,386,147	1,683,789	12,252,964	19,059,600
4.50	501.977	2740.49	15.10	3,425,327	1,702,869	13,955,833	19,173,050
5.00	584.796	3192.64	15.28	3,466,364	1,722,923	15,678,755	19,286,500
5.50	671.043	3663.49	15.47	3,509,099	1,743,866	17,422,621	19,399,950
6.00	760.435	4151.52	15.66	3,553,392	1,765,623	19,188,244	19,513,400
6.50	852.716	4655.32	15.86	3,599,117	1,788,127	20,976,371	19,626,850
7.00	947.656	5173.63	16.07	3,646,159	1,811,319	22,787,690	19,740,300
7.50	1045.042	5705.30	16.28	3,694,413	1,835,143	24,622,833	19,853,750
8.00	1144.679	6249.26	16.50	3,743,783	1,859,549	26,482,382	19,967,200

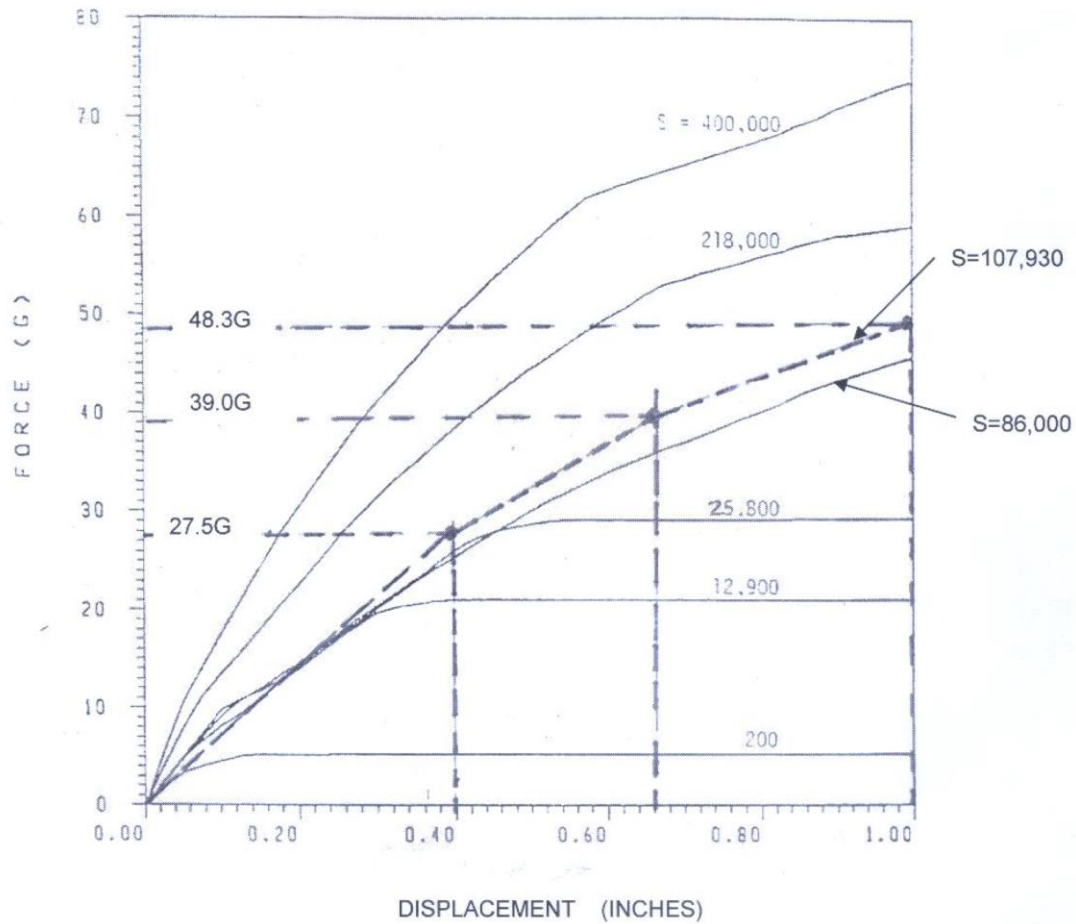


Figure 3.9.7-1
Force vs. Displacement – End Drop
(see Reference 1, Figure 14)

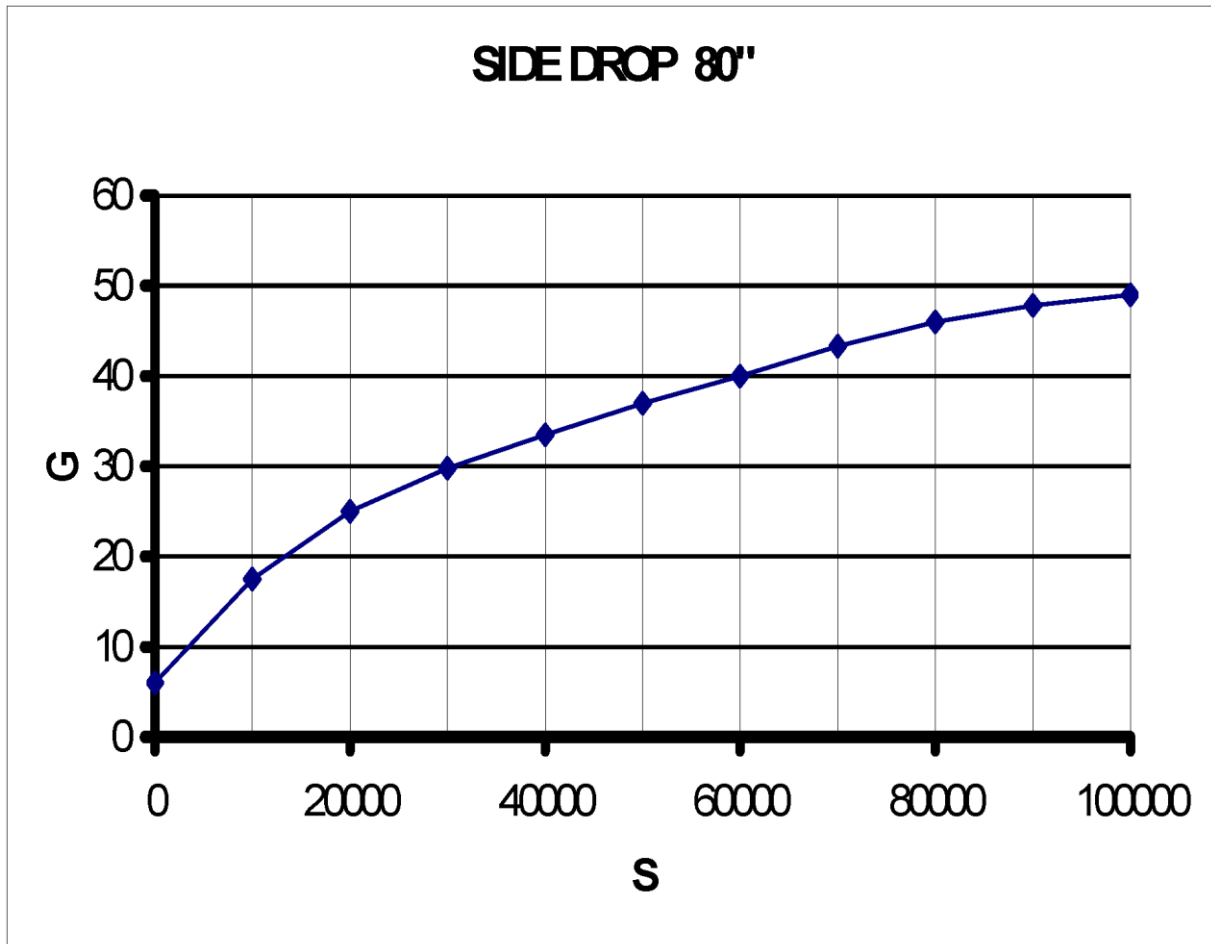
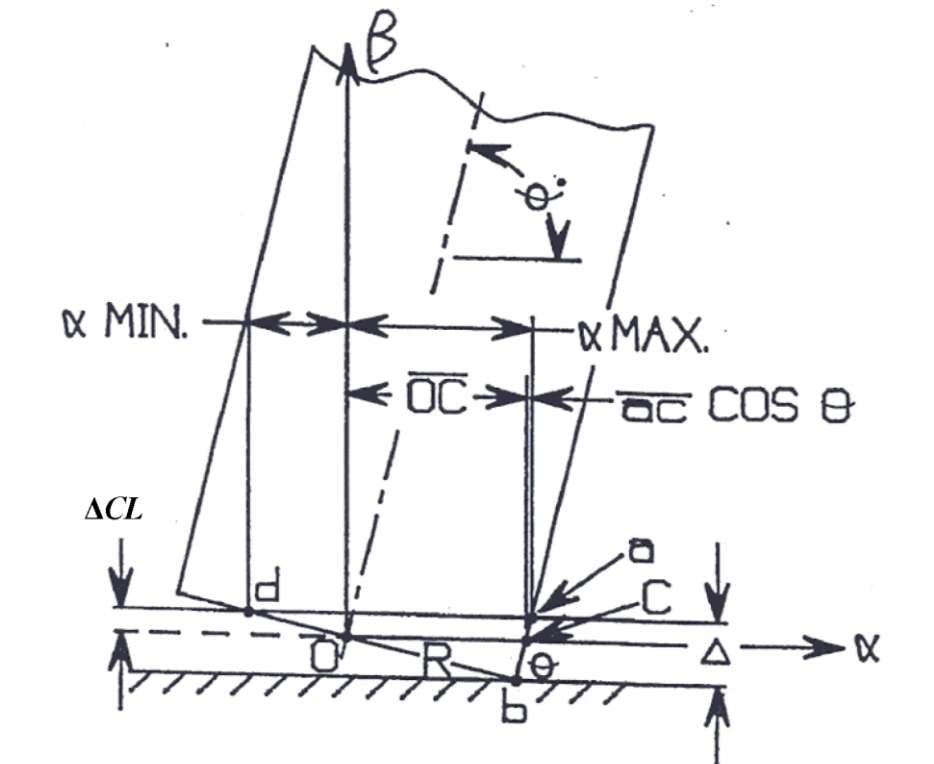


Figure 3.9.7-2
S vs. g Curve for 80 inch Height Side Drop



$$\sin \theta = \frac{R}{oc} \qquad \cos \theta = \frac{bc}{oc} \qquad \theta = \tan^{-1} \left(\frac{197.07}{81.7} \right) = 67.48^\circ$$

$$bc = oc \cos \theta = R \left(\frac{\cos \theta}{\sin \theta} \right)$$

$$ac = ab - bc = \frac{\Delta}{\sin \theta} - R \left(\frac{\cos \theta}{\sin \theta} \right)$$

$$ad = \frac{ab}{\cos \theta} = \frac{\Delta}{\sin \theta \cos \theta}$$

$$\Delta CL = \Delta - bc \sin \theta = \Delta - R \cos \theta$$

$$\begin{aligned}\alpha_{\max} &= oc + ac \cos \theta = \frac{R}{\sin \theta} + ac \cos \theta \\ &= \frac{R}{\sin \theta} + \Delta CL \left(\frac{\cos \theta}{\sin \theta} \right)\end{aligned}$$

$$\begin{aligned}\alpha_{\min} = ad - \alpha_{\max} &= \frac{\Delta}{\sin \theta \cos \theta} - \frac{R}{\sin \theta} - \Delta CL \left(\frac{\cos \theta}{\sin \theta} \right) \\ &= \Delta CL \left(\frac{1}{\sin \theta \cos \theta} - \frac{\cos \theta}{\sin \theta} \right)\end{aligned}$$

Figure 3.9.7-3
Geometry of C. G. Over Corner Drop

The area of the impact surface is obtained by first writing the equation for the intersection curves between the cylinder and plane surfaces. We set up the following coordinate systems with the origin at the bottom center of the cask.

By transforming coordinates:

$$\begin{aligned}\alpha &= x \sin \theta + z \cos \theta & x &= \alpha \sin \theta - \beta \cos \theta \\ \beta &= -x \cos \theta + z \sin \theta & z &= \alpha \cos \theta + \beta \sin \theta\end{aligned}$$

The equation for a cylinder is,

$$x^2 + y^2 = R^2$$

Or by transforming coordinates,

$$\alpha^2 \sin^2 \theta - 2\alpha\beta \sin \theta \cos \theta + \beta^2 \cos^2 \theta + y^2 = R^2$$

By setting the intersection of this surface with target surface, $\beta = \Delta CL$, the equation of the intersection curve becomes the following.

$$\alpha^2 \sin^2 \theta - 2\Delta CL \sin \theta \cos \theta + \Delta CL^2 \cos^2 \theta + y^2 = R^2$$

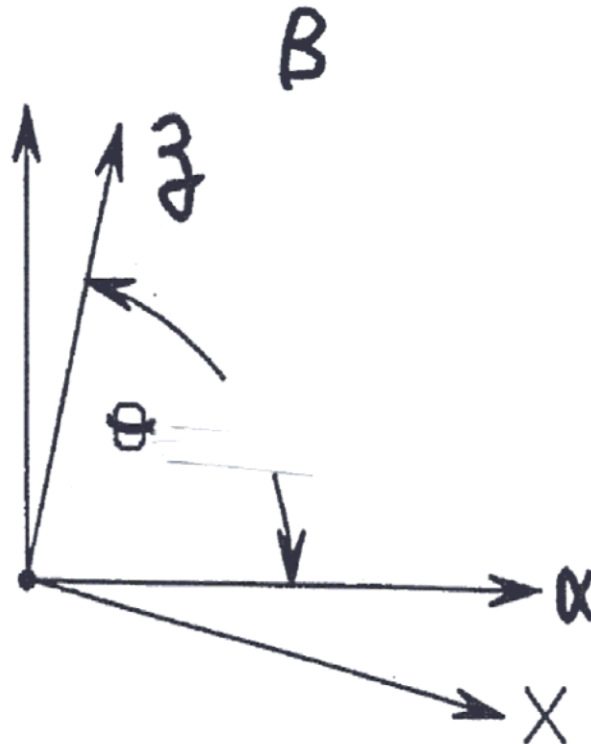


Figure 3.9.7-4
Geometry of C. G. Over Corner Drop

The area, A , as a function of the deformation is calculated by integrating the following.

$$\alpha^2 \sin^2 \theta - 2\alpha \Delta CL \sin \theta \cos \theta + \Delta CL^2 \cos^2 \theta + y^2 = R^2$$

$$A = 2 \int_{\alpha \min}^{\alpha \max} y d\alpha$$

Where y is given in above equation.

This is numerically integrated using 100 divisions and the trapezoidal rule. The results are tabulated in Table 3.9.7-4.

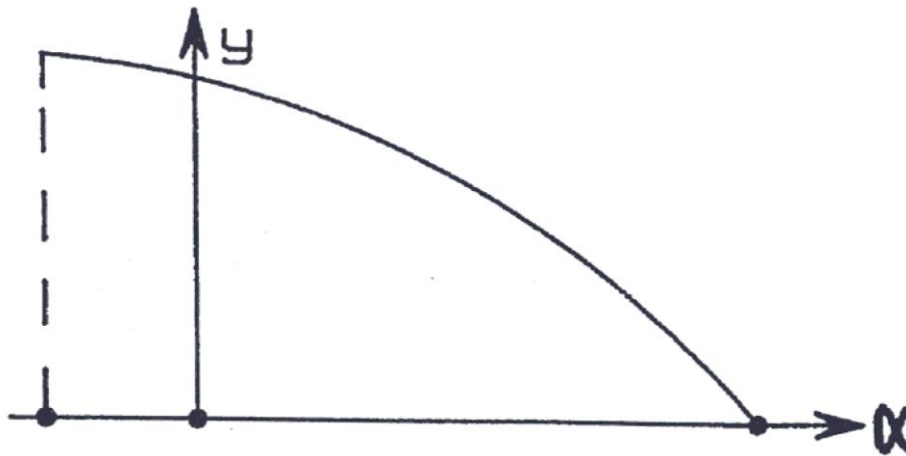


Figure 3.9.7-5
Geometry of the C. G. Over Corner Drop - Area Calculation

$$L = 2 \left[\left(\frac{2R\delta_e}{\cos\theta} \right) - \left(\frac{\delta_e^2}{\cos^2\theta} \right) \right]^{1/2}$$

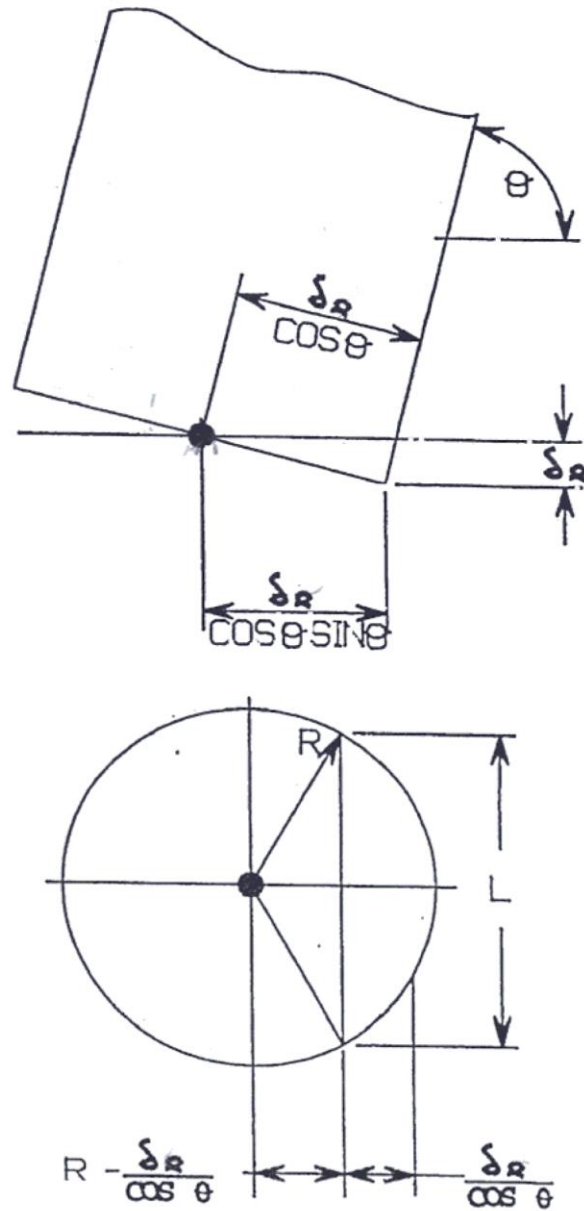


Figure 3.9.7-6
C. G. Over Corner Drop – L Dimension Calculation

APPENDIX 3.9.8
DAMAGED FUEL CLADDING STRUCTURAL EVALUATION

TABLE OF CONTENTS

3.9.8	DAMAGED FUEL CLADDING STRUCTURAL EVALUATION	3.9.8-1
3.9.8.1	Introduction.....	3.9.8-1
3.9.8.2	Design Input / Data	3.9.8-2
3.9.8.3	Loads	3.9.8-3
3.9.8.4	Evaluation Criteria	3.9.8-4
3.9.8.5	Evaluation Methodology	3.9.8-5
3.9.8.6	Trailer Acceleration from 0 mph to 5 mph during Transfer.....	3.9.8-7
3.9.8.7	Trailer Deceleration from 5 mph to 0 mph during Transfer.....	3.9.8-10
3.9.8.8	Normal Loading Condition during Insertion / Retrieval of DSC into / from HSM.....	3.9.8-12
3.9.8.9	Off-Normal Jammed Canister Loading during Insertion of DSC into HSM	3.9.8-13
3.9.8.10	One Foot End Drop Damaged Fuel Evaluation	3.9.8-14
3.9.8.11	One Foot Side Drop Damaged Fuel Evaluation	3.9.8-15
3.9.8.12	Conclusions.....	3.9.8-19
3.9.8.13	Derivation of Fuel Assembly Material Properties	3.9.8-20
3.9.8.14	DELETED	3.9.8-23
3.9.8.15	References	3.9.8-23

LIST OF TABLES

Table 3.9.8-1	WE & WES 15x15 - KI Calculation using Fracture Geometry #2.....	3.9.8-25
Table 3.9.8-2	WE 17x17 - KI Calculation using Fracture Geometry #2	3.9.8-26
Table 3.9.8-3	MK BW 17x17 - KI Calculation using Fracture Geometry #2.....	3.9.8-27
Table 3.9.8-4	WEV 17x17 - KI Calculation using Fracture Geometry #2	3.9.8-28
Table 3.9.8-5	WEO 17x17 - KI Calculation using Fracture Geometry #2	3.9.8-29
Table 3.9.8-6	CE 14x14 - KI Calculation using Fracture Geometry #2	3.9.8-30
Table 3.9.8-7	Summary - Maximum Fuel Rod Stresses and Stress Ratios.....	3.9.8-31
Table 3.9.8-8	Summary - Computed Fuel Tube Stress Intensity Factors and Ratios ..	3.9.8-32
Table 3.9.8-9	Derivation of Tensile Force (T) and Applied Moment (M) Relationship for a Circular Tube.....	3.9.8-33
Table 3.9.8-10	Tire Stiffness Calculation	3.9.8-35

LIST OF FIGURES

Figure 3.9.8-1	Fracture Geometry #1 - Ruptured Section	3.9.8-37
Figure 3.9.8-2	Fracture Geometry #2: Through-Wall Circumferential Crack in Cylinder under Bending.....	3.9.8-38
Figure 3.9.8-3	Stress Intensity Factor Solutions: For Several Specimen Configurations.....	3.9.8-39
Figure 3.9.8-4	Temperature Vs Tensile and Yield Strength for Low Burn up Fuel.....	3.9.8-40
Figure 3.9.8-5	Temperature Vs Tensile and Yield Strength for High Burn up Fuel	3.9.8-41

3.9.8 DAMAGED FUEL CLADDING STRUCTURAL EVALUATION

3.9.8.1 Introduction

The purpose of this appendix is to demonstrate structural integrity of the damaged fuel cladding in the NUHOMS[®] 32PTH DSC following normal and off-normal loading conditions of storage and onsite transfer (required for Part 72 License) and normal condition of offsite transport (required for Part 71 License).

In this appendix, the damaged fuel is defined as: “damaged PWR fuel assemblies are fuel assemblies containing missing or partial fuel rods or fuel rods with known or suspected cladding defects greater than hairline cracks or pinhole leaks. The extent of cladding damage in the fuel rods is to be limited such that a fuel pellet is not able to pass through the damaged cladding during handling and retrievability is assured following Normal/Off-Normal conditions”.

This appendix evaluates stresses in the fuel cladding associated with normal and off-normal conditions of on-site transfer/storage and off-site transport. It also presents a fracture mechanics assessment of the cladding using conservative assumptions regarding defect size geometry and amount of oxidation in the cladding material. These evaluations demonstrate the structural integrity of the damaged fuel cladding under normal and off-normal conditions.

The NUHOMS[®] 32PTH DSC is designed to store 32 intact fuel assemblies, or no more than 16 damaged and the remainder intact, for a total of 32 standard PWR fuel assemblies per canister. All the fuel assemblies, intact or damaged, consist of PWR fuel assemblies with Zircaloy cladding. Damaged fuel assemblies may only be stored in the center compartments of the NUHOMS[®] 32PTH DSC, as shown in Chapter 2, Figure 2-2.

3.9.8.2 Design Input / Data

The design inputs, taken from References [2] and [12], are modified to include the reduction in cladding thickness due to oxidation. They are documented in the following table.

Fuel Assembly Type	WE & WES 15x15	WE 17x17	MK BW 17x17	WE 17x17 Vantage 5H	WE 17x17 OFA	CE 14x14	Notes
Fuel Assembly Weight (lb)	1,555	1,575	1,575	1,575	1,575	1,450	(1,2)
No. of Rods	204	264	264	264	264	176	(1)
Active Fuel Length (in)	144.0	144.0	144.0	144.0	144.0	137.0	(1)
No. of Internal Spacers	6	6	6	6	6	7	(3)
Max. Fuel Rod Span (in)	27.0	25.0	25.0	25.0	25.0	17.0	(5)
Fuel Rod OD (in)	0.4193	0.3713	0.3713	0.3713	0.3573	0.4373	(1,4)
Clad Thickness (in)	0.0216	0.0198	0.0213	0.0198	0.0198	0.0253	(1,4)
Fuel Pellet OD (in)	0.3659	0.3225	0.3195	0.3225	0.3088	0.3765	(1)
Fuel Tube Area (in ²)	0.0270	0.0219	0.0234	0.0219	0.0210	0.0327	
Fuel Tube M.I. (in ⁴)	5.35E-04	3.39E-04	3.60E-04	3.39E-04	3.00E-04	6.97E-04	
Fuel Rod Weight (lb)	7.62	5.97	5.97	5.97	5.97	8.24	(6)
Irradiated Yield Stress (psi)	69,500	69,500	69,500	69,500	69,500	69,500	(7)
Young's Modulus (psi)	10.6E6	10.6E6	10.6E6	10.6E6	10.6E6	10.6E6	(8)

Notes:

1. Data are obtained from Chapter 2, Table 2-1.
2. The fuel assembly weight does not include BPRA weight.
3. The number of internal spacers is obtained from (Ref 12).
4. Include 0.00270 in thickness reduction to account for maximum oxide thickness.
5. Maximum fuel rod span is obtained from (Ref 12) and have been rounded up to whole number.
6. Fuel rod weight = Fuel Assembly Weight / No. of Rods.
7. Data are obtained from Figure 3.9.8-5 at 725 °F temperature.
8. Data is obtained from (Ref 3).

3.9.8.3 Loads

3.9.8.3.1 Part 72 Normal and Off-normal Condition Loads

The damaged fuel inside the DSC is subjected to following normal and off normal condition Part 72 loads:

- Dead Weight
- Internal Pressure
- Thermal
- Transfer Load (Inertia Loads associated with moving the DSC from the fuel loading area to the ISFSI site), which consists of 1g in the longitudinal, 1g in the transverse and 1g in the vertical direction.
- HSM Loading/Unloading (Normal loads associated with inserting the DSC into and retrieving the DSC from the HSM)
- Jammed Canister Load (Off normal loads associated with jamming the DSC during DSC insertion into the HSM)

The stresses due to the dead weight are insignificant. No internal pressure is assumed for the damaged fuel. The cladding is assumed to be able to expand due to thermal loads and thus no thermal-induced stresses are considered. However, the temperature of the cladding is considered for selection of allowable stresses at temperature. Therefore, the structural integrity of the damaged fuel is evaluated in this appendix only for the Transfer/Handling loads (DSC Loading/transfer to ISFSI, HSM Loading/Unloading, and Jammed Canister Load conditions).

3.9.8.3.2 Part 71 Normal Condition Loads

The structural integrity of the fuel cladding for the normal condition Part 71 load is evaluated only for the one-foot side drop condition in this application. The one-foot end drop and vibratory loads will be addressed in the 10CFR71 application.

Note that for the normal and accident off-site transport drops, the impact limiters are attached at both ends of the horizontal loaded cask.

3.9.8.4 Evaluation Criteria

The retrievability of the damaged fuel in the NUHOMS[®] 32PTH DSCs is assured if the damaged fuel cladding retains its structural integrity when subjected to normal and off normal loads. Per the damaged fuel definition in Section 3.9.8.1, the damaged fuel rods loaded in the 32PTH DSCs may have cladding defects greater than hairline cracks or pinhole leaks. However, under normal and off-normal loads, the original defects (such as cracks or pinholes) should not change significantly so that the damaged fuel can be retrieved.

The damaged fuel cladding needs to meet the following criteria to ensure their structural integrity and thus be retrievable:

- Fuel cladding stresses under normal and off-normal load conditions are less than the irradiated yield strength of the cladding material.
- Stability of the cladding tube is maintained (i.e., no buckling occurs).
- The stress intensity factor, K_I , of the fuel cladding tube geometry considering through-wall flaw is less than experimentally determined fracture toughness, K_{IC} , considering temperature and irradiation effects.

3.9.8.5 Evaluation Methodology

The onsite transfer of the fuel is accomplished using the OS 187H or Standard Transfer Cask loaded on a transfer trailer that is 10' 6" wide [8]. The transfer trailer has four axles with eight (8) 235/75 R17.5 SLR 184 tires per axle (total of 32 tires). The measured tire stiffness per tire is 1500 lbs/in [1].

During the on-site transfer operation, the trailer either accelerates from 0 initial velocity to a maximum velocity of 5 MPH [8] or decelerates from a maximum velocity of 5 MPH to 0 final velocity. Therefore, during the transfer operation the gap between the fuel assemblies and the DSC top or bottom plugs may close if friction is overcome. The kinetic energy during impact of the fuel assemblies' mass on the top or bottom plugs is absorbed as strain energy through the cask, skid, trailer, and ultimately in the tires, acting as springs.

The structural integrity of the fuel assembly is evaluated by using the principle of conservation of energy. Thus, for a spring/mass system the kinetic energy of the mass is equal to the strain energy absorbed by the spring at the time of impact.

Therefore: $(1/2) M \cdot V^2 = (1/2) K \cdot X^2$

Where:

M = Mass of the system (lb.sec²/in) = W/g

W = Weight of the system (lbs)

g = Acceleration due to gravity = 386.4 in/sec²

V = Velocity of the system (in/sec)

K = Stiffness of the spring (lbs/in)

F = Force acting on the mass and the spring (lbs)

X = Displacement of the spring (in) = F/K

Substituting F/K for X in the above equation and solving for F gives the force acting on the mass as:

$$F = (K \cdot M)^{1/2} \cdot V$$

Therefore, the equivalent g load acting on the mass = F/W

For the fuel rod once the force of impact (F) is known the stress may be computed knowing the area of cross section (A) of the cladding.

The following basic equations of kinematics relating distance, velocity, acceleration and time are used in this appendix:

$$s = u \cdot t + (1/2) \cdot a \cdot t^2$$

$$v = u + a \cdot t$$

where,

s = distance (in)

u = initial velocity (in/sec)
v = final velocity (in/sec)
a = acceleration or deceleration (in/sec²)
t = time (sec)

The structural integrity of the damaged fuel rods is evaluated for the following five loading events:

- Damaged fuel rod assemblies subjected to 1g acceleration when the trailer accelerates from 0 initial velocity to constant velocity of 5 mph [8] during onsite transfer.
- Damaged fuel rod assemblies subjected to 1g deceleration when the trailer decelerates from 5 mph [8] constant velocity to 0 final velocity during onsite transfer.
- Normal condition of loading during insertion or extraction of the DSC into or from the HSM for storage.
- Off normal jammed canister loading during insertion or extraction of the DSC into the HSM for storage.
- Damaged fuel rod assemblies subjected to 1-foot drops during normal condition of off site transport.

For each of the above five loading events, the integrity of the damaged fuel assemblies is evaluated in the following sections.

3.9.8.6 Trailer Acceleration from 0 mph to 5 mph during Transfer

During onsite transfer of the cask from the fuel building to the ISFSI the loaded trailer picks up the velocity from 0 mph to 5 mph (88 in/s). The fuel assemblies inside the canister are subjected to a maximum postulated 1g (386.4 in/s²) equivalent axial transfer load [1]. The maximum speed during this event is 5 mph and any sudden load on the fuel assemblies is transferred from the fuel assemblies to the cask, the support skid, the trailer, the rubber tires and to the road bed. The maximum transfer acceleration is +/- 1g.

Under the hot condition, the maximum gap between the fuel assemblies and the DSC plug = d (in)

Substituting in the kinematics equation $s = s_o + u_o t + a * t^2 / 2 = d$

Where:

Initial displacement, $s_o = 0$

Initial velocity, $u_o = 0$

Acceleration, $a = (1-0.3) g = 0.7g$

Where, 0.3 is the friction coefficient between the fuel assembly grid straps and the fuel compartment [9].

$$g = 386.4 \text{ in/s}^2$$

Solving for t

$$t = \{(2) * (d) / (0.7g)\}^{1/2}$$

At contact with top shield plug the velocity of the fuel assembly is

$$v = (0.7g) (t)$$

The contact force on the fuel assembly is equal to: $F = (K * M)^{1/2} * (v)$

Where:

M = total mass of the fuel assemblies = $(W * n) / g$

W = Weight of each fuel assembly

n = number of fuel assemblies/canister = 32

$K = k * 32$ lb/in, where k = stiffness of each of 32 rubber tires

k = stiffness of each tire is computed as follows:

Tire pressure = 135 psi,

For **235** (tire width mm)/**75** (height to width ratio in %) **R 17.5** (rim diameter inch) **SLR184** tires:

$$\text{Tire width} = (235 \text{ mm}) / (25.4 \text{ mm/in}) = 9.25 \text{ in}$$

$$\text{Height of the tire} = 75\% \text{ of } 9.25 \text{ in} = 6.94 \text{ in}$$

$$\text{Diameter of the tire} = (17.5 \text{ in}) + 2 * 6.94 \text{ in} = 31.4 \text{ in}$$

$$\text{Total loaded trailer weight} = \text{weight of (loaded cask + trailer + skid + ram)}$$

$$\text{Loaded Cask Weight (with impact limiters)} = 250,000 \text{ lbs. (conservative, see Chapter 3, Section 3.2.3)}$$

$$\begin{aligned} \text{Weight (trailer + skid + ram)} &= 39,700(\text{trailer}) + 26,500(\text{skid}) + 6,400(\text{ram}) \quad [1] \\ &= 72,600 \text{ lb} \end{aligned}$$

$$\text{Total Load} = 250,000 + 72,600 = 322,600 \text{ lb}$$

$$\text{Load per tire} = (322,600 \text{ lb}) / (32 \text{ tires}) = 10,081 \text{ lb}$$

$$\text{Area of contact of the tire} = (10,081 \text{ lbs} / 135 \text{ psi}) = 74.7 \text{ in}^2$$

$$\text{Length of compression of the tire} = 74.7 \text{ in}^2 / 9.25 \text{ in} = 8.08 \text{ in}$$

$$\text{Therefore, deflection of the tire} = (31.4/2) - \{(31.4/2)^2 - (8.08/2)^2\}^{1/2} = 0.5287 \text{ in}$$

$$\text{Tire stiffness/tire} = (10,081 \text{ lb}) / (0.5287 \text{ in}) = 19,068 \text{ lb/in}$$

$$\text{Total tire stiffness for 32 tires} = (19,068)(32) = 6.1 \times 10^5 \text{ lb/in}$$

$$\text{As per Table 3.9.8-9, the measured tire stiffness} = 1500 \times 32 = 4.8 \times 10^4 \text{ lb/in}$$

$$\text{Conservatively, use tire stiffness of } 6.1 \times 10^5 \text{ lb/in}$$

$$\text{The force in the fuel assemblies is } F = (K * M)^{1/2} * (v)$$

$$\text{Therefore, load per assembly} = F / 32 \text{ lb}$$

$$\text{Equivalent g load in the fuel rods} = F / 32 / W$$

$$\text{The axial stress in the rod is} = F / \text{Fuel Tube Area}$$

Using the methodology described above, the fuel tube axial stresses for the prescribed condition are computed and presented in the following table.

Fuel Assembly Type	WE & WES 15x15	WE 17x17	MK BW 17x17	WEV 17x17	WEO 17x17	CE 14x14
Total Fuel Weight (lb)	1,555	1,575	1,575	1,575	1,575	1,450
Fuel Tube Area (in ²)	0.0270	0.0219	0.0234	0.0219	0.0210	0.0327
gap (in) ⁽¹⁾	6.0	6.0	6.0	6.0	6.0	6.0
t (s)	0.211	0.211	0.211	0.211	0.211	0.211
v (in/s)	56.97	56.97	56.97	56.97	56.97	56.97
M (lb-s ² /in)	128.8	130.4	130.4	130.4	130.4	120.1
W (lb)	48.6	49.2	49.2	49.2	49.2	45.3
No. of Fuel Assemblies	32	32	32	32	32	32
K, lb/in	610,000	610,000	610,000	610,000	610,000	610,000
F (lb)	504,946	508,183	508,183	508,183	508,183	487,600
Force / Assembly (lb)	15,780	15,881	15,881	15,881	15,881	15,237
No of Rod / Assembly	204	264	264	264	264	176
Force / Rod (lb)	77.4	60.2	60.2	60.2	60.2	86.6
Equivalent g load	10.1	10.1	10.1	10.1	10.1	10.5
Axial Stress (lb)	2,865	2,747	2,571	2,747	2,864	2,648

Note:

- (1) The gap between the fuel assembly and the DSC end component is conservatively assumed to be 6" (the actual length is around 2 in.).

The axial stresses in the fuel rods are compressive stresses, and they are significantly less than the irradiated yield stress of the cladding material = 69,500 psi (Figure 3.9.8-5). Therefore, the fuel rods will maintain their structural integrity when subjected to the trailer acceleration during transfer.

3.9.8.7 Trailer Deceleration from 5 mph to 0 mph during Transfer

During onsite transfer of the cask from the fuel building to the ISFSI the loaded trailer travels at a maximum constant velocity of 5 mph (88 in/s). Any sudden loads, which may occur during an emergency stop, are transferred from the road bed through the rubber tires, the trailer, the support skid, and the cask to the fuel assemblies. The fuel assemblies inside the canister are subjected to maximum postulated 1g (386.4 in/s²) equivalent axial transfer load [7]. Therefore, the maximum transfer acceleration is +/- 1g.

The initial velocity is $v_i = 88$ in/s, the deceleration, $g = 386.4$ in/s²

The maximum velocity at impact of the fuel assemblies on the inner bottom cover plate is

$$v = 88 \text{ in/sec} - v_f \text{ (due to friction)} - v_d \text{ (due to deceleration)}$$

Where, v_f is a function of work done by the force due to friction (F_f).

$$\text{Therefore, } (M * v_f^2)/2 = F_f * d$$

Where:

M = mass of the fuel assemblies

$F_f = M * g * 0.3$ (where the coefficient of friction between grid straps and canister is 0.3 [9])

d = gap between fuel assembly and the DSC plug

$$v_f = \{(2 * F_f * d) / M\}^{1/2}$$

Conservatively assume that cask is tied to the trailer so that it does not move.

v_d is calculated as follows:

Substituting in the kinematics equation $s = s_o + ut + a * t^2 / 2$ (Section 3.9.8.5)

$$s_o = 0, \quad u = 88 \text{ in/sec}, \quad \text{Acceleration, } a = 386.4 \text{ in/s}^2 \text{ and solving for 't'}$$

$$v_d = u + a * t$$

Conservatively, ignoring v_d (change in velocity due to deceleration), at contact with the inner bottom cover plate of the DSC the velocity of the fuel assembly is

$$v = 88 - v_f$$

$$\text{The contact force on the fuel assembly} = F = (K * M)^{1/2} * (v)$$

Where:

M = total mass of the fuel assemblies = $(W * n) / g$

W = maximum weight of each fuel assembly

n = number of fuel assemblies/canister = 32

K = conservatively use tire stiffness of 6.1×10^5 lb/in (Section 3.9.8.6)

$$F = (M * K)^{1/2} * v$$

Therefore, load per assembly = $F / 32$

Equivalent g load in the fuel rods = $F / 32 / W$.

The axial stress in the rod is = $F / \text{Fuel Tube Area}$.

Using the methodology described above, the fuel tube axial stresses for the prescribed condition are computed and presented in the following table.

Fuel Assembly Type	WE & WES 15x15	WE 17x17	MK BW 17x17	WEV 17x17	WEO 17x17	CE 14x14
Total Fuel Weight (lb)	1,555	1,575	1,575	1,575	1,575	1,450
Fuel Tube Area (in ²)	0.0270	0.0219	0.0234	0.0219	0.0210	0.0327
gap (in) ⁽¹⁾	6.0	6.0	6.0	6.0	6.0	6.0
M (lb-s ² /in)	128.8	130.4	130.4	130.4	130.4	120.1
W (lb)	48.6	49.2	49.2	49.2	49.2	45.3
F _f (lb)	14,928	15,120	15,120	15,120	15,120	13,920
v _f (in/s)	37.3	37.3	37.3	37.3	37.3	37.3
v (in/s)	50.7	50.7	50.7	50.7	50.7	50.7
K, lb/in	610,000	610,000	610,000	610,000	610,000	610,000
F (lb)	449,390	452,271	452,271	452,271	452,271	433,952
Force / Assembly (lb)	14,043	14,133	14,133	14,133	14,133	13,561
No of Rod / Assembly	204	264	264	264	264	176
Force / Rod (lb)	68.8	53.5	53.5	53.5	53.5	77.1
Equivalent g load	9.0	9.0	9.0	9.0	9.0	9.4
Axial Stress (lb)	2,550	2,445	2,288	2,445	2,549	2,356

Note:

(1) The gap between the fuel assembly and the DSC end component is conservatively assumed to be 6".

The axial stresses in the fuel rods are compressive stresses, and they are significantly less than the irradiated yield strength of the cladding material = 69,500 psi (Figure 3.9.8-5). Therefore, the fuel rods will maintain their structural integrity when subjected to the trailer deceleration during transfer.

3.9.8.8 Normal Loading Condition during Insertion / Retrieval of DSC into / from HSM

The insertion or retrieval of the DSC into the HSM is a highly controlled procedure, and the process is conducted slowly. For normal loading condition, the maximum ram push force for DSC insertion and grapple pull force for DSC retrieval are 80 kips and 60 kips, respectively. These applied forces are monitored and controlled. The acceleration/deceleration resulting from the procedure will be small and bounded by the transfer acceleration and deceleration as reported in Sections 3.9.8.6 and 3.9.8.7, respectively.

3.9.8.9 Off-Normal Jammed Canister Loading during Insertion of DSC into HSM

The insertion or retrieval of the DSC into the HSM is a highly controlled procedure, and the process is conducted slowly. For off-normal jammed canister loading condition, the maximum ram push for DSC insertion and grapple pull force for DSC retrieval are both 80 kips. This applied force is monitored and controlled. Similar to the normal loading condition, the acceleration/deceleration resulting from the procedure will be small and bounded by the transfer acceleration and deceleration as reported in Sections 3.9.8.6 and 3.9.8.7, respectively.

3.9.8.10 One Foot End Drop Damaged Fuel Evaluation

The structural integrity of the fuel cladding due to the one-foot end drop loading condition will be analyzed in the 10CFR71 application.

3.9.8.11 One Foot Side Drop Damaged Fuel Evaluation

Note: The one-foot side drop analysis contained in this section has not been reviewed by the NRC staff because it is not needed to support a 10 CFR Part 72 certification. Therefore, the NRC staff expects the one-foot side drop and the one-foot end drop and vibratory loading conditions to be addressed in the 10 CFR Part 71 application.

During off site transport (Part 71) the damaged fuel assemblies need to be evaluated for 1 foot side drop. The transport operation is carried out using the MP 187H Cask, with the DSC and the impact limiters in the horizontal position.

The maximum g load acting on the damaged fuel rods under 1 foot side drop load = 30g. The damaged fuel rod structural integrity under 1 foot side drop load is assessed by computing the bending stress in the rod and comparing it with the yield stress of the cladding material. The fracture assessment of the damaged fuel rod structural integrity is made by using two fracture geometries (ruptured sections) as described below.

It is assumed that the damaged fuel tube is burst at the spacers (supports) location, which is the location of maximum bending moment. The loading assumed is on the opposite side of the rod at the burst location. The following two geometries, used for the fracture evaluation of the damaged fuel rods, are based on these assumptions.

Fracture Geometry #1: The first geometry is shown in Figure 3.9.8-1. In this damage mode the fuel tube is assumed to bulge from diameter D to diameter W ($W \geq D$) and rupture to a hole of diameter (2a) at the bulge location. It is assumed that $(2a/w) = 0.5$ for this geometry.

Fracture Geometry #2: The second geometry is shown in Figure 3.9.8-2. The stress intensities factors for this geometry are determined using the solution for a tube with a crack subjected to pure bending moment given in Reference 13. This evaluation is based on a crack length to diameter ratio of 0.47 (or $2a/D_m = 0.47$).

The basis for the 0.5 (ruptured hole to tube diameter ratio) for fracture geometry #1 and 0.47 (crack length to tube diameter ratio) for fracture geometry #2 are the experimental tests on “as received” Zircalloy fuel tubes with measured burst temperatures of up to 909°C, which showed flaw opening to diameter ratios of 0.4 to 0.5 [16].

3.9.8.11.1 Structural Integrity Evaluation with Fracture Geometry #1

The fracture geometry #1 (Ruptured Section) is shown in Figure 3.9.8-1. With reference to Figure 3.9.8-1, the methodology for computing the stress intensity factor K_I is as follows:

Fuel rod OD = D

Oxidized Clad Thickness = t

Average radius, $R = (D-t)/2$

I = net tube MI.

Span Length = S

Assume $(2a/W) = 0.5$, where $2a$ = ruptured hole diameter,

W = bulged fuel tube diameter $\geq D$.

Stress Intensity Factor, $K_I = (Y)(P*a^{1/2})/(t*W)$, [Reference 14, Fig. 8.7(c)]

Where:

$Y = 2.11$ {established using $(2a/W) = 0.5$ (for Forman et al. case) in Figure 3.9.8-3}

P = average tensile force at the crack which is expressed as a function of moment on the cross section as:

$$= (2MR^2t)/I \quad (\text{See Table 3.9.8-8})$$

$W = \pi R$

$M = 0.1058(W_s*S^2)$ (See Appendix 2 of Reference 3)

$W_s = 30g$ Fuel Rod Weight / Length

Bending Stress = $MD / 2I$

Using the methodology described above, the stress intensity factors, K_I , for the prescribed condition are computed and presented in the following table.

Fuel Assembly Type	WE & WES 15x15	WE 17x17	MK BW 17x17	WEV 17x17	WEO 17x17	CE 14x14
Fuel Rod OD, D (in)	0.4193	0.3713	0.3713	0.3713	0.3573	0.4373
Clad Thickness, t (in)	0.0216	0.0198	0.0213	0.0198	0.0198	0.0253
Average Radius, R (in)	0.1989	0.1758	0.1750	0.1758	0.1688	0.2060
Fuel Tube M.I. (in ⁴)	5.35E-04	3.39E-04	3.60E-04	3.39E-04	3.00E-04	6.97E-04
Span Length, S (in)	27.0	25.0	25.0	25.0	25.0	17.0
(2a/W)	0.5	0.5	0.5	0.5	0.5	0.5
Y	2.11	2.11	2.11	2.11	2.11	2.11
W (in)	0.62	0.55	0.55	0.55	0.53	0.65
Fuel Assembly Weight (lb)	1,555	1,575	1,575	1,575	1,575	1,450
No. of Rods	204	264	264	264	264	176
Active Fuel Length (in)	144.0	144.0	144.0	144.0	144.0	137.0
1-Foot Side Drop Equivalent g load	30	30	30	30	30	30
W_s (lb/in)	1.59	1.24	1.24	1.24	1.24	1.80
Moment, M (kip. in)	0.12	0.08	0.08	0.08	0.08	0.06
Bending Stress (psi)	47,990	45,040	42,390	45,040	48,950	17,300
P (kip)	0.391	0.297	0.298	0.297	0.309	0.170
K_I (ksi in ^{1/2})	24.2	21.3	19.9	21.3	22.6	8.8

The computed stress intensity factor is compared with experimentally obtained plane strain fracture toughness, K_{IC} of irradiated Zircaloy cladding material as reported in [15].

Reference 15 reports a $K_{IC} = 35 \text{ ksi in}^{1/2}$ at approximately 300°F which is greater than highest computed stress intensity factor, K_I of 24.2 ksi in^{1/2} presented in the above table.

Therefore, the structural integrity of the damaged fuel rods, which are conservatively assumed to rupture as shown in Figure 3.9.8-1, will be maintained.

3.9.8.11.2 Structural Integrity Evaluation with Fracture Geometry #2

This geometry is shown in Figure 3.9.8-2. Stress intensity factors are computed for a crack in a fuel tube subjected to a uniform bending moment (M) using formulas given in “The Stress Analysis of Cracks Handbook” [13]:

$$K_I = \sigma (\pi R_m \theta)^{1/2} F(\theta)$$

where,

$$F(\theta) = 1 + 6.8*(\theta/\pi)^{3/2} - 13.6*(\theta/\pi)^{5/2} + 20.0*(\theta/\pi)^{7/2}$$

σ = Bending Stress due to Uniform Moment ‘M’

R_m = Average radius of the fuel tube

2θ = Angle which the crack makes at the center of the tube

K_I = Stress Intensity Factor at the crack

The K_I is computed for all the different fuel assemblies, and the results for all the fuel assemblies are presented in Table 3.9.8-1, Table 3.9.8-2, Table 3.9.8-3, Table 3.9.8-4 and Table 3.9.8-5.

Based on the computed K_I using Fracture Geometries #1 & #2, a summary of the comparisons is presented as follows:

	Fracture Geometry #1 K_I	Fracture Geometry #2 K_I
WE & WES 15x15	24.2	33.8
WE 17x17	21.3	29.9
MK BW 17x17	19.9	28.0
WEV 17x17	21.3	29.9
WEO 17x17	22.6	31.8
CE 14x14	8.8	12.4

3.9.8.12 Conclusions

The maximum computed stresses in the fuel rods and their ratios to the irradiated yield stress of the cladding material are summarized in Table 3.9.8-6. From Table 3.9.8-6, it can be concluded that stresses for all load cases considered are significantly less than the yield stress of the Zircaloy cladding material (computed stresses are 4% to 49% of the yield stress).

It is important to note that, the stresses in the fuel rods for all analyzed normal and off normal load cases are compressive stresses (less than the critical buckling stress), except for the 1-foot transport condition side drop load.

For the 1-foot side drop it is demonstrated by using fracture mechanics procedures (by comparing computed stress intensity factors to critical crack initiation fracture toughness in Table 3.9.8-7), that the damaged fuel rods will maintain their structural integrity.

This calculation demonstrates that the fuel cladding in the NUHOMS® 32PTH DSC will retain its structural integrity when subjected to normal condition of storage and on site transfer loads. The fuel cladding will also maintain its integrity when subjected to a one-foot side drop during offsite transport. The fuel cladding integrity during the one-foot end drop and transport vibratory loads will be demonstrated in the 10CFR71 application. Therefore, the retrievability of the fuel assembly is assured when subjected to storage and transfer normal and off normal loads.

3.9.8.13 Derivation of Fuel Assembly Material Properties

Material property for low burnup fuel

The material properties used for the fuel cladding structural analysis is based on the LLNL report “Dynamic Impact Effects on Spent Fuel Assemblies” [3] and is for low burnup fuel. The material properties used for the drop analysis at elevated temperature are obtained from the following methodology.

Yield Strength of cladding: The yield stress vs. temperature is taken from Table 5 of [3, page 12] and is depicted in Figure 3.9.8-4. Since the relation between the yield strength vs. temperature is linear, the yield strength at higher temperature is obtained by extending the curve.

$$S_y = 81,500 \text{ psi (725 } ^\circ\text{F)}$$

$$S_y = 80,500 \text{ psi (750 } ^\circ\text{F)}$$

Tensile Strength of cladding: The tensile strength corresponding to the yield strength at the temperatures is obtained from Figure 5 of [3, page 17] and is also depicted in Figure 3.9.8-4.

$$S_u = 92,000 \text{ psi (725 } ^\circ\text{F)}$$

$$S_u = 91,800 \text{ psi (750 } ^\circ\text{F)}$$

Material property for high burnup fuel

In order to calculate the actual thickness of the cladding needed to be reduced, the oxide thickness accumulation needed to be corrected. A Pilling-Bedworth factor of 1.75 [18, page 426] is used in Chapter 3 calculation and is repeated as follows.

$$(120/1.75) \times 10^{-6} \times 39.372 = 0.0027 \text{ in.}$$

Proprietary Information on This Page
Withheld Pursuant to 10 CFR 2.390

3.9.8.14 DELETED3.9.8.15 References

1. Transnuclear Calculation No. NUH24PTH.0209 Rev. 0, “NUHOMS® 24PTH Damaged Fuel Cladding Structural Evaluation to Demonstrate the Retrievability of the Fuel Subject to Normal and Off-Normal Loads”.
2. Transnuclear, Inc., “Design Criteria Document (DCD) for the NUHOMS®-32PTH System for Transportation and Storage,” E-21621, Revision 5.
3. UCID – 21246, “Dynamic Impact Effects on Spent Fuel Assemblies,” Lawrence Livermore National Laboratory, October 20, 1987.
4. Transnuclear Calculation No. 10494-6, Rev. 2, “NUHOMS-32PTH DSC, Transfer Cask, and ‘Under Hook’ Nominal Weight Calculation.”
5. ANSI N14.23, “Draft American National Standard Design Basis for Resistance to Shock and Vibration of Radioactive Material Packages Greater than One Ton in Truck Transport”, May 1980.
6. NRC -12 , SAND76-0427, NUREG766510, “Shock and Vibration Environments for Large Shipping Containers on Rail Cars and Trucks”, June 1977.
7. Updated Final Safety Analysis Report for the Standardized NUHOMS® Horizontal Modular Storage System for Irradiated Nuclear Fuel, NUH-003-0103, Rev. 12.
8. Transnuclear, Inc., “Technical Specification for the NUHOMS® 10’ - 6” Wide Cask Transfer Trailer,” Report No. NUH-07-106, Revision 5.
9. Baumeister, T., “Mark’s Standard Handbook for Mechanical Engineers,” McGraw-Hill Book Company, 8th Edition.
10. Transnuclear Calculation No. 10494-20, Rev. 1, “NUHOMS-32PTH Thermal Analysis of DSC in the HSM for Normal, Off-Normal, and Accident Storage Conditions”.
11. Transnuclear Calculation No. 10494-46, Rev. 0, “NUHOMS-32PTH Thermal Expansions”.
12. OCRWM Database, “Characteristics of spent fuel, high level waste, and other radioactive wastes which may require long term isolation” Appendix 2A, Volume 3 of 6, DOE/RW-0184, December 1987.
13. “The Stress Analysis of Cracks Handbook” Third Edition by Hiroshi Tada et al., ASME Press, 2000.
14. R.W. Hertzberg,” Deformation and Fracture Mechanics of Engineering Material” John Wiley & Sons, New York, 1976.

15. T.J. Walker, et al., "Variation of Zircaloy Fracture Toughness in Irradiation" Zirconium in Nuclear Applications, ASTM STP 551, American Society for Testing and Materials, 1974, pp. 328-354.
16. Light-Water Reactor Safety Research Program: Quarterly Progress Report July - September 1976, Section III, "Mechanical Properties of Zircaloy Containing Oxygen", Figs III-29 to III-32, ANL-75-72 (September 1975).
17. EPRI Technical Report 1003218 "Hot Cell Examination of ZIRLO PWR Fuel, Irradiated to 70 GWd/MTU", December 2003.
18. Van Swam, L. F., Strasser A. A., Cook J. D., Burger J. M., "Behavior of Zircaloy-4 and Zirconium Linear Zircaloy-4 Cladding at High Burnup" Proceedings of the 1997 International Topical Meeting on LWR Fuel Performance, Portland, Oregon March 2-6, 1997.
19. North Anna Power Station UFSAR, rev. 40, 13/30/04.
20. John F. Harvey "Theory and Design of Modern Pressure Vessel" Second edition.
21. NUREG/CR-0497 "A handbook of Materials Properties for Use in the Analysis of Light Water Reactor Fuel Rod Behavior, MATPRO-Version 11" February 1979.

Table 3.9.8-1
WE & WES 15x15 - KI Calculation using Fracture Geometry #2

OD (in) =	0.4193
t (in) =	0.0216
R / t =	9.71
Rm (in) =	0.1989
M (kip-in) =	0.12
Theta (radian) =	0.47
I (in ⁴) =	5.34E-04
Bending Stress (ksi) =	47.99
E (ksi) =	10,600

Theta (rad)	Theta/pi	Half Length (in)	F(Theta)	K _I (ksi in ^{1/2})
0.05	0.0159	0.0099	1.0132	8.6
0.10	0.0318	0.0199	1.0363	12.4
0.15	0.0477	0.0298	1.0646	15.6
0.20	0.0637	0.0398	1.0966	18.6
0.25	0.0796	0.0497	1.1312	21.5
0.30	0.0955	0.0597	1.1677	24.3
0.35	0.1114	0.0696	1.2058	27.1
0.40	0.1273	0.0795	1.2450	29.9
0.45	0.1432	0.0895	1.2853	32.7
0.47	0.1496	0.0935	1.3017	33.8
0.51	0.1623	0.1014	1.3348	36.2
0.52	0.1655	0.1034	1.3432	36.7
0.55	0.1751	0.1094	1.3686	38.5
0.60	0.1910	0.1193	1.4117	41.5
0.65	0.2069	0.1293	1.4557	44.5
0.70	0.2228	0.1392	1.5009	47.6

Table 3.9.8-2
WE 17x17 - KI Calculation using Fracture Geometry #2

OD (in) =	0.3713
t (in) =	0.0198
R / t =	9.38
Rm (in) =	0.1758
M (kip-in) =	0.08
Theta (radian) =	0.47
I (in ⁴) =	3.39E-04
Bending Stress (ksi) =	45.04
E (ksi) =	10,600

Theta (rad)	Theta/pi	Half Length (in)	F(Theta)	K _I (ksi in ^{1/2})
0.05	0.0159	0.0088	1.0132	7.6
0.10	0.0318	0.0176	1.0363	11.0
0.15	0.0477	0.0264	1.0646	13.8
0.20	0.0637	0.0352	1.0966	16.4
0.25	0.0796	0.0439	1.1312	18.9
0.30	0.0955	0.0527	1.1677	21.4
0.35	0.1114	0.0615	1.2058	23.9
0.40	0.1273	0.0703	1.2450	26.4
0.45	0.1432	0.0791	1.2853	28.9
0.47	0.1496	0.0826	1.3017	29.9
0.51	0.1623	0.0896	1.3348	31.9
0.52	0.1655	0.0914	1.3432	32.4
0.55	0.1751	0.0967	1.3686	34.0
0.60	0.1910	0.1055	1.4117	36.6
0.65	0.2069	0.1142	1.4557	39.3
0.70	0.2228	0.1230	1.5009	42.0

Table 3.9.8-3
MK BW 17x17 - KI Calculation using Fracture Geometry #2

OD (in) =	0.3713
t (in) =	0.0213
R / t =	8.72
Rm (in) =	0.1750
M (kip-in) =	0.08
Theta (radian) =	0.47
I (in ⁴) =	3.60E-04
Bending Stress (ksi) =	42.39
E (ksi) =	10,600

Theta (rad)	Theta/pi	Half Length (in)	F(Theta)	K _I (ksi in ^{1/2})
0.05	0.0159	0.0088	1.0132	7.1
0.10	0.0318	0.0175	1.0363	10.3
0.15	0.0477	0.0263	1.0646	13.0
0.20	0.0637	0.0350	1.0966	15.4
0.25	0.0796	0.0438	1.1312	17.8
0.30	0.0955	0.0525	1.1677	20.1
0.35	0.1114	0.0613	1.2058	22.4
0.40	0.1273	0.0700	1.2450	24.7
0.45	0.1432	0.0788	1.2853	27.1
0.47	0.1496	0.0823	1.3017	28.0
0.51	0.1623	0.0893	1.3348	30.0
0.52	0.1655	0.0910	1.3432	30.4
0.55	0.1751	0.0963	1.3686	31.9
0.60	0.1910	0.1050	1.4117	34.4
0.65	0.2069	0.1138	1.4557	36.9
0.70	0.2228	0.1225	1.5009	39.5

Table 3.9.8-4
WEV 17x17 - KI Calculation using Fracture Geometry #2

OD (in) =	0.3713
t (in) =	0.0198
R / t =	9.38
Rm (in) =	0.1758
M (kip-in) =	0.08
Theta (radian) =	0.47
I (in ⁴) =	3.39E-04
Bending Stress (ksi) =	45.04
E (ksi) =	10,600

Theta (rad)	Theta/pi	Half Length (in)	F(Theta)	K _I (ksi in ^{1/2})
0.05	0.0159	0.0088	1.0132	7.6
0.10	0.0318	0.0176	1.0363	11.0
0.15	0.0477	0.0264	1.0646	13.8
0.20	0.0637	0.0352	1.0966	16.4
0.25	0.0796	0.0439	1.1312	18.9
0.30	0.0955	0.0527	1.1677	21.4
0.35	0.1114	0.0615	1.2058	23.9
0.40	0.1273	0.0703	1.2450	26.4
0.45	0.1432	0.0791	1.2853	28.9
0.47	0.1496	0.0826	1.3017	29.9
0.51	0.1623	0.0896	1.3348	31.9
0.52	0.1655	0.0914	1.3432	32.4
0.55	0.1751	0.0967	1.3686	34.0
0.60	0.1910	0.1055	1.4117	36.6
0.65	0.2069	0.1142	1.4557	39.3
0.70	0.2228	0.1230	1.5009	42.0

Table 3.9.8-5
WEO 17x17 - KI Calculation using Fracture Geometry #2

OD (in) =	0.3573
t (in) =	0.0198
R / t =	9.02
Rm (in) =	0.1688
M (kip-in) =	0.08
Theta (radian) =	0.47
I (in ⁴) =	3.00E-04
Bending Stress (ksi) =	48.95
E (ksi) =	10,600

Theta (rad)	Theta/pi	Half Length (in)	F(Theta)	K _I (ksi in ^{1/2})
0.05	0.0159	0.0084	1.0132	8.1
0.10	0.0318	0.0169	1.0363	11.7
0.15	0.0477	0.0253	1.0646	14.7
0.20	0.0637	0.0338	1.0966	17.5
0.25	0.0796	0.0422	1.1312	20.2
0.30	0.0955	0.0506	1.1677	22.8
0.35	0.1114	0.0591	1.2058	25.4
0.40	0.1273	0.0675	1.2450	28.1
0.45	0.1432	0.0759	1.2853	30.7
0.47	0.1496	0.0793	1.3017	31.8
0.51	0.1623	0.0861	1.3348	34.0
0.52	0.1655	0.0878	1.3432	34.5
0.55	0.1751	0.0928	1.3686	36.2
0.60	0.1910	0.1013	1.4117	39.0
0.65	0.2069	0.1097	1.4557	41.8
0.70	0.2228	0.1181	1.5009	44.8

Table 3.9.8-6
CE 14x14 - KI Calculation using Fracture Geometry #2

OD (in) =	0.4373
t (in) =	0.0253
R / t =	8.64
Rm (in) =	0.2060
M (kip-in) =	0.06
Theta (radian) =	0.47
I (in ⁴) =	6.97E-04
Bending Stress (ksi) =	17.30
E (ksi) =	10,600

Theta (rad)	Theta/pi	Half Length (in)	F(Theta)	K _I (ksi in ^{1/2})
0.05	0.0159	0.0103	1.0132	3.2
0.10	0.0318	0.0206	1.0363	4.6
0.15	0.0477	0.0309	1.0646	5.7
0.20	0.0637	0.0412	1.0966	6.8
0.25	0.0796	0.0515	1.1312	7.9
0.30	0.0955	0.0618	1.1677	8.9
0.35	0.1114	0.0721	1.2058	9.9
0.40	0.1273	0.0824	1.2450	11.0
0.45	0.1432	0.0927	1.2853	12.0
0.47	0.1496	0.0968	1.3017	12.4
0.51	0.1623	0.1051	1.3348	13.3
0.52	0.1655	0.1071	1.3432	13.5
0.55	0.1751	0.1133	1.3686	14.1
0.60	0.1910	0.1236	1.4117	15.2
0.65	0.2069	0.1339	1.4557	16.3
0.70	0.2228	0.1442	1.5009	17.5

Table 3.9.8-7
Summary - Maximum Fuel Rod Stresses and Stress Ratios

Normal and Off Normal Load Case	Maximum⁽¹⁾ Stress (psi)	Stress⁽²⁾ Ratio
On site Transport and Transfer Operations	2,865	0.04
One-foot Side Drop (Part 71)	48,950	0.70

Notes:

1. Maximum stress for all fuel assemblies.
2. Stress ratio = maximum stress / 69,500 (yield stress for Zircaloy cladding).

Table 3.9.8-8
Summary - Computed Fuel Tube Stress Intensity Factors and Ratios

Fracture Geometry	Max K_I⁽¹⁾ (ksi in^{1/2})	K_{IC}⁽²⁾ (ksi in^{1/2})	Ratio Max K_I / K_{IC}
Geometry #1	24.2	35.0	0.69
Geometry #2	33.8	35.0	0.97

Notes:

1. Maximum K_I for all fuel assemblies.
2. K_{IC} = Crack initiation fracture toughness (plane strain fracture toughness).

Table 3.9.8-9
Derivation of Tensile Force (T) and Applied Moment (M) Relationship for a Circular Tube

Consider a circular tube of average radius “R”, thickness “t” subjected to a bending moment “M”.

At angle “θ” from the neutral axis (N/A), for a segment of the tube with angle “dθ”

$$\text{Area} = A = t \cdot R \cdot d\theta,$$

$$\text{Tensile stress} = \sigma = (M \cdot R \cdot \sin\theta) / I$$

Where, I = moment of inertia of the section

Therefore,

$$\text{Tensile Force} = \Delta P = (M \cdot R \cdot \sin\theta / I) \cdot (t \cdot R \cdot d\theta)$$

$$\text{Total Tensile Force} = P = \int (M \cdot R \cdot \sin\theta / I) \cdot (t \cdot R \cdot d\theta)$$

Where, limits of integral are from angle “θ = 0” to angle “θ = π”

Therefore,

$$\begin{aligned} P &= (M \cdot R^2 \cdot t / I) \int \sin\theta \, d\theta \\ &= (M \cdot R^2 \cdot t / I) [-\cos\theta]_0^\pi \\ &= 2 \cdot M \cdot R^2 \cdot t / I \end{aligned}$$

Table 3.9.8-9 (concluded)
Derivation of Tensile Force (T) and Applied Moment (M) Relationship for a Circular Tube

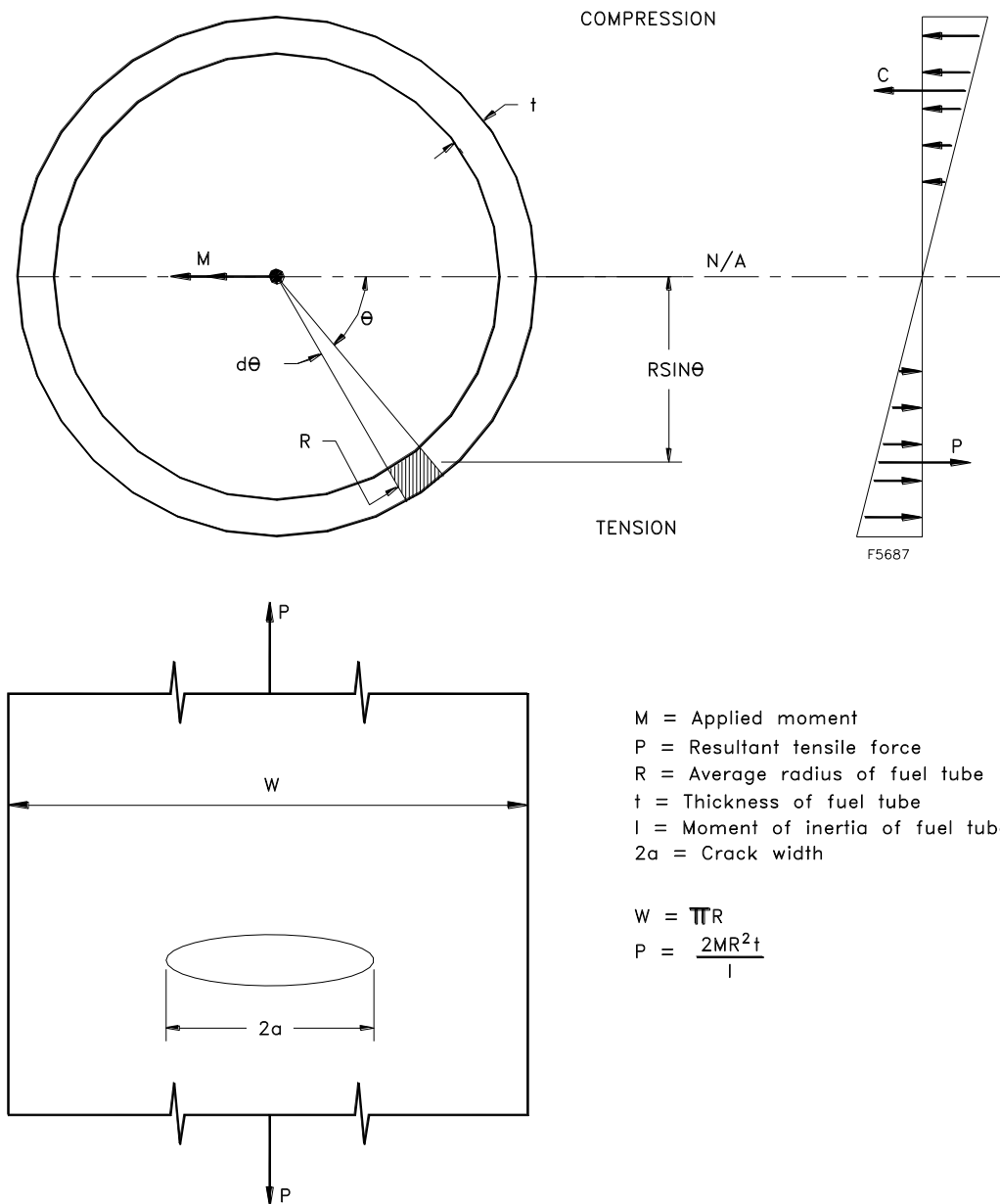


Table 3.9.8-10
Tire Stiffness Calculation

The on-site transfer trailer has four axles with eight 235/75R 17.5 SLR 184 tires per axle (total of 32 tires). The tire stiffness is estimated based on tire measurements as follows:

For 235 (tire width in mm)/75 (height-to-width ratio in %) R 17.5 (rim diameter in inches) SLR184:

Tire width 235mm/25.4mm/in =9.25 inch

Height of tire = 75% of 9.25= 6.94 inch

Tire diameter = 17.5+2*6.94= 31.4 inch.

From trailer tire measurements:

	a (height) - in	b (width) - in	c (ground top) - in
A (front right tire)	6.5	7.4	30.0
B (front left tire)	7.3	7.4	30.8
C (rear right tire)	4.8	7.3	31.3
D (rear left tire)	4.0	7.2	31.4

Tire pressure: 140-145 psi

Trailer weight: 39,700 lbs.

Skid weight: 26,500 lbs

RAM weight: 6,400 lbs.

Average c dimension at front= (30+30.8)/2=30.4 inches

Average c dimension at rear = (31.3+31.4)/2=31.4 inches

Tire height: 33 inches, at approximately 145 psi pressure

Weight per tire (excluding RAM weight): 66,200/32=2070 lbs/tire

Weight per tire (assuming RAM weight is distributed on 8 tires): 6400/8= 1600 lb/tire

Front 8 tires: 2070+1600=3670 lbs/tire.

Table 3.9.8-10 (concluded)
Tire Stiffness Calculation

All other tires: 2070 lbs/tire

Stiffness is determined as:

$$K_{\text{front}} = 3670 / (33 - 30.4) = 1411 \text{ lbs/in}$$

$$K_{\text{all others}} = 2070 / (33 - 31.4) = 1294 \text{ lbs/in}$$

Use $K/\text{tire} = 1500 \text{ lbs/inch}$.

$$\text{Total stiffness} = 32 \times 1500 = 4.8 \times 10^4 \text{ lbs/in}$$

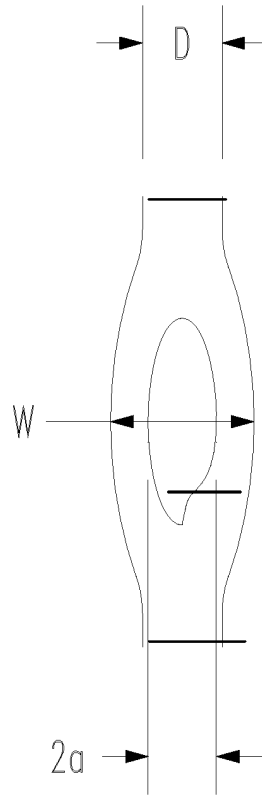
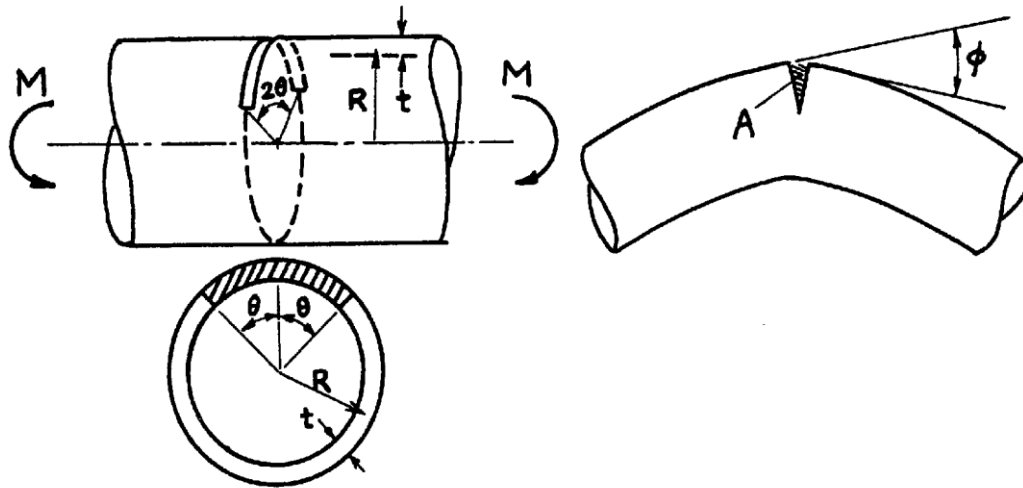


Figure 3.9.8-1
Fracture Geometry #1 - Ruptured Section



$$\frac{R}{t} \simeq 10 \quad (\theta < 110^\circ)$$

$$\sigma = M / (\pi R^2 t)$$

$$K_I = \sigma \sqrt{\pi(R\theta)} \cdot F(\theta)$$

$$F(\theta) = 1 + 6.8 \left(\frac{\theta}{\pi} \right)^{3/2} - 13.6 \left(\frac{\theta}{\pi} \right)^{5/2} + 20.0 \left(\frac{\theta}{\pi} \right)^{7/2}$$

Figure 3.9.8-2
Fracture Geometry #2: Through-Wall Circumferential Crack in Cylinder under Bending

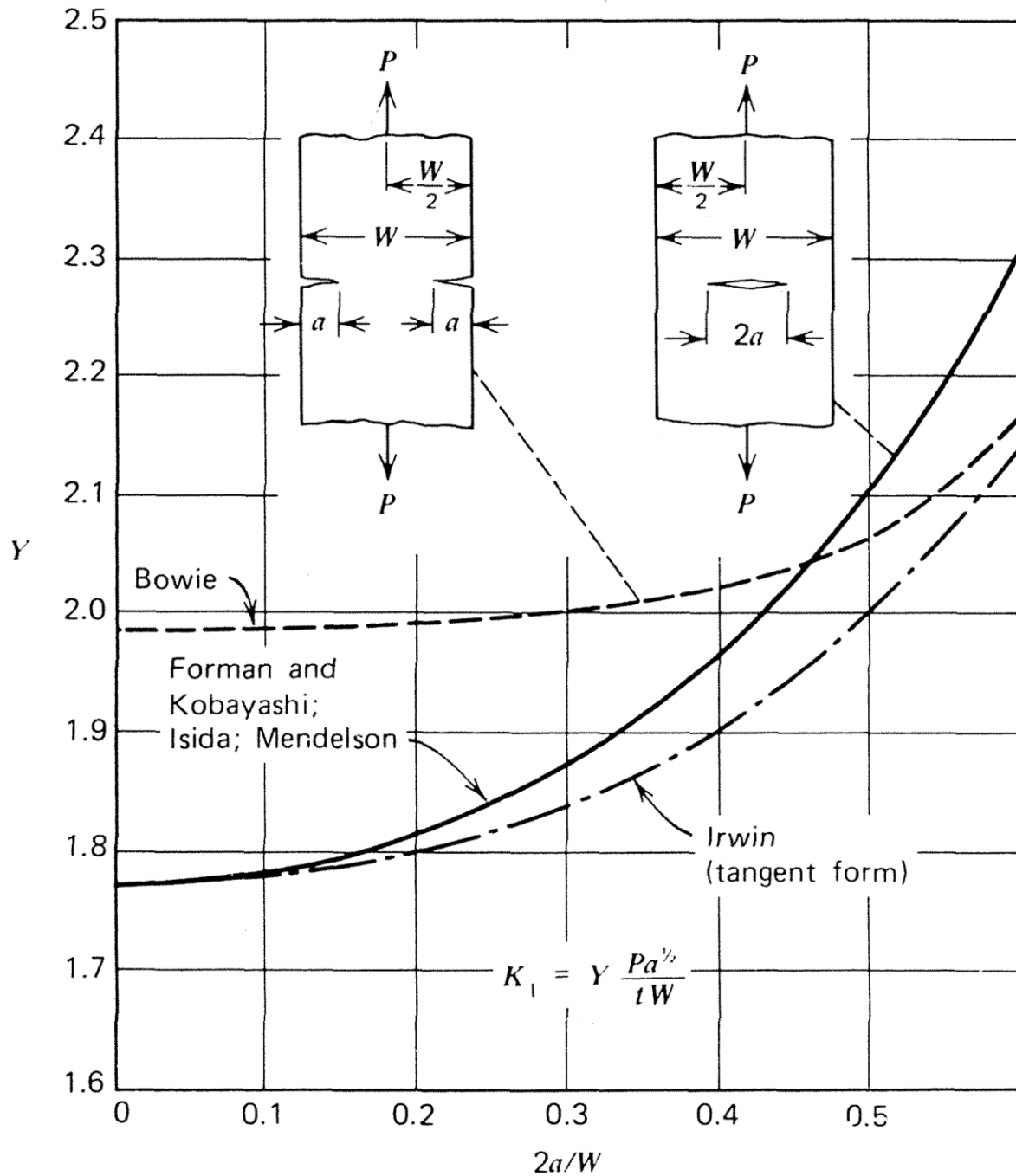
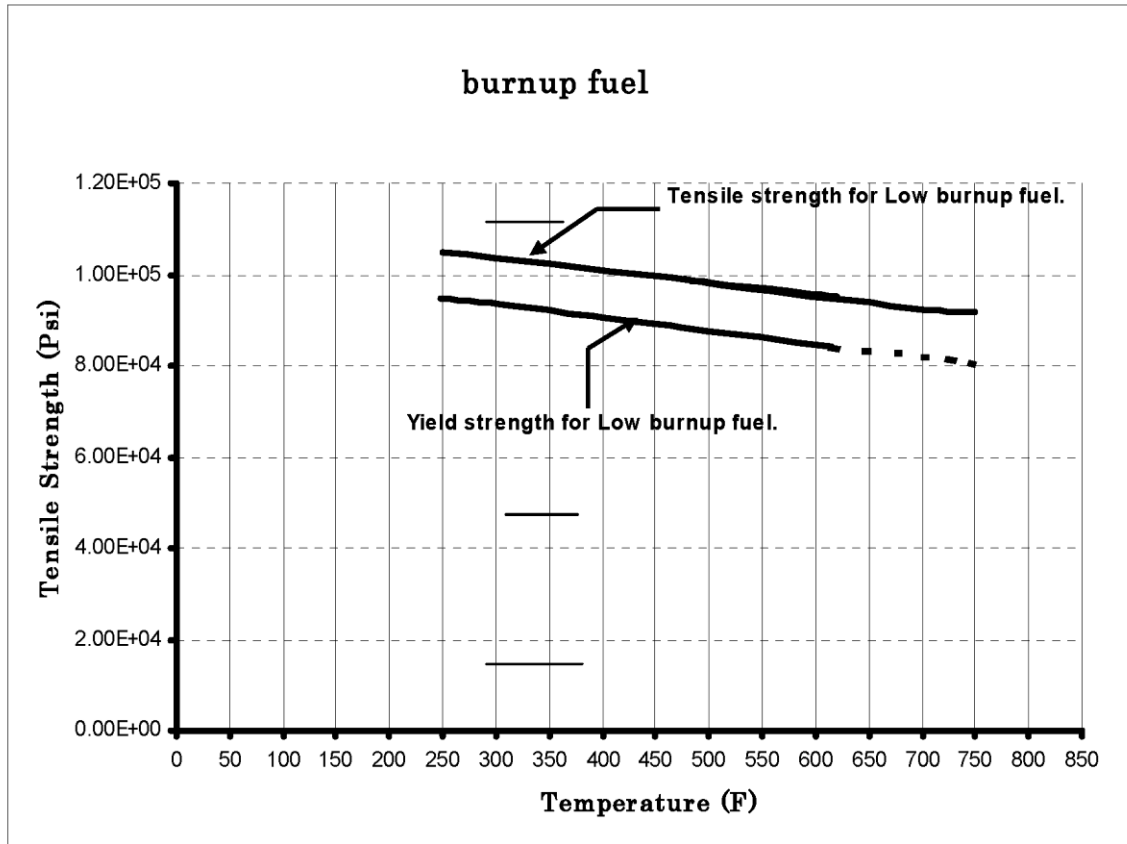


Figure 3.9.8-3
Stress Intensity Factor Solutions: For Several Specimen Configurations



Yield Strength (Low Burn Up)	Temp F
9.49E+04	248
9.44E+04	264
9.39E+04	284
9.33E+04	304
9.24E+04	334
9.14E+04	369
9.01E+04	415
8.81E+04	486
8.44E+04	615
8.15E+04	725
8.05E+04	750

Tensile Strength (Low Burn Up)	Temp F
1.05E+05	250
9.52E+04	615
9.85E+04	486
9.20E+04	725
9.18E+04	750

Figure 3.9.8-4
Temperature Vs Tensile and Yield Strength for Low Burn up Fuel

Proprietary Information on This Page
Withheld Pursuant to 10 CFR 2.390

APPENDIX 3.9.9
HSM-H STRUCTURAL ANALYSIS

TABLE OF CONTENTS

3.9.9	HSM-H STRUCTURAL ANALYSIS	3.9.9-1
3.9.9.1	Introduction.....	3.9.9-1
3.9.9.2	General Description of the HSM-H.....	3.9.9-1
3.9.9.3	Material Properties	3.9.9-3
3.9.9.4	Component Weights.....	3.9.9-4
3.9.9.5	Design Criteria	3.9.9-5
3.9.9.6	Load Cases.....	3.9.9-8
3.9.9.7	Finite Element Model	3.9.9-13
3.9.9.8	Normal Operation Structural Analysis.....	3.9.9-16
3.9.9.9	Off-Normal Operation Structural Analysis.....	3.9.9-18
3.9.9.10	Accident Condition Structural Analysis	3.9.9-20
3.9.9.11	Load Combination	3.9.9-27
3.9.9.12	Conclusions.....	3.9.9-28
3.9.9.13	References	3.9.9-29

LIST OF TABLES

Table 3.9.9-1	Summary of HSM-H Component Design Loadings.....	3.9.9-30
Table 3.9.9-2	Summary of 32PTH DSC Support Structure Design Loadings.....	3.9.9-31
Table 3.9.9-3	HSM-H Concrete Load Combinations.....	3.9.9-32
Table 3.9.9-4	Ultimate Capacities of Concrete Components.....	3.9.9-33
Table 3.9.9-5	Structural Design Criteria for DSC Support Structure	3.9.9-34
Table 3.9.9-6	HSM-H Support Steel Structure Load Combinations.....	3.9.9-35
Table 3.9.9-7	Design Pressures for Tornado Wind Loading.....	3.9.9-36
Table 3.9.9-8	Maximum NUHOMS® HSM-H Concrete Component Forces and Moment for Normal and Off-Normal Loads	3.9.9-37
Table 3.9.9-9	Summary of Thermal Forces and Moments in the HSM-H Concrete Components	3.9.9-38
Table 3.9.9-10	Maximum HSM-H Concrete Component Forces and Moments for Accident Loads	3.9.9-39
Table 3.9.9-11	Comparison of Highest Combined Shear Forces/Moments with the Capacities.....	3.9.9-40
Table 3.9.9-12	Maximum/Minimum Forces/Moments in the Rail Components in the Local System.....	3.9.9-41
Table 3.9.9-13	Maximum/Minimum Forces/Moments in the Rail Extension Plates in the Local System.....	3.9.9-42
Table 3.9.9-14	Maximum/Minimum Axial Forces in the Cross Member Components	3.9.9-43
Table 3.9.9-15	Rail Component Results	3.9.9-44
Table 3.9.9-16	Extension Plates and Cross Members Results	3.9.9-45

LIST OF FIGURES

Figure 3.9.9-1	Analytical Model of the W12x96 Beam with Slotted, Nitronic and Stiffener Plates	3.9.9-46
Figure 3.9.9-2	Analytical Model of the HSM-H for Mechanical Load Analysis	3.9.9-47
Figure 3.9.9-3	Analytical Model of the 32PTH DSC Support Structure.....	3.9.9-48
Figure 3.9.9-4	Analytical Model of the HSM-H for Thermal Load Analysis	3.9.9-49
Figure 3.9.9-5	Symbolic Notations of Force and Moment Capacities (Also for Computed Forces and Moments)	3.9.9-50
Figure 3.9.9-6	Components of Support Structure.....	3.9.9-51

3.9.9 HSM-H STRUCTURAL ANALYSIS

3.9.9.1 Introduction

The purpose of this appendix is to present the structural evaluation of the HSM-H due to all applied loads during storage loading operations.

The design of the HSM-H for 32PTH DSC is the same as the HSM-H which is under NRC review as Amendment 8 to CoC 1004 for 24PTH DSC. Analyses performed for HSM-H with 24PTH DSC used bounding values to envelop both 24PTH DSC and 32PTH DSC.

The HSM-H module design for 32PTH canister is identical to the HSM-H design for 24PTH canister except the following modifications:

1. The module for the 32PTH canister is designed such that the center line of the loaded 32PTH canister is approximately four inches higher compared to that of the 24PTH canister.
2. The diameter of the door openings in the front and rear of the front wall are approximately four inches and two inches larger for the 32PTH canister compared to those of the 24PTH canister.
3. The transfer cask docking surface in the module for the 32PTH canister transfer cask is approximately half inch wider compared to the cask docking surface for the 24PTH canister transfer cask.
4. The diameters of the front inner circular steel plate and rear circular concrete block of the shielded door for the 32PTH canister are approximately four inches and two inches larger compared to those of the 24PTH canisters.
5. For the 32PTH design the spacers at the canister stop plate of the module will be provided similar to the 24PTH short cavity design.

Analyses performed for HSM-H with 24PTH DSC used bounding values to envelop both 24PTH DSC and 32PTH DSC. The structural evaluation provided in this appendix is identical as the information provided in Amendment 8 to CoC 1004 for 24PTH DSC. Amendment 8 reference sections are indicated in this appendix for cross reference.

3.9.9.2 General Description of the HSM-H

The HSM-H is a free standing reinforced concrete structure designed to provide environmental protection and radiological shielding for the 32PTH DSC. Each HSM-H provides a self-contained modular structure for the storage of a 32PTH DSC containing up to 32 PWR spent fuel

assemblies. The HSM-H provides heat rejection from the spent fuel decay heat by a combination of radiation, conduction and convection. Schematic sketch of the HSM-H showing the different components is provided in Chapter 1, Figure 1-1. The drawings in Chapter 1, Section 1.5 provide the principal dimensions and design parameters of the HSM-H.

The HSM-H is a reinforced concrete structure comprised of a base unit, where the 32 PTH DSC is stored and a roof unit that serves to provide environmental protection and radiation shielding. These two units are assembled together to form a single module.

The HSM-H modules may be prefabricated off-site, then transported to the ISFSI site and installed on a reinforced concrete basemat. The HSM-H is placed next to, and in contact with, adjacent module(s) to form a continuous single or double row arrays.

The 32PTH DSC is supported inside the HSM-H by the DSC support structure. The DSC support structure (rail support assembly) is comprised of two rail sections, two slotted plates and two rail support plates. The rail support assembly provides support for the DSC during storage and act as a sliding surface during DSC insertion and retrieval.

The air inlet vents are extending through the front on both sides of the front wall. The front wall and the rear wall of the base unit provide support for the rails and the rail extension flanges. The roof unit rests on the front, rear and side walls of the base unit. The air outlet vents are provided in the roof unit.

The HSM-H front standard door is a composite door, which consists of a rectangular steel face plate at the front attached to a circular thick steel plate and a circular reinforced concrete block at the rear. The rectangular steel face plate of the door is attached to the front wall concrete using four bolts anchored through four embedments. The alternate circular door is similar to the standard door except that the front face is a circular steel plate. The circular steel plate of the door is attached to the front wall concrete by four clamps which are located at the 45° line in each quadrant of the door. The clamps consist of four “L” shaped clips which are bolted to the front wall concrete through four embedments. The door provides missile protection and shielding for the DSC.

The concrete door provides missile protection and shielding. End shield walls are provided at the ends of a module array to provide the required missile and shielding protection. Similarly, an additional shield wall is used at the rear of the module for single module rows.

The side heat shields (with fins) consist of three panels. Each panel consists of anodized aluminum fins mounted on the stainless steel base plates. The base plates are provided with aluminum backing plates on the surface facing the concrete. The alternate side heat shields are made of stainless steel and consist of four flat panels. The top louvered heat shield under the roof consists of six panels. Each panel has two aluminum mounting bars. Horizontal louvers are mounted on these bars. The alternate top heat shields are made of stainless steel and consist of two flat panels. The heat shields provide thermal protection for the HSM-H concrete.

During DSC insertion/retrieval operations, the transfer cask is docked with the HSM-H docking surface and mechanically secured to the embedment provided in the front wall. The embedments are equally spaced on either side of the HSM-H access opening.

The drawings in Chapter 1, Section 1.5 provide the principal dimensions and design parameters of the HSM-H. The dimension differences between the HSM-H to be used for storing the 32PTH canister and 24PTH canister are listed in the following tables.

TN drawing No. 10494-72-104 (for 32PTH data)

HSM-H		
Dimension	System Type	
	For 32PTH Canister	For 24PTH Canister [13]
A	8' – 10"	8' – 6"
B	Ø 5' – 11 5/8"	Ø 5' – 9"
C	Ø 7' – 5"	Ø 7' – 1 1/2"

TN drawing No. 10494-72-107 (for 32PTH data)

HSM-H		
Dimension	System Type	
	For 32PTH Canister	For 24PTH Canister [13]
A	34.88"	33.60"

TN drawing No. 10494-72-108 (for 32PTH data)

HSM-H		
Dimension	System Type	
	For 32PTH Canister	For 24PTH Canister [13]
A	8' – 1 1/2"	7' – 3 3/4"
B	Ø 7' – 3"	Ø 6' – 11 1/2"
C	Ø 5' – 8 5/8"	Ø 5' – 6"
D	Ø 7' – 7 1/4"	Ø 7' – 3 3/4"
E	1' – 10 1/2"	1' – 10 1/2"

3.9.9.3 Material Properties

The temperature dependent material properties for concrete and reinforcing steel are provided in Chapter 3, Tables 3-6, 3-7 and 3-7A. The material properties of the Type 304 Stainless Steel rails are identical to the ASME Code properties listed in Chapter 3, Table 3-5.

3.9.9.4 Component Weights

The following table summarizes the weight of the loaded HSM-H.

Component Description	CALCULATED WEIGHT (kips)
32PTH DSC Empty Weight	58.04
32 PWR Spent Fuel Assemblies	51.52
Total Loaded DSC Weight (Dry)	109.56
HSM-H Single Module Weight (Empty)	306.1
HSM-H Single Module Weight (Loaded)	415.66

3.9.9.5 Design Criteria

Codes and Standards

The reinforced concrete HSM-H, including the 32PTH-DSC support structures, are important to safety NUHOMS® HD system components. Consequently, they are designed and analyzed to perform their intended functions under the extreme environmental and natural phenomena specified in 10CFR 72.122 [1] and ANSI 57.9 [2]. These include tornado, wind, seismic, and flood design criteria.

The following table summarizes Codes and Standards for design and fabrication of these components.

Component	Code of Construction
HSM-H and 32PTH DSC Support Structures	<ul style="list-style-type: none"> • ACI 349-97 (Concrete); ACI 318-95 (construction) • AISC Ninth Edition (Structural Steel) • AWS D1.1 (Structural Welds) • ASCE 7-95 (Loads) • ANSI 57.9-84 (Loads & Load Combinations)

Loadings

The loadings are listed in Tables 3.9.9-1 & 3.9.9-2 and discussed in details in Section 3.9.9.6.

Loading Criteria

The ultimate strength method of ACI 349 [3] is used for the design of the HSM-H reinforced concrete structural components. Required reinforcement is provided to meet the minimum flexural and shear reinforcement requirements of ACI 349 and to ensure that the provided design strength exceeds that required for the factored design loads specified in Table 3.9.9-3.

The following relationships from the ACI code are used to compute capacities of the concrete components:

Ultimate Moment Capacity (M_u)

$$M_u = \phi M_n = \phi A_s f_y (d-a/2)$$

where $a = (A_s f_y) / (0.85 f'_c b)$

Ultimate Tension Capacity (P_{tu})

$$P_{tu} = \phi A_{st} f_y$$

$$\phi = 0.9$$

$$A_{st} = 2A_s \text{ (The reinforcement in two opposite faces are assumed to be same)}$$

Ultimate Compression Capacity (P_{cu})

$$P_{cu} = \phi P_n = 0.8\phi[0.85f'_c (A_g - A_{st}) + f_y A_{st}]$$

$$A_{st} = 2A_s, \phi = 0.7$$

Ultimate In-Plane Shear Capacity (V_{ui})

$$V_{ui} = \phi A_g (2\sqrt{f'_c} + \rho_n f_y)$$

$$\phi = 0.85, \rho_n = (2A_s / bT)$$

Ultimate Out-Plane Shear Capacity (V_{uo})

$$V_{uo} = \phi 2 \sqrt{f'_c} (bd)$$

$$\phi = 0.85$$

where:

ϕ = Strength reduction factor

A_s = Area of reinforcing steel in tension

A_{st} = Total area of the reinforcing steel

A_g = Gross area of concrete section

f_y = Yield strength of reinforcing steel

f'_c = Compressive strength of concrete

d = Distance of the top fiber of concrete from the center of the rebar

b = Width of the section = 12"

T = Depth of the section

The computed shear and moment capacities for all the concrete components of the HSM-H, calculated based on the preceding equations from ACI 349 [3] are provided in Table 3.9.9-4.

The capacities calculated in Table 3.9.9-4 for the accident condition consider a 10% reduction in compressive strength of the concrete and yield strength of the reinforcing rebar materials due to concrete temperatures exceeding 350 °F.

The required steel strength, S , and required shear strength, S_v for critical sections of steel structure are calculated in accordance with the requirements of AISC Allowable Stress Design (ASD) method [4].

In addition to deadweight and normal and off normal handling loads, the steel support structure components are subjected to the normal operating thermal loads (TN), off-normal operating thermal loads (TO) and accident thermal loads (TA), which cause additional stresses. However, the steel support structure is protected from design wind load (WW), Tornado wind and missile impact loads (WT) and Flood loads (FL) by the concrete components of the HSM-H. Therefore, these loads do not cause stresses in the steel support structure.

The corresponding structural design criteria for the DSC support structure are summarized in Table 3.9.9-5 and 3.9.9-6.

3.9.9.6 Load Cases

3.9.9.6.1 HSM-H Normal Loads (*Section P.2.2.5.2.1 from CoC 1004 Amendment #8*)

A. Dead Loads (DW)

Dead load includes the weight of the HSM-H concrete structure and the steel structure (the DSC weight is considered as a live load rather than a dead load).

The dead load is varied by +5% from the estimated value to simulate the most adverse loading condition in accordance with ANSI-57.9 [2].

B. Live Loads (LL)

Live loads include the roof design basis snow and ice load of 110 psf conservatively derived from ASCE 7-95 [5]. A total live load of 200 psf (which includes snow and ice load) is used to envelope all postulated live loading, including such items as ladders, handrails, conduits, etc. added for personnel protection. In addition, the normal handling loads (RO), and off-normal handling loads (RA), and the DSC weight are treated as live loads for the concrete component evaluation.

In accordance with ANSI-57.9 [2], the live load is varied between 0% and 100% of the estimated load to simulate the most adverse conditions for the structure.

C. Normal Operating Thermal Loads (TN)

The normal thermal loads on HSM-H include the effects of design basis internal heat load (40.8 kW maximum heat load) generated by the canister plus the effects of normal ambient conditions (0 °F and 100 °F).

D. Normal Handling Loads (RO)

The most significant normal operational loading condition for the HSM-H components is the sliding of the DSC from the TC into the HSM-H. Friction forces are developed between the sliding surfaces of the DSC, the TC and the HSM-H support rails. Normal operation assumes the canister is sliding over the support structure due to a hydraulic ram force of up to 80,000 lbs (insertion) and 60,000 lbs (extraction) applied to the DSC base. It is assumed that the 80 or 60 kips load is resisted by an axial load (40 or 30 kips) in each support rail and front embedments. In addition the DSC weight is applied as a distributed load on both the rails. The normal handling loads are considered as live loads for the design of the concrete components.

E. Design Basis Wind Load (WW)

Conservatively, this load case is assumed to be enveloped by tornado generated wind load (WT) described in Section 3.9.9.6.3.

3.9.9.6.2 HSM-H Off-Normal Loads (*Section P.2.2.5.2.2 from CoC 1004 Amendment #8*)

A. Off-Normal Operating Thermal Loads (TO)

This load case is the same as the normal thermal load but with an ambient temperature range from -40°F to 117°F. The temperature distribution for the extreme ambient conditions is used in the analysis for the concrete and steel component evaluation.

B. Off-Normal Handling Loads (RA)

This load case assumes that the TC is not accurately aligned with respect to the HSM-H resulting in binding of the DSC during a transfer operation causing the hydraulic pressure in the ram to increase. The ram force is limited to a maximum load of 80 kips during insertion and 80 kips during retrieval. Therefore, for the steel support structure, the off-normal jammed canister load (RA) is defined as an axial load on one rail of 80 kips during insertion and 80 kips during retrieval, plus a vertical load of one half the DSC weight (on both rails) at the most critical location. The off-normal operating handling loads are considered as live loads for the design of the concrete components.

3.9.9.6.3 HSM-H Accident Loads (*Section P.2.2.5.2.3 from CoC 1004 Amendment #8*)

A. Accident Thermal Loads (TA)

The postulated accident thermal event occurs due to blockage of either the air inlet or outlet vents under off-normal ambient temperatures range from -40°F to 117°F .

B. Tornado Wind and Tornado Missiles (WT, WM)

The design basis tornado (DBT) wind intensities used for the HSM-H design are obtained from NRC Regulatory Guide 1.76 [6]. Region I intensities are utilized since they result in the most severe loading parameters. For this region, the maximum wind speed is 360 mph, the rotational speed is 290 mph and the maximum translational speed is 70 mph. The radius of the maximum rotational speed is 150 ft, the pressure drop across the tornado is 3 psi and the rate of pressure drop is 2 psi per second [6].

Determination of Forces on Structure

Tornado loads are generated for three separate loading phenomena:

- Pressure or suction forces created by drag as air impinges and flows past the HSM-H. These pressure or suction forces are due to tornado generated wind with maximum wind speed of 360 mph.
- Pressure or suction forces created by tornado generated pressure drop or differential pressure load of 3 psi.
- Impact, penetration and spalling forces created by tornado-generated missiles impacting on the HSM-H.

The DBT velocity pressure is computed based on the following equation specified in ASCE 7-95 [5].

$$q_v = 0.00256 K_z * K_{zt} * I * V^2 \text{ lb/sq ft}$$

Where:

K_z = velocity pressure exposure coefficient equal to 0.9 applied to the full HSM-H height of 18.5 ft for level C exposure (Table 6-3 of [5]).

K_{zt} = 1.0 for level C exposure and structures with height less than 30 ft. (Section 6.5.5 of [5]).

I = Importance Factor equal to 1.15 (Table 6-2 of [5]).

Since the generic design basis HSM-H dimensions are relatively small compared to 150 ft rotational radius of the DBT, the velocity value of combined rotational and translational wind velocity of 360 mph is conservatively used in the above equation to compute the DBT velocity pressure of 344 psf.

The design pressures for the tornado wind load are shown in Table 3.9.9-7.

Tornado Missiles

The determination of impact forces created by DBT generated missiles for the HSM-H is based on the criteria provided by NUREG-0800, Section 3.5.1.4, III.4 [7]. Accordingly, eight types of missiles are postulated:

1. The utility wooden pole, 13.5" diameter, 35' long missile weighing 1500 lbs at a horizontal velocity of 294 fps.
2. The armor piercing artillery shell 8" diameter, weighing 276 lbs at a horizontal velocity of 185 fps.
3. The steel pipe missile 12" diameter, Schedule 40, 30' long weighing 1500 lbs at a horizontal velocity of 205 fps.
4. The massive automobile missile weighing 4000 lbs at a horizontal velocity of 195 fps traveling through the air not more than 25 ft above the ground and having contact area of 20 square ft.
5. Wood plank missiles traveling end on, 200 lbs, traveling at 440 fps.
6. Steel Pipe 3" diameter, Sch 40, weighing 115 lbs, traveling at 268 fps.
7. Steel Pipe 6" diameter, Sch 40, 285 lbs, traveling at 230 fps.
8. Steel rod, 1" diameter, 3' long weighing 8 lbs traveling at 317 fps.

For the overall effects of a DBT missile impact, overturning and sliding of the HSM-H, the force due to the deformable massive missile impact is applied to the structure at the most adverse location. Conservation of momentum is assumed to demonstrate that sliding and/or tipping of the module will not result in an unacceptable condition for the module. The coefficient of restitution is assumed to be zero and the missile energy is transferred to the module to be dissipated as sliding friction, or an increase in potential energy due to raising the center of gravity. The force is evenly distributed over the impact area. The magnitude of the impact force for design of the local reinforcing is calculated in accordance with Bechtel Topical Report "Design of Structures for Missile Impact" [8].

For the local damage analysis of the HSM-H for DBT missiles, three governing missiles are used for the evaluation of concrete penetration, spalling, scabbing and perforation thickness. The modified National Defense Research Committee (NDRC) empirical formula is used for this evaluation as recommended in NUREG-0800, Section 3.5.3 [7]. The results of these evaluations are reported in Chapter 11.

C. Flood Load (FL) (Section P.2.2.2 from CoC 1004 Amendment #8)

Flooding of the NUHOMS® ISFSI greater than 0.46 m (1'-6") above grade results in blockage of the HSM inlet vents. Flooding of the NUHOMS® ISFSI greater than 1.7 m (5'-8") above grade results in wetting of the DSC. Greater flood heights result in submersion of the DSC and blockage of the HSM outlet vents.

The DSC and HSM are conservatively designed for an enveloping design basis flood, postulated to result from natural phenomena such as a tsunami, and seiches, as specified by 10CFR72.122(b). For the purpose of this bounding generic evaluation, a 15 m (50 foot) flood height and water velocity of 4.6 m/sec (15 fps) is used. The HSM-H is evaluated for the effects of a water current of 4.6 m/sec (15 fps) impinging upon the side of a submerged HSM-H. The DSC is subjected to an external pressure equivalent to a 15 m (50 foot) head of water.

The calculated effects of the enveloping design basis flood are included in the load combinations and reported stresses presented in Section 3.9.9.10.3. The plant specific design basis flood (if the possibility for flooding exists at a particular ISFSI site) should be evaluated by the licensee and shown to be enveloped by the flooding conditions used for this generic evaluation of the NUHOMS[®] DSC and HSM-H.

D. Seismic Load (EQ) (Section P.2.2.3 from CoC 1004 Amendment #8)

The design basis response spectra of NRC Regulatory Guide 1.60 [9] are selected as the design earthquake for qualifying different component of HSM-H. A damping value of seven percent of damping is used for the concrete structure [12]. The response spectra are anchored to a maximum ground acceleration of 0.3g for the horizontal component and 0.2g for the vertical component. The results of the frequency analysis of the HSM-H structure (which includes a simplified model of the DSC) yield a lowest frequency of 23.2 Hz in the transverse direction and 28.4 Hz in the longitudinal direction. The lowest vertical frequency exceeds 33 Hz. Thus, based on the R.G. 1.60 response spectra amplifications, the corresponding seismic accelerations used for the design of the HSM-H are 0.37g and 0.33g in the transverse and longitudinal directions respectively and 0.20g in the vertical direction. The corresponding accelerations applicable to the DSC are 0.41g and 0.36g in the transverse and longitudinal directions, respectively, and 0.20g in the vertical direction. The seismic analysis of the HSM-H is further discussed in Section 3.9.9.10.

3.9.9.6.4 Combined Load Criteria (*Section P.2.2.5 from CoC 1004 Amendment #8*)

A summary of the design loads for the HSM-H System is provided in Tables 3.9.9-1 and 3.9.9-2. These tables also present the applicable codes and standards for development of these loads. Table 3.9.9-3 and 3.9.9-6 summary the load combination requirements of the HSM-H module design. These tables comply with the requirements of 10 CFR 72.122, and ANSI 57.9.

3.9.9.7 Finite Element Model

3.9.9.7.1 ANSYS Finite Element Model of the Rail Assembly

Description of the Rail Assembly

The HSM-H support structure consists of two rail assemblies, each at 30 degrees from the vertical center line of the DSC. Two welded cross members connect the two rail assemblies by four gusset plates welded to the rail web and flanges. The steel support structure supports the DSC stored inside the module. Each rail assembly of the DSC support structure consists of the following components:

1. W 12x96 Rail Section 187" long made from ASTM A992 material and with twelve (12) 6" diameter holes for airflow cooling of the DSC. The depth of the section is 12.71", thickness of the web is 0.55", width of the flange is 12.16" and thickness of the flange is 0.9" (Ref. 4).
2. A 1" thick slotted rail support plate made from A572 Grade 50 material with 1/2"x2" slots normal to the plate axis.
3. A 3/16" thick support plate made from Nitronic 60 (UNS S21800) material which provides a smooth support for the DSC to slide.
4. A rail extension baseplate which consists of 1" thick plate ASTM A36 material.

The rail extension baseplate is attached to 1-1/2" diameter threaded embedments by two bolts.

Finite Element Model of the Rail Assembly

A three dimensional finite element model of the rail section, slotted plate, rail support plate and rail extension flange was developed for the computer program ANSYS [10]. The rail sections, slotted plates, rail support plates and extension plates were modeled using SOLID 73 element. Each element has 8 nodes with six degrees of freedom (three translational and three rotational) per node. The web of the W section and the stiffeners were modeled using Shell 63 element. In order to establish compatibility of the degrees of freedom between solid and plate elements, the ANSYS option for activating realistic in-plane rotational stiffness (Allman rotational stiffness, KEYOPT(3)=2) is used for the plate elements. The model is inclined by 30 degrees from the vertical. A plot of the partial model (front end) is shown in Figure 3.9.9-1.

The model is completely restrained at the bottom end of the extension plate and supported vertically and transversely approximately 6" from the end to simulate the connection between the

extension plate and the front wall. The model also is supported in the vertical and transverse directions at approximately 12" on either side of the W section at the bottom flange (to simulate the simple support condition of the concrete pedestals at the front and rear walls).

Finite element analysis of the above rail assembly model was performed to compute the maximum displacements of the model, subjected to unit load normal to rail axis in and out of plane of the curb and in the axial direction. The equivalent beam element properties such as area (A), moment of inertia about the major axis (I_{x-x}) and moment of inertia about the minor axis (I_{y-y}) are determined by equating the maximum deflection of the beam to displacement obtained from the finite element model.

3.9.9.7.2 ANSYS Finite Element Model of the HSM-H Combined Concrete and Steel Structure for Structural Analysis

The structural analysis of an individual module provides a conservative estimate of the response of the HSM-H structural elements under various static and dynamic loads for any HSM-H array configuration. Therefore, analytical models of a single free standing HSM-H is developed in this section for the computer program ANSYS [10]. The frame and shear wall action of the HSM-H concrete components are considered to be the primary structural system resisting the loads. The analytical models are evaluated for normal operating, off-normal and postulated accident loads acting on the HSM-H.

A three dimensional finite element model of the HSM-H which includes all the concrete components (rear wall, front wall, two side walls and the roof) was developed for the computer program ANSYS [10]. The eight node brick element type SOLID 73 element was used to model the concrete structure. Four layers of brick elements were used to model the concrete components. Each node of the eight node brick element has six degrees of freedom. The DSC was modeled using the beam elements (ANSYS element type BEAM4). The rails and the lateral bracing between the rails (Cross beams) were also modeled using beam elements with appropriate stiffness. The mass of the DSC was lumped at the nodes representing the DSC using lumped mass elements (ANSYS element type MASS21). Plots of the model which includes the concrete structure and the support structure are shown in Figures 3.9.9-2. A plot of the support structure model (which includes the DSC, rails and the cross beams) is shown in Figure 3.9.9-3.

The material properties used in the DSC support structure model are provided in Chapter 3. The DSC support structure model is attached to the concrete at several locations (four locations at the rear shelf, four locations in the front shelf and two locations on the front wall opening.) Each node of the support structure has three translational and three rotational degrees of freedoms. The rails are supported such that they are completely restrained at the front extension plate locations and free to rotate in all three directions and free to translate only in axial direction at the other supports in the rear and the front shelf locations.

The DSC support structure analytical model is incorporated into the HSM-H analytical model. The various normal, off-normal and accident loads are applied to the analytical model and

internal forces and moments were computed in different members by performing a linear elastic finite element analysis.

The node coupling option of ANSYS was used to represent the appropriate connection between the different concrete components of the HSM-H model. The connections of the support structure to the concrete structure were modeled also using the node coupling option.

For the analysis performed in this calculation, due to applied loading, the model is assumed neither to uplift from the basemat (because of its dead weight) nor to slide on the basemat (because of friction). Therefore, the model is restrained vertically at all nodes on the bottom of the model, and also restrained laterally and axially at all nodes on the bottom of the model to prevent rigid body movement.

3.9.9.7.3 ANSYS Finite Element Model of the HSM-H for Thermal Stress Analysis

The thermal stress analysis of the HSM-H was performed using the three dimensional finite element model (developed for ANSYS) which includes the concrete and support steel components. The eight node brick elements of type SOLID73 were used to model the concrete structure. Four layers of brick elements were used to model the concrete components. Each node of the brick element has three translational and three rotational degrees of freedom. The connections between the HSM-H concrete structure and the door are designed such that free thermal growth is permitted in the door, when the HSM-H is subjected to thermal loads. Because of the free thermal growth, the door does not induce stresses in the concrete components of the HSM-H. Therefore, the analytical model of the HSM-H for thermal stress analysis of the concrete components does not include the door. The ANSYS model used to perform thermal stress analysis of the concrete and support steel components is shown in Figures 3.9.9-4. Conservatively, the roof and the base unit are coupled in this model. However, the DSC beam model is uncoupled from the support steel beam model.

The model base is restrained at one set of end nodes (in axial and lateral directions) and friction forces are applied in the axial and lateral directions at the opposite set of end nodes. For the thermal load analysis all the nodes at the base are restrained in the vertical direction.

3.9.9.8 Normal Operation Structural Analysis

The evaluation of the HSM-H for 32PTH DSC is the same as the HSM-H which is under NRC review as Amendment 8 to CoC 1004 for the 24PTH DSC [13]. Analyses performed for the HSM-H with 24PTH DSC used bounding values to envelop both the 24PTH DSC and the 32PTH DSC. The following table shows how the bounding loads are used for structural evaluation of the HSM-H.

	Weight	Thermal
24PTH DSC (loaded weight)	93.7 kips	40.8 kw
32PTH DSC (loaded weight)	109.56 kips	34.8 kw
Weight used for HSM-H structural evaluation to envelop both 24PTH & 32PTH	110.0 kips (max.) ⁽¹⁾ 72.0 kips (min.) ⁽²⁾	
Thermal load used for HSM-H structural evaluation to envelop both 24PTH & 32PTH		40.8 kw

Notes:

1. Maximum weight is used for structural evaluation of the HSM-H.
2. Minimum weight is used for stability evaluation of the HSM-H.

The following table shows the normal operating loads for which the HSM-H components are designed. The table also lists the individual NUHOMS® HSM-H components which are affected by each loading.

Load Type	Affected Component	
	DSC Support Structure	HSM-H
Dead Weight	X	X
Normal Thermal	X	X
Normal Handling	X	X
Live Loads		X

The reinforced concrete and the support steel structure of the HSM-H are analyzed for the normal, off-normal, and postulated accident conditions using finite element models described in Section 3.9.9.7. These models are used to evaluate concrete and support structure forces and moments due to dead load, live load, normal thermal loads, and normal handling loads. The methodology used to evaluate the effects of these normal loads is addressed in the following paragraphs.

A. HSM-H Dead Load (DW) Analysis (Section P.3.6.1.4(A) from CoC 1004 Amendment #8)

Dead loads are applied to the analytical model by application of 1.05g where g is the gravitational acceleration in the vertical direction (386.4 in/sec²). The 5% variation in the dead

load is in accordance with ANSI/ANS 57.9. The results of the HSM-H concrete components dead load analysis are presented in Table 3.9.9-8.

B. HSM-H Live load (LL) Analysis (Section P.3.6.1.4(B) from CoC 1004 Amendment #8)

Live load analysis is performed by applying 200 psf pressure on the roof and the DSC weight as a distributed load on the support structure. The normal handling load of 80 kips during DSC insertion and 60 kips during DSC retrieval is included as a live load for the concrete component evaluation. The results of the HSM-H concrete components live load analysis are presented in Table 3.9.9-8.

C. HSM-H Normal Operating Thermal (TN) Stress Analysis (Section P.3.6.1.4(C) from CoC 1004 Amendment #8)

Normal operating thermal stress analysis of the concrete and steel support structure is performed for the enveloping thermal load case which is 40.8 kW heat load with ambient temperature of 100°F. An additional thermal load case with -40 °F ambient and 40.8 kW heat load is also considered as a bounding case for the end module in an array of HSM-H. The thermal tests of the HSM-H documented in [15] showed that the HSM-H thermal analysis methodology as described in Chapter 4 conservatively predicts HSM-H component temperatures. The HSM-H thermal stress analysis was performed using thermal profiles and maximum temperatures that bounds those reported in Chapter 4. The results of the HSM-H concrete components thermal load analysis are presented in Table 3.9.9-9.

D. HSM-H Operational Handling Load (RO) Analysis (Section P.3.6.1.4(D) from CoC 1004 Amendment #8)

The operation handling loads of 80 kips during DSC insertion and 60 kips during DSC retrieval are applied to the rail support structure in the axial direction. In addition, the DSC weight is applied as a distributed load on both rails of the HSM-H.

The normal operating handling loads are considered as live loads for the design of the concrete components. The results of the HSM-H concrete components operational handling load analysis are presented in Table 3.9.9-8.

E. HSM-H Design Basis Wind Load (WW) Analysis (Section P.3.6.1.4(E) from CoC 1004 Amendment #8)

The DSC support structure and DSC inside the HSM-H are not affected by wind load. The concrete structure forces and moments due to design basis wind load are bounded by the result of tornado generated wind load discussed in Section 3.9.9.10. Therefore, no separate analysis is performed for this case.

The results of the HSM-H concrete components design basis wind load analysis are presented in Table 3.9.9-8.

3.9.9.9 Off-Normal Operation Structural Analysis

This section describes the design basis off-normal events for the HSM-H modules and presents analyses which demonstrate the adequacy of the design safety features of the HSM-H modules.

The following table shows the off-normal operating loads for which the HSM-H components are designed.

Load Type	Affected Component	
	DSC Support Structure	HSM-H
Off-Normal Thermal	X	X
Off-Normal Handling	X	X

For an operating NUHOMS[®] HD system, off-normal events could occur during fuel loading, transfer cask handling, trailer towing, canister transfer and other operational events. Two off-normal events are defined which bound the range of off-normal conditions. The limiting off-normal events are defined as a jammed DSC during loading or unloading from the HSM-H and the extreme ambient temperatures of -40 °F (winter) and +117 °F (summer). These events envelope the range of expected off-normal structural loads and temperatures acting on the HSM-H. ANSYS finite element models described in Section 3.9.9.7 are used to evaluate concrete and support structure forces and moments due to these loads.

A. HSM-H Off-Normal Thermal Loads (TO) Analysis (Section P.3.6.2.3 (A) from CoC 1004 Amendment #8)

This load case is the same as the normal thermal load but with an ambient temperature range from -40°F to 117°F. The temperature distributions for the extreme ambient conditions are used in the analysis for the concrete component evaluation. The results of the HSM-H concrete components thermal load analysis are presented in Table 3.9.9-9.

B. HSM-H Off-Normal Handling Loads (RA) Analysis (Section P.3.6.2.3 (B) from CoC 1004 Amendment #8)

This load case assumes that the transfer cask is not accurately aligned with respect to the HSM-H resulting in binding of the DSC during a transfer operation causing the hydraulic pressure in the ram to increase. The ram force is limited to a maximum load of 80 kips during insertion and 80 kips during retrieval. Therefore, for the steel support structure, the off-normal jammed canister load (RA) is defined as an axial load on one rail of 80 kips during insertion and 80 kips during retrieval, plus a vertical load of one half the DSC weight (on both rails) at the most critical

location. The off-normal operating handling loads are considered as live loads for the design of the concrete components.

The results of the HSM-H concrete components for off-normal load analysis are presented in Table 3.9.9-8.

3.9.9.10 Accident Condition Structural Analysis

The design basis accident events specified by ANSI/ANS 57.9-1984, and other credible accidents postulated to affect the normal safe operation of the NUHOMS® HSM-H are addressed in this section.

In the following sections, each accident condition is analyzed to demonstrate that the requirements of 10CFR72.122 are met and that adequate safety margins exist for the HSM-H design. The resulting accident condition stresses in the HSM-H components are evaluated and compared with the applicable code limits set forth in Section 3.9.9.5. Load combination results for the HSM-H are presented in Section 3.9.9.11. The postulated accident conditions addressed in this section include:

- Tornado winds and tornado generated missiles (WT, WM)
- Design basis earthquake (EQ)
- Design basis flood (FL)
- Block Vent Thermal (TA)

ANSYS finite element models described in Section 3.9.9.7 are used to evaluate concrete and support structure forces and moments due to these loads.

3.9.9.10.1 Tornado Winds/Tornado Missile (WT, WM) (*Section P.3.7.1 from CoC 1004 Amendment #8*)

Stability and stress analyses are performed to determine the response of the HSM-H to tornado wind pressure loads. The stability analyses are performed using manual calculation methods to determine sliding and overturning response of the HSM-H array. A single HSM-H with both the end and the rear shield walls is conservatively selected for the analyses. The stress analyses are performed using the ANSYS finite element model of a single HSM-H to determine design forces and moments. These conservative generic analyses envelop the effects of wind pressures on the HSM-H array. Thus, the requirements of 10CFR 72.122 are met.

In addition, the HSM-H is evaluated for tornado missiles.

Effect of DBT Wind Pressure Loads on HSM-H

The HSM-H is qualified for maximum DBT generated design wind loads of 234 lb/ft² and 148 lb/ft² on the windward and leeward HSM-H walls (Table 3.9.9-7), respectively and a pressure drop of 3 psi.

A single stand-alone HSM-H is protected by shield walls on either side and at the rear. For an HSM-H array, the critical module is on the windward end of the array. This module has an end shield wall to protect the module from tornado missile impacts. The shield wall is also subjected to the 234 lb/ft² windward pressure load. The leeward side of the same end module in the array

has no appreciable suction load due to the presence of the adjacent module. The 148 lb/ft² suction load is applicable to the end shield wall on the opposite end module in the array. A suction of 207 lb/ft² is also applied to the roof of each HSM-H in the array.

For the stress analyses, the DBT wind pressures are applied to the HSM-H as uniformly distributed loads. The rigidity of the HSM-H in the transverse direction, due to frame and shear wall action of the HSM-H, is the primary load transfer mechanism assumed in the analysis. The bending moments and shear forces at critical locations in the HSM-H concrete components are calculated by performing an analysis using the ANSYS analytical model of the HSM-H. The resulting moments and shear forces are shown in Table 3.9.9-10 and are included in the HSM-H load combination results reported in Section 3.9.9.11.

For conservatism, the design basis operating wind pressure loads are assumed to be equal to those calculated for the DBT in the formulation of HSM-H load combination results.

A stability analysis is performed to evaluate the effects of overturning and sliding due to the postulated DBT. A single, freestanding HSM-H with end shield walls and rear shield wall is used for this analysis.

The pressure drop has no effect on the HSM-H, since the HSM-H is an open structure, due to the presence of the inlet and outlet vents.

HSM-H Overturning Analysis (Section P.3.7.1.1.1 from CoC 1004 Amendment #8)

For the DBT wind overturning analysis, the overturning moment and the resulting stabilizing moments are calculated.

A lower bound estimate of the stabilizing moment (M_{st}) for the windward module is:

$$M_{st} = Wd = 18,824 \text{ k-in.}$$

Where:

$$\begin{aligned} W &= 362 \text{ K, [Lower bound weight of HSM-H (290 kips) + Lowest envelope of any DSC weight (72 kips)]} \\ d &= 52 \text{ in., Horizontal distance between center of gravity of HSM-H to the outer edge of the module.} \end{aligned}$$

and the overturning moment (M_{ot}) for the windward module due to DBT wind pressure is:

$$M_{ot} = [(W_1) A_w h/2 + W_3 A_r d]12$$

Where:

$$\begin{aligned} W_1 &= 0.148 \text{ K/ft.}^2, \text{ Wind load, leeward wall} \\ h &= 18.5 \text{ ft, Wall height} \\ W_3 &= 0.207 \text{ K/ft.}^2, \text{ Wind uplift on roof} \\ A_r &= 199.9 \text{ ft.}^2, \text{ Roof area} \\ A_w &= 382.4 \text{ ft.}^2, \text{ Wall area} \\ d &= 4.34 \text{ ft., Half of the transverse dimension of the roof} \end{aligned}$$

Therefore: $M_{ot} = 8437.0 \text{ K-in.}$

Because the overturning moment is smaller than the stabilizing moment, the freestanding HSM-H will not overturn. The resulting factor of safety against overturning effects for the DBT wind loads is > 2.23 .

HSM-H Sliding Analysis (Section P.3.7.1.1.2 from CoC 1004 Amendment #8)

To evaluate the potential for sliding of a single, freestanding HSM-H, the sliding force generated by the postulated DBT wind pressure is compared to the sliding resistance provided by friction between the base of the HSM-H and the ISFSI basemat.

The force (F_{sl}) required to slide the end module in an array is:

$$F_{sl} = [W - W_3 A_r] \mu$$

Where:

$\mu = 0.6$, coefficient of friction
 W , W_3 and A_r are defined above.

Substituting gives:

$$F_{sl} = 192.4 \text{ K}$$

The sliding force (F_{hw}) generated by DBT wind pressure for a single HSM-H is:

$$F_{hw} = (W_1 + W_2) A_w$$

Where:

$W_2 = 0.234 \text{ k/ft}^2$ wind load, windward wall
 W_1 , and A_w are as defined above.

Substituting gives:

$$F_{hw} = 146.1 \text{ K}$$

Because the horizontal force generated by the postulated DBT is smaller than the force required to slide the end module in an HSM-H array, the HSM-H will not slide. The factor of safety against sliding of the HSM-H due to DBT wind loads is 1.32.

3.9.9.10.2 Earthquake (Seismic) (Section P.3.7.2 from CoC 1004 Amendment #8)

The peak horizontal ground acceleration of 0.30g and the peak vertical ground acceleration of 0.20g are utilized for the design basis seismic analysis of the HSM-H components. Based on NRC Reg. Guide 1.61 [12], a damping value of three (3) percent is used for the DSC seismic analysis. Similarly, a damping value of seven (7) percent for DSC support steel and concrete is utilized for the HSM-H. An evaluation of the frequency content of the loaded HSM-H is performed to determine the amplified accelerations associated with the design basis seismic response spectra for the NUHOMS[®] HSM-H and DSC.

HSM-H Seismic Evaluation (Section P.3.7.2.3 from CoC 1004 Amendment #8)

Seismic Loads (EQ)

As described in Section 3.9.9.6.3, the design basis accelerations for the HSM-H are 0.3g in the horizontal directions and 0.2g in the vertical direction. These seismic accelerations are amplified based on the results of the frequency analysis of the HSM-H, as documented in Section 3.9.9.6.3. The resulting amplified accelerations are 0.37g and 0.33g in the transverse and longitudinal directions, respectively and 0.20g in the vertical direction. For conservatism, a value of 0.37g is used for both horizontal directions in the seismic analysis of the HSM-H.

Seismic Stress Analysis

An equivalent static analysis of the HSM-H is performed using the ANSYS model described in Section 3.9.9.7 and the seismic accelerations of 0.37g horizontally (longitudinal and transverse directions) and 0.2g vertically. These amplified accelerations are determined based on the frequency analysis of the HSM-H.

The responses for each orthogonal direction are combined using the SRSS method.

The seismic analysis results are shown in Table 3.9.9-10 and are incorporated in the loading combination C4C (Table 3.9.9-3) and C4S (Table 3.9.9-6) for the concrete and support structure components, respectively.

HSM-H Seismic Overturning Analysis

The following conservative analysis is performed to show that a single freestanding HSM-H without an end shield wall (in an array of two or more loaded modules) will not overturn due to seismic loads. Overturning about the long axis (i.e., in the short direction of the module) is considered.

Stabilizing moment = $M_{st} = (W_{hsm} + W_{dsc}) b/2$

Overturning moment = $M_{ot} = (W_{hsm} 0.4a_{v1} + W_{dsc} 0.4a_{v2})b/2 + W_{hsm} d_1 a_{h1} + W_{dsc} d_2 a_{h2}$

(100% of horizontal acceleration is combined with 40% of vertical acceleration, Ref. [11])

Where:

W_{hsm} = 310 K, Weight of the HSM-H (conservatively assumed)

W_{dsc} = 110 K, Weight of DSC (conservatively assumed)

$b/2$ = 52 in, Horizontal distance from CG to corner(half width of the HSM-H)

d_1 = 123.45 in, Height of CG of HSM-H without the DSC

d_2 = 106 in, Height of the DSC center line

a_{v1} = 0.20g, HSM-H peak vertical seismic acceleration

a_{v2} = 0.20g, DSC peak vertical seismic acceleration

a_{h1} = 0.37g, HSM-H peak horizontal seismic acceleration

a_{h2} = 0.43g, DSC peak horizontal seismic acceleration (conservatively assumed)

M_{st} = 21,840 K-in

M_{ot} = 20,921 K-in

Because stabilizing moment is greater than the overturning moment the HSM-H will not overturn during the seismic event.

HSM-H Seismic Sliding Analysis

The friction force resisting sliding = $F_{st} = W_{hsm}(1-0.4*a_{v1}) + W_{dsc}(1-0.4*a_{v2})\mu$

The applied horizontal seismic force = $F_{hs} = [W_{hsm}a_{h1} + W_{dsc}a_{h2}]$

Where:

μ = coefficient of friction between concrete HSM-H base on concrete basemat = 0.6.

W_{hsm} , W_{dsc} , a_{v1} , a_{v2} , a_{h1} , a_{h2} are defined above.

$F_{st} = 231.8K$

$F_{hs} = 162.0K$

The force required to slide the HSM-H is larger than the resulting lateral seismic force and therefore, the loaded HSM-H will not slide.

3.9.9.10.3 Flood Load (FL) *(Section P.3.7.3 from CoC 1004 Amendment #8)*

Since the source of flooding is site specific, the exact source, or quantity of flood water, should be established by the licensee. However, for this generic evaluation of the HSM-H, bounding flooding conditions are specified that envelop those that are postulated for most plant sites. As described in Section 3.9.9.6.3, the design basis flooding load is specified as a 50 foot static head of water and a maximum flow velocity of 15 feet per second. Each licensee should confirm that this represents a bounding design basis for their specific ISFSI site.

HSM-H Flooding Analysis

Because the HSM-H is open to the atmosphere, static differential pressure due to flooding is not a design load.

The maximum drag force, F , acting on the HSM-H due to a 15 fps flood water velocity is calculated as follows:

Where:

$F = (v^2/2g) C_D A \rho_w [14]$

$v = 15$ fps, Flood water velocity

$C_D = 2.0$, Drag coefficient for flat plate

$A = 18.5$ ft²/ft, HSM-H area per foot length

$\rho_w = 62.4$ lb./ft.³, Flood water density

$F =$ Drag force (lb.)

$$g = 32.2 \text{ ft./s}^2 = \text{Acceleration due to gravity}$$

The resulting flood induced load is: $F = 8.07 \text{ K/ft.}$

The following four flood load cases are considered:

Case 1: Flood water flow from front of HSM-H to rear of HSM-H

Case 2: Flood water flow from rear of HSM-H to front of HSM-H

Case 3: Flood water flow from left side of HSM-H to right side

Case 4: Flood water flow from right side of HSM-H to left side

Flood water flow from front of HSM-H to rear or rear of HSM-H to front (Cases 1 and 2)

$$\text{Front/Rear wall, } F_w = 8070 \times 9' 8'' = 78010 \text{ lbs}$$

Conservatively, the total drag load on the front concrete components of the HSM-H is applied as a normal pressure load of magnitude $(78010)/(18'6'' \times 9'8'' \times 144) = 3.1 \text{ psi.}$

Flood water flow in left side of HSM-H to right side or right side of HSM-H to left (Cases 3 and 4)

$$\text{Side walls, } F_w = 8070 \times 20'8'' = 166780 \text{ lbs}$$

Conservatively, the total drag load on the left side concrete components of the HSM-H is applied as a normal pressure load of magnitude $(166780)/(18'6'' \times 20'8'' \times 144) = 3.1 \text{ psi.}$

ANSYS finite element model described in Section 3.9.9.7 is used for the structural evaluation. The results for flood load case are obtained by enveloping results from above 4 load cases and shown on Table 3.9.9-10.

HSM-H Overturning Analysis

The factor of safety against overturning for the postulated flooding conditions is calculated using the stabilizing moment for a single HSM-H (with shield walls included) by summing moments about the bottom outside corner of a free-standing HSM-H. A net weight of 253.7 kips for a loaded HSM-H plus 100.4 kips for the upstream end shield wall, including buoyancy effects, is used to calculate the stabilizing moment that resists the overturning moment applied to the HSM-H by the flood water drag force. The stabilizing moment is:

$$\begin{aligned} M_{st} &= 253.7 \times 52 + 100.4 \times 18 \\ &= 15,000 \text{ K-in.} \end{aligned}$$

The maximum drag force due to the postulated water current velocity of 15 fps is 8.07 k/ft (see calculation above). The overturning moment due to the postulated flood current is based on drag

forces acting on a minimum of two modules in an array. The overturning moment is estimated as:

$$\begin{aligned} M_{ot} &= 0.5 \times 8.07 \text{ K/ft.} \times 20.67 \text{ ft.} \times (18.5 \times 12/2) \\ &= 9,258 \text{ K-in.} \end{aligned}$$

The factor of safety (F.S.) against overturning for a freestanding HSM-H due to the postulated design basis flood water velocity is given by:

$$\text{F.S.} = 15,000 / 9,258 = 1.62$$

Therefore, a minimum of two (2) HSM-Hs adjacent to each other are required to prevent overturning.

HSM-H Sliding Analysis

The factor of safety against sliding of a freestanding HSM-H due to the maximum postulated flood water velocity of 15 fps is calculated using methods similar to those described above. The effective weight of the HSM-H including the DSC and end shield wall acting vertically downward, less the effects of buoyancy acting vertically upward is 354 K. The friction force resisting sliding of the HSM-H is equal to the product of the net weight of the HSM-H and the DSC and the coefficient of friction for concrete placed against another concrete surface such as that between the HSM-H and basemat, which is 0.6 [3]. Therefore, the force resisting sliding of the HSM-H is 0.6×354 or 212.5 kips. The drag force acting on a HSM-H (considering a minimum of two modules in an array) is $0.5 \times 8.07 \text{ kips/ft} \times 20.67 = 83.4$ kips total acting on the side wall of a single HSM-H, due to a flood velocity of 15 fps. The resulting factor of safety against sliding of a free standing HSM-H due to the design basis flood water velocity is 2.55.

Therefore, a minimum of two (2) HSM-Hs adjacent to each other are required to prevent sliding.

3.9.9.10.4 Blocked Vent Thermal (TA) *(Section P.3.7.6 from CoC 1004 Amendment #8)*

This accident conservatively postulates the complete blockage of the HSM-H ventilation air inlet and outlet openings on the HSM-H side walls.

Since the NUHOMS® HSM-Hs are located outdoors; there is a remote probability that the ventilation air inlet and outlet vent openings could become blocked by debris. The NUHOMS® design features such as the perimeter security fence and the redundant protected location of the air inlet and outlet vent openings and the screens reduces the probability of occurrence of such an accident. Nevertheless, for this conservative generic analysis, such an accident is postulated to occur and is analyzed.

The postulated accident thermal event occurs due to blockage of either the air inlet or outlet vents under off-normal ambient temperatures range from -40°F to 117°F . The results of the HSM-H concrete components blockage thermal load analysis are presented in Table 3.9.9-9.

3.9.9.11 Load Combination

Concrete Components

To determine the required strength (internal axial forces, shear forces, and bending moments) for each HSM-H concrete component, linear elastic finite element analyses are performed for the normal, off-normal, and accident loads using the analytical models described in Section 3.9.9.7 for mechanical and thermal loads.

The individual load analysis results of the HSM-H concrete structure are presented in Table 3.9.9-8, 9 and 3.9.9-10. The load combination results for each component are presented in Table 3.9.9-11 for the load combinations defined in Table 3.9.9-3. The notations for the components of forces and moments and the concrete component planes in which capacities are computed are shown in Figure 3.9.9-5. The HSM-H concrete components thermal stresses used in the load combination results, summarized in Table 3.9.9-11, are based on thermal results that bound those reported in Chapter 4. All load combination results are below the computed section capacities.

Support Steel Structure

The support rails, rail stiffener plates, extension plates and cross members of the DSC support structure, shown in Figure 3.9.9-6 are evaluated using the allowable stress design method of the AISC Manual of Steel Construction [4]. The load combination results for each of these components are provided in Table 3.9.9-12 to 14. The maximum temperature used in the stress analysis of the support steel bounds the maximum temperature reported in Chapter 4.

The support rail stress comparison results are presented in Table 3.9.9-15. The extension plate and cross member stress comparison results are presented in Table 3.9.9-16.

HSM-H Shield Door

The shield door is free to grow in the radial direction when subjected to thermal loads. Therefore, there will be no stresses in the door due to thermal growth. The dead weight, tornado wind, differential pressure and flood loads cause insignificant stresses in the door compared to stresses due to missile impact load. Therefore, the door is evaluated only for the missile impact load. The computed maximum ductility ratio for the door is less than 5 (compared to the allowable ductility of 20).

For the door anchorage, the controlling load is tornado generated differential pressure drop load. The maximum tensile force per bolt (four door attachment bolts), is 4.5 kips. This is less than the allowable of 44.3 kips. The concrete pull-out strength is conservatively estimated as 24 kips. Half of the concrete pull-out strength (12 kips) is greater than the tension load of 4.5 kips per bolt, thus satisfying the ductility requirements of the ACI Code.

HSM-H Heat Shield

The top heat shield (louvers) consists of six panels. Each panel has two aluminum mounting bars. The aluminum louvers are mounted on the mounting bars. Each mounting bar is suspended from the roof by two threaded rods. The natural lateral frequency of a typical rod is conservatively estimated to be 9.0 Hz. The combined axial and bending stress in the hanger rods is 24.0 ksi. The allowable axial and bending stress is 84.3 ksi.

The alternate top heat shield consists of two panels made of stainless steel plate. The panels are suspended from the roof by fifteen 1/2" diameter rods threaded into concrete embedments. The combined axial and bending stress in the rods is 59.5 ksi. The allowable stress is 70.2 ksi.

The side heat shields consists of three panels. Each panel is suspended from the roof by two threaded rods, and supported laterally and longitudinally by four rods. The maximum axial plus bending stress in the lateral and longitudinal support rods is 83.7 ksi. The allowable axial and bending stress is 84.3 ksi. The maximum temperature used in the stress analysis of the heat shields bounds the maximum temperatures reported in Chapter 4.

The alternate side heat shields consists of four panels, attached to the base unit side wall by 34 threaded rod stand-offs. The maximum axial and bending stress in the rods is about 1.4 ksi and 79.3 ksi, respectively. The axial and bending stress allowable for the rods is 67.9 ksi and 112.3 ksi, respectively.

HSM-H Seismic Retainers

The seismic retainer consists of a capped tube steel embedment located within the bottom center of the round access opening of the HSM-H, and a tube steel retainer that drops into the embedment cavity after DSC transfer is complete. The drop-in retainer extends approximately 4" above the rail to provide axial restraint of the DSC. The maximum seismically induced shear load in the retainer is 61 kips. The maximum shear stress in the retainer is 15.25 ksi. The allowable shear stress is 17.8 ksi.

3.9.9.12 Conclusions

The load categories associated with normal operating conditions, off-normal conditions and postulated accident conditions are described and analyzed in previous sections. The load combination results for HSM-H components important to safety are also presented. Comparison of the results with the corresponding design capacity shows that the design strength of the HSM-H is greater than the strength required for the most critical load combination.

3.9.9.13 References

1. Title 10, Code of Federal Regulations, Part 72 (10CFR72), "Licensing Requirements for the Storage of Spent Fuel in the Independent Spent Fuel Storage Installation," U.S. Nuclear Regulatory Commission, August 31, 1988.
2. ANSI/ANS 57.9-1984, "Design Criteria for an Independent Spent Fuel Storage Installation (Dry Storage Type)," American Nuclear Society.
3. "Code Requirements for Nuclear Safety Related Concrete Structures," ACI 349-97, American Concrete Institute, Detroit, MI.
4. "Manual of Steel Construction," American Institute of Steel Construction, Ninth Edition, 1989.
5. American Society of Civil Engineers, ASCE 7-95, "Minimum Design Loads for Buildings and Other Structures" (formerly ANSI A58.1).
6. "Design Basis Tornado for Nuclear Power Plants," Regulatory Guide 1.76, U.S. Atomic Energy Commission, April 1974.
7. "Missiles Generated by Natural Phenomenon," Standard Review Plan, NUREG-0800, U.S. Nuclear Regulatory Commission
8. Bechtel Topical Report, "Design of Structures for Missile Impact," BC-TOP-9-A, Revision 2, September 1974.
9. Regulatory Guide 1.60, "Design Response Spectra for Seismic Design of Nuclear Power Plants," U.S. Atomic Energy Commission, Revision 1, December 1973.
10. ANSYS Users Manual Rev. 5.6 and 7.0.
11. "Structural Analysis and Design of Nuclear Plant Facilities," ASCE Publication No. 58.
12. Regulatory Guide 1.61, "Damping Values for Seismic Design of Nuclear Power Plants," U.S. Atomic Energy Commission, October 1973.
13. Amendment No. 8 to NUHOMS® CoC 1004, addition of 24PTH DSC to Standardized NUHOMS® System.
14. "Fluid Mechanics", Raymond C. Binder, 4th Edition, Prentice-Hall, Inc.
15. "Thermal testing of the NUHOMS® Horizontal Storage Module, Model HSM-H", Transnuclear Report No. E-21625, Rev 1.

Table 3.9.9-1
Summary of HSM-H Component Design Loadings

Component	Design Load Type	Design Parameters	Applicable Codes
HSM-H Module	Dead Load (DW)	150 pcf concrete structure and weight of support steel structure	ANSI 57.9-1984 [2]
	Live Load (LL)	200 psf (including snow and ice load) on the roof DSC weight (110 kips)	ANSI-57.9-1984 [2] ASCE 7-95 [5]
	Normal Operating Temperature (TN)	Normal: Ambient air temperature 0 °F -100 °F	ANSI 57.9-1984 [2]
	Off-Normal Operating Temperature (TO)	Off Normal: Ambient air temperature -40 °F to 117 °F	
	Normal Handling Loads(RO)	Hydraulic ram load of 80,000 lb.(DSC HSM insertion) 60,000 lb (DSC HSM extraction) on the rails	ANSI 57.9-1984 [2]
	Design Basis Wind Load(WW)	Conservatively assumed to be same as tornado generated wind load.	ASCE 7-95 [5]
	Off-Normal Handling Loads (RA)	Hydraulic ram load of: 80,000 lb (DSC insertion) 80,000 lb (DSC extraction) on each rail, one rail at a time.	ANSI-57.9-1984 [2]
	Accident Temperature (TA)	Ambient air temperature of -40 °F and 117 °F with inlet and outlet vents blocked.	10CFR72.122(n) [1]
	Tornado Wind Load (WT)	Maximum wind speed of 360 mph and a pressure drop of 3 psi	ASCE 7-95 [5] NRC Regulatory Guide 1.76 [6]
	Tornado Missile Load (WM)	See Section T.2.2.1.3 for missiles considered.	NUREG-0800 Section 3.5.1.4 [7]
	Flood (FL)	Maximum water height: 50 ft. Maximum velocity of water 15'/sec.	10CFR72.122(b) [1]
	Seismic (EQ)	Horizontal ground acc: 0.30g Vertical ground acc.: 0.20g	NRC Reg. Guides 1.60 & 1.61 [9] and [12]

Table 3.9.9-2
Summary of 32PTH DSC Support Structure Design Loadings

Component	Design Load Type	Design Parameters	Applicable Codes
32PTH DSC Support Structure	Live Load (LL)	DSC weight (110 kips)	ANSI-57.9-1984 [2]
	Normal Operating Temperature (TN)	Normal: Ambient air temperature 0 °F -100 °F	ANSI 57.9-1984 [2]
	Off-Normal Operating Temperature (TO)	Off Normal: Ambient air temperature -40 °F to 117 °F	
	Normal Handling Loads (RO)	Hydraulic ram load of 80,000 lb.(DSC insertion) 60,000 lb (DSC extraction) on the rails	ANSI 57.9-1984 [2]
	Off-Normal Handling Loads (RA)	Hydraulic ram load of: 80,000 lb (DSC insertion) 80,000 lb (DSC extraction) on each rail. One rail at a time.	ANSI-57.9-1984 [2]
	Accident Temperature (TA)	Ambient air temperature of -40 °F and 117 °F with inlet and outlet vents blocked.	10CFR72.122(n) [1]
	Seismic (EQ)	Horizontal ground acc: 0.30g Vertical ground acc.: 0.20g	NRC Reg. Guides 1.60 & 1.61 [9] and [12]

Table 3.9.9-3
HSM-H Concrete Load Combinations

Load Combination No.	Combination Identifier	Load Combination
C1C	COMB1C	$U > 1.4*DW + 1.7*(LL + RO)$
C2C	COMB2C	$U > 1.05*DW + 1.275*(LL + TN + WW)$
C3C	COMB3C	$U > 1.05*DW + 1.275*(LL + TN + RA)$
C4C	COMB4C	$U > DW + LL + TN + EQ$
C5C	COMB5C	$U > DW + LL + TN + WT$
C6C	COMB6C	$U > DW + LL + TN + FL$
C7C	COMB7C	$U > DW + LL + \text{MAX}(TO \text{ and } TA)$

Note: For definition of individual load cases see Table 3.9.9-1

Table 3.9.9-4
Ultimate Capacities of Concrete Components

Component	Thermal Condition	$V_{ui}^{(1)}$ Kips/ft	$V_{uo1}^{(1)}$ Kips/ft	$V_{uo2}^{(1)}$ kips/ft	$M_{u1}^{(1)}$ Kip-in/ft	$M_{u2}^{(1)}$ kip-in/ft
Rear Wall (upper)	Normal	75.2	14.5	14.5	298.2	298.2
	Accident	69.6	13.8	13.8	273.8	273.8
Rear Wall (lower)	Normal	96.8	36.2	36.2	757.9	757.9
	Accident	90.1	34.3	34.3	696.3	696.3
Side Walls (upper)	Normal	55.4	14.8	14.8	196.9	196.9
	Accident	50.5	14.0	14.0	180.8	180.8
Side Walls (lower)	Normal	64.0	23.4	23.4	314.6	314.6
	Accident	58.7	22.2	22.2	289.0	289.0
Roof	Normal	177.6	59.1	59.1	2375.0	2375.0
	Accident	162.4	56.1	56.1	2181.7	2181.7
Front Wall (upper)	Normal	174.7	56.3	56.3	2257.3	2257.3
	Accident	159.6	53.4	53.4	2073.5	2073.5
Front Wall (lower)	Normal	192.1	73.6	73.6	2963.4	2963.4
	Accident	176.0	69.8	69.8	2722.4	2722.4

Notes:

- (1) V_{ui} = Minimum of ultimate in plane shear capacities in planes 1 and 2
 V_{uo1} = Minimum Ultimate out of plane shear capacity in plane 1
 V_{uo2} = Minimum Ultimate out of plane shear capacity in plane 2
 M_{u1} = Minimum Ultimate moment capacity in plane 1
 M_{u2} = Minimum Ultimate moment capacity in plane 2

Table 3.9.9-5
Structural Design Criteria for DSC Support Structure

Allowable Stress (S)	
Stress Type	Stress Value
Tensile	$0.60 S_y$
Compressive	(See Note 1)
Bending	$0.60 S_y^{(2)}$
Shear	$0.40 S_y$
Interaction	(See Note 3)

Notes:

- (1) Equations E2-1 or E2-2 of the AISC Specification (Ref. 4) are used as appropriate.
- (2) For properly braced non-compact sections, for other cases see AISC Specification Chapter F.
- (3) Interaction equations per the AISC Specification are used as appropriate.
- (4) S_y = Yield strength of the material

Table 3.9.9-6
HSM-H Support Steel Structure Load Combinations

Load Combination No.	Combination Identifier	Load Combination
C1S	COMB1S	$(1.5S \text{ or } 1.4 S_v) > DW+LL+TN^{(1), (2)}$
C2S	COMB2S	$S > DW+RO^{(3), (4)}$
C3S	COMB3S	$1.3S > DW+TN+RA^{(3), (4)}$
C4S	COMB4S	$(1.6S \text{ or } 1.4S_v) > DW+LL+TN+EQ^{(2)}$
C5S	COMB5S	$(1.7S \text{ or } 1.4S_v) > DW+LL+MAX (TO \text{ and } TA)^{(2)}$

Notes:

- (1) This normal operating load combination applies to DSC storage condition.
- (2) DSC weight is included as live load (LL) for this condition; the DSC spans between end supports
- (3) These load combinations represent normal and off-normal handling conditions.
- (4) DSC weight is included as a direct load on the rail.

Table 3.9.9-7
Design Pressures for Tornado Wind Loading

HSM-H Wall Orientation⁽¹⁾	Velocity Pressure (psf)	Pressure Coefficient⁽²⁾	Max/Min Design Pressure (psf)
Front	344	+0.68	234
Left	344	-0.60	-207
Rear	344	-0.43	-148
Right	344	-0.60	-207
Roof	344	-0.60	-207

Notes:

1. Wind direction assumed to be from front. Wind load from other directions may be found by rotating table values to desired wind directions.
2. Pressure coefficient = guest factor (0.85) x max/min pressure coefficient from Figure 6-3 of reference 5.

Table 3.9.9-8
Maximum NUHOMS® HSM-H Concrete Component Forces and Moment for Normal and Off-Normal Loads

Load Case	Concrete Component	Forces/Moments			
		Shear, V_{01} (kips/ft)	Shear, V_{02} (kips/ft)	Moment, M_1 (kip-in/ft)	Moment, M_2 (kip-in/ft)
Dead Load (DW)	Rear Wall	1.20	0.60	5.40	20.10
	Side Wall	4.40	2.80	24.80	20.40
	Front Wall	5.30	5.10	75.30	190.80
	Roof	2.80	3.50	45.20	136.20
Live Load (LL)	Rear Wall	1.40	0.60	6.70	20.10
	Side Wall	1.20	0.80	8.50	9.60
	Front Wall	30.20	23.80	344.60	510.60
	Roof	0.90	1.30	16.00	47.20
Operational Handling Load (RO)	Rear Wall	Included in Live Load (LL)			
	Side Wall				
	Front Wall				
	Roof				
Off-Normal Handling Load (RA)	Rear Wall	Included in Live Load (LL)			
	Side Wall				
	Front Wall				
	Roof				
Design Wind Load (WW)	Rear Wall	4.88	2.20	81.50	124.88
	Side Wall	27.00	10.87	190.50	135.00
	Front Wall	12.75	12.12	179.00	289.12
	Roof	3.25	2.50	135.50	80.88

Table 3.9.9-9
Summary of Thermal Forces and Moments in the HSM-H Concrete Components

Thermal Case	Concrete Component	Forces/Moments			
		Shear, $V_{o1}^{(1)}$ (kips/ft)	Shear, $V_{o2}^{(1)}$ (kips/ft)	Moment, $M_1^{(2)}$ (kip-in/ft)	Moment, $M_2^{(2)}$ (kip-in/ft)
Normal Thermal (TN)	Rear Wall	4	6	104	228
	Side Wall	7	7	185	71
	Front Wall	30	23	1318	2025
	Roof	6	5	111	234
Off-Normal Thermal (TO)	Rear Wall	4	5	100	207
	Side Wall	6	6	160	67
	Front Wall	30	23	1315	1938
	Roof	6	5	93	233
Accident Thermal (TA)	Rear Wall	9	19	140	272
	Side Wall	92	32	184	340
	Front Wall	41	38	1772	3325
	Roof	11	24	404	830

Notes:

1. V_{o1} and V_{o2} are out of plane shear
2. M_1 and M_2 are out of plane moment

Table 3.9.9-10
Maximum HSM-H Concrete Component Forces and Moments for Accident Loads

Load Case	Concrete Component	Forces/Moments			
		Shear, $V_{01}^{(1)}$ (kips/ft)	Shear, $V_{02}^{(1)}$ (kips/ft)	Moment, $M_1^{(2)}$ (kip-in/ft)	Moment, $M_2^{(2)}$ (kip-in/ft)
Earthquake (EQ)	Rear Wall	4.71	1.31	23.92	89.41
	Side Wall	7.30	5.47	49.13	64.12
	Front Wall	17.71	13.37	133.16	498.61
	Roof	3.05	1.83	230.46	75.03
Flood (FL)	Rear Wall	6.34	3.42	146.03	106.63
	Side Wall	49.04	19.28	340.62	248.39
	Front Wall	20.5	17.57	309.27	351.48
	Roof	3.05	1.83	230.46	75.03
Tornado Wind (WT)	Rear Wall	4.88	3.81	151.94	124.88
	Side Wall	51.75	21.25	349.75	259.50
	Front Wall	16.62	13.94	295.69	289.12
	Roof	5.75	4.25	248.06	112.25

Notes:

(1) V_{01} and V_{02} are out of plane shears.

(2) M_1 and M_2 are out of plane moments.

Table 3.9.9-11
Comparison of Highest Combined Shear Forces/Moments with the Capacities

Component	Load Comb. ⁽¹⁾	Quantity	V ₁ kips/ft	V ₀₁ kips/ft	V ₀₂ kips/ft	M ₁ kip-in/ft	M ₂ kip-in/ft
Rear Wall (Upper)	Comb 1c thru 6c	Computed	14.52	7.71	9.16	147.35	267.10
		Capacity	75.2	14.5	14.5	298.2	298.2
		Ratio	0.19	0.53	0.63	0.49	0.90
	Comb 7c	Computed	18.44	11.37	6.08	131.14	264.5
		Capacity	69.6	13.8	13.8	273.8	273.8
		Ratio	0.26	0.82	0.44	0.48	0.97
Rear Wall (Lower)	Comb 1c thru 6c	Computed	17.34	9.48	13.25	159.40	167.70
		Capacity	96.8	36.2	36.2	757.9	757.9
		Ratio	0.18	0.26	0.37	0.21	0.22
	Comb 7c	Computed	9.49	6.40	20.84	154.30	251.80
		Capacity	90.1	34.3	34.3	696.3	696.3
		Ratio	0.11	0.19	0.61	0.22	0.36
Side Walls (Upper)	Comb 1c thru 6c	Computed	18.92	12.05	13.19	177.76	163.10
		Capacity	54.4	14.8	14.8	196.9	196.9
		Ratio	0.35	0.82	0.89	0.90	0.83
	Comb 7c	Computed	22.37	12.08	9.10	120.24	91.05
		Capacity	50.5	14.0	14.0	180.8	180.8
		Ratio	0.44	0.86	0.265	0.67	0.50
Side Walls (Lower)	Comb 1c thru 6c	Computed	36.17	22.33	21.12	308.10	261.55
		Capacity	63.0	23.4	23.4	314.6	314.6
		Ratio	0.57	0.95	0.91	0.98	0.83
	Comb 7c	Computed	19.28	21.12	15.34	97.25	180.24
		Capacity	58.7	22.2	22.2	289.0	289.0
		Ratio	0.33	0.95	0.69	0.34	0.63
Roof	Comb 1c thru 6c	Computed	13.18	9.44	28.73	487.01	1022.49
		Capacity	174.6	59.1	59.10	2475.0	2375.0
		Ratio	0.08	0.16	0.49	0.21	0.43
	Comb 7c	Computed	7.69	11.48	28.38	386.48	897.67
		Capacity	162.4	56.1	56.10	2181.7	2181.70
		Ratio	0.05	0.21	0.51	0.18	0.41
Front Wall (Upper)	Comb 1c thru 6c	Computed	41.82	44.83	37.00	1393.19	1895.08
		Capacity	174.7	56.3	56.3	2257.3	2317.3
		Ratio	0.24	0.80	0.66	0.62	0.84
	Comb 7c	Computed	32.63	48.95	26.29	1853.0	1906.74
		Capacity	159.6	53.4	53.4	2073.5	2073.5
		Ratio	0.20	0.92	0.49	0.89	0.92
Front Wall (Lower)	Comb 1c thru 6c	Computed	29.29	30.43	37.83	1783.50	836.92
		Capacity	189.0	73.6	73.6	2963.4	2963.4
		Ratio	0.16	0.42	0.52	0.60	0.28
	Comb 7c	Computed	48.04	45.95	41.38	1908.90	507.22
		Capacity	176.0	69.8	69.8	2722.4	2722.4
		Ratio	0.27	0.66	0.59	0.70	0.19

Note:

1. Comb 1c thru 6c includes normal thermal. Comb 7c includes accident thermal (see Table 3.9.9-3)

Table 3.9.9-12
Maximum/Minimum Forces/Moments in the Rail Components in the Local System

Load Combination		F_x Kips	F_y Kips	F_z Kips	M_x kip-in	M_y kip-in	M_z Kip-in
C1S	MAX	0.0	33.0	65.2	63.5	231.1	213.7
	MIN	0.0	-41.0	-61.3	-52.4	-1146.7	-236.2
C2S	MAX	38.5	39.8	77.0	0.22	428.2	247.8
	MIN	-28.9	-39.8	-60.9	-0.32	-1137.6	-247.8
C3S	MAX	86.5	30.7	89.6	63.6	592.7	199.4
	MIN	-86.5	-38.1	-63.0	-52.4	-1422.4	-230.4
C4S	MAX	22.3	38.2	102.1	63.6	562.5	-267.6
	MIN	-22.3	-46.3	-98.3	-52.4	-1869.0	-290.2
C5S	MAX	0.	49.6	82.1	183.7	264.8	267.3
	MIN	0.	-54.1	-80.9	-159.3	-143.4	-267.1

Table 3.9.9-13
Maximum/Minimum Forces/Moments in the Rail Extension Plates in the Local System

Load Combination		F_x Kips	F_y Kips	F_z Kips	M_x kip-in	M_y kip-in	M_z Kip-in
C1S	MAX	0.0	0.85	-0.25	2.7	6.8	13.8
	MIN	0.0	-4.0	-0.73	-2.7	-4.3	-45.9
C2S	MAX	40.0	2.6	-0.4	0.1	5.3	26.1
	MIN	-30.0	-2.6	-0.5	-0.1	-2.6	-26.1
C3S	MAX	80.0	0.8	-0.2	2.7	7.2	13.6
	MIN	-79.9	-3.9	-0.8	-2.8	-4.2	-44.9
C4S	MAX	38.5	1.5	-0.0	2.7	9.3	17.0
	MIN	-38.5	-4.7	-1.0	-2.8	-5.8	-53.2
C5S	MAX	0.1	1.02	0.34	9.4	12.3	18.2
	MIN	0.1	-7.6	-1.5	-9.5	-9.7	-94.7

Table 3.9.9-14
Maximum/Minimum Axial Forces in the Cross Member Components

Load Combination		F _x Kips
C1S	MAX	6.2
	MIN	5.2
C2S	MAX	8.1
	MIN	5.8
C3S	MAX	5.2
	MIN	2.6
C4S	MAX	6.2
	MIN	5.2
C5S	MAX	7.1
	MIN	5.1

Table 3.9.9-15
Rail Component Results

Load Comb.	Interaction Ratio⁽¹⁾	Shear Stress Ratio⁽²⁾	Stiffener Plate Stress Ratio⁽³⁾
C1S	0.35	0.67	0.19
C2S	0.58	0.84	0.00
C3S	0.58	0.93	0.22
C4S	0.51	0.96	0.18
C5S	0.40	0.63	0.55

Notes:

- (1) Axial and bending stresses are computed using axial (F_x) and bending moment (M_y , M_z) results from Table 3.9.9-12. Interaction ratios are based on appropriate equations from Chapter H of AISC [4].
- (2) Shear stresses are computed using shear forces (F_y , F_z) from Table 3.9.9-12. Shear stress ratio is the computed shear stress/shear stress allowable.
- (3) Flexural stresses in the stiffener plates are computed using torsional moment (M_x) result from Table 3.9.9-12. Stiffener plate stress ratio is the bending stress in the plate/bending allowable stress.

Table 3.9.9-16
Extension Plates and Cross Members Results

Load Comb.	Extension Plates Interaction Ratio⁽¹⁾	Cross Members Stress Ratio(2)
C1S	0.77	0.25
C2S	0.77	0.32
C3S	0.71	0.21
C4S	0.60	0.25
C5S	0.71	0.33

Notes:

- (1) Axial and bending stresses are computed using axial (F_x) and bending moment (M_y , M_z) results from Table 3.9.9-13. Interaction ratios are based on appropriate equations from Chapter H of AISC [4].
- (2) Axial stresses in the cross members are computed using axial (F_x) force results from Table 3.9.9-14. Cross member stress ratio is the axial stress in the member/axial allowable stress.

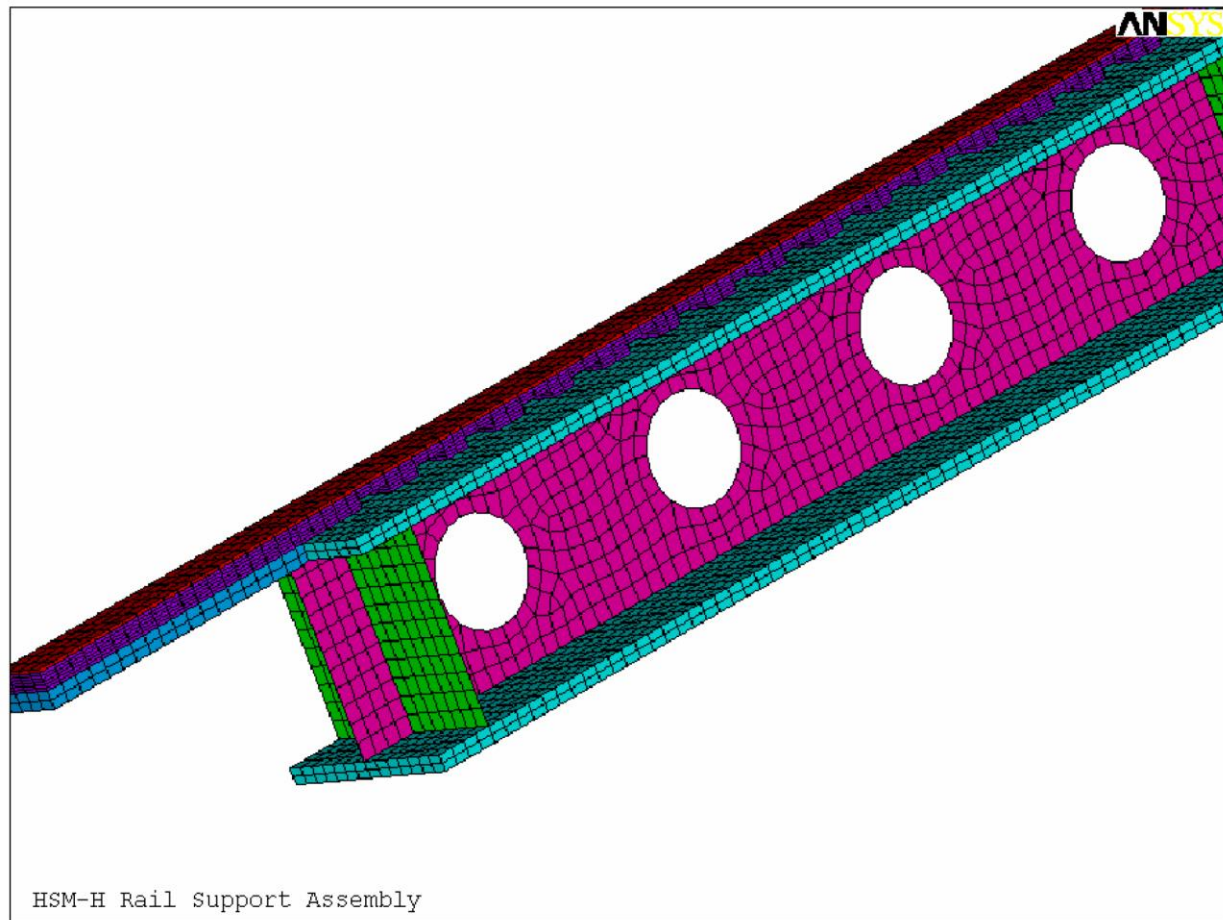


Figure 3.9.9-1
Analytical Model of the W12x96 Beam with Slotted, Nitronic and Stiffener Plates

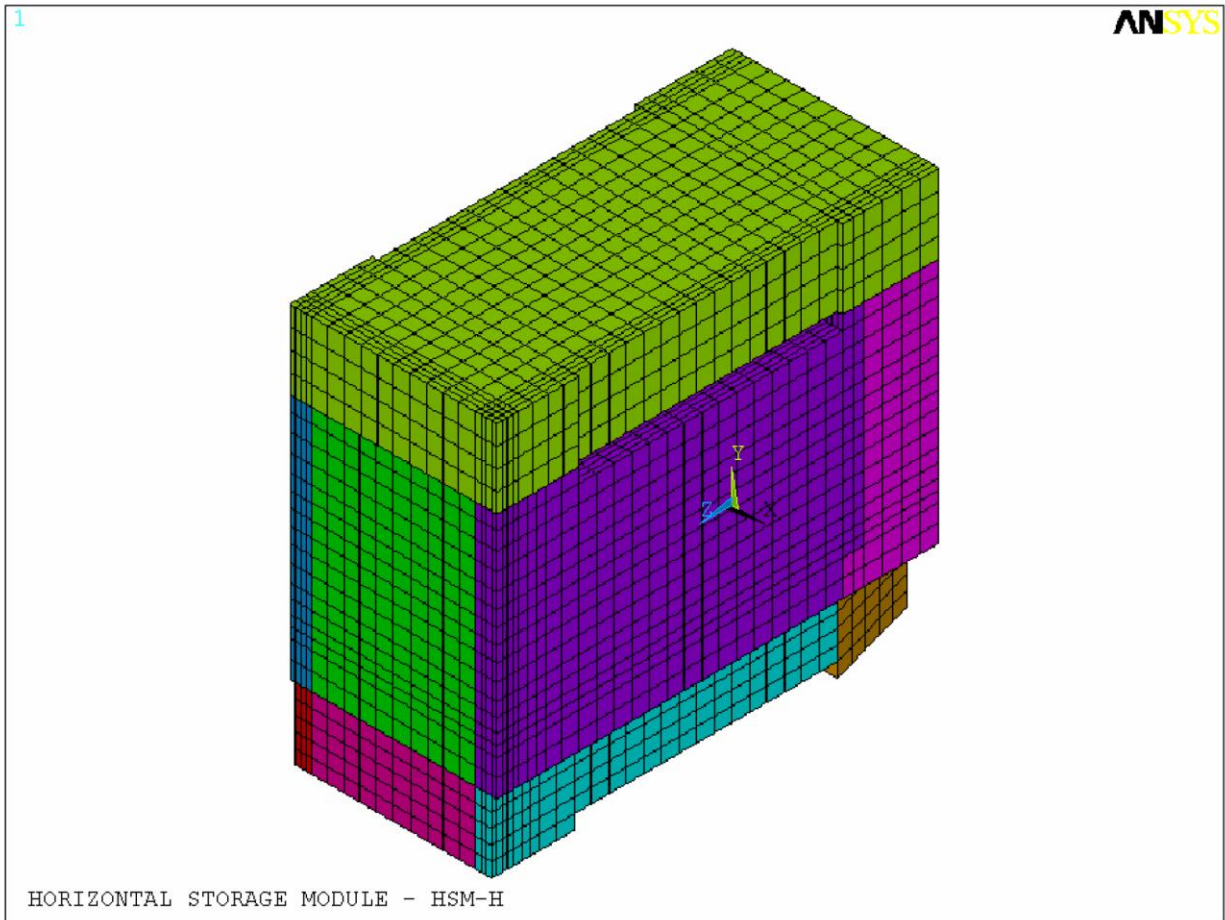


Figure 3.9.9-2
Analytical Model of the HSM-H for Mechanical Load Analysis

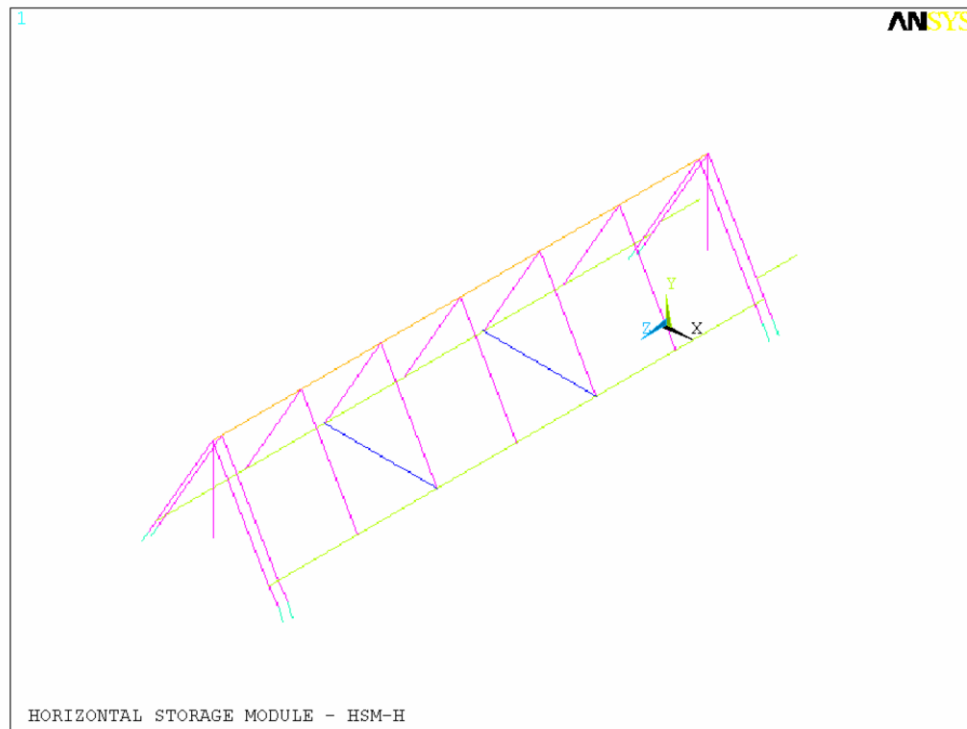


Figure 3.9.9-3
Analytical Model of the 32PTH DSC Support Structure

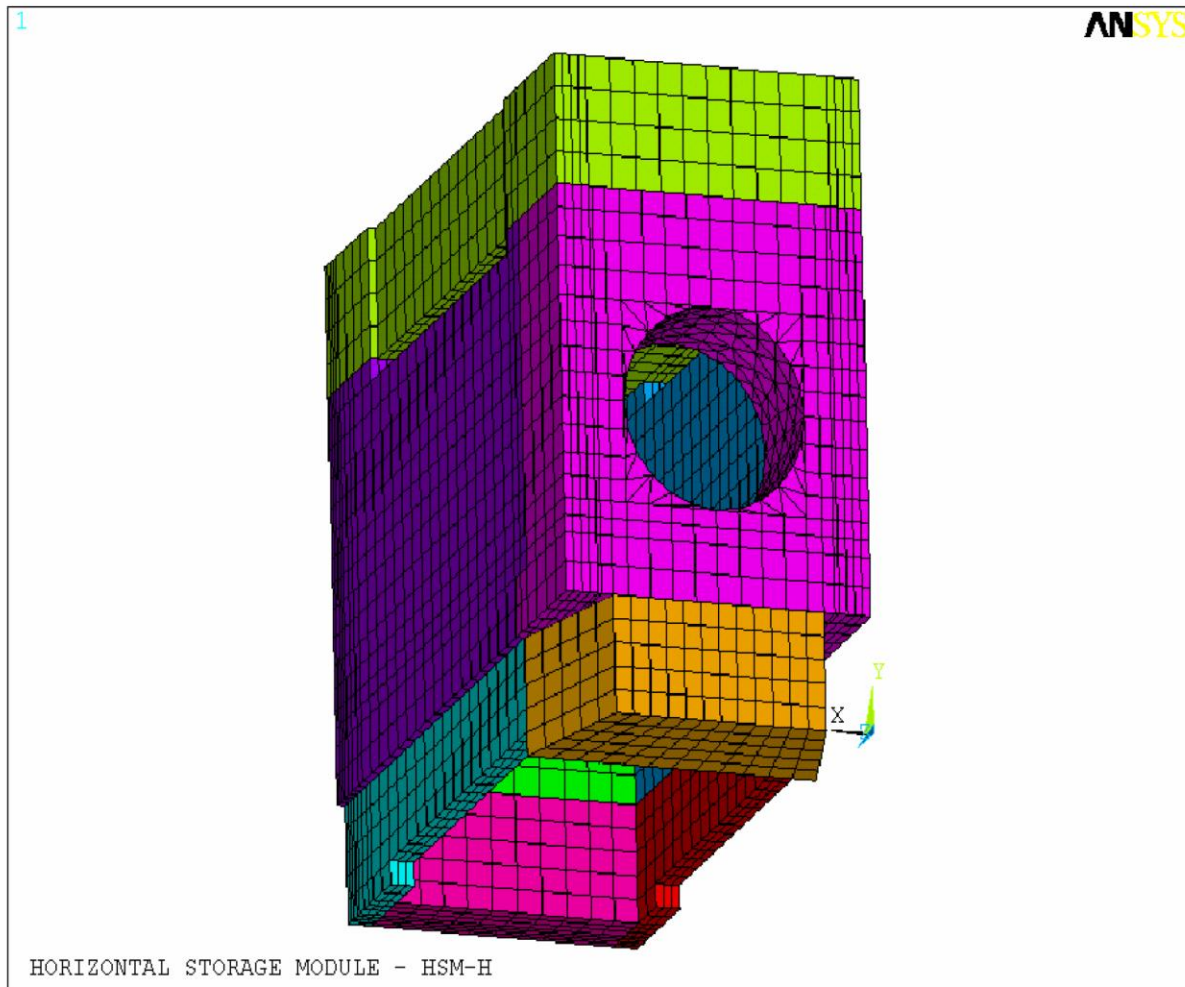


Figure 3.9.9-4
Analytical Model of the HSM-H for Thermal Load Analysis

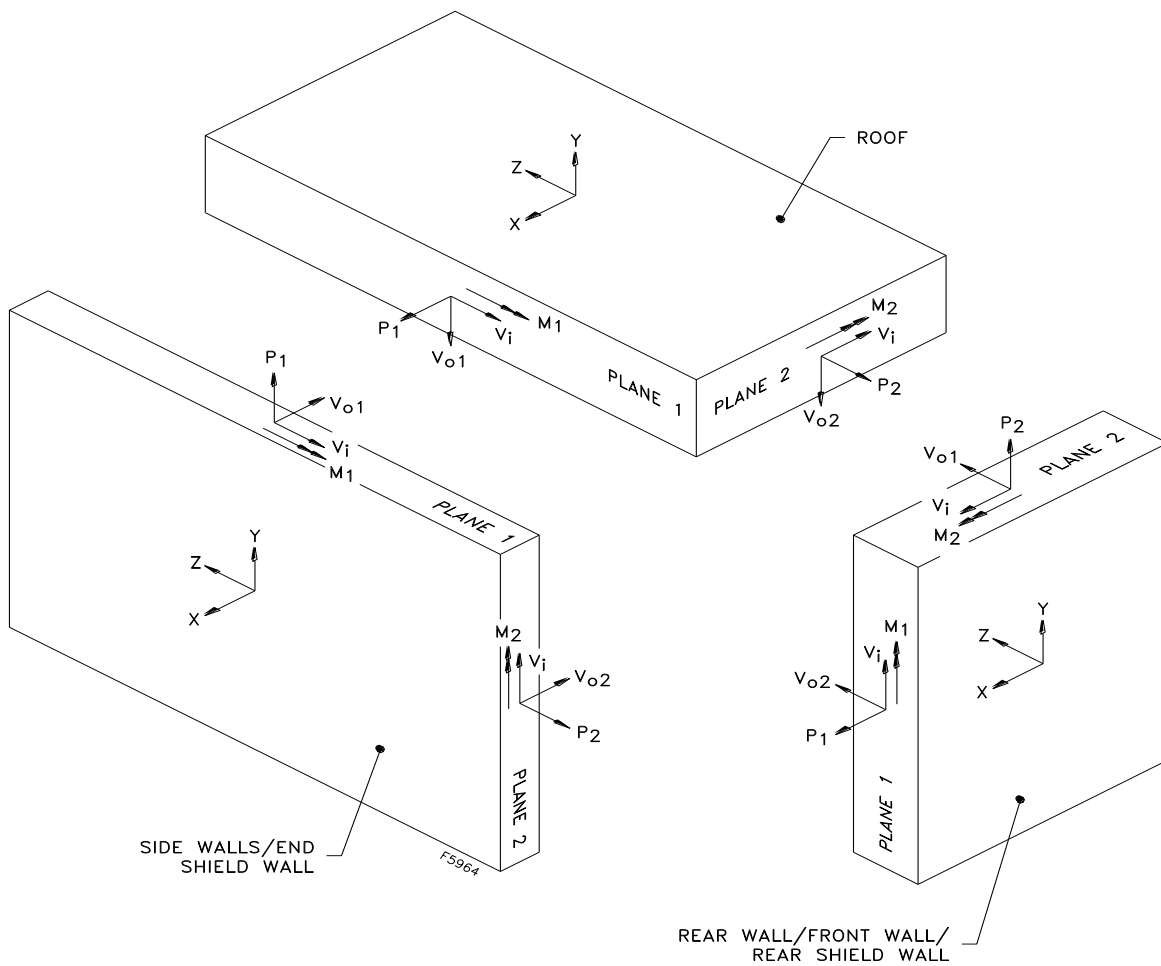


Figure 3.9.9-5
Symbolic Notations of Force and Moment Capacities
(Also for Computed Forces and Moments)

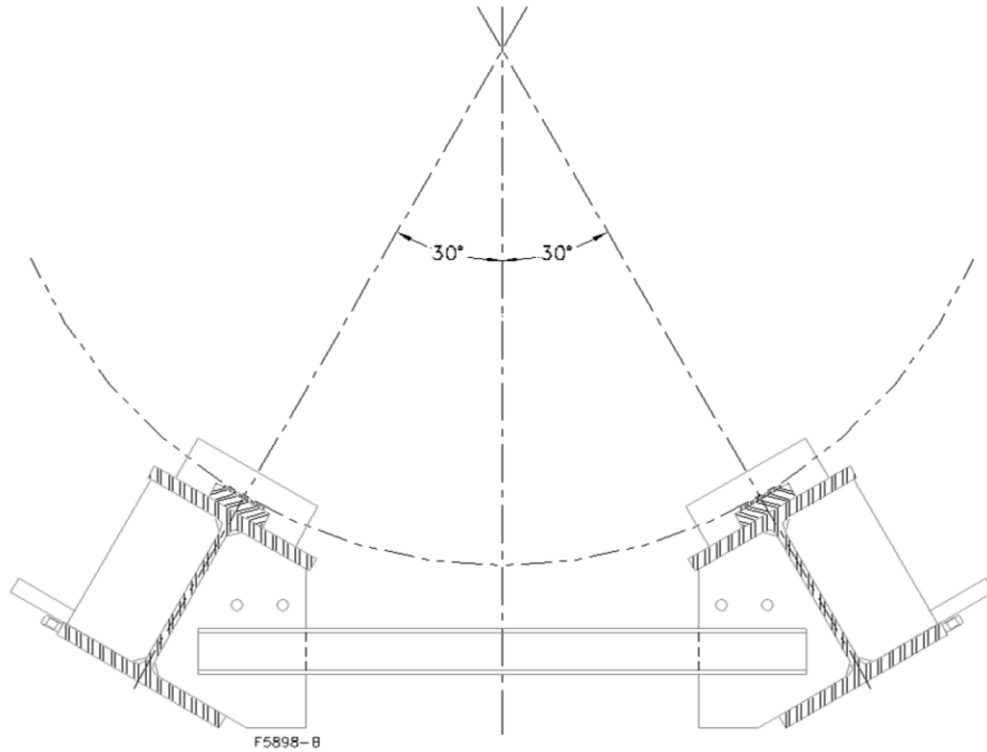


Figure 3.9.9-6
Components of Support Structure

APPENDIX 3.9.10 OS187H TRANSFER CASK DYNAMIC IMPACT ANALYSIS

TABLE OF CONTENTS

3.9.10 OS187H TRANSFER CASK DYNAMIC IMPACT ANALYSIS	3.9.10-1
3.9.10.1 Introduction.....	3.9.10-1
3.9.10.2 Analysis Software.....	3.9.10-1
3.9.10.3 Validation of the LS-DYNA Impact Analysis	3.9.10-2
3.9.10.4 OS187H Transfer Cask Impact Analysis.....	3.9.10-8
3.9.10.5 Summary of g-Loads for the OS187H Transfer Cask Body and Lid Bolt Stress	3.9.10-13
3.9.10.6 References	3.9.10-16

LIST OF FIGURES

Figure 3.9.10-1	Finite Element Model of “GENERIC” Storage Cask, Side Drop and Tip Over Onto Concrete Pad And Soil (Reproduced From LLNL Report)	3.9.10-17
Figure 3.9.10-2	TN-32 Cask Tipover Analysis Finite Element Model	3.9.10-18
Figure 3.9.10-3	TN-32 Cask Tipover Analysis Finite Element Model (Enlarged view of the TN-32 Cask).....	3.9.10-19
Figure 3.9.10-4	TN-32 Transfer Cask Deformed Shape-Mode 1	3.9.10-20
Figure 3.9.10-5	TN-32 Transfer Cask Deformed Shape-Mode 02.....	3.9.10-21
Figure 3.9.10-6	OS187H Transfer Cask Side Drop Dynamic Impact Finite Element Model	3.9.10-22
Figure 3.9.10-7	OS187H Transfer Cask Side Drop Dynamic Impact Finite Element Model	3.9.10-23
Figure 3.9.10-8	OS187H Transfer Cask CG Over Corner Drop Dynamic Impact Finite Element Model	3.9.10-24
Figure 3.9.10-9	OS187H Transfer Cask CG Over Corner Drop Dynamic Impact Finite Element Model	3.9.10-25
Figure 3.9.10-10	OS187H Transfer Cask Finite Element Model without the Internals..	3.9.10-26
Figure 3.9.10-11	OS187H Transfer Cask Internals Finite Element Model	3.9.10-27

Figure 3.9.10-12	OS187H Transfer Cask Side Drop Nodal Sections Analyzed	3.9.10-28
Figure 3.9.10-13	OS187H Transfer Cask CG Over Corner Drop Nodal Sections Analyzed	3.9.10-29
Figure 3.9.10-14	OS187H Transfer Cask Finite Element Model used for Modal Analysis, Elements.....	3.9.10-30
Figure 3.9.10-15	OS187H Transfer Cask Finite Element Model used for Modal Analysis, Boundary Conditions	3.9.10-31
Figure 3.9.10-16	OS187H Transfer Cask Deformed Shape – Mode 2.....	3.9.10-32
Figure 3.9.10-17	OS187H Transfer Cask Deformed Shape – Mode 3.....	3.9.10-33
Figure 3.9.10-18	OS187H Transfer Cask Deformed Shape – Mode 4.....	3.9.10-34
Figure 3.9.10-19	OS187H Transfer Cask, Side Drop,.....	3.9.10-35
Figure 3.9.10-20	OS187H Transfer Cask, Side Drop,.....	3.9.10-36
Figure 3.9.10-21	OS187H Transfer Cask, Side Drop,.....	3.9.10-37
Figure 3.9.10-22	OS187H Transfer Cask, CG Over Corner Drop,	3.9.10-38
Figure 3.9.10-23	OS187H Transfer Cask, CG Over Corner Drop,	3.9.10-39

3.9.10 OS187H TRANSFER CASK DYNAMIC IMPACT ANALYSIS

3.9.10.1 Introduction

The purpose of this calculation is to determine the rigid body accelerations for the NUHOMS[®] - OS187H Transfer Cask during the hypothetical accident condition 80 inch free drop during fuel transfer. The drop orientations analyzed in this appendix are the 80 inch side drop (10 CFR 72) and the 80 inch corner drop (10 CFR 50).

The rigid body transfer cask accelerations are predicted numerically by the LS-DYNA 3D explicit nonlinear dynamic analysis finite element solver, Version 970 [1]. The methodology used in performing this analysis is based on work conducted at the Lawrence Livermore National Laboratory, where an analysis methodology is developed and validated through comparisons with test data [2][3]. Validation of the dynamic impact analyses presented herein is achieved through comparison of a previous TN-32 Dry Storage Cask Tipover Analysis with a similar analysis performed by Lawrence Livermore National Labs (LLNL). The results of these analyses are used as input to the detailed static analyses for the cask body presented in Appendix 3.9.2.

The results of these analyses are also used as input to the static analyses of the cask internal basket and canister structures (presented in Appendix 3.9.1) by including dynamic application factors (See Appendix 3.9.11).

3.9.10.2 Analysis Software

The LS-DYNA [1] finite element program was used for the analyses presented in this Appendix. Model generation was performed using the ANSYS [4] finite element program. Data filtering was performed using the LS-PREPOST software supplied with LS-DYNA.

LS-DYNA is a general purpose, explicit finite element program used to model the nonlinear dynamic response of three-dimensional models. Applications of LS-DYNA include crash worthiness, sheet metal forming, high velocity impact, explosive phenomena, drop tests, etc.

ANSYS is a general purpose program capable of solving structural, mechanical, electrical, electromagnetic, electronic, thermal, fluid, and biomedical problems. It has extensive preprocessing (model generation), solution, postprocessing, and graphics capabilities.

3.9.10.3 Validation of the LS-DYNA Impact Analysis

In order to validate the accuracy of the HUNOMS[®]-OS187H Transfer Cask impact analysis, a tipover analysis of the TN-32 cask is performed and compared with the LLNL [2] results based on the TN-32 cask geometry.

The following table lists key dimensions and weights of the LLNL and Transnuclear TN-32 Model3.

	LLNL Model	TN-32 Model
Cask ID	68.75"	68.75"
Cask OD	87.75"	87.75"
Cask Cavity Length	163.25"	163.25"
Cask Overall Length	184"	184"
Weight Including Internals	232,000 lb	232,000 lb
Cask Material	Carbon Steel	Carbon Steel

These two models have the same geometry and weight, therefore it is a reasonable approach to use the TN-32 model to validate the accuracy of the LS-DYNA impact analysis.

LLNL Model

The finite element model of the LLNL model is described in the LLNL report [2]. A plot of the finite element model is shown in Figure 3.9.10-1 of this Appendix for reference.

TN-32 Model

The finite element model of the TN-32 is developed in a similar manner to those models represented in LLNL report. The cask and basket meshes are simplified and totally independent of each other with surface-to-surface contact elements transferring load between the two components. Contact surfaces are also used between the cask and concrete pad and between the concrete pad and the soil.

The TN-32 finite element model is made up of four components: cask body, cask internals, concrete and soil. Each of these components is modeled using 3-D 8-node brick elements. The finite element models were developed in ANSYS and transferred to LS-DYNA through the ANSYS-LS-DYNA interface. Modifications were made to the LS-DYNA input to add the material definition and state variables since they are not available through the ANSYS translator. The geometries of the cask and basket have been simplified since the purpose of the analysis is to predict the rigid body response of the cask. Features on the cask such as the trunnions, neutron shield and weather cover are neglected in terms of stiffness but their weight is lumped into the density of the cask. Figures 3.9.10-2 and 3.9.10-3 illustrate the finite element model of the cask, basket, concrete, and soil. Mesh sizes in this analysis are in reasonable agreement with those represented in LLNL report [2]. The concrete material is modeled with all elements having a constant length of 10 inches since the concrete material law can be dependent on mesh size.

TN-32 Material Properties

The material properties required to perform the analysis include modulus of elasticity, E , Poisson's Ratio, ν , and material density (ρ) for the cask body, basket, concrete, and soil. The concrete pad requires a more detailed material model since all of the significant nonlinear deformations occur in the concrete. Material properties used for the concrete and soil are based on those developed at Lawrence Livermore National Labs [2].

All material properties are taken at room temperature. This is considered conservative because the cask loaded with spent fuel will typically reach temperatures higher than room temperature, and the lower modulus of elasticity at higher temperatures tends to soften the impact and consequently lower the computed g-loads.

TN-32 Cask Material

The same modulus of elasticity used in the LLNL report is used for the TN-32 tipover analysis. The density of the cask was adjusted to match the mass properties of those entities not explicitly modeled. The material properties used for the casks are as follows:

$$E = 30 \times 10^6 \text{ psi}$$

$$\nu = 0.3$$

$$\rho = 0.865 \times 10^{-3} \text{ lb-sec}^2/\text{in}^4$$

Note that the density of each cask has been adjusted so that the weight of the TN-32 cask minus the basket and fuel is 166,200 lbs.

TN-32 Fuel and Basket Material

The fuel and basket were modeled as a set of hollow cylinders inside the cask walls (similar manner to those models represented in Reference [2]). The material properties of the fuel/basket were defined to match the correct weight and approximate the stiffness of the basket. The cask and basket finite element model meshes are totally independent of each other with surface-to-surface contact elements transferring load between the two components. Because the cask stiffness is so much greater than the basket stiffness this simplification is reasonable. The modulus of elasticity used for the basket is adjusted such that the fundamental frequency of the approximate basket matches the fundamental frequency of the detailed basket analysis. Material properties used for the basket are as follows:

$$E = 8.1 \times 10^6 \text{ psi}$$

$$\nu = 0.3$$

$$\rho = 0.863 \times 10^{-3} \text{ lb-sec}^2/\text{in}^4$$

Again the density of the basket has been adjusted to account for the weight of the fuel. The weight of the basket plus fuel for TN-32 cask is 65,800 lbs.

Concrete Material

The concrete is modeled using material law 16 in LS-DYNA [1], which was developed specifically for granular type materials. The concrete data used in the analysis was originally designed by LLNL for the Shippingport Station Decommissioning Project in 1988. This model is also used in the LLNL [2] cask drop analysis. Material constants are implemented into Material Model 16, Mode II.B in LS-DYNA. The material represents 4,200 psi compressive strength concrete. A summary of the input used in the analysis is as follows.

$$\rho = 2.09675 \times 10^{-4} \text{ lb sec}^2 / \text{in}^4$$

$$\nu = 0.22$$

$$a_0 = 1606$$

$$a_1 = 0.418$$

$$a_2 = 8.35 \times 10^{-5} \text{ psi}^{-1}$$

$$b_1 = 0$$

$$a_{0f} = 0.0 \text{ psi}$$

$$a_{1f} = 0.385$$

Effective Plastic Strain versus Scale Factor for Concrete Material

Effective Plastic Strain	Scale Factor, ν
0	0
0.00094	0.289
0.00296	0.465
0.00837	0.629
0.01317	0.774
0.0234	0.893
0.04034	1.0
1.0	1.0

The maximum principal stress tensile failure cutoff is set at 870 psi. Strain rate effects are neglected in the analysis. Dilger [9] suggests that the major impact of strain rate effects is in the softening part of the stress-strain curve. Since the purpose of these analyses is primarily to predict the peak accelerations, we can neglect the strain rate effects on the material behavior.

The pressure-volume behavior of the concrete is modeled with the following tabulated pressure versus volumetric strain rate relationship using the equation of state feature in LS-DYNA [1].

Tabulated Pressure versus Volumetric Strain Rate for the Concrete Material

Volumetric Strain, ϵ	Pressure (psi)
0	0
-0.006	4,600
-0.075	5,400
-0.01	6,200
-0.012	6,600
-0.02	7,800
-0.038	10,000
-0.06	12,600
-0.0755	15,000
-0.097	18,700

An unloading bulk modulus of 700,000 psi is assumed to be constant at any volumetric strain, as was assumed in Reference [2].

One percent deformation is assumed in the concrete pad to account for the pad reinforcement. The one percent reinforcement is also used in the analyses presented in EPRI [10].

The material properties used for the reinforcing bar are as follows.

$$E = 30 \times 10^6 \text{ psi [2]}$$

$$\nu = 0.3 \text{ [2]}$$

$$S_y = 30,000 \text{ psi [2]}$$

$$\text{Tangent Modulus, } E_T = 30 \times 10^4 \text{ psi [2]}$$

Soil Material

The Lawrence Livermore National Labs report [2] indicates that the stiffness of the soil has little impact on the peak accelerations predicted in the cask. Thus for the purpose of the TN-32 impact analysis, the same soil model is assumed as that used in the Livermore report. The soil material properties assumed for the analysis are:

$$E = 6,000 \text{ psi [2]}$$

$$\nu = 0.3 \text{ [2]}$$

$$\rho = 0.225 \times 10^{-3} \text{ lb-sec}^2 / \text{in}^4 \text{ [2]}$$

Boundary Conditions

A ½ model is also used in the TN-32 analysis, with symmetry boundary conditions used to simulate the full structure. Non-reflecting boundaries were used around the soil non-symmetry boundaries to prevent artificial stress waves from reflecting from the boundaries of the soil.

Damping Factor

The true damping characteristics of the cask impact event are very hard to quantify. Typical values for reinforced concrete structures subjected to dynamic loads are in the 5 to 10% range [11][12]. During the tipover drop events, the concrete, cask and soil absorb energy as a result of damping. Since the response of the concrete is nonlinear, a single damping ratio can not be defined. In order to define a relatively uniform damping ratio over a range of frequencies, damping is defined proportional to both the stiffness and mass matrices. Known as Rayleigh damping [16], two factors can be defined relative to mass and stiffness proportional damping to provide a range of damping. A uniform damping rate of 5% of critical is assumed between the frequencies of 50 and 1000 Hz in developing the initial damping coefficients. Since the damping ratio must be assumed, both an upper and lower bound ratio of damping is used in the preliminary analyses. However, based on the results presented in the LLNL report [2], the 6% critical damping results appear to be most realistic. The Damping ratio and parameters α and β used for the TN-32 Cask tipover verification analysis are summarized as follows.

Damping Ratio = 6%

$\alpha = 122$

$\beta = 1.5 \times 10^{-5}$

LS-DYNA Analysis and Results

For the TN-32 tipover verification analysis, an angular velocity is applied based on a non-mechanistic cask tipover accident. The center of rotation is set at the edge of the cask bottom located at the center of the coordinate system. LS-DYNA calculates the initial velocity components associated with each node for this rotational motion. The initial angular velocity applied to the TN-32 Cask model was 1.729 radian/sec.

LS-DYNA computes the nodal accelerations at 0.4 msec intervals. Therefore, by the Nyquist theorem, the frequency content of the nodal acceleration data, computed by LS-DYNA, ranges from zero Hz, up to the following maximum frequency, f_{\max} .

$$f_{\max} = \frac{1}{2} \times \frac{1}{(4 \times 10^{-4})} = 1,250 \text{ Hz}$$

The lowest natural frequencies of the TN-32 Cask model, which can be excited by an impact event, are much lower than this. These natural modes of the cask involve small displacements (and therefore low stresses) at frequencies higher than that of the rigid body motion of the cask. These high frequency accelerations mask the true rigid body motion of the cask, because both the low frequency rigid body acceleration and the high frequency natural vibration accelerations superimpose. The net acceleration is contained in the raw data computed by LS-DYNA. Therefore, filtering is necessary to remove these high frequency accelerations.

In order to estimate the natural frequencies of the cask model, a modal analysis is performed by using the ANSYS 3D finite element model. The weight densities are all changed to mass densities ($\rho_m = \rho_w / 386.4$).

The cask is oriented in the horizontal orientation and supported at the bottom. The cask finite element model and boundary conditions are shown in Figures 3.9.10-2 and 3.9.10-3.

The first two significant mode frequencies resulting from the ANSYS modal analysis are tabulated below:

Frequencies of the First Two Natural Modes of the TN-32 Cask Model

Mode Number	Frequency (Hz)
1	177.86
2	291.41

The mode shapes corresponding to these frequencies are plotted in Figures 3.9.10-4 and 3.9.10-5.

The averaged raw data for each cross section is filtered using a low pass Butterworth filter with a cutoff frequency of 350 Hz in order to recover the actual rigid body acceleration of the cask. The Butterworth filter used in this analysis is characterized by its large number of coefficients, small pass band ripple, and slow roll off. The cutoff frequency of 350 Hz is conservative, because it is higher than at least the first two dominant modes of the TN-32 Cask computed above (350 Hz also used in LLNL report for cutoff frequency). Therefore, the response predicted by the filtered results includes more dynamics than simply the rigid body motion of the transfer cask.

The results of the TN-32 tipover analyses provide reasonable agreement with LLNL results presented in LLNL report [2]. The following table compares the LLNL and Transnuclear TN-32 analysis results.

Comparison of LLNL Analysis and TN-32 Analysis

	LLNL LS-DYNA Analysis	Transnuclear LS-DYNA Analysis
Peak Acceleration (350 Hz Filter)	66.7 g	67 g
Duration of Pulse	0.003 sec	0.003 sec
Pulse Shape	Triangle	Triangle

3.9.10.4 OS187H Transfer Cask Impact Analysis

OS187H Transfer Cask Finite Element Model Description

The ANSYS finite element model of the OS187H Transfer Cask developed for the transfer cask stress analysis (Appendix 3.9.2) is simplified for use in the dynamic impact analysis. The OS187H Transfer Cask model consists of the transfer cask body, including the lead gamma shielding, the DSC, and the concrete pad and soil. Each of these components is modeled using 3D 8-node brick elements. Full Integration (Flanagan and Belytschko, 1981 [1]) with exact volume integration is used for all elements to reduce the risk of hourglassing problems.

The finite element models are developed with ANSYS and transferred to LS-DYNA through the use of an ANSYS macro. Modifications were made to the LS-DYNA input file to add the material definitions, non-reflecting boundaries and equation of state into LS-DYNA, since these input variables are not available through the ANSYS macro. Features of the transfer cask, such as the trunnions, neutron shield, and top neutron shield are neglected in terms of stiffness but their weight is lumped into the density of the transfer cask.

A simplified model of the DSC is placed inside the transfer cask in order to model the effect of the cask internals. Automatic surface to surface contact elements are placed between the external surface of the DSC and the internal surface of the transfer cask, between the transfer cask shells and lead gamma shielding, between the transfer cask outer surface and the concrete pad, and between the concrete pad and the soil.

The geometry of the transfer cask finite element model including the cask internals, concrete and base soil is shown in Figures 3.9.10-6 through 3.9.10-11. Figures 3.9.10-6 and 3.9.10-7 show the arrangement of the side drop impact analysis, and Figures 3.9.10-8 and 3.9.10-9 show the arrangement of the CG over corner drop impact analysis. Figure 3.9.10-10 is an enlarged view of the transfer cask without the internals, and Figure 3.9.10-11 is an enlarged view of the cask internals themselves.

Only $\frac{1}{2}$ of the transfer cask, internals, concrete and soil are modeled, because the entire arrangement is symmetric about the x - y plane. The $\frac{1}{2}$ slab of concrete modeled is 600 inches \times 200 inches \times 36 inches thick, and the $\frac{1}{2}$ soil modeled is 1,200 inches \times 400 inches \times 500 inches deep.

Mesh sizes in this analysis are in reasonable agreement with those used in LLNL report [2]. The finite element sizes between the contact surfaces of the concrete and soil are refined to have better match (see Figure 3.9.10-3 for LLNL model and 3.9.10-7 for OS187H model).

OS187H Transfer Cask Material

The following material properties are used for the transfer cask body.

Stainless Steel (SA-240 Type 304)

$$E = 28.3 \times 10^6 \text{ psi [5]}$$

$$\nu = 0.3$$

$$S_y = 30.0 \text{ ksi. [5]}$$

$$\text{Tangent Modulus, } E_T = 1.13 \times 10^5 \text{ psi}$$

The density of the transfer cask body is adjusted to account for the weight of unmodeled components, including the trunnions and outer radial neutron shield. The effective density is computed in the following way.

$$\begin{aligned} \text{Weight of Transfer Cask} &= \frac{1}{2} \times [119,891 \text{ lb (transfer cask weight)} - 62,369 \text{ lb (lead weight)}] \\ &= 28,761 \text{ lb} \end{aligned}$$

$$\text{Volume of F.E.M.} = 68,923.2 \text{ in}^3 \text{ (from ANSYS model)}$$

$$\rho_{eff} = 28,761 \text{ lb} / 68,923.2 \text{ in}^3 / (386.4 \text{ in/sec}^2) = 1.080 \times 10^{-3} \text{ lb-sec/in}^4$$

Lead Gamma Shield Material

The following material properties are used for the transfer cask lead gamma shield.

Chemical Lead (ASTM B-29)

$$E = 2.35 \times 10^6 \text{ psi [5]}$$

$$\nu = 0.45 \text{ [6]}$$

$$S_y = 1,140 \text{ psi [8]}$$

$$\text{Tangent Modulus, } E_T = 8.93 \times 10^3 \text{ psi}$$

The density of the lead gamma shield is computed in the following way.

$$\text{Weight of lead gamma shield} = \frac{1}{2} \times 62,369 \text{ lb} = 31,184.5 \text{ lb}$$

$$\text{Volume of F.E.M. Lead} = 75,358.5 \text{ in}^3 \text{ (from ANSYS model)}$$

$$\rho_{eff} = 31,184.5 \text{ lb} / 75,358.5 \text{ in}^3 / (386.4 \text{ in/sec}^2) = 1.071 \times 10^{-3} \text{ lb-sec/in}^4$$

DSC (basket and canister) Material

The following material properties are used for the DSC.

Stainless Steel (SA-240 Type 304)

$$E = 28.3 \times 10^6 \text{ psi}$$
$$\nu = 0.3$$

The density of the DSC is adjusted so that the actual weight of the DSC is properly accounted for. The effective density is computed in the following way.

$$\text{Weight of DSC} = \frac{1}{2} \times [28,191 \text{ lb (canister weight)} + 29,854 \text{ lb (basket weight)} + 51,520 \text{ lb (fuel weight)}] = 54,782.5 \text{ lb}$$

$$\text{Volume of F.E.M.} = 69,807.6 \text{ in}^3 \text{ (from ANSYS model)}$$

$$\rho_{eff} = 54,782.5 \text{ lb} / 69,807.6 \text{ in}^3 / (386.4 \text{ in/sec}^2) = 2.016 \times 10^{-3} \text{ lb-sec/in}^4$$

Concrete Material

The same concrete material properties used in the LLNL and TN-32 analyses, presented in Section 3.9.10.3, are also used for the OS187H transfer cask analysis. The concrete material properties used in the analysis are representative and do not constitute limits for the ISFSI Pad design or any other concrete which the loaded OS187H transfer cask is transported over. The OS187H transfer cask g-loads used for the stress evaluation given in the Table in Section 3.9.10.5 represent the limits that must be maintained for an 80 inch drop of the loaded OS187H transfer cask.

Soil Material

The same soil material properties used in the LLNL and TN-32 analyses, presented in Section 3.9.10.3, are also used for the OS187H transfer cask analysis. The soil material properties used in the analysis are representative and do not constitute limits for the ISFSI Pad design or any other concrete which the loaded OS187H transfer cask is transported over. The OS187H transfer cask g-loads used for the stress evaluation given in the Table in Section 3.9.10.5 represent the limits that must be maintained for an 80 inch drop of the loaded OS187H transfer cask.

Boundary Conditions

A $\frac{1}{2}$ model is employed with symmetry boundary conditions used to simulate the full structure. Non-reflecting boundaries are used around the soil non-symmetry boundaries (bottom, left side, right side, and back) to prevent artificial stress waves from reflecting from the boundaries of the soil. Both dilatation and shear waves are damped as described in the LS-DYNA *BOUNDARY command [1].

Contact boundaries between the cask and DSC, cask and lead, cask and concrete, and concrete

and soil are modeled using surface-to surface contact elements in LS-DYNA. These contacts are defined using part numbers defined by the ANSYS macro that transfers the ANSYS finite element to the LS-DYNA model. A description of the LS-DYNA surface-to-surface contact elements are provided in Reference [1].

Damping Factor

As described in the above LLNL and TN-32 impact analyses (Section 3.9.10.3), the true damping characteristics of the cask impact event are very hard to quantify. Typical values for reinforced concrete structures subjected to dynamic loads are in the 5 to 10% range. A 6% damping factor is used for the LLNL and TN-32 impact analyses, for conservatism a lower bound damping factor of 5% is used for OS187H transfer cask impact analysis.

OS187H Transfer Cask Model LS-DYNA Impact Analysis

Two accident condition drop scenarios are evaluated which are considered to bound all credible transfer cask drops during fuel transfer:

- 80 inch, 0° side drop, and
- 80 inch, 60° CG over corner drop

The cask outer surface is initially placed in contact with the concrete pad, and an initial velocity is applied to the cask, lead, and DSC, to simulate the non-mechanistic drop events. The initial velocity is computed by equating potential and kinetic energies.

$$V = \text{potential energy} = mgh$$

$$T = \text{kinetic energy} = \frac{1}{2}mv^2$$

$$\Rightarrow mgh = \frac{1}{2}mv^2$$

$$\Rightarrow v = \sqrt{2gh} = \sqrt{2(386.4)(80)} = 248.644 \text{ in /sec}$$

With the above model, boundary conditions and initial conditions, the LS-DYNA program was run from $t_0 = 0$ seconds to $t_f = 0.04$ seconds for both the Side Drop and the C.G. over corner drop runs. The time step was automatically chosen by the LS-DYNA program based on the minimum model element sizes.

Transfer Cask Sections Evaluated

The resulting nodal acceleration time histories, computed in the drop direction by LS-DYNA, are averaged over several cross sections of the transfer cask. For the side drop analysis, only the accelerations transverse to the transfer cask axis are computed since the resulting accelerations in the direction of the cask axis are negligible. For the CG over corner drop however, the accelerations in the drop direction are decomposed into accelerations in the longitudinal (parallel to the cask axis) and transverse directions, since significant impact accelerations are expected in both orthogonal directions. Different nodal sections are selected as appropriate for each drop orientation.

Figures 3.9.10-12 and 3.9.10-13 show the nodal sections analyzed for the side drop and CG over corner drop.

Raw Data Filtering

As described in the TN-32 model LS-DYNA analysis, the LS-DYNA computes the nodal accelerations at 0.4 msec intervals. Therefore, by the Nyquist theorem, the frequency content of the nodal acceleration data, computed by LS-DYNA, ranges from zero Hz, up to the following maximum frequency, f_{\max} .

$$f_{\max} = 1/2 \times 1/(4 \times 10^{-4}) = 1,250 \text{ Hz}$$

The lowest natural frequencies of the OS187H Transfer Cask, which can be excited by an impact event, are much lower than this. These natural modes of the transfer cask involve small displacements (and therefore low stresses) at frequencies higher than that of the rigid body motion of the transfer cask. These high frequency accelerations mask the true rigid body motion of the transfer cask, because both the low frequency rigid body acceleration and the high frequency natural vibration accelerations superimpose. The net acceleration is contained in the raw data computed by LS-DYNA. Therefore, filtering is necessary to remove these high frequency accelerations.

In order to estimate the natural frequencies of the OS187H transfer cask, a modal analysis is performed by using the ANSYS 3D finite element model described in Appendix 3.9.2. The weight densities used in Appendix 3.9.2 file are all changed to mass densities ($\rho_m = \rho_w / 386.4$).

The cask is oriented in the horizontal orientation and supported at the bottom. The cask finite element model and boundary conditions are shown in Figures 3.9.10-14 and 3.9.10-15.

The first five mode frequencies resulting from the ANSYS modal analysis are tabulated below:

Frequencies of the First Five Natural Modes of the OS187H Transfer Cask

Mode Number	Frequency (Hz)
1	69.17
2	125.00
3	130.52
4	141.07
5	147.23

The mode shapes of Mode 2, 3, and 4 are plotted in Figures 3.9.10-16 through 3.9.10-18.

The averaged raw data for each cross section is filtered using a low pass Butterworth filter with a cutoff frequency of 180 Hz in order to recover the actual rigid body acceleration of the Transfer Cask. The Butterworth filter used in this analysis is characterized by its large number of coefficients, small pass band ripple, and slow roll off. The cutoff frequency of 180 Hz is conservative, because it is higher than at least the first five dominant modes of the OS187H

Transfer Cask computed above. Therefore, the response predicted by the filtered results includes more dynamics than simply the rigid body motion of the transfer cask.

Results of LS-DYNA Analyses

The following table lists the LS-DYNA side drop results.

Summary of Impact g Load Due to Side Drop

Transfer Cask Section (see Figure 3.9.10-12)	G Load
Lid Section	62.9g
Top Trunnion Section	55.8g
Middle Section	57.3g
Bottom Trunnion Section	46.9g
Bottom Plate Section	44.0g

Based on the Results shown in above table, the maximum acceleration in the OS187H Transfer Cask during the 80 inch accident condition side drop event is 62.9g and occurs in the transfer cask lid section. Also from this table, the highest acceleration in the region of the transfer cask where the DSC rests is 57.3g during an 80 inch side drop event.

Figure 3.9.10-19 and 3.9.10-20 show the acceleration time history of the transfer cask lid section and middle section. Figure 3.9.10-21 shows the maximum effective stress of the transfer cask during the side drop event as computed by LS-DYNA.

The following table lists the LS-DYNA CG over corner drop results.

Summary of Impact g Load Due to CG Over Corner Drop

Transfer Cask Section (see Figure 3.9.10-13)	Axial Accelerations
Lid Section	15.5g

This table shows that the maximum axial acceleration during an 80 inch CG over corner drop accident event is 15.5g. Figure 3.9.10-23 shows the axial acceleration time history of the transfer cask lid section. Figure 3.9.10-23 shows the maximum effective stress of the transfer cask during the CG over corner drop event as computed by LS-DYNA.

3.9.10.5 Summary of g-Loads for the OS187H Transfer Cask Body and Lid Bolt Stress

Analyses

Based on the dynamic analysis results shown on the above table, the following table summarizes the g loads to be used for the stress analyses of the transfer cask body and lid bolts.

Component	Drop Orientation	Maximum G Load Computed by LS-DYNA	G Load used for Stress Evaluation
Cask Body	Side Drop	62.9	75
	Corner Drop	15.5 ⁽¹⁾	75 ⁽¹⁾
Lid Bolt	Corner Drop	15.5	21.65 ⁽²⁾

Note:

1. The transfer cask is transferred in a horizontal position held by the transfer trailer. In the axial direction it is possible to slide into the ground and incur a corner drop. The maximum stress resulting from DYNA corner impact analysis is plot in Figure 3.9.10-23 of this Appendix and also compared with ASME code allowable as described in item 5 below. Additionally, a conservative 75g end drop analysis of the cask body was also performed in Appendix 3.9.2.
2. A conservative 21.65g was used in the lid bolt corner drop analysis (Appendix 3.9.3).

The g loads used for the static stress analyses of the cask and lid bolts are reasonable and conservative for following reasons:

1. The casks of OS187H and LLNL/TN-32 are very similar in both geometry and weight. However, the OS187H (0.5" SS + 4.5" lead + 2.5" SS) is less rigid than the LLNL/TN-32 (9.5" thick CS shell). The less rigidity results in a lower calculated g load for the OS187H cask than for the LLNL/TN32 cask from LS-DYNA analyses.
2. Like LLNL/TN-32 models, the OS187H model does not include the outer shell and resin. In reality, these relatively soft components will deform and absorb energy during a drop and will slow down the rate of deceleration to produce a lower g load.
3. All material properties at room temperature are used in the LS-DYNA analyses. In reality, the transfer cask loaded with spent fuels will be at temperatures higher than room temperature. The modulus of elasticity for the cask material decreases while its temperature increases. The lower modulus of elasticity for the cask materials at the real temperatures will produce a lower impact g-load than that calculated in this analysis for the cask at room temperature.
4. During the drop accident, the g loads vary along the cask length from the minimum occurred at the bottom end to the maximum occurred at the top surface of the lid. However, a uniform 75 g load along the cask length is conservatively used in the cask static stress analysis. The maximum stress intensity in the cask structural shell is calculated to be 58.17 ksi (see Table 3.9.2-1 of Appendix 3.9.2, structural shell) from the static stress analysis.
5. Comparably, the maximum effective stress (Von Mises stress) in the cask structure shell is calculated to be 29.12 ksi (see Figure 3.9.10-21 of this Appendix) from the LS-DYNA dynamic analysis. This indicates that the static stress analysis using drop load of 75g is a very conservative approach, which produces about twice stress value of that produced by the dynamic LS-DYNA analysis.
6. Figure 3.9.10-23 shows the maximum effective stress (Von Mises stress) in transfer cask due to CG over corner drop from LS-DYNA analysis. The maximum effective stress at cask top cover plate is about 34.49 ksi, which is less than its allowable stress of 94.2 ksi (SA-240, Type XM 19 at 300 °F). The maximum effective stress in the structural shell is about 24.0 ksi, which is less than its allowable stress of 66.2 ksi (SA-240, Type 304 at 300 °F).

The g loads (including dynamic load factor) to be used for canister and basket structural analyses are described in Appendix 3.9.11.

3.9.10.6 References

1. LS-DYNA Keyword User's Manual, Volumes 1 & 2, Version 970, April 2003, Livermore Software Technology Corporation.
2. Witte, M. et al., Evaluation of Low-Velocity Impact Testing of Solid Steel Billet onto Concrete Pads and Application to Generic ISFSI Storage Cask for Tipover and Side Drop, Lawrence Livermore National Laboratory, UCRL-ID-126295, Livermore, California. March 1997.
3. NUREG/CR-6608, UCRL-1D-12911, "Summary and Evaluation of Low-Velocity Impact Tests of Solid Steel/Billet onto Concrete Pad," LLNL, February, 1998
4. ANSYS User's Manual, Rev 5.6.
5. American Society of Mechanical Engineers, ASME Boiler and Pressure Vessel Code, Section II, Part D, 1998, through 2000 addenda.
6. Baumeister & Marks, Standard Handbook for Mechanical Engineers, 7th Edition.
7. American Society of Mechanical Engineers, ASME Boiler and Pressure Vessel Code, Section II, Part A, 1998, through 2000 addenda.
8. A Survey of Strain Rate Effects for some Common Structural Materials Used in Radioactive Material Packaging and Transportation Systems, U.S. Energy Research and Development Administration, Battelle Columbus Laboratories, August 1976.
9. Dilger, etc., Ductility of Plain and Confined Concrete under Different Stain Rates, ACI Journal, January-February, 1984.
10. Structural Design of Concrete Storage Pads for Spent Fuel Casks, Electric Power Research Institute, EPRI NP-7551, RP 2813-28, August 1991.
11. Matthiesen, R. B., Observations of Strong Motions from Earthquakes, ASCE Convention and Exposition, Portland, Oregon, April 1980.
12. Dove, R. C., Endebrock, E. G., Dunwoody, W. E., Bennet, J. G., Seismic Tests on Models of Reinforced-Concrete Category 1 Buildings, Structural Mechanics in Reactor Technology, SMIRT 8, Brussels, Belgium 1985.
13. ANSYS User's Manual, Rev 6.0.
14. Harris and Crede, Shock and Vibration Handbook, Second Edition, McGraw-Hill.
15. Methods for Impact Analysis of Shipping Containers, NUREG/CR-3966, UCID-20639, LLNL, 1987.
16. Clough and Penzien, "Dynamics of Structures" McGraw-Hill, 2nd Edition, 1993.

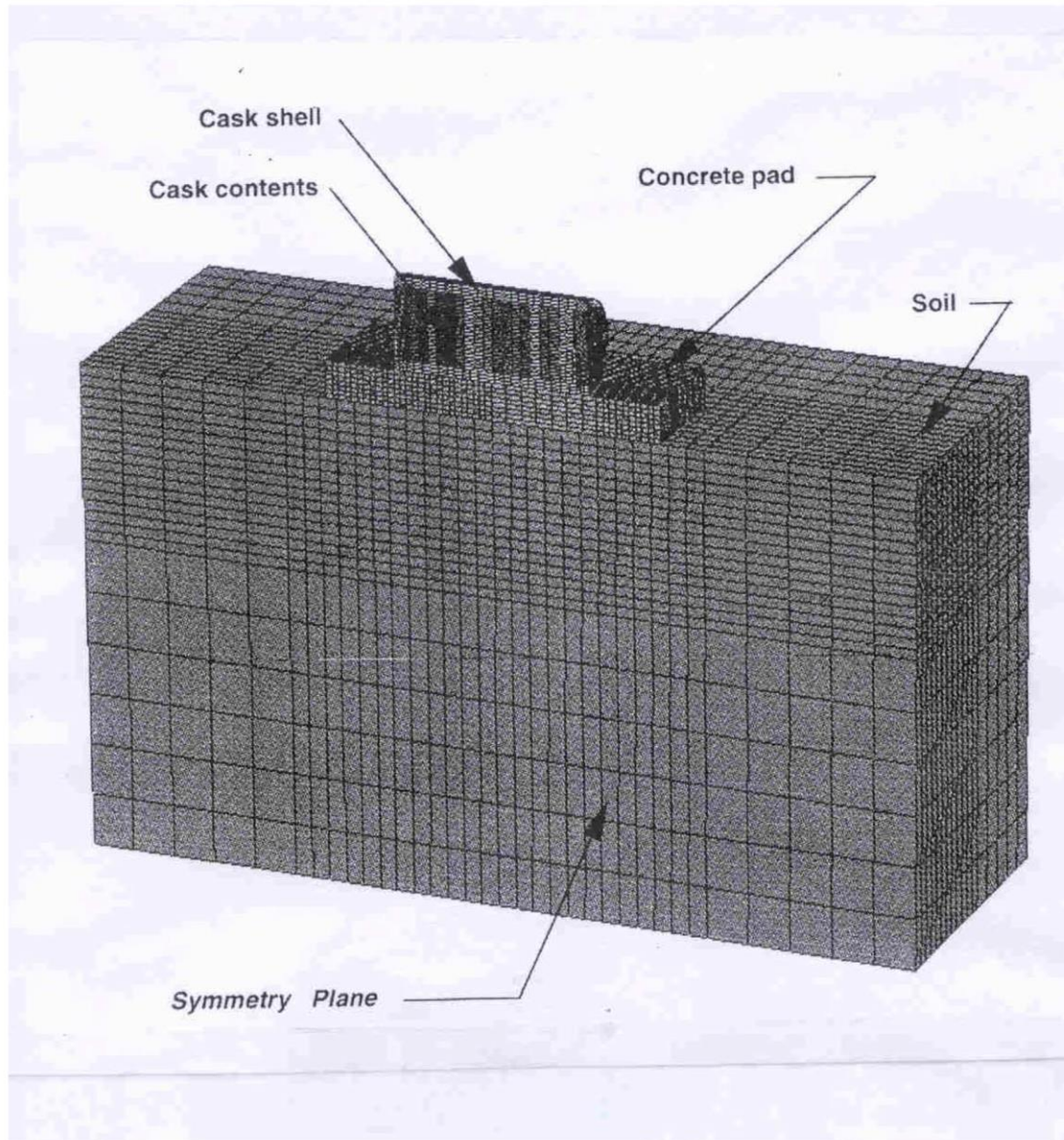


Figure 3.9.10-1
Finite Element Model of “GENERIC” Storage Cask, Side Drop and Tip Over Onto Concrete Pad And Soil (Reproduced From LLNL Report)

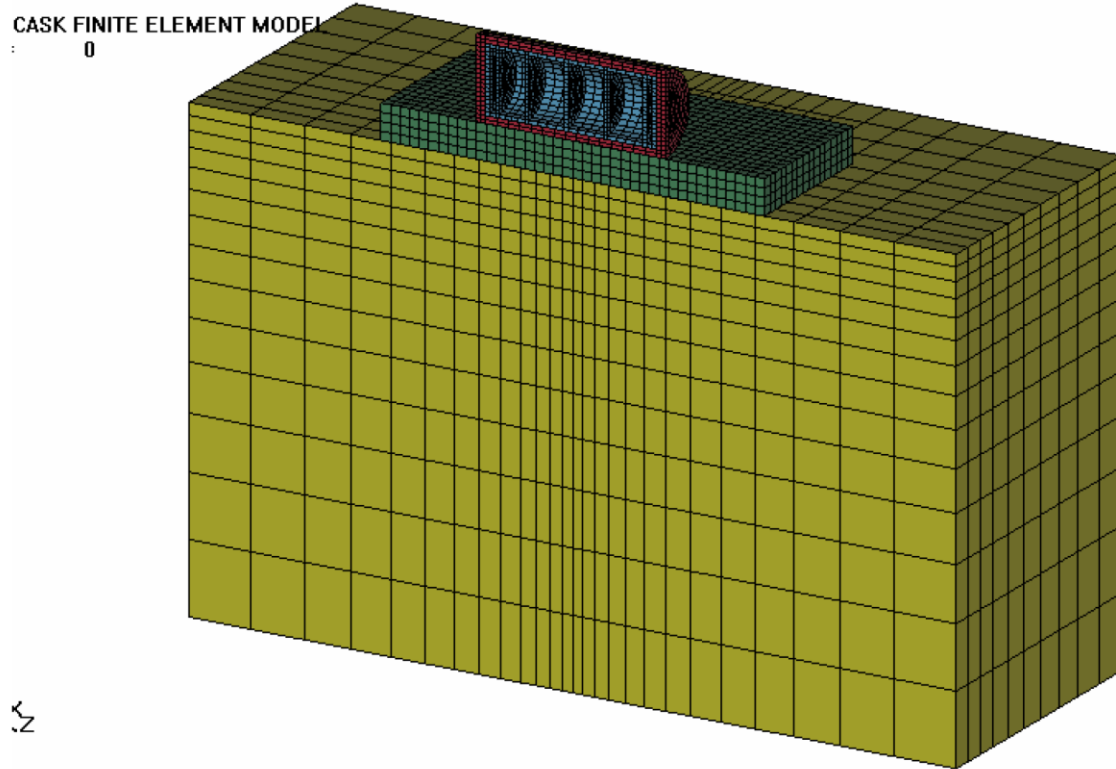


Figure 3.9.10-2
TN-32 Cask Tipover Analysis Finite Element Model

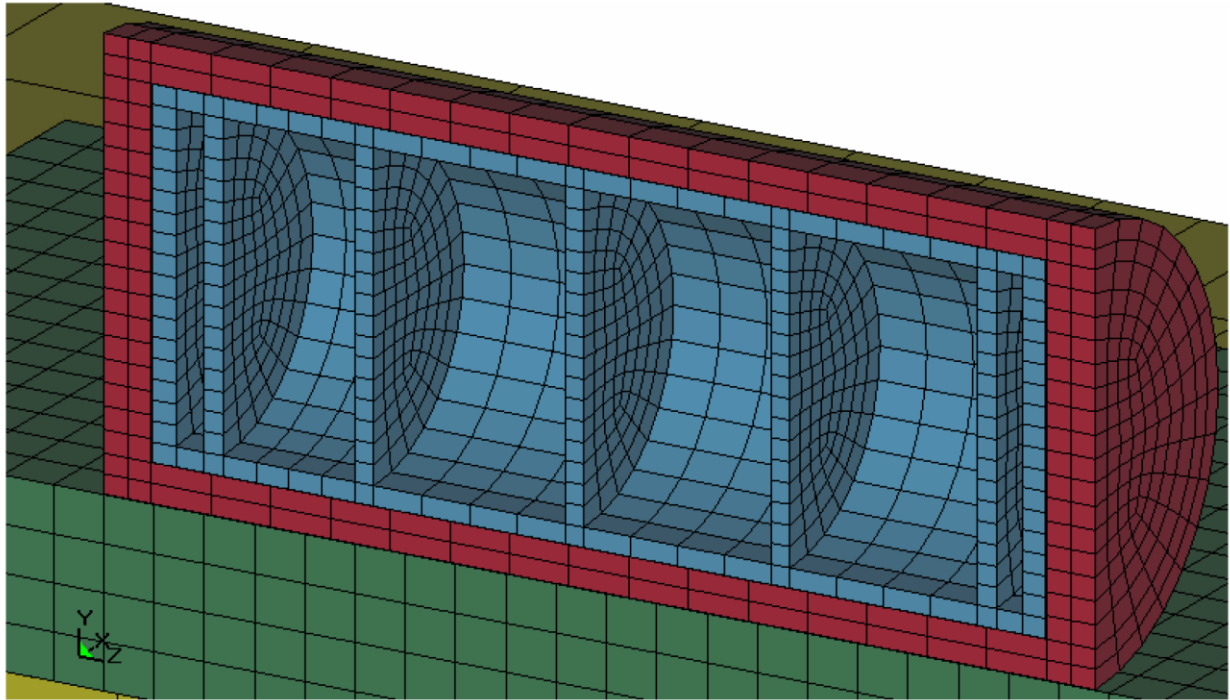


Figure 3.9.10-3
TN-32 Cask Tipover Analysis Finite Element Model (Enlarged view of the TN-32 Cask)

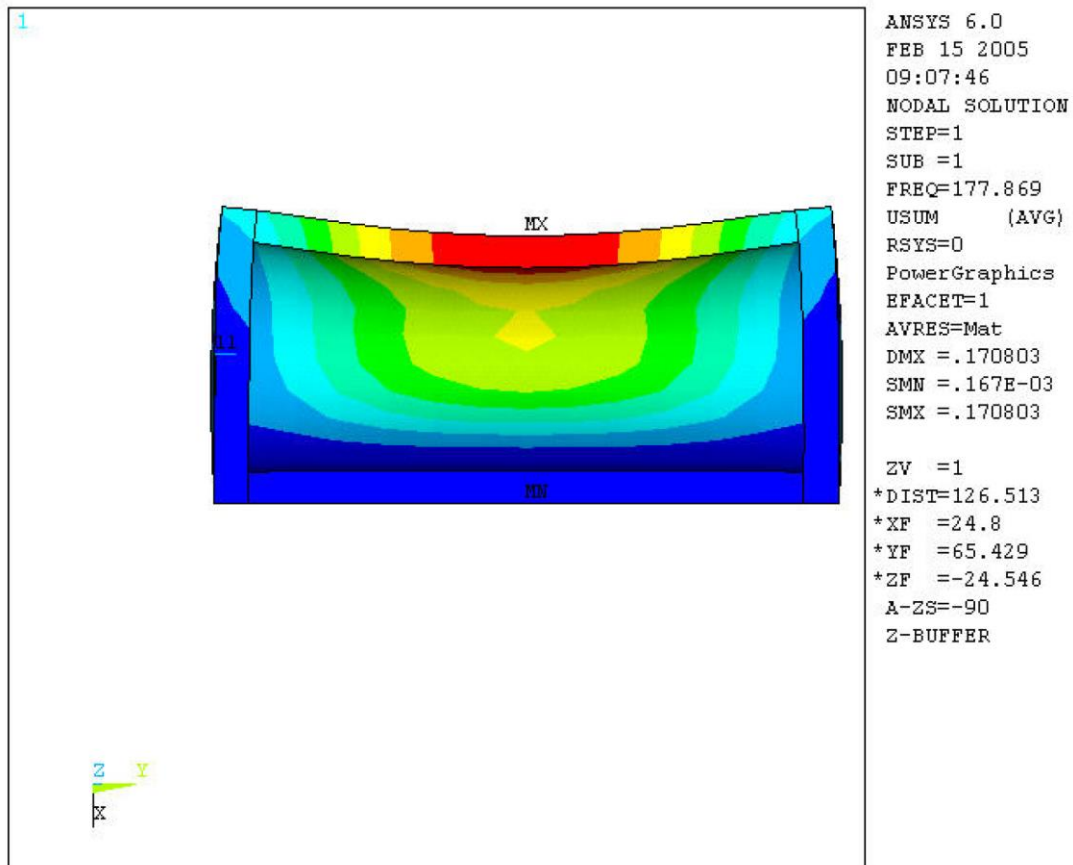


Figure 3.9.10-4
TN-32 Transfer Cask Deformed Shape-Mode 1

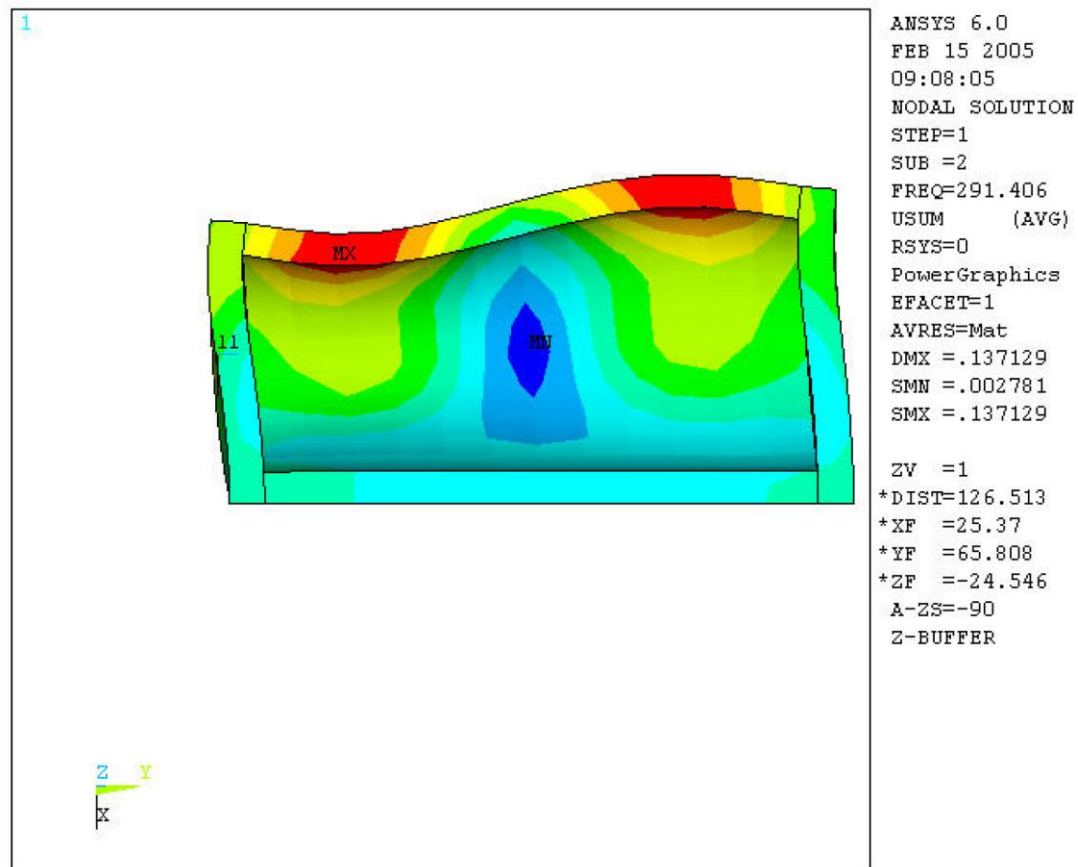


Figure 3.9.10-5
TN-32 Transfer Cask Deformed Shape-Mode 02

OS187H TRANSFER CASK IMPACT ANALYSIS
Time = 0

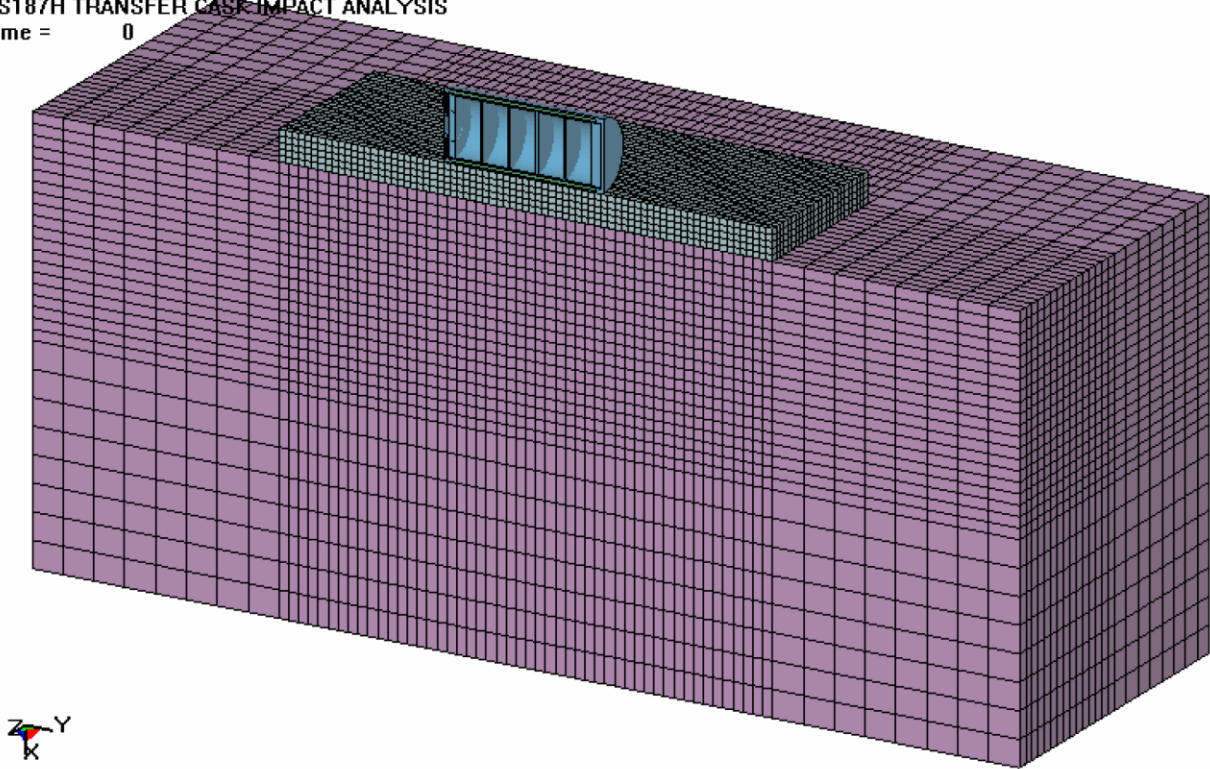


Figure 3.9.10-6
OS187H Transfer Cask Side Drop Dynamic Impact Finite Element Model

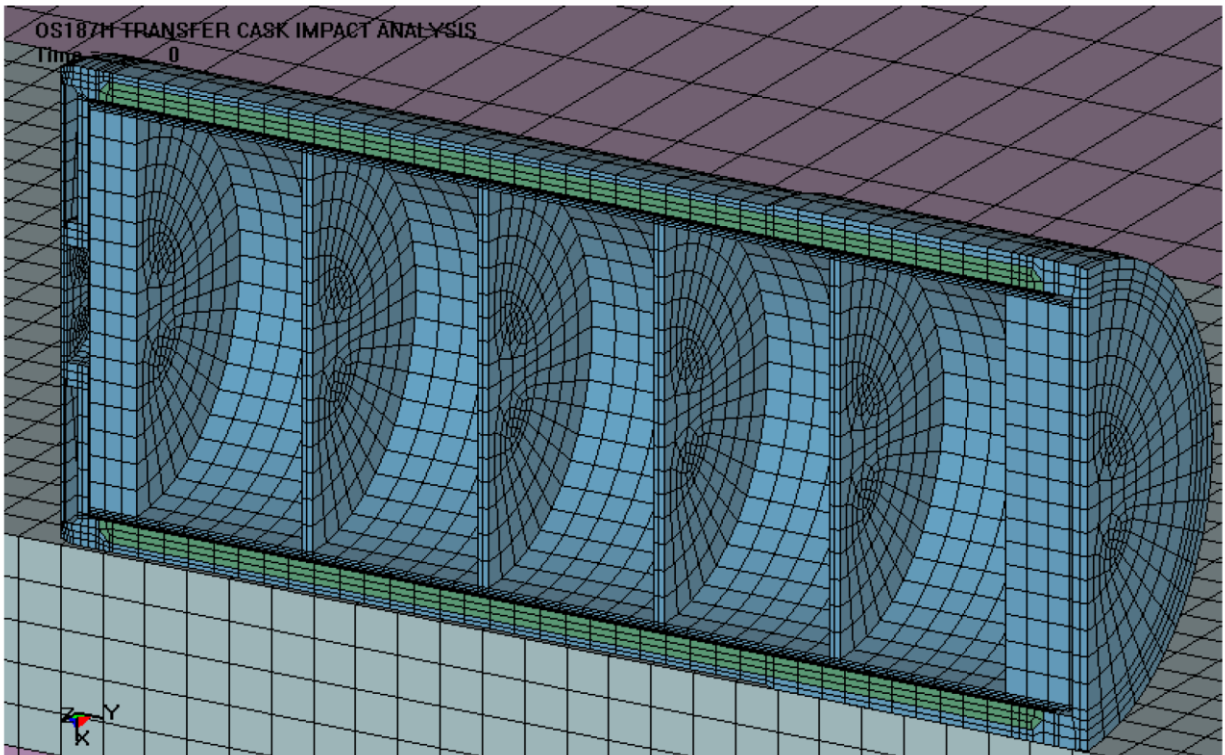


Figure 3.9.10-7
OS187H Transfer Cask Side Drop Dynamic Impact Finite Element Model
(Enlarged view of the Transfer Cask)

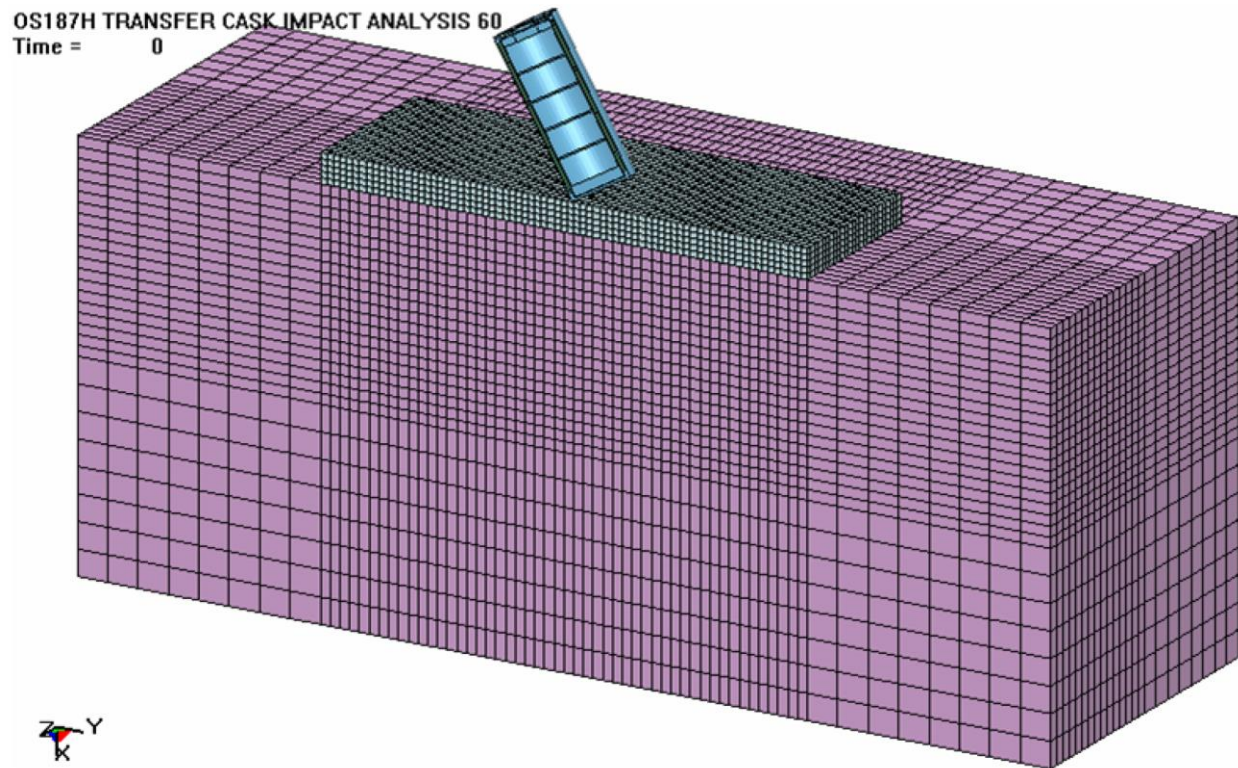


Figure 3.9.10-8
OS187H Transfer Cask CG Over Corner Drop Dynamic Impact Finite Element Model

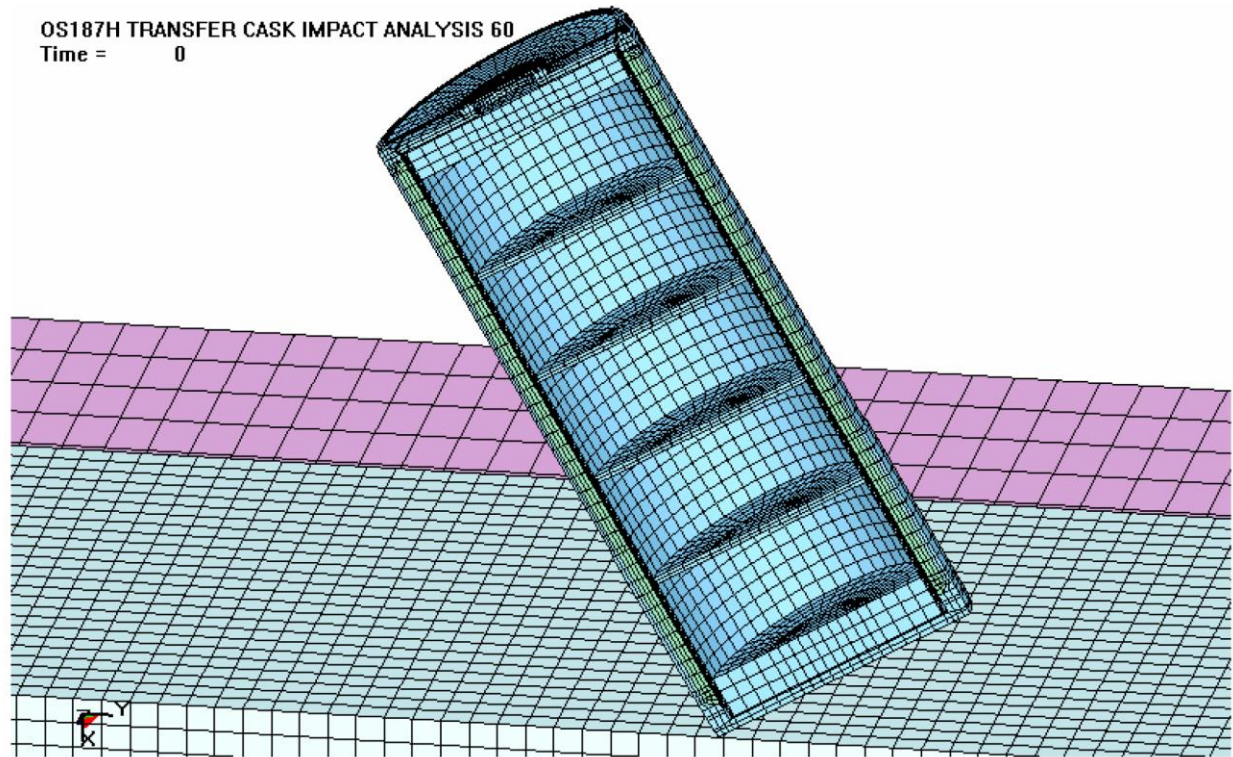


Figure 3.9.10-9
OS187H Transfer Cask CG Over Corner Drop Dynamic Impact Finite Element Model
(Enlarged View of the Transfer Cask)

OS187H TRANSFER CASK IMPACT ANALYSIS
Time = 0

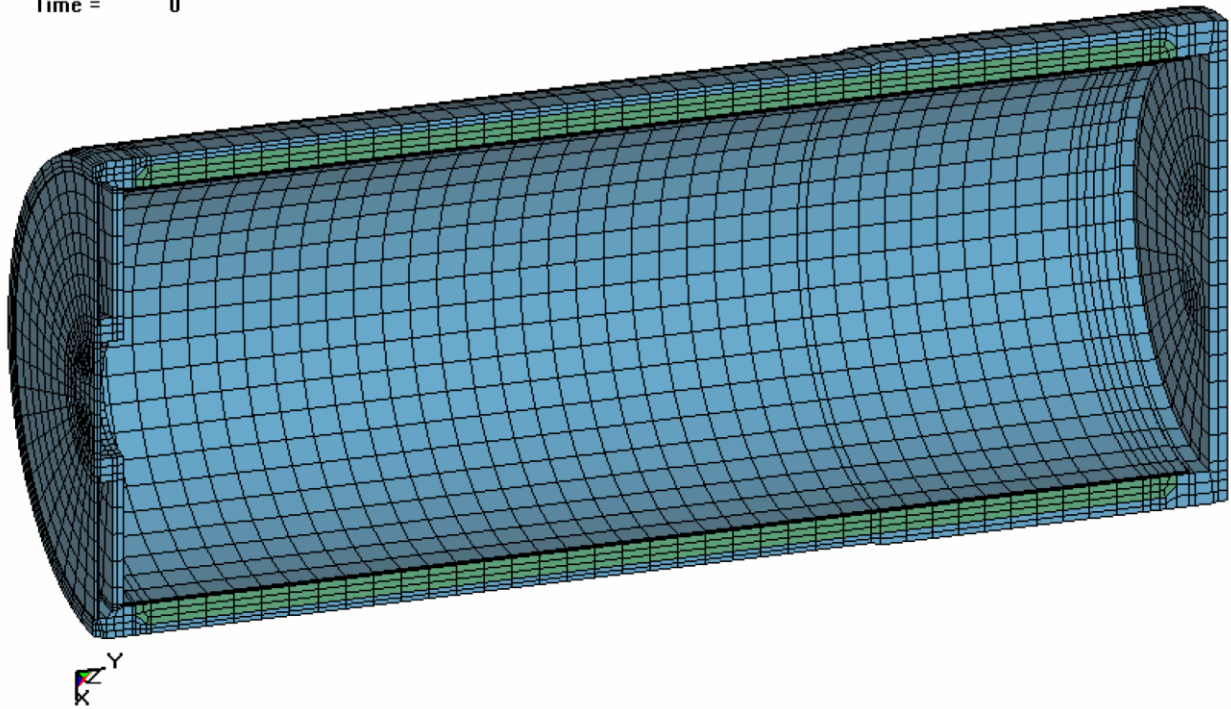


Figure 3.9.10-10
OS187H Transfer Cask Finite Element Model without the Internals

OS187H TRANSFER CASK IMPACT ANALYSIS
Time = 0

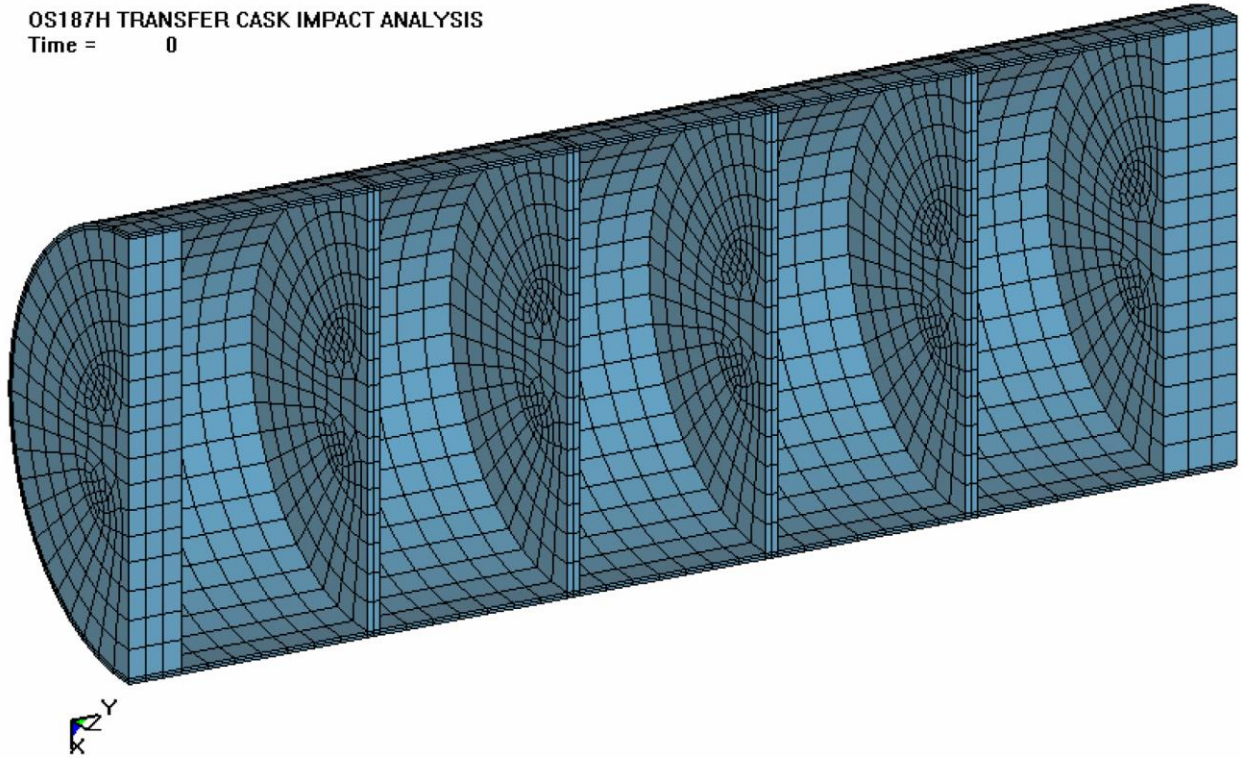


Figure 3.9.10-11
OS187H Transfer Cask Internals Finite Element Model

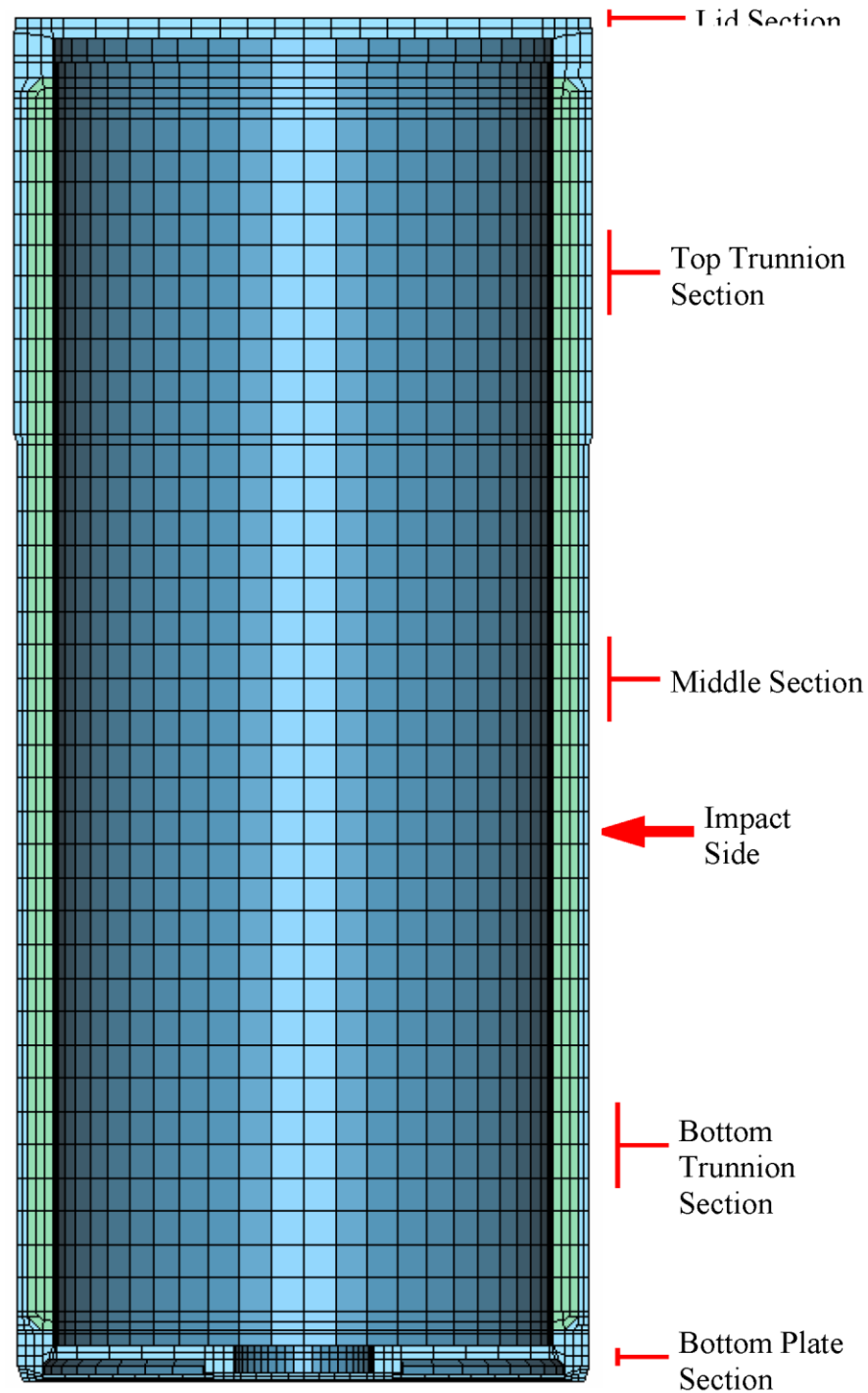


Figure 3.9.10-12
OS187H Transfer Cask Side Drop Nodal Sections Analyzed

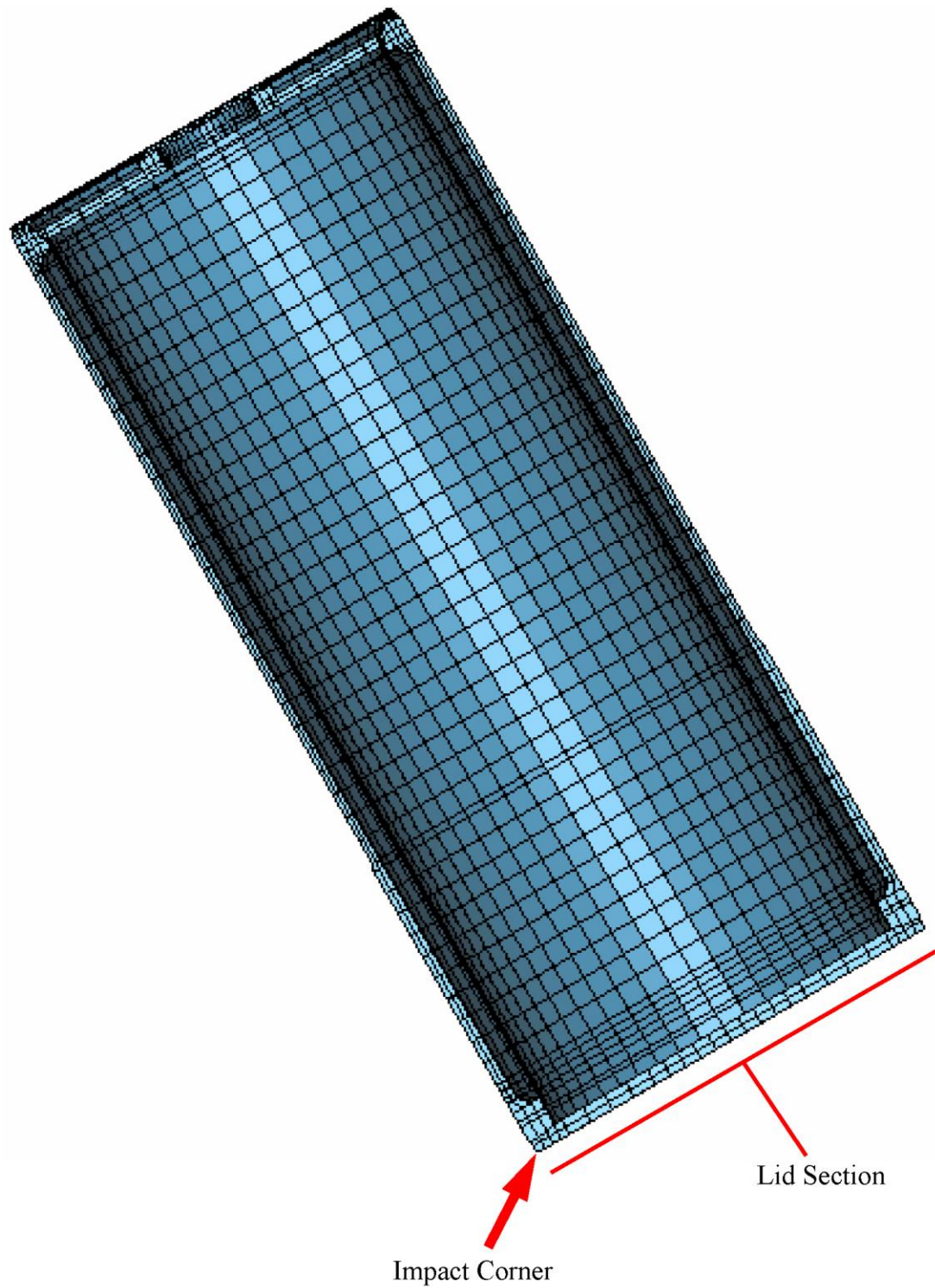


Figure 3.9.10-13
OS187H Transfer Cask CG Over Corner Drop Nodal Sections Analyzed

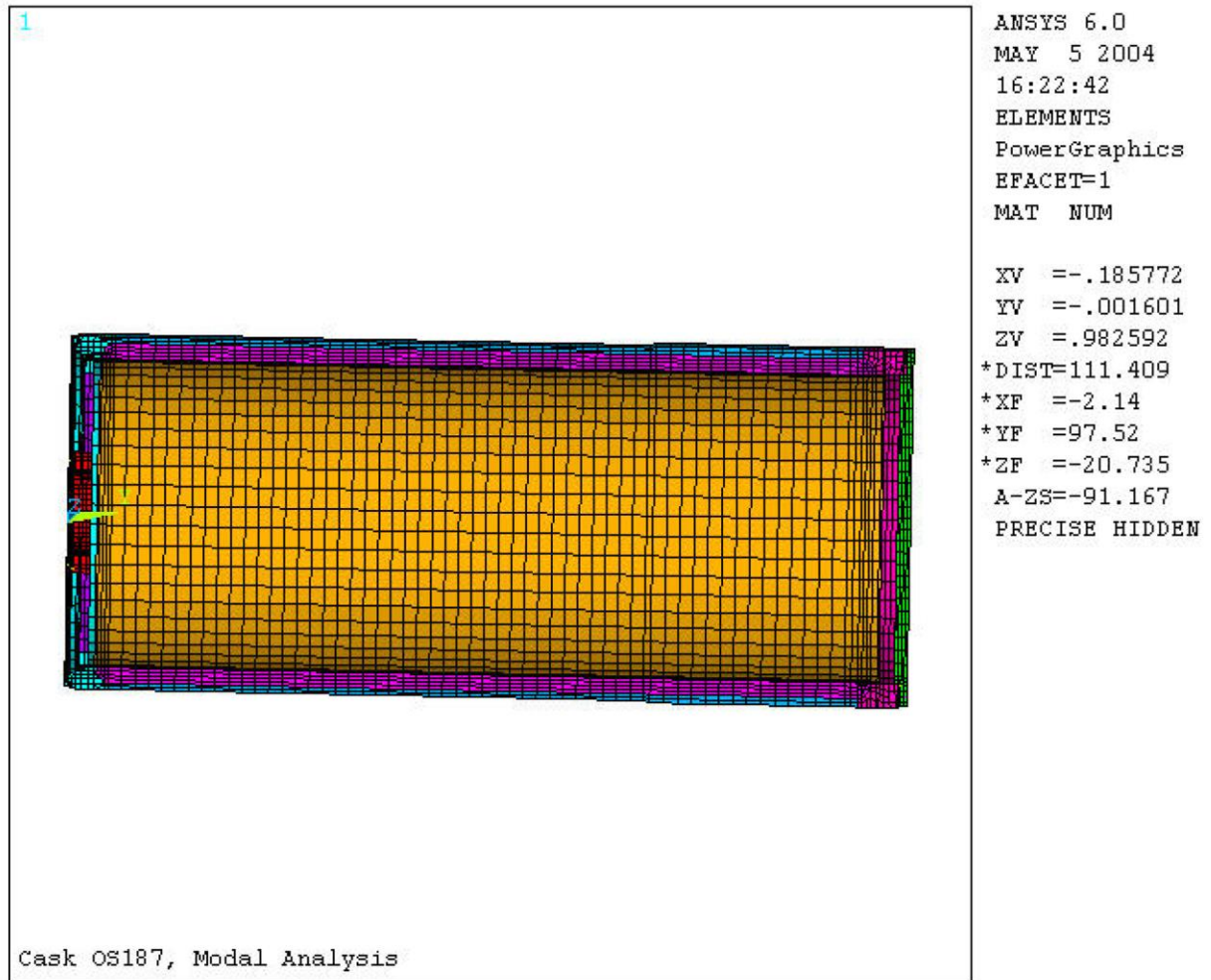


Figure 3.9.10-14
OS187H Transfer Cask Finite Element Model used for Modal Analysis, Elements

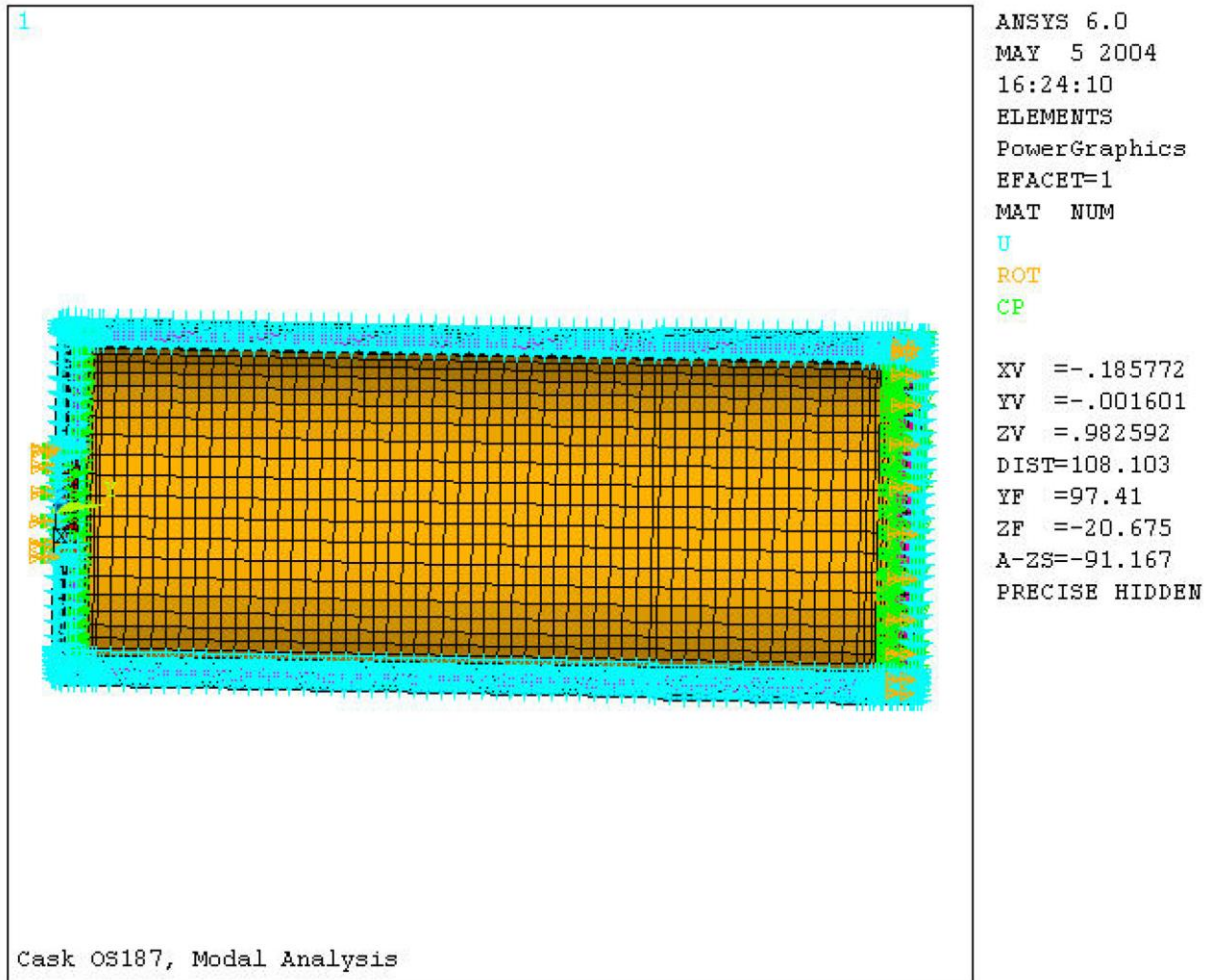


Figure 3.9.10-15
OS187H Transfer Cask Finite Element Model used for Modal Analysis, Boundary Conditions

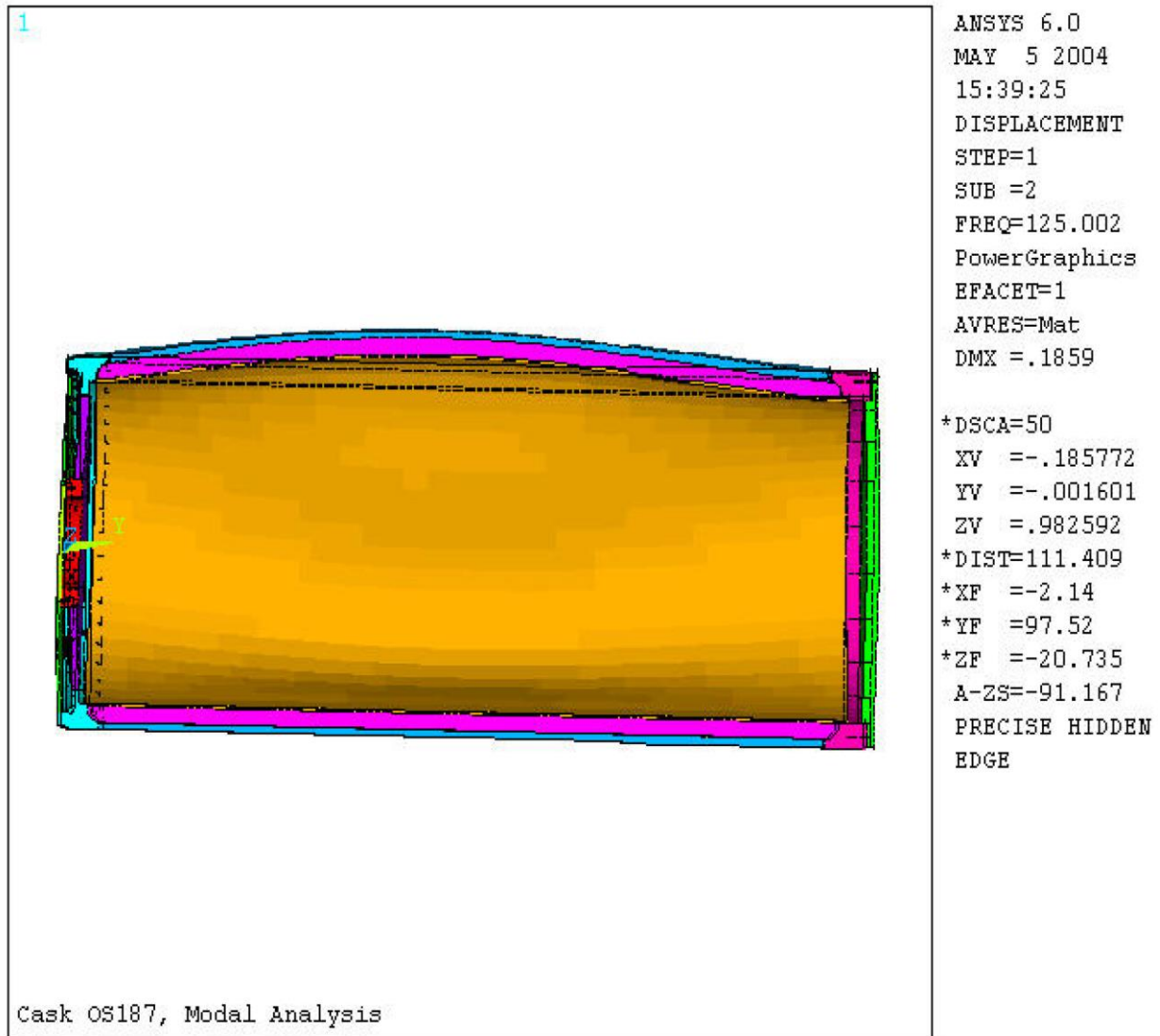


Figure 3.9.10-16
OS187H Transfer Cask Deformed Shape – Mode 2

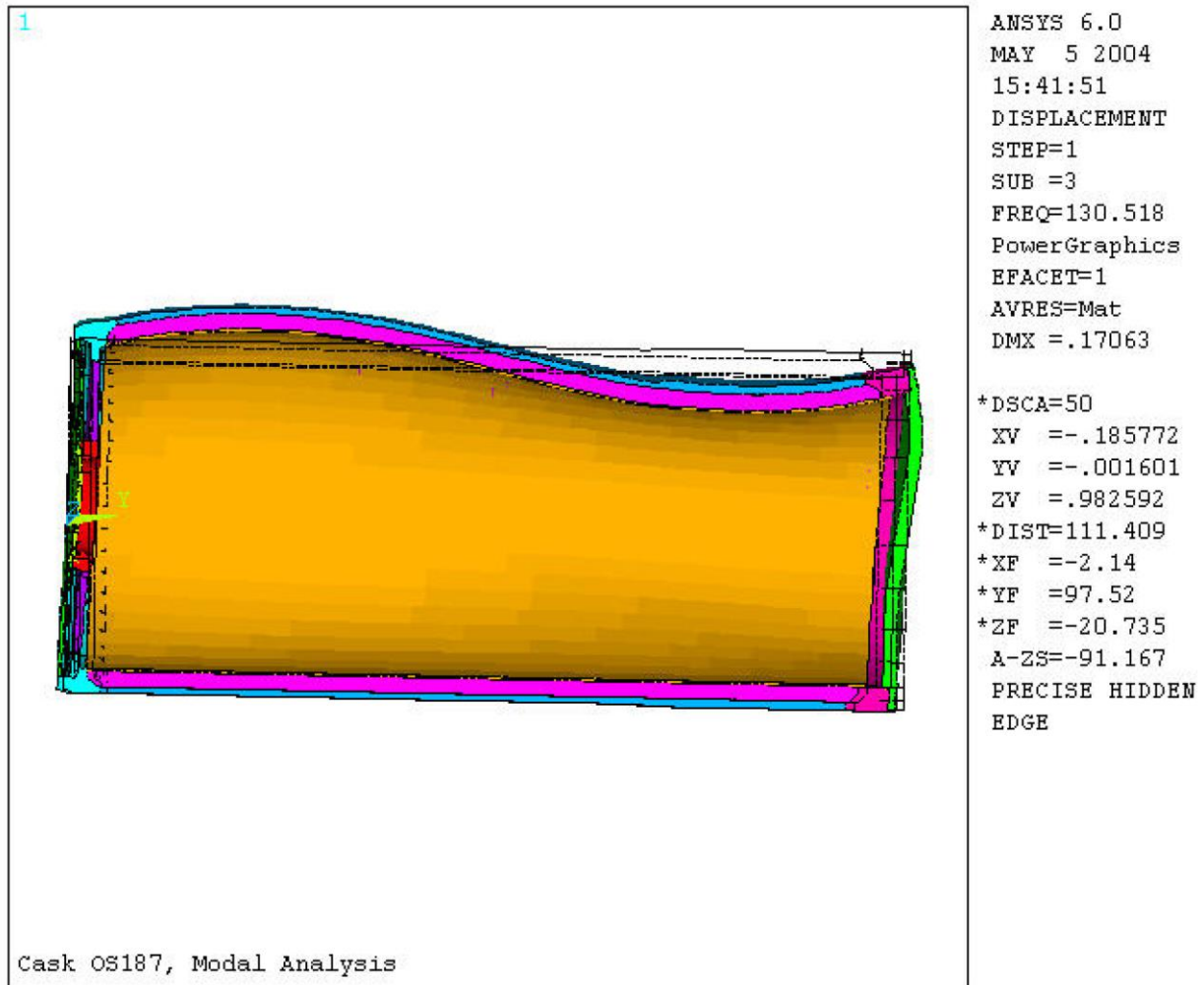


Figure 3.9.10-17
OS187H Transfer Cask Deformed Shape – Mode 3

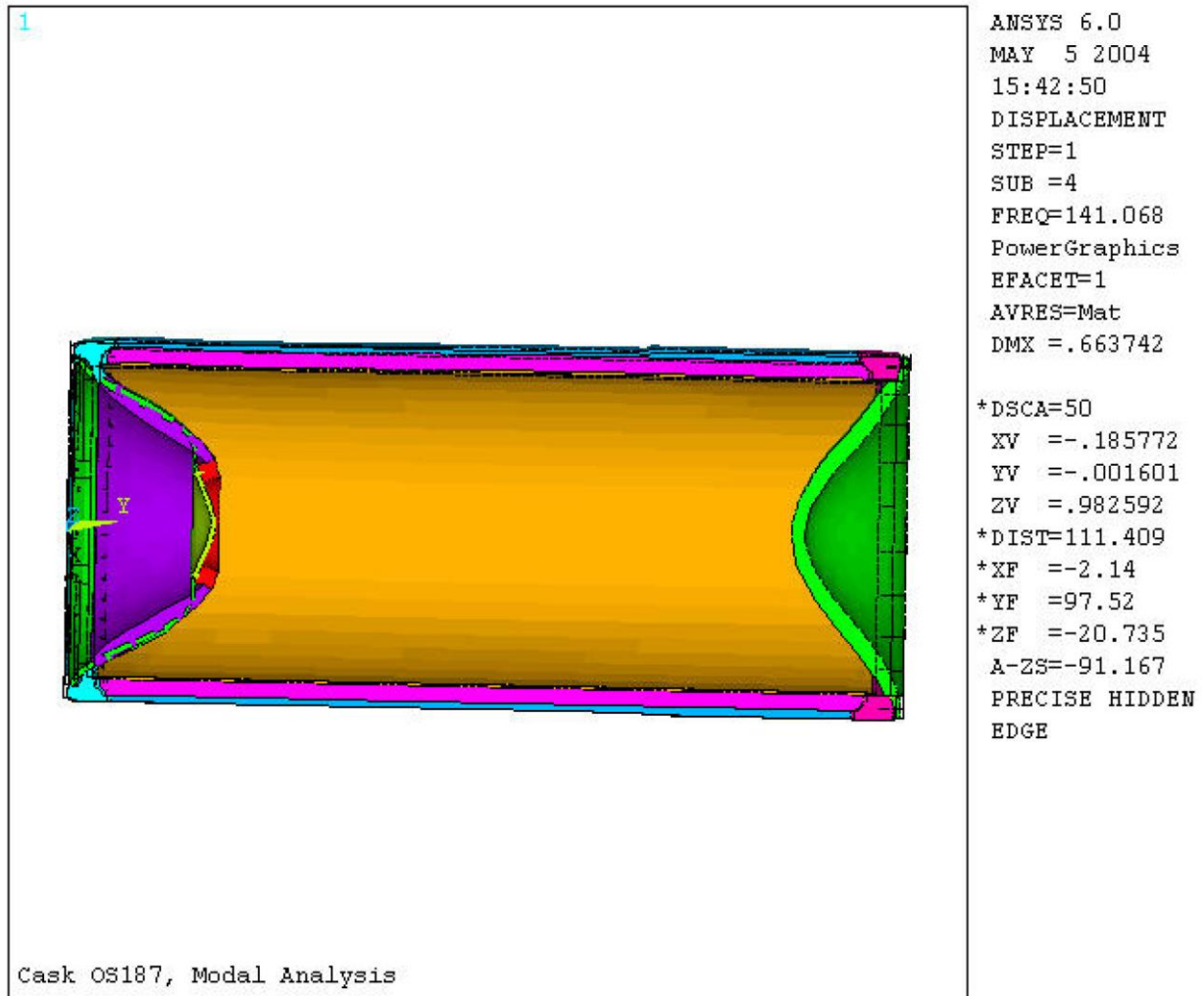


Figure 3.9.10-18
OS187H Transfer Cask Deformed Shape – Mode 4

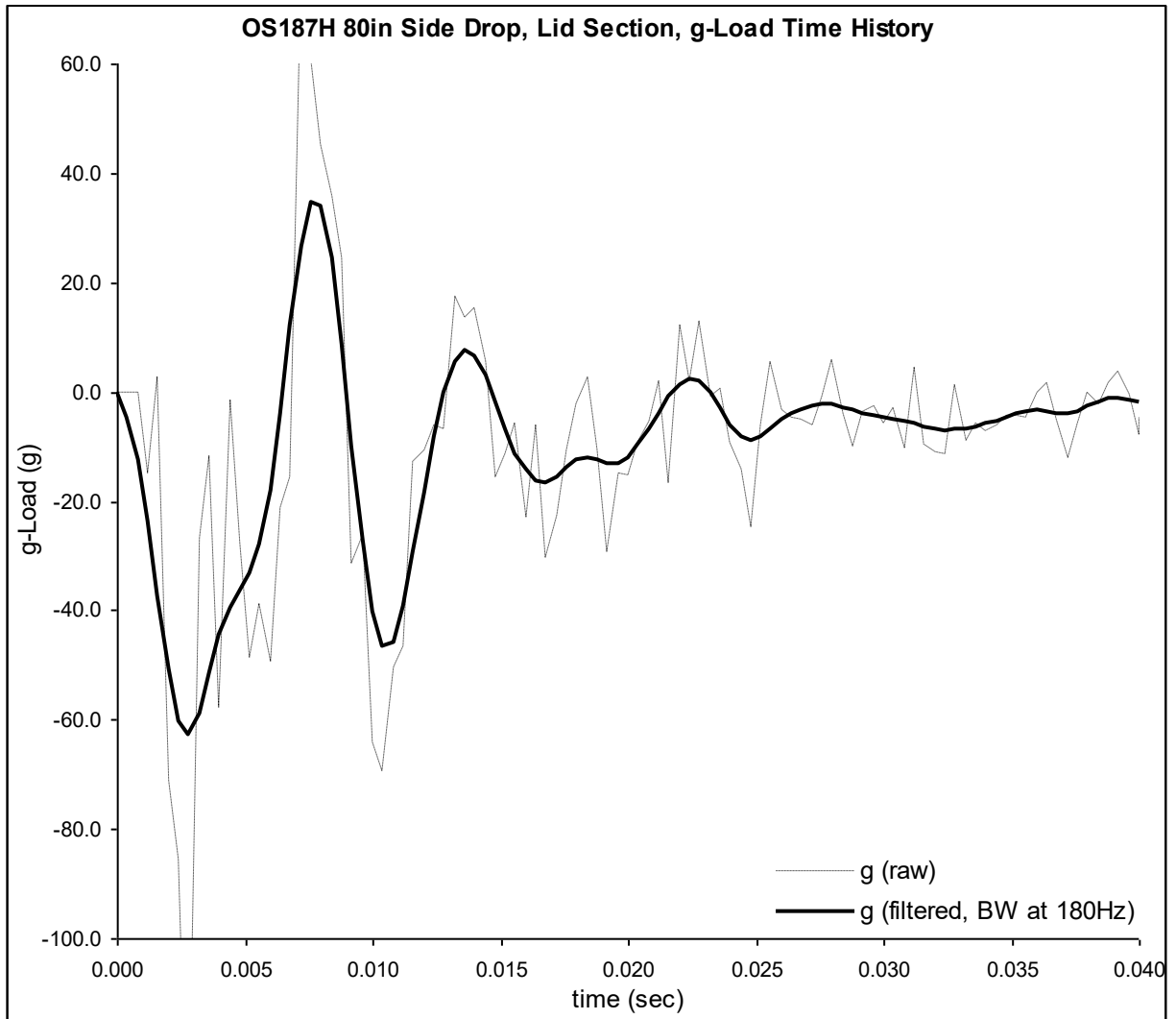


Figure 3.9.10-19
OS187H Transfer Cask, Side Drop,
Lid Section Acceleration Time History

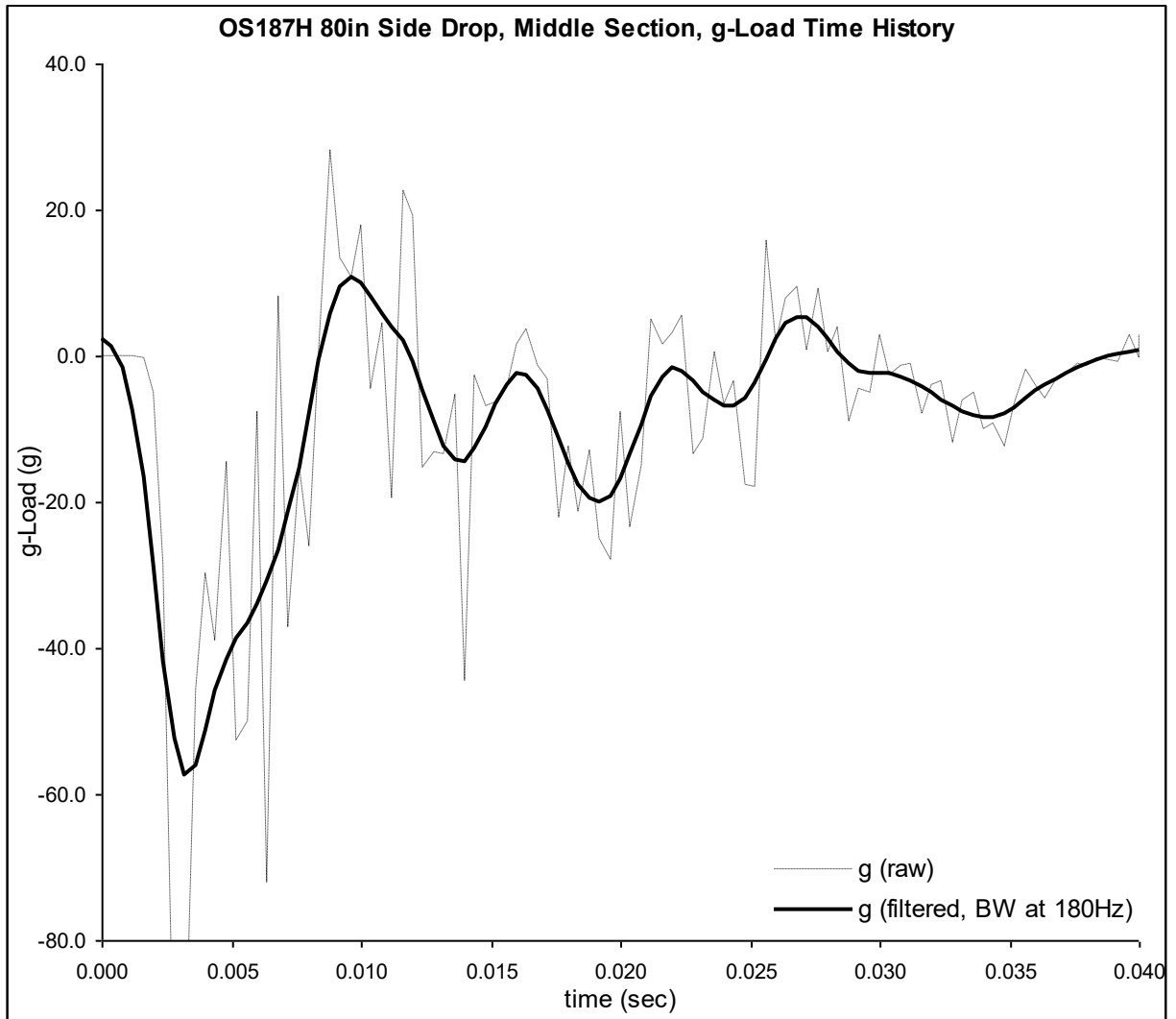


Figure 3.9.10-20
OS187H Transfer Cask, Side Drop,
Middle Section Acceleration Time History

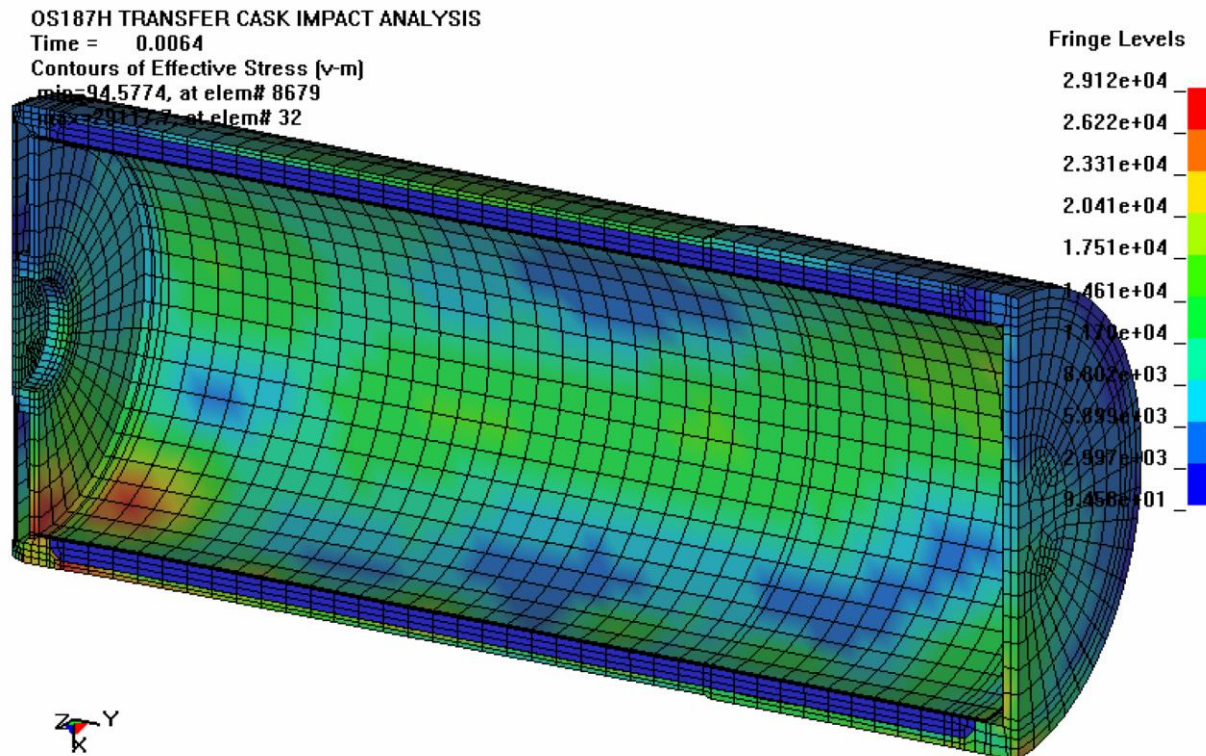


Figure 3.9.10-21
OS187H Transfer Cask, Side Drop,
Maximum Effective Stress Distribution

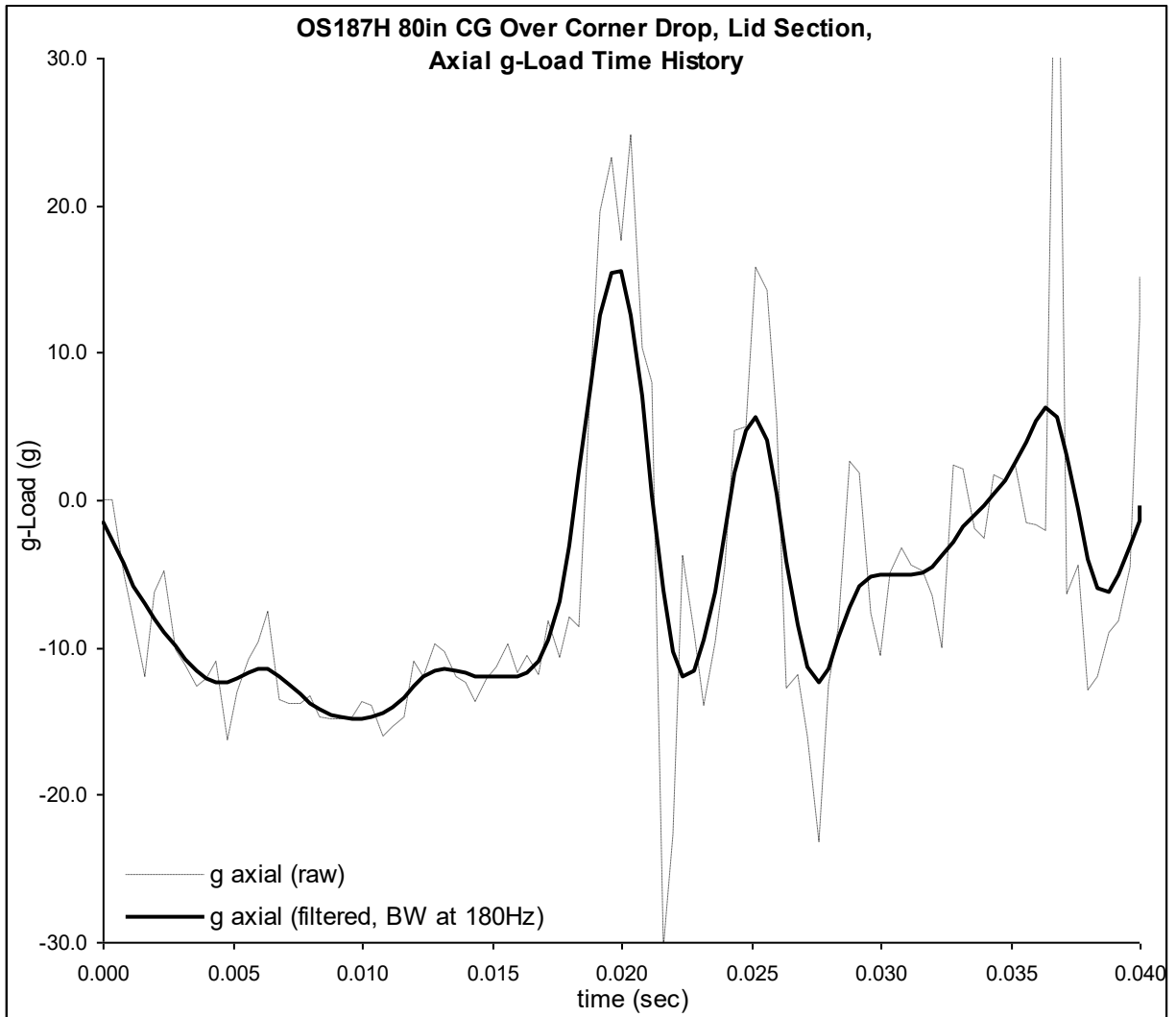


Figure 3.9.10-22
OS187H Transfer Cask, CG Over Corner Drop,
Lid Section Axial Acceleration Time History

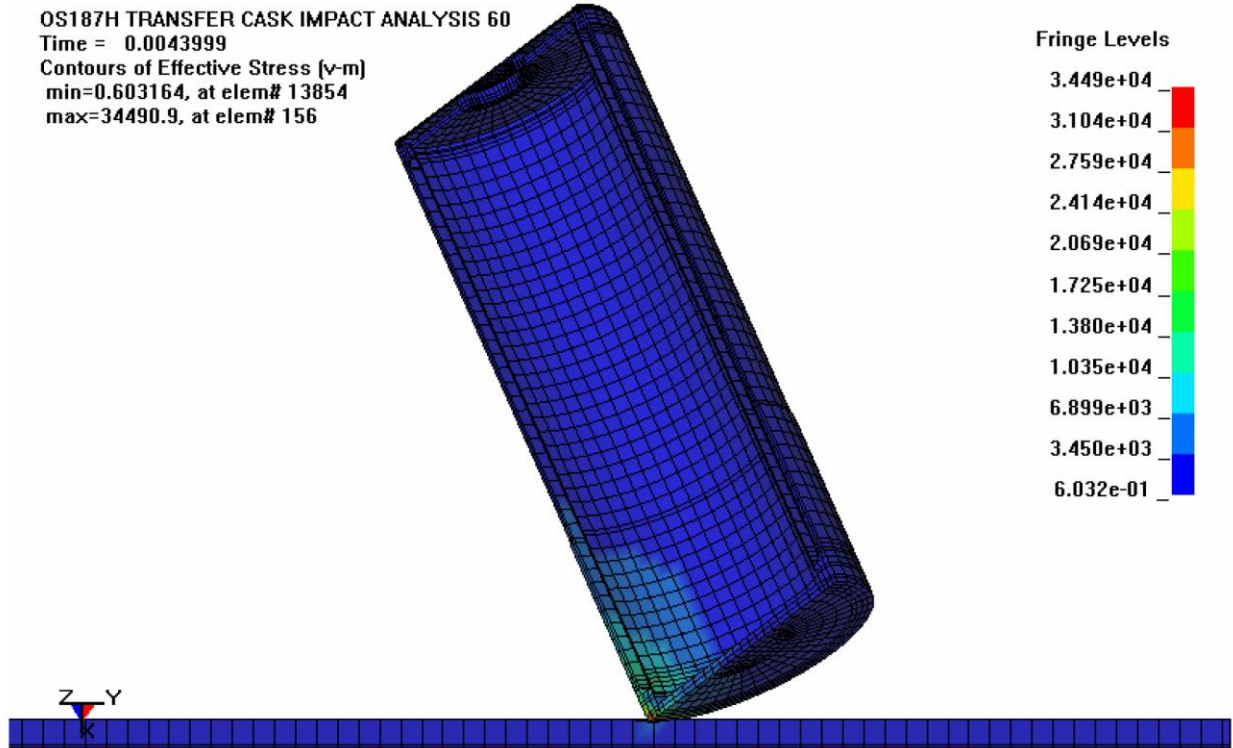


Figure 3.9.10-23
OS187H Transfer Cask, CG Over Corner Drop,
Maximum Effective Stress Distribution

APPENDIX 3.9.11 32PTH DSC DYNAMIC AMPLIFICATION FACTOR (DAF) CALCULATION

TABLE OF CONTENTS

3.9.11 32PTH DSC DYNAMIC AMPLIFICATION FACTOR (DAF) CALCULATION.....	3.9.11-1
3.9.11.1 DAF Analysis Introduction	3.9.11-1
3.9.11.2 DAF Analysis Notations.....	3.9.11-2
3.9.11.3 End Drop Modal Analysis	3.9.11-2
3.9.11.4 Side Drop Modal Analysis	3.9.11-3
3.9.11.5 Dynamic Load Factor Calculations.....	3.9.11-5
3.9.11.6 Summary of g-Loads for 32PTH Canister and Basket Impact Analyses.....	3.9.11-6
3.9.11.7 References	3.9.11-7

LIST OF FIGURES

Figure 3.9.11-1	NUHOMS 32 PTH Basket – Finite Element Model.....	3.9.11-8
Figure 3.9.11-2	NUHOMS 32 PTH Basket – First Mode Shape, 0 Degree Orientation.....	3.9.11-9
Figure 3.9.11-3	NUHOMS 32 PTH Basket – First Mode Shape, 45 Degree Orientation.....	3.9.11-10
Figure 3.9.11-4	Spring - Mass Finite Element Model	3.9.11-11

3.9.11 32PTH DSC DYNAMIC AMPLIFICATION FACTOR (DAF) CALCULATION

3.9.11.1 DAF Analysis Introduction

The two components of the OS187H Transfer Cask internals with the longest and most significant natural periods are the Canister and Fuel Basket (with fuel assemblies). Each component is analyzed separately. The Dynamic Amplification Factor used for the entire structure is conservatively taken to be the higher of the two computed individual dynamic amplification factors.

Two load cases will be evaluated in this analysis; one due to longitudinal loading and one due to transverse loading. During an end drop, the fundamental natural periods of the 32PTH DSC components are taken to be that of simply supported cylindrical shells without axial constraint, under longitudinal vibration. During a side drop, the fundamental natural period of the 32PTH canister shell is taken to be that of a cylinder in an ovaling mode and a simply supported cylindrical shell without axial constraint. For the basket, a modal analysis is conducted using ANSYS [1]. The fuel and aluminum plates mass is lumped with the steel compartment plates.

Since the canister and basket are not modeled in detail in the transfer cask dynamic analysis it is necessary to transfer the loads from the cask dynamic analysis model to the detailed models of canister and basket. The canister and basket structures are evaluated using quasi-static analyses with a dynamic amplification factor (DAF) computed from the transient dynamic analysis. The value of dynamic amplification factors are representative of the magnitude of the displacement of the 32PTH canister and basket relative to the displacement in the OS187H Transfer Cask.

Since the side drop is the only credible accident during storage or transfer operations as discussed in Section 3.1.1.4, the dynamic amplification factors of canister and basket are computed only for the side drop event in this section using ANSYS transient dynamic analyses. The acceleration time-history from LS-DYNA cask analyses in Appendix 3.9.10 is used as a forcing function in canister and basket spring-mass models to get the dynamic response. The ratio of the dynamic deflection to the static deflection is used to determine the DAF for the canister and basket.

3.9.11.2 DAF Analysis Notations

The notations used in this analysis are taken from Blevins [2], and are as follows.

E ,	Modulus of Elasticity, (psi).
f_1, f_{11} ,	Fundamental natural frequency, (Hz.).
I ,	Moment of inertia of the beam, (in. ⁴).
L ,	Length of beam or cylindrical shell, (in.).
m ,	Mass per unit length of the beam, (lbm.in. ⁻¹).
μ ,	Mass density, (lbm.in. ⁻³).
ν ,	Poisson's ratio.
R ,	Outer radius of the cylindrical shell, (in.).

3.9.11.3 End Drop Modal Analysis

A. Canister Shell

The maximum normal conditions transportable canister temperature is 475 °F (Chapter 4). However, the canister material properties are conservatively taken at 500 °F. The canister shell is constructed from SA-240 Type 304, which has a modulus of elasticity of 25.8×10^6 psi. at 500 °F [3]. The length of the canister between the top and bottom shield plugs is 164.5 inches.

Weight of the entire Canister = 28,191 lb.

Weight of bottom shield plug = 9,420 lb.

Section area of cylinder = $(\pi/4)(69.75^2 - 68.75^2) = 108.78 \text{ in.}^2$

Maximum static vertical deflection, $\Delta = WL/AE = \frac{(28,191 - 9,420)164.5}{(108.78)(25.8 \times 10^6)} = 0.0011 \text{ in}$

Therefore,

$$\text{Natural Frequency, } f_1 = \frac{1}{2\pi} \left(\frac{g}{\Delta} \right)^{1/2},$$

$$f_1 = \frac{1}{2\pi} \left(\frac{386.4}{0.0011} \right)^{1/2} = 94.3 \text{ Hz.}$$

The natural period of the canister shell is then $1/f_1$ or $T = 0.0106 \text{ s}$.

B. Basket

The fundamental natural frequency of a simply supported basket structure under axial vibration simplifies to that of a uniform beam, axially free at both ends. The fundamental natural frequency of a uniform beam free at both ends, under longitudinal vibration is as follows. ([2], p. 183, Table 8-16, Frame 1)

$$f_1 = \frac{\lambda_1}{2\pi L} \left(\frac{E}{\mu} \right)^{1/2}$$

Where $\lambda_1 = \pi$.

The maximum normal condition of transfer fuel basket temperature is 697 °F. The peripheral rail temperature is 561 °F. However, the basket material properties are taken at the average temperature of the basket, which is roughly 650 °F. The modulus of elasticity is taken to be that of SA-240 Type 304 stainless steel at 650 °F, or 25.1×10^6 psi. [3]. The length of the basket is 162.00 inches.

Based on component weights and volumes of the 32PTH basket (stainless steel density of 0.29 lb. in.⁻³ and an aluminum density of 0.098 lb. in.⁻³), the average weight density is calculated to be 0.226 lb.in⁻³ and the average mass density is calculated as follow:

$$\text{Average mass density, } \mu = \frac{0.226}{386.4} = 0.000586 \text{ lbm. in.}^{-3}$$

Therefore,

$$f_1 = \frac{\pi}{2\pi(162)} \left(\frac{25.1 \times 10^6}{0.000586} \right)^{1/2} = 639 \text{ Hz.}$$

The natural period of the fuel compartments is then $1/f_1$ or $T = 0.00157$ sec. It may be noted that for vertical vibration due to end drop, the weight of fuel is not lumped with the basket. However, the weight of fuel is considered during side drop vibrations.

3.9.11.4 Side Drop Modal Analysis

A. Canister Shell

The fundamental natural frequency of the canister is assumed to be caused by a cylindrical shell ovalling mode. The fundamental natural frequency of the canister shell ovalling (Radial-Axial) mode is determined assuming the cylindrical shell is simply supported without axial constraint. The natural frequency of the cylindrical shell ovalling mode is given by the following [2], p. 305, Table 12-2, Frame 5:

$$f_{ij} = \frac{\lambda_{ij}}{2\pi R} \left(\frac{E}{\mu(1-\nu^2)} \right)^{1/2}$$

Where L is taken to be the length between the top and bottom shield plugs, which is roughly 164.5 in, $E = 25.8 \times 10^6$ psi. (for SA-240 Type 304 stainless steel at 500 °F [3]), R is the average shell radius, 34.625 in., ν is Poisson's ratio, which is 0.305 for stainless steel [4], page 5-6, $\mu = 0.29/386.4 = 0.000751$ lbm. in⁻³, and thickness $h = 0.5$ in.

$$\lambda_{ij} = \frac{\left\{ (1-\nu^2)(j\pi R/L)^4 + (h^2/12R^2)[i^2 + (j\pi R/L)^2]^4 \right\}^{1/2}}{(j\pi R/L)^2 + i^2}$$

For the fundamental mode, $i = 2$ and $j = 1$.

$$\lambda_{ij} = \frac{\left\{ (1-.305^2)(\pi \times 34.625 / 164.5)^4 + (0.5^2 / 12 \times 34.625^2)[2^2 + (\pi 34.625 / 164.5)^2]^4 \right\}^{1/2}}{(\pi 34.625 / 164.5)^2 + 2^2} = 0.09617$$

$$f_{21} = \frac{0.09617}{2\pi \times 34.625} \left(\frac{25.8 \times 10^6}{0.000751(1-0.305^2)} \right)^{1/2} = 86 \text{ Hz}$$

The natural period of the canister is then $1/f_{21}$ or $T = 0.01162$ s.

B. Basket with Fuel Assemblies

Basket Finite Element Modal Description

The 32PTH fuel basket finite element model described in Appendix 3.9.1 is used to perform the modal analyses. ANSYS computer program [1] is used for the analysis. All assumptions used in that appendix for modeling are, therefore, applicable to this analysis. The outer canister shell and gap elements are removed from the finite element model and boundary conditions are applied directly to the rails. The basket finite element model is shown on Figure 3.9.11-1.

The basket is assumed supported at the rails periphery for the modal analysis. This assumption causes the basket natural frequencies to be strongly dependent on the inertial mass of the fuel compartment plates.

Material Properties

Material properties taken from Reference [3] based on a basket temperature of 700° F and a periphery rail temperature of 550° F is used. Weight densities are changed to mass densities ($\rho_m = \rho_w / 386.4$).

Boundary Conditions

Since modal analysis is a linear analysis, all gap elements (and canister shell elements) used in the Appendix 3.9.1 finite element model are deleted and the rails are supported at periphery. Thus this model yields only the natural frequencies of the fuel supporting basket plates and the rail panels.

For the 0° basket orientation, fuel is supported only by the horizontal panels, but for the 45° basket orientation, fuel is supported by both horizontal and vertical panels. Since only the lateral modes of vibration are significant, the master degree-of-freedom are applied on horizontal panels in *y*-direction and on vertical panels in *x*-direction.

Resulting Modes and Frequencies from the ANSYS Analysis

The first four natural frequencies of the 32PTH basket, resulting from the ANSYS modal analysis are tabulated below.

32PTH Finite Element Modal Analysis Results

Mode Number	Frequency for the 0° Analysis (Hz)	Frequency for the 45° Analysis (Hz)
1	110.29	112.32
2	113.58	112.95
3	114.54	117.44
4	115.86	117.47

The first mode shape of the 0° and 45° modal analyses are plotted on Figures 3.9.11- 2 and 3.9.11-3, respectively.

3.9.11.5 Dynamic Load Factor Calculations

An ANSYS [1] spring-mass model is developed using COMBIN14 Spring-Damper element and MASS21 Structural Mass element (See Figure 3.9.11-4). The spring stiffness and mass are adjusted to produce fundamental natural frequencies for canister and basket in axial and transverse orientations. Acceleration time-history for the cask side drop from Figures 3.9.10-19, Appendix 3.9.10, is impressed on the canister and basket spring-mass models in a transient dynamic analysis. Based on discussions in NUHOMS® MP187 SAR [5], Section 2.10.10.2, a damping ratio of 20% is used in these transient dynamic analyses. These analyses determine the dynamic and static deflections of an oscillator with a single degree of freedom for a given dynamic load and calculate the DAFs as the ratio of the dynamic responses to the static responses.

$$DAF = U_{\max \text{ dynamic}} / U_{\max \text{ static}}$$

Where,

$U_{\max \text{ dynamic}}$ = Calculated by ANSYS

$U_{\max \text{ static}}$ = Calculated by mass "g" load * mass/stiffness

The resulting DAFs for the canister and basket at their respective natural frequencies are presented in the following table.

Dynamic Amplification Factor Calculation Results

Drop Orientation	Component	Natural Frequency (Hz)	Dynamic Amplification Factor
Side Drop	Basket	110.29	1.24
	Canister	86.0	1.15

Conservatively, an overall DAF of 1.24 is used to calculate the side drop g loads both for the canister and the basket.

3.9.11.6 Summary of g-Loads for 32PTH Canister and Basket Impact Analyses

Appendix 3.9.10 summarizes the maximum g-loads computed for the OS187H Transfer Cask during an 80 inch side drop event. The DAF of 1.24 is used to compute g-loads for canister and basket impact loads for side drop. The impact load is computed in the following table:

Drop Orientation	Acceleration Direction	Maximum G-Load From LS-DYNA Analysis	Maximum Basket and Canister G-Load	G-Load Used for Canister and Basket Evaluation
Side Drop	Transverse	57.3G ⁽¹⁾	57.3 G x 1.24 = 71.1G	75G

Note:

1. A total of five sections ranging from the lid down to the bottom plate (see Figure 3.9.10-12 of Appendix 3.9.10) are selected in order to capture all possible g-load ranges seen by the OS187H Transfer Cask. However, only the middle three sections (top trunnion, middle, and bottom trunnion sections) will transmit inertial loads to the canister and basket. Therefore, only the maximum g load in these sections is used to compute the g-loads seen by the canister and basket.

3.9.11.7 References

1. ANSYS User's Manual, Rev 6.0, 8.0 and 10.0A1.
2. Blevins, Formulas for Natural Frequency and Mode Shape, Krieger Publishing Company, 1995.
3. American Society of Mechanical Engineers, ASME Boiler and Pressure Vessel Code, Section II, Part D, 1998, through 2000 addenda.
4. Baumeister & Marks, Standard Handbook for Mechanical Engineers. 7th Edition.
5. Transportation Package Safety Analysis Report for NUHOMS® MP187 Multi-Purpose Cask, Transnuclear Document No. NUH-05-151, Rev. 17, CoC 9255, Rev. 9.

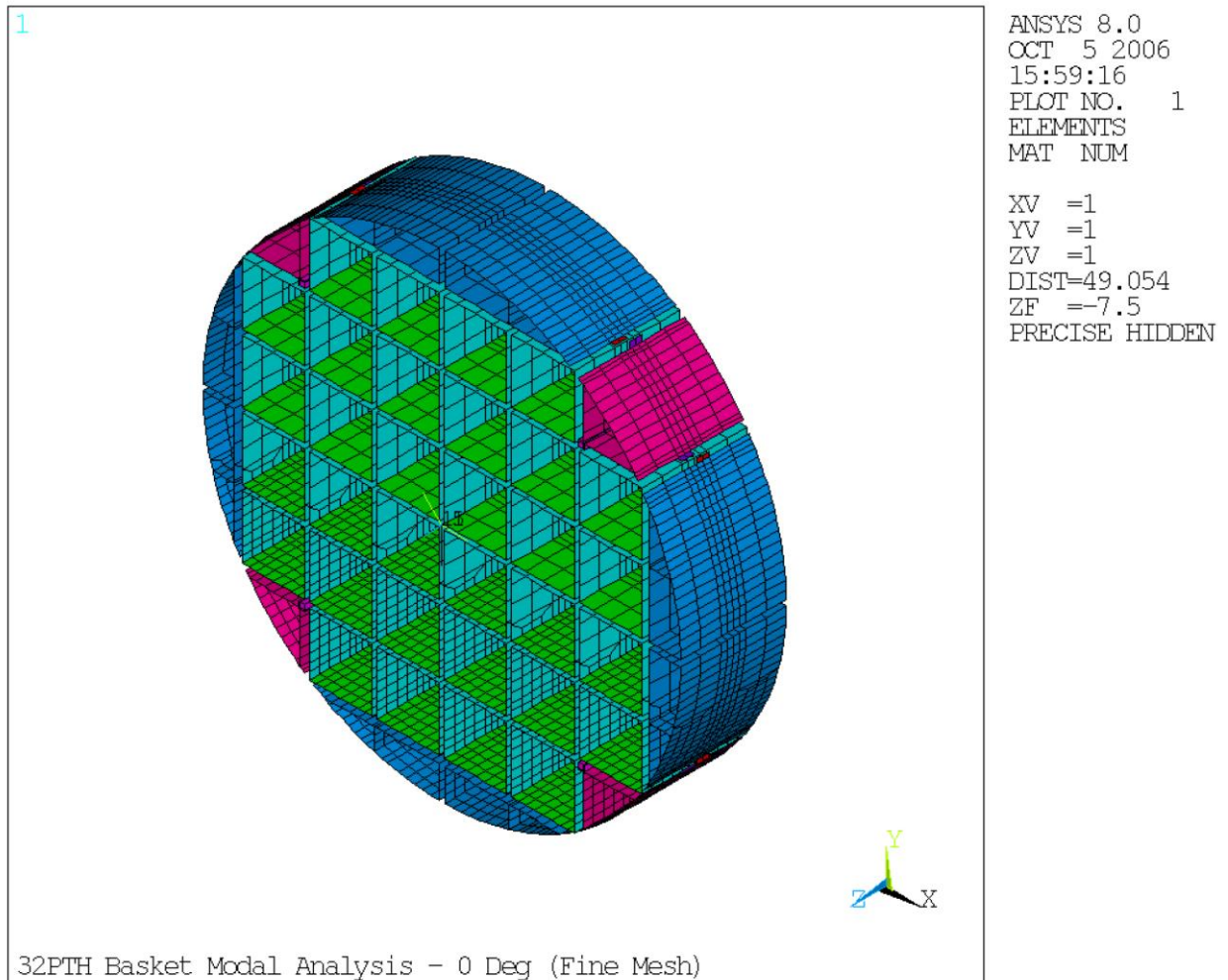


Figure 3.9.11-1
NUHOMS 32 PTH Basket – Finite Element Model

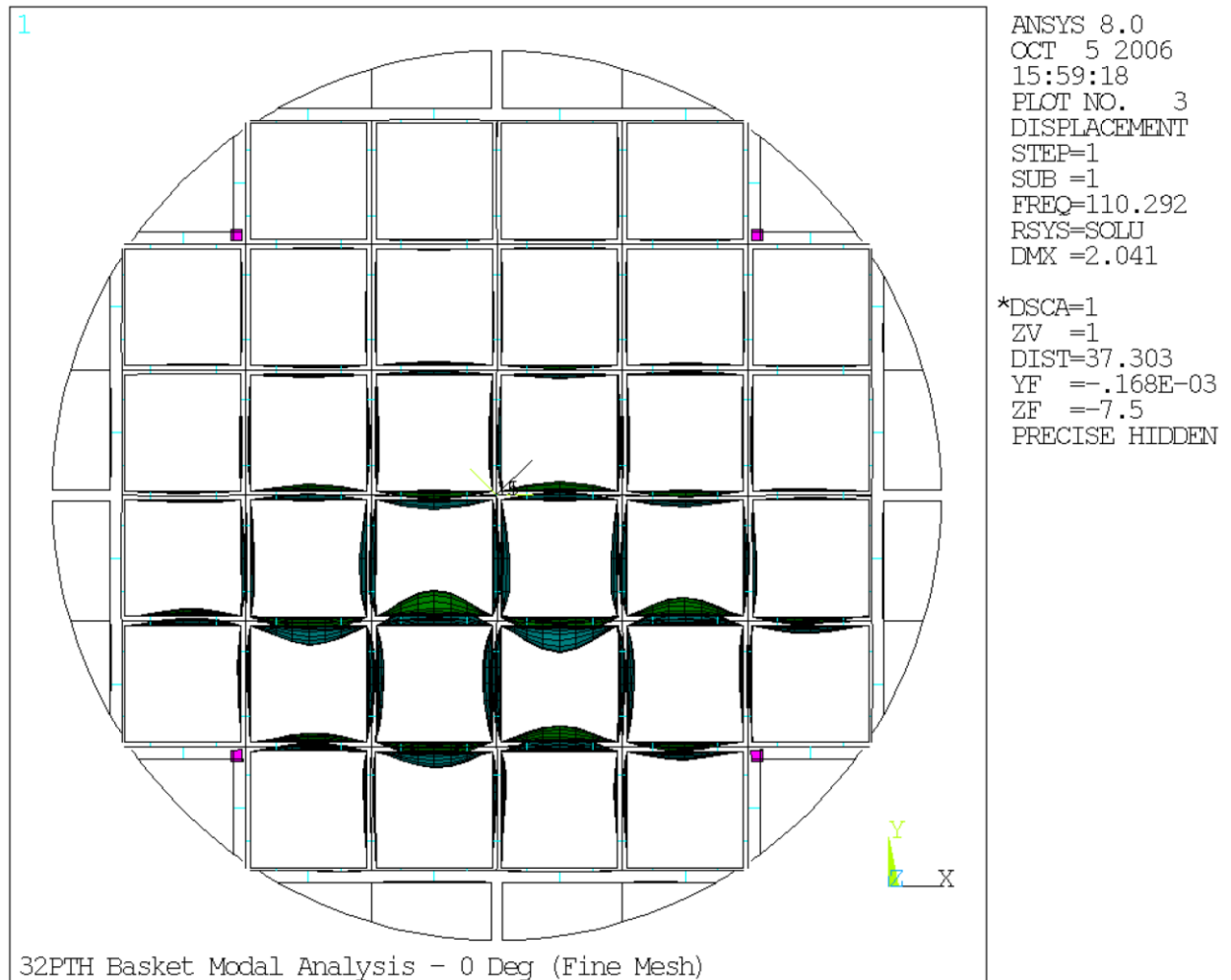


Figure 3.9.11-2
NUHOMS 32 PTH Basket – First Mode Shape, 0 Degree Orientation

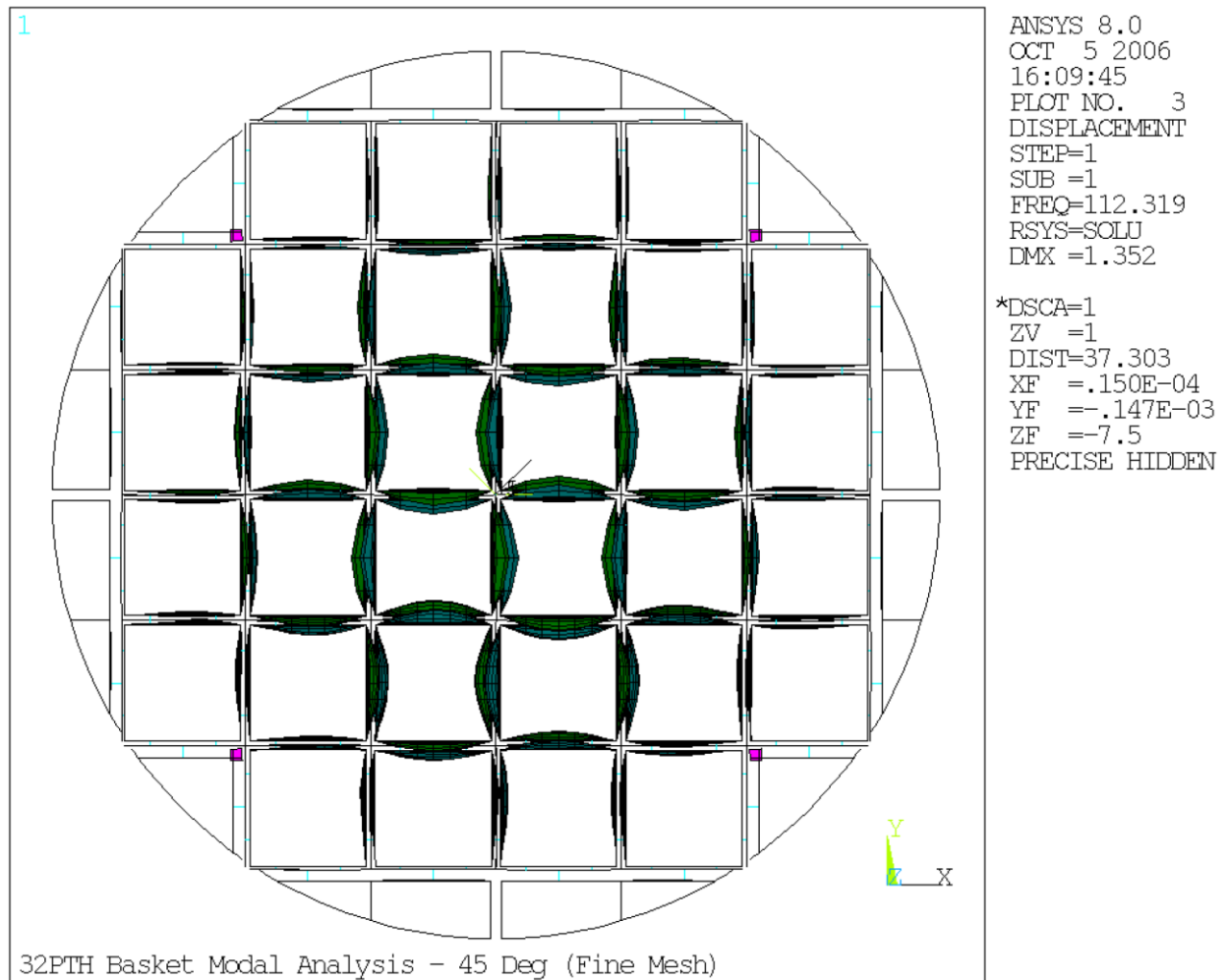


Figure 3.9.11-3
NUHOMS 32 PTH Basket – First Mode Shape, 45 Degree Orientation

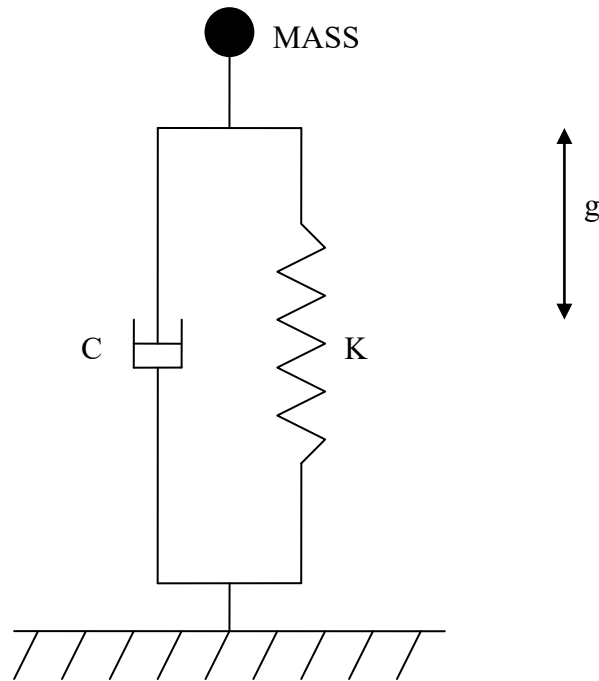


Figure 3.9.11-4
Spring - Mass Finite Element Model

CHAPTER 4 THERMAL EVALUATION

TABLE OF CONTENTS

4.	THERMAL EVALUATION	4-1
4.1	Discussion.....	4-1
4.2	Summary of Thermal Properties of Materials	4-3
4.3	Thermal Evaluation for Normal and Off-Normal Conditions	4-9
4.3.1	Thermal Models for Normal and Off-Normal Conditions.....	4-9
4.3.2	Maximum Temperatures for Normal and Off-Normal Conditions.....	4-20
4.3.3	Minimum Temperatures for Normal and Off-Normal Conditions	4-21
4.3.4	Maximum Internal Pressures for Normal and Off-Normal Conditions	4-21
4.3.5	Maximum Thermal Stresses for Normal and Off-Normal Conditions	4-21
4.3.6	Evaluation of Thermal Performance for Normal and Off-Normal Conditions	4-21
4.4	Thermal Evaluation for Accident Conditions	4-23
4.4.1	Thermal Models for Accident Conditions	4-23
4.4.2	Maximum Temperatures for Accident Conditions	4-28
4.4.3	Maximum Internal Pressures for Accident Conditions.....	4-29
4.4.4	Maximum Thermal Stresses for Accident Conditions.....	4-29
4.4.5	Evaluation of Thermal Performance for Accident Conditions	4-29
4.5	Thermal Evaluation for Loading and Unloading Conditions.....	4-30
4.5.1	Vacuum Drying.....	4-30
4.5.2	Reflooding.....	4-34
4.6	Maximum Internal Pressure.....	4-36
4.6.1	Average Gas Temperature	4-37
4.6.2	Amount of Initial Helium Backfill.....	4-38
4.6.3	Free Gas within Fuel Assemblies / BPRA.....	4-39
4.6.4	Total Amount of Gas within DSC	4-39
4.6.5	Maximum DSC Internal Pressures.....	4-40
4.6.6	Maximum Pressure in Annulus.....	4-40
4.7	Axial Decay Heat Profile	4-41
4.8	Effective Fuel Properties	4-44
4.8.1	Discussion	4-44
4.8.2	Summary of Material Properties	4-44
4.8.3	Effective Fuel Conductivity	4-46
4.8.4	Effective Fuel Density and Specific Heat	4-47
4.8.5	Conclusion	4-48

4.8.6	Effect of Irradiation on UO ₂ Thermal Conductivity	4-50
4.9	Effective Conductivity of Fluids in the Transfer Cask.....	4-53
4.9.1	Effective Conductivity in the Shielding Panel.....	4-53
4.9.2	Effective Water Conductivity in Annulus between TC and DSC.....	4-55
4.10	Justification of the Assumed Hot Gap Sizes	4-57
4.10.1	Radial Gap between Basket Rails and DSC shell	4-57
4.10.2	Radial Gap between Lead and the Cask Structural Shell	4-58
4.11	Heat Transfer Coefficients	4-60
4.11.1	Total heat Transfer Coefficient to Ambient.....	4-60
4.11.2	Free Convection Coefficients	4-60
4.12	Effective Conductivity of Air in Closed Cavity of HSM-H.....	4-68
4.13	Thermal-Hydraulic Equations for the HSM-H.....	4-69
4.14	Thermal Evaluation of DSC Containing Damaged Fuel.....	4-72
4.14.1	Normal / Off-Normal Conditions.....	4-72
4.14.2	Accident Conditions.....	4-72
4.14.3	Effective Properties of Damaged Fuel	4-74
4.14.4	Evaluation of DSC Thermal Performance with Damaged Fuel.....	4-75
4.15	References	4-77
4.16	Appendices.....	4-79
Appendix 4.16.1	Heat Transfer Coefficient Macros	
Appendix 4.16.2	Heat Generation Rate as a Function of Spent Fuel Parameters	
Appendix 4.16.3	Addition of CE 16x16 Fuel Assemblies	
Appendix 4.16.4	Effect of Change in Minimum Off-Normal Ambient Temperature to -21°F	
Appendix 4.16.5	Effect of Dose Reduction Hardware on Airflow Analysis for HSM-H	

LIST OF TABLES

Table 4-1	Maximum Component Temperatures during Transfer Operations at 115°F ambient	4-80
Table 4-2	Maximum Component Temperatures for Storage Conditions at 115°F ambient	4-81
Table 4-3	Maximum Component Temperatures during Transfer Operations at -20°F ambient	4-82
Table 4-4	Maximum Component Temperatures for Storage Conditions at -20°F ambient, 34.8 kW	4-82
Table 4-5	Maximum Component Temperatures for Fire Accident Case Transfer Cask, 34.8 kW	4-83
Table 4-6	Maximum Component Temperatures for Blocked Vent Accident Case	4-83
Table 4-7	Average Heat up Rates	4-84
Table 4-8	Maximum Temperatures during Vacuum Drying Process	4-85
Table 4-9	Maximum Decay Heat Load without Time Limitation for Vacuum Drying	4-85
Table 4-10	32PTH DSC Internal Pressure	4-86
Table 4-11	Average Peaking Factors for Active Fuel Length of 144”	4-87
Table 4-12	Characteristics of Fuel Assemblies	4-89
Table 4-13	Effective Fuel Properties	4-90
Table 4-14	Effective Conductivity of Liquid Neutron Shielding – Sections 1 and 16	4-94
Table 4-15	Verification of the Calculated Effective Conductivities for Liquid Neutron Shielding	4-97
Table 4-16	Effective Conductivity of Liquid Neutron Shield during Burning Period	4-99
Table 4-17	Effective Conductivity of Air within Shielding Panel during Cool Down Period	4-100
Table 4-18	Verification of the selected k_{eff} value for Water in the Annulus	4-102
Table 4-19	Total Heat Transfer Coefficient during Fire	4-103
Table 4-20	Table Is Deleted In Its Entirety	4-104

Table 4-21	Summary of the Energy-Hydraulic Calculation Results for 34.8 kW	4-105
Table 4-22	Summary of the Energy-Hydraulic Calculation Results for 32.0 kW	4-109
Table 4-23	Summary of the Energy-Hydraulic Calculation Results for 26.1 kW	4-110
Table 4-24	Minimum Height of the Fuel Rubble	4-111
Table 4-25	Transverse Effective Fuel Conductivity at Various Fuel Rod Pitches	4-112
Table 4-26	Transverse Effective Conductivity of Damaged Fuel	4-113
Table 4-27	Maximum Component Temperatures in DSC containing 16 Damaged Fuel Assemblies.....	4-114
Table 4-28	Internal DSC Pressure during Transferring of Damaged Fuel	4-115

LIST OF FIGURES

Figure 4-1	Position of the DSC in the Transfer Cask	4-116
Figure 4-2	Finite element Model of Transfer Cask OS187H.....	4-117
Figure 4-3	FEM of Transfer Cask OS187H, Details.....	4-118
Figure 4-4	Top and Bottom Sub-Models of Transfer Cask OS187H	4-119
Figure 4-5	Typical Boundary Conditions on the TC Model	4-120
Figure 4-6	Finite Element Model of HSM-H.....	4-121
Figure 4-7	FEM of HSM-H, Concrete Structure.....	4-122
Figure 4-8	FEM of HSM-H, DSC and Support Rails	4-123
Figure 4-9	DSC Circumferential Convection Regions in the HSM-H Model	4-124
Figure 4-10	Typical Convection Boundary Conditions in the HSM-H Model.....	4-126
Figure 4-11	Typical Heat Flux and Fixed Temperature Boundary Conditions for the HSM-H Model.....	4-128
Figure 4-12	Finite Element Model of the DSC	4-129
Figure 4-13	FEM of DSC Basket, Details.....	4-130
Figure 4-14	FEM of DSC Rails, Details	4-131
Figure 4-15	Thermally Bounding Loading Configurations Considered in the DSC Model For Total Decay Heat Load of 34.8 kW	4-132
Figure 4-16	Typical Boundary Conditions in the DSC Model	4-134
Figure 4-17	Transfer Cask Temperature Distributions, 115°F Ambient	4-135
Figure 4-18	Temperature Distributions in Transfer Cask Sub-Models.....	4-136
Figure 4-19	DSC Temperature Distribution during Transfer Operation Basket Type I, Loading Configuration 1, 115°F Ambient	4-137
Figure 4-20	Temperature Distribution of DSC and Fuel Assemblies during Transfer Operations, 115°F Ambient.....	4-138
Figure 4-21	HSM-H Temperature Distribution 115°F Ambient with Finned Aluminum Side Heat Shields, 34.8 kW	4-139

Figure 4-22	HSM-H Temperature Distribution 115°F Ambient with Un-finned Side Heat Shields.....	4-140
Figure 4-23	DSC Temperature Distribution during Storage, 115°F Ambient, 34.8 kW in HSM-H with Finned Aluminum Side Heat Shields	4-141
Figure 4-24	Temperature Distributions during Transfer Operations, Ambient -20°F	4-142
Figure 4-25	Temperature Distribution during Storage, Ambient -20°F, 34.8 kW	4-143
Figure 4-26	FEM of Transfer Cask for Fire Accident Case.....	4-144
Figure 4-27	Basket Model for Calculation of Effective Conductivities (HSM-H Model Blocked Vent Accident Case)	4-145
Figure 4-28	Temperature Distribution on TC Slice Model for Fire Accident Case	4-146
Figure 4-29	Time-History of TC Component Temperatures for the Fire Accident Case	4-147
Figure 4-30	Temperature Distribution for HSM-H 34 hours after Blockage of the Vents, 34.8 kW	4-148
Figure 4-31	DELETED	4-150
Figure 4-32	Temperature Distribution of DSC Model for Blocked Vent Accident Case	4-151
Figure 4-33	Temperature-Time History of HSM-H Components for Blocked Vent Accident Case.....	4-152
Figure 4-34	Temperature Distribution for TC Backfill Operations	4-153
Figure 4-35	DELETED	4-154
Figure 4-36	DELETED	4-155
Figure 4-37	Time-Temperature History for TC Backfill Operations.....	4-156
Figure 4-38	Total Free Gas Volume versus Burnup Rate	4-157
Figure 4-39	Comparison of the Axial Heat Profiles in the FE Model and in Ref. [4]	4-158
Figure 4-40	Finite Element Model of Fuel Assemblies	4-159
Figure 4-41	Effective Transverse Fuel Conductivity in Helium.....	4-160
Figure 4-42	Effective Transverse Fuel Conductivity for Vacuum Conditions	4-161
Figure 4-43	Effective Axial Fuel Conductivity.....	4-162

Figure 4-44	Schematic Flow Paths through HSM-H	4-163
Figure 4-45	DELETED	4-164
Figure 4-46	Location of the Damaged Fuel Assemblies in the Basket	4-165
Figure 4-47	Typical FE Models of Damaged (Reconfigured) Fuel WEO 17x17	4-166
Figure 4-48	Transverse Effective Fuel Conductivity versus Pitch Size.....	4-167
Figure 4-49	Effective Transverse Conductivity of Damaged (Reconfigured) Fuel.....	4-168
Figure 4-50	Temperature Distributions in the DSC containing 16 Damaged Fuel Assemblies for Normal / Off-Normal Transfer Conditions	4-169
Figure 4-51	Temperature Distributions in the DSC Containing 16 Damaged (Rubble) Fuel Assemblies for Accident Conditions	4-170

4. THERMAL EVALUATION

The thermal evaluation described in this chapter 4.0 is applicable to the 32PTH DSC loaded inside the OS187H TC and HSM-H. See Appendix A, Chapter A.4 for discussion of applicability of these analyses for the 32PTH Type 1 DSC inside the OS187H Type 1 TC and HSM-H. See Appendix B, Chapter B.4 for discussion of applicability of these analyses for the 32PTH Type 2 inside the OS187H Type 2 TC and HSM-H.

4.1 Discussion

The NUHOMS[®]-32PTH DSC is designed to passively reject decay heat during storage and transfer for normal, off-normal, and accident conditions while maintaining temperatures and pressures within specified limits. Objectives of the thermal analyses performed for this evaluation include:

- Determination of maximum and minimum temperatures with respect to material limits to ensure components perform their intended safety functions,
- Determination of temperature distributions to support the calculation of thermal stresses,
- Determination of maximum DSC internal pressures for normal, off-normal, and accident conditions, and
- Determination of the maximum fuel cladding temperature, and to confirm that this temperature will remain sufficiently low to prevent unacceptable degradation of the fuel during storage.

To establish the heat removal capability, several thermal design criteria are established for the System. These are:

- Maximum temperatures of the containment structural components must not adversely affect the containment function.
- To maintain the stability of the neutron shield resin in the transfer cask (TC) during normal transfer conditions, a maximum allowable temperature of 300°F is set for the neutron shield material [1].
- A maximum fuel cladding temperature limit of 400°C (752°F) has been established for normal conditions of storage and for short-term storage operations such as transfer and vacuum drying [2]. During off-normal storage and accident conditions, the fuel cladding temperature limit is 570°C (1058°F) [2].
- A maximum temperature limit of 327°C (620°F) is considered for the lead in the transfer cask, corresponding to the melting point [3].

- The ambient temperature range for normal operation is 0 to 100°F (-18 to 38°C). The minimum and maximum off-normal ambient temperatures are -21°F (-29.4°C) and 115°F (46°C) respectively. In general, all the thermal criteria are associated with maximum temperature limits and not minimum temperatures. All materials can be subjected to a minimum environment temperature of -21°F (-29.4°C) without adverse effects.
- The maximum DSC internal pressure during normal and off-normal conditions must be below the design pressures of 15 psig and 20 psig respectively. For accident cases, the maximum DSC internal pressure must be lower than 70 psig during storage and lower than 120 psig during transfer operation.

The NUHOMS[®]-32PTH DSC is analyzed based on a maximum heat load of 34.8 kW from 32 fuel assemblies with a maximum heat load of 1.5 kW per assembly. For CE 14x14 fuel assembly the maximum total heat load is limited to 33.8 kW. The loading requirements described in Section 4.3.1.3 are used to develop the bounding load configurations.

Appendix 4.16.3 describes the analysis performed to include the CE 16X16 fuel assembly to the authorized content of the NUHOMS[®] HD System. Appendix 4.16.4 describes the analysis performed to change the minimum off-normal ambient temperature from -20°F to -21°F.

A description of the detailed analyses performed for normal/off-normal conditions is provided in Section 4.3, and accident conditions in Section 4.4. The thermal analyses performed for the loading and unloading conditions are described in Section 4.5. DSC internal pressures are discussed in Section 4.6.

The analyses consider the effect of the decay heat flux varying axially along a fuel assembly. The axial decay heat profile for a PWR fuel assembly is based on [4]. Section 4.7 describes the calculated peaking factors and the methodology to apply the axial heat profile in the model.

Fuel assemblies are considered as homogenized materials in the fuel compartments. The effective thermal conductivity of the fuel assemblies used in the thermal analysis is based on the conservative assumption that heat transfer within the fuel region occurs only by conduction and radiation where any convection heat transfer is neglected. The lowest effective properties among the applicable fuel assemblies are selected to perform the thermal analysis. Section 4.8 presents the calculation that determines the bounding effective thermal properties of the applicable fuel assemblies.

WE 15x15 and WE 17x17 class fuel assemblies containing Instrument Tube Tie Rods (ITTRs) are also qualified for storage in the NUHOMS[®] HD System as demonstrated in Section 4.6.

The thermal evaluation concludes that with a design basis heat load of 34.8 kW and the loading requirements described in Section 4.3.1.3, all design criteria are satisfied.

4.2 Summary of Thermal Properties of Materials

The analyses use interpolated values when appropriate for intermediate temperatures where the temperature dependency of a specific parameter is deemed significant. The interpolation assumes a linear relationship between the reported values.

1. Homogenized PWR Fuel with Helium Backfill¹

Temp (°F)	Transverse conductivity in Helium (Btu/hr-in-°F)	Temp (°F)	Axial Conductivity (Btu/hr-in-°F)	Temp (°F)	C _{p, eff} (Btu/lbm-°F)	ρ _{eff} (lbm/in ³)
137	0.0188	212	0.0576	80	0.0593	0.1248
231	0.0221	392	0.0606	260	0.0654	
327	0.0258	572	0.0644	692	0.0726	
423	0.0304	752	0.0695	1502	0.0779	
520	0.0350	932	0.0763			
617	0.0406	1112	0.0852			
715	0.0468					
813	0.0542					
1010	0.0684					

2. PWR Fuel with Air Backfill at low pressures for vacuum drying conditions

Temp (°F)	Transverse Conductivity for Vacuum Conditions (Btu/hr-in-°F)
188	0.0079
270	0.0099
355	0.0126
444	0.0157
535	0.0197
629	0.0242
723	0.0300
819	0.0363

3. Helium [5]

Temperature		Conductivity	
(K)	(°F)	(W/m-K)	(Btu/hr-in-°F)
200	-100	0.1151	0.0055
250	-10	0.1338	0.0064
300	80	0.1500	0.0072
400	260	0.1800	0.0087
500	440	0.2110	0.0102
600	620	0.2470	0.0119
800	980	0.3070	0.0148
1000	1340	0.3630	0.0175

Density and specific heat of helium is set to zero for transient runs.

¹ See Section 4.8 for calculation of the effective fuel properties

4. Air [5]

Temperature (K)	Conductivity (W/m-K)	ν (m ² /kg)	Prandtl No. (---)	Dyn. Visc. (Pa-s)
100	0.0093	---	---	---
200	0.0180	0.573	0.740	1.33E-05
300	0.0263	0.861	0.708	1.85E-05
400	0.0336	1.148	0.694	2.30E-05
500	0.0403	1.436	0.688	2.70E-05
600	0.0466	1.723	0.690	3.06E-05
800	0.0577	2.298	0.705	3.70E-05
1000	0.0681	2.872	0.707	4.24E-05

Temperature (°F)	Conductivity (Btu/hr-in-°F)	ρ (lbm/ft ³)	Prandtl No. (---)	Kin. Visc. (ft ² /hr)
-280	0.0004	---	---	---
-100	0.0009	0.109	0.740	0.2953
80	0.0013	0.073	0.708	0.6172
260	0.0016	0.054	0.694	1.0232
440	0.0019	0.043	0.688	1.5024
620	0.0022	0.036	0.690	2.0430
980	0.0028	0.027	0.705	3.2948
1340	0.0033	0.022	0.707	4.7187

Density and specific heat of air is set to zero for transient runs. Prandtl number, kinematic viscosity, and density of air are used to calculate the convection coefficients in Section 4.11.

5. Solid Neutron Shield [1]

Temp (°C)	k (W/m-K)	Temp (°F)	k_{min} (Btu/hr-in-°F)
20	0.815	68	0.039
50	0.806	122	0.039
75	0.823	167	0.040
100	0.852	212	0.041
125	0.858	257	0.041
150	0.828	302	0.040
170	0.815	338	0.039

6. SA-240, Type 304 Stainless Steel

Temperature (°F)	Conductivity (Btu/hr-ft-°F) [6]	Conductivity (Btu/hr-in-°F)	Diffusivity (ft ² /hr) [6]	Specific Heat (Btu/lbm-°F) ¹	Density (lbm/in ³) [3]
70	8.6	0.717	0.151	0.117	0.29
100	8.7	0.725	0.152	0.117	
150	9.0	0.750	0.154	0.120	
200	9.3	0.775	0.156	0.122	
250	9.6	0.800	0.158	0.125	
300	9.8	0.817	0.160	0.126	
350	10.1	0.842	0.162	0.128	
400	10.4	0.867	0.165	0.129	
450	10.6	0.883	0.167	0.130	
500	10.9	0.908	0.170	0.131	
550	11.1	0.925	0.172	0.132	
600	11.3	0.942	0.174	0.133	
650	11.6	0.967	0.177	0.134	
700	11.8	0.983	0.179	0.135	
750	12.0	1.000	0.181	0.136	
800	12.2	1.017	0.184	0.136	

7. Aluminum

Al-1100

Temperature (°F)	Conductivity (Btu/hr-ft-°F) [6]	Conductivity (Btu/hr-in-°F)	Diffusivity (ft ² /hr) [6]	Specific Heat (Btu/lbm-°F) ²	Density (lbm/in ³) [6]
70	133.1	11.092	3.67	0.214	0.098
100	131.8	10.983	3.61	0.216	
150	130.0	10.833	3.50	0.219	
200	128.5	10.708	3.42	0.222	
250	127.3	10.608	3.35	0.224	
300	126.2	10.517	3.28	0.227	
350	125.3	10.442	3.23	0.229	
400	124.5	10.375	3.17	0.232	

Al-6061

Temperature (°F)	70	100	150	200	250	300	350	400
Conductivity (Btu/hr-ft-°F) [6]	96.1	96.9	98.0	99.0	99.8	100.6	101.3	101.9
Conductivity (Btu/hr-in-°F)	8.00	8.08	8.17	8.25	8.32	8.38	8.44	8.49

8. Lead

Temperature (K)	Conductivity (W/m-K) [5]	Temperature (°F)	Conductivity (Btu/hr-in-°F)	Specific Heat (Btu/lbm-°F) [3]	Density (lbm/in ³) [3]
200	36.7	-100	1.767	0.03	0.393
250	36.0	10	1.733		
300	35.3	80	1.700		
400	34.0	260	1.637		
500	32.8	440	1.579		
600	31.4	620	1.512		

¹ Thermal diffusivity is $\alpha = \frac{k}{\rho c_p}$, this equation is used to calculate the specific heat.

9. Poison Plates

Neutron poison plates in the basket type I are borated aluminum alloy or MMC. The minimum conductivity of the borated material must be equal or larger than the 145 W/m-K at 100°C. It is assumed that the conductivity of the borated aluminum alloy/MMC remains unchanged at higher temperatures. The measured conductivities of the available borated aluminum alloys for the entire range of 20°C to 400°C are much higher than the above requirement [7 and 8].

Basket type II is designed to use Boral[®] absorber as neutron poison plate. The Boral[®] absorber possesses orthotropic thermal conductivity. To avoid any uncertainty, conductivity values of Boral[®] are set conservatively to zero. An equivalent conductivity is calculated for a pair of Boral[®] and aluminum-1100 plates in thermal analyses. For calculation of the equivalent conductivity, the paired plates are considered as parallel thermal resistances. Since the temperature gradients along the plates are much higher than the temperature gradients across the plates, this assumption is reasonable. The following equation is used to calculate the equivalent thermal conductivity of paired plates.

$$k_{eq} = \frac{k_{Al} t_{Al} + k_p t_p}{t_{total}} = \frac{k_{Al} t_{Al}}{t_{total}}$$

t_{total} = Total thickness of the basket plate = 0.5"

k_{Al} = Thermal conductivity of aluminum plate (Al 1100)

t_{Al} = Thickness of the aluminum plate ($t_{total} - t_p$ -tolerance)

t_p = Thickness of the Boral[®] plate = 0.075"

Temp (°F)	k - Al-1100 [6] (Btu/hr-ft-°F)	k_{eq} for Basket Type II (Btu/hr-in-°F)
70	133.1	9.34
100	131.8	9.25
150	130.0	9.12
200	128.5	9.02
250	127.3	8.93
300	126.2	8.86
350	125.3	8.79
400	124.5	8.74
650	121.3 ¹	8.51

Basket type II contains Boral[®] plates with a nominal core thickness of 0.05 in.

Total Boral[®] plate thickness is 0.075±0.004 in. from Reference [9]

The minimum thickness of the Al-1100 plate (0.421") is considered to calculate the equivalent conductivity.

The minimum required thermal conductivities of the paired aluminum and poison plates will be verified via testing as described in Chapter 9.

To minimize the thermal resistance of the basket during fire period, the conductivity of poison plate is considered to be equal to the aluminum conductivity. Conductivity of the poison plate is set equal to the minimum value of 145 W/m-K (6.98 Btu/hr-in-°F) during the cool down period to maximize the thermal resistance. Specific heat and density of poison plate is set equal to those of aluminum for transient runs.

¹ Extrapolated from the values in [ASME]

10. Water [5]

Temp (K)	ν (m ³ /kg)	μ (N.s/m ²)	k (W/m-K)	β (1/K)	ν (m ² /s)	Pr (---)
275	1.000E-03	1.65E-03	0.574	1.196E-04	1.652E-06	12.22
300	1.003E-03	8.55E-04	0.613	1.200E-04	8.576E-07	5.83
325	1.013E-03	5.28E-04	0.645	3.988E-04	5.349E-07	3.42
350	1.027E-03	3.65E-04	0.668	5.528E-04	3.749E-07	2.29
375	1.045E-03	2.74E-04	0.681	7.011E-04	2.863E-07	1.70
400	1.067E-03	2.17E-04	0.688	8.421E-04	2.315E-07	1.34
420	1.088E-03	1.85E-04	0.688	9.841E-04	2.013E-07	1.16
450	1.123E-03	1.52E-04	0.678	1.072E-03	1.707E-07	0.99
480	1.167E-03	1.29E-04	0.660	1.306E-03	1.505E-07	0.89
500	1.203E-03	1.18E-04	0.642	1.542E-03	1.420E-07	0.86

The expansion coefficient is defined as:
$$\beta = \frac{-1}{\rho} \left(\frac{\partial \rho}{\partial T} \right)_p$$

For the thermal analyses, the expansion coefficient is calculated for each interval given in the above table as:

$$\beta = \frac{-1}{\rho} \left(\frac{\rho_2 - \rho_1}{T_2 - T_1} \right)$$

Thermal properties of water are used to calculate the effective conductivity of water in shielding panel of the transfer cask. Section 4.9 describes the methodology to calculate the effective conductivity of the fluids in the shielding panel.

11. Concrete

The thermal conductivity of normal, saturated concrete varies from 1.2 to 2.0 Btu/ft-hr-°F at temperature ranging from 50 to 150°F [10]. The conductivity of concrete decreases rapidly with the rise in temperature and assumes, at 750°C (1382°F) a conductivity value equal approximately to 50 percent of that of normal temperature [10]. For the thermal analyses a thermal conductivity of 1.15 Btu/hr-ft-°F (0.0958 Btu/hr-in-°F) is considered for concrete at 70°F. This conductivity is reduced by half to a value of 0.0479 Btu/hr-in-°F at 1382°F.

The density of concrete is considered to be 145 lbm/ft³ (0.084 lbm/in³). The nominal density of the concrete for the HSM-H is 150 lbm/ft³. Practical thermal conductivity of concrete in this density range is 10.0 to 16.5 Btu/hr-ft²-(°F/in) (0.0694 to 0.1145 Btu/hr-in-°F) [11]. This shows that the assumed concrete conductivity is within this range and therefore acceptable.

The specific heat of concrete is considered to be 0.22 Btu/lbm-°F in the thermal analyses [11]

12. Soil

The following properties are considered for soil from Reference [12]:

Thermal conductivity = 0.3 W/m-K (0.0144 Btu/hr-in-°F)

Density = 1600 kg/m³ (0.0578 lbm/in³)

Specific heat = 800 J/kg-°C (0.191 Btu/lbm-°F)

13. Emissivities and Absorptivities

Reference [13] gives an emissivity between 0.92 to 0.96 and a solar absorptivity between 0.09 to 0.23 for white paints. To account for dust and dirt and to bound the problem, the thermal analysis uses a solar absorptivity of 0.3 and an emissivity of 0.9 for white painted surfaces.

The unpainted surfaces are weathered stainless steel. The measured emissivity of stainless steel is 0.46 [14]. It is assumed that the absorptivity and the emissivity of stainless steel are equal. Solar absorptivity and emissivity of 0.46 are applied in the thermal analysis for the stainless steel surfaces exposed to ambient. The emissivity value of 0.46 is also considered for radiation exchange between the DSC shell and the transfer cask inner shell. The emissivity of the DSC shell is set to 0.587 for storage conditions within the HSM-H cavity as concluded in the thermal test report [25]. For conservatism, an emissivity of 0.3 is considered for the fuel compartments in calculation of the transverse effective fuel conductivity in Section 4.8.

The emissivity of the TC surface is set to 0.8 as required in [22] during the fire burning time. It is assumed that the cask surface is covered with soot after the fire. The solar absorptivity of soot is 0.95 [13]. To bound the problem, the thermal analysis uses a solar absorptivity of 1.0 and an emissivity of 0.9 for TC surfaces during the cool down period.

Emissivity of concrete is reportedly 0.9 to 0.94 [12 and 13]. An emissivity of 0.90 is considered for concrete surfaces in the analyses. The absorptivity of the concrete surface is 0.73 - 0.91 at 300K [13]. For conservatism a solar absorptivity of 1.0 is considered for concrete surface.

Emissivity of anodized aluminum is reported to be 0.88 to 0.94 [13.and 15] at moderate temperatures and decreases rapidly at high temperatures. An emissivity of 0.80 is considered for anodized aluminum surfaces in the thermal analyses of the HSM-H to cover the expected temperature range. Emissivity of non-anodized aluminum surfaces is set to 0.1 [3].

References [5] and [13] report emissivities of 0.21 to 0.28 for galvanized steel in a temperature range from 68°F to 200°F. To bound the concrete temperature, an emissivity of 0.3 is considered for the galvanized steel in the HSM-H.

4.3 Thermal Evaluation for Normal and Off-Normal Conditions

4.3.1 Thermal Models for Normal and Off-Normal Conditions

The finite element models are developed using the ANSYS computer code [16]. ANSYS is a comprehensive thermal, structural, and fluid flow analysis package. It is a finite element analysis code capable of solving steady-state and transient thermal analysis problems in one, two, and three dimensions. Heat transfer via a combination of conduction, radiation, and convection can be modeled by ANSYS.

Three finite element models are used for evaluation of the normal and off-normal storage and transfer conditions:

- A transfer cask model (OS-187H) to determine temperature distributions within the cask body and neutron shielding. This model also includes the DSC shell and the helium gap between the DSC and the cask inner surface.
- A DSC model including the basket and the homogenized fuel assemblies to determine temperature distributions within the DSC and its contents.
- A HSM-H model including the DSC shell and shield plugs to determine temperature distribution in the HSM-H concrete structure, the supporting rails, and the DSC shell.

The analysis starts first with evaluating the transfer cask or the HSM-H model. The resultant temperatures of the DSC shell are then applied as boundary conditions to the exterior nodes of the DSC model. This approach allows modeling of sufficient detail within the DSC while keeping the overall size of the individual models reasonable.

Ambient temperatures between 0 and 100°F are considered as normal, long-term transfer and storage conditions. Minimum and maximum off-normal ambient temperatures are -20°F and 115°F. Should these extreme temperatures ever occur, they would be expected to last for a short period of time. Nevertheless, these ambient temperatures are conservatively assumed to occur for a significant duration to result in a steady-state temperature distribution in the NUHOMS[®]-32PTH system components.

Since the normal conditions are bounded by the off-normal conditions, the finite element models are evaluated only for off-normal conditions. The thermal stresses and the DSC internal pressures for the normal conditions are therefore conservatively calculated based on the resultant temperatures for the off-normal conditions.

4.3.1.1 Steady State Transfer Cask Model (OS187H)

OS187H transfer cask is designed to provide structural and radiological protection for the DSC during transfer operation while providing passive heat removal for the canisterized spent fuel. The three-dimensional finite element model of the OS187H transfer cask represents a 180° symmetric section of the TC and includes the geometry and material properties of the DSC shell and shield plugs, inner shell, gamma shell (lead), and structural shell of the transfer cask, as well as the shielding panel, cask lid, cask bottom plate, and the solid neutron shields. Properties of pure water are assumed for the liquid neutron shield contained in the shielding panel.

The neutron shield panel consists of a cylindrical shell welded to the cask structural shell and supported by 17 rings. Each of the 15 inner supporting rings has four holes to allow filling and draining of water in or out of the panel. The water in the neutron shield panel is modeled as 16 individual, cylindrical segments using SOLID70 elements. Effective conductivities are calculated for individual segments in Section 4.9 to model the combination of the conduction and convection heat transfer through the water contained in the shielding panel.

Radiation between the DSC outer shell and the cask inner shell is modeled using radiation LINK31 elements. The LINK elements connect the outermost nodes of the DSC shell to the inner most nodes of the transfer cask in the radial and axial directions. A macro¹ is written to retrieve the average surface area of the elements attached to each LINK31 element and apply it as a real constant to the corresponding LINK31 element.

Since the outer diameter of DSC is very close to the inner diameter of the cask, the radiating surfaces of the DSC and cask can be considered as parallel planes. The effective emissivity for the radiation exchange between the parallel planes is calculated as follows and applied as real constant to radiation LINK31 elements.

$$\varepsilon_{eff} = \frac{1}{\left(\frac{1}{\varepsilon_1} + \frac{1}{\varepsilon_2} - 1\right)} = 0.2987$$

A surface emissivity of 0.46 for stainless steel (see Section 4.2) is used for ε_1 , ε_2 in the above equation to calculate the real constant of ε_{eff} . The value of ε_{eff} remains unchanged for all the radiation LINK elements.

Following assumptions are considered in developing the model:

- DSC is centered axially in the transfer cask. This assumption reduces the axial heat transfer and hence maximizes the DSC shell temperature, which in turn results in higher fuel cladding temperature in the DSC model.
- The total decay heat load (34.8 kW) is considered evenly distributed over the radial inner surface of the DSC cavity. The applied heat flux is:

$$\text{Decay heat flux} = \frac{Q}{\pi D_i L} = 3.34 \text{ Btu/hr-in}^2 \quad \text{or} \quad 3.25 \text{ Btu/hr-in}^2 \text{ for CE 14x14 only}$$

¹ See Appendix 4.16.1 for macros

where,

Q = total decay heat load = 34.8 kW = (118,748 Btu/hr) or 33.8 kW (115,336 Btu/hr) for CE 14x14 only

D_i = inner DSC diameter = 68.75"

L = DSC cavity length = 164.5"

- c) The view factor of the radiation LINK elements is set to one, which implies that each node on the DSC outer surface views only one node on the inner surface of the transfer cask. This assumption reduces the distribution effect of radiation heat transfer slightly but it simplifies the modeling efforts enormously. This assumption is justified since the gap between the transfer cask and the DSC is very small.
- d) Since the transfer operation occurs in horizontal position, the lower halves of the cask cylindrical surfaces are in shade. No solar radiation is considered over these surfaces. To remove any uncertainty about the solar impact on the vertical surfaces, the entire surface area of vertical plates is considered for application of the solar heat flux.

Although assumption "a" is conservative regarding the fuel cladding temperature, it is less conservative for calculating the maximum temperatures for the seals and the solid neutron shield at the top and bottom of the TC. Therefore, two sub-models of the TC are developed, in which the DSC is touching either the cask bottom plate or the cask lid with a maximum gap of 0.01". Heat flux to the top and bottom surfaces of the DSC shield plugs in the sub-models are considered to be 5% of the maximum decay heat load distributed evenly over the corresponding surface (1.60 Btu/hr-in^2). The remaining heat load is distributed over the radial inner surface of the DSC. The sub-models calculate conservative temperatures for the seals and solid neutron shield.

The DSC shell rests on four rails in the transfer cask during the transfer operation. These rails are flat stainless steel plates welded to the inner shell of the transfer cask. The thickness of these rails is 0.12". Considering the rail configuration shown in Figure 4-1, the gap between the DSC shell and cask inner shell is calculated. The nodes of the DSC shell and the cask inner shell are coupled only at the location of the two middle rails to represent the contact area at these locations.

The following gaps are considered between components in the model at thermal equilibrium:

- 0.01" axial air gaps are considered on both sides of solid neutron shielding to simulate the contact resistance.
- 0.03" radial air gap is considered between the gamma shell (lead) and the structural shell to take account for the difference in thermal expansion behavior of stainless steel and lead. See Section 4.10 for justification.
- 0.01" axial and radial gap between the cask lid and the cask body
- 0.01" axial gap between the bottom cover plate and the ram access penetration ring

Details of the OS187H transfer cask finite element model and sub-models are shown in Figure 4-2 to Figure 4-4.

Steady State Boundary Conditions for the Transfer Cask Model

Ambient temperature of 115°F is considered for both normal and off-normal conditions. The minimum ambient temperature of -20°F is considered to maximize the temperature gradients.

Convection and radiation to the ambient are combined together to form a total heat transfer coefficient, which is defined as a temperature dependent material property in the model. The total heat transfer coefficient is used to apply the boundary conditions on the outer surface of the cask. Section 4.11 describes the correlations to calculate the total heat transfer coefficients applied on the outer surface of the transfer cask.

Solar radiation is considered as a constant heat flux applied on the SURF152 elements overlaid on the outer surface of the transfer cask. Reference [17] reports the total values for insolation over a 12-hour solar day. These values are used to calculate the solar heat flux on the outer surface of the transfer cask. Although NUREG 1536 [22] allows averaging the insolation over a 24 hour period, it is not considered in the transfer cask thermal model for conservatism.

The outer surface of the shielding panel is painted white. The other surfaces are considered unpainted. The insolation values from [17] are considered as the maximum amount of solar radiation that is available for absorption on any surface. These values are multiplied by the absorptivity factor of each surface to calculate the amount of solar heat flux that each surface absorbs. The resultant value is applied as a constant heat flux to the corresponding surface.

Surface shape	Insolation [17] (gcal/cm ²)	Total solar heat flux average over 12 h (Btu/hr-in ²)	Absorptivity ¹	Solar heat flux in the model (Btu/hr-in ²)
Curved, Painted	400	0.853	0.3	0.256
Curved, Unpainted	400	0.853	0.46	0.392
Flat, Vertical, Painted	200	0.427	0.3	0.128
Flat, Vertical, Unpainted	200	0.427	0.46	0.196

Solar radiation is only considered for the maximum normal and off-normal conditions with ambient temperature of 115°F.

Typical boundary conditions for the transfer cask model are shown in Figure 4-5.

¹ See Section 4.2 for discussion

4.3.1.2 Steady State HSM-H Model

Horizontal Storage Module (HSM-H) is designed to provide an independent, passive system with substantial structural capacity to ensure safe storage of spent fuel assemblies in NUHOMS® - 32PTH canisters. The decay heat load from stored canisters is removed via radiation, free convection and conduction. Natural draft of air within the HSM-H cavity is created by the temperature difference between ambient and the DSC surface, and the height difference between the HSM-H vents. Ambient air enters the HSM-H through the inlet openings in the lower part of the HSM-H side walls and circulates around the DSC and the side heat shields. Warm air passes through or around the top heat shield and exits the HSM-H through the outlet openings in the upper part of the HSM-H side walls.

Decay heat is rejected from the DSC to the HSM-H air space by convection and then is removed from the HSM-H by natural air circulation. Heat is also radiated from the DSC surface to the heat shields and HSM-H walls, where again natural air circulation and conduction through the walls remove the heat. Typical flow paths are shown in Figure 4-44.

A half symmetric, three dimensional, finite element model of the HSM-H is developed using ANSYS [16]. The model represents one module among adjacent HSM-H's containing DSCs with the maximum heat load of 34.8kW. Therefore, adiabatic boundary conditions are applied over the outer surfaces of the HSM-H side walls and back wall. The HSM-H model includes the DSC shell and shield plugs, the concrete structure, and the heat shields. The DSC content is not considered for the steady state runs. The basket and its content are homogenized for the transient runs. The homogenized basket properties are discussed in Section 4.4.1.1.

Conduction through components is modeled using SOLID70 elements. Conduction through air within the HSM-H cavity is not considered for the steady state runs. Radiation between the DSC shell, heat shields, and HSM-H walls is modeled using /AUX12 methodology. SHELL57 elements were superimposed on radiating surfaces to create the Super-element MATRIX50. The SHELL57 elements were unselected prior to solving the model. The finite element model of HSM-H is shown in Figure 4-6 to Figure 4-8.

For the design basis heat load, 34.8 kW, the side heat shields are equipped with fins on the surface facing the DSC. In this case, the fins and the surface facing the DSC are anodized. The side shields are modeled as flat plates with a thickness of 0.3125" at the position of shield base plate. Convection from the fins attached to the side shields is modeled using equivalent convection coefficient. Calculation of the effective convection coefficients is discussed in Section 4.11. Optionally, the alternative side heat shields without the fins may be utilized. For this un-finned configuration, the convection coefficient for a flat, vertical plate replaces the effective convection coefficient over the fins. Flat side heat shields may be made from stainless steel, aluminum or galvanized steel. If aluminum is used, the surface of the side heat shield facing the DSC is anodized.

The top heat shield is a louver plate attached to the ceiling or a flat stainless steel plate for HSM-H modules with stainless steel side heat shields. The louvered heat shield is modeled in its exact geometry. The convection coefficient for the louvered top heat shield is discussed in

Section 4.11. The convection coefficients for flat, horizontal plate facing up or downwards are considered for the flat stainless steel top heat shield. These convection coefficients are discussed in Section 4.11 as well.

The HSM-H design includes optional hardware to reduce the dose rates at the inlet or outlet vents. The effect of dose reduction hardware on airflow is discussed in Appendix 4.16.5.

Steady State Boundary conditions for the HSM-H Model

Ambient temperatures between 0 and 100 °F are considered as normal storage conditions. The maximum day temperature of 115 °F and the minimum temperature of -20 °F are considered as the maximum and minimum off-normal storage condition, respectively.

Because of the large thermal inertia, the temperature responses of the HSM-H and DSC to maximum day temperature are relatively slow. Therefore, considering an average maximum temperature over a 24-hour period is reasonable to calculate the maximum component temperatures during storage using steady state boundary conditions.

In order to calculate a daily average temperature given a maximum day temperature, a minimum daily range must be specified. Reference [18] shows that the minimum daily range in the contiguous United States is 27 °F for a maximum summer ambient above 110 °F. the hourly temperature is defined in [18] as:

$$T_{\text{hour}} = T_{\text{max}} - (\text{percentage of the daily range}) \times (\text{min daily range})$$

The percentages of the daily range are shown as a function of day time in [18]. The average of the hourly temperatures over the 24-hour period gives the daily average temperature. The following table shows the calculated daily average temperature for a maximum day temperature of 115 °F and a daily minimum range of 27 °F.

Maximum day temperature = 115 °F

Minimum daily range = 27 °F

Time, hr	% daily range [16]	T_{hour} (°F)	Time, hr	% daily range [16]	T_{hour} (°F)
1	87	91.5	13	11	112.0
2	92	90.2	14	3	114.2
3	96	89.1	15	0	115.0
4	99	88.3	16	3	114.2
5	100	88.0	17	10	112.3
6	98	88.5	18	21	109.3
7	93	89.9	19	34	105.8
8	84	92.3	20	47	102.3
9	71	95.8	21	58	99.3
10	56	99.9	22	68	96.6
11	39	104.5	23	76	94.5
12	23	108.8	24	82	92.9

Daily average temperature = 100 °F

A daily average temperature 105 °F is used in this analysis to bound the maximum temperatures for normal and off-normal storage conditions. To maximize the temperature gradients in the

HSM-H concrete structure, only the off-normal storage condition of -20°F ambient is considered for the evaluation.

The circumference of the DSC model is divided into three regions for convection boundary conditions as shown in Figure 4-9. If the bar located on the supporting beam is slotted, the surface of the DSC shell from -64.2° to -60° is located above the upper edge of the slots in the slotted plate. The free convection is therefore restricted over this area. For conservatism, this area is considered as a dead zone with no free convection. In the case that no slot is provided on the supporting bar, the dead zone is increased to 18.9° as shown in Figure 4-9. Calculation of free convection coefficients for the DSC regions is discussed in Section 4.11.

Similar to the DSC circumference, the cross section of the HSM-H cavity is divided into different regions to apply the convection boundary conditions. Energy and hydraulic equations are combined to calculate the exit and the average bulk air temperatures for various ambient temperatures. Section 4.13 shows the regions and describes briefly the methodology to calculate the exit and the average bulk air temperatures in the HSM-H cavity.

Convection on HSM-H end walls is calculated using free convection correlations for vertical surfaces at HSM-H average bulk air temperature (T_c). Convection on the lower part of the side wall, below the side heat shield, is determined using free convection correlation for vertical surfaces at ambient temperature (T_c). For the space between the side wall and the side heat shield, free convection correlation for a narrow channel is used to determine the free convection coefficient. For the HSM-H ceiling and the HSM-H basemat, correlations for flat horizontal surfaces are used to determine free convection coefficients. Air temperatures for the convection on the basemat and ceiling are ambient temperature (T_c) and exit air temperature (T_{exit}) respectively. The calculation methods of free convection coefficients are discussed in detail in Section 4.11. Figure 4-10 shows the convection boundary conditions applied in the HSM-H model.

The thermal test reported in Reference [25] shows that the HSM-H thermal analysis methodology conservatively predicts the DSC and the HSM-H component temperatures.

Insolance is applied as a constant heat flux on the roof and front wall of the HSM-H, which are exposed to the ambient. The value of the solar heat flux is taken from [17] averaged over a 24 hour period. The insolance is applied as a constant heat flux over the SURF152 elements superimposed on the SOLID70 elements on the HSM-H roof and front wall. A solar absorptivity of 1.0 is assumed for the concrete surface. The values of the applied heat fluxes are listed below:

Shape	Insolance [17] (gcal/cm ²)	Averaged over 24 hr (Btu/hr-in ²)
HSM roof	800	0.8537
HSM front wall	200	0.2134

Insolance is not considered for the minimum ambient temperature of -20°F.

Convection and radiation from the roof and the front wall are combined together as a total convection coefficient. The calculation of the total convection coefficient is discussed in Section 4.11.

The decay heat load is considered to be distributed evenly on the radial inner surface of the DSC for the steady state runs in this analysis. The applied decay heat flux is:

$$\text{Decay heat flux} = \frac{Q}{\pi D_i L} = 3.34 \text{ Btu/hr-in}^2 \text{ or } 3.25 \text{ Btu/hr-in}^2 \text{ for CE 14x14 only}$$

where,

Q = total decay heat load = 34.8 kW = (118,748 Btu/hr) or 33.8 kW (115,336 Btu/hr) for CE 14x14 only

D_i = inner DSC diameter = 68.75"

L = DSC cavity length = 164.5"

HSM-H modules with finned aluminum side shields and HSM-H modules with stainless steel heat shields are evaluated with the maximum decay heat load of 34.8 kW. In order to limit the maximum concrete temperature below the values considered for the HSM-H with finned aluminum side heat shields, the maximum decay heat load is decreased for the HSM-H modules with flat aluminum or flat galvanized steel side heat shields. The maximum decay heat load for the HSM-H modules with un-finned aluminum side heat shields is 32.0 kW, which gives a uniform heat flux of 3.07 Btu/hr-in².

$$\text{Decay heat flux} = \frac{Q}{\pi D_i L} = 3.07 \text{ Btu/hr-in}^2 \text{ for HSM-H with un-finned aluminum side heat shields}$$

Q₁ = 32.0 kW = 109,194 Btu/hr

For the HSM-H modules with galvanized side heat shields, the maximum decay heat load is limited to 26.1 kW.

$$\text{Decay heat flux} = \frac{Q}{\pi D_i L} = 2.51 \text{ Btu/hr-in}^2 \text{ for HSM-H with galvanized steel side heat shields}$$

Q₂ = 26.1 kW = 89,061 Btu/hr

It is assumed that soil has a temperature of 70°F at 10' below the HSM-H basemat for hot conditions. The soil temperature for cold condition (-20°F) is assumed to be 45°F. These assumptions are consistent with the assumptions in the thermal analysis of the standardized HSM design [19]. The HSM-H basemat is considered to be a 4' thick concrete slab. Due to low conductivity of concrete and soil, the model is insensitive to the thickness of the basemat / soil and the soil temperature. The heat flux and fixed temperature boundary conditions applied in the model are shown in Figure 4-11.

4.3.1.3 Steady State 32PTH DSC Model

The 32PTH DSC is a high integrity stainless steel welded pressure vessel that provides confinement of radioactive material, encapsulates the fuel in a helium atmosphere, and when placed in the transfer cask, provides radiological shielding.

A three dimensional finite element model of the 32PTH DSC is developed using ANSYS [16] to determine the maximum fuel cladding temperature. The DSC model includes the DSC shell, shield plugs, basket rails, basket, and fuel assemblies. The fuel assemblies are modeled as

homogenized regions within the fuel compartments. The effective thermal properties for the homogenized fuel are calculated in Section 4.8.

The following conservative assumptions are considered in developing the finite element model to maximize the fuel cladding temperature:

- No convection occurs within the DSC cavity,
- The basket containing the fuel assemblies is centered axially in the DSC cavity,
- Heat transfer across the contact gaps within the basket occurs only by gaseous conduction.

The following gaps are considered between components in the model at thermal equilibrium:

- 0.010" gap between each two adjacent basket plates except for the following cases:
 - between the aluminum inserts and the stainless steel rails – this gap is considered to be at least 0.020"
 - between the aluminum and the poison plates, when applicable. The aluminum plate and the poison plate are sandwiched between fuel compartments. For ease of modeling the 0.010" gaps are placed on both sides of the paired plates. These gaps account for the total contact resistance between the four plates shown in Figure 4-13, Detail B.
- 0.010" gap between the basket plates and aluminum rails
- 0.100" radial gap between rails and inner shell (see Section 4.11 for justification)

The axial cold gap of 0.07" between the stainless steel support plates and the aluminum plates is divided into a 0.01" axial gap at the bottom and a 0.060" axial gap at the top of the stainless steel plate. All dimensions of the canister are at nominal values. Details of the finite element model are shown in Figure 4-12 to Figure 4-14.

Five basket types in two categories are designed for NUHOMS-32PTH DSC. Relevant characteristics of these basket types are listed below.

Basket type	I	II
A	Boron Aluminum, or Metal Matrix Composites (MMC) Maximum thickness 0.187"	Boral [®]
B		Maximum thickness 0.075"
C		
D		Not applicable
E		Not applicable

Aluminum plates are to be paired with the poison plates to make a nominal thickness of 0.5". The conductivity of the borated aluminum/MMC plate depends on the boron content and the fabrication procedure. To bound the maximum component temperature, the maximum thickness of the boron containing plate (0.1875") is considered in the model for basket type I.

Paired Boral[®] / aluminum plates are used in basket type II. An effective conductivity is calculated for the paired Boral[®] / aluminum plates, as discussed in Section 4.2. Other combination of aluminum and poison plates that satisfies the conductivity requirements in Chapter 9 can be used in the basket.

Heat transfer from the fuel regions occurs only by conduction through the basket plates and the rails. Conduction and radiation heat transfer are considered between the rails and the DSC shell. Conduction through components is modeled using SOLID70 elements.

Radiation between the rails and the DSC shell is modeled using radiation LINK31 elements using the same methodology as described in Section 4.3.1.1. Axial radiation is also considered between the top and bottom surfaces of the fuel assemblies to the shield plugs. The emissivity of the heavily oxidized top and bottom surfaces of the fuel assemblies are considered to be 0.9.

The material properties of Al-1100 are considered for the rail inserts and back plates in the DSC model. Alternately, Al-6061 can be used to fabricate these components.

The DSC model is modified to evaluate the thermal effects of using alternate material Al-6061. The conductivity of rail inserts and back plate is changed from Al-1100 to Al-6061 in the modified model. All other material properties and boundary conditions remain unchanged. The results are discussed in Section 4.3.2.

Steady State Boundary conditions for the DSC Model

The nodal temperatures of the DSC shell are retrieved from the transfer cask or HSM-H models described in Sections 4.3.1.1 and 4.3.1.2, and applied to the corresponding nodes in the DSC model via a macro described in Appendix 4.16.1.

The SOLID70 elements representing the homogenized fuel are given heat generating boundary conditions in the region of the active fuel length. Active fuel length is considered to be 144" [20] beginning at approximately 4.0" above the bottom of the fuel assembly [20]. Fuel assembly has a total length of 162" in the model. Peaking factors to apply the axial decay heat profile for the homogenized fuel region are calculated in Section 4.7.

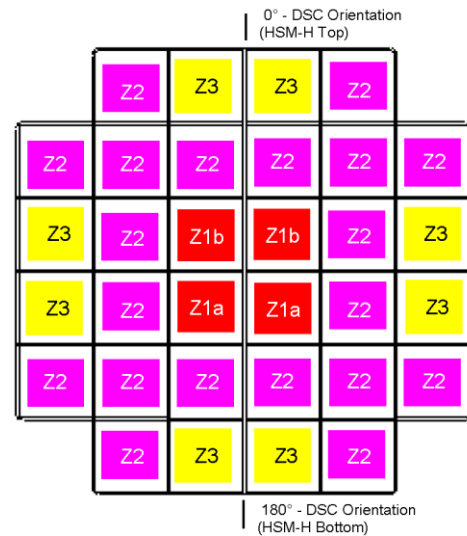
The maximum heat load per canister is 33.8 kW for CE 14x14 fuel assemblies and 34.8 kW for other fuel assemblies. Since CE 14x14 fuel assembly has a shorter active fuel length than the other assemblies, a lower total heat load is considered for CE 14x14 assembly to avoid a high heat generating rate. The maximum decay heat per assembly is 1.5 kW. Heat load zoning, as illustrated below, is used to maximize the number of higher heat load assemblies per DSC. The loading requirements are as follows.

For CE 14x14 Assemblies

- Q_{zi} is the maximum decay heat per assembly in zone i
- Total Decay Heat ≤ 33.8 kW
- 4 fuel assemblies in zone 1 with $Q_{z1} \leq 0.775$ kW
- 20 fuel assemblies in zone 2 with $Q_{z2} \leq 1.068$ kW
- 8 fuel assemblies in zone 3 with $Q_{z3} \leq 1.5$ kW

For other fuel Assemblies

- Q_{zi} is the maximum decay heat per assembly in zone i
- Total Decay Heat ≤ 34.8 kW
- 4 fuel assemblies in zone 1 with
 - total decay heat ≤ 3.2 kW
 - $Q_{z1a} \leq 1.05$ kW in the lower compartments
 - $Q_{z1b} \leq 0.8$ kW in the upper compartments
- 20 fuel assemblies in zone 2 with $Q_{z2} \leq 1.1$ kW
- 8 fuel assemblies in zone 3 with $Q_{z3} \leq 1.5$ kW



Heat generation rates as a function of spent fuel parameters are calculated in Appendix 4.16.2.

Five extreme loading configurations are considered to bound the maximum component temperatures. The loading configurations are shown in Figure 4-15. In the first configuration, the heat load in the core compartments is maximized, so that zone 1 has a uniform heat load of 0.8 kW per assembly and zone 2 has a heat load of 1.1 kW per assembly. Since the total heat load is limited to 34.8 kW, the heat load of zone 3 is 1.2 kW per assembly.

The heat load in the peripheral compartments is maximized in loading configuration 2, so that zone 3 has a heat load of 1.5 kW per assembly and zone 2 has a heat load of 1.1 kW per assembly. Since the total heat load is limited to 34.8 kW, the heat load of zone 1 is 0.2 kW per assembly. A heat load of 0.2 kW per assembly for a fuel assembly in zone 1 is rather unrealistic.

To have a more realistic estimation of maximum component temperatures loading configuration 3 is considered, in which zone 1 has a heat load of 0.55 kW per assembly and zone 3 has a heat load of 1.5 kW per assembly. Zone 2 is divided into two subdivisions. The first subdivision includes the fuel assemblies around the central assemblies with a heat load of 0.925 kW per assembly and the second subdivision located at the periphery has a heat load of 1.1 kW per assembly.

In loading configuration 4, the heat load in zone 1 and zone 3 are maximized, so that the central and peripheral compartments have maximum heat load. The heat load is 1.5 kW per assembly in zone 3 and 0.8 kW per assembly in zone 1. The remaining heat load is divided uniformly over assemblies in zone 2, which gives a heat load of 0.98 kW per assembly.

To investigate the effect of non-uniform loading in zone 1, loading configuration 5 is considered, in which the two lower compartments in zone 1 have a heat load of 1.05 kW per assembly. It gives a heat load of 0.55 kW per assembly for the two upper compartments in zone 1 based on the loading restrictions.

Similar to load configuration 1, the heat load in the core compartments is maximized for CE 14x14 assemblies in load configuration 6. The heat load of zone 3 is 1.17 kW per assembly.

Load configuration 7 is similar to configuration 4, the heat load in zones 1 and 3 are maximized to investigate the effect of the maximum heat load in zone 3 on the cladding temperature.

The seven loading configurations discussed above are considered only for the maximum ambient temperature of 115°F during transfer operation. For the other conditions loading configuration 1 is evaluated, which gives the maximum DSC component temperatures for high enriched fuel assemblies in basket type I. The maximum temperatures for the type II basket represent a slight deviation from the temperatures in configuration 1. The deviation is small enough to consider configuration 1 to still be bounding. Configuration 1A is bounded by the type II basket type temperatures.

Heat generating rate for each segment of the active fuel region is calculated as follows:

$$\dot{q}''' = \frac{\left(\frac{Q}{4a^2 L_a} \right)}{0.984}$$

where

Q = Heat load per assembly defined for each loading zone

a = half width of fuel compartment = Width of the modeled fuel assembly = 8.7"/2 = 4.35"

L_a = Active fuel length = 137 for CE 14x14 / 144" for other assemblies

PF = Peaking Factor from Section 4.7

The area beneath the peaking factor curve shown in Section 4.7 is 0.984. The heat generating value is divided by this factor to avoid any reduction of the total heat load in the model. The total heat load applied in the model is verified by retrieving the reaction solution from the solved model and comparing it to the maximum heat load value. Typical applied boundary conditions are shown in Figure 4-16.

4.3.2 Maximum Temperatures for Normal and Off-Normal Conditions

Steady state thermal analyses are performed using the maximum decay heat load of 34.8 kW (33.8 kW for CE 14x14) per canister, 115°F ambient temperature, and the maximum insolation per Reference [17]. Insolation is averaged over a 12 hour period for transfer conditions and over a 24 hour period for storage conditions.

The temperature distributions within the TC, the HSM-H, and the DSC models are shown in Figure 4-17 to Figure 4-23. Summaries of the maximum component temperatures are listed in Table 4-1 and Table 4-2. The maximum component temperatures for 34.8 kW heat load bounds the temperatures calculated for 33.8 kW heat load as shown in Table 4-1.

The maximum basket component temperatures for normal and off-normal storage conditions in Table 4-2 and Table 4-4 are calculated based on DSC shell temperature profiles with the maximum temperature of 422°F and 319°F for off-normal hot and cold conditions, respectively. These maximum temperatures bound the maximum DSC shell temperatures resulted for HSM-H with stainless steel heat shields. Therefore, the maximum basket component temperatures including the maximum fuel cladding temperatures reported in Table 4-2 and Table 4-4 are the bounding temperatures for all HSM-H variations discussed in Section 4.3.1.2.

As seen from Table 4-2, using Al-6061 instead of Al-1100 for rail inserts and back plates increases the maximum cladding temperature by 4 °F. The temperature increase for the basket components due to use of Al-6061 is bounded by 4 °F as well.

The maximum temperatures calculated for off-normal conditions bound the values for the normal conditions. Therefore, thermal stress and DSC internal pressures for both normal and off-normal conditions are calculated based on the temperatures resulted from the maximum off-normal conditions (115°F ambient) for conservatism.

4.3.3 Minimum Temperatures for Normal and Off-Normal Conditions

Temperature distributions under the minimum ambient temperatures of -20°F with no insolation and the maximum design heat load are determined under steady state conditions to maximize the temperature gradients in the TC, the HSM-H and the DSC. Figure 4-24 and Figure 4-25 show the temperature distributions for transfer operations and storage conditions at -20°F respectively. Table 4-3 and Table 4-4 summarize the results of these analyses.

The resultant DSC and transfer cask temperatures for the -20°F ambient during transfer and storage are used to calculate the thermal stresses for the normal conditions at 0°F ambient.

4.3.4 Maximum Internal Pressures for Normal and Off-Normal Conditions

Maximum internal pressure within the NUHOMS[®]-32PTH DSC is calculated in Section 4.6.

4.3.5 Maximum Thermal Stresses for Normal and Off-Normal Conditions

Maximum thermal stresses during normal and off-normal conditions of storage and transfer are calculated in Chapter 3.

4.3.6 Evaluation of Thermal Performance for Normal and Off-Normal Conditions

The thermal analysis for normal and off-normal conditions of transfer and storage concludes that the NUHOMS[®]-32PTH System design meets all applicable requirements.

The maximum component temperatures calculated using conservative assumptions are lower than the allowable limits. The maximum TC seal temperature (255°F / 124°C) during off-normal transfer conditions is well below the 400°F long-term limit specified for continued seal function. The maximum solid neutron shield temperature (265°F / 129°C) is below allowable limit of 300°F (149°C) and no degradation of the solid neutron shielding material is expected. The maximum pressure within the neutron shielding panel (38.5 psia / 23.8 psig) corresponding to the average temperature of the liquid neutron shield (265°F / 129°C) is below the set point of the pressure relief valve (54.7 psia / 40 psig).

For all the side heat shield configurations, the maximum local temperature of the HSM-H concrete structure is lower than 300°F as required in [22]. The concrete structure of the HSM-H is made using Type II cement with fine aggregates satisfying ASTM C33 or equivalents as defined in NUREG-1536 [22].

The calculated maximum fuel cladding temperature is lower than the temperature limit of 752°F (400°C) considered for normal conditions of storage and short-term operations in [2]. The comparison of the resultant maximum temperatures with the allowable limits is listed below:

Component	Transfer Conditions ¹	Allowable / Design Limit
Cask Lid Seal	205°F	400°F
Cask Bottom Plate Seal	190°F	400°F
Lead	337°F	621°F
Liquid Neutron Shield (Temp / Press)	265°F / 23.8 psig	45 psig
Solid Neutron Shield	213 °F	300°F
Fuel Cladding	727°F	752°F

Component	Storage Conditions ₆	Allowable / Design Limit
Concrete in module with finned aluminum side heat shields @ 34.8 kW	213°F	300°F
Concrete in module with flat stainless side heat shields @ 34.8 kW	248°F	300°F
Concrete in module with un-finned aluminum side heat shields @ 32.0 kW	219°F	300°F
Concrete in module with un-finned galvanized steel side heat shields @ 26.1 kW	213°F	300°F
Fuel Cladding @ 34.8 kW	684°F	752°F for normal conditions / 1058°F for off-normal conditions

The maximum DSC internal pressures for normal and off-normal storage conditions are 5.9 and 10.7 psig respectively. The maximum DSC internal pressure for normal transfer conditions is 6.4 psig and for off-normal transfer conditions is 11.2 psig. The DSC internal pressures are lower than the design pressure limits of 15 psig for normal and 20 psig for off-normal storage and transfer conditions.

¹ The TC and HSM-H models are run only with off-normal conditions at 115°F ambient. The resultant temperatures are used to evaluate the thermal performance for both normal and off-normal conditions. The fuel cladding temperature remains in all cases below the normal allowable limit of 752°F.

4.4 Thermal Evaluation for Accident Conditions

Three hypothetical accident cases during transfer operation are relevant for thermal evaluation:

- Loss of the TC liquid neutron shield due to damages on the shielding panel
- Loss of helium gas in annulus between the DSC and the TC
- Postulated fire engulfing the TC

It is considered in all the above cases that the transfer cask contains a fully loaded DSC. The fire accident is postulated in which maximum amount of 300 gallons of diesel fuel is spilled onto the ground in such a way as to completely engulf the transfer cask. Subsequent to the fire accident, it is assumed that the seals for the TC lid and the bottom cover plate will burn, and the liquid neutron shield will be released and evaporates completely. Therefore, the fire accident scenario bounds the loss of liquid neutron shield and the loss of helium gas in the accident cases. The fire accident case is analyzed to give the bounding fuel cladding temperature for the transfer accident cases.

Since the HSM-H is located outdoors, there is a remote probability that the air inlet and outlet openings will become blocked by snow or by debris from events such as flooding, high wind, and tornados. The perimeter security fence around ISFSI and the location of the air inlet and outlet openings reduces the probability of such an event. Nevertheless, it is conservatively considered in this analysis that all the inlet and outlet openings become blocked.

The thermal mass of the HSM-H, the construction of the vent openings, and the location of the fuel on the transfer vehicle limit the effect of a fire accident for the HSM-H. Therefore, the worst case fire accident is bounded by the fire accident case during transfer operation.

A new model is developed to evaluate the fire accident case during transfer operation. The HSM-H model described in Section 4.3 is slightly modified to evaluate the blocked vent accident case during storage. The DSC model is unchanged for this evaluation. Details of the models are discussed in Section 4.4.1.

4.4.1 Thermal Models for Accident Conditions

4.4.1.1 Transient Transfer Cask Model

To determine the temperature distribution in the transfer cask and the DSC for fire accident case, a three dimensional model is developed using ANSYS [16]. This model is created by selecting the nodes and elements of the DSC model described in Section 4.3 at z-axis from 56.06" to 86.07". The shells of TC including the annulus are then modeled around the DSC using SOLID70 elements. LINK31 elements are created using the same methodology as described in Section 4.3.1.1 to simulate the radiation between the DSC shell and the TC inner shell. The three dimensional model represents a slice of the DSC within the transfer cask. The TC slice model is shown in Figure 4-26. Axial length of the slice model is 30".

It is assumed that the helium gas in the annulus will remain in place during the burning period to maximize the heat input from fire into the transfer cask. For the same reason, the 0.030" air gap assumed between the lead and the structural shell in the transfer cask is removed during the burning period. To eliminate the uncertainties about the maximum poison plate conductivity, the conductivity of poison plate is set equal to that of aluminum 1100 during the fire.

The liquid neutron shield (water) will be released at high temperatures when its saturation pressure exceeds the set point of the pressure relief value (40 psig). The average temperature of liquid neutron shield drops to 212°F (boiling point of water) when the pressure relief valve opens. After this point, the energy of fire will be consumed to evaporate the liquid neutron shield and the temperatures remain constant until the liquid shield is evaporated completely. Nevertheless, during the burning fire period, it is conservatively assumed that the water remains in the shield panel which will conduct the fire better than air. Using the methodology in Section 4.9, an effective conductivity of 2.25 Btu/hr-in-°F is considered for the liquid neutron shield to bound the problem and to maximize the heat input from the fire into the transfer cask.

During the cool down period the air gap in the transfer cask, between the gamma shield and the structural shell, is returned to the model. Subsequent to the fire, during the cool down period, it is assumed that the TC seals are burned and the shielding panel is emptied. The properties of air are therefore given to the elements in the annulus between the DSC and the transfer cask during the cool down period. Convection and radiation through the air in the shielding panel are combined together in form of an effective conductivity. Section 4.9 describes the calculation of the effective conductivity for the air within the shielding panel. Convection is not considered for the air in the annulus. As mentioned in Section 4.3.1.1, radiation in annulus is modeled using LINK31 elements.

Boundary Conditions for the Fire Accident Case

Initial temperatures for the transfer cask slice model are transferred from the steady-state models at 115°F ambient conditions.

Fire is assumed to have an average flame temperature of 1475°F and an emissivity of 0.9. The cask surface emissivity is set to 0.8 during the fire. These assumptions are in compliance with 10CFR71.73 [17].

It is assumed that the diesel fuel creates a pool diameter of about 200 inches, which is the approximate length of the transfer cask. Considering a volume of 300 gallons and a minimum burning rate of 0.15 in/min [23] give a burning time of 14.5 minutes for diesel fuel. A burning time of 15 minutes is considered conservatively for analytical purposes.

A forced convection value of 4.5 Btu/hr-ft²-F is considered during the burning time as concluded in [23]. The calculation of the heat transfer coefficients on the transfer cask during fire accident are described in Section 4.11.1.

Heat generation corresponding to loading configuration 1 is considered for the solid elements representing the homogenized fuel during the burning time and the cool down period.

A peaking factor of 1.1 is considered for this evaluation. Adiabatic boundary conditions are applied over the vertical end surfaces of the slice model. This model is conservative regarding the fuel cladding temperature since the axial heat transfer is restricted and the maximum peaking factor is applied to the heat generating rate.

4.4.1.2 Transient HSM-H Model

A slightly modified HSM-H model discussed in Section 4.3.1 is used to determine the temperature distribution in the HSM-H and the 32PTH DSC shell for the blocked vent accident case. The basket and its content including the fuel assemblies are homogenized for the transient run required for the blocked vent analysis. The effective thermal properties of the homogenized DSC content are calculated as follows.

Effective Properties of the Homogenized Basket

Volume and weight of the basket components are calculated in chapter 3. The relevant values are listed below for calculation of the effective basket properties.

Component	Volume in ³	Weight lbm	C _p Btu/lbm-°F	C _p x M Btu/°F
Fuel Assemblies	148488	50720	0.068	3449
Basket, Stainless Steel	75928	22019	0.116	2554
Basket, Aluminum	79952	7835	0.218	1708
Total	304368	80574	---	7711

The equations for calculating the average basket density and heat capacity are:

$$\bar{\rho} = \frac{\text{basket weight} + \text{fuel assemblies weight}}{\text{total cavity volume}}$$

$$\bar{C}_p = \frac{\text{weight of SS} \times C_{p,ss} + \text{weight of Al} \times C_{p,ss} + \text{weight of fuel} \times C_{p,fuel}}{\text{basket weight} + \text{fuel assemblies weight}}$$

$$\text{total cavity volume} = \pi/4 \times D_i^2 \times L$$

$$D_i = \text{DSC inner diameter} = 68.75''$$

$$L = \text{cavity length} = 164.5''$$

$$C_{p,ss} = 0.114 \text{ Btu/lbm-°F @ } 100^\circ\text{F [6]}$$

$$C_{p,Al} = 0.216 \text{ Btu/lbm-°F @ } 100^\circ\text{F [6]}$$

$$C_{p,fuel} = 0.068 \text{ Btu/lbm-°F @ } 400^\circ\text{F [Section 4.8]}$$

Specific heat capacities of stainless steel and aluminum increase at higher temperatures as shown in Section 4.2. Initial basket temperature for blocked vent case is higher than 100°F. Selecting lower heat capacity values for stainless steel and aluminum at 100°F is conservative since it reduces the amount of stored heat in the basket and results in a higher fuel cladding temperature.

The heat capacity of the fuel assembly is selected at 400°F, which is lower than the average off-normal temperature of the fuel assemblies in the 32PTH DSC model. Similar to stainless steel and aluminum, selecting lower heat capacity values for fuel assemblies is conservative.

The resultant effective density and specific heat capacity of the basket are:

$$\bar{\rho} = 0.132 \quad \text{lbm/in}^3$$

$$\bar{C}_p = 0.096 \quad \text{Btu/lbm-}^\circ\text{F}$$

To calculate the axial and the transverse effective conductivities of the basket a 15” long slice of the basket is created by selecting the nodes and elements of the 32PTH DSC shell and basket from the finite element model described in Section 4.3.1.3. DSC shell elements are unselected prior to run the slice model. The basket slice model is shown in Figure 4-27.

To calculate the axial effective conductivity of the basket, constant temperature boundary conditions are applied at the top and bottom of the slice model. No heat generation is considered for the fuel elements in this case. The axial effective conductivity is calculated using the following equation:

$$k_{eff,axl} = \frac{Q \times L}{A \times \Delta T}$$

where,

Q = Amount of heat leaving the upper face of the slice model – reaction solution of the uppermost nodes (Btu/hr)

L = Length of the model = 15”

A = Surface area of the upper (or bottom) face of the model = $\pi/2 \times r_i^2 = 1856 \text{ in}^2$

r_i = Inner radius of the DSC shell = 34.375”

$\Delta T = (T_1 - T_2)$ = Temperature difference between upper and lower faces of the model (°F)

T_1 = Constant temperature applied on the lower face of the model (°F)

T_2 = Constant temperature applied on the upper face of the model (°F)

In determining the temperature dependent axial effective conductivities an average temperature, equal to $(T_1 + T_2)/2$, is used for the basket temperature. The resulting axial effective conductivities of the basket are listed below.

T_1 (°F)	T_2 (°F)	T_{avg} (°F)	$Q_{reaction}$ (Btu/hr)	$k_{eff,axl}$ (Btu/hr-in-°F)
300	400	350	12380	1.0005
400	500	450	12533	1.0128
500	600	550	12734	1.0291
600	700	650	12928	1.0448
700	800	750	13096	1.0583
800	900	850	13280	1.0732
900	1000	950	13449	1.0869
1000	1100	1050	13627	1.1013
1100	1200	1150	13762	1.1122

To calculate the transverse effective conductivity of the basket, constant temperature boundary conditions are applied on the outermost nodes of the slice model and heat generating conditions

are applied on the fuel elements. The heat generation rates are calculated based on the loading configuration 1 shown in Figure 4-15 with a peaking factor of 1.1.

The following equation from [15] determines the maximum temperature for long solid cylinders with uniformly distributed heat sources.

$$T = T_o + \frac{\dot{q} r_o^2}{4k} \left[1 - \left(\frac{r}{r_o} \right)^2 \right]$$

with T_o = Temperature at the outer surface of the cylinder (°F)

T = Maximum temperature of cylinder (°F)

\dot{q} = Heat generation rate (Btu/hr-in³)

r_o = Outer radius = 34.375"

r = Inner radius = 0 for slice model

k = Conductivity (Btu/hr-in-°F)

The above equation is rearranged to calculate the transverse effective conductivity of the basket.

$$\dot{q} = \frac{Q}{V} = \frac{Q}{\frac{\pi r_o^2}{2} L} \rightarrow k_{eff,rad} = \frac{2 Q}{4 \pi L \Delta T}$$

with

Q = Amount of heat leaving the periphery of the slice model – reaction solution of the outermost nodes (Btu/hr)

L = length of the model = 15"

$\Delta T = (T - T_o)$ = Difference between maximum and the outer surface temperatures in (°F)

Since the surface area of the fuel assemblies at the basket cross section is much larger than the other components, assuming a uniform heat generation is a reasonable approximation to calculate the radial, effective conductivity. In determining the temperature dependent transverse effective conductivities an average temperature, equal to $(T_{max} + T_o)/2$, is used for the basket temperature. The resulting transverse effective conductivities of the basket are listed below.

T_o (°F)	T_{max} (°F)	T_{avg} (°F)	$Q_{reaction}$ (Btu/hr)	$k_{eff,rad}$ (Btu/hr-in-°F)
100	491	296	6914	0.1876
200	568	384	6914	0.1993
300	647	474	6914	0.2114
400	728	564	6914	0.2237
500	810	655	6914	0.2366
600	894	747	6914	0.2495
700	980	840	6914	0.2620
800	1068	934	6914	0.2737
900	1160	1030	6914	0.2821
1000	1254	1127	6914	0.2888

Boundary Conditions for the Blocked Vent Case

The initial temperatures for the HSM-H model are calculated using the same convection and radiation boundary conditions as described in Section 4.3.1.2 for the maximum ambient temperature of 115°F (105°F daily average temperature).

The insolation on the HSM-H surfaces exposed to the ambient and the soil temperature are applied also in the same way as described in Section 4.3.1.2. Uniform heat generating boundary conditions are applied over the elements representing the homogenized basket. The heat generating rate for the basket elements is calculated as follows.

$$\text{Heat generating rate} = \frac{Q}{\left(\frac{\pi}{4} D_i^2 L\right)} = 0.1945 \quad \text{Btu/hr-in}^3$$

where,

Q = total decay heat load = 34.8 kW = 118748 Btu/hr

Di = inner DSC diameter = 68.75"

L = DSC cavity length = 164.5"

During the blockage of the vents, air within the HSM-H cavity is trapped. The convection heat transfer under these circumstances reduces to free convection in closed cavities. However, closed cavity convection is conservatively ignored and all convection boundary conditions within the HSM-H cavity are removed. Only the conductivity of air is considered for this analysis. The effect of the thermal radiation exchange between the top heat shield and the DSC is studied to calculate the bounding component temperatures for the blocked vent conditions.

The DSC shell temperatures are retrieved from the transient HSM-H model and applied as steady state boundary conditions to the 32PTH DSC model. This methodology over predicts the fuel cladding temperature since the fuel assemblies heat up faster than the DSC shell. The heat generating rates and peaking factors for the homogenized fuel regions in the DSC model are calculated in the same way as described in 4.3.1.3. The maximum decay heat load of 34.8 kW and loading configuration 1 (Figure 4-15) are considered for this evaluation. The DSC temperatures for 34.8 kW decay heat load bound the temperatures for lower decay heat loads of 32.0 and 26.1 kW cases.

4.4.2 Maximum Temperatures for Accident Conditions

The maximum component temperatures resulted from the transient run of the transfer cask model are listed in Table 4-5. Figure 4-28 shows the temperature distributions for the transfer cask fire accident. The temperature-time histories of major components in the transfer cask OS187H during fire accident are shown in Figure 4-29.

The transient model of the HSM-H simulates 36 hours of the blocked vents accident case. 34 hours after complete blockage of the inlet and outlet vents, the maximum concrete temperature rises to 364°F for the HSM-H equipped with finned aluminum side heat shields and to 377°F for the HSM-H equipped with flat stainless steel heat shields. Since lower heat loads are specified for the HSM-H with un-finned side heat shields (aluminum or galvanized steel), it takes longer

than 34 hours of vent blockage until the maximum concrete temperature of these modules exceed the above temperature. Typical temperature distributions for the HSM-H model during blockage of the vents are shown in Figure 4-30.

The DSC shell temperatures at 34 hours after blockage of the vents are retrieved from the transient model and applied as steady-state boundary conditions to the DSC model. The typical resultant temperature distributions are shown in Figure 4-32.

The maximum component temperatures for the blocked vent cases are listed in Table 4-6. Since the DSC shell temperature resulted for HSM-H with finned aluminum side heat shields is higher, the maximum basket component temperatures including the maximum fuel cladding temperature are bounded by this case. Figure 4-33 shows the temperature-time history of major components in the HSM-H during blockage of the vents, for the bounding case.

4.4.3 Maximum Internal Pressures for Accident Conditions

Maximum internal pressure within the NUHOMS®-32PTH DSC is calculated in Section 4.6.

4.4.4 Maximum Thermal Stresses for Accident Conditions

Maximum thermal stresses during accident conditions of storage and transfer are calculated in Chapter 3.

4.4.5 Evaluation of Thermal Performance for Accident Conditions

The thermal analysis for the accident conditions during storage or transfer operation concludes that the NUHOMS®-32PTH System design meets all applicable requirements.

The conservative model of the transfer cask for the fire accident case shows that the maximum fuel cladding temperature does not exceed 1036°F. This maximum temperature is lower than the allowable limit of 1058°F.

The maximum fuel cladding temperature after blockage of the vents for 34 hours is 823°F in the HSM-H with the design basis heat load of 34.8 kW. This temperature is well below the maximum allowable limit of 1058°F set for fuel cladding in accident conditions.

The analysis for the blocked vent accident conditions limits the block vent duration to 34 hours. This time limit is adequate for a combination of inspection and reaction times to remove any vent blockage. Since the maximum concrete temperature is higher than 350°F suggested in Reference [21], the strength of the concrete structure will be verified by a test as described in Chapter 12.

The maximum DSC internal pressure 34 hours after blockage of the HSM-H vents is 14.1 psig, which is lower than the design pressure of 70 psig. The maximum DSC internal pressure for fire accident case during transfer operation is 91.0 psig, which is well below 120 psig design pressure considered for the transfer accident cases.

4.5 Thermal Evaluation for Loading and Unloading Conditions

Fuel loading and unloading operations occur in the fuel handling building. During loading operation fuel assemblies are submerged in pool water permitting heat dissipation. After fuel loading is complete, the TC and 32PTH DSC are removed from the pool and the DSC is drained (helium is used to assist removal of water), dried, backfilled with helium and sealed. The TC will be sealed and backfilled with helium after sealing the DSC.

4.5.1 Vacuum Drying

The loading condition evaluated is the heatup of the DSC before transfer to the storage site. The 32PTH DSC heatup occurs during draining, vacuum drying, backfilling, and sealing of the DSC, when the DSC is contained in the TC in the vertical position inside the fuel handling building. The water level in the annulus between the DSC and TC is monitored during the above operations to be approximately 12 inches below the top of the DSC shell. Water in the annulus is replenished, if required, to maintain the water in the annulus during vacuum drying operations.

It is assumed in this evaluation that the complete drainage of water from the 32PTH DSC cavity may occur either before or after welding the DSC top shield plug. Partial drainage of water from the DSC cavity and from the annulus between the DSC and the TC (approximately 12 inches below the top of the DSC shell) is required to perform the welding. Helium is used to assist removal of water from the DSC cavity and during backfilling. Maintaining a helium atmosphere within the DSC cavity is required after drainage of water.

Fuel cladding temperature must be maintained below 752°F as required in [2].

Since the DSC is backfilled with helium after drainage of water and water is maintained in the annulus between the DSC and TC, there is no time limit for completion of the vacuum drying process. The reason is the DSC shell temperature is maintained at temperatures lower than the values calculated for the storage conditions. With helium in the DSC cavity, the fuel cladding temperature is well below the values calculated for the off-normal storage conditions in Section 4.3.6, and would never approach the allowable limit of 752°F.

4.5.1.1 Transfer Cask Annulus Backfill

After completion of the vacuum drying, the DSC must be sealed, the annulus between the DSC and the transfer cask must be drained, the cask must be sealed and backfilled with helium. To ensure the integrity of the fuel cladding, a time limit is considered for performing the activities after drainage of the annulus water until backfilling of the transfer cask starts. This time limit is calculated in this section, as follows:

In the calculational model, the water in the annulus is assumed to be drained as soon as its temperature exceeds 180°F (conservative assumption). Two time limits are calculated for this scenario. The first time limit starts after complete DSC drainage. The second time limit includes the activities after drainage of the annulus water to the point that DSC backfilling starts. Even though helium is required as a cover gas during water draindown from the DSC cavity, to be

conservative, it is assumed that backfilling of the DSC with helium starts not immediately after drainage of the DSC water, but occurs after drainage of the annulus water.

Transient thermal analyses are performed to determine the time limits. A bounding initial average temperature is considered to start the transient analysis.

The three-dimensional model of the 32PTH DSC within the TC described in Section 4.4.1.1 is slightly modified to analyze this operation. The model contains a half slice of the 32PTH DSC within the TC. The modifications are:

- The DSC is centered in the transfer cask cavity
- The effective conductivity of fuel assemblies are changed to the values reported for vacuum conditions in Section 4.2
- Air conductivity is given to the elements representing the gas and gaps within the basket
- It is considered that the annulus between the DSC and the TC is initially filled with water
- Radiation is not considered between the basket rails and the DSC shell

All the other material properties remain unchanged.

Free convection and radiation are combined together to calculate the total heat transfer coefficient from the TC outer surface to the ambient. Due to the large outer diameter of the TC, the free convection coefficient approaches that for a vertical flat plate. The correlations to calculate the free convection coefficient on vertical plates are discussed in Section 4.11. Following inputs are considered to calculate the total heat transfer coefficient on the outer surface of the transfer cask in this evaluation.

- Ambient temperature in the fuel handling building is 100°F.
- Height of the cylinder is 173", which is approximately the length of the neutron shield panel.
- Surface emissivity of the transfer cask is 0.9 (see Section 4.2 for painted surfaces)

A decay heat load of 34.8 kW is considered for the transient runs. The decay heat is applied as heat generating boundary conditions on the elements representing the homogenized fuel assemblies with a peaking factor of 1.1. Loading configuration 1 is considered for this purpose. Adiabatic boundary conditions are applied on the top and bottom faces of the slice model for conservatism.

Conduction and free convection heat transfer are combined together to calculate an effective conductivity for the water in the annulus. The calculation of the effective conductivity for the water in the annulus is discussed in detail in Section 4.9.

After draining the water from the annulus, thermal properties of air (conduction only) are considered for the elements in the annulus between the 32PTH DSC and the TC. Free convection and radiation boundary conditions are applied on the outer surface of the TC using the total heat transfer coefficient described in Section 4.11.

As described earlier, helium is required as a cover gas during water draindown from the DSC cavity. However, to be conservative the following assumptions are made. To calculate the time limit to backfill the transfer cask with helium after completion of the vacuum drying, the properties of the DSC backfill gas is changed to that of helium, and the fuel effective conductivities are changed to those calculated for helium atmosphere. Time of this change is 14 hours after complete drainage of DSC water. It is considered that it takes three hours until the helium replaces the water vapor within the DSC cavity completely. After the three hour period, the conductivity of back fill gas is changed to that of helium, and the fuel effective conductivities are changed to those calculated for helium atmosphere.

An average, initial temperature at the beginning of the transient runs is calculated for the 32PTH DSC and transfer cask as follows.

$$\begin{aligned} \text{Initial Temperature 1} = & \text{initial pool temperature} + \\ & \text{average heat up rate with water in DSC} \times \text{duration of lifting} + \\ & \text{average heat up rate without water in DSC} \times \text{duration of drainage} \\ & \text{when water from the DSC cavity is drained completely before the welding process} \end{aligned}$$

and

$$\begin{aligned} \text{Initial Temperature 2} = & \text{initial pool temperature} + \\ & \text{average heat up rate with water in DSC} \times \text{duration of lifting} + \\ & \text{average heat up rate with water in DSC} \times \text{duration of welding} \\ & \text{when water from the DSC cavity is drained completely after the welding process} \end{aligned}$$

Following assumptions are considered to calculate the initial temperature:

- Initial pool temperature is 115°F
- No heat dissipation occurs from the transfer cask outer surface
- All the decay heat is used to heat up the transfer cask and its content
- Lifting the transfer cask from the pool to the fuel handling building and performing the required inspections take 2 hours
- Drainage (pumping) of water from the DSC takes 4 hours

The average heat up rate is defined as:

$$\text{heat up rate} = \frac{Q}{M \bar{C}_p}$$

Q = total decay heat load = 34.8 kW (118748 Btu/hr)

M = total weight (lbm)

\bar{C}_p = average specific heat (Btu/lbm-°F)

The average specific heat is the mass average specific heat of all of the components.

$$\bar{C}_p = \frac{\sum m_i C_{p,i}}{M}$$

The components volumes and weights are taken from Chapter 3. Specific heat values increase generally at higher temperatures. Specific heats of the components are taken at about 100°F, which results in higher initial temperature and increases the conservatism in the model. A summary of the heat up rate calculation is shown in Table 4-7. The initial average temperature of the transfer cask and its content is then:

$$\begin{aligned} \text{Initial average temp 1} &= 115 + 3.2 \times 2 + 4.5 \times 4 = 139.4^{\circ}\text{F} \\ \text{with } &\begin{aligned} &\text{initial pool temperature} = 115^{\circ}\text{F} \\ &\text{average heat up rate during lifting} = 3.2^{\circ}\text{F/hr (see Table 1)} \\ &\text{duration of lifting} = 2 \text{ hrs} \\ &\text{average heat up rate after drainage of DSC} = 4.5^{\circ}\text{F/hr (see Table 1)} \\ &\text{duration of draining water from DSC} = 4 \text{ hrs} \end{aligned} \end{aligned}$$

$$\begin{aligned} \text{Initial average temp 2} &= 115 + 3.2 \times 2 + 3.2 \times 10 = 153.4^{\circ}\text{F} \\ \text{with } &\begin{aligned} &\text{initial pool temperature} = 115^{\circ}\text{F} \\ &\text{average heat up rate during lifting} = 3.2^{\circ}\text{F/hr (see Table 1)} \\ &\text{duration of lifting} = 2 \text{ hrs} \\ &\text{average heat up rate before drainage of DSC} = 3.2^{\circ}\text{F/hr (see Table 1)} \\ &\text{duration of welding the DSC shield plug} = 10 \text{ hrs} \end{aligned} \end{aligned}$$

For conservatism, an initial temperature of 160°F is considered for the TC and its content at the start of the transient runs.

4.5.1.2 Evaluation of Vacuum Drying and TC Backfill Operations

The maximum fuel cladding temperatures during TC backfill operations are summarized in Table 4-8. Typical temperature distributions at the end of vacuum drying process are shown in Figure 4-34. Histories of the maximum component temperatures are shown in Figure 4-37.

The time limit to start backfilling of the transfer cask with helium must be within 28 hours after drainage of the annulus water based on the time-temperature history curve shown in Figure 4-37.

Vacuum drying operations preclude any thermal cycling of fuel cladding. Backfilling the DSC with helium gas causes a one time temperature drop, which is not considered as a repeated thermal cycling. Re-evacuation of the DSC under helium atmosphere does not reduce the pressure sufficiently to decrease the thermal conductivity of helium. Therefore, evacuation and re-pressurizing the DSC under helium atmosphere proceed on a descending curve to the minimum steady state temperatures, and does not include any thermal cycling. It concludes that the limit of 65°C (118°F) considered for thermal cycling is not applicable for NUHOMS[®]-32PTH system.

As discussed in Section 4.5.1, there is no time limit for completion of the DSC vacuum drying process because helium is used to assist drainage of water from DSC. In this case the maximum fuel cladding temperature remains below the allowable limit of 752°F (400°C).

The time limit for the helium backfilling of the DSC/TC annulus is 28 hours starting from the time of drainage of the annulus water.

4.5.2 Reflooding

For unloading operations, the DSC will be filled with the spend fuel pool water through the siphon port. During this filling, the DSC vent port is maintained open with effluents routed to the plant's off-gas monitoring system.

When the pool water is added to a DSC cavity containing hot fuel and basket components, some of the water will flash to steam causing internal cavity pressure to rise. The steam pressure is released through the vent port. The initial flow rate of the reflood water must be controlled such that the internal pressure in the DSC cavity does not exceed 20 psig. This is assured by monitoring the maximum internal pressure in the DSC cavity during reflood event. The reflood of the DSC is considered as a "Service Level D" event and the design pressure of the DSC is 120 psig. Therefore, there is sufficient margin in the DSC internal pressure during the reflooding event to ensure that the DSC will not be over pressurized.

The maximum fuel cladding temperature during reflooding process is significantly less than the vacuum drying condition owing to the presence of water/steam in the DSC cavity. Hence, the peak cladding temperature during the reflooding operation will be less than 734°F calculated for procedure A in Section 4.5.1 when water circulates in the annulus between the DSC and transfer cask.

To evaluate the effects of the thermal loads on the fuel cladding during reflooding operations, a conservative high fuel rod temperature of 750°F and a conservative low quench water temperature of 50°F are used.

The following material properties, corresponding to 750°F, are used in the evaluation.

Modulus of elasticity, $E = 10.4 \times 10^6$ psi = 7.17×10^{10}	(Pa)	[26]
Modulus of rigidity, $G = 2.47 \times 10^{10}$	(PaPa)	[31]
Thermal expansion coefficient, $\alpha = 6.72 \times 10^{-6}$	(1/K)	[31]
Yield stress, $S_y = 80,500$ psi = 5.55×10^8	(Pa)	[26]
Poisson's ratio, $\nu = \frac{E}{2G} - 1$		[27]

The fuel cladding stress is evaluated as a hollow cylinder with an outer surface temperature of T (50°F), and the inner surface temperature of T+ΔT (750°F) using the following equations from [27].

Maximum circumferential stresses are:

$$\text{(outer surface) } \sigma_{to} = \frac{\Delta T \cdot \alpha \cdot E}{2(1-\nu) \ln(r_o / r_i)} \left(1 - \frac{2 r_i^2}{(r_o^2 - r_i^2)} \ln\left(\frac{r_o}{r_i}\right) \right) \quad \text{tension}$$

$$\text{(inner surface) } \sigma_{ti} = \frac{\Delta T \cdot \alpha \cdot E}{2(1-\nu) \ln(r_o / r_i)} \left(1 - \frac{2 r_o^2}{(r_o^2 - r_i^2)} \ln\left(\frac{r_o}{r_i}\right) \right) \quad \text{compression}$$

The longitudinal stresses are equal to the tangential stresses [27]. The maximum stresses calculated for the fuel assembly types to be stored in the NUHOMS-32PTH are summarized in the following table.

	WE & WES 15x15	WE 17x17	MK BW 17x17	WEO 17x17	CE 14x14
OD fuel rod (in)	0.422	0.374	0.374	0.360	0.440
Clad thickness (in)	0.0243	0.0225	0.0240	0.0225	0.028
ID Clad (in)	0.3734	0.3290	0.3260	0.3150	0.3840
σ_{to} max (Pa)	1.64E+08	1.64E+08	1.63E+08	1.63E+08	1.63E+08
σ_{to} max (psi)	23,768	23,719	23,644	23,676	23,654
σ_{ti} max (Pa)	1.78E+08	1.78E+08	1.79E+08	1.78E+08	1.79E+08
σ_{ti} max (psi)	25,787	25,835	25,910	25,879	25,900
σ_{max} (psi) =	25,910				

The maximum stress is 25,910 psi. The calculated maximum stress is much less than the yield stress of 80,500 psi. Therefore, cladding integrity is maintained during reflooding operation.

4.6 Maximum Internal Pressure

The following methodology is used to determine the maximum pressures within the 32PTH DSC during storage and transfer conditions:

- Average cavity gas temperatures are derived from component temperatures.
- The amount of helium present within the canister after the initial backfilling is determined via the ideal gas law.
- The total amount of free gas within the fuel assemblies, including both fill and fission gases, is calculated based on data reported in [28].
- The amount of released gas from the fuel rods into the DSC cavity is determined based on the maximum fraction of the ruptured fuel rods considered in NUREG 1536 [22].
- The amount of helium gas is added to the amount of released gases to make the total amount of gases in the 32PTH DSC cavity.
- Finally, the maximum cavity pressures are determined via the ideal gas law.

The design pressures for the NUHOMS[®]-32PTH DSC are summarized in the following table.

Condition	Maximum Allowable Pressure For Storage (psig)	Maximum Allowable Pressure for Transfer (psig)
Normal	15	15
Off-Normal	20	20
Accident	70	120

Based on the ideal gas law, the internal pressure of the DSC increases as the average gas temperature increases. Since the DSC normal operating temperatures are bounded by the off-normal temperatures, the maximum internal pressure of the DSC is conservatively calculated based on the off-normal temperatures for both the normal and the off-normal conditions. The average cavity gas temperatures are calculated for transfer and storage conditions with 34.8 kW, which give the bounding maximum component temperatures. (See Table 4-1 and Table 4-2.)

The maximum fractions of the fuel rods that can rupture and release their free gases to DSC cavity for normal, off-normal, and accident cases are 1, 10, and 100% respectively as considered in NUREG 1536 [22].

For WE 15x15 and WE 17x17 class fuel assemblies containing ITTRs, the ITTR volume per fuel assembly and the total fuel assembly volume are as follows:

	WE15x15	WE17x17	Design Basis Fuel Assembly
ITTR volume per fuel assembly, in ³	34	34	-
Volume per fuel assembly with ITTR, in ³	4,237	4,386	-
Number of fuel assembly per DSC	32	32	32
Total fuel assembly volume per DSC, in ³	135,584	140,352	148,488

As shown in the above table, the total FA volume per DSC for WE 15x15 and WE 17x17 FAs with ITTRs is smaller than the total design basis fuel assemblies volume per DSC. Therefore, the total DSC cavity volumes for the WE 15x15 and WE 17x17 fuel assemblies with ITTRs are larger

than the design basis DSC cavity volume used in this section for DSC maximum internal pressure calculation. Hence the maximum internal pressure in 32PTH DSC cavity calculated in this section remains bounding for the WE 15x15 and WE 17x17 class fuel assemblies containing ITTRs.

As shown in Section 4.8, the effective fuel conductivities in the transverse and axial direction for WE 15x15 and WE 17x17 class fuel assemblies containing ITTRs are bounded by the values presented in Section 4.2. Hence, the maximum fuel cladding temperatures determined in Section 4.0 remain bounding for WE 15x15 and WE 17x17 class fuel assemblies containing ITTRs.

4.6.1 Average Gas Temperature

To determine the average gas temperature, volume average temperatures of the elements representing the helium gaps (T_{void}) and the homogenized fuel assemblies (T_{fuel}) are calculated discretely from the thermal models. Although the average temperature of the homogenized fuel elements includes the fuel rods and the helium gas between them, this average temperature is considered as the average gas temperature within fuel compartments. The following volumes are considered to calculate the gas average temperature:

$$\begin{aligned}\text{Gas volume in the fuel compartments} &= \text{Volume of the fuel compartments} - \text{Volume of the fuel rods} \\ \text{Volume of the fuel compartment} &= 8.7 \times 8.7 \times 162 \times 32 = 392,377 \text{ in}^3 \\ \text{Volume of the fuel rods} &= 148,488 \text{ in}^3 \quad [\text{Chapter 3}] \\ \text{Gas volume in the fuel compartments (V}_{\text{He,comp}}) &= 243,889 \text{ in}^3\end{aligned}$$

Gas volume in the void space of DSC = Total DSC cavity volume – Gas volume in the fuel compartments
Total DSC cavity volume (V_{cavity}) = 308,146 in³ [Chapter 3]
Gas volume in fuel compartments = 243,889 in³
Gas volume in void space of DSC (V_{void}) = 64,257 in³

The average gas temperature in the 32PTH DSC is calculated as follows:

$$\bar{T}_{DSC} = \frac{T_{\text{avg,fuel}} \times V_{\text{He,comp}} - T_{\text{avg,void}} \times V_{\text{void}}}{V_{\text{cavity}}}$$

For an average gas temperature, the mass and volume average temperatures are equal. The results are summarized below.

Operating Condition		$\bar{T}_{DSC}(^{\circ}F)$
Storage	Normal	515
	Off-Normal	515
	Accident ¹	647
Transfer	Normal	537
	Off-Normal	537
	Accident ²	961

Using Al-6061 instead of Al-1100 for rail inserts and back plates increases the DSC component temperature by at most 4 °F as discussed in Section 4.3.2. As noted in Table 4-2, the DSC component temperatures for normal and off-normal storage conditions are based on maximum DSC shell temperature of 422°F instead of 407°F for conservatism. This conservatism compensates more than adequate the temperature increase due to use of Al-6061. Therefore, the average gas temperatures in the above table remain bounding for storage conditions.

The temperature increase of 4°F for transfer conditions results in an increase of at most 0.3% for absolute average gas temperature within DSC cavity.

Temp. Increase / Absolute Fuel Cladding Temp. [Table 4-2] = 4/(723 + 460) = 0.3%

4.6.2 Amount of Initial Helium Backfill

The initial helium fill pressure within the canister is 2.5±1.0 psig after vacuum drying. An initial pressure of 3.5 psig (18.2 psia) is considered here to maximize the amount of helium gas. The finite element model developed to analyze the vacuum drying process (Section 4.5.1) is run for steady state conditions with helium atmosphere to consider the minimum initial DSC temperature before backfilling, which gives the maximize amount of initial helium gas. The average gas temperature is then calculated using the same methodology described in Section 4.6.1. The initial temperature of the backfill gas within the canister is 469°F.

¹ After 48 hours of vent blockage

² At the end of cool down period, 120 hours after beginning of the fire

From the backfill pressure and initial backfill gas temperature, the amount of helium backfill gas can be calculated using the ideal gas law.

$$n = \frac{PV}{RT}$$

P = maximum initial canister fill pressure = 18.2 psia

V = DSC cavity volume (loaded) = 308,146 in³ = 178.3 ft³ [Chapter 3]

T = initial fill temperature = 469°F = 929 R

R = universal gas constant = 10.730 psia-ft³/lbmoles-R [3]

n_{back} = 0.326 lb-moles

4.6.3 Free Gas within Fuel Assemblies / BPRA

Maximum volume of free gas per assembly is bounded by WE 15x15 fuel assembly with 204 fuel rods for burnup rates from 35,000 to 55,000 MWd/MTU as concluded in [28]. The reported total free gas volumes from Reference [28] are extrapolated to evaluate the free gas volume at the maximum design burnup rate of to 60,000 MWd/MTU. Figure 4-38 illustrates this extrapolation. Based on extrapolation results, the total free gas volume at 60,000 MWd/MTU burnup rate is 1123 cc per fuel rod at standard pressure and temperature (0°C and 760 mmHg). The amount of free gases in the fuel rods based on the ideal gas law is then:

$$\begin{aligned} n_{\text{fuel}} &= (204 \text{ rods/assy})(32 \text{ assy})[(760 \times 1123/1000)/ (62.361 \times 273.15)] (2.2046\text{E-}3 \text{ lbm/g}) \\ &= 0.721 \text{ lbmoles} \end{aligned}$$

with R = 62.361 (mmHg-lit/gmoles-K)

Customer supplied data [29] states that the Westinghouse BPRA has the largest displacement volume and the most amount of free gas among the applicable BPRA types. The amount of free gas in each BPRA rod is 2.0E-4 lbmoles per Reference [29].

The amount of free gas in the BPRA rods is:

$$\begin{aligned} n_{\text{BPRA}} &= (2.0\text{E-}4 \text{ lbmole/rod})(20 \text{ rod/assy})(32 \text{ assy}) \\ &= 0.128 \text{ lbmoles} \end{aligned}$$

Total amount of free gas is:

$$n_{\text{free}} = n_{\text{fuel}} + n_{\text{BPRA}}$$

4.6.4 Total Amount of Gas within DSC

The total amount of gas within the DSC is equal to the amount of the initial helium backfill gas plus any free gases within the ruptured fuel assembly rods or BPRA. All free gases within the ruptured fuel rods/BPRAs will be released into the canister. It is assumed that the fractions of the ruptured BPRA rods are the same as those considered for the fuel rods, i.e., 1, 10, and 100% for normal, off-normal, and accident case respectively.

Total amount of free gas released to the DSC cavity is:

$$n_{\text{total}} = n_{\text{back}} + f_B (n_{\text{free}})$$

n_{total} = total amount of gas (lbmoles)
 f_B = fraction of the ruptured fuel rods

4.6.5 Maximum DSC Internal Pressures

Displacement volume of the BPRA is 480 in³ per Reference [29]. Maximum DSC internal pressures are determined via the ideal gas law:

$$P = (n_{\text{total}} R \bar{T}_{\text{DSC}}) / V$$

P = pressure (psia)
 V = Cavity volume = 178.3 (ft³) without BPRAs
 V = Cavity volume – BPRA volume = (308,146 – 32*480)/12³ = 169.4 (ft³) with BPRAs
 R = universal gas constant = 10.73 (psia-ft³/lbmoles-R)

The results are summarized in Table 4-10.

The temperature increase of 0.3% for transfer conditions discussed in Section 4.6.1 due to use of Al-6061 for rail inserts and back plates increases the DSC internal pressure by the same ratio according to the above equation. This small increase remains bounded by the design pressures in Table 4-10.

4.6.6 Maximum Pressure in Annulus

The pressure in the annulus between the transfer cask and the DSC is calculated using the ideal gas law:

$$P_{\text{ann}} = P_{\text{init}} \frac{T}{T_{\text{init}}}$$

P_{ann} = Annulus pressure (psia)
 P_{init} = initial pressure = 3.0 psig = 16.7 psia
 T = annulus average temperature (R)
 T_{init} = annulus initial temperature = 70°F = 530 R

Average annulus temperature is the volume average temperature of the annulus elements retrieved from the transfer cask model. The results are summarized below.

Transfer Condition	\bar{T}_{ann}	P_{ann}	P_{ann}
	(°F)	(psia)	(psig)
Normal and Off-Normal	349	27.0	12.3
Accident	682	38.1	23.4

4.7 Axial Decay Heat Profile

The normalized axial burnup profile for typical PWR fuels with burnups higher than 30 GWd/MTU from Reference [4] is shown below. An active fuel length of 144" is considered for the evaluation.

% of Core Height	Corresponding Length from Bottom of Active Fuel (in)	Peaking Factor	Area under the Profile
0.00	0.00	0	
2.78	4.00	0.652	1.31
8.33	12.00	0.967	6.47
13.89	20.00	1.074	8.17
19.44	27.99	1.103	8.70
25.00	36.00	1.108	8.85
30.56	44.01	1.106	8.86
36.11	52.00	1.102	8.82
41.67	60.00	1.097	8.80
47.22	68.00	1.094	8.76
52.78	76.00	1.094	8.76
58.33	84.00	1.095	8.75
63.89	92.00	1.096	8.77
69.44	99.99	1.095	8.76
75.00	108.00	1.086	8.73
80.56	116.01	1.059	8.59
86.11	124.00	0.971	8.11
91.67	132.00	0.738	6.84
97.22	140.00	0.462	4.80
100.00	144.00	0	0.92
Sum			141.76
Average			0.984

The average value in the above table is the total area under the axial decay heat profile divided by the active fuel length. This value must be equal to 1. Since it differs from one, a correction factor of 1/0.984 is multiplied by the heat generating rate to avoid any degradation of the applied heat in the model.

14 axial fuel regions are defined for the fuel assembly in the finite element model. An average peaking factor is calculated for each region so that the resultant axial profile is identical to the profile resulted from the above table.

The average peaking factor of each fuel region is set equal to the area underneath the peaking factor curve divided by the height of the corresponding region. The area underneath the peaking factor curve is calculated as follows.

$$A_j = \sum_{i=1}^n \frac{(P_{i+1} + P_i)}{2(l_{i+1} - l_i)}$$

Where,

A_j = area underneath the profile in fuel region j

P_i = Local peaking factors at location i in fuel region j

l_i = Corresponding length to the local peaking factor P_i

Average peaking factor is:

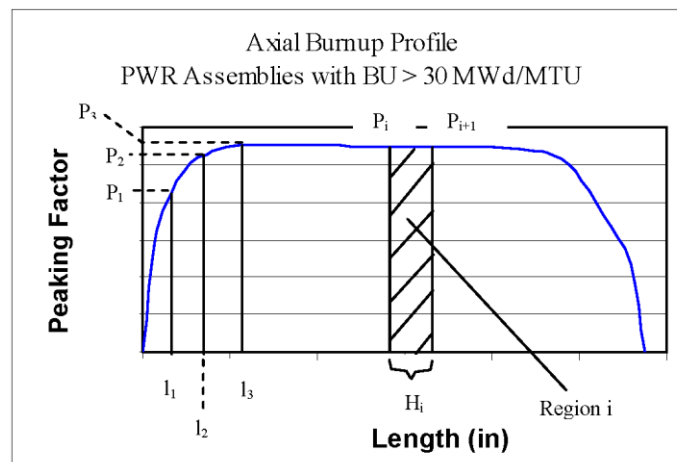
$$P_j = \frac{A_j}{H_j}$$

P_j = Average peaking factors of fuel region j

H_j = Height of fuel region i

The following Figure depicts this methodology. The resultant average peaking factors for active fuel length of 144" are listed in Table 4-11.

Calculation of the Average Peaking Factor



The height of each region is converted to the corresponding local coordination in the finite element model to apply the peaking factors in the model. The peaking factors applied in the model are listed below.

For WE and MK BW Fuel Assemblies (Active Fuel Length = 144")

Region No.	Height from bottom of active fuel		Z-axis in FEM		Peaking Factor
	from	To	from	to	
1	0	1.32	4	5.32	0.107
2	1.32	7.0675	5.32	11.0675	0.582
3	7.0675	14.5	11.0675	18.5	0.908
4	14.5	22.0675	18.5	26.0675	1.048
5	22.0675	37.0675	26.0675	41.0675	1.100
6	37.0675	57.69	41.0675	61.69	1.104
7	57.69	66.9425	61.69	70.9425	1.096
8	66.9425	82.0675	70.9425	86.0675	1.094
9	82.0675	97.0675	86.0675	101.0675	1.095
10	97.0675	111.9425	101.0675	115.9425	1.088
11	111.9425	121.26	115.9425	125.26	1.046
12	121.26	127.0675	125.26	131.0675	0.955
13	127.0675	136.26	131.0675	140.26	0.743
14	136.26	144	140.26	148	0.374

For CE 14x14 Fuel Assembly (Active Fuel Length =137")

Region No.	Height from bottom of active fuel		Z-axis in FEM		Peaking Factor
	from	To	from	to	
1	0	5.5	5.5	11.0675	0.441
2	5.5	11.0675	11.0675	18.5	0.874
3	11.0675	18.5	18.5	26.0675	1.041
4	18.5	26.0675	26.0675	41.0675	1.100
5	26.0675	41.0675	41.0675	61.69	1.103
6	41.0675	61.69	61.69	65.32	1.097
7	61.69	65.32	65.32	78.51	1.094
8	65.32	78.51	78.51	95.32	1.095
9	78.51	95.32	95.32	110.32	1.091
10	95.32	110.32	110.32	120	1.054
11	110.32	120	120	125.32	0.974
12	120	125.32	125.32	136.75	0.732
13	125.32	137	136.75	142.5	0.321

A comparison between the axial burnup profile from Reference [4] and the axial burnup profile used in the finite element model is shown in the Figure 4-39.

Figure 4-39 shows that the calculated axial profile perfectly matches the data from Reference [4] except for the very ends of the active fuel. The small discrepancy at the very ends is due to the size of the regions and has a minimum effect on the thermal evaluation.

4.8 Effective Fuel Properties

4.8.1 Discussion

The NUHOMS[®]-32PTH DSC finite element models simulate the effective thermal properties of the fuel with a homogenized material occupying the volume within the basket where the fuel assemblies are stored. Effective values for density, specific heat, and conductivity are determined for this homogenized material for use in the finite element models.

The 32PTH DSC is capable of handling a variety of spent PWR fuel assemblies. In order to determine conservative thermal properties of the homogenized fuel assembly, all of the PWR fuel assemblies types to be stored in the 32PTH DSC are studied. WE and MK BW fuel assemblies are considered in one category with active fuel length of 144". The lowest effective thermal conductivity, density, and specific heat of these studied fuel assembly groupings are selected to apply in the finite element model. Use of these properties would conservatively predict bounding maximum temperatures for the components of the NUHOMS[®]-32PTH DSC. The effective fuel properties for CE 14x14 assembly are considered separately since CE 14x14 assembly has a shorter active fuel length.

The characteristics of the fuel assemblies to be stored in the 32PTH DSC are listed in Table 4-12.

4.8.2 Summary of Material Properties

1. UO₂, Fuel Pellets

Conductivity and specific heat for fuel pellets are taken from [30] and listed below.

Temperature (°C)	k (cal/s-cm-°C) [30]	Temperature (°F)	K* (Btu/hr-in-°F)
25	0.025	77	0.503
100	0.021	212	0.423
200	0.018	392	0.362
300	0.015	572	0.302
500	0.0132	932	0.266
700	0.0123	1292	0.248
800	0.0124	1472	0.250

Temperature (°C)	C _p (cal/g-°C) [30]	Temperature (°F)	C _p (Btu/lbm-°F)
0	0.056	32	0.056
100	0.063	212	0.063
200	0.0675	392	0.068
400	0.0722	752	0.072
1200	0.079	2192	0.079

* See Section 4.8.6 for effect of irradiation on thermal conductivity of UO₂.

The density of fuel pellets (UO₂) is 10.96 g/cc = 0.396 lbm/in³ [30].

2. Zircaloy-4, Cladding

Table B-2.I of Reference [31] lists measured and calculated values of thermal conductivity for zircaloy-4 at various temperatures. The measured values used in this calculation are listed below.

Temperature (K)	k (W/m-K) [31]	Temperature (°F)	k (Btu/hr-in-°F)
373.2	13.6	212	0.655
473.2	14.3	392	0.689
573.2	15.2	572	0.732
673.2	16.4	752	0.790
773.2	18.0	932	0.867
873.2	20.1	1112	0.968

Table B-1.1 of [31] lists specific heat values for Zircaloy as a function of temperature.

Temperature (K)	C _p (J/kg-K) [31]	Temperature (°F)	C _p (Btu/lbm-°F)
300	281	80	0.067
400	302	260	0.072
640	331	692	0.079
1090	375	1502	0.090

The density of Zircaloy is $6.56 \text{ g/cm}^3 = 0.237 \text{ lbm/in}^3$, as defined in [30].

Table B-3.11 of [31] lists the measured emissivity values for fuel cladding. For ease of calculation a temperature independent emissivity of 0.8 is set for zircaloy4 in this calculation.

$$\epsilon_{\text{zirc}} = 0.80$$

3. Helium

Temperature (K)	Conductivity [5] (W/m-k)	Temperature (°F)	Conductivity (Btu/hr-in-°F)
200	0.1151	-100	0.0055
250	0.1338	-10	0.0064
300	0.150	80	0.0072
400	0.180	260	0.0087
500	0.211	440	0.0102
600	0.247	620	0.0119
800	0.307	980	0.0148
1000	0.363	1340	0.0175

4. Air at low pressure (0.1 bar)

Temperature (K)	Conductivity [5] (W/m-k)	Temperature (°F)	Conductivity (Btu/hr-in-°F)
200	0.0180	-100	0.0009
300	0.0263	80	0.0013
400	0.0336	260	0.0016
500	0.0403	440	0.0019
600	0.0466	620	0.0022
800	0.0577	980	0.0028
1000	0.0681	1340	0.0033

The air conductivity at low pressure is used to calculate the effective transverse conductivity for vacuum drying conditions. Air is not allowed for blowdown operations. Only helium is allowed. For conservatism, air conductivity is utilized in the calculational models (for 14 hours) for vacuum drying and transfer cask backfill operations.

5. Stainless Steel SA-240, Type 304

A stainless steel emissivity of 0.3, a value lower than the measured values from Reference [14] is used in the analysis for conservatism.

4.8.3 Effective Fuel Conductivity4.8.3.1 Transverse Effective Conductivity

The purpose of the effective conductivity in the transverse direction of a fuel assembly is to relate the temperature drop of a homogeneous heat generating square to the temperature drop across an actual assembly cross section for a given heat load. This relationship is established by the following equation obtained from Reference [32]:

$$k_{eff} = \frac{Q}{4L_a (T_c - T_o)} (0.29468)$$

where:

k_{eff} = Effective thermal conductivity (Btu/hr-in.-°F)

Q = Assembly head generation (Btu/hr)

Q_{react} = Reaction solution retrieved from quarter model (Btu/hr)

$$Q = 4 \times Q_{react} \times L_a \quad \text{for WE and MK BW assemblies with quarter symmetric models}$$

$$Q = Q_{react} \times L_a \quad \text{for CE 14x14 assembly with full-scale model}$$

Q_{react} = Reaction solution retrieved from the ANSYS model (Btu/hr-in)

L_a = Assembly active length (in.)

T_o = Maximum temperature (°F)

T_s = Surface temperature (°F)

Discrete finite element models of the fuel assemblies to be stored in the NUHOMS®-32PTH DSC are developed using the ANSYS computer code [16]. These two-dimensional models simulate heat transfer by radiation and conduction and include the geometry of the fuel rods and

fuel pellets. Helium or air properties are used as the fill gas in the fuel assembly. A fuel assembly decay heat load of 0.8 kW¹ is used for heat generation. An active length of 144" is assumed for WE and MK BW assemblies. The active fuel length of CE 14x14 assembly is considered to be 137".

For WE 15x15 and WE 17x17 class fuel assemblies containing ITTRs, the inserted ITTR in the instrument tube void will enhance heat transfer within the fuel assembly and are bounded by the values presented in Section 4.2.

The finite element models are used to calculate the maximum radial temperature difference with isothermal boundary conditions. All components are modeled using 2-D PLANE55 thermal solid elements. LINK32 elements are placed on the exteriors of the fuel assembly components to set up the creation of the radiation super-element. The compartment wall is modeled using LINK32 elements and used only to set up the surrounding surface for the creation of the radiation matrix super-element using the /AUX12 processor in ANSYS. All LINK32 elements are unselected prior to solution of the thermal problem. The thermal properties used in the model are described in Section 4.8.2, and the fuel assembly geometries are shown in Table 4-12. A typical ANSYS finite element model of fuel assemblies is shown in Figure 4-40 for fuel assemblies WE 17x17 and CE 14x14.

Several computational runs were made for each model using isothermal boundary temperatures ranging from 100 to 1000°F. In determining the temperature dependent effective conductivities of the fuel assemblies an average temperature, equal to $(T_o + T_s)/2$, is used for the fuel temperature. The transverse effective conductivity is calculated in helium for storage and transfer conditions. For vacuum drying conditions, the conductivity of helium is replaced by air conductivity at low pressure. The vacuum drying of the DSC generally does not reduce the pressure sufficiently to reduce the thermal conductivity of the water vapor and air in the DSC cavity [33]. Therefore, air conductivity at low pressures is assumed for the backfill gas for vacuum drying conditions and the effect of water vapor conductivity is neglected.

4.8.3.2 Axial Effective Conductivity

The backfill gas, fuel pellets, and zircaloy behave like resistors in parallel. However, due to the small conductivity of the fill gas and the axial gaps between fuel pellets, credit is only taken for the zircaloy in the determination of the axial effective conductivities.

$$k_{axial} = \frac{\text{cladding area}}{4a^2} \times \text{cladding conductivity}$$

with $a = \text{half of compartment width} = 8.7''/2 = 4.35''$

The insertion of ITTR in WE 15x15 and WE 17x17 class fuel assemblies does not affect the axial effective conductivities presented in Section 4.2 since only the fuel cladding material in the fuel assembly is considered in determining the axial effective conductivities.

4.8.4 Effective Fuel Density and Specific Heat

¹ 0.8 kW is the maximum decay heat load for the fuel assemblies in the center of the basket.

Volume average density and weight average specific heat are calculated to determine the effective density and specific heat for each fuel assembly type separately. The equations to determine the effective density and specific heat are shown below.

$$\rho_{eff} = \frac{\sum \rho_i V_i}{V_{assembly}} = \frac{\rho_{UO2} V_{UO2} + \rho_{Zr4} V_{Zr4}}{4a^2 L_a}$$

$$C_{p,eff} = \frac{\sum \rho_i V_i C_{Pi}}{\sum \rho_i V_i} = \frac{\rho_{UO2} V_{UO2} C_{p,UO2} + \rho_{Zr4} V_{Zr4} C_{p,Zr4}}{\rho_{UO2} V_{UO2} + \rho_{Zr4} V_{Zr4}}$$

4.8.5 Conclusion

The effective transverse conductivity values are plotted in Figure 4-41. Among WE and MK BW assemblies, fuel type WEO 17x17 has the lowest conductivity for the range of 100 to 700°F under helium atmosphere. For temperatures higher than 700°F, fuel assembly MK BW 17x17 has the lowest transverse conductivity. To bound the transverse effective conductivity, the lowest effective conductivity value in each temperature range is selected to apply in the thermal analysis. The effective transverse conductivity of CE 14x14 is used separately in a DSC model with 137" active fuel length.

The calculated transverse effective conductivities for vacuum drying conditions are plotted in Figure 4-42. As Figure 4-42 shows, fuel assembly MK BW 17x17 has the lowest conductivity for vacuum drying conditions, which are used in thermal analysis for vacuum conditions.

The axial effective conductivity for each fuel type is calculated using the equation from Section 4.8.3.2. The resultant values are listed in Table 4-13 and plotted in Figure 4-43. The lowest axial effective conductivity belongs to fuel type WE 15x15 among WE and MK BW assemblies. This value is used in all DSC models except for the DSC model containing CE 14x14 fuel assemblies. The latest model uses the CE 14x14 axial conductivity shown separately in Figure 4-43.

Effective density of each fuel type is calculated using the corresponding equation from Section 4.8.4. Since using the lowest density results in the highest cladding temperature for accident conditions, the density of fuel assembly WEO 17x17 is the bounding density. The calculated effective density values are listed in Table 4-13.

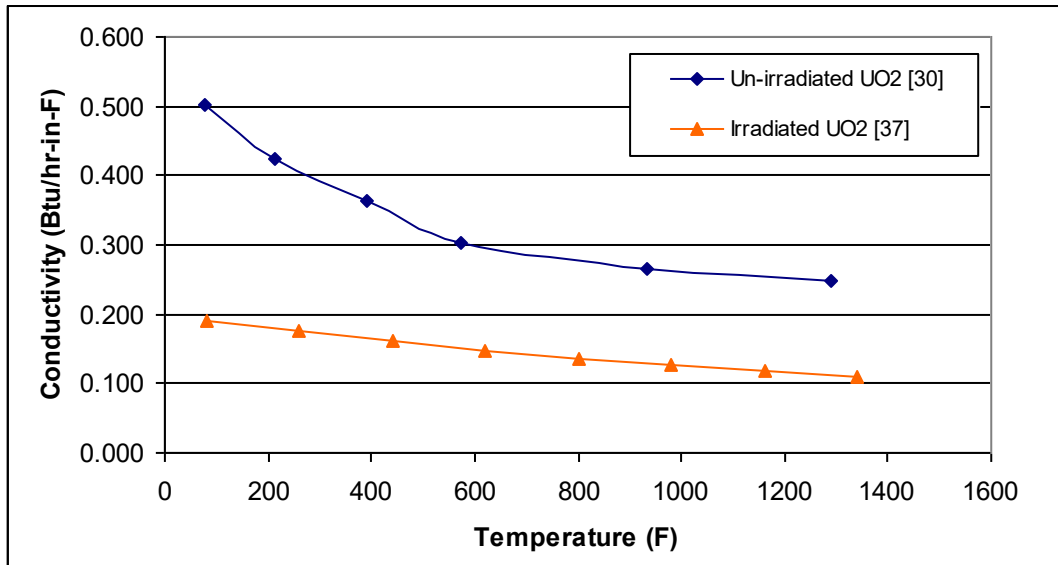
Effective specific heat values are calculated as a function of temperature using the corresponding equation from Section 4.8.4. Properties of fuel pellets and fuel cladding from Section 4.8.2 are linearly interpolated for this purpose. The lowest specific heat belongs to the fuel type WE 15x15 (and WES 15x15). Since the lowest specific heat results in the highest cladding temperature for transient calculations, specific heat of fuel type WE 15x15 (and WES 15x15) is selected for thermal analysis as the bounding property. The calculated effective specific heat values are listed in Table 4-13.

Since CE 14x14 fuel assembly is analyzed only for steady state transfer conditions, the effective density and the effective specific heat are not calculated for this fuel type.

The bounding effective fuel properties used in the finite element models for WE and MK BW assemblies are listed in Section 4.2.

4.8.6 Effect of Irradiation on UO₂ Thermal Conductivity

Based on Ronchi study [37], UO₂ thermal conductivity of irradiated UO₂ with ~62 GWd/t and irradiation temperature $T_{irr} \geq 1300K$ drops significantly (more than 50%) compared to un-irradiated UO₂. The thermal conductivity values of UO₂ in Section 4.8.2 [30] are compared to the values obtained from [37] study in the figure below.



Irradiated and Un-irradiated UO₂ Thermal Conductivity

The comparison shows that the [30] values in the fuel assembly temperature range of interest are higher by approximately a factor of two compared to values obtained from Ronchi study [37].

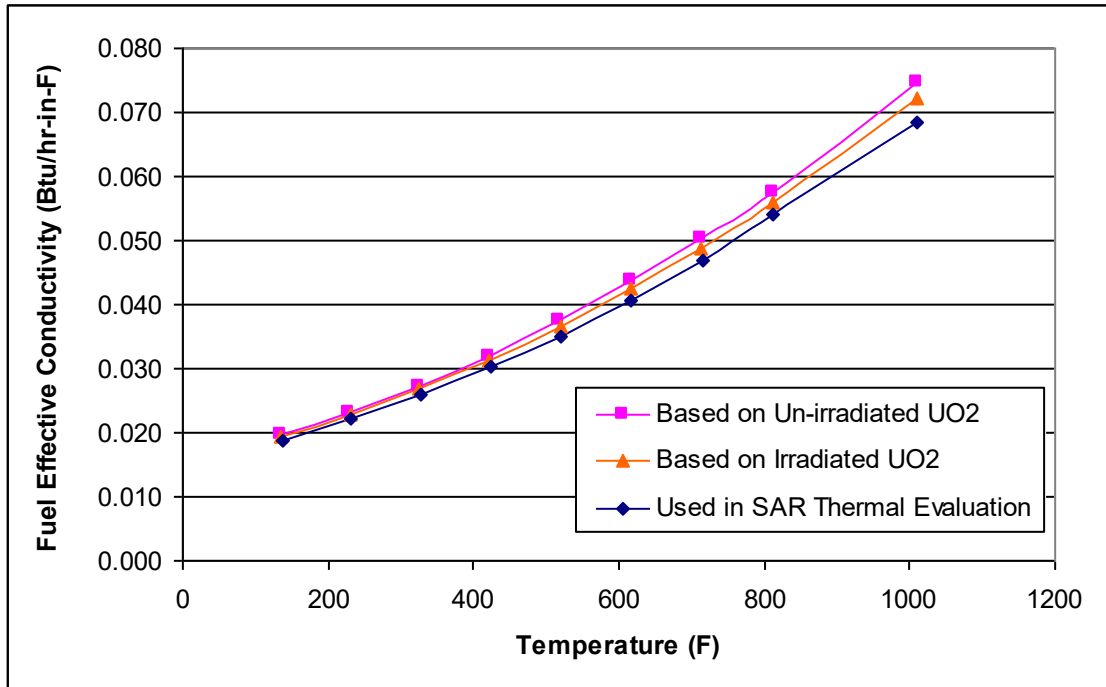
Using irradiated UO₂ conductivity decreases the effective conductivity of fuel assembly in transverse direction. Note that as discussed in Section 4.8.3.2, axial effective thermal conductivity of fuel assembly is calculated based on the fuel cladding material only and does not include the UO₂ fuel pellet thermal conductivity. Therefore, the axial effective conductivity of fuel assembly is not impacted.

A sensitivity analysis is performed to determine the impact of the irradiated UO₂ conductivity on the maximum fuel cladding temperatures. A sensitivity analysis includes two steps. In the first step, the transverse effective conductivity for fuel assemblies with irradiated and un-irradiated UO₂ conductivities are calculated based on the methodology described in Section 4.8.3.1.

In the second step, the calculated fuel assembly effective conductivities from the first step are used in the 32PTH DSC model from Section 4.3.1.3 to determine the maximum fuel cladding temperature. Normal transfer conditions for 32PTH DSC in OS187H transfer cask with heat load zoning configuration 1 at 115°F ambient is selected for this analysis.

The transverse effective conductivity for fuel assemblies calculated based on irradiated [37] and un-irradiated [30] UO₂ thermal conductivities are compared in the figure below. The transverse

effective conductivity for fuel assemblies used in the evaluation based on UO₂ properties used in the ANSYS model for fuel assembly effective conductivity calculation documented in the Section 4.2 (1) is also added to the figure below for reference.



Transverse Effective Conductivity for Fuel Assembly

As seen in the figure above, the fuel assembly effective thermal conductivity calculated with irradiated UO₂ conductivity is approximately 3% lower than the one calculated with un-irradiated UO₂ conductivity at the fuel cladding temperature of 700°F. The results of the sensitivity runs for the maximum fuel cladding temperature calculation using the DSC model from Section 4.3.1.3 are summarized in the table below.

Maximum Component Temperatures - Sensitivity Analysis
(32PTH DSC in OS187H, HLZC #1, 115°F Ambient)

Component	(1)	(2)
Fuel Cladding	716	717
Fuel Compartment	691	692
Basket Al Plates	691	691
Basket Rails	560	560
DSC Shell	475	475

Notes:

- (1) Effective conductivity for fuel assembly is based on un-irradiated UO₂ conductivity as shown in Section 4.2, subsection 1.
- (2) Effective conductivity for fuel assembly is based on irradiated UO₂ conductivity values from Ronchi study [37].

The sensitivity analysis results show that values for both cases are comparable to those shown in Table 4-1, 2nd Part for Config. # 1. It also shows that the maximum fuel cladding temperature changes by approximately 1°F (0.14%) which is negligible. These results show that the fuel cladding temperatures are not sensitive to change in UO₂ thermal conductivity due to irradiation. Therefore, use of UO₂ fuel pellets conductivity from [30] is reasonable for irradiated UO₂.

4.8.6.1 UO₂ Thermal Conductivity used in ANSYS Fuel Assembly Model

The ANSYS model described in Section 4.8.3.1 erroneously but conservatively used UO₂ conductivity values which are lower than those shown in Section 4.8.2 (1). A comparison of these values is shown in the table below.

UO₂ Thermal Conductivity

Section 4.8 (1)		Used in ANSYS Model Described in Section 4.8.3.1	
Temperature (°F)	k (Btu/hr-in-°F)	Temperature (°F)	k (Btu/hr-in-°F)
77	0.503	32	0.056
212	0.423	212	0.063
392	0.362	392	0.068
572	0.302	752	0.072
932	0.266		
1292	0.248		
1472	0.250		

As seen from the table above, the UO₂ conductivity values used in the ANSYS model are at least 30% lower than the values obtained from Ronchi study [37]. Use of lower UO₂ thermal conductivity values in the ANSYS model of the fuel assembly results in conservatively lower values of effective thermal conductivity for fuel assembly. This in turn results in higher calculated fuel cladding and DSC component temperatures which are conservative. The transverse effective thermal conductivity for fuel assembly used in the thermal analysis is compared to the corresponding values from sensitivity analysis in the second figure in Section 4.8.6.

Since the effective thermal conductivity for fuel assembly used in thermal analyses of this SAR is lower than the effective thermal conductivity for fuel assembly with irradiated UO₂, the calculated maximum component temperatures are conservative and the difference in irradiated and un-irradiated UO₂ fuel pellet thermal conductivity values does not affect thermal analysis results reported in this SAR.

4.9 Effective Conductivity of Fluids in the Transfer Cask

4.9.1 Effective Conductivity in the Shielding Panel

Heat transfer in the shielding panel occurs by conduction and convection through the fluid (water) contained in the shielding. The shielding panel consists of 16 cylindrical segments. Each segment can be considered as two concentric, horizontal cylinders. The following correlation from [5] is used to calculate the free convection coefficient for water within each of the panel segments.

$$k_{con} = Nu \ k_w$$

k_{con} = effective conductivity for conduction and convection from inner to outer cylinder

k_w = conductivity of water

$$Nu = [Nu_{COND}, Nu_l]_{\max}$$

$$Nu_{COND} = \frac{\ln(D_o / D_i)}{\cosh^{-1} \left[\left((D_o^2 + D_i^2 - 4E^2) / 2D_o D_i \right) \right]} \quad \text{conduction}$$

$$Nu_l = 0.603 \bar{C}_l \frac{\ln(D_o / D_i) Ra^{1/4}}{\left[(L / D_i)^{3/5} + (L / D_o)^{3/5} \right]^{5/4}} \quad \text{laminar flow}$$

where,

$$Ra = \frac{g\beta(T_i - T_o)L^3}{\nu^2} \times Pr \quad \text{with} \quad L = (D_o - D_i)/2 \quad \text{and}$$

$$\bar{C}_l = \frac{0.503}{\left[1 + (0.492 / Pr)^{1/6} \right]^{4/9}}$$

All water properties are evaluated at average temperature:

$$T_{avg} = (T_o + T_i) / 2$$

T_o = average temperature of the outer cylinder

T_i = average temperature of the inner cylinder

Diameter of the inner cylinder is 81.7", and diameter of outer cylinder is 91.825". The average inner and outer temperatures are initially unknown. Iterative solution of the ANSYS [16] model combined with the above correlations determines the inner and outer temperatures, and the effective conductivity. The iteration continues until the difference between the applied coefficient in the ANSYS model and the calculated coefficient is less than 5% for the off-normal conditions at 115°F ambient. To ease the analysis, this criterion is increased to 10% for the off-normal conditions at -20°F ambient, which is less sensitive for thermal evaluations.

Water properties are reported in Section 4.2. The calculated effective conductivity values and their verifications are shown in the Table 4-14 and Table 4-15 for normal and off-normal transfer conditions.

The same methodology as described above is used to calculate the effective conductivity of liquid neutron shield during the burning period of fire accident case

The calculated values are listed in Table 4-16. These values are bounded by a value of 2.25 Btu/hr-in-F used in the thermal analysis to maximize the fire heat flux toward the interior of the transfer cask

It is assumed that water in the shielding panel evaporates completely subsequent to the hypothetical fire accident. Heat transfer in the empty (filled with air) shielding panel occurs by conduction, convection, and radiation through air during the cool-down period. Conduction and convection are combined together using the same methodology described above, with the exception that the water properties are replaced with the air properties from Section 4.2.

Radiation between two concentric, horizontal cylinders can be described as follows [5].

$$q_r = \frac{\sigma A_1 (T_1^4 - T_2^4)}{\frac{1}{\varepsilon_1} + \frac{A_1}{A_2} \left(\frac{1}{\varepsilon_2} - 1 \right)} \quad (4.9-1)$$

Where

q_r = radiation heat transfer rate (Btu/hr)

σ = Stefan-Boltzmann constant = 0.1714×10^{-8} (Btu/hr-ft²-R⁴)

A_1 = area of the inner surface = $\pi D_1 L$ (ft²)

A_2 = area of the outer surface = $\pi D_2 L$ (ft²)

ε_1 = emissivity of the inner surface = 0.46 for stainless steel [Section 4.2]

ε_2 = emissivity of the outer surface = 0.46 for stainless steel [Section 4.2]

T_1 = temperature of the inner surface (R)

T_2 = temperature of the outer surface (R)

Conduction in cylindrical shells is [5]:

$$q_{cond} = \frac{2\pi k L (T_1 - T_2)}{\ln \left(\frac{D_2}{D_1} \right)} \quad (4.9-2)$$

Comparing equation (4.9-1) with equation (4.9-2) gives the equation for effective radiation conductivity:

$$k_r = \frac{\sigma D_1}{2 \left[\frac{1}{\varepsilon_1} + \left(\frac{D_1}{D_2} \right) \left(\frac{1}{\varepsilon_2} - 1 \right) \right]} \cdot \frac{(T_1^4 - T_2^4)}{(T_1 - T_2)} \cdot \ln \left(\frac{D_2}{D_1} \right) \quad (4.9-3)$$

Adding k_r to k_{con} results in the total effective conductivity for the air inside the shielding panel. The total effective conductivity values are calculated iteratively using the results of the ANSYS model. The final results are shown in Table 4-17. This table shows that the effective conductivity values applied in the ANSYS model deviates less than 10% from the final calculated values. The applied effective conductivities are lower than the calculated values. The applied effective conductivities are therefore conservative regarding the fuel cladding temperature.

4.9.2 Effective Water Conductivity in Annulus between TC and DSC

At the beginning of the vacuum process, the annulus between the transfer cask and the DSC is filled with fresh water. During vacuum drying, the DSC and the transfer cask remain in vertical position. Due to the large size of the DSC outer diameter and transfer cask inner diameter, the curvature effects are minimal and the convection in the annulus can be approximated as convection in a vertical rectangular cavity. Reference [5] introduces the following correlations to calculate the combination of the convection and conduction heat transfer in vertical rectangular cavities.

For $Pr \approx 0.7$ (4.9-4)

$$Nu = [Nu_{ct}, Nu_l, Nu_t]_{\max}$$

where

$$Nu_{ct} = \left[1 + \left\{ \frac{0.104 Ra^{0.293}}{1 + (6310 / Ra)^{1.36}} \right\}^3 \right]^{1/3}$$

$$Nu_l = 0.242 \left(\frac{Ra L}{H} \right)^{0.273}$$

$$Nu_t = 0.0605 Ra^{1/3}$$

For $Pr \geq 4$ (4.9-5)

If $Ra (H/L)^3 < 4 \times 10^{12}$ then

$$Nu = \left[1, 0.36 Pr^{0.051} \left(\frac{L}{H} \right)^{0.36} Ra^{0.25}, 0.084 Pr^{0.051} \left(\frac{L}{H} \right)^{0.1} Ra^{0.3} \right]_{\max}$$

and for $Ra (H/L)^3 > 4 \times 10^{12}$

$$Nu = 0.039 Ra^{1/3}$$

with

$$Ra = \frac{g \beta (T_h - T_c) \Pr}{\nu^2}$$

Since the Pr number of water in the annulus is between 0.7 and 4.0, the Nu is calculated as the linear interpolation between Nu numbers from correlations (4.9-4) and (4.9-5). The combined convection and conduction heat transfer can be expressed as an effective conductivity as defined in [5]. The effective conductivity of water in annulus is:

$$k_{eff} = Nu k_w$$

k_{eff} = effective conductivity of water in the annulus

Nu = calculated Nusselt number

k_w = water conductivity

All water properties are considered at average water temperature. The thermal properties of water are listed in Section 4.2.

The temperature difference between hot and cold surfaces is initially unknown. The k_{eff} value is calculated iteratively and verified after solving the model. For the first hour of simulation, the k_{eff} value is set equal to the water conductivity (k_w) for conservatism. To verify the applied values in the model, k_{eff} is calculated based on the average hot and cold surface temperatures of the annulus retrieved from the results of the model as shown in the first part of Table 4-18. The applied k_{eff} values are lower than all the calculated values for the entire simulation time, as shown in the second part of Table 4-18.

Using lower effective conductivities for water in annulus is conservative, since lower effective conductivity values result in higher fuel cladding temperature for the vacuum drying analysis.

4.10 Justification of the Assumed Hot Gap Sizes

4.10.1 Radial Gap between Basket Rails and DSC shell

The radial cold gap between the rails and the 32PTH DSC shell is 0.125". The nominal DSC inner diameter is 68.75". This gives a nominal basket outer diameter of 68.5". The diameters of the basket and the DSC shell can be calculated after the thermal equilibrium using the following equation:

$$D_{hot} = D_{cold} (1 + \alpha (T_{avg} - 70)) \quad (4.10-1)$$

α = mean coefficient of thermal expansion

T_{avg} = average component temperature

To calculate the average basket temperature only stainless steel components of the basket are considered. Adequate gaps exist between the aluminum plates and the stainless steel structure of the basket to avoid deformation. The size of the radial, hot gap can be calculated as follows:

$$\text{Hot gap} = (D_{i, \text{DSC, hot}} - D_{o, \text{basket, hot}})/2$$

The maximum and minimum temperatures are taken from result files of the DSC model (Section 4.3) at hottest ($71.067 \leq Z \leq 86.067$) and coolest ($4.0 \leq Z \leq 20.32$) sections for 115°F ambient during transfer operation. The calculated hot dimensions are listed below.

Hottest Cross Section	Cold Dimension	T_{max}	T_{min}	T_{avg}	Material	α^1	Hot Dimension
	(in)	(°F)	(°F)	(°F)	---	(in/in-°F)	(in)
$D_{o, \text{basket}}$	68.50	693	345	519	SA 240, type 304	9.738×10^{-6}	68.800
$D_{i, \text{DSC}}$	68.75	474	339	407	SA 240, type 304	9.514×10^{-6}	68.970
Radial Gap	0.125	---	---	---	---	---	0.085

Coolest Cross Section	Cold Dimension	T_{max}	T_{min}	T_{avg}	Material	α^{10}	Hot Dimension
	(in)	(°F)	(°F)	(°F)	---	(in/in-°F)	(in)
$D_{o, \text{basket}}$	68.50	611	303	457	SA 240, type 304	9.614×10^{-6}	68.755
$D_{i, \text{DSC}}$	68.75	452	271	362	SA 240, type 304	9.224×10^{-6}	68.935
Radial Gap	0.125	---	---	---	---	---	0.090

A radial, hot gap of 0.1" is considered in the model. This assumption is conservative, since the average gaps calculated in the above table are smaller than the assumed gap.

¹ Interpolated from values in Reference [6]

4.10.2 Radial Gap between Lead and the Cask Structural Shell

A 0.030" radial air gap is assumed between the lead and the TC structural shell in the finite element model described in Section 4.3.1.1. This air gap might occur due to different thermal expansion factors of stainless steel lead after the lead is poured.

The following assumptions are made for the verification of the lead gap:

1. The TC body has nominal dimension at 70°F.
2. During the lead pour the cask body and lead are at 620°F.
3. The inner diameter of the gamma shell (lead) is equal to the outer diameter of the inner cask shell at thermal equilibrium.

The average coefficients of thermal expansion for SA-240, type 304 stainless steel are:

Temperature (°F) [6]	α (in/in-°F) [6]
70	8.5×10^{-6}
100	8.6×10^{-6}
150	8.8×10^{-6}
200	8.9×10^{-6}
250	9.1×10^{-6}
300	9.2×10^{-6}
350	9.3×10^{-6}
400	9.5×10^{-6}
450	9.6×10^{-6}
500	9.7×10^{-6}
550	9.8×10^{-6}
600	9.8×10^{-6}
650	9.9×10^{-6}

The density of lead as a function of temperature is found below.

Temperature (K) [5]	Density (kg/m ³) [5]	Temperature (°F)	Density (lbm/in ³)
50	11,570	-370	0.4180
100	11,520	-280	0.4162
150	11,470	-190	0.4144
200	11,430	-100	0.4129
250	11,380	-10	0.4111
300	11,330	80	0.4093
400	11,230	260	0.4057
500	11,130	440	0.4021
600	11,010	620	0.3978

The volume within the "lead cavity" is found by determining the stainless steel body dimensions at 620°F. Since no gaps will be present between the molten lead and the stainless steel body, this volume is equal to the volume of lead at 620°F. The mass of the lead filled the lead cavity at 620°F is then determined.

Maximum cask inner shell temperature is 340°F during normal condition of transfer (see Table 4-1). The dimensions of the "lead cavity" at 340°F are determined using similar equations to equation (4.10-1). From the mass of the lead, the lead volume is determined using the lead density at 340°F. Conservatively assuming the maximum possible axial length for the lead, the lead volume is used to determine the maximum size of the air gap adjacent to the lead.

Determination of Lead Mass

$$\alpha = 9.84 \times 10^{-6} \text{ in/in-}^\circ\text{F @ } 620^\circ\text{F (via linear interpolation for SA240, type 304)}$$

$$R_{in} = \text{inner radius of lead cavity} = 35.75"$$

$$R_{out} = \text{outer radius of lead cavity} = 39.35"$$

$$L = \text{length of lead cavity} = 179.1"$$

$$R_{in, 620} = (R_{in})(1+(\alpha)(\Delta T)) = (35.75)(1+(9.84\text{E-}6)(620-70)) = 35.9438"$$

$$R_{out, 620} = (R_{out})(1+(\alpha)(\Delta T)) = (39.35)(1+(9.84\text{E-}6)(620-70)) = 39.5630"$$

$$L_{620} = (L)(1+(\alpha)(\Delta T)) = (179.1)(1+(9.84\text{E-}6)(620-70)) = 180.0693"$$

$$V_{cavity} = V_{lead} = (\pi)(R_{out,620}^2 - R_{in,620}^2)(L_{620}) = 154,603.8 \text{ in}^3$$

$$M_{lead} = (V_{lead})(\rho_{lead}) = (154,603.8 \text{ in}^3)(0.3978 \text{ lbm/in}^3) = 61,501.4 \text{ lbm}$$

Lead gap determination

$$\rho_{lead} = 0.4037 \text{ lbm/in}^3 \text{ at } 340^\circ\text{F, via linear interpolation}$$

$$R_{in, ss, 340} = (R_{in})(1+(\alpha)(\Delta T)) = (35.75)(1+(9.28\text{E-}6)(340-70)) = 35.8396"$$

$$R_{out, ss, 340} = (R_{out})(1+(\alpha)(\Delta T)) = (39.35)(1+(9.28\text{E-}6)(340-70)) = 39.4486"$$

$$L_{ss, 340} = (L)(1+(\alpha)(\Delta T)) = (179.1)(1+(9.28\text{E-}6)(340-70)) = 179.5487"$$

$$V_{lead, 340} = M_{lead} / \rho_{lead} = 61,501.4 / 0.4037 = 152,344.3 \text{ in}^3$$

Since $R_{in,ss,340} = R_{in,lead,340}$, then :

$$V_{lead,340} = (\pi)(R_{out, lead,340}^2 - R_{in, ss, 340}^2)(L_{ss, 340})$$

It gives:

$$R_{out,lead,340} = 39.4279"$$

The difference between the cavity outer radius and the lead outer radius gives the maximum radial gap size.

$$\text{Air gap} = R_{out,ss,340} - R_{out, lead,340} = 0.021"$$

The assumed air gap of 0.03" is conservative to maximize the DSC shell temperature.

4.11 Heat Transfer Coefficients

4.11.1 Total heat Transfer Coefficient to Ambient

The outer surfaces of the transfer cask or the HSM-H dissipate heat to the ambient via free convection and radiation. Total heat transfer coefficient is defined as:

$$H_t = h_r + h_c$$

where,

h_r = radiation heat transfer coefficient

h_c = free convection heat transfer coefficient

The radiation heat transfer coefficient, h_r , is given by the equation:

$$h_r = \varepsilon F_{12} \left[\frac{\sigma(T_1^4 - T_2^4)}{T_1 - T_2} \right] \text{ Btu/hr} \cdot \text{ft}^2 \cdot ^\circ\text{F}$$

where,

ε = surface emissivity

F_{12} = view factor from surface 1 to ambient

$\sigma = 0.1714 \times 10^{-8} \text{ Btu/hr} \cdot \text{ft}^2 \cdot \text{R}^4$

T_1 = surface temperature, R

T_2 = ambient temperature, R

The free convection coefficients are calculated based on the surface shape and position in Section 4.11.2. The above correlations are incorporated in ANSYS [16] model via macros “HTOT_VPL.mac” and “HTOT_HCL.mac” for the transfer cask and “HC_ROOF.mac” and “HC_FRONT.mac” for the HSM-H model. Air properties reported in Section 4.2 are used in these macros. The macros are listed in Appendix 4.16.1.

The free convection heat transfer at the outer surface of the transfer cask is replaced with forced convection to analyze the fire accident case. A forced convection value of $4.5 \text{ Btu/hr} \cdot \text{ft}^2 \cdot \text{F}$ is considered during the burning time from Reference [23]. The calculated total heat transfer coefficients for the outer cask surfaces during the fire are listed in the Table 4-19.

4.11.2 Free Convection Coefficients

The free convection coefficients are calculated based on the shape and position of the convective surface using correlations from Reference [5]. The convection correlations are described in the following sections.

4.11.2.1 Horizontal Cylinder

$$Ra = Gr \text{ Pr} \quad ; \quad Gr = \frac{g \beta (T_w - T_\infty) D^3}{\nu^2}$$

$$Nu_l = \frac{2f}{\ln(1 + 2f / Nu^T)} \quad \text{Nusselt number for laminar flow with}$$

$$Nu^T = 0.772 \bar{C}_l Ra^{1/4}, \quad f = 1 - \frac{0.13}{(Nu^T)^{0.16}}, \quad \text{and } \bar{C}_l = 0.515 \text{ for gases [5]}$$

$$Nu_t = \bar{C}_l Ra^{1/3} \quad \text{Nusselt number for turbulent flow}$$

$$\bar{C}_l = 0.103 \quad \text{for horizontal cylinders [34]}$$

$$Nu = \left[(Nu_l)^m + (Nu_t)^m \right]^{1/m} \quad \text{with } m = 3.3 \text{ for } 10^{-10} < Ra < 10^{10}$$

$$h_c = \frac{Nu k}{D} \text{ with}$$

D = diameter of the horizontal cylinder

k = air conductivity

The above correlations are incorporated in ANSYS [16] model via macro "HC_HCL.mac" listed in Appendix 4.16.1.

4.11.2.2 Vertical Flat Plate

$$Ra = Gr Pr \quad ; \quad Gr = \frac{g \beta (T_w - T_\infty) L^3}{\nu^2}$$

$$Nu_l = \frac{2.8}{\ln(1 + 2.8 / Nu^T)} \quad \text{Nusselt number for laminar flow with}$$

$$Nu^T = \bar{C}_l Ra^{1/4}, \quad \bar{C}_l = 0.515 \quad \text{for gases [5]}$$

$$Nu_t = C_l^V Ra^{1/3} \quad \text{Nusselt number for turbulent flow with}$$

$$C_l^V = \frac{0.13 Pr^{0.22}}{(1 + 0.61 Pr^{0.81})^{0.42}}$$

$$Nu = \left[(Nu_l)^m + (Nu_t)^m \right]^{1/m} \quad \text{with } m = 6 \text{ for } 1 < Ra < 10^{12}$$

$$h_c = \frac{Nu k}{L} \text{ with}$$

L = height of the vertical surface

k = air conductivity

The above correlations are incorporated in ANSYS [16] model via macro "HC_VPL.mac" in Appendix 4.16.1.

4.11.2.3 Horizontal Flat Plate Facing Upwards

$$Ra = Gr Pr \quad ; \quad Gr = \frac{g \beta (T_w - T_\infty) L^3}{\nu^2}$$

$$Nu_l = \frac{1.4}{\ln(1 + 1.4 / Nu^T)} \quad \text{Nusselt number for laminar flow with}$$

$$Nu^T = 0.835 \bar{C}_l Ra^{1/4} \quad , \quad \text{and } \bar{C}_l = 0.515 \quad \text{for gases [5]}$$

$$Nu_t = C_t^H Ra^{1/3} \quad \text{Nusselt number for turbulent flow with}$$

$$C_t^H \approx 0.14 \quad \text{for } Pr < 100 \quad [5]$$

$$Nu = \left[(Nu_l)^m + (Nu_t)^m \right]^{1/m} \quad \text{with } m = 10 \quad \text{for } Ra > 1$$

$$h_c = \frac{Nu \, k}{L} \quad \text{with}$$

$$L = A/P$$

A=surface area of heated surface

P= perimeter of the heated surface

k = air conductivity

The above correlations are incorporated in ANSYS [16] model via macro "HC_HPLU.mac" in Appendix 4.16.1.

4.11.2.4 Horizontal Flat Plate Facing Downwards

$$Ra = Gr \, Pr \quad ; \quad Gr = \frac{g \, \beta (T_w - T_\infty) L^3}{\nu^2}$$

$$Nu_l = \frac{0.527 Ra^{1/5}}{[1 + (1.9/Pr)^{9/10}]^{2/9}} \quad \text{for laminar flow}$$

$$Nu = Nu_l$$

$$h_c = \frac{Nu \, k}{L} \quad \text{with}$$

$$L = A/P$$

A=surface area of heated surface

P= perimeter of the heated surface

k = air conductivity

The above correlations are incorporated in ANSYS [16] model via macro "HC_HPLD.mac" in Appendix 4.16.1.

4.11.2.5 Inclined Flat Plate, Positive Angled

Reference [5] gives the following correlations for free convection over inclined flat, plates. The angle of inclined surface is measured from vertical line. The positive or negative sign of the angle is defined in the following figure.

$$Ra = Gr \, Pr \quad ; \quad Gr = \frac{g \, \beta (T_w - T_\infty) L^3}{\nu^2} \cos \phi$$

$$Nu_l = \frac{2.8}{\ln(1 + 2.8/Nu^T)} \quad \text{Nusselt number for laminar flow with}$$

$$Nu^T = \bar{C}_l Ra^{1/4} \quad , \quad \bar{C}_l = 0.515 \quad \text{for gases [5]}$$

$$Nu_t = C_t^H Ra^{1/3} \quad \text{Nusselt number for turbulent flow with}$$

$$C_t = C_t^V \cos^{1/3} \phi \quad \text{for} \quad -90^\circ \leq \phi \leq \tan^{-1} \left(\frac{C_t^V}{C_t^H} \right)^3$$

$$C_t = C_t^H \sin^{1/3} \phi \quad \text{for} \quad \tan^{-1} \left(\frac{C_t^V}{C_t^H} \right)^3 \leq \phi \leq 90^\circ$$

with

$$C_t^V \approx \frac{0.13 \text{Pr}^{0.22}}{(1 + 0.61 \text{Pr}^{0.81})^{0.42}}$$

$$C_t^H \approx 0.14 \quad \text{for} \quad \text{Pr} < 100$$

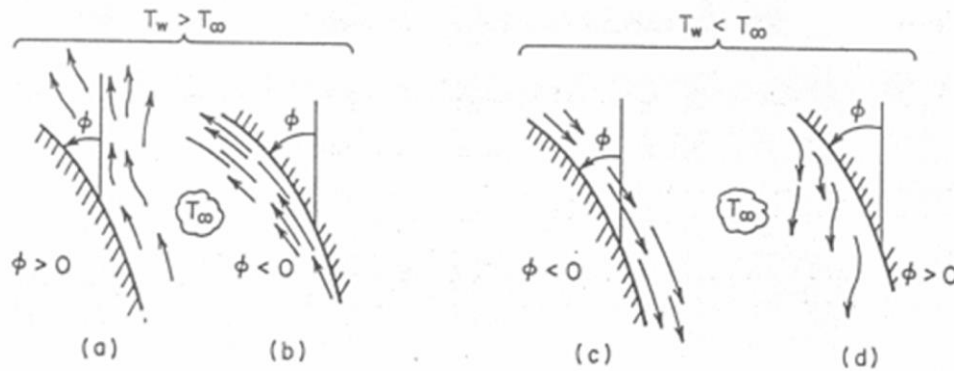
$$Nu = \left[(Nu_l)^m + (Nu_t)^m \right]^{1/m} \quad \text{with} \quad m = 6 \quad \text{for} \quad 1 < Ra < 10^{12}$$

$$h_c = \frac{Nu \, k}{L} \quad \text{with}$$

L = length of the inclined plate

k = air conductivity

The above correlations are incorporated in ANSYS [16] model via macros "HC_IPLU.mac" and "HCIPLUm.mac" listed in Appendix 4.16.1.



Definition of surface angle ϕ for a heated wall (a and b), and a cooled wall (c and d). If the flow is turbulent, a and d depict detached flow, b and c attached flow.

4.11.2.6 Inclined Flat Plate, Negative Angled

$$Ra = Gr \, \text{Pr} \quad ; \quad Gr = \frac{g \beta (T_w - T_\infty) L^3}{\nu^2} \times \cos \phi$$

$$Nu_{l,v} = \frac{2.8}{\ln(1 + 2.8 / Nu^T)}$$

$$Nu^T = \bar{C}_l \, Ra^{1/4} \quad , \quad \bar{C}_l = 0.515 \quad \text{for gases [5]}$$

$$Nu_{l,H} = \frac{0.527 Ra^{1/5}}{[1 + (1.9 / Pr)^{9/10}]^{2/9}}$$

$$Nu_l = \max[Nu_{l,V}, Nu_{l,H}] \quad \text{Nusselt number for laminar flow}$$

$$Nu_t = C_t Ra^{1/3} \quad \text{Nusselt number for turbulent flow with}$$

$$C_t = C_t^V \cos^{1/3} \phi \quad \text{for} \quad -90^\circ \leq \phi \leq \tan^{-1} \left(\frac{C_t^V}{C_t^H} \right)^3$$

$$C_t = C_t^H \sin^{1/3} \phi \quad \text{for} \quad \tan^{-1} \left(\frac{C_t^V}{C_t^H} \right)^3 \leq \phi \leq 90^\circ$$

$$\text{with} \quad C_t^V \approx \frac{0.13 Pr^{0.22}}{(1 + 0.61 Pr^{0.81})^{0.42}}$$

$$C_t^H \approx 0.14 \quad \text{for} \quad Pr < 100$$

$$Nu = [(Nu_l)^m + (Nu_t)^m]^{1/m} \quad \text{with} \quad m = 6 \quad \text{for} \quad 1 < Ra < 10^{12}$$

$$h_c = \frac{Nu k}{L} \quad \text{with}$$

L = length of the inclined plate

k = air conductivity

The above correlations are incorporated in ANSYS [16] model via macro "HC_IPLD.mac" listed in Appendix 4.16.1.

4.11.2.7 Convection Coefficient for the Louvered Top Heat Shield

The louvered top shield consists of six pieces each containing 70 inclined plates. Because of the relatively large opening between the plates and their short length, the interference of the thermal boundary layers is minimal, so that a convection coefficient can be calculated separately for each plate as follows.

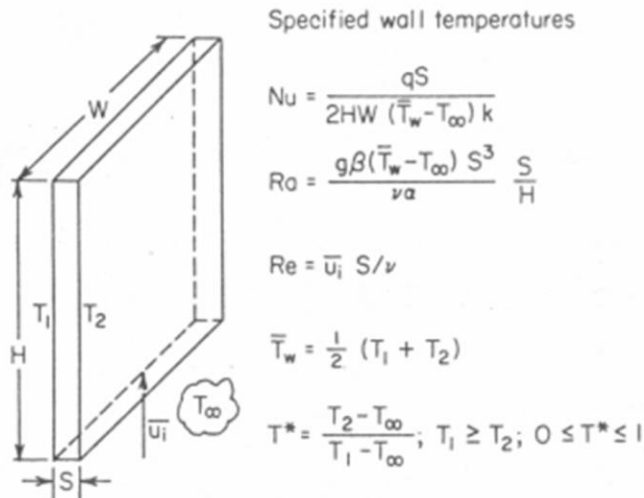
h_{up} = convection coefficient on upper surface of louver plates (positive angled)

h_{down} = convection coefficient on lower surface of louver plates (negative angled)

h_{up} and h_{down} are calculated using the correlations described in Sections 4.11.2.5 and 4.11.2.6 for inclined plates. The above correlations are incorporated in ANSYS [16] model via macro "HC_LL.mac" listed in Appendix 4.16.1.

4.11.2.8 Effective convection Coefficient for Side Heat Shield with Fins

Cross section of the side heat shield shows that the fin width, W , is much larger than the distance between the parallel fin plates, S . Reference [5] states that when $W/S \geq 5$, the convection coefficient through the fins is the same as for the parallel-plate channel shown below.



Geometry and nomenclature for natural-convection heat transfer from a wide ($W \gg S$), rectangular cooling slot with temperature-specified conditions on the walls.

The following correlations for parallel-plate channels are specified in Reference [5], when $W/S \geq 5$.

$$W=2.5'', S=0.5''$$

$$Nu \approx \frac{Ra}{24} \quad \text{for } Ra \leq 10$$

$$Nu = 0.62 Ra^{1/4} \quad \text{for } 10 < Ra < 1000$$

$$Nu = \left[\left(\frac{Ra}{24} \right)^m + \left(0.62 Ra^{1/4} \right)^m \right]^{1/m} \quad \text{with } m=-1.9 \quad \text{for } Ra < 10^5$$

Rayleigh number for the above correlations is defined in above figure. Since the average plate temperature is first unknown, the model is solved iteratively. The final results are:

For off-normal conditions (115°F maximum day temperature):

Average side heat shield temperature = 164°F (retrieved from HSM-H model results)

Average air temperature within HSM = 136°F (Section 4.13)

For off-normal conditions (-20°F minimum temperature):

Average side heat shield temperature = 22°F (retrieved from HSM-H model results)

Average air temperature within the HSM = 3.2°F (Section 4.13)

T _w	T _{amb}	T _{avg}	T _{avg}	k [5]	β	ν [5]	Pr [5]	C _l	Ra	Nu	h _{fin}
(°F)	(°F)	(°F)	(K)	(W/m-K)	(1/K)	(m ² /s)	(---)	(---)	(---)	(---)	(Btu/hr-in ² -°F)
164	136	150	339	0.029	2.95E-03	2.000E-05	0.70	0.514	40.5	1.56	0.0044
22	3.2	13	263	0.023	3.81E-03	1.282E-05	0.72	0.516	87.6	1.90	0.0042

The fins are modeled as a flat plat to reduce the number of SHELL57 elements in creation of radiation super-element. To compensate for the reduced area, an effective convection coefficient is calculated for the fins.

$$h_{fin,eff} = h_{fin} \cdot \frac{A_{fins}}{A_{model}}$$

$$A_{fin} = (2 n_{up} \times 4 + 2 n_{down}) H W$$

$$\text{number of fins at upper half: } n_{up} = (15'2'' - 4'') / (0.5'' + 0.125'') + 1 = 285 \quad [2]$$

$$\text{number of fins at lower half: } n_{down} = (15'2'' - 44'') / (0.5'' + 0.125'') + 1 = 221 \quad [2]$$

$$H = 20''$$

$$W = 2.5''$$

$$A_{fin} = 136100 \quad \text{in}^2$$

$$A_{model} = [15'2'' \times 7'2'' + 1'10'' \times (15'2'' - 2 \times 1'8'')] = 18776 \quad \text{in}^2$$

$$h_{fin,eff} = 0.0044 \cdot \frac{136100}{18776} = 0.032 \quad \text{Btu/hr-in-}^\circ\text{F} \quad \text{for } 115^\circ\text{F ambient}$$

$$h_{fin,eff} = 0.0042 \cdot \frac{136100}{18776} = 0.031 \quad \text{Btu/hr-in-}^\circ\text{F} \quad \text{for } -20^\circ\text{F ambient}$$

The h_{fin} value used in the HSM-H model is 0.030 Btu/hr-in-°F.

Distance between the base plate of the side heat shield and the HSM-H side wall is 2''. The base plate and the HSM-H side wall create a narrow channel behind the side heat shield. The convection coefficient for this narrow channel is calculated using the same methodology described above. The dimensions of the narrow channel behind the side heat shield used to calculate the convection coefficient are:

$$S = 2''$$

$$H = 108''$$

$$W = 182''$$

The final surface temperature of the narrow channel is verified after iterative solution of the model. The final results are:

For off-normal conditions (115°F maximum day temperature):

Average nodal temperature of narrow channel = 154°F (retrieved from model results HSM-H)

Entering air temperature into channel = 110°F (Section 4.13)

For off-Normal conditions (-20°F minimum day temperature):

Average nodal temperature of narrow channel = 12.8°F (retrieved from HSM-H model results)

Entering air temperature into channel = -17°F (Section 4.13)

T_w	T_{amb}	T_{avg}	T_{avg}	k [5]	β	ν [5]	Pr [5]	C_l	Ra	Nu	$h_{channel}$
(°F)	(°F)	(°F)	(K)	(W/m-K)	(1/K)	(m ² /s)	(---)	(---)	(---)	(---)	(Btu/hr-in ² -°F)
154	110	132	329	0.028	3.04E-03	1.90E-05	0.70	0.514	3468	4.75	0.003
12.8	-17	-2	254	0.023	3.93E-03	1.21E-05	0.72	0.516	7600	5.79	0.003

The $h_{channel}$ value used in the HSM-H model is 0.003 Btu/hr-in-°F.

4.12 Effective Conductivity of Air in Closed Cavity of HSM-H

When the inlet and outlet vents are blocked, the air surrounding the DSC in the HSM-H cavity is trapped. The temperature difference between the DSC surface and the cooler surrounding surfaces of the concrete and heat shield results in closed cavity convection. However, closed cavity convection during the blockage of the vents is conservatively ignored. The blocked vent thermal analysis considers only the thermal conductivity of air for evaluation of the HSM-H accident conditions.

4.13 Thermal-Hydraulic Equations for the HSM-H

Energy and hydraulic equations are combined together to calculate the exit air temperatures in the HSM-H cavity. For this purpose, it is assumed that the total decay heat load will be transferred out of the HSM-H only by free convection to the air flowing through the cavity. Since the thermal conduction through the concrete structure is minimal, this assumption is conservative.

The air flow paths inside the HSM-H are designed, so that the pressure difference due to buoyancy effects is greater than the pressure losses due to friction, area, and flow direction changes. The pressure difference due to buoyancy effect (stack pressure) is driven by the density differences between indoor and outdoor air and is given by:

$$\Delta P_s = \left(\frac{g}{g_c}\right)(\rho_c - \rho_s)(\Delta h) = \left(\frac{g}{g_c}\right)(\Delta \rho)(\Delta h)$$

where:

ΔP_s = stack pressure
 ρ_c = ambient air density
 ρ_s = stack average air density
 g = local gravity
 g_c = universal gravitational constant
 Δh = HSM-H cavity height

The expansion coefficient is defined as follows:

$$\beta = \frac{-1}{\rho} \left(\frac{\partial \rho}{\partial T} \right)_p \rightarrow \frac{\Delta \rho}{\rho_s} = \beta \cdot \Delta T_{avg}$$

where:

$\Delta T_{avg} = (T_s - T_c)$
 T_c = ambient air temperature (absolute temperature)
 T_s = stack average air temperature (absolute temperature)
 ρ_s = air density at stack average temperature T_s

Considering air as an ideal gas the expansion coefficient is defined:

$$\beta = \frac{1}{T}$$

Then it follows:

$$\frac{\Delta \rho}{\rho_s} = \frac{\Delta T_{avg}}{T_s}$$

Substituting the above equation into stack pressure equation gives:

$$\Delta P_s = \frac{g}{g_c} \cdot \frac{\rho_s}{T_s} \cdot \Delta T_{avg} \cdot \Delta h$$

The dynamic pressure loss is given by:

$$\Delta P_{loss} = \sum \left(K \cdot \frac{1}{2} \cdot \rho \cdot \frac{V^2}{g_c} \right) = \sum \left(K_{Ei} \cdot \frac{1}{2} \cdot \frac{1}{gc \cdot \bar{\rho}} \cdot \frac{\dot{m}_{Ei}^2}{A_{Ei}^2} \right)$$

where:

ΔP_{loss} = dynamic pressure loss
 \dot{m}_{Ei} = air mass flow rate

K_{Ei} = dynamic loss coefficient through a specific flow path

A_{Ei} = cross sectional flow area

$\bar{\rho}$ = average density for the flow path

If the air mass flow rate is equal for all paths, then:

$$\Delta P_{loss} = \frac{\dot{m}_E^2}{2g_c \cdot \bar{\rho}} \sum \frac{K_{Ei}}{A_{Ei}^2} \quad \text{with } \bar{\rho} = (\rho_c + \rho_{exit})/2$$

The energy balance requires:

$$Q = \dot{m}_E C_p (T_{exit} - T_c) = \dot{m}_E C_p \Delta T_{HSM-H}$$

with Q = total decay heat load

Setting ΔP_s equal to ΔP_{loss} , substituting \dot{m}_E from energy balance, and solving for ΔT_{HSM-H} gives:

$$\Delta T_{HSM-H} = \left[\frac{T_s Q^2}{2 \rho_s \bar{\rho} g \Delta h C_p^2 \Delta T_{avg}} \cdot \sum \frac{K_{Ei}}{A_{Ei}^2} \right]^{1/2}$$

The dynamic loss coefficients (K_{Ei}) depend on the air velocity (air mass flow rate) and the flow path shape. Iterative solution of the above equation using dynamic loss coefficient correlations gives the ΔT_{HSM-H} and the T_{exit} . Schematic views of flow paths through the HSM-H module are shown in Figure 4-44.

The stack average air temperature (T_s) in the above equation is considered as the volumetric average temperature within the HSM-H cavity. The following equation determines the stack average temperature.

$$T_s = \frac{\sum_0^i (T_i \cdot V_i)}{\sum_0^i (V_i)}$$

V_i = Volume of air region = $A_i \cdot L_{DSC}$

A_i = (HSM-H cavity cross sectional area) – (DSC cross sectional area)

Length of the air region is set equal to the overall DSC length (185.25”).

The average bulk temperature (T_{mean}) is calculated as follows to use for the convection boundary conditions within the HSM-H cavity.

$$T_{\text{mean}} = (T_c + T_{\text{exit}})/2$$

The HSM-H is divided into three following sections to calculate the dynamic loss coefficients.

- 1: from air entrance opening to the inlet vent at the lower part of the HSM-H sidewall
- 2: HSM-H cavity from inlet opening to outlet opening
- 3: from outlet opening at the upper part of the HSM-H sidewall to the exhaust opening on the roof.

Each section is divided into subsections. Hydraulic loss coefficients in subsections are calculated using corresponding correlations from [35] and [36]. Serial loss coefficients of subsections are

added together to make the equivalent total loss coefficient ($\sum \frac{K_{Ei}}{A_{Ei}^2}$). For calculation of the

equivalent loss coefficient for parallel flow paths see footnote on Table 4-21. Table 4-21 summarizes the results for 34.8 kW decay heat load for both HSM-H with louvered top heat shield and finned aluminum side heat shields and for HSM-H with flat stainless steel top and side heat shields. The results for 32.0 kW and 26.1 kW decay heat loads are listed in Table 4-22 and Table 4-23, respectively.

4.14 Thermal Evaluation of DSC Containing Damaged Fuel

Maximum 16 damaged fuel assemblies can be stored in the basket of the NUHOMS[®]-32PTH DSC. Damaged fuel is defined as fuel assemblies with one or more non-adjacent damaged grid spacer(s) and /or containing fuel rods with known or suspected cladding defects greater than hairline cracks or pinhole leaks. Missing cladding and/or crack size in the fuel pins is to be limited such that a fuel pellet is not able to pass through the gap created by the cladding opening during handling. Retrievability of the damaged fuel must be assured following normal and off-normal conditions.

Location of the damaged fuel assemblies in the 32PTH DSC basket is shown in Figure 4-46. To ensure the retrievability of the fuels, the maximum cladding temperature of the intact fuel rods must remain below the allowable temperature limits established in [2].

Thermal analyses of the 32PTH DSC for normal and off-normal conditions (Section 4.3) show that the fuel cladding temperature has the highest value during transfer operation. For the accident conditions also, the maximum fuel temperature is resulted for transfer operation (Section 4.4). Hence, transfer conditions are considered to evaluate the effects of the damaged fuel assemblies on the thermal performance of NUHOMS-32PTH System.

4.14.1 Normal / Off-Normal Conditions

The 32PTH DSC model described in Section 4.3 is used for this evaluation. Loading configuration 1 and maximum heat load of 34.8 kW are considered to analyze the transfer operation with 16 damaged fuel assemblies in the DSC. Identical decay heat profiles from Section 4.7 are considered for both the damaged and the intact fuel assemblies for this analysis. Due to these conditions, the heat flux on the transfer cask inner shell remains unchanged in comparison to values discussed in Section 4.3. Therefore, the DSC shell temperatures resulted from the transfer cask model in Section 4.3 is applicable to the DSC model containing 16 damaged fuel assemblies.

Transverse effective conductivity for the damaged fuel is discussed in Section 4.14.3. To bound the reduction in axial conductivity of damaged fuel due to the cladding defects, the axial effective conductivity of the fuel calculated in Section 4.8 is decreased by 10% to use for the damaged fuel elements. All other material properties remain the same as those described in Section 4.3. The model is run steady state to determine the maximum temperature of the intact fuel.

4.14.2 Accident Conditions

Due to presence of damaged fuel assemblies, an extra hypothetical accident case is considered for evaluation. Although unlikely, but it is postulated that the defected cladding of damaged fuel assemblies might break entirely in consequence of a drop accident. In that event, the fuel pellets could be released in the compartment space. The end caps will hold the fuel rubble within the compartment volume, though the decay heat profile is changed subsequently.

The concentration of the decay heat for the rubble fuels is maximized, when the rubble is compressed to a minimum height at one end of the fuel compartment.

To bound the maximum cladding temperature of the intact fuel assemblies, it is assumed that all the 16 damaged fuel assemblies transform to rubble. The cladding is considered as powder but the pellets are assumed to keep their shape in the rubble. An approximate void volume between the pellets can be evaluated considering the area ratio of the pellet cross-section to the square area with a width equal to the pellet outer diameter. The increased volume due to the void spaces between pellets is then:

$$\{(\text{OD}_{\text{pellet}}^2 - \pi \text{OD}_{\text{pellet}}^2 / 4) / (\pi \text{OD}_{\text{pellet}}^2 / 4)\} \times 100 = (4/\pi - 1) \times 100 = 27.32 \%$$

The minimum height of the fuel rubble is calculated as follows.

$$H_{\min} = \frac{V_{\text{UO}_2} \times 1.2732 + V_{\text{Zr}_4}}{A}$$

where

A = cross-sectional area of the fuel compartment = $8.7 \times 8.7 = 75.69 \text{ in}^2$

V_{UO_2} = volume of fuel pellets from Section 4.8

V_{Zr_4} = volume of fuel cladding from Section 4.8

Table 4-24 summarizes the calculation of H_{\min} for all the fuel types. The shortest height of 61” is used for the fuel rubble.

The thermal model of the transfer cask described in Section 4.3 is modified for the purpose of the evaluation. It is assumed that the seals of the transfer cask and the shielding shell will be damaged as a consequence of the hypothetical drop accident. In this event, the helium in the annulus and the water in the shielding shell will be released to the ambient. To evaluate the thermal effects of this accident, the transfer cask model developed in Section 4.3 is used to determine the DSC shell temperature when the DSC contains fuel rubble. Helium conductivity in the annulus is replaced with air conductivity. The effective conductivity in the shielding panel is also recalculated based on air properties.

To stabilize the ANSYS run and shorten the run time, the LINK31 elements simulating the radiation between the DSC and transfer cask are replaced with equivalent effective conductivity. Calculations of the effective conductivities for air in annulus and in the shielding shell are based on the methodologies described in Section 4.9. The equivalency of the applied effective conductivities to the radiation elements (LINK31) is verified by hand comparison of the maximum temperatures resulting from separate runs of the transfer cask slice model using LINK31 elements and equivalent effective conductivities.

Steady state boundary conditions are used to run the transfer cask model. Total heat load of 34.8 kW is applied uniformly on the DSC inner radial surface. The resultant DSC shell temperatures are transferred then to the DSC model to determine the maximum fuel temperature for this accident case.

The 32PTH DSC model described in Section 4.3 is also slightly modified to include the fuel rubble. The height of the elements in the core compartments are adjusted, so that a region with the height of 61" (H_{min}) is created. This region is assigned as fuel rubble region. All the elements beyond the fuel rubble region, which previously represented homogenized fuel within the core compartments, are deleted. The decay heat load of the damaged fuel assemblies are applied as a uniform heat generation rate without peaking factor to the elements in the fuel rubble region. Thermal properties of helium are considered for the elements representing the fuel rubble to eliminate the uncertainties regarding the fuel rubble conductivity. The decay heat profile from Section 4.7 is considered for the intact fuels in the peripheral compartments for this analysis. The DSC model is run steady state to determine the maximum component temperatures.

Except for those mentioned above, the geometry and material properties of all the other elements in the DSC and the transfer cask models remain unchanged.

In the drop accident case considered above, it was assumed that the liquid neutron shield and the helium in the transfer cask were lost. Since the 15 min fire has only a short term effect on the neutron shield panel as shown in Figure 4-29, and the transfer cask and the DSC models are run steady state, the drop accident case bounds the fire accident case temperatures.

4.14.3 Effective Properties of Damaged Fuel

Defected spacer or grids might change the fuel rod pitch and hence change the effective fuel conductivity. It is assumed that the fuel rods in the assembly with defected grids can move in axial and in transverse directions. The axial moving of the fuel rods has no impact on the thermal conductivity in either direction. To determine the impact of the transverse moving on the fuel effective conductivity, the fuel assemblies WEO 17x17 and Framatome MK BW 17x17 are investigated. The reason to investigate these assemblies is that the intact assembly WEO 17x17 has the lowest transverse conductivity in temperature range from 100 to 700°F and the intact assembly MK BW 17x17 has the lowest transverse conductivity for temperatures higher than 700°F as shown in Section 4.8.

For the investigation, the effective transverse fuel conductivity is determined using the same methodology described in Section 4.8.

The effect of the transverse moving of the fuel rods is investigated by changing the pitch size of the fuel rods. The pitch size is changed from the minimum closest packed pitch to the maximum most spread out pitch. A 0.01" gap has been added to the minimum and maximum pitch to account for contact resistance. Typical finite element models of reconfigured fuel assemblies are shown in Figure 4-47.

Each pitch is evaluated for two different compartment wall temperatures and then the average conductivity is determined. Compartment wall temperatures of 200°F and 300°F are considered for various pitch sizes of WEO 17x17 assembly. For MK BW 17x17 assembly, compartment wall temperatures of 700°F and 800°F are considered. The effective transverse conductivities are interpolated to average temperatures of 300°F for WEO 17x17 and 800°F for MK BW 17x17.

The results of the investigation are summarized in Table 4-25 and plotted in Figure 4-48. As Figure 4-48 shows, the minimum transverse conductivities occur at a pitch sizes of 0.387" for WEO 17x17 and 0.402" for MK BW 17x17.

Finite element models of WEO 17x17 and MK BW 17x17 with minimum conductivity pitch sizes are created to determine the minimum effective transverse conductivity of reconfigured fuel for the temperature range of 100 to 1000°F. The results are listed in Table 4-26 and plotted in Figure 4-49. WEO 17x17 assembly provides lower transverse conductivities for the entire temperature range. Following values calculated for reconfigured WEO 17x17 are used in the model for the effective transverse conductivity of damaged fuel.

Temperature (°F)	Transverse Effective Conductivity (Btu/hr-in-°F)
150	0.0138
243	0.0161
337	0.0187
432	0.0217
527	0.0252
624	0.0290
721	0.0331
818	0.0376
916	0.0426
1014	0.0481

Reconfiguration of the fuel rods as a consequence of damaged grids does not have any impact on the other effective fuel properties such as density, specific heat, and axial conductivity.

4.14.4 Evaluation of DSC Thermal Performance with Damaged Fuel

To establish the heat removal capability and the integrity of the intact fuel cladding, maximum fuel cladding temperature limit of 752°F is considered for normal / off-normal transfer conditions [2]. For the accident conditions, a maximum fuel cladding temperature limit of 1058°F is considered [2].

Temperature distributions for the normal / off-normal, and accident cases are shown in Figure 4-50 and Figure 4-51. A comparison between the maximum component temperatures resulted for a DSC with 32 intact fuel assemblies and a DSC with 16 damaged fuel assemblies are shown in Table 4-27.

As Table 4-27 shows, the maximum fuel cladding temperature remains below the allowable limit for the DSC containing 16 damaged fuel assemblies. The basket temperature increases only by 3°F for this case. Regarding the margin to the allowable limit this temperature increase is not significant. Similar behavior is expected for storage conditions.

The maximum temperature of intact fuels, when the damaged fuel is transformed to rubble in consequence of an accident is lower than the maximum fuel temperature resulted from fire accident case with 32 intact fuel assemblies.

Due to the increased fuel and basket temperatures during transfer of damaged fuel, the inner DSC pressure increases in comparison to transfer of 32 intact fuel assemblies. Using the same methodology as described in Section 4.6, the internal pressure of DSC containing damaged fuels is calculated. The results of pressure calculation are shown in Table 4-28. As Table 4-28 shows, the DSC pressure increase due to transfer of damaged fuels is minimal (about 0.1 psi). Similar behavior is expected to occur for the normal / off-normal storage conditions.

Table 4-27 shows that the maximum fuel and basket temperatures drop when the damaged fuel is transformed to rubble in consequence of an accident. Therefore, the 32PTH DSC inner pressure in this case is bounded by the pressure calculated for the fire accident case in Section 4.6.

4.15 References

1. Cogema Logistics, Personnel Communication.
2. USNRC, SFPO, Interim Staff Guidance – 11, Rev. 3, “Cladding Considerations for the Transportation and Storage of Spent Fuel.”
3. Perry, R. H., Chilton, C. H., “Chemical Engineers’ Handbook,” 5th Edition, 1973.
4. USDOE, “Topical Report on Actinide-Only Burnup Credit for PWR Spent Nuclear Fuel Packages,” Department of Energy, Report No. DOE / RW0472, Rev. 2, 1998.
5. Rohsenow, W. M., Hartnett, J. P., Ganic, E. N. , “Handbook of Heat Transfer Fundamentals,” 2nd Edition, 1985.
6. ASME Boiler and Pressure Vessel Code, Section II, Part D, “Material Properties,” 1998 and 2000 addenda.
7. Issard, Herve, “ACL Progress on Boralyn Development,” Cogema Logistics presented in “Transnuclear Group Technical Exchange Meeting,” October 11, 2002.
8. Final Documentation Package TN-68, P.O. # EP-2001-022, Section G, “Thermal Conductivity Measurements of Borated Aluminum Specimens,” Rev. 0.
9. AAR Brooks & Perkins Advanced Structures Division, “Boral® The Neutron Absorber – Product Performance,” Report 624.
10. Zoldners, N. G., “Thermal Properties of Concrete under Sustained Elevated Temperatures,” ACI Publications, Paper SP 25-1, American Concrete Institute, Detroit, MI, 1970.
11. Cavanaugh, Kevin, “Guide to Thermal Properties of Concrete and Masonry Systems,” Reported by ACI Committee 122, Report # ACI 122R-02, American Concrete Institute, Detroit, MI, 2002.
12. Bentz, D. P., “A Computer Model to Predict the Surface Temperature and Time-of-wetness of Concrete Pavements and Bridge Decks,” Report # NISTIR 6551, National Institute of Standards and Technology, 2000.
13. Siegel, Robert, Howell, R. H., “Thermal Radiation Heat Transfer,” 4th Edition, 2002.
14. Azzazy Technology Inc., “Emissivity Measurements of 304 Stainless Steel,” Report Number ATI-2000-09-601, 2000.
15. Kreith, Frank, “Principles of Heat Transfer,” 3rd Edition, 1973.
16. ANSYS Computer Code and User’s Manuals, Rev. 6.0.
17. USNRC, Code of Federal Regulations, Part 71, “Packaging and Transportation of Radioactive Material,” 2003.
18. “ASHRAE Handbook Fundamentals,” 4th Edition, 1983.
19. Updated Final Safety Analysis Report, Standardized NUHOMS® Horizontal Modular Storage System for Irradiated Nuclear Fuel, Rev. 9, Feb. 2006.
20. Viebrock, J. M., Douglas, H. M., “Domestic Light Water Reactor Fuel Design Evolution,” Vol. III, Nuclear Assurance Corporation, 1981.
21. American Concrete Institute, “Code Requirements for Nuclear Safety Related Concrete Structures (ACI 349-97) and Commentary (ACI 349R-97),” 1997.
22. USNRC, SFPO, NUREG-1536, “Standard Review Plan for Dry Cask Storage Systems - Final Report,” 1997.
23. Gregory, J. J., Mata, R., Keltner, N. R., “Thermal Measurements in a Series of Long Pool Fires,” SANDIA Report, SAND 85-0196, TTC-0659, 1987.
24. Parker O-Ring Handbook, 5700, Y2000 Edition, 1999.

25. Transnuclear, Inc., “Thermal Testing of the NUHOMS[®] Horizontal Storage Module, Model HSM-H,” Doc. No. E-21625, Rev. 1.
26. Chun, R., Witte, M., Schwartz, M., “Dynamic Impact Effects on Spent Fuel Assemblies,” Lawrence Livermore National Laboratory, Report UCID-21246, 1987.
27. Young, W. C., “Roark’s Formulas for Stress and Strain,” 6th Edition, 1989.
28. Plannel, et al., “Extended Fuel Burnup Demonstration Program – Topical Report – Transport Considerations for Transnuclear Casks,” DOE/ET 34014-11, TN-E4226, Transnuclear, Inc. 1983.
29. Brookmire, et al., “Storage of Burnable Poison Rod Assemblies and Thimble Plug Devices in Dry Storage Casks Surry ISFSI,” NE-1162, Rev. 0, 1998.
30. Oak Ridge National Laboratory, RSIC Computer Code Collection, “SCALE, A Modular Code System for Performing Standardized Computer Analysis for Licensing Evaluation for Workstations and Personal Computers,” NUREG/CR-0200, Rev. 6, ORNL/NUREG/CSD-2/V3/R6.
31. USNRC, SFPO, NUREG/CR-0497, “A Handbook of Materials Properties for Use in the Analysis of Light Water Reactor Fuel Rod Behavior,” MATPRO - Version 11, EG&G Idaho, Inc., TREE-1280, 1979.
32. SANDIA Report, SAND90-2406, “A Method for Determining the Spent Fuel Contribution to Transport Cask Containment Requirements,” 1992.
33. Dament, R.M.E., “Thermal and Acoustic Insulation,” 1986.
34. Kreith, Frank, “The CRC Handbook of Thermal Engineering,” 2000.
35. “ASHRAE Handbook, Fundamentals,” – SI Edition, 1997.
36. I.E. Idelchik, “Handbook of Hydraulic Resistance,” 3rd Edition, 1994.
37. C. Ronchi, M. Sheindlin, D. Staicu, M. Kinoshita, Effect of Burn-up on the Thermal Conductivity of Uranium Dioxide up to 1000.000 MWdt⁻¹, Journal of Nuclear Materials, 327 (2004), 58 – 76.

4.16 Appendices

The ANSYS [16] macros for:

- Calculation of heat transfer coefficients,
- Creation of the radiation LINK31 elements between the DSC shell and the transfer cask inner shell, and
- Transferring of the nodal temperatures from the transfer cask or the HSM-H model to the DSC model

are listed in Appendix 4.16.1.

The calculation of the heat generation rates as a function of fuel parameters is shown in Appendix 4.16.2.

The addition of CE 16x16 fuel assemblies is presented in Appendix 4.16.3.

The effect of change in minimum off-normal ambient temperature to 21 °F is presented in Appendix 4.16.4.

The effect of dose reduction hardware on the HSM-H airflow is discussed in Appendix 4.16.5.

Table 4-1
Maximum Component Temperatures during Transfer Operations at 115°F ambient

Component	Maximum Temperature 34.8 kW (°F)	Allowable Maximum Temperature (°F)
DSC shell	475	
Cask inner shell	340	
Lead gamma shielding	337	621 [3]
Cask structural shell	280	
Neutron shield panel	263	
Cask lid inner plate ¹	275	
Cask lid outer plate	217	
Solid neutron shield	265	300 [1]
Cask lid seal ²	240	400 [24]
Bottom plate seal ³	255	400 [24]
Liquid neutron shield (Bulk temperature) ⁴	265	286.9 ⁵
Liquid neutron shield (Maximum temperature)	275	

	Maximum Temperature (°F) 34.8 kW							Allowable Max. Temp. (°F)
Basket Type	Type I					Type II		
Component	Conf. #1	Conf. #1A[¶]	Conf. # 2	Conf. # 3	Conf. # 4	⁶	⁷	
Fuel cladding	719	726	705	700	715	723	727	752 [2]
Fuel compartment	693	700	667	673	689	697	700	
Basket Al plates	692	699	666	672	688	696	699	
Basket rails	561	561	559	559	558	561	565	

	Maximum Temperature (°F) 33.8 kW for CE 14x14 Fuel Assembly		Allowable Max. Temp. (°F)
Basket Type	Type I		
Component	Configuration # 6	Configuration # 7	
Fuel cladding	717	712	752 [2]
Fuel compartment	689	685	
Basket Al plates	689	684	
Basket rails	555	552	
DSC Shell	467	467	

¹ Temperatures of cask lid, solid neutron absorber, and seals are from the transfer cask sub-models.

² Maximum temperature of cask body at seal location

³ Maximum temperature of ram access ring at seal location

⁴ Bulk temperature is the volumetric average temperature of the elements in shielding segments 8 and 9, see Figure 4-2.

⁵ 286.9°F is the saturated water temperature at 40 psig.

[¶] Conf. 1 with MMC thermal conductivity of 190 W/m-K

⁶ Conf. #1 with Al-1100 for rail inserts and back-plates

⁷ Conf. #1 with Al-6061 for rail inserts and back-plates

Table 4-2
Maximum Component Temperatures for Storage Conditions at 115°F ambient

HSM-H with Finned Aluminum Side Heat Shields		
Component	Maximum Temperature @ 34.8 kW (°F)	Allowable Max. Temp. (°F)
Fuel cladding	684 ¹	752 [2] ²
Fuel compartment	656	
Basket Al plates	655	
Basket rails	511	
DSC shell	407	
Concrete structure	213	300 ³
Top heat shield	199	
Side heat shield	188	
DSC supporting structure	268	

	Flat Stainless Side Heat Shields @ 34.8 kW	Un-finned Aluminum Side Heat Shields @ 32.0 kW	Un-finned Galvanized Steel Side Heat Shields @ 26.1 kW	
Component	Maximum Temperature (°F)	Maximum Temperature (°F)	Maximum Temperature (°F)	Allowable Max. Temp. (°F)
Fuel cladding	⁴	[§]	[§]	752 [2]
DSC shell	420	394	368	
Concrete structure	248	219	213	300
Top heat shield	245	196	186	
Side heat shield	239	241	190	
DSC supporting structure	311	264	247	

¹ The fuel cladding temperature is calculated based on bounding DSC shell temperatures with the maximum temperature of 422°F.

² The ambient temperature of 115°F is the maximum off-normal temperature. Based on Reference [2], maximum allowable fuel cladding temperature is 1058°F (570°C) for off-normal storage conditions and 752°F (400°C) for normal storage conditions. The maximum fuel cladding temperatures in Table 4-2 are all below 752°F.

³ The cement type and concrete aggregates satisfy the guidelines in NUREG 1536, Section V.2 [22]

⁴ Bounded by 34.8 kW case in the upper part of the table

Table 4-3
Maximum Component Temperatures during Transfer Operations
at -20°F ambient

Component	Maximum Temperature (°F)
Fuel cladding	650
Fuel compartment	620
Basket Al plates	619
Basket rails	487
DSC shell	398
Cask inner shell	249
Lead gamma shielding	245
Cask structural shell	178
Neutron shield panel	157
Cask lid inner plate	76
Cask lid outer plate	65
Solid neutron shield	97
Cask lid seal	88
Cask bottom plate seal	70
Liquid neutron shield (Bulk temperature)	162
Liquid neutron shield (Maximum temperature)	172

Table 4-4
Maximum Component Temperatures for Storage Conditions
at -20°F ambient, 34.8 kW

Component	Maximum Temperature (°F) (Finned Aluminum Side Heat Shields)	Maximum Temperature (°F) (Flat Stainless Steel Side Heat Shields)
Fuel cladding ¹	596	²
Fuel compartment	565	†
Basket Al plates	564	†
Basket rails	418	†
DSC shell	292	306
Concrete structure	49	117
Top heat shield	50	91
Side heat shield	41	85
DSC supporting structure	135	183

¹ The fuel cladding temperature is calculated based on bounding DSC shell temperatures with the maximum temperature of 319°F

² Bounded by the values for HSM-H with finned aluminum side heat shields since the maximum DSC shell temperature is lower than 319°F.

Table 4-5
Maximum Component Temperatures for Fire Accident Case
Transfer Cask, 34.8 kW

Component	Maximum Temperature (°F)	Time (hr)	Allowable Max. Temp. (°F)
Fuel cladding	1036	200	1058 [2]
Basket Al plates	1021	200	
Basket rails	878	200	
DSC shell	790	200	
Gamma shell (lead)	618	200	
Cask structural shell	553	200	
Shielding shell	598	0.25	

Table 4-6
Maximum Component Temperatures for Blocked Vent Accident Case

	HSM-H with Finned Aluminum Side Heat Shields, 34.8 kW	HSM-H with Flat Stainless Steel Heat Shields, 34.8 kW	
Component	Max. Temp (°F) 34 hours after complete blockage		Allowable Max. Temp. (°F)
Fuel Cladding	823	-	1058 [2]
Fuel Compartment	801	¹	
Basket Al Plates	800	*	
Basket Rails	662	*	
DSC Shell	600	582	
Concrete Structure	364	377	350 [21] ²
Top Heat Shield	366	431	
Side Heat Shield	471	385	
DSC support Str.	497	505	

¹ These temperatures are bounded by the values resulted for HSM-H with finned aluminum side heat shields.

² Capability of concrete will be verified at elevated temperatures above 350°F via test, see Chapter 12.

Table 4-7
Average Heat up Rates

Average Heat up Rate of Transfer Cask and DSC with Water in DSC

Component	Volume (in ³)	Mass (lbm)	Cp (Btu/lbm-°F)	Cp x M (Btu/°F)
Fuel Assemblies	148488	50720	0.06 ^{1*}	3043
DSC w/o cover pl.	89838	26053	0.114 ^{2†}	2970
Basket,ss	75928	22019	0.114	2510
Basket,Al	79952	7835	0.216 ^{3‡}	1692
TC,ss	149276	43290	0.114	4935
TC,resin	8927	579	0.256 ^{4§}	148
TC,lead	152121	62369	0.030 ^{5**}	1871
Tc,water	234294	8458	1.0 ^{6††}	8458
Water in DSC	308146	11124	1.0	11124
Water in annulus	15350	554	1.0	554
Total	1262320	233002		37306

$$\bar{C}_p = \frac{37306}{233002} = 0.160 \text{ Btu/lbm-°F, heat up rate} = \frac{118748}{(233002 \times 0.16)} = 3.2 \text{ °F/hr}$$

Average Heat up Rate of Transfer Cask and DSC without Water in DSC

Component	Volume (in3)	Mass (lbm)	Cp (Btu/lbm-°F)	Cp x M (Btu/°F)
Fuel Assemblies	148488	50720	0.06	3043
DSC w/o cover pl.	89837	26053	0.114	2970
Basket,ss	75928	22019	0.114	2510
Basket,Al	79952	7835	0.216	1692
TC,ss	149276	43290	0.114	4935
TC,resin	8927	579	0.256	148
TC,lead	152121	62369	0.030	1871
Tc,water	234294	8458	1.0	8458
Water in DSC	0	0	1.0	0
Water in annulus	14358	518	1.0	518
Total	953181	221841		26146

$$\bar{C}_p = \frac{26146}{221841} = 0.118 \text{ Btu/lbm-°F, heat up rate} = \frac{118748}{(221841 \times 0.118)} = 4.5 \text{ °F/hr}$$

¹ Effective Cp of fuel assembly at 400°F from Section 4.8

² Cp of SA240, type 304 at 100°F from [6]

³ Cp of Aluminum at 100°F from [6]

⁴ Cp of solid neutron absorber at 104°F from [1]

⁵ Cp of lead from [3]

⁶ Cp of water from Section 3

Table 4-8
Maximum Temperatures during Vacuum Drying Process

Component	TC Backfill^a T_{max} (°F)	Allowable Limit (°F)
Fuel assembly	734	752 [2]
Basket Al plates	714	---
Basket rails	591	---
DSC shell	515	---
TC inner shell	278	---
Lead gamma shield	275	---
TC Structural shell	219	---
Liquid neutron shield - T_{max}	215	---
Liquid neutron shield – T_{bulk}	208	---
Neutron shield panel	205	---

Note:

^a 28 hours after drainage of the annulus water with helium in the DSC cavity.

Table 4-9
Maximum Decay Heat Load without Time Limitation for Vacuum Drying

DELETED

Table 4-10
32PTH DSC Internal Pressure

Operating Condition Without BPRA		n_{back}	f_B	n_{free}	n_{total}	\bar{T}_{DSC}	P_{DSC}		Design Pressure
		(lbmoles)	(---)	(lbmoles)	(lbmoles)	(°F)	(psia)	(psig)	(psig)
Storage	Normal	0.326	0.01	0.721	0.333	515	19.5	4.8	15
	Off-Normal	0.326	0.1	0.721	0.398	515	23.3	8.6	20
	Accident	0.326	0.1	0.721	0.398	647	26.5	11.8	70
Transfer ¹	Normal	0.326	0.01	0.721	0.333	537	20.0	5.3	15
	Off-Normal	0.326	0.1	0.721	0.398	537	23.9	9.2	20
	Accident	0.326	1.0	0.721	1.047	961	89.5	74.8	120

Operating Condition With BPRA		n_{back}	f_B	n_{free}	n_{total}	\bar{T}_{DSC}	P_{DSC}		Design Pressure
		(lbmoles)	(---)	(lbmoles)	(lbmoles)	(°F)	(psia)	(psig)	(psig)
Storage	Normal	0.326	0.01	0.849	0.334	515	20.6	5.9	15
	Off-Normal	0.326	0.1	0.849	0.411	515	25.4	10.7	20
	Accident	0.326	0.1	0.849	0.411	647	28.8	14.1	70
Transfer*	Normal	0.326	0.01	0.849	0.334	537	21.1	6.4	15
	Off-Normal	0.326	0.1	0.849	0.411	537	25.9	11.2	20
	Accident	0.326	1.0	0.849	1.175	961	105.7	91.0	120

¹ The average gas temperature within DSC cavity for transfer conditions increase by 0.3% if Al-6061 is used for rail inserts and back-plates as discussed in Section 4.6.1. The DSC absolute pressure will be increased by the same ratio. This small change remains bounded by the design pressures.

Table 4-11
Average Peaking Factors for Active Fuel Length of 144"

	Height from Bottom of Active Fuel (in)	P_i [4]	P_i (interpolated)	A_i	$P_{avg, i}$
1	0	0.000			
	1.32		0.215	0.142	0.107
2	4.00	0.652			
	7.0675		0.773	3.346	0.582
3	12.00	0.967			
	14.5		1.000	6.751	0.908
4	20.00	1.074			
	22.0675		1.081	7.933	1.048
5	27.99	1.103			
6	36.00	1.108			
	37.0675		1.108	16.506	1.100
7	44.01	1.106			
8	52.00	1.102			
	57.69		1.098	22.766	1.104
9	60.00	1.097			
	66.9425		1.094	10.143	1.096
10	68.00	1.094			
11	76.00	1.094			
	82.0675		1.095	16.549	1.094
12	84.00	1.095			
13	92.00	1.096			
	97.0675		1.095	16.432	1.095
14	99.99	1.095			
15	108.00	1.086			
	111.943		1.073	16.191	1.088
16	116.01	1.059			
	121.26		1.001	9.743	1.046
17	124.00	0.971			
	127.068		0.882	5.543	0.955
18	132.00	0.738			
	136.26		0.591	6.826	0.743
19	140.00	0.462			
	144		0.000	2.892	0.374
20	144.00	0.000			

**Table 4-11 – Concluded
Average Peaking Factors for Active Fuel Length of 137”**

	Height from Bottom of Active Fuel (in)	P_i [4]	P_i (interpolated)	A_i	$P_{avg, i}$
1	0	0.000			
	5.5675		0.725	2.452	0.441
2	11.41	0.967			
	13		0.989	6.497	0.874
3	19.03	1.074			
	20.5675		1.080	7.877	1.041
4	26.63	1.103			
	34.25	1.108			
5	35.5675		1.108	16.500	1.100
6	41.87	1.106			
	49.47	1.102			
7	56.19		1.098	22.757	1.103
8	57.09	1.097			
	59.82		1.096	3.981	1.097
9	64.69	1.094			
	72.31	1.094			
10	73.01		1.094	14.435	1.094
11	79.91	1.095			
	87.53	1.096			
12	89.82		1.096	18.410	1.095
13	95.13	1.095			
	102.75	1.086			
14	104.82		1.079	16.366	1.091
15	110.37	1.059			
	114.5		1.011	10.207	1.054
16	117.97	0.971			
	119.82		0.914	5.183	0.974
17	125.59	0.738			
	131.25		0.532	8.362	0.732
18	133.19	0.462			
	137		0.000	1.845	0.321
19	137	0.000			

Table 4-12
Characteristics of Fuel Assemblies

Fuel Type	WE & WES 15x15	WE & WEV 17x17	MK BW 17x17	WEO 17x17	CE 14x14
Active fuel length	142-144	144	144	144	137
Pellet OD	0.3649- 0.3669	0.3225	0.3195	0.3088	0.3765
Rod OD	0.422	0.374	0.374	0.360	0.440
Clad wall thickness	0.0243	0.0225	0.0240	0.0225	0.028
Rod pitch	0.563	0.496	0.496	0.496	0.580
No. of fuel rods	204	264	264	264	176
No. of Guide/Instrument tubes	21	25	25	25	5
Guide tube OD	0.484-0.545	0.429-0.482	0.482	0.429- 0.482	1.115
Guide tube wall thickness	0.015	0.016	0.016	0.016	0.04
Instrument tube OD	0.545	0.474-0.545	0.482	0.474- 0.545	---
Instrument tube wall thickness	0.015	0.015-.016	0.016	0.015-.016	---

All Dimensions are in inches

Table 4-13
Effective Fuel Properties

Transverse Effective Fuel Conductivity in Helium

Fuel Type	WE & WES 15x15			WE 17x17			Fuel Type	MK BW 17x17			WEO 17x17		
T _o (°F)	T _c (°F)	T _{avg} (°F)	k (Btu/hr-in-°F)	T _c (°F)	T _{avg} (°F)	k (Btu/hr-in-°F)	T _o (°F)	T _c (°F)	T _{avg} (°F)	k (Btu/hr-in-°F)	T _c (°F)	T _{avg} (°F)	k (Btu/hr-in-°F)
100	172	136	0.0194	171	136	0.0194	100	170	135	0.0197	173	137	0.0189
200	261	231	0.0230	261	231	0.0226	200	260	230	0.0230	262	231	0.0223
300	352	326	0.0269	352	326	0.0266	300	352	326	0.0266	353	327	0.0260
400	445	423	0.0311	445	423	0.0307	400	445	423	0.0307	445	423	0.0307
500	538	519	0.0368	539	520	0.0354	500	539	520	0.0354	539	520	0.0354
600	633	617	0.0424	633	617	0.0418	600	633	617	0.0418	633	617	0.0418
700	729	714	0.0490	729	715	0.0476	700	729	715	0.0476	729	715	0.0476
800	825	813	0.0560	825	813	0.0552	800	825	813	0.0552	825	813	0.0552
1000	1019	1010	0.0737	1019	1010	0.0727	1000	1020	1010	0.0690	1019	1010	0.0727
Q _{react} (Btu/hr-in)	4.751			4.685			Q _{react} (Btu/hr-in)	4.685			4.685		
Q (Btu/hr) / kW	2699 / 0.8			2699 / 0.8			Q (Btu/hr) / kW	2699 / 0.8			2699 / 0.8		

Transverse Effective Fuel Conductivity for Vacuum Conditions

Fuel Type	WE & WES 15x15			WE 17x17			Fuel Type	MK BW 17x17			WEO 17x17		
T _o (°F)	T _c (°F)	T _{avg} (°F)	k (Btu/hr-in-°F)	T _c (°F)	T _{avg} (°F)	k (Btu/hr-in-°F)	T _o (°F)	T _c (°F)	T _{avg} (°F)	k (Btu/hr-in-°F)	T _c (°F)	T _{avg} (°F)	k (Btu/hr-in-°F)
100	272	186	0.0081	275	188	0.0079	100	276	188	0.0078	275	188	0.0079
200	336	268	0.0103	340	270	0.0099	200	340	270	0.0099	339	270	0.0099
300	408	354	0.0130	411	356	0.0124	300	412	356	0.0123	410	355	0.0126
400	486	443	0.0163	489	445	0.0155	400	490	445	0.0153	488	444	0.0157
500	569	535	0.0203	572	536	0.0192	500	572	536	0.0192	570	535	0.0197
600	656	628	0.0250	658	629	0.0238	600	659	630	0.0234	657	629	0.0242
700	746	723	0.0304	748	724	0.0288	700	748	724	0.0288	746	723	0.0300
800	838	819	0.0368	839	820	0.0354	800	840	820	0.0345	838	819	0.0363
Q _{react} (Btu/hr-in)	4.685			4.685			Q _{react} (Btu/hr-in)	4.685			4.685		
Q (Btu/hr) / kW	2699 / 0.8			2699 / 0.8			Q (Btu/hr) / kW	2699 / 0.8			2699 / 0.8		

Table 4-13 – Continued
Effective Fuel Properties

Axial Effective Fuel Conductivity in Helium or Vacuum

Fuel type	WE & WES 15x15	WE & WEV 17x17	MK BW 17x17	WEO 17x17
No of fuel rods	204	264	264	264
OD fuel rod (in)	0.422	0.374	0.374	0.360
Clad thickness (in)	0.0243	0.0225	0.0240	0.0225
No of guides tubes	20	24	24	24
OD guide tubes (in)	0.484	0.429	0.482	0.429
Wall thickness (in)	0.015	0.016	0.016	0.016
No of Instrument tubes	1	1	1	1
OD Instrument tube (in)	0.545	0.474	0.482	0.474
Wall thickness (in)	0.015	0.015	0.016	0.015

Fuel type	WE & WES 15x15	WE & WEV 17x17	MK BW 17x17	WEO 17x17
Cladding area (in ²)	6.66	7.08	7.55	6.82
Compartment area (in ²)	75.69	75.69	75.69	75.69
Temperature	k-axial	k-axial	k-axial	k-axial
(°F)	(Btu/hr-in-°F)	(Btu/hr-in-°F)	(Btu/hr-in-°F)	(Btu/hr-in-°F)
212	0.0576	0.0612	0.0653	0.0590
392	0.0606	0.0644	0.0687	0.0620
572	0.0644	0.0685	0.0730	0.0659
752	0.0695	0.0739	0.0788	0.0711
932	0.0763	0.0811	0.0865	0.0781
1112	0.0852	0.0905	0.0966	0.0872

**Table 4-13 – Continued
Effective Fuel Properties**

Effective Fuel Density					Effective Specific Heat of Fuel				
Fuel Type	WE & WES 15x15	WE 17x17	MK BW 17x17	WEO 17x17	Fuel Type	WE & WES 15x15	WE 17x17	MK BW 17x17	WEO 17x17
No of fuel rods	204	264	264	264	No of fuel rods	204	264	264	264
OD fuel rod (in)	0.422	0.374	0.374	0.360	OD fuel rod (in)	0.422	0.374	0.374	0.360
Clad thickness (in)	0.0243	0.0225	0.0240	0.0225	Clad thickness (in)	0.0243	0.0225	0.0240	0.0225
No of guides tubes	20	24	24	24	No of guides tubes	20	24	24	24
OD guide tubes (in)	0.484	0.429	0.482	0.429	OD guide tubes (in)	0.484	0.429	0.482	0.429
Wall thickness (in)	0.015	0.016	0.016	0.016	Wall thickness (in)	0.015	0.016	0.016	0.016
No of Instrument tubes	1	1	1	1	No of Instrument tubes	1	1	1	1
OD Instrument tube (in)	0.545	0.474	0.482	0.474	OD Instrument tube (in)	0.545	0.474	0.482	0.474
Wall thickness (in)	0.015	0.015	0.016	0.015	Wall thickness (in)	0.015	0.015	0.016	0.015
Active fuel length (in)	142	144	144	144	Active fuel length (in)	142	144	144	144
Pellet OD (in)	0.3649	0.3225	0.3195	0.3088	Pellet OD (in)	0.3649	0.3225	0.3195	0.3088

Fuel Type	WE & WES 15x15	WE 17x17	MK BW 17x17	WEO 17x17		WE & WES 15x15	WE 17x17	MK BW 17x17	WEO 17x17
Cladding area (in ²)	6.66	7.08	7.55	6.82	Cladding area (in ²)	6.66	7.08	7.55	6.82
Cladding volume (in ³)	946	1019	1088	982	Cladding volume (in ³)	946	1019	1088	982
Pellet area (in ²)	21.33	21.57	21.17	19.77	Pellet area (in ²)	21.33	21.57	21.17	19.77
UO ₂ volume (in ³)	3029	3105	3048	2847	UO ₂ volume (in ³)	3029	3105	3048	2847
ρ eff (lbm/in ³)	0.1325	0.1350	0.1344	0.1248	Temperature	Cp eff	Cp eff	Cp eff	Cp eff
					(°F)	(Btu/lbm-°F)	(Btu/lbm-°F)	(Btu/lbm-°F)	(Btu/lbm-°F)
					80	0.0593	0.0594	0.0595	0.0594
					260	0.0654	0.0655	0.0656	0.0656
					692	0.0726	0.0727	0.0728	0.0727
					1502	0.0779	0.0780	0.0782	0.0781

**Table 4-13 – Concluded
Effective Fuel Properties for CE 14x14**

Transverse Effective Fuel Conductivity in Helium					Axial Effective Conductivity	
Fuel Type			CE 14x14		Fuel type	CE 14x14
T _o (°F)	T _c (°F)	T _{avg} (°F)	Q _{react} (Btu/hr-in)	k (Btu/hr-in-°F)	No of fuel rods	176
100	181	140	19.968	0.0182	OD fuel rod (in)	0.440
225	291	258	19.969	0.0222	Clad thickness (in)	0.028
350	404	377	19.969	0.0271	No of guide tubes	5
475	519	497	19.970	0.0331	OD guide tubes (in)	1.115
600	637	618	19.970	0.0402	Wall thickness (in)	0.04
725	755	740	19.970	0.0483	No of instrument tubes	---
850	875	863	19.970	0.0577	OD instrument tube (in)	---
					Wall thickness (in)	---

Fuel type	CE 14x14
Cladding area (in ²)	7.05
Compartment area (in ²)	75.69
Temperature (°F)	k-axial (Btu/hr-in-°F)
212	0.0610
392	0.0642
572	0.0682
752	0.0736
932	0.0808

Table 4-14
Effective Conductivity of Liquid Neutron Shielding – Sections 1 and 16

Ti	To	Tavg	Tavg	k	β	ν	Pr	C _I	Ra	Nu_COND	Nu_I	Nu	k_eff
(°F)	(°F)	(°F)	(K)	(W/m-K)	(1/K)	(m ² /s)	(---)	(---)	(---)	(---)	(---)	(---)	(Btu/hr-in-°F)
134	126	130	328	0.648	4.159E-04	5.171E-07	3.29	0.5883	4.751E+08	1.00	21.62	21.62	0.674
144	136	140	333	0.653	4.501E-04	4.815E-07	3.04	0.5852	5.477E+08	1.00	22.29	22.29	0.701
154	146	150	339	0.658	4.844E-04	4.460E-07	2.79	0.5819	6.304E+08	1.00	22.96	22.96	0.727
164	156	160	344	0.663	5.186E-04	4.104E-07	2.54	0.5780	7.253E+08	1.00	23.62	23.62	0.754
174	166	170	350	0.668	5.528E-04	3.749E-07	2.29	0.5737	8.352E+08	1.00	24.28	24.28	0.781
184	176	180	356	0.671	5.858E-04	3.552E-07	2.16	0.5712	9.292E+08	1.00	24.83	24.83	0.802
194	186	190	361	0.674	6.187E-04	3.355E-07	2.03	0.5684	1.033E+09	1.00	25.37	25.37	0.823
204	196	200	367	0.677	6.517E-04	3.158E-07	1.90	0.5654	1.149E+09	1.00	25.92	25.92	0.844
214	206	210	372	0.680	6.846E-04	2.962E-07	1.77	0.5622	1.277E+09	1.00	26.46	26.46	0.866
224	216	220	378	0.682	7.167E-04	2.802E-07	1.66	0.5593	1.404E+09	1.00	26.96	26.96	0.885
234	226	230	383	0.683	7.481E-04	2.681E-07	1.58	0.5570	1.525E+09	1.00	27.40	27.40	0.902
244	236	240	389	0.685	7.794E-04	2.559E-07	1.50	0.5545	1.655E+09	1.00	27.85	27.85	0.918
254	246	250	394	0.686	8.108E-04	2.437E-07	1.42	0.5518	1.797E+09	1.00	28.29	28.29	0.935
264	256	260	400	0.688	8.421E-04	2.315E-07	1.34	0.5490	1.951E+09	1.00	28.73	28.73	0.952
274	266	270	406	0.688	8.815E-04	2.231E-07	1.29	0.5471	2.117E+09	1.00	29.22	29.22	0.968
284	276	280	411	0.688	9.210E-04	2.147E-07	1.24	0.5451	2.296E+09	1.00	29.71	29.71	0.984
294	286	290	417	0.688	9.604E-04	2.063E-07	1.19	0.5430	2.489E+09	1.00	30.20	30.20	1.000
304	296	300	422	0.687	9.906E-04	1.990E-07	1.15	0.5411	2.660E+09	1.00	30.60	30.60	1.012

Table 4-14 – Continued
Effective Conductivity of Liquid Neutron Shielding – Sections 2 to 12

Ti	To	Tavg	Tavg	k	β	ν	Pr	C _I	Ra	Nu_COND	Nu _I	Nu	k _{eff}
(°F)	(°F)	(°F)	(K)	(W/m-K)	(1/K)	(m ² /s)	(---)	(---)	(---)	(---)	(---)	(---)	(Btu/hr-in-°F)
156.5	143.5	150	339	0.658	4.844E-04	4.460E-07	2.79	0.5819	1.024E+09	1.00	25.92	25.92	0.821
166.5	153.5	160	344	0.663	5.186E-04	4.104E-07	2.54	0.5780	1.179E+09	1.00	26.67	26.67	0.851
176.5	163.5	170	350	0.668	5.528E-04	3.749E-07	2.29	0.5737	1.357E+09	1.00	27.42	27.42	0.882
186.5	173.5	180	356	0.671	5.858E-04	3.552E-07	2.16	0.5712	1.510E+09	1.00	28.03	28.03	0.906
196.5	183.5	190	361	0.674	6.187E-04	3.355E-07	2.03	0.5684	1.679E+09	1.00	28.65	28.65	0.929
206.5	193.5	200	367	0.677	6.517E-04	3.158E-07	1.90	0.5654	1.866E+09	1.00	29.26	29.26	0.953
216.5	203.5	210	372	0.680	6.846E-04	2.962E-07	1.77	0.5622	2.076E+09	1.00	29.88	29.88	0.978
226.5	213.5	220	378	0.682	7.167E-04	2.802E-07	1.66	0.5593	2.282E+09	1.00	30.44	30.44	0.999
236.5	223.5	230	383	0.683	7.481E-04	2.681E-07	1.58	0.5570	2.478E+09	1.00	30.94	30.94	1.018
246.5	233.5	240	389	0.685	7.794E-04	2.559E-07	1.50	0.5545	2.690E+09	1.00	31.44	31.44	1.037
256.5	243.5	250	394	0.686	8.108E-04	2.437E-07	1.42	0.5518	2.920E+09	1.00	31.94	31.94	1.056
266.5	253.5	260	400	0.688	8.421E-04	2.315E-07	1.34	0.5490	3.171E+09	1.00	32.43	32.43	1.074
276.5	263.5	270	406	0.688	8.815E-04	2.231E-07	1.29	0.5471	3.441E+09	1.00	32.99	32.99	1.093
286.5	273.5	280	411	0.688	9.210E-04	2.147E-07	1.24	0.5451	3.731E+09	1.00	33.54	33.54	1.111
296.5	283.5	290	417	0.688	9.604E-04	2.063E-07	1.19	0.5430	4.044E+09	1.00	34.09	34.09	1.129
306.5	293.5	300	422	0.687	9.906E-04	1.990E-07	1.15	0.5411	4.323E+09	1.00	34.54	34.54	1.143
316.5	303.5	310	428	0.685	1.007E-03	1.934E-07	1.12	0.5396	4.528E+09	1.00	34.85	34.85	1.150
326.5	313.5	320	433	0.684	1.023E-03	1.877E-07	1.08	0.5381	4.745E+09	1.00	35.17	35.17	1.157

Table 4-14 – Concluded
Effective Conductivity of Liquid Neutron Shielding – Sections 13 to 15

Ti	To	Tavg	Tavg	k	β	ν	Pr	C _I	Ra	Nu_COND	Nu_I	Nu	k _{eff}
(°F)	(°F)	(°F)	(K)	(W/m-K)	(1/K)	(m ² /s)	(---)	(---)	(---)	(---)	(---)	(---)	(Btu/hr-in-°F)
135	125	130	328	0.648	4.159E-04	5.171E-07	3.29	0.5883	5.938E+08	1.00	22.83	22.83	0.712
145	135	140	333	0.653	4.501E-04	4.815E-07	3.04	0.5852	6.846E+08	1.00	23.54	23.54	0.740
155	145	150	339	0.658	4.844E-04	4.460E-07	2.79	0.5819	7.880E+08	1.00	24.24	24.24	0.768
165	155	160	344	0.663	5.186E-04	4.104E-07	2.54	0.5780	9.066E+08	1.00	24.94	24.94	0.796
175	165	170	350	0.668	5.528E-04	3.749E-07	2.29	0.5737	1.044E+09	1.00	25.64	25.64	0.825
185	175	180	356	0.671	5.858E-04	3.552E-07	2.16	0.5712	1.162E+09	1.00	26.22	26.22	0.847
195	185	190	361	0.674	6.187E-04	3.355E-07	2.03	0.5684	1.291E+09	1.00	26.79	26.79	0.869
205	195	200	367	0.677	6.517E-04	3.158E-07	1.90	0.5654	1.436E+09	1.00	27.37	27.37	0.892
215	205	210	372	0.680	6.846E-04	2.962E-07	1.77	0.5622	1.597E+09	1.00	27.94	27.94	0.914
225	215	220	378	0.682	7.167E-04	2.802E-07	1.66	0.5593	1.755E+09	1.00	28.46	28.46	0.934
235	225	230	383	0.683	7.481E-04	2.681E-07	1.58	0.5570	1.906E+09	1.00	28.94	28.94	0.952
245	235	240	389	0.685	7.794E-04	2.559E-07	1.50	0.5545	2.069E+09	1.00	29.40	29.40	0.970
255	245	250	394	0.686	8.108E-04	2.437E-07	1.42	0.5518	2.246E+09	1.00	29.87	29.87	0.987
265	255	260	400	0.688	8.421E-04	2.315E-07	1.34	0.5490	2.439E+09	1.00	30.33	30.33	1.005
275	265	270	406	0.688	8.815E-04	2.231E-07	1.29	0.5471	2.647E+09	1.00	30.85	30.85	1.022
285	275	280	411	0.688	9.210E-04	2.147E-07	1.24	0.5451	2.870E+09	1.00	31.37	31.37	1.039
295	285	290	417	0.688	9.604E-04	2.063E-07	1.19	0.5430	3.111E+09	1.00	31.88	31.88	1.056
305	295	300	422	0.687	9.906E-04	1.990E-07	1.15	0.5411	3.325E+09	1.00	32.31	32.31	1.069

Table 4-15
Verification of the Calculated Effective Conductivities for Liquid Neutron Shielding

At 115°F Ambient Temperature

Sec. #	Ti ¹	To ²	\overline{T} ³	\overline{T} ⁴	k	β	ν	Pr	C _I	Ra	Nu	Calculated. k _{eff} ⁵	k _{eff} in Model ⁶	Diff. %
(---)	(°F)	(°F)	(°F)	(K)	(W/m-K)	(1/K)	(m ² /s)	(---)	(---)	(---)	(---)	(Btu/hr-in-°F)	(Btu/hr-in-°F)	(---)
1	213	205	209	372	0.679	6.83E-04	2.974E-07	1.77	0.5624	1.245E+09	26.30	0.860	0.865	0.5%
2	231	220	225	381	0.683	7.35E-04	2.731E-07	1.61	0.5580	2.047E+09	29.55	0.971	1.008	3.7%
3	245	234	239	389	0.685	7.78E-04	2.565E-07	1.50	0.5546	2.325E+09	30.32	1.000	1.035	3.5%
4	256	244	249	395	0.686	8.11E-04	2.436E-07	1.42	0.5518	2.780E+09	31.55	1.043	1.055	1.1%
5	264	251	256	398	0.688	8.33E-04	2.350E-07	1.36	0.5498	3.091E+09	32.28	1.069	1.068	0.1%
6	268	255	261	401	0.688	8.48E-04	2.302E-07	1.33	0.5487	3.294E+09	32.73	1.084	1.076	0.7%
7	271	257	263	402	0.688	8.58E-04	2.281E-07	1.32	0.5482	3.412E+09	32.99	1.093	1.081	1.1%
8	272	258	265	403	0.688	8.63E-04	2.271E-07	1.31	0.5480	3.469E+09	33.11	1.097	1.083	1.3%
9	272	259	265	403	0.688	8.64E-04	2.270E-07	1.31	0.5479	3.475E+09	33.12	1.097	1.083	1.3%
10	271	258	264	403	0.688	8.60E-04	2.277E-07	1.32	0.5481	3.433E+09	33.03	1.094	1.081	1.2%
11	269	256	262	401	0.688	8.52E-04	2.295E-07	1.33	0.5485	3.328E+09	32.80	1.087	1.078	0.8%
12	265	252	258	399	0.688	8.37E-04	2.336E-07	1.35	0.5495	3.016E+09	32.06	1.062	1.070	0.8%
13	257	245	251	395	0.687	8.14E-04	2.424E-07	1.41	0.5515	2.600E+09	30.97	1.024	0.988	3.5%
14	246	236	241	389	0.685	7.83E-04	2.546E-07	1.49	0.5542	2.235E+09	29.96	0.988	0.971	1.8%
15	232	223	227	382	0.683	7.39E-04	2.716E-07	1.60	0.5577	1.689E+09	28.11	0.924	0.946	2.4%
16	215	207	211	373	0.680	6.87E-04	2.947E-07	1.76	0.5619	1.225E+09	26.17	0.857	0.865	0.9%

¹ This value is the average temperature of the structural shell retrieved from the solid elements in the model

² This value is the average temperature of the shielding shell retrieved from the solid elements in the model

³ This value is the average temperature of the water within the shielding shell retrieved from the model

⁴ This value is the calculated average temperature (Ti+To)/2 converted to Kelvin

⁵ This value is calculated using the correlations discussed in Section 4.9.1

⁶ This value is resulted from interpolation between the values used in the ANSYS model

Table 4-15 – Concluded
Verification of the Calculated Effective Conductivities for Liquid Neutron Shielding

At -20°F Ambient Temperature

Sec. #	T _i	T _o	\overline{T}	\overline{T}	k	β	ν	Pr	C _l	Ra	Nu	Calculated k _{eff}	k _{eff} in Model	Diff. %
(---)	(°F)	(°F)	(°F)	(K)	(W/m-K)	(1/K)	(m ² /s)	(---)	(---)	(---)	(---)	(Btu/hr-in-°F)	(Btu/hr-in-°F)	(---)
1	100	90	95	308	0.623	2.11E-04	7.519E-07	5.04	0.6030	2.232E+08	18.35	0.551	0.674	22.4%
2	121	107	113	319	0.637	3.33E-04	6.117E-07	3.99	0.5952	5.807E+08	23.01	0.706	0.761	7.8%
3	138	124	130	328	0.648	4.19E-04	5.141E-07	3.27	0.5880	8.705E+08	25.15	0.785	0.762	2.9%
4	152	136	143	336	0.655	4.64E-04	4.672E-07	2.94	0.5839	1.134E+09	26.68	0.841	0.801	4.8%
5	161	145	152	340	0.659	4.94E-04	4.359E-07	2.72	0.5808	1.325E+09	27.59	0.876	0.827	5.5%
6	167	150	158	344	0.662	5.13E-04	4.162E-07	2.58	0.5787	1.457E+09	28.15	0.897	0.844	6.0%
7	170	153	161	345	0.664	5.24E-04	4.047E-07	2.50	0.5774	1.539E+09	28.48	0.910	0.854	6.2%
8	171	155	162	346	0.664	5.29E-04	3.992E-07	2.46	0.5767	1.580E+09	28.63	0.916	0.858	6.3%
9	172	155	163	346	0.665	5.30E-04	3.986E-07	2.46	0.5767	1.585E+09	28.65	0.917	0.859	6.3%
10	170	154	161	346	0.664	5.26E-04	4.028E-07	2.49	0.5772	1.554E+09	28.53	0.912	0.855	6.2%
11	168	151	159	344	0.663	5.17E-04	4.126E-07	2.56	0.5783	1.479E+09	28.24	0.901	0.847	6.0%
12	162	146	154	341	0.660	4.99E-04	4.311E-07	2.69	0.5803	1.293E+09	27.40	0.871	0.832	4.5%
13	153	138	145	336	0.655	4.68E-04	4.627E-07	2.91	0.5835	1.073E+09	26.26	0.829	0.753	9.1%
14	140	126	133	329	0.649	4.26E-04	5.065E-07	3.22	0.5874	8.544E+08	24.97	0.780	0.719	7.9%
15	122	110	116	320	0.639	3.44E-04	5.985E-07	3.90	0.5944	5.077E+08	22.18	0.682	0.712	4.4%
16	102	92	97	309	0.625	2.25E-04	7.357E-07	4.92	0.6023	2.361E+08	18.59	0.559	0.674	20.5%

Note: The applied k_{eff} values in the model for sections 1 and 16 at -20°F ambient are accepted, because these values are higher than the calculated values, which cause higher temperature gradient in the model for minimum ambient conditions.

Table 4-16
Effective Conductivity of Liquid Neutron Shield during Burning Period

Ti (°F)	To (°F)	Tavg (°F)	Tavg (K)	k (W/m-K)	β (1/K)	ν (m ² /s)	Pr (---)	C _I (---)	Ra (---)	Nu_COND (---)	Nu_I (---)	Nu (---)	k_eff (Btu/hr-in-°F)
680	700	212	373	0.680	6.91E-04	2.92E-07	1.74	0.561	3.26E+09	1.00	33.4	33.4	1.09
650	700	212	373	0.680	6.91E-04	2.92E-07	1.74	0.561	8.16E+09	1.00	42.0	42.0	1.37
620	700	212	373	0.680	6.91E-04	2.92E-07	1.74	0.561	1.30E+10	1.00	47.2	47.2	1.55
580	600	212	373	0.680	6.91E-04	2.92E-07	1.74	0.561	3.26E+09	1.00	33.4	33.4	1.09
550	600	212	373	0.680	6.91E-04	2.92E-07	1.74	0.561	8.16E+09	1.00	42.0	42.0	1.37
500	600	212	373	0.680	6.91E-04	2.92E-07	1.74	0.561	1.63E+10	1.00	49.9	49.9	1.63
480	500	212	373	0.680	6.91E-04	2.92E-07	1.74	0.561	3.26E+09	1.00	33.4	33.4	1.09
450	500	212	373	0.680	6.91E-04	2.92E-07	1.74	0.561	8.16E+09	1.00	42.0	42.0	1.37
420	500	212	373	0.680	6.91E-04	2.92E-07	1.74	0.561	1.30E+10	1.00	47.2	47.2	1.55
380	400	390	472	0.665	1.25E-03	1.56E-07	0.92	0.529	1.09E+10	1.00	42.5	42.5	1.36
350	400	375	464	0.670	1.18E-03	1.61E-07	0.94	0.531	2.48E+10	1.00	52.4	52.4	1.69
320	400	360	456	0.675	1.12E-03	1.67E-07	0.97	0.532	3.60E+10	1.00	57.7	57.7	1.87
280	300	290	417	0.688	9.60E-04	2.06E-07	1.19	0.543	6.22E+09	1.00	37.9	37.9	1.26
250	300	275	408	0.688	9.01E-04	2.19E-07	1.27	0.546	1.38E+10	1.00	46.5	46.5	1.54
220	300	260	400	0.688	8.42E-04	2.32E-07	1.34	0.549	1.95E+10	1.00	51.0	51.0	1.69

Table 4-17
Effective Conductivity of Air within Shielding Panel during Cool Down Period

T _i	T _o	T _{avg}	k	β	ν	Pr	C _i	Ra	Nu _{COND}	Nu _i	Nu	k _{conv}	k _r	k _{eff} ¹
(°F)	(°F)	(K)	(W/m-K)	(1/K)	(m ² /s)	(---)	(---)	(---)	(---)	(---)	(---)	(Btu/hr-in-°F)	(Btu/hr-in-°F)	(Btu/hr-in-°F)
540	1200	870	0.054	1.38E-03	7.52E-05	0.70	0.514	1.31E+06	1.00	4.3	4.3	0.01	0.18	0.19
480	1200	840	0.053	1.41E-03	7.25E-05	0.70	0.514	1.57E+06	1.00	4.5	4.5	0.01	0.17	0.18
500	1000	750	0.051	1.52E-03	6.44E-05	0.70	0.514	1.47E+06	1.00	4.5	4.5	0.01	0.13	0.14
400	1000	700	0.049	1.57E-03	5.99E-05	0.69	0.513	2.11E+06	1.00	4.9	4.9	0.01	0.12	0.13
460	800	630	0.047	1.66E-03	5.36E-05	0.69	0.513	1.57E+06	1.00	4.5	4.5	0.01	0.09	0.11
410	800	605	0.046	1.69E-03	5.16E-05	0.69	0.513	1.99E+06	1.00	4.8	4.8	0.01	0.09	0.10
310	800	555	0.044	1.79E-03	4.77E-05	0.69	0.513	3.08E+06	1.00	5.3	5.3	0.01	0.08	0.09
420	600	510	0.043	1.87E-03	4.42E-05	0.69	0.513	1.38E+06	1.00	4.4	4.4	0.01	0.06	0.08
370	600	485	0.042	1.92E-03	4.23E-05	0.69	0.513	1.97E+06	1.00	4.8	4.8	0.01	0.06	0.07
270	600	435	0.040	2.01E-03	3.84E-05	0.69	0.513	3.59E+06	1.00	5.6	5.6	0.01	0.05	0.06
330	450	390	0.039	2.14E-03	3.53E-05	0.69	0.513	1.64E+06	1.00	4.6	4.6	0.01	0.04	0.05
340	300	320	0.036	2.33E-03	3.05E-05	0.69	0.513	8.03E+05	1.00	3.8	3.8	0.01	0.03	0.04
190	300	245	0.033	2.57E-03	2.55E-05	0.70	0.514	3.49E+06	1.00	5.5	5.5	0.01	0.02	0.03
160	150	155	0.029	2.99E-03	2.03E-05	0.70	0.514	5.90E+05	1.00	3.5	3.5	0.01	0.02	0.02

¹ The calculated k_{eff} values are smoothed to use in the ANSYS model

Table 4-17 – Concluded
Effective Conductivity of Air within Shielding Panel during Cool Down Period – Verification

time	Ti ¹	To ²	T _{avg} ³	T _{avg}	k	β	ν	Pr	C _I	Ra	Nu	Calculate d k _{eff} ⁴	k _{eff} in Model ⁵	Diff. %
(hr)	(°F)	(°F)	(°F)	(K)	(W/m-K)	(1/K)	(m ² /s)	(---	(---	(---	(---	(Btu/hr-in-°F)	(Btu/hr-in-°F)	(---
0.26	370	559	456	509	0.041	120E-03	4.00E-05	0.69	0.513	1.86E+06	4.7	0.066	0.064	2.3%
1	356	255	308	427	0.035	2.4E-03	2.97E-05	0.69	0.513	2.18E+06	4.9	0.040	0.038	4.4%
2	352	227	292	418	0.035	2.4E-03	2.86E-05	0.69	0.513	2.97E+06	5.3	0.039	0.036	6.7%
5	357	219	290	417	0.035	2.4E-03	2.85E-05	0.69	0.513	3.30E+06	5.4	0.039	0.036	7.4%
10	378	227	305	425	0.035	2.4E-03	2.95E-05	0.69	0.513	3.29E+06	5.4	0.041	0.038	6.9%
15	399	235	320	433	0.036	2.3E-03	3.05E-05	0.69	0.513	3.27E+06	5.4	0.043	0.040	6.6%
20	415	243	333	440	0.036	2.3E-03	3.14E-05	0.69	0.513	3.22E+06	5.4	0.045	0.042	6.2%
50	491	277	391	473	0.039	2.1E-03	3.54E-05	0.69	0.513	2.92E+06	5.3	0.053	0.050	5.3%
80	521	292	415	486	0.039	2.1E-03	3.70E-05	0.69	0.513	2.76E+06	5.2	0.057	0.055	2.0%
120	535	299	426	492	0.040	2.0E-03	3.78E-05	0.69	0.513	2.68E+06	5.2	0.058	0.058	0.6%
175	540	302	430	494	0.040	2.0E-03	3.81E-05	0.69	0.513	2.65E+06	5.2	0.059	0.059	0.3%
200	540	302	430	495	0.040	2.0E-03	3.81E-05	0.69	0.513	2.65E+06	5.2	0.059	0.059	0.2%

¹ This value is the average temperature of the structural shell retrieved from the solid elements in the model

² This value is the average temperature of the shielding shell retrieved from the solid elements in the model

³ This value is the average temperature of the air within the shielding shell retrieved from the model

⁴ This value is calculated using the correlations discussed in Section 4.9.

⁵ This value is resulted from interpolation between the values used in the ANSYS model

Table 4-18
Verification of the selected k_{eff} value for Water in the Annulus

time (hr)	T_h ¹ (°F)	T_c ² (°F)	T_{avg} ³ (°F)	T_{avg} (K)	k (W/m-K)	β (1/K)	ν (m ² /s)	Pr (---)	Ra (---)
1	160.0	159.6	159.8	344	0.663	5.175E-04	4.111E-07	1.83	1.058E+04
2	160.0	158.9	159.4	344	0.663	5.162E-04	4.125E-07	1.84	2.889E+04
3	160.0	158.4	159.2	344	0.662	5.155E-04	4.133E-07	1.84	4.189E+04
5	161.5	158.7	160.1	345	0.663	5.186E-04	4.101E-07	1.83	7.442E+04
8	166.9	162.5	164.7	347	0.665	5.345E-04	3.937E-07	1.77	1.264E+05
12	177.8	171.9	174.9	353	0.669	5.690E-04	3.652E-07	1.66	1.969E+05
17	194.5	187.2	190.9	362	0.674	6.217E-04	3.337E-07	1.53	2.941E+05

$Ra(H/L)^3$ (---)	Nu _{ct} (---)	Nu _l (---)	Nu _t (---)	Nu _{0.7} (---)	Nu _c (---)	Nu _l (---)	Nu _t (---)	Nu _{4.0} (---)	Nu ⁴ (---)	k_{eff} (Btu/hr-in-°F)
1.11E+12	1.3	0.6	1.3	1.3	1.0	0.4	0.8	1.0	1.1	0.036
3.04E+12	2.0	0.7	1.9	2.0	1.0	0.5	1.0	1.0	1.3	0.043
4.40E+12	2.3	0.8	2.1	2.3	1.0	0.6	1.1	1.4	1.7	0.053
7.83E+12	2.7	1.0	2.5	2.7	1.0	0.6	1.4	1.6	2.0	0.064
1.33E+13	3.2	1.1	3.0	3.2	1.0	0.7	1.6	2.0	2.4	0.076
2.07E+13	3.7	1.3	3.5	3.7	1.0	0.8	1.8	2.3	2.7	0.086
3.09E+13	4.2	1.4	4.0	4.2	1.0	0.9	2.0	2.6	3.0	0.097

time (hr)	Calculated k_{eff} (Btu/hr-in-°F)	k_{eff} in Model (Btu/hr-in-°F)
1	0.036	0.030
2	0.043	0.040
3	0.053	0.050
5	0.064	0.060
8	0.076	0.070
12	0.086	0.080
17	0.097	0.090

¹ Average temperature of the DSC shell retrieved from the model

² Average temperature of the cask inner shell retrieved from the model

³ Average temperature of water in the annulus retrieved from the model

⁴ Linear interpolation between Nu-0.7 and Nu_{4.0} based on the Pr number

Table 4-19
Total Heat Transfer Coefficient during Fire

$T_{amb} = 1475$ °F
 $L = 92.2$ in
 $F_{12} = 1.0$
 $\varepsilon = 0.9$

T_s	T_f	h_c	h_r	H_t
(°F)	(°F)	(Btu/hr-ft ² -°F)	(Btu/hr-in ² -°F)	(Btu/hr-in ² -°F)
226	1475	4.5	0.095	0.126
251	1475	4.5	0.096	0.127
276	1475	4.5	0.098	0.129
301	1475	4.5	0.100	0.131
326	1475	4.5	0.101	0.133
351	1475	4.5	0.103	0.134
376	1475	4.5	0.105	0.136
401	1475	4.5	0.107	0.138
426	1475	4.5	0.109	0.140
451	1475	4.5	0.111	0.142
476	1475	4.5	0.113	0.144
501	1475	4.5	0.115	0.146
526	1475	4.5	0.117	0.148
551	1475	4.5	0.119	0.151
576	1475	4.5	0.121	0.153
601	1475	4.5	0.124	0.155
626	1475	4.5	0.126	0.157
651	1475	4.5	0.128	0.159
676	1475	4.5	0.131	0.162
701	1475	4.5	0.133	0.164
726	1475	4.5	0.135	0.167
751	1475	4.5	0.138	0.169
776	1475	4.5	0.140	0.171
801	1475	4.5	0.143	0.174
826	1475	4.5	0.145	0.176
851	1475	4.5	0.147	0.179
876	1475	4.5	0.150	0.181
901	1475	4.5	0.152	0.184
926	1475	4.5	0.155	0.186
951	1475	4.5	0.155	0.186

Table 4-20
Table Is Deleted In Its Entirety

Table 4-21
Summary of the Energy-Hydraulic Calculation Results for 34.8 kW
(HSM-H with Finned Aluminum Side Shields)

Section	No. of Flow Paths	Subsection	Type of Flow Resistance	Ref.	K_{Ei} at 115°F	K_{Ei} at -20°F	$\Sigma(K_{Ei}/A_{Ei}^2)$ at 115°F (in ⁻⁴)	$\Sigma(K_{Ei}/A_{Ei}^2)$ at -20°F (in ⁻⁴)
1	Two parallel flows *	Entrance $A_0 = 30 \times 36 = 1080 \text{ in}^2$	Entrance effect	[35]	0.5	0.5	9.26×10^{-7}	9.26×10^{-7}
			Screen	[35]	0.58	0.58		
		Inlet channel $A_{0,1} = 12 \times 30 = 360 \text{ in}^2$ $A_{0,2} = 8 \times 12 = 96 \text{ in}^2$	First Contraction & Friction	[36]	0.03	0.03	7.84×10^{-6}	7.68×10^{-6}
			Second Contraction & Friction	[36]	0.04	0.02		
			Splitting	[36]	0.63	0.63		
		Inlet opening $A_0 = 8 \times 148 = 1184 \text{ in}^2$	Friction thru Sidewall **	[35]	0.04	0.04	7.43×10^{-6}	7.41×10^{-6}
			Discharge	[35]	1	1		
Equivalent Losses in Section 1 for two parallel flows							2.38×10^{-6}	2.34×10^{-6}
2	Two parallel flows	Flow direction change $A_0 = 8 \times 148 = 1184 \text{ in}^2$	Bend	[36]	0.75	0.71	1.35×10^{-7}	1.27×10^{-7}
	One flow	Lower part of HSM-H cavity $A_0 = 68 \times 185.25 = 12597 \text{ in}^2$	Friction through lower part	[35]	0.01	0.01	6.26×10^{-11}	5.64×10^{-11}
	One flow	HSM-H cavity below DSC $A_0 = 82.4 \times 185.25 = 15260 \text{ in}^2$	Expansion	[36]	0.03	0.03	1.57×10^{-10}	1.54×10^{-10}
			Friction after expansion	[35]	0.006	0.005		
	3 parallel flow couples	Flow thru holes of the beam $A_0 = 12.7 \times 185.25 = 2355 \text{ in}^2$	Orifice or perforated plates	[36]	112.5	112.5	2.07×10^{-9}	2.07×10^{-9}
		Flow through slotted bar $A_0 = 1 \times 185.25 = 185.25 \text{ in}^2$	Orifice or perforated plates	[36]	18.19	18.19		
		Flow bypassing Support rails $A_0 = 12 \times 185.25 = 2223 \text{ in}^2$	Contraction with $\alpha = 30^\circ$	[36]	0.04	0.04		
	One flow	Middle part of HSM-H cavity $A_0 = 82.375 \times 185.25 = 15260 \text{ in}^2$	DSC as solid object in flow	[36]	4.20	4.65	1.82×10^{-8}	2.01×10^{-8}
			Friction on side heat shields	[35]	0.03	0.03		
	One flow	Upper part of HSM-H cavity $A_0 = 82.375 \times 185.25 = 15260 \text{ in}^2$	Top heat shields as louver	[36]	5.44	5.44	2.61×10^{-8}	2.61×10^{-8}
			Splitting to outlets	[36]	0.63	0.63		
Equivalent Losses in Section 2 for one flow path							1.81×10^{-7}	1.76×10^{-7}

Table 4-21 – Continued
Summary of the Energy-Hydraulic Calculation Results for 34.8 kW
(HSM-H with Finned Aluminum Side Shields)

Section	No. of Flow Paths	Subsection	Type of Flow Resistance	Ref.	K _{Ei} at 115°F	K _{Ei} at -20°F	Σ(K _{Ei} /A _{Ei} ²) at 115°F (in ⁻⁴)	Σ(K _{Ei} /A _{Ei} ²) at -20°F (in ⁻⁴)
3	Two parallel flows	Outlet opening A ₀ = 8 x148 = 1184 in ²	Entrance	[35]	0.5	0.5	1.86x10 ⁻⁶	1.78x10 ⁻⁶
			Friction thru sidewall	[35]	0.03	0.03		
			First bend (friction included)	[36]	2.08	1.97		
		Exhaust channel A ₀ = 4 x 148 = 592 in ²	Friction	[35]	0.25	0.24	3.14x10 ⁻⁶	2.97x10 ⁻⁶
			Second bend (friction included)	[36]	0.85	0.81		
		Exhaust to Ambient A ₀ = 6 x 148 = 888 in ²	Screen	[35]	0.58	0.58	2.00x10 ⁻⁶	2.00x10 ⁻⁶
			Discharge	[35]	1	1		
Equivalent Losses in Section 3 for two Parallel Flows							1.75x10 ⁻⁶	1.69x10 ⁻⁶
Total Equivalent Losses (in-4)							4.31x10-6	4.20x10-6
Total Equivalent Losses (ft-4)							0.089	0.087

Ambient (°F)	$\Sigma(K_{Ei}/A_{Ei}^2)$ (ft ⁻⁴)	T_{exit} (°F)	T_{mean} (°F)
115	0.089	188	147
-20	0.087	43	12

* The equivalent loss coefficient for parallel flow paths can be expressed as follows:

$$\frac{K_E}{A_E^2} = \frac{1}{\left(\sum \frac{A_j}{\sqrt{K_j}} \right)^2} \quad \text{using continuity and pressure loss equations. } \Delta p_E = \Delta p_j = K_j \frac{\rho V_j^2}{2}; \dot{m}_j = \rho A_j V_j$$

** Friction loss coefficient is $K_f = f \frac{L}{D_h}$ with L=channel length, Dh = hydraulic diameter,

$$f = \begin{cases} f' & \text{if } f' \geq 0.018 \\ \frac{f'}{0.85 f' + 0.0028} & \text{if } f' < 0.018 \end{cases}, \text{ and } f' = 0.11 \left[\frac{\varepsilon}{D_h} + \frac{64}{\text{Re}} \right]^{0.25} \quad [35]$$

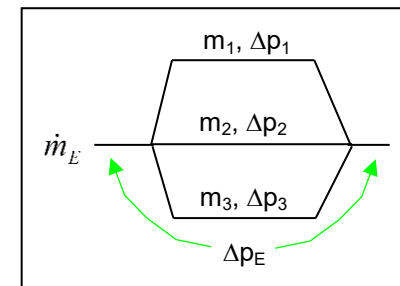


Table 4-21 – Continued
Summary of the Energy-Hydraulic Calculation Results for 34.8 kW
(HSM-H with Flat Stainless Steel Shields)

Section	No. of Flow Paths	Subsection	Type of Flow Resistance	Ref.	K_{Ei} at 115°F	K_{Ei} at -20°F	$\Sigma(K_{Ei}/A_{Ei}^2)$ at 115°F (in ⁻⁴)	$\Sigma(K_{Ei}/A_{Ei}^2)$ at -20°F (in ⁻⁴)
1	Two parallel flows *	Entrance $A_0 = 30 \times 36 = 1080 \text{ in}^2$	Entrance effect	[35]	0.5	0.5	9.26×10^{-7}	9.26×10^{-7}
			Screen	[35]	0.58	0.58		
		Inlet channel $A_{0,1} = 12 \times 30 = 360 \text{ in}^2$ $A_{0,2} = 8 \times 12 = 96 \text{ in}^2$	First Contraction & Friction	[36]	0.02	0.02	7.86×10^{-6}	7.69×10^{-6}
			Second Contraction & Friction	[36]	0.02	0.01		
			Splitting	[36]	0.63	0.63		
		Inlet opening $A_0 = 8 \times 148 = 1184 \text{ in}^2$	Friction thru Sidewall **	[35]	0.04	0.04	7.44×10^{-7}	7.42×10^{-7}
			Discharge	[35]	1	1		
Equivalent Losses in Section 1 for two parallel flows							2.38×10^{-6}	2.34×10^{-6}
2	Two parallel flows	Flow direction change $A_0 = 8 \times 148 = 1184 \text{ in}^2$	Bend	[36]	0.76	0.72	1.35×10^{-7}	1.28×10^{-7}
	One flow	Lower part of HSM-H cavity $A_0 = 68 \times 179.75 = 12223 \text{ in}^2$	Friction through lower part	[35]	0.01	0.01	6.74×10^{-11}	6.06×10^{-11}
	One flow	HSM-H cavity below DSC $A_0 = 87.5 \times 179.75 = 15773 \text{ in}^2$	Expansion	[36]	0.05	0.05	2.27×10^{-10}	2.25×10^{-10}
			Friction after expansion	[35]	0.006	0.005		
	Two parallel flow couples	Flow thru holes of the beam $A_0 = 12.7 \times 179.75 = 2283 \text{ in}^2$	Orifice or perforated plates	[36]	105.4	105.4	2.24×10^{-9}	2.24×10^{-9}
		Flow through slotted bar $A_0 = 0 \text{ in}^2$	Orifice or perforated plates	[36]	0	0		
		Flow bypassing Support rails $A_0 = 12 \times 179.75 = 2157 \text{ in}^2$	Contraction with $\alpha = 30^\circ$	[36]	0.04	0.04		
	One flow	Middle part of HSM-H cavity $A_0 = 87.5 \times 179.75 = 15773 \text{ in}^2$	DSC as solid object in flow	[36]	3.40	3.81	1.38×10^{-8}	1.54×10^{-8}
			Friction on side heat shields	[35]	0.03	0.03		
	One flow	Upper part of HSM-H cavity $A_0 = 87.75 \times 179.75 = 15260 \text{ in}^2$	Splitting below top heat shield	[36]	0.63	0.63	2.53×10^{-9}	2.53×10^{-9}
	Two parallel flows	$A_0 = 4.88 \times 179.75 = 1753 \text{ in}^2$	Contraction between shields	[36]	0.62	0.62	2.02×10^{-7}	2.02×10^{-7}
	Two parallel flows	$A_0 = 4.88 \times 148 = 722 \text{ in}^2$	Bend toward outlet	[36]	0.84	0.79	4.03×10^{-7}	3.81×10^{-7}
	Equivalent Losses in Section 2 for one flow path							7.59×10^{-7}

Table 4-21 – Concluded
Summary of the Energy-Hydraulic Calculation Results for 34.8 kW
(HSM-H with Flat Stainless Steel Shields)

Section	No. of Flow Paths	Subsection	Type of Flow Resistance	Ref.	K_{Ei} at 115°F	K_{Ei} at -20°F	$\Sigma(K_{Ei}/A_{Ei}^2)$ at 115°F (in ⁻⁴)	$\Sigma(K_{Ei}/A_{Ei}^2)$ at -20°F (in ⁻⁴)
3	Two parallel flows	Outlet opening $A_0 = 8 \times 148 = 1184 \text{ in}^2$	Entrance	[35]	0.5	0.5	1.87×10^{-6}	1.79×10^{-6}
			Friction thru sidewall	[35]	0.03	0.03		
			First bend (friction included)	[36]	2.09	1.98		
		Exhaust channel $A_0 = 4 \times 148 = 592 \text{ in}^2$	Friction	[35]	0.25	0.24	3.15×10^{-6}	2.99×10^{-6}
			Second bend (friction included)	[36]	0.86	0.81		
		Exhaust to Ambient $A_0 = 6 \times 148 = 888 \text{ in}^2$	Screen	[35]	0.58	0.58	2.00×10^{-6}	2.00×10^{-6}
			Discharge	[35]	1	1		
Equivalent Losses in Section 3 for two Parallel Flows							1.76×10^{-6}	1.70×10^{-6}
Total Equivalent Losses (in ⁻⁴)							4.90×10^{-6}	4.77×10^{-6}
Total Equivalent Losses (ft ⁻⁴)							0.102	0.099

Ambient t (°F)	$\Sigma(K_{Ei}/A_{Ei}^2)$ (ft ⁻⁴)	T _{exit} (°F)	T _{mean} (°F)
115	0.102	192	148
-20	0.099	46	13

* The equivalent loss coefficient for parallel flow paths can be expressed as follows:

$$\frac{K_E}{A_E^2} = \frac{1}{\left(\sum \frac{A_j}{\sqrt{K_j}} \right)^2} \quad \text{using continuity and pressure loss equations. } \Delta p_E = \Delta p_j = K_j \frac{\rho V_j^2}{2}; \dot{m}_j = \rho A_j V_j$$

** Friction loss coefficient is $K_f = f \frac{L}{D_h}$ with L=channel length, Dh = hydraulic diameter,

$$f = \begin{cases} f' & \text{if } f' \geq 0.018 \\ \frac{f'}{0.85 f' + 0.0028} & \text{if } f' < 0.018 \end{cases}, \text{ and } f' = 0.11 \left[\frac{\varepsilon}{D_h} + \frac{64}{\text{Re}} \right]^{0.25} \quad [35]$$

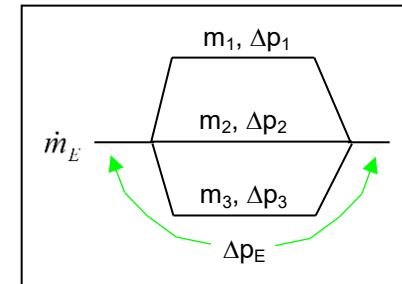


Table 4-22
Summary of the Energy-Hydraulic Calculation Results for 32.0 kW

Section	No. of Flow Paths	Subsection	Type of Flow Resistance	Ref.	K_{Ei} at 115°F	$\Sigma(K_{Ei}/A_{Ei}^2)$ at 115°F (in ⁻⁴)
1	Two parallel flows	Entrance $A_0 = 30 \times 36 = 1080 \text{ in}^2$	Entrance effect	[35]	0.5	9.26E-07
			Screen	[35]	0.58	
		Inlet channel $A_{0,1} = 12 \times 30 = 360 \text{ in}^2$ $A_{0,2} = 8 \times 12 = 96 \text{ in}^2$	1 st Contraction & Friction	[36]	0.03	7.85E-06
			2 nd Contraction & Friction	[36]	0.03	
			Splitting (Tee)	[36]	0.63	
		Inlet opening $A_0 = 8 \times 148 = 1184 \text{ in}^2$	Friction thru Sidewall	[35]	0.04	7.43E-07
			Discharge	[35]	1.0	
Equivalent Losses in Section 1 for two Parallel Flows						2.38E-06
2	Two parallel flows	Flow direction change $A_0 = 8 \times 148 = 1184 \text{ in}^2$	Bend	[36]	0.76	1.35E-07
	One flow	Lower part of HSM-H cavity $A_0 = 68 \times 185.25 = 12597 \text{ in}^2$	Friction through lower part	[35]	0.01	6.29E-11
	One flow	HSM-H cavity below DSC $A_0 = 87.4 \times 185.25 = 16186 \text{ in}^2$	Expansion	[36]	0.05	2.10E-10
			Friction after expansion	[35]	0.006	
	3 parallel flow couples	Flow thru holes of the beam $A_0 = 12.7 \times 185.25 = 2355 \text{ in}^2$	Orifice or perforated plates	[36]	112.5	2.09E-09
		Flow through slotted bar $A_0 = 1 \times 185.25 = 185.25 \text{ in}^2$	Orifice or perforated plates	[36]	18.19	
		Flow bypassing Support rails $A_0 = 12 \times 185.25 = 2223 \text{ in}^2$	Contraction with $\alpha = 30^\circ$	[36]	0.04	
	One flow	Middle part of HSM-H cavity $A_0 = 87.4 \times 185.25 = 16186 \text{ in}^2$	DSC as solid object in flow	[36]	3.44	1.33E-08
			Friction on side heat shields	[35]	0.03	
	One flow	Upper part of HSM-H cavity $A_0 = 87.4 \times 185.25 = 16186 \text{ in}^2$	Top heat shields as louver	[36]	5.44	2.32E-08
			Splitting to outlets	[36]	0.63	
Equivalent Losses in Section 2 for one Flow Path						1.74E-07
3	Two parallel flows	Outlet opening $A_0 = 8 \times 148 = 1184 \text{ in}^2$	Entrance	[35]	0.5	1.87E-06
			Friction thru sidewall	[35]	0.03	
			First bend (friction included)	[36]	2.09	
		Exhaust channel $A_0 = 4 \times 148 = 592 \text{ in}^2$	Friction	[35]	0.25	3.14E-06
			Second bend (friction included)	[36]	0.85	
		Exhaust to Ambient $A_0 = 6 \times 148 = 888 \text{ in}^2$	Screen	[35]	0.58	2.00E-06
			Discharge	[35]	1.0	
Equivalent Losses in Section 3 for two Parallel Flows						1.75E-06
Total Equivalent Losses (in ⁻⁴)						4.31E-06
Total Equivalent Losses (ft ⁻⁴)						0.089

Ambient (°F)	Decayeat (kW)	$\Sigma(K_{Ei}/A_{Ei}^2)$ (ft ⁻⁴)	T_{exit} (°F)	T_s (°F)
115	32.0	0.0897	183	144

Table 4-23
Summary of the Energy-Hydraulic Calculation Results for 26.1 kW

Section	No. of Flow Paths	Subsection	Type of Flow Resistance	Ref.	K_{Ei} at 115°F	$\Sigma(K_{Ei}/A_{Ei}^2)$ at 115°F (in ⁻⁴)
1	Two parallel flows	Entrance $A_0 = 30 \times 36 = 1080 \text{ in}^2$	Entrance effect	[35]	0.5	9.26E-07
			Screen	[35]	0.58	
		Inlet channel $A_{0,1} = 12 \times 30 = 360 \text{ in}^2$ $A_{0,2} = 8 \times 12 = 96 \text{ in}^2$	1 st Contraction & Friction	[36]	0.03	7.88E-06
			2 nd Contraction & Friction	[35]	0.03	
			Splitting (Tee)	[36]	0.63	
		Inlet opening $A_0 = 8 \times 148 = 1184 \text{ in}^2$	Friction thru Sidewall	[35]	0.04	7.44E-07
			Discharge	[35]	1.0	
Equivalent Losses in Section 1 for two Parallel Flows						2.39E-06
2	Two parallel flows	Flow direction change $A_0 = 8 \times 148 = 1184 \text{ in}^2$	Bend	[36]	0.76	1.35E-07
	One flow	Lower part of HSM-H cavity $A_0 = 68 \times 185.25 = 12597 \text{ in}^2$	Friction through lower part	[35]	0.01	6.38E-11
	One flow	HSM-H cavity below DSC $A_0 = 87.4 \times 185.25 = 16186 \text{ in}^2$	Expansion	[36]	0.05	2.10E-10
			Friction after expansion	[35]	0.006	
	3 parallel flow couples	Flow thru holes of the beam $A_0 = 12.7 \times 185.25 = 2355 \text{ in}^2$	Orifice or perforated plates	[36]	112.5	2.09E-09
		Flow through slotted bar $A_0 = 1 \times 185.25 = 185.25 \text{ in}^2$	Orifice or perforated plates	[36]	18.19	
		Flow bypassing Support rails $A_0 = 12 \times 185.25 = 2223 \text{ in}^2$	Contraction with $\alpha = 30^\circ$	[36]	0.04	
	One flow	Middle part of HSM-H cavity $A_0 = 87.4 \times 185.25 = 16186 \text{ in}^2$	DSC as solid object in flow	[36]	3.41	1.31E-08
			Friction on side heat shields	[35]	0.03	
	One flow	Upper part of HSM-H cavity $A_0 = 87.4 \times 185.25 = 16186 \text{ in}^2$	Top heat shields as louver	[36]	5.44	2.32E-08
			Splitting to outlets	[36]	0.63	
Equivalent Losses in Section 2 for one Flow Path						1.75E-07
3	Two parallel flows	Outlet opening $A_0 = 8 \times 148 = 1184 \text{ in}^2$	Entrance	[35]	0.5	1.87E-06
			Friction thru sidewall	[35]	0.03	
			First bend (friction included)	[36]	2.10	
		Exhaust channel $A_0 = 4 \times 148 = 592 \text{ in}^2$	Friction	[35]	0.25	3.16E-06
			Second bend (friction included)	[36]	0.86	
		Exhaust to Ambient $A_0 = 6 \times 148 = 888 \text{ in}^2$	Screen	[35]	0.58	2.00E-06
			Discharge	[35]	1.0	
			Equivalent Losses in Section 3 for two Parallel Flows			
Total Equivalent Losses (in ⁻⁴)						4.32E-06
Total Equivalent Losses (ft ⁻⁴)						0.090

Ambient (°F)	Decayeat (kW)	$\Sigma(K_{Ei}/A_{Ei}^2)$ (ft ⁻⁴)	T_{exit} (°F)	T_{mean} (°F)
115	26.1	0.090	173	139

Table 4-24
Minimum Height of the Fuel Rubble

ρ_{UO_2} = 0.396 lb/in³
 ρ_{Zr_4} = 0.237 lb/in³
 Fuel Comp width = 8.70 In

Fuel Type	WE & WES 15x15	WE & WEV 17x17	MK BW 17x17	WEO 17x17
No of fuel rods	204	264	264	264
OD fuel rod (in)	0.422	0.374	0.374	0.360
Clad thickness (in)	0.0243	0.0225	0.0240	0.0225
No of guides tubes	20	24	24	24
OD guide tubes (in)	0.484	0.429	0.482	0.429
Wall thickness (in)	0.015	0.016	0.016	0.016
No of Instrument tubes	1	1	1	1
OD Instrument tube (in)	0.545	0.474	0.482	0.474
Wall thickness (in)	0.015	0.015	0.016	0.015
Active fuel length (in)	142	144	144	144
Pellet OD (in)	0.3649	0.3225	0.3195	0.3088
Cladding area (in ²)	6.66	7.08	7.55	6.82
Cladding volume (in ³)	946	1019	1088	982
Pellet area (in ²)	21.33	21.57	21.17	19.77
UO ₂ volume (in ³)	3029	3105	3048	2847
H _{min} (in)	63	66	66	61

Table 4-25
Transverse Effective Fuel Conductivity at Various Fuel Rod Pitches

Assembly Type MK BW 17x17						
Pitch (in)	T_o (°F)	T_c (°F)	T_{avg} (°F)	Q_{react} (Btu/hr-in)	k (Btu/hr-in-°F)	k @ 800°F (Btu/hr-in-°F)
0.384	700	739	719	4.6770	0.0357	0.0396
	800	834	817	4.6770	0.0405	
0.4	700	740	720	4.6770	0.0347	0.0385
	800	835	818	4.6770	0.0393	
0.438	700	738	719	4.6770	0.0362	0.0405
	800	833	817	4.6770	0.0413	
0.446225	700	737	719	4.6770	0.0371	0.0415
	800	833	816	4.6770	0.0424	
0.46445	700	735	717	4.6770	0.0398	0.0446
	800	830	815	4.6770	0.0455	
0.482675	700	732	716	4.6780	0.0434	0.0488
	800	828	814	4.6787	0.0496	
0.5009	700	728	714	4.6783	0.0493	0.0556
	800	824	812	4.6788	0.0565	
0.519125	700	722	711	4.6786	0.0637	0.0728
	800	819	809	4.6791	0.0738	

Assembly Type WEO 17x17						
Pitch (in)	T_o (°F)	T_c (°F)	T_{avg} (°F)	Q_{react} (Btu/hr-in)	k (Btu/hr-in-°F)	k @ 300°F (Btu/hr-in-°F)
0.37	200	286	243	4.6761	0.0159	0.0176
	300	374	337	4.6769	0.0187	
0.4	200	287	244	4.6761	0.0158	0.0174
	300	375	337	4.6769	0.0184	
0.427	200	283	242	4.6762	0.0166	0.0182
	300	372	336	4.6768	0.0193	
0.4501	200	278	239	4.6763	0.0177	0.0195
	300	367	334	4.6768	0.0205	
0.4732	200	271	236	4.6764	0.0194	0.0215
	300	361	331	4.6768	0.0226	
0.4963	200	263	231	4.6767	0.0219	0.0246
	300	354	327	4.6769	0.0256	
0.5194	200	252	226	4.6770	0.0266	0.0305
	300	344	322	4.6769	0.0316	

Table 4-26
Transverse Effective Conductivity of Damaged Fuel

	T_o (°F)	T_c (°F)	T_{avg} (°F)	Q_{react} (Btu/hr-in)	k (Btu/hr-in-°F)
WEO 17x17	100	200	150	4.6770	1.38E-02
	200	285	243	4.6769	1.61E-02
	300	374	337	4.6769	1.87E-02
	400	463	432	4.6769	2.17E-02
	500	555	527	4.6769	2.52E-02
	600	648	624	4.6769	2.90E-02
	700	742	721	4.6769	3.31E-02
	800	837	818	4.6769	3.76E-02
	900	932	916	4.6769	4.26E-02
	1000	1029	1014	4.6769	4.81E-02
MK BW 17x17	100	194	147	4.6762	1.47E-02
	200	281	240	4.6762	1.70E-02
	300	370	335	4.6762	1.98E-02
	400	460	430	4.6762	2.28E-02
	500	552	526	4.6769	2.64E-02
	600	645	623	4.6769	3.04E-02
	700	740	720	4.6770	3.46E-02
	800	835	818	4.6770	3.93E-02
	900	931	916	4.6770	4.44E-02
	1000	1028	1014	4.6770	5.01E-02

Table 4-27
Maximum Component Temperatures in DSC containing 16 Damaged Fuel Assemblies

Normal / Off-Normal Transfer Conditions

for Ambient 115°F, Loading Configuration 1, Basket Type I

Component	Maximum Temperature (°F)		Temp. Limit (°F)
	32 Intact Fuel (Section 4.3)	16 Damaged Fuel	
Fuel Cladding	719	738	752 [2]
Fuel Compartment	693	696	
Basket Al Plates	692	695	
Basket Rails	561	561	
DSC Shell	475	475	

Accident Conditions during Transfer Operation

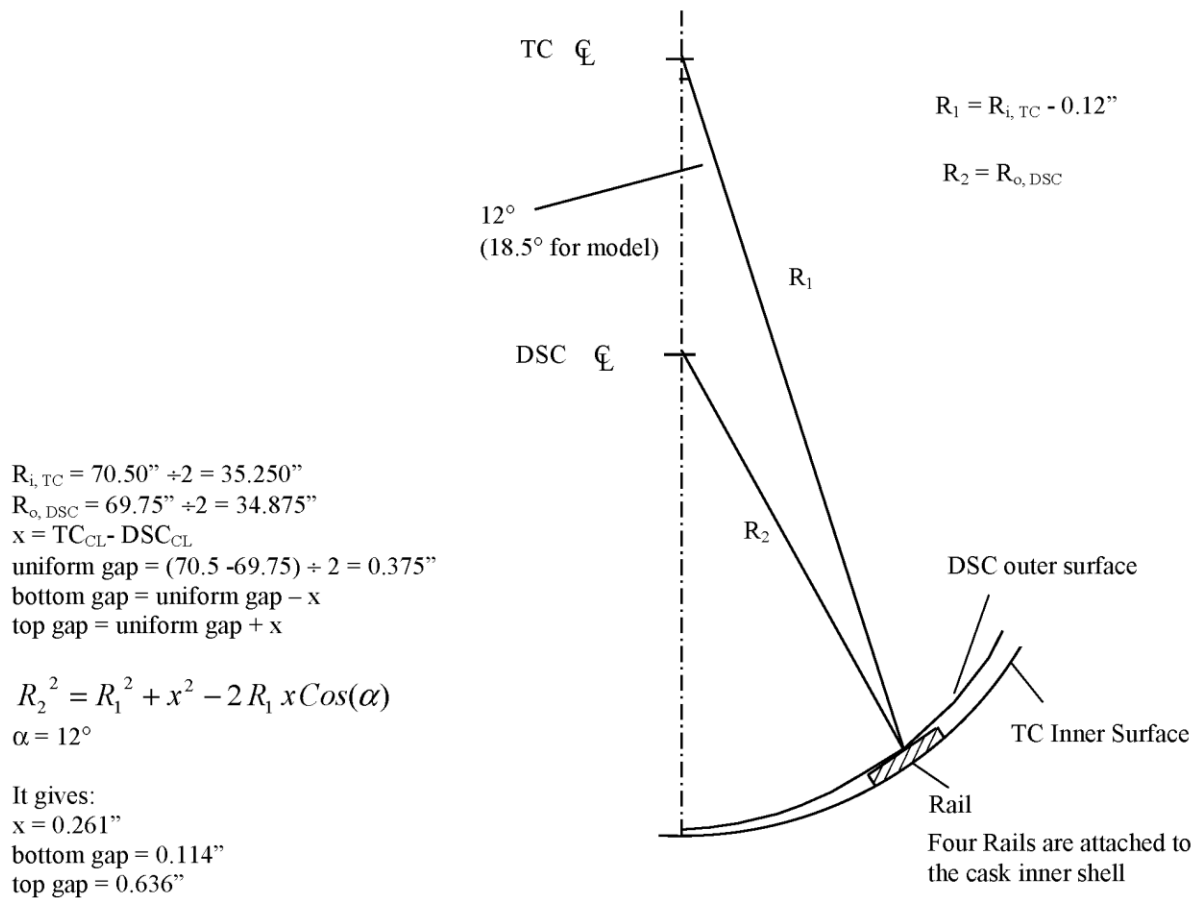
for Ambient 115°F, Loading Configuration 1, Basket Type I

	32 Intact Fuel (Section 4.3)	16 Damaged Fuel (Fuel Rubble)	
Component	Maximum Temperature (°F)		Temp. Limit (°F)
Intact Fuel cladding	1036	924	1058 [2]
Basket plates	1021	1008	
Basket rails	878	797	
DSC shell	790	737	
Gamma shell (lead)	618	522	621 [3]
Cask structural shell	553	469	
Shielding shell	598	260	

Table 4-28
Internal DSC Pressure during Transferring of Damaged Fuel

Transfer Operation		n_{total} [Section 4.6]	\overline{T}_{DSC}^1	P_{DSC} 16 Damaged Fuel		P_{DSC} 32 Intact Fuel [Section 4.6]	Design Pressure
		(lbmoles)	(°F)	(psia)	(psig)	(psig)	(psig)
Without BPRA	Normal	0.333	540	20.0	5.3	5.3	15
	Off-Normal	0.398	540	24.0	9.3	9.2	20
With BPRA	Normal	0.334	540	21.2	6.5	6.4	15
	Off-Normal	0.411	540	26.0	11.3	11.2	20

¹ The following temperatures are resulted from the DSC model containing 16 damaged fuel assemblies:
 $T_{avg, fuel} = 577^{\circ}F$, $T_{avg, void} = 401^{\circ}F$



Considering the above configuration, the gap between the DSC shell and cask inner shell will be 0.114" at the bottom and 0.636" at the top. The transfer cask model considers a slightly different configuration with an angle of 18.5 degree between the lower rail and the vertical plane. Therefore, the calculated gap between the DSC shell and cask inner shell is 0.106" at the bottom and 0.644" at the top. The nodes of the DSC shell and the cask inner shell are coupled only at the location of the two middle rails to represent the contact area at these locations. The slight difference in temperature profile caused by the smaller gap size in the model will be more than compensated by the fact that the relative thin shell of the DSC will rest on all four rails, which provide more contact area as considered in the model.

Figure 4-1
Position of the DSC in the Transfer Cask

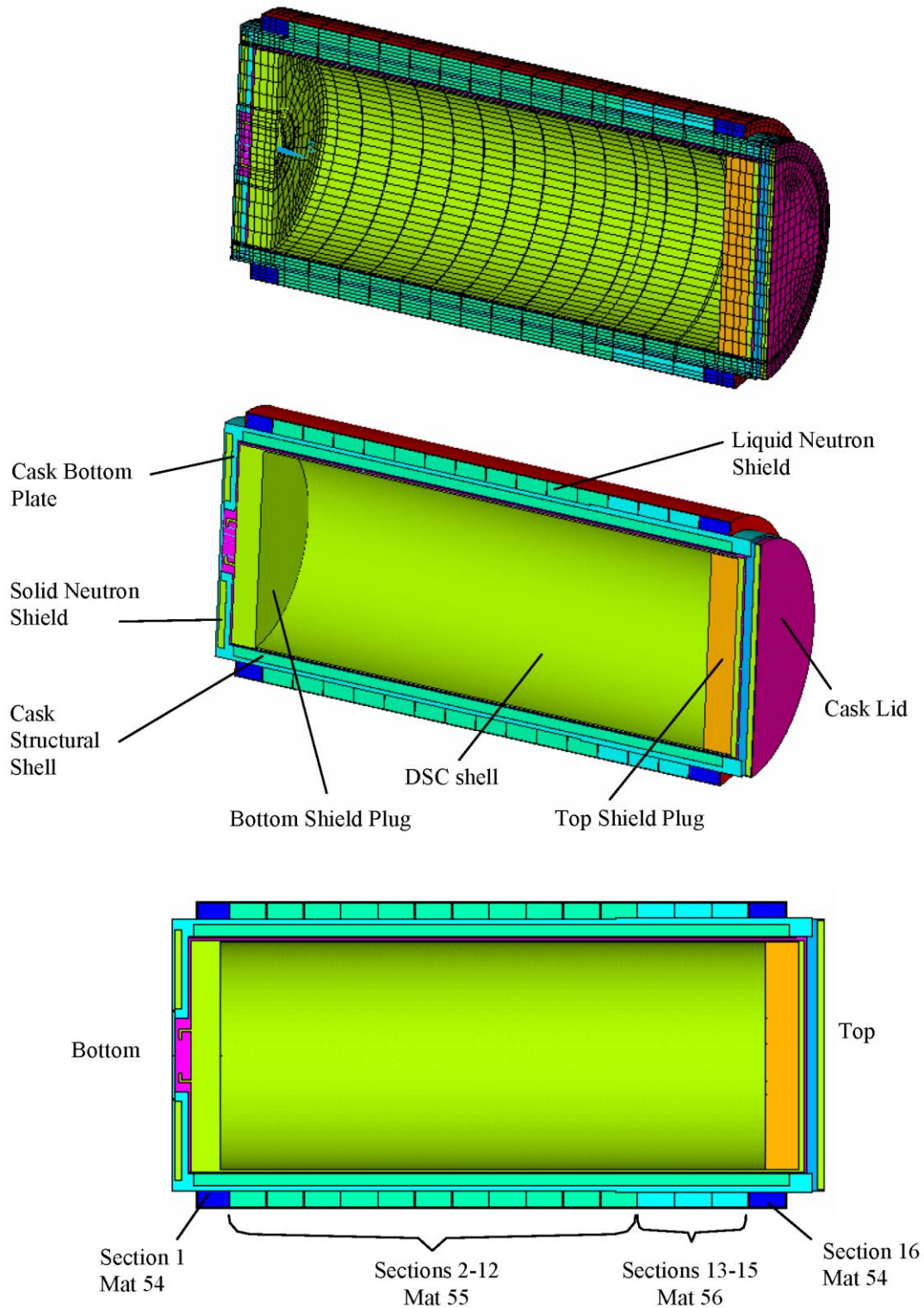


Figure 4-2
Finite element Model of Transfer Cask OS187H

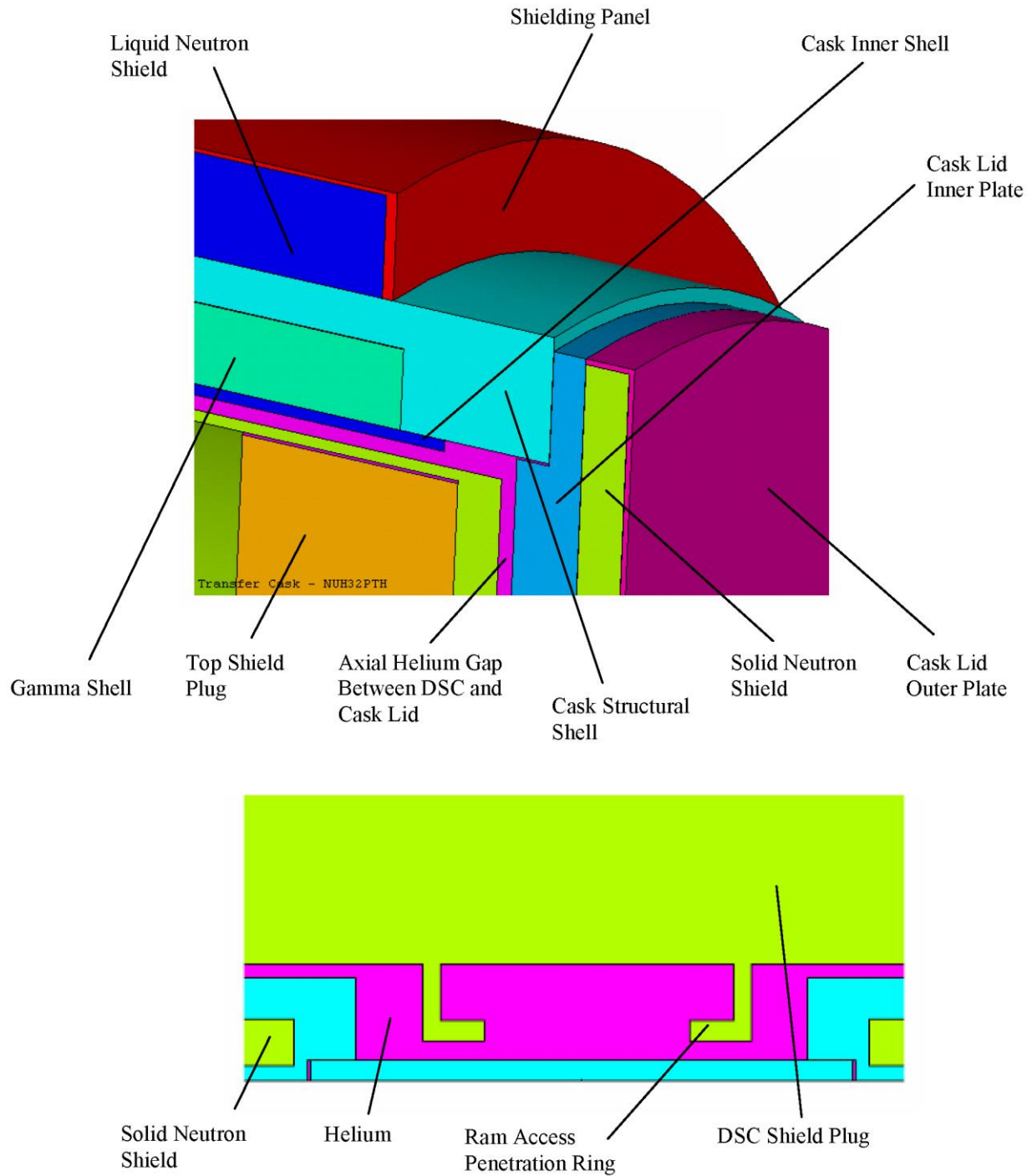


Figure 4-3
FEM of Transfer Cask OS187H, Details

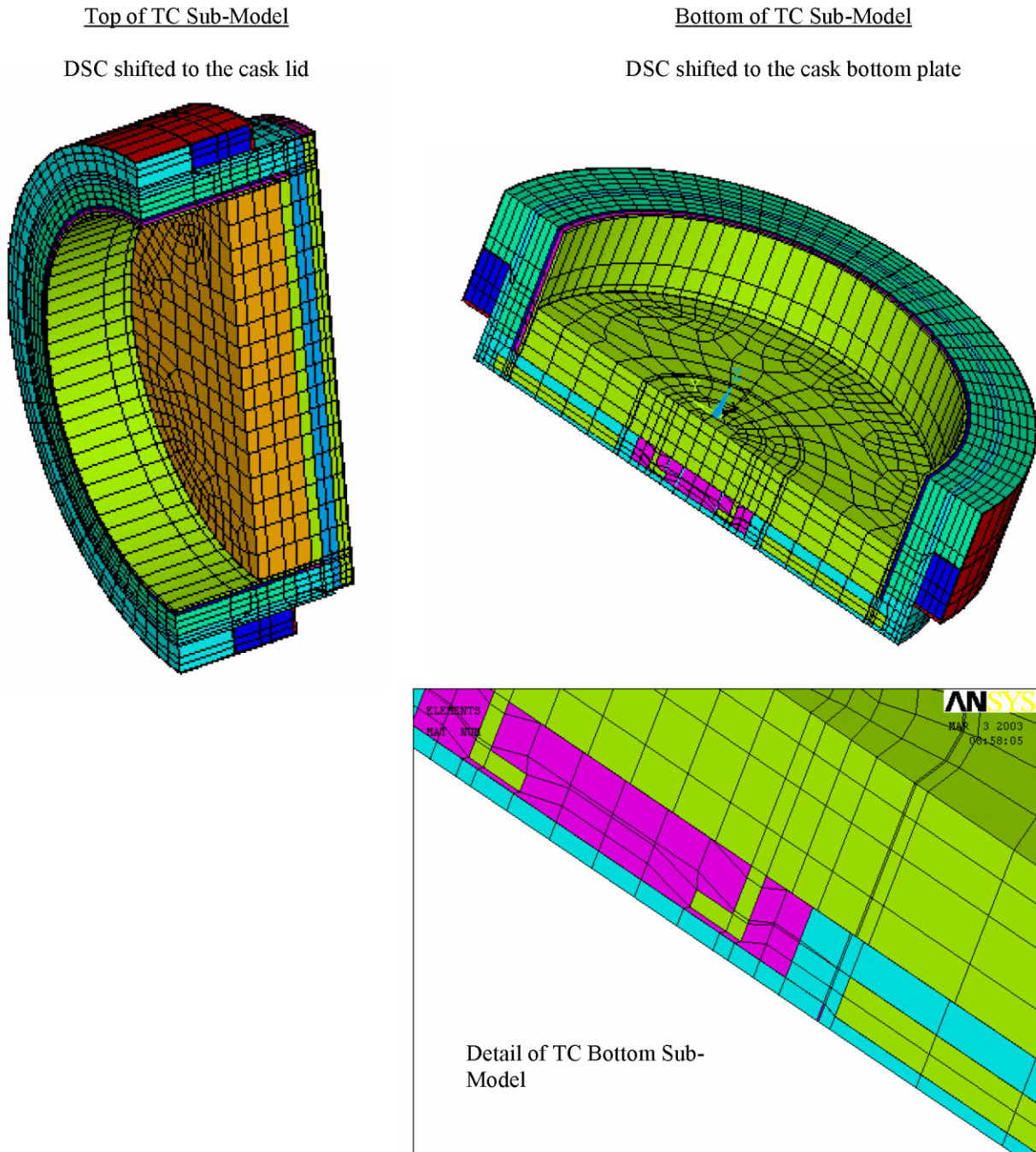


Figure 4-4
Top and Bottom Sub-Models of Transfer Cask OS187H

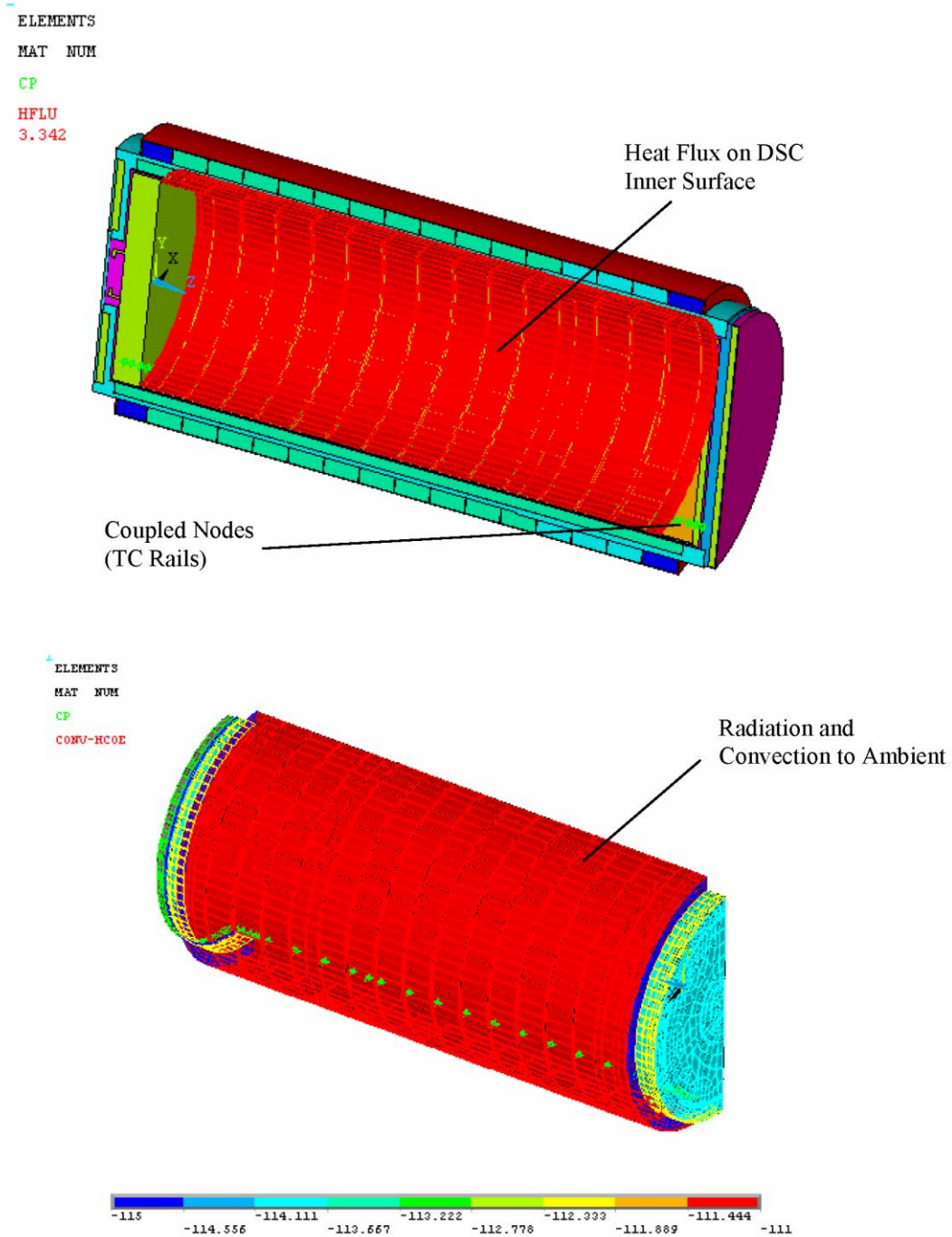


Figure 4-5
Typical Boundary Conditions on the TC Model

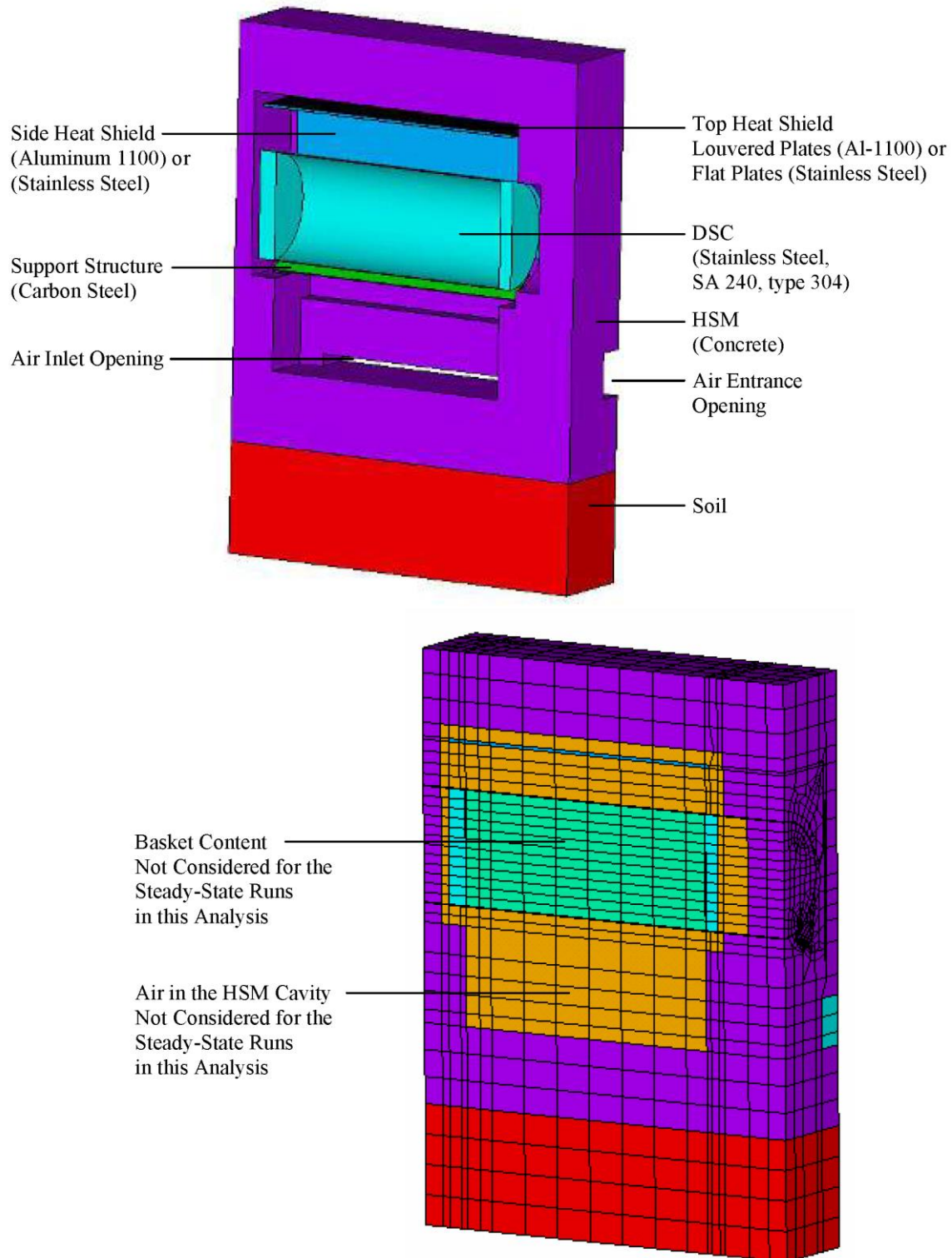


Figure 4-6
Finite Element Model of HSM-H

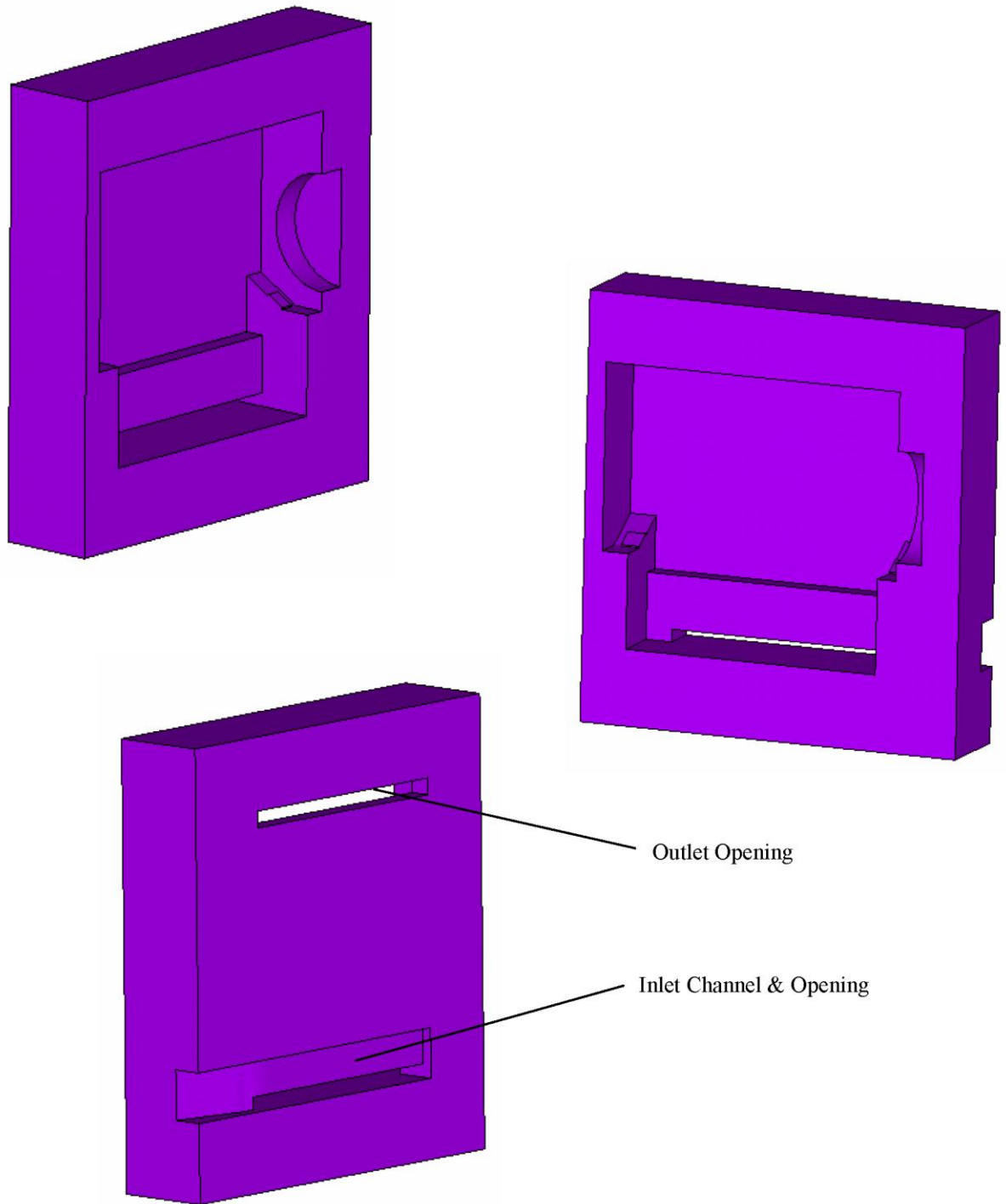


Figure 4-7
FEM of HSM-H, Concrete Structure

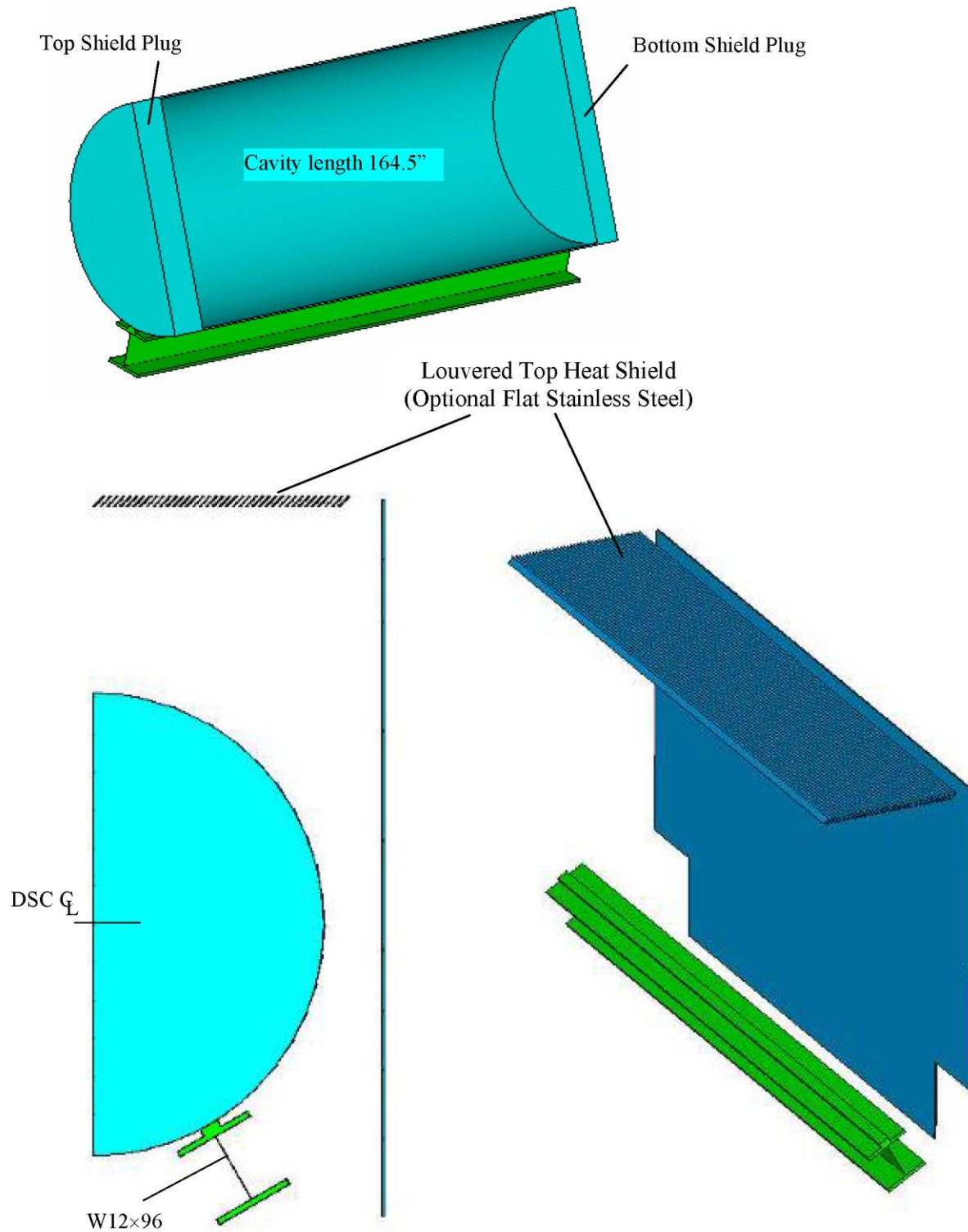
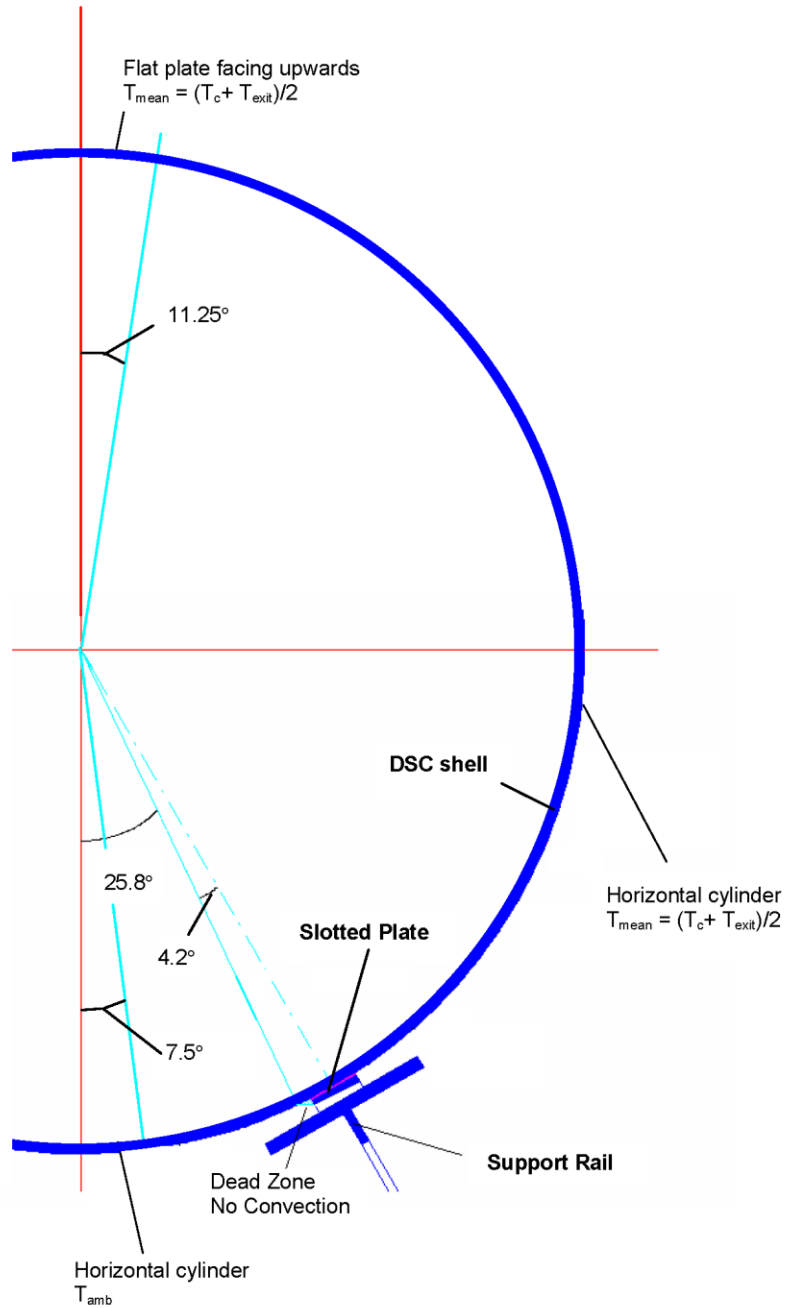


Figure 4-8
FEM of HSM-H, DSC and Support Rails



For option with slotted plate on support rail

Figure 4-9
DSC Circumferential Convection Regions in the HSM-H Model

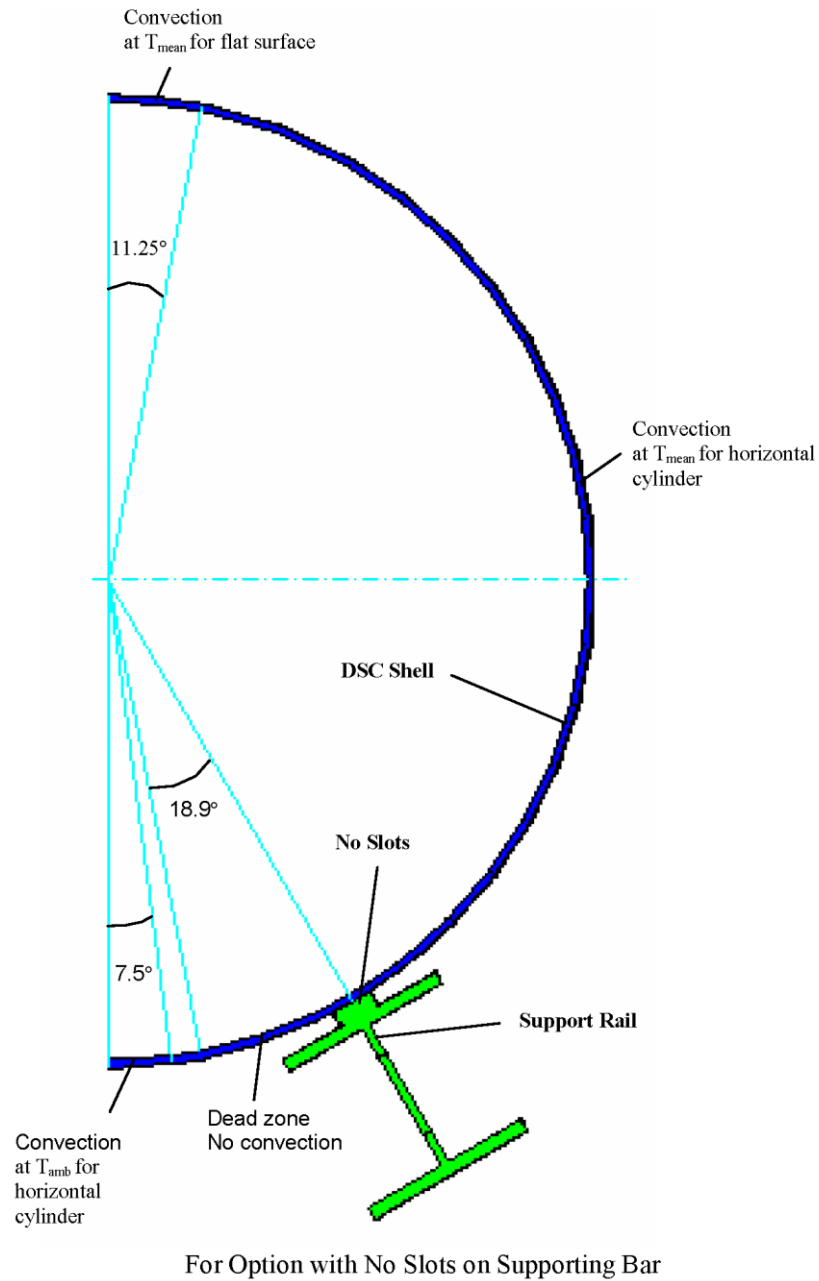


Figure 4-9-continued
DSC Circumferential Convection Regions in the HSM-H Model

Convection for a narrow strip (22.5°) at top as flat plate to T_{mean}
 Convection at a narrow strip (15°) at bottom to T_c
 Convection on other areas as horizontal cylinder to T_{mean}

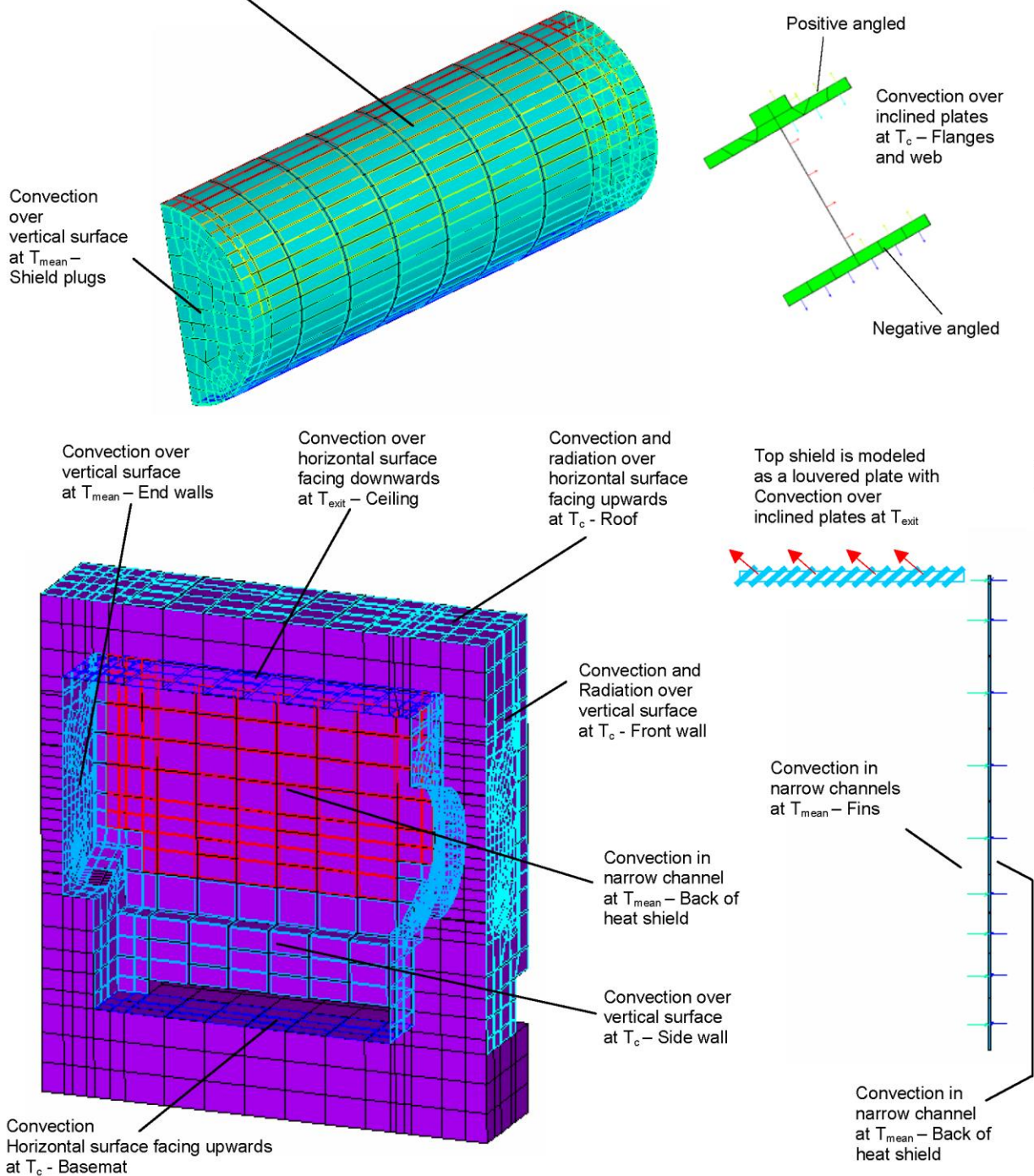


Figure 4-10
Typical Convection Boundary Conditions in the HSM-H Model

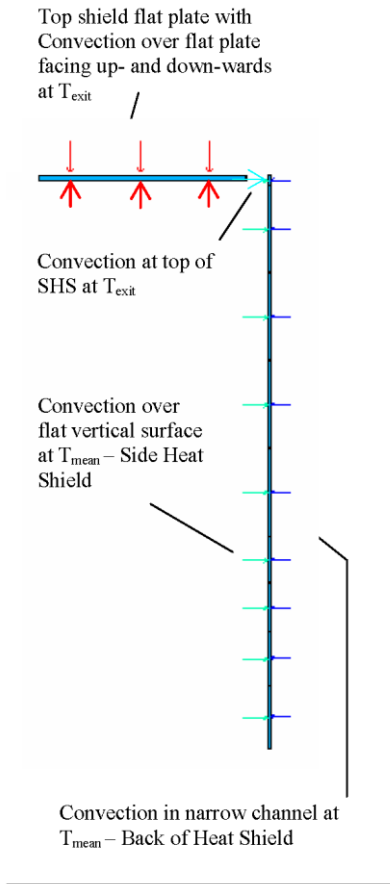


Figure 4-10– continued
Typical Convection boundary Conditions in the HSM-H Model

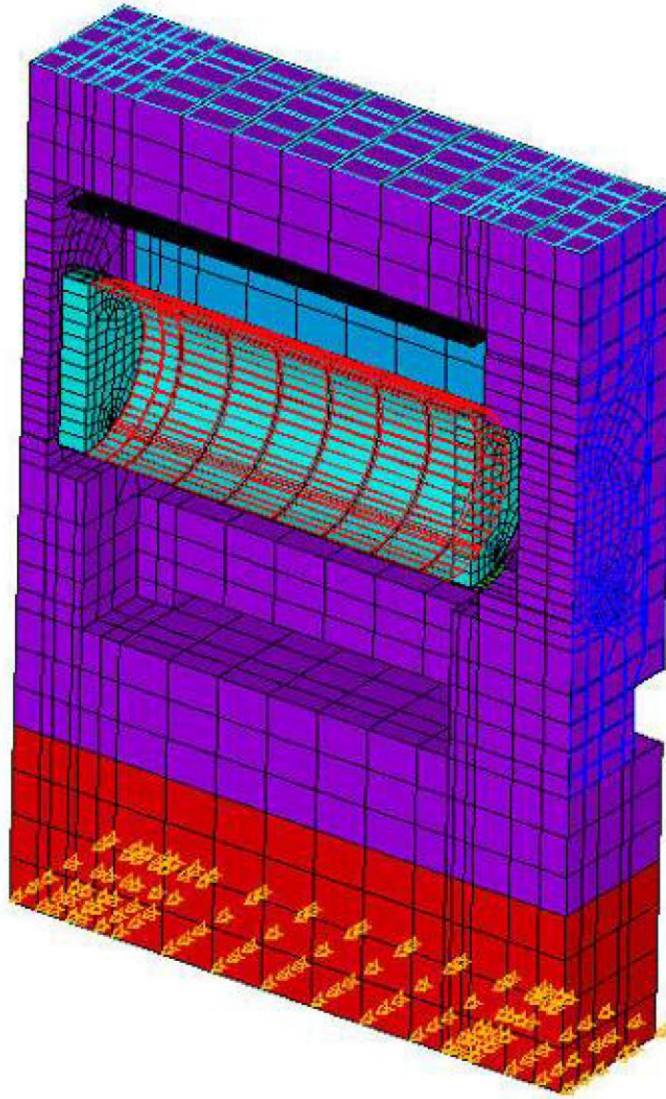


Figure 4-11
Typical Heat Flux and Fixed Temperature Boundary Conditions for the HSM-H Model

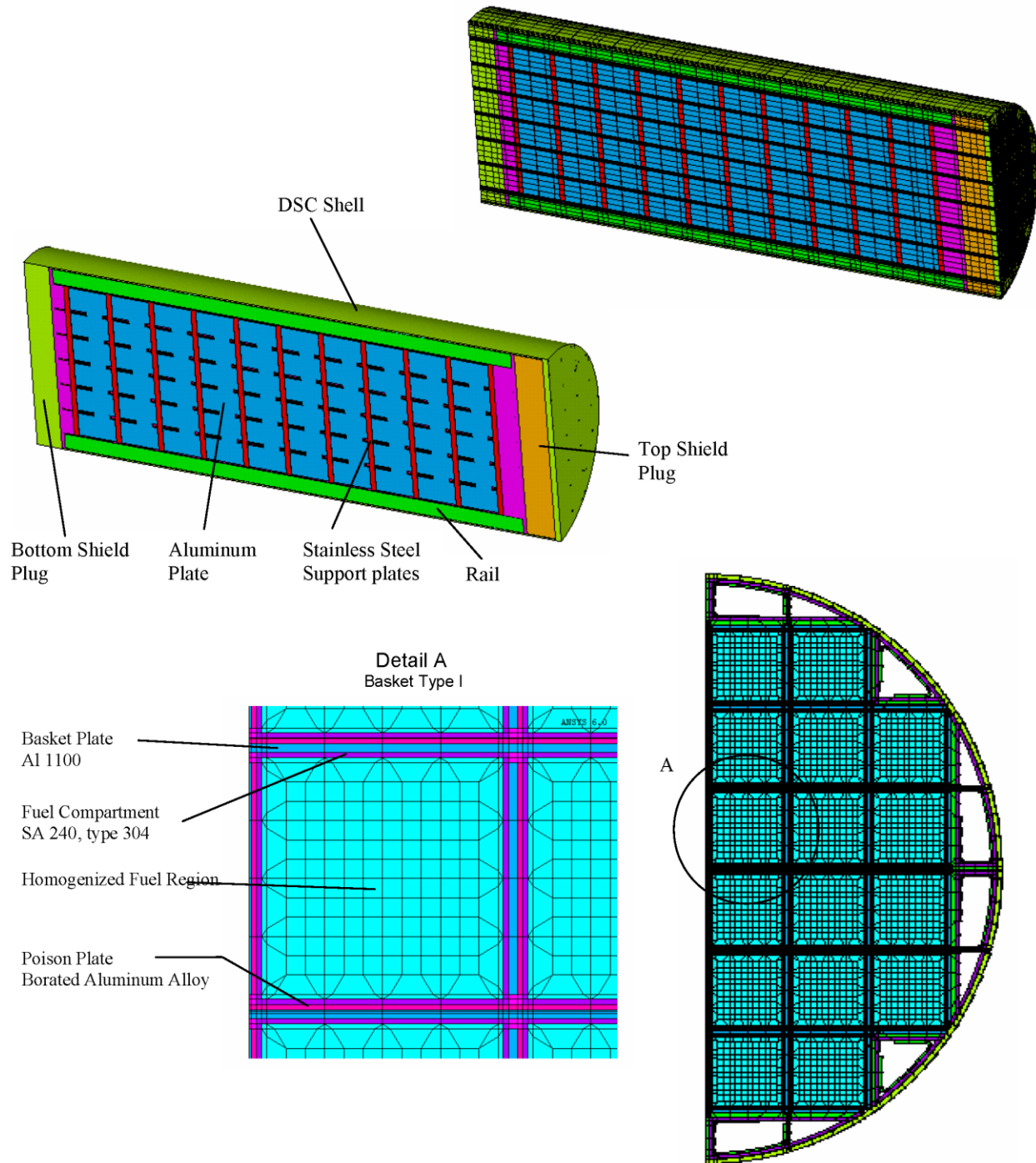


Figure 4-12
Finite Element Model of the DSC

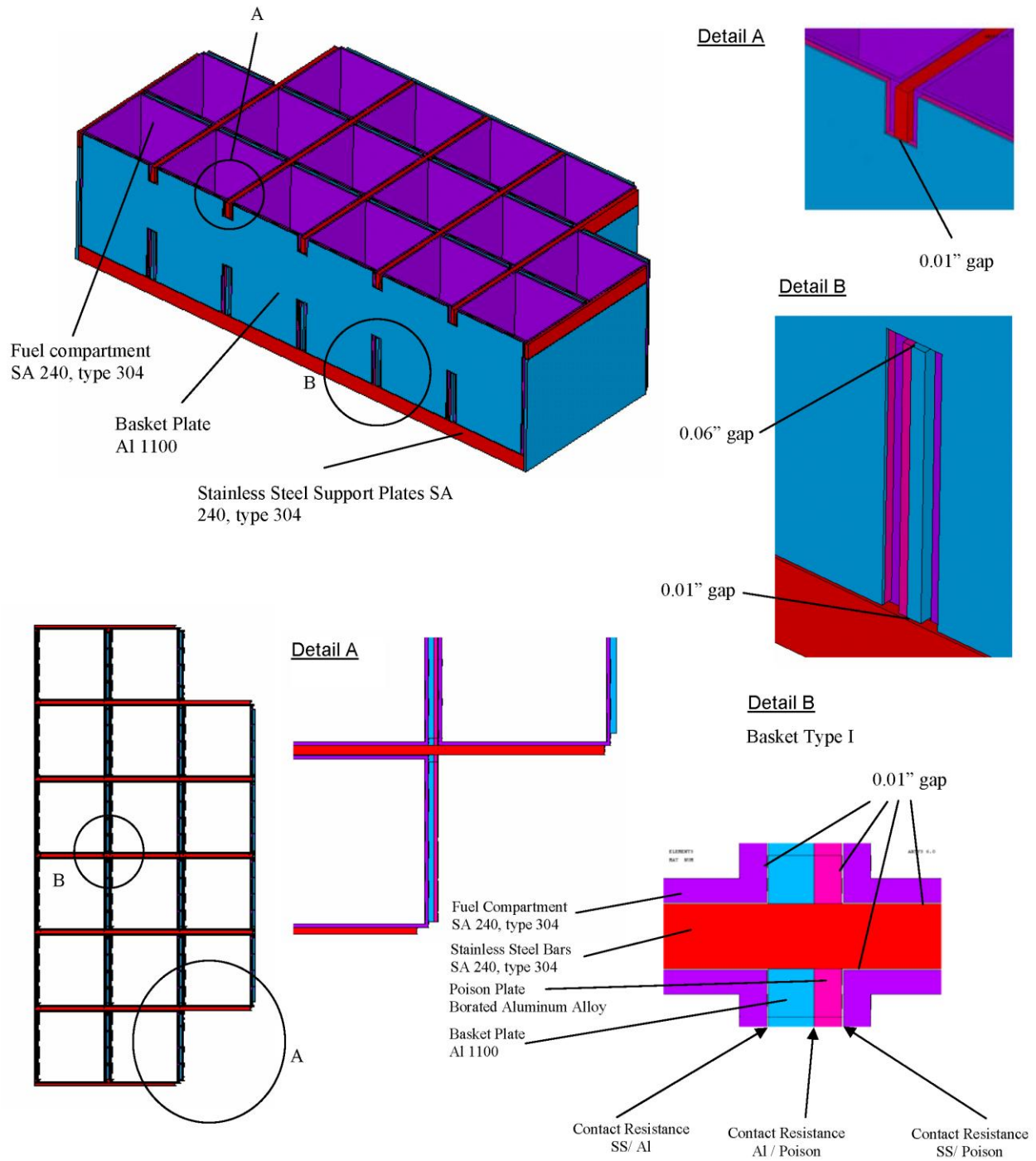


Figure 4-13
FEM of DSC Basket, Details

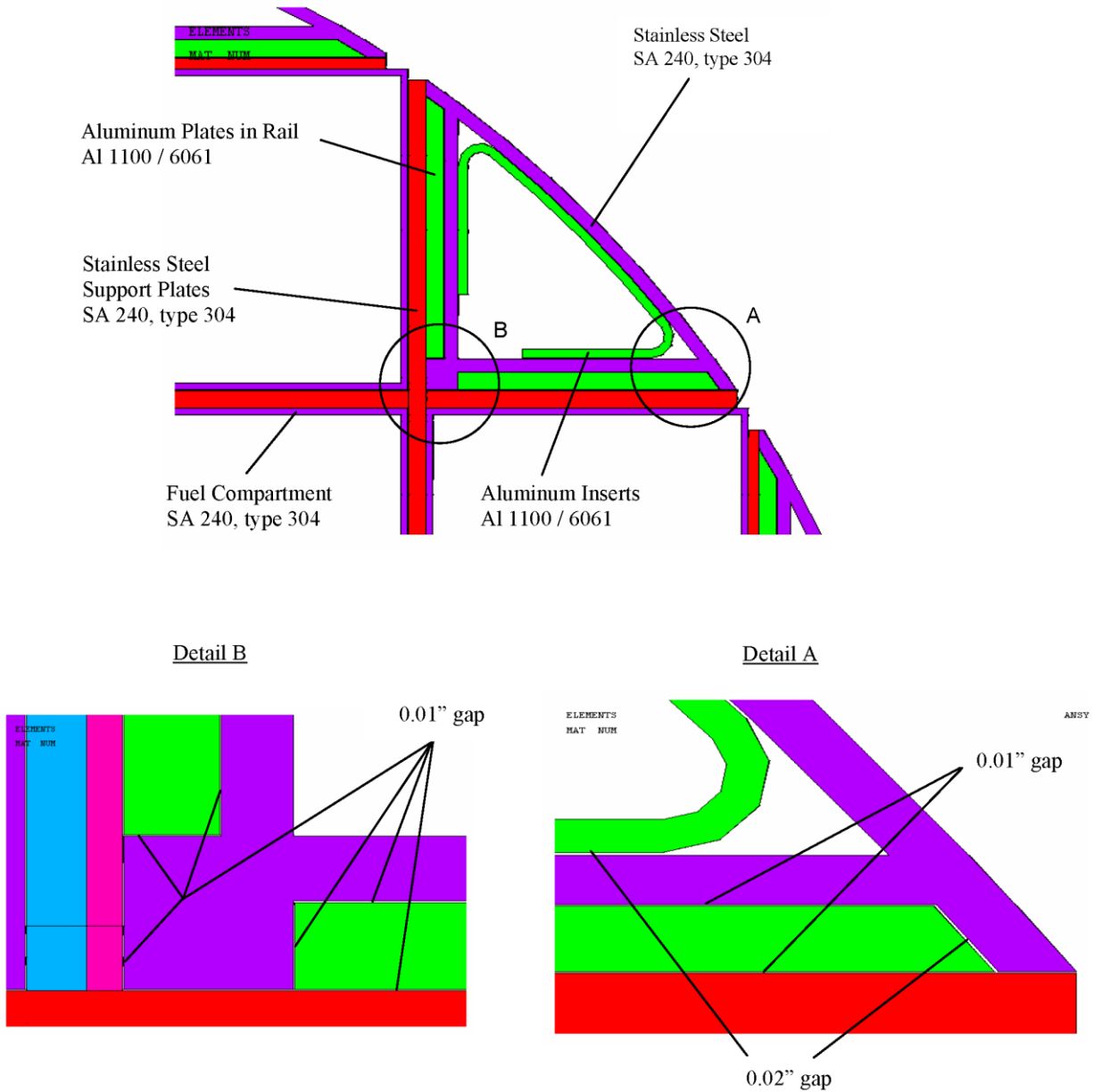


Figure 4-14
FEM of DSC Rails, Details

Configuration 1

	1.1	1.2	1.2	1.1	
1.1	1.1	1.1	1.1	1.1	1.1
1.2	1.1	0.8	0.8	1.1	1.2
1.2	1.1	0.8	0.8	1.1	1.2
1.1	1.1	1.1	1.1	1.1	1.1
	1.1	1.2	1.2	1.1	

Configuration 2

	1.1	1.5	1.5	1.1	
1.1	1.1	1.1	1.1	1.1	1.1
1.5	1.1	0.2	0.2	1.1	1.5
1.5	1.1	0.2	0.2	1.1	1.5
1.1	1.1	1.1	1.1	1.1	1.1
	1.1	1.5	1.5	1.1	

Configuration 3

	1.1	1.5	1.5	1.1	
1.1	1.1	0.925	0.925	1.1	1.1
1.5	0.925	0.55	0.55	0.925	1.5
1.5	0.925	0.55	0.55	0.925	1.5
1.1	1.1	0.925	0.925	1.1	1.1
	1.1	1.5	1.5	1.1	

Configuration 4

	0.98	1.5	1.5	0.98	
0.98	0.98	0.98	0.98	0.98	0.98
1.5	0.98	0.80	0.80	0.98	1.5
1.5	0.98	0.80	0.80	0.98	1.5
0.98	0.98	0.98	0.98	0.98	0.98
	0.98	1.5	1.5	0.98	

Configuration 5

	1.1	1.2	1.2	1.1	
1.1	1.1	1.1	1.1	1.1	1.1
1.2	1.1	0.55	0.55	1.1	1.2
1.2	1.1	1.05	1.05	1.1	1.2
1.1	1.1	1.1	1.1	1.1	1.1
	1.1	1.2	1.2	1.1	

Figure 4-15
Thermally Bounding Loading Configurations Considered in the DSC Model
For Total Decay Heat Load of 34.8 kW

Configuration 6

	1.068	1.168	1.168	1.068	
1.068	1.068	1.068	1.068	1.068	1.068
1.168	1.068	0.755	0.755	1.068	1.168
1.168	1.068	0.755	0.755	1.068	1.168
1.068	1.068	1.068	1.068	1.068	1.068
	1.068	1.168	1.168	1.068	

Configuration 7

	0.935	1.5	1.5	0.935	
0.935	0.935	0.935	0.935	0.935	0.935
1.5	0.935	0.775	0.775	0.935	1.5
1.5	0.935	0.775	0.775	0.935	1.5
0.935	0.935	0.935	0.935	0.935	0.935
	0.935	1.5	1.5	0.935	

Figure 4-15 – Concluded
Thermally Bounding Loading Configurations Considered in the DSC Model
For Total Decay Heat Load of 33.8 kW, CE14x14 Fuel Assemblies

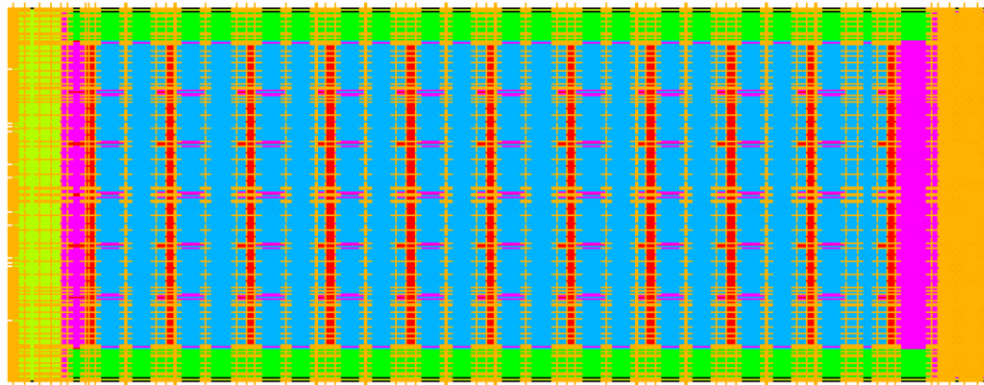
Temperature Boundary Conditions

ELEMENTS

ANSYS 6.0

MAT NUM

TEMP

Heat Generating Boundary Conditions

ELEMENTS

ANSYS 6.0

HGEN RATES

QMIN=0

QMAX=.421504

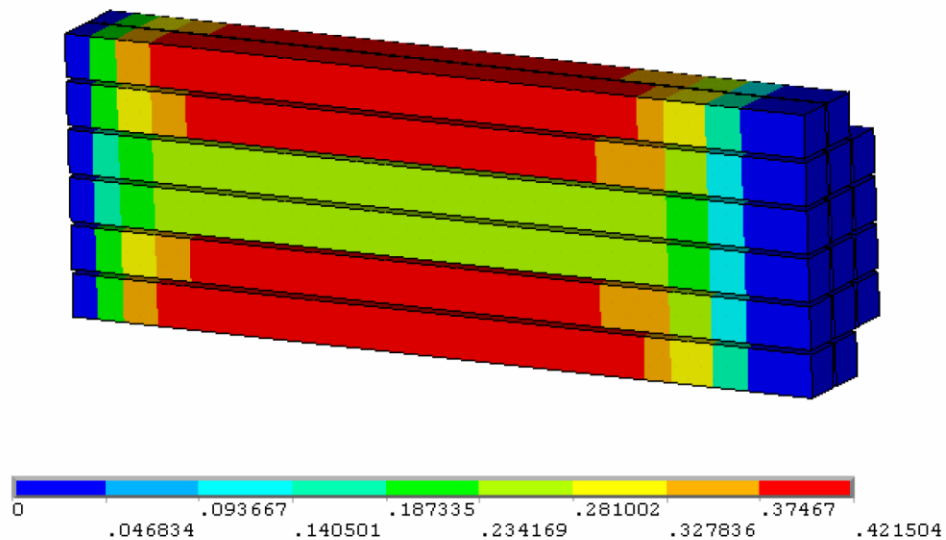


Figure 4-16
Typical Boundary Conditions in the DSC Model

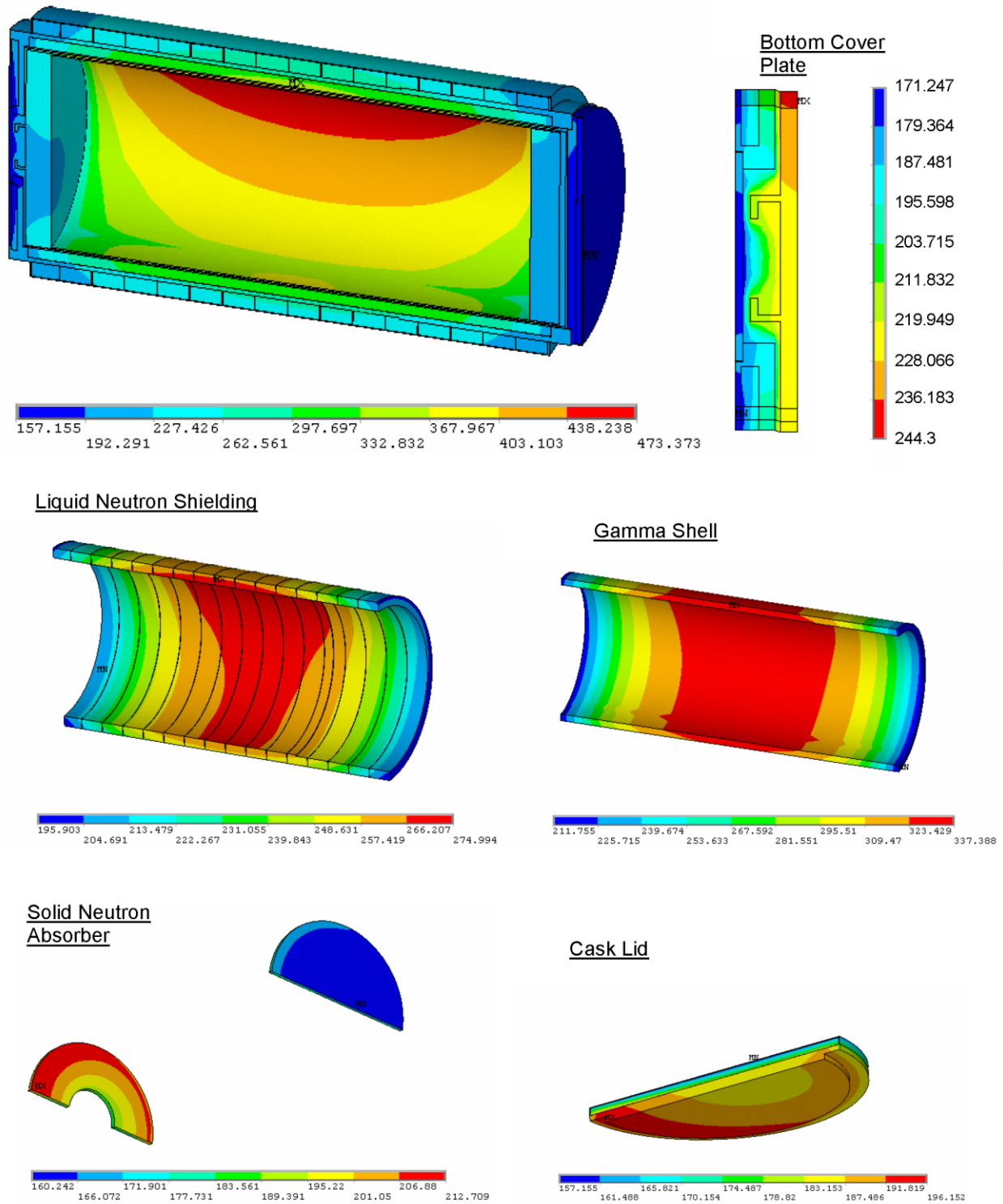


Figure 4-17
Transfer Cask Temperature Distributions, 115°F Ambient

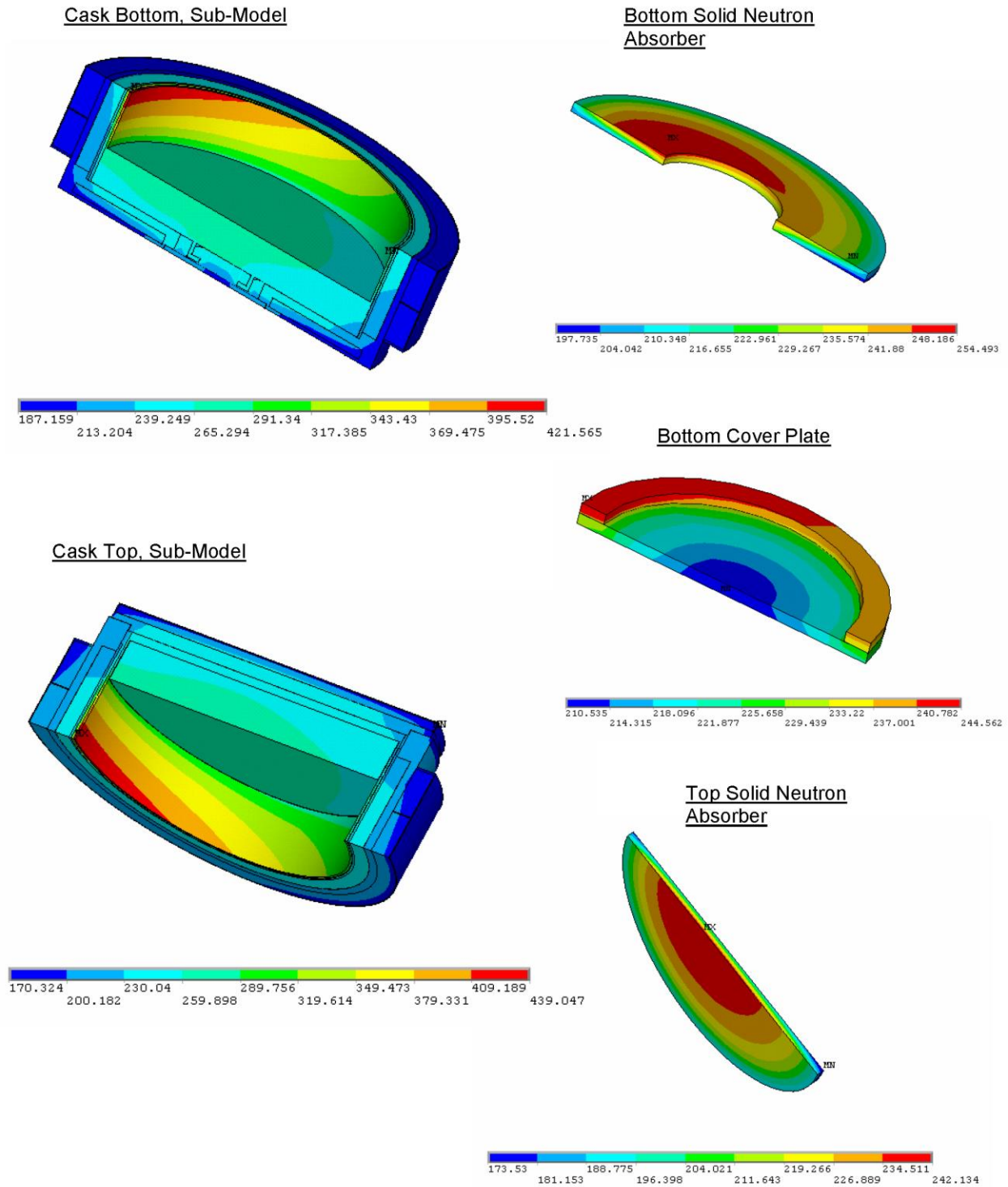


Figure 4-18
Temperature Distributions in Transfer Cask Sub-Models

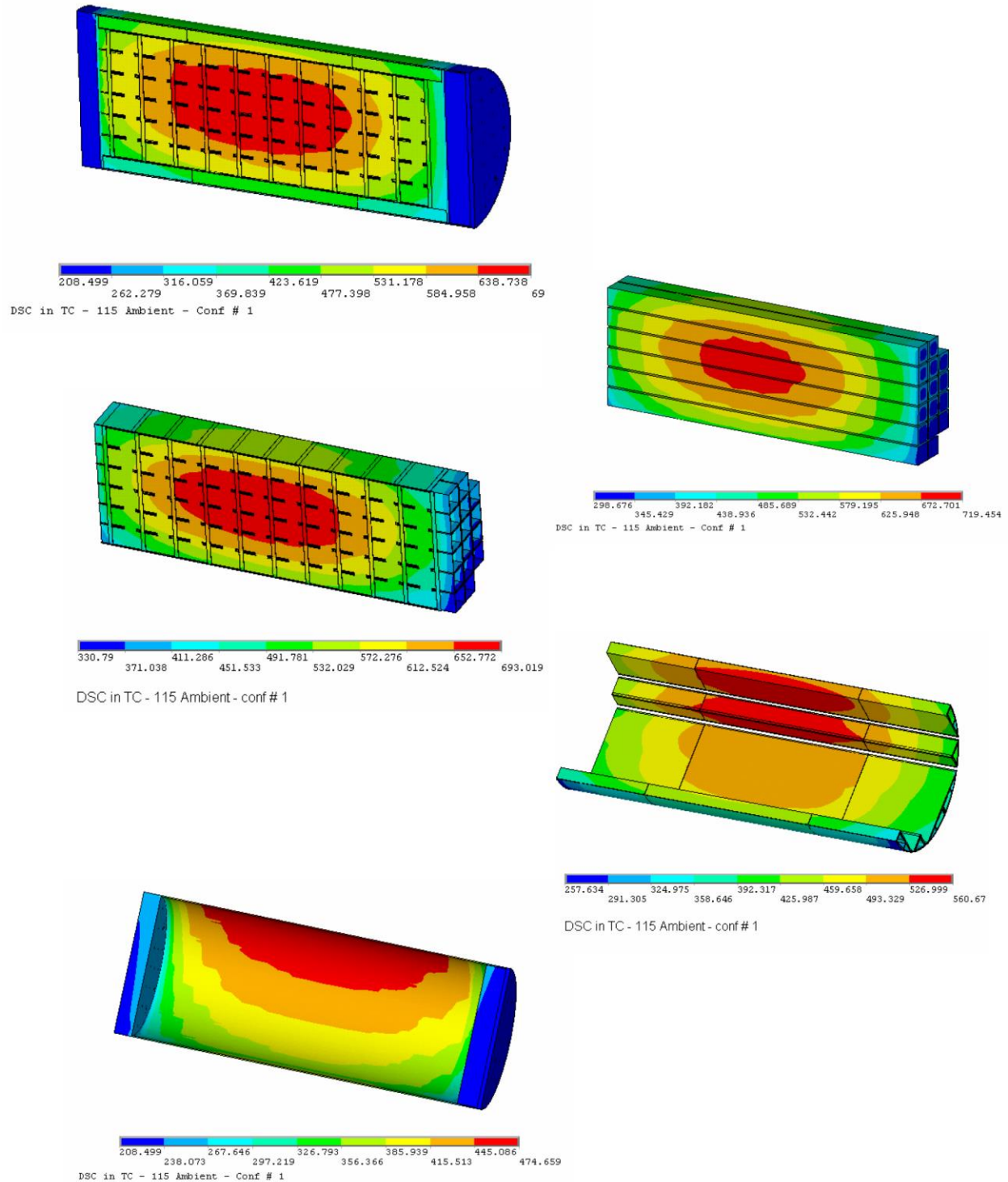


Figure 4-19
DSC Temperature Distribution during Transfer Operation
Basket Type I, Loading Configuration 1, 115°F Ambient

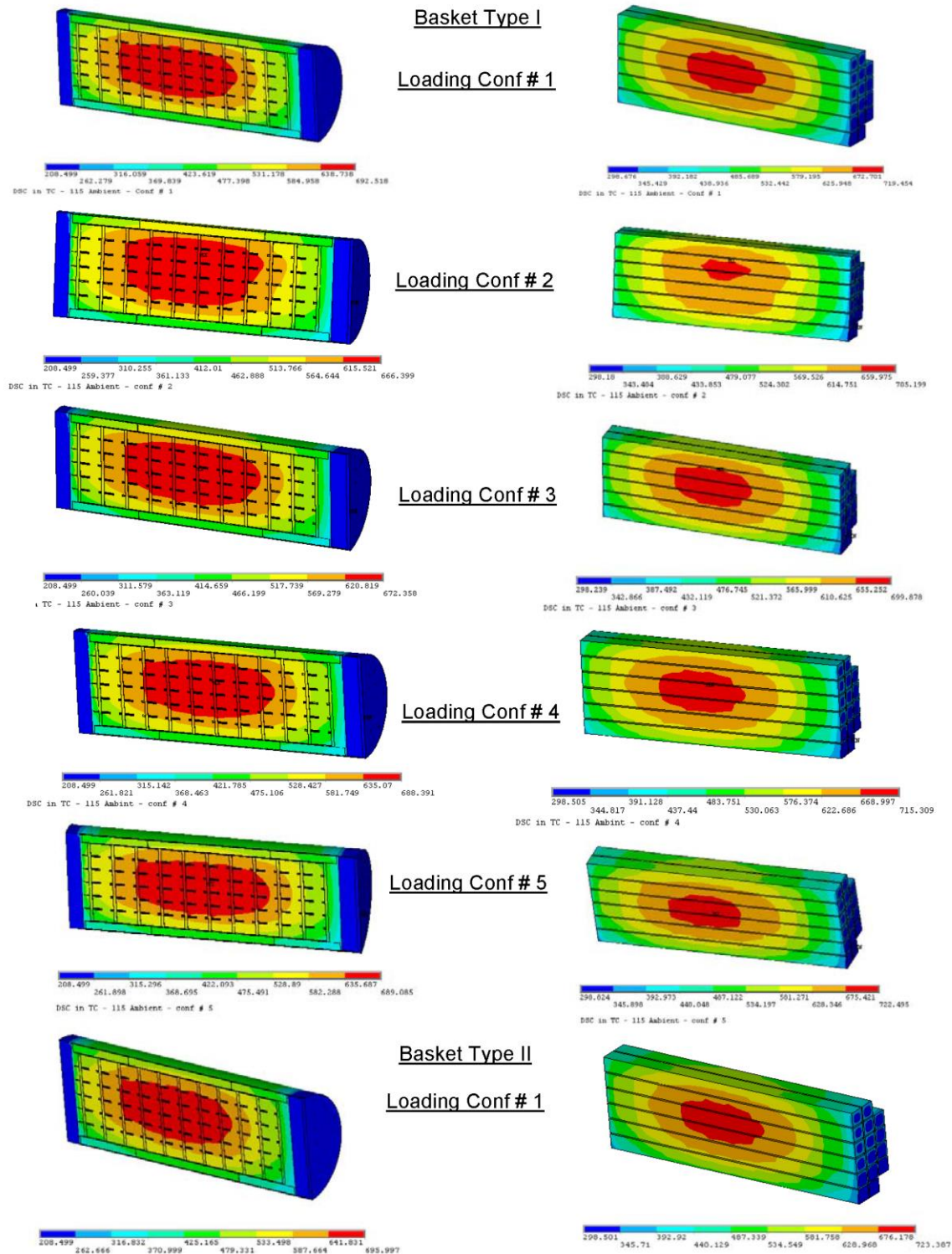


Figure 4-20
Temperature Distribution of DSC and Fuel Assemblies
during Transfer Operations, 115°F Ambient

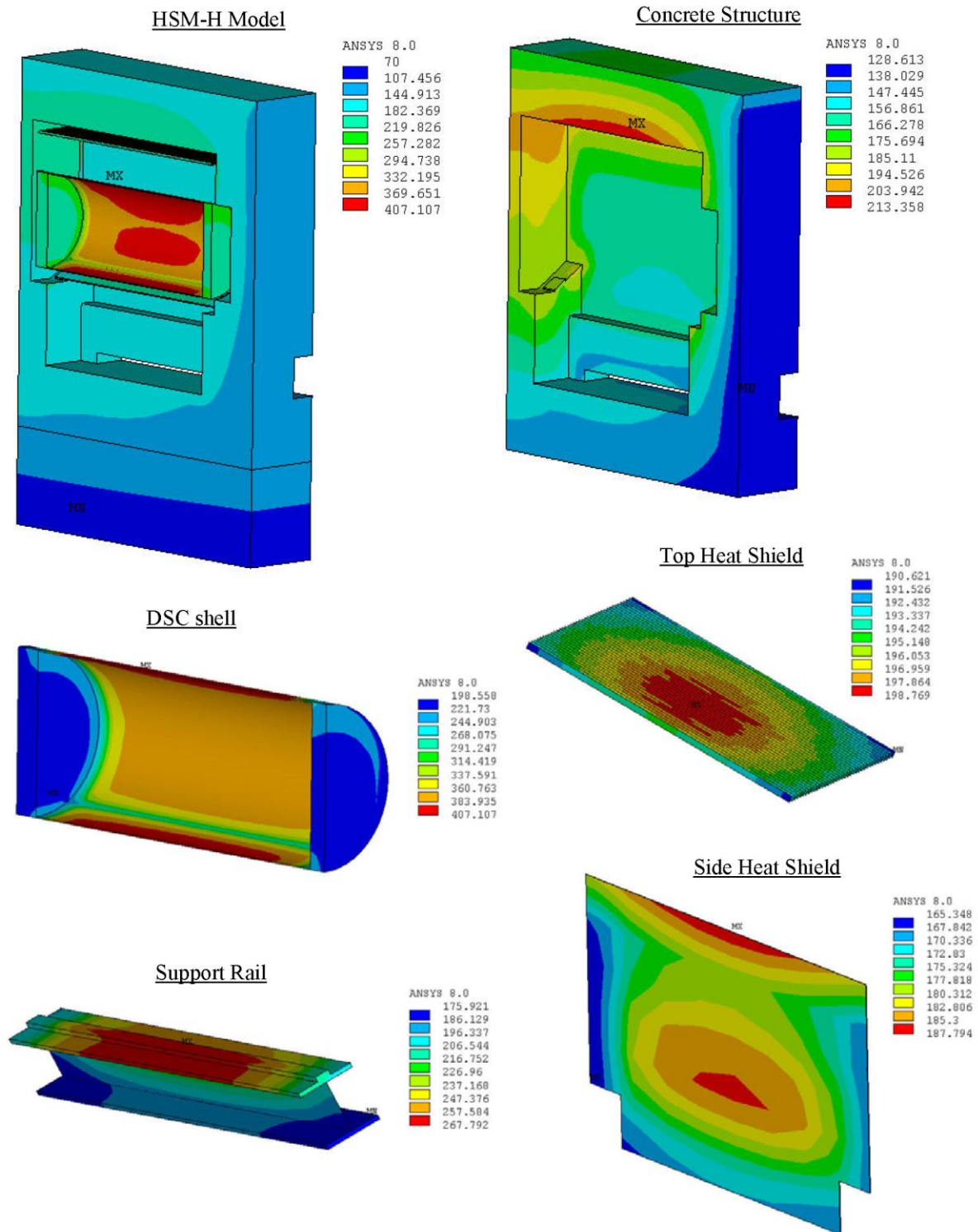
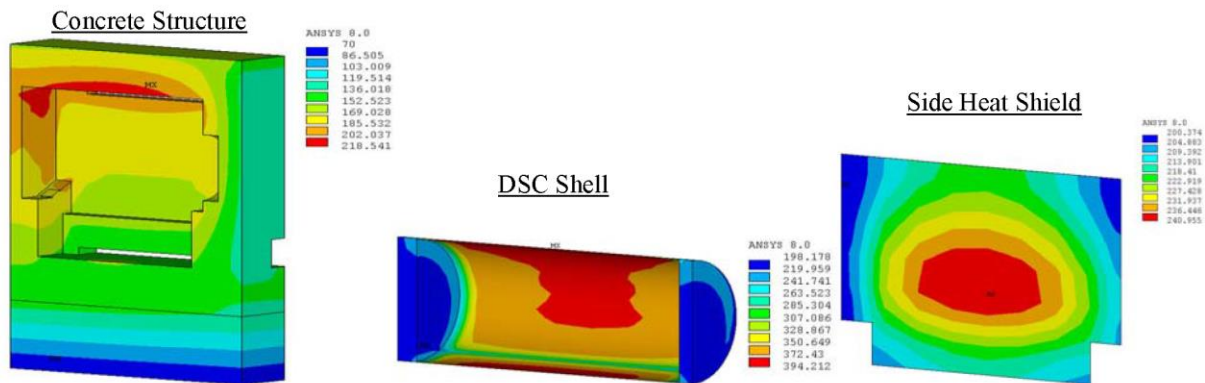
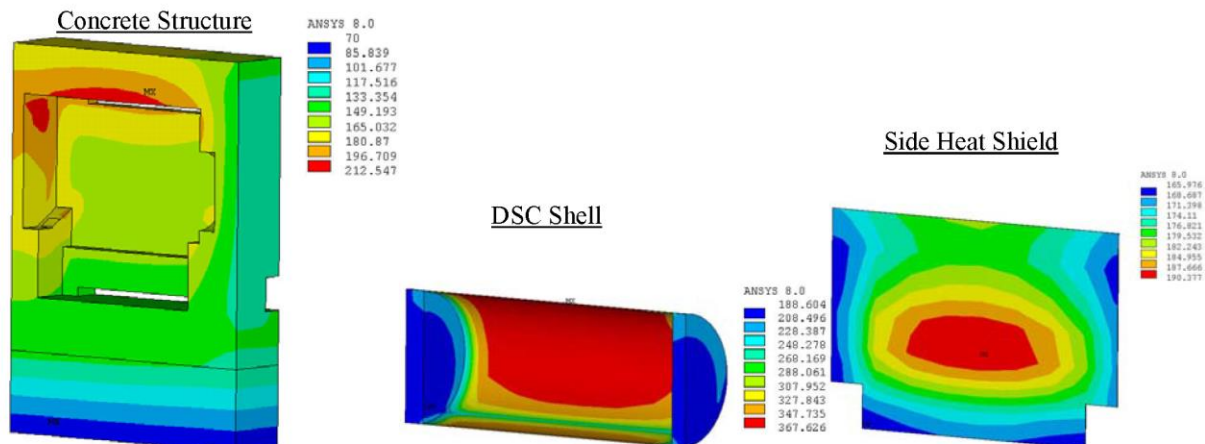


Figure 4-21
HSM-H Temperature Distribution 115°F Ambient
with Finned Aluminum Side Heat Shields, 34.8 kW

HSM-H with Un-finned Aluminum Side Heat Shield – 32.0 kW



HSM-H with Un-finned Galvanized Steel Side Heat Shield – 26.1 kW



HSM-H with Flat Stainless Steel Top & Side Heat Shields – 34.8 kW

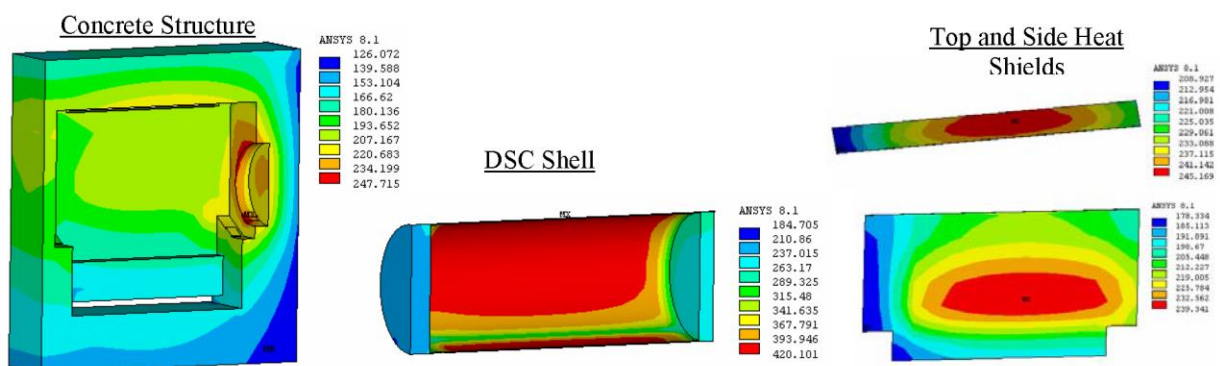


Figure 4-22
HSM-H Temperature Distribution 115°F Ambient
with Un-finned Side Heat Shields

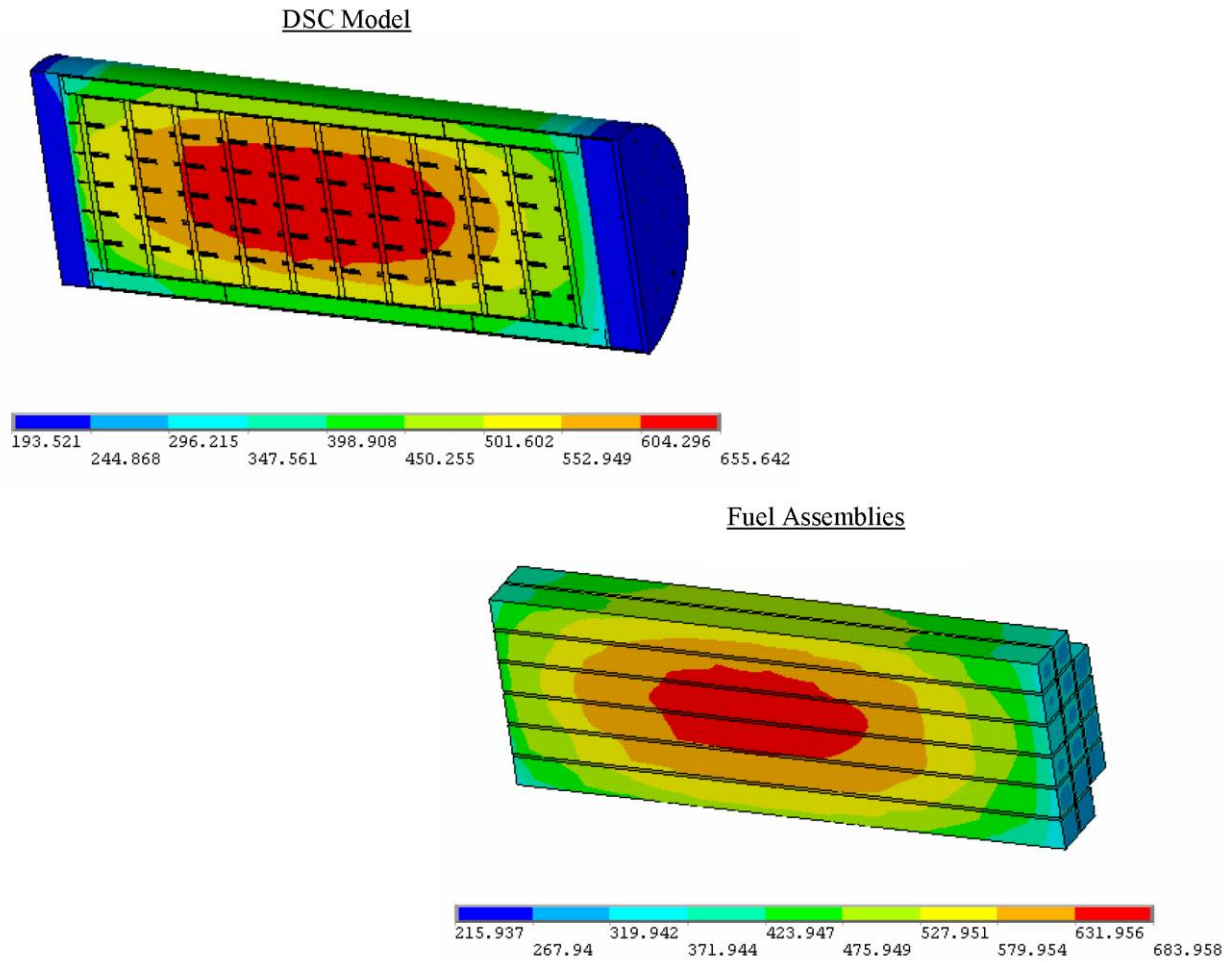


Figure 4-23
DSC Temperature Distribution during Storage, 115°F Ambient, 34.8 kW
in HSM-H with Finned Aluminum Side Heat Shields*

* These temperature distributions are calculated based on DSC maximum shell temperature of 422°F. Therefore, these profiles are bounding for the HSM-H with flat stainless steel heat shields with maximum DSC shell temperature of 420°F reported in Table 4-2.

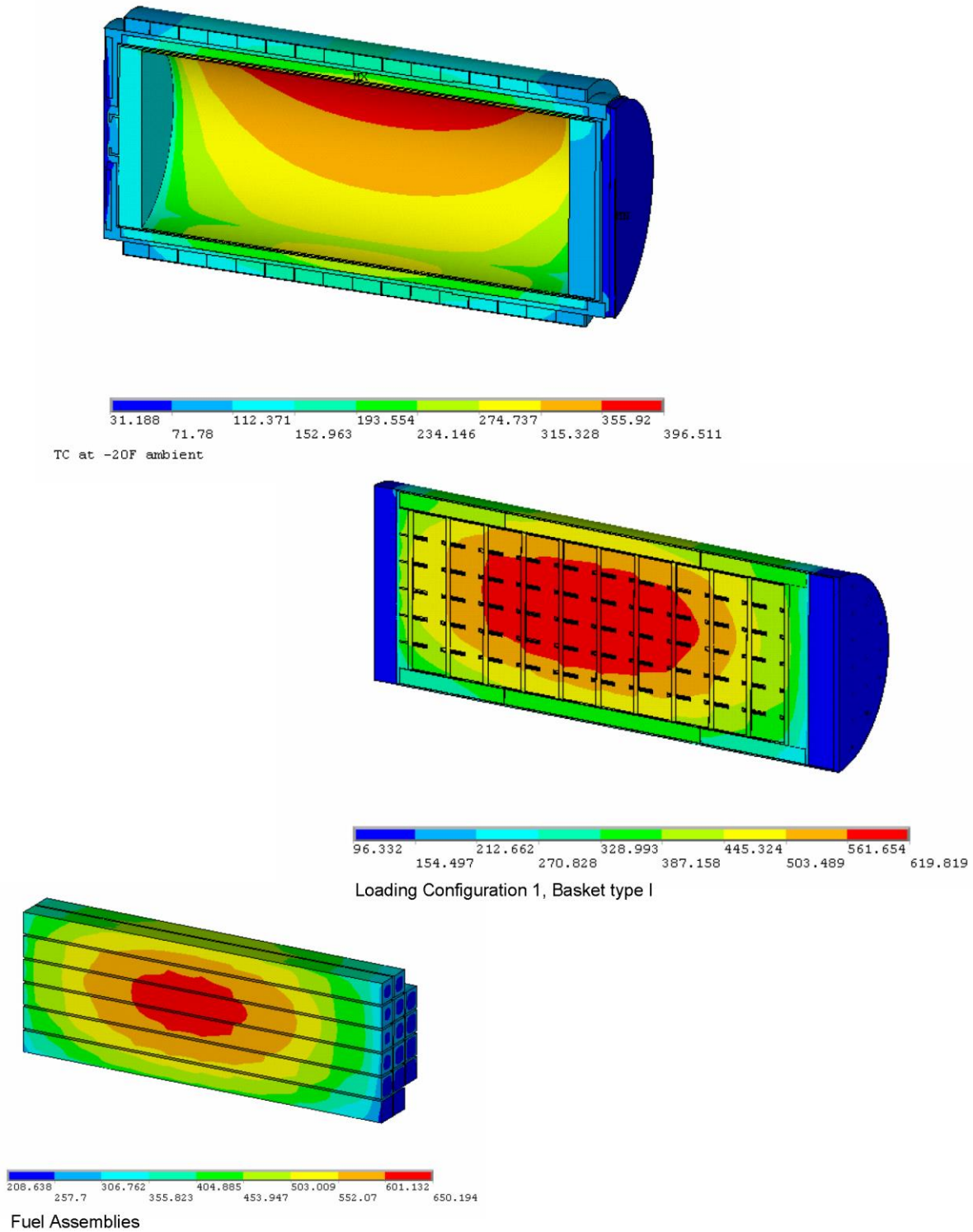


Figure 4-24
Temperature Distributions during Transfer Operations, Ambient -20°F

HSM-H with Finned Aluminum Side Heat Shields

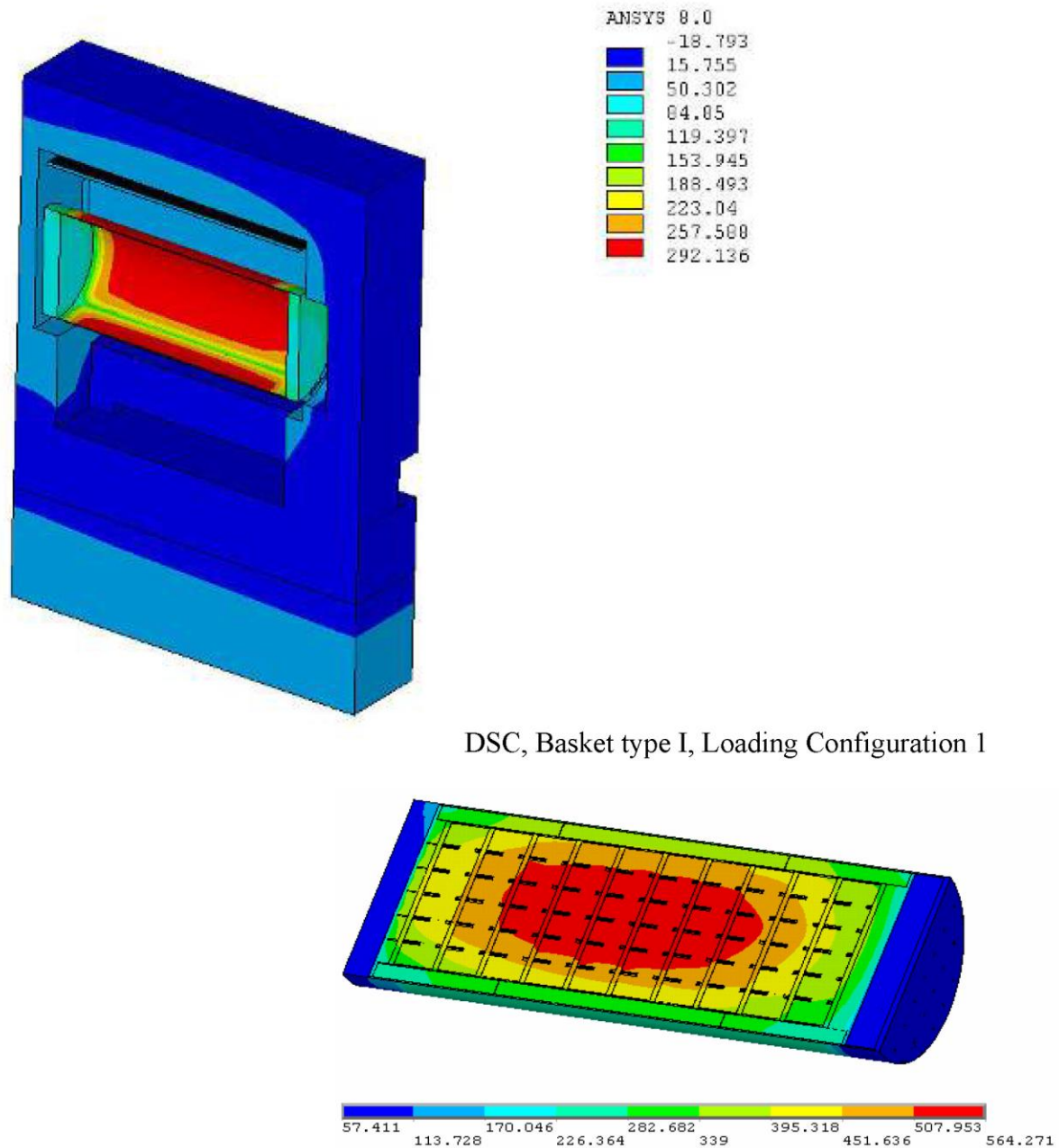


Figure 4-25
Temperature Distribution during Storage, Ambient -20°F, 34.8 kW

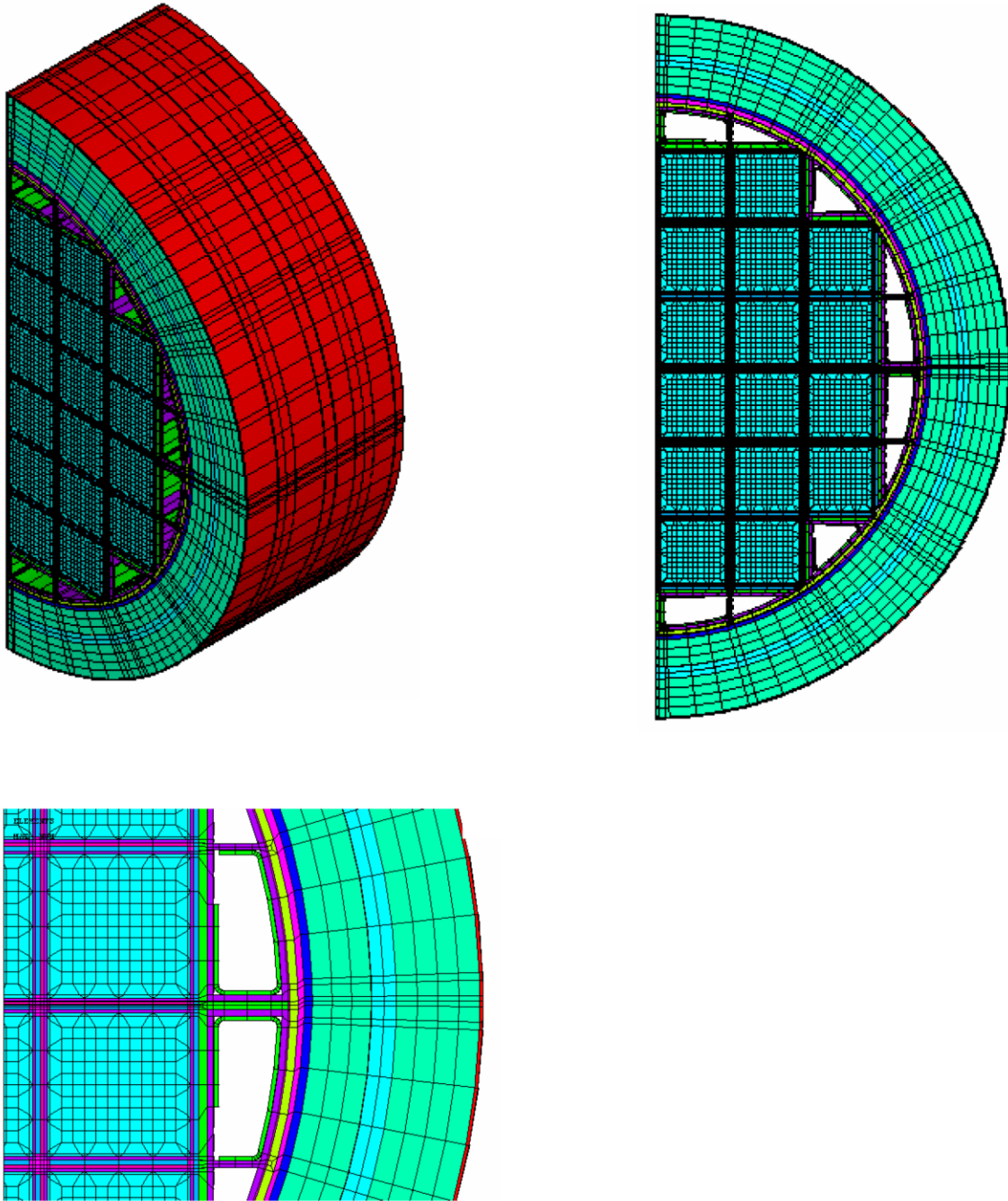


Figure 4-26
FEM of Transfer Cask for Fire Accident Case

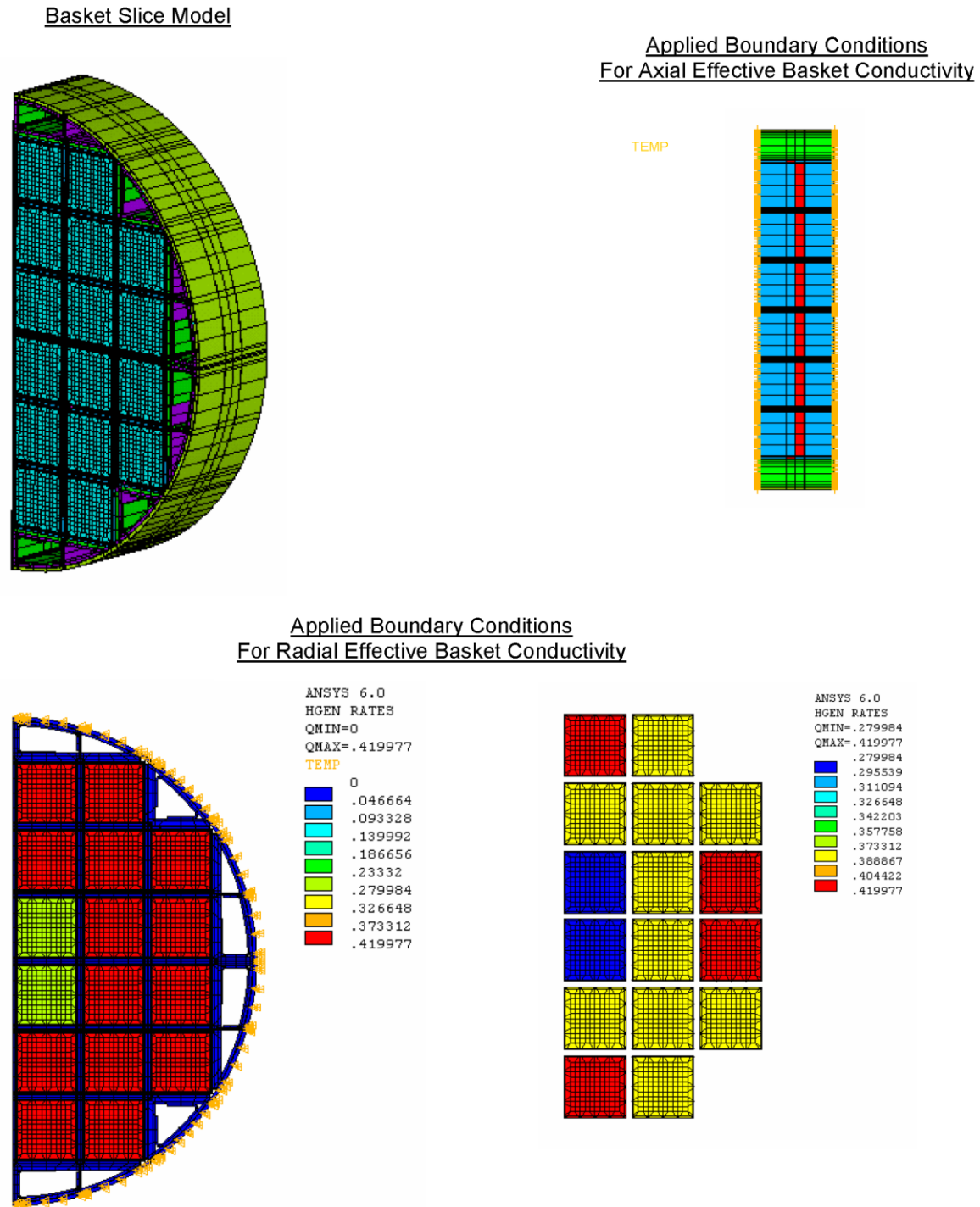


Figure 4-27
Basket Model for Calculation of Effective Conductivities
(HSM-H Model Blocked Vent Accident Case)

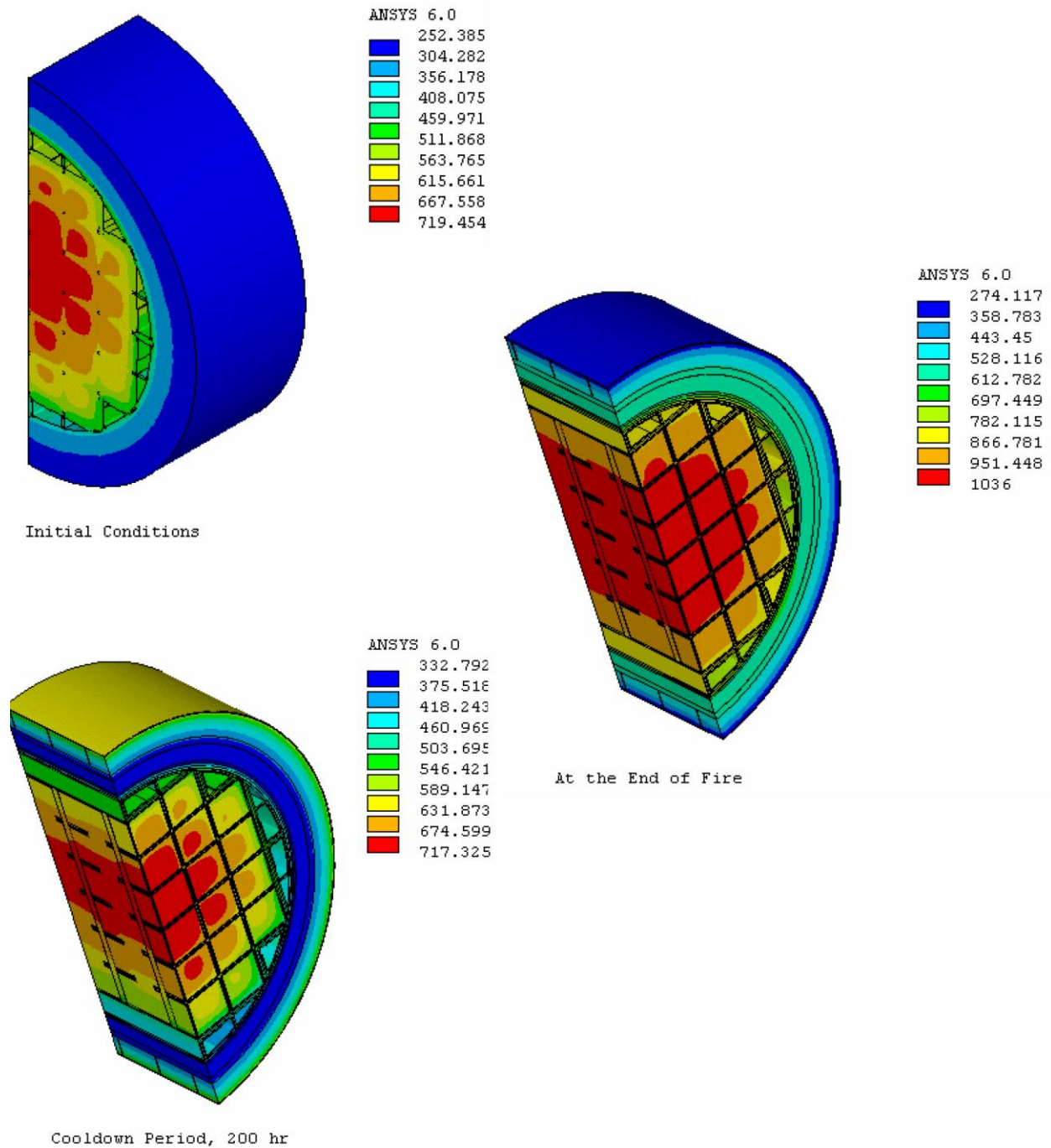


Figure 4-28
Temperature Distribution on TC Slice Model for Fire Accident Case

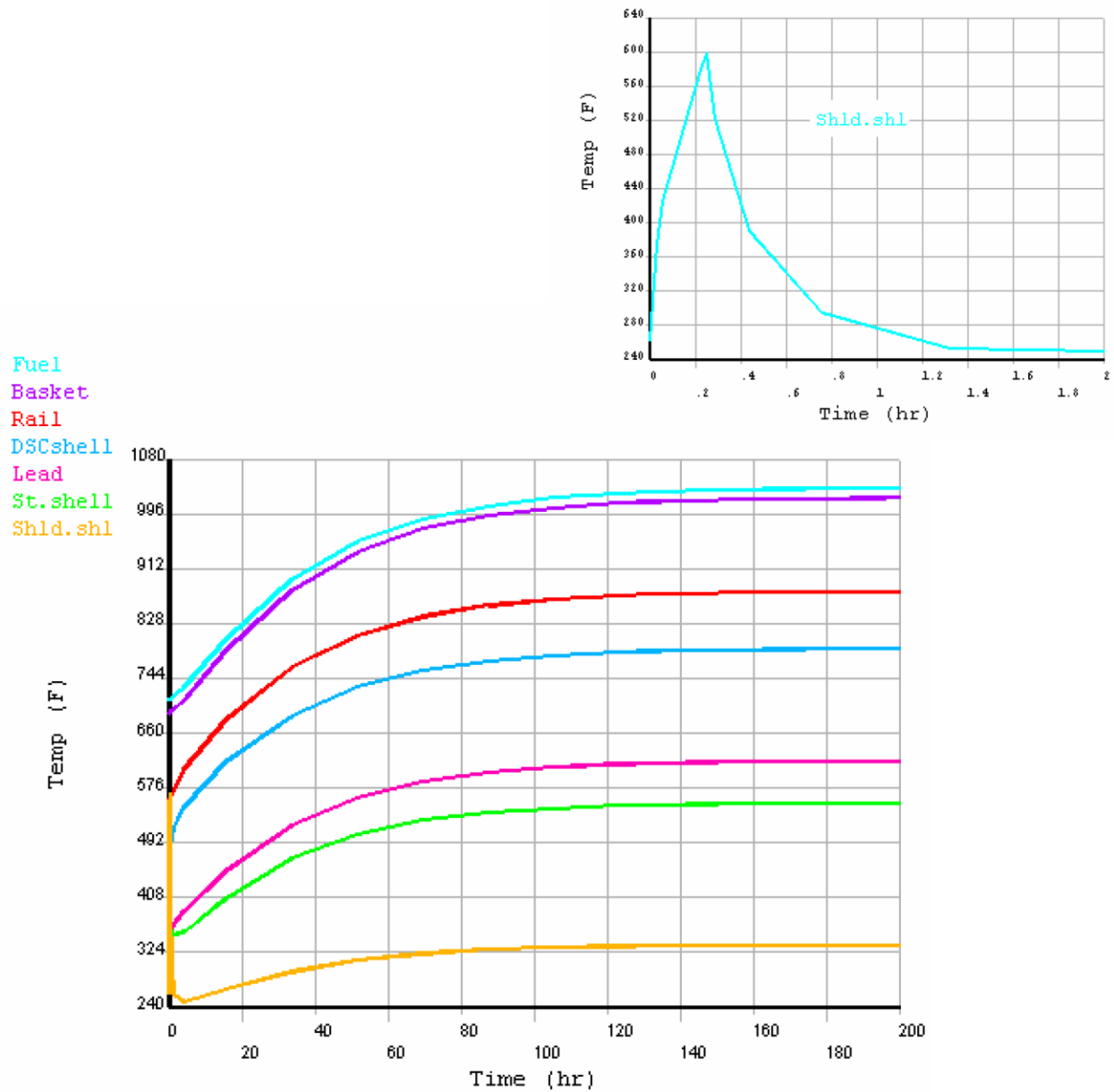


Figure 4-29
Time-History of TC Component Temperatures for the Fire Accident Case

HSM-H with Finned Aluminum Side Heat Shields and Louvered Top Heat Shield

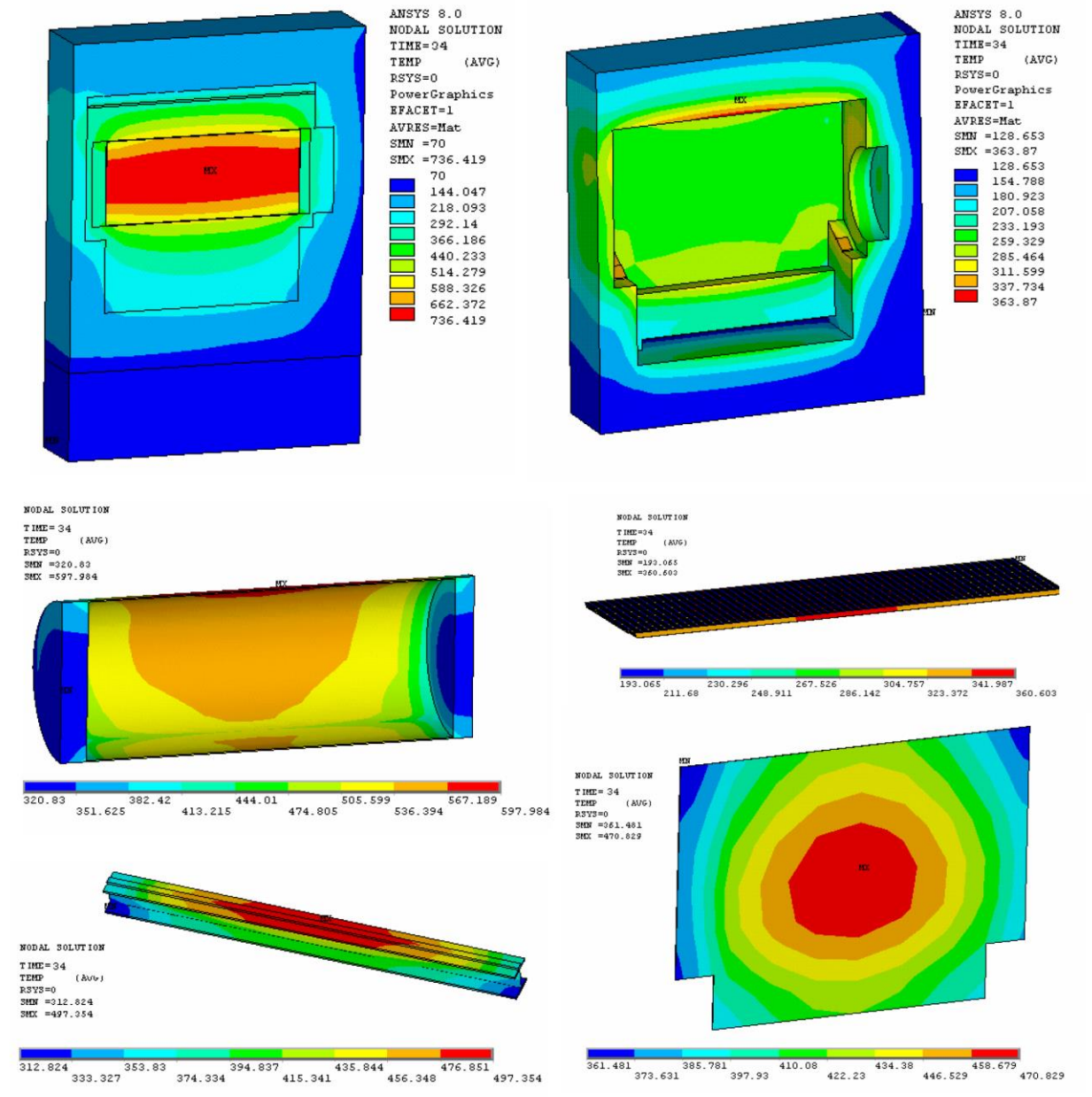


Figure 4-30
Temperature Distribution for HSM-H 34 hours after Blockage of the Vents,
34.8 kW

HSM-H with Flat Stainless Steel Top and Side Heat Shields

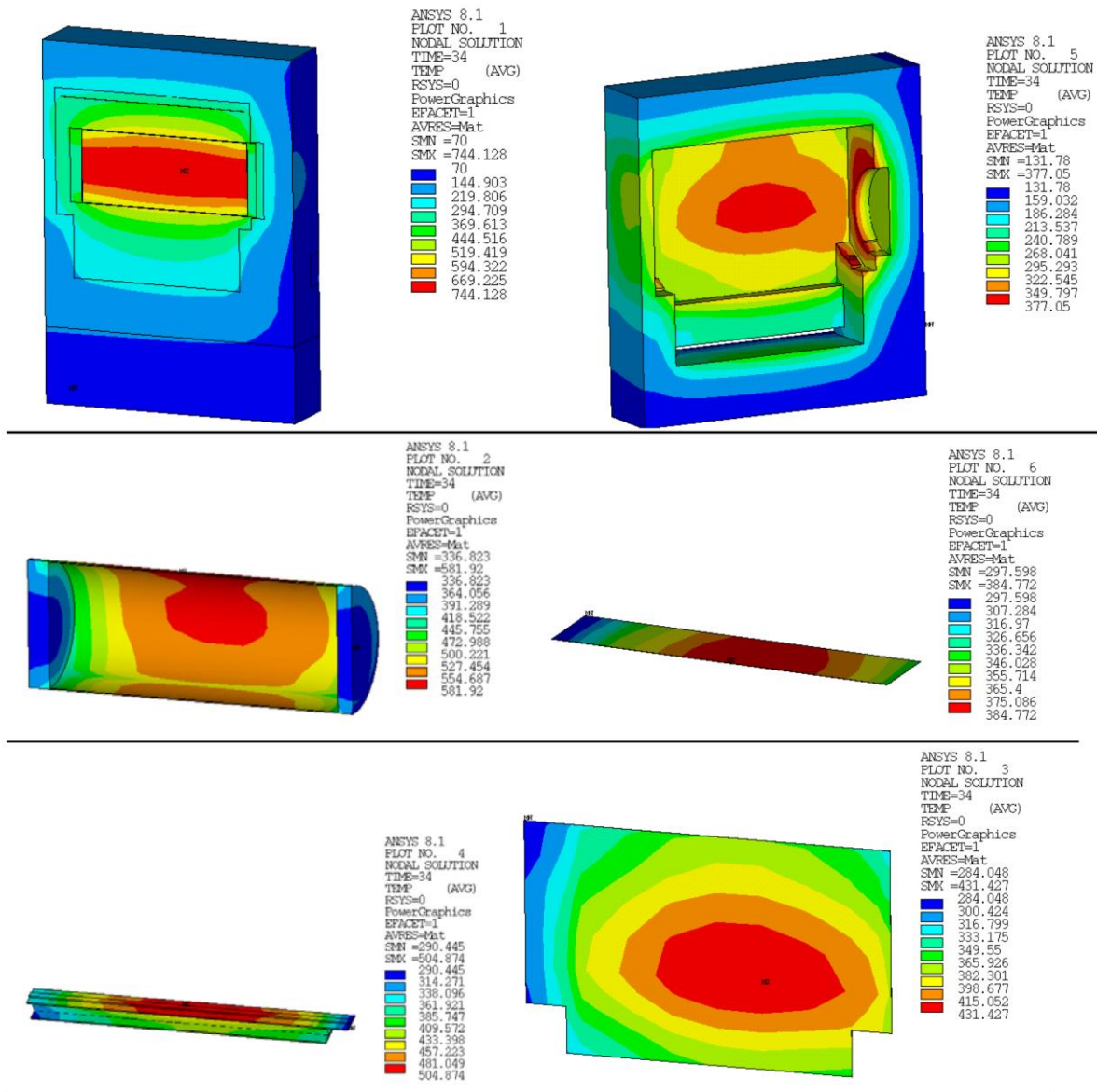


Figure 4-30—continued
Temperature Distribution for HSM-H 34 hours after Blockage of the Vents,
34.8 kW

FIGURE IS DELETED IN ITS ENTIRETY

**Figure 4-31
DELETED**

In HSM-H with Finned Aluminum Side Heat Shields
34 hours after Vent Blockage, 34.8 kW

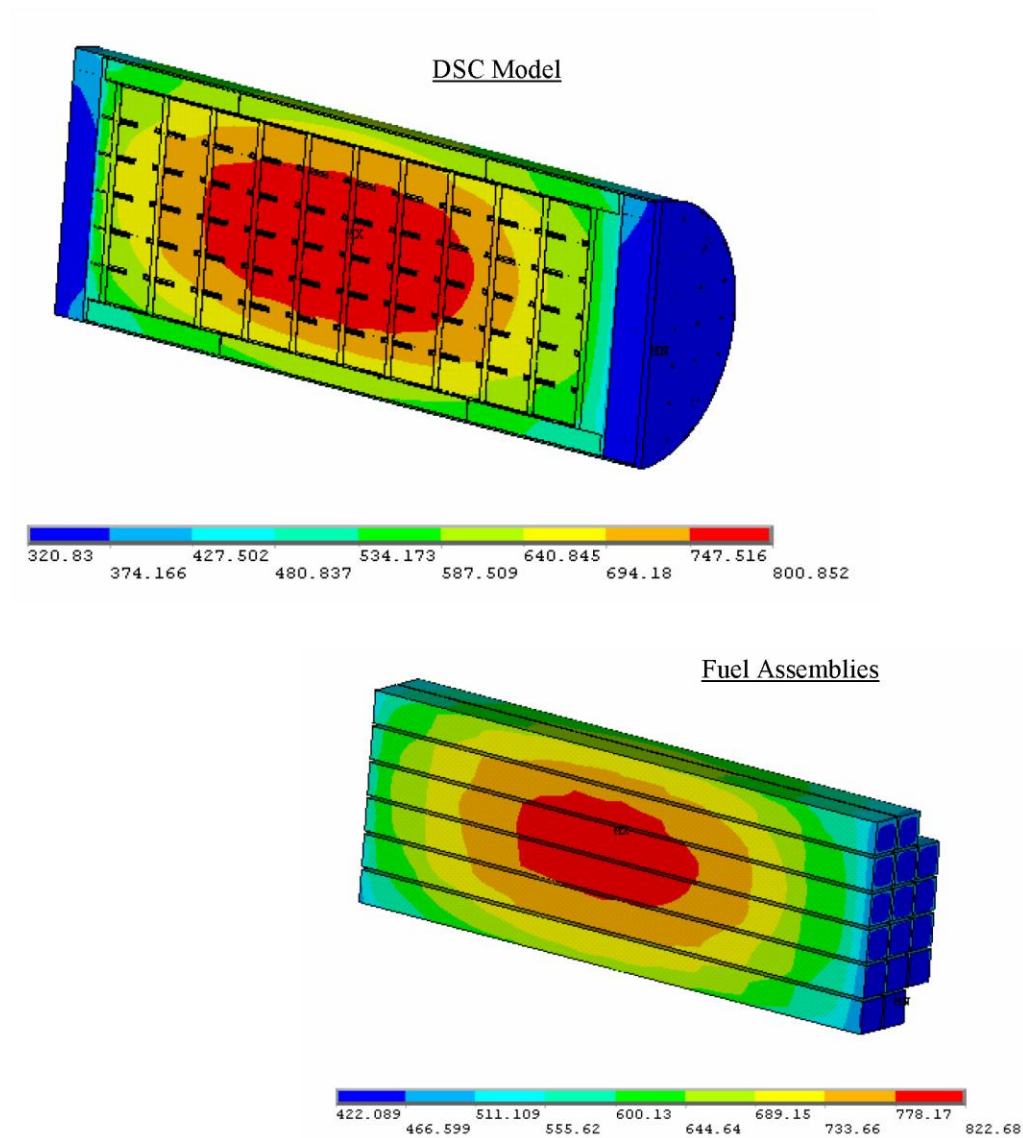


Figure 4-32
Temperature Distribution of DSC Model for Blocked Vent Accident Case

HSM-H Model with Finned Aluminum Side Heat
Shields, 34.8 kW

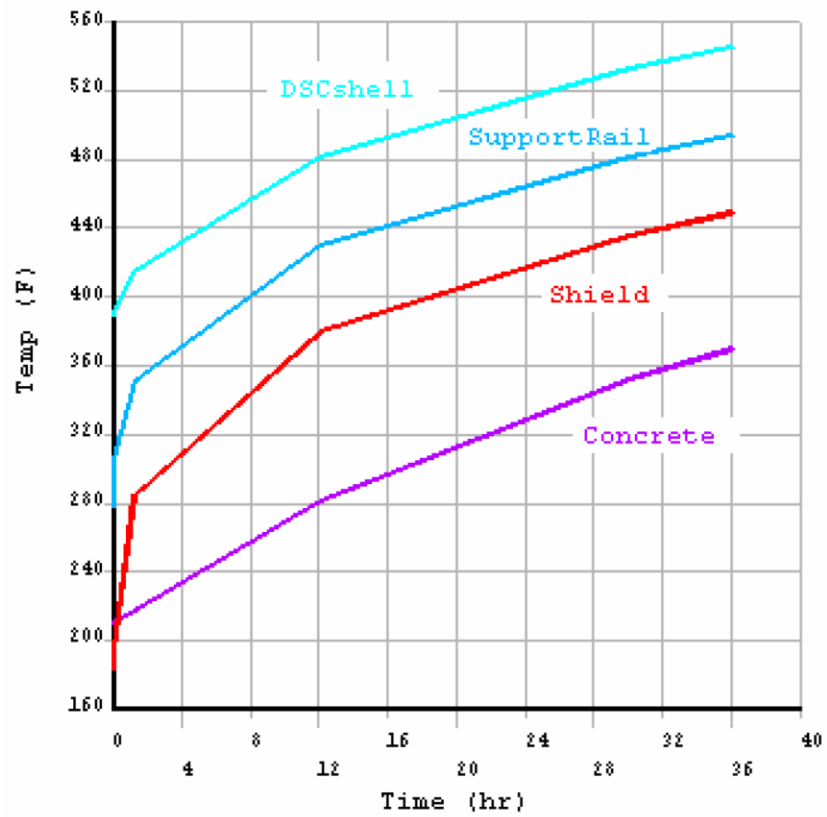


Figure 4-33
Temperature-Time History of HSM-H Components for Blocked Vent Accident Case

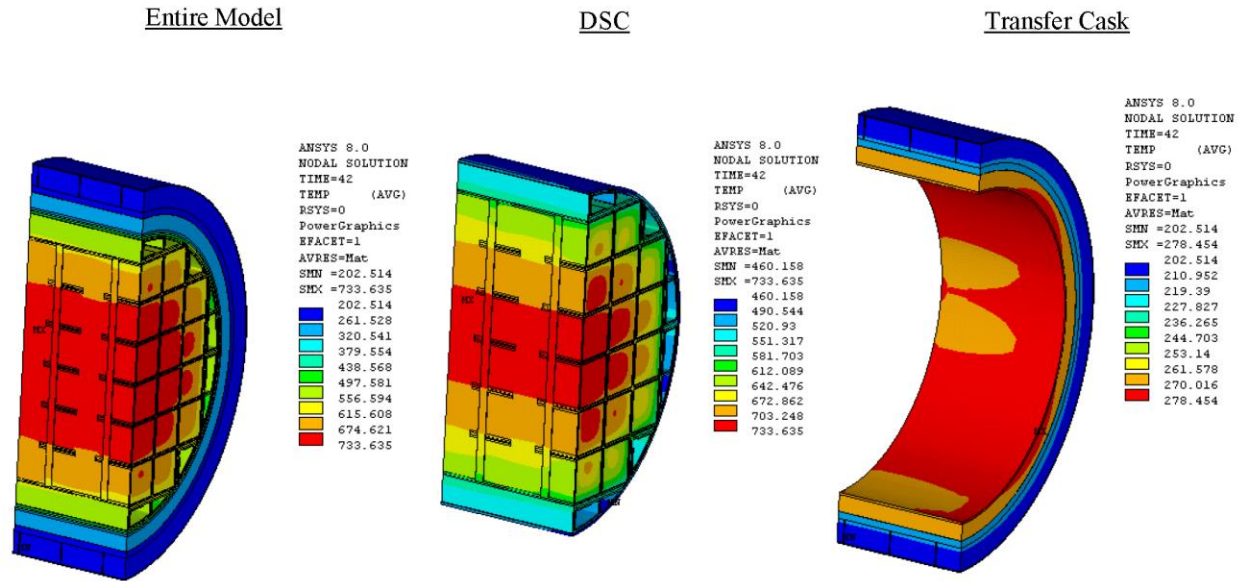


Figure 4-34
Temperature Distribution for TC Backfill Operations

FIGURE IS DELETED IN ITS ENTIRETY.

**Figure 4-35
DELETED**

FIGURE IS DELETED IN ITS ENTIRETY.

**Figure 4-36
DELETED**

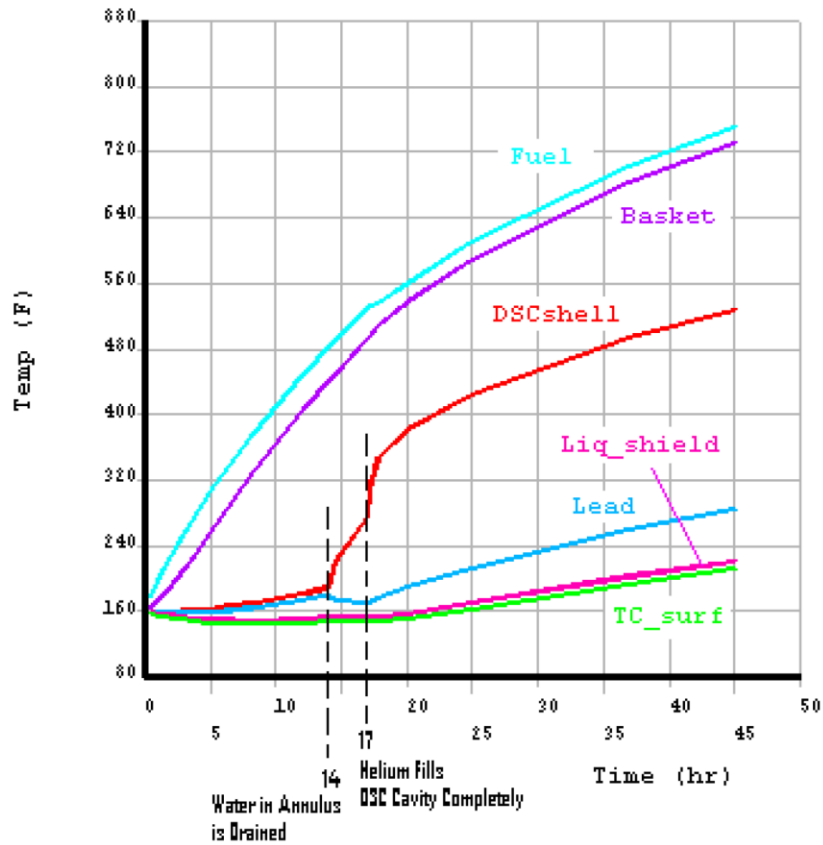


Figure 4-37
Time-Temperature History for TC Backfill Operations

Burnup rate MWD/MTU	Total Free Gas (cc/fuel rod)
35000	760
45000	939
55000	1073
60000	1123

← extrapolated

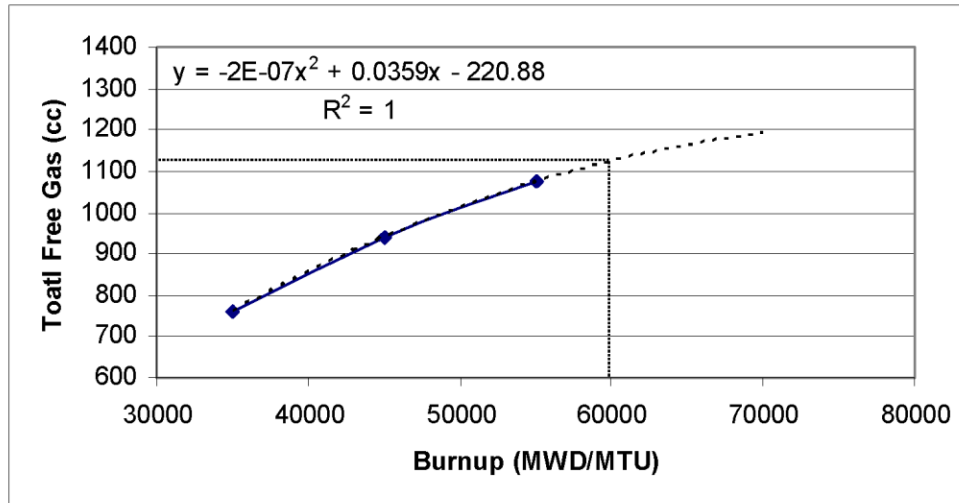
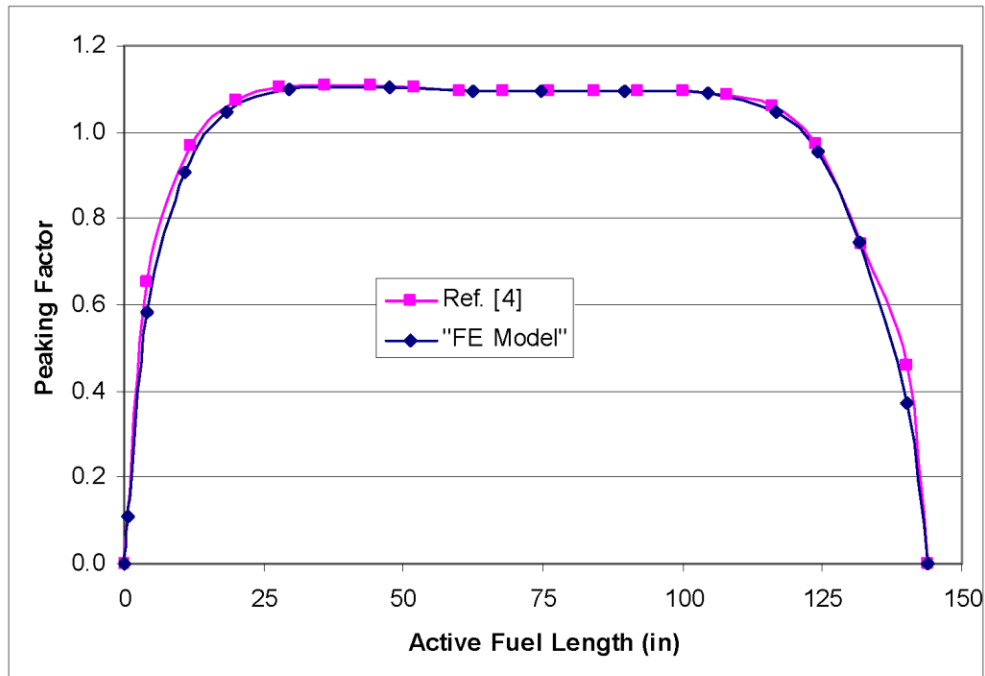


Figure 4-38
Total Free Gas Volume versus Burnup Rate



For Total Decay Heat of 33.8 kW, CE 14x14 Fuel Assemblies

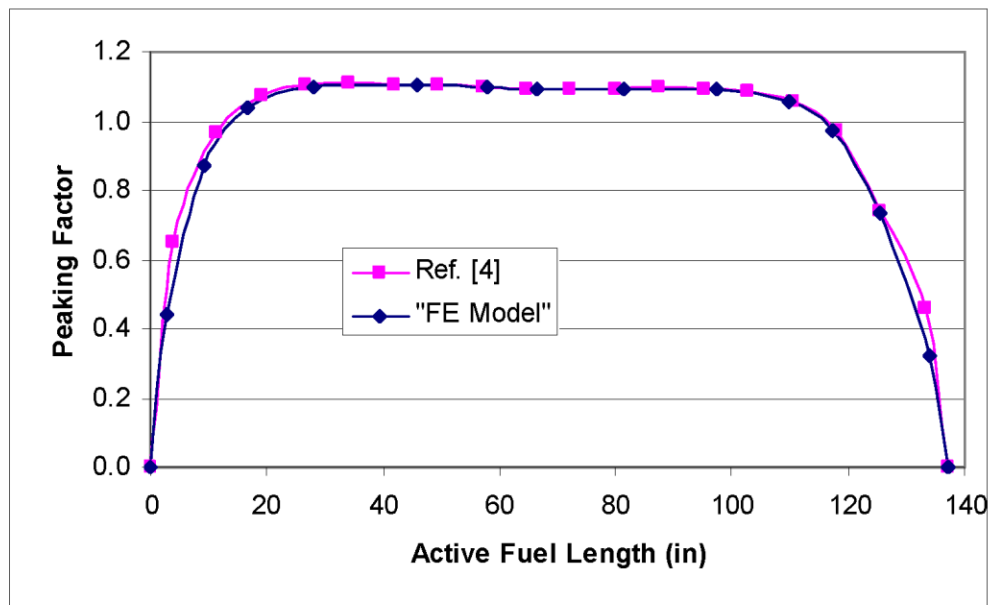


Figure 4-39
Comparison of the Axial Heat Profiles in the FE Model and in Ref. [4]

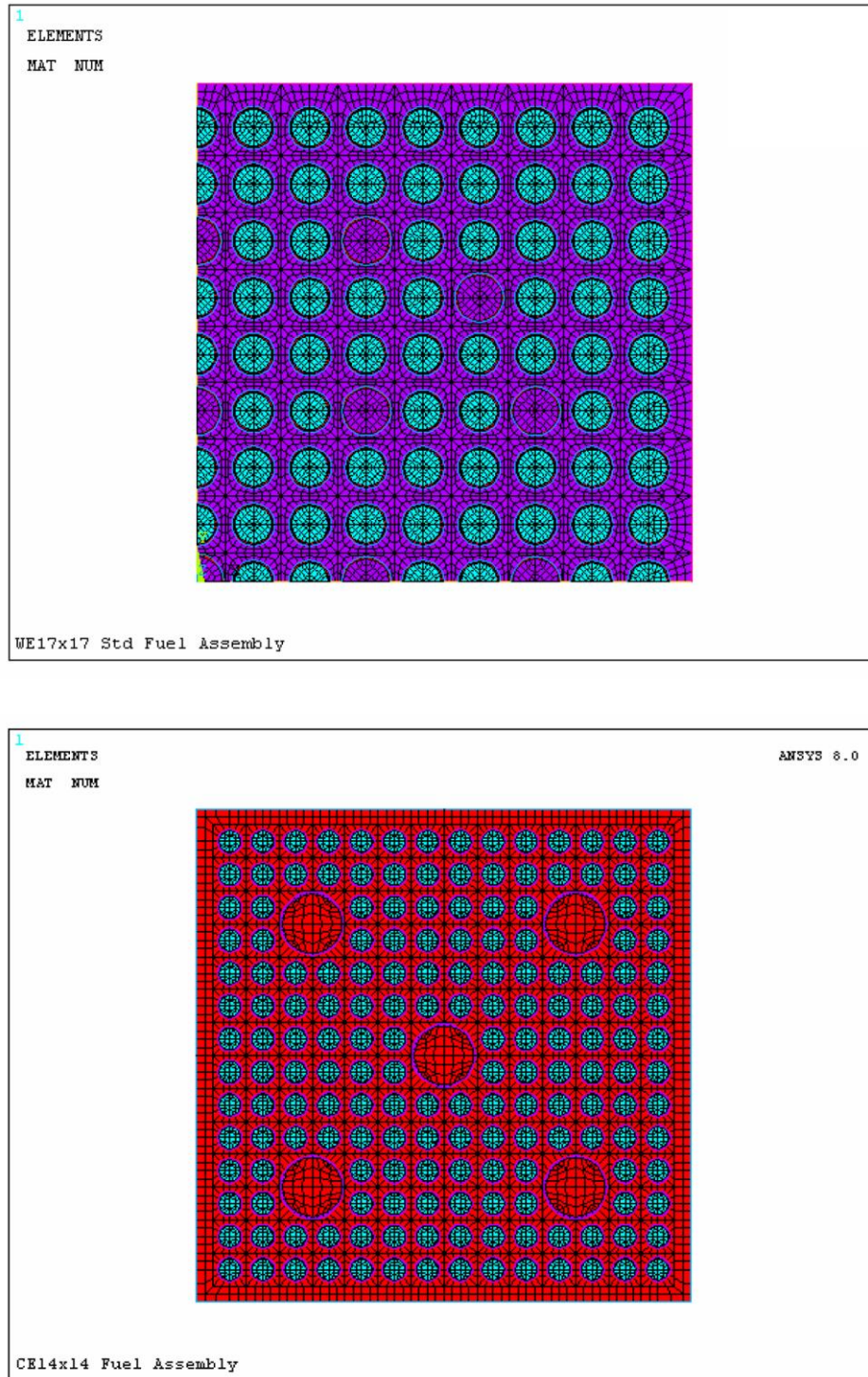


Figure 4-40
Finite Element Model of Fuel Assemblies

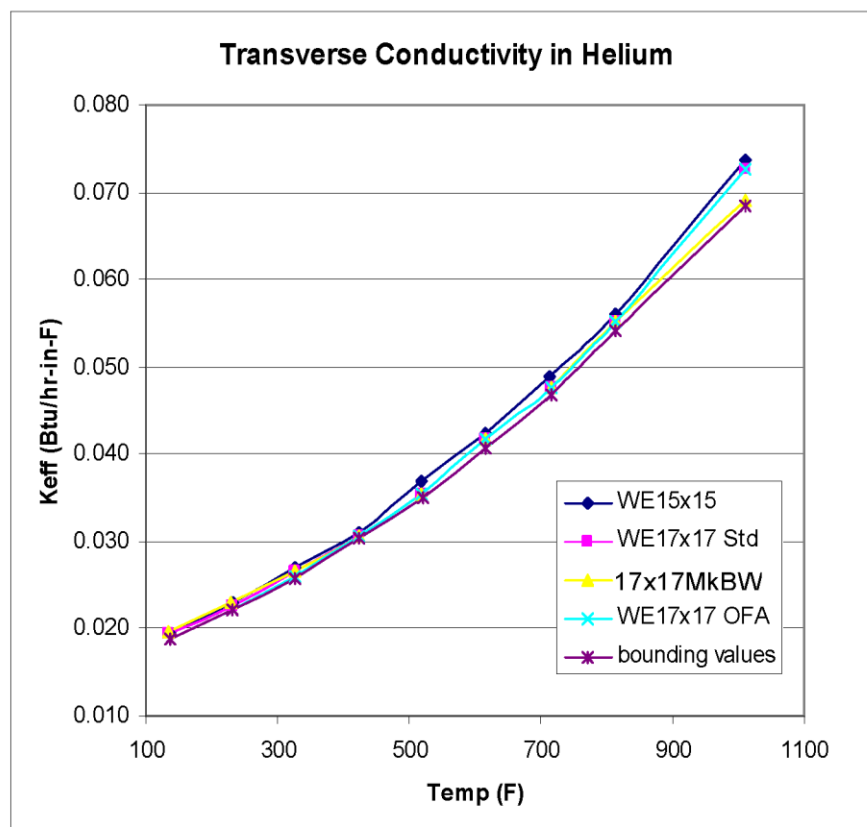
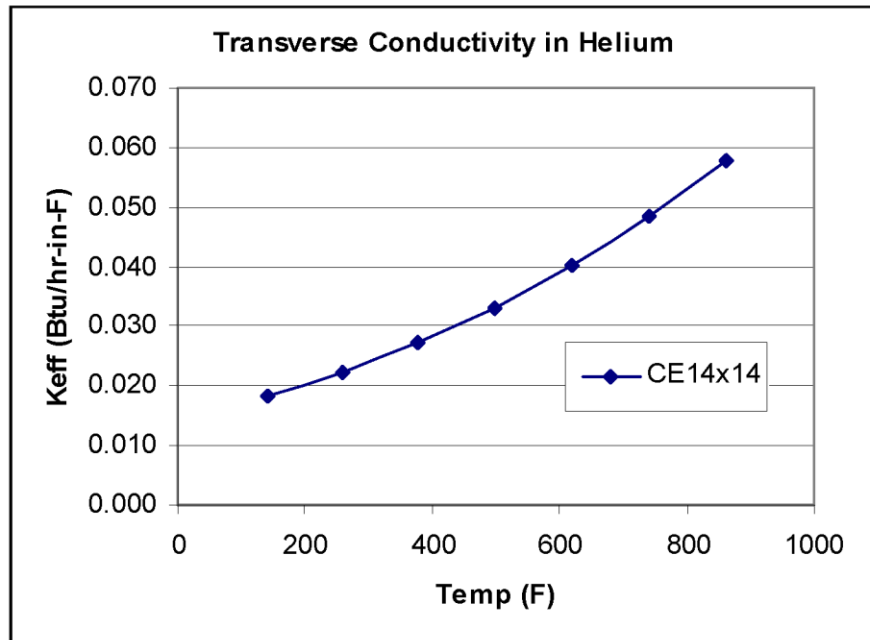


Figure 4-41
Effective Transverse Fuel Conductivity in Helium

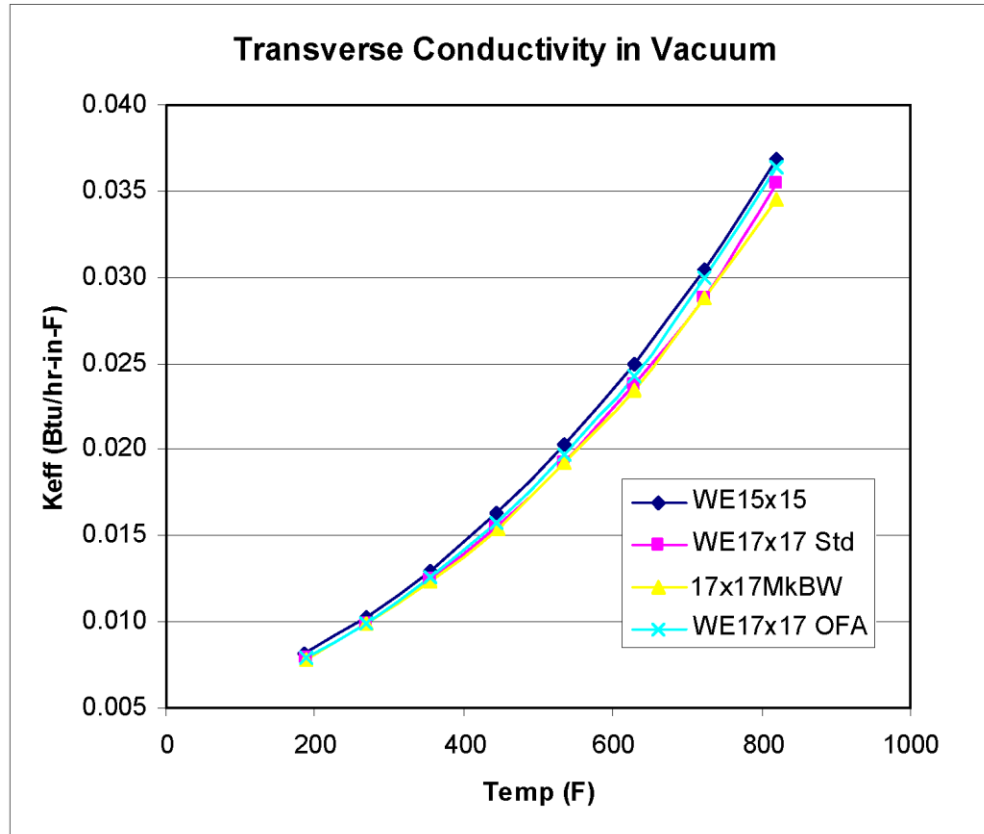


Figure 4-42
Effective Transverse Fuel Conductivity for Vacuum Conditions

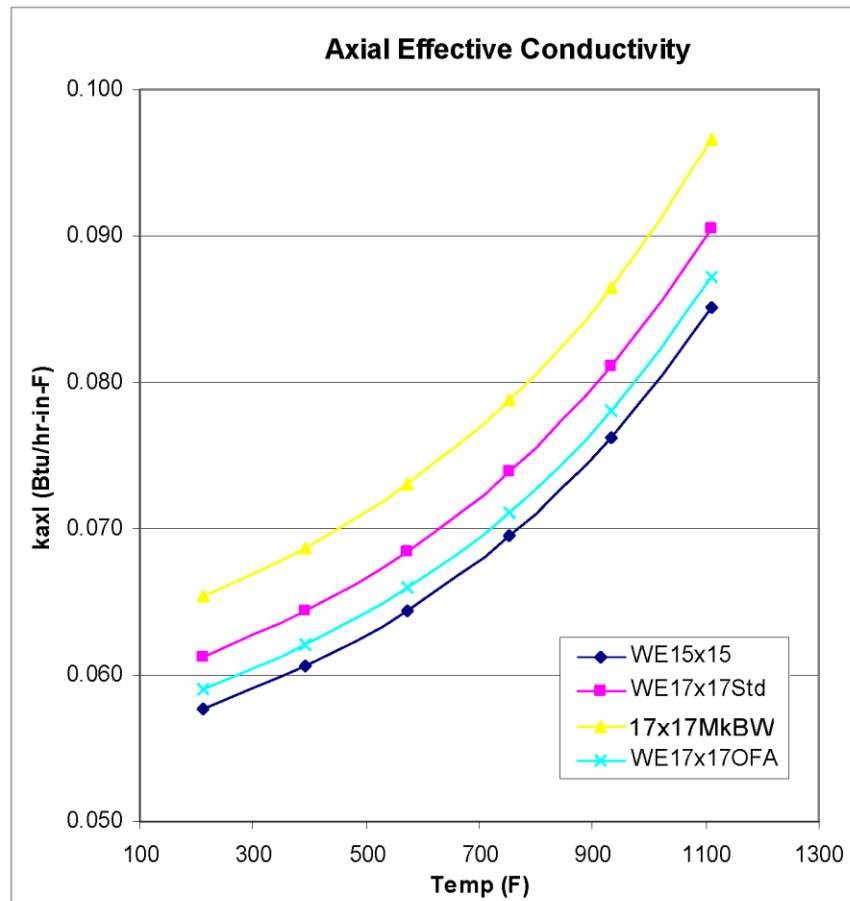
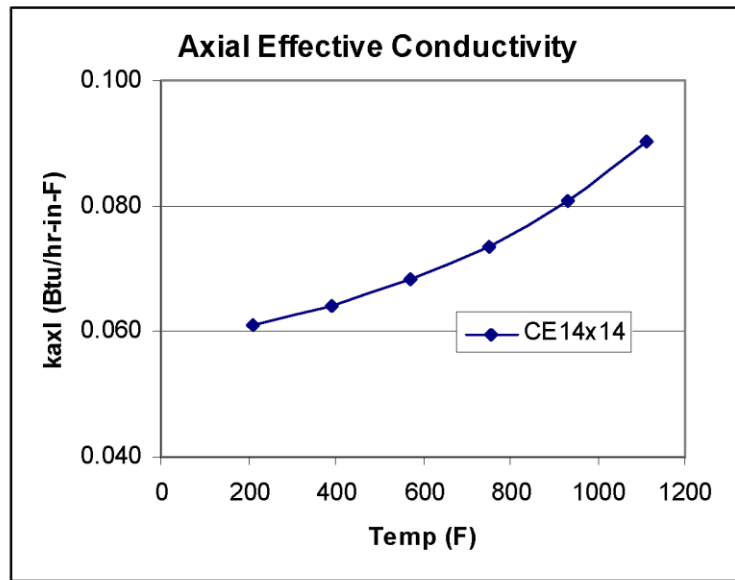


Figure 4-43
Effective Axial Fuel Conductivity

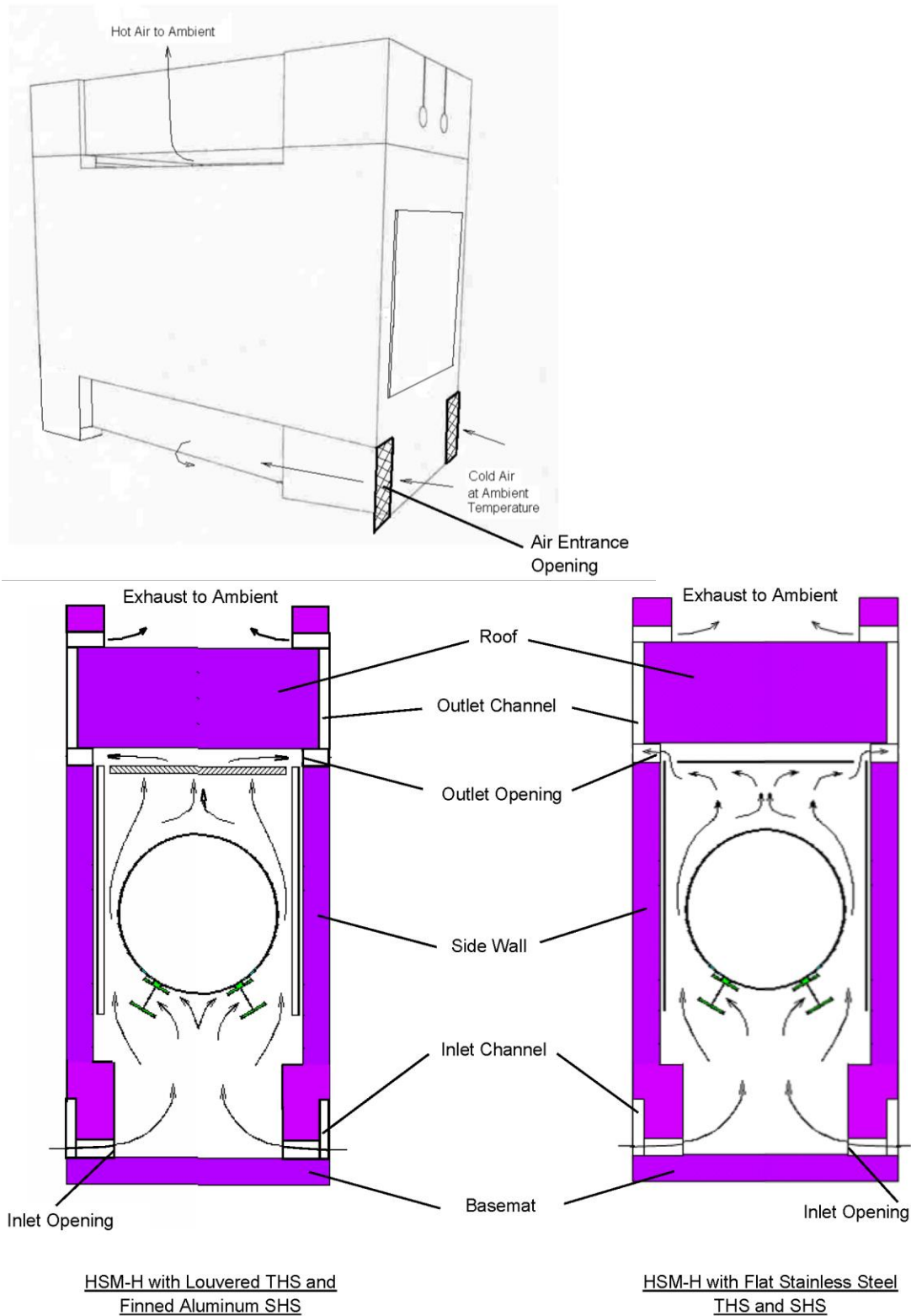


Figure 4-44
Schematic Flow Paths through HSM-H

FIGURE IS DELETED IN ITS ENTIRETY

**Figure 4-45
DELETED**

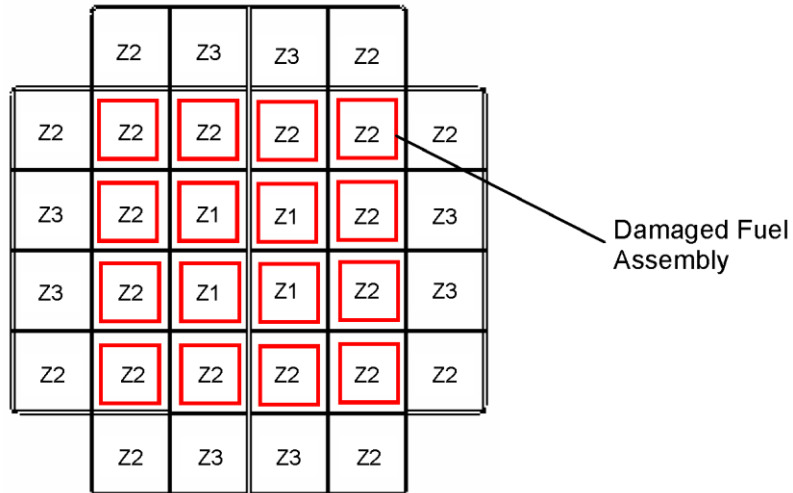


Figure 4-46
Location of the Damaged Fuel Assemblies in the Basket

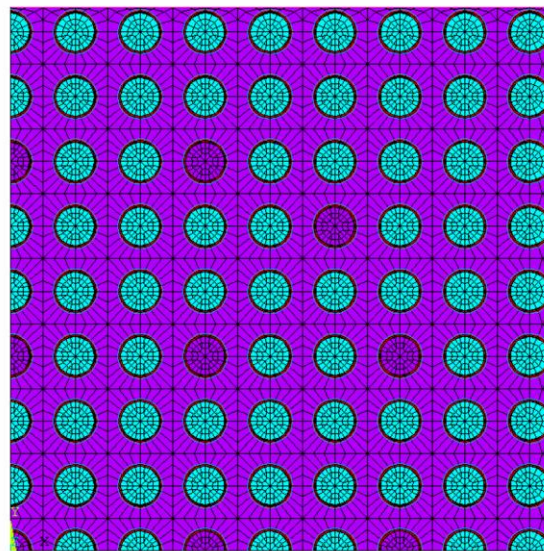
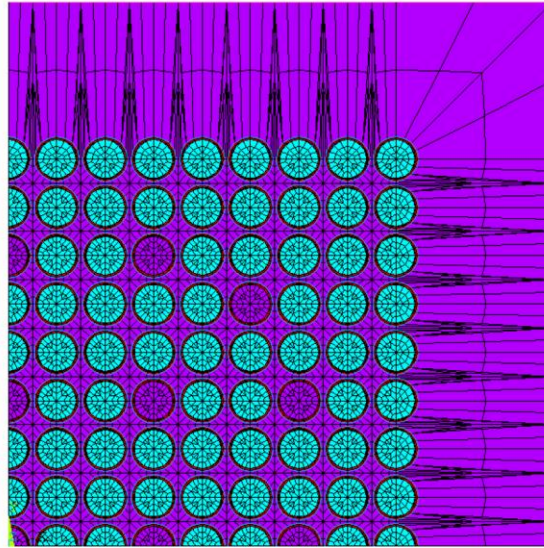


Figure 4-47
Typical FE Models of Damaged (Reconfigured) Fuel WEO 17x17

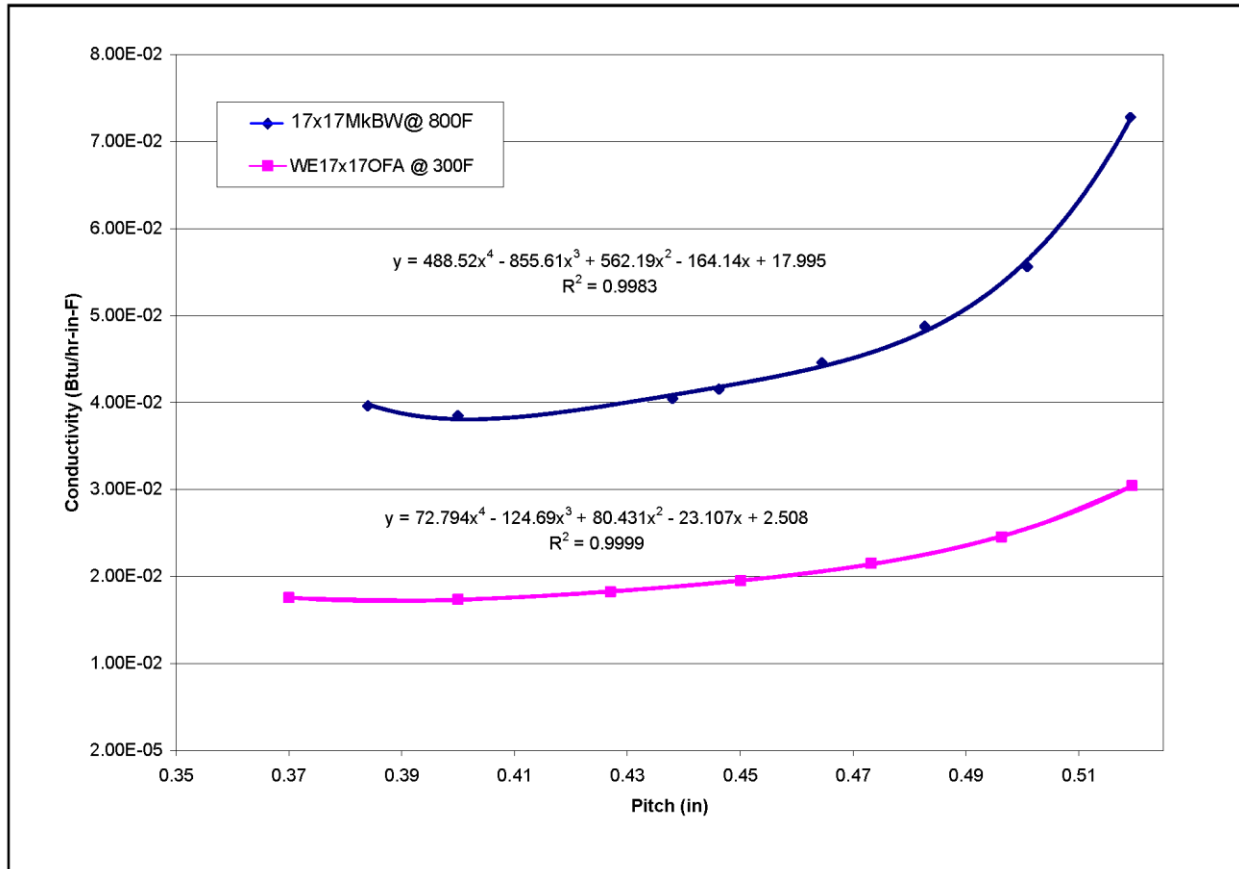


Figure 4-48
Transverse Effective Fuel Conductivity versus Pitch Size

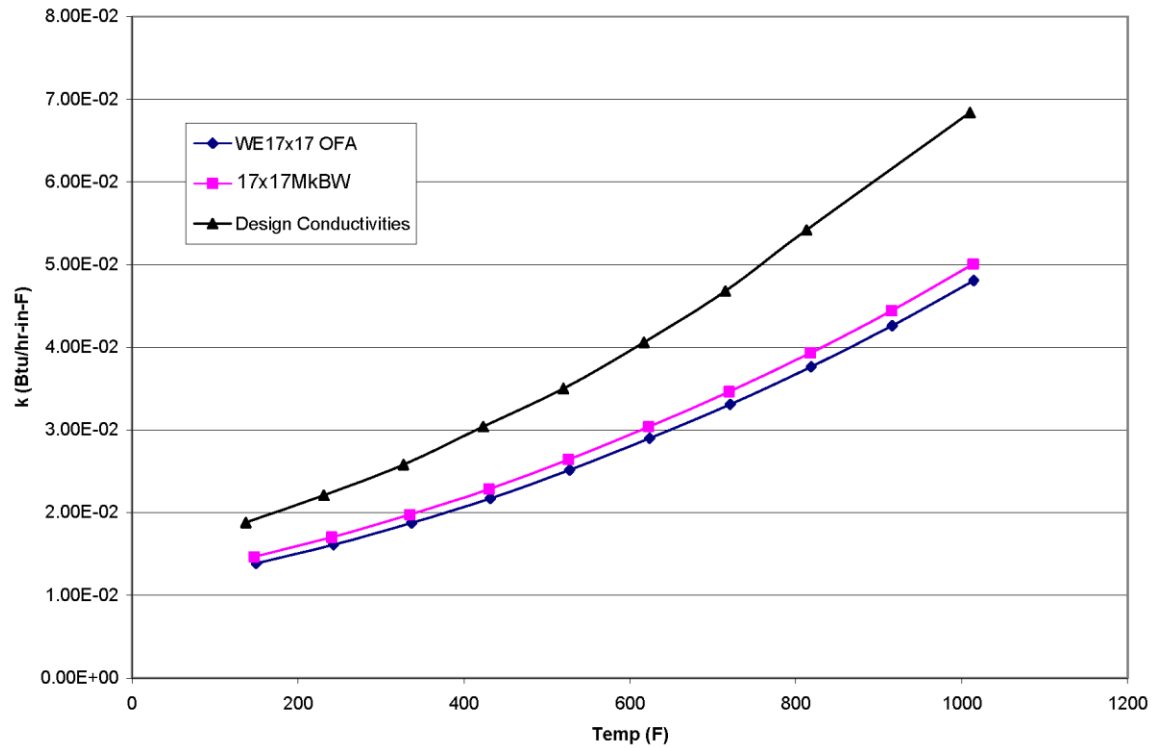


Figure 4-49
Effective Transverse Conductivity of Damaged (Reconfigured) Fuel

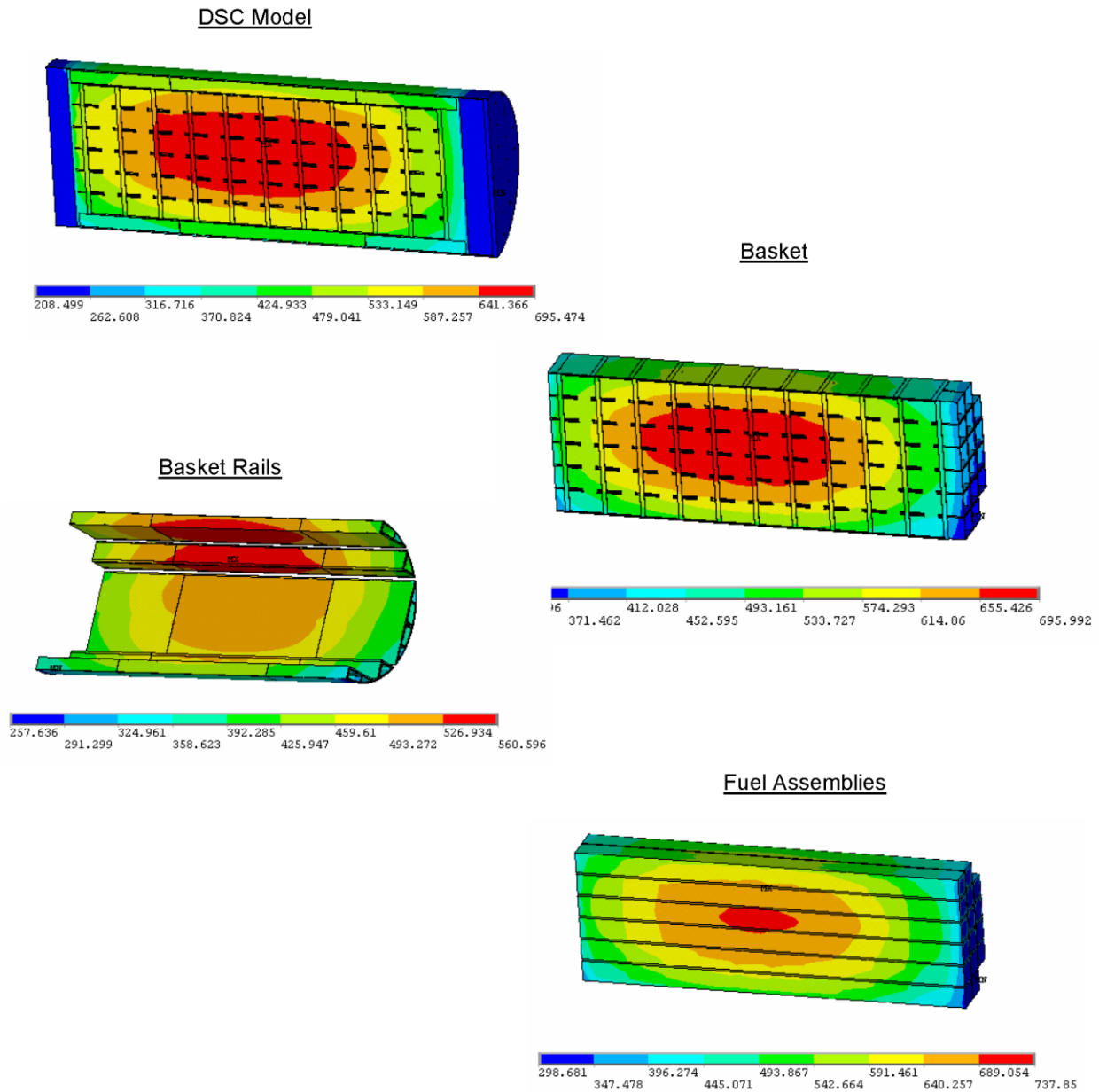


Figure 4-50
Temperature Distributions in the DSC containing 16 Damaged Fuel Assemblies
for Normal / Off-Normal Transfer Conditions

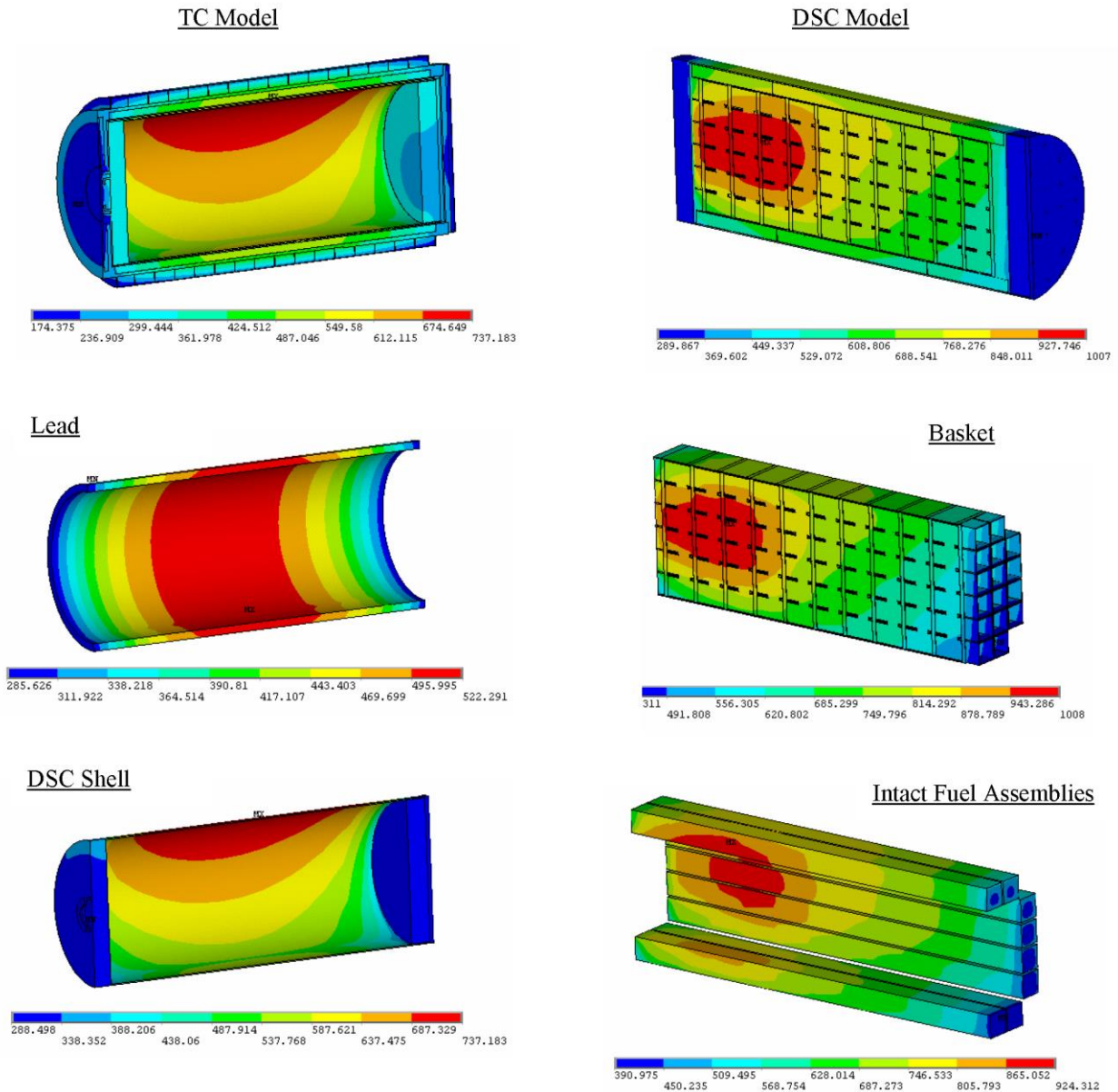


Figure 4-51
Temperature Distributions in the DSC Containing 16 Damaged (Rubble) Fuel Assemblies for Accident Conditions

Proprietary Information on Pages 4.16.1-i and Pages 4.16.1-1 through 4.16.1-13
Withheld Pursuant to 10 CFR 2.390

Proprietary Information on Page 4.16.2-i and Pages 4.16.2-1 through 4.16.2-21
Withheld Pursuant to 10 CFR 2.390

APPENDIX 4.16.3
ADDITION OF CE 16x16 FUEL ASSEMBLIES4.16.3.1 Effective Thermal Conductivity

CE 16x16 fuel assembly effective properties are calculated using the methodology described in Chapter 4, Section 4.8. The values calculated in Section 4.8 are lower than the values for the CE 16x16 fuel assemblies. Therefore, the thermal analysis results calculated using the existing thermal properties also remain bounding for the CE 16x16 Fuel Assemblies. Therefore, there is no change in thermal properties used for 32PTH system thermal analyses and 32PTH bounding thermal results remain unchanged.

The effective transverse conductivity of fuel assemblies are plotted in Figure 4.16.3-1, which includes CE 16x16 fuel. The bounding values shown herein correspond to those from Chapter 4, Figure 4-41.

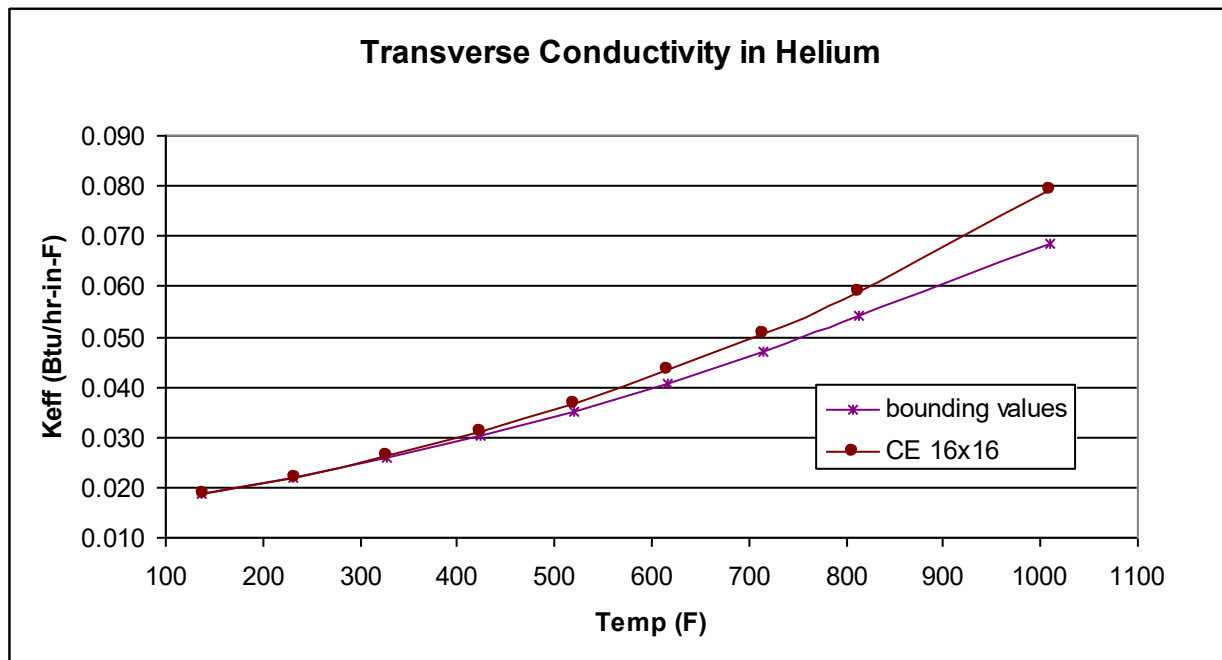


Figure 4.16.3-1
Existing Bounding Fuel and CE 16x16 Fuel Effective Transverse Fuel Conductivity in Helium

APPENDIX 4.16.4
EFFECT OF CHANGE IN MINIMUM OFF-NORMAL
AMBIENT TEMPERATURE TO -21°F

The analysis provided below shows that the effect of a 1°F reduction in the minimum off-normal ambient temperature is bounded by the conservatism included in the -20°F minimum ambient temperature case.

The air flow calculation for minimum ambient conditions is described in Section 4.13 for a minimum ambient temperature of -20°F. The thermal response of the HSM and DSC for temperature variations during the day is relatively slow because of the large thermal inertia of the system. Therefore, consideration of an average minimum temperature over a 24-hour period is reasonable to calculate temperatures and thermal gradients for the HSM, TC, and DSC using steady state boundary conditions. For a day with a minimum temperature of -21°F, a 24-hour average ambient temperature will be higher than -20°F (since the minimum mean daily temperature range is about 10°F as shown in Chapter 24, Table 1 of the ASHRAE Handbook—Reference 4.18). Therefore, the air flow, HSM-H, TC, and DSC temperature and internal DSC pressure values calculated for a minimum ambient temperature of -20°F in Section 4.13 bound those for a minimum ambient temperature of -21°F, due to the conservatisms included in the current analyses.

APPENDIX 4.16.5 EFFECT OF DOSE REDUCTION HARDWARE ON AIRFLOW ANALYSIS FOR HSM-H

TABLE OF CONTENTS

4.16.5 EFFECT OF DOSE REDUCTION HARDWARE ON AIRFLOW ANALYSIS FOR HSM-H	4.16.5-1
4.16.5.1 Introduction.....	4.16.5-1
4.16.5.2 Methodology	4.16.5-2
4.16.5.3 References	4.16.5-4

LIST OF TABLES

Table 4.16.5-1 Summary of Airflow Calculation Results.....	4.16.5-5
--	----------

LIST OF FIGURES

Figure 4.16.5-1 Schematic Configuration of the Dose Reduction Assembly Type A	4.16.5-6
Figure 4.16.5-2 Schematic Configuration of Dose Reduction Assembly Type B and Type C.....	4.16.5-7

4.16.5 EFFECT OF DOSE REDUCTION HARDWARE ON AIRFLOW ANALYSIS FOR HSM-H

4.16.5.1 Introduction

The HSM-H design may include optional hardware assemblies to reduce the dose rates at the inlet and outlet vents. The optional dose reduction hardware (DRH) assemblies can be installed at three locations:

- Type A: Staggered circular pipes attached to the bird screen and inserted into the inlet vents.
- Type B: One row of circular pipes attached to each of the two HSM-H cavity inlets.
- Type C: One row of circular pipes attached to the bird screen and inserted into the outlet vents.

Since the dose reduction assembly Type A is installed downstream from the bird screen and the pipe openings are larger than the mesh size of the bird screen, the large size debris will be blocked by the bird screen and the small size particles, such as dust that passes through the wire mesh of the bird screen cannot block the pipe openings. Therefore, the likelihood of a vent blockage is not increased and the operation of the HSM-H remains unaffected.

This appendix evaluates the effect of the DRH on the airflow and air temperatures used for evaluation of HSM-H design.

The HSM-H model loaded with the 32PTH DSC with flat, stainless steel heat shields as described in Chapter 4, Section 4.3.1.2 is selected as a baseline for this evaluation since it includes the maximum heat load of 34.8 kW and presents the bounding temperatures for the HSM-H design as reported in Chapter 4, Table 4-2. The assumptions, conservatism, and methodology for the HSM-H airflow analysis are identical to those described in Chapter 4, Section 4.13.

The dose reduction assembly Type A in the inlet vents consists of three staggered, stainless steel pipes with nominal outer diameter of 14 in. The thickness and the length of the pipes are 0.25 in. and 6 in., respectively. The configuration of the inlet vent dose reduction assembly Type A is shown schematically in Figure 4.16.5-1.

The dose reduction assembly Type B in the HSM-H cavity inlets consists of one row of 19 stainless steel tubes with nominal outer diameter of 7.5 in. The thickness and the length of the tubes are 0.25 in. and 6 in., respectively. The configuration of the HSM-H cavity inlet dose reduction assembly Type B is shown schematically in Figure 4.16.5-2.

The dose reduction assembly Type C in the HSM-H outlet vents consists of one row of 26 stainless steel tubes with nominal outer diameter of 5.5 in. The thickness and the length of the tubes are 0.25 in. and 6 in., respectively. The schematic configuration of the HSM-H cavity outlet dose reduction assembly Type C is also shown in Figure 4.16.5-2.

4.16.5.2 Methodology

The additional resistance associated with the dose reduction hardware is evaluated by considering them as thick perforated area at the entrance of the inlet vents or at the discharge of HSM-H cavity inlets. The flow resistance for this configuration is given in Diagram 8-3 of Idelchik Handbook [1]. The following parameters are defined in this diagram.

$$\xi = \left[0.5(1 - \bar{f})^{0.75} + \tau(1 - \bar{f})^{1.375} + (1 - \bar{f})^2 + \lambda \frac{l}{d_h} \right] / \bar{f}^2 \quad (1)$$

$$\bar{l} = \frac{l}{d_h}, \quad d_h = \frac{4F_0}{\Pi_0}, \quad \bar{f} = \frac{F_0}{F_1},$$

- ξ = local loss coefficient,
 l = width of the thick perforated area (length of the pipes),
 d_h = hydraulic diameter,
 F_0 = free surface area,
 F_1 = total cross-sectional area,
 Π_0 = perimeter of the free surface area,
 A_{pipe} = cross section area of one pipe,
 τ = parameter from following table taken from [1], Diagram 8-3.

\bar{l}	0	0.2	0.4	0.6	0.8	1.0	1.4	2.0	3.0	4.0
τ	1.35	1.22	1.10	0.84	0.42	0.24	0.1	0.02	0	0

Based on the data provided in Figure 4.16.5-1, the parameters for the dose reduction hardware at the entrance of the inlet vents (Type A) can be calculated as follows:

- y = width of the inlet vent at back of staggered pipes
 $y = 12 + 2 \times m = 33.3$,
 m = auxiliary dimension shown in Figure 4.16.5-1,
 $m = (36 - 12)/2 \times (54 - 12/2)/54 = 10.67$,
 $F_1 = 33.3 \times 30 \approx 1,000 \text{ in}^2$,
 $A_{\text{pipe-vent}} = \pi/4 [\text{OD}^2 - (\text{OD} - 2 \times t)^2] = \pi/4 [14^2 - (14 - 2 \times 0.25)^2] = 10.8 \text{ in}^2$,
 $F_0 = F_1 - 3 \times A_{\text{pipe}} = 1,000 - 3 \times 10.8 = 967.6 \text{ in}^2$ for Dose Reduction Hardware Type A,
 $\Pi_0 = 3 \times [\pi \times \text{OD} + \pi (\text{OD} - 2 \times t)] + 2 \times (30 + 33.3) = 385.8 \text{ in}$,
 $\bar{f} = 967.6 / 1,000 = 0.9676$,
 $d_h = 4 \times 967.6 / 385.8 = 10 \text{ in}$,
 $\bar{l} = 6 / 10 = 0.60$,
 $\tau = 0.84$ (calculated at $\bar{l} = 0.60$ based on the above table).

The parameters for the dose reduction hardware at the discharge of the HSM-H cavity inlets (Type B – shown in Figure 4.16.5-2) are calculated as follows:

$$\begin{aligned}
 F_1 &= 148 \times 8 = 1,184 \text{ in}^2, \\
 A_{\text{pipe-cavity}} &= \pi/4 [\text{OD}^2 - (\text{OD} - 2 \times t)^2] = \pi/4 [7.5^2 - (7.5 - 2 \times 0.25)^2] = 5.7 \text{ in}^2, \\
 F_0 &= F_1 - 19 \times A_{\text{pipe}} = 1,184 - 19 \times 5.7 = 1,075.7 \text{ in}^2 \text{ for Dose Reduction Hardware Type B,} \\
 \Pi_0 &= 19 \times [\pi \times \text{OD} + \pi (\text{OD} - 2 \times t)] + 2 \times (148 + 8) = 1,177.5 \text{ in,} \\
 \bar{f} &= 1,075.7 / 1,184 = 0.909, \\
 d_h &= 4 \times 1,075.7 / 1,177.5 = 3.7 \text{ in,} \\
 \bar{l} &= 6 / 3.7 = 1.62 \text{ (precise evaluation in spreadsheet shows a value of 1.64),} \\
 \tau &= 0.07 \text{ (calculated at } \bar{l} = 1.64 \text{ based on the above table).}
 \end{aligned}$$

Similarly, the parameters for the dose reduction hardware at the HSM-H outlet vents (Type C – shown in Figure 4.16.5-2) are calculated as follows:

$$\begin{aligned}
 F_1 &= 154 \times 6 = 924 \text{ in}^2, \\
 A_{\text{pipe-cavity}} &= \pi/4 [\text{OD}^2 - (\text{OD} - 2 \times t)^2] = \pi/4 [5.5^2 - (5.5 - 2 \times 0.25)^2] = 4.1 \text{ in}^2, \\
 F_0 &= F_1 - 27 \times A_{\text{pipe}} = 924 - 27 \times 4.1 = 813.3 \text{ in}^2 \text{ for Dose Reduction Hardware Type C,} \\
 \Pi_0 &= 27 \times [\pi \times \text{OD} + \pi (\text{OD} - 2 \times t)] + 2 \times (154 + 6) = 1,210.6 \text{ in,} \\
 \bar{f} &= 813.3 / 924 = 0.880, \\
 d_h &= 4 \times 813.3 / 1,210.6 = 2.7 \text{ in,} \\
 \bar{l} &= 6 / 2.7 = 2.22 \text{ (precise evaluation in spreadsheet shows a value of 2.23),} \\
 \tau &= 0.02 \text{ (calculated at } \bar{l} = 2.23 \text{ based on the above table).}
 \end{aligned}$$

λ is the frictional resistance coefficient and is given in [1], Chapter 2, Equation 2-10 as follows.

$$\lambda = 0.11 \times \left(\frac{\Delta}{d_h} + \frac{68}{\text{Re}} \right)^{0.25} \quad (2)$$

$$\text{Re} = \text{Reynolds number, } \text{Re} = \frac{\rho v d_h}{\mu} = \frac{\dot{m} d_h}{F_0 \mu} \quad (3)$$

With:

$$\begin{aligned}
 \dot{m} &= \text{mass flow rate, lb/s,} \\
 F_0 &= \text{free surface area} = 967.6 \text{ in}^2 \text{ for the Dose Reduction Hardware Type A,} \\
 &= 1,075.7 \text{ in}^2 \text{ for the Dose Reduction Hardware Type B,} \\
 &= 813.3 \text{ in}^2 \text{ for the Dose Reduction Hardware Type C} \\
 \rho &= \text{density, lb/in}^3, \\
 v &= \text{velocity, in/s,} \\
 \mu &= \text{dynamic viscosity, lb/in-s,} \\
 \Delta &= \text{surface roughness} = 0.2 \text{ mm} \approx 0.01 \text{ in. [1], Table 2-5}
 \end{aligned}$$

The surface roughness value is based on concrete roughness, which is higher than stainless steel roughness and is conservative to use in this calculation. The loss coefficient for the dose reduction hardware is:

$$K = \frac{\xi}{A^2} = \frac{\xi}{F_1^2} \quad (4)$$

ξ = local loss coefficient from equation (1),

$A = F_1$ = cross-sectional area for airflow at the location of dose reduction hardware, in².

Equations (1) through (4) are integrated into the airflow calculation used in Section 4.13 to determine the overall flow resistance and air temperatures for the HSM-H with dose reduction hardware. The results of airflow evaluation for the HSM-H with 34.8 kW heat load and with or without dose reduction hardware are shown in Table 4.16.5-1.

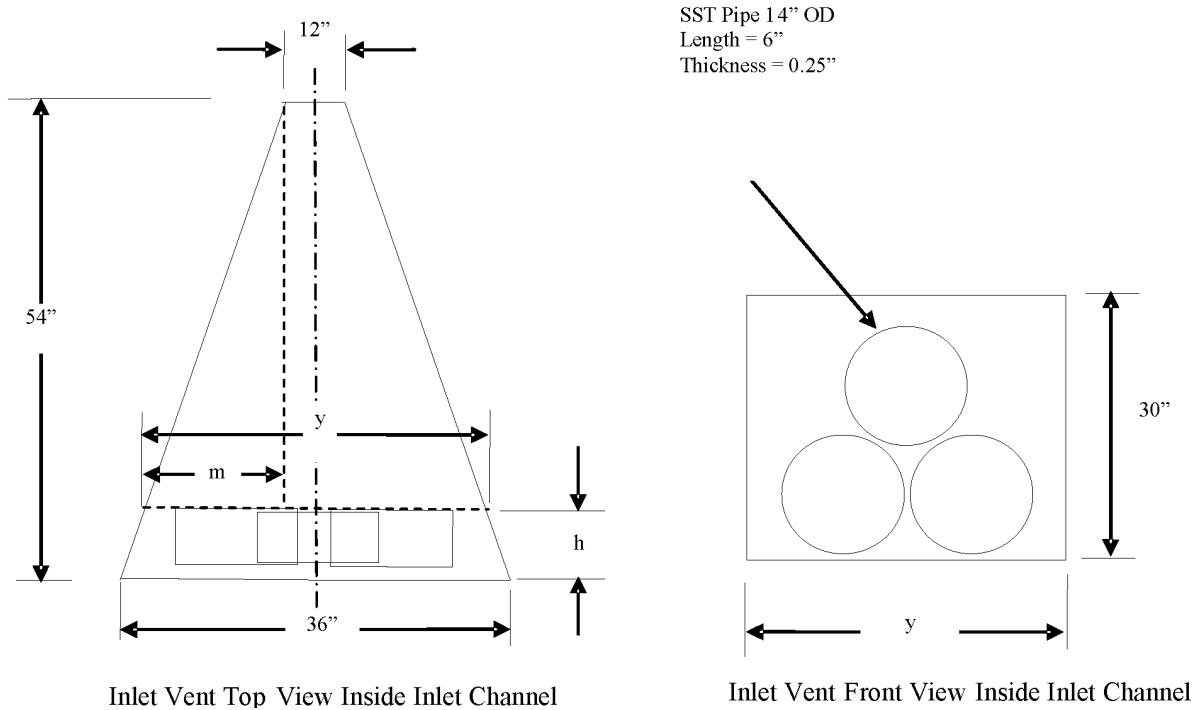
As seen in Table 4.16.5-1, the exit and mean air temperatures change by approximately 1 °F when the HSM-H is equipped with dose reduction hardware Types A, B, and C. These changes were resulted for the bounding off-normal condition with maximum ambient temperature of 115 °F and maximum heat load of 34.8 kW. Therefore, this change is bounding for all other storage conditions. The effect of 1 °F change for the exit or average air temperature is less than 1 °F on the HSM-H components temperatures and on the DSC shell temperature. The change of less than 1 °F for the HSM-H and DSC components temperatures is negligible. It concludes that the effect of dose reduction hardware on the thermal performance of the HSM-H loaded with 32PTH DSC is insignificant and therefore the results for HSM-H evaluation reported in Chapter 4 remain valid.

4.16.5.3 References

1. I.E. Idelchik, "Handbook of Hydraulic Resistance," 3rd Edition, 1994.

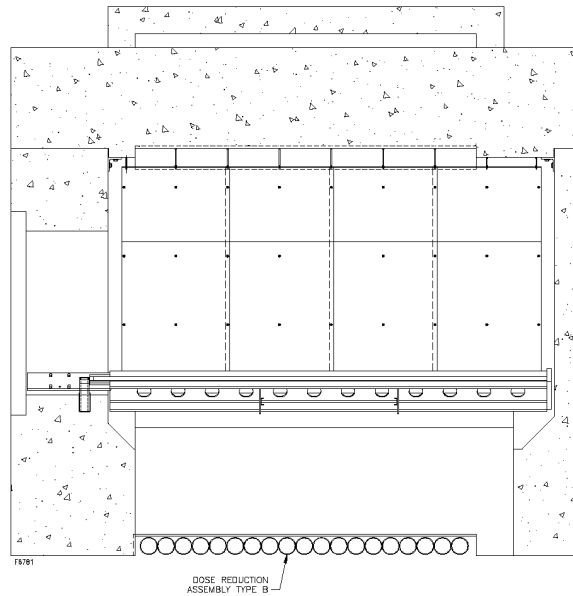
Table 4.16.5-1
Summary of Airflow Calculation Results

HSM-H Design Option	Flat Stainless Steel Heat Shields without Dose Reduction Hardware (from Table 4-21)	Flat Stainless Steel Heat Shields with Dose Reduction Hardware Type A, B, and C
T_{amb} , (°F)	115	115
T_{Exit} , (°F)	192	193
T_{mean} , (°F)	148	149
ΣK , (ft ⁻⁴)	0.102	0.107
Mass Flow Rate, (lbm/s)	1.574	1.547

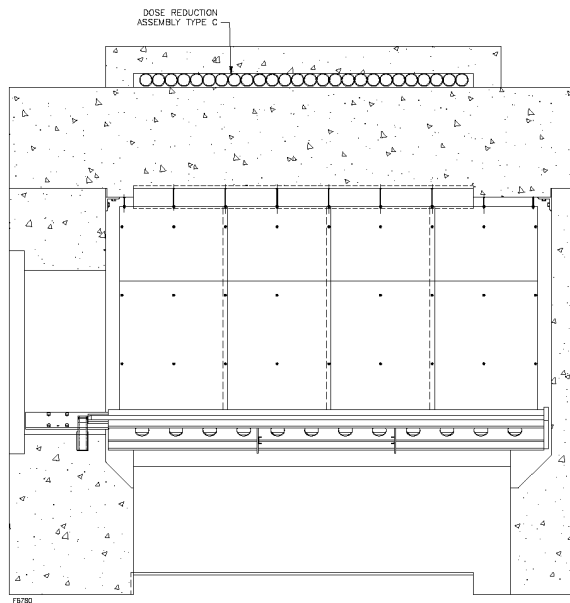


Dimensions are:
 54 in. – Inlet vent length
 36 in. – Inlet vent width
 30 in. – Inlet vent height
 12 in. – Narrow inlet width

Figure 4.16.5-1
Schematic Configuration of the Dose Reduction Assembly Type A



Dose Reduction Assembly Type B



Dose Reduction Assembly Type C

**Figure 4.16.5-2
Schematic Configuration of Dose Reduction Assembly
Type B and Type C**

CHAPTER 5
SHIELDING EVALUATION

TABLE OF CONTENTS

5. SHIELDING EVALUATION	5-1
5.1 Discussion and Results.....	5-3
5.2 Source Specification.....	5-5
5.2.1 Gamma Sources	5-8
5.2.2 Neutron Source	5-8
5.2.3 Fuel Qualification	5-9
5.3 Model Specification.....	5-14
5.3.1 Description of the Radial and Axial Shielding Configurations	5-14
5.3.2 Shield Regional Densities	5-15
5.4 Shielding Evaluation.....	5-17
5.4.1 Computer Programs	5-17
5.4.2 Spatial Source Distribution	5-17
5.4.3 Cross-Section Data.....	5-18
5.4.4 Flux-to-Dose-Rate Conversion	5-18
5.4.5 Model Geometry	5-18
5.4.6 Methodology	5-18
5.4.7 Assumptions.....	5-19
5.4.8 Normal Condition Models	5-20
5.4.9 Impact on Dose Rates from Gaps between HSM-Hs in the ISFSI	5-24
5.4.10 Impact on Dose Rates with the Addition of Dose Reduction Hardware (DRH).....	5-25
5.5 Supplemental Information	5-26
5.5.1 References.....	5-26
5.5.2 Sample Input Files	5-27

LIST OF TABLES

Table 5-1	NUHOMS® HD 32PTH System Shielding Materials	5-69
Table 5-2	Summary HSM-H Dose Rates.....	5-70
Table 5-3	Transfer Cask (Loading/Unloading/Transfer Operations) Side Dose Rate Summary	5-71
Table 5-4	Transfer Cask (Loading/Unloading/Transfer Operations) Top End Dose Rate Summary	5-72
Table 5-5	Cask (Loading/Unloading/Transfer Operations) Bottom End Dose Rate Summary	5-72
Table 5-6	Flux Factor By Fuel Assembly Region	5-73
Table 5-7	Fuel Assembly Materials and Masses	5-73
Table 5-8	NFAH Materials and Masses.....	5-75
Table 5-9	Fuel Assembly Material Masses.....	5-76
Table 5-10	SAS2H Gamma Sources for 60 GWd/MTU, 7-Year Cooled MK BW 17x17 Fuel Assembly.....	5-77
Table 5-11	SAS2H Gamma Sources for 210 GWd/MTU, 20-Year Cooled TPA	5-78
Table 5-12	SAS2H Gamma Sources for 30 GWd/MTU, 4-day Cooled BPRA	5-78
Table 5-13	SAS2H Neutron Sources for 60 GWD/MTU, 7-10 yr Cooled Fuel MK BW 17x17 Fuel Assembly	5-79
Table 5-14	ANSI Standard-6.1.1-1977 Flux-to-Dose Factors.....	5-80
Table 5-15	Material Densities for Fuel Assembly Regions (dry).....	5-81
Table 5-16	Material Densities for Fuel Assembly Regions (wet)	5-82
Table 5-17	NUHOMS® HD 32PTH DSC and OS-187H Material Composition	5-83
Table 5-18	NUHOMS® HD 32PTH DSC and OS-187H Material Composition	5-83
Table 5-19	Composition and Densities for HSM-H Concrete.....	5-84
Table 5-20	Source Axial Profile	5-85
Table 5-21	Summary of NUHOMS® HD 32PTH DSC in the HSM-H, Maximum and Average Dose Rates	5-86

Table 5-22	Summary of NUHOMS® HD 32PTH DSC in the OS187H TC, Maximum Dose Rates During Decontamination and Welding Operations	5-87
Table 5-23	Summary of NUHOMS® HD 32PTH DSC in the OS187H TC, Maximum Dose Rates During Transfer Operations (Configuration C).....	5-88
Table 5-24	Dose Rate Comparison for Fuel Qualification	5-89
Table 5-25	Fuel Qualification with Reconstituted Fuel Assemblies	5-93
Table 5-26	Summary of Results, Side-to-Side Gaps	5-94
Table 5-27	Fuel Qualification Evaluation for Fuel Assemblies Containing BLEU Fuel Material	5-95
Table 5-28	Dose Reduction Hardware Properties	5-96
Table 5-29	Dose Reduction Hardware Summary of Results	5-97

LIST OF FIGURES

Figure 5-1	NUHOMS [®] HD 32PTH System Shielding Configuration (HSM-H)	5-98
Figure 5-2	Dry Shielded Canister Shielding Configuration	5-99
Figure 5-3	Right Elevation Cross Section View of HSM-H	5-100
Figure 5-4	Shielding Configuration of the OS187H Transfer Cask	5-101
Figure 5-5	OS187H DSC and Annulus Flooded	5-102
Figure 5-6	One Quarter Cross Section DSC/Basket in Transfer Cask	5-103
Figure 5-7	OS187H Lids Installed (DSC and Annulus Dry)	5-104
Figure 5-8	HSM-H Side View at DSC Centerline	5-105
Figure 5-9	HSM-H Head-on View at X=0	5-106
Figure 5-10	HSM-H Head-on View at DSC Lid End (X=225)	5-107
Figure 5-11	HSM-H Head-on View at DSC Bottom End (X=-225)	5-108
Figure 5-12	HSM-H Detector Locations Head-on View	5-109
Figure 5-13	HSM-H Detector Locations Side View	5-110
Figure 5-14	Dose Rates Around the Top of the TC/32PTH-DSC (Configuration A)	5-111
Figure 5-15	Dose Rates Around the Top of the TC/32PTH-DSC (Configuration B)	5-112
Figure 5-16	Dose Rates Around TC/32PTH-DSC (Transfer Configuration)	5-113
Figure 5-17	Dose Rates On the HSM-H Roof	5-114
Figure 5-18	Dose Rates On the HSM-H Front and Side	5-115
Figure 5-19	HSM-H Array Showing Maximum As-Modeled Gaps	5-116
Figure 5-20	HSM-H Model for 1.25 Inch Side-to-Side Gap (x-y view)	5-117
Figure 5-21	HSM-H Model with Back-to-Back Gap	5-118
Figure 5-22	Front Birdscreens Dose Reduction Hardware Type A	5-119
Figure 5-23	Inlets to Front Vents Dose Reduction Hardware Type B	5-119
Figure 5-24	Roof Outlet Vent Cap Dose Reduction Hardware Type C	5-120

5. SHIELDING EVALUATION

The shielding evaluation presented for the NUHOMS[®] 32PTH System demonstrates adequacy of the shielding design for the payload described in Chapter 2. The geometry of the NUHOMS[®] System is described in Chapter 1. The heavy concrete walls and roof of the Horizontal Storage Module (HSM-H) provide the bulk of the shielding for the payload in the storage condition. During fuel loading and transfer operations, the combination of thick steel shield plugs at the ends of the 32PTH-DSC and heavy steel/lead/neutron shield material of the OS187H transfer cask provide shielding for personnel loading and transferring the 32PTH-DSC to the HSM-H. Figure 5-1 through Figure 5-4 and Table 5-1 provide the general configuration and material thicknesses of the important components of the NUHOMS[®] 32PTH System.

The NUHOMS[®] HD System is capable of storing CE 14x14 class, WE 15x15 class, CE 16x16 class, and WE 17x17 class of PWR fuel assemblies.

For this shielding evaluation, source terms are calculated for the bounding Framatome ANP Advanced MK BW 17x17 (MK BW 17x17) fuel assembly, a WE 17x17 class fuel assembly. This fuel assembly is bounding because it contains the greatest mass of fuel.

The NUHOMS[®] HD System is also authorized to store fuel assemblies containing Blended Low Enriched Uranium (BLEU) fuel material. [

]

The 32PTH DSC is also designed to store up to 32 intact standard PWR fuel assemblies with or without Control Components (CCs) such as Burnable Poison Rod Assemblies (BPRAs), Control Rod Assemblies (CRAs), Control Element Assemblies (CEAs), Rod Cluster Control Assemblies (RCCAs), Thimble Plug Assemblies (TPAs), Axial Power Shaping Rod Assemblies (APSRAs), Orifice Rod Assemblies (ORAs), Vibration Suppression Inserts (VSIs), Neutron Sources, and Neutron Source Assemblies (NSAs). The design basis CC for shielding evaluation is the BPRA.

Several burnup/enrichment combinations with minimum 5 year cooling times are addressed for the fuel to provide more flexibility in qualifying fuel for storage. These combinations form the basis for the NUHOMS[®] 32PTH System fuel specifications in Chapter 12. Bounding operating histories are assumed for the BPRA with a minimum cooling time of 4 days. The methodology, assumptions, and criteria used in this evaluation are summarized in the following subsections.

Section 5.4 provides a three dimensional (3-D) shielding analysis for the NUHOMS[®] 32PTH System using MCNP [2,6]

The shielding evaluation described in this chapter 5.0 is applicable to the 32PTH DSC in the OS187H TC and HSM-H. See Appendix A, Chapter A.5 for discussion of applicability of these analyses for the 32PTH Type 1 DSC in the OS187H Type 1 TC and HSM-H. See Appendix B, Chapter B.5 for discussion of applicability of these analyses for the 32PTH Type 2 DSC in the OS187H Type 2 TC and HSM-HS.

5.1 Discussion and Results

The maximum and average dose rates due to 32 design basis PWR fuel assemblies stored with 32 design basis CCs (BPRA) in the NUHOMS[®] 32PTH System are summarized in Table 5-2 through Table 5-5. Table 5-2 provides the dose rates on the surface of the HSM-H while Table 5-3 through Table 5-5 provide the dose rates on and around the Transfer Cask (top, bottom and sides) during fuel loading, and transfer operations.

As previously stated, the NUHOMS[®] HD System is capable of storing PWR spent fuel, and CCs. Based on the source term calculations presented in Section 5.2, the design basis fuel source term is the Framatome MK BW 17x17 fuel assembly with 60 GWD/MTU burnup, a minimum initial enrichment of 4.0 weight % U-235 and a cooling time of 7 years. The design basis CC source term is a BPRA assembly irradiated to 30 GWD/MTU and a cooled for 4 days.

WE 15x15 and WE 17x17 class fuel assemblies containing Instrument Tube Tie Rods (ITTRs) are also qualified for storage in the NUHOMS[®] HD System. The design basis shielding calculations are performed using source terms from fuel assemblies and control components that are inserted in the guide tubes as described in Section 5.2. The ITTR is an unirradiated non-fuel hardware and therefore, does not generate radioactive source terms and therefore, there is no effect on the shielding analyses of the NUHOMS[®] HD System.

Fuel qualification tables are developed (based on a decay heat equation) that determine the eligibility of fuel assemblies to be stored in the 32PTH DSC. Since bounding parameters are utilized in all the 32 fuel assembly locations in the shielding evaluation, fuel qualification is limited only by the heat capacity of the DSC. This qualification covers fuel assemblies with a minimum enrichment of 0.2 wt. % U-235 and a minimum cooling time of 5 years. Fuel assemblies with enrichment between 0.2 wt. % U-235 and 1.5 wt. % U-235 are qualified by limiting their burnup. This ensures that the shielding analysis is also bounding for these fuel assemblies.

Fuel assemblies containing Blended Low Enriched Uranium (BLEU) with a minimum enrichment of 0.2 wt. % U-235 are qualified. Calculations are performed with the bounding Low Enriched Uranium (LEU) cases of Table 5-24 and Table 5-25 by adding the isotopic profile of BLEU fuel. The results are compared to the bounding cases of Table 5-24 and Table 5-25 in Table 5-27. The comparison demonstrates that BLEU fuel assemblies that are otherwise identical to LEU fuel assemblies are qualified by adding 2.5 years of cooling time to the LEU fuel cool time value.

Reconstituted fuel assemblies where fuel pins that are replaced by lower-enriched pins or non-fuel pins are also authorized for storage. A discussion on the fuel qualification methodology is provided in Section 5.2.3.

A discussion of the method used to determine the design basis fuel and CC source terms is included in Section 5.2. The model specification and shielding material densities are given in Section 5.3. The method used to determine the dose rates due to 32 design basis fuel assemblies with 32 design basis CC in the NUHOMS[®] 32PTH System is provided in Section 5.4.

Normal and off-normal conditions are modeled with the NUHOMS[®] 32PTH System intact, including the filled neutron shield in the transfer cask. The shielding calculations are performed using the MCNP Monte Carlo transport code [2]. Average and peak dose rates on the front, side, top and back of the HSM-H and the OS187H Transfer Cask System are calculated. Occupational doses during loading, transfer to the ISFSI, and maintenance and surveillance operations are provided in Chapter 10. The areas of highest operational dose are the front of a loaded HSM-H at the air inlet vent, at the cask side or DSC top with a partially or completely drained DSC (cover welding, transfer operations), and at the cask/DSC annulus. Operating procedures, temporary shielding, and personnel training should minimize personnel exposure in these areas.

For accident conditions (e.g., cask drop, fire), the transfer cask neutron shield water (shown in Figure 5-4 is assumed to be removed and a 1 inch void in the lead due to “lead slump” is also assumed at the top and/or bottom. Site dose and occupational dose analyses are addressed in Chapter 10 (including requirements for site specific 72.104 and 72.106 analyses).

5.2 Source Specification

Source terms are calculated with the SAS2H (ORIGEN-S) module of SCALE 4.4 [1]. The following sub-sections provide a discussion of the fuel assembly and CC material weights and composition, gamma and neutron source terms and energy spectrum. The SAS2H results are used to develop source terms suitable for use in the shielding calculations.

There are five principal sources of radiation associated with the NUHOMS[®] 32PTH System that are of concern for radiation protection. These are:

1. Primary gamma radiation from the spent fuel
2. Primary gamma radiation from activation products in the structural materials found in the spent fuel assembly and the CC
3. Primary neutron radiation from the spent fuel
4. Neutrons produced from sub-critical multiplication in the fuel
5. Capture gammas from (n, γ) reactions in the NUHOMS[®] 32PTH System materials

The first three sources of radiation are evaluated using SAS2H. The capture gamma radiation and sub-critical multiplication are handled as part of the shielding analysis which is performed with MCNP.

The neutron flux during reactor operation is peaked in the active fuel (in-core) region of the fuel assembly and drops off rapidly outside the in-core region. Much of the fuel assembly hardware is outside of the in-core region of the fuel assembly. To account for this reduction in neutron flux, each fuel assembly type is divided into four exposure zones. A neutron flux (fluence) correction is applied to each region to account for this reduction in neutron flux outside the in-core region. The correction factors are given in Table 5-6. The four exposure zones, or regions are [4]:

Bottom—location of fuel assembly bottom nozzle and fuel rod end plugs

In-core—location of active fuel

Plenum—location of fuel rod plenum spring and top plug

Top—location of top nozzle

The Framatome MK BW 17x17 assembly is the bounding fuel assembly design for shielding purposes because it has the highest initial heavy metal loading as compared to the 14x14, 15x15, 16x16 and other 17x17 fuel assemblies which are also authorized contents of the NUHOMS[®]-32PTH DSC and described in Chapter 2. The SAS2H/ORIGEN-S modules of the SCALE code with the 44 group ENDF/B-V library are used to generate the gamma and neutron source terms. For the bounding MK BW 17x17 fuel assembly, an initial enrichment of 4.0 wt% U-235 is assumed. The fuel assembly is irradiated with a constant specific power of 25 MW/assy to a total burnup of 60 GWD/MTU. A conservative three-cycle operating history is utilized with a 20 day down time between each cycle. The fuel assembly masses for each irradiation region are listed in Table 5-7.

Data for the WE 17x17 assembly is from Reference [7]. Some values for the WE 15x15 were assumed to be the same as the WE 17x17. The fuel assembly masses for each irradiation region of the CE 16x16 fuel assembly are also shown in Table 5-7. The design-basis heavy metal weight is 0.476 MTU. These masses are irradiated in the appropriate fuel assembly region in the SAS2H/ORIGEN-S models. The mass of hardware for the MK BW 17x17 assembly is the greatest; however, the source term from the irradiated hardware for the WE 17x17 is bounding.

The maximum burnup of fuel assemblies with enrichments between 0.7 wt% U-235 and 1.5 wt % U-235 is limited to 32 GWD/MTU to ensure that their gamma and neutron source terms are bounded by those of the design basis fuel assembly. Similarly, the maximum burnup of fuel assemblies with enrichments between 0.3 wt.% U-235 and 0.7 wt.% U-235 is limited to 25 GWD/MTU. The maximum burnup of fuel assemblies with enrichments between 0.2 wt.% U-235 and 0.3 wt.% U-235 is limited to 20 GWD/MTU.

Reconstituted Fuel Assemblies

A detailed discussion on the definition, qualification methodology, and evaluations for reconstituted fuel assemblies is provided in Section 5.2.3.

If reconstituted fuel assemblies (considered as intact fuel in the criticality analyses) with stainless steel rods undergo further irradiation, their gamma source term on a per DSC basis shall be bounded by the total design basis gamma source terms shown (on an assembly basis) in Table 5-10 for the design basis fuel assembly.

As explained above, reconstituted fuel assemblies may contain up to 10 irradiated stainless steel rods that replace damaged fuel rods. Because steel rods replace fuel rods, the decay heat of a reconstituted assembly is typically less than the decay heat of an equivalent standard assembly. Conversely, because steel contains Co-59 which activates to form Co-60, for low cooling times a reconstituted assembly typically generates higher dose rates than an equivalent standard assembly. As the half-life of Co-60 is 5.27 years, after 10 years the Co-60 activity has reduced by almost a factor of four and a reconstituted assembly no longer generates higher dose rates than an equivalent standard assembly. To bound this effect, the fuel qualification tables require that for fuel assembly with irradiated reconstituted steel rods with cooling times less than 10 years, additional one year of cooling time is required. For cooling times of 10 years or greater, no additional cooling time is required to bound the reconstituted fuel with steel rods.

TPA

The TPA materials and masses for each irradiation zone are listed in Table 5-8. These materials are irradiated in the appropriate zone for fourteen cycles of operation. The TPA is irradiated to an equivalent assembly life burnup of 210 GWd/MTU over 14 cycles. The model assumes that the TPA is irradiated in an assembly each with an initial enrichment of 3.50 weight % U-235. The fuel assembly, containing the TPA, is burned for three cycles with a burnup of 15 GWd/MTU per cycle. This is equivalent to an assembly life burnup of 45 GWd/MTU over the three cycles. The results for a cooling time of 20 years are increased by the ratio of 14/3 to achieve the equivalent 210 GWD/MTU source.

BPRA

The BPRA materials and masses for each irradiation zone are also listed in Table 5-8. These materials are irradiated in the appropriate zone for three cycles of operation. The model assumes that the BPRA is irradiated in an assembly each with an initial enrichment of 3.50 weight % U-235. The fuel assembly containing the BPRA is burned for three cycles with a burnup of 10 GWd/MTU per cycle. This is equivalent to an assembly life burnup of 30 GWd/MTU over the three cycles. The source term for the BPRA is taken at 4 days cooling time.

VSI

VSIs are very similar in design to burnable poison rod assemblies: the stainless steel baseplate and hold-down spring assembly designs are identical to those used on older Westinghouse BPRAs. Each VSI contains 24 solid Zircalloy-4 damper rods that are attached to the hold-down assembly using a crimp nut top connector. The damper rods are the same diameter and length as BPRA rodlets. The VSIs are assumed to be equivalent in source strength to BPRAs.

Neutron Sources

Neutron sources usually consist of a single pin containing the source material. They are typically irradiated for several cycles prior to final discharge. The neutron source term from these series is several orders of magnitude lower than that of the spent fuel. The gamma source term is bounded by that of a BPRA.

Other CCs

All other CCs listed in Section 5 are not evaluated explicitly. The cladding material for the CCs include, stainless steel, inconel, zirconium based alloys such as zircaloy, M5 or zirlo. The internal component materials include non fuel materials like inconel, B₄C, Ag-In-Cd, Al₂O₃ etc. All these CCs consist of one or several rodlets similar to BPRAs. However, the resulting source terms from these CCs are required to be bounded by that of the design basis BPRA as described above.

Elemental Compositions of Structural Materials

To account for the source terms due to the elemental composition of the fuel assembly and CC structural materials the following methodology is used:

1. The material composition for each irradiation region is determined for the assembly and CC type.
2. The elemental compositions for each of the structural materials present in each region is determined by multiplying the total weight of each material in a specific irradiation zone (Table 5-7) by the elemental compositions. The fuel assembly and NFAH elemental composition, including impurities, for each material are taken from Reference [7].
3. The results of each material are summed to determine the total elemental composition for each irradiation zone.

4. The elemental composition is multiplied by the appropriate flux factor given in Table 5-6.
5. Finally, the elemental composition is entered in the light element card of the SAS2H input. The elemental composition for the fuel assembly is shown in Table 5-9.

A comparison of the fuel assembly hardware (scaled elemental composition from Table 5-9) data for the WE 15x15, WE 17x17 and CE 16x16 indicates that the CE 16x16 fuel assembly has the lowest cobalt content. The Cobalt content in the CE 16x16 fuel assembly is 2.5 times lower than that of both the WE 15x15, WE 17x17 designs. Therefore, for the purpose of calculation of source terms, the fuel assembly with the highest material mass (e.g., steel, inconel) – the WE 17x17 is selected to be the design basis fuel assembly for modeling the hardware.

The MkBW 17x17 fuel assembly with the highest MTU loading is the design basis fuel assembly for irradiation purposes.

The SAS2H model of the design basis fuel assembly will be based on a geometry and material design of the MkBW 17x17 fuel assembly and the hardware design of the WE 17x17 fuel assembly.

The SAS2H calculation applies the total flux to the light elements; therefore, the total composition must be adjusted by the appropriate flux factor in the input. A SAS2H input is created for each irradiation zone of each fuel assembly and CC type. An example input file for the active fuel zone is shown in Section 5.5.2.

5.2.1 Gamma Sources

Source terms for the fuel bounding Framatome MK BW 17x17 fuel assembly and associated burnup/initial enrichment/cooling times and CCs are calculated with SAS2H module and the 44 group ENDF/B-V library. The SAS2H calculated contributions from actinides, fission products, and activation products, as applicable, are included for each irradiation region. The 7-year post irradiation cooling time results for the MK BW 17x17 fuel with 60 GWD/MTU burnup, and 4.0 wt % U-235 initial enrichment are shown in Table 5-10. The post irradiation cooling time results for the TPA, and BPRA are shown in Table 5-11, and Table 5-12, respectively.

Based on the results presented in Table 5-11 and Table 5-12 (maximum gamma source term) the design basis CC is the BPRA. The spectrum is dominated by Co-60 for all CC. These design basis fuel assembly sources with the BPRA source are used in the MCNP calculations to determine the bounding dose rates on and around the NUHOMS® 32PTH System, including the Transfer Cask.

5.2.2 Neutron Source

The total neutron source for the NUHOMS® 32PTH System is also calculated with SAS2H. The total neutron sources for the MK BW 17x17 assembly is summarized in Table 5-13. Again, the design basis source term is for 60 GWd/MTU burnup, 4.00 weight % U-235 initial enrichment and 7-year cooling time. The neutron source term consists primarily of spontaneous fission neutrons (largely from Cm-244) with (α ,O-18) sources of lesser importance, both causing

secondary fission neutrons. The overall spectrum is well represented by the Cm-244 fission spectrum.

5.2.3 Fuel Qualification

This section provides the basis for qualification of the design basis fuel to be loaded in the NUHOMS[®] HD System from a shielding perspective. The analyses are performed to demonstrate that the fuel assemblies with the parameters corresponding to the design basis fuel result in the highest calculated dose rate so that bounding shielding analysis can be performed by utilizing these design basis source terms. In order to determine the bounding spent fuel parameters (design basis fuel assembly), the candidate assembly parameters are ranked by their relative radiation source strengths. A simple 1-D shielding calculation based on the OS 187H transfer cask is performed and the radiation dose rates at the cask side surface are determined. The spent fuel parameters that yield the highest total dose rate (gamma + neutron) are considered the design basis for shielding calculations.

The SAS2H module of the SCALE 4.4 [1] computer code system is utilized to determine the dose rates for fuel qualification purposes. The mathematical function developed to determine the heat generation from the spent fuel as a function of enrichment, burnup and cooling time (the decay heat equation) is described in Appendix 4.16.2. The representative fuel qualification tables (FQT) are developed for each heat loading zone based on the decay heat equation and are also shown in Appendix 4.16.2 (Table 4.16.2-2 through Table 4.16.2-5).

The FQT data shown in Table 4.16.2-2 through Table 4.16.2-5 of Appendix 4.16.2 are based on limiting thermal sources. It does not necessarily mean that these fuel parameters also result in limiting radiation sources. The SAS2H dose comparison runs with the spent fuel parameters from these tables are utilized to generate additional restrictions (allowable combinations of burnup and enrichment) on the FQT such that these spent fuel parameters are bounded by the design basis assembly parameters. In other words, the FQT for radiation doses are developed such that the doses due to the fuel assemblies considered as acceptable for loading into the NUHOMS[®]-32PTH DSC are bounded by those determined for the design basis assembly.

The results of the surface dose rate comparison are shown in Table 5-24. In calculating the surface dose rates, it is assumed that the NUHOMS[®]-32PTH DSC is loaded with 32 fuel assemblies with the same characteristics. This dose rate comparison is only performed at the active fuel region. It is assumed that the contribution from fuel assembly hardware (end fittings and plenum regions) to the surface dose rate is low enough to assure that the fuel region dose rate comparison is adequate.

The SAS2H model is based on a homogenization of the basket and rail material. Further, the water in the DSC/TC annulus is not modeled as the DSC shell and the TC inner shell are merged into a single shell. The calculation of the dose rate with design basis source term with SAS2H essentially creates a “normalized” design basis dose rate which can then be compared to determine limiting parameters. A conservative specific power of 25 MW is utilized for all burnup values including at 20 and 25 GWD/MTU. The SAS2H input file utilized to perform the fuel qualification calculations is listed in Section 5.5.2.

In order to make a complete and thorough determination of the design basis spent fuel assembly, dose rates from the potential entries in the FQTs shown in Appendix 4.16.2 have to be determined. However, basic shielding analysis principles can be utilized to reduce the number of SAS2H cask analysis calculations. A total of 42 burnup, enrichment, cooling time combinations have been utilized to perform the surface dose rate comparison studies. The selection of these candidate assembly parameters is based on the following principles:

- The parameters that affect the dose rates in the increasing order of importance are burnup, enrichment and cooling time. This means that for a given heat load, the fuel assembly with the lowest enrichment and cooling time is expected to produce the largest dose rates.
- For the 5 years cooling time, the minimum and maximum burnup cases are analyzed.
- The maximum credited burnup (60 GWd/MTU) at the minimum possible cooling time is analyzed.
- Remaining cases that are analyzed are representative for each cooling time.
- Cases are also analyzed at a low enrichment (as low as 0.2 wt % U235) to determine any other restrictions for loading lower enriched fuel.

These results indicate that the doses for spent fuel loadings with some of the parameters at a thermal power of 1500 watts per assembly have surface dose rates that exceed the design basis dose rate shown as Case 1. The total doses for those cases that exceed the design basis dose rates are shaded in grey in Table 5-24. These results imply that certain restrictions maybe placed when loading spent fuel at higher thermal power, specifically for loading in Zone 3.

A realistic, yet conservative approach to dose evaluation based on the results from Table 5-24 would indicate that the fuel loading in Zone 3 can be unrestricted. This is due to the fact that only 8 fuel assemblies with a decay heat load of 1500 watts per assembly are authorized be loaded in the NUHOMS[®]-32PTH canister while all the results (and restrictions) are based on a loading of 32 Zone 3 fuel assemblies. Therefore, any restriction to the Zone 3 fuel loading can only be applied by comparing the surface dose rate from a canister based on a multi-zone fuel loading to that of the design basis fuel. Calculations from other NUHOMS[®] DSCs indicate that the peripheral locations (16 fuel assemblies) contribute to approximately 80% of the total dose rate while the interior locations (16 fuel assemblies) contribute to the remaining 20%. Assuming that the Zone 2 and Zone 3 fuel assembly locations contribute equally to the dose rates due to the 16 outer locations, the contribution from Zone 3 and Zone 2 locations are approximately 40% and 60% respectively, to the total dose rates. Note that this approach is also conservative since it does not include Zone 1 fuel assemblies.

The average total surface dose rate for a conservative loading, based on 55% of the dose from the worst Zone 3 fuel (Case 2, 261.6 mrem/hour) and 45% of the dose from the worst Zone 2 fuel (Case 35, 215.1 mrem/hour), is 240.7 mrem/hour and is bounded by the design basis value of 241.7 mrem/hour. Moreover, the estimated dose rate from the worst Zone 3 fuel (Case 2, 261.6 mrem/hour) is higher than that from the design basis fuel (Case 1, 241.7 mrem/hour) by less than 10%. Therefore, it can be argued that based on a conservative yet realistic zone loading of fuel assemblies, the design basis fuel assembly analyzed for radiation dose rates is bounding.

All the dose rate comparisons for the fuel assemblies with lower enrichment (as low as 1.2 wt. % U-235, Table 5-24, Case 27 through Case 37) are made with Zone 1A and Zone 2 fuel only. These results conservatively encompass all of the Zone 1B results. These results indicate that the doses for spent fuel loadings with low enrichments and high burnups have surface dose rates that exceed the design basis dose rate shown as Case 1 and are shaded in grey in Table 5-24. Note that some of the burnup, enrichment and cooling time combinations evaluated in Table 5-24 have heat loads that exceed the maximum allowable value of 1500 watts. These cases are intended to be illustrative and demonstrate that the evaluation performed is reasonably encompassing. These results imply that certain restrictions may be placed when loading spent fuel at very low enrichments combined with impractically high burnups.

For the cases with very low enrichment (less than 1.2 wt. % U-235, Table 5-24, Case 38 through Case 42), only bounding cases at the lowest enrichment, highest allowable burnup and lowest allowable cooling time are considered. Because of the low enrichment, small changes need to be made to the SAS2H models to ensure that the source calculations have converged. This is ensured by setting the NLIB/CYC to 2 for cases with enrichments of 0.7 wt. % U-235 and NLIB/CYC to 5 for cases with enrichments of 0.3 and 0.2 wt. % U-235.

The following is a summary of the significant results of this fuel qualification evaluation:

- The spent fuel parameters utilized to determine the design basis source terms result in the design basis dose rates on and around the HD system, provided some restrictions are placed.
- The decay heat equation can be used to determine the decay heat for fuel assemblies with initial enrichments greater than or equal to 1.5 wt. % U-235. The minimum enrichments for loading in the various zones using the decay heat equation are: Zone 1- 1.5 wt. % U-235, Zone 2- 1.6 wt. % U-235 and Zone 3- 2.5 wt. % U-235.
- The maximum burnup for fuel assemblies with initial enrichment between 1.5 wt. % U-235 and 2.5 wt. % U-235 is 55 GWD/MTU.
- The maximum burnup for fuel assemblies with initial enrichment between 0.7 wt. % U-235 and 1.5 wt. % U-235 is 32 GWD/MTU.
- The maximum burnup for fuel assemblies with initial enrichment between 0.3 wt. % U-235 and 0.7 wt. % U-235 is 25 GWD/MTU.
- The maximum burnup for fuel assemblies with initial enrichment between 0.2 wt. % U-235 and 0.3 wt. % U-235 is 20 GWD/MTU.

The evaluation to determine the cooling time requirements for fuel assemblies with reconstituted rods is documented herein. Reconstituted fuel assemblies are those where one or more fuel rods are replaced by rods that displace the same amount of water in the active fuel region. The material for these replacement rods can be solid zirconium alloy rods, low enriched UO₂ rods (with zirconium alloy cladding), solid or hollow stainless steel rods, etc. For fuel assemblies that do not undergo further irradiation in the reactor following the replacement of these rods, no other cooling time restrictions are needed. Further, no restrictions on the material or the number of replacement rods are placed for such fuel assemblies.

For fuel assemblies that undergo further irradiation in the reactor following the replacement of these rods, restrictions on the cooling time of the fuel assemblies and in the material and number of the replacement rods is required. Replacement rods made up of zirconium alloy clad low enriched UO₂ or solid zirconium alloys that undergo further irradiation in the reactor do not result in source terms that are greater than that of the original UO₂ rods. Therefore, no restrictions in their number or cooling time are necessary for their qualification – the thermal and source term qualification (from above) is sufficient.

Fuel assemblies with replacement stainless steel rods that undergo subsequent irradiation are restricted to a maximum of 10 replacement rods. Further, such fuel assemblies need to be cooled for an additional amount of time to ensure that the resulting source terms are bounded by those of the design basis fuel. There is no effect on the source terms/shielding due to the position of the reconstituted rods in the fuel rod array. Reconstituted fuel has a rather small effect on the dose rate such that for fuel assemblies with cooling times less than 10 years, an additional year of cooling time is required if reconstituted rods (with irradiated stainless steel) are present in fuel assemblies.

The remainder of this section documents the analysis performed to determine the cooling time restrictions for these fuel assemblies. This analysis is also performed using the SAS2H module and is similar to the analyses performed for the fuel qualification evaluation documented above.

The irradiation history utilized in these calculations is based on three cycles of equal duration. For the fuel assemblies with reconstituted rods, the first cycle assumes that no replacement of rods have taken place. The second and third cycles assume that 10 stainless steel rods have replaced the original UO₂ rods. For these cycles, the mass of Uranium in the fuel is reduced to 0.458 MTU from 0.476 MTU which corresponds to 10 rods. The mass of stainless steel is increased by 20.58 kg to account for the mass of 10 solid stainless steel rods.

The results of these evaluations are shown in Table 5-25. A total of 15 individual dose rate calculations are performed grouped under 6 case numbers. Case #s ending with “A” are based on fuel assembly without reconstituted rods. Case #s ending with “B” and “C” are based on fuel assembly with 10 reconstituted stainless steel rods that undergo additional 2 cycles of irradiation. These results indicate that for cooling times at or below 10 years, the dose rate from a reconstituted fuel assembly with reconstituted rods is greater than that of an un-reconstituted fuel assembly. This indicates that a cooling time of 10 years can represent a possible limit for fuel assemblies containing reconstituted rods. A comparison of the three SAS2H runs that constitute Case #1, indicate that the dose rate for the design basis fuel assembly increases from 241.7 mrem/hour to 253.0 mrem/hour when it is reconstituted. However, this dose rate drops to 226.5 mrem/hour when this fuel assembly is cooled by an additional year which represents a reduction of 10%. This indicates that an additional year of cooling time can also represent a conservative limit for reconstituted fuel assemblies.

The following is a summary of the significant results of the reconstituted fuel evaluation that provides the limits on the qualification of these fuel assemblies. The restrictions are applicable only to fuel assemblies that contain no more than 10 replacement rods and that undergo further irradiation following reconstitution.

- An additional cooling time of 1 year is needed to load reconstituted fuel assemblies in Zone 2 and Zone 3 that would have otherwise qualified based purely on thermal loading requirements.
- The cooling time restrictions are limited to reconstituted fuel assemblies with cooling times less than or equal to ten years.

5.3 Model Specification

The neutron and gamma dose rates on the surface of the HSM-H, and on the surface, and at 1.5 and 3 feet from the surface of the OS187H Transfer Cask are evaluated with the Monte Carlo transport code MCNP [2, 6]. The flux-to-dose conversion factors specified by the ANSI/ANS 6.1.1-1977 [5], are used and provided in Table 5-14.

5.3.1 Description of the Radial and Axial Shielding Configurations

Figure 5-1 is a sketch of an HSM-H cut away at the mid-vertical plane. Figure 5-3 is also a cut through the vertical mid-plane, the 32PTH-DSC is shown in phantom lines, and the front door is at the left hand side. The rear wall of the HSM-H module has a minimum thickness of 1 foot. A 3-foot shield wall is placed along the rear and sides of the HSM-H, as shown in Figure 5-1.

The MCNP computer models are built to evaluate the dose rate along the front wall surface, the rear shield wall surface, the vent openings, the roof surface, and on the side shield walls.

Figure 5-4 shows the shielding configuration of the OS187H transfer cask.

5.3.1.1 Storage Configuration

A three-dimensional MCNP model was developed for the HSM-H Model. The HSM length was designated as the x axis (North-South direction), the width as the y axis (East-West direction), and the HSM height as the z axis. The HSM door is designated as the S side and the -x direction, with the E wall as the -y direction. The roof is the +z direction. The E wall is designated as a reflective boundary and an end shield wall (3 ft thick) is attached to the W wall. The geometry of nearly all components of the HSM is Cartesian, except for the 32PTH-DSC, which is cylindrical. The MCNP model is a full 3-D representation of a single DSC inside the HSM-H with the reflective boundary, end and side shield walls. A three foot thick concrete shield wall is placed at the rear of the HSM. A NUHOMS[®]-32PTH-DSC MCNP model was developed for the transfer cask analysis, discussed below. This model was revised slightly and located within the HSM model. The DSC support rails are not included in the model. The heat shields are modeled as flat plates without fins or louvers and horizontal vent "liner" plates (2cm thk) are modeled in the top side vents.

Two liners are used for gamma dose attenuation at the bottom vents. The "top" liner is a 1-inch steel plate, positioned at the roof of the bottom vent. The "front" liner is a 1-inch steel plate, at the side of the inlet vent (near the HSM front). Due to modeling constraints the "front" liner is modeled as part of the vent. This simplification does not impact the overall gamma dose rates.

5.3.1.2 Loading/Unloading Configurations

The dose rates on the surface, and at 1.5 and 3 feet from the surface of the 32PTH-DSC/ Transfer Cask are evaluated with MCNP. Three different key configurations in the loading/unloading of the spent fuel are analyzed. The three different stages modeled are: (1) Decontamination, (2) Dry Welding and (3) Transfer. Calculations are performed assuming no temporary shielding is utilized for in the configurations, which is normally done at the sites.

Definition of Transfer Cask and 32PTH-DSC Loading Stages

1. Decontamination. The water level in the 32PTH-DSC cavity is assumed to be lowered four inches below the bottom of the top shield plug. The Cask/32PTH-DSC annulus is assumed to remain completely filled with water. (No DSC top cover or cask lid)
2. Dry welding. The 32PTH-DSC cavity is assumed to be completely dry, the 32PTH-DSC inner and outer top cover plates have been installed. The Cask/32PTH-DSC annulus is assumed to remain completely filled with water. (no cask lid)
3. Transfer. The 32PTH-DSC and 32PTH-DSC/Cask annulus are dry.

Dose analysis results for the above conditions are provided in Table 5-22 and Table 5-23.

5.3.1.3 Transfer Configuration

For the transfer configuration the Transfer Cask/32PTH-DSC annulus is completely dry. The 32PTH-DSC inner and outer top cover plates are installed. The top end of the Transfer Cask is in place which consists of a 3" thick steel cover plate and a 2" thick solid neutron shield, and a 1/4" thick steel plate cover is over the solid neutron shield.

A three-dimensional MCNP model was developed for the OS-187H transfer cask containing the NUHOMS[®]-32PTH DSC. The cask/canister length was designated as the z axis (axial direction), the radial direction as the x and y axis. The 32PTH-DSC basket compartments and rails were discretely modeled in MCNP. The basket was simply modeled as the 8.70" sq, 0.187" thk SS compartments, each compartment surrounded by 0.5" of aluminum. Conservatively, neither boron in the aluminum, nor the SS strips were included in the MCNP basket model. Each of the 32 fuel assemblies was modeled in four axial regions; bottom fitting, fuel, plenum, and top fitting. The axial length of each fuel assembly region modeled was; 4.17", 14.4", 6.95", and 6.17", respectively. The lead thickness (3.60" nom) in the OS-187H is modeled as 3.56" of lead with a 0.04" void and the density of the lead is reduced to 0.985 TD.

The neutron shield support rings provide support for the skin, which contains the water for the neutron shield. The rings are modeled explicitly in the water filled neutron shield. The trunnions penetrate the neutron shield, which locally changes the shielding configuration of the neutron shield. The trunnions which are explicitly modeled are thick steel structures filled with solid resin neutron shielding material. These structures provide more gamma and neutron shielding than the water that they replace, because they protrude well past the neutron shield and are made of materials which provide more gamma shielding and comparable neutron shielding as compared to the water that they replace.

5.3.2 Shield Regional Densities

Table 5-7 shows the material masses for the four fuel assembly regions. Based on these material masses, and the material compositions [7], material densities for the fuel assembly regions are determined and provided in Tables 5-15 and 5-16 (loading configuration 1 above).

The mass of materials in each fuel assembly region is homogenized over the volume of the region (x-section = 71 in²). Tables 5-17 and 5-18 provide the shield regional densities for the 32PTH-DSC and OS187H TC.

The concrete for the HSM-H is chosen to be “plain” concrete with a density of 143 lbs/ft³ with the rebar conservatively neglected. Table 5-19 provides the concrete densities.

The actual fuel layout in the 32PTH-DSC is a cartesian array of fuel assemblies inside stainless steel compartments surrounded by sheets of aluminum material. These regions are modeled discretely as are the rails on the periphery of the basket. A source is modeled for each of the four homogenized fuel assembly regions for all 32 fuel assemblies. The source regions are cuboid in shape with the same 8.426” x 8.426” (17 times the Pitch) x-section and the appropriate axial length.

When the transfer cask/32PTH-DSC annulus and 32PTH-DSC are filled with water, the wet axial densities are used for the homogenized regions.

5.4 Shielding Evaluation

5.4.1 Computer Programs

MCNP [2, 6] is a general-purpose Monte Carlo N-Particle code that can be used for neutron, photon, electron, or coupled neutron/photon/electron transport. The code treats an arbitrary three-dimensional configuration of materials in geometric cells bounded by first- and second-degree surfaces and some special fourth-degree surfaces. Pointwise (continuous energy) cross-section data are used. For neutrons, all reactions given in a particular cross-section evaluation are accounted for in the cross section set. For photons, the code takes account of incoherent and coherent scattering, the possibility of fluorescent emission after photoelectric absorption, absorption in pair production with local emission of annihilation radiation, and bremsstrahlung. Important standard features that make MCNP very versatile and easy to use include a powerful general source; an extensive collection of cross-section data; and an extensive collection of variance reduction techniques that can be employed to track particles through very complex deep penetration problems.

5.4.2 Spatial Source Distribution

The source components are:

- A neutron source due to the active fuel regions of the 32 fuel assemblies,
- A gamma source due to the active fuel regions of the 32 fuel assemblies,
- A gamma source due to the plenum regions of the 32 fuel assemblies,
- A gamma source due to the top nozzle regions of the 32 fuel assemblies,
- A gamma source due to the bottom nozzle region of the 32 fuel assemblies,
- A gamma source due to the 32 BPRAs in the top nozzle, plenum and fuel regions of the 32 fuel assemblies

Axial burnup peaking factors for PWR fuel are taken from Reference [4]. These peaking factors are assumed to match the gamma axial source distribution because the gamma source is proportional to burnup. The neutron source is approximately proportional to the fourth power of the burnup. Therefore, the axial neutron source distribution may be determined as the fourth power of the axial burnup profile.

Axial peaking changes with increasing burnup. The axial peaking factors used are provided in Table 5-20. The OS187H TC and HSM-H calculations use peaking factors for a burnup >46 GWd/MTU because the design basis source occurs at a burnup of 60 GWd/MTU. The neutron and gamma peaking factors are shown as a function of the core height in Table 5-20. These factors are directly applied to each MCNP interval in the fuel region.

The average values of the axial peaking distributions are also provided in Table 5-20. For the gamma distribution, the average value is 1.00. However, for the neutron distribution, the average value of the distribution is greater than 1.00. The average value of the axial neutron distribution may be interpreted as the ratio of the true total neutron source in an assembly to the neutron source calculated by SAS2H/ORIGEN-S for an average assembly burnup.

Therefore, to properly correct the magnitude of the neutron source, the neutron source per assembly as reported in Table 5-13 is multiplied by the average value of the neutron source distribution as reported in Table 5-20.

5.4.3 Cross-Section Data

The cross-section data used is the continuous energy ENDF/B provided with the MCNP code. The cross-section data allows coupled neutron/gamma-ray dose rate evaluation to be made to account for secondary gamma radiation (n,γ), if desired. All of the transfer cask dose rate calculations account for the dose rate due to secondary gamma radiation. For the HSM-H dose rate calculation, the dose rate contribution from the secondary gamma radiation is ignored because it is insignificant.

5.4.4 Flux-to-Dose-Rate Conversion

The flux distribution calculated by the MCNP code is converted to dose rates using flux-to-dose rate conversion factors from ANSI/ANS-6.1.1-1977 [5] given in Table 5-14.

5.4.5 Model Geometry

Figure 5-5 through Figure 5-7 are the MCNP models for the Transfer Cask (TC) containing the 32PTH-DSC. Figures 5-8 through Figure 5-11 are the MCNP models of the HSM-H with the DSC. The figures show dimensions in cm with MCNP surface numbers in brackets. Figures 5-12 and 5-13 show the location of the detectors cells on the HSM surfaces.

5.4.6 Methodology

The methodology used in the shielding analysis of the 32PTH system utilizes the 3-D MCNP code. MCNP allows for explicit 3-D modeling of any shielding configuration and reduces the number of approximations needed. The methodology used herein is summarized below.

1. Sources are developed for all fuel regions using the source term data developed in Section 5.2. Source regions include the active fuel region, bottom end fitting (including all materials below the active fuel region), plenum, and top end fitting (including all materials above the active fuel region). Sources for CC are added group-by-group to the fuel sources.
2. Suitable shielding material densities are calculated for all regions modeled.
3. The 3-D Monte Carlo transport code MCNP is used to calculate dose rates on and around the HSM-H and the OS187H TC. The MCNP4 code is selected because of its ability to handle thick, multi-layered shields and account for streaming through both the HSM-H air vents and cask/DSC annulus using 3-D geometry. MCNP4C2 results are used to calculate offsite exposures (see Chapter 10).
4. For the TC, weight windows are utilized for variance reduction. Segmented surface (ring) detectors are used to tally surfaces for dose rate determinations.

For the HSM-H, importance biasing is utilized for variance reduction and tally cells and segmented tally cells are used to determine average and maximum dose rates around the HSM-H.

5. MCNP models are also generated to determine the effects of accident scenarios, such as loss of cask neutron shield, for the OS187H TC.

5.4.7 Assumptions

The following general assumptions are used in the analyses.

5.4.7.1 Source Term Assumptions

1. The primary neutron source in LWR spent fuel is the spontaneous fission of ^{244}Cm . For the ranges of exposures, enrichments, and cooling times in the fuel qualification tables, ^{244}Cm represents more than 85% of the total neutron source. The neutron spectrum is, therefore, relatively constant for the fuel parameters addressed herein and is assumed to follow the ^{244}Cm fission spectrum.
2. Surface gamma dose rates are calculated for the HSM and cask surfaces using the actual photon spectrum applicable for each case.
3. The PWR heavy metal weight is assumed to be 0.476 MTU per assembly to bound existing PWR fuel designs.
4. The source term associated with the BPRAs are bounding for all CCs.
5. The source terms for an assembly reconstituted with stainless steel pins are bounding for all other reconstituted assemblies.

5.4.7.2 HSM-H Dose Rate Analysis Assumptions

1. Planes of reflection are used to simulate adjacent HSM-Hs.
2. Embedments and rebar in the HSM-H concrete are conservatively neglected.
3. The borated neutron absorber sheets in the 32PTH-DSC are modeled as aluminum.
4. Axial source distribution assumed as shown in Table 5-20.
5. Fuel is homogenized within the fuel compartment and source region, although the 32PTH-DSC basket is modeled explicitly.
6. The steel on the front door is conservatively modeled using a thickness of 3 7/8" while the actual thickness is 7 7/8".

5.4.7.3 OS187H TC Dose Rate Analysis Assumptions

1. The 32PTH-DSC is modeled within the OS187H TC.
2. The OS187H is modeled for the welding operation. No supplemental neutron shielding is assumed to be placed on top of the 32PTH-DSC cover plates during welding.
3. During the accident case, the cask neutron shield (water) is assumed to be lost and a lead slump of 1" is assumed in the cask end.
4. The borated neutron absorber sheets in the 32PTH- DSC are modeled as aluminum.
5. The stainless steel strip plates are conservatively modeled as aluminum.
6. Axial source distribution assumed as shown in Table 5-20.
7. Fuel is homogenized within the fuel compartments and the source regions, although the 32PTH-DSC baskets are modeled explicitly.
8. In the OS187H TC model, the lead shield is assumed at the minimum thickness and with reduced density.

5.4.8 Normal Condition Models

Two basic MCNP models are developed: (1) 32PTH- DSC in the HSM-H and (2) 32PTH-DSC in the OS187H TC. These models are described in subsequent sections.

5.4.8.1 32PTH DSC in HSM-H

Two, three-dimensional MCNP4C2 models are developed for the 32PTH-DSC within a HSM-H, one model for neutrons and the other for gammas. These models are presented in Figures 5-8 through Figure 5-11. The HSM-H length is designated as the x axis, the width as the y axis, and the height as the z axis. The HSM-H door is designated as the south side and the -x direction, with the east wall as the -y direction. The roof is the +z direction. The east wall is designated as a reflective boundary and an end shield wall (3 ft thick) is attached to the west wall.

The bottom (bottom of bottom fitting) of the fuel assembly is assigned to an x plane at -213.84 cm. The center of the HSM-H is at y=0 and z=0. The 32PTH-DSC lid is located 5" from the HSM-H rear wall (x=254.84 cm) which places the bottom of the DSC at x=-215.69 cm, about 20 inches from the door interior. The 32PTH-DSC support rails are not included in the model. The heat shields are modeled as flat plates without fins or louvers, and horizontal vent "liner" plates (2 cm thick) are modeled in the top side vents.

Dose rates are calculated on thin cells surrounding the HSM-H and are segmented into 30 cm increments to capture the peak dose rates. Dose rates are also calculated at the inlet and outlet vents. Dose rates for this scenario are provided in Table 5-21. Dose rates for the front, roof, and side shield wall surface at DSC centerline of the HSM-H are also plotted as a function of distance in Figures 5-17 and 5-18 respectively.

A sample MCNP4C2 model input file of HSM-H with 32PTH-DSC is included in Section 5.5.2.

The use of an optional door design with a steel thickness of 3 inches (instead of 3.875 inches in the shielding models) and a concrete thickness of 29.375 inches (instead of 22.5 inches in the shielding models) will have no impact on the shielding of the HSM-H. The results shown in Table 5-21 indicate that the door dose rates are mostly due to neutrons (approximately 62%) and an increase in the neutron shielding will offset the reduction in the gamma shielding. Overall, minor changes to the door design that involve changes to the steel thickness within 1 inch and concrete thickness within 6 inches do not result in a significant change in the HSM-H front surface dose rate because the average door dose rates are approximately 15 times lower than the front average dose rates.

5.4.8.2 32PTH- DSC in OS187H TC

Two three-dimensional MCNP4B models are employed for shielding analyses of the 32PTH-DSC within an OS187H TC, one model for neutrons and the other for gammas. These models are presented in Figure 5-5 through Figure 5-7. The DSC/TC length was designated as the z-axis in the MCNP models. Select features within the cask and on its surface are neglected because they produce only localized effects and have minimal impact on operational dose rates. Examples of neglected features include relief valves, clevises, and eyebolts.

These items are local features that increase the shielding in a small area without replacing any of the shielding material which is included in the model. The additional shielding material that these features provide is not smeared into the bulk shielding, nor is any credit taken for it in the occupational exposure calculation. The neutron shield support rings provide support for the neutron shield skin, which contains the water for the neutron shield. The fifteen rings are modeled explicitly within the neutron shield.

The trunnions penetrate the neutron shield, which locally changes the shielding configuration of the neutron shield. The trunnions are thick steel structures filled with solid neutron shielding material. These structures protrude well past the neutron shield and are made of materials which provide more gamma shielding and comparable neutron shielding as compared to the 0.96 g/cm³ water that these replace. The trunnions are also modeled explicitly in MCNP.

Design features relevant to the shielding analysis of the OS187H TC and 32PTH-DSC are modeled in MCNP4B. The overall length of the OS187H TC is 193.32". The outer diameter of the OS187H TC is 92.20" (neutron shield included). The outer diameter excluding the neutron shield is 82.70". The bottom of the OS187H TC is designed to mate with a 32PTH-DSC. The overall length of the 32PTH-DSC is 185.75" (excluding the grapple) and its outer diameter is 69.75". The bottom end of the 32PTH-DSC is in contact with the structural shell assembly of the transfer cask.

In section 5.3.1.2 and 5.3.1.3, the three transfer cask scenarios are described. The basic MCNP models for the OS187H TC described above are modified as described below to represent the loading/transfer configurations.

A. Cask Decontamination

The 32PTH-DSC and the OS187H TC are assumed to be filled with water, including the region between 32PTH-DSC and cask, which is referred to as the “cask/32PTH-DSC annulus.” The water in the DSC is assumed to be approximately 4” below the shield plug. The 32PTH-DSC shield plug is assumed to be in place and the temporary shielding has not yet been installed. The DSC top cover and cask lid are not installed. Results for this case are provided in Table 5-22.

B. Welding and DSC Draining

Before the start of welding operation, water in the DSC cavity is removed to reduce the potential due to hydrogen generation. A dry DSC cavity is assumed in all welding models to be conservative. Temporary shielding is not installed. In addition, the cask lid is not installed. The cask/32PTH-DSC annulus is assumed to remain completely filled with water. Results for this case are provided in Table 5-22.

C. Transfer

In preparation for transfer to the HSM-H, the DSC is drained, dried, the tops welded on, the annulus drained, and the cask lid installed. Results for this case are provided in Table 5-23 along with accident dose rates (loss of water in neutron shield tank and 1” lead slump).

Dose rates at the sides, top, and bottom of this cask are presented graphically in Figure 5-14 through Figure 5-16.

A sample MCNP4B model input file for OS187H TC with 32PTH-DSC is included in Section 5.2.2.

Proprietary Information on Pages 5-24 and 5-25
Withheld Pursuant to 10 CFR 2.390

5.5 Supplemental Information

5.5.1 References

1. Oak Ridge National Laboratory, RSIC Computer Code Collection, "SCALE: A Modular Code System for Performing Standardized Computer Analysis for Licensing Evaluations for Workstations and Personal Computers," NUREG/CR-0200, Revision 6, ORNL/NUREG/CSD-2/V2/R6.
2. MCNP4B2, "Monte Carlo N-Particle Transport Code System," Los Alamos National Laboratory, CCC-660, RSIC, January 1998.
3. Radiation Shielding, J. Kenneth Shultis and Richard E. Faw, Pretence Hall, 1996.
4. "Recommendations for Addressing Axial Burnup in PWR Burnup Credit Analyses," NUREG/CR-6801, March 2003.
5. "American National Standard Neutron and Gamma-Ray Flux-to-Dose Rate Factors". ANSI/ANS-6.1.1-1977, American Nuclear Society, La Grange Park, Illinois. March 1977.
6. MCNP4C2, "Monte Carlo N-Particle Transport Code System," Los Alamos National Laboratory, CCC-701, RSIC, June 2001.
7. Ludwig, S.B., and J.P. Renier, "Standard- and Extended-Burnup PWR and BWR Reactor Models for the ORIGEN2 Computer Code," ORNL/TM-11018, Oak Ridge National Laboratory, December 1989.

Proprietary Information on Pages 5-27 through 5-68
Withheld Pursuant to 10 CFR 2.390

Table 5-1
NUHOMS[®] HD 32PTH System Shielding Materials

HSM-H

Components	Thickness/Material Modeled
Side Walls	1' concrete
Side Shield Wall	3' concrete
Roof	4' concrete
Rear Wall	Minimum thickness 1' concrete
Rear Shield Wall	3' concrete
Front Door/Front Wall	2.5'/3.5' thick concrete

32PTH-DSC

Components	Thickness/Material Modeled
Bottom Shield Plugs/Cover Plates	8.75" Steel
Top Shield Plugs/Cover Plates	12.00" Steel
Cylindrical shell	0.50" Steel
Basket (main components)	32 Stainless Steel Fuel compartments, 3/16" thick each, and aluminum/ borated aluminum plates total 1/2" thk

OS187H Transfer Cask

Components	Thickness/Material Modeled
Top Cover Plate	2" resin and 3.25" Steel
Bottom Cover Plate	2.25" resin and 2.75" Steel
<u>Radial walls</u>	
Inner Shell	0.5" Steel
Lead Gamma Shield	3.56" Lead
Structural Shell	1.5"/2.00" Steel
Neutron Shield	4.56" Water
Skin	0.19" Steel

Table 5-2
Summary HSM-H Dose Rates ⁽³⁾

Surface	Dose Rate Component	Average Surface Dose Rate ⁽²⁾ , mrem/hr
Rear ⁽¹⁾	Gamma	0.5
	Neutron	<0.1
Front	Gamma	5.5
	Neutron	0.5
Roof	Gamma	13.9
	Neutron	1.9
Side ⁽¹⁾	Gamma	0.4
	Neutron	0.2

⁽¹⁾ Rear and side dose rates are on the outer surfaces of the shield walls.

⁽²⁾ These dose rates are bounding for 1 meter occupational exposures during transfer operations.

⁽³⁾ Dose rates can be higher by 6% to account for the use of grout during HSM fabrication and installation.

Table 5-3
Transfer Cask (Loading/Unloading/Transfer Operations) Side Dose Rate Summary

Stage of TC/32PTH-DSC Processing	Dose Rate mrem/hr	On Outside Surface		1.5' from Surface		3' from Surface	
		Gamma	Neutron	Gamma	Neutron	Gamma	Neutron
Decontamination	Maximum	241	158	153	95.7	107	65.4
	Minimum	7.8	0.4	26.0	4.0	29.4	8.8
	Average ⁽¹⁾ Surface	162	93.9	105	61.2	75.0	43.6
Welding	Maximum	310	95.8	198	59.0	139	40.9
	Minimum	12.3	10.9	27.4	4.2	37.3	10.7
	Average ⁽¹⁾ Surface	206	59.3	136	37.3	97.5	26.9
Transfer	Maximum	384	125	238	77.0	165	54.7
	Minimum	15.1	22.2	31.8	7.5	44.2	13.0
	Average ⁽¹⁾ Surface	254	81.4	163	50.0	116	35.5

Notes:

(1) Surface weighted average of ring detectors used as tally surfaces

Table 5-4
Transfer Cask (Loading/Unloading/Transfer Operations) Top End Dose Rate Summary

Stage of TC/32PTH-DSC Processing	Dose Rate mrem/hr	On Outside Surface		1.5' from Surface		3' from Surface	
		Gamma	Neutron	Gamma	Neutron	Gamma	Neutron
Decontamination	Maximum	933	118	688	52.0	513	27.5
	Minimum	314	31.7	337	15.1	281	12.2
	Average ⁽¹⁾ Surface	646	66.8	430	26.5	361	17.0
Welding	Maximum	95.5	328	77.6	192	52.5	102
	Minimum	39.4	63.1	41.0	66.9	32.0	53.1
	Average ⁽¹⁾ Surface	58.9	145	52.7	106	43.3	69.7
Transfer-Storage	Maximum	8.8	24.5	5.2	14.1	3.5	8.7
	Minimum	5.0	11.5	3.9	5.5	2.8	4.5
	Average ⁽¹⁾ Surface	6.1	14.1	4.2	8.1	3.0	5.7

Notes:

(1) Surface weighted average of ring detectors used as tally surfaces

Table 5-5
Cask (Loading/Unloading/Transfer Operations) Bottom End Dose Rate Summary

Stage of TC/32PTH-DSC Processing	Dose Rate mrem/hr	On Outside Surface		One Foot from Surface		Three Feet from Surface	
		Gamma	Neutron	Gamma	Neutron	Gamma	Neutron
Transfer	Maximum	475	1350	118	305	53.1	117
	Minimum	9.5	43.3	13.6	40.4	14.0	39.5
	Average ⁽¹⁾ Surface	36.5	134	29.7	86.9	23.3	58.9

Notes:

(1) Surface weighted average of ring detectors used as tally surfaces

Table 5-6
Flux Factor By Fuel Assembly Region

Fuel Assembly Region	Flux Factor
Bottom	0.20
In-Core	1.00
Plenum	0.20
Top	0.10

Table 5-7
Fuel Assembly Materials and Masses
(Page 1 of 2)

Region	Material	Mass (kg/assembly)		
		WE 15x15	WE 17x17	MK BW 17x17
Top Fitting				
Upper Tie Plate	SS 304	6.8	6.8	7.0
Hold Down Springs	Inconel 718	1.1	1.37	1.1
Plenum				
Cladding & Guide Tubes	Zr-4	6.1	5.5	6.3
Plenum Spring	SS 302	1.5	1.9	4.7
Fuel Zone				
Cladding & Guide Tubes	Zr-4	99.2	102.9	109.9*
Grids	Zr-4			8.2
	Inconel-718	5.9	5.9	0.8
Grid Brazing Material	Microbraz 50	1.2	1.2	-
Miscellaneous	SS 304	4.6	4.6	0.1*
Bottom Fitting				
Bottom Tie Plate	SS 304	5.7	5.7	4.3
Total		132.1	135.6	142.4

* Clad is M5™ which is treated as Zr-4

Table 5-7
Fuel Assembly Materials and Masses
 (Page 2 of 2)

CE 16x16 Fuel Assembly Hardware Materials and Masses

Item	Material	Average Weight (lb./assembly)	Average Weight (kg/assembly)
Active Fuel Zone			
Guide Tubes	Zircaloy-4	21	9.53
Spacer Grids	Zircaloy-4	23.4	10.62
Spacer Grid	Inconel 625	2.6	1.18
Cladding	Zircaloy-4	235.2	106.78
Fuel Rods	UO ₂	1137	Total U = 455.5 kg
Plenum Zone			
Guide Tubes	Zircaloy-4	1.5	0.68
Spacer Grid	Zircaloy-4	1.8	0.82
Upper End Cap	Zircaloy-4	1.9	0.86
Cladding	Zircaloy-4	15.7	7.13
Plenum Springs	Stainless Steel 302	16.5	7.49
Spacer Discs	Al ₂ O ₃	1.3	0.59
Top Fitting Zone			
Holddown Plate	Stainless Steel 304	24.6	11.17
Flow Plate	Stainless Steel 304		
Outer Posts	Stainless Steel 304		
Center Guide Post	Stainless Steel 304		
Guide Tubes	Zircaloy-4	0.3	0.14
Holddown springs	Inconel X-750	11.4	5.18
Bottom Fitting Zone			
Guide Tubes	Zircaloy-4	0.9	0.41
Locking Discs/Sleeve	Stainless Steel 304	0.2	0.09
Spacer Grid	Inconel 625	2.6	1.18
Spacer Discs	Al ₂ O ₃	1.3	0.59
Cladding	Zircaloy-4	0.4	0.18
Bottom End Cap	Zircaloy-4	20.6	9.35
Lower End Fitting	Stainless Steel 304	13.1	5.95

Fuel Assembly Zone	Zircaloy	Steel	Inconel
Component Mass (Kg)			
Bottom Fitting	9.94	6.04	1.18
Active Fuel	126.94	-	1.18
Plenum	9.49	7.49	-
Top Fitting	0.14	11.17	5.18

Table 5-8
NFAH Materials and Masses

Component	Region	Material	Mass (kg)
TPA	<u>Top Fitting</u>		
	Baseplate, yoke, holddown bar, etc.	Type 304 SS	2.5
	spring	Inconel 718	0.36
BPRA/ VSI	<u>Plenum</u>		
	Thimble plugs	Type 304 SS	3.3
	<u>Top Fitting</u>		
	Baseplate, yoke, holddown bar, etc	Type 304 SS	2.5
	spring	Inconel 718	0.36
	<u>Plenum</u>		
	Cladding & liner	Type 304 SS	0.80
	<u>Fuel Zone</u>		
	Cladding & liner	Type 304 SS	15.0

Table 5-9
Fuel Assembly Material Masses

(kg/assembly)

Scaling Factors	0.1	0.2	1	0.2	
	Top Fitting	Plenum	Active Fuel	Bottom Fitting	Total
15x15					
Chromium	0.1501	0.0555	2.2972	0.2166	2.7194
Manganese	0.0138	0.0060	0.1059	0.0228	0.1485
Iron	0.4879	0.2121	4.4512	0.7848	5.9360
Cobalt	0.0011	0.0003	0.0328	0.0009	0.0350
Nickel	0.1178	0.0268	4.3714	0.1017	4.6177
Zirconium	0.0000	1.1945	97.128	0.0000	98.322
Aluminum	0.0007	0.0000	0.0380	0.0000	0.0387
Silicon	0.0070	0.0030	0.0124	0.0000	0.0224
Titanium	0.0009	0.0000	0.0473	0.0000	0.0481
Niobium	0.0061	0.0000	0.3272	0.0000	0.3333
Molybdenum	0.0033	0.0000	0.1768	0.0000	0.1801
Tin	0.0000	0.0195	1.6608	0.0182	1.6986
17x17					
Chromium	0.1551	0.0698	2.3018	0.2166	2.7433
Manganese	0.0139	0.0076	0.1060	0.0228	0.1503
Iron	0.4927	0.2676	4.4595	0.7848	6.0047
Cobalt	0.0012	0.0003	0.0329	0.0009	0.0353
Nickel	0.1317	0.0339	4.3715	0.1017	4.6388
Zirconium	0.0000	1.0770	100.75	0.0000	101.83
Aluminum	0.0008	0.0000	0.0381	0.0000	0.0389
Silicon	0.0071	0.0038	0.0124	0.0182	0.0415
Titanium	0.0011	0.0000	0.0473	0.0000	0.0484
Niobium	0.0076	0.0000	0.3272	0.0000	0.3348
Molybdenum	0.0041	0.0000	0.1768	0.0000	0.1809
Tin	0.0000	0.0176	1.7200	0.0182	1.7558
16 x 16					
Chromium	0.3104	0.2720	0.3827	0.2767	1.2419
Manganese	0.0234	0.0300	0.0049	0.0247	0.0829
Iron	0.8619	1.0496	0.4978	0.8783	3.2877
Cobalt	0.0033	0.0012	0.0068	0.0021	0.0134
Nickel	0.3686	0.1337	0.6159	0.2304	1.3486
Zirconium	0.0133	1.8581	124.2867	1.9559	128.114
Aluminum	0.0031	0.0000	0.0101	0.0015	0.0147
Silicon	0.0010	0.0150	0.0024	0.0005	0.0188
Titanium	0.0041	0.0000	0.0094	0.0019	0.0155
Niobium	0.0287	0.0000	0.0655	0.0131	0.1073
Molybdenum	0.0155	0.0000	0.0354	0.0071	0.0579
Tin	0.0181	0.0304	2.0310	0.0513	2.1307

Table 5-10
SAS2H Gamma Sources for 60 GWd/MTU, 7-Year Cooled
MK BW 17x17 Fuel Assembly

(γ/s/assembly)

Energy Interval (meV)			Fuel	Bottom	Plenum	Top
1.000E-02	to	5.000E-02	1.532E+15	1.298E+11	1.499E+11	1.096E+11
5.000E-02	to	1.000E-01	4.151E+14	1.643E+10	2.080E+10	2.136E+10
1.000E-01	to	2.000E-01	3.240E+14	8.873E+09	9.762E+09	5.155E+09
2.000E-01	to	3.000E-01	9.290E+13	4.910E+08	5.335E+08	2.563E+08
3.000E-01	to	4.000E-01	6.066E+13	1.432E+09	1.462E+09	3.356E+08
4.000E-01	to	6.000E-01	7.102E+14	2.627E+10	2.539E+10	2.121E+07
6.000E-01	to	8.000E-01	3.087E+15	1.360E+10	1.314E+10	9.567E+08
8.000E-01	to	1.000E+00	3.374E+14	1.819E+10	6.393E+09	1.248E+10
1.000E+00	to	1.330E+00	2.748E+14	4.704E+12	5.982E+12	6.234E+12
1.330E+00	to	1.660E+00	7.314E+13	1.328E+12	1.689E+12	1.760E+12
1.660E+00	to	2.000E+00	5.506E+11	3.493E-01	4.747E+01	4.592E-01
2.000E+00	to	2.500E+00	7.537E+11	3.152E+07	4.009E+07	4.178E+07
2.500E+00	to	3.000E+00	3.712E+10	4.888E+04	6.217E+04	6.478E+04
3.000E+00	to	4.000E+00	4.718E+09	1.175E-14	3.835E-15	1.289E-09
4.000E+00	to	5.000E+00	3.768E+07			
5.000E+00	to	6.500E+00	1.512E+07			
6.500E+00	to	8.000E+00	2.966E+06			
8.000E+00	to	1.000E+01	6.298E+05			
Total:			6.908E+15	6.247E+12	7.899E+12	8.144E+12

Table 5-11
SAS2H Gamma Sources for 210 GWd/MTU, 20-Year Cooled
TPA

light elements - TPA - plenum zone						
	<u>energy interval</u>			<u>3 cycles</u> <u>y/second</u>	<u>Fraction</u>	<u>14 cycles</u> <u>y/second</u>
36	1.33E+00	to	1.660E+00	1.03E+11	2.202E-01	4.814E+11
37	1.00E+00	to	1.330E+00	3.65E+11	7.798E-01	1.705E+12
Total:				4.685E+11		2.186E+12
light elements - TPA - Top Fitting Zone						
	<u>energy interval</u>			<u>y/second</u>		<u>y/second</u>
36	1.33E+00	to	1.660E+00	8.19E+10	2.202E-01	3.823E+11
37	1.00E+00	to	1.330E+00	2.90E+11	7.798E-01	1.354E+12
Total:				3.720E+11		1.736E+12

Table 5-12
SAS2H Gamma Sources for 30 GWd/MTU, 4-day Cooled
BPRA

BPRA Source (y/s/BPRA)

E_{min}, MeV		E_{max}, MeV	Top Region	Plenum Region	In-core Region
0.00E+00	to	5.00E-02	1.170E+11	3.328E+10	3.14E+12
5.00E-02	to	1.00E-01	3.261E+10	9.260E+09	8.73E+11
1.00E-01	to	2.00E-01	1.736E+10	4.906E+09	4.63E+11
2.00E-01	to	3.00E-01	4.695E+09	1.316E+09	1.24E+11
3.00E-01	to	4.00E-01	1.128E+12	5.018E+11	4.74E+13
4.00E-01	to	6.00E-01	5.321E+11	1.474E+11	1.39E+13
6.00E-01	to	8.00E-01	5.487E+08	1.521E+08	1.44E+10
8.00E-01	to	1.00E+00	2.224E+12	7.587E+11	7.16E+13
1.00E+00	to	1.33E+00	2.702E+12	6.848E+11	6.44E+13
1.33E+00	to	1.66E+00	7.630E+11	1.934E+11	1.82E+13
1.66E+00	to	2.00E+00	8.185E+09	2.267E+09	2.14E+11
2.00E+00	to	2.50E+00	1.811E+07	4.590E+06	4.31E+08
2.50E+00	to	3.00E+00	2.808E+04	7.119E+03	6.69E+05
3.00E+00	to	4.00E+00	3.434E-01	1.718E-01	1.63E+01
4.00E+00	to	5.00E+00	0.000E+00	0.000E+00	0.00E+00
5.00E+00	to	6.50E+00	0.000E+00	0.000E+00	0.00E+00
6.50E+00	to	8.00E+00	0.000E+00	0.000E+00	0.00E+00
8.00E+00	to	1.00E+01	0.000E+00	0.000E+00	0.00E+00
Total:			7.529E+12	2.337E+12	2.20E+14

Table 5-13
SAS2H Neutron Sources for 60 GWD/MTU, 7-10 yr Cooled Fuel
MK BW 17x17 Fuel Assembly

(n/sec/assembly)

Grp	Energy Interval (meV)		7 yr	8 yr	9 yr	10 yr
1	6.43	- 20.0	2.036E+07	1.957E+07	1.882E+07	1.810E+07
2	3.00	- 6.43	2.297E+08	2.209E+08	2.124E+08	2.044E+08
3	1.85	- 3.00	2.519E+08	2.423E+08	2.331E+08	2.244E+08
4	1.40	- 1.85	1.433E+08	1.377E+08	1.325E+08	1.275E+08
5	0.90	- 1.40	1.948E+08	1.872E+08	1.800E+08	1.732E+08
6	0.40	- 0.90	2.129E+08	2.047E+08	1.968E+08	1.893E+08
7	0.10	- 0.40	4.168E+07	4.007E+07	3.853E+07	3.706E+07
Total:			1.095E+09	1.052E+09	1.012E+09	9.740E+08

Table 5-14
ANSI Standard-6.1.1-1977 Flux-to-Dose Factors

Photon energy (MeV)	Response Function (rem/hr)/(γ/cm ² -s)	Neutron energy (MeV)	Response Function ((rem/hr)/(n/cm ² -s)
0.01	3.96E-06	2.5E-08	3.67E-06
0.03	5.82E-07	1.0E -07	3.67E-06
0.05	2.90E-07	1.0E-06	4.46E-06
0.07	2.58E-07	1.0E-05	4.54E-06
0.10	2.83E-07	1.0E-04	4.18E-06
0.15	3.79E-07	1.0E-03	3.76E-06
0.20	5.01E-07	1.0E-02	3.56E-06
0.25	6.31E-07	1.0E-01	2.17E-05
0.30	7.59E-07	5.0E-01	9.26E-05
0.35	8.78E-07	1.0	1.32E-04
0.40	9.85E-07	2.5	1.25E-04
0.45	1.08E-06	5.0	1.56E-04
0.50	1.17E-06	7.0	1.47E-04
0.55	1.27E-06	10.0	1.47E-04
0.60	1.36E-06	14.0	2.08E-04
0.65	1.44E-06	20.0	2.27E-04
0.70	1.52E-06		
0.80	1.68E-06		
1.0	1.98E-06		
1.4	2.51E-06		
1.8	2.99E-06		
2.2	3.42E-06		
2.6	3.82E-06		
2.8	4.01E-06		
3.25	4.41E-06		
3.75	4.83E-06		
4.25	5.23E-06		
4.75	5.60E-06		
5.0	5.80E-06		
5.25	6.01E-06		
5.75	6.37E-06		
6.25	6.74E-06		
6.75	7.11E-06		
7.5	7.66E-06		
9.0	8.77E-06		
11.0	1.03E-05		
13.0	1.18E-05		
15.0	1.33E-05		

Table 5-15
Material Densities for Fuel Assembly Regions (dry)

Region	In-Core		Plenum		Top		Bottom	
Element	Gram Density g/cm	Atom Density a/bn-cm	Gram Density g/cm	Atom Density a/bn-cm	Gram Density g/cm	Atom Density a/bn-cm	Gram Density g/cm	Atom Density a/bn-cm
O	4.243E-01	1.597E-02	6.462E-04	2.432E-05	0.000E+00	0.000E+00	0.000E+00	0.000E+00
Al	2.264E-04	5.053E-06	1.632E-05	3.644E-07	1.143E-03	2.551E-05	0.000E+00	0.000E+00
Ti	2.944E-04	3.701E-06	1.360E-05	1.710E-07	1.525E-03	1.917E-05	0.000E+00	0.000E+00
Si	3.487E-04	7.476E-06	2.350E-03	5.038E-05	9.855E-03	2.113E-04	1.175E-02	2.519E-04
Cr	1.375E-02	1.592E-04	4.550E-02	5.269E-04	2.162E-01	2.504E-03	2.232E-01	2.585E-03
Fe	2.661E-02	2.885E-04	1.653E-01	1.792E-03	6.861E-01	7.438E-03	8.083E-01	8.763E-03
Ni	2.611E-02	2.678E-04	2.097E-02	2.151E-04	1.837E-01	1.885E-03	1.048E-01	1.075E-03
Mn	6.326E-04	6.934E-06	4.713E-03	5.166E-05	1.933E-02	2.119E-04	2.350E-02	2.576E-04
Zr	6.013E-01	3.970E-03	6.659E-01	4.396E-03	0.000E+00	0.000E+00	0.000E+00	0.000E+00
Mo	1.056E-03	6.631E-06	0.000E+00	0.000E+00	5.725E-03	3.594E-05	0.000E+00	0.000E+00
U-235	1.115E-01	2.857E-04	5.442E-09	1.394E-11	0.000E+00	0.000E+00	0.000E+00	0.000E+00
U-238	2.676E+00	6.771E-03	1.306E-07	3.304E-10	0.000E+00	0.000E+00	0.000E+00	0.000E+00
Total	3.882	2.774E-02	0.905	7.057E-03	1.124	1.233E-02	1.172	1.293E-02

Table 5-16
Material Densities for Fuel Assembly Regions (wet)

Region	In-Core		Plenum		Top(wet)		Bottom	
Element	Gram Density g/cm ³	Atom Density a/bn-cm	Gram Density g/cm ³	Atom Density a/bn-cm	Gram Density g/cm ³	Atom Density a/bn-cm	Gram Density g/cm ³	Atom Density a/bn-cm
H	1.717E-02	1.026E-02	6.481E-02	3.872E-02	1.956E-01	1.169E-01	7.856E-02	4.693E-02
O	5.127E-01	1.930E-02	5.191E-01	1.954E-02	1.565E+00	5.889E-02	6.285E-01	2.365E-02
Al	2.264E-04	5.053E-06	1.632E-05	3.644E-07	1.143E-03	2.551E-05	0.000E+00	0.000E+00
Ti	2.944E-04	3.701E-06	1.360E-05	1.710E-07	1.525E-03	1.917E-05	0.000E+00	0.000E+00
Si	3.487E-04	7.476E-06	2.350E-03	5.038E-05	9.855E-03	2.113E-04	1.175E-02	2.519E-04
Cr	1.375E-02	1.592E-04	4.550E-02	5.269E-04	2.162E-01	2.504E-03	2.232E-01	2.585E-03
Fe	2.661E-02	2.885E-04	1.653E-01	1.792E-03	6.861E-01	7.438E-03	8.083E-01	8.763E-03
Ni	2.611E-02	2.678E-04	2.097E-02	2.151E-04	1.837E-01	1.885E-03	1.048E-01	1.075E-03
Mn	6.326E-04	6.934E-06	4.713E-03	5.166E-05	1.933E-02	2.119E-04	2.350E-02	2.576E-04
Zr	6.013E-01	3.970E-03	6.659E-01	4.396E-03	0.000E+00	0.000E+00	0.000E+00	0.000E+00
Mo	1.056E-03	6.631E-06	0.000E+00	0.000E+00	5.725E-03	3.594E-05	0.000E+00	0.000E+00
U-235	1.115E-01	2.857E-04	0.000E+00	0.000E+00	0.000E+00	0.000E+00	0.000E+00	0.000E+00
U-238	2.676E+00	6.771E-03	0.000E+00	0.000E+00	0.000E+00	0.000E+00	0.000E+00	0.000E+00
Total	3.970	4.133E-02	1.424	6.529E-02	2.688	1.881E-01	1.800	8.352E-02

Region	Top (dry)	
Element	Gram Density g/cm ³	Atom Density a/bn-cm
H	0.000E+00	0.000E+00
O	0.000E+00	0.000E+00
Al	1.143E-03	2.551E-05
Ti	1.525E-03	1.917E-05
Si	9.855E-03	2.113E-04
Cr	2.162E-01	2.504E-03
Fe	6.861E-01	7.438E-03
Ni	1.837E-01	1.885E-03
Mn	1.933E-02	2.119E-04
Zr	0.000E+00	0.000E+00
Mo	5.725E-03	3.594E-05
U-235	0.000E+00	0.000E+00
U-238	0.000E+00	0.000E+00
Total	1.124	1.233E-02

Table 5-17
NUHOMS® HD 32PTH DSC and OS-187H Material Composition

(% weight)

Element	Atomic Weight	Carbon Steel ¹	Stainless Steel 304 ¹	Aluminum ¹	Lead ¹	Water ¹ (atm fraction)	Air ²	Polyester Resin ³
H	1.008					0.666		5.05
B	10.811							1.05
C	12.011	1.00					0.01	35.1
N	14.0067						75.53	
O	15.9994					0.333	23.18	41.7
Al	26.9815			100.00				14.9
Ar	39.948						1.28	
Cr	51.996		19.00					
Mn	54.938		2.00					
Fe	55.847	99.00	68.375					
Ni	58.71		9.50					
Zn	65.37							2.11
Pb	207.19				100.00			
density (g/cc)		7.8212	7.92	2.702	11.17 ⁴	0.9982	0.0012	1.58

Ref [1], 2. Ref [3], 3. Proprietary resin formulation, 4. Use 98.5% of TD (11.344 g/cc)

Table 5-18
NUHOMS® HD 32PTH DSC and OS-187H Material Composition

(atm/b-cm)

Element	Carbon Steel	Stainless Steel 304	Aluminum	Lead	Water	Dry Air	Polyester Resin
H					6.673E-02		4.767E-02
B-10							2.098E-04
C	3.921E-03					6.016E-09	3.168E-02
N						3.897E-05	
O					3.337E-02	1.047E-05	2.825E-02
Al			6.031E-02				5.986E-03
Ar						2.315E-07	
Cr		1.743E-02					
Mn		1.736E-03					
Fe	8.349E-02	5.935E-02					
Ni		7.718E-03					
Zn*							3.499E-04
Pb				3.248E-02			

*- Ignored,

Table 5-19
Composition and Densities for HSM-H Concrete

Element	Concrete (atm/b·cm)
H	7.767×10^{-3}
O	4.317×10^{-2}
Na	1.022×10^{-3}
Al	2.343×10^{-3}
Si	1.559×10^{-2}
K	6.776×10^{-4}
Ca	2.855×10^{-3}
Fe	3.019×10^{-4}
total	7.363×10^{-2}

Table 5-20
Source Axial Profile

Zone No.	Zone Center (% of height)	Lower Model Bound (cm)	Upper Model Bound (cm)	Gamma Profile	Neutron Profile	Neutron Normal Factor*	Gamma Normal Factor*
1	2.78	-182.880	-162.544	0.573	0.108	0.00599	0.03186
2	8.33	-162.544	-142.281	0.917	0.707	0.03917	0.05080
3	13.89	-142.281	-121.871	1.066	1.291	0.07205	0.05948
4	19.44	-121.871	-101.681	1.106	1.496	0.08260	0.06105
5	25.00	-101.681	-81.199	1.114	1.540	0.08624	0.06238
6	30.56	-81.199	-61.009	1.111	1.524	0.08410	0.06133
7	36.11	-61.009	-40.599	1.106	1.496	0.08349	0.06171
8	41.69	-40.599	-20.190	1.101	1.469	0.08199	0.06144
9	47.22	-20.190	-0.146	1.097	1.448	0.07936	0.06012
10	52.80	-0.146	20.629	1.093	1.427	0.08106	0.06208
11	58.33	20.629	40.307	1.089	1.406	0.07566	0.05859
12	63.89	40.307	61.301	1.086	1.391	0.07984	0.06234
13	69.44	61.301	80.906	1.081	1.366	0.07319	0.05794
14	75.00	80.906	101.974	1.073	1.326	0.07635	0.06180
15	80.56	101.974	121.579	1.051	1.220	0.06540	0.05633
16	86.11	121.579	142.573	0.993	0.972	0.05581	0.05700
17	91.67	142.573	162.251	0.932	0.755	0.04059	0.05014
18	97.22	162.251	182.880	0.512	0.069	0.00388	0.02888
average						1.167	1.00

* - Zone weighted profile

Table 5-21
Summary of NUHOMS® HD 32PTH DSC in the HSM-H, Maximum and Average Dose Rates⁽²⁾

Dose Rate Location	Maximum Gamma (mrem/hour)	Gamma MCNP 1σ Error	Maximum Neutron (mrem/hour)	Neutron MCNP 1σ Error	Maximum Total⁽¹⁾ (mrem/hour)	Total MCNP 1σ Error
HSM-H Roof (centerline)	13.2	0.043	1.9	0.021	15.1	0.038
HSM-H Roof Birdscreen	152.0	0.021	18.5	0.014	170.0	0.019
HSM-H End (Side) Shield Wall Surface	0.9	0.041	0.5	0.016	1.4 (4.3) ⁽³⁾	0.022
HSM-H Door Exterior Surface (centerline)	0.5	0.106	1.0	0.120	1.6 (0.8) ⁽³⁾	0.162
HSM-H Front Birdscreen	736.0	0.140	16.1	0.070	752.0 (356.7) ⁽³⁾	0.137

Dose Rate Location	Average Gamma (mrem/hour)	Gamma MCNP 1σ Error	Average Neutron (mrem/hour)	Neutron MCNP 1σ Error	Average Total (mrem/hour)	Total MCNP 1σ Error
HSM-H Roof	13.9	0.012	1.9	0.007	15.8	0.010
HSM-H End (Side) Shield Wall Surface	0.4	0.011	0.2	0.053	0.6	0.019
HSM-H Front	20.3	0.130	0.5	0.054	20.8	0.127
HSM-H Back Shield Wall	0.5	0.060	<0.1	0.025	0.5	0.060

Notes:

- Gamma and Neutron dose rate peaks do not always occur at same location; therefore, the total dose rate is not always the sum of the maximum gamma plus maximum neutron dose rate.
- Dose rates can be higher by 6% to account for the use of grout during HSM-H fabrication and installation.
- Maximum dose rate results from the HSM-H gap analysis.

Table 5-22
Summary of NUHOMS® HD 32PTH DSC in the OS187H TC, Maximum Dose Rates During
Decontamination and Welding Operations

Dose Rate Location	Maximum Gamma ⁽³⁾ (mrem/hr)	Gamma MCNP 1 σ Error	Maximum Neutron (mrem/hr)	Neutron MCNP 1 σ Error	Maximum Total ⁽¹⁾ (mrem/hr)	Total MCNP 1 σ Error
Decontamination (Configuration A)						
Cask Side Surface (Radial)	241	0.034	158	0.081	399	0.053
Top Axial Surface (@ shield plug)	933	0.183	118	0.405	1050	0.189
Cask Bottom Axial Surface ⁽²⁾	397	0.129	1430	0.127	1825	0.127
1.5 ft from Cask Side (Radial)	153	0.027	95.7	0.067	249	0.043
1.5 ft from Top Axial Surface	688	0.090	52.0	0.299	739	0.092
1.5 ft from Cask Bottom Axial Surface	95.3	0.173	300	0.120	389	0.129
3 ft from Cask Side (Radial)	107	0.025	65.4	0.063	172	0.039
3 ft from Top Axial Surface	513	0.122	27.5	0.262	539	0.123
Welding (Configuration B)						
Cask Side Surface (Radial)	310	0.027	95.8	0.042	397	0.027
Top Axial Surface	95.5	0.062	328	0.028	421	0.032
Cask Bottom Axial Surface ⁽²⁾	490	0.125	1240	0.033	1730	0.056
1.5 ft from Cask Side (Radial)	198	0.015	59.0	0.036	256	0.017
1.5 ft from Top Axial Surface	77.6	0.058	192	0.031	269	0.036
1.5 ft from Cask Bottom Axial Surface	136	0.255	279	0.041	415	0.118
3 ft from Cask Side (Radial)	139	0.013	40.9	0.031	179	0.015
3 ft from Top Axial Surface	52.5	0.055	102	0.027	154	0.035

Notes:

- (1) Gamma and Neutron dose rate peaks do not always occur at same location; therefore, the total dose rate is not always the sum of the maximum gamma plus maximum neutron dose rate.
- (2) The peak bottom surface dose rate is directly below the grapple ring cut out approximately 1" below the bottom of the cask.
- (3) Gamma dose rates include secondary gamma.

Table 5-23
Summary of NUHOMS® HD 32PTH DSC in the OS187H TC, Maximum Dose Rates During Transfer Operations (Configuration C)

Dose Rate Location	Maximum Gamma⁽³⁾ (mrem/hr)	Gamma MCNP 1σ Error	Maximum Neutron (mrem/hr)	Neutron MCNP 1σ Error	Maximum Total⁽¹⁾ (mrem/hr)	Total MCNP 1σ Error
Cask Side Surface (Radial)	384	0.018	125	0.040	508	0.021
Cask Top Axial Surface	8.1	0.029	24.5	0.136	32.1	0.130
Cask Bottom Axial Surface ⁽²⁾	475	0.112	1350	0.028	1820	0.045
1.5 ft from Cask Side (Radial)	238	0.015	77.0	0.035	315	0.018
1.5 ft from Cask Top Axial Surface	5.2	0.029	14.1	0.158	19.3	0.149
1.5 ft from Cask Bottom Axial Surface	118	0.154	305	0.031	423	0.063
3 ft from Cask Side (Radial)	165	0.013	54.7	0.034	219	0.016
3 ft from Cask Top Axial Surface	3.5	0.054	8.7	0.203	12.1	0.189
3 ft from Cask Bottom Axial Surface	53.1	0.118	117	0.029	170	0.056
Cask 1 m (Radial) Accident Condition	186	0.012	2200	0.003	2390	0.003
Cask 100 m (Radial) Accident Condition	0.1	0.01	1.2	0.004	1.3	0.004

Notes:

- (1) Gamma and Neutron dose rate peaks do not always occur at same location therefore the total dose rate is not always the sum of the maximum gamma plus maximum neutron dose rate.
- (2) The peak bottom surface dose rate is 1" below the bottom of the cask in the grapple ring area.. The max bottom dose rates, with the RAM access open are 1090 mrem/hr gamma, 1525 mrem/hr neutron.
- (3) Gamma dose rates include secondary gamma.

Table 5-24
Dose Rate Comparison for Fuel Qualification

(Page 1 of 4)

Case ID	Description	Surface Dose Rate (mrem/hour)		
		Neutron	Gamma	Total
1	Enrichment 4.00 wt. % U-235 Burnup 60.0 GWD/MTU Cooling Time 7 Years Design Basis	48.2	193.5	241.7
2	Enrichment 2.50 wt. % U-235 Burnup 46.0 GWD/MTU Cooling Time 5 Years Thermal Power ~ 1500 Watts	36.6	225.0	261.6
3	Enrichment 2.50 wt. % U-235 Burnup 44.0 GWD/MTU Cooling Time 5 Years Thermal Power 1404 Watts	31.2	208.4	239.6
4	Enrichment 2.50 wt. % U-235 Burnup 40.0 GWD/MTU Cooling Time 5 Years Thermal Power 1236 Watts	21.9	177.7	199.6
5	Enrichment 2.50 wt. % U-235 Burnup 50.0 GWD/MTU Cooling Time 7 Years Thermal Power ~ 1278 Watts	45.3	186.4	231.7
6	Enrichment 2.75 wt. % U-235 Burnup 45.0 GWD/MTU Cooling Time 7 Years Thermal Power ~ 1088 Watts	27.7	140.5	168.2
7	Enrichment 3.00 wt. % U-235 Burnup 47.0 GWD/MTU Cooling Time 5 Years Thermal Power ~ 1500 Watts	31.4	209.5	240.9
8	Enrichment 3.00 wt. % U-235 Burnup 52.4 GWD/MTU Cooling Time 6 Years Thermal Power ~ 1500 Watts	45.0	210.5	255.5
9	Enrichment 3.00 wt. % U-235 Burnup 51.2 GWD/MTU Cooling Time 6 Years Thermal Power 1432 Watts	41.2	200.4	241.6
10	Enrichment 3.00 wt. % U-235 Burnup 52.4 GWD/MTU Cooling Time 10 Years Thermal Power 1069 Watts	38.4	130.0	168.4
11	Enrichment 3.00 wt. % U-235 Burnup 55.0 GWD/MTU Cooling Time 8 Years Thermal Power 1299 Watts	49.3	178.1	227.4

Table 5-24
Dose Rate Comparison for Fuel Qualification

(Page 2 of 4)

Case ID	Description	Surface Dose Rate (mrem/hour)		
		Neutron	Gamma	Total
12	Enrichment 3.00 wt. % U-235 Burnup 59.5 GWD/MTU Cooling Time 15 Years Thermal Power 1069 Watts	48.9	122.5	171.4
13	Enrichment 3.50 wt. % U-235 Burnup 53.5 GWD/MTU Cooling Time 6 Years Thermal Power ~ 1500 Watts	39.6	196.3	235.9
14	Enrichment 3.50 wt. % U-235 Burnup 58.0 GWD/MTU Cooling Time 7 Years Thermal Power ~ 1500 Watts	51.1	200.5	251.6
15	Enrichment 3.50 wt. % U-235 Burnup 50.0 GWD/MTU Cooling Time 5 Years Thermal Power 1566 Watts	31.9	211.7	243.6
16	Enrichment 3.50 wt. % U-235 Burnup 56.6 GWD/MTU Cooling Time 7 Years Thermal Power 1433 Watts	46.8	189.8	236.6
17	Enrichment 3.75 wt. % U-235 Burnup 48.4 GWD/MTU Cooling Time 5 Years Thermal Power ~ 1500 Watts	25.3	190.9	216.2
18	Enrichment 3.75 wt. % U-235 Burnup 54.0 GWD/MTU Cooling Time 6 Years Thermal Power 1500 Watts	37.1	189.7	226.8
19	Enrichment 3.75 wt. % U-235 Burnup 58.5 GWD/MTU Cooling Time 7 Years Thermal Power ~ 1500 Watts	48.1	193.1	241.2
20	Enrichment 4.00 wt. % U-235 Burnup 48.8 GWD/MTU Cooling Time 5 Years Thermal Power ~ 1500 Watts	23.6	185.3	208.9
21	Enrichment 4.00 wt. % U-235 Burnup 54.5 GWD/MTU Cooling Time 6 Years Thermal Power ~ 1500 Watts	34.9	183.8	218.7

Table 5-24
Dose Rate Comparison for Fuel Qualification

(Page 3 of 4)

Case ID	Description	Surface Dose Rate (mrem/hour)		
		Neutron	Gamma	Total
22	Enrichment 4.25 wt. % U-235 Burnup 55.0 GWD/MTU Cooling Time 6 Years Thermal Power 1475 Watts	32.9	178.4	211.3
23	Enrichment 4.50 wt. % U-235 Burnup 55.0 GWD/MTU Cooling Time 5 Years Thermal Power 1689 Watts	31.3	211.4	242.7
24	Enrichment 4.50 wt. % U-235 Burnup 60.0 GWD/MTU Cooling Time 6 Years Thermal Power 1646 Watts	42.1	204.0	246.1
25	Enrichment 4.75 wt. % U-235 Burnup 55.0 GWD/MTU Cooling Time 5 Years Thermal Power 1668 Watts	28.6	203.3	231.9
26	Enrichment 4.75 wt. % U-235 Burnup 60.0 GWD/MTU Cooling Time 6 Years Thermal Power 1625 Watts	38.7	195.0.9	233.7
27	Enrichment 1.20 wt. % U-235 Burnup 33.4 GWD/MTU Cooling Time 5 Years Thermal Power ~ 1082 Watts	24.9	187.0	211.9
28	Enrichment 1.50 wt. % U-235 Burnup 34.1 GWD/MTU Cooling Time 5 Years Thermal Power 1083 Watts	22.0	177.2	199.2
29	Enrichment 2.00 wt. % U-235 Burnup 35.1 GWD/MTU Cooling Time 5 Years Thermal Power 1080 Watts	17.8	162.5	180.3
31	Enrichment 1.50 wt. % U-235 Burnup 42.2 GWD/MTU Cooling Time 7 Years Thermal Power ~ 1081 Watts	41.5	177.5	219.0
32	Enrichment 2.00 wt. % U-235 Burnup 43.3 GWD/MTU Cooling Time 7 Years Thermal Power ~ 1082 Watts	35.0	160.4	195.4

Table 5-24
Dose Rate Comparison for Fuel Qualification

(Page 4 of 4)

Case ID	Description	Surface Dose Rate (mrem/hour)		
		Neutron	Gamma	Total
33	Enrichment 1.50 wt. % U-235 Burnup 49.8 GWD/MTU Cooling Time 10 Years Thermal Power 1080 Watts	61.5	181.8	243.3
34	Enrichment 1.60 wt. % U-235 Burnup 50.0 GWD/MTU Cooling Time 10 Years Thermal Power 1080 Watts	59.6	177.6	237.2
35	Enrichment 2.00 wt. % U-235 Burnup 50.8 GWD/MTU Cooling Time 10 Years Thermal Power 1081 Watts	52.7	162.4	215.1
36	Enrichment 1.50 wt. % U-235 Burnup 48.1 GWD/MTU Cooling Time 10 Years Thermal Power 1029 Watts	55.4	168.7	224.1
37	Enrichment 1.60 wt. % U-235 Burnup 57.3 GWD/MTU Cooling Time 15 Years Thermal Power ~ 1080 Watts	72.4	169.2	241.6
38	Enrichment 0.70 wt. % U-235 Burnup 26.0 GWD/MTU Cooling Time 5 Years Thermal Power < 1000 Watts	15.9	156	171.9
39	Enrichment 0.70 wt. % U-235 Burnup 32.0 GWD/MTU Cooling Time 5 Years Thermal Power ~ 1100 Watts	29.3	202	231.3
40	Enrichment 0.30 wt. % U-235 Burnup 15.0 GWD/MTU Cooling Time 5 Years Thermal Power < 1000 Watts	3.3	92.0	95.4
41	Enrichment 0.30 wt. % U-235 Burnup 25.0 GWD/MTU Cooling Time 5 Years Thermal Power ~ 1000 Watts	26.9	194	220.9
42	Enrichment 0.20 wt. % U-235 Burnup 20.0 GWD/MTU Cooling Time 5 Years Thermal Power < 800 Watts	10.5	133.1	143.6

Table 5-25
Fuel Qualification with Reconstituted Fuel Assemblies

SAS2H Case #	Burn-up (GWd/MTU)	Enrichment (wt. % U-235)	Cooling Time (years)	Total Dose Rate (mrem/hour)	Decay Heat (watts/FA)
1A	60.0	4.0	7.0	241.7	1515
1B	60.0	4.0	7.0	253.0	<1515
1C	60.0	4.0	8.0	226.5	<1392
2A	32.0	0.7	5.0	226.8	1074
2B	32.0	0.7	5.0	241.4	<1074
3A	57.25	1.6	15.0	241.6	1080
3B	57.25	1.6	15.0	239.8	<1080
4A	57.25	2.0	14.5	218.2	1076
4B	57.25	2.0	14.5	217.5	<1076
5A	50.8	2.0	10.0	215.1	1081
5B	50.8	2.0	10.0	213.0	<1081
6A	60.0	2.5	16.5	189.1	1070
6B	60.0	2.5	16.5	186.7	<1070

Note: Case #s ending with "A" are based on fuel assembly without reconstituted rods. Case #s ending with "B" and "C" are based on fuel assembly with 10 reconstituted stainless steel rods that undergo an additional 2 cycles of irradiation.

Table 5-26
Summary of Results, Side-to-Side Gaps

Maximum Dose Rates			
Dose Rate Location	No Gap (mrem/hour)	0.5 inch Gap (mrem/hour)	1.25 inch Gap (mrem/hour)
Roof (centerline)	11.6	12.8	13.7
Roof Birdscreen	219.8	241.4	270.6
End (Side) Shield Wall Surface	0.9	0.9	1.0
Door Exterior Surface (centerline)	0.8	0.8	0.8
Front Birdscreen	324.2	324.2	356.7
Front Gap (excluding vent)	NA	86.7	108.5
Roof Gap (excluding vent)	NA	519.4	899.9
Average Dose Rates			
Dose Rate Location	No Gap (mrem/hour)	0.5 inch Gap (mrem/hour)	1.25 inch Gap (mrem/hour)
Roof	11.6	12.6	14.4
End (Side) Shield Wall Surface	0.3	0.3	0.3
Front	10.4	11.3	13.1
Back Shield Wall	0.08	0.14	0.49

Table 5-27
Fuel Qualification Evaluation for Fuel Assemblies Containing BLEU Fuel Material

Case Description	Cooling Time (years)	Total Dose Rate (millirem/hour)
0.7 wt. % U-235, 33.0 GWd/MTU	5.00	243.0
Above Case with BLEU Fuel Material	7.32	243.0
Additional Cooling Time Needed	2.32	-
1.2 wt. % U-235, 49.3 GWd/MTU	10.00	265.9
Above Case with BLEU Fuel Material	12.50	265.9
Additional Cooling Time Needed	2.50	-
Table 5-24 Case 2 Cool Time	5.00	261.6
Above Case with BLEU Fuel Material	6.83	261.6
Additional Cooling Time Needed	1.83	-
Table 5-24 Case 1 Cool Time	7.00	241.7
Above Case with BLEU Fuel Material	9.26	241.7
Additional Cooling Time Needed	2.26	-

Proprietary Information on This Page
Withheld Pursuant to 10 CFR 2.390

Table 5-29
Dose Reduction Hardware Summary of Results

Cell Tally Dose Rates (millirem/hour)	DRH Type	Base HSM-H	w/DRH	Reduction	% Reduction
Left average dose rate on roof	C	11.1	6.0	5.1	46%
Left average dose rate on front	A & B	10.4	3.4	7.1	68%
Average dose rate, left vent	A & B	198.4	60.4	138.1	70%
Average dose rate, right vent	A & B	33.4	15.2	18.2	54%
Mesh Tally Dose Rates (millirem/hour)	DRH Type	Base HSM-H	w/DRH	Reduction	% Reduction
Roof HSM-H Centerline	C	11.3	7.15	4.1	37%
LHS Front Vent	A & B	330.0	68.4	261.7	79%
RHS Front Vent	A & B	36.0	18.3	17.7	49%
Left Roof Birdscreen Max	C	213.4	88.2	125.2	59%

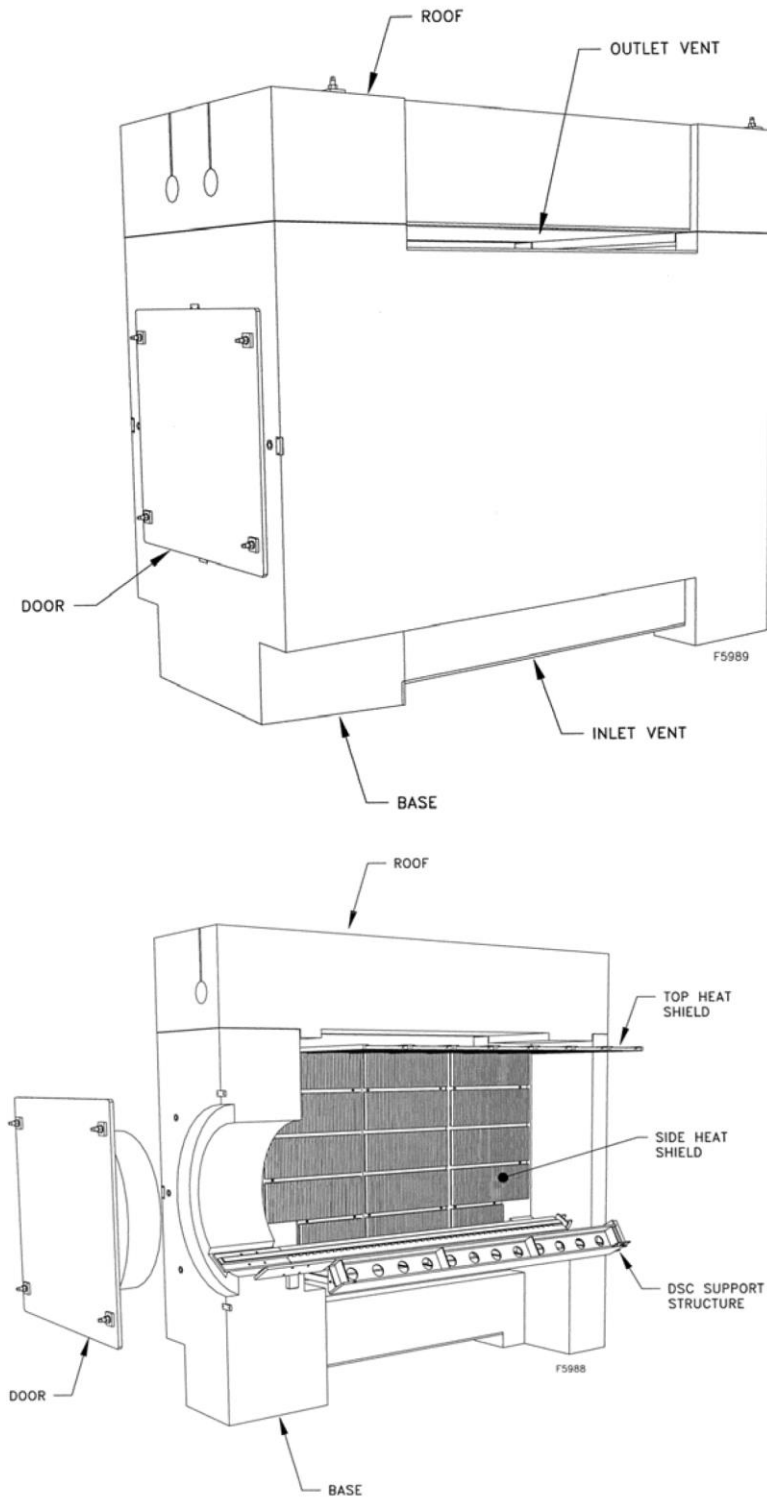


Figure 5-1
NUHOMS® HD 32PTH System Shielding Configuration (HSM-H)

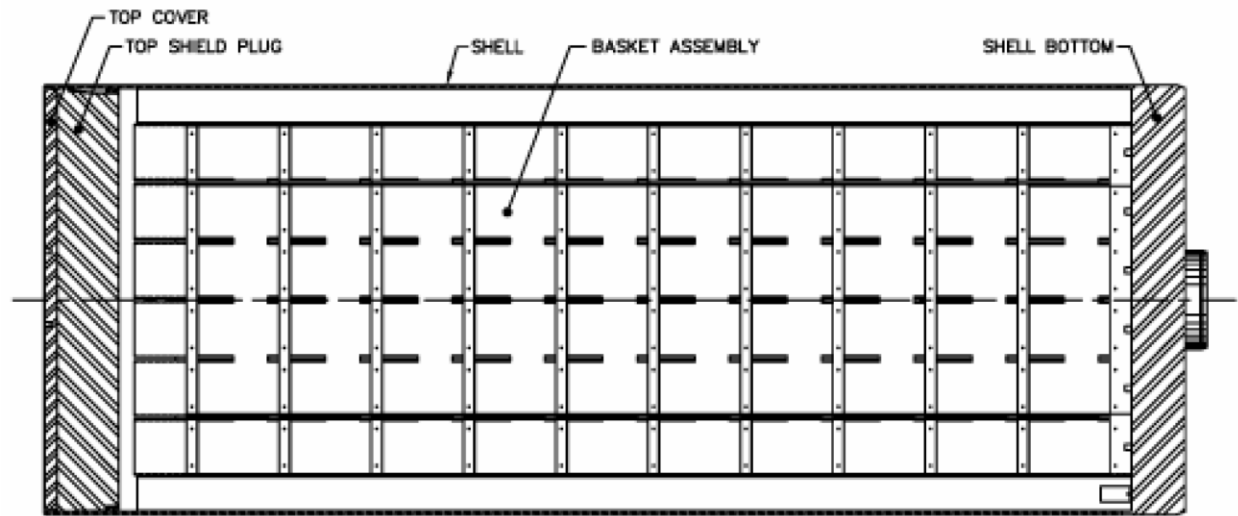


Figure 5-2
Dry Shielded Canister Shielding Configuration

Proprietary Information on This Page
Withheld Pursuant to 10 CFR 2.390

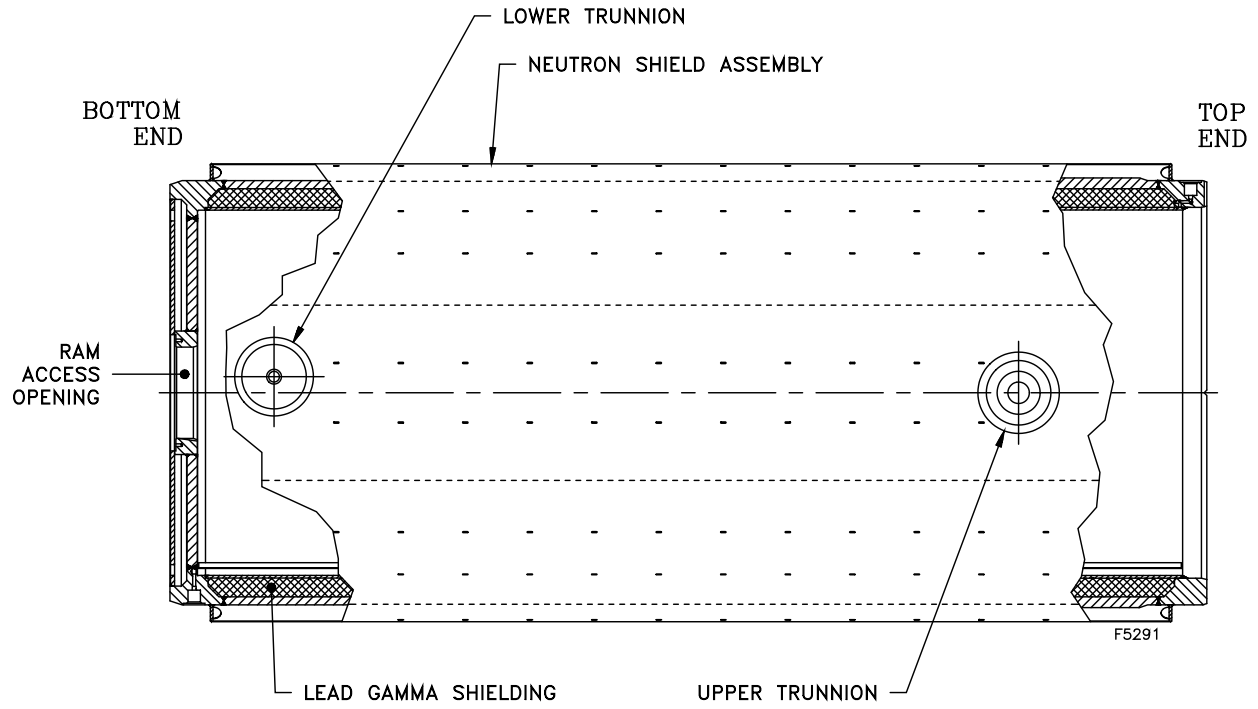


Figure 5-4
Shielding Configuration of the OS187H Transfer Cask

Proprietary Information on Pages 5-102 through 5-106
Withheld Pursuant to 10 CFR 2.390

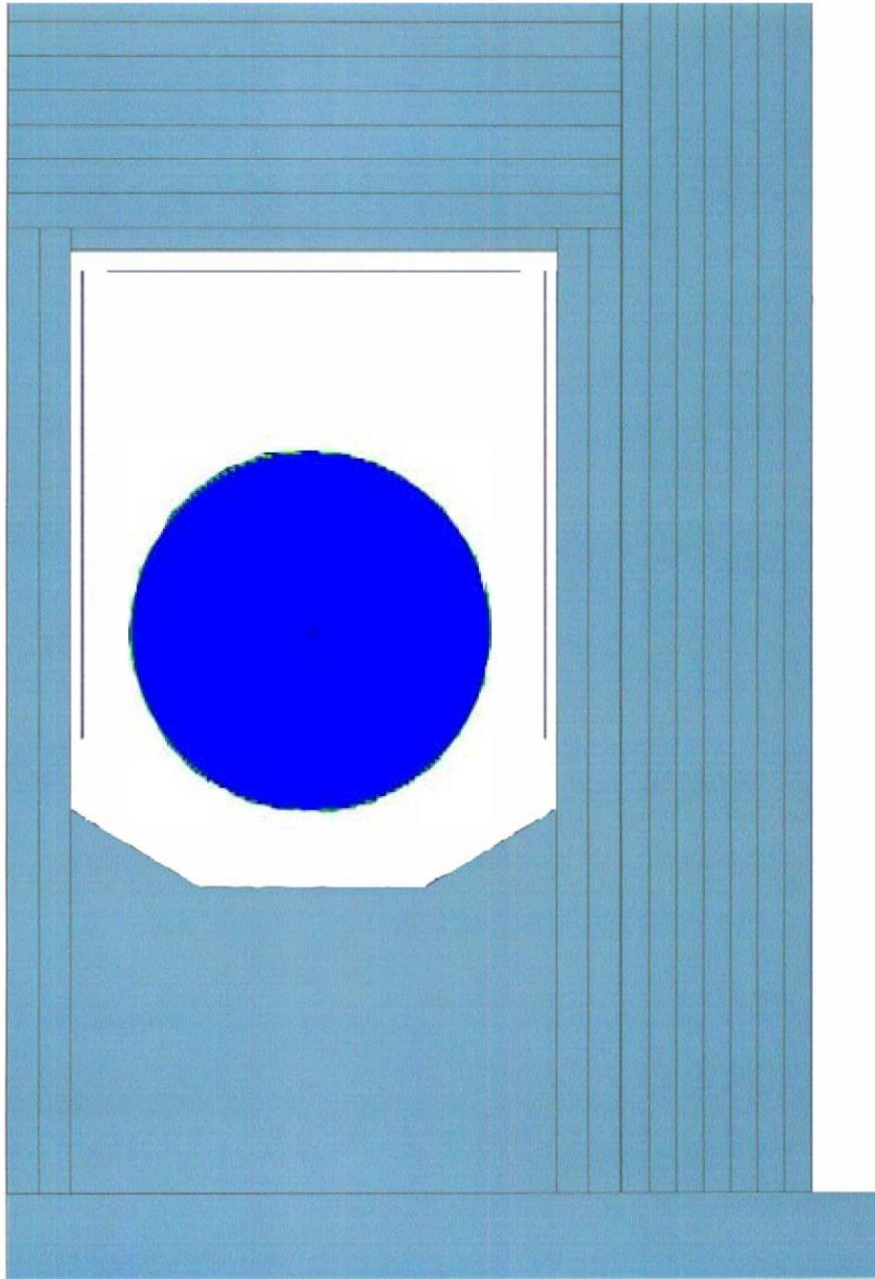


Figure 5-10
HSM-H Head-on View at DSC Lid End (X=225)

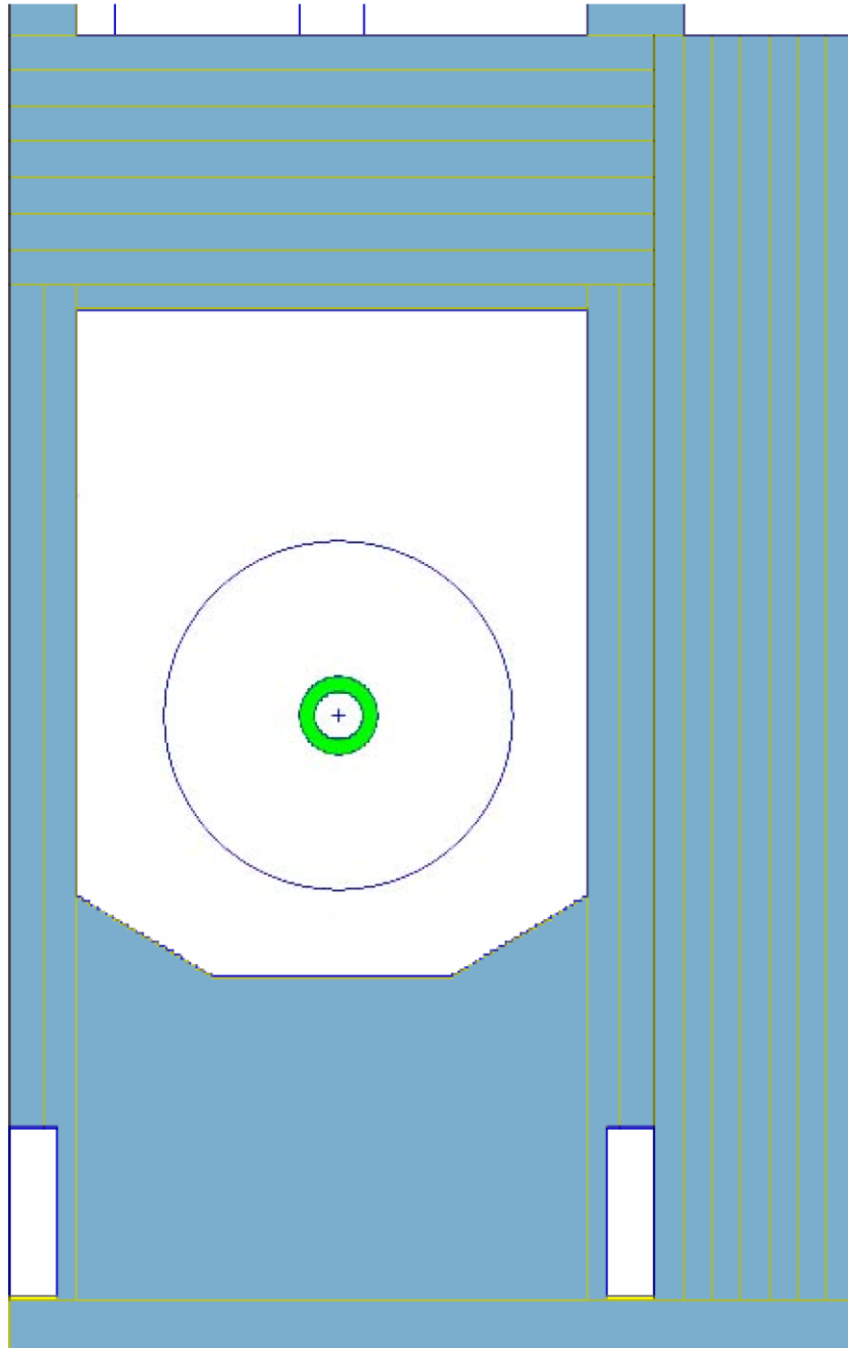


Figure 5-11
HSM-H Head-on View at DSC Bottom End (X=-225)

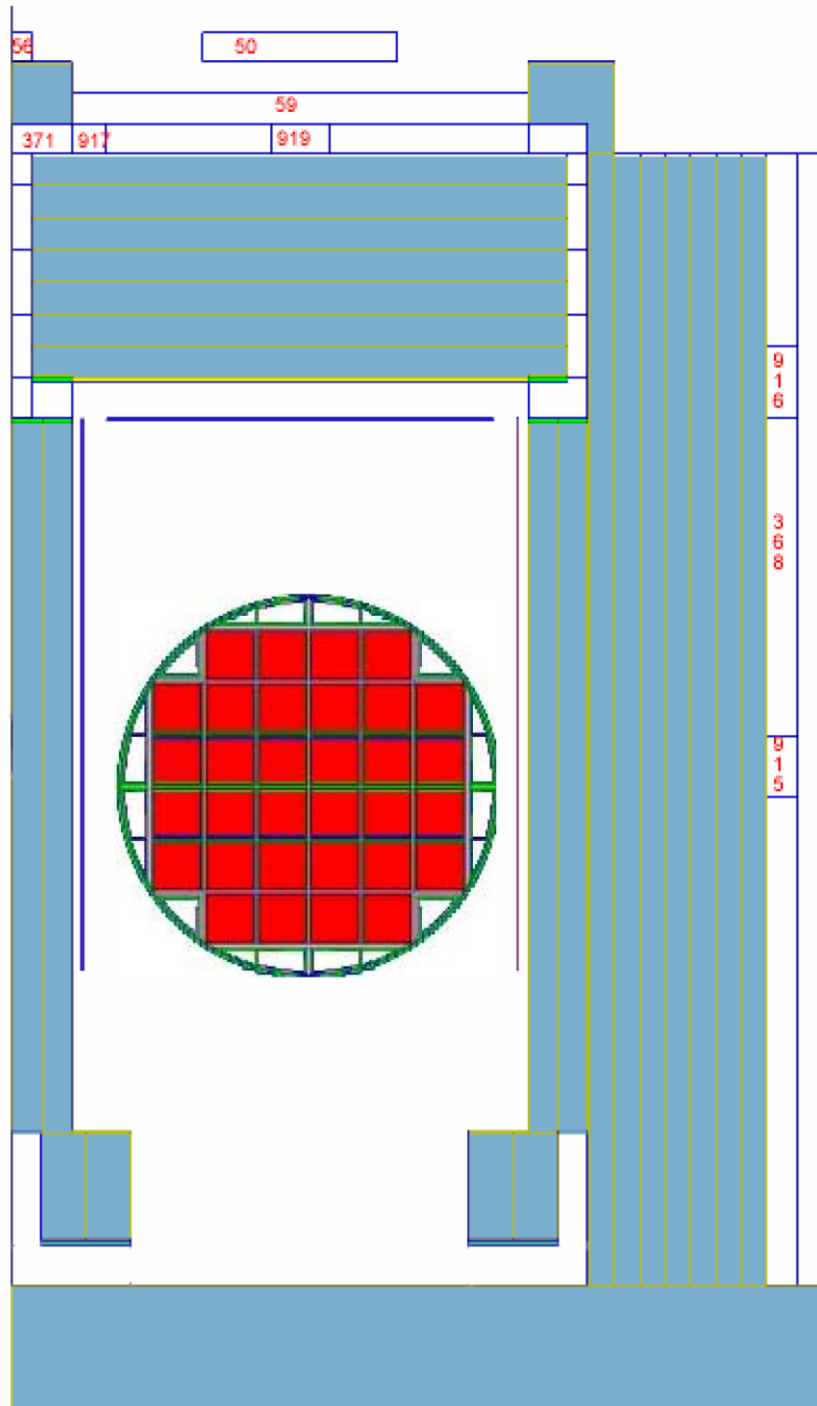


Figure 5-12
HSM-H Detector Locations Head-on View

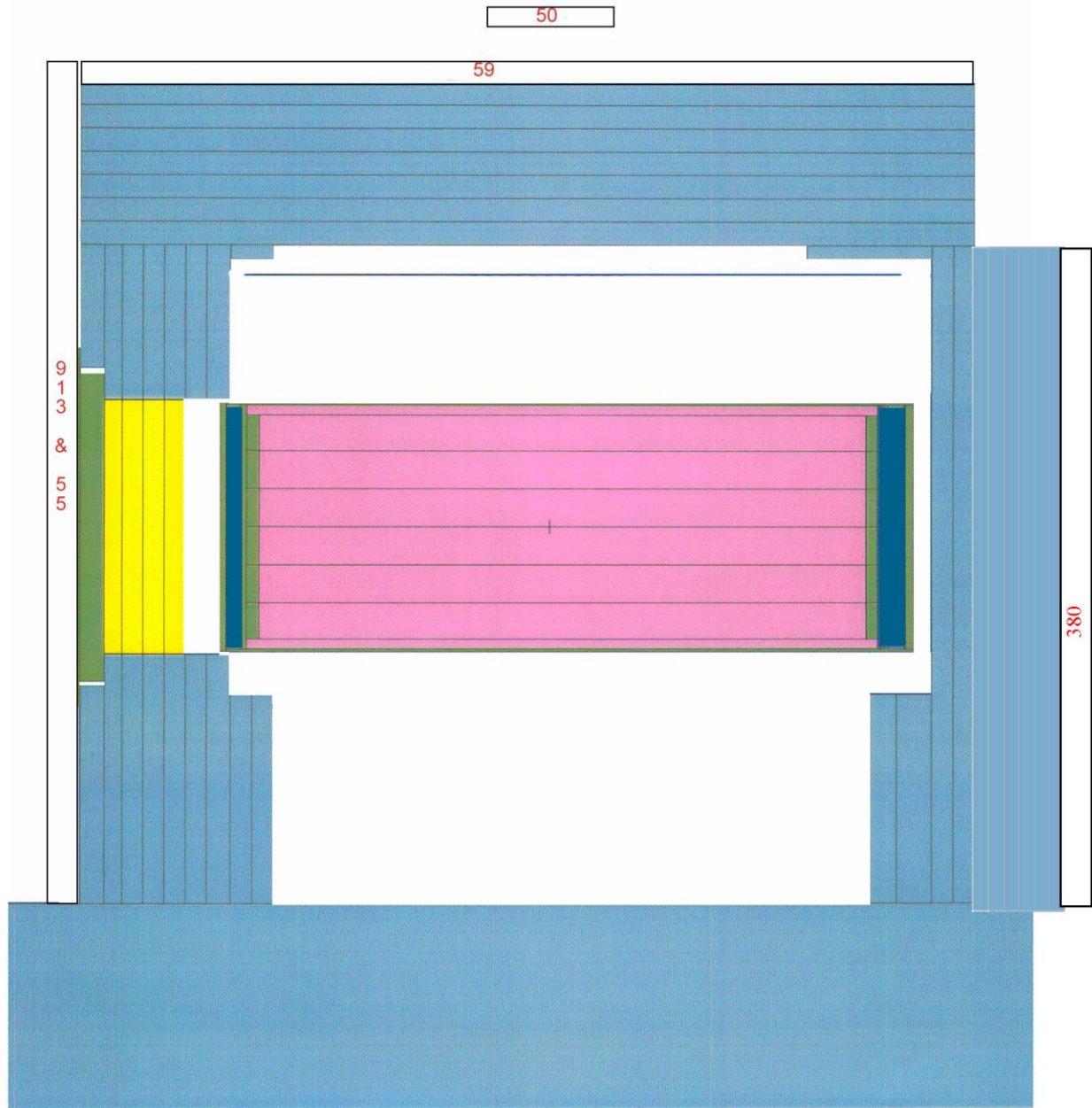


Figure 5-13
HSM-H Detector Locations Side View

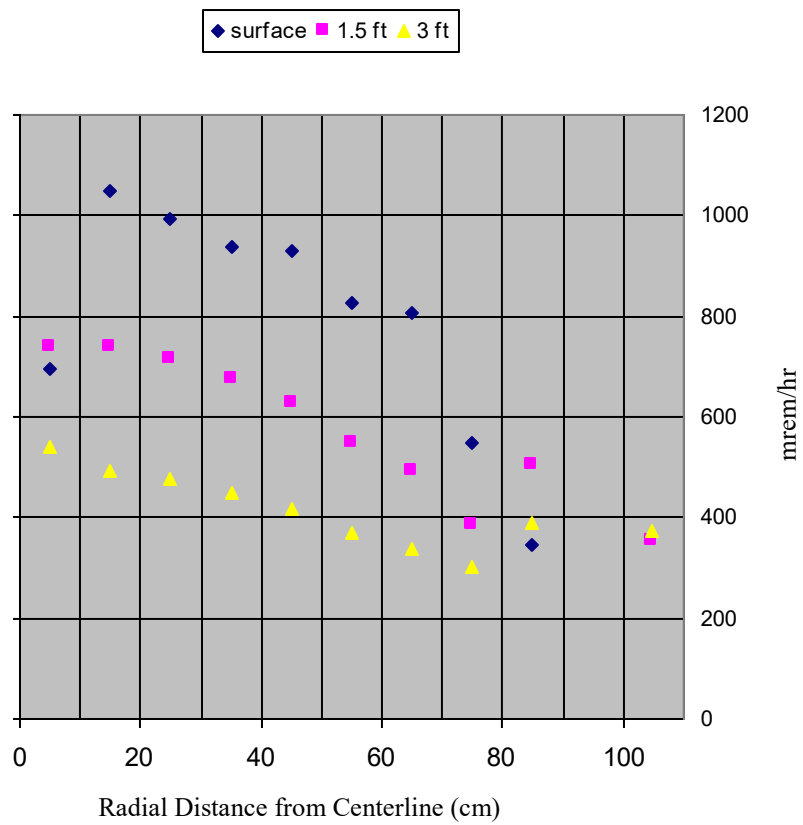


Figure 5-14
Dose Rates Around the Top of the TC/32PTH-DSC
(Configuration A)

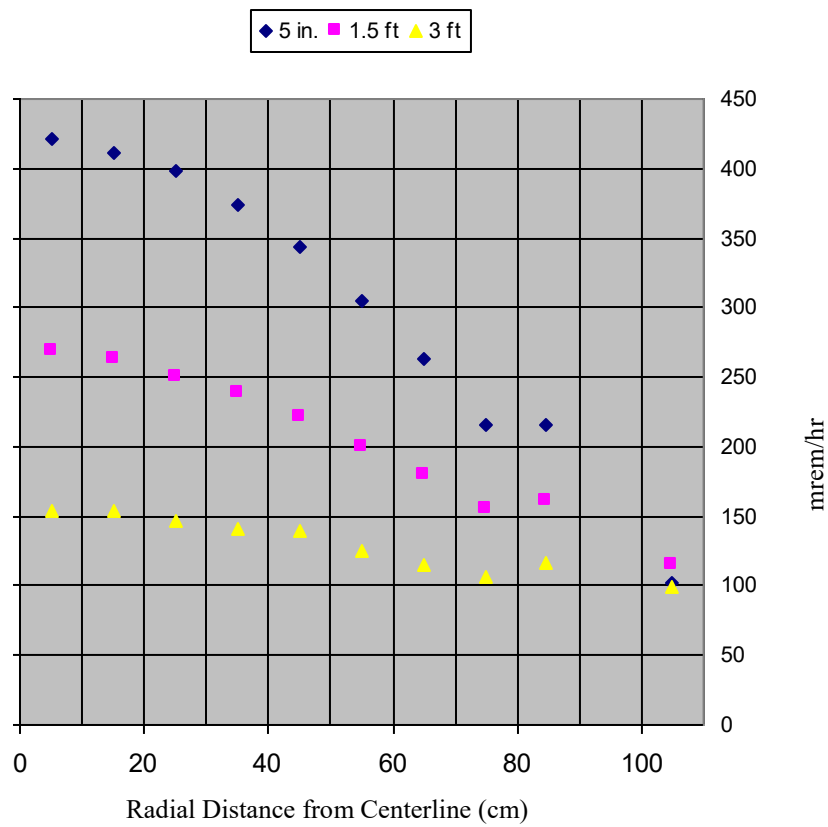


Figure 5-15
Dose Rates Around the Top of the TC/32PTH-DSC
(Configuration B)

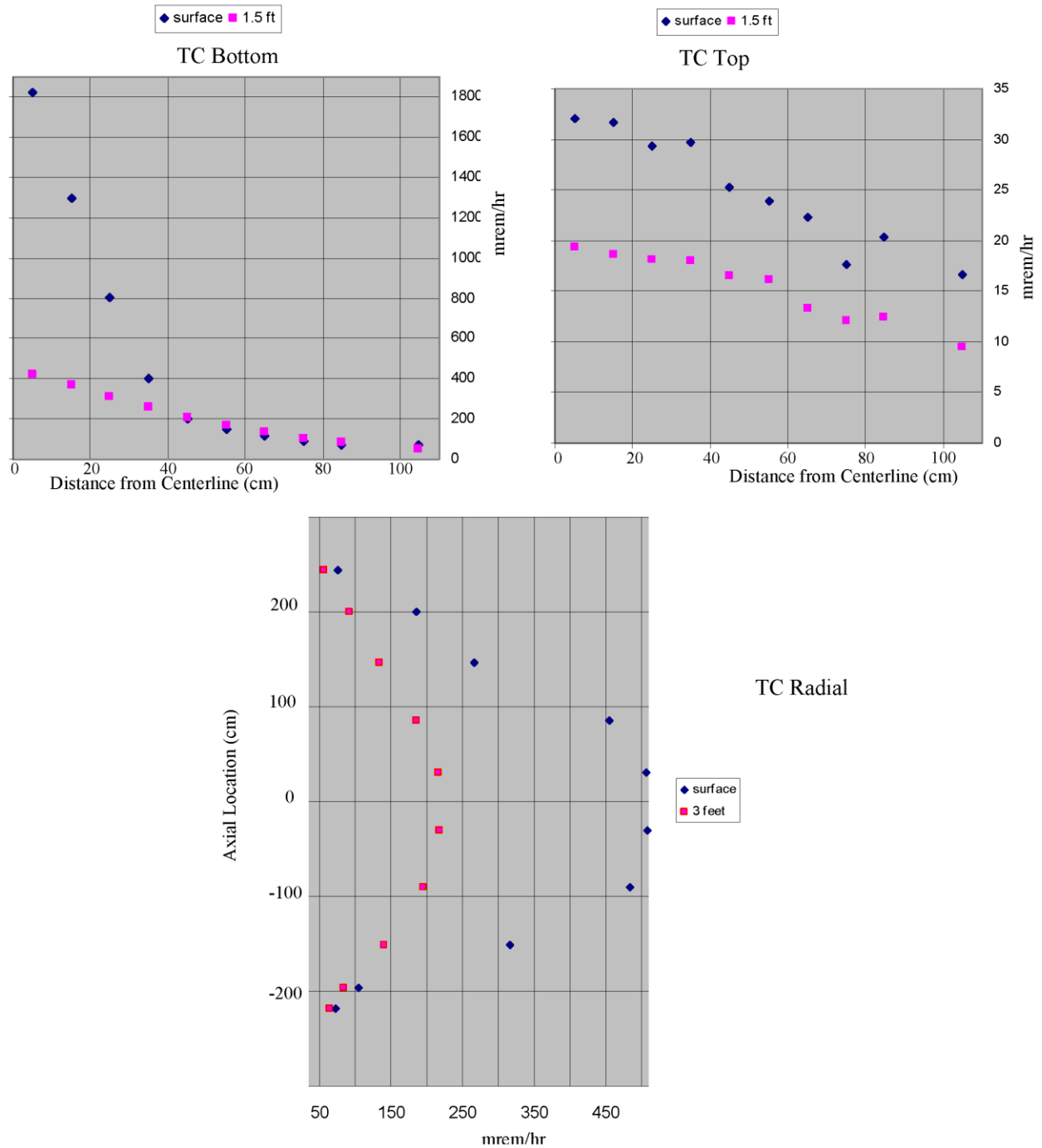


Figure 5-16
Dose Rates Around TC/32PTH-DSC (Transfer Configuration)

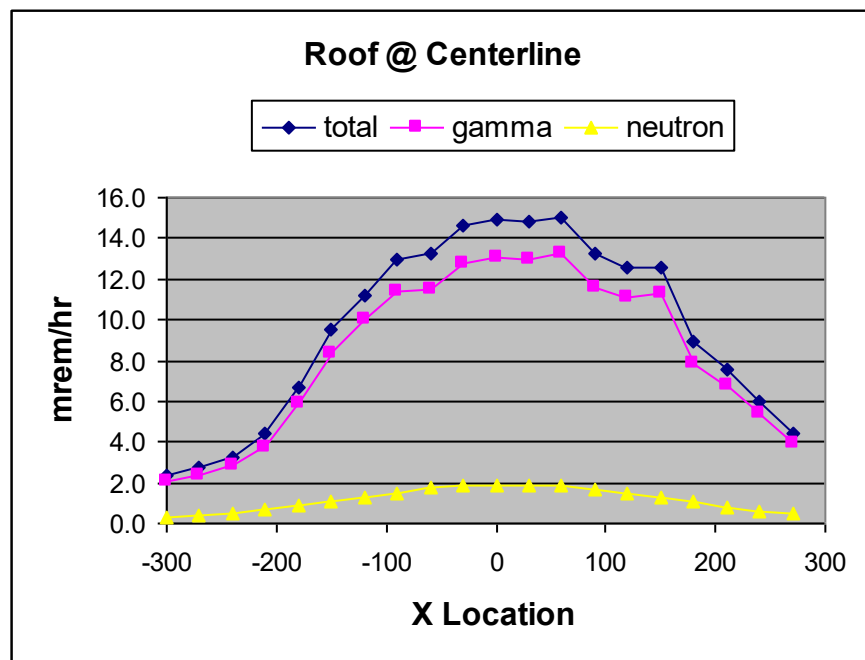
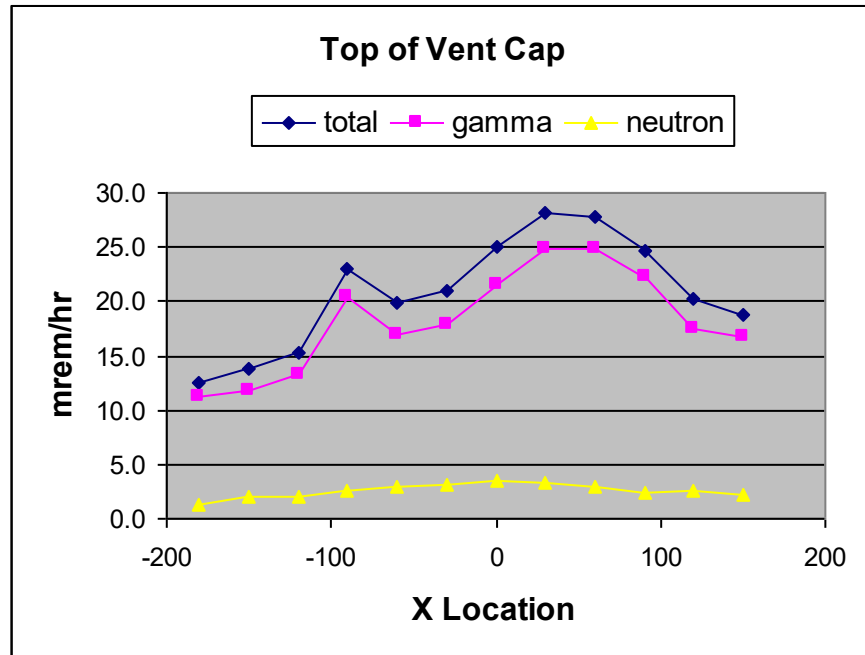


Figure 5-17
Dose Rates On the HSM-H Roof

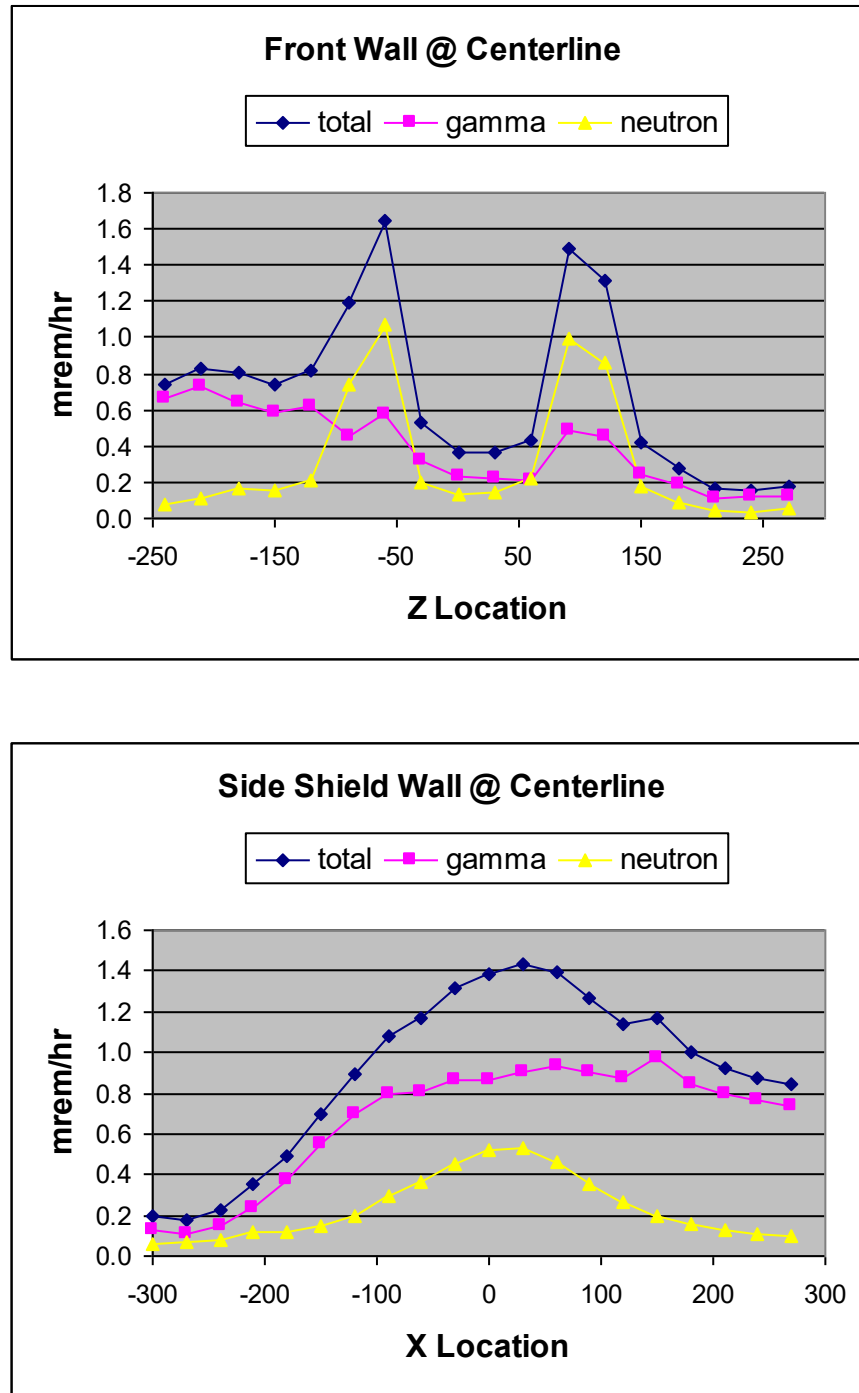


Figure 5-18
Dose Rates On the HSM-H Front and Side

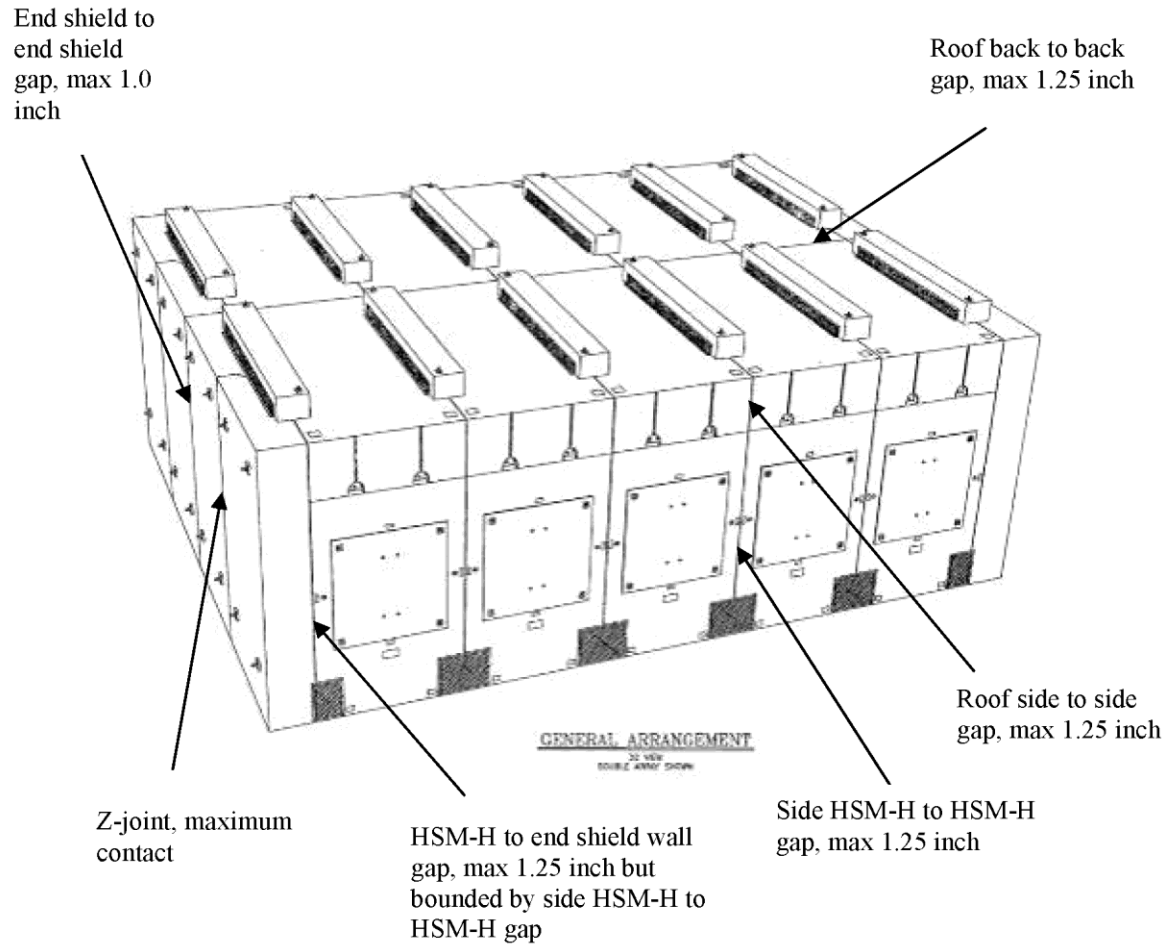


Figure 5-19
HSM-H Array Showing Maximum As-Modeled Gaps

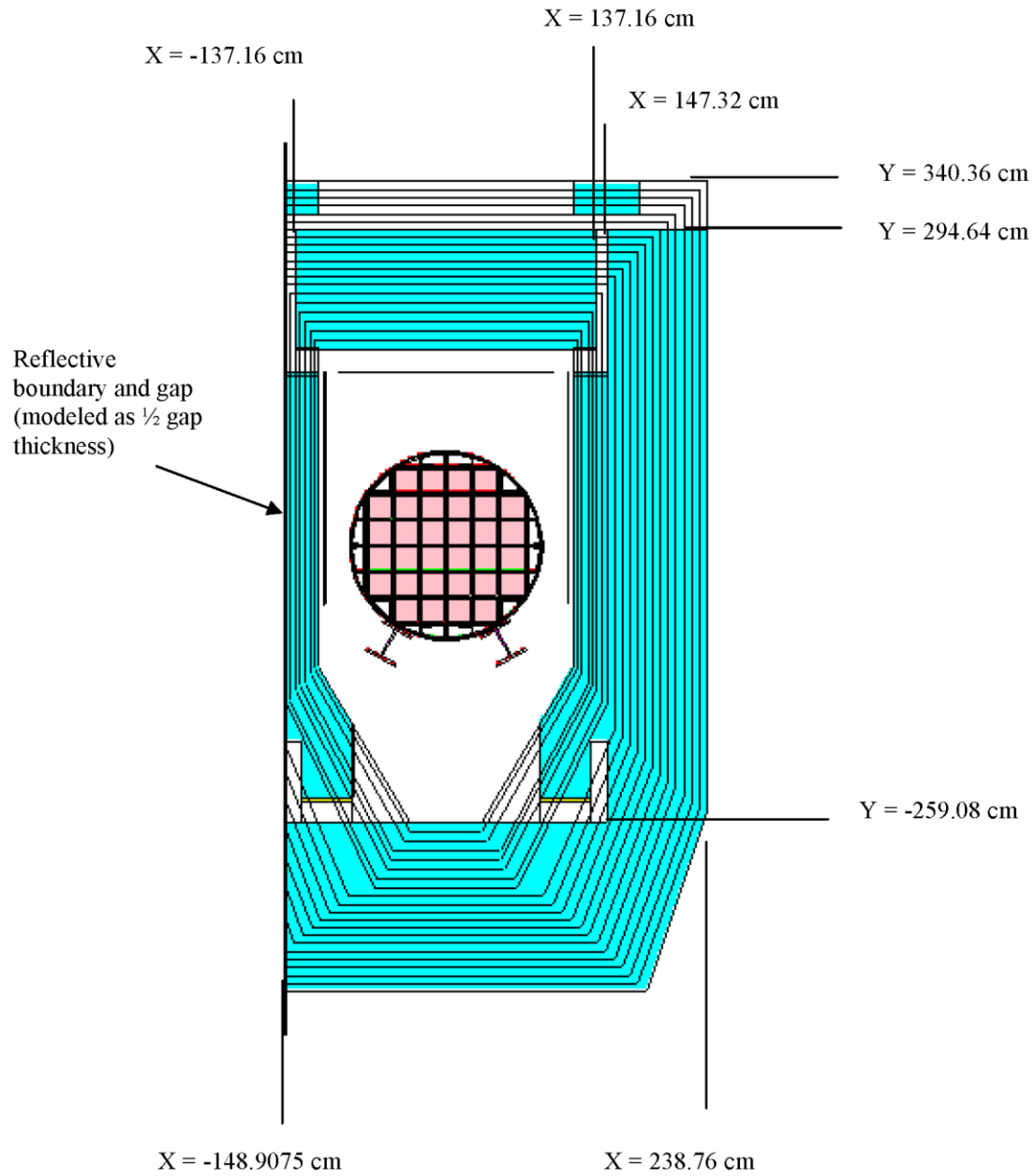


Figure 5-20
HSM-H Model for 1.25 Inch Side-to-Side Gap (x-y view)

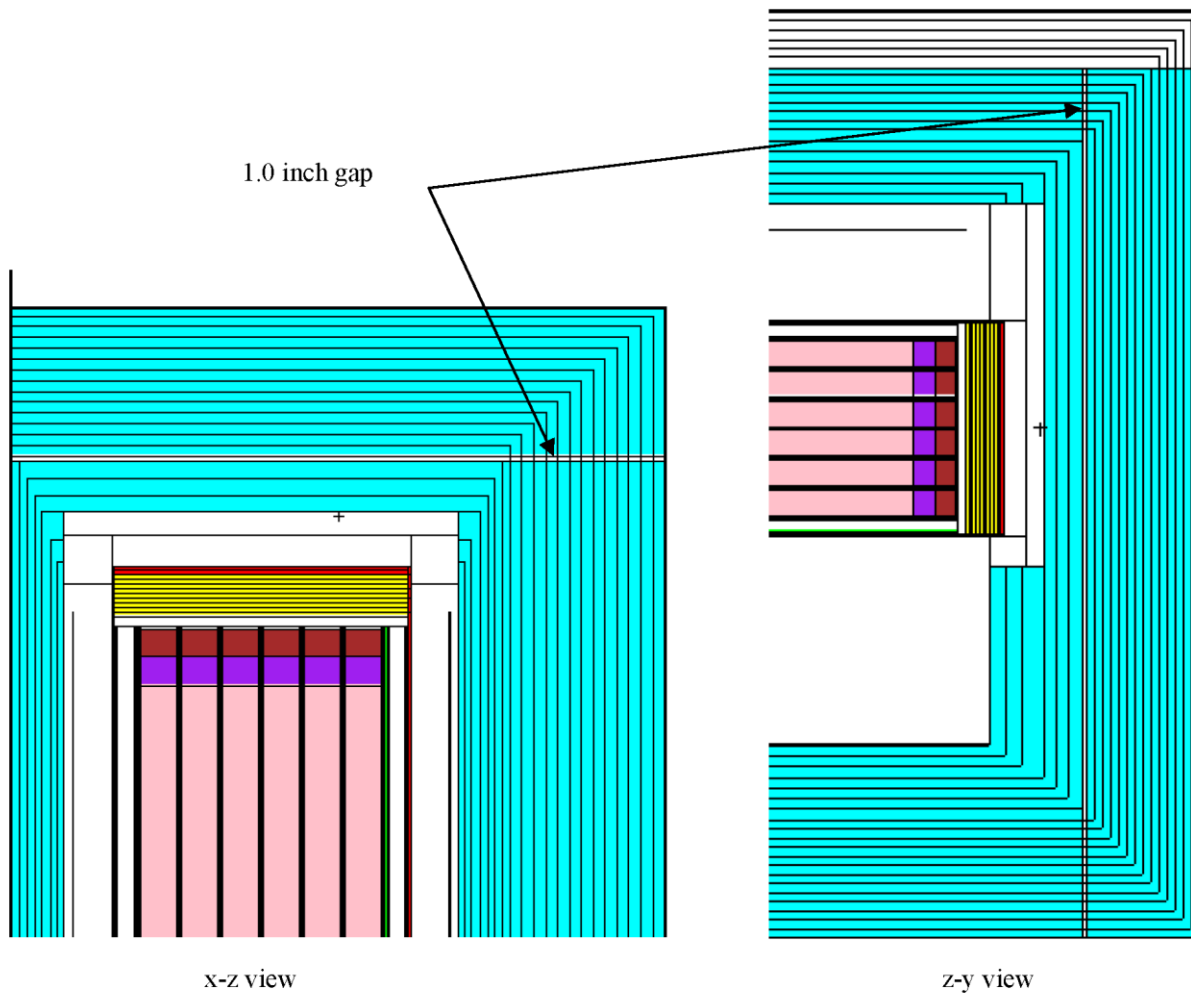


Figure 5-21
HSM-H Model with Back-to-Back Gap

Proprietary Information on Pages 5-119 and 5-120
Withheld Pursuant to 10 CFR 2.390

CHAPTER 6
CRITICALITY EVALUATION

TABLE OF CONTENTS

6. CRITICALITY EVALUATION.....	6-1
6.1 Discussion and Results.....	6-2
6.2 Spent Fuel Loading	6-4
6.3 Model Specification.....	6-6
6.3.1 Description of Criticality Analysis Model	6-6
6.3.2 Package Regional Densities	6-8
6.4 Criticality Calculation	6-9
6.4.1 Calculational Method	6-9
6.4.2 Fuel Loading Optimization	6-14
6.4.3 Criticality Results	6-26
6.5 Critical Benchmark Experiments.....	6-28
6.5.1 Benchmark Experiments and Applicability	6-28
6.5.2 Results of the Benchmark Calculations.....	6-29
6.6 Supplemental Information	6-30
6.6.1 References	6-30
6.6.2 KENO Input Files.....	6-31

LIST OF TABLES

Table 6-1	Maximum Planar Average Initial Enrichment for Intact and Damaged Fuel Loading.....	6-60
Table 6-2	Summary of Limiting Criticality Evaluations for all Fuel Assemblies.....	6-62
Table 6-3	Authorized Contents for NUHOMS [®] -32PTH DSC	6-63
Table 6-4	Fuel Assembly Design Parameters for Criticality Analysis	6-64
Table 6-5	NUHOMS [®] -32PTH - Basket and DSC Dimensions	6-65
Table 6-6	NUHOMS [®] OS187H Transfer Cask Dimensions	6-65
Table 6-7	NUHOMS [®] -32PTH - Fixed Poison Loading Requirements	6-66
Table 6-8	Description of the Basic KENO Model Units	6-67
Table 6-9	Material Property Data	6-68
Table 6-10	Results of the Fuel Assembly Positioning Studies	6-69
Table 6-11	Results of the Rail Material Variation Studies	6-71
Table 6-12	Results of the Poison Plate Thickness Variation Studies	6-72
Table 6-13	Results of the Fuel Compartment Width Variation Studies	6-72
Table 6-14	Results of the Fuel Compartment Thickness Variation Studies.....	6-73
Table 6-15	WE 15x15 Class Intact Assemblies Without BPRAs - Final Results	6-74
Table 6-16	WE 15x15 Class Intact Assemblies With BPRAs - Final Results	6-77
Table 6-17	WE 17x17 Class Intact Assemblies Without BPRAs - Final Results	6-81
Table 6-18	WE 17x17 Class Intact Assemblies with BPRAs - Final Results	6-84
Table 6-19	Limiting Parameters for Damaged Fuel Calculations	6-88
Table 6-20	Results of Optimum Pitch Studies.....	6-89
Table 6-21	Results of the Single Ended Rod Shear Studies	6-93
Table 6-22	Results of the Double Ended Rod Shear Studies.....	6-97
Table 6-23	Evaluation of the Shifting of Fuel Rods Beyond the Poison.....	6-100
Table 6-24	Most Reactive Damaged Assembly Configuration	6-101

Table 6-25	Double Ended Rod Shear Study with BPRAs	6-102
Table 6-26	WE 15x15 Class Damaged Assemblies With BPRAs - Final Results	6-103
Table 6-27	WE 17x17 Class Damaged Assemblies With BPRAs - Final Results	6-107
Table 6-28	Maximum k_{eff} for Intact Fuel Assemblies - Final Results	6-112
Table 6-29	Maximum k_{eff} for Damaged Assemblies - Final Results	6-113
Table 6-30	Benchmark Results	6-114
Table 6-31	USL-1 Results	6-117
Table 6-32	USL Determination for Criticality Analysis	6-118
Table 6-33	CE 14x14 Class Intact Assemblies without BPRAs - Final Results	6-119
Table 6-34	CE 14x14 Class Assembly Final Results with BPRAs (Intact)	6-121
Table 6-35	Intact CE 16x16 Class Assembly without BPRAs, Final Results	6-124
Table 6-36	Intact CE 16x16 Class Assembly with BPRAs, Final Results	6-128
Table 6-37	CE 14x14 Class Damaged Assemblies without BPRAs - Final Results	6-132
Table 6-38	CE 14x14 Class Assembly Final Results with BPRAs (Damaged)	6-135
Table 6-39	Damaged CE 16x16 Class Assembly without BPRAs, Final Results	6-139
Table 6-40	Damaged CE 16x16 Class Assembly with BPRAs, Final Results	6-144
Table 6-41	Criticality Results for the WE 15x15 STD Fuel	6-149
Table 6-42	Criticality Results for the WE 15x15 OFA	6-149
Table 6-43	Intact WE 15x15 and WE 17x17 Fuel Assemblies with ITTR Inserted	6-150
Table 6-44	Damaged WE 15x15 and WE 17x17 Fuel Assemblies with ITTR Inserted	6-151

LIST OF FIGURES

Figure 6-1	Basket Views and Dimensions	6-152
Figure 6-2	Basket Model Compartment Wall (View G).....	6-153
Figure 6-3	Basket Model Compartment Wall (View F)	6-154
Figure 6-4	Basket Model Compartment Wall With Fuel Assembly (View G).....	6-155
Figure 6-5	Basket Model Compartment Wall With Fuel Assembly (View F)	6-156
Figure 6-6	Basket Compartment With Fuel (Section A).....	6-157
Figure 6-7	Basket Compartment With Fuel (Section B).....	6-158
Figure 6-8	Fuel Assembly Positions and Poison Plate Locations in the Basket	6-159
Figure 6-9	Fuel Assembly Positions by KENO Unit ID	6-160
Figure 6-10	Canister and Transfer Cask Description in the KENO Model	6-161
Figure 6-11	Radial Cross Section of the Detailed KENO Model	6-162
Figure 6-12	WE 15x15 Fuel Assemblies in the Centered Position.....	6-163
Figure 6-13	WE 15x15 Fuel Assemblies in the Inward Position.....	6-164
Figure 6-14	CE 14x14 Fuel Assembly : Optimum Pitch Study.....	6-165
Figure 6-15	WE 17x17 Fuel Assembly : Single Ended Rod Shear Study	6-166
Figure 6-16	WE 15x15 Fuel Assembly : Double Ended Rod Shear Study.....	6-167
Figure 6-17	WE 17x17 Fuel Assembly : 4-inch Shift of Fuel Assembly	6-168
Figure 6-18	WE 15x15 Fuel Assembly : 6-inch Shift of Fuel Rods	6-169
Figure 6-19	WE 15x15 Fuel Assembly : Double Ended Rod Shear with BPRAs.....	6-170
Figure 6-20	CE 16x16 Class Assembly – Optimum Pitch KENO Model with BPRAs	6-171

6. CRITICALITY EVALUATION

The NUHOMS[®] HD System is designed to meet 10 CFR 72.124 criticality safety limits during worst case wet loading/unloading operations with the use of fixed neutron absorbing materials (poisons) in the flooded Dry Shielded Canister (32PTH DSC) and credit for soluble boron in the spent fuel pool. The design assures criticality safety under all normal, off-normal and accident conditions associated with fuel handling, 32PTH DSC handling, on-site transfer and 32PTH DSC storage.

The NUHOMS[®] 32PTH DSC criticality safety is ensured by fixed neutron absorbers, soluble boron in the pool and favorable geometry. Burnup credit is not taken in this criticality evaluation. The basket uses a Borated-Aluminum alloy, Aluminum/B₄C metal matrix composite, or Boral[®] as its fixed neutron poison material. These materials are ideal for long-term use in the radiation and thermal environments of a DSC. The minimum required boron-10 loading for the metallic plates is 7.0 mg/cm² (90% credit taken in the criticality analysis or 6.3 mg/cm²). Metal Matrix Composites (MMCs) at a minimum areal density of 7.0 mg/cm² have been qualified for use as a neutron absorber with 90% credit as justified in Section 9.1.7.2 of this UFSAR. Similarly, Section 9.1.7.1 provides the justification for the use of 90% credit for borated aluminum. The maximum poison loading for the metallic plates is 50.0 mg B-10/cm² (90% credit taken in the analysis or 45.0 mg B-10/cm²). The minimum required poison loading for Boral[®] plates is 9.0 mg B-10/cm² (75% credit). The maximum poison loading for Boral[®] plates is 25.0 mg B-10/cm² (75% credit). In addition to utilizing five different fixed poison loadings, the soluble boron concentration credited in the analysis is also varied from a minimum of 2000 ppm to a maximum of 2800 ppm.

The results of the detailed analyses demonstrate that the NUHOMS[®] HD System is criticality safe under normal, off normal and accident conditions including all applicable biases and uncertainties.

The criticality evaluation described in this chapter 6.0 is applicable to the 32PTH DSC and the OS187H TC. See Appendix A, Chapter A.6 for discussion of applicability of these analyses for the 32PTH Type 1 DSC and OS187H Type 1 TC. See Appendix B, Chapter B.6 for discussion of applicability of these analyses for the 32PTH Type 2 DSC and OS187H Type 2 TC.

6.1 Discussion and Results

The NUHOMS[®]-32PTH DSC stainless steel basket consists of an egg-crate plate design. The fuel assemblies are housed in 32 stainless steel fuel compartments with the damaged fuel assemblies occupying the positions shown in Chapter 12. The basket structure, including the fuel compartments, is held together with stainless steel insert plates and the poison and aluminum plates that form the egg crate structure. The basket compartment structure is connected to perimeter rail assemblies, portions of it comprising of a solid aluminum interface. The fuel compartment structure is connected to perimeter transition rail assemblies as described shown on the drawings in Section 1.5. The poison/aluminum plates are located between the fuel compartments.

The analysis presented herein is performed for a NUHOMS[®]-32PTH DSC in the NUHOMS[®]-OS187H transfer cask (TC) during normal and accident loading conditions. The NUHOMS[®]-OS187H TC consists of an inner stainless steel shell, lead gamma shield, a stainless steel structural shell and a water neutron shield. This analysis is applicable to any licensed cask of similar construction. The NUHOMS[®]-32PTH DSC/TC configuration is shown to be subcritical under normal and accident conditions of loading, transfer and storage.

The 32PTH DSC contents are limited to the fuel designs listed in Section 6.1. Computer models of the 32PTH DSC are discussed in Section 6.3. The criticality evaluation is presented in Section 6.4. The 32PTH DSC was evaluated for the following conditions that bound normal conditions and the off-normal and accident events listed in Chapter 11:

- varied internal moderator density (IMD) within the basket with borated water (water density evaluated includes steam which may be generated during loading and unloading operations),
- variations in material tolerances,
- variations in fuel assembly position in the compartment tubes,
- fresh water in the fuel pellet - cladding annulus,
- postulated change of pin pitch due to fuel grid crushing in a drop accident,
- postulated failures for damaged fuel payloads.

The various effects are evaluated individually, and are combined as required to demonstrate compliance with the requirement of 10CFR 72.124 that "before a criticality accident is possible, at least two unlikely, independent, and concurrent or sequential changes have occurred in the conditions essential to nuclear criticality safety."

The criticality analysis determines the most reactive configuration for the basket and fuel assembly position. Then criticality calculations evaluate a variety of fuel assembly types, initial enrichments and poison loadings (fixed and soluble poison). Finally, the maximum allowed initial enrichment for each fuel assembly type as a function of soluble boron concentration and fixed poison loading is determined and is listed in Table 6-1.

Additionally, calculations are carried out to determine the most reactive damaged fuel assembly (design basis damaged fuel assembly) configuration for each fuel assembly class.

Then criticality calculations evaluate a variety of fuel assembly types, initial enrichments and poison loadings (fixed and soluble poison). Finally, the maximum planar average initial enrichment is also shown in Table 6-1.

These calculations determine k_{eff} with the CSAS25 control module of SCALE-4.4 [3] for each assembly type and initial enrichment, including all uncertainties to assure criticality safety under all credible conditions.

The results of these calculations demonstrate that the maximum expected k_{eff} , including statistical uncertainty, will be less than the Upper Subcritical Limit (USL) determined from a statistical analysis of benchmark criticality experiments. The statistical analysis procedure includes a confidence band with an administrative safety margin of 0.05. A series of benchmark calculations were performed with the SCALE 4.4 PC/CSAS25 [3] package using the 44-group cross-section library as presented in Section 6.5. The minimum value of the Upper Subcritical Limit (USL) was determined to be 0.9419.

The results of the limiting criticality analyses are summarized in Table 6-2. The maximum k_{eff} for the normal fuel geometry is 0.9407 ($k_{\text{eff}}+2\sigma$) and is based on the Combustion Engineering (CE 16x16) class fuel assembly design. The maximum k_{eff} for the damaged fuel geometry is 0.9402 ($k_{\text{eff}}+2\sigma$) and is based on the WE 17x17 fuel assembly design.

6.2 Spent Fuel Loading

This section provides a summary of the maximum spent fuel loading and spent fuel parameters for the 32PTH DSC.

The NUHOMS[®]-32PTH DSC is capable of transferring and storing a maximum 32 intact PWR fuel assemblies. Additionally, a maximum of 16 locations (out of the 32 locations) per DSC can be loaded with damaged PWR fuel assemblies with the remaining locations loaded with intact PWR fuel assemblies. The required placement of the damaged fuel assemblies is defined in Chapter 12. Damaged fuel includes assemblies with known or suspected cladding defects greater than hairline cracks or pinhole leaks. The reactivity of a DSC loaded with less than 32 PWR fuel assemblies is expected to be lower than that calculated in this report since the more absorbing borated water replaces the fuel in the empty locations. Reconstituted fuel assemblies, where the fuel pins are replaced by lower enriched fuel pins or non-fuel (prior to initial irradiation or following initial irradiation) pins that displace the same amount of borated water, are considered intact fuel assemblies. Table 6-3 lists the fuel assemblies considered as authorized contents of the NUHOMS[®]-32PTH DSC.

WE 15x15 and WE 17x17 class fuel assemblies containing ITTRs are also qualified for storage in the 32PTH DSC.

Table 6-4 lists the fuel design parameters for the PWR fuel assemblies. Reload fuel from other manufacturers with the same parameters are also considered as authorized contents. For WE 15x15 fuel assembly class two additional fuel types at smaller fuel diameters and different guide tube dimensions as indicated in Table 6-4 are also qualified as reload fuel.

For the fuel assemblies to be loaded in the NUHOMS[®]-32PTH DSC control components (CCs) are also included as authorized contents. The only change to the package fuel loading is the addition of CCs that are modeled as $^{11}\text{B}_4\text{C}$. Since CCs displace borated moderator in the assembly guide tubes, an evaluation is performed to determine the potential impact of the storage of CCs such as BPRAs, CRAs that extend into the active fuel region, on the system reactivity. For these CCs (bounded by BPRA) no credit is taken for BPRA cladding and absorbers; rather the BPRA is modeled as $^{11}\text{B}_4\text{C}$ in the entire guide tube of the respective design. Thus, the highly borated moderator between the guide tube and the BPRA rodlet is modeled as $^{11}\text{B}_4\text{C}$. The inclusion of more Boron-11 and carbon enhances neutron scattering causing the neutron population in the fuel assembly to be slightly increased which increases reactivity. Therefore, these calculations bound any CC design that is compatible with WE 17x17, CE 16x16, WE 15x15 and CE 14x14 class assemblies. CCs that do not extend into the active fuel region of the assembly do not have any effect on the reactivity of the system as evaluated because only the active fuel region is modeled in this evaluation with periodic boundary conditions making the model infinite in the axial direction. The fuel assembly dimensions reported in Table 6-4 remains unchanged for the BPRA cases. The models that include BPRAs only differ in that the region inside the guide tubes and instrument tube are modeled as $^{11}\text{B}_4\text{C}$ instead of moderator. Additionally, the presences of non-multiplying sources like the NSAs have no impact on criticality calculations. Therefore all CCs are bounded by the BPRAs for criticality purposes and will be referred to as BPRAs for the rest of the report. Since the criticality analysis models simulate on the active fuel height, any CC that is inserted into the fuel assembly such that it does not extend into the active fuel region is considered as authorized for storage without adjustment to the soluble boron content or initial enrichment as required for control components that extend

into the active fuel region. For example, TPAs or ORAs are permitted for storage within a fuel assembly without adjusting the maximum initial enrichment or minimum soluble boron content given in Table 6-1, since TPAs or ORAs do not extend into the active fuel region.

6.3 Model Specification

The following subsections describe the physical models and materials of the NUHOMS[®]-32PTH DSC as loaded and transferred in the NUHOMS[®] OS187H TC used for input to the CSAS25 module of SCALE-4.4 3 to perform the criticality evaluation. The reactivity of the DSC under storage conditions is bounded by the TC analysis with zero internal moderator density case. The TC analysis with zero internal moderator density case bounds the storage conditions in the HSM because (1) the DSC internals are always dry (purged and backfilled with He) while in the HSM, and (2) the TC contains materials such as steel and lead which provide close reflection of fast neutrons back into the fueled basket while the HSM materials (concrete) are much further from the sides of the DSC and thereby tend to reflect thermalized neutrons back to the DSC which are absorbed in the DSC materials reducing the system reactivity.

6.3.1 Description of Criticality Analysis Model

The transfer cask and DSC are explicitly modeled using the appropriate geometry options in KENO V.a of the CSAS25 module in SCALE-4.4. Several models are developed to evaluate the fabrication tolerances of the DSC, fuel assembly locations, fuel assembly type, initial enrichments, fixed poison loading, soluble boron concentration and storage of CCs.

The basket design modeled in the calculation is based on the 32PTH basket detailed in Chapter 1 with a section length of 15.03" (13.28" basket section + 1.75" steel plate). The key basket dimensions utilized in the calculation are shown in Table 6-5. The key transfer cask dimensions utilized in the calculation are shown in Table 6-6. The fixed poison modeled in the calculation is based on borated aluminum alloy. A credit of 90% is taken for the fixed poison loading in the analysis. Alternatively, Boral[®] can be used as a fixed poison. However, the criticality analysis with Boral[®] assumes crediting only 75% of the fixed poison loading. Therefore, the Boral[®] loading requirements are appropriately (and conservatively) adjusted and the fixed poison loading requirements are shown in Table 6-7.

The basic calculational KENO model is a 15.03-inch axial section and full-radial cross section of the DSC and cask with periodic boundary conditions at the axial boundaries (top and bottom) and reflective boundary conditions at the radial boundaries (sides). This axial section essentially models one building block of the egg crate basket structure. Periodic boundary conditions ensure that the resulting KENO model is essentially infinite in the axial direction. The model does not explicitly include the water neutron shield; however the infinite array of casks without the neutron shield does contain unborated water between the casks and in the canister - transfer cask gap. This basic building block is shown in Figure 6-1.

The fuel assemblies within the basket are modeled explicitly. The fuel compartment surrounds each fuel assembly which is bounded by the basket plates consisting of 0.50" Aluminum/Borated Aluminum plates (modeled as two 0.25"-thick plates). These plates are arranged to represent an egg-crate design with the 0.075" or 0.187"-Borated Aluminum and the remaining-Aluminum plate. The thermal expansion and egg-crate slot gaps are not modeled (conservative) assuming plate continuity, thus replacing the more absorbing internal moderator with aluminum plate. KENO model plots in 2D for the various views of the basket compartment are shown in Figure 6-2 through Figure 6-7.

There are a total of 10 poison plates in the NUHOMS[®]-32PTH basket. They are located at all the faces where six fuel assemblies are lined up. Thus, all the interior 16 fuel assemblies are surrounded by poison plates on all four faces and the outer 16 fuel assemblies do not have poison plates on the radially outward looking face. The fuel assembly and poison plate positions (and the aluminum plate positions) in the KENO model of the basket is shown in Figure 6-8. Even though the poison and aluminum plates have been shown as discrete plates around the fuel compartment, they are all continuous running from one end of the basket to the other.

The basket structure is connected to the DSC shell by perimeter rail assemblies. The rail material is aluminum and SS304 and provide for a heat conduction path from the basket to the DSC shell. These rails are not modeled explicitly in the basic KENO model. They are, however, modeled in KENO as a homogenous (as illustrated in Figure 6-9) mixture of unborated water, Aluminum and SS304. The KENO unit numbers used for the fuel assembly positions are shown in Figure 6-9.

A list of all the geometry units used in the basic KENO model is shown in Table 6-8. Figure 6-10 shows the various radial “cylinders” utilized in the KENO model surrounding the fuel assemblies. Basically, this shows the canister and transfer cask details. For the parametric calculations to determine the most reactive geometry, the fuel assemblies are modeled with an initial enrichment of 4.30 wt. % U-235, a soluble boron concentration of 2500 ppm and a fixed poison loading of 15 mg B-10/cm² (Type B basket with a 90% credit for Borated Aluminum poison in the analysis).

In addition, a detailed KENO model with explicit representation of the rail structure, within the limitations of the KENO geometry, is also developed to demonstrate the adequacy and conservatism of the simplified KENO model with “homogenous” rail structure. A radial cross section of the basket with the “detailed” KENO model is shown in Figure 6-11.

The basic KENO model is used to determine the most reactive fuel assembly for a given enrichment, most reactive assembly-to-assembly pitch, and to determine the most reactive DSC configuration accounting for manufacturing tolerances including rail material homogenization. The second model is of the most reactive configuration identified above. This model is used to determine the maximum allowable initial enrichment for each assembly type as a function of the soluble boron concentration and fixed poison loading, as appropriate.

A slightly different, yet a more conservative 32PTH basket model is used in the evaluation of the CE 16x16 fuel assemblies as well as the WE 15x15, WE 17x17 and CE 14x14 at soluble boron concentrations of 2800 ppm. This model is discussed in Section 6.4.

This basic KENO model is modified to model the various damaged fuel configurations like single shear, double shear, optimum pitch and axial fuel shifting. These models are analyzed to determine the most reactive damaged fuel configuration for each fuel assembly class. The second model is based on the most reactive configuration identified above. This model is used to determine the maximum number of damaged fuel assemblies per DSC and the maximum allowable initial enrichment for each assembly type as a function of the soluble boron concentration and fixed poison loading, as appropriate.

6.3.2 Package Regional Densities

The Oak Ridge National Laboratory (ORNL) SCALE code package 3 contains a standard material data library for common elements, compounds, and mixtures. All the materials used for the TC and canister analysis are available in this data library.

Table 6-9 provides a complete list of all the relevant materials used for the criticality evaluation. The material density for the B-10 in the poison plates includes a 10% reduction.

6.4 Criticality Calculation

This section describes the analysis methodology utilized for the criticality analysis. The analyses are performed with the CSAS25 module of the SCALE system. A series of calculations are performed to determine the relative reactivity of the various fuel assembly designs evaluated and to determine the most reactive configuration without BPRAs. The most reactive intact fuel design, for a given enrichment, as demonstrated by the analyses, is the WE 17x17 standard assembly. The most reactive credible configuration is an infinite array of flooded casks, each containing 32 fuel assemblies, with minimum fuel compartment ID, minimum basket structure thickness and minimum assembly-to-assembly pitch.

A series of calculations are also performed to determine the relative reactivity of the various damaged fuel configurations for each fuel assembly class. The most reactive damaged fuel configuration for the WE 17x17 and WE 15x15 class occurs due to a postulated double-ended shear. The most reactive damaged fuel configuration for the CE 14x14 and CE 16x16 class occurs when the fuel rods are arranged in an optimum pitch configuration. The most reactive credible configuration analyzed in this calculation is an infinite array of flooded casks, each containing a maximum of 32 damaged fuel assemblies with BPRAs, with minimum fuel compartment ID, minimum basket structure thickness and minimum assembly-to-assembly pitch.

As mentioned in Section 6.1, the NUHOMS[®]-32PTH DSC is evaluated to determine the maximum initial enrichment of the fuel assemblies (both damaged and intact) per DSC for each assembly class as a function of fixed poison loading and soluble boron concentration levels.

6.4.1 Calculational Method

6.4.1.1 Computer Codes

Criticality analyses were performed using the microcomputer application KENO-Va and the 44 neutron group library based on ENDF-B Version 5 cross-section data that are part of the SCALE 4.4 code package [3]. Validation and benchmarking of these codes is performed in accordance with applicable QA program requirements (see Chapter 13) and is discussed in Section 6.5.

SCALE 4.4 [3] is an extensive computer package which has many applications including cross section processing, criticality studies, and heat transfer analyses among others. The package is comprised of many functional modules, which can be run independently of each other. Control Modules were created to combine certain functional modules in order to make the input requirements less complex. For the purpose of criticality analysis, only four functional modules are used and one control module. These Modules are CSAS25, which includes the three dimensional criticality code KENO-Va and the preprocessing codes BONAMI-S, NITAWL-II and XSDRNPM-S.

KENO-Va, in conjunction with a suitable working library of nuclear cross section data, is used to calculate the multiplication factor, k_{eff} , of systems of fissile material. It can also compute lifetime and generation time, energy dependent leakages, energy and region-dependent absorptions, fissions, fluxes, and fission densities. KENO-Va utilizes a three-dimensional Monte-Carlo computation scheme. KENO-Va is capable of modeling complex geometries including facilities for handling arrays, arrays of arrays, and holes.

SCALE 4.4 is set up so that any number of cross-section libraries may be used with the preprocessing functional and control modules. For the purpose of this analysis, only the 44-group ENDF/B Version 5 library is used.

The preprocessing codes used for this analysis are the functional modules BONAMI-S, NITAWL-II and XSDRNPM-S. They are consolidated into the control module CSAS25. BONAMI-S has the function of performing Bondarenko calculations for resonance self-shielding. The cross sections and Bondarenko factor data are pulled from an AMPX master library. The output is placed into a master library as well. Dancoff approximations allow for different fuel lattice cell geometries. The main function of NITAWL-II is to change the format of the master cross-section libraries to one which the criticality code (KENO-Va) can access. It also provides the Nordheim Integral Treatment for resonance self-shielding. XSDRNPM-S provides cell-weighted cross sections based on the specified unit cell.

The criticality analysis, using the above computer codes, is performed in compliance with the 10CFR 72 [1] requirements. Specifically, all cases are analyzed assuming that the basket is fully flooded with borated water and the neutron shield of the transfer cask is eliminated and the cask is flooded with fresh water. Finally, KENO V.a calculates the k_{eff} of the system that is modeled. A sufficiently large number of neutron histories are run so that the standard deviation is below 0.0010 for all calculations.

6.4.1.2 Physical and Nuclear Data

The physical and nuclear data required for the criticality analysis include the fuel assembly data and cross-section data as described below.

Table 6-4 provides the pertinent data for criticality analysis for each fuel assembly evaluated for the NUHOMS[®] HD System.

The criticality analysis used the 44-group cross-section library built into the SCALE system. ORNL used ENDF/B-V data to develop this broad-group library specifically for criticality analysis of a wide variety of thermal systems.

6.4.1.3 Bases and Assumptions

The analytical results reported in Section 3.7 demonstrate that the TC containment boundary and canister basket structure do not experience any significant distortion under hypothetical accident conditions. Therefore, for both normal and hypothetical accident conditions the TC geometry is identical except for the neutron shield and skin. As discussed above, the neutron shield and skin are conservatively removed and the interstitial space modeled as water.

The TC is modeled with KENO V.a using the available geometry input. This option allows a model to be constructed that uses regular geometric shapes to define the material boundaries. The following conservative assumptions are also incorporated into the criticality calculations:

1. No burnable poisons like IFBA, Gadolinia, Erbia, B₄C or any other absorber, accounted for in the fuel.
2. CCs like BPRA, TPA, and VSI are conservatively assumed to exhibit neutronic properties similar to ¹¹B₄C. There is no neutron absorption from any of these hardware and are collectively referred to as BPRAs.
3. Water density at optimum moderator density.
4. Unirradiated fuel – no credit taken for fissile depletion due to burnup or fission product poisoning.
5. The fuel pins are modeled assuming a stack density of 97.5% theoretical density with no allowance for dishing or chamfer. This assumption conservatively increases the total fuel content in the model.
6. Temperature at 20°C (293K).
7. The maximum fuel enrichment is modeled as uniform everywhere throughout the assembly. Natural Uranium blankets and axial or radial enrichment zones are modeled as enriched uranium with an average enrichment.
8. All fuel rods are filled with full density water in the pellet/cladding gap.
9. Only a 15.03-inch (for the CE 16x16 models, this section is 13.48 inch) section of the basket with fuel assemblies is explicitly modeled with periodic axial boundary conditions, therefore the model is effectively infinitely long.
10. It is assumed that for all cases the neutron shield and stainless steel skin of the cask are stripped away and the infinite array of casks are pushed close together with moderator in the interstitial spaces.

11. The thermal expansion and egg-crate gaps are conservatively replaced with the basket material wherever present. This results in replacing the soluble boron moderator in the gap regions with Aluminum thereby decreasing the neutron absorption around the fuel.
12. The transition rails between the basket and the canister shell are modeled as a homogenous material consisting of 30% full density water, 35% aluminum and 35% SS304 by volume. This homogenous rail structure assumption will be shown to be adequate and conservative with comparisons using a “detailed” model.
13. The fixed poison inside the basket is based on either Boral[®] or a Borated Aluminum alloy material design. A credit of 90% of the absorber material (B-10) is assumed in the analysis. When Boral[®] is used as the fixed poison, a credit of 75% for the absorber material is utilized.
14. All steel materials are modeled as SS304. The small differences in the composition of the various stainless steels have no effect on results of the calculation.
15. All zirconium based materials in the fuel are modeled as Zircalloy-4. The small differences in the composition of the various clad / guide tube materials have no effect on the results of the calculation.
16. No calculations are performed that model the uncovering of poison in the active fuel region of the basket. Even though the size of the cavity in the DSC is larger than the size of the basket, accidents involving a relative shift of the basket and the fuel assemblies at the bottom are not considered credible when the basket (and the DSC) is flooded with borated water and the DSC/TC system is in the vertical position. Therefore, all calculations are carried out with the active fuel region axially surrounded by fixed poison in the basket.

The following are the additional assumptions that are relevant to the damaged fuel assembly calculations:

1. The cask containment boundary and canister basket structure do not experience any significant distortion under hypothetical accident conditions.
2. The worst case gross damage resulting from a cask-drop accident is assumed to be either a single-ended or double-ended rod shear with flooding in borated water. A maximum of 4 inches of fuel may be uncovered by the poison plates due to shifting of the sheared rods.
3. The cases with bare fuel and rubble are not modeled since replacing the clad with borated water results in an increase in absorption. Hence, damaged fuel cases are modeled with the presence of the clad around the fuel pellet.
4. The bent or bowed fuel rod cases assume that the fuel is intact but that the rod pitch is allowed to vary from its nominal fuel rod pitch.

5. The single-ended fuel rod shear cases assume that fuel rods that form one assembly face shear in one place and are displaced to new locations. The fuel pellets are assumed to remain in the fuel rods.
6. The double-ended fuel rod shear cases assume that the fuel rods that form one assembly face shear in two places and the intact fuel rod pieces are separated from the parent fuel rods.
7. Although only 16 damaged fuel assemblies are authorized contents for the DSC, all 32 fuel assemblies are considered to be damaged in the criticality analyses for damaged fuel.

6.4.1.4 Determination of k_{eff}

The Monte Carlo calculations performed with CSAS25 (KENO V.a) use a flat neutron starting distribution. The total number of histories traced for each calculation is approximately 800,000. This number of histories is sufficient to achieve source convergence and produce standard deviations of less than 0.0010% in Δk_{eff} . The maximum k_{eff} for the calculation is determined with the following formula:

$$k_{\text{eff}} = k_{\text{KENO}} + 2\sigma_{\text{KENO}}.$$

6.4.2 Fuel Loading Optimization

The criticality analysis is performed for the 32PTH DSC loaded with 32 intact or 32 damaged fuel assemblies. The following sub-sections describe the various analyses performed with the intact and damaged fuel assemblies.

The design basis intact and damaged fuel criticality analysis models employed in the 32PTH1 DSC described in Appendix U.6 of the Standardized NUHOMS[®] System UFSAR [10] are utilized herein for the evaluations at a boron concentration of 2800 ppm for the four fuel assembly classes. Further, these models are also employed in all the calculations for the CE 16x16 class fuel assemblies. From a criticality standpoint, the 32PTH1 DSC is identical to the 32PTH DSC for all conditions of loading, transfer and storage.

The design basis models for the 32PTH1 DSC employ a more conservative representation of the basket where the basic egg-crate section is modeled with a height of 13.48 inches (poison + 1.75 inches steel) instead of 15.03 inches (poison + 1.75 inches steel). This results in a slightly lower amount of poison in the axial direction for the 32PTH1 DSC model. Further, the basket periphery of the 32PTH1 DSC is modeled with solid aluminum, while the 32PTH DSC periphery contains a mixture of aluminum, steel and water, which results in a slightly higher reactivity for the 32PTH1 model. Due to these modeling differences, the most reactive damaged configuration for the WE 17x17 class fuel assemblies at 2800 ppm boron concentration is due to optimum pitch based on the 32PTH1 model while that at other boron concentrations is due to double shear for the 32PTH model. This results in a conservative calculation of the k_{eff} at 2800 ppm.

The maximum allowable enrichment for each fuel assembly class as a function of basket type and soluble boron concentration for the 32PTH1 DSC is shown in Table U.6-3 of Appendix U.6 of reference [10] for intact fuel assemblies and Table U.6-4 of Appendix U.6 of reference [10] for damaged fuel assemblies. The maximum allowable enrichment for each fuel assembly class as a function of basket type and soluble boron concentration for the 32PTH DSC is calculated to be higher than those for the 32PTH1 DSC as shown in Table 6-1 for both intact and damaged fuel assemblies. This indicates that the reactivity of the 32PTH1 model is higher than that of the 32PTH model and therefore provides the justification that this model is applicable and conservative.

6.4.2.1 Most Reactive Fuel Assembly and Assembly Position Studies

The first series of analyses determines the most reactive fuel assembly design and the most reactive fuel positioning within the steel tubes. The first KENO run models the fuel assemblies as being centered within the basket compartment tubes. The off-center fuel assembly positioning is modeled by shifting all the fuel assemblies radially inward such that the fuel pins come in contact with the two faces of the compartment tubes. This is “inward” positioning and the fuel assemblies are at the closest approach relative to the center of the basket.

These calculations are repeated for all four fuel assembly classes listed in Table 6-3. These runs are carried out at nominal compartment dimensions with varying internal moderator density assuming a Type B basket and fuel at 4.30 wt. % U-235 and a boron concentration of 2500 ppm. The CE 16x16 calculations are carried out at an enrichment of 4.25 wt. % U-235, a fixed poison loading of 18.75 mg B-10/cm². All input and output files are included on the attached compact disk. In all other respects, the model is the same as that described in Sections 6.3.1 and 6.3.2. The 2D KENO plots are shown in Figure 6-12 and Figure 6-13 and the results are shown in Table 6-10.

The peripheral rails were not modeled for these calculations. The rail material was assumed to be completely replaced by the internal moderator (borated water at 2500 ppm). This assumption does not affect this parametric study. For the CE 16x16 calculations, the rail structure was modeled with solid aluminum. The rail structure was also modeled with solid aluminum for all assembly classes at 2800 ppm soluble boron.

The most reactive fuel assembly design is the WE 17x17 standard fuel assembly for the WE 17x17 class, the WE 15x15 standard fuel assembly for the WE 15x15 class, the CE 16x16 System 80 fuel assembly for the CE 16x16 class and the CE 14x14 Fort Calhoun Fuel assembly for the CE 14x14 class of fuel assemblies. The “inward” positioning of fuel assemblies is most reactive.

Table 6-41 presents the results of the criticality analysis performed for the WE 15x15 standard fuel with fuel OD of 0.3669”, and guide tube OD of 0.546” and ID of 0.512”, and fuel OD of 0.3659”, and guide tube OD of 0.546” and ID of 0.512”, for intact fuel with and without BPRAs, and damaged fuels with BPRAs. These results, in comparison with the design basis intact and damaged fuel analysis performed for standard fuel, with fuel OD of 0.3669”, guide tube OD of 0.545” and ID of 0.510”, with and without BPRAs demonstrate that the reactivity differences between the additional dimension combinations for the standard fuel and the design basis fuel are statistically insignificant, and standard fuel with the two additional dimension combinations are acceptable as reload fuel.

The results in Table 6-42 presented for the WE 15x15 OFA fuel with fuel OD of 0.3659” and guide tube OD of 0.533” and ID of 0.499” also demonstrate that the OFA fuel is acceptable as reload fuel.

6.4.2.2 Determination of the Most Reactive Configuration

The fuel loading configuration of the canister/cask affects the reactivity of the package. Several series of analyses determined the most reactive configuration for the canister/cask.

For this analysis, the most reactive fuel type is used to determine the most reactive configuration. The canister/cask is modeled, with the WE 17x17 standard assembly, over a 15.03-inch axial section with periodic axial boundary conditions and reflective radial boundary conditions. This represents an infinite array in the x-y direction of canister/casks that are infinite in length, which is conservative for criticality analysis. The starting model is identical to the model used above. The canister/cask model for this evaluation differs from the actual design in the following ways:

- The boron 10 content in the poison plates is 10% lower than the minimum required,
- The stainless steel and aluminum basket rails, which provide support to the fuel compartment grid, are modeled using a homogenized material and,

- The neutron shield and the skin of the cask are conservatively replaced with water between the casks.

Each evaluation is performed at various internal moderator density (IMD) values to determine the optimum moderator density where the reactivity is maximized. All input and output files are included on the attached compact disk.

The first set of analyses determines the effect of rail material composition variation on the reactivity of the basket. The most reactive configuration from the previous section is utilized as the base case for this evaluation. Four different variations in the rail material compositions are considered in this evaluation. The previous evaluation utilized borated water as the rail material. In this evaluation, the rail materials used are unborated water at 100% density, composition 3 (30% water, 35% aluminum, 35% ss304 by volume), composition 4 (40% water, 30% aluminum, 30% ss304 by volume) and composition 5 (50% water, 25% aluminum, 25% ss304 by volume). The rails are also modeled discretely based on the detailed model, as shown in Figure 6-11, for a comparison of the results.

Based on the actual volume fraction of rail materials, it is expected that the volume of water does not go below 30%. Also, such a variation (composition 3 through 5) adequately accounts for the fabrication tolerances associated with the rail materials. The results of this evaluation are shown in Table 6-11 including the most reactive results from the previous study and the results based on the detailed model. These results indicate that the most reactive rail composition is the one based on composition 3. The results also indicate that the change in k_{eff} due to variation in composition is statistically insignificant. The comparison of k_{eff} results with composition 3 and detailed model indicates that the simplified model (based on homogenous rail) is both adequate and conservative. Therefore, for the rest of the calculation, the rail assemblies will be modeled with a homogenous rail assumption with the material based on composition 3.

The next set of calculations determines the effect of variation in the poison plate thickness in the reactivity of the system. The poison plate thickness is varied from a maximum of 0.187 inches (for the Type D basket) to a minimum of 0.050 inches (for the Type A basket) based on a poison loading of 15.0 mg B-10/cm² (Borated Aluminum poison, Type B basket loading). Even though, this large variation in thickness is not expected for a single basket type, these calculations are intended to demonstrate that the effect of variation is statistically insignificant. The variation in the poison plate thickness also results in a compensatory variation in the aluminum plate thickness in order to maintain the total thickness of 0.25 inches. Therefore, the study also indirectly evaluates the effect of variation in the aluminum plate thickness. The results of these calculations are shown in Table 6-12 along with the most reactive results from the previous evaluation.

The results of this evaluation indicate that the effect of variation in the poison plate thickness is statistically insignificant and that the maximum k_{eff} values at all plate thicknesses are about the same. As stated above, the variation in the thickness considered in this evaluation is not expected to represent physical reality; however, the results demonstrate that within the tolerance band for the thicknesses of various basket types, the variation in k_{eff} is statistically insignificant.

These results also indicate that there would be no significant effect on k_{eff} due to the presence of aluminum cladding Boral[®] poison because this study also evaluates the effect of aluminum plate thickness.

The next set of analyses determines the effect of fuel compartment size on the system reactivity. The model starts with the most reactive geometry determined from the previous study. For this evaluation, the compartment size is varied from 8.650 inches (square) to 8.750 inches (square). These results are shown in Table 6-13. These results indicate that the most reactive configuration is with the minimum fuel compartment size because the assembly-to-assembly pitch is minimized.

The next set of analyses determines the effect of fuel compartment box thickness on the system reactivity. The model starts with the minimum fuel compartment width from the previous study and the compartment thickness is varied from 0.1775 inches to 0.2325 inches. The results in Table 6-14 show that the most reactive calculated condition occurs with nominal compartment box thickness. The results indicate that the system reactivity is not very sensitive to the box thickness and that the difference in k_{eff} between the nominal and minimum thickness cases is within statistical uncertainty. The balance of this evaluation uses the nominal box thickness because it represents the most reactive configuration from this study.

For the CE 16x16 models, as discussed in Section 6.4.2.1, the basket transition rails are modeled, conservatively, with solid aluminum. The 2800 ppm soluble boron evaluations for all assembly classes also conservatively model the basket transition rails with solid aluminum. This is conservative because the presence of aluminum allows for the neutrons to scatter through to the adjacent cask and interact with the fuel rather than being absorbed in the water/steel mixture. Another difference is that the basket is modeled with a section height of 13.48 in. instead of 15.03 in. This modeling feature is also slightly conservative because this results in a slight reduction in the amount of poison per unit length of the basket. In addition, other minor differences that are expected to have no significant impact on criticality are listed below:

- the inner shell radius is modeled as 34.5 in. instead of 35 in.
- the TC/DSC gap is modeled as 0.37 in instead of 0.50 in.
- the inner shell thickness is modeled as 0.63 in. instead of 0.50 in.

6.4.2.3 Determination of Maximum Initial Enrichment for Intact Assemblies

The most reactive configuration determined based on parametric studies is with the rail structure represented with Composition 3, poison and aluminum plates at nominal thickness, fuel compartment at minimum width and nominal thickness and the fuel assemblies positioned in the “inward” position. The following analysis uses this configuration to determine the maximum allowable initial enrichment as a function of poison plate loading and soluble boron concentration for the three (WE 17x17, WE 15x15 and CE 14x14) fuel assembly classes. For the CE 16x16 fuel assembly class, the model with solid aluminum rails described above is utilized. The 2800 ppm soluble boron evaluations for all assembly classes also utilize the solid aluminum rails in their models. Only the fuel assembly type, the fixed and soluble poison loading is changed for each model. In addition, the internal moderator density is varied to determine the peak reactivity for the specific configuration.

The canister / cask model for this evaluation differs from the actual design in the following ways:

- the boron-10 content in the borated aluminum poison plates is 10% lower than the minimum required and the boron-10 content in the Boral[®] poison plates is 25% lower than the minimum required
- the neutron shield and the skin of the cask are conservatively replaced with water between the casks, and
- the worst case geometry and material conditions, as determined in the previous sections, are modeled.

Five different fixed poison loadings are analyzed in the criticality calculations as described in Section 6.3, corresponding to the five different types of basket based on fixed poison loading (Type A, B, C, D and E). Five different soluble boron concentration levels are analyzed: 2000 ppm, 2300 ppm, 2400 ppm, 2500 ppm, and 2800 ppm. The maximum analyzed initial enrichment is 5.0 wt. % U-235. The calculational models for the 2800 ppm soluble boron cases for all assembly classes are directly obtained from Chapter U.6 of [10].

Calculations are also performed with the presence of BPRAs (bounding for all CCs) in the guide tubes to determine the maximum allowable enrichment for the WE 15x15 and WE 17x17 fuel assembly classes with CCs. These calculations are applicable to intact fuel assemblies only. Reconstituted fuel assemblies, where the fuel pins are replaced by non-fuel pins are also considered intact fuel assemblies provided they displace the same amount of moderator. The CE 14x14 and CE 16x16 fuel assembly classes are evaluated separately with and without BPRAs.

CE 14x14 Class Assemblies

The most reactive CE 14x14 class assembly is the CE 14x14 Fort Calhoun type fuel assembly with the larger fuel pellet OD. The results for the CE 14x14 class of fuel assemblies without BPRAs are shown in Table 6-33. The results for CE 14x14 class of fuel assemblies with BPRAs are shown in Table 6-34. These results indicate that the presence of BPRAs increases the reactivity of the system and consequently a reduction in the allowable enrichment.

WE 15x15 Class Assemblies

The most reactive WE 15x15 class assembly is the WE 15x15 standard fuel assembly. The results for the WE 15x15 class of fuel assemblies without BPRAs are shown in Table 6-15. The results for WE 15x15 class of fuel assemblies with BPRAs are shown in Table 6-16. These results indicate that the presence of BPRAs increases the reactivity of the system and consequently a reduction in the allowable enrichment.

WE 17x17 Class Assemblies

The most reactive WE 17x17 class assembly is the WE 17x17 standard fuel assembly. The results for the WE 17x17 class of fuel assemblies without BPRAs are shown in Table 6-17. The results for WE 17x17 class of fuel assemblies with BPRAs are shown in Table 6-18. These results also indicate that the presence of BPRAs increases the reactivity of the system and consequently a reduction in the allowable enrichment. For calculations with Type C basket, the WE 17x17 assembly results are conservatively applied to WE 15x15 assembly.

CE 16x16 Class Assemblies

The most reactive CE 16x16 class assembly is the CE 16x16 System 80 type fuel assembly with the larger fuel pellet OD. The results for the CE 16x16 class of fuel assemblies without BPRAs are shown in Table 6-35. The results for the CE 16x16 class of fuel assemblies with BPRAs are shown in Table 6-36. These results indicate that the presence of BPRAs increases the reactivity of the system and consequently a reduction in the allowable enrichment.

6.4.2.4 Determination of the Most Reactive Damaged Fuel Configuration

There are several mechanisms by which a fuel rod may be breached. These mechanisms may occur while the fuel is loaded in the reactor core, in the spent fuel pool, during transport, while in temporary dry storage, and while in permanent dry storage. In addition, the type and extent of fuel rod breach can be broken down into several categories. For this calculation, the method by which the fuel rod is breached is not as important as the extent of the resultant damage. The worst case gross damage resulting from a cask drop accident is assumed to be either a single-ended or double-ended rod shear with moderator intrusion. The bent or bowed fuel rod cases assume that the fuel is intact but not in its nominal fuel rod pitch. It is possible that the fuel rods may be crushed inwards or bowed outwards to a certain degree. Therefore, this will be evaluated by varying the fuel rod pitch from a minimum pitch (based on clad OD) to a maximum based on the fuel compartment size for each fuel assembly class. All pitch variations assume a uniform rod pitch throughout the entire fuel matrix.

The single-ended fuel rod shear cases assume that a fuel rod shears in one place and is displaced to a new location. The fuel pellets are assumed to remain in the fuel rod. This case will be evaluated by displacing one row of rods from the base fuel assembly matrix at small increments towards the side of the fuel compartment. The base fuel assembly matrix will be at nominal pitch and positioned in the “inward” position within the 32PTH DSC to maximize the separation distance between the fuel array and the sheared row of fuel rods. A smaller rod pitch for the base fuel assembly matrix was not chosen because it has been shown from the pitch cases that decreasing the rod pitch decreases reactivity. Increasing the base fuel assembly rod pitch will increase reactivity, however, the resulting model is similar to and is bounded by the rod pitch varying cases presented above and therefore will not be duplicated here. The single shear cases are analyzed for the two fuel assembly classes.

The double-ended fuel rod shear cases assume that the fuel rod shears in two places and the intact fuel rod piece is separated from the parent fuel rod. Three resulting conditions are exhibited by the occurrence of a double-ended rod shear. These are, the fuel rod piece can remain in place, it can be displaced in the same plane, or it can be displaced to a different plane. The “remain in place” situation results in no deviation from the base fuel assembly matrix, and is therefore considered trivial and will not be evaluated separately. The fuel rod piece displaced in the same plane is equivalent to the single-ended rod shear case discussed above and will not be reevaluated in these cases. The fuel rod piece displaced in a different plane results in two possibilities: an added rod or a removed rod. As in the single-ended shear cases, the base fuel assembly matrix will be positioned in the “inward” position of the 32PTH DSC to allow room for a row of displaced fuel rods. One row of fuel rods of different lengths will be removed from a section of the assembly and added to another to determine if the system exhibits any trends.

The nominal rod pitch is used for the base fuel matrix just as in the single-ended shear rod cases. The two fuel assembly classes are analyzed for the double-ended shear configuration.

In order to determine the effect of an axial shift in the fuel assemblies beyond the poison during transfer, bounding calculations that consider a 4" axial shift of fuel assemblies are performed. The nominal rod pitch is used for these cases and both the fuel assembly classes are analyzed for this configuration.

The first step is to determine the most reactive damaged fuel assembly geometry. This was completed using limiting fixed poison loading, soluble boron concentration and assembly enrichment for the various fuel assembly classes. The limiting parameters used for this study are shown in Table 6-19. All 32 assembly locations were filled with damaged fuel assemblies. The intent of these calculations was to determine the most reactive geometry, not to meet the USL. The following is a breakdown of runs made in this analysis:

- Optimum Rod Pitch Study (for fuel assemblies and rod storage baskets).
- Single-ended Shear Study.
- Double-ended Shear Study.
- Shifting of fuel assemblies beyond (4 inches above) the poison sheet height.

With the selection of the most reactive damaged fuel assembly geometry, the next set of analyses determined the maximum k_{eff} for various damaged fuel assembly loading configurations in the NUHOMS[®] 32PTH DSC. The most reactive damaged fuel assembly geometry for each fuel assembly class determined will be used to determine the maximum enrichment as a function of fixed poison loading and soluble boron concentration for loading 32 damaged fuel assemblies in the basket. In other words, cases are analyzed for all the configurations described in Table 6-1.

Rod Pitch Study:

The first set of damaged fuel analyses involved a study on the effect of the fuel rod pitch on system reactivity. KENO models with rod pitches ranging from a minimum corresponding to the clad OD to a maximum limited by the fuel compartment size are developed for each fuel assembly class. The results of the rod pitch study are shown in Table 6-20.

This study also bounds damaged fuel configurations with missing rods. A separate study to determine the effect on reactivity due to removal of fuel rods at optimum pitch is not necessary due to the presence of soluble boron in the moderator. The removal of fuel rods would ensure that the fissile fuel rods are replaced with boron poison and would result in a reduction in k_{eff} . Therefore, the rod pitch study is completed by determining the optimum pitch and the associated maximum k_{eff} at optimum moderator density. The 2D KENO plot for the CE 14x14 fuel assembly (without BPRAs) is shown in Figure 6-14. The 2D KENO plot for the CE 16x16 fuel assembly (with BPRAs) is shown in Figure 6-20.

Single Ended Rod Shear Study:

The next set of analyses performed is for the Single-ended rod shear. The Single-ended rod shear study depicts the fuel assembly with its last row of rods separated from the rest of the assembly. The displacement of the sheared row of rods varies radially from fuel assembly up to a maximum that is governed by the fuel assembly width and the fuel compartment size.

To model this in KENO, the base case was slightly modified. First, for a given fuel lattice, the fuel assemblies are modeled as a XX by (XX-1) array where XX corresponds to the fuel assembly class. For example, the WE 15 fuel assembly is modeled as a 15x14 array. Unit 200 is a XX by 1 array comprising of the single sheared row of rods. The units 201, 204, 211 and 214, therefore consist of two arrays, the array describing the truncated fuel assembly and the sheared row of fuel rods. The displaced row of rod array is then shifted (separation distance is “d”) away from the fuel assembly. The amount of fuel remains the same, i.e. no new fuel is added to the system. Nominal rod pitch for all of the fuel assembly classes is used for the base XX by (XX-1) fuel assembly. In the cask drop accident scenarios, it is more likely that the fuel assembly will be crushed as a result of the drop and therefore cause local decreases in the rod pitch of the assembly. However, the rod pitch studies outlined above show that a decrease in the fuel rod pitch results in a decrease in system reactivity, therefore for the single-ended rod shear study runs, rod pitch is modeled at nominal value. The study is repeated for all the fuel assembly classes and at varying moderator density for important separation distances. An example plot of a single ended shear configuration with WE 17x17 fuel assembly is shown in Figure 6-15. The results of this evaluation are shown in Table 6-21. The results indicate that there exists an optimum shear row separation distance for each class of fuel assembly where the reactivity is highest.

Double Ended Rod Shear Study:

The three Double-ended Rod Shear cases model a row (XX by 1 array) of dislocated rods severed at different sections axially and then displacing to other sections of the DSC in order to define a conservative bounding condition for fuel rod location subsequent to a double-ended rod shear. To model this in KENO, the base case was accordingly modified. A new KENO unit, UNIT 11 forms one axial section of the basket that models the un-sheared fuel assemblies. The sheared fuel assemblies depleted by one row of fuel rods are modeled as a XX by (XX-1) array where XX corresponds to the fuel assembly class. The corresponding KENO units for the fuel assembly positions are 301, 304, 311, 314, 302, 303, 305 and 312. The unit 12 forms the axial section of the basket that models this depleted array of fuel assemblies. The fuel assemblies that contain the sheared-migrated row of fuel rods are modeled as a XX by (XX+1) array where XX corresponds to the fuel assembly class. The corresponding KENO units for the fuel assembly positions are 401, 404, 411 414, 402, 403, 405 and 412. The unit 13 forms the axial section of the basket that models this depleted array of fuel assemblies. Depending on the fraction of double shear, the array 11 (an axial array of units 11, 12 and 13) is constructed to calculate the reactivity effect. Due to the height of a single axial segment (15.03"), the total axial height of the model for these studies is 150.30" (15.03*10). However, periodic axial boundary conditions are applied making the model essentially infinite. The same rod pitch assumptions made for the Single-ended Shear runs also apply here.

Basically three types of double ended shear studies are evaluated. The first is a half shear where the sheared row breaks into two equal sections resulting in one-half of the fuel assembly being defined by a rod array containing an extra row of fuel rods while the other half is defined by an array depleted by one row of fuel rods. The half shear is represented in this calculation as a $(5/10)^{\text{th}}$ shear. The second is a one-third shear where the sheared row breaks into two unequal sections measuring a third of the fuel assembly length and two-third of the fuel assembly length respectively. Therefore, the fuel assembly can be defined by three axially equal sections, one with a regular array of fuel rods, one with an extra row of fuel rods and the other with a depleted row of fuel rods. This is modeled as $(3/10)^{\text{th}}$ which is about the same as one-third. The same mechanism can be extended to other shear ratios but the effect on reactivity is expected to reduce with reduction in the shear ratio. The one-fifth shear is also analyzed in this study as $(2/10)^{\text{th}}$ shear. The internal moderator density is varied to determine the k_{eff} at optimum density.

Results of the double-ended rod shear study show that the movement of one exterior row of half of the fuel assembly length is the most reactive. The CE 14x14 and CE 16x16 fuel is only evaluated for the half shear condition since the evaluation results show this is the most reactive. An example plot of a double ended shear configuration with WE 15x15 fuel assembly is shown in Figure 6-16. The results of the evaluation are shown Table 6-22.

Shifting of Fuel Beyond Fixed Poison:

This study analyzes the effect of shifting of loose rods beyond the height of the poison plates. Two types of shifting of fuel rods beyond the poison plates are analyzed in this study. The first calculational model assumes that a four-inch axial section of the entire fuel assembly shifts beyond the poison plates. The height of the axial shift, four-inches, is more than the maximum difference between the basket height and the canister cavity height (about 2.5 inches). The second calculational model involves a shifting of 8 of the outermost rows of fuel rods (basically two concentric rings of fuel rods) beyond the poison plates by six inches. In KENO, this six-inch section is modeled like a regular fuel assembly with fuel pins defining the 8 outer most rows (and columns) with aluminum occupying the space in the middle. This is done to simulate the sliding of fuel rods around the inlet or outlet nozzle during an accident. These models conservatively bound all the cases associated with the shifting of fuel rods beyond poison like sliding of a single rod, sliding of a row of single sheared rods etc.

To model these in KENO, the base case was modified. First, a new KENO unit, UNIT 11 forms one axial section of the basket that models the fuel assemblies covered with poison. For the shifting of fuel assemblies (first model), a four-inch axial section of the fuel assemblies containing the uncovered fuel assemblies are modeled with the KENO units 301, 304, 311 and 314. The unit 12 forms the axial section of the basket that models this uncovered section of fuel assemblies. Finally, the array 11 (an axial array of units 11 and 12) is constructed to calculate the reactivity effect. Periodic axial boundary conditions are utilized to make this model essentially infinite in length. For the sliding of fuel assemblies (second model), a six-inch axial section of the fuel assemblies containing the eight uncovered rows of fuel rods with aluminum in the middle portion are modeled with the KENO units 301, 304, 311 and 314. The unit 12 forms the axial section of the basket that models this uncovered section of fuel assemblies. Finally, the

array 11 (an axial array of units 11 and 12) is constructed to calculate the reactivity effect. Periodic axial boundary conditions are utilized to make this model essentially infinite in length. This study is performed for the two fuel assembly classes with varying moderator density. Since the four-inch shift configuration is always found to be more reactive than the six-inch slide configuration, only the four-inch shift configuration was evaluated for the CE 16x16 fuel assembly class.

The results of these evaluations are shown in Table 6-23. An example plot of a shifting configuration with WE 17x17 fuel assembly is shown in Figure 6-17. An example plot of a sliding configuration with WE 15x15 fuel assembly is shown in Figure 6-18.

6.4.2.5 Determination of the Most Reactive Damaged Fuel Assembly Configuration

The fuel-loading configuration of the canister/cask affects the reactivity of the package. Several series of analyses performed in the previous sections evaluated the various damaged fuel assembly configurations. A comparison of the maximum k_{eff} due to the various damaged fuel assembly configurations is shown in Table 6-24. The most reactive damaged fuel assembly configuration for the CE 14x14 and CE 16x16 fuel is the optimum pitch configuration of the rods.

For the CE 14x14 fuel assembly class, the optimum pitch was calculated to be 0.620 in. For the CE 16x16 fuel assembly class, the optimum pitch was calculated to be 0.545 in. For the WE 15x15 and WE 17x17 fuel classes, the double ended rod shear is the most reactive damaged fuel assembly configuration, with the exception of the WE 17x17 assemblies modeled at 2800 ppm. The most reactive damaged configuration modeled on the WE 17x17 class at 2800 ppm is based on the sensitivity calculations documented in Appendix U.6 of [10]. The WE 17x17 models at 2800 ppm soluble boron were modeled using the more conservative solid aluminum rail structure and their most reactive damaged configuration is the optimum pitch of 0.5125 in. The maximum k_{eff} for the optimum pitch WE 17x17 damaged assemblies at 2800 ppm is less than the maximum k_{eff} of all other WE 17x17 double ended shear cases, and therefore, provides for additional margin.

Additionally, the one-half (5/10) double-ended shear configuration is modified to include BPRAs to obtain a bounding damaged assembly configuration. The results of this evaluation, shown in Table 6-25, demonstrate that the configuration with BPRAs is bounding. Therefore, this configuration is the design basis configuration for the WE 15x15 and WE 17x17 fuel assembly classes and will be utilized to determine the k_{eff} of the NUHOMS[®]-32PTH DSC containing damaged fuel assemblies. An example plot of a double ended shear configuration with WE 15x15 fuel assembly with BPRAs is shown in Figure 6-19.

6.4.2.6 Determination of Maximum Initial Enrichment for Damaged Fuel Assemblies

The most reactive damaged fuel assembly configuration for the WE 15x15 and WE 17x17 fuel is based on the double-ended shear model with a shear ratio of one-half with BPRAs while the most reactive damaged assembly configuration for the CE 14x14 and CE 16x16 fuel is based on an optimum pitch arrangement of rods. The following analysis uses these configurations to determine the maximum allowable initial enrichment as a function of poison plate loading and

soluble boron concentration for all the fuel assembly classes. The analysis is carried out with the NUHOMS[®]-32PTH DSC containing 32 design basis damaged fuel assemblies. Only the fuel assembly type, the fixed and soluble poison loading is changed for each model. In addition, the internal moderator density is varied to determine the peak reactivity for the specific configuration. All calculations for the WE 15x15 and WE 17x17 fuel are performed with the presence of BPRAs (bounding for all CC and no CC cases) in the guide tubes to determine the maximum allowable enrichment for these two fuel assembly classes with and without CCs. The CE 14x14 and CE 16x16 fuel assembly classes are evaluated separately with and without BPRAs. For ease of modeling the guide tubes and BPRAs are modeled as cuboids with an equivalent area rather than cylinders.

The canister / cask model for this evaluation differs from the actual design in the following ways:

- the boron-10 content in the borated aluminum poison plates is 10% lower than the minimum required and the boron-10 content in the Boral[®] poison plates is 25% lower than the minimum required
- the neutron shield and the skin of the cask are conservatively replaced with water between the casks, and
- the worst case geometry and material conditions as determined in Section 6.4.2.2 and the worst case damaged fuel assembly configuration as determined in Section 6.4.2.5, are modeled.

Five different fixed poison loadings are analyzed in the criticality calculations as described in Section 4.2, corresponding to the four different types of basket based on fixed poison loading (Type A, B, C, D and E). Five different soluble boron concentration levels are analyzed - 2000 ppm, 2300 ppm, 2400 ppm, 2500 ppm, and 2800 ppm. The maximum analyzed initial enrichment is 5.0 wt. % U-235. The calculational models for the 2800 ppm soluble boron cases for all assembly classes are directly obtained from Chapter U.6 of [10].

CE 14x14 Class Assemblies

The most reactive CE 14x14 class assembly is the CE 14x14 Ft. Calhoun fuel assembly. The results for CE 14x14 class of fuel assemblies without BPRAs are shown in Table 6-37. The results for the CE 14x14 class of fuel assemblies with BPRAs are shown in Table 6-38.

CE 16x16 Class Assemblies

The most reactive CE 16x16 class assembly is the CE 16x16 System 80 fuel assembly. The results for CE 16x16 class of fuel assemblies without BPRAs are shown in Table 6-39. The results for the CE 16x16 class of fuel assemblies with BPRAs are shown in Table 6-40.

WE 15x15 Class Assemblies

The most reactive WE 15x15 class assembly is the WE 15x15 standard fuel assembly. The results for WE 15x15 class of fuel assemblies with BPRAs are shown in Table 6-26. For calculations with Type C basket, the WE 17x17 assembly results are conservatively applied to the WE 15x15 assembly.

WE 17x17 Class Assemblies

The most reactive WE 17x17 class assembly is the WE 17x17 standard fuel assembly. The results for the WE 17x17 class of fuel assemblies with BPRAs are shown in Table 6-27.

6.4.3 Criticality Results

This section presents the results of the analyses used to demonstrate the acceptability of storing qualified fuel in the 32PTH DSC under normal, off-normal, and accident conditions for fuel loading, handling, and storage.

Table 6-28 lists the bounding results for intact fuel assemblies for all conditions of storage. The highest calculated k_{eff} , including 2σ uncertainty, is for the CE 16x16 class fuel assembly with an initial enrichment of 4.80 wt. % U-235, 2000 ppm soluble boron and a poison loading of 28.8 mg B-10/cm² (Type D Basket) without BPRAs. The maximum allowable initial enrichment with BPRAs for the WE 15x15 and WE 17x17 (bounding for cases without BPRAs) fuel assembly types and with and without BPRAs for the CE 14x14 and CE 16x16 fuel assembly type as a function of fixed poison loading and soluble boron concentration is given in Table 6-1. The input files for the cases with the highest calculated reactivity (with and without BPRAs) are included in the Appendix A.

Table 6-29 lists the bounding results for damaged fuel assemblies for all conditions of storage. The highest calculated k_{eff} , including 2σ uncertainty for the damaged assembly calculations, is 0.9402 and it occurs for the WE 17x17 Standard fuel assembly with an initial enrichment of 4.80 wt. % U-235, 2400 ppm soluble boron and a poison loading of 50.0 mg B-10/cm² (Type E Basket). The maximum allowable initial enrichment with BPRAs for the WE 15x15 and WE 17x17 (bounding for cases without BPRAs) fuel assembly types and without BPRAs for the CE 14x14 fuel assembly type as a function of fixed poison loading and soluble boron concentration is given in Table 6-1.

The effect on criticality due to the addition of an ITTR to a WE 15x15 and WE 17x17 class fuel assembly is equivalent to the addition of a mild neutron absorber material (steel) which will cause a slight reduction in reactivity. An ITTR also displaces a small amount of moderator which has been credited in the criticality analysis.

Multiple representative cases were chosen for WE 15x15 and WE 17x17 class fuel assemblies (damaged and intact) for performing the criticality analysis with ITTRs added to the model. The ITTR is modeled both as a solid stainless steel rod and as an annular stainless steel rod inserted in the instrument tube to determine the sensitivity of the system due to displacement of borated water. This evaluation uses identical methodology and assumptions as described above in Sections 6.4.1 and 6.4.2.

The results of these evaluations are shown in Table 6-43 and Table 6-44. These results indicate that the effect on criticality due to the addition of an ITTR is statistically insignificant with a small reduction in the maximum calculated k_{eff} .

ANS/ANSI-8.1 [5] recommends that calculational methods used in determining criticality safety limits for applications outside reactors be validated by comparison with appropriate critical experiments. An Upper Subcritical Limit (USL) provides a high degree of confidence that a given system is subcritical if a criticality calculation based on the system yields a k_{eff} below the USL.

The criterion for subcriticality is that

$$k_{\text{KENO}} + 2\sigma_{\text{KENO}} \leq \text{USL},$$

Where USL is the upper subcritical limit established by an analysis of benchmark criticality experiments. In Section 6.5, the minimum USL over the parameter range is determined to be 0.9419. From Table 6-28 and Table 6-29, for the most reactive case,

$$k_{\text{KENO}} + 2\sigma_{\text{KENO}} = 0.9391 + 2(0.0008) = 0.9407 \leq 0.9419.$$

This indicates that the fuel will remain subcritical. Conclusions regarding specific aspects of the methods used or the analyses presented can be drawn from the quantitative results presented in the associated tables.

6.5 Critical Benchmark Experiments

The criticality safety analysis of the NUHOMS[®] OS 187H TC containing the NUHOMS[®] - 32PTH DSC uses the CSAS25 module of the SCALE system of codes. The CSAS25 control module allows simplified data input to the functional modules BONAMI-S, NITAWL-II, and KENO V.a. These modules process the required cross-section data and calculate the k_{eff} of the system. BONAMI-S performs resonance self-shielding calculations for nuclides that have Bondarenko data associated with their cross sections. NITAWL-II applies a Nordheim resonance self-shielding correction to nuclides having resonance parameters. Finally, KENO V.a calculates the effective neutron multiplication (k_{eff}) of a 3-D system.

The analysis presented herein uses the fresh fuel assumption for criticality analysis. The analysis employs the 44-group ENDF/B-V cross-section library because it has a small bias, as determined by 121 benchmark calculations. The Upper Subcritical Limit (USL-1) was determined using the results of these 121 benchmark calculations.

The benchmark problems used in this verification are representative of benchmarks of commercial light water reactor (LWR) fuels with the following characteristics:

- A. water moderation
- B. boron neutron absorbers
- C. unirradiated light water reactor type fuel (no fission products or “burnup credit”)
- D. close reflection
- E. near room temperature (vs. reactor operating temperature)
- F. Uranium oxide fuels.

Criticality codes are verified by comparing benchmark calculations to actual critical benchmark experiments. The difference between the calculated reactivity and the experimental reactivity is referred to as ‘calculational’ bias. This bias may be a function of system parameters such as fuel lattice separation, fuel enrichment, neutron absorber properties, reflector properties, or fuel/moderator volume ratio; or, there may be no specific correlation with system parameters. These experiments are discussed in detail in reference 6.

6.5.1 Benchmark Experiments and Applicability

The benchmark data used for determination of the USL is provided in Table 6.5-1. The set of criticality experiments used as benchmarks are representative of the composition, configuration, and nuclear characteristics of the system modeled. Six parameters were selected in order to demonstrate the applicability of the SCALE 44-group ENDF/B-V cross-section library for the range of conditions spanned by the calculation models. The results of these evaluations are provided in Table 6.5-2. Only those experiments with the parameter in question were used to determine the USL for that parameter. The methodology used to calculate the USL is based on NUREG/CR-6361 6, USL method 1.

USL-1 applies a statistical calculation of the bias and its uncertainty plus an administrative margin ($0.05 \Delta k$) to the linear fit of results of the experimental benchmark data developed. The

USL from the data set with the best correlation is used as the acceptance criteria for subsequent criticality evaluations. Since there was not a strong correlation for any of the data sets, i.e., the correlation was essentially random and the lowest possible USL-1 result was used as the USL.

The uncertainty due to modeling approximations does not impact the calculated k_{eff} . Worst case tolerances (as specified in the design drawings presented in Chapter 1) are used in the analysis to maximize k_{eff} . Only the tolerances of those dimensions that had a positive effect on k_{eff} were included in the SCALE geometry models.

6.5.2 Results of the Benchmark Calculations

A summary of all of the pertinent parameters for each experiment along with the results of each case is included in Table 6-30. The USL benchmark calculations are also shown in Table 6-30. The best correlation (linear regression correlation for each parameter vs. k_{eff}) is observed for fuel assembly separation distance, with a correlation of 0.656. All other parameters show much lower correlation ratios indicating no real correlation. All parameters were evaluated for trends and to determine the most conservative USL. Since there was no observable correlation, the worst case USL was selected for the identified parameters. Results from the USL evaluation are presented in Table 6-31.

The criticality evaluation presented here used the same cross section library, fuel materials and similar material/geometry options that were used in the 121 benchmark calculations as shown in Table 6-30. The modeling techniques and the applicable parameters for the actual criticality evaluations fall within the range of those addressed by the benchmarks in Table 6-31. The results from the comparisons of physical parameters of each of the fuel assembly types to the applicable USL value are presented in Table 6-32. The minimum value of the USL-1 was determined to be 0.9419 based on comparisons to the most limiting assembly parameters.

6.6 Supplemental Information

6.6.1 References

1. Title 10 Code of Federal Regulations, Part 72, "Licensing Requirements for the Independent Storage of Spent Nuclear Fuel and High-Level Radioactive Waste."
2. Not Used
3. "SCALE, A Modular Code System for Performing Standardized Computer Analyses for Licensing Evaluation," NUREG/CR-0200, Rev. 6 (ORNL/NUREG/CSD-2/R6), Vol. I-III, September 1998.
4. Not Used.
5. ANS/ANSI-8.1, American National Standard for Nuclear Criticality Safety in Operations with Fissionable Materials Outside Reactors, 1983.
6. Not Used.
7. Not Used.
8. Not Used.
9. Not Used.
10. Updated Final Safety Analysis Report for the Standardized NUHOMS[®] Horizontal Modular Storage System for Irradiated Nuclear Fuel, NUH-003, Rev. 12.

Proprietary Information on Pages 6-31 through 6-59
Withheld Pursuant to 10 CFR 2.390

Table 6-1
Maximum Planar Average Initial Enrichment for Intact and Damaged Fuel Loading

Assembly Class	Maximum Planar Average Initial Enrichment ⁽²⁾ of U-235 as a Function of Soluble Boron Concentration and Fixed Poison Loading (Basket Type)					
	Basket Type ⁽¹⁾	Minimum Soluble Boron Concentration				
		2000 ppm	2300 ppm	2400 ppm	2500 ppm	2800 ppm
CE 14x14 Intact Fuel Assembly (without CCs)	A	4.05	4.40	4.45	4.55	4.60
	B	4.55	4.90	5.00	5.00	5.00
	C	4.70	5.00	5.00	5.00	5.00
	D	5.00	5.00	5.00	5.00	5.00
	E	5.00	5.00	5.00	5.00	5.00
CE 14x14 Intact Fuel Assembly (with ⁽³⁾ CCs)	A	3.95	4.25	4.35	4.45	4.55
	B	4.35	4.70	4.80	4.90	5.00 ⁽⁴⁾
	C	4.50	4.85	5.00	5.00	5.00
	D	4.75	5.00	5.00	5.00	5.00
	E	5.00	5.00	5.00	5.00	5.00
CE 16x16 Intact Fuel Assembly (without CCs)	A	3.90	4.10	4.20	4.30	4.60
	B	4.30	4.60	4.70	4.80	5.00
	C	4.50	4.80	4.90	5.00	5.00
	D	4.80	5.00	5.00	5.00	5.00
	E	5.00	5.00	5.00	5.00	5.00
CE 16x16 Intact Fuel Assembly (with ⁽³⁾ CCs)	A	3.80	4.00	4.10	4.20	4.50
	B	4.20	4.50	4.60	4.70	5.00
	C	4.40	4.70	4.80	4.90	5.00
	D	4.70	4.90	5.00	5.00	5.00
	E	4.90	5.00	5.00	5.00	5.00
WE 15x15 Intact Fuel Assembly (with and without CCs)	A	3.50	3.70	3.80	3.90	4.05
	B	3.80	4.10	4.20	4.30	4.50
	C	3.95	4.25	4.35	4.45	4.70
	D	4.20	4.50	4.70	4.80	5.00
	E	4.50	4.80	4.90	5.00	5.00
WE 17x17 Intact Fuel Assembly (with and without CCs)	A	3.50	3.70	3.80	3.90	4.00
	B	3.80	4.10	4.20	4.30	4.45
	C	3.95	4.25	4.35	4.45	4.65
	D	4.20	4.50	4.60	4.70	4.95
	E	4.45	4.70	4.90	5.00	5.00

Table 6-1
Maximum Planar Average Initial Enrichment for Intact and Damaged Fuel Loading
(Concluded)

Assembly Class	Maximum Planar Average Initial Enrichment ⁽²⁾ of U-235 as a Function of Soluble Boron Concentration and Fixed Poison Loading (Basket Type)					
	Basket Type ⁽¹⁾	Minimum Soluble Boron Concentration				
		2000 ppm	2300 ppm	2400 ppm	2500 ppm	2800 ppm
CE 14x14 Damaged Fuel Assembly (without CCs)	A	3.90	4.20	4.25	4.35	4.40
	B	4.35	4.70	4.80	4.90	4.90
	C	4.50	4.85	4.95	5.00	5.00
	D	4.85	5.00	5.00	5.00	5.00
	E	5.00	5.00	5.00	5.00	5.00
CE 14x14 Damaged Fuel Assembly (with ⁽³⁾ CCs)	A	3.70	3.95	4.05	4.10	4.20
	B	4.10	4.40	4.50	4.60	4.65
	C	4.20	4.55	4.65	4.75	4.90
	D	4.50	4.85	5.00	5.00	5.00
	E	4.75	5.00	5.00	5.00	5.00
CE 16x16 Damaged Fuel Assembly (without CCs)	A	3.65	3.90	4.00	4.05	4.30
	B	4.05	4.30	4.40	4.50	4.80
	C	4.20	4.50	4.60	4.70	5.00
	D	4.50	4.80	4.90	5.00	5.00
	E	4.75	5.00	5.00	5.00	5.00
CE 16x16 Damaged Fuel Assembly (with ⁽³⁾ CCs)	A	3.60	3.80	3.90	4.00	4.20
	B	3.95	4.20	4.30	4.40	4.70
	C	4.10	4.40	4.50	4.60	4.90
	D	4.40	4.70	4.80	4.90	5.00 ⁽⁴⁾
	E	4.65	4.90	5.00	5.00	5.00
WE 15x15 Damaged Fuel Assembly (with and without CCs)	A	3.40	3.60	3.70	3.80	3.95
	B	3.75	4.00	4.10	4.20	4.35
	C	3.85	4.15	4.25	4.35	4.50
	D	4.10	4.40	4.50	4.60	4.80
	E	4.35	4.70	4.80	4.90	5.00
WE 17x17 Damaged Fuel Assembly (with and without CCs)	A	3.40	3.60	3.70	3.80	3.95
	B	3.75	4.00	4.10	4.20	4.35
	C	3.85	4.15	4.25	4.35	4.55
	D	4.10	4.40	4.50	4.60	4.80
	E	4.30	4.65	4.80	4.90	5.00

Notes:

1. The fixed poison loading requirements as a function of basket type is a function of Basket Type are specified in Table 6-7.
2. Linear interpolation is allowed between adjacent maximum planar average initial enrichments and soluble boron concentration levels.
3. Applicable for fuel assemblies with CCs that extend into the active fuel region. Refer to Section 6.2.
4. Represents a value that was not explicitly analyzed. Based on the trends seen in other fuel classes and poison types, the increase in boron concentration between poison types will allow for the loading up fuel up to 5.0 wt. %.

Table 6-2
Summary of Limiting Criticality Evaluations for all Fuel Assemblies

Limiting Assembly Position- The fuel assembly is located in the corner of each compartment tube closest to the 32PTH DSC centerline.				
CE 14x14 Fuel Assembly				
Case	K_{keno}	σ_{keno}	K_{eff}	USL
Intact Fuel - 90% IMD, Type B Basket (15.0 mg B-10/cm ²), 2300 ppm Boron, 4.7 wt. % U-235	0.9383	0.0009	0.9401	0.9419
Damaged Fuel – Optimum Pitch, 70% IMD Type B Basket (15.0 mg B-10/cm ²), 2400 ppm Boron, 4.8 wt. % U-235	0.9386	0.0007	0.9400	0.9419
WE 15x15 Fuel Assembly				
Case	K_{keno}	σ_{keno}	K_{eff}	USL
Intact Fuel - 80% IMD, With BPRA, Type C Basket (20.0 mg B-10/cm ²), 2800 ppm Boron, 4.7 wt. % U-235	0.9391	0.0007	0.9405	0.9419
Damaged Fuel - Double Ended Shear Full IMD, With BPRA, Type B Basket (15.0 mg B-10/cm ²), 2000 ppm Boron, 4.7 wt. % U-235	0.9372	0.0007	0.9386	0.9419
WE 17x17 Fuel Assembly				
Case	K_{keno}	σ_{keno}	K_{eff}	USL
Intact Fuel - 80% IMD, No BPRA, Type C Basket (20.0 mg B-10/cm ²), 2800 ppm Boron, 4.7 wt. % U-235 ⁽¹⁾	0.9391	0.0007	0.9405	0.9419
Damaged Fuel - Double Ended Shear Full IMD, With BPRA, Type E Basket (50.0 mg B-10/cm ²), 2400 ppm Boron, 4.8 wt. % U-235	0.9388	0.0007	0.9402	0.9419
CE 16x16 Fuel Assembly				
Case	K_{keno}	σ_{keno}	K_{eff}	USL
Intact Fuel, IMD 80% No BPRA, Type D Basket, 2000 ppm, 4.80 wt. %	0.9391	0.0008	0.9407	0.9419
Damaged Fuel, IMD 90% with BPRA Type E Basket, 2000 ppm Boron, 4.65 wt% U-235	0.9384	0.0007	0.9398	0.9419

Note:

- These cases were modeled as Westinghouse 17x17 RFA assemblies, which conservatively bound all Westinghouse 17x17 class assemblies that are authorized for loading.

Table 6-3
Authorized Contents for NUHOMS®-32PTH DSC

Assembly Type⁽¹⁾	Array/Class
Westinghouse 17x17 Standard (WE 17x17) Vantage 5H/OFA	17x17
Framatome ANP Advanced MK BW 17x17 (MK BW 17x17)	17x17
Westinghouse 15x15 Standard (WE 15x15) Westinghouse 15x15 Surry Improved (WES 15x15)	15x15
CE 14x14 Standard (CE 14x14)	14x14
CE 16x16 Standard/System 80 (CE 16x16)	16x16

(1) Equivalent reload fuel assemblies that are enveloped by the fuel assembly design characteristics listed above are also acceptable.

Table 6-4
Fuel Assembly Design Parameters for Criticality Analysis

Manufacturer⁽¹⁾	Array	Version	Active Fuel Length (inches)	# Fuel Rods per Assembly	Pitch (inches)	Fuel Pellet OD (inches)
Westinghouse	17x17	Standard Vantage	144	264	0.4960	0.3225
Westinghouse	17x17	OFA	144	264	0.4960	0.3088
Framatome	17x17	MK BW	144	264	0.4960	0.3195
Westinghouse	15x15 ⁽²⁾	Std / Surry	144	204	0.5630	0.3669
CE	14x14	Std	137	176	0.5800	0.3765
CE	14x14	Ft. Calhoun	128	176	0.5800	0.3815
CE	16x16	System 80	150	236	0.506	0.3255
CE	16x16	Standard	150	236	0.506	0.3255
Manufacturer⁽¹⁾	Array	Version	Clad Thickness (inches)	Clad OD (inches)	Guide Tube OD Inst. Tube OD (inches)	Guide Tube ID Inst. Tube ID (inches)
Westinghouse	17x17	Standard Vantage	0.0225	0.374	24 @ 0.4820 1 @ 0.4740	24 @ 0.4500 1 @ 0.4440
Westinghouse	17x17	OFA	0.0225	0.360	24 @ 0.4820 1 @ 0.4740	24 @ 0.4500 1 @ 0.4440
Framatome	17x17	MK BW	0.0225	0.374	24 @ 0.4820 1 @ 0.4820	24 @ 0.4500 1 @ 0.4500
Westinghouse	15x15 ⁽³⁾	Std / Surry	0.0243	0.422	20 @ 0.5450 1 @ 0.5450	20 @ 0.5100 1 @ 0.5100
CE	14x14	Std	0.0280	0.440	5 @ 1.115	5 @ 1.035
CE	14x14	Ft. Calhoun	0.0280	0.440	5 @ 1.115	5 @ 1.035
CE	16x16	System 80	0.0230	0.382	5@0.768	5@0.687
CE	16x16	Standard	0.0250	0.382	5@0.768	5@0.687

Note: All dimensions shown are nominal

- (1) Equivalent reload fuel assemblies that are enveloped by the fuel assembly design characteristics listed above are also acceptable.
- (2) STD and OFA fuel are also qualified with 0.3659" fuel pellet OD.
- (3) STD fuel with guide tube dimensions of 0.546" (OD) and 0.512" (ID) and OFA fuel with guide dimensions of 0.533" (OD) and 0.499" (ID) are also qualified.

Table 6-5
NUHOMS® -32PTH - Basket and DSC Dimensions

Parameter	Actual inches	Model inches (cm)
Compartment Inside (Nominal)	8.700	8.700 (22.0980)
Compartment Inside (Maximum)	8.750	8.750 (22.2250)
Compartment Inside (Minimum)	8.650	8.650 (21.9710)
Compartment wall (Nominal)	0.1875	0.1875 (0.47625)
Compartment wall (Maximum)	0.2325	0.2325 (0.59055)
Compartment wall (Minimum)	0.1775	0.1775 (0.45085)
Stainless steel strip height	1.75	1.75 (4.445)
Stainless steel strip thickness	0.50	0.50 (1.27)
Poison/Al plates height	13.18	13.18 (33.477)
Poison/Al plates thickness	0.50	0.50 (1.27)
horizontal gap	0.07	No Gap (replaced with Aluminum)
vertical slot width / height	1.00 / 5.75	No Slot (replaced with Aluminum)
DSC inside radius	34.375	34.500 (87.630)
DSC wall thickness	0.500	0.500 (1.270)

Table 6-6
NUHOMS® OS187H Transfer Cask Dimensions

Parameter	Actual	Model
DSC Shell Radius (OR)	34.875 inches	35.000 inches
Water Gap Radius	34.875" to 35.25"	35.000" to 35.375"
Inner Shell Radius (0.50" thick)	35.25" to 35.75"	35.375" to 35.875"
Gamma Shield Radius (3.56" thick)	35.75" to 39.31"	35.875" to 39.435"
Structural Shell Radius (1.50" thick)	39.31" to 40.81"	39.435" to 40.935"
Neutron Shield Radius (5.00" thick)	40.81" to 45.81"	Not modeled
Neutron Shield Skin Radius (0.188")	45.81" to 46.00"	Not modeled

Table 6-7
NUHOMS®-32PTH - Fixed Poison Loading Requirements

Basket Type	Borated Aluminum Loading	Boral® Loading
A	7.0 mg B-10/cm ² Thickness = 0.050"	9.0 mg B-10/cm ² Thickness = 0.075"
B	15.0 mg B-10/cm ² Thickness = 0.075"	19.0 mg B-10/cm ² Thickness = 0.075"
C	20.0 mg B-10/cm ² Thickness = 0.075"	25.0 mg B-10/cm ² Thickness = 0.075"
D	32.0 mg B-10/cm ² Thickness = 0.125"	Not Applicable
E	50.0 mg B-10/cm ² Thickness = 0.187"	Not Applicable

Note: New neutron absorbers or changes to existing absorbers will be qualified as per information provided in Chapter 9.

Table 6-8
Description of the Basic KENO Model Units

Geometry Units	Description
1	Fuel Pin Cell
2	Guide Tube
3	Instrument Tube
21 - 23	Basket Cells with Poison along the West Face of F/A
31 - 33	Basket Cells without Poison along North Face of F/A
41 - 43	Basket Cells without Poison along the East Face of F/A
51 - 53	Basket Cells with Poison along the South Face of F/A
25,35,45,55	Arrays that define the West, North, East and South Faces of the Basket Cell without fuel
61 - 63	Basket Cells without Poison along the West Face of F/A
71 - 73	Basket Cells without Poison along North Face of F/A
81 - 83	Basket Cells without Poison along the East Face of F/A
91 - 93	Basket Cells without Poison along the South Face of F/A
65,75,85,95	Arrays that define the West, North, East and South Faces of the Basket Cell without fuel and poison
201	Basket Cell with Fuel Assembly Positions 201, 202, 205, 206 representing the South West Interior Positions
204	Basket Cell with Fuel Assembly Positions 203, 204, 207, 208, 235, 236 representing the South East Positions
211	Basket Cell with Fuel Assembly Positions 211, 212, 215, 216, 231, 232 representing the North West Positions
214	Basket Cell with Fuel Assembly Positions 213, 214, 217, 218, 233, 234, 237, 238 representing the North East Positions
202	Basket Cell with Fuel Assembly Positions 225, 226 representing West Facing Corner (South West) Positions
203	Basket Cell with Fuel Assembly Positions 221, 222 representing South Facing Corner (South West) Positions
205	Basket Cell with Fuel Assembly Positions 223, 224 representing the South Facing Corner (South East) Positions
212	Basket Cell with Fuel Assembly Positions 227, 228 representing West Facing Corner (North West) Positions
241 - 245	Array of Basket Cells defining the outer 16 locations
245	Array of Basket Cells defining the inner 16 locations
10	Global Unit

Table 6-9
Material Property Data

Material	ID	Density g/cm ³	Element	Weight %	Atom Density (atoms/b-cm)
UO ₂ (Enrichment - 5.0 wt%)	1	10.686	U-235	4.407	1.20673E-03
			U-238	83.743	2.26382E-02
			O	11.850	4.76898E-02
Zircaloy-4	2	6.56	Zr	98.23	4.2541E-02
			Sn	1.45	4.8254E-04
			Fe	0.21	1.4856E-04
			Cr	0.10	7.5978E-05
			Hf	0.01	2.2133E-06
Water (Pellet Clad Gap)	3	0.998	H	11.1	6.6769E-02
			O	88.9	3.3385E-02
Stainless Steel (SS304)	4	7.94	C	0.080	3.1877E-04
			Si	1.000	1.7025E-03
			P	0.045	6.9468E-05
			Cr	19.000	1.7473E-02
			Mn	2.000	1.7407E-03
			Fe	68.375	5.8545E-02
			Ni	9.500	7.7402E-03
Borated Water (2500 ppm Boron)	5	1.000	H	11.165	6.67692E-02
			O	88.586	3.33846E-02
			B-10	4.605E-02	2.77126E-05
			B-11	2.038E-01	1.11547E-04
UO ₂ (Extra Fuel) (Enrichment - 5.0 wt%)	6	10.686	U-235	4.407	1.20673E-03
			U-238	83.743	2.26382E-02
			O	11.850	4.76898E-02
¹¹ B ₄ C in BPRA	7	2.555	B-11	78.56	1.0988E-01
			C	21.44	2.7470E-02
Aluminum	8	2.70	Al	100.0	6.0307E-02
Type A Borated Aluminum Poison Plate (6.30 mg B-10/cm ²)	9	2.693	B-10	1.842	2.98348E-03
			B-11	0.205	3.01496E-04
			Al	97.953	5.88756E-02
Water	10	0.998	H	11.1	6.6769E-02
			O	88.9	3.3385E-02
Lead	11	11.34	Pb	100.0	3.2969E-02
Rail Material	12	4.024	Water	7.44	
			SS304	69.04	
			Aluminum	23.50	
Type B Borated Aluminum Poison Plate (13.5 mg B-10/cm ²)	9	2.693	B-10	2.632	4.26218E-03
			B-11	0.292	4.30715E-04
			Al	97.076	5.83483E-02
Type D Borated Aluminum Poison Plate (28.8 mg B-10/cm ²)	9	2.693	B-10	3.368	5.45561E-03
			B-11	0.374	5.51316E-04
			Al	96.258	5.78562E-02

Table 6-10
Results of the Fuel Assembly Positioning Studies

Description	K_{keno}	σ_{keno}	K_{eff}	Filename
Framatome 17x17 MK BW Fuel Assembly				
Centered, 70% IMD	0.9216	0.0008	0.9232	adfr17mkb_c070.out:
Centered, 80% IMD	0.9235	0.0006	0.9247	adfr17mkb_c080.out:
Centered, 90% IMD	0.9219	0.0008	0.9235	adfr17mkb_c090.out:
Centered, 100% IMD	0.9153	0.0008	0.9169	adfr17mkb_c100.out:
Inward, 70% IMD	0.9239	0.0008	0.9255	adfr17mkb_o070.out:
Inward, 80% IMD	0.9263	0.0007	0.9277	adfr17mkb_o080.out:
Inward, 90% IMD	0.9250	0.0007	0.9264	adfr17mkb_o090.out:
Inward, 100% IMD	0.9194	0.0007	0.9208	adfr17mkb_o100.out:
Westinghouse 5x15 Standard Fuel Assembly				
Centered, 70% IMD	0.9210	0.0007	0.9224	we15std_c070.out:
Centered, 80% IMD	0.9220	0.0007	0.9234	we15std_c080.out:
Centered, 90% IMD	0.9187	0.0007	0.9201	we15std_c090.out:
Centered, 100% IMD	0.9101	0.0007	0.9115	we15std_c100.out:
Inward, 70% IMD	0.9242	0.0008	0.9258	we15std_o070.out:
Inward, 80% IMD	0.9231	0.0008	0.9247	we15std_o080.out:
Inward, 90% IMD	0.9231	0.0008	0.9247	we15std_o090.out:
Inward, 100% IMD	0.9148	0.0008	0.9164	we15std_o100.out:
Westinghouse 17x17 OFA Fuel Assembly				
Centered, 70% IMD	0.9069	0.0007	0.9083	we17ofa_c070.out:
Centered, 80% IMD	0.9057	0.0008	0.9073	we17ofa_c080.out:
Centered, 90% IMD	0.9027	0.0007	0.9041	we17ofa_c090.out:
Centered, 100% IMD	0.8955	0.0007	0.8969	we17ofa_c100.out:
Inward, 70% IMD	0.9106	0.0007	0.9120	we17ofa_o070.out:
Inward, 80% IMD	0.9108	0.0006	0.9120	we17ofa_o080.out:
Inward, 90% IMD	0.9050	0.0007	0.9064	we17ofa_o090.out:
Inward, 100% IMD	0.8984	0.0006	0.8996	we17ofa_o100.out:
Combustion Engineering 16x16 Fuel Assembly				
CE 16x16 System 80 Centered, 100% IMD	0.8676	0.0007	0.8690	
CE 16x16 Standard Centered 100% IMD	0.8666	0.0006	0.8678	

Table 6-10
Results of the Fuel Assembly Positioning Studies
(Concluded)

Description	K_{keno}	σ_{keno}	K_{eff}	Filename
Westinghouse 17x17 Standard Fuel Assembly				
Centered, 70% IMD	0.9212	0.0008	0.9228	we17std_c070.out:
Centered, 80% IMD	0.9264	0.0007	0.9278	we17std_c080.out:
Centered, 90% IMD	0.9233	0.0007	0.9247	we17std_c090.out:
Centered, 100% IMD	0.9194	0.0007	0.9208	we17std_c100.out:
Inward, 70% IMD	0.9245	0.0008	0.9261	we17std_o070.out:
Inward, 80% IMD	0.9289	0.0008	0.9305	we17std_o080.out:
Inward, 90% IMD	0.9277	0.0007	0.9291	we17std_o090.out:
Inward, 100% IMD	0.9217	0.0007	0.9231	we17std_o100.out:
CE 14x14 Standard Fuel Assembly				
Centered, 60% IMD	0.8799	0.0007	0.8813	ce14std_c060.out:
Centered, 70% IMD	0.8834	0.0007	0.8848	ce14std_c070.out:
Centered, 80% IMD	0.8807	0.0007	0.8821	ce14std_c080.out:
Centered, 90% IMD	0.8723	0.0007	0.8737	ce14std_c090.out:
Centered, 100% IMD	0.8619	0.0007	0.8633	ce14std_c100.out:
Inward, 60% IMD	0.8826	0.0008	0.8842	ce14std_o060.out:
Inward, 70% IMD	0.8862	0.0007	0.8876	ce14std_o070.out:
Inward, 80% IMD	0.8842	0.0007	0.8856	ce14std_o080.out:
Inward, 90% IMD	0.8772	0.0008	0.8788	ce14std_o090.out:
Inward, 100% IMD	0.8676	0.0007	0.8690	ce14std_o100.out:
CE 14x14 Fort Calhoun Fuel Assembly				
Centered, 60% IMD	0.8808	0.0008	0.8824	ce14ftc_c060.out:
Centered, 70% IMD	0.8851	0.0007	0.8865	ce14ftc_c070.out:
Centered, 80% IMD	0.8828	0.0007	0.8842	ce14ftc_c080.out:
Centered, 90% IMD	0.8756	0.0008	0.8772	ce14ftc_c090.out:
Centered, 100% IMD	0.8679	0.0007	0.8693	ce14ftc_c100.out:
Inward, 60% IMD	0.8826	0.0008	0.8842	ce14ftc_o060.out:
Inward, 70% IMD	0.8883	0.0007	0.8897	ce14ftc_o070.out:
Inward, 80% IMD	0.8865	0.0008	0.8881	ce14ftc_o080.out:
Inward, 90% IMD	0.8815	0.0008	0.8831	ce14ftc_o090.out:
Inward, 100% IMD	0.8717	0.0008	0.8733	ce14ftc_o100.out:

Table 6-11
Results of the Rail Material Variation Studies

Description	K_{keno}	σ_{keno}	K_{eff}	Filename
Detailed Model, 70% IMD	0.9285	0.0008	0.9301	rail_act_070.out:
Detailed Model, 80% IMD	0.9317	0.0007	0.9331	rail_act_080.out:
Detailed Model, 90% IMD	0.9290	0.0007	0.9304	rail_act_090.out:
Detailed Model, 100% IMD	0.9239	0.0007	0.9253	rail_act_100.out:
Water Rail, 70% IMD	0.9271	0.0009	0.9289	rail_h2o_070.out:
Water Rail, 80% IMD	0.9292	0.0008	0.9308	rail_h2o_080.out:
Water Rail, 90% IMD	0.9288	0.0008	0.9304	rail_h2o_090.out:
Water Rail, 100% IMD	0.9230	0.0008	0.9246	rail_h2o_100.out:
Composition 3, 70% IMD	0.9298	0.0008	0.9314	rail_h3o_070.out:
Composition 3, 80% IMD	0.9324	0.0007	0.9338	rail_h3o_080.out:
Composition 3, 90% IMD	0.9319	0.0008	0.9335	rail_h3o_090.out:
Composition 3, 100% IMD	0.9244	0.0007	0.9258	rail_h3o_100.out:
Composition 4, 70% IMD	0.9273	0.0007	0.9287	rail_h4o_070.out:
Composition 4, 80% IMD	0.9309	0.0007	0.9323	rail_h4o_080.out:
Composition 4, 90% IMD	0.9298	0.0007	0.9312	rail_h4o_090.out:
Composition 4 100% IMD	0.9232	0.0007	0.9246	rail_h4o_100.out:
Composition 5, 70% IMD	0.9287	0.0008	0.9303	rail_h5o_070.out:
Composition 5, 80% IMD	0.9312	0.0007	0.9326	rail_h5o_080.out:
Composition 5, 90% IMD	0.9279	0.0007	0.9293	rail_h5o_090.out:
Composition 5, 100% IMD	0.9244	0.0007	0.9258	rail_h5o_100.out:
Borated Water, 70% IMD	0.9245	0.0008	0.9261	we17std_o070.out:
Borated Water, 80% IMD	0.9289	0.0008	0.9305	we17std_o080.out:
Borated Water, 90% IMD	0.9277	0.0007	0.9291	we17std_o090.out:
Borated Water, 100% IMD	0.9217	0.0007	0.9231	we17std_o100.out:

Table 6-12
Results of the Poison Plate Thickness Variation Studies

Description	K_{keno}	σ_{keno}	K_{eff}	Filename
0.187", Max Thickness, 70% IMD	0.9299	0.0008	0.9315	poison_max_070.out:
0.187", Max Thickness, 80% IMD	0.9322	0.0008	0.9338	poison_max_080.out:
0.187", Max Thickness, 90% IMD	0.9304	0.0008	0.9320	poison_max_090.out:
0.187", Max Thickness, 100% IMD	0.9237	0.0008	0.9253	poison_max_100.out:
0.050", Min Thickness, 70% IMD	0.9292	0.0007	0.9306	poison_min_070.out:
0.050", Min Thickness, 80% IMD	0.9323	0.0007	0.9337	poison_min_080.out:
0.050", Min Thickness, 90% IMD	0.9294	0.0008	0.9310	poison_min_090.out:
0.050", Min Thickness, 100% IMD	0.9245	0.0007	0.9259	poison_min_100.out:
0.075", Nom Thickness, 70% IMD	0.9298	0.0008	0.9314	rail_h3o_070.out:
0.075", Nom Thickness, 80% IMD	0.9324	0.0007	0.9338	rail_h3o_080.out:
0.075", Nom Thickness, 90% IMD	0.9319	0.0008	0.9335	rail_h3o_090.out:
0.075", Nom Thickness, 100% IMD	0.9244	0.0007	0.9258	rail_h3o_100.out:

Table 6-13
Results of the Fuel Compartment Width Variation Studies

Description	K_{keno}	σ_{keno}	K_{eff}	Filename
8.750", Max Width, 70% IMD	0.9270	0.0007	0.9284	boxid_max_070.out:
8.750", Max Width, 80% IMD	0.9301	0.0008	0.9317	boxid_max_080.out:
8.750", Max Width, 90% IMD	0.9283	0.0008	0.9299	boxid_max_090.out:
8.750", Max Width, 100% IMD	0.9203	0.0007	0.9217	boxid_max_100.out:
8.650", Min Width, 70% IMD	0.9327	0.0007	0.9341	boxid_min_070.out:
8.650", Min Width, 80% IMD	0.9341	0.0007	0.9355	boxid_min_080.out:
8.650", Min Width, 90% IMD	0.9325	0.0007	0.9339	boxid_min_090.out:
8.650", Min Width, 100% IMD	0.9279	0.0008	0.9295	boxid_min_100.out:
8.700", Nom Width, 70% IMD	0.9298	0.0008	0.9314	rail_h3o_070.out:
8.700", Nom Width, 80% IMD	0.9324	0.0007	0.9338	rail_h3o_080.out:
8.700", Nom Width, 90% IMD	0.9319	0.0008	0.9335	rail_h3o_090.out:
8.700", Nom Width, 100% IMD	0.9244	0.0007	0.9258	rail_h3o_100.out:

Table 6-14
Results of the Fuel Compartment Thickness Variation Studies

Description	K_{keno}	σ_{keno}	K_{eff}	Filename
0.2325", Max Thickness, 70% IMD	0.9308	0.0007	0.9322	boxod_max_070.out:
0.2325", Max Thickness, 80% IMD	0.9334	0.0007	0.9348	boxod_max_080.out:
0.2325", Max Thickness, 90% IMD	0.9318	0.0007	0.9332	boxod_max_090.out:
0.2325", Max Thickness, 100% IMD	0.9258	0.0007	0.9272	boxod_max_100.out:
0.1775", Min Thickness, 70% IMD	0.9321	0.0008	0.9337	boxod_min_070.out:
0.1775", Min Thickness, 80% IMD	0.9333	0.0007	0.9347	boxod_min_080.out:
0.1775", Min Thickness, 90% IMD	0.9318	0.0008	0.9334	boxod_min_090.out:
0.1775", Min Thickness, 100% IMD	0.9272	0.0007	0.9286	boxod_min_100.out:
0.1875", Nom Thickness, 70% IMD	0.9327	0.0007	0.9341	boxid_min_070.out:
0.1875", Nom Thickness, 80% IMD	0.9341	0.0007	0.9355	boxid_min_080.out:
0.1875", Nom Thickness, 90% IMD	0.9325	0.0007	0.9339	boxid_min_090.out:
0.1875", Nom Thickness, 100% IMD	0.9279	0.0008	0.9295	boxid_min_100.out:

Table 6-15
WE 15x15 Class Intact Assemblies Without BPRAs - Final Results

Description	K_{keno}	σ_{keno}	K_{eff}	Filename
Type A Basket (7.0 mg B-10/cm ²), 2300 ppm Boron, 3.8 wt. % U-235				
60% IMD	0.9326	0.0007	0.9340	we15b23_p07e38_060.out:
70% IMD	0.9360	0.0006	0.9372	we15b23_p07e38_070.out:
80% IMD	0.9356	0.0007	0.9370	we15b23_p07e38_080.out:
90% IMD	0.9295	0.0008	0.9311	we15b23_p07e38_090.out:
100% IMD	0.9198	0.0007	0.9212	we15b23_p07e38_100.out:
Type B Basket (15.0 mg B-10/cm ²), 2300 ppm Boron, 4.2 wt. % U-235				
60% IMD	0.9234	0.0007	0.9248	we15b23_p15e42_060.out:
70% IMD	0.9340	0.0008	0.9356	we15b23_p15e42_070.out:
80% IMD	0.9367	0.0007	0.9381	we15b23_p15e42_080.out:
90% IMD	0.9361	0.0007	0.9375	we15b23_p15e42_090.out:
100% IMD	0.9294	0.0008	0.9310	we15b23_p15e42_100.out:
Type D Basket (32.0 mg B-10/cm ²), 2300 ppm Boron, 4.6 wt. % U-235				
60% IMD	0.9090	0.0008	0.9106	we15b23_p32e46_060.out:
70% IMD	0.9246	0.0007	0.9260	we15b23_p32e46_070.out:
80% IMD	0.9315	0.0007	0.9329	we15b23_p32e46_080.out:
90% IMD	0.9342	0.0006	0.9354	we15b23_p32e46_090.out:
100% IMD	0.9320	0.0007	0.9334	we15b23_p32e46_100.out:
Type E Basket (50.0 mg B-10/cm ²), 2300 ppm Boron, 4.9 wt. % U-235				
60% IMD	0.9034	0.0007	0.9048	we15b23_p50e49_060.out:
70% IMD	0.9216	0.0007	0.9230	we15b23_p50e49_070.out:
80% IMD	0.9304	0.0007	0.9318	we15b23_p50e49_080.out:
90% IMD	0.9362	0.0007	0.9376	we15b23_p50e49_090.out:
100% IMD	0.9341	0.0007	0.9355	we15b23_p50e49_100.out:
Type A Basket (7.0 mg B-10/cm ²), 2400 ppm Boron, 3.9 wt. % U-235				
60% IMD	0.9333	0.0007	0.9347	we15b24_p07e39_060.out:
70% IMD	0.9373	0.0008	0.9389	we15b24_p07e39_070.out:
80% IMD	0.9355	0.0007	0.9369	we15b24_p07e39_080.out:
90% IMD	0.9299	0.0008	0.9315	we15b24_p07e39_090.out:
100% IMD	0.9203	0.0008	0.9219	we15b24_p07e39_100.out:
Type B Basket (15.0 mg B-10/cm ²), 2400 ppm Boron, 4.3 wt. % U-235				
60% IMD	0.9259	0.0007	0.9273	we15b24_p15e43_060.out:
70% IMD	0.9344	0.0008	0.9360	we15b24_p15e43_070.out:
80% IMD	0.9373	0.0007	0.9387	we15b24_p15e43_080.out:
90% IMD	0.9340	0.0007	0.9354	we15b24_p15e43_090.out:
100% IMD	0.9278	0.0007	0.9292	we15b24_p15e43_100.out:

Table 6-15
WE 15x15 Class Intact Assemblies Without BPRAs - Final Results
(Continued)

Description	K_{keno}	σ_{keno}	K_{eff}	Filename
Type D Basket (32.0 mg B-10/cm ²), 2400 ppm Boron, 4.7 wt. % U-235				
60% IMD	0.9115	0.0007	0.9129	we15b24_p32e47_060.out:
70% IMD	0.9263	0.0008	0.9279	we15b24_p32e47_070.out:
80% IMD	0.9338	0.0007	0.9352	we15b24_p32e47_080.out:
90% IMD	0.9333	0.0007	0.9347	we15b24_p32e47_090.out:
100% IMD	0.9305	0.0008	0.9321	we15b24_p32e47_100.out:
Type E Basket (50.0 mg B-10/cm ²), 2400 ppm Boron, 5.0 wt. % U-235				
60% IMD	0.9050	0.0009	0.9068	we15b24_p50e50_060.out:
70% IMD	0.9219	0.0010	0.9239	we15b24_p50e50_070.out:
80% IMD	0.9299	0.0009	0.9317	we15b24_p50e50_080.out:
90% IMD	0.9340	0.0011	0.9362	we15b24_p50e50_090.out:
100% IMD	0.9319	0.0010	0.9339	we15b24_p50e50_100.out:
Type A Basket (7.0 mg B-10/cm ²), 2500 ppm Boron, 3.9 wt. % U-235				
60% IMD	0.9270	0.0007	0.9284	we15b25_p07e39_060.out:
70% IMD	0.9326	0.0007	0.9340	we15b25_p07e39_070.out:
80% IMD	0.9301	0.0007	0.9315	we15b25_p07e39_080.out:
90% IMD	0.9215	0.0008	0.9231	we15b25_p07e39_090.out:
100% IMD	0.9119	0.0008	0.9135	we15b25_p07e39_100.out:
Type B Basket (15.0 mg B-10/cm ²), 2500 ppm Boron, 4.4 wt. % U-235				
60% IMD	0.9282	0.0008	0.9298	we15b25_p15e44_060.out:
70% IMD	0.9355	0.0007	0.9369	we15b25_p15e44_070.out:
80% IMD	0.9357	0.0008	0.9373	we15b25_p15e44_080.out:
90% IMD	0.9353	0.0006	0.9365	we15b25_p15e44_090.out:
100% IMD	0.9273	0.0008	0.9289	we15b25_p15e44_100.out:
Type D Basket (32.0 mg B-10/cm ²), 2500 ppm Boron, 4.9 wt. % U-235				
60% IMD	0.9171	0.0008	0.9187	we15b25_p32e49_060.out:
70% IMD	0.9316	0.0007	0.9330	we15b25_p32e49_070.out:
80% IMD	0.9364	0.0007	0.9378	we15b25_p32e49_080.out:
90% IMD	0.9383	0.0008	0.9399	we15b25_p32e49_090.out:
100% IMD	0.9336	0.0008	0.9352	we15b25_p32e49_100.out:
Type A Basket (7.0 mg B-10/cm ²), 2800 ppm Boron, 4.10 wt. % U-235				
60 % IMD	0.9355	0.0008	0.9371	
70 % IMD	0.9371	0.0006	0.9383	
80 % IMD	0.9299	0.0006	0.9311	
90 % IMD	0.9195	0.0006	0.9207	
100 % IMD	0.9082	0.0006	0.9094	

Table 6-15
WE 15x15 Class Intact Assemblies Without BPRAs - Final Results
(Concluded)

Description	K_{keno}	σ_{keno}	K_{eff}	Filename
Type B Basket (15.0 mg B-10/cm ²), 2800 ppm Boron, 4.50 wt. % U-235				
60 % IMD	0.9305	0.0007	0.9319	
70 % IMD	0.9345	0.0008	0.9361	
80 % IMD	0.9318	0.0007	0.9332	
90 % IMD	0.9229	0.0006	0.9241	
100 % IMD	0.9193	0.0008	0.9209	
Type C Basket (20.0 mg B-10/cm ²), 2800 ppm Boron, 4.70 wt. % U-235				
60 % IMD	0.9291	0.0007	0.9305	
70 % IMD	0.9333	0.0007	0.9347	
80 % IMD	0.9336	0.0007	0.9350	
90 % IMD	0.9282	0.0008	0.9298	
100 % IMD	0.9192	0.0007	0.9206	
Type D Basket (32.0 mg B-10/cm ²), 2800 ppm Boron, 5.00 wt. % U-235				
60 % IMD	0.9227	0.0007	0.9241	
70 % IMD	0.9319	0.0007	0.9333	
80 % IMD	0.9328	0.0007	0.9342	
90 % IMD	0.9309	0.0007	0.9323	
100 % IMD	0.9235	0.0007	0.9249	

Table 6-16
WE 15x15 Class Intact Assemblies With BPRAs - Final Results

Description	K_{keno}	σ_{keno}	K_{eff}	Filename
Type A Basket (7.0 mg B-10/cm ²), 2300 ppm Boron, 3.7 wt. % U-235				
60% IMD	0.9187	0.0007	0.9201	we15bp23_p07e37_060.out:
70% IMD	0.9290	0.0008	0.9306	we15bp23_p07e37_070.out:
80% IMD	0.9315	0.0007	0.9329	we15bp23_p07e37_080.out:
90% IMD	0.9302	0.0007	0.9316	we15bp23_p07e37_090.out:
100% IMD	0.9260	0.0007	0.9274	we15bp23_p07e37_100.out:
Type B Basket (15.0 mg B-10/cm ²), 2300 ppm Boron, 4.1 wt. % U-235				
60% IMD	0.9105	0.0007	0.9119	we15bp23_p15e41_060.out:
70% IMD	0.9239	0.0007	0.9253	we15bp23_p15e41_070.out:
80% IMD	0.9324	0.0007	0.9338	we15bp23_p15e41_080.out:
90% IMD	0.9342	0.0007	0.9356	we15bp23_p15e41_090.out:
100% IMD	0.9338	0.0007	0.9352	we15bp23_p15e41_100.out:
Type D Basket (32.0 mg B-10/cm ²), 2300 ppm Boron, 4.5 wt. % U-235				
60% IMD	0.8947	0.0008	0.8963	we15bp23_p32e45_060.out:
70% IMD	0.9124	0.0008	0.9140	we15bp23_p32e45_070.out:
80% IMD	0.9263	0.0008	0.9279	we15bp23_p32e45_080.out:
90% IMD	0.9324	0.0008	0.9340	we15bp23_p32e45_090.out:
100% IMD	0.9335	0.0008	0.9351	we15bp23_p32e45_100.out:
Type E Basket (50.0 mg B-10/cm ²), 2300 ppm Boron, 4.8 wt. % U-235				
60% IMD	0.8869	0.0008	0.8885	we15bp23_p50e48_060.out:
70% IMD	0.9087	0.0008	0.9103	we15bp23_p50e48_070.out:
80% IMD	0.9218	0.0007	0.9232	we15bp23_p50e48_080.out:
90% IMD	0.9296	0.0008	0.9312	we15bp23_p50e48_090.out:
100% IMD	0.9358	0.0008	0.9374	we15bp23_p50e48_100.out:
Type A Basket (7.0 mg B-10/cm ²), 2400 ppm Boron, 3.8 wt. % U-235				
60% IMD	0.9222	0.0008	0.9238	we15bp24_p07e38_060.out:
70% IMD	0.9309	0.0008	0.9325	we15bp24_p07e38_070.out:
80% IMD	0.9344	0.0007	0.9358	we15bp24_p07e38_080.out:
90% IMD	0.9312	0.0006	0.9324	we15bp24_p07e38_090.out:
100% IMD	0.9252	0.0007	0.9266	we15bp24_p07e38_100.out:
Type B Basket (15.0 mg B-10/cm ²), 2400 ppm Boron, 4.2 wt. % U-235				
60% IMD	0.9140	0.0009	0.9158	we15bp24_p15e42_060.out:
70% IMD	0.9266	0.0007	0.9280	we15bp24_p15e42_070.out:
80% IMD	0.9319	0.0007	0.9333	we15bp24_p15e42_080.out:
90% IMD	0.9335	0.0007	0.9349	we15bp24_p15e42_090.out:
100% IMD	0.9322	0.0007	0.9336	we15bp24_p15e42_100.out:

Table 6-16
WE 15x15 Class Intact Assemblies With BPRAs - Final Results
(Continued)

Description	K_{keno}	σ_{keno}	K_{eff}	Filename
Type D Basket (32.0 mg B-10/cm ²), 2400 ppm Boron, 4.7 wt. % U-235				
60% IMD	0.9016	0.0009	0.9034	we15bp24_p32e47_060.out:
70% IMD	0.9200	0.0007	0.9214	we15bp24_p32e47_070.out:
80% IMD	0.9317	0.0007	0.9331	we15bp24_p32e47_080.out:
90% IMD	0.9368	0.0008	0.9384	we15bp24_p32e47_090.out:
100% IMD	0.9388	0.0007	0.9402	we15bp24_p32e47_100.out:
Type E Basket (50.0 mg B-10/cm ²), 2400 ppm Boron, 4.9 wt. % U-235				
60% IMD	0.8862	0.0008	0.8878	we15bp24_p50e49_060.out:
70% IMD	0.9083	0.0009	0.9101	we15bp24_p50e49_070.out:
80% IMD	0.9219	0.0010	0.9239	we15bp24_p50e49_080.out:
90% IMD	0.9298	0.0009	0.9316	we15bp24_p50e49_090.out:
100% IMD	0.9351	0.0010	0.9371	we15bp24_p50e49_100.out:
Type A Basket (7.0 mg B-10/cm ²), 2500 ppm Boron, 3.9 wt. % U-235				
60% IMD	0.9251	0.0007	0.9265	we15bp25_p07e39_060.out:
70% IMD	0.9330	0.0008	0.9346	we15bp25_p07e39_070.out:
80% IMD	0.9358	0.0007	0.9372	we15bp25_p07e39_080.out:
90% IMD	0.9342	0.0007	0.9356	we15bp25_p07e39_090.out:
100% IMD	0.9276	0.0007	0.9290	we15bp25_p07e39_100.out:
Type B Basket (15.0 mg B-10/cm ²), 2500 ppm Boron, 4.3 wt. % U-235				
60% IMD	0.9154	0.0008	0.9170	we15bp25_p15e43_060.out:
70% IMD	0.9273	0.0007	0.9287	we15bp25_p15e43_070.out:
80% IMD	0.9339	0.0008	0.9355	we15bp25_p15e43_080.out:
90% IMD	0.9338	0.0007	0.9352	we15bp25_p15e43_090.out:
100% IMD	0.9319	0.0006	0.9331	we15bp25_p15e43_100.out:
Type D Basket (32.0 mg B-10/cm ²), 2500 ppm Boron, 4.8 wt. % U-235				
60% IMD	0.9051	0.0008	0.9067	we15bp25_p32e48_060.out:
70% IMD	0.9221	0.0008	0.9237	we15bp25_p32e48_070.out:
80% IMD	0.9314	0.0007	0.9328	we15bp25_p32e48_080.out:
90% IMD	0.9371	0.0007	0.9385	we15bp25_p32e48_090.out:
100% IMD	0.9371	0.0008	0.9387	we15bp25_p32e48_100.out:
Type E Basket (50.0 mg B-10/cm ²), 2500 ppm Boron, 5.0 wt. % U-235				
60% IMD	0.8903	0.0010	0.8923	we15bp25_p50e50_060.out:
70% IMD	0.9105	0.0009	0.9123	we15bp25_p50e50_070.out:
80% IMD	0.9224	0.0009	0.9242	we15bp25_p50e50_080.out:
90% IMD	0.9306	0.0010	0.9326	we15bp25_p50e50_090.out:
100% IMD	0.9334	0.0009	0.9352	we15bp25_p50e50_100.out:

Table 6-16
WE 15x15 Class Intact Assemblies With BPRAs - Final Results
(Continued)

Description	K_{keno}	σ_{keno}	K_{eff}	Filename
Type A Basket (7.0 mg B-10/cm ²), 2000 ppm Boron, 3.50 wt. % U-235				
60% IMD	0.9200	0.0007	0.9214	we15bp20_p07e35_060.out:
70% IMD	0.9312	0.0008	0.9328	we15bp20_p07e35_070.out:
80% IMD	0.9362	0.0007	0.9376	we15bp20_p07e35_080.out:
90% IMD	0.9370	0.0007	0.9384	we15bp20_p07e35_090.out:
100% IMD	0.9318	0.0007	0.9332	we15bp20_p07e35_100.out:
Type B Basket (15.0 mg B-10/cm ²), 2000 ppm Boron, 3.80 wt. % U-235				
60% IMD	0.9037	0.0008	0.9053	we15bp20_p15e38_060.out:
70% IMD	0.9204	0.0009	0.9222	we15bp20_p15e38_070.out:
80% IMD	0.9290	0.0007	0.9304	we15bp20_p15e38_080.out:
90% IMD	0.9335	0.0008	0.9351	we15bp20_p15e38_090.out:
100% IMD	0.9328	0.0007	0.9342	we15bp20_p15e38_100.out:
Type D Basket (32.0 mg B-10/cm ²), 2000 ppm Boron, 4.20 wt. % U-235				
60% IMD	0.8903	0.0007	0.8917	we15bp20_p32e42_060.out:
70% IMD	0.9105	0.0007	0.9119	we15bp20_p32e42_070.out:
80% IMD	0.9255	0.0007	0.9269	we15bp20_p32e42_080.out:
90% IMD	0.9324	0.0007	0.9338	we15bp20_p32e42_090.out:
100% IMD	0.9354	0.0007	0.9368	we15bp20_p32e42_100.out:
Type E Basket (50.0 mg B-10/cm ²), 2000 ppm Boron, 4.50 wt. % U-235				
60% IMD	0.8827	0.0008	0.8843	we15bp20_p50e45_060.out:
70% IMD	0.9063	0.0008	0.9079	we15bp20_p50e45_070.out:
80% IMD	0.9236	0.0008	0.9252	we15bp20_p50e45_080.out:
90% IMD	0.9320	0.0008	0.9336	we15bp20_p50e45_090.out:
100% IMD	0.9380	0.0008	0.9396	we15bp20_p50e45_100.out:
Type A Basket (7.0 mg B-10/cm ²), 2800 ppm Boron, 4.05 wt. % U-235				
60 % IMD	0.9326	0.0008	0.9342	
70 % IMD	0.9368	0.0008	0.9384	
80 % IMD	0.9351	0.0008	0.9367	
90 % IMD	0.9285	0.0008	0.9301	
100 % IMD	0.9225	0.0006	0.9237	
Type B Basket (15.0 mg B-10/cm ²), 2800 ppm Boron, 4.50 wt. % U-235				
60 % IMD	0.9254	0.0007	0.9268	
70 % IMD	0.9338	0.0007	0.9352	
80 % IMD	0.9357	0.0007	0.9371	
90 % IMD	0.9348	0.0007	0.9362	
100 % IMD	0.931	0.0006	0.9322	

Table 6-16
WE 15x15 Class Intact Assemblies With BPRAs - Final Results
(Concluded)

Description	K_{keno}	σ_{keno}	K_{eff}	Filename
Type C Basket (20.0 mg B-10/cm ²), 2800 ppm Boron, 4.70 wt. % U-235				
60 % IMD	0.9219	0.0008	0.9235	
70 % IMD	0.9342	0.0007	0.9356	
80 % IMD	0.9391	0.0007	0.9405	
90 % IMD	0.9372	0.0007	0.9386	
100 % IMD	0.9344	0.0007	0.9358	
Type D Basket (32.0 mg B-10/cm ²), 2800 ppm Boron, 5.00 wt. % U-235				
60 % IMD	0.9143	0.0006	0.9155	
70 % IMD	0.9285	0.0008	0.9301	
80 % IMD	0.935	0.0007	0.9364	
90 % IMD	0.9378	0.0007	0.9392	
100 % IMD	0.9368	0.0009	0.9386	

Table 6-17
WE 17x17 Class Intact Assemblies Without BPRAs - Final Results

Description	K_{keno}	σ_{keno}	K_{eff}	Filename
Type A Basket (7.0 mg B-10/cm ²), 2300 ppm Boron, 3.8 wt. % U-235				
60% IMD	0.9303	0.0007	0.9317	we17b23_p07e38_060.out:
70% IMD	0.9390	0.0007	0.9404	we17b23_p07e38_070.out:
80% IMD	0.9376	0.0007	0.9390	we17b23_p07e38_080.out:
90% IMD	0.9355	0.0008	0.9371	we17b23_p07e38_090.out:
100% IMD	0.9279	0.0006	0.9291	we17b23_p07e38_100.out:
Type B Basket (15.0 mg B-10/cm ²), 2300 ppm Boron, 4.1 wt. % U-235				
60% IMD	0.9177	0.0007	0.9191	we17b23_p15e41_060.out:
70% IMD	0.9292	0.0008	0.9308	we17b23_p15e41_070.out:
80% IMD	0.9340	0.0008	0.9356	we17b23_p15e41_080.out:
90% IMD	0.9320	0.0008	0.9336	we17b23_p15e41_090.out:
100% IMD	0.9271	0.0007	0.9285	we17b23_p15e41_100.out:
Type D Basket (32.0 mg B-10/cm ²), 2300 ppm Boron, 4.55 wt. % U-235				
60% IMD	0.9082	0.0008	0.9098	we17b23_p32e46_060.out:
70% IMD	0.9233	0.0008	0.9249	we17b23_p32e46_070.out:
80% IMD	0.9335	0.0008	0.9351	we17b23_p32e46_080.out:
90% IMD	0.9352	0.0007	0.9366	we17b23_p32e46_090.out:
100% IMD	0.9346	0.0007	0.9360	we17b23_p32e46_100.out:
Type E Basket (50.0 mg B-10/cm ²), 2300 ppm Boron, 4.8 wt. % U-235				
60% IMD	0.8977	0.0008	0.8993	we17b23_p50e48_060.out:
70% IMD	0.9163	0.0007	0.9177	we17b23_p50e48_070.out:
80% IMD	0.9283	0.0008	0.9299	we17b23_p50e48_080.out:
90% IMD	0.9330	0.0007	0.9344	we17b23_p50e48_090.out:
100% IMD	0.9350	0.0008	0.9366	we17b23_p50e48_100.out:
Type A Basket (7.0 mg B-10/cm ²), 2400 ppm Boron, 3.8 wt. % U-235				
60% IMD	0.9261	0.0007	0.9275	we17b24_p07e38_060.out:
70% IMD	0.9317	0.0007	0.9331	we17b24_p07e38_070.out:
80% IMD	0.9328	0.0008	0.9344	we17b24_p07e38_080.out:
90% IMD	0.9275	0.0007	0.9289	we17b24_p07e38_090.out:
100% IMD	0.9189	0.0007	0.9203	we17b24_p07e38_100.out:
Type B Basket (15.0 mg B-10/cm ²), 2400 ppm Boron, 4.2 wt. % U-235				
60% IMD	0.9193	0.0006	0.9205	we17b24_p15e42_060.out:
70% IMD	0.9316	0.0007	0.9330	we17b24_p15e42_070.out:
80% IMD	0.9335	0.0008	0.9351	we17b24_p15e42_080.out:
90% IMD	0.9326	0.0007	0.9340	we17b24_p15e42_090.out:
100% IMD	0.9296	0.0008	0.9312	we17b24_p15e42_100.out:

Table 6-17
WE 17x17 Class Intact Assemblies Without BPRAs - Final Results
(Continued)

Description	K_{keno}	σ_{keno}	K_{eff}	Filename
Type D Basket (32.0 mg B-10/cm ²), 2400 ppm Boron, 4.7 wt. % U-235				
60% IMD	0.9122	0.0007	0.9136	we17b24_p32e47_060.out:
70% IMD	0.9271	0.0009	0.9289	we17b24_p32e47_070.out:
80% IMD	0.9360	0.0008	0.9376	we17b24_p32e47_080.out:
90% IMD	0.9383	0.0007	0.9397	we17b24_p32e47_090.out:
100% IMD	0.9373	0.0008	0.9389	we17b24_p32e47_100.out:
Type E Basket (50.0 mg B-10/cm ²), 2400 ppm Boron, 4.9 wt. % U-235				
60% IMD	0.8992	0.0007	0.9006	we17b24_p50e49_060.out:
70% IMD	0.9165	0.0008	0.9181	we17b24_p50e49_070.out:
80% IMD	0.9285	0.0007	0.9299	we17b24_p50e49_080.out:
90% IMD	0.9335	0.0007	0.9349	we17b24_p50e49_090.out:
100% IMD	0.9339	0.0007	0.9353	we17b24_p50e49_100.out:
Type A Basket (7.0 mg B-10/cm ²), 2500 ppm Boron, 3.9 wt. % U-235				
60% IMD	0.9299	0.0006	0.9311	we17b25_p07e39_060.out:
70% IMD	0.9350	0.0008	0.9366	we17b25_p07e39_070.out:
80% IMD	0.9333	0.0008	0.9349	we17b25_p07e39_080.out:
90% IMD	0.9278	0.0007	0.9292	we17b25_p07e39_090.out:
100% IMD	0.9193	0.0007	0.9207	we17b25_p07e39_100.out:
Type B Basket (15.0 mg B-10/cm ²), 2500 ppm Boron, 4.3 wt. % U-235				
60% IMD	0.9224	0.0007	0.9238	we17b25_p15e43_060.out:
70% IMD	0.9327	0.0007	0.9341	we17b25_p15e43_070.out:
80% IMD	0.9341	0.0007	0.9355	we17b25_p15e43_080.out:
90% IMD	0.9325	0.0007	0.9339	we17b25_p15e43_090.out:
100% IMD	0.9279	0.0008	0.9295	we17b25_p15e43_100.out:
Type D Basket (32.0 mg B-10/cm ²), 2500 ppm Boron, 4.8 wt. % U-235				
60% IMD	0.9137	0.0009	0.9155	we17b25_p32e48_060.out:
70% IMD	0.9282	0.0009	0.9300	we17b25_p32e48_070.out:
80% IMD	0.9358	0.0008	0.9374	we17b25_p32e48_080.out:
90% IMD	0.9373	0.0007	0.9387	we17b25_p32e48_090.out:
100% IMD	0.9356	0.0007	0.9370	we17b25_p32e48_100.out:
Type E Basket (50.0 mg B-10/cm ²), 2500 ppm Boron, 5.0 wt. % U-235				
60% IMD	0.8996	0.0007	0.9010	we17b25_p50e50_060.out:
70% IMD	0.9174	0.0008	0.9190	we17b25_p50e50_070.out:
80% IMD	0.9273	0.0009	0.9291	we17b25_p50e50_080.out:
90% IMD	0.9326	0.0008	0.9342	we17b25_p50e50_090.out:
100% IMD	0.9329	0.0008	0.9345	we17b25_p50e50_100.out:

Table 6-17
WE 17x17 Class Intact Assemblies Without BPRAs - Final Results
(Concluded)

Description	K_{keno}	σ_{keno}	K_{eff}	Filename
Type A Basket (7.0 mg B-10/cm ²), 2800 ppm Boron, 4.00 wt. % U-235				
60 % IMD	0.9308	0.0007	0.9322	
70 % IMD	0.9330	0.0007	0.9344	
80 % IMD	0.9283	0.0006	0.9295	
90 % IMD	0.9192	0.0007	0.9206	
100 % IMD	0.9083	0.0007	0.9097	
Type B Basket (15.0 mg B-10/cm ²), 2800 ppm Boron, 4.50 wt. % U-235				
60 % IMD	0.9309	0.0007	0.9323	
70 % IMD	0.9376	0.0007	0.9390	
80 % IMD	0.9368	0.0007	0.9382	
90 % IMD	0.9319	0.0006	0.9331	
100 % IMD	0.9242	0.0007	0.9256	
Type C Basket (20.0 mg B-10/cm ²), 2800 ppm Boron, 4.70 wt. % U-235				
60 % IMD	0.9294	0.0007	0.9308	
70 % IMD	0.9389	0.0008	0.9405	
80 % IMD	0.9391	0.0007	0.9405	
90 % IMD	0.9250	0.0007	0.9264	
100 % IMD	0.9291	0.0007	0.9305	
Type D Basket (32.0 mg B-10/cm ²), 2800 ppm Boron, 5.00 wt. % U-235				
60 % IMD	0.9215	0.0008	0.9231	
70 % IMD	0.9335	0.0007	0.9349	
80 % IMD	0.9379	0.0007	0.9393	
90 % IMD	0.9387	0.0007	0.9401	
100 % IMD	0.9326	0.0008	0.9342	
Type E Basket (50.0 mg B-10/cm ²), 2800 ppm Boron, 5.00 wt. % U-235				
60 % IMD	0.9020	0.0007	0.9034	
70 % IMD	0.9145	0.0007	0.9159	
80 % IMD	0.9202	0.0007	0.9216	
90 % IMD	0.9205	0.0007	0.9219	
100 % IMD	0.9186	0.0007	0.9200	

Table 6-18
WE 17x17 Class Intact Assemblies with BPRAs - Final Results

Description	K_{keno}	σ_{keno}	K_{eff}	Filename
Type A Basket (7.0 mg B-10/cm ²), 2000 ppm Boron, 3.50 wt. % U-235				
60% IMD	0.9184	0.0007	0.9198	we17bp20_p07e35_060.out:
70% IMD	0.9302	0.0007	0.9316	we17bp20_p07e35_070.out:
80% IMD	0.9370	0.0008	0.9386	we17bp20_p07e35_080.out:
90% IMD	0.9377	0.0006	0.9389	we17bp20_p07e35_090.out:
100% IMD	0.9355	0.0007	0.9369	we17bp20_p07e35_100.out:
Type B Basket (15.0 mg B-10/cm ²), 2000 ppm Boron, 3.80 wt. % U-235				
60% IMD	0.9045	0.0007	0.9059	we17bp20_p15e38_060.out:
70% IMD	0.9198	0.0007	0.9212	we17bp20_p15e38_070.out:
80% IMD	0.9300	0.0007	0.9314	we17bp20_p15e38_080.out:
90% IMD	0.9339	0.0009	0.9357	we17bp20_p15e38_090.out:
100% IMD	0.9359	0.0007	0.9373	we17bp20_p15e38_100.out:
Type C Basket (20.0 mg B-10/cm ²), 2000 ppm Boron, 3.95 wt. % U-235				
60% IMD	0.8982	0.0007	0.8996	we17bp20_p20e40_060.out:
70% IMD	0.9174	0.0008	0.9190	we17bp20_p20e40_070.out:
80% IMD	0.9295	0.0007	0.9309	we17bp20_p20e40_080.out:
90% IMD	0.9338	0.0008	0.9354	we17bp20_p20e40_090.out:
100% IMD	0.9366	0.0008	0.9382	we17bp20_p20e40_100.out:
Type D Basket (32.0 mg B-10/cm ²), 2000 ppm Boron, 4.20 wt. % U-235				
60% IMD	0.8890	0.0007	0.8904	we17bp20_p32e42_060.out:
70% IMD	0.9110	0.0007	0.9124	we17bp20_p32e42_070.out:
80% IMD	0.9257	0.0009	0.9275	we17bp20_p32e42_080.out:
90% IMD	0.9338	0.0007	0.9352	we17bp20_p32e42_090.out:
100% IMD	0.9375	0.0008	0.9391	we17bp20_p32e42_100.out:
Type E Basket (50.0 mg B-10/cm ²), 2000 ppm Boron, 4.45 wt. % U-235				
60% IMD	0.8771	0.0008	0.8787	we17bp20_p50e45_060.out:
70% IMD	0.9020	0.0007	0.9034	we17bp20_p50e45_070.out:
80% IMD	0.9203	0.0009	0.9221	we17bp20_p50e45_080.out:
90% IMD	0.9324	0.0008	0.9340	we17bp20_p50e45_090.out:
100% IMD	0.9372	0.0007	0.9386	we17bp20_p50e45_100.out:
Type A Basket (7.0 mg B-10/cm ²), 2300 ppm Boron, 3.7 wt. % U-235				
60% IMD	0.9195	0.0007	0.9209	we17bp23_p07e37_060.out:
70% IMD	0.9298	0.0008	0.9314	we17bp23_p07e37_070.out:
80% IMD	0.9328	0.0007	0.9342	we17bp23_p07e37_080.out:
90% IMD	0.9338	0.0007	0.9352	we17bp23_p07e37_090.out:
100% IMD	0.9292	0.0007	0.9306	we17bp23_p07e37_100.out:

Table 6-18
WE 17x17 Class Intact Assemblies with BPRAs - Final Results
(Continued)

Description	K_{keno}	σ_{keno}	K_{eff}	Filename
Type B Basket (15.0 mg B-10/cm ²), 2300 ppm Boron, 4.1 wt. % U-235				
60% IMD	0.9105	0.0008	0.9121	we17bp23_p15e41_060.out:
70% IMD	0.9243	0.0008	0.9259	we17bp23_p15e41_070.out:
80% IMD	0.9332	0.0007	0.9346	we17bp23_p15e41_080.out:
90% IMD	0.9375	0.0007	0.9389	we17bp23_p15e41_090.out:
100% IMD	0.9358	0.0007	0.9372	we17bp23_p15e41_100.out:
Type C Basket (20.0 mg B-10/cm ²), 2300 ppm Boron, 4.25 wt. % U-235				
60% IMD	0.9046	0.0007	0.9060	we17bp23_p20e43_060.out:
70% IMD	0.9219	0.0007	0.9233	we17bp23_p20e43_070.out:
80% IMD	0.9314	0.0007	0.9328	we17bp23_p20e43_080.out:
90% IMD	0.9355	0.0007	0.9369	we17bp23_p20e43_090.out:
100% IMD	0.9369	0.0007	0.9383	we17bp23_p20e43_100.out:
Type D Basket (32.0 mg B-10/cm ²), 2300 ppm Boron, 4.5 wt. % U-235				
60% IMD	0.8936	0.0009	0.8954	we17bp23_p32e45_060.out:
70% IMD	0.9137	0.0009	0.9155	we17bp23_p32e45_070.out:
80% IMD	0.9276	0.0007	0.9290	we17bp23_p32e45_080.out:
90% IMD	0.9340	0.0007	0.9354	we17bp23_p32e45_090.out:
100% IMD	0.9376	0.0008	0.9392	we17bp23_p32e45_100.out:
Type E Basket (50.0 mg B-10/cm ²), 2300 ppm Boron, 4.7 wt. % U-235				
60% IMD	0.8813	0.0007	0.8827	we17bp23_p50e47_060.out:
70% IMD	0.9005	0.0008	0.9021	we17bp23_p50e47_070.out:
80% IMD	0.9181	0.0008	0.9197	we17bp23_p50e47_080.out:
90% IMD	0.9281	0.0008	0.9297	we17bp23_p50e47_090.out:
100% IMD	0.9337	0.0007	0.9351	we17bp23_p50e47_100.out:
Type A Basket (7.0 mg B-10/cm ²), 2400 ppm Boron, 3.8 wt. % U-235				
60% IMD	0.9227	0.0007	0.9241	we17bp24_p07e38_060.out:
70% IMD	0.9308	0.0007	0.9322	we17bp24_p07e38_070.out:
80% IMD	0.9348	0.0007	0.9362	we17bp24_p07e38_080.out:
90% IMD	0.9344	0.0008	0.9360	we17bp24_p07e38_090.out:
100% IMD	0.9319	0.0008	0.9335	we17bp24_p07e38_100.out:
Type B Basket (15.0 mg B-10/cm ²), 2400 ppm Boron, 4.2 wt. % U-235				
60% IMD	0.9119	0.0007	0.9133	we17bp24_p15e42_060.out:
70% IMD	0.9275	0.0007	0.9289	we17bp24_p15e42_070.out:
80% IMD	0.9333	0.0008	0.9349	we17bp24_p15e42_080.out:
90% IMD	0.9361	0.0008	0.9377	we17bp24_p15e42_090.out:
100% IMD	0.9367	0.0007	0.9381	we17bp24_p15e42_100.out:

Table 6-18
WE 17x17 Class Intact Assemblies with BPRAs - Final Results
(Continued)

Description	K_{keno}	σ_{keno}	K_{eff}	Filename
Type C Basket (20.0 mg B-10/cm ²), 2400 ppm Boron, 4.35 wt. % U-235				
60% IMD	0.9074	0.0008	0.9090	we17bp24_p20e44_060.out:
70% IMD	0.9234	0.0008	0.9250	we17bp24_p20e44_070.out:
80% IMD	0.9318	0.0008	0.9334	we17bp24_p20e44_080.out:
90% IMD	0.9364	0.0007	0.9378	we17bp24_p20e44_090.out:
100% IMD	0.9366	0.0007	0.9380	we17bp24_p20e44_100.out:
Type D Basket (32.0 mg B-10/cm ²), 2400 ppm Boron, 4.6 wt. % U-235				
60% IMD	0.8958	0.0008	0.8974	we17bp24_p32e46_060.out:
70% IMD	0.9152	0.0009	0.9170	we17bp24_p32e46_070.out:
80% IMD	0.9266	0.0008	0.9282	we17bp24_p32e46_080.out:
90% IMD	0.9335	0.0008	0.9351	we17bp24_p32e46_090.out:
100% IMD	0.9348	0.0007	0.9362	we17bp24_p32e46_100.out:
Type E Basket (50.0 mg B-10/cm ²), 2400 ppm Boron, 4.9 wt. % U-235				
60% IMD	0.8873	0.0008	0.8889	we17bp24_p50e49_060.out:
70% IMD	0.9093	0.0007	0.9107	we17bp24_p50e49_070.out:
80% IMD	0.9241	0.0008	0.9257	we17bp24_p50e49_080.out:
90% IMD	0.9314	0.0008	0.9330	we17bp24_p50e49_090.out:
100% IMD	0.9381	0.0007	0.9395	we17bp24_p50e49_100.out:
Type A Basket (7.0 mg B-10/cm ²), 2500 ppm Boron, 3.9 wt. % U-235				
60% IMD	0.9243	0.0007	0.9257	we17bp25_p07e39_060.out:
70% IMD	0.9338	0.0008	0.9354	we17bp25_p07e39_070.out:
80% IMD	0.9381	0.0008	0.9397	we17bp25_p07e39_080.out:
90% IMD	0.9362	0.0009	0.9380	we17bp25_p07e39_090.out:
100% IMD	0.9295	0.0007	0.9309	we17bp25_p07e39_100.out:
Type B Basket (15.0 mg B-10/cm ²), 2500 ppm Boron, 4.3 wt. % U-235				
60% IMD	0.9141	0.0007	0.9155	we17bp25_p15e43_060.out:
70% IMD	0.9277	0.0007	0.9291	we17bp25_p15e43_070.out:
80% IMD	0.9357	0.0008	0.9373	we17bp25_p15e43_080.out:
90% IMD	0.9374	0.0007	0.9388	we17bp25_p15e43_090.out:
100% IMD	0.9358	0.0007	0.9372	we17bp25_p15e43_100.out:
Type C Basket (20.0 mg B-10/cm ²), 2500 ppm Boron, 4.45 wt. % U-235				
60% IMD	0.9094	0.0006	0.9106	we17bp25_p20e45_060.out:
70% IMD	0.9242	0.0007	0.9256	we17bp25_p20e45_070.out:
80% IMD	0.9335	0.0008	0.9351	we17bp25_p20e45_080.out:
90% IMD	0.9358	0.0007	0.9372	we17bp25_p20e45_090.out:
100% IMD	0.9372	0.0008	0.9388	we17bp25_p20e45_100.out:

Table 6-18
WE 17x17 Class Intact Assemblies with BPRAs - Final Results
(Continued)

Description	K_{keno}	σ_{keno}	K_{eff}	Filename
Type D Basket (32.0 mg B-10/cm ²), 2500 ppm Boron, 4.7 wt. % U-235				
60% IMD	0.8992	0.0007	0.9006	we17bp25_p32e47_060.out:
70% IMD	0.9154	0.0007	0.9168	we17bp25_p32e47_070.out:
80% IMD	0.9272	0.0007	0.9286	we17bp25_p32e47_080.out:
90% IMD	0.9341	0.0007	0.9355	we17bp25_p32e47_090.out:
100% IMD	0.9356	0.0008	0.9372	we17bp25_p32e47_100.out:
Type E Basket (50.0 mg B-10/cm ²), 2500 ppm Boron, 5.0 wt. % U-235				
60% IMD	0.8871	0.0008	0.8887	we17bp25_p50e50_060.out:
70% IMD	0.9102	0.0007	0.9116	we17bp25_p50e50_070.out:
80% IMD	0.9260	0.0007	0.9274	we17bp25_p50e50_080.out:
90% IMD	0.9343	0.0008	0.9359	we17bp25_p50e50_090.out:
100% IMD	0.9379	0.0008	0.9395	we17bp25_p50e50_100.out:
Type A Basket (7.0 mg B-10/cm ²), 2800 ppm Boron, 4.00 wt. % U-235				
60 % IMD	0.9289	0.0007	0.9303	
70 % IMD	0.9347	0.0007	0.9361	
80 % IMD	0.9329	0.0006	0.9341	
90 % IMD	0.9297	0.0007	0.9311	
100 % IMD	0.9227	0.0007	0.9241	
Type B Basket (15.0 mg B-10/cm ²), 2800 ppm Boron, 4.45 wt. % U-235				
60 % IMD	0.9221	0.0006	0.9233	
70 % IMD	0.9318	0.0007	0.9332	
80 % IMD	0.9358	0.0007	0.9372	
90 % IMD	0.9348	0.0006	0.9360	
100 % IMD	0.9317	0.0007	0.9331	
Type C Basket (20.0 mg B-10/cm ²), 2800 ppm Boron, 4.65 wt. % U-235				
60 % IMD	0.9201	0.0007	0.9215	
70 % IMD	0.9309	0.0009	0.9327	
80 % IMD	0.9367	0.0007	0.9381	
90 % IMD	0.9375	0.0007	0.9389	
100 % IMD	0.9366	0.0006	0.9378	
Type D Basket (32.0 mg B-10/cm ²), 2800 ppm Boron, 4.95 wt. % U-235				
60 % IMD	0.9111	0.0007	0.9125	
70 % IMD	0.9262	0.0007	0.9276	
80 % IMD	0.9353	0.0008	0.9369	
90 % IMD	0.9387	0.0007	0.9401	
100 % IMD	0.9380	0.0007	0.9394	

Table 6-18
WE 17x17 Class Intact Assemblies with BPRAs - Final Results
(Concluded)

Description	K_{keno}	σ_{keno}	K_{eff}	Filename
Type E Basket (50.0 mg B-10/cm ²), 2800 ppm Boron, 5.00 wt. % U-235				
60 % IMD	0.8907	0.0007	0.8921	
70 % IMD	0.9079	0.0008	0.9095	
80 % IMD	0.9189	0.0007	0.9203	
90 % IMD	0.9244	0.0007	0.9258	
100 % IMD	0.9265	0.0007	0.9279	

Table 6-19
Limiting Parameters for Damaged Fuel Calculations

Fuel Assembly Type	Enrichment	Boron Concentration	Fixed Poison Loading
CE 14x14	4.90 wt. % U-235	2300 ppm	15 mg B-10/cm ²
Westinghouse 15x15	4.90 wt. % U-235	2500 ppm	32 mg B-10/cm ²
Westinghouse 17x17	4.80 wt. % U-235	2500 ppm	32 mg B-10/cm ²
CE 16x16	4.90 wt. % U-235	2400 ppm	25 mg B-10/cm ²

Table 6-20
Results of Optimum Pitch Studies

Description	K_{keno}	σ_{keno}	K_{eff}	Filename
WE 15x15, 4.9 wt. % U-235, 2500 ppm, 32 mg B-10/cm ² (Type D Basket)				
Pitch = 0.4220", 90% IMD	0.7062	0.0009	0.7080	we15_pitch4220_090.out:
Pitch = 0.4500", 90% IMD	0.7766	0.0009	0.7784	we15_pitch4500_090.out:
Pitch = 0.4750", 90% IMD	0.8280	0.0007	0.8294	we15_pitch4750_090.out:
Pitch = 0.5000", 90% IMD	0.8741	0.0009	0.8759	we15_pitch5000_090.out:
Pitch = 0.5250", 90% IMD	0.9106	0.0009	0.9124	we15_pitch5250_090.out:
Pitch = 0.5500", 90% IMD	0.9324	0.0007	0.9338	we15_pitch5500_090.out:
Pitch = 0.5630", 60% IMD	0.9208	0.0007	0.9222	we15_pitch5630_060.out:
Pitch = 0.5630", 70% IMD	0.9327	0.0007	0.9341	we15_pitch5630_070.out:
Pitch = 0.5630", 80% IMD	0.9398	0.0007	0.9412	we15_pitch5630_080.out:
Pitch = 0.5630", 90% IMD	0.9381	0.0008	0.9397	we15_pitch5630_090.out:
Pitch = 0.5630", 100% IMD	0.9323	0.0007	0.9337	we15_pitch5630_100.out:
Pitch = 0.5750", 60% IMD	0.9251	0.0007	0.9265	we15_pitch5750_060.out:
Pitch = 0.5750", 70% IMD	0.9359	0.0007	0.9373	we15_pitch5750_070.out:
Pitch = 0.5750", 80% IMD	0.9397	0.0007	0.9411	we15_pitch5750_080.out:
Pitch = 0.5750", 90% IMD	0.9381	0.0007	0.9395	we15_pitch5750_090.out:
Pitch = 0.5750", 100% IMD	0.9327	0.0008	0.9343	we15_pitch5750_100.out:
Pitch = 0.5877", 60% IMD	0.9304	0.0007	0.9318	we15_pitch5877_060.out:
Pitch = 0.5877", 70% IMD	0.9399	0.0008	0.9415	we15_pitch5877_070.out:
Pitch = 0.5877", 80% IMD	0.9417	0.0007	0.9431	we15_pitch5877_080.out:
Pitch = 0.5877", 90% IMD	0.9361	0.0007	0.9375	we15_pitch5877_090.out:
Pitch = 0.5877", 100% IMD	0.9291	0.0007	0.9305	we15_pitch5877_100.out:

Table 6-20
Results of Optimum Pitch Studies
(Continued)

Description	K_{keno}	σ_{keno}	K_{eff}	Filename
WE 17x17, 4.8 wt. % U-235, 2500 ppm, 32 mg B-10/cm ² (Type D Basket)				
Pitch = 0.3740", 90% IMD	0.7028	0.0007	0.7042	we17_pitch3740_090.out:
Pitch = 0.4000", 90% IMD	0.7757	0.0007	0.7771	we17_pitch4000_090.out:
Pitch = 0.4250", 90% IMD	0.8372	0.0008	0.8388	we17_pitch4250_090.out:
Pitch = 0.4500", 90% IMD	0.8859	0.0008	0.8875	we17_pitch4500_090.out:
Pitch = 0.47500", 90% IMD	0.9215	0.0008	0.9231	we17_pitch4750_090.out:
Pitch = 0.4960", 60% IMD	0.9164	0.0008	0.9180	we17_pitch4960_060.out:
Pitch = 0.4960", 70% IMD	0.9308	0.0008	0.9324	we17_pitch4960_070.out:
Pitch = 0.4960", 80% IMD	0.9377	0.0008	0.9393	we17_pitch4960_080.out:
Pitch = 0.4960", 90% IMD	0.9376	0.0008	0.9392	we17_pitch4960_090.out:
Pitch = 0.4960", 100% IMD	0.9355	0.0008	0.9371	we17_pitch4960_100.out:
Pitch = 0.5100", 60% IMD	0.9233	0.0008	0.9249	we17_pitch5100_060.out:
Pitch = 0.5100", 70% IMD	0.9348	0.0009	0.9366	we17_pitch5100_070.out:
Pitch = 0.5100", 80% IMD	0.9404	0.0008	0.9420	we17_pitch5100_080.out:
Pitch = 0.5100", 90% IMD	0.9405	0.0008	0.9421	we17_pitch5100_090.out:
Pitch = 0.5100", 100% IMD	0.9351	0.0007	0.9365	we17_pitch5100_100.out:
Pitch = 0.5172", 60% IMD	0.9258	0.0007	0.9272	we17_pitch5172_060.out:
Pitch = 0.5172", 70% IMD	0.9371	0.0007	0.9385	we17_pitch5172_070.out:
Pitch = 0.5172", 80% IMD	0.9402	0.0007	0.9416	we17_pitch5172_080.out:
Pitch = 0.5172", 90% IMD	0.9386	0.0007	0.9400	we17_pitch5172_090.out:
Pitch = 0.5172", 100% IMD	0.9312	0.0006	0.9324	we17_pitch5172_100.out:

Table 6-20
Results of Optimum Pitch Studies
(Continued)

Description	K_{keno}	σ_{keno}	K_{eff}	Filename
CE 14x14, 4.9 wt. % U-235, 2300 ppm, 15 mg B-10/cm ² (Type B Basket)				
Pitch = 0.4400", 70% IMD	0.6852	0.0007	0.6866	ce14_pitch_min_070.out:
Pitch = 0.4400", 80% IMD	0.6915	0.0008	0.6931	ce14_pitch_min_080.out:
Pitch = 0.4700", 70% IMD	0.7560	0.0008	0.7576	ce14_pitch_470_070.out:
Pitch = 0.4700", 80% IMD	0.7626	0.0009	0.7644	ce14_pitch_470_080.out:
Pitch = 0.5000", 70% IMD	0.8196	0.0008	0.8212	ce14_pitch_500_070.out:
Pitch = 0.5000", 80% IMD	0.8245	0.0008	0.8261	ce14_pitch_500_080.out:
Pitch = 0.5400", 70% IMD	0.8872	0.0008	0.8888	ce14_pitch_540_070.out:
Pitch = 0.5400", 80% IMD	0.8886	0.0009	0.8904	ce14_pitch_540_080.out:
Pitch = 0.5800", 70% IMD	0.9337	0.0007	0.9351	ce14_pitch_nom_070.out:
Pitch = 0.5800", 80% IMD	0.9336	0.0007	0.9350	ce14_pitch_nom_080.out:
Pitch = 0.6000", 70% IMD	0.9473	0.0007	0.9487	ce14_pitch_600_070.out:
Pitch = 0.6000", 80% IMD	0.9468	0.0007	0.9482	ce14_pitch_600_080.out:
Pitch = 0.6100", 60% IMD	0.9457	0.0008	0.9473	ce14_pitch_610_060.out:
Pitch = 0.6100", 70% IMD	0.9491	0.0008	0.9507	ce14_pitch_610_070.out:
Pitch = 0.6100", 80% IMD	0.9467	0.0007	0.9481	ce14_pitch_610_080.out:
Pitch = 0.6100", 90% IMD	0.9383	0.0008	0.9399	ce14_pitch_610_090.out:
Pitch = 0.6100", 100% IMD	0.9290	0.0007	0.9304	ce14_pitch_610_100.out:
Pitch = 0.6200", 60% IMD	0.9500	0.0007	0.9514	ce14_pitch_620_060.out:
Pitch = 0.6200", 70% IMD	0.9512	0.0007	0.9526	ce14_pitch_620_070.out:
Pitch = 0.6200", 80% IMD	0.9471	0.0007	0.9485	ce14_pitch_620_080.out:
Pitch = 0.6200", 90% IMD	0.9368	0.0008	0.9384	ce14_pitch_620_090.out:
Pitch = 0.6200", 100% IMD	0.9250	0.0007	0.9264	ce14_pitch_620_100.out:
Pitch = 0.6250", 60% IMD	0.9499	0.0007	0.9513	ce14_pitch_625_060.out:
Pitch = 0.6250", 70% IMD	0.9506	0.0007	0.9520	ce14_pitch_625_070.out:
Pitch = 0.6250", 80% IMD	0.9476	0.0008	0.9492	ce14_pitch_625_080.out:
Pitch = 0.6250", 90% IMD	0.9372	0.0007	0.9386	ce14_pitch_625_090.out:
Pitch = 0.6250", 100% IMD	0.9234	0.0008	0.9250	ce14_pitch_625_100.out:
Pitch = 0.6315", 60% IMD	0.9499	0.0007	0.9513	ce14_pitch_max_060.out:
Pitch = 0.6315", 70% IMD	0.9500	0.0008	0.9516	ce14_pitch_max_070.out:
Pitch = 0.6315", 80% IMD	0.9445	0.0007	0.9459	ce14_pitch_max_080.out:
Pitch = 0.6315", 90% IMD	0.9340	0.0008	0.9356	ce14_pitch_max_090.out:
Pitch = 0.6315", 100% IMD	0.9187	0.0007	0.9201	ce14_pitch_max_100.out:

Table 6-20
Results of Optimum Pitch Studies
(Concluded)

Model Description	k_{KENO}	1σ	k_{eff}
CE 16x16, 4.90 wt. % U-235, 2400 ppm, Type C Basket			
Pitch=0.3820", IMD=080%	0.6889	0.0008	0.6905
Pitch=0.4000", IMD=080%	0.7389	0.0008	0.7405
Pitch=0.4250", IMD=080%	0.7971	0.0009	0.7989
Pitch=0.4500", IMD=080%	0.8476	0.0007	0.8490
Pitch=0.4750", IMD=080%	0.8938	0.0008	0.8954
Pitch=0.5060", IMD=080%	0.9338	0.0007	0.9352
Pitch=0.5200", IMD=050%	0.9278	0.0007	0.9292
Pitch=0.5200", IMD=060%	0.9397	0.0009	0.9415
Pitch=0.5200", IMD=070%	0.9455	0.0008	0.9471
Pitch=0.5200", IMD=080%	0.9431	0.0007	0.9445
Pitch=0.5200", IMD=090%	0.9382	0.0007	0.9396
Pitch=0.5450", IMD=050%	0.9405	0.0007	0.9419
Pitch=0.5450", IMD=060%	0.9501	0.0008	0.9517
Pitch=0.5450", IMD=070%	0.9537	0.0007	0.9551
Pitch=0.5450", IMD=080%	0.9470	0.0007	0.9484
Pitch=0.5450", IMD=090%	0.9399	0.0007	0.9413
Pitch=0.5511", IMD=050%	0.9406	0.0008	0.9422
Pitch=0.5511", IMD=060%	0.9517	0.0007	0.9531
Pitch=0.5511", IMD=070%	0.9509	0.0007	0.9523
Pitch=0.5511", IMD=080%	0.9448	0.0006	0.9460
Pitch=0.5511", IMD=090%	0.9358	0.0006	0.9370

Table 6-21
Results of the Single Ended Rod Shear Studies

Description	K_{keno}	σ_{keno}	K_{eff}	Filename
WE 15x15, 4.9 wt. % U-235, 2500 ppm, 32 mg B-10/cm ² (Type D Basket)				
D=0.00 cm, 60% IMD	0.9224	0.0008	0.9240	we15_ss000_060.out:
D=0.00 cm, 70% IMD	0.9334	0.0007	0.9348	we15_ss000_070.out:
D=0.00 cm, 80% IMD	0.9381	0.0007	0.9395	we15_ss000_080.out:
D=0.00 cm, 90% IMD	0.9374	0.0007	0.9388	we15_ss000_090.out:
D=0.00 cm, 100% IMD	0.9326	0.0007	0.9340	we15_ss000_100.out:
D=0.15 cm, 60% IMD	0.9222	0.0008	0.9238	we15_ss015_060.out:
D=0.15 cm, 70% IMD	0.9344	0.0008	0.9360	we15_ss015_070.out:
D=0.15 cm, 80% IMD	0.9388	0.0007	0.9402	we15_ss015_080.out:
D=0.15 cm, 90% IMD	0.9378	0.0007	0.9392	we15_ss015_090.out:
D=0.15 cm, 100% IMD	0.9341	0.0007	0.9355	we15_ss015_100.out:
D=0.25 cm, 60% IMD	0.9212	0.0009	0.9230	we15_ss025_060.out:
D=0.25 cm, 70% IMD	0.9359	0.0007	0.9373	we15_ss025_070.out:
D=0.25 cm, 80% IMD	0.9394	0.0008	0.9410	we15_ss025_080.out:
D=0.25 cm, 90% IMD	0.9382	0.0007	0.9396	we15_ss025_090.out:
D=0.25 cm, 100% IMD	0.9352	0.0008	0.9368	we15_ss025_100.out:
D=0.35 cm, 60% IMD	0.9225	0.0008	0.9241	we15_ss035_060.out:
D=0.35 cm, 70% IMD	0.9355	0.0007	0.9369	we15_ss035_070.out:
D=0.35 cm, 80% IMD	0.9403	0.0007	0.9417	we15_ss035_080.out:
D=0.35 cm, 90% IMD	0.9391	0.0007	0.9405	we15_ss035_090.out:
D=0.35 cm, 100% IMD	0.9333	0.0007	0.9347	we15_ss035_100.out:
D=0.45 cm, 60% IMD	0.9238	0.0008	0.9254	we15_ss045_060.out:
D=0.45 cm, 70% IMD	0.9335	0.0008	0.9351	we15_ss045_070.out:
D=0.45 cm, 80% IMD	0.9378	0.0008	0.9394	we15_ss045_080.out:
D=0.45 cm, 90% IMD	0.9381	0.0008	0.9397	we15_ss045_090.out:
D=0.45 cm, 100% IMD	0.9330	0.0007	0.9344	we15_ss045_100.out:
D=0.52 cm (max), 60% IMD	0.9224	0.0007	0.9238	we15_ssmax_060.out:
D=0.52 cm (max), 70% IMD	0.9333	0.0008	0.9349	we15_ssmax_070.out:
D=0.52 cm (max), 80% IMD	0.9396	0.0008	0.9412	we15_ssmax_080.out:
D=0.52 cm (max), 90% IMD	0.9376	0.0007	0.9390	we15_ssmax_090.out:
D=0.52 cm (max), 100% IMD	0.9346	0.0007	0.9360	we15_ssmax_100.out:

Table 6-21
Results of the Single Ended Rod Shear Studies
(Continued)

Description	K_{keno}	σ_{keno}	K_{eff}	Filename
WE 17x17, 4.8 wt. % U-235, 2500 ppm, 32 mg B-10/cm ² (Type D Basket)				
D=0.00 cm, 60% IMD	0.9155	0.0007	0.9169	we17_ss000_060.out:
D=0.00 cm, 70% IMD	0.9294	0.0008	0.9310	we17_ss000_070.out:
D=0.00 cm, 80% IMD	0.9366	0.0007	0.9380	we17_ss000_080.out:
D=0.00 cm, 90% IMD	0.9381	0.0007	0.9395	we17_ss000_090.out:
D=0.00 cm, 100% IMD	0.9327	0.0007	0.9341	we17_ss000_100.out:
D=0.15 cm, 60% IMD	0.9165	0.0007	0.9179	we17_ss015_060.out:
D=0.15 cm, 70% IMD	0.9300	0.0007	0.9314	we17_ss015_070.out:
D=0.15 cm, 80% IMD	0.9360	0.0007	0.9374	we17_ss015_080.out:
D=0.15 cm, 90% IMD	0.9398	0.0008	0.9414	we17_ss015_090.out:
D=0.15 cm, 100% IMD	0.9366	0.0007	0.9380	we17_ss015_100.out:
D=0.25 cm, 60% IMD	0.9168	0.0008	0.9184	we17_ss025_060.out:
D=0.25 cm, 70% IMD	0.9298	0.0009	0.9316	we17_ss025_070.out:
D=0.25 cm, 80% IMD	0.9381	0.0008	0.9397	we17_ss025_080.out:
D=0.25 cm, 90% IMD	0.9391	0.0008	0.9407	we17_ss025_090.out:
D=0.25 cm, 100% IMD	0.9370	0.0007	0.9384	we17_ss025_100.out:
D=0.35 cm, 60% IMD	0.9167	0.0007	0.9181	we17_ss035_060.out:
D=0.35 cm, 70% IMD	0.9318	0.0008	0.9334	we17_ss035_070.out:
D=0.35 cm, 80% IMD	0.9370	0.0007	0.9384	we17_ss035_080.out:
D=0.35 cm, 90% IMD	0.9389	0.0007	0.9403	we17_ss035_090.out:
D=0.35 cm, 100% IMD	0.9356	0.0007	0.9370	we17_ss035_100.out:
D=0.45 cm, 60% IMD	0.9160	0.0007	0.9174	we17_ss045_060.out:
D=0.45 cm, 70% IMD	0.9311	0.0008	0.9327	we17_ss045_070.out:
D=0.45 cm, 80% IMD	0.9378	0.0007	0.9392	we17_ss045_080.out:
D=0.45 cm, 90% IMD	0.9398	0.0007	0.9412	we17_ss045_090.out:
D=0.45 cm, 100% IMD	0.9363	0.0007	0.9377	we17_ss045_100.out:
D=0.55 cm (max), 60% IMD	0.9176	0.0008	0.9192	we17_ssmax_060.out:
D=0.55 cm (max), 70% IMD	0.9332	0.0007	0.9346	we17_ssmax_070.out:
D=0.55 cm (max), 80% IMD	0.9381	0.0006	0.9393	we17_ssmax_080.out:
D=0.55 cm (max), 90% IMD	0.9389	0.0007	0.9403	we17_ssmax_090.out:
D=0.55 cm (max), 100% IMD	0.9360	0.0007	0.9374	we17_ssmax_100.out:

Table 6-21
Results of the Single Ended Rod Shear Studies
(Continued)

Description	K_{keno}	σ_{keno}	K_{eff}	Filename
CE 14x14, 4.9 wt. % U-235, 2300 ppm, 15 mg B-10/cm ² (Type B Basket)				
D=0.00 cm, 60% IMD	0.9309	0.0008	0.9325	ce14_ss000_060.out:
D=0.00 cm, 70% IMD	0.9348	0.0009	0.9366	ce14_ss000_070.out:
D=0.00 cm, 80% IMD	0.9343	0.0007	0.9357	ce14_ss000_080.out:
D=0.00 cm, 90% IMD	0.9289	0.0007	0.9303	ce14_ss000_090.out:
D=0.00 cm, 100% IMD	0.9214	0.0008	0.9230	ce14_ss000_100.out:
D=0.20 cm, 60% IMD	0.9303	0.0007	0.9317	ce14_ss020_060.out:
D=0.20 cm, 70% IMD	0.9383	0.0007	0.9397	ce14_ss020_070.out:
D=0.20 cm, 80% IMD	0.9357	0.0007	0.9371	ce14_ss020_080.out:
D=0.20 cm, 90% IMD	0.9311	0.0008	0.9327	ce14_ss020_090.out:
D=0.20 cm, 100% IMD	0.9230	0.0007	0.9244	ce14_ss020_100.out:
D=0.40 cm, 60% IMD	0.9336	0.0008	0.9352	ce14_ss040_060.out:
D=0.40 cm, 70% IMD	0.9391	0.0008	0.9407	ce14_ss040_070.out:
D=0.40 cm, 80% IMD	0.9400	0.0008	0.9416	ce14_ss040_080.out:
D=0.40 cm, 90% IMD	0.9335	0.0007	0.9349	ce14_ss040_090.out:
D=0.40 cm, 100% IMD	0.9254	0.0007	0.9268	ce14_ss040_100.out:
D=0.60 cm, 60% IMD	0.9335	0.0008	0.9351	ce14_ss060_060.out:
D=0.60 cm, 70% IMD	0.9407	0.0008	0.9423	ce14_ss060_070.out:
D=0.60 cm, 80% IMD	0.9402	0.0008	0.9418	ce14_ss060_080.out:
D=0.60 cm, 90% IMD	0.9345	0.0007	0.9359	ce14_ss060_090.out:
D=0.60 cm, 100% IMD	0.9248	0.0007	0.9262	ce14_ss060_100.out:
D=0.80 cm, 60% IMD	0.9340	0.0008	0.9356	ce14_ss080_060.out:
D=0.80 cm, 70% IMD	0.9403	0.0007	0.9417	ce14_ss080_070.out:
D=0.80 cm, 80% IMD	0.9411	0.0008	0.9427	ce14_ss080_080.out:
D=0.80 cm, 90% IMD	0.9342	0.0007	0.9356	ce14_ss080_090.out:
D=0.80 cm, 100% IMD	0.9252	0.0007	0.9266	ce14_ss080_100.out:
D=1.00 cm, 60% IMD	0.9351	0.0008	0.9367	ce14_ss100_060.out:
D=1.00 cm, 70% IMD	0.9410	0.0008	0.9426	ce14_ss100_070.out:
D=1.00 cm, 80% IMD	0.9401	0.0008	0.9417	ce14_ss100_080.out:
D=1.00 cm, 90% IMD	0.9336	0.0007	0.9350	ce14_ss100_090.out:
D=1.00 cm, 100% IMD	0.9233	0.0008	0.9249	ce14_ss100_100.out:

Table 6-21
Results of the Single Ended Rod Shear Studies
(Concluded)

Description	K_{keno}	σ_{keno}	K_{eff}	Filename
CE 14x14, 4.9 wt. % U-235, 2300 ppm, 15 mg B-10/cm ² (Type B Basket)				
D=1.20 cm, 60% IMD	0.9336	0.0007	0.9350	ce14_ss120_060.out:
D=1.20 cm, 70% IMD	0.9402	0.0008	0.9418	ce14_ss120_070.out:
D=1.20 cm, 80% IMD	0.9384	0.0007	0.9398	ce14_ss120_080.out:
D=1.20 cm, 90% IMD	0.9325	0.0007	0.9339	ce14_ss120_090.out:
D=1.20 cm, 100% IMD	0.9235	0.0007	0.9249	ce14_ss120_100.out:
D=1.35 cm, 60% IMD	0.9341	0.0007	0.9355	ce14_ssmax_060.out:
D=1.35 cm, 70% IMD	0.9386	0.0007	0.9400	ce14_ssmax_070.out:
D=1.35 cm, 80% IMD	0.9363	0.0008	0.9379	ce14_ssmax_080.out:
D=1.35 cm, 90% IMD	0.9291	0.0008	0.9307	ce14_ssmax_090.out:
D=1.35 cm, 100% IMD	0.9203	0.0007	0.9217	ce14_ssmax_100.out:
Model Description	K_{keno}	σ_{keno}	K_{eff}	
CE 16x16 4.90 wt. % U-235, 2400 ppm, Type C Basket				
Nominal Pitch, IMD=080%	0.9338	0.0007	0.9352	
D=0.000 cm, IMD=080%	0.9339	0.0008	0.9355	
D=0.300 cm, IMD=080%	0.9364	0.0007	0.9378	
D=0.600 cm, IMD=080%	0.9377	0.0007	0.9391	
D=0.900 cm, IMD=080%	0.9370	0.0007	0.9384	
D=1.200 cm, IMD=080%	0.9374	0.0008	0.9390	
D=1.407 cm, IMD=080%	0.9348	0.0007	0.9362	

Table 6-22
Results of the Double Ended Rod Shear Studies

CE 14x14, 4.9 wt. % U-235, 2300 ppm, 15 mg B-10/cm ² (Type B Basket)				
Description	K _{keno}	σ_{keno}	K _{eff}	Filename
No Shear				
Ratio=0, 60% IMD	0.9289	0.0008	0.9305	ce14_ds000_060.out:
Ratio=0, 70% IMD	0.9340	0.0008	0.9356	ce14_ds000_070.out:
Ratio=0, 80% IMD	0.9336	0.0007	0.9350	ce14_ds000_080.out:
Ratio=0, 90% IMD	0.9284	0.0008	0.9300	ce14_ds000_090.out:
Ratio=0, 100% IMD	0.9224	0.0007	0.9238	ce14_ds000_100.out:
Double Ended Shear with Minimum Distance Between the Sheared and Intact Rows				
Ratio=5/10, 60% IMD	0.9349	0.0007	0.9363	ce14_ds001_060.out:
Ratio=5/10, 70% IMD	0.9406	0.0009	0.9424	ce14_ds001_070.out:
Ratio=5/10, 80% IMD	0.9442	0.0007	0.9456	ce14_ds001_080.out:
Ratio=5/10, 90% IMD	0.9398	0.0008	0.9414	ce14_ds001_090.out:
Ratio=5/10, 100% IMD	0.9328	0.0008	0.9344	ce14_ds001_100.out:
Double Ended Shear with Maximum Distance Between the Sheared and Intact Rows				
Ratio=5/10, 60% IMD	0.9373	0.0007	0.9387	ce14_ds011_060.out:
Ratio=5/10, 70% IMD	0.9453	0.0008	0.9469	ce14_ds011_070.out:
Ratio=5/10, 80% IMD	0.9492	0.0008	0.9508	ce14_ds011_080.out:
Ratio=5/10, 90% IMD	0.9443	0.0007	0.9457	ce14_ds011_090.out:
Ratio=5/10, 100% IMD	0.9365	0.0007	0.9379	ce14_ds011_100.out:

Table 6-22
Results of the Double Ended Rod Shear Studies
(Continued)

Description	K_{keno}	σ_{keno}	K_{eff}	Filename
WE 15x15, 4.9 wt. % U-235, 2500 ppm, 32 mg B-10/cm ² (Type D Basket)				
Ratio=0, 60% IMD	0.9209	0.0007	0.9223	we15_ds000_060.out:
Ratio=0, 70% IMD	0.9320	0.0008	0.9336	we15_ds000_070.out:
Ratio=0, 80% IMD	0.9382	0.0007	0.9396	we15_ds000_080.out:
Ratio=0, 90% IMD	0.9384	0.0007	0.9398	we15_ds000_090.out:
Ratio=0, 100% IMD	0.9335	0.0008	0.9351	we15_ds000_100.out:
Ratio=2/10, 60% IMD	0.9204	0.0007	0.9218	we15_ds210_060.out:
Ratio=2/10, 70% IMD	0.9321	0.0008	0.9337	we15_ds210_070.out:
Ratio=2/10, 80% IMD	0.9388	0.0008	0.9404	we15_ds210_080.out:
Ratio=2/10, 90% IMD	0.9381	0.0008	0.9397	we15_ds210_090.out:
Ratio=2/10, 100% IMD	0.9334	0.0007	0.9348	we15_ds210_100.out:
Ratio=3/10, 60% IMD	0.9214	0.0008	0.9230	we15_ds310_060.out:
Ratio=3/10, 70% IMD	0.9350	0.0008	0.9366	we15_ds310_070.out:
Ratio=3/10, 80% IMD	0.9408	0.0008	0.9424	we15_ds310_080.out:
Ratio=3/10, 90% IMD	0.9421	0.0008	0.9437	we15_ds310_090.out:
Ratio=3/10, 100% IMD	0.9367	0.0008	0.9383	we15_ds310_100.out:
Ratio=5/10, 60% IMD	0.9239	0.0008	0.9255	we15_ds510_060.out:
Ratio=5/10, 70% IMD	0.9371	0.0007	0.9385	we15_ds510_070.out:
Ratio=5/10, 80% IMD	0.9438	0.0008	0.9454	we15_ds510_080.out:
Ratio=5/10, 90% IMD	0.9425	0.0007	0.9439	we15_ds510_090.out:
Ratio=5/10, 100% IMD	0.9404	0.0009	0.9422	we15_ds510_100.out:

Table 6-22
Results of the Double Ended Rod Shear Studies
(Concluded)

Description	K_{keno}	σ_{keno}	K_{eff}	Filename
WE 17x17, 4.8 wt. % U-235, 2500 ppm, 32 mg B-10/cm ² (Type D Basket)				
Ratio=0, 60% IMD	0.9149	0.0007	0.9163	we17_ds000_060.out:
Ratio=0, 70% IMD	0.9304	0.0009	0.9322	we17_ds000_070.out:
Ratio=0, 80% IMD	0.9354	0.0007	0.9368	we17_ds000_080.out:
Ratio=0, 90% IMD	0.9369	0.0007	0.9383	we17_ds000_090.out:
Ratio=0, 100% IMD	0.9355	0.0008	0.9371	we17_ds000_100.out:
Ratio=2/10, 60% IMD	0.9159	0.0008	0.9175	we17_ds210_060.out:
Ratio=2/10, 70% IMD	0.9299	0.0007	0.9313	we17_ds210_070.out:
Ratio=2/10, 80% IMD	0.9371	0.0008	0.9387	we17_ds210_080.out:
Ratio=2/10, 90% IMD	0.9386	0.0008	0.9402	we17_ds210_090.out:
Ratio=2/10, 100% IMD	0.9372	0.0008	0.9388	we17_ds210_100.out:
Ratio=3/10, 60% IMD	0.9184	0.0008	0.9200	we17_ds310_060.out:
Ratio=3/10, 70% IMD	0.9319	0.0008	0.9335	we17_ds310_070.out:
Ratio=3/10, 80% IMD	0.9382	0.0007	0.9396	we17_ds310_080.out:
Ratio=3/10, 90% IMD	0.9415	0.0007	0.9429	we17_ds310_090.out:
Ratio=3/10, 100% IMD	0.9386	0.0008	0.9402	we17_ds310_100.out:
Ratio=5/10, 60% IMD	0.9179	0.0008	0.9195	we17_ds510_060.out:
Ratio=5/10, 70% IMD	0.9324	0.0008	0.9340	we17_ds510_070.out:
Ratio=5/10, 80% IMD	0.9404	0.0007	0.9418	we17_ds510_080.out:
Ratio=5/10, 90% IMD	0.9444	0.0008	0.9460	we17_ds510_090.out:
Ratio=5/10, 100% IMD	0.9403	0.0007	0.9417	we17_ds510_100.out:
Model Description	K_{keno}	σ_{keno}	K_{eff}	Filename
CE 16x16, 4.9 wt. % U-235, 2400 ppm, Type C Basket				
IMD=060%	0.9372	0.0007	0.9386	
IMD=070%	0.9457	0.0008	0.9473	
IMD=080%	0.9449	0.0008	0.9465	
IMD=090%	0.9413	0.0009	0.9431	

Table 6-23
Evaluation of the Shifting of Fuel Rods Beyond the Poison

Description	K_{keno}	σ_{keno}	K_{eff}	Filename
CE 14x14, 4.9 wt. % U-235, 2300 ppm, 15 mg B-10/cm ² (Type B Basket)				
Shift 4-inches, 60% IMD	0.9320	0.0008	0.9336	ce14_nopoison_04_060.out
Shift 4-inches, 70% IMD	0.9372	0.0008	0.9388	ce14_nopoison_04_070.out
Shift 4-inches, 80% IMD	0.9371	0.0009	0.9389	ce14_nopoison_04_080.out
Shift 4-inches, 90% IMD	0.9321	0.0008	0.9337	ce14_nopoison_04_090.out
Shift 4-inches, 100% IMD	0.9224	0.0008	0.9240	ce14_nopoison_04_100.out
Slide 6-inches, 60% IMD	0.9279	0.0008	0.9295	ce14_slide_06_060.out:
Slide 6-inches, 70% IMD	0.9341	0.0007	0.9355	ce14_slide_06_070.out:
Slide 6-inches, 80% IMD	0.9329	0.0008	0.9345	ce14_slide_06_080.out:
Slide 6-inches, 90% IMD	0.9276	0.0007	0.9290	ce14_slide_06_090.out:
Slide 6-inches, 100% IMD	0.9198	0.0007	0.9212	ce14_slide_06_100.out:
4" Shifting, WE 15x15, 4.9 wt. % U-235, 2500 ppm, 32 mg B-10/cm ² (Type D Basket)				
Shift 4-inches, 60% IMD	0.9271	0.0009	0.9289	we15_np004_060.out:
Shift 4-inches, 70% IMD	0.9382	0.0008	0.9398	we15_np004_070.out:
Shift 4-inches, 80% IMD	0.9424	0.0008	0.9440	we15_np004_080.out:
Shift 4-inches, 90% IMD	0.9397	0.0008	0.9413	we15_np004_090.out:
Shift 4-inches, 100% IMD	0.9341	0.0007	0.9355	we15_np004_100.out:
6" Sliding, WE 15x15, 4.9 wt. % U-235, 2500 ppm, 32 mg B-10/cm ² (Type D Basket)				
Slide 6-inches, 60% IMD	0.9190	0.0007	0.9204	we15_sl006_060.out:
Slide 6-inches, 70% IMD	0.9324	0.0008	0.9340	we15_sl006_070.out:
Slide 6-inches, 80% IMD	0.9378	0.0008	0.9394	we15_sl006_080.out:
Slide 6-inches, 90% IMD	0.9372	0.0008	0.9388	we15_sl006_090.out:
Slide 6-inches, 100% IMD	0.9319	0.0007	0.9333	we15_sl006_100.out:
WE 17x17, 4.8 wt. % U-235, 2500 ppm, 32 mg B-10/cm ² (Type D Basket)				
Shift 4-inches, 60% IMD	0.9241	0.0009	0.9259	we17_np004_060.out:
Shift 4-inches, 70% IMD	0.9362	0.0007	0.9376	we17_np004_070.out:
Shift 4-inches, 80% IMD	0.9407	0.0007	0.9421	we17_np004_080.out:
Shift 4-inches, 90% IMD	0.9411	0.0007	0.9425	we17_np004_090.out:
Shift 4-inches, 100% IMD	0.9366	0.0008	0.9382	we17_np004_100.out:
6" Sliding, WE 17x17, 4.8 wt. % U-235, 2500 ppm, 32 mg B-10/cm ² (Type D Basket)				
Slide 6-inches, 60% IMD	0.9153	0.0007	0.9167	we17_sl006_060.out:
Slide 6-inches, 70% IMD	0.9283	0.0007	0.9297	we17_sl006_070.out:
Slide 6-inches, 80% IMD	0.9344	0.0007	0.9358	we17_sl006_080.out:
Slide 6-inches, 90% IMD	0.9364	0.0008	0.9380	we17_sl006_090.out:
Slide 6-inches, 100% IMD	0.9346	0.0008	0.9362	we17_sl006_100.out:

Table 6-23
Evaluation of the Shifting of Fuel Rods Beyond the Poison
(Concluded)

Model Description	k_{KENO}	1σ	k_{eff}	
CE 16x16, 4.9 wt. % U-235, 2400 ppm, Type C Basket				
IMD=060%	0.9323	0.0008	0.9339	
IMD=070%	0.9375	0.0007	0.9389	
IMD=080%	0.9355	0.0007	0.9369	
IMD=090%	0.9288	0.0007	0.9302	

Table 6-24
Most Reactive Damaged Assembly Configuration

Description	K_{keno}	σ_{keno}	K_{eff}	Filename
CE 14x14, 4.9 wt. % U-235, 2300 ppm, 15 mg B-10/cm ² (Type B Basket)				
Optimum Pitch	0.9512	0.0007	0.9526	ce14_pitch_620_070.out:
Single Ended Shear	0.9411	0.0008	0.9427	ce14_ss080_080.out:
Double Ended Shear	0.9492	0.0008	0.9508	ce14_ds011_080.out:
Shift 4-inches	0.9371	0.0009	0.9389	ce14_nopoison_04_080.out
Slide 6-inches	0.9341	0.0007	0.9355	ce14_slide_06_070.out:
WE 15x15, 4.9 wt. % U-235, 2500 ppm, 32 mg B-10/cm ² (Type D Basket), No BPRA				
Optimum Pitch	0.9417	0.0007	0.9431	we15_pitch5877_080.out:
Single Ended Shear	0.9403	0.0007	0.9417	we15_ss035_080.out:
Double Ended Shear	0.9438	0.0008	0.9454	we15_ds510_080.out:
Shift 4-inches	0.9424	0.0008	0.9440	we15_np004_080.out:
Slide 6-inches	0.9378	0.0008	0.9394	we15_sl006_080.out:
WE 17x17, 4.8 wt. % U-235, 2500 ppm, 32 mg B-10/cm ² (Type D Basket), No BPRA				
Optimum Pitch	0.9405	0.0008	0.9421	we17_pitch5100_090.out:
Single Ended Shear	0.9398	0.0008	0.9414	we17_ss015_090.out:
Double Ended Shear	0.9444	0.0008	0.9460	we17_ds510_090.out:
Shift 4-inches	0.9411	0.0007	0.9425	we17_np004_090.out:
Slide 6-inches	0.9364	0.0008	0.9380	we17_sl006_090.out:
Model Description	K_{keno}	σ_{keno}	K_{eff}	Filename
CE 16x16, 4.9 wt. % U-235, 2400 ppm, Type C Basket				
Optimum Pitch	0.9537	0.0007	0.9551	
Single Shear	0.9377	0.0007	0.9391	
Double Shear	0.9457	0.0008	0.9473	
4" Shift	0.9375	0.0007	0.9389	

Table 6-25
Double Ended Rod Shear Study with BPRAs

Description	K_{keno}	σ_{keno}	K_{eff}	Filename
WE 15x15, 4.9 wt. % U-235, 2500 ppm, 32 mg B-10/cm ² (Type D Basket), BPRA				
Ratio=5/10, 60% IMD	0.9132	0.0008	0.9148	we15bp_ds510_060.out:
Ratio=5/10, 70% IMD	0.9316	0.0008	0.9332	we15bp_ds510_070.out:
Ratio=5/10, 80% IMD	0.9410	0.0009	0.9428	we15bp_ds510_080.out:
Ratio=5/10, 90% IMD	0.9483	0.0008	0.9499	we15bp_ds510_090.out:
Ratio=5/10, 100% IMD	0.9514	0.0007	0.9528	we15bp_ds510_100.out:
WE 17x17, 4.8 wt. % U-235, 2500 ppm, 32 mg B-10/cm ² (Type D Basket), BPRA				
Ratio=5/10, 60% IMD	0.9052	0.0008	0.9068	we17bp_ds510_060.out:
Ratio=5/10, 70% IMD	0.9257	0.0007	0.9271	we17bp_ds510_070.out:
Ratio=5/10, 80% IMD	0.9387	0.0007	0.9401	we17bp_ds510_080.out:
Ratio=5/10, 90% IMD	0.9462	0.0008	0.9478	we17bp_ds510_090.out:
Ratio=5/10, 100% IMD	0.9478	0.0008	0.9494	we17bp_ds510_100.out:

Table 6-26
WE 15x15 Class Damaged Assemblies With BPRAs - Final Results

Description	K_{keno}	σ_{keno}	K_{eff}	Filename
Type A Basket (7.0 mg B-10/cm ²), 2300 ppm Boron, 3.6 wt. % U-235				
60% IMD	0.9131	0.0007	0.9145	we15bpds_p07e36_060.out:
70% IMD	0.9249	0.0007	0.9263	we15bpds_p07e36_070.out:
80% IMD	0.9296	0.0007	0.9310	we15bpds_p07e36_080.out:
90% IMD	0.9267	0.0008	0.9283	we15bpds_p07e36_090.out:
100% IMD	0.9255	0.0007	0.9269	we15bpds_p07e36_100.out:
Type B Basket (15.0 mg B-10/cm ²), 2300 ppm Boron, 4.0 wt. % U-235				
60% IMD	0.9053	0.0007	0.9067	we15bpds_p15e40_060.out:
70% IMD	0.9223	0.0008	0.9239	we15bpds_p15e40_070.out:
80% IMD	0.9288	0.0008	0.9304	we15bpds_p15e40_080.out:
90% IMD	0.9314	0.0008	0.9330	we15bpds_p15e40_090.out:
100% IMD	0.9340	0.0007	0.9354	we15bpds_p15e40_100.out:
Type D Basket (32.0 mg B-10/cm ²), 2300 ppm Boron, 4.4 wt. % U-235				
60% IMD	0.8923	0.0008	0.8939	we15bpds_p32e44_060.out:
70% IMD	0.9121	0.0009	0.9139	we15bpds_p32e44_070.out:
80% IMD	0.9232	0.0007	0.9246	we15bpds_p32e44_080.out:
90% IMD	0.9324	0.0007	0.9338	we15bpds_p32e44_090.out:
100% IMD	0.9333	0.0008	0.9349	we15bpds_p32e44_100.out:
Type E Basket (50.0 mg B-10/cm ²), 2300 ppm Boron, 4.7 wt. % U-235				
60% IMD	0.8825	0.0008	0.8841	we15bpds_p50e47_060.out:
70% IMD	0.9068	0.0008	0.9084	we15bpds_p50e47_070.out:
80% IMD	0.9210	0.0008	0.9226	we15bpds_p50e47_080.out:
90% IMD	0.9316	0.0008	0.9332	we15bpds_p50e47_090.out:
100% IMD	0.9361	0.0007	0.9375	we15bpds_p50e47_100.out:
Type A Basket (7.0 mg B-10/cm ²), 2400 ppm Boron, 3.7 wt. % U-235				
60% IMD	0.9158	0.0008	0.9174	we15bpds_p07e37_060.out:
70% IMD	0.9264	0.0007	0.9278	we15bpds_p07e37_070.out:
80% IMD	0.9305	0.0007	0.9319	we15bpds_p07e37_080.out:
90% IMD	0.9288	0.0006	0.9300	we15bpds_p07e37_090.out:
100% IMD	0.9254	0.0008	0.9270	we15bpds_p07e37_100.out:
Type B Basket (15.0 mg B-10/cm ²), 2400 ppm Boron, 4.1 wt. % U-235				
60% IMD	0.9079	0.0007	0.9093	we15bpds_p15e41_060.out:
70% IMD	0.9230	0.0007	0.9244	we15bpds_p15e41_070.out:
80% IMD	0.9324	0.0009	0.9342	we15bpds_p15e41_080.out:
90% IMD	0.9332	0.0008	0.9348	we15bpds_p15e41_090.out:
100% IMD	0.9326	0.0007	0.9340	we15bpds_p15e41_100.out:

Table 6-26
WE 15x15 Class Damaged Assemblies With BPRAs - Final Results
(Continued)

Description	K_{keno}	σ_{keno}	K_{eff}	Filename
Type D Basket (32.0 mg B-10/cm ²), 2400 ppm Boron, 4.5 wt. % U-235				
60% IMD	0.8942	0.0007	0.8956	we15bpds_p32e45_060.out:
70% IMD	0.9139	0.0007	0.9153	we15bpds_p32e45_070.out:
80% IMD	0.9239	0.0007	0.9253	we15bpds_p32e45_080.out:
90% IMD	0.9309	0.0007	0.9323	we15bpds_p32e45_090.out:
100% IMD	0.9333	0.0007	0.9347	we15bpds_p32e45_100.out:
Type E Basket (50.0 mg B-10/cm ²), 2400 ppm Boron, 4.8 wt. % U-235				
60% IMD	0.8851	0.0009	0.8869	we15bpds_p50e48_060.out:
70% IMD	0.9078	0.0009	0.9096	we15bpds_p50e48_070.out:
80% IMD	0.9221	0.0008	0.9237	we15bpds_p50e48_080.out:
90% IMD	0.9318	0.0008	0.9334	we15bpds_p50e48_090.out:
100% IMD	0.9353	0.0007	0.9367	we15bpds_p50e48_100.out:
Type A Basket (7.0 mg B-10/cm ²), 2500 ppm Boron, 3.8 wt. % U-235				
60% IMD	0.9194	0.0007	0.9208	we15bpds_p07e38_060.out:
70% IMD	0.9286	0.0007	0.9300	we15bpds_p07e38_070.out:
80% IMD	0.9322	0.0008	0.9338	we15bpds_p07e38_080.out:
90% IMD	0.9327	0.0008	0.9343	we15bpds_p07e38_090.out:
100% IMD	0.9265	0.0007	0.9279	we15bpds_p07e38_100.out:
Type B Basket (15.0 mg B-10/cm ²), 2500 ppm Boron, 4.2 wt. % U-235				
60% IMD	0.9125	0.0007	0.9139	we15bpds_p15e42_060.out:
70% IMD	0.9240	0.0009	0.9258	we15bpds_p15e42_070.out:
80% IMD	0.9311	0.0007	0.9325	we15bpds_p15e42_080.out:
90% IMD	0.9349	0.0008	0.9365	we15bpds_p15e42_090.out:
100% IMD	0.9334	0.0007	0.9348	we15bpds_p15e42_100.out:
Type D Basket (32.0 mg B-10/cm ²), 2500 ppm Boron, 4.6 wt. % U-235				
60% IMD	0.8965	0.0008	0.8981	we15bpds_p32e46_060.out:
70% IMD	0.9144	0.0008	0.9160	we15bpds_p32e46_070.out:
80% IMD	0.9236	0.0007	0.9250	we15bpds_p32e46_080.out:
90% IMD	0.9315	0.0008	0.9331	we15bpds_p32e46_090.out:
100% IMD	0.9312	0.0009	0.9330	we15bpds_p32e46_100.out:
Type E Basket (50.0 mg B-10/cm ²), 2500 ppm Boron, 4.9 wt. % U-235				
60% IMD	0.8873	0.0007	0.8887	we15bpds_p50e49_060.out:
70% IMD	0.9084	0.0008	0.9100	we15bpds_p50e49_070.out:
80% IMD	0.9233	0.0009	0.9251	we15bpds_p50e49_080.out:
90% IMD	0.9295	0.0007	0.9309	we15bpds_p50e49_090.out:
100% IMD	0.9358	0.0008	0.9374	we15bpds_p50e49_100.out:

Table 6-26
WE 15x15 Class Damaged Assemblies With BPRAs - Final Results
(Continued)

Description	K_{keno}	σ_{keno}	K_{eff}	Filename
Type A Basket (7.0 mg B-10/cm ²), 2000 ppm Boron, 3.40 wt. % U-235				
60% IMD	0.9101	0.0008	0.9117	we15bpds_p07e34_060.out:
70% IMD	0.9249	0.0007	0.9263	we15bpds_p07e34_070.out:
80% IMD	0.9321	0.0008	0.9337	we15bpds_p07e34_080.out:
90% IMD	0.9324	0.0007	0.9338	we15bpds_p07e34_090.out:
100% IMD	0.9297	0.0008	0.9313	we15bpds_p07e34_100.out:
Type B Basket (15.0 mg B-10/cm ²), 2000 ppm Boron, 3.75 wt. % U-235				
60% IMD	0.9007	0.0007	0.9021	we15bpds_p15e38_060.out:
70% IMD	0.9205	0.0007	0.9219	we15bpds_p15e38_070.out:
80% IMD	0.9290	0.0007	0.9304	we15bpds_p15e38_080.out:
90% IMD	0.9352	0.0007	0.9366	we15bpds_p15e38_090.out:
100% IMD	0.9372	0.0007	0.9386	we15bpds_p15e38_100.out:
Type D Basket (32.0 mg B-10/cm ²), 2000 ppm Boron, 4.10 wt. % U-235				
60% IMD	0.8863	0.0008	0.8879	we15bpds_p32e41_060.out:
70% IMD	0.9088	0.0008	0.9104	we15bpds_p32e41_070.out:
80% IMD	0.9211	0.0008	0.9227	we15bpds_p32e41_080.out:
90% IMD	0.9307	0.0007	0.9321	we15bpds_p32e41_090.out:
100% IMD	0.9337	0.0008	0.9353	we15bpds_p32e41_100.out:
Type E Basket (50.0 mg B-10/cm ²), 2000 ppm Boron, 4.35 wt. % U-235				
60% IMD	0.8760	0.0007	0.8774	we15bpds_p50e44_060.out:
70% IMD	0.9020	0.0008	0.9036	we15bpds_p50e44_070.out:
80% IMD	0.9177	0.0008	0.9193	we15bpds_p50e44_080.out:
90% IMD	0.9274	0.0007	0.9288	we15bpds_p50e44_090.out:
100% IMD	0.9336	0.0008	0.9352	we15bpds_p50e44_100.out:
Type A Basket (7.0 mg B-10/cm ²), 2800 ppm Boron, 3.95 wt. % U-235				
60% IMD	0.9267	0.0007	0.9281	
70% IMD	0.9339	0.0008	0.9355	
80% IMD	0.9341	0.0009	0.9359	
90% IMD	0.9306	0.0006	0.9318	
100% IMD	0.9240	0.0008	0.9256	
Type B Basket (15.0 mg B-10/cm ²), 2800 ppm Boron, 4.35 wt. % U-235				
60% IMD	0.9184	0.0008	0.9200	
70% IMD	0.9295	0.0008	0.9311	
80% IMD	0.9353	0.0007	0.9367	
90% IMD	0.9327	0.0008	0.9343	
100% IMD	0.9305	0.0007	0.9319	

Table 6-26
WE 15x15 Class Damaged Assemblies With BPRAs - Final Results
(Concluded)

Description	K_{keno}	σ_{keno}	K_{eff}	Filename
Type C Basket (20.0 mg B-10/cm ²), 2800 ppm Boron, 4.50 wt. % U-235				
60% IMD	0.9146	0.0009	0.9164	
70% IMD	0.9250	0.0007	0.9264	
80% IMD	0.9316	0.0008	0.9332	
90% IMD	0.9327	0.0008	0.9343	
100% IMD	0.9292	0.0008	0.9308	
Type D Basket (32.0 mg B-10/cm ²), 2800 ppm Boron, 4.80 wt. % U-235				
60% IMD	0.9102	0.0008	0.9118	
70% IMD	0.9237	0.0007	0.9251	
80% IMD	0.9320	0.0008	0.9336	
90% IMD	0.9350	0.0007	0.9364	
100% IMD	0.9352	0.0008	0.9368	
Type E Basket (50.0 mg B-10/cm ²), 2800 ppm Boron, 5.00 wt. % U-235				
60% IMD	0.8936	0.0007	0.8950	
70% IMD	0.9119	0.0008	0.9135	
80% IMD	0.9229	0.0007	0.9243	
90% IMD	0.9276	0.0008	0.9292	
100% IMD	0.9292	0.0008	0.9308	

Table 6-27
WE 17x17 Class Damaged Assemblies With BPRAs - Final Results

Description	K_{keno}	σ_{keno}	K_{eff}	Filename
Type A Basket (7.0 mg B-10/cm ²), 2000 ppm Boron, 3.40 wt. % U-235				
60% IMD	0.9111	0.0008	0.9127	we17bpds_p07e34_060.out:
70% IMD	0.9238	0.0007	0.9252	we17bpds_p07e34_070.out:
80% IMD	0.9320	0.0007	0.9334	we17bpds_p07e34_080.out:
90% IMD	0.9340	0.0008	0.9356	we17bpds_p07e34_090.out:
100% IMD	0.9347	0.0006	0.9359	we17bpds_p07e34_100.out:
Type B Basket (15.0 mg B-10/cm ²), 2000 ppm Boron, 3.75 wt. % U-235				
60% IMD	0.8999	0.0007	0.9013	we17bpds_p15e38_060.out:
70% IMD	0.9188	0.0008	0.9204	we17bpds_p15e38_070.out:
80% IMD	0.9301	0.0007	0.9315	we17bpds_p15e38_080.out:
90% IMD	0.9357	0.0008	0.9373	we17bpds_p15e38_090.out:
100% IMD	0.9379	0.0006	0.9391	we17bpds_p15e38_100.out:
Type C Basket (20.0 mg B-10/cm ²), 2000 ppm Boron, 3.85 wt. % U-235				
60% IMD	0.8922	0.0008	0.8938	we17bpds_p20e39_060.out:
70% IMD	0.9125	0.0008	0.9141	we17bpds_p20e39_070.out:
80% IMD	0.9241	0.0008	0.9257	we17bpds_p20e39_080.out:
90% IMD	0.9321	0.0007	0.9335	we17bpds_p20e39_090.out:
100% IMD	0.9343	0.0007	0.9357	we17bpds_p20e39_100.out:
Type D Basket (32.0 mg B-10/cm ²), 2000 ppm Boron, 4.10 wt. % U-235				
60% IMD	0.8851	0.0007	0.8865	we17bpds_p32e41_060.out:
70% IMD	0.9075	0.0009	0.9093	we17bpds_p32e41_070.out:
80% IMD	0.9203	0.0008	0.9219	we17bpds_p32e41_080.out:
90% IMD	0.9327	0.0008	0.9343	we17bpds_p32e41_090.out:
100% IMD	0.9362	0.0007	0.9376	we17bpds_p32e41_100.out:
Type E Basket (50.0 mg B-10/cm ²), 2000 ppm Boron, 4.30 wt. % U-235				
60% IMD	0.8721	0.0008	0.8737	we17bpds_p50e44_060.out:
70% IMD	0.8977	0.0008	0.8993	we17bpds_p50e44_070.out:
80% IMD	0.9150	0.0007	0.9164	we17bpds_p50e44_080.out:
90% IMD	0.9270	0.0008	0.9286	we17bpds_p50e44_090.out:
100% IMD	0.9336	0.0008	0.9352	we17bpds_p50e44_100.out:
Type A Basket (7.0 mg B-10/cm ²), 2300 ppm Boron, 3.6 wt. % U-235				
60% IMD	0.9102	0.0007	0.9116	we17bpds_p07e36_060.out:
70% IMD	0.9227	0.0007	0.9241	we17bpds_p07e36_070.out:
80% IMD	0.9293	0.0008	0.9309	we17bpds_p07e36_080.out:
90% IMD	0.9303	0.0007	0.9317	we17bpds_p07e36_090.out:
100% IMD	0.9275	0.0008	0.9291	we17bpds_p07e36_100.out:

Table 6-27
WE 17x17 Class Damaged Assemblies With BPRAs - Final Results
(Continued)

Description	K_{keno}	σ_{keno}	K_{eff}	Filename
Type B Basket (15.0 mg B-10/cm ²), 2300 ppm Boron, 4.0 wt. % U-235				
60% IMD	0.9047	0.0007	0.9061	we17bpds_p15e40_060.out:
70% IMD	0.9211	0.0007	0.9225	we17bpds_p15e40_070.out:
80% IMD	0.9295	0.0008	0.9311	we17bpds_p15e40_080.out:
90% IMD	0.9349	0.0007	0.9363	we17bpds_p15e40_090.out:
100% IMD	0.9352	0.0008	0.9368	we17bpds_p15e40_100.out:
Type C Basket (20.0 mg B-10/cm ²), 2300 ppm Boron, 4.15 wt. % U-235				
60% IMD	0.8995	0.0008	0.9011	we17bpds_p20e42_060.out:
70% IMD	0.9191	0.0008	0.9207	we17bpds_p20e42_070.out:
80% IMD	0.9282	0.0008	0.9298	we17bpds_p20e42_080.out:
90% IMD	0.9349	0.0008	0.9365	we17bpds_p20e42_090.out:
100% IMD	0.9361	0.0008	0.9377	we17bpds_p20e42_100.out:
Type D Basket (32.0 mg B-10/cm ²), 2300 ppm Boron, 4.4 wt. % U-235				
60% IMD	0.8914	0.0008	0.8930	we17bpds_p32e44_060.out:
70% IMD	0.9107	0.0009	0.9125	we17bpds_p32e44_070.out:
80% IMD	0.9257	0.0007	0.9271	we17bpds_p32e44_080.out:
90% IMD	0.9333	0.0008	0.9349	we17bpds_p32e44_090.out:
100% IMD	0.9352	0.0007	0.9366	we17bpds_p32e44_100.out:
Type E Basket (50.0 mg B-10/cm ²), 2300 ppm Boron, 4.65 wt. % U-235				
60% IMD	0.8792	0.0008	0.8808	we17bpds_p50e47_060.out:
70% IMD	0.9040	0.0008	0.9056	we17bpds_p50e47_070.out:
80% IMD	0.9201	0.0008	0.9217	we17bpds_p50e47_080.out:
90% IMD	0.9290	0.0008	0.9306	we17bpds_p50e47_090.out:
100% IMD	0.9365	0.0008	0.9381	we17bpds_p50e47_100.out:
Type A Basket (7.0 mg B-10/cm ²), 2400 ppm Boron, 3.7 wt. % U-235				
60% IMD	0.9173	0.0007	0.9187	we17bpds_p07e37_060.out:
70% IMD	0.9271	0.0008	0.9287	we17bpds_p07e37_070.out:
80% IMD	0.9308	0.0007	0.9322	we17bpds_p07e37_080.out:
90% IMD	0.9335	0.0007	0.9349	we17bpds_p07e37_090.out:
100% IMD	0.9289	0.0008	0.9305	we17bpds_p07e37_100.out:
Type B Basket (15.0 mg B-10/cm ²), 2400 ppm Boron, 4.1 wt. % U-235				
60% IMD	0.9071	0.0007	0.9085	we17bpds_p15e41_060.out:
70% IMD	0.9216	0.0008	0.9232	we17bpds_p15e41_070.out:
80% IMD	0.9315	0.0009	0.9333	we17bpds_p15e41_080.out:
90% IMD	0.9363	0.0007	0.9377	we17bpds_p15e41_090.out:
100% IMD	0.9354	0.0008	0.9370	we17bpds_p15e41_100.out:

Table 6-27
WE 17x17 Class Damaged Assemblies With BPRAs - Final Results
(Continued)

Description	K_{keno}	σ_{keno}	K_{eff}	Filename
Type C Basket (20.0 mg B-10/cm ²), 2400 ppm Boron, 4.25 wt. % U-235				
60% IMD	0.9016	0.0009	0.9034	we17bpds_p20e43_060.out:
70% IMD	0.9184	0.0008	0.9200	we17bpds_p20e43_070.out:
80% IMD	0.9306	0.0008	0.9322	we17bpds_p20e43_080.out:
90% IMD	0.9351	0.0007	0.9365	we17bpds_p20e43_090.out:
100% IMD	0.9352	0.0008	0.9368	we17bpds_p20e43_100.out:
Type D Basket (32.0 mg B-10/cm ²), 2400 ppm Boron, 4.50 wt. % U-235				
60% IMD	0.8917	0.0008	0.8933	we17bpds_p32e45_060.out:
70% IMD	0.9133	0.0007	0.9147	we17bpds_p32e45_070.out:
80% IMD	0.9245	0.0008	0.9261	we17bpds_p32e45_080.out:
90% IMD	0.9350	0.0008	0.9366	we17bpds_p32e45_090.out:
100% IMD	0.9364	0.0008	0.9380	we17bpds_p32e45_100.out:
Type E Basket (50.0 mg B-10/cm ²), 2400 ppm Boron, 4.80 wt. % U-235				
60% IMD	0.8843	0.0008	0.8859	we17bpds_p50e48_060.out:
70% IMD	0.9074	0.0009	0.9092	we17bpds_p50e48_070.out:
80% IMD	0.9227	0.0008	0.9243	we17bpds_p50e48_080.out:
90% IMD	0.9325	0.0009	0.9343	we17bpds_p50e48_090.out:
100% IMD	0.9388	0.0007	0.9402	we17bpds_p50e48_100.out:
Type A Basket (7.0 mg B-10/cm ²), 2500 ppm Boron, 3.80 wt. % U-235				
60% IMD	0.9159	0.0008	0.9175	we17bpds_p07e38_060.out:
70% IMD	0.9302	0.0008	0.9318	we17bpds_p07e38_070.out:
80% IMD	0.9329	0.0007	0.9343	we17bpds_p07e38_080.out:
90% IMD	0.9334	0.0006	0.9346	we17bpds_p07e38_090.out:
100% IMD	0.9305	0.0006	0.9317	we17bpds_p07e38_100.out:
Type B Basket (15.0 mg B-10/cm ²), 2500 ppm Boron, 4.20 wt. % U-235				
60% IMD	0.9086	0.0009	0.9104	we17bpds_p15e42_060.out:
70% IMD	0.9228	0.0008	0.9244	we17bpds_p15e42_070.out:
80% IMD	0.9328	0.0008	0.9344	we17bpds_p15e42_080.out:
90% IMD	0.9364	0.0007	0.9378	we17bpds_p15e42_090.out:
100% IMD	0.9349	0.0007	0.9363	we17bpds_p15e42_100.out:
Type C Basket (20.0 mg B-10/cm ²), 2500 ppm Boron, 4.35 wt. % U-235				
60% IMD	0.9059	0.0008	0.9075	we17bpds_p20e44_060.out:
70% IMD	0.9210	0.0007	0.9224	we17bpds_p20e44_070.out:
80% IMD	0.9302	0.0007	0.9316	we17bpds_p20e44_080.out:
90% IMD	0.9353	0.0007	0.9367	we17bpds_p20e44_090.out:
100% IMD	0.9369	0.0006	0.9381	we17bpds_p20e44_100.out:

Table 6-27
WE 17x17 Class Damaged Assemblies With BPRAs - Final Results
(Continued)

Description	K_{keno}	σ_{keno}	K_{eff}	Filename
Type D Basket (32.0 mg B-10/cm ²), 2500 ppm Boron, 4.60 wt. % U-235				
60% IMD	60% IMD	60% IMD	60% IMD	60% IMD
70% IMD	70% IMD	70% IMD	70% IMD	70% IMD
80% IMD	80% IMD	80% IMD	80% IMD	80% IMD
90% IMD	90% IMD	90% IMD	90% IMD	90% IMD
100% IMD	100% IMD	100% IMD	100% IMD	100% IMD
Type E Basket (50.0 mg B-10/cm ²), 2500 ppm Boron, 4.9 wt. % U-235				
60% IMD	60% IMD	60% IMD	60% IMD	60% IMD
70% IMD	70% IMD	70% IMD	70% IMD	70% IMD
80% IMD	80% IMD	80% IMD	80% IMD	80% IMD
90% IMD	90% IMD	90% IMD	90% IMD	90% IMD
100% IMD	100% IMD	100% IMD	100% IMD	100% IMD
Type A Basket (7.0 mg B-10/cm ²), 2800 ppm Boron, 3.95 wt. % U-235				
60% IMD	0.9328	0.0007	0.9342	
70% IMD	0.9369	0.0006	0.9381	
80% IMD	0.9336	0.0007	0.9350	
90% IMD	0.9285	0.0007	0.9299	
100% IMD	0.9191	0.0006	0.9203	
Type B Basket (15.0 mg B-10/cm ²), 2800 ppm Boron, 4.35 wt. % U-235				
60% IMD	0.9264	0.0006	0.9276	
70% IMD	0.9343	0.0006	0.9355	
80% IMD	0.9361	0.0007	0.9375	
90% IMD	0.9323	0.0008	0.9339	
100% IMD	0.9265	0.0006	0.9277	
Type C Basket (20.0 mg B-10/cm ²), 2800 ppm Boron, 4.55 wt. % U-235				
60% IMD	0.9241	0.0007	0.9255	
70% IMD	0.9344	0.0007	0.9358	
80% IMD	0.9376	0.0007	0.9390	
90% IMD	0.9365	0.0007	0.9379	
100% IMD	0.9303	0.0007	0.9317	
Type D Basket (32.0 mg B-10/cm ²), 2800 ppm Boron, 4.80 wt. % U-235				
60% IMD	0.9154	0.0007	0.9168	
70% IMD	0.9279	0.0006	0.9291	
80% IMD	0.9353	0.0006	0.9365	
90% IMD	0.9346	0.0007	0.9360	
100% IMD	0.9313	0.0007	0.9327	

Table 6-27
WE 17x17 Class Damaged Assemblies With BPRAs - Final Results
(Concluded)

Description	K_{keno}	σ_{keno}	K_{eff}	Filename
Type E Basket (50.0 mg B-10/cm ²), 2800 ppm Boron, 5.00 wt. % U-235				
60% IMD	0.9035	0.0007	0.9049	
70% IMD	0.9181	0.0007	0.9195	
80% IMD	0.9278	0.0007	0.9292	
90% IMD	0.9307	0.0007	0.9321	
100% IMD	0.9286	0.0007	0.9300	

NOTE: The cases evaluated at 2800 ppm boron were modeled using the 32PTH1 DSC, as described in Section 6.4.2.1. These models represent the most reactive damaged configuration for the 32PTH1 basket as analyzed in Reference [10], which is the optimum pitch configuration. As the 32PTH1 optimum pitch configuration bounds the 32PTH1 double shear configuration; these cases conservatively bound the 32PTH double shear configuration at 2800 ppm for the various basket types.

Table 6-28
Maximum k_{eff} for Intact Fuel Assemblies - Final Results

Description	K_{keno}	σ_{keno}	K_{eff}
CE 14x14, BPRA, Type B Basket (15.0 mg B-10/cm ²), 2300 ppm Boron, 4.7 wt. % U-235			
90% IMD	0.9383	0.0009	0.9401
WE 15x15, BPRA, Type C Basket (20.0 mg B-10/cm ²), 2800 ppm Boron, 4.7 wt. % U-235			
80% IMD	0.9391	0.0007	0.9405
WE 17x17, No BPRA, Type C Basket (20.0 mg B-10/cm ²), 2800 ppm Boron, 4.7 wt. % U-235			
80% IMD	0.9391	0.0007	0.9405
CE 16x16, No BPRA, Type D Basket, 2000 ppm Boron, 4.80 wt. % U-235			
80% IMD	0.9391	0.0008	0.9407
Regulatory Requirements			
Dry Storage : Bounded by Infinite array of Dry Casks	0.5554	0.0004	0.5562
Normal Conditions: Wet Loading	0.9388	0.0007	0.9402
Accident Conditions: Damaged Transfer Cask While Fuel Still Wet	0.9391	0.0008	0.9407

Note:

- These cases were modeled as Westinghouse 17x17 RFA assemblies, which conservatively bound all Westinghouse 17x17 class assemblies that are authorized for loading.

Table 6-29
Maximum k_{eff} for Damaged Assemblies - Final Results

Description	K_{keno}	σ_{keno}	K_{eff}	Filename
CE 14x14, No BPRA, Type D Basket (15.0 mg B-10/cm ²), 2400 ppm Boron, 4.8 wt. % U-235				
70% IMD	0.9386	0.0007	0.9400	ce14d24_p15e48_070.out:
WE 15x15, BPRA, Type B Basket (15.0 mg B-10/cm ²), 2000 ppm Boron, 3.75 wt. % U-235				
100% IMD	0.9372	0.0007	0.9386	we15bpds_p15e38_100.out:
WE 17x17, BPRA, Type E Basket (50.0 mg B-10/cm ²), 2400 ppm Boron, 4.8 wt. % U-235				
100% IMD	0.9388	0.0007	0.9402	we17bpds_p50e48_100.out:
Dry	0.5264	0.0004	0.5272	we17bpds_p50e48_000.out:
CE 16x16, BPRA, Type E Basket, 2000 ppm Boron, 4.65 wt. % U-235				
90% IMD	0.9384	0.0007	0.9398	
Regulatory Requirements				
Dry Storage : Bounded by Infinite array of Dry Casks	0.5264	0.0004	0.5272	we17bpds_p50e48_000.out:
Normal Conditions: Wet Loading	0.9388	0.0007	0.9402	we17bpds_p50e48_100.out:
Accident Conditions: Damaged Transfer Cask While Fuel Still Wet	0.9386	0.0007	0.9400	ce14d24_p15e48_070.out:

**Table 6-30
Benchmark Results**

Run ID	U-235 Enrich. Wt. %	Pitch (cm)	H2O/Fuel volume	Assembly Separation (cm)	AEG	K _{eff}	1 σ
B1645SO1	2.46	1.410	1.015	1.78	32.8118	0.9965	0.0008
B1645SO2	2.46	1.410	1.015	1.78	32.7528	1.0006	0.0008
BW1231B1	4.02	1.511	1.139		31.1429	0.9966	0.0009
BW1231B2	4.02	1.511	1.139		29.8872	0.9990	0.0007
BW1273M	2.46	1.511	1.376		32.2213	0.9961	0.0007
BW1484A1	2.46	1.636	1.841	1.64	34.5373	0.9975	0.0008
BW1484A2	2.46	1.636	1.841	4.92	35.1630	0.9934	0.0008
BW1484B1	2.46	1.636	1.841		33.9415	0.9984	0.0008
BW1484B2	2.46	1.636	1.841	1.64	34.5780	0.9961	0.0009
BW1484B3	2.46	1.636	1.841	4.92	35.2638	0.9978	0.0008
BW1484C1	2.46	1.636	1.841	1.64	34.6547	0.9936	0.0009
BW1484C2	2.46	1.636	1.841	1.64	35.2469	0.9944	0.0010
BW1484S1	2.46	1.636	1.841	1.64	34.5159	1.0002	0.0008
BW1484S2	2.46	1.636	1.841	1.64	34.5530	0.9990	0.0008
BW1484SL	2.46	1.636	1.841	6.54	35.4203	0.9944	0.0009
BW1645S1	2.46	1.209	0.383	1.78	30.1060	0.9987	0.0008
BW1645S2	2.46	1.209	0.383	1.78	29.9920	1.0049	0.0008
BW1810A	2.46	1.636	1.841		33.9524	0.9987	0.0006
BW1810B	2.46	1.636	1.841		33.9711	0.9995	0.0006
BW1810C	2.46	1.636	1.841		33.1503	0.9998	0.0008
BW1810D	2.46	1.636	1.841		33.0876	0.9981	0.0010
BW1810E	2.46	1.636	1.841		33.1520	0.9991	0.0007
BW1810F	2.46	1.636	1.841		33.9581	1.0029	0.0007
BW1810G	2.46	1.636	1.841		32.9414	0.9974	0.0008
BW1810H	2.46	1.636	1.841		32.9370	0.9981	0.0008
BW1810I	2.46	1.636	1.841		33.9613	1.0028	0.0007
BW1810J	2.46	1.636	1.841		33.1379	0.9995	0.0008
EPRU65	2.35	1.562	1.196		33.9138	0.9959	0.0008
EPRU65B	2.35	1.562	1.196		33.4073	1.0000	0.0009
EPRU75	2.35	1.905	2.408		35.8676	0.9968	0.0009
EPRU75B	2.35	1.905	2.408		35.3074	1.0002	0.0008
EPRU87	2.35	2.210	3.687		36.6120	1.0011	0.0009
EPRU87B	2.35	2.210	3.687		36.3460	1.0003	0.0008
NSE71SQ	4.74	1.260	1.823		33.7627	0.9978	0.0009
NSE71W1	4.74	1.260	1.823		34.0088	0.9981	0.0010
NSE71W2	4.74	1.260	1.823		34.3856	0.9995	0.0010
P2438BA	2.35	2.032	2.918	5.05	36.2244	0.9973	0.0009
P2438SLG	2.35	2.032	2.918	8.39	36.2906	0.9985	0.0009
P2438SS	2.35	2.032	2.918	6.88	36.2690	0.9979	0.0009
P2438ZR	2.35	2.032	2.918	8.79	36.2891	0.9976	0.0009
P2615BA	4.31	2.540	3.883	6.72	35.7276	1.0005	0.0011
P2615SS	4.31	2.540	3.883	8.58	35.7456	0.9959	0.0011
P2615ZR	4.31	2.540	3.883	10.92	35.7709	0.9980	0.0010
P2827L1	2.35	2.032	2.918	13.72	36.2491	1.0051	0.0008

**Table 6-30
Benchmark Results
(Continued)**

Run ID	U-235 Enrich. Wt. %	Pitch (cm)	H2O/Fuel volume	Assembly Separation (cm)	AEG	K _{eff}	1 σ
P2827L2	2.35	2.032	2.918	11.25	36.2939	1.0005	0.0010
P2827L3	4.31	2.540	3.883	20.78	35.6740	1.0095	0.0009
P2827L4	4.31	2.540	3.883	19.04	35.7173	1.0066	0.0010
P2827SLG	2.35	2.032	2.918	8.31	36.3010	0.9957	0.0008
P3314BA	4.31	1.892	1.600	2.83	33.1874	1.0000	0.0009
P3314BC	4.31	1.892	1.600	2.83	33.2334	0.9992	0.0009
P3314BF1	4.31	1.892	1.600	2.83	33.2422	1.0024	0.0009
P3314BF2	4.31	1.892	1.600	2.83	33.2121	1.0001	0.0010
P3314BS1	2.35	1.684	1.600	3.86	34.8545	0.9957	0.0010
P3314BS2	2.35	1.684	1.600	3.46	34.8324	0.9940	0.0008
P3314BS3	4.31	1.892	1.600	7.23	33.4328	0.9996	0.0009
P3314BS4	4.31	1.892	1.600	6.63	33.4152	1.0000	0.0008
P3314SLG	4.31	1.892	1.600	2.83	34.0109	0.9971	0.0010
P3314SS1	4.31	1.892	1.600	2.83	33.9613	0.9984	0.0010
P3314SS2	4.31	1.892	1.600	2.83	33.7719	1.0014	0.0009
P3314SS3	4.31	1.892	1.600	2.83	33.8956	0.9995	0.0010
P3314SS4	4.31	1.892	1.600	2.83	33.7604	0.9962	0.0009
P3314SS5	2.35	1.684	1.600	7.80	34.9476	0.9947	0.0010
P3314SS6	4.31	1.892	1.600	10.52	33.5406	1.0010	0.0008
P3314W1	4.31	1.892	1.600		34.3962	1.0009	0.0010
P3314W2	2.35	1.684	1.600		35.2153	0.9972	0.0008
P3314ZR	4.31	1.892	1.600	2.83	33.9897	0.9977	0.0010
P3602BB	4.31	1.892	1.600	8.30	33.3198	1.0031	0.0010
P3602BS1	2.35	1.684	1.600	4.80	34.7746	1.0034	0.0009
P3602BS2	4.31	1.892	1.600	9.83	33.3649	1.0047	0.0010
P3602N11	2.35	1.684	1.600	8.98	34.7410	1.0025	0.0008
P3602N12	2.35	1.684	1.600	9.58	34.8378	1.0048	0.0009
P3602N13	2.35	1.684	1.600	9.66	34.9334	1.0006	0.0009
P3602N14	2.35	1.684	1.600	8.54	35.0287	0.9969	0.0010
P3602N21	2.35	2.032	2.918	10.36	36.2787	0.9999	0.0009
P3602N22	2.35	2.032	2.918	11.20	36.1963	1.0014	0.0008
P3602N31	4.31	1.892	1.600	14.87	33.2015	1.0063	0.0010
P3602N32	4.31	1.892	1.600	15.74	33.3085	1.0072	0.0010
P3602N33	4.31	1.892	1.600	15.87	33.4168	1.0084	0.0010
P3602N34	4.31	1.892	1.600	15.84	33.4653	1.0028	0.0010
P3602N35	4.31	1.892	1.600	15.45	33.5169	1.0030	0.0009
P3602N36	4.31	1.892	1.600	13.82	33.5832	1.0003	0.0010
P3602N41	4.31	2.540	3.883	12.89	35.5269	1.0127	0.0010
P3602N42	4.31	2.540	3.883	14.12	35.6711	1.0068	0.0009
P3602N43	4.31	2.540	3.883	12.44	35.7505	1.0049	0.0009
P3602SS1	2.35	1.684	1.600	8.28	34.8708	1.0007	0.0009
P3602SS2	4.31	1.892	1.600	13.75	33.4133	1.0026	0.0010
P3926L1	2.35	1.684	1.600	10.06	34.8569	1.0003	0.0009
P3926L2	2.35	1.684	1.600	10.11	34.9374	1.0020	0.0008

**Table 6-30
Benchmark Results
(Concluded)**

Run ID	U-235 Enrich. Wt. %	Pitch (cm)	H2O/Fuel volume	Assembly Separation (cm)	AEG	K _{eff}	1 σ
P3926L3	2.35	1.684	1.600	8.50	35.0657	0.9967	0.0010
P3926L4	4.31	1.892	1.600	17.74	33.3262	1.0066	0.0009
P3926L5	4.31	1.892	1.600	18.18	33.4035	1.0054	0.0010
P3926L6	4.31	1.892	1.600	17.43	33.5141	1.0038	0.0009
P3926SL1	2.35	1.684	1.600	6.59	35.0674	0.9950	0.0009
P3926SL2	4.31	1.892	1.600	12.79	33.5810	0.9998	0.0009
P4267B1	4.31	1.890	1.590		31.7989	0.9992	0.0008
P4267B2	4.31	0.890	1.590		31.5288	1.0027	0.0007
P4267B3	4.31	1.715	1.090		30.9907	1.0057	0.0009
P4267B4	4.31	1.715	1.090		30.5098	0.9993	0.0008
P4267B5	4.31	1.715	1.090		30.1008	1.0009	0.0008
P4267SL1	4.31	1.890	1.590		33.4692	0.9987	0.0011
P4267SL2	4.31	1.715	1.090		31.9346	0.9995	0.0011
P62FT231	4.31	1.891	1.600	5.67	32.9228	1.0020	0.0009
P71F14F3	4.31	1.891	1.600	5.19	32.8227	1.0009	0.0010
P71F14V3	4.31	1.891	1.600	5.19	32.8587	0.9977	0.0010
P71F14V5	4.31	1.891	1.600	5.19	32.8662	0.9980	0.0010
P71F214R	4.31	1.891	1.600	5.19	32.8669	0.9976	0.0009
PAT80L1	4.74	1.600	3.807	2.00	35.0276	1.0014	0.0009
PAT80L2	4.74	1.600	3.807	2.00	35.1079	0.9986	0.0011
PAT80SS1	4.74	1.600	3.807	2.00	35.0125	0.9998	0.0009
PAT80SS2	4.74	1.600	3.807	2.00	35.1128	0.9967	0.0010
W3269A	5.70	1.422	1.930		33.1383	0.9976	0.0009
W3269B1	3.70	1.105	1.432		32.4010	0.9962	0.0008
W3269B2	3.70	1.105	1.432		32.3940	0.9965	0.0008
W3269B3	3.70	1.105	1.432		32.2464	0.9945	0.0008
W3269C	2.72	1.524	1.494		33.7731	0.9979	0.0009
W3269SL1	2.72	1.524	1.494		33.3854	0.9973	0.0010
W3269SL2	5.70	1.422	1.930		33.1006	1.0024	0.0010
W3269W1	2.72	1.524	1.494		33.5160	0.9972	0.0012
W3269W2	5.70	1.422	1.930		33.1786	1.0015	0.0010
W3385SL1	5.74	1.422	1.932		33.2320	1.0004	0.0009
W3385SL2	5.74	2.012	5.067		35.8876	1.0014	0.0010
Correlation	0.321	0.379	0.187	0.656	0.036	N/A	N/A

Table 6-31
USL-1 Results

Parameter	Range of Applicability	Formula to Determine USL
Pin Pitch (cm)	0.890 - 2.540	$0.9366 + (4.2438\text{E-}03)*X$ ($X < 1.796$) 0.9442 ($X \geq 1.796$)
Water to Fuel Volume Ratio	0.383 - 5.067	$0.9421 + (7.6076\text{E-}04)*X$ ($X < 2.146$) 0.9438 ($X \geq 2.146$)
Average Energy Group Causing Fission (AEG)	29.89 - 36.61	$0.9466 - (8.5090\text{E-}05)*X$ ($X < 32.548$) 0.9438 ($X \geq 32.548$)
Assembly Separation (cm)	1.640 - 20.78	$0.9409 + (5.0514\text{E-}04)*X$ ($X < 7.118$) 0.9445 ($X \geq 7.118$)
Boron Concentration (ppm)	15 - 3389	$0.9435 + (5.3999\text{E-}07)*X$ ($X < 2450$) 0.9449 ($X \geq 2450$)
Enrichment (wt. % U-235)	2.350 - 5.740	$0.9403 + (1.0614\text{E-}03)*X$ ($X < 3.597$) 0.9442 ($X \geq 3.597$)

Table 6-32
USL Determination for Criticality Analysis

Parameter	Value from Limiting WE 17x17 Analysis	Bounding USL-1
Pin Pitch (cm)	1.25984	0.9419
Water to Fuel Volume Ratio	1.667	0.9434
Average Energy Group Causing Fission (AEG)	30.6011	0.9440
Assembly Separation (cm)	2.1717 (min)	0.9420
Boron Concentration (ppm)	2800	0.9449
Enrichment (wt. % U-235)	3.70 (min)	0.9442
Parameter	Value from Limiting WE 15x15 Analysis	Bounding USL
Pin Pitch (cm)	1.43002	0.9426
Water to Fuel Volume Ratio	1.6751	0.9433
Average Energy Group Causing Fission (AEG)	31.3557	0.9438
Assembly Separation (cm)	2.222	0.9420
Boron Concentration (ppm)	2400	0.9448
Enrichment (wt. % U-235)	3.700 (min)	0.9442
Parameter	Value from Limiting CE 14x14 Analysis	Bounding USL
Pin Pitch (cm)	1.4732	0.9428
Water to Fuel Volume Ratio	1.6127	0.9433
Average Energy Group Causing Fission (AEG)	30.5980	0.9440
Assembly Separation (cm)	2.222	0.9420
Boron Concentration (ppm)	2400	0.9448
Enrichment (wt. % U-235)	3.700 (min)	0.9442
Parameter	Value from Limiting CE 16x16 Analysis	Bounding USL
Pin Pitch (cm)	1.28524	0.9421
Water to Fuel Volume Ratio	1.700	0.9424
Average Energy Group Causing Fission (AEG)	31.1626	0.9439
Assembly Separation (cm)	2.222	0.9420
Boron Concentration (ppm)	2000	0.9446
Enrichment (wt. % U-235)	3.700 (min)	0.9442

Table 6-33
CE 14x14 Class Intact Assemblies without BPRAs - Final Results

Description	K_{keno}	σ_{keno}	K_{eff}	Filename
Type A Basket (7.0 mg B-10/cm ²), 2000 ppm Boron, 4.05 wt. % U-235				
60% IMD	0.9290	0.0008	0.9306	ce14b20_p07e40_060.out:
70% IMD	0.9344	0.0009	0.9362	ce14b20_p07e40_070.out:
80% IMD	0.9338	0.0008	0.9354	ce14b20_p07e40_080.out:
90% IMD	0.9281	0.0007	0.9295	ce14b20_p07e40_090.out:
100% IMD	0.9192	0.0007	0.9206	ce14b20_p07e40_100.out:
Type B Basket (15.0 mg B-10/cm ²), 2000 ppm Boron, 4.55 wt. % U-235				
60% IMD	0.9239	0.0009	0.9257	ce14b20_p15e45_060.out:
70% IMD	0.9349	0.0008	0.9365	ce14b20_p15e45_070.out:
80% IMD	0.9364	0.0007	0.9378	ce14b20_p15e45_080.out:
90% IMD	0.9359	0.0008	0.9375	ce14b20_p15e45_090.out:
100% IMD	0.9299	0.0007	0.9313	ce14b20_p15e45_100.out:
Type C Basket (20.0 mg B-10/cm ²), 2000 ppm Boron, 4.70 wt. % U-235				
60% IMD	0.9183	0.0009	0.9201	ce14b20_p20e47_060.out:
70% IMD	0.9311	0.0007	0.9325	ce14b20_p20e47_070.out:
80% IMD	0.9357	0.0007	0.9371	ce14b20_p20e47_080.out:
90% IMD	0.9324	0.0007	0.9338	ce14b20_p20e47_090.out:
100% IMD	0.9294	0.0009	0.9312	ce14b20_p20e47_100.out:
Type D Basket (32.0 mg B-10/cm ²), 2000 ppm Boron, 5.00 wt. % U-235				
60% IMD	0.9091	0.0007	0.9105	ce14b20_p32e50_060.out:
70% IMD	0.9242	0.0009	0.9260	ce14b20_p32e50_070.out:
80% IMD	0.9320	0.0007	0.9334	ce14b20_p32e50_080.out:
90% IMD	0.9347	0.0008	0.9363	ce14b20_p32e50_090.out:
100% IMD	0.9317	0.0007	0.9331	ce14b20_p32e50_100.out:
Type A Basket (7.0 mg B-10/cm ²), 2300 ppm Boron, 4.40 wt. % U-235				
60% IMD	0.9356	0.0008	0.9372	ce14b23_p07e44_060.out:
70% IMD	0.9383	0.0007	0.9397	ce14b23_p07e44_070.out:
80% IMD	0.9338	0.0007	0.9352	ce14b23_p07e44_080.out:
90% IMD	0.9282	0.0008	0.9298	ce14b23_p07e44_090.out:
100% IMD	0.9159	0.0008	0.9175	ce14b23_p07e44_100.out:
Type B Basket (15.0 mg B-10/cm ²), 2300 ppm Boron, 4.90 wt. % U-235				
60% IMD	0.9286	0.0007	0.9300	ce14b23_p15e49_060.out:
70% IMD	0.9359	0.0009	0.9377	ce14b23_p15e49_070.out:
80% IMD	0.9377	0.0008	0.9393	ce14b23_p15e49_080.out:
90% IMD	0.9327	0.0007	0.9341	ce14b23_p15e49_090.out:
100% IMD	0.9256	0.0007	0.9270	ce14b23_p15e49_100.out:

Table 6-33
CE 14x14 Class Intact Assemblies without BPRAs - Final Results
(Concluded)

Description	K_{keno}	σ_{keno}	K_{eff}	Filename
Type C Basket (20.0 mg B-10/cm ²), 2300 ppm Boron, 5.00 wt. % U-235				
60% IMD	0.9196	0.0007	0.9210	ce14b23_p20e50_060.out:
70% IMD	0.9295	0.0007	0.9309	ce14b23_p20e50_070.out:
80% IMD	0.9305	0.0008	0.9321	ce14b23_p20e50_080.out:
90% IMD	0.9285	0.0008	0.9301	ce14b23_p20e50_090.out:
100% IMD	0.9223	0.0007	0.9237	ce14b23_p20e50_100.out:
Type A Basket (07.0 mg B-10/cm ²), 2400 ppm Boron, 4.45 wt. % U-235				
60% IMD	0.9317	0.0007	0.9331	ce14b24_p07e44_060.out:
70% IMD	0.9347	0.0007	0.9361	ce14b24_p07e44_070.out:
80% IMD	0.9305	0.0008	0.9321	ce14b24_p07e44_080.out:
90% IMD	0.9221	0.0007	0.9235	ce14b24_p07e44_090.out:
100% IMD	0.9124	0.0008	0.9140	ce14b24_p07e44_100.out:
Type B Basket (15.0 mg B-10/cm ²), 2400 ppm Boron, 5.00 wt. % U-235				
60% IMD	0.9290	0.0007	0.9304	ce14b24_p15e50_060.out:
70% IMD	0.9358	0.0008	0.9374	ce14b24_p15e50_070.out:
80% IMD	0.9358	0.0007	0.9372	ce14b24_p15e50_080.out:
90% IMD	0.9306	0.0007	0.9320	ce14b24_p15e50_090.out:
100% IMD	0.9238	0.0007	0.9252	ce14b24_p15e50_100.out:
Type A Basket (07.0 mg B-10/cm ²), 2500 ppm Boron, 4.55 wt. % U-235				
60% IMD	0.9345	0.0007	0.9359	ce14b25_p07e45_060.out:
70% IMD	0.9370	0.0008	0.9386	ce14b25_p07e45_070.out:
80% IMD	0.9295	0.0008	0.9311	ce14b25_p07e45_080.out:
90% IMD	0.9237	0.0007	0.9251	ce14b25_p07e45_090.out:
100% IMD	0.9139	0.0007	0.9153	ce14b25_p07e45_100.out:
Type A Basket (7.0 mg B-10/cm ²), 2800 ppm Boron, 4.60 wt. % U-235				
50 % IMD	0.9296	0.0007	0.9310	C14_A_2800_050.in
60 % IMD	0.9346	0.0007	0.9360	C14_A_2800_060.in
70 % IMD	0.9302	0.0007	0.9316	C14_A_2800_070.in
80 % IMD	0.9214	0.0007	0.9228	C14_A_2800_080.in
90 % IMD	0.9081	0.0006	0.9093	C14_A_2800_090.in

Table 6-34
CE 14x14 Class Assembly Final Results with BPRAs (Intact)

Description	K_{keno}	σ_{keno}	K_{eff}
Type A Basket (7.0 mg B-10/cm ²), 2000 ppm Boron, 3.95 wt. % U-235			
60% IMD	0.9213	0.0006	0.9225
70% IMD	0.9323	0.0007	0.9337
80% IMD	0.9363	0.0007	0.9377
90% IMD	0.9376	0.0007	0.9390
100% IMD	0.9349	0.0007	0.9363
Type B Basket (15.0 mg B-10/cm ²), 2000 ppm Boron, 4.35 wt. % U-235			
60% IMD	0.9081	0.0008	0.9097
70% IMD	0.9229	0.0008	0.9245
80% IMD	0.9331	0.0008	0.9347
90% IMD	0.9353	0.0007	0.9367
100% IMD	0.9374	0.0008	0.9390
Type C Basket (20.0 mg B-10/cm ²), 2000 ppm Boron, 4.50 wt. % U-235			
60% IMD	0.9012	0.0007	0.9026
70% IMD	0.9190	0.0008	0.9206
80% IMD	0.9294	0.0009	0.9312
90% IMD	0.9359	0.0007	0.9373
100% IMD	0.9372	0.0009	0.9390
Type D Basket (32.0 mg B-10/cm ²), 2000 ppm Boron, 4.75 wt. % U-235			
60% IMD	0.8882	0.0008	0.8898
70% IMD	0.9083	0.0008	0.9099
80% IMD	0.9224	0.0007	0.9238
90% IMD	0.9322	0.0007	0.9336
100% IMD	0.9340	0.0008	0.9356
Type E Basket (50.0 mg B-10/cm ²), 2000 ppm Boron, 5.00 wt. % U-235			
60% IMD	0.8762	0.0008	0.8778
70% IMD	0.9006	0.0009	0.9024
80% IMD	0.9156	0.0007	0.9170
90% IMD	0.9268	0.0008	0.9284
100% IMD	0.9316	0.0008	0.9332

Table 6-34
CE 14x14 Class Assembly Final Results with BPRAs (Intact)
(Continued)

Description	K_{keno}	σ_{keno}	K_{eff}
Type A Basket (7.0 mg B-10/cm ²), 2300 ppm Boron, 4.25 wt. % U-235			
60% IMD	0.9265	0.0007	0.9279
70% IMD	0.9361	0.0008	0.9377
80% IMD	0.9380	0.0007	0.9394
90% IMD	0.9370	0.0007	0.9384
100% IMD	0.9320	0.0008	0.9336
Type B Basket (15.0 mg B-10/cm ²), 2300 ppm Boron, 4.70 wt. % U-235			
60% IMD	0.9138	0.0008	0.9154
70% IMD	0.9270	0.0008	0.9286
80% IMD	0.9345	0.0007	0.9359
90% IMD	0.9383	0.0009	0.9401
100% IMD	0.9356	0.0008	0.9372
Type C Basket (20.0 mg B-10/cm ²), 2300 ppm Boron, 4.85 wt. % U-235			
60% IMD	0.9087	0.0008	0.9103
70% IMD	0.9227	0.0007	0.9241
80% IMD	0.9310	0.0009	0.9328
90% IMD	0.9361	0.0009	0.9379
100% IMD	0.9347	0.0008	0.9363
Type D Basket (32.0 mg B-10/cm ²), 2300 ppm Boron, 5.00 wt. % U-235			
60% IMD	0.8952	0.0009	0.8970
70% IMD	0.9072	0.0008	0.9088
80% IMD	0.9109	0.0007	0.9123
90% IMD	0.9119	0.0007	0.9133
100% IMD	0.9081	0.0007	0.9095
Type A Basket (7.0 mg B-10/cm ²), 2400 ppm Boron, 4.35 wt. % U-235			
60% IMD	0.9277	0.0008	0.9293
70% IMD	0.9369	0.0007	0.9383
80% IMD	0.9382	0.0007	0.9396
90% IMD	0.9349	0.0008	0.9365
100% IMD	0.9318	0.0007	0.9332

Table 6-34
CE 14x14 Class Assembly Final Results with BPRAs (Intact)
(Concluded)

Description	K_{keno}	σ_{keno}	K_{eff}
Type B Basket (15.0 mg B-10/cm²), 2400 ppm Boron, 4.80 wt. % U-235			
60% IMD	0.9153	0.0008	0.9169
70% IMD	0.9275	0.0009	0.9293
80% IMD	0.9341	0.0007	0.9355
90% IMD	0.9372	0.0006	0.9384
100% IMD	0.9352	0.0007	0.9366
Type C Basket (20.0 mg B-10/cm²), 2400 ppm Boron, 5.00 wt. % U-235			
60% IMD	0.9108	0.0008	0.9124
70% IMD	0.9272	0.0008	0.9288
80% IMD	0.9351	0.0008	0.9367
90% IMD	0.9368	0.0008	0.9384
100% IMD	0.9372	0.0008	0.9388
Type A Basket (7.0 mg B-10/cm²), 2500 ppm Boron, 4.45 wt. % U-235			
60% IMD	0.9289	0.0008	0.9305
70% IMD	0.9374	0.0008	0.9390
80% IMD	0.9376	0.0007	0.9390
90% IMD	0.9352	0.0008	0.9368
100% IMD	0.9309	0.0008	0.9325
Type B Basket (15.0 mg B-10/cm²), 2500 ppm Boron, 4.90 wt. % U-235			
60% IMD	0.9173	0.0008	0.9189
70% IMD	0.9290	0.0007	0.9304
80% IMD	0.9349	0.0008	0.9365
90% IMD	0.9354	0.0008	0.9370
100% IMD	0.9332	0.0009	0.9350
Type A Basket (7.0 mg B-10/cm²), 2800 ppm Boron, 4.55 wt. % U-235			
50 % IMD	0.9254	0.0009	0.9272
60 % IMD	0.9341	0.0008	0.9357
70 % IMD	0.9358	0.0007	0.9372
80 % IMD	0.9324	0.0006	0.9336
90 % IMD	0.9287	0.0007	0.9301

Table 6-35
Intact CE 16x16 Class Assembly without BPRAs, Final Results

Model Description	k_{KENO}	1σ	k_{eff}
Enrichment = 3.90 wt. % U-235, Soluble Boron = 2000 ppm, Type A Basket			
Internal Moderator Density = 90 %	0.9306	0.0008	0.9322
Internal Moderator Density = 80 %	0.9367	0.0007	0.9381
Internal Moderator Density = 70 %	0.9383	0.0007	0.9397
Internal Moderator Density = 60 %	0.9368	0.0007	0.9382
Internal Moderator Density = 50 %	0.9248	0.0008	0.9264
Enrichment = 4.30 wt. % U-235, Soluble Boron = 2000 ppm, Type B Basket			
Internal Moderator Density = 90 %	0.9353	0.0007	0.9367
Internal Moderator Density = 80 %	0.9364	0.0008	0.9380
Internal Moderator Density = 70 %	0.9357	0.0007	0.9371
Internal Moderator Density = 60 %	0.9274	0.0007	0.9288
Internal Moderator Density = 50 %	0.9120	0.0007	0.9134
Enrichment = 4.50 wt. % U-235, Soluble Boron = 2000 ppm, Type C Basket			
Internal Moderator Density = 90 %	0.9359	0.0007	0.9373
Internal Moderator Density = 80 %	0.9388	0.0008	0.9404
Internal Moderator Density = 70 %	0.9348	0.0008	0.9364
Internal Moderator Density = 60 %	0.9244	0.0008	0.9260
Internal Moderator Density = 50 %	0.9081	0.0007	0.9095
Enrichment = 4.80 wt. % U-235, Soluble Boron = 2000 ppm, Type D Basket			
Internal Moderator Density = 100 %	0.9347	0.0008	0.9363
Internal Moderator Density = 90 %	0.9382	0.0008	0.9398
Internal Moderator Density = 80 %	0.9391	0.0008	0.9407
Internal Moderator Density = 70 %	0.9317	0.0008	0.9333
Internal Moderator Density = 60 %	0.9185	0.0008	0.9201
Enrichment = 5.00 wt. % U-235, Soluble Boron = 2000 ppm, Type E Basket			
Internal Moderator Density = 100 %	0.9334	0.0008	0.9350
Internal Moderator Density = 90 %	0.9340	0.0008	0.9356
Internal Moderator Density = 80 %	0.9306	0.0008	0.9322
Internal Moderator Density = 70 %	0.9212	0.0009	0.9230
Internal Moderator Density = 60 %	0.9065	0.0008	0.9081

Table 6-35
Intact CE 16x16 Class Assembly without BPRAs, Final Results
(Continued)

Model Description	k_{KENO}	1σ	k_{eff}
Enrichment = 4.10 wt. % U-235, Soluble Boron = 2300 ppm, Type A Basket			
Internal Moderator Density = 90 %	0.9199	0.0007	0.9213
Internal Moderator Density = 80 %	0.9270	0.0007	0.9284
Internal Moderator Density = 70 %	0.9320	0.0009	0.9338
Internal Moderator Density = 60 %	0.9327	0.0007	0.9341
Internal Moderator Density = 50 %	0.9245	0.0007	0.9259
Enrichment = 4.60 wt. % U-235, Soluble Boron = 2300 ppm, Type B Basket			
Internal Moderator Density = 90 %	0.9303	0.0007	0.9317
Internal Moderator Density = 80 %	0.9359	0.0007	0.9373
Internal Moderator Density = 70 %	0.9358	0.0008	0.9374
Internal Moderator Density = 60 %	0.9295	0.0009	0.9313
Internal Moderator Density = 50 %	0.9179	0.0008	0.9195
Enrichment = 4.80 wt. % U-235, Soluble Boron = 2300 ppm, Type C Basket			
Internal Moderator Density = 90 %	0.9314	0.0007	0.9328
Internal Moderator Density = 80 %	0.9352	0.0007	0.9366
Internal Moderator Density = 70 %	0.9340	0.0007	0.9354
Internal Moderator Density = 60 %	0.9271	0.0009	0.9289
Internal Moderator Density = 50 %	0.9133	0.0008	0.9149
Enrichment = 5.00 wt. % U-235, Soluble Boron = 2300 ppm, Type D Basket			
Internal Moderator Density = 100 %	0.9231	0.0009	0.9249
Internal Moderator Density = 90 %	0.9275	0.0008	0.9291
Internal Moderator Density = 80 %	0.9268	0.0007	0.9282
Internal Moderator Density = 70 %	0.9235	0.0007	0.9249
Internal Moderator Density = 60 %	0.9163	0.0008	0.9179

Table 6-35
Intact CE 16x16 Class Assembly without BPRAs, Final Results
(Continued)

Model Description	k_{KENO}	1σ	k_{eff}
Enrichment = 4.20 wt. % U-235, Soluble Boron = 2400 ppm, Type A Basket			
Internal Moderator Density = 90 %	0.9210	0.0007	0.9224
Internal Moderator Density = 80 %	0.9286	0.0007	0.9300
Internal Moderator Density = 70 %	0.9333	0.0008	0.9349
Internal Moderator Density = 60 %	0.9338	0.0008	0.9354
Internal Moderator Density = 50 %	0.9268	0.0007	0.9282
Enrichment = 4.70 wt. % U-235, Soluble Boron = 2400 ppm, Type B Basket			
Internal Moderator Density = 90 %	0.9284	0.0007	0.9298
Internal Moderator Density = 80 %	0.9344	0.0007	0.9358
Internal Moderator Density = 70 %	0.9348	0.0008	0.9364
Internal Moderator Density = 60 %	0.9317	0.0009	0.9335
Internal Moderator Density = 50 %	0.9191	0.0007	0.9205
Enrichment = 4.90 wt. % U-235, Soluble Boron = 2400 ppm, Type C Basket			
Internal Moderator Density = 90 %	0.9313	0.0008	0.9329
Internal Moderator Density = 80 %	0.9344	0.0007	0.9358
Internal Moderator Density = 70 %	0.9342	0.0007	0.9356
Internal Moderator Density = 60 %	0.9295	0.0007	0.9309
Internal Moderator Density = 50 %	0.9134	0.0007	0.9148

Table 6-35
Intact CE 16x16 Class Assembly without BPRAs, Final Results
(Concluded)

Model Description	k_{KENO}	1σ	k_{eff}
Enrichment = 4.30 wt. % U-235, Soluble Boron = 2500 ppm, Type A Basket			
Internal Moderator Density = 90 %	0.9176	0.0009	0.9194
Internal Moderator Density = 80 %	0.9288	0.0008	0.9304
Internal Moderator Density = 70 %	0.9338	0.0006	0.9350
Internal Moderator Density = 60 %	0.9359	0.0006	0.9371
Internal Moderator Density = 50 %	0.9301	0.0006	0.9313
Enrichment = 4.80 wt. % U-235, Soluble Boron = 2500 ppm, Type B Basket			
Internal Moderator Density = 90 %	0.9282	0.0007	0.9296
Internal Moderator Density = 80 %	0.9324	0.0007	0.9338
Internal Moderator Density = 70 %	0.9353	0.0007	0.9367
Internal Moderator Density = 60 %	0.9302	0.0007	0.9316
Internal Moderator Density = 50 %	0.9211	0.0008	0.9227
Enrichment = 5.00 wt. % U-235, Soluble Boron = 2500 ppm, Type C Basket			
Internal Moderator Density = 90 %	0.9298	0.0007	0.9312
Internal Moderator Density = 80 %	0.9345	0.0008	0.9361
Internal Moderator Density = 70 %	0.9360	0.0008	0.9376
Internal Moderator Density = 60 %	0.9283	0.0010	0.9303
Internal Moderator Density = 50 %	0.9142	0.0007	0.9156
Enrichment = 4.60 wt. % U-235, Soluble Boron = 2800 ppm, Type A Basket			
Internal Moderator Density = 90 %	0.9181	0.0007	0.9195
Internal Moderator Density = 80 %	0.9281	0.0007	0.9295
Internal Moderator Density = 70 %	0.9347	0.0008	0.9363
Internal Moderator Density = 60 %	0.9375	0.0008	0.9391
Internal Moderator Density = 50 %	0.9337	0.0007	0.9351
Enrichment = 5.00 wt. % U-235, Soluble Boron = 2800 ppm, Type B Basket			
Internal Moderator Density = 90 %	0.9185	0.0008	0.9201
Internal Moderator Density = 80 %	0.9252	0.0008	0.9268
Internal Moderator Density = 70 %	0.9289	0.0008	0.9305
Internal Moderator Density = 60 %	0.9288	0.0007	0.9302
Internal Moderator Density = 50 %	0.9199	0.0007	0.9213

Table 6-36
Intact CE 16x16 Class Assembly with BPRAs, Final Results

Model Description	k_{KENO}	1σ	k_{eff}
Enrichment = 3.85 wt. % U-235, Soluble Boron = 2000 ppm, Type A Basket			
Internal Moderator Density = 90 %	0.9351	0.0007	0.9365
Internal Moderator Density = 80 %	0.9379	0.0008	0.9395
Internal Moderator Density = 70 %	0.9381	0.0007	0.9395
Internal Moderator Density = 60 %	0.9326	0.0008	0.9342
Internal Moderator Density = 50 %	0.9191	0.0006	0.9203
Enrichment = 4.25 wt. % U-235, Soluble Boron = 2000 ppm, Type B Basket			
Internal Moderator Density = 90 %	0.9380	0.0008	0.9396
Internal Moderator Density = 80 %	0.9380	0.0008	0.9396
Internal Moderator Density = 70 %	0.9337	0.0007	0.9351
Internal Moderator Density = 60 %	0.9241	0.0007	0.9255
Internal Moderator Density = 50 %	0.9044	0.0008	0.9060
Enrichment = 4.40 wt. % U-235, Soluble Boron = 2000 ppm, Type C Basket			
Internal Moderator Density = 100 %	0.9358	0.0008	0.9374
Internal Moderator Density = 90 %	0.9371	0.0009	0.9389
Internal Moderator Density = 80 %	0.9355	0.0007	0.9369
Internal Moderator Density = 70 %	0.9294	0.0007	0.9308
Internal Moderator Density = 60 %	0.9188	0.0008	0.9204
Enrichment = 4.70 wt. % U-235, Soluble Boron = 2000 ppm, Type D Basket			
Internal Moderator Density = 100 %	0.9389	0.0007	0.9403
Internal Moderator Density = 90 %	0.9389	0.0008	0.9405
Internal Moderator Density = 80 %	0.9360	0.0008	0.9376
Internal Moderator Density = 70 %	0.9262	0.0008	0.9278
Internal Moderator Density = 60 %	0.9115	0.0007	0.9129
Enrichment = 4.90 wt. % U-235, Soluble Boron = 2000 ppm, Type E Basket			
Internal Moderator Density = 100 %	0.9358	0.0008	0.9374
Internal Moderator Density = 90 %	0.9339	0.0007	0.9353
Internal Moderator Density = 80 %	0.9282	0.0007	0.9296
Internal Moderator Density = 70 %	0.9154	0.0009	0.9172
Internal Moderator Density = 60 %	0.8984	0.0008	0.9000

Table 6-36
Intact CE 16x16 Class Assembly with BPRAs, Final Results
(Continued)

Model Description	k_{KENO}	1σ	k_{eff}
Enrichment = 4.10 wt. % U-235, Soluble Boron = 2300 ppm, Type A Basket			
Internal Moderator Density = 90 %	0.9318	0.0007	0.9332
Internal Moderator Density = 80 %	0.9347	0.0008	0.9363
Internal Moderator Density = 70 %	0.9371	0.0007	0.9385
Internal Moderator Density = 60 %	0.9344	0.0007	0.9358
Internal Moderator Density = 50 %	0.9225	0.0007	0.9239
Enrichment = 4.55 wt. % U-235, Soluble Boron = 2300 ppm, Type B Basket			
Internal Moderator Density = 90 %	0.9343	0.0007	0.9357
Internal Moderator Density = 80 %	0.9374	0.0007	0.9388
Internal Moderator Density = 70 %	0.9369	0.0009	0.9387
Internal Moderator Density = 60 %	0.9258	0.0007	0.9272
Internal Moderator Density = 50 %	0.9108	0.0007	0.9122
Enrichment = 4.70 wt. % U-235, Soluble Boron = 2300 ppm, Type C Basket			
Internal Moderator Density = 100 %	0.9298	0.0007	0.9312
Internal Moderator Density = 90 %	0.9348	0.0007	0.9362
Internal Moderator Density = 80 %	0.9346	0.0007	0.9360
Internal Moderator Density = 70 %	0.9296	0.0007	0.9310
Internal Moderator Density = 60 %	0.9216	0.0007	0.9230
Enrichment = 5.00 wt. % U-235, Soluble Boron = 2300 ppm, Type D Basket			
Internal Moderator Density = 100 %	0.9333	0.0009	0.9351
Internal Moderator Density = 90 %	0.9349	0.0008	0.9365
Internal Moderator Density = 80 %	0.9333	0.0008	0.9349
Internal Moderator Density = 70 %	0.9266	0.0007	0.9280
Internal Moderator Density = 60 %	0.9124	0.0008	0.9140

Table 6-36
Intact CE 16x16 Class Assembly with BPRAs, Final Results
(Continued)

Model Description	k_{KENO}	1σ	k_{eff}
Enrichment = 4.20 wt. % U-235, Soluble Boron = 2400 ppm, Type A Basket			
Internal Moderator Density = 90 %	0.9294	0.0008	0.9310
Internal Moderator Density = 80 %	0.9343	0.0008	0.9359
Internal Moderator Density = 70 %	0.9374	0.0008	0.9390
Internal Moderator Density = 60 %	0.9343	0.0008	0.9359
Internal Moderator Density = 50 %	0.9257	0.0008	0.9273
Enrichment = 4.65 wt. % U-235, Soluble Boron = 2400 ppm, Type B Basket			
Internal Moderator Density = 100 %	0.9307	0.0008	0.9323
Internal Moderator Density = 90 %	0.9349	0.0009	0.9367
Internal Moderator Density = 80 %	0.9371	0.0007	0.9385
Internal Moderator Density = 70 %	0.9361	0.0007	0.9375
Internal Moderator Density = 60 %	0.9285	0.0007	0.9299
Enrichment = 4.85 wt. % U-235, Soluble Boron = 2400 ppm, Type C Basket			
Internal Moderator Density = 100 %	0.9322	0.0007	0.9336
Internal Moderator Density = 90 %	0.9367	0.0007	0.9381
Internal Moderator Density = 80 %	0.9369	0.0007	0.9383
Internal Moderator Density = 70 %	0.9331	0.0007	0.9345
Internal Moderator Density = 60 %	0.9242	0.0008	0.9258

Table 6-36
Intact CE 16x16 Class Assembly with BPRAs, Final Results
(Concluded)

Model Description	k_{KENO}	1σ	k_{eff}
Enrichment = 4.30 wt. % U-235, Soluble Boron = 2500 ppm, Type A Basket			
Internal Moderator Density = 90 %	0.9290	0.0008	0.9306
Internal Moderator Density = 80 %	0.9350	0.0007	0.9364
Internal Moderator Density = 70 %	0.9395	0.0008	0.9411
Internal Moderator Density = 60 %	0.9357	0.0007	0.9371
Internal Moderator Density = 50 %	0.9285	0.0007	0.9299
Enrichment = 4.80 wt. % U-235, Soluble Boron = 2500 ppm, Type B Basket			
Internal Moderator Density = 90 %	0.9369	0.0008	0.9385
Internal Moderator Density = 80 %	0.9391	0.0008	0.9407
Internal Moderator Density = 70 %	0.9380	0.0006	0.9392
Internal Moderator Density = 60 %	0.9303	0.0007	0.9317
Internal Moderator Density = 50 %	0.9174	0.0007	0.9188
Enrichment = 4.95 wt. % U-235, Soluble Boron = 2500 ppm, Type C Basket			
Internal Moderator Density = 100 %	0.9306	0.0008	0.9322
Internal Moderator Density = 90 %	0.9366	0.0008	0.9382
Internal Moderator Density = 80 %	0.9367	0.0007	0.9381
Internal Moderator Density = 70 %	0.9334	0.0008	0.9350
Internal Moderator Density = 60 %	0.9258	0.0007	0.9272
Enrichment = 4.50 wt. % U-235, Soluble Boron = 2800 ppm, Type A Basket			
Internal Moderator Density = 90 %	0.9211	0.0007	0.9225
Internal Moderator Density = 80 %	0.9313	0.0007	0.9327
Internal Moderator Density = 70 %	0.9350	0.0007	0.9364
Internal Moderator Density = 60 %	0.9340	0.0008	0.9356
Internal Moderator Density = 50 %	0.9276	0.0008	0.9292
Enrichment = 5.00 wt. % U-235, Soluble Boron = 2800 ppm, Type B Basket			
Internal Moderator Density = 90 %	0.9288	0.0008	0.9304
Internal Moderator Density = 80 %	0.9323	0.0009	0.9341
Internal Moderator Density = 70 %	0.9336	0.0008	0.9352
Internal Moderator Density = 60 %	0.9290	0.0008	0.9306
Internal Moderator Density = 50 %	0.9166	0.0007	0.9180

Table 6-37
CE 14x14 Class Damaged Assemblies without BPRAs - Final Results

Description	K_{keno}	σ_{keno}	K_{eff}	Filename
Type A Basket (7.0 mg B-10/cm ²), 2000 ppm Boron, 3.90 wt. % U-235				
60% IMD	0.9371	0.0007	0.9385	ce14d20_p07e39_060.out:
70% IMD	0.9375	0.0007	0.9389	ce14d20_p07e39_070.out:
80% IMD	0.9304	0.0007	0.9318	ce14d20_p07e39_080.out:
90% IMD	0.9181	0.0007	0.9195	ce14d20_p07e39_090.out:
100% IMD	0.9046	0.0008	0.9062	ce14d20_p07e39_100.out:
Type B Basket (15.0 mg B-10/cm ²), 2000 ppm Boron, 4.35 wt. % U-235				
60% IMD	0.9331	0.0008	0.9347	ce14d20_p15e43_060.out:
70% IMD	0.9381	0.0007	0.9395	ce14d20_p15e43_070.out:
80% IMD	0.9354	0.0008	0.9370	ce14d20_p15e43_080.out:
90% IMD	0.9282	0.0007	0.9296	ce14d20_p15e43_090.out:
100% IMD	0.9180	0.0007	0.9194	ce14d20_p15e43_100.out:
Type C Basket (20.0 mg B-10/cm ²), 2000 ppm Boron, 4.50 wt. % U-235				
60% IMD	0.9293	0.0007	0.9307	ce14d20_p20e45_060.out:
70% IMD	0.9348	0.0007	0.9362	ce14d20_p20e45_070.out:
80% IMD	0.9342	0.0007	0.9356	ce14d20_p20e45_080.out:
90% IMD	0.9273	0.0007	0.9287	ce14d20_p20e45_090.out:
100% IMD	0.9187	0.0007	0.9201	ce14d20_p20e45_100.out:
Type D Basket (32.0 mg B-10/cm ²), 2000 ppm Boron, 4.85 wt. % U-235				
60% IMD	0.9263	0.0007	0.9277	ce14d20_p32e48_060.out:
70% IMD	0.9370	0.0008	0.9386	ce14d20_p32e48_070.out:
80% IMD	0.9385	0.0006	0.9397	ce14d20_p32e48_080.out:
90% IMD	0.9338	0.0007	0.9352	ce14d20_p32e48_090.out:
100% IMD	0.9257	0.0008	0.9273	ce14d20_p32e48_100.out:
Type E Basket (50.0 mg B-10/cm ²), 2000 ppm Boron, 5.00 wt. % U-235				
60% IMD	0.9111	0.0007	0.9125	ce14d20_p50e50_060.out:
70% IMD	0.9240	0.0008	0.9256	ce14d20_p50e50_070.out:
80% IMD	0.9296	0.0008	0.9312	ce14d20_p50e50_080.out:
90% IMD	0.9253	0.0007	0.9267	ce14d20_p50e50_090.out:
100% IMD	0.9197	0.0008	0.9213	ce14d20_p50e50_100.out:
Type A Basket (7.0 mg B-10/cm ²), 2300 ppm Boron, 4.20 wt. % U-235				
60% IMD	0.9382	0.0007	0.9396	ce14d23_p07e42_060.out:
70% IMD	0.9363	0.0007	0.9377	ce14d23_p07e42_070.out:
80% IMD	0.9280	0.0008	0.9296	ce14d23_p07e42_080.out:
90% IMD	0.9161	0.0007	0.9175	ce14d23_p07e42_090.out:
100% IMD	0.8999	0.0007	0.9013	ce14d23_p07e42_100.out:

Table 6-37
CE 14x14 Class Damaged Assemblies without BPRAs - Final Results
(Continued)

Description	K_{keno}	σ_{keno}	K_{eff}	Filename
Type B Basket (15.0 mg B-10/cm ²), 2300 ppm Boron, 4.70 wt. % U-235				
60% IMD	0.9369	0.0009	0.9387	ce14d23_p15e47_060.out:
70% IMD	0.9380	0.0007	0.9394	ce14d23_p15e47_070.out:
80% IMD	0.9349	0.0007	0.9363	ce14d23_p15e47_080.out:
90% IMD	0.9242	0.0007	0.9256	ce14d23_p15e47_090.out:
100% IMD	0.9118	0.0008	0.9134	ce14d23_p15e47_100.out:
Type C Basket (20.0 mg B-10/cm ²), 2300 ppm Boron, 4.85 wt. % U-235				
60% IMD	0.9314	0.0008	0.9330	ce14d23_p20e48_060.out:
70% IMD	0.9357	0.0008	0.9373	ce14d23_p20e48_070.out:
80% IMD	0.9346	0.0008	0.9362	ce14d23_p20e48_080.out:
90% IMD	0.9260	0.0007	0.9274	ce14d23_p20e48_090.out:
100% IMD	0.9135	0.0007	0.9149	ce14d23_p20e48_100.out:
Type D Basket (32.0 mg B-10/cm ²), 2300 ppm Boron, 5.00 wt. % U-235				
60% IMD	0.9170	0.0007	0.9184	ce14d23_p32e50_060.out:
70% IMD	0.9231	0.0007	0.9245	ce14d23_p32e50_070.out:
80% IMD	0.9237	0.0007	0.9251	ce14d23_p32e50_080.out:
90% IMD	0.9173	0.0007	0.9187	ce14d23_p32e50_090.out:
100% IMD	0.9081	0.0007	0.9095	ce14d23_p32e50_100.out:
Type A Basket (07.0 mg B-10/cm ²), 2400 ppm Boron, 4.25 wt. % U-235				
60% IMD	0.9356	0.0007	0.9370	ce14d24_p07e42_060.out:
70% IMD	0.9322	0.0007	0.9336	ce14d24_p07e42_070.out:
80% IMD	0.9235	0.0007	0.9249	ce14d24_p07e42_080.out:
90% IMD	0.9113	0.0007	0.9127	ce14d24_p07e42_090.out:
100% IMD	0.8952	0.0006	0.8964	ce14d24_p07e42_100.out:
Type B Basket (15.0 mg B-10/cm ²), 2400 ppm Boron, 4.80 wt. % U-235				
60% IMD	0.9366	0.0007	0.9380	ce14d24_p15e48_060.out:
70% IMD	0.9386	0.0007	0.9400	ce14d24_p15e48_070.out:
80% IMD	0.9323	0.0007	0.9337	ce14d24_p15e48_080.out:
90% IMD	0.9242	0.0007	0.9256	ce14d24_p15e48_090.out:
100% IMD	0.9115	0.0007	0.9129	ce14d24_p15e48_100.out:
Type C Basket (20.0 mg B-10/cm ²), 2400 ppm Boron, 4.95 wt. % U-235				
60% IMD	0.9318	0.0008	0.9334	ce14d24_p20e49_060.out:
70% IMD	0.9354	0.0008	0.9370	ce14d24_p20e49_070.out:
80% IMD	0.9313	0.0008	0.9329	ce14d24_p20e49_080.out:
90% IMD	0.9247	0.0007	0.9261	ce14d24_p20e49_090.out:
100% IMD	0.9121	0.0007	0.9135	ce14d24_p20e49_100.out:

Table 6-37
CE 14x14 Class Damaged Assemblies without BPRAs - Final Results
(Concluded)

Description	K_{keno}	σ_{keno}	K_{eff}	Filename
Type A Basket (07.0 mg B-10/cm ²), 2500 ppm Boron, 4.35 wt. % U-235				
60% IMD	0.9364	0.0007	0.9378	Ce14d25_p07e43_060.out:
70% IMD	0.9323	0.0007	0.9337	Ce14d25_p07e43_070.out:
80% IMD	0.9235	0.0006	0.9247	Ce14d25_p07e43_080.out:
90% IMD	0.9087	0.0007	0.9101	Ce14d25_p07e43_090.out:
100% IMD	0.8926	0.0007	0.8940	Ce14d25_p07e43_100.out:
Type B Basket (15.0 mg B-10/cm ²), 2500 ppm Boron, 4.90 wt. % U-235				
60% IMD	0.9375	0.0009	0.9393	Ce14d25_p15e49_060.out:
70% IMD	0.9380	0.0007	0.9394	ce14d25_p15e49_070.out:
80% IMD	0.9327	0.0008	0.9343	ce14d25_p15e49_080.out:
90% IMD	0.9220	0.0007	0.9234	ce14d25_p15e49_090.out:
100% IMD	0.9077	0.0008	0.9093	ce14d25_p15e49_100.out:
Type C Basket (20.0 mg B-10/cm ²), 2500 ppm Boron, 5.00 wt. % U-235				
60% IMD	0.9297	0.0007	0.9311	ce14d25_p20e50_060.out:
70% IMD	0.9326	0.0007	0.9340	ce14d25_p20e50_070.out:
80% IMD	0.9277	0.0007	0.9291	ce14d25_p20e50_080.out:
90% IMD	0.9178	0.0007	0.9192	ce14d25_p20e50_090.out:
100% IMD	0.9059	0.0007	0.9073	ce14d25_p20e50_100.out:
Type A Basket (7.0 mg B-10/cm ²), 2800 ppm Boron, 4.40 wt. % U-235				
40% IMD	0.9257	0.0007	0.9271	
50% IMD	0.9361	0.0007	0.9375	
60% IMD	0.9357	0.0006	0.9369	
70% IMD	0.9283	0.0007	0.9297	
80% IMD	0.9153	0.0007	0.9167	
Type B Basket (15.0 mg B-10/cm ²), 2800 ppm Boron, 4.90 wt. % U-235				
50% IMD	0.9322	0.0007	0.9336	
60% IMD	0.9362	0.0006	0.9374	
70% IMD	0.9305	0.0007	0.9319	
80% IMD	0.9220	0.0006	0.9232	
90% IMD	0.9074	0.0007	0.9088	
Type C Basket (20.0 mg B-10/cm ²), 2800 ppm Boron, 5.00 wt. % U-235				
50% IMD	0.9201	0.0007	0.9215	
60% IMD	0.9285	0.0007	0.9299	
70% IMD	0.9272	0.0007	0.9286	
80% IMD	0.9174	0.0008	0.9190	
90% IMD	0.9071	0.0007	0.9085	

Table 6-38
CE 14x14 Class Assembly Final Results with BPRAs (Damaged)

Description	K_{keno}	σ_{keno}	K_{eff}
Type A Basket (7.0 mg B-10/cm²), 2000 ppm Boron, 3.70 wt. % U-235			
60% IMD	0.9287	0.0006	0.9299
70% IMD	0.9352	0.0007	0.9366
80% IMD	0.9367	0.0006	0.9379
90% IMD	0.9333	0.0007	0.9347
100% IMD	0.9246	0.0007	0.9260
Type B Basket (15.0 mg B-10/cm²), 2000 ppm Boron, 4.10 wt. % U-235			
60% IMD	0.9212	0.0007	0.9226
70% IMD	0.9323	0.0008	0.9339
80% IMD	0.9379	0.0008	0.9395
90% IMD	0.9381	0.0008	0.9397
100% IMD	0.9327	0.0008	0.9343
Type C Basket (20.0 mg B-10/cm²), 2000 ppm Boron, 4.20 wt. % U-235			
60% IMD	0.9132	0.0007	0.9146
70% IMD	0.9261	0.0007	0.9275
80% IMD	0.9332	0.0008	0.9348
90% IMD	0.9350	0.0007	0.9364
100% IMD	0.9315	0.0007	0.9329
Type D Basket (32.0 mg B-10/cm²), 2000 ppm Boron, 4.50 wt. % U-235			
60% IMD	0.9079	0.0007	0.9093
70% IMD	0.9236	0.0007	0.9250
80% IMD	0.9352	0.0007	0.9366
90% IMD	0.9365	0.0007	0.9379
100% IMD	0.9364	0.0007	0.9378
Type E Basket (50.0 mg B-10/cm²), 2000 ppm Boron, 4.75 wt. % U-235			
60% IMD	0.8951	0.0007	0.8965
70% IMD	0.9159	0.0008	0.9175
80% IMD	0.9301	0.0008	0.9317
90% IMD	0.9350	0.0007	0.9364
100% IMD	0.9363	0.0008	0.9379

Table 6-38
CE 14x14 Class Assembly Final Results with BPRAs (Damaged)
(Continued)

Description	K_{keno}	σ_{keno}	K_{eff}
Type A Basket (7.0 mg B-10/cm ²), 2300 ppm Boron, 3.95 wt. % U-235			
60% IMD	0.9295	0.0007	0.9309
70% IMD	0.9372	0.0007	0.9386
80% IMD	0.9356	0.0008	0.9372
90% IMD	0.9289	0.0006	0.9301
100% IMD	0.9201	0.0008	0.9217
Type B Basket (15.0 mg B-10/cm ²), 2300 ppm Boron, 4.40 wt. % U-235			
60% IMD	0.9239	0.0007	0.9253
70% IMD	0.9331	0.0007	0.9345
80% IMD	0.9374	0.0008	0.9390
90% IMD	0.9343	0.0008	0.9359
100% IMD	0.9293	0.0007	0.9307
Type C Basket (20.0 mg B-10/cm ²), 2300 ppm Boron, 4.55 wt. % U-235			
60% IMD	0.9185	0.0008	0.9201
70% IMD	0.9315	0.0008	0.9331
80% IMD	0.9362	0.0008	0.9378
90% IMD	0.9360	0.0007	0.9374
100% IMD	0.9303	0.0007	0.9317
Type D Basket (32.0 mg B-10/cm ²), 2300 ppm Boron, 4.85 wt. % U-235			
60% IMD	0.9113	0.0007	0.9127
70% IMD	0.9288	0.0008	0.9304
80% IMD	0.9336	0.0007	0.9350
90% IMD	0.9368	0.0007	0.9382
100% IMD	0.9333	0.0007	0.9347
Type E Basket (50.0 mg B-10/cm ²), 2300 ppm Boron, 5.00 wt. % U-235			
60% IMD	0.8956	0.0007	0.8970
70% IMD	0.9147	0.0008	0.9163
80% IMD	0.9236	0.0008	0.9252
90% IMD	0.9262	0.0007	0.9276
100% IMD	0.9259	0.0008	0.9275

Table 6-38
CE 14x14 Class Assembly Final Results with BPRAs (Damaged)
(Continued)

Description	K_{keno}	σ_{keno}	K_{eff}
Type A Basket (7.0 mg B-10/cm²), 2400 ppm Boron, 4.05 wt. % U-235			
60% IMD	0.9323	0.0008	0.9339
70% IMD	0.9369	0.0007	0.9383
80% IMD	0.9362	0.0006	0.9374
90% IMD	0.9297	0.0006	0.9309
100% IMD	0.9192	0.0006	0.9204
Type B Basket (15.0 mg B-10/cm²), 2400 ppm Boron, 4.50 wt. % U-235			
60% IMD	0.9248	0.0008	0.9264
70% IMD	0.9349	0.0009	0.9367
80% IMD	0.9382	0.0007	0.9396
90% IMD	0.9380	0.0008	0.9396
100% IMD	0.9278	0.0008	0.9294
Type C Basket (20.0 mg B-10/cm²), 2400 ppm Boron, 4.65 wt. % U-235			
60% IMD	0.9206	0.0008	0.9222
70% IMD	0.9311	0.0007	0.9325
80% IMD	0.9356	0.0006	0.9368
90% IMD	0.9340	0.0007	0.9354
100% IMD	0.9304	0.0007	0.9318
Type D Basket (32.0 mg B-10/cm²), 2400 ppm Boron, 5.00 wt. % U-235			
60% IMD	0.9155	0.0008	0.9171
70% IMD	0.9287	0.0008	0.9303
80% IMD	0.9361	0.0008	0.9377
90% IMD	0.9371	0.0008	0.9387
100% IMD	0.9341	0.0007	0.9355
Type A Basket (7.0 mg B-10/cm²), 2500 ppm Boron, 4.10 wt. % U-235			
60% IMD	0.9304	0.0007	0.9318
70% IMD	0.9353	0.0007	0.9367
80% IMD	0.9322	0.0007	0.9336
90% IMD	0.9232	0.0008	0.9248
100% IMD	0.9154	0.0007	0.9168

Table 6-38
CE 14x14 Class Assembly Final Results with BPRAs (Damaged)
(Concluded)

Description	K_{keno}	σ_{keno}	K_{eff}
Type B Basket (15.0 mg B-10/cm²), 2500 ppm Boron, 4.60 wt. % U-235			
60% IMD	0.9263	0.0007	0.9277
70% IMD	0.9375	0.0007	0.9389
80% IMD	0.9370	0.0007	0.9384
90% IMD	0.9342	0.0007	0.9356
100% IMD	0.9275	0.0007	0.9289
Type C Basket (20.0 mg B-10/cm²), 2500 ppm Boron, 4.75 wt. % U-235			
60% IMD	0.9206	0.0007	0.9220
70% IMD	0.9329	0.0007	0.9343
80% IMD	0.9355	0.0007	0.9369
90% IMD	0.9339	0.0008	0.9355
100% IMD	0.9254	0.0009	0.9272
Type A Basket (7.0 mg B-10/cm²), 2800 ppm Boron, 4.20 wt. % U-235			
50% IMD	0.9273	0.0007	0.9287
60% IMD	0.9358	0.0007	0.9372
70% IMD	0.9342	0.0006	0.9354
80% IMD	0.9261	0.0007	0.9275
90% IMD	0.9148	0.0007	0.9162
Type B Basket (15.0 mg B-10/cm²), 2800 ppm Boron, 4.65 wt. % U-235			
60% IMD	0.9311	0.0007	0.9325
70% IMD	0.9350	0.0006	0.9362
80% IMD	0.9306	0.0007	0.9320
90% IMD	0.9226	0.0007	0.9240
100% IMD	0.9116	0.0006	0.9128
Type C Basket (20.0 mg B-10/cm²), 2800 ppm Boron, 4.90 wt. % U-235			
60% IMD	0.9331	0.0007	0.9345
70% IMD	0.9359	0.0008	0.9375
80% IMD	0.9346	0.0007	0.9360
90% IMD	0.9289	0.0008	0.9305
100% IMD	0.9182	0.0007	0.9196

Table 6-39
Damaged CE 16x16 Class Assembly without BPRAs, Final Results

Model Description	k_{KENO}	1σ	k_{eff}
Enrichment = 3.65 wt. % U-235, Soluble Boron = 2000 ppm, Type A Basket			
Internal Moderator Density = 050 %	0.9289	0.0007	0.9303
Internal Moderator Density = 060 %	0.9369	0.0007	0.9383
Internal Moderator Density = 070 %	0.9347	0.0007	0.9361
Internal Moderator Density = 080 %	0.9298	0.0007	0.9312
Internal Moderator Density = 090 %	0.9176	0.0006	0.9188
Enrichment = 4.05 wt. % U-235, Soluble Boron = 2000 ppm, Type B Basket			
Internal Moderator Density = 060 %	0.9334	0.0007	0.9348
Internal Moderator Density = 070 %	0.9363	0.0007	0.9377
Internal Moderator Density = 080 %	0.9329	0.0007	0.9343
Internal Moderator Density = 090 %	0.9280	0.0007	0.9294
Internal Moderator Density = 100 %	0.9159	0.0007	0.9173
Enrichment = 4.20 wt. % U-235, Soluble Boron = 2000 ppm, Type C Basket			
Internal Moderator Density = 060 %	0.9313	0.0008	0.9329
Internal Moderator Density = 070 %	0.9365	0.0007	0.9379
Internal Moderator Density = 080 %	0.9338	0.0007	0.9352
Internal Moderator Density = 090 %	0.9286	0.0007	0.9300
Internal Moderator Density = 100 %	0.9189	0.0007	0.9203
Enrichment = 4.50 wt. % U-235, Soluble Boron = 2000 ppm, Type D Basket			
Internal Moderator Density = 060 %	0.9278	0.0007	0.9292
Internal Moderator Density = 070 %	0.9357	0.0007	0.9371
Internal Moderator Density = 080 %	0.9378	0.0007	0.9392
Internal Moderator Density = 090 %	0.9338	0.0007	0.9352
Internal Moderator Density = 100 %	0.9275	0.0007	0.9289
Enrichment = 4.75 wt. % U-235, Soluble Boron = 2000 ppm, Type E Basket			
Internal Moderator Density = 060 %	0.9213	0.0007	0.9227
Internal Moderator Density = 070 %	0.9307	0.0007	0.9321
Internal Moderator Density = 080 %	0.9376	0.0007	0.9390
Internal Moderator Density = 090 %	0.9354	0.0008	0.9370
Internal Moderator Density = 100 %	0.9289	0.0007	0.9303

Table 6-39
Damaged CE 16x16 Class Assembly without BPRAs, Final Results
(Continued)

Model Description	k_{KENO}	1σ	k_{eff}
Enrichment = 3.90 wt. % U-235, Soluble Boron = 2300 ppm, Type A Basket			
Internal Moderator Density = 050 %	0.9325	0.0007	0.9339
Internal Moderator Density = 060 %	0.9369	0.0006	0.9381
Internal Moderator Density = 070 %	0.9328	0.0007	0.9342
Internal Moderator Density = 080 %	0.9238	0.0008	0.9254
Internal Moderator Density = 090 %	0.9116	0.0007	0.9130
Enrichment = 4.30 wt. % U-235, Soluble Boron = 2300 ppm, Type B Basket			
Internal Moderator Density = 060 %	0.9323	0.0006	0.9335
Internal Moderator Density = 070 %	0.9329	0.0007	0.9343
Internal Moderator Density = 080 %	0.9284	0.0008	0.9300
Internal Moderator Density = 090 %	0.9198	0.0007	0.9212
Internal Moderator Density = 100 %	0.9068	0.0007	0.9082
Enrichment = 4.50 wt. % U-235, Soluble Boron = 2300 ppm, Type C Basket			
Internal Moderator Density = 060 %	0.9308	0.0006	0.9320
Internal Moderator Density = 070 %	0.9343	0.0007	0.9357
Internal Moderator Density = 080 %	0.9315	0.0008	0.9331
Internal Moderator Density = 090 %	0.9240	0.0007	0.9254
Internal Moderator Density = 100 %	0.9119	0.0006	0.9131
Enrichment = 4.80 wt. % U-235, Soluble Boron = 2300 ppm, Type D Basket			
Internal Moderator Density = 060 %	0.9292	0.0007	0.9306
Internal Moderator Density = 070 %	0.9345	0.0008	0.9361
Internal Moderator Density = 080 %	0.9340	0.0007	0.9354
Internal Moderator Density = 090 %	0.9284	0.0007	0.9298
Internal Moderator Density = 100 %	0.9190	0.0007	0.9204
Enrichment = 5.00 wt. % U-235, Soluble Boron = 2300 ppm, Type E Basket			
Internal Moderator Density = 060 %	0.9184	0.0008	0.9200
Internal Moderator Density = 070 %	0.9269	0.0008	0.9285
Internal Moderator Density = 080 %	0.9278	0.0008	0.9294
Internal Moderator Density = 090 %	0.9236	0.0007	0.9250
Internal Moderator Density = 100 %	0.9169	0.0006	0.9181

Table 6-39
Damaged CE 16x16 Class Assembly without BPRAs, Final Results
(Continued)

Model Description	k_{KENO}	1σ	k_{eff}
Enrichment = 4.00 wt. % U-235, Soluble Boron = 2400 ppm, Type A Basket			
Internal Moderator Density = 050 %	0.9343	0.0007	0.9357
Internal Moderator Density = 060 %	0.9368	0.0007	0.9382
Internal Moderator Density = 070 %	0.9327	0.0006	0.9339
Internal Moderator Density = 080 %	0.9236	0.0006	0.9248
Internal Moderator Density = 090 %	0.9107	0.0006	0.9119
Enrichment = 4.40 wt. % U-235, Soluble Boron = 2400 ppm, Type B Basket			
Internal Moderator Density = 060 %	0.9334	0.0007	0.9348
Internal Moderator Density = 070 %	0.9339	0.0006	0.9351
Internal Moderator Density = 080 %	0.9275	0.0007	0.9289
Internal Moderator Density = 090 %	0.9188	0.0007	0.9202
Internal Moderator Density = 100 %	0.9060	0.0006	0.9072
Enrichment = 4.60 wt. % U-235, Soluble Boron = 2400 ppm, Type C Basket			
Internal Moderator Density = 060 %	0.9326	0.0007	0.9340
Internal Moderator Density = 070 %	0.9336	0.0007	0.9350
Internal Moderator Density = 080 %	0.9315	0.0006	0.9327
Internal Moderator Density = 090 %	0.9231	0.0008	0.9247
Internal Moderator Density = 100 %	0.9107	0.0007	0.9121
Enrichment = 4.90 wt. % U-235, Soluble Boron = 2400 ppm, Type D Basket			
Internal Moderator Density = 060 %	0.9269	0.0007	0.9283
Internal Moderator Density = 070 %	0.9333	0.0007	0.9347
Internal Moderator Density = 080 %	0.9325	0.0007	0.9339
Internal Moderator Density = 090 %	0.9259	0.0007	0.9273
Internal Moderator Density = 100 %	0.9162	0.0007	0.9176
Enrichment = 5.00 wt. % U-235, Soluble Boron = 2400 ppm, Type E Basket			
Internal Moderator Density = 060 %	0.9127	0.0007	0.9141
Internal Moderator Density = 070 %	0.9198	0.0008	0.9214
Internal Moderator Density = 080 %	0.9203	0.0008	0.9219
Internal Moderator Density = 090 %	0.9164	0.0007	0.9178
Internal Moderator Density = 100 %	0.9088	0.0007	0.9102

Table 6-39
Damaged CE 16x16 Class Assembly without BPRAs, Final Results
(Continued)

Model Description	k_{KENO}	1σ	k_{eff}
Enrichment = 4.05 wt. % U-235, Soluble Boron = 2500 ppm, Type A Basket			
Internal Moderator Density = 050 %	0.9308	0.0007	0.9322
Internal Moderator Density = 060 %	0.9348	0.0006	0.9360
Internal Moderator Density = 070 %	0.9304	0.0006	0.9316
Internal Moderator Density = 080 %	0.9199	0.0007	0.9213
Internal Moderator Density = 090 %	0.9062	0.0006	0.9074
Enrichment = 4.50 wt. % U-235, Soluble Boron = 2500 ppm, Type B Basket			
Internal Moderator Density = 060 %	0.9329	0.0008	0.9345
Internal Moderator Density = 070 %	0.9336	0.0008	0.9352
Internal Moderator Density = 080 %	0.9272	0.0007	0.9286
Internal Moderator Density = 090 %	0.9161	0.0006	0.9173
Internal Moderator Density = 100 %	0.9036	0.0007	0.9050
Enrichment = 4.70 wt. % U-235, Soluble Boron = 2500 ppm, Type C Basket			
Internal Moderator Density = 060 %	0.9318	0.0007	0.9332
Internal Moderator Density = 070 %	0.9343	0.0008	0.9359
Internal Moderator Density = 080 %	0.9305	0.0007	0.9319
Internal Moderator Density = 090 %	0.9204	0.0008	0.9220
Internal Moderator Density = 100 %	0.9086	0.0007	0.9100
Enrichment = 5.00 wt. % U-235, Soluble Boron = 2500 ppm, Type D Basket			
Internal Moderator Density = 060 %	0.9287	0.0007	0.9301
Internal Moderator Density = 070 %	0.9321	0.0008	0.9337
Internal Moderator Density = 080 %	0.9316	0.0007	0.9330
Internal Moderator Density = 090 %	0.9246	0.0007	0.9260
Internal Moderator Density = 100 %	0.9131	0.0007	0.9145
Enrichment = 5.00 wt. % U-235, Soluble Boron = 2500 ppm, Type E Basket			
Internal Moderator Density = 060 %	0.9077	0.0007	0.9091
Internal Moderator Density = 070 %	0.9138	0.0007	0.9152
Internal Moderator Density = 080 %	0.9138	0.0008	0.9154
Internal Moderator Density = 090 %	0.9093	0.0007	0.9107
Internal Moderator Density = 100 %	0.9003	0.0008	0.9019

Table 6-39
Damaged CE 16x16 Class Assembly without BPRAs, Final Results
(Concluded)

Model Description	k_{KENO}	1σ	k_{eff}
Enrichment = 4.30 wt. % U-235, Soluble Boron = 2800 ppm, Type A Basket			
Internal Moderator Density = 050 %	0.9359	0.0007	0.9373
Internal Moderator Density = 060 %	0.9357	0.0007	0.9371
Internal Moderator Density = 070 %	0.9290	0.0007	0.9304
Internal Moderator Density = 080 %	0.9172	0.0007	0.9186
Internal Moderator Density = 090 %	0.9015	0.0006	0.9027
Enrichment = 4.80 wt. % U-235, Soluble Boron = 2800 ppm, Type B Basket			
Internal Moderator Density = 050 %	0.9308	0.0007	0.9322
Internal Moderator Density = 060 %	0.9350	0.0008	0.9366
Internal Moderator Density = 070 %	0.9328	0.0009	0.9346
Internal Moderator Density = 080 %	0.9267	0.0007	0.9281
Internal Moderator Density = 090 %	0.9149	0.0007	0.9163
Enrichment = 5.00 wt. % U-235, Soluble Boron = 2800 ppm, Type C Basket			
Internal Moderator Density = 050 %	0.9263	0.0006	0.9275
Internal Moderator Density = 060 %	0.9352	0.0007	0.9366
Internal Moderator Density = 070 %	0.9330	0.0007	0.9344
Internal Moderator Density = 080 %	0.9271	0.0007	0.9285
Internal Moderator Density = 090 %	0.9181	0.0007	0.9195

Table 6-40
Damaged CE 16x16 Class Assembly with BPRAs, Final Results

Model Description	k_{KENO}	1σ	k_{eff}
Enrichment = 3.60 wt. % U-235, Soluble Boron = 2000 ppm, Type A Basket			
Internal Moderator Density = 050 %	0.9255	0.0007	0.9269
Internal Moderator Density = 060 %	0.9353	0.0008	0.9369
Internal Moderator Density = 070 %	0.9380	0.0007	0.9394
Internal Moderator Density = 080 %	0.9347	0.0006	0.9359
Internal Moderator Density = 090 %	0.9261	0.0006	0.9273
Enrichment = 3.95 wt. % U-235, Soluble Boron = 2000 ppm, Type B Basket			
Internal Moderator Density = 060 %	0.9274	0.0007	0.9288
Internal Moderator Density = 070 %	0.9354	0.0007	0.9368
Internal Moderator Density = 080 %	0.9353	0.0008	0.9369
Internal Moderator Density = 090 %	0.9303	0.0008	0.9319
Internal Moderator Density = 100 %	0.9220	0.0007	0.9234
Enrichment = 4.10 wt. % U-235, Soluble Boron = 2000 ppm, Type C Basket			
Internal Moderator Density = 060 %	0.9245	0.0006	0.9257
Internal Moderator Density = 070 %	0.9334	0.0007	0.9348
Internal Moderator Density = 080 %	0.9358	0.0006	0.9370
Internal Moderator Density = 090 %	0.9312	0.0007	0.9326
Internal Moderator Density = 100 %	0.9245	0.0007	0.9259
Enrichment = 4.40 wt. % U-235, Soluble Boron = 2000 ppm, Type D Basket			
Internal Moderator Density = 060 %	0.9218	0.0007	0.9232
Internal Moderator Density = 070 %	0.9337	0.0007	0.9351
Internal Moderator Density = 080 %	0.9383	0.0007	0.9397
Internal Moderator Density = 090 %	0.9364	0.0007	0.9378
Internal Moderator Density = 100 %	0.9322	0.0008	0.9338
Enrichment = 4.65 wt. % U-235, Soluble Boron = 2000 ppm, Type E Basket			
Internal Moderator Density = 060 %	0.9155	0.0007	0.9169
Internal Moderator Density = 070 %	0.9293	0.0007	0.9307
Internal Moderator Density = 080 %	0.9380	0.0007	0.9394
Internal Moderator Density = 090 %	0.9384	0.0007	0.9398
Internal Moderator Density = 100 %	0.9353	0.0007	0.9367

Table 6-40
Damaged CE 16x16 Class Assembly with BPRAs, Final Results
(Continued)

Model Description	k_{KENO}	1σ	k_{eff}
Enrichment = 3.80 wt. % U-235, Soluble Boron = 2300 ppm, Type A Basket			
Internal Moderator Density = 050 %	0.9238	0.0007	0.9252
Internal Moderator Density = 060 %	0.9330	0.0008	0.9346
Internal Moderator Density = 070 %	0.9321	0.0006	0.9333
Internal Moderator Density = 080 %	0.9275	0.0007	0.9289
Internal Moderator Density = 090 %	0.9169	0.0007	0.9183
Enrichment = 4.20 wt. % U-235, Soluble Boron = 2300 ppm, Type B Basket			
Internal Moderator Density = 060 %	0.9282	0.0007	0.9296
Internal Moderator Density = 070 %	0.9321	0.0006	0.9333
Internal Moderator Density = 080 %	0.9302	0.0008	0.9318
Internal Moderator Density = 090 %	0.9242	0.0007	0.9256
Internal Moderator Density = 100 %	0.9141	0.0007	0.9155
Enrichment = 4.40 wt. % U-235, Soluble Boron = 2300 ppm, Type C Basket			
Internal Moderator Density = 060 %	0.9298	0.0008	0.9314
Internal Moderator Density = 070 %	0.9337	0.0007	0.9351
Internal Moderator Density = 080 %	0.9344	0.0007	0.9358
Internal Moderator Density = 090 %	0.9288	0.0007	0.9302
Internal Moderator Density = 100 %	0.9206	0.0007	0.9220
Enrichment = 4.70 wt. % U-235, Soluble Boron = 2300 ppm, Type D Basket			
Internal Moderator Density = 060 %	0.9247	0.0007	0.9261
Internal Moderator Density = 070 %	0.9332	0.0008	0.9348
Internal Moderator Density = 080 %	0.9360	0.0007	0.9374
Internal Moderator Density = 090 %	0.9325	0.0008	0.9341
Internal Moderator Density = 100 %	0.9252	0.0008	0.9268
Enrichment = 4.90 wt. % U-235, Soluble Boron = 2300 ppm, Type E Basket			
Internal Moderator Density = 060 %	0.9125	0.0007	0.9139
Internal Moderator Density = 070 %	0.9267	0.0008	0.9283
Internal Moderator Density = 080 %	0.9317	0.0007	0.9331
Internal Moderator Density = 090 %	0.9302	0.0007	0.9316
Internal Moderator Density = 100 %	0.9268	0.0008	0.9284

Table 6-40
Damaged CE 16x16 Class Assembly with BPRAs, Final Results
(Continued)

Model Description	k_{KENO}	1σ	k_{eff}
Enrichment = 3.90 wt. % U-235, Soluble Boron = 2400 ppm, Type A Basket			
Internal Moderator Density = 050 %	0.9281	0.0007	0.9295
Internal Moderator Density = 060 %	0.9346	0.0007	0.9360
Internal Moderator Density = 070 %	0.9329	0.0007	0.9343
Internal Moderator Density = 080 %	0.9270	0.0007	0.9284
Internal Moderator Density = 090 %	0.9158	0.0006	0.9170
Enrichment = 4.30 wt. % U-235, Soluble Boron = 2400 ppm, Type B Basket			
Internal Moderator Density = 060 %	0.9298	0.0007	0.9312
Internal Moderator Density = 070 %	0.9331	0.0007	0.9345
Internal Moderator Density = 080 %	0.9314	0.0006	0.9326
Internal Moderator Density = 090 %	0.9231	0.0007	0.9245
Internal Moderator Density = 100 %	0.9138	0.0007	0.9152
Enrichment = 4.50 wt. % U-235, Soluble Boron = 2400 ppm, Type C Basket			
Internal Moderator Density = 060 %	0.9288	0.0007	0.9302
Internal Moderator Density = 070 %	0.9355	0.0007	0.9369
Internal Moderator Density = 080 %	0.9327	0.0006	0.9339
Internal Moderator Density = 090 %	0.9273	0.0007	0.9287
Internal Moderator Density = 100 %	0.9185	0.0007	0.9199
Enrichment = 4.80 wt. % U-235, Soluble Boron = 2400 ppm, Type D Basket			
Internal Moderator Density = 060 %	0.9247	0.0007	0.9261
Internal Moderator Density = 070 %	0.9343	0.0007	0.9357
Internal Moderator Density = 080 %	0.9347	0.0008	0.9363
Internal Moderator Density = 090 %	0.9322	0.0008	0.9338
Internal Moderator Density = 100 %	0.9247	0.0007	0.9261
Enrichment = 5.00 wt. % U-235, Soluble Boron = 2400 ppm, Type E Basket			
Internal Moderator Density = 060 %	0.9079	0.0007	0.9093
Internal Moderator Density = 070 %	0.9193	0.0007	0.9207
Internal Moderator Density = 080 %	0.9236	0.0007	0.9250
Internal Moderator Density = 090 %	0.9217	0.0007	0.9231
Internal Moderator Density = 100 %	0.9157	0.0007	0.9171

Table 6-40
Damaged CE 16x16 Class Assembly with BPRAs, Final Results
(Continued)

Model Description	k_{KENO}	1σ	k_{eff}
Enrichment = 4.00 wt. % U-235, Soluble Boron = 2500 ppm, Type A Basket			
Internal Moderator Density = 050 %	0.9310	0.0007	0.9324
Internal Moderator Density = 060 %	0.9365	0.0008	0.9381
Internal Moderator Density = 070 %	0.9348	0.0007	0.9362
Internal Moderator Density = 080 %	0.9278	0.0006	0.9290
Internal Moderator Density = 090 %	0.9170	0.0007	0.9184
Enrichment = 4.40 wt. % U-235, Soluble Boron = 2500 ppm, Type B Basket			
Internal Moderator Density = 060 %	0.9318	0.0006	0.9330
Internal Moderator Density = 070 %	0.9344	0.0007	0.9358
Internal Moderator Density = 080 %	0.9299	0.0007	0.9313
Internal Moderator Density = 090 %	0.9223	0.0006	0.9235
Internal Moderator Density = 100 %	0.9127	0.0007	0.9141
Enrichment = 4.60 wt. % U-235, Soluble Boron = 2500 ppm, Type C Basket			
Internal Moderator Density = 060 %	0.9298	0.0006	0.9310
Internal Moderator Density = 070 %	0.9338	0.0009	0.9356
Internal Moderator Density = 080 %	0.9330	0.0007	0.9344
Internal Moderator Density = 090 %	0.9271	0.0007	0.9285
Internal Moderator Density = 100 %	0.9181	0.0006	0.9193
Enrichment = 4.90 wt. % U-235, Soluble Boron = 2500 ppm, Type D Basket			
Internal Moderator Density = 060 %	0.9257	0.0007	0.9271
Internal Moderator Density = 070 %	0.9336	0.0007	0.9350
Internal Moderator Density = 080 %	0.9351	0.0007	0.9365
Internal Moderator Density = 090 %	0.9310	0.0007	0.9324
Internal Moderator Density = 100 %	0.9235	0.0008	0.9251
Enrichment = 5.00 wt. % U-235, Soluble Boron = 2500 ppm, Type E Basket			
Internal Moderator Density = 060 %	0.9087	0.0008	0.9103
Internal Moderator Density = 070 %	0.9203	0.0008	0.9219
Internal Moderator Density = 080 %	0.9240	0.0008	0.9256
Internal Moderator Density = 090 %	0.9215	0.0007	0.9229
Internal Moderator Density = 100 %	0.9140	0.0007	0.9154

Table 6-40
Damaged CE 16x16 Class Assembly with BPRAs, Final Results
(Concluded)

Model Description	k_{KENO}	1σ	k_{eff}
Enrichment = 4.20 wt. % U-235, Soluble Boron = 2800 ppm, Type A Basket			
Internal Moderator Density = 050 %	0.9304	0.0008	0.9320
Internal Moderator Density = 060 %	0.9343	0.0007	0.9357
Internal Moderator Density = 070 %	0.9311	0.0007	0.9325
Internal Moderator Density = 080 %	0.9221	0.0007	0.9235
Internal Moderator Density = 090 %	0.9088	0.0007	0.9102
Enrichment = 4.70 wt. % U-235, Soluble Boron = 2800 ppm, Type B Basket			
Internal Moderator Density = 060 %	0.9341	0.0007	0.9355
Internal Moderator Density = 070 %	0.9358	0.0007	0.9372
Internal Moderator Density = 080 %	0.9308	0.0007	0.9322
Internal Moderator Density = 090 %	0.9202	0.0006	0.9214
Internal Moderator Density = 100 %	0.9080	0.0007	0.9094
Enrichment = 4.90 wt. % U-235, Soluble Boron = 2800 ppm, Type C Basket			
Internal Moderator Density = 060 %	0.9337	0.0006	0.9349
Internal Moderator Density = 070 %	0.9363	0.0007	0.9377
Internal Moderator Density = 080 %	0.9324	0.0007	0.9338
Internal Moderator Density = 090 %	0.9245	0.0007	0.9259
Internal Moderator Density = 100 %	0.9131	0.0007	0.9145

Table 6-41
Criticality Results for the WE 15x15 STD Fuel

Description	k_{keno}	σ	k_{eff}	Output file
Pellet OD - 0.3669", GT - 0.546" (OD), 0.512" (ID) - w/o BPRAs				
70% IMD	0.9249	0.0007	0.9263	we15std-gt-o070.out
80% IMD	0.9257	0.0008	0.9273	we15std-gt-o080.out
Pellet OD - 0.3669", GT - 0.546" (OD), 0.512" (ID) w/ BPRAs				
80% IMD	0.9320	0.0008	0.9336	we15bp24_p32e47-gt-080.out
90% IMD	0.9370	0.0008	0.9386	we15bp24_p32e47-gt-090.out
100%IMD	0.9388	0.0007	0.9402	we15bp24_p32e47-gt-100.out
Pellet OD - 0.3669", GT - 0.546" (OD), 0.512" (ID) w/ BPRAs Damaged Fuel				
80% IMD	0.9307	0.0007	0.9321	we15bpds-p15e38-gt-080.out
90% IMD	0.9338	0.0007	0.9352	we15bpds-p15e38-gt-090.out
100%IMD	0.9362	0.0008	0.9378	we15bpds-p15e38-gt-100.out
Pellet OD - 0.3659", GT - 0.546" (OD), 0.512" (ID) w/o BPRAs				
70% IMD	0.9212	0.0008	0.9228	we15std-gt2-o070.out
80% IMD	0.9252	0.0007	0.9266	we15std-gt2-o080.out
Pellet OD - 0.3659", GT - 0.546" (OD), 0.512" (ID) w/ BPRAs				
80% IMD	0.9318	0.0008	0.9334	we15bp24_p32e47-gt2-080.out
90% IMD	0.9384	0.0007	0.9398	we15bp24_p32e47-gt2-090.out
100%IMD	0.9384	0.0008	0.9400	we15bp24_p32e47-gt2-100.out

Table 6-42
Criticality Results for the WE 15x15 OFA

Description	k_{keno}	σ	k_{eff}	Output file
Pellet OD - 0.3659", GT - 0.533" (OD), 0.499" (ID) - w/o BPRAS				
70% IMD	0.9233	0.0007	0.9247	we15std-gt1-o070.out
80% IMD	0.9242	0.0008	0.9258	we15std-gt1-o080.out

Proprietary Information on Pages 6-150 through 6-151
Withheld Pursuant to 10 CFR 2.390

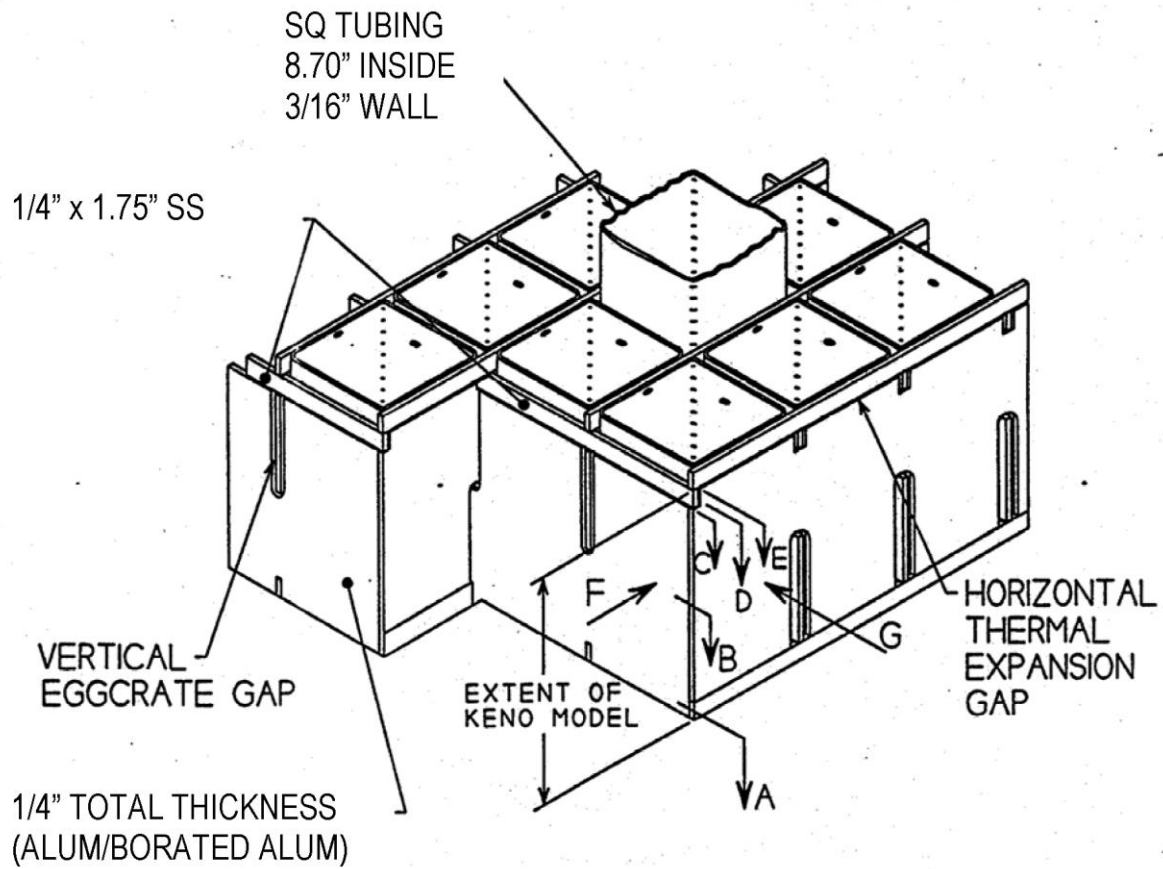


Figure 6-1
Basket Views and Dimensions

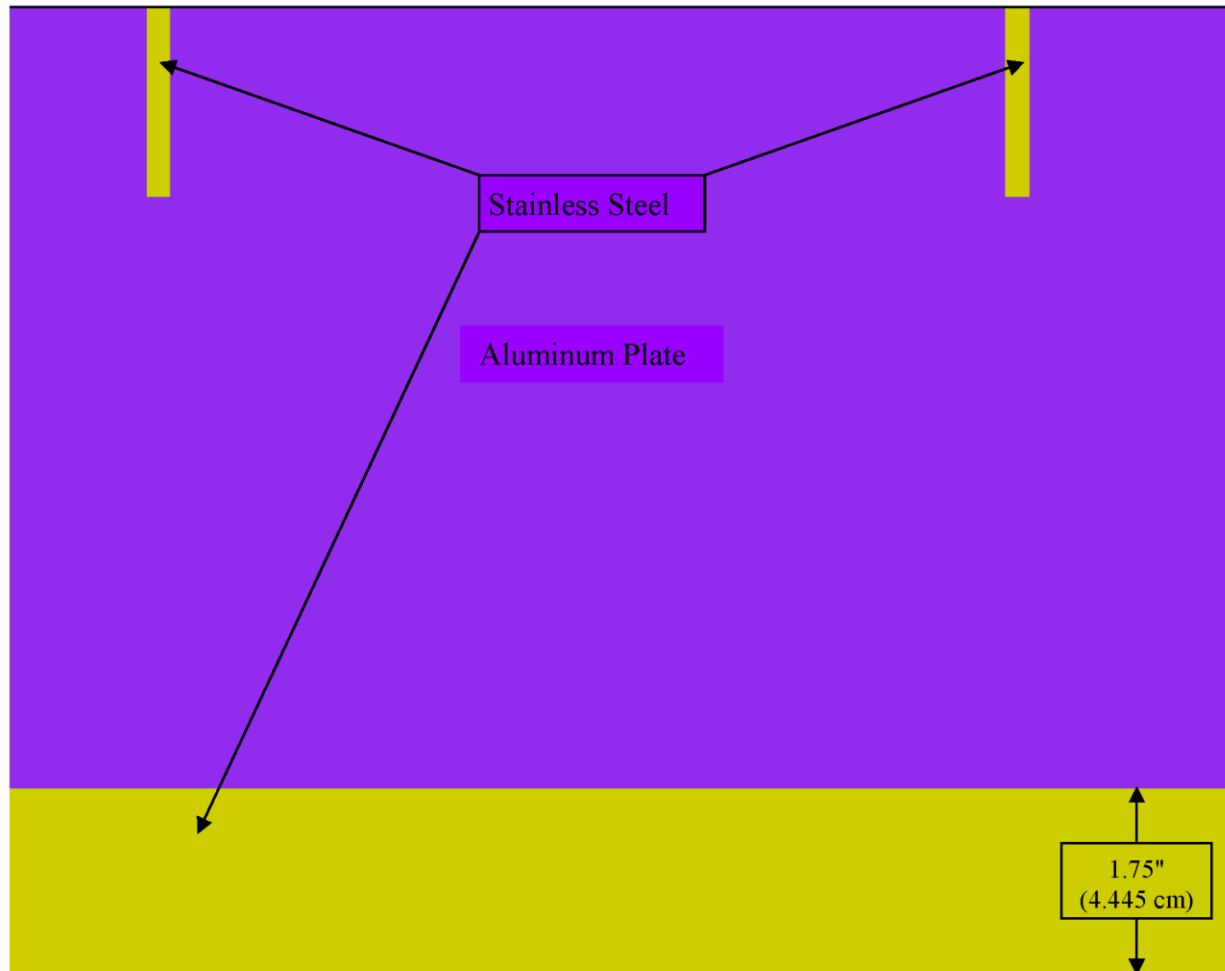


Figure 6-2
Basket Model Compartment Wall (View G)

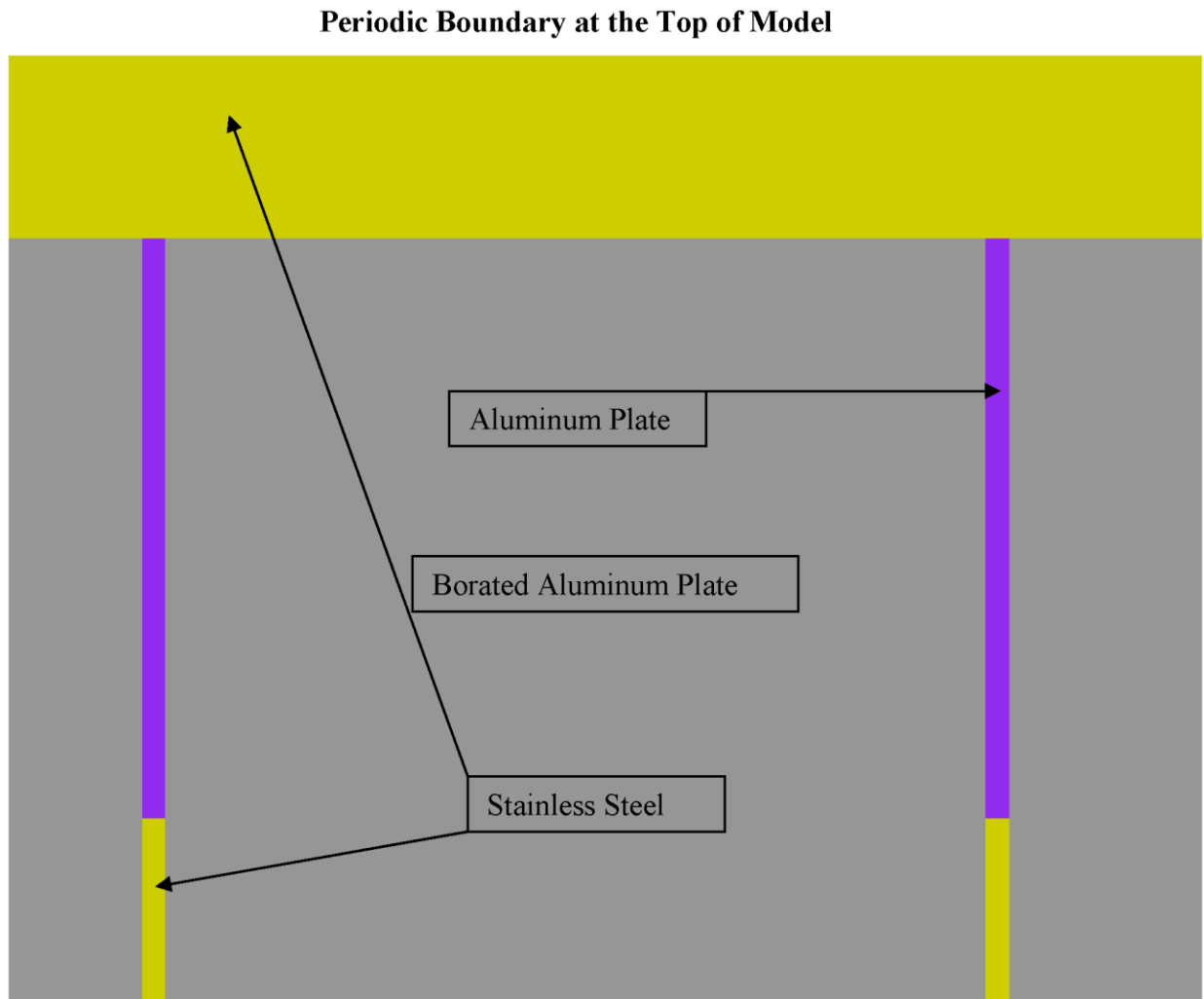


Figure 6-3
Basket Model Compartment Wall (View F)

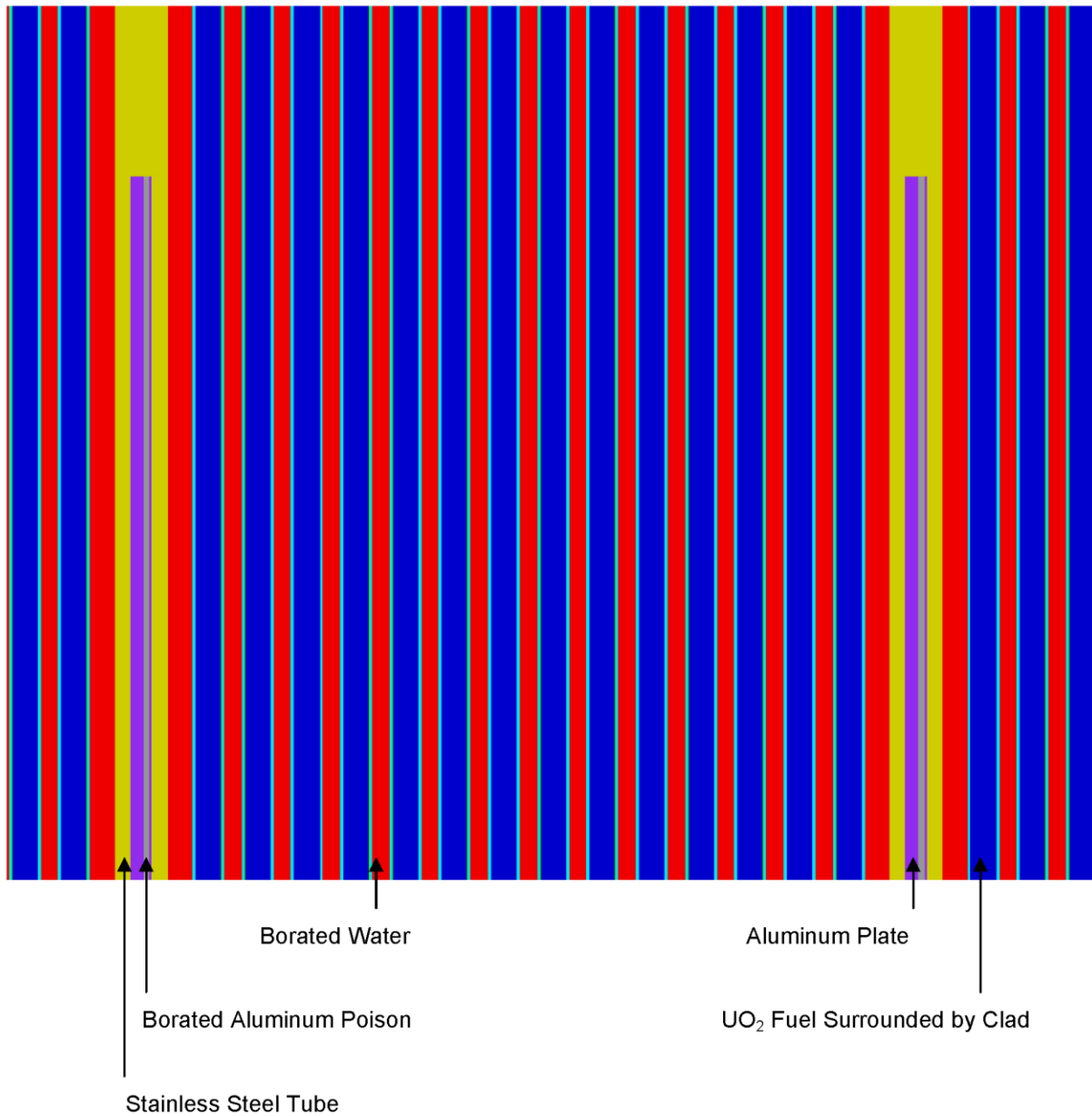


Figure 6-4
Basket Model Compartment Wall With Fuel Assembly (View G)

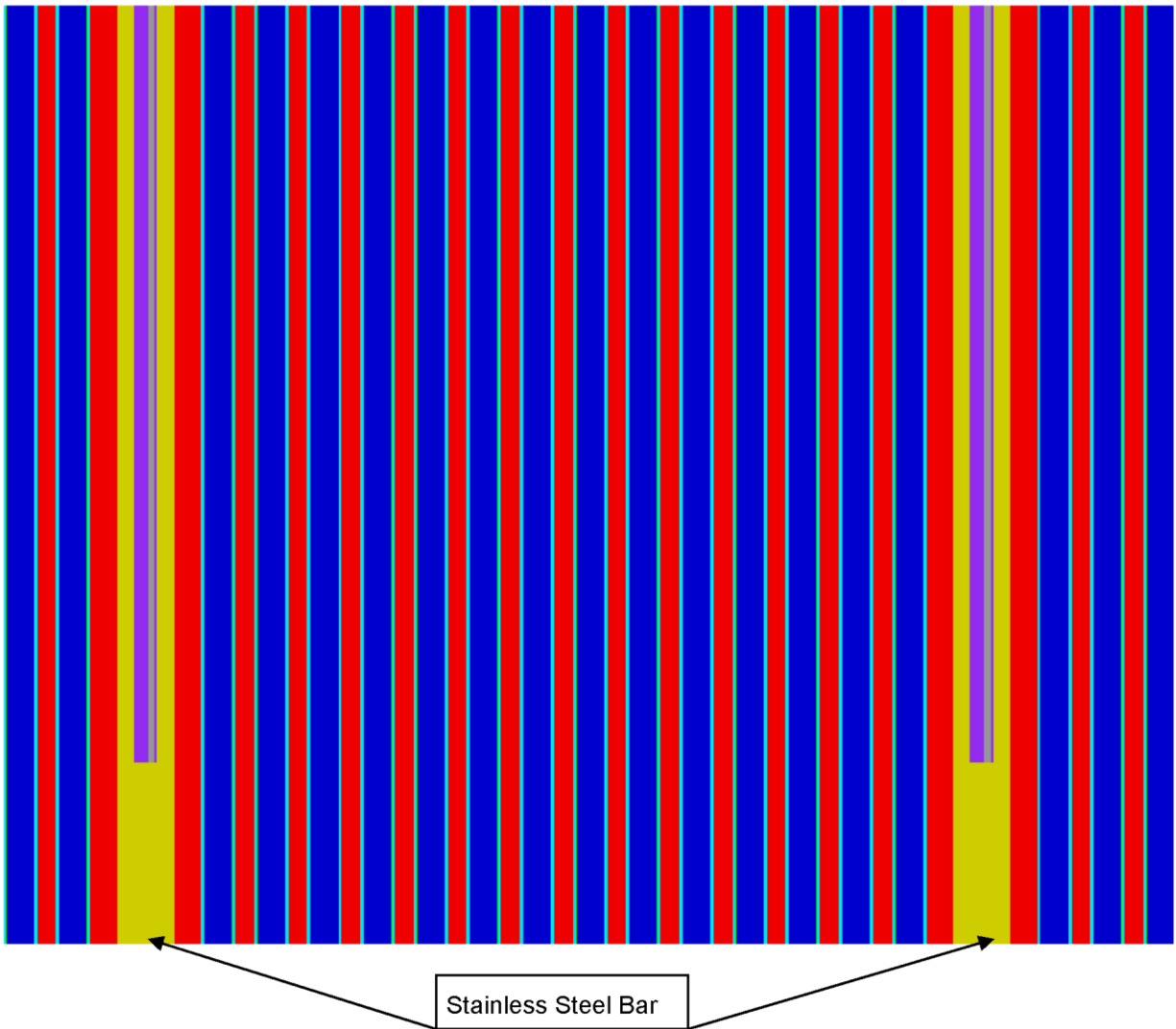


Figure 6-5
Basket Model Compartment Wall With Fuel Assembly (View F)

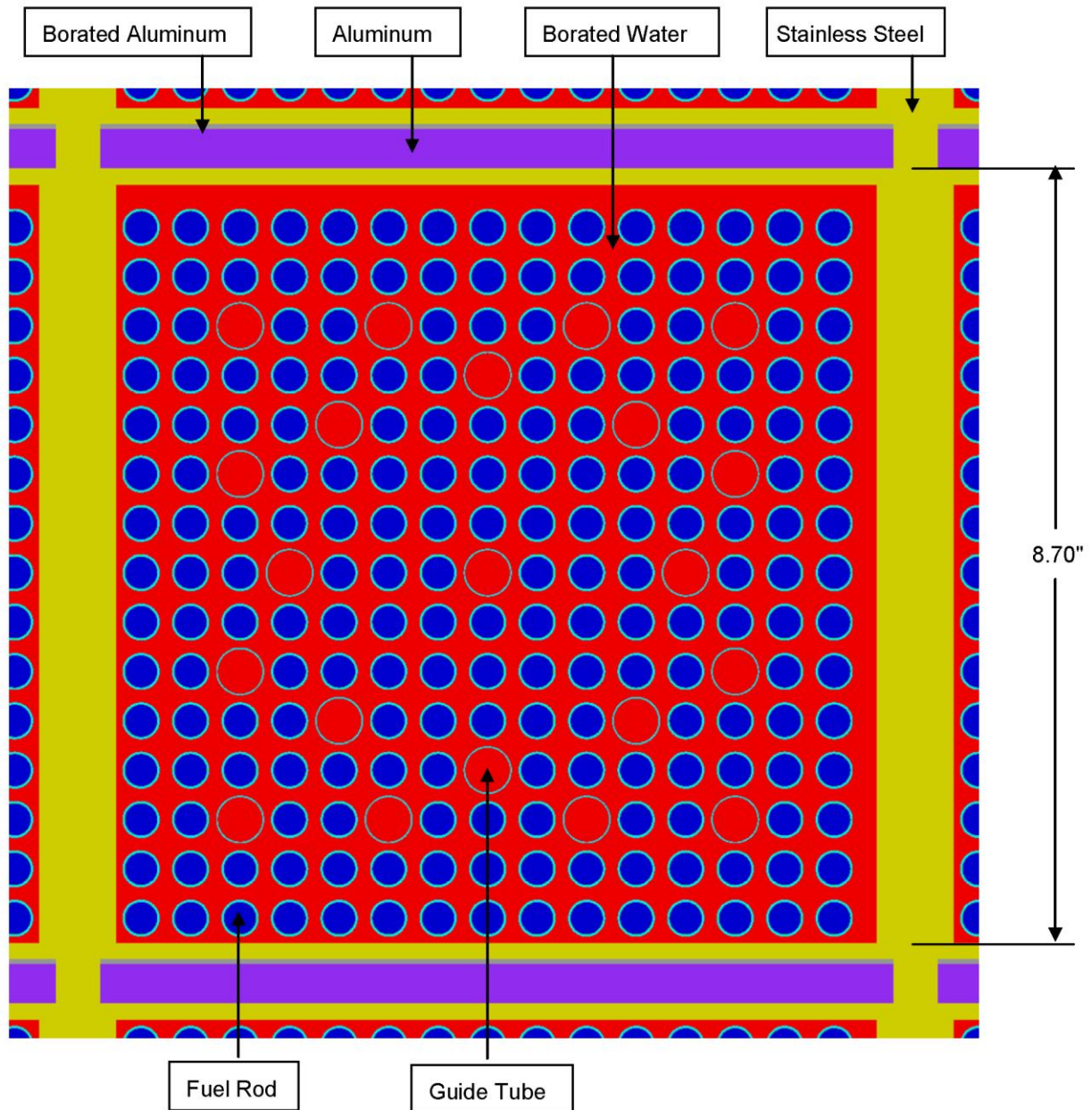


Figure 6-6
Basket Compartment With Fuel (Section A)

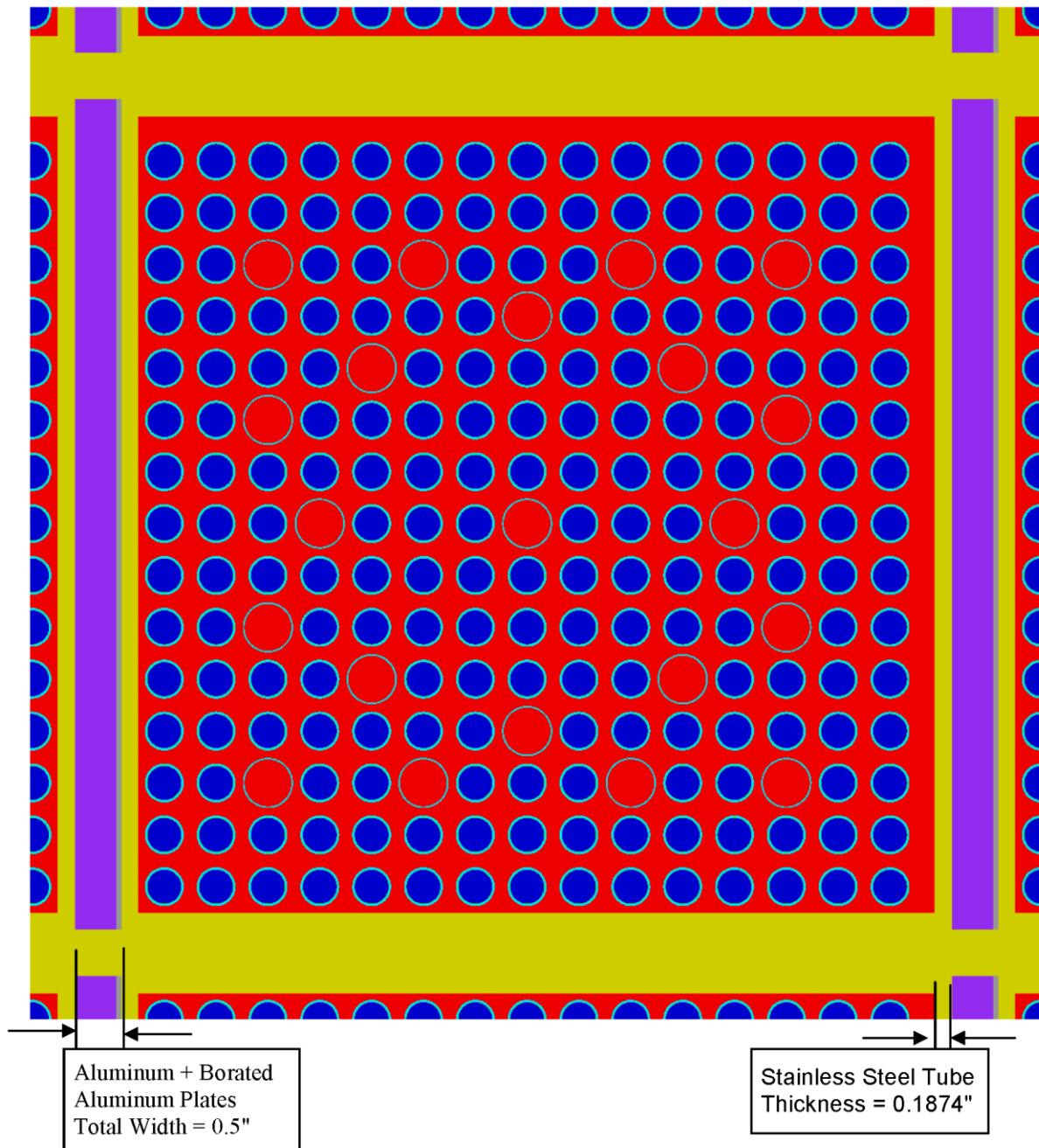


Figure 6-7
Basket Compartment With Fuel (Section B)

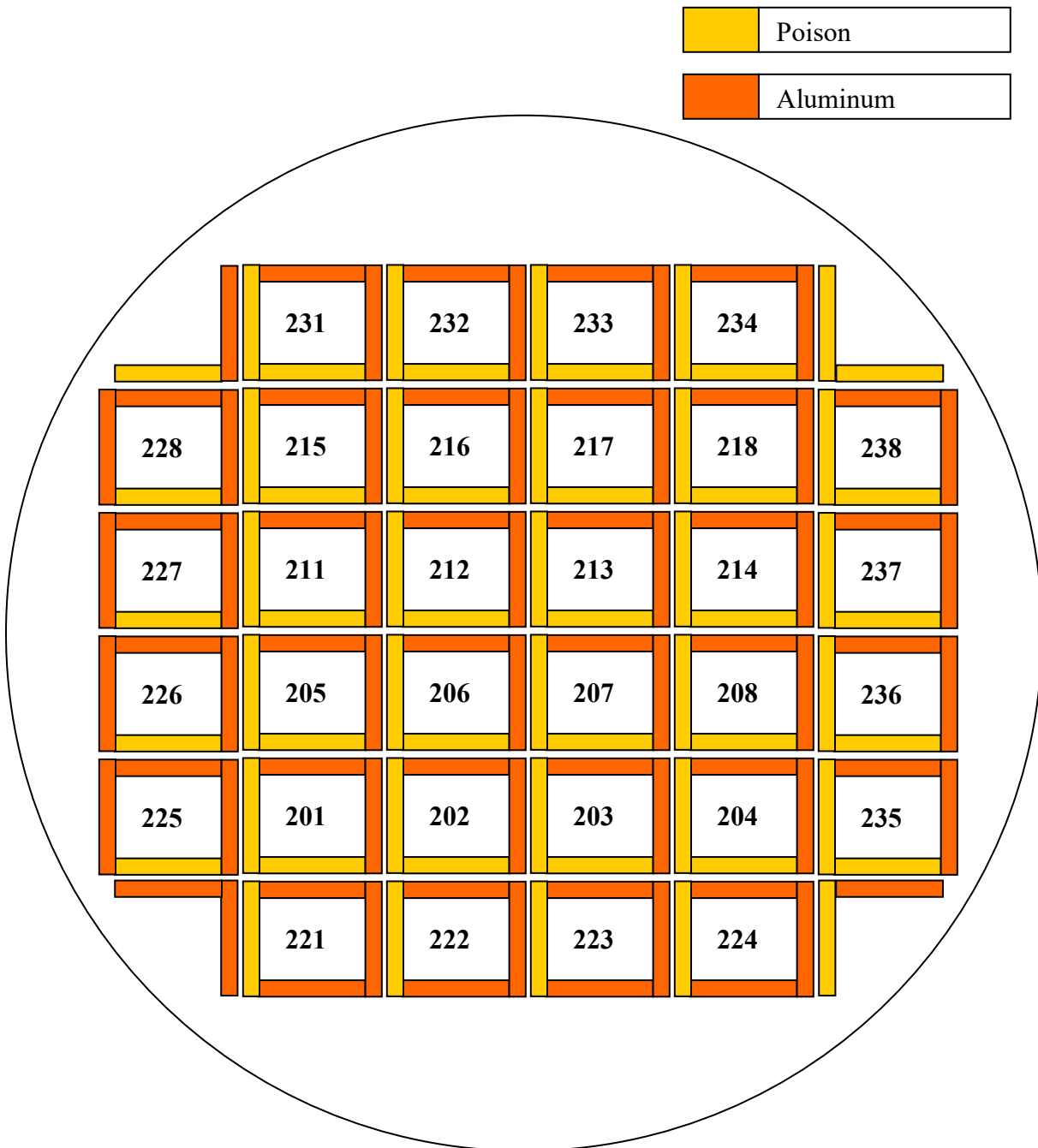


Figure 6-8
Fuel Assembly Positions and Poison Plate Locations in the Basket

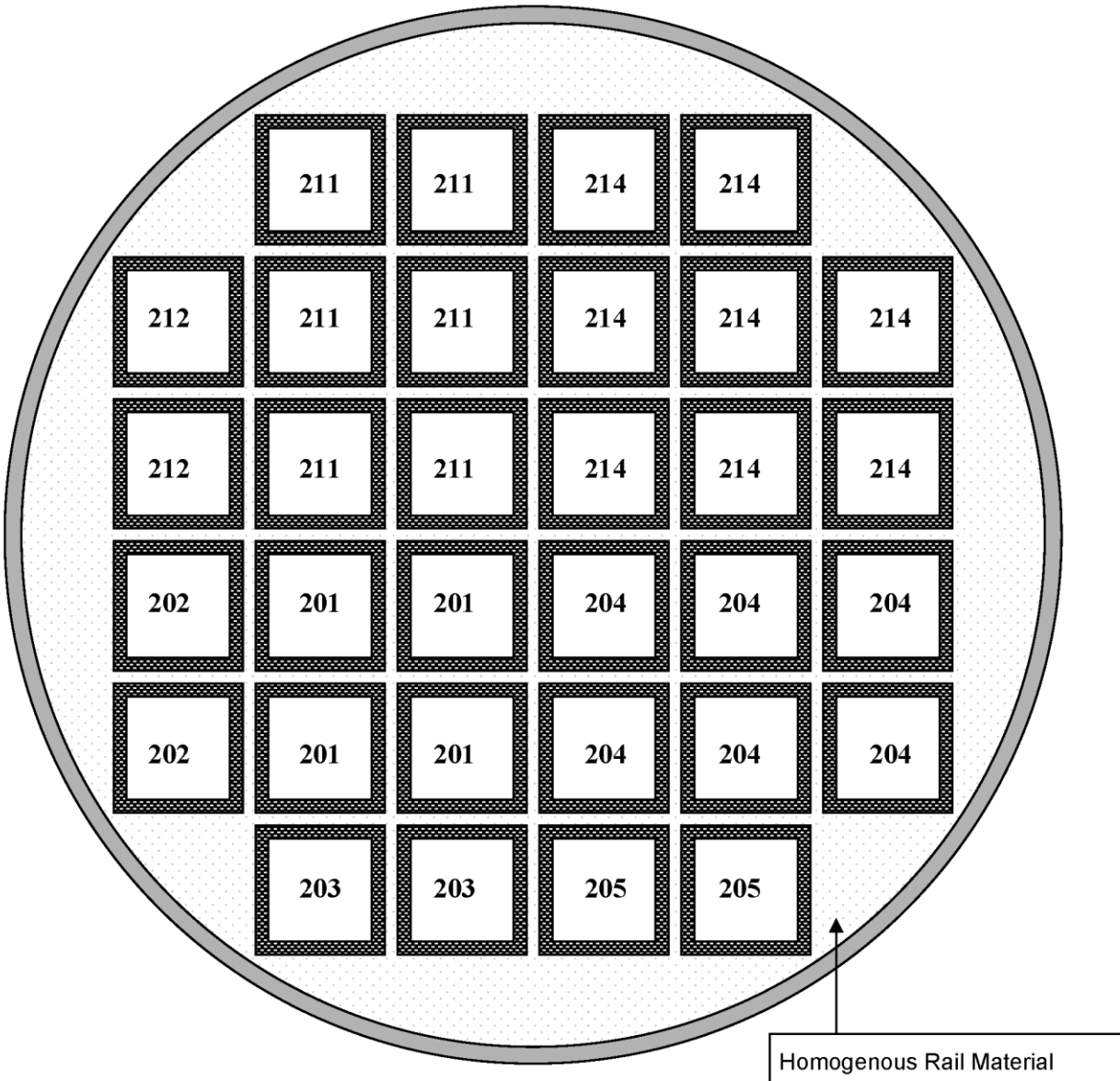


Figure 6-9
Fuel Assembly Positions by KENO Unit ID

Proprietary Information on This Page
Withheld Pursuant to 10 CFR 2.390

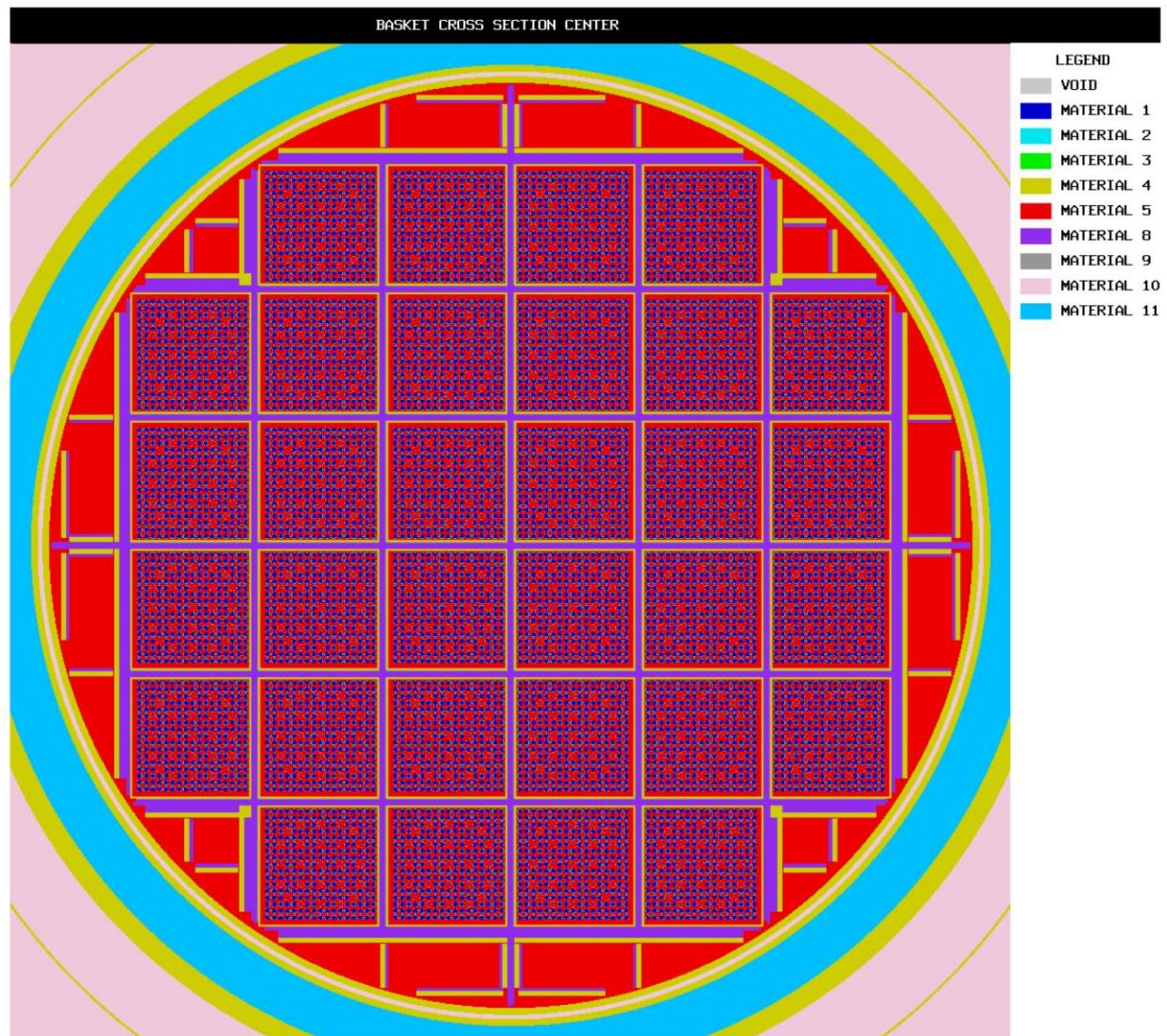


Figure 6-11
Radial Cross Section of the Detailed KENO Model

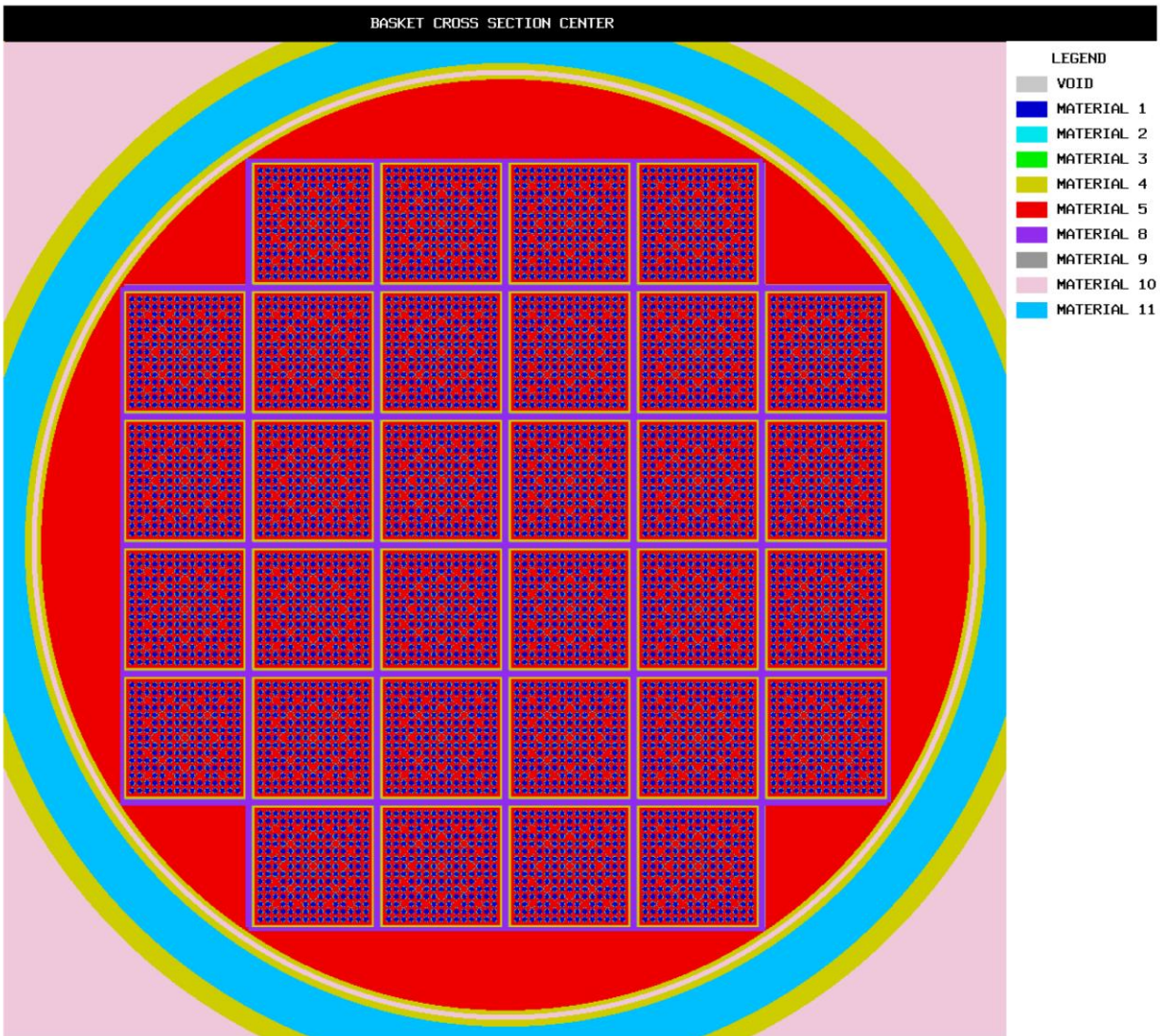


Figure 6-12
WE 15x15 Fuel Assemblies in the Centered Position

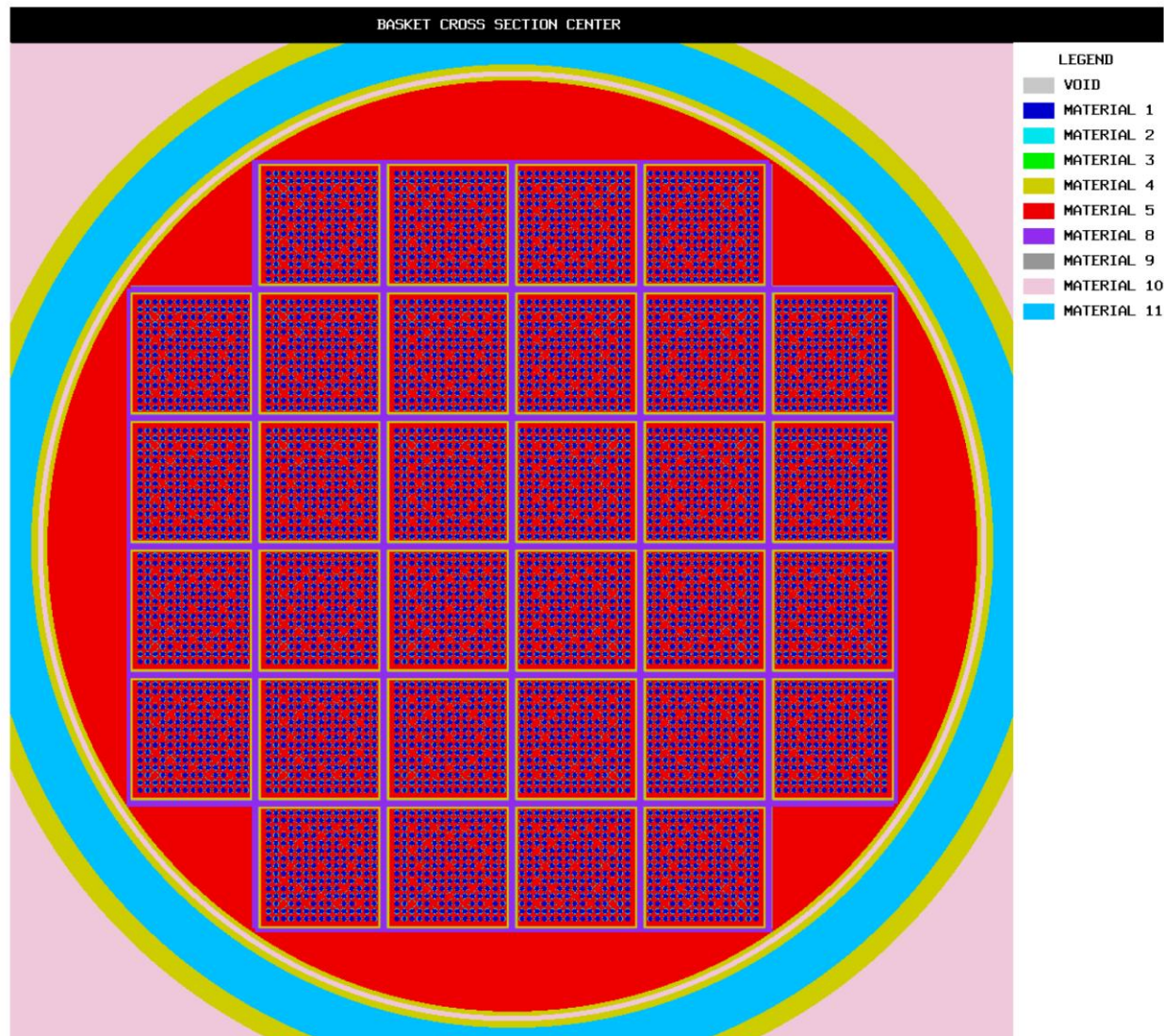


Figure 6-13
WE 15x15 Fuel Assemblies in the Inward Position

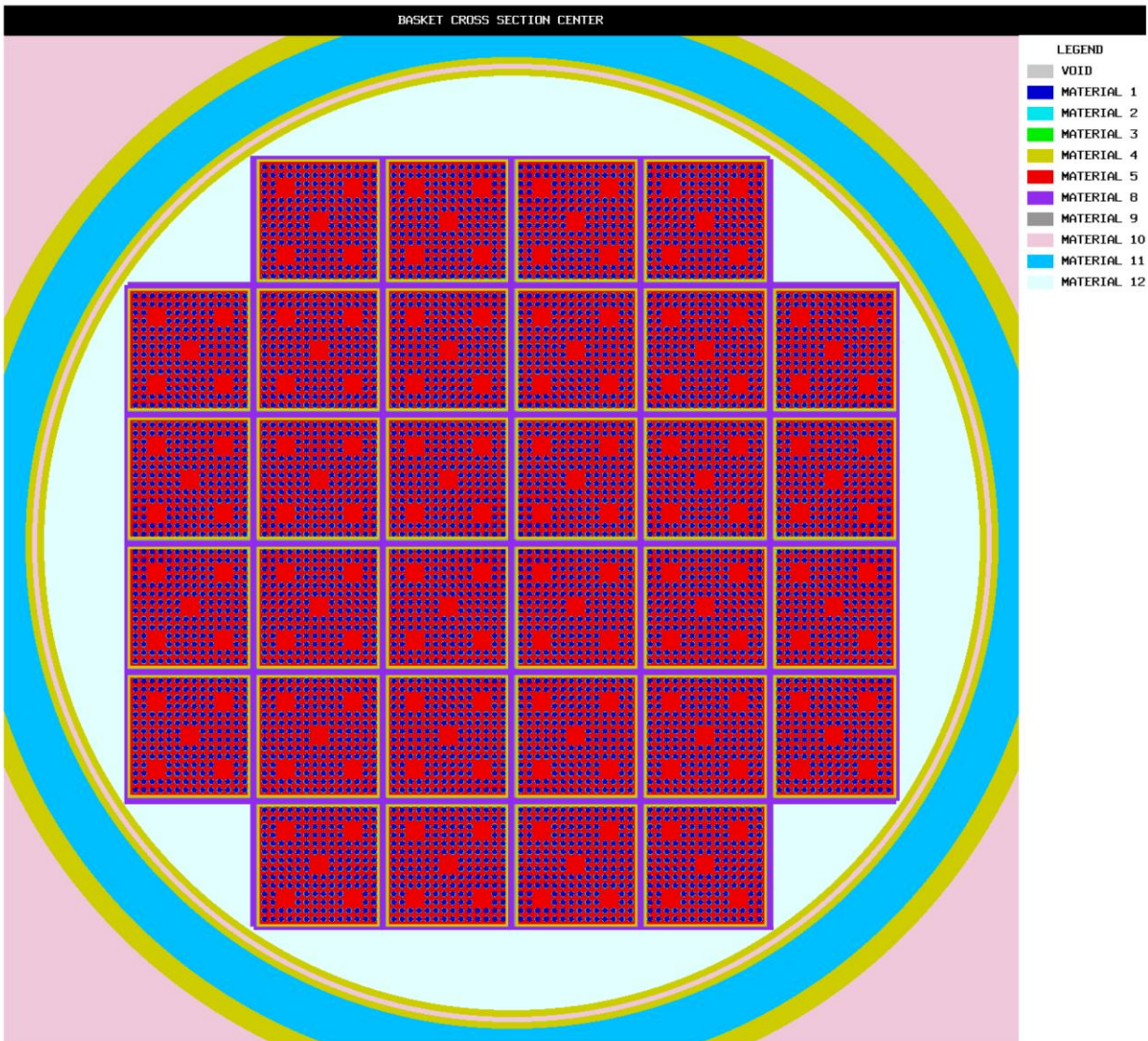


Figure 6-14
CE 14x14 Fuel Assembly : Optimum Pitch Study

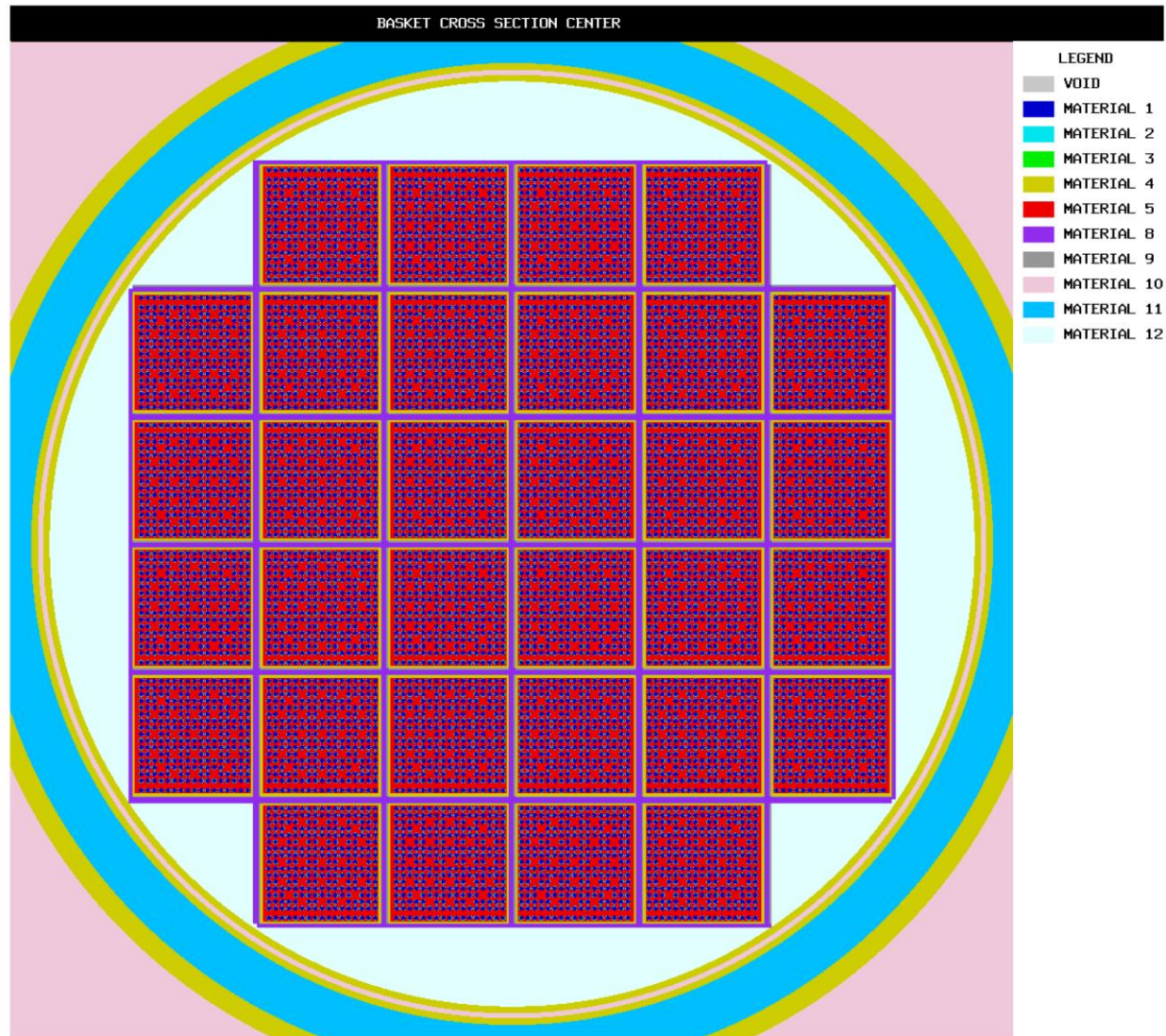


Figure 6-15
WE 17x17 Fuel Assembly : Single Ended Rod Shear Study

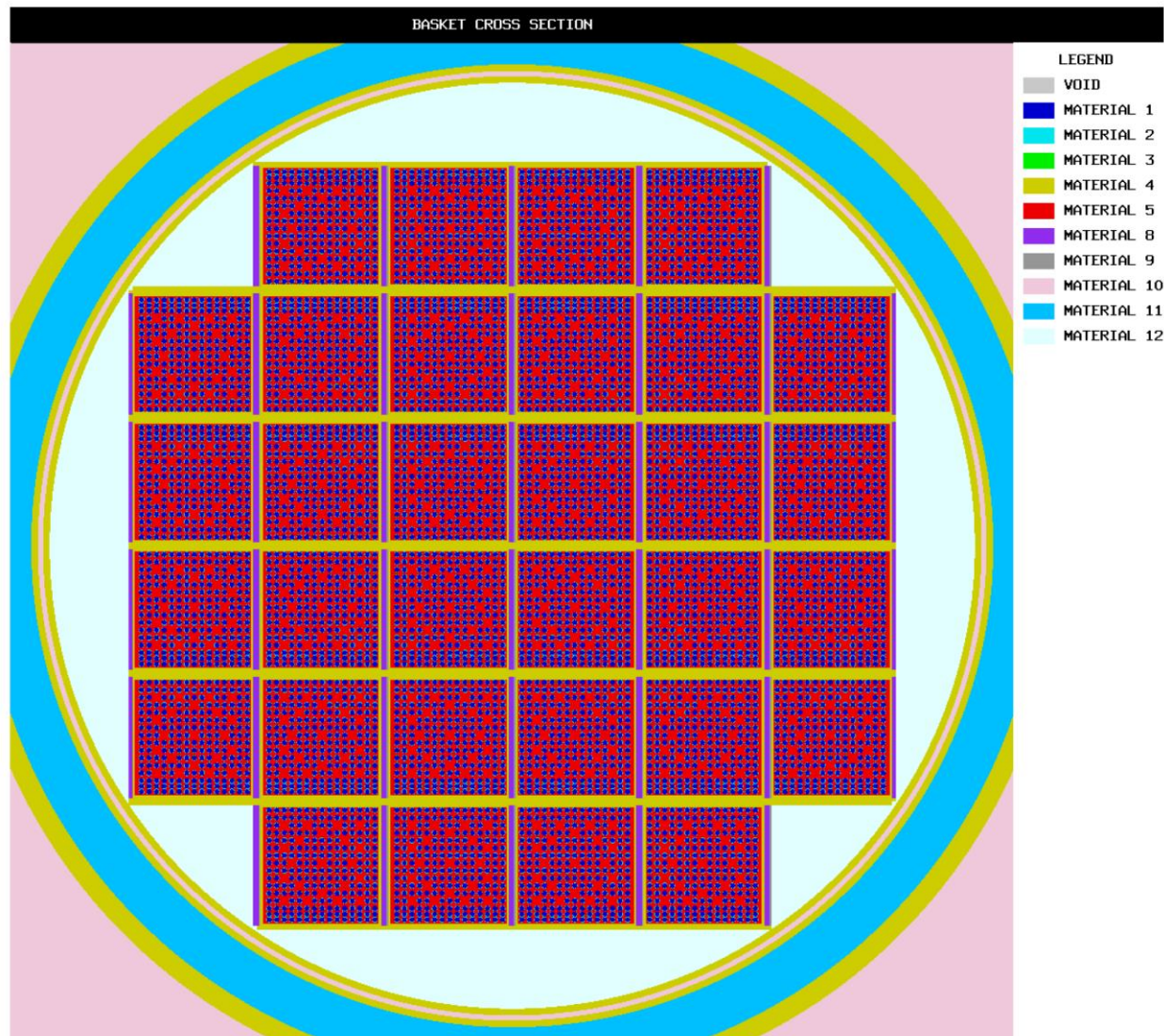


Figure 6-16
WE 15x15 Fuel Assembly : Double Ended Rod Shear Study

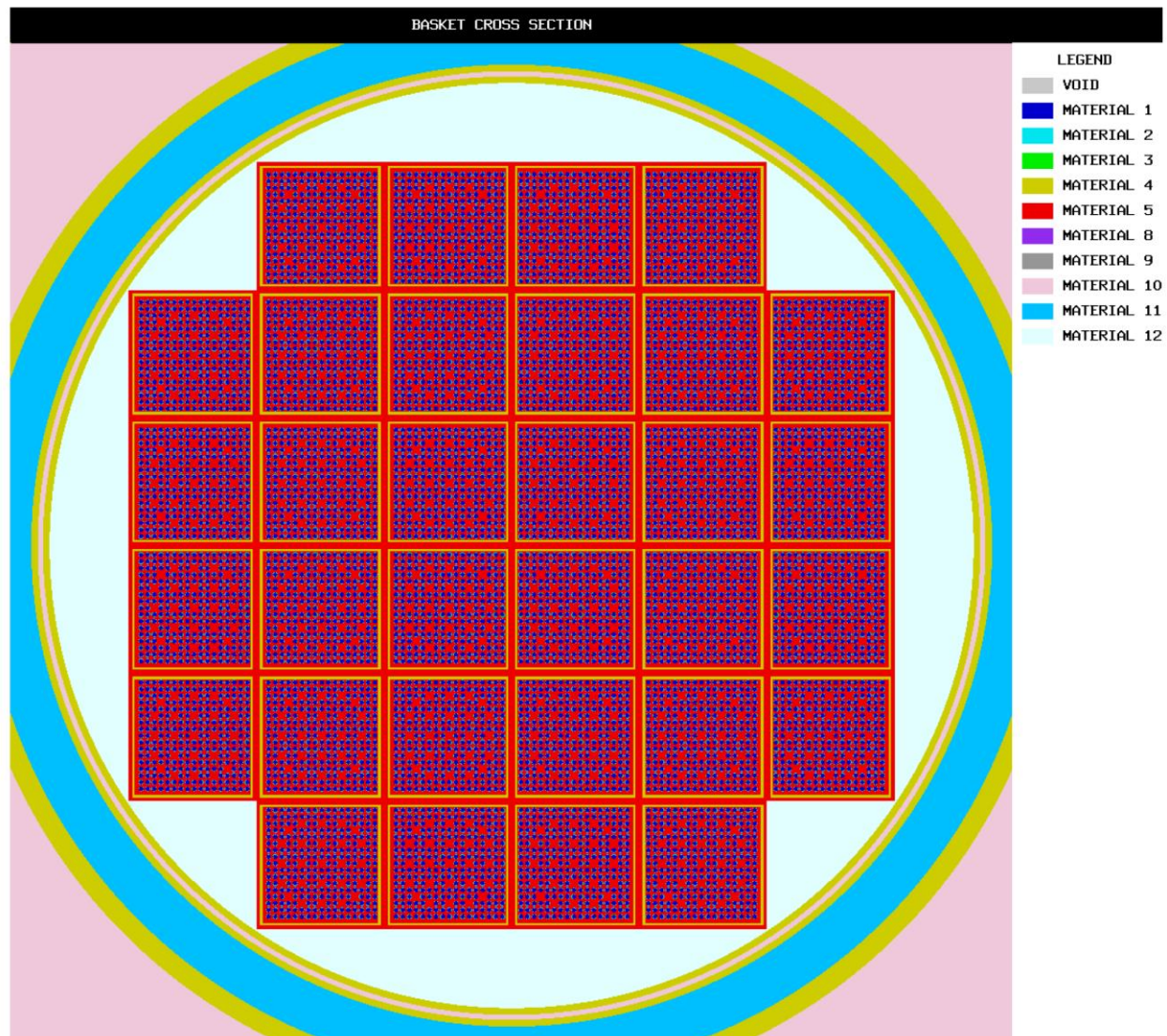


Figure 6-17
WE 17x17 Fuel Assembly : 4-inch Shift of Fuel Assembly

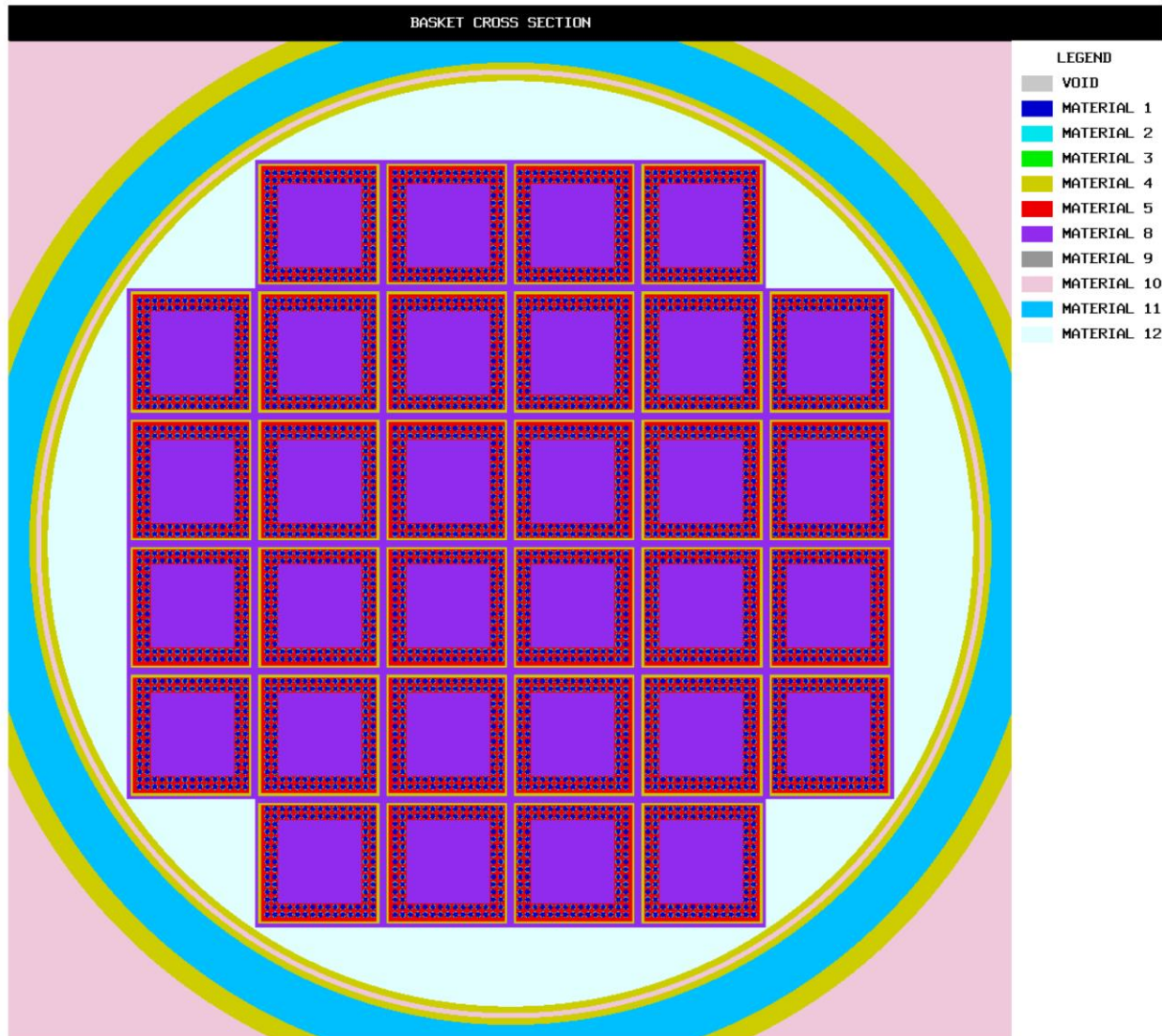


Figure 6-18
WE 15x15 Fuel Assembly : 6-inch Shift of Fuel Rods

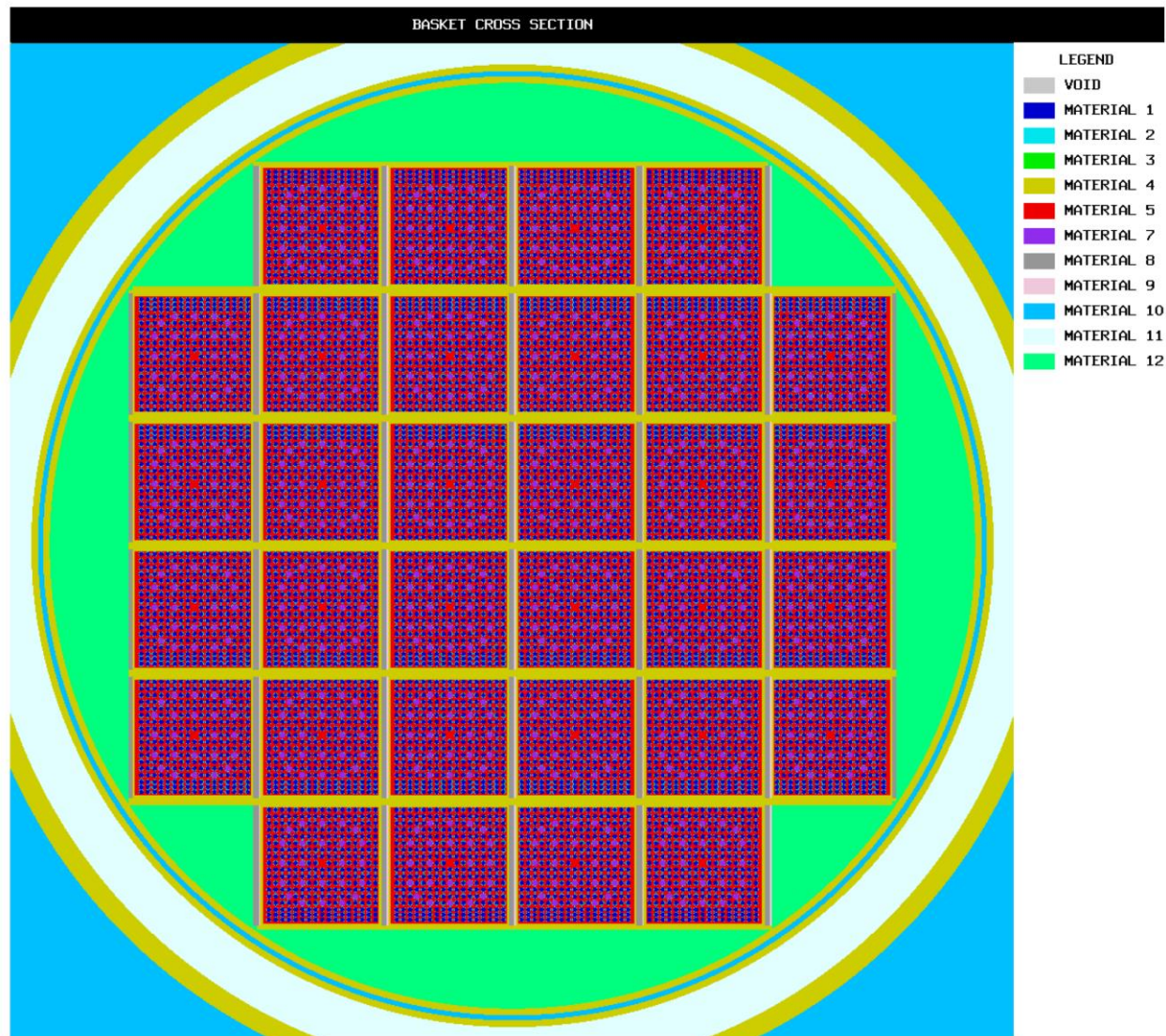


Figure 6-19
WE 15x15 Fuel Assembly : Double Ended Rod Shear with BPRAs

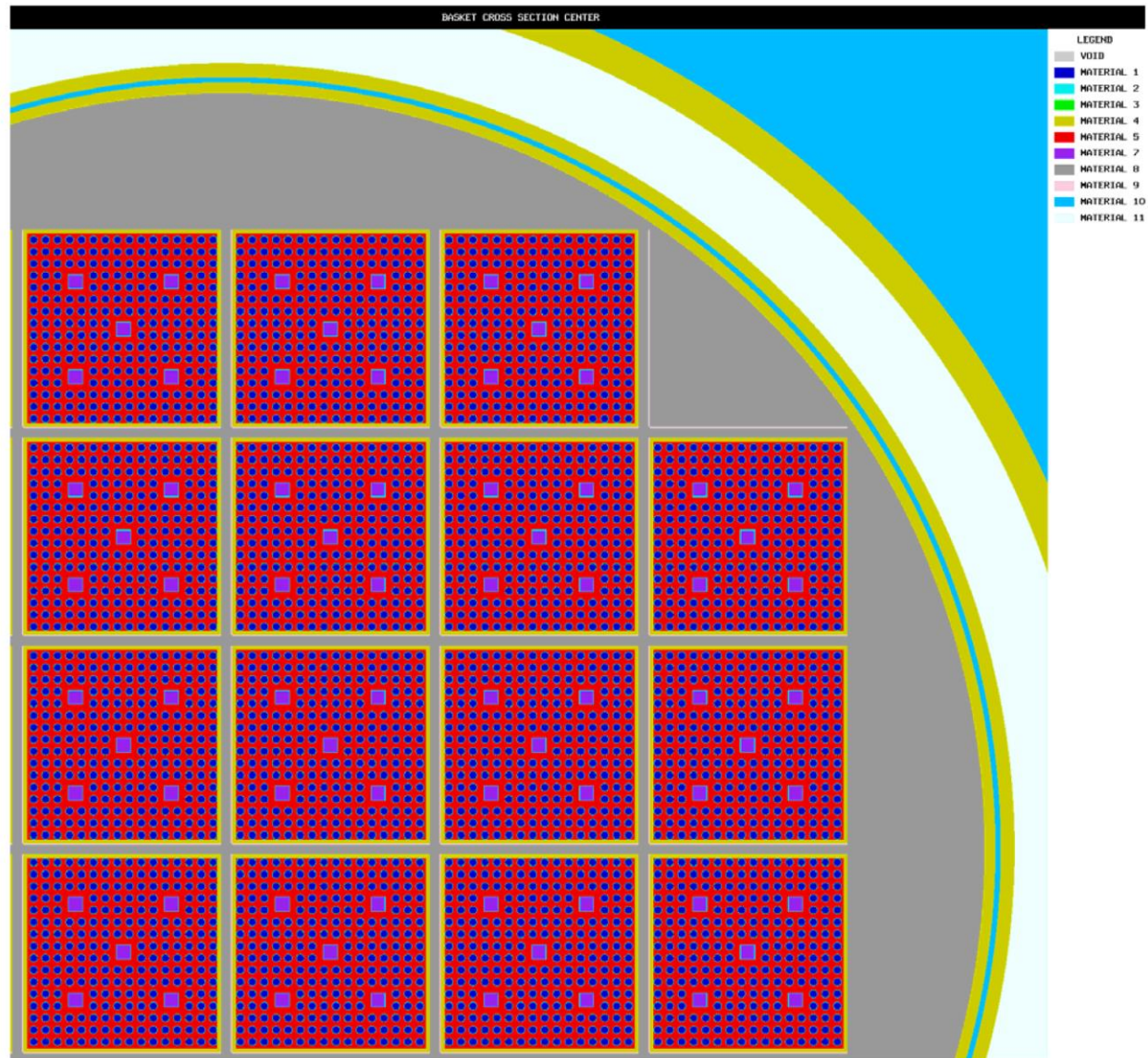


Figure 6-20
CE 16x16 Class Assembly – Optimum Pitch KENO Model with BPRAs

CHAPTER 7 CONFINEMENT

TABLE OF CONTENTS

7. CONFINEMENT	7-1
7.1 Confinement Boundary	7-1
7.1.1 Confinement Vessel	7-1
7.1.2 Confinement Penetrations	7-2
7.1.3 Seals and Welds	7-2
7.1.4 Closure	7-2
7.2 Requirements for Normal Conditions of Storage	7-3
7.2.1 Release of Radioactive Material	7-3
7.2.2 Pressurization of Confinement Vessel	7-3
7.3 Confinement Requirements for Hypothetical Accident Conditions	7-4
7.3.1 Fission Gas Products	7-4
7.3.2 Release of Contents	7-4
7.4 Supplemental Data	7-5
7.4.1 Confinement Monitoring Capability	7-5
7.4.2 References	7-5

LIST OF FIGURES

Figure 7-1	Typical 32PTH DSC Confinement Boundary	7-6
------------	--	-----

7. CONFINEMENT

The confinement evaluation described in this chapter 7.0 is applicable to the 32PTH DSC. See Appendix A, Chapter A.7, for discussion of applicability of these analyses to the 32PTH Type 1 DSC. See Appendix B, Chapter 7.B, for discussion of applicability of these analyses to the 32PTH Type 2 DSC.

7.1 Confinement Boundary

The 32PTH DSC is a high integrity stainless steel welded vessel that provides confinement of radioactive materials encapsulates the fuel in a helium atmosphere and provides biological shielding during 32PTH DSC closure and transfer and storage operations. The 32PTH DSC is designed to maintain confinement of radioactive material within the limits of 10CFR 72.104(a), 10CFR 72.106(b) and 10CFR 20 under normal, off-normal, and credible accident conditions. Chapter 3 concludes that the design including the helium atmosphere within the 32PTH DSC will adequately protect the spent fuel cladding against degradation that might otherwise lead to gross ruptures during storage. The design ensures that fuel degradation during storage will not pose operational safety problems with respect to removal of the fuel from storage.

The DSC cylindrical shell, the inner top cover/shield plug¹, and shell bottom form the confinement boundary for the spent fuel. The vent and siphon covers and welds are also included in the confinement boundary. The outer top cover plate is a structural attachment to the confinement boundary. The dimensions and material descriptions for the confinement boundary assemblies and the redundantly welded barriers are discussed in Chapter 1. The components important to safety are identified in Chapter 2.

7.1.1 Confinement Vessel

The cylindrical shell and inner shell to bottom cover plate welds are made during fabrication of the 32PTH DSC and are fully compliant to ASME Section III, Subsection NB. The welds between the shell and inner top cover/shield plug¹ (including siphon and vent cover welds and option 2 or option 3 design welds shown in Figure 7-1) are made after fuel loading. These welds are designed, fabricated, inspected and tested using alternatives to the ASME code specified in SAR Section 3.10.

Stringent design and fabrication requirements ensure that the confinement function of the 32PTH DSC is maintained. The cylindrical shell and shell bottom are pressure tested in accordance with the ASME Code, Section III, Subarticle NB-6300. This pressure test is performed after installation of the shell bottom at the fabricator's facility and may be performed concurrently with the leak test, provided the requirements of NB-6300 are met.

¹ For option 2 design (described in Chapter 1 drawings): Top casing plate, siphon/vent block, alignment pin block and lifting post are included in the confinement boundary

For option 3 design (described in Chapter 1 drawings): Top shield plug outer plate is included in the confinement boundary

A leak test of the shell assembly, including the shell bottom, is performed in accordance with ANSI N14.5 [2] and the ASME Code, Section V, Article 10. These tests are typically performed at the fabricator's facility. The acceptance criteria for the test are "leaktight" as defined in [2].

The process involved in leak testing the 32PTH DSC involves temporarily sealing the shell from the top end. The gas filled envelope and evacuated envelope testing methodologies have the required nominal test sensitivity for leaktight construction and are used for leak testing. A helium mass spectrometer is used to detect any leakage as defined in [2]. During final drying and sealing operations of the 32PTH DSC, the top closure confinement welds are applied to confine radioactive materials within the cavity.

The inner top cover/shield plug weld (including option 2 or option 3 inner top cover welds discussed in Figure 7-1) is welded to the DSC shell using automated welding equipment. Once the 32PTH DSC has been vacuum dried, a pressure test is performed by backfilling the DSC cavity with helium. Following a satisfactory completion of the pressure test, the siphon/vent covers are welded and a leak test is performed to verify that the weld between the DSC shell and the inner top cover/shield plug (including option 2 or option 3 design welds shown in Figure 7-1) and the siphon/vent cover welds meet the leak-tight criteria of [2]. The outer top cover plate is also welded in place using automated welding equipment. The outer top cover plate is a structural attachment to the confinement boundary.

7.1.2 Confinement Penetrations

All penetrations in the 32PTH DSC confinement boundary are welded closed. The 32PTH DSC is designed to have no credible leakage as described above.

7.1.3 Seals and Welds

The welds made during fabrication of the 32PTH DSC that affect the confinement boundary include the weld applied to the shell bottom and the circumferential and longitudinal seam welds applied to the cylindrical shell. These welds are inspected (radiographic or ultrasonic inspection, and liquid penetrant inspection) according to the requirements of Subsection NB of the ASME Code.

The welds applied to the vent and siphon port covers and the inner top cover/shield plug (including option 2 or option 3 inner cover) during closure operations, define the confinement boundary at the top end of the 32PTH DSC. These welds are applied using a multiple-layer technique with multi-level PT in accordance with alternatives to the ASME code as specified in SAR Section 3.10. This effectively eliminates any pinhole leak which might occur in a single-pass weld, since the chance of pinholes being in alignment on successive weld passes is negligibly small. Figure 7-1 provides a graphic representation of the confinement boundaries and welds.

7.1.4 Closure

The 32PTH DSC is closed entirely by welding and thus, no closure devices are utilized for confinement.

7.2 Requirements for Normal Conditions of Storage

The 32PTH DSC shell is designed to prevent the leakage of radioactive materials. No discernable undetected leakage is credible and the dose at the controlled area boundary from atmospheric release is negligible.

7.2.1 Release of Radioactive Material

Analyses for determining the annual dose equivalent to an individual located at the site boundary or outside the controlled area resulting from releases of radioactive material are not required in accordance with NRC Spent Fuel Project Office Interim Staff Guidance-5 (ISG-5) [3], since the 32PTH DSC is designed to have no credible leakage. Analyses required for determining the annual dose equivalent based on direct radiation for normal, off-normal, and accident conditions are discussed in Chapter 10.

7.2.2 Pressurization of Confinement Vessel

The design provides for drying and evacuation of the 32PTH DSC interior as part of the loading operations. The design is acceptable for the pressures that may be experienced during these operations as discussed in Chapter 4. On completion of fuel loading, the gas fill of the 32PTH DSC interior is at a pressure level that will maintain a non-reactive environment for at least the 40 year storage life of the 32PTH DSC interior under normal, off-normal, and accident conditions.

7.3 Confinement Requirements for Hypothetical Accident Conditions

7.3.1 Fission Gas Products

The 32PTH DSC confinement boundary is designed to prevent the leakage of radioactive materials. The analyses presented in Chapters 3 and 11 demonstrate that the confinement boundary is not compromised following hypothetical accident conditions. Therefore, estimating the maximum quantity of fission gas products is not necessary in accordance with ISG-5 [3].

7.3.2 Release of Contents

The 32PTH DSC confinement boundary is designed to prevent the leakage of radioactive materials. The analyses presented in Chapters 3 and 11 demonstrate that the confinement boundary is not compromised following hypothetical accident conditions. End and corner drops are not considered credible events during storage and transfer. However, the DSC and transfer cask have been evaluated for these drops to support evaluations required for postulated events under 10CFR50 and 10CFR71. The cladding integrity must be demonstrated by the user for 10CFR50 postulated end drops and will be evaluated in the 10CFR71 transport safety analysis report for hypothetical accidents during transports. Therefore, confinement analyses for the release of radioactive materials are not necessary in accordance with ISG-5 [3].

7.4 Supplemental Data

7.4.1 Confinement Monitoring Capability

The NUHOMS® HD System is a self-contained passive system that does not produce routine, solid, liquid or gaseous effluents. Effluent processing systems, or monitoring for airborne or liquid radioactivity, are not required to protect personnel or the environment during storage conditions. Since the 32PTH DSC is closed entirely by welding, a closure monitoring system is not utilized in accordance with NRC ISG-5 [3].

7.4.2 References

1. American Society of Mechanical Engineers, Boiler & Pressure Vessel Code, Section III, 1998 Edition with Addenda through 2000.
2. American National Standards Institute, ANSI N14.5-1997, Leakage Tests on Packages for Shipment of Radioactive Materials.
3. NRC Spent Fuel Project Office, Interim Staff Guidance, ISG-5, Revision 1, Confinement Evaluation.

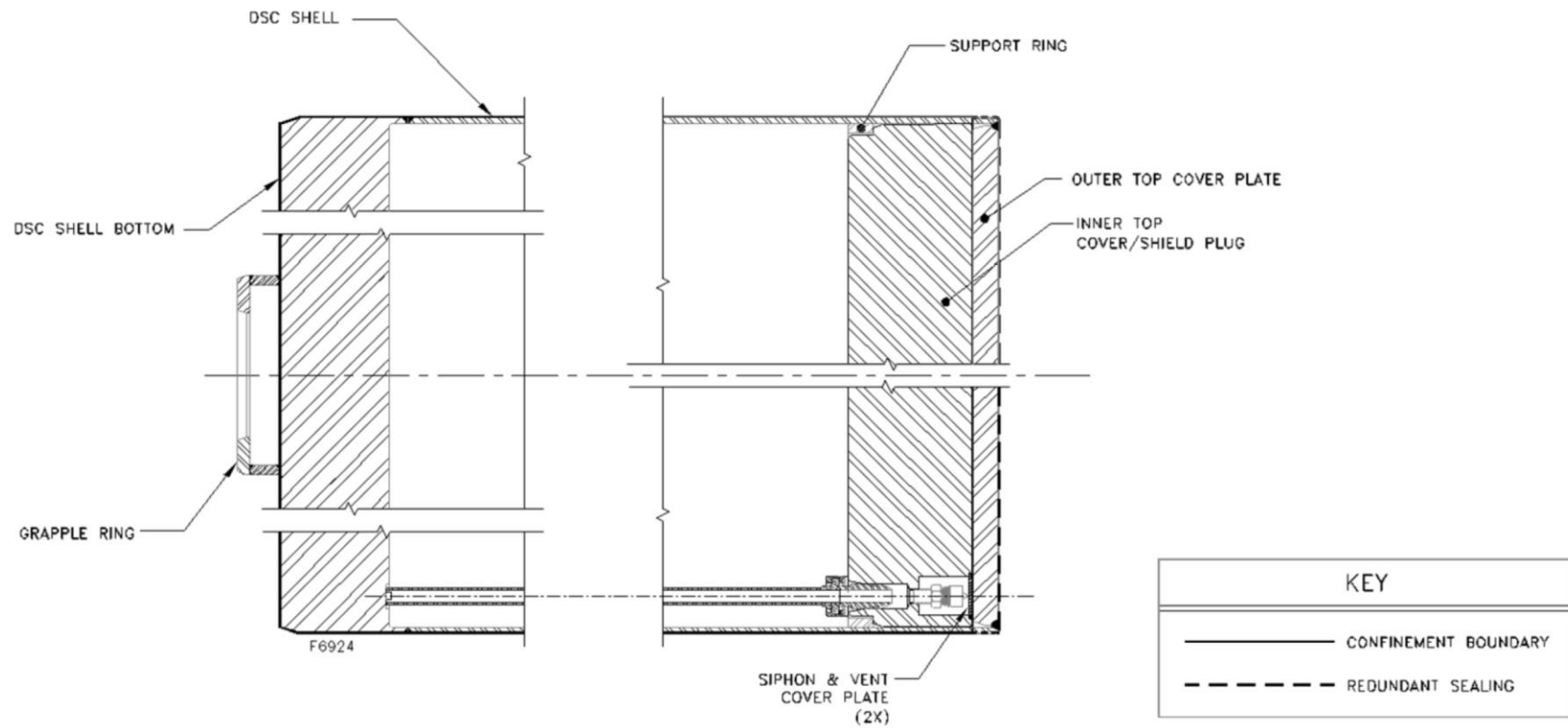


Figure 7-1
Typical 32PTH DSC Confinement Boundary

CHAPTER 8
OPERATING PROCEDURES
TABLE OF CONTENTS

8. OPERATING PROCEDURES	8-1
8.1 Procedures for Loading the DSC and Transfer to the HSM-H.....	8-1
8.1.1 Narrative Description.....	8-1
8.2 Procedures for Unloading the DSC	8-10
8.2.1 DSC Retrieval from the HSM-H.....	8-10
8.2.2 Removal of Fuel from the DSC	8-11
8.3 Supplemental Information	8-14
8.3.1 Other Operating Systems	8-14
8.3.2 Operation Support System	8-14
8.3.3 Surveillance and Maintenance	8-14
8.4 References	8-15

LIST OF TABLES

Table 8-1	Major Equipment Used During NUHOMS® HD System Loading and Unloading Operations.....	8-16
-----------	---	------

LIST OF FIGURES

Figure 8-1	NUHOMS® HD System Loading Operations	8-17
------------	--	------

8. OPERATING PROCEDURES

This chapter outlines a sequence of operations to be incorporated into procedures for preparation of the NUHOMS[®] HD System DSC, loading of fuel, closure of the DSC, transport to the ISFSI, transfer into the HSM-H, monitoring operations, and retrieval and unloading. Operations are presented in their anticipated approximate performance sequence. Alternate sequencing that achieves the same purpose is acceptable. Temporary shielding may be used throughout as appropriate to maintain doses as low as reasonably achievable (ALARA). Only the use of helium is authorized to assist in removal of water. After water is drained from the DSC, (sections 8.1.1.2 & 8.1.1.3), the DSC shall be backfilled only with helium.

As stated in Appendix A, Chapter A.8, the operational steps described here in Chapter 8 apply in their entirety and without change to the 32PTH Type 1 DSC (described in Appendix A), or to the 32PTH Type 2 DSC (described in Appendix B) when the optional two-part top end closure assembly (which is similar to the 32PTH DSC) is used. The 32PTH Type 1 DSC and 32PTH Type 2 DSC also features a three-part top end closure assembly. Appendix A, Chapter A.8 provides a description of the changes in operational sequences that are applicable when using that alternative.

8.1 Procedures for Loading the DSC and Transfer to the HSM-H

8.1.1 Narrative Description

The following steps describe the recommended generic operating procedures for the NUHOMS[®] System. A list of major equipment used during loading and unloading operations is provided in Table 8-1. A pictorial representation of key phases of this process is provided in Figure 8-1.

8.1.1.1 Transfer Cask and DSC Preparation

1. Verify by plant records or other means that candidate fuel assemblies meet the physical, thermal and radiological criteria specified in the Technical Specifications.
2. Clean or decontaminate the transfer cask as necessary to meet licensee pool and ALARA requirements, and to minimize transfer of contamination from the cask cavity to the DSC exterior.
3. Examine the transfer cask cavity for any physical damage.
4. Verify specified lubrication of the transfer cask rails.
5. Examine the DSC for any physical damage and for cleanliness. Verify that bottom fuel spacers or damaged fuel bottom end caps, if required, are present in all fuel compartments. Remove damaged fuel top end caps if they are in place. Record the DSC serial number which is located on the grappling ring. Verify the basket type by identifying the last character in the serial number.
6. If not already installed, install lifting rods into the four threaded sockets in the bottom of the DSC cavity in accordance with the design drawing.
7. Lift the DSC into the cask cavity and rotate the DSC to match the transfer cask alignment marks.

8. Remove the lifting rods.
9. Fill the transfer cask/DSC annulus with clean water.
10. Seal the top of the annulus, using for example an inflatable seal.
11. A tank filled with clean water, and kept above the pool surface may be connected to the top vent port of the transfer cask via a hose to provide a positive pressure in the annulus. This is an optional arrangement, which provides additional assurance that contaminated water from the fuel pool will not enter the annulus. Do not pressurize this tank, nor raise it sufficiently high to float the DSC. For the 32PTH DSC with a 69.75 inch OD, and an empty weight of 49,000 lb, a differential pressure of 12.8 psi, equivalent to 29.6 ft of pure water, would be sufficient to lift the DSC.
12. If the DSC top covers were trial fitted, they must be removed prior to filling the DSC with water. The vent port quick connect fitting in the inner top cover may be removed to facilitate hydrogen monitoring later. The drain port fitting may be either left in place or removed – water may be pumped from the DSC either with or without the fitting.
13. The licensee shall develop procedures to verify that the boron content of the water added to the DSC conforms to the Technical Specifications. Fill the DSC with water from the fuel pool or an equivalent source meeting the minimum boron concentration required by the Technical Specifications. Optionally, this may be done at the time of immersing the cask in the pool. If the pool water is allowed flow over the transfer cask lip and into the DSC, provision must be made to protect the annulus seal from being dislodged by the water running over it.
- 14a. Optionally, secure a sheet of suitable material to the bottom of the cask to minimize the potential for ground-in contamination. This step may be done at any convenient time prior to immersion.
- 14b. Drain or fill the transfer cask liquid neutron shield, as required by licensee ALARA requirements and crane weight limits. This step may be done at any convenient time prior to immersion.
15. Prior to the cask being lifted into the fuel pool, the water level in the pool should be adjusted as necessary to accommodate the transfer cask and DSC volume. If the water placed in the DSC cavity was obtained from the fuel pool, a level adjustment may not be necessary.

8.1.1.2 DSC Fuel Loading

1. Verify proper engagement of the lifting yoke with the transfer cask lifting trunnions.
2. Lift the transfer cask / DSC and position them over the cask loading area of the spent fuel pool.
3. Lower the cask into the fuel pool until the bottom of the cask is at the height of the fuel pool surface. As the cask is lowered into the pool, spray the exterior surface of the cask with clean water to minimize surface adhesion of contamination.

4. Place the cask in the location of the fuel pool designated as the cask loading area.
5. Disengage the lifting yoke from the transfer cask lifting trunnions and move the yoke clear of the cask. Spray the lifting yoke with clean water if it is raised out of the fuel pool.
6. Load pre-selected spent fuel assemblies into the DSC basket compartments. The licensee shall develop procedures to verify that the boron content of the water conforms to the Technical Specifications, and that fuel identifications are verified and documented. The loading plan must be developed according to Figure 2-1 for the orientation of the fuel assemblies. Damaged fuel must be loaded only in designated compartments fitted with a damaged fuel bottom end cap.
7. After all the fuel assemblies have been placed into the DSC and their identities verified, install damaged fuel top end caps into designated compartments containing damaged fuel.
8. Lower the inner top cover/shield plug¹ in the DSC, aligning it with the guide on the DSC wall, and engaging the drain tube, until it seats on its support ring.
9. Visually verify that the inner top cover/shield plug is properly seated in the DSC. Reseat if necessary.
10. Position the lifting yoke and verify that it is properly engaged with the transfer cask trunnions.
11. Lift the transfer cask to the pool surface and spray the exposed portion of the cask with clean water.
12. Drain any water from above the inner top cover/shield plug back to the spent fuel pool. Up to 1300 gallons of water may be removed from the DSC prior to lifting the transfer cask clear of the pool surface. Up to 15 psig of helium may only be used to assist the removal of water. The DSC shall be backfilled only with helium after drainage of bulk water.
13. Lift the cask from the fuel pool, continuing to spray the cask with clean water. Provisions shall be made to assure that air will not enter the DSC cavity. One way to achieve this is by replenishing the helium in the DSC cavity during cask movement from the fuel pool to the decon area in case of malfunction of equipment used for cask movement.
14. Move the cask with loaded DSC to the area designated for DSC draining and closure operations. The set-down area should be level, or if slightly sloped, the transfer cask and DSC should be placed with the slope down toward the DSC drain/siphon tube.

¹ Including option 2 or option 3 inner top cover as described in Chapter 1 drawings.

8.1.1.3 DSC Closing, Drying, and Backfilling

1. Fill the transfer cask liquid neutron shield if it was drained for weight reduction during preceding operations.
2. Decontaminate the transfer cask exterior.
3. Disengage the rigging from the inner top cover/shield plug, and remove the eyebolts. Disengage the lifting yoke from the trunnions.
4. Disconnect the annulus overpressure tank if one was used, decontaminate the exposed surfaces of the DSC shell perimeter, remove any remaining water from the top of the annulus seal, and remove the seal.
5. Open the cask cavity drain port and allow water from the annulus to drain out until the water level is approximately twelve inches below the top of the DSC shell. Take swipes around the outer surface of the DSC shell to verify conformance with Technical Specification limits.
6. Cover the transfer cask / DSC annulus to prevent debris and weld splatter from entering the annulus.
7. If water was not drained from the DSC earlier, connect a pump to the DSC drain port and remove up to 1300 gallons of water. Consistent with ISG-22 [3] guidance and Technical Specification 3.1.1, helium at 1-3 psig is used to backfill the DSC with an inert gas as water is being removed from the DSC. This lowers the water sufficiently to allow welding of the inner top cover/shield plug. Up to 15 psig of helium gas may be applied at the vent port to assist the water pump down.

CAUTION: Verify that no inadvertent draining of the TC Neutron Shield water has occurred.

CAUTION: Radiation dose rates are expected to be high at the vent and siphon port locations. Use proper ALARA practices (e.g., use of temporary shielding, appropriate positioning of personnel, etc.) to minimize personnel exposure.

- 7a. Monitor TC/DSC annulus water level to be approximately twelve inches below the top of the DSC shell and replenish as necessary until drained.
8. Install the automated welding machine onto the inner top cover/shield plug.
9. Hydrogen monitoring is required prior to commencing and continuously during the welding of the inner top cover / shield plug per Technical Specification 5.6. Install hydrogen monitoring equipment that samples the atmosphere below the shield plug.
10. Verify that the hydrogen concentration does not exceed 2.4% [1]. If this limit is exceeded, stop all welding operations and purge the DSC cavity with helium to reduce hydrogen concentration safely below the 2.4% limit before resuming welding operations.

11. Complete the inner top cover/shield plug welding and perform the non-destructive examinations as required by the Technical Specifications. The weld must be made in at least two layers.
12. Remove the automated welding machine.
13. Pump remaining water from the DSC. Remove as much free standing water as possible to shorten vacuum drying time. Use of helium is required per Technical Specification 3.1.1. Up to 15 psig of helium gas may be applied at the vent port to assist the water pump down. All helium used in backfilling operations shall be at least 99.99% pure (this may be done as part of step 15).

NOTE: Proceed cautiously when evacuating the dry shielded canister (DSC) to avoid freezing consequences.

14. DELETED

15. Connect a vacuum pump / helium backfill manifold to the vent port or to both the vent and drain ports. The quick connect fittings may be removed and replaced with stainless steel pipe nipple / vacuum hose adapters to improve vacuum conductance. Make provision to prevent icing, for example by avoiding traps (low sections) in the vacuum line. Provide appropriate measures as required to control any airborne radionuclides in the vacuum pump exhaust. Purge air from the helium backfill manifold.

Optionally, leak test the manifold and the connections to the DSC. The DSC may be pressurized to no more than 15 psig for leak testing.

CAUTION: Radiation dose rates are expected to be high at the vent and siphon port locations. Use proper ALARA practices (e.g., use of temporary shielding, appropriate positioning of personnel, etc.) to minimize personnel exposure.

CAUTION: During the vacuum drying evolution, personnel should be in the area of loading operations, or in nearby low dose areas, in order to take proper action in the event of a malfunction.

16. Evacuate the DSC to the pressure required by the Technical Specification for vacuum drying, and isolate the vacuum pump. The isolation valve should be as near to the DSC as practicable, with a pressure gauge on the DSC side of the valve. Prior to performing the vacuum hold for 30 minutes as required by the Technical Specification, the vacuum pump must be turned off; or if the pump is not turned off, provide a tee and valve (or other means) to open the line to atmosphere between the pump and the DSC isolation valve.

Note: The user shall ensure that the vacuum pump is isolated from the DSC cavity when demonstrating compliance with Technical Specification 3.1.1 requirements. Simply closing the valve between the DSC and the vacuum pump is not sufficient, as a faulty valve allows the vacuum pump to continue to draw a vacuum on the DSC. Turning off the pump, or opening the suction side of the pump to atmosphere are examples of ways to assure that the pump is not continuing to draw a vacuum on the DSC.

17. DELETED

18. If the Technical Specification is satisfied, i.e., if the pressure remains below the specified limit for the required duration with the pump isolated, continue to the next step. If not, repeat step 16.

19a. Purge air from the backfill manifold, open the isolation valve, and backfill the DSC cavity with helium to 16.5 to 18 psig and hold for 10 minutes.

19b. Reduce the DSC cavity pressure to atmospheric pressure, or slightly over.

20. If the quick connect fittings were removed for vacuum drying, remove the vacuum line adapters from the ports, and re-install the quick connect fittings using suitable pipe thread sealant.

CAUTION: Radiation dose rates are expected to be high at the vent and siphon port locations. Use proper ALARA practices (e.g., use of temporary shielding, appropriate positioning of personnel, etc.) to minimize personnel exposure.

21. Evacuate the DSC through the vent port quick connect fitting to a pressure 100 mbar or less.

Note: The user shall ensure that the vacuum pump is isolated from the DSC cavity when demonstrating compliance with Technical Specification 3.1.1 requirements. Simply closing the valve between the DSC and the vacuum pump is not sufficient, as a faulty valve allows the vacuum pump to continue to draw a vacuum on the DSC. Turning off the pump, or opening the suction side of the pump to atmosphere are examples of ways to ensure that the pump is not continuing to draw a vacuum on the DSC.

22. Backfill the DSC with helium to the pressure specified in the Technical Specifications, and disconnect the vacuum / backfill manifold from the DSC.

23. DELETED

24a. Weld the covers over the vent and drain ports, performing non-destructive examination as required by the Technical Specifications. The welds shall have at least two layers.

24b. Install a temporary test head fixture (or any other alternative means). Perform a leak test of the inner top cover/shield plug to the DSC shell welds and siphon/vent cover welds in accordance with the Technical Specification limits. Verify that the personnel performing the leak test are qualified in accordance with SNT-TC-1A.

25. Place the outer top cover plate onto the DSC and verify correct rotational alignment of the cover and the DSC shell. Install the automated welding machine onto the outer top cover plate. As an option, the welding machine may be mounted onto the cover plate and then placed together on the DSC.

26. Complete the outer top cover welding and perform the non-destructive examinations as required by the Technical Specifications. The weld must be made in at least two layers.

27. Remove everything except the DSC from the transfer cask cavity: welding machine, protective covering from the transfer cask / DSC annulus, temporary shielding, etc., and drain the water from the transfer cask/DSC annulus.

28. Install the transfer cask lid and bolt it.
29. Evacuate the transfer cask cavity to below 100 mbar, and backfill the transfer cask annulus with helium in accordance with the Technical Specifications pressure tolerance and time limit.

CAUTION: Monitor the applicable time limits of the Technical specifications for transfer cask annulus helium backfill.

8.1.1.4 Transfer Cask Downending and Transport to ISFSI

1. Deleted.
2. The transfer trailer should be positioned so that the cask support skid is accessible to the crane with the trailer supported on its vertical jacks. If required due to space limitations, the crane may remain in a stationary position while the cask support skid and trailer translate underneath the cask as it is downended, (the trailer cannot be supported on the vertical jacks.)
3. Engage the lifting yoke and lift the transfer cask over the cask support skid onto the transfer trailer.
4. Position the cask lower trunnions onto the transfer trailer support skid pillow blocks.
5. Move the crane while simultaneously lowering the cask until the cask upper trunnions are just above the support skid upper trunnion pillow blocks. Alternatively, if the crane is to remain stationary as identified above, slowly move the trailer and support skid as the cask is lowered until the upper trunnions are just above the support skid upper trunnion pillow blocks.
6. Verify that the cask and trunnion pillow blocks are properly aligned.
7. Lower the cask onto the skid until the weight of the cask is distributed to the trunnion pillow blocks.
8. Verify the trunnions are properly seated onto the skid. Install the trunnion tower closure plates (optional).

8.1.1.5 DSC Transfer to the HSM-H

1. The maximum lifting height and ambient temperature requirements of the Technical Specifications must be met during transfer from the fuel building to the HSM-H.
2. Prior to loading the DSC into the HSM-H, verify that there is no debris in the HSM-H, the air inlet and outlets are not blocked, the air inlet and outlet screens are not damaged, and the rails are lubricated as specified.

CAUTION: The insides of empty modules have the potential for high dose rates due to adjacent loaded modules. Proper ALARA practices should be followed for operations inside these modules and in the areas outside these modules whenever the door from the empty HSM has been removed.

3. Tow the transfer trailer with the loaded cask to the ISFSI.
4. Position the transfer trailer to within a few feet of the HSM-H to maintain doses ALARA when the cask lid is removed.
5. Verify that the centerline of the HSM-H and cask approximately coincide. Reposition the trailer as necessary following appropriate ALARA practices.
6. Using a portable crane, unbolt and remove the cask lid.
7. Back the trailer to within a few inches of the HSM-H, set the trailer brakes and disengage the tractor. Drive the tractor clear of the trailer and extend the transfer trailer vertical jacks.
8. Remove the skid tie-down bracket fasteners and use the hydraulic skid positioning system to bring the cask into approximate vertical and horizontal alignment with the HSM-H. Using optical survey equipment and the alignment marks on the cask and the HSM-H, adjust the position of the cask until it is aligned with the HSM-H.
9. Using the skid positioning system, fully insert the cask into the HSM-H access opening docking collar.
10. Secure the cask to the front wall embedments of the HSM-H using the cask restraints.
11. Verify the alignment of the transfer cask is within specified tolerance using the optical survey equipment.
12. Remove the bottom ram access cover plate from the transfer cask. Extend the ram through the bottom cask opening into the DSC grapple ring.

13. Activate the hydraulic cylinder on the ram grapple and engage the grapple arms with the grapple ring.
14. Activate the hydraulic ram to initiate insertion of the DSC into the HSM-H. Stop the ram when the DSC reaches the support rail stops at the back of the module.
15. Disengage the ram grapple mechanism from the DDC grapple ring, and retract the hydraulic ram system from the transfer cask.
16. Remove the cask restraints from the HSM-H. Replace the bottom ram access cover plate. Optionally, a temporary cover may be used to cover the ram access opening.
17. Using the skid positioning system, disengage the cask from the HSM-H access opening.
18. Install the DSC seismic restraint.
19. Secure the skid to the trailer, retract the vertical jacks. Tow the trailer and cask a few feet to provide access for door installation.
20. Install the HSM-H door and secure it in place.
21. Replace the transfer cask lid.
22. Tow the trailer and cask from the ISFSI.

8.1.1.6 Monitoring Operations

1. Perform routine security surveillance in accordance with the licensee's ISFSI security plan.
2. Perform a daily visual surveillance of the HSM-H air inlets and outlets (bird screens) to verify that no debris is obstructing the HSM-H vents in accordance with Technical Specification requirements.
3. Perform a temperature measurement for each HSM-H in accordance with Technical Specification requirements.

8.2 Procedures for Unloading the DSC

The following section outlines the procedures for retrieving the DSC from the HSM-H and for removing the fuel assemblies from the DSC.

8.2.1 DSC Retrieval from the HSM-H

1. The maximum lifting height and ambient temperature requirements of the Technical Specifications must be met during transfer from the HSM-H to the fuel building.
2. Ready the transfer cask, transfer trailer, and support skid for service and tow the trailer to the HSM-H. Fill the transfer cask liquid neutron shield and remove the bottom access plate from the transfer cask.
3. Remove HSM-H door and seismic restraint. Remove the transfer cask lid. Back the trailer to within a few inches of the HSM-H.
4. Using the skid positioning system align the transfer cask with the HSM-H and position the skid until the transfer cask is docked with the HSM-H access opening.
5. Using optical survey equipment verify alignment of the transfer cask with respect to the HSM-H within specified tolerance. Install the transfer cask restraints.
6. Install and align the hydraulic ram with the transfer cask.
7. Extend the ram through the transfer cask into the HSM-H until it is inserted in the DSC grapple ring.
8. Activate the arms on the ram grapple mechanism to engage the grapple ring.
9. Retract the ram and pull the DSC into the transfer cask.
10. Disengage the ram grapple arms.
11. Retract the ram from the transfer cask.
12. Replace the cask ram access cover plate and remove the transfer cask restraints.
13. Using the skid positioning system, disengage the transfer cask from the HSM-H.
- 14a. Install the transfer cask top cover plate and ready the trailer for transfer/transport.

14b. Evacuate the transfer cask cavity to below 100 mbar, and backfill with helium in accordance with the Technical Specifications pressure tolerance and time limit, if using a transfer cask. If using a transportation cask, follow applicable requirements for the transportation cask.

15. Replace the door and seismic restraint on the HSM-H.

8.2.2 Removal of Fuel from the DSC

If it is necessary to remove fuel from the DSC, it can be removed in dry transfer facility or the initial fuel loading sequence can be reversed and the plant's spent fuel pool utilized.

Procedures for wet unloading of the DSC are presented here. Dry unloading procedures are essentially identical up to the removal of the DSC vent and drain port covers.

1. Tow the trailer with the loaded cask to the cask handling area inside the plant's fuel handling building. Drain the transfer cask liquid neutron shield as required by licensee ALARA requirements and crane weight limits.
2. Position and ready the trailer for access by the crane.
3. Engage the lifting yoke with the trunnions of the transfer cask.
4. Verify that the yoke lifting hooks are properly aligned and engaged onto the transfer cask trunnions.
5. Lift the transfer cask approximately one inch off the trunnion supports. Verify that the yoke lifting hooks are properly positioned on the trunnions.
6. Move the crane in a horizontal motion while simultaneously raising the crane hook vertically and lift the transfer cask off the trailer. Move the transfer cask to the cask decontamination area.
7. Lower the transfer cask into the cask staging area in the vertical position.
8. Unbolt the transfer cask lid and remove it.
9. Install temporary shielding to reduce personnel exposure as required. Fill the transfer cask/DSC annulus with clean water and seal the top of the annulus, using, for example, an inflatable seal.
10. Locate the drain and vent port using the indications on the outer top cover plate. Place a portable drill press on the top of the DSC. Align the drill over the drain port.
11. Cut or drill a hole through the top cover plate to expose the drain port on the inner top cover. Remove the drain port cover plate with an annular hole cutter. Repeat for the vent port.

CAUTION: Radiation dose rates are expected to be high at the vent and siphon port locations. Use proper ALARA practices (e.g., use of temporary shielding, appropriate positioning of personnel, etc.) to minimize personnel exposure.

12. Obtain a sample of the DSC atmosphere. Confirm acceptable hydrogen concentration and check for presence of fission gas indicative of degraded fuel cladding.
13. If degraded fuel is suspected, additional measures appropriate for the specific conditions are to be planned, reviewed, and implemented to minimize exposures to workers and radiological releases to the environment.
14. Verify that the boron content of the fill water conforms to the Technical Specifications. Fill the DSC with water from the fuel pool or equivalent source through the drain port with the vent port open. The vented cavity gas may include steam, water, and radioactive material, and should be routed accordingly. Monitor the vent pressure and regulate the water fill rate to ensure that the pressure does not exceed 15 psig.
15. Provide for continuous hydrogen monitoring of the DSC cavity atmosphere during all subsequent cutting operations, per Technical Specifications 5.6, to ensure that hydrogen concentration does not exceed 2.4%. Purge with helium as necessary to maintain the hydrogen concentration below this limit before resuming cutting operations.
16. Provide suitable protection for the transfer cask during cutting operations.
17. Using a suitable method, such as mechanical cutting, remove the weld of the outer top cover plate to the DSC shell.
18. Remove the outer top cover plate.
19. Remove the weld of the inner top cover/shield plug to the shell in the same manner as the outer cover plate. Do not remove the inner top cover/shield plug at this time unless the removal is being done remotely in a dry transfer system.
20. Remove any remaining excess material on the inside shell surface by grinding.
21. Clean the transfer cask surface of dirt and any debris which may be on the transfer cask surface as a result of the weld removal operation.
22. Engage the yoke onto the trunnions, install eyebolts or other lifting attachment(s) into the inner top cover/shield plug, and connect the rigging cables to the eyebolts/lifting attachment(s).
23. Verify that the lifting hooks of the yoke are properly positioned on the trunnions.

24. Lift the transfer cask just far enough to allow the weight of the transfer cask to be distributed onto the yoke lifting hooks. Verify that the lifting hooks are properly positioned on the trunnions.
25. Optionally install suitable protective material onto the bottom of the transfer cask to minimize cask contamination. Move the transfer cask to the spent fuel pool.
26. Prior to lowering the transfer cask into the pool, adjust the pool water level, if necessary, to accommodate the volume of water which will be displaced by the transfer cask during the operation.
27. Position the transfer cask over the cask loading area in the spent fuel pool.
28. Lower the transfer cask into the pool. As the transfer cask is being lowered, the exterior surface of the transfer cask should be sprayed with clean water.
29. Disengage the lifting yoke from the transfer cask and lift the inner top cover/shield plug from the DSC.
30. Remove any failed fuel top end caps.
31. Remove the fuel from the DSC.

8.3 Supplemental Information

8.3.1 Other Operating Systems

The NUHOMS[®] System is a passive storage system and requires no operating systems other than those systems used in transferring the DSC to and from the HSM-H.

8.3.2 Operation Support System

The NUHOMS[®] System is a self contained passive system and requires no effluent processing systems during storage conditions.

8.3.3 Surveillance and Maintenance

Surveillance and maintenance requirements are discussed in Chapters 9 and 12. The only required surveillances during storage are monitoring of the HSM-H air exhaust temperature, and visual verification that the inlet and outlet vents are not blocked. There is no normally required maintenance of the HSM-H or DSC.

8.4 References

1. U.S. Nuclear Regulatory Commission, Office of the Nuclear Material Safety and Safeguards, "Safety Evaluation of VECTRA Technologies' Response to Nuclear Regulatory Commission Bulletin 96-04 for NUHOMS[®]-24P and NUHOMS[®]-7P Dry Spent Fuel Storage System," November 1997 (Dockets 72-1004, 72-3, 72-4, 72-8, and 72-14).
2. NUREG-0612, "Control of Heavy Loads at Nuclear Power Plants," USNRC, July 1980.
3. U.S. Nuclear Regulatory Commission, Interim Staff Guidance (ISG-22), "Potential Rod Splitting due to Exposures to an Oxidizing Atmosphere during Short-term Cask Loading Operations in LWR of Other Uranium Oxide Based Fuel."

Table 8-1
Major Equipment Used During NUHOMS® HD System Loading and Unloading Operations

NUHOMS® HD System	Function
Dry Shielded Canister (DSC)	Fuel confinement.
Horizontal Storage Module (HSM-H)	Shielding, physical protection
Transfer Cask	Handling and transport of loaded DSC
Transfer trailer with support frame, ram, alignment system, and hydraulic power pack, pressure gauges and pressure relief	Transport of loaded transfer cask, and transfer of DSC into or retrieval from HSM-H; monitor and limit force applied to DSC by ram

Other Equipment and Instruments	Function
Lift yoke	Lifting transfer cask empty or loaded, in conformance to NUREG-0612 [2]
Lifting eyes, slings, rigging, etc.	Lifting the empty DSC, DSC covers, and the transfer cask lid in conformance to NUREG-0612 [2]
Water pump, hoses, connectors, fittings	Draining the DSC
Transfer cask / DSC annulus seal	Contamination control of the DSC exterior by pool water
Small water tank and hose	Maintaining positive pressure in annulus
Vacuum pump / helium backfill manifold, valves, hoses, fittings, adapters, pressure and vacuum gauges, etc.	Pressure test, vacuum drying and backfill of DSC; helium backfill of transfer cask cavity
Helium leak test equipment, including test head	Leak test closure welds
Gas bottles	Pressurize canister cavity for blowdown pressure test, helium backfill, etc.
Tractor	Towing the transfer trailer
Mobile crane and rigging	Removal of HSM-H door and transfer cask lid at ISFSI
Scaffolding, manlifts, etc	As required for easy access during operations
Temporary shielding	As required to maintain doses ALARA
Automatic welder	Remote welding of inner and outer top covers
Manual or automatic welder	Welding of vent and drain cover plates
Radiation detectors	Surveys to maintain doses ALARA
Transit with platform	Align transfer cask and ram with HSM-H
Hydrogen detector	Monitoring DSC cavity hydrogen during welding (loading) or cutting (unloading) of inner top cover
Temperature sensor and/or water circulation system	Optional, monitoring or circulation of water in transfer cask / DSC annulus

DSC Opening Equipment and Instruments	Function
Plasma torch or other cutting machine	Removal of lids for unloading of fuel
Portable drill press and annular cutters	Removal of vent and siphon covers
Gas sampling cylinder with quick connect adapter	Sampling of cavity gas prior to opening of DSC
Pressure gauge and water flow control valve	Limiting DSC pressure during reflooding

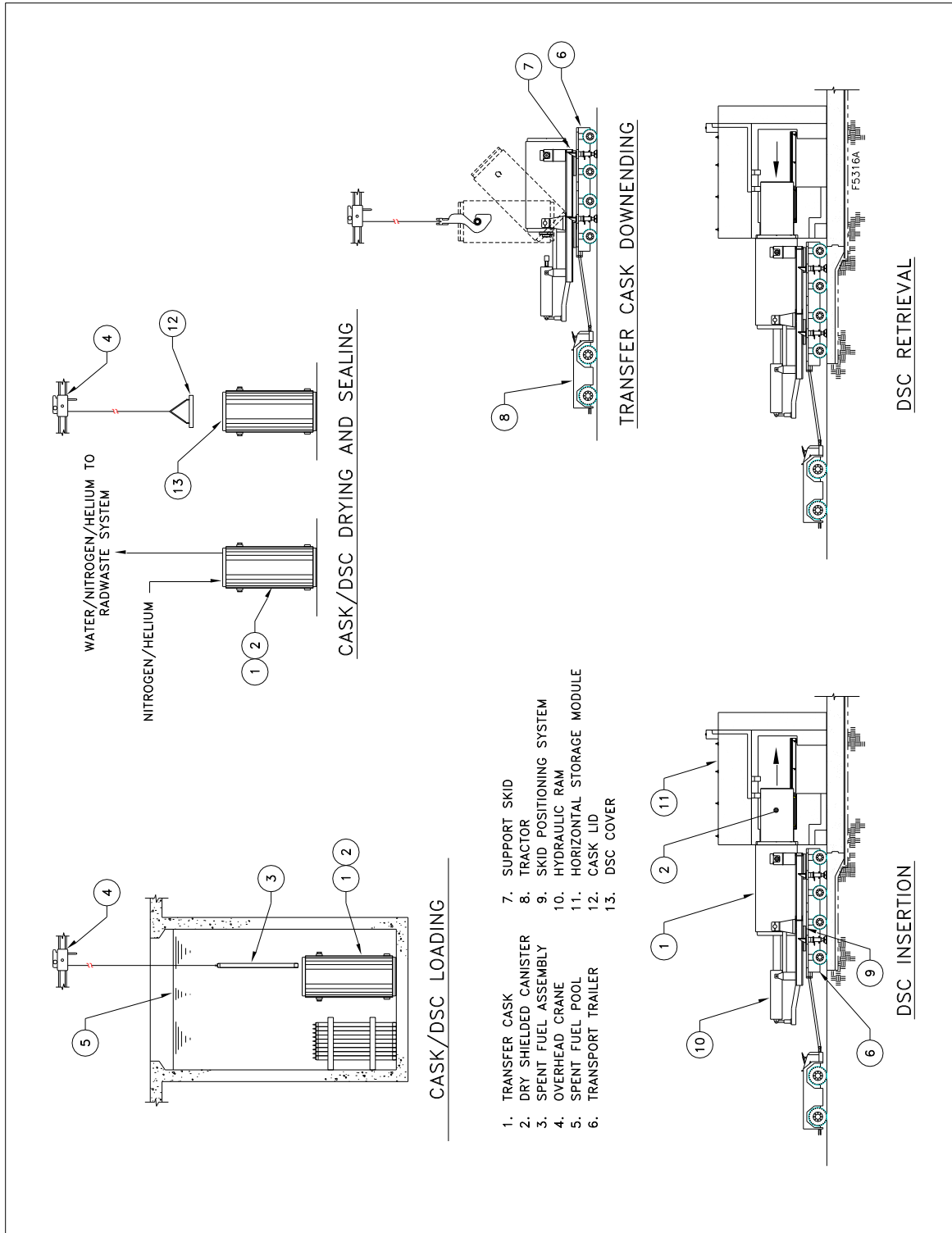


Figure 8-1
NUHOMS® HD System Loading Operations

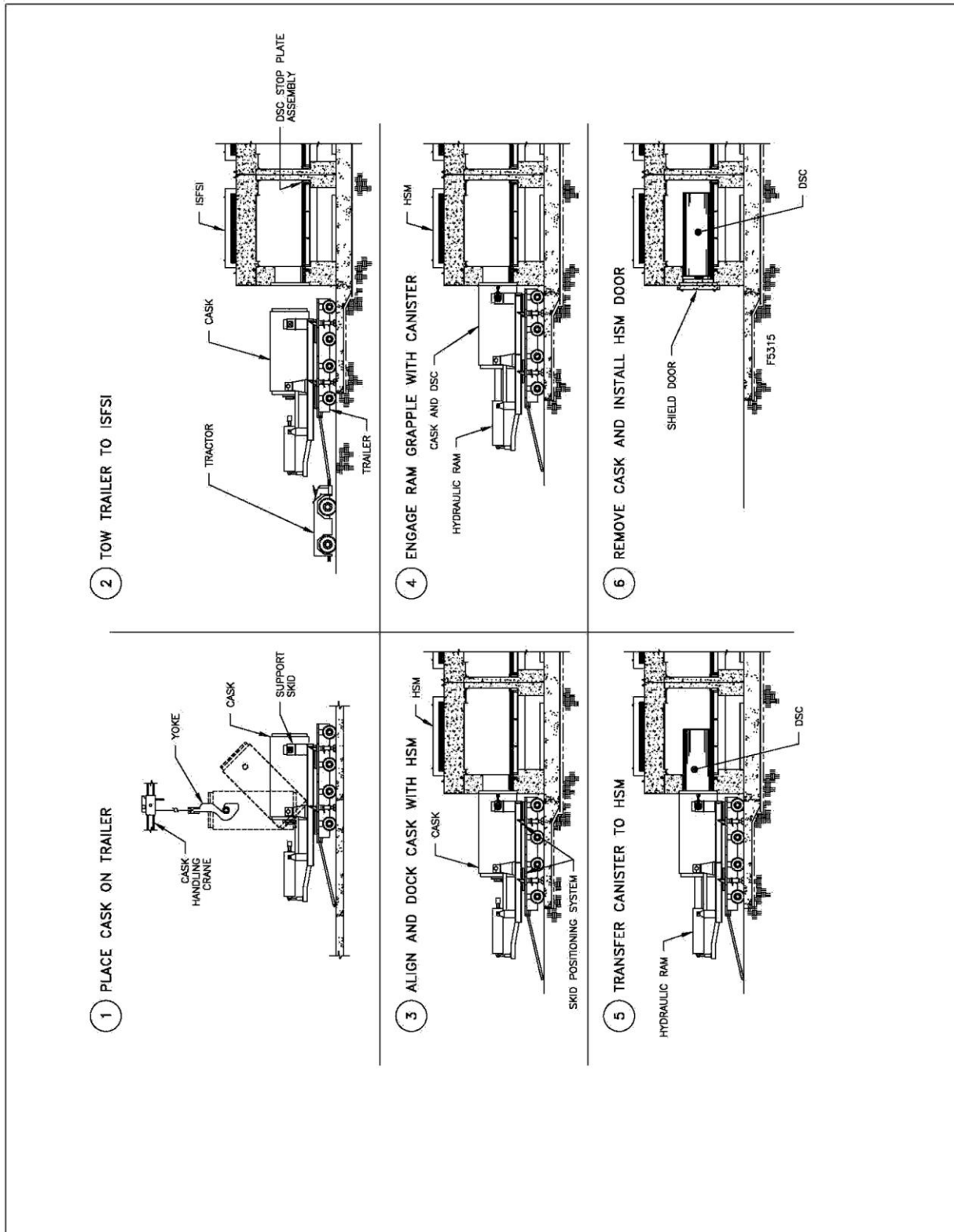


Figure 8-1
NUHOMS® HD System Loading Operations
(concluded)

CHAPTER 9 ACCEPTANCE TESTS AND MAINTENANCE PROGRAM

TABLE OF CONTENTS

9. ACCEPTANCE TESTS AND MAINTENANCE PROGRAM	9-1
9.1 Acceptance Criteria	9-1
9.1.1 Visual Inspection and Non-Destructive Examination (NDE).....	9-1
9.1.2 Structural and Pressure Tests	9-1
9.1.3 Leak Tests	9-2
9.1.4 Components	9-3
9.1.5 Shielding Integrity	9-3
9.1.6 Thermal Acceptance	9-3
9.1.7 Neutron Absorber Tests	9-4
9.2 Maintenance Program	9-6
9.2.1 Inspection.....	9-6
9.2.2 Tests	9-7
9.2.3 Repair, Replacement, and Maintenance.....	9-8
9.3 Marking	9-8
9.4 Pre-Operational Testing and Training Exercise.....	9-8
9.5 Specification for Neutron Absorbers	9-9
9.5.1 Specification for Thermal Conductivity Testing of Neutron Absorbers	9-9
9.5.2 Specification for Acceptance Testing of Neutron Absorbers by Neutron Transmission.....	9-10
9.5.3 Specification for Qualification Testing of Metal Matrix Composites.....	9-12
9.5.4 Specification for Process Controls for Metal Matrix Composites	9-14
9.6 References	9-16

LIST OF TABLES

Table 9-1 Boron Content of Neutron Absorbers.....	9-17
Table 9-2 Thermal Conductivity as a Function of Temperature for Sample Neutron Absorbers.....	9-18
Table 9-3 Sample Determination of Thermal Conductivity Acceptance Criterion	9-19

9. ACCEPTANCE TESTS AND MAINTENANCE PROGRAM

As noted in Chapter A.9, this chapter is also applicable to the 32PTH Type 1 DSC and OS187H Type 1 TC. As noted in Chapter B.9, this chapter is also applicable to the 32PTH Type 2 DSC and OS187H Type 2 TC.

9.1 Acceptance Criteria

9.1.1 Visual Inspection and Non-Destructive Examination (NDE)

Visual inspections are performed at the fabricator's facility to ensure that the 32PTH DSC, the OS187H Transfer Cask and the HSM-H conform to the drawings and specifications. The visual inspections include weld, dimensional, surface finish, and cleanliness inspections. Visual inspections specified by codes applicable to a component are performed in accordance with the requirements and acceptance criteria of those codes.

All weld inspection is performed using qualified processes and qualified personnel according to the applicable code requirements, e.g., ASME or AWS. Non-destructive examination (NDE) requirements for welds are specified on the drawings provided in Chapter 1; acceptance criteria are as specified by the governing code. NDE personnel are qualified in accordance with SNT-TC-1A [2].

The confinement welds on the DSC are inspected in accordance with ASME B&PV Code Subsection NB [1] including alternatives to ASME Code specified in UFSAR Section 3.10.

DSC non-confinement welds are inspected to the NDE acceptance criteria of ASME B&PV Code Subsection NG or NF, based on the applicable code for the components welded.

Upon arrival at the licensee's site, the DSCs and HSM-Hs are again inspected to ensure that they have not been damaged during shipment. Conditions that are not in conformance with the drawings and specifications will be repaired, or evaluated in accordance with 10 CFR 72.48 for the effect of the condition on the safety function of the components.

The Transfer Cask welds are inspected in accordance with ASME B&PV Code Subsection NC for class 2 components, as modified by code alternates identified in Section 3.10 of Chapter 3.

9.1.2 Structural and Pressure Tests

The DSC confinement boundary except inner top cover/shield plug (including option 2 or option 3 inner top cover as described in the UFSAR) to the DSC shell weld is pressure tested at the fabricator's shop in accordance with ASME Article NB-6300.

The inner top cover/shield plug (including option 2 or option 3 inner top cover) to the DSC shell weld is also pressure tested between 16.5 to 18 psig at the field after the fuel assemblies are loaded in the canister. This test is in accordance with the alternatives to the ASME code specified in UFSAR Section 3.10.

HSM-H reinforcement and concrete are tested as described in Section 2.5.2 and footnotes to Tables 4.1-5 and 4.4-3.

The Transfer Cask lifting (top) trunnions will be load tested in accordance with ANSI N14.6 [3] for a single failure proof design, i.e., three times the design load. The design load is conservatively set at 250,000 lb (Section 3.2.2); therefore, the test load is 750,000 lb (375,000 lb/trunnion).

9.1.3 Leak Tests

The 32PTH DSC confinement boundary is tested using two procedures described below. Personnel performing the leakage test are qualified in accordance with SNT-TC-1A [2], or more recent edition.

Procedure 1 is accomplished during fabrication:

Upon completion of all 32PTH DSC shell welding and attachment of the inner bottom cover plate to the DSC shell, a temporary seal plate is placed over the open end of the 32PTH DSC. A bag or other enclosure is placed around the outside of the entire 32PTH DSC and it is filled with helium. The 32PTH DSC cavity is evacuated and a helium leakage test is performed using a port in the seal plate. This test is used to show that the entire 32PTH DSC confinement boundary tested is leak tight (1×10^{-7} ref cm³/s) [4].

Procedure 2 occurs after the 32PTH DSC has been loaded with fuel assemblies:

The 32PTH DSC cavity has been dried, back filled with helium and the top shield plate and the vent and siphon port cover plates have been welded in place. After these welds are completed, a temporary test cover is installed with at least the root pass of the full weld. The cavity between the top shield plate and the temporary test cover is evacuated and a helium leakage test is performed using a test port in the temporary test cover. The leakage test thus includes the weld attaching the top shield plate to the 32PTH DSC shell, the vent and siphon port cover plate welds, and the base metal of the top shield plate and vent and siphon port cover plates. The vent and siphon ports are filled with helium prior to welding the vent and siphon port covers. This test verifies that the tested welds and cover plates are leak tight (1×10^{-7} ref cm³/s) [4].

The weld between the DSC shell and inner top cover/shield plug (including option 2 or option 3 inner top cover) and siphon/vent cover welds are also leak tested to an acceptance criteria of 1×10^{-7} ref cm³/s at the field after the fuel assemblies are loaded in the canister.

The Transfer Cask lid, ram access, vent, and drain cover o-rings, vent and drain quick connect fittings, neutron shield welds, and neutron shield fittings are leak tested prior to first use.

If bubble leak testing is used, no leak indication is allowed. If pressure drop or helium leak testing is used, the maximum allowable leak for each of the components listed is 10^{-3} ref cm³/s.

9.1.4 Components

The NUHOMS® System does not include any components such as valves, rupture discs, pumps, or blowers. The gaskets in the Transfer Cask do not require acceptance testing other than the leak testing cited above. No other components of the NUHOMS® System require testing, except as discussed in this chapter.

9.1.5 Shielding Integrity

The Transfer Cask poured lead shielding integrity will be confirmed via gamma scanning or approved equivalent prior to first use. The detector and examination grid will be matched to provide coverage of the entire lead-shielded surface area. The acceptance criterion is attenuation greater than or equal to that of a test block matching the cask through-wall configuration with lead and steel thicknesses equal to the design minimum less 5%.

The radial neutron shielding is provided by filling the neutron shield shell with water during operations. No testing is necessary. The neutron shield material in the lid and bottom end is a proprietary polymer resin. The shielding performance of the resin will be assured by written procedures controlling temperature, measuring, and mixing of the components, degassing of the resin, and verification of the mass or volume of resin installed.

The gamma and neutron shielding materials of the storage system itself are limited to concrete HSM components and steel shield plugs in the DSC. The integrity of these shielding materials is ensured by the control of their fabrication in accordance with the appropriate ASME, ASTM or ACI criteria. No additional acceptance testing is required.

9.1.6 Thermal Acceptance

No thermal acceptance testing is required to verify the performance of each storage unit other than that specified in the Technical Specifications for initial loading of each HSM-H.

The heat transfer analysis for the basket includes credit for the thermal conductivity of neutron-absorbing materials, as specified in Section 4.3. Because these materials do not have publicly documented values for thermal conductivity, testing of such materials will be performed in accordance with Section 9.5.1.

9.1.7 Neutron Absorber Tests

CAUTION

Sections 9.1.7.1 through 9.1.7.4 below are incorporated by reference into the NUHOMS[®] CoC 1030 Technical Specifications (paragraph 4.3.1) and shall not be deleted or altered in any way without a CoC amendment approval from the NRC. The text of these sections is shown in bold type to distinguish them from other sections.

The neutron absorber used for criticality control in the DSC basket may consist any of the following types of material:

- a) Boron-aluminum alloy (borated aluminum)
- b) Boron carbide/Aluminum metal matrix composite (MMC)
- c) Boral[®]

The 32PTH DSC safety analyses do not rely upon the tensile strength of these materials. The radiation and temperature environment in the cask is not sufficiently severe to damage these metallic/ceramic materials. To assure performance of the neutron absorber's design function only the presence of B10 and the uniformity of its distribution need to be verified, with testing requirements specific to each material. The boron content of these materials is given in Table 9-1.

References to metal matrix composites throughout this chapter are not intended to refer to Boral[®].

9.1.7.1 Boron Aluminum Alloy (Borated Aluminum)

See the Caution in Section 9.1.7 before deletion or modification to this section.

The material is produced by direct chill (DC) or permanent mold casting with boron precipitating primarily as a uniform fine dispersion of discrete AlB₂ or TiB₂ particles in the matrix of aluminum or aluminum alloy (other boron compounds, such as AlB₁₂, can also occur). For extruded products, the TiB₂ form of the alloy shall be used. For rolled products, either the AlB₂, the TiB₂, or a hybrid may be used.

Boron is added to the aluminum in the quantity necessary to provide the specified minimum B10 areal density in the final product. The amount required to achieve the specified minimum B10 areal density will depend on whether boron with the natural isotopic distribution of the isotopes B10 and B11, or boron enriched in B10 is used. In no case shall the boron content in the aluminum or aluminum alloy exceed 5% by weight.

The criticality calculations take credit for 90% of the minimum specified B10 areal density of borated aluminum. The basis for this credit is the B10 areal density acceptance testing, which shall be as specified in Section 9.5.2. The specified acceptance testing assures that at any location in the material, the minimum specified areal density of B10 will be found with 95% probability and 95% confidence.

9.1.7.2 Boron Carbide / Aluminum Metal Matrix Composites (MMC)

See the Caution in Section 9.1.7 before deletion or modification to this section.

The material is a composite of fine boron carbide particles in an aluminum or aluminum alloy matrix. The material shall be produced by direct chill casting, permanent mold casting, powder metallurgy, molten metal infiltration, or thermal spray techniques. The boron carbide content shall not exceed 40% by volume except for MMCs with an integral aluminum cladding or produced by molten metal infiltration, which shall not exceed 50% by volume.

The final MMC product shall have density greater than 98% of theoretical density demonstrated by qualification testing, with no more than 0.5 volume % interconnected porosity. For MMC with an integral cladding, the final density of the core shall be greater than 97% of theoretical density demonstrated by qualification testing, with no more than 0.5 volume % interconnected porosity of the core and cladding as a unit of the final product.

At least 50% by weight of the B₄C particles in MMCs shall be smaller than 40 microns. No more than 10% of the particles shall be over 60 microns.

Prior to use in the 32PTH DSC, MMCs shall pass the qualification testing specified in Section 9.5.3, and shall subsequently be subject to the process controls specified in Section 9.5.4.

The criticality calculations take credit for 90% of the minimum specified B10 areal density of MMCs. The basis for this credit is the B10 areal density acceptance testing, which is specified in Section 9.5.2. The specified acceptance testing assures that at any location in the final product, the minimum specified areal density of B10 will be found with 95% probability and 95% confidence.

9.1.7.3 Boral[®]

See the Caution in Section 9.1.7 before deletion or modification to this section.

This material consists of a core of aluminum and boron carbide powders between two outer layers of aluminum, mechanically bonded by hot rolling an “ingot” consisting of an aluminum box filled with blended boron carbide and aluminum powders. The core, which is exposed at the edges of the sheet, is slightly porous. Before rolling, at least 80% by weight of the B₄C particles in Boral[®] shall be smaller than 200 microns. The nominal boron carbide content shall be limited to 65% (+ 2% tolerance limit) of the core by weight.

The criticality calculations take credit for 75% of the minimum specified B10 areal density of Boral[®]. B10 areal density will be verified by chemical analysis and by certification of the B10 isotopic fraction for the boron carbide powder, or by neutron transmission testing. Areal density testing is performed on a coupon taken from the sheet produced from each ingot. If the measured areal density is below that specified, all the material produced from that ingot will be either rejected, or accepted only on the basis of alternate verification of B10 areal density for each of the final pieces produced from that ingot.

9.1.7.4 Visual Inspections of Neutron Absorbers

Neutron absorbers shall be 100% visually inspected in accordance with the Certificate Holder's QA procedures. Material that does not meet the following acceptance criteria shall be reworked, repaired, or scrapped. Blisters shall be treated as non-conforming. Inspection of MMCs with an integral aluminum cladding shall also include verification that the matrix is not exposed through the faces of the aluminum cladding and that solid aluminum is not present at the edges. For Boral[®], visual inspection shall verify that there are no cracks through the cladding, exposed core on the face of the sheet, or solid aluminum at the edge of the sheet. Material that does not meet these criteria shall be reworked, repaired, or scrapped.

9.1.7.5 Other Visual Inspections Criteria (non-Technical Specifications)

For borated aluminum and MMCs, visual inspections shall follow the recommendations in Aluminum Standards and Data, Chapter 4 "Quality Control, Visual Inspection of Aluminum Mill Products" [5]. Local or cosmetic conditions such as scratches, nicks, die lines, inclusions, abrasion, isolated pores, or discoloration are acceptable.

9.2 Maintenance Program

The NUHOMS[®] HD System is designed to be totally passive with minimal maintenance requirements. The 32PTH DSC does not require any maintenance once it is loaded into the HSM-H. The HSM-H does not require any maintenance other than that indicated in off-normal operations, Chapter 11, such as clearing of blocked air inlets. Periodic inspection is therefore limited to the Transfer Cask.

9.2.1 Inspection

The following inspections of the transfer cask should be performed prior to each fuel loading or unloading campaign:

- A. Visual inspection of the transfer cask trunnions for damaged bearing surfaces
- B. Visual or functional inspection of all taps, threaded inserts, and bolts
- C. Functional inspection of all quick-connect fittings
- D. Visual inspection of the interior surface of the cask for any indications of excessive wear.
- E. Visual inspection of the neutron shield jacket for indications of damage
- F. Visual inspection of all Transfer Cask o-rings for indications of damage

Within the year prior to any loading or unloading campaign, the top trunnion bearing surfaces and accessible welds shall be examined by dye penetrant. No linear indications shall be acceptable other than surface scratches and wear.

9.2.2 Tests

The Transfer Cask lid and ram access cover o-rings, vent and drain quick connect fittings, and neutron shield fittings shall be leak tested within the year before the start of any fuel loading or unloading campaign. If bubble leak testing is used, no leak indication is allowed. If pressure drop or helium leak testing is used, the maximum allowable leak for each of the components listed is 10^{-3} ref cm³/s. If any of the listed components is replaced, that component shall be leak tested before use in fuel loading or unloading operations.

No periodic testing of the 32PTH DSC, HSM-H or routine support equipment is required.

Temperature and radiation monitoring is provided in accordance with the Technical Specifications. Periodic calibration of the monitoring equipment shall be as required by the licensee's quality program.

9.2.3 Repair, Replacement, and Maintenance

Any parts which fail inspections listed in 9.1.2 shall be repaired or replaced. Such parts may also be accepted as-is if determined appropriate by engineering and licensing review.

9.3 Marking

The HSM-H and 32PTH DSC are marked with the model number, unique identification number, and empty weight in accordance with 10 CFR 72.236(k). The 32PTH DSC nameplate is shown in drawing 10494-72-7.

9.4 Pre-Operational Testing and Training Exercise

A dry run training exercise of the loading, closure, handling, unloading, and transfer of the NUHOMS® HD System shall be performed by each licensee prior to their first use of the system to load spent fuel assemblies. The dry run shall be conducted with simulated fuel to match the weight of the actual fuel. The dry run need not be performed in the sequence of operations in Chapter 8. The dry run shall include:

- a) Loading of mock-up fuel
- b) DSC draining, vacuum drying, welding, and backfilling
- c) Loading of the Transfer Cask onto the Transfer Trailer, and transfer to the ISFSI
- d) DSC transfer to the HSM-H
- e) DSC retrieval from the HSM-H
- f) Re-flooding of a sealed 32PTH DSC
- g) Removal of the covers from a sealed 32PTH DSC

The dry run will simulate, as nearly as possible, the detailed written procedures developed by the licensee for NUHOMS® HD System operations. Guidelines for the dry run follow.

- A. An actual or a mock-up 32PTH DSC loaded with mock-up fuel is typically utilized. The 32PTH DSC is loaded into the transfer cask; the transfer cask/DSC annulus seal is installed.
- B. Functional testing is performed with the transfer cask and lifting equipment. These tests are to ensure that the transfer cask can be safely lifted from the plant's cask receiving area to the cask washdown area. The cask is partially lowered into the spent fuel pool and positioned in the cask loading area to verify clearances and travel path. The inner top cover is installed to verify handling and alignment operations.

- C. The transfer cask is placed on the transfer trailer, which is moved to the ISFSI aligned with an HSM-H. Compatibility of the transfer trailer with the transfer cask, verification of the transfer route to the ISFSI, and maneuverability within the confines of the ISFSI are verified.
- D. The transfer trailer is aligned and docked with the HSM-H. The hydraulic ram is used to insert the 32PTH DSC loaded with mock-up fuel assemblies into the HSM-H and then to retrieve it. Transfer of the 32PTH DSC to the HSM-H will verify that the support skid positioning system and the hydraulic ram system operate safely for both insertion and retrieval.
- E. A weld mockup, typically a shortened 32PTH DSC mockup modeling the top end, covers, and drain tube, is used to demonstrate closure welding, draining, drying, backfill, re-flooding, and canister opening operations.
- F. The dry run is deemed successful if the expected results are achieved safely and without damage to any of the components or associated equipment.
- G. Should any equipment or components require modification in order to achieve the expected results, it will be retested, as necessary, to confirm that the modification is adequate. Should the dry run indicate that procedures require change in order to achieve the expected results, the changes will be incorporated into the appropriate operating procedures prior to use for fuel transfer.

9.5 Specification for Neutron Absorbers

9.5.1 Specification for Thermal Conductivity Testing of Neutron Absorbers

Testing shall conform to ASTM E1225¹, ASTM E1461², or equivalent method, performed at room temperature on coupons taken from the rolled or extruded production material. Previous testing of borated aluminum and metal matrix composite, Table 9-2, shows that thermal conductivity increases slightly with temperature. Initial sampling shall be one test per lot, defined by the heat or ingot, and may be reduced if the first five tests meet the specified minimum thermal conductivity.

If a thermal conductivity test result is below the specified minimum, at least four additional tests shall be performed on the material from that lot. If the mean value of those tests, including the original test, falls below the specified minimum, the associated lot shall be rejected.

After twenty five tests of a single type of material, with the same aluminum alloy matrix, the same boron content, and the same primary boron phase, e.g., B₄C, TiB₂, or AlB₂, if the mean value of all the test results less two standard deviations meets the specified thermal conductivity, no further testing of that material is required. This exemption may also be applied to the same type of material if the matrix of the material changes to a more thermally conductive alloy (e.g., from 6000 to 1000 series aluminum), or if the boron content is reduced without changing the boron phase.

¹ ASTM E1225, "Thermal Conductivity of Solids by Means of the Guarded-Comparative-Longitudinal Heat Flow Technique"

² ASTM E1461, "Thermal Diffusivity of Solids by the Flash Method"

The thermal analysis in Chapter 4 assumes a 3/16 inch thick neutron absorber paired with a 5/16 inch aluminum 1100 plate. The specified thickness of the neutron absorber may vary, and the thermal conductivity acceptance criterion for the neutron absorber will be based on the nominal thickness specified. The minimum thermal conductivity shall be such that the total thermal conductance (sum of conductivity * thickness) of the neutron absorber and the aluminum 1100 plate shall equal the conductance assumed in the analysis, 4.774 BTU/hr.F, as shown in Table 9-3, where the acceptance criterion is highlighted.

The aluminum 1100 plate does not need to be tested for thermal conductivity; the material may be credited with the values published in the ASME Code Section II part D. The neutron absorber material need not be tested for thermal conductivity if the nominal thickness of the aluminum 1100 plate is 0.425 inch or greater. This case is examined explicitly in chapter 4, where no credit is taken for the thermal conductivity of Boral[®].

9.5.2 Specification for Acceptance Testing of Neutron Absorbers by Neutron Transmission

CAUTION

Section 9.5.2a and portions of 9.5.2b are incorporated by reference into the NUHOMS[®] CoC 1030 Technical Specifications (paragraph 4.3.1) and shall not be deleted or altered in any way without a CoC amendment approval from the NRC. The text of information incorporated by reference in these sections is shown in bold type to distinguish it from other sections.

- a. **Neutron Transmission acceptance testing procedures shall be subject to approval by the Certificate Holder. Test coupons shall be removed from the rolled or extruded production material at locations that are systematically or probabilistically distributed throughout the lot. Test coupons shall not exhibit physical defects that would not be acceptable in the finished product, or that would preclude an accurate measurement of the coupon's physical thickness.**

A lot is defined as all the pieces produced from a single ingot or heat or from a group of billets from the same heat. If this definition results in lot size too small to provide a meaningful statistical analysis of results, an alternate larger lot definition may be used, so long as it results in accumulating material that is uniform for sampling purposes.

The sampling rate for neutron transmission measurements shall be such that there is at least one neutron transmission measurement for each 2000 square inches of final product in each lot.

The B10 areal density is measured using a collimated thermal neutron beam up to 1.1 inch diameter.

The neutron transmission through the test coupons is converted to B10 areal density by comparison with transmission through calibrated standards. These standards are composed of a homogeneous boron compound without other significant neutron absorbers. For example, boron carbide, zirconium diboride or titanium diboride sheets are acceptable standards. These standards are paired with aluminum shims sized to match the effect of neutron scattering by aluminum in the test coupons.

Uniform but non-homogeneous materials such as metal matrix composites may be used for standards, provided that testing shows them to provide neutron attenuation equivalent to a homogeneous standard. Standards will be calibrated, traceable to nationally recognized standards, or by attenuation of a monoenergetic neutron beam correlated to the known cross section of boron 10 at that energy.

The minimum areal density specified shall be verified for each lot at the 95% probability, 95% confidence level or better. If a goodness-of-fit test demonstrates that the sample comes from a normal population, the one-sided tolerance limit for a normal distribution may be used for this purpose. Otherwise, a non-parametric (distribution-free) method of determining the one-sided tolerance limit may be used. Demonstration of the one-sided tolerance limit shall be evaluated for acceptance in accordance with the Certificate Holder's QA procedures.

- b. The following illustrates one acceptable method and is intended to be utilized as an example. Therefore, the following text is not part of the Technical Specifications.

The acceptance criterion for individual plates is determined from a statistical analysis of the test results for their lot. The B10 areal densities determined by neutron transmission are converted to volume density, i.e., the B10 areal density is divided by the thickness at the location of the neutron transmission measurement or the maximum thickness of the coupon. The lower tolerance limit of B10 volume density is then determined, defined as the mean value of B10 volume density for the sample, less K times the standard deviation, where K is the one-sided tolerance limit factor for a normal distribution with 95% probability and 95% confidence [7].

Finally, the minimum specified value of B10 areal density is divided by the lower tolerance limit of B10 volume density to arrive at the minimum plate thickness, which provides the specified B10 areal density.

Any plate that is thinner than the statistically derived minimum thickness from 9.5.2 a) or the minimum design thickness, whichever is greater, shall be treated as non-conforming, with the following exception. Local depressions are acceptable, so long as they total no more than 0.5% of the area on any given plate, and the thickness at their location is not less than 90% of the minimum design thickness. Edge effects due to manufacturing operations such as shearing, deburring, and chamfering need not be included in this determination.

Non-conforming material shall be evaluated for acceptance in accordance with the Certificate Holder's QA procedures.

9.5.3 Specification for Qualification Testing of Metal Matrix Composites

CAUTION

Section 9.5.3.4 and Section 9.5.3.5 are incorporated by reference into the NUHOMS[®] CoC 1030 Technical Specifications (paragraph 4.3.1) and shall not be deleted or altered in any way without a CoC amendment approval from the NRC. The text of these sections is shown in bold type to distinguish them from other sections.

9.5.3.1 Applicability and Scope

Metal matrix composites (MMCs) acceptable for use in the 32PTH DSC are described in Section 9.1.7.2.

Prior to initial use in a spent fuel dry storage or transport system, such MMCs shall be subjected to qualification testing that will verify that the product satisfies the design function. Key process controls shall be identified per Section 9.5.4 so that the production material is equivalent to or better than the qualification test material. Changes to key processes shall be subject to qualification before use of such material in a spent fuel dry storage or transport system.

ASTM test methods and practices are referenced below for guidance. Alternative methods may be used with the approval of the certificate holder.

9.5.3.2 Design Requirements

In order to perform its design functions the product must have at a minimum sufficient strength and ductility for manufacturing and for the normal and accident conditions of the storage/transport system. This is demonstrated by the tests in Section 9.5.3.4. It must have a uniform distribution of boron carbide. This is demonstrated by the tests in Section 9.5.3.5.

9.5.3.3 Durability

There is no need to include accelerated radiation damage testing in the qualification. Such testing has already been performed on MMCs, and the results confirm what would be expected of materials that fall within the limits of applicability cited above. Metals and ceramics do not experience measurable changes in mechanical properties due to fast neutron fluences typical over the lifetime of spent fuel storage, about 10^{15} neutrons/cm².

Thermal damage and corrosion (hydrogen generation) testing shall be performed unless such tests on materials of the same chemical composition have already been performed and found acceptable. The following paragraphs illustrate two cases where such testing is not required.

Thermal damage testing is not required for unclad MMCs consisting only of boron carbide in an aluminum 1100 matrix, because there is no reaction between aluminum and boron carbide below 842°F, well above the basket temperature under normal conditions of storage or transport³.

³ Sung, C., "Microstructural Observation of Thermally Aged and Irradiated Aluminum/Boron Carbide (B₄C) Metal

Corrosion testing is not required for full density MMCs (clad or unclad) consisting only of boron carbide in an aluminum 1100 matrix, because testing on one such material has already been performed by Transnuclear⁴.

9.5.3.4 Required Qualification Tests and Examinations to Demonstrate Mechanical Integrity

At least three samples, one each from approximately the two ends and middle of the qualification material shall be subject to:

a) Room temperature tensile testing (ASTM- B557⁵) demonstrating that the material has the following tensile properties:

- Minimum yield strength, 0.2% offset: 1.5 ksi
- Minimum ultimate strength: 5 ksi
- Minimum elongation in 2 inches: 0.5%

As an alternative to the elongation requirement, ductility may be demonstrated by bend testing per ASTM E290⁶. The radius of the pin or mandrel shall be no greater than three times the material thickness, and the material shall be bent at least 90 degrees without complete fracture,

b) Testing to verify more than 98% of theoretical density for non-clad MMCs and 97% for the matrix of clad MMCs. Testing or examination for interconnected porosity on the faces and edges of unclad MMC, and on the edges of clad MMC, shall be performed by a means to be approved by the Certificate Holder. The maximum interconnected porosity is 0.5 volume %,

c) Clad MMCs shall be subjected to thermal damage testing following water immersion to ensure that delamination does not occur under normal conditions of storage.

An example of such a test would be: (1) immerse a specimen at least 6 x 6 inches in water under pressure ≥ 30 psig for at least 24 hours, (2) place the specimen in a vacuum furnace preheated to at least 300 °F and evacuate the furnace. Acceptance criterion: no blistering or delamination of the cladding.

9.5.3.5 Required Tests and Examinations to Demonstrate B10 Uniformity

Uniformity of the boron distribution shall be verified either by:

⁴ Boralyn testing submitted to the NRC under docket 71-1027, 1998

⁵ ASTM B557 Standard Test Methods of Tension Testing Wrought and Cast Aluminum and Magnesium-Alloy Products.

⁶ ASTM E290, Standard Methods for Bend Testing of Materials for Ductility

- (a) **Neutron radioscopy or radiography (ASTM E94 [8], E142 [9], and E545 [10]) of material from the ends and middle of the test material production run, verifying no more than 10% difference between the minimum and maximum B10 areal density, or**
- (b) **Quantitative testing for the B10 areal density, B10 density, or the boron carbide weight fraction, on locations distributed over the test material production run, verifying that one standard deviation in the sample is less than 10% of the sample mean. Testing may be performed by a neutron transmission method similar to that specified in Section 9.5.2, or by chemical analysis for boron carbide content in the composite.**

9.5.3.6 Approval of Procedures

Qualification report shall be prepared by, or subject to approval by the Certificate Holder.

9.5.4 Specification for Process Controls for Metal Matrix Composites

This section provides process controls to ensure that the material delivered for use is equivalent to the qualification test material.

CAUTION

Sections 9.5.4.1 and 9.5.4.2 are incorporated by reference into the NUHOMS® CoC 1030 Technical Specifications (paragraph 4.3.1) and shall not be deleted or altered in any way without a CoC amendment approval from the NRC. The text of these sections is shown in bold type to distinguish them from other sections.

9.5.4.1 Applicability and Scope

Key processing changes shall be subject to qualification prior to use of the material produced by the revised process. The Certificate Holder shall determine whether a complete or partial re-qualification program per Section 9.5.3 is required, depending on the characteristics of the material that could be affected by the process change.

9.5.4.2 Definition of Key Process Changes

Key process changes are those that could adversely affect the uniform distribution of the boron carbide in the aluminum, reduce density, reduce corrosion resistance, or reduce the mechanical strength or ductility of the MMC.

9.5.4.3 Identification and Control of Key Process Changes

The manufacturer shall provide the Certificate Holder with a description of materials and process controls used in producing the MMC. The Certificate Holder and manufacturer shall identify key process changes as defined in Section 9.5.4.2.

An increase in nominal boron carbide content over that previously qualified shall always be regarded as a key process change. The following are examples of other changes that are established as key process changes, as determined by the Certificate Holder's review of the specific applications and production processes:

- a) Changes in the boron carbide particle size specification that increase the average d50 particle size by more than 5 microns or that increase the amount of particles larger than 60 microns from the previously qualified material by more than 5% of the total distribution but less than the 10% limit,
- b) Change of the billet production process, e.g., from vacuum hot pressing to cold isostatic pressing followed by vacuum sintering,
- c) Change in the nominal matrix alloy,
- d) Changes in mechanical processing that could result in reduced density of the final product, e.g., for PM or thermal spray MMCs that were qualified with extruded material, a change to direct rolling from the billet,
- e) For MMCs using a magnesium-alloyed aluminum matrix, changes in the billet formation process that could increase the likelihood of magnesium reaction with the boron carbide, such as an increase in the maximum temperature or time at maximum temperature, and
- f) Changes in powder blending or melt stirring processes that could result in less uniform distribution of boron carbide, e.g., change in duration of powder blending.
- g) For MMCs with an integral aluminum cladding, a change greater than 25% in the ratio of the nominal aluminum cladding thickness (sum of two sides of cladding) and the nominal matrix thickness could result in changes in the mechanical properties of the final product.

In no case shall process changes be accepted if they result in a product outside the limits in Sections 9.5.3.1 and 9.5.3.4.

9.6 References

1. ASME Boiler and Pressure Vessel Code, Section III, 1998 Edition through 2000 addenda.
2. SNT-TC-1A, "American Society for Nondestructive Testing, Personnel Qualification and Certification in Nondestructive Testing," 1992.
3. ANSI N14.6, "American National Standard for Special Lifting Devices for Shipping Containers Weighing 10,000 Pounds or More for Nuclear Materials," New York, 1996.
4. ANSI N14.5-1997, "American National Standard for Leakage Tests on Packages for Shipment of Radioactive Materials," February 1998.
5. "Aluminum Standards and Data, 2003" The Aluminum Association.
6. Not used.
7. Natrella, "Experimental Statistics," Dover, 2005
8. ASTM E94, Recommended Practice for Radiographic Testing.
9. ASTM E142, Controlling Quality of Radiographic Testing.
10. ASTM E545, Standard Method for Determining Image Quality in Thermal Neutron Radiographic Testing.

Table 9-1
Boron Content of Neutron Absorbers

Borated Aluminum and Metal Matrix Composites, 90% B10 credit

NUHOMS [®] - 32PTH DSC Basket Type	B10 Areal Density, (g/cm ²)	Nom wt % boron in enriched borated aluminum 0.187" thk (notes 1, 2, 3)	Nom wt % boron in natural borated aluminum 0.187" thk (notes 2, 3)	Nominal vol % B ₄ C in MMC, 0.187" thick (notes 2, 3)
AI	0.007	0.6	3.1	4.1
BI	0.015	1.3	Note 4	8.9
CI	0.020	1.7		11.8
DI	0.032	2.7		18.9
EI	0.050	4.2		29.5

0.075 inch thick Boral[®], 75% B10 credit

NUHOMS [®] -32PTH DSC Basket Type	B10 Areal Density, (g/cm ²)	Boral [®] nominal core thickness, inch
AII	0.009	0.0535 (note 5)
BII	0.019	
CII	0.025	
DII	N/A	Note 6
EII	N/A	

Notes:

1. Enriched boron is nominally 95 atom % B10
2. The neutron absorber manufacturer may increase this value to provide margin against rejection of the product
3. If a neutron absorber thinner than 0.187 inch is used, the boron content varies in inverse proportion to the thickness to maintain the same areal density
4. The necessary boron content in this range is too high (>5%) to use boron with its naturally-occurring isotopic distribution (nominal 20 atom % B10) in borated aluminum
5. Boral[®] sheet and core thickness remain the same; boron carbide / aluminum powder ratio is varied to achieve the required areal density
6. Boral[®] in this range requires a sheet thicker than 0.075 inches

Table 9-2
Thermal Conductivity as a Function of Temperature for Sample Neutron Absorbers

Material >	1	2	3	4
20	193	170	194	194
100	203	183	207	201
200	208	-	-	
250	-	201	218	206
300	211	204	220	203
314	-	-	-	202
342	-	-	-	202

Units: W/mK

Materials:

- 1) Boralyn[®] MMC, aluminum 1100 with 15% B₄C
- 2) Borated aluminum 1100, 2.5% boron as TiB₂
- 3) Borated aluminum 1100, 2.0% boron as TiB₂
- 4) Borated aluminum 1100, 4.3% boron as AlB₂

Sources:

Thermal Conductivity Measurements of Boron Carbide/Aluminum Specimens, Oct 1998, testing by Precision Measurements and Instruments Corp. for Transnuclear, Inc.

Qualification of Thermal Conductivity, Borated Aluminum 1100, Eagle Picher Report AAQR06, May 2001

Table 9-3
Sample Determination of Thermal Conductivity Acceptance Criterion

	Al 1100	n absorber	total	
thickness (inch)	0.3125	0.1875	0.5	as modeled
conductivity at 70 F (Btu/hr.in.F)	11.09	6.98	n/a	
conductance (Btu/hr.F)	3.466	1.309	4.774	
thickness (inch)	0.28	0.22	0.5	thicker neutron absorber
conductivity at 70 F (Btu/hr.in.F)	11.09	7.59	n/a	
conductance (Btu/hr.F)	3.105	1.670	4.775	
thickness (inch)	0.35	0.15	0.5	thinner neutron absorber
conductivity at 70 F (Btu/hr.in.F)	11.09	5.95	n/a	
conductance (Btu/hr.F)	3.882	0.893	4.774	

The acceptance criterion is identified by boldface type for each thickness.

CHAPTER 10
RADIATION PROTECTION

TABLE OF CONTENTS

10. RADIATION PROTECTION.....	10-1
10.1 Ensuring That Occupational Radiation Exposures Are As Low As Reasonably Achievable (ALARA).....	10-1
10.1.1 Policy Considerations	10-1
10.1.2 Design Considerations	10-1
10.1.3 Operational Considerations.....	10-3
10.2 Radiation Protection Design Features	10-4
10.2.1 NUHOMS® HD System Design Features.....	10-4
10.2.2 Offsite Dose Calculations	10-4
10.3 Estimated Onsite Collective Dose Assessment	10-8
10.3.1 DSC Loading, Transfer and Storage Operations	10-8
10.3.2 DSC Retrieval Operations.....	10-8
10.3.3 Fuel Unloading Operations	10-9
10.3.4 Maintenance Operations	10-9
10.3.5 Doses During ISFSI Array Expansion.....	10-9
10.4 References.....	10-10

LIST OF TABLES

Table 10-1	Occupational Exposure Summary, NUHOMS [®] HD System.....	10-11
Table 10-2	Total Annual Exposure from 32PTH DSC in HSM-H.....	10-12
Table 10-3	NUHOMS [®] HD System, 32PTH DSC / HSM-H Spectra.....	10-13
Table 10-4	Summary of ISFSI Surface Activities, 32PTH DSC in HSM-H.....	10-14
Table 10-5	MCNP Front Detector Dose Rates for 2x10 Array, 32PTH DSC in HSM-H..	10-15
Table 10-6	MCNP Back Detector Dose Rates for the Two 1x10 Arrays, 32PTH DSC in HSM-H	10-16
Table 10-7	MCNP Side Detector Dose Rates, 32PTH DSC in HSM-H	10-17

LIST OF FIGURES

Figure 10-1	Annual Exposure from the ISFSI as a Function of Distance, 32PTH DSC in HSM-H	10-18
-------------	---	-------

10. RADIATION PROTECTION

The applicability of these analyses to the 32PTH Type 1 DSC and OS187H Type 1 TC described in Appendix A are discussed in Appendix A, Chapter A.10, and the applicability of these analyses to the 32PTH Type 2 DSC and OS187H Type 2 described in Appendix B are discussed in Appendix B, Chapter B.10, along with any necessary additional details.

10.1 Ensuring That Occupational Radiation Exposures Are As Low As Reasonably Achievable (ALARA)

10.1.1 Policy Considerations

The licensee's radiation safety and ALARA policies should be applied to the ISFSI. The ALARA program should follow the general guidelines of Regulatory Guides 1.8 [4], 8.8 [1], 8.10 [3] and 10 CFR 20 [6]. ISFSI personnel should be trained in the proper operation, inspection, repair and maintenance of the NUHOMS® HD System and updated on ALARA practices and dose reduction techniques. Implementation of ISFSI procedures should be reviewed by the licensee to ensure ALARA exposure.

10.1.2 Design Considerations

The thick inner cover of the DSC is designed to minimize exposure during draining, drying, and closure operations. The vent and drain ports are designed for maximum water flow rate and vacuum conductance to minimize the time (and thereby the exposure) associated with draining and vacuum drying. The design of the cover welds minimizes exposure during closure operations. The welds are designed to be easily performed by remote welding equipment. Because the cover welds are not used to lift the canister, they are relatively small, reducing the time needed to complete them. Because they are austenitic welds, no pre-heating is required. These welds are tested to be leak-tight as described in Chapter 7. Therefore, exposure associated with a leaking DSC is eliminated.

Lead, steel, water, and borated plastic in the transfer cask provide required gamma and neutron shielding during transfer activities. The exterior of the transfer cask is decontaminated prior to transfer to the ISFSI, thereby minimizing exposure of personnel to surface contamination.

The NUHOMS® HSM-H storage modules include no active components which require periodic maintenance thereby minimizing potential personnel dose due to maintenance activities.

The shielding design features of the storage modules storage minimize occupational exposure for any activities on or near the ISFSI. These features are:

- The DSCs are loaded and sealed prior to transfer to the ISFSI. Seals are austenitic stainless welds with at least two layers.
- The fuel will not be unloaded nor will the DSCs be opened at the ISFSI unless the ISFSI is specifically licensed for these purposes.
- The fuel is stored in a dry inert environment inside the DSCs so that no radioactive liquid is available for leakage.

- The DSCs are sealed with a helium atmosphere to prevent oxidation of the fuel. The leaktight design features are described in Chapter 7.
- The DSCs are heavily shielded on both ends to reduce external dose rates. The shielding design features are discussed in Chapter 5.
- No radioactive material will be discharged during storage since the DSC is designed, fabricated, and tested to be leaktight.
- The DSC outside surface is contamination free due to the use of clean water sealed in the annulus between the cask and DSC during loading operations.
- HSMs provide thick concrete shielding, while placement of modules immediately adjacent to one another enhances the effectiveness of this shielding.

Regulatory Position 2 of Regulatory Guide 8.8 [1], is incorporated into the design considerations, as described below:

- Regulatory Position 2a on access control is met by use of a fence with a locked gate that surrounds the ISFSI and prevents unauthorized access.
- Regulatory Position 2b on radiation shielding is met by the heavy shielding of the NUHOMS[®] System which minimizes personnel exposures.
- Regulatory Position 2c on process instrumentation and controls is met by designing the instrumentation for a long service life and locating readouts in a low dose rate location. The use of temperature sensors for temperature measurements located in embedded thermowells provides reliable, easily maintainable instrumentation for this monitoring function.
- Regulatory Position 2d on control of airborne contaminants may be applicable for vacuum drying operations of DSCs containing damaged fuel. Diversion of the vacuum pump exhaust to an appropriate filtration system is recommended in the Chapter 8 operations. The regulatory position does not apply during transfer or storage because neither gaseous releases nor significant surface contamination are expected.
- Regulatory Position 2e on crud control is not applicable to the ISFSI because there are no systems at the ISFSI that could transport crud. The leaktight DSC design ensures that spent fuel crud will not be released or transferred from the DSC. Draining back to the spent fuel pool provides control over any crud that could be entrained in the outflow from the DSC draining operations.
- Regulatory Position 2f on decontamination is met because the transfer cask is decontaminated prior to transfer to the ISFSI. The transfer cask accessible surfaces are designed to facilitate decontamination.
- Regulatory Position 2g on radiation monitoring does not apply. There is no need for airborne radioactivity monitoring because the DSCs are sealed by leaktight welds. Airborne radioactivity due to damaged fuel is discussed under Regulatory Position 2d above. Area radiation monitors are not required because the ISFSI will not be occupied on a regular basis.

- Regulatory Position 2h on resin and sludge treatment systems is not applicable to the ISFSI because there are no radioactive systems containing resins or sludge associated with the ISFSI.
- Regulatory Position 2i concerning other miscellaneous ALARA items is not applicable because these items refer to radioactive systems not present at the ISFSI.

10.1.3 Operational Considerations

The operations description in Chapter 8 makes provision for measures which can minimize doses during operations including:

- using temporary shielding,
- wetting equipment with clean water prior to pool immersion to improve ease of decontamination,
- preventing contamination of the DSC exterior by the use of clean water in a sealed transfer cask/DSC annulus,
- using remote equipment for welding, long-handled tools for decontamination, etc., and
- controlling gases and liquids removed from the DSC during DSC vacuum drying and during fuel unloading.

The areas of highest operational dose are the front of a loaded HSM-H at the air inlet vent, at the cask side or DSC top with a partially or completely drained DSC (cover welding, transfer operations) and at the cask/DSC annulus. Operating procedures, temporary shielding, and personnel training should minimize personnel exposure in these areas.

The DSCs contain no radioactive liquids and, for intact fuel assemblies, are not expected to contain any radioactive gases. The DSC is designed and welded to be leaktight.

The NUHOMS[®] HD System HSM-H and 32PTH DSC are designed to be essentially maintenance free. It is a passive system without any moving parts. The only anticipated maintenance procedures are the visual inspection of the bird screens on the HSM ventilation inlet and outlet openings, and periodic maintenance of the temperature sensors. Maintenance operations on the transfer cask, transfer equipment and other auxiliary equipment are normally performed in a low dose environment during periods when fuel movement is not occurring.

The ISFSI contains no systems that process liquids or gases or contain, collect, store, or transport radioactive liquids or solids other than payloads identified in Chapter 2. Therefore, the ISFSI meets ALARA requirements since there are no systems to be maintained other than the transfer and auxiliary equipment.

10.2 Radiation Protection Design Features

10.2.1 NUHOMS[®] HD System Design Features

The NUHOMS[®] HD System has design features which ensure a high degree of integrity for the confinement of radioactive materials and reduction of direct radiation exposures during storage. Those features are described in Section 10.1.2.

10.2.2 Offsite Dose Calculations

Calculated dose rates in the immediate vicinity of the NUHOMS[®] HD System are presented in Chapter 5, which provides a detailed description of source term configuration, analysis models and bounding dose rates. Off-site dose rates and doses are presented in this section. This evaluation determines the neutron and gamma-ray off-site dose rates including skyshine in the vicinity of the two generic ISFSI layouts containing design-basis contents in the DSCs.

The first generic ISFSI evaluated is a 2x10 back-to-back array of HSM-Hs loaded with design-basis fuel and control components (NFAH) in NUHOMS[®] 32PTH DSCs. The second generic layout evaluated is two 1x10 front-to-front arrays. This evaluation provides results for distances ranging from 6.1 to 600 meters from each face of the two arrays.

The total annual exposure for each ISFSI layout as a function of distance from each face is given in Table 10-2 and plotted in Figure 10-1. The total annual exposure estimates assume 100% occupancy for 365 days.

The Monte Carlo computer code MCNP 2 calculates the dose rates at the specified locations around the arrays of HSMs. The results of this calculation provide an example of how to demonstrate compliance with the relevant radiological requirements of 10 CFR 20 [6], 10 CFR 72 [5], and 40 CFR 190 [8] for a specific site. Each site must perform specific site calculations to account for the actual layout of the HSMs and fuel source.

The assumptions for the MCNP analyses are summarized below.

- The 20 HSMs in the 2x10 back-to-back array are modeled as a box enveloping the 2x10 array of HSMs including the 3-foot shield walls on the two ends of the array. MCNP starts the source particles on the surfaces of the box.
- The 20 HSMs in the two 1x10 front-to-front arrays are modeled as two boxes which envelope each 1x10 array of HSMs including the 3-foot shield walls on the two ends and back of each array. MCNP starts the source particles on the surfaces of one of the boxes.
- The ISFSI approach slab is modeled as concrete. Because the ground composition has, at best, only a secondary impact on the dose rates at the detectors, any differences between this assumed layout and the actual layout would not have a significant affect on the site dose rates.

- For the 2x10 array, the interiors of the HSMs and shield walls are modeled as air. Most particles that enter the interiors of the HSMs and shield walls will therefore pass through unhindered.
- For the two 1x10 arrays, the interiors of one array of HSMs and shield walls are modeled as air. Most particles that enter the interiors of these HSMs and shield walls will therefore pass through unhindered. The other 1x10 array is modeled as concrete to simulate the shielding provided by the second array of HSMs for the direct radiation from the front of the opposing 1x10 array.
- The “universe” is a sphere surrounding the ISFSI. To account for skyshine radius of this sphere ($r=500,000$ cm) is more than 10 mean free paths for neutrons and 50 mean free paths for gammas greater than that of the outermost surface, thus ensuring that the model is of a sufficient size to include all interactions, including skyshine, affecting the dose rate at the detectors.
- The HSM-H surface sources are bootstrapped (input to provide an equivalent boundary condition) using the surface average dose rates calculated in Section 5.4 and shown in Table 5-2.
- MCNP starts the source particles on the ISFSI array surface with initial directions following a cosine distribution. Radiation fluxes outside thick shields such as the HSM walls and roof tend to have forward peaked angular distributions; therefore, a cosine function is a reasonable approximation for the starting direction distribution. Vents through shielding regions such as the HSM vents tend to collimate particles such that a semi-isotropic assumption would not be appropriate.
- Point detectors determine the dose rates on the four sides of the ISFSI as a function of distance from the ISFSI. All detectors represent the dose rate at three feet above ground level.
- Source information required by MCNP includes gamma-ray and neutron spectra for the HSM array surfaces, total gamma-ray and neutron activities for each HSM-H array face and total gamma-ray and neutron activities for the entire ISFSI. The neutron and gamma-ray spectra are determined using the MCNP spectra determined in the HSM-H dose calculations (from Section 5.4) using the design-basis in-core neutron and gamma fuel sources. Use of the roof is conservative because it represents the thickest cross section of the HSM-H shield. The thicker shield increases the dose rate importance of the higher energy neutrons and gamma-rays from the fuel because the thicker shield filters out the lower energy particles. Therefore, use of the thickest part of the shield results in a harder spectrum for all of the other surfaces. The HSM-H spectra as determined from MCNP are normalized to a one mrem/hour source using the flux-to-dose-factors from ANSI/ANS 6.1.1-1977 9. These normalized spectra are then input in the MCNP ERG source variable.

- The probability of a particle being born on a given surface is proportional to the total activity of that surface. The activity of each surface is determined by multiplying the sum of the normalized group fluxes, calculated above, by the average surface dose rate and by the area of the surface. This calculation is performed for the roof, sides, back and front of the HSM-H. The sum of the surface activities is then input as the tally multiplier for each of the MCNP tallies to convert the tally results to fluxes (particles per second per square centimeter).
- Neutron and gamma-ray spectra are shown in Table 10-3. The group fluxes on the roof are taken from the MCNP run. The dose rate contribution from each group is the product of the flux and the flux-to-dose factor. The “Input Current” column in the tables is simply the roof flux in each group, divided by half the total dose rate and represents the roof current normalized to one mrem per hour.

10.2.2.1 Activity Calculations

The surface activities are summarized in Table 10-4.

10.2.2.2 Dose Rates

Dose rates are calculated for distances of 6.1 meters (20 feet) to 600 meters from the edges of the two ISFSI designs.

Neutron and gamma-ray sources are placed on each surface using the spectra and activities determined above. The angular distribution of source particles is modeled as a cosine distribution. The contribution of capture gamma-rays has been neglected, as has the contribution of bremsstrahlung electrons. The inclusion of coherent scattering greatly increases the variance in a problem with point detector tallies without improving the accuracy of the calculation. Thus, coherent scattering of photons is ignored.

For the 2x10 back-to-back array with end shield walls, the “box” dimensions are 1260 cm wide, 3129 cm long, and 564 cm high.

For the two 1x10 front-to-front arrays with end and back shield walls, the “box” dimensions for each array are 721 cm wide, 3129 cm long, and 564 cm high. The two 1x10 arrays are 1026 cm (34 feet) apart.

Point detectors are placed at the following locations as measured from each face of the “box”: 6.095 m (20 feet), 10 m, 20 m, 30 m, 40 m, 50 m, 60 m, 70 m, 80 m, 90 m, 100 m, 200 m, 300 m, 400 m, 500 m, and 600 m. Each point detector is placed 91.4 cm (3 feet) above the ground.

The MCNP results for each detector from the front of 2x10 back-to-back array are summarized in Table 10-5. The MCNP results as a function of distance from the back of the two 1x10 front-to-front arrays are summarized in Table 10-6. The MCNP results as a function of distance from the side of the 2x10 back-to-back array and the two 1x10 front-to-front arrays are summarized in Table 10-7.

The preceding analyses and results are intended to provide high estimates of dose rates for generic ISFSI layouts. The written evaluations performed by a licensee for an actual ISFSI must consider the type and number of storage units, layout, characteristics of the irradiated fuel to be stored, site characteristics (e.g., berms, distance to the controlled area boundary, etc.), and reactor operations at the site in order to demonstrate compliance with 10 CFR 72.104.

10.3 Estimated Onsite Collective Dose Assessment

This section provides estimates of occupational for typical ISFSI operations. Offsite dose rates for normal and anticipated conditions controlled by 10 CFR 72.104 are addressed in Section 10.2. Dose rates from accident conditions controlled by 10 CFR 72.106 are addressed in Chapters 5 and 11.

Assumed annual occupancy times, including the anticipated maximum total hours per year for any individual and total person-hours per year for all personnel for each radiation area during normal operation and anticipated operational occurrences will be evaluated by the licensee in a 10 CFR 72.212 evaluation to address the site specific ISFSI layout, inspection, and maintenance requirements. In addition, the estimated annual collective doses associated with loading operations will be addressed by the licensee in a 10 CFR 72.212 evaluation.

10.3.1 DSC Loading, Transfer and Storage Operations

The estimated occupational exposures to ISFSI personnel during loading, transfer, and storage of the DSC (time and manpower may vary depending on individual ISFSI practices) is shown in Table 10-1. The task times, number of personnel required and total doses are listed in this table. The total dose is estimated to be 2.2 rem per loaded canister. This is a bounding estimate; measured doses from Standardized NUHOMS[®] System loading campaigns have been 600 mrem or lower per canister for normal operations.

The average distance for a given operation takes into account that the operator may be in contact with the transfer cask, but this duration will be limited. For draining activities and vacuum drying the attachment of fittings will take place closer to the cask than the operation of the pumps. For decontamination activities, although operators could be near the cask for some activities, other parts of the operation could be performed from farther away. For this reason, 1 foot or 3 feet is an appropriate average distance for these operations.

The operator's hands may be in a high dose rate location momentarily, for example when connecting fittings at the ports. This does not translate into a whole-body dose, and therefore, these localized streaming effects are not considered here.

For operations near the top end of the 32PTH DSC, most of the work will take place around the perimeter and a smaller portion will take place directly over the shielded inner top cover.

Regulatory Guide 8.34 [7] is to be employed in defining the on-site occupational dose and monitoring requirements.

10.3.2 DSC Retrieval Operations

Occupational exposures to ISFSI personnel during 32PTH DSC retrieval are similar to those exposures calculated for 32PTH DSC insertion. Dose rates for retrieval operations will be lower than those for insertion operations due to radioactive decay of the spent fuel inside the HSM. Therefore, the dose rates for 32PTH DSC retrieval are bounded by the dose rates calculated for insertion.

10.3.3 Fuel Unloading Operations

The process of unloading the 32PTH DSC is similar to that used for loading the 32PTH DSC. The identical ALARA procedures utilized for loading should also be applied to unloading.

Occupational exposures to plant personnel are bounded by those exposures calculated for 32PTH DSC loading.

10.3.4 Maintenance Operations

The dose rate for surveillance activities is obtained from Table 10-5, Table 10-6, and Table 10-7 for dose rates 6.1 meters from the front of an HSM-H. The 6.1 meter dose rate is a conservative estimate for surveillance activities. The HSM-H surface dose rate provided in Chapter 5 is a conservative estimate for temperature sensor maintenance activities including calibration and repair. The surface dose rate calculated in Chapter 5 also provides a conservative estimate of a dose rate at 3 feet from the HSM-H which may be encountered during operations associated with removal of debris from HSM-H vents.

The ISFSI license applicant will evaluate the additional dose to station personnel from ISFSI operations, based on the particular storage configuration and site personnel requirements.

10.3.5 Doses During ISFSI Array Expansion

ISFSI expansion should be planned to eliminate the need for entry into a module adjacent to a loaded module. Similarly, during array expansion, when the shield wall is removed, personnel access to the area should be controlled. For a module separated from a loaded HSM-H by an empty module, with temporary shielding at the vent ports of the empty module, the resulting dose will be less than that calculated in Chapter 5 for the side dose rate of an array with an installed shield wall.

10.4 References

1. U.S. Nuclear Regulatory Commission, Regulatory Guide 8.8, Information Relevant to Ensuring That Occupational Exposures at Nuclear Power Stations will be As Low As Is Reasonably Achievable, Revision 3, June 1978.
2. MCNP4C2, Monte Carlo N-Particle Transport Code System, Oak Ridge National Laboratory, CCC-701, RSICC Computer Code Collection, June 2001.
3. U.S. Nuclear Regulatory Commission, Regulatory Guide 8.10, Operating Philosophy for Maintaining Occupational Radiation Exposures as low as is reasonably Achievable, Revision 1-R, May 1977.
4. U.S. Nuclear Regulatory Commission, Regulatory Guide 1.8, Qualification and Training of Personnel for Nuclear Power Plants, Revision 2, April 1987.
5. Title 10 Code of Federal Regulations Part 72, Licensing Requirements for the Independent Storage of Spent Nuclear Fuel and High-Level Radioactive Waste.
6. Title 10 Code of Federal Regulations Part 20, Standards for Protection Against Radiation.
7. U.S. Nuclear Regulatory Commission, Regulatory Guide 8.34, Monitoring Criteria and Methods to Calculate Occupational Radiation Doses, July 1992.
8. Title 40 Code of Federal Regulations Part 190, Environmental Radiation Protection Standards for Nuclear Power Operations.
9. American National Standard Neutron and Gamma-Ray Fluence-to-Dose Factors, ANSI/ANS-6.1.1-1977, American Nuclear Society, LaGrange Park, Illinois, March 1977.
10. US Nuclear Regulatory Commission Interim Staff Guidance ISG-18, The Design/Qualification of Final Closure Welds on Austenitic Stainless Steel Canisters as Confinement Boundary for Spent Fuel Storage and Containment Boundary for Spent Fuel Transportation.

Table 10-1
Occupational Exposure Summary, NUHOMS® HD System

Location	Task Description	Number of workers	Duration (hr)	Total exposure (person-mrem)	Fraction of the Total Time	Fraction of the Total Dose
Auxiliary Building and Fuel Pool	Place the DSC into the transfer cask	3	1	6	0.016	0.003
	Fill the cask/DSC annulus with clean water and Install the annulus seal	2	2	8	0.031	0.004
	Fill the DSC cavity with water	1	6	12	0.094	0.005
	Place the cask containing the DSC in the fuel pool	5	0.5	5	0.008	0.002
	Load the fuel assemblies into the DSC	3	5	39	0.102	0.018
	Place the inner top cover on the DSC	2	1	4	0.016	0.002
	Remove the cask/DSC from the fuel pool and place them in the decon area	5	0.5	5	0.008	0.002
		1	0.033	9(84)*	0.001	0.004
		1	1	119 (1140)*	0.016	0.053
Cask Decontamination Area	Decontaminate the outer surface of the transfer cask	1	1.75	208	0.028	0.093
		1	1	2	0.016	0.001
	Decontaminate the top region of the cask and DSC	2	0.5	457	0.008	0.205
		1	1	2	0.016	0.001
	Drain water from the DSC	1	0.083	21	0.001	0.009
	Remove cask/DSC annulus seal and set-up welding machine	1	0.25	51	0.004	0.023
		1	1.25	141	0.020	0.063
	Weld the inner top cover to the DSC shell and Perform NDE (PT)	1	1.5	3	0.024	0.001
		2	6	24	0.094	0.011
	Drain the cask/DSC annulus and the DSC cavity	1	0.5	57	0.008	0.026
		1	0.25	28	0.004	0.013
	Vacuum dry and backfill the DSC with helium	1	0.017	3	0.000	0.001
		1	0.5	1	0.008	0.000
	Weld vent and drain port covers and perform NDE (PT)	As above	0.78	33	0.012	0.015
		1	0.5	57	0.008	0.026
	Fit-up the DSC outer top cover plate	1	0.5	1	0.008	0.000
		1	0.5	57	0.008	0.026
Reactor/Fuel Building Bay	Weld the outer top cover plate to DSC shell and perform NDE (PT)	1	1.25	141	0.020	0.063
		1	1.5	3	0.024	0.001
	Install the transfer cask lid	2	14	56	0.220	0.025
		1	0.5	57	0.008	0.026
	Install the transfer cask lid	2	1	18	0.016	0.008
Reactor/Fuel Building Bay	Prepare the cask support skid and transport trailer	2	2	8	0.031	0.004
	Place the cask onto the skid and trailer	2	0.5	152 (1600)*	0.008	0.068
	Secure the cask to the skid	1	0.25	38 (400)*	0.004	0.017
ISFSI Site	Prepare the HSM-H and hydraulic ram	2	2	0	0.031	0.000
	Transport the Cask to ISFSI	6	1	0	0.016	0.000
	Position the Cask in Close Proximity with the HSM-H	3	1	0	0.016	0.000
	Remove the Cask Lid	2	1	68	0.016	0.031
	Align and Dock the Cask with the HSM-H	2	0.25	87	0.004	0.039
	Position and Align Ram with Cask	2	0.5	173	0.008	0.078
	Remove Ram Access Cover Plate	1	0.25	21	0.004	0.009
	Transfer the DSC from the Cask to the HSM-H	3	0.5	0	0.008	0.000
	Lift the Ram Back onto the Trailer and Un-Dock the Cask from the	2	0.083	29	0.001	0.013
	Install HSM-H Access Door	2	0.5	21	0.008	0.009
	Totals	N/A	63.5	2225	1	1

* Exposure if the transfer cask liquid neutron shield is drained. For this condition, the duration and number of workers should be minimized, the working distance from the cask increased and temporary shielding utilized as required to meet ALARA.

Table 10-2
Total Annual Exposure from 32PTH DSC in HSM-H

Two 1x10 Front To Front Array

Distance (meters)	Back Total Dose (mrem)	1 σ Uncertainty (mrem)	1 σ Relative Uncertainty
6.1	5850	13	0.002
10	4720	13	0.003
20	2970	10	0.003
30	2070	10	0.005
40	1510	8	0.005
50	1140	7	0.006
60	876	6	0.006
70	691	5	0.007
80	553	4	0.007
90	440	3	0.007
100	362	4	0.010
200	63	2	0.027
300	13	0.5	0.035
400	3.8	0.3	0.069
500	0.9	0.03	0.040
600	0.3	0.02	0.066

Distance (meters)	Side Total Dose (mrem)	1 σ Uncertainty (mrem)	1 σ Relative Uncertainty
6.1	21100	34	0.002
10	11600	25	0.002
20	4460	15	0.003
30	2530	14	0.005
40	1680	10	0.006
50	1210	10	0.008
60	889	7	0.007
70	691	6	0.009
80	543	6	0.012
90	434	6	0.013
100	348	5	0.014
200	56	1	0.022
300	13	1	0.050
400	3.1	0.2	0.061
500	0.7	0.04	0.049
600	0.2	0.01	0.031

2x10 Back To Back Array

Distance (meters)	Front Total Dose (mrem)	1 σ Uncertainty (mrem)	1 σ Relative Uncertainty
6.1	57900	46	0.001
10	35500	35	0.001
20	13800	21	0.002
30	7030	14	0.002
40	4210	11	0.003
50	2760	9	0.003
60	1910	7	0.004
70	1400	7	0.005
80	1039	5	0.005
90	812	5	0.006
100	623	4	0.006
200	89	1	0.013
300	18	0.4	0.020
400	4.4	0.1	0.026
500	1.3	0.1	0.052
600	0.4	0.03	0.062

Distance (meters)	Side Total Dose (mrem)	1 σ Uncertainty (mrem)	1 σ Relative Uncertainty
6.1	6080	14	0.002
10	4530	14	0.003
20	2710	13	0.005
30	1840	11	0.006
40	1340	8	0.006
50	1000	6	0.006
60	769	6	0.007
70	615	6	0.009
80	493	5	0.011
90	395	5	0.012
100	319	4	0.012
200	57	2	0.038
300	12	1	0.068
400	2.6	0.1	0.034
500	0.7	0.03	0.036
600	0.2	0.02	0.104

Table 10-3
NUHOMS[®] HD System, 32PTH DSC / HSM-H Spectra

Neutron

Group Number	E_{upper} (MeV)	E_{mean} (MeV)	Flux-Dose (Ref. [10]) (mR/hr)/(n/cm²-sec)	Roof Flux (n/cm²-sec)	Dose Rate (mR/hr)	Input Current (n/cm²-sec per mrem/hr)
1	1.00E-02	5.00E-03	3.575E-03	3.48E+02	1.24E+00	9.020E+01
2	1.00E-01	5.50E-02	3.675E-03	2.40E+01	8.83E-02	6.223E+00
3	2.50E-01	1.75E-01	3.598E-02	3.12E+00	1.12E-01	8.086E-01
4	5.00E-01	3.75E-01	7.146E-02	1.64E+00	1.17E-01	4.259E-01
5	1.00E+00	7.50E-01	1.137E-01	1.42E+00	1.61E-01	3.670E-01
6	1.50E+00	1.25E+00	1.299E-01	5.39E-01	7.00E-02	1.395E-01
7	2.00E+00	1.75E+00	1.275E-01	3.47E-01	4.42E-02	8.978E-02
8	4.00E+00	3.00E+00	1.326E-01	5.77E-01	7.64E-02	1.494E-01
9	6.00E+00	5.00E+00	1.562E-01	7.55E-02	1.18E-02	1.957E-02
10	1.00E+01	8.00E+00	1.471E-01	1.43E-02	2.10E-03	3.705E-03
11	1.50E+01	1.25E+01	1.853E-01	3.19E-03	5.92E-04	8.269E-04
12	2.00E+01	1.75E+01	2.200E-01	3.41E-03	7.51E-04	8.842E-04
Totals				3.80E+02	1.93E+00	98.4

Gamma

Group Number	E_{upper} (MeV)	E_{mean} (MeV)	Flux-Dose (Ref. [10]) (mR/hr)/(γ/cm²-sec)	Roof Flux (γ/cm²-sec)	Dose Rate (mR/hr)	Input Current (γ/cm²-sec per mrem/hr)
1	5.00E-02	2.50E-02	8.002E-04	3.60E+02	2.88E-01	1.292E+01
2	1.00E-01	7.50E-02	2.583E-04	1.73E+04	4.48E+00	6.230E+02
3	2.00E-01	1.50E-01	3.793E-04	1.16E+04	4.38E+00	4.150E+02
4	3.00E-01	2.50E-01	6.310E-04	3.21E+03	2.03E+00	1.153E+02
5	4.00E-01	3.50E-01	8.780E-04	1.28E+03	1.12E+00	4.583E+01
6	6.00E-01	5.00E-01	1.153E-03	7.21E+02	8.31E-01	2.590E+01
7	8.00E-01	7.00E-01	1.304E-03	2.33E+02	3.03E-01	8.355E+00
8	1.00E+00	9.00E-01	1.268E-03	1.46E+02	1.86E-01	5.260E+00
9	1.33E+00	1.17E+00	1.079E-03	1.75E+02	1.89E-01	6.297E+00
10	1.66E+00	1.50E+00	7.918E-04	1.20E+02	9.49E-02	4.304E+00
11	2.00E+00	1.83E+00	5.430E-04	2.05E+01	1.11E-02	7.358E-01
12	2.50E+00	2.25E+00	3.241E-04	2.77E+01	8.98E-03	9.946E-01
Totals				3.52E+04	1.39E+01	1263.9

Table 10-4
Summary of ISFSI Surface Activities, 32PTH DSC in HSM-H

2x10 Back-To-Back Array

Source	Area (cm²)	Neutron Activity (neutrons/sec)	Gamma-Ray Activity (γ/sec)
Roof	3.942E+06	7.490E+08	6.936E+10
Front 1	1.765E+06	8.598E+07	4.523E+10
Front 2	1.765E+06	8.598E+07	4.523E+10
Side 1	7.104E+05	1.294E+07	3.430E+08
Side 2	7.104E+05	1.294E+07	3.430E+08
Total	8.892E+06	9.468E+08	1.605E+11

Two 1x10 Front-to-Front Arrays

Source	Area (cm²)	Neutron Activity (neutrons/sec)	Gamma-Ray Activity (γ/sec)
Roof	2.257E+06	4.288E+08	3.971E+10
Front 1	1.765E+06	8.598E+07	4.523E+10
Front 2	1.765E+06	4.104E+05	1.079E+09
Side 1	4.068E+05	7.407E+06	1.964E+08
Side 2	4.068E+05	7.407E+06	1.964E+08
Total	6.600E+06	5.300E+08	8.641E+10

Table 10-5
MCNP Front Detector Dose Rates for 2x10 Array, 32PTH DSC in HSM-H

Distance (meters)	Gamma Dose Rate (mrem/hr)	Gamma MCNP 1 σ error ⁽¹⁾	Neutron Dose Rate (mrem/hr)	Neutron MCNP 1 σ error ⁽¹⁾	Total Dose Rate (mrem/hr) ⁽²⁾	Combined MCNP 1 σ error ⁽³⁾
6.10E+00	6.24E+00	8.00E-04	3.68E-01	4.10E-03	6.61E+00	0.0008
1.00E+01	3.79E+00	1.00E-03	2.57E-01	4.90E-03	4.05E+00	0.0010
2.00E+01	1.44E+00	1.50E-03	1.34E-01	7.30E-03	1.58E+00	0.0015
3.00E+01	7.17E-01	1.80E-03	8.53E-02	9.90E-03	8.02E-01	0.0019
4.00E+01	4.20E-01	2.20E-03	6.06E-02	1.41E-02	4.81E-01	0.0026
5.00E+01	2.71E-01	3.20E-03	4.32E-02	1.36E-02	3.15E-01	0.0033
6.00E+01	1.85E-01	3.10E-03	3.23E-02	1.59E-02	2.18E-01	0.0035
7.00E+01	1.35E-01	4.50E-03	2.53E-02	1.77E-02	1.60E-01	0.0047
8.00E+01	9.92E-02	4.10E-03	1.94E-02	1.83E-02	1.19E-01	0.0046
9.00E+01	7.63E-02	5.50E-03	1.64E-02	2.59E-02	9.27E-02	0.0064
1.00E+02	5.90E-02	5.90E-03	1.21E-02	2.16E-02	7.11E-02	0.0061
2.00E+02	8.25E-03	1.31E-02	1.86E-03	4.21E-02	1.01E-02	0.0132
3.00E+02	1.70E-03	2.21E-02	3.28E-04	4.42E-02	2.03E-03	0.0199
4.00E+02	4.18E-04	2.05E-02	8.92E-05	1.16E-01	5.07E-04	0.0265
5.00E+02	1.20E-04	5.38E-02	2.36E-05	1.61E-01	1.43E-04	0.0521
6.00E+02	3.88E-05	5.99E-02	9.45E-06	1.99E-01	4.83E-05	0.0620

(1) Fractional Error from MCNP

(2) Sum of columns 2 and 4

(3) Quadrature sum of columns 3 and 5 (weighted by means)

Table 10-6
MCNP Back Detector Dose Rates for the Two 1x10 Arrays, 32PTH DSC in HSM-H

Distance (meters)	Gamma Dose Rate (mrem/hr)	Gamma MCNP 1 σ error ⁽¹⁾	Neutron Dose Rate (mrem/hr)	Neutron MCNP 1 σ error ⁽¹⁾	Total Dose Rate (mrem/hr) ⁽²⁾	Combined MCNP 1 σ error ⁽³⁾
6.10E+00	5.13E-01	0.0019	1.55E-01	0.0074	6.67E-01	0.0022
1.00E+01	4.07E-01	0.0025	1.33E-01	0.0085	5.39E-01	0.0028
2.00E+01	2.49E-01	0.0029	9.08E-02	0.0093	3.39E-01	0.0033
3.00E+01	1.72E-01	0.0047	6.48E-02	0.0113	2.37E-01	0.0046
4.00E+01	1.24E-01	0.0046	4.86E-02	0.0138	1.72E-01	0.0051
5.00E+01	9.29E-02	0.0061	3.67E-02	0.0167	1.30E-01	0.0064
6.00E+01	7.10E-02	0.0058	2.90E-02	0.0173	1.00E-01	0.0065
7.00E+01	5.64E-02	0.0055	2.25E-02	0.0199	7.88E-02	0.0069
8.00E+01	4.47E-02	0.0061	1.85E-02	0.0198	6.32E-02	0.0072
9.00E+01	3.58E-02	0.0057	1.44E-02	0.0206	5.02E-02	0.0072
1.00E+02	2.95E-02	0.0099	1.18E-02	0.0238	4.13E-02	0.0098
2.00E+02	4.99E-03	0.0239	2.18E-03	0.0691	7.17E-03	0.0268
3.00E+02	1.10E-03	0.0355	4.18E-04	0.0860	1.52E-03	0.0350
4.00E+02	3.01E-04	0.0705	1.33E-04	0.1589	4.33E-04	0.0690
5.00E+02	7.80E-05	0.0469	2.01E-05	0.0726	9.82E-05	0.0402
6.00E+02	2.31E-05	0.0833	6.89E-06	0.0674	3.00E-05	0.0660

(1) Fractional Error from MCNP

(2) Sum of columns 2 and 4

(3) Quadrature sum of columns 3 and 5 (weighted by means)

Table 10-7
MCNP Side Detector Dose Rates, 32PTH DSC in HSM-H

2x10 Back-to-Back Array

Distance (meters)	Gamma Dose Rate (mrem/hr)	Gamma MCNP 1 σ error ⁽¹⁾	Neutron Dose Rate (mrem/hr)	Neutron MCNP 1 σ error ⁽¹⁾	Total Dose Rate (mrem/hr) ⁽²⁾	Combined MCNP 1 σ error ⁽³⁾
6.10E+00	4.96E-01	2.20E-03	1.97E-01	6.10E-03	6.94E-01	0.0023
1.00E+01	3.73E-01	3.20E-03	1.44E-01	7.50E-03	5.17E-01	0.0031
2.00E+01	2.21E-01	3.90E-03	8.80E-02	1.32E-02	3.09E-01	0.0047
3.00E+01	1.50E-01	5.50E-03	5.97E-02	1.49E-02	2.10E-01	0.0058
4.00E+01	1.09E-01	5.90E-03	4.37E-02	1.49E-02	1.53E-01	0.0060
5.00E+01	8.12E-02	6.30E-03	3.31E-02	1.62E-02	1.14E-01	0.0065
6.00E+01	6.31E-02	7.50E-03	2.47E-02	1.73E-02	8.77E-02	0.0073
7.00E+01	5.00E-02	8.50E-03	2.02E-02	2.53E-02	7.02E-02	0.0095
8.00E+01	4.01E-02	1.14E-02	1.62E-02	2.40E-02	5.63E-02	0.0107
9.00E+01	3.24E-02	1.30E-02	1.27E-02	2.52E-02	4.51E-02	0.0117
1.00E+02	2.59E-02	8.20E-03	1.05E-02	3.60E-02	3.64E-02	0.0119
2.00E+02	4.46E-03	2.24E-02	2.09E-03	1.08E-01	6.55E-03	0.0378
3.00E+02	9.34E-04	2.84E-02	4.03E-04	2.16E-01	1.34E-03	0.0680
4.00E+02	2.22E-04	4.09E-02	7.07E-05	6.02E-02	2.92E-04	0.0343
5.00E+02	5.89E-05	3.50E-02	2.03E-05	9.88E-02	7.92E-05	0.0363
6.00E+02	1.91E-05	1.34E-01	6.41E-06	1.07E-01	2.55E-05	0.1039

Two 1x10 Front-To-Front Arrays

Distance (meters)	Gamma Dose Rate (mrem/hr)	Gamma MCNP 1 σ error ⁽¹⁾	Neutron Dose Rate (mrem/hr)	Neutron MCNP 1 σ error ⁽¹⁾	Total Dose Rate (mrem/hr) ⁽²⁾	Combined MCNP 1 σ error ⁽³⁾
6.10E+00	2.18E+00	1.60E-03	2.32E-01	6.80E-03	2.41E+00	0.0016
1.00E+01	1.16E+00	2.00E-03	1.70E-01	9.50E-03	1.33E+00	0.0021
2.00E+01	4.13E-01	3.30E-03	9.68E-02	1.11E-02	5.10E-01	0.0034
3.00E+01	2.24E-01	5.60E-03	6.51E-02	1.45E-02	2.89E-01	0.0054
4.00E+01	1.43E-01	5.00E-03	4.90E-02	1.92E-02	1.92E-01	0.0062
5.00E+01	1.01E-01	7.10E-03	3.68E-02	2.43E-02	1.38E-01	0.0083
6.00E+01	7.42E-02	7.30E-03	2.73E-02	1.88E-02	1.02E-01	0.0074
7.00E+01	5.68E-02	7.80E-03	2.21E-02	2.65E-02	7.89E-02	0.0093
8.00E+01	4.49E-02	1.21E-02	1.71E-02	2.89E-02	6.19E-02	0.0118
9.00E+01	3.55E-02	1.29E-02	1.40E-02	3.27E-02	4.96E-02	0.0131
1.00E+02	2.81E-02	9.10E-03	1.17E-02	4.22E-02	3.98E-02	0.0139
2.00E+02	4.36E-03	1.34E-02	2.04E-03	6.41E-02	6.40E-03	0.0224
3.00E+02	9.96E-04	3.71E-02	4.41E-04	1.41E-01	1.44E-03	0.0504
4.00E+02	2.69E-04	6.74E-02	8.04E-05	1.35E-01	3.50E-04	0.0605
5.00E+02	6.37E-05	6.20E-02	1.92E-05	5.53E-02	8.29E-05	0.0493
6.00E+02	1.71E-05	3.27E-02	6.16E-06	7.19E-02	2.32E-05	0.0307

(1) Fractional error from MCNP

(2) Sum of columns 2 and 4

(3) Quadrature sum of columns 3 and 5 (weighted by means)

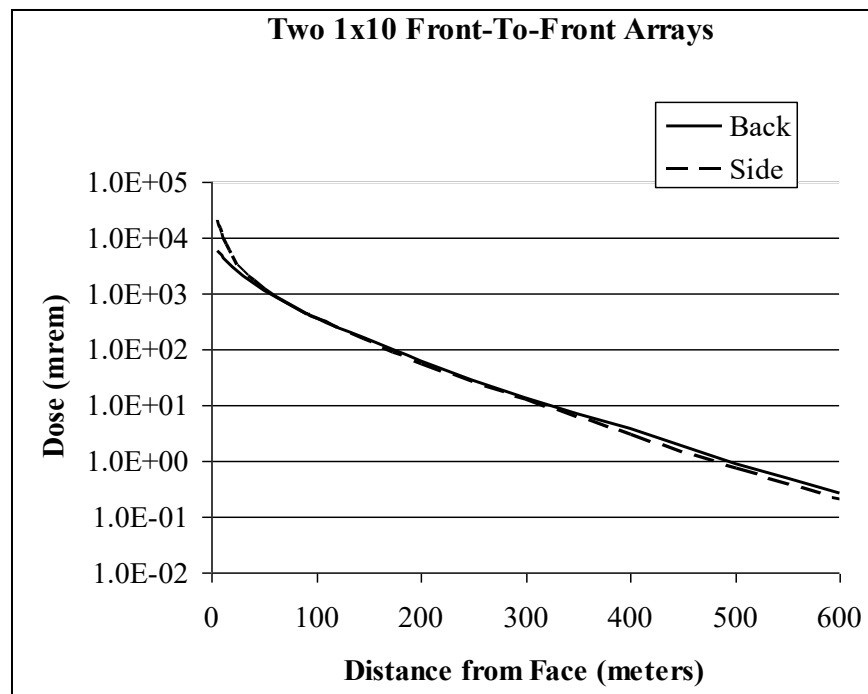
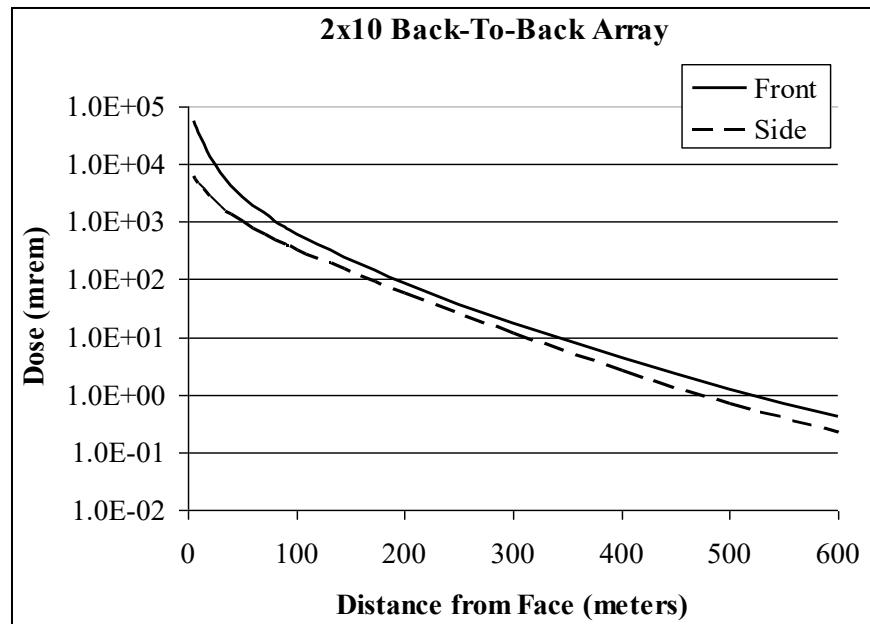


Figure 10-1
Annual Exposure from the ISFSI as a Function of Distance, 32PTH DSC in HSM-H

CHAPTER 11 ACCIDENT ANALYSIS

TABLE OF CONTENTS

11. ACCIDENT ANALYSIS	11-1
11.1 Introduction.....	11-1
11.2 Off-Normal Operation.....	11-2
11.2.1 Off-Normal Transfer Load.....	11-3
11.2.2 Extreme Temperature.....	11-5
11.2.3 Radiological Impact from Off-Normal Operations.....	11-6
11.3 Postulated Accident	11-7
11.3.1 Cask Drop	11-8
11.3.2 Earthquake	11-10
11.3.3 Tornado Wind and Tornado Missiles Effect on HSM-H.....	11-11
11.3.4 Tornado Wind and Tornado Missiles Effect on Transfer Cask	11-18
11.3.5 Flood	11-25
11.3.6 Blockage of HSM-H Air Inlet and Outlet Openings	11-25
11.3.7 Lightning.....	11-26
11.3.8 Fire/Explosion.....	11-27
11.4 References	11-28

LIST OF FIGURES

Figure 11-1 HSM-H Dimensions for Missile Impact Stability Analysis	11-29
--	-------

11. ACCIDENT ANALYSIS

The applicability of these analyses to the 32PTH Type 1 DSC and OS187H Type 1 TC described in Appendix A are discussed in Appendix A, Chapter A.11, and the applicability of these analyses to the 32PTH Type 2 DSC and OS187H Type 2 TC described in Appendix B are discussed in Appendix B, Chapter B.11, including additional evaluations specific to the OS187H Type 1 TC.

11.1 Introduction

This Chapter describes the postulated off-normal and accident events that might occur during transfer/storage of the 32PTH DSC in an HSM-H at an ISFSI. In addition, this chapter also addresses the potential causes of these events, their detection and consequences, and the corrective course of action to be taken by ISFSI personnel. Accident analyses demonstrate that the functional integrity of the system is maintained by:

1. Maintaining sub-criticality within margins defined in Chapter 6.
2. Maintaining confinement boundary integrity
3. Ensuring fuel retrievability and
4. Maintaining doses within 10CFR 72.106 [1] limits (<5 rem).

The Accident Dose Calculations sections report the expected doses resulting from the postulated event in terms of whole body doses only. The leaktight canister design and the maintenance of confinement boundary integrity under all credible off-normal and accident scenarios ensures no radiation leakage from the 32PTH DSC, thereby limiting dose consequences to direct and scattered radiation doses without any associated inhalation or ingestion doses.

11.2 Off-Normal Operation

Off-normal operations are design events of the second type (Design Event II) as defined in ANSI/ANS 57.9 [2]. Design Event II conditions consist of that set of events that, although not occurring regularly, can be expected to occur with moderate frequency, or on the order of once during a calendar year of ISFSI operation.

For the NUHOMS[®] HD System, off-normal events could occur during fuel loading, trailer towing, 32PTH DSC transfer and other operational events. The two off-normal events, which bound the range of off-normal conditions, are:

1. A “jammed” 32PTH DSC during loading or unloading from the HSM-H
2. The extreme ambient temperatures of -20 °F (winter) and +115 °F (summer)**

These two events envelope the range of expected off-normal structural loads and temperatures acting on the NUHOMS[®] HD System.

** The HSM-H structural evaluation is conservative using an extreme ambient temperature of -40 °F (winter) and +117 °F (summer)

11.2.1 Off-Normal Transfer Load

Although unlikely, the postulated off-normal handling event assumes that the leading edge of the 32PTH DSC becomes jammed against some element of the support structure during transfer between the transfer cask and the HSM-H.

Cause of the Event

It is postulated that if the transfer cask is not accurately aligned with respect to the HSM-H, the 32PTH DSC could bind or jam during transfer operations.

The interiors of the transfer cask and the HSM-H are inspected prior to transfer operations to ensure there are no obstacles, and the 32PTH DSC has beveled lead-ins on each end, designed to avoid binding or sticking on small (less than 1/4 inch) obstacles. The transfer cask and the 32PTH DSC support rails inside the HSM-H are also designed with lead-ins to minimize binding or obstruction during 32PTH DSC transfer. The postulated off-normal handling load event assumes that the leading edge of the 32PTH DSC becomes jammed against some element of the support structure because of gross misalignment of the transfer cask.

The interfacing dimensions of the top end of the transfer cask and the HSM-H access opening sleeve are specified such that docking of the transfer cask with the HSM-H is not possible should gross misalignments between the transfer cask and HSM-H exist.

Detection of the Event

The normal load to push/pull the DSC in and out of the Transfer Cask/HSM-H is less than 32 kips ($110 \text{ kips} \times 0.2/\cos 30$). This movement is performed at a very low speed. System operating procedures and technical specification limits defining the safeguards to be provided ensure that the system design margins are not compromised. If the 32PTH DSC were to jam or bind during transfer, the hydraulic pressure in the ram would increase. The off-normal load set for the “jammed 32PTH DSC” for both push/pull is 80 kips. This load is administrative controlled to ensure that during the transfer operation this load will not be exceeded.

NOTE: Even though the DSC and HSM are designed and analyzed for off-normal transfer loads of 80 kips, the DSC is conservatively analyzed for accident transfer loads of 110 kips.

During the transfer operation, the force exerted on the 32PTH DSC by the hydraulic ram is that required to first overcome the static frictional resisting force between the transfer cask rails and the 32PTH DSC. Once the 32PTH DSC begins to slide, the resisting force is a function of the sliding friction coefficient between the 32PTH DSC and the transfer cask rails and/or between the 32PTH-DSC and the HSM-H support rails. If motion is prevented, the hydraulic pressure increases, thereby increasing the force on the 32PTH DSC until the hydraulic ram system pressure limit is reached. This limit is controlled so that adequate force is available to overcome variations in surface finish, etc., but is sufficiently low to ensure that component damage does not occur.

Analysis of Effects and Consequences

The 32PTH DSC and the HSM-H are designed and analyzed for off-normal transfer loads of 80 kips during insertion (loading) and during retrieval (unloading) operations. These analyses are discussed in Chapter 3, Appendix 3.9.1, Load Cases 21 & 22 for off-normal conditions. For either loading or unloading of the 32PTH DSC under off-normal conditions, the stresses on the shell assembly components are demonstrated to be within the ASME allowable stress limits. Therefore, permanent deformation of the 32PTH DSC shell components does not occur. The internal basket assembly components are unaffected by these loads based on clearances provided between support rods and 32PTH DSC internal envelope.

There is no breach of the confinement pressure boundary and, therefore, no potential for release of radioactive material exists.

Corrective Actions

The required corrective action is to reverse the direction of the force being applied to the 32PTH DSC by the ram, and return the 32PTH DSC to its previous position. Since no permanent deformation of the 32PTH DSC occurs, the sliding of the 32PTH DSC back to its previous position is unimpeded. The transfer cask alignment is then rechecked, and the transfer cask repositioned as necessary before attempts at transfer are renewed.

11.2.2 Extreme Temperature

The NUHOMS® HD System is designed for use at ambient temperatures of -20°F (winter) and 115°F (summer). The structural evaluation of the HSM-H concrete module is conservatively based on ambient temperatures of -40°F (winter) and 117°F (summer). Even though these extreme temperatures would likely occur for a short period of time, it is conservatively assumed that these temperatures occur for a sufficient duration to produce steady state temperature distributions in each of the affected NUHOMS® components. Each licensee should verify that this range of ambient temperatures envelopes the design basis ambient temperatures for the ISFSI site. The NUHOMS® HD system components affected by the postulated extreme ambient temperatures are the transfer cask and DSC during their transfer from the plant's fuel/reactor building to the ISFSI site, and the HSM-H during storage of a DSC.

Cause of the Event

Off-normal ambient temperatures are natural phenomena.

Detection of Event

Off-normal ambient temperature conditions will be confirmed by the licensee to be bounding for their site.

Analysis of Effects and Consequences

Thermal analysis of the Advanced NUHOMS® System for extreme ambient conditions is presented in Chapter 4. The effects of extreme ambient temperatures on the NUHOMS® HD System are analyzed as follows:

Components	SAR Sections
Basket	Appendix 3.9.1, Section 3.9.1.2.3
Canister	Appendix 3.9.1, Load Cases 4 & 5
Transfer Cask	Appendix 3.9.2, Load Cases 4 & 5
HSM-H	Appendix 3.9.9, Section 3.9.9.9

Corrective Actions

None

11.2.3 Radiological Impact from Off-Normal Operations

For loading and unloading operations under off-normal conditions, the stresses on the 32PTH DSC shell assembly components are demonstrated to be within the ASME Code stress limits. Therefore, there is no permanent deformation of the shell. Since there is no potential for breach of the confinement pressure boundary, there is no potential for release of radioactive material.

The 32PTH DSC shell assembly stresses due to extreme ambient temperature conditions are also demonstrated to be less than the ASME Code stress limits as shown in Chapter 3, Appendix 3.9.1. The HSM-H stresses due to extreme ambient temperature conditions are within the provisions of the ACI Code (Appendix 3.9.9). Therefore, no damage will occur in the shell assembly or the HSM-H. There is no potential for breach of the confinement boundary and therefore, no potential for release of radioactive material.

11.3 Postulated Accident

The design basis accident events specified by ANSI/ANS 57.9-1984 [2] and other postulated accidents that may affect the normal safe operation of the NUHOMS[®] HD System are addressed in this section.

The following sections provide descriptions of the analyses performed for each accident condition. The analyses demonstrate that the requirements of 10CFR 72.122 are met and that adequate safety margins exist for the NUHOMS[®] HD System design. The resulting accident condition stresses in the NUHOMS[®] HD System components are evaluated and compared with the applicable code limits set forth in Chapter 2.

Radiological calculations are performed to confirm that on-site and off-site dose rates are within acceptable limits.

The postulated accident conditions addressed in this section include:

- Cask Drop
- Earthquake
- Tornado Wind Pressure and Tornado Generated Missiles
- Flood
- Blockage of HSM-H Air Inlet and Outlet Openings
- Lightning
- Fire/Explosion

11.3.1 Cask Drop

Cause of Accident

As described in Chapter 8, handling operations involving hoisting and movement of the on-site transfer cask and 32PTH DSC are typically performed inside the plant's fuel handling building. These include utilizing the crane for placement of the empty 32PTH DSC into the transfer cask cavity, lifting the transfer cask/32PTH DSC into and out of the plant's spent fuel pool, and placement of the transfer cask/32PTH DSC onto the transport skid/trailer. An analysis of the plant's lifting devices used for these operations, including the crane and lifting yoke, is needed to address a postulated drop accident for the transfer cask and its contents. The postulated drop accident scenarios addressed in the plant's 10CFR 50 licensing basis are plant specific and should be addressed by the licensee.

Once the transfer cask is loaded onto the transport skid/trailer and secured, it is pulled to the HSM-H site by a tractor vehicle. A predetermined route is chosen to minimize the potential hazards that could occur during transport. This movement is performed at very low speeds. System operating procedures and technical specification limits defining the safeguards to be provided ensure that the system design margins are not compromised. As a result, it is highly unlikely that any plausible incidents leading to a transfer cask drop accident could occur. Similarly, at the ISFSI site, the transport skid/trailer is backed-up to, and aligned with, the HSM-H using hydraulic positioning equipment. The transfer cask is then docked with, and secured to, the HSM-H access opening. The loaded 32PTH DSC is transferred to or from the HSM-H using a hydraulic ram system. The bolts that secure the transfer skid to the transfer trailer remain in place at all times during the 32PT DSC transfer. The transfer cask is secured to the transfer skid by the trunnion towers, whose pockets are deeper than the trunnion diameter. As a result, there is no reasonable way during these operations for a cask drop accident to occur.

Lifts of the transfer cask loaded with the dry storage canister are made within the existing heavy loads requirements and procedures of the licensed nuclear power plant. The transfer cask design meets requirements of NUREG-0612 and ANSI N14.6.

The transfer cask is transported to the ISFAI in a horizontal configuration. Therefore, the only credible drop accident during storage or transfer operations is a side drop.

The transfer cask and dry storage canister are evaluated for a postulated end and corner drops to demonstrate structural integrity during transport and plant handling. However, the fuel cladding structural integrity has not been demonstrated for these scenarios. Therefore, the user is required to demonstrate fuel cladding structural integrity under 10CFR50 postulated drop accidents or demonstrate that the drop accidents are not credible.

Accident Analysis

The stress analyses are performed in Chapter 3, Appendix 3.9.1 for 32PTH DSC and Appendix 3.9.2 for the Transfer Cask.

Components	SAR Sections
Basket	Appendix 3.9.1, Section 3.9.1.2.3
Canister	Appendix 3.9.1, Load Cases 6 through 17
Transfer Cask	Appendix 3.9.2, Load Cases 7 through 9
Fuel Cladding	Section 3.5.3, Appendix 3.9.8

Accident Dose Calculation

Based on analysis results presented in Appendix 3.9.1 and Appendix 3.9.2, the accidental transfer cask drop scenarios do not breach the transfer cask/32PTH DSC confinement boundaries. The function of transfer cask lead shielding is not compromised by these drops. The transfer cask neutron shield, however, may be damaged in an accidental drop.

The transfer cask surface dose rate, with the neutron shield intact for the 32PTH DSC in the transfer cask is calculated in Chapter 5 of this SAR as 384 mrem/hr gamma and 125 mrem/hr neutron.

The dose rate at the transfer cask surface due to the loss of the neutron shield is also calculated; at 1 meter from the cask, the peak dose is 186 mrem/hr gamma and 2200 mrem/hr neutron. *Table 5-23 provides a dose rate at 100 meters from the cask of 0.1 mrem/hr gamma and 1.2 mrem/hr neutron for the accident condition. For a duration of 8 hours, this corresponds to a received exposure of less than 10.4 mrem at 100 meters and this meets the acceptance criteria of 5 rem.*

Corrective Actions

The DSC will be inspected for damage, and the DSC opened and the fuel removed for inspection, as necessary. Removal of the transfer cask top cover plate may require cutting of the bolts in the event of a corner drop onto the top end. These operations will take place in the plant fuel building decontamination area and spent fuel pool after recovery of the transfer cask.

Following recovery of the transfer cask and unloading of the DSC, the transfer cask will be inspected, repaired and tested as appropriate prior to reuse.

For recovery of the cask and contents, it may be necessary to develop a special sling/lifting apparatus to move the transfer cask from the drop site to the fuel pool. This may require several weeks of planning to ensure all steps are correctly organized. During this time, lead blankets may be added to the transfer cask to minimize on-site exposure to site operations personnel. The transfer cask would be roped off to ensure the safety of the site personnel.

11.3.2 Earthquake

Cause of Accident

The seismic design criteria for the NUHOMS[®] HD System is consistent with the criteria set forth in Chapter 2, Section 2.2.3, with the exception that the NRC Regulatory Guide 1.60 (R.G. 1.60) [3] response spectra is anchored to a maximum ground acceleration of 0.30g (instead of 0.25g) for the horizontal components and 0.20g (instead of 0.17g) for the vertical component. The results of the frequency analysis of the HSM-H structure (which includes a simplified model of the DSC) yield a lowest frequency of 23.2 Hz in the transverse direction and 28.4 Hz in the longitudinal direction. The lowest vertical frequency exceeds 33 Hz. Thus, based on the R.G. 1.60 response spectra amplifications, the corresponding seismic accelerations used for the design of the HSM-H are 0.37g and 0.33g in the transverse and longitudinal directions respectively and 0.20g in the vertical direction. The corresponding accelerations applicable to the DSC are 0.41g and 0.36g in the transverse and longitudinal directions, respectively, and 0.20g in the vertical direction.

Accident Analysis

The seismic analyses of the components which are important to safety are analyzed as follows:

Components	SAR Sections
Basket	Appendix 3.9.1, Section 3.9.1.2.3
Canister	Appendix 3.9.1, Section 3.9.1.3.2
Transfer Cask	Appendix 3.9.2, Load Case 6
HSM-H	Appendix 3.9.9, Section 3.9.9.2

The results of these analyses show that seismic stresses are well below ASME code allowables.

Accident Dose Calculations

All the components which are important to safety are designed and analyzed to withstand the design basis earthquake accident. Hence, no radiation is released and there is no associated dose increase due to this event.

Corrective Actions

After a seismic event, all components would be inspected for damage. Any debris would be removed. An evaluation would be performed to determine if the system components were still within the licensed design basis.

11.3.3 Tornado Wind and Tornado Missiles Effect on HSM-H

11.3.3.1 Cause of Accident

In accordance with ANSI-57.9 [2] and 10CFR 72.122 [1], the NUHOMS® HD System is designed for tornado effects including tornado wind loads. In addition, the NUHOMS® HD System is also designed for tornado missile effects. The NUHOMS® HD System is designed to be located anywhere within the United States; therefore, the most severe tornado wind and missile loadings specified by NUREG-0800 [4] and NRC Regulatory Guide 1.76 [5] are selected as a design basis for this postulated accident. The determination of the tornado wind pressures and tornado missile loads acting on the NUHOMS® HD System are detailed in Chapter 2, Section 2.2.1.

11.3.3.2 Stability and Stress Analysis

Stability and stress analyses are performed to determine the response of the HSM-H to tornado wind pressure loads. The stability analyses are performed using closed-form calculation methods to determine the sliding and overturning response of the HSM-H array. A single HSM-H with both the end and the rear shield walls is conservatively selected for the analyses. The stress analyses are performed using the ANSYS [6] finite element model of a single HSM-H to determine design forces and moments. These conservative generic analyses envelop the effects of wind pressures on the HSM-H array. These analyses are described in details in Appendix 3.9.9, Section 3.9.9.10.1. Thus, the requirements of 10CFR 72.122 are met.

In addition, the HSM-H is evaluated for tornado missiles. The adequacy of the HSM-H to resist tornado missile loads is addressed using empirical formulae [7]. These evaluations are described in the following sections.

11.3.3.3 Local Damage Evaluation

Local missile impact effects consist of (a) missile penetration into the target, (b) missile perforation through the target and (c) spalling and scabbing of the target. This also includes punching shear in the region of the target. As per the ACI code [8] if the concrete thickness is at least 20% greater than that required to prevent perforation, the punching shear requirement of the code need not be checked. Several empirical formulas are available and are used to predict local damage effects.

The following enveloping missiles (based on the mass of the missile) are considered for local damage:

- Utility pole
- Armor piercing artillery shell
- 12" diameter steel pipe missile
- Large deformable missiles such as automobiles do not penetrate the structure. Therefore, the local effects from an automobile are evaluated using punching shear criteria of the ACI Code [8].

The following empirical formulas are used to determine the local damage effects:

Reinforced Concrete Target

A. Modified National Defense Research Committee (NDRC) formulas for penetration depth [7]:

$$X = [4KNWd^{-0.8}(v_o/1000d)^{1.8}]^{0.5} \quad \text{for } x/d \leq 2.0$$

$$X = \{[KNW (v_o/1000d)^{1.8}] + d\} \quad \text{for } x/d > 2.0$$

where,

x = Missile penetration depth, inches

K = concrete penetrability factor = $180/\sqrt{f_c}$

N = projectile shape factor

= 0.72 flat nosed

= 0.84 blunt nosed

= 1.0 bullet nosed (spherical end)

= 1.14 very sharp nose

W = weight of missile, lbs

v_o = striking velocity of missile, fps

d = effective projectile diameter, inches.

for a solid cylinder, d = diameter of projectile and

for a non-solid cylinder, $d = (4A_c/\pi)^{1/2}$

A_c = projectile impact area, in²

B. Modified NDRC formula for perforation thickness [7]:

$$(e/d) = 3.19(x/d) - 0.718(x/d)^2 \quad \text{for } x/d \leq 1.35$$

$$(e/d) = 1.32 + 1.24 (x/d) \quad \text{for } 1.35 \leq x/d \leq 13.5$$

where

e = perforation thickness, in.

In order to provide an adequate margin of safety, the design thickness $t_d = 1.2 e$ [8]

C. Modified NDRC formula for scabbing thickness [7]:

$$(s/d) = 7.91(x/d) - 5.06(x/d)^2 \quad \text{for } x/d \leq 0.65$$

$$(s/d) = 2.12 + 1.36 (x/d) \quad \text{for } 0.65 \leq x/d \leq 11.75$$

where

s = scabbing thickness, in.

In order to provide an adequate margin of safety, the design thickness $t_d = 1.2 s$ [8]

The concrete targets of the HSM-H which may be subjected to local damage due to missile impact are:

- 44” thick roof
- 42” thick (minimum) front wall
- 36” thick end shield wall with 12” thick side wall (No gap between shield wall and side wall)
- 36” thick rear shield wall with 12” thick (minimum) rear wall
- 36” thick end shield wall at the side of the roof (with vent opening) and at the bottom with 6” gap between the shield wall and the side wall.
- 30.375” thick composite shielding door (7.875” steel in front, 22.5” concrete at rear)

The missile evaluations of the shielded composite door, presented in this section, require a minimum steel thickness of 1.45”. Therefore, the shielded door evaluations remain applicable for the optional door with reduced steel thickness.

Steel Targets

The steel barriers subjected to missile impact are designed to preclude perforation. The steel plate thickness for threshold of perforation is [9]:

$$T_p = (E_k)^{2/3} / 672D$$

Where:

$$E_k = M_m v_o^2 / 2$$

$$T_p = \text{steel plate thickness for threshold of perforation (in)}$$

$$E_k = \text{missile kinetic energy (ft-lbs)}$$

$$M_m = \text{mass of the missile (lb-sec}^2 \text{ /ft)}$$

$$v_o = \text{missile striking velocity (fps)}$$

$$D = \text{missile diameter (in), for pipe missiles, D is the outside diameter of the pipe}$$

The design thickness to prevent perforation is $t_p = 1.25 T_p$ [9].

The steel target of the HSM-H which may be subjected to local damage due to missile impact is the composite steel door (7.875” steel in front).

A. Local Missile Impact Effects of Utility Pole Missile

The wood missiles (utility pole missile) do not have sufficient strength to penetrate a concrete target and the scabbing thickness required for wood missiles is substantially less than that required for a steel missile with the same mass and velocity. Practical wooden pole missiles are not capable of causing local damage to walls 12 inches thick, or greater for the missile velocities considered. Because none of the concrete targets are less than 12 inch thick, the postulated wood missiles will not cause any local damage to the HSM-H concrete structure. Steel targets are also resistant to penetration which implies that only nondeformable missiles can perforate a steel target.

B. Local Missile Impact Effects of Armor Piercing Artillery Shell

Concrete Wall Evaluation:

$$\begin{aligned}
 d &= \text{diameter of missile} = 8'' \\
 W &= 280 \text{ lbs (conservatively assumed)} \\
 V_o &= 185 \text{ fps} \\
 f_c' &= 5000 \text{ psi} \\
 K &= 180/\sqrt{5000} = 2.55 \\
 N &= 0.84 \text{ blunt nosed}
 \end{aligned}$$

$$\begin{aligned}
 \text{Penetration thickness} \quad x &= 4.67 \text{ in for } x/d = 0.584 \leq 2 \\
 \text{Perforation thickness} \quad e &= 12.95'' \\
 \text{Required Perforation thickness} &= 1.2 * 12.95 = 15.5'' \\
 \text{Scabbing thickness} \quad s &= 23.1'' \text{ inches} \\
 \text{Required scabbing thickness} &= 1.2 * 23.2 = 27.7''
 \end{aligned}$$

Shielded Door Evaluation:

Required perforation thickness of steel is 0.66'' which is less than 7.875''. Therefore, the missile will not perforate the steel in the shielded door.

C. Local Missile Impact Effects of 12 Inch Diameter Steel Pipe Missile

Concrete Wall Evaluation:

$$\begin{aligned}
 \text{Diameter of missile} &= 12.75'' \text{ (Outer diameter of 12'' dia Sch 40 pipe)} \\
 \text{Contact surface area} &= A_c = 15.7 \text{ in}^2 \text{ (cross section metal area of 12'' dia Sch 40 pipe)} \\
 \text{Effective diameter} &= d = (4 * 15.7 / \pi)^{1/2} = 4.47 \text{ inches}
 \end{aligned}$$

$$\begin{aligned}
 W &= 1500 \text{ lbs} \\
 v_o &= 205 \text{ fps} \\
 f_c' &= 5000 \text{ psi} \\
 K &= 180/\sqrt{5000} = 2.55 \\
 N &= 0.72 \text{ flat nosed}
 \end{aligned}$$

$$\begin{aligned}
 \text{Perforation thickness} \quad x &= 15.2 \text{ in for } x/d > 2 \\
 \text{Perforation thickness} \quad e &= 24.75 \text{ in} \\
 \text{Required perforation thickness} &= 1.2 * 24.75 = 29.7'' \\
 \text{Scabbing thickness} \quad s &= 30.15 \text{ inches} \\
 \text{Required scabbing thickness} &= 1.2 * 30.15 = 36.2 \text{ inches}
 \end{aligned}$$

The roof (44'' thick), front wall (42'' thick) and the shield walls (36'' thick) will not be perforated. However, the missile may produce scabbing in the end shield wall above the side walls and lower 40'' of the end shield wall. Assuming some scabbed concrete from the end

shield will fall into the vent openings, it will not cause any problem in the safe retrieval of the DSC from the module.

Composite Shield Door Evaluation

$$M_m = 1500/32.2 = 46.6 \text{ lb-sec}^2/\text{ft}$$

$$v_s = 205 \text{ fps}$$

$$E_k = 46.6 * 205 * 205 / 2 = 979182$$

$$D = 12.75 \text{ in}$$

$$T_p = (979182)^{2/3} / (672 * 12.75) = 1.16 \text{ inches}$$

$$\text{The required thickness} = 1.25 T_p = 1.25 * 1.16 = 1.45 \text{ inches}$$

The composite shield door will not be perforated by this missile.

11.3.3.4 Missile Impact Analysis

The HSM-H stability and potential damage due to impact of the postulated DBT massive missile consisting of a 4000 lb. automobile, 20 sq. ft. frontal area traveling at 195 ft/sec., is evaluated. The massive missile is assumed to impact the shield wall of an end module in an array. Using the principles of conservation of momentum with a coefficient of restitution of zero, the analysis presented below demonstrates that the end module remains stable and the missile energy is dissipated by sliding or slight tipping of the module.

Using conservation of momentum, the missile impact force equals the change in linear (sliding) or angular (overturning) momentum of the HSM-H. The HSM-H velocities immediately after impact are:

$$\text{Sliding: } V = (m * v_i) / (M + m) \quad (\text{Eq. 11.3-1})$$

$$\text{Overturning: } \omega_b = (m * d_m * v_i) / (m * d_m^2 + I_B) \quad (\text{Eq. 11.3-2})$$

Where,

V = initial linear velocity of module after impact

v_i = 195 ft/sec = initial velocity of missile (conservative)

ω_B = initial rotational velocity about bottom right corner of the module and end shield walls (Figure 11-1)

d_m = Vertical distance of the CG of the missile from B (Figure 11-1) = 198 inches

m = $4000/386.4 = 10.35 \text{ lb-sec}^2/\text{in}$ = mass of the missile

M = $(290.0 + 110 + 2 * 172.0) * 1000 / 386.4 = 1925.5 \text{ lb-sec}^2/\text{in}$ = Mass of loaded HSM-H + End Shield walls

d = 118.77, Elevation of the CG of the loaded HSM-H

I_B = Mass moment of inertia of loaded HSM-H about point B (Figure 11-1)
= $3.85 \times 10^7 \text{ lb-sec}^2\text{-in}$ (conservatively used)

Sliding:

From Eq. 11.3-1: $V = 12.51 \text{ in/sec} = 1.043 \text{ ft/sec}$

For an impact at the bottom of the HSM-H wall, the kinetic energy imparted to the HSM-H is absorbed by sliding friction between the concrete of the HSM-H and the basemat. Coefficient of friction is 0.6 [8].

Assuming that the missile impact load results in sliding of the HSM-H and equating the kinetic energy generated by the moving module to the work done by sliding friction force gives:

$$\mu * g * (M+m) * \Delta = (M+m)*V^2/2$$

$$\Delta = 0.0281 \text{ ft} = 0.34 \text{ inch}$$

Therefore, a massive missile impact on a single HSM-H will slide the complete module approximately 0.34 inches sideways. The sliding distance will be significantly reduced due to presence of more than one module side by side.

Therefore, the sliding displacement of the modules due to a massive missile impact is insignificant and will not cause any structural damage.

Overtipping:

When the massive missile impacts at the top of the HSM-H, the missile energy is absorbed by plastic deformation of the missile and in rotation of the HSM-H. Therefore, equating the loss of kinetic energy to increase in the potential energy:

$$I_B \omega_B^2 / 2 = M * g * d [\cos(\beta + \alpha - 90) - \cos\beta] \text{ (Figure 11-1)}$$

From Eq. 11.2-2: $\omega_B = 0.12372 \text{ rad/sec}$

$$\beta = \tan^{-1} \{(52)/118.77\} = 24.65^\circ$$

$$M = 1480 \text{ lb-sec}^2/\text{in}$$

$$\cos(24.65 + \alpha - 90) - \cos(24.65) = 0.00433$$

$$\cos(24.65 + \alpha - 90) = 0.00433 + 0.907411 = 0.911741$$

$$90 - \alpha = 24.85 - 24.25 = 0.60$$

Therefore, a loaded HSM-H rotates a maximum of 0.60° from vertical. The loaded HSM-H is stable against overturning as tip-over does not occur until the CG rotates past the edge point (point B, Figure 11-1) to an angle of more than $24.65^\circ [= \tan^{-1}(52.0/118.77)]$.

11.3.3.5 Accident Dose Calculation

As shown in the above evaluation, the tornado wind and tornado missiles do not breach the confinement boundary. Localized scabbing of the end shield wall may be possible. Table 10-2 presents dose rates for an ISFSI array of HSM-Hs. Side and/or back annual doses at 100 meters are shown to be around 300 - 350 mrem (corresponding to a dose rate of approximately 0.04 mrem/hour). Localized scabbing of the end/back shield wall (one HSM-H unit), where a couple of inches of concrete may be removed, would have a negligible effect on the dose at 100 meters (site boundary) from the ISFSI.

The increase in exposure due to the loss of vent caps from an array of 20 HSM-H modules is evaluated. The roof dose rate increases from 11.1 mrem/hr to 143.6 mrem/hr. This corresponds to a 13-fold increase in the roof surface dose rate. Since the dose rate from the front of the HSM-H array has the largest contribution from the roof, and the largest dose rates over a given distance, the front array dose rate is considered for this analysis. Assuming the contribution to the dose rate increases by a factor of 13, the dose rate from the face of a 2x10 back to back array of HSM-Hs as tabulated in Section 10.3, Table 10-7 would increase from 3.64E-02 mrem/hr to 0.47 mrem/hr at 100 m, and would increase from 7.92E-05 mrem/hr to 1.03E-3 mrem/hr at 500 m. For a duration of 8 hours, this corresponds to a received exposure of less than 3.8 mrem at 100 m and less than 8.2E-03 mrem at 500 m.

11.3.3.6 Corrective Action

After excessive high winds or a tornado, the HSM-Hs would be inspected for damage. Any debris would be removed. Any damage resulting from impact with a missile would be evaluated to determine if the system was still within the licensed design basis.

The need for temporary shielding would be evaluated and HSM-H repairs would be performed to return the HSM-H to pre-accident design conditions.

11.3.4 Tornado Wind and Tornado Missiles Effect on Transfer Cask

The transfer cask is evaluated for the tornado wind speed and missile specified in Chapter 2, Section 2.2.1. The maximum DBT tornado wind speed of 360 mph produces a design pressure of 304 psf. The 4000 pound automobile and 276 pound eight inch diameter shell missiles were also considered. The other types of missiles are enveloped by the eight inch shell missile.

This analysis is performed for the cask secured in the horizontal position on the support skid. The following criteria are used to evaluate the adequacy of the transfer cask for the loads described above.

- Penetration Resistance
- Impact Stress Analysis

Stability analysis is not required since the cask is already evaluated for a design basis cask drop accident.

11.3.4.1 Penetration Resistance

There are two equations available from literatures for calculating the penetration, T , into the transfer cask outer structural shell and its end covers when the cask is impacted by the armor piercing artillery missile. The neutron shield shell outside the cask structural shell is conservatively ignored for absorbing any impact energy.

$$T_1 = [KE / (2.4S_u D^{1.6})]^{0.71} \quad [10]$$

$$T_2 = (KE^{2/3}) / (672D) \quad [11]$$

Where,

$$KE = \frac{1}{2}(mV^2)$$

m = Mass of missile, lb_m

V = Velocity of missile, in/sec

D = Missile diameter, in

S_u = 94,200 psi (cask top cover, SA-240 Gr. XM-19)

= 66,200 psi (cask structural shell and bottom cover, SA-240 Gr.304)

The penetration and stress calculations for the cask under impact of missile 8" diameter, 276 lbs armor piercing artillery shell are as follows:

$$m = 276 \text{ lb}_m$$

$$V = 185 \text{ ft/sec}$$

$$D = 8 \text{ in}$$

$$KE = \frac{1}{2} \times m \times V^2$$

$$= [\frac{1}{2} \times 276 \text{ lb}_m \times (185 \times 12)^2 \text{ in}^2 / \text{sec}^2] \times [1 \text{ lb}_f / (386.4 \text{ lb}_m \times \text{in} / \text{sec}^2)]$$

$$= 1,760,143 \text{ in-lb}_f$$

$$= 146,678 \text{ ft-lb}_f$$

$$\begin{aligned}
 T1 &= [KE / (2.4Su D1.6)]^{0.71} \\
 &= [1,760,143 / (2.4 \times 66,200 \times 8^{1.6})]^{0.71} \\
 &= 0.52'' < 1.5''
 \end{aligned}$$

The thickness of the cask outer structural shell is 1.5 ", which is greater than the calculated missile penetration of 0.52". Therefore the missile will not penetrate through the cask structural outer shell. A second equation is also used for calculation of the missile penetration into the cask shell and provides a matching result as follows.

$$\begin{aligned}
 T_2 &= (KE^{2/3}) / (672D) \\
 &= (146,678^{2/3}) / (672 \times 8) \\
 &= 0.52'' < 1.5''
 \end{aligned}$$

11.3.4.2 Impact Stress Analysis

Tornado Wind Load

Chapter 2, Section 2.2.1.1 specifies a maximum tornado wind speed at 360 mph. The corresponding velocity pressure, q_z , can be calculated by Eq. 6-1 of [12].

$$q_z = 0.00256 K_z K_{zt} V^2 I \quad (\text{lb/ft}^2)$$

Where,

$$\begin{aligned}
 K_z &= \text{Velocity pressure exposure coefficient} \\
 &= 1.03 \text{ (Height above ground } < 15 \text{ ft in Exposure D, Table 6-3 of [12])} \\
 K_{zt} &= \text{Topographic factor} \\
 &= 1 \\
 V &= \text{Basic wind speed} \\
 &= 360 \text{ mph} \\
 I &= \text{Importance factor} \\
 &= 1.15 \text{ (Category IV, Table 6-2 of [12])}
 \end{aligned}$$

$$q_z = 0.00256 \times 1.03 \times 1 \times 1.15 = 393 \text{ lb/ft}^2$$

A. Transverse wind pressure acting on cask shell surface

The projected area of the transfer cask normal to the wind is equal to the OD (92.2 inch) of the neutron shield multiplied to the length of the cask. The total wind force is then equal to the wind pressure multiplied to this projected area. This total wind force is equivalent to a line force, p , acting at the elevation of the cask centerline and along the entire cask length. This wind force will be assumed to be solely resisted only by the cask outer structural shell, which has a length of 193.2" with an OD of 82.7" and a thickness of 1.5".

$$\begin{aligned}
 p &= q_z \times (\text{OD of neutron shield}) \\
 &= 393 \text{ lb/ft}^2 \times (92.2 / 12) \text{ ft} \\
 &= 3019.6 \text{ lb/ft} \\
 &= 251.63 \text{ lb/in}
 \end{aligned}$$

Case 9c in Table 31 of [13] provides stress formula for a thin-walled cylindrical vessel supported at both ends and subjected to a uniform load over the entire length of its top element as follows.

$$B = [12(1-\nu^2)]^{1/8} = 1.348, \quad \nu = 0.3$$

Maximum hoop membrane stress,

$$\begin{aligned}\sigma_2 &= -0.492 B p R^{3/4} L^{-1/2} t^{-5/4} \\ &= -0.492 \times (1.348) \times 251.63 \times (82.7/2)^{3/4} \times (193.32)^{-1/2} \times (1.5)^{-5/4} \\ &= -117.9 \text{ psi}\end{aligned}$$

Maximum hoop bending stress,

$$\begin{aligned}\sigma_2' &= -1.217 B^{-1} p R^{1/4} L^{1/2} t^{-7/4} \\ &= -1.217 \times (1.348)^{-1} \times 251.63 \times (82.7/2)^{1/4} \times (193.32)^{1/2} \times (1.5)^{-7/4} \\ &= -3939.7 \text{ psi}\end{aligned}$$

Maximum hoop membrane plus bending stress,

$$(\sigma_2)_{\text{Total}} = \sigma_2 + \sigma_2' = -117.9 \text{ psi} - 3939.7 \text{ psi} = -4058 \text{ psi}$$

Maximum axial membrane stress,

$$\begin{aligned}\sigma_1 &= \text{Axial membrane stress} \\ &= -0.1188 B^3 p R^{1/4} L^{1/2} t^{-7/4} \\ &= -0.1188 \times (1.348)^3 \times 251.63 \times (82.7/2)^{1/4} \times 193.32^{1/2} \times (1.5)^{-7/4} \\ &= -1270 \text{ psi}\end{aligned}$$

Maximum axial bending stress,

$$\sigma_1' \approx \nu \times \sigma_2' = 0.3 \times (-3939.7 \text{ psi}) = -1181.9 \text{ psi}$$

Maximum axial membrane plus bending stress,

$$(\sigma_1)_{\text{Total}} = \sigma_1 + \sigma_1' = -1270 \text{ psi} + (-1181.9 \text{ psi}) = -2451.7 \text{ psi}$$

Maximum membrane plus bending stress intensity = $0 - (-4058) = 4058 \text{ psi}$

The ASME code allowable stress for the general membrane stress intensity will be conservatively used for evaluation of the above calculated maximum membrane plus bending stress intensity. The Service Level D allowable stress for the membrane stress intensity is the lesser of $2.4S_m$ and $0.7S_u$. For SA-240 Gr. 304 cask structural shell material, $S_m = 20,000 \text{ psi}$ at 300°F and $S_u = 66,200 \text{ psi}$. Thus the allowable stress is $0.7S_u = 46,340 \text{ psi}$.

Therefore the maximum calculated membrane plus bending stress intensity, under tornado wind load, in the cask shell is acceptable.

B. Axial wind pressure acting on the top end cover of the transfer cask

Case 10b in Table 24 of [13] provides formula for calculating the resultant moment on the 1.5" recessed flange thickness of the fixed cask top end plate under the wind pressure.

Maximum bending moment,

$$\begin{aligned} M_{ra} &= -q_z a^2 / 8 \\ &= -393 \text{ lb/ft}^2 \times (1 \text{ ft}^2 / 144 \text{ in}^2) \times (82.7/2 \text{ in})^2 / 8 \\ &= -583.3 \text{ in-lb/in} \end{aligned}$$

Maximum bending stress,

$$\begin{aligned} \sigma &= 6M_{ra} / t^2 \\ &= 6 \times (583.3 \text{ in-lb/in}) / (1.5 \text{ in})^2 \\ &= 1555 \text{ psi} < 46,340 \text{ psi} \quad \text{OK} \end{aligned}$$

C. Axial wind pressure acting on the bottom end cover of the transfer cask

Case 2f in Table 24 of [13] provides formula for calculating the resultant moment on the 2" thick fixed bottom end plate of the cask under the wind pressure.

$$\begin{aligned} b &= 14" = \text{radius of the cask bottom ram penetration ring} \\ a &= 81.7" / 2 = 40.85" = \text{Outer radius of bottom end plate} \\ b/a &= .3427 \Rightarrow K_{Mra} = -0.0888 \quad (\text{By interpolation}) \end{aligned}$$

Maximum bending moment,

$$M_{ra} = K_{Mra} q_z a^2 = -0.0888 \times 393/144 \times 40.85^2 = -404.4 \text{ in-lb/in}$$

Maximum bending stress,

$$\sigma = 6M_{ra} / t^2 = 6 \times (404.4 \text{ in-lb/in}) / (2 \text{ in})^2 = 607 \text{ psi} < 46,340 \text{ psi} \quad \text{OK}$$

Massive Automobile Missile

The impact forces applied to the cask as it is struck by the automobile missile is determined as follows:

The massive automobile missile is assumed to crush 3 feet under a constant force during the impact. The loss of kinetic energy is assumed to be dissipated by crushing of the missile. The frontal contact area of the automobile is specified to be 20 sq. ft.

$$F_a \times 3\text{ft} = \frac{1}{2} [m_a v_o^2]$$

$$P_a = F_a / 20 \text{ ft}^2$$

where:

$$m_a = \text{mass of missile} = 4,000 \text{ lb}$$

v_o = missile initial velocity = 195 ft/sec

F_a = Impact force on cask by missile automobile

p_a = Impact pressure on cask by missile automobile

$$\begin{aligned} F_a &= \frac{1}{2} \times \{4,000 \text{ lbm} \times [(195 \times 12) \text{ in/sec}]^2\} / (3 \times 12) \text{ in} \\ &= 3.042 \times 10^8 \text{ lbm} \cdot \text{in/sec}^2 \\ &= 3.042 \times 10^8 \text{ lb}_m \cdot \text{in/sec}^2 \times [1 \text{ lb}_f / (386.4 \text{ lb}_m \cdot \text{in/sec}^2)] \\ &= 787,267 \text{ lb}_f \end{aligned}$$

$$\begin{aligned} P_a &= 787,267 \text{ lb}_f / [20 \times (12)^2 \text{ in}^2] \\ &= 273.4 \text{ psi} \end{aligned}$$

The automobile missile deforms and is crushed during the impact. The shear stress in the cask wall is conservatively calculated below. It is assumed that the impact force is concentrated on a small curved section of the cask wall having dimensions $w \times L$. It is also assumed that only two side edges of the impact section are tending to shear. Edges above and below the impact section are assumed to bend, not shear. It is also assumed that the concentrated impact section is 3 foot wide, half of the automotive width. The impact area is then 36" wide by 80" high (equals to 20 ft² area).

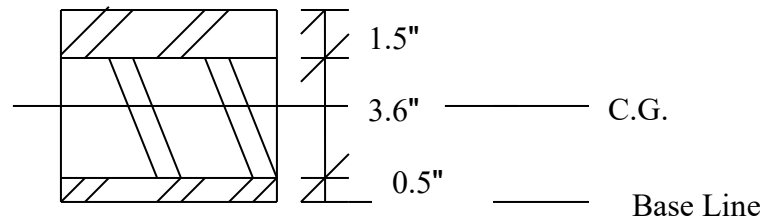
$$\begin{aligned} \text{Shear Area} &= 2 \times (20 \text{ ft}^2 / 3 \text{ ft}) \times \text{the thickness of the cask outer structural shell} \\ &= 2 \times 80" \times 1.5" = 240 \text{ in}^2 \end{aligned}$$

$$\text{The shear stress, } \tau = \text{Force/area} = 787,267 \text{ lb} / 240 \text{ in}^2 = 3,280 \text{ psi}.$$

The level D allowable shear stress for the cask shell is $0.42 S_u = 0.42 \times 66,200 = 26,480 \text{ psi}$. The shear stress is well below the allowable shear stress.

Assuming that the impact on the side of the cask is reacted by a 36"×80" section of the cask shell, Case 1c from Table 26 of [13] is used to calculate the resulted stresses in the shell. This case represents a flat plate with simply supported edges under a uniform load over central rectangular area. It is conservative for this Case to represent the automotive crushing onto a curved section of the cask.

The transfer cask shell is made of a three-layer composite. It consists of a 1.5" outer structural shell, a 3.6" lead gamma shield, and a 0.5" inner liner (see sketch below). This sandwiched composite plate may be represented by an equivalent one-piece plate which has a thickness producing the same moment of inertia as that of the composite. The thickness of its equivalent one-piece plate is calculated as follows.



For unit length of the composite plate,

Neglecting the strength of the 3.6" thick lead,

The distance from Base Line to C.G.

$$\begin{aligned}
 &= [(1.5" \times 1") \times (1.5"/2 + 3.6" + 0.5") + (0.5" \times 1") \times (0.5"/2)] \div \\
 &\quad [(1.5" \times 1") + (0.5" \times 1")] \\
 &= 7.4" \div 2 \\
 &= 3.7"
 \end{aligned}$$

The combined moment of inertia of the composite structural plates, I_{comb}

$$\begin{aligned}
 I_{\text{comb}} &= (1 \times 1.5^3 / 12) + (1.5 \times 1) \times (1.5/2 + 3.6 + 0.5 - 3.7)^2 + (1 \times 0.5^3 / 12) + (0.5 \times 1) \times (3.7 - 0.5/2)^2 \\
 &= 8.23 \text{ in}^4
 \end{aligned}$$

The thickness of the equivalent one-piece plate, t_{eq}

$$I_{\text{comb}} = 8.23 \text{ in}^4 = (1 \times t_{\text{eq}}^3) / 12 \Rightarrow t_{\text{eq}} = 4.62"$$

An automobile missile crushing into the horizontal cylindrical canister with an impact area of 36" wide by 80" high is conservatively analyzed by a case that the same impact is applied to a rectangular plate of dimensions at the cask length by the cask OD. All edges of the rectangular plate are assumed simply supported. Case 1c in Table 26 of [13] provides maximum stress calculation of this rectangular plate as follows.

$$\text{Max } \sigma = (\beta W) / t^2$$

$$W = F_a = 787,267 \text{ lb}$$

$$t = t_{\text{eq}} = 4.62"$$

$$a_1 = 36", b_1 = 80"$$

$$a = 193.32" \text{ (cask length)}$$

$$b = 82.7" \text{ (cask OD)}$$

$$a_1 / b = 0.4353$$

$$b_1 / b = 0.967$$

$$a / b = 2.337$$

Use $(b_1 / b) = 0.8$, and $(a_1 / b) = 0.4$ for the table given under the Case 1c in Table 26 of [13];

From this table,

$\beta = 0.68$ for $(a / b) = 1.4$, and $\beta = 0.76$ for $(a / b) = 2$

By extrapolation, $\beta = 0.81$ for $(a / b) = 2.337$

$\therefore \text{Max } \sigma = (0.81 \times 787,267 \text{ lb}) / (4.62^2) = 29,876 \text{ psi}$

The ASME code allowable stress for the general membrane stress intensity will be conservatively used for evaluation of the above calculated maximum membrane plus bending stress intensity. The Service Level D allowable stress for the membrane stress intensity is the lesser of $2.4S_m$ and $0.7S_u$. For SA-240 Gr. 304 cask structural shell material, $S_m = 20,000 \text{ psi}$ at 300°F and $S_u = 66,200 \text{ psi}$. Thus the allowable stress is $0.7S_u = 46,340 \text{ psi}$. Therefore the maximum membrane plus bending stress of $29,876 \text{ psi}$ is acceptable.

11.3.4.3 Accident Dose Calculation

Based on the above analyses, the 32PTH DSC confinement boundary will not be breached as a result of the missile impacts. Accordingly, no 32PTH DSC damage or release of radioactivity is postulated.

The missile impact scenario may result in the loss of cask neutron shielding and local deformation/damage of the gamma shielding. The effect of loss of the neutron shielding due to a missile impact is bounded by that resulting from a cask drop scenario. The radiation dose due to local deformation/damage of the gamma shielding is negligible.

11.3.4.4 Corrective Action

The transfer cask will be inspected for damage. These operations will take place in the plant fuel building decontamination area and spent fuel pool after recovery of the transfer cask. Following recovery of the transfer cask and unloading of the DSC, the transfer cask will be inspected, repaired and tested as appropriate prior to reuse.

For recovery of the cask and contents, it may be necessary to develop a special sling/lifting apparatus to move the transfer cask from the site to the fuel pool. This may require several weeks of planning to ensure all steps are correctly organized. During this time, lead blankets may be added to the transfer cask to minimize on-site exposure to site operations personnel. The transfer cask would be roped off to ensure the safety of the site personnel.

11.3.5 Flood

Cause of Accident

Flooding conditions simulating a range of flood types, such as tsunami and seiches as specified in 10CFR72.122 (b) are considered. In addition, floods resulting from other sources, such as high water from a river or a broken dam, are postulated as the cause of the accident.

Accident Analysis

The HSM-H is evaluated for flooding in Appendix 3.9.9, Section 3.9.9.10.3. Based on the evaluation presented in that section, the HSM-H will withstand the design basis flood.

Accident Dose Calculation

The radiation dose due to flooding of the HSM-H is negligible. Flooding does not breach the confinement boundary. Therefore radioactive material inside the DSC will remain sealed in the DSC and, therefore, will not contaminate the encroaching flood water.

Corrective Actions

Because of the location and geometry of the HSM-H vents, it is unlikely that any significant amount of silt would enter an HSM-H should flooding occur. Any silt deposits would be removed using a pump suction hose or fire hose inserted through the inlet vent to suck the silt out, or produce a high velocity water flow to flush the silt through the HSM-H inlet vents.

11.3.6 Blockage of HSM-H Air Inlet and Outlet Openings

This accident conservatively postulates the complete blockage of the ventilation air inlet and outlet openings of the HSM-H.

Cause of Accident

Since the NUHOMS[®] HSM-Hs are located outdoors; there is a remote probability that the ventilation air inlet and outlet openings could become blocked by debris from such unlikely events as floods and tornados. The NUHOMS[®] design features such as the perimeter security fence and the redundant protected location of the air inlet and outlet openings reduce the probability of occurrence of such an accident. Nevertheless, for this conservative generic analysis, such an accident is postulated to occur and is analyzed.

Accident Analysis

The thermal evaluation of this event is presented in Chapter 4, Section 4 for 32PTH DSC (34.8 kw) and Amendment #8, Section P.4 for 24PTH DSC (40.8 kw). The analysis performed for HSM-H with 24PTH DSC bounding the values for HSM-H with 32PTH DSC. Therefore, the temperatures determined in Amendment #8, Section P.4 are used in the HSM-H structural evaluation of this event, which is presented in Appendix 3.9.9, Section 3.9.9.10.4. The structural

evaluation of the 32PTH DSC based on the thermal evaluation presented in Chapter 4 of this SAR is presented in Appendix 3.9.1, storage load case 6.

Accident Dose Calculation

There are no off-site dose consequences as a result of this accident. The only significant dose increase is that related to the recovery operation where it is conservatively estimated that the on-site workers will receive an additional dose of no more than one man-rem during the eight hour period it is estimated may be required for removal of debris from the air inlet and outlet openings in the HSM-H.

Corrective Actions

Debris removal is all that is required to recover from a postulated blockage of the HSM ventilation air inlets and outlets. Cooling will begin immediately following removal of the debris from the inlets and outlets. The amount and nature of debris can vary, but even in the most extreme case, manual means or readily available equipment can be used to remove debris.

The debris is conservatively assumed to remain in place for 34 hours. The last seven hours of this period are assumed to be the time required to completely remove all the debris before the natural circulation air flow can be restored.

11.3.7 Lightning

Cause of Accident

The likelihood of lightning striking the HSM-H and causing an off-normal condition is not considered to be a credible event. Lightning protection system requirements are site specific and depend upon the frequency of occurrences of lightning storms in the proposed ISFSI location and the degree of protection offered by other grounded structures in the proximity of the HSM-Hs. The addition of simple lightning protection equipment, required by plant criteria, to HSM-H structures (i.e., grounded handrails, ladders, etc.) is considered a miscellaneous attachment.

Accident Analysis

Should lightning strike in the vicinity of the HSM-H the normal storage operations of the HSM-H will not be affected. The current discharged by the lightning will follow the low impedance path offered by the surrounding structures. Therefore, the HSM-H will not be damaged by the heat or mechanical forces generated by current passing through the higher impedance concrete. Since the HSM-H requires no equipment for its continued operation, the resulting current surge from the lightning will not affect the normal operation of the HSM-H.

Corrective Actions

Since no off-normal condition will develop as the result of lightning striking in the vicinity of the HSM-H, no corrective action would be necessary. Also, there would be no radiological consequences.

11.3.8 Fire/Explosion

Cause of Accident

Combustible materials will not normally be stored at an ISFSI. Therefore, a credible fire would be very small and of short duration such as that due to a fire or explosion from a vehicle or portable crane.

Direct engulfment of the HSM-H is highly unlikely. Any fire within the ISFSI boundary while the DSC is in the HSM would be bounded by the fire during transfer cask movement. The HSM-H concrete acts as a significant insulating fire wall to protect the DSC from the high temperatures of the fire.

Accident Analysis

The evaluation of the hypothetical fire event is presented in Chapter 4, Section 4. The fire thermal evaluation is performed primarily to demonstrate the confinement integrity and fuel retrievability of the 32PTH DSC. Peak temperatures for the NUHOMS[®]-32PTH System components are summarized in Table 4-5 of Chapter 4. Temperatures in this table are used for structural evaluations of the transfer Cask. The results of this analysis are presented in Appendix 3.9.2, Section 3.9.2.2.4, Load Case 10.

Accident Dose Calculation

The 32PTH-DSC confinement boundary will not be breached as a result of the postulated fire/explosion scenario. Accordingly, no 32PTH-DSC damage or release of radioactivity is postulated. Because no radioactivity is released, no resultant dose increase is associated with this event.

The fire scenario may result in the loss of transfer cask neutron shielding should the fire occur while the 32PTH-DSC is in the cask. The effect of loss of the neutron shielding due to a fire is bounded by that resulting from a cask drop scenario. See Section 11.3.1 of this Chapter for evaluation of dose consequences of a cask drop.

Corrective Actions

Evaluation of transfer cask neutron shield damage as a result of a fire is to be performed to assess the need for temporary shielding (if fire occurs during transfer operations) and repairs to restore the transfer cask to pre-fire design conditions.

11.4 References

1. 10CFR Part 72, Licensing Requirement for Storage of Spent Fuel in an Independent Spent Fuel Storage Installation.
2. American Nuclear Society, ANSI/ANS-57.9-1984, Design Criteria for an Independent Spent Fuel Storage Installation (Dry Storage Type).
3. Regulatory Guide 1.60, "Design Response Spectra for Seismic Design of Nuclear Power Plants," U.S. Atomic Energy Commission, Revision 1, December 1973.
4. "Missiles Generated by Natural Phenomenon," Standard Review Plan, NUREG-0800, U.S. Nuclear Regulatory Commission
5. "Design Basis Tornado for Nuclear Power Plants," Regulatory Guide 1.76, U.S. Atomic Energy Commission, April 1974.
6. ANSYS Engineering Analysis System, Users Manual for ANSYS Rev. 5.6 and 6.0, Swanson Analysis Systems, Inc., Houston, PA.
7. "Structural Analysis and Design of Nuclear Plant Facilities," ASCE Publication No. 58.
8. "Code Requirements for Nuclear Safety Related Concrete Structures," ACI 349-97, American Concrete Institute, Detroit, MI.
9. "Design of Structures for Missile Impact", BC-TOP-9A, Revision 2, September 1974, Bechtel Power Corporation.
10. H.A. Nelms, "Structural Analysis of Shipping Casks, Effects of Jacket Physical Properties and Curvature and Puncture Resistance," Vol. 3, ORNL TM-1312, Oak Ridge National Laboratory, Oak ridge Tennessee, June 1968.
11. Gwaltney, R. C., "Missile Generation and Protection in Light-Water Cooled Power Reactor Plants", ORNL NSIC-22, Oak Ridge National Laboratory, Oak Ridge, TN, for the USAEC, September 1968.
12. American Society of Civil Engineers, ASCE 7-95, Minimum Design Loads for Buildings and Other Structures, Approved June 6, 1996
13. "Formulas for Stress and Strain", 5th Edition, R. J. Roark and W. C. Young

Proprietary Information on This Page
Withheld Pursuant to 10 CFR 2.390

12. OPERATING CONTROLS AND LIMITS

The original application for approval of the NUHOMS® HD System provided proposed Technical Specifications (TS) and TS Bases as Chapter 12 of this Safety Analysis Report (SAR). Upon approval of Certificate of Compliance (CoC) No. 1030, Amendment 0, dated January 10, 2007, the TS were listed as Appendix A of the CoC, and were therefore removed from this SAR with the issuance of Final Safety Analysis Report (FSAR) Revision 0, dated February 23, 2007.

NUHOMS® HD SYSTEM TECHNICAL SPECIFICATION BASES

TABLE OF CONTENTS

B.12.2 FUNCTIONAL AND OPERATING LIMITS.....	B12-1
B.12.3 LIMITING CONDITION FOR OPERATION (LCO) APPLICABILITY	B12-2
B.12.3 SURVEILLANCE REQUIREMENT (SR) APPLICABILITY	B12-5
B.12.3.1 FUEL INTEGRITY.....	B12-9
B.12.3.2 CASK CRITICALITY CONTROL	B12-15

B.12.2 FUNCTIONAL AND OPERATING LIMITS

BASES

BACKGROUND

The 32PTH DSC design requires certain limits on spent fuel parameters, including fuel type, maximum allowable enrichment prior to irradiation, maximum burnup, minimum acceptable cooling time prior to storage in the 32PTH DSC, and physical condition of the spent fuel (i.e., intact or damaged fuel assemblies). Other important limitations are the radiological source terms from Control Components (CCs) associated Burnable Poison Rod Assemblies (BPRAs), Vibration Suppressor Inserts (VSIs), and Thimble Plug Assemblies (TPAs). These limitations are included in the thermal, structural, radiological, and criticality evaluations performed for the canister.

APPLICABLE SAFETY ANALYSIS

Various analyses have been performed that use these fuel parameters as assumptions. These assumptions are included in the thermal, criticality, structural, shielding and confinement analyses.

Technical Specification Tables 1, 2, 3, 4, and 5 provide the key fuel parameters that require confirmation prior to 32PTH DSC loading.

FUNCTIONAL AND OPERATING LIMITS VIOLATIONS

If Functional and Operating Limits are violated, the limitations on the fuel assemblies in the canister have not been met. Actions must be taken to place the affected fuel assemblies in a safe condition. This safe condition may be established by returning the affected fuel assemblies to the spent fuel pool. However, it is acceptable for the affected fuel assemblies to remain in the canister if that is determined to be a safe condition.

Notification of the violation of a Functional and Operating Limit to the NRC is required within 24 hours. Written reporting of the violation must be accomplished within 60 days. This notification and written report are independent of any reports and notification that may be required by 10CFR 72.75.

REFERENCES

SAR Chapter 2

B.12.3 LIMITING CONDITION FOR OPERATION (LCO) APPLICABILITYBASES

LCOs	LCO 3.0.1, 3.0.2, 3.0.4 and 3.0.5 establish the general requirements applicable to all Specifications and apply at all times, unless otherwise stated.
------	--

LCO 3.0.1	LCO 3.0.1 establishes the Applicability statement within each individual Specification as the requirement for when the LCO is required to be met (i.e., when the canister is in the specified conditions of the Applicability statement of each Specification).
-----------	---

LCO 3.0.2	LCO 3.0.2 establishes that upon discovery of a failure to meet an LCO, the associated ACTIONS shall be met. The Completion Time of each Required Action for an ACTIONS Condition is applicable from the point in time that an ACTIONS Condition is entered. The Required Actions establish those remedial measures that must be taken within specified Completion Times when the requirements of an LCO are not met. This Specification establishes that:
-----------	---

- a. Completion of the Required Actions within the specified Completion Times constitutes compliance with a Specification; and
- b. Completion of the Required Actions is not required when an LCO is met within the specified Completion Time, unless otherwise specified.

There are two basic types of Required Actions. The first type of Required Action specifies a time limit in which the LCO must be met. This time limit is the Completion Time to restore a system or component or to restore variables to within specified limits. If this type of Required Action is not completed within the specified Completion Time, the canister may have to be placed in the spent fuel pool and unloaded. (Whether stated as a Required Action or not, correction of the entered Condition is an action that may always be considered upon entering ACTIONS.) The second type of Required Action specifies the remedial measures that permit continued operation of the unit that is not further restricted by the Completion Time. In this case, compliance with the Required Actions provides an acceptable level of safety for continued operation.

Completing the Required Actions is not required when an LCO is met or is no longer applicable, unless otherwise stated in the individual Specifications.

The Completion Times of the Required Actions are also applicable when a system or component is removed from service intentionally. The reasons for intentionally relying on the ACTIONS include, but are not limited to, performance of Surveillances, preventive maintenance, corrective maintenance, or investigation of operational problems. Entering ACTIONS for these reasons must be done in a manner that does not compromise safety. Intentional entry into ACTIONS should not be made for operational convenience.

Individual Specifications may specify a time limit for performing an SR when equipment is removed from service or bypassed for testing. In this case, the Completion Times of the Required Actions are applicable when this time limit expires if the equipment remains removed from service or bypassed.

When a change in specified condition is required to comply with Required Actions, the equipment may enter a specified condition in which another Specification becomes applicable. In this case, the Completion Times of the associated Required Actions would apply from the point in time that the new Specification becomes applicable and the ACTIONS Condition(s) are entered.

LCO 3.0.3	THIS SPECIFICATION IS NOT APPLICABLE TO THE NUHOMS [®] HD SYSTEM. THE PLACEHOLDER IS RETAINED FOR CONSISTENCY WITH THE POWER REACTOR TECHNICAL SPECIFICATIONS.
-----------	---

LCO 3.0.4	<p>LCO 3.0.4 ESTABLISHES LIMITATIONS ON CHANGES IN SPECIFIED CONDITIONS IN THE APPLICABILITY WHEN AN LCO IS NOT MET. IT PRECLUDES PLACING THE NUHOMS[®] HD SYSTEM IN A SPECIFIED CONDITION STATED IN THAT APPLICABILITY (E.G., Applicability desired to be entered) when the following exist:</p> <ul style="list-style-type: none">a. Conditions are such that the requirements of the LCO would not be met in the Applicability desired to be entered; andb. Continued noncompliance with the LCO requirements, if the Applicability were entered, would result in the equipment being required to exit the Applicability desired to be entered to comply with the Required Actions.
-----------	--

Compliance with Required Actions that permit continued operation of the equipment for an unlimited period of time in specified condition provides an acceptable level of safety for continued operation. Therefore, in such cases, entry into a specified condition in the Applicability may be made in accordance with the provisions of the Required Actions. The provisions of this Specification should not be interpreted as endorsing the failure to exercise the good practice of restoring systems or components before entering an associated specified condition in the Applicability.

The provisions of LCO 3.0.4 shall not prevent changes in specified conditions in the Applicability that are required to comply with ACTIONS. In addition, the provisions of LCO 3.0.4 shall not prevent changes in specified conditions in the Applicability that are related to the unloading of a canister.

Exceptions to LCO 3.0.4 are stated in the individual Specifications.

Exceptions may apply to all the ACTIONS or to a specific Required Action of a Specification.

Surveillances do not have to be performed on the associated equipment out of service (or on variables outside the specified limits), as permitted by SR 3.0.1. Therefore, changing specified conditions while in an ACTIONS Condition, either in compliance with LCO 3.0.4 or where an exception to LCO 3.0.4 is stated, is not a violation of SR 3.0.1 or SR 3.0.4 for those Surveillances that do not have to be performed due to the associated out of service equipment.

LCO 3.0.5	LCO 3.0.5 establishes the allowance for restoring equipment to service under administrative controls when it has been removed from service or not in service in compliance with ACTIONS. The sole purpose of this Specification is to provide an exception to LCO 3.0.2 (e.g., to not comply with the applicable Required Action(s)) to allow the performance of required testing to demonstrate:
-----------	---

- a. The equipment being returned to service meets the LCO; or
- b. Other equipment meets the applicable LCOs.

The administrative controls ensure the time the equipment is returned to service in conflict with the requirements of the ACTIONS is limited to the time absolutely necessary to perform the allowed required testing. This Specification does not provide time to perform any other preventive or corrective maintenance.

LCO 3.0.6	This specification is not applicable to the NUHOMS® HD System. The placeholder is retained for consistency with the power reactor technical specifications.
-----------	---

LCO 3.0.7	This specification is not applicable to the NUHOMS® HD System. The placeholder is retained for consistency with the power reactor technical specifications.
-----------	---

B.12.3 SURVEILLANCE REQUIREMENT (SR) APPLICABILITYBASES

SRs	SR 3.0.1 through SR 3.0.4 establish the general requirements applicable to all Specifications in Sections 3.1, 3.2 and 3.3 and apply at all times, unless otherwise stated.
-----	---

SR 3.0.1	SR 3.0.1 establishes the requirement that SRs must be met during the specified conditions in the Applicability for which the requirements of the LCO apply, unless otherwise specified in the individual SRs. This Specification is to ensure that Surveillances are performed to verify systems and components, and that variables are within specified limits. Failure to meet a Surveillance within the specified Frequency, in accordance with SR 3.0.2, constitutes a failure to meet an LCO.
----------	--

Systems and components are assumed to meet the LCO when the associated SRs have been met. Nothing in this Specification, however, is to be construed as implying that systems or components meet the associated LCO when:

- a. The systems or components are known to not meet the LCO, although still meeting the SRs; or
- b. The requirements of the Surveillance(s) are known to be not met between required Surveillance performances.

Surveillances do not have to be performed when the equipment is in a specified condition for which the requirements of the associated LCO are not applicable, unless otherwise specified.

Surveillances, including Surveillances invoked by Required Actions, do not have to be performed on equipment that has been determined to not meet the LCO because the ACTIONS define the remedial measures that apply. Surveillances have to be met and performed in accordance with SR 3.0.2, prior to returning equipment to service.

Upon completion of maintenance, appropriate post maintenance testing is required to declare equipment within its LCO. This includes ensuring applicable Surveillances are not failed and their most recent performance is in accordance with SR 3.0.2. Post maintenance testing may not be possible in the current specified conditions in the Applicability due to the necessary equipment parameters not having been established. In these situations, the equipment may be considered to meet the LCO provided testing has been satisfactorily completed to the extent possible and the equipment is not otherwise believed to be incapable of performing its function.

This will allow operation to proceed to a specified condition where other necessary post maintenance tests can be completed.

- SR 3.0.2 SR 3.0.2 establishes the requirements for meeting the specified Frequency for Surveillances and any Required Action with a Completion Time that requires the periodic performance of the Required Action on a "once per..." interval.
- SR 3.0.2 permits a 25% extension of the interval specified in the Frequency. This extension facilitates Surveillance scheduling and considers plant operating conditions that may not be suitable for conducting the Surveillance (e.g., transient conditions or other ongoing Surveillance or maintenance activities).
- The 25% extension does not significantly degrade the reliability that results from performing the Surveillance at its specified Frequency. This is based on the recognition that the most probable result of any particular Surveillance being performed is the verification of conformance with the SRs. The exceptions to SR 3.0.2 are those Surveillances for which the 25% extension of the interval specified in the Frequency does not apply. These exceptions are stated in the individual Specifications. The requirements of regulations take precedence over the TS. Therefore, when a test interval is specified in the regulations, the test interval cannot be extended by the TS, and the SR includes a Note in the Frequency stating, "SR 3.0.2 is not applicable".
- As stated in SR 3.0.2, the 25% extension also does not apply to the initial portion of a periodic Completion Time that requires performance on a "once per..." basis. The 25% extension applies to each performance after the initial performance. The initial performance of the Required Action, whether it is a particular Surveillance or some other remedial action, is considered a single action with a single Completion Time. One reason for not allowing the 25% extension to this Completion Time is that such an action usually verifies that no loss of function has occurred by checking the status of redundant or diverse components or accomplishes the function of the equipment in an alternative manner.
- The provisions of SR 3.0.2 are not intended to be used repeatedly merely as an operational convenience to extend Surveillance intervals (other than those consistent with refueling intervals) or periodic Completion Time intervals beyond those specified.
-

- SR 3.0.3 SR 3.0.3 establishes the flexibility to defer declaring affected equipment as not meeting the LCO or an affected variable outside the specified limits when a Surveillance has not been completed within the specified Frequency. A delay period of up to 24 hours or up to the limit of the specified Frequency, whichever is less, applies from the point in time that it is discovered that the

Surveillance has not been performed in accordance with SR 3.0.2, and not at the time that the specified Frequency was not met.

This delay period provides adequate time to complete Surveillances that have been missed. This delay period permits the completion of a surveillance before complying with Required Actions or other remedial measures that might preclude completion of the Surveillance. The basis for this delay period includes consideration of unit conditions, adequate planning, availability of personnel, the time required to perform the Surveillance, the safety significance of the delay in completing the required Surveillance, and the recognition that the most probable result of any particular Surveillance being performed is the verification of conformance with the requirements.

When a Surveillance with a Frequency based not on time intervals, but upon specified unit conditions or operational situations, is discovered not to have been performed when specified, SR 3.0.3 allows the full delay period of 24 hours to perform the Surveillance.

SR 3.0.3 also provides a time limit for completion of Surveillances that become applicable as a consequence of changes in the specified conditions in the Applicability imposed by Required Actions.

Failure to comply with specified Frequencies for SRs is expected to be an infrequent occurrence. Use of the delay period established by SR 3.0.3 is a flexibility which is not intended to be used as an operational convenience to extend Surveillance intervals.

If a Surveillance is not completed within the allowed delay period, then the equipment is considered not in service or the variable is considered outside the specified limits and the Completion Times of the Required Actions for the applicable LCO Conditions begin immediately upon expiration of the delay period. If a Surveillance is failed within the delay period, then the equipment is not in service, or the variable is outside the specified limits and the Completion Times of the Required Actions for the applicable LCO Conditions begin immediately upon the failure of the Surveillance. Completion of the Surveillance within the delay period allowed by this Specification, or within the Completion Time of the ACTIONS, restores compliance with SR 3.0.1.

SR 3.0.4 SR 3.0.4 establishes the requirement that all applicable SRs must be met before entry into a specified condition in the Applicability.

This Specification ensures that system and component requirements and variable limits are met before entry in the Applicability for which these systems and components ensure safe operation of the facility.

The provisions of this Specification should not be interpreted as endorsing the failure to exercise the good practice of restoring systems or components to an appropriate status before entering an associated specified condition in the Applicability. However, in certain circumstances, failing to meet an SR will not result in SR 3.0.4 restricting a change in specified condition. When a system, subsystem, division, component, device, or variable is outside its specified limits, the associated SR(s) are not required to be performed, per SR 3.0.1, which states that Surveillances do not have to be performed on such equipment. When equipment does not meet the LCO, SR 3.0.4 does not apply to the associated SR(s) since the requirement for the SR(s) to be performed is removed. Therefore, failing to perform the Surveillance(s) within the specified Frequency does not result in an SR 3.0.4 restriction to changing specified conditions of the Applicability. However, since the LCO is not met in this instance, LCO 3.0.4 will govern any restrictions that may (or may not) apply to specified condition changes.

The provisions of SR 3.0.4 shall not prevent changes in specified conditions in the Applicability that are required to comply with ACTIONS. In addition, the provisions of SR 3.0.4 shall not prevent changes in specified conditions in the Applicability that are related to the unloading of a HSM-H or 32PTH DSC.

The precise requirements for performance of SRs are specified such that exceptions to SR 3.0.4 are not necessary. The specific time frames and conditions necessary for meeting the SRs are specified in the Frequency, in the Surveillance, or both. This allows performance of Surveillances when the prerequisite condition(s) specified in a Surveillance procedure require entry into the specified condition in the Applicability of the associated LCO prior to the performance or completion of a Surveillance. A Surveillance that could not be performed until after entering the LCO Applicability would have its Frequency specified such that it is not "due" until the specific conditions needed are met. Alternatively, the Surveillance may be stated in the form of a Note as not required (to be met or performed) until a particular event, condition, or time has been reached. Further discussion of the specific formats of SR annotation is found in Technical Specifications Section 1.4, operation to proceed to a specified condition where other necessary post maintenance tests can be completed.

B.12.3.1 FUEL INTEGRITY

B.12.3.1.1 DSC Bulkwater Removal Medium and Vacuum Drying Pressure

BASES

BACKGROUND

A 32PTH DSC is placed in the spent fuel pool and loaded with fuel assemblies meeting the requirements of the Functional and Operating Limits. An inner top cover/shield plug assembly or shield plug is then placed on the 32PTH DSC. Subsequent operations involve moving the 32PTH DSC to the decontamination area and removing water from the 32PTH DSC (using helium as a cover gas for assisting in the drainage of bulk water). After the 32PTH DSC inner top cover/shield plug is secured, vacuum drying of the 32PTH DSC is performed, and the 32PTH DSC is backfilled with helium. During normal storage conditions, the fuel assemblies are stored in the 32PTH DSC with an inert helium atmosphere, which results in lower fuel clad temperatures and provides an inert atmosphere during storage conditions.

32PTH DSC vacuum drying is utilized to remove residual moisture from the cavity after the 32PTH DSC has been drained of water. Any water which was not drained from the 32PTH DSC evaporates from fuel or basket surfaces due to the vacuum. This vacuum drying operation is aided by the temperature increase due to the heat generation of the fuel.

APPLICABLE SAFETY ANALYSIS

The confinement of radioactivity during the storage of spent fuel in a 32PTH DSC is ensured by the use of multiple confinement barriers and systems. The barriers relied upon are the fuel pellet matrix, the fuel cladding tubes in which the fuel pellets are contained, and the 32PTH DSC in which the fuel assemblies are stored. Long-term integrity of the fuel cladding depends on storage in an inert atmosphere. This protective environment is accomplished by removing water from the 32PTH DSC (using helium for assisting in the drainage of bulk water) and backfilling the 32PTH DSC with helium. The removal of water is necessary to prevent phase change–related pressure increase upon heatup. The analysis in Chapter 4 demonstrates that if helium is used as a cover gas for bulk water removal operations, the conductivity of helium during vacuum drying operations assure that cladding temperature remains below the cladding temperature limit. The DSC/transfer cask annulus contains water during the vacuum drying process. This SAR evaluates and documents that the 32PTH DSC confinement boundary is not compromised due to any normal, off-normal or accident condition postulated (SAR Chapter 3 and 11 structural analyses) and the fuel clad temperature remains below allowable values (SAR Chapter 4).

LCO

Utilizing helium as the medium to assist during drainage of bulk water ensures that the fuel cladding remains under the limits during the entire vacuum drying operations.

A stable vacuum pressure of < 3 torr further ensures that all liquid water has evaporated in the 32PTH DSC cavity, and that the resulting inventory of oxidizing gases in the 32PTH DSC is below 0.25 volume %.

Technical Specification 3.1 requires the use of helium during the bulkwater removal process. Therefore, water from the DSC cavity is replaced by helium during the bulkwater removal process. Fuel cladding temperatures are low during this short duration process due to the presence of liquid water and helium.

Therefore use of helium during bulkwater removal, vacuum drying and long term storage operations assures that the fuel assemblies will have limited (or no) exposure to the oxidizing environment.

APPLICABILITY

This is applicable to all 32PTH DSCs during LOADING OPERATIONS but before TRANSFER OPERATIONS.

ACTIONS

The actions specified require checking for any leaks in the vacuum drying system or welds and correcting them or establishment of a helium pressure of at least 0.5 atmosphere within the time limits specified in the LCO. The timeframe specified applies to the vacuum drying operations and the helium backfill operations. If the required vacuum can not be established within the timeframe specified in the Condition column of the Actions table, a helium atmosphere (with a pressure of at least 0.5 atmosphere) is to be established within 30 days or perform an assessment and implementation of corrective actions to return the 32PTH DSC to an analyzed condition or reflood the DSC submerging all fuel assemblies. The 15 psig limit in the action section is conservatively below the maximum analyzed blowdown pressure.

SURVEILLANCE REQUIREMENTS

Ensure a minimum oxidizing gas content and maintain cladding integrity.

REFERENCES

SAR Chapters 3 and 4

B 12.3.1 FUEL INTEGRITY

B.12.3.1.2 32PTH DSC Helium Backfill Pressure

BASES

BACKGROUND

A 32PTH DSC is placed in the spent fuel pool and loaded with fuel assemblies meeting the requirements of the Functional and Operating Limits. An inner top cover/shield plug assembly or shield plug is then placed on the 32PTH DSC. Subsequent operations involve moving the 32PTH DSC to the decontamination area and removing water from the 32PTH DSC using helium to assist in the drainage of bulk water. After the 32PTH DSC inner top cover/shield plug is welded, vacuum drying of the 32PTH DSC is performed, and the 32PTH DSC is backfilled with helium. During normal storage conditions, the 32PTH DSC is backfilled with helium, which results in lower fuel clad temperatures. The inert helium environment protects the fuel from potential oxidizing environments.

APPLICABLE SAFETY ANALYSIS

Long-term integrity of the fuel cladding depends on storage in an inert atmosphere. SAR section 3.5 evaluates the effect of long term storage and short term temperature transients on fuel cladding integrity. Credit for the helium backfill pressure is taken to limit the potential for corrosion of the fuel cladding. SAR Chapter 4 evaluates the 32PTH DSC maximum pressure under normal, off-normal, and accident conditions.

LCO

32PTH DSC backpressure is maintained within a range of pressure that will ensure maintenance of the helium backfill pressure over time and will not result in excessive 32PTH DSC pressure in normal, off-normal and accident conditions.

APPLICABILITY

This specification is applicable to all 32PTH DSCs during LOADING OPERATIONS but before TRANSFER OPERATIONS.

ACTIONS

The actions required and associated completion times are associated with the time limits established in Technical Specification 3.1.2. The total time for vacuum drying and helium backfill is specified in Technical Specification 3.1.2. The thermal analysis in Chapter 4 demonstrates that with water in the DSC/cask annulus and helium atmosphere in the DSC cavity, fuel cladding temperatures are below the cladding material temperature limits. These time limits are imposed to ensure that there is sufficient time to complete the required actions and the 32PTH DSC fuel cladding will not exceed maximum allowable temperatures.

SURVEILLANCE REQUIREMENTS

To ensure that: (1) the atmosphere surrounding the irradiated fuel is a non-oxidizing inert gas; (2) the atmosphere is favorable for the transfer of decay heat.

REFERENCES

SAR Chapters 3 and 4

B 12.3.1 FUEL INTEGRITY

B.12.3.1.3 Transfer Cask Cavity Helium Backfill Pressure

BASES

BACKGROUND

A 32PTH DSC is placed in the spent fuel pool and loaded with fuel assemblies meeting the requirements of the Functional and Operating Limits. An inner top cover/shield plug assembly or shield plug is then placed on the 32PTH DSC. Subsequent operations involve moving the 32PTH DSC to the decontamination area and removing water from the 32PTH DSC using helium to assist in the drainage of bulk water. After the 32PTH DSC inner top cover/shield plug is welded, vacuum drying of the 32PTH DSC is performed, and the 32PTH DSC is backfilled with helium. The 32PTH DSC outer top cover plate is welded, and subsequently, the water drained from the transfer cask (TC) annulus. After installation of the TC lid, the TC cavity is backfilled with helium to assure adequate heat transfer which maintains the fuel cladding temperatures below the maximum allowable temperature.

APPLICABLE SAFETY ANALYSIS

Long-term integrity of the fuel cladding depends on storage in an inert atmosphere and maintaining fuel cladding temperature below an acceptable limit. SAR Chapter 4 evaluates the 32PTH DSC temperatures under normal, off-normal, and accident conditions. The thermal analysis in SAR Chapter 4 demonstrates that with helium in the DSC/TC annulus and helium in the DSC cavity, the fuel cladding temperatures are below the cladding material temperature limits. Monitoring of the TC cavity annulus pressure during transfer operation or verification after filling ensures that helium will be present in the annulus during transfer operations to keep the temperatures within analyzed conditions.

LCO

The OS187H cavity is maintained within a range of pressure that will ensure maintenance of the helium backfill pressure over the transfer time and will not result in excessive pressure in normal, off-normal and accident conditions. The cavity helium backfill must commence within 26 hours after the drainage of the water in the annulus.

APPLICABILITY

This specification is applicable to OS187H transfer cask with loaded 32PTH DSC during LOADING, TRANSFER, and UNLOADING OPERATIONS.

ACTIONS

Should the helium pressure not meet the requirements of this specification, the TC/32PTH DSC must be returned to an analyzed condition.

SURVEILLANCE REQUIREMENTS

To ensure the transfer cask cavity is in a helium environment during LOADING, UNLOADING, and TRANSFER OPERATIONS.

REFERENCES

SAR Chapter 4

B.12.3.2 CASK CRITICALITY CONTROL

BASES

BACKGROUND

During loading and unloading of the 32PTH DSC, the DSC cavity is filled with borated water having a minimum boron concentration of which is a function of the basket type, fuel assembly class, maximum planar average enrichment and the condition of fuel assemblies (intact or damaged). This specification ensures that a subcritical configuration is maintained in the event of an accidental loading of the DSC with unirradiated fuel.

APPLICABLE SAFETY ANALYSIS

The 32PTH DSC has been designed for unirradiated fuel with a specified maximum planar average initial enrichment while taking credit for the soluble boron concentration in the DSC cavity water and the boron content in the neutron absorber plates. The criticality analysis provided in Chapter 6 of the UFSAR evaluates the DSC to ensure that a subcritical configuration is maintained.

LCO

The minimum boron concentration limits of the water in the DSC cavity as specified in the LCO to ensure that a subcritical configuration is maintained in the event of an accidental loading of the DSC with unirradiated fuel.

APPLICABILITY

This specification is applicable to the 32PTH DSC during loading and unloading operations.

ACTIONS

The actions required and the specified completion times for the required actions are associated with ensuring that either the dissolved boron concentration is restored above the specified minimum or the fuel is removed from the DSC.

SURVEILLANCE REQUIREMENTS

Performance of two separate independent analysis of the water used to fill the DSC cavity (a) within 4 hours of initiation of loading/unloading operations and (b) subsequent analysis at intervals not exceeding 48 hours until the conclusion of such loading/unloading operations provides assurance that a subcritical DSC configuration is always maintained.

REFERENCES

UFSAR Chapter 6

CHAPTER 13 QUALITY ASSURANCE

TABLE OF CONTENTS

13. QUALITY ASSURANCE.....	13-1
13.1 Introduction.....	13-2
13.2 “Important-to-Safety & “Safety Related” NUHOMS® HD System Components	13-3
13.3 Description of TN 10CFR 72, Subpart G QA Program	13-5
13.3.1 Project Organization.....	13-5
13.3.2 QA Program	13-5
13.3.3 Design Control	13-5
13.3.4 Procurement Document Control.....	13-6
13.3.5 Procedures, Instructions, and Drawings	13-6
13.3.6 Document Control	13-6
13.3.7 Control of Purchased Items and Services.....	13-6
13.3.8 Identification and Control of Materials, Parts, and Components	13-7
13.3.9 Control of Special Processes	13-7
13.3.10 Inspection	13-7
13.3.11 Test Control.....	13-7
13.3.12 Control of Measuring and Test Equipment	13-7
13.3.13 Handling, Storage and Shipping.....	13-7
13.3.14 Inspection and Test Status	13-8
13.3.15 Control of Nonconforming Items	13-8
13.3.16 Corrective Action	13-8
13.3.17 Records.....	13-8
13.3.18 Audits and Surveillances	13-8
13.4 Conditions of Approval Records	13-9
13.5 Supplemental Information	13-10
13.5.1 References	13-10

LIST OF TABLES

Table 13-1	TN QA Program Description Manual and Implementing Procedures Manual.....	13-11
------------	---	-------

LIST OF FIGURES

Figure 13-1	Project Organization Chart	13-12
-------------	----------------------------------	-------

13. QUALITY ASSURANCE

TN's Quality Assurance (QA) program has been established in accordance with the requirements of 10CFR 72, Subpart G [1]. The QA program applies to the design, purchase, fabrication, handling, shipping, storing, cleaning, assembly, inspection, testing, operation, maintenance, repair, and modification of the NUHOMS® HD System and components identified as "important to safety" and "safety related." These components and systems are defined in Chapter 2 of the SAR.

13.1 Introduction

The complete description and specific commitments of the TN QA program are contained in the TN QA Program Description Manual [2]. This manual has been approved by the Nuclear Regulatory Commission (NRC) for performing 10CFR 72 related activities. Changes to the TN QA program shall be submitted to the NRC for approval within thirty (30) days of implementation. Changes to the TN QA program which decrease or delete previously approved QA commitments shall be submitted to the NRC for approval prior to implementation.

The matrix in Table 13-1 shows the 10CFR 72, Subpart G criteria and the respective sections of the TN QA Program Description Manual and TN Implementing Procedures Manual [3] that address the criteria.

Figure 13-1 shows the organization structure for the NUHOMS® HD System project.

13.2 “Important-to-Safety & “Safety Related” NUHOMS® HD System Components

TN will apply its QA program to the NUHOMS® HD System components within its scope of responsibility which are defined as "important to safety" and "safety related" as delineated in Section 2.5. QA procedures are used to establish the quality category of components, subassemblies, and piece parts according to each item's importance to safety.

In Section 2.5, each component is identified as "important to safety," "not important to safety," or "safety related". During the design process, items that are considered "important to safety" are further categorized using a graded quality approach. When the graded quality approach is used, a list shall be developed for each "important to safety" item which includes an assigned quality category consistent with the item's importance to safety. Quality categories are determined based on the following and the guidance provided in NUREG/CR-6407 [4]:

Category A items are critical to safe operation. These items include structures, components and systems whose failure or malfunction could directly result in a condition adversely affecting public health and safety. This would include conditions such as loss of primary containment with subsequent release of radioactive material, loss of shielding or an unsafe geometry compromising criticality control.

Category B items have a major impact on safety. These items include structures, components, and systems whose failure or malfunction could indirectly result in a condition adversely affecting public health and safety. An unsafe operation could result only if a primary event occurs in conjunction with a secondary event or other failure or environmental occurrence.

Category C items have a minor impact on safety. These items include structures, components, and systems whose failure or malfunction would not significantly reduce the packaging effectiveness and would be unlikely to create a condition adversely affecting public health and safety.

For "safety related" items the Quality Assurance program is applied as described for Category A items. The Quality Assurance program as described in Section 13.3 is applied to each "important to safety" graded category and is limited as follows.

Category A

- A. The design is based on the most stringent industrial codes or standards. Design verification shall be accomplished by prototype testing or formal design review.
- B. Vendors for items and services for this category may only be selected from the Approved Suppliers List.
- C. TN suppliers and sub-tier suppliers must have a QA program based on applicable criteria in Subpart G to 10CFR 72, or equivalent.
- D. Complete traceability of raw materials and the use of certified welders and processes is required.
- E. All personnel performing Quality Assurance related inspections, tests, and examinations shall be qualified and certified in accordance with the requirements of the QA program.

- F. Only qualified and certified auditors and lead auditors shall perform audits.
- G. TN QA personnel shall be required to inspect and/or approve supplier fabricated components prior to authorizing shipment release.
- H. Welding consumables shall be procured as a Category A item if the intended use is unknown. If purchased for a specific Category B or C application, the material must be identified and its use restricted to fabrication of the same level.

Category B

- A. The design is based on the most stringent industrial codes and standards. But design verification may be accomplished by use of alternate calculations or computer codes.
- B. The procurement of items may be from suppliers on the Approved Suppliers List or QA program requirements for the supplier may be based upon the inspection and test requirements of the procured item.
- C. Traceability of materials is not required; however, specified welds require completion by qualified, certified welders.
- D. Quality Assurance verification activities shall be performed by personnel qualified and certified in accordance with the requirements of the QA program.
- E. Only lead auditor personnel require certification in accordance with the QA program.

Category C

- A. Items may be purchased from a catalog or "off-the-shelf."
- B. When received, the item shall be identified and checked for compliance with the purchase order and for damage.

Items not considered important-to-safety will be controlled in accordance with good industrial practices.

If a utility elects to perform construction, and has an NRC approved QA program (10CFR 50) [5] that is equivalent to or exceeds TN's program, then the utility QA program is considered an acceptable substitute for their scope of responsibility.

13.3 Description of TN 10CFR 72, Subpart G QA Program

13.3.1 Project Organization

The NUHOMS[®] HD System has been designed by a dedicated TN project organization.

QA duties are performed by the TN project organization, the QA Manager, and QA Specialists.

The organization structure for the NUHOMS[®] HD System project is presented in Table 13-1. A description of TN's organizational structure, functional responsibilities, levels of authority, and lines of internal and external (client and supplier) communication may be found in the TN QA Program Description Manual.

Project QA controls are determined by the Project Manager and approved by QA. All Project Plans, regardless of the indicated applicability of QA requirements, are reviewed by QA to assure that QA controls are commensurate with the specific activity, item complexity, importance to safety and client-imposed contractual requirements.

Project personnel are indoctrinated, trained, and qualified in accordance with the TN QA program.

13.3.2 QA Program

TN will apply the QA program to components defined in Section 2.5 as "important to safety" and "safety related" in accordance with the TN QA Program Description Manual.

TN has established and implemented a QA program for the control of quality in the design, purchase, fabrication, handling, shipping, storing, cleaning, assembly, inspection, testing, operation, maintenance, repair, and modification of storage containers for nuclear products. Training and/or evaluation of personnel qualifications in accordance with written procedures are required for personnel performing activities affecting quality. The QA program assures that all quality requirements, engineering specifications and specific provisions of any package design approval are met. Those characteristics critical to safety are emphasized.

The TN QA Manager regularly evaluates the TN QA program for adherence to the 18 point criteria in scope, implementation and effectiveness. Further, the TN President requires that the QA program, including the QA Program Description Manual and Implementing Procedures Manual, be implemented and enforced on all applicable projects at TN.

13.3.3 Design Control

"Important to safety" and "safety related" NUHOMS[®] HD System design activities shall be implemented in accordance with the TN QA Manual. Design verification will be performed by a competent individual with the appropriate skill level. However, this individual's skill level may not be the same as the originator but must be equivalent.

Errors and deficiencies in the design, including the design process, are documented in the form of Corrective Action Reports.

Industry standards and specifications are used for the selection of suitable materials, parts, equipment and processes for “important to safety” and “safety related” structures, systems, or components as defined in the various chapters and sections of this SAR.

13.3.4 Procurement Document Control

Procurement documents are prepared in accordance with the TN QA program which delineates the actions to be accomplished in the preparation, review, approval, and control of procurement documents. Review and approval of procurement documents by QA are documented on the procurement documents prior to release to assure the adequacy of quality requirements stated therein. This review determines that quality requirements are correctly stated, inspectable, and controllable; that there are adequate acceptance and rejection criteria; and that the procurement document has been prepared, reviewed, and approved in accordance with QA program requirements. Refer to Section 13.2 for supplier selection requirements.

The procurement documents shall identify the documentation required to be submitted for information, review, or approval by TN or TN’s client. The time of submittal shall also be established. When TN requires the supplier to maintain specific QA records, the retention times and disposition requirements shall be prescribed.

13.3.5 Procedures, Instructions, and Drawings

As required by the TN QA program, activities affecting quality are prescribed in approved, written procedures, instructions, or drawings and these procedures, instructions, and drawings shall be followed.

13.3.6 Document Control

The issuance, distribution, and receipt of documents which prescribe activities affecting quality are controlled in accordance with the TN QA program. Controlled documents include, but are not limited to, the TN design specifications and criteria documents, drawings, instructions, and test procedures.

The individuals or groups responsible for reviewing, approving, and issuing documents and revisions thereto are identified in the "Responsibilities" sections of the TN QA implementing procedures.

13.3.7 Control of Purchased Items and Services

The control of purchased items and services shall be implemented in accordance with the TN QA program.

Surveillance of subcontracted activities is planned and performed in accordance with written procedures to assure conformance to the purchase order. These procedures provide for instructions that specify the characteristics to be witnessed, inspected or verified, and accepted; the method of surveillance and the extent of documentation required; and those responsible for implementing these instructions.

TN suppliers shall furnish documentation that identifies any procurement requirements which have not been met, together with a description of those nonconformances dispositioned as "use-as-is" or "repair."

Documentation from TN suppliers which demonstrates compliance with procurement requirements (such as material test reports, NDE results, performance test results, etc.) is periodically evaluated by audits, independent inspections, or tests as necessary to assure its validity.

13.3.8 Identification and Control of Materials, Parts, and Components

Materials, parts, and components shall be identified and controlled in accordance with the TN QA program. Hardware identification requirements are determined during generation of design drawings and specifications such that the location and method of identification do not affect the form, fit, function, or quality of the item being identified.

13.3.9 Control of Special Processes

The control of special processes, such as nondestructive examination, chemical cleaning, welding, and heat treating shall be performed in accordance with the TN QA program.

13.3.10 Inspection

Receipt inspections, and in-process and final inspections of TN-fabricated, constructed, or erected items, systems, components, or structures shall be performed in accordance with the TN QA program.

13.3.11 Test Control

Test control shall be accomplished in accordance with the TN QA program.

13.3.12 Control of Measuring and Test Equipment

The TN QA program defines the requirements for calibration of measuring and test equipment. Calibration is against certified measurement standards which have known relationships to national standards, where such standards exist. Where such standards do not exist, the basis for calibration shall be documented.

13.3.13 Handling, Storage and Shipping

Handling, storage, and shipping shall be conducted in accordance with the TN QA program. Special handling, preservation, storage, cleaning, packaging, and shipping requirements are established and accomplished by qualified individuals in accordance with predetermined work and inspection instructions.

13.3.14 Inspection and Test Status

The use of inspection and test status tags shall be implemented in accordance with the TN QA program.

13.3.15 Control of Nonconforming Items

The TN QA program defines the requirements and assigns the responsibilities for the control, identification, segregation, documentation, and close-out of nonconforming items to prevent their inadvertent installation or use in fabrication, construction, or erection.

Nonconformance reports identify the item description and quantity, the disposition of the nonconformance, the inspection requirements, and signature approval of the disposition. They are periodically analyzed to show quality trends and help identify root causes of nonconformances. Significant results are reported to responsible management for review and assessment.

Nonconforming items are segregated from acceptable items and tagged to prevent inadvertent use until properly dispositioned and closed out.

13.3.16 Corrective Action

Corrective action for conditions adverse to quality shall be taken in accordance with the TN QA program. For significant conditions adverse to quality the cause is determined and action to preclude recurrence is taken and reported to the appropriate levels of management.

13.3.17 Records

The TN QA program defines the scope of the records program such that sufficient records are maintained to provide documentary evidence of the quality of items and activities affecting quality.

13.3.18 Audits and Surveillances

A comprehensive system of planned and documented audits, including audits of suppliers and site construction activities, verifies compliance with all aspects of the TN QA program and determines the effectiveness of the program.

Audits are performed by certified lead auditors and are planned, performed, and documented in accordance with the TN QA program.

Unannounced QA surveillances may be performed on activities affecting quality by the TN QA Manager, or his designee, on an as-needed basis to further assure compliance with QA requirements.

13.4 Conditions of Approval Records

As required by 10CFR 72, Subpart L, TN will establish and maintain records for each storage component fabricated under a certificate of compliance as required by §72.234(d). The records will be available for inspection as required by §72.234(e). Written procedures and appropriate tests will be established prior to use of the storage components which will be provided to each NUHOMS[®] HD System user as required by §72.234(f).

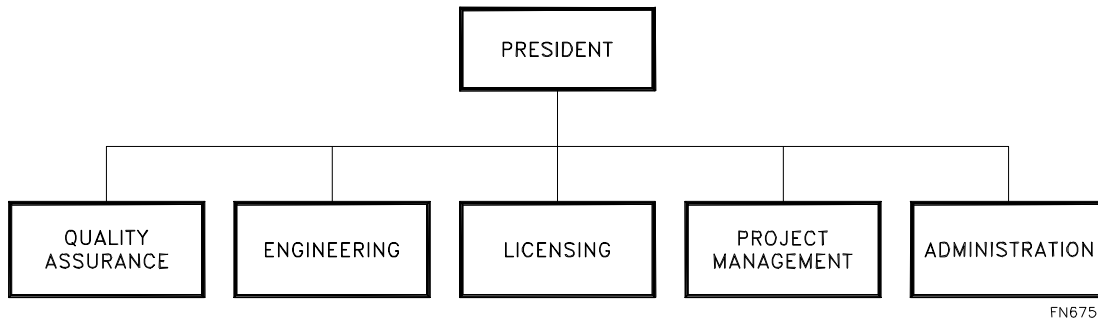
13.5 Supplemental Information

13.5.1 References

1. CFR Title 10, Part 72, Licensing Requirements for the Independent Storage of Spent Nuclear Fuel and High-Level Radioactive Waste.
2. “Transnuclear Quality Assurance Program Description Manual,” current revision.
3. “Transnuclear Quality Implementing Procedures Manual,” current revision.
4. NUREG/CR-6407, “Classification of Transportation Packaging and Dry Spent Fuel Storage System Components According to Importance to Safety,” February 1996.
5. CFR Title 10, Part 50, Domestic Licensing of Production and Utilization Facilities.

Table 13-1
TN QA Program Description Manual and Implementing Procedures Manual

10CFR 72, Subpart G	QA Program
.142	1.0 Organization
.144	2.0 QA Program
.146	3.0 Design Control
.148	4.0 Procurement Document Control
.150	5.0 Procedures, Instructions, and Drawings
.152	6.0 Document Control
.154	7.0 Control of Purchased Items and Services
.156	8.0 Identification and Control of Materials, Parts, and Components
.158	9.0 Control of Special Processes
.160	10.0 Inspection
.162	11.0 Test Control
.164	12.0 Control of Measuring and Test Equipment
.166	13.0 Handling, Storage, and Shipping
.168	14.0 Inspection and Test Status
.170	15.0 Control of Nonconforming Items
.172	16.0 Corrective Action
.174	17.0 Records
.176	18.0 Audits



- Notes: 1. Licensing may report to Engineering.
 2. Administration activities may report to the various other organizations.

Figure 13-1
Project Organization Chart

CHAPTER 14
DECOMMISSIONING

TABLE OF CONTENTS

14. DECOMMISSIONING.....	14-1
14.1 Decommissioning Considerations.....	14-1
14.2 Supplemental Information	14-4
14.2.1 References	14-4

14. DECOMMISSIONING

14.1 Decommissioning Considerations

The NUHOMS[®] HD System design features inherent ease and simplicity for decommissioning by providing easily decontaminable surfaces and isolating the external surfaces of the 32PH1-DSC from contact with the fuel pool. At the end of its service life, the 32PTH DSC decommissioning could be performed by one of the options listed below:

- Option 1, the 32PTH DSC, including stored spent fuel, could be shipped to either a monitored retrievable storage system (MRS) or a geological repository for final disposal, or
- Option 2, the spent fuel could be removed from the 32PTH DSC (either at the ISFSI site or at another off site location) and shipped in an NRC approved transportation cask.

The first option requires that the 32PTH DSC be licensed to current Part 71 regulations. The design and licensing of a transport packaging for the 32PTH is planned.

The first option does not require any decommissioning of the 32PTH DSC. No residual contamination is expected to be left behind on the concrete HSM-H. The HSM-H, fence, and peripheral utility structures will require no decontamination or special handling after the last 32PTH DSC is removed. The HSM-H, fence, and peripheral utility structures could be demolished and recycled with normal construction techniques.

The second option would require decontamination of the 32PTH DSC and transfer cask (if applicable). The sources of contamination in the interior of the 32PTH DSC or transfer cask would be the primary contamination left from the spent fuel pool water; or crud, hot particles and fines from the spent fuel pins. This contamination could be removed with a high pressure water spray. If further surface decontamination of the 32PH1-DSC or transfer cask is necessary, electropolishing or chemical etching can be used to clean the contaminated surface. After decontamination, the 32PTH DSC and/or transfer cask could be cut up for scrap, partially scrapped, or refurbished for reuse. Any activated metal would be shipped as low level radioactive waste to a near surface disposal facility.

A review of cask activation analyses previously performed for similar systems (TN-32 cask [3] and NUHOMS[®] site license storage system) indicates that the levels of activation of the 32PTH DSC, HSM-H and transfer cask would be orders of magnitude below the specific activity of the isotopes listed in Tables 1 and 2 of 10CFR 61.55 [2]. A comparison of the source terms for this application to those referenced above including the activation analysis summary for the above applications is provided below. Although the 32PTH radiation sources are larger than the other systems, a detailed analysis is not considered necessary based on the significant margins determined from these analyses.

Comparison of Source Terms for Activation Analyses

Source Term (including Control Components)	32PTH DSC	TN-32 (Metal Cask)	NUHOMS® Site License HSM
γ (γ /sec/assy)	6.9×10^{15}	5.3×10^{15}	1.53×10^{15}
n (n/sec/assy)	1.1×10^9	3.3×10^8	2.23×10^8

TN 32 and NUHOMS® Site License HSM Activation Analysis Results

Nuclide	Activity Ci/m ³			
	HSM Concrete	HSM Steel	TN-32	10CFR 61.55 Limit
H-3			8.3×10^{-11}	40
C-14			2.3×10^{-10}	8
Co-60	4.4×10^{-5}	8.1×10^{-2}	7.7×10^{-6}	700
Ni-59	1.4×10^{-10}	3.1×10^{-6}	2.5×10^{-6}	220
Ni-63	8.3×10^{-8}	3.2×10^{-4}	3.4×10^{-4}	3.5
Nb-94		3.9×10^{-8}		.2
<5 year half life	4.6×10^{-3}	2.0×10^{-1}	2.3×10^{-2}	700

Following surface decontamination, the radiation levels in the 32PTH DSC or transfer cask due to activation will be below the acceptable limits of Regulatory Guide 1.86 [1]. The activation levels of the 32PTH DSC or transfer cask materials will be far below the specific activity limits for both short and long lived nuclides for Class A waste. A detailed evaluation will be performed at the time of decommissioning to determine the appropriate mode of disposal, should refurbishment not be elected.

The procedure for decommissioning a 32PTH DSC or transfer cask not being returned to service is summarized below:

- Remove fuel in accordance with the unloading procedures of Chapter 8.
- Survey interior of 32PTH DSC or transfer cask. Wash down the inside of the 32PTH DSC or transfer cask. Pump out and filter contaminated water and cleaning agent. Survey interior of 32PTH DSC or transfer cask again, decontaminate as required. It is expected that surface decontamination will be minimal. If so, dispose of the 32PTH DSC or transfer cask body as scrap metal. If unable to decontaminate to acceptable levels, the 32PTH DSC and/or transfer cask body can be disposed of as low level radioactive waste.
- Decontaminate the top inner and outer cover plates until able to dispose of as scrap metal. If unable to achieve acceptable levels, dispose of them as low level radioactive waste.

The fuel unloading and decontamination steps for 32PTH DSC, HSM-H, or cask refurbishment are as outlined for the scrap choices, discussed above. However, the only pieces discarded are components damaged by unloading or that are considered to be difficult to decontaminate. Following a comprehensive survey to confirm continued 32PTH DSC, HSM-H or transfer cask functionality within design basis, the components will be eligible for returning to spent fuel storage service.

The volume of waste material produced incidental to ISFSI decommissioning is expected to be limited to that necessary to accomplish surface decontamination of the 32PTH DSCs, if the spent

fuel elements are removed. No chemical or mixed waste is anticipated. The licensee is responsible for the disposal of any waste generated by decontamination. Furthermore, it is estimated that the 32PTH DSC materials will be slightly activated as a result of their long term exposure to the relatively small neutron flux emanating from the spent fuel, and that the resultant activation level will be well below the allowable limits for general release as noncontrolled material. Therefore, it is anticipated that the 32PTH DSCs may be decommissioned from nuclear service by surface decontamination alone. This activity could be performed at the utility, or other suitable facility.

A detailed decommissioning plan will be submitted prior to the commencement of decommissioning activities. The costs of decommissioning the ISFSI are expected to represent a small and negligible fraction of the cost of decommissioning a nuclear power station.

14.2 Supplemental Information

14.2.1 References

1. Regulatory Guide 1.86, "Termination of Operating Licenses for Nuclear Reactors."
2. U.S. Nuclear Regulatory Commission, Title 10 Code of Federal Regulations, Part 61, "Licensing Requirements for Land Disposal or Radioactive Waste."
3. Safety Analysis Report for the TN-32 Cask, Docket 72-1021, Revision 0, January 2000.

APPENDIX A

32PTH Type 1 DSC and OS187H Type 1 TC

Chapter A.1 General Information

TABLE OF CONTENTS

A.1	GENERAL INFORMATION	A.1-1
A.1.1	Introduction.....	A.1-2
A.1.2	General Description of the NUHOMS® HD System with the 32PTH Type 1 DSC and OS187H Type 1 TC.....	A.1-3
A.1.2.1	NUHOMS® HD System Characteristics	A.1-3
A.1.2.2	Operational Features	A.1-4
A.1.2.3	32PTH Type 1 DSC Contents.....	A.1-5
A.1.3	Identification of Agents and Contractors	A.1-6
A.1.4	Generic Cask Arrays	A.1-7
A.1.5	Supplemental Data.....	A.1-8
A.1.5.1	References.....	A.1-8
A.1.5.2	Drawings	A.1-8

LIST OF TABLES

Table A.1-1	Key Design Parameters of the NUHOMS® HD System Components	A.1-9
-------------	---	-------

LIST OF FIGURES

Figure A.1-1	32PTH Type 1 Dry Shielded Canister (Optional two-part top end configuration shown)	A.1-10
Figure A.1-2	OS187H Type 1 On-Site Transfer Cask	A.1-11

A.1 GENERAL INFORMATION

Appendix A to this NUHOMS[®] HD System Final Safety Analysis Report (FSAR) documents the addition of the 32PTH Type 1 dry shielded canister (DSC) and the OS187H Type 1 transfer cask (TC) to the NUHOMS[®] HD System. These two components are similar but longer length versions of the 32PTH DSC and the OS187H TC described in the main body of this FSAR.

The general information presented in Chapter 1 remains applicable when the 32PTH Type 1 DSC and the OS187H Type 1 TC are added to the NUHOMS[®] HD System.

The format and content of this appendix follows the format and content of the main body of this FSAR. Generally, the same chapters and section numbers as in the main body have been kept in this appendix, preceded with a letter A. In addition, in several sections of this appendix reference is made to the corresponding section/chapter in the main body of the FSAR to avoid repetition of documentation that is also applicable to this appendix. For the sections in this appendix which have been identified as “No change,” the description or analysis presented in the corresponding sections of the FSAR for the 32PTH and OS187H are also applicable to the 32PTH Type 1 DSC or the OS187H Type 1 transfer cask. Table and figures presented in the FSAR which remain unchanged due to the addition of the 32PTH Type 1 DSC and OS187H Type 1 transfer cask are not repeated in this appendix.

Note: References to sections or chapters within this appendix are identified with a prefix A (e.g., Section A.2.1 or Chapter A.2). References to sections or chapters of the FSAR outside of this appendix (main body of the FSAR) are identified with the applicable FSAR section or chapter number (e.g., Section 2.1 or Chapter 2).

A.1.1 Introduction

There is no change to the generic description presented in Section 1.1 of the FSAR when the 32PTH Type 1 dry shielded canister (DSC) and the OS187H Type 1 transfer cask (TC) are used instead of the 32PTH DSC and the OS187H TC. When used with the Type 1 components, the NUHOMS[®] HD System consists of the 32PTH Type 1 DSC, the OS187H Type 1 TC, and the HSM-H Horizontal Storage Module. Sketches for the 32PTH Type 1 DSC and the OS187H Type 1 TC are shown in Figure A.1-1 and Figure A.1-2.

The 32PTH Type 1 DSC and the OS187H Type 1 TC are similar to but longer length versions of the 32PTH DSC and OS187H TC described in the main body of this FSAR. The main design changes associated with these longer length NUHOMS[®] HD System components are summarized in Sections A.1.2.1.1 and A.1.2.1.3.1 for the 32PTH Type 1 DSC and OS187H Type 1 TC, respectively. The authorized contents and overall design criteria as described in the main body of this FSAR is the same for these added components with the exception that an elastic-plastic analysis methodology is used for the accident pressure load case evaluation of the 32PTH Type 1 DSC (instead of elastic analysis methodology used for the 32PTH DSC). The application of the elastic-plastic analysis methodology to the 32PTH Type 1 DSC is similar to that used for the NUHOMS[®] 32P DSC in Reference [2].

A.1.2 General Description of the NUHOMS[®] HD System with the 32PTH Type 1 DSC and OS187H Type 1 TC

The general arrangement of NUHOMS[®] HD System shown in Figure 1-3 and Figure 1-4 and the general description presented in Section 1.2 remain applicable when the 32PTH Type 1 DSC and the OS187H Type 1 TC are used instead of the 32PTH DSC and OS187H TC. The confinement boundary of the 32PTH Type 1 DSC is shown in Figure A.7-1 when the standard three-piece top end assembly configuration is used. For the optional two-piece top end assembly configuration, the confinement boundary is the same as that for the 32PTH DSC as shown in Figure 7-1.

The 32PTH Type 1 DSC is identified as follows: XXX-32PTH-YYY-Z-1, where XXX, YYY, and Z are as described in Section 1.2. The basket types are the same as for the 32PTH DSC and are described in drawing 10494-72-2003-SAR.

A.1.2.1 NUHOMS[®] HD System Characteristics

A.1.2.1.1 Dry Shielded Canister (32PTH Type 1 DSC)

No change to the generic description for the 32PTH DSC presented in Section 1.2.1.1. Table A.1-1 summarizes the key design parameters for the 32PTH Type 1 DSC.

The major changes implemented in the 32PTH Type 1 DSC relative to the 32PTH DSC are as follows:

- The interior cavity length of the 32PTH Type 1 DSC is increased, approximately 7½", with a corresponding increase in basket length.
- Since the thicknesses of the top and bottom shield assemblies remain unchanged, the overall DSC length also is increased. The DSC diameter is unchanged.
- The top end assembly of the 32PTH Type 1 DSC consists of a three-part closure design (top shield plug, inner top cover, and outer top cover). This design is the same as other standardized NUHOMS[®] canister designs described in Reference [1]. The two-part top end closure design of the 32PTH DSC is an alternate design in the 32PTH Type 1 DSC.
- Lifting lugs are used to lift the empty 32PTH Type 1 DSC into the OS187H Type 1 transfer cask. The lifting lugs are welded to the shell and are located at the support ring elevation, similar to other standardized NUHOMS[®] canister designs [1]. Lifting lugs are used in lieu of the lifting rods with welded bosses, located at the inner bottom cover plate, in the 32PTH design. The lifting lugs are non-safety components as they are used to lift the DSC prior to fuel load.

The 32PTH Type 1 DSC is shown on drawings 10494-2001-SAR through 10494-2005-SAR in Section A.1.5.2.

A.1.2.1.2 Horizontal Storage Module (HSM-H)

No change to the generic description presented in Section 1.2.1.2. Only a small ($\frac{1}{2}$ "") increase in the overall length of the DSC support rail is required to accommodate the 32PTH Type 1 DSC. The key design parameters for the HSM-H as presented in Table 1-1 are not changed.

A.1.2.1.3 Transfer Systems

A.1.2.1.3.1 OS187H Type 1 On-Site Transfer Cask

No change to the generic description presented in Section 1.2.1.3.1 for the OS187H TC. Table A.1-1 summarizes the key design parameters for the OS187H Type 1 TC. The major changes incorporated into the OS187H Type 1 transfer cask are:

- In order to accommodate the longer 32PTH Type 1 DSC, the minimum internal cavity length of the TC is increased from 186.60" (OS187H) to 198.75" (OS187H Type 1). As a result of the increased cavity length, the overall length is increased and the distance between upper and lower trunnions is also increased. The 70.5" inside diameter and the thicknesses of the top and bottom end assemblies are unchanged.
- The thickness of the inner liner is increased from $\frac{1}{2}$ " to a nominal $\frac{5}{8}$ ". The thickness of the upper shell course is increased from 2.00" to $2\frac{3}{8}$ ".
- The transfer cask trunnions are revised to remove the resin-filled voids. The material for the lower trunnions is changed from SA-182 Type F304 to SA-182 Type F304N.
- The separate resin-filled and removable upper trunnion pocket shielding has been deleted and the water neutron shield extended to mate with the trunnion.

The OS187H Type 1 TC has a payload capacity of 120,000 lbs (determined based on its evaluated capacity of 250,000 lbs and its total weight of 130,000 lbs).

A.1.2.1.3.2 Transfer Equipment

No change to the transfer equipment description presented in Section 1.2.1.3.2.

A.1.2.2 Operational Features

A.1.2.2.1 Dry Run Operations

No change.

A.1.2.2.2 SFA Loading Operations

No change in the primary operations (in sequence of occurrence) for the NUHOMS[®] HD System described in Section 1.2.2.2, except for placement of the cask spacer (if required) prior to placing the 32PTH Type 1 DSC into the transfer cask, and, for a 32PTH Type 1 DSC with a three-part top end closure, the inner top cover plate is placed following placement of the top shield plug (step 8) and lifting of the transfer cask from the pool (step 9). The inner top cover is sealed in Step 10 instead of the top shield plug.

A.1.2.2.3 Identification of Subjects for Safety and Reliability Analysis

A.1.2.2.3.1 Criticality Prevention

No change.

A.1.2.2.3.2 Chemical Safety

No change.

A.1.2.2.3.3 Operation Shutdown Modes

The NUHOMS[®] HD System is a totally passive system so that consideration of operation shutdown modes is unnecessary.

A.1.2.2.3.4 Instrumentation

No change.

A.1.2.2.3.5 Maintenance and Surveillance

No change. All maintenance and surveillance tasks are described in Chapter A.9.

A.1.2.3 32PTH Type 1 DSC Contents

No change. The DSC contents described in Section 1.2.3 for the 32PTH DSC are applicable for the 32PTH Type 1 DSC.

A.1.3 Identification of Agents and Contractors

No change.

A.1.4 Generic Cask Arrays

No change.

A.1.5 Supplemental Data

A.1.5.1 References

1. Updated Final Safety Analysis Report, Standardized NUHOMS[®] Horizontal Modular Storage System for Irradiated Nuclear Fuel, Revision 9, February 2006, USNRC Docket No. 72-1004.
2. USNRC Safety Evaluation Report, SNM-2505, Amendment 7, Dated 11/2/2005, Docket 72-8

A.1.5.2 Drawings

32PTH Type 1 DSC:

- 10494-72-2001-SAR, (3 sheets), (PROPRIETARY)
- 10494-72-2002-SAR, (2 sheets), (PROPRIETARY)
- 10494-72-2003-SAR, (5 sheets), (PROPRIETARY)
- 10494-72-2004-SAR, (3 sheets), (PROPRIETARY)
- 10494-72-2005-SAR, (5 sheets) (PROPRIETARY)

OS187H Type 1 TC:

- 10494-72-9001-SAR, (3 sheets), (PROPRIETARY)
- 10494-72-9002-SAR, (3 sheets), (PROPRIETARY)
- 10494-72-9003-SAR, (3 sheets) (PROPRIETARY)

Table A.1-1
Key Design Parameters of the NUHOMS® HD System Components

Dry Shielded Canister (32PTH Type 1 DSC)	
Overall length (in.)	193.00 (max), increased from 185.75 (max)
Outside diameter (in.)	69.75 (unchanged)
Cavity length (in.)	171.63 (min), increased from 164.5 (min.)
Shell thickness (in.)	0.5 (unchanged)
Design weight of loaded 32PTH Type 1 DSC (lb)	109,000 ⁽¹⁾
Materials of construction	Stainless steel shell assembly and internals, carbon steel and/or stainless steel shield plugs, aluminum
Neutron absorbing material	Boral™, borated aluminum, metal matrix composite (MMC)
Internal atmosphere	Helium

Horizontal Storage Module (HSM-H)	
Overall length (without back shield wall)	20'-8"
Overall width (without end shield walls)	9'-8"
Overall height	18' 6"
Total weight (not including 32PTH Type 1 DSC) (lbs.)	307,200 ⁽¹⁾
Materials of construction	Reinforced concrete and structural steel
Heat removal	Conduction, convection, and radiation

On-Site Transfer Cask (OS187H Type 1)	
Overall length (in.)	210.50, increased from 197.1
Outside diameter (in.)	92.11, changed from 92.2
Cavity length (in.)	198.75, increased from 186.6
Lead thickness (in.)	3.56 (nom), changed from 3.60 (nom)
Gross weight (including 32PTH Type 1 DSC) (tons)	120.0 ⁽¹⁾ (increased from 114.5)
Materials of construction	Stainless steel shell assemblies and closures with lead shielding
Internal atmosphere	Helium

Note:

(1) Rounded up values

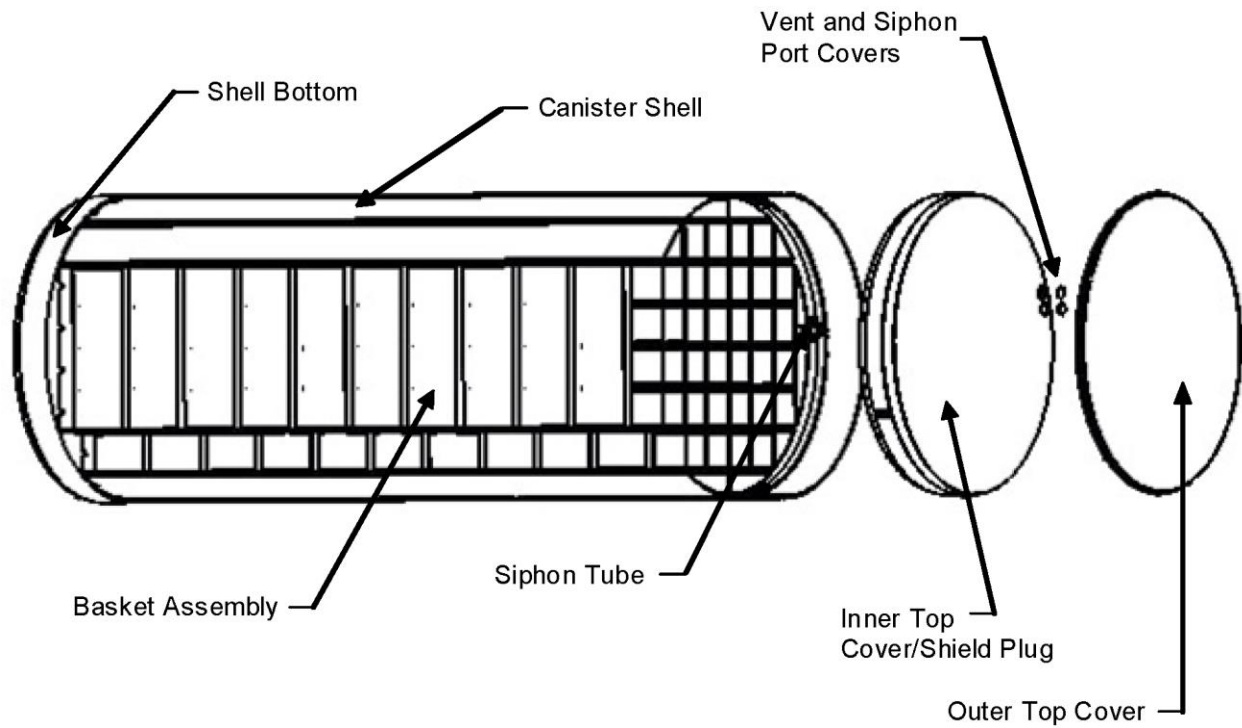


Figure A.1-1
32PTH Type 1 Dry Shielded Canister
(Optional two-part top end configuration shown)

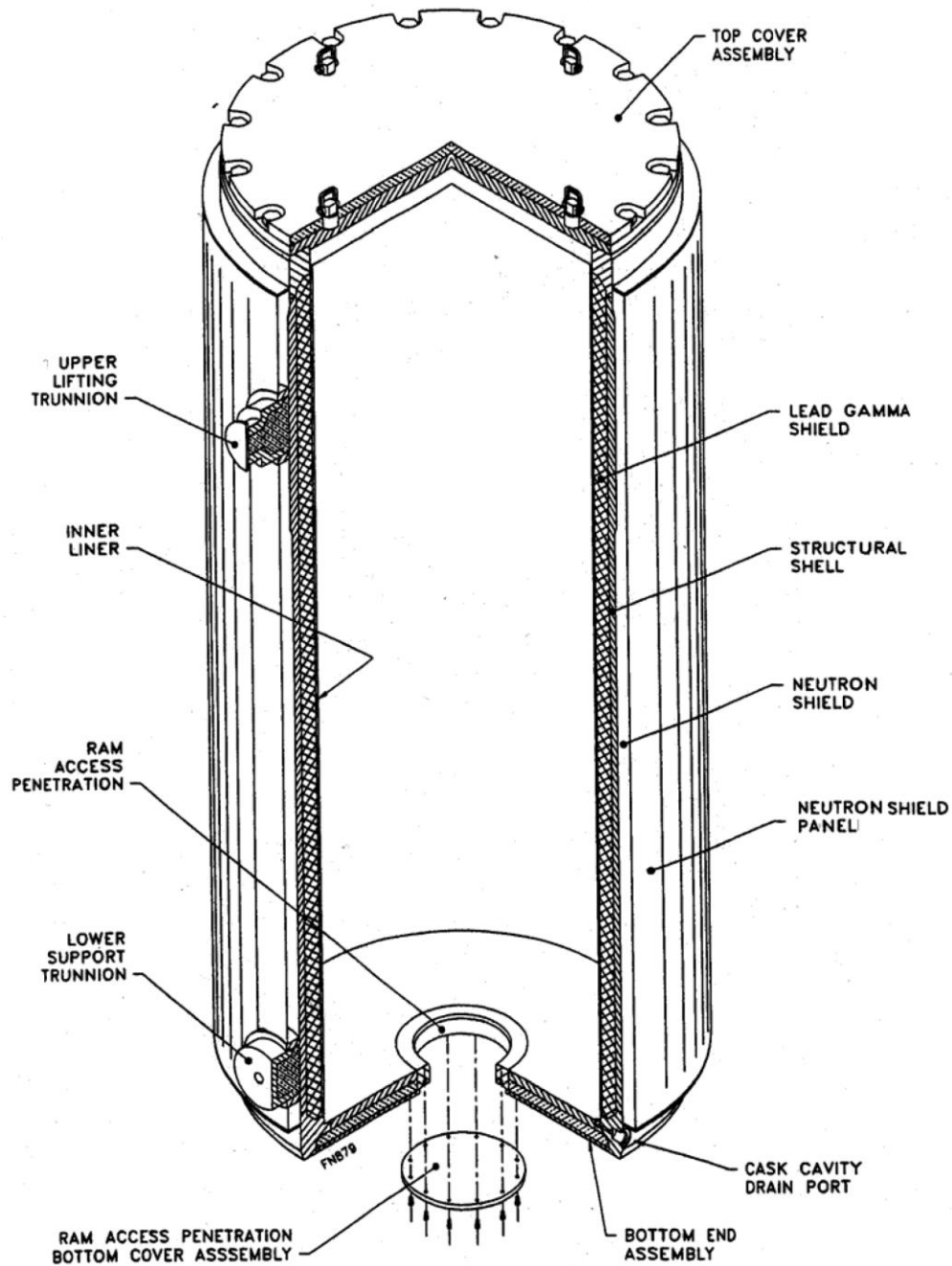


Figure A.1-2
OS187H Type 1 On-Site Transfer Cask

**Proprietary and Security Related Information
for Drawing 10494-72-2001, Rev. 4
Withheld Pursuant to 10 CFR 2.390**

**Proprietary and Security Related Information
for Drawing 10494-72-2002, Rev. 0
Withheld Pursuant to 10 CFR 2.390**

**Proprietary and Security Related Information
for Drawing 10494-72-2003-SAR, Rev. 3
Withheld Pursuant to 10 CFR 2.390**

**Proprietary and Security Related Information
for Drawing 10494-72-2004-SAR, Rev. 2
Withheld Pursuant to 10 CFR 2.390**

**Proprietary and Security Related Information
for Drawing 10494-72-2005, Rev. 1
Withheld Pursuant to 10 CFR 2.390**

**Proprietary and Security Related Information
for Drawing 10494-72-9001, Rev. 1
Withheld Pursuant to 10 CFR 2.390**

**Proprietary and Security Related Information
for Drawing 10494-72-9002, Rev. 1
Withheld Pursuant to 10 CFR 2.390**

**Proprietary and Security Related Information
for Drawing 10494-72-9003, Rev. 3
Withheld Pursuant to 10 CFR 2.390**

Chapter A.2

Principal Design Criteria

No change. The design criteria described in Chapter 2 for the 32PTH DSC and OS187H TC are applicable to the 32PTH Type 1 DSC and the OS187H Type 1 TC. The contents authorized for storage in the 32PTH Type 1 DSC are the same as the authorized contents for the 32PTH DSC described in Section 2.1. The number of fuel assemblies per DSC, maximum heat load per DSC and heat load configurations, basket poison types, and basket geometric configuration are not changed. Similarly, there is no change to the design criteria for environmental conditions and natural phenomena as described in Section 2.2, or to the safety protection systems as described in Section 2.3. Section 2.4 (Decommissioning Considerations), Section 2.5 (Structures, Systems and Components Important to Safety), and Section 2.6 (References) are not changed. As described in Section A.1.1, an elastic-plastic analysis methodology is used for the accident pressure load case of the 32PTH Type 1 DSC. As with the 32PTH DSC, the details of the 32PTH Type 1 DSC evaluation criteria are described in Chapter A.3.

Chapter A.3 Structural Evaluation

TABLE OF CONTENTS

A.3	STRUCTURAL EVALUATION	A.3-1
A.3.1	Structural Design.....	A.3-1
	A.3.1.1 Discussion	A.3-1
	A.3.1.2 Design Criteria	A.3-6
A.3.2	Weights.....	A.3-7
	A.3.2.1 32PTH Type 1 DSC Weight.....	A.3-7
	A.3.2.2 OS187H Type 1 Transfer Cask Weight	A.3-8
	A.3.2.3 HSM-H Weight	A.3-8
A.3.3	Mechanical Properties of Materials.....	A.3-9
A.3.4	General Standards for 32PTH Type 1 DSC, HSM-H, and OS187H Type 1 TC.....	A.3-10
	A.3.4.1 Chemical and Galvanic Reactions.....	A.3-10
	A.3.4.2 Positive Closure.....	A.3-10
	A.3.4.3 Lifting Devices	A.3-10
	A.3.4.4 Heat	A.3-10
	A.3.4.5 Cold	A.3-11
A.3.5	Fuel Rods General Standards for 32PTH Type 1 DSC	A.3-12
A.3.6	Normal Conditions of Storage and Transfer	A.3-13
	A.3.6.1 32PTH Type 1 DSC Normal Conditions Structural Analysis	A.3-13
	A.3.6.2 HSM-H Normal Conditions Structural Analysis.....	A.3-15
	A.3.6.3 OS187H Type 1 Transfer Cask Normal Conditions Structural Analysis	A.3-15
A.3.7	Off-Normal and Hypothetical Accident Conditions.....	A.3-18
	A.3.7.1 32PTH Type 1 DSC Off-Normal and Accident Conditions Structural Analysis	A.3-18
	A.3.7.2 HSM-H Off-Normal and Accident Conditions Structural Analysis	A.3-21
	A.3.7.3 OS187H Type 1 Transfer Cask Off Normal and Accident Conditions Structural Analysis.....	A.3-22

A.3.8	References	A.3-24
A.3.9	Appendices	A.3-25
A.3.10	ASME Code Alternatives.....	A.3-25

A.3 STRUCTURAL EVALUATION

A.3.1 Structural Design

This chapter, including its appendices, summarizes the structural evaluation of the NUHOMS[®] HD System Type 1 components, i.e., the 32PTH Type 1 DSC and the OS187H Type 1 transfer cask (TC).

The 32PTH Type 1 DSC is similar to but a longer version of the 32PTH DSC documented in the main body of this FSAR. As with the 32PTH DSC, the 32PTH Type 1 DSC is designed to accommodate up to 32 intact PWR fuel assemblies (or up to 16 damaged assemblies, with the remaining intact) with the same total heat load of up to 34.8 kW. Similarly, the OS187H Type 1 TC is similar to but a longer version of the OS187H TC.

The structural evaluation criteria for the 32PTH Type 1 DSC and the OS187H Type 1 TC are the same as the evaluation criteria for the 32PTH DSC and OS187H TC described in the main body of this FSAR, with the exception of the analysis methodology used for the evaluation of the accident pressure load case in the 32PTH Type 1 DSC, where an elastic-plastic analysis was used instead of an elastic analysis used for the 32PTH DSC.

A.3.1.1 Discussion

No change.

A.3.1.1.1 General Description of the 32PTH Type 1 DSC

The principal characteristics of the 32PTH Type 1 DSC are described in Chapter A.1, Section A.1.2.1, including the changes implemented in the 32PTH Type 1 DSC relative to the 32PTH DSC. The 32PTH Type 1 DSC is shown on drawings 10494-72-2001-SAR to 10494-72-2005-SAR in Section A.1.5.

For purposes of the structural analysis, the 32PTH Type 1 DSC is divided into the 32PTH Type 1 DSC shell assembly and the internal basket assembly.

A. DSC Shell Assembly Description

The 32PTH Type 1 canister shell assembly and design details are shown on drawings 10494-72-2001-SAR (main assembly), 10494-72-2002-SAR (shell assembly), and 10494-72-2005-SAR (alternate two-piece top end assembly design) in Section A1.5. As with the 32PTH DSC, the 32PTH Type 1 DSC shell assembly is a high integrity stainless steel (SA-240 Type 304 or SA-182 Type F304) welded vessel that provides confinement of radioactive materials, encapsulates the fuel in an inert atmosphere (the canister is backfilled with helium before being seal welded closed), and provides biological shielding (in axial direction).

The 32PTH Type 1 main structural components include the welded cylindrical shell and the top and bottom end assemblies. The top end assembly may be a three-piece assembly, (a solid shield plug, made of A36 carbon steel, and the inner cover and outer cover plates, both made of SA-240 Type 304 stainless steel) or, as an alternate, a two-piece assembly, consisting of a combined top

shield plug/inner cover assembly, and an outer cover plate. The combined top shield plug/inner cover may be a single stainless steel piece (SA-240 Type 304 or SA-182 Type F304), or two stainless steel plates welded together, or a carbon steel shield plug encased within welded stainless steel plates. The various top end assembly design options for the alternate design are similar to those of the 32PTH DSC, as described in Section 3.1.1.1. For the bottom end assembly, the four optional design configurations present in the 32PTH are kept for the 32PTH Type 1 DSC. Although the total thickness of the bottom end assembly remains the same (8.75"), the minimum thicknesses of the bottom end inner and outer cover plates have increased from 1.69" and 1.70", respectively, in the 32PTH DSC to 2.25" and 2.00" in the 32PTH Type 1 DSC.

The remaining 32PTH Type 1 shell assembly structural components include the grapple ring assembly, the support ring and the lifting lugs (in the three-piece top end assembly design), or lifting blocks (in the two-piece alternate top end assembly design). The grapple ring assembly, which is welded to the shell bottom or outer bottom cover plate, is used to insert/extract the DSC to and from the Horizontal Storage Module (HSM-H). The grapple ring minimum thickness is increased from 1.00" to 1.20" in the 32PTH Type 1 DSC. The support ring, welded to the cylindrical shell, supports the shield plug. The 32PTH Type 1 DSC with the three-piece top end assembly design option incorporates four lifting lugs (welded to the shell and to the support ring) in lieu of the four lifting blocks which are welded to the inside of the shell bottom in the alternate design. The lifting lugs/lifting blocks are used to lift the DSC into the transfer cask prior to fuel loading operations.

The 32PTH Type 1 DSC shell assembly is designed, fabricated, examined, and tested in accordance with the same ASME Code Subsection NB [6] requirements as for the 32PTH DSC presented in Section 3.1.1.1.A. The 32PTH Type 1 DSC top closure is designed, fabricated, and inspected using the same alternatives to the ASME code specified in Section 3.10. The outer top cover plate and inner top cover plate are sealed by separate, redundant closure welds. The inner top cover (or inner top cover/top shield plug in the alternate two-piece top end design) is welded to the 32PTH Type 1 DSC shell to form the confinement boundary at the top end of the 32PTH Type 1 DSC, as shown in Chapter A.7, Figure A.7-1 (or Chapter 7, Figure 7-1 for the alternate top end design). The outer top cover plate provides structural support to the confinement boundary. All closure welds are multiple layer welds. Both, the inner and outer top cover plates to shell welds are examined by multi-level liquid penetrant to effectively eliminate through wall leaks. The three-piece top end assembly incorporates a vent and siphon block, welded to the shell, that is similar to that in other NUHOMS® canister designs [9]. The vent and siphon block weld to the shell and the inner top cover plate weld to the vent and siphon block are part of the confinement boundary. These welds are also multiple layer welds and receive multi-level liquid penetrant examination.

The leak test and the acceptance criterion of 1×10^{-7} ref. cm^3/sec as defined in ANSI N14.5 [2] of the DSC shell and bottom end assembly during fabrication and of the inner top closure weld (including vent/siphon cover welds) after loading of the fuel assemblies, have not changed from those of the 32PTH DSC.

The use of a strongback is not required during fuel loading operations when using the 32PTH Type 1 DSC.

B. Fuel Basket Assembly Description

The details of the 32PTH Type 1 basket assembly are shown in drawings 10494-72-2003-SAR and 10494-72-2004-SAR, provided in Section A.1.5. The overall length of the 32PTH Type 1 DSC basket is increased from 162.00" to 169.00". The internal canister cavity length is also increased from 164.50" minimum to 171.63" minimum to allow for thermal expansion, tolerances, and access to the top of the fuel assemblies.

The description for the basket assembly presented in Section 3.1.1.1 (B) for the 32PTH basket is applicable to the 32PTH Type 1 basket assembly. Additionally, when lifting blocks are not used, the circumferential orientation of the basket is maintained by the use of a key welded to the inside diameter of the shell at two opposite azimuths, and two accompanying slots in the basket rails. The purpose of the basket key is non-safety and is intended to prevent rotation during fabrication and during shipment of the empty canister.

A.3.1.1.2 General Description of the HSM-H

The general description of the HSM-H presented in Section 3.1.1.2 is applicable when the HSM-H is loaded with a 32PTH Type 1 DSC. The spacer mounted on the support rails used to accommodate shorter length DSCs is not needed for storage of the 32PTH Type 1 DSC. Additionally, the HSM-H support rail structure length has been slightly increased. The changes to the HSM-H support rail are shown in drawings 10494-72-100 and 10494-72-107.

A.3.1.1.3 General Description of the OS187H On-Site Transfer Cask

The NUHOMS® OS187H Type 1 On-Site transfer cask consists of a structural shell, gamma shielding material, and solid and liquid (water) neutron shield. The OS187H Type 1 TC is similar to the OS187H TC described in Section 3.1.1.3. The OS187H Type 1 TC is approximately 13 inches longer than the OS187H TC due to an increase in the interior cavity length to accommodate the longer 32PTH Type 1 DSC. Other main changes include:

- The OS187H Type 1 TC trunnions are made of monolithic solid steel forgings (the OS187H trunnions have a cutout that is filled with resin material) to accommodate the increased weight of the 32PTH Type 1 DSC and provide additional margins. The lower trunnion material is changed from SA-182 Type F304 to SA-182 Type F304N.
- The upper course of the structural shell thickness is increased from 2.00" to 2.38". Similarly, the upper trunnions pad plate is increased from 1.00" to 1.375".
- The inner liner thickness is increased from ½" to 5/8".

The overall dimensions of the OS187H Type 1 TC are 210.50" long and 92.11" in diameter. The TC structural shell is 83.63" in diameter (upper course). The TC cavity is 198.75" long and 70.50" in diameter. Detailed design drawings for the OS187H Type 1 TC are provided in drawings 10494-72-9001-SAR through 10494-72-9003-SAR on Chapter A.1, Section A.1.5. The materials used to fabricate the TC are shown in the parts list on each drawing. Where more than one material has been specified for a component, the most limiting properties are used in the analyses in the subsequent chapters of this Final Safety Analysis Report.

The gross weight of the loaded transfer cask is approximately 120.0 tons including a DSC payload of 54.3 tons. Section A.3.2.2 summarizes the weights of the NUHOMS® OS187H Type 1 packaging components.

The TC is fabricated primarily of stainless steel. Non-stainless steel members include the cast lead shielding between the inner radial shell and the structural shell, the O-ring seals, the NS-3 shielding material in the top and bottom end assemblies, and the carbon steel closure bolts. The top cover is bolted to the top flange by 24-1 1/2 in. diameter high strength bolts and sealed with O-ring. A cover plate is provided to seal the bottom hydraulic ram access penetration of the cask (by 12-1/2 in. high strength bolts with O-ring) during fuel loading and transferring the canister to the ISFSI. The dimensions and design details of the OS187H Type 1 TC are provided in drawings 10494-72-9001-SAR through 10494-72-9003-SAR in Chapter A.1, Section A.1.5.

The geometry and dimensions of the OS176H Type 1 TC trunnions are shown on Sheet 2 of Drawing 10494-72-9002-SAR. Some details/features of the OS187H Type 1 TC trunnions are different from those of the OS187H TC, e.g., the bearing width in each trunnion cylinder has been increased for ease of operations. In addition, the trunnion shielding pockets which are machined cavities filled with resin shielding material in the OS187H TC are deleted. Instead, the OS187H Type 1 TC trunnions are solid steel components.

The following sections provide physical and functional descriptions of each major component of the transfer cask.

A. Transfer Cask Body and Structural Components

The shell or cask body cylinder assembly is an open ended (at the top) cylindrical unit with an integral closed bottom end. This assembly consists of concentric inner shell and outer shell (both SA-240 Type 304), welded to massive closure flanges (SA-182 Type F304N) at the top and bottom ends. The inner shell is 0.625 inches thick and has a 70.50 inch inside diameter. The outer shell is the primary structural shell and is 1.5 inches (lower course) to 2.38 inches thick (upper course), and has a 78.87 inch inside diameter. The annulus between the shells is filled with lead shielding. The lead gamma shield is 3.56 inches (nominal) thick and is poured into the annulus in a molten state using a carefully controlled procedure.

The transfer cask bottom end assembly and top cover assembly are similar to the OS187H transfer cask with the exception that the resin neutron shield in the OS187H transfer cask is replaced with NS-3, a castable neutron shielding material. As with the OS187H, the OS187H Type 1 transfer cask is designed to maintain a helium atmosphere in the cask cavity.

The OS187H Type 1 transfer cask is designed, fabricated, examined, and tested in accordance with the requirements of Subsection NC [3] of the ASME Code to the maximum practical extent. The alternatives to the ASME Code presented in Section 3.10 for the OS187H TC are also applicable to the OS187H Type 1 TC.

B. Gamma and Radial Neutron Shielding

The description provided in Section 3.1.1.3 (B) is applicable to the OS187H Type 1 TC except that the resin material in the top and bottom assemblies, which provides axial neutron shielding in

the OS187H, is replaced with NS-3, a castable cementitious material. NS-3 has been used in other NUHOMS® applications, e.g., the OS197 transfer cask [9]. The radial neutron shielding provided by liquid water enclosed in a radial outer stainless steel shell welded to the structural shell is of similar design as the OS187H transfer cask.

C. Tiedown and Lifting Devices

The description provided in Section 3.1.1. 3 (C) is applicable to the OS187H Type 1 TC. The OS187H Type 1 trunnions are solid steel forgings as opposed to the OS187H trunnions that incorporate a neutron shield plug. The top trunnions are designed, fabricated, and tested in accordance with ANSI N14.6 [4] as single failure proof lifting devices. Consequently, they are designed with a factor of safety of 6 against the material yield strength and a factor of safety of 10 against the material ultimate strength.

D. Operational Features

The NUHOMS® OS187H Type 1 transfer cask is not considered to be operationally complex and is designed to be compatible with spent fuel pool loading/unloading methods. All operational features are readily apparent from inspection of the General Arrangement Drawings provided in Chapter A.1, Section A.1.5. The sequential steps to be followed for cask loading, testing, and unloading operations are provided in Chapter A.8.

A.3.1.1.4 Discussion of NUHOMS® HD System Drop Analysis

All lifting of the TC loaded with the DSC must be made within the existing heavy loads requirements and procedures of the licensed nuclear power plant.

The transfer cask is transported to the ISFSI in a horizontal configuration. Therefore, the only credible drop accident during storage or transfer operations is a side drop. The transfer cask, canister and basket assemblies and fuel cladding are analyzed for this accident in the following sections.

In addition, a vertical drop or corner drop accident scenarios may need to be evaluated under 10CFR50 should the user not be able to demonstrate that this accident drop is not credible during loading operations, or during transport operations governed under 10CFR71. Similarly, the fuel cladding integrity has not been demonstrated for this accident scenario. An additional safety review by the user is required to demonstrate fuel cladding integrity under 10CFR50 or to demonstrate that the end drop accidents are not credible.

The drop analyses of the NUHOMS® HD 32PTH Type 1 DSC and OS187H Type 1 transfer cask components are performed in the following appendices.

Appendix A.3.9.1

This appendix describes the detailed analysis of the 32PTH Type 1 DSC shell assembly and basket assembly for all the loading conditions. For the drop loads, the DSC shell assembly is analyzed for the 75g side and end drops. The basket assembly is also analyzed for the 75g side

and end drops. The 75g side drop in conjunction with the 75g end drop is considered to bound the 22g corner drop.

Appendix A.3.9.2

This appendix describes the detailed analysis of the OS187H Type 1 TC for all the loading conditions. For the drop loads, the TC is analyzed for the 75g side and end drops. The results for the TC side drop using LS-DYNA are reported in Appendix A.3.9.10.

Appendix A.3.9.3

This appendix describes the detailed analysis of the TC top cover bolt and ram cover bolt due to the 22g corner drop. The stress analysis is performed in accordance with NUREG/CR-6007.

Appendix A.3.9.4

Since the end and corner drops are not credible under 10CFR Part 72 the OS187H Type 1 TC lead slump and inner shell buckling analysis for the 75g end drop load are not evaluated. Vertical drop or corner drop accident scenarios may need to be evaluated under 10CFR50 should the user not be able to demonstrate that this accident drop is not credible during loading operations, or during transport operations governed under 10CFR71.

Appendix A.3.9.8

No change to the structural evaluations of the fuel cladding presented in Appendix 3.9.8.

Appendix A.3.9.10

This appendix provides the justification for the rigid body accident drop accelerations applicable to the OS187H Type 1 TC based on the LS-DYNA accident drop analysis documented in Appendix 3.9.10.

Appendix A.3.9.11

This appendix computes the dynamic amplification factor (DAF) to be applied to the response accelerations obtained from the side drop accident dynamic analysis of the transfer cask (TC) when applying those accelerations as input to an equivalent static analysis of the 32PTH Type 1 DSC.

A.3.1.2 Design Criteria

No change. The design criteria described in Section 3.1.2 is not changed and remains applicable to the 32PTH Type 1 DSC and OS187H Type 1 TC.

A.3.2 Weights

The nominal 32PTH Type 1 DSC, HSM-H and OS187H Type 1 transfer cask geometry is used to compute the weights of the NUHOMS® HD system components. Material densities are unchanged and are provided in Chapter 3.

A.3.2.1 32PTH Type 1 DSC Weight

The bounding weight of the loaded 32PTH Type 1 DSC is 108.61 kips (54.3 tons). The weights of the major individual subassemblies are listed in following table.

32PTH Type 1 DSC Summary of Nominal Component Weights

Component	Nominal Weight (lb x 1000)
Canister shell	5.81
Outer top cover plate	2.14
Inner top cover plate	2.15
Top shield plug and support ring	8.57
Bottom end assembly	9.70
Grapple ring	0.075
Total canister assembly	28.44
Fuel compartments (32)	10.48
Aluminum/poison plates	4.67
Stainless steel plates	2.36
Small support rails	3.08
Large support rails	8.86
Total Fuel Basket	29.45
Total Empty DSC (Basket & Canister)	57.89
Fuel assembly weight (32) @ 1585 lb/assembly	50.72
Total loaded DSC weight	108.61

A.3.2.2 OS187H Type 1 Transfer Cask Weight

The total weight of the loaded NUHOMS® OS187H Type 1 transfer cask is 239.47 kips (119.7 tons). The weights of the major individual subassemblies are listed in following table.

OS187H Type 1 Transfer Cask Summary of Nominal Component Weights

Component	Nominal Weight (lb x 1000)
Structural shell	23.73
Inner shell	7.89
Lead gamma shield	66.65
Top flange	2.63
Bottom flange	3.40
Top cover assembly	5.36
Bottom assembly	3.94
Neutron shield panel assembly	5.14
Radial neutron shield (water)	8.67
Upper trunnion pair	1.45
Lower trunnion pair	1.06
Total Empty Transfer Cask Weight	130.00⁽¹⁾
Total Transfer Cask with Empty DSC Weight	188.00⁽¹⁾
Total Transfer Cask with Loaded DSC Weight (Dry)	240.00^{(1) (2) (3)}

Notes:

(1) Rounded up to nearest 1,000 lbs.

(2) Includes a cask spacer with an approximate weight of 900 lbs.

(3) 250.0 kips is conservatively used for the trunnion analysis.

A.3.2.3 HSM-H Weight

No change. See Section 3.2.3 for details of the HSM-H weight.

A.3.3 Mechanical Properties of Materials

No change. The material properties described in Section 3.3 remain applicable to the 32PTH Type 1 DSC and OS187H Type 1 TC. The properties for the resin shielding material used in the stress analysis of the OS187H TC are similar to those of the NS-3 material in the OS187H Type 1 TC.

A.3.4 General Standards for 32PTH Type 1 DSC, HSM-H, and OS187H Type 1 TC

A.3.4.1 Chemical and Galvanic Reactions

No change. The information provided in Section 3.4.1 is unchanged and applicable to the 32PTH Type 1 DSC and OS187H Type 1 TC.

A.3.4.2 Positive Closure

No change. The information provided in Section 3.4.2 is unchanged and applicable to the 32PTH Type 1 DSC and OS187H Type 1 TC.

A.3.4.3 Lifting Devices

No change. The information provided in Section 3.4.3 is unchanged and applicable to the 32PTH Type 1 DSC and OS187H Type 1 TC.

A.3.4.4 Heat

A.3.4.4.1 Summary of Pressures and Temperatures

No change. As documented in Chapter A.4, the heat transfer analyses documented in Chapter 4 for the 32PTH DSC inside the OS187H TC during transfer and in the HSM-H during storage are bounding relative to the 32PTH Type 1 DSC in the HSM-H and in the OS187H Type 1 TC.

Therefore, the pressures and temperatures used for the stress analyses of the 32PTH DSC and the OS187H TC in Chapter 3 are also applicable for the 32PTH Type 1 DSC and the OS187H Type 1 TC. As discussed in Section A.3.6 and Section A.3.7, the Chapter 4 temperature distributions are conservatively applied (considering the longer length of the 32PTH Type 1 DSC and OS187H Type 1 TC) for the structural evaluations.

Thus, the maximum and minimum temperatures for the various components for normal, off-normal, and accident conditions are the same as those summarized in Tables 4-1 to Table 4-6. Similarly, the maximum pressures are the same as those summarized in Table 4-10. The Table 4-10 pressures bound those used in the structural analysis of the 32PTH Type 1 DSC.

A.3.4.4.2 Differential Thermal Expansion

Potential interference due to differential thermal expansion between the 32PTH Type 1 DSC shell assembly, the basket assembly, and transfer cask components is evaluated in Appendix A.3.9.1, Section A.3.9.1.4.

A.3.4.4.3 Stress Calculations

The stress analyses have been performed using the acceptance criteria presented in Section 3.1.2. The structural analyses for the 32PTH Type 1 DSC and OS187H Type 1 TC are summarized in Sections A.3.6 and A.3.7, for normal, off-normal, and hypothetical accident conditions, respectively.

A.3.4.5 Cold

No change.

A.3.5 Fuel Rods General Standards for 32PTH Type 1 DSC

No change. The fuel rod evaluations presented in Section 3.5 are unchanged for the 32PTH Type 1 DSC.

A.3.6 Normal Conditions of Storage and Transfer

This section presents the structural analyses of the 32PTH Type 1 DSC, and the OS187H Type 1 TC subjected to normal conditions of storage and transfer. The analyses performed evaluate these two major NUHOMS® HD System components for the design criteria described in Section A.3.1.2 of this appendix. The structural analyses of the HSM-H presented in Chapter 3.6 are bounding and thus, not changed.

The 32PTH Type 1 DSC is subjected to both storage and transfer loading conditions and the OS187H Type 1 TC is only subjected to transfer loading conditions.

Numerical analyses have been performed for the normal and accident conditions, as well as for the lifting loads. In general, numerical analyses have been performed for the regulatory events. These analyses are summarized in Section A.3.6 and Section A.3.7, and described in detail in the Appendices A.3.9.1 through A.3.9.10 listed below.

The detailed structural analysis of the NUHOMS® HD System is included in the following appendices:

Appendix A.3.9.1	32PTH Type 1 DSC (Canister and Basket) Structural Analysis
Appendix A.3.9.2	OS187H Type 1 Transfer Cask Body Structural Analysis
Appendix A.3.9.3	OS187H Type 1 Transfer Cask Top Cover and Ram Access Cover Bolts Analyses
Appendix A.3.9.4	Not used (since the end and corner drops are not credible under 10CFR Part 72, the lead slump and inner shell buckling analysis of the OS187H Type 1 TC for the 75g end drop load are not documented).
Appendix A.3.9.5	OS187H Type 1 Transfer Cask Trunnion Analysis
Appendix A.3.9.6	OS187H Type 1 Transfer Cask Shield Panel Structural Analysis
Appendix A.3.9.7	Deleted (superseded by Appendix A.3.9.10)
Appendix A.3.9.8	No change. (Damaged Fuel Cladding Structural Evaluation)
Appendix A.3.9.9	No change. (HSM-H Structural Analysis)
Appendix A.3.9.10	OS187H Type 1 Transfer Cask Dynamic Impact Analysis
Appendix A.3.9.11	32PTH Type 1 DSC Dynamic Amplification Factors

A.3.6.1 32PTH Type 1 DSC Normal Conditions Structural Analysis

Details of the structural analysis of the 32PTH Type 1 DSC are provided in Appendix A.3.9.1. The fuel basket assembly and canister shell assembly are analyzed independently. The structural evaluation of the 32PTH Type 1 fuel basket assembly is described in Section A.3.6.1.1. The structural evaluation of the canister shell assembly is described in Section A.3.6.1.2.

A.3.6.1.1 32PTH Type 1 DSC Fuel Basket Assembly Normal Condition Structural Evaluation

No change. As described in Appendix A.3.9.1, Section A.3.9.1.2, the ANSYS models, material properties, and design criteria used for the evaluation of the fuel basket assembly are the same between the 32PTH and the 32PTH Type 1 DSCs, and, therefore, the stress analysis results documented in Section 3.9.1.2 for the 32PTH fuel basket assembly are applicable to the 32PTH

Type 1 fuel basket assembly. As described in Section 3.9.1.2, a 360° finite element model of a 15 inch segment of the basket assembly is constructed for the structural evaluation of the basket assembly.

Based on the results of these analyses, the design of the 32PTH Type 1 DSC basket is structurally adequate with respect to normal condition transfer and storage loads.

A.3.6.1.2 32PTH Type 1 DSC Canister Shell Assembly Normal Condition Structural Evaluation

This section summarizes the evaluation of the structural adequacy of the 32PTH Type 1 DSC canister shell assembly under all applied normal condition loads. Detailed evaluation of the stresses generated in the canister is presented in Appendix A.3.9.1, Section A.3.9.1.3.2. The DSC canister shell buckling evaluation is presented in Appendix A.3.9.1, Section A.3.9.1.3.3.

Elastic and elastic-plastic analyses are performed to calculate the stresses in the 32PTH Type 1 DSC canister under the transfer and storage loads. These detailed load cases are summarized in Appendix A.3.9.1, Tables A.3.9.1-3, A.3.9.1-4 and A.3.9.1-13.

The calculated stresses in the canister shell due to normal transfer loading conditions are summarized in Appendix A.3.9.1, Tables A.3.9.1-5, A.3.9.1-6, A.3.9.1-9, and A.3.9.1-10. The stresses due to normal storage loading conditions are summarized in Appendix A.3.9.1, Tables A.3.9.1-14, and A.3.9.1-15.

The 32PTH Type 1 DSC with the three-piece top end assembly configuration (separate inner cover plate, shield plug, and outer cover plate) is considered to bound the alternate design with a two-piece top end assembly (combined top shield plug/inner cover plate and outer cover plate). Similarly, the bottom end assembly configuration, consisting of separate inner bottom, shield plug and outer bottom plates is considered the bounding configuration relative to that of a DSC with the optional single or two piece bottom end configurations. See discussion in Section A.3.9.1.3.4.

As described in Chapter A.8, Section A.8.1.1.3, operation steps 7 and 13, a maximum of 15.0 psig air pressure may be applied at the canister vent port to assist draining of the water. The canister is structurally evaluated for a bounding 25 psig internal pressure using the 2-D ANSYS finite element model described in Appendix A.3.9.1, Section A.3.9.1.3.2. The outer cover plate of the canister is removed from the 2-D model, since it is not yet installed during the application of this 25 psig air pressure. The maximum stress intensity in the canister is calculated to as 7.09 ksi. The stress limit for membrane stress per ASME B&PV Code Subsection NB [6] is 16.40 ksi. Therefore, the application of 25 psig air pressure to the canister is acceptable.

Based on the results of these analyses, the design of the 32PTH Type 1 DSC canister is structurally adequate with respect to both transfer and storage loads under the normal conditions.

A.3.6.2 HSM-H Normal Conditions Structural Analysis

No change. The DSC weight used for the structural evaluation of the HSM-H (110,000 lb) bounds the calculated weight of the 32PTH Type 1 DSC (108,610 lb). In addition, as discussed in Chapter A.4, the temperature distributions of the HSM-H loaded with a 32PTH Type 1 DSC are bounded by those of the HSM-H loaded with a 32PTH DSC documented in Chapter 4. Therefore, the structural evaluation of the HSM-H loaded with a 32PTH DSC, as documented in Section 3.6.2 and Appendix 3.9.9, are applicable for a HSM-H loaded with the 32PTH Type 1 DSC.

A.3.6.3 OS187H Type 1 Transfer Cask Normal Conditions Structural Analysis

Details of the structural analysis of the OS187H Type 1 transfer cask are provided in Appendices A.3.9.2 through A.3.9.6. The contents of each of these appendices are as follows.

Appendix A.3.9.2	OS187H Type 1 Transfer Cask Body Structural Analysis
Appendix A.3.9.3	OS187H Type 1 Transfer Cask Lid and Ram Access Cover Bolt Analyses
Appendix A.3.9.5	OS187H Type 1 Transfer Cask Trunnion Analysis
Appendix A.3.9.6	OS187H Type 1 Transfer Cask Shield Panel Structural Analysis

A.3.6.3.1 Structural Analysis of the Transfer Cask Body under Normal Conditions

The details of the structural analyses of the NUHOMS® OS187H Type 1 TC body including the cylindrical shell assembly and bottom assembly, the top cover, and the local stresses at the trunnion/cask body interface are presented in Appendix A.3.9.2. The specific methods, models and assumptions used to analyze the cask body for the various individual loading conditions specified in 10CFR72 [1] are described in that appendix.

The OS187H Type 1 TC body structural analyses for normal conditions use static or quasistatic linear elastic methods. The stresses and deformations due to the applied loads are generally determined using the ANSYS [7] computer program.

Table A.3.9.2-1 of Appendix A.3.9.2 summarizes the maximum stresses in the transfer cask body computed for normal conditions of transfer. The maximum stresses in each component are listed along with the normal loading condition that generates the stress. The results are evaluated against the ASME Code [3] design criteria described in Section A.3.1.2 of this chapter.

Based on the results of these analyses, the design of the OS187H Type 1 TC is structurally adequate with respect to normal condition (Level A) transfer loads.

A.3.6.3.2 Transfer Cask Top Cover and Ram Access Cover Bolt Normal Condition Analysis

The detailed calculations for the top cover and ram access cover bolts are presented in Appendix A.3.9.3. The analysis is based on NUREG/CR-6007 [8]. The bolts are analyzed for the following normal loading conditions: operating pre-load, gasket seating load, internal pressure, and temperature changes.

The bolt preload is calculated to withstand the worst case load combination and to maintain a clamping (compressive) force on the closure joint, under normal conditions. Based upon the load

combination results (see Appendix A.3.9.3, Sections A.3.9.3.3 and A.3.9.3.8), it is shown that a positive (compressive) load is maintained on the clamped joint for all normal condition load combinations.

A summary of the calculated top cover bolt stresses is provided in Appendix A.3.9.3, Section A.3.9.3.5. The calculations result in a maximum average tensile stress of 37.4 ksi, which is below the allowable tensile stress of 92.4 ksi for normal conditions. The maximum average shear stress in the bolts is due to torsion during pre-loading. This stress is 6.8 ksi, which is well below the allowable shear stress of 55.4 ksi. The maximum combined stress intensity due to tension plus shear plus bending is 72.9 ksi, which is also less than the maximum allowable stress intensity of 124.7 ksi.

A summary of the calculated ram access bolt stresses is provided in Appendix A.3.9.3, Section A.3.9.3.10. The analysis results in a maximum average tensile stress of 70.8 ksi, which is below the allowable tensile stress of 92.4 ksi for normal conditions. The maximum normal condition shear stress is 15.9 ksi, which is well below the allowable shear stress of 55.4 ksi. The maximum combined stress intensity due to tension plus shear plus bending is 97.3 ksi, which is also less than the maximum allowable stress intensity of 124.7 ksi.

A.3.6.3.3 Transfer Cask Normal Condition Trunnion Analysis

Appendix A.3.9.5 presents the evaluation of the trunnion stresses in the NUHOMS® OS187H Type 1 TC due to all applied loads during fuel loading and transfer operations.

The NUHOMS® OS187H Type 1 TC has two upper trunnions constructed from SA-182 Type FXM-19 and two lower trunnions constructed from SA-182 Type F304N stainless steel material. Both sets of trunnions are solid forged components welded to the structural shell of the transfer cask, which is constructed from SA240 Type 304 stainless steel. The upper trunnions are used to lift the cask with an empty DSC into a fuel pool. After the spent fuel has been loaded into the DSC, the upper trunnions are used to lift the cask to the decontamination area. After draining, drying, and closure welding of the DSC, the cask lid is bolted onto the transfer cask and the cask is vertically lifted to the transfer trailer where the cask is mated with the transfer skid front trunnion towers and pivoted about the lower trunnions into its horizontal position. In its horizontal position, the cask is supported by its four trunnions which are mounted on the four trunnion towers of the transfer skid.

Based on the loading and transfer scenario described above, the top trunnions are analyzed for 6g vertical lifting loads, and both sets of trunnions are evaluated for a prescribed set of transfer handling loads.

The transfer cask shell and trunnions are assumed to be at 300 °F during transfer. This assumption is conservative based on the thermal evaluation performed in Chapter 4.

The calculated maximum trunnion stresses are summarized in Appendix A.3.9.5, Table A.3.9.5-1 and compared with their corresponding allowable stresses. Table A.3.9.5-1 shows that all calculated trunnion stresses are less than their corresponding allowable stresses. Therefore, the

NUHOMS® OS187H Type 1 TC top and bottom trunnions are structurally adequate to withstand loads during lifting and transfer operations.

A.3.6.3.4 Transfer Cask Shield Panel Structural Analysis for Normal Conditions

Appendix A.3.9.6 presents the evaluation of the stresses in the NUHOMS® OS187H Type 1 TC neutron shield shell due to all applied loads during fuel loading and transfer operations.

A finite element model, similar to that of the OS187H TC neutron shield panel, is developed for the structural analysis of the outer neutron shield shell, end closure, central plates and structural shell. These structural components were modeled with two dimensional axisymmetric elements. The same finite element model is used for all loading conditions.

Table A.3.9.6-1 of Appendix A.3.9.6 summarizes the calculated stresses for the transfer cask lifting and transfer loads. Based on the results of the analysis, it is concluded that the outer shell structure is structurally adequate for the specified transfer loads.

A.3.7 Off-Normal and Hypothetical Accident Conditions

This section presents the structural analyses of the 32PTH Type 1 DSC, the HSM-H and the OS187H Type 1 TC subjected to off normal and hypothetical accident conditions of storage and transfer. The analyses are summarized in Sections A.3.7.1, A.3.7.2 and A.3.7.3 of this appendix and are evaluated against the design criteria described in Section A.3.1.2 of this chapter.

The 32PTH Type 1 DSC is subjected to both storage and transfer loading conditions, while the HSM-H is only subjected to storage loading conditions and the OS187H Type 1 TC is only subjected to transfer loading conditions.

A.3.7.1 32PTH Type 1 DSC Off-Normal and Accident Conditions Structural Analysis

Details of the structural analysis of the 32PTH Type 1 DSC are provided in Appendix A.3.9.1. The fuel basket assembly and canister shell assembly are analyzed independently. The structural analysis of the fuel basket assembly is described in Appendix A.3.9.1, Section A.3.9.1.2, while the structural analysis of the canister shell assembly is described in Section A.3.9.1.3. A 360° finite element model of a 15" segment of the basket assembly is constructed for the structural evaluation of the fuel basket assembly. Four finite element models are used for the structural evaluation of the canister shell assembly. A 2-D axisymmetric model used for the analysis of axisymmetric loads, two 3-D models modeling the top and bottom halves of the shell assembly, respectively, used for the analysis of non-axisymmetric loads, and a 3-D local model of the lifting lugs welded to the shell assembly to evaluate stresses during lifting of the DSC and placement into the transfer cask prior to fuel loading.

A.3.7.1.1 32PTH Type 1 DSC Fuel Basket Assembly Off Normal and Accident Condition Structural Analysis

A.3.7.1.1.1 32PTH Type 1 Fuel Basket Off-Normal and Accident Condition Stress Analysis

The fuel basket assembly stress analyses are performed for off-normal and accident condition loads during fuel transfer and storage.

The mechanical properties of structural materials used in the basket and canister are shown in Section 3, Table 3-5, and Appendix 3.9.1, Table 3.9.1-1, as a function of temperature. All structural components of the fuel basket and support rails are constructed from SA-240, Type 304 stainless steel, with properties taken from AMSE B&PV Code [5].

The load cases used for the analyses of the 32PTH Type 1 fuel basket assembly are the same as for the 32PTH fuel basket assembly and are as summarized in Section 3.9.1.2.2.

The details of the stress analysis of the basket assembly, as presented in Appendix 3.9.1, Section 3.9.1.2.3 are applicable without change to the 32PTH Type 1 fuel basket assembly. As discussed in Section 3.9.1.2.3, the basket stress analyses are performed using a 3-dimensional finite element model of the cross section of the basket assembly. The model is a 15" long segment of the basket assembly and is described in detail in Appendix 3.9.1, Section 3.9.1.2.3 (A). This model is used for the analysis of the transfer side drop impact loads, storage seismic loads, and both, transfer

and storage thermal load cases. Hand calculations are used for the evaluation of the transfer end drop load cases.

The stresses calculated for the 32PTH DSC fuel basket assembly and summarized in Tables 3.9.1-4a and 3.9.1-4b for the transfer accident loads and Table 3.9.1-5 for the storage accident loads are applicable to the 32PTH Type 1 basket assembly.

The maximum shear load in the fusion welds for the 75g side drop accident loading condition is calculated in Appendix 3.9.1, Section 3.9.1.2.3.B.5. The calculated maximum shear force during side drop is 7,208 lb. The fusion weld is qualified by a pull test (shear). The minimum test load is 17.1 kips. This test load includes a safety factor of 2 and a correction for material strength for room temperature testing.

Based on the results of these analyses, the design of the 32PTH Type 1 DSC basket is structurally adequate with respect to off-normal and accident conditions of transfer and storage loads.

A.3.7.1.1.2 32PTH Type 1 DSC Fuel Basket Accident Condition Buckling Analysis

As stated in Section A.3.9.1.2.4, the details of the buckling analysis is presented in detail in Appendix 3.9.1, Section 3.9.1.2.4 are applicable without change to the 32PTH Type 1 fuel basket assembly. The results for the buckling analysis are also described in Section 3.9.1.2.4.

Since the critical collapse load for the 32PTH Type 1 DSC basket (83.9g for the 30° orientation) is greater than the maximum design acceleration of 75g, the basket will not fail in buckling during the accident condition events.

A.3.7.1.1.3 32PTH Type 1 DSC Fuel Basket Support Rail Accident Condition Buckling Analysis

No change.

A.3.7.1.2 32PTH Type 1 DSC Canister Shell Off Normal and Accident Condition Structural Evaluation

A.3.7.1.2.1 32PTH Type 1 Canister Shell Assembly Off-Normal and Accident Condition Stress Analysis

The description of the off-normal and accident analysis for the 32PTH DSC shell assembly presented in Section 3.7.1.2.1 is applicable without change to the 32PTH Type 1 canister shell assembly.

Elastic and elastic-plastic analyses are performed to calculate the stresses in the 32PTH Type 1 DSC shell assembly under the transfer and storage loads. These load cases are summarized in Appendix A.3.9.1, Tables A.3.9.1-3, A.3.9.1-4 and A.3.9.1-13. The accident side drop load case and the accident pressure load case are analyzed by elastic-plastic analyses and the rest by elastic analyses.

Two finite element model types are used for the analysis of the 32PTH Type 1 DSC shell assembly. The first type is a 2-Dimensional axisymmetric model used for the analysis of symmetric loads (e.g., pressure, dead weight). The second type is a 3-Dimensional model of the top and bottom halves of the shell assembly and is used for the analysis of non-axisymmetric loads (e.g., side drops). The 2-D model is shown in Figures A.3.9.1-1. The 3-D models are shown in Figure A.3.9.1-4 and A.3.9.1-5 for the top and bottom halves, respectively. As shown in Figure A.3.9.1-2, the three-part top end assembly is modeled (separate shield plug, inner cover, and outer cover plates). Similarly, as shown in Figure A.3.9.1-3, the design option with separate inner bottom cover plate, bottom shield plug, and outer bottom cover plate is modeled. This configuration is expected to be the bounding as the pressure load is resisted by the inner top and inner bottom plates, and supported by the outer top cover plate (at the top) and, through the stiff bottom shield plug by the outer bottom cover plate (at the bottom).

The calculated stresses in the canister shell assembly due to off-normal and accident transfer loading conditions are summarized in Appendix A.3.9.1, Tables A.3.9.1-6, 7, 8, 10, 11, and 12. The stresses due to accident storage loading conditions are summarized in Appendix A.3.9.1, Tables A.3.9.1-14, and 15.

The alternate top closure assembly of the 32PTH Type 1 DSC which consists of the two-part combined shield plug/inner cover assembly (including the optional configurations), as well as the optional bottom end configurations are not analyzed explicitly. The results of the 32PTH DSC for the side drop accident load case are applicable for these alternate configurations. See discussion in Section A.3.9.1.3.4.

Based on the results of these analyses, the design of the 32PTH Type 1 DSC canister is structurally adequate with respect to off-normal and accident condition transfer and storage loads.

A.3.7.1.2.2 32PTH Type 1 DSC Canister Shell Accident Condition Buckling Analysis

This section summarizes the evaluation of the 32PTH Type 1 DSC canister against buckling under a vertical end drop during transfer operations. The details of the DSC canister shell buckling analysis are provided in Appendix A.3.9.1, Section A.3.9.1.3.3. A finite element elastic-plastic analysis with large displacement option is performed to monitor occurrence of canister shell buckling under the specified loads.

The thermal evaluation presented in Chapter 4 shows that the metal temperatures of the entire canister are below 500 °F during transfer operations. The material properties of the canister at 500 °F are therefore conservatively used for the canister buckling analysis.

The following three hypothetical accident load cases for the canister are considered in this buckling analysis.

- Buckling Load Case 1:* 15 psig external pressure and 75g axial acceleration due to end drop
- Buckling Load Case 2:* 30 psig internal pressure and 75g axial acceleration due to end drop
- Buckling Load Case 3:* 0 psig internal pressure and 75g axial acceleration due to end drop

The same two-dimensional axisymmetric finite element model used for the stress analysis of the canister shell assembly and described in Appendix A.3.9.1, Section A.3.9.1.3.2.D.2 is used for the buckling accident analysis. Since the top end of the canister is heavier than the bottom end, it is a more severe case when the canister drops on its bottom end. A bottom end drop is therefore chosen for analysis in this calculation.

Load Case 1 converged at 173.5g load. Load Case 2 converged at 174.9g load. Load Case 3 converged at a load corresponding to 174.0g. This load is much higher than the required 75g load in either Load Case 1 or 2. The analysis shows that the canister does not buckle up to an end drop load of 173.5g, which is well beyond the design 75g load. It is, therefore, concluded that buckling of the canister will not occur during a hypothetical accident end drop.

A.3.7.2 HSM-H Off-Normal and Accident Conditions Structural Analysis

No change. As discussed in Section 3.7.2, the HSM-H is evaluated for a DSC weight and heat loads that bound those of the 32PTH Type 1 DSC. Thus, the evaluations of the 32PTH inside the HSM-H documented in Section 3.7.2 are bounding for the 32PTH Type 1 DSC inside the HSM-H.

A.3.7.3 OS187H Type 1 Transfer Cask Off Normal and Accident Conditions Structural Analysis

A.3.7.3.1 Structural Analysis of the Transfer Cask Body for Off Normal and Accident Conditions

The details of the structural analyses of the NUHOMS[®] OS187H Type 1 TC body including the cylindrical shell assembly and bottom assembly, the top cover, and the local stresses at the trunnion/cask body interface are presented in Appendix A.3.9.2. The specific methods, models and assumptions used to analyze the cask body for the various individual loading conditions specified in 10CFR72 [1] are described in that appendix.

The OS187H transfer cask body structural analyses generally use static or quasistatic linear elastic methods. The stresses and deformations due to the applied loads are generally determined using the ANSYS [7] computer program.

The maximum stresses in each of the major components of the transfer cask are reported for each load case and load combination in Appendix A.3.9.2, Table A.3.9.2-1. The results are evaluated against the ASME Code [3] design criteria described in Section A.3.1.2 of this chapter.

Based on the results of these analyses, the design of the OS187H Type 1 TC is structurally adequate with respect to off normal and hypothetical accident transfer loads.

A.3.7.3.2 Transfer Cask Top Cover and Ram Access Cover Bolt Accident Condition Analysis

The detailed calculations for the top cover and ram access cover bolts are presented in Appendix A.3.9.3. The analysis is based on NUREG/CR-6007 [8]. The bolts are analyzed for the hypothetical accident condition impact loads and load combinations.

A summary of the calculated top cover bolt stresses is listed in Appendix A.3.9.3, Section A.3.9.3.5. The calculations result in a maximum average tensile stress of 110.6 ksi, which is below the allowable tensile stress of 115.5 ksi for accident conditions. The maximum average shear stress in the bolts is due to torsion during pre-loading. This stress is 6.8 ksi, which is well below the allowable shear stress of 69.3 ksi.

A summary of the calculated ram access bolt stresses is listed in Appendix A.3.9.3, Section A.3.9.3.10. The analysis results in a maximum average tensile stress of 70.8 ksi, which is below the allowable tensile stress of 115.5 ksi for accident conditions. The maximum accident shear stress is 15.9 ksi, which is well below the allowable shear stress of 69.3 ksi.

A.3.7.3.3 Transfer Cask Lead Slump Analysis

As described in Section 3.1.1.4, the only credible drop accident during storage or transfer operations is a side drop. Thus, lead slump evaluation under top or bottom end drop accident is not performed for the OS187H Type 1 TC.

A.3.7.3.4 Transfer Cask Inner Containment Buckling Analysis

As described in Section 3.1.1.4, the only credible drop accident during storage or transfer operations is a side drop. Thus, inner liner buckling evaluation under top or bottom end drop accidents is not performed for the OS187H Type 1 TC.

A.3.7.3.5 Transfer Cask Trunnion Analysis

Appendix A.3.9.5 presents the evaluation of the trunnion stresses in the NUHOMS® OS187H Type 1 TC due to all applied loads during fuel loading and transfer operations. The calculated maximum normal condition trunnion stresses are summarized in Table A.3.9.5-1 and compared with their corresponding allowable stresses.

A.3.7.3.6 Transfer Cask Shield Panel Structural Analysis for Accident Conditions

Appendix A.3.9.6 presents the evaluation of the stresses in the NUHOMS® OS187H Type 1 TC neutron shield shell due to all applied loads during fuel loading and transfer operations. The calculated maximum normal condition neutron shield shell stresses are summarized in Table A.3.9.6-1 of Appendix A.3.9.6.

A.3.7.3.7 Transfer Cask Impact Analysis

Appendix A.3.9.10 presents the computation of the peak decelerations of NUHOMS® OS187H Type 1 TC during impact, subsequent to the hypothetical accident drop onto the concrete pad/soil system during transfer operations.

A.3.8 References

1. Title 10, Code of Federal Regulations, Part 72, "Licensing Requirements for the Storage of Spent Fuel in an Independent Spent Fuel Storage Installation."
2. American National Standards Institute, ANSI N14.5-1997, Leakage Tests on Packages for Shipment of Radioactive Materials.
3. American Society of Mechanical Engineers, ASME Boiler and Pressure Vessel Code, Section III, Subsection NC, 1998 through 2000 addenda.
4. American National Standards Institute, ANSI N14.6, American National Standard for Special Lifting Devices for Shipping Containers Weighing 10,000 Pounds or More for Nuclear Materials, 1993.
5. American Society of Mechanical Engineers, ASME Boiler and Pressure Vessel Code, Section II, Parts A, B, C and D, 1998, through 2000 addenda.
6. American Society of Mechanical Engineers, ASME Boiler and Pressure Vessel Code, Section III, Subsection NB, 1998 through 2000 addenda.
7. ANSYS Users Manual, Rev. 5.6 and 6.0, 8.0, 8.1, and 10A1
8. NUREG/CR-6007 "Stress Analysis of Closure Bolts for Shipping Casks", By Mok, Fischer, and Hsu, Lawrence Livermore National Laboratory, 1992.
9. Updated Final Safety Analysis Report (UFSAR) for the Standardized NUHOMS[®] Horizontal Modular Storage System for Irradiated Nuclear Fuel, NUH003.0103 Rev. 12.

A.3.9 Appendices

The detailed structural analyses of the NUHOMS[®] HD system Type 1 components are included in the following appendices:

Appendix A.3.9.1	32PTH Type 1 DSC (Canister and Basket) Structural Analysis
Appendix A.3.9.2	OS187H Type 1 Transfer Cask Body Structural Analysis
Appendix A.3.9.3	OS187H Type 1 Transfer Cask Top Cover and Ram Access Cover Bolts Analyses
Appendix A.3.9.4	Not used (since the end and corner drops are not credible under 10CFR Part 72, the lead slump and inner shell buckling analysis of the OS187H Type 1 TC for the 75g end drop load are not documented).
Appendix A.3.9.5	OS187H Type 1 Transfer Cask Trunnion Analysis
Appendix A.3.9.6	OS187H Type 1 Transfer Cask Shield Panel Structural Analysis
Appendix A.3.9.7	Deleted (superseded by Appendix A.3.9.10)
Appendix A.3.9.8	No change (Damaged Fuel Cladding Structural Evaluation)
Appendix A.3.9.9	No change (HSM-H Structural Analysis)
Appendix A.3.9.10	OS187H Type 1 Transfer Cask Dynamic Impact Analysis
Appendix A.3.9.11	32PTH Type 1 DSC Dynamic Amplification Factors

A.3.10 ASME Code Alternatives

No change to the ASME Code Alternatives provided in Section 3.10.

Appendix A.3.9.1

32PTH Type 1 Type 1 DSC (Canister and Basket) Structural Analysis

TABLE OF CONTENTS

A.3.9.1	32PTH TYPE 1 DSC (CANISTER AND BASKET) STRUCTURAL ANALYSIS	A.3.9.1-1
A.3.9.1.1	Introduction.....	A.3.9.1-1
A.3.9.1.2	32PTH Type 1 DSC Fuel Basket Assembly Structural Evaluation.....	A.3.9.1-2
	A.3.9.1.2.1 Approach.....	A.3.9.1-2
	A.3.9.1.2.2 Loading Conditions.....	A.3.9.1-2
	A.3.9.1.2.3 Fuel Basket Assembly Stress Analysis	A.3.9.1-2
	A.3.9.1.2.4 32PTH Type 1 Fuel Basket Assembly Buckling Analysis.....	A.3.9.1-2
A.3.9.1.3	32PTH Type 1 DSC Shell Assembly Structural Evaluation	A.3.9.1-3
	A.3.9.1.3.1 Approach.....	A.3.9.1-3
	A.3.9.1.3.2 DSC Canister Shell Assembly Stress Analysis.....	A.3.9.1-3
	A.3.9.1.3.3 DSC Shell Buckling Evaluation.....	A.3.9.1-20
	A.3.9.1.3.4 Evaluation of Alternate DSC Top and Bottom Closure Assembly Design.....	A.3.9.1-23
A.3.9.1.4	32PTH Type 1 DSC and OS187H Type 1 Transfer Cask Thermal Expansion Evaluation	A.3.9.1-24
	A.3.9.1.4.1 Introduction.....	A.3.9.1-24
	A.3.9.1.4.2 Approach.....	A.3.9.1-24
	A.3.9.1.4.3 Mechanical Properties of Materials	A.3.9.1-24
	A.3.9.1.4.4 Thermal Expansion Computation	A.3.9.1-24
	A.3.9.1.4.5 Thermal Expansion Analysis Conclusions	A.3.9.1-27
A.3.9.1.5	References	A.3.9.1-28

LIST OF TABLES

Table A.3.9.1-1	Temperature Dependent Material Properties for ASTM A-36	A.3.9.1-29
Table A.3.9.1-2	Material Stress Limits for 32PTH Type 1 DSC SA-240/SA-479 304 & SA-182 F304.....	A.3.9.1-30
Table A.3.9.1-3	32PTH Type 1 DSC Canister Load Combinations during Transfer	A.3.9.1-31
Table A.3.9.1-4	32PTH Type 1 DSC Canister Load Combinations during Lifting, Testing, and Hydraulic Loads	A.3.9.1-32
Table A.3.9.1-5	Summary of Calculated Stresses for Testing Condition Loads	A.3.9.1-33
Table A.3.9.1-6	Summary of Calculated Stress for Normal and Off-Normal Condition Transfer Loads	A.3.9.1-34
Table A.3.9.1-7	Summary of Calculated Stress for Accident Condition Transfer Loads (Axisymmetric Loads)	A.3.9.1-35
Table A.3.9.1-8	Summary of Stresses for Accident Condition Transfer Loads (3-D Inertial Loads).....	A.3.9.1-36
Table A.3.9.1-9	Summary of Calculated Stress at End Closure Welds for Testing Condition Loads.....	A.3.9.1-37
Table A.3.9.1-10	Summary of Calculated Stress at the End Closure Welds for Normal and Off-Normal Condition Transfer Loads	A.3.9.1-38
Table A.3.9.1-11	Summary of Calculated Stresses at End Closure Welds for Accident Condition Transfer Loads (Axisymmetric Loads).....	A.3.9.1-39
Table A.3.9.1-12	Summary of Calculated Stresses at End Closure Welds for Accident Condition Transfer Loads (3-D Inertial Loads).....	A.3.9.1-40
Table A.3.9.1-13	32PTH Type 1 DSC Canister Load Combinations during Storage	A.3.9.1-41
Table A.3.9.1-14	Summary of Calculated Stresses for Normal and Accident Condition Loads (canister in horizontal position)	A.3.9.1-42
Table A.3.9.1-15	Summary of Calculated Stresses at the End Closure Welds for Normal and Accident Condition Storage Loads	A.3.9.1-43

LIST OF FIGURES

Figure A.3.9.1-1	2-D Canister Axisymmetrical Thermal and Stress Finite Element Model	A.3.9.1-44
Figure A.3.9.1-2	Top End of the 2-D Axisymmetrical Canister Model.....	A.3.9.1-45
Figure A.3.9.1-3	Bottom End of the 2-D Axisymmetrical Canister Model	A.3.9.1-46
Figure A.3.9.1-4	3-D DSC Canister Top End Assembly Finite Element Model	A.3.9.1-47
Figure A.3.9.1-5	3-D DSC Canister Bottom End Assembly Finite Element Model..	A.3.9.1-48
Figure A.3.9.1-6	32PTH Type 1 DSC Canister Finite Element Model used for Pressure Test Analysis	A.3.9.1-49

A.3.9.1 32PTH TYPE 1 DSC (CANISTER AND BASKET) STRUCTURAL ANALYSIS

A.3.9.1.1 Introduction

The NUHOMS[®] 32PTH Type 1 DSC consists of a fuel basket assembly and a canister shell assembly. The canister shell assembly consists of a cylindrical shell, top end assembly (outer top cover plate, inner top cover plate, top shield plug), and a bottom end assembly (inner bottom cover plate, bottom shield plug, outer bottom cover plate). An alternate design for the top end assembly includes a two-part top end (combined shield plug/inner top cover and the outer cover plate). Similarly, the bottom end may consist of a single forged piece or two-piece, or three-piece assembly. The primary confinement boundary for the 32PTH Type 1 DSC consists of the DSC shell, the inner top cover plate, and shell bottom or inner bottom cover plate of the shell bottom assembly.

The canister shell thickness is 0.50 inches, and the top and bottom closure assemblies are 12.0 inches and 8.75 inches, respectively. The canister is constructed entirely from SA-240 Type 304 stainless steel and SA-182 Type F304. The shield plugs are constructed from ASTM A-36. There are no penetrations through the confinement vessel. The draining and venting systems are covered by the port plugs, and the outer top cover plate and the inner top cover plate are welded to the cylindrical shell with multi-layer welds. The canister cavity is pressurized above atmospheric pressure with helium. The 32PTH Type 1 DSC shell assembly geometry and the materials used for its analysis and fabrication are shown on drawings 10492-72-2001-SAR to 2005-SAR included in Chapter A.1.

The basket structure consists of assemblies of stainless steel fuel compartments and support rails. The borated aluminum or boron carbide/aluminum metal matrix composite plates (neutron poison plates) provide the necessary criticality control and also provide a portion of the heat conduction paths from the fuel assemblies to the cask cavity wall. This method of construction forms a very strong structure of compartment assemblies which provide for storage of 32 PWR fuel assemblies. The open dimension of each fuel compartment is 8.70 in. × 8.70 in., which provides clearance around the fuel assemblies.

The fuel basket assembly and the canister assembly are analyzed separately. The fuel basket assembly is analyzed in Section A.3.9.1.2, while the canister shell assembly is analyzed in Section A.3.9.1.3. The full 360° 3-dimensional finite element model of the basket assembly used for the evaluation of the 32PTH basket is applicable to the 32PTH Type 1 basket assembly. The analyses performed in Section 3.9.1.2 for the 32PTH basket are applicable for the 32PTH Type 1 basket (See Section A.3.9.1.2 for details).

Three finite element models are used for the structural evaluation of the canister shell assembly. A 2-dimensional axisymmetric model of the DSC canister shell assembly is used to evaluate axial inertial loads as well as internal pressure, external pressure, and thermal loads. Two 3-dimensional finite element models of the DSC shell assembly are used to evaluate the effects of transverse inertial loads (e.g., side drop). These are separate models of the top half and bottom half assemblies of the 32PTH Type 1 DSC.

A.3.9.1.2 32PTH Type 1 DSC Fuel Basket Assembly Structural Evaluation

A.3.9.1.2.1 Approach

The basket design for the NUHOMS® 32PTH Type 1 DSC is identical to the 32PTH DSC except that the length of the 32PTH Type 1 basket is longer (the length of the 32PTH DSC basket is 162 inches, whereas the length of the 32PTH Type 1 DSC basket is 169 inches). In addition, the fuel compartment tubes at the top of the basket are also connected with support bars and fusion welds in the 32PTH Type 1 design. The 15 inch pitch between support bars (where the fuel compartments are connected to each other by fusion welds), which is the basis for the selection of the axial length of the analysis model, is the same for the 32PTH and 32PTH Type 1 baskets. The material properties, maximum fuel assembly weight, and the temperature profiles used in the 32PTH basket analyses (Section 3.9.1.2) have not changed. Thus, the analyses performed for the 32PTH basket assembly, documented in Section 3.9.1.2, are also applicable for the 32PTH Type 1 basket.

Therefore, the analysis results for the 32PTH basket in Section 3.9.1.2 are also applicable to the 32PTH Type 1 basket.

A. Material Properties

No change. The material properties for the 32PTH DSC in Section 3.9.1.2.1(A) are also applicable to the 32PTH Type 1 DSC.

B. Design Criteria

No change. The design criteria for the 32PTH DSC described in Section 3.9.1.2.1 (B) are also applicable to the 32PTH Type 1 DSC.

A.3.9.1.2.2 Loading Conditions

No change. The loading conditions for the 32PTH DSC described in Section 3.9.1.2.2 are also applicable to the 32PTH Type 1 DSC.

A.3.9.1.2.3 Fuel Basket Assembly Stress Analysis

No change. The 32PTH basket stress analysis model and analysis results in Section 3.9.1.2.3 are applicable to the 32PTH Type 1.

A.3.9.1.2.4 32PTH Type 1 Fuel Basket Assembly Buckling Analysis

The buckling evaluation for the 32PTH DSC performed using the full 360° 3-dimensional model of the basket assembly documented in Section 3.9.1.2.4 (A.3) is also applicable to the 32PTH Type 1 DSC.

A.3.9.1.3 32PTH Type 1 DSC Shell Assembly Structural Evaluation

A.3.9.1.3.1 Approach

This section evaluates the structural adequacy of the 32PTH Type 1 DSC canister under all applicable normal and hypothetical accident condition loads. Evaluation of the stresses generated in the DSC is presented in Section A.3.9.1.3.2, and the DSC shell assembly buckling evaluation is presented in Section A.3.9.1.3.3.

A.3.9.1.3.2 DSC Canister Shell Assembly Stress Analysis

A. Methodology

An enveloping technique of combining various individual loads in a single analysis is used in this evaluation for several load combinations. This approach greatly reduces the number of computer runs while remaining conservative. However, for some load combinations, the stress intensities under individual loads are added to obtain resultant stress intensities for the specified combined loads. This stress addition at the stress intensity level for the combined loads, instead of at component stress level, is also a conservative way to reduce the number of analyses runs.

The ANSYS calculated stresses are the total stresses of the combined membrane, bending, and peak stresses. These total stresses are conservatively taken to be membrane stresses (P_m) as well as membrane plus bending stresses ($P_L + P_b$) and are evaluated against their corresponding ASME code stress limits. In the case where the total stresses, evaluated in this manner, exceed the ASME allowable stresses, a detailed stress linearization is performed to separate the membrane, bending, and peak stresses. The linearized stresses are then compared to their proper Code allowable stresses. ASME B&PV Code Subsection NB [8] is used for evaluation of loads under normal conditions and Appendix F [3] for evaluation of loads under hypothetical accident conditions.

The thermal stress intensities are classified as secondary stress intensities, Q , for code evaluations.

B. Canister Material Properties

Temperature dependent material properties obtained from Reference 1 for the NUHOMS[®] 32PTH Type 1 canister materials are summarized as follows.

Elastic Material Properties

Elastic properties are tabulated in Table 3-5 for SA-240 Type 304/SA-182 F304 (DSC Shell, Support Ring, Outer Top Cover, Inner Top Cover, Bottom Grapple Ring, Inner Bottom Cover and Outer Bottom Cover) and in Table A.3.9.1-1 for ASTM A-36 (top and bottom shield plugs).

Elastic-Plastic Material Properties

The ANSYS Bilinear Kinematic Hardening option of inelastic analysis is employed for Transfer Load Case 4 (120 psig internal pressure and hypothetical accident fire). Tangent modulus of 5% of elastic modulus is assumed after yield stress.

The ANSYS Multilinear Kinematic Hardening material option of inelastic analysis is employed in the analyses of all canister accident side drops. A multi-linear stress-strain curve for Type 304 stainless steel at 500 °F is constructed using the yield and tensile stress values taken from Reference 1 and the elongation value from Reference 9. The stress-strain curve used for all canister materials is as follows.

Point	1	2	3	4	5
Strain (in/in)	0.0004845	0.000768	0.001164	0.00275	0.46
Stress (psi)	12,500	14,660	17,120	19,400	63,400

C. DSC Shell Assembly Stress Criteria

Allowable stresses given in ASME B&PV Code Subsection NB [8] and Appendix F [3] are used to evaluate the calculated stresses in the canister under normal, off-normal, and accident conditions, respectively. The stress criteria are summarized in Table 3-2. The allowable stresses are summarized in Table A.3.9.1-2. The closure welds between the inner top cover to the shell and the outer top cover to the shell use a stress reduction factor of 0.8 in accordance with ISG-15 [14].

D. DSC Shell Assembly Stress Analysis for Transfer Loads

The evaluation of the stresses generated in the NUHOMS[®] 32PTH Type 1 canister during transfer operations is presented here. During fuel transfer, the canister is oriented horizontally inside the OS187H Type 1 Transfer Cask. The OS187H Type 1 Transfer Cask is mounted to the transfer skid and transferred from the fuel building to the ISFSI.

The maximum temperature in the canister under vacuum drying operation is calculated to be 522 °F in the thermal stress analysis (see Chapter 4). This temperature occurs in the shell center where stresses are low. The maximum temperature in critical stress areas (top and bottom canister regions) are below 500 °F. However, the stress evaluations are conservatively performed at 500 °F.

D.1. DSC Shell Assembly Transfer Load Cases

Elastic and elastic-plastic analyses are performed to calculate the stresses in the NUHOMS[®] 32PTH Type 1 canister under the transfer loads. These load cases are summarized in Table A.3.9.1-3 and Table A.3.9.1-4. The accident side drop and the accident pressure load cases are analyzed by elastic-plastic analyses and the rest by elastic analyses.

D.2. DSC Shell Assembly Finite Element Model Descriptions

DSC Temperature Distribution

The DSC metal temperatures which are calculated in Chapter 4 are extracted and directly applied as temperature loads to the 2-D stress model using ANSYS macros. Since the 32PTH Type 1 DSC is longer than the 32PTH DSC, the temperature distribution at the maximum temperature location was extended in the middle of the canister, thus maximizing thermal gradients and hence thermal stresses at the top and bottom of the canister shell.

2-D Canister Stress Models

A two-dimensional (2-D) axisymmetric ANSYS finite element model, constructed from PLANE42 elements, is used for the elastic analyses of all axisymmetrical loading on the canister. ANSYS contact elements CONTAC12 are generated by connecting the nodes of two adjacent solids along their boundary. The real constant of each contact element is defined for the initial gap at each contact element.

At the weld locations between two joined solids, the contacting nodes are coupled in all directions. These coupled-nodes are applied to the welds between the shell and the support ring and between the shell and the inner top cover plate. The larger ½ inch weld between the shell and the top cover is modeled with PLANE42 elements. The normal stiffness of all contact elements are calculated using guidelines in the ANSYS manual [10]. The applied boundary conditions for this 2-D model under each load case are described in the following sections. Figure A.3.9.1-1, Figure A.3.9.1-2, and Figure A.3.9.1-3 show the ANSYS 2-D finite element model, which includes the canister shell, outer and inner top covers, support ring and outer and inner bottom covers. This model is used for analyses of all axisymmetric loads during the transfer operations of the canister.

The normal stiffness, K_N , for the contact elements were estimated according to the ANSYS manual [10] as follows.

$$KN \approx f E h$$

Where, f = Factor that controls contact compatibility (ranging between 0.01 to 100), use 1

E = Young's modulus, use 25.8×10^6 psi

h = average radius where contact to occur (for 2-D axisymmetrical model), use 34 in.

$K_N = 1 \times 25.8 \times 10^6 \times 34 = 8.8 \times 10^8$ lb/in. Conservatively used 1×10^9 lb/in.

3-D Canister Stress Model

A three-dimensional (3-D) ANSYS stress model is created using ANSYS elements SOLID45 and CONTAC178. The 3-D model is used for the analysis of accident side drops. To help reduce the ANSYS run time and assure numerical convergence, the whole canister is split into two portions, namely, the top and the bottom end sections. These two sections are represented by two different ANSYS models. Each end model includes the canister shell at a length beyond which the un-modeled shell will have no significant impact on the stress levels at the junction between the shell and its end closures. The DSC canister top end assembly finite element model is shown in Figure A.3.9.1-4 and the canister bottom end assembly model is shown in Figure A.3.9.1-5.

These 3-D models are used for analyses of side drops only. The postulated side drops will occur when the canister is resting inside the OS187H Type 1 transfer cask during transfer. Two side drops with the impact points located at 0° (i.e., the cask drops onto a target at 180° opposite to its four canister support pads) and at 180° (i.e., the cask drops onto a target between its two bottom canister support pads) are analyzed.

Load cases 6, 7, 10, and 11 consider the side drop loads at 0° and load cases 8, 9, 12, and 13 at 180° (see Table A.3.9.1-3). Elastic-plastic analyses, using multi-linear hardening material properties, are performed for both side drops. In addition to the contact areas generated from the 2-D model, new contact elements are generated connecting the inner diameter of the cask and the outer diameter of the canister in the radial direction. The nodes of these contact elements are located either on the inner diameter of the cask or on the outer diameter of the canister at the moment when the cask hits the side drop target. The actual gaps for these contact elements are defined by their initial location in conjunction with the contact element real constants. The contact element nodes located on the inner diameter of the cask are held fixed in all directions, simulating a rigid cask on which the canister drops.

Weak link elements are added to each contact element in the model to help numerical convergence. Zero density of these link elements is used to avoid adding any non-existing weights. This model does not calculate the stress levels in the middle section of the canister shell, which are calculated and evaluated as part of the basket stress analysis in Section 3.9.1.2.3.

Only half of the canister in circumferential direction is included in the 3-D model. Symmetry boundary conditions are applied to the plane of symmetry (global Cartesian x - z plane) during a side drop. Symmetry boundary conditions are also applied to the cut-off plane at the canister shell to provide proper diametrical rigidity of the shell during side drops.

During the 75 g side drop, the canister internals are accounted for by applying a cosine varying pressure distribution on the inside surface of the canister shell. Assuming that the canister internals react upon a 90° arc of the inside surface, then the inertial load of the internals, $P_{(\theta)}$, which varies with angle, θ , ($\theta = 0$ is at the impact point), is governed by the following expression.

$$P_{(\theta)} = P_{max} \cos(2\theta) \quad (0^\circ < \theta < 45^\circ)$$

Where P_{max} is the maximum pressure at the impact point ($\theta = 0$). Assuming the axial length of the applied load is L , the inside radius of the canister shell is R , and the load distribution, $P_{(\theta)}$ above, then the total inertial load generated by the internals, F , is the following.

$$F = \int_{-\frac{\pi}{4}}^{\frac{\pi}{4}} P_{max} \cos(2\theta) \cos(\theta) LR d\theta$$

or,

$$F = \frac{P_{max} LR}{2} \int_{-\frac{\pi}{4}}^{\frac{\pi}{4}} \cos((2+1)\theta) + \cos((2-1)\theta) d\theta$$

By integrating we get the following:

$$F = \left[\frac{P_{\max} LR}{2} \right] \left[\frac{\sin(3\theta)}{3} + \sin(\theta) \right] \Bigg|_{-\frac{\pi}{4}}^{\frac{\pi}{4}}$$

Therefore,

$$F = \left[\frac{P_{\max} LR}{2} \right] \left[\frac{\sin\left(\frac{3\pi}{4}\right)}{3} + \sin\left(\frac{\pi}{4}\right) - \frac{\sin\left(\frac{-3\pi}{4}\right)}{3} - \sin\left(\frac{-\pi}{4}\right) \right]$$

$$F = P_{\max} LR \left[\frac{\sin\left(\frac{3\pi}{4}\right)}{3} + \sin\left(\frac{\pi}{4}\right) \right]$$

The canister shell inner diameter, $R = 34.375$ in., the axial length of the applied load, $L = 169$ in. The total applied force, F , is equal to the inertial load of the canister internals, which is the following.

Basket weight = 29,451 lb,

Fuel assembly weight = 51,520 lb

Total weight of canister internals = 29,451 lb + 51,520 lb = 80,971 lb (use 83,000 lb).

Then,

$$F = 83,000 \times 75 \text{ g} = 6,225,000 \text{ lb.}$$

Therefore, P_{\max} is the following:

$$P_{\max} = \frac{6,225,000}{(169)(34.375)} \left[\frac{\sin\left(\frac{3\pi}{4}\right)}{3} + \sin\left(\frac{\pi}{4}\right) \right]^{-1} = 1136.54 \text{ psi.}$$

The equivalent pressure applied on the canister inside shell surface is therefore,

$$P_{(\theta)} = 1136.54 \cos(2\theta),$$

Where, θ is the angle from the bottom ($\theta = 0$) of the horizontal canister shell to the center of the shell element, up to 45° .

D.3. DSC Shell Assembly Stress Evaluation for Transfer Loads

All analyzed load cases in this section are identified in Table A.3.9.1-3 and Table A.3.9.1-4 and are described in detail in the following sections.

Transfer Load Case 1: Deadweight + 15 psig external pressure + thermal (vacuum drying)

The temperature profile utilized for the analysis of Transfer Load Case 1 for the 32PTH DSC described in Section 3.9.1.3.2 (D.3) was adjusted by linearly scaling to the maximum vacuum drying temperature of 522 °F, which is greater than the maximum temperature for vacuum drying 511 °F, as calculated in Chapter 4. This adjusted temperature profile is used for the analysis of Transfer Load Case 1 for the 32PTH Type 1 DSC.

The weight of the canister internals (basket and fuel assemblies) is accounted for by applying equivalent pressures on the support surfaces of the canister. The actual weights of the basket and fuel assemblies are 29,451 lb and 51,520 lb, respectively (see Section A.3.2.1). Therefore, the total weight of the canister internals is 80,971 lb. A weight of 83,000 lb is conservatively used in this analysis. The canister cavity inner radius is 34.375 in. Therefore, the pressure load equivalent to the inertial load of the internals, P_{ia} , is,

$$P_{ia} = [83,000 / (\pi \times 34.375^2)] = 22.36 \text{ psi}$$

An elastic analysis is performed using the ANSYS 2-D axisymmetric model. The analysis was run in two load steps. The first load step includes dead weight, 15 psig external pressure, and the temperature profile discussed above, but it does not include coefficient of thermal expansion. The second load step includes the coefficient of thermal expansion and all of the above-mentioned loads. The results from the first load step are compared against the P_m and $P_m + P_b$ allowable stresses and the results from the second load step are compared against the $P_m + P_b + Q$ allowable stresses.

The maximum primary stress intensity in the canister was calculated to be 2.05 ksi in Load Step 1. The maximum primary stress intensity in the closure welds is calculated to be 1.52 ksi.

The maximum primary plus secondary stress intensity in the canister was calculated to be 22.69 ksi in Load Step 2. These stresses are summarized in Table A.3.9.1-6. The maximum primary stress intensity in the closure welds is calculated to be 2.07 ksi.

Transfer Load Case 2: Handling, 2 g axial + 2 g transverse + 2 g vertical + 30 psig int. pressure + thermal (115 °F ambient)

The handling 2 g inertial loads applied to the canister when inside the transfer cask in the horizontal orientation are analyzed as part of the basket model described in Section 3.9.1.2.3 (B.2) (the basket model includes a segment of the canister shell). It is judged that under the relatively light handling loads the maximum stresses in the canister will occur in the shell section and can be obtained from the results calculated in Section 3.9.1.2.3 (B.2). The maximum primary membrane stress intensity and primary membrane plus bending stress intensity in the canister shell due to the handling load of 2 g, calculated in Section 3.9.1.2.3 (B.2), are 880 psi and 9740 psi, respectively. These stresses are summarized in Table A.3.9.1-6.

The stress intensities calculated in Section 3.9.1.2.3 (B.2) for the canister shell due to the 2 g handling loads are combined with the stresses due to internal pressure of 30 psig, and the 115 °F ambient environment temperature loads resulting from the thermal analysis in Chapter 4.

The stress analysis for the 30 psig internal pressure and 115 °F thermal loads is performed using the ANSYS 2-D axisymmetric model. The stress analysis contains two load steps. Load step 1 includes the primary loads of 30 psig internal pressure. Load step 2 includes the primary pressure load plus the secondary thermal load.

The maximum primary stress intensity in the canister was calculated to be 14.97 ksi in Load Step 1 analysis. The maximum primary stress intensity in the closure welds is calculated to be 11.75 ksi. The maximum primary plus secondary stress intensity in the canister is calculated to be 41.70 ksi under load step 2. The maximum primary plus secondary stress intensity in the closure welds is calculated to be 14.94 ksi.

The maximum primary stress intensities in the canister shell calculated in Section 3.9.1.2.3 (B.2) are added to the maximum primary and primary plus secondary stress intensities calculated from the 2-D axisymmetric model and the combined results are evaluated against the corresponding ASME stress limits (See Table A.3.9.1-6). The direct addition of stresses at the stress intensities level, instead of at the component level, as well as the addition of the maximum stress intensities at different locations is very conservative. This enveloping technique is used to minimize the computer runs.

Transfer Load Case 3: Handling 2 g axial + 2 g transverse + 2 g vertical + 15 psig ext. pressure + thermal (-20 °F ambient)

The same methodology described for load case 2 is used in this load case.

The maximum stress intensity in the canister for the primary load of 15 psig external pressure in load step 1 is calculated to be 2.75 ksi. The maximum stress intensity in the closure welds is calculated to be 1.46 ksi.

The maximum stress intensity in the canister for the primary load of 15 psig external pressure plus the secondary temperature load in load step 2, is calculated to be 31.63 ksi. These stresses combined with the stresses due to the handling loads as well as the evaluation against the ASME stress limits are summarized in Table A.3.9.1-6. The maximum stress intensity in the closure welds is calculated to be 2.32 ksi.

Transfer Load Case 4: 120 psig internal pressure and hypothetical accident fire

Stresses in the canister under an internal pressure of 120 psig are calculated in this load case. ASME code [3] requires only primary stresses be evaluated under accident conditions. The secondary thermal stresses are therefore not calculated. The ANSYS 2-D axisymmetric model is used for analysis of this accident pressure load. This is an elastic-plastic analysis with large deformations.

The maximum calculated stress in the entire canister for the pressure load is 23.92 ksi. This maximum stress intensity is conservatively treated both as primary membrane stress intensity

and as primary membrane plus bending stress intensity and so evaluated against ASME code limits at the maximum metal temperature of the canister (See Table A.3.9.1-7).

The maximum metal temperature in the canister during fire accident is calculated to be 790 °F (see Chapter 4). Canister material properties at 800 °F are used for the ANSYS model. The maximum stress intensity in the closure welds is calculated to be 21.71 ksi.

Transfer Load Case 5: 25 psig external pressure and flood hypothetical accident

The external pressure of 25 psig on the canister is analyzed using material properties taken at 500 °F for the entire model.

The maximum stress intensity in the canister for this load case is calculated to be 4.56 ksi. The maximum stress intensity in the closure welds is calculated to be 2.42 ksi.

Transfer Load Case 6: Accident condition 75 g side drop at 0° (no rail) at ambient temperature of 115 °F (75 g side drop + 30 psig internal pressure)—top end portion of canister

The canister internal pressure of 30 psig plus a side acceleration of 75 g is analyzed in this load case. A multi-linear elastic-plastic stress-strain curve for material 304 SS at 500 °F is applied to all materials. The stress-strain curve is obtained from Reference 9. ASME code requires only primary stresses be evaluated under accident conditions. The values of the thermal expansion coefficients for all materials are therefore set to 0 to eliminate any secondary thermal stresses in the canister.

The maximum stress intensity in the canister for this load case is calculated to be 25.5 ksi. The maximum stress intensity in the closure welds is calculated to be 23.3 ksi.

Transfer Load Case 7: Accident condition 75 g side drop at 0° (no rail) at ambient temperature of 115 °F (75 g side drop + 30 psig internal pressure)—bottom end portion of canister

The methodology of the analysis and stress evaluation used in this load case is the same as that described for Load Case 6.

The maximum stress intensity in the canister for this load case is calculated to be 24.0 ksi.

Transfer Load Case 8: Accident 75 g side drop at 180° (drop between two transfer cask bottom support pads) at ambient temperature of 115 °F (75 g side drop + 30 psig internal pressure)—top end portion of canister

The same methodology of the analysis and stress evaluation used for Load Case 6 is used for this load case except that the gaps between the canister and the rigid cask are different due to the orientation of the transfer cask support pads.

The maximum stress intensity in the canister for this load case is calculated to be 27.3 ksi. The maximum stress intensity in the closure welds is calculated to be 24.3 ksi.

Transfer Load Case 9: Accident 75 g side drop at 180° (drop between two cask bottom rails) at ambient temperature of 115 °F (75 g side drop + 30 psig internal pressure)—bottom end portion of canister

The same methodology of the analysis and stress evaluation used for Load Case 7 is used for this load case except that the gaps between the canister and the rigid cask are different.

The maximum stress intensity in the canister for this load case is calculated to be 24.7 ksi.

Transfer Load Case 10: Accident 75 g side drop at 0° (drop at no cask rail) at ambient temperature of -20 °F (75 g side drop + 15 psig external pressure)—top end portion of canister

The same methodology of the analysis and stress evaluation used for Load Case 6 is used for this load case except that external pressure instead of internal pressure is applied.

The maximum stress intensity in the canister for this load case is calculated to be 25.9 ksi. The maximum stress intensity in the closure welds is calculated to be 23.4 ksi.

Transfer Load Case 11: Accident 75 g side drop at 0° (drop at no cask rail) at ambient temperature of -20 °F (75 g side drop + 15 psig external pressure)—bottom end portion of canister

The same methodology of the analysis and stress evaluation used for Load Case 7 are used for this load case except external pressure instead of internal pressure is applied.

The maximum stress intensity in the canister for this load case is calculated to be 24.1 ksi.

Transfer Load Case 12: Accident 75 g side drop at 180° (drop between two cask bottom rails) at ambient temperature of -20 °F (75 g side drop + 15 psig external pressure)—top end portion of canister

The same methodology of the analysis and stress evaluation used for Load Case 8 is used for this load case except that external pressure instead of internal pressure is applied.

The maximum stress intensity in the canister for this load case is calculated to be 27.3 ksi. The maximum stress intensity in the closure welds is calculated to be 24.2 ksi.

Transfer Load Case 13: Accident 75 g side drop at 180° (drop between two cask bottom rails) at ambient temperature of -20 °F (75 g side drop + 15 psig external pressure)—bottom end portion of canister

The same methodology of the analysis and stress evaluation used for Load Case 9 is used for this load case except that the external pressure instead of the internal pressure is applied.

The maximum stress intensity in the canister is calculated to be 24.9 ksi.

Transfer Load Case 14: Accident 75 g top end drop (75 g + internal pressure of 30 psig)

The top end drop is not considered credible during storage and transfer operations under 10 CFR Part 72 because the transfer cask is always in the horizontal orientation. The top end drop

evaluation documented below is performed in support of a 10 CFR Part 50 evaluation that may be performed by the user if the user cannot demonstrate that this accident drop is not credible.

The weight of the canister internals (basket and fuel assemblies) during end drop is accounted for by applying equivalent pressures on canister components that support them. The actual weights of the canister basket and fuel assemblies are 29,451 lb and 51,520 lb (see Section A.3.2.1). Therefore, the total actual weight of the canister internals is 80,971 lb. The weight of the canister internals used in this analysis is conservatively increased to 83,000 lb.

The canister cavity inner radius at the top end is 34.375 in. The pressure load equivalent to the inertial load of the internals at 75 g under accident condition, P_{ia} , is,

$$P_{ia} = [83,000 / (\pi \times 34.375^2)] \times 75 g = 1676.89 \text{ psi}$$

The top face of the canister outer top cover is held in the axial direction in order to simulate the rigid support provided by the transfer cask top cover. An inertial load of 75 g in the negative y-direction is applied to the model. An internal pressure of 30 psig and the metal temperatures from the 115 °F ambient condition are also included in this analysis. Temperature-dependent material properties are selected based on the temperature distribution in the canister. The values of thermal expansion coefficients for all materials are set to zero so that secondary thermal stresses, which are not required for evaluation under an accident condition per Reference 3, are not calculated.

The maximum stress intensity in the canister for this load case is calculated to be 17.68 ksi. The maximum stress intensity in the closure welds is calculated to be 6.43 ksi.

Transfer Load Case 15: Accident 75 g bottom end drop (75 g + internal pressure of 30 psig)

The bottom end drop is not considered credible during storage and transfer operations under 10 CFR Part 72 because the transfer cask is always in the horizontal orientation. The bottom end drop evaluation documented below is performed in support of a 10 CFR Part 50 evaluation that may be performed by the user if the user cannot demonstrate that this accident drop is not credible.

The weight of the canister internals used in this analysis is 83,000 lb. The canister cavity inner radius at the bottom end is 34.375 in. The pressure load equivalent to the weight of the internals under the accident condition 75 g drop, P_{ia} , is,

$$P_{ia} = [83,000 / (\pi \times 34.375^2)] \times 75 g = 1676.89 \text{ psi}$$

The bottom face of the canister is held in the axial direction in order to simulate the rigid support provided by the transfer cask bottom. An inertial load of 75 g in the positive y-direction is applied to the model. An internal pressure of 30 psig and the metal temperatures from the 115 °F ambient condition are included in this analysis. Temperature-dependent material properties are selected based on the temperature distribution in the canister. The values of thermal expansion coefficients for all materials are set to zero so that secondary thermal stresses, which are not required for evaluation under an accident condition per Reference 3, are not calculated.

The maximum stress intensity in the canister for this load case is calculated to be 21.05 ksi. The maximum stress intensity in the closure welds is calculated to be 4.27 ksi.

Transfer Load Case 16: Accident 75 g top end drop (75 g + external pressure of 15 psig)

The top end drop is not considered credible during storage and transfer operations under 10 CFR Part 72 because the transfer cask is always in the horizontal orientation. The top end drop evaluation documented below is performed in support of a 10 CFR Part 50 evaluation that may be performed by the user if the user cannot demonstrate that this accident drop is not credible.

This load case is similar to Load Case 14 with different pressure loadings and metal temperatures. An external pressure of 15 psig and material properties at 500 °F are used in this analysis. The values of thermal expansion coefficients for all materials are set to zero so that secondary thermal stresses, which are not required for evaluation under an accident condition per Reference 3, are not calculated.

The maximum stress intensity in the canister for this load case is calculated to be 30.7 ksi. The maximum stress intensity in the closure welds is calculated to be 8.7 ksi.

Transfer Load Case 17: Accident 75 g bottom end drop in accident condition (75 g + external pressure of 15 psig)

The bottom end drop is not considered credible during storage and transfer operations under 10 CFR Part 72 because the transfer cask is always in the horizontal orientation. The bottom end drop evaluation documented below is performed in support of a 10 CFR Part 50 evaluation that may be performed by the user if the user cannot demonstrate that this accident drop is not credible.

This load case is similar to Load Case 15 with different pressure loadings and metal temperatures. An external pressure of 15 psig and material properties at 500 °F are used in this analysis. The values of thermal expansion coefficients for all materials are set to zero so that secondary thermal stresses, which are not required for evaluation under an accident condition per Reference 3, are not calculated.

The maximum stress intensity in the canister for this load case is calculated to be 26.1 ksi. The maximum stress intensity in the closure welds is calculated to be 6.1 ksi.

Transfer Load Case 18: Fabrication test condition (DW + 25 psig internal pressure + 155 kips axial load)

After the canister bottom is welded to the shell a pressure test is conducted by applying an internal pressure of 25 psig with a top seal plate being held by an axial force of 155 kips. The canister bottom may be made, as an option, of composite plates. For each of these options the bottom inner plate, which is to be first welded to the shell and tested, has a minimum thickness of 2.25 inches. An ANSYS model, shown in Figure A.3.9.1-6, is generated that simulates the canister shell with the bottom inner plate for analysis of pressure and axial loads under the test condition. The deadweight load on the horizontal canister is manually analyzed using Roark's formulas [7]. The stresses calculated from both manual and ANSYS analyses are conservatively added for ASME Code stress evaluation.

(1) 1g deadweight load

It is conservatively assumed that the horizontal shell's own weight is line supported at its base.

From Case 15 of Table 9.2 in Roark's Formulas for Stress & Strains, 7th Edition:

$$R \text{ (mean radius)} = \frac{1}{2} (69.75 \text{ in.} - 0.5 \text{ in.}) = 34.625 \text{ in.}$$

$$t \text{ (wall thickness)} = 0.5 \text{ in.}$$

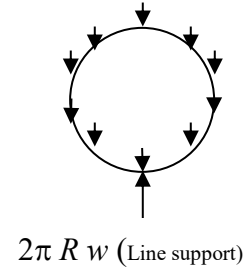
$$\rho \text{ (density)} = 0.29 \text{ lb/in}^3$$

Take unit length ($L = 1 \text{ in.}$) of shell,

The weight per unit length of circumference of shell, w , is,

$$\begin{aligned} w &= (2 \times \pi \times R \times t \times L \times \rho) / (2 \times \pi \times R) \\ &= t \times L \times \rho = 0.5 \times 1 \text{ in.} \times 0.29 \text{ lb/in}^3 = 0.145 \text{ lb/in} \end{aligned}$$

For a thin ring, $I = \frac{t^3}{12(1-\nu^2)} = 0.01145$, where $\nu = 0.3$



$$K_T = 1 + \frac{I}{AR^2} \approx 1 \quad K_2 = 1 - \alpha = 1 - \frac{I}{AR^2} \approx 1$$

$$\text{Max. } -M = -wR^2(1.6408 - K_2) = -0.145 \times 34.625^2 (1.6408 - 1) = -111.4 \text{ in-lb/in}$$

or,

$$\text{Max. } +M = (3/2) wR^2 = 1.5 \times 0.145 \times 34.625^2 = 260.76 \text{ in-lb/in}$$

$$\text{Max. bending stress, } \sigma_b = (6M)/(t^2) = (6 \times 260.76) / (0.5^2) = 6,258 \text{ psi}$$

$$N = N_A \cos(x) + V_A \sin(x) + LT_N$$

$$V_A = 0$$

$$LT_N = -Wr(x)(\sin(x))$$

$$N_A = wR/2 = 2.51 \text{ lb/in}$$

$$N = 2.51 \cos(x) - 0.145 \times 34.625 \times (x) \times \sin(x) \text{ lb/in}$$

$$N_{\max} = 2.51 \text{ lb/in at } x = 0^\circ$$

$$\text{Max. membrane stress, } \sigma_m = N_{\max} / t = (2.51 \text{ lb/in}) / (0.5 \text{ in}) = 5 \text{ psi}$$

(2) 25 psig internal pressure + 155 kips axial load

An internal pressure of 25 psig is applied while an axial force of 155 kips is applied to a seal plate on the top of the shell. An equivalent pressure of 933 psig is applied at the top of the shell to represent the axial load of 155 kips less the pressure load on the temporary test lid. Figure A.3.9.1-6 shows the model with the applied boundary conditions.

The maximum stress intensity in the canister is calculated to be 12.86 ksi under these testing loads.

The resultant stresses calculated in (1) and (2) above are conservatively added and evaluated against ASME Code allowable stresses in Table A.3.9.1-5.

Transfer Load Case 19: Normal 80 kip push hydraulic load (internal pressure of 30 psig + 80 kip push + thermal load of 115 °F ambient)

During transfer of the canister from the transfer cask to the HSM a normal maximum push force of 80 kip is applied by a hydraulic ram over an area of 9 inch diameter on the canister bottom. A uniform pressure of 1258 psig [= 80,000 lb / (($\pi/4$) \times 9²)] is applied over this area. The periphery of the top cover outer surface is held as boundary condition. The sustained loads of an internal pressure of 30 psig plus the equivalent push load pressure of 1,258 psi are applied in load step 1. The sustained loads plus the temperature load from fuel decay heat are applied in load step 2.

The maximum stress intensity for load step 1 is calculated to be 15.73 ksi. The maximum stress intensity in the closure welds is calculated to be 10.75 ksi.

The maximum stress intensity in the canister for load step 2 is calculated to be 38.19 ksi. The maximum stress intensity in the closure welds is calculated to be 14.91 ksi.

Transfer Load Case 20: Normal 60 kip pull hydraulic load (internal pressure of 30 psig + 60 kip pull + thermal of 115 °F ambient)

During retrieval of the canister from the HSM into the transfer cask a normal maximum pull force of 60 kips is applied by a hydraulic ram over an annulus area of 12.62 inches outer diameter and 10 inches inner diameter on the inside surface of grapple ring. A uniform pressure of 1,289 psig [= 60,000 lb / (($\pi/4$) \times (12.62² – 10²))] is applied over this area. The periphery of the top cover outer surface is held as boundary condition. The sustained loads of an internal pressure of 30 psig plus the equivalent pull load pressure of 1,289 psi are applied in load step 1. The sustained loads plus the temperature load from fuel decay heat are applied in load step 2.

Stresses in the grapple ring, outer bottom cover plate, and the bottom 2 inches of the canister shell are linearized in ANSYS. The membrane stress results are compared against the general membrane stress, P_m , stress limits. The membrane plus bending stress results are compared against the primary membrane plus bending, $P_m/P_L + P_B$, stress limits. The maximum stress intensity in the rest of the canister is compared against the general membrane stress, P_m , and primary membrane plus bending stress, $P_m/P_L + P_B$, stress limit.

The maximum membrane and membrane plus bending stress in the grapple ring, outer bottom cover plate, and the bottom 2 inches of the canister shell are 9.30 ksi and 25.80 ksi, respectively for Load Case 1. Maximum stress intensity in all other components is 14.97 ksi for Load Case 1. The maximum stress intensity in the closure welds is calculated to be 11.75 ksi.

The maximum stress intensity in the canister is calculated to be 41.64 ksi for load step 2. The maximum stress intensity in the closure welds is calculated to be 14.94 ksi.

Transfer Load Case 21: Off-normal 80 kip push hydraulic load (internal pressure of 30 psig + 80 kip push + thermal load of 115 °F ambient)

The same 80 kip push hydraulic load analyzed in Load Case 19 is also designated as an off-normal condition. Evaluation of this load in Load Case 19 as normal condition covers this off-normal condition.

Transfer Load Case 22: Off-normal 80 kip pull hydraulic load (internal pressure of 30 psig + 80 kip pull + thermal of 115 °F ambient)

During retrieval, the canister from the HSM into the transfer cask a normal maximum pull force of 80 kips is applied by a hydraulic ram over an annulus area of 12.62 inches outer diameter and 10 inches inner diameter on the inside surface of grapple ring. A uniform pressure of 1,719 psig $[= 80,000 \text{ lb} / ((\pi/4) \times (12.62^2 - 10^2))]$ is applied over this area. The periphery of the top cover outer surface is held as boundary condition. The sustained loads of an internal pressure of 30 psig plus the equivalent pull load pressure of 1,719 psi are applied as the loading. ASME code requires only primary stresses to be evaluated under off-normal condition Service Level C, therefore the secondary thermal stresses are not evaluated.

Stresses in the grapple ring, outer bottom cover plate, and the bottom 2 inches of the canister shell are linearized in ANSYS. The membrane stress results are compared against the general membrane stress, P_m , stress limits. The membrane plus bending stress results are compared against the primary membrane plus bending, $P_m/P_L + P_B$, stress limits. The maximum stress intensity in the rest of the canister is compared against the general membrane stress, P_m , and primary membrane plus bending stress, $P_m/P_L + P_B$, stress limit.

The maximum membrane and membrane plus bending stress in the grapple ring, outer bottom cover plate, and the bottom 2 inches of the canister shell are 12.41 ksi and 34.43 ksi, respectively. The maximum stress intensity in all other components is 14.97 ksi. The maximum stress intensity in the closure welds is calculated to be 11.75 ksi.

Transfer Load Case 23: Accident 110 kip push hydraulic load (internal pressure of 30 psig + 110 kip push)

The maximum accident hydraulic force applied by the ram to push the canister from its transfer cask to the HSM is set at 110 kips. The load will be applied over an area with a 9 inch diameter on the canister bottom. A uniform pressure of 1,729.1 psig $[= 110,000 \text{ lb} / ((\pi/4) \times 9^2)]$ is applied over this area in the 2-D ANSYS canister model. The periphery of the canister top cover outer surface is held as boundary condition. The sustained loads of an internal pressure of 30 psig plus the equivalent push force pressure of 1,729 psi are applied as the loading. The secondary temperature load is not required by ASME code for an accident condition analysis.

The maximum stress intensity in the canister for this load case is calculated to be 16.36 ksi. The maximum stress intensity in the closure welds is calculated to be 10.49 ksi.

Transfer Load Case 24: Accident 110 kip pull hydraulic load (internal pressure of 30 psig + 110 kip pull)

The maximum accident condition hydraulic force applied by the ram to pull the canister out of the HSM into the transfer cask is set at 110 kips. This pull force is applied over an annulus area of 12.62 inches outer diameter and 10 inches inner diameter on the inside surface of grapple ring. A uniform pressure of 2,363 psig $[=110,000 \text{ lb} / ((\pi/4) \times (12.62^2 - 10^2))]$ is applied over this area in the 2-D ANSYS canister model. The periphery of the top cover outer surface is held as a boundary condition. The sustained loads of an internal pressure of 30 psig plus the equivalent pull force pressure of 2,363 psi are applied as loading. The secondary temperature load is not required by ASME code for an accident condition analysis.

Stresses in the grapple ring, outer bottom cover plate, and the bottom 2 inches of the canister shell are linearized in ANSYS. The membrane stress results are compared against the general membrane stress, P_m , stress limits. The membrane plus bending stress results are compared against the primary membrane plus bending, $P_m/P_L + P_B$, stress limits. The maximum stress intensity in the rest of the canister is compared against the general membrane stress, P_m , and primary membrane plus bending stress, $P_m/P_L + P_B$, stress limit.

The maximum membrane and membrane plus bending stress in the grapple ring, outer bottom cover plate, and the bottom 2 inches of the canister shell are 17.03 ksi and 47.25 ksi, respectively. The maximum stress intensity in all other components is 15.99 ksi. The maximum stress intensity in the closure welds is calculated to be 11.75 ksi.

Transfer Load Case 25: Canister lifting**Three-Piece Top End Assembly Design**

For the three-piece top end assembly design, four lifting lugs are used for lifting the empty canister into the transfer cask. The lifting lugs, support ring, reinforcing pad, connecting welds, and local stresses in the canister shell are evaluated using an empty DSC weight and a dynamic load factor of 1.15.

Since lifting using internal lugs is an infrequent event (normally the DSC would be lifted for placement into the cask only once prior to fuel loading and will never occur after the DSC is in service), Service Level B allowable stresses are applied. Level B allowables are identical to Level A allowables for the components (shell, support ring, and lug). However, for the welds, Level B allowables are 33% greater than Level A values.

The evaluation is performed using a combination of hand calculations and ANSYS finite element analyses. Hand calculations are used to evaluate the local stresses in the lifting lugs near the pin-hole; finite element analyses are used to determine loads and/or stresses in all other components.

The shell, support ring and lug components are modeled using ANSYS solid elements and welds are modeled by coupling the translational degrees of freedom for the coincident nodes.

Results of the stress evaluation are calculated for different lifting configurations. The maximum stress ratio is 0.909 for the spreader bar assembly, 8' sling, and 10' sling lifting configurations. Therefore, the lug design and required welds are acceptable for the 32PTH Type 1 DSC.

Alternate Two-piece Top End Assembly Design

For the alternate two-piece top end assembly design, the evaluations performed for the 32PTH DSC are bounding.

Canister Corner Drop Analysis

As stated in [16], the end and corner drops are generally not considered credible during storage and transfer operations because the transfer cask will always be in horizontal orientation. Thus, corner drop load cases are not evaluated.

D.4. Summary of Results for DSC Shell Assembly Stress Evaluation for Transfer Loads

The calculated maximum stress intensities in the DSC shell assembly components are summarized in Table A.3.9.1-5 through Table A.3.9.1-8. These tables also show that the stress intensity results are below the ASME code stress intensity allowables.

The stresses in the closure welds are summarized in Table A.3.9.1-9 through Table A.3.9.1-12. These tables also show that the stress results are below the ASME code stress allowables.

Based on the results of these analyses, the design of the 32PTH Type 1 DSC shell assembly is structurally adequate under transfer loads of testing, normal (Service Level A), and accident (Level D) conditions.

E. DSC Shell Assembly Stress Evaluation for Storage Loads

This section evaluates the structural adequacy of the 32PTH Type 1 DSC shell assembly when it is in the horizontal storage position within an HSM-H. This section considers storage loads on the canister under both normal and hypothetical accident conditions.

The evaluation of the stresses in the canister for storage loads employs an ANSYS 2-D axisymmetrical model to analyze three thermal conditions specified for the canister during storage. This 2-D model is the same model described in Section A.3.9.1.3.2 (D.2) used to compute stresses due to axisymmetric transfer loads. The analyses of axisymmetric loads such as internal and external pressure loads for transfer conditions are also valid for a horizontal storage canister. Their results are therefore used in this section for stress combinations and evaluations.

The fuel basket stress analysis for storage loads (Section 3.9.1.2.3 (C)) uses an ANSYS 3-D model, which includes the DSC canister shell, to calculate the non-axisymmetrical seismic and deadweight loads. The calculated stress intensities in the canister under the seismic and deadweight loads from Section 3.9.1.2.3 (C) are used in this section for stress combinations and evaluations.

The temperatures in the canister under 115 °F and -20 °F ambient conditions of and under HSH-H blocked vent conditions for 34 hours are computed in Chapter 4. These temperatures are imposed on the stress model in this evaluation for thermal stress calculations.

E.1. DSC Shell Assembly Storage Load Cases

The storage load cases considered in this section are summarized in Table A.3.9.1-13.

E.2. DSC Shell Assembly Finite Element Model Descriptions

The 2-D axisymmetrical stress models described in Section A.3.9.1.3.2 (D.2) for the transfer load analysis are also used for the storage load analysis. Figure A.3.9.1-1, Figure A.3.9.1-2, and Figure A.3.9.1-3 show this model. This model is used to evaluate the three specified thermal cases for storage, which are the -20 °F and 115 °F ambient conditions, and the blocked vent hypothetical accident condition. The temperature profiles in the canister for the three storage thermal cases are calculated in Chapter 4.

E.3. DSC Shell Assembly Stress Analysis for Storage Loads

All individual load cases specified in Table A.3.9.1-13 are described in detail in the following sections.

Storage Load Case 1: Deadweight (1 g down)

The canister shell and fuel basket containing the fuel assemblies, resting horizontally on the rails of an HSM-H is analyzed in Section 3.9.1.2.3 (C) for storage loads. The maximum primary membrane and membrane plus bending stress intensities in the canister shell due to the deadweight load are calculated to be 0.4 ksi, and 4.05 ksi, respectively (see Table 3.9.1-5). These stress intensities are also used as maximum stress intensities at closures welds (see Table A.3.9.1-15).

Storage Load Case 2: Internal pressure of 30 psig

The internal pressure of 30 psig applied on the canister is analyzed in load step 1 of Transfer Load Case 2 in Section A.3.9.1.3.2 (D). The maximum membrane plus bending stress intensities in the canister, calculated in Section A.3.9.1.3.2 (D) is 14.97 ksi. The maximum stress intensity in the closure welds is calculated to be 11.75 ksi calculated in Section A.3.9.1.3.2 (D).

Storage Load Case 3: Seismic loads (0.65 g axial + 0.65 g transverse + 1.3g vertical down)

The seismic loads on the canister, containing the basket and the fuel assemblies and resting on the rails of an HSM-H, are analyzed in Section 3.9.1.2.3 (C). The maximum primary membrane and membrane plus bending stress intensities are calculated in Section 3.9.1.2.3 (C) to be 0.63 ksi, and 6.08 ksi, respectively (see Table 3.9.1-5). This specified seismic load includes a 1g deadweight load.

Storage Load Case 4: Thermal load at -20 °F ambient

The maximum temperature in the canister for this thermal case is calculated in Chapter 4 to be 318 °F. The temperatures in the canister calculated in Chapter 4 are applied to the stress model in order to compute the thermal stress intensities in the canister. The maximum secondary thermal stress intensity is calculated to be 22.49 ksi. The 22.49 ksi stress is calculated based on canister maximum temperature of 324 °F. Since the revised temperature of 318 °F is less than 324 °F, 22.49 ksi is conservatively used for load combination and compared with the allowables. The maximum stress intensity in the closure welds is calculated to be 2.47 ksi.

Storage Load Case 5: Thermal load at 115 °F ambient

The thermal load case with the canister stored in the HSM-H with fins, described in Chapter 4, is selected for this evaluation. The maximum temperature in the canister for this thermal case is calculated in Chapter 4 to be 407 °F. The same procedure used for calculating the thermal stress intensities for the Load Case 4 is repeated for the 115 °F ambient thermal load. The secondary thermal stress intensity is calculated to be 20.51 ksi. The 20.51 ksi stress is calculated based on canister maximum temperature of 434 °F. Since the revised temperature of 407 °F is less than 434 °F, 20.51 ksi is conservatively used for load combination and compare with the allowables. The maximum stress intensity in the closure welds is calculated to be 2.50 ksi.

Storage Load Case 6: Blocked vent thermal accident condition

The thermal evaluation presented in Chapter 4 reports four thermal cases for the canister stored in the HSM with blocked vent. The maximum temperature of 600 °F in the canister is reached after 34 hours of complete vent blockage in an HSM with fins. The 34 hour vent blockage is a conservative scenario, since the vent is visually checked at least every 24 hours. However, this case is reported in the thermal evaluation and is therefore selected for analysis in this section. The same procedure used for obtaining the thermal load in Load Case 4 is used in this load case. The secondary thermal stress intensity is calculated to be 20.96 ksi. The maximum stress intensity in the closure welds is calculated to be 7.12 ksi.

Storage Load Case 7: Accident internal pressure of 70 psig (in the event of blocked vent)

The internal pressure of 70 psig in the canister is analyzed for enveloping the accident condition internal pressures during the blocked vent scenario. The maximum primary membrane plus bending stress intensity in the canister is calculated to be 34.96 ksi. The maximum stress intensity in the closure welds is calculated to be 27.44 ksi.

Storage Load Case 8: Accident flood load (enveloped by external pressure of 30 psig)

The hypothetical accident condition flood load is enveloped by an external pressure of 30 psig. The maximum primary membrane plus bending stress intensity in canister is calculated to be 5.48 ksi. The maximum stress intensity in the closure welds is calculated to be 2.90 ksi.

E.4. Summary of the Stress Calculation Results for All Storage Load Cases

Table A.3.9.1-14 and Table A.3.9.1-15 summarize the calculated stresses in the entire canister and their corresponding ASME code evaluations.

Based on the results of this calculation, the 32PTH Type 1 DSC canister is structurally adequate under all normal (Service Level A), off-normal (Service Level C), and hypothetical accident (Service Level D) conditions during storage.

A.3.9.1.3.3 DSC Shell Buckling Evaluation

This section evaluates the structural adequacy of the 32PTH Type 1 DSC canister against buckling during a vertical end drop during transfer operations.

For the NUHOMS HD[®] System, the vertical end drops are not considered credible during storage and transfer operations under 10 CFR Part 72 because the transfer cask is always in the horizontal orientation. The vertical end drop buckling evaluation documented below is performed in support of a 10 CFR Part 50 evaluation that may be performed by the user if the user cannot demonstrate that this accident drop is not credible.

A. Approach

A finite element plastic analysis with large displacement option is performed to monitor occurrence of canister shell buckling under the specified loads.

The thermal evaluation presented in Chapter 4 shows that the metal temperatures of the entire canister are below 500 °F during the transfer operations. The material properties of canister at 500 °F are therefore conservatively used in this calculation.

B. Material Properties used for Canister Buckling Evaluation

The material properties of the canister materials, SA-240 Type 304 stainless steel, at 500 °F are as follows.

Property	@ 500 °F
S_m (ksi)	17.5
S_y (ksi)	19.4
S_u (ksi)	63.4
E (psi)	25.8×10^6

For the elastic-plastic finite element analysis, bilinear kinematic hardening material properties are used. Tangent modulus of 5% of elastic modulus is assumed after yield stress.

The material properties for the top and bottom shield plug, A-36, at 500 °F are as follows:

Property	@ 500 °F
S_m (ksi)	19.3
S_y (ksi)	29.3
S_u (ksi)	58.0
E (psi)	27.3×10^6

C. Finite Element Buckling Analysis

The following three hypothetical accident load cases for the canister are considered in this buckling analysis.

Buckling Load Case 1: End drop + 15 psig external pressure

Buckling Load Case 2: End drop + 30 psig internal pressure

Buckling Load Case 3: End drop + 0 psig internal pressure

The two-dimensional axisymmetric finite element model of the canister described in Appendix A.3.9.1, Section A.3.9.1.3.2 (D.2) for the DSC canister stress analysis is used for this analysis.

The gap element real constants, node couplings and displacement boundary conditions are also the same as those used in Section A.3.9.1.3.2 (D.2). The weight of the canister's outer and inner top cover plus the top shield plug and its support ring is 12,856 lb, and the bottom shield plug is 9,696 lb (see Section A.3.2.1). Since the top end of the canister is heavier than the bottom end, it is a more severe case when the canister drops on its bottom end. A drop on the bottom end is therefore chosen for analysis in this calculation.

For load case with external pressure or internal pressure, a quasi-static plastic analysis consisting of two load steps is performed to monitor buckling of the canister. The first load step applies external pressure or internal pressure alone. A subsequent inertial load of 300g is added in the second load step. The outer surface of the canister bottom is held in order to simulate the case that the canister drops on a rigid cask bottom face.

In the load step 1, the stepped external or internal pressure is applied as a static load.

In the load step 2, the weight of the canister internals (basket and fuel assemblies) is accounted for by applying an equivalent internal pressure on the canister bottom. The actual total weight of the canister internals is 80,971 lb (basket 29,451 lb + fuel assemblies 51,520 lb) (Chapter A.3, Section A.3.2.1). A total weight of 83,000 lb for the canister internals is conservatively used in this analysis. This inertial load is uniformly distributed over the bottom surface of the canister cavity with a radius of 34.375 in. This equivalent uniform pressure, P_{in} , exerted on the canister bottom by the weight of the internals under a 1 g load is calculated as follows.

$$P_{in} = [83,000 / (\pi \times 34.375^2)] = 22.3585 \text{ psi}$$

An equivalent pressure of 6707.55 psig on the canister bottom corresponding to the 300g load ($P_{in} = 300 \times 22.3585 = 6707.55 \text{ psi}$) is, therefore, applied to the canister bottom along with the 300g acceleration load in the load step 2.

A bilinear stress-strain relationship (with kinematic hardening) is used to obtain stresses and deflections beyond the elastic limit of the material. The large displacement option in ANSYS is activated to monitor the buckling response.

D. Summary Canister Buckling Analysis Results

The following table summarizes the last converged load for the three load cases:

Load Case	Last Converged Load (g)	g Load Used for Basket Structural Analysis	Factor of Safety
1	173.5	75	2.31
2	174.9	75	2.33
3	174.0	75	2.32

The analysis shows that the critical buckling load for the canister end drop is 173.5g, which is well beyond the design 75g load. Therefore, it is concluded that buckling of the canister will not occur during a hypothetical accident end drop.

A.3.9.1.3.4 Evaluation of Alternate DSC Top and Bottom Closure Assembly Design

The alternate top closure assembly of the 32PTH Type 1 DSC which consists of the two-part combined shield plug /inner cover assembly (including the optional configurations), as well as the optional bottom end configurations (consisting of two-plate or single forging bottom assembly) are not analyzed explicitly.

The evaluations for the 32PTH Type 1 DSC consider a DSC with a three-part top end configuration (with separate inner cover plate, shield plug, and outer cover plate) and a three-part bottom end configuration (with separate inner bottom cover, bottom shield plug, outer bottom cover plate). The results from these evaluations are documented in Sections A.3.9.1.3.2 and A.3.9.1.3.3, and are considered to be bounding relative to those for a DSC with the alternate two-part top end assembly or the optional bottom end configurations for cases involving internal pressure and handling loads. For side drop accident loads, the results of the 32PTH DSC for the side drop accident load case are also applicable for the alternate top end and the optional bottom end configurations of the 32PTH Type 1 DSC. This is justified because the side drop analyses are performed using two separate 3-D models which model the top and the bottom regions of the DSC shell assembly, respectively. These models include a segment of the DSC shell and are intended to capture the maximum stresses that occur near the transition between the shell and the stiffer top and bottom ends, and, therefore, are not sensitive to the length differences between the 32PTH and 32PTH Type 1 DSCs. Furthermore, the loaded canister weight used in the 32PTH DSC analysis is the same as in the 32PTH Type 1 analyses.

A.3.9.1.4 32PTH Type 1 DSC and OS187H Type 1 Transfer Cask Thermal Expansion Evaluation

A.3.9.1.4.1 Introduction

The purpose of this section is to determine the thermal growths among components of fuel cladding, basket, canister, and transfer cask in the 32PTH Type 1 DSC and OS187H Type 1 TC. This thermal expansion calculation covers events of vacuum drying, transfer, storage, and storage with blocked vent.

A.3.9.1.4.2 Approach

The temperatures of the fuel cladding, basket, canister, and transfer cask under various events calculated in the thermal analyses of Chapter 4 are applicable for the 32PTH Type 1 DSC and OS187H Type 1 transfer cask. Transient thermal analyses are conducted for the vacuum drying and blocked vent events. Steady-state thermal analyses are conducted for the normal and off-normal conditions during transfer and storage. This section computes the thermal expansions at the steady-state temperatures in the events of transfer and storage.

In the vacuum drying load case, the profiles of transient temperature versus time computed in Chapter 4 are studied for selection of the critical time points at which the corresponding component temperatures would generate a minimum clearance between two nested components. For the blocked vent load case, the maximum temperatures from Chapter 4 are used in this calculation.

The cold dimensions of each pair of nested components are so determined, based on design tolerances, which generates a minimum cold clearance between the two components.

Unless otherwise stated, nominal dimensions of basket, canister, and cask are used for the thermal expansion calculations.

A.3.9.1.4.3 Mechanical Properties of Materials

The coefficient of thermal expansion of structural materials used for the fuel basket, canister shell, and transfer cask are provided in Table 3.9.1-6 as a function of temperature. The properties of SA-240 Type 304 are taken from Reference 1, and the zircaloy properties are taken from Reference 4.

A.3.9.1.4.4 Thermal Expansion Computation

A. Thermal Expansion between the Length of Fuel Assembly and Canister Cavity

The maximum length of fuel assemblies in 32PTH Type 1 DSC is 170.0 inches and the minimum cavity length of the 32PTH Type 1 DSC is 171.63 inches. The clearance between the fuel assembly and the DSC cavity for 32PTH Type 1 DSC is calculated using the same methodology and data as described in Appendix 3.9.1, Section 3.9.1.4.4(A).

An irradiation growth of 1.25 inches is considered in Appendix 3.9.1, Section 3.9.1.4.4(A) for the fuel assemblies with a maximum length of 162.4 inches with a maximum burnup of 60 GWd/MTU. The fuel assemblies in 32PTH Type 1 have a maximum length of 170.0 inches with the same maximum burnup of 60 GWd/MTU. Since the irradiation growth is proportional to the fuel assembly length for a given burnup, an irradiation growth of 1.31 inches is considered for the fuel assemblies in the 32PTH Type 1 DSC as calculated below.

$$\Delta L_{\text{irrad}} = \frac{170.0''}{162.4''} \times 1.25'' = 1.31''$$

The results of the calculation for the clearance between the fuel assembly and the DSC cavity for 32PTH Type 1 DSC are summarized below using the same nomenclature as used in Appendix 3.9.1, Section 3.9.1.4.4(A).

Event	T _F (°F)	α _Z (in/in-°F)	α _S (in/in-°F)	T _C (°F)	α _C (in/in-°F)	L _F (in)	L _{F, irrad} (in)	L _{CH} (in)	L _{CH} - L _{FHT} (in)
Vacuum Drying	760	3.01E-06	10.0E-06	210	8.94E-06	170.48	171.79	171.84	0.05
Transfer	730	3.00E-06	10.0E-06	390	9.46E-06	170.46	171.77	172.15	0.38
Storage, Off-Normal	700	3.00E-06	10.0E-06	280	9.16E-06	170.44	171.75	171.96	0.21
Storage Accident	830	3.01E-06	10.1E-06	590	9.80E-06	170.53	171.84	172.50	0.66

As seen in the above table, adequate clearance has been provided to permit free thermal expansion of the fuel assemblies within 32PTH Type 1 DSC cavity.

B. Thermal Expansion between the Outer Diameter of the Basket and the Inner Diameter of the Canister Cavity

The diametrical gap between the outer diameter of the basket and the inner diameter of the canister remains the same as for the 32PTH DSC. With the same radial temperature profile, the thermal expansion values calculated in Section 3.9.1.4.4.B are applicable for the 32PTH Type 1 DSC. These calculations show that the gap will allow free thermal expansion.

C. Thermal Expansion between the Length of Basket and Canister Cavity

The maximum length of the 32PTH Type 1 basket and the minimum cavity length of the 32PTH Type 1 DSC are 169.0 inches and 171.63 inches, respectively at room temperature. The clearance between the basket and the DSC cavity for 32PTH Type 1 DSC is calculated using the same methodology and data as described in Appendix 3.9.1, Section 3.9.1.4.4(C).

The results of the calculation for the clearance between the basket and the DSC cavity for 32PTH Type 1 DSC are summarized below using the same nomenclature as used in Appendix 3.9.1, Section 3.9.1.4.4(C).

Event	Case	T _{CNH} (°F)	α _{CN} (in/in-°F)	T _{BKH} (°F)	α _{BK} (in/in-°F)	L _{CNH} (in)	L _{BKH} (in)	L _{CNH} - L _{BKH} (in)
Vacuum Drying	TC Backfill	500	9.70E-06	550	9.80E-06	172.346	169.795	2.551
Transfer	115°F Amb. Basket Type I, Conf. # 1	460	9.62E-06	640	9.88E-06	172.274	169.952	2.322
	115°F Amb. Basket Type I, Conf. # 2	460	9.62E-06	625	9.85E-06	172.274	169.924	2.350
	115°F Amb. Basket Type I, Conf. # 3	460	9.62E-06	630	9.86E-06	172.274	169.933	2.341
	115°F Amb. Basket Type I, Conf. # 4	460	9.62E-06	640	9.88E-06	172.274	169.952	2.322
	-20°F Amb. Basket Type I, Conf. # 1	390	9.46E-06	570	9.80E-06	172.150	169.828	2.321
	115°F Amb. Basket Type II, Conf. # 1	460	9.62E-06	640	9.88E-06	172.274	169.952	2.322
Storage	115°F Amb. HSM-H w/ Finned Side Shield	400	9.50E-06	600	9.80E-06	172.168	169.878	2.290
	-20°F Amb. HSM-H w/ Finned Side Shield	280	9.16E-06	505	9.71E-06	171.960	169.714	2.246
	34 hours after Blockage HSM-H w/ Finned Side Shield	590	9.80E-06	740	10.0E-06	172.505	170.132	2.373

D. Thermal Expansion between the Outer Diameter of the Canister and the Inner Diameter of the Cask Body

The diametrical gap between the outer diameter of the canister and the inner diameter of the cask remains the same as for the 32PTH DSC and OS187H transfer cask. With the same radial temperature profile, the thermal expansion values calculated in Section 3.9.1.4.4.D are applicable for the 32PTH Type 1 DSC and OS187H Type 1 transfer cask. These values show that the current gap will allow free thermal expansion.

E. Thermal Expansion between the Length of the Canister and the Transfer Cask Cavity

The maximum outer length of the 32PTH Type 1 DSC and the minimum cavity length of the OS187H Type 1 TC are 193.0 inches and 198.75 inches, respectively, at room temperature. The clearance between the DSC and the TC cavity for 32PTH Type 1 DSC is calculated using the same methodology and data as described in Appendix 3.9.1, Section 3.9.1.4.4(E).

The results of the calculation for the clearance between the DSC and TC cavity for 32PTH Type 1 DSC are summarized below using the same nomenclature as used in Appendix 3.9.1, Section 3.9.1.4.4(E).

Event	Case	T _{CKH} (°F)	α _{CK} (in/in-°F)	T _{CNH} (°F)	α _{CN} (in/in-°F)	L _{CKH} (in)	L _{CNH} (in)	L _{CKH} - L _{CNH} (in)
Vacuum Drying	TC Backfill	265	9.13E-06	525	9.75E-06	199.104	193.856	5.248
Transfer	115°F Amb.	330	9.26E-06	485	9.67E-06	199.229	193.775	5.454
	-20°F Amb.	240	9.06E-06	500	9.70E-06	199.056	193.805	5.251

As seen in the above table, the smallest clearance between the 32PTH Type 1 DSC and OS187H Type 1 TC is larger than 5.248 inches. A cask spacer with the height of 5 to 5.125 inches will be adequate to raise the DSC and enable welding operation and to maintain adequate clearance to permit free thermal expansion of the 32PTH Type 1 DSC within OS187H Type 1 TC.

A.3.9.1.4.5 Thermal Expansion Analysis Conclusions

This evaluation demonstrates that adequate clearance is provided between the 32PTH Type 1 DSC fuel basket and canister shell, and between the 32PTH Type 1 DSC canister and the OS187H Type 1 transfer cask to permit free thermal expansions among these components due to all specified design and service conditions.

A.3.9.1.5 References

1. American Society of Mechanical Engineers, ASME Boiler and Pressure Vessel Code, Section II, Part D, 1998, through 2000 addenda.
2. Not used.
3. American Society of Mechanical Engineers, ASME Boiler and Pressure Vessel Code, Section III, Appendix F, 1998 through 2000 addenda.
4. NUREG/CR-0497-Rev 2, MATPRO-Version 11 (Revision 2), A handbook of materials properties for use in the analysis of light water reactor fuel rod behavior.
5. Not used.
6. Manual of Steel Construction, Ninth Edition, American Institute of Steel Construction, Inc., 1989.
7. Roark, Formulas for Stress and Strain, Seventh Edition.
8. American Society of Mechanical Engineers, ASME Boiler and Pressure Vessel Code, Section III, Division 1, Subsection NB, 1998, through 2000 addenda.
9. NUREG/CR-0481 SAND77-1872 R-7, "An Assessment of Stress-Strain Data Suitable for Finite-Element Elastic-Plastic Analysis of Shipping Containers," September 1978.
10. ANSYS Users Manual, Release 8.0 and 10.0A1.
11. Not used.
12. Not used.
13. Not used.
14. USNRC Spent Fuel Project Office, Interim Staff Guidance – 15, "Materials Evaluation."
15. Roark, Formulas for Stress and Strain, Sixth Edition.
16. Safety Evaluation Report, Transnuclear, Inc., NUHOMS[®] HD Horizontal Modular Storage System for Irradiated Nuclear fuel, Docket No. 72-1030.

Table A.3.9.1-1
Temperature Dependent Material Properties for ASTM A-36

Temp (°F)	E (10³ ksi)	S_m (ksi)	S_y (ksi)	S_u (ksi)	α_{INST} (10⁻⁶°F⁻¹)	α_{AVG} (10⁻⁶°F⁻¹)
70	29.5	19.3	36.0	58.0	6.4	6.4
200	28.8	19.3	33.0	58.0	6.9	6.7
300	28.3	19.3	31.8	58.0	7.3	6.9
400	27.7	19.3	30.8	58.0	7.7	7.1
500	27.3	19.3	29.3	58.0	8.0	7.3
600	26.7	17.7	27.6	58.0	8.4	7.4
700	25.5	17.3	25.8	58.0	8.6	7.6

Table A.3.9.1-2
Material Stress Limits for 32PTH Type 1 DSC
SA-240/SA-479 304 & SA-182 F304

Temp	Level A			Level C		Level D			
						Elastic		Elastic-Plastic	
(°F)	P _m	P _m + P _b	P _m + P _b + Q	P _m	P _m + P _b	P _m	P _m + P _b	P _m	P _m + P _b
70	20.0	30.0	60.0	30.0	45.0	48.0	72.0	52.5	67.5
200	20.0	30.0	60.0	25.0	37.5	48.0	71.0	49.7	63.9
300	20.0	30.0	60.0	24.0	36.0	46.3	66.2	46.3	59.6
400	18.7	28.1	56.1	22.4	33.7	44.8	64.0	44.8	57.6
500	17.5	26.3	52.5	21.0	31.5	42.0	63.0	44.4	57.1
600	16.4	24.6	49.2	19.7	29.5	39.4	59.0	44.4	57.1
700	16.0	24.0	48.0	19.2	28.8	38.4	57.6	44.4	57.1
800	15.2	22.8	45.6	18.2	27.4	36.5	54.7	44.0	56.5

Table A.3.9.1-3
32PTH Type 1 DSC Canister Load Combinations during Transfer

Loading	Canister w/Transfer Cask Orientation	Service Level	Load for Analysis	Load Combinations	Analyzed Load Case No.	ANSYS Model
Dead weight	Vertical ⁽¹⁾	A	1 g down (axial)	1 g down + 15 psig ext. press. + thermal (vacuum dry)	1	2-D
External pressure	Vertical ⁽¹⁾	A	15 psig			
Thermal	Vertical ⁽¹⁾	A	Vacuum dry			
Dead weight	Horizontal ⁽²⁾	A	2 g axial + 2 g trans. + 2 g vertical	A = 2 g axial + 2 g trans. + 2 g vertical	2	2-D
Handling load in transfer cask	Horizontal ⁽²⁾	A		A+ 30 psig int. pressure + thermal (115 °F) A+ 15 psig ext. pressure + thermal (-20 °F)	3	2-D
Internal pressure	Horizontal ⁽²⁾	A	30 psig ⁽⁶⁾	Pressure stress	[2] ⁽⁵⁾	2-D
External pressure	Horizontal ⁽²⁾	A	15 psig	Pressure stress	[3] ⁽⁵⁾	2-D
Thermal	Horizontal ⁽²⁾	A	Thermal stress (-20 °F Ambient)	Thermal stress	[3] ⁽⁵⁾	2-D
Thermal	Horizontal ⁽²⁾	A	Thermal stress (115 °F ambient)	Thermal stress	[2] ⁽⁵⁾	2-D
Internal pressure	Horizontal	D	120 psig ⁽³⁾	Pressure stress	4	2-D
External pressure	Horizontal	D	25 psig ⁽⁴⁾	Pressure stress	5	2-D
Side drop	Horizontal	D	75 g multiple orientations (0°, 30°, 45°, impact on two rails, impact on one rail) Drop angles are enveloped by 0° (no rail) and 180° (two rails)	75 g side drop at 0° (no rail) + 30 psig int. press. of top/bottom ends	6/7	3-D
				75 g side drop at 180° (two rails) + 30 psig int. press. of top/bottom ends	8/9	3-D
				75 g side drop at 0° (no rail) + 15 psig ext. press. of top/bottom ends	10/11	3-D
				75 g side drop at 180° (two rails) + 15 psig ext. press. of top/bottom ends	12/13	3-D
Corner drop	Horizontal	D	Enveloped by 75 g Side Drop and 75 g End Drop			
End drop	Vertical	D	75 g End Drop	75 g top/bottom + 30 psig int. pressure	14/15	2-D
				75 g top/bottom + 15 psig ext. pressure	16/17	2-D

Notes:

- (1) Transfer cask supported at the bottom.
- (2) Transfer cask supported at 4 trunnion location.
- (3) Under accident fire condition.
- (4) Under accident flood condition.
- (5) [#] indicates this individual load case is enveloped in the analyzed load case No.
- (6) From Chapter 4, Table 4-10, the maximum normal operating pressure is 6.4 psig during transfer operation. However, a design pressure of 15 psig is used. Conservatively, 30 psig is used for structural evaluation of the canister.

Table A.3.9.1-4
32PTH Type 1 DSC Canister Load Combinations during Lifting, Testing, and Hydraulic Loads

Loading	Canister w/Transfer Cask Orientation	Service Level	Load for Analysis	Load Combinations	Analyzed Load Case No.	ANSYS Model
Dead weight	Horizontal	A	1 g	1 g + 25 psig int. pressure + 155 kips axial loads	18	2-D
Test pressure	Horizontal	A	25 psig ⁽³⁾			
Seal plate axial load	Horizontal	A	155 kips			
Hydraulic loads ^{(1) (2)} (push/pull)	Horizontal	A	80/60 kips	30 psig int. pressure + 80 kips push/60 kips pull + thermal (115 °F)	19/20	2-D
Hydraulic loads ^{(1) (2)} (push/pull)	Horizontal	C	80/80 kips	30 psig int. pressure + 80 kips + thermal (115 °F)	21/22	2-D
Hydraulic loads ^{(1) (2)} (push/pull)	Horizontal	D	110/110 kips	30 psig int. pressure + 110 kips	23/24	2-D
Lifting	Vertical	A	1g	1 g	25	3-D

Notes:

- (1) The hydraulic push loads are applied at the canister bottom surface within the grapple ring support.
- (2) The hydraulic pull loads are applied at the inner surface of the grapple ring.
- (3) From Chapter 4, Table 4-10, the maximum normal operating pressure is 6.4 psig during transfer operation. The canister is conservatively evaluated at higher test pressures.

Table A.3.9.1-5
Summary of Calculated Stresses for Testing Condition Loads

Load Case	Combination of Loads	Canister Orientation	Service Level	Component	Stress Category	Stress (ksi)	Stress Limit (ksi)
18	DW + 25 psig int. press. + 155 kip axial load	Horizontal	A	All ⁽¹⁾	P_m	12.86 ⁽²⁾	24 ⁽⁴⁾
					$P_m + P_b$	19.12 ksi ⁽³⁾	40.5 ⁽⁵⁾

Notes:

- (1) Yield stress, $S_y = 30,000$ psi, is taken at test temperature of 100 °F for both material SA-240 GR.304 and SA-182 F304
(2) $P_m = 12.86$ ksi + 0.005 ksi (dead weight, in load case 18) = 12.86 ksi
(3) $P_m + P_b = 12.86$ ksi + 6.26 ksi (dead weight, in load case 18) = 19.12 ksi
(4) $P_m < 0.8 S_y = 24$ ksi
(5) $P_m + P_b < 1.35 S_y = 40.5$ ksi

Table A.3.9.1-6
Summary of Calculated Stress for Normal and Off-Normal
Condition Transfer Loads

Load Case	Combination of Loads	Canister Orientation	Service Level	Components	Stress Category	Stress ⁽³⁾ (ksi)	Stress Limit (ksi)
1	1 g down + 15 psig ext. press. + vacuum drying thermal	Vertical	A	All ⁽²⁾	P _m	2.05	17.5
					P _m + P _b	2.05	26.3
					P _m + P _b + Q	22.69	52.5
2	Handling 2 g + 30 psig int. press. + thermal (115 °F)	Horizontal	A	All ⁽²⁾	P _m	14.97+0.88 = 15.85	17.5
					P _m + P _b	14.97+9.74 = 24.71	26.3
					P _m + P _b + Q	41.70+9.74 = 51.44	52.5
3	Handling 2 g + 15 psig ext. press. + thermal (-20 °F)	Horizontal	A	All ⁽²⁾	P _m	2.75+0.88 = 3.63	17.5
					P _m + P _b	2.75+9.74 = 12.49	26.3
					P _m + P _b + Q	31.63+9.74 = 41.37	52.5
19	30 psig int. press + 80 kips push + thermal (115 °F)	Horizontal	A	All ⁽²⁾	P _m	15.73	17.5
					P _m + P _b	15.73	26.3
					P _m + P _b + Q	38.19	52.5
20	30 psig int. press + 60 kips pull + thermal (115 °F)	Horizontal	A	GR, BOCP, and bottom 2" CS ⁽¹⁾	P _m	9.30	20.0
					P _m + P _b	25.80	30.0
					P _m + P _b + Q	27.45	60.0
				All except GR, BOCP, and bottom 2" CS ⁽³⁾	P _m	14.97	17.5
					P _m + P _b	14.97	26.3
					P _m + P _b + Q	41.64	52.5
21	30 psig int. press + 80 kips push + thermal (115 °F)	Horizontal	C	All ⁽²⁾	P _m	15.73	21.0
					P _m + P _b	15.73	31.5
					P _m + P _b + Q	-	-
22	30 psig int. press + 80 kips pull + thermal (115 °F)	Horizontal	C	GR, BOCP, and bottom 2" CS ⁽¹⁾	P _m	12.41	24.0
					P _m + P _b	34.43	36.0
					P _m + P _b + Q	-	-
				All except GR, BOCP, and bottom 2" CS ⁽³⁾	P _m	14.97	21.0
					P _m + P _b	14.97	31.5
					P _m + P _b + Q	-	-

Notes:

- (1) GR—grapple ring; BOCP—bottom outer cover plate; CS—canister shell. Except for the vacuum drying and fire accident load cases, the temperature in the grapple ring, the bottom outer cover plate and the bottom 2 inches of the canister shell do not exceed 300 °F. Conservatively stress limits at 300 °F are used.
- (2) Conservatively the stress limits at 500 °F are used.
- (3) Conservatively the maximum stress intensity was used for both P_m and P_m + P_b stresses for all analyses except for grapple pull load cases, 20 and 22, where the stresses were linearized in the grapple ring, bottom outer cover plate and bottom 2 in of the canister shell.

Table A.3.9.1-7
Summary of Calculated Stress for Accident Condition Transfer Loads (Axisymmetric Loads)

Load Case	Combination of Loads	Canister Orientation	Service Level	Components	Stress Category	Stress ⁽⁴⁾ (ksi)	Stress Limit (ksi)
4	120 psig int. press. under fire accident	Horizontal	D	All ⁽²⁾	P_m	23.92	44.0
					$P_m + P_b$	23.92	56.5
5	25 psig ext. press. under flood accident	Horizontal	D	All ⁽³⁾	P_m	4.56	42.0
					$P_m + P_b$	4.56	63.0
14	75 g top end drop + 30 psig int. press.	Vertical	D	All ⁽³⁾	P_m	17.68	42.0
					$P_m + P_b$	17.68	63.0
15	75 g bottom end drop + 30 psig int. press.	Vertical	D	All ⁽³⁾	P_m	21.05	42.0
					$P_m + P_b$	21.05	63.0
16	75 g top end drop + 15 psig ext. press.	Vertical	D	All ⁽³⁾	P_m	30.68	42.0
					$P_m + P_b$	30.68	63.0
17	75 g bottom end drop + 15 psig ext. press.	Vertical	D	All ⁽³⁾	P_m	26.09	42.0
					$P_m + P_n$	26.9	63.0
23	30 psig int. press. + 110 kips push	Horizontal	D	All ⁽³⁾	P_m	16.36	42.0
					$P_m + P_b$	16.36	63.0
24	30 psig int. press. + 110 kips pull	Horizontal	D	GR, BOC _P , and bottom 2" CS ⁽¹⁾	P_m	17.03	46.3
					$P_m + P_b$	47.25	66.2
				All except GR, BOC _P , and bottom 2" CS ⁽³⁾	P_m	15.99	42.0
					$P_m + P_b$	15.99	63.0

Notes:

- (1) GR—grapple ring; BOC_P—bottom outer cover plate; CS—canister shell. Except for the vacuum drying and fire accident load cases, the temperature in the grapple ring, the bottom outer cover plate, and bottom 2 inches of the canister shell do not exceed 300 °F. Conservatively stress limits at 300 °F are used for elastic analysis.
- (2) Conservatively the stress limits at 800 °F are used for elastic-plastic analysis.
- (3) Conservatively the stress limits at 500 °F are used for elastic analysis.
- (4) Conservatively the maximum stress intensity was used for both P_m and $P_m + P_b$ stresses for all analyses except for grapple pull load cases, 23, where the stresses were linearized in the grapple ring, bottom outer cover plate and bottom 2 inches of the canister shell.

Table A.3.9.1-8
Summary of Stresses for Accident Condition Transfer Loads (3-D Inertial Loads)

Load Case	Load Combination	Canister	Maximum Stress Intensity ⁽¹⁾ [ksi]	Stress Limits	
				PM	PM+PB
6	Side drop 75 g + 30 psig internal pressure	Top end, no rails (orientation 0°)	25.5	44.4 ksi	57.1 ksi
7	Side drop 75 g + 30 psig internal pressure	Bottom end, no rails (orientation 0°)	24.0	44.4 ksi	57.1 ksi
8	Side drop 75 g + 30 psig internal pressure	Top end, rails (orientation 180°)	27.3	44.4 ksi	57.1 ksi
9	Side drop 75 g + 30 psig internal pressure	Bottom end, rails (orientation 180°)	24.7	44.4 ksi	57.1 ksi
10	Side drop 75 g + 15 psig external pressure	Top end, no rails (orientation 0°)	25.9	44.4 ksi	57.1 ksi
11	Side drop 75 g + 15 psig external pressure	Bottom end, no rails (orientation 0°)	24.1	44.4 ksi	57.1 ksi
12	Side drop 75 g + 15 psig external pressure	Top end, rails (orientation 180°)	27.3	44.4 ksi	57.1 ksi
13	Side drop 75 g + 15 psig external pressure	Bottom end, rails (orientation 180°)	24.9	44.4 ksi	57.1 ksi

Note:

(1) Shield plug component excluded in stress evaluation.

Table A.3.9.1-9
Summary of Calculated Stress at End Closure Welds for Testing Condition Loads

Load Case	Combination of Loads	Canister Orientation	Service Level	Stress Category	Stress ⁽¹⁾ (ksi)	Stress Limit (ksi)
18	DW + 25 psig int. press. + 155 kip axial load	Horizontal	A	P _m	-	-
				P _m + P _b	-	-

Note:

(1) There are no closure welds during pressure test.

Table A.3.9.1-10
Summary of Calculated Stress at the End Closure Welds for Normal and Off-Normal
Condition Transfer Loads

Load Case	Combination of Loads	Canister Orientation	Service Level	Stress Category	Stress ⁽²⁾ (ksi)	Stress Limit ⁽¹⁾ (ksi)
1	1 g down + 15 psig ext. press. + vacc. dry thermal	Vertical	A	P_m	1.52	16
				$P_m + P_b$	1.52	24
				$P_m + P_b + Q$	2.07	48
2	Handling 2 g + 30 psig int. press. + thermal (115 °F)	Horizontal	A	P_m	$11.75+0.88 = 12.63$	16
				$P_m + P_b$	$11.75+9.74 = 21.49$	24
				$P_m + P_b + Q$	$14.94+9.74 = 24.68$	48
3	Handling 2 g + 15 psig ext. press. + thermal (-20 °F)	Horizontal	A	P_m	$1.46+0.88 = 2.34$	16
				$P_m + P_b$	$1.46+9.74 = 11.20$	24
				$P_m + P_b + Q$	$2.32+9.74 = 12.06$	48
19	30 psig int. press + 80 kips push + thermal (115 °F)	Horizontal	A	P_m	10.75	16
				$P_m + P_b$	10.75	24
				$P_m + P_b + Q$	14.91	48
20	30 psig int. press + 60 kips pull + thermal (115 °F)	Horizontal	A	P_m	11.75	16
				$P_m + P_b$	11.75	24
				$P_m + P_b + Q$	14.94	48
21	30 psig int. press + 80 kips push + thermal (115 °F)	Horizontal	C	P_m	10.75	19.2
				$P_m + P_b$	10.75	28.8
				$P_m + P_b + Q$	-	-
22	30 psig int. press + 80 kips pull + thermal (115 °F)	Horizontal	C	P_m	11.75	19.2
				$P_m + P_b$	11.75	28.8
				$P_m + P_b + Q$	-	-

Notes:

- (1) Since the temperatures at the closure welds do not exceed 300 °F, the allowable stresses at 300 °F are used.
(2) Conservatively the maximum stress intensity was used for both P_m and $P_m + P_b$ stresses for all analyses

Table A.3.9.1-11
Summary of Calculated Stresses at End Closure Welds for Accident Condition Transfer
Loads (Axisymmetric Loads)

Load Case	Combination of Loads	Canister Orientation	Service Level	Stress Category	Stress ⁽²⁾ (ksi)	Stress Limit ⁽¹⁾ (ksi)
4	120 psig int. press. under fire accident	Horizontal	D	P_m	21.71	37.04
				$P_m + P_b$	21.71	47.68
5	25 psig ext. press. under flood accident	Horizontal	D	P_m	2.42	37.04
				$P_m + P_b$	2.42	52.96
14	75 g top end drop + 30 psig int. press.	Vertical	D	P_m	6.43	37.04
				$P_m + P_b$	6.43	52.96
15	75 g bottom end drop + 30 psig int. press.	Vertical	D	P_m	4.27	37.04
				$P_m + P_b$	4.27	52.96
16	75 g top end drop + 15 psig ext. press.	Vertical	D	P_m	8.67	37.04
				$P_m + P_b$	8.67	52.96
17	75 g bottom end drop + 15 psig ext. press.	Vertical	D	P_m	6.10	37.04
				$P_m + P_b$	6.10	52.96
23	30 psig int. press. + 110 kips push	Horizontal	D	P_m	10.49	37.04
				$P_m + P_b$	10.49	52.96
24	30 psig int. press. + 110 kips pull	Horizontal	D	P_m	11.75	37.04
				$P_m + P_b$	11.75	52.96

Notes:

- (1) Since the temperatures at the closure welds do not exceed 300 °F, the allowable stresses at 300 °F are used.
- (2) Conservatively the maximum stress intensity was used for both P_m and $P_m + P_b$ stresses for all analyses.

Table A.3.9.1-12
Summary of Calculated Stresses at End Closure Welds for Accident Condition Transfer
Loads (3-D Inertial Loads)

Load Case	Load Combination	Canister	Maximum Stress Intensity (ksi)	Stress Limits
6	Side drop 75 <i>g</i> + 30 psig internal pressure	Top end, no rails (orientation 0°)	23.3	35.52 ksi
8	Side drop 75 <i>g</i> + 30 psig internal pressure	Top end, rails (orientation 180°)	24.3	35.52 ksi
10	Side drop 75 <i>g</i> + 15 psig external pressure	Top end, no rails (orientation 0°)	23.4	35.52 ksi
12	Side drop 75 <i>g</i> + 15 psig external pressure	Top end, rails (orientation 180°)	24.2	35.52 ksi

Table A.3.9.1-13
32PTH Type 1 DSC Canister Load Combinations during Storage

Loading	Canister Orientation	Service Level	Load	Enveloped Load for Analysis	Load Combinations
Dead weight	Horizontal ⁽¹⁾	A	1 g down	.65 g axial + .65 g trans.	.65 g axial + .65 g trans. + 1.3 g vertical down
Seismic loads	Horizontal ⁽¹⁾	C ⁽²⁾	0.43 g axial + 0.43 g trans. +0.20 g vertical	+ 1.3 g vertical	.65 g axial + .65 g trans. + 1.3 g vertical down + 30 psig + thermal (115 F) .65 g axial + .65 g trans. + 1.3 g vertical down + 30 psig + thermal (-20 °F)
Internal pressure	Horizontal ⁽¹⁾	A	15 psig	30 psig	Pressure
Thermal	Horizontal ⁽¹⁾	A	Thermal (-20 °F ambient)	Thermal (-20 °F ambient)	Thermal
Thermal	Horizontal ⁽¹⁾	A	Thermal (115 °F ambient)	Thermal (115 °F ambient)	Thermal
Thermal	Horizontal ⁽¹⁾	D	Blocked vent	Blocked vent	1 g down + 70 psig int. pressure + thermal (blocked vent)
Internal pressure	Horizontal ⁽¹⁾	D	< 67 psig due to blocked vent	Enveloped by 70 psig internal pressure	
Flood	Horizontal ⁽¹⁾	D ^(c)	50 ft water (≈22 psig)	Enveloped by 30 psig external pressure design	

Notes:

- (1) Canister supported at HSM rails and axial restrained by the seismic restraint devices.
(2) Levels C loads are conservatively treated as Level A loads and so evaluated.

Table A.3.9.1-14
Summary of Calculated Stresses for Normal and Accident Condition Loads (canister in horizontal position)

Load Case	Combination of Loads	Canister Orientation	Service Level	Components	Stress Category	Stress (ksi)	Stress Limit (ksi)
S1	Dead weight (1 g down)	Horizontal	A	All ⁽²⁾	P_m	0.40	17.5
					$P_m + P_b$	4.05	26.3
S2	30 psig internal pressure	Horizontal	A	All ⁽²⁾	$P_m^{(3)}$	14.97	17.5
					$P_m + P_b^{(3)}$	14.97	26.3
S3	Seismic (0.65 g axial + 0.65 trans. + 1.3 vert. down)	Horizontal	A ⁽¹⁾	All ⁽²⁾	P_m	0.63	17.5
					$P_m + P_b$	6.08	26.3
S4	Thermal (-20 °F amb.)	Horizontal	A	All ⁽²⁾	Q	22.49	52.5
S5	Thermal (115 °F amb.)	Horizontal	A	All ⁽²⁾	Q	20.51	52.5
S6	Thermal (blocked vent)	Horizontal	D	All ⁽⁴⁾	Q	20.96	63.0
S7	Accident 70 psig internal pressure	Horizontal	D	All ⁽²⁾	$P_m^{(3)}$	34.96	42.0
					$P_m + P_b^{(3)}$	34.96	63.0
S8	Accident flood (enveloped by 30 psig ext. pressure)	Horizontal	D	All ⁽²⁾	$P_m^{(3)}$	5.48	42.0
					$P_m + P_b^{(3)}$	5.48	63.0
SC1	S2 + S3 + S4	Horizontal	A ⁽¹⁾	All ⁽²⁾	P_m	15.60	17.5
					$P_m + P_b$	21.05	26.3
					$P_m + P_b + Q$	43.54	52.5
SC2	S2 + S3 + S5	Horizontal	A ⁽¹⁾	All ⁽²⁾	P_m	15.60	17.5
					$P_m + P_b$	21.05	26.3
					$P_m + P_b + Q$	41.56	52.5
SC3	S1 + S7 + S6	Horizontal	D	All ⁽⁴⁾	P_m	35.36	42.0
					$P_m + P_b$	39.01	63.0
					$P_m + P_b + Q$	59.97	63.0
SC4	S1 + S8	Horizontal	D	All ⁽²⁾	P_m	5.88	42.0
					$P_m + P_b$	9.53	63.0

Notes:

- (1) Seismic loads are conservatively treated as Level A loads.
- (2) Conservatively the stress limits at 500 °F are used.
- (3) Conservatively the maximum stress intensity was used for both P_m and $P_m + P_b$ stresses for all analyses.
- (4) ASME code requires only primary stresses be evaluated under accident conditions, conservatively secondary stresses were evaluated and compared against the $P_m + P_b$ stress limits. The peak stresses occur at the top and bottom of the canister where the maximum temperature is lower than 500 °F. The stress limits at 500 °F are used.

Table A.3.9.1-15
Summary of Calculated Stresses at the End Closure Welds for Normal and Accident
Condition Storage Loads

Load Case	Combination of Loads	Canister Orientation	Service Level	Stress Category	Stress (ksi)	Stress Limit ⁽²⁾ (ksi)
S1	Dead weight (1 g down)	Horizontal	A	P_m	0.40	16
				$P_m + P_b$	4.05	24
S2	30 psig internal pressure	Horizontal	A	$P_m^{(3)}$	11.75	16
				$P_m + P_b^{(3)}$	11.75	24
S3	Seismic (0.65 g axial + 0.65 trans. + 1.3 vert. down)	Horizontal	A ⁽¹⁾	P_m	0.63	16
				$P_m + P_b$	6.08	24
S4	Thermal (-20 °F amb.)	Horizontal	A	Q	2.47	48
S5	Thermal (115 °F amb.)	Horizontal	A	Q	2.50	48
S6	Thermal (blocked vent)	Horizontal	D	Q ⁽⁴⁾	7.12	52.96
S7	Accident 70 psig internal pressure	Horizontal	D	$P_m^{(3)}$	27.44	37.04
				$P_m + P_b^{(3)}$	27.44	52.96
S8	Accident flood (enveloped by 30 psig ext. pressure)	Horizontal	D	$P_m^{(3)}$	2.90	37.04
				$P_m + P_b^{(3)}$	2.90	52.96
SC1	S2 + S3 + S4	Horizontal	A ⁽¹⁾	P_m	12.38	16
				$P_m + P_b$	17.83	24
				$P_m + P_b + Q$	20.30	48
SC2	S2 + S3 + S5	Horizontal	A ⁽¹⁾	P_m	12.38	16
				$P_m + P_b$	17.83	24
				$P_m + P_b + Q$	20.33	48
SC3	S1 + S7 + S6	Horizontal	D	P_m	27.84	37.04
				$P_m + P_b$	31.49	52.96
				$P_m + P_b + Q^{(4)}$	38.61	52.96
SC4	S1 + S8	Horizontal	D	P_m	3.30	37.04
				$P_m + P_b$	6.95	52.96

Notes:

- (1) Seismic loads are conservatively treated as Level A loads.
- (2) Since the temperatures at the closure welds do not exceed 300 °F, the stress limits at 300 °F are used.
- (3) Conservatively the maximum stress intensity was used for both P_m and $P_m + P_b$ stresses for all analyses.
- (4) ASME code requires only primary stresses be evaluated under accident conditions, conservatively secondary stresses were also included and compared against the $P_m + P_b$ stress limits.

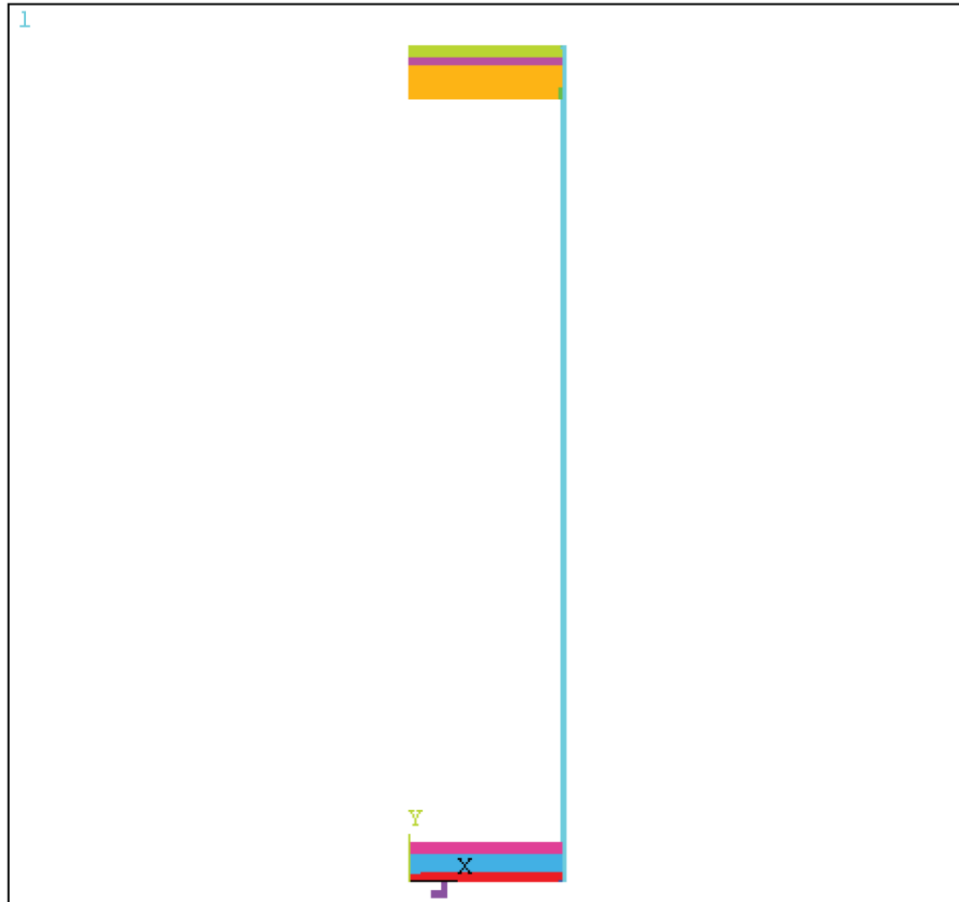


Figure A.3.9.1-1
2-D Canister Axisymmetrical Thermal and Stress Finite Element Model

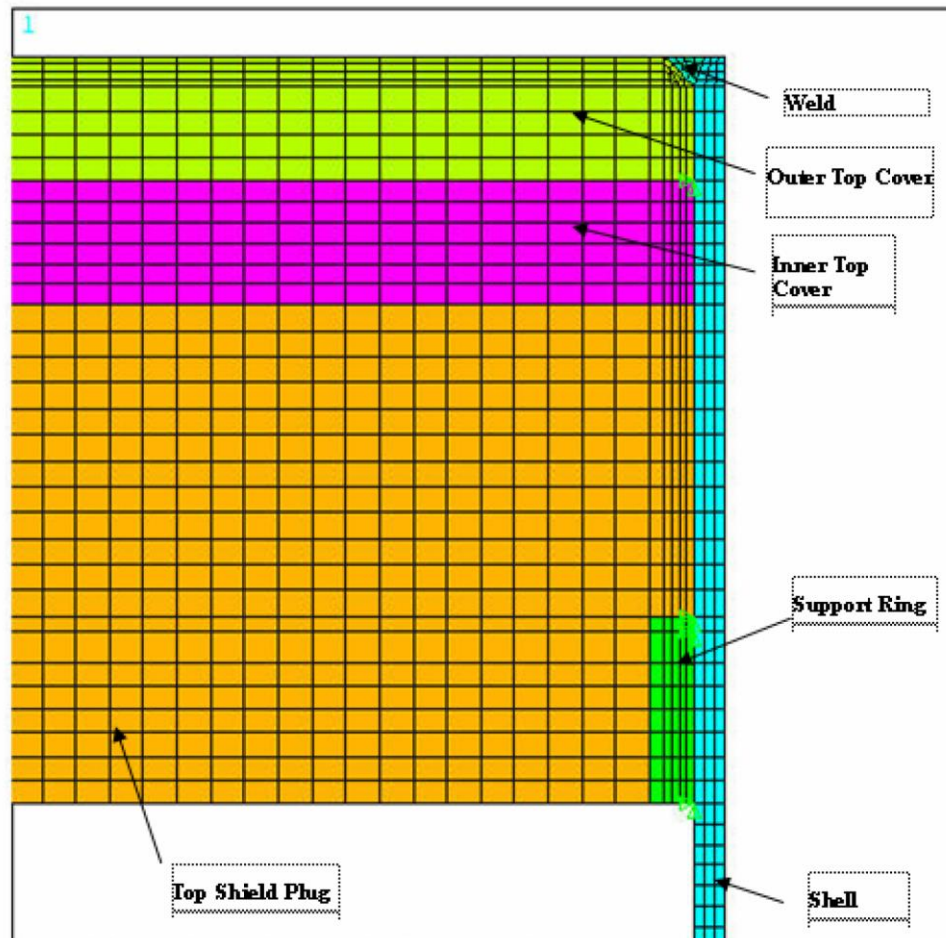


Figure A.3.9.1-2
Top End of the 2-D Axisymmetrical Canister Model

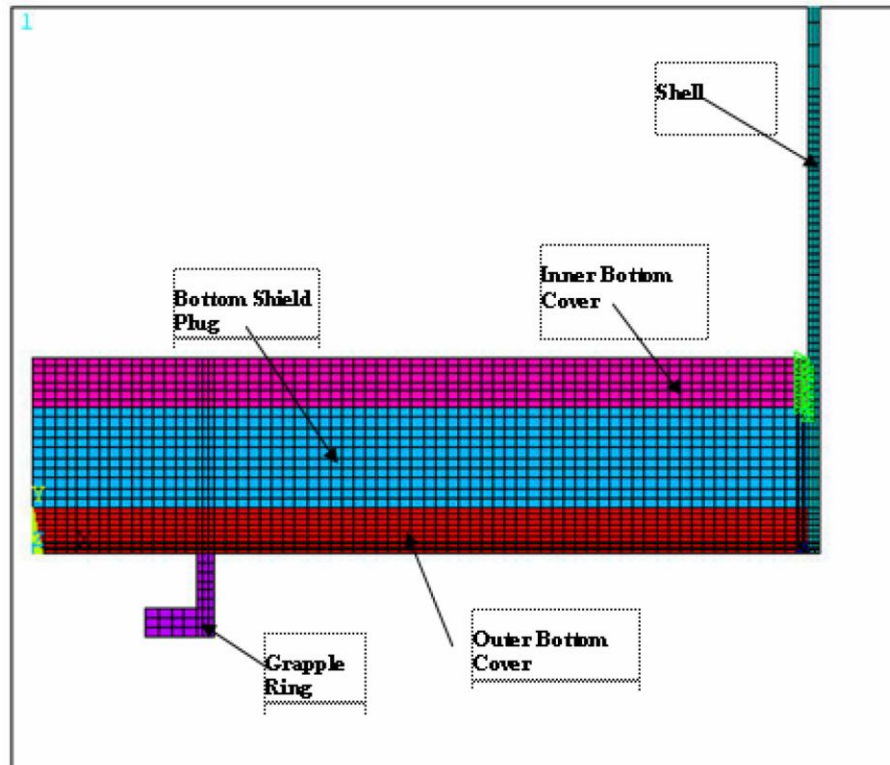


Figure A.3.9.1-3
Bottom End of the 2-D Axisymmetrical Canister Model

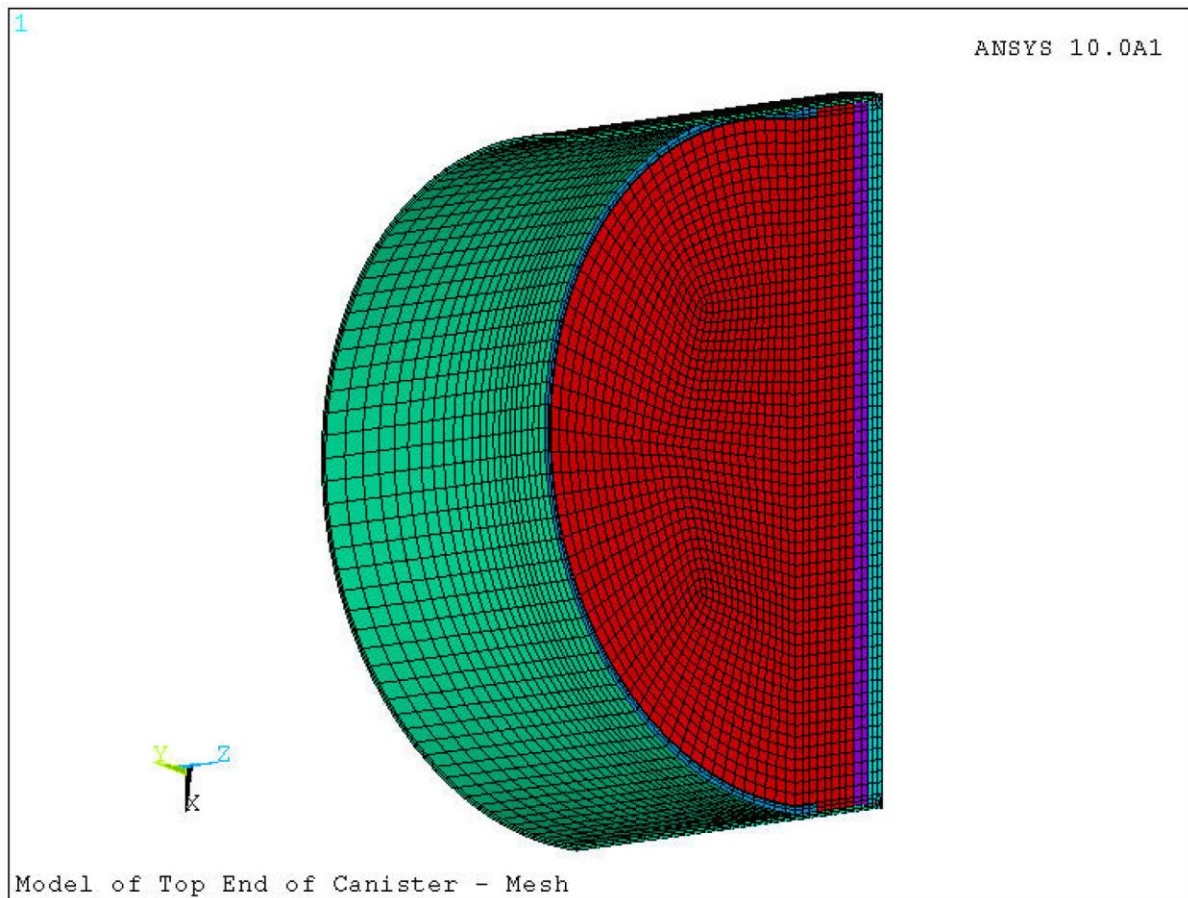


Figure A.3.9.1-4
3-D DSC Canister Top End Assembly Finite Element Model

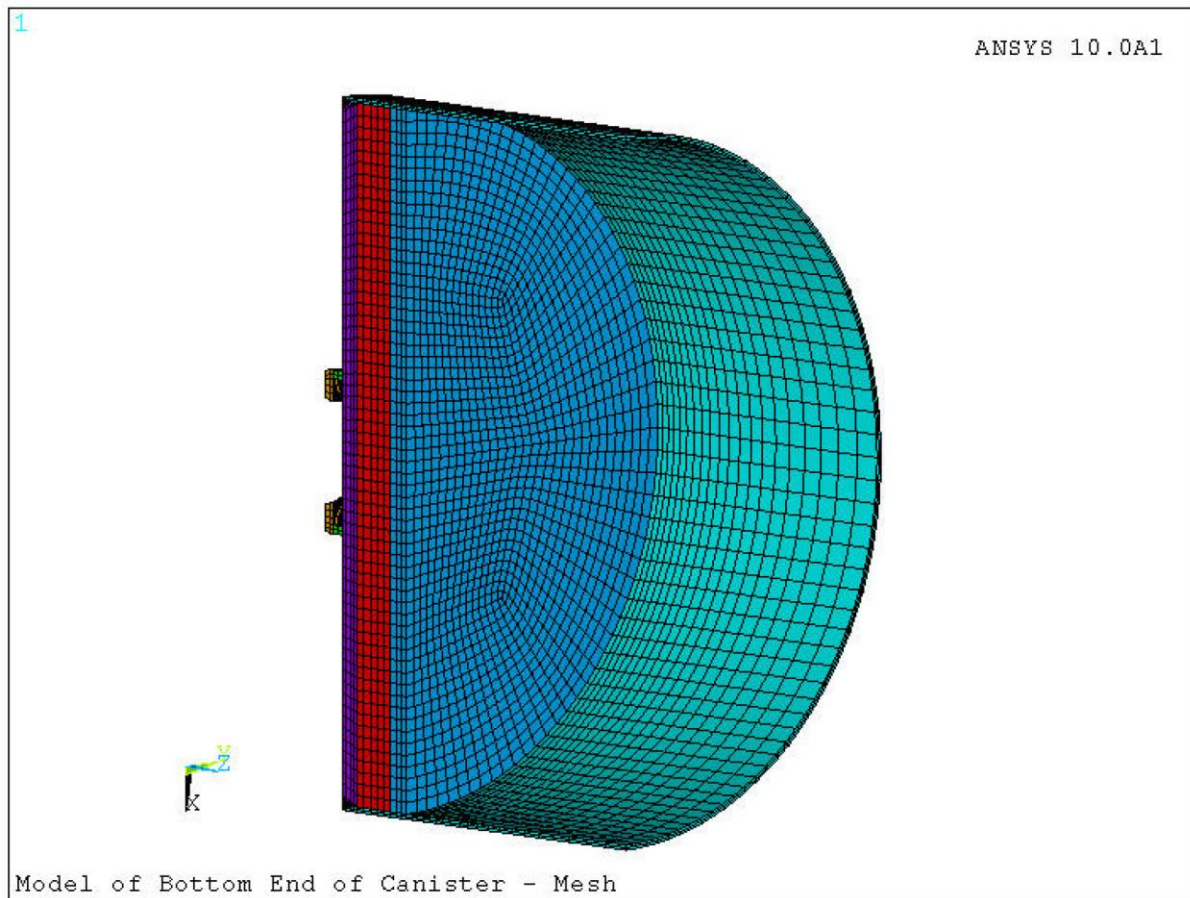


Figure A.3.9.1-5
3-D DSC Canister Bottom End Assembly Finite Element Model

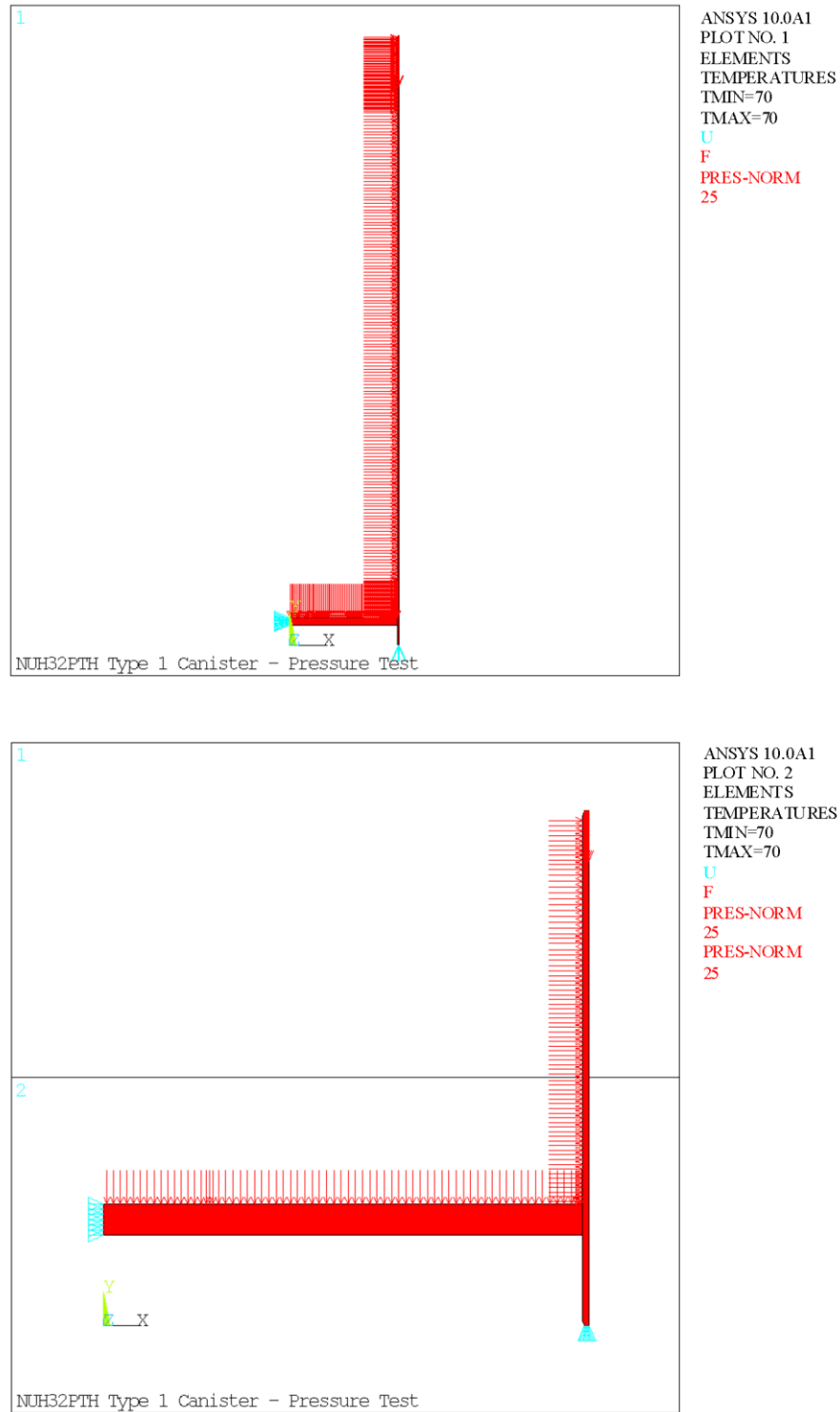


Figure A.3.9.1-6
32PTH Type 1 DSC Canister Finite Element Model used for Pressure Test Analysis

Appendix A.3.9.2

OS187H Type 1 Transfer Cask Body Structural Analysis

TABLE OF CONTENTS

A.3.9.2	OS187H TYPE 1 TRANSFER CASK BODY STRUCTURAL ANALYSIS	A.3.9.2-1
A.3.9.2.1	Introduction.....	A.3.9.2-1
A.3.9.2.1.1	OS187H Type 1 Transfer Cask Geometry Description.....	A.3.9.2-1
A.3.9.2.1.2	Transfer Cask Component Weights	A.3.9.2-2
A.3.9.2.1.3	Stress Criteria.....	A.3.9.2-3
A.3.9.2.1.4	Material Properties.....	A.3.9.2-3
A.3.9.2.2	ANSYS Analysis.....	A.3.9.2-4
A.3.9.2.2.1	Geometry Description.....	A.3.9.2-4
A.3.9.2.2.2	Allowable Stresses	A.3.9.2-4
A.3.9.2.2.3	OS187H Type 1 Transfer Cask Finite Element Models.....	A.3.9.2-4
A.3.9.2.2.4	Load Cases	A.3.9.2-7
A.3.9.2.3	ANSYS Analysis Results and Reporting Methodology	A.3.9.2-18
A.3.9.2.4	Evaluation of OS187H Type 1 Transfer Cask Trunnion Local Stresses	A.3.9.2-19
A.3.9.2.4.1	Approach.....	A.3.9.2-19
A.3.9.2.4.2	Load Cases	A.3.9.2-20
A.3.9.2.4.3	Material Properties.....	A.3.9.2-22
A.3.9.2.4.4	Stress Criteria.....	A.3.9.2-22
A.3.9.2.4.5	Stress Computation	A.3.9.2-23
A.3.9.2.4.6	Stress Intensity Calculation.....	A.3.9.2-25
A.3.9.2.4.7	Local Shell Stress Results.....	A.3.9.2-25
A.3.9.2.4.8	Local Shell Stress Conclusions.....	A.3.9.2-25
A.3.9.2.5	Stress and Deflection of Transfer Cask Inner Shell Support Rails.....	A.3.9.2-26
A.3.9.2.6	References.....	A.3.9.2-28

LIST OF TABLES

Table A.3.9.2-1	Transfer Cask Components Stress—Summary of Results	A.3.9.2-29
Table A.3.9.2-2	Local Shell Stress at Trunnion Locations—Computation Spreadsheet for Case UT1	A.3.9.2-32
Table A.3.9.2-3	Local Shell Stress at Trunnion Locations—Computation Spreadsheet for Case UT2	A.3.9.2-33
Table A.3.9.2-4	Local Shell Stress at Trunnion Locations—Computation Spreadsheet for Case UT3	A.3.9.2-34
Table A.3.9.2-5	Local Shell Stress at Trunnion Locations—Computation Spreadsheet for Case UT4	A.3.9.2-35
Table A.3.9.2-6	Local Shell Stress at Trunnion Locations—Computation Spreadsheet for Case UT5	A.3.9.2-36
Table A.3.9.2-7	Local Shell Stress at Trunnion Locations—Computation Spreadsheet for Case UT6	A.3.9.2-37
Table A.3.9.2-8	Local Shell Stress at Trunnion Locations—Computation Spreadsheet for Case UT7	A.3.9.2-38
Table A.3.9.2-9	Local Shell Stress at Trunnion Locations—Computation Spreadsheet for Case UT8	A.3.9.2-39
Table A.3.9.2-10	Local Shell Stress at Trunnion Locations—Computation Spreadsheet for Case UT9	A.3.9.2-40
Table A.3.9.2-11	Local Shell Stress at Trunnion Locations—Computation Spreadsheet for Case UT10	A.3.9.2-41
Table A.3.9.2-12	Local Shell Stress at Trunnion Locations—Computation Spreadsheet for Case LT1	A.3.9.2-42
Table A.3.9.2-13	Local Shell Stress at Trunnion Locations—Computation Spreadsheet for Case LT2	A.3.9.2-43
Table A.3.9.2-14	Local Shell Stress at Trunnion Locations—Computation Spreadsheet for Case LT3	A.3.9.2-44
Table A.3.9.2-15	Local Shell Stress at Trunnion Locations—Computation Spreadsheet for Case LT4	A.3.9.2-45
Table A.3.9.2-16	Local Shell Stress at Trunnion Locations—Summary of Results ..	A.3.9.2-46

LIST OF FIGURES

Figure A.3.9.2-1	Transfer Cask Key Components and Dimensions	A.3.9.2-47
Figure A.3.9.2-2	2-Dimensional Finite Element Model, Element Plot.....	A.3.9.2-48
Figure A.3.9.2-3	3-Dimensional Finite Element Model, Element Plot.....	A.3.9.2-49
Figure A.3.9.2-4	115 °F Ambient Temperature Distribution.....	A.3.9.2-50
Figure A.3.9.2-5	-20 °F Ambient Temperature Distribution.....	A.3.9.2-51
Figure A.3.9.2-6	6 g Lifting Boundary Conditions (3D Half Model)	A.3.9.2-52
Figure A.3.9.2-7	30 psi Internal Pressure Boundary Conditions (2D Model)	A.3.9.2-53
Figure A.3.9.2-8	Transfer Loads Boundary Conditions (3D Full Model)	A.3.9.2-54
Figure A.3.9.2-9	75 g Bottom End Drop Boundary Conditions (2D Model).....	A.3.9.2-55
Figure A.3.9.2-10	75 g Top End Drop Boundary Conditions (2D Model)	A.3.9.2-56
Figure A.3.9.2-11	75 g Side Drop Boundary Conditions (3D Model).....	A.3.9.2-57
Figure A.3.9.2-12	Computational Worksheet for WRC 107 Bulletin Evaluation	A.3.9.2-58
Figure A.3.9.2-13	NUHOMS OS187H Type 1 Transfer Cask Side Drop– 3D Finite Element Model.....	A.3.9.2-59
Figure A.3.9.2-14	Transfer Cask Side Drop Model Top Cover/Flange/Lead Interface	A.3.9.2-60
Figure A.3.9.2-15	Transfer Cask Side Drop Model Canister/Cask Shell/Lead/Interface	A.3.9.2-61
Figure A.3.9.2-16	Transfer Cask Side Drop Model Canister/ Bottom Access Ram/Lead/Interface.....	A.3.9.2-62
Figure A.3.9.2-17	Transfer Cask Side Drop Model—Rail Locations for Load Case 1	A.3.9.2-63
Figure A.3.9.2-18	Transfer Cask Side Drop Model—Rail Locations for Load Case 2	A.3.9.2-64
Figure A.3.9.2-19	Transfer Cask Side Drop—Sketch of Drop Modeling for Load Case 1.....	A.3.9.2-65
Figure A.3.9.2-20	Transfer Cask Side Drop—Sketch of Drop Modeling for Load Case 2.....	A.3.9.2-66
Figure A.3.9.2-21	Transfer Cask Side Drop Results—Inner Shell Stress Intensity for Load Case 1.....	A.3.9.2-67
Figure A.3.9.2-22	Transfer Cask Side Drop Results—Outer Shell Stress Intensity for Load Case 1.....	A.3.9.2-68
Figure A.3.9.2-23	Transfer Cask Side Drop Results—Inner Shell Stress Intensity for Load Case 2.....	A.3.9.2-69
Figure A.3.9.2-24	Transfer Cask Side Drop Results—Outer Shell Stress Intensity for Load Case 2.....	A.3.9.2-70

A.3.9.2 OS187H TYPE 1 TRANSFER CASK BODY STRUCTURAL ANALYSIS

A.3.9.2.1 Introduction

This appendix presents the structural analyses of the NUHOMS® OS187H Type 1 transfer cask (TC) body including the top cover, cylindrical shell assembly, bottom assembly, and the local stresses at the trunnion/cask body interface. The specific methods, models, and assumptions used to analyze the cask body for the various individual loading conditions specified in 10CFR72 [1] are described. The maximum stresses in each of the major components of the TC are reported in Section A.3.9.2.2.4 for each analyzed load case and load combination. The results are evaluated against the ASME Code [2] design criteria described in Section A.3.9.2.1.3.

The OS187H Type 1 TC body structural analyses use static linear elastic analysis and elastic-plastic analysis methods. The stresses and deformations due to the applied loads are determined using finite element models developed using the ANSYS [4] computer program and/or hand calculations.

Other components associated with the TC are described and analyzed in the following appendices:

- Appendix A.3.9.3 OS187H Type 1 Transfer Cask Top Cover and Ram Access Cover Bolt Analyses
- Appendix A.3.9.4 Not used (since the end and corner drops are not credible under 10CFR Part 72, the lead slump and inner shell buckling analysis of the OS187H Type 1 TC for the 75g end drop load are not documented).
- Appendix A.3.9.5 OS187H Type 1 Transfer Cask Trunnion Analysis
- Appendix A.3.9.6 OS187H Type 1 Transfer Cask Shield Shell Panel Structural Analyses

A.3.9.2.1.1 OS187H Type 1 Transfer Cask Geometry Description

Key dimensions of the OS187H Type 1 TC are shown in Figure A.3.9.2-1. As with the OS187H TC described in Section 3.9.2.1, the shell, or cask body of the cylinder assembly, is an open ended (at the top) cylindrical unit with an integral closed bottom end. This assembly consists of a concentric inner shell (SA-240, Type 304) and an outer shell (SA-240, Type 304) welded to a massive closure flange (SA-182, Type F304N) at the top and bottom ends. The annulus between the shells is filled with lead shielding. The top cover is bolted to the top flange by 24-1 1/2 in. diameter high strength bolts and sealed with an O-ring. A cover plate is provided to seal the bottom hydraulic ram access penetration of the cask (by 12-1/2 in. high strength bolts with an O-ring) during fuel loading and transferring of the canister to the ISFSI.

Two upper trunnions are provided for handling the TC in the plant's fuel/reactor building using a lifting yoke and an overhead crane. Two lower support trunnions are provided for pivoting the TC from/to the vertical and horizontal positions on the support skid/transport trailer.

The overall dimensions of the OS187H Type 1 TC are 210.5 inches long and 92.11 inches in diameter. The TC structural shell is 83.63 inches in diameter. The TC cavity is 198.75 inches long and 70.50 inches in diameter. A detailed physical description of the TC is provided in

Chapter A.1. Section A.1.5 also contains reference drawings of the NUHOMS[®] OS187H Type 1 TC which are the source of dimensions and other information used to develop analysis models.

The gross weight of the loaded TC is approximately 120 tons (240 kips) including a 32PTH Type 1 DSC payload (dry) of 54.70 tons (109.410 kips), and a cask spacer (0.89 kips). Sections A.3.9.2.1.2 and Figure A.3.9.2-1 summarize the component weights and key dimensions of the NUHOMS[®] OS187H Type 1 TC, respectively.

This appendix evaluates the structural integrity of the OS187H Type 1 TC main structural members during all normal and hypothetical accident condition loadings.

A.3.9.2.1.2 Transfer Cask Component Weights

The following tables summarize the component weights of the NUHOMS[®] OS187H Type 1 TC as well as the dry loaded NUHOMS[®]-DSC weight, that are used for the TC structural evaluation.

OS187H Type 1 Transfer Cask Component Weights

Transfer Cask Component	Weight (lb x 1000)
Structural shell	23.73
Inner shell	7.89
Lead gamma shield	66.65
Top flange	2.63
Bottom flange	3.40
Top cover	5.36
Bottom assembly	3.94
Neutron shield panel (including water)	13.81
Upper trunnions (2)	1.45
Lower trunnions (2)	1.06
Total Transfer Cask Empty Weight	130.00⁽¹⁾
Total 32PTH Type 1 Weight (dry)	109.410
Cask Spacer	0.89
Total Transfer Cask Loaded Weight (dry)	240.00⁽¹⁾

Note:

1. Rounded up to the nearest 1000 lb.

Dry Loaded 32PTH Type 1 DSC Weight

Transfer Cask Payload	Weight (lb x 1000)	Weight Used for Analysis (lb x 1000)
32PTH Type 1 canister	28.44	
32PTH Type 1 basket	29.45	
Fuel assemblies (32)	51.52	
Total 32PTH Type 1 DSC Weight	109.41	110.00
Cask spacer	0.89	5.00
Total Payload	110.30	115.00

A.3.9.2.1.3 Stress Criteria

The stress criteria used for the OS187H Type 1 TC is summarized in the table below. The resulting stresses are compared with the allowable stresses set forth by ASME B&PV Code, Section III, Subsection NC [2] for normal conditions and ASME B&PV Code, Section III, Appendix F [3] for accident conditions.

Service Level	Analysis Method	Stress Category	Stress Criteria
A (Normal Conditions)	Elastic Analysis	Primary Membrane Stress, P_m	S_m
		Primary Membrane + Bending Stress, $P_m + P_b$	$1.5 S_m$
		Primary + Secondary Stress, $P_m + P_b + Q$	$3 S_m$
D (Accident Conditions)	Elastic Analysis	Primary Membrane Stress, P_m	Lesser of $2.4 S_m$ or $0.7 S_u$
		Primary Local Membrane Stress, P_L	Lesser of 150% of P_m Stress Limit, or S_u
		Primary Membrane + Bending Stress, $P_m + P_b$	Lesser of $3.6 S_m$ or S_u
	Elastic Plastic Analysis	Primary Membrane Stress, P_m	Greater of $0.7 S_u$ and $S_y + 1/3(S_u - S_y)$
		Primary Membrane + Bending Stress, $P_m + P_b$	$0.9 S_u$

A.3.9.2.1.4 Material Properties

The material properties used for the analysis of the OS187H Type 1 TC are the same as those provided in Section 3.3 and Section 3.9.2.1.4 for the OS187H TC with the exception of the shielding material used in the top and bottom covers of the OS187H Type 1 TC, which uses a castable neutron shielding (NS-3) material instead of the resin material used in the OS187H TC. As discussed in Section A.3.3, the mechanical properties of these two shielding materials are not significantly different.

The NUHOMS[®] OS187H Type 1 TC is primarily constructed from SA-240 Type 304 stainless steel. The massive flanges at the top and bottom ends are machined forgings made of SA-182 Type 304N. The upper and lower trunnions are solid monolithic steel components made of SA-182 Type FXM-19 and SA-182 Type 304N, respectively. The top cover is constructed from SA-240 Type XM-19, or SA-182 Type FXM-19 (material properties for SA 240 Type XM-19 are bounding and used in the analysis). SA-540 Grade B23 Class 1 is used for the top cover and bottom cover bolts. Chemical lead is used for radial gamma shielding; NS-3 [5] is used for the solid axial neutron shielding, and liquid water is used for radial neutron shielding.

A.3.9.2.2 ANSYS Analysis

A.3.9.2.2.1 Geometry Description

The top cover, inner shell, structural shell, and bottom assembly are the primary structural members of the cask. Key components and dimensions of the confinement vessel are shown in Figure A.3.9.2-1. Chapter A.1 contains reference drawings of the NUHOMS® OS187H Type 1 TC which are the source of dimensions and other information used to develop analysis models.

A.3.9.2.2.2 Allowable Stresses

No change. The allowable stresses used for the stress evaluation of the OS187H Type 1 TC are the same as those for the OS187H TC, documented in Section 3.9.2.2.2. These allowables are based on conservative bounding temperatures of 300 °F and 400 °F for the outer and inner shells, respectively (the maximum temperatures from Chapter 4 thermal analysis are 280 °F and 340 °F, respectively). For the elastic-plastic analysis documented in Section A.3.9.2.5, the allowable stresses for the outer and inner shells are based on a bounding temperatures of 350 °F.

A.3.9.2.2.3 OS187H Type 1 Transfer Cask Finite Element Models

Three separate finite element models (FEMs) were constructed. The first is a 2-dimensional, axisymmetric representation of the cask, which is constructed with plane elements. The second model is a 180° (or half-symmetry model) 3-dimensional representation of the TC using “brick” elements. The third model is a 360° (or full model) 3-dimensional representation using “brick” elements.

A. 2-Dimensional Finite Element Model Description

A 2-dimensional axisymmetric ANSYS [4] finite element model, constructed primarily from PLANE42 elements, is used to analyze all axisymmetric load cases. The basic dimensions of the OS187H Type 1 TC are provided in Figure A.3.9.2-1. An element plot of the 2-dimensional FEM is shown in Figure A.3.9.2-2.

Model Material Properties

No change. The temperature dependent material properties used for the analysis of the OS187H Type 1 TC are based on the same temperature distributions applied to the OS187H TC. The temperature distributions applied to the OS187H Type 1 TC are shown in Figure A.3.9.2-4 and Figure A.3.9.2-5 for the 115 °F and -20 °F ambient conditions.

Unmodeled Components

As with the OS187H TC, only the structural steel section of the top cover (3 in. thick.) is modeled. The top neutron shield material, the ¼ in. thickness top cover outer plate, and hoist ring standoffs are not modeled since they are not intended to provide any structural support. However, their inertial load is accounted for by increasing the density of the structural portion of the top cover.

The weight of the unmodeled top cover components (neutron shield, ¼” top cover, and hoisting standoffs) is approximately 1,114 lb. The weight of the structural steel portion of the top cover is 4,246 lb. Thus, the total top cover weight, including the unmodeled components, is 5,360 lb. The density of the top cover is calculated in the ANSYS model based on this total weight.

The radial neutron shield (water) and neutron shield panel are also not modeled, because they are not considered structural components of the transfer cask. Therefore, the density of the structural shell of the transfer cask is increased to account for these unmodeled components. The weight of the unmodeled radial neutron shield assembly is 13,806 lb. The weight of the structural shell is 23,729 lb. Thus, the total weight, including the unmodeled neutron shield assembly is 37,535 lb. This total weight is used to calculate the density of the structural shell in the ANSYS model.

Top Cover and Ram Access Cover Bolts

No change. The top cover and ram access cover bolts are modeled with axisymmetric BEAM3 elements, and are only used in the model to simulate the overall behavior of the closure joints. The stresses in the top cover and ram access cover bolts are evaluated separately in Appendix A.3.9.3. The element real constants for the top cover and the ram access cover bolts used in the ANSYS analysis are not changed from those used in the OS187H analysis.

The initial strains in BEAM3 elements are adjusted to match the minimum preload values of 27,270 lb and 6,364 lb for the top cover bolts and for the ram access cover bolts, respectively.

Contact Elements

CONTAC12 elements are placed between all surfaces of the top flange and top cover, between the ram access cover and ram access penetration that contact each other, and between the lead gamma shielding and the inner and structural shells. These contact elements are used to model the reaction forces that occur between these surfaces.

The contact elements introduce nonlinearities in the analysis depending on whether they are open or closed. Initially, at all contact surfaces, the gaps are closed. The contact element spring constant, K_n , is calculated in the following way.

$$K_n = f E h [4]$$

Where,

f = A factor usually between 0.01 to 100.

E = Modulus of elasticity (27.0×10^6 psi for SA-240, Type 304 @ 300 °F)

E_{lead} = Modulus of Elasticity (2.06×10^6 psi for ASTM B-29 chemical lead @ 300 °F)

h = contact target length.

Average radius of lead, $h \approx 37.66$ in.

Therefore,

$$K_n = 27.0 \times 10^6 \times 37.66 \times f \approx 1.0 \times 10^7 \text{ to } 1.0 \times 10^{11} \text{ lb/in. for steel}$$

$$K_n = 2.06 \times 10^6 \times 37.66 \times f \approx 7.8 \times 10^5 \text{ to } 7.8 \times 10^9 \text{ lb/in. for lead}$$

Thus, there is a very wide range for the K_n value. For the 2-D finite element model, the structure responded well with a spring constant value of 1.0×10^6 lb/in. for the lead shield contact elements and 1.0×10^7 lb/in. for the top cover and ram access cover contact elements.

Boundary Conditions

Separate sets of boundary conditions are required for the various loading cases analyzed. The boundary condition sets are used to prevent rigid body motion and are assigned based on the specific loading configuration. In each of the boundary condition sets, displacement constraints are fixed such that no displacement is permitted in the prescribed direction.

B. 3-Dimensional Finite Element Models Description

A 3-dimensional ANSYS [4] finite element model, constructed primarily from SOLID45 elements, is used to analyze all non-axisymmetric load cases. A 180° version (half symmetry model) is used for symmetric load cases such as the 6 g lifting and side drop load cases. A 360° version (full model) is used for asymmetric load cases such as the transfer load cases. A plot of the 3-dimensional FEM (half model) is shown in Figure A.3.9.2-3.

Model Material Properties

No change. As in the 2-dimensional model, the temperature dependent material properties used for the analysis of the OS187H Type 1 TC are based on the same temperature distributions applied to the OS187H TC.

Unmodeled Components Weights

Only the structural steel section of the top cover (3 in. thick.) is modeled. The top neutron shield material, the $\frac{1}{4}$ in. thickness top cover outer plate, and hoist ring standoffs are not modeled since they are not intended to provide any structural support. However, their inertial load is accounted for by increasing the density of the structural portion of the top cover.

The weight of the unmodeled top cover components (neutron shield, $\frac{1}{4}$ " top cover, and hoisting standoffs) is approximately 1,114 lb. The weight of the structural steel portion of the top cover is 4,246 lb. Thus, the total top cover weight including the unmodeled components is 5,360 lb. The density of the top cover is calculated in the ANSYS model based on this total weight.

The radial neutron shield (water) and neutron shield panel are also not modeled, because they are not considered structural components of the TC. The weight of the unmodeled radial neutron shield assembly is 13,806 lb. Therefore, the density of the structural shell of the TC is increased by 13,806 lb to account for the unmodeled components.

The NS-3 material in the bottom cask cover weights 554 lb and is not modeled. Therefore, the densities of the bottom end plate, the bottom neutron shield plate, and the bottom flange components in the ANSYS model are increased in proportion to their respective weights to account for the unmodeled bottom neutron shield weight.

Top Cover and Ram Access Cover Bolts

No change. The top cover and ram access cover bolts are modeled with BEAM4 elements, and are only used in the model to simulate the overall behavior of the closure joints. The stresses in the top cover and ram access cover bolts are evaluated separately in Appendix A.3.9.3. The element real constants for the top cover and the ram access cover bolts used in the ANSYS analysis are not changed from those used in the OS187H analysis.

The initial strains in BEAM4 elements are adjusted to match the minimum preload values of 27,270 lb and 6,364 lb for the top cover bolts and for the ram access cover bolts, respectively.

Contact Elements

CONTAC52 elements are placed between all surfaces of the top flange and top cover, between the ram access cover and ram access penetration that contact each other, and between the lead gamma shielding and the inner and structural shells. These contact elements are used to model the reaction forces that occur between closure surfaces. LINK8 elements with a very low modulus of elasticity and density are placed in all locations where CONTAC52 elements exist in order to maintain overall stability of the model. This is only required in the 3-dimensional model.

The contact elements introduce nonlinearities in the analysis depending on whether they are open or closed. Initially, at all contact surfaces, the gaps are closed. The contact element spring constant, K_n , is calculated in the following way [4].

$$K_n = f E h$$

Where,

f = A factor usually between 0.01 to 100.

E = Modulus of elasticity (27.0×10^6 psi for SA-240, type 304 @ 300 °F)

h = contact target length (i.e., the square root of target area).

Typical element length $\approx 1/2$ in.

Typical element width ≈ 1 in.

Typical target length, $h = (0.5 \times 1.0)^{0.5} = 1.22$ in.

Therefore,

$$K_n = 25.8 \times 10^6 \times 1.22 \times f \approx 3.39 \times 10^5 \text{ to } 3.39 \times 10^9 \text{ lb/in.}$$

Thus, there is a very wide range for the K_n value. For the 3-D finite element model, the structure responded well with a spring constant value of 1.0×10^7 lb/in. for the lead shield contact elements and 1.0×10^8 lb/in. for the top cover and ram access cover contact elements.

A.3.9.2.2.4 Load Cases

The following two tables describe the normal (Level A) and accident (Level D) condition load cases analyzed in this calculation. The load cases considered consist of 115 °F hot ambient and -20 °F cold ambient environments, 30 psig internal, vacuum drying conditions, transfer

loads, and 75 g accident condition end and side drops. The normal and accident load conditions are summarized in the following table.

Summary of Normal and Accident Load Conditions

Load Case Number	Loading Condition	Service Level	Case Description
1A	6 g vertical lifting	A	Cask vertical, supported at top trunnions, 6 g vertical acceleration + 30 psi internal pressure
1B	6 g vertical lifting + thermal loads	A	Cask vertical, supported at top trunnions, 6 g vertical acceleration + 30 psi internal pressure + 115 °F ambient
2	Vacuum drying	A	Cask vertical, supported at cask bottom, 15 psi external pressure + vacuum drying thermal loads
3	30 psi internal pressure	A	30 psi internal pressure
4	115 °F ambient hot thermal environment	A	115 °F ambient temperature
5	-20 °F ambient cold thermal environment	A	-20 °F ambient temperature
6A	Transfer inertial loads—axial accel. toward bottom	A	Cask horizontal, 2 g acceleration in all directions—axial acceleration toward the bottom of the cask
6B	Transfer inertial loads—axial accel. toward top	A	Cask horizontal, 2 g acceleration in all directions—axial acceleration toward the top of the cask
7A	Transfer loads—axial accel. toward bottom + internal pressure	A	Cask horizontal, 2 g acceleration in all directions—axial acceleration toward the bottom of the cask + 30 psi internal pressure
7B	Transfer loads—axial accel. toward top + internal pressure	A	Cask horizontal, 2 g acceleration in all directions—axial acceleration toward the top of the cask + 30 psi internal pressure
7C	Transfer loads + 115 °F ambient + internal pressure	A	Cask horizontal, supported at top and bottom trunnions, 2 g acceleration in all directions + 30 psi internal pressure + 115 °F ambient
8	Transfer loads + -20 °F ambient + internal pressure	A	Cask horizontal, supported at top and bottom trunnions, 2 g acceleration in all directions + 30 psi internal pressure + -20 °F ambient
9	75 g bottom end drop + internal pressure	D	Cask vertical, supported at bottom, 75 g vertical up acceleration + 30 psi internal pressure
10	75 g top end drop + internal pressure	D	Cask vertical, supported at top, 75 g vertical down acceleration + 30 psi internal pressure
11	75 g side drop + internal pressure	D	Cask horizontal, supported on side, 75 g transverse acceleration + 30 psi internal pressure
12	Transfer thermal accident (Fire)	D	30 psi internal pressure + thermal accident loads

Method of Applying Load to the Cask Body

Pressures applied in the axial direction are calculated based on load divided by pressure area calculation.

Pressures applied in the radial direction in the 3-dimensional finite element model are based on cosine distributed pressure functions. These pressure distributions simulate the internal cask contents applying pressure to the inner cask wall. The pressure distribution is assumed to be in the longitudinal direction over a specified length and vary with a cosine distribution around the circumference of the cask.

The following sections describe the boundary conditions used for each individual load case and load combination.

Load Case 1: 6 g Lifting (3-D FEM)

The 6 g Lifting Load case consists of the loaded OS187H Type 1 TC in the vertical position, supported by the two top trunnions. A 6 g vertical acceleration is conservatively used to bound the normal lifting load. An internal pressure of 30 psi is also applied.

The weight of the TC internals (canister, basket, and fuel assemblies) is accounted for by applying equivalent pressures. The weight of the cask internals used in this analysis is 115,000 lb. The TC inner radius is 35.25 in., and the inner radius of the ram access penetration is 11.00 in. The inertial load of the TC internals reacts against the annular surface bounded by these two radii during lifting. Therefore the area of the reaction surface, A_{6gl} , is as follows.

$$A_{6gl} = \pi(35.25^2 - 11.00^2) = 3,523.49 \text{ in}^2.$$

The pressure equivalent to the inertial load of the internals during a 6 g lift, P_{6gi} , is,

$$P_{6gl} = [115,000/3,523.49] \times 6 \text{ gs} = 195.83 \text{ psi}$$

Symmetry displacement boundary conditions are applied along the y-axis of the 3-dimensional axisymmetric model.

A depiction of the 6 g lifting load case boundary conditions is provided in Figure A.3.9.2-6.

Load Case 2: Vacuum Drying

The applied loads used to calculate the maximum stress in the TC during vacuum drying include a 15 psi external pressure, a maximum radial temperature gradient, and a 1g axial (gravity) load. The stresses generated in the TC shell by these three loads are computed using hand calculations. Since the primary load during vacuum drying is caused by the radial temperature gradient, the maximum TC stress is computed for the outer radial structural shell.

A uniform 15 psi pressure is applied to the external radial surface of the cask, generating a hoop stress in the cask structural shell. The hoop stress, σ_p , in the shell is computed in the following way.

$$\begin{aligned}\sigma_p &= \text{external pressure} \times \text{the mean structural shell radius} / \text{the minimum structural shell thickness} \\ &= 15 \text{ psi} \times (78.87 + 1.50)/2 \text{ in.} / 1.50 \text{ in.} = 402 \text{ psi}\end{aligned}$$

The stress generated in the structural shell by the 1g axial load is conservatively computed assuming that the weight of the entire TC is taken by the cross sectional area of the structural shell. The weight of the TC is conservatively taken to be 250,000 lb. The 1g axial stress in the structural shell, σ_g , is computed as follows.

$$\begin{aligned}\sigma_g &= 1g \times \text{maximum TC weight} / \text{minimum cross sectional area of the structural shell} \\ &= 1g \times 250,000 / [(\pi/4) \times (81.87^2 - 78.87^2)] = 660 \text{ psi}\end{aligned}$$

The maximum hoop stress generated by the radial thermal gradient during the vacuum drying process will occur in the outer structural shell due to the thermal expansion of the lead gamma shield. From Chapter 4, the maximum temperature difference between the lead gamma shield and the structural shell occurs during the drying process, when the lead and structural shell are at 275 °F and 219 °F, respectively.

The change in the outer radius of the lead gamma shield, ΔR_l , is computed as follows.

$$\begin{aligned}\Delta R_l &= R_l \times \alpha_l \times \Delta T_l = 39.435 \text{ in.} \times 17.34 \times 10^{-6} \text{ in./in. } ^\circ\text{F} (@300 ^\circ\text{F}) \times (275 - 70) ^\circ\text{F} \\ &= 0.1402 \text{ in.}\end{aligned}$$

The change in the inner radius of the structural shell, ΔR_s , is computed as follows.

$$\begin{aligned}\Delta R_s &= R_s \times \alpha_s \times \Delta T_s = 39.435 \text{ in.} \times 8.9 \times 10^{-6} \text{ in./in. } ^\circ\text{F} (@200 ^\circ\text{F}) \times (219 - 70) ^\circ\text{F} \\ &= 0.0523 \text{ in.}\end{aligned}$$

Therefore the differential radial expansion between the lead and structural shell, ΔR , is as follows.

$$\Delta R = 0.1402 \text{ in.} - 0.0523 \text{ in.} = 0.0879 \text{ in.}$$

Therefore, the lead cylinder, if it were free, would grow 0.0879 in. more than the inner surface of the structural shell. If all of the differential expansion is accommodated in the lead, the lead strain, ε_l , would be the following.

$$\varepsilon_l = \Delta R / R_l = 0.0879 \text{ in.} / 39.435 \text{ in.} = 0.00223 \text{ in./in.}$$

If the lead remained linear elastic, the maximum hoop stress in the lead would be,

$$\sigma_l = E_l \times \varepsilon_l = 2.06 \times 10^6 \text{ psi} (@300 ^\circ\text{F}) \times 0.00223 \text{ in./in.} = 4,594 \text{ psi}$$

Conservatively assuming that the lead remains linear elastic, the interference pressure on the outer structural shell required to exert an average hoop stress of 4,594 psi in the lead can be determined in the following way.

$$P_{\text{interface}} = \sigma_l \times \text{lead thickness} / R_{\text{interface}} = 4,594 \text{ psi} \times 3.56 \text{ in.} / 39.435 \text{ in.} = 415 \text{ psi}$$

This interference pressure would generate the following hoop stress in the structural shell.

$$\sigma_s = P_{interface} \times R_{interface}/\text{shell thickness} = 415 \text{ psi} \times 39.435/1.50 = 10,910 \text{ psi}$$

The total combine maximum stress intensity, σ , in the TC during vacuum drying operations is then,

$$\sigma = 402 \text{ psi} + 660 \text{ psi} + 10,910 \text{ psi} = 11,972 \text{ psi}$$

Load Case 3: 30 psi Internal Pressure (2-D FEM)

A uniform 30 psi pressure is applied to the internal surface of the OS187H Type 1 TC up to the top cover and ram access cover seal locations. Symmetry displacement boundary conditions are applied along the y-axis of the 2-dimensional axisymmetric model, and the TC is held in the y-direction at one location to prevent rigid body motion. A depiction of the internal pressure load case boundary conditions is provided in Figure A.3.9.2-7.

Load Case 4: 115 °F Ambient Hot Thermal Environment (2-D FEM)

The temperature distribution resulting from a 115 °F ambient environment is shown in Figure A.3.9.2-4. The distribution is based on the temperature profile used in the OS187H TC which is bounding when applied to the OS187H Type 1 TC. The temperature dependent coefficients of thermal expansion are applied to each corresponding material type, in order to induce thermal stresses in the model.

Symmetry displacement boundary conditions are applied along the cut boundary of the 2-dimensional axisymmetric model, and the TC is held in the axial direction at one location to prevent rigid body motion.

Load Case 5: -20 °F Ambient Cold Thermal Environment (2-D FEM)

The temperature distribution resulting from a -20 °F ambient environment is shown in Figure A.3.9.2-5. The distribution is based on the temperature profile used in the OS187H TC which is bounding when applied to the OS187H Type 1 TC. The temperature dependent coefficients of thermal expansion are applied to each corresponding material type, in order to induce thermal stresses in the model.

Symmetry displacement boundary conditions are applied along the cut boundary of the 2-dimensional axisymmetric model, and the TC is held in the axial direction at one location to prevent rigid body motion.

Load Case 6-8: Transfer Loads (3-D FEM)

The transfer load cases consist of the loaded TC in the horizontal position, supported at both upper and lower trunnions in the vertical direction, supported at the bottom two trunnions in the axial direction, and supported at one side of the trunnion towers of the skid (the loaded side) in the lateral (transverse) direction.

An acceleration of 2 g in all directions (axial, vertical, and transverse) is applied to the TC model in order to bound all possible transfer accelerations. For the transverse and vertical directions, the weights of the DSC and spacer are accounted for by applying a cosine varying pressure on the inside surface of the inner shell. The approach is explained below.

The vertical and transverse accelerations are combined, so that a single horizontal acceleration is applied to the finite element model in the following way.

$$\text{Resultant Acceleration} = [2 g^2 \text{ transverse} + 2 g^2 \text{ vertical}]^{1/2} = 2.828 g$$

The resultant inertial load of the TC internals is accounted for by applying a cosine varying pressure on the inside surface of the cask inner shell. Assuming that the TC internals react upon 90° arc of the inside surface, then the inertial load of the internals, $P_{(\theta)}$, which varies with angle, θ , ($\theta = 0$ is at the impact point), is governed by the following expression.

$$P_{(\theta)} = P_{\max} \cos(2\theta)$$

Where P_{\max} is the maximum load at the impact point ($\theta = 0$). Assuming the axial length of the applied load is L , the inside radius of the cask inner shell is R , and the load distribution, $P_{(\theta)}$ above, then the total inertial load generated by the internals, F , is the following.

$$F = \int_{-\frac{\pi}{4}}^{\frac{\pi}{4}} P_{\max} \cos(2\theta) \cos(\theta) LR d\theta$$

or,

$$F = \frac{P_{\max} LR}{2} \int_{-\frac{\pi}{4}}^{\frac{\pi}{4}} \cos((2+1)\theta) + \cos((2-1)\theta) d\theta$$

By integrating we get the following.

$$F = \left[\frac{P_{\max} LR}{2} \right] \left[\frac{\sin(3\theta)}{3} + \sin(\theta) \right] \Bigg|_{-\frac{\pi}{4}}^{\frac{\pi}{4}}$$

Therefore,

$$F = \left[\frac{P_{\max} LR}{2} \right] \left[\frac{\sin\left(\frac{3\pi}{4}\right)}{3} + \sin\left(\frac{\pi}{4}\right) - \frac{\sin\left(\frac{-3\pi}{4}\right)}{3} - \sin\left(\frac{-\pi}{4}\right) \right]$$

$$F = P_{\max} LR \left[\frac{\sin\left(\frac{3\pi}{4}\right)}{3} + \sin\left(\frac{\pi}{4}\right) \right]$$

The applied forces are the inertial load of the DSC, F_i , and the inertial load of the spacer and air wedges, F_s :

$$F_i = 110,000 \text{ lb} \times 2.828 \text{ g} = 311,080 \text{ lb},$$

$$F_s = 5,000 \text{ lb} \times 2.828 \text{ g} = 14,140 \text{ lb. (spacer weight of 5,000 lb is bounding; see section A.3.9.2.1.2)}$$

Additional input data are:

TC inner shell inner diameter,	$R = 35.25 \text{ in.},$
axial length of the applied DSC load,	$L_i = 190.25 \text{ in.},$ and
axial length of the applied spacer load,	$L_s = 5.0 \text{ in.},$ are applied

Therefore, P_{\max} for the DSC and spacer are the following:

$$P_{i\max} = \frac{311,080}{(190.25)(35.25)} \left[\frac{\sin\left(\frac{3\pi}{4}\right)}{3} + \sin\left(\frac{\pi}{4}\right) \right]^{-1} = 49.2 \text{ psi}$$

$$P_{s\max} = \frac{14,140}{(6)(35.25)} \left[\frac{\sin\left(\frac{3\pi}{4}\right)}{3} + \sin\left(\frac{\pi}{4}\right) \right]^{-1} = 70.9 \text{ psi}$$

The axial inertial load of the TC internals is accounted for by applying a pressure on the inside surface of the cask lid. For a 2 g inertial load, the applied axial pressure, P_a , is as follows.

$$P_{aBOT} = 115,000 \text{ lb} \times 2 \text{ g} / [\pi \times (35.25^2 - 11^2)] = 65.28 \text{ psi} - \text{Cases 6A and 7A}$$

$$P_{aTOP} = 115,000 \text{ lb} \times 2 \text{ g} / [\pi \times 35.83^2] = 57.03 \text{ psi} - \text{Cases 6B and 7B}$$

Transfer loads are run with and without internal pressure of 30 psi to bound any possible pressure build up inside the cask. Displacement constraints are applied at the trunnion locations to the 3-dimensional full model.

A depiction of the transfer loads load case boundary conditions is provided in Figure A.3.9.2-8.

Load Case 9: 75 g Bottom End Drop (2-D FEM)

The bottom end drop is not considered credible during storage and transfer operations under 10 CFR Part 72 because the TC will always be in the horizontal orientation. The bottom drop evaluation documented below is performed in support of a 10 CFR Part 50 evaluation that may be performed by the user if the user cannot demonstrate that this accident drop is not credible.

The weight of the TC internals (canister, basket, spacer, and fuel assemblies) is accounted for by applying equivalent pressures. The total actual weight of the cask internals is 109.50 kips. For conservatism, the weight of the cask internals used in this analysis is increased to 115 kips. The TC inner radius is 35.25 in., and the inner radius of the ram access penetration is 11.00 in. The inertial load of the TC internals reacts against the annular surface bounded by these two radii during a bottom end drop. The area of this reaction surface, A_{bi} , is as follows.

$$A_{bi} = \pi(35.25^2 - 11.00^2) = 3,523 \text{ in}^2.$$

The pressure equivalent to the inertial load of the internals under accident conditions, P_{bi} , is,

$$P_{in} = [115,000 / 3,523] \times 75 \text{ gs} = 2,447.86 \text{ psi}$$

Internal pressure of 30 psi is applied.

Symmetry displacement boundary conditions are applied along the y -axis of the 2-dimensional axisymmetric model. The bottom end of the TC is held in the axial direction in order to simulate the rigid reaction force generated by the impact target. A 75 g inertial load in the positive y -direction is also applied to the model for the accident condition load case.

A depiction of the Bottom End Drop load case boundary conditions is provided in Figure A.3.9.2-9.

Load Case 10: 75 g Top End Drop (2-D FEM)

The top end drop is not considered credible during storage and transfer operations under 10 CFR Part 72 because the TC will always be in the horizontal orientation. The top end drop evaluation documented below is performed in support of a 10 CFR Part 50 evaluation that may be performed by the user if the user cannot demonstrate that this accident drop is not credible.

The weight of the TC internals (canister, basket, spacer, and fuel assemblies) is accounted for by applying equivalent pressures. The weight of the canister internals used in this analysis is 115,000 lb. The inertial load of the TC internals reacts against the inside surface of the top cover assembly during a top end drop. The outer radius of the inside surface of the TC top cover assembly is 35.675 in. Therefore the area of the reaction surface, A_{bi} , is as follows.

$$A_{bi} = \pi(35.675^2) = 3,998.32 \text{ in}^2.$$

The pressure equivalent to the inertial load of the internals under accident conditions, P_{bi} , is,

$$P_{in} = [115,000/3,998.32] \times 75 \text{ gs} = 2,157.16 \text{ psi}$$

The internal pressure of 30 psi is also applied to the model.

Symmetry displacement boundary conditions are applied along the y-axis of the 2-dimensional axisymmetric model. The outer surface of the top cover is held in the axial direction in order to simulate the rigid reaction force generated by the impact target. A 75 g inertial load in the negative y-direction is also applied to the model for the accident condition load case.

A depiction of the top end drop load case boundary conditions is provided in Figure A.3.9.2-10.

Since the top end vertical drop will induce much higher shear stress in the weld between the TC inner shell and top flange, this load case is used to calculate the weld stresses. The ANSYS run result file from this load case is post processed to get the maximum shear stress at this weld location.

The maximum shear stress is 7,991 psi and the allowable shear stress is $0.42 S_u$ ($0.42 \times 64,000 = 26,880$ psi, for 304 SS at 400 °F). Factor of safety = $26,880/7,991 = 3.36$.

Load Case 11: 75 g Side Drop (3-D FEM)

During the 75 g side drop load case, the loaded TC is dropped onto a concrete target generating a transverse acceleration of 75 g.

The impact side of the TC is supported in the cask radial direction along the entire length of the cask. The radial support spans 15° of the 180° model. The radial support is intended to model the reaction of the concrete target during impact.

The inertial load of the TC internals is accounted for by applying a cosine varying pressure on the inside surface of the cask inner shell using the same method that was used for the transfer loads case. The applied forces are the inertial load of the DSC, F_i , and the inertial load of the spacer and air wedges, F_s :

$$F_i = 110,000 \text{ lb} \times 75 \text{ g} = 8,250,000 \text{ lb},$$

$$F_s = 5,000 \text{ lb} \times 75 \text{ g} = 375,000 \text{ lb}.$$

Therefore, P_{\max} for the DSC and spacer are the following:

$$P_{i \max} = \frac{8,250,000}{(190.25)(35.25)} \left[\frac{\sin\left(\frac{3\pi}{4}\right)}{3} + \sin\left(\frac{\pi}{4}\right) \right]^{-1} = 1,304.8 \text{ psi}$$

$$P_{s \max} = \frac{375,000}{(6)(35.25)} \left[\frac{\sin\left(\frac{3\pi}{4}\right)}{3} + \sin\left(\frac{\pi}{4}\right) \right]^{-1} = 1,880.6 \text{ psi}$$

Symmetry displacement boundary conditions are applied along the cut boundary of the 3-dimensional half model. An internal pressure of 30 psi is also applied to the model.

A depiction of the 75 g side drop load case boundary conditions is provided in Figure A.3.9.2-11.

Load Case 12: Transfer Thermal Accident (Fire)

The applied loads used to calculate the maximum stress in the transfer during fire accident event include a maximum radial temperature gradient and normal conditions transfer loads. The stresses generated in the TC shell by the temperature gradient are computed using hand calculations. The resulting stresses caused by the thermal temperature gradient are added to the stresses computed for the transfer load case. Since the primary load for the fire accident is caused by the radial temperature gradient, the maximum TC stress is computed for the outer radial structural shell.

The maximum stress generated by the radial thermal gradient fire accident will occur in the outer structural shell due to the thermal expansion of the lead gamma shield. From Chapter 4, the maximum temperature difference between the lead gamma shield and the structural shell occurs when the lead and structural shell are at 618 °F and 553 °F, respectively.

The change in the outer radius of the lead gamma shield, ΔR_l , is computed as follows.

$$\Delta R_l = R_l \times \alpha_l \times \Delta T_l = 39.435 \text{ in.} \times 19.68 \times 10^{-6} \text{ in./in. } ^\circ\text{F} (@600 ^\circ\text{F}) \times (618 - 70) ^\circ\text{F} \\ = 0.4253 \text{ in.}$$

The change in the inner radius of the structural shell, ΔR_s , is computed as follows.

$$\Delta R_s = R_s \times \alpha_s \times \Delta T_s = 39.435 \text{ in.} \times 9.7 \times 10^{-6} \text{ in./in. } ^\circ\text{F} (@500 ^\circ\text{F}) \times (553 - 70) ^\circ\text{F} \\ = 0.1848 \text{ in.}$$

Therefore the differential radial expansion between the lead and structural shell, ΔR , is as follows:

$$\Delta R = 0.4253 \text{ in.} - 0.1848 \text{ in.} = 0.241 \text{ in.}$$

Therefore, the lead cylinder, if it were free, would grow 0.241 in. more than the inner surface of the structural shell. If all of the differential expansion is accommodated in the lead, the lead strain, ϵ_l , would be the following.

$$\epsilon_l = \Delta R / R_l = 0.241 \text{ in.} / 39.435 \text{ in.} = 0.006 \text{ in./in.}$$

If the lead remained linear elastic, the residual hoop stress in the lead would be,

$$\sigma_l = E_l \times \epsilon_l = 1.64 \times 10^6 \text{ psi} (@600 ^\circ\text{F}) \times 0.006 \text{ in./in.} = 9,840 \text{ psi}$$

Conservatively assuming that the lead remains linear elastic, the interference pressure on the outer structural shell required to exert an average hoop stress of 9,840 psi in the lead can be determined in the following way.

$$P_{interface} = \sigma_l \times \text{lead thickness} / R_{interface} = 9,840 \text{ psi} \times 3.56 \text{ in.} / 39.435 \text{ in.} = 888 \text{ psi}$$

This interference pressure would generate the following hoop stress in the structural shell.

$$\sigma_s = P_{interface} \times R_{interface} / t_s = 888 \text{ psi} \times 39.435 / 1.50 = 23,346 \text{ psi} \approx 23.35 \text{ ksi}$$

The total combined maximum stress, σ , in the TC during the fire accident is then,

$$\begin{aligned} \sigma &= 5.06 \text{ ksi (stress due to 30 psi internal pressure from load case 3)} + 23.35 \text{ ksi} \\ &= 28.41 \text{ ksi} \end{aligned}$$

A.3.9.2.3 ANSYS Analysis Results and Reporting Methodology

The maximum nodal stress intensities in various components of the NUHOMS® OS187H Type 1 TC are extracted from the ANSYS results files for all load cases. These stresses are compared to the normal and accident condition allowable stresses set forth by ASME B&PV Code Section III, Subsection NC [2] and Appendix F [3]. Allowable stresses are derived from material properties taken from Reference 6 at the various component temperatures listed in the Material Properties section. A summary of the maximum TC component stresses and corresponding allowable stresses is presented in Table A.3.9.2-1.

The maximum nodal stress intensities ($P_m + P_b$) are conservatively compared to the allowable membrane stress intensities, unless otherwise stated. In load cases where the nodal stress intensity exceeds the membrane allowable stress, individual membrane and membrane plus bending stresses are computed by linearizing the maximum component stresses through the thickness of the component. The resulting linearized stresses are then compared to their corresponding P_m and $P_m + P_b$ allowable stresses.

For the load combinations involving mechanical loads and thermal loads (i.e., 6 g lifting plus 115 °F ambient), the maximum stresses from the mechanical load case and the maximum stress from the thermal load case are simply summed for each of the major cask components. This method of computing the maximum load combination stresses is very conservative, because, in general, the maximum stress caused by a mechanical load and the maximum stress caused by a thermal load will not occur at the same location in the TC.

Typically, fictitious stresses at nodes where point contact exists are ignored. These unrealistic stresses usually occur in the top cover at locations where the top cover bolts are fixed to the cover by node coupling (in all degrees of freedom) at a single node. Similarly, in the transfer loads analysis, the TC is held at the trunnion locations. This boundary condition creates fictitious stresses in the structural shell around the trunnions. Thus, stresses 4-inches around the trunnions are not evaluated. Local stresses in the shell due to trunnion loads are evaluated separately and are documented in Section A.3.9.2.4. For the 75 g side drop, high fictitious stresses are created due to the boundary condition discontinuity at the contact location. These stresses are also not evaluated.

A.3.9.2.4 Evaluation of OS187H Type 1 Transfer Cask Trunnion Local Stresses

The purpose of this section is to evaluate the local stress intensities in the NUHOMS[®] OS187H Type 1 TC radial shells near the upper and lower trunnions, due to all applied loads during fuel loading and transfer operations.

A.3.9.2.4.1 Approach

The NUHOMS[®] OS187H Type 1 TC has two upper trunnions made of SA-182 Gr. FXM19 forging and two lower trunnions made of SA-182 Gr. F304N. The OS187H Type 1 TC cylindrical shell and the reinforcing pad are made of SA-240 Type 304 stainless steel.

The two top trunnions are used to first lift the cask, containing an empty DSC, into a fuel pool for loading of the spent fuel. After the spent fuel has been loaded into the DSC, the cask is lifted to a decontamination area. After draining and drying of the pool water, welding of the canister cover, and bolting of the cask top cover, the cask is placed on a trailer for transfer to an onsite HSM-H.

The TC is vertically lifted into the trailer and rests its bottom trunnions on a support frame mounted to the top of the trailer. Then the cask is allowed to rotate, using the bottom trunnion supports as the pivot points, into a horizontal position until the top trunnions rest on their supports on the trailer. Throughout the operation the maximum total load is applied to the cask top trunnions. After the cask has been placed in the trailer, it is supported by all four trunnions and is subject to a set of specified handling loads.

The following two load cases are analyzed for the four cask trunnions and adjoining shell:

1. Lifting Loads (cask is in vertical position, lifted from the pool to the decontamination area and then to the trailer). The two top trunnions and interfacing structural shell are analyzed for vertical 6g load. The two bottom trunnions are not used during lifting of the cask.
2. Handling Loads (cask is in a horizontal position mounted on the trailer). All four trunnions rest on the supports in the trailer.

These four trunnion-shell interfaces are designed to resist the following transfer load combinations:

1. DW (dead weight) + 1 g axial (load resisted by lower trunnions only)
2. DW + 1 g transverse (load is resisted by trunnions on one side of the cask)
3. DW + 1 g vertical (load is distributed to all four trunnions)
4. DW + 1/2 g axial + 1/2 g transverse + 1/2 g vertical
(Directions of transfer loads are relative to a horizontal cask)

In load combination 4, the load components are distributed according to the direction used in load cases 1 through 3 above.

HSM insertion/withdrawal loads are bounded by the analyzed transfer loads. For the OS187H Type 1 TC, the maximum load that may be reacted by the trunnions during insertion/withdrawal of the DSC to/from the HSM is 80 kips. The evaluation of local stresses near the upper trunnions considers loads exceeding that magnitude.

The trunnions and cask shells are assumed to be at a 400° F uniform temperature during transfer, which is conservative compared to the maximum temperature computed in Chapter 4 for the 115 °F ambient environment condition (see Figure A.3.9.2-4).

The following calculations are based on the method described in Reference 10. A spreadsheet based on Figure 3.9.2-12, which implements the Reference 10 method, was developed to aid in the computations. The computation spreadsheets presented in Table A.3.9.2-2 through Table A.3.9.2-15 document the evaluation of local shell stresses for the various load cases analyzed.

A.3.9.2.4.2 Load Cases

The weights of NUHOMS® OS187H Type 1 TC components are listed in Section A.3.9.2.1.2. The weight of the NUHOMS® OS187H Type 1 TC loaded with a 32PTH Type 1 DSC (dry) is 240,000 lbs. The wet weight of a loaded OS187H Type 1 TC (includes the weight of water in the DSC and TC/DSC annulus and excludes the weight of the TC lid and DSC top covers) is approximately 244,500 lbs. However, for conservatism, a weight of 250,000 lb is used in this analysis.

In the estimation of the magnitude of trunnion reactions it is assumed that:

- a) Maximal load considered for vertical lift is 125 kips (per trunnion) plus the 15% allowance, or 143.75 kips.
- b) The moment arm is measured from the center of the yoke of the (lifting) hook to the middle surface of the TC structural shell.
- c) The cask weight is distributed proportionally between the upper and lower trunnions and the cask is analyzed as a simply supported beam.

The requirement given in (b) above is consistent with the methodology in WRC-107 Bulletin [10]. Based on geometry relations the median radius of cask shell, R_m , can be defined as:

$$R_m = R_I + (T_{\text{shell}} + T_{\text{pad}})/2$$

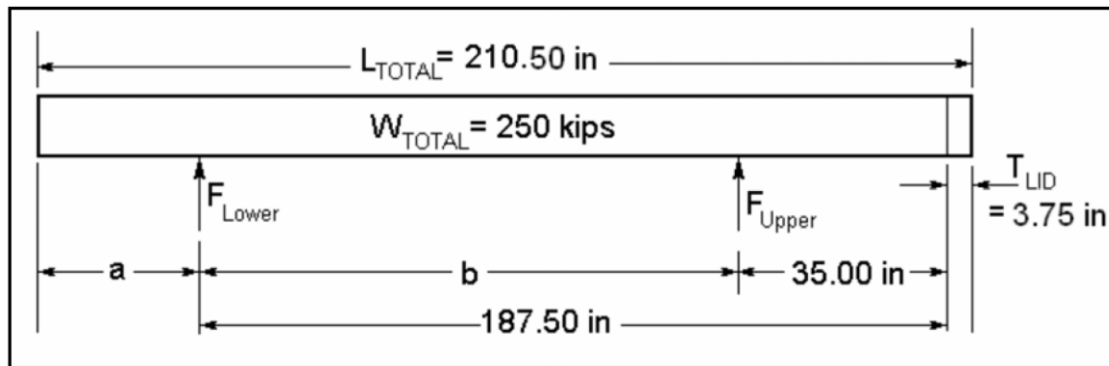
where:

- T_{shell} is nominal thickness of cask shell at trunnion location
- T_{pad} is the thickness of reinforcement pad
- R_I = 39.44 inch is inner radius of cask shell

The table below provides values of median radius of cask shell R_m and moment arms used in this calculation. Reinforcement pad thickness $T_{\text{pad}} = 1.31$ inches is used conservatively in the calculations (actual design thickness = 1.375 inches).

Upper Trunnion - Input Data for Reinforcement Pad-Trunnion Joint (Load Cases UT 1-5)						
R _l [in]	R _m [in]	T _{shell} [in]	T _{pad} [in]	Load Type	Moment Arm Definition	Moment Arm[in]
39.44	41.29	2.38	1.31	6g Lifting Load	46.3+3.75+ 3.25/2-R _m	10.390
				Transfer Loads	46.3+3.75/2-R _m	6.8900
Upper Trunnion - Input Data for Reinforcement Pad - Shell Joint (Load Cases UT 6-10)						
39.44	40.63	2.38	0	6g Lifting Load	46.3+3.75+ 3.25/2-R _m	11.045
				Transfer Loads	46.3+3.75/2-R _m	7.5450
Lower Trunnion Input Data for Trunnion-Shell Joint - No Reinforcement Pad (Load Cases LT 1- 4)						
39.44	40.19	1.5	0	Transfer Loads	46.3+3.5/2-R _m	7.8600

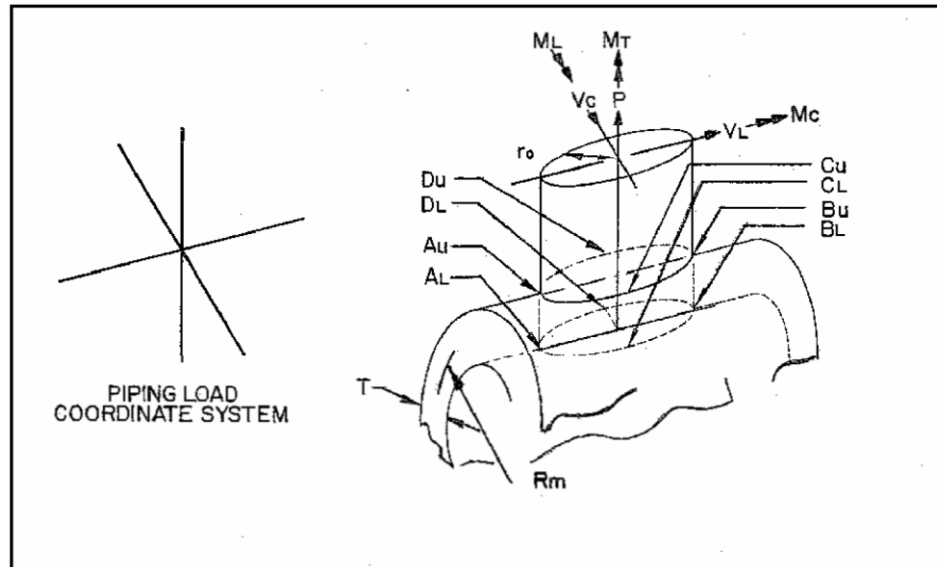
The figure below shows basic geometry relations, derived from the OS187H Type 1 TC drawings.



The above geometrical relations are used in the calculation of reaction forces for the upper and lower trunnions. The total length of the cask is 210.50 inches. The dimension $T_{LID} = 3.75$ inches denotes the thickness of the top cover above the top edge of the cask. Distance $a = 19.25$ inches, distance $b = 152.5$ inches.

Assuming a total weight of 250 kips, the reaction forces at trunnion locations can be calculated as $F_{upper} = 71$ kips for the upper trunnion, and $F_{lower} = 54$ kips for the lower trunnion.

The stress classification locations (A_U , B_U , C_U , D_U and A_L , B_L , C_L , D_L) as well as basic parameters used in WRC-107 Bulletin [10] are illustrated in the figure below:



In the WRC-107 Bulletin coordinate system convention, the radial load P is assumed positive when directed away from cylinder centerline. Axial loads (e.g., critical lifting loads for upper trunnions, axial transport loads for lower trunnions) are represented as V_L loads. When the transfer cask is supported in the horizontal position the vertical transfer loads and deadweight loads acting on the transfer cask are tangential loads V_C . The M_L loads are force moments generated by V_L loads, while M_C loads are force moments generated by V_C loads.

A.3.9.2.4.3 Material Properties

The following pertinent material properties are taken from Reference 6 corresponding to a (conservative) temperature of 400 °F.

Property	SA-240, Type 304 stainless steel (cask shells and pad)
S_m	18.7 ksi
S_y	20.7 ksi
S_u	64.0 ksi

A.3.9.2.4.4 Stress Criteria

All load cases analyzed are Service Level A load cases. According to ASME Code, Section III, Subsection NC [2], for Service Level A conditions, the maximum allowable general primary membrane stresses (P_m) shall be limited to S_m . Local primary membrane stresses (P_L) shall be limited to $1.5 S_m$, while maximum allowable primary plus secondary stresses, $P_L + P_b + Q$, shall be limited to $3.0 S_m$.

Primary stresses result from an imposed loading for which it is necessary to satisfy the laws of equilibrium between external and internal forces and moments. The basic characteristic of primary stress is that it is not self-limiting. If the primary stress exceeds yield through the entire thickness of the wall, the failure of the design depends entirely on strain hardening properties of

material. In the case of trunnion load, the primary stress is the membrane stress occurring near the trunnion, caused by mechanical load.

General primary stresses (P_m) are stresses that are located remote from any structural discontinuity. Such stresses should be derived as the average stresses through the thickness of the cask shell at the location remote from discontinuity. No redistribution of load occurs as a result of yielding of material of general primary stress.

Local primary stress (P_L) is also average stress across a solid section, but it includes the effect of gross structural discontinuities. This type of stress is self-limiting when it exceeds yield because the load is resisted by other parts of the structure, but it may result in excessive distortion of the structure because of the shift of the load to other parts. In the case of the WRC-107 methodology, the example of local primary stress is stress in the vicinity of a nozzle (trunnion) occurring as a result of external loads.

Secondary stresses (Q) are developed as a result of the strain pattern induced by the maintaining of structural continuity between structural members of the design. The basic characteristic of secondary stresses is that they are self-limiting. In the case of external loads imposed onto trunnions the secondary stresses are surface stresses caused by mechanical load in the vicinity of the trunnion. In the case of the WRC-107 methodology, these stresses are surface stresses at stress classification locations A_U , B_U , C_U , D_U and A_L , B_L , C_L , D_L .

For the upper trunnions region, stress levels for primary membrane and secondary stresses are checked in the trunnion to reinforcement pad juncture and the reinforcement pad to cask shell juncture. For the lower trunnions region, the primary membrane and secondary stresses are checked at the trunnion-to-shell juncture.

The TC shells and pad are constructed from stainless steel, SA-240, Type 304. The material properties are taken at 400 °F, which bounds the maximum inner shell and structural shell temperatures generated during 150 °F ambient transfer condition.

The table below shows a summary of stress acceptance criteria used in the stress evaluation:

Stress Location	Stress Description	Stress Classification	Criteria Limit	Criteria Limit [ksi]
Cask shell at both trunnion locations	Local membrane	P_L	$1.5 \cdot S_m$	28.1
	Surface stress	$P_L + P_b + Q$	$3.0 \cdot S_m$	56.1

A.3.9.2.4.5 Stress Computation

For the upper trunnion, stress levels for primary membrane and secondary stresses are checked in the trunnion-to-reinforcement pad juncture and the reinforcement pad-to-cask shell juncture. For the lower trunnion, the primary membrane and secondary stresses are checked at the trunnion-to-shell juncture. The detailed information about input loads V_L , M_L , V_C , M_C , and P at these locations is provided below. The definition of these input loads is presented in section A.3.9.2.4.2.

Stress results for the load combinations presented below are calculated in the attached spreadsheets (Table A.3.9.2-2 through Table A.3.9.2-15). Each spreadsheet contains the specification of all input parameters used in the stress calculation. The summary of stress results is provided in Table A.3.9.2-16.

The specification of input loads at the juncture of the upper trunnion and reinforcement pad is presented in the table below. Stress calculations for load cases UT1, UT2 UT3, UT4, and UT5 are documented in Table A.3.9.2-2 through Table A.3.9.2-6.

Load Type	Load Combination	Case ID	Axial Load	Axial Load Moment	Tangential Load	Tangential Load Moment	Radial Load
			V_L [kips]	M_L [in-kips]	V_C [kips]	M_C [in-kips]	P [kips]
Lifting Loads	Critical lifts	UT1	862.5	8961.4	0.0	0.0	0.0
Transfer Handling Loads	DW+1g Axial	UT2	0.0	0.0	71.0	489.2	0.0
	DW+1g Transverse	UT3	0.0	0.0	71.0	489.2	-142.0
	DW+1g Vertical	UT4	0.0	0.0	142.0	978.4	0.0
	1/2g Axial + 1/2g Transverse + 1/2g Vertical + DW	UT5	0.0	0.0	106.5	733.8	-71.0

The specification of input load at the juncture of the upper trunnion reinforcement pad and cask shell is shown in the following table. Stress calculations for load cases UT6, UT7 UT8, UT9, and UT10 are documented in Table A.3.9.2-7 through Table A.3.9.2-11.

Load Type	Load Combination	Case ID	Axial Load	Axial Load Moment	Tangential Load	Tangential Load Moment	Radial Load
			V_L [kips]	M_L [in-kips]	V_C [kips]	M_C [in-kips]	P [kips]
Lifting Loads	Critical lifts	UT6	862.5	9526.3	0.0	0.0	0.0
Transfer Handling Loads	DW+1g Axial	UT7	0.0	0.0	71.0	535.7	0.0
	DW+1g Transverse	UT8	0.0	0.0	71.0	535.7	-142.0
	DW+1g Vertical	UT9	0.0	0.0	142.0	1071.4	0.0
	1/2g Axial + 1/2g Transverse + 1/2g Vertical + DW	UT10	0.0	0.0	106.5	803.5	-71.0

Finally, the specification of input loads at the interface of the lower trunnion and cask shell is presented in the table below. Stress calculations for load cases LT1, LT2, LT3, and LT4 are documented in Table A.3.9.2-12 through Table A.3.9.2-15.

Load Type	Load Combination	Case ID	Axial Load	Axial Load Moment	Tangential Load	Tangential Load Moment	Radial Load
			V _L [kips]	M _L [in-kips]	V _C [kips]	M _C [in-kips]	P [kips]
Transfer Handling Loads	DW+1g Axial	LT1	125.0	982.5	54.0	424.4	0.0
	DW+1g Transverse	LT2	0.0	0.0	54.0	424.4	-108.0
	DW+1g Vertical	LT3	0.0	0.0	108.0	848.9	0.0
	1/2g Axial + 1/2g Transverse + 1/2g Vertical + DW	LT4	62.5	491.3	81.0	636.7	-54.0

A.3.9.2.4.6 Stress Intensity Calculation

Membrane plus bending stress intensities are calculated in the following way.

$$S.I. = \text{Max. of} \left\{ \begin{array}{l} \frac{1}{2} \left[(\sigma_x + \sigma_\phi) \pm \sqrt{(\sigma_x - \sigma_\phi)^2 + 4\tau^2} \right] \\ \sqrt{(\sigma_x - \sigma_\phi)^2 + 4\tau^2} \end{array} \right.$$

In order to calculate the membrane or bending stress intensity, only those components associated with membrane or bending stress, respectively, are summed to calculate σ_ϕ , σ_x and τ .

A.3.9.2.4.7 Local Shell Stress Results

Table A.3.9.2-16 summarizes the maximum stress intensities and compares them against applicable allowables.

A.3.9.2.4.8 Local Shell Stress Conclusions

All calculated local membrane stresses are less than the allowable local membrane stress of 28.1 ksi, and all local membrane plus bending stress intensities are less than the allowable local membrane plus bending stress of 56.1 ksi. Therefore, the NUHOMS® OS187H Type 1 TC shells adjoining the trunnions are structurally adequate with respect to local stresses generated during lifting and transfer operations.

A.3.9.2.5 Stress and Deflection of Transfer Cask Inner Shell Support Rails

The 3D finite element model used for side drop analyses as described in Appendix A.3.9.2, Section A.3.9.2.2.3 (B) is modified as follows and used to calculate the stresses and deflections of the transfer cask inner shell along the support rail locations.

Finite Element Model Modifications

1. Include the 3" wide x 0.12" thick rails in the 3-D TC inner shell (SHELL 43 element)
2. Include canister shell (SOLID 45 element) in the 3-D model
3. Gap elements (CONTACT 52) are used between the canister shell and transfer cask inner shell and between the canister shell and inner shell rail

Radial gap elements (CONTACT 52) are used to simulate the interface between the outer radius of the canister and inner radius of the cask inner shell. Each gap element contains two nodes; one on each surface of the structure. The gap size at each gap element is determined by the difference between the canister outer radius and the inside radius of the cask (canister outer radius = 34.875" and cask inner radius = 35.25" to give a 0.375 inch mean gap). Radial gap elements are generated using an ANSYS macro. Actual gap sizes for the gap element, at each radial location, were determined and input into the model as real constants using another ANSYS macro. This macro accepts the drop orientation and model geometry as inputs and determines the circumferential position of each gap element. The macro then computes the appropriate real constants and applies to appropriate gap elements.

During drops on cask rails (180° side drop), the initial gaps between the canister and the cask are modified using the ANSYS macro. Two 3 inch wide and 0.12 inch thick rails are welded to the cask inner shell at 12° on both sides of the vertical center line of the model and another set of two rails are welded at 38° on both sides of the same vertical center line. For the 180° side drop onto the rails, the initial gaps at the two inner rail locations are assumed closed (0 gap). In-between these two rail locations, the initial gaps are set to 0.12 inches. On the other two rail locations, the gaps are initially set to open, and the gap sizes are generated by macro with consideration of the rail thickness.

The ANSYS 3-D finite element models including cask shell, lead, rails, canister, and gap elements are shown on Figure A.3.9.2-13 through Figure A.3.9.2-18.

Loadings

Pressures applied in the radial direction to the inner surface of the canister in the 3-dimensional finite element model are based on a cosine distribution. This pressure distribution simulates the load which the internal canister contents exert on the inner canister wall. Two drop cases are analyzed: impact on two rails (Figure A.3.9.2-19) and impact on one rail (Figure A.3.9.2-20).

Materials

In order to properly calculate the deflections of the rails, elastic and inelastic material properties of the canister and cask at the temperatures are used for the analysis.

Results

The following table summarizes the maximum stress intensities at the TC inner and outer shells for the above two drop load cases.

Summary of Maximum Stress Intensities and Allowables

Load Case	Component	Stress Category	Calculated Max. Stress Intensity (ksi)	Allowable Membrane Stress Intensity (ksi) ⁽¹⁾	Factor of Safety
Impact on two rails	Inner Shell	$P_L + P_b$	43.786	45.57	1.04
	Outer Shell	$P_L + P_b$	37.674	45.57	1.21
Impact on one rail	Inner Shell	$P_L + P_b$	45.282	45.57	1.01
	Outer Shell	$P_L + P_b$	37.805	45.57	1.21

Note:

- (1) Since the calculated maximum stress intensity is less than the allowable membrane stress intensity (P_m), therefore only maximum stress intensity is reported.

The calculated stresses are less than the code allowables and the calculated maximum deflection in the rail is 0.0725". This small deflection will not affect the retrieving of the canister from the TC after an accident drop.

The maximum stress intensity plots of the cask inner shell and outer shell for the impact to the two rails load case are shown on Figure A.3.9.2-21 and Figure A.3.9.2-22, respectively. The maximum stress intensity plots of the inner shell and outer shell for the impact to the one rail load case are shown on Figure A.3.9.2-23 and Figure A.3.9.2-24, respectively.

A.3.9.2.6 References

1. 10CFR Part 72, Licensing Requirement for Storage of Spent Fuel in an Independent Spent Fuel Storage Installation.
2. ASME Code Section III, Subsection NC and Appendices, 1998, through 2000 addenda.
3. American Society of Mechanical Engineers, ASME Boiler and Pressure Vessel Code, Section III, Appendix F, 1998, through 2000 addenda.
4. ANSYS Users Manual, Rev. 8.0 and Rev. 8.1.
5. Technical Report N3-3-012, Bisco Products Inc., April 1984.
6. American Society of Mechanical Engineers, ASME Boiler and Pressure Vessel Code, Section II, Part D, 1998, through 2000 addenda.
7. Not Used.
8. Not Used.
9. Not Used.
10. Welding Research Council (WRC), Local Stresses in Spherical and Cylindrical Shells Due to External Loadings, Bulletin 107, March 1979.
11. Not Used.

Table A.3.9.2-1
Transfer Cask Components Stress—Summary of Results

Load Case Number	Loading Condition	Service Level	Component ⁽⁶⁾		Maximum Stress Intensity (ksi)	Allowable Stress (ksi)
1A	6 g vertical lifting	A	Structural shell	P_m	8.71	20.00
				$P_m + P_b$	27.48	30.00
			Top cover		8.92	31.40
			Inner shell		15.08	18.70
			Bottom end plates	P_m	15.22	20.00
				$P_m + P_b$	27.34	30.00
			Ram acc. and cover	P_m	19.51	20.00
				$P_m + P_b$	21.45	30.00
1B	6 g vertical lifting + thermal loads	A	Structural shell		53.6	60.00 ⁽¹⁾
			Top cover		19.54	94.20 ⁽¹⁾
			Inner shell		41.83	56.10 ⁽¹⁾
			Bottom end plates		39.79	60.00 ⁽¹⁾
			Ram access and cover		36.44	60.00 ⁽¹⁾
2	Vacuum drying	A	Structural shell		11.97	60.00 ⁽¹⁾
3	30 psi internal pressure	A	Structural shell		5.06	20.00
			Top cover		6.31	31.40
			Inner shell		3.89	18.70
			Bottom end plates		5.06	20.00
			Ram access and cover		3.93	20.00
4	115 °F ambient hot thermal environment	A	Structural shell		26.12	60.00 ⁽¹⁾
			Top cover		10.62	94.20 ⁽¹⁾
			Inner shell		23.70	56.10 ⁽¹⁾
			Bottom end plates		12.45	60.00 ⁽¹⁾
			Ram access and cover		14.99	60.00 ⁽¹⁾
5	-20 °F ambient cold thermal environment	A	Structural shell		10.97	60.00 ⁽¹⁾
			Top cover		9.34	94.20 ⁽¹⁾
			Inner shell		26.75	56.10 ⁽¹⁾
			Bottom end plates		11.83	60.00 ⁽¹⁾
			Ram access and cover		12.43	60.00 ⁽¹⁾
A	Transfer inertial loads—axial accel. toward bottom	A	Structural shell		18.90	20.00
			Top cover		8.55	31.40
			Inner shell		12.81	18.70
			Bottom end plates		10.70	20.00
			Ram access and cover		9.09	20.00

Table A.3.9.2-1
Transfer Cask Components Stress—Summary of Results (continued)

Load Case Number	Loading Condition	Service Level	Component ⁽⁶⁾		Maximum Stress Intensity (ksi)	Allowable Stress (ksi)
6B	Transfer inertial loads—axial accel. toward top	A	Structural shell	P_m	9.27	20.00
				$P_m + P_b$	22.85	30.00
			Top cover		12.14	31.40
			Inner shell	P_m	8.48	18.70
				$P_m + P_b$	17.66	28.05
			Bottom end plates		7.43	20.00
			Ram access and cover		6.50	20.00
7A	Transfer loads—axial accel. toward bottom + internal pressure	A	Structural shell		18.37	20.00
			Top cover		11.92	31.40
			Inner shell		12.38	18.70
			Bottom end plates		14.89	20.00
			Ram access and cover		12.23	20.00
7B	Transfer loads—axial accel. toward top + internal pressure	A	Structural shell	P_m	9.12	20.00
				$P_m + P_b$	21.17	30.00
			Top cover		15.74	31.40
			Inner shell		18.50	18.70
			Bottom end plates		6.85	20.00
7C ⁽⁷⁾	Transfer loads + 115 °F ambient + internal pressure	A	Structural shell		48.97	60.00 ⁽¹⁾
			Top cover		26.36	94.20 ⁽¹⁾
			Inner shell		42.70	56.10 ⁽¹⁾
			Bottom end plates		27.34	60.00 ⁽¹⁾
			Ram access and cover		27.22	60.00 ⁽¹⁾
8 ⁽⁷⁾	Transfer loads + -20 °F ambient + internal pressure	A	Structural shell		33.82	60.00 ⁽¹⁾
			Top cover		25.08	94.20 ⁽¹⁾
			Inner shell		45.25	56.10 ⁽¹⁾
			Bottom end plates		26.72	60.00 ⁽¹⁾
			Ram access and cover		24.66	60.00 ⁽¹⁾
9	75 g bottom end drop + internal pressure	D	Structural shell		39.62	46.34
			Top cover		46.41	65.94
			Inner shell		16.69	44.80
			Bottom end plates		26.50	46.34
			Ram access and cover		43.86	48.00

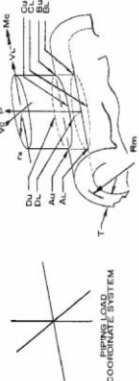
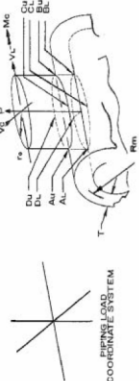
Table A.3.9.2-1
Transfer Cask Components Stress—Summary of Results (concluded)

Load Case Number	Loading Condition	Service Level	Component ⁽⁶⁾		Maximum Stress Intensity (ksi)	Allowable Stress (ksi)
10	75 g top end drop + internal pressure	D	Structural shell		43.61	46.34
			Top cover		39.44	65.94
			Inner shell		18.11	44.80
			Bottom end plates		5.93	46.34
			Ram access and cover		4.87	48.00
11	75 g side drop + internal pressure	D	Structural shell ⁽⁵⁾	P_m	45.06	46.34
				$(P_m \text{ or } P_L) + P_b$	61.64	66.20 ⁽³⁾
			Top cover ⁽⁵⁾	P_m	63.82	65.94
				$(P_m \text{ or } P_L) + P_b$	79.79	94.20 ⁽³⁾
			Inner shell	P_m	35.43	44.80
				$(P_m \text{ or } P_L) + P_b$	44.35	64.00 ⁽³⁾
			Bottom end plates ⁽⁴⁾	P_m	45.96	46.34
				P_L	50.73	66.20
				$(P_m \text{ or } P_L) + P_b$	51.21	66.20 ⁽³⁾
			Ram access and cover	P_m	44.47	48.00
				$(P_m \text{ or } P_L) + P_b$	54.42	71.00 ⁽³⁾
12	Transfer thermal accident (fire)	D	Structural shell		28.41	58.32 ⁽²⁾

Notes

- (1) $P_L + P_b + Q$ allowable stress.
- (2) $S_m = 16.2$ ksi. For SA-240 type 304 at a temperature of 650 °F. (the maximum TC temperature is 618° during the thermal accident condition). The allowable stress is taken as $3.6S_m$.
- (3) Membrane plus bending [$(P_m \text{ or } P_L) + P_b$] allowable stress.
- (4) Stresses at the edge of the impact target support at the 15° location is considered local and are compared to P_L allowable stresses.
- (5) High stresses due to boundary condition discontinuity and bearing stresses at contact locations are not evaluated for top cover and top flange.
- (6) See Figure A.3.9.2-1 for the stress reporting components. Structural Shell component includes the structural shell, the top flange and the bottom support ring components shown in Figure A.3.9.2-1. Bottom end plates component includes the bottom end plate and bottom neutron shield plate components.
- (7) Load cases 6A and 6B are transfer handling load cases without internal pressure; load cases 7A and 7B are transfer handling load cases with internal pressure. If the component stresses for transfer handling load cases without internal pressure is higher, conservatively the higher stress is used for load combination in load cases 7C and 8.

Table A.3.9.2-3
Local Shell Stress at Trunnion Locations—Computation Spreadsheet
for Case UT2

Applied Loads		Geometry									
				1	2	3	4	5	6	7	8
V_L	0.0	[kips]	I [in]	A_U	A_L	B_U	B_L	C_U	C_L	D_U	D_L
M_L	0.0	[in-kips]	R_m [in]	0.0	0.0	0.0	0.0	0.0	0.0	0.0	0.0
V_C	71.0	[kips]	r_0 [in]	0.0	0.0	0.0	0.0	0.0	0.0	0.0	0.0
M_C	489.2	[in-kips]	$\beta=0.875 \cdot d_0/R_m$	0.0	0.0	0.0	0.0	0.0	0.0	0.0	0.0
P	0.0	[kips]	$\gamma=R_m/T$	0.0	0.0	0.0	0.0	0.0	0.0	0.0	0.0
M_T	0	[in-kips]	$\lambda=d/D/(\pi)^{1/2}$	0.0	0.0	0.0	0.0	0.0	0.0	0.0	0.0
Figures											
Read curves for				values							
3C AND 4C				0.0							
1C AND 2C-1				0.0							
3A				0.0							
1A				0.1							
3B				28.7							
1B (OR 1B-1)				0.0							
Summation of circumferential stresses $\sigma_\theta \Rightarrow$				0.0							
4C AND 3C				0.0							
2C AND 1C-1				0.0							
4A				0.2							
2A				1.6							
4B				0.0							
2B (OR 2B-1)				0.0							
Summation of longitudinal stresses $\sigma_x \Rightarrow$				0.0							
Shear stress τ due to V_L				0							
Shear stress τ due to V_C				0.71							
Shear stress τ due to M_T				0.00							
Summation of shear stress $\tau \Rightarrow$				0.7							
Membrane components of $\sigma_\theta \Rightarrow$				0.0							
Membrane components of $\sigma_x \Rightarrow$				0.0							
Membrane stress intensities $S_I \Rightarrow$				1.4							
Stress intensities $S_I \Rightarrow$				1.4							
σ_1				0.7							
σ_2				-0.7							
$[\sigma_1 - \sigma_2]$				1.4							
$[\sigma_1 + \sigma_2]$				0.0							

WRC-107

S_m	18.7	[kips]
S_v	20.7	[kips]
Allowable	28.05	[kips]
Allowable	56.1	[kips]

- Curves 1B and 2B apply to rigid attachments
- If $d(D/T)/2 > 2.0$, then use 2c-1 for 1c and 1c-1 for 2c

[Ref: Stearns Roger "Analysis of External Loadings on Pressure Vessels"]

OS187H Type 1 Trunnions WRC-107 Calculation

wrc107-case UT2

Table A.3.9.2-4
Local Shell Stress at Trunnion Locations—Computation Spreadsheet
for Case UT3

Applied Loads		Geometry		 COORDINATE SYSTEM												
V _L	0.0	[kips]	I [in]	3.690												
M _L	0.0	[in-kips]	R _m [in]	41.285												
V _C	71.0	[kips]	t ₀ [in]	8.575												
M _C	489.2	[in-kips]	β=0.875·t ₀ /R _m	0.182												
P	-142.0	[kips]	γ=R _m /T	11.188												
M _T	0	[in-kips]	λ=dD/(D _T) ^{1/2}	0.983												
Read curves for				multiplier	abs. stress values											
Figures	3C AND 4C	1.578	2.006	-0.9	-1.5	-1.9	-1.9	-1.9	-1.5	-1.5	-1.5	-1.5	-1.5	1		
	1C AND 2C-1	0.116	0.085	-62.6	-7.3	-5.3	5.3	-7.3	7.3	-7.3	7.3	-7.3	7.3	2		
	3A	0.324		0.4	0.1									3		
	1A	0.097		28.7	2.8									4		
	3B	1.161		0.0	0.0									5		
	1B (OR 1B-1)	0.048		0.0	0.0									6		
Summation of circumferential stresses σ _φ =>				-7.2	3.5	-7.2	3.5	-11.7	8.5	-5.8	3.2	7				
	4C AND 3C	2.006	1.578	-0.9	-1.5	-1.5	-1.5	-1.5	-1.9	-1.9	-1.9	-1.9	8			
	2C AND 1C-1	0.085	0.116	-62.6 <td>-5.3</td> <td>-7.3</td> <td>7.3</td> <td>-7.3</td> <td>7.3</td> <td>-5.3</td> <td>5.3</td> <td>-5.3</td> <td>9</td>	-5.3	-7.3	7.3	-7.3	7.3	-5.3	5.3	-5.3	9			
	4A	0.498		0.4 <td>0.2<td></td><td></td><td></td><td></td><td>-0.2</td><td>-0.2</td><td>0.2</td><td>10</td></td>	0.2 <td></td> <td></td> <td></td> <td></td> <td>-0.2</td> <td>-0.2</td> <td>0.2</td> <td>10</td>					-0.2	-0.2	0.2	10			
	2A	0.057		28.7	1.6 <td></td> <td></td> <td></td> <td></td> <td>-1.6</td> <td>1.6</td> <td>1.6</td> <td>11</td>					-1.6	1.6	1.6	11			
	4B	0.330		0.0 <td>0.0<td></td><td></td><td></td><td></td><td>0.0</td><td>0.0</td><td>0.0</td><td>12</td></td>	0.0 <td></td> <td></td> <td></td> <td></td> <td>0.0</td> <td>0.0</td> <td>0.0</td> <td>12</td>					0.0	0.0	0.0	12			
	2B (OR 2B-1)	0.076		0.0 <td>0.0<td></td><td></td><td></td><td></td><td>0.0</td><td>0.0</td><td>0.0</td><td>13</td></td>	0.0 <td></td> <td></td> <td></td> <td></td> <td>0.0</td> <td>0.0</td> <td>0.0</td> <td>13</td>					0.0	0.0	0.0	13			
Summation of longitudinal stresses σ _x =>				-8.7	5.8	-8.7	5.8	-9.0	4.9	-5.4	2.1	14				
Shear stress τ due to V _L				0				0.00	0.00	0.00	0.00	15				
Shear stress τ due to V _C				0.7142				-0.71	-0.71			16				
Shear stress τ due to M _T				0.00				0.00	0.00	0.00	0.00	17				
Summation of shear stress τ =>				0.7	0.7	-0.7	-0.7	0.0	0.0	0.0	0.0	18				
Membrane components of σ _φ =>				-1.9	-1.9	-1.9	-1.9	-1.9	-1.6	-1.6	-1.3	19				
Membrane components of σ _x =>				-1.5	-1.5	-1.5	-1.5	-2.1	-2.1	-1.7	-1.7	20				
Membrane stress intensities S _m =>				2.4	2.4	2.4	2.4	2.1	2.1	1.7	1.7	21				
Stress intensities S _I =>				9.0	6.0	9.0	6.0	11.7	8.5	5.8	3.2	22				
S _m				6.9	6.0	6.9	6.0	9.0	8.5	-5.4	3.2					
S _I				9.0	3.3	9.0	3.3	-11.7	4.9	-5.8	2.1					
Allowable				2.1	2.7	2.1	2.7	2.6	3.6	0.4	1.1					
Allowable				16.0	9.3	16.0	9.3	20.7	13.3	11.2	5.2					

WRC-107

1. Curves 1B and 2B apply to rigid attachments

2. If dD/(D_T)^{1/2} > 2.0, then use 2C-1 for 1c and 1c-1 for 2c

wrc107-case UT3

OS187H Type 1 Trunnions WRC-107 Calculation

Table A.3.9.2-5
Local Shell Stress at Trunnion Locations—Computation Spreadsheet
for Case UT4

Applied Loads		Geometry		COORDINATE SYSTEM											
V_L	0.0	[kips]	I	[in]											
M_L	0.0	[in-kips]	R_m	[in]											
V_C	142.0	[kips]	f_0	[in]											
M_C	978.4	[in-kips]	$\beta=0.875 \cdot f_0 / R_m$												
P	0.0	[kips]	$y=R_m/T$												
M_T	0	[in-kips]	$\lambda=d(D/D_T)^{1/2}$												
Figures		Read curves for		multiplier		abs. stress values									
3C AND 4C	1.578	2.006	0.0	0.0	0.0	0.0	0.0	A_u	A_l	B_u	B_l	C_u	C_l	D_u	D_l
1C AND 2C-1	0.116	0.085	0.0	0.0	0.0	0.0	0.0								
3A	0.324		0.9	0.3	0.0	0.0	0.0								
1A	0.097		57.5	5.6	0.0	0.0	0.0								
3B	1.161		0.0	0.0	0.0	0.0	0.0								
1B (OR 1B-1)	0.048		0.0	0.0	0.0	0.0	0.0								
Summation of circumferential stresses $\sigma_\theta \Rightarrow$															
4C AND 3C	2.006	1.578	0.0	0.0	0.0	0.0	0.0								
2C AND 1C-1	0.085	0.116	0.0	0.0	0.0	0.0	0.0								
4A	0.498		0.9	0.4	0.0	0.0	0.0								
2A	0.057		57.5	3.2	0.0	0.0	0.0								
4B	0.330		0.0	0.0	0.0	0.0	0.0								
2B (OR 2B-1)	0.076		0.0	0.0	0.0	0.0	0.0								
Summation of longitudinal stresses $\sigma_x \Rightarrow$															
Shear stress τ due to V_L															
Shear stress τ due to V_C															
Shear stress τ due to M_T															
Summation of shear stress $\tau \Rightarrow$															
Membrane components of $\sigma_\theta \Rightarrow$															
Membrane components of $\sigma_x \Rightarrow$															
Membrane stress intensities $S_I \Rightarrow$															
Stress intensities $S_I \Rightarrow$															
S_m	18.7	[kips]													
S_v	20.7	[kips]													
Allowable	28.05	[kips]													
Allowable	56.1	[kips]													

WRC-107

1. Curves 1B and 2B apply to rigid attachments

2. If $d(D/D_T)^{1/2} > 2.0$, then use 2c-1 for 1c and 1c-1 for 2c

3. See Design Manual of External Loadings on Vessels

1. Curves 1B and 2B apply to rigid attachments
2. If $d(D/D_T)^{1/2} > 2.0$, then use 2C-1 for 1c and 1c-1 for 2c
Ref: Stearns Roger "Analysis of External Loadings on Pressure Vessels"

OS187H Type 1 Trunnions WRC-107 Calculation

WRC107-case UT4

Table A.3.9.2-6
Local Shell Stress at Trunnion Locations—Computation Spreadsheet
for Case UT5

Applied Loads		Geometry										
V_L	0.0	[kips]	I	[in]								
M_L	0.0	[in-kips]	R_m	[in]								
V_C	106.5	[kips]	f_0	[in]								
M_C	733.8	[in-kips]	$\beta=0.875+f_0/R_m$	0.182								
P	-71.0	[kips]	$\gamma=R_m/T$	11.188								
M_T	0	[in-kips]	$\lambda=0.010/T^{1/2}$	0.983								
Figures	Read curves for	multiplier	abs. stress	values	1	2	3	4	5	6	7	8
3C AND 4C	1.578	2.006	-0.5	-0.9	-0.9	-0.9	-0.9	-0.9	-0.7	-0.7	-0.7	-0.7
1C AND 2C-1	0.116	0.085	-31.3	-3.6	-2.7	2.7	-2.7	2.7	-3.6	3.6	-3.6	3.6
3A	0.324		0.6	0.2								
1A	0.097		43.1	4.2						-4.2	4.2	-4.2
3B	1.161		0.0	0.0	0.0	0.0	0.0	0.0				
1B (OR 1B-1)	0.048		0.0	0.0	0.0	0.0	0.0	0.0				
Summation of circumferential stresses $\sigma_c \gg$					-3.6	1.7	-3.6	1.7	-8.8	6.9	0.0	-1.1
4C AND 3C	2.006	1.578	-0.5	-0.9	-0.7	-0.7	-0.7	-0.7	-0.9	-0.9	-0.9	-0.9
2C AND 1C-1	0.085	0.116	-31.3	-3.6	-3.6	3.6	-3.6	3.6	-2.7	2.7	-2.7	2.7
4A	0.498		0.6	0.3								
2A	0.057		43.1	2.4					-0.3	-0.3	0.3	0.3
4B	0.330		0.0	0.0	0.0	0.0	0.0	0.0	-2.4	2.4	2.4	-2.4
2B (OR 2B-1)	0.076		0.0	0.0	0.0	0.0	0.0	0.0				
Summation of longitudinal stresses $\sigma_L \gg$					-4.4	2.9	-4.4	2.9	-6.4	3.9	-0.8	-0.4
Shear stress τ due to V_L					0							
Shear stress τ due to V_C					1.0714							
Shear stress τ due to M_T					0.00							
Summation of shear stress $\tau \gg$					1.1	1.1	-1.1	-1.1	0.0	0.0	0.0	0.0
Membrane components of $\sigma_c \gg$					-0.9	-0.9	-0.9	-0.9	-0.9	-0.9	-0.5	-0.5
Membrane components of $\sigma_L \gg$					-0.7	-0.7	-0.7	-0.7	-1.3	-1.3	-0.6	-0.6
Membrane stress intensities \gg					2.2	2.2	2.2	2.2	1.3	1.3	0.6	0.6
Stress intensities $SI \gg$					5.1	3.5	5.1	3.5	8.8	6.9	0.9	1.1
G_1					-2.9	3.5	-2.9	3.5	-6.4	6.9	0.0	-0.4
G_2					-5.1	1.1	-5.1	1.1	-8.8	3.9	-0.8	-1.1
G_3					2.3	2.4	2.3	2.4	2.4	3.0	0.7	0.7
G_4					8.0	4.5	8.0	4.5	15.1	10.7	0.8	1.4

WRC-107

1. Curves 1B and 2B apply to rigid attachments

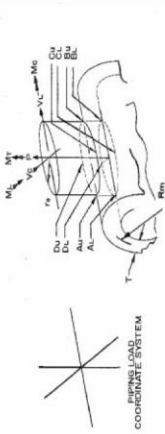
2. If $d(D/D_T)^{1/2} > 2.0$, then use 2c-1 for 1c and 1c-1 for 2c

3. For Stress-Block Mechanics of External Loading on Ducts

Table A.3.9.2-7
Local Shell Stress at Trunnion Locations—Computation Spreadsheet
for Case UT6

Applied Loads		Geometry																				
Figures		Read curves for		multiplier		abs. stress		values														

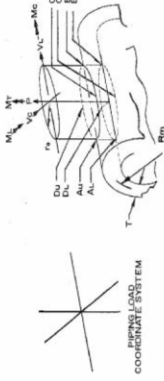
Table A.3.9.2-8
Local Shell Stress at Trunnion Locations—Computation Spreadsheet
for Case UT7

Applied Loads		Geometry									
				1	2	3	4	5	6	7	8
				A _u	A _t	B _u	B _t	C _u	C _t	D _u	D _t
V _L	0.0	[in]	2.380	0.0	0.0	0.0	0.0	0.0	0.0	0.0	0.0
M _L	0.0	[in-kips]	40.630	0.0	0.0	0.0	0.0	0.0	0.0	0.0	0.0
V _C	71.0	[kips]	15.000	0.0	0.0	0.0	0.0	0.0	0.0	0.0	0.0
M _C	535.7	[in-kips]	0.323	0.0	0.0	0.0	0.0	0.0	0.0	0.0	0.0
P	0.0	[kips]	17.071	0.0	0.0	0.0	0.0	0.0	0.0	0.0	0.0
M _T	0	[in-kips]	2.157	0.0	0.0	0.0	0.0	0.0	0.0	0.0	0.0
Figures				abs. stress values							
Read curves for				multiplier							
3C AND 4C	1.718	2.346		0.0	0.0	0.0	0.0	0.0	0.0	0.0	0.0
1C AND 2C-1	0.056	0.032		0.0	0.0	0.0	0.0	0.0	0.0	0.0	0.0
3A	0.734			0.4	0.3	0.3	0.3	0.3	0.3	0.3	0.3
1A	0.077			43.2	3.3	3.3	3.3	3.3	3.3	3.3	3.3
3B	1.759			0.0	0.0	0.0	0.0	0.0	0.0	0.0	0.0
1B (OR 1B-1)	0.024			0.0	0.0	0.0	0.0	0.0	0.0	0.0	0.0
Summation of circumferential stresses $\sigma_c \Rightarrow$				0.0	0.0	0.0	0.0	-3.6	3.0	3.6	-3.0
4C AND 3C	2.346	1.718		0.0	0.0	0.0	0.0	0.0	0.0	0.0	0.0
2C AND 1C-1	0.032	0.057		0.0	0.0	0.0	0.0	0.0	0.0	0.0	0.0
4A	1.459			0.4	0.6	0.6	0.6	0.6	0.6	0.6	0.6
2A	0.038			43.2	1.7	1.7	1.7	1.7	1.7	1.7	1.7
4B	0.709			0.0	0.0	0.0	0.0	0.0	0.0	0.0	0.0
2B (OR 2B-1)	0.042			0.0	0.0	0.0	0.0	0.0	0.0	0.0	0.0
Summation of longitudinal stresses $\sigma_L \Rightarrow$				0.0	0.0	0.0	0.0	-2.3	1.0	2.3	-1.0
WRC-107				0.63	0.63	-0.63	-0.63	0.00	0.00	0.00	0.00
Shear stress τ due to V _L				0.00	0.00	0.00	0.00	0.00	0.00	0.00	0.00
Shear stress τ due to V _C				0.00	0.00	0.00	0.00	0.00	0.00	0.00	0.00
Shear stress τ due to M _T				0.00	0.00	0.00	0.00	0.00	0.00	0.00	0.00
Summation of shear stress $\tau \Rightarrow$				0.6	0.6	-0.6	-0.6	0.0	0.0	0.0	0.0
Membrane components of $\sigma_c \Rightarrow$				0.0	0.0	0.0	0.0	-0.3	-0.3	0.3	0.3
Membrane components of $\sigma_L \Rightarrow$				0.0	0.0	0.0	0.0	-0.6	-0.6	0.6	0.6
Membrane stress intensities $S_I \Rightarrow$				1.3	1.3	1.3	1.3	0.6	0.6	0.6	0.6
Stress intensities $S_I \Rightarrow$				1.3	1.3	1.3	1.3	3.6	3.0	3.6	3.0
S _m				0.6	0.6	0.6	0.6	-2.3	3.0	3.6	-1.0
S _t				-0.6	-0.6	-0.6	-0.6	-3.6	1.0	2.3	-3.0
Allowable				1.3	1.3	1.3	1.3	1.4	2.0	1.4	2.0
Allowable				0.0	0.0	0.0	0.0	5.9	4.0	5.9	4.0

WRC-107-case UT7

OS187H Type 1 Trunnions WRC-107 Calculation

Table A.3.9.2-9
Local Shell Stress at Trunnion Locations—Computation Spreadsheet
for Case UT8

Applied Loads		Geometry									
				1	2	3	4	5	6	7	8
				A _U	A _L	B _U	B _L	C _U	C _L	D _U	D _L
V _L	0.0	[kips]	I [in]	abs. stress values							
M _L	0.0	[in-kips]	R _m [in]	-3.4	-3.4	-3.4	-3.4	-2.5	-2.5	-2.5	-2.5
V _C	71.0	[kips]	I ₀ [in]	-4.8	4.8	-4.8	4.8	-8.5	8.5	-8.5	8.5
M _C	535.7	[in-kips]	$\beta=0.875 \cdot d_0/R_m$	0.3	0.3	0.3	0.3	-0.3	-0.3	0.3	0.3
P	-142.0	[kips]	$\gamma=R_m/T$	3.3	3.3	3.3	3.3	-3.3	-3.3	3.3	3.3
M _T	0	[in-kips]	$\lambda=d/D \cdot \pi^{1/2}$	0.0	0.0	0.0	0.0	0.0	0.0	0.0	0.0
Read curves for				multiplier							
3C AND 4C	1.718	2.346	-1.5	-2.5	-2.5	-2.5	-2.5	-3.4	-3.4	-3.4	-3.4
1C AND 2C-1	0.056	0.032	-150.4	-8.5	-8.5	-8.5	-8.5	-8.5	-8.5	-8.5	-8.5
3A	0.734	0.4	0.4	0.3	0.3	0.3	0.3	-0.3	-0.3	0.3	0.3
1A	0.077	43.2	43.2	3.3	3.3	3.3	3.3	-3.3	-3.3	3.3	3.3
3B	1.759	0.0	0.0	0.0	0.0	0.0	0.0	0.0	0.0	0.0	0.0
1B (OR 1B-1)	0.024	0.0	0.0	0.0	0.0	0.0	0.0	0.0	0.0	0.0	0.0
Summation of circumferential stresses $\sigma_\theta \Rightarrow$				-8.2	1.3	-8.2	1.3	-14.5	9.0	-7.4	2.9
4C AND 3C	2.346	1.718	-1.5	-3.4	-3.4	-3.4	-3.4	-2.5	-2.5	-2.5	-2.5
2C AND 1C-1	0.032	0.057	-150.4	-8.5	-8.5	-8.5	-8.5	-8.5	-8.5	-8.5	-8.5
4A	1.459	0.4	0.4	0.6	0.6	0.6	0.6	-0.6	-0.6	0.6	0.6
2A	0.038	43.2	43.2	1.7	1.7	1.7	1.7	-1.7	-1.7	1.7	1.7
4B	0.709	0.0	0.0	0.0	0.0	0.0	0.0	0.0	0.0	0.0	0.0
2B (OR 2B-1)	0.042	0.0	0.0	0.0	0.0	0.0	0.0	0.0	0.0	0.0	0.0
Summation of longitudinal stresses $\sigma_x \Rightarrow$				-11.0	6.0	-11.0	6.0	-10.5	2.4	-6.0	0.3
Shear stress τ due to V _L				0	0	0	0	0	0	0	0
Shear stress τ due to V _C				0.6331	0.63	-0.63	-0.63	0.00	0.00	0.00	0.00
Shear stress τ due to M _T				0.00	0.00	0.00	0.00	0.00	0.00	0.00	0.00
Summation of shear stress $\tau \Rightarrow$				0.6	0.6	-0.6	-0.6	0.0	0.0	0.0	0.0
Membrane components of $\sigma_\theta \Rightarrow$				-3.4	-3.4	-3.4	-3.4	-2.8	-2.8	-2.2	-2.2
Membrane components of $\sigma_x \Rightarrow$				-2.5	-2.5	-2.5	-2.5	-4.1	-4.1	-2.8	-2.8
Membrane stress intensities $S_I \Rightarrow$				3.8	3.8	3.8	3.8	4.1	4.1	2.8	2.8
Stress intensities $S_I \Rightarrow$				11.2	6.1	11.2	6.1	14.6	9.0	7.4	2.9
S_1				-8.1	6.1	-8.1	6.1	-10.5	9.0	-6.0	2.9
S_2				1.3	1.3	-11.2	1.3	-14.6	2.4	-7.4	0.3
$ S_1 - S_2 $				3.1	4.8	3.1	4.8	4.1	6.6	1.4	2.6
$ S_1 + S_2 $				19.3	7.3	19.3	7.3	25.1	11.3	13.3	3.3

1. Curves 1B and 2B apply to rigid attachments
 2. If $d(D/4T)^{1/2} > 2.0$, then use 2c-1 for 1c and 1c-1 for 2c
 Ref: Stearns Roger "Analysis of External Loadings on Pressure Vessels"

OS187H Type 1 Trunnions WRC-107 Calculation

WRC107-case UT8

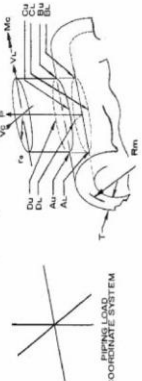
Table A.3.9.2-10
Local Shell Stress at Trunnion Locations—Computation Spreadsheet
for Case UT9

Applied Loads		Geometry									
				1	2	3	4	5	6	7	8
				A _U	A _L	B _U	B _L	C _U	C _L	D _U	D _L
V _L	0.0	[kips]	2.380	0.0	0.0	0.0	0.0	0.0	0.0	0.0	0.0
M _L	0.0	[in-kips]	40.630	0.0	0.0	0.0	0.0	0.0	0.0	0.0	0.0
V _C	142.0	[kips]	15.000	0.0	0.0	0.0	0.0	0.0	0.0	0.0	0.0
M _C	1071.4	[in-kips]	0.323	0.0	0.0	0.0	0.0	0.0	0.0	0.0	0.0
P	0.0	[kips]	17.071	0.0	0.0	0.0	0.0	0.0	0.0	0.0	0.0
M _T	0	[in-kips]	2.157	0.0	0.0	0.0	0.0	0.0	0.0	0.0	0.0
Figures				abs. stress values							
Read curves for				multiplier							
3C AND 4C				0.0							
1C AND 2C-1				0.0							
3A				0.8							
1A				86.5							
3B				0.0							
1B (OR 1B-1)				0.0							
Summation of circumferential stresses σ_{θ}				=>							
4C AND 3C				0.0							
2C AND 1C-1				0.0							
4A				0.8							
2A				86.5							
4B				0.0							
2B (OR 2B-1)				0.0							
Summation of longitudinal stresses σ_z				=>							
Shear stress τ due to V _L				0							
Shear stress τ due to V _C				1.27							
Shear stress τ due to M _T				0.00							
Summation of shear stress τ				=>							
Membrane components of σ_{θ}				=>							
Membrane components of σ_z				=>							
Membrane stress intensities S_I				=>							
Stress intensities S_I				=>							
1. Curves 1B and 2B apply to rigid attachments											
2. If $d(D/D_T)^{1/2} > 2.0$, then use 2C-1 for 1C and 1C-1 for 2C											
Ref: Stearns Roger "Analysis of External Loadings on Pressure Vessels"											

WRC107-case UT9

OS187H Type 1 Trunnions WRC-107 Calculation

Table A.3.9.2-12
Local Shell Stress at Trunnion Locations—Computation Spreadsheet
for Case LT1

Applied Loads			Geometry																																																				
V_L	125.0 [kips]	I [in]	1,500	A_U	A_L	B_U	B_L	C_U	C_L	D_U	D_L																																												
M_L	982.5 [in-kips]	R_m [in]	40,190	0.0	0.0	0.0	0.0	0.0	0.0	0.0	0.0	1																																											
V_C	54.0 [kips]	r_0 [in]	7,315	0.0	0.0	0.0	0.0	0.0	0.0	0.0	0.0	2																																											
M_C	424.4 [in-kips]	$\beta=0.875 \cdot r_0 / R_m$	0.159	0.0	0.0	0.0	0.0	0.0	0.0	0.0	0.0	3																																											
P	0.0 [kips]	$\gamma=R_m/T$	26,793	0.0	0.0	0.0	0.0	-1.1	-1.1	1.1	1.1	4																																											
M_T	0 [in-kips]	$\lambda=d(D/D_T)^{1/2}$	1,332	-7.6	-7.6	7.6	7.6	-16.1	16.1	16.1	-16.1	5																																											
				-16.1	16.1	16.1	-16.1					6																																											
Figures				-23.6	8.5	23.6	-8.5	-17.2	15.0	17.2	-15.0	7																																											
3C AND 4C			0.0	0.0	0.0	0.0	0.0	0.0	0.0	0.0	0.0	8																																											
1C AND 2C-1			0.0	0.0	0.0	0.0	0.0	0.0	0.0	0.0	0.0	9																																											
3A			1.1	1.1	1.1	1.1	1.1	-1.1	-1.1	1.1	1.1	10																																											
1A			176.8	16.1	16.1	16.1	16.1	-16.1	16.1	16.1	-16.1	11																																											
3B			2.5	7.6	7.6	7.6	7.6	-16.1	16.1	16.1	-16.1	12																																											
1B (OR 1B-1)			409.3	16.1	16.1	16.1	16.1	-16.1	16.1	16.1	-16.1	13																																											
				Summation of circumferential stresses $\sigma_\phi \Rightarrow$																																																			
4C AND 3C			4.336	3.154	0.0	0.0	0.0	0.0	0.0	0.0	0.0	14																																											
2C AND 1C-1			0.065	0.102	0.0	0.0	0.0	0.0	0.0	0.0	0.0	15																																											
4A			1.506	1.1	1.1	1.1	1.1	-1.1	-1.1	1.1	1.1	16																																											
2A			0.047	176.8	8.4	8.4	8.4	-8.4	8.4	8.4	-8.4	17																																											
4B			0.932	2.5	2.4	2.4	2.4	-2.4	2.4	2.4	-2.4	18																																											
2B (OR 2B-1)			0.064	409.3	26.1	26.1	26.1	-26.1	26.1	26.1	-26.1	19																																											
				Summation of longitudinal stresses $\sigma_x \Rightarrow$																																																			
WRC-107			Shear stress τ due to V_L 3,6262																																																				
			Shear stress τ due to V_C 1,5665																																																				
			Shear stress τ due to M_T 0.00																																																				
			Summation of shear stress $\tau \Rightarrow$																																																				
			Membrane components of $\sigma_\phi \Rightarrow$																																																				
			Membrane components of $\sigma_x \Rightarrow$																																																				
			Membrane stress intensities $S_I \Rightarrow$																																																				
			Stress intensities $S_I \Rightarrow$																																																				
S_m	18.7 [kips]																																																						
S_v	20.7 [kips]																																																						
Allowable	28.05 [kips]																																																						
Allowable	56.1 [kips]																																																						
			σ_1																																																				
			σ_2																																																				
			$[\sigma_1 - \sigma_2]$																																																				
			$[\sigma_1 + \sigma_2]$																																																				

1. Curves 1B and 2B apply to rigid attachments
2. If $d(D/D_T)^{1/2} > 2.0$, then use 2c-1 for 1c and 1c-1 for 2c
Ref: Stearns Roger "Analysis of External Loadings on Pressure Vessels"

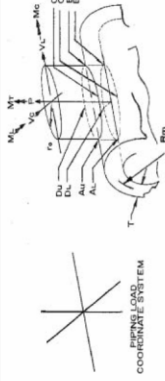
OS187H Type 1 Trunnions WRC-107 Calculation

WRC 107-case LT1

WRC-107-case LT1

OS187H Type 1 Trunnions WRC-107 Calculation

Table A.3.9.2-14
Local Shell Stress at Trunnion Locations—Computation Spreadsheet
for Case LT3

Applied Loads		Geometry									
				1	2	3	4	5	6	7	8
V_L	0.0	[kips]	I [in]	A_U	A_L	B_U	B_L	C_U	C_L	D_U	D_L
M_L	0.0	[in-kips]	R_m [in]	0.0	0.0	0.0	0.0	0.0	0.0	0.0	0.0
V_C	108.0	[kips]	r_0 [in]	0.0	0.0	0.0	0.0	0.0	0.0	0.0	0.0
M_C	848.9	[in-kips]	$\beta=0.875 \cdot d_0 R_m$	0.0	0.0	0.0	0.0	0.0	0.0	0.0	0.0
P	0.0	[kips]	$y=R_m/T$	0.0	0.0	0.0	0.0	0.0	0.0	0.0	0.0
M_T	0	[in-kips]	$\lambda=d/D \cdot \pi^{1/2}$	0.0	0.0	0.0	0.0	0.0	0.0	0.0	0.0
Read curves for				abs. stress values							
Figures				multiplier							
3C AND 4C				3.154	4.336	0.099	0.065	0.0	0.0	0.0	0.0
1C AND 2C-1				0.0	0.0	0.0	0.0	0.0	0.0	0.0	0.0
3A				0.972	0.065	0.0	0.0	0.0	0.0	0.0	0.0
1A				0.091	0.065	2.2	353.7	2.1	-2.1	2.1	2.1
3B				2.971	0.0	0.0	0.0	32.2	32.2	32.2	-32.2
1B (OR 1B-1)				0.039	0.0	0.0	0.0	0.0	0.0	0.0	0.0
4C AND 3C				4.336	3.154	0.0	0.0	-34.4	30.1	34.4	-30.1
2C AND 1C-1				0.065	0.102	0.0	0.0	0.0	0.0	0.0	0.0
4A				1.506	0.065	0.0	0.0	0.0	0.0	0.0	0.0
2A				0.047	0.065	2.2	353.7	-3.3	-3.3	3.3	3.3
4B				0.932	0.0	0.0	0.0	-16.7	16.7	16.7	-16.7
2B (OR 2B-1)				0.064	0.0	0.0	0.0	0.0	0.0	0.0	0.0
WRC-107				Summation of longitudinal stresses σ_x							
				Shear stress τ due to V_L							
				Shear stress τ due to V_C							
				Shear stress τ due to M_T							
				Summation of shear stress τ							
				Membrane components of σ_θ							
				Membrane stress intensities S_I							
				Stress intensities S_I							
				σ_1							
				σ_2							
				$ \sigma_1 - \sigma_2 $							
				$ \sigma_1 + \sigma_2 $							
				1. Curves 1B and 2B apply to rigid attachments							
				2. If $d/D \cdot \pi^{1/2} > 2.0$, then use 2C-1 for 1C and 1C-1 for 2C							
				Ref: Stearns Roger "Analysis of External Loadings on Pressure Vessels"							

WRC107-case LT3

OS187H Type 1 Trunnions WRC-107 Calculation

Table A.3.9.2-15
Local Shell Stress at Trunnion Locations—Computation Spreadsheet
for Case LT4

Applied Loads		Geometry									
V_L	62.5 [kips]	I	[in]	multiplier		abs. stress		values			
M_L	491.3 [in-kips]	R_m	[in]								
V_C	81.0 [kips]	t_0	[in]								
M_C	636.7 [in-kips]	$\beta=0.875 \cdot d_0/R_m$									
P	-54.0 [kips]	$\gamma=R_m/T$									
M_T	0 [in-kips]	$\lambda=d/D \cdot (\pi)^{1/2}$									
Figures				1	2	3	4	5	6	7	8
Read curves for				A_U	A_L	B_U	B_L	C_U	C_L	D_U	D_L
3C AND 4C				3.154	4.3	-0.9	-2.8	-3.9	-3.9	-2.8	-2.8
1C AND 2C-1				0.099	0.065	-144.0	-9.4	-9.4	-14.2	-14.2	-14.2
3A				0.972		1.6					
1A				0.091		265.2					
3B				2.971		1.3					
1B (OR 1B-1)				0.039		204.7					
Summation of circumferential stresses $\sigma_\theta \Rightarrow$				-3.8	-3.8	3.8	3.8				
4C AND 3C				4.336	3.2	-0.9	-2.8	-2.8	-3.9	-3.9	-3.9
2C AND 1C-1				0.065	0.102	-144.0	-9.4	-9.4	-14.7	-14.7	-14.7
4A				1.506		1.6					
2A				0.047		265.2					
4B				0.932		1.3					
2B (OR 2B-1)				0.064		204.7					
Summation of longitudinal stresses $\sigma_x \Rightarrow$				-13.0	-13.0	13.0	13.0				
WRC-107				-31.8	23.7	-3.3	0.0	-28.3	15.6	1.7	-4.5
Shear stress τ due to V_L				2.35	2.35	-2.35	-2.35				
Shear stress τ due to V_C				0.00	0.00	0.00	0.00				
Shear stress τ due to M_T				2.3	2.3	-2.3	-2.3	1.8	1.8	-1.8	-1.8
Summation of shear stress $\tau \Rightarrow$				-7.7	-7.7	-0.1	-0.1	-4.4	-4.4	-1.2	-1.2
Membrane components of $\sigma_\theta \Rightarrow$				-4.0	-4.0	-1.6	-1.6	-6.4	-6.4	-1.4	-1.4
Membrane components of $\sigma_x \Rightarrow$				8.8	8.8	4.9	4.9	7.5	7.5	3.6	3.6
Membrane stress intensities $S_I \Rightarrow$				32.5	24.1	5.0	4.9	43.0	34.1	9.2	11.7
Allowable				28.05	28.05	28.05	28.05	28.05	28.05	28.05	28.05
Allowable				56.1	56.1	56.1	56.1	56.1	56.1	56.1	56.1
1. Curves 1B and 2B apply to rigid attachments											
2. If $d/D \cdot (\pi)^{1/2} > 2.0$, then use 2c-1 for 1c and 1c-1 for 2c											
Ref: Stearns Roger "Analysis of External Loadings on Pressure Vessels"											

wrc107-case LT4

OS187H Type 1 Trunnions WRC-107 Calculation

Table A.3.9.2-16
Local Shell Stress at Trunnion Locations—Summary of Results

Case ID.	Location	Load Combination	Maximum Stress		Allowable [ksi]	Reference Table
			Type	Value [ksi]		
UT1	Upper trunnion pad	Critical lifting 6g axial	P_L	17.4	28.1	Table A.3.9.2-2
			P_L+P_b+Q	42.7	56.1	Table A.3.9.2-2
UT6	Upper trunnion shell	Critical lifting 6g axial	P_L	15.4	28.1	Table A.3.9.2-7
			P_L+P_b+Q	37.9	56.1	Table A.3.9.2-7
UT2	Upper trunnion pad	Transfer load DW+1g axial	P_L	1.4	28.1	Table A.3.9.2-3
			P_L+P_b+Q	2.9	56.1	Table A.3.9.2-3
UT7	Upper trunnion shell	Transfer load DW+1g axial	P_L	1.3	28.1	Table A.3.9.2-8
			P_L+P_b+Q	3.6	56.1	Table A.3.9.2-8
UT3	Upper trunnion pad	Transfer load DW+1g transverse	P_L	2.4	28.1	Table A.3.9.2-4
			P_L+P_b+Q	11.7	56.1	Table A.3.9.2-4
UT8	Upper trunnion shell	Transfer load DW+1g transverse	P_L	4.1	28.1	Table A.3.9.2-9
			P_L+P_b+Q	14.6	56.1	Table A.3.9.2-9
UT4	Upper trunnion pad	Transfer load DW+1g vertical	P_L	2.9	28.1	Table A.3.9.2-5
			P_L+P_b+Q	5.8	56.1	Table A.3.9.2-5
UT9	Upper trunnion shell	Transfer load DW+1g vertical	P_L	2.5	28.1	Table A.3.9.2-10
			P_L+P_b+Q	7.3	56.1	Table A.3.9.2-10
UT5	Upper trunnion pad	Transfer load $1/2g A+1/2gT+1/2gV +DW$	P_L	2.2	28.1	Table A.3.9.2-6
			P_L+P_b+Q	8.8	56.1	Table A.3.9.2-6
UT10	Upper trunnion shell	Transfer load $1/2g A+1/2gT+1/2g V+DW$	P_L	2.6	28.1	Table A.3.9.2-11
			P_L+P_b+Q	10.9	56.1	Table A.3.9.2-11
LT1	Lower trunnion shell	Transfer load DW+1g axial	P_L	8.0	28.1	Table A.3.9.2-12
			P_L+P_b+Q	28.9	56.1	Table A.3.9.2-12
LT2	Lower trunnion shell	Transfer load DW+1g transverse	P_L	9.4	28.1	Table A.3.9.2-13
			P_L+P_b+Q	51.2	56.1	Table A.3.9.2-13
LT3	Lower trunnion shell	Transfer load DW+1g vertical	P_L	6.3	28.1	Table A.3.9.2-14
			P_L+P_b+Q	34.4	56.1	Table A.3.9.2-14
LT4	Lower trunnion shell	Transfer load $1/2g A+1/2gT+1/2gV +DW$	P_L	8.8	28.1	Table A.3.9.2-15
			P_L+P_b+Q	43.0	56.1	Table A.3.9.2-15

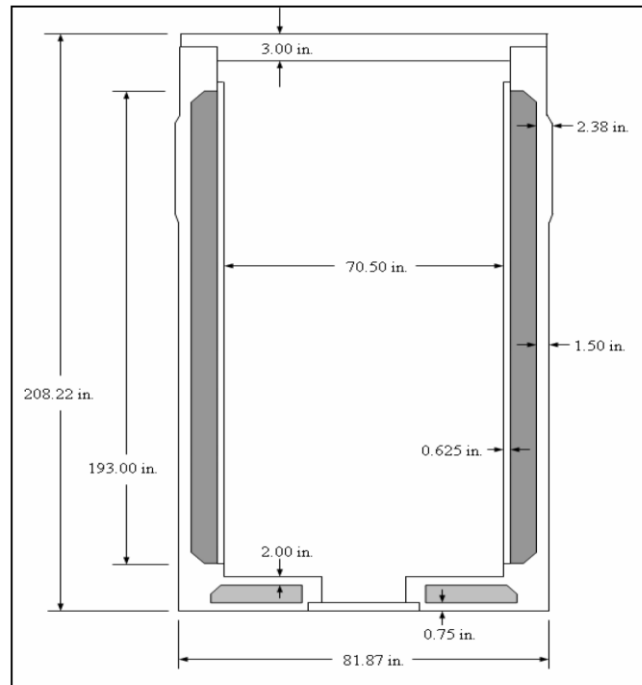
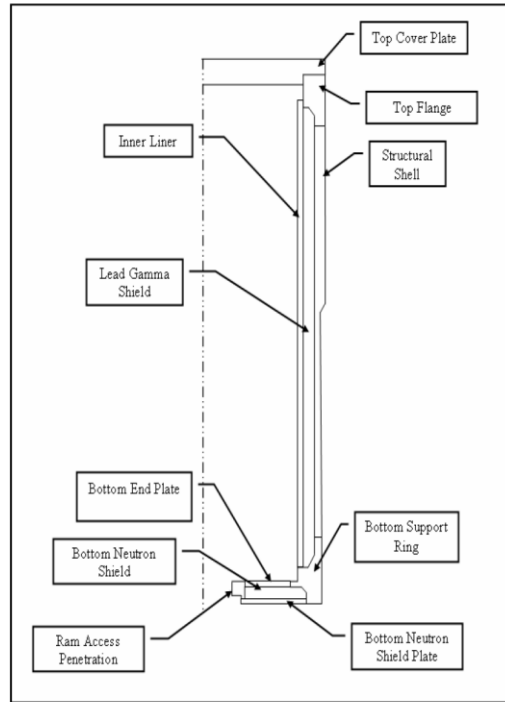


Figure A.3.9.2-1
Transfer Cask Key Components and Dimensions
 (Drawing Not to Scale)

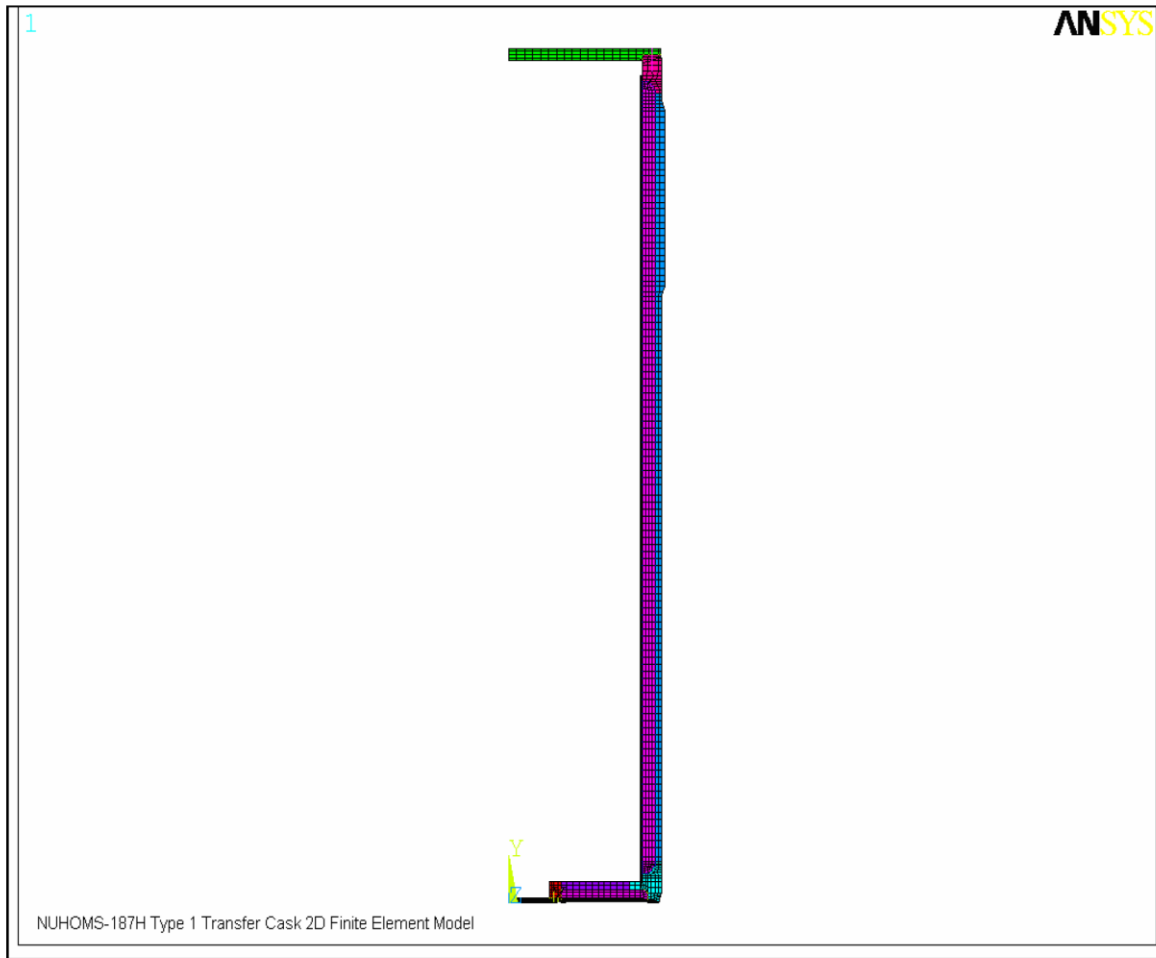


Figure A.3.9.2-2
2-Dimensional Finite Element Model, Element Plot

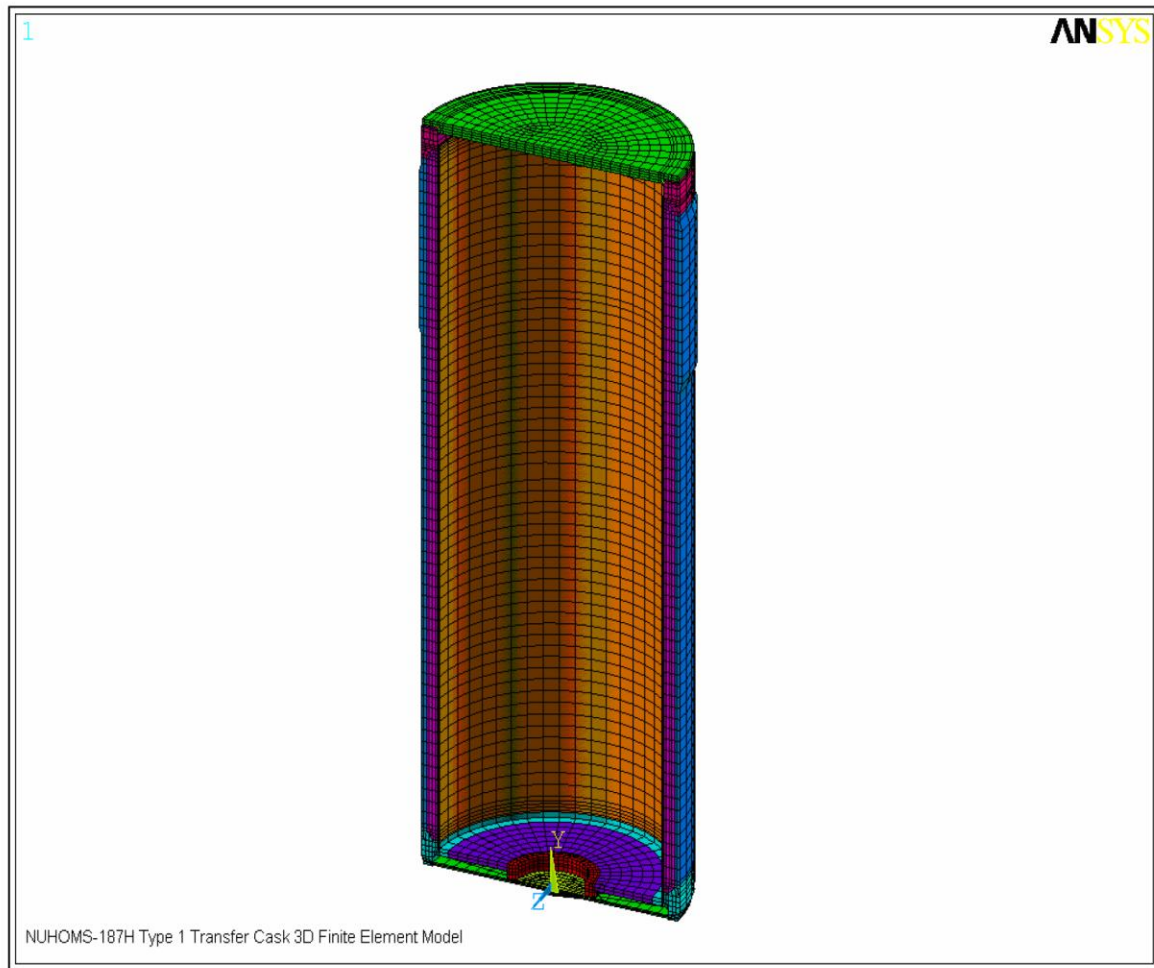


Figure A.3.9.2-3
3-Dimensional Finite Element Model, Element Plot

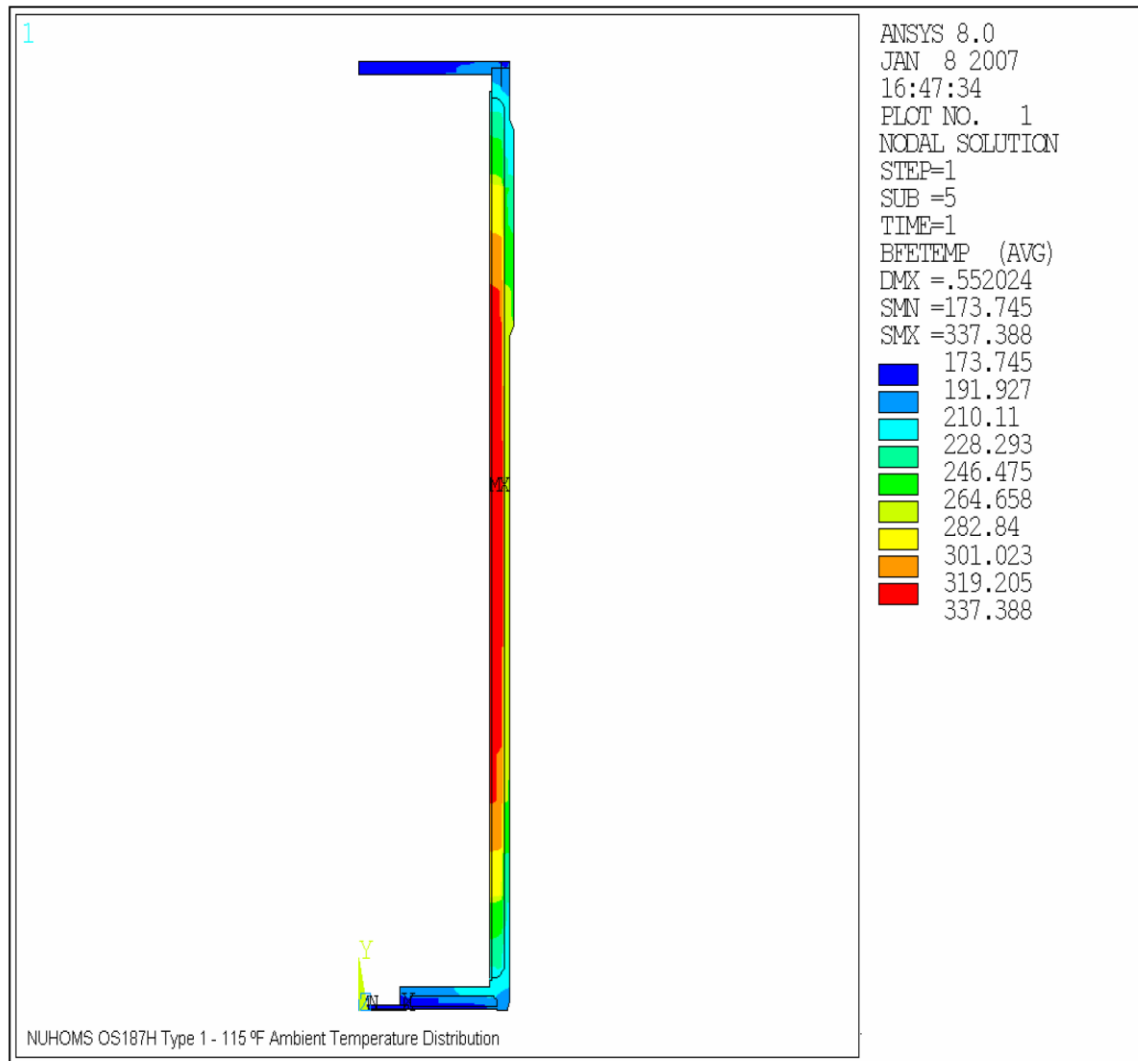


Figure A.3.9.2-4
115 °F Ambient Temperature Distribution

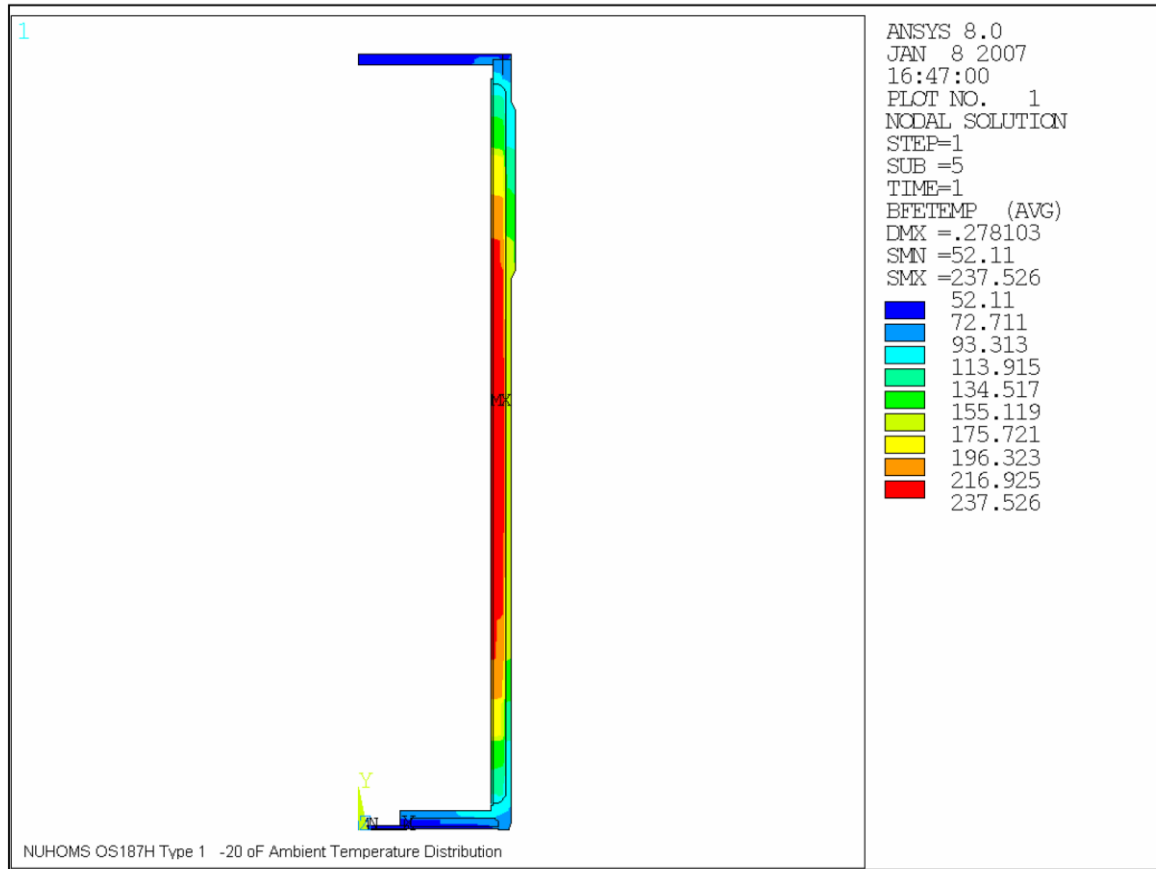


Figure A.3.9.2-5
-20 °F Ambient Temperature Distribution

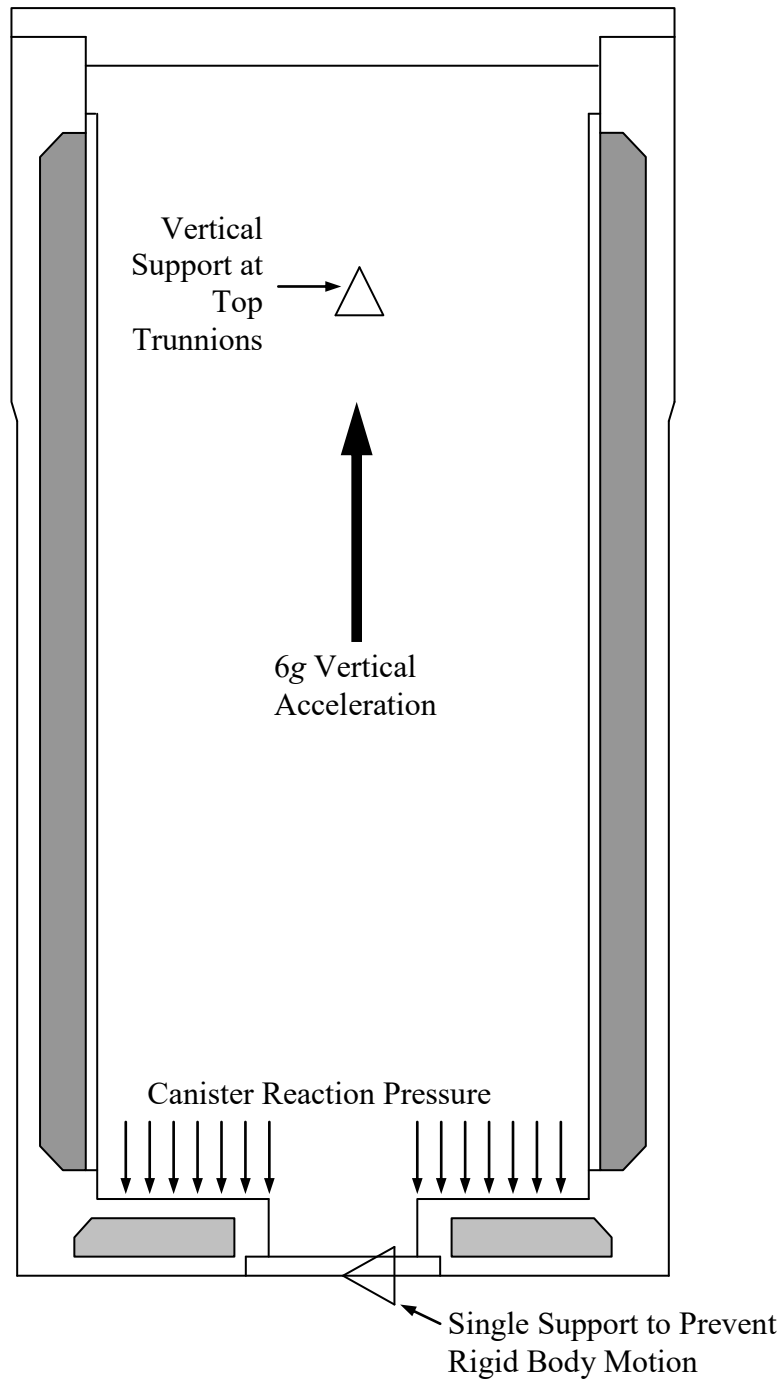


Figure A.3.9.2-6
6 g Lifting Boundary Conditions (3D Half Model)

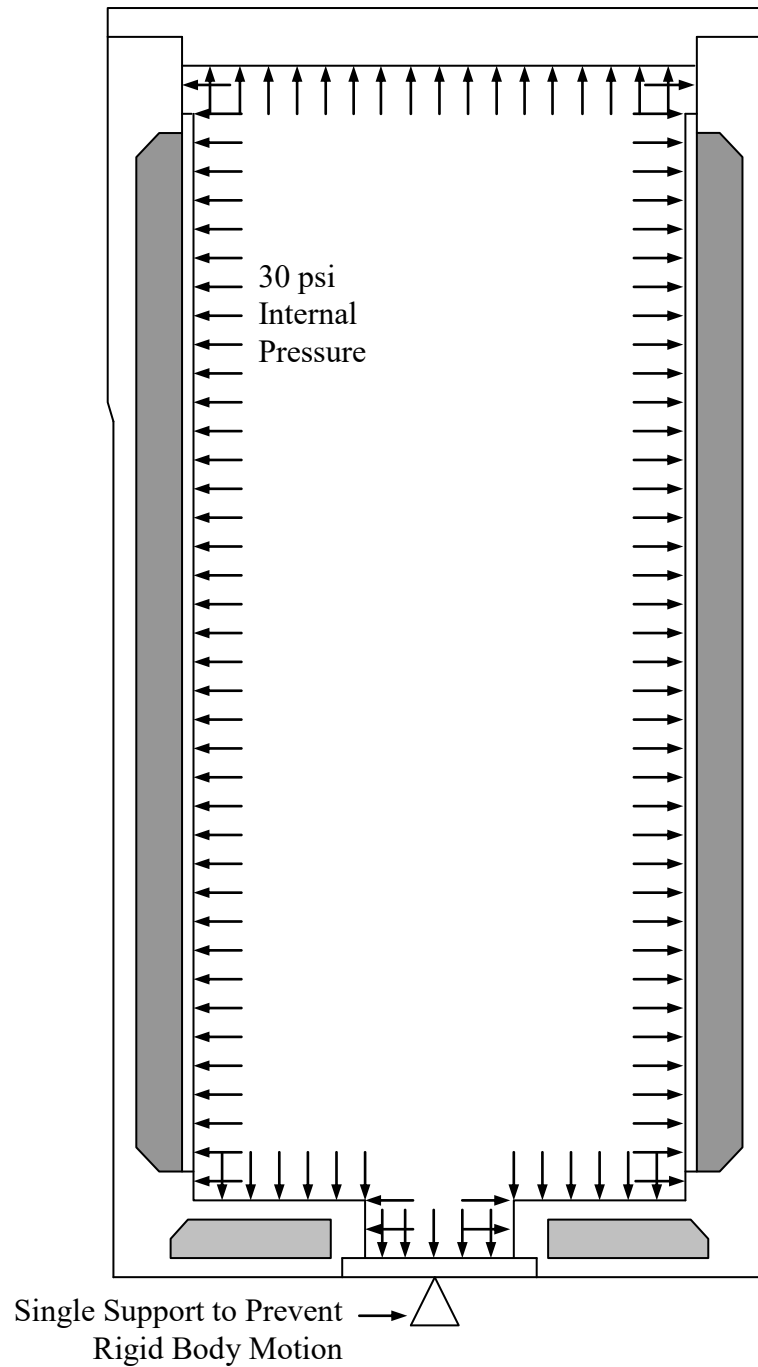


Figure A.3.9.2-7
30 psi Internal Pressure Boundary Conditions (2D Model)

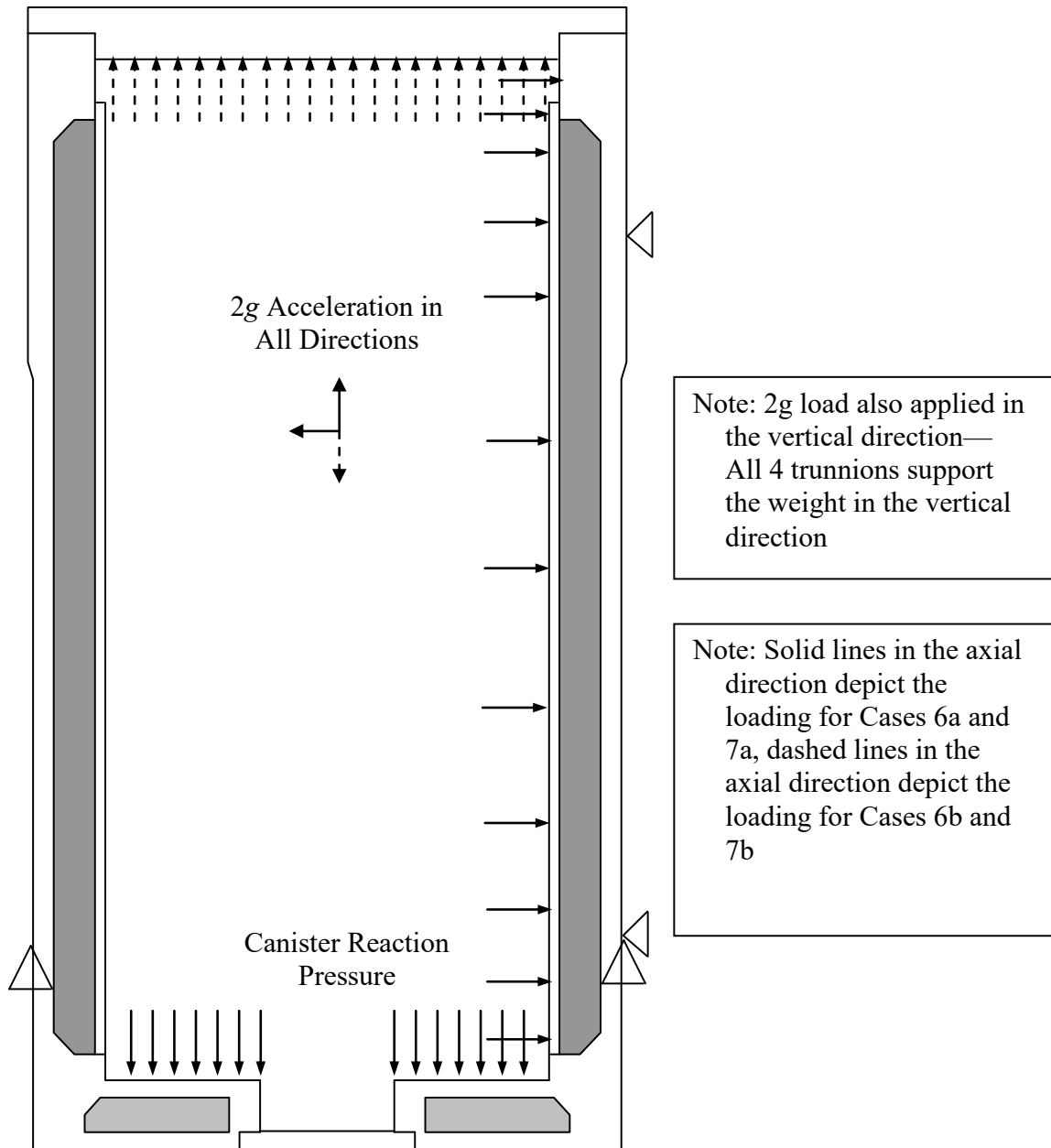


Figure A.3.9.2-8
Transfer Loads Boundary Conditions (3D Full Model)

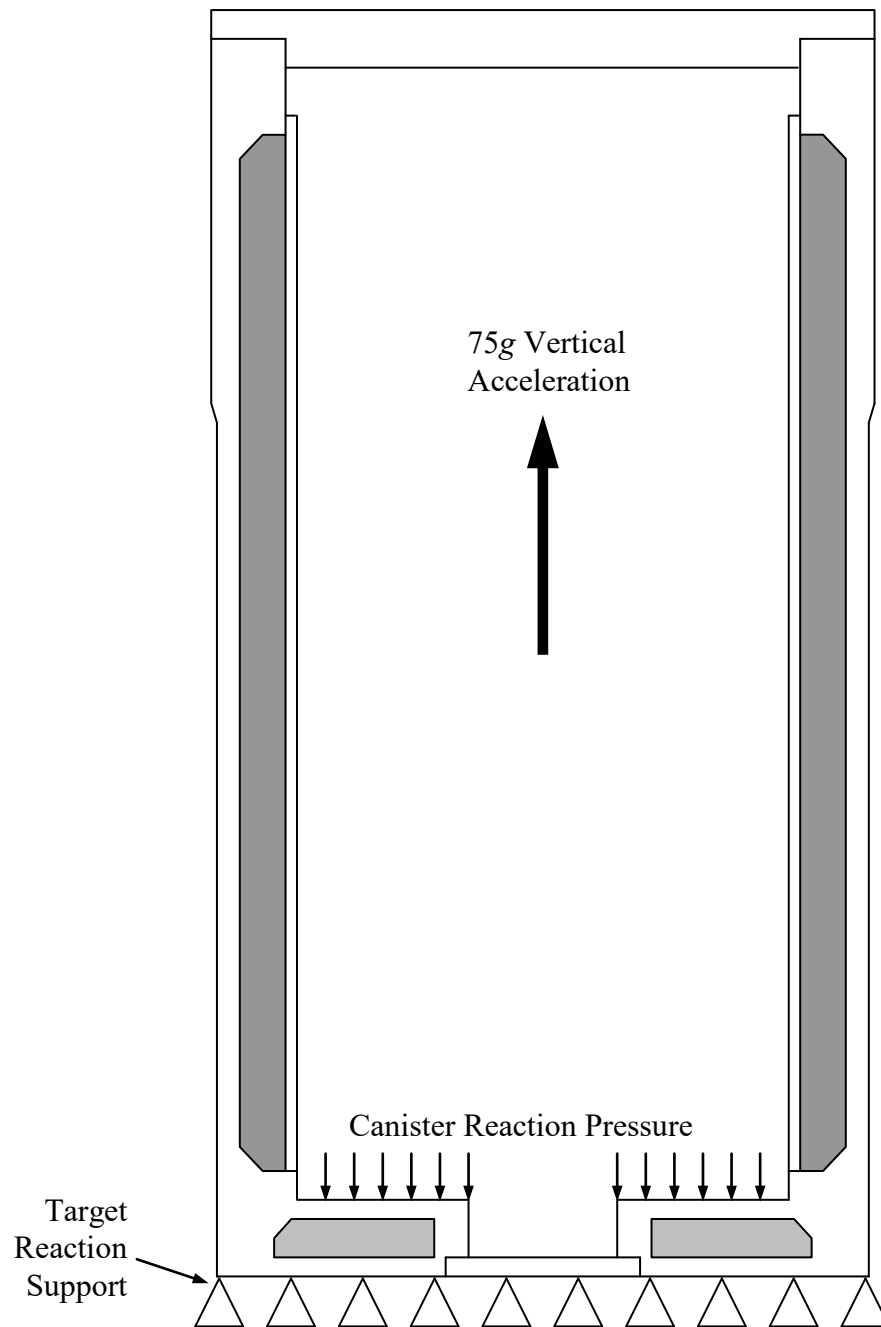


Figure A.3.9.2-9
75 g Bottom End Drop Boundary Conditions (2D Model)

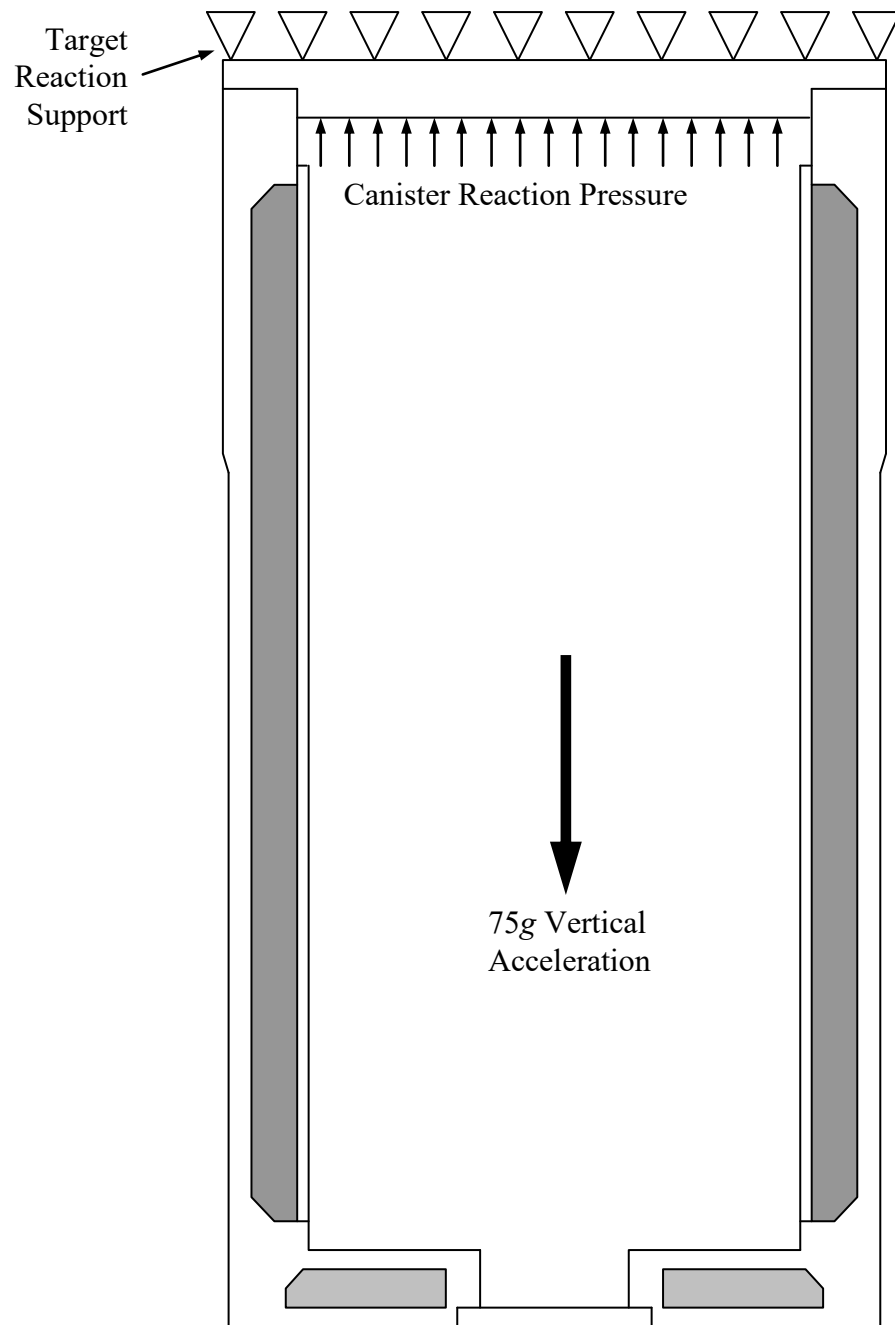


Figure A.3.9.2-10
75 g Top End Drop Boundary Conditions (2D Model)

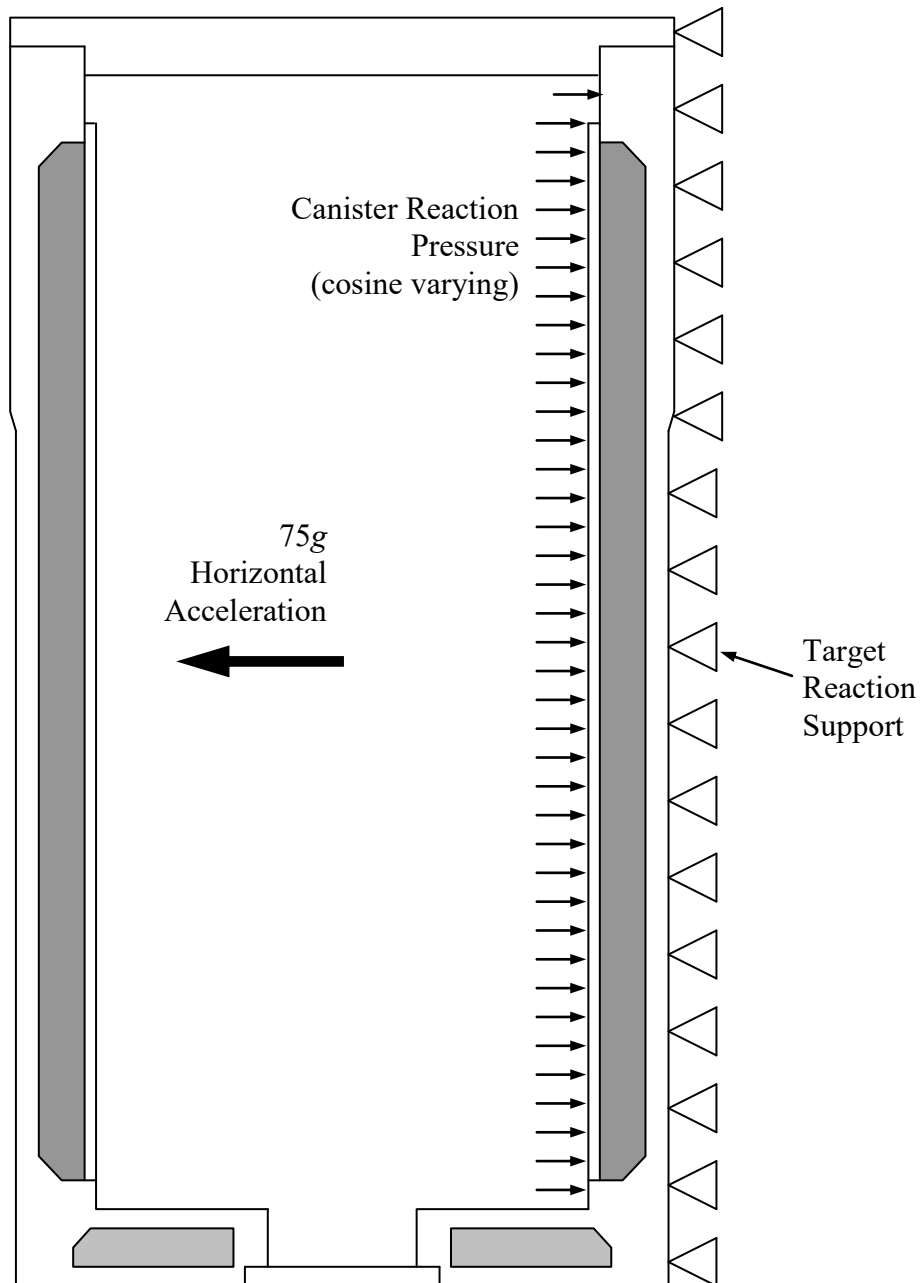


Figure A.3.9.2-11
75 g Side Drop Boundary Conditions (3D Model)

*** APPLIED LOADS**

NOZZLE LOAD P _____ LB. VESSEL THICKNESS T _____ IN. $7 \cdot \frac{P}{T}$ _____

CIRC. MOMENT M _____ IN-LB. ATTACHMENT RADII r_1 _____ IN. r_2 _____ IN. r_3 _____ IN. r_4 _____ IN.

LONG. MOMENT M_L _____ IN-LB. VESSEL RADII R_1 _____ IN. R_2 _____ IN. R_3 _____ IN. R_4 _____ IN.

TORSION MOMENT M_T _____ IN-LB.

SHEAR LOAD W _____ LB.

SHEAR LOAD V _____ LB.

*** NOTE: ENTER ALL FORCE VALUES IN ACCORDANCE WITH SIGN CONVENTION**

2. GEOMETRY

3. GEOMETRIC PARAMETERS

PRINCIPAL LOAD COORDINATE SYSTEM

FROM FILE	READ DATA FOR	COMPUTE ABSOLUTE VALUES OF STRESS AND ENTER RESULTS	STRESSES - IF LOADS OPPOSITE THAN SHOWN, REVERSE SIGNS SHOWN							
			M_1	M_2	M_3	M_4	M_5	M_6	M_7	
3C AND 4C	$\frac{M}{\pi R^2 T}$	$\left(\frac{M}{\pi R^2 T}\right) \cdot \frac{P}{T}$	+	+	+	+	+	+	+	
1C AND 2C-1	$\frac{M}{\pi R^2 T}$	$\left(\frac{M}{\pi R^2 T}\right) \cdot \frac{P}{T}$	+	+	+	+	+	+	+	
3A	$\frac{M}{\pi R^2 T}$	$\left(\frac{M}{\pi R^2 T}\right) \cdot \frac{P}{T}$	+	+	+	+	+	+	+	
1A	$\frac{M}{\pi R^2 T}$	$\left(\frac{M}{\pi R^2 T}\right) \cdot \frac{P}{T}$	+	+	+	+	+	+	+	
3B	$\frac{M}{\pi R^2 T}$	$\left(\frac{M}{\pi R^2 T}\right) \cdot \frac{P}{T}$	+	+	+	+	+	+	+	
1B OR 1B-1	$\frac{M}{\pi R^2 T}$	$\left(\frac{M}{\pi R^2 T}\right) \cdot \frac{P}{T}$	+	+	+	+	+	+	+	
ADD ALGEBRAICALLY FOR SUMMATION OF 8 STRESSES OF 1.										
3C AND 4C	$\frac{M}{\pi R^2 T}$	$\left(\frac{M}{\pi R^2 T}\right) \cdot \frac{P}{T}$	+	+	+	+	+	+	+	
1C-1 AND 2C	$\frac{M}{\pi R^2 T}$	$\left(\frac{M}{\pi R^2 T}\right) \cdot \frac{P}{T}$	+	+	+	+	+	+	+	
4A	$\frac{M}{\pi R^2 T}$	$\left(\frac{M}{\pi R^2 T}\right) \cdot \frac{P}{T}$	+	+	+	+	+	+	+	
2A	$\frac{M}{\pi R^2 T}$	$\left(\frac{M}{\pi R^2 T}\right) \cdot \frac{P}{T}$	+	+	+	+	+	+	+	
4B	$\frac{M}{\pi R^2 T}$	$\left(\frac{M}{\pi R^2 T}\right) \cdot \frac{P}{T}$	+	+	+	+	+	+	+	
2B OR 2B-1	$\frac{M}{\pi R^2 T}$	$\left(\frac{M}{\pi R^2 T}\right) \cdot \frac{P}{T}$	+	+	+	+	+	+	+	
ADD ALGEBRAICALLY FOR SUMMATION OF 8 STRESSES OF 1.										
SHEAR STRESS DUE TO TORSION M_T			$7 \cdot \frac{M_T}{T}$	$7 \cdot \frac{M_T}{T}$	$7 \cdot \frac{M_T}{T}$	$7 \cdot \frac{M_T}{T}$	$7 \cdot \frac{M_T}{T}$	$7 \cdot \frac{M_T}{T}$	$7 \cdot \frac{M_T}{T}$	
SHEAR STRESS DUE TO TORSION M_T			$7 \cdot \frac{M_T}{T}$	$7 \cdot \frac{M_T}{T}$	$7 \cdot \frac{M_T}{T}$	$7 \cdot \frac{M_T}{T}$	$7 \cdot \frac{M_T}{T}$	$7 \cdot \frac{M_T}{T}$	$7 \cdot \frac{M_T}{T}$	
SHEAR STRESS DUE TO LOAD W			$7 \cdot \frac{W}{T}$	$7 \cdot \frac{W}{T}$	$7 \cdot \frac{W}{T}$	$7 \cdot \frac{W}{T}$	$7 \cdot \frac{W}{T}$	$7 \cdot \frac{W}{T}$	$7 \cdot \frac{W}{T}$	
SHEAR STRESS DUE TO LOAD W			$7 \cdot \frac{W}{T}$	$7 \cdot \frac{W}{T}$	$7 \cdot \frac{W}{T}$	$7 \cdot \frac{W}{T}$	$7 \cdot \frac{W}{T}$	$7 \cdot \frac{W}{T}$	$7 \cdot \frac{W}{T}$	
ADD ALGEBRAICALLY FOR SUMMATION OF SHEAR STRESSES 2.										

PRESSURE STRESS

LONGITUDINAL, BENDING STRESS

TOTAL MEMBRANE STRESS

TOTAL SURFACE STRESS

LONGITUDINAL, σ_L

BENDING, σ_B

CHROMATOPHORE, σ_C

NOZZLE NO. _____

PIPING LOAD CODE _____

ANALYSIS POINT _____

COMPUTATION SHEET FOR LOCAL STRESSES

IN CYLINDRICAL SHELLS

Figure A.3.9.2-12
Computational Worksheet for WRC 107 Bulletin Evaluation

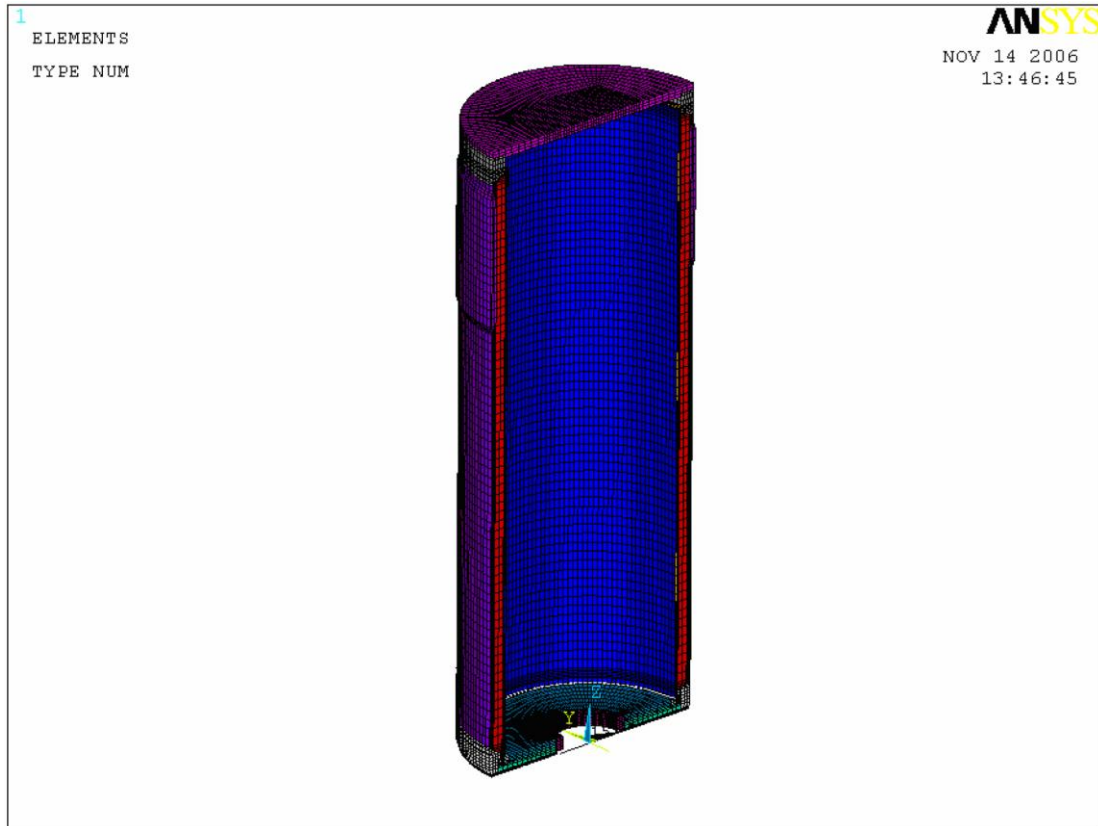


Figure A.3.9.2-13
NUHOMS OS187H Type 1 Transfer Cask Side Drop– 3D Finite Element Model

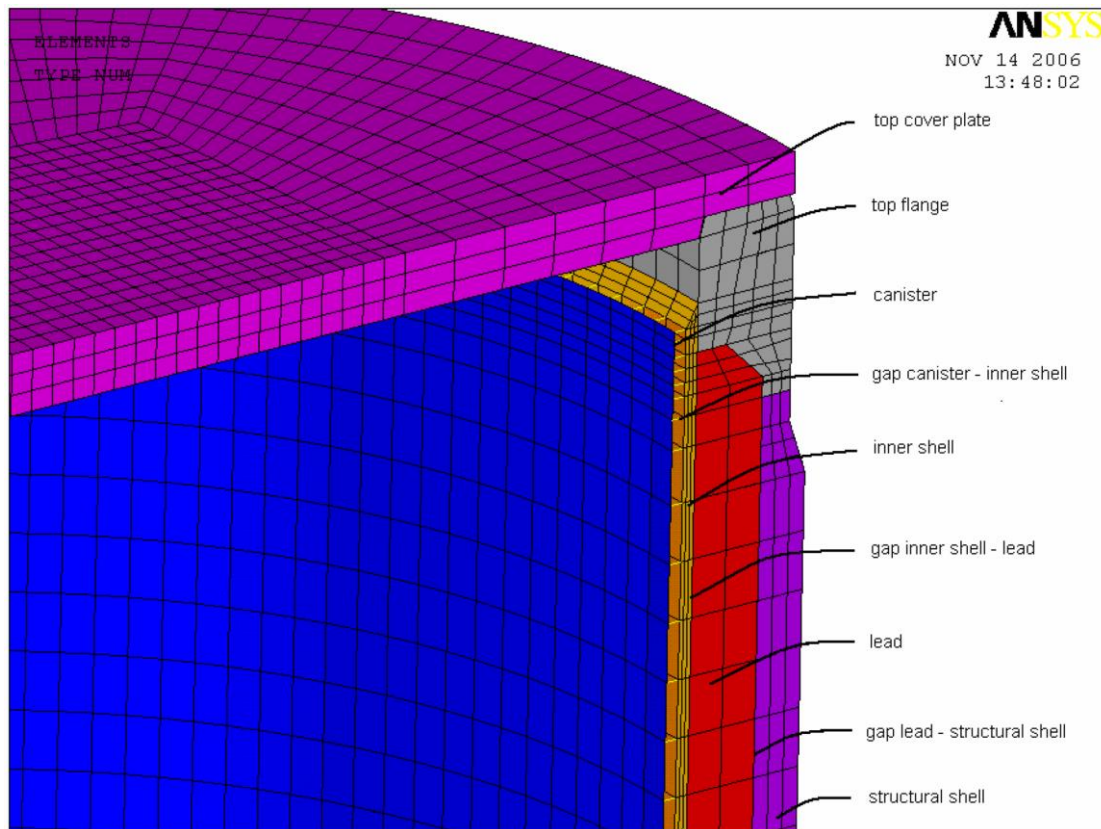


Figure A.3.9.2-14
Transfer Cask Side Drop Model Top Cover/Flange/Lead Interface

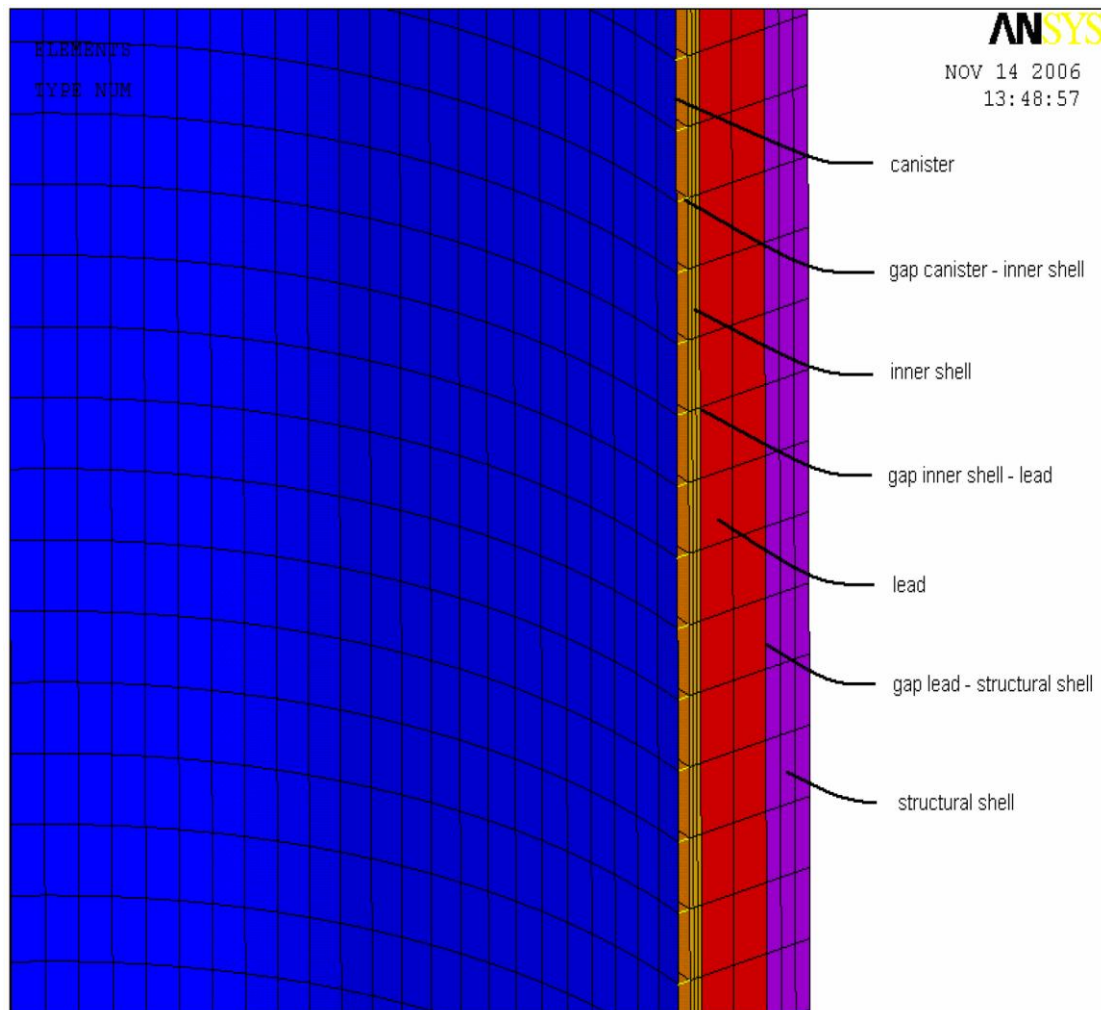


Figure A.3.9.2-15
Transfer Cask Side Drop Model Canister/Cask Shell/Lead/Interface

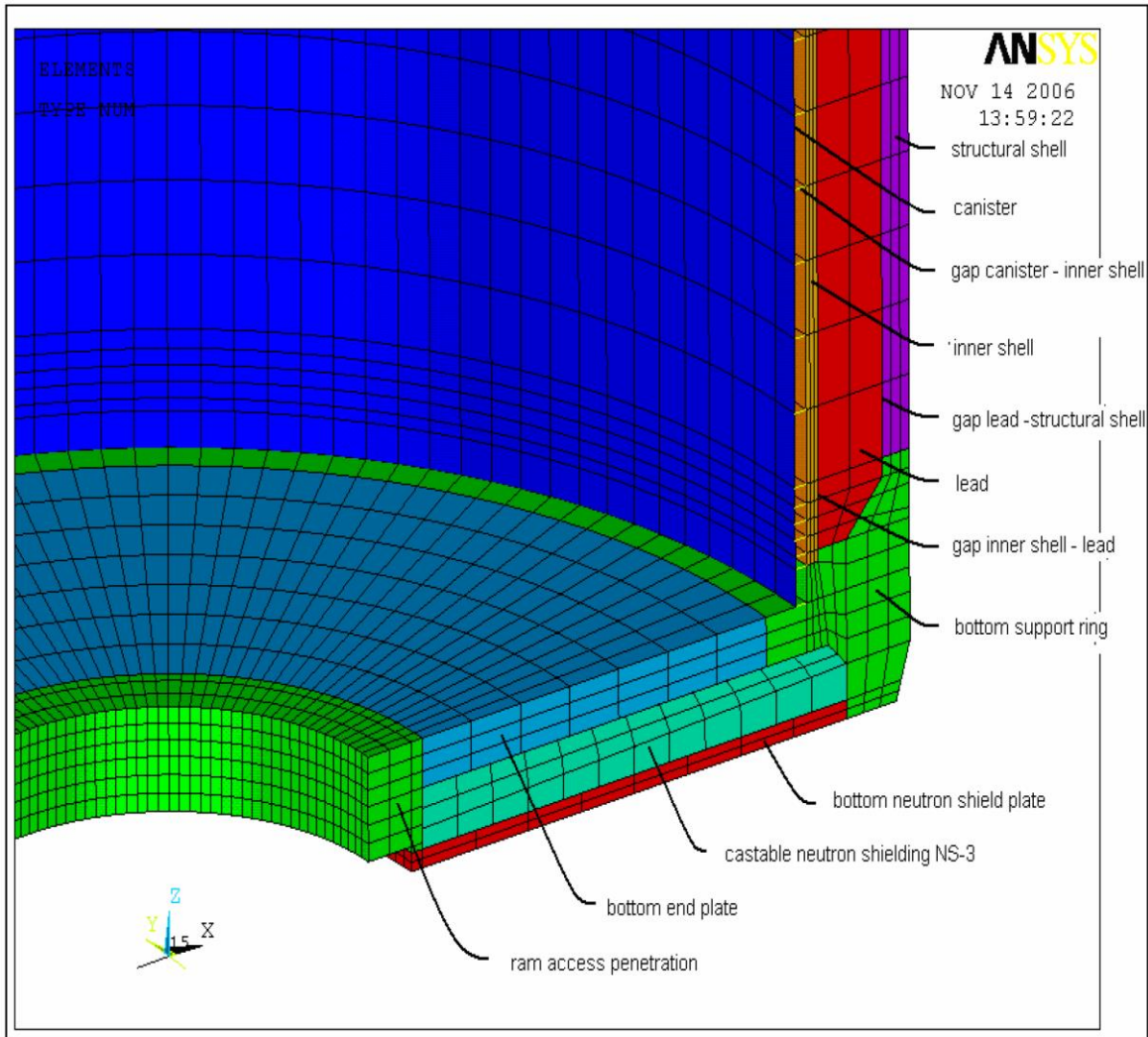


Figure A.3.9.2-16
Transfer Cask Side Drop Model Canister/ Bottom Access Ram/Lead/Interface

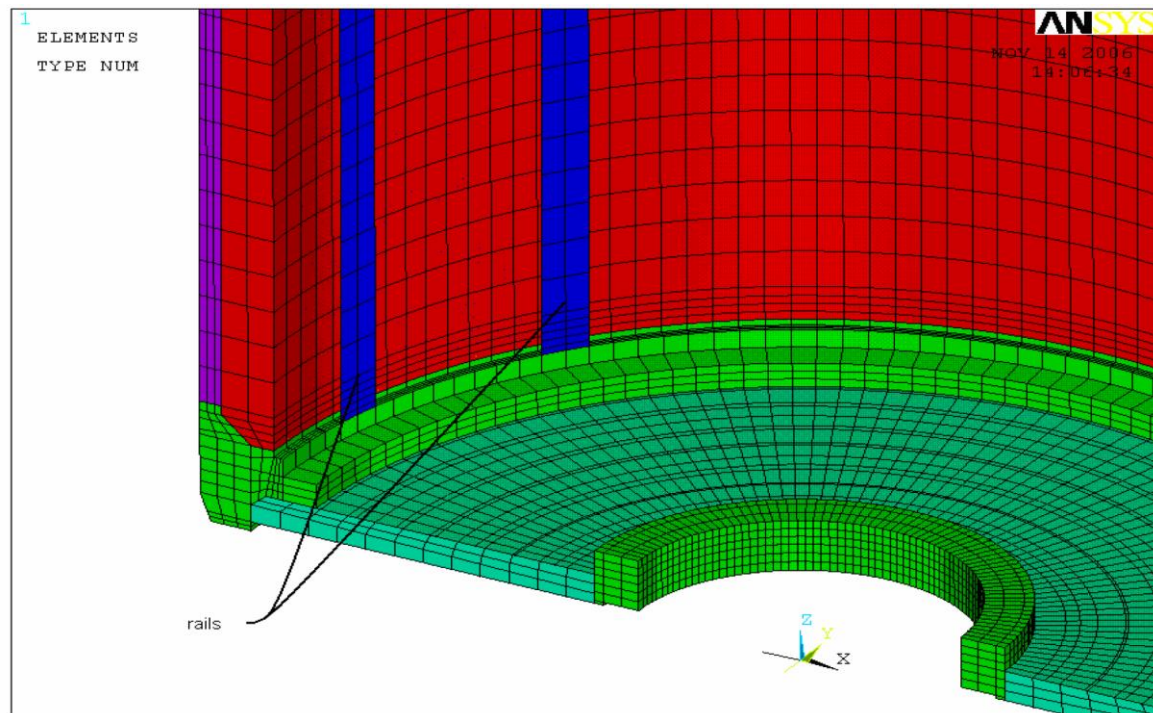
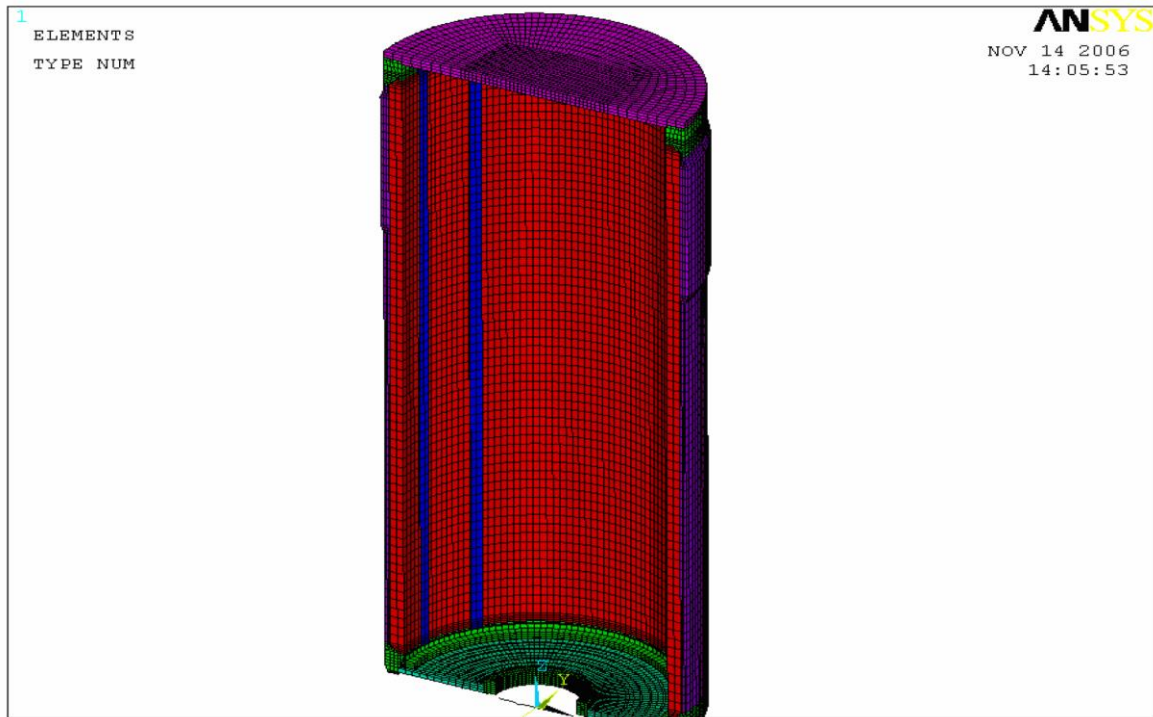


Figure A.3.9.2-17
Transfer Cask Side Drop Model—Rail Locations for Load Case 1

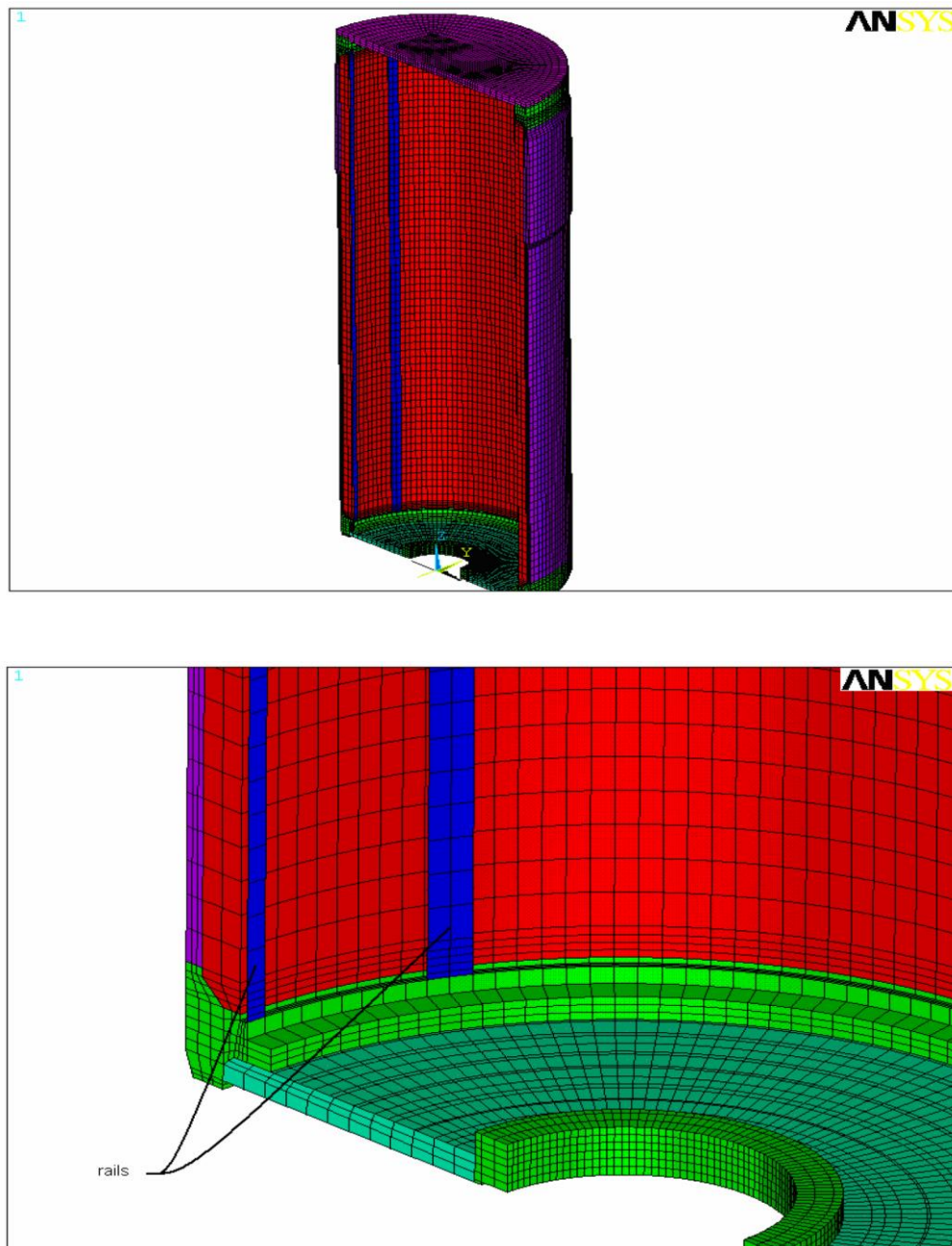


Figure A.3.9.2-18
Transfer Cask Side Drop Model—Rail Locations for Load Case 2

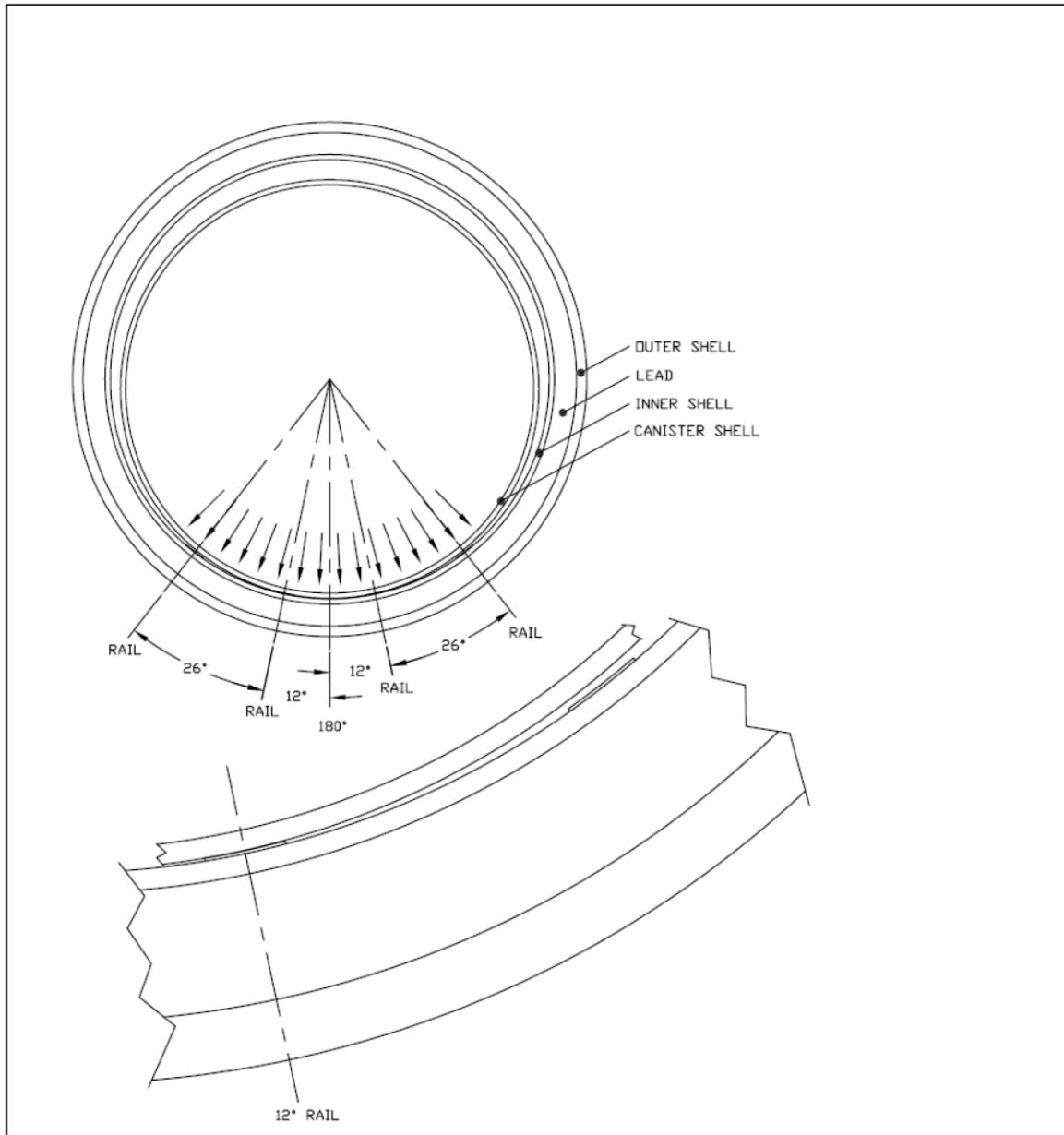


Figure A.3.9.2-19
Transfer Cask Side Drop—Sketch of Drop Modeling for Load Case 1

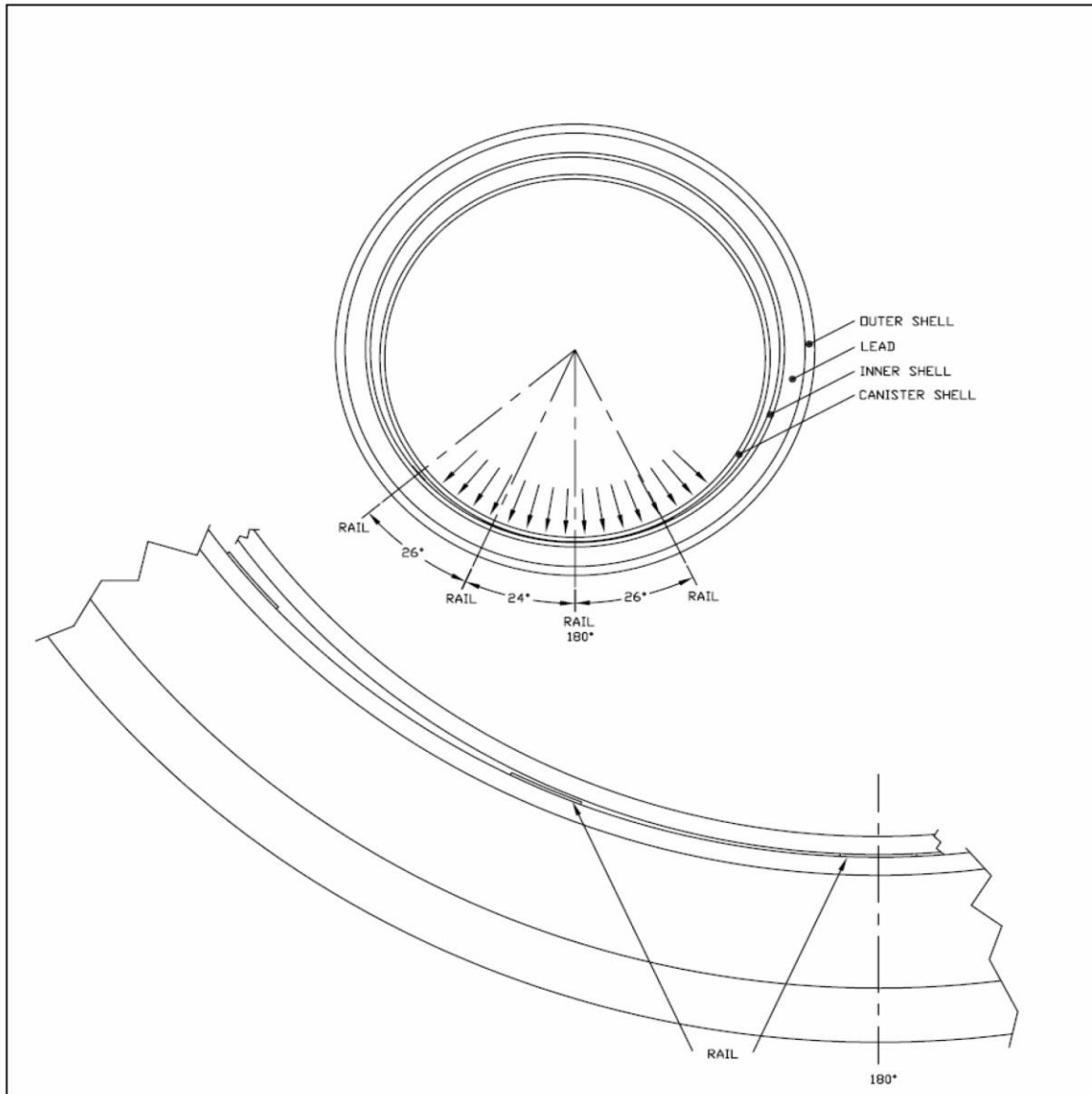


Figure A.3.9.2-20
Transfer Cask Side Drop—Sketch of Drop Modeling for Load Case 2

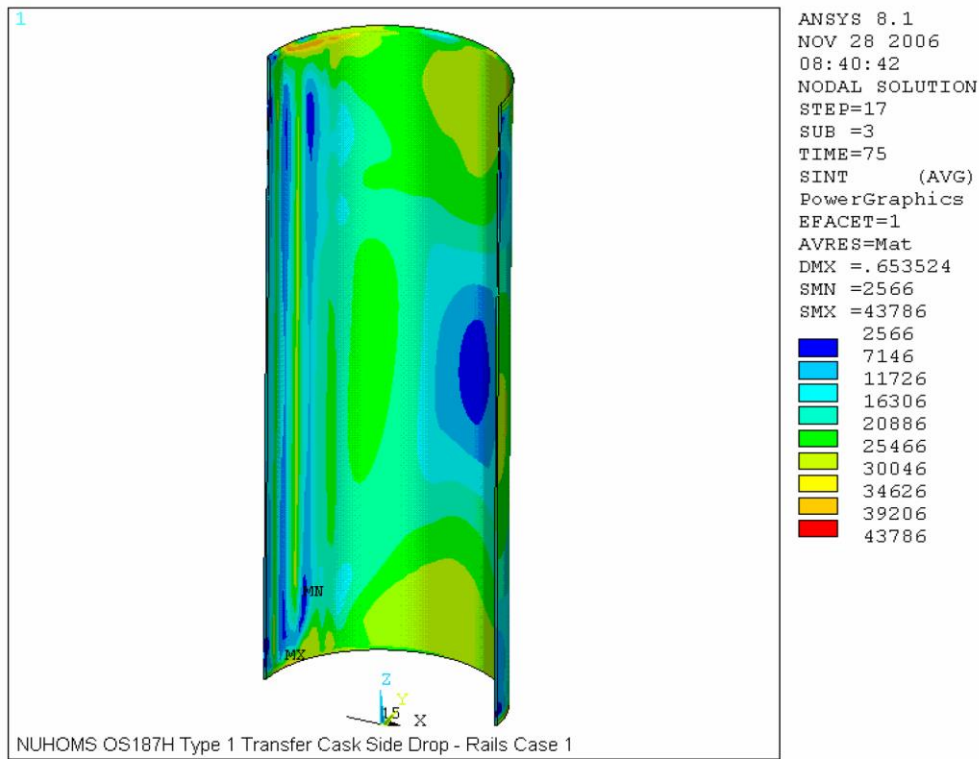


Figure A.3.9.2-21
Transfer Cask Side Drop Results—Inner Shell Stress Intensity for Load Case 1

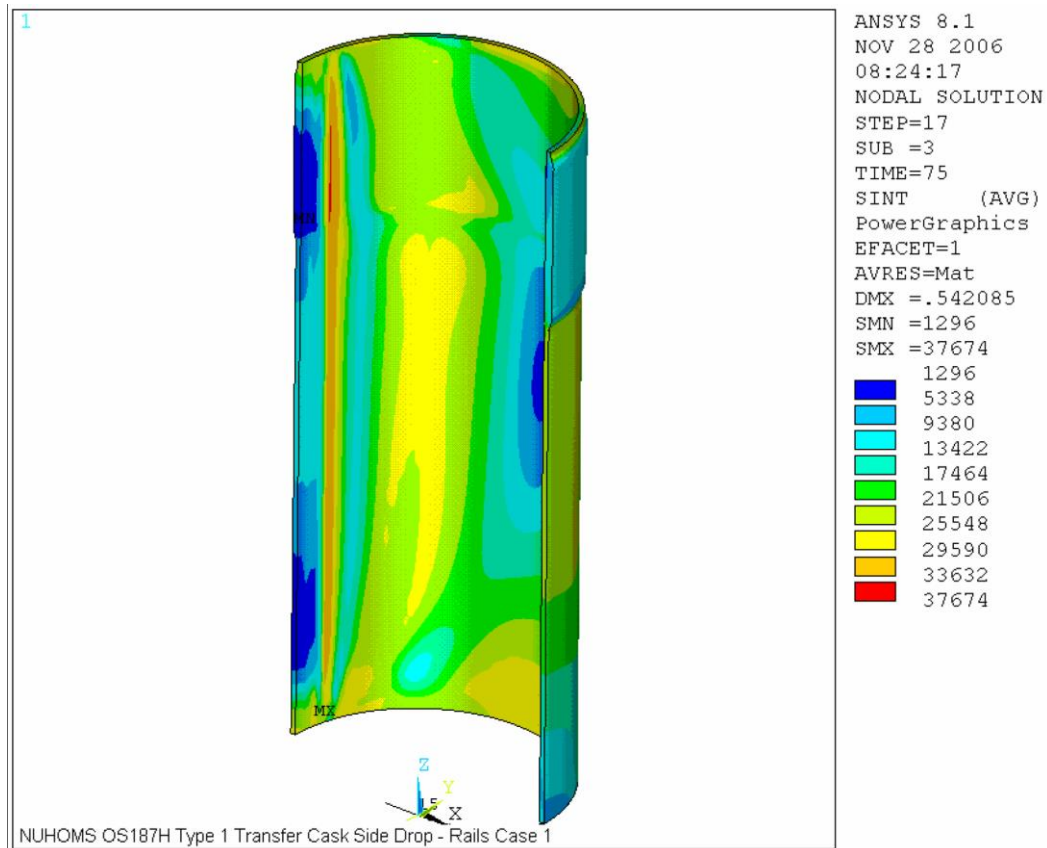


Figure A.3.9.2-22
Transfer Cask Side Drop Results—Outer Shell Stress Intensity for Load Case 1

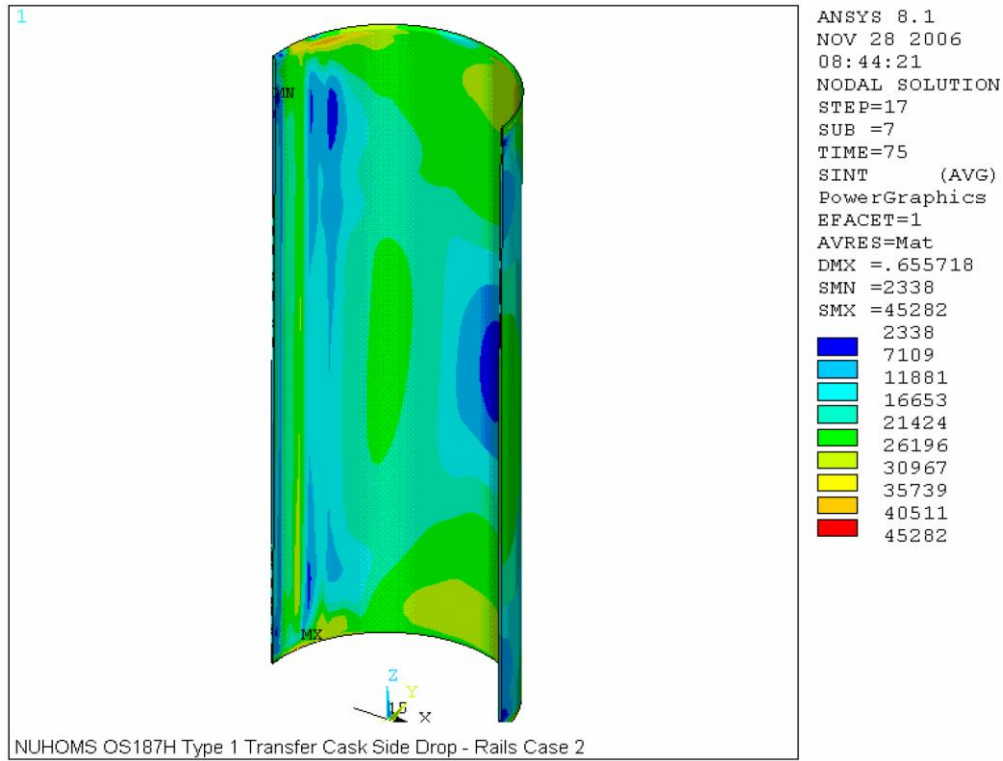


Figure A.3.9.2-23
Transfer Cask Side Drop Results—Inner Shell Stress Intensity for Load Case 2

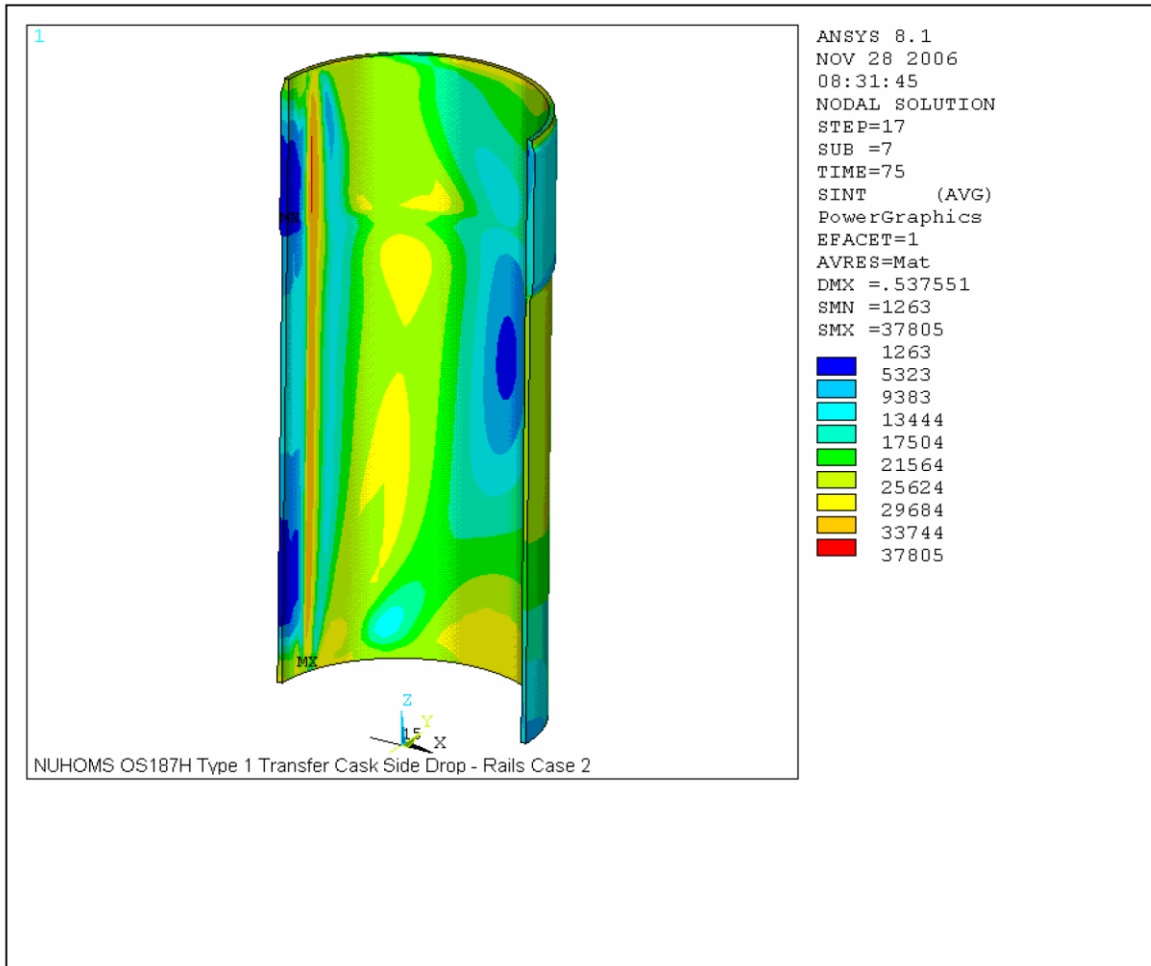


Figure A.3.9.2-24
Transfer Cask Side Drop Results—Outer Shell Stress Intensity for Load Case 2

Appendix A.3.9.3 OS187H Type 1 Transfer Cask Top Cover and Ram Cover Bolt Analyses

TABLE OF CONTENTS

A.3.9.3	OS187H TYPE 1 TRANSFER CASK TOP COVER AND RAM ACCESS COVER BOLT ANALYSES.....	A.3.9.3-1
A.3.9.3.1	Introduction.....	A.3.9.3-1
A.3.9.3.2	Top Cover Bolt Load Calculations.....	A.3.9.3-3
A.3.9.3.2.1	Top Cover Bolt Preload and Bolt Torque	A.3.9.3-3
A.3.9.3.2.2	Top Cover Gasket Seating Load	A.3.9.3-4
A.3.9.3.2.3	Pressure Loads	A.3.9.3-4
A.3.9.3.2.4	Temperature Loads	A.3.9.3-5
A.3.9.3.2.5	Impact Loads.....	A.3.9.3-5
A.3.9.3.3	Top Cover Bolt Load Combinations	A.3.9.3-7
A.3.9.3.4	Top Cover Bolt Stress Calculations.....	A.3.9.3-8
A.3.9.3.4.1	Average Tensile Stress.....	A.3.9.3-8
A.3.9.3.4.2	Bending Stress	A.3.9.3-9
A.3.9.3.4.3	Shear Stress.....	A.3.9.3-9
A.3.9.3.4.4	Maximum Combined Stress Intensity.....	A.3.9.3-9
A.3.9.3.4.5	Stress Ratios.....	A.3.9.3-10
A.3.9.3.4.6	Bearing Stress (Under Bolt Head)	A.3.9.3-10
A.3.9.3.5	Top Cover Bolt Analysis Results	A.3.9.3-11
A.3.9.3.6	Minimum Engagement Length for Top Cover Bolt and Flange.....	A.3.9.3-12
A.3.9.3.7	Ram Access Cover Bolt Calculations	A.3.9.3-14
A.3.9.3.7.1	Ram Access Cover Bolt Preload and Bolt Torque..	A.3.9.3-14
A.3.9.3.7.2	Ram Access Cover Gasket Seating Load.....	A.3.9.3-14
A.3.9.3.7.3	Pressure Loads	A.3.9.3-15
A.3.9.3.7.4	Temperature Loads	A.3.9.3-16
A.3.9.3.7.5	Impact Loads.....	A.3.9.3-16
A.3.9.3.8	Ram Access Cover Bolt Load Combinations	A.3.9.3-19
A.3.9.3.9	Ram Access Cover Bolt Stress Calculations.....	A.3.9.3-20
A.3.9.3.9.1	Average Tensile Stress.....	A.3.9.3-21
A.3.9.3.9.2	Bending Stress	A.3.9.3-22
A.3.9.3.9.3	Shear Stress.....	A.3.9.3-22
A.3.9.3.9.4	Maximum Combined Stress Intensity.....	A.3.9.3-22

A.3.9.3.9.5 Stress Ratios.....	A.3.9.3-22
A.3.9.3.9.6 Bearing Stress (Under Bolt Head)	A.3.9.3-23
A.3.9.3.10 Ram Access Cover Bolt Analysis Results.....	A.3.9.3-24
A.3.9.3.11 Minimum Engagement Length for Ram Access Cover Bolt..	A.3.9.3-25
A.3.9.3.12 Brittle Fracture Analysis of Top Cover Bolt	A.3.9.3-27
A.3.9.3.13 Conclusions.....	A.3.9.3-30
A.3.9.3.14 References	A.3.9.3-31

LIST OF TABLES

Table A.3.9.3-1	Design Parameters for Top Cover Bolt Analysis.....	A.3.9.3-32
Table A.3.9.3-2	Design Parameters for Ram Access Cover Bolt Analysis	A.3.9.3-33
Table A.3.9.3-3	Bolt Data	A.3.9.3-34
Table A.3.9.3-4	Allowable Stresses in Closure Bolts for Normal Conditions.....	A.3.9.3-35
Table A.3.9.3-5	Allowable Stresses in Closure Bolts for Hypothetical Accident Conditions	A.3.9.3-36

LIST OF FIGURES

Figure A.3.9.3-1	Effect of Tempering Temperature on Notch Toughness	A.3.9.3-37
Figure A.3.9.3-2	Correlation between Notch Toughness and Yield Strength.....	A.3.9.3-38
Figure A.3.9.3-3	Singular Integral Equation and Asymptotic Approximation for Brittle Fracture Evaluation.....	A.3.9.3-39

A.3.9.3 OS187H TYPE 1 TRANSFER CASK TOP COVER AND RAM ACCESS COVER BOLT ANALYSES

A.3.9.3.1 Introduction

This section documents the evaluation of the top cover bolts and ram access cover bolts of the NUHOMS[®] OS187H Type 1 transfer cask (TC) under normal and accident conditions. The criteria and methods of evaluation used are the same as those of the OS187H TC documented in Section 3.9.3. The stress analysis is performed in accordance with NUREG/CR-6007 [1].

The NUHOMS[®] OS187H Type 1 TC top cover closure and ram access cover design, including bolts type and mechanical properties of the bolt material are the same as the OS187H TC. As shown in drawing 10494-72-9003-SAR, the 3.0 inch thick top cover is bolted to the top flange of the TC using twenty four 1½ inch diameter bolts. As shown in drawings 10494-72-9001-SAR and 10494-72-9003-SAR, the 1.0 inch thick ram access cover is bolted to the ram access penetration ring using twelve ½ inch diameter bolts. The bolt material for both applications is SA-540 Gr. B23 Class 1, which has a minimum yield strength of 150 ksi at room temperature [2].

Table A.3.9.3-1 and Table A.3.9.3-2 summarize the design parameters used for the evaluation of the OS187H Type 1 TC top cover bolts and the ram access cover bolts, respectively. These tables are similar to Tables 3.9.3-1 and 3.9.3-2 for the OS187H TC. Based on a comparison between these sets of tables, the table below summarizes the differences that affect the evaluation of the top cover and ram access cover bolts between the two TCs. The evaluations documented in the following sections of this appendix are performed to address the effect of these differences.

Top Lid Closure Parameter	OS187H (See Table 3.9.3-1)	OS187H Type 1 (See Table A.3.9.3-1)
Closure lid diameter (at bolt circle), in.	77.61	76.85
Closure lid diameter (at the seal), in.	74.19	73.61
Closure lid diameter (outer edge), in.	82.20	81.37
Flange thickness, in.	5.575	6.50
Payload weight, lb	110,300	120,000

Ram Access Cover Parameter	OS187H (See Table 3.9.3-2)	OS187H Type 1 (See Table A.3.9.3-2)
Ram access cover diameter (at bolt circle), in.	23.50	24.50
Ram access cover diameter (at the seal), in.	21.16	23.16
Ram access cover diameter (outer edge), in.	25.45	26.45
Ram access cover diameter (at inner edge), in.	20.00	22.00
Ram access penetration thickness, in.	4.00	3.00

As with the OS187H TC, the following evaluations are presented in this section:

- Top cover and ram cover bolt torque
- Bolt preload
- Gasket seating load

- Pressure load
- Temperature load
- Impact load
- Thread engagement length evaluation
- Bearing stress
- Load combinations for normal and accident conditions
- Bolt stresses and allowable stresses

A.3.9.3.2 Top Cover Bolt Load Calculations

The design parameters of the top cover are summarized in Table A.3.9.3-1. The top cover bolt data and material allowables are presented in Table A.3.9.3-3 through Table A.3.9.3-5. These tables are the same as Table 3.9.3-3 through Table 3.9.3-5 and are presented here for completeness of presentation. The temperature of 300 °F is used in the top cover bolt region during normal and accident conditions. The following load cases are considered in the analysis.

- Preload + temperature load (normal condition)
- Pressure load (normal condition)
- Pressure + 80 inch corner drop (accident condition)

Symbols and terminology used in this analysis are taken from NUREG/CR-6007 [1] and are reproduced in Table A.3.9.3-1.

A.3.9.3.2.1 Top Cover Bolt Preload and Bolt Torque

This evaluation is not changed from that presented in Section 3.9.3.2.1 for the OS187H TC and is presented here for purposes of completeness of presentation.

A bolt torque range of 450 to 580 ft. lb. has been selected.

Using the minimum torque,

$$F_a = Q/KD_b = 450 \times 12 / (0.132 \times 1.50) = 27,270 \text{ lb.}, \text{ and}$$

$$\text{Preload stress} = F_a / \text{Stress Area} = 27,270 / 1.406 = 19,400 \text{ psi}$$

Where:

$$\text{Stress Area} = 1.491 \text{ in}^2 \text{ (Table A.3.9.3-3; conservatively, used } 1.406 \text{ in}^2 \text{).}$$

Using the maximum torque,

$$F_a = Q/KD_b = 580 \times 12 / (0.132 \times 1.50) = 35,150 \text{ lb.}, \text{ and}$$

$$\text{Preload stress} = F_a / \text{Stress Area} = 35,150 / 1.406 = 25,000 \text{ psi}$$

Where:

$$\text{Stress Area} = 1.491 \text{ in}^2 \text{ (Table A.3.9.3-3; conservatively, used } 1.406 \text{ in}^2 \text{).}$$

Residual torsional moment for minimum torque of 450 ft. lb. is,

$$M_{tr} = 0.5Q = .5(450 \times 12) = 2,700 \text{ in. lb.}$$

Residual torsional moment for maximum torque of 580 ft. lb. is,

$$M_{tr} = 0.5Q = .5(580 \times 12) = 3,480 \text{ in. lb.}$$

Residual tensile bolt force for maximum torque,

$$F_{ar} = F_a = 35,150 \text{ lb.}$$

A.3.9.3.2.2 Top Cover Gasket Seating Load

Since a self energizing O-ring is used, the gasket seating load is negligible.

A.3.9.3.2.3 Pressure Loads

The methodology of Reference 1, Table 4.3, is used. Axial force per bolt due to internal pressure is

$$F_a = \frac{\pi D_{lg}^2 (P_{li} - P_{lo})}{4N_b}$$

D_{lg} (median lid seal diameter) = 73.61 in. Then,

$$F_a = \frac{\pi(73.61^2)(30 - 0)}{4(24)} = 5,320 \text{ lb./bolt}$$

The fixed edge closure lid force is,

$$F_f = \frac{D_{lb}(P_{li} - P_{lo})}{4} = \frac{76.85(30)}{4} = 576.40 \text{ lb. in.}^{-1}$$

The fixed edge closure lid moment is,

$$M_f = \frac{(P_{li} - P_{lo})D_{lb}^2}{32} = \frac{30(76.85^2)}{32} = 5,537 \text{ in. lb. in.}^{-1}$$

The shear bolt force per bolt is,

$$F_s = \frac{\pi E_l t_l (P_{li} - P_{lo}) D_{lb}^2}{2 N_b E_c t_c (1 - N_{ul})} = \frac{\pi (27.0 \times 10^6) (3.0) (30) (76.85)^2}{2 (24) (27.0 \times 10^6) (5.06) (1 - 0.3)} = 9,822 \text{ lb./bolt}$$

The top cover shoulder takes this shear force, so that $F_s = 0$.

A.3.9.3.2.4 Temperature Loads

The top cover bolt material is SA-540, Grade B23. The top cover is constructed from SA-240 Type XM-19 or SA-182 Type FXM-19, and the flange is constructed from SA-182 Type F304N. The bolts have a coefficient of thermal expansion of 6.9×10^{-6} in./in.°F⁻¹ at 300 °F, the lid has a coefficient of thermal expansion of 8.8×10^{-6} in./in.°F⁻¹ at 300 °F, and the flange has a coefficient of thermal expansion of 9.2×10^{-6} in./in.°F⁻¹ at 300 °F [2].

Therefore, the tensile load in the bolt due to different thermal expansion is,

$$F_a = 0.25 \pi D_b^2 E_b (a_l T_l - a_b T_b)$$

$$F_a = 0.25(\pi)(1.50^2)(26.7 \times 10^6) \{ (8.8 \times 10^{-6})(230) - (6.9 \times 10^{-6})(230) \} = 20,620 \text{ lb.}$$

Even though the top cover and flange are constructed from different materials, the shear force per bolt, F_s , due to a temperature change of 230 °F is, 0 psi, since the clearance holes in the lid are oversized (1.88 in. diameter) allowing the lid to grow in the radial direction.

$$F_s = 0$$

The temperature difference between the inside and outside of the top cover will always be less than one degree (see Chapter A.4). Consequently, the resulting bending moment is negligible.

$$M_f = 0$$

A.3.9.3.2.5 Impact Loads

Per Reference 1, Table 4.5, the non-prying tensile bolt force per bolt, F_a ,

$$F_a = \frac{1.34 \sin(xi)(DLF)(ai)(W_l + W_c)}{N_b} = \frac{1.34 \sin(xi)(1.1)(ai)(120,000)}{24} = 7,370(ai) \sin(xi) \text{ lb./bolt}$$

Note: $W_l + W_c$ is conservatively assumed to be 120,000 lb. (see Table A.3.9.3-1)

The shear bolt force is,

$$F_s = \frac{\cos(xi)(ai)(W_l)}{N_b} = \frac{5,500(ai) \cos(xi)}{24} = 229.2(ai) \cos(xi) \text{ lb./bolt}$$

The lid shoulder during normal and accident condition drops takes shear force. Therefore,

$$F_s = 0$$

The fixed-edge closure lid force, F_f , is,

$$F_f = \frac{1.34 \sin(xi)(DLF)(ai)(W_l + W_c)}{\pi D_{lb}} = \frac{1.34 \sin(xi)(1.1)(ai)(120,000)}{\pi(76.85)} = 732.6 \sin(xi)(ai) \text{ lb. in.}^{-1}$$

The fixed-edge closure lid moment, M_f , is,

$$M_f = \frac{1.34 \sin(xi)(DLF)(ai)(W_l + W_c)}{8\pi} = \frac{1.34 \sin(xi)(1.1)(ai)(120,000)}{8\pi} = 7,038 \sin(xi)(ai) \text{ in.lb.in}^{-1}$$

The accident condition impact load is taken to be the axial acceleration due to corner drop. As described in Section 3.1.1.4, end and corner drops are not considered credible during transfer operations under 10 CFR Part 72 because the transfer cask is always in the horizontal orientation. The evaluation below is performed in support of a 10 CFR Part 50 evaluation that may be performed by the user if the user cannot demonstrate that these accident drops are not credible. The following corner drop acceleration and impact angle are assumed to bound any possible corner drop accident scenario:

$$ai = 25 \text{ gs, and } xi = 60^\circ$$

Therefore,

$$F_a = 7,370 \times 25 \times \sin(60^\circ) = 159,565 \text{ lb./bolt}$$

$$F_s = 0 \text{ lb./bolt}$$

$$F_f = 732.6 \times 25 \times \sin(60^\circ) = 15,861 \text{ lb./bolt, and}$$

$$M_f = 7,038 \times 25 \times \sin(60^\circ) = 152,373 \text{ lb./bolt}$$

The top cover individual load is summarized in the following table.

Top Cover Bolt Individual Load Summary

Load Case	Applied Load		Non-Prying Tensile Force, F_a (lb.)	Torsional Moment, M_t (in. lb.)	Prying Force, F_f (lb.in. ⁻¹)	Prying Moment, M_f (in. lb. in. ⁻¹)
Preload	Residual	Minimum torque	27,270	2,700	0	0
		Maximum torque	35,150	3,480	0	0
Gasket	Seating load		0	0	0	0
Pressure	50 psig internal		5,320	0	576.4	5,537
Thermal	300 °F		20,620	0	0	0
Impact	Accident condition drop		159,565	0	15,861	152,373

A.3.9.3.3 Top Cover Bolt Load Combinations

A summary of normal and accident condition load combinations ([1], Table 4.9) is presented in the following table.

Top Cover Bolt Normal and Accident Load Combinations

Load Case	Combination Description		Non-Prying Tensile Force, F_a (lb.)	Torsional Moment, M_t (in. lb.)	Prying Force, F_f (lb.in. ⁻¹)	Prying Moment, M_f (in. lb. in. ⁻¹)
1	Preload + temperature (normal condition)	Minimum torque	47,890	2,700	0	0
		Maximum torque	55,770	3,480	0	0
2	Pressure (normal condition)		5,320	0	576.4	5,537
3	Pressure + accident impact (accident condition)		164,885	0	16,437	157,910

A.3.9.3.4 Top Cover Bolt Stress Calculations

Additional Prying Bolt Force

Table *Top Cover Bolt Normal and Accident Load Combinations* above shows that all loading conditions cause outward acting loads only. Outward acting loads generate no additional prying bolt forces, because the gap between the lid and flange at the outer edge prevents the creation of a prying moment.

Bolt Bending Moment

The maximum bending bolt moment, M_{bb} , generated by the applied load is evaluated as follows:

$$M_{bb} = \left(\frac{\pi D_{lb}}{N_b} \right) \left[\frac{K_b}{K_b + K_l} \right] M_f$$

The K_b and K_l are based on geometry and material properties and are defined in Reference 1, Table 2.2. By substituting the values given above,

$$K_b = \left(\frac{N_b}{L_b} \right) \left(\frac{E_b}{D_{lb}} \right) \left(\frac{D_b^4}{64} \right) = \left(\frac{24}{1.5} \right) \left(\frac{26.7 \times 10^6}{76.85} \right) \left(\frac{1.50^4}{64} \right) = 4.397 \times 10^5, \text{ and}$$

$$K_l = \frac{E_l t_l^3}{3 \left[(1 - N_{ul}^2) + (1 - N_{ul})^2 \left(\frac{D_{lb}}{D_{lo}} \right)^2 \right] D_{lb}} = \frac{27.0 \times 10^6 (3.0^3)}{3 \left[(1 - 0.3^2) + (1 - 0.3)^2 \left(\frac{76.85}{81.37} \right)^2 \right] 76.85}$$

$$= 2.347 \times 10^6$$

Therefore,

$$M_{bb} = \left(\frac{\pi 76.85}{24} \right) \left[\frac{4.397 \times 10^5}{4.397 \times 10^5 + 2.347 \times 10^6} \right] M_f = 1.587 M_f.$$

For load case 2, $M_f = 5,537$ in. lb. Substituting this value into the equation above gives,

$$M_{bb} = 8,789 \text{ in. lb./bolt}$$

A.3.9.3.4.1 Average Tensile Stress

A summary of the applied loads for the transfer cask lid bolts is provided in Section A.3.9.3.3, in the table *Top Cover Bolt Normal and Accident Load Combinations*.

For the normal condition load cases, the applied bolt preload maintains closure of the transfer cask top cover. The closure force per bolt generated by the minimum lid bolt torque, with or without the additional closure force generated by thermal loads, is greater than the normal condition forces trying to open the top cover.

For accident conditions, the impact loads may instantaneously relax pressure on the top cover seals. However the accident condition loads will not cause lid bolt failure, as shown below, and immediately following the accident impact the top closure seal will be reseated by the bolt preload.

Per Reference 1, Table 5.1,

Normal Condition

$$S_{ba} = 1.2732 \frac{F_a}{D_{ba}^2} = 1.2732 \frac{55,770}{1.378^2} = 37,390 \text{ psi} = 37.4 \text{ ksi}$$

Accident Condition

$$S_{ba} = 1.2732 \frac{F_a}{D_{ba}^2} = 1.2732 \frac{164,885}{1.378^2} = 110,555 \text{ psi} = 110.6 \text{ ksi}$$

A.3.9.3.4.2 Bending Stress

Normal Condition

$$S_{bb} = 10.186 \frac{M_{bb}}{D_{ba}^3} = 10.186 \frac{8,789}{1.378^3} = 34,213 \text{ psi} = 34.2 \text{ ksi}$$

A.3.9.3.4.3 Shear Stress

For both normal and accident conditions, the average shear stress caused by shear bolt force F_s is,

$$S_{bs} = 0$$

For normal and accident conditions the maximum shear stress caused by the torsional moment M_t is,

$$S_{bt} = 5.093 \frac{M_t}{D_{ba}^3} = 5.093 \frac{3,480}{1.378^3} = 6,773 \text{ psi} = 6.8 \text{ ksi}$$

A.3.9.3.4.4 Maximum Combined Stress Intensity

The maximum combined stress intensity is calculated in the following way (Ref. [1], Table 5.1).

$$S_{bi} = \{(S_{ba} + S_{bb})^2 + 4(S_{bs} + S_{bt})^2\}^{0.5}$$

For normal conditions combine tension, shear, bending, and residual torsion.

$$S_{bi} = \{(37,390 + 34,213)^2 + 4(0 + 6,773)^2\}^{0.5} = 72,873 \text{ psi} = 72.9 \text{ ksi}$$

A.3.9.3.4.5 Stress Ratios

In order to meet the stress ratio requirement, the following relationship must hold for both normal and accident conditions.

$$R_t^2 + R_s^2 < 1$$

Where R_t is the ratio of average tensile stress to allowable average tensile stress, and R_s is the ratio of average shear stress to allowable average shear stress.

For normal conditions

$$R_t = 37,390/92,400 = 0.405$$

$$R_s = 6,773/55,400 = 0.122$$

$$R_t^2 + R_s^2 = (0.405)^2 + (0.122)^2 = 0.179 < 1$$

For accident conditions

$$R_t = 110,555/115,500 = 0.957$$

$$R_s = 6,773/69,300 = 0.098$$

$$R_t^2 + R_s^2 = (0.957)^2 + (0.098)^2 = 0.925 < 1$$

A.3.9.3.4.6 Bearing Stress (Under Bolt Head)

A standard 1.50 in. washer is placed under the head of each top cover bolt. The inside and outside diameter of a standard 1.50 in. washer is 1.50 in. and 3.00 in. respectively. The diameter of the bolt clearance hole in the top cover is 1.88 in. Therefore, the total bearing area under the top cover bolts, A_b , is the following.

$$A_b = (\pi/4) [3.00^2 - 1.88^2] = 4.293 \text{ in.}^2$$

According to Reference 1, bearing stress evaluation is required for normal condition loads only. For normal conditions, the maximum bearing stress under the washer, σ_b , is the following.

$$\sigma_b = 55,770 \text{ lb.} / 4.293 \text{ in.}^2 = 12,991 \text{ psi}$$

The normal condition allowable bearing stress on the cover is taken to be the yield stress of the cover material at 300 °F. The cover is manufactured out of SA-240 Type XM-19 or SA-182 Type FXM19, which have a yield stress of 43.3 ksi at 300 °F.

A.3.9.3.5 Top Cover Bolt Analysis Results

A summary of the stresses calculated above is listed in the following table:

Summary of Top Cover Bolt Stresses and Allowables

Stress Type	Normal Condition		Accident Condition	
	Stress	Allowable	Stress	Allowable
Average tensile (ksi)	37.4	92.4	110.6	115.5
Shear (ksi)	6.8	55.4	6.8	69.3
Combined (ksi)	72.9	124.7	Not Required [1]	
Interaction equation $R_t^2 + R_s^2 < 1$	0.179	1	0.925	1
Bearing (ksi) allowable (ksi) (S_y of lid material)	13.0	43.3	Not Required [1]	

A.3.9.3.6 Minimum Engagement Length for Top Cover Bolt and Flange

The top cover bolt and flange minimum engagement length evaluation is not changed from that presented in Section 3.9.3.6 for the OS187H TC and is presented here for purposes of completeness of presentation.

For a 1 1/2"– 8UN – 2A bolt, the material is SA-540 Grade B23 Class 1, with

$$S_u = 165 \text{ ksi and}$$

$$S_y = 150 \text{ ksi (at room temperature)}$$

The helicoil insert is neglected in the thread engagement length computation. It is conservative to neglect the helicoil insert, because it has a much higher tensile strength (200 ksi, [3]) than the flange material. The flange material is constructed from Type 304 stainless steel and has the following material properties.

$$S_u = 75 \text{ ksi and}$$

$$S_y = 30 \text{ ksi (at room temperature)}$$

The minimum engagement length, L_e , for the bolt and flange is ([4], p. 1149),

$$L_e = \frac{2A_t}{3.1416 K_{n \max} \left[\frac{1}{2} + .57735 n (E_{s \min} - K_{n \max}) \right]}$$

Where,

$$A_t = \text{tensile stress area} = 1.491 \text{ in.}^2,$$

$$n = \text{number of threads per inch} = 8,$$

$$K_{n \max} = \text{maximum minor diameter of internal threads} = 1.390 \text{ in. ([4], p. 1292)}$$

$$E_{s \min} = \text{minimum pitch diameter of external threads} = 1.4093 \text{ in. ([4], p. 1292)}$$

Substituting the values given above,

$$L_e = \frac{2(1.491)}{(3.1416)1.390 \left[\frac{1}{2} + .57735 (8)(1.4093 - 1.390) \right]} = 1.159 \text{ in.}$$

$$J = \frac{A_s \times S_{ue}}{A_n \times S_{ui}} \quad [4]$$

Where, S_{ue} is the tensile strength of external thread material, and S_{ui} is the tensile strength of internal thread material.

$$A_s = \text{shear area of external threads} = 3.1416 n L_e K_{n \max} \{1/(2n) + .57735 (E_{s \min} - K_{n \max})\}$$

$$A_n = \text{shear area of internal threads} = 3.1416 n L_e D_{s \min} \{1/(2n) + .57735(D_{s \min} - E_{n \max})\}$$

For the bolt/Helicoil insert connection:

$$E_{n \max} = \text{maximum pitch diameter of internal threads} = 1.4283 \text{ in. ([4], p.1292)}$$

$$D_{s \min} = \text{minimum major diameter of external threads} = 1.4828 \text{ in. ([4], p. 1292)}$$

Therefore,

$$A_s = 3.1416(8)(1.159)(1.390)\{1/(2 \times 8) + .57735 (1.4093 - 1.390)\} = 2.982 \text{ in.}^2$$

$$A_n = 3.1416(8)(1.159)(1.4828)\{1/(2 \times 8) + .57735 (1.4828 - 1.4283)\} = 4.059 \text{ in.}^2$$

So,

$$J = \frac{2.982(165.0)}{4.059(75.0)} = 1.616$$

$$Q = L_e J = (1.159)(1.616) = 1.873 \text{ in.}$$

The actual engagement length can be calculated as:

$$4.50 \text{ in. bolt length} - 1.50 \text{ in. cover thickness} - 0.180 \text{ in. washer thickness} = 2.82 \text{ in.} > 1.873 \text{ in.}$$

A.3.9.3.7 Ram Access Cover Bolt Calculations

The design parameters of the ram access cover bolts are summarized in Table A.3.9.3-2. The ram access cover bolt data and material allowables are presented in Table A.3.9.3-3 through Table A.3.9.3-5. A temperature of 300 °F is used in the ram access cover bolt region during normal and accident conditions. The following load cases are considered in the analysis.

- Preload + temperature load (normal condition)
- Pressure load (normal condition)
- Pressure + 80 inch corner drop (accident condition)

Symbols and terminology used in this analysis are taken from NUREG/CR-6007 [1] and are reproduced in Table A.3.9.3-2.

A.3.9.3.7.1 Ram Access Cover Bolt Preload and Bolt Torque

A bolt torque range of 35 to 40 ft. lb. has been selected.

Using the minimum torque,

$$F_a = Q/KD_b = 35 \times 12 / (0.132 \times 0.50) = 6,363.6 \text{ lb.}, \text{ and}$$

$$\text{Preload stress} = F_a / \text{Stress Area (Table A.3.9.3-3)} = 6,364 / 0.142 = 44,814 \text{ psi}$$

Using the maximum torque,

$$F_a = Q/KD_b = 40 \times 12 / (0.132 \times 0.50) = 7,273 \text{ lb.}, \text{ and}$$

$$\text{Preload stress} = F_a / \text{Stress Area (Table A.3.9.3-3)} = 7,273 / 0.142 = 51,216 \text{ psi}$$

Residual torsional moment for minimum torque of 35 ft. lb. is,

$$M_{tr} = 0.5Q = .5(35 \times 12) = 210 \text{ in. lb.}$$

Residual torsional moment for maximum torque of 40 ft. lb. is,

$$M_{tr} = 0.5Q = .5(40 \times 12) = 240 \text{ in. lb.}$$

Residual tensile bolt force for maximum torque,

$$F_{ar} = F_a = 7,273 \text{ lb.}$$

A.3.9.3.7.2 Ram Access Cover Gasket Seating Load

Since a self-energizing O-ring is used, the gasket seating load is negligible.

A.3.9.3.7.3 Pressure Loads

Axial force per bolt due to internal pressure is (per Reference 1, Table 4.3),

$$F_a = \frac{\pi D_{lg}^2 (P_{li} - P_{lo})}{4 N_b}$$

D_{lg} (median cover seal diameter) = 23.16 in. Then,

$$F_a = \frac{\pi (23.16^2) (30 - 0)}{4(12)} = 1053.2 \text{ lb./bolt}$$

The fixed edge cover force is,

$$F_f = \frac{D_{lb} (P_{li} - P_{lo})}{4} = \frac{24.50(30)}{4} = 183.8 \text{ lb. in.}^{-1}$$

The fixed edge cover moment is,

$$M_f = \frac{(P_{li} - P_{lo}) D_{lb}^2}{32} = \frac{30(24.50^2)}{32} = 562.7 \text{ in. lb. in.}^{-1}$$

The shear bolt force per bolt is,

$$F_s = \frac{\pi E_l t_l (P_{li} - P_{lo}) D_{lb}^2}{2 N_b E_c t_c (1 - N_{ul})} = \frac{\pi (27.0 \times 10^6) (1.0) (30) (24.50)^2}{2(12) (27.0 \times 10^6) (3.0) (1 - 0.3)} = 1122.5 \text{ lb./bolt}$$

The radial growth of the access ring due to an internal pressure of 30 psi, δ_r , is given by the following equation.

$$\delta_r = \frac{Pr^2}{Et_c}$$

Where, P is the applied pressure (30 psi), r is the mean radius of the ram access penetration ring (12.00 in.), E is the material modulus of elasticity (27.0×10^6 psi @ 300° F [2]), and $t_c = 3.0$ in. is the thickness of the ram access penetration (Table A.3.9.3-2).

Therefore,

$$\delta_r = \frac{(30)(12.00)^2}{(27 \times 10^6)(3.00)} = 5.33 \times 10^{-5} \text{ in.}$$

Since the radial growth due to internal pressure is less than the ram access bolt clearance (0.563 in. – 0.5 in. = 0.063 in.), no shear force is generated in the ram access cover bolts. Therefore,

$$F_s = 0$$

A.3.9.3.7.4 Temperature Loads

The cover bolt material is SA-540 Grade B23 Class 1. The ram access penetration and ram access cover are both constructed from SA-240 Type 304. The bolts have a coefficient of thermal expansion of 6.9×10^{-6} in./in. °F⁻¹ at 300 °F, and the ram access penetration and ram access cover have a coefficient of thermal expansion of 9.2×10^{-6} in./in. °F⁻¹ at 300 °F. The tensile load in the bolt due to different thermal expansion is,

$$F_a = 0.25 \pi D_b^2 E_b (a_l T_l - a_b T_b)$$

$$F_a = 0.25(\pi)(0.50^2)(26.7 \times 10^6) \{ (9.2 \times 10^{-6})(230) - (6.9 \times 10^{-6})(230) \} = 2,773 \text{ lb./bolt}$$

The shear force per bolt, F_s , due to a temperature change of 230 °F is 0 lb, since there is negligible differential thermal expansion between the ram access penetration and ram access cover, which are both constructed from the same material, and since the clearance holes in the cover are oversized (0.563 in. diameter). Therefore,

$$F_s = 0$$

The temperature difference between the inside and outside of the cover will always be less than one degree (see Chapter A4). Consequently, the resulting bending moment is negligible.

$$M_f = 0$$

A.3.9.3.7.5 Impact Loads

The DSC inside the NUHOMS® OS187H Type 1 transfer cask is supported in the axial direction at the bottom of the cask by the bottom end plate. During a free drop event, the inertial load of the transfer cask internals is transferred through the bottom end plate, bottom neutron shield, and neutron shield plate to the impact target. Consequently, only the inertial load of the ram access cover itself generates loads in the bolts.

The non-prying tensile bolt force per bolt, F_a , is (per Reference 1, Table 4.5),

$$F_a = \frac{1.34 \sin(xi)(DLF)(ai)(W_l + W_c)}{N_b} = \frac{1.34 \sin(xi)(1.1)(ai)(200)}{12} = 24.57(ai) \sin(xi) \text{ lb./bolt}$$

Note: $W_l + W_c$ is assumed to be only the weight of the ram access cover, $W_c = 200$ lb. [see Table A.3.9.3-2]

The shear bolt force is,

$$F_s = \frac{\cos(xi)(ai)(W_l)}{N_b} = \frac{200(ai)\cos(xi)}{12} = 16.67(ai)\cos(xi) \text{ lb./bolt}$$

The cover shoulder during normal and accident condition drops takes shear force. Therefore,

$$F_s = 0$$

The fixed-edge cover force, F_f , is,

$$F_f = \frac{1.34 \sin(xi)(DLF)(ai)(W_l + W_c)}{\pi D_{lb}} = \frac{1.34 \sin(xi)(1.1)(ai)(200)}{\pi(24.50)} = 3.83 \sin(xi)(ai) \text{ lb. in.}^{-1}$$

The fixed-edge cover moment, M_f , is,

$$M_f = \frac{1.34 \sin(xi)(DLF)(ai)(W_l + W_c)}{8\pi} = \frac{1.34 \sin(xi)(1.1)(ai)(200)}{8\pi} = 11.73 \sin(xi)(ai) \text{ in.lb.in.}^{-1}$$

The accident condition impact load is taken to be the axial acceleration due to corner drop. As described in Section 3.1.1.4, end and corner drops are not considered credible during transfer operations under 10 CFR Part 72 because the transfer cask is always in the horizontal orientation. The evaluation below is performed in support of a 10 CFR Part 50 evaluation that may be performed by the user if the user cannot demonstrate that these accident drops are not credible. The following corner drop acceleration and impact angle are assumed to bound any possible corner drop accident scenario:

$$ai = 25 \text{ gs, and } xi = 60^\circ$$

Therefore,

$$F_a = 24.57 \times 25 \times \sin(60^\circ) = 532.0 \text{ lb./bolt,}$$

$$F_s = 0.0 \text{ lb./bolt,}$$

$$F_f = 3.83 \times 25 \times \sin(60^\circ) = 82.92 \text{ lb./in., and}$$

$$M_f = 11.73 \times 25 \times \sin(60^\circ) = 254.0 \text{ in.lb./in.}$$

The ram cover bolt individual load is summarized in the following table.

Ram Access Cover Bolt Individual Load Summary

Load Case	Applied Load		Non-Prying Tensile Force, F_a (lb.)	Torsional Moment, M_t (in. lb.)	Prying Force, F_f (lb.in.⁻¹)	Prying Moment, M_f (in. lb. in.⁻¹)
Preload	Residual	Minimum torque	6,364	210	0	0
		Maximum torque	7,273	240	0	0
Gasket	Seating load		0	0	0	0
Pressure	30 psig internal		1053.2	0	183.8	562.7
Thermal	300 °F		2,773	0	0	0
Impact	Accident condition drop		532	0	82.92	254.0

A.3.9.3.8 Ram Access Cover Bolt Load Combinations

A summary of normal and accident condition load combinations (Reference 1, Table 4.9) is presented in the following table.

Ram Access Cover Bolt Normal And Accident Load Combinations

Load Case	Combination Description		Non-Prying Tensile Force, F_a (lb.)	Torsional Moment, M_t (in. lb.)	Prying Force, F_f (lb.in.⁻¹)	Prying Moment, M_f (in. lb. in.⁻¹)
1	Preload + Temperature (Normal Condition)	Minimum torque	9,134	210	0	0
		Maximum torque	10,043	240	0	0
2	Pressure (Normal Condition)		1053.2	0	183.8	562.7
3	Pressure + Accident Impact (Accident Condition)		1585.2	0	266.7	816.7

A.3.9.3.9 Ram Access Cover Bolt Stress Calculations

Additional Prying Bolt Force (Ref. [1], Table 2.1)

The additional prying bolt force, F_{ap} , is calculated in the following way.

$$F_{ap} = -\left(\frac{\pi D_{lb}}{N_b}\right) \left[\frac{\frac{2M_f}{(D_{lo}^* - D_{lb})} - C_1(B - F_f) - C_2(B - P)}{C_1 + C_2} \right]$$

where,

$$\begin{aligned} C_1 &= 1, \\ C_2 &= \left(\frac{8}{3(D_{lo} - D_{lb})^2} \right) \left[\frac{E_l t_l^3}{1 - N_{ul}} + \frac{(D_{lo} - D_{li}) E_{lf} t_{lf}^3}{D_{lb}} \right] \left(\frac{L_b}{N_b D_b^2 E_b} \right) \\ &= \left(\frac{8}{3(26.45 - 24.50)^2} \right) \left[\frac{27.0 \times 10^6 (1.0^3)}{1 - 0.3} + \frac{(26.45 - 22.00)(27.0 \times 10^6)(3.0)^3}{24.50} \right] \left(\frac{1.00}{(12)(0.50^2)(26.7 \times 10^6)} \right) \\ &= 1.50, \end{aligned}$$

B is the non-prying tensile bolt force, and P is the bolt preload. Since $F_f = 0$, then $F_f < P$, and therefore $B = P$. Parameters B , P , F_f , and M_f are quantities per unit length of bolt circle. The equations above show that it is conservative to use the bolt preload, P , using the minimum bolt torque. For the applied inward force,

$$P = B = \frac{F_a N_b}{\pi D_{lb}} = \frac{(6,364)(12)}{\pi(24.50)} = 992.2 \text{ lb. in.}^{-1},$$

$$M_f = 816.7 \text{ in.lb. in.}^{-1}, \text{ and } F_f = 266.7 \text{ lb. in.}^{-1}.$$

Therefore,

$$\begin{aligned} F_{ap} &= -\left(\frac{\pi(24.50)}{12}\right) \left[\frac{\frac{2(266.7)}{(26.45 - 24.50)} - 1(992.2 - 266.7) - 1.50(992.2 - 992.2)}{1 + 1.50} \right] \\ &= 1159.6 \text{ lb./bolt} \end{aligned}$$

It is observed that the additional tensile bolt force due to prying plus the maximum combined accident condition load is less than the minimum applied bolt preload. Therefore the additional prying bolt force is not critical for the bolt stress evaluation.

Bolt Bending Moment ([1], Table 2.2)

The maximum bending bolt moment, M_{bb} , evaluated for normal conditions only, is evaluated as follows:

$$M_{bb} = \left(\frac{\pi D_{lb}}{N_b} \right) \left[\frac{K_b}{K_b + K_l} \right] M_f$$

K_b and K_l are based on geometry and material properties and are defined in Reference 1, Table 2.2. By substituting the values given above,

$$K_b = \left(\frac{N_b}{L_b} \right) \left(\frac{E_b}{D_{lb}} \right) \left(\frac{D_b^4}{64} \right) = \left(\frac{12}{1.00} \right) \left(\frac{26.7 \times 10^6}{24.50} \right) \left(\frac{0.50^4}{64} \right) = 1.277 \times 10^4, \text{ and}$$

$$K_l = \frac{E_l t_l^3}{3 \left[(1 - N_{ul}^2) + (1 - N_{ul})^2 \left(\frac{D_{lb}}{D_{lo}} \right)^2 \right] D_{lb}} = \frac{27.0 \times 10^6 (1.00^3)}{3 \left[(1 - 0.3^2) + (1 - 0.3)^2 \left(\frac{24.50}{26.45} \right)^2 \right] 24.50}$$

$$= 2.761 \times 10^5$$

Therefore,

$$M_{bb} = \left(\frac{\pi 24.50}{12} \right) \left[\frac{1.277 \times 10^4}{1.277 \times 10^4 + 2.761 \times 10^5} \right] M_f = 0.2836 M_f$$

For load case 2, $M_f = 562.7$ in.lb./in. Substituting this value into the equation above gives,

$$M_{bb} = 159.6 \text{ in. lb./bolt}$$

A.3.9.3.9.1 Average Tensile Stress

A summary of the applied loads for the transfer cask ram access cover bolts is provided in Section A.3.9.3.8, in the table *Ram Access Cover Bolt Normal and Accident Load Combinations*.

For both normal and accident condition load cases, the applied bolt preload maintains closure of the transfer cask ram access cover. The closure force per bolt generated by the minimum ram access cover bolt torque, with or without the additional closure force generated by thermal loads, is greater than all loads trying to open the ram access cover.

Per Reference 1, Table 5.1,

Normal and Accident Condition

$$S_{ba} = 1.2732 \frac{F_a}{D_{ba}^2} = 1.2732 \frac{10,043}{0.425^2} = 70,792 \text{ psi} = 70.8 \text{ ksi}$$

A.3.9.3.9.2 Bending Stress**Normal Condition**

$$S_{bb} = 10.186 \frac{M_{bb}}{D_{ba}^3} = 10.186 \frac{159.6}{0.425^3} = 21,177 \text{ psi} = 21.2 \text{ ksi}$$

A.3.9.3.9.3 Shear Stress

For normal conditions and for accident conditions, the average shear stress caused by shear bolt force F_s is,

$$S_{bs} = 0$$

For normal and accident conditions the maximum shear stress caused by the torsional moment M_t is,

$$S_{bt} = 5.093 \frac{M_t}{D_{ba}^3} = 5.093 \frac{240}{0.425^3} = 15,922 \text{ psi} = 15.9 \text{ ksi}$$

A.3.9.3.9.4 Maximum Combined Stress Intensity

The maximum combined stress intensity is calculated in the following way (Ref. [1], Table 5.1).

$$S_{bi} = [(S_{ba} + S_{bb})^2 + 4(S_{bs} + S_{bt})^2]^{0.5}$$

For normal conditions combine tension, shear, bending, and residual torsion.

$$S_{bi} = [(70,792 + 21,177)^2 + 4(0 + 15,922)^2]^{0.5} = 97,326 \text{ psi} = 97.3 \text{ ksi}$$

A.3.9.3.9.5 Stress Ratios

In order to meet the stress ratio requirement, the following relationship must hold for both normal and accident conditions.

$$R_t^2 + R_s^2 < 1$$

Where R_t is the ratio of average tensile stress to allowable average tensile stress, and R_s is the ratio of average shear stress to allowable average shear stress.

For normal conditions

$$R_t = 70,792/92,400 = 0.766$$

$$R_s = 15,922/55,400 = 0.287$$

$$R_t^2 + R_s^2 = (0.766)^2 + (0.287)^2 = 0.669 < 1$$

For accident conditions

$$R_t = 70,792/115,500 = 0.613$$

$$R_s = 15,922/69,300 = 0.23$$

$$R_t^2 + R_s^2 = (0.613)^2 + (0.23)^2 = 0.429 < 1$$

A.3.9.3.9.6 Bearing Stress (Under Bolt Head)

A 0.5 in. standard washer is placed under the head of each ram access cover bolt. The inside and outside diameter of the washer are 0.531 in. and 1.062 in. respectively. The diameter of the bolt clearance hole in the cover is 0.563 in. Therefore, the total bearing area under the top cover bolts, A_b , is the following.

$$A_b = (\pi/4) [1.062^2 - 0.563^2] = 0.637 \text{ in.}^2$$

According to Reference 1, bearing stress evaluation is required for normal condition loads only. For normal conditions, the maximum bearing stress under the washer, σ_b , is the following.

$$\sigma_b = 10,043 \text{ lb.} / 0.637 \text{ in.}^2 = 15,766 \text{ psi} = 15.8 \text{ ksi}$$

The normal condition allowable bearing stress on the cover is taken to be the yield stress of the cover material at 300 °F. The cover is manufactured out of SA-240 Type 304, which has a yield stress of 22.4 ksi at 300 °F.

A.3.9.3.10 Ram Access Cover Bolt Analysis Results

A summary of the stresses calculated above is given in the following table:

Summary of Stresses and Allowables

Stress Type	Normal Condition		Accident Condition	
	Stress	Allowable	Stress	Allowable
Average tensile (ksi)	70.8	92.4	70.8	115.5
Shear (ksi)	15.9	55.4	15.9	69.3
Combined (ksi)	97.3	124.7	Not Required [1]	
Interaction E.Q. $Rt2 + Rs2 < 1$	0.669	1	0.429	1
Bearing (ksi) allowable (ksi) (Sy of cover material)	15.8	22.4	Not Required [1]	

Note: The preload load case controls for both normal and accident conditions

A.3.9.3.11 Minimum Engagement Length for Ram Access Cover Bolt

The ram access cover bolt minimum engagement length evaluation is not changed from that presented in Section 3.9.3.11 for the OS187H TC and is presented here for purposes of completeness of presentation.

For a 1/2"– 13UNC – 2A bolt, the material is SA-540 Grade B23 Class 1, with

$$S_u = 165 \text{ ksi, and}$$

$$S_y = 150 \text{ ksi (at room temperature)}$$

The ram access penetration and threaded insert material are both constructed from Type 304 stainless steel and have the following material properties.

$$S_u = 75 \text{ ksi, and}$$

$$S_y = 30 \text{ ksi (at room temperature)}$$

The minimum engagement length, L_e , for the bolt and flange is ([4], p. 119)

$$L_e = \frac{2A_t}{3.1416 K_{n \max} \left[\frac{1}{2} + .57735 n (E_{s \min} - K_{n \max}) \right]}$$

Where,

A_t = tensile stress area = 0.142 in.²

n = number of threads per inch = 13

$K_{n \max}$ = maximum minor diameter of internal threads = 0.434 in. ([4], p. 1283)

$E_{s \min}$ = minimum pitch diameter of external threads = 0.4435 in. ([4], p. 1283)

Substituting the values given above,

$$L_e = \frac{2(0.142)}{(3.1416)0.434 \left[\frac{1}{2} + .57735 (13)(0.4435 - 0.434) \right]} = 0.365 \text{ in.}$$

$$J = \frac{A_s \times S_{ue}}{A_n \times S_{ui}} [4]$$

Where, S_{ue} is the tensile strength of external thread material, and S_{ui} is the tensile strength of internal thread material.

A_s = shear area of external threads = $3.1416 n L_e K_{n \max} \{1/(2n) + .57735 (E_{s \min} - K_{n \max})\}$

A_n = shear area of internal threads = $3.1416 n L_e D_{s \min} \{1/(2n) + .57735 (D_{s \min} - E_{n \max})\}$

For the bolt/Helicoil insert connection:

$E_{n\ max}$ = maximum pitch diameter of internal threads = 0.4565 in. ([4], p. 1283)

$D_{s\ min}$ = minimum major diameter of external threads = 0.4876 in. ([4], p. 1283)

Therefore,

$$A_s = 3.1416(13)(0.365)(0.434)\{1/(2 \times 13) + .57735(0.4435 - 0.434)\} = 0.2843\ \text{in.}^2$$

$$A_n = 3.1416(13)(0.365)(0.4876)\{1/(2 \times 13) + .57735(0.4876 - 0.4565)\} = 0.4101\ \text{in.}^2$$

So,

$$J = \frac{0.2843(165.0)}{0.4101(75.0)} = 1.525$$

$$Q = L_e J = (0.365)(1.525) = 0.557\ \text{in.}$$

The actual engagement length can be calculated as:

1.25 in. bolt length – 1.00 in. cover thickness + 0.66 in. cover counter bore – 0.125 in. washer thickness = 0.785 in. > 0.557 in.

A.3.9.3.12 Brittle Fracture Analysis of Top Cover Bolt

The transfer cask and its attachment bolts are designed and fabricated per ASME Subsection NC Code [6]. The fracture toughness requirements for the bolting material are specified in Section NC-2332.3, which indicates that in order to meet the fracture toughness requirements, a Charpy V-notch test shall be performed. The test shall be performed at or below the lowest service metal temperature, and all three specimens shall meet the requirements of [6], Table NC-2332.3-1. The size of the top cover bolt is 1.5" diameter, and based on [6], Table NC-2332.3-1, the required C_v value is 25 mil (lateral expansions).

In addition to the above Charpy V-notch test, a brittle fracture evaluation is performed to demonstrate that brittle fracture is not a concern for the top cover bolts.

The top cover bolts are fabricated from SA-540 Grade B23 Class 1 and have the following material properties.

Material Grade	Yield Strength, ksi (Room Temperature)	Ultimate Tensile Strength, ksi (Room Temperature)
SA-540 Grade B23 Class 1	150	165

In accordance with the ASME Code, Section II, Part A [7], the bar stocks of these materials are quenched and fully tempered (1000 – 1100 °F or higher) to produce a strong and tough microstructure.

ASM Metal Handbook [8], Figure 26 (reproduced here in Figure A.3.9.3-1) shows that a 4340 steel tempered at 1035 °F for 1 ½ hours to produce a yield strength of 158 ksi exhibits a very low Charpy impact transition temperature (< -20 °F) and an upper shelf energy of about 45 ft-lb at – 20 °F.

Reference 8, p. 705, Figure 31 (reproduced here in Figure A.3.9.3-2) shows that a medium carbon low alloy steel tempered to a yield strength of 107 ksi (like SA-193, Grade B7) would have an upper shelf energy of about 52 ft-lb and absorb about 48 ft-lb at –20 °F while material at a yield strength of 149 ksi (like SA-540 Grade B23 Class 1) would have an upper shelf energy of 35 ft-lb and absorb about 30 ft-lb at -20 °F.

The following table summarizes the equivalent impact energy of the SA-540 Grade B23 Class 1 at -20 °F and the Charpy values used for the brittle fracture evaluation.

Summary of the Equivalent Impact Energy

Material Grade	Yield Strength (ksi)	Charpy Value, -20 °F (ft-lb)	Charpy Value Used for Brittle Fracture Evaluation (ft-lb)
4340 steel tempered at 1035 °F for 1½ hours (Figure A.3.9.3-1)	158	45	
Medium-carbon low alloy (Figure A.3.9.3-2)	149	30	
SA-540 Grade B23 Class 1	150		20*

* By comparison with the similar yield strength materials, lower values are conservatively used for SA-540 Grade B23 Class 1 brittle fracture evaluations.

A brittle fracture evaluation of the top cover bolt is performed based on a service temperature of -20 °F. The work includes the following:

- Methodology
- Stress
- Material fracture toughness
- Fracture toughness criteria
- Allowable flaw calculations
- NDE Inspection Plan

Methodology

The allowable flaw sizes were performed using the Singular Integral Equation and Asymptotic Approximation [9] (see Figure A.3.9.3-3). The total applied stress intensity K_{applied} is calculated based on the following equations.

$$\sigma_{\text{net}} = P/(\pi a^2)$$

$$K_{\text{applied}} = \sigma_{\text{net}} (\pi a)^{1/2} F_1(a/b) \text{ (see Figure A.3.9.3-3 for definitions)}$$

Stress

The maximum tensile stress for the top cover bolts is 110.6 ksi and is calculated in Section A.3.9.3.5. The maximum net tensile stress is calculated based on 0.025" deep 360° circumferential crack.

$$\sigma_{\text{net}} = 110.6 \{1.5/(1.5-2 \times 0.025)\}^2 = 118.36 \text{ ksi}$$

Material Fracture Toughness

The Charpy impact value may be transformed into a fracture toughness value by using the empirical relation developed in Section 4.2 of NUREG/CR-1815 [10] as follows:

$$K_{\text{id}} = \{5E(C_v)\}^{1/2}$$

Where

K_{id} = Dynamic Fracture Toughness, psi-(in)^{1/2}

E = Modulus of Elasticity, 26.7×10^6 psi

C_v = Charpy Impact Value, 20 ft-lb

Substituting the values given above,

$$K_{id} = \{5E(C_v)\}^{1/2} = \{5 \times 26.7 \times 10^6 (20)\}^{1/2} = 51,672 \text{ psi-in}^{1/2}$$

Fracture Toughness Criteria

Using the method described in the ASME Code, Section XI, IWB-3613 [11], the limiting fracture toughness values are reduced by a factor of $\sqrt{2}$ for the accident condition and are calculated as follows:

$$K_{\text{allowable}} \leq 51,672/\sqrt{2} = 36.54 \text{ ksi-}\sqrt{\text{in}}$$

Allowable Flaw Size Calculation

Using the above load definitions, fracture toughness values and assumed flaw size (0.025"), the total applied stress intensity K_I (applied) is calculated based on the singular integral equation and asymptotic approximation (see Figure A.3.9.3-3).

$$K_{\text{applied}} = \sigma_{\text{net}} (\pi a)^{1/2} F_1(a/b)$$

$$2b = 1.5 \text{ in.} \quad b = 0.75 \text{ in.}$$

$$2a = 1.5 \text{ in.} - 2 \times 0.025 \text{ in.} = 1.45 \text{ in.} \quad a = 0.725 \text{ in.}$$

$$a/b = 0.725/0.75 = 0.97 \quad F_1(a/b) = 0.18$$

$$K_{\text{applied}} = 118.36 (\pi \times 0.725)^{1/2} (0.18) = 32.15 \text{ ksi-}\sqrt{\text{in}} \leq 36.54 \text{ ksi-}\sqrt{\text{in}}$$

NDE Inspection Plan

The results of the fracture toughness analysis show that the critical flaws in the attachment bolts which would result in unstable crack growth or brittle fracture are larger than those generally observed in the bolt and bar stock.

The allowable flaw size for the attachment bolts is 0.025 in. The attachment bolts are fabricated per ASME Subsection NC code and only visual inspection is required by this code. In order to detect the surface indication, a PT or MT will be performed using NB code paragraph NB-2583.3. The requirement is that any linear nonaxial indications are unacceptable and therefore assuming 0.025" deep 360° circumferential crack for brittle fracture evaluation is conservative.

The liquid penetrant or magnetic particle method will be used in accordance with Section V, Article 6 of the ASME Code [12].

A.3.9.3.13 Conclusions

Top cover and ram access cover bolt stresses meet the acceptance criteria of NUREG/CR-6007 *Stress Analysis of Closure Bolts for Shipping Casks* [1].

The top cover and ram cover bolt, insert, and flange thread engagement length is acceptable.

The calculated stress intensity factor for a maximum flaw size 0.025 in. is less than the allowable stress intensity factor. Hence, there is no potential for top cover bolt brittle fracture failure up to this flaw size.

A.3.9.3.14 References

1. Stress Analysis of Closure Bolts for Shipping Casks, NUREG/CR-6007, 1992.
2. American Society of Mechanical Engineers, ASME Boiler and Pressure Vessel Code, Section II, Part D, 1998 through 2000 addenda.
3. Helicoil Catalog, Heli-Coil 8-Pitch Inserts, Bulletin 913B.
4. Machinery Handbook, 21st Ed, Industrial Press, 1979.
5. Baumeister, T., Marks, L. S., *Standard Handbook for Mechanical Engineers*, 7th Edition, McGraw-Hill, 1967.
6. American Society of Mechanical Engineers, ASME Boiler and Pressure Vessel Code, Section III, Division 1, Subsection NC, 1998, through 2000 addenda.
7. American Society of Mechanical Engineers, ASME Boiler and Pressure Vessel Code, Section II, Part A, 1998, through 2000 addenda.
8. American Society for Metals (ASM) Metal Handbook (Volume 1), Notch Toughness of Steels Section, 9th Edition, 1978.
9. Singular Integral Equation (Bueckner) and Asymptotic Approximation (Benthem).
10. NUREG/CR-1815 "Recommendation for Protecting Against Failure by Brittle Fracture in Ferritic Steel Shipping Containers Up to Four Inches Thick" Lawrence Livermore National Laboratory, June 15, 1981.
11. American Society of Mechanical Engineers, ASME Boiler and Pressure Vessel Code, Section XI, 1998 through 2000 addenda.
12. American Society of Mechanical Engineers, ASME Boiler and Pressure Vessel Code, Section V, Article 6, 1998 through 2000 addenda.

Table A.3.9.3-1
Design Parameters for Top Cover Bolt Analysis

D_b	Nominal diameter of closure bolt; 1.500 in.
K	Nut factor for empirical relation between the applied torque and achieved preload is 0.132
Q	Applied torque for the preload (in.-lb)
D_{lb}	Closure lid diameter at bolt circle, 76.85 in.
D_{lg}	Closure lid diameter at the seal = 73.61 in.
E_c	Young's modulus of cask wall material, 27.0×10^6 psi @ 300 °F
E_l	Young's modulus of lid material, 27.0×10^6 psi @ 300 °F
N_b	Total number of closure bolts, 24
N_{ul}	Poisson's ratio of closure lid, 0.3, ([5]. p. 5-6)
P_{ei}	Inside pressure of cask, 30 psig
D_{lo}	Closure lid diameter at outer edge, 81.37 in.
P_{li}	Pressure inside the closure lid, 30 psig
t_c	Thickness of flange, 6.50 in.
t_l	Thickness of lid, 3.0in./1.5 in.
a_b	Thermal coefficient of expansion, bolt material, 6.9×10^{-6} in. in. ⁻¹ °F ⁻¹ at 300 °F
a_c	Thermal coefficient of expansion, cask, 9.2×10^{-6} in. in. ⁻¹ °F ⁻¹ at 300 °F
a_l	Thermal coefficient of expansion, lid, 8.8×10^{-6} in. in. ⁻¹ °F ⁻¹ at 300 °F
E_b	Young's modulus of bolt material, 26.7×10^6 psi at 300 °F
a_i	Maximum rigid-body impact acceleration (g) of the cask
DLF	Dynamic load factor to account for any difference between the rigid body acceleration and the acceleration of the contents and closure lid = 1.1
W_c	Weight of contents = 51,520 lb (fuel) + 29450 lb (basket) + 28,440 lb (canister) + 888 lb (cask spacer) = 110,298 lb
W_l	Weight of closure lid = 5,360 lb, conservatively use 5,500 lb
W_c+W_l	$110,298 + 5,500 = 115,798$ lb, conservatively use 120,000 lb
α_i	Impact angle between the cask axis and target surface
S_{yl}	Yield strength of closure lid material, 43.3 ksi @ 300 °F
S_{ul}	Ultimate strength of closure lid, 94.2 ksi @ 300 °F
S_{yb}	Yield strength of bolt material (see Table A.3.9.3-4)
S_{ub}	Ultimate strength of bolt material (see Table A.3.9.3-5)
P_{lo}	Pressure outside the cover
P_{co}	Pressure outside the cask, 0 psig (worst case scenario)
L_b	Bolt length between the top and bottom surfaces of closure, 1.50 in.

Table A.3.9.3-2
Design Parameters for Ram Access Cover Bolt Analysis

D_b	Nominal diameter of closure bolt, 0.50 in.
K	Nut factor for empirical relation between the applied torque and achieved preload is 0.132
Q	Applied torque for the preload (in.-lb.)
D_{lb}	Ram access cover diameter at bolt circle, 24.50 in.
D_{lg}	Ram access cover diameter at the seal = 23.16 in.
E_c	Young's modulus of ram access penetration wall material, 27.0×10^6 psi @ 300 °F
E_l	Young's modulus of cover material, 27.0×10^6 psi @ 300 °F
N_b	Total number of closure bolts, 12
N_{ul}	Poisson's ratio of closure ram access cover, 0.3 ([5], pp 5-6)
P_{ci}	Inside pressure of ram access penetration, 30 psig
D_{lo}	Cover diameter at outer edge, 26.45 in.
D_{li}	Cover diameter at inner edge, 22.00 in.
P_{li}	Pressure inside the cover, 30 psig
t_c	Thickness of the ram access penetration, 3.00 in.
t_l	Thickness of cover, 1.0 in.
a_b	Thermal coefficient of expansion, bolt material, 6.9×10^{-6} in. in. ⁻¹ °F ⁻¹ at 300 °F
a_c	Thermal coefficient of expansion, ram access penetration, 9.2×10^{-6} in. in. ⁻¹ °F ⁻¹ at 300 °F
a_l	Thermal coefficient of expansion, ram access cover, 9.2×10^{-6} in. in. ⁻¹ °F ⁻¹ at 300 °F
E_b	Young's modulus of bolt material, 26.7×10^6 psi at 300 °F
a_i	Maximum rigid-body impact acceleration (g) of the cask
DLF	Dynamic load factor to account for any difference between the rigid body acceleration and the acceleration of the contents and cover = 1.1
W_c	The inertial load of the transfer cask contents does not affect the cover bolts
W_l	Weight of ram access cover = 157 lb., conservatively use 200 lb.
W_c+W_l	$0 + 200 = 200$ lb.
ξ	Impact angle between the cask axis and target surface
S_{yl}	Yield strength of closure cover material, 22.4 ksi @ 300 °F
S_{ul}	Ultimate strength of closure lid, 66.2 ksi @ 300 °F
S_{yb}	Yield strength of bolt material (see Table A.3.9.3-4)
S_{ub}	Ultimate strength of bolt material (see Table A.3.9.3-5)
P_{lo}	Pressure outside the cover, 0 psig (worst case scenario)
P_{co}	Pressure outside the ram access penetration, 0 psig (worst case scenario)
L_b	Bolt length between the top and bottom surfaces of closure, 1.00 in.

**Table A.3.9.3-3
Bolt Data**

Parameter	Top cover bolts (1 1/2"– 8UN – 2A)	Ram closure bolts (1/2"– 13UNC – 2A)
N (no of threads per inch)	8	13
p (pitch)	$1/8" = .125$ in.	$1/13" = .0769$ in.
D_b (nominal diameter)	1.50 in.	0.50 in.
D_{ba} (bolt diameter for stress calculations)	$D_b - .9743p = 1.50 - .9743(0.125) = 1.378$ in.	$D_b - .9743p = 0.50 - .9743(0.0769) = 0.425$ in.
Stress area	$\pi/4 (1.378)^2 = 1.491$ in ²	$\pi/4 (0.425)^2 = 0.142$ in ²

Data from [1], Table 5.1

Table A.3.9.3-4
Allowable Stresses in Closure Bolts for Normal Conditions

(Material: SA-540 Grade B23 Class 1)

Temperature (°F)	Yield Stress ⁽¹⁾ (ksi)	Normal Condition Allowables		
		F_{tb} ^(2,4) (ksi)	F_{vb} ^(3,4) (ksi)	$S.I.$ ⁽⁵⁾ (ksi)
100	150	100.0	60.0	135.0
200	143.4	95.6	57.4	129.1
300	138.6	92.4	55.4	124.7
400	134.4	89.6	53.8	121.0
500	130.2	86.8	52.1	117.2
600	124.2	82.8	49.7	111.8

Notes:

- (1) Yield stress values are from ASME Code, Section II, Table 4 (Ratio: $S_y = 3S_m$) [2]
- (2) Allowable Tensile stress, $F_{tb} = 2/3 S_y$ (Ref. [1], Table 6.1)
- (3) Allowable shear stress, $F_{vb} = 0.4 S_y$ (Ref. [1], Table 6.1)
- (4) Tension and shear stress must be combined using the following interaction equation:

$$\frac{\sigma_{tb}^2}{F_{tb}^2} + \frac{\tau_{vb}^2}{F_{vb}^2} \leq 1.0 \quad [1]$$

Stress intensity from combined tensile, shear and residual torsion loads, $S.I. \leq 0.9 S_y$ (Ref. [1], Table 6.1)

Table A.3.9.3-5
Allowable Stresses in Closure Bolts for Hypothetical Accident Conditions

(Material: SA-540 Grade B23 Class 1)

Temperature (°F)	Yield Stress ⁽¹⁾ (ksi)	Accident Condition Allowables		
		$0.6 S_y^{(3)}$ (ksi)	$F_{tb}^{(2,4)}$ (ksi)	$F_{vb}^{(3,4)}$ (ksi)
100	150.0	90.0	115.5	69.3
200	143.4	86.0	115.5	69.3
300	138.6	83.2	115.5	69.3
400	134.4	80.6	115.5	69.3
500	130.2	78.1	115.5	69.3
600	124.2	74.5	115.5	69.3

Notes:

- (1) Yield and tensile stress values are from ASME Code, [2], Table 4, Note that S_u is 165.0 ksi at all temperatures of interest.
- (2) Allowable Tensile stress, $F_{tb} = \text{MINIMUM}(0.7 S_u, S_y)$, where $0.7 S_u = 0.7 (165.0) = 115.5$ ksi (Ref. [1], Table 6.3)
- (3) Allowable shear stress, $F_{vb} = \text{MINIMUM}(0.42 S_u, 0.6 S_y)$, where $0.42 S_u = 0.42 (165.0) = 69.3$ ksi (Ref. [1], Table 6.3)
- (4) Tension and shear stresses must be combined using the following interaction equation:

$$\frac{\sigma_{tb}^2}{F_{tb}^2} + \frac{\tau_{vb}^2}{F_{vb}^2} \leq 1.0 \quad [1]$$

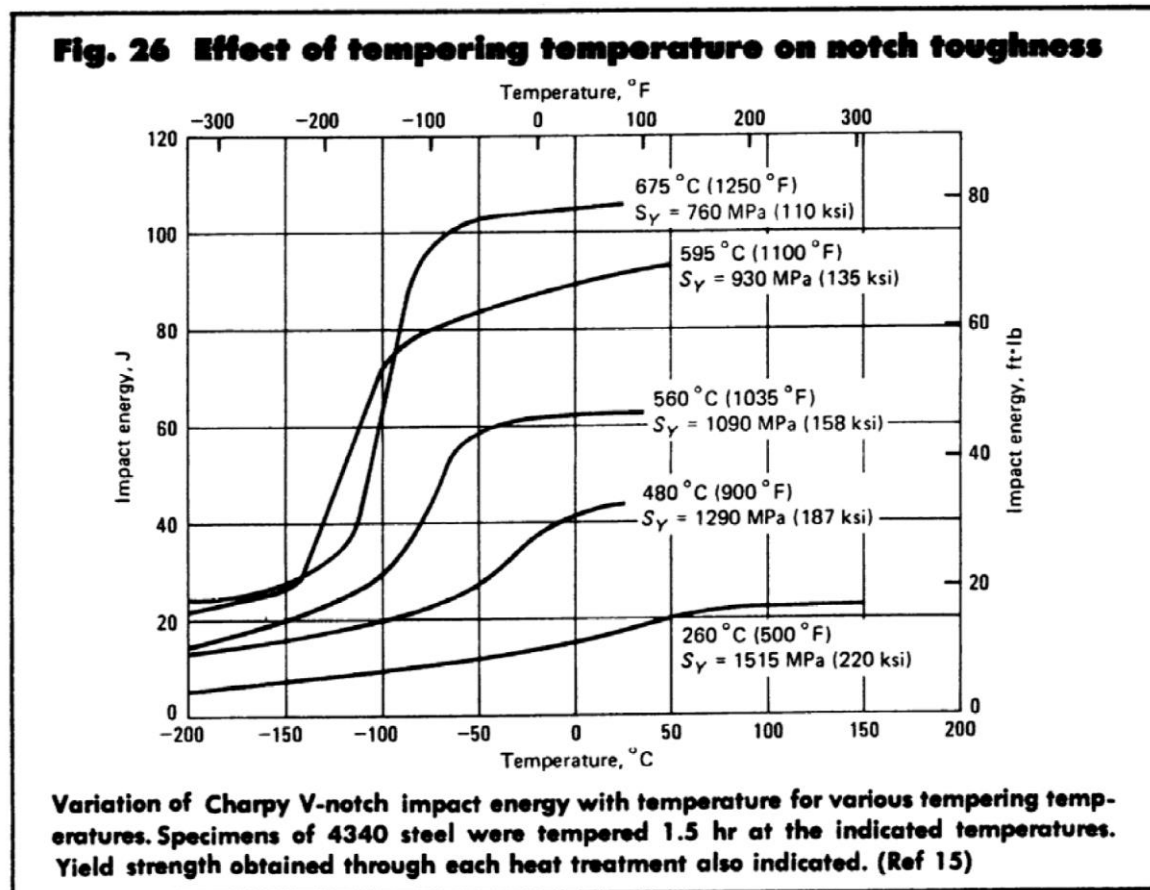


Figure A.3.9.3-1
Effect of Tempering Temperature on Notch Toughness

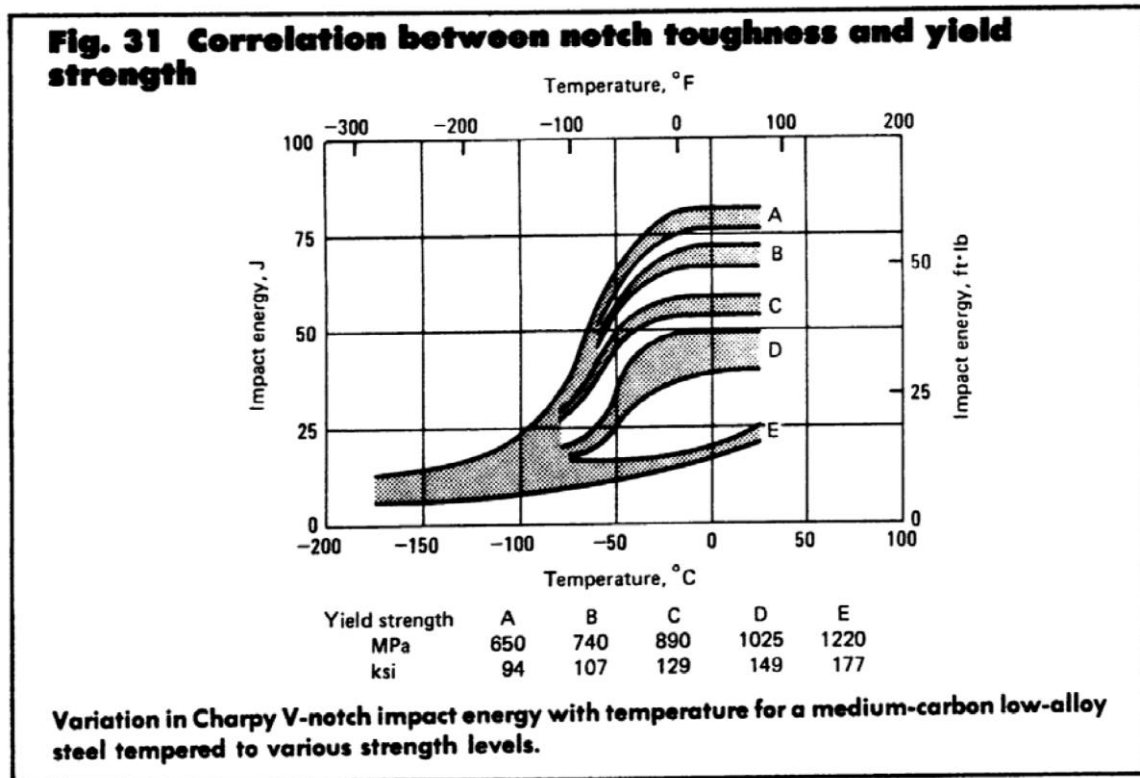


Figure A.3.9.3-2
Correlation between Notch Toughness and Yield Strength

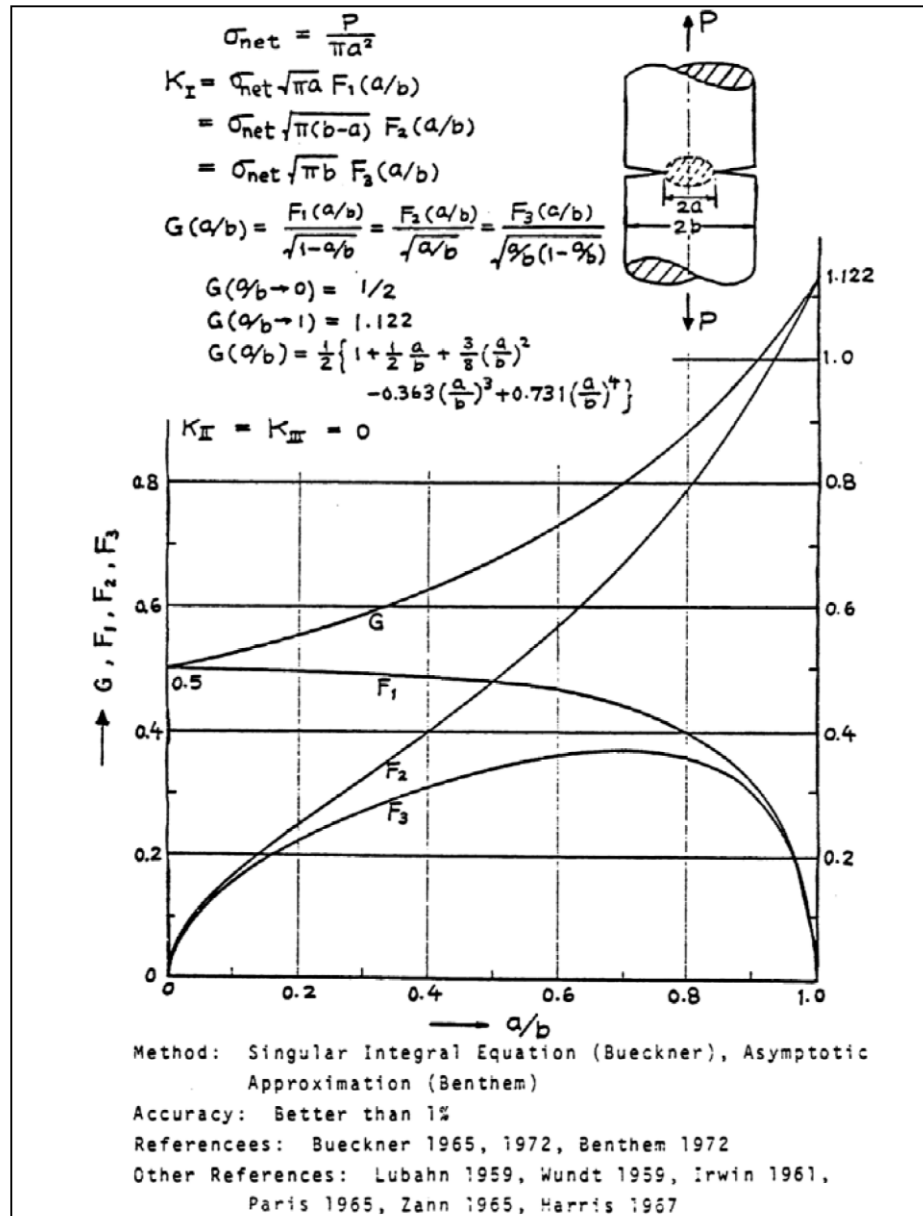


Figure A.3.9.3-3
Singular Integral Equation and Asymptotic Approximation for Brittle Fracture Evaluation

APPENDIX A.3.9.4
OS187H TYPE 1 TRANSFER CASK LEAD SLUMP AND INNER SHELL
BUCKLING ANALYSIS

In accordance with the HD System Safety Evaluation Report (SER), the top and bottom end accident drops and the corner accident drop are not credible under 10CFR Part 72 because the OS187H Type 1 transfer cask (TC) is always in the horizontal orientation. Therefore, the OS187H Type 1 TC lead slump and shell buckling analysis are not evaluated and, thus, this appendix has been deleted. These analyses may need to be evaluated under 10CFR Part 50 should the user not be able to demonstrate that the top and bottom end and the corner drops are not credible during loading operations, or during transport operations governed under 10CFR Part 71.

Appendix A.3.9.5 OS187H Type 1 Transfer Cask Trunnion Analysis

TABLE OF CONTENTS

A.3.9.5	OS187H TYPE 1 TRANSFER CASK TRUNNION ANALYSIS.....	A.3.9.5-1
A.3.9.5.1	Introduction.....	A.3.9.5-1
A.3.9.5.2	Component Weights.....	A.3.9.5-2
A.3.9.5.3	Material Properties.....	A.3.9.5-3
A.3.9.5.4	Stress Criteria.....	A.3.9.5-4
A.3.9.5.5	Load Cases.....	A.3.9.5-5
	A.3.9.5.5.1 Critical Lifts.....	A.3.9.5-5
	A.3.9.5.5.2 Transfer Handling Loads	A.3.9.5-6
A.3.9.5.6	Stress Calculation.....	A.3.9.5-7
A.3.9.5.7	Summary of Computed Stresses.....	A.3.9.5-9
A.3.9.5.8	Conclusions.....	A.3.9.5-10
A.3.9.5.9	References.....	A.3.9.5-11

LIST OF TABLES

Table A.3.9.5-1	Summary of Computed and Allowable Trunnion Stresses.....	A.3.9.5-12
-----------------	--	------------

LIST OF FIGURES

Figure A.3.9.5-1	Upper trunnion, general arrangement	A.3.9.5-13
Figure A.3.9.5-2	Lower trunnion, general arrangement.....	A.3.9.5-13
Figure A.3.9.5-3	Loads and stress sections at upper trunnion.....	A.3.9.5-14
Figure A.3.9.5-4	Loads and stress sections at lower trunnion.....	A.3.9.5-14

A.3.9.5 OS187H TYPE 1 TRANSFER CASK TRUNNION ANALYSIS

A.3.9.5.1 Introduction

This appendix presents the evaluation of the NUHOMS® OS187H Type 1 transfer cask (TC) trunnion stresses due to all applied loads during fuel loading and transfer/handling operations at normal (Service Level A) conditions.

The OS187H Type 1 TC has two upper trunnions and two lower trunnions made of monolithic forged stainless steel, SA-182 Type FXM-19 and Type F304N, respectively. Schematic representation of the upper trunnion is shown in Figure A.3.9.5-1, while the lower trunnion is shown in Figure A.3.9.5-2. The design details for both sets of trunnions are provided in Drawing 10494-72-9002-SAR in Section A.1.5.

The two upper trunnions are used to lift the TC containing a canister and an empty basket into a fuel pool prior to loading spent fuel assemblies. After the spent fuel has been loaded into the basket, the TC is lifted to a decontamination area. There, after water has been removed from the TC and the canister, the canister is sealed by welding the canister cover in place. The TC lid is lowered onto the TC and bolted in place. The TC is then placed on a trailer/transfer skid for transfer to an onsite HSM. The TC is vertically lifted above the transfer skid and then lowered until the lower trunnions rest in matching trunnion towers support pockets of the skid. The TC is downended, using the lower trunnion supports as the pivot points, to a horizontal position when the upper trunnions rest on their support pockets. Prior to the downending operation the weight of the TC is carried by the upper trunnions. During the downending, the TC weight is shared by both upper and lower trunnions. After completion of the process, the TC is supported by all four trunnions. After securing the TC onto the skid's trunnion towers, the TC is towed to the ISFSI. At the ISFSI, the TC is aligned to the HSM opening and the DSC is pushed into the HSM. During this operation, the upper trunnions take the reaction force required to push the DSC into the HSM.

Analyzed loads include lifting loads and transfer/handling loads. Acceptance criteria and applicable stress limits for upper and lower trunnions are listed in Section A.3.9.5.4. Stresses caused by handling loads are assessed against the ASME Service Level A criteria [3]. Critical lift load stresses for the upper trunnions are evaluated against ANSI N14.6 [1] criteria.

The TC shell and trunnions are assumed to be at 300 °F during transfer. This assumption is conservative based on the thermal evaluation performed in Chapter A.4.

A.3.9.5.2 Component Weights

The weight of the OS187H Type 1 TC is 240 kips, including the loaded canister (Section A.3.2.2). However, for conservatism, a weight of 250.00 kips is used in the analysis.

A.3.9.5.3 Material Properties

The following material properties, used in the trunnion stress analysis, are taken from Reference [2], for temperature 300 °F.

Material Property	SA-182, Type FXM-19 (upper trunnions)	SA-182, Type F304N (lower trunnions)
S _m	31.4 ksi	22.5 ksi
S _y	43.3 ksi	25.0 ksi
S _u	94.2 ksi	76.1 ksi

A.3.9.5.4 Stress Criteria

Critical lift load stresses at the upper trunnions are assessed against ANSI N14.6 criteria [1]. Upper and lower trunnion stresses caused by transfer and handling loads are assessed against ASME Service Level A criteria [3]. Acceptance criteria and applicable stress limits for upper trunnions and lower trunnions are listed in the table below:

	Lift Loads				Handling Loads			
Component	Upper trunnion		Lower trunnion		Upper trunnion		Lower trunnion	
Basis	ANSI N14.6		ASME Level A		ASME Level A		ASME Level A	
Stress classification	Maximum tensile	Combined shear	P_M	$P_M + P_B$	P_M	$P_M + P_B$	P_M	$P_M + P_B$
Criteria	Smaller of S_y , $0.6S_u$	Smaller of S_y , $0.6S_u$	S_m	$1.5 S_m$	S_m	$1.5 S_m$	S_m	$1.5 S_m$
Allowable stress	43.3 ksi	43.3 ksi	22.5 ksi	33.8 ksi	31.4 ksi	47.1 ksi	22.5 ksi	33.8 ksi

A.3.9.5.5 Load Cases

The trunnion design is evaluated against the following two load types:

- A. **Lifting loads**—(The OS187H Type 1 TC is in vertical position, lifted from the pool to the decontamination area and then to the trailer). The two upper trunnions are analyzed for this critical lifting load.

The two bottom trunnions are not used for lifting of the TC. However, when the vertical TC is lowered and placed onto the transfer skid, a portion of the TC weight is reacted by the lower trunnions during downending of the TC to its horizontal position.

The lifting loads for upper trunnions and lower trunnions are described in Section A.3.9.5.5.1.

- B. **Transfer handling loads**—(The OS187H Type 1 TC is in a horizontal position on the transfer trailer/skid). All four trunnions rest on the trunnion tower supports. The trunnions are designed to withstand the following transfer handling load combinations, listed below:

- 1) DW + 1g axial—axial load resisted by lower trunnions only
- 2) DW + 1g transverse—transverse load resisted by trunnions on one side of TC
- 3) DW + 1g vertical—vertical load shared by all four trunnions
- 4) DW + 1/2g axial + 1/2g transverse + 1/2g vertical

In load combination 4, the load components are distributed as defined in load combinations 1 through 3 above.

The distribution of deadweight loads onto upper trunnions and lower trunnions is described in Section A.3.9.5.5.2. In addition to the combinations listed above, the trunnion stresses are also evaluated for the envelope of all four transfer load combinations.

A.3.9.5.5.1 Critical Lifts

ANSI N14.6-1993 [1] imposes two requirements on the upper trunnion design. The first is to withstand six times the weight of the lifted TC (6g load) without generating a combined shear stress or maximum tensile stress at any point in excess of the yield strength of the trunnion material, S_y . The second is to withstand ten times the weight of the lifted TC (10g load) without generating a combined shear stress, or maximum tensile stress at any point in excess of the ultimate strength of the trunnion material, S_u .

In the evaluation, the two requirements are reduced to a single criterion for tensile/shear stress limit: the minimum of S_y and $0.6S_u$ ($0.6S_u = 6g / 10g S_u$), applied to the 6g load.

For the lifting load case, the TC weight is increased by a dynamic load factor of 15% to account for dynamic effects that may be experienced during lifting of the TC. The resulting loads are:

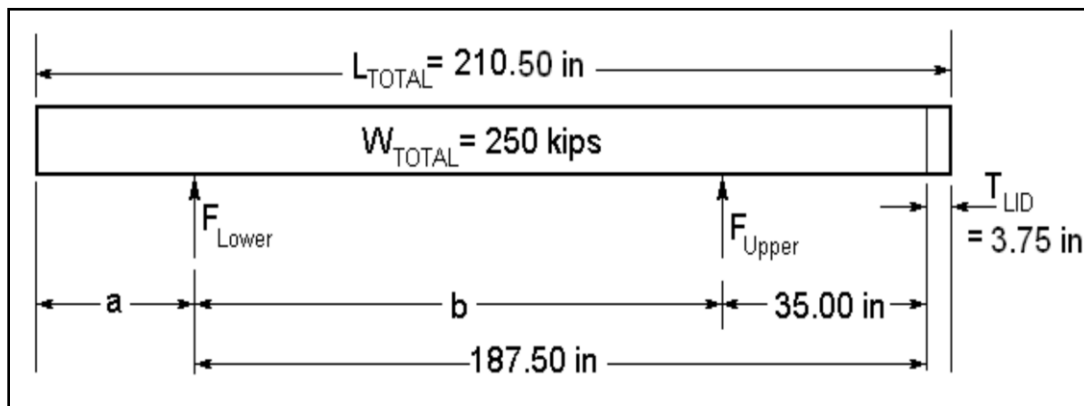
$$F_L (\text{upper trunnion}) = 1.15 \times 6 \times DW/2 = 1.15 \times 6 \times 250.0 / 2 = 862.5 \text{ kips/trunnion}$$

As discussed above, the two bottom trunnions are not used for lifting of the TC. However, the bottom trunnions react a portion of the TC weight during downending of the TC to its horizontal position. For evaluation purposes, it is conservatively assumed that the lower trunnions will react the entire weight of the cask:

$$F_L (\text{lower trunnion}) = 1.15 \times DW / 2 = 1.15 \times 250 / 2 = 143.75 \text{ kips/trunnion}$$

A.3.9.5.5.2 Transfer Handling Loads

The figure below shows the geometry derived from the OS187H Type 1 TC drawings.



These dimensions are used to calculate the reaction forces for the upper and lower trunnions. Dimensions “a” (distance from TC bottom to centerline of lower trunnion) and “b” (distance between upper and lower trunnions) are 19.25 in., and 152.5 in., respectively.

Conservatively assuming a total weight of 250 kips, the support reaction forces at the trunnions can be calculated as $F_{Upper} = 71 \text{ kips}$ for each upper trunnion, and $F_{Lower} = 54 \text{ kips}$ for each lower trunnion.

A.3.9.5.6 Stress Calculation

The geometry and major dimensions used in the stress evaluation of the upper and lower trunnions are shown in Figure A.3.9.5-1 and Figure A.3.9.5-2, respectively. Materials used for each part are listed in Section A.3.9.5.3.

Section properties and moment arms are calculated at the trunnion sections shown in Figure A.3.9.5-3 and Figure A.3.9.5-4 for the upper and lower trunnions, respectively. The following assumptions are used in the specification of loads acting on trunnions:

1. Loads from the skid and lifting yoke are assumed to act at the center of the bearing surface.
2. The lifting load is the total weight of 250 kips times a dynamic load factor of 1.15.
3. All axial and vertical loads on the lower trunnion act through the part of the trunnion that rests on the transfer skid.
4. Transverse (radial) loads are resisted by bearing of the trunnion against the skid support towers. Therefore, the radial load is resisted by Section 1-1 (see table below).

Trunnion moment arms and section properties used in calculations are presented in the table below:

Upper Trunnion

Section	OD	A	I	S	L _{SKID}	L _{LIFT}	L _{HSM}
1 - 1	17.15 in	231.0 in ²	4,246 in ⁴	495.2 in ³	7.88 in	11.38 in	13.00 in
2 - 2	12.00 in	113.1 in ²	1,018 in ⁴	169.7 in ³	1.88 in	5.38 in	7.00 in
3 - 3	8.00 in	50.27 in ²	201.1 in ⁴	50.28 in ³	n/a	1.63 in	3.25 in

Lower Trunnion

Section	OD	A	I	S	L _{SKID}	L _{LIFT}	L _{HSM}
1 - 1	14.63 in	168.1 in ²	2,249 in ⁴	307.5 in ³	8.75 in	n/a	10.5 in
2 - 2	12.00 in	113.1 in ²	1,018 in ⁴	169.7 in ³	1.75 in	n/a	3.5 in

Definitions used in the table above are explained below:

OD section diameter

A section area $A = \pi \times OD^2 / 4$

I section moment of inertia $I = \pi \times OD^4 / 64$

S section modulus $S = I \times 2 / OD$

In order to illustrate the calculation method, DW + 1g axial load case, calculated at Section 2-2 of upper trunnion (UT) is detailed below. The load for this case consists of the axial force $F_L = 0$ kips (axial load per upper trunnion) because of the sliding trunnion support, the tangential force $F_T = 71$ kips (deadweight) and the bending moment caused by the tangential force. (Radial load F_R for this case is zero, $F_R = 0$).

The acting moment arm of deadweight is $L_{SKID} = 1.88$ inches, therefore the moment induced by this force is

$$F_T \times L_{SKID} = 71 \times 1.88 = 133.5 \text{ in.-kips}$$

The total shear force acting on section 2-2 is

$$F_v = (F_L^2 + F_T^2)^{0.5} = (0^2 + 71^2)^{0.5} = 71 \text{ kips}$$

The total moment at section 2-2 is

$$M_B = (M_L^2 + M_T^2)^{0.5} = (0^2 + 133.5^2)^{0.5} = 133.5 \text{ in.-kips}$$

The maximum shear stress for a solid circular section is $4/3 \times (\text{Shear Force})/(\text{Section Area})$ (Reference [4], page 129). The area of section 2-2 is $A = 113.1 \text{ in}^2$, so the maximum shear stress at section 2-2 is

$$S_v = 4 \times F_v / (A \times 3) = 4 \times 71 / (113.1 \times 3) = 0.837 \text{ ksi}$$

The maximum bending stress is calculated as $S_B = (\text{Total Acting Moment})/(\text{Section Modulus})$. The section modulus of section 2-2 is $S = 169.7 \text{ in}^3$. The resulting bending stress is then

$$S_B = M_B / S = 133.5 / 169.7 = 0.787 \text{ ksi}$$

Maximum normal stress for section 2-2 is calculated as

$$S_R = S_B + F_R / A = 0.787 + 0.0 / 113.1 = 0.787 \text{ ksi}$$

Maximum combined shear stress is calculated as

$$S_v^{\max} = ((S_R/2)^2 + S_v^2)^{0.5} = ((0.787 / 2)^2 + 0.837^2)^{0.5} = 0.925 \text{ ksi}$$

Maximum tensile stress is calculated as

$$S_{\max} = S_B/2 + S_v^{\max} = 0.787 / 2 + 0.925 = 1.319 \text{ ksi}$$

Finally, membrane stress intensity P_M and membrane plus bending stress intensity $P_M + P_B$ are calculated respectively as:

$$P_M = ((F_R/A)^2 + 4 \times S_v^2)^{0.5} = ((0.0 / 113.1)^2 + 4 \times (0.837)^2)^{0.5} = 1.674 \text{ ksi}$$

$$P_M + P_B = 2 \times S_v^{\max} = 2 \times 0.925 = 1.850 \text{ ksi}$$

A.3.9.5.7 Summary of Computed Stresses

The calculated maximum trunnion stresses are summarized in Table A.3.9.5-1 and compared with their corresponding allowable stresses.

A.3.9.5.8 Conclusions

Table A.3.9.5-1 shows that all calculated trunnion stresses are less than their corresponding allowable stresses. Therefore, the NUHOMS[®] OS187H Type 1 TC trunnions are structurally adequate to withstand loads during lifting and transfer operations.

A.3.9.5.9 References

1. “Special Lifting Devices for Shipping Containers Weighing 10,000 Pounds or More,” ANSI N14.6, 1993.
2. American Society of Mechanical Engineers, ASME Boiler and Pressure Vessel Code, Section II, Part D, 1998, through 2000 addenda.
3. American Society of Mechanical Engineers, ASME Boiler and Pressure Vessel Code, Section III, Division 1, Subsection NC, 1998, through 2000 addenda.
4. Warren C. Young, Richard G. Budynas, “Roark’s Formulas for Stress and Strain,” Seventh Edition, 2002, McGraw-Hill.

Table A.3.9.5-1
Summary of Computed and Allowable Trunnion Stresses

Upper Trunnions

Load type	Load combination	Maximum Stress [ksi]		Allowable (ksi)	Stress ratio
		Type	Magnitude		
Lifting loads	Critical lift	Combined shear	26.81	43.3	0.62
		Max tensile	40.79	43.3	0.94
Handling loads	DW+1g axial	PM	1.67	31.4	0.05
		PM+PB	1.85	47.1	0.04
	DW+1g transverse	PM	1.67	31.4	0.05
		PM+PB	1.93	47.1	0.04
	DW+1g vertical	PM	3.35	31.4	0.11
		PM+PB	3.70	47.1	0.08
	1/2g axial + 1/2g transverse + 1/2g vertical + DW	PM	2.51	31.4	0.08
		PM+PB	2.78	47.1	0.06

Lower Trunnions

Load type	Load combination	Maximum stress [ksi]		Allowable (ksi)	Stress ratio
		Type	Magnitude		
Lifting loads	Critical lift	PM	3.39	22.5	0.15
		PM+PB	4.69	33.8	0.14
Handling loads	DW+1g axial	PM	3.21	22.5	0.14
		PM+PB	4.44	33.8	0.13
	DW+1g transverse	PM	1.27	22.5	0.06
		PM+PB	2.34	33.8	0.07
	DW+1g vertical	PM	2.55	22.5	0.11
		PM+PB	3.52	33.8	0.10
	1/2g axial + 1/2g transverse + 1/2g vertical + DW	PM	2.41	22.5	0.11
		PM+PB	3.62	33.8	0.11

Proprietary Information on This Page
Withheld Pursuant to 10 CFR 2.390

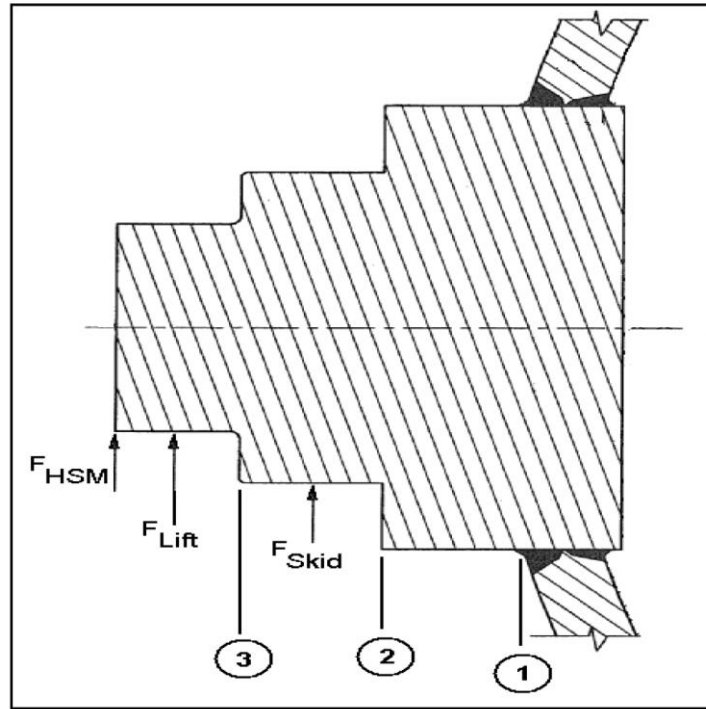


Figure A.3.9.5-3
Loads and stress sections at upper trunnion

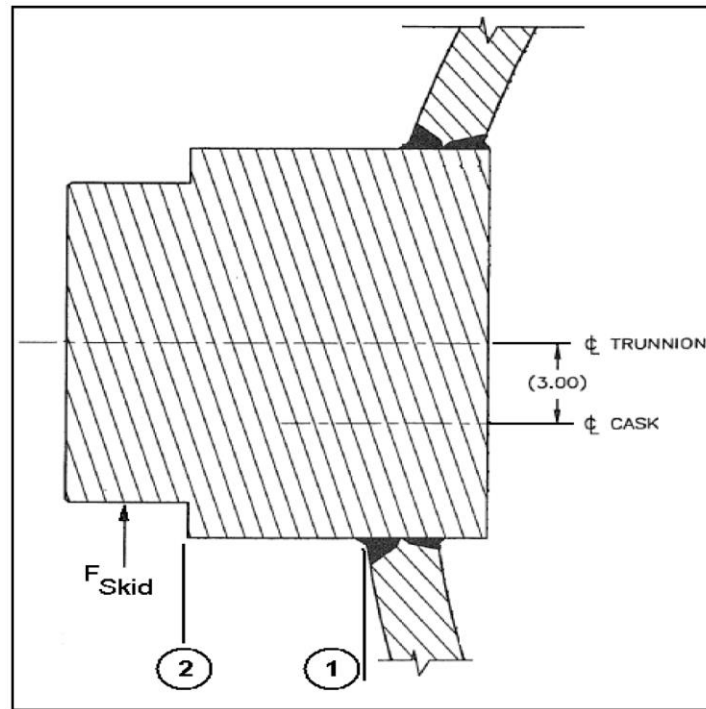


Figure A.3.9.5-4
Loads and stress sections at lower trunnion

Appendix A.3.9.6

OS187H TYPE 1 Transfer Cask Shield Panel Structural Analysis

TABLE OF CONTENTS

A.3.9.6	OS187H TYPE 1 TRANSFER CASK SHIELD PANEL STRUCTURAL ANALYSIS	A.3.9.6-1
A.3.9.6.1	Introduction.....	A.3.9.6-1
A.3.9.6.2	Material Properties.....	A.3.9.6-2
A.3.9.6.3	Component Weights.....	A.3.9.6-3
A.3.9.6.4	Stress Criteria.....	A.3.9.6-4
A.3.9.6.5	Load Cases.....	A.3.9.6-5
A.3.9.6.6	Stress Calculations	A.3.9.6-6
	A.3.9.6.6.1 3 g Lifting Load Case	A.3.9.6-6
	A.3.9.6.6.2 Transfer Load Condition.....	A.3.9.6-6
	A.3.9.6.6.3 Thermal Analyses	A.3.9.6-7
	A.3.9.6.6.4 Thermal Stress Analyses.....	A.3.9.6-7
	A.3.9.6.6.5 Weld Stresses	A.3.9.6-7
A.3.9.6.7	Conclusions.....	A.3.9.6-8
A.3.9.6.8	References.....	A.3.9.6-9

LIST OF TABLES

Table A.3.9.6-1	Summary of Calculated and Allowable Neutron Shield Shell Stresses	A.3.9.6-10
Table A.3.9.6-2	Summary of Weld Stresses (3 g Lifting)	A.3.9.6-10
Table A.3.9.6-3	Summary of Weld Stresses (Transfer Load).....	A.3.9.6-11

LIST OF FIGURES

Figure A.3.9.6-1	Neutron Shield Shell Finite Element Model.....	A.3.9.6-12
Figure A.3.9.6-2	Neutron Shield Shell Finite Element Model, Top Plate Region	A.3.9.6-13
Figure A.3.9.6-3	Neutron Shield Shell Finite Element Model, Bottom Plate Region	A.3.9.6-14
Figure A.3.9.6-4	Neutron Shield Shell Finite Element Model, 3 g Lifting Loads	A.3.9.6-15
Figure A.3.9.6-5	3 g Lifting Stress Intensity Distribution.....	A.3.9.6-16
Figure A.3.9.6-6	Neutron Shield Shell Finite Element Model, Transfer Loads.....	A.3.9.6-17
Figure A.3.9.6-7	Transfer Loads Stress Intensity Distribution	A.3.9.6-18
Figure A.3.9.6-8	Cold Ambient Environment Temperature Distribution	A.3.9.6-19
Figure A.3.9.6-9	Hot Ambient Environment Temperature Distribution	A.3.9.6-20
Figure A.3.9.6-10	Transfer Loads plus Cold Ambient Condition Stress Intensity Distribution	A.3.9.6-21
Figure A.3.9.6-11	Transfer Loads plus Hot Ambient Condition Stress Intensity Distribution	A.3.9.6-22

A.3.9.6 OS187H TYPE 1 TRANSFER CASK SHIELD PANEL STRUCTURAL ANALYSIS

A.3.9.6.1 Introduction

The purpose of this appendix is to present the evaluation of the stresses in the NUHOMS[®] OS187H Type 1 transfer cask (TC) neutron shield shell assembly due to all applied loads during fuel loading and transfer operations.

A finite element model of the neutron shield shell assembly was built for the structural analysis. The model includes the outer neutron shield panel, the top and bottom support ring plates, the shield panel stiffener plates, and the structural shell. These components were modeled with the ANSYS 2D Structural Solid PLANE42 elements with axisymmetric option. Double nodes were created at all weld locations. These nodes were coupled in x and y directions to simulate the weld effect. Figure A.3.9.6-1, Figure A.3.9.6-2 and Figure A.3.9.6-3 show the overall finite element model and its details. The same finite element model is used for all loading conditions.

A.3.9.6.2 Material Properties

The TC neutron shield shell is assumed to be at a 300 °F uniform temperature during transfer operations. This assumption is based on the thermal evaluations performed in Chapter 4. Material allowables are conservatively taken at 350 °F.

All shell components are constructed from stainless steel SA-240, Grade 304. The following mechanical and thermal material properties taken from Reference 1 are used in the analysis:

Material	Temp. °F	S_u (ksi)	S_y (ksi)	S_m (ksi)	E (106 psi)	α (10-6) (in/in/°F)	Conductivity (Btu/hr-in-°F)	Density (lb/in³)
SA-240 Stainless Steel 304	70	75.0	30.0	20.0	28.3	8.5	0.7217	0.29
	200	71.0	25.0	20.0	27.6	8.9	0.775	0.29
	300	66.2	22.4	20.0	27.0	9.2	0.8167	0.29
	400	64.0	20.7	18.7	26.5	9.5	0.8667	0.29

A.3.9.6.3 Component Weights

The weight of the NUHOMS® OS187H Type 1 TC neutron shield shell, including the cylindrical shell, the top and bottom support rings, and the 16 central support rings is 5,134 lb. The weight of the neutron shield shell water is 8,671 lb (the transfer component weights are tabulated in Section A.3.2). However, for conservatism, a bounding weight of 8,900 lb. is used for the weight of water in this analysis.

For the TC in the vertical orientation, the inertial force due to water weight is applied as pressure in the following way.

The weight of the neutron shield water, W is 8,900 lb. The maximum hydrostatic pressure at the bottom of the neutron shield shell, W_h , is,

$$W_h = 62.4 \text{ lb/ft}^3 \times 190.1 \text{ in} / 12^3 = 6.86 \text{ psi}$$

This hydrostatic pressure is uniformly applied to the entire internal region of the neutron shield.

In addition to the water weight pressure, an additional internal uniform pressure of 45 psig is used in all load cases.

A.3.9.6.4 Stress Criteria

All load cases are analyzed and results evaluated to the requirements of ASME Code, Subsection NC [2] as normal condition (Level A) load cases. According to Reference 2, the maximum allowable membrane (P_m) and membrane plus bending ($P_m + P_b$) stress intensities for normal conditions are S_m and $1.5 S_m$, respectively. Also, average pure shear is limited to $0.6 S_m$. The maximum primary plus secondary stress is limited to $3.0 S_m$.

The components of the neutron shield shell assembly are constructed from SA-240, Type 304 stainless steel. Therefore, the maximum allowable membrane and membrane plus bending stress intensities (conservatively taken at 350 °F) are as follows:

Stress Category	Stress Criteria	Maximum Allowable Stress
P_m	S_m	19.35 ksi
$P_m + P_b$	$1.5 S_m$	29.03 ksi
$P_m + P_b + Q$	$3.0 S_m$	58.05 ksi
Pure Shear	$0.6 S_m$	11.61 ksi

A.3.9.6.5 Load Cases

The following load cases are considered. When transferring the loaded cask to the ISFSI, the transfer loads are 1 g axial, 1 g transverse, and 1 g vertical. For conservatism, a bounding 2 g axial + 2 g transverse + 2 g vertical is used for stress calculations.

Load Case	Applied Load
3 g Lifting (cask vertical)	45 psi pressure + hydrostatic pressure + 3 g longitudinal
Transfer loads (cask horizontal)	45 psi pressure + water pressure + 2 g longitudinal + 2 g vertical + 2 g transverse + dead weight 45 psi pressure + water pressure + 2 g longitudinal + 2 g vertical + 2 g transverse + cold thermal + dead weight 45 psi pressure + water pressure + 2 g longitudinal + 2 g vertical + 2 g transverse + hot thermal + dead weight

A.3.9.6.6 Stress Calculations

A.3.9.6.6.1 3 g Lifting Load Case

The pressure at the bottom plate due to the 3 g lifting load for water = $3 \times 6.86 = 20.58$ psi (use 21 psi).

The ANSYS elastic stress run is made by applying a 45 psi internal pressure and a 21 psi hydrostatic pressure. The loading applied to the model is shown in Figure A.3.9.6-4. A 3 g vertical acceleration is applied to account for the inertia loads. As shown in Figure A.3.9.6-4, an internal pressure of 66.0 psi (45 psi + 21 psi) is uniformly applied to the entire internal region of the neutron shield.

The resulting stress intensity distribution in the various shell components is shown in Figure A.3.9.6-5. It is seen that the maximum nodal stress intensity in the shell model is 28,058 psi. This maximum stress occurs near the weld between the center support ring and the neutron shield panel. In the stress evaluation, nodal stresses corresponding to the centerline nodes (through the component's plate thicknesses) are considered membrane stresses. Conservatively, membrane plus bending stresses are taken as the maximum stress at any node in the various structural components. These stresses are presented in Table A.3.9.6-1.

A.3.9.6.6.2 Transfer Load Condition

During transfer operations, the cask is in the horizontal position and the neutron shield shell is subjected to 45 psi internal pressure, transfer handling loads (2 g vertical + 2 g lateral + 2 g axial) and dead weight.

The vertical and lateral loads are combined in the following way.

$$g_{transverse} = (3.0^2 + 2.0^2)^{1/2} = 3.61 \text{ g}$$

The stress due to the 3.61 g inertia load conservatively assumes that the weight of the shell structure (5,134 lb.) and water (8,900 lb.) are uniformly distributed only over the 190.1 inch length and a 60° arc. Therefore, the equivalent pressure applied to the outer shell is,

$$p_{vl} = [(5,134 + 8,900) \times 3.61] / [2 \pi (45.87)(190.1) \times (60^\circ/360^\circ)] = 5.55 \text{ psi}$$

Again, the 5.55 psi load on the 60° sector is conservatively assumed to act on the full 360°. This pressure is added to 45 psi pressure and applied to the shield shell.

For 2 g axial acceleration, the pressure due to the water inertial load on the top plate is,

$$p_a = 8,900 \times 2.0 / [\pi \times (45.87^2 - 40.935^2)] = 13.23 \text{ psi}$$

Therefore, a pressure of 58.23 psi (45 + 13.23) is applied to the top plate. Also, there is a 45 psi pressure applied to the bottom plate.

An ANSYS elastic stress run is made by applying the above calculated pressures to the finite element model. The loading is shown in Figure A.3.9.6-6. The resulting stress intensity distribution is shown in Figure A.3.9.6-7. It is seen that the maximum nodal stress intensity in the shell model is 21,458 psi. This maximum stress occurs in the outer shell near the bottom plate weld. Nodal stresses at the middle thickness (considered P_m) and the maximum stresses (considered $P_m + P_b$) are summarized and evaluated in Table A.3.9.6-1.

A.3.9.6.6.3 Thermal Analyses

The thermal analysis of the neutron shield shell assembly model is conducted for both cold and hot environmental conditions. Steady-state ANSYS thermal analyses of the model are conducted to obtain the nodal temperature distribution in the structural model by mapping the temperatures from the thermal heat transfer analysis model as the boundary conditions for both cold and hot conditions. The mapped temperature distribution bounds that resulting from the Chapter 4 thermal analysis. Two-dimensional thermal elements (PLANE55) are used in the analyses. Temperature dependent thermal material properties are also used in the analysis.

The resulting temperature distributions for cold and hot ambient cases are shown in Figure A.3.9.6-8 and Figure A.3.9.6-9, respectively.

A.3.9.6.6.4 Thermal Stress Analyses

Elastic stress analyses of the neutron shield shell structure are conducted in order to evaluate the transfer plus thermal loads. The transfer condition loading as shown in Figure A.3.9.6-6 and the nodal temperature distribution from the above thermal analyses results are combined and applied to the stress model to obtain the transfer plus thermal stresses in the model.

The nodal stress intensity distribution is shown in Figure A.3.9.6-10 for the cold condition analysis case and in Figure A.3.9.6-11 for the 115 °F hot ambient condition case. The critical stress intensities (considered $P_m + P_b + Q$ stresses) are summarized in Table A.3.9.6-1.

It is seen from Figure A.3.9.6-10 and Figure A.3.9.6-11 that the maximum thermal stress intensities are generated in the cold ambient case. The maximum nodal stress intensity in the neutron shield shell assembly model is 26,805 psi. This maximum stress occurs in the outer shell near the bottom support ring plate weld. Cold and hot nodal stresses maximum stresses are summarized and evaluated in Table A.3.9.6-1.

A.3.9.6.6.5 Weld Stresses

Per Section A.3.9.6.4, the pure shear allowable stress in the fillet and plug welds is 0.6 times the base material allowable membrane stress. The analysis utilizes an axisymmetric model for which loads and force results are applied on a 360-degree basis, the weld stress is based on the total area of the weld around the circumference of the structure. The weld stresses are summarized in Table A.3.9.6-2 for the 3 g lifting load case and Table A.3.9.6-3 for the transfer load cases.

A.3.9.6.7 Conclusions

Based on the results of the analyses, it is concluded that the outer shell structure is structurally adequate for the specified lifting and transfer loads.

A.3.9.6.8 References

1. American Society of Mechanical Engineers, ASME Boiler and Pressure Vessel Code, Section II, Part D, 1998, including 2000 addenda.
2. American Society of Mechanical Engineers, ASME Boiler and Pressure Vessel Code, Section III, Division 1, Subsection NC, 1998, including 2000 addenda.

Table A.3.9.6-1
Summary of Calculated and Allowable Neutron Shield Shell Stresses

Load Case	Stress Category	Maximum Stress (ksi)	Allowable Stress (ksi)
3 g lifting	P_m	17.73	19.35
	$P_m + P_b$	28.06	29.02
Transfer load	P_m	13.64	19.35
	$P_m + P_b$	21.46	29.02
	$P_m + P_b + Q$ (Cold)	26.81	58.05
	$P_m + P_b + Q$ (Hot)	24.78	58.05

Table A.3.9.6-2
Summary of Weld Stresses (3 g Lifting)

Stress	Weld Locations				
	Top and Bottom Support Rings, Structural Shell	Central Support Rings, Structural Shell	Central Support Rings, T Section	Neutron Shield Shell Plug Welds	Neutron Shield Shell, Top and Bottom Rings
Max. shear (S) [kips]	41.85	32.92	19.74	2.6	97.6
Max. tension (T)[kips]	265.76	74.89	68.07	72.36	17.3
Weld area (A) [in ²]	56.8	11.4	7.58	4.5	38.3
Tensile stress (S1=T/A) [ksi]	4.68	6.57	8.98	16.08	0.45
Shear stress (S2=S/A) [ksi]	0.74	2.89	2.60	0.58	2.55
Max. stress intensity ($S=(S1^2+4S2^2)^{1/2}$) [ksi]	4.91	8.75	10.38	16.12	5.12
Pure shear allowable stress 0.6 S_m (Sa1) [ksi]	11.61	11.61	11.61	11.61	11.61
Weld allowable stress (Sa2) S_m [ksi]	19.35	19.35	19.35	19.35	19.35
Shear stress ratio (S2/Sa1)	0.06	0.25	0.22	0.05	0.22
Stress ratio (S/Sa2)	0.25	0.45	0.54	0.83	0.26

Table A.3.9.6-3
Summary of Weld Stresses (Transfer Load)

Stress	Weld Location				
	Top and Bottom Support Rings, Structural Shell	Central Support Rings, Structural Shell	Central Support Rings, T Section	Neutron Shield Shell Plug Welds	Neutron Shield Shell, Top and Bottom Rings
Max. shear (S) [kips]	36.92	32.95	1.36	2.71	92.68
Max. tension (T)[kips]	239.56	77.86	73.19	80.69	17.38
Weld area (A) [in ²]	56.8	11.4	7.58	4.5	38.3
Tensile stress (S1=T/A) [ksi]	4.22	6.83	9.66	17.93	0.45
Shear stress (S2=S/A) [ksi]	0.65	2.89	0.18	0.60	2.42
Max. stress intensity ($S=(S1^2+4S2^2)^{1/2}$) [ksi]	4.41	8.95	9.66	17.97	4.86
Pure shear allowable stress $0.6S_m$ (Sa1) [ksi]	11.61	11.61	11.61	11.61	11.61
Weld allowable stress (Sa2) S_m [ksi]	19.35	19.35	19.35	19.35	19.35
Shear stress ratio (S2/Sa1)	0.06	0.25	0.02	0.05	0.21
Stress ratio (S/Sa2)	0.23	0.46	0.50	0.93	0.25

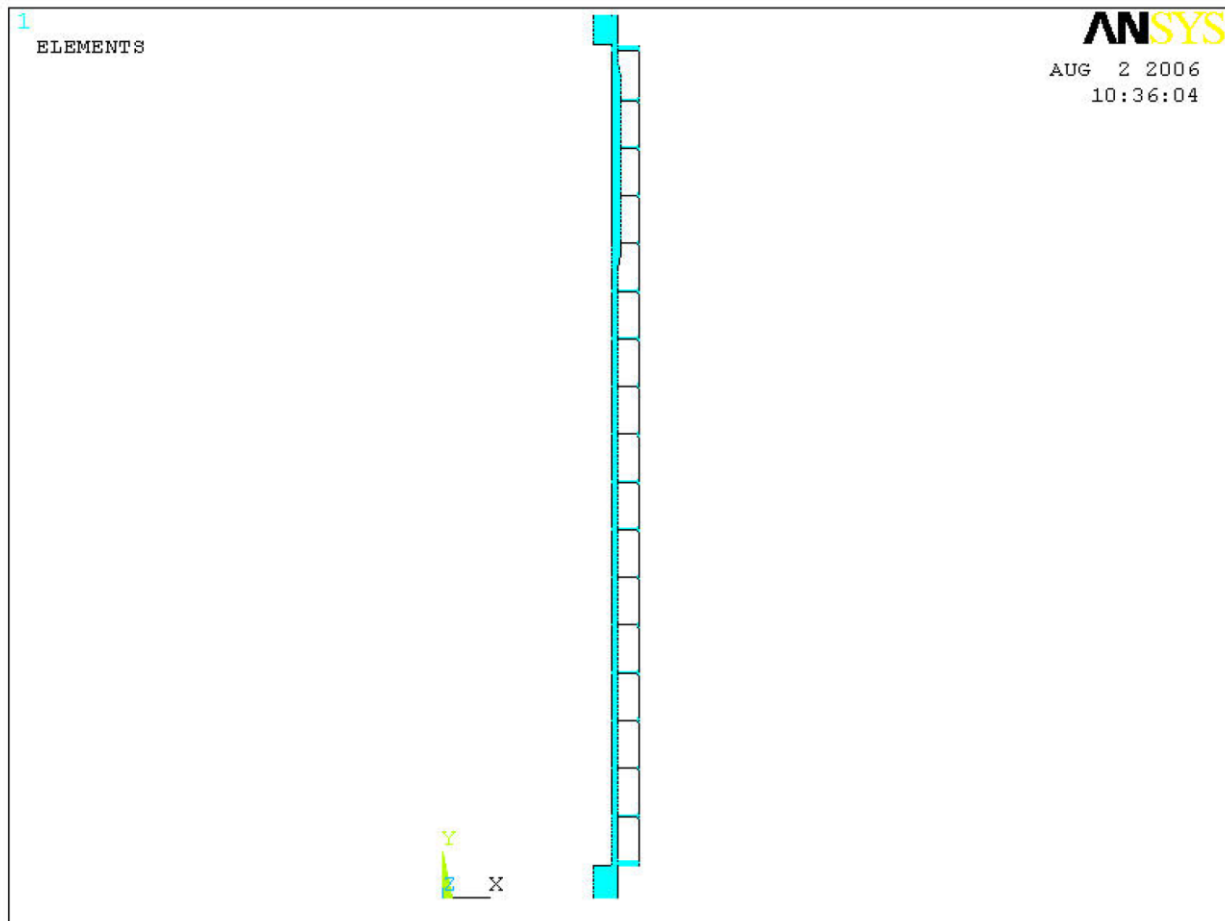


Figure A.3.9.6-1
Neutron Shield Shell Finite Element Model

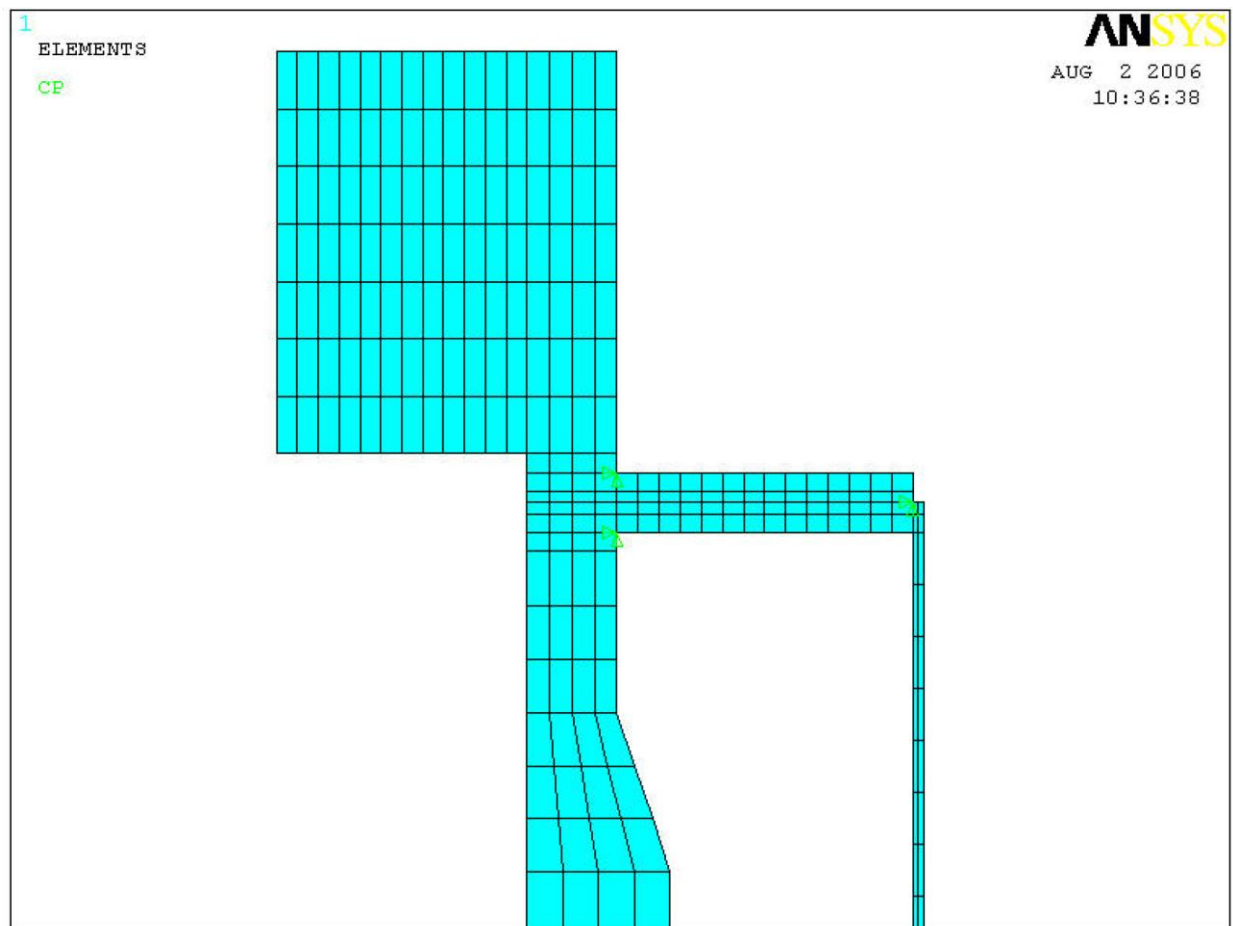


Figure A.3.9.6-2
Neutron Shield Shell Finite Element Model, Top Plate Region

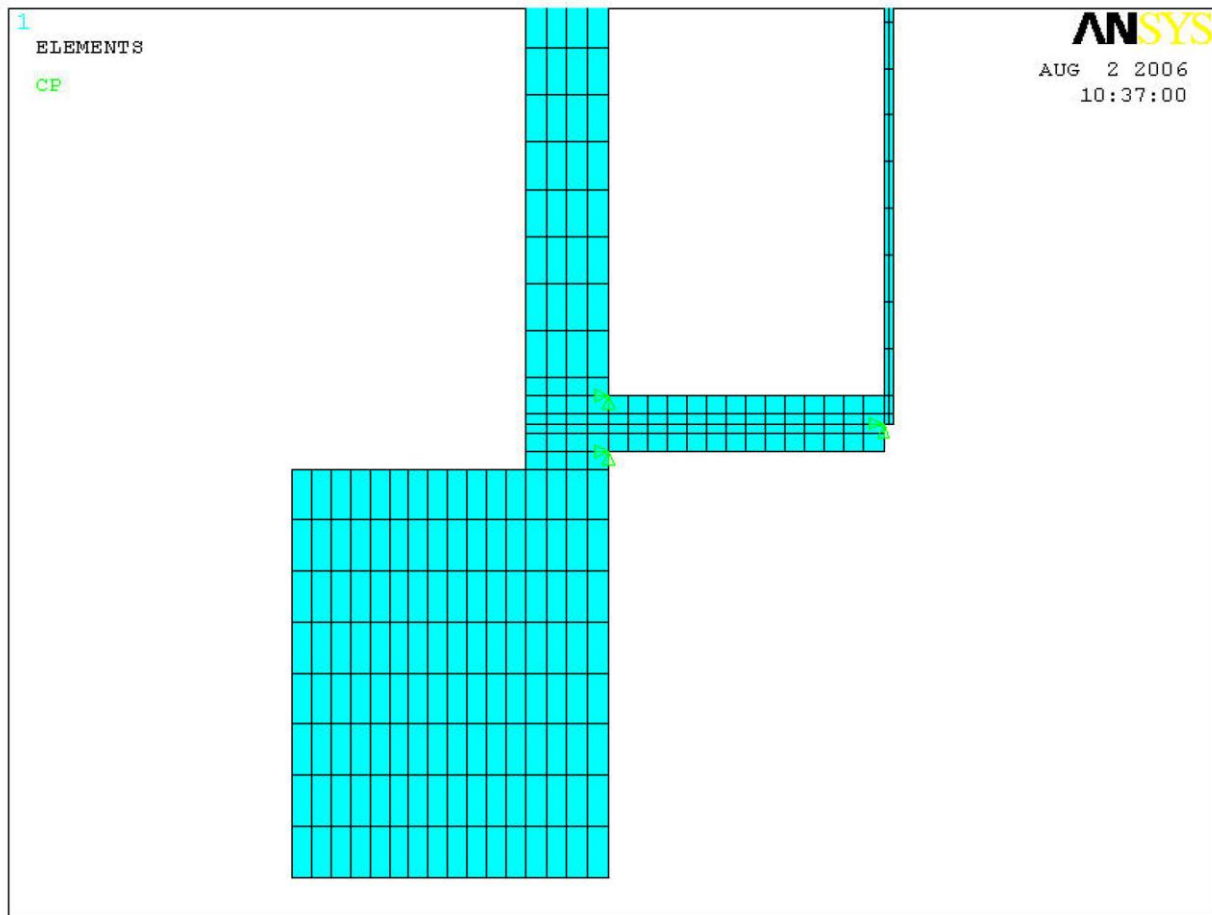


Figure A.3.9.6-3
Neutron Shield Shell Finite Element Model, Bottom Plate Region

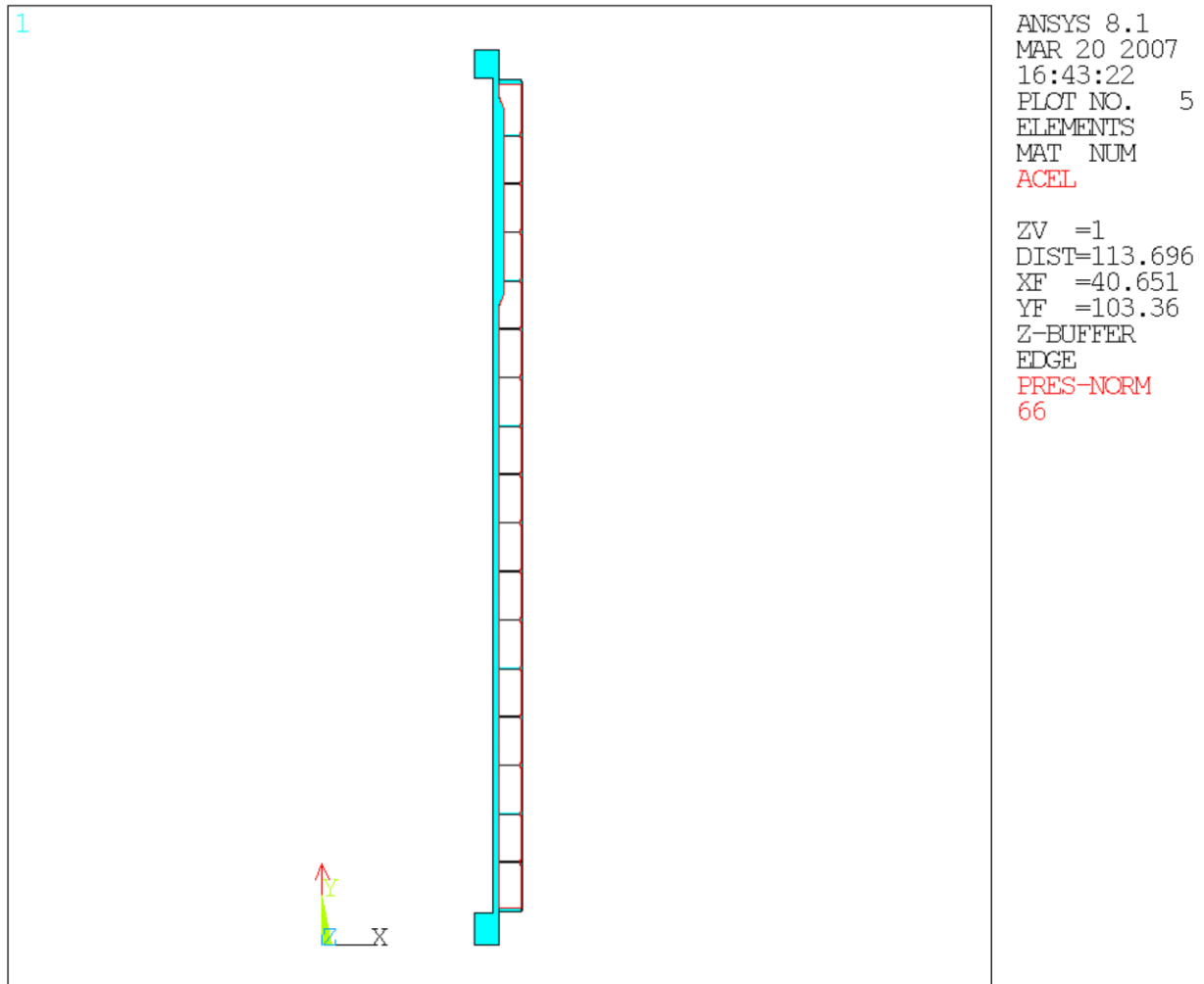


Figure A.3.9.6-4
Neutron Shield Shell Finite Element Model, 3 g Lifting Loads

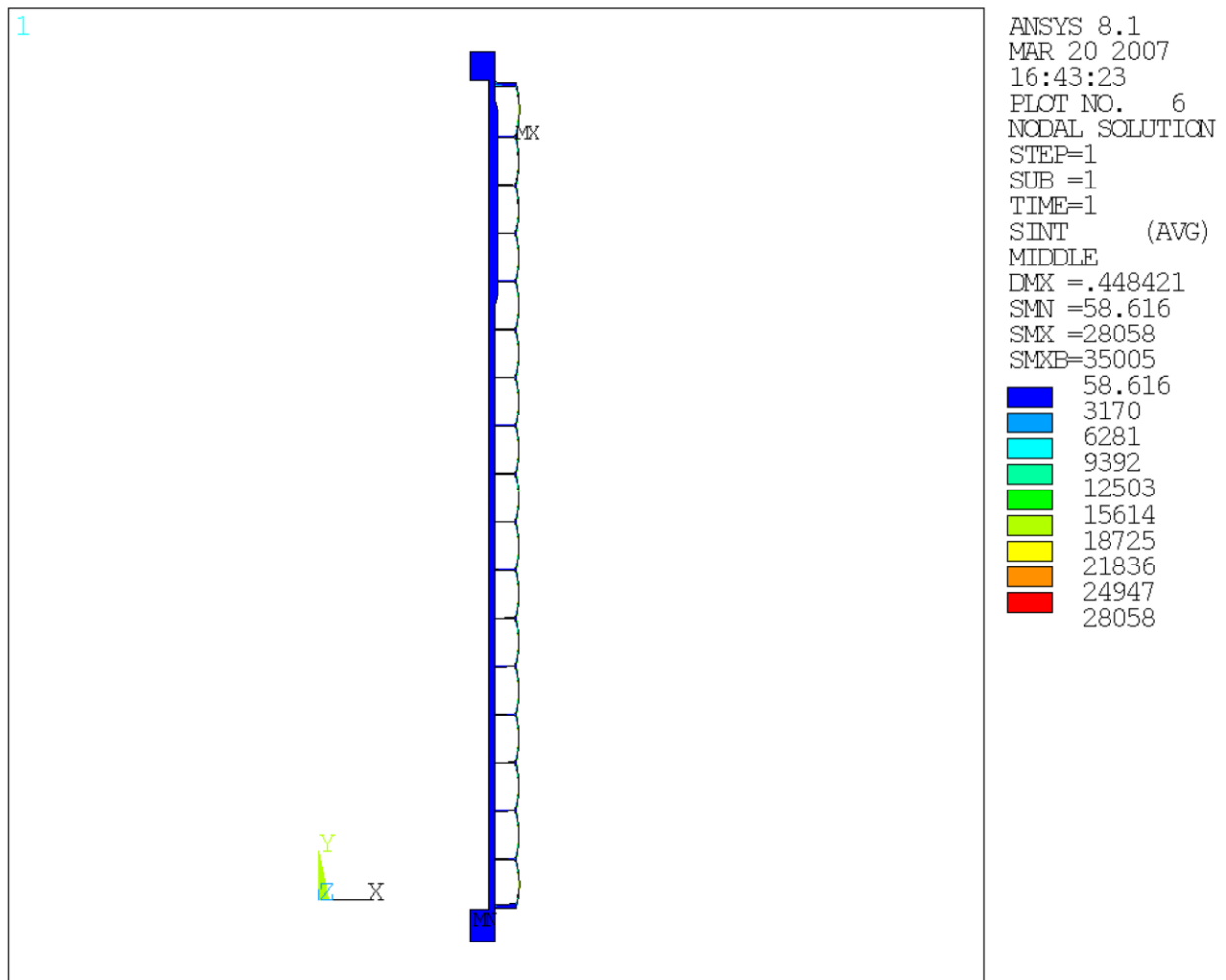


Figure A.3.9.6-5
3 g Lifting Stress Intensity Distribution

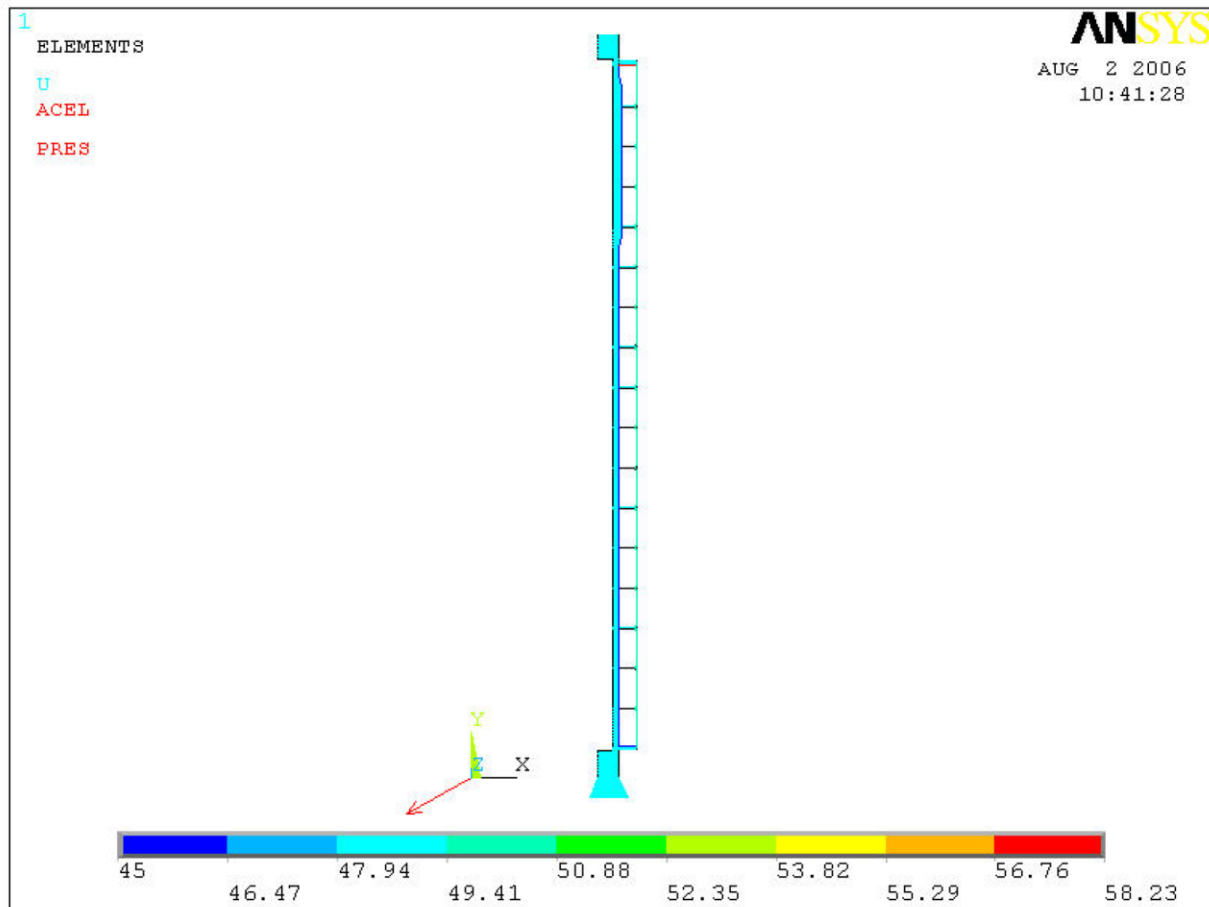


Figure A.3.9.6-6
Neutron Shield Shell Finite Element Model, Transfer Loads

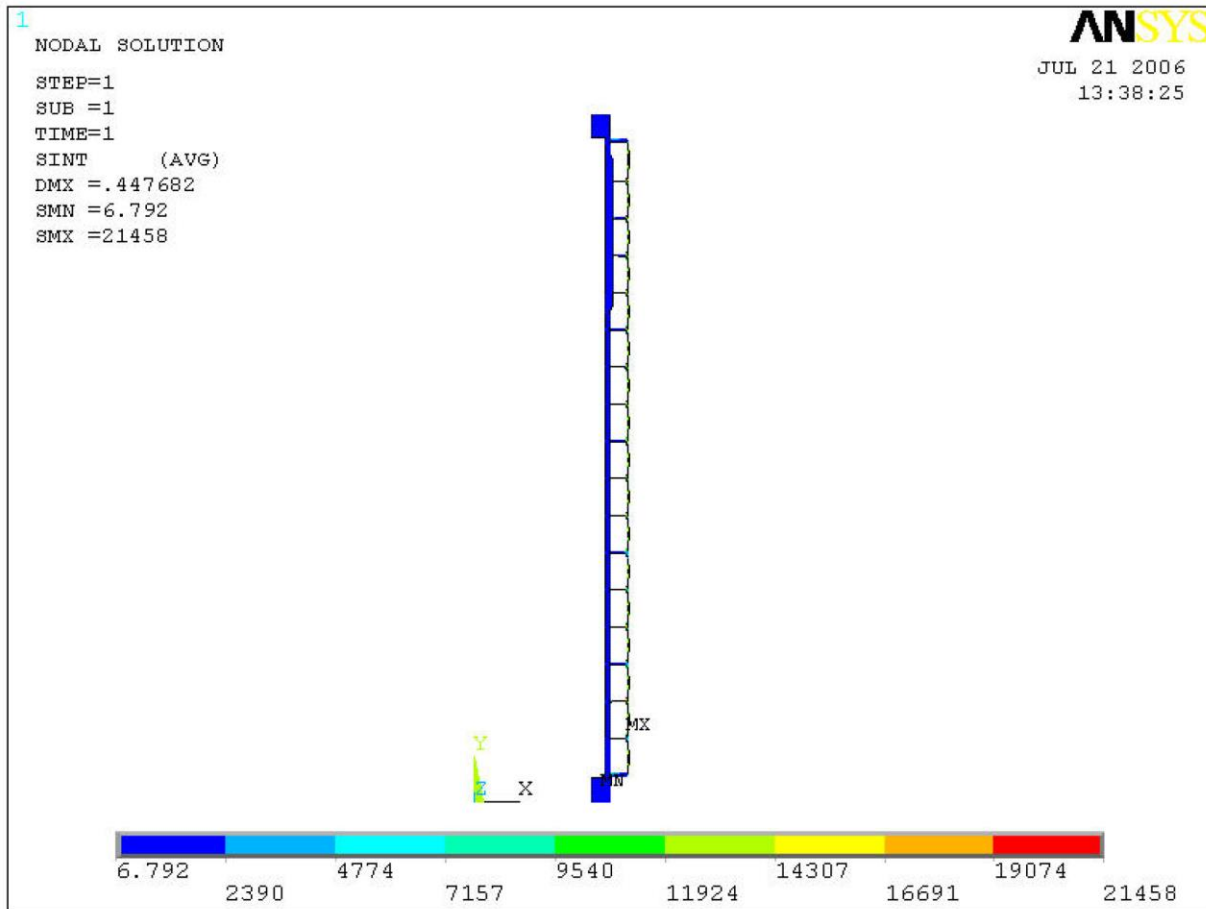


Figure A.3.9.6-7
Transfer Loads Stress Intensity Distribution

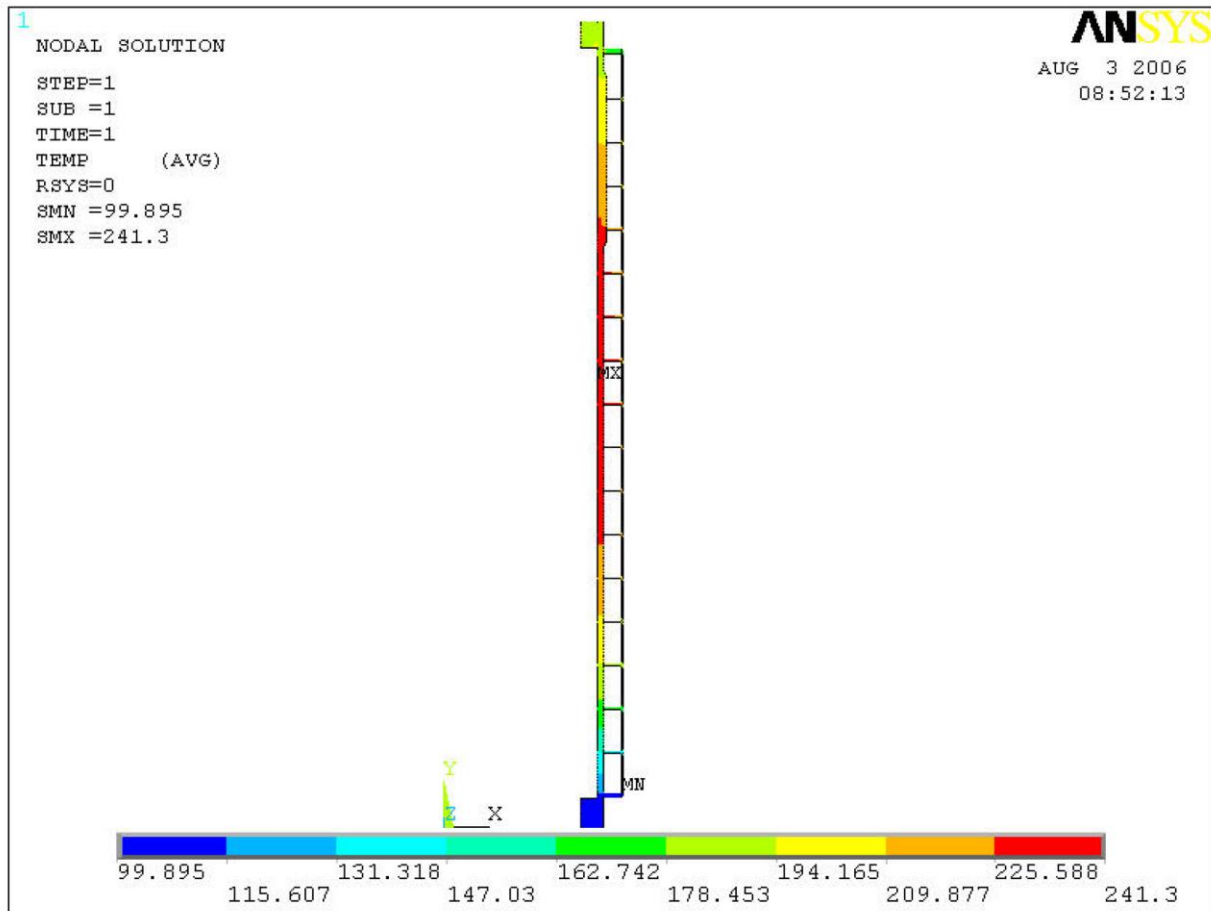


Figure A.3.9.6-8
Cold Ambient Environment Temperature Distribution

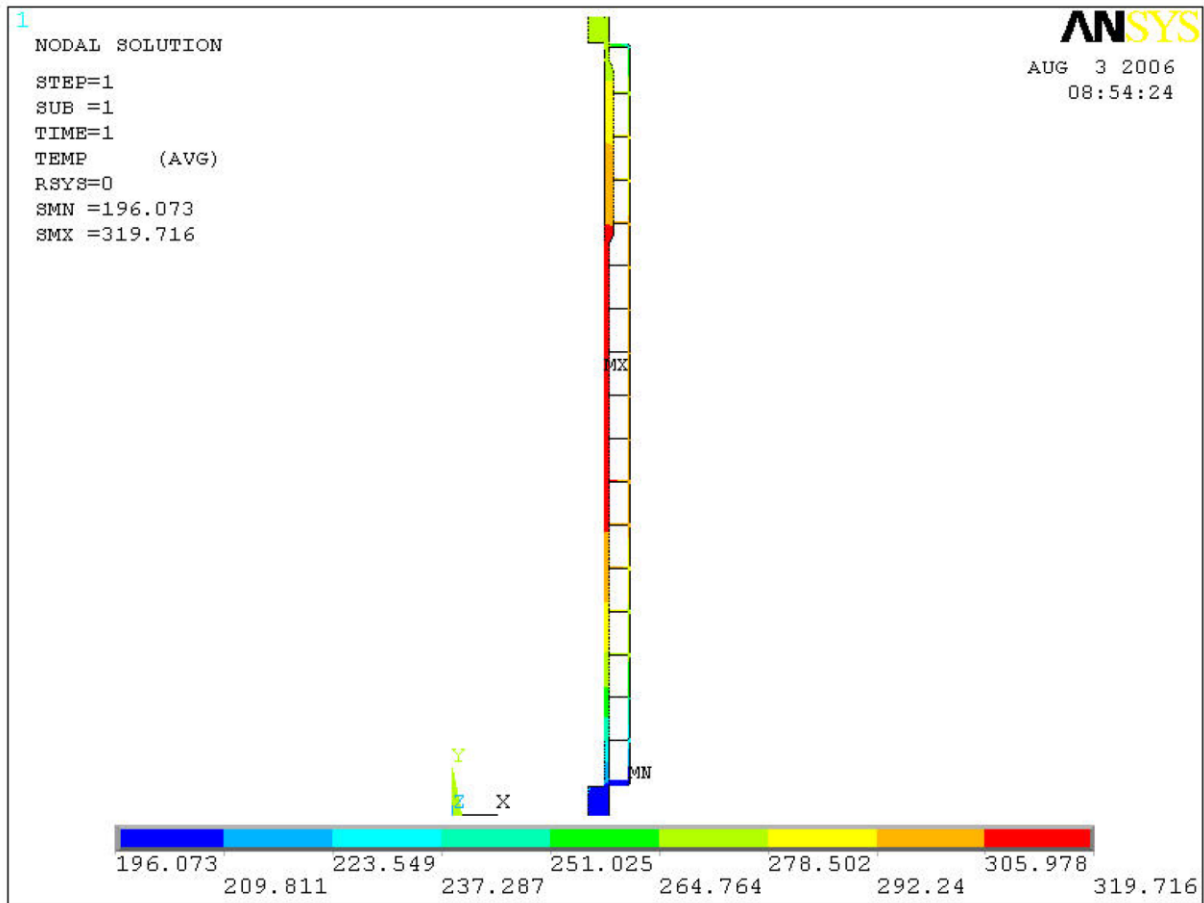


Figure A.3.9.6-9
Hot Ambient Environment Temperature Distribution

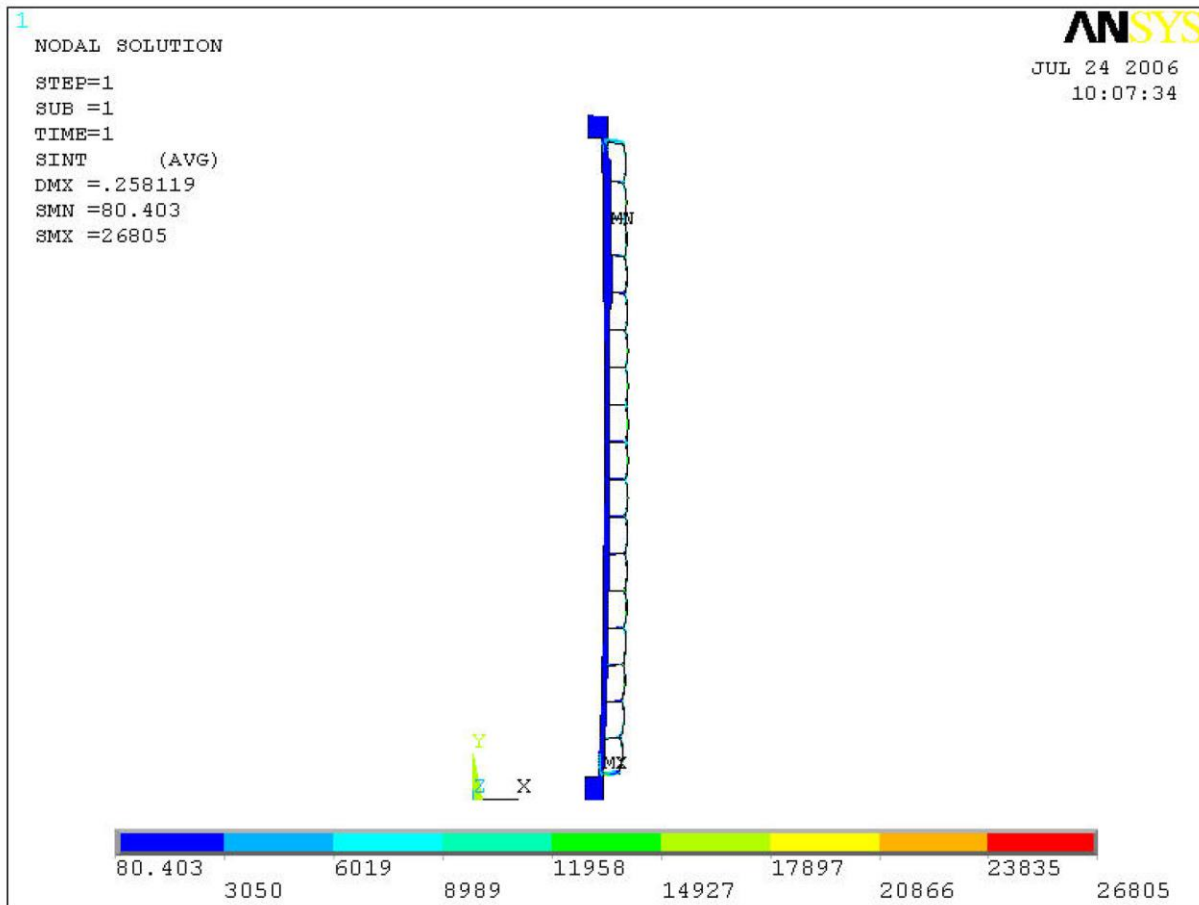


Figure A.3.9.6-10
Transfer Loads plus Cold Ambient Condition Stress Intensity Distribution

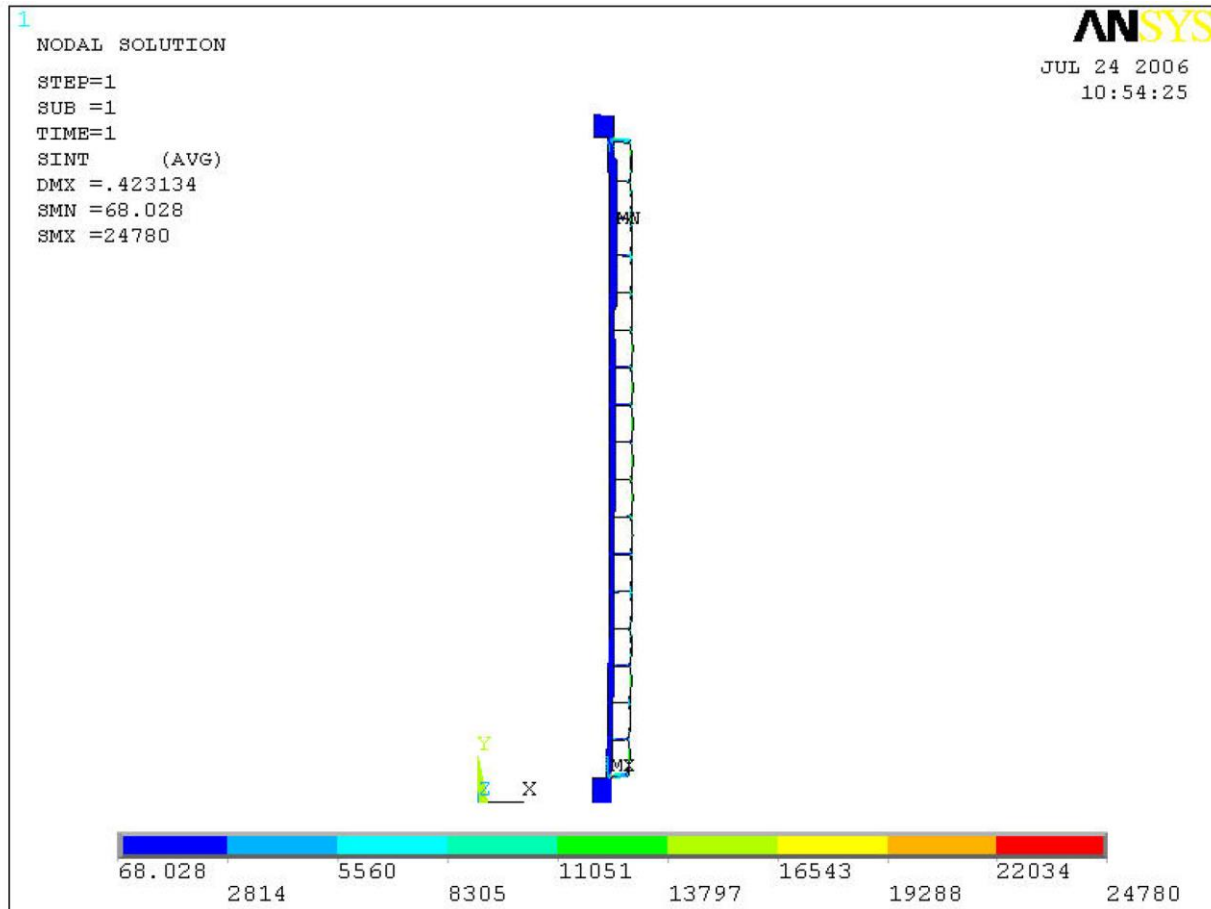


Figure A.3.9.6-11
Transfer Loads plus Hot Ambient Condition Stress Intensity Distribution

Appendix A.3.9.7

OS187H Type 1 Transfer Cask Impact Analysis

Appendix 3.9.7 describes the evaluations originally performed to substantiate the 75g accident drop decelerations used for the structural evaluation of the NUHOMS® HD System components. During the licensing of the 32PTH System and as part of the RAI process, TN performed an accident drop analysis of the OS187H TC using the LS-DYNA computer code. This LS-DYNA evaluation is documented in Appendix 3.9.10 and forms the basis for the acceleration values used for evaluation of the NUHOMS® HD System components. The justification for applicability of the Appendix 3.9.7 to the 32PTH Type 1 DSC and OS187H Type 1 TC is provided in Appendix A.3.9.10. Therefore, Appendix A.3.9.7 is deleted.

Appendix A.3.9.8

Damaged Fuel Cladding Structural Evaluation

No change. The damaged fuel cladding evaluations documented in Appendix 3.9.8 are applicable without change to the 32PTH Type 1 DSC.

Appendix A.3.9.9 HSM-H Structural Analysis

The structural evaluation of the HSM-H documented in Appendix 3.9.9 remains applicable when the HSM-H is loaded with a 32PTH Type 1 DSC. The HSM-H evaluation in Appendix 3.9.9 is based on a DSC weight of 110 kips which bounds the weight of the loaded 32PTH Type 1 DSC of 109,410 kips. Also, as documented in Chapter 4, the HSM-H design is based on temperature distributions resulting from thermal analysis using a bounding heat load of 40.8 kW which is higher than the 32PTH Type 1 maximum heat load of 34.8 kW. As documented in Chapter A.4, the longer 32PTH Type 1 DSC is not expected to change significantly the HSM-H temperature distributions documented in Chapter 4 for the HSM-H loaded with a 32PTH DSC.

Two minor design modifications are made to the HSM-H to accommodate the 32PTH Type 1 DSC. These consist of a small ($\frac{1}{2}$ ") increase in the length of the support rail structure, and, to accommodate the rail length increase, an alternate design of the DSC stop plate at the rear of the rail support structure is implemented (the 1" thick stiffened canister stop plate assembly is replaced with a single 2" thick plate welded to the top flange of the support rail structure). These design modifications are shown in drawings 10494-72-100-SAR and 10494-72-107-SAR. These modifications do not affect the overall structural qualification of the HSM-H as documented in Appendix 3.9.9. The increased length provides additional bearing area for the support rail structure on its concrete support on the rear wall of the module and, thus, has no effect on the structural qualification of the rail support structure. The alternate DSC stop plate is evaluated using the same loads and allowables as the original stop plate design and is shown to meet the same stress allowable criteria. The maximum bending and shear stresses are on the order of 13.0 ksi and 2.5 ksi, respectively, versus allowable stresses of 18.9 ksi and 12.5 ksi, respectively. The weld between the stop plate and the top flange of the rail is conservatively specified as a full penetration weld.

Therefore, the HSM-H as evaluated in Appendix 3.9.9 with the minor design modifications described above is qualified to store a 32PTH Type 1 DSC.

Appendix A.3.9.10

OS187H Type 1 Transfer Cask Dynamic Impact Analysis

The analysis to determine the rigid body accelerations for the NUHOMS® OS187H transfer cask (TC) documented in Appendix 3.9.10 is applicable to the OS187H Type 1 TC. This is based on the overall similarity of the two transfer cask designs. Both the OS187H and the OS187H Type 1 TCs have similar geometric and mass configuration and are fabricated using the same materials of construction. The OS187H Type 1 has the same diameter, its overall length is approximately 14” longer (210.5” versus 197.07”, about a 7% difference) and its maximum weight, including payload, is about 10 kips heavier (239 kips versus 229 kips, about a 4% difference).

Overall, the magnitude of the noted differences is not significant enough to alter appreciably the resulting rigid body accelerations determined from the LS-DYNA analysis documented in Appendix 3.9.10. This is confirmed by energy balance considerations, whereby the increased potential energy resulting from the increased weight of the OS187H Type 1 TC is equated to the strain energy of the TC. Based on these energy balance considerations, it is estimated that the OS187H Type 1 TC drop accelerations would be on the order of 2% to 2.5% higher than the OS187H TC accelerations.

Therefore, the maximum accelerations obtained for the various components of the OS187H TC by the LS-DYNA analysis are conservatively increased by 2.5%. The table below summarizes the OS187H TC and the OS187H Type 1 TC maximum accelerations. These accelerations are well below the acceleration of 75 g used in the accident drop evaluations, and therefore, have no effect on the structural evaluations of the NUHOMS® HD 32PTH Type 1 and OS187H Type 1 components, documented in Chapter A.3, and Appendices A.3.9.1 and A.3.9.2.

Transfer Cask Section	OS187H TC (LS-DYNA) Maximum Accelerations	OS187H Type 1 TC (Estimated) Maximum Accelerations
Lid section	62.9 g	64.5 g
Top trunnion section	55.8 g	57.2 g
Middle section	57.3 g	58.7 g
Bottom trunnion section	46.9 g	48.1 g
Bottom plate section	44.0 g	45.1 g

Appendix A.3.9.11

NUHOMS® 32PTH Type 1 DSC Dynamic Amplification Factor Analysis

TABLE OF CONTENTS

A.3.9.11	NUHOMS® 32PTH TYPE 1 DSC DYNAMIC AMPLIFICATION FACTOR ANALYSIS	A.3.9.11-1
A.3.9.11.1	Introduction	A.3.9.11-1
A.3.9.11.2	Side Drop Modal Analysis.....	A.3.9.11-2
A.3.9.11.3	Dynamic Load Factor Calculations.....	A.3.9.11-3
A.3.9.11.4	Summary of <i>g</i>-Loads for 32PTH Type 1 DSC Impact Analyses	A.3.9.11-4
A.3.9.11.5	References	A.3.9.11-5

A.3.9.11 NUHOMS[®] 32PTH TYPE 1 DSC DYNAMIC AMPLIFICATION FACTOR ANALYSIS

A.3.9.11.1 Introduction

This appendix computes the dynamic amplification factor (DAF) to be applied to the response accelerations obtained from the drop accident dynamic analysis of the OS187H Type 1 transfer cask (TC) when applying those accelerations as input to an equivalent static analysis of the 32PTH Type 1 DSC of the same postulated drop accident event.

The DAF is computed for the loaded 32PTH Type 1 DSC in the horizontal orientation. Vertical and corner drop accidents are not credible events since the TC is always in the horizontal configuration.

A.3.9.11.2 Side Drop Modal AnalysisA. Canister Shell

The fundamental natural frequency of the 32PTH Type 1 DSC shell corresponding to an ovalling (radial-axial) mode is determined assuming the cylindrical shell is simply supported without axial constraint. The natural frequency of the cylindrical shell ovalling mode is given by the following [1, p. 305, Table 12-2, Frame 5]:

$$f_{ij} = \frac{\lambda_{ij}}{2\pi R} \left(\frac{E}{\mu(1-\nu^2)} \right)^{1/2}$$

$$\lambda_{ij} = \frac{\left\{ (1-\nu^2)(j\pi R/L)^4 + (h^2/12R^2) \left[i^2 + (j\pi R/L)^2 \right]^4 \right\}^{1/2}}{(j\pi R/L)^2 + i^2}$$

Where L is taken to be the length between the top and bottom shield plugs, which is roughly 171.63 in, $E = 25.8 \times 10^6$ psi (for SA-240 Type 304 stainless steel at 500 °F [2]), R is the average shell radius, 34.625 in., ν is Poisson's ratio, which is 0.305 for stainless steel [3, page 5-6], $\mu = 0.29/386.4 = 0.000751$ lbm. in⁻³, and thickness $h = 0.5$ in.

For the fundamental mode, $i = 2$ and $j = 1$.

$$\lambda_{ij} = \frac{\left\{ (1-.305^2)(\pi \times 34.625 / 171.63)^4 + (0.5^2 / 12 \times 34.625^2) \left[2^2 + (\pi 34.625 / 171.63)^2 \right]^4 \right\}^{1/2}}{(\pi 34.625 / 171.63)^2 + 2^2}$$

$$= 0.0888$$

$$f_{21} = \frac{0.0888}{2\pi \times 34.625} \left(\frac{25.8 \times 10^6}{0.000751(1-0.305^2)} \right)^{1/2} = 79.4 \text{ Hz}$$

B. Basket with Fuel Assemblies

The basket for the 32PTH Type 1 DSC is identical to the 32PTH DSC, except that the length of the basket is longer in the 32PTH Type 1 DSC and the fuel tubes at the top of the basket are also connected with crossbars and fusion welds. The length of the 32PTH DSC basket is 162 inches and the length of the 32PTH Type 1 DSC is 169 inches. The weight of the fuel remains the same. As discussed in Appendix A.3.9.1, the axial length of the finite element model of the 32PTH basket assembly is based on a 15 inch segment which corresponds to the pitch of the cross bars where the compartment tubes are welded together. This basket model and analysis results are also applicable to the 32PTH Type 1 basket. Thus, the DAF for the 32PTH DSC basket assembly computed in Appendix 3.9.11 are also applicable to the 32PTH Type 1 basket assembly.

A.3.9.11.3 Dynamic Load Factor Calculations

The natural frequency of the 32PTH Type 1 canister (79.4 Hz) is lower than the 32PTH canister (86.0 Hz) in the horizontal orientation. It is concluded from the results in Section 3.9.11.5 and the amplification factor results for a half sine wave [4, Figure 2.15] that frequencies lower than 86 Hz will result in a lower DAF than 1.03. Thus the DAF calculated for the 32PTH canister side drop bounds the DAF for the 32PTH Type 1 canister.

Since the natural frequencies of the NUHOMS[®] 32PTH Type 1 basket are the same as the NUHOMS[®] 32PTH basket, the DAF for the NUHOMS[®] 32PTH Type 1 will also be the same as the DAF for the NUHOMS[®] 32PTH basket, which is 1.18.

A.3.9.11.4 Summary of g-Loads for 32PTH Type 1 DSC Impact Analyses

Appendix A.3.9.10 summarizes the maximum g-loads computed for the OS187H Type 1 transfer cask during an 80 inch side drop. A DAF of 1.18 is used to compute g-loads for canister and basket impact loads for side drops. These impact loads are computed in the following table:

Drop Orientation	Acceleration Direction	Maximum Transfer cask g-Load	Maximum DSC g-Load	g-Load Used for Canister and Basket Analyses
Side drop	Transverse	58.73 g ⁽¹⁾	58.73 g x 1.18 = 69.30 g	75 g

Note:

- (1) A total of five sections ranging from the lid down to the bottom plate are reported in A.3.9.10. However, only the middle three sections (top trunnion, middle, and bottom trunnion sections) will transmit loads to the canister and basket. Therefore, only the maximum g load in these sections is used to compute the g load seen by the canister and basket.

A.3.9.11.5 References

1. Blevins, Formulas for Natural Frequency and Mode Shape, Krieger Publishing Company, 1995.
2. American Society of Mechanical Engineers, ASME Boiler and Pressure Vessel Code, Section II, Part D, 1998 through 2000 addenda.
3. Baumeister & Marks, Standard Handbook for Mechanical Engineers, 7th Edition.
4. Methods for Impact Analysis of Shipping Containers, NUREG/CR-3966, UCID-20639, LLNL, 1987.

Chapter A.4 Thermal Evaluation

TABLE OF CONTENTS

A.4	THERMAL EVALUATION.....	A.4-1
A.4.1	Discussion.....	A.4-1
A.4.1.1	Air Flow Evaluation for 32PTH Type 1 DSC in HSM-H	A.4-1
A.4.1.2	Thermal Evaluation of 32PTH Type 1 DSC in HSM-H.....	A.4-2
A.4.1.3	Thermal Evaluation of 32PTH Type 1 DSC in OS187H Type 1 TC	A.4-2
A.4.1.4	Maximum 32PTH Type 1 DSC Internal Pressure for Storage and Transfer Conditions	A.4-3

LIST OF TABLES

Table A.4-1	Airflow Calculation Results for HSM-H Loaded with 32PTH Type 1 DSC	A.4-1
Table A.4-2	Applied Decay Heat Load and Heat Generation Rate within 32PTH DSC and 32PTH Type 1 DSC in HSM-H	A.4-2

A.4 THERMAL EVALUATION

A.4.1 Discussion

The NUHOMS[®] 32PTH Type 1 DSC is designed to passively reject decay heat during storage and transfer for normal, off-normal, and accident conditions while maintaining temperatures and pressures within specified limits. There are changes to the thermal evaluation as discussed in Chapter 4 of the SAR.

In general, the thermal evaluations and results documented in Chapter 4 for the 32PTH DSC inside the HSM-H and OS187H TC are bounding for the 32PTH Type 1 DSC inside the HSM-H and the OS187H Type 1 TC.

As shown in Table A.1-1, the main differences between the 32PTH DSC and the 32PTH Type 1 DSC consist of a longer overall DSC length and a corresponding longer internal cavity length to accommodate an increased basket length. The effect of these differences is addressed below and shown to have a negligible effect on the overall thermal performance of the 32PTH Type 1 DSC as compared to the 32PTH DSC.

The longer length of the 32PTH Type 1 DSC affects the HSM-H air flow calculation, and the longer cavity length affects the decay heat flux and heat generation rate of the 32PTH Type 1 DSC.

A.4.1.1 Air Flow Evaluation for 32PTH Type 1 DSC in HSM-H

The mass flow rates, exit and average air temperatures, and total loss coefficients for the 32PTH Type 1 DSC in the HSM-H are calculated for the bounding off-normal conditions using the same methodology used for the 32PTH DSC described in Chapter 4. Table A.4-1 shows the results of the air flow calculations in comparison to those from the 32PTH DSC.

Table A.4-1 Airflow Calculation Results for HSM-H Loaded with 32PTH Type 1 DSC

Parameter	32PTH Type 1 DSC	32PTH DSC	32PTH Type 1 DSC	32PTH DSC
Ambient temperature, T_{amb} , (°F)	-20	-20	115*	115*
Exit air temperature, T_{Exit} , (°F)	46.1	46.2	191.8	191.9
Average air temperature, T_{aver} , (°F)	13.0	13.1	148.4	148.4
Total loss coefficient, ΣK , (ft ⁻⁴)	0.0984	0.0988	0.1012	0.1016
Mass flow rate, (lbm/s)	2.076	2.073	1.577	1.574

*24-hour average of 105 °F used

As seen from Table A.4-1, the differences in the air flow calculation results for HSM-H loaded with 32PTH Type 1 DSC or 32PTH DSC are insignificant. The exit air temperatures for 32PTH Type 1 DSC are bounded by those of the 32PTH DSC due to the longer DSC length which results in a lower decay heat flux at the DSC surface and a larger heat transfer surface. The reduced air temperature difference from the exit to the inlet of the HSM-H results in increasing

air mass flow rate through the HSM-H cavity. Thus, the air flow calculation results used for the thermal evaluation of the 32PTH DSC in the HSM-H can be conservatively used for thermal evaluation of the 32PTH Type 1 DSC in the HSM-H.

A.4.1.2 Thermal Evaluation of 32PTH Type 1 DSC in HSM-H

The main design differences between the 32PTH DSC and the 32PTH Type 1 DSC listed in Table A.1-1 only affect applied decay heat load used for normal and off-normal conditions and heat generation rate within the DSC used for blocked vent accident conditions. Table A.4-2 summarizes the applied decay heat load and heat generation rate for 32PTH DSC and 32PTH Type 1 DSC in the HSM-H.

Table A.4-2 Applied Decay Heat Load and Heat Generation Rate within 32PTH DSC and 32PTH Type 1 DSC in HSM-H

Parameter	32PTH Type 1 DSC	32PTH DSC
Total decay heat load, Q	118748 Btu/hr (34.8kW)	
DSC inner diameter, D_i , (in.)	68.75	
DSC cavity length, L, (in.)	171.63	164.5
Decay heat flux = $Q/(\pi D_i L)$, (Btu/hr-in. ²)	3.2034	3.3422
Heat generation rate = $Q/(\pi D_i^2 L/4)$, (Btu/hr-in. ³)	0.1864	0.1945

As seen from Table A.4-2, both the decay heat flux and the heat generation rate for the 32PTH Type 1 DSC are bounded by those used for 32PTH DSC in HSM-H. The 32PTH Type 1 DSC is longer, which provides larger heat transfer surface for DSC outer shell than 32PTH DSC. The added length of the 32PTH Type 1 DSC basket increases the heat rejection capacity of the basket. Therefore, the temperatures of 32PTH Type 1 DSC in HSM-H for storage conditions are bounded by those calculated for 32PTH DSC.

Due to the longer length of the 32PTH Type 1 DSC, the HSM-H is exposed to a lower heat flux/heat generation rate than the 32PTH DSC. Thus, the temperature distribution in the HSM-H concrete structure and steel support structure will correspondingly decrease with the lower heat flux/heat generation rate. Therefore, the temperatures in the HSM-H loaded with a 32PTH DSC as calculated in Chapter 4 are bounding.

A.4.1.3 Thermal Evaluation of 32PTH Type 1 DSC in OS187H Type 1 TC

Since the 32PTH Type 1 DSC cavity and OS187H Type 1 TC cavity are longer than that of 32PTH DSC and OS187H TC, the total decay heat load (34.8kW) would be distributed over a larger radial inner surface of the DSC cavity than the one considered in the Chapter 4 thermal analysis for transfer conditions. This means the applied heat fluxes and heat generation rates considered in Chapter 4 bound those for the 32PTH Type 1 DSC and OS187H Type 1 TC. Furthermore, the longer DSC/TC length provide large heat transfer surface for heat rejection from the DSC to the ambient. The maximum DSC/TC component temperatures decrease with a lower heat flux/heat generation rate and a larger DSC/TC heat transfer surface, and therefore the

results of the 32PTH DSC in OS187H thermal analysis bound those for the 32PTH Type 1 DSC and OS187H Type 1 TC.

A.4.1.4 Maximum 32PTH Type 1 DSC Internal Pressure for Storage and Transfer Conditions

The 32PTH Type 1 DSC has a longer cavity length in comparison to 32PTH DSC, which provides an additional 4.3% of cavity volume. The overall 32PTH Type 1 DSC cavity gas volume with the increased basket length is still higher than that of 32PTH DSC. Furthermore, the authorized fuel assembly types and decay heat loads are the same for 32PTH Type 1 DSC, and, therefore, the volumes of fission and fill gas calculated for 32PTH DSC are unchanged. As discussed in Sections A.4.1.2 and A.4.1.3, the average cavity gas temperatures for 32PTH Type 1 DSC for both storage and transfer conditions are bounded by the 32PTH DSC. Therefore, the maximum internal pressures within the 32PTH Type 1 DSC are bounded by those for 32PTH DSC design and the pressure design criteria are satisfied for the 32PTH Type 1 DSC.

Chapter A.5 Shielding Evaluation

TABLE OF CONTENTS

A.5	SHIELDING EVALUATION.....	A.5-1
------------	----------------------------------	--------------

LIST OF TABLES

Table A.5-1	Material Composition of NS-3 Neutron Shielding Resin.....	A.5-3
Table A.5-2	Type 1 Transfer Cask Top and Bottom Dose Rate Summary During Transfer Operations	A.5-3

A.5 SHIELDING EVALUATION

The NUHOMS® 32PTH Type 1 DSC and the OS187H Type 1 transfer cask (TC) are designed to be equivalent to the NUHOMS® 32PTH DSC and OS187H TC from a shielding standpoint for all conditions of loading, storage and transfer. In general, the shielding evaluation documented in Chapter 5 for the 32PTH DSC and OS187H TC is applicable and bounding for the 32PTH Type 1 DSC and OS187H Type 1 TC.

The effect on shielding due to the small changes in the geometry and material design of the 32PTH Type 1 DSC and OS187H Type 1 TC is evaluated herein. The 32PTH Type 1 DSC and OS187H Type 1 TC are designed to be longer than the 32PTH DSC and OS187H TC. Since there is no change in the authorized fuel contents of the NUHOMS® HD System, all the source terms and fuel qualification tables determined in Chapter 5 remain unchanged. The computational model of the DSC inside the HSM-H for long term storage described in Chapter 5 is insensitive to the length of the DSC. Therefore, the shielding evaluations for the 32PTH DSC inside the HSM-H documented in Section 5.4.8.1 are applicable to the 32PTH Type 1 DSC. The differences between the 32PTH and 32PTH Type 1 DSCs inside the OS187H TC and the OS187H Type 1 TCs, respectively, that are relevant to the calculation of dose rates during loading and transfer are evaluated and discussed below:

- The OS187H Type 1 TC inner liner thickness is increased from 0.500" to 0.625". This change results in a reduction in radial dose rates and is an improvement in the shielding design.
- The OS187H Type 1 TC lead shielding thickness is reduced from 3.60" to 3.56". The shielding calculations documented in Chapter 5 utilize a lead shield thickness of 3.56" and therefore, the results from Chapter 5 radial dose rate calculations are applicable for the Type 1 DSC and Type 1 TC.
- Type 1 TC water (radial) neutron shield is extended to mate with the upper trunnion. This design change is an improvement and results in a reduction in the neutron dose rates below the upper trunnion as there are no pocket-to-neutron shield gaps.
- Type 1 TC trunnions utilize a monolithic forging (solid steel) with removal of the solid neutron shield resin inside the trunnions. This is an improvement in design since it results in a significant reduction in the gamma dose rates around the trunnions. The slight increase in the neutron dose rates due to the removal of the solid neutron shield resin inside the trunnions is more than compensated by the increase in the gamma shielding due to the stainless steel. Note that the dose rates around the transfer cask are mostly due to contribution from gamma sources.
- The solid neutron shielding material (resin) at the top and bottom of the OS187H Type 1 TC is changed from TN Proprietary Polyester Resin to NS-3. The material composition of the resin material is shown in Table 5-17. The material composition of the NS-3 material is shown in Table A.5-1. The shielding characteristics of these materials are similar and do not result in a substantial change in the dose rate magnitude and distribution at the top and bottom of the transfer cask.

A shielding evaluation with the MCNP computer code (described in Chapter 5, Section 5.4) is performed to determine the effect of the change of the solid neutron shield material for the OS187H Type 1 TC. The MCNP model for this evaluation is identical to that described in Chapter 5, Section 5.3.1.3 for the transfer configuration (shown in Figures 5-5 through 5-7) except for the use of NS-3 as the solid neutron shield material at the axial ends of the TC. The results of this evaluation are shown in Table A.5-2. A comparison of the dose rates at the top and bottom ends of the Type 1 TC with those shown in Table 5-4 and Table 5-5 for the OS187H TC indicates that the differences in dose rates from use of NS-3 vary from being up to 33% higher at the top end to being statistically insignificant at the bottom end. The dose rate increase at the top end of the OS187H Type 1 TC due to the use of NS-3 as the solid neutron shielding material is relatively insignificant in comparison to the dose rates at the side and bottom of the TC. More specifically, the average dose rates at the top end during the transfer operations (approximately 30 mrem/hr at the surface) are significantly lower than the average dose rates at the bottom end (approximately 180 mrem/hr at the surface) or the TC side (approximately 330 mrem/hr at the surface, Table 5-3).

Further, the average dose rates at the top end of the TC during transfer operations (approximately 30 mrem/hr at the top surface) are significantly lower than those during welding operations (approximately 200 mrem/hr at the top surface, Table 5-4) or during decontamination operations (approximately 700 mrem/hr at the top surface, Table 5-4). Therefore, even a 33% increase in the top end dose rates during transfer operations is a statistically insignificant increase in comparison to all of the loading and transfer operations involving the OS187H Type 1 TC.

- The 32PTH Type 1 DSC top shielding design includes a two-piece assembly, consisting of separate top shield plug and the inner top cover plate. This configuration is equivalent to the single piece top shield plug/inner top cover plate assembly modeled in the Chapter 5 shielding calculations for all operations following decontamination. During decontamination, the 32PTH Type 1 DSC top shielding configuration consists of the shield plug only which results in a reduction of the amount of steel at the top of the DSC (during decontamination operations) by 2". The shielding models for decontamination are described in Chapter 5, Section 5.3.1.2. Due to the two-piece top shield plug and inner top cover plate assembly design, it is not necessary to decontaminate the top surface of the shield plug (as opposed to the single piece design where it is required). Therefore, top dose rates during this stage of operation do not significantly impact total occupational exposure and are not calculated. The radial dose results for these operations from Chapter 5, Section 5.4.8 are applicable for both the 32PTH Type 1 DSC and OS187H Type 1 TC.

In summary, the shielding evaluation documented in Chapter 5 for the 32PTH DSC and OS187H TC is applicable and bounding for the 32PTH Type 1 DSC and OS187H Type 1 TC for all conditions of loading, storage and transfer, except for the TC top end dose rate calculation with NS3 which is documented herein. However, it has been shown that the increase in dose rates due to the change in the neutron shielding material has a relatively insignificant impact in comparison to the dose rates around the TC during loading and transfer operations.

Table A.5-1 Material Composition of NS-3 Neutron Shielding Resin

Element	Weight %
Hydrogen	4.85
Carbon	9.35
Calcium	5.61
Oxygen	57.05
Silicon	3.36
Aluminum	17.89
Iron	0.56
Trace ⁽¹⁾	1.33
Density (g/cm ³)	1.76

Note:

(1) Trace elements were modeled as oxygen in the shielding analysis

Table A.5-2 Type 1 Transfer Cask Top and Bottom Dose Rate Summary During Transfer Operations

Location	Dose Rate mrem/hr	On Outside Surface		1.5 Feet from Surface		Three Feet from Surface	
		Gamma	Neutron	Gamma	Neutron	Gamma	Neutron
Top end	Maximum	19.8	34.4	9.55	21.2	5.07	12.6
	Minimum	6.16	12.1	5.16	7.49	3.69	6.20
	Average ⁽¹⁾ surface	10.9	18.6	6.37	11.5	4.10	8.08

Location	Dose Rate mrem/hr	On Outside Surface		One Foot from Surface		Three Feet from Surface	
		Gamma	Neutron	Gamma	Neutron	Gamma	Neutron
Bottom end	Maximum	460	1318	119	289	57.1	113
	Minimum	13.7	47.2	18.6	41.1	16.9	39.2
	Average ⁽¹⁾ surface	48.4	133	36.2	86.9	26.8	58.3

Note:

(1) Surface weighted average of ring detectors used as tally surfaces

Chapter A.6 Criticality Evaluation

The NUHOMS[®] 32PTH Type 1 DSC and the OS187H Type 1 transfer cask (TC) are designed to be identical to the NUHOMS[®] 32PTH DSC and OS187H TC from a criticality standpoint for all conditions of loading, storage and transfer. In general, the criticality analysis documented in Chapter 6 for the 32PTH DSC in the OS187H TC is applicable and bounding for the 32PTH Type 1 DSC in the OS187H Type 1 TC.

The effect on criticality due to the small changes in the geometry of the Type 1 DSC and Type 1 TC is determined by investigating the effect due to the geometry modeling employed in the criticality calculations documented in Chapter 6. These considerations are listed below:

- The height of the individual egg-crate sections in the active fuel region of the basket of the 32PTH Type 1 DSC does not change. The increase in overall height of the 32PTH Type 1 DSC is due to an increase in the number of egg-crate sections. Though the height of the top egg-crate section of the Type 1 DSC is different from that of the 32PTH DSC, the top section of the Type 1 DSC contains more neutron poison than that of the 32PTH DSC. Therefore, the criticality analysis model in Chapter 6, that considers an infinite axial array of egg-crate sections, is applicable, conservatively, to the Type 1 DSC. Note that the gap between the top of the neutron poison sheets and the bottom of the top shield plug is decreased for the 32PTH Type 1 DSC.
- The difference between the basket length and the DSC cavity length for the Type 1 DSC is greater than that of the 32PTH DSC by approximately 0.15 inches. However, this difference is well within the conservatism employed in the damaged fuel criticality calculations documented in Section 6.4.2.4 (shifting of fuel assemblies beyond fixed the poison sheet height) of Chapter 6.

In summary, the criticality analysis documented in Chapter 6 for the 32PTH DSC in the OS187H TC is applicable and bounding for the 32PTH Type 1 DSC in the OS187H Type 1 TC for all conditions of loading, storage, and transfer.

Chapter A.7 Confinement

TABLE OF CONTENTS

A.7	CONFINEMENT	A.7-1
A.7.1	Confinement Boundary	A.7-1
A.7.2	Requirements for Normal Conditions of Storage	A.7-2
A.7.3	Confinement Requirements for Hypothetical Accident Conditions	A.7-3
A.7.4	Supplemental Data.....	A.7-4
	A.7.4.1 Confinement Monitoring Capability.....	A.7-4
A.7.5	References.....	A.7-5

LIST OF FIGURES

Figure A.7-1	32PTH Type 1 DSC Confinement Boundaries and Welds for Three-Part Top End Configuration	A.7-6
--------------	---	-------

A.7 CONFINEMENT

A.7.1 Confinement Boundary

No change. Section 7.1 applies in its entirety to the 32PTH Type 1 DSC. The 32PTH DSC confinement boundary described in Section 7.1 and shown in Figure 7-1 is applicable without change to the 32PTH Type 1 DSC design when the optional two-part top end closure assembly is used. In addition, as described in Chapter A.1, the 32PTH Type 1 DSC also features a three-part top end closure assembly, consisting of separate top shield plug, inner top cover and outer top cover plates. This three-part closure design is the same as that used in other NUHOMS[®] canister designs [1] and includes a vent and siphon block which is welded to the shell during fabrication.

The confinement boundary for the three-part closure consists of the DSC cylindrical shell, the inner top cover plate, the siphon and vent block, the inner bottom cover plate, and the associated welds. At the top, the inner top cover plate, the siphon and vent block, and the DSC shell are welded to each other using partial penetration welds, which are subject to multi-level PT examination. The vent and siphon block contains two ports which are used for draining, vacuum drying, and backfilling. These ports are closed with welded cover plates which are also subject to multi-level PT. Along the shell and at the bottom end of the DSC, the confinement boundary is the same as for the 32PTH DSC.

The confinement boundary for the three-part top end closure configuration is shown in Figure A.7-1.

A.7.2 Requirements for Normal Conditions of Storage

No change.

A.7.3 Confinement Requirements for Hypothetical Accident Conditions

No change.

A.7.4 Supplemental Data

A.7.4.1 Confinement Monitoring Capability

No change.

A.7.5 References

1. Updated Final Safety Analysis Report, Standardized NUHOMS® Horizontal Modular Storage System for Irradiated Nuclear Fuel, Revision 9, February 2006, USNRC Docket No. 72-1004.

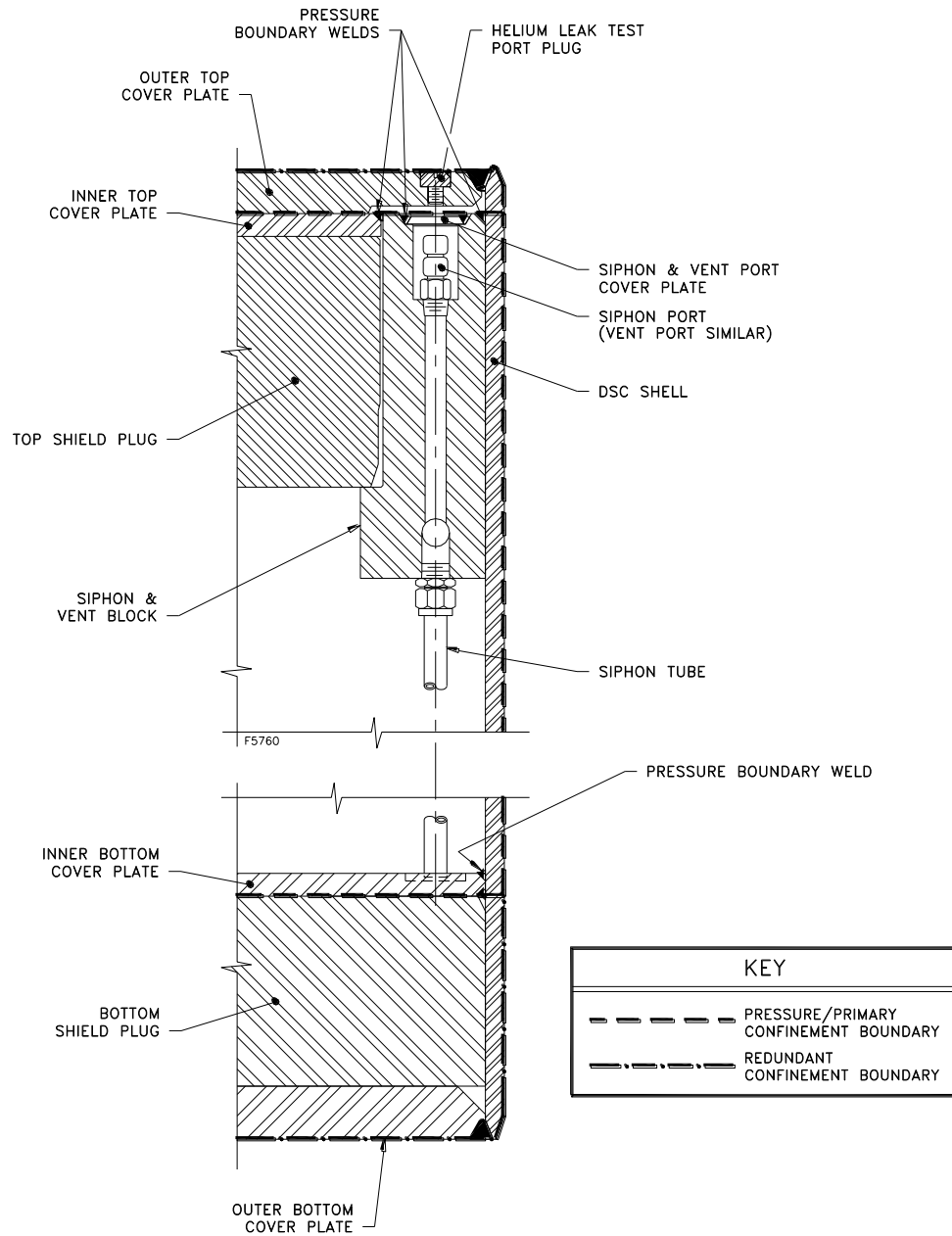


Figure A.7-1
32PTH Type 1 DSC Confinement Boundaries and Welds for Three-Part Top End Configuration

Chapter A.8 Operation Procedures

TABLE OF CONTENTS

A.8	OPERATING PROCEDURES.....	A.8-1
A.8.1	Procedures for Loading the DSC and Transfer to the HSM-H.....	A.8-2
	A.8.1.1 Narrative Description.....	A.8-2
A.8.2	Procedures for Unloading the DSC	A.8-9
	A.8.2.1 DSC Retrieval from the HSM-H.....	A.8-9
	A.8.2.2 Removal of Fuel from the DSC	A.8-9
A.8.3	Supplemental Information	A.8-12
A.8.4	References	A.8-13

A.8 OPERATING PROCEDURES

Chapter 8 applies in its entirety and without change to the 32PTH Type 1 DSC when the optional two-part top end closure assembly (which is similar to the 32PTH DSC) is used. In addition, as described in Chapter A.1, the 32PTH Type 1 DSC also features a three-part top end closure assembly, consisting of separate top shield plug, inner top cover and outer top covers. The modifications to the operating procedures described in this chapter apply to the three-part closure design and are based on the similar three-part closure used in other NUHOMS[®] canister designs [3].

A.8.1 Procedures for Loading the DSC and Transfer to the HSM-H

A.8.1.1 Narrative Description

The following steps describe the recommended modifications to the generic operating procedures described in Sections 8.1 and 8.2, and are applicable when the standard three-part top end closure assembly is implemented in the 32PTH Type 1 DSC. For purposes of completeness of presentation, the entire sequence of operational steps is presented whenever a modification has been introduced in any particular operation. When no changes are made to a section, “No Change” is indicated and a reference is listed to the applicable section in Chapter 8.

A.8.1.1.1 Transfer Cask and DSC Preparation

1. Verify by plant records or other means that candidate fuel assemblies meet the physical, thermal and radiological criteria specified in the Technical Specifications.
2. Clean or decontaminate the transfer cask as necessary to meet licensee pool and ALARA requirements, and to minimize transfer of contamination from the cask cavity to the DSC exterior.
3. Examine the transfer cask cavity for any physical damage. Insert cask spacer at the bottom of the transfer cask, if required.
4. Verify specified lubrication of the transfer cask rails.
5. Examine the DSC for any physical damage and for cleanliness. Verify that bottom fuel spacers or damaged fuel bottom end caps, if required, are present in all fuel compartments. Remove damaged fuel top end caps if they are in place. Record the DSC serial number which is located on the grappling ring. Verify the basket type by identifying the “Z” character in the XXX-32PTH-YYY-Z-1 serial number.
6. Not used.
7. Lift the DSC by the internal lifting lugs and lower it into the cask cavity. Rotate the DSC to match the transfer cask alignment marks.
8. Not used.
9. Fill the transfer cask/DSC annulus with clean water.
10. Seal the top of the annulus, using for example an inflatable seal.
11. A tank filled with clean water, and kept above the pool surface may be connected to the top vent port of the transfer cask via a hose to provide a positive pressure in the annulus. This is an optional arrangement, which provides additional assurance that contaminated water from the fuel pool will not enter the annulus. Do not pressurize this tank, nor raise it sufficiently high to float the DSC. For the 32PTH Type 1 DSC with a 69.75 inch OD, and an empty weight of 45,000 lb, a differential pressure of approximately 11.7 psi, equivalent to 27.1 ft of pure water, would be sufficient to lift the DSC.

12. If the DSC top shield plug and top cover plates were trial fitted, they must be removed prior to filling the DSC with water. The vent port quick connect fitting in the inner top cover may be removed to facilitate hydrogen monitoring later. The drain port fitting may be either left in place or removed—water may be pumped from the DSC either with or without the fitting.
13. The licensee shall develop procedures to verify that the boron content of the water added to the DSC conforms to the Technical Specifications. Fill the DSC with water from the fuel pool or an equivalent source meeting the minimum boron concentration required by the Technical Specifications. Optionally, this may be done at the time of immersing the cask in the pool. If the pool water is allowed to flow over the transfer cask lip and into the DSC, provision must be made to protect the annulus seal from being dislodged by the water running over it.
- 14a. Optionally, secure a sheet of suitable material to the bottom of the cask to minimize the potential for ground-in contamination. This step may be done at any convenient time prior to immersion.
- 14b. Drain or fill the transfer cask liquid neutron shield, as required by licensee ALARA requirements and crane weight limits. This step may be done at any convenient time prior to immersion.
15. Prior to the cask being lifted into the fuel pool, the water level in the pool should be adjusted as necessary to accommodate the transfer cask and DSC volume. If the water placed in the DSC cavity was obtained from the fuel pool, a level adjustment may not be necessary.

A.8.1.1.2 DSC Fuel Loading

1. Verify proper engagement of the lifting yoke with the transfer cask lifting trunnions.
2. Lift the transfer cask/DSC and position them over the cask loading area of the spent fuel pool.
3. Lower the cask into the fuel pool until the bottom of the cask is at the height of the fuel pool surface. As the cask is lowered into the pool, spray the exterior surface of the cask with clean water to minimize surface adhesion of contamination.
4. Place the cask in the location of the fuel pool designated as the cask loading area.
5. Disengage the lifting yoke from the transfer cask lifting trunnions and move the yoke clear of the cask. Spray the lifting yoke with clean water if it is raised out of the fuel pool.

6. Load pre-selected spent fuel assemblies into the DSC basket compartments. The licensee shall develop procedures to verify that the boron content of the water conforms to the Technical Specifications, and that fuel identifications are verified and documented. The loading plan must be developed according to Figure 2-1 for the orientation of the fuel assemblies. Damaged fuel must be loaded only in designated compartments fitted with a damaged fuel bottom end cap.
7. After all the fuel assemblies have been placed into the DSC and their identities verified, install damaged fuel top end caps into designated compartments containing damaged fuel.
8. Lower the top shield plug into the DSC.
9. Visually verify that the top shield plug is properly seated in the DSC. Reseat if necessary.
10. Position the lifting yoke and verify that it is properly engaged with the transfer cask trunnions.
11. Lift the transfer cask to the pool surface and spray the exposed portion of the cask with clean water.
12. Drain any water from above the top shield plug back to the spent fuel pool. Up to 1300 gallons of water may be removed from the DSC prior to lifting the transfer cask clear of the pool surface. Up to 15 psig of helium may only be used to assist the removal of water. The DSC shall be backfilled only with helium after drainage of bulk water.
13. Lift the cask from the fuel pool, continuing to spray the cask with clean water.
14. Move the cask with loaded DSC to the area designated for DSC draining and closure operations. The set-down area should be level, or if slightly sloped, the transfer cask and DSC should be placed with the slope down toward the DSC drain/siphon tube.

A.8.1.1.3 DSC Closing, Drying, and Backfilling

1. Fill the transfer cask liquid neutron shield if it was drained for weight reduction during preceding operations.
2. Decontaminate the transfer cask exterior.
3. Disengage the rigging from the top shield plug, and remove the eyebolts. Disengage the lifting yoke from the trunnions.
4. Disconnect the annulus overpressure tank if one was used, decontaminate the exposed surfaces of the DSC shell perimeter, remove any remaining water from the top of the annulus seal, and remove the seal.

5. Open the cask cavity drain port and allow water from the annulus to drain out until the water level is approximately twelve inches below the top of the DSC shell. Take swipes around the outer surface of the DSC shell to verify conformance with Technical Specification limits.
6. Cover the transfer cask/DSC annulus to prevent debris and weld splatter from entering the annulus.
7. If water was not drained from the DSC earlier, connect a pump to the DSC drain port and remove up to 1,300 gallons of water. Consistent with ISG-22 [4] guidance and Technical Specification 3.1.1, helium at 1-3 psig is used to backfill the DSC with an inert gas (helium) as water is being removed from the DSC. This lowers the water sufficiently to allow welding of the inner top cover, while keeping a sufficient volume of water in the DSC to cool the spent fuel. Up to 15 psig of helium gas may be applied at the vent port to assist the water pump down.

CAUTION: Verify that no inadvertent draining of the TC Neutron Shield has occurred.

CAUTION: Radiation dose rates are expected to be high at the vent and siphon port locations. Use proper ALARA practices (e.g., use of temporary shielding, appropriate positioning of personnel, etc.) to minimize personnel exposure.

- 7a. Monitor TC/DSC annulus water level to be approximately twelve inches below the top of the DSC shell and replenish as necessary until drained.
8. Install the automated welding machine onto the inner top cover and place the inner top cover with the automatic welding machine onto the DSC. Optionally, the inner top cover and the automatic welding machine can be placed separately. Verify proper fit up of the inner top cover with the DSC shell.
9. Hydrogen monitoring is required prior to commencing and continuously during the welding of the inner top cover. Install hydrogen monitoring equipment that samples the atmosphere below the shield plug.
10. Verify that the hydrogen concentration does not exceed 2.4% [1]. If this limit is exceeded, stop all welding operations and purge the DSC cavity with helium to reduce hydrogen concentration safely below the 2.4% limit.
11. Complete the inner top cover welding and perform the non-destructive examinations as required by the Technical Specifications. The weld must be made in at least two layers.
12. Remove the automated welding machine.
13. Pump remaining water from the DSC. Remove as much free standing water as possible to shorten vacuum drying time. Use of helium is required per Technical Specification 3.1.1. Up to 15 psig of helium gas may be applied at the vent port to assist the water pump down. All helium used in backfilling operations shall be at least 99.99% pure (this may be done as part of step 15).

(NOTE: Proceed cautiously when evacuating the dry shielded canister (DSC) to avoid freezing consequences.)

14. DELETED.

15. Connect a vacuum pump/helium backfill manifold to the vent port or to both the vent and drain ports. The quick connect fittings may be removed and replaced with stainless steel pipe nipple/vacuum hose adapters to improve vacuum conductance. Make provision to prevent icing, for example by avoiding traps (low sections) in the vacuum line. Provide appropriate measures as required to control any airborne radionuclides in the vacuum pump exhaust. Purge air from the helium backfill manifold.

Optionally, leak test the manifold and the connections to the DSC. The DSC may be pressurized to no more than 15 psig for leak testing.

CAUTION: Radiation dose rates are expected to be high at the vent and siphon port locations. Use proper ALARA practices (e.g., use of temporary shielding, appropriate positioning of personnel, etc.) to minimize personnel exposure.

CAUTION: During the vacuum drying evolution, personnel should be in the area of loading operations, or in nearby low dose areas, in order to take proper action in the event of a malfunction.

16. Evacuate the DSC to the pressure required by the Technical Specification for vacuum drying, and isolate the vacuum pump. The isolation valve should be as near to the DSC as practicable, with a pressure gauge on the DSC side of the valve. Prior to performing the vacuum hold for 30 minutes as required by the Technical Specification, the vacuum pump must be turned off; or if the pump is **not** turned off, provide a tee and valve (or other means) to open the line to atmosphere between the pump and the DSC isolation valve.

Note: The user shall ensure that the vacuum pump is isolated from the DSC cavity when demonstrating compliance with Technical Specification 3.1.1 requirements. Simply closing the valve between the DSC and the vacuum pump is not sufficient, as a faulty valve allows the vacuum pump to continue to draw a vacuum on the DSC. Turning off the pump, or opening the suction side of the pump to atmosphere are examples of ways to assure that the pump is not continuing to draw a vacuum on the DSC.

17. DELETED.

18. If the Technical Specification is satisfied, i.e., if the pressure remains below the specified limit for the required duration with the pump isolated, continue to the next step. If not, repeat step 16.

- 19a. Purge air from the backfill manifold, open the isolation valve, and backfill the DSC cavity with helium to 16.5 to 18 psig and hold for 10 minutes.

- 19b. Reduce the DSC cavity pressure to atmospheric pressure, or slightly over.

20. If the quick connect fittings were removed for vacuum drying, remove the vacuum line adapters from the ports, and re-install the quick connect fittings using suitable pipe thread sealant.

CAUTION: Radiation dose rates are expected to be high at the vent and siphon port locations. Use proper ALARA practices (e.g., use of temporary shielding, appropriate positioning of personnel, etc.) to minimize personnel exposure.

21. Evacuate the DSC through the vent port quick connect fitting to a pressure of 100 mbar or less.

Note: The user shall ensure that the vacuum pump is isolated from the DSC cavity when demonstrating compliance with Technical Specification 3.1.1 requirements. Simply closing the valve between the DSC and the vacuum pump is not sufficient, as a faulty valve allows the vacuum pump to continue to draw a vacuum on the DSC. Turning off the pump, or opening the suction side of the pump to atmosphere are examples of ways to assure that the pump is not continuing to draw a vacuum on the DSC.

22. Backfill the DSC with helium to the pressure specified in the Technical Specifications, and disconnect the vacuum/backfill manifold from the DSC.

23. DELETED.

- 24a. Weld the covers over the vent and drain ports, performing non-destructive examination as required by the Technical Specifications. The welds shall have at least two layers.

- 24b. Install a temporary test head fixture (or any other alternative means). Perform a leak test of the inner top cover to the DSC shell welds and siphon/vent cover welds in accordance with the Technical Specification limits. Verify that the personnel performing the leak test are qualified in accordance with SNT-TC-1A.

25. Place the outer top cover plate onto the DSC and verify correct rotational alignment of the cover and the DSC shell. Install the automated welding machine onto the outer top cover plate. As an option, the welding machine may be mounted onto the cover plate and then placed together on the DSC.

26. Complete the outer top cover welding and perform the non-destructive examinations as required by the Technical Specifications. The weld must be made in at least two layers.

27. Remove everything except the DSC from the transfer cask cavity: welding machine, protective covering from the transfer cask / DSC annulus, temporary shielding, etc., and drain the water from the transfer cask/DSC annulus.

28. Install the transfer cask lid and bolt it.

29. Evacuate the transfer cask cavity to below 100 mbar, and backfill the transfer cask annulus with helium in accordance with the Technical Specifications pressure tolerance and time limit.

CAUTION: Monitor the applicable time limits of the Technical Specifications for transfer cask annulus helium backfill.

A.8.1.1.4 Transfer Cask Downending and Transport to ISFSI

No change. See Section 8.1.1.4.

A.8.1.1.5 DSC Transfer to the HSM-H

No change. See Section 8.1.1.5.

A.8.1.1.6 Monitoring Operations

No change. See Section 8.1.1.6.

A.8.2 Procedures for Unloading the DSC

The following section outlines the procedures for retrieving the DSC from the HSM-H and for removing the fuel assemblies from the DSC.

A.8.2.1 DSC Retrieval from the HSM-H

No change. See Section 8.2.1.

A.8.2.2 Removal of Fuel from the DSC

If it is necessary to remove fuel from the DSC, it can be removed in a dry transfer facility or the initial fuel loading sequence can be reversed and the plant's spent fuel pool utilized.

Procedures for wet unloading of the DSC are presented here. Dry unloading procedures are essentially identical up to the removal of the DSC vent and drain port covers.

1. Tow the trailer with the loaded cask to the cask handling area inside the plant's fuel handling building. Drain the transfer cask liquid neutron shield as required by licensee ALARA requirements and crane weight limits.
2. Position and ready the trailer for access by the crane.
3. Engage the lifting yoke with the trunnions of the transfer cask.
4. Verify that the yoke lifting hooks are properly aligned and engaged onto the transfer cask trunnions.
5. Lift the transfer cask approximately one inch off the trunnion supports. Verify that the yoke lifting hooks are properly positioned on the trunnions.
6. Move the crane in a horizontal motion while simultaneously raising the crane hook vertically and lift the transfer cask off the trailer. Move the transfer cask to the cask decontamination area.
7. Lower the transfer cask into the cask staging area in the vertical position.
8. Unbolt the transfer cask lid and remove it.
9. Install temporary shielding to reduce personnel exposure as required. Fill the transfer cask/DSC annulus with clean water and seal the top of the annulus, using, for example, an inflatable seal.
10. Locate the drain and vent port using the indications on the outer top cover plate. Place a portable drill press on the top of the DSC. Align the drill over the drain port.
11. Cut or drill a hole through the top cover plate to expose the drain port on the inner top cover. Remove the drain port cover plate with an annular hole cutter. Repeat for the vent port.

CAUTION: Radiation dose rates are expected to be high at the vent and siphon port locations. Use proper ALARA practices (e.g., use of temporary shielding, appropriate positioning of personnel, etc.) to minimize personnel exposure.

12. Obtain a sample of the DSC atmosphere. Confirm acceptable hydrogen concentration and check for presence of fission gas indicative of degraded fuel cladding.
13. If degraded fuel is suspected, additional measures appropriate for the specific conditions are to be planned, reviewed, and implemented to minimize exposures to workers and radiological releases to the environment.
14. Verify that the boron content of the fill water conforms to the Technical Specifications. Fill the DSC with water from the fuel pool or equivalent source through the drain port with the vent port open. The vented cavity gas may include steam, water, and radioactive material, and should be routed accordingly. Monitor the vent pressure and regulate the water fill rate to ensure that the pressure does not exceed 15 psig.
15. Provide for continuous hydrogen monitoring of the DSC cavity atmosphere during all subsequent cutting operations to ensure that hydrogen concentration does not exceed 2.4%. Purge with helium as necessary to maintain the hydrogen concentration below this limit.
16. Provide suitable protection for the transfer cask during cutting operations.
17. Using a suitable method, such as mechanical cutting, remove the weld of the outer top cover plate to the DSC shell.
18. Remove the outer top cover plate.
19. Remove the weld of the inner top cover to the shell in the same manner as the outer cover plate. Remove the inner top cover. Do not remove the top shield plug at this time unless the removal is being done remotely in a dry transfer system.
20. Remove any remaining excess material on the inside shell surface by grinding.
21. Clean the transfer cask surface of dirt and any debris which may be on the transfer cask surface as a result of the weld removal operation.
22. Engage the yoke onto the trunnions, install eyebolts or other lifting attachment(s) into the top shield plug, and connect the rigging cables to the eyebolts/lifting attachment(s).
23. Verify that the lifting hooks of the yoke are properly positioned on the trunnions.
24. Lift the transfer cask just far enough to allow the weight of the transfer cask to be distributed onto the yoke lifting hooks. Verify that the lifting hooks are properly positioned on the trunnions.

25. Optionally install suitable protective material onto the bottom of the transfer cask to minimize cask contamination. Move the transfer cask to the spent fuel pool.
26. Prior to lowering the transfer cask into the pool, adjust the pool water level, if necessary, to accommodate the volume of water which will be displaced by the transfer cask during the operation.
27. Position the transfer cask over the cask loading area in the spent fuel pool.
28. Lower the transfer cask into the pool. As the transfer cask is being lowered, the exterior surface of the transfer cask should be sprayed with clean water.
29. Disengage the lifting yoke from the transfer cask and lift the top shield plug from the DSC.
30. Remove any failed fuel top end caps.
31. Remove the fuel from the DSC.

A.8.3 Supplemental Information

No change. See Section 8.3.

A.8.4 References

1. U.S. Nuclear Regulatory Commission, Office of the Nuclear Material Safety and Safeguards, "Safety Evaluation of VECTRA Technologies' Response to Nuclear Regulatory Commission Bulletin 96-04 for NUHOMS[®]-24P and NUHOMS[®] 7P Dry Spent Fuel Storage System," November 1997 (Dockets 72-1004, 72-3, 72-4, 72-8, and 72-14).
2. NUREG-0612, "Control of Heavy Loads at Nuclear Power Plants," USNRC, July 1980.
3. Transnuclear Inc., UFSAR, Standardized NUHOMS[®] Horizontal Modular Storage Systems for Irradiated Nuclear Fuel, Revision 9, Docket 72-1004.
4. U.S. Nuclear Regulatory Commission, Interim Staff Guidance (ISG-22), "Potential Rod Splitting due to Exposures to an Oxidizing Atmosphere during Short-term Cask Loading Operations in LWR of Other Uranium Oxide Based Fuel."

A.9 ACCEPTANCE TESTS AND MAINTENANCE PROGRAM

Chapter 9 applies in its entirety to this chapter, except for the leakage tests described in Section 9.1.3. The 32PTH Type 1 DSC design contains an inner and outer top cover, and a separate top shield plug; therefore, the leakage test procedure has been revised to reflect this geometry. This three-part closure design is the same as that is used in other NUHOMS[®] DSC canister designs.

A.9.1 Acceptance Criteria

A.9.1.1 Visual Inspection and Non-Destructive Examination (NDE)

No change from Chapter 9, Section 9.1.1.

A.9.1.2 Structural and Pressure Tests

No change from Chapter 9, Section 9.1.2.

A.9.1.3 Leak Tests

The 32PTH-Type 1 DSC confinement boundary is tested using two procedures described below. Personnel performing the leakage test are qualified in accordance with SNT-TC-1A [1].

Procedure 1 is accomplished during fabrication:

Upon completion of all 32PTH-Type 1 DSC shell welding and attachment of the inner bottom cover plate to the DSC shell, a temporary seal plate is placed over the open end of the 32PTH-Type 1 DSC. A bag or other enclosure is placed around the outside of the entire 32PTH-Type 1 DSC and it is filled with helium. The 32PTH-Type 1 DSC cavity is evacuated and a helium leakage test is performed using a port in the seal plate. This test is used to show that the entire 32PTH-Type 1 DSC confinement boundary tested is leak tight (1×10^{-7} ref cm³/s).

Procedure 2 occurs after the 32PTH-Type 1 DSC has been loaded with fuel assemblies:

The 32PTH-Type 1 DSC cavity has been dried, back filled with helium, and the inner top cover plate and the vent and siphon port cover plates have been welded in place. After these welds are completed, a temporary test cover is installed or the outer top cover plate is welded in place with at least the root pass of the full weld. The cavity between the inner top cover plate and the temporary test cover or outer top cover plate is evacuated and a helium leakage test is performed using a test port in the temporary test cover or in the outer top cover plate. The leakage test thus includes the weld attaching the inner top cover plate to the 32PTH-Type 1 DSC shell, the vent and siphon port cover plate welds, and the base metal of the inner top cover plate and vent and siphon port cover plates. The vent and siphon ports are filled with helium prior to welding the vent and siphon port covers. This test verifies that the tested welds and cover plates are leak tight (1×10^{-7} ref cm³/s).

A.9.1.4 Components

No change from Chapter 9, Section 9.1.4.

A.9.1.5 Shielding Integrity

No change from Chapter 9, Section 9.1.5.

A.9.1.6 Thermal Acceptance

No change from Chapter 9, Section 9.1.6.

A.9.1.7 Neutron Absorber Tests

No change from Chapter 9, Section 9.1.7.

A.9.2 Maintenance Program

No change from Chapter 9, Section 9.2.

A.9.3 Marking

No change from Chapter 9, Section 9.3.

A.9.4 Pre-Operational Testing and Training Exercise

No change from Chapter 9, Section 9.4.

A.9.5 Specification for Neutron Absorbers

No change from Chapter 9, Section 9.5.

A.9.6 References

1. SNT-TC-1A, “American Society for Nondestructive Testing, Personnel Qualification and Certification in Nondestructive Testing,” 1992.

Chapter A.10 Radiation Protection

TABLE OF CONTENTS

A.10	RADIATION PROTECTION	A.10-1
A.10.1	Ensuring That Occupational Radiation Exposures Are As Low As Reasonably Achievable (ALARA)	A.10-1
A.10.2	Radiation Protection Design Features	A.10-2
A.10.3	Estimated Onsite Collective Dose Assessment	A.10-3

A.10 RADIATION PROTECTION

A.10.1 Ensuring That Occupational Radiation Exposures Are As Low As Reasonably Achievable (ALARA)

No change.

A.10.2 Radiation Protection Design Features

The estimates of off-site dose rates in and around an ISFSI containing arrays (two generic arrays – 2x10 back-to-back array and 2-1x10 front-to-front array) of loaded HSM-Hs (each HSM-H containing a 32PTH DSC fully loaded with design basis fuel) during long term storage are presented in Section 10.2 of Chapter 10. As described in Chapter A.5, the authorized fuel content has not changed, the top and bottom canister shielding thicknesses are not changed, and therefore there is no change in the dose rates in and around the HSM-H loaded with a 32PTH Type 1 DSC. Therefore, the off-site dose estimates presented in Chapter 10 are applicable to the 32PTH Type 1 DSC.

A.10.3 Estimated Onsite Collective Dose Assessment

The estimates of occupational dose during the loading of a 32PTH DSC fully loaded with design basis fuel for long term storage in an HSM-H using an OS187H TC during transfer are presented in Section 10.3 of Chapter 10. As described in Chapter A.5, the differences in the design of the 32PTH Type 1 DSC and the OS187H Type 1 TC do not result in a substantial change in the dose rates in and around the TC during loading and transfer operations. Some of the design changes result in a reduction in these near field dose rates. For the top end design option with separate shield plug and inner cover plate, the occupational exposure during decontamination operations is expected to be lower because the DSC top shield plug is not required to be decontaminated. Overall, the occupational exposure estimates presented in Chapter 10 are applicable and bounding to the Type 1 DSC and Type 1 TC.

Chapter A.11

Accident Analysis

TABLE OF CONTENTS

A.11	ACCIDENT ANALYSIS	A.11-1
A.11.1	Introduction.....	A.11-1
A.11.2	Off-Normal Operation.....	A.11-2
A.11.3	Postulated Accident	A.11-3
A.11.3.1	Cask Drop	A.11-3
A.11.3.2	Earthquake	A.11-3
A.11.3.3	Tornado Wind and Tornado Missiles Effect on HSM-H.....	A.11-3
A.11.3.4	Tornado Wind and Tornado Missiles Effect on Transfer Cask.....	A.11-3
A.11.3.5	Flood	A.11-9
A.11.3.6	Blockage of HSM-H Air Inlet and Outlet Openings	A.11-9
A.11.3.7	Lightning.....	A.11-9
A.11.3.8	Fire/Explosion.....	A.11-9
A.11.4	References	A.11-10

A.11 ACCIDENT ANALYSIS

A.11.1 Introduction

No change.

A.11.2 Off-Normal Operation

No change.

A.11.3 Postulated Accident

No change.

A.11.3.1 Cask Drop

No change.

A.11.3.2 Earthquake

No change.

A.11.3.3 Tornado Wind and Tornado Missiles Effect on HSM-H

No change.

A.11.3.4 Tornado Wind and Tornado Missiles Effect on Transfer Cask

This section summarizes the evaluation of the OS187H Type 1 transfer cask (TC) for tornado wind speed and tornado missile spectrum specified in Chapter 2, Section 2.2.1. This evaluation is similar to the evaluation for the OS187H presented in Section 11.3.4 and is performed to reconcile the changes in geometry parameters between the two TCs as documented in the table below. Subsections which are not affected by the changes in TC geometry are not repeated and are indicated as “No change.”

Parameter	OS187H TC	OS187H Type 1
Length of structural shell, in.	193.2	206.7
OD of structural shell, in.	82.70	81.87
OD of neutron shield, in.	92.20	92.11
Thickness of lead shielding, in.	3.60	3.56
Thickness of inner liner, in.	0.50	0.625

The maximum DBT tornado wind speed of 360 mph produces a design pressure of 304 psi. The 4,000 pound automobile and 276 pound eight inch diameter shell missiles were also considered. The other types of missiles are enveloped by the eight inch shell missile.

This analysis is performed for the cask secured in the horizontal position on the support skid. The following criteria are used to evaluate the adequacy of the transfer cask for the loads described above.

- Penetration resistance
- Impact stress analysis

Stability analysis is not required since the cask is already evaluated for a design basis cask drop accident.

A.11.3.4.1 Penetration Resistance

No change.

A.11.3.4.2 Impact Stress Analysis*Tornado Wind Load*

Chapter 2, Section 2.2.1.1 specifies a maximum tornado wind speed at 360 mph. The corresponding velocity pressure, q_z , can be calculated by Eq. 6-1 of [12].

$$q_z = 0.00256 K_z K_{zt} V^2 I \text{ (lb/ft}^2\text{)}$$

Where,

K_z = velocity pressure exposure coefficient

= 1.03 (height above ground < 15 ft in Exposure D, Table 6-3 of [12])

K_{zt} = topographic factor

= 1

V = basic wind speed

= 360 mph

I = importance factor

= 1.15 (Category IV, Table 6-2 of [12])

$$q_z = 0.00256 \times 1.03 \times 1 \times 1.15 = 393 \text{ lb/ft}^2$$

(a) Transverse wind pressure acting on cask shell surface

The projected area of the transfer cask normal to the wind is equal to the OD (92.11 inch) of the neutron shield multiplied by the length of the cask. The total wind force is then equal to the wind pressure multiplied by this projected area. This total wind force is equivalent to a line force, p , acting at the elevation of the cask centerline and along the entire cask length. This wind force will be assumed to be solely resisted only by the cask outer structural shell, which has a length of 206.7" with an OD of 81.87" and a thickness of 1.5".

$$p = q_z \times (\text{OD of neutron shield})$$

$$= 393 \text{ lb/ft}^2 \times (92.11 / 12) \text{ ft}$$

$$= 3016.6 \text{ lb/ft}$$

$$= 251.4 \text{ lb/in}$$

Case 9c in Table 31 of [13] provides stress formula for a thin-walled cylindrical vessel supported at both ends and subjected to a uniform load over the entire length of its top element as follows.

$$B = [12(1-\nu^2)]^{1/8} = 1.348, \nu = 0.3$$

Maximum hoop membrane stress,

$$\sigma_2 = -0.492 B p R^{3/4} L^{-1/2} t^{-5/4}$$

$$= -0.492 \times (1.348) \times 251.4 \times (81.87/2)^{3/4} \times (206.7)^{-1/2} \times (1.5)^{-5/4}$$

$$= -113.1 \text{ psi}$$

Maximum hoop bending stress,

$$\begin{aligned}\sigma_2' &= -1.217 B^{-1} p R^{1/4} L^{1/2} t^{-7/4} \\ &= -1.217 \times (1.348)^{-1} \times 251.4 \times (81.87/2)^{1/4} \times (206.7)^{1/2} \times (1.5)^{-7/4} \\ &= -4059.8 \text{ psi}\end{aligned}$$

Maximum hoop membrane plus bending stress,

$$(\sigma_2)_{\text{Total}} = \sigma_2 + \sigma_2' = -113.1 \text{ psi} - 4059.8 \text{ psi} = -4172.9 \text{ psi}$$

Maximum axial membrane stress,

$$\begin{aligned}\sigma_1 &= \text{axial membrane stress} \\ &= -0.1188 B^3 p R^{1/4} L^{1/2} t^{-7/4} \\ &= -0.1188 \times (1.348)^3 \times 251.4 \times (81.87/2)^{1/4} \times 206.7^{1/2} \times (1.5)^{-7/4} \\ &= -1308.5 \text{ psi}\end{aligned}$$

Maximum axial bending stress,

$$\sigma_1' \approx \nu \times \sigma_2' = 0.3 \times (-4059.8 \text{ psi}) = -1217.9 \text{ psi}$$

Maximum axial membrane plus bending stress,

$$(\sigma_1)_{\text{Total}} = \sigma_1 + \sigma_1' = -1308.5 \text{ psi} + (-1217.9 \text{ psi}) = -2526.4 \text{ psi}$$

Maximum membrane plus bending stress intensity = $0 - (-4172.9) = 4172.9 \text{ psi}$

The ASME code allowable stress for the general membrane stress intensity will be conservatively used for evaluation of the above calculated maximum membrane plus bending stress intensity. The Service Level D allowable stress for the membrane stress intensity is the lesser of $2.4S_m$ and $0.7S_u$. For SA-240 Gr. 304 cask structural shell material, $S_m = 20,000 \text{ psi}$ at 300°F and $S_u = 66,200 \text{ psi}$. Thus the allowable stress is $0.7S_u = 46,340 \text{ psi}$.

Therefore the maximum calculated membrane plus bending stress intensity, under tornado wind load, in the cask shell is acceptable.

(b) Axial wind pressure acting on the top end cover of the transfer cask

Case 10b in Table 24 of [13] provides a formula for calculating the resultant moment on the 1.5" recessed flange thickness of the fixed cask top end plate under the wind pressure.

Maximum bending moment,

$$\begin{aligned}M_{ra} &= -q_z a^2 / 8 \\ &= -393 \text{ lb/ft}^2 \times (1 \text{ ft}^2 / 144 \text{ in}^2) \times (81.87/2 \text{ in})^2 / 8 \\ &= -571.6 \text{ in-lb/in}\end{aligned}$$

Maximum bending stress,

$$\begin{aligned}\sigma &= 6M_{ra} / t^2 \\ &= 6 \times (571.6 \text{ in-lb/in}) / (1.5 \text{ in})^2 \\ &= 1524.4 \text{ psi} < 46,340 \text{ psi OK}\end{aligned}$$

(c) Axial wind pressure acting on the bottom end cover of the transfer cask

Case 2f in Table 24 of [13] provides a formula for calculating the resultant moment on the 2" thick fixed bottom end plate of the cask under the wind pressure.

$$\begin{aligned}b &= 14" = \text{radius of the cask bottom ram penetration ring} \\ a &= 81.87" / 2 = 40.935" = \text{outer radius of bottom end plate} \\ b/a &= .3420 \Rightarrow K_{Mra} = -0.0889 \text{ (by interpolation)}\end{aligned}$$

Maximum bending moment,

$$M_{ra} = K_{Mra} q_z a^2 = -0.0889 \times 393/144 \times 40.935^2 = -406.6 \text{ in-lb/in}$$

Maximum bending stress,

$$\sigma = 6M_{ra} / t^2 = 6 \times (406.6 \text{ in-lb/in}) / (2 \text{ in})^2 = 609.9 \text{ psi} < 46,340 \text{ psi OK}$$

Massive Automobile Missile

The impact forces applied to the cask as it is struck by the automobile missile is determined as follows:

The massive automobile missile is assumed to crush 3 feet under a constant force during the impact. The loss of kinetic energy is assumed to be dissipated by crushing of the missile. The frontal contact area of the automobile is specified to be 20 sq. ft.

$$\begin{aligned}F_a \times 3\text{ft} &= \frac{1}{2} [m_a v_o^2] \\ P_a &= F_a / 20 \text{ ft}^2\end{aligned}$$

where:

$$\begin{aligned}m_a &= \text{mass of missile} = 4,000 \text{ lb} \\ v_o &= \text{missile initial velocity} = 195 \text{ ft/sec} \\ F_a &= \text{impact force on cask by missile automobile} \\ p_a &= \text{impact pressure on cask by missile automobile}\end{aligned}$$

$$\begin{aligned}F_a &= \frac{1}{2} \times \{4,000 \text{ lbm} \times [(195 \times 12) \text{ in/sec}]^2\} / (3 \times 12) \text{ in} \\ &= 3.042 \times 10^8 \text{ lbm-in/sec}^2 \\ &= 3.042 \times 10^8 \text{ lb}_m\text{-in/sec}^2 \times [1 \text{ lb}_f / (386.4 \text{ lb}_m\text{-in/sec}^2)] \\ &= 787,267 \text{ lb}_f\end{aligned}$$

$$P_a = 787,267 \text{ lb}_f / [20 \times (12)^2 \text{ in}^2]$$

$$= 273.4 \text{ psi}$$

The automobile missile deforms and is crushed during the impact. The shear stress in the cask wall is conservatively calculated below. It is assumed that the impact force is concentrated on a small curved section of the cask wall having dimensions $w \times L$. It is also assumed that only two side edges of the impact section are tending to shear. Edges above and below the impact section are assumed to bend, not shear. It is also assumed that the concentrated impact section is 3 ft wide, half of the automotive width. The impact area is then 36" wide by 80" high (equal to 20 ft² area).

$$\text{Shear area} = 2 \times (20 \text{ ft}^2 / 3\text{ft}) \times \text{the thickness of the cask outer structural shell}$$

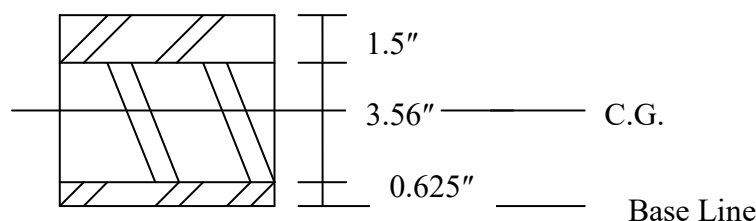
$$= 2 \times 80" \times 1.5" = 240 \text{ in}^2$$

$$\text{The shear stress, } \tau = \text{force/area} = 787,267 \text{ lb} / 240 \text{ in}^2 = 3,280 \text{ psi}$$

The level D allowable shear stress for the cask shell is $0.42 S_u = 0.42 \times 66,200 = 26,480 \text{ psi}$. The shear stress is well below the allowable shear stress.

Assuming that the impact on the side of the cask is reacted by a 36"×80" section of the cask shell, Case 1c from Table 26 of [13] is used to calculate the resulted stresses in the shell. This case represents a flat plate with simply supported edges under a uniform load over a central rectangular area. It is conservative for this case to represent the automotive crushing onto a curved section of the cask.

The transfer cask shell is made of a three-layer composite. It consists of a 1.5" outer structural shell, a 3.56" lead gamma shield, and a 0.625" inner liner (see sketch below). This sandwiched composite plate may be represented by an equivalent one-piece plate which has a thickness producing the same moment of inertia as that of the composite. The thickness of its equivalent one-piece plate is calculated as follows.



For unit length of the composite plate,
neglecting the strength of the 3.6" thick lead,
the distance from base line to C.G.

$$= [(1.5" \times 1") \times (1.5"/2 + 3.56" + 0.625") + (0.625" \times 1") \times (0.625"/2)] \div$$

$$[(1.5" \times 1") + (0.625" \times 1")]$$

$$= 7.6" \div 2.125$$

$$= 3.58"$$

The combined moment of inertia of the composite structural plates, I_{comb}

$$I_{\text{comb}} = (1 \times 1.5^3 / 12) + (1.5 \times 1) \times (1.5/2 + 3.56 + 0.625 - 3.58)^2 + (1 \times 0.625^3 / 12) + (0.625 \times 1) \times (3.58 - 0.625/2)^2 \\ = 9.73 \text{ in}^4$$

The thickness of the equivalent one-piece plate, t_{eq}

$$I_{\text{comb}} = 9.73 \text{ in}^4 = (1 \times t_{\text{eq}}^3) / 12 \Rightarrow t_{\text{eq}} = 4.89''$$

An automobile missile crushing into the horizontal cylindrical canister with an impact area of 36'' wide by 80'' high is conservatively analyzed by a case that the same impact is applied to a rectangular plate of dimensions at the cask length by the cask OD. All edges of the rectangular plate are assumed simply supported. Case 1c in Table 26 of [13] provides maximum stress calculation of this rectangular plate as follows.

$$\text{Max } \sigma = (\beta W) / t^2 \\ W = F_a = 787,267 \text{ lb, calculated in Section 11.3.4.2} \\ t = t_{\text{eq}} = 4.89''$$

$$a_1 = 36'', b_1 = 80'' \\ a = 206.7'' \text{ (cask length)} \\ b = 81.87'' \text{ (cask OD)} \\ a_1 / b = 0.4397 \\ b_1 / b = 0.977 \\ a / b = 2.525$$

Use $(b_1 / b) = 0.8$, and $(a_1 / b) = 0.4$ for the table given under the Case 1c in Table 26 of [13];

From this table,

$$\beta = 0.68 \text{ for } (a / b) = 1.4, \text{ and } \beta = 0.76 \text{ for } (a / b) = 2$$

By extrapolation, $\beta = 0.83$ for $(a / b) = 2.525$

$$\therefore \text{Max } \sigma = (0.83 \times 787,267 \text{ lb}) / (4.89^2) = 27,326 \text{ psi}$$

The ASME code allowable stress for the general membrane stress intensity will be conservatively used for evaluation of the above calculated maximum membrane plus bending stress intensity. The Service Level D allowable stress for the membrane stress intensity is the lesser of $2.4S_m$ and $0.7S_u$. For SA-240 Gr. 304 cask structural shell material, $S_m = 20,000$ psi at 300°F and $S_u = 66,200$ psi. Thus the allowable stress is $0.7S_u = 46,340$ psi. Therefore the maximum membrane plus bending stress of 27,326 psi is acceptable.

A.11.3.4.3 Accident Dose Calculation

Based on the above analyses, the 32PTH Type 1 DSC confinement boundary will not be breached as a result of the missile impacts. Accordingly, no 32PTH Type 1 DSC damage or release of radioactivity is postulated.

The missile impact scenario may result in the loss of cask neutron shielding and local deformation/damage of the gamma shielding. The effect of loss of the neutron shielding due to a missile impact is bounded by that resulting from a cask drop scenario. The radiation dose due to local deformation/damage of the gamma shielding is negligible.

A.11.3.4.4 Corrective Action

The transfer cask will be inspected for damage. These operations will take place in the plant fuel building decontamination area and spent fuel pool after recovery of the transfer cask.

Following recovery of the transfer cask and unloading of the DSC, the transfer cask will be inspected, repaired and tested as appropriate prior to reuse.

For recovery of the cask and contents, it may be necessary to develop a special sling/lifting apparatus to move the transfer cask from the site to the fuel pool. This may require several weeks of planning to ensure all steps are correctly organized. During this time, lead blankets may be added to the transfer cask to minimize on-site exposure to site operations personnel. The transfer cask would be roped off to ensure the safety of the site personnel.

A.11.3.5 Flood

No change.

A.11.3.6 Blockage of HSM-H Air Inlet and Outlet Openings

No change.

A.11.3.7 Lightning

No change.

A.11.3.8 Fire/Explosion

No change.

A.11.4 References

No change.

Chapter A.12

Operating Controls and Limits

No change.

Chapter A.13

Quality Assurance

No change.

Chapter A.14 Decommissioning

No change.

APPENDIX B

32PTH Type 2 DSC and OS187H Type 2 TC

APPENDIX B.1 GENERAL INFORMATION

TABLE OF CONTENTS

B.1	GENERAL INFORMATION	B.1-1
B.1.1	Introduction.....	B.1-2
B.1.2	General Description of the NUHOMS® HD System with the 32PTH Type 2 DSC and OS187H Type 2 TC.....	B.1-3
	B.1.2.1 NUHOMS® HD System Characteristics.....	B.1-3
	B.1.2.2 Operational Features	B.1-4
	B.1.2.3 32PTH Type 2 DSC Contents.....	B.1-5
B.1.3	Identification of Agents and Contractors	B.1-6
B.1.4	Generic Cask Arrays	B.1-7
B.1.5	Supplemental Data.....	B.1-8
	B.1.5.1 References.....	B.1-8
	B.1.5.2 Drawings	B.1-8

LIST OF TABLES

Table B.1-1	Key Design Parameters of the NUHOMS® HD System Components ...	B.1-9
-------------	---	-------

LIST OF FIGURES

Figure B.1-1	32PTH Type 2 Dry Shielded Canister (Optional two-part top end configuration shown)	B.1-10
Figure B.1-2	OS187H Type 2 On-Site Transfer Cask	B.1-11

B.1 GENERAL INFORMATION

Appendix B to this NUHOMS[®] HD System updated Final Safety Analysis Report (UFSAR) documents the addition of the 32PTH Type 2 dry shielded canister (DSC) and the OS187H Type 2 transfer cask (TC) to the NUHOMS[®] HD System. These two components are similar but longer length versions of the 32PTH DSC and the OS187H TC described in the main body of this UFSAR.

The general information presented in Chapter 1 remains applicable for 32PTH Type 2 DSC and OS187H Type 2 TC, which are added to the NUHOMS[®] HD System.

The format and content of this appendix follows the format and content of the main body of this UFSAR. Generally, the same chapters and section numbers as in the main body have been kept in this appendix, preceded with a letter B. In addition, in several sections of this appendix reference is made to the corresponding section/chapter in the main body of the FSAR to avoid repetition of documentation that is also applicable to this appendix. For the sections in this appendix which have been identified as “No change,” the description or analysis presented in the corresponding sections of the UFSAR for the 32PTH and OS187H or 32PTH Type 1 and OS187H Type 1 are also applicable to the 32PTH Type 2 DSC or the OS187H Type 2 transfer cask. The Tables and figures presented in the UFSAR, which remain unchanged due to the addition of the 32PTH Type 2 DSC and OS187H Type 2 TC, are not repeated in this Appendix B.

Note: References to sections or chapters within this appendix are identified with a prefix B (e.g., Section B.2.1 or Chapter B.2). References to sections or chapters of the UFSAR outside of this appendix (main body of the UFSAR) are identified with the applicable UFSAR section, chapter number or prefix A (e.g., Section 2.1, Chapter 2, Section A.2.1 or Chapter A.2).

B.1.1 Introduction

There is no change to the generic description presented in Section 1.1 of the UFSAR when the 32PTH Type 2 DSC and the OS187H Type 2 TC are used instead of the 32PTH DSC and the OS187H TC. When used with the Type 2 components, the NUHOMS[®] HD System consists of the 32PTH Type 2 DSC, the OS187H Type 2 TC, and the HSM-H Horizontal Storage Module. Sketches for the 32PTH Type 2 DSC and the OS187H Type 2 TC are shown in Figure B.1-1 and Figure B.1-2.

The 32PTH Type 2 DSC and the OS187H Type 2 TC are similar to, but longer length versions of, the 32PTH DSC and OS187H TC described in the main body of this UFSAR. The main design changes associated with these longer length NUHOMS[®] HD System components are summarized in Sections B.1.2.1.1 and B.1.2.1.3.1 for the 32PTH Type 2 DSC and OS187H Type 2 TC, respectively. The authorized contents and overall design criteria as described in the main body of this UFSAR is the same for these added components with the exception that an elastic-plastic analysis methodology is used for the accident pressure load case evaluation of the 32PTH Type 2 DSC (instead of elastic analysis methodology used for the 32PTH DSC). The application of the elastic-plastic analysis methodology to the 32PTH Type 2 DSC is similar to that used for the NUHOMS[®] 32P DSC in Reference [2].

B.1.2 General Description of the NUHOMS[®] HD System with the 32PTH Type 2 DSC and OS187H Type 2 TC

The general arrangement of NUHOMS[®] HD System shown in Figure 1-3 and Figure 1-4 and the general description presented in Section 1.2 remain applicable when the 32PTH Type 2 DSC and the OS187H Type 2 TC are used instead of the 32PTH DSC and OS187H TC. The confinement boundary of the 32PTH Type 2 DSC is shown in Figure B.7-1 when the standard three-piece top end assembly configuration is used. For the optional two-piece top end assembly configuration, the confinement boundary is the same as that for the 32PTH DSC as shown in Figure 7-1.

The 32PTH Type 2 DSC is identified as follows: XXX-32PTH-YYY-Z-1, where XXX, YYY, and Z are as described in Section 1.2. The basket types are the same as for the 32PTH DSC and are described in drawing 10494-72-2008-SAR.

B.1.2.1 NUHOMS[®] HD System Characteristics

B.1.2.1.1 Dry Shielded Canister (32PTH Type 2 DSC)

No change to the generic description for the 32PTH DSC presented in Section 1.2.1.1. Table A.1-1 summarizes the key design parameters for the 32PTH Type 2 DSC.

The major changes implemented in the 32PTH Type 2 DSC relative to the 32PTH DSC are as follows:

- The interior cavity length of the 32PTH Type 2 DSC is increased, approximately 17 in., with a corresponding increase in basket length.
- The thickness of the top shield assembly is reduced from 12.0 in. to 10.0 in. whereas the thickness of the bottom shield assembly is reduced from 8.75 in. to 6.5 in. The overall DSC length also is increased. The DSC diameter is unchanged.
- The top end assembly of the 32PTH Type 2 DSC consists of a three-part closure design (top shield plug, inner top cover, and outer top cover). This design is the same as other standardized NUHOMS[®] canister designs described in Reference [1]. The two-part top end closure design of the 32PTH DSC is an alternate design in the 32PTH Type 2 DSC.
- Lifting lugs are used to lift the empty 32PTH Type 2 DSC into the OS187H Type 2 TC. The lifting lugs are welded to the shell and are located at the support ring elevation, similar to other standardized NUHOMS[®] canister designs [1]. Lifting lugs are used in lieu of the lifting rods with welded bosses, located at the inner bottom cover plate, in the 32PTH design. The lifting lugs are non-safety components as they are used to lift the DSC prior to fuel load.

The 32PTH Type 2 DSC is shown on drawings 10494-72-2006-SAR through 10494-72-2010-SAR in Section B.1.5.2.

B.1.2.1.2 Horizontal Storage Module (HSM-H)

No change to the generic description presented in Section 1.2.1.2. Only a small (2.5 in.) increase in the overall length of the DSC support rail is required to accommodate the 32PTH Type 2 DSC. The key design parameters for the HSM-H as presented in Table 1-1 are not changed.

B.1.2.1.3 Transfer Systems

B.1.2.1.3.1 OS187H Type 2 On-Site Transfer Cask

No change to the generic description presented in Section A.1.2.1.3.1 for the OS187H Type 1 TC. Table B.1-1 summarizes the key design parameters for the OS187H Type 2 TC. The major changes incorporated into the OS187H Type 2 transfer cask are:

- In order to accommodate the longer 32PTH Type 2 DSC, the minimum internal cavity length of the TC is increased from 198.75 in. (OS187H Type 1) to 199.05 in. (OS187H Type 2). The increased cavity length is achieved by reducing the thickness of the bottom air flow wedge plate. The 70.5 in. inside diameter and the thicknesses of the top and bottom end assemblies are unchanged.
- There are no other changes (except cavity) in the OS187H Type 2 TC compared to OS187H Type 1 TC.

The OS187H Type 2 TC has a payload capacity of 120,000 lb (determined based on its evaluated capacity of 250,000 lb and its total weight of 130,000 lb).

B.1.2.1.3.2 Transfer Equipment

No change to the transfer equipment description presented in Section 1.2.1.3.2.

B.1.2.2 Operational Features

B.1.2.2.1 Dry Run Operations

No change to the dry run operations description present in Section 1.2.2.1.

B.1.2.2.2 SFA Loading Operations

No change in the primary operations (in sequence of occurrence) for the NUHOMS[®] HD System described in Section 1.2.2.2, except for placement of the cask spacer (if required) prior to placing the 32PTH Type 2 DSC into the TC, and, for a 32PTH Type 2 DSC with a three-part top end closure, the inner top cover plate is placed following placement of the top shield plug (Step 8) and lifting of the transfer cask from the pool (Step 9). The inner top cover is sealed in Step 10 instead of the top shield plug

B.1.2.2.3 Identification of Subjects for Safety and Reliability Analysis

B.1.2.2.3.1 Criticality Prevention

No change in criticality prevention present in Section 1.2.2.3.1.

B.1.2.2.3.2 Chemical Safety

No change in chemical safety present in Section 1.2.2.3.2.

B.1.2.2.3.3 Operation Shutdown Modes

The NUHOMS[®] HD System is a totally passive system so that consideration of operation shutdown modes is unnecessary.

B.1.2.2.3.4 Instrumentation

No change in instrumentation present in Section 1.2.2.3.4.

B.1.2.2.3.5 Maintenance and Surveillance

No change. All maintenance and surveillance tasks are described in Chapter A.9.

B.1.2.3 32PTH Type 2 DSC Contents

No change. The DSC contents described in Section 1.2.3 for the 32PTH DSC are applicable for the 32PTH Type 2 DSC.

B.1.3 Identification of Agents and Contractors

No change to identification of agents and contractors present in Section 1.3.

B.1.4 Generic Cask Arrays

No change to Generic Cask Arrays present in Section 1.4.

B.1.5 Supplemental Data

B.1.5.1 References

1. Updated Final Safety Analysis Report (UFSAR), Standardized NUHOMS[®] Horizontal Modular Storage System for Irradiated Nuclear Fuel, NUH003.0103 Revision 14, USNRC Docket No. 72-1004.
2. USNRC Safety Evaluation Report, SNM-2505, Amendment 7, Dated 11/2/2005, Docket 72-8

B.1.5.2 Drawings

32PTH Type 2 DSC:

- 10494-72-2006-SAR, (3 sheets), (PROPRIETARY)
- 10494-72-2007-SAR, (2 sheets), (PROPRIETARY)
- 10494-72-2008-SAR, (5 sheets), (PROPRIETARY)
- 10494-72-2009-SAR, (3 sheets), (PROPRIETARY)
- 10494-72-2010-SAR, (5 sheets) (PROPRIETARY)

OS187H Type 2 TC:

- 10494-72-9004-SAR, (3 sheets), (PROPRIETARY)
- 10494-72-9005-SAR, (3 sheets), (PROPRIETARY)
- 10494-72-9006-SAR, (3 sheets) (PROPRIETARY)

Table B.1-1
Key Design Parameters of the NUHOMS[®] HD System Components

Dry Shielded Canister (32PTH Type 2 DSC)	
Overall length (in.)	198.50 (max)
Outside diameter (in.)	69.75 (unchanged)
Cavity length (in.)	181.38 (min)
Shell thickness (in.)	0.5 (unchanged)
Design weight of loaded 32PTH Type 2 DSC (lb)	108,000 ⁽¹⁾
Materials of construction	Stainless steel shell assembly and internals, carbon steel and/or stainless steel shield plugs, aluminum
Neutron absorbing material	Boral [™] , borated aluminum, metal matrix composite (MMC)
Internal atmosphere	Helium

Horizontal Storage Module (HSM-H)	
Overall length (without back shield wall)	20'-8"
Overall width (without end shield walls)	9'-8"
Overall height	18' 6"
Total weight (not including 32PTH Type 2 DSC) (lbs.)	307,200 ⁽¹⁾
Materials of construction	Reinforced concrete and structural steel
Heat removal	Conduction, convection, and radiation

On-Site Transfer Cask (OS187H Type 2)	
Overall length (in.)	210.50
Outside diameter (in.)	92.11
Cavity length (in.)	199.05
Lead thickness (in.)	3.56 (nom)
Gross weight (including 32PTH Type 1 DSC) (tons)	120.0 ⁽¹⁾
Materials of construction	Stainless steel shell assemblies and closures with lead shielding
Internal atmosphere	Helium

Note:

(1) Rounded up values

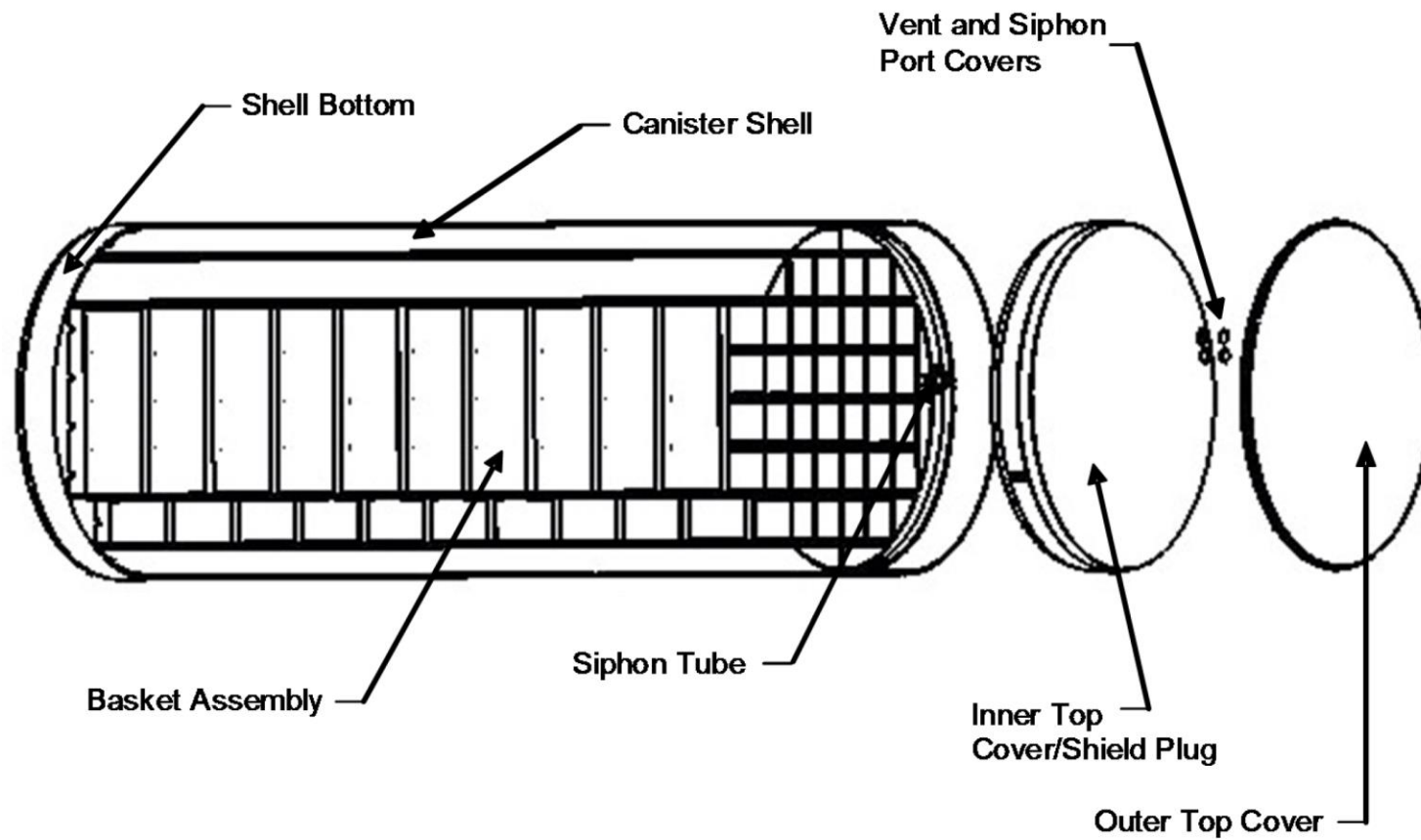


Figure B.1-1
32PTH Type 2 Dry Shielded Canister
(Optional two-part top end configuration shown)

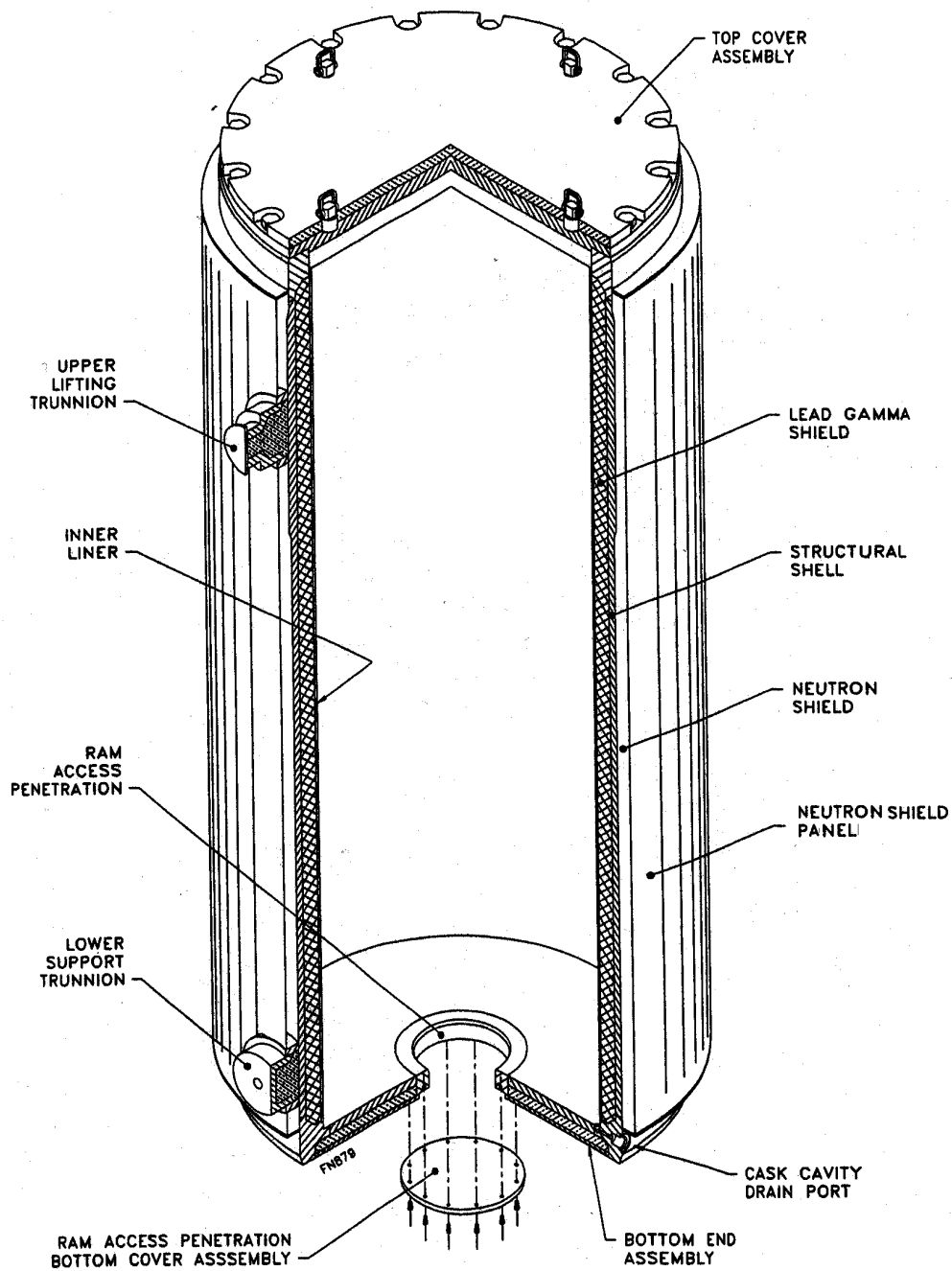


Figure B.1-2
OS187H Type 2 On-Site Transfer Cask

**Proprietary and Security Related Information
for Drawing 10494-72-2006, Rev. 0
Withheld Pursuant to 10 CFR 2.390**

**Proprietary and Security Related Information
for Drawing 10494-72-2007, Rev. 0
Withheld Pursuant to 10 CFR 2.390**

**Proprietary and Security Related Information
for Drawing 10494-72-2008, Rev. 0
Withheld Pursuant to 10 CFR 2.390**

**Proprietary and Security Related Information
for Drawing 10494-72-2009, Rev. 0
Withheld Pursuant to 10 CFR 2.390**

**Proprietary and Security Related Information
for Drawing 10494-72-2010, Rev. 0
Withheld Pursuant to 10 CFR 2.390**

**Proprietary and Security Related Information
for Drawing 10494-72-9004, Rev. 0
Withheld Pursuant to 10 CFR 2.390**

**Proprietary and Security Related Information
for Drawing 10494-72-9005, Rev. 0
Withheld Pursuant to 10 CFR 2.390**

**Proprietary and Security Related Information
for Drawing 10494-72-9006, Rev. 0
Withheld Pursuant to 10 CFR 2.390**

APPENDIX B.2

PRINCIPAL DESIGN CRITERIA

No change. The design criteria described in Chapter 2 for the 32PTH DSC and OS187H transfer cask (TC) are applicable to the 32PTH Type 2 DSC and the OS187H Type 2 TC. The contents authorized for storage in the 32PTH Type 2 DSC are the same as the authorized contents for the 32PTH DSC described in Section 2.1. The number of fuel assemblies per DSC, maximum heat load per DSC and heat load configurations, basket poison types, and basket geometric configuration are not changed. Similarly, there is no change to the design criteria for environmental conditions and natural phenomena as described in Section 2.2, or to the safety protection systems as described in Section 2.3. Section 2.4 (Decommissioning Considerations), Section 2.5 (Structures, Systems and Components Important to Safety), and Section 2.6 (References) are not changed. As described in Section B.1.1, an elastic-plastic analysis methodology is used for the accident pressure load case of the 32PTH Type 2 DSC. As with the 32PTH DSC, the details of the 32PTH Type 2 DSC evaluation criteria are described in Chapter B.3.

APPENDIX B.3 STRUCTURAL EVALUATION

TABLE OF CONTENTS

B.3	STRUCTURAL EVALUATION	B.3-1
B.3.1	Structural Design	B.3-1
	B.3.1.1 Discussion	B.3-1
	B.3.1.2 Design Criteria	B.3-6
B.3.2	Weights.....	B.3-7
	B.3.2.1 32PTH Type 2 DSC Weight	B.3-7
	B.3.2.2 OS187H Type 2 TC Weight	B.3-8
	B.3.2.3 HSM-H Weight.....	B.3-8
B.3.3	Mechanical Properties of Materials	B.3-9
B.3.4	General Standards for 32PTH Type 2 DSC, HSM-H, and OS187H Type 2 TC	B.3-10
	B.3.4.1 Chemical and Galvanic Reactions	B.3-10
	B.3.4.2 Positive Closure	B.3-10
	B.3.4.3 Lifting Devices.....	B.3-10
	B.3.4.4 Heat	B.3-10
	B.3.4.5 Cold.....	B.3-11
B.3.5	Fuel Rods General Standards for 32PTH Type 1 DSC	B.3-12
B.3.6	Normal Conditions of Storage and Transfer.....	B.3-13
	B.3.6.1 32PTH Type 2 DSC Normal Conditions Structural Analysis.....	B.3-13
	B.3.6.2 HSM-H Normal Conditions Structural Analysis	B.3-15
	B.3.6.3 OS187H Type 2 TC Normal Conditions Structural Analysis.....	B.3-15
B.3.7	Off-Normal and Hypothetical Accident Conditions	B.3-17
	B.3.7.1 32PTH Type 2 DSC Off-Normal and Accident Conditions Structural Analysis	B.3-17
	B.3.7.2 HSM-H Off-Normal and Accident Conditions Structural Analysis.....	B.3-20
	B.3.7.3 OS187H Type 2 TC Off-Normal and Accident Conditions Structural Analysis	B.3-20

B.3.8	References	B.3-22
B.3.9	Appendices.....	B.3-23
B.3.10	ASME Code Alternatives	B.3-24

B.3 STRUCTURAL EVALUATION

B.3.1 Structural Design

This chapter, including its appendices, summarizes the structural evaluation of the NUHOMS[®] HD System Type 2 components, i.e., the 32PTH Type 2 dry shielded canister (DSC) and the OS187H Type 2 transfer cask (TC).

The 32PTH Type 2 DSC is similar to, but a longer version of, the 32PTH DSC documented in the main chapter of this UFSAR. As with the 32PTH DSC, the 32PTH Type 2 DSC is designed to accommodate up to 32 intact pressurized water reactor (PWR) fuel assemblies (or up to 16 damaged assemblies, with the remaining intact) with the same total heat load of up to 34.8 kW. The OS187H Type 2 TC is identical to OS187H Type 1 TC with the exception of a slightly longer cavity length. The cavity length is increased from the 198.75 in. of the OS187H Type 1 TC to 199.05 in. for the OS187H Type 2 TC.

The structural evaluation criteria for the 32PTH Type 2 DSC and the OS187H Type 2 TC are the same as the evaluation criteria for the 32PTH DSC and OS187H Type 1 TC described in the main chapter and Appendix A, respectively, of this UFSAR, with no exception to the analysis methodology.

B.3.1.1 Discussion

No change.

B.3.1.1.1 General Description of the 32PTH Type 2 DSC

The principal characteristics of the 32PTH Type 2 DSC are described in Chapter B.1, Section B.1.2.1, including the changes implemented in the 32PTH Type 2 DSC relative to the 32PTH DSC. The 32PTH Type 2 DSC is shown on drawings attached in Section B.1.5.

For purposes of the structural analysis, the 32PTH Type 2 DSC is divided into the 32PTH Type 2 DSC shell assembly and the internal basket assembly.

A. DSC Shell Assembly Description

The 32PTH Type 2 canister shell assembly and design details are shown on drawings in Section B1.5. As with the 32PTH DSC, the 32PTH Type 2 DSC shell assembly is a high integrity stainless steel (SA-240 Type 304 or SA-182 Type F304) welded vessel that provides confinement of radioactive materials, encapsulates the fuel in an inert atmosphere (the canister is backfilled with helium before being seal welded closed), and provides biological shielding (in axial direction).

The 32PTH Type 2 main structural components include the welded cylindrical shell and the top and bottom end assemblies. The top end assembly may be a three-piece assembly, (a solid shield plug, made of A36 carbon steel, and the inner cover and outer cover plates, both made of SA-240 Type 304 stainless steel) or, as an alternate, a two-piece assembly, consisting of a combined top shield plug/inner cover assembly, and an outer cover plate. The combined top shield plug/inner cover may be a single stainless steel piece (SA-240 Type 304 or SA-182 Type F304), or two stainless steel plates welded together, or a carbon steel shield plug encased within welded stainless steel plates. The various top end assembly optional design configurations are similar to those of the 32PTH DSC, as described in Section 3.1.1.1. Although the total thicknesses of top end assembly is reduced from 12 in. for the 32PTH DSC to 10 in. for the 32PTH Type 2 DSC. For the bottom end assembly, the four optional design configurations present in the 32PTH are kept for the 32PTH Type 2 DSC. The total thickness of the bottom end assembly is reduced from 8.75 in. for the 32PTH DSC to 6.50 in. for the 32PTH Type 2 DSC.

The remaining 32PTH Type 2 shell assembly structural components include the grapple ring assembly, the support ring and the lifting lugs (in the three-piece top end assembly design), or lifting blocks (in the two-piece alternate top end assembly design). The grapple ring assembly, which is welded to the shell bottom or outer bottom cover plate, is used to insert/extract the DSC to and from the horizontal storage module (HSM-H). The grapple ring minimum thickness is same as 32PTH DSC. The support ring, welded to the cylindrical shell, supports the shield plug. The 32PTH Type 2 DSC with the three-piece top end assembly design option incorporates four lifting lugs (welded to the shell and to the support ring) in lieu of the four lifting blocks, which are welded to the inside of the shell bottom in the alternate design. The lifting lugs/lifting blocks are used to lift the DSC into the TC prior to fuel loading operations.

The 32PTH Type 2 DSC shell assembly is designed, fabricated, examined, and tested in accordance with the same ASME Code Subsection NB [6] requirements as for the 32PTH DSC. The 32PTH Type 2 DSC top closure is designed, fabricated, and inspected using the same alternatives to the ASME code specified for 32PTH DSC. The outer top cover plate and inner top cover plate are sealed by separate, redundant closure welds. The inner top cover (or inner top cover/top shield plug in the alternate two-piece top end design) is welded to the 32PTH Type 2 DSC shell to form the confinement boundary at the top end of the 32PTH Type 2 DSC, as shown in Chapter B.7, Figure B.7-1 (or Chapter 7, Figure 7-1 for the alternate top end design). The outer top cover plate provides structural support to the confinement boundary. All closure welds are multiple layer welds. Both, the inner and outer top cover plates to shell welds are examined by multi-level liquid penetrant to effectively eliminate through wall leaks. The three-piece top end assembly incorporates a vent and siphon block welded to the shell, which is similar to that in other NUHOMS[®] canister designs [9]. The vent and siphon block weld to the shell and the inner top cover plate weld to the vent and siphon block are part of the confinement boundary. These welds are also multiple layer welds and receive multi-level liquid penetrant examination.

The leak test and the acceptance criterion of 1×10^{-7} ref. cm³/sec as defined in ANSI N14.5 [2] of the DSC shell and bottom end assembly during fabrication and of the inner top closure weld (including vent/siphon cover welds) after loading of the fuel assemblies, have not changed from those of the 32PTH DSC.

The use of a strong back is not required during fuel loading operations when using the 32PTH Type 2 DSC.

B. Fuel Basket Assembly Description

The details of the 32PTH Type 1 basket assembly are shown in drawings provided in Section B.1.5. The overall length of the basket is increased from the 162.00 in. of the 32PTH DSC to 178.75 in. for the 32PTH Type 2 DSC. The internal canister cavity length is also increased from 164.38 in. for 32PTH DSC minimum to 181.38 in. minimum for 32PTH Type 2 DSC to allow for thermal expansion, tolerances, and access to the top of the fuel assemblies.

The description for the basket assembly presented in Section 3.1.1.1 (B) for the 32PTH basket is applicable to the 32PTH Type 2 basket assembly. Additionally, when lifting blocks are not used, the circumferential orientation of the basket is maintained by the use of a key welded to the inside diameter of the shell at two opposite azimuths, and two accompanying slots in the basket rails. The purpose of the basket key is non-safety and is intended to prevent rotation during fabrication and during shipment of the empty canister.

B.3.1.1.2 General Description of the HSM-H

The general description of the HSM-H presented in Section 3.1.1.2 is applicable when the HSM-H is loaded with a 32PTH Type 2 DSC. The spacer mounted on the support rails used to accommodate shorter length DSCs is not needed for storage of the 32PTH Type 2 DSC. Additionally, the HSM-H support rail structure length for 32PTH DSC has been increased by 2.5 in., and the thickness of the door is reduced to 2 ft.- 4 3/8 in. to accommodate the longer length 32PTH Type 2 DSC. The optional or alternate optional, square or round, doors with 3" metal plate can be used with the 32PTH Type 2 DSC. The changes to the HSM-H drawings are provided in Chapter B.1, Section B.1.5

B.3.1.1.3 General Description of the OS187H Type 2 On-Site TC

The NUHOMS[®] OS187H Type 2 on-site TC consists of a structural shell, gamma shielding material, and solid and liquid (water) neutron shield. The OS187H Type 2 TC is exactly similar to the OS187H Type 1 TC described in Section A.3.1.1.3 except the minimum cavity length. The minimum cavity length of the OS187H Type 2 TC is increased to 199.05 in. to accommodate the longer 32PTH Type 2 DSC. This increased cavity length is achieved by reducing the thickness of the wedge plates. Drawings for the OS187H Type 2 TC are provided in Chapter B.1, Section B.1.5.

The gross weight of the loaded TC is approximately 120 tons including a DSC payload of 54.02 tons. Section B.3.2.2 summarizes the weights of the NUHOMS[®] OS187H Type 2 packaging components.

The TC is fabricated and assembled in a exactly same manner as described in Section A.3.1.1.3 for OS187H Type 1 TC. The dimensions and design details of the OS187H Type 2 TC are provided in Chapter B.1, Section B.1.5.

The geometry and dimensions of the OS187H Type 2 TC trunnions are exactly same as that of OS187H Type 1 TC trunnions as explained in Chapter A.3, Section A.3.1.1.3.

The following sections provide physical and functional descriptions of each major component of the TC.

A. Transfer Cask Body and Structural Components

The shell or cask body cylinder assembly is an open ended (at the top) cylindrical unit with an integral closed bottom end. This assembly consists of concentric inner shell and outer shell (both SA-240 Type 304), welded to massive closure flanges (SA-182 Type F304N) at the top and bottom ends. The inner shell is 0.625 in. thick and has a 70.50 in. inside diameter. The outer shell is the primary structural shell and is 1.5 in. (lower course) to 2.38 in. thick (upper course), and has a 78.87 in. inside diameter. The annulus between the shells is filled with lead shielding. The lead gamma shielding is 3.56 in. (nominal) thick and is poured into the annulus in a molten state using a carefully controlled procedure.

The TC bottom end assembly and top cover assembly are similar to OS187H Type 1 TC with the exception that the minimum inner cavity length of the OS187H Type 2 TC is increased from 198.75 in. to 199.05 in. to accommodate longer 32PTH Type 2 DSC. This is achieved by reducing the thickness of the bottom wedge. As with the OS187H Type 1 TC, the OS187H Type 2 TC is designed to maintain a helium atmosphere in the cask cavity.

The OS187H Type 2 TC is designed, fabricated, examined, and tested in accordance with the requirements of Subsection NC [3] of the ASME code to the maximum practical extent. The alternatives to the ASME code presented in Section 3.10 for the OS187H TC are also applicable to the OS187H Type 2 TC.

B. Gamma and Radial Neutron Shielding

The description provided in Section 3.1.1.3 (B) is applicable to the OS187H Type 2 TC except that the resin material in the top and bottom assemblies, which provides axial neutron shielding in the OS187H TC, is replaced with NS-3, a castable cementitious material. NS-3 has been used in other NUHOMS applications, e.g., the OS197 TC[9]. The radial neutron shielding provided by liquid water enclosed in a radial outer stainless steel shell welded to the structural shell is of similar design as the OS187H TC.

C. Tiedown and Lifting Devices

The description provided in Section 3.1.1.3 (C) is applicable to the OS187H Type 2 TC. The OS187H Type 2 TC trunnions are the same as the OS187H TC. The top trunnions are designed, fabricated, and tested in accordance with ANSI N14.6 [4] as single-failure-proof lifting devices. Consequently, they are designed with a factor of safety of 6 against the material yield strength and a factor of safety of 10 against the material ultimate strength.

D. Operational Features

The NUHOMS® OS187H Type 2 TC is not considered to be operationally complex and is designed to be compatible with spent fuel pool loading/unloading methods. All operational features are readily apparent from inspection of the General Arrangement Drawings provided in Chapter B.1, Section B.1.5. The sequential steps to be followed for cask loading, testing, and unloading operations are provided in Chapter B.8.

B.3.1.1.4 Discussion of NUHOMS® HD System Drop Analysis

All lifting of the TC loaded with the DSC must be done within the existing heavy loads requirements and procedures of the licensed nuclear power plant.

The TC is transported to the independent spent fuel storage installation (ISFSI) in a horizontal configuration. Therefore, the only credible drop accident during storage or transfer operations is a side drop. The TC, canister and basket assemblies and fuel cladding are analyzed for this accident in the following sections.

In addition, vertical drop or corner drop accident scenarios may need to be evaluated under 10 CFR Part 50 if the user is unable to demonstrate that this accident drop is not credible during loading operations, or during transport operations governed under 10 CFR Part 71. Similarly, the fuel cladding integrity has not been demonstrated for this accident scenario. An additional safety review by the user is required to demonstrate fuel cladding integrity under 10 CFR Part 50 or to demonstrate that the end drop accidents are not credible.

The drop analyses of the NUHOMS® HD 32PTH Type 2 DSC and OS187H Type 2 TC components are performed in the following appendices.

Appendix B.3.9.1

This appendix describes the detailed analysis of the 32PTH Type 2 DSC shell assembly and basket assembly for all the loading conditions. For the drop loads, the DSC shell assembly is analyzed for the 75g side and end drops. The basket assembly is also analyzed for the 75g side and end drops. The 75g side drop in conjunction with the 75g end drop is considered to bound the 22g corner drop.

Appendix B.3.9.2

This appendix describes the detailed analysis of the OS187H Type 2 TC for all the loading conditions. No change to the structural evaluation of the OS187H Type 2 TC for side and end drop presented in Appendix A.3.9.10.

Appendix B.3.9.3

No change to the structural evaluations of the TC top cover bolt and ram cover bolt due to corner drop presented in Appendix A.3.9.3.

Appendix B.3.9.4

Since the end and corner drops are not credible under 10 CFR Part 72, the OS187H Type 2 TC lead slump and inner shell buckling analysis for the 75g end drop load are not evaluated. Vertical drop or corner drop accident scenarios may need to be evaluated under 10 CFR Part 50 if the user is unable to demonstrate that this accident drop is not credible during loading operations, or during transport operations governed under 10 CFR Part 71.

Appendix B.3.9.8

No change to the structural evaluations of the fuel cladding presented in Appendix A.3.9.8.

Appendix B.3.9.10

No change to the drop accelerations presented in Appendix A.3.9.10.

Appendix B.3.9.11

This appendix computes the dynamic amplification factor (DAF) to be applied to the response acceleration obtained from side drop accident dynamic analysis of the TC when applying those acceleration as input to an equivalent static analysis of the 32PTH Type 2 DSC.

B.3.1.2 Design Criteria

No change. The design criteria described in Section 3.1.2 is not changed and remains applicable to the 32PTH Type 2 DSC and OS187H Type 2 TC.

B.3.2 Weights

The nominal 32PTH Type 2 DSC, HSM-H and OS187H Type 2 TC geometry is used to compute the weights of the NUHOMS® HD System components. Material densities are unchanged and are provided in Chapter 3.

B.3.2.1 32PTH Type 2 DSC Weight

The bounding weight of the loaded 32PTH Type 2 DSC is 108.03 kips (54.02 tons). The weights of the major individual subassemblies are listed in following table.

32PTH Type 2 DSC Summary of Nominal Component Weights

Component	Nominal Weight (lb x 1000)
Canister shell	6.06
Outer top cover plate	2.14
Inner top cover plate	2.15
Top shield plug and support ring	6.43
Bottom end assembly	7.20
Grapple ring	0.075
Total canister assembly	24.05
Fuel compartments (32)	11.09
Aluminum/poison plates	4.92
Stainless steel plates	2.36
Small support rails	3.26
Large support rails	9.37
Total Fuel Basket	31.00
Basket Fuel spacer	1.46
Total Empty DSC (Basket and Canister)	56.51
Fuel assembly weight (32) @ 1610 lb/assembly	51.52
Total loaded DSC weight	108.03

B.3.2.2 OS187H Type 2 TC Weight

The total weight of the loaded NUHOMS® OS187H Type 2 TC is 239.47 kips (119.7 tons). The weights of the major individual subassemblies are listed in following table.

OS187H Type 2 TC Summary of Nominal Component Weights

Component	Nominal Weight (lb x 1000)
Structural shell	23.73
Inner shell	7.89
Lead gamma shield	66.65
Top flange	2.63
Bottom flange	3.40
Top cover assembly	5.36
Bottom assembly	3.94
Neutron shield panel assembly	5.14
Radial neutron shield (water)	8.67
Upper trunnion pair	1.45
Lower trunnion pair	1.06
Total Empty TC Weight	130.00⁽¹⁾
Total TC with Empty DSC Weight	187.00⁽¹⁾
Total TC with Loaded DSC Weight (Dry)	240.00^{(1) (2)}

Notes:

(1) Rounded up to the nearest 1,000 lbs.

(2) 250.0 kips is conservatively used for the trunnion analysis.

B.3.2.3 HSM-H Weight

No change. See Section 3.2.3 for details of the HSM-H weight.

B.3.3 Mechanical Properties of Materials

No change. The material properties described in Section 3.3 remain applicable to the 32PTH Type 2 DSC and the OS187H Type 2 TC.

B.3.4 General Standards for 32PTH Type 2 DSC, HSM-H, and OS187H Type 2 TC

B.3.4.1 Chemical and Galvanic Reactions

No change. The information provided in Section 3.4.1 is unchanged and applicable to the 32PTH Type 2 DSC and OS187H Type 2 TC.

B.3.4.2 Positive Closure

No change. The information provided in Section 3.4.2 is unchanged and applicable to the 32PTH Type 2 DSC and OS187H Type 2 TC.

B.3.4.3 Lifting Devices

No change. The information provided in Section 3.4.3 is unchanged and applicable to the 32PTH Type 2 DSC and OS187H Type 2 TC.

B.3.4.4 Heat

B.3.4.4.1 Summary of Pressures and Temperatures

No change. As documented in Chapter B.4, the heat transfer analyses documented in Chapter 4 for the 32PTH DSC inside the OS187H TC during transfer, and in the HSM-H during storage are bounding relative to the 32PTH Type 2 DSC in the HSM-H and in the OS187H Type 2 TC. Therefore, the pressures and temperatures used for the stress analyses of the 32PTH DSC and the OS187H TC in Chapter 3 are also applicable for the 32PTH Type 2 DSC and the OS187H Type 2 TC. As discussed in Section B.3.6 and Section B.3.7, the Chapter 4 temperature distributions are conservatively applied (considering the longer length of the 32PTH Type 2 DSC and OS187H Type 2 TC) for the structural evaluations.

Thus, the maximum and minimum temperatures for the various components for normal, off-normal, and accident conditions are the same as those summarized in Tables 4-1 to 4-6. Similarly, the maximum pressures are the same as those summarized in Table 4-10. The Table 4-10 pressures bound those used in the structural analysis of the 32PTH Type 2 DSC.

B.3.4.4.2 Differential Thermal Expansion

Potential interference due to differential thermal expansion between the 32PTH Type 2 DSC shell assembly, the basket assembly, and TC components is evaluated in Appendix B.3.9.1, Section B.3.9.1.4.

B.3.4.4.3 Stress Calculations

The stress analyses have been performed using the acceptance criteria presented in Section 3.1.2. The structural analyses for the 32PTH Type 2 DSC and OS187H Type 2 TC are summarized in Sections B.3.6 and B.3.7, for normal, off-normal, and hypothetical accident conditions, respectively.

B.3.4.5 Cold

No change. The limits on low temperature for operations that are provided in Section 3.4.5 are unchanged for the 32PTH Type 2 DSC.

B.3.5 Fuel Rods General Standards for 32PTH Type 1 DSC

No change. The fuel rod evaluations presented in Section 3.5 are unchanged for the 32PTH Type 2 DSC.

B.3.6 Normal Conditions of Storage and Transfer

This section presents the structural analyses of the 32PTH Type 2 DSC, and the OS187H Type 2 TC subjected to normal conditions of storage and transfer. The analyses performed evaluate these two major NUHOMS[®] HD System components for the design criteria described in Section B.3.1.2 of this appendix. The structural analyses of the HSM-H presented in Chapter 3.6 are bounding and, therefore, not changed.

The 32PTH Type 2 DSC is subjected to both storage and transfer loading conditions and the OS187H Type 2 TC is only subjected to transfer loading conditions.

Numerical analyses have been performed for the normal and accident conditions loads. In general, numerical analyses have been performed for the regulatory events. These analyses are summarized in Section A.3.6 and Section A.3.7, and described in detail in the Appendices B.3.9.1 through B.3.9.10 listed below.

The detailed structural analysis of the NUHOMS[®] HD System is included in the following appendices:

- Appendix B.3.9.1 32PTH Type 2 DSC (Canister and Basket) Structural Analysis
- Appendix B.3.9.2 OS187H Type 2 Transfer Cask Body Structural Analysis
- Appendix B.3.9.3 OS187H Type 2 Transfer Cask Top Cover and Ram Access Cover Bolts Analyses
- Appendix B.3.9.4 Not used (since the end and corner drops are not credible under 10CFR Part 72, the lead slump and inner shell buckling analysis of the OS187H Type 2 TC for the 75g end drop load are not documented).
- Appendix B.3.9.5 OS187H Type 2 Transfer Cask Trunnion Analysis
- Appendix B.3.9.6 OS187H Type 2 Transfer Cask Shield Panel Structural Analysis
- Appendix B.3.9.7 Not used (See Appendix B.3.9.10)
- Appendix B.3.9.8 Damaged Fuel Cladding Structural Evaluation
- Appendix B.3.9.9 HSM-H Structural Analysis
- Appendix B.3.9.10 OS187H Type 2 Transfer Cask Dynamic Impact Analysis
- Appendix B.3.9.11 32PTH Type 2 DSC Dynamic Amplification Factors

B.3.6.1 32PTH Type 2 DSC Normal Conditions Structural Analysis

Details of the structural analysis of the 32PTH Type 2 DSC are provided in Appendix B.3.9.1. The fuel basket assembly and canister shell assembly are analyzed independently. The structural evaluation of the 32PTH Type 2 fuel basket assembly is described in Section B.3.6.1.1. The structural evaluation of the canister shell assembly is described in Section B.3.6.1.2.

B.3.6.1.1 32PTH Type 2 DSC Fuel Basket Assembly Normal Condition Structural Evaluation

No change. As described in Appendix B.3.9.1, Section B.3.9.1.2, the ANSYS models, material properties, and design criteria used for the evaluation of the fuel basket assembly are the same between the 32PTH and the 32PTH Type 2 DSCs and, therefore, the stress analysis results documented in Section 3.9.1.2 for the 32PTH fuel basket assembly are applicable to the 32PTH Type 2 fuel basket assembly. As described in Section 3.9.1.2, a 360° finite element model (FEM) of a 15-inch segment of the basket assembly is constructed for the structural evaluation of the basket assembly.

Based on the results of these analyses, the design of the 32PTH Type 2 DSC basket is structurally adequate with respect to normal condition transfer and storage loads.

B.3.6.1.2 32PTH Type 2 DSC Canister Shell Assembly Normal Condition Structural Evaluation

This section summarizes the evaluation of the structural adequacy of the 32PTH Type 2 DSC canister shell assembly under all applied normal condition loads. Detailed evaluation of the stresses generated in the canister is presented in Appendix B.3.9.1, Section B.3.9.1.3.2. The DSC canister shell buckling evaluation is presented in Appendix B.3.9.1, Section B.3.9.1.3.3.

Elastic and elastic-plastic analyses are performed to calculate the stresses in the 32PTH Type 2 DSC canister under the transfer and storage loads. These detailed load cases are summarized in Appendix B.3.9.1, Tables B.3.9.1-3, B.3.9.1-4 and B.3.9.1-13.

The calculated stresses in the canister shell due to normal transfer loading conditions are summarized in Appendix B.3.9.1, Tables B.3.9.1-5, B.3.9.1-6, B.3.9.1-9, and B.3.9.1-10. The stresses due to normal storage loading conditions are summarized in Appendix B.3.9.1, Tables B.3.9.1-14, and B.3.9.1-15.

The 32PTH Type 2 DSC with the three-piece top end assembly configuration (separate inner cover plate, shield plug, and outer cover plate) is considered to bound the alternate design with a two-piece top end assembly (combined top shield plug/inner cover plate and outer cover plate). Similarly, the bottom end assembly configuration, consisting of separate inner bottom, shield plug and outer bottom plates is considered the bounding configuration relative to that of a DSC with the optional single or two-piece bottom end configurations. See discussion in Section B.3.9.1.3.4.

As described in Chapter B.8, Section B.8.1.1.3, Operation Steps 7 and 13, a maximum of 15.0 psig air pressure may be applied at the canister vent port to assist draining of the water. The canister is structurally evaluated for a bounding 25 psig internal pressure using the 2-D ANSYS FEM described in Appendix B.3.9.1, Section B.3.9.1.3.2. The outer cover plate of the canister is removed from the two-dimensional (2-D) model, since it is not yet installed during the application of this 25 psig air pressure. The maximum stress intensity in the canister is calculated as 14.46 ksi. The stress limit for membrane stress per ASME B&PV Code Subsection NB [6] is 24.0 ksi.

Based on the results of these analyses, the design of the 32PTH Type 2 DSC canister is structurally adequate with respect to both transfer and storage loads under the normal conditions.

B.3.6.2 HSM-H Normal Conditions Structural Analysis

No change. The DSC weight used for the structural evaluation of the HSM-H (110,000 lb) bounds the calculated weight of the 32PTH Type 2 DSC (108.03 kips). In addition, as discussed in Chapter B.4, the temperature distributions of the HSM-H loaded with a 32PTH Type 2 DSC are bounded by those of the HSM-H loaded with a 32PTH DSC documented in Chapter 4. Therefore, the structural evaluation of the HSM-H loaded with a 32PTH DSC, as documented in Section 3.6.2 and Appendix B.3.9.9 are applicable for a HSM-H loaded with the 32PTH Type 2 DSC.

B.3.6.3 OS187H Type 2 TC Normal Conditions Structural Analysis

Details of the structural analysis of the OS187H Type 2 TC are provided in Appendices B.3.9.2 through B.3.9.6. The contents of each of these appendices are as follows.

- Appendix B.3.9.2 OS187H Type 2 Transfer Cask Body Structural Analysis
- Appendix B.3.9.3 OS187H Type 2 Transfer Cask Lid and Ram Access Cover Bolt Analyses
- Appendix B.3.9.5 OS187H Type 2 Transfer Cask Trunnion Analysis
- Appendix B.3.9.6 OS187H Type 2 Transfer Cask Shield Panel Structural Analysis

B.3.6.3.1 Structural Analysis of the TC Body under Normal Conditions

The TC body evaluations documented in Appendix A.3.9.2 for OS187H Type 1 TC are applicable without change to the OS187H Type 2 TC. The details of the structural analyses of the NUHOMS® OS187H Type 1 TC body, including the cylindrical shell assembly and bottom assembly, the top cover, and the local stresses at the trunnion/cask body interface, are presented in Appendix A.3.9.2. The specific methods, models and assumptions used to analyze the cask body for the various individual loading conditions specified in 10 CFR Part 72 [1] are described in that appendix.

The NUHOMS® OS187H Type 2 on-site TC consists of a structural shell, gamma shielding material, and solid and liquid (water) neutron shield. The OS187H Type 2 TC is identical to the OS187H Type 1 TC described in Section A.3.1.1.3, with the exception of the minimum cavity length. The minimum cavity length of the OS187H Type 2 TC is increased to 199.05 in. to accommodate the longer 32PTH Type 2 DSC. This increased cavity length is achieved by reducing the thickness of the wedge plates. Detailed design drawings for the OS187H Type 2 TC are provided in Chapter B.1, Section B.1.5.

The wedge plates (Item 7, 10494-72-9004-SAR) thickness is reduced from 1.0 in. to 0.5 in. to increase the cavity. These forced air cooling wedge plates that go inside the cask cavity are not accounted for in the structural evaluation. There are no other changes made to the TC.

B.3.6.3.2 TC Top Cover and Ram Access Cover Bolt Normal Condition Analysis

No change. The TC top cover and ram cover bolt evaluations documented in Appendix A.3.9.3 for OS187H Type 1 are applicable without change to the OS187H Type 2 TC.

B.3.6.3.3 TC Normal Condition Trunnion Analysis

No change. The TC trunnion evaluations documented in Appendix A.3.9.5 for OS187H Type 1 are applicable without change to the OS187H Type 2 TC.

B.3.6.3.4 TC Shield Panel Structural Analysis for Normal Conditions

No change. The TC shield panel structural evaluations documented in Appendix A.3.9.5 for OS187H Type 1 are applicable without change to the OS187H Type 2 TC.

B.3.7 Off-Normal and Hypothetical Accident Conditions

This section presents the structural analyses of the 32PTH Type 2 DSC, the HSM-H and the OS187H Type 2 TC subjected to off-normal and hypothetical accident conditions of storage and transfer. The analyses are summarized in Sections B.3.7.1, B.3.7.2 and B.3.7.3 of this appendix and are evaluated against the design criteria described in Section B.3.1.2 of this chapter.

The 32PTH Type 2 DSC is subjected to both storage and transfer loading conditions, while the HSM-H is only subjected to storage loading conditions and the OS187H Type 2 TC is only subjected to transfer loading conditions.

B.3.7.1 32PTH Type 2 DSC Off-Normal and Accident Conditions Structural Analysis

Details of the structural analysis of the 32PTH Type 2 DSC are provided in Appendix B.3.9.1. The fuel basket assembly and canister shell assembly are analyzed independently. The structural analysis of the fuel basket assembly is described in Appendix B.3.9.1, Section B.3.9.1.2, while the structural analysis of the canister shell assembly is described in Section B.3.9.1.3. A 360° FEM of a 15-inch segment of the basket assembly is constructed for the structural evaluation of the fuel basket assembly. Three FEMs are used for the structural evaluation of the canister shell assembly. A 2-D axisymmetric model used for the analysis of axisymmetric loads, two three-dimensional (3-D) models modeling the top and bottom halves of the shell assembly, respectively, used for the analysis of non-axisymmetric loads.

B.3.7.1.1 32PTH Type 2 DSC Fuel Basket Assembly Off-Normal and Accident Condition Structural Analysis

B.3.7.1.1.1 32PTH Type 2 Fuel Basket Off-Normal and Accident Condition Stress Analysis

The fuel basket assembly stress analyses are performed for off-normal and accident condition loads during fuel transfer and storage.

The mechanical properties of structural materials used in the basket and canister are shown in Section 3, Table 3-5, and Appendix 3.9.1, Table 3.9.1-1, as a function of temperature. All structural components of the fuel basket and support rails are constructed from SA-240, Type 304 stainless steel, with properties taken from AMSE B&PV Code [5].

The load cases used for the analyses of the 32PTH Type 2 fuel basket assembly are the same as for the 32PTH fuel basket assembly and are as summarized in Section 3.9.1.2.2.

The details of the stress analysis of the basket assembly, as presented in Appendix 3.9.1, Section 3.9.1.2.3, are applicable without change to the 32PTH Type 2 fuel basket assembly. As discussed in Section 3.9.1.2.3, the basket stress analyses are performed using a 3-D FEM of the cross section of the basket assembly. The model is a 15-inch long segment of the basket assembly and is described in detail in Appendix 3.9.1, Section 3.9.1.2.3 (A). This model is used for the analysis of the transfer side drop impact loads, storage seismic loads, and both transfer and storage thermal load cases. Hand calculations are used for the evaluation of the transfer end drop load cases.

The stresses calculated for the 32PTH DSC fuel basket assembly and summarized in Tables 3.9.1-4a and 3.9.1-4b for the transfer accident loads and Table 3.9.1-5 for the storage accident loads are applicable to the 32PTH Type 2 basket assembly.

The maximum shear load in the fusion welds for the 75g side drop accident loading condition is calculated in Appendix 3.9.1, Section 3.9.1.2.3.B.5. The calculated maximum shear force during side drop is 7,208 lb. The fusion weld is qualified by a pull test (shear). The minimum test load is 17.1 kips. This test load includes a safety factor of 2 and a correction for material strength for room temperature testing.

Based on the results of these analyses, the design of the 32PTH Type 2 DSC basket is structurally adequate with respect to off-normal and accident conditions of transfer and storage loads.

B.3.7.1.1.2 32PTH Type 2 DSC Fuel Basket Accident Condition Buckling Analysis

As stated in Section B.3.9.1.2.4, the details of the buckling analysis presented in detail in Appendix 3.9.1, Section 3.9.1.2.4 are applicable without change to the 32PTH Type 2 fuel basket assembly. The results for the buckling analysis are also described in Section 3.9.1.2.4.

Since the critical collapse load for the 32PTH DSC basket (83.9g for the 30° orientation) is greater than the maximum design acceleration of 75g, the basket will not fail in buckling during the accident condition events.

B.3.7.1.1.3 32PTH Type 2 DSC Fuel Basket Support Rail Accident Condition Buckling Analysis

The NUHOMS[®] 32PTH1 basket with stainless steel rail design provided for the standardized NUHOMS[®] system in CoC 1004 (see UFSAR [9]) is identical to the NUHOMS[®] 32PTH basket design for the NUHOMS[®] HD system. The buckling evaluation for the 32PTH1 basket performed in Section U.3.7.4.3.3 [9] of the CoC 1004 UFSAR is applicable also to the NUHOMS[®] HD system. The used pressure on the basket panel due to the final assembly load for the evaluation is 1.24 psi. However, the actual fuel assembly load calculated in Section 3.9.1.2.3, B.2 is 1.1856 psi. Therefore, the basket support rail accident condition buckling analysis is applicable to 32PTH Type 2 DSC.

B.3.7.1.2 32PTH Type 2 DSC Canister Shell Off-Normal and Accident Condition Structural Evaluation

B.3.7.1.2.1 32PTH Type 2 Canister Shell Assembly Off-Normal and Accident Condition Stress Analysis

The description of the off-normal and accident analysis for the 32PTH DSC shell assembly presented in Section 3.7.1.2.1 is applicable without change to the 32PTH Type 2 canister shell assembly.

Elastic and elastic-plastic analyses are performed to calculate the stresses in the 32PTH Type 2 DSC shell assembly under the transfer and storage loads. These load cases are summarized in Appendix B.3.9.1, Tables B.3.9.1-3, B.3.9.1-4 and B.3.9.1-13. The accident side drop load case and the accident pressure load case are analyzed by elastic-plastic analyses and the rest by elastic analyses.

Two FEM types are used for the analysis of the 32PTH Type 2 DSC shell assembly. The first type is a 2-D axisymmetric model used for the analysis of symmetric loads (e.g., pressure, dead weight). The second type is a 3-D model of the top and bottom halves of the shell assembly and is used for the analysis of non-axisymmetric loads (e.g., side drops). The 2-D model is shown in Figures B.3.9.1-1. The 3-D models are shown in Figure B.3.9.1-4 and B.3.9.1-5 for the top and bottom halves, respectively. As shown in Figure B.3.9.1-2, the three-part top end assembly is modeled (separate shield plug, inner cover, and outer cover plates). Similarly, as shown in Figure B.3.9.1-3, the design option with separate inner bottom cover plate, bottom shield plug, and outer bottom cover plate is modeled. This configuration is expected to be the bounding as the pressure load is resisted by the inner top and inner bottom plates, and supported by the outer top cover plate (at the top) and, through the stiff bottom shield plug by the outer bottom cover plate (at the bottom).

The calculated stresses in the canister shell assembly due to off-normal and accident transfer loading conditions are summarized in Appendix B.3.9.1, Tables B.3.9.1-6, 7, 8, 10, 11, and 12. The stresses due to accident storage loading conditions are summarized in Appendix B.3.9.1, Tables B.3.9.1-14, and 15.

The alternate top closure assembly of the 32PTH Type 2 DSC, which consists of the two-part combined shield plug/inner cover assembly (including the optional configurations), as well as the optional bottom end configurations, are not analyzed explicitly. The results of the 32PTH DSC for the side drop accident load case are applicable for these alternate configurations. See discussion in Section B.3.9.1.3.4.

Based on the results of these analyses, the design of the 32PTH Type 2 DSC canister is structurally adequate with respect to off-normal and accident condition transfer and storage loads.

B.3.7.1.2.2 32PTH Type 2 DSC Canister Shell Accident Condition Buckling Analysis

This section summarizes the evaluation of the 32PTH Type 2 DSC canister against buckling under a vertical end drop during transfer operations. The details of the DSC canister shell buckling analysis are provided in Appendix B.3.9.1, Section B.3.9.1.3.3. A finite element elastic-plastic analysis with large displacement option is performed to monitor occurrence of canister shell buckling under the specified loads.

The thermal evaluation presented in Chapter 4 shows that the metal temperatures of the entire canister are below 500 °F during transfer operations. The material properties of the canister at 500 °F are, therefore, conservatively used for the canister buckling analysis.

The following three hypothetical accident load cases for the canister are considered in this buckling analysis.

Buckling Load Case 1: 15 psig external pressure and 75g axial acceleration due to end drop

Buckling Load Case 2: 30 psig internal pressure and 75g axial acceleration due to end drop

Buckling Load Case 3: 0 psig internal pressure and 75g axial acceleration due to end drop

The same 2-D axisymmetric FEM used for the stress analysis of the canister shell assembly and described in Appendix B.3.9.1, Section B.3.9.1.3.2.D.2 is used for the buckling accident analysis. Since the top end of the canister is heavier than the bottom end, it is a more severe case when the canister drops on its bottom end. A bottom end drop is, therefore, chosen for analysis in this calculation.

Load Case 1 converged at 181.0g load. Load Case 2 converged at 187.7g load. Load Case 3 converged at a load corresponding to 195.0g. This load is much higher than the required 75g load in either Load Case 1 or 2. The analysis shows that the canister does not buckle up to an end drop load of 181.0g, which is well beyond the design 75g load. It is, therefore, concluded that buckling of the canister will not occur during a hypothetical accident end drop.

B.3.7.2 HSM-H Off-Normal and Accident Conditions Structural Analysis

No change. As discussed in Section 3.7.2, the HSM-H is evaluated for a DSC weight and heat loads that bound those of the 32PTH Type 2 DSC. Thus, the evaluations of the 32PTH inside the HSM-H documented in Section 3.7.2 are bounding for the 32PTH Type 2 DSC inside the HSM-H.

B.3.7.3 OS187H Type 2 TC Off-Normal and Accident Conditions Structural Analysis

B.3.7.3.1 Structural Analysis of the TC Body for Off-Normal and Accident Conditions

No change. The TC body evaluations documented in Appendix A.3.9.2 for OS187H Type 1 are applicable without change to the OS187H Type 2 TC.

B.3.7.3.2 TC Top Cover and Ram Access Cover Bolt Accident Condition Analysis

No change. The TC top cover and ram cover bolt evaluations documented in Appendix A.3.9.3 for OS187H Type 1 are applicable without change to the OS187H Type 2 TC.

B.3.7.3.3 TC Lead Slump Analysis

As described in Section 3.1.1.4, the only credible drop accident during storage or transfer operations is a side drop. Thus, lead slump evaluation under top or bottom end drop accident is not performed for the OS187H Type 2 TC.

B.3.7.3.4 TC Inner Containment Buckling Analysis

As described in Section 3.1.1.4, the only credible drop accident during storage or transfer operations is a side drop. Thus, inner liner buckling evaluation under top or bottom end drop accidents is not performed for the OS187H Type 2 TC.

B.3.7.3.5 TC Trunnion Analysis

No change. The TC trunnion evaluations documented in Appendix A.3.9.5 for OS187H Type 1 are applicable without change to the OS187H Type 2 TC.

B.3.7.3.6 TC Shield Panel Structural Analysis for Accident Conditions

No change. The TC shield panel structural evaluations documented in Appendix A.3.9.5 for OS187H Type 1 are applicable without change to the OS187H Type 2 TC.

B.3.7.3.7 TC Impact Analysis

No change. The TC impact evaluation documented in Appendix 3.9.7 is applicable to 32PTH Type 2 DSC and OS187H Type 2 TC.

B.3.8 References

1. Title 10, Code of Federal Regulations, Part 72, “Licensing Requirements for the Storage of Spent Fuel in an Independent Spent Fuel Storage Installation.”
2. American National Standards Institute, ANSI N14.5-1997, Leakage Tests on Packages for Shipment of Radioactive Materials.
3. American Society of Mechanical Engineers, ASME Boiler and Pressure Vessel Code, Section III, Subsection NC, 1998 through 2000 addenda.
4. American National Standards Institute, ANSI N14.6, American National Standard for Special Lifting Devices for Shipping Containers Weighing 10,000 Pounds or More for Nuclear Materials, 1993.
5. American Society of Mechanical Engineers, ASME Boiler and Pressure Vessel Code, Section II, Parts A, B, C and D, 1998, through 2000 addenda.
6. American Society of Mechanical Engineers, ASME Boiler and Pressure Vessel Code, Section III, Subsection NB, 1998 through 2000 addenda.
7. ANSYS Users Manual, Rev. 5.6 and 6.0, 8.0, 8.1, 10A1, 14.0, 14.0.3.
8. NUREG/CR-6007 “Stress Analysis of Closure Bolts for Shipping Casks,” By Mok, Fischer, and Hsu, Lawrence Livermore National Laboratory, 1992.
9. Updated Final Safety Analysis Report (UFSAR) for the Standardized NUHOMS[®] Horizontal Modular Storage System for Irradiated Nuclear Fuel, NUH003.0103 Rev. 14, USNRC Docket No. 72-1004.

B.3.9 Appendices

The detailed structural analyses of the NUHOMS[®] HD System Type 2 components are included in the following appendices:

- Appendix B.3.9.1 32PTH Type 2 DSC (Canister and Basket) Structural Analysis
- Appendix B.3.9.2 OS187H Type 2 Transfer Cask Body Structural Analysis
- Appendix B.3.9.3 OS187H Type 2 Transfer Cask Top Cover and Ram Access Cover Bolts Analyses
- Appendix B.3.9.4 Not used (since the end and corner drops are not credible under 10 CFR Part 72, the lead slump and inner shell buckling analysis of the OS187H Type 2 TC for the 75g end drop load are not documented).
- Appendix B.3.9.5 OS187H Type 2 Transfer Cask Trunnion Analysis
- Appendix B.3.9.6 OS187H Type 2 Transfer Cask Shield Panel Structural Analysis
- Appendix B.3.9.7 Not used (See Appendix B.3.9.10)
- Appendix B.3.9.8 Damaged Fuel Cladding Structural Evaluation
- Appendix B.3.9.9 HSM-H Structural Analysis
- Appendix B.3.9.10 OS187H Type 2 Transfer Cask Dynamic Impact Analysis
- Appendix B.3.9.11 32PTH Type 2 DSC Dynamic Amplification Factors

B.3.10 ASME Code Alternatives

No change to the ASME Code Alternatives provided in Section 3.10.

APPENDIX B.3.9.1
32PTH TYPE 2 DSC (CANISTER AND BASKET) STRUCTURAL ANALYSIS

TABLE OF CONTENTS

B.3.9.1 32PTH TYPE 2 DSC (CANISTER AND BASKET) STRUCTURAL ANALYSIS	B.3.9.1-1
B.3.9.1.1 Introduction	B.3.9.1-1
B.3.9.1.2 32PTH Type 2 DSC Fuel Basket Assembly Structural Evaluation	B.3.9.1-2
B.3.9.1.2.1 Approach.....	B.3.9.1-2
B.3.9.1.2.2 Loading Conditions.....	B.3.9.1-2
B.3.9.1.2.3 Fuel Basket Assembly Stress Analysis	B.3.9.1-2
B.3.9.1.2.4 32PTH Type 2 Fuel Basket Assembly Buckling Analysis.....	B.3.9.1-2
B.3.9.1.3 32PTH Type 2 DSC Shell Assembly Structural Evaluation.....	B.3.9.1-3
B.3.9.1.3.1 Approach.....	B.3.9.1-3
B.3.9.1.3.2 DSC Canister Shell Assembly Stress Analysis.....	B.3.9.1-3
B.3.9.1.3.3 DSC Shell Buckling Evaluation.....	B.3.9.1-21
B.3.9.1.3.4 Evaluation of Alternate DSC Top and Bottom Closure Assembly Design	B.3.9.1-24
B.3.9.1.4 32PTH Type 2 DSC and OS187H Type 2 TC Thermal Expansion Evaluation	B.3.9.1-25
B.3.9.1.4.1 Introduction.....	B.3.9.1-25
B.3.9.1.4.2 Approach.....	B.3.9.1-25
B.3.9.1.4.3 Mechanical Properties of Materials	B.3.9.1-25
B.3.9.1.4.4 Thermal Expansion Computation	B.3.9.1-25
B.3.9.1.4.5 Thermal Expansion Analysis Conclusions	B.3.9.1-28
B.3.9.1.5 References	B.3.9.1-29

LIST OF TABLES

Table B.3.9.1-1	Temperature Dependent Material Properties for ASTM A-36	B.3.9.1-30
Table B.3.9.1-2	Material Stress Limits for 32PTH Type 2 DSC SA-240/SA-479 304 & SA-182 F304.....	B.3.9.1-31
Table B.3.9.1-3	32PTH Type 2 DSC Canister Load Combinations during Transfer	B.3.9.1-32
Table B.3.9.1-4	32PTH Type 2 DSC Canister Load Combinations during Lifting, Testing, and Hydraulic Loads	B.3.9.1-33
Table B.3.9.1-5	Summary of Calculated Stresses for Testing Condition Loads	B.3.9.1-34
Table B.3.9.1-6	Summary of Calculated Stress for Normal and Off-Normal Condition Transfer Loads	B.3.9.1-35
Table B.3.9.1-7	Summary of Calculated Stress for Accident Condition Transfer Loads (Axisymmetric Loads)	B.3.9.1-36
Table B.3.9.1-8	Summary of Stresses for Accident Condition Transfer Loads (3-D Inertial Loads).....	B.3.9.1-37
Table B.3.9.1-9	Summary of Calculated Stress at End Closure Welds for Testing Condition Loads.....	B.3.9.1-38
Table B.3.9.1-10	Summary of Calculated Stress at the End Closure Welds for Normal and Off-Normal Condition Transfer Loads	B.3.9.1-39
Table B.3.9.1-11	Summary of Calculated Stresses at End Closure Welds for Accident Condition Transfer Loads (Axisymmetric Loads).....	B.3.9.1-40
Table B.3.9.1-12	Summary of Calculated Stresses at End Closure Welds for Accident Condition Transfer Loads (3-D Inertial Loads).....	B.3.9.1-41
Table B.3.9.1-13	32PTH Type 2 DSC Canister Load Combinations during Storage	B.3.9.1-42
Table B.3.9.1-14	Summary of Calculated Stresses for Normal and Accident Condition Loads (canister in horizontal position)	B.3.9.1-43
Table B.3.9.1-15	Summary of Calculated Stresses at the End Closure Welds for Normal and Accident Condition Storage Loads	B.3.9.1-44

LIST OF FIGURES

Figure B.3.9.1-1	2-D Canister Axisymmetrical Thermal and Stress Finite Element Model	B.3.9.1-45
Figure B.3.9.1-2	Top End of the 2-D Axisymmetrical Canister Model.....	B.3.9.1-46
Figure B.3.9.1-3	Bottom End of the 2-D Axisymmetrical Canister Model	B.3.9.1-47
Figure B.3.9.1-4	3-D DSC Canister Top End Assembly Finite Element Model	B.3.9.1-48
Figure B.3.9.1-5	3-D DSC Canister Bottom End Assembly Finite Element Model...	B.3.9.1-49

Figure B.3.9.1-6	32PTH Type 2 DSC Canister Finite Element Model used for Pressure Test Analysis	B.3.9.1-50
------------------	---	------------

B.3.9.1 32PTH Type 2 DSC (Canister and Basket) Structural Analysis

B.3.9.1.1 Introduction

The NUHOMS® 32PTH Type 2 dry shielded canister (DSC) consists of a fuel basket assembly and a canister shell assembly. The canister shell assembly consists of a cylindrical shell, top end assembly (outer top cover plate, inner top cover plate, top shield plug), and a bottom end assembly (inner bottom cover plate, bottom shield plug, outer bottom cover plate). An alternate design for the top end assembly includes a two-part top end (combined shield plug/inner top cover and the outer cover plate). Similarly, the bottom end may consist of a single forged piece or two-piece or three-piece assembly. The primary confinement boundary for the 32PTH Type 2 DSC consists of the DSC shell, the inner top cover plate, and shell bottom or inner bottom cover plate of the shell bottom assembly.

The canister shell thickness is 0.50 in., and the top and bottom closure assemblies are 10.0 in. and 6.50 in., respectively. The canister is constructed entirely from SA-240 Type 304 stainless steel and SA-182 Type F304. The shield plugs are constructed from ASTM A-36. There are no penetrations through the confinement vessel. The draining and venting systems are covered by the port plugs, and the outer top cover plate and the inner top cover plate are welded to the cylindrical shell with multi-layer welds. The canister cavity is pressurized above atmospheric pressure with helium. The 32PTH Type 2 DSC shell assembly geometry and the materials used for its analysis and fabrication are shown on drawings 10494-72-2006-SAR to 2010-SAR included in Chapter B.1.

The basket structure consists of assemblies of stainless steel fuel compartments and support rails. The borated aluminum or boron carbide/aluminum metal matrix composite plates (neutron poison plates) provide the necessary criticality control and also provide a portion of the heat conduction paths from the fuel assemblies to the cask cavity wall. This method of construction forms a very strong structure of compartment assemblies that provide for storage of 32 PWR fuel assemblies. The open dimension of each fuel compartment is 8.70 in. × 8.70 in., which provides clearance around the fuel assemblies.

The fuel basket assembly and the canister assembly are analyzed separately. The fuel basket assembly is analyzed in Section B.3.9.1.2, and the canister shell assembly is analyzed in Section B.3.9.1.3. The full 360° three-dimensional (3-D) finite element model (FEM) of the basket assembly used for the evaluation of the 32PTH basket is applicable to the 32PTH Type 2 basket assembly. The analyses performed in Section 3.9.1.2 for the 32PTH basket are applicable for the 32PTH Type 2 basket (See Section B.3.9.1.2 for details).

Three FEMs are used for the structural evaluation of the canister shell assembly. A two-dimensional (2-D) axisymmetric model of the DSC canister shell assembly is used to evaluate axial inertial loads as well as internal pressure, external pressure, and thermal loads. Two 3-D FEMs of the DSC shell assembly are used to evaluate the effects of transverse inertial loads (e.g., side drop). These are separate models of the top half and bottom half assemblies of the 32PTH Type 2 DSC.

B.3.9.1.2 32PTH Type 2 DSC Fuel Basket Assembly Structural Evaluation

B.3.9.1.2.1 Approach

The basket design for the NUHOMS® 32PTH Type 2 DSC is identical to the 32PTH DSC except that the length of the 32PTH Type 2 basket is longer (the length of the 32PTH DSC basket is 162 in., whereas the length of the 32PTH Type 2 DSC basket is 178.75 in.) with one additional full height layer of neutron poison/thermal aluminum cross bars. In addition, the fuel compartment tubes at the top of the basket are also connected with support bars and fusion welds in the 32PTH Type 2 design. The 15-inch pitch between support bars (where the fuel compartments are connected to each other by fusion welds), which is the basis for the selection of the axial length of the analysis model, is the same for the 32PTH and 32PTH Type 2 baskets. The material properties, maximum fuel assembly weight, and the temperature profiles used in the 32PTH basket analyses (Section 3.9.1.2) have not changed. Thus, the analyses performed for the 32PTH basket assembly, documented in Section 3.9.1.2, are also applicable for the 32PTH Type 2 basket.

Therefore, the analysis results for the 32PTH basket in Section 3.9.1.2 are also applicable to the 32PTH Type 2 basket.

A. Material Properties

No change. The material properties for the 32PTH DSC in Section 3.9.1.2.1(A) are also applicable to the 32PTH Type 2 DSC.

B. Design Criteria

No change. The design criteria for the 32PTH DSC described in Section 3.9.1.2.1 (B) are also applicable to the 32PTH Type 2 DSC.

B.3.9.1.2.2 Loading Conditions

No change. The loading conditions for the 32PTH DSC described in Section 3.9.1.2.2 are also applicable to the 32PTH Type 2 DSC.

B.3.9.1.2.3 Fuel Basket Assembly Stress Analysis

No change. The 32PTH basket stress analysis model and analysis results in Section 3.9.1.2.3 are applicable to the 32PTH Type 2.

B.3.9.1.2.4 32PTH Type 2 Fuel Basket Assembly Buckling Analysis

The buckling evaluation for the 32PTH DSC performed using the full 360° 3-D model of the basket assembly documented in Section 3.9.1.2.4 (A.3) is also applicable to the 32PTH Type 2 DSC.

B.3.9.1.3 32PTH Type 2 DSC Shell Assembly Structural Evaluation

B.3.9.1.3.1 Approach

This section evaluates the structural adequacy of the 32PTH Type 2 DSC canister under all applicable normal and hypothetical accident condition loads. Evaluation of the stresses generated in the DSC is presented in Section B.3.9.1.3.2, and the DSC shell assembly buckling evaluation is presented in Section B.3.9.1.3.3.

B.3.9.1.3.2 DSC Canister Shell Assembly Stress Analysis

A. Methodology

An enveloping technique of combining various individual loads in a single analysis is used in this evaluation for several load combinations. This approach greatly reduces the number of computer runs while remaining conservative. However, for some load combinations, the stress intensities under individual loads are added to obtain resultant stress intensities for the specified combined loads. This stress addition at the stress intensity level for the combined loads, instead of at component stress level, is also a conservative way to reduce the number of analyses runs.

The ANSYS calculated stresses are the total stresses of the combined membrane, bending, and peak stresses. These total stresses are conservatively taken to be membrane stresses (P_m), as well as membrane plus bending stresses ($P_L + P_b$), and are evaluated against their corresponding ASME code stress limits. In the case where the total stresses, evaluated in this manner, exceed the ASME allowable stresses, a detailed stress linearization is performed to separate the membrane, bending, and peak stresses. The linearized stresses are then compared to their proper Code allowable stresses. ASME B&PV Code Subsection NB [8] is used for evaluation of loads under normal conditions and Appendix F [3] for evaluation of loads under hypothetical accident conditions.

The thermal stress intensities are classified as secondary stress intensities, Q , for code evaluations.

B. Canister Material Properties

Temperature dependent material properties obtained from Reference 1 for the NUHOMS[®] 32PTH Type 2 canister materials are summarized as follows.

Elastic Material Properties

Elastic properties are tabulated in Table 3-5 for SA-240 Type 304/SA-182 F304 (DSC shell, support ring, outer top cover, inner top cover, bottom grapple ring, inner bottom cover and outer bottom cover) and in Table B.3.9.1-1 for ASTM A-36 (top and bottom shield plugs).

Elastic-Plastic Material Properties

The ANSYS Bilinear Kinematic Hardening option of inelastic analysis is employed for Transfer Load Case 4 (120 psig internal pressure and hypothetical accident fire). Tangent modulus of 5% of elastic modulus is assumed after yield stress.

The ANSYS Multilinear Kinematic Hardening material option of inelastic analysis is employed in the analyses of all canister accident side drops. A multi-linear stress-strain curve for Type 304 stainless steel at 500 °F is constructed using the yield and tensile stress values taken from Reference 1 and the elongation value from Reference [9]. The stress-strain curve used for all canister materials is as follows.

Point	1	2	3	4	5
Strain (in/in)	0.0004845	0.000768	0.001164	0.00275	0.46
Stress (psi)	12,500	14,660	17,120	19,400	63,400

C. DSC Shell Assembly Stress Criteria

Allowable stresses given in ASME B&PV Code Subsection NB [8] and Appendix F [3] are used to evaluate the calculated stresses in the canister under normal, off-normal, and accident conditions, respectively. The stress criteria are summarized in Table 3-2. The allowable stresses are summarized in Table B.3.9.1-2. The closure welds between the inner top cover to the shell and the outer top cover to the shell use a stress reduction factor of 0.8 in accordance with ISG-15 [14].

D. DSC Shell Assembly Stress Analysis for Transfer Loads

The evaluation of the stresses generated in the NUHOMS[®] 32PTH Type 2 canister during transfer operations is presented here. During fuel transfer, the canister is oriented horizontally inside the OS187H Type 2 Transfer Cask (TC). The OS187H Type 2 TC is mounted to the transfer skid and transferred from the fuel building to the independent spent fuel storage installation (ISFSI).

The maximum temperature in the canister under vacuum drying operation is calculated to be 522 °F in the thermal stress analysis (see Chapter 4). This temperature occurs in the shell center where stresses are low. The maximum temperature in critical stress areas (top and bottom canister regions) are below 500 °F. However, the stress evaluations are conservatively performed at 500 °F.

D.1 DSC Shell Assembly Transfer Load Cases

Elastic and elastic-plastic analyses are performed to calculate the stresses in the NUHOMS[®] 32PTH Type 2 canister under the transfer loads. These load cases are summarized in Table B.3.9.1-3 and Table B.3.9.1-4. The accident side drop and the accident pressure load cases are analyzed by elastic-plastic analyses and the rest by elastic analyses.

D.2 DSC Shell Assembly Finite Element Model Descriptions

DSC Temperature Distribution

The DSC metal temperatures that are calculated in Chapter 4 are extracted and directly applied as temperature loads to the 2-D stress model using ANSYS macros. Since the 32PTH Type 2 DSC is longer than the 32PTH DSC, the temperature distribution at the maximum temperature location was extended in the middle of the canister, thus maximizing thermal gradients and hence thermal stresses at the top and bottom of the canister shell.

2-D Canister Stress Models

A 2-D axisymmetric ANSYS FEM, constructed from PLANE42 elements, is used for the elastic analyses of all axisymmetrical loading on the canister. ANSYS contact elements CONTAC12 are generated by connecting the nodes of two adjacent solids along their boundary. The real constant of each contact element is defined for the initial gap at each contact element.

At the weld locations between two joined solids, the contacting nodes are coupled in all directions. These coupled-nodes are applied to the welds between the shell and the support ring and between the shell and the inner top cover plate. The larger 0.5- inch weld between the shell and the top cover is modeled with PLANE42 elements. The normal stiffness of all contact elements are calculated using guidelines in the ANSYS manual [10]. The applied boundary conditions for this 2-D model under each load case are described in the following sections. Figures B.3.9.1-1, B.3.9.1-2, and B.3.9.1-3 show the ANSYS 2-D FEM, which includes the canister shell, outer and inner top covers, support ring and outer and inner bottom covers. This model is used for analyses of all axisymmetric loads during the transfer operations of the canister.

The normal stiffness, K_N , for the contact elements were estimated according to the ANSYS manual [10] as follows.

$$K_N \approx f E h$$

Where:

- f = Factor that controls contact compatibility (ranging between 0.01 to 100), use 1
- E = Young's modulus, use 25.8×10^6 psi
- h = average radius where contact to occur (for 2-D axisymmetrical model), use 34 in.
- K_N = $1 \times 25.8 \times 10^6 \times 34 = 8.8 \times 10^8$ lb/in. Conservatively used 1×10^9 lb/in.

3-D Canister Stress Model

A 3-D ANSYS stress model is created using ANSYS elements SOLID45 and CONTAC178. The 3-D model is used for the analysis of accident side drops. To help reduce the ANSYS run time and assure numerical convergence, the whole canister is split into two portions, namely, the top and the bottom end sections. These two sections are represented by two different ANSYS models. Each end model includes the canister shell at a length beyond which the un-modeled shell will have no significant impact on the stress levels at the junction between the shell and its end closures. The DSC canister top end assembly FEM is shown in Figure B.3.9.1-4 and the canister bottom end assembly model is shown in Figure B.3.9.1-5.

These 3-D models are used for analyses of side drops only. The postulated side drops will occur when the canister is resting inside the OS187H Type 2 TC during transfer. Two side drops with the impact points located at 0° (i.e., the cask drops onto a target at 180° opposite to its four canister support pads) and at 180° (i.e., the cask drops onto a target between its two bottom canister support pads) are analyzed.

Load cases 6, 7, 10, and 11 consider the side drop loads at 0° and load cases 8, 9, 12, and 13 at 180° (see Table B.3.9.1-8). Elastic-plastic analyses, using multi-linear hardening material properties, are performed for both side drops. In addition to the contact areas generated from the 2-D model, new contact elements are generated connecting the inner diameter of the cask and the outer diameter of the canister in the radial direction. The nodes of these contact elements are located either on the inner diameter of the cask or on the outer diameter of the canister at the moment when the cask hits the side drop target. The actual gaps for these contact elements are defined by their initial location in conjunction with the contact element real constants. The contact element nodes located on the inner diameter of the cask are held fixed in all directions, simulating a rigid cask on which the canister drops.

Weak link elements are added to each contact element in the model to help numerical convergence. Zero density of these link elements is used to avoid adding any non-existing weights. This model does not calculate the stress levels in the middle section of the canister shell, which are calculated and evaluated as part of the basket stress analysis in Section 3.9.1.2.3.

Only half of the canister in circumferential direction is included in the 3-D model. Symmetry boundary conditions are applied to the plane of symmetry (global Cartesian x - z plane) during a side drop. Symmetry boundary conditions are also applied to the cut-off plane at the canister shell to provide proper diametrical rigidity of the shell during side drops.

During the 75 g side drop, the canister internals are accounted for by applying a cosine varying pressure distribution on the inside surface of the canister shell. Assuming that the canister internals react upon a 90° arc of the inside surface, then the inertial load of the internals, $P_{(\theta)}$, which varies with angle, θ , ($\theta = 0$ is at the impact point), is governed by the following expression.

$$P_{(\theta)} = P_{max} \cos(2\theta) \quad (0^\circ < \theta < 45^\circ)$$

Where P_{max} is the maximum pressure at the impact point ($\theta = 0$). Assuming the axial length of the applied load is L , the inside radius of the canister shell is R , and the load distribution, $P_{(\theta)}$ above, then the total inertial load generated by the internals, F , is the following.

$$F = \int_{-\frac{\pi}{4}}^{\frac{\pi}{4}} P_{max} \cos(2\theta) \cos(\theta) LR d\theta$$

or,

$$F = \frac{P_{max} LR}{2} \int_{-\frac{\pi}{4}}^{\frac{\pi}{4}} \cos((2+1)\theta) + \cos((2-1)\theta) d\theta$$

By integrating we get the following:

$$F = \left[\frac{P_{max} LR}{2} \right] \left[\frac{\sin(3\theta)}{3} + \sin(\theta) \right] \Bigg|_{-\frac{\pi}{4}}^{\frac{\pi}{4}}$$

Therefore,

$$F = \left[\frac{P_{max} LR}{2} \right] \left[\frac{\sin\left(\frac{3\pi}{4}\right)}{3} + \sin\left(\frac{\pi}{4}\right) - \frac{\sin\left(\frac{-3\pi}{4}\right)}{3} - \sin\left(\frac{-\pi}{4}\right) \right]$$

$$F = P_{max} LR \left[\frac{\sin\left(\frac{3\pi}{4}\right)}{3} + \sin\left(\frac{\pi}{4}\right) \right]$$

The canister shell inner diameter, $R = 34.375$ in., the axial length of the applied load, $L = 178.75$ in. The total applied force, F , is equal to the inertial load of the canister internals, which is the following.

- Basket weight = 31,000 lb
- Fuel assembly weight = 51,520 lb
- Total weight of canister internals = 31,000 lb + 51,520 lb = 82,520 lb (use 85,000 lb)

Then,

$$F = 85,000 \times 75 g = 6,375,000 \text{ lb.}$$

Therefore, P_{\max} is the following:

$$P_{\max} = \frac{6,375,000}{(178.75)(34.375)} \left[\frac{\sin\left(\frac{3\pi}{4}\right)}{3} + \sin\left(\frac{\pi}{4}\right) \right]^{-1} = 1163.93 \text{ psi.}$$

The equivalent pressure applied on the canister inside shell surface is, therefore:

$$P_{(\theta)} = 1163.93 \cos(2\theta),$$

Where, θ is the angle from the bottom ($\theta = 0$) of the horizontal canister shell to the center of the shell element, up to 45° .

D.3 DSC Shell Assembly Stress Evaluation for Transfer Loads

All analyzed load cases in this section are identified in Tables B.3.9.1-3 and B.3.9.1-4 and are described in detail in the following sections.

Transfer Load Case 1: Deadweight + 15 psig external pressure + thermal (vacuum drying)

The temperature profile utilized for the analysis of Transfer Load Case 1 for the 32PTH DSC described in Section 3.9.1.3.2 (D.3) was adjusted by linearly scaling to the maximum vacuum drying temperature of 522°F , which is greater than the maximum temperature for vacuum drying 511°F , as calculated in Chapter 4. This adjusted temperature profile is used for the analysis of Transfer Load Case 1 for the 32PTH Type 2 DSC.

The weight of the canister internals (basket and fuel assemblies) is accounted for by applying equivalent pressures on the support surfaces of the canister. The actual weights of the basket and fuel assemblies are 31,000 lb and 51,520 lb, respectively (see Section B.3.2.1). Therefore, the total weight of the canister internals is 82,520 lb. A weight of 85,000 lb is conservatively used in this analysis. The canister cavity inner radius is 34.375 in. Therefore, the pressure load equivalent to the inertial load of the internals, P_{ia} , is,

$$P_{ia} = [85,000 / (\pi \times 34.375^2)] = 22.90 \text{ psi}$$

An elastic analysis is performed using the ANSYS 2-D axisymmetric model. The analysis was run in two load steps. The first load step includes dead weight, 15 psig external pressure, and the temperature profile discussed above, but it does not include coefficient of thermal expansion.

The second load step includes the coefficient of thermal expansion and all of the above-mentioned loads. The results from the first load step are compared against the P_m and $P_m + P_b$ allowable stresses and the results from the second load step are compared against the $P_m + P_b + Q$ allowable stresses.

The maximum primary stress intensity in the canister was calculated to be 1.95 ksi in Load Step 1. The maximum primary stress intensity in the closure welds is calculated to be 1.56 ksi.

The maximum primary plus secondary stress intensity in the canister was calculated to be 18.82 ksi in Load Step 2. These stresses are summarized in Table B.3.9.1-6. The maximum primary stress intensity in the closure welds is calculated to be 1.75 ksi.

Transfer Load Case 2: Handling, 2 g axial + 2 g transverse + 2 g vertical + 30 psig int. pressure + thermal (115 °F ambient)

The handling 2 g inertial loads applied to the canister when inside the TC in the horizontal orientation are analyzed as part of the basket model described in Section 3.9.1.2.3 (B.2) (the basket model includes a segment of the canister shell). It is judged that under the relatively light handling loads the maximum stresses in the canister will occur in the shell section and can be obtained from the results calculated in Section 3.9.1.2.3 (B.2). The maximum primary membrane stress intensity and primary membrane plus bending stress intensity in the canister shell due to the handling load of 2 g, calculated in Section 3.9.1.2.3 (B.2), are 880 psi and 9740 psi, respectively. These stresses are summarized in Table B.3.9.1-6.

The stress intensities calculated in Section 3.9.1.2.3 (B.2) for the canister shell due to the 2 g handling loads are combined with the stresses due to internal pressure of 30 psig, and the 115 °F ambient environment temperature loads resulting from the thermal analysis in Chapter 4.

The stress analysis for the 30 psig internal pressure and 115 °F thermal loads is performed using the ANSYS 2-D axisymmetric model. The stress analysis contains two load steps. Load step 1 includes the primary loads of 30 psig internal pressure. Load Step 2 includes the primary pressure load plus the secondary thermal load.

The maximum primary stress intensity in the canister was calculated to be 14.81 ksi in Load Step 1 analysis. The maximum primary stress intensity in the closure welds is calculated to be 11.72 ksi. The maximum primary plus secondary stress intensity in the canister is calculated to be 38.35 ksi under load Step 2. The maximum primary plus secondary stress intensity in the closure welds is calculated to be 15.25 ksi.

The maximum primary stress intensities in the canister shell calculated in Section 3.9.1.2.3 (B.2) are added to the maximum primary and primary plus secondary stress intensities calculated from the 2-D axisymmetric model and the combined results are evaluated against the corresponding ASME stress limits (See Table B.3.9.1-6). The direct addition of stresses at the stress intensities level, instead of at the component level, as well as the addition of the maximum stress intensities at different locations is very conservative. This enveloping technique is used to minimize the computer runs.

Transfer Load Case 3: Handling 2 g axial + 2 g transverse + 2 g vertical + 15 psig ext. pressure + thermal (-20 °F ambient)

The same methodology described for load case 2 is used in this load case.

The maximum stress intensity in the canister for the primary load of 15 psig external pressure in Load Step 1 is calculated to be 5.83 ksi. The maximum stress intensity in the closure welds is calculated to be 1.48 ksi.

The maximum stress intensity in the canister for the primary load of 15 psig external pressure plus the secondary temperature load in Load Step 2, is calculated to be 28.84 ksi. These stresses combined with the stresses due to the handling loads as well as the evaluation against the ASME stress limits are summarized in Table B.3.9.1-6. The maximum stress intensity in the closure welds is calculated to be 3.02 ksi.

Transfer Load Case 4: 120 psig internal pressure and hypothetical accident fire

Stresses in the canister under an internal pressure of 120 psig are calculated in this load case. ASME code [3] requires only primary stresses be evaluated under accident conditions. The secondary thermal stresses are therefore not calculated. The ANSYS 2-D axisymmetric model is used for analysis of this accident pressure load. This is an elastic-plastic analysis with large deformations.

The maximum calculated stress in the entire canister for the pressure load is 23.87 ksi. This maximum stress intensity is conservatively treated both as primary membrane stress intensity and as primary membrane plus bending stress intensity and so evaluated against ASME code limits at the maximum metal temperature of the canister (See Table B.3.9.1-7).

The maximum metal temperature in the canister during fire accident is calculated to be 790 °F (see Chapter 4). Canister material properties at 800 °F are used for the ANSYS model. The maximum stress intensity in the closure welds is calculated to be 21.76 ksi.

Transfer Load Case 5: 25 psig external pressure and flood hypothetical accident

The external pressure of 25 psig on the canister is analyzed using material properties taken at 500 °F for the entire model.

The maximum stress intensity in the canister for this load case is calculated to be 9.73 ksi. The maximum stress intensity in the closure welds is calculated to be 2.45 ksi.

Transfer Load Case 6: Accident condition 75 g side drop at 0° (no rail) at ambient temperature of 115 °F (75 g side drop + 30 psig internal pressure)—top end portion of canister

The canister internal pressure of 30 psig plus a side acceleration of 75 g is analyzed in this load case. A multi-linear elastic-plastic stress-strain curve for material 304 SS at 500 °F is applied to all materials. The stress-strain curve is obtained from Reference 9. ASME code requires only primary stresses be evaluated under accident conditions. The values of the thermal expansion coefficients for all materials are therefore set to 0 to eliminate any secondary thermal stresses in the canister.

The maximum stress intensity in the canister for this load case is calculated to be 25.31 ksi. The maximum stress intensity in the closure welds is calculated to be 21.81 ksi.

Transfer Load Case 7: Accident condition 75 g side drop at 0° (no rail) at ambient temperature of 115 °F (75 g side drop + 30 psig internal pressure)—bottom end portion of canister

The methodology of the analysis and stress evaluation used in this load case is the same as that described for Load Case 6.

The maximum stress intensity in the canister for this load case is calculated to be 23.96 ksi.

Transfer Load Case 8: Accident 75 g side drop at 180° (drop between two TC bottom support pads) at ambient temperature of 115 °F (75 g side drop + 30 psig internal pressure)—top end portion of canister

The same methodology of the analysis and stress evaluation used for Load Case 6 is used for this load case except that the gaps between the canister and the rigid cask are different due to the orientation of the TC support pads.

The maximum stress intensity in the canister for this load case is calculated to be 26.89 ksi. The maximum stress intensity in the closure welds is calculated to be 23.63 ksi.

Transfer Load Case 9: Accident 75 g side drop at 180° (drop between two cask bottom rails) at ambient temperature of 115 °F (75 g side drop + 30 psig internal pressure)—bottom end portion of canister

The same methodology of the analysis and stress evaluation used for Load Case 7 is used for this load case except that the gaps between the canister and the rigid cask are different.

The maximum stress intensity in the canister for this load case is calculated to be 24.59 ksi.

Transfer Load Case 10: Accident 75 g side drop at 0° (drop at no cask rail) at ambient temperature of -20 °F (75 g side drop + 15 psig external pressure)—top end portion of canister

The same methodology of the analysis and stress evaluation used for Load Case 6 is used for this load case except that external pressure instead of internal pressure is applied.

The maximum stress intensity in the canister for this load case is calculated to be 25.65 ksi. The maximum stress intensity in the closure welds is calculated to be 21.27 ksi.

Transfer Load Case 11: Accident 75 g side drop at 0° (drop at no cask rail) at ambient temperature of -20 °F (75 g side drop + 15 psig external pressure)—bottom end portion of canister

The same methodology of the analysis and stress evaluation used for Load Case 7 are used for this load case except external pressure instead of internal pressure is applied.

The maximum stress intensity in the canister for this load case is calculated to be 23.95 ksi.

Transfer Load Case 12: Accident 75 g side drop at 180° (drop between two cask bottom rails) at ambient temperature of -20 °F (75 g side drop + 15 psig external pressure)—top end portion of canister

The same methodology of the analysis and stress evaluation used for Load Case 8 is used for this load case except that external pressure instead of internal pressure is applied.

The maximum stress intensity in the canister for this load case is calculated to be 26.86 ksi. The maximum stress intensity in the closure welds is calculated to be 23.49 ksi.

Transfer Load Case 13: Accident 75 g side drop at 180° (drop between two cask bottom rails) at ambient temperature of -20 °F (75 g side drop + 15 psig external pressure)—bottom end portion of canister

The same methodology of the analysis and stress evaluation used for Load Case 9 is used for this load case except that the external pressure instead of the internal pressure is applied.

The maximum stress intensity in the canister is calculated to be 24.71 ksi.

Transfer Load Case 14: Accident 75 g top end drop (75 g + internal pressure of 30 psig)

The top end drop is not considered credible during storage and transfer operations under 10 CFR Part 72 because the TC is always in the horizontal orientation. The top end drop evaluation documented below is performed in support of a 10 CFR Part 50 evaluation that may be performed by the user if the user cannot demonstrate that this accident drop is not credible.

The weight of the canister internals (basket and fuel assemblies) during end drop is accounted for by applying equivalent pressures on canister components that support them. The actual weights of the canister basket and fuel assemblies are 31,000 lb and 51,520 lb (see Section B.3.2.1). Therefore, the total actual weight of the canister internals is 82,520 lb. The weight of the canister internals used in this analysis is conservatively increased to 85,000 lb.

The canister cavity inner radius at the top end is 34.375 in. The pressure load equivalent to the inertial load of the internals at 75 g under accident condition, P_{ia} , is,

$$P_{ia} = [85,000 / (\pi \times 34.375^2)] \times 75 g = 1717.30 \text{ psi}$$

The top face of the canister outer top cover is held in the axial direction in order to simulate the rigid support provided by the TC top cover. An inertial load of 75 g in the negative y-direction is applied to the model. An internal pressure of 30 psig and the metal temperatures from the 115 °F ambient condition are also included in this analysis. Temperature-dependent material properties are selected based on the temperature distribution in the canister. The values of thermal expansion coefficients for all materials are set to zero so that secondary thermal stresses, which are not required for evaluation under an accident condition per Reference 3, are not calculated.

The maximum stress intensity in the canister for this load case is calculated to be 43.19 ksi. The maximum stress intensity in the closure welds is calculated to be 10.76 ksi.

Transfer Load Case 15: Accident 75 g bottom end drop (75 g + internal pressure of 30 psig)

The bottom end drop is not considered credible during storage and transfer operations under 10 CFR Part 72 because the TC is always in the horizontal orientation. The bottom end drop evaluation documented below is performed in support of a 10 CFR Part 50 evaluation that may be performed by the user if the user cannot demonstrate that this accident drop is not credible.

The weight of the canister internals used in this analysis is 85,000 lb. The canister cavity inner radius at the bottom end is 34.375 in. The pressure load equivalent to the weight of the internals under the accident condition 75 g drop, P_{ia} , is,

$$P_{ia} = [85,000 / (\pi \times 34.375^2)] \times 75 \text{ g} = 1717.30 \text{ psi}$$

The bottom face of the canister is held in the axial direction in order to simulate the rigid support provided by the TC bottom. An inertial load of 75 g in the positive y-direction is applied to the model. An internal pressure of 30 psig and the metal temperatures from the 115 °F ambient condition are included in this analysis. Temperature-dependent material properties are selected based on the temperature distribution in the canister. The values of thermal expansion coefficients for all materials are set to zero so that secondary thermal stresses, which are not required for evaluation under an accident condition per Reference 3, are not calculated.

The maximum stress intensity in the canister for this load case is calculated to be 17.71 ksi. The maximum stress intensity in the closure welds is calculated to be 13.57 ksi.

Transfer Load Case 16: Accident 75 g top end drop (75 g + external pressure of 15 psig)

The top end drop is not considered credible during storage and transfer operations under 10 CFR Part 72 because the TC is always in the horizontal orientation. The top end drop evaluation documented below is performed in support of a 10 CFR Part 50 evaluation that may be performed by the user if the user cannot demonstrate that this accident drop is not credible.

This load case is similar to Load Case 14 with different pressure loadings and metal temperatures. An external pressure of 15 psig and material properties at 500 °F are used in this analysis. The values of thermal expansion coefficients for all materials are set to zero so that secondary thermal stresses, which are not required for evaluation under an accident condition per Reference 3, are not calculated.

The maximum stress intensity in the canister for this load case is calculated to be 59.29 ksi. The maximum stress intensity in the closure welds is calculated to be 12.22 ksi.

Transfer Load Case 17: Accident 75 g bottom end drop in accident condition (75 g + external pressure of 15 psig)

The bottom end drop is not considered credible during storage and transfer operations under 10 CFR Part 72 because the TC is always in the horizontal orientation. The bottom end drop evaluation documented below is performed in support of a 10 CFR Part 50 evaluation that may be performed by the user if the user cannot demonstrate that this accident drop is not credible.

This load case is similar to Load Case 15 with different pressure loadings and metal temperatures. An external pressure of 15 psig and material properties at 500 °F are used in this analysis. The values of thermal expansion coefficients for all materials are set to zero so that secondary thermal stresses, which are not required for evaluation under an accident condition per Reference 3, are not calculated.

The maximum stress intensity in the canister for this load case is calculated to be 22.63 ksi. The maximum stress intensity in the closure welds is calculated to be 14.80 ksi.

Transfer Load Case 18: Fabrication test condition (DW + 25 psig internal pressure + 155 kips axial load)

After the canister bottom is welded to the shell a pressure test is conducted by applying an internal pressure of 25 psig with a top seal plate being held by an axial force of 155 kips. The canister bottom may be made, as an option, of composite plates. For each of these options the bottom inner plate, which is to be first welded to the shell and tested, has a minimum thickness of 2.25 in. An ANSYS model, shown in Figure B.3.9.1-6, is generated that simulates the canister shell with the bottom inner plate for analysis of pressure and axial loads under the test condition. The deadweight load on the horizontal canister is manually analyzed using Roark's formulas [7]. The stresses calculated from both manual and ANSYS analyses are conservatively added for ASME Code stress evaluation.

1. 1g deadweight load

It is conservatively assumed that the horizontal shell's own weight is line supported at its base.

From Case 15 of Table 9.2 in Roark's Formulas for Stress & Strains, 7th Edition :

$$R \text{ (mean radius)} = \frac{1}{2} (69.75 \text{ in.} - 0.5 \text{ in.}) = 34.625 \text{ in.}$$

$$t \text{ (wall thickness)} = 0.5 \text{ in.}$$

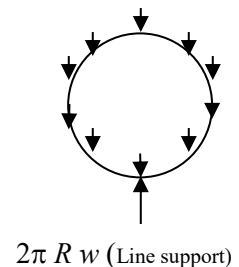
$$\rho \text{ (density)} = 0.29 \text{ lb/in}^3$$

Take unit length ($L = 1 \text{ in.}$) of shell,

The weight per unit length of circumference of shell, w , is,

$$\begin{aligned} w &= (2 \times \pi \times R \times t \times L \times \rho) / (2 \times \pi \times R) \\ &= t \times L \times \rho = 0.5 \times 1 \text{ in.} \times 0.29 \text{ lb/in}^3 = 0.145 \text{ lb/in} \end{aligned}$$

$$\text{For a thin ring, } I = \frac{t^3}{12(1-\nu^2)} = 0.01145, \text{ where } \nu = 0.3$$



$$K_T = 1 + \frac{I}{AR^2} \approx 1 \quad K_2 = 1 - \alpha = 1 - \frac{I}{AR^2} \approx 1$$

$$\text{Max. } -M = -wR^2(1.6408 - K_2) = -0.145 \times 34.625^2 (1.6408 - 1) = -111.4 \text{ in-lb/in}$$

or,

$$\text{Max. } +M = (3/2) wR^2 = 1.5 \times .145 \times 34.625^2 = 260.76 \text{ in-lb/in}$$

$$\text{Max. bending stress, } \sigma_b = (6M)/(t^2) = (6 \times 260.76) / (0.5^2) = 6,258 \text{ psi}$$

$$N = N_A \cos(x) + V_A \sin(x) + LT_N$$

$$V_A = 0$$

$$LT_N = -Wr(x)(\sin(x))$$

$$N_A = w R/2 = 2.51 \text{ lb/in}$$

$$N = 2.51 \cos(x) - 0.145 \times 34.625 \times (x) \times \sin(x) \text{ lb/in}$$

$$N_{\max} = 2.51 \text{ lb/in at } x = 0^\circ$$

$$\text{Max. membrane stress, } \sigma_m = N_{\max} / t = (2.51 \text{ lb/in}) / (0.5 \text{ in}) = 5 \text{ psi}$$

2. 25 psig internal pressure + 155 kips axial load

An internal pressure of 25 psig was applied while an axial force of 155 kips is applied to a seal plate on the top of the shell. The net force applied to the entire circumference of the shell at top will be 62,195 lb (155,000 lb – 25 lb/in² × [$\pi/4 \times 68.752$] in² = 62,195 lb). A nodal force of 15,548.75 lb (62,195 / 4 = 15,548.75 lb) was applied at each node on the top end of the shell.

Figure B.3.9.1-6 shows the model with the applied boundary conditions.

The maximum stress intensity in the canister is calculated to be 8.0 ksi under these testing loads.

The resultant stresses calculated in (1) and (2) above are conservatively added and evaluated against ASME Code allowable stresses in Table B.3.9.1-5.

Transfer Load Case 19: Normal 80 kip push hydraulic load (internal pressure of 30 psig + 80 kip push + thermal load of 115 °F ambient)

During transfer of the canister from the TC to the HSM a normal maximum push force of 80 kip is applied by a hydraulic ram over an area of 9-inch diameter on the canister bottom. A uniform pressure of 1258 psig [= 80,000 lb / (($\pi/4 \times 9^2$))] is applied over this area. The periphery of the top cover outer surface is held as boundary condition. The sustained loads of an internal pressure of 30 psig plus the equivalent push load pressure of 1,258 psi are applied in Load Step 1. The sustained loads plus the temperature load from fuel decay heat are applied in Load Step 2.

The maximum stress intensity for Load Step 1 is calculated to be 15.65 ksi. The maximum stress intensity in the closure welds is calculated to be 10.72 ksi.

The maximum stress intensity in the canister for Load Step 2 is calculated to be 31.35 ksi. The maximum stress intensity in the closure welds is calculated to be 15.21 ksi.

Transfer Load Case 20: Normal 60 kip pull hydraulic load (internal pressure of 30 psig + 60 kip pull + thermal of 115 °F ambient)

During retrieval of the canister from the HSM into the TC a normal maximum pull force of 60 kips is applied by a hydraulic ram over an annulus area of 12.62 in. outer diameter and 10 in. inner diameter on the inside surface of grapple ring. A uniform pressure of 1,289 psig [= 60,000 lb / (($\pi/4$) × (12.62² – 10²))] is applied over this area. The periphery of the top cover outer surface is held as boundary condition. The sustained loads of an internal pressure of 30 psig plus the equivalent pull load pressure of 1,289 psi are applied in Load Step 1. The sustained loads plus the temperature load from fuel decay heat are applied in Load Step 2.

Stresses in the grapple ring, outer bottom cover plate, and the bottom 2 in. of the canister shell are linearized in ANSYS. The membrane stress results are compared against the general membrane stress, P_m , stress limits. The membrane plus bending stress results are compared against the primary membrane plus bending, $P_m/P_L + P_B$, stress limits. The maximum stress intensity in the rest of the canister is compared against the general membrane stress, P_m , and primary membrane plus bending stress, $P_m/P_L + P_B$, stress limit.

The maximum membrane and membrane plus bending stress in the grapple ring, outer bottom cover plate, and the bottom 2 in. of the canister shell are 9.24 ksi and 25.57 ksi, respectively for Load Case 1. Maximum stress intensity in all other components is 14.81 ksi for Load Case 1. The maximum stress intensity in the closure welds is calculated to be 11.73 ksi.

The maximum stress intensity in the canister is calculated to be 38.73 ksi for Load Step 2. The maximum stress intensity in the closure welds is calculated to be 15.25 ksi.

Transfer Load Case 21: Off-normal 80 kip push hydraulic load (internal pressure of 30 psig + 80 kip push + thermal load of 115 °F ambient)

The same 80 kip push hydraulic load analyzed in Load Case 19 is also designated as an off-normal condition. Evaluation of this load in Load Case 19 as normal condition covers this off-normal condition.

Transfer Load Case 22: Off-normal 80 kip pull hydraulic load (internal pressure of 30 psig + 80 kip pull + thermal of 115 °F ambient)

During retrieval, the canister from the HSM into the TC a normal maximum pull force of 80 kips is applied by a hydraulic ram over an annulus area of 12.62 in. outer diameter, and 10-inch inner diameter on the inside surface of grapple ring. A uniform pressure of 1,719 psig [= 80,000 lb / (($\pi/4$) × (12.62² – 10²))] is applied over this area. The periphery of the top cover outer surface is held as boundary condition. The sustained loads of an internal pressure of 30 psig plus the equivalent pull load pressure of 1,719 psi are applied as the loading. The ASME code requires only primary stresses to be evaluated under off-normal condition Service Level C; therefore, the secondary thermal stresses are not evaluated.

Stresses in the grapple ring, outer bottom cover plate, and the bottom 2 in. of the canister shell are linearized in ANSYS. The membrane stress results are compared against the general membrane stress, P_m , stress limits. The membrane plus bending stress results are compared against the primary membrane plus bending, $P_m/P_L + P_B$, stress limits. The maximum stress intensity in the rest of the canister is compared against the general membrane stress, P_m , and primary membrane plus bending stress, $P_m/P_L + P_B$, stress limit.

The maximum membrane and membrane plus bending stress in the grapple ring, outer bottom cover plate, and the bottom 2 in. of the canister shell are 12.32 ksi and 34.13 ksi, respectively. The maximum stress intensity in all other components is 14.81 ksi. The maximum stress intensity in the closure welds is calculated to be 11.72 ksi.

Transfer Load Case 23: Accident 110 kip push hydraulic load (internal pressure of 30 psig + 110 kip push)

The maximum accident hydraulic force applied by the ram to push the canister from its TC to the HSM is set at 110 kips. The load will be applied over an area with a 9-inch diameter on the canister bottom. A uniform pressure of 1,729.1 psig $[= 110,000 \text{ lb} / ((\pi/4) \times 9^2)]$ is applied over this area in the 2-D ANSYS canister model. The periphery of the canister top cover outer surface is held as boundary condition. The sustained loads of an internal pressure of 30 psig plus the equivalent push force pressure of 1,729 psi are applied as the loading. The secondary temperature load is not required by ASME code for an accident condition analysis.

The maximum stress intensity in the canister for this load case is calculated to be 16.25 ksi. The maximum stress intensity in the closure welds is calculated to be 10.45 ksi.

Transfer Load Case 24: Accident 110 kip pull hydraulic load (internal pressure of 30 psig + 110 kip pull)

The maximum accident condition hydraulic force applied by the ram to pull the canister out of the HSM into the TC is set at 110 kips. This pull force is applied over an annulus area of 12.62 in. outer diameter and 10 in. inner diameter on the inside surface of grapple ring. A uniform pressure of 2,363 psig $[= 110,000 \text{ lb} / ((\pi/4) \times (12.62^2 - 10^2))]$ is applied over this area in the 2-D ANSYS canister model. The periphery of the top cover outer surface is held as a boundary condition. The sustained loads of an internal pressure of 30 psig plus the equivalent pull force pressure of 2,363 psi are applied as loading. The secondary temperature load is not required by ASME code for an accident condition analysis.

Stresses in the grapple ring, outer bottom cover plate, and the bottom 2 in. of the canister shell are linearized in ANSYS. The membrane stress results are compared against the general membrane stress, P_m , stress limits. The membrane plus bending stress results are compared against the primary membrane plus bending, $P_m/P_L + P_B$, stress limits. The maximum stress intensity in the rest of the canister is compared against the general membrane stress, P_m , and primary membrane plus bending stress, $P_m/P_L + P_B$, stress limit.

The maximum membrane and membrane plus bending stress in the grapple ring, outer bottom cover plate, and the bottom 2 in. of the canister shell are 16.96 ksi and 46.98 ksi, respectively. The maximum stress intensity in all other components is 14.81 ksi. The maximum stress intensity in the closure welds is calculated to be 11.72 ksi.

Transfer Load Case 25: Canister lifting

Three-Piece Top End Assembly Design

For the three-piece top end assembly design, four lifting lugs are used for lifting the empty canister into the TC. The lifting lugs, support ring, reinforcing pad, connecting welds, and local stresses in the canister shell are evaluated using an empty DSC bounding weight and a dynamic load factor of 1.15.

Since lifting using internal lugs is an infrequent event (normally the DSC would be lifted for placement into the cask only once prior to fuel loading and will never occur after the DSC is in service), Service Level B allowable stresses are applied. Level B allowables are identical to Level A allowables for the components (shell, support ring, and lug). However, for the welds, Level B allowables are 33% greater than Level A values.

The evaluation is performed using a combination of hand calculations and ANSYS finite element analyses. Hand calculations are used to evaluate the local stresses in the lifting lugs near the pin-hole; finite element analyses are used to determine loads and/or stresses in all other components.

The shell, support ring and lug components are modeled using ANSYS solid elements and welds are modeled by coupling the translational degrees of freedom for the coincident nodes.

Results of the stress evaluation are calculated for different lifting configurations. The maximum stress ratio is 0.909 for the spreader bar assembly, 8-foot sling, and 10-foot sling lifting configurations. Therefore, the lug design and required welds are acceptable for the 32PTH Type 2 DSC.

Alternate Two-piece Top End Assembly Design

For the alternate two-piece top end assembly design, the evaluations performed for the 32PTH DSC are bounding.

Canister Corner Drop Analysis

As stated in [16], the end and corner drops are generally not considered credible during storage and transfer operations because the TC will always be in horizontal orientation. Thus, corner drop load cases are not evaluated.

D.4 Summary of Results for DSC Shell Assembly Stress Evaluation for Transfer Loads

The calculated maximum stress intensities in the DSC shell assembly components are summarized in Tables B.3.9.1-5 through B.3.9.1-8. These tables also show that the stress intensity results are below the ASME code stress intensity allowables.

The stresses in the closure welds are summarized in Tables B.3.9.1-9 through B.3.9.1-12. These tables also show that the stress results are below the ASME code stress allowables.

Based on the results of these analyses, the design of the 32PTH Type 2 DSC shell assembly is structurally adequate under transfer loads of testing, normal (Service Level A), and accident (Level D) conditions.

E. DSC Shell Assembly Stress Evaluation for Storage Loads

This section evaluates the structural adequacy of the 32PTH Type 2 DSC shell assembly when it is in the horizontal storage position within an HSM-H. This section considers storage loads on the canister under both normal and hypothetical accident conditions.

The evaluation of the stresses in the canister for storage loads employs an ANSYS 2-D axisymmetrical model to analyze three thermal conditions specified for the canister during storage. This 2-D model is the same model described in Section B.3.9.1.3.2 (D.2) used to compute stresses due to axisymmetric transfer loads. The analyses of axisymmetric loads, such as internal and external pressure loads for transfer conditions, are also valid for a horizontal storage canister. Their results are, therefore, used in this section for stress combinations and evaluations.

The fuel basket stress analysis for storage loads (Section 3.9.1.2.3 (C)) uses an ANSYS 3-D model, which includes the DSC canister shell, to calculate the non-axisymmetrical seismic and deadweight loads. The calculated stress intensities in the canister under the seismic and deadweight loads from Section 3.9.1.2.3 (C) are used in this section for stress combinations and evaluations.

The temperatures in the canister under 115 °F and -20 °F ambient conditions of and under HSM-H blocked vent conditions for 34 hours are computed in Chapter 4. These temperatures are imposed on the stress model in this evaluation for thermal stress calculations.

E.1 DSC Shell Assembly Storage Load Cases

The storage load cases considered in this section are summarized in Table B.3.9.1-13.

E.2 DSC Shell Assembly Finite Element Model Descriptions

The 2-D axisymmetrical stress models described in Section B.3.9.1.3.2 (D.2) for the transfer load analysis are also used for the storage load analysis. Figures B.3.9.1-1, B.3.9.1-2 and B.3.9.1-3 show this model. This model is used to evaluate the three specified thermal cases for storage, which are the -20 °F and 115 °F ambient conditions, and the blocked vent hypothetical accident condition. The temperature profiles in the canister for the three storage thermal cases are calculated in Chapter 4.

E.3 DSC Shell Assembly Stress Analysis for Storage Loads

All individual load cases specified in Table B.3.9.1-13 are described in detail in the following sections.

Storage Load Case 1: Deadweight (1g down)

The canister shell and fuel basket containing the fuel assemblies, resting horizontally on the rails of an HSM-H is analyzed in Section 3.9.1.2.3 (C) for storage loads. The maximum primary membrane and membrane plus bending stress intensities in the canister shell due to the deadweight load are calculated to be 0.4 ksi, and 4.05 ksi, respectively (see Table 3.9.1-14). These stress intensities are also used as maximum stress intensities at closures welds (see Table B.3.9.1-15).

Storage Load Case 2: Internal pressure of 30 psig

The internal pressure of 30 psig applied on the canister is analyzed in Load Step 1 of Transfer Load Case 2 in Section B.3.9.1.3.2 (D). The maximum membrane plus bending stress intensities in the canister, calculated in Section B.3.9.1.3.2.D is 14.97 ksi. The maximum stress intensity in the closure welds is calculated to be 11.75 ksi calculated in section B.3.9.1.3.2 (D).

Storage Load Case 3: Seismic loads (0.65g axial + 0.65g transverse + 1.3g vertical down)

The seismic loads on the canister, containing the basket and the fuel assemblies and resting on the rails of an HSM-H, are analyzed in Section 3.9.1.2.3 (C). The maximum primary membrane and membrane plus bending stress intensities are calculated in Section 3.9.1.2.3 (C) to be 0.63 ksi, and 6.08 ksi, respectively (see Table 3.9.1-14). This specified seismic load includes a 1g deadweight load.

Storage Load Case 4: Thermal load at -20 °F ambient

The maximum temperature in the canister for this thermal case is calculated in Chapter 4 to be 318 °F. The temperatures in the canister calculated in Chapter 4 are applied to the stress model in order to compute the thermal stress intensities in the canister. The maximum secondary thermal stress intensity is calculated to be 20.91 ksi. The 20.91 ksi stress is calculated based on canister maximum temperature of 324 °F. Since the revised temperature of 318 °F is less than 324 °F, 20.91 ksi is conservatively used for load combination and compared with the allowables. The maximum stress intensity in the closure welds is calculated to be 3.67 ksi.

Storage Load Case 5: Thermal load at 115 °F ambient

The thermal load case with the canister stored in the HSM-H with fins, described in Chapter 4, is selected for this evaluation. The maximum temperature in the canister for this thermal case is calculated in Chapter 4 to be 407 °F. The same procedure used for calculating the thermal stress intensities for the Load Case 4 is repeated for the 115 °F ambient thermal load. The secondary thermal stress intensity is calculated to be 18.95 ksi. The 18.95 ksi stress is calculated based on canister maximum temperature of 434 °F. Since the revised temperature of 407 °F is less than 434 °F, 18.95 ksi is conservatively used for load combination and compare with the allowables. The maximum stress intensity in the closure welds is calculated to be 3.62 ksi.

Storage Load Case 6: Blocked vent thermal accident condition

The thermal evaluation presented in Chapter 4 reports four thermal cases for the canister stored in the HSM with blocked vent. The maximum temperature of 600 °F in the 24-hour canister is reached after 34 hours of complete vent blockage in an HSM with fins. The 34-hour vent blockage is a conservative scenario, since the vent is visually checked at least every 24 hours. However, this case is reported in the thermal evaluation and is therefore selected for analysis in this section. The same procedure used for obtaining the thermal load in Load Case 4 is used in this load case. The secondary thermal stress intensity is calculated to be 18.48 ksi. The maximum stress intensity in the closure welds is calculated to be 8.19 ksi.

Storage Load Case 7: Accident internal pressure of 70 psig (in the event of blocked vent)

The internal pressure of 70 psig in the canister is analyzed for enveloping the accident condition internal pressures during the blocked vent scenario. The maximum primary membrane plus bending stress intensity in the canister is calculated to be 34.56 ksi. The maximum stress intensity in the closure welds is calculated to be 27.38 ksi.

Storage Load Case 8: Accident flood load (enveloped by external pressure of 30 psig)

The hypothetical accident condition flood load is enveloped by an external pressure of 30 psig. The maximum primary membrane plus bending stress intensity in canister is calculated to be 11.67 ksi. The maximum stress intensity in the closure welds is calculated to be 2.94 ksi.

E.4 Summary of the Stress Calculation Results for All Storage Load Cases

Tables B.3.9.1-14 and B.3.9.1-15 summarize the calculated stresses in the entire canister and their corresponding ASME code evaluations.

Based on the results of this calculation, the 32PTH Type 2 DSC canister is structurally adequate under all normal (Service Level A), off-normal (Service Level C), and hypothetical accident (Service Level D) conditions during storage.

B.3.9.1.3.3 DSC Shell Buckling Evaluation

This section evaluates the structural adequacy of the 32PTH Type 2 DSC canister against buckling during a vertical end drop during transfer operations.

For the NUHOMS HD[®] System, the vertical end drops are not considered credible during storage and transfer operations under 10 CFR Part 72 because the TC is always in the horizontal orientation. The vertical end drop buckling evaluation documented below is performed in support of a 10 CFR Part 50 evaluation that may be performed by the user if the user cannot demonstrate that this accident drop is not credible.

A. Approach

A finite element plastic analysis with large displacement option is performed to monitor occurrence of canister shell buckling under the specified loads.

The thermal evaluation presented in Chapter 4 shows that the metal temperatures of the entire canister are below 500 °F during the transfer operations. The material properties of canister at 500 °F are, therefore, conservatively used in this calculation.

B. Material Properties used for Canister Buckling Evaluation

The material properties of the canister materials, SA-240 Type 304 stainless steel, at 500 °F are as follows.

Property	@ 500 °F
S_m (ksi)	17.5
S_y (ksi)	19.4
S_u (ksi)	63.4
E (psi)	25.8×10^6

For the elastic-plastic finite element analysis, bilinear kinematic hardening material properties are used. Tangent modulus of 5% of elastic modulus is assumed after yield stress.

The material properties for the top and bottom shield plug, A-36, at 500 °F are as follows:

Property	@ 500 °F
S_m (ksi)	19.3
S_y (ksi)	29.3
S_u (ksi)	58.0
E (psi)	27.3×10^6

C. Finite Element Buckling Analysis

The following three hypothetical accident load cases for the canister are considered in this buckling analysis.

Buckling Load Case 1: End drop + 15 psig external pressure

Buckling Load Case 2: End drop + 30 psig internal pressure

Buckling Load Case 3: End drop + 0 psig internal pressure

The 2-D axisymmetric FEM of the canister described in Appendix B.3.9.1, Section B.3.9.1.3.2 (D.2) for the DSC canister stress analysis is used for this analysis.

The gap element real constants, node couplings and displacement boundary conditions are also the same as those used in Section B.3.9.1.3.2 (D.2). The weight of the canister's outer and inner top cover plus the top shield plug and its support ring is 10,720 lb, and the bottom shield plug is 7,200 lb (see Section B.3.2.1). Since the top end of the canister is heavier than the bottom end, it is a more severe case when the canister drops on its bottom end. A drop on the bottom end is, therefore, chosen for analysis in this calculation.

For load case with external pressure or internal pressure, a quasi-static plastic analysis consisting of two load steps is performed to monitor buckling of the canister. The first load step applies external pressure or internal pressure alone. A subsequent inertial load of 300g is added in the second load step. The outer surface of the canister bottom is held in order to simulate the case that the canister drops on a rigid cask bottom face.

In the Load Step 1, the stepped external or internal pressure is applied as a static load.

In the Load Step 2, the weight of the canister internals (basket and fuel assemblies) is accounted for by applying an equivalent internal pressure on the canister bottom. The actual total weight of the canister internals is 82,520 lb (basket 31,000 lb + fuel assemblies 51,520 lb) (Chapter B.3, Section B.3.2.1). A total weight of 85,000 lb for the canister internals is conservatively used in this analysis. This inertial load is uniformly distributed over the bottom surface of the canister cavity with a radius of 34.375 in. This equivalent uniform pressure, P_{in} , exerted on the canister bottom by the weight of the internals under a 1g load is calculated as follows.

$$P_{in} = [85,000 / (\pi \times 34.375^2)] = 22.8972 \text{ psi}$$

An equivalent pressure of 6870.0 psig on the canister bottom corresponding to the 300g load ($P_{in} = 300 \times 22.8972 = 6870.0 \text{ psi}$) is, therefore, applied to the canister bottom along with the 300g acceleration load in the Load Step 2.

A bilinear stress-strain relationship (with kinematic hardening) is used to obtain stresses and deflections beyond the elastic limit of the material. The large displacement option in ANSYS is activated to monitor the buckling response.

D. Summary Canister Buckling Analysis Results

The following table summarizes the last converged load for the three load cases:

Load Case	Last Converged Load (g)	g Load Used for Basket Structural Analysis	Factor of Safety
1	181.0	75	2.41
2	187.7	75	2.50
3	195.0	75	2.60

The analysis shows that the critical buckling load for the canister end drop is 181.0g, which is well beyond the design 75g load. Therefore, it is concluded that buckling of the canister will not occur during a hypothetical accident end drop.

B.3.9.1.3.4 Evaluation of Alternate DSC Top and Bottom Closure Assembly Design

The alternate top closure assembly of the 32PTH Type 2 DSC, which consists of the two-part combined shield plug /inner cover assembly (including the optional configurations), as well as the optional bottom end configurations (consisting of two-plate or single forging bottom assembly), are not analyzed explicitly.

The evaluations for the 32PTH Type 2 DSC consider a DSC with a three-part top end configuration (with separate inner cover plate, shield plug, and outer cover plate) and a three-part bottom end configuration (with separate inner bottom cover, bottom shield plug, outer bottom cover plate). The results from these evaluations are documented in Sections B.3.9.1.3.2 and B.3.9.1.3.3, and are considered to be bounding relative to those for a DSC with the alternate two-part top end assembly or the optional bottom end configurations for cases involving internal pressure and handling loads. For side drop accident loads, the results of the 32PTH DSC for the side drop accident load case are also applicable for the alternate top end and the optional bottom end configurations of the 32PTH Type 2 DSC. This is justified because the side drop analyses are performed using two separate 3-D models, which model the top and the bottom regions of the DSC shell assembly, respectively. These models include a segment of the DSC shell and are intended to capture the maximum stresses that occur near the transition between the shell and the stiffer top and bottom ends and, therefore, are not sensitive to the length differences between the 32PTH and 32PTH Type 2 DSCs. Furthermore, the loaded canister weight used in the 32PTH DSC analysis bounds the 32PTH Type 2 analyses.

B.3.9.1.4 32PTH Type 2 DSC and OS187H Type 2 TC Thermal Expansion Evaluation

B.3.9.1.4.1 Introduction

The purpose of this section is to determine the thermal growths among fuel assembly, basket, canister, and TC in the 32PTH Type 2 DSC and OS187H Type 2 TC. This thermal expansion calculation covers events of vacuum drying, transfer, storage, and storage with blocked vent.

B.3.9.1.4.2 Approach

The temperatures of the fuel cladding, basket, canister, and TC under various events calculated in the thermal analyses of Chapter 4 are applicable for the 32PTH Type 2 DSC and OS187H Type 2 TC. Transient thermal analyses are conducted for the vacuum drying and blocked vent events. Steady-state thermal analyses are conducted for the normal and off-normal conditions during transfer and storage. This section evaluates the thermal expansions at the steady-state temperatures in the events of transfer and storage.

In the vacuum drying load case, the profiles of transient temperature versus time computed in Chapter 4 are studied for selection of the critical time points at which the corresponding component temperatures would generate a minimum clearance between two nested components. For the blocked vent load case, the maximum temperatures from Chapter 4 are used in this evaluation.

The cold dimensions of each pair of nested components are so determined, based on design tolerances, which generates a minimum cold clearance between the two components.

Unless otherwise stated, nominal dimensions of basket, canister, and cask are used for the thermal expansion calculations.

B.3.9.1.4.3 Mechanical Properties of Materials

The coefficient of thermal expansion of structural materials used for the fuel basket, canister shell, and TC are provided in Table 3.9.1-6 as a function of temperature. The properties of SA-240 Type 304 and the zircaloy are taken from References 1 and 4 listed in Section 3.9.1.5.

B.3.9.1.4.4 Thermal Expansion Computation

A. Thermal Expansion between the Length of Fuel Assembly and DSC Cavity

The maximum length of fuel assemblies in 32PTH Type 2 DSC is 170.0 in and the minimum cavity length of the 32PTH Type 2 DSC is 181.38 in. The clearance between the fuel assembly and the 32PTH Type 2 DSC cavity is calculated using the same methodology and data as described in Appendix 3.9.1, Section 3.9.1.4.4.A.

An irradiation growth of 1.25 in. is considered in Appendix 3.9.1, Section 3.9.1.4.4.A for the fuel assemblies with a maximum length of 162.4 in. with a maximum burnup of 60 GWd/MTU. The fuel assemblies in 32PTH Type 2 DSC have a maximum length of 170.0 in. with the same maximum burnup of 60 GWd/MTU. Since the irradiation growth is proportional to the fuel assembly length for a given burnup, an irradiation growth of 1.31 in is considered for the fuel assemblies in the 32PTH Type 2 DSC as calculated below.

$$\Delta L_{\text{irrad}} = \frac{170.0''}{162.4''} \times 1.25'' = 1.31''$$

The calculated clearances between the fuel assembly and the DSC cavity for 32PTH Type 2 DSC are summarized below using the same nomenclature as used in Appendix 3.9.1, Section 3.9.1.4.4.A.

Event	T _F (°F)	α _z (in/in-°F)	α _s (in/in-°F)	T _C (°F)	α _C (in/in-°F)	L _F (in)	L _{F, irrad} (in)	L _{CH} (in)	L _{CH} - L _{FHT} (in)
Vacuum Drying	760	3.01E-06	10.0E-06	210	8.94E-06	170.48	171.79	181.61	9.82
Transfer	730	3.00E-06	10.0E-06	390	9.46E-06	170.46	171.77	181.93	10.16
Storage, Off-Normal	700	3.00E-06	10.0E-06	280	9.16E-06	170.44	171.75	181.73	9.98
Storage Accident	830	3.01E-06	10.1E-06	590	9.80E-06	170.53	171.84	182.30	10.46

As shown in the above table, the minimum clearance between the fuel assemblies and the 32PTH Type 2 DSC cavity is 9.82 in. Fuel space is required to minimize the axial fuel gap while maintain the adequate clearance to permit free thermal expansion of the fuel assemblies in the 32PTH Type 2 DSC.

B. Thermal Expansion between the Outer Diameter of the Basket and the Inner Diameter of the DSC Cavity

The diametrical gap between the outer diameter of the basket and the inner diameter of the canister remains the same as for the 32PTH DSC. With the same radial temperature profile, the thermal expansion values calculated in Section 3.9.1.4.4.B are applicable for the 32PTH Type 2 DSC. These calculations show that the gap will allow free thermal expansion.

C. Thermal Expansion between the Length of Basket and DSC Cavity

The maximum length of the 32PTH Type 2 basket and the minimum cavity length of the 32PTH Type 2 DSC are 178.75 in. and 181.38 in., respectively, at room temperature. The clearance between the basket and the DSC cavity for 32PTH Type 2 DSC is calculated using the same methodology and data as described in Appendix 3.9.1, Section 3.9.1.4.4.C.

The calculated clearances between the basket and the 32PTH Type 2 DSC cavity are summarized below using the same nomenclature as used in Appendix 3.9.1, Section 3.9.1.4.4.C.

Event	Case	T _{CNH} (°F)	α _{CN} (in/in-°F)	T _{BKH} (°F)	α _{BK} (in/in-°F)	L _{CNH} (in)	L _{BKH} (in)	L _{CNH} – L _{BKH} (in)
Vacuum Drying	TC Backfill	500	9.70E-06	550	9.80E-06	182.137	179.591	2.546
Transfer	115 °F Amb. Basket Type I, Conf. # 1	460	9.62E-06	640	9.88E-06	182.061	179.757	2.304
	115 °F Amb. Basket Type I, Conf. # 2	460	9.62E-06	625	9.85E-06	182.061	179.727	2.334
	115 °F Amb. Basket Type I, Conf. # 3	460	9.62E-06	630	9.86E-06	182.061	179.737	2.324
	115 °F Amb. Basket Type I, Conf. # 4	460	9.62E-06	640	9.88E-06	182.061	179.757	2.304
	-20 °F Amb. Basket Type I, Conf. # 1	390	9.46E-06	570	9.80E-06	181.929	179.626	2.303
	115 °F Amb. Basket Type II, Conf. # 1	460	9.62E-06	640	9.88E-06	182.061	179.757	2.304
Storage	115 °F Amb. HSM-H w/ Finned Side Shield	400	9.50E-06	600	9.80E-06	181.949	179.678	2.271
	-20°F Amb. HSM-H w/ Finned Side Shield	280	9.16E-06	505	9.71E-06	181.729	179.505	2.224
	34 hours after Blockage HSM-H w/ Finned Side Shield	590	9.80E-06	740	10.0E-06	182.304	179.948	2.356

As shown in the above table, adequate clearance has been provided to permit free thermal expansion of the basket within 32PTH Type 2 DSC cavity.

D. Thermal Expansion between the Outer Diameter of the DSC and the Inner Diameter of the TC

The diametrical gap between the outer diameter of the canister and the inner diameter of the cask remains the same as for the 32PTH DSC and OS187H TC. With the same radial temperature profile, the thermal expansion values calculated in Section 3.9.1.4.4.D are applicable for the 32PTH Type 2 DSC and OS187H Type 2 TC. These values show that the current gap will allow free thermal expansion.

E. Thermal Expansion between the Length of the DSC and the TC Cavity

The maximum length of the 32PTH Type 2 DSC and the minimum cavity length of the OS187H Type 2 TC are 198.50 in. and 199.05 in., respectively, at room temperature. The clearance between the DSC and the TC cavity for 32PTH Type 2 DSC is calculated using the same methodology and data as described in Appendix 3.9.1, Section 3.9.1.4.4.E.

The calculated clearances between the 32PTH Type 2 DSC and OS187H Type 2 TC cavity are summarized below using the same nomenclature as used in Appendix 3.9.1, Section 3.9.1.4.4.E.

Event	Case	T _{CKH} (°F)	α _{CK} (in/in-°F)	T _{CNH} (°F)	α _{CN} (in/in-°F)	L _{CKH} (in)	L _{CNH} (in)	L _{CKH} - L _{CNH} (in)
Vacuum Drying	TC Backfill	265	9.13E-06	525	9.75E-06	199.404	193.381	0.023
Transfer	115°F Amb.	330	9.26E-06	485	9.67E-06	199.529	199.297	0.232
	-20°F Amb.	240	9.06E-06	500	9.70E-06	199.357	199.328	0.029

As seen in the above table, an adequate clearance has been provided to permit free thermal expansion of the 32PTH Type 2 DSC within the OS187H Type 2 TC.

B.3.9.1.4.5 Thermal Expansion Analysis Conclusions

This evaluation demonstrates that adequate clearance is provided between the 32PTH Type 2 DSC fuel basket and canister shell, and between the 32PTH Type 2 DSC canister and the OS187H Type 2 TC to permit free thermal expansions among these components due to all specified design and service conditions.

B.3.9.1.5 References

1. American Society of Mechanical Engineers, ASME Boiler and Pressure Vessel Code, Section II, Part D, 1998, through 2000 addenda.
2. Not used.
3. American Society of Mechanical Engineers, ASME Boiler and Pressure Vessel Code, Section III, Appendix F, 1998 through 2000 addenda.
4. NUREG/CR-0497-Rev 2, MATPRO-Version 11 (Revision 2), A handbook of materials properties for use in the analysis of light water reactor fuel rod behavior.
5. Not used.
6. Manual of Steel Construction, Ninth Edition, American Institute of Steel Construction, Inc., 1989.
7. Roark, Formulas for Stress and Strain, Seventh Edition.
8. American Society of Mechanical Engineers, ASME Boiler and Pressure Vessel Code, Section III, Division 1, Subsection NB, 1998, through 2000 addenda.
9. NUREG/CR-0481 SAND77-1872 R-7, "An Assessment of Stress-Strain Data Suitable for Finite-Element Elastic-Plastic Analysis of Shipping Containers," September 1978.
10. ANSYS Users Manual, Release 8.0 and 10.0A1 and 14.0
11. Not used.
12. Not used.
13. Not used.
14. USNRC Spent Fuel Project Office, Interim Staff Guidance – 15, "Materials Evaluation."
15. Roark, Formulas for Stress and Strain, Sixth Edition.
16. Safety Evaluation Report, Transnuclear, Inc., NUHOMS[®] HD Horizontal Modular Storage System for Irradiated Nuclear fuel, Docket No. 72-1030.

Table B.3.9.1-1
Temperature Dependent Material Properties for ASTM A-36

Temp (°F)	E (10³ ksi)	S_m (ksi)	S_y (ksi)	S_u (ksi)	α_{INST} (10⁻⁶ °F⁻¹)	α_{AVG} (10⁻⁶ °F⁻¹)
70	29.5	19.3	36.0	58.0	6.4	6.4
200	28.8	19.3	33.0	58.0	6.9	6.7
300	28.3	19.3	31.8	58.0	7.3	6.9
400	27.7	19.3	30.8	58.0	7.7	7.1
500	27.3	19.3	29.3	58.0	8.0	7.3
600	26.7	17.7	27.6	58.0	8.4	7.4
700	25.5	17.3	25.8	58.0	8.6	7.6

Table B.3.9.1-2
Material Stress Limits for 32PTH Type 2 DSC
SA-240/SA-479 304 & SA-182 F304

Temp (°F)	Level A			Level C		Level D			
						Elastic		Elastic-Plastic	
	P_m	$P_m + P_b$	$P_m + P_b + Q$	P_m	$P_m + P_b$	P_m	$P_m + P_b$	P_m	$P_m + P_b$
70	20.0	30.0	60.0	30.0	45.0	48.0	72.0	52.5	67.5
200	20.0	30.0	60.0	25.0	37.5	48.0	71.0	49.7	63.9
300	20.0	30.0	60.0	24.0	36.0	46.3	66.2	46.3	59.6
400	18.7	28.1	56.1	22.4	33.7	44.8	64.0	44.8	57.6
500	17.5	26.3	52.5	21.0	31.5	42.0	63.0	44.4	57.1
600	16.4	24.6	49.2	19.7	29.5	39.4	59.0	44.4	57.1
700	16.0	24.0	48.0	19.2	28.8	38.4	57.6	44.4	57.1
800	15.2	22.8	45.6	18.2	27.4	36.5	54.7	44.0	56.5

Table B.3.9.1-3
32PTH Type 2 DSC Canister Load Combinations during Transfer

Loading	Canister w/TC Orientation	Service Level	Load for Analysis	Load Combinations	Analyzed Load Case No.	ANSYS Model
Dead weight	Vertical ⁽¹⁾	A	1g down (axial)	1g down + 15 psig ext. press. + thermal (vacuum dry)	1	2-D
External pressure	Vertical ⁽¹⁾	A	15 psig			
Thermal	Vertical ⁽¹⁾	A	Vacuum dry			
Dead weight	Horizontal ⁽²⁾	A	2g axial + 2g trans. + 2g vertical	A = 2g axial + 2g trans. + 2g vertical A+ 30 psig int. pressure + thermal (115 °F)	2	2-D
Handling load in TC	Horizontal ⁽²⁾	A			3	2-D
Internal pressure	Horizontal ⁽²⁾	A	30 psig ⁽⁶⁾	Pressure stress	[2] ⁽⁵⁾	2-D
External pressure	Horizontal ⁽²⁾	A	15 psig	Pressure stress	[3] ⁽⁵⁾	2-D
Thermal	Horizontal ⁽²⁾	A	Thermal stress (-20 °F Ambient)	Thermal stress	[3] ⁽⁵⁾	2-D
Thermal	Horizontal ⁽²⁾	A	Thermal stress (115 °F ambient)	Thermal stress	[2] ⁽⁵⁾	2-D
Internal pressure	Horizontal	D	120 psig ⁽³⁾	Pressure stress	4	2-D
External pressure	Horizontal	D	25 psig ⁽⁴⁾	Pressure stress	5	2-D
Side drop	Horizontal	D	75g multiple orientations (0°, 30°, 45°, impact on two rails, impact on one rail) Drop angles are enveloped by 0° (no rail) and 180° (two rails)	75g side drop at 0° (no rail) + 30 psig int. press. of top/bottom ends	6/7	3-D
				75g side drop at 180° (two rails) + 30 psig int. press. of top/bottom ends	8/9	3-D
				75g side drop at 0° (no rail) + 15 psig ext. press. of top/bottom ends	10/11	3-D
				75g side drop at 180° (two rails) + 15 psig ext. press. of top/bottom ends	12/13	3-D
Corner drop	Horizontal	D	Enveloped by 75 g Side Drop and 75 g End Drop			
End drop	Vertical	D	75g End Drop	75g top/bottom + 30 psig int. pressure	14/15	2-D
				75g top/bottom + 15 psig ext. pressure	16/17	2-D

Notes:

- (1) TC supported at the bottom.
- (2) TC supported at 4 trunnion location.
- (3) Under accident fire condition.
- (4) Under accident flood condition.
- (5) [#] indicates this individual load case is enveloped in the analyzed load case No.
- (6) From Chapter 4, Table 4-10, the maximum normal operating pressure is 6.4 psig during transfer operation. However, a design pressure of 15 psig is used. Conservatively, 30 psig is used for structural evaluation of the canister.

Table B.3.9.1-4
32PTH Type 2 DSC Canister Load Combinations during Lifting, Testing, and Hydraulic Loads

Loading	Canister w/TC Orientation	Service Level	Load for Analysis	Load Combinations	Analyzed Load Case No.	ANSYS Model
Dead weight	Horizontal	A	1g	1g + 25 psig int. pressure + 155 kips axial loads	18	2-D
Test pressure	Horizontal	A	25 psig ⁽³⁾			
Seal plate axial load	Horizontal	A	155 kips			
Hydraulic loads ^{(1) (2)} (push/pull)	Horizontal	A	80/60 kips	30 psig int. pressure + 80 kips push/60 kips pull + thermal (115 °F)	19/20	2-D
Hydraulic loads ^{(1) (2)} (push/pull)	Horizontal	C	80/80 kips	30 psig int. pressure + 80 kips + thermal (115 °F)	21/22	2-D
Hydraulic loads ^{(1) (2)} (push/pull)	Horizontal	D	110/110 kips	30 psig int. pressure + 110 kips	23/24	2-D
Lifting	Vertical	A	1g	1g	25	3-D

Notes:

- (1) The hydraulic push loads are applied at the canister bottom surface within the grapple ring support.
- (2) The hydraulic pull loads are applied at the inner surface of the grapple ring.
- (3) From Chapter 4, Table 4-10, the maximum normal operating pressure is 6.4 psig during transfer operation. The canister is conservatively evaluated at higher test pressures.

Table B.3.9.1-5
Summary of Calculated Stresses for Testing Condition Loads

Load Case	Combination of Loads	Canister Orientation	Service Level	Component	Stress Category	Stress (ksi)	Stress Limit (ksi)
T8(a)	DW + 25 psig int. press. + 155 kip axial load	Horizontal	A	All ⁽¹⁾	P _m	8.0 ⁽²⁾	24 ⁽⁴⁾
					P _m + P _b	14.26 ksi ⁽³⁾	40.5 ⁽⁵⁾

Notes:

- (1) Yield stress, $S_y = 30,000$ psi, is taken at test temperature of 100 °F for both material SA-240 GR.304 and SA-182 F304
- (2) $P_m = 8.0$ ksi + 0.005 ksi (dead weight, in load case 18) = 8 ksi
- (3) $P_m + P_b = 8$ ksi + 6.26 ksi (dead weight, in load case 18) = 14.26 ksi
- (4) $P_m < 0.8 S_y = 24$ ksi
- (5) $P_m + P_b < 1.35 S_y = 40.5$ ksi

Table B.3.9.1-6
Summary of Calculated Stress for Normal and Off-Normal
Condition Transfer Loads

Load Case	Combination of Loads	Canister Orientation	Service Level	Components	Stress Category	Stress ⁽³⁾ (ksi)	Stress Limit (ksi)
T1	1g down + 15 psig ext. press. + vacuum drying thermal	Vertical	A	All ⁽²⁾	P_m	1.95	17.5
					$P_m + P_b$	1.95	26.3
					$P_m + P_b + Q$	18.82	52.5
T2	Handling 2g + 30 psig int. press. + thermal (115 °F)	Horizontal	A	All ⁽²⁾	P_m	14.81+0.88 = 15.69	17.5
					$P_m + P_b$	14.81+9.74 = 24.55	26.3
					$P_m + P_b + Q$	38.35+9.74 = 48.09	52.5
T3	Handling 2g + 15 psig ext. press. + thermal (-20 °F)	Horizontal	A	All ⁽²⁾	P_m	5.83+0.88 = 6.71	17.5
					$P_m + P_b$	5.83+9.74 = 15.57	26.3
					$P_m + P_b + Q$	28.84+9.74 = 38.58	52.5
T9	30 psig int. press + 80 kips push + thermal (115 °F)	Horizontal	A	All ⁽²⁾	P_m	15.65	17.5
					$P_m + P_b$	15.65	26.3
					$P_m + P_b + Q$	31.35	52.5
T10	30 psig int. press + 60 kips pull + thermal (115 °F)	Horizontal	A	GR, BOCP, and bottom 2" CS ⁽¹⁾	P_m	9.24	20.0
					$P_m + P_b$	25.57	30.0
					$P_m + P_b + Q$	27.23	60.0
				All except GR, BOCP, and bottom 2" CS ⁽³⁾	P_m	14.81	17.5
					$P_m + P_b$	14.81	26.3
					$P_m + P_b + Q$	38.73	52.5
T11	30 psig int. press + 80 kips push + thermal (115 °F)	Horizontal	C	All ⁽²⁾	P_m	15.65	21.0
					$P_m + P_b$	15.65	31.5
					$P_m + P_b + Q$	-	-
T12	30 psig int. press + 80 kips pull + thermal (115 °F)	Horizontal	C	GR, BOCP, and bottom 2" CS ⁽¹⁾	P_m	12.32	24.0
					$P_m + P_b$	34.13	36.0
					$P_m + P_b + Q$	-	-
				All except GR, BOCP, and bottom 2" CS ⁽³⁾	P_m	14.81	21.0
					$P_m + P_b$	14.81	31.5
					$P_m + P_b + Q$	-	-

Notes:

- (1) GR—grapple ring; BOCP—bottom outer cover plate; CS—canister shell. Except for the vacuum drying and fire accident load cases, the temperature in the grapple ring, the bottom outer cover plate and the bottom 2 in. of the canister shell do not exceed 300 °F. Conservatively stress limits at 300 °F are used.
- (2) Conservatively the stress limits at 500 °F are used.
- (3) Conservatively the maximum stress intensity was used for both P_m and $P_m + P_b$ stresses for all analyses except for grapple pull load cases, 20 and 22, where the stresses were linearized in the grapple ring, bottom outer cover plate and bottom 2 in. of the canister shell.

Table B.3.9.1-7
Summary of Calculated Stress for Accident Condition Transfer Loads (Axisymmetric Loads)

Load Case	Combination of Loads	Canister Orientation	Service Level	Components	Stress Category	Stress ⁽⁴⁾ (ksi)	Stress Limit (ksi)
T4	120 psig int. press. under fire accident	Horizontal	D	All ⁽²⁾	P_m	23.87	44.0
					$P_m + P_b$	23.87	56.5
T5	25 psig ext. press. under flood accident	Horizontal	D	All ⁽³⁾	P_m	9.73	42.0
					$P_m + P_b$	9.73	63.0
T6	75 g top end drop + 30 psig int. press.	Vertical	D	All ⁽³⁾	P_m	6.39	42.0
					$P_m + P_b$	43.19	63.0
T7	75 g bottom end drop + 30 psig int. press.	Vertical	D	All ⁽³⁾	P_m	17.71	42.0
					$P_m + P_b$	17.71	63.0
T16	75 g top end drop + 15 psig ext. press.	Vertical	D	All ⁽³⁾	P_m	8.90	42.0
					$P_m + P_b$	59.29	63.0
T15	75 g bottom end drop + 15 psig ext. press.	Vertical	D	All ⁽³⁾	P_m	22.63	42.0
					$P_m + P_n$	22.63	63.0
T13	30 psig int. press. + 110 kips push	Horizontal	D	All ⁽³⁾	P_m	16.25	42.0
					$P_m + P_b$	16.25	63.0
T14	30 psig int. press. + 110 kips pull	Horizontal	D	GR, BOCP, and bottom 2" CS ⁽¹⁾	P_m	16.96	46.3
					$P_m + P_b$	46.98	66.2
				All except GR, BOCP, and bottom 2" CS ⁽³⁾	P_m	14.81	42.0
					$P_m + P_b$	14.81	63.0

Notes:

- (1) GR—grapple ring; BOCP—bottom outer cover plate; CS—canister shell. Except for the vacuum drying and fire accident load cases, the temperature in the grapple ring, the bottom outer cover plate, and bottom 2 in. of the canister shell do not exceed 300 °F. Conservatively stress limits at 300 °F are used for elastic analysis.
- (2) Conservatively the stress limits at 800 °F are used for elastic-plastic analysis.
- (3) Conservatively the stress limits at 500 °F are used for elastic analysis.
- (4) Conservatively the maximum stress intensity was used for both P_m and $P_m + P_b$ stresses for all analyses except for grapple pull load cases, 23, where the stresses were linearized in the grapple ring, bottom outer cover plate and bottom 2 in. of the canister shell.

Table B.3.9.1-8
Summary of Stresses for Accident Condition Transfer Loads (3-D Inertial Loads)

Load Case	Load Combination	Canister	Maximum Stress Intensity ⁽¹⁾ [ksi]	Stress Limits	
				P _m	P _m +P _b
SD1	Side drop 75g + 30 psig internal pressure	Top end, no rails (orientation 0°)	25.31	44.4 ksi	57.1 ksi
SD2	Side drop 75g + 30 psig internal pressure	Bottom end, no rails (orientation 0°)	23.96	44.4 ksi	57.1 ksi
SD3	Side drop 75g + 30 psig internal pressure	Top end, rails (orientation 180°)	26.89	44.4 ksi	57.1 ksi
SD4	Side drop 75g + 30 psig internal pressure	Bottom end, rails (orientation 180°)	24.59	44.4 ksi	57.1 ksi
SD5	Side drop 75g + 15 psig external pressure	Top end, no rails (orientation 0°)	25.65	44.4 ksi	57.1 ksi
SD6	Side drop 75g + 15 psig external pressure	Bottom end, no rails (orientation 0°)	23.95	44.4 ksi	57.1 ksi
SD7	Side drop 75g + 15 psig external pressure	Top end, rails (orientation 180°)	26.86	44.4 ksi	57.1 ksi
SD8	Side drop 75g + 15 psig external pressure	Bottom end, rails (orientation 180°)	24.71	44.4 ksi	57.1 ksi

Note:

(1) Shield plug component excluded in stress evaluation.

Table B.3.9.1-9
Summary of Calculated Stress at End Closure Welds for Testing Condition Loads

Load Case	Combination of Loads	Canister Orientation	Service Level	Stress Category	Stress ⁽¹⁾ (ksi)	Stress Limit (ksi)
18	DW + 25 psig int. press. + 155 kip axial load	Horizontal	A	P _m	-	-
				P _m + P _b	-	-

Note:

(1) There are no closure welds during pressure test.

Table B.3.9.1-10
Summary of Calculated Stress at the End Closure Welds for Normal and Off-Normal Condition Transfer Loads

Load Case	Combination of Loads	Canister Orientation	Service Level	Stress Category	Stress ⁽²⁾ (ksi)	Stress Limit ⁽¹⁾ (ksi)
T1	1g down + 15 psig ext. press. + vacc. dry thermal	Vertical	A	P _m	1.56	16
				P _m + P _b	1.56	24
				P _m + P _b + Q	1.75	48
T2	Handling 2g + 30 psig int. press. + thermal (115 °F)	Horizontal	A	P _m	11.72+0.88 = 12.60	16
				P _m + P _b	11.72+9.74 = 21.46	24
				P _m + P _b + Q	15.25+9.74 = 24.99	48
T3	Handling 2g + 15 psig ext. press. + thermal (-20 °F)	Horizontal	A	P _m	1.48+0.88 = 2.36	16
				P _m + P _b	1.48+9.74 = 11.22	24
				P _m + P _b + Q	3.02+9.74 = 12.76	48
T9	30 psig int. press + 80 kips push + thermal (115 °F)	Horizontal	A	P _m	10.72	16
				P _m + P _b	10.72	24
				P _m + P _b + Q	15.21	48
T10	30 psig int. press + 60 kips pull + thermal (115 °F)	Horizontal	A	P _m	11.73	16
				P _m + P _b	11.73	24
				P _m + P _b + Q	15.25	48
T11	30 psig int. press + 80 kips push + thermal (115 °F)	Horizontal	C	P _m	10.72	19.2
				P _m + P _b	10.72	28.8
				P _m + P _b + Q	-	-
T12	30 psig int. press + 80 kips pull + thermal (115 °F)	Horizontal	C	P _m	11.72	19.2
				P _m + P _b	11.72	28.8
				P _m + P _b + Q	-	-

Notes:

- (1) Since the temperatures at the closure welds do not exceed 300 °F, the allowable stresses at 300 °F are used.
- (2) Conservatively, the maximum stress intensity was used for both P_m and P_m + P_b stresses for all analyses.

Table B.3.9.1-11
Summary of Calculated Stresses at End Closure Welds for Accident Condition Transfer
Loads (Axisymmetric Loads)

Load Case	Combination of Loads	Canister Orientation	Service Level	Stress Category	Stress ⁽²⁾ (ksi)	Stress Limit ⁽¹⁾ (ksi)
T4	120 psig int. press. under fire accident	Horizontal	D	P_m	21.76	37.04
				$P_m + P_b$	21.76	47.68
T5	25 psig ext. press. under flood accident	Horizontal	D	P_m	2.45	37.04
				$P_m + P_b$	2.45	52.96
T6	75g top end drop + 30 psig int. press.	Vertical	D	P_m	10.76	37.04
				$P_m + P_b$	10.76	52.96
T7	75g bottom end drop + 30 psig int. press.	Vertical	D	P_m	13.57	37.04
				$P_m + P_b$	13.57	52.96
T16	75g top end drop + 15 psig ext. press.	Vertical	D	P_m	12.22	37.04
				$P_m + P_b$	12.22	52.96
T15	75g bottom end drop + 15 psig ext. press.	Vertical	D	P_m	14.80	37.04
				$P_m + P_b$	14.80	52.96
T13	30 psig int. press. + 110 kips push	Horizontal	D	P_m	10.45	37.04
				$P_m + P_b$	10.45	52.96
T14	30 psig int. press. + 110 kips pull	Horizontal	D	P_m	11.72	37.04
				$P_m + P_b$	11.72	52.96

Notes:

- (1) Since the temperatures at the closure welds do not exceed 300 °F, the allowable stresses at 300 °F are used.
- (2) Conservatively, the maximum stress intensity was used for both P_m and $P_m + P_b$ stresses for all analyses.

Table B.3.9.1-12
Summary of Calculated Stresses at End Closure Welds for Accident Condition Transfer
Loads (3-D Inertial Loads)

Load Case	Load Combination	Canister	Maximum Stress Intensity (ksi)	Stress Limits
SD1	Side drop 75g + 30 psig internal pressure	Top end, no rails (orientation 0°)	21.81	35.52 ksi
SD3	Side drop 75g + 30 psig internal pressure	Top end, rails (orientation 180°)	23.63	35.52 ksi
SD5	Side drop 75g + 15 psig external pressure	Top end, no rails (orientation 0°)	21.27	35.52 ksi
SD7	Side drop 75g + 15 psig external pressure	Top end, rails (orientation 180°)	23.49	35.52 ksi

Table B.3.9.1-13
32PTH Type 2 DSC Canister Load Combinations during Storage

Loading	Canister Orientation	Service Level	Load	Enveloped Load for Analysis	Load Combinations
Dead weight	Horizontal ⁽¹⁾	A	1g down	0.65g axial + 0.65 g trans. + 1.3 g vertical	0.65g axial + 0.65g trans. + 1.3g vertical down
Seismic loads	Horizontal ⁽¹⁾	C ⁽²⁾	0.43g axial + 0.43g trans. +0.20g vertical		0.65g axial + 0.65g trans. + 1.3 g vertical down + 30 psig + thermal (115 °F)
					0.65g axial + 0.65g trans. + 1.3 g vertical down + 30 psig + thermal (-20 °F)
Internal pressure	Horizontal ⁽¹⁾	A	15 psig	30 psig	Pressure
Thermal	Horizontal ⁽¹⁾	A	Thermal (-20 °F ambient)	Thermal (-20 °F ambient)	Thermal
Thermal	Horizontal ⁽¹⁾	A	Thermal (115 °F ambient)	Thermal (115 °F ambient)	Thermal
Thermal	Horizontal ⁽¹⁾	D	Blocked vent	Blocked vent	1g down + 70 psig int. pressure + thermal (blocked vent)
Internal pressure	Horizontal ⁽¹⁾	D	< 67 psig due to blocked vent	Enveloped by 70 psig internal pressure	
Flood	Horizontal ⁽¹⁾	D ⁽¹⁾	50 ft water (≈22 psig)	Enveloped by 30 psig external pressure design	

Notes:

- (1) Canister supported at HSM rails and axial restrained by the seismic restraint devices.
(2) Levels C loads are conservatively treated as Level A loads and evaluated as such.

Table B.3.9.1-14
Summary of Calculated Stresses for Normal and Accident Condition Loads (canister in horizontal position)

Load Case	Combination of Loads	Canister Orientation	Service Level	Components	Stress Category	Stress (ksi)	Stress Limit (ksi)
S1	Dead weight (1g down)	Horizontal	A	All ⁽²⁾	P_m	0.40	17.5
					$P_m + P_b$	4.05	26.3
S2	30 psig internal pressure	Horizontal	A	All ⁽²⁾	$P_m^{(3)}$	14.97	17.5
					$P_m + P_b^{(3)}$	14.97	26.3
S3	Seismic (0.65g axial + 0.65 trans. + 1.3 vert. down)	Horizontal	A ⁽¹⁾	All ⁽²⁾	P_m	0.63	17.5
					$P_m + P_b$	6.08	26.3
S4	Thermal (-20 °F amb.)	Horizontal	A	All ⁽²⁾	Q	20.91	52.5
S5	Thermal (115 °F amb.)	Horizontal	A	All ⁽²⁾	Q	18.95	52.5
S6	Thermal (blocked vent)	Horizontal	D	All ⁽⁴⁾	Q	18.48	63.0
S7	Accident 70 psig internal pressure	Horizontal	D	All ⁽²⁾	$P_m^{(3)}$	34.56	42.0
					$P_m + P_b^{(3)}$	34.56	63.0
S8	Accident flood (enveloped by 30 psig ext. pressure)	Horizontal	D	All ⁽²⁾	$P_m^{(3)}$	11.67	42.0
					$P_m + P_b^{(3)}$	11.67	63.0
SC1	S2 + S3 + S4	Horizontal	A ⁽¹⁾	All ⁽²⁾	P_m	15.56	17.5
					$P_m + P_b$	21.05	26.3
					$P_m + P_b + Q$	41.96	52.5
SC2	S2 + S3 + S5	Horizontal	A ⁽¹⁾	All ⁽²⁾	P_m	15.60	17.5
					$P_m + P_b$	21.05	26.3
					$P_m + P_b + Q$	40.0	52.5
SC3	S1 + S7 + S6	Horizontal	D	All ⁽⁴⁾	P_m	34.96	42.0
					$P_m + P_b$	38.61	63.0
					$P_m + P_b + Q$	57.09	63.0
SC4	S1 + S8	Horizontal	D	All ⁽²⁾	P_m	12.07	42.0
					$P_m + P_b$	15.72	63.0

Notes:

- (1) Seismic loads are conservatively treated as Level A loads.
- (3) Conservatively the stress limits at 500 °F are used.
- (3) Conservatively the maximum stress intensity was used for both P_m and $P_m + P_b$ stresses for all analyses.
- (4) ASME code requires only primary stresses be evaluated under accident conditions, conservatively secondary stresses were evaluated and compared against the $P_m + P_b$ stress limits. The peak stresses occur at the top and bottom of the canister where the maximum temperature is lower than 500 °F. The stress limits at 500 °F are used.

Table B.3.9.1-15
Summary of Calculated Stresses at the End Closure Welds for Normal and Accident
Condition Storage Loads

Load Case	Combination of Loads	Canister Orientation	Service Level	Stress Category	Stress (ksi)	Stress Limit ⁽²⁾ (ksi)
S1	Dead weight (1g down)	Horizontal	A	P_m	0.40	16
				$P_m + P_b$	4.05	24
S2	30 psig internal pressure	Horizontal	A	$P_m^{(3)}$	11.75	16
				$P_m + P_b^{(3)}$	11.75	24
S3	Seismic (0.65 g axial + 0.65 trans. + 1.3 vert. down)	Horizontal	A ⁽¹⁾	P_m	0.63	16
				$P_m + P_b$	6.08	24
S4	Thermal (-20 °F amb.)	Horizontal	A	Q	3.67	48
S5	Thermal (115 °F amb.)	Horizontal	A	Q	3.62	48
S6	Thermal (blocked vent)	Horizontal	D	Q ⁽⁴⁾	8.19	52.96
S7	Accident 70 psig internal pressure	Horizontal	D	$P_m^{(3)}$	27.38	37.04
				$P_m + P_b^{(3)}$	27.38	52.96
S8	Accident flood (enveloped by 30 psig ext. pressure)	Horizontal	D	$P_m^{(3)}$	2.94	37.04
				$P_m + P_b^{(3)}$	2.94	52.96
SC1	S2 + S3 + S4	Horizontal	A ⁽¹⁾	P_m	12.38	16
				$P_m + P_b$	17.83	24
				$P_m + P_b + Q$	21.50	48
SC2	S2 + S3 + S5	Horizontal	A ⁽¹⁾	P_m	12.38	16
				$P_m + P_b$	17.83	24
				$P_m + P_b + Q$	21.45	48
SC3	S1 + S7 + S6	Horizontal	D	P_m	27.78	37.04
				$P_m + P_b$	31.43	52.96
				$P_m + P_b + Q^{(4)}$	39.62	52.96
SC4	S1 + S8	Horizontal	D	P_m	3.34	37.04
				$P_m + P_b$	6.99	52.96

Notes:

- (1) Seismic loads are conservatively treated as Level A loads.
- (2) Since the temperatures at the closure welds do not exceed 300 °F, the stress limits at 300 °F are used.
- (3) Conservatively, the maximum stress intensity was used for both P_m and $P_m + P_b$ stresses for all analyses.
- (4) ASME code requires only primary stresses be evaluated under accident conditions, conservatively secondary stresses were also included and compared against the $P_m + P_b$ stress limits.

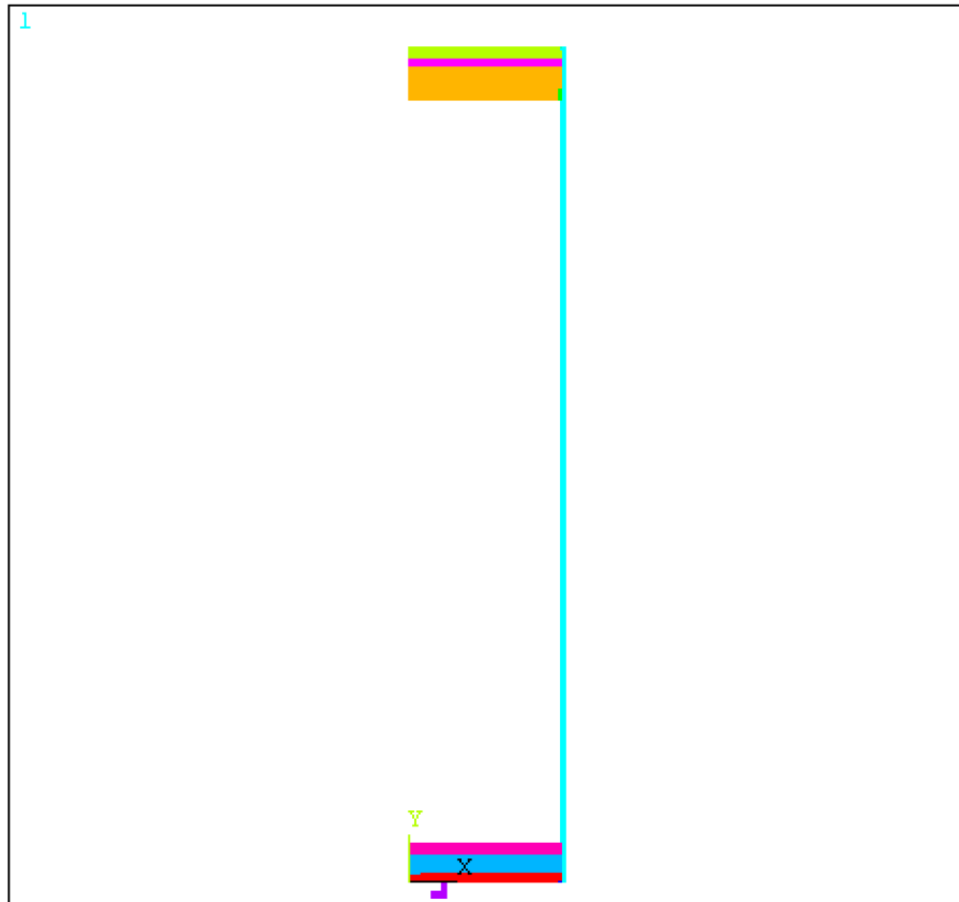


Figure B.3.9.1-1
2-D Canister Axisymmetrical Thermal and Stress Finite Element Model

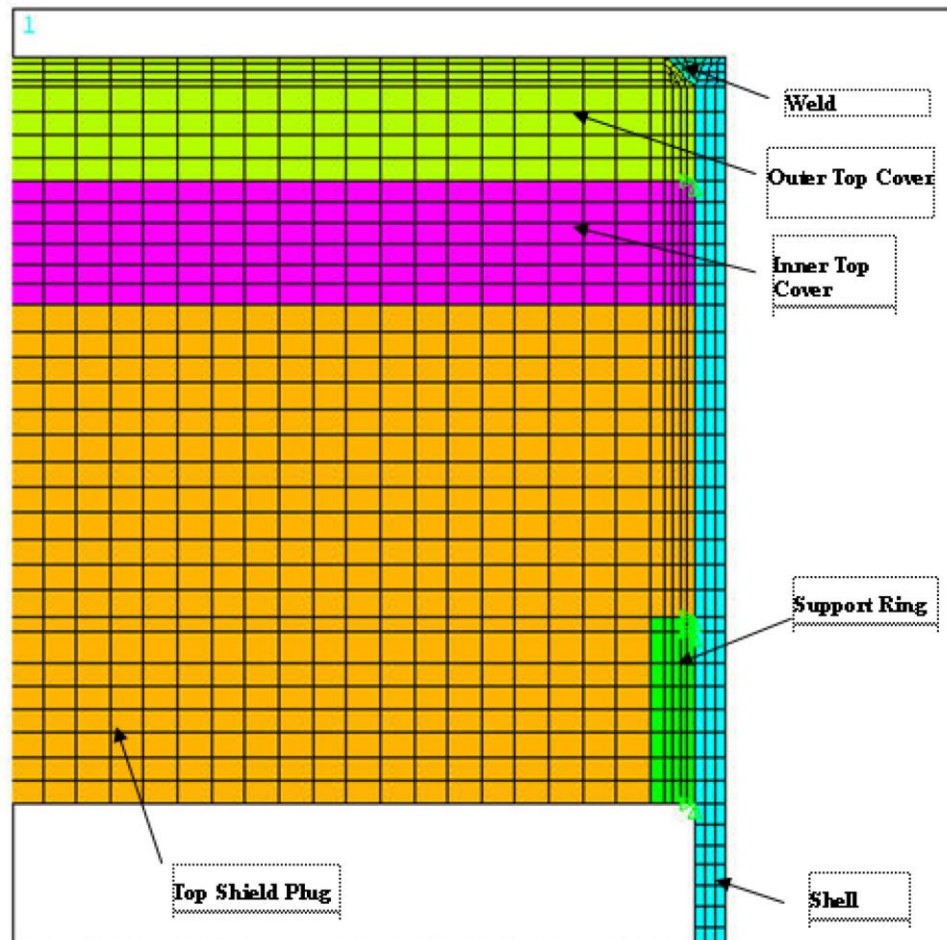


Figure B.3.9.1-2
Top End of the 2-D Axisymmetrical Canister Model

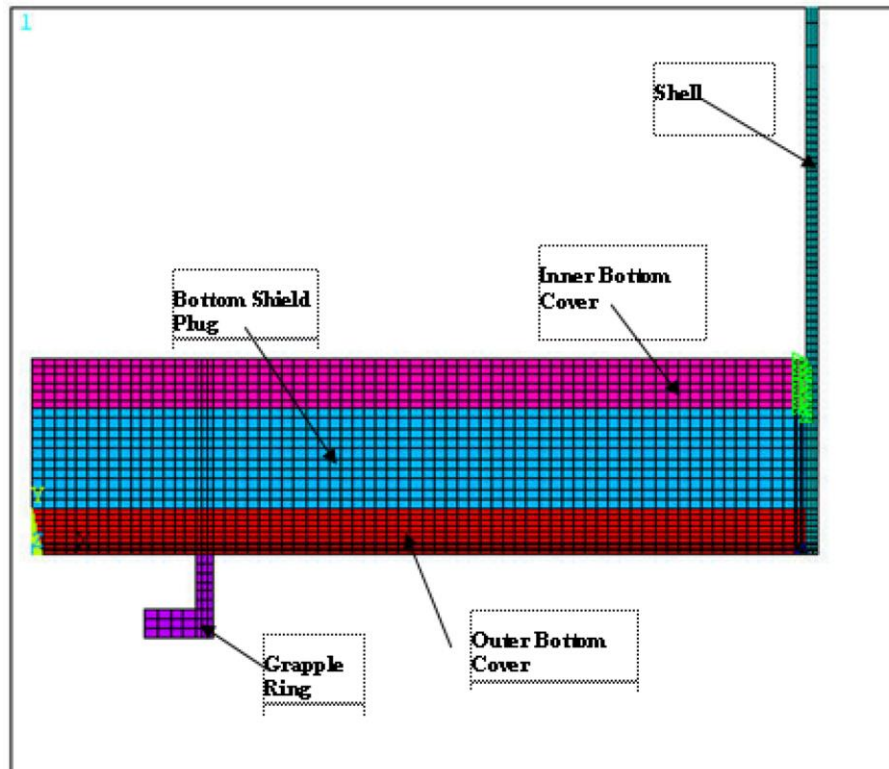


Figure B.3.9.1-3
Bottom End of the 2-D Axisymmetrical Canister Model

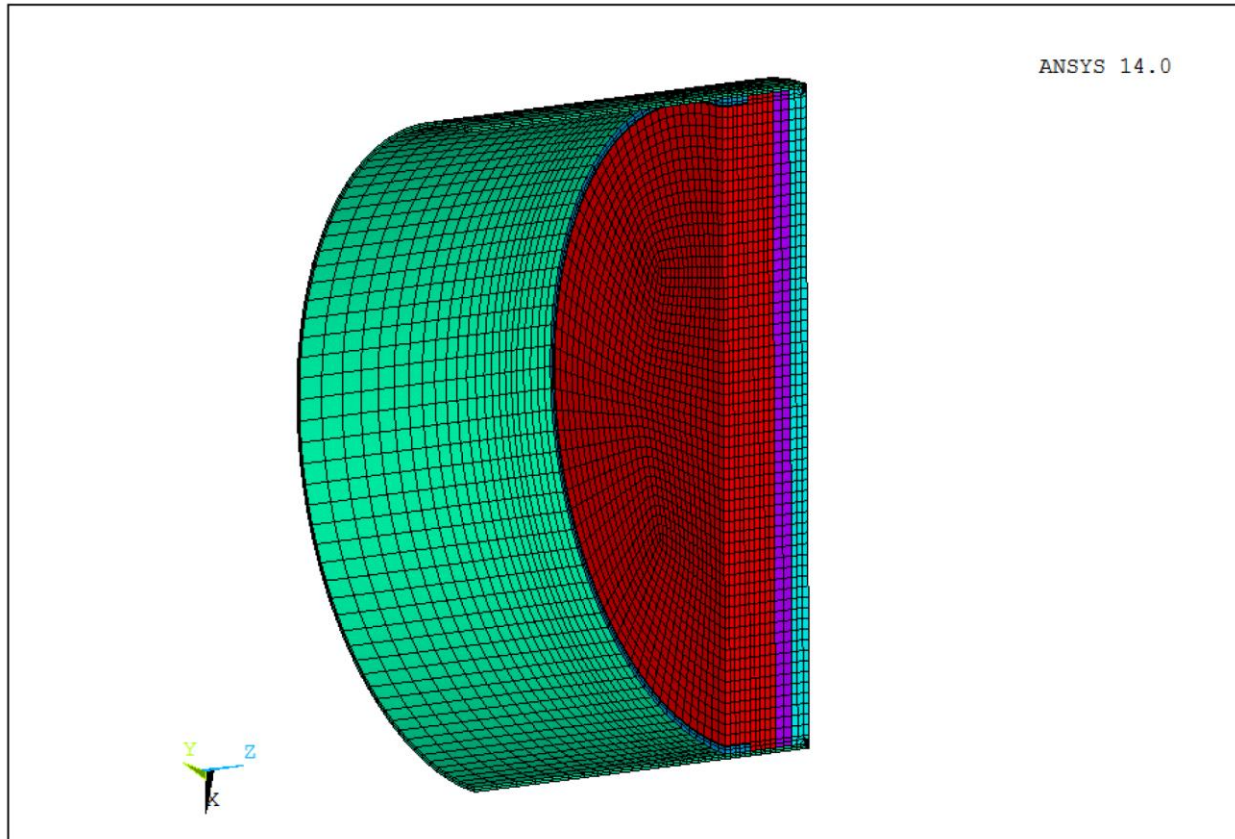


Figure B.3.9.1-4
3-D DSC Canister Top End Assembly Finite Element Model

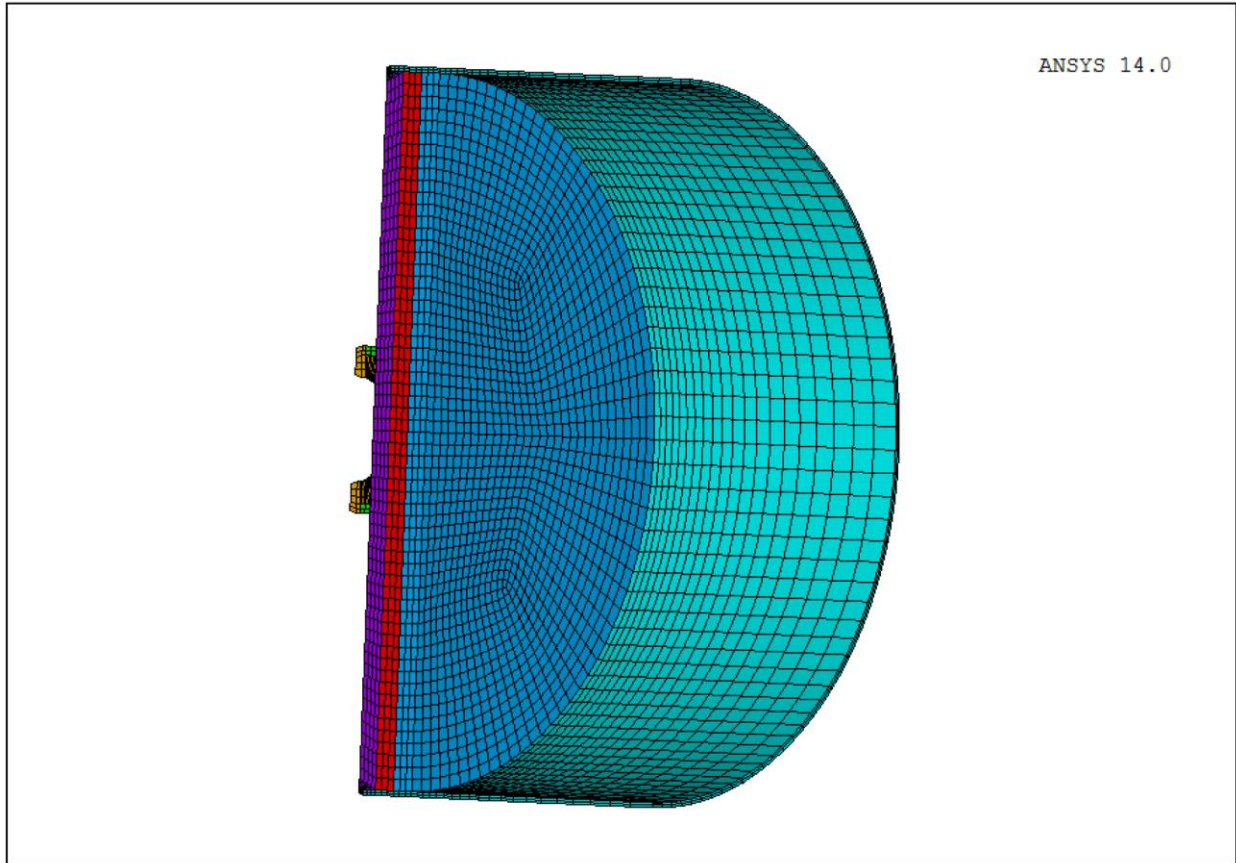


Figure B.3.9.1-5
3-D DSC Canister Bottom End Assembly Finite Element Model

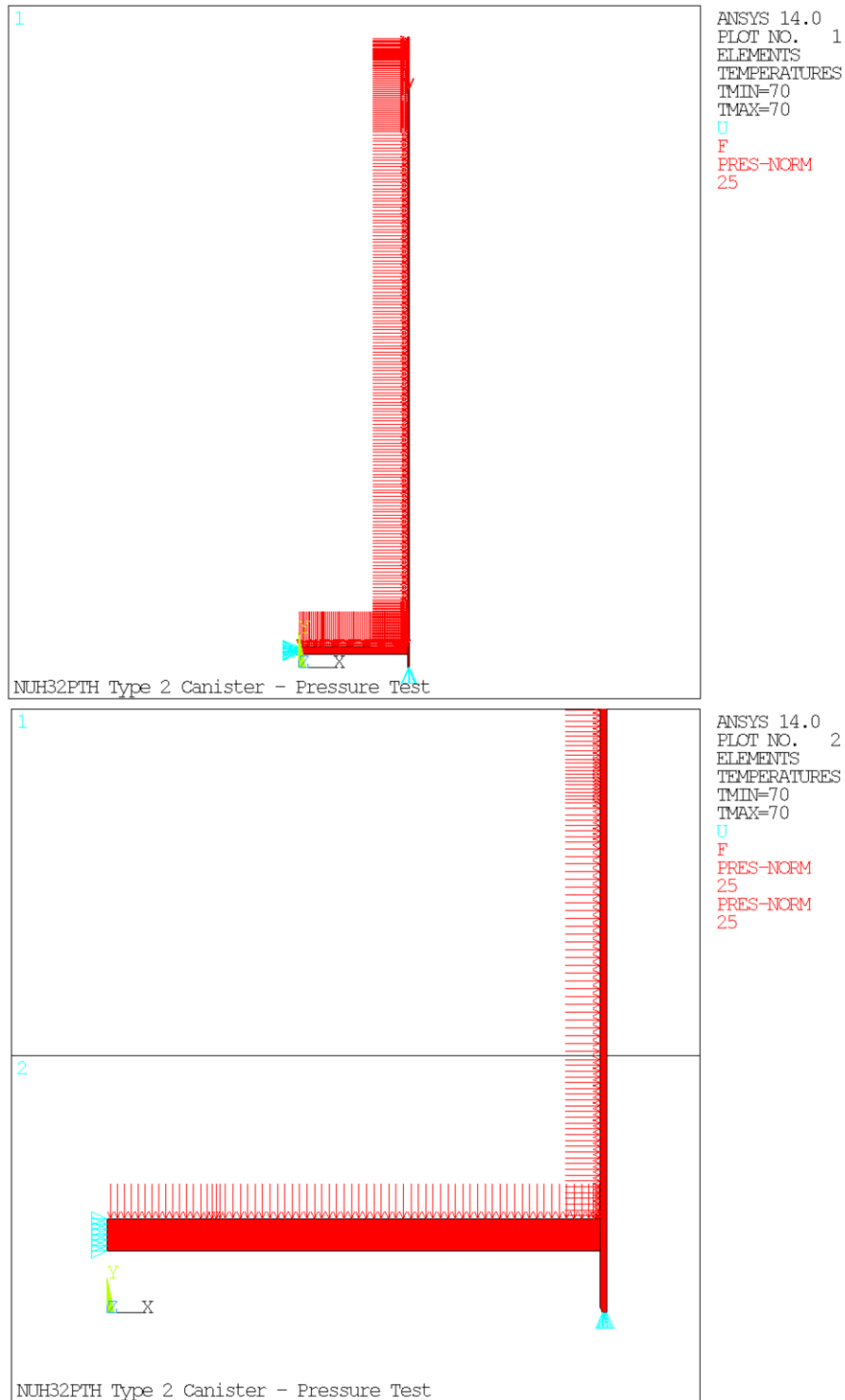


Figure B.3.9.1-6
32PTH Type 2 DSC Canister Finite Element Model used for Pressure Test Analysis

Appendix B.3.9.2
OS187H Type 2 Transfer Cask Body Structural Analysis

No change. The clearance to permit free thermal expansion of the 32PTH Type 2 DSC within the OS187H Type 2 transfer cask (TC) requires a minimum cavity length of 199.05 in. The air flow wedge thickness is reduced to 0.5 in. to achieve this cavity length. There is no structural credit taken for these wedges. There are no other changes made to the TC. The TC evaluations documented in Appendix A.3.9.2 for OS187H TYPE 1 TC are applicable without change to the OS187H TYPE 2 TC.

Appendix B.3.9.3OS187H Type 2 Transfer Cask Top Cover and Ram Cover Bolt Analyses

No change. There are no changes to the transfer cask (TC) top cover or ram bolts. The TC Top Cover and Ram Cover Bolt evaluations documented in Appendix A.3.9.3 for OS187H Type 1 are applicable without change to the OS187H Type 2 TC.

Appendix B.3.9.4OS187H Type 2 Transfer Cask Lead Slump and Inner Shell Buckling Analysis

In accordance with the NUHOMS[®] HD System Safety Evaluation Report (SER), the top and bottom end accident drops and the corner accident drop are not credible under 10 CFR Part 72 because the OS187H Type 2 transfer cask (TC) is always in the horizontal orientation. Therefore, the OS187H Type 2 TC lead slump and shell buckling analysis are not evaluated and, thus, this appendix has been deleted. These analyses may need to be evaluated under 10 CFR Part 50 should the user not be able to demonstrate that the top and bottom end and the corner drops are not credible during loading operations, or during transport operations governed under 10 CFR Part 71.

Appendix B.3.9.5
OS187H Type 2 Transfer Cask Trunnion Analysis

No change. There are no changes to the transfer cask (TC) trunnion. The TC Trunnion evaluations documented in Appendix A.3.9.5 for OS187H Type 1 are applicable without change to the OS187H Type 2 TC.

Appendix B.3.9.6
OS187H TYPE 2 Transfer Cask Shield Panel Structural Analysis

No change. There are no changes to the transfer cask (TC) shield panel. The TC Shield Panel structural evaluations documented in Appendix A.3.9.5 for the OS187H Type 1 TC are applicable without change to the OS187H Type 2 TC.

Appendix B.3.9.7
OS187H Type 2 Transfer Cask Impact Analysis

Appendix 3.9.7 describes the evaluations originally performed to substantiate the 75g accident drop decelerations used for the structural evaluation of the NUHOMS® HD System components. During the licensing of the 32PTH System and as part of the request for additional information response process, TN performed an accident drop analysis of the OS187H TC using the LS-DYNA computer code. This LS-DYNA evaluation is documented in Appendix 3.9.10 and forms the basis for the acceleration values used for evaluation of the NUHOMS® HD System components. The justification for applicability of the Appendix 3.9.7 to the 32PTH Type 2 DSC and OS187H Type 2 TC is provided in Appendix B.3.9.10. Therefore, Appendix B.3.9.7 is deleted.

Appendix B.3.9.8
Damaged Fuel Cladding Structural Evaluation

No change. The damaged fuel cladding evaluations documented in Appendix 3.9.8 are applicable without change to the 32PTH Type 2 DSC.

Appendix B.3.9.9
HSM-H Structural Analysis

The structural evaluation of the HSM-H documented in Appendix 3.9.9 remains applicable when the HSM-H is loaded with a 32PTH Type 2 DSC. The HSM-H evaluation in Appendix 3.9.9 is based on a dry shielded canister (DSC) weight of 110 kips, which bounds the weight of the loaded 32PTH Type 2 DSC of 108.03 kips. Also, as documented in Chapter 4, the HSM-H design is based on temperature distributions resulting from thermal analysis using a bounding heat load of 40.8 kW, which is higher than the 32PTH Type 2 DSC maximum heat load of 34.8 kW. As documented in Chapter A.4, the longer 32PTH Type 2 DSC is not expected to change significantly the HSM-H temperature distributions documented in Chapter 4 for the HSM-H loaded with a 32PTH DSC.

Two minor design modifications are made to the HSM-H to accommodate the 32PTH Type 2 DSC. These consist of a small (2.5 in.) increase in the length of the support rail structure, and, to accommodate the rail length increase, an alternate design of the DSC stop plate at the rear of the rail support structure is implemented (the 1-inch thick stiffened canister stop plate assembly is replaced with a single 2-inch thick plate welded to the top flange of the support rail structure). These design modifications are shown in drawings provided in Chapter B.1, Section B.1.5. These modifications do not affect the overall structural qualification of the HSM-H as documented in Appendix 3.9.9. The increased length provides additional bearing area for the support rail structure on its concrete support on the rear wall of the module and, thus, has no effect on the structural qualification of the rail support structure. The alternate DSC stop plate is evaluated using the same loads and allowables as the original stop plate design and is shown to meet the same stress allowable criteria. The maximum bending and shear stresses are on the order of 13.0 ksi and 2.5 ksi, respectively, versus allowable stresses of 18.9 ksi and 12.5 ksi, respectively. The weld between the stop plate and the top flange of the rail is conservatively specified as a full penetration weld.

Therefore, the HSM-H as evaluated in Appendix 3.9.9 with the minor design modifications described above is qualified to store a 32PTH Type 2 DSC.

Appendix B.3.9.10
OS187H Type 2 Transfer Cask Dynamic Impact Analysis

No change. There are no changes to the transfer cask (TC) top design except change in the cavity length. The Transfer Cask Dynamic Impact assessment documented in Appendix A.3.9.10 for the OS187H Type 1 TC is applicable without change to the OS187H Type 2 TC.

APPENDIX B.3.9.11
NUHOMS® 32PTH TYPE 2 DSC DYNAMIC AMPLIFICATION FACTOR ANALYSIS

TABLE OF CONTENTS

B.3.9.11 NUHOMS® 32PTH TYPE 2 DSC DYNAMIC AMPLIFICATION FACTOR ANALYSIS	B.3.9.11-1
B.3.9.11.1 Introduction.....	B.3.9.11-1
B.3.9.11.2 Side Drop Modal Analysis.....	B.3.9.11-1
B.3.9.11.3 Dynamic Load Factor Calculations.....	B.3.9.11-2
B.3.9.11.4 Summary of g-Loads for 32PTH Type 2 DSC Impact Analyses	B.3.9.11-2
B.3.9.11.5 References	B.3.9.11-3

B.3.9.11 NUHOMS® 32PTH Type 2 DSC Dynamic Amplification Factor Analysis

B.3.9.11.1 Introduction

This appendix computes the dynamic amplification factor (DAF) to be applied to the response accelerations obtained from the drop accident dynamic analysis of the OS187H Type 2 transfer cask (TC) when applying those accelerations as input to an equivalent static analysis of the 32PTH Type 2 DSC of the same postulated drop accident event.

The DAF is computed for the loaded 32PTH Type 2 DSC in the horizontal orientation. Vertical and corner drop accidents are not credible events since the TC is always in the horizontal configuration.

B.3.9.11.2 Side Drop Modal Analysis

A. Canister Shell

The fundamental natural frequency of the 32PTH Type 2 DSC shell corresponding to an ovaling (radial-axial) mode is determined assuming the cylindrical shell is simply supported without axial constraint. The natural frequency of the cylindrical shell ovaling mode is given by the following [1, p. 305, Table 12-2, Frame 5]:

$$f_{ij} = \frac{\lambda_{ij}}{2\pi R} \left(\frac{E}{\mu(1-\nu^2)} \right)^{1/2}$$

$$\lambda_{ij} = \frac{\left\{ (1-\nu^2)(j\pi R/L)^4 + (h^2/12R^2)[i^2 + (j\pi R/L)^2]^4 \right\}^{1/2}}{(j\pi R/L)^2 + i^2}$$

Where L is taken to be the length between the top and bottom shield plugs, which is roughly 181.38 in., $E = 25.8 \times 10^6$ psi (for SA-240 Type 304 stainless steel at 500 °F [2]), R is the average shell radius, 34.625 in., ν is Poisson's ratio, which is 0.305 for stainless steel [3, page 5-6], $\mu = 0.29/386.4 = 0.000751$ lbm. in⁻³, and thickness $h = 0.5$ in.

For the fundamental mode, $i = 2$ and $j = 1$.

$$\lambda_{ij} = \frac{\left\{ (1-.305^2)(\pi \times 34.625 / 171.63)^4 + (0.5^2 / 12 \times 34.625^2)[2^2 + (\pi 34.625 / 171.63)^2]^4 \right\}^{1/2}}{(\pi 34.625 / 181.38)^2 + 2^2}$$

$$= 0.081$$

$$f_{21} = \frac{0.081}{2\pi \times 34.625} \left(\frac{25.8 \times 10^6}{0.000751(1-0.305^2)} \right)^{1/2} = 72.46 \text{ Hz}$$

B. Basket with Fuel Assemblies

The basket for the 32PTH Type 2 DSC is identical to the 32PTH DSC, except that the length of the basket is 15 in. longer in the 32PTH Type 2 DSC with one additional full height layer of neutron poison/thermal aluminum cross bars and the fuel tubes at the top of the basket are also connected with crossbars and fusion welds. The length of the 32PTH DSC basket is 162 in. and the length of the 32PTH Type 2 DSC is 178.75 in. The weight of the fuel remains the same. As discussed in Appendix B.3.9.1, the axial length of the finite element model of the 32PTH basket assembly is based on a 15-inch segment, which corresponds to the pitch of the cross bars where the compartment tubes are welded together. This basket model and analysis results are also applicable to the 32PTH Type 2 basket. Thus, the DAF for the 32PTH DSC basket assembly computed in Appendix 3.9.11 are also applicable to the 32PTH Type 2 basket assembly.

B.3.9.11.3 Dynamic Load Factor Calculations

The natural frequency of the 32PTH Type 2 canister (72.46 Hz) is lower than the 32PTH canister (86.0 Hz) in the horizontal orientation. It is concluded from the results in Section 3.9.11.5 and the amplification factor results for a half sine wave [4, Figure 2.15] that frequencies lower than 86 Hz will result in a lower DAF than 1.03. Thus the DAF calculated for the 32PTH canister side drop bounds the DAF for the 32PTH Type 1 canister.

Since the natural frequencies of the NUHOMS[®] 32PTH Type 2 basket are the same as the NUHOMS[®] 32PTH basket, the DAF for the NUHOMS[®] 32PTH Type 2 will also be the same as the DAF for the NUHOMS[®] 32PTH basket, which is 1.18.

B.3.9.11.4 Summary of g-Loads for 32PTH Type 2 DSC Impact Analyses

Appendix A.3.9.10 summarizes the maximum g-loads computed for the OS187H Type 1 transfer cask (TC) during an 80-inch side drop is applicable without change to the OS187H Type 2 TC.

B.3.9.11.5 References

1. Blevins, R. D., "Formulas for Natural Frequency and Mode Shape," Krieger Publishing Company, 1995.
2. American Society of Mechanical Engineers, ASME Boiler and Pressure Vessel Code, Section II, Part D, 1998 through 2000 addenda.
3. Baumeister, T. and L. S. Marks, "Standard Handbook for Mechanical Engineers," Seventh Edition, McGraw-Hill Book Company, December 1967.
4. Nelson, T. A. and R. C. Chun, "Methods for Impact Analysis of Shipping Containers," NUREG/CR-3966, UCID-20639, Lawrence Livermore National Lab (LLNL), CA, 1987.

APPENDIX B.4 THERMAL EVALUATION

TABLE OF CONTENTS

B.4	THERMAL EVALUATION.....	B.4-1
B.4.1	Discussion.....	B.4-1
B.4.1.1	Air Flow Evaluation for 32PTH Type 2 DSC in HSM-H	B.4-1
B.4.1.2	Thermal Evaluation of 32PTH Type 2 DSC in HSM-H.....	B.4-1
B.4.1.3	Thermal Evaluation of 32PTH Type 2 DSC in OS187H Type 2 TC	B.4-2
B.4.1.4	Maximum 32PTH Type 2 DSC Internal Pressure for Storage and Transfer Conditions	B.4-2

LIST OF TABLES

Table B.4-1	Airflow Calculation Results for HSM-H Loaded with 32PTH Type 2 DSC.....	B.4-3
Table B.4-2	Applied Decay Heat Load and Heat Generation Rate within 32PTH DSC and 32PTH Type 2 DSC in HSM-H	B.4-4

B.4 THERMAL EVALUATION

B.4.1 Discussion

The NUHOMS[®] 32PTH Type 2 DSC is designed to passively reject decay heat during storage and transfer for normal, off-normal, and accident conditions while maintaining temperatures and dry shielded canister (DSC) internal pressures within specified limits.

In general, the thermal evaluations and results documented in Chapter 4 for the 32PTH DSC inside the HSM-H and OS187H TC are bounding for the 32PTH Type 2 DSC inside the HSM-H and the OS187H Type 2 TC.

As shown in Table B.1-1, the main differences between the 32PTH DSC and the 32PTH Type 2 DSC consist of a longer overall DSC length and a corresponding longer internal cavity length to accommodate an increased basket length. The effect of these differences is addressed in this chapter and shows a negligible effect on the overall thermal performance of the 32PTH Type 2 DSC compared to the 32PTH DSC.

The longer length of the 32PTH Type 2 DSC affects the HSM-H air flow evaluation, and the longer cavity length affects the decay heat flux and heat generation rate used for thermal evaluation of the 32PTH Type 2 DSC.

B.4.1.1 Air Flow Evaluation for 32PTH Type 2 DSC in HSM-H

The mass flow rates, exit and average air temperatures, and total loss coefficients for the 32PTH Type 2 DSC in the HSM-H are calculated for the bounding off-normal conditions using the same methodology used for the 32PTH DSC described in Chapter 4. Table B.4-1 shows the results of the air flow calculations for 32PTH Type 2 DSC in comparison to those for the 32PTH DSC.

As shown in Table B.4-1, the differences in the air flow calculation results for HSM-H loaded with 32PTH Type 2 DSC or 32PTH DSC are insignificant. The exit air temperatures for 32PTH Type 2 DSC are bounded by those of the 32PTH DSC due to the longer DSC length, which results in a lower decay heat flux at the DSC surface and a larger heat transfer surface. The reduced air temperature difference from the exit to the inlet of the HSM-H results in increasing air mass flow rate through the HSM-H cavity. Thus, the air flow calculation results used for the thermal evaluation of the 32PTH DSC in the HSM-H can be conservatively used for thermal evaluation of the 32PTH Type 2 DSC in the HSM-H.

B.4.1.2 Thermal Evaluation of 32PTH Type 2 DSC in HSM-H

The main design differences between the 32PTH DSC and the 32PTH Type 2 DSC listed in Table B.1-1 only affect applied decay heat load used for normal and off-normal conditions and heat generation rate within the DSC used for blocked vent accident conditions. Table B.4-2 summarizes the applied decay heat load and heat generation rate for 32PTH DSC and 32PTH Type 2 DSC in the HSM-H.

As shown in Table B.4-2, both the decay heat flux and the heat generation rate for the 32PTH Type 2 DSC are bounded by those used for 32PTH DSC in HSM-H. The 32PTH Type 2 DSC is longer, which provides larger heat transfer surface for DSC outer shell than 32PTH DSC. The added length of the 32PTH Type 2 DSC basket increases the heat rejection capacity of the basket. Therefore, the temperatures of 32PTH Type 2 DSC in HSM-H for storage conditions are bounded by those calculated for 32PTH DSC in Chapter 4.

Due to the longer length of the 32PTH Type 2 DSC, the HSM-H is exposed to a lower heat flux/heat generation rate than the 32PTH DSC. Thus, the temperature distribution in the HSM-H concrete structure and steel support structure will correspondingly decrease with the lower heat flux/heat generation rate. Therefore, the thermal analysis results of the 32PTH DSC in HSM-H as calculated in Chapter 4 (see Table 4-2, Table 4-4 and Table 4-6) are bounding.

B.4.1.3 Thermal Evaluation of 32PTH Type 2 DSC in OS187H Type 2 TC

To accommodate the longer length of the 32PTH Type 2 DSC in the OS187H Type 2 TC, the air flow wedge in the TC is reduced from 1.0 in. to 0.5 in. to increase TC cavity length. The wedges support forced air cooling option, which is not used for the OS187H Type 2 TC. However, the overall TC length does not change. So, this change has no impact on TC thermal performance.

Since the 32PTH Type 2 DSC cavity and OS187H Type 2 TC cavity are longer than that of 32PTH DSC and OS187H TC, the total decay heat load (34.8 kW) would be distributed over a larger radial inner surface of the DSC cavity than the one considered in the Chapter 4 thermal analysis for transfer conditions. This means the applied heat fluxes and heat generation rates considered in Chapter 4 bound those for the 32PTH Type 2 DSC and OS187H Type 2 TC. Furthermore, the longer DSC/TC length provide large heat transfer surface for heat rejection from the DSC to the ambient. The maximum DSC/TC component temperatures decrease with a lower heat flux/heat generation rate and a larger DSC/TC heat transfer surface and, therefore, the thermal analysis results of the 32PTH DSC in OS187H TC (see Table 4-1, Table 4-3 and Table 4-5) bound those for the 32PTH Type 2 DSC and OS187H Type 2 TC.

B.4.1.4 Maximum 32PTH Type 2 DSC Internal Pressure for Storage and Transfer Conditions

The 32PTH Type 2 DSC has a longer cavity length in comparison to 32PTH DSC, which provides an additional 10.3% of cavity volume. The overall 32PTH Type 2 DSC cavity gas volume with the increased basket length is still higher than that of 32PTH DSC. Furthermore, the authorized fuel assembly types and decay heat loads are the same for both 32PTH DSC and 32PTH Type 2 DSC. Therefore, the volumes of fission and fill gas calculated for 32PTH DSC are unchanged for 32PTH Type 2 DSC. As discussed in Sections B.4.1.2 and B.4.1.3, the average cavity gas temperatures for 32PTH Type 2 DSC for both storage and transfer conditions are bounded by those for the 32PTH DSC. Therefore, the maximum internal pressures within the 32PTH Type 2 DSC are bounded by those for 32PTH DSC design (see Table 4-10) and the pressure design criteria are satisfied for the 32PTH Type 2 DSC.

Table B.4-1
Airflow Calculation Results for HSM-H Loaded with 32PTH Type 2 DSC

Parameter	32PTH DSC	32PTH Type 2 DSC	32PTH DSC	32PTH Type 2 DSC
Ambient temperature, T_{amb} , (°F)	-20		115*	
Exit air temperature, T_{Exit} , (°F)	46.2	46.0	191.9	191.7
Average air temperature, T_{aver} , (°F)	13.1	13.0	148.4	148.4
Total loss coefficient, ΣK , (ft ⁻⁴)	0.0988	0.0982	0.1016	0.1009
Mass flow rate, (lbm/s)	2.073	2.078	1.574	1.578

*24-hour average of 105 °F used

Table B.4-2
Applied Decay Heat Load and Heat Generation Rate
within 32PTH DSC and 32PTH Type 2 DSC in HSM-H

Parameter	32PTH DSC	32PTH Type 2 DSC
Total decay heat load, Q	118748 Btu/hr (34.8 kW)	
DSC inner diameter, D_i , (in)	68.75	
DSC cavity length, L , (in)	164.5	181.38
Decay heat flux = $Q/(\pi D_i L)$, (Btu/hr-in ²)	3.3422	3.0312
Heat generation rate = $Q/(\pi D_i^2 L/4)$, (Btu/hr-in ³)	0.1945	0.1764

APPENDIX B.5 SHIELDING EVALUATION

TABLE OF CONTENTS

B.5	SHIELDING EVALUATION.....	B.5-1
------------	----------------------------------	--------------

LIST OF TABLES

Table B.5-1	Material Composition of NS-3 Neutron Shielding Resin.....	B.5-5
Table B.5-2	32PTH Type 2 Transfer Cask Top and Bottom Dose Rate Summary During Transfer Operations	B.5-6
Table B.5-3	32PTH Type 2 DSC in HSM, Maximum and Average Dose Rates	B.5-7

LIST OF FIGURES

Figure B.5-1	Geometry Comparison for 32PTH DSC in OS187H TC and 32PTH Type 2 DSC in OS187H Type 2 TC	B.5-8
Figure B.5-2	Geometry Comparison of 32PTH DSC in HSM-H Using the Original Shield Door and 32PTH Type 2 DSC in HSM-H Using the Optional or Alternate Optional (Square or Round) Shield Door	B.5-9

B.5 SHIELDING EVALUATION

The NUHOMS[®] 32PTH Type 2 DSC and the OS187H Type 2 transfer cask (TC) are designed to be comparable to the NUHOMS[®] 32PTH DSC and the OS187H TC from a shielding standpoint for all conditions of loading and transfer. The shielding evaluation documented in Chapter 5 for the 32PTH DSC and OS187H TC is applicable but not bounding for the 32PTH Type 2 DSC and OS187H Type 2 TC for loading and transfer conditions. Additional analysis is evaluated herein for the 32PTH Type 2 DSC and OS187H Type 2 TC for loading and transfer conditions.

The NUHOMS[®] 32PTH Type 2 DSC and the HSM-H using the 32PTH Type 2 HSM-H optional or alternate optional (square or round) door are designed to be comparable to the NUHOMS[®] 32PTH DSC and the HSM-H using the 32PTH and 32PTH Type 1 HSM-H original door from a shielding standpoint for all conditions of storage. In general, the shielding evaluation documented in Chapter 5 for the 32PTH DSC and the HSM-H using the 32PTH and 32PTH Type 1 HSM-H original door is applicable and bounding for the 32PTH optional or alternate optional (square or round) DSC and the HSM-H using the 32PTH Type 2 HSM-H door for storage conditions.

DSC, TC, and HSM Physics Parameters

The effect on shielding due to the changes in the geometry and material design of the 32PTH Type 2 DSC, the OS187H Type 2 TC, and the HSM-H using the 32PTH Type 2 HSM-H optional or alternate optional (square or round) door with 3 inch inner steel plate is evaluated herein. The 32PTH Type 2 DSC and OS187H Type 2 TC are designed to be longer than the 32PTH DSC and OS187H TC with thickness reductions incorporated into the top shield plug and bottom lid of 32PTH Type 2 DSC. The 32PTH Type 2 HSM-H optional or alternate optional (square or round) door is designed to be thinner than the 32PTH and 32PTH Type 1 HSM-H original door. Since there is no change in the authorized fuel contents of the NUHOMS[®] HD System, all the source terms and fuel qualification tables determined in Chapter 5 remain unchanged.

DSC and TC Geometry and Material Design Changes

The computational models of the DSC inside the TC for loading and transfer described in Chapter 5 are impacted by the reduction in thickness of the DSC top shield plug and bottom lid. Therefore, the shielding evaluations for the 32PTH DSC inside the OS187H TC documented in Section 5.4.8.2 are reevaluated for the 32PTH Type 2 DSC inside the OS187H Type 2 TC. The differences between the 32PTH and 32PTH Type 2 DSCs, and the OS187H and the OS187H Type 2 TCs, respectively, that are relevant to the calculation of dose rates during loading and transfer are evaluated and discussed below:

- The OS187H Type 2 TC inner liner thickness is increased from the OS187H TC 0.50 in. to 0.625 in. This change results in a small reduction in radial dose rates and is an improvement in the shielding design.

- The OS187H Type 2 TC lead shielding thickness is reduced from the OS187H TC 3.60 in. to 3.56 in. The shielding calculations documented in Chapter 5 utilize a lead shield thickness of 3.56 in. and, therefore, the results from the Chapter 5 radial dose rate calculations are applicable for the Type 2 TC.
- The Type 2 TC water (radial) neutron shield is extended to mate with the upper trunnion. This design change is an improvement over the OS187H TC and results in a reduction in the neutron dose rates below the upper trunnion as there are no pocket-to-neutron shield gaps.
- The Type 2 TC trunnions utilize a monolithic forging (solid steel) with removal of the solid neutron shield resin inside the trunnions. This is an improvement in design over the OS187H TC since it results in a significant reduction in the gamma dose rates around the trunnions. The slight increase in the neutron dose rates due to the removal of the solid neutron shield resin inside the trunnions is more than compensated by the increase in the gamma shielding due to the stainless steel. Note that the dose rates around the TC are mostly due to contribution from gamma sources.
- The solid neutron shielding material (resin) at the top and bottom of the OS187H Type 2 TC is changed from TN Proprietary Polyester Resin of the OS187H TC to NS-3. The material composition of the TN Proprietary Polyester Resin material is shown in Table 5-17. The material composition of the NS-3 material is shown in Table B.5.1. The shielding characteristics of these materials are similar and do not result in a substantial change in the dose rate magnitude and distribution at the top and bottom of the TC.

A shielding evaluation with the Monte Carlo N-Particle (MCNP) computer code (described in Chapter 5, Section 5.4) is performed to determine the effect of the change of the solid neutron shield material for the OS187H Type 2 TC and the reduction of shielding materials at both ends. The results of this evaluation are shown in Table B.5-2. A comparison of the dose rates at the top and bottom ends of the Type 2 TC with those shown in Table 5-4 and Table 5-5 for the OS187H TC indicates that the differences in dose rates vary from 1.5 times at the surface top end to about three times at the bottom end. The dose rate increase at the top end and bottom end of the OS187H Type 2 TC is due to the use of NS-3 as the solid neutron shielding material and the reduction of the shielding material.

- The 32PTH Type 2 DSC top shielding design includes a two-piece assembly, consisting of a separate top shield plug and inner top cover plate. This configuration is similar to, but 2 in. less thick than the single piece top shield plug/inner top cover plate assembly modeled in the Chapter 5 shielding calculations. During some steps in the decontamination process, the 32PTH Type 2 DSC top shielding configuration consists of the shield plug only which results in a reduction of the amount of steel at the top of the DSC (during decontamination operations) by 4 in. compared to the 32PTH DSC. During additional steps in decontamination, the 32PTH Type 2 DSC top shielding configuration consists of the shield plug and the inner top cover plate, which results in a reduction of the amount of steel at the top of the DSC by 4 in. compared to the 32PTH DSC. The shielding models for decontamination are described in Chapter 5, Section 5.3.1.2.

Due to the two-piece top shield plug and inner top cover plate assembly design, it is not necessary to decontaminate the top surface of the shield plug (as opposed to the single piece design where it is required). Therefore, top dose rates during this stage of operation do not significantly impact total occupational exposure. The radial dose results are used for these operations steps for the 32PTH Type 2 DSC and OS187H Type 2 TC.

An additional welding configuration model is introduced for the Type 2 TC, which calculates dose rates during the welding operations of the outer top cover plate. This second configuration reduces the top dose rates further by modelling the shield plug and both top cover plates during several steps in decontamination.

- The 32PTH Type 2 DSC bottom shielding design is 2.25 in. less thick than the 32PTH DSC modeled in the Chapter 5 shielding calculations. All transfer process steps that place personnel at the bottom of the 32PTH Type 2 DSC will be exposed to higher dose rates when compared to either the 32PTH DSC or 32PTH Type 1 DSC.

The modeling differences discussed for the 32PTH Type 2 DSC in the OS187H Type 2 TC are illustrated in Figure B.5-1.

DSC and HSM Geometry and Material Design Changes

The computational model of the 32PTH DSC inside the HSM-H using the original shield door documented in Section 5.4.8.1 contains significant conservatism in how the HSM-H base unit shielding concrete is modeled, especially around the lower cavity and inlet vents. It would be expected that the reduction in thickness of the 32PTH Type 2 DSC top shield plug and bottom lid, and the reduction in thickness of the HSM-H shield door would result in an increase in dose rates calculated at the HSM surfaces. However, the shielding models used for the 32PTH Type 2 DSC inside the HSM-H using the optional or alternate optional (square or round) shield door incorporate improvements to the modeling details of the HSM-H base unit, which results in noticeably lower HSM surface dose rates. With the modeling improvements incorporated into the Type 2 system analysis, the resulting dose rates including the thickness reductions in the DSC shield plug, bottom lid, and the HSM shield door, Table B.5-3, are bounded by the storage system dose rate analysis documented in Table 5-21.

The differences between the 32PTH and 32PTH Type 2 DSCs detailed in the DSC and TC section are also applicable to the DSC and HSM evaluation. The differences between the HSM-H 32PTH Type 1 with the original shield door and the HSM-H 32PTH Type 2 with the optional or alternate optional (square or round) shield door that are relevant to the calculation of dose rates during long term storage are evaluated and discussed below:

- Both shield doors for the HSM-H consist of a 3-inch thick (square or round) steel plate fastened to the front concrete wall, and both have a stepped circular reinforced concrete block at the rear of the 3-inch thick steel plate. The reinforced concrete block for both shield doors consists of a block at the front which is 6-7/8-inch thick. However, the rear block for the 32PTH Type 1 original door is 1-foot-10 ½-in. thick and rear block for the 32PTH Type 2 optional or alternate optional (square or round) door is 1-foot-6 ½ in. thick. This reduction in thickness of 4 in. of concrete will have an impact on storage system dose rates.

In summary, the shielding evaluation documented in Chapter 5 for the 32PTH DSC and OS187H TC is applicable but not bounding for the 32PTH Type 2 DSC and OS187H Type 2 TC for all conditions of loading and transfer. The occupational dose for pool-to-pad operations with the Type 2 system is estimated to be 3.6 rem comparing to 2.2 rem for the 32PTH system. Improvements such as using additional temporary shielding or performing evolutions at different locations or remotely would yield significant exposure dose improvements. The shielding evaluation documented in Chapter 5 for the 32PTH DSC and the HSM-H using the original shield door is applicable and bounding for the 32PTH Type 2 DSC and the HSM-H using the shield door for all conditions of storage.

Table B.5-1
Material Composition of NS-3 Neutron Shielding Resin

Element	Weight %
Hydrogen	4.85
Carbon	9.35
Calcium	5.61
Oxygen	57.05
Silicon	3.36
Aluminum	17.89
Iron	0.56
Trace ⁽¹⁾	1.33
Density (g/cm ³)	1.76

Note:

- (1) Trace elements were modeled as oxygen
in the shielding analysis

Table B.5-2
32PTH Type 2 Transfer Cask Top and Bottom Dose Rate Summary
During Transfer Operations

Location	Dose Rate mrem/hr	On Outside Surface		1.5 Feet from Surface		Three Feet from Surface	
		Gamma	Neutron	Gamma	Neutron	Gamma	Neutron
Top end	Average surface	13.51	16.83	9.98	9.69	7.48	6.87

Location	Dose Rate mrem/hr	On Outside Surface		1.5 Feet from Surface		Three Feet from Surface	
		Gamma	Neutron	Gamma	Neutron	Gamma	Neutron
Bottom end	Average surface	287.51	171.50	243.82	112.65	194.66	76.25

Table B.5-3
32PTH Type 2 DSC in HSM, Maximum and Average Dose Rates

Dose Rate Location	Total Maximum Dose Rates (mrem/hour)
HSM-H End (Side) Shield Wall Surface	0.93
HSM-H Door Exterior Surface (centerline)	1.42
HSM-H Front Bird Screen	318.64
Dose Rate Location	Total Average Dose Rates (mrem/hour)
HSM-H End (Side) Shield Wall Surface	0.32
HSM-H Front	10.17
HSM-H Back Shield Wall Surface	0.07

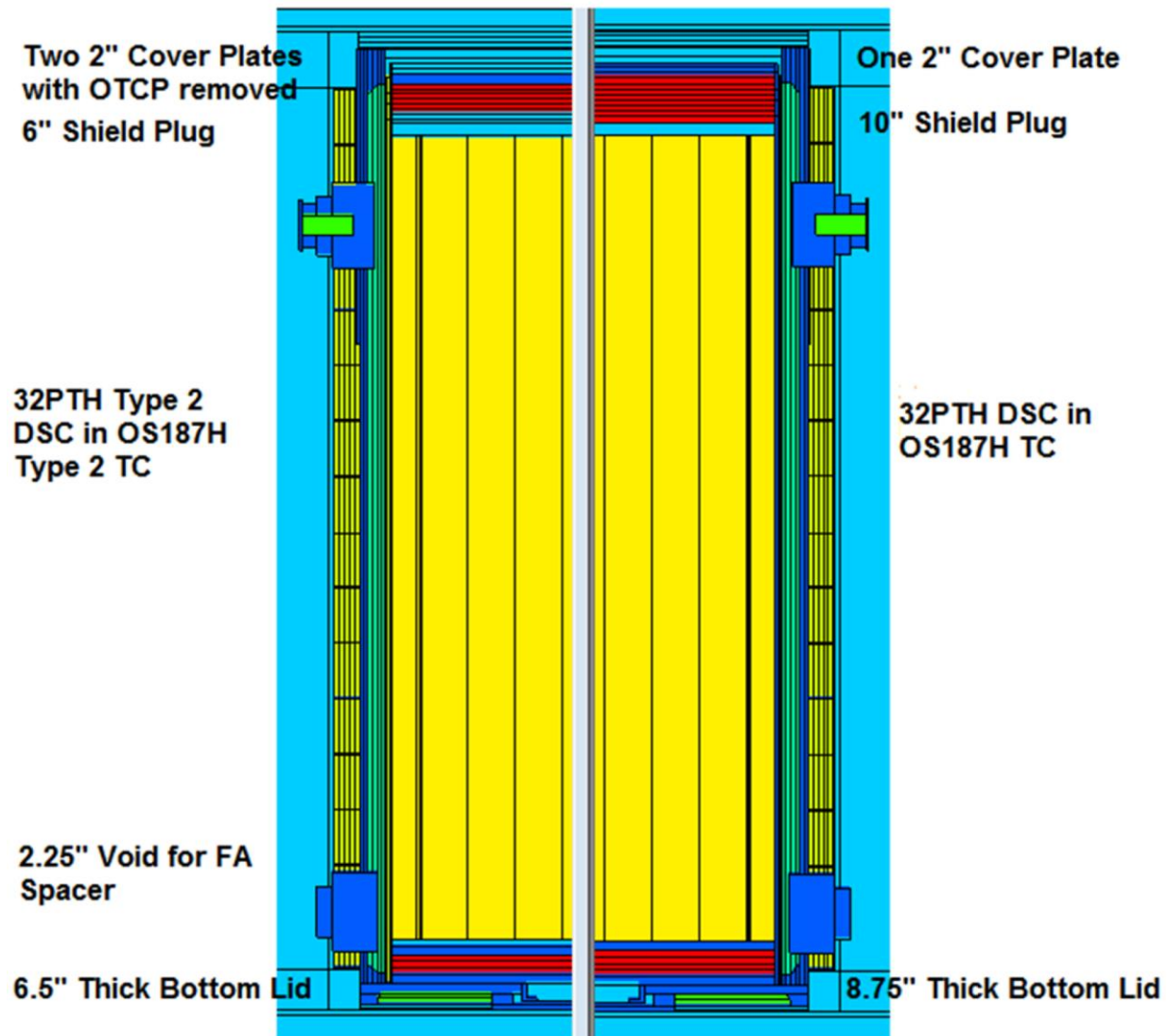


Figure B.5-1
Geometry Comparison for 32PTH DSC in OS187H TC and 32PTH Type 2 DSC in OS187H Type 2 TC

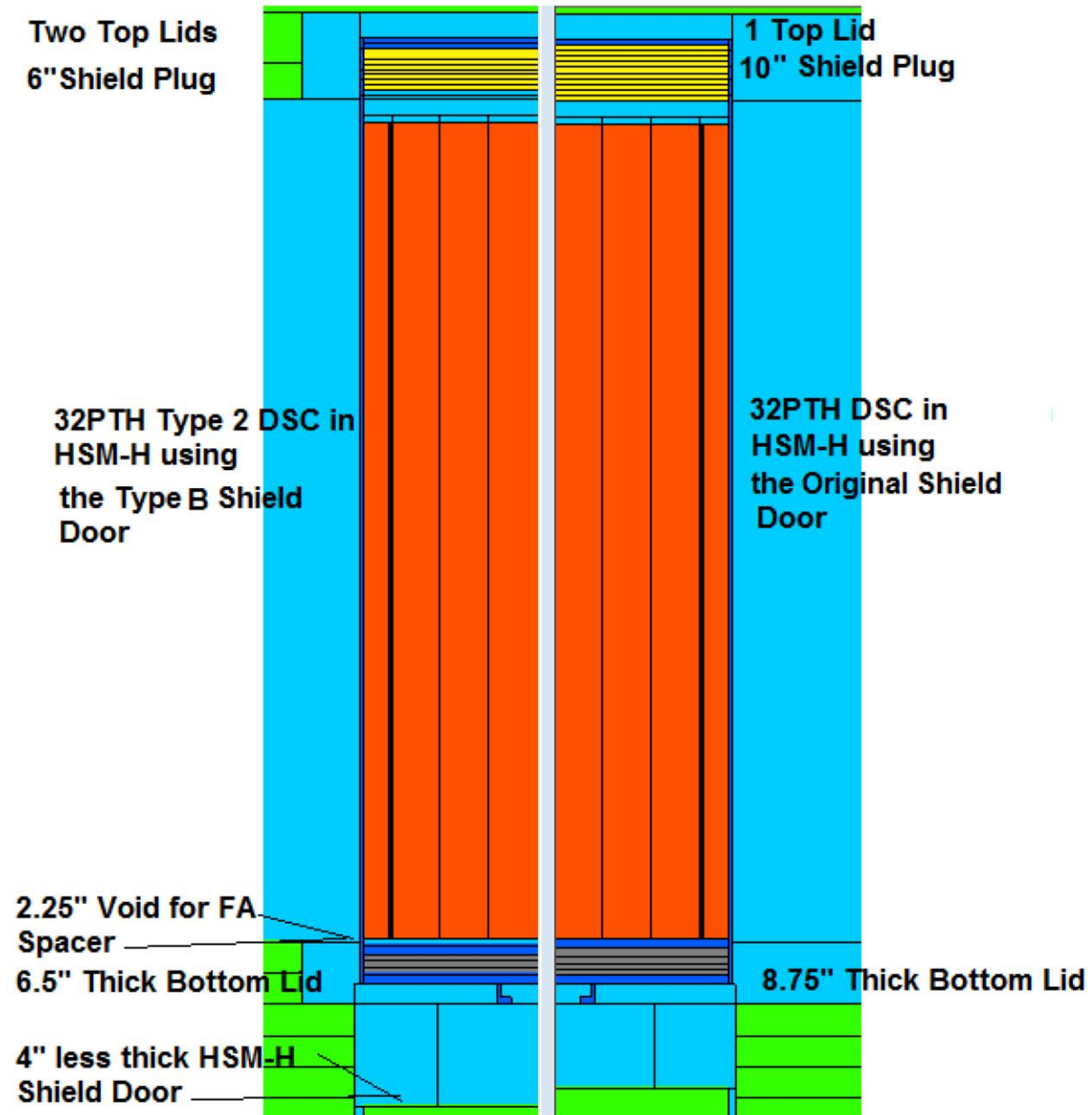


Figure B.5-2
Geometry Comparison of 32PTH DSC in HSM-H Using the Original Shield Door and 32PTH Type 2 DSC in HSM-H Using the Optional or Alternate Optional (Square or Round) Shield Door

APPENDIX B.6

CRITICALITY EVALUATION

The NUHOMS[®] 32PTH Type 2 dry shielded canister (DSC) and the OS187H Type 2 transfer cask (TC) are designed to be identical to the NUHOMS[®] 32PTH DSC and OS187H TC from a criticality standpoint for all conditions of loading, storage, and transfer. In general, the criticality analysis documented in Chapter 6 for the 32PTH DSC in the OS187H TC is applicable and bounding for the 32PTH Type 2 DSC in the OS187H Type 2 TC.

The effect on criticality due to the small changes in the geometry of the Type 2 DSC and Type 2 TC is determined by investigating the effect due to the geometry modeling employed in the criticality calculations documented in Chapter 6. These considerations are listed below:

- The height of the individual egg-crate sections in the active fuel region of the basket of the 32PTH Type 2 DSC does not change. The increase in overall height of the 32PTH Type 2 DSC is due to an increase in the number of egg-crate sections. Though the height of the top egg-crate section of the Type 2 DSC is different from that of the 32PTH DSC, the top section of the Type 2 DSC contains more neutron poison than that of the 32PTH DSC. Therefore, the criticality analysis model in Chapter 6, that considers an infinite axial array of egg-crate sections, is applicable, conservatively, to the Type 2 DSC. Note that the gap between the top of the neutron poison sheets and the bottom of the top shield plug is decreased for the 32PTH Type 2 DSC.
- The Type 2 DSC is 12.75 in. longer than the 32PTH DSC and has 17 more inches of basket and poison plates. The top layer of basket plates in the Type 2 DSC contain integral neutron poison material whereas the top layer of basket plates in the 32PTH DSC do not.

In summary, the criticality analysis documented in Chapter 6 for the 32PTH DSC in the OS187H TC is applicable and bounding for the 32PTH Type 2 DSC in the OS187H Type 2 TC for all conditions of loading, storage, and transfer.

APPENDIX B.7 CONFINEMENT

TABLE OF CONTENTS

B.7	CONFINEMENT	B.7-1
B.7.1	Confinement Boundary	B.7-1
B.7.2	Requirements for Normal Conditions of Storage	B.7-2
B.7.3	Confinement Requirements for Hypothetical Accident Conditions	B.7-3
B.7.4	Supplemental Data.....	B.7-4
	B.7.4.1 Confinement Monitoring Capability.....	B.7-4
B.7.5	References.....	B.7-5

LIST OF FIGURES

Figure B.7-1	32PTH Type 2 DSC Confinement Boundaries and Welds for Three- Part Top End Configuration.....	B.7-6
--------------	---	-------

B.7 CONFINEMENT

B.7.1 Confinement Boundary

No change. Section 7.1 applies in its entirety to the 32PTH Type 2 DSC. The 32PTH DSC confinement boundary described in Section 7.1 and shown in Figure 7-1 is applicable without change to the 32PTH Type 2 DSC design when the optional two-part top end closure assembly is used. In addition, as described in Chapter B.1, the 32PTH Type 2 DSC also features a three-part top end closure assembly, consisting of separate top shield plug, inner top cover and outer top cover plates. This three-part closure design is the same as that used in other NUHOMS[®] canister designs [1] and includes a vent and siphon block which is welded to the shell during fabrication.

The confinement boundary for the three-part closure consists of the DSC cylindrical shell, the inner top cover plate, the siphon and vent block, the inner bottom cover plate, and the associated welds. At the top, the inner top cover plate, the siphon and vent block, and the DSC shell are welded to each other using partial penetration welds, which are subject to multi-level penetrant testing (PT) examination. The vent and siphon block contains two ports, which are used for draining, vacuum drying, and backfilling. These ports are closed with welded cover plates, which are also subject to multi-level PT. Along the shell and at the bottom end of the DSC, the confinement boundary is the same as for the 32PTH DSC. The 32PTH Type 2 DSC top shield design is 2 in. thinner than the 32PTH DSC. The Type 2 DSC bottom lid is also 2.25 in. thinner than that of the 32PTH DSC.

The confinement boundary for the three-part top end closure configuration is shown in Figure B.7-1.

B.7.2 Requirements for Normal Conditions of Storage

No change.

B.7.3 Confinement Requirements for Hypothetical Accident Conditions

No change.

B.7.4 Supplemental Data

B.7.4.1 Confinement Monitoring Capability

No change.

B.7.5 References

1. Updated Final Safety Analysis Report, “Standardized NUHOMS[®] Horizontal Modular Storage System for Irradiated Nuclear Fuel,” Revision 14, August 2014, U.S. Nuclear Regulatory Commission, Docket No. 72-1004.

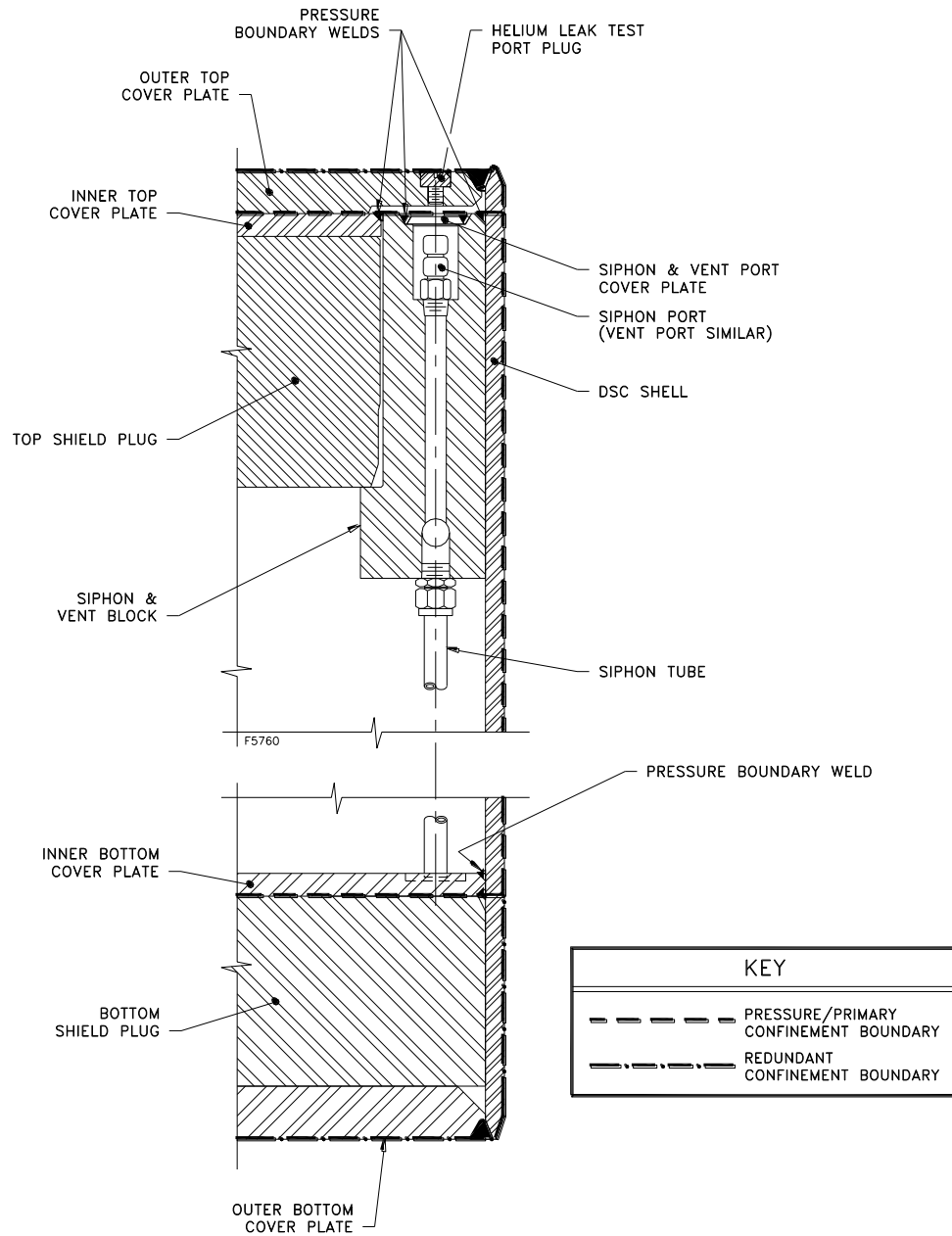


Figure B.7-1
32PTH Type 2 DSC Confinement Boundaries and Welds for Three-Part Top End Configuration

APPENDIX B.8 OPERATION PROCEDURES

TABLE OF CONTENTS

B.8	OPERATION PROCEDURES.....	B.8-1
B.8.1	Procedures for Loading the DSC and Transfer to the HSM-H.....	B.8-2
	B.8.1.1 Narrative Description.....	B.8-2
B.8.2	Procedures for Unloading the DSC	B.8-10
	B.8.2.1 DSC Retrieval from the HSM-H.....	B.8-10
	B.8.2.2 Removal of Fuel from the DSC	B.8-10
B.8.3	Supplemental Information	B.8-13
B.8.4	References	B.8-14

B.8 OPERATION PROCEDURES

Chapter 8 applies in its entirety and without change to the 32PTH Type 2 DSC when the optional two-part top end closure assembly (which is similar to the 32PTH DSC) is used. In addition, as described in Chapter B.1, the 32PTH Type 2 DSC also features a three-part top end closure assembly, consisting of separate top shield plug, inner top cover, and outer top covers. The modifications to the operating procedures described in this chapter apply to the three-part closure design and are based on the similar three-part closure used in other NUHOMS[®] canister designs [3].

B.8.1 Procedures for Loading the DSC and Transfer to the HSM-H

B.8.1.1 Narrative Description

The following steps describe the recommended modifications to the generic operating procedures described in Sections 8.1 and 8.2, and are applicable when the standard three-part top end closure assembly is implemented in the 32PTH Type 2 DSC. For purposes of completeness of presentation, the entire sequence of operational steps is presented whenever a modification has been introduced in any particular operation. When no changes are made to a section, “No Change” is indicated and a reference is listed to the applicable section in Chapter 8.

B.8.1.1.1 Transfer Cask and DSC Preparation

1. Verify by plant records or other means that candidate fuel assemblies meet the physical, thermal and radiological criteria specified in the Technical Specifications.
2. Clean or decontaminate the transfer cask as necessary to meet licensee pool and ALARA requirements, and to minimize transfer of contamination from the cask cavity to the DSC exterior.
3. Examine the transfer cask cavity for any physical damage.
4. Verify specified lubrication of the transfer cask rails.
5. Examine the DSC for any physical damage and for cleanliness. Verify that bottom fuel spacers or damaged fuel bottom end caps, if required, are present in all fuel compartments. Remove damaged fuel top end caps if they are in place. Record the DSC serial number, which is located on the grappling ring. Verify the basket type by identifying the “Z” character in the XXX- 32PTH-YYY-Z-1 serial number.
6. Lift the DSC into the cask cavity and rotate the DSC to match the transfer cask alignment marks.
7. Fill the transfer cask/DSC annulus with clean water.
8. Seal the top of the annulus, using for example an inflatable seal.
9. A tank filled with clean water, and kept above the pool surface may be connected to the top vent port of the transfer cask via a hose to provide a positive pressure in the annulus. This is an optional arrangement, which provides additional assurance that contaminated water from the fuel pool will not enter the annulus. Do not pressurize this tank, nor raise it sufficiently high to float the DSC. For the 32PTH Type 2 DSC with a 69.75-inch OD, and an empty weight of 46,000 lb, a differential pressure of 11.7 psi, equivalent to 27.1 ft of pure water, would be sufficient to lift the DSC.
10. If the DSC top covers were trial fitted, they must be removed prior to filling the DSC with water. The vent port quick connect fitting in the inner top cover may be removed to facilitate hydrogen monitoring later. The drain port fitting may be either left in place or removed – water may be pumped from the DSC either with or without the fitting.

11. The licensee shall develop procedures to verify that the boron content of the water added to the DSC conforms to the Technical Specifications. Fill the DSC with water from the fuel pool or an equivalent source meeting the minimum boron concentration required by the Technical Specifications. Optionally, this may be done at the time of immersing the cask in the pool. If the pool water is allowed flow over the transfer cask lip and into the DSC, provision must be made to protect the annulus seal from being dislodged by the water running over it.
- 12a. Optionally, secure a sheet of suitable material to the bottom of the cask to minimize the potential for ground-in contamination. This step may be done at any convenient time prior to immersion.
- 12b. Drain or fill the transfer cask liquid neutron shield, as required by licensee ALARA requirements and crane weight limits. This step may be done at any convenient time prior to immersion.
13. Prior to the cask being lifted into the fuel pool, the water level in the pool should be adjusted as necessary to accommodate the transfer cask and DSC volume. If the water placed in the DSC cavity was obtained from the fuel pool, a level adjustment may not be necessary.

B.8.1.1.2 DSC Fuel Loading

1. Verify proper engagement of the lifting yoke with the transfer cask lifting trunnions.
2. Lift the transfer cask / DSC and position them over the cask loading area of the spent fuel pool.
3. Lower the cask into the fuel pool until the bottom of the cask is at the height of the fuel pool surface. As the cask is lowered into the pool, spray the exterior surface of the cask with clean water to minimize surface adhesion of contamination.
4. Place the cask in the location of the fuel pool designated as the cask loading area.
5. Disengage the lifting yoke from the transfer cask lifting trunnions and move the yoke clear of the cask. Spray the lifting yoke with clean water if it is raised out of the fuel pool.
6. Load pre-selected spent fuel assemblies into the DSC basket compartments. The licensee shall develop procedures to verify that the boron content of the water conforms to the Technical Specifications, and that fuel identifications are verified and documented. The loading plan must be developed according to Figure 2-1 for the orientation of the fuel assemblies. Damaged fuel must be loaded only in designated compartments fitted with a damaged fuel bottom end cap.
7. After all the fuel assemblies have been placed into the DSC and their identities verified, install damaged fuel top end caps into designated compartments containing damaged fuel.
8. Lower the top shield plug into the DSC.
9. Visually verify that the inner top cover/shield plug is properly seated in the DSC. Reseat if necessary.
10. Position the lifting yoke and verify that it is properly engaged with the transfer cask trunnions.

11. Lift the transfer cask to the pool surface and spray the exposed portion of the cask with clean water.
12. Drain any water from above the inner top cover/shield plug back to the spent fuel pool. Up to 1300 gallons of water may be removed from the DSC prior to lifting the transfer cask clear of the pool surface. Up to 15 psig of helium may only be used to assist the removal of water. The DSC shall be backfilled only with helium after drainage of bulk water.
13. Lift the cask from the fuel pool, continuing to spray the cask with clean water.
14. Move the cask with loaded DSC to the area designated for DSC draining and closure operations. The set-down area should be level, or if slightly sloped, the transfer cask and DSC should be placed with the slope down toward the DSC drain/siphon tube.

B.8.1.1.3 DSC Closing, Drying, and Backfilling

1. Fill the transfer cask liquid neutron shield if it was drained for weight reduction during preceding operations.
2. Decontaminate the transfer cask exterior.
3. Disengage the rigging from the top shield plug, and remove the eyebolts. Disengage the lifting yoke from the trunnions.
4. Disconnect the annulus overpressure tank if one was used, decontaminate the exposed surfaces of the DSC shell perimeter, remove any remaining water from the top of the annulus seal, and remove the seal.
5. Open the cask cavity drain port and allow water from the annulus to drain out until the water level is approximately twelve inches below the top of the DSC shell. Take swipes around the outer surface of the DSC shell to verify conformance with Technical Specification limits.
6. Cover the transfer cask / DSC annulus to prevent debris and weld splatter from entering the annulus.
7. If water was not drained from the DSC earlier, connect a pump to the DSC drain port and remove up to 1300 gallons of water. Consistent with ISG-22 [4] guidance and Technical Specification 3.1.1, helium at 1-3 psig is used to backfill the DSC with an inert gas (helium) as water is being removed from the DSC. This lowers the water sufficiently to allow welding of the inner top cover/shield plug. Up to 15 psig of helium gas may be applied at the vent port to assist the water pump down.

CAUTION: Verify that no inadvertent draining of the TC Neutron Shield water has occurred.

CAUTION: Radiation dose rates are expected to be high at the vent and siphon port locations. Use proper ALARA practices (e.g., use of temporary shielding, appropriate positioning of personnel, etc.) to minimize personnel exposure.

- 7a. Monitor TC/DSC annulus water level to be approximately twelve inches below the top of the DSC shell and replenish as necessary until drained.

8. Install the automated welding machine onto the inner top cover and place the inner top cover with the automatic welding machine onto the DSC. Optionally, the inner top cover and the automatic welding machine can be place separately. Verify proper fit up of the inner top cover with the DSC shell.
9. Hydrogen monitoring is required prior to commencing and continuously during the welding of the inner top cover / shield plug per Technical Specification 5.6. Install hydrogen monitoring equipment that samples the atmosphere below the shield plug.
10. Verify that the hydrogen concentration does not exceed 2.4% [1]. If this limit is exceeded, stop all welding operations and purge the DSC cavity with helium to reduce hydrogen concentration safely below the 2.4% limit before resuming welding operations.
11. Complete the inner top cover/shield plug welding and perform the non-destructive examinations as required by the Technical Specifications. The weld must be made in at least two layers.
12. Remove the automated welding machine.
13. Pump remaining water from the DSC. Remove as much free standing water as possible to shorten vacuum drying time. Use of helium is required per Technical Specification 3.1.1. Up to 15 psig of helium gas may be applied at the vent port to assist the water pump down. All helium used in backfilling operations shall be at least 99.99% pure (this may be done as part of Step 15).

NOTE: Proceed cautiously when evacuating the DSC to avoid freezing consequences.

14. Connect a vacuum pump / helium backfill manifold to the vent port or to both the vent and drain ports. The quick connect fittings may be removed and replaced with stainless steel pipe nipple / vacuum hose adapters to improve vacuum conductance. Make provision to prevent icing, for example by avoiding traps (low sections) in the vacuum line. Provide appropriate measures as required to control any airborne radionuclides in the vacuum pump exhaust. Purge air from the helium backfill manifold.

Optionally, leak test the manifold and the connections to the DSC. The DSC may be pressurized to no more than 15 psig for leak testing.

CAUTION: Radiation dose rates are expected to be high at the vent and siphon port locations. Use proper ALARA practices (e.g., use of temporary shielding, appropriate positioning of personnel, etc.) to minimize personnel exposure.

CAUTION: During the vacuum drying evolution, personnel should be in the area of loading operations, or in nearby low dose areas, in order to take proper action in the event of a malfunction.

15. Connect a vacuum pump / helium backfill manifold to the vent port or to both the vent and drain ports. The quick connect fittings may be removed and replaced with stainless steel pipe nipple / vacuum hose adapters to improve vacuum conductance. Make provision to prevent icing, for example by avoiding traps (low sections) in the vacuum line. Provide appropriate measures as required to control any airborne radionuclides in the vacuum pump exhaust. Purge air from the helium backfill manifold.

Optionally, leak test the manifold and the connections to the DSC. The DSC may be pressurized to no more than 15 psig for leak testing.

CAUTION: Radiation dose rates are expected to be high at the vent and siphon port locations. Use proper ALARA practices (e.g., use of temporary shielding, appropriate positioning of personnel, etc.) to minimize personnel exposure.

CAUTION: During the vacuum drying evolution, personnel should be in the area of loading operations, or in nearby low dose areas, in order to take proper action in the event of a malfunction.

16. Evacuate the DSC to the pressure required by the Technical Specification for vacuum drying, and isolate the vacuum pump. The isolation valve should be as near to the DSC as practicable, with a pressure gauge on the DSC side of the valve. Prior to performing the vacuum hold for 30 minutes as required by the Technical Specification, the vacuum pump must be turned off; or if the pump is not turned off, provide a tee and valve (or other means) to open the line to atmosphere between the pump and the DSC isolation valve.

NOTE: The user shall ensure that the vacuum pump is isolated from the DSC cavity when demonstrating compliance with Technical Specification 3.1.1 requirements. Simply closing the valve between the DSC and the vacuum pump is not sufficient, as a faulty valve allows the vacuum pump to continue to draw a vacuum on the DSC. Turning off the pump, or opening the suction side of the pump to atmosphere are examples of ways to ensure that the pump is not continuing to draw a vacuum on the DSC.

17. If the Technical Specification is satisfied, i.e., if the pressure remains below the specified limit for the required duration with the pump isolated, continue to the next step. If not, repeat Step 16.
18. Purge air from the backfill manifold, open the isolation valve, and backfill the DSC cavity with helium to 16.5 to 18 psig and hold for 10 minutes.
19. Reduce the DSC cavity pressure to atmospheric pressure, or slightly over.
20. If the quick connect fittings were removed for vacuum drying, remove the vacuum line adapters from the ports, and re-install the quick connect fittings using suitable pipe thread sealant.

CAUTION: Radiation dose rates are expected to be high at the vent and siphon port locations. Use proper ALARA practices (e.g., use of temporary shielding, appropriate positioning of personnel, etc.) to minimize personnel exposure.

21. Evacuate the DSC through the vent port quick connect fitting to a pressure 100 mbar or less.

NOTE: The user shall ensure that the vacuum pump is isolated from the DSC cavity when demonstrating compliance with Technical Specification 3.1.1 requirements. Simply closing the valve between the DSC and the vacuum pump is not sufficient, as a faulty valve allows the vacuum pump to continue to draw a vacuum on the DSC. Turning off the pump, or opening the suction side of the pump to atmosphere are examples of ways to assure that the pump is not continuing to draw a vacuum on the DSC.

22. Backfill the DSC with helium to the pressure specified in the Technical Specifications, and disconnect the vacuum / backfill manifold from the DSC.
23. Weld the covers over the vent and drain ports, performing non-destructive examination as required by the Technical Specifications. The welds shall have at least two layers.
24. Install a temporary test head fixture (or any other alternative means). Perform a leak test of the inner top cover/shield plug to the DSC shell welds and siphon/vent cover welds in accordance with the Technical Specification limits. Verify that the personnel performing the leak test are qualified in accordance with SNT-TC-1A.
25. Place the outer top cover plate onto the DSC and verify correct rotational alignment of the cover and the DSC shell. Install the automated welding machine onto the outer top cover plate. As an option, the welding machine may be mounted onto the cover plate and then placed together on the DSC.
26. Complete the outer top cover welding and perform the non-destructive examinations as required by the Technical Specifications. The weld must be made in at least two layers.
27. Remove everything except the DSC from the transfer cask cavity: welding machine, protective covering from the transfer cask / DSC annulus, temporary shielding, etc., and drain the water from the transfer cask/DSC annulus.
28. Install the transfer cask lid and bolt it.
29. Evacuate the transfer cask cavity to below 100 mbar, and backfill the transfer cask annulus with helium in accordance with the Technical Specifications pressure tolerance and time limit.

CAUTION: Monitor the applicable time limits of the Technical specifications for transfer cask annulus helium backfill.

B.8.1.1.4 Transfer Cask Downending and Transport to ISFSI

1. The transfer trailer should be positioned so that the cask support skid is accessible to the crane with the trailer supported on its vertical jacks. If required due to space limitations, the crane may remain in a stationary position while the cask support skid and trailer translate underneath the cask as it is downended, (the trailer cannot be supported on the vertical jacks.)
2. Engage the lifting yoke and lift the transfer cask over the cask support skid onto the transfer trailer.
3. Position the cask lower trunnions onto the transfer trailer support skid pillow blocks.
4. Move the crane while simultaneously lowering the cask until the cask upper trunnions are just above the support skid upper trunnion pillow blocks. Alternatively, if the crane is to remain stationary as identified above, slowly move the trailer and support skid as the cask is lowered until the upper trunnions are just above the support skid upper trunnion pillow blocks.
5. Verify that the cask and trunnion pillow blocks are properly aligned.
6. Lower the cask onto the skid until the weight of the cask is distributed to the trunnion pillow blocks.

7. Verify the trunnions are properly seated onto the skid. Install the trunnion tower closure plates (optional).

B.8.1.1.5 DSC Transfer to the HSM-H

1. The maximum lifting height and ambient temperature requirements of the Technical Specifications must be met during transfer from the fuel building to the HSM-H.
2. Prior to loading the DSC into the HSM-H, verify that there is no debris in the HSM-H, the air inlet and outlets are not blocked, the air inlet and outlet screens are not damaged, and the rails are lubricated as specified.

CAUTION: The insides of empty modules have the potential for high dose rates due to adjacent loaded modules. Proper ALARA practices should be followed for operations inside these modules and in the areas outside these modules whenever the door from the empty HSM has been removed.

3. Tow the transfer trailer with the loaded cask to the ISFSI.
4. Position the transfer trailer to within a few feet of the HSM-H to maintain doses ALARA when the cask lid is removed.
5. Verify that the centerline of the HSM-H and cask approximately coincide. Reposition the trailer as necessary following appropriate ALARA practices.
6. Using a portable crane, unbolt and remove the cask lid.
7. Back the trailer to within a few inches of the HSM-H, set the trailer brakes and disengage the tractor. Drive the tractor clear of the trailer and extend the transfer trailer vertical jacks.
8. Remove the skid tie-down bracket fasteners and use the hydraulic skid positioning system to bring the cask into approximate vertical and horizontal alignment with the HSM-H. Using optical survey equipment and the alignment marks on the cask and the HSM-H, adjust the position of the cask until it is aligned with the HSM-H.
9. Using the skid positioning system, fully insert the cask into the HSM-H access opening docking collar.
10. Secure the cask to the front wall embedments of the HSM-H using the cask restraints.
11. Verify the alignment of the transfer cask is within specified tolerance using the optical survey equipment.
12. Remove the bottom ram access cover plate from the transfer cask. Extend the ram through the bottom cask opening into the DSC grapple ring.
13. Activate the hydraulic cylinder on the ram grapple and engage the grapple arms with the grapple ring.
14. Activate the hydraulic ram to initiate insertion of the DSC into the HSM-H. Stop the ram when the DSC reaches the support rail stops at the back of the module.
15. Disengage the ram grapple mechanism from the DDC grapple ring, and retract the hydraulic ram system from the transfer cask.

16. Remove the cask restraints from the HSM-H. Replace the bottom ram access cover plate. Optionally, a temporary cover may be used to cover the ram access opening.
17. Using the skid positioning system, disengage the cask from the HSM-H access opening.
18. Install the DSC seismic restraint.
19. Secure the skid to the trailer, retract the vertical jacks. Tow the trailer and cask a few feet to provide access for door installation.
20. Install the HSM-H door and secure it in place.
21. Replace the transfer cask lid.
22. Tow the trailer and cask from the ISFSI.

B.8.1.1.6 Monitoring Operations

1. Perform routine security surveillance in accordance with the licensee's ISFSI security plan.
2. Perform a daily visual surveillance of the HSM-H air inlets and outlets (bird screens) to verify that no debris is obstructing the HSM-H vents in accordance with Technical Specification requirements.
3. Perform a temperature measurement for each HSM-H in accordance with Technical Specification requirements.

B.8.2 Procedures for Unloading the DSC

The following section outlines the procedures for retrieving the DSC from the HSM-H and for removing the fuel assemblies from the DSC.

B.8.2.1 DSC Retrieval from the HSM-H

1. The maximum lifting height and ambient temperature requirements of the Technical Specifications must be met during transfer from the HSM-H to the fuel building.
2. Ready the transfer cask, transfer trailer, and support skid for service and tow the trailer to the HSM-H. Fill the transfer cask liquid neutron shield and remove the bottom access plate from the transfer cask.
3. Remove HSM-H door and seismic restraint. Remove the transfer cask lid. Back the trailer to within a few inches of the HSM-H.
4. Using the skid positioning system, align the transfer cask with the HSM-H and position the skid until the transfer cask is docked with the HSM-H access opening.
5. Using optical survey equipment, verify alignment of the transfer cask with respect to the HSM-H within specified tolerance. Install the transfer cask restraints.
6. Install and align the hydraulic ram with the transfer cask.
7. Extend the ram through the transfer cask into the HSM-H until it is inserted in the DSC grapple ring.
8. Activate the arms on the ram grapple mechanism to engage the grapple ring.
9. Retract the ram and pull the DSC into the transfer cask.
10. Disengage the ram grapple arms.
11. Retract the ram from the transfer cask.
12. Replace the cask ram access cover plate and remove the transfer cask restraints.
13. Using the skid positioning system, disengage the transfer cask from the HSM-H.
14. Install the transfer cask top cover plate and ready the trailer for transfer/transport.
15. Evacuate the transfer cask cavity to below 100 mbar, and backfill with helium in accordance with the Technical Specifications pressure tolerance and time limit, if using a transfer cask. If using a transportation cask, follow applicable requirements for the transportation cask.
16. Replace the door and seismic restraint on the HSM-H.

B.8.2.2 Removal of Fuel from the DSC

If it is necessary to remove fuel from the DSC, it can be removed in dry transfer facility or the initial fuel loading sequence can be reversed and the plant's spent fuel pool utilized.

Procedures for wet unloading of the DSC are presented here. Dry unloading procedures are essentially identical up to the removal of the DSC vent and drain port covers.

1. Tow the trailer with the loaded cask to the cask handling area inside the plant's fuel handling building. Drain the transfer cask liquid neutron shield as required by licensee ALARA requirements and crane weight limits.
2. Position and ready the trailer for access by the crane.
3. Engage the lifting yoke with the trunnions of the transfer cask.
4. Verify that the yoke lifting hooks are properly aligned and engaged onto the transfer cask trunnions.
5. Lift the transfer cask approximately one inch off the trunnion supports. Verify that the yoke lifting hooks are properly positioned on the trunnions.
6. Move the crane in a horizontal motion while simultaneously raising the crane hook vertically and lift the transfer cask off the trailer. Move the transfer cask to the cask decontamination area.
7. Lower the transfer cask into the cask staging area in the vertical position.
8. Unbolt the transfer cask lid and remove it.
9. Install temporary shielding to reduce personnel exposure as required. Fill the transfer cask/DSC annulus with clean water and seal the top of the annulus, using, for example, an inflatable seal.
10. Locate the drain and vent port using the indications on the outer top cover plate. Place a portable drill press on the top of the DSC. Align the drill over the drain port.
11. Cut or drill a hole through the top cover plate to expose the drain port on the inner top cover. Remove the drain port cover plate with an annular hole cutter. Repeat for the vent port.

CAUTION: Radiation dose rates are expected to be high at the vent and siphon port locations. Use proper ALARA practices (e.g., use of temporary shielding, appropriate positioning of personnel, etc.) to minimize personnel exposure.
12. Obtain a sample of the DSC atmosphere. Confirm acceptable hydrogen concentration and check for presence of fission gas indicative of degraded fuel cladding.
13. If degraded fuel is suspected, additional measures appropriate for the specific conditions are to be planned, reviewed, and implemented to minimize exposures to workers and radiological releases to the environment.
14. Verify that the boron content of the fill water conforms to the Technical Specifications. Fill the DSC with water from the fuel pool or equivalent source through the drain port with the vent port open. The vented cavity gas may include steam, water, and radioactive material, and should be routed accordingly. Monitor the vent pressure and regulate the water fill rate to ensure that the pressure does not exceed 15 psig.
15. Provide for continuous hydrogen monitoring of the DSC cavity atmosphere during all subsequent cutting operations to ensure that hydrogen concentration does not exceed 2.4%. Purge with helium as necessary to maintain the hydrogen concentration below this limit.
16. Provide suitable protection for the transfer cask during cutting operations.

17. Using a suitable method, such as mechanical cutting, remove the weld of the outer top cover plate to the DSC shell.
18. Remove the outer top cover plate.
19. Remove the weld of the inner top cover/shield plug to the shell in the same manner as the outer cover plate. Do not remove the inner top cover/shield plug at this time unless the removal is being done remotely in a dry transfer system.
20. Remove any remaining excess material on the inside shell surface by grinding.
21. Clean the transfer cask surface of dirt and any debris that may be on the transfer cask surface as a result of the weld removal operation.
22. Engage the yoke onto the trunnions, install eyebolts or other lifting attachment(s) into the inner top cover/shield plug, and connect the rigging cables to the eyebolts/lifting attachment(s).
23. Verify that the lifting hooks of the yoke are properly positioned on the trunnions.
24. Lift the transfer cask just far enough to allow the weight of the transfer cask to be distributed onto the yoke lifting hooks. Verify that the lifting hooks are properly positioned on the trunnions.
25. Optionally, install suitable protective material onto the bottom of the transfer cask to minimize cask contamination. Move the transfer cask to the spent fuel pool.
26. Prior to lowering the transfer cask into the pool, adjust the pool water level, if necessary, to accommodate the volume of water that will be displaced by the transfer cask during the operation.
27. Position the transfer cask over the cask loading area in the spent fuel pool.
28. Lower the transfer cask into the pool. As the transfer cask is being lowered, the exterior surface of the transfer cask should be sprayed with clean water.
29. Disengage the lifting yoke from the transfer cask and lift the inner top cover/shield plug from the DSC.
30. Remove any failed fuel top end caps.
31. Remove the fuel from the DSC.

B.8.3 Supplemental Information

No change. See Section 8.3.

B.8.4 References

1. U.S. Nuclear Regulatory Commission, Office of the Nuclear Material Safety and Safeguards, "Safety Evaluation of VECTRA Technologies' Response to Nuclear Regulatory Commission Bulletin 96-04 for NUHOMS®-24P and NUHOMS® 7P Dry Spent Fuel Storage System," November 1997 (Dockets 72-1004, 72-3, 72-4, 72-8, and 72-14).
2. NUREG-0612, "Control of Heavy Loads at Nuclear Power Plants," U.S. Nuclear Regulatory Commission, July 1980.
3. Transnuclear, Inc., Updated Final Safety Analysis Report, "Standardized NUHOMS® Horizontal Modular Storage Systems for Irradiated Nuclear Fuel," Revision 14, Docket 72-1004.
4. U.S. Nuclear Regulatory Commission, Interim Staff Guidance (ISG-22), "Potential Rod Splitting due to Exposures to an Oxidizing Atmosphere during Short-term Cask Loading Operations in LWR of Other Uranium Oxide Based Fuel."

TABLE OF CONTENTS

Page B.9-i

B.9 ACCEPTANCE TESTS AND MAINTENANCE PROGRAM

Chapter 9 applies in its entirety to this chapter, except for the leakage tests described in Section 9.1.3. The 32PTH Type 2 DSC design contains an inner and outer top cover, and a separate top shield plug; therefore, the leakage test procedure has been revised to reflect this geometry. This three-part closure design is the same as that is used in other NUHOMS[®] DSC canister designs.

B.9.1 Acceptance Criteria

B.9.1.1 Visual Inspection and Non-Destructive Examination (NDE)

No change from Chapter 9, Section 9.1.1.

B.9.1.2 Structural and Pressure Tests

No change from Chapter 9, Section 9.1.2.

B.9.1.3 Leak Tests

No change from Chapter 9, Section 9.1.3.

B.9.1.4 Components

No change from Chapter 9, Section 9.1.4.

B.9.1.5 Shielding Integrity

No change from Chapter 9, Section 9.1.5.

B.9.1.6 Thermal Acceptance

No change from Chapter 9, Section 9.1.6.

B.9.1.7 Neutron Absorber Tests

No change from Chapter 9, Section 9.1.7.

B.9.2 Maintenance Program

No change from Chapter 9, Section 9.2.

B.9.3 Marking

No change from Chapter 9, Section 9.3.

B.9.4 Pre-Operational Testing and Training Exercise

No change from Chapter 9, Section 9.4.

B.9.5 Specification for Neutron Absorbers

No change from Chapter 9, Section 9.5.

B.9.6 References

1. American Society for Nondestructive Testing, "Personnel Qualification and Certification in Nondestructive Testing," SNT-TC-1A, 1992.

APPENDIX B.10 RADIATION PROTECTION

TABLE OF CONTENTS

B.10	RADIATION PROTECTION	B.10-1
B.10.1	Ensuring That Occupational Radiation Exposures Are As Low As Reasonably Achievable (ALARA)	B.10-1
B.10.2	Radiation Protection Design Features	B.10-2
B.10.3	Estimated Onsite Collective Dose Assessment	B.10-3

B.10 RADIATION PROTECTION

B.10.1 Ensuring That Occupational Radiation Exposures Are As Low As Reasonably Achievable (ALARA)

No change.

B.10.2 Radiation Protection Design Features

The estimates of off-site dose rates in and around an independent spent fuel storage installation containing arrays (two generic arrays – 2x10 back-to-back array and 2-1x10 front-to-front array) of loaded HSM-Hs (each HSM-H containing a 32PTH DSC fully loaded with design basis fuel) during long term storage are presented in Section 10.2 of Chapter 10. As described in Chapter B.5, the authorized fuel content has not changed. The top and bottom canister shielding thicknesses, including the HSM-H door, have decreased; however the average HSM-H surface dose rates remain bounded by those around the HSM-H loaded with a 32PTH DSC. Therefore, the off-site dose estimates presented in Chapter 10 are applicable to the 32PTH Type 2 DSC.

B.10.3 Estimated Onsite Collective Dose Assessment

The estimates of occupational dose during the loading of a 32PTH DSC fully loaded with design basis fuel for long term storage in an HSM-H using an OS187H TC during transfer are presented in Section 10.3 of Chapter 10. As described in Chapter B.5, the differences in the design of the 32PTH Type 2 DSC and the OS187H Type 2 TC result in an increase about 49% in the dose rates at the surface top end. Some of the design changes result in a reduction in these near field dose rates. For the top end design option with separate shield plug and inner cover plate, the occupational exposure during decontamination operations is expected to be lower because the DSC top shield plug is not required to be decontaminated. Overall, the occupational exposure estimate presented in Chapter 10 is expected to increase by 60% when loading Type 2 DSC and Type 2 TC; temporary shielding and ALARA practices (distances, duration and number of workers) could be employed to minimize the occupational exposure.

APPENDIX B.11 ACCIDENT ANALYSIS

TABLE OF CONTENTS

B.11	ACCIDENT ANALYSIS	B.11-1
B.11.1	Introduction.....	B.11-1
B.11.2	Off-Normal Operation	B.11-2
B.11.3	Postulated Accident	B.11-3
B.11.3.1	Cask Drop	B.11-3
B.11.3.2	Earthquake	B.11-3
B.11.3.3	Tornado Wind and Tornado Missiles Effect on HSM-H.....	B.11-3
B.11.3.4	Tornado Wind and Tornado Missiles Effect on Transfer Cask.....	B.11-3
B.11.3.5	Flood	B.11-3
B.11.3.6	Blockage of HSM-H Air Inlet and Outlet Openings	B.11-3
B.11.3.7	Lightning.....	B.11-3
B.11.3.8	Fire/Explosion.....	B.11-4
B.11.4	References	B.11-5

B.11 ACCIDENT ANALYSIS

B.11.1 Introduction

No change from Chapter 11, Section 11.1.

B.11.2 Off-Normal Operation

No change from Chapter 11, Section 11.2.

B.11.3 Postulated Accident

No change from Chapter 11, Section 11.3.

B.11.3.1 Cask Drop

No change from Chapter 11, Section 11.3.1.

B.11.3.2 Earthquake

No change from Chapter 11, Section 11.3.2.

B.11.3.3 Tornado Wind and Tornado Missiles Effect on HSM-H

No change from Chapter 11, Section 11.3.3.

B.11.3.4 Tornado Wind and Tornado Missiles Effect on Transfer Cask

No change from Chapter A.11, Section A.11.3.4.

B.11.3.4.1 Penetration Resistance

No change from Chapter 11, Section 11.3.4.1.

B.11.3.4.2 Impact Stress Analysis

No change from Chapter A.11, Section A.11.3.4.2.

B.11.3.4.3 Accident Dose Calculation

No change from Chapter A.11, Section A.11.3.4.3.

B.11.3.4.4 Corrective Action

No change from Chapter A.11, Section A.11.3.4.4.

B.11.3.5 Flood

No change from Chapter 11, Section 11.3.5.

B.11.3.6 Blockage of HSM-H Air Inlet and Outlet Openings

No change from Chapter 11, Section 11.3.6.

B.11.3.7 Lightning

No change from Chapter 11, Section 11.3.7.

B.11.3.8 Fire/Explosion

No change from Chapter 11, Section 11.3.8.

B.11.4 References

No change from Chapter 11, Section 11.4.

APPENDIX B.12 OPERATING CONTROLS AND LIMITS

No change from Chapter 12.

APPENDIX B.13 QUALITY ASSURANCE

No change from Chapter 13.

APPENDIX B.14 DECOMMISSIONING

No change from Chapter 14.